NAS 1.9/4:33/11

TECHNOLOGY & SCIENCE
DETROIT PUBLIC LIBRARY

Scientific and Technical Aerospace Reports

RED SEAL

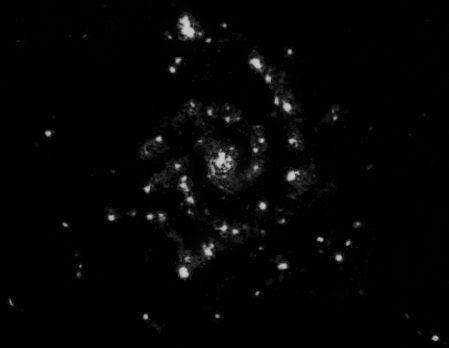

An Abstract Journal

NASA

Volume 33, Number 11
November 1995
N95-30358 to N95-32372

The NASA STI Office... in Profile

Since its founding, NASA has been dedicated to the advancement of aeronautics and space science. The NASA Scientific and Technical Information (STI) Office plays a key part in helping NASA maintain this important role.

The NASA STI Office provides access to the NASA STI Database, the largest collection of aeronautical and space science STI in the world. The Office is also NASA's institutional mechanism for disseminating the results of its research and development activities.

Specialized services that help round out the STI Office's diverse offerings include creating custom thesauri, building customized databases, organizing and publishing research results ... even providing videos.

For more information about the NASA STI Office, you can:

- **Phone** the NASA Access Help Desk at (301) 621-0390
- **Fax** your question to the NASA Access Help Desk at (301) 621-0134
- **E-mail** your question via the **Internet** to help@sti.nasa.gov
- **Write** to:

  NASA Access Help Desk
  NASA Center for AeroSpace Information
  800 Elkridge Landing Road
  Linthicum Heights, MD 21090-2934

DETROIT PUBLIC LIBRARY
3 5674 02477633 9

Scientific and Technical Aerospace Reports

Scientific and Technical Aerospace Reports (STAR), is published each month as a major product of the NASA Scientific and Technical Information (STI) Office.

Inside this issue you will find:

- **Front Matter** containing a typical citation and abstract sample explaining the standard format, including codes for ordering reports
- **An Abstract Section** containing citations and abstracts of reports and publications that provide comprehensive coverage of worldwide aerospace-related topics including aeronautics and space science technology. *STAR* lists published and publicly available reports entered into the NASA STI Database during the four weeks preceding publication of this issue. These citations and abstracts are listed by subject categories.
- **An Index Section**
  - Subject
  - Personal author
  - Corporate source
  - Contract number
  - Report number
- **An Appendix** containing a guide for ordering cited reports, registering with the NASA STI Office, and using the available products and services. Additionally, price schedules, phone numbers, and addresses are included in this information packed section.

NASA also sponsors the companion journal, *NASA Open Volumes on Aerospace (NOVA)*, which lists abstracts of the open literature on aerospace subjects available worldwide. *NOVA* is for internal NASA use only, available from the NASA Center for AeroSpace Information (CASI).

Entries found in *STAR* are available through the NASA online retrieval service, RECON.

The NASA STI Office gathers information through national and international agreements and exchanges and makes this information available to the NASA community and to the public in many forms through various outlets.

For additional information on the NASA STI Office, call the NASA Access Help Desk at (301) 621-0390, or write to:

NASA Center for AeroSpace Information
800 Elkridge Landing Road
Linthicum Heights, Maryland 21090-2934

US ISSN 0036-8741

DETROIT PUBLIC LIBRARY
DEC 1 2 1995
DEPOSITORY DOCUMENT

The New NASA Video Catalog is Here

Free!

To order your free copy call
the NASA Access Help Desk at
(301) 621-0390 or
fax to (301) 621-0134 or
e-mail to helpdesk@sti.nasa.gov

EXPLORE THE UNIVERSE

This publication was prepared by the NASA Center for AeroSpace Information,
800 Elkridge Landing Road, Linthicum Heights, MD 21090-2934, (301) 621-0390.

Volume 33 Number 11 / November 1995

TABLE OF CONTENTS

AERONAUTICS For related information see also *Astronautics.*

01 AERONAUTICS (GENERAL) **2741**

02 AERODYNAMICS **2742**
Includes aerodynamics of bodies, combinations, wings, rotors, and control surfaces; and internal flow in ducts and turbomachinery. For related information see also *34 Fluid Mechanics and Heat Transfer.*

03 AIR TRANSPORTATION AND SAFETY **2745**
Includes passenger and cargo air transport operations; and aircraft accidents. For related information see also *16 Space Transportation* and *85 Urban Technology and Transportation.*

04 AIRCRAFT COMMUNICATIONS AND NAVIGATION **2748**
Includes digital and voice communication with aircraft; air navigation systems (satellite and ground based); and air traffic control. For related information see also *17 Space Communications, Spacecraft Communications, Command and Tracking* and *32 Communications and Radar.*

05 AIRCRAFT DESIGN, TESTING AND PERFORMANCE **2750**
Includes aircraft simulation technology. For related information see also *18 Spacecraft Design, Testing and Performance* and *39 Structural Mechanics.* For land transportation vehicles see *85 Urban Technology and Transportation.*

06 AIRCRAFT INSTRUMENTATION **2753**
Includes cockpit and cabin display devices; and flight instruments. For related information see also *19 Spacecraft Instrumentation* and *35 Instrumentation and Photography.*

07 AIRCRAFT PROPULSION AND POWER **2753**
Includes prime propulsion systems and systems components, e.g., gas turbine engines and compressors; and onboard auxiliary power plants for aircraft. For related information see also *20 Spacecraft Propulsion and Power, 28 Propellants and Fuels,* and *44 Energy Production and Conversion.*

08 AIRCRAFT STABILITY AND CONTROL **2756**
Includes aircraft handling qualities; piloting; flight controls; and autopilots. For related information see also *05 Aircraft Design, Testing and Performance.*

09 RESEARCH AND SUPPORT FACILITIES (AIR) **2762**
Includes airports, hangars and runways; aircraft repair and overhaul facilities; wind tunnels; shock tubes; and aircraft engine test stands. For related information see also *14 Ground Support Systems and Facilities (Space).*

ASTRONAUTICS For related information see also *Aeronautics.*

12 ASTRONAUTICS (GENERAL) ..... **N.A.**
For extraterrestrial exploration see *91 Lunar and Planetary Exploration.*

13 ASTRODYNAMICS ..... **N.A.**
Includes powered and free-flight trajectories; and orbital and launching dynamics.

14 GROUND SUPPORT SYSTEMS AND FACILITIES (SPACE) ..... **N.A.**
Includes launch complexes, research and production facilities; ground support equipment, e.g., mobile transporters; and simulators. For related information see also *09 Research and Support Facilities (Air).*

15 LAUNCH VEHICLES AND SPACE VEHICLES **2764**
Includes boosters; operating problems of launch/space vehicle systems; and reusable vehicles. For related information see also *20 Spacecraft Propulsion and Power.*

16 SPACE TRANSPORTATION **2764**
Includes passenger and cargo space transportation, e.g., shuttle operations; and space rescue techniques. For related information see also *03 Air Transportation and Safety* and *18 Spacecraft Design, Testing and Performance.* For space suits see *54 Man/System Technology and Life Support.*

17 SPACE COMMUNICATIONS, SPACECRAFT COMMUNICATIONS, COMMAND AND TRACKING **2765**
Includes telemetry; space communications networks; astronavigation and guidance; and radio blackout. For related information see also *04 Aircraft Communications and Navigation* and *32 Communications and Radar.*

N.A.—No abstracts were assigned to this category for this issue.

18 SPACECRAFT DESIGN, TESTING AND PERFORMANCE **2765**
Includes satellites; space platforms; space stations; spacecraft systems and components such as thermal and environmental controls; and attitude controls. For life support systems see *54 Man/System Technology and Life Support.* For related information see also *05 Aircraft Design, Testing and Performance, 39 Structural Mechanics,* and *16 Space Transportation.*

19 SPACECRAFT INSTRUMENTATION ..... **N.A.**
For related information see also *06 Aircraft Instrumentation* and *35 Instrumentation and Photography.*

20 SPACECRAFT PROPULSION AND POWER **2768**
Includes main propulsion systems and components, e.g., rocket engines; and spacecraft auxiliary power sources. For related information see also *07 Aircraft Propulsion and Power, 28 Propellants and Fuels, 44 Energy Production and Conversion,* and *15 Launch Vehicles and Space Vehicles.*

CHEMISTRY AND MATERIALS

23 CHEMISTRY AND MATERIALS (GENERAL) **2771**

24 COMPOSITE MATERIALS **2783**
Includes physical, chemical, and mechanical properties of laminates and other composite materials. For ceramic materials see *27 Nonmetallic Materials.*

25 INORGANIC AND PHYSICAL CHEMISTRY **2791**
Includes chemical analysis, e.g., chromatography; combustion theory; electrochemistry; and photochemistry. For related information see also *77 Thermodynamics and Statistical Physics.*

26 METALLIC MATERIALS **2802**
Includes physical, chemical, and mechanical properties of metals, e.g., corrosion; and metallurgy.

27 NONMETALLIC MATERIALS **2811**
Includes physical, chemical, and mechanical properties of plastics, elastomers, lubricants, polymers, textiles, adhesives, and ceramic materials. For composite materials see *24 Composite Materials.*

28 PROPELLANTS AND FUELS **2825**
Includes rocket propellants, igniters and oxidizers; their storage and handling procedures; and aircraft fuels. For related information see also *07 Aircraft Propulsion and Power, 20 Spacecraft Propulsion and Power,* and *44 Energy Production and Conversion.*

29 MATERIALS PROCESSING **2837**
Includes space-based development of products and processes for commercial application. For biological materials see *55 Space Biology:*

ENGINEERING For related information see also *Physics.*

31 ENGINEERING (GENERAL) **2838**
Includes vacuum technology; control engineering; display engineering; cryogenics; and fire prevention.

32 COMMUNICATIONS AND RADAR **2845**
Includes radar; land and global communications; communications theory; and optical communications. For related information see also *04 Aircraft Communications and Navigation* and *17 Space Communications, Spacecraft Communications, Command and Tracking.* For search and rescue see *03 Air Transportation and Safety,* and *16 Space Transportation.*

33 ELECTRONICS AND ELECTRICAL ENGINEERING **2858**
Includes test equipment and maintainability; components, e.g., tunnel diodes and transistors; microminiaturization; and integrated circuitry. For related information see also *60 Computer Operations and Hardware* and *76 Solid-State Physics.*

34 FLUID MECHANICS AND HEAT TRANSFER **2866**
Includes boundary layers; hydrodynamics; fluidics; mass transfer and ablation cooling. For related information see also *02 Aerodynamics* and *77 Thermodynamics and Statistical Physics.*

35 INSTRUMENTATION AND PHOTOGRAPHY **2878**
Includes remote sensors; measuring instruments and gauges; detectors; cameras and photographic supplies; and holography. For aerial photography see *43 Earth Resources and Remote Sensing.* For related information see also *06 Aircraft Instrumentation* and *19 Spacecraft Instrumentation.*

36 LASERS AND MASERS **2882**
Includes parametric amplifiers. For related information see also *76 Solid-State Physics.*

37 MECHANICAL ENGINEERING **2887**
Includes auxiliary systems (nonpower); machine elements and processes; and mechanical equipment.

38 QUALITY ASSURANCE AND RELIABILITY **2891**
Includes product sampling procedures and techniques; and quality control.

39 STRUCTURAL MECHANICS **2892**
Includes structural element design and weight analysis; fatigue; and thermal stress. For applications see *05 Aircraft Design, Testing and Performance* and *18 Spacecraft Design, Testing and Performance.*

GEOSCIENCES For related information see also *Space Sciences.*

42 GEOSCIENCES (GENERAL) **2899**

43 EARTH RESOURCES AND REMOTE SENSING **2900**
Includes remote sensing of earth resources by aircraft and spacecraft; photogrammetry; and aerial photography. For instrumentation see *35 Instrumentation and Photography.*

44 ENERGY PRODUCTION AND CONVERSION **2902**
Includes specific energy conversion systems, e.g., fuel cells; global sources of energy; geophysical conversion; and windpower. For related information see also *07 Aircraft Propulsion and Power, 20 Spacecraft Propulsion and Power,* and *28 Propellants and Fuels.*

45 ENVIRONMENT POLLUTION **2907**
Includes atmospheric, noise, thermal, and water pollution.

46 GEOPHYSICS **2912**
Includes aeronomy; upper and lower atmosphere studies; ionospheric and magnetospheric physics; and geomagnetism. For space radiation see *93 Space Radiation.*

47 METEOROLOGY AND CLIMATOLOGY **2918**
Includes weather forecasting and modification.

48 OCEANOGRAPHY **2922**
Includes biological, dynamic, and physical oceanography; and marine resources. For related information see also *43 Earth Resources and Remote Sensing.*

LIFE SCIENCES

51 LIFE SCIENCES (GENERAL) **2925**

52 AEROSPACE MEDICINE **2926**
Includes physiological factors; biological effects of radiation; and effects of weightlessness on man and animals.

53 BEHAVIORAL SCIENCES **2928**
Includes psychological factors; individual and group behavior; crew training and evaluation; and psychiatric research.

54 MAN/SYSTEM TECHNOLOGY AND LIFE SUPPORT **2929**
Includes human engineering; biotechnology; and space suits and protective clothing. For related information see also *16 Space Transportation.*

55 SPACE BIOLOGY ..... **N.A.**
Includes exobiology; planetary biology; and extraterrestrial life.

MATHEMATICAL AND COMPUTER SCIENCES

59 MATHEMATICAL AND COMPUTER SCIENCES (GENERAL) **2931**

60 COMPUTER OPERATIONS AND HARDWARE **2931**
Includes hardware for computer graphics, firmware, and data processing. For components see *33 Electronics and Electrical Engineering.*

61 COMPUTER PROGRAMMING AND SOFTWARE **2932**
Includes computer programs, routines, algorithms, and specific applications, e.g., CAD/CAM.

62 COMPUTER SYSTEMS **2947**
Includes computer networks and special application computer systems.

63 CYBERNETICS **2949**
Includes feedback and control theory, artificial intelligence, robotics and expert systems. For related information see also *54 Man/System Technology and Life Support.*

64 NUMERICAL ANALYSIS **2954**
Includes iteration, difference equations, and numerical approximation.

65 STATISTICS AND PROBABILITY **2963**
Includes data sampling and smoothing; Monte Carlo method; and stochastic processes.

66 SYSTEMS ANALYSIS **2964**
Includes mathematical modeling; network analysis; and operations research.

67 THEORETICAL MATHEMATICS **2964**
Includes topology and number theory.

PHYSICS For related information see also *Engineering.*

70 PHYSICS (GENERAL) **2966**
For precision time and time interval (PTTI) see *35 Instrumentation and Photography*; for geophysics, astrophysics or solar physics see *46 Geophysics, 90 Astrophysics*, or *92 Solar Physics.*

71 ACOUSTICS **2973**
Includes sound generation, transmission, and attenuation. For noise pollution see *45 Environment Pollution.*

72 ATOMIC AND MOLECULAR PHYSICS **2975**
Includes atomic structure, electron properties, and molecular spectra.

73 NUCLEAR AND HIGH-ENERGY PHYSICS **2991**
Includes elementary and nuclear particles; and reactor theory. For space radiation see *93 Space Radiation.*

74 OPTICS **2995**
Includes light phenomena and optical devices. For lasers see *36 Lasers and Masers.*

75 PLASMA PHYSICS **3003**
Includes magnetohydrodynamics and plasma fusion. For ionospheric plasmas see *46 Geophysics.* For space plasmas see *90 Astrophysics.*

76 SOLID-STATE PHYSICS **3008**
Includes superconductivity. For related information see also *33 Electronics and Electrical Engineering* and *36 Lasers and Masers.*

77 THERMODYNAMICS AND STATISTICAL PHYSICS **3017**
Includes quantum mechanics; theoretical physics; and Bose and Fermi statistics. For related information see also *25 Inorganic and Physical Chemistry* and *34 Fluid Mechanics and Heat Transfer.*

SOCIAL SCIENCES

80 SOCIAL SCIENCES (GENERAL) **3021**
Includes educational matters.

81 ADMINISTRATION AND MANAGEMENT **3021**
Includes management planning and research.

82 DOCUMENTATION AND INFORMATION SCIENCE **3022**
Includes information management; information storage and retrieval technology; technical writing; graphic arts; and micrography. For computer documentation see *61 Computer Programming and Software.*

83 ECONOMICS AND COST ANALYSIS ..... **N.A.**
Includes cost effectiveness studies.

84 LAW, POLITICAL SCIENCE AND SPACE POLICY ..... **N.A.**
Includes NASA appropriation hearings; aviation law; space law and policy; international law; international cooperation; and patent policy.

85 URBAN TECHNOLOGY AND TRANSPORTATION **3027**
Includes applications of space technology to urban problems; technology transfer; technology assessment; and surface and mass transportation. For related information see *03 Air Transportation and Safety, 16 Space Transportation,* and *44 Energy Production and Conversion.*

SPACE SCIENCES For related information see also *Geosciences.*

88 SPACE SCIENCES (GENERAL) 3028

89 ASTRONOMY 3028
Includes radio, gamma-ray, and infrared astronomy; and astrometry.

90 ASTROPHYSICS 3028
Includes cosmology; celestial mechanics; space plasmas; and interstellar and interplanetary gases and dust. For related information see also *75 Plasma Physics.*

91 LUNAR AND PLANETARY EXPLORATION 3030
Includes planetology; and manned and unmanned flights. For spacecraft design or space stations see *18 Spacecraft Design, Testing and Performance.*

92 SOLAR PHYSICS 3030
Includes solar activity, solar flares, solar radiation and sunspots. For related information see also *93 Space Radiation.*

93 SPACE RADIATION 3032
Includes cosmic radiation; and inner and outer earth's radiation belts. For biological effects of radiation see *52 Aerospace Medicine.* For theory see *73 Nuclear and High-Energy Physics.*

GENERAL

Includes aeronautical, astronautical, and space science related histories, biographies, and pertinent reports too broad for categorization; histories or broad overviews of NASA programs.

99 GENERAL 3032

SUBJECT INDEX I-1

PERSONAL AUTHOR INDEX I-133

CORPORATE SOURCE INDEX I-147

CONTRACT NUMBER INDEX I-169

REPORT NUMBER INDEX I-173

APPENDIX A-1

TYPICAL CITATION AND ABSTRACT

NASA SPONSORED — ON MICROFICHE

ACCESSION NUMBER → N95-10148*# National Aeronautics and Space Administration. Lewis Research Center, Cleveland, OH. ← CORPORATE SOURCE

TITLE → **EFFECTS OF A FORWARD-SWEPT FRONT ROTOR ON THE FLOWFIELD OF A COUNTERROTATION PROPELLER**

AUTHORS → M. Nallasamy (NYMA, Inc., Brook Park, OH.) and Gary G. Podboy Aug. 1994 19 p Presented at the 30th Joint Propulsion Conference, Indianapolis, IN, 27-29 Jun. 1994; sponsored by AIAA, ASME, SAE, and ASEE ← PUBLICATION DATE

CONTRACT OR GRANT → (Contract NAS3-27186; RTOP 538-03-11)

REPORT NUMBERS → (NASA-TM-106671; E-8994; NAS 1.15:106671; AIAA Paper 94-2694) Avail: CASI HC A03/MF A01; 6 functional color pages ← AVAILABILITY SOURCE AND PRICE CODE

The effects of a forward-swept front rotor on the flowfield of a counterrotation model propeller at takeoff conditions at zero degree angle of attack are studied by solving the unsteady three-dimensional Euler equations. The configuration considered is an uneven blade count counterrotation model with twelve forward-swept blades on the fore rotor and ten aft-swept blades on the aft rotor. The flowfield is compared with that of a reference aft-swept counterrotation geometry and Laser Doppler Velocimeter (LDV) measurements. At the operating conditions considered, the forward-swept blade experiences a higher tip loading and produces a stronger tip vortex compared to the aft-swept blade, consistent with the LDV and acoustic measurements. Neither the solution nor the LDV data indicated the formation of a leading edge vortex. The predicted radial distribution of the circumferentially averaged axial velocity at the measurement station agreed very closely with LDV data, while crossflow velocities showed poor agreement. The discrepancy between prediction and LDV data of tangential and radial velocities is due in part to the insufficient mesh resolution in the region between the rotors and in the tip region to track the tip vortex. The vortex is diffused by the time it arrives at the measurement station. The uneven blade count configuration requires the solution to be carried out for six blade passages of the fore rotor and five passages of the aft rotor, thus making grid refinement prohibitive.

Author

VOLUME 33 NUMBER 11 / November 1995

Scientific and Technical Aerospace Reports

A Monthly Publication of the National Aeronautics and Space Administration

01 AERONAUTICS (GENERAL)

N95-31000*# National Aeronautics and Space Administration. Langley Research Center, Hampton, VA.
PATTERNS IN THE SKY: NATURAL VISUALIZATION OF AIRCRAFT FLOW FIELDS
James F. Campbell and Joseph R. Chambers 1994 162 p Original contains color illustrations
(NASA-SP-514; NAS 1.21:514) Avail: CASI HC A08/MF A02; 118 functional color pages

The objective of the current publication is to present the collection of flight photographs to illustrate the types of flow patterns that were visualized and to present qualitative correlations with computational and wind tunnel results. Initially in section 2, the condensation process is discussed, including a review of relative humidity, vapor pressure, and factors which determine the presence of visible condensate. Next, outputs from computer code calculations are postprocessed by using water-vapor relationships to determine if computed values of relative humidity in the local flow field correlate with the qualitative features of the in-flight condensation patterns. The photographs are then presented in section 3 by flow type and subsequently in section 4 by aircraft type to demonstrate the variety of condensed flow fields that was visualized for a wide range of aircraft and flight maneuvers. Author

N95-31598# Federal Aviation Administration, Washington, DC. Office of Aviation Policy and Plans.
FAA AVIATION FORECASTS: FISCAL YEAR 1995-2006
Mar. 1995 243 p
(AD-A293682; FAA-APO-95-1) Avail: CASI HC A11/MF A03

This report contains the Fiscal Years 1995-2006 Federal Aviation Administration (FAA) forecasts of aviation activity at FAA facilities. These include airports with FAA control towers, air route traffic control centers, and flight service stations. Detailed forecasts were made for the major users of the National Aviation System: air carriers, air taxi/ commuters, military, and general aviation. The forecasts have been prepared to meet the budget and planning needs of the constituent units of the FAA and to provide information that can be used by state and local authorities, the aviation industry, and the general public. The outlook for the 12-year forecast period is for moderate economic growth, stable real fuel prices, modest inflation, and continued moderate to strong growth in the demand for aviation services. Based on these assumptions, aviation activity is forecast to increase by 19.7 percent at FAA towered airports (352 airports) and 26.0 percent at air route traffic control centers. The general aviation active fleet is forecast to decline by 0.8 percent during the forecast period but increased utilization (hours flown by aircraft) results in a 12.0 percent increase in general aviation hours flown during same period. Scheduled domestic revenue passenger miles (RPM's) are forecast to increase 60.5 percent, scheduled international RPM's are forecast to increase by 97.2 percent, and regional/commuter RPM's are forecast to increase by 154.1 percent. DTIC

N95-32164# Lawrence Livermore National Lab., Livermore, CA.
MAPPING HIDDEN AIRCRAFT DEFECTS WITH DUAL-BAND INFRARED COMPUTED TOMOGRAPHY
Nancy K. DelGrande and Philip F. Durbin 3 Apr. 1995 14 p Presented at the Conference on Nondestructive Evaluation of Aging Infrastructure, Oakland, CA, 6-8 Jun. 1995
(Contract W-7405-eng-48)
(DE95-011531; UCRL-JC-120546; CONF-9506126-2) Avail: CASI HC A03/MF A01

Infrared computed tomography (IRCT) is a promising, non-contact, nondestructive evaluation tool used to inspect the mechanical integrity of large structures. We describe on-site, proof-of-principle demonstrations of IRCT to inspect defective metallic and composite structures. The IRCT system captures time sequences of heat-stimulated, dual-band infrared (DBIR) thermal maps for flash-heated and naturally-heated targets. Our VIEW algorithms produce co-registered thermal, thermal inertia, and thermal-timegram maps from which we quantify the percent metal-loss corrosion damage for airframes and the defect sites, depths, and host-material physical properties for composite structures. The IRCT method clarifies the type of defect, e.g., corrosion, fabrication, foreign-material insert, delamination, unbond, void, and quantifies the amount of damage from the defect, e.g., the percent metal-loss from corrosion in metal structures, the depth, thickness, and areal extent of heat damage in multi-layered composite materials. Potential long-term benefits of IRCT technology are in-service monitoring of incipient corrosion damage, to avoid catastrophic failure and production-monitoring of cure states for composite materials. DOE

N95-32194# General Accounting Office, Washington, DC. National Security and International Affairs Div.
REPORT TO THE CHAIRMAN, LEGISLATION AND NATIONAL SECURITY SUBCOMMITTEE, COMMITTEE ON GOVERNMENT OPERATIONS, HOUSE OF REPRESENTATIVES. C-17 AIRCRAFT PROGRAM: IMPROVEMENTS IN INITIAL PROVISIONING PROCESS
21 Jan. 1994 11 p
(GAO/NSIAD-94-63; B-255832) Avail: CASI HC A03/MF A01; GAO, PO Box 6015, Gaithersburg, MD 20877 HC

This GAO report is an updated review of the Air Force's initial provisioning of spare parts for the C-17 military transport aircraft. Since 1989, when it began initial provisioning for the C-17 aircraft program, the Air Force has frequently ordered spare parts prematurely. As of July 1993, the Air Force had $111.2 million of C-17 spare parts on order. These premature procurements were made under a DOD policy that called for maximizing procurement of support items for the provisioning period. Within the framework of this policy, this report finds that premature ordering occurred because the Air Force: used inaccurate and outdated information to determine how many spare parts to buy and when to buy them; bought quantities of spare parts that were higher than computed stockage levels justified; and failed to follow regulations that governed the initial provisioning process. DOD has recently revised its provisioning guidance to stress the need to limit the initial procurement of spare parts, thereby minimizing cost. Derived from text

N95-32198# General Accounting Office, Washington, DC. National Security and International Affairs Div.
REPORT TO CONGRESSIONAL COMMITTEES. MILITARY AIRLIFT: C-17 SETTLEMENT IS NOT A GOOD DEAL
15 Apr. 1994 18 p
(GAO/NSIAD-94-141; B-256721) Avail: CASI HC A03/MF A01; GAO, PO Box 6015, Gaithersburg, MD 20877 HC

This report deals with the status of the C-17 program, with emphasis on DoD's proposed settlement agreement with McDonnell Douglas, the prime contractor on the C-17 aircraft. It also discusses DOD's efforts to identify alternatives to the C-17 program. Rising program costs, less than anticipated performance, and lengthy delays in this concurrent acquisition

program raise serious doubts about the C-17's cost-effectiveness and undermine the program's credibility. Despite these problems, DOD has proposed a settlement with McDonnell Douglas that, in our opinion, is not in the best interest of the government. Although the true cost is not known, the settlement identifies the cost to the government and the contractor as $348 million and $454 million, respectively. Under the proposed settlement, DOD would delay the decision on the number of C-17's to be procured until November 1995; it would also, in effect, delay the decision on the most cost-effective mix of aircraft for meeting its airlift requirements until that time. Most of the benefits of the contractor's management and productivity improvements called for in the settlement will not be realized until 1996 or beyond. We are also concerned that DOD has not established specific cost, schedule, and performance criteria to evaluate McDonnell Douglas' performance and to decide whether to purchase more than 40 aircraft. CASI

02 AERODYNAMICS

Includes aerodynamics of bodies, combinations, wings, rotors, and control surfaces; and internal flow in ducts and turbomachinery.

For related information see also *34 Fluid Mechanics and Heat Transfer.*

N95-30448 University of Southern California, Los Angeles, CA.
FLOW MODELS FOR THE DESIGN OF A HYPERSONIC IODINE VAPOR WIND TUNNEL NOZZLE WITH CHEMICAL AND VIBRATIONAL NONEQUILIBRIUM EFFECTS Ph.D. Thesis
Marty Keith Bradley 1994
Avail: Issuing Activity (Univ. of Southern California, Doheny Library, Micrographics Dept., Los Angeles, CA 90089-0182)

A hypersonic iodine wind tunnel facility (H.I.T.) is being built at the University of Southern California (U.S.C.) to study hypersonic nonequilibrium flow. A detailed model for iodine nozzle flow with vibrational as well as chemical nonequilibrium has been developed to assess the impact of vibrational nonequilibrium in the wind tunnel nozzle. Each discrete vibrational level is treated as a separate species and reaction rate expressions are developed for vibration-vibration (V-V), vibration-translation (V-T), and dissociation reactions using various reaction rate models. Vibrational equilibrium, harmonic oscillator, SSH, and modified SSH thermodynamic and reaction rate models have been developed for iodine. One-dimensional and two-dimensional finite-rate chemistry nozzle calculations have been made using the LPP (Liquid Performance Program) nozzle analysis code. In the SSH and modified SSH models, V-T transitions were found to be dominant when compared to V-V transitions, and population inversions were created downstream in the nozzle in vibrational levels above about ten for the harmonic oscillator, SSH, and modified SSH models. Results from these calculations have been compared to data from an iodine freejet test. The sensitivity of the wind tunnel nozzle exit flow profile to the various nonequilibrium flow models has also been determined. Based on these results and considering the effects of vibrational nonequilibrium and boundary layer state, a nozzle contour has been designed that will produce near-uniform flow properties for the first H.I.T. nozzle, despite any uncertainties present in the chemistry, vibration, or boundary layer flow models. Dissert. Abstr.

N95-30611*# United Technologies Research Center, East Hartford, CT.
DEVELOPMENT OF A LINEARIZED UNSTEADY EULER ANALYSIS FOR TURBOMACHINERY BLADE ROWS Final Contractor Report
Joseph M. Verdon, Matthew D. Montgomery, and Kenneth A. Kousen Jun. 1995 107 p
(Contract NAS3-25425; RTOP 505-62-10)
(NASA-CR-4677; E-9575; NAS 1.26:4677; R95-970293) Avail: CASI HC A06/MF A02

A linearized unsteady aerodynamic analysis for axial-flow turbomachinery blading is described in this report. The linearization is based on the Euler equations of fluid motion and is motivated by the need for an efficient aerodynamic analysis that can be used in predicting the aeroelastic and aeroacoustic responses of blade rows. The field equations and surface conditions required for inviscid, nonlinear and linearized, unsteady aerodynamic analyses of three-dimensional flow through a single, blade row operating within a cylindrical duct, are derived. An existing numerical algorithm for determining time-accurate solutions of the nonlinear unsteady flow problem is described, and a numerical model, based upon this nonlinear flow solver, is formulated for the first-harmonic linear unsteady problem. The linearized aerodynamic and numerical models have been implemented into a first-harmonic unsteady flow code, called LINFLUX. At present this code applies only to two-dimensional flows, but an extension to three-dimensions is planned as future work. The three-dimensional aerodynamic and numerical formulations are described in this report. Numerical results for two-dimensional unsteady cascade flows, excited by prescribed blade motions and prescribed aerodynamic disturbances at inlet and exit, are also provided to illustrate the present capabilities of the LINFLUX analysis. Author

N95-30638# Technische Univ., Delft (Netherlands). Inst. for Wind Energy.
AXIAL LOADS ON YAWED ROTORS
G. J. W. vanBussel Nov. 1993 28 p
(PB95-214193; IW-93073R) Avail: CASI HC A03/MF A01

Under the assumption of incompressible, inviscid and irrotational flow, it can be shown that the pressure perturbation in the complete flow field is given by a Laplace equation and acts as an acceleration potential function. The rotor blades are represented in the model as discrete surfaces on which a pressure discontinuity is present. Spanwise and chordwise pressure distributions are present, which are composed of analytical asymptotic solutions for the Laplace equation. This model is implemented in the PREDICHAT and PREDICDYN computer code series for steady and dynamic inflow cases respectively. Dynamic inflow concerns with large scale unsteady rotor aerodynamics, such as coherent wind gusts, collective blade pitch and rotor speed variations. PREDICDYN is at present extended for the investigation of yawed flow. Axial induction velocities and axial load distributions are determined with this method and compared with yawed flow momentum theory extensions. NTIS

N95-30704*# National Aeronautics and Space Administration. Lewis Research Center, Cleveland, OH.
VALIDATION OF THE NPARC CODE FOR NOZZLE AFTERBODY FLOWS AT TRANSONIC SPEEDS
James R. DeBonis, Nicholas J. Georgiadis, and Crawford F. Smith (NYMA, Inc., Brook Park, OH.) Jul. 1995 28 p Presented at the 31st Joint Porpulsion Conference and Exhibit, San Diego, CA, 10-12 Jul. 1995; sponsored by AIAA, ASME, SAE, and ASEE
(Contract NAS3-27186; RTOP 537-02-00)
(NASA-TM-106971; E-9732; NAS 1.15:106971; AIAA Paper 95-2614)
Avail: CASI HC A03/MF A01

The NPARC code, a Reynolds-averaged full Navier-Stokes code, was validated for nozzle afterbody (boatail) flow fields at transonic speeds. The flow fields about three geometries were studied: an axisymmetric nozzle with attached flow; an axisymmetric nozzle with separated flow: and a two-dimensional (rectangular) nozzle with separated flow. Three turbulence models, Baldwin-Lomax, Baldwin-Barth, and Chien k-epsilon, were used to determine the effect of turbulence model selection on the flow field solution. Static pressure distributions on the nozzle surfaces and pitot pressure measurements in the exhaust plume were examined. Results from the NPARC code compared very well with experimental data for all cases. For attached flow fields, the effect of the turbulence models showed no discernable differences. The Baldwin-Barth model yielded better results than either the Chien k-epsilon or the Baldwin-Lomax model for separated flow fields. Author

N95-30712*# National Aeronautics and Space Administration. Marshall Space Flight Center, Huntsville, AL.
TRANSONIC AERODYNAMIC CHARACTERISTICS OF A PROPOSED WING-BODY REUSABLE LAUNCH VEHICLE CONCEPT
A. M. Springer Washington Mar. 1995 111 p
(NASA-TM-108489; NAS 1.15:108489) Avail: CASI HC A06/MF A02

A proposed wing-body reusable launch vehicle was tested in the NASA Marshall Space Flight Center's 14 x 14-inch trisonic wind tunnel during the winter of 1994. This test resulted in the vehicle's subsonic and transonic, Mach 0.3 to 1.96, longitudinal and lateral aerodynamic characteristics. The effects of control surface deflections on the basic vehicle's aerodynamics, including a body flap, elevons, ailerons, and tip fins, are presented. Author

N95-30788*# National Aeronautics and Space Administration. Ames Research Center, Moffett Field, CA.

FLIGHT TEST EVALUATION OF THE STANFORD UNIVERSITY/UNITED AIRLINES DIFFERENTIAL GPS CATEGORY 3 AUTOMATIC LANDING SYSTEM

David N. Kaufmann and B. David NcNally Jun. 1995 475 p
(RTOP 505-64-13)
(NASA-TM-110354; A-950066; NAS 1.15:110354) Avail: CASI HC A20/MF A04

Test flights were conducted to evaluate the capability of Differential Global Positioning System (DGPS) to provide the accuracy and integrity required for International Civil Aviation Organization (ICAO) Category (CAT) 3 precision approach and landings. These test flights were part of a Federal Aviation Administration (FAA) program to evaluate the technical feasibility of using DGPS based technology for CAT 3 precision approach and landing applications. A United Airlines Boeing 737-300 (N304UA) was equipped with DGPS receiving equipment and additional computing capability provided by Stanford University. The test flights were conducted at NASA Ames Research Center's Crows Landing Flight Facility, Crows Landing, California. The flight test evaluation was based on completing 100 approaches and autolandings; 90 touch and go, and 10 terminating with a full stop. Two types of accuracy requirements were evaluated: 1) Total system error, based on the Required Navigation Performance (RNP), and 2) Navigation sensor error, based on ICAO requirements for the Microwave Landing System (MLS). All of the approaches and autolandings were evaluated against ground truth reference data provided by a laser tracker. Analysis of these approaches and autolandings shows that the Stanford University/United Airlines system met the requirements for a successful approach and autolanding 98 out of 100 approaches and autolandings, based on the total system error requirements as specified in the FAA CAT 3 Level 2 Flight Test Plan. Author

N95-30814# National Aerospace Lab., Amsterdam (Netherlands).

MULTIGRID CONVERGENCE ACCELERATION FOR THE 2D EULER EQUATIONS APPLIED TO HIGH-LIFT SYSTEMS

K. M. J. deCock 6 Jul. 1993 35 p Sponsored by Nederlands Inst.
(Contract NIVR-01308N)
(PB95-198081; NLR-TP-93301-U) Avail: CASI HC A03/MF A01

In this paper, a multigrid convergence acceleration technique for the two-dimensional Euler equations will be described. Applications to high-lift flows are made. The multigrid method is tested for this type of flow. NTIS

N95-30837# Technische Univ., Delft (Netherlands).

NUMERICAL INVESTIGATION INTO VORTICAL FLOW ABOUT A DELTA-WING CONFIGURATION UP TO INCIDENCES AT WHICH VORTEX BREAKDOWN OCCURS IN EXPERIMENT

J. I. vandenBerg, H. W. M. Hoeijmakers, and F. J. Brandsma 11 Nov. 1993 21 p
(Contract NIVR-07302N)
(PB95-198024; NLR-TP-93511-U) Copyright Avail: CASI HC A03/MF A01

To contribute to the development and validation of Euler methods for complete fighter configurations, numerical investigations are carried out into the flow for two generic configurations. Results are presented about a wing-alone and a wing-body configuration with a sharp-edged cropped delta wing for incidences in the range at which vortex breakdown occurs in experiment. Above the aft part of the wing-alone configuration, the structure of the vortex core undergoes a remarkable change, i.e., there is a switch-over in the sign of the vorticity vector as well as a sharp reduction of the axial velocity component, in a way similar to what occurs during vortex breakdown in experiment. For the wing-body configuration similar flow features are found, but only in the near wake. NTIS

N95-30843 Stanford Univ., CA.

COMPUTATION OF HIGH-ALTITUDE HYPERSONIC FLOW-FIELD RADIATION Ph.D. Thesis

Stephane Moreau 1994 438 p
Avail: Univ. Microfilms Order No. DA9422110

Accurate calculations of radiation on and from transatmospheric flight vehicles are currently a challenge to computational aerodynamicists. Due to combined effects of low density and hypersonic flight conditions, the gas in the shock-layer is in a state of thermal and chemical nonequilibrium. The present work aims at gathering existing ideas together about how such flows should be modeled and comparing them to recent, more accurate experiments that probe the separate energy modes of the different species of the gas in a more direct way than previously reported. Two recent Bow-Shock-Ultra-Violet flight experiments, and two recent shock-tube experiments are used to test the validity of the flow-field models implemented in the current state-of-the-art numerical codes. They involve highly non-equilibrium flow regimes in nitrogen and air with negligible ionization and provide detailed spectra emitted by the hot gas. A recent plasma torch experiment at Stanford, and the Cochise experiments at the Geophysics Directorate laboratories, have been the ideal experimental counterpart to test and improve the radiation calculation in the UV-visible spectral range and the IR region respectively. Each spectral region is used to probe several different aspects of the thermal and chemical nonequilibrium. A hierarchy of flow-field codes has been developed in conjunction with a greatly enhanced radiation code, termed NEQAIR2, to simulate these experiments. The flow-field codes involve axisymmetric Navier-Stokes and Burnett simulations around blunt-nose cones for the flight experiments and quasi-ID Euler simulations for the shock-tube experiments. They include between 5 and 8 chemical species and between 3 and 6 separate internal energy modes. The corresponding system of conservation equations are solved with finite volume, flux split algorithms. Gauss-Siedel line relaxation is used to increase efficiency of the fully-implicit method and exact numerical jacobians have been derived to increase the rate of convergence. The radiation code involves a collisional-radiative model based on a quasi-steady-state (QSS) approximation and a detailed line-by-line calculation for several atomic systems and molecular band systems. Comparisons of numerical spectra with the flight data show good agreement at the lower altitudes but the predictions are only within an order of magnitude at higher altitudes. Dissert. Abstr.

N95-30885# Lockheed Corp., Fort Worth, TX.

UNSTEADY TRANSONIC WIND TUNNEL TEST ON A SEMISPAN STRAKED DELTA WING, OSCILLATING IN PITCH. PART 1: DESCRIPTION OF THE MODEL, TEST SETUP, DATA ACQUISITION, AND DATA PROCESSING Final Report, Mar. 1989 - Dec. 1993

A. M. Cunningham, Jr., R. G. DenBoer, C. S. Dogger, E. G. Geurts, and A. P. Retel Dec. 1994 93 p
(Contract F33657-84-C-0247)
(AD-A293113; NLR-CR-93570L; WL-TR-94-3094) Avail: CASI HC A05/MF A01

A wind tunnel investigation was conducted in 1992 to investigate the unsteady aerodynamic aspects of transonic high incidence flows over a simple straked wing model. This test was designed to show how low speed vortex type flows evolve into complicated shock vortex interacting flows at transonic speeds. Requirements for this test were based on a low speed test conducted in 1986 on a full span model in the NLR Low Speed Tunnel. The transonic model was a semispan version of the low speed model with some modifications. It was equipped with a three-component semispan balance to measure total wing loads, seven rows of high response pressure transducers to measure unsteady pressures, and 15 vertical accelerometers to measure model motion and vibrations. The model was oscillated sinusoidally in pitch at various amplitudes and frequencies for mean model incidences varying from 4 to 48 deg. In addition, maneuver type transient motions of the model were tested with amplitudes of 16 and 30 deg total rotation at various starting angles. The test was conducted in the NLR HST in the Mach range of 0.225 to 0.90 with some preliminary vapor screen flow visualization data taken at M = 0.6 and 0.9. This part of the report presents a description of the model, test setup, data acquisition, and data processing. DTIC

N95-30929# Naval Surface Warfare Center, Silver Spring, MD.

HYPERVELOCITY WIND TUNNEL NUMBER 9, HIGH MACH NUMBER DEVELOPMENT PROGRAM Final Report

Melissa A. Lederer 5 Dec. 1994 85 p
(AD-A289934; NSWCDD/TR-94/96) Avail: CASI HC A05/MF A01

This report describes the results of the high Mach Number Development program performed at the White Oak, Maryland site of the Dahlgren Division, Naval Surface Warfare Center. The goal of this program was to expand the capabilities of the Hypervelocity Wind Tunnel Number 9 (Tunnel 9) to include operation at Mach 18. The constraints of this program involved

using the existing Mach 14 setup with as little modification as necessary. There were two major areas of interest for this program, the heater and the nozzle. The required supply temperature for Mach 18 operation is above the current capabilities of the Tunnel 9 Mach 14 heater. Utilizing supercooled flow conditions lowered the required supply temperature to within the Mach 14 heater capability. The current Mach 14 nozzle was used and the throat section was replaced with a new hardware set designed to achieve the correct nozzle throat-to-exit area ratio to obtain the higher Mach number. Forty-one runs were carried out in Tunnel 9 in support of this program. The Mach number capability in Tunnel 9 has been extended to Mach 16.5. For this condition the flow has a 30-inch test core with Pitot pressure deviations of -1.1% to + 1.3% and 3.5 seconds of good run time. A Mach 18 capability has also been investigated. Research efforts to achieve acceptable Mach 18 conditions are continuing. DTIC

N95-31715# National Aerospace Lab., Tokyo (Japan). Aeroengine Div.
EFFECTS OF CAVITY BLEED AND ITS CONFIGURATION ON AERODYNAMIC CHARACTERISTICS OF SUPERSONIC INTERNAL FLOW
Akira Murakami, Sigemi Shindo, Fumio Komiyama (Japanese Patent Office, Tokyo, Japan.), and Kimio Sakata Sep. 1994 18 p In JAPANESE Original contains color illustrations
(ISSN 0389-4010)
(NAL-TR-1247) Avail: CASI HC A03/MF A01

This paper presents experimental results of the effects of cavity bleed and its configuration on the supersonic internal flow field and the aerodynamic characteristics. The experiments were conducted in the supersonic heat transfer test facility of NAL using the partial model to simulate the supersonic internal compression passage of the mixed compression air-intake. The pressure recovery characteristics of five cavity configurations was obtained for the bleed mass flow rates. It was found that the cavity bleed was effective for the starting of the air-intake but the excessive cavity bleed aggravated the pressure recovery. The cavity configuration affected the characteristics of the pressure in the cavity bleed plenum for the bleed mass flow rates. Therefore, the optimum bleed mass flow rates for the maximum pressure recovery depended on the cavity configuration. Author

N95-31741# National Aerospace Lab., Tokyo (Japan). Aerodynamics Div.
SIDE FORCE ACTING ON BLUNTED CIRCULAR CYLINDER BODIES AT HIGH ANGLES OF ATTACK IN SUPERSONIC FLOW
Atsushi Tate, Mitsunori Watanabe, Junichi Noda, Hideo Sekine, and Takashi Yoshinaga Dec. 1994 22 p In JAPANESE
(ISSN 0389-4010)
(NAL-TR-1255) Avail: CASI HC A03/MF A01

To obtain data for stable recovery of future rocket boosters and the rocket itself, measurements of side force acting on blunted circular cylinders were carried out at high angles of attack (alpha less than 32 deg) in supersonic flows of several Mach numbers. The blunted circular heads, including a flat face and semi-elliptic shapes, were tested to determine the effects of nose shapes on side force. Highly blunted bodies close to a flat-faced cylinder show large side force as the Mach number decreases, while a flat-faced cylinder shows large side force in the narrow regions between M(sub infinity) = 1.75 and 2.25. Author

N95-31984*# National Aeronautics and Space Administration. Langley Research Center, Hampton, VA.
AFTERBODY/NOZZLE PRESSURE DISTRIBUTIONS OF A TWIN-TAIL TWIN-ENGINE FIGHTER WITH AXISYMMETRIC NOZZLES AT MACH NUMBERS FROM 0.6 TO 1.2
David J. Wing May 1995 214 p
(RTOP 505-59-30-04)
(NASA-TP-3509; L-17438; NAS 1.60:3509) Avail: CASI HC A10/MF A03

Distributions of static pressure coefficient over the afterbody and axisymmetric nozzles of a generic, twin-tail twin-engine fighter were obtained in the Langley 16-Foot Transonic Tunnel. The longitudinal positions of the vertical and horizontal tails were varied for a total of six aft-end configurations. Static pressure coefficients were obtained at Mach numbers between 0.6 and 1.2, angles of attack between 0 deg and 8 deg, and nozzle pressure ratios ranging from jet-off to 8. The results of this investigation indicate that the influence of the vertical and horizontal tails extends beyond the vicinity of the tail-afterbody juncture. The pressure distribution affecting the aft-end drag is influenced more by the position of the vertical tails than by the position of the horizontal tails. Transonic tail-interference effects are seen at lower free-stream Mach numbers at positive angles of attack than at an angle of attack of 0 deg. Author

N95-32188*# National Aeronautics and Space Administration. Ames Research Center, Moffett Field, CA.
NUMERICAL SOLUTION OF THE FULL POTENTIAL EQUATION USING A CHIMERA GRID APPROACH
Terry L. Holst Jul. 1995 33 p
(RTOP 505-59-53)
(NASA-TM-110360; A-950082; NAS 1.15:110360) Avail: CASI HC A03/MF A01

A numerical scheme utilizing a chimera zonal grid approach for solving the full potential equation in two spatial dimensions is described. Within each grid zone a fully-implicit approximate factorization scheme is used to advance the solution one interaction. This is followed by the explicit advance of all common zonal grid boundaries using a bilinear interpolation of the velocity potential. The presentation is highlighted with numerical results simulating the flow about a two-dimensional, nonlifting, circular cylinder. For this problem, the flow domain is divided into two parts: an inner portion covered by a polar grid and an outer portion covered by a Cartesian grid. Both incompressible and compressible (transonic) flow solutions are included. Comparisons made with an analytic solution as well as single grid results indicate that the chimera zonal grid approach is a viable technique for solving the full potential equation. Author

N95-32193*# MCAT Inst., San Jose, CA.
CONTROL OF UNSTEADY SEPARATED FLOW ASSOCIATED WITH THE DYNAMIC STALL OF AIRFOILS Final Report
M. C. Wilder 31 Jan. 1995 41 p Original contains color illustrations
(Contract NCC2-637)
(NASA-CR-198972; NAS 1.26:198972; MCAT-95-09) Avail: CASI HC A03/MF A01; 1 functional color page

An effort to understand and control the unsteady separated flow associated with the dynamic stall of airfoils was funded for three years through the NASA cooperative agreement program. As part of this effort a substantial data base was compiled detailing the effects various parameters have on the development of the dynamic stall flow field. Parameters studied include Mach number, pitch rate, and pitch history, as well as Reynolds number (through two different model chord lengths) and the condition of the boundary layer at the leading edge of the airfoil (through application of surface roughness). It was found for free stream Mach numbers as low as 0.4 that a region of supersonic flow forms on the leading edge of the suction surface of the airfoil at moderate angles of attack. The shocks which form in this supersonic region induce boundary-layer separation and advance the dynamic stall process. Under such conditions a supercritical airfoil profile is called for to produce a flow field having a weaker leading-edge pressure gradient and no leading-edge shocks. An airfoil having an adaptive-geometry, or dynamically deformable leading edge (DDLE), is under development as a unique active flow-control device. The DDLE, formed of carbon-fiber composite and fiberglass, can be flexed between a NACA 0012 profile and a supercritical profile in a controllable fashion while the airfoil is executing an angle-of-attack pitch-up maneuver. The dynamic stall data were recorded using point diffraction interferometry (PDI), a noninvasive measurement technique. A new high-speed cinematography system was developed for recording interferometric images. The system is capable of phase-locking with the pitching airfoil motion for real-time documentation of the development of the dynamic stall flow field. Computer-aided image analysis algorithms were developed for fast and accurate reduction of the images, improving interpretation of the results. Author

03 AIR TRANSPORTATION AND SAFETY

Includes passenger and cargo air transport operations; and aircraft accidents.

For related information see also *16 Space Transportation* and *85 Urban Technology and Transportation.*

N95-31061# Advisory Group for Aerospace Research and Development, Neuilly-Sur-Seine (France). Flight Vehicle Integration Panel.

FLIGHT VEHICLE INTEGRATION PANEL WORKSHOP ON PILOT INDUCED OSCILLATIONS [ATELIER SUR LE POMPAGE PILOTE]

Feb. 1995 117 p Workshop on Pilot Induced Oscillations of the Symposium on Active Control Technology, Turin, Italy, May 1994 (AGARD-AR-335; ISBN-92-836-1013-X) Copyright Avail: CASI HC A06/MF A02

Instability of the pilot/airframe combination has been a problem of manned flight. Rapid advances made in aviation following World War 2 greatly increased the incidence of PIO problems and the amount of research and development work aimed at understanding and mitigating these difficulties. Criteria and requirements were developed to be used in design to obtain satisfactory PIO qualities, but, in spite of all this work and the great flexibility in available modern control design technologies, PIO problems still often occur with new aircraft. It is clear that a universal solution of the PIO problem still evades the engineering community. The cost of these problems financially and in program delay is significant. This AGARD Flight Mechanics Workshop summary report contains presentations and discussions that aim toward the elimination and avoidance of PIO's by increasing the knowledge of PIO's and the problems associated with them. For individual titles, see N95-31062 through N95-31072.

N95-31062*# National Aeronautics and Space Administration. Hugh L. Dryden Flight Research Facility, Edwards, CA.

PIO: A HISTORICAL PERSPECTIVE

Duane T. McRuer (Systems Technology, Inc., Manhatten Beach, CA.) and R. E. Smith *In* Advisory Group for Aerospace Research and Development, Flight Vehicle Integration Panel Workshop on Pilot Induced Oscillations Feb. 1995 4 p (For primary document see N95-31061 11-03)

Copyright Avail: CASI HC A01/MF A02

These problems relating to Pilot Induced Oscillations have manifested themselves since the earliest days of manned flight. The earliest recorded examples of PIO date back to the Wright brothers first aircraft. The earliest filmed records date back to just prior to World War 2, with the XB-19 aircraft which suffered a pitch PIO just prior to touchdown. Four classes of PIO have been identified, into which all of the known incidents can be grouped. These are: (1) Essentially Single Axis, Extended Rigid Body Effective Vehicle Dynamics; (2) Essentially Single Axis, Extended Rigid Body with Significant Feel-Systern Manipulator Mechanical Control Elements; (3) Multiple Axis, Extended Rigid Body Effective Vehicle Dynamics; and (4) PIO's Involving Higher Frequency Modes. Derived from text

N95-31063*# National Aeronautics and Space Administration, Washington, DC.

THE PROCESS FOR ADDRESSING THE CHALLENGES OF AIRCRAFT PILOT COUPLING

Ralph AHarrah *In* Advisory Group for Aerospace Research and Development, Flight Vehicle Integration Panel Workshop on Pilot Induced Oscillations Feb. 1995 3 p (For primary document see N95-31061 11-03)

Copyright Avail: CASI HC A01/MF A02

The term 'Pilot Induced Oscillation' is misleading in that it places an undue emphasis on the role of the pilot in the process. Clearly, the phenomenon cannot occur in the absence of the pilot, but the term PIO suggests that the pilot is in some way responsible for the occurrence. He is not. The phenomenon may be better described by the title 'Aircraft-Pilot Coupling', or A-PC. This may be considered to better describe what is actually occurring when the pilot is trying to perform his normal function, i.e., that of controlling the aircraft which he is flying. For a designer, the objective should be to ensure that there is no possibility of A-PC occurring. Associated with this, the goal should also be to achieve Level 1 handling qualities. The key is to understand the Process involved in design and test and to ensure that this is exercised to achieve the objective. This has to be set alongside the management goals of better, faster and cheaper, in order that the manufacturer can remain competitive in the market. Derived from text

N95-31064# High Plains Engineering, Tehachapi, CA.

OBSERVATIONS ON PIO

Ralph H. Smith *In* Advisory Group for Aerospace Research and Development, Flight Vehicle Integration Panel Workshop on Pilot Induced Oscillations Feb. 1995 9 p (For primary document see N95-31061 11-03)

Copyright Avail: CASI HC A02/MF A02

Comparison of the handling characteristics of a Porsche with those expected from a modern combat type aircraft indicate that we accept significantly poorer handling performance with the aircraft than we would with a high performance road vehicle. The work which led to the evolution of the Smith-Geddes criteria stems from work performed for the USAF in relation to the F-15 aircraft. The logic that arrived at the criteria stemmed from a belief that the existing handling qualities criteria were inadequate for assessing the Pilot Induced Oscillation (PIO) susceptibility of an aircraft, and that the only successful way to test for this was to use the methods of Handling Qualities During Tracking (HQDT). The work which was performed was offered for the update of Mil 1797, but was not incorporated. This presentation concentrated on the understanding of PIO and the process by which it originates, using a simple model to demonstrate the characteristics which are inherent. The presentation also provided an explanation of the Smith-Geddes criteria, without resorting to the detail of the theories which support the criteria. The major thrust relates to the application to the assessment of PIO susceptibility and includes a commentary on the state of the control law development, together with the associated flight test technology. Derived from text

N95-31065# Hoh Aeronautics, Inc., Lomita, CA.

UNIFIED CRITERIA FOR ACT AIRCRAFT LONGITUDINAL DYNAMICS c05

Roger H. Hoh *In* Advisory Group for Aerospace Research and Development, Flight Vehicle Integration Panel Workshop on Pilot Induced Oscillations Feb. 1995 9 p (For primary document see N95-31061 11-03)

Copyright Avail: CASI HC A02/MF A02

This paper reports research done by USAF to adequately predict the susceptibility to pilot induced oscillation (PIO) and AGARD's response to the research. It discusses different criteria and characteristics that help to analyze PIO: the concept of phase delay, triggers, the effects of rate limiting, response characteristics and appropriate analysis techniques, and feel system influence. From the evidence presented by USAF, AGARD concludes that there is sufficient evidence that a PIO could be predicted, as could the effects of the bobweight. However, the impact of the actuation behavior may have had a dominant effect on the overall behavior of the aircraft. CASI

N95-31066# Gibson (J. C.), Saint Annes (England).

LOOKING FOR THE SIMPLE PIO MODEL

John C. Gibson *In* Advisory Group for Aerospace Research and Development, Flight Vehicle Integration Panel Workshop on Pilot Induced Oscillations Feb. 1995 11 p (For primary document see N95-31061 11-03)

Copyright Avail: CASI HC A03/MF A02

Eighteen years after the Tornado PIO (Pilot induced Oscillation) was successfully resolved, it seems inexplicable that similar PIO problems can still occur. For whatever reason, current formal methods are not working. The Vista F-16 is a powerful tool which should be put to use in establishing a universally acceptable set of criteria for the prevention of PIO by design. It should do this by determining the PIO qualities of a sufficiently wide range of linear and non-linear dynamic qualities, both in pitch and in roll, to establish a customer-defined set of Level boundary limits on whatever parameters are found best to quantify PIO. Only by doing this will it be possible to resolve the claims of the many competing criteria and guarantee a PIO-free future for all. It is not particularly difficult to identify the means. Derived from text

N95-31067# McDonnell-Douglas Aerospace, Long Beach, CA. Transport Aircraft Unit.

THE RELATION OF HANDLING QUALITIES RATINGS TO AIRCRAFT SAFETY

John Hodgkinson *In* Advisory Group for Aerospace Research and Development, Flight Vehicle Integration Panel Workshop on Pilot Induced Oscillations Feb. 1995 3 p (For primary document see N95-31061 11-03)

Copyright Avail: CASI HC A01/MF A02

The main theme of this presentation, is that of relating the handling qualities issues, and specifically the PIO, to aircraft safety. It is essential that the programme managers recognize that PIO is safety critical in that it is loss of control, and that when it is encountered, it is as dangerous as a structural failure of the airframe. Derived from text

N95-31068# Deutsche Forschungsanstalt fuer Luft- und Raumfahrt, Brunswick (Germany). Inst. fuer Flugmechanik.

SCARLET: DLR RATE SATURATION FLIGHT EXPERIMENT

Jennifer R. Martin and Joerg J. Buchholz *In* Advisory Group for Aerospace Research and Development, Flight Vehicle Integration Panel Workshop on Pilot Induced Oscillations Feb. 1995 6 p (For primary document see N95-31061 11-03)

Copyright Avail: CASI HC A02/MF A02

The time delay which arises due to rate limiting in a control system has been identified as a contributing factor to the occurrence of pilot induced oscillations (PIO's). Recent discussions concerning PIO prevention measures have proposed the elimination of this time delay through an alternate control scheme. In response to this proposal, the SCARLET (Saturated Command And Rate Limited Elevator Time delay) project was initiated in order to study the effects of both the time delay and the elimination scheme on the handling qualities of a contemporary fly-by-wire aircraft. A flight experiment was carried out in 1992 using DLR's ATTAS In-Flight Simulator. The flight test included runs with two different control laws: a conventional control scheme and the alternate control scheme (ACS). Results of the experiment demonstrated both the negative effect of rate saturation and the effectiveness of ACS to reduce the equivalent time delay and improve tracking performance. In order to further validate the concept of an alternate control scheme, the algorithms were adapted for use with a model-following control system. Pilot-in-the-loop simulations have shown improved performance through the use of ACS during rate saturated conditions. A second flight test will be performed this year in order to further evaluate the use of the alternate control scheme to eliminate the rate limit induced time delay and reduce the danger of PIO. Derived from text

N95-31069# Saab-Scania, Linkoeping (Sweden). Flight Control.

SAAB EXPERIENCE WITH PIO

E. Kullberg and Per-Olov Elgerona *In* Advisory Group for Aerospace Research and Development, Flight Vehicle Integration Panel Workshop on Pilot Induced Oscillations Feb. 1995 9 p (For primary document see N95-31061 11-03)

Copyright Avail: CASI HC A02/MF A02

The past experience in Sweden with PIO is reviewed, which had been so publicly witnessed with the second accident to the JAS-39 aircraft at the Stockholm Water Festival. Prior to commencing on the JAS-39 project, SAAB's experience of the PIO phenomenon had commenced with the J-35 aircraft. This aircraft had high stick sensitivity combined with a linear gearing of the stick to elevon. Following the PIO, the solution devised was to add a nonlinear gearing and improve the stability augmentation of the system. For the next aircraft project, the AJ-37 Viggen, significant work was performed on the handling qualities and resistance to PIO, based upon new information received during the 1960's from Ashkenas, McRuer, and A'Harrah. By 1963, Sweden had developed its own specification for flight control system design and for handling qualities. The latest versions of this AJ-37 aircraft have a digital flight control system. The AJ-37 Viggen has never experienced a problem with PIO in its service to date. The JAS-39 flight control system originated from demonstration work performed by SAAB on a FBW AJ-37 Viggen aircraft. This aircraft had been flown with instability levels of up to 4 percent chord at low Mach Number. This was the limit for this aircraft. Although this aircraft was reported to have experienced Level 2 or 3 handling, due to excessive time delays within the flight control system, it never experienced rate limiting or PIO. On this basis, it was deemed that there was sufficient knowledge and confidence to proceed with the JAS-39 aircraft project, and the JAS-39 specification was written around this experience, with a demanding handling qualities requirement. Derived from text

N95-31070# Department of the Air Force, California City, CA.

AEROELASTIC PILOT-IN-THE-LOOP OSCILLATIONS

W. J. Norton *In* Advisory Group for Aerospace Research and Development, Flight Vehicle Integration Panel Workshop on Pilot Induced Oscillations Feb. 1995 14 p (For primary document see N95-31061 11-03)

Copyright Avail: CASI HC A03/MF A02

Pilot-induced oscillation (PIO) is an unwanted and inadvertent closed-loop coupling between the pilot and one or more independent response variables of an aircraft. PIO typically results when the pilot attempts to perform a high gain tracking task using the usual cues of acceleration or attitude. Control system and aircraft characteristics within the bandwidth in which the pilot is active can contribute to a coupling between the pilot response and aircraft dynamics. The result is a neutrally damped or undamped out-of-control condition in which the pilot is often making intentional extreme and repetitive inputs in an effort to damp the motion but only serves to enhance it. Pilot-augmented oscillation (PAO) is an unintentional closed-loop coupling which does not involve a tracking task. Another aircraft variable which may lead to PIO or PAO is aeroelastic deformation of the vehicle structure. This elastic response can produce pilot cues or aircraft rigid body motion which can be enhanced when the pilot attempts to damp the oscillation and PIO results. Or, the elastic oscillations alone may lead to PAO. The potential for aeroelastic pilot-in-the-loop coupling is not widely recognized, and this can mean resources expended in ineffectual or nonoptimal solutions to the problem until the aeroelastic source is recognized. This paper will characterize the aeroelastic/pilot coupling phenomena without reproducing the fundamental research which has already been published on more general PIO. Examples of aeroelastic PIO and PAO will be provided to illustrate the various ways in which the phenomena can manifest itself, including recent experiences with the C-17A and the V-22. An examination of the potential for predicting this coupling will also be provided. Lastly, recommendations for flight test methodology to uncover and investigate aeroelastic pilot-in-the-loop coupling will be provided. Author

N95-31071# Deutsche Forschungsanstalt fuer Luft- und Raumfahrt, Brunswick (Germany). Inst. fuer Flugmechanik.

HANDLING QUALITIES ANALYSIS ON RATE LIMITING ELEMENTS IN FLIGHT CONTROL SYSTEMS **c08**

Dietrich Hanke *In* Advisory Group for Aerospace Research and Development, Flight Vehicle Integration Panel Workshop on Pilot Induced Oscillations Feb. 1995 18 p (For primary document see N95-31061 11-03)

Copyright Avail: CASI HC A03/MF A02

Rate saturation conditions caused by rate limiting elements (RLE's) in flight control systems can contribute to severe pilot induced oscillation. In order to gain more theoretical insight in this problem the paper deals with the development of rate limiter describing functions in order to establish a theoretical basis for open and closed loop handling qualities analysis in the frequency domain. Although rate limitation produces nonlinear system behaviour it could be shown that rate limiter describing functions could be applied to existing methods used in handling qualities analysis of pilot/aircraft systems. A new handling quality parameter, the rate limiter onset frequency, is defined as a measure of input amplitude and frequency. Here the onset frequency in reference to the system bandwidth could be a suitable parameter in defining handling qualities boundaries for flight control systems with RLE's. The response in amplitude and phase is presented for different types of input signals such as triangle and sinusoidal oscillations. Rate limiter cascading is considered, too. Further, the suitability of various existing handling quality criteria are compared with the RLE results especially with respect to PIO. Finally, the improvements in system behavior by applying an alternate control scheme (ACS), as proposed by A'Harrah, will be discussed. Derived from text

N95-31072# Chalk (Charles R.), Williamsville, NY.

CALSPAN EXPERIENCE OF PIO AND THE EFFECTS OF RATE LIMITING

Charles R. Chalk *In* Advisory Group for Aerospace Research and Development, Flight Vehicle Integration Panel Workshop on Pilot Induced

Oscillations Feb. 1995 12 p (For primary document see N95-31061 11-03)
Copyright Avail: CASI HC A03/MF A02

The experience of PIO within the Calspan Corporation is considerable, following a long standing interest in the subject. During this experience, the major concern that has been uncovered is that of the attitude towards the pilot following a PIO incident. There is still a tendency in many areas of aviation to consider a PIO as a failure of the pilot, whereas it must be properly regarded as a failure of the control system and its design process. Over a period of some years, the Calspan Corporation has undertaken a series of experiments with the NT-33A and Lear Jet aircraft to examine the effects of rate limiting compensating devices. The notes which follow summarize the presentation given on some of the aspects which have been investigated both analytically and experimentally in flight tests.

Derived from text

N95-31428# Federal Aviation Administration, Cambridge, MA.
AVIATION CAPACITY ENHANCEMENT PLAN 1994
1 Oct. 1994 364 p Limited Reproducibility: Document partially illegible
(AD-A292758; DOT/FAA/ASC-94-1) Avail: CASI HC A16/MF A03

A comprehensive review of Federal Aviation Administration programs intended to improve the capacity of the National Air Transportation System. The Plan identifies the causes and extent of capacity and delay problems currently associated with air travel in the U.S. and outlines various planned and ongoing FAA projects with the potential to reduce the severity of the problems in the future. The major areas of discussion are: (1) Airport Development; (2) Airport Capacity; (3) Airspace Capacity; (4) New Instrument Approach Procedures; (5) Technology for Capacity Improvement; and (6) Marketplace Solutions. DTIC

N95-31454# Naval Research Lab., Monterey, CA.
ENVIRONMENTAL SUPPORT OF NAVAL AVIATION Final Report
Sam Brand and Steven B. Dresksler Feb. 1995 64 p
(AD-A292873; NRL/MR/7543-94-7218) Avail: CASI HC A04/MF A01

A two-pronged approach to providing environmental support to Navy aviation is described. One approach focuses on flight safety and efficiency, and the other focuses on support to the tactical mission planner. Products are discussed in terms of requirements and the technical issues associated with the development or implementation of the products. This insight should be useful not only to the operational, tactical, and environmental communities, but to the R&D community as well. DTIC

N95-31512# Air Force Inst. of Tech., Wright-Patterson AFB, OH. School of Engineering.
PATIENT/AIRCRAFT FORECASTING FOR THE STRATEGIC AEROMEDICAL EVACUATION LIFT-BED PROCESS M.S. Thesis
Donald F. Kimminau Mar. 1995 90 p
(AD-A293902; AFIT/GOA/ENS/95M-04) Avail: CASI HC A05/MF A01

The goal of this research is to develop a tool for the Global Patient Movement Requirements Center (GPMRC) to efficiently forecast Aeromedical Evacuation (AE) aircraft and schedule patients in the lift-bed process. During a contingency, GPMRC is responsible for requesting required airlift, and providing lift-bed candidates to the Theater Patient Movement Requirements Center. The objective is to evacuate all waiting patients while minimizing the number of C-141 aircraft which must to be dedicated to the AE mission. In the solution process, a short-term forecast of patient movement requirements is input, including number of patients, bed and aircraft availability, and hub preferences. A mixed integer linear program is formulated, and solved. Upon reaching optimality or a user-specified node limit, the user analyzes the solution and determines if the search will be continued. At process completion, a solution file is produced which contains a feasible schedule which minimizes the number of dedicated C-141s required. The programs developed to assist the solution process were tested with 16 data sets. While optimal solutions are not guaranteed to be found for every case, the process quickly produces good, feasible solutions and provides timely, valuable information to GPMRC so it can request airlift and provide lift-bed candidates to appropriate agencies. DTIC

N95-31569# Federal Aviation Administration, Atlantic City, NJ.
CHEMICAL OPTIONS TO HALONS FOR AIRCRAFT USE Final Report
Robert E. Tapscott Feb. 1995 62 p
(AD-A293741; DOT/FAA/CT-95/9) Avail: CASI HC A04/MF A01

This report contains a summary of available fire suppression agents, their properties, and their applicability in the various aircraft applications. Classes of agents, with presently available agents listed, are recommended for use in the development of test protocols. The test protocol developed for a class of agents can be used, with minor modifications, to test all agents belonging to that class. DTIC

N95-31687# Arnold Engineering Development Center, Arnold AFS, TN.
ICING SIMULATION IN THE AEROPROPULSION SYSTEMS TEST FACILITY PROPULSION DEVELOPMENT TEST CELL C-2 Final Report, 13 - 23 May 1994
C. S. Bartlett Jan. 1995 49 p
(AD-A293039; AEDC-TR-94-12) Avail: CASI HC A03/MF A01

The AEDC Propulsion Development Test Cell C-2 has been modified to provide simulated altitude icing conditions. Spray droplet clouds with droplet mass median diameters simulating natural icing clouds are produced with calibrated water atomizing spray nozzles. The proper amount of liquid water ingested by an engine in flight through icing clouds is simulated by injection of the proper water content into the airstream that enters a test engine. The addition of the icing simulation spray system provides the opportunity to conduct simulated icing testing in the large engine test cell. The system is capable of providing icing testing of large engines, inlets, windshields, wings, and other full-scale test articles. The results of system activation testing have been summarized. The system can be used to initiate clouds and reach steady controlled spray operation within 10 sec. The system is capable of varying the liquid water content (LWC) over a five-to-one range within 10 sec. The simulation spray can be terminated within 5 sec. The uniformity of the distribution of the supercooled water at the test section has been determined. The transient response of the spray system and the ability to operate at extreme cold conditions for icing testing are improvements beyond previous AEDC icing simulation system capabilities. DTIC

N95-31687# Mitre Corp., McLean, VA. Center for Advanced Aviation System Development.
EFFECTS OF CIVIL TILTROTOR SERVICE IN THE NORTHEAST CORRIDOR ON EN ROUTE AIRSPACE LOADS Final Report
William W. Trigeiro, Xavier P. Szebrat, and Stephanie B. Fraser Oct. 1994 70 p Prepared in cooperation with NYMA, Inc.
(Contract DTFA01-93-C-0001)
(AD-A293586; MTR-94W0000150; DOT/FAA/AOR-100/94/008) Avail: CASI HC A04/MF A01

This report documents an analysis of the effects of the introduction of civil tiltrotor (CTR) service on en route airspace loads. The analysis is intended as one in a set of analyses designed to provide information to senior decision makers and other interested parties on the potential effects of CTR service on National Airspace System performance. The analysis uses a demand scenario that addresses the introduction of CTR services into the Northeast Corridor of the United States using several simplifying assumptions. This report also includes an update on the previously published report 'Civil Tiltrotor Northeast Corridor Delay Analysis (Based on the Demand Scenario Described in Civil Tiltrotor and Applications Phase 2: The Commercial Passenger Market).' This document is based on briefing materials developed to report on the results of this analysis. These briefing materials have not been expanded to the full text more typical of technical reports. Instead, this document contains copies of the briefing slides and the associated briefing text. DTIC

N95-31712# National Transportation Safety Board, Washington, DC.
ANNUAL REVIEW OF AIRCRAFT ACCIDENT DATA: US GENERAL AVIATION CALENDAR YEAR 1993
12 May 1995 84 p
(PB95-215828; NTSB/ARG-95/01) Avail: CASI HC A05/MF A01

This report presents a statistical compilation and review of general aviation accidents which occurred in 1993 in the United States, its territories and possessions and in international waters. The accidents reported are all those involving U.S. registered aircraft not conducting operations under 14 CFR 121, 14 CFR 127, or 14 CFR 135. This report is divided into five sections: All Accidents; Fatal Accidents; Serious Injury Accidents; Property Damage Accidents; and Midair Collision Accidents. Several tables present accident parameters for 1993 accidents only, and each section includes

tabulations which present comparative statistics for 1993 and for the nine-year period 1984-1992. Author

N95-31845# Federal Aviation Administration, Oklahoma City, OK. Civil Aeromedical Institute.
AIRCRAFT EVACUATIONS THROUGH TYPE-3 EXITS I: EFFECTS OF SEAT PLACEMENT AT THE EXIT Final Report
G. A. McLean, M. H. George, C. B. Chittum, and G. E. Funkhouser Jul. 1995 13 p
(DOT/FAA/AM-95/22) Avail: CASI HC A03/MF A01

Simulated emergency egress from Type 3 over-wing exits was studied to support regulatory action by the FAA. Passageway width and seat encroachment distance adjacent to the Type-3 exit were the major variables of interest. Two subject groups of differing mean ages were employed in a repeated-measures evaluation of different passageway widths leading to the exit in the CAMI aircraft cabin evacuation facility. Main effects of passageway width and seat encroachment distance on egress rates were determined using analysis of variance (ANOVA). Main effects were found for passageway width (p less than .001), seat encroachment distance (p less than .001), and subject group (p less than .001). The passageway width resulted from slowed egress at 6 and 10 inch wide passageway relative to 13, 15, and 20 inch passageways; seat encroachment effects were found for maximum seat encroachments but not midpoint and minimum encroachment distances. The subject group effects were found to result from a general increase in egress time for the older subject group. The placement of seat assemblies at the Type-3 exit has significant effects on passenger egress through the exit opening. Narrow passageways and/or large encroachments of the seat into the area of the exit opening delay egress significantly. Relative to the younger subjects, older subjects were found to have a general increase in egress times at all seat placement configurations that did not appear to worsen as the access route to the exit was made more restrictive. Author

N95-32185# National Transportation Safety Board, Washington, DC.
SPECIAL INVESTIGATION REPORT: SAFETY OF THE AIR TOUR INDUSTRY IN THE UNITED STATES
1 Jun. 1995 63 p
(PB95-917004; NTSB/SIR-95/01) Avail: CASI HC A04/MF A01

This report explains the National Transportation Safety Board's concerns about the safety of the air tour industry in the United States. The safety issues involved the adequacy of regulations pertaining to the air tour industry, the adequacy of past corrective actions, the use of emergency equipment, and the effectiveness of the oversight and certification of air tour operators by the Federal Aviation Administration. Author

04 AIRCRAFT COMMUNICATIONS AND NAVIGATION

Includes digital and voice communication with aircraft; air navigation systems (satellite and ground based); and air traffic control.

For related information see also *17 Space Communications, Spacecraft Communications, Command and Tracking* and *Communications and Radar.*

N95-30486 Columbia Univ., New York, NY.
QUALITATIVE ENVIRONMENTAL NAVIGATION: THEORY AND PRACTICE Ph.D. Thesis
Il-Pyung Park 1994 173 p
Avail: Univ. Microfilms Order No. DA9421385

In this thesis we propose and investigate a new model for robot navigation in large unstructured environments. Current models which depend on metric information contain inherent mechanical and sensory uncertainties. Instead we supply the navigator with qualitative information. Our model consists of two parts, the map-maker and the navigator. Given a source and a goal, the map-maker derives a navigational path based on the topological relationships between landmarks. A navigational path is generated as a combination of 'parkway' and 'trajectory' paths, both of which are abstractions of the real world into topological data structures. Traversing within a parkway enables the navigator to follow visible landmarks. Traversing on a trajectory enables the navigator to move reliably into a homogeneous space, based on shapes formed by visible landmarks that are robust to positional and orientational errors. Reliability measures of parkway and trajectory traversals are defined by appropriate error models that account for the sensory errors of the navigator, the motor errors of the navigator, and the population of neighboring objects. Error detection and error recovery methods are also encoded into the generated path. The optimal path is further abstracted into a 'custom map,' which consists of a list of verbal directional instructions, the vocabulary of which is defined by our environmental description language. Based on the custom map generated by the map-maker, the navigating robot looks for events that are characterized by spatial properties of the environment. The map-maker and the navigator are implemented using two cameras, an IBM 7575 robot arm and PIPE (Pipelined Image Processing Engine). Various experiments show the effectiveness of navigation 'in the large' using the proposed methods. Dissert. Abstr.

N95-30597# Norwegian Inst. for Air Research, Kjeller (Norway).
RESULTS FROM TESTS OF THE HONEYWELL INTEGRATED FLIGHT MANAGEMENT UNIT
B. Jalving 8 Jan. 1995 48 p
(Proj. FFIE/633/131.1)
(PB95-211355) Avail: CASI HC A03/MF A01

The Norwegian Defense Research Establishment (NDRE) has tested Honeywell Military Avionics' Integrated Flight Management Unit (IFMU) as part of a program for investigating alternative technologies and vendors for the new antiship missile for the Royal Norwegian Navy. The HG1700 Inertial Measurement Unit (IMU) considered for use in the missile contains the same GG1308 ring laser gyros and Sundstrand RBA 500 accelerometers as the IFMU. Among the tests carried out were static navigation, gyro compassing, dynamic navigation, and impact of vibrations. It was observed that the performance was dependent upon the flight profile. Gyro biases, accelerometer biases, and random walk coefficients have been estimated. Additionally, the applicability of the IMU navigation data for seeker stabilization has been investigated. The HG1700 unit is suitable for the new antiship missile. NTIS

N95-30815# National Aerospace Lab., Amsterdam (Netherlands).
DEVELOPMENT OF ADVANCED APPROACH AND DEPARTURE PROCEDURES. FAILURE SCENARIOS
L. J. J. Erkelens and J. H. vanDronkelaar 15 Sep. 1994 18 p
(PB95-198123; NLR-TP-93348-U) Avail: CASI HC A03/MF A01

Under a joint contract awarded by the Federal Aviation Administration (FAA) and the Netherlands Department of Civil Aviation (RLD), a flight simulator program was carried out on National Aerospace Laboratory's (NLR's) Research Flight Simulator (RFS) with 19 airline crews to evaluate various test scenarios concerning curved approaches and departures. The test program was flown under full Microwave Landing System (MLS) guidance with a simulated Boeing 747-200 aircraft. The scenarios included procedures for both to New York Area (John F. Kennedy International and La Guardia Airports) and Amsterdam International Airport Schiphol. Four curved approaches and two MLS departures have been evaluated. Crew ability to detect insidious failures and to respond to them were investigated. Crew performance and perception data were also measured in case of a simulated failure of the flight management computer during execution of a curved approach. The workload during a one-engine inoperative flight was also evaluated. NTIS

N95-31013# Federal Aviation Administration, Atlantic City, NJ.
A NASPAC-BASED ANALYSIS OF THE DELAY AND COST EFFECTS OF THE WESTERN-PACIFIC REGION PRELIMINARY RESECTORIZATION EFFORT OF 1993 Technical Note
Joseph M. Richie and Douglas Baart Nov. 1994 145 p
(AD-A288696; DOT/FAA/CT-TN94/49; FAA-AOR-100-94-012) Avail: CASI HC A07/MF A02

This report contains the findings and analysis of the effects of the Western-Pacific Region (AWP) Preliminary Resectorization Plan of 1993 on local (AWP airports) and system-wide traffic delays. The National Airspace System Performance Analysis Capability (NASPAC) was used to perform this task, and calculates the local and system-wide delays with and without the AWP Resectorization Plan. Cost of delay was derived using the Cost of Delay Module based on these delays, on passenger cost, and on airline and aircraft specific cost. The results indicate that the proposed

resectorization will reduce the operational delay in years 1995 and 2000 at most AWP airports and system-wide with the maximum benefit occurring in the year 2000. On the other hand, resectorization does not favor the passengers for the future years modeled. However, in year 2000, the increase in passenger delay is less than for year 1995. DTIC

N95-31433# Minnesota Univ., Minneapolis, MN.
EMERGING APPLICATIONS IN PROBABILITY (SENSOR MANAGEMENT) Final Technical Report, May 1994 - Jan. 1995
Avner Friedman and Keith Kastella 22 Feb. 1995 2 p
(Contract F49620-94-1-0275)
(AD-A292781) Avail: CASI HC A01/MF A01

This grant from the Air Force Office of Scientific Research supported research in Sensor Management related to the IMA 1993-94 academic year program 'EMERGING APPLICATIONS OF PROBABILITY'. It provided partial support for residency of Keith Kastella, an industrial researcher at Unisys Government Systems, to pursue research on the use of discrimination gain optimization for sensor management in Air Traffic Control. Manufacturing, Robotics, Remote Sensing and Defense Applications. Grant AF/F49620-94-1-0275 supported the publication of a technical research report submitted by Dr Kastella for inclusion in the IMA Preprint Series. This paper has been submitted to the IEEE Transactions on Systems, Man and Cybernetics. DTIC

N95-31520# Massachusetts Inst. of Tech., Cambridge, MA.
AN EXPLORATORY SURVEY OF INFORMATION REQUIREMENTS FOR INSTRUMENT APPROACH CHARTS Final Report, Nov. 1990
R. J. Hansman, Jr. and Mark Mykityshyn Mar. 1995 126 p
(Contract DTRS57-88-C-0078)
(AD-A293882; DOTVNTSC-FAA-95/2) Avail: CASI HC A07/MF A02

This report documents a user centered survey and interview effort conducted to analyze the information content of current Instrument Approach Plates (IAP). In the pilot opinion survey of approach chart information requirements, respondents indicated their preferences for approach information and at what phase of the approach they preferred to see this information. Both precision and non-precision IAP formats were examined. In addition to the survey. focused interviews were conducted with pilots who represent the full spectrum of operational IAP user communities from major domestic air carriers to general aviation. DTIC

N95-31521# Massachusetts Inst. of Tech., Lexington, MA.
INTEGRATED TERMINAL WEATHER SYSTEM (ITWS) DEMONSTRATION AND VALIDATION OPERATIONAL TEST AND EVALUATION
Diana L. Klingle-Wilson 13 Apr. 1995 81 p
(Contract DTFA01-91-Z-02036)
(AD-A293932; ATC-234) Avail: CASI HC A05/MF A01

During summer 1994, MIT Lincoln Laboratory conducted the Operational Test and Evaluation Demonstration and Validation (Dem Val) of the Federal Aviation Administration's Integrated Terminal Weather System (ITWS). The purpose of the demonstration was to obtain user feedback on products and to prove that the ITWS products and concept were sufficiently mature to proceed with procurement. Dem Val was conducted at the Memphis international Airport from 23 May through 22 July and at the Orlando International Airport form 11 July through 19 August. Products were delivered to users at the Memphis Airport Traffic Control Tower (ATCT) and TRACON (Terminal Radar Approach Control), at the Memphis Air Route Traffic Control Center (ARTCC), at the Orlando international ATCT and TRACON, and at the Jacksonville ARTCC. in addition, ITWS displays were available to the National Weather Service forecast offices at Memphis, TN, and Melbourne, FL; to Northwest Airlines in Minneapolis, MN; and to Delta Airlines in Orlando, FL. This report documents the technical performance of the product generation algorithms. Each algorithm is described briefly, including the product operational and display concepts. The techniques by which the technical performance is assessed and the results of the assessment are presented. The performance of the algorithms is measured against the Minimum Operational Performance Requirements (MOPR), which products must meet to be considered operationally useful by the ATC user community. DTIC

N95-31572# Federal Aviation Administration, Cambridge, MA.
GUIDELINES FOR THE DESIGN OF GPS AND LORAN RECEIVER CONTROLS AND DISPLAYS Final Report
M. S. Huntley, Jr. Mar. 1995 128 p
(AD-A293753; DOT-VNTSC-FAA-95-7; DOT/FAA/RD-95-7) Avail: CASI HC A07/MF A02

Long range navigation (Loran) and global positioning system (GPS) receivers are widely used in aviation. The Loran and GPS receivers are similar in size and function but derive their navigation signals from different sources. The design of the controls, displays, and computer logic is usually similar for the two types of receivers from a single manufacturer, but differs substantially among manufacturers. Some or all of the designs may provide a suboptimal human-computer interface, which may result in simple time delays or in serious risks if the pilot cannot use the system effectively and efficiently. The design variations also make it difficult to certify receivers for different applications. As a result, the Volpe National Transportation Systems Center has sponsored a program of research to address issues in Loran and GPS receiver design. This report first reviews the literature on user experiences with Loran and GPS receivers and other types of similar, automated equipment. Second, the report reviews the major human factors references, texts, and individual journal articles that are relevant to the regulatory requirements for the receivers. Finally, specific human factors principles and guidelines are proposed for the design and certification of GPS and Loran receiver controls, displays, and control-display integration. DTIC

N95-31581# Air Force Inst. of Tech., Wright-Patterson AFB, OH. School of Engineering.
ANALYSIS AND MODELING OF AN AIRPORT DEPARTURE PROCESS M.S. Thesis
Joseph E. Hebert Mar. 1995 137 p
(AD-A293782; AFIT/GOA/ENS/95M-02) Avail: CASI HC A07/MF A02

This study analyzes departure delays at a major airport using probability models to represent this nonhomogeneous process. The models developed in this study expand on the Markovian models presently used by employing the method of stages to represent some of the model processes. This technique improves the user's ability to achieve a close fit for the service time probability distribution while maintaining the advantages of the Markovian model. The three types of models developed and compared all assume a Markovian system entry process. The first model uses an exponential distribution to model the service process. The second uses an Erlang distribution. The third models employs a unique server absence process to explicitly represents the periods of time when the server is unavailable to service departing aircraft. All three models generate results which correlate well with the delays actually observed. However, the Erlang model is preferred. Its results have lower variability than the exponential service time model. In addition, it generates solutions much faster than a typical application of the absence model. This model should be useful for improving capacity estimation and take-off delay prediction. DTIC

N95-32022# Federal Aviation Administration, Cambridge, MA.
INTEGRATION OF AIR TRAFFIC DATABASES: A CASE STUDY Final Report, Oct. - Nov. 1994
Charles T. Phillips Mar. 1995 62 p
(AD-A293691; DOT-VNTSC-FAA-94-29; DOT/FAA/AOR-100/95-01) Avail: CASI HC A04/MF A01

This report describes a case study to show the benefits from maximum utilization of existing air traffic databases. The study demonstrates the utility of integrating available data through developing and demonstrating a methodology addressing the issue of airport performance. The study utilized data bases which addressed the factors of airport capacity and aircraft delay, and focused on the single airport of Philadelphia International. Since avoidable delays impose major costs to the nation's airlines, the study objective was to better understand the conditions under which delays occur and their causal factors. This will provide guidance for decisions on airport investments which are justified with well-defined benefits. The report presents quantitative measures of average delay, number of delayed flights, and total delay. As expected, there were more delayed flights and longer average delays under poor weather conditions than under better weather conditions. However, total delay under good weather conditions considerably outweighs the total delay experienced under poor weather conditions. The report also

demonstrates a quantitative relationship between average delay and the demand/capacity ratio at the airport. This should prove to be especially useful in the investment analyses of airport improvements. DTIC

N95-32186# Tulsa Univ., OK. Dept. of Psychology.
CONTROLLER RESOURCE MANAGEMENT: WHAT CAN WE LEARN FROM AIRCREWS? Final Report
Charmine Haertel and Guenther F. Haertel (Colorado State Univ., Fort Collins, CO.) Jul. 1995 41 p
(Contract DTFA02-93-P-7913)
(DOT/FAA/AM-95/21) Avail: CASI HC A03/MF A01

This paper provides an overview of the scientific literature regarding Crew Resource Management (CRM). It reaponds to tasking from the Office of Air Traffic Program Management to conduct studies addressing the application of team training models such as CRM for air traffic operational and administrative tasks. The authors report that there is no single model for CRM per se. They formulate a model by integrating common dynamic elements found in many CRM programs. The literature reviewed points out that current CRM research: (a) is primarily focused on flight deck CRM; (b) is insufficient to establish the superiority of CRM training over other team training alternatives; (c) has not identified the critical components of CRM team training; and (d) is limited in part by weaknesses in assessment methods and outcome criteria. The authors identify alternative assessment methods and performance criteria currently being explored by behavioral scientists. Finally, the authors discuss potential CRM techniques for enhancing Air Traffic Control Specialists operational tasks. Author

N95-32197# General Accounting Office, Washington, DC. Resources, Community, and Economic Development Div.
FACT SHEET FOR CONGRESSIONAL COMMITTEES. AIR TRAFFIC CONTROL: STATUS OF FAA'S MODERNIZATION PROGRAM
15 Apr. 1994 80 p
(GAO/RCED-94-167FS; B-247729) Avail: CASI HC A05/MF A01; GAO, PO Box 6015, Gaithersburg, MD 20877 HC

This fact sheet is the fifth annual review of the Federal Aviation Administration's (FAA) comprehensive effort to modernize the nation's air traffic control system by acquiring new equipment, such as radars, computers, and communications systems. The fact sheet provides information on the status of modernization, giving special emphasis to 12 of the largest projects: Advanced Automation System, Air Route Surveillance Radar-4, Airport Surface Detection Equipment-3, Airport Surveillance Radar-9, Automated Weather Observing System, Central Weather Processor, Flight Service Automation System, Microwave Landing System, Mode Select, Radar Microwave Link Replacement and Expansion, Terminal Doppler Weather Radar, and Voice Switching and Control System. Derived from text

N95-32199# General Accounting Office, Washington, DC. Resources, Community, and Economic Development Div.
REPORT TO THE CHAIRMAN, SUBCOMMITTEE ON TRANSPORTATION AND RELATED AGENCIES, COMMITTEE ON APPROPRIATIONS, HOUSE OF REPRESENTATIVES. AIR TRAFFIC CONTROL: STATUS OF FAA'S PLANS TO CLOSE AND CONTRACT OUT LOW-ACTIVITY TOWERS
12 Sep. 1994 27 p
(GAO/RCED-94-265; B-257854) Avail: CASI HC A03/MF A01; GAO, PO Box 6015, Gaithersburg, MD 20877 HC

The objectives are (1) to determine the reasonableness of FAA's plans to close level 1 (low-activity) air traffic control towers and contract out the operations of other level 1 towers, (2) to assess the reasonableness of the potential savings that could result from such actions, (3) to identify the factors that could impede FAA's plans to close and contract out towers, and (4) to identify steps that FAA can take to enhance its strategy for reassigning controllers from closed or contracted out level 1 towers. Of the 151 level 1 towers, 36 do not meet FAA's benefit-cost criteria for continued operations. FAA is planning to permanently close 23 of these towers within the next 3 years, saving as much as $5 million annually. Of the remaining 127 towers, 32 are currently contracted out. FAA estimates that it could save as much as $120 million (in constant 1994 dollars) if it contracts out the operation of the remaining level 1 towers by fiscal year 1997. FAA will not realize immediate savings primarily because of the short-term costs to relocate controllers to other facilities. Several factors may affect FAA's efforts to close or contract out level 1 towers quickly. First, according to FAA program management officials, the agency is receiving mixed signals from the Congress regarding level 1 towers. Second, FAA cannot contract out towers until the Department of Labor completes its wage determinations for each tower location. The FAA does not have a strategy for reassigning controllers from towers to be closed or contracted out to higher level facilities after fiscal year 1994. Also, since a number of controllers at level 1 towers have not been able to perform required duties at other facilities, FAA could incur significant costs to relocate controllers a second time if they do not succeed at higher-level facilities. CASI

05 AIRCRAFT DESIGN, TESTING AND PERFORMANCE

Includes aircraft simulation technology.

For related information see also *18 Spacecraft Design, Testing and Performance* and *39 Structural Mechanics*.For land transportation vehicles see *85 Urban Technology and Transportation*.

N95-30497 Virginia Polytechnic Inst., Blacksburg, VA.
A GENERAL INVERSE DESIGN PROCEDURE FOR AERODYNAMIC BODIES Ph.D. Thesis
Michael Lawrence Papay 1994 103 p
Avail: Univ. Microfilms Order No. DA9425587

A general inverse design procedure has been developed to use optimization techniques and generic surface descriptions for the purpose of aerodynamic shape design. A variety of flow regimes are examined from 2D inviscid, subsonic cases to 3D turbulent, supersonic problems. Surface descriptions have been generalized through the use of B-splines to model a variety of curves and shapes with a minimum of parameters. The process uses a computational fluid dynamics program, GASP (the General Aerodynamic Simulation Program), and several iterative and optimization techniques to examine bodies of interest. A 2D inviscid, subsonic airfoil test case demonstrates the ability of the procedure to solve problems governed by elliptic equations. A 3D, viscous, compressible flow over a forebody/canopy model of a supersonic fighter and its comparison to test data establishes the ability of the method to solve practical problems of interest. Several other test cases are performed, including an axisymmetric power law body and a 3D elliptic cone. Unconstrained multiparameter optimizations have been quite successful in matching target pressure coefficients and reproducing target body shapes. Dissert. Abstr.

N95-30646*# National Aeronautics and Space Administration. Ames Research Center, Moffett Field, CA.
MOVING BASE SIMULATION OF AN INTEGRATED FLIGHT AND PROPULSION CONTROL SYSTEM FOR AN EJECTOR-AUGMENTOR STOVL AIRCRAFT IN HOVER
Walter McNeill, E., William W. Chung, and Michael W. Stortz Jun. 1995 31 p
(RTOP 505-68-32)
(NASA-TM-108867; A-950046; NAS 1.15:108867) Avail: CASI HC A03/MF A01

A piloted motion simulator evaluation, using the NASA Ames Vertical Motion Simulator, was conducted in support of a NASA Lewis Contractual study of the integration of flight and propulsion systems of a STOVL aircraft. Objectives of the study were to validate the Design Methods for Integrated Control Systems (DMICS) concept, to evaluate the handling qualities, and to assess control power usage. The E-7D ejector-augmentor STOVL fighter design served as the basis for the simulation. Handling-qualities ratings were obtained during precision hover and shipboard landing tasks. Handling-qualities ratings for these tasks ranged from satisfactory to adequate. Further improvement of the design process to fully validate the DMICS concept appears to be warranted. Author

N95-30827*# National Aeronautics and Space Administration. Langley Research Center, Hampton, VA.
A WIND TUNNEL INVESTIGATION OF THE EFFECTS OF MICRO-VORTEX GENERATORS AND GURNEY FLAPS ON THE HIGH-LIFT CHARACTERISTICS OF A BUSINESS JET WING M.S. Thesis

Michelle Therese Martuccio Aug. 1994 129 p
(NASA-TM-110626; NAS 1.15:110626) Avail: CASI HC A07/MF A02

A study of a full-scale, semi-span business jet wing has been conducted to investigate the potential of two types of high-lift devices for improving aircraft high-lift performance. The research effort involved low-speed wind-tunnel tests of micro-vortex generators and Gurney flaps applied to the flap system of the business jet wing and included force and moment measurements, surface pressure surveys and flow visualization on the wing and flap. Results showed that the micro-vortex generators tested had no beneficial effects on the longitudinal force characteristics in this particular application, while the Gurney flaps were an effective means of increasing lift. However, the Gurney flaps also caused an increase in drag in most circumstances. Author

N95-30838# National Aerospace Lab., Amsterdam (Netherlands). Fluid Dynamics Div.
VALIDATION OF THE HELICOPTER ROTOR CODE HERO
J. Bosschers 11 Oct. 1993 23 p
(PB95-198040; NLR-TP-93418-U) Avail: CASI HC A03/MF A01

Some improvements are shown for the helicopter rotor code HERO. The code is based on a blade element method using relative simple inflow models and is presently being improved with respect to aerodynamic modeling. Experimental results are used to validate the performance characteristics and the inflow modeling. Calculations with the unsteady aerodynamics model of Leishman & Beddoes are shown. A preliminary empirical formula is presented to take rotational effects into account. The formula is implemented in a semi-empirical dynamic stall program, and a dynamic stall loop showing the influence of rotation is presented. NTIS

N95-30923# Continuum Dynamics, Inc., Princeton, NJ.
A NOVEL INSTRUMENTATION SYSTEM FOR MEASUREMENT OF HELICOPTER ROTOR MOTIONS AND LOADS DATA, PHASE 1 Final Report, 10 Aug. 1994 - 10 Mar. 1995
Robert McKillip, Jr. Apr. 1995 61 p
(Contract N00600-94-C-3087)
(AD-A293309; CDI-95-03) Avail: CASI HC A04/MF A01

Results of a Phase-1 SBIR study directed at a novel instrumentation system for the measurement of helicopter rotor motion and loads are described. Background into the requirements and needs of the measurement system are provided, along with a summary of past activities in this area. Consideration is then given to a novel scheme that incorporates blade-mounted accelerometer sensors with a simplified signal processing scheme to extract both rotor motion measurements, and to a limited extent, blade loading information. Issues regarding sensitivity of the system to modeling errors, nonlinearities and sensor bias errors are examined through detailed simulation and analysis. Also, a demonstration of the system performance for reconstructing flapping motion measurements is provided using Froude-scaled model rotor test results. Finally, implementation issues are discussed, and a plan for continued work leading to prototype development for this system is outlined. DTIC

N95-30927# Naval Postgraduate School, Monterey, CA.
PROBABILISTIC RELIABILITY MODELING OF FATIGUE ON THE H-46 TIE BAR M.S. Thesis
John C. OConnor Sep. 1994 84 p
(AD-A289926) Avail: CASI HC A05/MF A01

The H-46 helicopter has experienced early in-service failures in its tie bar. The tie bar is a multi-component system that is a critical part of the linkage, which attaches the rotor blade to the rotating hub of the helicopter. This research developed methodology to predict the life of the tie bar under nominal operational flight loads. A probability model is indispensable because a revised design has yet to accumulate field data, and laboratory testing can never be sufficiently extensive for non-parametric reliability prediction. An algorithm was developed for three and four component systems that will generate the probability of system failure based on the probability of failure in its components. Finite element analysis was conducted on the tie bar to determine stress on each component for all possible damage configurations of the tie bar. A given set of flight loads was resolved into boundary conditions for the stress analysis. A methodology was developed to determine the probability of failure of each component using an idealized load history, based on the expected stress-life (S-N) relation of the component at the stress levels experienced by the component. The result is a prediction method that can fortify laboratory results to predict the probability of failure of a system given the system load history. This model will be verified using the early in-service failure statistics of the current design and can be used to assess revised designs. The model will provide a prediction of the failure distributions, (the bell-shaped distribution) as a fabrication of flight hours, or one, two, three, and four elements of failures within the leaves of the tie bar. DTIC

N95-31416# Department of Defense, Fort Meade, MD.
UNMANNED AERIAL VEHICLES. 1994 MASTER PLAN
31 May 1994 132 p Original contains color illustrations
Avail: CASI HC A07/MF A02

This 1994 Unmanned Aerial Vehicle (UAV) Master Plan is the sixth submission to Congress, providing the acquisition and technology strategies, management, and program plans for nonlethal UAVs. The UAV Joint Project Office is the single Department of Defense organization charged with management responsibility for UAV's; the United States Navy was designated as the Executive Service for nonlethal UAV programs. This plan is comprised of the following sections: executive summary; management; supporting the user; programs; commonality and interoperability; technology; analysis and simulation; integrated logistics support (ILS), training, and human systems integration (HSI); test and evaluation; international programs; resources; needs rationale; UAV characteristics; dual use of UAV's; and points of contact. CASI

N95-31451# Virginia Polytechnic Inst. and State Univ., Blacksburg, VA.
COMPUTATIONAL METHODS FOR CONTROL AND OPTIMAL DESIGN OF AEROSPACE SYSTEMS Final Technical Report, 1 Jan. 1992 - 31 Mar. 1994
J. A. Burns and E. M. Cliff 31 May 1994 16 p
(Contract F49620-92-J-0078)
(AD-A292861; ICAM-94-06-03) Avail: CASI HC A03/MF A01

This final technical report contains a summary of the research funded by AFOSR under Grant F49620-92J-0078, titled Computational Methods for Control and Optimal Design of Aerospace Systems, for the period 1 January 1992 to 31 March 1994. During this period, the investigators concentrated on five problems; optimal design of forebody simulators, control of highly maneuverable aircraft, control of fluid flows, modeling and identification of smart materials, and robust control of nonlinear conservation laws. A new sensitivity equation method was developed for shape optimization and flow tailoring. This method was transitioned into software at the Arnold Engineering Development Center and at Virginia Tech. A new mathematical model for aircraft agility was used to investigate feedback control laws for time optimal maneuvers. New vortex shedding patterns were discovered for unsteady flows about rotating cylinders. The work on smart materials produced new models and computational methods for the dynamics of shape memory alloys. In addition, robust control theory was applied to nonlinear conservation laws yielding a new approach to sensor location. The report contains a complete list of papers produced during this period. DTIC

N95-31525# Air Force Environmental Technical Applications Center, Scott AFB, IL.
ARTIFICIAL INTELLIGENCE TECHNIQUES FOR FLIGHT TEST PLANNING, PHASE 1 Final Report
Richard H. Stottler 28 Mar. 1995 52 p Limited Reproducibility: Document partially illegible
(Contract N00600-94-C-2972)
(AD-A293962; FR001) Avail: CASI HC A04/MF A01

We found that several AI techniques would be applicable to the development of a system to aid flight test engineers. Flight test engineers reported that test plan and test report creation to be their most time-consuming activities and that they often made informal use of similar plans and reports. Based on the requirements of the flight test engineers, we developed the design for the Automated Flight Test Engineering System (AFTES). To prove its feasibility we implemented and demonstrated critical portions in three Phase 1 prototypes. AFTES is feasible and will benefit the Navy substantially when it is implemented. The three prototypes showed that the most critical aspects could be implemented. Furthermore, the very positive response we received from flight test engineers over both the AFTES designs and the Phase 1 prototypes indicates that AFTES will be utilized when its implemented. Finally, the fact that the productivity of flight

test engineers will markedly improve is based on the fact that AFTES was designed with precisely this purpose, along with improving the quality of the plans and reports produced. For example, the test plan produced in a a few minutes by the prototype can take some less-experienced flight test engineers several days to produce. DTIC

N95-31544# Defence Science and Technology Organisation, Canberra (Australia).
PREPARATION OF S-70A-9 BLACK HAWK HELICOPTER FOR FLIGHT TESTS TO INVESTIGATE CAUSE OF CRACKING OF INNER FUSELAGE PANEL
D. C. Lombardo, A. K. Patterson, P. Ferrarotto, S. A. Dutton, and I. G. Powlesland Feb. 1995 50 p
(AD-A293891; DSTO-TN-0004; DODA-AR-009-205) Avail: CASI HC A03/MF A01

An Australian Army Black Hawk helicopter has been fitted with suitable flight test instrumentation at the Aeronautical and Maritime Research Laboratory to enable an investigation of the cause of cracking in an internal fuselage skin panel. Nine accelerometer channels and 46 strain gauge channels have been provided. Reasons for the choice of measurement type and location are provided together with details of the measuring system installed. Plans for the conduct of suitable flight tests and for the evaluation of the collected data are provided. DTIC

N95-31578# Naval Postgraduate School, Monterey, CA.
A CASE STUDY OF THE TEAMING CONCEPT IN THE PROCUREMENT OF THE V-22 AIRCRAFT M.S. Thesis
Richard D. Colvard Dec. 1994 68 p
(AD-A293770) Avail: CASI HC A04/MF A01

This thesis is a case study of the V-22 Osprey program. It examines dual-sourcing of major weapon systems which was the original acquisition strategy for the V-22. It examines the history of the V-22 program management. The chronology of the program is presented from the birth of the Joint Services Aircraft Program in 1981 through the engineering, manufacturing, and development phase in 1994. The focus of this thesis is to look at the relationship between the Joint Program Office, the parent companies of Bell Helicopter, Inc. and Boeing Helicopter, Inc., and the Government. The thesis also looks at other strategies that have been used in major weapon systems procurements such as the F/A-18 aircraft program which is being procured sole-source with the prime/subcontractor arrangement. This thesis concludes that the acquisition of the V-22 has not been efficient and that Bell and Boeing Aircraft Companies, operating under a teaming concept, have not presented a single face to the Government. DTIC

N95-31579# Naval Postgraduate School, Monterey, CA.
MODELING F/A-18 FLIGHT HOUR PROGRAM COSTS USING REGRESSION ANALYSIS M.S. Thesis
Larry E. Arkley Dec. 1994 123 p
(AD-A293771) Avail: CASI HC A06/MF A02

This thesis is an in depth analysis of cost variance in Naval Air Reserve units flying the McDonnell Douglas F/A-18. The purpose of the thesis is to identify, analyze, and quantify the effect of variances in the cost per flight hour of the Naval Air Reserve's Flying Hour Program. The study begins with a review of the planning, programming, and budgeting system which is used to justify and fund the Flying Hour Program. Then three different methods of determining Flying Hour Program requirements are described. The four components of cost per hour within the Flying Hour Program (fuel, organizational maintenance activity, intermediate maintenance activity, and aviation depot level repairables) are defined. Finally, using regression analysis techniques, these four components of F/A-18 cost data are analyzed on the basis of the intensity of aircraft utilization: flight hours. The analysis includes a regression model to provide budgeters at the headquarter or squadron level the means for predicting aircraft maintenance and fuel costs given a utilization rate. The thesis concludes with areas recommended for further research. DTIC

N95-31602# Virginia Polytechnic Inst. and State Univ., Blacksburg, VA.
PERFORMANCE IMPROVEMENT OF COMPOSITE WINGS THROUGH AEROELASTIC TAILORING AND MODERN CONTROL Final Report, 1 Sep. 1991 - 31 Aug. 1994
Leonard Meirovitch 23 Jan. 1995 110 p
(Grant AF-AFOSR-0351-91)
(AD-A293689; AFOSR-95-0326TR) Avail: CASI HC A06/MF A02

The research has been carried out simultaneously on three aspects of aircraft wings performance optimization, as follows: (1) Structural tailoring and modern control of thin-walled model of composite aircraft wings; (2) Structural tailoring of a low-aspect ratio plate model of composite aircraft wings; and (3) Integrated structural design and vibration control by multiobjective optimization. Significant progress has been made on all fronts. DTIC

N95-32196# General Accounting Office, Washington, DC. National Security and International Affairs Div.
REPORT TO THE CHAIRMAN, LEGISLATION AND NATIONAL SECURITY SUBCOMMITTEE, COMMITTEE ON GOVERNMENT OPERATIONS, HOUSE OF REPRESENTATIVES. UNMANNED AERIAL VEHICLES: PERFORMANCE OF SHORT-RANGE SYSTEM STILL IN QUESTION
15 Dec. 1993 19 p
(GAO/NSIAD-94-65; B-229489) Avail: CASI HC A03/MF A01; GAO, PO Box 6015, Gaithersburg, MD 20877 HC

The Department of Defense (DOD) is acquiring the Short-Range Unmanned Aerial Vehicle (UAV) at an estimated cost of $4.1 billion to meet the needs of the military services for reconnaissance, surveillance, target acquisition, and intelligence missions. The Short-Range UAV's performance capability as demonstrated in recent testing is evaluated. Although DOD considered the short-range system's preproduction test results to be sufficient to justify its low-rate production, the detailed test results showed deficiencies that could jeopardize the system's capability to meet military requirements. In addition, several important performance requirements were either not tested or were tested under unrealistic conditions. Thus, DOD has committed to acquiring an unproven and possibly deficient system. This condition occurred because DOD allowed the Short-Range UAV program to be driven by schedule requirements rather than by demonstrated accomplishments, as required by DOD's stated policy. CASI

N95-31065# Hoh Aeronautics, Inc., Lomita, CA.
UNIFIED CRITERIA FOR ACT AIRCRAFT LONGITUDINAL DYNAMICS
Roger H. Hoh *In* Advisory Group for Aerospace Research and Development, Flight Vehicle Integration Panel Workshop on Pilot Induced Oscillations Feb. 1995 9 p (For primary document see N95-31061 11-03)
Copyright Avail: CASI HC A02/MF A02

N95-32003# Wright Lab., Wright-Patterson AFB, OH. Flight Dynamics Directorate.
FLIGHT EVALUATION OF FOREBODY VORTEX CONTROL IN POST-STALL FLIGHT
Lawrence A. Walchli *In* AGARD, Active Control Technology: Applications and Lessons Learned 10 P (SEE N95-31989 11-08) Jan. 1995 (For primary document see N95-31989 11-08)
Copyright Avail: CASI HC A02/MF A04

N95-32007# Air Force Flight Test Center, Edwards AFB, CA.
FLIGHT TEST RESULTS OF THE F-16 AIRCRAFT MODIFIED WITH AXISYMMETRIC VECTORING EXHAUST NOZZLE
D. Kidman and D. Vanhoy *In* AGARD, Active Control Technology: Applications and Lessons Learned Jan. 1995 19 p (For primary document see N95-31989 11-08)
Copyright Avail: CASI HC A03/MF A04

N95-32008# Dassault Aviation, Saint-Cloud (France).
CATAPULT-LAUNCHING OF THE RAFALE DESIGN AND EXPERIMENTATION [CATAPULTAGE DU RAFALE CONCEPTION ET EXPERIMENTATION]
D. Fleygnac and L. Lequeux *In* AGARD, Active Control Technology: Applications and Lessons Learned Jan. 1995 12 p In FRENCH (For primary document see N95-31989 11-08)
Copyright Avail: CASI HC A03/MF A04

N95-32013# Deutsche Aerospace A.G., Munich (Germany). Military Aircraft Div.
X-31: A PROGRAM OVERVIEW AND FLIGHT TEST STATUS
H. Ross and U. Neuberger *In* AGARD, Active Control Technology: Applications and Lessons Learned Jan. 1995 7 p (For primary document see N95-31989 11-08)
Copyright Avail: CASI HC A02/MF A04

06 AIRCRAFT INSTRUMENTATION

Includes cockpit and cabin display devices; and flight instruments.

For related information see also *19 Spacecraft Instrumentation* and *35 Instrumentation and Photography.*

N95-30920# Air Force Environmental Technical Applications Center, Scott AFB, IL.
IMPROVED ALTIMETER SETTINGS FOR A-10 AIRCRAFT
Timothy D. Oram Feb. 1995 23 p
(AD-A293142; AWS/FM-95/001) Avail: CASI HC A03/MF A01

This forecaster memo describes a process designed to improve the bombing accuracy of A-10 aircraft equipped with the Low Altitude Safety and Targeting Enhancement (LASTE) system by improving altimeter setting accuracy. After finding unacceptable altitude errors during tests of LASTE Version 3.3 the 57th Test Group (57 TG) at Nellis AFB asked the 57 055/05W to develop a method for improving A-10 bombing accuracy by developing improved altimeter setting forecasts. The 57 TG also contracted for General Electric to include software in LASTE Version 4 to correct for these altitude errors automatically. This memo describes a method for improving altimeter setting forecasts in support of LASTE Version 3.3. It also explains basic altimetry theory and tells how the theory relates to the A-10 bombing problem. Finally, the memo provides weather forecasting tips for supporting the new LASTE Version 4. DTIC

N95-31180 Department of the Navy, Washington, DC.
APPARENT SIZE PASSIVE RANGE METHOD Patent
Walter L. Harriman, inventor (to Navy) 13 Dec. 1994 8 p Filed 15 Jul. 1993
(AD-D017360; US-Patent-5,373,318; US-Patent-Appl-SN-094663; US-Patent-Class-348-117) Avail: US Patent and Trademark Office

A method and apparatus provides instantaneous passive range measurement onboard an aircraft for determining the range between the aircraft and a target. The target may either be stationary or a slower moving vehicle. Calculation of the desired range is achieved using the formula: Range = (S/S')V(Cos a)(Cos b) where S = apparent target size; S' = rate of change of apparent size; V = round velocity; a = azimuth angle from aircraft eading to target; and b = elevation angle from the aircraft heading to the target. The apparatus consists of an automatic video tracker, a video camera, and a servo controlled aiming platform. The video tracker provides target size data. Resolvers on the aiming platform are utilized to determine the azimuth and elevation angles from the aircraft axis to the target. The azimuth angle is added to the aircraft drift angle to determine the total azimuth angle from the aircraft heading to the target. The drift angle and ground velocity are obtained from the aircraft inertial system. DTIC

N95-31463# Honeywell Technology Center, Minneapolis, MN.
SYNTHETIC TERRAIN IMAGERY FOR HELMET-MOUNTED DISPLAY. VOLUME 3: SOFTWARE USER'S MANUAL Final Report, 1 Jun. 1992 - 1 Mar. 1995
Rand Whillock, Bill Corwin, and Jeff Groat 15 Nov. 1994 16 p
(Contract F33615-92-C-3601)
(AD-A293613; WL-TR-95-3027) Avail: CASI HC A03/MF A01

The purpose of this document is to describe how to use the STI software program (STI). The software samples data from a preprocessed database created from the U.S. Defense Mapping Agency's Digital Terrain Elevation Data (DTED) database and renders, in perspective view, the visual scene. An NTSC video signal drives a helmet-mounted display. The Synthetic Terrain Imagery for Helmet Mounted Display program was written to present digital terrain elevation data to pilots in several different formats on an HMD. The program can be run stand-alone, in which case it behaves like the 'flight' program that is provided by Silicon Graphics, or it can be integrated into a simulation environment which communicates over the ethernet. DTIC

N95-31584# Air Force Inst. of Tech., Wright-Patterson AFB, OH. School of Engineering.
ANALYSIS OF HEADS-UP DISPLAY QUICKENING VERSUS HANDLING QUALITIES M.S. Thesis
Mar. 1995 133 p
(AD-A293797; AFIT/GAE/ENY/95M-01) Avail: CASI HC A07/MF A02

This study investigated an analytical means of selecting the quickening time constant for the standardized heads-up display flight path marker. The theoretically determined time constant allowed a faster, less resource intensive means of selecting the quickening time constant. The theoretically best time constant for pilot-aircraft handling qualities was equal to the airframe pitch attitude high frequency zero time constant, T(sub theta 2). Flight test indicated an empirical, more labor intensive method yielded better handling qualities, even though paper analysis indicated the theoretical method was better. The theoretically determined time constant gave slightly lower handling qualities, but was less costly to implement than the empirical method. DTIC

N95-31655# Honeywell Technology Center, Minneapolis, MN.
SYNTHETIC TERRAIN IMAGERY FOR HELMET-MOUNTED DISPLAY. VOLUME 2: SOFTWARE DESIGN DOCUMENT Final Report, 1 Jun. 1992 - 1 Mar. 1995
Rand Whillock, Bill Corwin, and Jeff Groat 15 Nov. 1994 106 p
(Contract F33615-92-C-3601)
(AD-A293611; WL-TR-95-3026) Avail: CASI HC A06/MF A02

The software that has been developed as part of the Synthetic Terrain Imagery (STI) Helmet-Mounted Display program is written in C and is designed to execute on a Silicon Graphics VGX Workstation. This software was developed for purposes of evaluating the utility of synthetically derived representations of the local terrain presented on a helmet mounted display. DTIC

N95-31656# Honeywell Technology Center, Minneapolis, MN.
SYNTHETIC TERRAIN IMAGERY FOR HELMET-MOUNTED DISPLAY, VOLUME 1 Final Report, 1 Jun. 1992 - 1 Mar. 1995
Bill Corwin, Rand Whillock, and Jeff Groat 15 Nov. 1994 77 p
(Contract F33615-92-C-3601)
(AD-A293612; WL-TR-95-3025) Avail: CASI HC A05/MF A01

In order to aggressively maneuver an aircraft at low altitude, the pilot must be aware of his attitude as well as the elevation of the surrounding terrain. Low altitude tactical maneuvering is difficult during day operations but becomes nearly impossible at night without an effective night attack system. A system that generates a terrain image from onboard data without the use of sensors would be valuable day or night under all weather conditions. Having a terrain image produced on a Helmet-Mounted Display (HMD) will provide a terrain reference wherever the pilot is looking, thus allowing for more aggressive tactical maneuvering at night. Therefore, with the advent of HMD technology, along with the ability to store a digital terrain data base on tactical aircraft, this capability can be realized. The overall objective of this program is to enhance tactical operations by utilizing a digital terrain system data base to generate a Synthetic Terrain Image(STI) on an HMD. DTIC

07 AIRCRAFT PROPULSION AND POWER

Includes prime propulsion systems and systems components, e.g., gas turbine engines and compressors; and onboard auxilliary power plants for aircraft.

For related information see also *20 Spacecraft Propulsion and Power, 28 Propellants and Fuels,* and *44 Energy Production and Conversion.*

N95-30514*# National Aeronautics and Space Administration. Lewis Research Center, Cleveland, OH.
A SYSTEM SIMULATION DEVELOPMENT PROJECT: LEVERAGING RESOURCES THROUGH PARTNERSHIPS
Colin K. Drummond, A. Karl Owen (Army Research Lab., Cleveland, OH.),

and Milt W. Davis (Sverdrup Technology, Inc., Arnold AFS, TN.) Jul. 1995 8 p Presented at the Aerospace Atlantic Conference, Dayton, OH, 23 May 1995; sponsored by SAE
(RTOP 505-62-10)
(NASA-TM-106962; E-9718; NAS 1.15:106962; ARL-TR-793) Avail: CASI HC A02/MF A01

Partnerships between government agencies are an intellectually attractive method of conducting scientific research; the goal is to establish mutually beneficial participant roles for technology exchange that ultimately pays-off in a stronger R&D program for each partner. Anticipated and current aerospace research budgetary pressures through the 90's provide additional impetus for Government research agencies to candidly assess their R&D for those simulation activities no longer unique enough to warrant 'going it alone,' or for those elements where partnerships or teams can offset development costs. This paper describes a specific inter-agency system simulation activity that leverages the development cost of mutually beneficial R&D. While the direct positive influence of partnerships on complex technology developments is our main thesis, we also address on-going teaming issues and hope to impart to the reader the immense indirect (sometimes immeasurable) benefits that meaningful interagency partnerships can produce. Author

N95-30517*# National Aeronautics and Space Administration. Lewis Research Center, Cleveland, OH.
WAVE ROTOR-ENHANCED GAS TURBINE ENGINES
Gerard E. Welch (Army Research Lab., Cleveland, OH.), Jones M. Scott, and Daniel E. Paxson Jun. 1995 15 p Presented at the 31st Joint Propulsion Conference and Exhibit, San Diego, CA, 10-12 Jul 1995; sponsored by AIAA, ASME, SAE, and ASEE
(RTOP 505-90-58)
(NASA-TM-106998; E-9777; NAS 1.15:106998; ARL-TR-806; AIAA Paper 95-2799) Avail: CASI HC A03/MF A01

The benefits of wave rotor-topping in small (400 to 600 hp-class) and intermediate (3000 to 4000 hp-class) turboshaft engines, and large (80,000 to 100,000 lb(sub f)-class) high bypass ratio turbofan engines are evaluated. Wave rotor performance levels are calculated using a one-dimensional design/analysis code. Baseline and wave rotor-enhanced engine performance levels are obtained from a cycle deck in which the wave rotor is represented as a burner with pressure gain. Wave rotor-toppings is shown to significantly enhance the specific fuel consumption and specific power of small and intermediate size turboshaft engines. The specific fuel consumption of the wave rotor-enhanced large turbofan engine can be reduced while operating at significantly reduced turbine inlet temperature. The wave rotor-enhanced engine is shown to behave off-design like a conventional engine. Discussion concerning the impact of the wave rotor/gas turbine engine integration identifies tenable technical challenges. Author

N95-30589*# National Aeronautics and Space Administration. Lewis Research Center, Cleveland, OH.
EFFECTS OF INITIAL CONDITIONS ON A SINGLE JET IN CROSSFLOW
D. S. Liscinsky (United Technologies Research Center, East Hartford, CT.), B. True (United Technologies Research Center, East Hartford, CT.), and J. D. Holdeman Jul. 1995 13 p Presented at the 31st Joint Propulsion Conference and Exhibit, San Diego, CA, 10-12 Jul 1995; sponsored by AIAA, ASME, SAE, and ASEE Original contains color illustrations
(RTOP 537-02-21)
(NASA-TM-107002; E-9782; NAS 1.15:107002; AIAA Paper 95-2998)
Avail: CASI HC A03/MF A01; 4 functional color pages

An experimental investigation of the effects of jet inlet flow conditions has been conducted for the isothermal mixing of a single jet injected into a crossflow. Jet penetration and mixing was studied using planar Mie scattering to measure time-averaged jet mixture fraction distributions. The effects of 'passive' control methods such as jet 'tabs' and jet swirl are reported. Mixing effectiveness, determined using a spatial unmixedness parameter based on the variance of the mean jet concentration distributions, was compared to a baseline case of a round jet injected into a uniform crossflow. All results are compared at a jet-to-mainstream momentum-flux ratio of 8.5. In the near-field, the mixing rates are similar to, or less than, the baseline configuration using this measure of mixedness. None of the tested configurations appear to significantly augment mixing within a downstream distance of 3 diameters of an equivalent-area round orifice. Author

N95-30594*# National Aeronautics and Space Administration. Lewis Research Center, Cleveland, OH.
OBJECT-ORIENTED APPROACH FOR GAS TURBINE ENGINE SIMULATION
Brian P. Curlett and James L. Felder Jul. 1995 34 p
(RTOP 505-69-50)
(NASA-TM-106970; E-9731; NAS 1.15:106970) Avail: CASI HC A03/MF A01

An object-oriented gas turbine engine simulation program was developed. This program is a prototype for a more complete, commercial grade engine performance program now being proposed as part of the Numerical Propulsion System Simulator (NPSS). This report discusses architectural issues of this complex software system and the lessons learned from developing the prototype code. The prototype code is a fully functional, general purpose engine simulation program, however, only the component models necessary to model a transient compressor test rig have been written. The production system will be capable of steady state and transient modeling of almost any turbine engine configuration. Chief among the architectural considerations for this code was the framework in which the various software modules will interact. These modules include the equation solver, simulation code, data model, event handler, and user interface. Also documented in this report is the component based design of the simulation module and the inter-component communication paradigm. Object class hierarchies for some of the code modules are given. Author

N95-30617*# National Aeronautics and Space Administration. Lewis Research Center, Cleveland, OH.
A NUMERICAL MODEL FOR DYNAMIC WAVE ROTOR ANALYSIS
D. E. Paxson Jul. 1995 13 p Presented at the 31st Joint Propulsion Conference and Exhibit, San Diego, CA, 10-12 Jul. 1995; sponsored by AIAA, ASME, SAE, and ASEE
(RTOP 505-62-50)
(NASA-TM-106997; E-9776; NAS 1.15:106997; AIAA Paper 95-2800)
Avail: CASI HC A03/MF A01

A numerical model has been developed which can predict the dynamic (and steady state) performance of a wave rotor, given the geometry and time dependent boundary conditions. The one-dimensional, perfect gas, CFD based code tracks the gasdynamics in each of the wave rotor passages as they rotate past the various ducts. The model can operate both on and off-design, allowing dynamic behavior to be studied throughout the operating range of the wave rotor. The model accounts for several major loss mechanisms including finite passage opening time, fluid friction, heat transfer to and from the passage walls, and leakage to and from the passage ends. In addition, it can calculate the amount of work transferred to and from the fluid when the flow in the ducts is not aligned with the passages such as occurs in off-design operation. Since it is one-dimensional, the model runs reasonably fast on a typical workstation. This paper will describe the model and present the results of some transient calculations for a conceptual four port wave rotor designed as a topping cycle for a small gas turbine engine. Author

N95-30632*# National Aeronautics and Space Administration. Lewis Research Center, Cleveland, OH.
PRELIMINARY ASSESSMENT OF COMBUSTION MODES FOR INTERNAL COMBUSTION WAVE ROTORS
M. Razi Nalim Jul. 1995 14 p Presented at the 31st Joint Propulsion Conference and Exhibit, San Diego, CA, 10-12 Jul. 1995; sponsored by AIAA, ASME, SAE, and ASEE
(RTOP 505-90-58)
(NASA-TM-107000; E-9779; NAS 1.15:107000; AIAA Paper 95-2801)
Avail: CASI HC A03/MF A01

Combustion within the channels of a wave rotor is examined as a means of obtaining pressure gain during heat addition in a gas turbine engine. Several modes of combustion are considered and the factors that determine the applicability of three modes are evaluated in detail; premixed autoignition/detonation, premixed deflagration, and non-premixed compression ignition. The last two will require strong turbulence for completion of combustion in a reasonable time in the wave rotor. The compression/autoignition modes will require inlet temperatures in excess

of 1500 R for reliable ignition with most hydrocarbon fuels; otherwise, a supplementary ignition method must be provided. Examples of combustion mode selection are presented for two core engine applications that had been previously designed with equivalent 4-port wave rotor topping cycles using external combustion. Author

N95-30698*# National Aeronautics and Space Administration. Lewis Research Center, Cleveland, OH.

JET MIXING AND EMISSION CHARACTERISTICS OF TRANSVERSE JETS IN ANNULAR AND CYLINDRICAL CONFINED CROSSFLOW

D. B. Bain (CFD Research Corp., Huntsville, AL.), C. E. Smith (CFD Research Corp., Huntsville, AL.), and J. D. Holdeman Jul. 1995 32 p Presented at the 31st Joint Propulsion Conference and Exhibit, San Diego, CA, 10-12 Jul. 1995; sponsored by AIAA, ASME, SAE, and ASEE Original contains color illustrations

(RTOP 537-02-21)

(NASA-TM-106976; E-9737; NAS 1.15:106976; AIAA Paper 95-2995)

Avail: CASI HC A03/MF A01; 11 functional color pages

Three dimensional turbulent reacting CFD analyses were performed on transverse jets injected into annular and cylindrical (can) confined crossflows. The goal was to identify and assess mixing differences between annular and can geometries. The approach taken was to optimize both annular and can configurations by systematically varying orifice spacing until lowest emissions were achieved, and then compare the results. Numerical test conditions consisted of a jet-to-mainstream mass-flow ratio of 3.2 and a jet-to-mainstream momentum-flux ratio (J) of 30. The computational results showed that the optimized geometries had similar emission levels at the exit of the mixing section although the annular configuration did mix-out faster. For lowest emissions, the density correlation parameter (C = (S/H) square root of J) was 2.35 for the annular geometry and 3.5 for the can geometry. For the annular geometry, the constant was about twice the value seen for jet mixing at low mass-flow ratios (i.e., MR less than 0.5). For the can geometry, the constant was about 1 1/2 times the value seen for low mass-flow ratios. Author

N95-30702*# National Aeronautics and Space Administration. Lewis Research Center, Cleveland, OH.

EFFECT OF VELOCITY AND TEMPERATURE DISTRIBUTION AT THE HOLE EXIT ON FILM COOLING OF TURBINE BLADES

Vijay K. Garg (AYT Corp., Brook Park, OH.) and Raymond E. Gaugler Jun. 1995 14 p Presented at the 40th Gas Turbine and Aeroengine Congress and Exposition, Houston, TX, 5-8 Jun. 1995; sponsored by ASME

(RTOP 505-62-52)

(NASA-TM-106954; E-9704; NAS 1.15:106954) Avail: CASI HC A03/MF A01

An existing three-dimensional Navier-Stokes code, modified to include film cooling considerations, has been used to study the effect of coolant velocity and temperature distribution at the hole exit on the heat transfer coefficient on three-film-cooled turbine blades, namely, the C3X vane, the VKI rotor, and the ACE rotor. Results are also compared with the experimental data for all the blades. Moreover, Mayle's transition criterion, Forest's model for augmentation of leading edge heat transfer due to freestream turbulence, and Crawford's model for augmentation of eddy viscosity due to film cooling are used. Use of Mayle's and Forest's models is relevant only for the ACE rotor due to the absence of showerhead cooling on this rotor. It is found that, in some cases, the effect of distribution of coolant velocity and temperature at the hole exit can be as much as 60% on the heat transfer coefficient at the blade suction surface, and 50% at the pressure surface. Also, different effects are observed on the pressure and suction surface depending upon the blade as well as upon the hole shape, conical or cylindrical. Author

N95-30779*# United Technologies Corp., East Hartford, CT.

METHOD FOR EXTRACTING FORWARD ACOUSTIC WAVE COMPONENTS FROM ROTATING MICROPHONE MEASUREMENTS IN THE INLETS OF TURBOFAN ENGINES Final Contractor Report

D. E. Cicon and T. G. Sofrin (Sofrin, T. G., Newington, CT.) May 1995 55 p

(Contract NAS3-26618; RTOP 538-03-11)

(NASA-CR-195457; E-9577; NAS 1.26:195457) Avail: CASI HC A04/MF A01

This report describes a procedure for enhancing the use of the basic rotating microphone system so as to determine the forward propagating mode components of the acoustic field in the inlet duct at the microphone plane in order to predict more accurate far-field radiation patterns. In addition, a modification was developed to obtain, from the same microphone readings, the forward acoustic modes generated at the fan face, which is generally some distance downstream of the microphone plane. Both these procedures employ computer-simulated calibrations of sound propagation in the inlet duct, based upon the current radiation code. These enhancement procedures were applied to previously obtained rotating microphone data for the 17-inch ADP fan. The forward mode components at the microphone plane were obtained and were used to compute corresponding far-field directivities. The second main task of the program involved finding the forward wave modes generated at the fan face in terms of the same total radial mode structure measured at the microphone plane. To obtain satisfactory results with the ADP geometry it was necessary to limit consideration to the propagating modes. Sensitivity studies were also conducted to establish guidelines for use in other fan configurations. Author

N95-30853*# National Aeronautics and Space Administration. Lewis Research Center, Cleveland, OH.

JET MIXING IN A REACTING CYLINDRICAL CROSSFLOW

M. Y. Leong (California Univ., Irvine, CA.), G. S. Samuelsen (California Univ., Irvine, CA.), and J. D. Holdeman Jul. 1995 24 p Presented at the 31st Joint Propulsion Conference and Exhibit, San Diego, CA, 10-12 Jul. 1995 nsored by AIAA, ASME, SAE, and ASEE Original contains color illustrations

(RTOP 537-02-20)

(NASA-TM-106975; E-9736; NAS 1.15:106975; AIAA Paper 95-3109)

Avail: CASI HC A03/MF A01; 10 functional color pages

This paper addresses the mixing of air jets into the hot, fuel-rich products of a gas turbine primary zone. The mixing, as a result, occurs in a reacting environment with chemical conversion and substantial heat release. The geometry is a crossflow confined in a cylindrical duct with side-wall injection of jets issuing from round orifices. A specially designed reactor, operating on propane, presents a uniform mixture without swirl to mixing modules consisting of 8, 9, 10, and 12 holes at a momentum-flux ratio of 57 and a jet-to-mainstream mass-flow ratio of 2.5. Concentrations of O2, CO2, CO, and HC are obtained upstream, downstream, and within the orifice plane. O2 profiles indicate jet penetration while CO2, CO, and HC profiles depict the extent of reaction. Jet penetration is observed to be a function of the number of orifices and is found to affect the mixing in the reacting system. The results demonstrate that one module (the 12-hole) produces near-optimal penetration defined here as a jet penetration closest to the module half-radius, and hence the best uniform mixture at a plane one duct radius from the orifice leading edge. Author

N95-30861*# National Aeronautics and Space Administration. Lewis Research Center, Cleveland, OH.

PARAMETRICS ON 2D NAVIER-STOKES ANALYSIS OF A MACH 2.68 BIFURCATED RECTANGULAR MIXED-COMPRESSION INLET

M. Mizukami and J. D. Saunders Jul. 1995 16 p Presented at the 31st Joint Propulsion Conference and Exhibit, San Diego, CA, 10-12 Jul. 1995; Sponsored by AIAA, ASME, SAE and ASEE

(RTOP 537-02-22)

(NASA-TM-107003; E-9784; NAS 1.15:107003) Avail: CASI HC A03/MF A01

The supersonic diffuser of a Mach 2.68 bifurcated, rectangular, mixed-compression inlet was analyzed using a two-dimensional (2D) Navier-Stokes flow solver. Parametric studies were performed on turbulence models, computational grids and bleed models. The computer flowfield was substantially different from the original inviscid design, due to interactions of shocks, boundary layers, and bleed. Good agreement with experimental data was obtained in many aspects. Many of the discrepancies were thought to originate primarily from 3D effects. Therefore, a balance should be struck between expending resources on a high fidelity 2D simulation, and the inherent limitations of 2D analysis. The solutions were fairly insensitive to turbulence models, grids and bleed models. Overall, the k-e turbulence model, and the bleed models based on unchoked bleed hole discharge coefficients or uniform velocity are recommended. The 2D Navier-Stokes methods appear to be a useful tool for the design and

analysis of supersonic inlets, by providing a higher fidelity simulation of the inlet flowfield than inviscid methods, in a reasonable turnaround time.
Author

N95-31191# BBN Systems and Technologies Corp., Cambridge, MA.
AN ACTIVE LINER SYSTEM FOR JET ENGINE EXHAUST SILENCERS, PHASE 1 Final Report, 1 Jul. 1993 - 30 Jun. 1994
Istvan L. Ver and Michael Dignan Jun. 1994 65 p
(AF Proj. 3037)
(AD-A293277; AL/OE-TR-1994-0130) Avail: CASI HC A04/MF A01

In the framework of the U.S. Air Force's Advanced Technology Active Noise Reduction Initiative - an experimental program was carried out to demonstrate the feasibility of a new concept of an Active Liner. Using a 1:4 scale model of a jet engine test cell augmenter 8 dB to 15 dB reduction of the low frequency (8 Hz to 80 Hz at full scale) was obtained by inserting one or two active liner segments into a typical lined augmenter. The topics covered in this report include: (1) problems caused by low frequency noise and their land use implications, (2) description of the active liner concept, (3) control strategies employed, (4) description of the model-scale augmenter including passive and active sections and the feedback control system, (5) experimental results, (6) full-scale ramifications and (7) risk assessment of full-scale implementation. DTIC

N95-31425*# National Aeronautics and Space Administration. Hugh L. Dryden Flight Research Center, Edwards, CA.
FLIGHT ASSESSMENT OF THE ONBOARD PROPULSION SYSTEM MODEL FOR THE PERFORMANCE SEEKING CONTROL ALGORITHM ON AN F-15 AIRCRAFT
John S. Orme and Gerard S. Schkolnik Washington Jul. 1995 20 p
Presented at 31st AIAA/ASME/SAE/ASEE Joint Propulsion Conference, San Diego, CA, 10-12 Jul. 1995
(RTOP 533-02-03)
(NASA-TM-4705; H-2060; NAS 1.15:4705; AIAA Paper 95-2361) Avail: CASI HC A03/MF A01

Performance Seeking Control (PSC), an onboard, adaptive, real-time optimization algorithm, relies upon an onboard propulsion system model. Flight results illustrated propulsion system performance improvements as calculated by the model. These improvements were subject to uncertainty arising from modeling error. Thus to quantify uncertainty in the PSC performance improvements, modeling accuracy must be assessed. A flight test approach to verify PSC-predicted increases in thrust (FNP) and absolute levels of fan stall margin is developed and applied to flight test data. Application of the excess thrust technique shows that increases of FNP agree to within 3 percent of full-scale measurements for most conditions. Accuracy to these levels is significant because uncertainty bands may now be applied to the performance improvements provided by PSC. Assessment of PSC fan stall margin modeling accuracy was completed with analysis of in-flight stall tests. Results indicate that the model overestimates the stall margin by between 5 to 10 percent. Because PSC achieves performance gains by using available stall margin, this overestimation may represent performance improvements to be recovered with increased modeling accuracy. Assessment of thrust and stall margin modeling accuracy provides a critical piece for a comprehensive understanding of PSC's capabilities and limitations. Author

N95-31985*# National Aeronautics and Space Administration. Lewis Research Center, Cleveland, OH.
LASER ANEMOMETER MEASUREMENTS OF THE THREE-DIMENSIONAL ROTOR FLOW FIELD IN THE NASA LOW-SPEED CENTRIFUGAL COMPRESSOR
Michael D. Hathaway (Army Research Lab., Cleveland, OH.), Randall M. Chriss, Anthony J. Strazisar, and Jerry R. Wood Jun. 1995 297 p
(RTOP 505-62-52; DA Proj. 1L1-61102-AH-45)
(NASA-TP-3527; E-9390; NAS 1.60:3527; ARL-TR-333) Avail: CASI HC A13/MF A03

A laser anemometer system was used to provide detailed surveys of the three-dimensional velocity field within the NASA low-speed centrifugal impeller operating with a vaneless diffuser. Both laser anemometer and aerodynamic performance data were acquired at the design flow rate and at a lower flow rate. Floor path coordinates, detailed blade geometry, and pneumatic probe survey results are presented in tabular form. The laser anemometer data are presented in the form of pitchwise distributions of axial, radial, and relative tangential velocity on blade-to-blade stream surfaces at 5-percent-of-span increments, starting at 95-percent-of-span from the hub. The laser anemometer data are also presented as contour and wire-frame plots of throughflow velocity and vector plots of secondary velocities at all measurement stations through the impeller. Author

N95-31199 Naval Postgraduate School, Monterey, CA.
AN INVESTIGATION OF THE SIDE-DUMP DUAL IN-LINE RAMJET COMBUSTOR
M. W. Deppe, R. F. Salyer, and D. W. Netzer *In* Johns Hopkins Univ., The 31st JANNAF Combustion Subcommittee Meeting, Volume 1 Oct. 1994 p 59-74 (For primary document see N95-31194 11-28)
Avail: CPIA, 10630 Little Patuxent Pkwy., Suite 202, Columbia, MD 21044-3200 HC

N95-31201 Naval Air Warfare Center, China Lake, CA.
A PULSED LIQUID FUEL RAMJET
K. J. Wilson, E. J. Gutmark, R. A. Smith, and K. C. Schadow *In* Johns Hopkins Univ., The 31st JANNAF Combustion Subcommittee Meeting, Volume 1 Oct. 1994 p 85-99 (For primary document see N95-31194 11-28)
Avail: CPIA, 10630 Little Patuxent Pkwy., Suite 202, Columbia, MD 21044-3200 HC

08 AIRCRAFT STABILITY AND CONTROL

Includes aircraft handling qualities; piloting; flight controls; and autopilots.

For related information see also *05 Aircraft Design, Testing and Performance.*

N95-30937# Carnegie-Mellon Univ., Pittsburgh, PA.
NEW ADAPTIVE METHODS FOR RECONFIGURABLE FLIGHT CONTROL SYSTEMS, APPENDIX 1 Final Report, 1 Jul. 1992 - 31 Dec. 1994
Marc Bodson 15 Feb. 1995 116 p
(Contract F49620-92-J-0386)
(AD-A292711; AFOSR-95-0174TR) Avail: CASI HC A06/MF A02

The report discusses methods for the design of reconfigurable flight control systems. Model reference adaptive control algorithms were developed which allow for the rapid identification of aircraft parameters after failures or damages and for automatic control redesign. These algorithms are simple enough that they can be implemented in real-time with existing computers. Simulation results were obtained using a detailed nonlinear model of a fighter aircraft. The results demonstrate the ability of the adaptive algorithms to automatically readjust trim values after failures, to restore tracking of the pilot commands despite the loss of actuator effectiveness, and to coordinate the use of the remaining surfaces in order to maintain the decoupling between the rotational axes. The report also discusses analytical results that were obtained during the course of the research regarding the stability and convergence properties of multivariable adaptive control algorithms, the use of averaging methods for the analysis of transient response and robustness, and the estimation of uncertainty in dynamic models. A modified recursive least-squares algorithm with forgetting factor is also described which gives fast adaptation under normal conditions while keeping the sensitivity to noise limited when signal to noise ratios are poor. DTIC

N95-31400 Nielsen Engineering and Research, Inc., Mountain View, CA.
VORTICITY DYNAMICS AND CONTROL OF DYNAMIC STALL Final Report, 15 Apr. 1992 - 14 Jun. 1994
Patrick H. Reisenthel 18 Aug. 1994 129 p Limited Reproducibility: More than 20% of this document may be affected by microfiche quality
(Contract DAAL03-92-C-0013)
(AD-A288658; NEAR-TR-482; ARO-29049.4-EG-S) Avail: Issuing Activity (Defense Technical Information Center (DTIC))

The goal of the research was to understand key issues of vorticity dynamics prior to, during, and after the initiation of dynamic stall. The first portion of this work examined the indicial theory to the prediction of dynamic applicability stall. The research focused on extending the semi-analytical formalism of indicial theory to predict the vorticity fluxes and the vorticity

accumulation at the leading edge during unsteady maneuver. In the second portion of this work, highly accurate two-dimensional solutions of the Navier-Stokes equation were used on a model problem to investigate the Reynolds number scaling of incipient flow separation between Re = 50,000 and Re = 800,000. This portion of the work was motivated by the suggestion that the appearance of eruptive plumes of vorticity at high Reynolds number might be critical to the formation of the dynamic stall vortex. The results of the research appear to contradict the hypothesis that a form of Reynolds number bifurcation must take place at some intermediate laminar Reynolds number. Instead, self-similar behavior was observed, at least up to the time of formation of the primary stall vortex. Author

N95-31846*# National Aeronautics and Space Administration. Hugh L. Dryden Flight Research Center, Edwards, CA.

FLIGHT TEST VALIDATION OF A FREQUENCY-BASED SYSTEM IDENTIFICATION METHOD ON AN F-15 AIRCRAFT

Gerard S. Schkolnik, John S. Orme, and Mark A. Hreha (McDonnell-Douglas Aerospace, Saint Louis, MO.) Washington Jul. 1995 18 p Presented at the 31st AIAA/ASME/SAE/ASEE Joint Propulsion Conference and Exhibit, San Diego, CA, 10-12 Jul. 1995

(RTOP 505-68-00)

(NASA-TM-4704; H-2059; NAS 1.15:4704; AIAA Paper 95-2362) Avail: CASI HC A03/MF A01

A frequency-based performance identification approach was evaluated using flight data from the NASA F-15 Highly Integrated Digital Electronic Control aircraft. The approach used frequency separation to identify the effectiveness of multiple controls simultaneously as an alternative to independent control identification methods. Fourier transformations converted measured control and response data into frequency domain representations. Performance gradients were formed using multiterm frequency matching of control and response frequency domain models. An objective function was generated using these performance gradients. This function was formally optimized to produce a coordinated control trim set. This algorithm was applied to longitudinal acceleration and evaluated using two control effectors: nozzle throat area and inlet first ramp. Three criteria were investigated to validate the approach: simultaneous gradient identification, gradient frequency dependency, and repeatability. This report describes the flight test results. These data demonstrate that the approach can accurately identify performance gradients during simultaneous control excitation independent of excitation frequency. Author

N95-31989# Advisory Group for Aerospace Research and Development, Neuilly-Sur-Seine (France). Flight Mechanics Panel.

ACTIVE CONTROL TECHNOLOGY: APPLICATIONS AND LESSONS LEARNED [LES TECHNOLOGIES DU SYSTEME DE CONTROLE ACTIF: APPLICATIONS ET ENSEIGNEMENTS]

Jan. 1995 400 p In ENGLISH and FRENCH Presented at the Flight Mechanics Panel Symposium, Turin, France, 9-13 May 1994

(AGARD-CP-560; ISBN-92-836-0007-X) Copyright Avail: CASI HC A17/MF A04

In the last decade, Active Control Technology (ACT) has emerged from the realm of theory and modest experimental applications to full-scale use on production aircraft, while more elaborate forms of ACT are under test for the future production of aircraft. New technologies have been applied in military fighters to maximize maneuverability and agility, and in civil transports to reduce trim drag, lower pilot workload and improve riding qualities. During this symposium the status of Active Control Technology was assessed in light of the experience gained over the last decade. The symposium was organized around four sessions comprising 28 technical papers in all. These sessions focused on: Specifications for flight control design, Design and analysis methods, System integration and Implementation of experience. For individual titles, see N95-31990 through N95-32017.

N95-31990# Hoh Aeronautics, Inc., Lomita, CA.

THE ROLE OF HANDLING QUALITIES SPECIFICATIONS IN FLIGHT CONTROL SYSTEM DESIGN

Roger H. Hoh and David G. Mitchell *In* AGARD, Active Control Technology: Applications and Lessons Learned Jan. 1995 12 p (For primary document see N95-31989 11-08)

Copyright Avail: CASI HC A03/MF A04

The handling qualities specification should be an essential element of the flight control system design and testing for an active control technology (ACT) aircraft. This is a significant departure from previous conventional aircraft where handling qualities depended more on the configuration (tail size, control surface sizing, etc.). The necessity for incorporating the handling qualities specification into the flight control system design process has not been recognized by the industry, as evidenced by the fact that most of the ACT aircraft do not meet the requirements of the current handling qualities specification. This has resulted in excessive phase lag in the flight controls, and numerous cases of pilot induced oscillation. This paper reviews key handling qualities criteria for ACT aircraft as well as lessons that should be incorporated into specification upgrades and flight control design efforts. Author

N95-31991# Gibson (J. C.), Saint Annes (England).

THE PREVENTION OF PIO BY DESIGN

J. C. Gibson *In* AGARD, Active Control Technology: Applications and Lessons Learned Jan. 1995 12 p (For primary document see N95-31989 11-08)

Copyright Avail: CASI HC A03/MF A04

Control problems caused by poor pilot-aircraft closed loop characteristics have existed for as long as aircraft have been flown. The majority of them have been the result of excessive response amplitudes and phase lags conflicting with simple stability margin requirements. Their solutions have been rather straightforward and often amount to the provision of K/S-like responses, or sufficiently similar, within the bandwidths of interest. Most high order Pilot Induced Oscillation (PIO) problems have-been introduced, not by more complex fly by wire control laws, but by unnecessary lags or sometimes by excessive gain placed between the pilot and the response. The pilot is forced to operate in a region of excessive phase lag and response gain, typically with the impression that the aircraft is not actually responding to the commands. The solutions address the provision of adequate stability margins in much the same way as in earlier problems. The high order PIO problem is identified in the open loop attitude behavior in the uniquely defined PIO frequency region, in which the response lags the stick by 180 degrees or more. It is not necessary to model the pilot, who is found to operate in a synchronous manner with the attitude oscillation. The dominant feature in this is the rate zero crossing which acts to trigger the reversals of the control input. The input itself may take the form of a sinusoid, a relay switching action, or a mixture of the two. A number of simple criteria can be applied to control law design which have been found to ensure the prevention of high order PIO. The existence of a PIO problem can be identified with great certainty before flight by specific test methods, which should be applied with rigor no matter how much confidence exists in the design methods. Finally, it is crucial for all concerned to understand that if the underlying problem is there, no matter how extreme the pilot inputs may have to be to excite it, then it can be expected to happen in flight. It will be impossible to prevent it by pilot briefings.

Derived from text

N95-31992# McDonnell-Douglas Aerospace, Long Beach, CA.

THE IMPORTANCE OF FLYING QUALITIES DESIGN SPECIFICATIONS FOR ACTIVE CONTROL SYSTEMS

J. Hodgkinson and K. F. Rossitto *In* AGARD, Active Control Technology: Applications and Lessons Learned Jan. 1995 15 p (For primary document see N95-31989 11-08)

Copyright Avail: CASI HC A03/MF A04

The first part of this paper consists of recollections of how some of the flying qualities specifications for active control fighters emerged. These recollections include some lessons learned. The second part, with these recollections and lessons as motivation, introduces new data on the much more recent developments in active control transports. Author

N95-31993# Deutsche Forschungsanstalt fuer Luft- und Raumfahrt, Brunswick (Germany). Inst. fuer Flugmechanik.

EXPERIENCES WITH ADS-33 HELICOPTER SPECIFICATION TESTING AND CONTRIBUTIONS TO REFINEMENT RESEARCH

C. J. Ockier and H.-J. Pausder *In* AGARD, Active Control Technology: Applications and Lessons Learned Jan. 1995 20 p (For primary document see N95-31989 11-08)

Copyright Avail: CASI HC A03/MF A04

The introduction of Active Control Technology in rotorcraft created the need for new handling qualities requirements. In response to this, a new helicopter handling qualities specification was developed under the leadership

of the U.S. Army and published as Aeronautical Design Standard 33 (ADS-33). Since its introduction, research has been conducted to expand the handling qualities database on which ADS-33 is based. This paper presents DLR contributions to this research. A standard BO 105 was used to evaluate the applicability and repeatability of the current ADS-33C criteria in forward flight. As a result of this study, some data gaps were recognized and the criteria that need further verification were identified. The in-flight simulator ATTHeS was used for an investigation of the effects of bandwidth and phase delay and pitch-roll coupling on helicopter handling qualities in a high gain slalom tracking task. Results are shown that indicate a need to more tightly constrain the phase delay for the roll axis than in the current ADS-33 requirements. For the pitch-roll coupling criterion it is shown that although the format of the current ADS-33 requirements is valid for control and rate coupling, it cannot be used for coupling types typical of actively controlled helicopters. A frequency domain criterion that offers more comprehensive coverage of all types of pitch-roll coupling is proposed. Author

N95-31994# Israel Aircraft Industries Ltd., Ben-Gurion Airport (Israel). Flight Operations.

LAVI FLIGHT CONTROL SYSTEM: DESIGN REQUIREMENTS, DEVELOPMENT AND FLIGHT TEST RESULTS

Menahem Shmul, Eli Erenthal, and Moshe Attar *In* AGARD, Active Control Technology: Applications and Lessons Learned Jan. 1995 13 p (For primary document see N95-31989 11-08)

Copyright Avail: CASI HC A03/MF A04

The flight control system of the Lavi Multimission fighter is described. The control laws design philosophy is given along with the control laws development, the flying qualities requirements and the final structure of the pitch axis (DFCS). The simulation phase is covered along with special control laws features. The question 'how does the Lavi fly?' is addressed. Problems uncovered during flights, and solutions found, are detailed and the flying qualities data are given. Finally, the program status is explained. Author

N95-31995# Technische Univ., Delft (Netherlands). Dept. of Aerospace Engineering.

ROBUST CONTROL: A STRUCTURED APPROACH TO SOLVE AIRCRAFT FLIGHT CONTROL PROBLEMS

S. Bennani, J. A. Mulder, and O. H. Bosgra *In* AGARD, Active Control Technology: Applications and Lessons Learned Jan. 1995 24 p Sponsored by NAL (For primary document see N95-31989 11-08)

Copyright Avail: CASI HC A03/MF A04

This paper discusses an application of several robust control methodologies such as H(sub infinity) optimal control, micro-synthesis and gain scheduling via linear fractional transformations applied to a flight control system. To illustrate the approach, a design model for the short period approximation of the Cessna Citation 500 has been chosen, for which certain handling quality requirements have to be met over a large set of operating conditions. For all these methods, the design framework remains the same, only the system 'norm' changes to the object to be minimized. The paper shows how these methods work and illustrates the features of the new approach. Author

N95-31996# Honeywell, Inc., Minneapolis, MN.

DYNAMIC INVERSION: AN EVOLVING METHODOLOGY FOR FLIGHT CONTROL DESIGN

Dale Enns, Dan Bugajski, Russ Hendrick, and Gunter Stein *In* AGARD, Active Control Technology: Applications and Lessons Learned Jan. 1995 12 p (For primary document see N95-31989 11-08)

Copyright Avail: CASI HC A03/MF A04

This paper describes nonlinear dynamic inversion as an alternative design method for flight controls. The method is illustrated with super-maneuvering control laws for the F-18 High Angle-of-Attack Research Vehicle (HARV). Author

N95-31997# Office National d'Etudes et de Recherches Aerospatiales, Toulouse (France). Dept. d'Etudes et de Recherches en automatique.

EVALUATION OF THE TECHNIQUES OF FUZZY CONTROL FOR THE PILOTING AN AIRCRAFT [EVALUATION DES TECHNIQUES DE CONTROLE FLOU POUR LE PILOTAGE D'AVION]

N. Imbert and A. Piquerau *In* AGARD, Active Control Technology: Applications and Lessons Learned Jan. 1995 10 p In FRENCH (For primary document see N95-31989 11-08)

Copyright Avail: CASI HC A02/MF A04

The characteristic of a fuzzy controller is to use a knowledge expressed in natural language in the forms of expert rules to calculate the value of the control starting from the numerical information from the sensors. The implementation of such a pilot requires the interpretation of the numerical field symbolically and reciprocally. This is carried out by the use of fuzzy assemblies. The associated theory allows starting from consideration of precise measurement, the whole of the stated expert rules, and choice of suitable operators to deduce a value from control. It results in a particular structure of the fuzzy controllers, whose main characteristics are the subject of the first part of the presentation. The implementation on the example of the longitudinal pilot control of an aircraft is then presented. Two approaches were adopted: the first uses the rules of manual piloting formulated in natural language by the 'experts' who are the pilots. The second uses the laws resulting from a conventional autopilot to build rules of piloting. The results are presented in the perspective from a comparison between the two types of controllers, conventional or fuzzy. Transl. by CASI

N95-31998# Wright Lab., Wright-Patterson AFB, OH.

THE CONTROL SYSTEM DESIGN METHODOLOGY OF THE STOL AND MANEUVER TECHNOLOGY DEMONSTRATOR

David J. Moorhouse and Kevin D. Citurs (McDonnell-Douglas Aerospace, Saint Louis, MO.) *In* AGARD, Active Control Technology: Applications and Lessons Learned Jan. 1995 11 p (For primary document see N95-31989 11-08)

Copyright Avail: CASI HC A03/MF A04

This paper documents the development of a full-envelope Integrated Flight/Propulsion Control system. A combination of classical and multivariable design methodologies was used, including a unique inverse procedure to produce second-order equivalent systems meeting specified flying qualities requirements. The implementation was based on a rational choice between the two methodologies. It is suggested that a parallel design approach in the beginning will produce efficient convergence on a practical optimum design. Finally, all control law revisions should be done analytically and only evaluated by simulation. Regardless of the design technique used, the process begins by specifying detailed design guidelines selected to meet the intent of MIL-F-8785C. Once the designs were complete and analyzed based on the design guidelines, manned flight simulation was used only to validate and demonstrate the flying qualities achieved prior to flight test. Problems encountered during simulation or flight testing were addressed first by reviewing the original design guidelines and evaluating the success achieved in implementing them. Derived from text

N95-31999# Aeronautica Macchi S.p.A., Varese (Italy).

CONTROL LAW DESIGN USING H-INFINITY AND MU-SYNTHESIS SHORT-PERIOD CONTROLLER FOR A TAIL-AIRPLANE

L. Mangiacasale *In* AGARD, Active Control Technology: Applications and Lessons Learned Jan. 1995 11 p (For primary document see N95-31989 11-08)

Copyright Avail: CASI HC A03/MF A04

The recently developed methods H-infinity and mu-Synthesis are used in the design of a control law for a tail controlled unstable airplane. The design procedure has been applied with success and seems to be very promising in order to solve control design problems in real applications. The (H-infinity) + mu controller, characterized by a very large order (namely 34th), has been successfully reduced to one having order 5th with a very low decay in the overall performance. The reduced-order controller meets all the servo technical specifications demanded to the full-order one. At present it is under test as part of a 6-DoF simulation program to verify its real robustness in face of structured and unstructured perturbations. Author

N95-32000# Deutsche Forschungsanstalt fuer Luft- und Raumfahrt, Brunswick (Germany). Inst. fuer Flugmechanik.

MODEL FOLLOWING CONTROL FOR TAILORING HANDLING QUALITIES: ACT EXPERIENCE WITH ATTHeS

Gerd Bouwer, Wolfgang vonGruenhagen, and Heinz-Juergen Pausder *In* AGARD, Active Control Technology: Applications and Lessons Learned Jan. 1995 15 p (For primary document see N95-31989 11-08)

Copyright Avail: CASI HC A03/MF A04

In-flight simulators will play an important and unique role in the development process of future helicopter systems and in generating credible handling qualities data which establish design guides for the integrated helicopter systems including sophisticated cockpit technologies and high authority control systems. The Institute for Flight Mechanics of DLR has developed the helicopter in-flight simulator ATTHeS (Advanced Technology Testing Helicopter System) which is based on a BO 105 helicopter. The testbed is equipped with a full authority nonredundant fly-by-wire control system for the main rotor and a fly-by-light system for the tail rotor. In the simulation mode the testbed requires a two-man crew, a simulation and a safety pilot. The onboard computer system consists of two computers to which are assigned the separated tasks, data collection and digital control system. With the implemented software structure the flexibility is achieved to change the control laws without any changes in the real time process. Before undergoing any flight test with a new or modified control system, a real-time hardware/software-in-the-loop ground-based simulation has to be successfully performed. For the purposes of in-flight simulation an explicit model following control system was developed and the model following performance was evaluated in flight. This control system is composed of a dynamic feedforward, based on an extended model of the host helicopter, and an optimized feedback control system. The capability and flexibility of ATTHeS has been demonstrated in different test programs which have been related to the use of the testbed for test pilot training, handling qualities research, helicopter simulation, and control law design and evaluation including automatic navigation and hover position hold. Author

N95-32001*# National Aeronautics and Space Administration. Hugh L. Dryden Flight Research Center, Edwards, CA.

X-29 FLIGHT CONTROL SYSTEM: LESSONS LEARNED

Robert Clarke, John J. Burken, John T. Bosworth, and Jeffrey E. Bauer *In* AGARD, Active Control Technology: Applications and Lessons Learned Jan. 1995 15 p (For primary document see N95-31989 11-08)

Copyright Avail: CASI HC A03/MF A04

Two X-29A aircraft were flown at the NASA Dryden Flight Research Center over a period of eight years. The airplanes' unique features are the forward-swept wing, variable incidence close-coupled canard and highly relaxed longitudinal static stability (up to 35-percent negative static margin at subsonic conditions). This paper describes the primary flight control system and significant modifications made to this system, flight test techniques used during envelope expansion, and results for the low- and high-angle-of-attack programs. Throughout the paper, lessons learned will be discussed to illustrate the problems associated with the implementation of complex flight control systems. Author

N95-32002# Deutsche Forschungsanstalt fuer Luft- und Raumfahrt, Brunswick (Germany). Inst. of Flight Mechanics.

ADVANCED GUST MANAGEMENT SYSTEMS: LESSONS LEARNED AND PERSPECTIVES

R. Koenig, K.-U. Hahn, and J. Winter (Dornier Luftfahrt G.m.b.H., Friedrichshafen, Germany.) *In* AGARD, Active Control Technology: Applications and Lessons Learned Jan. 1995 17 p (For primary document see N95-31989 11-08)

Copyright Avail: CASI HC A03/MF A04

Aircraft operations at low altitudes often are affected by strong gusts and turbulence producing additional aerodynamic forces and moments. This results in extra aircraft accelerations and therefore in an unpleasant impact on passenger comfort and pilot workload as well as in extra structural loads. Active Control Technology is able to suppress these effects partly. The knowledge about the potential for improvement, the parameters of influence and the performance requirements for such gust alleviation systems is still quite small. Since the mid-seventies Dornier and DLR (Institute of Flight Mechanics) have been working together on BMFT programs developing systems to improve the ride quality in gusty weather. The developed Open-Loop Gust Alleviation System OLGA was investigated through dynamic wind tunnel experiments and flight-tested onboard the experimental aircraft Do 128 TNT. This research was continued by DLR developing the Load Alleviation and Ride Smoothing System LARS using the modified VFW 614 aircraft ATTAS (Advanced Technologies Testing Aircraft System). The Deutsche Aerospace Dornier Luftfahrt GmbH has concentrated on simulation studies for their aircraft types Do 228 and Do 328. The presented paper provides a brief description of the advantages of overall gust management systems considering lift, drag and pitch control. The following topics will be presented in detail: (1) the basic flight mechanics of gust load alleviation; (2) the design of integrated gust management systems; (3) simulation and flight test results; and (4) lessons learned and general perspectives. Author

N95-32003# Wright Lab., Wright-Patterson AFB, OH. Flight Dynamics Directorate.

FLIGHT EVALUATION OF FOREBODY VORTEX CONTROL IN POST-STALL FLIGHT **c05**

Lawrence A. Walchli *In* AGARD, Active Control Technology: Applications and Lessons Learned 10 P (SEE N95-31989 11-08) Jan. 1995 (For primary document see N95-31989 11-08)

Copyright Avail: CASI HC A02/MF A04

Loss of directional stability in a post-stall flight environment has become a major design issue for future fighter aircraft. Numerous studies have addressed this issue, either from an aerodynamics perspective or through use of propulsive forces generated by vectoring exhaust nozzles. The X-29 aircraft, with its forward swept wing and other advanced technologies, suffers loss of directional power above 40 degrees angle of attack (AOA). An exploratory development program was undertaken on this configuration to regain the lost stability through use of a pneumatic system on the aircraft nose which influenced the external flow field, generating significant side forces useful for control. Wind tunnel test results were inserted into the X-29 flight simulator at NASA Dryden Flight Research Facility and the simulator was used to support a critical flight experiment of this technology. This experiment is the subject of this paper. Author

N95-32004# Dornier Luftfahrt G.m.b.H., Friedrichshafen (Germany).

AUTOMATIC FLIGHT CONTROL SYSTEM FOR AN UNMANNED HELICOPTER SYSTEM DESIGN AND FLIGHT TEST RESULTS

M. Weidel and W. Alles *In* AGARD, Active Control Technology: Applications and Lessons Learned Jan. 1995 p 10 (For primary document see N95-31989 11-08)

Copyright Avail: CASI HC A02/MF A04

The use of unmanned air vehicles (UAV) in support of the Navy from small ships to fulfill tasks such as reconnaissance of large areas will succeed only if the user gains a high amount of confidence in the reliable operation of such a system, especially during the take off and landing phase. Take off from and landing on small landing pads on aviation facility ships in all-weather conditions prefer the application of VTOL-UAV's (Vertical Take Off and Landing) with a coaxial rotor system. Manual take off and landing procedures which have to be applied during operational service both at day time and at night under all-weather conditions and ship motions overtax the service personnel already at low sea states. This fact requires automatic take off and landing procedures. The German Ministry of Defence commissioned Dornier (DASA) in November 1990 with the development, test and demonstration of an automatic take off and landing system on the basis of the Gyrodyne QH-50 drone helicopter in order to prove the feasibilty of such a system in general. The essential ship and sea state dependent motions of the landing pad - roll, pitch and heave - were simulated with a ship deck simulator. The customer's requirement consisted of ten automatic take offs and landings of the UAV from a 4 by 4 meters landing pad. The test and demonstration phase was performed on the airfield of Friedrichshafen in the presence of experts from several NATO-Countries by the end of 1991. Derived from text

N95-32005# British Aerospace Defence Ltd., Preston (England). Military Aircraft Div.

THE FCS-STRUCTURAL COUPLING PROBLEM AND ITS SOLUTION

B. D. Caldwell *In* AGARD, Active Control Technology: Applications and Lessons Learned Jan. 1995 13 p (For primary document see N95-31989 11-08)

Copyright Avail: CASI HC A03/MF A04

Implementation of ACT in aircraft is now almost routine, and often essential in realizing performance requirements. However, unless a proactive and thorough approach is taken to ensuring that the effects of the flexibility of the airframe structure and its interaction with the FCS (Flight Control System) are analyzed and accounted for, costly development delays and control system redesigns may ensue. This paper is intended to discuss the basis of the phenomenon referred to at BAe Warton as FCS-Structural Coupling, the evolution of the methodology evolved at Warton to ensure

freedom from its effects, and the development directions required to advance the state of art in this field. Author

N95-32006# Deutsche Forschungsanstalt fuer Luft- und Raumfahrt, Goettingen (Germany).
STRUCTURAL ASPECTS OF ACTIVE CONTROL TECHNOLOGY
H. Hoenlinger, H. Zimmermann (Deutsche Aerospace A.G., Bremen, Germany.), O. Sensburg (Deutsche Aerospace A.G., Munich, Germany.), and J. Becker (Deutsche Aerospace A.G., Munich, Germany.) *In* AGARD, Active Control Technology: Applications and Lessons Learned Jan. 1995 25 p (For primary document see N95-31989 11-08)
Copyright Avail: CASI HC A03/MF A04

A survey on the structural relevant applications of Active Control Technology is presented. The benefits and disadvantages of various active control systems for transport and fighter aircraft are discussed. The problem of adverse structural coupling is addressed and possible solutions are outlined. The Smart Structure Technology offers new applications for active control technology, but to exploit the full potential of this technology multidisciplinary design methods have to be improved. Author

N95-32007# Air Force Flight Test Center, Edwards AFB, CA.
FLIGHT TEST RESULTS OF THE F-16 AIRCRAFT MODIFIED WITH AXISYMMETRIC VECTORING EXHAUST NOZZLE **c05**
D. Kidman and D. Vanhoy *In* AGARD, Active Control Technology: Applications and Lessons Learned Jan. 1995 19 p (For primary document see N95-31989 11-08)
Copyright Avail: CASI HC A03/MF A04

This paper presents results from flight testing an F-16 aircraft modified with the Axisymmetric Vectoring Exhaust Nozzle (AVEN). This includes an assessment of the AVEN nozzle and the modified F-16 flight control system to provide stability and control power in an expanded maneuvering envelope, an assessment of flying qualities, and an overall assessment of tactical utility. Also included are lessons learned regarding the testing and implementations of active control technology. Author

N95-32008# Dassault Aviation, Saint-Cloud (France).
CATAPULT-LAUNCHING OF THE RAFALE DESIGN AND EXPERIMENTATION [CATAPULTAGE DU RAFALE CONCEPTION ET EXPERIMENTATION] **c05**
D. Fleygnac and L. Lequeux *In* AGARD, Active Control Technology: Applications and Lessons Learned Jan. 1995 12 p In FRENCH (For primary document see N95-31989 11-08)
Copyright Avail: CASI HC A03/MF A04

The RAFALE program was conceived from the beginning to define, develop and produce a general-purpose aircraft meeting the future needs of the State - the Army, Air Force, and Navy. The Navy version is intended to equip the French naval air forces by the end of the decade. It will operate starting from the conventional propulsion Foch and the Charles De Gaulle nuclear aircraft carrier. Furnished with a numerical flight control system, the RAFALE M01 prototype is the first aircraft with delta canards to be catapulted from an aircraft carrier (April 1993). It is also the first naval aircraft to use the original method of catapult-assisted dihedral launching. The study of naval aircraft catapult launching combines the technical disciplines implicit in the design of fighter aircraft: aerodynamics, structure, flight control, and aircraft systems. In the framework of this conference, the discussion has particularly focused on flight dynamics. It covers: the specifications of the RAFALE naval launching; some related aspects at the aircraft catapult design: flight control system, improved performance systems (dihedral launch, high-energy recovery rate); the ground tests; and the tests at sea. Transl. by CASI

N95-32009# Alenia Aeronautica, Turin (Italy). Flight Mechanics Group.
DIGITAL AUTOPILOT DESIGN FOR COMBAT AIRCRAFT IN ALENIA
Aldo Tonon and Pier Luigi Bellusti *In* AGARD, Active Control Technology: Applications and Lessons Learned Jan. 1995 13 p (For primary document see N95-31989 11-08)
Copyright Avail: CASI HC A03/MF A04

ALENIA - Aeronautica has been involved in Digital Autopilot design for the AMX and EF 2000 programs. The AMX is a subsonic attack aircraft whose Flight Control System is based on Fly-by-wire technology, incorporating an Hybrid Analog and Digital Flight Control Computer for Control and Stability augmentation in pitch, roll and yaw axes, which guarantees the aircraft capability of full performance; in addition the Flight Control System has also a conventional mechanical back-up in the pitch and roll axes, which guarantees aircraft safe re-entry after failure of both hydraulic and both electrical circuits. The paper deals with the development history of the AMX autopilot through design to flight test. In particular the paper addresses the design to specification relationship, the system development and clearance process and the flight test results. The EF 2000 programme is an international development for an agile, highly unstable Fly-by-Wire Air Superiority fighter. Within the EF 2000 consortium ALENIA has the responsibility for Basic Autopilot design. This design, currently in the early stages of development, poses peculiar problems due to the interaction of Autopilot (external) feedback loops and the basic stabilization (inner) loops. The paper address these peculiar aspects in conjunction with the specific design methodologies applied. Author

N95-32010# British Aerospace Defence Ltd., Warton (England).
EXPERIMENTAL AIRCRAFT PROGRAMME (EAP): FLIGHT CONTROL SYSTEM DESIGN AND TEST
A. McCuish *In* AGARD, Active Control Technology: Applications and Lessons Learned Jan. 1995 14 p (For primary document see N95-31989 11-08)
Copyright Avail: CASI HC A03/MF A04

The objectives of the Experimental Aircraft Programme were to demonstrate various technologies relevant to a future combat aircraft within the rigors imposed by having to achieve flight clearance and demonstration. Prime areas for demonstration, among others, were modern cockpit displays, avionics systems integration, advanced material construction, advanced aerodynamics and active flight control. Nearly all future combat aircraft will have an unstable basic airframe due to the advantages that are accrued: smaller, lighter, aerodynamically more efficient, etc. Necessary to such an aircraft is a full time active control system. This paper outlines the philosophy and method taken to design the flight control laws and relates their development through the life of the programme. The experience gained from the three phase, 259 flight test programme is summarized. The success of the flight programme has provided a wealth of experience from the operation of the aircraft. In particular, and most impressive to the pilots, was the carefree handling capability; this was considered remarkable. A further success was the complete absence of pilot induced oscillation (PIO) tendency throughout the whole of the flight programme. Author

N95-32011# Air Force Flight Test Center, Edwards AFB, CA.
AN INVESTIGATION OF PILOT INDUCED OSCILLATION PHENOMENA IN DIGITAL-FLIGHT CONTROL SYSTEMS
William A. Flynn and Robert E. Lee *In* AGARD, Active Control Technology: Applications and Lessons Learned Jan. 1995 6 p (For primary document see N95-31989 11-08)
Copyright Avail: CASI HC A02/MF A04

This paper summarizes the results of a technical review of pilot induced oscillations (PIO) in aircraft equipped with digital flight control systems. A review of the causes of PIO, the specific interaction of digital flight control systems, and an evaluation of the flight control development process was conducted. The paper discusses the highlights of the technical review and the recommendations for future development of flight control systems to reduce the occurrences of handling qualities problems in general and PIO in particular. Author

N95-32012# British Aerospace Defence Ltd., Warton (England). Aerodynamics Dept.
FLIGHT DEMONSTRATION OF AN ADVANCED PITCH CONTROL LAW IN THE VAAC HARRIER AIRCRAFT
C. Fielding, S. L. Gale (Defence Research Agency, Bedford, England.), and D. V. Griffith (Defence Research Agency, Bedford, England.) *In* AGARD, Active Control Technology: Applications and Lessons Learned Jan. 1995 12 p Sponsored by UK Ministry of Defence (For primary document see N95-31989 11-08)
Copyright Avail: CASI HC A03/MF A04

'Vectored thrust Aircraft Advanced flight Control' (VAAC) is a UK project, sponsored by the Ministry of Defence and managed by the Defence Research Agency (DRA). The project is investigating, through ground-based simulation and flight test on the VAAC Harrier research aircraft, the low speed flight control, handling and cockpit display concepts applicable to an aircraft replacing the Harrier. As part of the project, British Aerospace

Defence Limited have designed a revolutionary two-inceptor pitch plane control law for assessment on the project aircraft. This Control Law has now been flight tested and further developed 'in-flight' by the DRA, culminating in a series of successful flight demonstrations to guest pilots. During the latter stages of flight testing the Control Law was modified to allow single-inceptor operation. Flight testing has shown that both the two- and single-inceptor control strategies result in a large reduction in pilot workload, when compared with the VAAC Harrier's three-inceptor arrangement, during the transition from wing-borne to jet-borne flight and hover. This paper describes the Control Law's evolution from initial concept through to the results obtained from flight testing. Author

N95-32013# Deutsche Aerospace A.G., Munich (Germany). Military Aircraft Div.

X-31: A PROGRAM OVERVIEW AND FLIGHT TEST STATUS c05

H. Ross and U. Neuberger *In* AGARD, Active Control Technology: Applications and Lessons Learned Jan. 1995 7 p (For primary document see N95-31989 11-08)

Copyright Avail: CASI HC A02/MF A04

The objective of the X-31 program (the first international US/German experimental program) was to develop a new fighter that can execute tactical maneuvers up to an angle of attack (AOA) of 70 degrees (which is far beyond the stall AOA) without the pilot losing control of the aircraft (poststall capability, PST). This capability extends aircraft performance with respect to deceleration capability, turn rate and radius, and pointing capability for weapon firing considerably and results in a distinctive improvement of the tactical advantages in close-in combat. The prerequisite for these capabilities is the use of thrust vector control to boost or even replace the aerodynamic controls which lose their effectiveness at low speeds and in the poststall regime. The technical development of the PST capability requires the application of new technologies in the areas of aerodynamics (separated vortex flow), propulsion (inlet aerodynamics and jet deflection) and in particular, flight control (unstable configurations, digital flight control systems, integrated thrust vector control). Flight test results of the X-31 showed that the four important basic maneuvers (safe flight and maneuvering at 70 deg. AOA, 360 deg. rolls about the velocity at 70 deg. AOA, poststall maneuvers at high load factors, and the 180 deg. J (or Herbst) turn with extremely small turn radii and high turn rates) have been successfully demonstrated. In Nov./Dec. 1993 the flight envelope was extended into the supersonic and flights with a helmet mounted display (HMD) were conducted. This paper gives an overview of the X-31 program and the results of the test flights. CASI

N95-32014# Boeing Defense and Space Group, Philadelphia, PA. Helicopters Div.

ADVANCED FLIGHT CONTROL TECHNOLOGY ACHIEVEMENTS AT BOEING HELICOPTERS

Kenneth H. Landis, Charles Dabundo, James M. Davis, and James F. Keller *In* AGARD, Active Control Technology: Applications and Lessons Learned Jan. 1995 16 p (For primary document see N95-31989 11-08)

Copyright Avail: CASI HC A03/MF A04

Over the last two decades, flight control system requirements have been in a state of transition. Rotary wing missions have become more demanding, requiring vehicle management systems capable of conducting highly aggressive missions under night / adverse-weather conditions in severe electromagnetic environments. The digital, fly-by-wire / optics control system technologies developed at Boeing Defense and Space Group, Helicopters Division to meet these air vehicle requirements are overviewed. These technologies, which integrate digital multimode control laws and sidestick controllers within redundant-reconfigurable architectures, provide the rotorcraft capabilities required for the 21st century. The advances in flight control design, as developed during various technology demonstrator programs and applied in production of the V-22 Osprey tiltrotor and the RAH-66 Comanche scout / attack helicopter, are summarized. Author

N95-32015# National Research Council of Canada, Ottawa (Ontario). Flight Research Lab.

PRACTICAL EXPERIENCES IN CONTROL SYSTEMS DESIGN USING THE NCR BELL 205 AIRBORNE SIMULATOR

Stewart W. Baillie, J. Murray Morgan, and Kevin R. Goheen *In* AGARD, Active Control Technology: Applications and Lessons Learned Jan. 1995 12 p (For primary document see N95-31989 11-08)

Copyright Avail: CASI HC A03/MF A04

The objective of this paper is to describe a variety of examples of control system design and application on the NRC Bell 205 Airborne Simulator. For background, this paper will first examine the physical characteristics of the Bell 205 and the mathematical models which have been developed to describe them. The paper then reviews the classical control design techniques which have been used to develop high bandwidth rate and attitude response type systems on the aircraft, and describes the empirically determined fixes which have become standard elements of these types of systems. To complete the paper, two sections will deal with application of modern control theories; the first describes a limited effort to develop a translational rate command system using a six degree of freedom model of the Bell 205 and a publicly available software package, MATLAB/Simulink. The second modern control theory section deals with a more detailed study performed in collaboration with Carleton University and supported by DND/CRAD to devise modern control theory controllers for the Bell 205. All discussions of the paper are substantiated with actual in-flight validation data to clearly demonstrate design successes and failures. Author

N95-32016# Aerospatiale, Toulouse (France). Handling Qualities Dept.

FLYING QUALITIES OF CIVIL TRANSPORT AIRCRAFT WITH ELECTRICAL FLIGHT CONTROL [LES QUALITIES DE VOL DE AVIONS DE TRANSPORT: CIVIL A COMMANDES DE VOL ELECTRIQUES]

D. Chatrenet *In* AGARD, Active Control Technology: Applications and Lessons Learned Jan. 1995 5 p In FRENCH (For primary document see N95-31989 11-08)

Copyright Avail: CASI HC A01/MF A04

This conclusion to the the conference covers the flying qualities and flight control systems (FCS) of transport aircraft equipped with electrical flight control systems, as seen by Aerospatiale. A retrospective look at the related technological developments over the past 25 years precedes a comparison between the Airbus A340 and A320. The main points in the differences between the FCS in the A320 and the A340 are associated with the compensation effects of the more flexible structure of the A340, its design for long-range ('minimum drag'), and the inherent limitations in take-off performance. Derived from text

N95-32017# British Aerospace Defence Ltd., Preston (England). Military Aircraft Div.

PILOT INDUCED OSCILLATION: A REPORT ON THE AGARD WORKSHOP ON PIO

K. McKay *In* AGARD, Active Control Technology: Applications and Lessons Learned Jan. 1995 10 p Workshop held on 13 May 1994 (For primary document see N95-31989 11-08)

Copyright Avail: CASI HC A02/MF A04

Instability of the pilot/airframe combination has been a problem from the beginning of manned flight. The rapid advances made in aviation following the Second World War greatly increased the incidence of PIO problems and led to a large amount of research and development work aimed at understanding and mitigating these difficulties. Criteria and requirements were developed which could be used in design to obtain satisfactory PIO qualities. Nevertheless, in spite of all this work, and even with the great flexibility in modern control technologies available to the designer, PIO problems still often occur with new aircraft; in fact it is the power and responsiveness of modern control systems which makes them susceptible to various 'non-linear' effects such as time delays, rate limits, actuator saturation, etc., leading to unexpected PIO difficulties. With current experience, it is clear that a universal solution of the PIO problem still evades the engineering community. The cost of these problems in programme delay and financial terms is significant. The gathering together of specialists to discuss this problem, from their various points of view, has led to positive gains in the state of knowledge regarding PIOs; it has provided a significant step toward their elimination and contributed to the avoidance of PIO associated programme costs and penalties. This paper provides an overview of the results from the Workshop. Fuller details are to be published by AGARD in the proceedings of the Conference and Workshop in the near future and in a separate Advisory Report. Author

N95-32111 California Univ., Los Angeles, CA.
VIBRATION REDUCTION IN HELICOPTER ROTORS USING AN ACTIVELY CONTROLLED PARTIAL SPAN TRAILING EDGE FLAP LOCATED ON THE BLADE Ph.D. Thesis
Thomas Alexander Millott 1993 519 p
Avail: Univ. Microfilms Order No. DA9420455

This dissertation describes the development of an aeroelastic analysis of a four-bladed hingeless helicopter rotor configuration incorporating an individually controlled aerodynamic surface located on each blade, and its application to the simulation of helicopter vibration reduction through individual blade control (IBC). The structural, inertial, and aerodynamic loads on an isolated rotor blade and control surface combination with fully coupled flap-lag-torsional dynamics are developed explicitly using a symbolic computing facility. Two blade models are used: the first is a simple offset-hinged spring restrained rigid blade model, and the second is a more realistic fully elastic blade model. The inertial loads on the blade are developed using D'Alembert's principle and quasi-steady aerodynamics, including the effects of a partial span trailing edge flap, is used to formulate the aerodynamic loads. Four blades are combined in a FORTRAN code to represent a four-bladed fixed hub hingeless rotor blade configuration. The rotor trim and blade response solutions are treated in a fully coupled manner using the harmonic balance technique. Various open-loop and closed-loop controllers based on global and local system models are implemented to reduce 4/rev vibratory hub loads using both an actively controlled aerodynamic surface on each blade as well as conventional IBC, in which the complete blade undergoes cyclic pitch change. The effectiveness of the two approaches for the simultaneous reduction of the 4/rev hub shears and hub moments is compared. It was found that both approaches are very effective in producing substantial vibration reduction. Comparisons of power requirements to implement the control were carried out and it was discovered that conventional IBC requires 5 to 25 times more power to achieve approximately the same degree of vibration reduction. The effect of blade torsional flexibility on the vibration reduction effectiveness of the actively controlled aerodynamic surface was also considered and it was found that this parameter has a very substantial influence. This study clearly demonstrates the feasibility of this novel concept for vibration reduction. Based on the results obtained, this is potentially one of the most effective means for vibration reduction. Furthermore it has the unique feature that it does not utilize the conventional swashplate of the helicopter and thus it has no effect on its airworthiness characteristics.

Dissert. Abstr.

N95-31071# Deutsche Forschungsanstalt fuer Luft- und Raumfahrt, Brunswick (Germany). Inst. fuer Flugmechanik.
HANDLING QUALITIES ANALYSIS ON RATE LIMITING ELEMENTS IN FLIGHT CONTROL SYSTEMS
Dietrich Hanke *In* Advisory Group for Aerospace Research and Development, Flight Vehicle Integration Panel Workshop on Pilot Induced Oscillations Feb. 1995 18 p (For primary document see N95-31061 11-03)
Copyright Avail: CASI HC A03/MF A02

09 RESEARCH AND SUPPORT FACILITIES (AIR)

Includes airports, hangars and runways; aircraft repair and overhaul facilities; wind tunnels; shock tubes; and aircraft engine test stands.

For related information see also *14 Ground Support Systems and Facilities (Space).*

N95-30493 Maryland Univ., College Park, MD.
A NUMERICAL STUDY OF THE STARTING PROCESS IN A HYPERSONIC SHOCK TUNNEL Ph.D. Thesis
Jang-Yeon Lee 1993 217 p
Avail: Univ. Microfilms Order No. DA9425077

This dissertation represents the first time calculations have been made of the unsteady viscous simulation of the starting process in a hypersonic shock tunnel including the bifurcation phenomenon due to the interaction of the reflected shock with the boundary layer generated by the incident shock in the shock tube. In order to simulate the unsteady viscous flow in the NASA Ames 16-inch hypersonic shock tunnel, which consists of axisymmetric shapes (shock tube and nozzle), rectangular shape (test cabin), and octagonal shape (diffuser), a time-dependent ADI (alternating direction implicit) axisymmetric full Navier-Stokes code with a second order upwind TVD (total variation diminishing) scheme and a time-dependent three-dimensional thin layer Navier-Stokes code with an explicit MacCormack TVD scheme have been developed. As shown in the code validation study, these Navier-Stokes codes with the high resolution TVD algorithms give fair agreement with available experimental data and exact solutions. Numerical simulations of the starting process for the NASA Ames 16-inch hypersonic shock tunnel show that during the reflected shock interaction process at the end of the shock tube, the bifurcation phenomenon and the strong vortices become dominant features. The vortices due to the reflected shock interactions appear in the axisymmetric simulation but are not generated in the two-dimensional flow. For the nominal testing condition, the starting process in the NASA Ames shock tunnel takes 1700 microsec. The required total testing time consists of the time for the starting process, 1.7 m sec, and the time for the flow establishment over a model in the test cabin which strongly depends on the model shape and size and model mounting location. For a 10 deg-cone model, the minimum required testing time is estimated as at least 2.7 m sec for the steady state.

Dissert. Abstr.

N95-30592*# National Aeronautics and Space Administration. Lewis Research Center, Cleveland, OH.
NASA LEWIS RESEARCH CENTER'S PREHEATED COMBUSTOR AND MATERIALS TEST FACILITY
Steve A. Nemets (NYMA, Inc., Brook Park, OH.), Robert C. Ehlers (NYMA, Inc., Brook Park, OH.), and Edith Parrott Jun. 1995 11 p
(Contract NAS3-27186; RTOP 505-62-84)
(NASA-TM-106676; E-9012; NAS 1.15:106676) Avail: CASI HC A03/MF A01

The Preheated Combustor and Materials Test Facility (PCMTF) in the Engine Research Building (ERB) at the NASA Lewis Research Center is one of two unique combustor facilities that provide a nonvitiated air supply to two test stands, where the air can be used for research combustor testing and high-temperature materials testing. Stand A is used as a research combustor stand, whereas stand B is used for cyclic and survivability tests of aerospace materials at high temperatures. Both stands can accommodate in-house and private industry research programs. The PCMTF is capable of providing up to 30 lb/s (pps) of nonvitiated, 450 psig combustion air at temperatures ranging from 850 to 1150 g F. A 5000 gal tank located outdoors adjacent to the test facility can provide jet fuel at a pressure of 900 psig and a flow rate of 11 gal/min (gpm). Gaseous hydrogen from a 70,000 cu ft (CF) tuber is also available as a fuel. Approximately 500 gpm of cooling water cools the research hardware and exhaust gases. Such cooling is necessary because the air stream reaches temperatures as high as 3000 deg F. The PCMTF provides industry and Government with a facility for studying the combustion process and for obtaining valuable test information on advanced materials. This report describes the facility's support systems and unique capabilities. Author

N95-30926 Environmental Protection Agency, Research Triangle Park, NC. Office of Research and Development.
DEMONSTRATION OF SPLIT-FLOW VENTILATION AND RECIRCULATION AS FLOW-REDUCTION METHODS IN AN AIR FORCE PAINT SPRAY BOOTH, VOLUME 2 Final Report, 15 Feb. 1991 - 9 Jan. 1992
S. Hughes, J. Ayer, and R. Sutay 27 Jul. 1994 179 p Limited Reproducibility: More than 20% of this document may be affected by microfiche quality
(AF Proj. 2103)
(AD-A286808; EPA/600/R-94/214B) Avail: CASI HC A09

During a series of painting operations in a horizontal-flow paint spray booth at Travis AFB, CA, baseline concentrations of four classes of toxic airborne pollutants were measured at 24 locations across a plane immediately forward of the exhaust filters, in the exhaust duct, and inside and outside the respirator in the painter's breathing zone (BZ). The resulting data were analyzed and used to design a modified ventilation system that (1) separates a portion of the exhaust exiting the lower portion of the booth, which contains a concentration of toxic pollutants greater than the average at the exhaust plane (split-flow); and (2) provides an option to return the flow from the upper portion of the exhaust to the intake plenum for mixing with fresh air and recirculation through the booth (recirculation). After critical

review by cognizant Air Force offices, and an experimental demonstration showing that a flame ionization detector monitoring the air entering the booth is able to detect excursions above the equivalent exposure limit for the solvents in the paint, the exhaust duct was reconfigured for split-flow and recirculating ventilation. DTIC

N95-31101 Environmental Protection Agency, Research Triangle Park, NC. Office of Research and Development.

DEMONSTRATION OF SPLIT-FLOW VENTILATION AND RECIRCULATION AS FLOW-REDUCTION METHODS IN AN AIR FORCE PAINT SPRAY BOOTH, VOLUME 1 Final Report, 15 Feb. 1991 - 9 Jan. 1992

S. Hughes, J. Ayer, and R. Sutay 27 Jul. 1994 132 p Limited Reproducibility: More than 20% of this document may be affected by microfiche quality

(AF Proj. 2103)

(AD-A286807; EPA/600/R-94/214A) Avail: CASI HC A07

During a series of painting operations in a horizontal-flow paint spray booth at Travis AFB, CA, baseline concentrations of four classes of toxic airborne pollutants were measured at 24 locations across a plane immediately forward of the exhaust filters, in the exhaust duct, and inside and outside the respirator in the painter's breathing zone (BZ). The resulting data were analyzed and used to design a modified ventilation system that (1) separates a portion of the exhaust exiting the lower portion of the booth, which contains a concentration of toxic pollutants greater than the average at the exhaust plane (split-flow); and (2) provides an option to return the flow from the upper portion of the exhaust to the intake plenum for mixing with fresh air and recirculation through the booth (recirculation). After critical review by cognizant Air Force offices and an experimental demonstration showing that a flame ionization detector monitoring the air entering the booth is able to detect excursions above the equivalent exposure limit for the solvents in the paint the exhaust duct was reconfigured for split-flow and recirculating ventilation. DTIC

N95-31468# Federal Aviation Administration, Atlantic City, NJ.

EVALUATION OF ALTERNATIVE PAVEMENT MARKING MATERIALS Final Report

Keith W. Bagot Jan. 1995 50 p

(AD-A292973; DOT/FAA/CT-94/119) Avail: CASI HC A03/MF A01

This study was undertaken to evaluate potential alternative marking materials for use on airport pavement marking systems. The materials were evaluated for conspicuity, durability, rubber buildup, color retention, friction, environmental acceptability, and cost benefits. In all, five materials (two water-borne, two epoxies, and one methacrylic resin) were evaluated at three test airports around the country for a period of one year. The three test airports, chosen for their different climatic conditions, were Atlantic City, Greater Pittsburgh, and Phoenix Sky Harbor International airports. Epoxies and resins were more durable than water-borne paints in areas subject to heavy snowfall and snowplow activity, particularly when applied to Portland cement concrete surfaces. The epoxies tested, however, did show signs of yellowing after extensive ultraviolet exposure. It was also determined that the addition of silica and/or glass beads improved the conspicuity of the markings, improved friction, and minimized rubber adherence. The cost-benefit analysis showed that more durable materials and the addition of silica and/or beads does increase the initial cost of marking the airport surfaces but could reduce the number of painting cycles on many portions of the airport from several times per year to once every several years. DTIC

N95-31653*# NYMA, Inc., Brook Park, OH.

FLOW QUALITY IMPROVEMENTS IN THE NASA LEWIS RESEARCH CENTER 9- BY 15-FOOT LOW SPEED WIND TUNNEL Final Report

E. Allen Arrington and Jose C. Gonsalez Cleveland, OH NASA Jun. 1995 20 p Presented at the 31st Joint Propulsion Conference and Exhibit, San Diego, CA, 10-12 Jul. 1995; sponsored by AIAA, ASME, SAE, and ASEE

(Contract NAS3-27186; RTOP 505-62-82)

(NASA-CR-195439; E-9465; NAS 1.26:195439; AIAA Paper 95-2390)

Avail: CASI HC A03/MF A01

The NASA Lewis Research Center 9- by 15-Ft Low Speed Wind Tunnel (LSWT) was recently upgraded with the addition of several flow quality improvement devices: four 10-mesh turbulence reduction screens and a flow straightening honeycomb (3/8-in. cell, length to diameter ratio, L/D = 16) in the settling chamber upstream of the test section, and a diffuser extension fairing downstream of the test section. Test section flow quality was measured prior to and following the tunnel modifications. Comparison of the pre- (baseline) to post-tunnel modification flow quality data will provide a gage of the effectiveness of the flow quality devices. An instrumented rake was used to provide both calibration and flow-field survey data at several stations in the test section. The flow-field parameters measured included total and static pressure, total temperature, pitch and yaw components of flow angle, and turbulence; boundary layer total pressure surveys were also made. The data indicated very good flow quality in the test section at all survey stations in terms of total pressure, total temperature, Mach number and flow angularity distributions, and turbulence levels. The data compared with that collected before facility flow quality additions indicate improvement in the test section Mach number distribution, flow angle distribution, and turbulence levels as well as an increase in the usable test section width. The temperature distributions can be further improved by increasing the cooling water flow into the facility heat exchanger. Author

N95-32217*# National Aeronautics and Space Administration. Langley Research Center, Hampton, VA.

COMPUTER MODEL TO SIMULATE TESTING AT THE NATIONAL TRANSONIC FACILITY

Raymond E. Mineck, Lewis R. Owens, Jr., Richard A. Wahls, and Judith A. Hannon Aug. 1995 45 p Sponsored by NASA, Washington

(RTOP 505-59-10-31)

(NASA-TM-4664; L-17459; NAS 1.15:4664) Avail: CASI HC A03/MF A01

A computer model has been developed to simulate the processes involved in the operation of the National Transonic Facility (NTF), a large cryogenic wind tunnel at the Langley Research Center. The simulation was verified by comparing the simulated results with previously acquired data from three experimental wind tunnel test programs in the NTF. The comparisons suggest that the computer model simulates reasonably well the processes that determine the liquid nitrogen (LN2) consumption, electrical consumption, fan-on time, and the test time required to complete a test plan at the NTF. From these limited comparisons, it appears that the results from the simulation model are generally within about 10 percent of the actual NTF test results. The use of actual data acquisition times in the simulation produced better estimates of the LN2 usage, as expected. Additional comparisons are needed to refine the model constants. The model will typically produce optimistic results since the times and rates included in the model are typically the optimum values. Any deviation from the optimum values will lead to longer times or increased LN2 and electrical consumption for the proposed test plan. Computer code operating instructions and listings of sample input and output files have been included. Author

N95-32176# Esquimalt Defence Research Detachment, Victoria (British Columbia).

FACILITIES USED FOR PLASTIC MEDIA BLASTING

Terry Foster *In* AGARD, Environmentally Safe and Effective Processes for Paint Removal Apr. 1995 4 p (For primary document see N95-32165 11-31)

Copyright Avail: CASI HC A01/MF A01

12 ASTRONAUTICS (GENERAL)

For extraterrestrial exploration see *91 Lunar and Planetary Exploration.*

No abstracts in this category.

13 ASTRODYNAMICS

Includes powered and free-flight trajectories; and orbital and launching dynamics.

No abstracts in this category.

14 GROUND SUPPORT SYSTEMS AND FACILITIES (SPACE)

Includes launch complexes, research and production facilities; ground support equipment, e.g., mobile transporters; and simulators.

For related information see also *09 Research and Support Facilities (Air).*

No abstracts in this category.

15 LAUNCH VEHICLES AND SPACE VEHICLES

Includes boosters; operating problems of launch/space vehicle systems; and reusable vehicles.

For related information see also *20 Spacecraft Propulsion and Power.*

N95-30948# Army Research Lab., Aberdeen Proving Ground, MD.
A RASCAL IN-BORE DYNAMIC ANALYSIS OF THE TASK B AND TASK C ELECTROMAGNETIC RAILGUNS Report, Aug. - Sep. 1994
Lawrence W. Burton Apr. 1995 88 p
(AD-A292742; ARL-TR-726) Avail: CASI HC A05/MF A01

Previous RASCAL in-bore gun dynamics analyses 90-mm railguns have shown high transverse accelerations can be expected because of anomalies in the bore straightness. A request was made for similar analyses to be made for the Task B and Task C 90-mm railguns, with the Sabot Launched Electromagnetic Gun KE (SLEKE) 2 projectile design. Results of the RASCAL analyses showed the importance of matching the contact stiffness of the rear and front bore riders of the SLEKE 2 designs. Numerous cases were run to slow the effects of variations in contact stiffness. Mismatched contact stiffness resulted in elevated transverse accelerations at the less stiff of the two bore riding contacts. Comparisons of the results of this work are made against previous RASCAL analyses. These results verify the effect a kink in the bore centerline profile has on the projectile's in-bore response. DTIC

16 SPACE TRANSPORTATION

Includes passenger and cargo space transportation, e.g., shuttle operations; and space rescue techniques.

For related information see also *03 Air Transportation and Safety* and *18 Spacecraft Design, Testing and Performance.* For space suits see *54 Man/System Technology and Life Support.*

N95-30852* National Aeronautics and Space Administration. Lyndon B. Johnson Space Center, Houston, TX.
STS-71 POST FLIGHT PRESENTATION (Videotape)
18 Jul. 1995 Videotape: 31 min. 25 sec. playing time, in color, with sound
(NASA-TM-110658; JSC-1510; NONP-NASA-VT-95-59071) Avail: CASI VHS A02/BETA A22

The post flight presentation for the STS-71 Space Shuttle Atlantis Mission is featured on this video, with astronauts Gibson, Precourt, Baker, Harbough, Dunbar, Strekalov, Dezhurov, and Thagard, present for the press conference. They showed film footage and photographic slides of various pre-launch and launch activities, and onboard Shuttle activities and explained each of the different operations from the footage. CASI

N95-30873* National Aeronautics and Space Administration. Lyndon B. Johnson Space Center, Houston, TX.
STS-70 FLIGHT: DAY 8 (Videotape)
20 Jul. 1995 Videotape: 21 min. 30 sec. playing time, in color, with sound
(NASA-TM-110666; BRF1359H; NONP-NASA-VT-95-59164) Avail: CASI VHS A02/BETA A22

The eighth day of the STS-70 Space Shuttle Discovery mission is featured on this video. The crew is interviewed in orbit via satellite regarding their personal opinions about their mission before they return to Earth. CASI

N95-30874* National Aeronautics and Space Administration. Lyndon B. Johnson Space Center, Houston, TX.
STS-70 FLIGHT: DAY 7 (Videotape)
19 Jul. 1995 Videotape: 14 min. playing time, in color, with sound
(NASA-TM-110665; BRF1359G; NONP-NASA-VT-95-59165) Avail: CASI VHS A02/BETA A22

The seventh day of the STS-70 Space Shuttle Discovery mission is featured on this video. The astronauts obtained a successful alignment of the Hercules geo-locating camera and evaluated the manual setup procedures for the rotating wall Bioreactor. Specialist Don Thomas activated and deactivated the Microencapsulation in Space experiment, using a device that produces a timed-release of an antibiotic medication in a weightlessness environment. The Discovery crew begins to wrap up their experiments after a week of gathering data, ranging from observations of Earth's surface and atmosphere to biological studies. There are several minutes of Shuttle observations of Earth included. CASI

N95-30875* National Aeronautics and Space Administration. Lyndon B. Johnson Space Center, Houston, TX.
STS-70 FLIGHT: DAY 6 (Videotape)
18 Jul. 1995 Videotape: 31 min. playing time, in color, with sound
(NASA-TM-110664; BRF1359F; NONP-NASA-VT-95-59166) Avail: CASI VHS A02/BETA A22

The sixth day of the STS-70 Space Shuttle Discovery mission is featured on this video. During another trouble-free day, the crew again performed a variety of experiments ranging from optical studies to biological investigations. One such biological experiment showed orange colon cancer cells coalescing into globules. Using the Hercules Camera, the crew shot film footage of the Earth's surface and during the Windex experiment, several views of the Shuttle were shown. CASI

N95-30876* National Aeronautics and Space Administration. Lyndon B. Johnson Space Center, Houston, TX.
STS-70 FLIGHT: DAY 5 (Videotape)
17 Jul. 1995 Videotape: 25 min. 45 sec. playing time, in color, with sound
(NASA-TM-110663; BRF1359E; NONP-NASA-VT-95-59167) Avail: CASI VHS A02/BETA A22

The fifth day of the STS-70 Space Shuttle Discovery mission is contained on this video. The crew continues working on experiments, such as the Space Tissue Loss Analysis and the Bioreactor Development System. CNN reporter, John Holliman, interviewed the flight crew and the crew also answered questions posed by Internet users while on NASA's Shuttle Web. There are brief views of Earth's surface included. CASI

N95-30877* National Aeronautics and Space Administration. Lyndon B. Johnson Space Center, Houston, TX.
STS-70 FLIGHT: DAY 4 (Videotape)
16 Jul. 1995 Videotape: 30 min. playing time, in color, with sound
(NASA-TM-110662; BRF1359D; NONP-NASA-VT-95-59168) Avail: CASI VHS A02/BETA A22

The fourth day of STS-70 mission of Space Shuttle Discovery is contained on this video. With the spacecraft continuing to perform flawlessly, Discovery's crew begins work with various experiments, ranging from biological studies to use of earth-observing cameras. The crew held a press conference via satellite link and answered questions from reporters in Florida and Ohio. CASI

N95-30878* National Aeronautics and Space Administration. Lyndon B. Johnson Space Center, Houston, TX.
STS-70 FLIGHT: DAY 3 (Videotape)
15 Jul. 1995 Videotape: 30 min. playing time, in color, with sound
(NASA-TM-110661; BRF1359C; NONP-NASA-VT-95-59169) Avail: CASI VHS A02/BETA A22

The third day of the STS-70 mission of Space Shuttle Discovery is contained on this video. Astronauts Kregal and Thomas begin the day by working with the Hercules camera, which will record pinpoint data on the surface location of Earth observation imagery. Other work includes operations with an experiment that gauges astronauts' reflexes and hand-eye coordination. During the day, the crew spoke with World War 2 veteran, Harland Claussen,and ABC's Mike and Maty Show and the Toledo Blade newspaper (Toledo, Ohio) interviewed the astronauts via satellite link. CASI

N95-30879* National Aeronautics and Space Administration. Lyndon B. Johnson Space Center, Houston, TX.
STS-70 FLIGHT: DAY 2 (Videotape)
14 Jul. 1995 Videotape: 24 min. playing time, in color, with sound
(NASA-TM-110660; BRF1359B; NONP-NASA-VT-95-59170) Avail: CASI VHS A02/BETA A22

The second day of STS-70 Space Shuttle Discovery mission is contained on this video. The crew is shown onboard the Shuttle working on a variety of secondary experiments. These range from the Hercules camera, which imprints the latitude and longitude of areas photographed on Earth, to the Windex, which studies of the glow created as the Shuttle's surfaces interact with atomic oxygen in low Earth orbits. Also featured are astronauts Henricks, Kregal, and Weber answering questions from the general public via use of The New York Times On-Line Services. CASI

N95-30880* National Aeronautics and Space Administration. Lyndon B. Johnson Space Center, Houston, TX.
STS-70 FLIGHT: DAY 1 (Videotape)
13 Jul. 1995 Videotape: 29 min. 30 sec. playing time, in color, with sound
(NASA-TM-110659; BRF1359A; NONP-NASA-VT-95-59171) Avail: CASI VHS A02/BETA A22

The first day of the STS-70 flight of the Space Shuttle Discovery is contained on this video. This mission highlights the deploy of NASA's communications satellite, the sixth and last such satellite to be deployed from a space shuttle. The STS-70 crew consists of Commander Tom Henricke, Pilot Kevin Kregel, and Mission Specialists Don Thomas, Nancy Currie, and Mary Ellen Weber. Flight footage contains prelaunch and launch activities. CASI

17 SPACE COMM., SPACECRAFT COMM., COMMAND & TRACKING

Includes telemetry; space communications networks; astronavigation and guidance; and radio blackout.

For related information see also *04 Aircraft Communications and Navigation* and *32 Communications and Radar.*

N95-31849*# Communications Satellite Corp., Clarksburg, MD.
INFORMATION SWITCHING PROCESSOR (ISP) CONTENTION ANALYSIS AND CONTROL Final Report
Thomas Inukai Cleveland, OH NASA Jul. 1995 84 p
(Contract NAS3-25933; RTOP 506-72-21)
(NASA-CR-195471; E-9657; NAS 1.26:195471) Avail: CASI HC A05/MF A01

In designing a satellite system with on-board processing, the selection of a switching architecture is often critical. The on-board switching function can be implemented by circuit switching or packet switching. Destination-directed packet switching has several attractive features, such as self-routing without on-board switch reconfiguration, no switch control memory requirement, efficient bandwidth utilization for packet switched traffic, and accommodation of circuit switched traffic. Destination-directed packet switching, however, has two potential concerns: (1) contention and (2) congestion. And this report specifically deals with the first problem. It includes a description and analysis of various self-routing switch structures, the nature of contention problems, and contention and resolution techniques. Author

N95-32223*# Jet Propulsion Lab., California Inst. of Tech., Pasadena, CA.
RATE CONSIDERATIONS IN DEEP SPACE TELEMETRY
M. Costa, M. Belongie, and F. Pollara *In its* The Telecommunications and Data Acquisition Report 15 May 1995 p 9-15 (For primary document see N95-32221 11-32)
Avail: CASI HC A02/MF A03

N95-32225*# Jet Propulsion Lab., California Inst. of Tech., Pasadena, CA.
COMPUTER SIMULATION RESULTS FOR PCM/PM/NRZ RECEIVERS IN NONIDEAL CHANNELS
A. Anabtawi, T. M. Nguyen, and S. Million *In its* The Telecommunications and Data Acquisition Report 15 May 1995 p 27-53 (For primary document see N95-32221 11-32)
Avail: CASI HC A03/MF A03

N95-32226*# Jet Propulsion Lab., California Inst. of Tech., Pasadena, CA.
THE APPLICATION OF NONCOHERENT DOPPLER DATA TYPES FOR DEEP SPACE NAVIGATION
S. Bhaskaran *In its* The Telecommunications and Data Acquisition Report 15 May 1995 p 54-65 (For primary document see N95-32221 11-32)
Avail: CASI HC A03/MF A03

18 SPACECRAFT DESIGN, TESTING AND PERFORMANCE

Includes satellites; space platforms; space stations; spacecraft systems and components such as thermal and environmental controls; and attitude controls.

For life support systems see *54 Man/System Technology and Life Support.* For related information see also *05 Aircraft Design, Testing and Performance, 39 Structural Mechanics,* and *16 Space Transportation.*

N95-30841 Auburn Univ., AL.
A FEEDBACK LINEARIZATION APPROACH TO ORBITAL MANEUVERS Ph.D. Thesis
Sanguk Lee 1994 110 p
Avail: Univ. Microfilms Order No. DA9420253

New methods for obtaining optimal orbital maneuvers of a space vehicle in total velocity change are described and applied. The elegance of Lambert's Theorem is combined with feedback linearization and linear optimal control to obtain solutions to nonlinear orbital maneuver problems. In particular, geocentric orbital maneuvers with finite-thrust acceleration are studied. The full nonlinear equations of motion are transformed exactly into a controllable linear set in Brunovsky canonical form by using feedback linearization and choosing the position vector as the fully observable output vector. These equations are used to pose a linear optimal tracking problem with a solution to the Lambert's impulsive-thrust two-point boundary-value problem as the reference orbit. The same procedure is used to force the space vehicle to follow a linear analytical solution to the continuous low-thrust orbital maneuver problem between neighboring orbits. Limits on thrust magnitudes are enforced by adjusting the weights on the states in the performance index, which is chosen to be the sum of integrals of the square sum of new control variables and the square sum of state variable errors from the reference trajectory. For comparison purpose, the feedback linearized equations are used to obtain a simple closed-form solution to an orbital maneuver problem without the use of a reference trajectory. In this case, the performance index was chosen as the integral of the square sum of new control variables only. Three different examples, coplanar rendezvous between neighboring orbits, large coplanar orbit transfer, and non-coplanar orbit transfer, are used to show the advantages of using the new methods introduced in this dissertation. The minimum-eccentricity orbit,

Hohmann transfer orbit, and minimum energy orbit were used in turn as the reference trajectories. The principal problems encountered in using the new methods are the choices of the proper reference trajectory, a suitable time-dependent scalar weighting function, and appropriate constant weighting matrices. Dissert. Abstr.

N95-30854* National Aeronautics and Space Administration. Lyndon B. Johnson Space Center, Houston, TX.
MIR 18 POST FLIGHT PRESENTATION (Videotape)
18 Jul. 1995 Videotape: 29 min. 15 sec. playing time, in color, with sound
(NASA-TM-110657; JSC-1516; NONP-NASA-VT-95-59072) Avail: CASI VHS A02/BETA A22

The post flight presentation for the Mir 18 Mission is featured on this video, with both the American astronauts and Russian Cosmonauts present for the press conference. They included: Gibson; Precourt; Baker; Harbough; Dunbar; Strekalov; Dezhurov; and Thagard. Film footage and photographic slides of the various activities performed aboard the Mir Space Station and the spaceborne experiments accomplished during the flight mission are presented. Each of the operations are explained by the cosmonauts, with brief views of the Atlantis-Mir Earth orbital rendezvous over the Red Sea included. CASI

N95-30919# Naval Postgraduate School, Monterey, CA.
CONTROL OF FLEXIBLE SPACECRAFT STRUCTURES USING H-INFINITY WAVE ABSORBING CONTROL M.S. Thesis
Ronald E. Strong Dec. 1994 68 p
(AD-A293141) Avail: CASI HC A04/MF A01

This work studies the use of a wave absorbing control law for vibration suppression of flexible spacecraft structures. A major advantage of this method is that it does not involve truncation into a finite dimensional mathematical model. A closed loop scattering matrix was derived which gives the relationship between incoming waves, outgoing waves, sensor and actuator. The control law was determined by minimizing the H-infinity norm of this matrix. The control law was applied to the Naval Postgraduate School's Flexible Spacecraft Simulator (FSS) for vibration suppression. The simulator's flexible beam was controlled using piezoceramic wafers as sensors and actuators. The H-infinity wave absorbing controller contributed significant damping to the structure, especially at the first mode of 1 Hz. Therefore, wave absorbing control and piezoceramic sensors and actuators offer a viable approach for vibration suppression of space structures. DTIC

N95-31143# Orion International Technologies, Albuquerque, NM.
ASSESSMENT OF THE NASA ORBITAL DEBRIS ENGINEERING MODEL Final Report, Apr. - Jun. 1992
K. W. Yates and F. M. Jonas Feb. 1995 89 p
(Contract F29601-89-C-0001)
(AD-A293350; PL-TR-92-1032) Avail: CASI HC A05/MF A01

This report presents an assessment of the orbital debris engineering model which predicts near and long term orbit debris environments on spacecraft in low earth orbit. The model predicts debris flux environment, mass, and collision velocity distributions. The empirically based model is a curve fit to measured data and incorporates results derived from the NASA EVOLVE code. The data base includes US Space Command orbital element sets, Aricebo and Goldstone radar observations, MIT/Lincoln Laboratory Experimental Test System and Ground based Electrooptical Deep Space Surveillance optical data, and surface impact data from the Solar Maximum Mission. The model is most sensitive to the small debris particles and becomes undefined as the particle size approaches zero. The model is least sensitive to changes in orbital altitude. The model predicts essentially constant flux greator than 1000 km and does not reproduce measured data at these altitudes. The uncertainty is shown to be a factor of 2-4 for an altitude of 500 + 200 km (all particle sizes) and for sizes greater than 10 cm (for all altitudes), and at least an order of magnitude for all other sizes and altitudes. The collision-velocity distribution, and particle mass expressions represent extremely gross approximations of the environment. On the basis of the results of the analysis, it is recommended the model's use be restricted to altitudes le ss than 1000 km, debris sizes from 10(exp -4) to 10(exp -3) cm, and for projections through the year 2010. DTIC

N95-31358*# National Aeronautics and Space Administration. Langley Research Center, Hampton, VA.
A MANUAL FOR PYROTECHNIC DESIGN, DEVELOPMENT AND QUALIFICATION
Laurence J. Bement and Morry L. Schimmel (Schimmel Co., Saint Louis, MO.) Jun. 1995 82 p
(RTOP 297-50-00-02)
(NASA-TM-110172; NAS 1.15:110172) Avail: CASI HC A05/MF A01

Although pyrotechnic devices have been singularly responsible for the success of many of the critical mechanical functions in aerospace programs for over 30 years, ground and in-flight failures continue to occur. Subsequent investigations reveal that little or no quantitative information is available on measuring the effects on performance of system variables or on determining functional margins. Pyrotechnics are considered to be readily available and, therefore, can be managed by any subsystem in which they are applied, such as structure, propulsion, electric power, or life support. The primary purpose of this manual is to alter the concept that the use of pyrotechnics is an art and refute 'justifications' that applications do not need to be understood by providing information on pyrotechnic design, development, and qualification on an engineering basis. Included are approaches to demonstrate functional reliability with less than 10 units, how to manage pyrotechnic-unique requirements, and methods to assure that the system is properly assembled and will perform the required tasks. Author

N95-31388# Naval Postgraduate School, Monterey, CA.
COMPUTER INTERFACE DEVELOPMENT FOR THE PETITE AMATEUR NAVY SATELLITE (PANSAT) SIMULATOR M.S. Thesis
Thomas C. Calvert Dec. 1994 145 p
(AD-A293263) Avail: CASI HC A07/MF A02

This thesis describes the development of personal computer interfaces for the Digital Control Subsystem (DCS) and Electrical Power System (EPS) of the Naval Postgraduate School's Petite Amateur Navy Satellite Simulator project. The work includes a brief description of related PANSAT and PANSAT simulator subsystems. The laboratory activity that provided the information for this work, namely, programming in the LabVIEW software programs G graphical programming language, involved the generation of programming code for controlling and reading data from the simulators component subsystems. Where appropriate, there is limited discussion of key satellite and simulator component designs and installations. Through the use of documentation and illustrative figures, the programming and display components of the interfaces are shown to be functional in the simulator environment. Instructions for making anticipated design accommodations are included. DTIC

N95-31553# Amptek, Inc., Bedford, MA.
SPACE SYSTEMS ENVIRONMENTAL INTERACTION STUDIES
M. A. Morgan, Alan C. Huber, John O. McGarity, David J. Sperry, and Scott J. Moran 30 Aug. 1994 31 p
(Contract F19628-91-C-0112)
(AD-A293826; PL-TR-94-2215; SR-3) Avail: CASI HC A03/MF A01

The preparation of Ground Support Equipment (GSE) hardware and software, as well as, attending to launch support concerns prior to and after APEX launch, constitutes the extent of the effort expended on Task 1 (the Photovoltaic Array Space Power Plus Diagnostics (PASP Plus) experiment). Previously written test software was refined and new code generated, in order to accommodate real-time instrument performance monitoring during ground contact periods, and to facilitate the display of historical instrument performance data after a downlink opportunity. Under Task 2, the Charging Hazards and Wake Studies (CHAWS) program, Amptek, Inc. acted largely in a consultative and support role to PL/GPSG during this report period. Under Task 3 (the Space Wave Interactions with Plasmas Experiment (SWIPE)) GSE hardware was completed, and software was written and tested, for the electronics module of the EPI instrument on the OEDIPUS-C program. Two flight boxes are now in-house, fully assembled. Flight software for the constituent elements within the instrument was completed, and instrument functionality was fully exercised and checked. No additional change is envisaged to either hardware or software at this time. DTIC

N95-31980# National Aerospace Lab., Tokyo (Japan). Space Technology Research Group.

ON-ORBIT TRUSS STRUCTURE TELE-OPERATION EXPERIMENT BY ENGINEERING TEST SATELLITE-7

Isao Yamaguchi, Koutarou Matsumoto, and Takashi Kida Aug. 1994 21 p In JAPANESE

(ISSN 0389-4010)

(NAL-TR-1246) Avail: CASI HC A03/MF A01

This report describes a preliminary ground test using the laboratory model of a truss structure and small research manipulator system which is a scaled model of the on-orbit truss structure experiment on Engineering Test Satellite-7(ETS-7). ETS-7 will be launched into low earth orbit by the H-2 rocket in 1997. This experimental application satellite is now being developed to establish rendezvous and docking technologies and remote tele-robotics technologies. National Aerospace Laboratory will participate in on-orbit experiments of remote deployment and construction of truss structures by using an on-board manipulator system. Author

N95-32081# Sandia National Labs., Albuquerque, NM. Material and Structural Mechanics Dept.

STRUCTURAL ANALYSES OF THE JPL MARS PATHFINDER IMPACT

Kenneth W. Gwinn 1994 7 p Presented at the 13th AIAA Aerodynamic Decelerator Systems Technology Conference, Clearwater Beach, FL, 15-19 May 1995

(Contract DE-AC04-94AL-85000)

(DE95-009581; SAND-94-2324C; CONF-950582-1) Avail: CASI HC A02/MF A01

The purpose of this paper is to demonstrate that finite element analysis can be used in the design process for high performance fabric structures. These structures exhibit extreme geometric nonlinearity; specifically, the contact and interaction of fabric surfaces with the large deformation which necessarily results from membrane structures introduces great complexity to analyses of this type. All of these features are demonstrated here in the analysis of the Jet Propulsion Laboratory (JPL) Mars Pathfinder impact onto Mars. This lander system uses airbags to envelope the lander experiment package, protecting it with large deformation upon contact. Results from the analysis show the stress in the fabric airbags, forces in the internal tendon support system, forces in the latches and hinges which allow the lander to deploy after impact, and deceleration of the lander components. All of these results provide the JPL engineers with design guidance for the success of this novel lander system. DOE

N95-32110 Clarkson Univ., Potsdam, NY.

VIBRATION CONTROL OF SPACECRAFTS AND SPACE STRUCTURES FROM LIFT-OFF TO ON-ORBIT ENVIRONMENTS Ph.D. Thesis

Gina Jimo Lee-Glauser 1994 201 p

Avail: Univ. Microfilms Order No. DA9422826

Vibration suppression of spacecraft and large flexible space structures using passive and active vibration control mechanisms are studied. Part 1 of this thesis is concerned with developing effective passive vibration control systems for protection of payload during lift-off. Two new trunnion designs (linear rubber bearing and resilient friction) for protecting the space shuttle payload and its sensitive subsystem during lift-off are presented and their effectiveness is analyzed. The results are compared with those for pure friction (current method in use with a treated friction surface) trunnions and fixed base (rigidly attached) case. Deterministic excitations including sinusoidal and the Space Transportation System mission 41 lift-off acceleration are used as dynamic input of the orbiter. Effects of the trunnion friction and flexibility on vibrations of payload and its subsystem are evaluated. Sensitivity analyses related to the vibration control systems and the flexible payload parameters are also performed. In Part 2 of the thesis, the probabilistic performance analysis of various linear and nonlinear passive vibration control systems under random orbiter lift-off excitations is presented. A simple stochastic model for generating synthetic orbiter lift-off accelerations is developed. This method is based on a filtered Gaussian white noise model which accounts for the nonstationary time evolution of amplitude and frequency content of orbiter lift-off accelerations. The peak responses of the payload with various vibration control systems are evaluated. Statistically derived acceleration response spectra are compared with those for the actual flight data for a single degree-of-freedom payload model. System performance with and without the passive vibration control systems are analyzed, and the effectiveness of vibration isolation devices are discussed. Part 3 of the thesis is concerned with developing an optimal active vibration absorber for microgravity environment, as well as for protection of payload during shuttle lift-off. The developed active vibration absorber is a second-order dynamic system which can provide effective control of vibrations for large flexible space structures with collocated sensors/actuators while guaranteeing closed-loop stability. Two methods for optimizing the active vibration absorber parameters (minimum resonant amplitude and the frequency matched) were evaluated. Numerical and experimental results under sinusoidal and random excitations were used to evaluate the effectiveness of the active controller. Performances of the active and passive vibration control systems under orbiter lift-off environment are compared using a five degree-of-freedom lump parameter model of a satellite. The presented performance analyses of the deterministic and probabilistic results show that, with proper design, the passive vibration control systems significantly reduce the peak acceleration and displacement experienced by the payload and its subsystem at high to moderate frequencies. The active vibration absorber is very effective in suppressing both on-orbit and lift-off vibration environments. Dissert. Abstr.

N95-32189*# Boeing Defense and Space Group, Seattle, WA.

OPERATION OF THE COMPUTER MODEL FOR DIRECT ATOMIC OXYGEN EXPOSURE OF EARTH SATELLITES

R. J. Bourassa, P. E. Gruenbaum, J. R. Gillis, and C. R. Hargraves Aug. 1995 112 p

(Contracts NAS1-18224; NAS1-19247; RTOP 233-03-02-02)

(NASA-CR-198188; NAS 1.26:198188) Avail: CASI HC A06/MF A02

One of the primary causes of material degradation in low Earth orbit (LEO) is exposure to atomic oxygen. When atomic oxygen molecules collide with an orbiting spacecraft, the relative velocity is 7 to 8 km/sec and the collision energy is 4 to 5 eV per atom. Under these conditions, atomic oxygen may initiate a number of chemical and physical reactions with exposed materials. These reactions contribute to material degradation, surface erosion, and contamination. Interpretation of these effects on materials and the design of space hardware to withstand on-orbit conditions requires quantitative knowledge of the atomic oxygen exposure environment. Atomic oxygen flux is a function of orbit altitude, the orientation of the orbit plan to the Sun, solar and geomagnetic activity, and the angle between exposed surfaces and the spacecraft heading. We have developed a computer model to predict the atomic oxygen exposure of spacecraft in low Earth orbit. The application of this computer model is discussed. Author

N95-32204*# Colorado Univ., Boulder, CO. Dept. of Aerospace Engineering Sciences.

COMPUTATIONAL METHODS AND SOFTWARE SYSTEMS FOR DYNAMICS AND CONTROL OF LARGE SPACE STRUCTURES Final Report

K. C. Park, C. A. Felippa, C. Farhat, and E. Pramono Jul. 1990 265 p

(Grant NAG1-756)

(NASA-CR-199036; NAS 1.26:199036; CU-CSSC-90-17) Avail: CASI HC A12/MF A03

This final report on computational methods and software systems for dynamics and control of large space structures covers progress to date, projected developments in the final months of the grant, and conclusions. Pertinent reports and papers that have not appeared in scientific journals (or have not yet appeared in final form) are enclosed. The grant has supported research in two key areas of crucial importance to the computer-based simulation of large space structure. The first area involves multibody dynamics (MBD) of flexible space structures, with applications directed to deployment, construction, and maneuvering. The second area deals with advanced software systems, with emphasis on parallel processing. The latest research thrust in the second area, as reported here, involves massively parallel computers. Author

N95-32345*# Space Operations Squadron (2nd), Falcon AFB, CO.

SVN 9 END-OF-LIFE TESTING

Gregory E. Hatten *In* NASA. Goddard Space Flight Center, The 26th Annual Precise Time and Time Interval (PTTI) Applications and Planning Meeting May 1995 p 405-413 (For primary document see N95-32319 11-70)

Avail: CASI HC A02/MF A04

19 SPACECRAFT INSTRUMENTATION

For related information see also *06 Aircraft Instrumentation* and *35 Instrumentation and Photography.*

No abstracts in this category.

20 SPACECRAFT PROPULSION AND POWER

Includes main propulsion systems and components, e.g., rocket engines; and spacecraft auxiliary power sources.

For related information see also *07 Aircraft Propulsion and Power, 28 Propellants and Fuels, 44 Energy Production and Conversion,* and *15 Launch Vehicles and Space Vehicles.*

N95-30595*# National Aeronautics and Space Administration. Lewis Research Center, Cleveland, OH.

SUPPLEMENTAL MULTILAYER INSULATION RESEARCH FACILITY

P. J. Dempsey and R. J. Stochl Jul. 1995 7 p Presented at the 1995 Cryogenic Engineering Conference, Columbus, OH, 17-21 Jul. 1995; sponsored by Centennial Conferences

(RTOP 243-30-07)

(NASA-TM-106991; E-9766; NAS 1.15:106991) Avail: CASI HC A02/MF A01

The Supplemental Multilayer Insulation Research Facility (SMIRF) provides a small scale test bed for conducting cryogenic experiments in a vacuum environment. The facility vacuum system is capable of simulating a Space Shuttle launch pressure profile as well as providing a steady space vacuum environment of 1.3 x 10(exp -4) Newton/sq meter (1 x 10(exp -6) torr). Warm side boundary temperatures can be maintained constant between 111 K (200 R) and 361 K (650 R) using a temperature controlled shroud. The shroud can also simulate a typical lunar day-night temperature profile. The test hardware consists of a cryogenic calorimeter supported by the lid of the vacuum chamber. A 0.45 cu meter (120 gallon) vacuum jacketed storage/supply tank is available for conditioning the cryogen prior to use in the calorimeter. The facility was initially designed to evaluate the thermal performance of insulation systems for long-term storage in space. The facility has recently been used to evaluate the performance of various new insulation systems for LH2 and LN2 ground storage dewars. Author

N95-30674# Martin Marietta Astro Space, Philadelphia, PA.

GPHS-RTGs IN SUPPORT OF THE CASSINI RTG PROGRAM Semiannual Technical Progress Report, 26 Sep. 1994 - 2 Apr. 1995

20 Apr. 1995 73 p

(Contract DE-AC03-91SF-18852)

(DE95-010306; DOE/SF-18852/T50) Avail: CASI HC A04/MF A01

The technical progress achieved during the period 26 Sep. 1994 - 2 Apr. 1995 on Contract DE-AC03-91SF-18852 Radioisotope Thermoelectric Generators and Ancillary Activities is described herein. Monthly technical activity for the period 27 Feb. - 2 Apr. 1995 is included in this progress report. The report addresses tasks, including: spacecraft integration and liaison; engineering support; safety; qualified unicouple production; ETG fabrication, assembly, and test; ground support equipment; RTG shipping and launch support; designs, reviews, and mission applications; project management, quality assurance, reliability, contract changes, CAGO acquisition (operating funds), and CAGO maintenance and repair; and CAGO acquisition (capital funds). DOE

N95-30856*# National Aeronautics and Space Administration. Lewis Research Center, Cleveland, OH.

ELECTRICALLY HEATED TUBE INVESTIGATION OF COOLING CHANNEL GEOMETRY EFFECTS

Michael L. Meyer Jun. 1995 14 p Presented at the 31st Joint Propulsion Conference and Exhibit, San Diego, CA, 10-12 Jul. 1995; sponsored by AIAA, ASME, SAE and ASEE

(NASA-TM-106985; E-9760; NAS 1.15:106985; AIAA Paper 95-2500) Avail: CASI HC A03/MF A01

The results of an experimental investigation on the combined effects of cooling channel aspect ratio and curvature for rocket engines are presented. Symmetrically heated tubes with average heat fluxes up to 1.7 MW/m(exp 2) were used. The coolant was gaseous nitrogen at an inlet temperature of 280 K (500 R) and inlet pressures up to 1.0 x 10(exp 7) N/m(exp 2) (1500 psia). Two different tube geometries were tested: a straight, circular cross-section tube, and an aspect-ratio 10 cross-section tube with a 45 deg bend. The circular tube results are compared to classical models from the literature as validation of the system. The curvature effect data from the curved aspect-ratio 10 tube compare favorably to the empirical equations available in the literature for low aspect ratio tubes. This latter results suggest that thermal stratification of the coolant due to diminished curvature effect mixing may not be an issue for high aspect-ratio cooling channels. Author

N95-30860*# NYMA, Inc., Brook Park, OH.

EFFECTS OF THERMAL AND ELECTRICAL STRESSING ON THE BREAKDOWN BEHAVIOR OF SPACE WIRING Final Report

Ahmad Hammoud, Mark Stavnes, Jayant Suthar (State Univ. of New York, Buffalo, NY.), and Javaid Laghari (State Univ. of New York, Buffalo, NY.) Jun. 1995 6 p

(Contract NAS3-27186; NAG3-1345; RTOP 297-50-00)

(NASA-CR-198360; E-9750; NAS 1.26:198360) Avail: CASI HC A02/MF A01

Several failures in the electrical wiring systems of many aircraft and space vehicles have been attributed to arc tracking and damaged insulation. In some instances, these failures proved to be very costly as they have led to the loss of many aircraft and imperilment of space missions. Efforts are currently underway to develop lightweight, reliable, and arc track resistant wiring for aerospace applications. In this work, six wiring constructions were evaluated in terms of their breakdown behavior as a function of temperature. These hybrid constructions employed insulation consisting of Kapton, Teflon, and cross-linked Tefzel. The properties investigated included the 400 Hz AC dielectric strength at ambient and 200 C, and the lifetime at high temperature with an applied bias of 40, 60, and 80% of breakdown voltage level. The results obtained are discussed, and conclusions are made concerning the suitability of the wiring constructions investigated for aerospace applications. Author

N95-30864*# National Aeronautics and Space Administration. Lewis Research Center, Cleveland, OH.

KINETIC THEORY MODEL PREDICTIONS COMPARED WITH LOW-THRUST AXISYMMETRIC NOZZLE PLUME DATA

B. R. Riley (Evansville Univ., IN.), S. J. Fuhrman (Evansville Univ., IN.), and P. F. Penko American Inst. of Aeronautics and Astronautics 1993 9 p

(Grant NAG3-746)

(NASA-CR-198934; NAS 1.26:198934) Avail: CASI HC A02/MF A01

A system of nonlinear integral equations equivalent to the steady-state Krook kinetic equation was used to model the flow from a low-thrust axisymmetric nozzle. The mathematical model was used to numerically calculate the number density, temperature, and velocity of a simple gas as it expands into a near vacuum. With these quantities the gas pressure and flow directions of the gas near the exit plane were calculated and compared with experimental values for a low-thrust nozzle of the same geometry and mass flow rate. Author

N95-30881# Iranian Physics Society, Teheran (Iran).

ABSTRACTS OF ANNUAL PHYSICS CONFERENCE OF IRAN

Jahanshah Mirzabeygui, ed. Aug. 1994 91 p Conference held in Sanandaj, Iran, 19 Aug. - 1 Sep. 1994

(DE95-611717; INIS-MF-14440; CONF-9408203) Avail: CASI HC A05/MF A01 (US Sales Only)

Collection of separate abstracts written in the proceedings of Annual Physics Conference of Iran, 1373, covered the following topics: mathematical methods in physics, relativity, and gravitation; the physics of elementary particles; nuclear physics and nuclear engineering; atomic and molecular physics, optics, and magnetism; fluids, plasma, and electric discharges; condensed matter; and astronomy and astrophysics. DOE

N95-31169*# GenCorp Aerojet, Sacramento, CA.

ADVANCED SMALL ROCKET CHAMBERS. OPTION 3: 110 lbf Ir-Re ROCKET, VOLUME 1 Final Report

Donald M. Jassowski and Leonard Schoenman Feb. 1995 390 p
(Contract NAS3-25646; RTOP 242-70-02)
(NASA-CR-195435-Vol-1; E-9457-Vol-1; NAS 1.26:195435-Vol-1) Avail: CASI HC A17/MF A04

This report describes the AJ10-221, a high performance Iridium-coated Rhenium (Ir-Re) 110 lbf (490N) welded rocket chamber with 286:1 area ratio nozzle. This engine was designed, built, and hot fired for over 6 hours on this program. It demonstrated an I(s) of 321.8 sec, which is 10 sec higher than conventional 110 lbf silicide coated Cb chambers now in use. The approach used in this portion of the program was to demonstrate the performance improvement that can be made by the elimination of fuel film cooling and the use of a high temperature (4000F) (2200C) iridium-coated rhenium (Ir-Re) rocket chamber. Detailed thermal, performance, mechanical, and dynamic design analyses of the full engine were conducted by Aerojet. Two Ir-Re chambers were built to the Aerojet design by Ultramet, using the chemical vapor deposition (CVD) process. Incorporation of a secondary mixing device or Boundary Layer Trip (BLT) within the combustion chamber (Aerojet Patents 4882904 and 4936091) results in improvement in flow uniformity, and a significant life and performance increase. The 110 lbf engine design was verified in bolt-up hardware tests at sea level and altitude. The effects of injector design on performance were studied. Two duplicate injectors were fabricated matching the preferred design and were demonstrated to be interchangeable in operation. One of these units was fabricated matching the preferred design and was demonstrated to be interchangeable in operation. One of these units was welded into a flight type thruster which was tested for an accumulated duration of 22,590 sec in 93 firings, one of which was a continuous burn of two hours. A design deficiency in the C-103 nozzle near the Re-Cb transition joint was discovered, studied and corrected design has been prepared. Workhardening studies have been conducted to investigate methods for increasing the low yield strength of the Re in the annealed conditions. An advanced 490N high performance engine has been demonstrated which, when proven to be capable of withstanding launch vibration, is ready for flight qualification.

Author

N95-31170*# GenCorp Aerojet, Sacramento, CA.
ADVANCED SMALL ROCKET CHAMBERS. OPTION 3: 110 lbf Ir-Re ROCKET, VOLUME 2
Donald M. Jassowski and Leonard Schoenman Feb. 1995 290 p
(Contract NAS3-25646; RTOP 242-70-02)
(NASA-CR-195435-Vol-2; E-9457-Vol-2; NAS 1.26:195435-Vol-2) Avail: CASI HC A13/MF A03

This is the second part of a two-part report that describes the AJ10-221, a high performance iridium-coated rhenium (Ir-Re) 110 lbf (490N) welded rocket chamber with 286:1 area ratio nozzle. This engine was designed, built, and hot fired for over 6 hours on this program. It demonstrated an I(s) of 321.8 sec, which is 10 sec higher than conventional 110 lbf silicide coated Cb chambers now in use. The approach used in this portion of the program was to demonstrate the performance improvement that can be made by the elimination of fuel film cooling and the use of a high temperature (4000 F) (2200 C) iridium-coated rhenium (Ir-Re) rocket chamber. Detailed thermal, performance, mechanical, and dynamic design analyses of the full engine were conducted by Aerojet. Two Ir-Re chambers were built to the Aerojet design by Ultramet, using the chemical vapor deposition (CVD) process. Incorporation of a secondary mixing device or Boundary Layer Trip (BLT) within the combustion chamber (Aerojet Patents 4882904 and 4936091) results in improvement in flow uniformity, and a significant life and performance increase. The 110 lbf engine design was verified in bolt-up hardware tests at sea level and altitude. The effects of injector design on performance were studied. Two duplicate injectors were fabricated matching the preferred design and were demonstrated to be interchangeable in operation. One of these units were welded into a flight type thruster which was tested for an accumulated duration of 22,590 sec in 93 firings, one of which was a continuous burn of two hours. A design deficiency in the C-103 nozzle near the Re-Cb transition joint was discovered, studied and corrected design has been prepared. Workhardening studies have been conducted to investigate methods for increasing the low yield strength of the Re in the annealed conditions. An advanced 490N high performance engine has been demonstrated which, when proven to be capable of withstanding launch vibration, is ready for flight qualification.

Author (revised)

N95-31567# Aerospace Corp., El Segundo, CA.
BEAM-CENTROID TRACKING INSTRUMENT FOR ION THRUSTERS
J. E. Pollard 20 Mar. 1995 11 p
(Contract F04701-93-C-0094)
(AD-A293654; TR-94(4507)-1; SMC-TR-95-13) Avail: CASI HC A03/MF A01

Thrust vector stability for an electrostatic ion engine can be measured with improved sensitivity and time resolution by the method described here. Four double-wire Langmuir probes, aligned in the form of a cross, are placed in the exhaust plume and are translated by a motorized positioning system to balance the currents collected along two orthogonal axes. The thrust vector position is thereby measured with an angular resolution of less than 0.01 deg and a response time of less than 5 sec. DTIC

N95-31716 Pennsylvania State Univ., University Park, PA.
PRIMARY ATOMIZATION OF LIQUID JETS ISSUING FROM ROCKET ENGINE COAXIAL INJECTORS Ph.D. Thesis
Roger D. Woodward 1993 178 p
Avail: Univ. Microfilms Order No. DA9414399

The investigation of liquid jet breakup and spray development is critical to the understanding of combustion phenomena in liquid-propellant rocket engines. Much work has been done to characterize low-speed liquid jet breakup and dilute sprays, but atomizing jets and dense sprays have yielded few quantitative measurements due to their optical opacity. This work focuses on a characteristic of the primary breakup process of round liquid jets, namely the length of the intact liquid core. The specific application considered is that of shear-coaxial type rocket engine injectors. Real-time x-ray radiography, capable of imaging through the dense two-phase region surrounding the liquid core, has been used to make the measurements. Nitrogen and helium were employed as the fuel simulants while an x-ray absorbing potassium iodide aqueous solution was used as the liquid oxygen (LOX) simulant. The intact-liquid-core length data have been obtained and interpreted to illustrate the effects of chamber pressure (gas density), injected-gas and liquid velocities, and cavitation. The results clearly show that the effect of cavitation must be considered at low chamber pressures since it can be the dominant breakup mechanism. A correlation of intact core length in terms of gas-to-liquid density ratio, liquid jet Reynolds number, and Weber number is suggested. The gas-to-liquid density ratio appears to be the key parameter for aerodynamic shear breakup in this study. A small number of hot-fire, LOX/hydrogen tests were also conducted to attempt intact-LOX-core measurements under realistic conditions in a single-coaxial-element rocket engine. The tests were not successful in terms of measuring the intact core, but instantaneous imaging of LOX jets suggests that LOX jet breakup is qualitatively similar to that of cold-flow, propellant-simulant jets. The liquid oxygen jets survived in the hot-fire environment much longer than expected, and LOX was even visualized exiting the chamber nozzle under some conditions. This may be an effect of the single element configuration. Dissert. Abstr.

N95-31739# National Aerospace Lab., Tokyo (Japan). Ramjet Propulsin Research Div.
EXPERIMENT OF ROCKET-RAM COMBINED COMBUSTOR
Kazuo Sato, Hiroshi Sakamoto, Masaki Sasaki, Fumiei Ono, and Nobuyuki Yatsuyanagi Oct. 1994 20 p In JAPANESE
(ISSN 0389-4010)
(NAL-TR-1249) Avail: CASI HC A03/MF A01

There are limitations to achieve high specific impulse with rocket engine operations alone. However, in the flight at low altitude, combined engines with an airbreathing ramjet engine and a rocket engine can be expected to increase the specific impulse significantly in parallel operation. In this paper, the superiority in the specific impulse of the double-nozzle type of rocket-ram combined engine over the single-nozzle type combined engine was shown by performance calculations. Then, a double-nozzle type of rocket-ram combined combustor with a total thrust of 5kN was designed and experimentally tested with varying ratios of thrust produced by rocket and ramjet. The propellants are LOX/kerosene+ hydrogen for rocket combustion and air-hydrogen for ram combustion. With the thrust chamber having different diverging half-angles, namely 10 deg 18 min, and 6 deg 40 min, thrust and pressure distribution along the common expansion nozzle were measured to investigate the effect of interaction of the expanding gases of rocket and ram on thrust. Enhancement of the specific impulse was experimentally verified. That is, the specific impulse which was gained

in rocket-ram parallel operations, when the thrust ratio of rocket to ram was 50 to 50, was found to increase 90 percent over those in pure rocket operations. Author

N95-31972 Colorado Univ., Boulder, CO.
COMBUSTION RESPONSE TO ACOUSTIC PERTURBATION IN LIQUID ROCKET ENGINES Ph.D. Thesis
Akbar Ghafourian 1993 169 p
Avail: Univ. Microfilms Order No. DA9423489

An experimental study of the effect of acoustic perturbations on combustion behavior of a model liquid propellant rocket engine has been carried out. A pair of compression drivers were used to excite transverse and longitudinal acoustic fields at strengths of up to 156.6 dB and 159.5 dB respectively in the combustion chamber of the experimental rocket engine. Propellant simulants were injected into the combustion chamber through a single element shear coaxial injector. Water and air were used in cold flow studies and ethanol and oxygen-enriched air were used as fuel and oxidizer in reacting hot flow studies. In cold flow studies an imposed transverse acoustic field had a more pronounced effect on the spray pattern than a longitudinal acoustic fields. A transverse acoustic field widened the spray by as much as 33 percent and the plane of impingement of the spray with chamber walls moved up closer to the injection plane. The behavior was strongly influenced by the gas phase velocity but was less sensitive to changes in the liquid phase velocity. In reacting hot flow studies the effects of changes in equivalence ratio, excitation amplitude, excitation frequency, liquid and gas phase velocity and chamber pressure on the response of the injector to imposed high frequency transverse acoustic excitation were measured. Reducing the equivalence ratio from 7.4 to 3.8 increased the chamber pressure response to the imposed excitation at 3000 Hz. Increasing the excitation amplitude from 147 dB to 155.6 dB at 3000 Hz increased the chamber pressure response to the excitation. In the frequency range of 1240 Hz to 3220 Hz, an excitation frequency of 3000 Hz resulted in the largest response of the chamber pressure indicating the importance of fluid dynamic coupling. Increasing the liquid phase velocity from 9.2 m/sec to 22.7 m/sec, did not change the amplitude of the chamber pressure response to excitation. This implied the importance of local equivalence ratio and not the overall equivalence ratio on chamber pressure response to excitation. Increasing the chamber pressure from 1.5 atm to 3.1 atm and gas phase velocity from 93.2 m/sec to 105.1 m/sec significantly increased the chamber pressure response to acoustic excitation. This emphasized the significance of the gas phase density and velocity. Measurements of the free radical C2 emission zone and Schlieren images indicated that transverse acoustic excitation moved the combustion zone closer to the injection plane and longitudinal acoustic excitation widened the combustion zone. The histogram of these images indicates that the area over which combustion takes place in the chamber increases under imposed acoustic excitation. This implied that more propellants combust prior to exiting from the exhaust nozzle under unsteady conditions. Dissert. Abstr.

N95-32121*# National Aeronautics and Space Administration. Lewis Research Center, Cleveland, OH.
ROBUST ROCKET ENGINE CONCEPT
Carl F. Lorenzo Jul. 1995 11 p Presented at the 31st Joint Propulsion Conference and Exhibit, San Diego, CA, 10-12 Jul. 1995; cosponsored by AIAA, ASME, SAE, and ASEE
(RTOP 505-62-50)
(NASA-TM-107010; E-9794; NAS 1.15:107010) Avail: CASI HC A03/MF A01

The potential for a revolutionary step in the durability of reusable rocket engines is made possible by the combination of several emerging technologies. The recent creation and analytical demonstration of life extending (or damage mitigating) control technology enables rapid rocket engine transients with minimum fatigue and creep damage. This technology has been further enhanced by the formulation of very simple but conservative continuum damage models. These new ideas when combined with recent advances in multidisciplinary optimization provide the potential for a large (revolutionary) step in reusable rocket engine durability. This concept has been named the robust rocket engine concept (RREC) and is the basic contribution of this paper. The concept also includes consideration of design innovations to minimize critical point damage. Author

N95-30987 Analytical Methods, Inc., Ogden, UT.
SURVEY OF RECENT Al2O3 DROPLET SIZE DATA IN SOLID ROCKET CHAMBERS, NOZZLES, AND PLUMES
Mark Salita *In* JHU, The 21st JANNAF Exhaust Plume Technology Meeting, Volume 1 Oct. 1994 p 1-17 (For primary document see N95-30986 11-34)
Avail: CPIA, 10630 Little Patuxent Pkwy., Suite 202, Columbia, MD 21044-3200 HC

N95-30988 Georgia Inst. of Tech., Atlanta, GA.
THE Al AND A(LC)L2O3 DROPLET CLOUD IN SOLID ROCKET MOTORS
Ed W. Price and R. K. Sigman *In* JHU, The 21st JANNAF Exhaust Plume Technology Meeting, Volume 1 Oct. 1994 p 19-28 (For primary document see N95-30986 11-34)
(Contract N00014-89-J-1293)
Avail: CPIA, 10630 Little Patuxent Pkwy., Suite 202, Columbia, MD 21044-3200 HC

N95-30989*# Naval Air Warfare Center, China Lake, CA.
SHUTTLE REDESIGNED SOLID ROCKET MOTOR ALUMINUM OXIDE INVESTIGATIONS
Fred S. Blomshield, Karl J. Kraeutle, and Richard A. Stalnaker *In* JHU, The 21st JANNAF Exhaust Plume Technology Meeting, Volume 1 Oct. 1994 p 29-39 Sponsored by NASA. Marshall Space Flight Center (For primary document see N95-30986 11-34)
Avail: CPIA, 10630 Little Patuxent Pkwy., Suite 202, Columbia, MD 21044-3200 HC

N95-31195 Analytical Methods, Inc., Bellevue, WA.
SURVEY OF RECENT Al2O3 DROPLET SIZE DATA IN SOLID ROCKET CHAMBERS, NOZZLES, AND PLUMES
Mark Salita *In* Johns Hopkins Univ., The 31st JANNAF Combustion Subcommittee Meeting, Volume 1 Oct. 1994 p 1-18 (For primary document see N95-31194 11-28)
Avail: CPIA, 10630 Little Patuxent Pkwy., Suite 202, Columbia, MD 21044-3200 HC

N95-31196 Georgia Inst. of Tech., Atlanta, GA.
THE Al AND Al2O3 DROPLET CLOUD IN SOLID ROCKET MOTORS
E. W. Price and R. K. Sigman *In* Johns Hopkins Univ., The 31st JANNAF CombustionSubcommittee Meeting, Volume 1 Oct. 1994 p 19-28 (For primary document see N95-31194 11-28)
(Contract N00014-89-J-1293)
Avail: CPIA, 10630 Little Patuxent Pkwy., Suite 202, Columbia, MD 21044-3200 HC

N95-31197* Naval Air Warfare Center, China Lake, CA.
SHUTTLE REDESIGNED SOLID ROCKET MOTOR ALUMINUM OXIDE INVESTIGATIONS
Fred S. Blomshield, Karl J. Kraeutle, and Richard A. Stalnaker *In* Johns Hopkins Univ., The 31st JANNAF Combustion Subcommittee Meeting, Volume 1 Oct. 1994 p 29-40 (For primary document see N95-31194 11-28)
Avail: CPIA, 10630 Little Patuxent Pkwy., Suite 202, Columbia, MD 21044-3200 HC

N95-31756*# Sverdrup Technology, Inc., Huntsville, AL.
TECHNOLOGY TRANSFER INTO THE SOLID PROPULSION INDUSTRY
Ralph L. Campbell and Lawrence J. Thomson *In* NASA. Marshall Space Flight Center, Aerospace Environmental Technology Conference Mar. 1995 p 123-129 (For primary document see N95-31746 11-23)
Avail: CASI HC A02/MF A06

N95-31806*# Rockwell International Corp., Canoga Park, CA.
INVESTIGATION OF CLEANLINESS VERIFICATION TECHNIQUES FOR ROCKET ENGINE HARDWARE
Marilyn L. Fritzemeier and Raymund P. Skowronski *In* NASA. Marshall Space Flight Center, Aerospace Environmental Technology Conference Mar. 1995 p 593-602 (For primary document see N95-31746 11-23)
Avail: CASI HC A02/MF A06

23 CHEMISTRY AND MATERIALS (GENERAL)

N95-30418# Department of the Navy, Washington, DC.
PREPARATION OF DIISOPROPYL STIBINES AND USE THEREOF Patent
Robert Gedridge, Jr., inventor (to Navy) 6 Dec. 1994 4 p Filed 30 Nov. 1993
(AD-D017419; US-Patent-5,371,257; US-Patent-Appl-SN-159964; US-Patent-Class-556-70) Avail: US Patent and Trademark Office

The new compound diisopropyl stibine is prepared by reacting an diisopropyl antimony halide with a hydride or deuteride transferring agent. The reaction is preferably carried out below about 0 C, in an inert atmosphere, under darkened conditions. The diisopropyl stibine is used as a precursor in forming antimony-containing semiconductor material by chemical vapor deposition. DTIC

N95-30734# Technische Univ., Delft (Netherlands).
ENANTIOSELECTIVITY OF QUINOPROTEIN ALCOHOL DEHYDROGENASES: PRODUCTION OF ENANTIOMERICALLY PURE C3-ALCOHOL SYNTHONS Ph.D. Thesis
Arie Geerlof 27 Sep. 1994 153 p
(PB95-196960) Avail: CASI HC A08/MF A02

The aim of this thesis was to investigate the possibility of using alcohol oxidoreductases as catalyst in the kinetic resolution of racemic mixtures of alcohols. Therefore, a screening was performed to determine the enantioselectivity in the oxidation of a number of chiral alcohols by alcohol dehydrogenases (ADH's) and oxidases. In view of the availability of and know-how on quinoprotein (pyrroloquinoline quinone (PQQ)-containing) alcohol dehydrogenases (Q-ADH's) in the authors' laboratory, the attention was especially focussed on these enzymes. NTIS

N95-31350*# National Aeronautics and Space Administration. Marshall Space Flight Center, Huntsville, AL.
AEROSPACE ENVIRONMENTAL TECHNOLOGY CONFERENCE: EXECTUTIVE SUMMARY
A. F. Whitaker, ed. Washington Mar. 1995 47 p Conference held in Huntsville, AL, 10-11 Aug. 1994
(NASA-CP-3297; M-774; NAS 1.55:3297) Avail: CASI HC A03/MF A01

The mandated elimination of CFC's, Halons, TCA, and other ozone depleting chemicals and specific hazardous materials has required changes and new developments in aerospace materials and processes. The aerospace industry has been involved for several years in providing product substitutions, redesigning entire production processes, and developing new materials that minimize or eliminate damage to the environment. These activities emphasize replacement cleaning solvents and their application verifications, compliant coatings including corrosion protection systems, and removal techniques, chemical propulsion effects on the environment, and the initiation of modifications to relevant processing and manufacturing specifications and standards. The papers from this conference are being published in a separate volume as NASA CP-3298. Author

N95-31360# Joint Publications Research Service, Arlington, VA.
JPRS REPORT: SCIENCE AND TECHNOLOGY. CENTRAL EURASIA
20 Jun. 1995 88 p Transl. into ENGLISH from various Central Eurasian articles
(JPRS-UST-95-025) Avail: CASI HC A05/MF A01

Translated articles cover the following topics: effect of hydrogen annealing and ionizing radiation on electrophysical Si-SiO2 boundary parameters: experiment and models; surface segregation of principal components in A(3)B(5) solid solution segregational heterojunctions in GaAlAs subsurface layer; epitaxial growth of high-purity GaAs by metal-organic chemical method of hydride deposition after purification of arsine by cryofiltration; and reaction of energy redistribution along front of incident wave with external powerful impact on material object. Author

N95-31746*# National Aeronautics and Space Administration. Marshall Space Flight Center, Huntsville, AL.
AEROSPACE ENVIRONMENTAL TECHNOLOGY CONFERENCE
A. F. Whitaker, ed. Washington Mar. 1995 635 p Conference held in Huntsville, AL, 10-11 Aug. 1994
(NASA-CP-3298; M-775; NAS 1.55:3298) Avail: CASI HC A99/MF A08

The mandated elimination of CFC's, Halons, TCA, and other ozone depleting chemicals and specific hazardous materials has required changes and new developments in aerospace materials and processes. The aerospace industry has been involved for several years in providing product substitutions, redesigning entire production processes, and developing new materials that minimize or eliminate damage to the environment. These activities emphasize replacement cleaning solvents and their application verifications, compliant coatings including corrosion protection systems, and removal techniques, chemical propulsion effects on the environment, and the initiation of modifications to relevant processing and manufacturing specifications and standards. The Executive Summary of this Conference is published as NASA CP-3297. For individual titles, see N95-31747 through N95-31814.

N95-31747*# Thiokol Corp., Brigham City, UT. Space Operations.
ATMOSPHERIC ENVIRONMENTAL IMPLICATIONS OF PROPULSION SYSTEMS c45
Allan J. McDonald and Robert R. Bennett *In* NASA. Marshall Space Flight Center, Aerospace Environmental Technology Conference Mar. 1995 p 3-14 (For primary document see N95-31746 11-23)
Avail: CASI HC A03/MF A06

Three independent studies have been conducted for assessing the impact of rocket launches on the earth's environment. These studies have addressed issues of acid rain in the troposphere, ozone depletion in the stratosphere, toxicity of chemical rocket exhaust products, and the potential impact on global warming from carbon dioxide emissions from rocket launches. Local, regional, and global impact assessments were examined and compared with both natural sources and anthropogenic sources of known atmospheric pollutants with the following conclusions: (1) Neither solid nor liquid rocket launches have a significant impact on the earth's global environment, and there is no real significant difference between the two. (2) Regional and local atmospheric impacts are more significant than global impacts, but quickly return to normal background conditions within a few hours after launch. And (3) vastly increased space launch activities equivalent to 50 U.S. Space Shuttles or 50 Russian Energia launches per year would not significantly impact these conclusions. However, these assessments, for the most part, are based upon homogeneous gas phase chemistry analysis; heterogeneous chemistry from exhaust particulates, such as aluminum oxide, ice contrails, soot, etc., and the influence of plume temperature and afterburning of fuel-rich exhaust products, need to be further addressed. It was the consensus of these studies that computer modeling of interactive plume chemistry with the atmosphere needs to be improved and computer models need to be verified with experimental data. Rocket exhaust plume chemistry can be modified with propellant reformulation and changes in operating conditions, but, based upon the current state of knowledge, it does not appear that significant environmental improvements from propellant formulation changes can be made or are warranted. Flight safety, reliability, and cost improvements are paramount for any new rocket system, and these important aspects cannot be compromised. A detailed environmental cost-benefit-risk analysis must be conducted before any new chemistry or changes in rocket operating conditions should be seriously considered for any future space or defense applications. This paper presents a summary of the results of environmental assessments contained in these independent studies. Author

N95-31748*# National Aeronautics and Space Administration. Marshall Space Flight Center, Huntsville, AL.
MANUFACTURING WASTE DISPOSAL PRACTICES OF THE CHEMICAL PROPULSION INDUSTRY c45
Benjamin E. Goldberg, Daniel E. Adams, and Scott A. Schutzenhofer *In its* Aerospace Environmental Technology Conference Mar. 1995 p 15-24 (For primary document see N95-31746 11-23)
Avail: CASI HC A02/MF A06

The waste production, mitigation and disposal practices of the United States chemical propulsion industry have been investigated, delineated, and comparatively assessed to the U.S. industrial base. Special emphasis has been placed on examination of ozone depleting chemicals (ODC's). The research examines present and anticipated future practices and problems encountered in the manufacture of solid and liquid propulsion systems. Information collected includes current environmental laws and

regulations that guide the industry practices, processes in which ODC's are or have been used, quantities of waste produced, funding required to maintain environmentally compliant practices, and preventive efforts.
Author

N95-31749*# National Aeronautics and Space Administration. Marshall Space Flight Center, Huntsville, AL.
CFD ASSESSMENT OF THE POLLUTANT ENVIRONMENT FROM RD-170 PROPULSION SYSTEM TESTING **c45**
Ten-See Wang, Paul McConnaughey, Saif Warsi (Sverdrup Technology, Inc., Huntsville, AL.), and Yen-Sen Chen (Engineering-Science, Inc., Huntsville, AL.) *In its* Aerospace Environmental Technology Conference Mar. 1995 p 25-47 (For primary document see N95-31746 11-23)
Avail: CASI HC A03/MF A06

Computational Fluid Dynamics (CFD) technology has been used to assess the exhaust plume pollutant environment of the RD-170 engine hot-firing on the F1 Test Stand at Marshall Space Flight Center. Researchers know that rocket engine hot-firing has the potential for forming thermal nitric oxides (NO(x)), as well as producing carbon monoxide (CO) when hydrocarbon fuels are used. Because of the complicated physics involved, however, little attempt has been made to predict the pollutant emissions from ground-based engine testing, except for simplified methods which can grossly underpredict and/or overpredict the pollutant formations in a test environment. The objective of this work, therefore, has been to develop a technology using CFD to describe the underlying pollutant emission physics from ground-based rocket engine testing. This resultant technology is based on a three-dimensional (3D), viscous flow, pressure-based CFD formulation, where wet CO and thermal NO finite-rate chemistry mechanisms are solved with a Penalty Function method. A nominal hot-firing of a RD-170 engine on the F1 stand has been computed. Pertinent test stand flow physics such as the multiple-nozzle clustered engine plume interaction, air aspiration from base and aspirator, plume mixing with entrained air that resulted in contaminant dilution and afterburning, counter-afterburning due to flame bucket water-quenching, plume impingement on the flame bucket, and restricted multiple-plume expansion and turning have been captured. The predicted total emission rates compared reasonably well with those of the existing hydrocarbon engine hot-firing test data. Author

N95-31750*# National Aeronautics and Space Administration. Marshall Space Flight Center, Huntsville, AL.
ENVIRONMENTAL BENEFITS OF CHEMICAL PROPULSION **c45**
Joyce A. Hayes, Benjamin E. Goldberg, and David M. Anderson *In its* Aerospace Environmental Technology Conference Mar. 1995 p 49-63 (For primary document see N95-31746 11-23)
Avail: CASI HC A03/MF A06

This paper identifies the necessity of chemical propulsion to satellite usage and some of the benefits accrued through monitoring global resources and patterns, including the Global Climate Change Model (GCM). The paper also summarized how the satellite observations are used to affect national and international policies. Chemical propulsion, like all environmentally conscious industries, does provide limited, controlled pollutant sources through its manufacture and usage. However, chemical propulsion is the sole source which enables mankind to launch spacecraft and monitor the Earth. The information provided by remote sensing directly affects national and international policies designed to protect the environment and enhance the overall quality of life on Earth. The resultant of chemical propulsion is the capability to reduce overall pollutant emissions to the benefit of mankind. Derived from text

N95-31751*# Thiokol Corp., Brigham City, UT.
AP RECLAMATION AND REUSE IN RSRM PROPELLANT **c28**
Kathryn F. Miks and Stacey A. Harris (Phillips Lab., Edwards AFB, CA.) *In* NASA. Marshall Space Flight Center, Aerospace Environmental Technology Conference Mar. 1995 p 67-86 (For primary document see N95-31746 11-23)
Avail: CASI HC A03/MF A06

A solid propellant ingredient reclamation pilot plant has been evaluated at the Strategic Operations of Thiokol Corporation, located in Brigham City, Utah. The plant produces AP wet cake (95 percent AP, 5 percent water) for recycling at AP vendors. AP has been obtained from two standard propellant binder systems (PBAN and HTPB). Analytical work conducted at Thiokol indicates that the vendor-recrystallized AP meets Space Shuttle propellant specification requirements. Thiokol has processed 1-, 5-, and 600-gallon propellant mixes with the recrystallized AP. Processing, cast, cure, ballistic, mechanical, and safety properties have been evaluated. Phillips Laboratory static-test-fired 70-pound and 800-pound BATES motors. The data indicate that propellant processed with reclaimed AP has nominal properties. Author

N95-31752*# Stevens Inst. of Tech., Hoboken, NJ. Center for Environmental Engineering.
ENHANCED ALKALINE HYDROLYSIS AND BIODEGRADABILITY STUDIES OF NITROCELLULOSE-BEARING MISSILE PROPELLANT **c28**
Mohammed Sidhoum, Christos Christodoulatos, Tsan-Liang Su, and Mercurios Redis *In* NASA. Marshall Space Flight Center, Aerospace Environmental Technology Conference Mar. 1995 p 87-98 Sponsored by US Army Construction Research Lab. (For primary document see N95-31746 11-23)
Avail: CASI HC A03/MF A06

Large amounts of energetic materials which have been accumulated over the years in various manufacturing and military installations must be disposed of in an environmentally sound manner. Historically, the method of choice for destruction of obsolete or aging energetic materials has been open burning or open detonation (OB/OD). This destruction approach has become undesirable due to air pollution problems. Therefore, there is a need for new technologies which will effectively and economically deal with the disposal of energetic materials. Along those lines, we have investigated a chemical/biological process for the safe destruction and disposal of a double base solid rocket propellant (AHH), which was used in several 8 inch projectile systems. The solid propellant is made of nitrocellulose and nitroglycerin as energetic components, two lead salts which act as ballistic modifiers, triacetin as a plasticizer and 2-Nitrodiphenylamine (2-NDPA) as a stabilizer. A process train is being developed to convert the organic components of the propellant to biodegradable products and remove the lead from the process stream. The solid propellant is first hydrolyzed through an enhanced alkaline hydrolysis process step. Following lead removal and neutralization, the digested liquor rich in nitrates and nitrites is found to be easily biodegradable. The digestion rate of the intact ground propellant as well as the release of nitrite and nitrate groups were substantially increased when ultrasound were supplied to the alkaline reaction medium compared to the conventional alkaline hydrolysis. The effects of reaction time, temperature, sodium hydroxide concentration and other relevant parameters on the digestion efficiency and biodegradability have been studied. The present work indicates that the AHH propellant can be disposed of safely with a combination of physiochemical and biological processes. Author

N95-31753*# Hercules Aerospace Co., Magna, UT.
ENVIRONMENTALLY COMPATIBLE SOLID ROCKET PROPELLANTS **c28**
James L. Jacox and Daniel J. Bradford *In* NASA. Marshall Space Flight Center, Aerospace Environmental Technology Conference Mar. 1995 p 99-104 (For primary document see N95-31746 11-23)
Avail: CASI HC A02/MF A06

Hercules' clean propellant development research is exploring three major types of clean propellant: (1) chloride-free formulations (no chlorine containing ingredients), being developed on the Clean Propellant Development and Demonstration (CPDD) contract sponsored by Phillips Laboratory, Edwards Air Force Base, CA; (2) low HCl scavenged formulations (HCl-scavenger added to propellant oxidized with ammonium perchlorate (AP)); and (3) low HCl formulations oxidized with a combination of AN and AP (with or without an HCl scavenger) to provide a significant reduction (relative to current solid rocket boosters) in exhaust HCl. These propellants provide performance approaching that of current systems, with less than 2 percent HCl in the exhaust, a significant reduction (greater than or equal to 70 percent) in exhaust HCl levels. Excellent processing, safety, and mechanical properties were achieved using only readily available, low cost ingredients. Two formulations, a sodium nitrate (NaNO3) scavenged HTPB and a chloride-free hydroxy terminated polyether (HTPE) propellant, were characterized for ballistic, mechanical, and rheological properties. In addition, the hazards properties were demonstrated to provide two families of class 1.3, 'zero-card' propellants. Further characterization is planned which includes

demonstration of ballistic tailorability in subscale (one to 70 pound) motors over the range of burn rates required for retrofit into current Hercules space booster designs (Titan 4 SRMU and Delta 2 GEM). Author

N95-31754*# Thiokol Corp., Brigham City, UT.
LOW ACID PRODUCING SOLID PROPELLANTS **c28**
Robert R. Bennett *In* NASA. Marshall Space Flight Center, Aerospace Environmental Technology Conference Mar. 1995 p 105-114 (For primary document see N95-31746 11-23)
Avail: CASI HC A02/MF A06

The potential environmental effects of the exhaust products of conventional rocket propellants have been assessed by various groups. Areas of concern have included stratospheric ozone, acid rain, toxicity, air quality and global warming. Some of the studies which have been performed on this subject have concluded that while the impacts of rocket use are extremely small, there are propellant development options which have the potential to reduce those impacts even further. This paper discusses the various solid propellant options which have been proposed as being more environmentally benign than current systems by reducing HCl emissions. These options include acid neutralized, acid scavenged, and nonchlorine propellants. An assessment of the acid reducing potential and the viability of each of these options is made, based on current information. Such an assessment is needed in order to judge whether the potential improvements justify the expenditures of developing the new propellant systems. Author

N95-31755*# McDonnell-Douglas Aerospace, Huntsville, AL.
IMPROVED HYBRID ROCKET FUEL **c28**
David L. Dean *In* NASA. Marshall Space Flight Center, Aerospace Environmental Technology Conference Mar. 1995 p 115-121 Sponsored by MDA-HSV-IRAD (For primary document see N95-31746 11-23)
Avail: CASI HC A02/MF A06

McDonnell Douglas Aerospace, as part of its Independent R&D, has initiated development of a clean burning, high performance hybrid fuel for consideration as an alternative to the solid rocket thrust augmentation currently utilized by American space launch systems including Atlas, Delta, Pegasus, Space Shuttle, and Titan. It could also be used in single stage to orbit or as the only propulsion system in a new launch vehicle. Compared to solid propellants based on aluminum and ammonium perchlorate, this fuel is more environmentally benign in that it totally eliminates hydrogen chloride and aluminum oxide by products, producing only water, hydrogen, nitrogen, carbon oxides, and trace amounts of nitrogen oxides. Compared to other hybrid fuel formulations under development, this fuel is cheaper, denser, and faster burning. The specific impulse of this fuel is comparable to other hybrid fuels and is between that of solids and liquids. The fuel also requires less oxygen than similar hybrid fuels to produce maximum specific impulse, thus reducing oxygen delivery system requirements. Author

N95-31756*# Sverdrup Technology, Inc., Huntsville, AL.
TECHNOLOGY TRANSFER INTO THE SOLID PROPULSION INDUSTRY **c20**
Ralph L. Campbell and Lawrence J. Thomson *In* NASA. Marshall Space Flight Center, Aerospace Environmental Technology Conference Mar. 1995 p 123-129 (For primary document see N95-31746 11-23)
Avail: CASI HC A02/MF A06

This paper is a survey of the waste minimization efforts of industries outside of aerospace for possible applications in the manufacture of solid rocket motors (SRM) for NASA. The Redesigned Solid Rocket Motor (RSRM) manufacturing plan was used as the model for processes involved in the production of an SRM. A literature search was conducted to determine the recycling, waste minimization, and waste treatment methods used in the commercial sector that might find application in SRM production. Manufacturers, trade organizations, and professional associations were also contacted. Waste minimization efforts for current processes and replacement technologies, which might reduce the amount or severity of the wastes generated in SRM production, were investigated. An overview of the results of this effort are presented in this paper. Author

N95-31757*# National Aeronautics and Space Administration. Marshall Space Flight Center, Huntsville, AL.
PRIORITIZATION METHODOLOGY FOR CHEMICAL REPLACEMENT **c45**
Wendy Cruit, Ben Goldberg, and Scott Schutzenhofer *In its* Aerospace Environmental Technology Conference Mar. 1995 p 131-141 (For primary document see N95-31746 11-23)
Avail: CASI HC A03/MF A06

Since United States of America federal legislation has required ozone depleting chemicals (class 1 & 2) to be banned from production, The National Aeronautics and Space Administration (NASA) and industry have been required to find other chemicals and methods to replace these target chemicals. This project was initiated as a development of a prioritization methodology suitable for assessing and ranking existing processes for replacement 'urgency.' The methodology was produced in the form of a workbook (NASA Technical Paper 3421). The final workbook contains two tools, one for evaluation and one for prioritization. The two tools are interconnected in that they were developed from one central theme - chemical replacement due to imposed laws and regulations. This workbook provides matrices, detailed explanations of how to use them, and a detailed methodology for prioritization of replacement technology. The main objective is to provide a GUIDELINE to help direct the research for replacement technology. The approach for prioritization called for a system which would result in a numerical rating for the chemicals and processes being assessed. A Quality Function Deployment (QFD) technique was used in order to determine numerical values which would correspond to the concerns raised and their respective importance to the process. This workbook defines the approach and the application of the QFD matrix. This technique: (1) provides a standard database for technology that can be easily reviewed, and (2) provides a standard format for information when requesting resources for further research for chemical replacement technology. Originally, this workbook was to be used for Class 1 and Class 2 chemicals, but it was specifically designed to be flexible enough to be used for any chemical used in a process (if the chemical and/or process needs to be replaced). The methodology consists of comparison matrices (and the smaller comparison components) which allow replacement technology to be quantitatively compared in several categories, and a QFD matrix which allows process/chemical pairs to be rated against one another for importance (using consistent categories). Depending on the need for application, one can choose the part(s) needed or have the methodology completed in its entirety. For example, if a program needs to show the risk of changing a process/chemical one may choose to use part of Matrix A and Matrix C. If a chemical is being used, and the process must be changed; one might use the Process Concerns part of Matrix D for the existing process and all possible replacement processes. If an overall analysis of a program is needed, one may request the QFD to be completed. Author

N95-31758*# National Center for Mfg. Sciences, Ann Arbor, MI.
NATIONAL CENTER FOR MANUFACTURING SCIENCES: ENVIRONMENTALLY CONSCIOUS MANUFACTURING **c45**
Clare Vinton *In* NASA. Marshall Space Flight Center, Aerospace Environmental Technology Conference Mar. 1995 p 145-147 (For primary document see N95-31746 11-23)
Avail: CASI HC A01/MF A06

The purpose of this presentation is to share the results and some of the thinking of the Environmentally Conscious Manufacturing - Strategic Initiative Group (ECM-SIG) at the National Center for Manufacturing Sciences (NCMS). NCMS is a consortium of more than 185 North American Manufacturing organizations comprised of about 75 percent for profit manufacturing companies and about 25 percent nonprofit organizations that support manufacturing activities. NCMS conducts collaborative R&D programs designed to improve global competitiveness of its members and other North American manufacturers to address common issues that are important to manufacturing industries. NCMS is an industry driven organization whose agenda is established by industry with input from appropriate government agencies. Derived from text

N95-31759*# Pennsylvania State Univ., State College, PA. Applied Research Lab.
AIR POLLUTION CONTROL SYSTEM RESEARCH: AN ITERATIVE APPROACH TO DEVELOPING AFFORDABLE SYSTEMS **c45**
Lewis C. Watt, Fred S. Cannon, Robert J. Heinsohn, and Timothy A. Spaeder *In* NASA. Marshall Space Flight Center, Aerospace Environmental Technology Conference Mar. 1995 p 149-156 (For primary document see N95-31746 11-23)
Avail: CASI HC A02/MF A06

This paper describes a Strategic Environmental Research and Development Program (SERDP) funded project led jointly by the Marine Corps Multi-Commodity Maintenance Centers, and the Air and Energy Engineering Research Laboratory (AEERL) of the USEPA. The research focuses on paint booth exhaust minimization using recirculation, and on volatile organic compound (VOC) oxidation by the modules of a hybrid air pollution control system. The research team is applying bench, pilot and full scale systems to accomplish the goals of reduced cost and improved effectiveness of air treatment systems for paint booth exhaust.

Author (revised)

N95-31760*# Electronics Mfg. Productivity Facility, Indianapolis, IN.

THE SEARCH FOR CFC ALTERNATIVES IS OVER? c27

Tim Crawford *In* NASA. Marshall Space Flight Center, Aerospace Environmental Technology Conference Mar. 1995 p 157-161 (For primary document see N95-31746 11-23)

Avail: CASI HC A01/MF A06

The Electronics Manufacturing Productivity Facility (EMPF) is a U.S. Navy Center of Excellence tasked to do research in electronics manufacturing. For the past seven years, the EMPF has performed extensive research in various cleaning materials and processes that have recently been made available to printed circuit board assemblers. This paper outlines our research and points out the positive and negative aspects that need to be considered when choosing an alternative process. Author

N95-31761*# Air Force Civil Engineering Center, Tyndall AFB, FL. Directorate of Construction Cost Management.

MAJOR WEAPON SYSTEM ENVIRONMENTAL LIFE-CYCLE COST ESTIMATING FOR CONSERVATION, CLEANUP, COMPLIANCE AND POLLUTION PREVENTION (C3P2) c45

Wesley Hammond, Marland Thurston (Delta Research Corp., Niceville, FL.), and Christopher Hood (Delta Research Corp., Niceville, FL.) *In* NASA. Marshall Space Flight Center, Aerospace Environmental Technology Conference Mar. 1995 p 163-168 (For primary document see N95-31746 11-23)

Avail: CASI HC A02/MF A06

The Titan 4 Space Launch Vehicle Program is one of many major weapon system programs that have modified acquisition plans and operational procedures to meet new, stringent environmental rules and regulations. The Environmental Protection Agency (EPA) and the Department of Defense (DOD) mandate to reduce the use of ozone depleting chemicals (ODC's) is just one of the regulatory changes that has affected the program. In the last few years, public environmental awareness, coupled with stricter environmental regulations, has created the need for DOD to produce environmental life-cycle cost estimates (ELCCE) for every major weapon system acquisition program. The environmental impact of the weapon system must be assessed and budgeted, considering all costs, from cradle to grave. The Office of the Secretary of Defense (OSD) has proposed that organizations consider Conservation, Cleanup, Compliance and Pollution Prevention (C(sup 3)P(sup 2)) issues associated with each acquisition program to assess life-cycle impacts and costs. The Air Force selected the Titan 4 system as the pilot program for estimating life-cycle environmental costs. The estimating task required participants to develop an ELCCE methodology, collect data to test the methodology and produce a credible cost estimate within the DOD C(sup 3)P(sup 2) definition. The estimating methodology included using the Program Office weapon system description and work breakdown structure together with operational site and manufacturing plant visits to identify environmental cost drivers. The results of the Titan IV ELCCE process are discussed and expanded to demonstrate how they can be applied to satisfy any life-cycle environmental cost estimating requirement. Author

N95-31762*# United Technologies Corp., Huntsville, AL.

EVALUATING THE COST EFFECTIVENESS OF ENVIRONMENTAL PROJECTS: CASE STUDIES IN AEROSPACE AND DEFENSE c45

James F. Shunk *In* NASA. Marshall Space Flight Center, Aerospace Environmental Technology Conference Mar. 1995 p 169-177 (For primary document see N95-31746 11-23)

Avail: CASI HC A02/MF A06

Using the replacement technology of high pressure waterjet decoating systems as an example, a simple methodology is presented for developing a cost effectiveness model. The model uses a four-step process to formulate an economic justification designed for presentation to decision makers as an assessment of the value of the replacement technology over conventional methods. Three case studies from major U.S. and international airlines are used to illustrate the methodology and resulting model. Tax and depreciation impacts are also presented as potential additions to the model. Author

N95-31763*# Martin Marietta Energy Systems, Inc., Oak Ridge, TN.

THE OAK RIDGE REFRIGERANT MANAGEMENT PROGRAM c27

Thomas H. Kevil *In* NASA. Marshall Space Flight Center, Aerospace Environmental Technology Conference Mar. 1995 p 179-186 (For primary document see N95-31746 11-23)

(Contract DE-AC05-84OR-21400)

Avail: CASI HC A02/MF A06

For many years, chlorofluorocarbons (CFC's) have been used by the Department of Energy's (DOE) Oak Ridge Y-12 Plant in air conditioning and process refrigeration systems. However, Title 6 of the Clean Air Act Amendments (CAAA) and Executive Order 12843 (Procurement Requirements and Policies for Federal Agencies for Ozone Depleting Substances) signed by President Clinton require, as policy, that all federal agencies maximize their use of safe, alternate refrigerants and minimize, where economically practical, the use of Class 1 refrigerants. Unfortunately, many government facilities and industrial plants have no plan or strategy in place to make this changeover, even though their air conditioning and process refrigeration equipment may not be sustainable after CFC production ends December 31, 1995. The Y-12 Plant in Oak Ridge, Tennessee, has taken an aggressive approach to complying with the CAAA and is working with private industry and other government agencies to solve tough manufacturing and application problems associated with CFC and hydrochlorofluorocarbon (HCFC) alternatives. Y-12 was the first DOE Defense Program (DP) facility to develop a long-range Stratospheric Ozone Protection Plan for refrigerant management for compliance with the CAAA. It was also the first DOE DP facility to complete detailed engineering studies on retrofitting and replacing all air conditioning and process refrigeration equipment to enable operation with alternate refrigerants. The management plan and engineering studies are models for use by other government agencies, manufacturing plants, and private industry. This presentation identifies some of the hidden pitfalls to be encountered in the accelerated phaseout schedule of CFC's and explains how to overcome and prevent these problems. In addition, it outlines the general issues that must be considered when addressing the phase-out of ozone depleting substances and gives some 'lessons learned' by Y-12 from its Refrigerant Management Program. Discussion topics include requirements for developing a refrigerant management plan and establishing priorities for cost-effective compliance with the CAAA, as well as ways in which employees can be empowered to develop a comprehensive refrigerant management plan. The result of this employee empowerment was a cooperative labor-management effort that is beneficial for Y-12, DOE, and the environment. Author

N95-31764*# Glidco Organics Corp., Jacksonville, FL.

Prepsolv (TM): THE OPTIMUM ALTERNATIVE TO 1,1,1-TRICHLOROETHANE AND METHYL ETHYL KETONE FOR HAND-WIPE CLEANING OF AEROSPACE MATERIALS c27

R. Scott Gallagher, John A. Purvis (Hercules Aerospace Co., Magna, UT.), and Wade W. Moran (Hercules Aerospace Co., Magna, UT.) *In* NASA. Marshall Space Flight Center, Aerospace Environmental Technology Conference Mar. 1995 p 187-197 (For primary document see N95-31746 11-23)

Avail: CASI HC A03/MF A06

Engineers at Hercules Aerospace, a rocket motor manufacturer in Utah, have worked closely with chemists at Glidco Organics to study the feasibility of using terpenes for zero-residue wipe cleaning. The result of this work is a technological breakthrough, in which the barrier to ultra-low non-volatile residue formation has been broken. After 2 years of development and testing, SCM Glidco Organics has announced the availability of Glidsafe(registered trademark) Prepsolv(TM): a state-of-the-art ultra-low residue terpene wipe cleaning agent that does not require rinsing. Prepsolv(TM) can successfully be used in simple hand-wipe cleaning processes without fear of leaving surface residues. Industry testing has confirmed that Prepsolv(TM) is not only highly effective, but can even be less expensive to use than traditional cleaning solvents like methyl chloroform. This paper addresses the features and benefits of Prepsolv(TM), and presents performance and material compatibility data that characterizes

this unique cleaning agent. Since its commercialization, Hercules Aerospace has chosen Prepsolv(TM) as the optimum cleaning agent to replace ozone-depleting solvents in their weapons factory in Magna, UT. Likewise, Boeing has approved Prepsolv(TM) for cleaning components in the manufacture of commercial aircraft at their facilities in Seattle, WA and Wichita, KS. Additional approvals are forthcoming for this uniquely safe and effective solvent. Derived from text

N95-31765*# Martin Marietta Corp., Huntsville, AL.
A WATER BLOWN URETHANE INSULATION FOR USE IN CRYOGENIC ENVIRONMENTS **c27**
Elana Blevins and Jon Sharpe *In* NASA. Marshall Space Flight Center, Aerospace Environmental Technology Conference Mar. 1995 p 201-206 (For primary document see N95-31746 11-23)
(Contract NAS8-36200)
Avail: CASI HC A02/MF A06

Thermal Protection Systems (TPS) of NASA's Space Shuttle External Tank include polyurethane and polyisocyanurate modified polyurethane foam insulations. These insulations, currently foamed with CFC 11 blowing agent, serve to maintain cryogenic propellant quality, maintain the external tank structural temperature limits, and minimize the formation of ice and frost that could potentially damage the ceramic insulation on the space shuttle orbiter. During flight the external tank insulations are exposed to mechanical, thermal and acoustical stresses. TPS must pass cryogenic flexure and substrate adhesion tests at -253 C, aerothermal and radiant heating tests at fluxes up to approximately 14 kilowatts per square meter, and thermal conductivity tests at cryogenic and elevated temperatures. Due to environmental concerns, the polyurethane insulation industry and the External Tank Project are tasked with replacing CFC 11. The flight qualification of foam insulations employing HCFC 141b as a foaming agent is currently in progress; HCFC 141b blown insulations are scheduled for production implementation in 1995. Realizing that the second generation HCFC blowing agents are an interim solution, the evaluation of third generation blowing agents with zero ozone depletion potential is underway. NASA's TPS Materials Research Laboratory is evaluating third generation blowing agents in cryogenic insulations for the External Tank; one option being investigated is the use of water as a foaming agent. A dimensionally stable insulation with low friability, good adhesion to cryogenic substrates, and acceptable thermal conductivity has been developed with low viscosity materials that are easily processed in molding applications. The development criteria, statistical experimental approach, and resulting foam properties will be presented. Author

N95-31766*# Martin Marietta Corp., Huntsville, AL. Manned Space Systems.
EVALUATION OF HFC 245ca AND HFC 236ea AS FOAM BLOWING AGENTS **c27**
Jon Sharpe, Doug MacArthur, Tom Kollie (Oak Ridge National Lab., TN.), Ron Graves (Oak Ridge National Lab., TN.), Matthew Liu (Martin Marietta Corp., New Orleans, LA.), and Robert V. Hendriks (Environmental Protection Agency, Research Triangle Park, NC.) *In* NASA. Marshall Space Flight Center, Aerospace Environmental Technology Conference Mar. 1995 p 207-224 (For primary document see N95-31746 11-23)
(Contracts NAS8-36200; DE-AC05-84OR-21400; EPA-DW-899349-75)
Avail: CASI HC A03/MF A06

Hydrochlorofluorocarbon (HCFC) 141b has been selected as the interim blowing agent for use in urethane insulations on NASA's Space Shuttle External Tank. Due to the expected limited commercial lifetime of this material, research efforts at the NASA Thermal Protection Systems Materials Research Laboratory at the Marshall Space Flight Center are now being devoted to the identification and development of alternatives with zero ozone depletion potential. Physical blowing agents identified to date have included hydrocarbons, fluorocarbons, hydrofluoroethers, and more predominantly, hydrofluorocarbons (HFCs). The majority of the HFC evaluations in industry have focused on the more readily available, low boiling candidates such as HFC 134a. Higher boiling HFC candidates that could be handled at ambient conditions and use current processing equipment would be more desirable. This paper will describe results from a research program of two such candidate HFC's performed as a cooperative effort between Martin Marietta Manned Space Systems, the U.S. Environmental Protection Agency, and Oak Ridge National Laboratories. The purpose of this effort was to perform a cursory evaluation of the developmental HFC's 245ca and 236ea as blowing agents in urethane based insulations. These two materials were selected from screening tests of 37 C2, C3, and C4 isomers based on physical properties, atmospheric lifetime, flammability, estimated toxicity, difficulty of synthesis, suitability for dual use as a refrigerant, and other factors. Solubility of the two materials in typical foam components was tested, pour foaming trials were performed, and preliminary data were gathered regarding foam insulation performance. Author

N95-31767*# Battelle Memorial Inst., Columbus, OH.
ALTERNATIVES TO OZONE DEPLETING REFRIGERANTS IN TEST EQUIPMENT **c27**
Richard L. Hall and Madeleine R. Johnson (Aerospace Guidance and Metrology Center, Newark Air Force Station, OH.) *In* NASA. Marshall Space Flight Center, Aerospace Environmental Technology Conference Mar. 1995 p 225-232 (For primary document see N95-31746 11-23)
Avail: CASI HC A02/MF A06

This paper describes the initial results of a refrigerant retrofit project at the Aerospace Guidance and Metrology Center (AGMC) at Newark Air Force Base, Ohio. The objective is to convert selected types of test equipment to properly operate on hydrofluorocarbon (HFC) alternative refrigerants, having no ozone depleting potential, without compromising system reliability or durability. This paper discusses the primary technical issues and summarizes the test results for 17 different types of test equipment: ten environmental chambers, two ultralow temperature freezers, two coolant recirculators, one temperature control unit, one vapor degreaser, and one refrigerant recovery system. The postconversion performance test results have been very encouraging: system capacity and input power remained virtually unchanged. In some cases, the minimum operating temperature increased by a few degrees as a result of the conversion, but never beyond AGMC's functional requirements. Author

N95-31768*# Department of the Air Force, Wright-Patterson AFB, OH.
ENVIRONMENTALLY SAFE AVIATION FUELS **c28**
Patricia D. Liberio *In* NASA. Marshall Space Flight Center, Aerospace Environmental Technology Conference Mar. 1995 p 233-237 (For primary document see N95-31746 11-23)
Avail: CASI HC A01/MF A06

In response to the Air Force directive to remove Ozone Depleting Chemicals (ODC's) from military specifications and Defense Logistics Agency's Hazardous Waste Minimization Program, we are faced with how to ensure a quality aviation fuel without using such chemicals. Many of these chemicals are found throughout the fuel and fuel related military specifications and are part of test methods that help qualify the properties and quality of the fuels before they are procured. Many years ago there was a directive for military specifications to use commercially standard test methods in order to provide standard testing in private industry and government. As a result the test methods used in military specifications are governed by the American Society of Testing and Materials (ASTM). The Air Force has been very proactive in the removal or replacement of the ODC's and hazardous materials in these test methods. For example, ASTM D3703 (Standard Test Method for Peroxide Number of Aviation Turbine Fuels), requires the use of Freon 113, a known ODC. A new rapid, portable hydroperoxide test for jet fuels similar to ASTM D3703 that does not require the use of ODC's has been developed. This test has proved, in limited testing, to be a viable substitute method for ASTM D3703. The Air Force is currently conducting a round robin to allow the method to be accepted by ASTM and therefore replace the current method. This paper will describe the Air Force's initiatives to remove ODC's and hazardous materials from the fuel and fuel related military specifications that the Air Force Wright Laboratory. Author

N95-31769*# Spectrex, Inc., Cedar Gove, NJ.
NEXT GENERATION FIRE SUPPRESSANTS **c27**
Jerry A. Brown *In* NASA. Marshall Space Flight Center, Aerospace Environmental Technology Conference Mar. 1995 p 239-243 (For primary document see N95-31746 11-23)
Avail: CASI HC A01/MF A06

Spectrex, Inc., located in Cedar Grove, NJ is a manufacturer of fire detection and suppression equipment. Spectrex is one of the original pioneers in high speed fire detection and suppression systems for combat vehicles. Spectrex has installed fire suppressions systems in thousands of combat

vehicles and ships throughout the world. Additionally, they manufacture flame explosion detectors, ship damage control systems, and optical gas and vapor detectors. The culmination of several years of research and development has recently produced an innovative electro-optical continuous monitoring systems called SharpEye 20/20I IR(sup 3) and SAFEYE that provide fast and reliable gas, vapor, aerosol, flame, and explosion detection. SharpEye 20/20I IR(sup 3) is a self-contained triple spectrum flame detector which scans for oscillating IR radiation (1 to 10 Hz) in the spectral bands ranging from 4.0 to 5.0 microns and uses programmed algorithms to check the ratio and correlation of data received by the three sensors to make the system highly immune to false alarms. It is extremely sensitive as it can detect a 1 x 1 square foot gasoline pan fire at 200 feet in less than 3 seconds. The sensitivity is user programmable, offering 4 ranges of detection. SAFEYE is comprised of a selected number of multispectral ban microprocessors controlled detectors which are in communication with one or more radiation sources that is projected along a 600 feet optical path. The signals from the selected narrow bands are processed and analyzed by highly sophisticated algorithms. It is ideal for high risk, remote, large areas such as petroleum and chemical manufacturing sites, waste dumps, aircraft cargo bays, and ship compartments. The SAFEYE will perform direct readings of the presence or rate of rise of concentrations of gases, vapors, or aerosols at the range of parts per million and provide alarms at various set points at different levels of concentrations. Derived from text

N95-31770*# Great Lakes Chemical Corp., West Lafayette, IN.
F-200(TM): THE NEW SOLUTION FOR FIRE PROTECTION **c27**
Alfred J. Thornton and Gerald J. Walter *In* NASA. Marshall Space Flight Center, Aerospace Environmental Technology Conference Mar. 1995 p 245-248 (For primary document see N95-31746 11-23)
Avail: CASI HC A01/MF A06

For more than two decades, halon 1301 has been protecting personnel and valuable aircraft and aerospace equipment from the hazards of fire. Only halon 1301 offered the advantages of being clean, odorless, colorless, electrically non-conductive and safe for occupied areas. However, concerns about the depletion of stratospheric ozone and the resulting Montreal Protocol mandated the production phase-out of halon 1301 on December 31, 1993. Prior to this phase-out, Great Lakes Chemical Corporation, the world's leading manufacturer of halon, directed substantial research efforts toward the rapid development of a safe, clean, and effective halon replacement. Some of the criteria for the development of a clean agent included: that it be an effective fire extinguisher; that it be safe for personnel; that it be safe for the environment; that it be safe for valuable assets; that it be cost effective; and that it be able to withstand the rigors of independent approvals. As the result of this research, Great Lakes developed FM-200(TM) is 1, 1, 1, 2, 3, 3, 3-hepta-fluoropropane. This paper discusses the physical properties of FM-200(TM) and its efficiency as an extinguishant. Author

N95-31771*# National Center for Mfg. Sciences, Ann Arbor, MI.
ASSESSMENT OF POLLUTION PREVENTION AND CONTROL TECHNOLOGY FOR PLATING OPERATIONS **c27**
Paul D. Chalmer, William A. Sonntag (National Association of Metal Finishers, Chicago, IL.), and George C. Cushnie, Jr. (Chrome Application, Inc., Oakton, VA.) *In* NASA. Marshall Space Flight Center, Aerospace Environmental Technology Conference Mar. 1995 p 251-266 (For primary document see N95-31746 11-23)
Avail: CASI HC A03/MF A06

The National Center for Manufacturing Sciences (NCMS) is sponsoring an on-going project to assess pollution prevention and control technology available to the plating industry and to make this information available to those who can benefit from it. Completed project activities include extensive surveys of the plating industry and vendors of technologies and an indepth literature review. The plating industry survey was performed in cooperation with the National Association of Metal Finishers. The contractor that conducted the surveys and prepared the project products was CAI Engineering. The initial products of the project were made available in April, 1994. These products include an extensive report that presents the results of the surveys and literature review and an electronic database. The project results are useful for all those associated with pollution prevention and control in the plating industry. The results show which treatment, recovery and bath maintenance technologies have been most successful for different plating processes and the costs for purchasing and operating these technologies. The project results also cover trends in chemical substitution, the identification of compliance-problem pollutants, sludge generation rates, off-site sludge recovery and disposal options, and many other pertinent topics. Author

N95-31772*# Rockwell International Corp., Canoga Park, CA. Rocketdyne Div.
THIN-FILM SULFURIC ACID ANODIZING AS A REPLACEMENT FOR CHROMIC ACID ANODIZING **c27**
K. J. Kallenborn and J. R. Emmons *In* NASA. Marshall Space Flight Center, Aerospace Environmental Technology Conference Mar. 1995 p 267-276 (For primary document see N95-31746 11-23)
Avail: CASI HC A02/MF A06

Chromic acid has long been used to produce a thin, corrosion resistant (Type I) coating on aluminum. Following anodizing, the hardware was sealed using a sodium dichromate solution. Sealing closes up pores inherent in the anodized coating, thus improving corrosion resistance. The thinness of the brittle coating is desirable from a fatigue standpoint, and chromium was absorbed by the coating during the sealing process, further improving corrosion resistance. Unfortunately, both chromic acid and sodium dichromate contain carcinogenic hexavalent chromium. Sulfuric acid is being considered as a replacement for chromic acid. Sulfuric acid of 10-20 percent concentration has traditionally been used to produce relatively thick (Types II and III) or abrasion resistant (Type III) coatings. A more dilute, that is five weight percent, sulfuric acid anodizing process, which produces a thinner coating than Type II or III, with nickel acetate as the sealant has been developed. The process was evaluated in regard to corrosion resistance, throwing power, fatigue life, and processing variable sensitivity, and shows promise as a replacement for the chromic acid process. Author

N95-31773*# Boeing Defense and Space Group, Seattle, WA.
CADMIUM PLATING REPLACEMENTS **c27**
Mary J. Nelson and Earl C. Groshart *In* NASA. Marshall Space Flight Center, Aerospace Environmental Technology Conference Mar. 1995 p 277-284 (For primary document see N95-31746 11-23)
Avail: CASI HC A02/MF A06

The Boeing Company has been searching for replacements to cadmium plate. Two alloy plating systems seem close to meeting the needs of a cadmium replacement. The two alloys, zinc-nickel and tin-zinc are from alloy plating baths; both baths are neutral pH. The alloys meet the requirements for salt fog corrosion resistance, and both alloys excel as a paint base. Currently, tests are being performed on standard fasteners to compare zinc-nickel and tin-zinc on threaded hardware where cadmium is heavily used. The Hydrogen embrittlement propensity of the zinc-nickel bath has been tested, and just beginning for the tin-zinc bath. Another area of interest is the electrical properties on aluminum for tin-zinc and will be discussed. The zinc-nickel alloy plating bath is in production in Boeing Commercial Airplane Group for non-critical low strength steels. The outlook is promising that these two coatings will help. The Boeing Company significantly reduce its dependence on cadmium plating. Author

N95-31774*# National Aeronautics and Space Administration. Marshall Space Flight Center, Huntsville, AL.
REPLACEMENT OF CORROSION PROTECTION CHROMATE PRIMERS AND PAINTS USED IN CRYOGENIC APPLICATIONS ON THE SPACE SHUTTLE WITH WIRE ARC SPRAYED ALUMINUM COATINGS **c27**
R. L. Daniel (Rockwell International Corp., Huntsville, AL.), H. L. Sanders (Rockwell International Corp., Huntsville, AL.), and F. R. Zimmerman *In its* Aerospace Environmental Technology Conference Mar. 1995 p 285-291 (For primary document see N95-31746 11-23)
(Contract NAS8-40000)
Avail: CASI HC A02/MF A06

With the advent of new environmental laws restricting volatile organic compounds and hexavalent chrome emissions, 'environmentally safe' thermal spray coatings are being developed to replace the traditional corrosion protection chromate primers. A wire arc sprayed aluminum coating is being developed for corrosion protection of low pressure liquid hydrogen carrying ducts on the Space Shuttle Main Engine. Currently, this hardware utilizes a chromate primer to provide protection against corrosion pitting and stress corrosion cracking induced by the cryogenic operating environment. The wire are sprayed aluminum coating has been found to have good potential

to provide corrosion protection for flight hardware in cryogenic applications. The coating development, adhesion test, corrosion test and cryogenic flexibility test results will be presented. Author

N95-31775*# Northrop Grumman Corp., Pico Rivera, CA. Environmentally Technology Development.

ENVIRONMENTALLY REGULATED AEROSPACE COATINGS c27

Virginia L. Morris *In* NASA. Marshall Space Flight Center, Aerospace Environmental Technology Conference Mar. 1995 p 295-305 (For primary document see N95-31746 11-23)

Avail: CASI HC A03/MF A06

Aerospace coatings represent a complex technology which must meet stringent performance requirements in the protection of aerospace vehicles. Topcoats and primers are used, primarily, to protect the structural elements of the air vehicle from exposure to and subsequent degradation by environmental elements. There are also many coatings which perform special functions, i.e., chafing resistance, rain erosion resistance, radiation and electric effects, fuel tank coatings, maskants, wire and fastener coatings. The scheduled promulgation of federal environmental regulations for aerospace manufacture and rework materials and processes will regulate the emissions of photochemically reactive precursors to smog and air toxics. Aerospace organizations will be required to identify, qualify and implement less polluting materials. The elimination of ozone depleting chemicals (ODC's) and implementation of pollution prevention requirements are added constraints which must be addressed concurrently. The broad categories of operations affected are the manufacture, operation, maintenance, and repair of military, commercial, general aviation, and space vehicles. The federal aerospace regulations were developed around the precept that technology had to be available to support the reduction of organic and air toxic emissions, i.e., the regulations cannot be technology forcing. In many cases, the regulations which are currently in effect in the South Coast Air Quality Management District (SCAQMD), located in Southern California, were used as the baseline for the federal regulations. This paper addresses strategies used by Southern California aerospace organizations to cope with these regulatory impacts on aerospace productions programs. All of these regulatory changes are scheduled for implementation in 1993 and 1994, with varying compliance dates established. Author

N95-31776*# United Space Boosters, Inc., Huntsville, AL. Materials and Processes Lab.

CONVERGENT SPRAY PROCESS FOR ENVIRONMENTALLY FRIENDLY COATINGS c27

Jack Scarpa *In* NASA. Marshall Space Flight Center, Aerospace Environmental Technology Conference Mar. 1995 p 307-313 (For primary document see N95-31746 11-23)

Avail: CASI HC A02/MF A06

Conventional spray application processes have poor transfer efficiencies, resulting in an exorbitant loss in materials, solvents, and time. Also, with ever tightening Environmental Protection Agency (EPA) regulations and Occupational Safety and Health Administration requirements, the low transfer efficiencies have a significant impact on the quantities of materials and solvents that are released into the environment. High solids spray processes are also limited by material viscosities, thus requiring many passes over the surface to achieve a thickness in the 0.125 -inch range. This results in high application costs and a negative impact on the environment. Until recently, requirements for a 100 percent solid sprayable, environmentally friendly, lightweight thermal protection system that can be applied in a thick (greater than 0.125 inch) single-pass operation exceeded the capability of existing systems. Such coatings must be applied by hand lay-up techniques, especially for thermal and/or fire protection systems. The current formulation of these coatings has presented many problems such as worker safety, environmental hazards, waste, high cost, and application constraints. A system which can apply coatings without using hazardous materials would alleviate many of these problems. Potential applications include the aerospace thermal protective specialty coatings, chemical and petroleum industries that require fire-protection coatings that resist impact, chemicals, and weather. These markets can be penetrated by offering customized coatings applied by automated processes that are environmentally friendly. Author

N95-31777*# Rockwell International Corp., Canoga Park, CA. Rocketdyne Div.

SSME MAIN COMBUSTION CHAMBER (MCC) HOT OIL DEWAXING c27

Anthony U. Akpati *In* NASA. Marshall Space Flight Center, Aerospace Environmental Technology Conference Mar. 1995 p 315-323 (For primary document see N95-31746 11-23)

Avail: CASI HC A02/MF A06

In an attempt to comply with the changing environmental regulations, a process was developed for the replacement of perchloroethylene in the dewaxing of the Space Shuttle Main Engine (SSME) Main Combustion Chamber (MCC) and other associated hardware filled with the Rigidax (R) casting compound. Rigidax (R) is a hard blue-dyed, calcium carbonate filled thermoplastic casting compound (melting point 77 C) that is melted and poured into hardware cavities to prevent contamination during material removal processes, i.e. machining, grinding, drilling, and deburring. Additionally, it serves as a maskant for designated areas during electroforming processes. Laboratory testing was conducted to evaluate seven alternate fluids for the replacement of perchloroethylene in the dewaxing process. Based upon successful laboratory results, a mineral oil was selected for testing on actual hardware. The final process developed involves simultaneous immersion and flushing of the MCC channels using a distinct eight stage process. A nonvolatile hydrocarbon analysis of a solvent flush sample is performed to determine the hardware cleanliness for comparison to the previous perchloroethylene dewaxing process. Author

N95-31778*# San Antonio Air Logistics Center, Kelly AFB, TX. Aircraft Production Div.

BICARBONATE OF SODA PAINT STRIPPING PROCESS VALIDATION AND MATERIAL CHARACTERIZATION c27

Michael N. Haas *In* NASA. Marshall Space Flight Center, Aerospace Environmental Technology Conference Mar. 1995 p 325-329 (For primary document see N95-31746 11-23)

Avail: CASI HC A01/MF A06

The Aircraft Production Division at San Antonio Air Logistics Center has conducted extensive investigation into the replacement of hazardous chemicals in aircraft component cleaning, degreasing, and depainting. One of the most viable solutions is process substitution utilizing abrasive techniques. SA-ALC has incorporated the use of Bicarbonate of Soda Blasting as one such substitution. Previous utilization of methylene chloride based chemical strippers and carbon removal agents has been replaced by a walk-in blast booth in which we remove carbon from engine nozzles and various gas turbine engine parts, depaint cowlings, and perform various other functions on a variety of parts. Prior to implementation of this new process, validation of the process was performed, and materials and waste stream characterization studies were conducted. These characterization studies examined the effects of the blasting process on the integrity of the thin-skinned aluminum substrates, the effects of the process on both air emissions and effluent disposal, and the effects on the personnel exposed to the process. Author

N95-31779*# National Aeronautics and Space Administration. Marshall Space Flight Center, Huntsville, AL.

WATERJET PROCESSES FOR COATING REMOVAL c27

Fletcher Burgess (United Space Boosters, Inc., Huntsville, AL.), Steve Cosby (United Space Boosters, Inc., Huntsville, AL.), and David Hoppe *In its* Aerospace Environmental Technology Conference Mar. 1995 p 331-336 (For primary document see N95-31746 11-23)

Avail: CASI HC A02/MF A06

USBI and NASA have been testing and investigating the use of high pressure water for coating removal for approximately the past 12 years at the Automated TPS (Thermal Protection System - ablative materials used for thermal protection during ascent and descent of the solid rocket boosters) Removal Facility located in the Productivity Enhancement Complex at Marshall Space Flight Center. Originally the task was to develop and automate the removal process and transfer the technology to a production facility at Kennedy Space Center. Since that time more and more applications and support roles for the waterjet technology have been realized. The facility has become a vital part of development activities ongoing at MSFC. It supports the development of environmentally compliant insulations, sealants, and coatings. It also supports bonding programs, test motors,

and pressure vessels. The most recent role of the cell is supporting Thiokol Corporation's solid rocket motor program in the development of waterjet degreasing and paint stripping methods. Currently vapor degreasing methods use 500,000 lbs. of ozone depleting chemicals per year. This paper describes the major cell equipment, test methods practiced, and coatings that have been removed. Author

N95-31780*# Jet Edge, Inc., Minneapolis, MN.
ULTRA-HIGH PRESSURE WATER JETTING FOR COATING REMOVAL AND SURFACE PREPARATION **c27**
Spencer T. Johnson *In* NASA. Marshall Space Flight Center, Aerospace Environmental Technology Conference Mar. 1995 p 337-347 (For primary document see N95-31746 11-23)
Avail: CASI HC A03/MF A06

This paper shall examine the basics of water technology with particular attention paid to systems currently in use and some select new applications. By providing an overview of commercially available water jet systems in the context of recent case histories, potential users may evaluate the process for future applications. With the on going introduction of regulations prohibiting the use of chemical paint strippers, manual scrapping and dry abrasive media blasting, the need for an environmentally compliant coating removal process has been mandated. Water jet cleaning has been a traditional part of many industrial processed for year, although it has only been in the last few years that reliable pumping equipment capable of ultra-high pressure operation have become available. With the advent of water jet pumping equipment capable of sustaining pressures in excess of 36,000 psi. there has been shift away from lower pressure, high water volume systems. One of the major factors in driving industry to seek higher pressures is the ability to offer higher productivity rates while lowering the quantity of water used and subsequently reprocessed. Among benefits of the trend toward higher pressure/lower volume systems is the corresponding reduction in water jet reaction forces making hand held water jetting practical and safe. Other unique applications made possible by these new generation pumping systems include the use of alternative fluids including liquid ammonia for specialized and hazardous material removal applications. A review of the equipment used and the required modifications will be presented along with the conclusions reached reached during this test program. Author

N95-31781*# Forward Technology Industries, Inc., Minneapolis, MN.
AQUEOUS CLEANING DESIGN PRESENTATION **c27**
Peter F. Maltby *In* NASA. Marshall Space Flight Center, Aerospace Environmental Technology Conference Mar. 1995 p 351-363 (For primary document see N95-31746 11-23)
Avail: CASI HC A03/MF A06

The phase-out of CFC's and other ozone depleting chemicals has prompted industries to re-evaluate their present methods of cleaning. It has become necessary to find effective substitutes for their processes as well as to meet the new cleaning challenges of improved levels of cleanliness and to satisfy concerns about environmental impact of any alternative selected. One of the most popular alternatives being selected is aqueous cleaning. This method offers an alternative for removal of flux, grease/oil, buffing compound, particulates and other soils while minimizing environmental impact. What I will show are methods that can be employed in an aqueous cleaning system that will make it environmentally friendly, relatively simple to maintain and capable of yielding an even higher quality of cleanliness than previously obtained. I will also explore several drying techniques available for these systems and other alternatives along with recent improvements made in this technology. When considering any type of cleaning system, a number of variables should be determined before selecting the basic configuration. Some of these variables are: (1) Soil or contaminants being removed from your parts; (2) The level of cleanliness required; (3) The environmental considerations of your area; (4) Maintenance requirements; and (5) Operating costs. Derived from text

N95-31782*# National Aeronautics and Space Administration. Marshall Space Flight Center, Huntsville, AL.
EVALUATION OF PRESSURIZED WATER CLEANING SYSTEMS FOR HARDWARE REFURBISHMENT **c27**
Terry W. Dillard (Thiokol Corp., Huntsville, AL.), Charles D. DeWeese, David T. Hoppe, John H. Vickers, Gary J. Swenson (Thiokol Corp., Brigham City, UT.), and Dale E. Hutchens (Thiokol Corp., Huntsville, AL.) *In its* Aerospace Environmental Technology Conference Mar. 1995 p 365-368 (For primary document see N95-31746 11-23)
Avail: CASI HC A01/MF A06

Historically, refurbishment processes for RSRM motor cases and components have employed environmentally harmful materials. Specifically, vapor degreasing processes consume and emit large amounts of ozone depleting compounds. This program evaluates the use of pressurized water cleaning systems as a replacement for the vapor degreasing process. Tests have been conducted to determine if high pressure water washing, without any form of additive cleaner, is a viable candidate for replacing vapor degreasing processes. This paper discusses the findings thus far of Engineering Test Plan - 1168 (ETP-1168), 'Evaluation of Pressurized Water Cleaning Systems for Hardware Refurbishment.' Author

N95-31783*# Blackstone Corp., Jamestown, NY.
ULTRASONIC CLEANING: FUNDAMENTAL THEORY AND APPLICATION **c71**
F. John Fuchs *In* NASA. Marshall Space Flight Center, Aerospace Environmental Technology Conference Mar. 1995 p 369-378 (For primary document see N95-31746 11-23)
Avail: CASI HC A02/MF A06

This presentation describes: the theory of ultrasonics, cavitation and implosion; the importance and application of ultrasonics in precision cleaning; explanations of ultrasonic cleaning equipment options and their application; process parameters for ultrasonic cleaning; and proper operation of ultrasonic cleaning equipment to achieve maximum results. Author

N95-31784*# Oak Ridge National Lab., TN.
A CENTRIFUGE CO2 PELLET CLEANING SYSTEM **c37**
C. A. Foster, P. W. Fisher, W. D. Nelson, and D. E. Schechter *In* NASA. Marshall Space Flight Center, Aerospace Environmental Technology Conference Mar. 1995 p 379-389 (For primary document see N95-31746 11-23)
(Contract DE-AC05-84OR-21400)
Avail: CASI HC A03/MF A06

An advanced turbine/CO2 pellet accelerator is being evaluated as a depaint technology at Oak Ridge National Laboratory (ORNL). The program, sponsored by Warner Robins Air Logistics Center (ALC), Robins Air Force Base, Georgia, has developed a robot-compatible apparatus that efficiently accelerates pellets of dry ice with a high-speed rotating wheel. In comparison to the more conventional compressed air 'sandblast' pellet accelerators, the turbine system can achieve higher pellet speeds, has precise speed control, and is more than ten times as efficient. A preliminary study of the apparatus as a depaint technology has been undertaken. Depaint rates of military epoxy/urethane paint systems on 2024 and 7075 aluminum panels as a function of pellet speed and throughput have been measured. In addition, methods of enhancing the strip rate by combining infra-red heat lamps with pellet blasting and by combining the use of environmentally benign solvents with the pellet blasting have also been studied. The design and operation of the apparatus will be discussed along with data obtained from the depaint studies. Author

N95-31785*# Tomco Equipment Co., Loganville, GA.
CO2 (DRY ICE) CLEANING SYSTEM **c37**
Donald M. Barnett *In* NASA. Marshall Space Flight Center, Aerospace Environmental Technology Conference 391-398 (SEE N95-31746 11-23) Mar. 1995 (For primary document see N95-31746 11-23)
Avail: CASI HC A02/MF A06

Tomco Equipment Company has participated in the dry ice (solid carbon dioxide, CO2) cleaning industry for over ten years as a pioneer in the manufacturer of high density, dry ice cleaning pellet production equipment. For over four years Tomco high density pelletizers have been available to the dry ice cleaning industry. Approximately one year ago Tomco introduced the DI-250, a new dry ice blast unit making Tomco a single source supplier for sublimable media, particle blast, cleaning systems. This new blast unit is an all pneumatic, single discharge hose device. It meters the insertion of 1/8 inch diameter (or smaller), high density, dry ice pellets into a high pressure, propellant gas stream. The dry ice and propellant streams are controlled and mixed from the blast cabinet. From there the mixture is transported to the nozzle where the pellets are accelerated to an appropriate blasting velocity. When directed to impact upon a target area, these dry ice pellets have sufficient energy to effectively remove

most surface coatings through dry, abrasive contact. The meta-stable, dry ice pellets used for CO2 cleaning, while labeled 'high density,' are less dense than alternate, abrasive, particle blast media. In addition, after contacting the target surface, they return to their equilibrium condition: a superheated gas state. Most currently used grit blasting media are silicon dioxide based, which possess a sharp tetrahedral molecular structure. Silicon dioxide crystal structures will always produce smaller sharp-edged replicas of the original crystal upon fracture. Larger, softer dry ice pellets do not share the same sharp-edged crystalline structures as their non-sublimable counterparts when broken. In fact, upon contact with the target surface, dry ice pellets will plastically deform and break apart. As such, dry ice cleaning is less harmful to sensitive substrates, workers and the environment than chemical or abrasive cleaning systems. Dry ice cleaning system components include: a dry ice pellet supply, a non-reactive propellant gas source, a pellet and propellant metering device, and a media transport and acceleration hose and nozzle arrangement. Dry ice cleaning system operating parameters include: choice of propellant gas, its pressure and temperature, dry ice mass flow rate, dry ice pellet size and shape, and acceleration nozzle configuration. These parameters may be modified to fit different applications. The growth of the dry ice cleaning industry will depend upon timely data acquisition of the effects that independent changes in these parameters have on cleaning rates, with respect to different surface coating and substrate combinations. With this data, optimization of cleaning rates for particular applications will be possible. The analysis of the applicable range of modulation of these parameters, within system component mechanical constraints, has just begun. Author

N95-31786*# Oak Ridge National Lab., TN.

A MICROWAVE PLASMA CLEANING APPARATUS **c75**

C. C. Tsai, W. D. Nelson, D. E. Schechter, L. M. Thompson, and A. L. Glover *In* NASA. Marshall Space Flight Center, Aerospace Environmental Technology Conference Mar. 1995 p 399-408 (For primary document see N95-31746 11-23)

Avail: CASI HC A02/MF A06

In a microwave electron cyclotron resonance plasma source, reactive plasmas of oxygen and its mixtures of argon have been used for evaluating plasma cleaning technologies. Small aluminum samples (0.95 x 1.9 cm) were coated with thin films (less than or equal to 20 micrometers in thickness) of Shell Vitrea oil and cleaned with reactive plasmas. The discharge parameters, such as gas pressure, magnetic field, substrate biasing, and microwave power, were varied to change cleaning conditions. A mass spectroscopy (or residual gas analyzer) was used to monitor the status of plasma cleaning. Mass loss of the samples after plasma cleaning was measured to estimate cleaning rates. Measured cleaning rates of low-pressure (0.5-m torr) argon/oxygen plasmas were as high as 2.7 micrometers/min. X-ray photoelectron spectroscopy was used to determine cleanliness of the sample surfaces. In this paper, significant results of the plasma cleaning are reported and discussed. Author

N95-31787*# National Aeronautics and Space Administration. John F. Kennedy Space Center, Cocoa Beach, FL.

AQUEOUS CLEANING AND VERIFICATION PROCESSES FOR PRECISION CLEANING OF SMALL PARTS **c37**

Gale J. Allen and Kenneth A. Fishell (Wiltech Corp. of Florida, Inc., Cocoa Beach, FL.) *In* NASA. Marshall Space Flight Center, Aerospace Environmental Technology Conference Mar. 1995 p 411-419 (For primary document see N95-31746 11-23)

Avail: CASI HC A02/MF A06

The NASA Kennedy Space Center (KSC) Materials Science Laboratory (MSL) has developed a totally aqueous process for precision cleaning and verification of small components. In 1990 the Precision Cleaning Facility at KSC used approximately 228,000 kg (500,000 lbs) of chlorofluorocarbon (CFC) 113 in the cleaning operations. It is estimated that current CFC 113 usage has been reduced by 75 percent and it is projected that a 90 percent reduction will be achieved by the end of calendar year 1994. The cleaning process developed utilizes aqueous degreasers, aqueous surfactants, and ultrasonics in the cleaning operation and an aqueous surfactant, ultrasonics, and Total Organic Carbon Analyzer (TOCA) in the nonvolatile residue (NVR) and particulate analysis for verification of cleanliness. The cleaning and verification process is presented in its entirety, with comparison to the CFC 113 cleaning and verification process, including economic and labor costs/savings. Author

N95-31788*# Rockwell International Corp., Canoga Park, CA. Rocketdyne Div.

ULTRASONIC FREQUENCY SELECTION FOR AQUEOUS FINE CLEANING **c71**

Joann F. Becker *In* NASA. Marshall Space Flight Center, Aerospace Environmental Technology Conference Mar. 1995 p 421-430 (For primary document see N95-31746 11-23)

Avail: CASI HC A02/MF A06

A study was conducted to evaluate ultrasonic cleaning systems for precision cleaning effectiveness for oxygen service hardware. This evaluation was specific for Rocketdyne Division of Rockwell Aerospace alloys and machining soils. Machining lubricants and hydraulic fluid were applied as soils to standardized complex test specimens designed to simulate typical hardware. The study consisted of tests which included 20, 25, 30, 40, 50, and 65 kHz ultrasonic cleaning systems. Two size categories of cleaning systems were evaluated, 3- to 10-gal laboratory size tanks and 35- to 320-gal industrial size tanks. The system properties of cavitation, frequency vs. cleaning effectiveness, the two types of transducers, and the power level of the system vs. size of the cleaning tank were investigated. The data obtained from this study was used to select the ultrasonic tanks for the aqueous fine clean facility installed at Rocketdyne. Author

N95-31789*# Thiokol Corp., Brigham City, UT.

QFD ANALYSIS OF RSRM AQUEOUS CLEANERS **c27**

Roy D. Marrs and Randy K. Jones *In* NASA. Marshall Space Flight Center, Aerospace Environmental Technology Conference Mar. 1995 p 431-437 (For primary document see N95-31746 11-23)

Avail: CASI HC A02/MF A06

This paper presents a Quality Function Deployment (QFD) analysis of the final down-selected aqueous cleaners to be used on the Redesigned Solid Rocket Motor (RSRM) program. The new cleaner will replace solvent vapor degreasing. The RSRM Ozone Depleting Compound Elimination program is discontinuing the methyl chloroform vapor degreasing process and replacing it with a spray-in-air aqueous cleaning process. Previously, 15 cleaners were down-selected to two candidates by passing screening tests involving toxicity, flammability, cleaning efficiency, contaminant solubility, corrosion potential, cost, and bond strength. The two down-selected cleaners were further evaluated with more intensive testing and evaluated using QFD techniques to assess suitability for cleaning RSRM case and nozzle surfaces in preparation for adhesive bonding. Author

N95-31790*# National Aeronautics and Space Administration. Marshall Space Flight Center, Huntsville, AL.

A DESIGN OF EXPERIMENTS TEST TO DEFINE CRITICAL SPRAY CLEANING PARAMETERS FOR BRULIN 815 GD AND JETTACIN CLEANERS **c27**

Jill M. Keen (Thiokol Corp., Huntsville, AL.), Kurt B. Evans (Thiokol Corp., Brigham City, UT.), Robert L. Schiffman (Thiokol Corp., Brigham City, UT.), C. Darrell DeWeese, and Michael E. Prince *In its* Aerospace Environmental Technology Conference Mar. 1995 p 439-448 (For primary document see N95-31746 11-23)

Avail: CASI HC A02/MF A06

Experimental design testing was conducted to identify critical parameters of an aqueous spray process intended for cleaning solid rocket motor metal components (steel and aluminum). A two-level, six-parameter, fractional factorial matrix was constructed and conducted for two cleaners, Brulin 815 GD and Diversey Jettacin. The matrix parameters included cleaner temperature and concentration, wash density, wash pressure, rinse pressure, and dishwasher type. Other spray parameters: nozzle stand-off, rinse water temperature, wash and rinse time, dry conditions, and type of rinse water (deionized) were held constant. Matrix response testing utilized discriminating bond specimens (fracture energy and tensile adhesion strength) which represent critical production bond lines. Overall, Jettacin spray cleaning was insensitive to the range of conditions tested for all parameters and exhibited bond strengths significantly above the TCA test baseline for all bond lines tested. Brulin 815 was sensitive to cleaning temperature, but produced bond strengths above the TCA test baseline even at the lower temperatures. Ultimately, the experimental design database was utilized to recommend process parameter settings for future aqueous spray cleaning characterization work. Author

N95-31791*# Jet Propulsion Lab., California Inst. of Tech., Pasadena, CA.

DEGRADATION OF TCE USING SEQUENTIAL ANAEROBIC BIOFILM AND AEROBIC IMMOBILIZED BED REACTOR **c37**

Kirit D. Chapatwala (Selma Univ., AL.), G. R. V. Babu (Selma Univ., AL.), Larry Baresi, and Richard M. Trunzo *In* NASA. Marshall Space Flight Center, Aerospace Environmental Technology Conference Mar. 1995 p 449-457 (For primary document see N95-31746 11-23)

(Grant NAGw-3969)

Avail: CASI HC A02/MF A06

Bacteria capable of degrading trichloroethylene (TCE) were isolated from contaminated wastewaters and soil sites. The aerobic cultures were identified as Pseudomonas aeruginosa (four species) and Pseudomonas fluorescens. The optimal conditions for the growth of aerobic cultures were determined. The minimal inhibitory concentration values of TCE for Pseudomonas sps. were also determined. The aerobic cells were immobilized in calcium alginate in the form of beads. Degradation of TCE by the anaerobic and dichloroethylene (DCE) by aerobic cultures was studied using dual reactors - anaerobic biofilm and aerobic immobilized bed reactor. The minimal mineral salt (MMS) medium saturated with TCE was pumped at the rate of 1 ml per hour into the anaerobic reactor. The MMS medium saturated with DCE and supplemented with xylenes and toluene (3 ppm each) was pumped at the rate of 1 ml per hour into the fluidized air-uplift-type reactor containing the immobilized aerobic cells. The concentrations of TCE and DCE and the metabolites formed during their degradation by the anaerobic and aerobic cultures were monitored by GC. The preliminary study suggests that the anaerobic and aerobic cultures of our isolates can degrade TCE and DCE. Author

N95-31792*# Martin Marietta Energy Systems, Inc., Oak Ridge, TN.

CLEANING WITHOUT CHLORINATED SOLVENTS **c27**

L. M. Thompson and R. F. Simandl *In* NASA. Marshall Space Flight Center, Aerospace Environmental Technology Conference Mar. 1995 p 461-470 (For primary document see N95-31746 11-23)

(Contract DE-AC05-84OR-21400)

Avail: CASI HC A02/MF A06

Because of health and environmental concerns, many regulations have been passed in recent years regarding the use of chlorinated solvents. The Oak Ridge Y-12 Plant has had an active program to find alternatives for these solvents used in cleaning applications for the past 7 years. During this time frame, the quantity of solvents purchased has been reduced by 92 percent. The program has been a twofold effort. Vapor degreasers used in batch cleaning operations have been replaced by ultrasonic cleaning with aqueous detergent, and other organic solvents have been identified for use in hand-wiping or specialty operations. In order to qualify these alternatives for use, experimentation was conducted on cleaning ability as well as effects on subsequent operations such as welding, painting, and bonding. Cleaning ability was determined using techniques such as x-ray photoelectron spectroscopy (XPS) and Fourier transform infrared spectroscopy (FTIR) which are capable of examining monolayer levels of contamination on a surface. Solvents have been identified for removal of rust preventative oils, lapping oils, machining coolants, lubricants, greases, and mold releases. Solvents have also been evaluated for cleaning urethane foam spray guns, swelling of urethanes, and swelling of epoxies. Author

N95-31793*# Aerospace Corp., El Segundo, CA. Mechanics and Materials Technology Center.

REPLACEMENT OF OZONE DEPLETING AND TOXIC CHEMICALS IN GRAVIMETRIC ANALYSIS OF NON-VOLATILE RESIDUE **c27**

G. S. Arnold, J. C. Uht, and F. B. Sinsheimer *In* NASA. Marshall Space Flight Center, Aerospace Environmental Technology Conference Mar. 1995 p 471-480 (For primary document see N95-31746 11-23)

(Contract F04701-92-C-0021)

Avail: CASI HC A02/MF A06

The standard tests for determining nonvolatile residue accretion on spacecraft surfaces and in clean processing facilities rely on the use of halogenated solvents that are targeted for elimination because of their toxic or ozone-depleting natures. This paper presents a literature-based screening survey for candidate replacement solvents. Potential replacements were evaluated for their vapor pressure, toxicity, and solvent properties. Three likely candidates were identified: ethyl acetate, methyl acetate, and acetone. Laboratory tests are presented that evaluate the suitability of these candidate replacement solvents. Author

N95-31794*# National Aeronautics and Space Administration. Marshall Space Flight Center, Huntsville, AL.

EVALUATION OF CONTROL PARAMETERS FOR SPRAY-IN-AIR (SIA) AQUEOUS CLEANING FOR SHUTTLE RSRM HARDWARE **c37**

S. J. Davis (Micro Craft, Inc., Huntsville, AL.) and C. D. DeWeese *In its* Aerospace Environmental Technology Conference Mar. 1995 p 481-490 (For primary document see N95-31746 11-23)

Avail: CASI HC A02/MF A06

HD-2 grease is deliberately applied to Shuttle Redesigned Solid Rocket Motor (RSRM) D6AC steel hardware parts as a temporary protective coating for storage and shipping. This HD-2 grease is the most common form of surface contamination on RSRM hardware and must be removed prior to subsequent surface treatment. Failure to achieve an acceptable level of cleanliness (HD-2 calcium grease removal) is a common cause of defect incidence. Common failures from ineffective cleaning include poor adhesion of surface coatings, reduced bond performance of structural adhesives, and failure to pass cleanliness inspection standards. The RSRM hardware is currently cleaned and refurbished using methyl chloroform (1,1,1-trichloroethane). This chlorinated solvent is mandated for elimination due to its ozone depleting characteristics. This report describes an experimental study of an aqueous cleaning system (which uses Brulin 815 GD) as a replacement for methyl chloroform. Evaluation of process control parameters for this cleaner are discussed as well as cleaning mechanisms for a spray-in-air process. Author

N95-31795*# United Space Boosters, Inc., Huntsville, AL. Materials and Processes Dept.

ENVIRONMENTALLY COMPATIBLE HAND WIPE CLEANING SOLVENTS **c27**

Catherine P. Clayton and Michael P. Kovach *In* NASA. Marshall Space Flight Center, Aerospace Environmental Technology Conference Mar. 1995 p 491-497 (For primary document see N95-31746 11-23)

Avail: CASI HC A02/MF A06

Several solvents of environmental concern have previously been used for hand wipe cleaning of SRB surfaces, including 1,1,1-trichloroethane, perchloroethylene, toluene, xylene, and MEK. USBI determined the major types of surfaces involved, and qualification requirements of replacement cleaning agents. Nineteen environmentally compatible candidates were tested on 33 material substrates with 26 types of potential surface contaminants, involving over 7,000 individual evaluations. In addition to the cleaning performance evaluation, bonding, compatibility, and corrosion tests were conducted. Results showed that one cleaner was not optimum for all surfaces. In most instances, some of the candidates cleaned better than the 1,1,1-trichloroethane baseline control. Aqueous cleaners generally cleaned better, and were more compatible with nonmetallic materials, such as paints, plastics, and elastomers. Organic base cleaners were better on metal surfaces. Five cleaners have been qualified and are now being implemented in SRB hand wipe cleaning operations. Author

N95-31796*# National Aeronautics and Space Administration. Marshall Space Flight Center, Huntsville, AL.

IMPLEMENTATION OF ENVIRONMENTALLY COMPLIANT CLEANING AND INSULATION BONDING FOR MNASA **c27**

Dale E. Hutchens (Thiokol Corp., Huntsville, AL.), Jill M. Keen (Thiokol Corp., Huntsville, AL.), Gary M. Smith (Thiokol Corp., Huntsville, AL.), Terry W. Dillard (Thiokol Corp., Huntsville, AL.), C. Darrell DeWeese, and Seth W. Lawson *In its* Aerospace Environmental Technology Conference Mar. 1995 p 499-506 (For primary document see N95-31746 11-23)

(Contract NAS8-38100)

Avail: CASI HC A02/MF A06

Historically, many subscale and full-scale rocket motors have employed environmentally and physiologically harmful chemicals during the manufacturing process. This program examines the synergy and interdependency between environmentally acceptable materials for solid rocket motor insulation applications, bonding, corrosion inhibiting, painting, priming, and cleaning, and then implements new materials and processes in subscale motors. Tests have been conducted to eliminate or minimize hazardous chemicals used in the manufacture of modified-NASA materials test motor (MNASA) components and identify alternate materials and/or

processes following NASA Operational Environmental Team (NOET) priorities. This presentation describes implementation of high pressure water refurbishment cleaning, aqueous precision cleaning using both Brulin 815 GD and Jettacin, and insulation case bonding using ozone depleting chemical (ODC) compliant primers and adhesives. Author

N95-31797*# National Aeronautics and Space Administration. Marshall Space Flight Center, Huntsville, AL.

SURFACE CONTAMINATION ANALYSIS TECHNOLOGY TEAM OVERVIEW c25

H. DeWitt Burns *In its* Aerospace Environmental Technology Conference Mar. 1995 p 509-515 (For primary document see N95-31746 11-23)

Avail: CASI HC A02/MF A06

A team was established which consisted of representatives from NASA (Marshall Space Flight Center and Langley Research Center), Thiokol Corporation, the University of Alabama in Huntsville, AC Engineering, SAIC, Martin Marietta, and Aerojet. The team's purpose was to bring together the appropriate personnel to determine what surface inspection techniques were applicable to multiprogram bonding surface cleanliness inspection. In order to identify appropriate techniques and their sensitivity to various contaminant families, calibration standards were developed. Producing standards included development of consistent low level contamination application techniques. Oxidation was also considered for effect on inspection equipment response. Ellipsometry was used for oxidation characterization. Verification testing was then accomplished to show that selected inspection techniques could detect subject contaminants at levels found to be detrimental to critical bond systems of interest. Once feasibility of identified techniques was shown, selected techniques and instrumentation could then be incorporated into a multipurpose inspection head and integrated with a robot for critical surface inspection. Inspection techniques currently being evaluated include optically stimulated electron emission (OSEE); near infrared (NIR) spectroscopy utilizing fiber optics; Fourier transform infrared (FTIR) spectroscopy; and ultraviolet (UV) fluorescence. Current plans are to demonstrate an integrated system in MSFC's Productivity Enhancement Complex within five years from initiation of this effort in 1992 assuming appropriate funding levels are maintained. This paper gives an overview of work accomplished by the team and future plans. Author

N95-31798*# AC Engineering, Inc., Huntsville, AL.

STANDARDIZATION OF SURFACE CONTAMINATION ANALYSIS SYSTEMS c25

Richard E. Boothe *In* NASA. Marshall Space Flight Center, Aerospace Environmental Technology Conference Mar. 1995 p 517-524 (For primary document see N95-31746 11-23)

Avail: CASI HC A02/MF A06

Corrosion products, oils and greases can potentially degrade material bonding properties. The Marshall Space Flight Center (MSFC) Surface Contamination Analysis Team (SCAT) utilizes a variety of analytical equipment to detect identify and quantify contamination on metallic and non-metallic substrates. Analysis techniques include FT-IR Microscopy (FT-IR), Near Infrared Optical Fiber Spectrometry (NIR), Optically Stimulated Electron Emission (OSEE), Ultraviolet Fluorescence (UVF) and Ellipsometry. To insure that consistent qualitative and quantitative information are obtained, standards are required to develop analysis techniques, to establish instrument sensitivity to potential contaminants, and to develop calibration curves. This paper describes techniques for preparing and preserving contamination standards. Calibration of surface contamination analysis systems is discussed, and methods are presented for evaluating the effects of potential contaminants on bonding properties. Author

N95-31799*# Thiokol Corp., Huntsville, AL. Space Operations.

CLEANLINESS INSPECTION TOOL FOR RSRM BOND SURFACES c38

Robert A. Mattes *In* NASA. Marshall Space Flight Center, Aerospace Environmental Technology Conference Mar. 1995 p 525-531 (For primary document see N95-31746 11-23)

Avail: CASI HC A02/MF A06

Using optically stimulated electron emission (OSEE), Thiokol has monitored bond surfaces in process for contamination on the Redesigned Solid Rocket Motor (RSRM). This technique provides process control information to help assure bond surface quality and repeatability prior to bonding. This paper will describe OSEE theory of operation and the instrumentation implemented at Thiokol Corporation since 1987. Data from process hardware will be presented. Author

N95-31800*# National Aeronautics and Space Administration. Langley Research Center, Hampton, VA.

THE DESIGN AND DEVELOPMENT OF A THIRD GENERATION OSEE INSTRUMENT c74

D. F. Perey, W. T. Yost, F. D. Stone, C. S. Welch (College of William and Mary, Williamsburg, VA.), E. Scales (Analytical Services and Materials, Inc., Hampton, VA.), E. S. Gasser (Analytical Services and Materials, Inc., Hampton, VA.), E. Joe (Analytical Services and Materials, Inc., Hampton, VA.), T. Goodman (Analytical Services and Materials, Inc., Hampton, VA.), X. Pascual (Analytical Services and Materials, Inc., Hampton, VA.), and B. Hefner (Analytical Services and Materials, Inc., Hampton, VA.) et al *In* NASA. Marshall Space Flight Center, Aerospace Environmental Technology Conference Mar. 1995 p 533-540 (For primary document see N95-31746 11-23)

Avail: CASI HC A02/MF A06

Optically Stimulated Electron Emission (OSEE) has been used to quantify surface contamination in the aerospace community. As advances are made towards the understanding of OSEE, it is desirable to incorporate technological advances with succeeding generations of instrumentation, so that improvements in the practical application of OSEE may be disseminated among the user community. Several studies undertaken by Yost, Welch, Abedin and others have expanded the knowledge base related to the underlying principles of OSEE. The conclusions of these studies, together with inputs from the user community were the foundation upon which the development of a third generation OSEE instrument was based. This manuscript describes the significant improvements incorporated into a third generation OSEE instrument as well as the elements unique to its design. Author

N95-31801*# Alabama Univ., Huntsville, AL.

STUDY OF SURFACES USING NEAR INFRARED OPTICAL FIBER SPECTROMETRY c74

G. L. Workman, W. A. Arendale, and C. Hughes *In* NASA. Marshall Space Flight Center, Aerospace Environmental Technology Conference Mar. 1995 p 541-549 Sponsored by Thiokol (For primary document see N95-31746 11-23)

(Contract NAS8-38609)

Avail: CASI HC A02/MF A06

The measurement and control of cleanliness for critical surfaces during manufacturing and in service provides a unique challenge for fulfillment of environmentally benign operations. Of particular interest has been work performed in maintaining quality in the production of bondline surfaces in propulsion systems and the identification of possible contaminants. This work requires an in-depth study of the possible sources of contamination, methodologies to identify contaminants, discrimination between contaminants and chemical species caused by environment, and the effect of particular contaminants on the bondline integrity of the critical surfaces. This presentation will provide an introduction to the use of optical fiber spectrometry in a nondestructive measurement system for process monitoring and how it can be used to help clarify issues concerning surface chemistry. Correlation of the Near Infrared (NIR) spectroscopic results with Optical Stimulated Electron Emission (OSEE) and ellipsometry will also be presented. Author

N95-31802*# Physical Sciences, Inc., Andover, MA.

CONTAMINATION DETECTION NDE FOR CLEANING PROCESS INSPECTION c38

W. J. Marinelli, V. DiCristina, D. Sonnenfroh, and D. Blair *In* NASA. Marshall Space Flight Center, Aerospace Environmental Technology Conference Mar. 1995 p 551-560 Sponsored by NASA. Langley Research Center (For primary document see N95-31746 11-23)

Avail: CASI HC A02/MF A06

In the joining of multilayer materials, and in welding, the cleanliness of the joining surface may play a large role in the quality of the resulting bond. No non-intrusive techniques are currently available for the rapid measurement of contamination on large or irregularly shaped structures prior to the joining process. An innovative technique for the measurement of contaminant levels in these structures using laser based imaging is

presented. The approach uses an ultraviolet excimer laser to illuminate large and/or irregular surface areas. The UV light induces fluorescence and is scattered from the contaminants. The illuminated area is viewed by an image-intensified CCD (charge coupled device) camera interfaced to a PC-based computer. The camera measures the fluorescence and/or scattering from the contaminants for comparison with established standards. Single shot measurements of contamination levels are possible. Hence, the technique may be used for on-line NDE testing during manufacturing processes. Author

N95-31803*# Martin Marietta Energy Systems, Inc., Oak Ridge, TN.
SURFACE INSPECTION USING FTIR SPECTROSCOPY **c74**
G. L. Powell, N. R. Smyrl, D. M. Williams, H. M. Meyers, III, T. E. Barber (Oak Ridge Inst. for Science and Education, TN.), and M. Marrero-Rivera (Oak Ridge Inst. for Science and Education, TN.) *In* NASA. Marshall Space Flight Center, Aerospace Environmental Technology Conference Mar. 1995 p 563-571 (For primary document see N95-31746 11-23)
(Contract DE-AC05-84OR-21400)
Avail: CASI HC A02/MF A06

The use of reflectance Fourier transform infrared (FTIR) spectroscopy as a tool for surface inspection is described. Laboratory instruments and portable instruments can support remote sensing probes that can map chemical contaminants on surfaces with detection limits under the best of conditions in the sub-nanometer range, i.e.. near absolute cleanliness, excellent performance in the sub-micrometer range, and useful performance for films tens of microns thick. Examples of discovering and quantifying contamination such as mineral oils and greases, vegetable oils, and silicone oils on aluminum foil, galvanized sheet steel, smooth aluminum tubing, and sandblasted 7075 aluminum alloy and D6AC steel. The ability to map in time and space the distribution of oil stains on metals is demonstrated. Techniques associated with quantitatively applying oils to metals, subsequently verifying the application, and non-linear relationships between reflectance and the quantity oil are described. Author

N95-31804*# Thiokol Corp., Brigham City, UT.
CLEANLINESS EVALUATION OF ROUGH SURFACES WITH DIFFUSE IR REFLECTANCE **c74**
L. H. Pearson *In* NASA. Marshall Space Flight Center, Aerospace Environmental Technology Conference Mar. 1995 p 573-581 (For primary document see N95-31746 11-23)
Avail: CASI HC A02/MF A06

Contamination on bonding surfaces has been determined to be a primary cause for degraded bond strength in certain solid rocket motor bondlines. Hydrocarbon and silicone based organic contaminants that are airborne or directly introduced to a surface are a significant source of contamination. Diffuse infrared (IR) reflectance has historically been used as an effective technique for detection of organic contaminants, however, common laboratory methods involving the use of a Fourier transform IR spectrometer (FTIR) are impractical for inspecting the large bonding surface areas found on solid rocket motors. Optical methods involving the use of acousto-optic tunable filters and fixed bandpass optical filters are recommended for increased data acquisition speed. Testing and signal analysis methods are presented which provide for simultaneous measurement of contamination concentration and roughness level on rough metal surfaces contaminated with hydrocarbons. Author

N95-31805*# National Aeronautics and Space Administration. John F. Kennedy Space Center, Cocoa Beach, FL.
CLEANING VERIFICATION BY AIR/WATER IMPINGEMENT **c37**
Lisa L. Jones, Maria D. Littlefield, Gregory S. Melton, Raoul E. B. Caimi, and Eric A. Thaxton *In* NASA. Marshall Space Flight Center, Aerospace Environmental Technology Conference Mar. 1995 p 583-591 (For primary document see N95-31746 11-23)
Avail: CASI HC A02/MF A06

This paper will discuss how the Kennedy Space Center intends to perform precision cleaning verification by Air/Water Impingement in lieu of chlorofluorocarbon-113 gravimetric nonvolatile residue analysis (NVR). Test results will be given that demonstrate the effectiveness of the Air/Water system. A brief discussion of the Total Carbon method via the use of a high temperature combustion analyzer will also be given. The necessary equipment for impingement will be shown along with other possible applications of this technology. Author

N95-31806*# Rockwell International Corp., Canoga Park, CA.
INVESTIGATION OF CLEANLINESS VERIFICATION TECHNIQUES FOR ROCKET ENGINE HARDWARE **c20**
Marilyn L. Fritzemeier and Raymund P. Skowronski *In* NASA. Marshall Space Flight Center, Aerospace Environmental Technology Conference Mar. 1995 p 593-602 (For primary document see N95-31746 11-23)
Avail: CASI HC A02/MF A06

Oxidizer propellant systems for liquid-fueled rocket engines must meet stringent cleanliness requirements for particulate and nonvolatile residue. These requirements were established to limit residual contaminants which could block small orifices or ignite in the oxidizer system during engine operation. Limiting organic residues in high pressure oxygen systems is particularly important. The current method of cleanliness verification used by Rocketdyne requires an organic solvent flush of the critical hardware surfaces. The solvent is filtered and analyzed for particulate matter, followed by gravimetric determination of the nonvolatile residue (NVR) content of the filtered solvent. The organic solvents currently specified for use (1,1,1-trichloroethane and CFC-113) are ozone-depleting chemicals slated for elimination by December 1995. A test program is in progress to evaluate alternative methods for cleanliness verification that do not require the use of ozone-depleting chemicals and that minimize or eliminate the use of solvents regulated as hazardous air pollutants or smog precursors. Initial results from the laboratory test program to evaluate aqueous-based methods and organic solvent flush methods for NVR verification are provided and compared with results obtained using the current method. Evaluation of the alternative methods was conducted using a range of contaminants encountered in the manufacture of rocket engine hardware. Author

N95-31807*# United Space Boosters, Inc., Huntsville, AL.
VERIFICATION OF SURFACE PREPARATION FOR ADHESIVE BONDING **c25**
Rodney S. Myers *In* NASA. Marshall Space Flight Center, Aerospace Environmental Technology Conference Mar. 1995 p 603-612 (For primary document see N95-31746 11-23)
Avail: CASI HC A02/MF A06

A survey of solid rocket booster (SRB) production operations identified potential contaminants which might adversely affect bonding operations. Lap shear tests quantified these contaminants' effects on adhesive strength. The most potent contaminants were selected for additional studies on SRB thermal protection system (TPS) bonding processes.. Test panels were prepared with predetermined levels of contamination, visually inspected using white and black light, then bonded with three different TPS materials over the unremoved contamination. Bond test data showed that white and black light inspections are adequate inspection methods for TPS bonding operations. Extreme levels of contamination (higher than expected on flight hardware) had an insignificant effect on TPS bond strengths because of the apparent insensitivity of the adhesive system to contamination effects, and the comparatively weak cohesive strength of the TPS materials.
Author

N95-31808*# Nebraska Univ., Lincoln, NE. Dept. of Electrical Engineering.
SPECTROSCOPIC ELLIPSOMETRY AS A SENSITIVE MONITOR OF MATERIALS CONTAMINATION **c25**
Jeffrey S. Hale, James N. Hilfiker, Blaine Spady, R. Synowicki, and John A. Woollam *In* NASA. Marshall Space Flight Center, Aerospace Environmental Technology Conference Mar. 1995 p 613-618 (For primary document see N95-31746 11-23)
Avail: CASI HC A02/MF A06

Spectroscopic ellipsometry is demonstrated to be extremely sensitive to contamination layers in the thickness range from 0.1 nm to 10 microns. In the present experiments we deposit either a thin lubricating oil (WD-40) or mineral oil continuously onto Ir, Cu, Al, Au, and V substrates from a bubbler, and monitor its thickness growth from sub-nanometer to tens of nanometers as a function of time. Re-evaporation of contaminant oils is also monitored in real-time by ellipsometry. Author

N95-31809*# Thiokol Corp., Brigham City, UT. Science and Engineering Analytical Labs. Dept.
THE ROLE OF SURFACE CHEMICAL ANALYSIS IN A STUDY TO SELECT REPLACEMENT PROCESSES FOR TCA VAPOR DEGREASING **c37**

Michael W. Lesley, Lawrence E. Davis (Physical Electronics Labs., Eden Prairie, MN.), John F. Moulder (Physical Electronics Labs., Eden Prairie, MN.), and Brad A. Carlson (Physical Electronics Labs., Eden Prairie, MN.) *In* NASA. Marshall Space Flight Center, Aerospace Environmental Technology Conference Mar. 1995 p 619-630 (For primary document see N95-31746 11-23)
Avail: CASI HC A03/MF A06

The role of surface-sensitive chemical analysis (ESCA, AES, and SIMS) in a study to select a process to replace 1, 1, 1-trichloroethane (TCA) vapor degreasing as a steel and aluminum bonding surface preparation method is described. The effort was primarily concerned with spray-in-air cleaning processes involving aqueous alkaline and semi-aqueous cleaners and a contamination sensitive epoxy-to-metal bondline. While all five cleaners tested produced bonding strength results equal to or better than those produced by vapor degreasing, the aqueous alkaline cleaners yielded results which were superior to those produced by the semi-aqueous cleaners. The main reason for the enhanced performance appears to be a silicate layer left behind by the aqueous alkaline cleaners. The silicate layer increases the polarity of the surface and enhances epoxy-to-metal bonding. On the other hand, one of the semi-aqueous cleaners left a nonpolar carbonaceous residue which appeared to have a negative effect on epoxy-to-metal bonding. Differences in cleaning efficiency between cleaners/processes were also identified. These differences in surface chemistry, which were sufficient to affect bonding, were not detected by conventional chemical analysis techniques. Author

N95-31810*# National Aeronautics and Space Administration. Marshall Space Flight Center, Huntsville, AL.
ENVIRONMENTAL DATABASES AND OTHER COMPUTERIZED INFORMATION TOOLS **c82**
Marceia Clark-Ingram *In its* Aerospace Environmental Technology Conference Mar. 1995 p 633-641 (For primary document see N95-31746 11-23)
Avail: CASI HC A02/MF A06

Increasing environmental legislation has brought about the development of many new environmental databases and software application packages to aid in the quest for environmental compliance. These databases and software packages are useful tools and applicable to a wide range of environmental areas from atmospheric modeling to materials replacement technology. The great abundance of such products and services can be very overwhelming when trying to identify the tools which best meet specific needs. This paper will discuss the types of environmental databases and software packages available. This discussion will also encompass the affected environmental areas of concern, product capabilities, and hardware requirements for product utilization. Author

N95-31811*# National Aeronautics and Space Administration. Marshall Space Flight Center, Huntsville, AL.
NEIS (NASA ENVIRONMENTAL INFORMATION SYSTEM) **c82**
Beth Cook *In its* Aerospace Environmental Technology Conference Mar. 1995 p 643-647 (For primary document see N95-31746 11-23)
Avail: CASI HC A01/MF A06

The NASA Environmental Information System (NEIS) is a tool to support the functions of the NASA Operational Environment Team (NOET). The NEIS is designed to provide a central environmental technology resource drawing on all NASA centers' capabilities, and to support program managers who must ultimately deliver hardware compliant with performance specifications and environmental requirements. The NEIS also tracks environmental regulations, usages of materials and processes, and new technology developments. It has proven to be a useful instrument for channeling information throughout the aerospace community, NASA, other federal agencies, educational institutions, and contractors. The associated paper will discuss the dynamic databases within the NEIS, and the usefulness it provides for environmental compliance efforts. Author

N95-31812*# National Aeronautics and Space Administration. Marshall Space Flight Center, Huntsville, AL.
THE EFFECT OF ENVIRONMENTAL INITIATIVES ON NASA SPECIFICATIONS AND STANDARDS ACTIVITIES **c45**
Dennis Griffin, David Webb, and Beth Cook *In its* Aerospace Environmental Technology Conference Mar. 1995 p 649-659 (For primary document see N95-31746 11-23)
Avail: CASI HC A03/MF A06

The NASA Operational Environment Team (NOET) has conducted a survey of NASA centers specifications and standards that require the use of Ozone Depleting Substances (ODS's) (Chlorofluorocarbons (CFCs), Halons, and chlorinated solvents). The results of this survey are presented here, along with a pathfinder approach utilized at Marshall Space Flight Center (MSFC) to eliminate the use of ODS's in targeted specifications and standards. Presented here are the lessons learned from a pathfinder effort to replace CFC-113 in a significant MSFC specification for cleaning and cleanliness verification methods for oxygen, fuel and pneumatic service, including Shuttle propulsion elements. Author

N95-31813*# National Aeronautics and Space Administration. Marshall Space Flight Center, Huntsville, AL.
AN OVERVIEW OF NASA TESTING REQUIREMENTS FOR ALTERNATE CLEANING SOLVENTS USED IN LIQUID AND GASEOUS OXYGEN ENVIRONMENTS **c25**
John W. Strickland (BAMSI, Inc., Huntsville, AL.) and S. Eddie Davis *In its* Aerospace Environmental Technology Conference Mar. 1995 p 661-665 (For primary document see N95-31746 11-23)
Avail: CASI HC A01/MF A06

The elimination of CFC-containing cleaning solvents for oxygen systems has prompted the development of a number of alternative cleaning solvents that must now be evaluated not only for cleanability, but compatibility as well. NASA Handbook 8060.1(NHB 8060.1) establishes the requirements for evaluation, testing, and selection of materials for use in oxygen rich environments. Materials intended for use in space vehicles, specified test facilities, and ground support equipment must meet the requirements of this document. In addition to the requirements of NHB 8060.1 for oxygen service, alternative cleaning solvents must also be evaluated in other areas (such as corrosivity, non-metals compatibility, non-volatile residue contamination, etc.). This paper will discuss the testing requirements of NHB 8060.1 and present preliminary results from early screening tests performed at Marshall Space Flight Center's Materials Combustion Research Facility. Author

N95-31814*# Athens State Coll., AL. Dept. of Management of Technology.
DEVELOPMENT OF A CFC CRITICAL AREA RESPONSE (CAR) PACKAGE **c45**
J. Wayne McCain *In* NASA. Marshall Space Flight Center, Aerospace Environmental Technology Conference Mar. 1995 p 667-671 (For primary document see N95-31746 11-23)
Avail: CASI HC A01/MF A06

During the past two years, the NASA Marshall Space Flight Center (MSFC) has studied means to improve the transfer of technology from a major federal lab to a significant portion of an industrial segment. In the past, technology transfers had taken place with individual firms, or small groups of firms. This method of 'customized' transfer is often time consuming and can reduce the effectiveness of a response. Thus, a method was achieved to develop a standardized package on replacement of Chlorofluorocarbons (CFC's) that could be sent out to a large number of firms with minimum follow-up. Author

24 COMPOSITE MATERIALS

Includes physical, chemical, and mechanical properties of laminates and other composite materials.

For ceramic materials see *27 Nonmetallic Materials*.

N95-30433# United Technologies Research Center, East Hartford, CT.
INTERFACIAL STUDIES OF COATED FIBER REINFORCED GLASS-CERAMIC MATRIX COMPOSITES Final Report, 1 Nov. 1992 - 31 Oct. 1994
John Brennan, Steven Nutt (Brown Univ., Providence, RI.), and Ellen Sun (Brown Univ., Providence, RI.) 31 Dec. 1994 138 p
(Contract F49620-92-C-0001)
(AD-A290780; R94-970150-3; AFOSR-95-0074TR) Avail: CASI HC A07/MF A02

The objective of this program is to develop an understanding of the

relationships between the fiber, fiber coating or coatings, and the glass-ceramic matrix, that will lead to a composite system exhibiting high strength, high toughness, and good thermal and environmental stability to temperatures of 1200 C. To meet this objective, the chemistry and microstructure of the fiber/coating(s)/matrix interfacial region and how these influence the interfacial bonding, strength, and toughness of the particular composite system was investigated. During the course of this program, emphasis was placed on the determination of the high temperature mechanical properties of the BMAS matrix/SiC over BN coated Nicalon fiber composite system, and how these properties relate to changes that may occur in the matrix, fiber coatings, or Nicalon fiber chemistry and microstructure. Specifically, short time flexural, short time tensile, tensile creep, and tensile fatigue testing was conducted in air to temperatures of 1200 C, all on the same composite sample. Flexural creep was also performed on similar composite samples and compared to the tensile creep results. In addition, Si3N4 over SN and BN by itself were evaluated as fiber coatings in the BMAS matrix/Nicalon fiber composite system. The effect of long-time heat-treatments in oxidizing and non- oxidizing environments were conducted on composites with different interface chemistries. With the collaboration of Brown University, SEM (scanning electron microscopy) and TEM (tunneling electron microscopy) analyses of the composites after being subjected to the various stress and temperature conditions were conducted. From these studies, damage modes and microstructural and chemical changes that occurred as a result of these tests were determined. Results of these studies are presented. DTIC

N95-30460# Technische Univ., Delft (Netherlands). Faculty of Aerospace Engineering.
DESIGN OF FIBRE REINFORCED COMPOSITE PANELS FOR AEROSPACE APPLICATIONS Ph.D. Thesis
P. G. vanBladel 31 Jan. 1995 150 p
(PB95-197851; ISBN-90-9007838-X) Avail: CASI HC A07/MF A02

This thesis is a contribution to the design of fiber composite panels, in particular for aerospace applications. As composite structures are increasingly used in practice, experience is also gained in manufacture, maintenance and repair. However, the preliminary design of these structures, where only the loading and general requirements on the structure are given while the actual form and layup have yet to be defined, has not received as much attention. This has prompted the research leading to this thesis. Two specific types of panels are chosen as subjects of the research: sandwich panels and corrugated panels. As part of this work two computer programs have been developed as software tools for the designer: SAPANO for sandwich panels and COPANO for corrugated panels. This thesis can be seen as the theoretical manual for the programs, while separate user's manuals are available to assist in their use. NTIS

N95-30491 Purdue Univ., West Lafayette, IN.
FATIGUE CRACK GROWTH BEHAVIOR OF A TITANIUM MATRIX COMPOSITE UNDER THERMOMECHANICAL LOADING Ph.D. Thesis
Paul Andrew Blatt 1993 239 p
Avail: Univ. Microfilms Order No. DA9420785

The fatigue crack growth characteristics of a 4-ply, unidirectional, titanium matrix composite, SCS-6/Ti-6Al-2Sn-4Zr-Mo, subjected to thermomechanical loading was investigated. The majority of work conducted for this research project was of an experimental nature. A test frame was assembled to perform the fully-automated, computer-controlled thermomechanical fatigue crack growth tests. A series of isothermal, in-phase, and out-of-phase crack growth tests were run. The test temperatures ranged from 150 deg C to 538 deg C and the fastest thermal frequency was 0.0083 Hz. The baseline isothermal and TMF data suggested that the time-at-temperature and the maximum temperature experienced by the composite significantly influenced the fatigue crack growth rates. Isothermal conditions produced higher crack growth rates than either in-phase or out-of-phase conditions for equivalent mechanical frequencies. Fiber bridging during both the isothermal and TMF tests was limited to a region of approximately 2-3 fibers directly behind the advancing crack tip. A linear summation approach was developed to model the effect of isothermal and thermomechanical cycling on the crack growth rates of the SCS-6/Ti-6Al-2Sn-4Zr-2Mo composite. The total fatigue crack growth rate was decomposed into cycle-dependent and time-dependent components. The model was able to correlate all the baseline fatigue crack growth tests as well predict the fatigue crack growth rate of a test which began under isothermal conditions and ended under in-phase conditions.
Dissert. Abstr.

N95-30661 Department of the Navy, Washington, DC.
VIBRATION-DAMPING STRUCTURAL COMPONENT Patent
David J. Barrett, inventor (to Navy) 29 Nov. 1994 6 p Filed 3 Mar. 1993
(AD-D017376; US-Patent-5,368,914; US-Patent-Appl-SN-025535; US-Patent-Class-428-201) Avail: US Patent and Trademark Office

An improvement to a vibration-damping structural component of the type having viscoelastic material sandwiched between two outer structural layers of stiffness material is disclosed. An inner layer of stiffness material having two predominant surfaces is positioned between the two outer structural layers of stiffness material and is fixed along an edge of one of the two pre-dominant surfaces to one of the two outer structural layers of stiffness material along a line thereon corresponding to a nodal line of vibration. The remainder of the two predominant surfaces is fixed to the viscoelastic material. During flexural vibrations, the inner layer displaces in-plane with respect to the inner surfaces of the outer layers, causing greater shearing in the viscoelastic material, and therefore causing greater vibration damping in the structural component. DTIC

N95-30694 Rutherford Appleton Lab., Oxford (England).
THERMOVISCOELASTIC BEHAVIOUR OF SOLIDS
A. D. Irving, T. Dewson, S. J. Watson, and L. J. Speet Dec. 1994 26 p Prepared in cooperation with Technische Univ., Delft, Netherlands, and Bristol Univ., England
(PB95-196226; RAL-94-124) Avail: Issuing Activity (National Technical Information Service (NTIS))

The thermoviscoelastic behavior of a composite material is represented as a mixed linear-nonlinear convolution form of the Onsager equations. A vector multidimensional Volterra functional series expansion is used to describe the thermoviscoelastic constitutive relationships. Linear and mixed linear-nonlinear moment hierarchy time series analyses are performed to investigate the nature of the thermoviscoelastic phenomena. A tractable set of simultaneous equations with well behaved coefficients can be generated by taking time series moments of a suitably truncated Volterra series expansion. This moment hierarchy is used to determine the dynamic and steady state thermoviscoelastic properties of the composite. Statistical analyses on out of sample predictions made using the estimated response functions demonstrate that the characterization provides a good description of the thermoviscoelastic process. The transport coefficients are estimated and used to determine the flux-force surfaces which characterizes the behavior of the composite. These surfaces illustrate that Curie's principle for combined thermodynamic phenomena does not hold for the thermoviscoelastic process. The thermoviscoelastic behavior of composite materials under fatigue loadings is weakly nonlinear. NTIS

N95-30731# Oak Ridge National Lab., TN.
FABRICATION AND MODIFICATION OF METAL NANOCLUSTER COMPOSITES USING ION AND LASER BEAMS
R. F. Haglund, Jr. (Vanderbilt Univ., Nashville, TN.), D. H. Osborne, Jr. (Vanderbilt Univ., Nashville, TN.), R. H. Magruder, III (Vanderbilt Univ., Nashville, TN.), C. W. White (Oak Ridge National Lab., TN.), R. A. Zuhr (Oak Ridge National Lab., TN.), P. D. Townsend (Sussex Univ., Brighton, England.), D. E. Hole (Sussex Univ., Brighton, England.), and R. E. Leuchtner (New Hampshire Univ., Durham, NH.) Dec. 1994 12 p Presented at the 1994 Fall Meeting of the Materials Research Society, Boston, MA, 28 Nov. - 2 Dec. 1994
(Contract DE-AC05-84OR-21400)
(DE95-009131; CONF-941144-104) Avail: CASI HC A03/MF A01

Metal nanocluster composites have attractive properties for applications in nonlinear optics. However, traditional fabrication techniques, using melt-glass substrates, are severely constrained by equilibrium thermodynamics and kinetics. This paper describes the fabrication of metal nanoclusters in both crystalline and glassy hosts by ion implantation and pulsed laser deposition. The size and size distribution of the metal nanoclusters can be modified by controlling substrate temperature during implantation, by subsequent thermal annealing, or by laser irradiation. The authors have characterized the optical response of the composites by absorption and third-order nonlinear-optical spectroscopies; electron and

scanning-probe microscopies have been used to benchmark the physical characteristics of the composites. The outlook for controlling the structure and nonlinear optical response properties of these nanophase materials appears increasingly promising. DOE

N95-30749 Department of the Navy, Washington, DC.
COMPOSITE STRUCTURE FORMING A WEAR SURFACE Patent
Edward I. Cohen, inventor (to Navy) 14 Feb. 1995 6 p Filed 24 Sep. 1993
(AD-D017462; US-Patent-5,389,411; US-Patent-Appl-SN-125715; US-Patent-Class-428-34) Avail: US Patent and Trademark Office

This patent discloses a pre-stressed composite liner structure is provided for tribological systems typically associated a pump engine, compressor or systems having bearings rotating within a journal. A hollowed ceramic core is concentrically wound with cladding material in the form of a filament or braid. The ceramic core and the wound cladding form an interference fit with one another to pre-stress the ceramic core in terms of tensile strength. DTIC

N95-30768 Rensselaer Polytechnic Inst., Troy, NY.
A THEORY FOR PREDICTING AND MINIMIZING THE EFFECTS OF MATRIX DEGRADATION ON THE THERMOMECHANICAL PROPERTIES OF GENERAL LAMINATES Ph.D. Thesis
Stephen C. Hill 1993 379 p
Avail: Univ. Microfilms Order No. DA9420328

The effects of matrix degradation on the properties of general composite laminates are investigated. The changes in matrix properties due to hygrothermal environment and the presence of microcracking are considered. The matrix-dominated properties of constituent laminate plies are affected by these changes. Laminates dependent on matrix behavior, such as those with coupling, will exhibit the largest variation due to these effects. Models are developed for the effects on ply properties. Hygrothermally-induced effects are modeled as variations in shear modulus. A model for microcracking is developed which considers variations in all ply properties due to microcracking. Both of these models are easily incorporated into laminate analyses based on classical laminated plate theory. A model for predicting the potential distributions of crack density through the laminate thickness for given applied loads is developed. This model is used to analyze laminate behavior. The effects of matrix property variation on laminate moduli and compliances are investigated with an emphasis on extension-shear coupling. Hybrid laminates are presented for which the variation of coupling due to hygrothermal and microcracking effects is reduced or eliminated. Overall variations in properties are reduced with these laminates. The effects of microcracking on laminate coefficients of thermal expansion are investigated. Laminates which are initially thermally isotropic and shear stable may lose these properties due to microcracking. The effects of crack closure on laminate behavior are discussed. As laminate loads (or thermal stresses) vary, ply cracks may be forced open or closed. It is assumed that plies with closed cracks can be treated as uncracked plies. The resulting properties for these laminates become functions of the applied load and may behave nonlinearly. In general, the behavior of laminates changes when cracking develops. For example, initially symmetric laminates will become unsymmetric under certain loading conditions. Except in special cases, cracked laminates must be treated as general laminates with no special symmetries. Dissert. Abstr.

N95-30787*# General Electric Co., Cincinnati, OH. Aircraft Engines.
THE EFFECT OF INTERFACE PROPERTIES ON NICKEL BASE ALLOY COMPOSITES Final Report
M. Groves, T. Grossman, M. Senemeier, and K. Wright Jul. 1995 89 p
(Contract NAS3-26501; RTOP 505-63-12)
(NASA-CR-198363; E-9769; NAS 1.26:198363) Avail: CASI HC A05/MF A01

This program was performed to assess the extent to which mechanical behavior models can predict the properties of sapphire fiber/nickel aluminide matrix composites and help guide their development by defining improved combinations of matrix and interface coating. The program consisted of four tasks: 1) selection of the matrices and interface coating constituents using a modeling-based approach; 2) fabrication of the selected materials; 3) testing and evaluation of the materials; and 4) evaluation of the behavior models to develop recommendations. Ni-50Al and Ni-20Al-30Fe (a/o) matrices were selected which gave brittle and ductile behavior, respectively, and an interface coating of PVD YSZ was selected which provided strong bonding to the sapphire fiber. Significant fiber damage and strength loss was observed in the composites which made straightforward comparison of properties with models difficult. Nevertheless, the models selected generally provided property predictions which agreed well with results when fiber degradation was incorporated. The presence of a strong interface bond was felt to be detrimental in the NiAl MMC system where low toughness and low strength were observed. Author

N95-30823 Ohio State Univ., Columbus, OH.
ULTRASONIC CHARACTERIZATION OF FIBER-MATRIX INTERPHASIAL PROPERTIES AND DAMAGE IN HIGH-TEMPERATURE COMPOSITES Ph.D. Thesis
Ya-Cherng Chu 1994 370 p
Avail: Univ. Microfilms Order No. DA9420938

This study addresses ultrasonic characterization of fiber-matrix interphasial properties and damage in high-temperature composites. To accomplish this, experimental techniques for measurements of ultrasonic phase velocities and methodology for calculation of composite elastic moduli from velocity data are first developed and applied to unidirectional ceramic and intermetallic matrix composites. It is shown that computational error in the composite moduli is comparable to experimental error in the velocity data. For cross-ply composites, a novel method for determination of lamina elastic moduli from measurements on a (0/90)(8) composite is developed and validated experimentally. Second, a method to determine the elastic moduli of interphasial layers in high-temperature composites from the measured composite moduli is developed and applied to characterization of 3-micron thick carbon interphasial layers in ceramic and intermetallic matrix composites. Third, the techniques developed are used for assessment of oxidation and fatigue damage in ceramic and metal matrix composites. It is shown that ultrasonic phase velocities are very sensitive to damage and can effectively quantify damage severity. Appropriate models are applied to describe the effect of damage on the measured ultrasonic data, and they show reasonable agreement with experiments. Dissert. Abstr.

N95-30824 Stanford Univ., CA.
RESPONSE OF MECHANICALLY FASTENED COMPOSITE JOINTS UNDER MULTIPLE BYPASS LOADS Ph.D. Thesis
Chang-Li Hung 1994 193 p
Avail: Univ. Microfilms Order No. DA9422093

An analytical and experimental investigation was performed to study the response of laminated composites containing a mechanical fastener. The mechanics and mechanisms of bearing damage in fiber-reinforced laminated composites were the primary focuses of the experimental study. A specially designed semi-circular notched specimen was proposed to characterize pin bearing damage in the experiments. Double shear-lap bolted joints were also tested to evaluate the effects of bolt clamping on the mechanisms of bearing damage and the response of the laminates. A progressive failure model was developed to predict the bearing damage in the laminates as well as to estimate the mechanical response of the joints. The model consists of two parts: stress analysis and failure analysis. Stresses and deformations in the laminates were calculated by a nonlinear finite element analysis based on a finite deformation theory. In the failure analysis, damage accumulation criteria were proposed to determine the type and the state of damage in composites as functions of the given stress state. In order to describe the progressive degradation of composites, constitutive relations for damaged laminates were developed. To facilitate the use of the model, a computer code designated as 'BJSTAT' was developed for predicting the response and the strengths of bolted composite joints under multiple bypass loads. Data obtained from the present investigation and existing literature were used to validate the model. Overall, the predictions agreed with the data very well. Utilizing the code, numerical simulations were also conducted to generate the strength envelope for a bolted composite joint under multi-axial bypass loads. The envelope can provide information on the strength as well as the failure type of the joint as functions of the bypass loads and, therefore, is extremely useful in the joint design. Dissert. Abstr.

N95-30826 Clemson Univ., SC.
CHARACTERIZATION AND PREDICTION OF POST-IMPACT FATIGUE DAMAGE IN STITCHED COMPOSITES Ph.D. Thesis

Darwin Gregory Moon 1993 322 p
Avail: Univ. Microfilms Order No. DA9419666

The post-impact fatigue response of stitched carbon/epoxy composite materials was characterized and modeled in this investigation. The five material configurations evaluated were composed of uni-woven AS4 graphite lamina arranged in a (45/0/ - 45/90)(sub 6s) preform. Four preforms were reinforced by a modified lock stitch process, and each material was fabricated with a specific stitch row spacing of either 1/4, 3/16, or 1/8 inches. An unstitched baseline laminate was the fifth configuration. A brittle resin system was used to consolidate three stitched and the unstitched preforms, while a toughened resin system was used in a second preform which was also stitched with 1/4-inch rows. Short-block compression and compression-after-impact tests were conducted on every material to establish their baseline performances. All the impacts were performed with a 10-lb drop-weight impacter with a 1/2-inch hemispherical tup set to deliver a uniform 1500-in.-lb/in. energy level. Impacted fatigue specimens were tested at a 4-Hz frequency with a tension-compression stress ratio of R = -5. Dye-enhanced radiographic techniques and extensometers were used to monitor both the post-impact condition and the fatigue damage propagation. Destructive sectioning and pyrolysis methods were also used to quantify the damage states. Statistical analysis of the undamaged compressive properties shows no strength penalty associated with the stitching process. However, stitching reinforcement is found to have statistically significant affects on the elastic moduli and ultimate compressive strains. Lower elastic moduli and higher compression strains are found in the stitched materials compared to the unstitched baseline. All the post-impact fatigue coupons display stable damage growth. While circular delaminations elongate into ellipses in the unstitched samples, the stitched materials develop narrow damage zones transverse to the loading direction. These narrow zones are characterized by extensive regions of transverse shear failure surfaces. Critical damage zone length is predicted using a point-stress failure criterion based on an open-hole stress distribution. The propagation of these narrow zones is empirically predicted with a non-dimensional parameter, P, which allows the post-impact fatigue data to be correlated with an exponential damage growth model. Dissert. Abstr.

N95-30839 Drexel Univ., Philadelphia, PA.
A VISCOELASTIC ANISOTROPIC WAVE PROPAGATION MODEL FOR COMPOSITE CURE EVALUATION Ph.D. Thesis
James E. Eder 1994 173 p
Avail: Univ. Microfilms Order No. DA9420297

Current composite processing methods rely heavily upon traditional temperature, pressure and vacuum sensors to provide process feedback to cure controllers. These sensors are not capable of directly measuring the composite's physical properties, and thus limit the feedback potential for this process. This thesis investigates the sensitivity of ultrasonic sensors for measuring physical changes exhibited by a curing composite, considering both anisotropy and viscoelasticity. A material model is proposed to predict the time-dependent mechanical properties of a curing composite. This effective moduli model combines the properties of a viscoelastic curing resin, whose properties are a function of cure time, with those of an elastic fiber, whose properties are assumed independent of cure time to produce the viscoelastic moduli of a curing composite. Using the predicted time-dependent material properties, two significant boundary value problems are formulated and solved to predict ultrasonic measurements which are sensitive to the expected changes encountered during cure. These problems are: the reflection and refraction of obliquely incident ultrasonic waves on the interface between an isotropic elastic half-space and a viscoelastic anisotropic half-space (half-space case), as well as reflection and refraction of obliquely incident ultrasonic waves on a viscoelastic anisotropic layer bounded by two identical elastic isotropic half-spaces (layer case). Finally, some experimental verifications are presented demonstrating the utility of the theoretical formulations for both the half-space and layer cases. Increased sensitivity to changes in a curing laminate using oblique incidence is demonstrated both theoretically and experimentally for the half-space case. The layer results demonstrate the ability of the theoretical formulation to adequately predict the time dependence of the reflection factors at several different incident angles and frequencies, provided the wavelength is large enough to neglect scattering from the fibers. Some possible ultrasonic measurements are evaluated for their utility to monitor composite curing, along with some practical considerations for implementation of this technology. Dissert. Abstr.

N95-30866# Florida Univ., Gainesville, FL. Dept. of Materials Science and Engineering.
INNOVATIVE PROCESSING OF COMPOSITES FOR ULTRA-HIGH TEMPERATURE APPLICATIONS, BOOK 3 Final Report
Reza Abbaschian Sep. 1994 106 p
(Contract N00014-91-J-4075)
(AD-A290891) Avail: CASI HC A06/MF A02

The objective of this program is to provide a fundamental understanding of the processing science and technology necessary to fabricate ceramic-matrix, intermetallic matrix, and metal-matrix composites with superior mechanical properties in high temperature and oxidizing environment. The composites are intended for use as structural materials for advance aerospace applications at temperatures exceeding 1200 C. In this book, book 3 (of 4), the discussion is focused on processing of Ceramic Matrix Composites and BaO-Al2O3-2SiO2 Fibers. DTIC

N95-30867# Florida Univ., Gainesville, FL. Dept. of Materials Science and Engineering.
INNOVATIVE PROCESSING OF COMPOSITES FOR ULTRA-HIGH TEMPERATURE APPLICATIONS, BOOK 4 Final Report
Reza Abbaschian Sep. 1994 90 p
(Contract N00014-91-J-4075)
(AD-A290892) Avail: CASI HC A05/MF A01

The objective of this program is to provide a fundamental understanding of the processing science and technology necessary to fabricate ceramic-matrix, intermetallic matrix, and metal-matrix composites with superior mechanical properties in high temperature and oxidizing environment. The composites are intended for use as structural materials for advance aerospace applications at temperatures exceeding 1200 C. In this book, book 4 (of 4), the discussion is focused on processing and Mechanical Property Characterization of Tape Cast, Multilayer, and Alumina/Nickel Laminated Composites. DTIC

N95-30898# Florida Univ., Gainesville, FL. Dept. of Materials Science and Engineering.
INNOVATIVE PROCESSING OF COMPOSITES FOR ULTRA-HIGH TEMPERATURE APPLICATIONS, BOOK 2 Final Report
Reza Abbaschian Sep. 1994 188 p
(Contract N00014-91-J-4075)
(AD-A290890) Avail: CASI HC A09/MF A02

The objective of this program is to provide a fundamental understanding of the processing science and technology necessary to fabricate ceramic-matrix, intermetallic matrix, and metal-matrix composites with superior mechanical properties in high temperature and oxidizing environment. The composites are intended for use as structural materials for advance aerospace applications at temperatures exceeding 1200 C. In this book, book 2 (of 4), the discussion is focused on the processing and properties of Intermetallic Matrix Composites. DTIC

N95-30934# Florida Univ., Gainesville, FL.
VISIBLE LIGHT EMITTING MATERIALS AND INJECTION DEVICES Quarterly Progress Report
Paul H. Holloway 28 Feb. 1995 18 p
(Contract N00014-92-J-1895)
(AD-A292701) Avail: CASI HC A03/MF A01

We performed real-time, in-situ CL intensity measurements this quarter during the MBE growth of Cd(x)Zn(1-x)Se/ZnSe MQW structures in which we varied the barrier and/or well widths for a fixed Cd(x)Zn(1-x)Se composition (x=0.2). In each case we quantified the integrated intensity of the CL emission observed during the growth. For the MQW structures grown thus far, the most intense integrated CL emission was detected from a structure comprised of 200A thick ZnSe barriers and 50A thick Cd(0.2)Zn(0.8)Se quantum wells. The 200A ZnSe/50 A CdZnSe MQW structure also exhibited strong room temperature exciton emission when ex-situ photoluminescence (PL) was performed on the sample. The PL intensity was measured by Dr. Simmons' group. Consequently, it appears that real-time, in-situ CL monitoring could have interesting applications with regard to the design and production of MQW structures and we plan to continue working in this area. DTIC

N95-30963# Army Research Lab., Aberdeen Proving Ground, MD.
EFFECTS OF HYDROSTATIC PRESSURE ON THE MECHANICAL BEHAVIOR OF COMPOSITE MATERIALS Final Report, Mar. 1993 - Jan. 1994
Christopher P. Hoppel, Travis A. Bogetti, and John W. Gillespie, Jr. Apr. 1995 64 p
(AD-A293162; ARL-TR-727) Avail: CASI HC A04/MF A01

Hydrostatic pressure can cause significant changes in the mechanical properties of composite materials. A thorough understanding of these effects is essential for the effective design of composite structures for high-pressure applications. In this report, the literature on the effects of hydrostatic pressure on the mechanical behavior of composite materials is reviewed. This includes a general description of the effects of hydrostatic pressure on unreinforced polymers and a detailed critique of the experimental work that has been done on composite materials. The section on composites is divided into three parts: compressive, tensile, and shear testing. For each type of testing, the test materials and techniques and the physical and quantitative results are discussed. DTIC

N95-30975# Southwest Research Inst., San Antonio, TX.
CHARACTERIZATION OF COMPRESSIVE DAMAGE MECHANISMS IN CERAMIC AND POLYMERIC MATRIX COMPOSITE MATERIALS Final Report, Oct. 1993 - Feb. 1995
James Lankford, Jr. Feb. 1995 78 p
(Contract N00014-92-C-0093)
(AD-A293171; Rept-06-5035) Avail: CASI HC A05/MF A01

Experiments involving expansion of the dynamic strain rate capabilities of the split Hopkinson pressure bar were performed. Unusually high strain rate hardening was obtained for the compressive failure of silicon nitride, while for silicon carbide, failure followed a lower rate of hardening, crack kinetics criterion. The silicon nitride results were interpreted in terms of plastic deformation, which changed the mode of failure from that observed at low strain rates, and altered the strength-strain rate dependency, apparently through the influence of dislocation generation upon microcrack nucleation. Recent experiments involved the response of monolithic ceramics and fiber-reinforced ceramic matrix composites to dynamic loading under hydrostatic confinement. Curious results were obtained for monolithic ceramics, which appeared to derive from crack initiation/growth kinetics and the stability of confined microcrack ensembles. Composites under confinement were found to reflect both dilatational and shear aspects of damage development, which are primarily a function of the matrix phase, while the effect of the fibers was to alter the relative kinetics and, under certain circumstances, the sequence of events involved in the macroscale growth of damage through the eventual zone of failure. Considerable effort has been devoted to new approaches to capturing the critical events associated with compressive kink band nucleation and development in polymeric matrix, fiber reinforced composites. DTIC

N95-30978# David Sarnoff Research Center, Princeton, NJ.
CERAMIC/METAL COMPOSITE CIRCUIT-BOARD-LEVEL TECHNOLOGY FOR APPLICATION SPECIFIC ELECTRONIC MODULES (ASEM'S) Technical Report, 22 Sep. 1994 - 14 Mar. 1995
Barry J. Thaler, A. H. Kumar, and A. N. Prabhu 13 Mar. 1995 38 p
(Contract DAAB07-94-C-C009; ARPA Order A840)
(AD-A293183) Avail: CASI HC A03/MF A01

The quarterly progress for the Ceramic/Metal Composite Circuit-Board-Level Technology for Application Specific Electronic Modules is described in this report. Data is reported for the following tasks: Metal Core Fabrication; LTCC Ceramic Development; Thin Film Interconnect Structure Integration; Multilayer Interaction; and Reliability Studies. DTIC

N95-31110 Georgia Inst. of Tech., Atlanta, GA.
MODELING OF FIBER-REINFORCED COMPOSITES INCORPORATING DISTINCT INTERFACE PROPERTIES Ph.D. Thesis
David Robert Veazie 1993 250 p
Avail: Univ. Microfilms Order No. DA9415674

A framework has been established to characterize the effects of distinct interphases in the study of fiber reinforced composites. On the basis of this framework, a rigorous analysis has been carried out for the transverse loading, both tensile normal and simple shear, of a unidirectional fiber reinforced composite. It is assumed that such an interphase is due to interfacial damage or is created deliberately by coating the fibers. By the use of the finite element method, a numerical analysis for a basic cell provides results for the micromechanical fields of stress and the micromechanical properties, with and without partial interphase failure. An analytical model is also developed to predict the macroscopic stress-strain behavior. The main objectives of this research are: (1) to develop micromechanics-based continuum models for transversely loaded fiber reinforced composites that incorporate distinct interphase properties; (2) to study the effects of distinct interphases on the local stress fields, the effective moduli, and along the matrix side of the interphase; and (3) to examine the effects of residual stresses on fiber composites with distinct interphases. The results of this work will enable the effect of interphase parameters on the overall elastic moduli to be determined prior to, as well as subsequent to, the development of interphase failure. Dissert. Abstr.

N95-31146# Naval Command, Control and Ocean Surveillance Center, San Diego, CA. RDT and E Div.
INTERMODULATION INTERFERENCE (IMI) TESTING OF COMPOSITE MATERIALS Final Report
J. W. Rockway, J. C. Logan, J. H. Schukantz, and T. A. Danielson Sep. 1994 16 p
(AD-A288621; NRAD-TD-2705) Avail: CASI HC A03/MF A01

With the possibility of the large-scale use of graphite-bearing composites for topside structures and masts, some concern has been expressed as to whether these materials might be intermodulation interference (IMI) generators. To resolve this question, tests were performed to compare the relative signal levels of intermodulation generated by two graphite fiber composite material samples to a steel sample and to a brass sample. The graphite fiber composite material samples were representative of the materials that will be used in the Advanced Enclosed Mast/Sensor (AEM/S) System. The results of these tests were evaluated in terms of the potential of graphite-loaded composite structures to be significant generators of IMI on board Navy ships. With the possibility of the large-scale use of graphite-bearing composites for topside structures and masts, some concern has been expressed as to whether these materials might be intermodulation interference (IMI) generators. To resolve this question, tests were performed to compare the relative signal levels of intermodulation generated by two graphite fiber composite material samples to a steel sample and to a brass sample. The graphite fiber composite material samples were representative of the materials that will be used in the Advanced Enclosed Mast/Sensor (AEM/S) System. The results of these tests were evaluated in terms of the potential of graphite-loaded composite structures to be significant generators of IMI on board Navy ships. DTIC

N95-31347 Rensselaer Polytechnic Inst., Troy, NY.
ELASTIC AND INELASTIC MICROMECHANICAL ANALYSIS OF FUNCTIONALLY GRADED MATERIALS AND LAMINATED STRUCTURES USING TRANSFORMATION FIELDS Ph.D. Thesis
Joseph Robert Zuiker 1993 377 p
Avail: Univ. Microfilms Order No. DA9420377

Micromechanical analysis of composites generally considers a representative volume of the composite subjected to boundary conditions derived from constant stress or strain fields. Certain microstructures can not be accurately analyzed by such methods. These include cases of composite plate bending, and functionally graded composites in which severe gradients in local reinforcement volume fraction may affect the effective properties. In this thesis, the problem of a representative volume element (RVE) of the composite medium subjected to boundary conditions derived from linearly varying stress or strain fields is considered. Constraints on the form of the applied field are identified which produce simple solutions throughout the RVE. Constitutive relations are derived which relate stress and strain averages as well as stress and strain gradients in the RVE. Existing micromechanical techniques, including the Mori-Tanaka method, are extended to generate estimates of these new stiffness matrices. This extended Mori-Tanaka formulation is used to estimate effective stiffness and thermal expansion of statistically homogeneous composites. The results reduce to the standard Mori-Tanaka solutions under appropriate conditions. Deviations from standard Mori-Tanaka estimates exist for certain microstructures and are in agreement with experimental results. Further generalizations are incorporated in order to consider severe reinforcement volume fraction gradients. Results indicate differences of as much as 25 percent in the effective properties for extreme cases when reinforcement volume fraction gradient effects are considered. While the above results

are useful in the elastic analysis of composites, transformation field analysis methods have certain advantages over other techniques in the inelastic analysis of composites. In this thesis, the fundamental concepts of transformation field analysis are extended to the case of boundary conditions derived from linearly varying stress or strain for cases in which the boundary conditions and applied transformation fields satisfy certain equilibrium constraints. A simplified form of the generalized relations is used within the assumptions of classical laminated plate theory to obtain closed form estimates of all required concentration factors. Further refinement of the method has the potential for efficient accurate plate analysis algorithms.
Dissert. Abstr.

N95-31369# Pennsylvania State Univ., University Park, PA. Materials Research Lab.
MATERIALS FOR ADAPTIVE STRUCTURAL ACOUSTIC CONTROL, VOLUME 1 Annual Report, 1 Feb. 1994 - 31 Jan. 1995
L. Eric Cross 6 Apr. 1995 214 p
(Contract N00014-92-J-1510)
(AD-A293444) Avail: CASI HC A10/MF A03

The objectives of this ONR sponsored University Research Initiative (URI) entitled 'Materials for Adaptive Structural Acoustic Control' concern both basic fundamental studies and highly applied development of the piezoelectric and electrostrictive ferroelectric ceramics which carry both the sensing and actuation functions for adaptive control. The report documents work over the third year of this five year program. For convenience and continuity, the activities are grouped under the headings General Summary Papers, Materials Studies, Composite Sensors, Actuator Studies, Integration Issues, Processing Studies, Thin Film Ferroelectrics, and the Abstracts of graduating students on the program. The first general papers illustrate the educational role undertaken by MRL faculty both in the basic understanding of ferroics, and in the philosophy of their application in 'smart' systems. It is interesting that through work pioneered on earlier ONR programs in MRL, it is now possible to measure both direct and converse electrostrictive response in simple solids, and to thus explore models to explain the signs and magnitudes of these striction constants. The relaxor ferroelectrics have been a topic of study for more than 30 years in the laboratory, but recent breakthroughs have revolutionized the level of understanding and opened a vista for further potential application of size (scale) effects in ferroics. Electrical control of shape memory has been achieved in a number of electro-ferroic solids, but full exploitation will need more complete understanding of both ferroelectric and ferroelastic:ferroelectric domain wall processes. DTIC

N95-31370# Pennsylvania State Univ., University Park, PA. Materials Research Lab.
MATERIALS FOR ADAPTIVE STRUCTURAL ACOUSTIC CONTROL, VOLUME 2 Annual Report, 1 Feb. 1994 - 31 Jan. 1995
L. Eric Cross 6 Apr. 1995 208 p
(Contract N00014-92-J-1510)
(AD-A293445) Avail: CASI HC A10/MF A03

The objectives of this ONR sponsored University Research Initiative (URI) entitled 'Materials for Adaptive Structural Acoustic Control' concern both basic fundamental studies and highly applied development of the piezoelectric and electrostrictive ferroelectric ceramics which carry both the sensing and actuation functions for adaptive control. The report documents work over the third year of this five year program. For convenience and continuity, the activities are grouped under the headings General Summary Papers, Materials Studies, Composite Sensors, Actuator Studies, Integration Issues, Processing Studies, Thin Film Ferroelectrics, and the Abstracts of graduating students on the program. This second volum picks up with Materials Studies and goes through Composite Sensors, and Actuator studies. DTIC

N95-31371# Pennsylvania State Univ., University Park, PA. Materials Research Lab.
MATERIALS FOR ADAPTIVE STRUCTURAL ACOUSTIC CONTROL, VOLUME 3 Annual Report, 1 Feb. 1994 - 31 Jan. 1995
L. Eric Cross 6 Apr. 1995 206 p
(Contract N00014-92-J-1510)
(AD-A293446) Avail: CASI HC A10/MF A03

The objectives of this ONR sponsored University Research Initiative (URI) entitled 'Materials for Adaptive Structural Acoustic Control' concern both basic fundamental studies and highly applied development of the piezoelectric and electrostrictive ferroelectric ceramics which carry both the sensing and actuation functions for adaptive control. The report documents work over the third year of this five year program. For convenience and continuity, the activities are grouped under the headings General Summary Papers, Materials Studies, Composite Sensors, Actuator Studies, Integration Issues, Processing Studies, Thin Film Ferroelectrics, and the Abstracts of graduating students on the program. This volume picks up with Actuator Studies and goes therough Integration Issues. DTIC

N95-31372# Pennsylvania State Univ., University Park, PA. Materials Research Lab.
MATERIALS FOR ADAPTIVE STRUCTURAL ACOUSTIC CONTROL, VOLUME 4 Annual Report, 1 Feb. 1994 - 31 Jan. 1995
L. Eric Cross 6 Apr. 1995 126 p
(Contract N00014-92-J-1510)
(AD-A293447) Avail: CASI HC A07/MF A02

The objectives of this ONR sponsored University Research Initiative (URI) entitled 'Materials for Adaptive Structural Acoustic Control' concern both basic fundamental studies and highly applied development of the piezoelectric and electrostrictive ferroelectric ceramics which carry both the sensing and actuation functions for adaptive control. The report documents work over the third year of this five year program. For convenience and continuity, the activities are grouped under the headings General Summary Papers, Materials Studies, Composite Sensors, Actuator Studies, Integration Issues, Processing Studies, Thin Film Ferroelectrics, and the Abstracts of graduating students on the program. This volume picks up with integration issues and moves on to Processing Studies, Thin Film Ferroelectrics, and graduating students in the program. DTIC

N95-31384# Columbia Univ., New York, NY. Dept. of Electrical Engineering.
PSEUDOMORPHIC HETEROSTRUCTURE MATERIALS FOR HIGH PERFORMANCE DEVICES Final Technical Report, 15 Dec. 1992 - 14 Dec. 1994
Wen I. Wang 21 Mar. 1995 12 p
(Contract N00014-90-J-1536)
(AD-A292906) Avail: CASI HC A03/MF A01

Using the planar-doping technique, Si has been shown to be amphoteric on (311)A InAlAs/InGaAs/InP grown by molecular beam epitaxy and excellent modulation-doped field effect transistors have been demonstrated. Through the use of an AlN/GaN strained superlattice buffer layer, high quality GaN layers were obtained. Crystalline SiC thin layers have been grown on 125 mm silicon-on-insulator (SOI) substrates. These two techniques have also been combined to synthesize the first GaN on SiC on SOI structure. Normal incidence infrared photodetectors using intersubband transitions in GaSb L-valley quantum wells have been demonstrated. Enhancement of normal incidence intervalence subband absorption in GaSb quantum wells coupled to a neighboring InAs has been observed. DTIC

N95-31403# Oak Ridge National Lab., TN.
SELF-LUBRICATING, TIN-MoS2 COMPOSITE COATINGS PRODUCED BY SIMULTANEOUS DEPOSITION FROM Ti((CH3))2N4/NH3/MoF6H2S GAS MIXTURE
Y. W. Bae, W. Y. Lee, T. M. Besmann, P. J. Blau, K. L. More, and D. N. Braski 1994 6 p Presented at the 1994 Fall Meeting of the Materials Research Society (MRS), Boston, MA, 28 Nov. - 2 Dec. 1994
(Contract DE-AC05-84OR-21400)
(DE95-010359; CONF-941144-137) Avail: CASI HC A02/MF A01

Composite coatings consisting of discrete phases of TiN and MoS2 were codeposited on graphite substrates from Ti(CH3)2N4/NH3/MoF6/H2S gas mixtures in a cold-wall reactor at 1,073 K and 1.3 kPa. Chemical composition and microstructure of the coatings were characterized by Auger electron spectroscopy, X-ray diffraction, and transmission electron microscopy. Kinetic friction coefficients of the coatings were determined by a computer-controlled friction microprobe and values less than 0.2 were obtained with a type-440 C stainless-steel counterface under ambient condition. DOE

N95-31421*# McDonnell-Douglas Aerospace, Long Beach, CA. Transport Aircraft.
DEVELOPMENT OF STITCHED/RTM PRIMARY STRUCTURES FOR TRANSPORT AIRCRAFT Report, 1 Apr. 1989 - 30 Apr. 1991
Arthur V. Hawley Jul. 1993 73 p
(Contract NAS1-18862; RTOP 510-02-11-08)
(NASA-CR-191441; NAS 1.26:191441; MDC-93K0265) Avail: CASI HC A04/MF A01

This report covers work accomplished in the Innovative Composite Aircraft Primary Structure (ICAPS) program. An account is given of the design criteria and philosophy that guides the development. Wing and fuselage components used as a baseline for development are described. The major thrust of the program is to achieve a major cost breakthrough through development of stitched dry preforms and resin transfer molding (RTM), and progress on these processes is reported. A full description is provided on the fabrication of the stitched RTM wing panels. Test data are presented. Author

N95-31469# Naval Postgraduate School, Monterey, CA.
MICROSTRUCTURE AND AGING RESPONSE OF SiCp REINFORCED A356 Al METAL MATRIX COMPOSITE SUBJECT TO POST FABRICATION THERMOMECHANICAL PROCESSING M.S. Thesis
Donald V. Avenger Dec. 1994 45 p
(AD-A292975) Avail: CASI HC A03/MF A01

The microstructure and aging behavior of a centrifugally cast A356 Al-SiCp metal matrix composite was studied as a function of post-fabrication processing via transmission electron microscopy (TEM) and differential scanning caloritemetry (DSO). The effects of total rolling strain, strain per rolling pass and rolling temperature on both microstructure and precipitation behavior were investigated. It was found that post fabrication processing had relatively little effect on the kinetics of the various precipitation processes that constitute aging, although they affected the amounts of the various precipitates significantly. DTIC

N95-31509# Quest Integrated, Inc., Kent, WA.
IN SITU COMPOSITES IN THE ALUMINUM NITRIDE-ALUMINA SYSTEM Final Report, 19 Sep. 1994 - 19 Apr. 1995
Ender Savron Apr. 1995 33 p
(Contract N00014-94-C-0263)
(AD-A293776; QUEST-TR-650) Avail: CASI HC A03/MF A01

An attempt was made to produce in situ composites in an aluminum nitride-alumina system via pressureless reaction sintering. Different aluminum nitride-alumina compositions were prepared and fired at temperatures between 1900 C and 2200 C. Phase compositions were determined by x-ray diffraction, and microstructure development was evaluated by scanning electron microscopy. Elongated grains in an equiaxed matrix were achieved. However, the expected improvement in mechanical properties was offset by excessive grain growth and porosity. The high mobility of grain boundaries causes abnormal growth and pore entrapment without full densification. Suggestions for further work are offered to remedy the problems. DTIC

N95-31668# Naval Undersea Warfare Center, Newport, RI.
AN INVERSE METHOD TO MEASURE THE AXIAL MODULUS OF COMPOSITE MATERIALS UNDER TENSION Final Report
Andrew J. Hull 3 Jan. 1995 22 p
(AD-A293042; NUWC-NPt-TR-10801) Avail: CASI HC A03/MF A01

An inverse method is developed to measure the axial modulus of materials subjected to tensile loads. The approach is intended for use on long composite structures whose modulus is frequency dependent. The governing differential equations of a laboratory test configuration are solved and then inverted at three locations that correspond to sensor transfer functions. These three equations are next combined in such a way that the complex-valued axial modulus is equal to a function of the measured data and the known system parameters. This expression is a closed-form measurement of the modulus at each test frequency. An experiment is included to validate the method. Comparisons between the transfer function data and the model expressed with the measured modulus are in close agreement. DTIC

N95-31731 McMaster Univ., Hamilton (Ontario).
FINITE ELEMENT ANALYSIS OF DAMPED VIBRATIONS OF LAMINATED COMPOSITE PLATES Ph.D. Thesis
Baogang Hu 1993 190 p
(ISBN-0-315-84928-2) Avail: Univ. Microfilms Order No. DANN84928

In this thesis, the damped free vibrations of composites are treated from the viewpoint of macromechanical analysis. Two damping models are developed, namely: the viscoelastic damping (VED) model and the specific damping capacity (SDC) model. The important symmetry property of the damping matrix is retained in both models. A modified modal strain energy method is proposed for the evaluation of modal damping in the VED model using a real, instead of a complex, eigenvalue problem solution. Numerical studies of multi-degree-of-freedom systems are conducted to illustrate the better accuracy of the method compared to the modal strain energy method. The experimental data reported in the literature for damped free vibrations, in both polymer-matrix and metal-matrix composites, were used in the finite element analysis to test and compare the damping models. The natural frequencies and modal damping were obtained using both the VED and the SDC models. It was shown that the results from both models are in satisfactory agreement with the experimental data. Both models were found to be reasonably accurate for systems with low damping. Parametric studies were conducted to study the effects on damping of the side-to-thickness ratio, the principal moduli ratio, the total number of layers, the ply-angle, and boundary conditions. Dissert. Abstr.

N95-31740# National Aerospace Lab., Tokyo (Japan). Airframe Div.
EVALUATION OF STATIC STRENGTH OF T800H/PMR-15 CARBON/POLYIMIDE LAMINATES AT ROOM TEMPERATURE AND 300 C
Yoshiaki Kakuta, Toshiyuki Shimokawa, Masataka Yamamoto, Shigeo Sanbongi, Yasumasa Hamaguchi, Masataka Yamamoto (National Space Development Agency, Tokyo, Japan.), and Hidehiko Mitsuma (National Space Development Agency, Tsukuba, Japan.) Nov. 1994 31 p In JAPANESE Original contains color illustrations
(ISSN 0389-4010)
(NAL-TR-1254) Avail: CASI HC A03/MF A01

The objective of this study is to evaluate the material properties and laminate strength of a T800H/PMR-15 carbon/polyimide composite, which is selected as a candidate material for the primary structures of the unmanned small space vehicle HOPE (H-II Orbiting Plane). Various static tests were conducted to obtain data on the material properties and the laminate strengths for the unnotched and circular-holenotched specimens of a quasi-isotropic laminate. These tests were conducted at room temperature and a high temperature (300 C). The material property data include tension, compression, and short beam shear strengths, failure strain, elastic modulus, and Poisson's ratio. The first ply failure and the last ply failure strengths of the unnotched laminate are computed using the material property data obtained and the maximum stress and Tsai-Wu failure criteria. The strength of the laminate with a circular hole is predicted on the basis of the point stress and the average stress criteria. These analytical results are compared with the test results and discussed. Author

N95-31973 California Univ., Santa Barbara, CA.
PROCESSING AND MICROSTRUCTURAL EVOLUTION OF ALUMINA/ALUMINUM ALLOY AND ALUMINUM NITRIDE/ALUMINUM ALLOY COMPOSITES BY DIRECTED MELT OXIDATION Ph.D. Thesis
Scott David Crudele 1994 251 p
Avail: Univ. Microfilms Order No. DA9423864

An experimental investigation on the directed oxidation of aluminum-zinc alloys to produce alumina/aluminum alloy composites with and without alumina preforms has been conducted. It has been suggested in the literature that Al-Mg alloys grow composites by the dissolution of a magnesia surface layer and reprecipitation of alumina in the composite. The intent of this investigation is to reveal relevant distinctions in the proposed dissolution-reprecipitation process as they apply to a more commercially interesting Zn containing alloy with a reinforcing preform. The TGA behavior and microstructural observations on the oxidation of Al-10Zn-8Si alloys were coupled with a thermodynamic and kinetic analysis to develop a composite growth model. Experiments were carried out in air at 1000-1200 C. At the higher temperatures (greater than 1100 C), Al2O3/Al composites grow by dissolving a ZnAl2O4 (spinel) surface layer. The dissolution process releases oxygen that reprecipitates in the form of Al2O3 on the existing composite, and also releases Zn and Al which migrate upward through the spinel to regenerate the surface oxide. Composite growth may only occur

when the surface regenerates at a rate comparable with that of the dissolution process. At the lower temperatures, 1000 C, the composite growth is limited by the spinel regeneration process, and becomes intermittent. The addition of Mg to this alloy allows normal composite growth by the dissolution of a surface (Zn,Mg)Al2O4 layer at the lower temperatures, 980-1060 C, but leads to heterogeneous microstructures with voids as the temperature increases above approximately 1060 C. The directed oxidation of an Al-Zn alloy into porous alumina preforms yields an Al2O3/Al composite matrix which fills the preform interstices. Al-10Zn-8Si-0.25Mg alloys that are oxidized from 960-1100 C, and Al-10Zn-8Si alloys that are oxidized at 800-1000 C climb up the preform particle. This climb process results in an extended oxidation front and voids in the composite. Elimination of Mg from the alloy suppresses climbing and void formation, but composite growth must be carried out at greater than or equal to 1100 C. An experimental investigation on the directed nitridation of aluminum-strontium alloys to produce aluminum nitride/aluminum alloy composites was also conducted with the intent of extending the directed oxidation knowledge to the nitridation process. Al-Sr-Si alloys exposed to N2 at 950-1200 C produce AlN/Al composites which can be partly explained by the dissolution of a strontium nitride surface layer. The lack of thermodynamic and kinetic information hinders the elaboration of the nitridation mechanism; although, it is clear that the basic principles to those operating in the directed oxidation process.

Dissert. Abstr.

N95-31976 Minnesota Univ., Minneapolis, MN.
CONTROL OF INTERFACIAL CHEMISTRY AND MECHANICAL PROPERTIES IN METAL/CERAMIC COMPOSITES Ph.D. Thesis
Hsin-Fu Wang 1994 152 p
Avail: Univ. Microfilms Order No. DA9424341

Evaluation of the mechanical properties of metal/ceramic interfaces (Ti/Al2O3) was accomplished by using four-point bending tests, nanoindentation tests and fiber pushout tests. At first, the interfacial fracture energy of composites with different applied bonding temperatures from 700 C to 1000 C and thickness of the metal interlayers were measured by four-point bending tests. The mixed mode interfacial fracture energy of the Ti/Al2O3 interface was found to increase with increasing bonding temperatures up to 950 C. There is increasing interdiffusion of the constituent atoms across the interfaces with increasing temperature as verified by X-ray mapping. Thus, a stronger chemical bond forms between the Ti and the Al2O3. Above this temperature, the interfacial fracture energy drops due to the formation of a continuous brittle intermetallic compound (Ti3Al) at the Ti/Al2O3 interface. Modification of the interface was achieved with a diffusion barrier consisting of a refractory metal and Y2O3 duplex coating prepared by r.f. sputtering methods. The diffusion barrier significantly reduces the diffusion of the constituent atoms and prevents the formation of a continuous Ti3Al reaction layer, thus maintaining the chemical integrity and stability at the Ti/Al2O3 interface. The interfacial fracture energy can be further reduced by providing thinner Ti interlayers. The contribution of the energy dissipation process to the interfacial fracture energy is due to plastic energy absorption in the Ti interlayer during the fracture process. The interfacial shear strength, interfacial frictional stress and mode II interfacial fracture energy of the fiber composites were obtained by performing the fiber pushout tests. Using the Atomic Force Microscope (AFM), the surface roughness and texture of the three different Al2O3 fibers were evaluated. Incorporation of the experimental data and the theory gives the calculated frictional coefficient to be 0.35. The distribution of the frictional force on the refractory metal coated Al2O3 surfaces was also measured by the Lateral Force Microscope (LFM) with frictional coefficient ranging from 0.2 to 0.8, the average frictional coefficient being 0.38.

Dissert. Abstr.

N95-32060*# Argonne National Lab., IL. Energy Technology Div.
INFLUENCE OF FIBER CONTENT ON MECHANICAL PERFORMANCE OF SIC-FIBER-REINFORCED REACTION-BONDED SILICON NITRIDE COMPOSITES
D. Singh, J. P. Singh, and R. T. Bhatt Jan. 1995 14 p Presented at the 19th Annual Conference on Advanced Ceramics, Materials and Structures, Cocoa Beach, FL, 9-12 Jan. 1995 Prepared in cooperation with NASA. Lewis Research Center, Cleveland, OH
(Contract W-31-109-eng-38)
(NASA-TM-110639; NAS 1.15:110639; DE95-009903; ANL/ET/CP-83786; CONF-950129-5) Avail: CASI HC A03/MF A01

The effect of fiber content on the resulting mechanical properties (first matrix cracking stress, ultimate strength, and work-of-fracture) of silicon carbide (SiC)-fiber-reinforced reaction-bonded silicon nitride (RBSN) matrix composites was investigated. Flexure tests were used to evaluate mechanical properties of composites containing various fiber contents. The first matrix cracking stress, ultimate strength, and work-of-fracture of the composites increased with increasing fiber content, reaching a peak value at a fiber content of (approximately) 16 vol.%. Further increases in fiber content degraded the mechanical properties of the composites. The variations in mechanical properties with fiber contents were correlated to the residual stresses in the matrix phase, processing related flaws, and failure modes observed in these composites. DOE

N95-32108 Michigan Univ., Ann Arbor, MI.
FAILURE MECHANISMS IN COMPOSITE PLATES SUBJECTED TO IN-PLANE COMPRESSIVE LOADING Ph.D. Thesis
Amir Reza Khamseh 1994 157 p
Avail: Univ. Microfilms Order No. DA9423229

An experimental investigation into the failure mechanisms of composite plates in the presence of stress gradients, generated by circular cutouts, subjected to uniaxial/biaxial compressive loading was carried out. The focus of the study was identification and analysis of the failure initiation mechanisms in laminated plates as a function of the centrally located circular hole and loading parameters. The experimental investigation was divided into two parts, the first dealing with single axis loading and the second addressing biaxial loading. The materials under investigation were comprised of a set of specially designed single layer unidirectional composites, as well as a series of 48 layer graphite/epoxy specimens with varying stacking ply orientation, provided by NASA Langley. Test specimens containing plies oriented in the direction of loading subjected to uniaxial loading exhibited failure initiation along the edge of the hole, perpendicular to the fiber and loading direction, traversing into the specimen in the form of fiber kinking, followed by delamination (i.e. several of the specimens exhibited fiber kinking failure with no evidence of delamination, or delamination growth lagging behind the kink tip). The above mentioned specimens subjected to biaxial loading exhibited similar failure mechanisms as their uniaxial counterparts, but failure initiation was in the form of fiber-matrix debonding. Shear dominated specimens, which have fibers oriented at 45 deg angles to the loading direction, exhibited highly nonlinear strain to failure values with no indication of localized fiber failure. The failure mode for these type of composites was shear induced delamination caused by large wavelength in-plane fiber microbuckling. A computational approach was employed to simulate some of the uniaxial experimental results, through the use of of the finite element method. The finite element analysis software HKS-ABAQUS was used, taking into account material nonlinearities. The computational analysis revealed the roles of fiber failure strain and hole gradient in the in-plane failure analysis of composite plates. This investigation has yielded results and shown trends in the failure patterns of composites and the results reported herein can be incorporated in developing their micromechanics based failure criteria. Dissert. Abstr.

N95-32113 Michigan Univ., Ann Arbor, MI.
CONTRIBUTIONS TO THE DESIGN OF NEUTRAL CUTOUTS IN LAMINATED PLATES AND SHELLS Ph.D. Thesis
Erol Senocak 1994 106 p
Avail: Univ. Microfilms Order No. DA9423314

The problem of designing a cutout and a suitable cutout edge reinforcement (termed neutral hole) in a load bearing structural member in the form of a plate or shell, such that the cut structure maintains its stress state with a minimal departure from the stress state of the uncut structure, is addressed. A particular class of structural optimization for laminated thin walled structures is considered, in which the geometry of the structure is obtained as a solution to a particular problem, for known states of stress, strain, boundary conditions, and appropriate constraints (sometimes called inverse problems in elasticity for some specific cases). In this category, either stress concentrations are reduced (optimized) by determining the shape of the openings (harmonic holes), or stress states in the cut structure with reinforcement are maintained unchanged compared to that of the uncut structure (neutral holes). Symmetrically laminated composite plates and circular cylindrical shells are considered. Planar loading

and pure bending cases for laminated plates, and hydrostatic pressure and axial compression loading cases for the shells are assumed. Unsymmetrically laminated plates are also studied and material coupling (bending-stretching coupling due to material elastic properties) has been investigated. Plates are analyzed using classical lamination theory, and the Donnell shallow thin shell model is applied to investigate laminated shells. An intermediate class of deformation theory, the von Karman model for plates, is considered for the unsymmetrically laminated plates. The reinforcement is modeled as a one-dimensional rod/beam type structural element. In the reinforcements that were considered, the fibers are tangential to the edge of the cutout. This is not a restriction, as the solution presented could very well accommodate other types of constitutive models as well. The shape of the cutout and the cross-sectional area of the reinforcement are determined in closed form. A novel approach is introduced for the determination of the optimum reinforcement when the analytical solution fails to produce a neutral condition. The original (uncut) stiffness of the plate and shell structures are restored by appropriately designing an edge reinforcement around the cutout. The buckling load of the designed shells are analyzed via the finite element method. It is shown that the resistance to buckling is almost completely recovered. An experimental investigation has been carried out to verify some of the results for the shell structures, and the results are presented. Dissert. Abstr.

N95-32209*# National Aeronautics and Space Administration. Lewis Research Center, Cleveland, OH.

A STUDY OF ELEVATED TEMPERATURE TESTING TECHNIQUES FOR THE FATIGUE BEHAVIOR OF PMCS: APPLICATION TO T650-35/AMB21

Andrew L. Gyekenyesi (Cleveland State Univ., OH.), Michael G. Gastelli (NYMA, Inc., Brook Park, OH.), John R. Ellis, and Christopher S. Burke (NYMA, Inc., Brook Park, OH.) Jul. 1995 22 p

(Contract NAS3-27186; RTOP 538-06-15)

(NASA-TM-106927; E-9648; NAS 1.15:106927) Avail: CASI HC A03/MF A01

An experimental study was conducted to investigate the mechanical behavior of a T650-35/AMB21 eight-harness satin weave polymer composite system. Emphasis was placed on the development and refinement of techniques used in elevated temperature uniaxial PMC testing. Issues such as specimen design, gripping, strain measurement, and temperature control and measurement were addressed. Quasi-static tensile and fatigue properties (R(sub sigma) = 0.1) were examined at room and elevated temperatures. Stiffness degradation and strain accumulation during fatigue cycling were recorded to monitor damage progression and provide insight for future analytical modeling efforts. Accomplishments included an untabbed dog-bone specimen design which consistently failed in the gage section, accurate temperature control and assessment, and continuous in-situ strain measurement capability during fatigue loading at elevated temperatures. Finally, strain accumulation and stiffness degradation during fatigue cycling appeared to be good indicators of damage progression. Author

25 INORGANIC AND PHYSICAL CHEMISTRY

Includes chemical analysis, e.g., chromatography; combustion theory; electrochemistry; and photochemistry.

For related information see also *77 Thermodynamics and Statistical Physics.*.

N95-30409# Phillips Lab., Edwards AFB, CA.

THEORETICAL ABSORPTION SPECTROSCOPY OF HIGH-TEMPERATURE METAL VAPORS: MODEL AND EXPERIMENT COMPARED Final Report

Jeffrey D. Mills Dec. 1994 36 p

(AF Proj. 2308)

(AD-A290872; PL-TR-94-3001) Avail: CASI HC A03/MF A01

Theoretical calculations in support of absorption spectroscopy of buffered metallic vapors in the Plasma Spectroscopy Cell are described. After a brief exposition of the theoretical principles and ingredients of the quantum-mechanical, state-to-state treatment of transition processes in atoms and diatoms at thermodynamic equilibrium, various aspects of the model and experimental absorption spectra for the lithium system are compared and discussed. Special emphasis is given to outlining those spectral characteristics which are most relevant to the energy transfer properties of the sample but are as yet incompletely understood and to determining the minimal computational algorithm sufficient to rapidly and accurately calculate absorption by these materials. An account of the modelling of the aluminum/lithium system preparative to a search for a heretofore unobserved molecule, aluminum lithium, is also included. DTIC

N95-30420# Pakistan Inst. of Nuclear Science and Technology, Islamabad.

STANDARDIZATION OF (13)CO2 PRODUCTION PROCEDURE FROM ORGANIC MATTER FOR MASS SPECTROMETRIC ANALYSIS

M. I. Sajjad, Z. Latif, M. A. Tasneem, M. Ali, and R. Bilal Nov. 1993 16 p

(DE95-614629; PINSTECH-RIAD-138) Avail: CASI HC A03/MF A01 (US Sales Only)

This report summarizes the ways and means by which (13)CO2 production procedure from organic matter can be standardized. Optimum sample preparation conditions were determined to get reproducible results. Plant combustion for six minutes at 900-1000 C with pure O2 and ten minutes for conversion of CO to CO2 over CUO gauze at 850 C have been found optimum conditions. Internal standards: PINSTECH wheat straw, PINSTECH grass sample, Glucose-D glaxo PINSTECH and polyethylene foil PINSTECH were selected, and calibrated against IAEA Sucrose and polyethylene foil standards. These internal standards have been used for correction of delta C-13 results. The mechanisms for the correction of results has been described. Causes of isotope fractionation of plant samples were determined. Statistical summary of measured results for delta C-13 standards has also been given. DOE

N95-30537# Helsinki Univ. of Technology, Espoo (Finland). Dept. of Chemical Engineering.

CATALYTIC REACTIONS OF SYNTHESIS GAS. PART 4: HETEROGENEOUS HYDROFORMYLATION

M. Niemelae 1994 28 p

(PB95-195558; ISBN-951-22-2369-4) Avail: CASI HC A03/MF A01

Rhodium and cobalt exhibit superior performance in homogeneous hydroformylation compared with other metal catalysts. Thus far heterogeneous hydroformylation catalysts have not been commercialized. Decomposed carbonyls on various inorganic supports have been studied in hydroformylation reaction as a probe reaction for the Fischer-Tropsch synthesis. Addition of ethylene and propylene to the reaction mixture of CO and H2 has resulted in the formation of typical hydroformylation products particularly on Rh and Co catalysts. In conclusion, ethylene or propylene hydroformylation is a suitable test reaction for molecular activation of CO, and it supplements well the catalyst characterizations by dissociative activation of CO in synthesis gas reaction. NTIS

N95-30541# Pennsylvania State Univ., University Park, PA. Dept. of Mechanical Engineering.

SIMULATION OF CHEMICAL KINETICS IN TURBULENT NATURAL GAS COMBUSTION. VOLUME 2: EXPERIMENTAL STUDIES OF NITRIC OXIDE PRODUCTION IN GAS FLAMES Annual Report, Sep. 1993 - Jun. 1994

S. R. Turns, R. V. Bandaru, and G. J. Nathan (Adelaide Univ., Australia.) Jul. 1994 45 p See also PB92-238799

(Contracts GRI-5086-260-1308; GRI-5092-260-2596)

(PB95-196721; GRI-94/0421.2) Avail: CASI HC A03/MF A01

One major focus of the work during the report was the design, fabrication, and installation of the necessary apparatus to conduct an investigation of jet flames in a crossflow. A second focus was a parametric investigation of precessing jet flames in an unconfined, quiescent ambient. Parameters varied include nozzle diameter, jet deflection angle, initial jet velocity (Reynolds number), dimensionless precession frequency (Strouhal number), and fuel type. The overall objective of this study is to provide an increased understanding of the combined effects of fluid mechanics and chemical kinetics in the production and emission of oxides of nitrogen from gas-burning combustion systems. NTIS

N95-30554 Department of the Navy, Washington, DC.

SONIC APPARATUS FOR DEGASSING LIQUIDS Patent

Patrick J. Monahan, inventor (to Navy) 13 Dec. 1994 4 p Filed 1

Jun. 1993
(AD-D017352; US-Patent-5,372,634; US-Patent-Appl-SN-069817; US-Patent-Class-96-175) Avail: US Patent and Trademark Office

A sonic apparatus for degassing liquids is presented. The apparatus includes a vessel for receiving and releasably retaining an open-top container and adapted to be closed with the container therein, transducer suspension structure positioned in the vessel, an ultrasonic transducer suspended from the structure and disposed in the container spaced from the walls and bottom of the container and beneath the surface of a liquid contained therein. The apparatus further includes a signal generated outside of the vessel for transmitting power to the transducer, and a vacuum pump for maintaining the vessel interior at a vacuum. DTIC

N95-30614# Rice Univ., Houston, TX.
APPLICATION OF SPIN-SENSITIVE ELECTRON SPECTROSCOPIES TO INVESTIGATIONS OF ELECTRONIC AND MAGNETIC PROPERTIES OF SOLID SURFACES AND EPITAXIAL SYSTEMS Final Report, 1 Jan. 1986 - 31 Oct. 1994
G. K. Walters and F. B. Dunning Feb. 1995 13 p
(Contract DE-FG05-86ER-45233)
(DE95-010154; DOE/ER-45233/10) Avail: CASI HC A03/MF A01

The principal objectives of the research have been improved understanding and characterization of electronic and magnetic properties of surfaces, adsorbates, and epitaxially-grown systems. Toward this end, substantial effort has also been directed toward better elucidation of the dynamical processes involved in electron-surface and atom-surface interactions, since these provide the bases for electron spectroscopies commonly used for probing surface properties. To accomplish these objectives, three novel spin-sensitive electron spectroscopies have been developed in this laboratory, and these have been exploited to provide new information not accessible using the corresponding conventional (non-spin-sensitive) spectroscopies. These spectroscopies and the new knowledge that has resulted from their application are discussed briefly in the following three sections of the report: spin polarized low energy electron diffraction (SPLEED); spin polarized electron energy loss spectroscopy (SPEELS); and spin polarized (metastable atom) deexcitation spectroscopy (SPMDS). DOE

N95-30670 Michigan Technological Univ., Houghton, MI.
AN EXPERIMENTAL AND NUMERICAL STUDY ON THE STRUCTURE AND EXTINCTION OF LAMINAR PREMIXED FLAMES Ph.D. Thesis
Chao Fu Daniels 1994 202 p
Avail: Univ. Microfilms Order No. DA9425336

The laminar premixed flames are studied to obtain the flame speed and flame thickness under the influence of stretch and preferential diffusion. A new concept of flame thickness which is defined by velocity profile of the flame structure is used. The extinction mechanism for the flames with different preferential diffusion effect is also studied and the extinction criterion is established for the adiabatic flames under stretch. The laminar premixed flames are studied by both experimentation and numerical calculation. Experimentally, the counterflow configuration technique is applied to establish the adiabatic, planar twin flames. The velocity profiles for methane/air and propane/air flames with different equivalence ratios are measured by laser Doppler velocimetry to obtain the flame speed and flame thickness under different stretch and preferential diffusion conditions. The numerical calculations based on different chemical mechanisms for methane/air and propane/air flames are also carried out to obtain the flame speed, flame thickness, and detailed flame structure in terms of different stretch rates and Le numbers for comparison with the experimental results. The comparison between the new concept of flame thickness and the existing widely used flame thickness has shown that the new flame thickness defined by the velocity profile can be used as the definition of the flame thickness. Based on the experimentation and calculation results, the local flame speed and local flame thickness are used to analyze the extinction behavior of the flames. The local Karlovitz number is proposed based on the local flame speed and local flame thickness, which can truly represent the influence of the stretch on the flame. A new nondimensional KT number is formed based on the local Karlovitz number and a temperature term, where the temperature term is the ratio between the temperature difference for the combustion and the flame temperature. The extinction will occur when the KT number is about unity. Dissert. Abstr.

N95-30709# Texas A&M Univ., College Station, TX.
FISCHER-TROPSCH SYNTHESIS IN SUPERCRITICAL FLUIDS Quarterly Technical Progress Report, 1 Oct. 1994 - - 21 Dec. 1994
A. Akgerman and D. B. Bukur 31 Jan. 1995 7 p
(Contract DE-FG22-92PC-92545)
(DE95-009631; DOE/PC-92545/9) Avail: CASI HC A02/MF A01

Progress reports are presented for the following two tasks: (1) diffusion coefficients of F-T products in supercritical fluids; and (2) Fischer-Tropsch reaction related studies. The objectives for this quarter for task 1 were to measure molecular diffusion coefficients and effective diffusivities at the same conditions. The objectives for task 2 were to conduct two additional tests with the Ruhrchemie catalyst and a catalyst synthesized in our laboratory under supercritical conditions. DOE

N95-30714# Lawrence Livermore National Lab., Livermore, CA.
SMART ACTIVE MULTIWAVE SENSING WITH ZERO BACKGROUND AMPLITUDE MODULATED PROBES
A. J. Ruggiero, R. A. Young, and L. Jelsma Jul. 1994 16 p Presented at the 1994 Chemical Analysis By Laser Interrogation of Proliferation Effluents (CALIOPE ITR) Interim Technical Review, Livermore, CA, 26-28 1994
(Contract W-7405-eng-48)
(DE95-008813; UCRL-JC-118286; CONF-9404162-19) Avail: CASI HC A03/MF A01

Recently, a new approach to multi-wavelength remote sensing has been proposed based on the generation and detection of spectral 'pickets' synthesized from the frequency filtered bandwidth of a modelocked laser. Using linear array liquid crystal spatial light modulator (SLM) technology for spectral filtering permits real time grey scale control of individual picket amplitudes and phases, making it possible to independently modulate picket characteristics in the kHz to MHz regime. Due to the versatility of this approach, a whole suite of spectroscopies based on detection techniques that are similar to conventional sideband spectroscopies can be implemented. These techniques not only inherit the S/N advantages of their conventional counterparts, they can also be easily extended to simultaneous multi-wavelength operation using frequency multiplex techniques and configured for real time adaptive data acquisition. We report the laboratory demonstration and theoretical development of a new class of zero background AM modulated spectroscopic probes for differential absorption measurements. Preliminary detection sensitivities on the order of 10(exp -6) can be inferred from our measurements. Application of this technique to realistic remote sensing scenarios, advantages over other modulation and direct detection approaches, as well as the present limitations and theoretical limits to detection sensitivity will be discussed. DOE

N95-30735# Los Alamos National Lab., NM.
ON-LINE SURFACTANT MONITORING
Ken I. Mullen, Everett E. Neal, Patrick D. Soran, and Barbara Smith 1995 8 p Presented at the International Forum Process Analytical Chemistry Conference, Houston, TX, 22-25 Jan. 1995
(Contract W-7405-eng-36)
(DE95-009417; LA-UR-95-966; CONF-950158-2) Avail: CASI HC A02/MF A01

This group has developed a process to extract metal ions from dilute aqueous solutions. The process uses water soluble polymers to complex metal ions. The metal/polymer complex is concentrated by ultrafiltration and the metals are recovered by a pH adjustment that frees the metal ions. The metal ions pass through the ultrafiltration membrane and are recovered in a concentrated form suitable for reuse. Surfactants are present in one of the target waste streams. Surfactants foul the costly ultrafiltration membranes. It was necessary to remove the surfactants before processing the waste stream. This paper discusses an on-line device the authors fabricated to monitor the process stream to assure that all the surfactant had been removed. The device is inexpensive and sensitive to very low levels of surfactants. DOE

N95-30762# Department of Energy, Morgantown, WV.
ACHIEVING IMPROVED CYCLE EFFICIENCY VIA PRESSURE GAIN COMBUSTORS
Randall S. Gemmen, Michael C. Janus, George A. Richards, Thomas S. Norton, and William A. Rogers 1995 14 p Presented at the ASME International Gas Turbine and Aeroengine Congress and Exposition: Land,

Sea and Air, Houston, TX, 5-8 Jun. 1995
(DE95-008945; DOE/METC-C/95/7183; CONF-950629-2) Avail: CASI HC A03/MF A01

As part of the Department of Energy's Advanced Gas Turbine Systems Program, an investigation is being performed to evaluate 'pressure gain' combustion systems for gas turbine applications. This paper presents experimental pressure gain and pollutant emission data from such combustion systems. Numerical predictions for certain combustor geometries are also presented. It is reported that for suitable aerovalved pulse combustor geometries studied experimentally, an overall combustor pressure gain of nearly 1 percent can be achieved. It is also shown that for one combustion system operating under typical gas turbine conditions, NO(x) and CO emissions, are about 30 ppmv and 8 ppmv, respectively. DOE

N95-30766# Texas A&M Univ., College Station, TX. Dept. of Chemistry.
A STUDY OF CATALYSTS AND MECHANISMS IN SYNTHESIS REACTIONS Final Report
Jack H. Lunsford Feb. 1995 12 p
(Contract DE-FG05-88ER-13829)
(DE95-010177; DOE/ER-13829/T1) Avail: CASI HC A03/MF A01

During the catalytic oxidation of hydrocarbons over many metal oxides, radicals are formed on the surface and these intermediates emanate into the gas phase where they become involved in homogeneous reactions. Examples include methyl radicals formed during the oxidative coupling of methane, allyl radicals formed during the partial oxidation of propylene, and hydroxyl radicals formed during the reaction of water with molecular oxygen. Higher temperatures (greater than 600 C) generally favor radical formation. Other factors that effect radical formation, as well as secondary reactions of the radicals with surfaces, have been investigated. A matrix isolation electron spin resonance (MIESR) system and a laser-induced fluorescence (LIF) system have been used to study hydrocarbon and hydroxyl radicals, respectively. The goal of the research is to understand the role that these surface generated intermediates play in catalytic reactions, with emphasis on the partial and complete oxidation of hydrocarbons. The results will find application in the utilization of natural gas reserves in an efficient and nonpolluting manner. DOE

N95-30936# Ohio State Univ., Columbus, OH.
THE 49TH INTERNATIONAL SYMPOSIUM ON MOLECULAR SPECTROSCOPY Final Report, 3 Jan. 1992 - 2 Dec. 1994
Terry A. Miller 2 Dec. 1994 280 p Symposium held in Columbus, OH, 13-27 Jun. 1994
(Contract DAAL03-92-G-0281)
(AD-A292708; ARO-30089.1-PH-GF) Avail: CASI HC A13/MF A03

The Ohio State University International Symposium on Molecular Spectroscopy is one of the longest running and most successful scientific conferences in the United States today. It plays a unique role in the educational development of large number of graduate students in the physical sciences. The Conferences subject area underlies many items of direct interest to ARO, such as interactions of electromagnetic radiation with molecules, characterization and quantification of low-level molecular concentrations, such as contaminants, pollutants, reactive intermediates in combustion, etc. DTIC

N95-30938# Colorado State Univ., Fort Collins, CO.
METAL NANOTUBULE MEMBRANES WITH ELECTROCHEMICALLY SWITCHABLE ION-TRANSPORT SELECTIVITY Interim Report
Matsuhiko Nishizawa, Vinod P. Menon, and Charles R. Martin Mar. 1995 20 p
(Contract N00014-82-K-0162)
(AD-A292712; TR-100) Avail: CASI HC A03/MF A01

Membranes that contain cylindrical metal nanotubules that span the complete thickness of the membrane are described. The inside radius of the nanotubules can be varied at will; nanotubule radii as small as 0.8 nm are reported here. These metal nanotubule membranes show selective ion transport analogous to that observed in ion-exchange polymers. Ion permselectivity is observed because excess charge density can be present on the inner walls of the metal tubules. The membranes reject ions of the same sign, and transport ions of the opposite sign, as this excess charge. Because the sign of the excess charge on the tubule can be changed potentiostatically, a metal nanotubule membrane can be either cation selective or anion selective, depending on the potential applied to the membrane. DTIC

N95-30971# Simons Research Associates, Lynnfield, MA.
EXTENSION OF THE PORE TREE MODEL TO DESCRIBE PORE INTERCONNECTIVITY
Girard A. Simons 31 Oct. 1994 15 p
(Contract DAAH04-94-C-0075)
(AD-A290366; ARO-32900.2-GS-S) Avail: CASI HC A03/MF A01

The 'pore tree' model of pore structure (Simons and Finson, 1979; Simons, 1982) was developed for catalysts and sorbents to allow diffusion within a porous media in the absence of convection through the media. The pore tree model is extended herein to describe the permeable pore structure which characterizes the subsurface flow of water in soil, the dispersion of contaminants and the in-situ remediation of contaminated sites. Permeability requires a statistical determination of the 'branches' that are common to several trees to allow percolation through the large scale (mobile) structure in addition to diffusion through the smaller scale (immobile) structure. While permeability is dominated by the largest pores, it is important to determine the level of convection that is occurring at the intermediate scales in order to accurately describe transport. This and subcequent interim technical reports will be self contained in that each report will contain the previous report plus new work described in the last 34 pages of each report. DTIC

N95-31009# Department of the Navy, Washington, DC.
HYDROGEN SULFIDE ANALYZER WITH PROTECTIVE BARRIER Patent Application
Rex A. Neihof, inventor (to Navy) 29 Sep. 1994 26 p
(AD-D017412; US-Patent-Appl-SN-321182) Avail: CASI HC A03/MF A01

A field test kit for determining quantity of hydrogen sulfide in a liquid test sample. The test kit includes a test container with an opening for a liquid test sample containing hydrogen sulfide gas and a cap provided over the opening. The cap has colorimetric particulate indicator on its top inside surface. A silicone barrier disposed over the indicator protects the indicator from contact with the test sample. DTIC

N95-31014# Bowling Green State Univ., OH. Center for Photochemical Sciences.
SPECIFIC RATE COEFFICIENTS FROM VIBRATIONAL OVERTONE ACTIVATION OF 1-METHYLCYCLOPROPENE
Deanne Snavely, Oleg Grinevich, Salah Hassoon, and Geoff Snavely 1 Dec. 1994 25 p
(Contract N00014-91-J-4130)
(AD-A288755; TR-16) Avail: CASI HC A03/MF A01

Laser vibrational overtone activation has been used to investigate the reaction channel competition in the isomerization of 1-methylcyclopropene (MCPene). The vibrational overtone activation of three types of CH stretches (methyl, methlenic and olefinic) in the 5v sub CH and 6v sub CH transitions was initiated and all three products (2-butyne, 1,3-butadiene and 1,2-butadiene) were detected by gas chromatography. Stern Volmer plots were constructed for the appearance of each individual product and the derived experimental specific rate coefficients were compared to those of RRKM theory. The rate coefficients at high energy were 10% higher than predicted and those at low energy were 60 to 80% high. Product ratios of 1,3-butadiene to 2-butyne were independent of pressure. These ratios were compared to the RRKM ratios. The product yield ratio for the lowest energy photolysis compared well with the RRKM ratio but the two higher energy product yield ratios were approximately 35% lower than the RRKM ratio. The implications of these comparisons are discussed. DTIC

N95-31113# Sandia National Labs., Albuquerque, NM.
AQUEOUS TIO2 PHOTOCATALYSIS OF METAL-EDTA COMPLEXES
Tom Madden, Abhaya K. Datye (New Mexico Univ., Albuquerque, NM.), Michael R. Prairie, and Bertha M. Stange 1995 10 p Presented at the 5th Annual Waste-management Education and Research Consortium (WERC) Technology Development Conference, Las Cruces, NM, 18-20 Apr. 1995
(Contract DE-AC04-94AL-85000)
(DE95-011058; SAND-95-0763C; CONF-9504135-2) Avail: CASI HC A02/MF A01

This report describes the results of experiments performed to determine the viability of titanium dioxide photocatalysis towards the treatment of water contaminated with different metal-EDTA (ethylene diamine tetraacetic acid) complexes. Both the Pb-EDTA and Ni-EDTA complexes were chosen for study, as they represent respectivcly metals that are and are not capable of photodeposition onto the TiO2 catalyst during the photoreaction. Batch reactions were carried out in a jacketed glass pot reactor using 300 ml of 50 mg/l metal chelated with an equimolar amount of EDTA and 0.1wt% of TiO2 in the solution. The UV source used was a 100 W low-pressure Hg spot lamp. The two systems were studied using Degussa P-25 titanium dioxide, and Aldrich titanium dioxide loaded with Pt and Au. Around 80% removal of the Ni-EDTA complex was attained after 120 min using both catalysts with no photodeposition of Ni onto the catalyst. However, pH precipitation treatment of the reacted solutions indicated that the Ni was still complexed, probably to complexing agents that were EDTA oxidation products. Apparent zero-order kinetics was observed in the P-25 catalyst reaction, whereas apparent first-order kinetics was observed in the metal-loaded TiO2 catalyst. In contrast the Pb-EDTA complex was completely removed in 10 min using both catalysts. Also, complete Pb deposition onto the catalyst was attained in 30 min for both catalysts. The Pb deposition seemed to first require the degradation of the complex. Total organic carbon was reduced in the Ni-EDTA system 15-21% using both catalysts, and about 33% in the Pb-EDTA system using both catalysts. No reduction of either metal or metal complex was observed when no catalyst was present and the other conditions held constant. DOE

N95-31268 Combustion Inst., Pittsburgh, PA.
THE 25TH INTERNATIONAL SYMPOSIUM ON COMBUSTION
1994 1824 p Symposium held in Irvine, CA, 31 Jul. - 5 Aug. 1994; sponsored by AFOSR, DOE, NASA, National Institute of Standards & Technology, NSF, ONR, AeroChem Research Laboratories, Inc. Limited Reproducibility: More than 20% of this document may be affected by microfiche quality
(ISSN 0082-0784)
(AD-A286825) Avail: Issuing Activity (Defense Technical Information Center (DTIC))

The following topics are discussed: (1) Gasdynamic Enhancement of Nonpremixed Combustion; (2) Navier-Stokes Numerical Simulation of Supersonic Hydrogen-Flourine Combustion in CW Chemical Lasers; (3) Numerical Modeling of Combustion Processes Induced by a Supersonic Conical Blunt Body; (4) Numerical Simulation of Supersonic Mixing and Combustion; (5) The Influence of Equivalence Ratio and Soret Effect on the Ignition of Hydrogen-Air Mixtures in Supersonic Boundary Layers; (6) Cavity-Actuated Supersonic Mixing and Combustion Control; (7) The Application of New Combustion and Turbulence Models to H2-Air Non-premixed Supersonic Combustion; (8) Reduced Kinetic Mechanism of Ignition for Non-Premixed Hydrogen/Air in a Supersonic Mixing Layer; (9) Accumulating Sequence of Ignitions from a Propagating Pulse; (10) On Deviations from Ideal Chapman-Jouguet Detonation Velocity; (11) Theoretical and Numerical Analysis of the Photochemical Initiation of Detonations in Hydrogen-Oxygen Mixtures; and (12) H2-Air and CH4-Air Detonations and Combustions behind Oblique Shock Waves. DTIC

N95-31271 Department of the Navy, Washington, DC.
ELECTRIFIED MICROHETEROGENEOUS CATALYSIS Patent
Debra R. Rolison, inventor (to Navy) and Joseph Z. Stemple, inventor (to Navy) 14 Mar. 1995 12 p Filed 24 Nov. 1993
(AD-D017446; US-Patent-Appl-SN-156752; US-Patent-Class-204-275)
Avail: US Patent and Trademark Office

In a system and method for enhancing chemical reactions, a reactant is brought in contact with a stable, non-soluble, porous, electronically non-conductive solid (reaction enhancer) in a fluidic medium to form a reaction mixture of low ionic strength. The reaction mixture so formed is then subjected to an electrifying force thereby enhancing the chemical reaction. Reaction products are then collected. DTIC

N95-31333 Case Western Reserve Univ., Cleveland, OH.
SPECTRAL ELEMENT METHOD FOR NUMERICAL SIMULATION OF UNSTEADY LAMINAR DIFFUSION FLAMES Ph.D. Thesis
Richard Allen Wessel, Jr. 1993 281 p
Avail: Univ. Microfilms Order No. DA9406237

A numerical method was developed for simulation of unsteady flow with combustion. The spectral element method is used to solve the Navier-Stokes equations for conservation of mass, momentum, energy, and species. The method by Korczak and Patera was extended to include variable transport properties and Arrhenius rate chemical reaction. A variable density formulation was developed, but was found to be numerically unstable using fractional time splitting and an implicit formulation of the pressure solution to satisfy the mass continuity constraint. Therefore, the choice of constant density flow was made for practical reasons rather than physical. Time accurate simulations of a diffusion flame were conducted for initially separate co-flowing streams of fuel and oxidant in a two dimensional duct. Flow regimes and transitional states for a attached flame, unsteady attached flame, and blow-off were investigated. An increase in air velocity has the effect of making the flame shorter. Eventually the wake type flow becomes unstable and begins to oscillate. As vortices alternately form and shed from the fuel channel, the flow stretches the flame between eddies and compresses the flame within the eddies. Increasing fuel velocity effects flame detachment and subsequent blowoff as the streamwise velocity exceeds the laminar flame speed. Results are in qualitative agreement with experimental observations in the literature. Dissert. Abstr.

N95-31356# Royal Inst. of Tech., Stockholm (Sweden). Center for Computational Mathematics and Mechanics.
ON CONVECTIVE EFFECTS IN SEDIMENTATION OF CONCENTRATED SUSPENSIONS WITH HIGH EFFECTIVE GRAVITY
Jacob Ystroem 1 Dec. 1993 21 p Prepared in cooperation with Stockholm Univ., Sweden
(TRITA-NA-9316) Avail: CASI HC A03/MF A01

Momentum balance for the continuum formulation of sedimentation is considered. A linear combination of the two momentum equations is formally treated as a system of ordinary differential equations. This results in a slightly different form of Darcy's law together with a momentum equation containing convective terms. These equations together with conservation of mass and constitutive equations for colloidally stable suspensions of hard spheres are solved numerically. It is found that the discrepancy due to convective terms is independent of the Peclet number and that the effect is very small. Author

N95-31368# Army Tank-Automotive Command, Warren, MI.
FUEL-TYPE CLASSIFICATION AND PARAMETERS PREDICTION BY GAS LIQUID CHROMATOGRAPHY ANALYSIS Final Report
Donald K. Minus Mar. 1995 84 p
(AD-A293442; TARDEC-TR-13641) Avail: CASI HC A05/MF A01

There is a research effort that envisions having a vehicle mounted petroleum analysis system that could travel close to the frontlines and would provide rapid test results. This system would quicken results feedback time and increase the scope of analyses by using new technologies that could predict several fuel properties and parameters. One approach under consideration for use in this system is Gas Liquid-Phase Chromatography (GLC). To simplify the GLC chromatograph of fuel samples, the data was collected as a series of time-segmented regions. These regions were defined to simulate separations by normal alkanes carbon chain length. The GLC data was analyzed with PIROUETTE correlation software (INFOMETRIX, Seattle, WA) to assign the fuel's type and to predict a selected number of fuel's physical properties. To conduct this study, sixty-seven (67) fuel samples were used of which fifteen were JET A-1/JET As, twelve were JP-4s, nine were JP-8s seven were MOGAS, and three were DF-2s. Preliminary results have included a 100% correct classification as to fuel type and predictions of the 10%, 50%, and 90% distillation. and final boiling point temperatures; and the densities of the samples with relatively low errors of prediction. DTIC

N95-31393# Sandia National Labs., Albuquerque, NM.
X-RAY DIFFRACTION STUDY OF CLUSTERS IN a-tC FILMS
L. J. Martinez-Miranda (Kent State Univ., OH.), M. P. Siegal, T. A. Friedmann, J. P. Sullivan, T. W. Mercer (Drexel Univ., Philadelphia, PA.), N. J. DiNardo (Drexel Univ., Philadelphia, PA.), and F. Fang (Pennsylvania Univ., Philadelphia, PA.) 1995 8 p Presented at the 1994 Fall Meeting of the Materials Research Society (MRS), Boston, MA, 28 Nov. - 2 Dec. 1994
(Contract DE-AC04-94AL-85000)
(DE95-010860; SAND-94-2987C; CONF-941144-144) Avail: CASI HC A02/MF A01

The authors performed an x-ray diffraction study of tetrahedral-coordinated-amorpous carbon (a-tC) films prepared by pulsed laser deposition (PLD). Samples properties were analyzed as a function of laser energy and thickness. For all thicknesses and laser energies, films were made up of clusters with a basic unit size of 7 - 11 nm. Thicker films, as well as films prepared at higher laser densities exhibit larger clusters, in the tens of nanometers. The clusters are not readily observable by AFM, which may indicate the presence of a flat (graphitized) top film surface. DOE

N95-31437# North Carolina Univ., Chapel Hill, NC. Dept. of Chemistry.
CONSEQUENCES OF KINETIC DISPERSION ON THE ELECTROCHEMISTRY OF AN ADSORBED REDOX-ACTIVE MONOLAYER Interim Technical Report
Gary K. Rowe, Michael T. Carter, John N. Richardson, and Royce W. Murray 1 Apr. 1995 49 p
(Contract N00014-90-J-1230)
(AD-A292794; TR-66) Avail: CASI HC A03/MF A01

Mixed monolayers of (ferrocenylcarboxy)-alkanethiol/n-alkanethiol have been investigated electrochemically in 2:1 (v:v) chloroethane:butyronitrile solvent in the temperature range of 120K to 150K. Cyclic voltammetry of these monolayers shows large oxidation-reduction peak potential separations indicative of electron transfer rate control. The voltammetric waveshapes are also broadened; this and curved log I vs. time transients observed in potential step experiments are interpreted as a dispersion in the reaction rates of the ferrocene sites. This paper considers origins and three models for such kinetic dispersion. DTIC

N95-31439# Stanford Univ., CA. Edward L Ginzton Lab. of Physics.
ADVANCED THIN-FILM DEPOSITION AND PHYSICAL PROPERTIES OF HIGH-TEMPERATURE AND OTHER NOVEL SUPERCONDUCTING MATERIALS Final Report, 15 Oct. 1991 - 30 Sep. 1994
M. R. Beasley, T. H. Geballe, and A. Kapitulnik 28 Feb. 1995 17 p
(Contract F49620-92-C-0004)
(AD-A292798; AFOSR-95-0173TR) Avail: CASI HC A03/MF A01

The aims of this program were to synthesize increasingly high-quality thin film and single crystals of the high Tc and other novel superconductors. We also proposed to study their physical properties, understand the nature of their superconductivity, and search for new superconducting devices and device concepts, with a primary objective of developing a better understanding of the limits of the occurrence of superconductors with high transition temperatures. DTIC

N95-31440# Illinois Univ., Urbana, IL. Dept. of Chemistry.
THE STRUCTURE AND REACTIVITY OF BORON AND CARBON SURFACES Final Technical Report, 15 Mar. 1992 - 14 Sep. 1994
Michael Trenary 22 Feb. 1995 6 p
(Contract F49620-92-J-0179)
(AD-A292804; AFOSR-95-0168TR) Avail: CASI HC A02/MF A01

Research funded by this grant focused on three areas: First, we have explored the surface chemistry associated with reactions of O2, D2O, B2O2 and B2O3 with boron thin films grown on Ta(110) through the thermal decomposition of diborane. These reactions were studied mainly with the techniques of X-ray photoelectron spectroscopy and mass analyzed thermal desorption. We find that both O2 and D2O form a B2O3-like oxide on the surface but that the oxide desorbs mainly as B2O2. Second, we have studied the reaction of B2O3 and O2 with graphitic carbon deposited on the Pt(111) surface. Although B2O3 is known to inhibit the oxidation of carbon/carbon composites, we found that B2O3 deposited on a carbon layer on Pt(111) completely removes the surface carbon by oxidizing it at 1000 K to CO(g). Although we also observe the desorption of B2O2(g) from the surface, we determined that the B2O3 is reduced in the process to elemental boron. Third, we finished some experiments during the first few months of the grant on the oxidation of the LaB6(100) surface. DTIC

N95-31473# Naval Research Lab., Washington, DC.
AN ANALYSIS OF GAS PHASE ETHANOL/WATER CHEMISTRY FOR DIAMOND CVD
Robert S. Sinkovits, Richard C. DeVore, Vasgen A. Shamamian, and Charles K. Westbrook 29 Mar. 1995 46 p
(AD-A293009; NRL/MR/6410-95-7662) Avail: CASI HC A03/MF A01

Chemical kinetics calculations have been carried out on ethanol (EtOH)water mixtures at a range of temperatures, pressures and EtOH/H2O ratios. The results show that the mole fractions of many chemical species depend very sensitively on the initial EtOH/H20 ratio and diverge sharply after an induction time which depends both on pressure and temperature. We explain this divergence primarily in terms of the stability of carbon monoxide and show that the rate-limiting steps that dictate the induction time are the molecular hydrogen dissociation reactions. Our calculations also predict the dependence of the concentrations of potential growth (C, CH3, C2H2) and etching (O, OH, O2) species for diamond chemical vapor deposition (CVD) on operating conditions. DTIC

N95-31580# Army Research Lab., Aberdeen Proving Ground, MD.
EVALUATION OF HALON ALTERNATIVES IN INERTING EXPERIMENTS Final Report, Oct. 1992 - Dec. 1994
Anthony E. Finnerty and Dawnn M. Saunders Apr. 1995 33 p
(AD-A293774; ARL-TR-733) Avail: CASI HC A03/MF A01

Inerting experiments were conducted in a 20-liter stainless steel chamber. Eight potential Halon 1301 replacement agents were used to inert butane-air mixtures. The agents were ranked on the amount required to completely inert the system and on their tendencies to form hydrogen fluoride. A specific ion electrode was used to determine the amount of hydrogen fluoride formed when less than the amount of agent required for complete inertion was used in an experiment. The two iodine-containing agents, perfluoroethyl iodide and perfluoromethyl iodide, were superior to the other potential replacement agents in that less concentration was required for inertion and less hydrogen fluoride formed than with the others. The ability of perfluoroethyl iodide and perfluoromethyl iodide, which are chemical fire-extinguishing agents, to act as inerting agents is attributed to the ease of breaking of the relatively weak (ca. 57 kcal/mole) carbon to iodine bond at low temperatures. This enabled the iodine-containing agents to act as energy-absorbing agents, which is important in preventing ignition of fuel-air-agent mixtures. DTIC

N95-31593# Lawrence Livermore National Lab., Livermore, CA.
RATIONALE AND SUMMARY OF METHODS FOR DETERMINING ULTRASONIC PROPERTIES OF MATERIALS AT LAWRENCE LIVERMORE NATIONAL LABORATORY
A. E. Brown Feb. 1995 36 p
(Contract W-7405-eng-48)
(DE95-009475; UCRL-ID-119958) Avail: CASI HC A03/MF A01

This report is a summary of the methods used to determine ultrasonic velocities through the many materials tested at the Acoustic Properties of Materials Laboratory. Ultrasonic velocity techniques enable the determination of material properties, including elastic moduli, without harming the materials being tested, an advantage some over mechanical methods. Ultrasonic modulus determination has other advantages as well: (1) relative ease and low cost of material preparation; and (2) comparative analysis to physical testing as a function of material loading rate dependence. In addition, ultrasonic measurement provides clues to determine grain size and orientation, and provides a relative indication of material anisotropy with respect to the material geometry. The authors usually perform ultrasonic measurements on materials in ambient atmospheric conditions, and in a relatively free-free condition. However, the authors can perform them in other environments, as required. This paper describes some of the techniques used in this laboratory and shows how ultrasonic velocities are used to establish elastic constants. It also includes a sample test report for a homogeneous isotropic solid. DOE

N95-31595# Florida Univ., Gainesville, FL. Quantum Theory Project.
A THEORETICAL TREATMENT OF THE ABSORPTION AND EMISSION PROPERTIES OF Cu(2) PORPHYRIN Interim Report
Krassimir K. Stavrev and Michael C. Zerner 18 Apr. 1995 21 p
Submitted for publication in the Chem. Phys. Letters
(Contract N00014-90-J-1608)
(AD-A293669; TR-30) Avail: CASI HC A03/MF A01

We examine the electronic spectrum of Cu(2) Porphyrin using the Intermediate Neglect of Differential Overlap (INDO) model that has been specifically parametrized for spectroscopy at the configuration interaction level of theory. The isolated molecule is predicted to have a trip-doublet absorption, corresponding to porphyrin triplets, at about 9,000/cm and 13,900/cm. The Q band is calculated at 15,900/cm, in good accord with experimental values. We predict a normal emission in this case, as is

observed. We find that chelating in the fifth position with a strong ligand such as pyridine leads to a state in energy below the Q band that is mostly d(z squared) greater than d(x squared-y squared) but with appreciable a2u(Pi) greater than d(x squared-y squared) character. We postulate that it is the presence of this state that quenches the emission when Cu(2) porphyrins are complexed with strong fifth or fifth and sixth position ligands. DTIC

N95-31596# Florida Univ., Gainesville, FL. Quantum Theory Project.
CALCULATED STRUCTURES AND ELECTRONIC ABSORPTION SPECTROSCOPY FOR MAGNESIUM PHTHALOCYANINE AND ITS ANION RADICAL Interim Report
Marshall G. Cory, Horoaki Hirose, and Michael C. Zerner 19 Apr. 1995 39 p Submitted for publication in the Inorg. Chemistry
(Contract N00014-90-J-1608)
(AD-A293672; TR-33) Avail: CASI HC A03/MF A01

Structures are calculated for Magnesium Phthalocyanine (MgPc) and its radical anion doublet (MgPc-), using both ab-initio (6-13G**) and semiemperical (INDO/1) self-consistent field approaches. The anion is first order Jahn-Teller distorted, and the various distortions that are possible are examined. The electronic absorption spectra of both molecular species, and the effect varying the degree of distortion has on the computed anion spectrum are diacussed. These results suggest that the four-orbital model often applied to porphyrin systems in interpreting the low energy spectrum is incomplete for the anion case. We further conclude that the Jahn-Teller distortions calculated by either ab-initio or semiemperical models may be too great. DTIC

N95-31633# Oak Ridge National Lab., TN.
DIFFERENCES IN CREEP PERFORMANCE OF A HIPED SILICON NITRIDE IN AMBIENT AIR AND INERT ENVIRONMENTS
A. A. Wereszczak, T. P. Kirkland, and M. K. Ferber 1995 9 p Presented at the 19th Annual Conference on Advanced Ceramics, Materials and Structures, Cocoa Beach, FL, 9-12 Jan. 1995
(Contract DE-AC05-84OR-21400)
(DE95-009172; CONF-950129-3) Avail: CASI HC A02/MF A01

High temperature tensile creep studies of a commercially available hot isostatically pressed (HIPed) silicon nitride were conducted in ambient air and argon environments. The creep performance of this HIPed silicon nitride was found to be different in these environments. The material crept faster (and had a consequentially shorter lifetime) in argon than in ambient air at 1370 C at tensile stresses between 110-140 MPa. The stress dependence of the minimum creep rate was found to be approx. 6 in argon and approx. 3.5 in air, while the minimum creep rates were almost an order of magnitude faster in argon than in air at equivalent tensile stresses. Differences in the creep performance are explained with reference to the presence or absence of oxygen in the two environments. DOE

N95-31660*# Jet Propulsion Lab., California Inst. of Tech., Pasadena, CA.
THE NASA/JPL EVALUATION OF OXYGEN INTERACTIONS WITH MATERIALS-3 (EOIM-3) Final Report
David E. Brinza, Shirley Y. Chung, Timothy K. Minton, and Ranty H. Liang Dec. 1994 107 p Original contains color illustrations
(Contract NAS7-1260; RTOP 233-03-02-08-28)
(NASA-CR-198865; JPL-Publ-94-31; NAS 1.26:198865) Avail: CASI HC A06/MF A02; 2 functional color pages

The deleterious effects of hyperthermal atomic oxygen (AO) found in low-earth-orbit (LEO) environments on critical flight materials has been known since early shuttle flights. This corrosive effect is of considerable concern because it compromises the performance and longevity of spacecraft/satellite materials deployed for extended periods in LEO. The NASA Evaluation of Oxygen Interactions with Materials-3 (EOIM-3) experiment served as a testbed for a variety of candidate flight materials for space assets. A total of 57 JPL test specimens were present in six subexperiments aboard EOIM-3. In addition to a number of passive exposure materials for flight and advanced technology programs, several subexperiments were included to provide data for understanding the details of atomic oxygen interactions with materials. Data and interpretations are presented for the heated tray, heated strips, solar ultraviolet exposure, and scatterometer subexperiments, along with a detailed description of the exposure conditions experienced by materials in the various experiments. Mass spectra of products emerging from identical samples of a (sup 13)C-enriched polyimide polymer (chemically equivalent to Kapton) under atomic oxygen bombardment in space and in the laboratory were collected. Reaction products unambiguously detected in space were (sup 13)CO, NO, (sup 12)CO2, and (sup 13)CO2. These reaction products and two others, H2O and (sup 12)CO, were detected in the laboratory, along with inelastically scattered atomic and molecular oxygen. Qualitative agreement was seen in the mass spectra taken in space and in the laboratory; the agreement may be improved by reducing the fraction of O2 in the laboratory molecular beam. Author

N95-31670# Army Research Lab., Aberdeen Proving Ground, MD.
FOURIER TRANSFORM (FT) RAMAN SPECTROSCOPY OF NITROGEN AT HIGH PRESSURE Final Report, Sep. - Dec. 1994
K. L. McNesby and J. B. Morris Mar. 1995 28 p
(AD-A293051; ARL-TR-718) Avail: CASI HC A03/MF A01

Rovibrational and rotational Raman spectra of nitrogen gas at 300 K over the pressure range 3 MPa to 24 MPa (500 to 3,500 psi) have been measured using a Fourier transform (FT) spectrometer employing 1064 nm laser radiation as the scattering source. It is shown that the pressure-induced narrowing and peak shift of the Raman spectrum of N2 observed in these experiments agrees within experimental error with data obtained by other investigators using different techniques. DTIC

N95-31691# Florida Univ., Gainesville, FL. Quantum Theory Project.
ABSORPTION AND IONIZATION SPECTRA OF MODEL RUBREDOXINS
Krassimir K. Stavrev and Michael C. Zerner 18 Apr. 1995 17 p Submitted for publication in the Intern. J. Quantum Chem.
(Contract N00014-90-J-1608)
(AD-A293668; TR-31) Avail: CASI HC A03/MF A01

We examine here spectroscopic properties of oxidized rubredoxin (Rdx) within the intermediate neglect of differential overlap method parameterized for spectroscopy. The Rdx structures are modeled using different length -SR residues bound to the Fe atom and the resulting effect on the absorption spectrum is examined. The corresponding ionization potentials are also calculated and their dependence on the molecular charge is studied. This study suggests that models used to reproduce the redox properties of these important electron-transfer compounds must be carefully chosen. DTIC

N95-31709 Pennsylvania State Univ., University Park, PA.
THE STUDY OF FLAME-VORTEX INTERACTIONS USING A PARTICLE IMAGE VELOCIMETER Ph.D. Thesis
David A. Nye 1993 201 p
Avail: Univ. Microfilms Order No. DA9414347

An experiment has been devised to examine the evolution of flame stretch, flame curvature, and flow strain rate during the interaction of a premixed (lean, methane-air) laminar V-flame and a Karman Vortex Street. The experimental technique relies heavily upon the use of a particle image velocimeter both to make strain rate measurements and also to quantify vortex structure. Thirty flame realizations are studied at a single operating condition. A sequence of events occurring during the interaction was constructed from flow visualization results and flame stretch measurements. A large region of positive flame curvature (convex to the reactants) bordered by cusps (small areas of large negative curvature) is formed by a pair of counter-rotating vortices that produces a local velocity deficit into which the flame propagates. The action of the flame tends to spread the pair apart while distorting and weakening individual vortices, thus signaling the end of the interaction. Velocity, vorticity, flame stretch rate, flame curvature, and flame strain rate plots are provided for several realizations. In addition, probability density functions (pdf) and scatter plots for these quantities are provided for the entire set of thirty flame realizations. Scatter plots indicate that the flame curvature and flow strain rate are found to be statistically independent, and that the average flame stretch rate for an individual flame is determined directly from the average flame curvature. Average flow strain is found to be nearly zero in accordance with the periodic flow pattern surrounding the vortex street. Results further indicate that flame properties such as flame speed and temperature will not be significantly affected by flame stretch. This condition provides an ideal baseline comparison for additional PIV system measurements and is an excellent test case for numerical code development. Comparison between these results and the action of large scales in premixed turbulent combustion is

also discussed. The action flow scales much larger than the flame thickness in a turbulent flame is inferred from the interaction of laminar vortices with a laminar flame front. Dissert. Abstr.

N95-31717 Pennsylvania State Univ., University Park, PA.
COMBUSTION OF LOX WITH H2(SUB g) UNDER SUBCRITICAL AND SUPERCRITICAL CONDITIONS Ph.D. Thesis
An-Shik Yang 1993 145 p
Avail: Univ. Microfilms Order No. DA9414403

The objective of this investigation is to study the evaporation and combustion of LOX under supercritical and subcritical conditions both experimentally and theoretically. In the evaporation studies, evaporation rate and surface temperature were measured when LOX vaporizing in helium environments at pressures ranging from 5 to 68 atm. A Varian 3700 gas chromatograph was employed to measure the oxygen concentration above the LOX surface. For the combustion tests, high magnification video photography was used to record direct images of the flame shape of a LOX/H2/He laminar diffusion flame. The gas composition in the post-flame region was also measured with the gas sampling and chromatography analysis. These data can be used to validate the theoretical model. A comprehensive theoretical model with the consideration of the solubility of ambient gases as well as variable thermophysical properties was formulated and solved numerically to study the gasification and burning of LOX at elevated pressures. The calculated flame shape agreed reasonably well with the edge of the observed luminous flame surface. The effect of gravity on the flame structure of laminar diffusion flames was found to be significant. In addition, the predicted results using the flame sheet model were compared with those based upon full equilibrium calculations (which considered the formation of intermediate species) at supercritical pressures. Except at the flame front where temperature exceeded 2,800 K, the flame-sheet and equilibrium solutions in terms of temperature distributions were in very close agreement. The temperature deviation in the neighborhood of the flame front is caused by the effect of high-temperature dissociation. Dissert. Abstr.

N95-31732 Pennsylvania State Univ., University Park, PA.
NON-INTRUSIVE COMBUSTION DIAGNOSTICS OF PREMIXED HYDROCARBON FLAMES USING FT-IR SPECTROMETRY Ph.D. Thesis
I.-Te Huang 1993 122 p
Avail: Univ. Microfilms Order No. DA9414304

Many of the current limitations in the knowledge of combustion of hydrocarbon fuels can be attributed to the inability to experimentally probe the flame zone of such fuels. As a result, there has been a considerable effort devoted to the development of both intrusive and nonintrusive diagnostic techniques. Intrusive techniques have limitations which include, among others, the following: (1) disturbances are introduced in the medium; (2) the probe is consumed by the hostile environment; and (3) the temporal response and spatial resolution are typically insufficient to follow the event. In this work, the use of FT-IR spectrometry for probing nonintrusively the premixed flame zone of hydrocarbon flames is described. The application of this technique yields spatial profiles of temperature, species concentrations, and relative soot concentration. Fuel-rich methane/oxygen/nitrogen flames are used to develop the combustion diagnostic technique. A Fortran package, PREMIX, which is capable of predicting temperature and species concentration profiles using user-supplied chemical kinetic information, is utilized for comparison purposes and to obtain information of major chemical reactions. Studies of liquid hydrocarbon fuels, such as benzene and toluene, are also proposed. Dissert. Abstr.

N95-31824# Sandia National Labs., Livermore, CA.
EFFECTS OF GAS-PHASE THERMAL EXPANSION ON THE STABILITY OF DEFLAGRATION THROUGH A POROUS ENERGETIC MATERIAL
S. B. Margolis and F. A. Williams (California Univ., San Diego, La Jolla, CA.) 1995 42 p Presented at the 30th AIAA/SAE/ASME Joint Propulsion Conference and Exhibit, San Diego, CA, 10-12 Jul. 1995
(Contract DE-AC04-94AL-85000)
(DE95-004382; SAND-95-8456C; CONF-950720-1) Avail: CASI HC A03/MF A01

The propagation of a deflagration wave through porous energetic materials, as in the case of strictly condensed-phase combustion, is subject to intrinsic diffusional/thermal instabilities that can lead to various oscillatory modes of burning. Under the assumption that the gas phase may be regarded as ideal but quasi-steady, asymptotic analyses are developed for the nonsteady, nonplanar deflagration of porous energetic solids, such as degraded nitramine propellants, that experience significant gas flow in the solid preheat region and are characterized by the presence of exothermic reactions in a bubbling melt layer at their surfaces. Relative motion between the gas and condensed phases is taken into account in both regions, and the derived asymptotic model is analyzed to obtain an explicit solution for steady, planar deflagration and a dispersion relation describing its linear stability. The present analysis parallels a similar study by the authors that allowed for a fully nonsteady gas phase, but neglected the effects of gas-phase thermal expansion. Nonetheless, qualitatively similar results are obtained, predicting a pulsating neutral stability boundary in the nondimensional activation energy - disturbance wavenumber plane beyond which nonsteady, nonplanar solutions are anticipated. Focusing on the realistic limit of small ratios of gas-phase to condensed-phase density and thermal conductivity, it is demonstrated that the effect of a nonzero porosity alpha(sub s) of the unburned solid material is generally destabilizing, by an amount proportional to alpha(sub s) (1 - alpha(sub s))(exp -1), relative to the nonporous case. The effect of gas-phase thermal expansion is also shown to be destabilizing, further suggesting that degraded propellants, which exhibit greater porosity than the pristine material, may be especially prone to nonsteady deflagration. DOE

N95-31830# Florida Univ., Gainesville, FL.
ON THE JAHN-TELLER EFFECT OF Mn(2+) IN ZINC-BLENDE ZnS CRYSTAL Interim Report
Krassimir K. Stavrev and Michael C. Zerner 18 Apr. 1995 26 p
(Contract N00014-90-J-1608)
(AD-A293711; TR-29) Avail: CASI HC A03/MF A01

The excited states of Mn(2+) in zinc-blende ZnS crystal have been studied by the Intermediate Neglect of Differential Overlap model parameterized for spectroscopy (INDO/S) within the Restricted Open-Shell Hartree-Fock (ROHF)-Configuration Interaction (CI) approximation. The effect of the Jahn-Teller (JT) active e-mode on the first excited state (a(4)T1) has been examined with respect to energy barriers and geometric distortions. The dynamical JT effect has been studied and the excited state absorption (ESA) profiles for different e-mode conformations have been calculated. Good reproduction of the experimental ESA spectrum has been obtained for nuclear arrangements corresponding to small S-Mn-S angle distortions. The off-center Tau 2-mode vibrations were found to promote the JT coupling by reducing the barriers between the stable structures. DTIC

N95-31840# Oak Ridge Y-12 Plant, TN.
DETERMINATION OF HALOGENS IN A PETROLEUM PRODUCT BY ION CHROMATOGRAPHY
H. L. Tucker 15 Jul. 1994 7 p Presented at the 36th Rocky Mountain Conference on Analytical Chemistry, Denver, CO, 31 Jul. - 5 Aug. 1995
(Contract DE-AC05-84OS-21400)
(DE95-002056; Y/DK-1043; CONF-950737-1) Avail: CASI HC A02/MF A01

A rapid, high-performance ion chromatography (HPIC) method with isocratic separation and the anion self-regenerating suppressor (in the chemical suppression mode, specifically for the determination of fluoride, chloride, bromide, and iodide in a petroleum product) is discussed. This is a proposed new method for a production laboratory within the Analytical Services Organization at the Oak Ridge Y-12 Plant. DOE

N95-32061# Argonne National Lab., IL. Environmental Research and Chemical Technology Div.
FASTER, CHEAPER RADIOANALYTICAL METHODS
M. D. Erickson, J. H. Aldstadt, J. S. Alvarado, J. S. Crain, K. A. Orlandini, and L. L. Smith 1995 8 p Presented at the Waste Management 1995 Conference, Tucson, AZ, 26 Feb. - 2 Mar. 1995
(Contract W-31-109-eng-38)
(DE95-009913; ANL/ER/CP-84530; CONF-950216-115) Avail: CASI HC A02/MF A01

This project focuses on improvement of radioanalytical methods, with an emphasis on faster and cheaper routine methods. The authors have developed improved methods for the separation of environmental levels of technetium-99, radium, and actinides from soil and water; separation of actinides from soil and water matrix interferences; and isolation of strontium.

Among the novel techniques for separation that are being used are element and class-specific resins and membranes. The authors have also developed methods for the simultaneous detection of multiple isotopes by using inductively coupled plasma-mass spectrometry (ICP-MS). Because of its mass-selective mode of detection, ICP-MS requires less rigorous chemical separations than does radiochemical analysis. In addition, improvements in the limits of detection, the volume of the sample and the time of analysis were obtained by using other techniques of sample introduction, such as ultrasonic nebulization, automated batch separation and electrothermal vaporization. Investigation of integration and automation of the separation methods with the ICP-MS method using flow injection analysis is underway. A solid scintillation device has been developed and tested for measurement and identification of low-energy beta-emitting radionuclides; application of this technique will eliminate the generation of mixed-waste counting cocktails. The final product of all activities will be methods that are available and are acceptable for use in regulatory situations. Concerted efforts are being made to facilitate implementation of the methods at DOE sites to realize the improvements offered. DOE

N95-32086# Oak Ridge National Lab., TN. Chemical and Analytical Sciences Div.

ULTRASENSITIVE FLUORESCENCE DETECTION AND PHOTOPHYSICS IN MICRODROPLETS

Michael D. Barnes, William B. Whitten, and J. Michael Ramsey 1995 10 p Presented at the SPIE 1995: SPIE Conference on Optics, Electro-óptics, and Laser Application in Science, Engineering and Medicine, San Jose, CA, 5-10 Feb. 1995

(Contract DE-AC05-84OR-21400)

(DE95-010283; CONF-950226-36) Avail: CASI HC A02/MF A01

Fluorescence detection of single molecules in room temperature liquids is usually plagued by many difficulties such as finite saturated absorption rate, finite laser-analyte interaction time, and analyte diffusion. Our approach to single molecule detection in liquids has been to use microdroplets as the sample medium which has many advantages over conventional 'bulk' techniques such as extended laser-analyte interaction time, a probe volume defined by the droplet, and modified radiative properties of molecules due to interactions with droplet resonances. We have demonstrated detection of single rhodamine molecules with signal-to-noise ratios on the order of 30 using levitated microdroplets as the sample medium. The focus of current work is on single molecule detection in falling droplet streams with analysis rates on the order of 5-10 kHz. DOE

N95-32091# Westinghouse Hanford Co., Richland, WA.

LLW SOLIDIFICATION IN CEMENT: EFFECT OF DILUTION

A. A. Kruger, A. Katz, A. R. Brough, T. Bakharev, R. J. Kirkpatrick, L. J. Struble, and J. F. Young Feb. 1995 8 p Presented at the 1994 Fall Meeting of the Materials Research Society (MRS), Boston, MA, 28 Nov. - 2 Dec. 1994

(Contract DE-AC06-87RL-10930)

(DE95-010108; WHC-SA-2675; CONF-941144-120) Avail: CASI HC A02/MF A01

A simulated Low Level nuclear Waste (LLW) solution was tested for long term solidification in a cement-based matrix. The waste is characterized by high pH and high concentrations of sodium, aluminum, nitrate, nitrite, phosphate and carbonate. The effect of diluting the waste with additional water was studied. The cementitious matrix was composed of cement, fly-ash and clay (21%, 68% and 11% respectively) with high solution to solid ratio (1 liter /1 kg.). Mixes were prepared at 45 C and cured at 90 C for 28 days. Maximum 28 day compressive strengths and early age heat evolution were achieved by diluting the LLW solution to approximately 67% of its original concentration. More dilution led to a lower heat evolution and compressive strength. No dilution was found to give lower compressive strength, and a heat evolution that was delayed, and lower in intensity. XRD spectra showed formation of zeolites and tobermorite at the higher concentrations (67, 85, and 100% of the concentration of the undiluted simulated LLW), with a change from Na-PI zeolite for 67% of the undiluted concentration to a sodalite at 100%. SEM observations showed a porous system for the low and high dilution rates but a less porous one for an intermediate level of dilution. DOE

N95-32258# Army Research Lab., Aberdeen Proving Ground, MD.

THE THEORETICAL CALCULATION OF VIBRATIONAL CIRCULAR DICHROISM SPECTRA Final Report, 1 Jan. 1993 - 1 Sep. 1994

P. J. Stevens, F. J. Devlin, C. S. Ashvar, C. F. Chabalowski, and M. J. Frisch Apr. 1995 48 p Prepared in cooperation with University of Southern California, Los Angeles, and Lorentzian, Inc., North Haven, CT

(DA Proj. 1L1-61102-AH-43)

(AD-A293614; ARL-TR-732) Avail: CASI HC A03/MF A01

We report calculations of the mid-IR unpolarized absorption and circular dichroism spectra of 4-methyl-2-oxetanone, 6,8-dioxabicyclo (3.2.1) octane and 1,7,7-trimethylbicyclo (2.2.1) heptan-2-one (camphor) based on harmonic force fields calculated using Density Functional Theory (DFT). A hybrid density functional -- Becke3LYP -- is used. The basis set is 6-31G. The results are in impressive agreement with experimental spectral calculations using the LSDA and BLYP functionals are much less successful. Our results using Becke3LYP/DFT are compared to the predictions of SCF and MP2 calculations. At the present time, the Becke3LYP/DFT methodology is clearly to be preferred in predicting mid-IR vibrational spectra. DTIC

N95-32318# Bettis Atomic Power Lab., West Mifflin, PA.

LABORATORY ROBOTICS: AN AUTOMATED TOOL FOR PREPARING ION CHROMATOGRAPHY CALIBRATION STANDARDS

James L. Chadwick 1995 11 p Presented at the Pittsburgh Conference and Exhibition on Analytical Chemistry and Applied Spectroscopy: Stimulating the Minds of Today's and Tomorrow's Scientists, New Orleans, LA, 5-10 Mar. 1995

(Contract DE-AC11-93PN-38195)

(DE95-009441; WAPD-T-3041; CONF-950389-1) Avail: CASI HC A03/MF A01

This paper describes the use of a laboratory robot as an automated tool for preparing multi-level calibration standards for On-Line Ion Chromatography (IC) Systems. The robot is designed for preparation of up to six levels of standards, with each level containing up to eleven ionic species in aqueous solution. The robot is required to add the standards' constituents as both a liquid and solid additions and to keep a record of exactly what goes into making up every standard. Utilizing a laboratory robot to prepare calibration standards provides significant benefits to the testing environment. These benefits include: accurate and precise calibration standards in individually capped containers with preparation traceability; automated and unattended multi-specie preparation for both anion and cation analytical channels; the ability to free up a test operator from a repetitive routine and re-apply those efforts to test operations; The robot uses a single channel IC to analyze each prepared standard for specie content and concentration. Those results are later used as a measure of quality control. System requirements and configurations, robotic operations, manpower requirements, analytical verification, accuracy and precision of prepared solutions, and robotic downtime are discussed in detail. DOE

N95-32360# Argonne National Lab., IL. Analytical Chemistry Lab.

WASTE MINIMIZATION VIA PREPARATIVE SCALE HIGH PERFORMANCE GEL PERMEATION CHROMATOGRAPHY

Amrit S. Boparai, Kathleen J. Parish, Stephen D. Kent, Yifen Tsai, and David A. Joe 1995 16 p Presented at the Pittsburgh Conference and Exhibition on Analytical Chemistry and Applied Spectroscopy: Stimulating the Minds of Today's and Tomorrow's Scientists, New Orleans, LA, 5-10 Mar. 1995

(Contract W-31-109-eng-38)

(DE95-011797; ANL/CMT-ACL/VU-83809; CONF-950389-2-Vugraphs)

Avail: CASI HC A03/MF A01

The procedures developed here allow removal of radioactivity, as judged by removal of (sup 152)Europium (III) from methylene chloride solutions of CLP analytes without significantly reducing recovery of organic compounds. This allows analysis of nonradioactive extracts on instrumentation maintained in a regular nonradioactive laboratory, resulting in a significant savings in cost. DOE

N95-32372 Selskapet for Industriell og Teknisk Forskning, Trondheim (Norway). Div. of Applied Chemistry.

SYNTHESIS OF SEPARATION SYSTEMS: METHODS AND APPLICATIONS IN DOWNSTREAM GAS PROCESSES

J. Sogge 1994 111 p

(PB95-208518; STF21-A94014) Avail: Issuing Activity (National Technical Information Service (NTIS))

In this work, the different separation processes applied in the downstream gas processing industry for separation of gaseous products have been described based upon information found in the literature. Furthermore, an overview of characteristics, simple design considerations/methods and cost data of the different gas separation technologies (e.g. distillation) has been made. The main purpose of this work is to increase the level of competence within synthesis of gas separation systems. The increased competence can be utilized to enhance the quality of the technical and economic evaluations of petrochemical processes, where the separation systems greatly influences the economics of these processes. NTIS

N95-30990 Brigham Young Univ., Provo, UT.
BURN TIME MEASUREMENTS OF SINGLE ALUMINUM PARTICLES IN STEAM AND CARBON DIOXIDE MIXTURES
Shane E. Olsen and Merrill W. Beckstead *In* JHU, The 21st JANNAF Exhaust Plume Technology Meeting, Volume 1 Oct. 1994 p 41-58 (For primary document see N95-30986 11-34)
(Grant AF-AFOSR-0152-91)
Avail: CPIA, 10630 Little Patuxent Pkwy., Suite 202, Columbia, MD 21044-3200 HC

N95-31198 Brigham Young Univ., Provo, UT.
BURN TIME MEASUREMENTS OF SINGLE ALUMINUM PARTICLES IN STEAM AND CARBON DIOXIDE MIXTURES
S. E. Olsen and M. W. Beckstead *In* Johns Hopkins Univ., The 31st JANNAF Combustion Subcommittee Meeting, Volume 1 Oct. 1994 p 41-58 (For primary document see N95-31194 11-28)
(Grant AF-AFOSR-0152-91)
Avail: CPIA, 10630 Little Patuxent Pkwy., Suite 202, Columbia, MD 21044-3200 HC

N95-31200 Naval Air Warfare Center, China Lake, CA.
ENHANCED ENERGY RELEASE AND SOOT REDUCTION IN ACTIVELY CONTROLLED FLAMES
E. J. Gutmark, T. P. Parr, D. M. Hanson-Parr, and K. C. Schadow *In* Johns Hopkins Univ., The 31st JANNAF Combustion Subcommittee Meeting, Volume 1 Oct. 1994 p 75-84 (For primary document see N95-31194 11-28)
(Contract N00014-93-WX-24268)
Avail: CPIA, 10630 Little Patuxent Pkwy., Suite 202, Columbia, MD 21044-3200 HC

N95-31202 Army Research Lab., Aberdeen Proving Ground, MD. Propulsion and Flight Div.
EXPERIMENTS IN A 120-mm RAM ACCELERATOR INCLUDING FLOW VISUALIZATION
David L. Kruczynski *In* Johns Hopkins Univ., The 31st JANNAF Combustion Subcommittee Meeting, Volume 1 Oct. 1994 p 101-114 (For primary document see N95-31194 11-28)
Avail: CPIA, 10630 Little Patuxent Pkwy., Suite 202, Columbia, MD 21044-3200 HC

N95-31203 Army Research Lab., Aberdeen Proving Ground, MD. Propulsion and Flight Div.
NUMERICAL SIMULATION OF RAM ACCELERATOR PERFORMANCE INCLUDING TRANSIENT EFFECTS DURING INITIATION OF COMBUSTION AND SENSITIVITY STUDIES
Michael J. Nusca *In* Johns Hopkins Univ., The 31st JANNAF Combustion Subcommittee Meeting, Volume 1 Oct. 1994 p 115-128 (For primary document see N95-31194 11-28)
Avail: CPIA, 10630 Little Patuxent Pkwy., Suite 202, Columbia, MD 21044-3200 HC

N95-31204 Washington Univ., Seattle, WA. Aerospace and Energetics Research Program.
INVESTIGATION OF RAM ACCELERATOR PERFORMANCE CAPABILITIES
A. J. Higgins, C. Knowlen, and A. P. Bruckner *In* Johns Hopkins Univ., The 31st JANNAF Combustion Subcommittee Meeting, Volume 1 Oct. 1994 p 165-176 (For primary document see N95-31194 11-28)
(Contracts F49620-92-J-0375; DAAL03-92-G-0110)
Avail: CPIA, 10630 Little Patuxent Pkwy., Suite 202, Columbia, MD 21044-3200 HC

N95-31205 Army Research Lab., Aberdeen Proving Ground, MD. Weapons Technology Directorate.
PULSE FORMING NETWORK IN THE ETC COMBUSTION CHARACTERIZATION OF PLASMA AUGMENTED SOLID PROPELLANTS
M. DelGuercio, H. Burden, I. Stobie, K. White, G. Katulka, and S. Driesen *In* Johns Hopkins Univ., The 31st JANNAF Combustion Subcommittee Meeting, Volume 1 Oct. 1994 p 177-188 (For primary document see N95-31194 11-28)
Avail: CPIA, 10630 Little Patuxent Pkwy., Suite 202, Columbia, MD 21044-3200 HC

N95-31208 Army Research Lab., Aberdeen Proving Ground, MD.
WORKSHOP REPORT: MEASUREMENT TECHNIQUES IN HIGHLY TRANSIENT, SPECTRALLY RICH COMBUSTION ENVIRONMENTS
Todd E. Rosenberger *In* Johns Hopkins Univ., The 31st JANNAF Combustion Subcommittee Meeting, Volume 1 Oct. 1994 p 345-354 (For primary document see N95-31194 11-28)
Avail: CPIA, 10630 Little Patuxent Pkwy., Suite 202, Columbia, MD 21044-3200 HC

N95-31209 Army Research Lab., Aberdeen Proving Ground, MD. Weapons Technology Directorate.
PRESSURE TRANSDUCER PERFORMANCE AND MEASUREMENT TRADE-OFFS IN A TRANSIENT, HIGH TEMPERATURE, COMBUSTION ENVIRONMENT
Todd E. Rosenberger, Joseph W. Colburn, Carl R. Ruth, John R. Hewitt, Melvin B. Ridgley, James F. Tuerk, and Arthur A. Koszoru *In* Johns Hopkins Univ., The 31st JANNAF Combustion Subcommittee Meeting, Volume 1 Oct. 1994 p 355-374 (For primary document see N95-31194 11-28)
Avail: CPIA, 10630 Little Patuxent Pkwy., Suite 202, Columbia, MD 21044-3200 HC

N95-31211* Spectral Sciences, Inc., Burlington, MA.
DEVELOPMENT OF A NEW INSTRUMENT FOR ROCKET ENGINE COMBUSTION DIAGNOSTICS
M. Gersh, N. Goldstein, L. Bernstein, and J. Lee *In* Johns Hopkins Univ., The 31st JANNAF Combustion Subcommittee Meeting, Volume 1 Oct. 1994 p 387-400 (For primary document see N95-31194 11-28)
(Contract NAS8-40162)
Avail: CPIA, 10630 Little Patuxent Pkwy., Suite 202, Columbia, MD 21044-3200 HC

N95-31212 Rockwell International Corp., Canoga Park, CA. Rocketdyne Div.
DESIGN AND TESTING OF AN OXIDIZER-RICH PREBURNER
S. Farhangi, K. Hunt, L. Tuegel, and D. Matthews *In* Johns Hopkins Univ., The 31st JANNAF Combustion Subcommittee Meeting, Volume 1 Oct. 1994 p 401-408 (For primary document see N95-31194 11-28)
Avail: CPIA, 10630 Little Patuxent Pkwy., Suite 202, Columbia, MD 21044-3200 HC

N95-31283 Tennessee Univ., Tullahoma, TN. Space Inst.
STABILITY PREDICTION WITH ROTATIONAL FLOW EFFECTS
G. A. Flandro *In* JHU, The 31st JANNAF Combustion Subcommittee Meeting, Volume 2 Oct. 1994 p 1-26 (For primary document see N95-31282 11-28)
Avail: CPIA, 10630 Little Patuxent Pkwy., Suite 202, Columbia, MD 21044-3200 HC

N95-31284 Illinois Univ. at Urbana-Champaign, Savoy, IL. Dept. of Mechanical and Industrial Enineering.
UNSTEADY LASER AUGMENTED COMBUSTION OF PURE OXIDIZERS AP AND RDX
T. B. Schroeder and M. Q. Brewster *In* JHU, The 31st JANNAF Combustion Subcommittee Meeting, Volume 2 Oct. 1994 p 27-34 (For primary document see N95-31282 11-28)

(Contract N00014-91-J-1977)
Avail: CPIA, 10630 Little Patuxent Pkwy., Suite 202, Columbia, MD 21044-3200 HC

N95-31285 Illinois Univ., Urbana, IL.
THEORY OF UNSTEADY COMBUSTION OF SOLIDS: INVESTIGATION OF QUASI-STEADY ASSUMPTION
M. A. Zebrowski and M. Q. Brewster *In* JHU, The 31st JANNAF Combustion Subcommittee Meeting, Volume 2 Oct. 1994 p 35-50 (For primary document see N95-31282 11-28)
(Contract N00014-91-J-1977)
Avail: CPIA, 10630 Little Patuxent Pkwy., Suite 202, Columbia, MD 21044-3200 HC

N95-31286 Illinois Univ., Urbana, IL.
OSCILLATORY COMBUSTION OF ALUMINIZED AP/HTPB PROPELLANTS
S. R. Hickman and M. Q. Brewster *In* JHU, The 31st JANNAF Combusrion Subcommittee Meeting, Volume 2 Oct. 1994 p 51-61 (For primary document see N95-31282 11-28)
(Contract N00014-91-C-1977)
Avail: CPIA, 10630 Little Patuxent Pkwy., Suite 202, Columbia, MD 21044-3200 HC

N95-31287 Brigham Young Univ., Provo, UT.
CHARACTERIZATION OF AN IMPROVED RIJKE BURNER AS PRELUDE TO MEASUREMENTS OF ALUMINUM DISTRIBUTED COMBUSTION
B. R. Newbold, M. W. Beckstead, W. Erikson, and S. Olsen *In* JHU, The 31st JANNAF Combustion Subcommittee Meeting, Volume 2 Oct. 1994 p 63-77 (For primary document see N95-31282 11-28)
(Grant AF-AFOSR-91-0152)
Avail: CPIA, 10630 Little Patuxent Pkwy., Suite 202, Columbia, MD 21044-3200 HC

N95-31288 Naval Air Warfare Center, China Lake, CA. Research and Technology Div.
ACTIVE CONTROL OF COMBUSTION INSTABILITY USING INJECTION TECHNIQUES
C. J. Bicker, Fred S. Blomshield, and Richard Stalnaker *In* JHU, The 31st JANNAF Combustion Subcommittee Meeting, Volume 2 Oct. 1994 p 79-88 (For primary document see N95-31282 11-28)
Avail: CPIA, 10630 Little Patuxent Pkwy., Suite 202, Columbia, MD 21044-3200 HC

N95-31290 United Technologies Corp., San Jose, CA.
MODEL FOR DEFINING PROPELLANT BURN RATE PERFORMANCE BOUNDARIES
W. M. Fisher and R. R. Miller *In* JHU, The 31st JANNAF Combustion Subcommittee Meeting, Volume 2 Oct. 1994 p 123-131 (For primary document see N95-31282 11-28)
Avail: CPIA, 10630 Little Patuxent Pkwy., Suite 202, Columbia, MD 21044-3200 HC

N95-31291 Johns Hopkins Univ., Columbia, MD. Chemical Propulsion Information Agency.
SURVEY OF US BURNING RATE MEASUREMENT METHODS FOR SOLID PROPULSION APPLICATIONS
Ronald S. Fry *In* JHU, The 31st JANNAF Combustion Subcommittee Meeting, Volume 2 Oct. 1994 p 123-131 (For primary document see N95-31282 11-28)
Avail: CPIA, 10630 Little Patuxent Pkwy., Suite 202, Columbia, MD 21044-3200 HC

N95-31292 Brigham Young Univ., Provo, UT.
AN IGNITION MODEL FOR MODERN DOUBLE BASE PROPELLANTS
M. W. Beckstead *In* JHU, The 31st JANNAF Combustion Subcommittee Meeting, Volume 2 Oct. 1994 p 163-180 Sponsored in cooperation with LMSC (For primary document see N95-31282 11-28)
Avail: CPIA, 10630 Little Patuxent Pkwy., Suite 202, Columbia, MD 21044-3200 HC

N95-31294 Hercules, Inc., Magna, UT.
ESTIMATING HEAT OF FORMATION OF ENERGETIC COMPOUNDS USING CORRECTED SEMIEMPIRICAL MOLECULAR ORBITAL THEORY
R. L. Raun and A. G. Butcher *In* JHU, The 31st JANNAF Combustion Subcommittee Meeting, Volume 2 Oct. 1994 p 185-196 (For primary document see N95-31282 11-28)
(Contract DAAH01-90-C-0833)
Avail: CPIA, 10630 Little Patuxent Pkwy., Suite 202, Columbia, MD 21044-3200 HC

N95-31295 Army Research Lab., Aberdeen Proving Ground, MD.
CONDENSED-PHASE PROCESSES DURING SOLID PROPELLANT COMBUSTION. 5: FURTHER OBSERVATIONS ON DEPTH PROFILING OF BURNED SURFACES OF XM39 AND M43 PROPELLANTS
M. A. Schroeder, R. A. Fifer, M. S. Miller, R. A. Pesce-Rodriguez, and J. M. Widder *In* JHU, The 31st JANNAF Combustion Subcommittee Meeting, Volume 2 Oct. 1994 p 211-220 (For primary document see N95-31282 11-28)
Avail: CPIA, 10630 Little Patuxent Pkwy., Suite 202, Columbia, MD 21044-3200 HC

N95-31296 Pennsylvania State Univ., University Park, PA.
OBSERVATION AND CHARACTERIZATION OF BURNING SURFACE REACTION ZONES OF SOLID PROPELLANTS
Ericefan T. Boyer, Yeu-Cherng Lu, Kevin Desmarais, and Kenneth K. Kuo *In* JHU, The 31st JANNAF Combustion Subcommittee Meeting, Volume 2 Oct. 1994 p 211-220 (For primary document see N95-31282 11-28)
(Contracts DAAL04-93-G-0364; DAAL03-92-G-0118)
Avail: CPIA, 10630 Little Patuxent Pkwy., Suite 202, Columbia, MD 21044-3200 HC

N95-31297 Pennsylvania State Univ., University Park, PA. Dept. of Mechanical Engineering.
MODELING OF THERMAL RESPONSE OF FILAMENT USED IN T-JUMP EXPERIMENT
Stefan T. Thynell, Polly E. Gongwer (Delaware Univ., Newark, DE.), and Thomas B. Brill (Delaware Univ., Newark, DE.) *In* JHU, The 31st JANNAF Combustion Subcommittee Meeting, Volume 2 Oct. 1994 p 221-232 (For primary document see N95-31282 11-28)
(Contract DAAL03-92-G-0118)
Avail: CPIA, 10630 Little Patuxent Pkwy., Suite 202, Columbia, MD 21044-3200 HC

N95-31298 Illinois Univ., Urbana, IL.
LASER PYROLYSIS OF HTPB
D. R. Esker and M. Q. Brewster *In* JHU, The 31st JANNAF Combustion Subcommittee Meeting, Volume 2 Oct. 1994 p 235-245 (For primary document see N95-31282 11-28)
(Contract N00014-91-J-1977; NSF CTS-91-13151)
Avail: CPIA, 10630 Little Patuxent Pkwy., Suite 202, Columbia, MD 21044-3200 HC

N95-31299 Pennsylvania State Univ., University Park, PA. Dept. of Mechanical Engineering.
ASSESSMENT OF DYNAMIC BURNING BEHAVIOR FOR JA-2 PROPELLANT RODS
T. J. Watson, K. K. Kuo, and S. T. Thynell *In* JHU, The 31st JANNAF Combustion Subcommittee Meeting, Volume 2 Oct. 1994 p 247-257 (For primary document see N95-31282 11-28)
(Contract DAAL03-92-G-0020)
Avail: CPIA, 10630 Little Patuxent Pkwy., Suite 202, Columbia, MD 21044-3200 HC

N95-31300 Princeton Scientific Enterprises, NJ.
PROGRESS IN DEVELOPING PROPELLANT IGNITION SYSTEMS BASED UPON ELECTRICALLY CONDUCTIVE POLYMERS
David W. Blair *In* JHU, The 31st JANNAF Combustion Subcommittee Meeting, Volume 2 Oct. 1994 p 259-268 (For primary document see N95-31282 11-28)
(Contract DAAL01-94-C-0073)
Avail: CPIA, 10630 Little Patuxent Pkwy., Suite 202, Columbia, MD 21044-3200 HC

N95-31302 Pennsylvania State Univ., University Park, PA. Dept. of Mechanical Engineering.
MEASUREMENT OF TEMPERATURES AND OH CONCENTRATIONS OF SOLID PROPELLANT FLAMES USING ABSORPTION SPECTROSCOPY
Yeu-Cherng Lu, Todd Freyman, and Kenneth K. Kuo *In* JHU, The 31st JANNAF Combustion Subcommittee Meeting, Volume 2 Oct. 1994 p 277-290 (For primary document see N95-31282 11-28)
(Contract DAAL03-92-G-0118)
Avail: CPIA, 10630 Little Patuxent Pkwy., Suite 202, Columbia, MD 21044-3200 HC

N95-31303 Pennsylvania State Univ., University Park, PA. Dept. of Mechanical Engineering.
SPECIES AND TEMPERATURE PROFILES OF PROPELLANT FLAMES OBTAINED FROM FTIR ABSORPTION SPECTROSCOPY
C. F. Mallery and S. T. Thynell *In* JHU, The 31st JANNAF Combustion Subcommittee Meeting, Volume 2 Oct. 1994 p 291-305 (For primary document see N95-31282 11-28)
(Contract DAAL03-92-G-0118)
Avail: CPIA, 10630 Little Patuxent Pkwy., Suite 202, Columbia, MD 21044-3200 HC

N95-31304 Pennsylvania State Univ., University Park, PA.
A STUDY OF GAS-PHASE PROCESSES DURING THE DEFLAGRATION OF RDX COMPOSITE PROPELLANTS USING A TRIPLE QUADRUPOLE MASS SPECTROMETER
Ching-Jen Tang, Young Joo Lee, and Thomas A. Litzinger *In* JHU, The 31st JANNAF Combustion Subcommittee Meeting, Volume 2 Oct. 1994 p 307-316 (For primary document see N95-31282 11-28)
(Contract DAAL03-92-G-0118)
Avail: CPIA, 10630 Little Patuxent Pkwy., Suite 202, Columbia, MD 21044-3200 HC

N95-31305 Aerodyne Research, Inc., Billerica, MA. Center for Chemical and Environmental Physics.
EMBEDDED INFRARED FIBER OPTIC ABSORPTION STUDIES OF NITRAMINE PROPELLANT STRAND BURNING
J. Wormhoudt and P Kebabian, L. *In* JHU, The 31st JANNAF Combustion Subcommittee Meeting, Volume 2 Oct. 1994 p 317-324 (For primary document see N95-31282 11-28)
(Contract DAAH04-93-C-0053)
Avail: CPIA, 10630 Little Patuxent Pkwy., Suite 202, Columbia, MD 21044-3200 HC

N95-31306 Army Research Lab., Aberdeen Proving Ground, MD.
IMPROVEMENTS IN INFRARED ABSORPTION OF SOLID PROPELLANT FLAMES
S. H. Modiano and J. A. Vanderhoff *In* JHU, The 31st JANNAF Combustion Subcommittee Meeting, Volume 2 Oct. 1994 p 325-332 (For primary document see N95-31282 11-28)
Avail: CPIA, 10630 Little Patuxent Pkwy., Suite 202, Columbia, MD 21044-3200 HC

N95-31307 Naval Air Warfare Center, China Lake, CA. Combustion Diagnostics Lab.
ADVANCED OXIDIZERS DIFFUSION FLAMES STRUCTURE
Tim Parr and Donna Hanson-Parr *In* JHU, The 31st JANNAF Combustion Subcommittee Meeting, Volume 2 Oct. 1994 p 333-344 (For primary document see N95-31282 11-28)
(Contract N00014-92-WX-24097)
Avail: CPIA, 10630 Little Patuxent Pkwy., Suite 202, Columbia, MD 21044-3200 HC

N95-31308 Army Research Lab., Aberdeen Proving Ground, MD.
AN ab Initio STUDY OF THE REACTION HNO+NO YIELDS OH+N2O: PRELIMINARY RESULTS
Steven W. Bunte, Cary F. Chabalowski, and Betsy M. Rice *In* JHU, The 31st JANNAF Combustion Subcommittee Meeting, Volume 2 Oct. 1994 p 345-354 (For primary document see N95-31282 11-28)
Avail: CPIA, 10630 Little Patuxent Pkwy., Suite 202, Columbia, MD 21044-3200 HC

N95-31309 Princeton Univ., NJ. Dept. of Mechanical and Aerospace Engineering.
THE OXIDATION OF CARBON MONOXIDE BY NITROUS OXIDE
M. T. Allen, R. A. Yetter, and F. L. Dryer *In* JHU, The 31st JANNAF Combustion Subcommittee Meeting, Volume 2 Oct. 1994 p 355-365 (For primary document see N95-31282 11-28)
(Contract N00014-90-J-4062)
Avail: CPIA, 10630 Little Patuxent Pkwy., Suite 202, Columbia, MD 21044-3200 HC

N95-31310 Princeton Univ., NJ. Dept. of Mechanical and Aerospace Engineering.
THE OXIDATION OF CARBON MONOXIDE BY NITROGEN DIOXIDE
J. L. Gatto, R. A. Yetter, and F. L. Dryer *In* JHU, The 31st JANNAF Combustion Subcommittee Meeting, Volume 2 Oct. 1994 p 367-375 (For primary document see N95-31282 11-28)
(Contract N00014-90-J-4062)
Avail: CPIA, 10630 Little Patuxent Pkwy., Suite 202, Columbia, MD 21044-3200 HC

N95-31311 Naval Research Lab., Washington, DC. Chemistry Div.
DETAILED CHEMICAL KINETIC MODELING OF PREMIXED HYDROCARBON FLAMES SUPPORTED BY NO2
Bradley A. Williams and James W. Fleming *In* JHU, The 31st JANNAF Combustion Subcommittee Meeting, Volume 2 Oct. 1994 p 377-386 (For primary document see N95-31282 11-28)
(Contract N00014-94-WX-2D001)
Avail: CPIA, 10630 Little Patuxent Pkwy., Suite 202, Columbia, MD 21044-3200 HC

N95-31312 Army Research Lab., Aberdeen Proving Ground, MD.
STUDIES OF REACTIONS PERTAINING TO AND DEVELOPMENT OF A REDUCED MECHANISM FOR THE DOUBLE BASE PROPELLANT DARK ZONE
W. R Anderson, N. Ilincic (California Univ., La Jolla, CA.), and K. Seshadri (California Univ., La Jolla, CA.) *In* JHU, The 31st JANNAF Combustion Subcommittee Meeting, Volume 2 Oct. 1994 p 387-397 (For primary document see N95-31282 11-28)
(Contract DAAL03-90-G-0084)
Avail: CPIA, 10630 Little Patuxent Pkwy., Suite 202, Columbia, MD 21044-3200 HC

N95-31313 Army Research Lab., Aberdeen Proving Ground, MD.
FLAME STRUCTURE STUDIES OF NEAT AND NH3 DOPED H2/N2O FLAMES EMPLOYING MOLECULAR BEAM MASS SPECTROMETRY AND MODELING
R. C. Sausa, G. Singh, G. W. Lemire, and W. R. Anderson *In* JHU, The 31st JANNAF Combustion Subcommittee Meeting, Volume 2 Oct. 1994 p 399-406 Sponsored in cooperation with NRC/NAS (For primary document see N95-31282 11-28)
Avail: CPIA, 10630 Little Patuxent Pkwy., Suite 202, Columbia, MD 21044-3200 HC

N95-31314 Naval Air Warfare Center, China Lake, CA. Research and Technology Div.
RDX LASER-ASSISTED FLAME STRUCTURE
Donna Hanson-Parr and Tim Parr *In* JHU, The 31st JANNAF Combustion Subcommittee Meeting, Volume 2 Oct. 1994 p 407-423 (For primary document see N95-31282 11-28)
(Contract N00014-92-WX-24097)
Avail: CPIA, 10630 Little Patuxent Pkwy., Suite 202, Columbia, MD 21044-3200 HC

N95-31315 Pennsylvania State Univ., University Park, PA.
A STUDY OF THE GAS-PHASE PROCESSES OF RDX COMBUSTION USING A TRIPLE QUADRUPOLE MASS-SPECTROMETER
Young Joo Lee, Ching-Jen Tang, and Thomas A. Litzinger *In* JHU, The 31st JANNAF Combustion Subcommittee Meeting, Volume 2 Oct. 1994 p 425-437 (For primary document see N95-31282 11-28)
(Contract N00014-93-1-0080)
Avail: CPIA, 10630 Little Patuxent Pkwy., Suite 202, Columbia, MD 21044-3200 HC

N95-31797*# National Aeronautics and Space Administration. Marshall Space Flight Center, Huntsville, AL.
SURFACE CONTAMINATION ANALYSIS TECHNOLOGY TEAM OVERVIEW
H. DeWitt Burns *In its* Aerospace Environmental Technology Conference Mar. 1995 p 509-515 (For primary document see N95-31746 11-23)
Avail: CASI HC A02/MF A06

N95-31798*# AC Engineering, Inc., Huntsville, AL.
STANDARDIZATION OF SURFACE CONTAMINATION ANALYSIS SYSTEMS
Richard E. Boothe *In* NASA. Marshall Space Flight Center, Aerospace Environmental Technology Conference Mar. 1995 p 517-524 (For primary document see N95-31746 11-23)
Avail: CASI HC A02/MF A06

N95-31807*# United Space Boosters, Inc., Huntsville, AL.
VERIFICATION OF SURFACE PREPARATION FOR ADHESIVE BONDING
Rodney S. Myers *In* NASA. Marshall Space Flight Center, Aerospace Environmental Technology Conference Mar. 1995 p 603-612 (For primary document see N95-31746 11-23)
Avail: CASI HC A02/MF A06

N95-31808*# Nebraska Univ., Lincoln, NE. Dept. of Electrical Engineering.
SPECTROSCOPIC ELLIPSOMETRY AS A SENSITIVE MONITOR OF MATERIALS CONTAMINATION
Jeffrey S. Hale, James N. Hilfiker, Blaine Spady, R. Synowicki, and John A. Woollam *In* NASA. Marshall Space Flight Center, Aerospace Environmental Technology Conference Mar. 1995 p 613-618 (For primary document see N95-31746 11-23)
Avail: CASI HC A02/MF A06

N95-31813*# National Aeronautics and Space Administration. Marshall Space Flight Center, Huntsville, AL.
AN OVERVIEW OF NASA TESTING REQUIREMENTS FOR ALTERNATE CLEANING SOLVENTS USED IN LIQUID AND GASEOUS OXYGEN ENVIRONMENTS
John W. Strickland (BAMSI, Inc., Huntsville, AL.) and S. Eddie Davis *In its* Aerospace Environmental Technology Conference Mar. 1995 p 661-665 (For primary document see N95-31746 11-23)
Avail: CASI HC A01/MF A06

26 METALLIC MATERIALS

Includes physical, chemical, and mechanical properties of metals, e.g., corrosion; and metallurgy.

N95-30404# Michigan Technological Univ., Houghton, MI. Dept. of Metallurgical and Materials Engineering.
MECHANICAL ALLOYING PROCESSING WITH APPLICATION TO STRUCTURAL MATERIALS Final Report, 1 Feb. 1993 - 30 Sep. 1994
T. H. Courtney 26 Sep. 1994 13 p
(Contract DAAH04-93-G-0057)
(AD-A290788; ARO-30920.9-MS) Avail: CASI HC A03/MF A01

This report summarizes efforts and accomplishments relative to modeling of the mechanical alloying processing and in synthesis and consolidation of structural materials made by mechanical alloying. Models depicting the extent of deformation and the fracture and welding frequencies of powders subjected to mechanical alloying are encapsulated. A description of an improved attritor processing scheme is given. In addition, we describe the means of synthesizing nanocermets of the Cu-NbC system. The structure and properties of these materials are described, as they are know at this time. Finally, a description of consolidated heavy metals and their properties as they are found when prepared from mechanically alloyed precursor powders is given. DTIC

N95-30518 Selskapet for Industriell og Teknisk Forskning, Trondheim (Norway). Dept. for Materials Technology.
WETTABILITY OF BORON CARBIDE
T. Torvund, O. M. Akselsen, O. Grong, and J. H. Ulvensoen 2 Jun. 1994 13 p
(PB95-196358; STF24-S94001) Avail: Issuing Activity (National Technical Information Service (NTIS))

The work was presented at the conference, Advanced Joining Technologies for New Materials II, which was held in Cocoa Beach, USA, 2-4 March. The conference proceedings will be published in 1994. The wettability of boron carbide has been examined by means of the sessile drop method, using the following candidate alloys: (96 wt percent Ag - 4 wt percent Ti), (Ag - 26.5 wt percent Cu - 3 wt percent Ti), (Sn - 10 wt percent AG - 4 wt percent Ti), Sn(99.95 wt percent) and Al(99.99 wt percent). The results show that B4C is completely wetted by the Ag-based alloys. Sn - 10 wt percent Ag - 4 wt pecrent Ti alloy and pure Al partly wet the B4C surface, while pure Sn does not wet B4C at all. NTIS

N95-30531*# Electroformed Nickel, Inc., Huntsville, AL.
HIGH TEMPERATURE BARRIER COATINGS FOR REFRACTORY METALS
G. A. Malone and T. Walech Cleveland, OH NASA Jun. 1995 133 p
(Contract NAS3-26256; SBIR-11.01-4707; RTOP 242-70-02)
(NASA-CR-195475; E-9682; NAS 1.26:195475) Avail: CASI HC A07/MF A02

Improvements in high temperature oxidation resistant metal coating technology will allow NASA and commercial entities to develop competitive civil space transport and communication systems. The success of investigations completed in this program will have a positive impact on broadening the technology base for high temperature materials. The work reported herein describes processes and procedures for successfully depositing coherent oxidation barrier coatings on refractory metals to prevent degradation under very severe operating environments. Application of the new technology developed is now being utilized in numerous Phase 3 applications through several prominent aerospace firms. Major achievements have included: (1) development of means to deposit thick platinum and rhodium coatings with lower stress and fewer microcracks than could be previously achieved; (2) development of processes to deposit thick adherent coatings of platinum group metals on refractory substrates that remain bonded through high temperature excursions and without need for intermediate coatings (bonding processes unique to specific refractory metals and alloys have been defined; (3) demonstration that useful alloys of refractory and platinum coatings can be made through thermal diffusion means; (4) demonstration that selected barrier coatings on refractory substrates can withstand severe oxidizing environments in the range of 1260 deg and 1760 deg C for long time periods essential to the life requirements of the hardware; and (5) successful application of the processes and procedures to prototype hardware. The results of these studies have been instrumental in improved thermal oxidation barrier coatings for the NASP propulsion system. Other Phase 3 applications currently being exploited include small uncooled thrusters for spacecraft and microsatellite maneuvering systems. Author

N95-30534 Selskapet for Industriell og Teknisk Forskning, Trondheim (Norway). Div. of Applied Physics.
OBSERVATION OF A LOW-BINDING-ENERGY PEAK IN THE 2p CORE-LEVEL PHOTOEMISSION FROM OXIDIZED Al(111)
C. Berg, S. Raaen, A. Borg, J. N. Andersen, and E. Lundgren 19 May 1994 6 p Prepared in cooperation with Lund Univ., Sweden and Technical Univ. of Norway, Trondheim
(PB95-195350; STF19-S94004) Copyright Avail: Issuing Activity (National Technical Information Service (NTIS))

High-resolution photoemission studies of oxidation of the Al(111) surface have been performed. The appearance of a component at lower binding energy than the metallic bulk Al emission in the Al 2p spectrum at oxygen exposures above approx. 50 langmuir (1 L = 10(exp -6) Torr s) is argued to be due to Al atoms which do not bond directly to oxygen atoms at the oxide-metal interface. Low-energy electron diffraction initially shows a 1 x 1 structure, which subsequently fades away at higher oxygen exposures, approximately equal or greater than or 400 L. NTIS

N95-30547# Oak Ridge National Lab., TN.
APPLICATIONS OF SXPS FOR STUDYING SURFACE STRUCTURE, REACTION MECHANISMS AND KINETICS
D. R. Mullins, D. R. Huntley, and S. H. Overbury 1994 6 p Presented at the 1994 Fall Meeting of the Materials Research Society (MRS), Boston, MA, 28 Nov. - 2 Dec. 1994
(Contracts DE-AC05-84OR-21400; DE-AC02-76CH-00016)
(DE95-008903; CONF-941144-94) Avail: CASI HC A02/MF A01

Soft x-ray photoelectron spectroscopy (SXPS) from the S 2p core level has been used to study adsorbate induced reconstruction, identify reaction intermediates and study reaction kinetics on the Ni(111) surface. The S 2p binding energy is affected by the nature of the surface adsorption site. It has been determined from the number of S 2p states and their relative binding energies that adsorbed S induces a reconstruction of the Ni(111) surface and that the S adsorbs in fourfold sites on terraces and in troughs. S 2p SXPS has also been used to identify adsorbed species during the thermal decomposition of methanethiol on Ni(111). CH3SH adsorbs as CH3S(minus) at low temperatures. Above 200 K, the CH3S(minus) changes adsorption site and the C-S bond begins to cleave. The relative concentrations of CH3S(minus) in the two different sites and of atomic S have been monitored as a function of temperature and initial coverage. As a result of the sensitivity and resolution available in SXPS, reaction rates and kinetic parameters have been obtained for the decomposition of benzenethiol on Ni(111) by monitoring the changes in the surface composition continuously as a function of temperature and time. DOE

N95-30551 Department of the Navy, Washington, DC.
TRIVALENT CHROMIUM SOLUTIONS FOR SEALING ANODIZED ALUMINUM Patent
Fred Pearlstein, inventor (to Navy) and Vinod S. Agarwala, inventor (to Navy) 20 Dec. 1994 7 p Filed 1 Oct. 1993
(AD-D017349; US-Patent-5,374,347; US-Patent-Appl-SN-134762; US-Patent-Class-205-203) Avail: US Patent and Trademark Office

Corrosion resistant seal-coatings are formed on anodized aluminum by immersion in aqueous solutions containing trivalent chromic compounds with an alkali added near or slightly beyond the precipitation of insoluble basic compounds. Trivalent chromium seals formed on the anodized aluminum when tested in 5% NaCl salt spray chamber showed improved corrosion resistance. After a post-treatment in a peroxide or permanganate solution, the corrosion resistance for the anodized aluminum showed even greater improvement in the salt chamber. DTIC

N95-30575# Oak Ridge National Lab., TN.
REACTION SYNTHESIS OF INTERMETALLICS
S. C. Deevi and V. K. Sikka 1994 6 p Presented at the 1994 Fall Meeting of the Materials Research Society (MRS), Boston, MA, 28 Nov. - 2 Dec. 1994
(Contract DE-AC05-84OR-21400)
(DE95-009029; CONF-941144-111) Avail: CASI HC A02/MF A01

Exothermicity associated with the synthesis of aluminides was utilized to obtain nickel, iron, and cobalt aluminides. Combustion synthesis, extrusion, and hot pressing were utilized to obtain intermetallics and their composites. Extrusion conditions, reduction ratios, and hot-pressing conditions of the intermetallics and their composites are discussed. DOE

N95-30593*# National Aeronautics and Space Administration. Lewis Research Center, Cleveland, OH.
HIGH-TEMPERATURE OXIDATION BEHAVIOR OF IRIDIUM-RHENIUM ALLOYS
Brian D. Reed Jul. 1995 15 p Presented at the 30th Joint Propulsion Conference, Indianapolis, IN, 27-29 Jun. 1994; sponsored by AIAA, ASME, SAE, and ASEE
(RTOP 506-42-31)
(NASA-TM-106720; E-9086; NAS 1.15:106720) Avail: CASI HC A03/MF A01

The life-limiting mechanism for radiation-cooled rockets made from iridium-coated rhenium (Ir/Re) is the diffusion of Re into the Ir layer and the subsequent oxidation of the resulting Ir-Re alloy from the inner surface. In a previous study, a life model for Ir/Re rockets was developed. It incorporated Ir-Re diffusion and oxidation data to predict chamber lifetimes as a function of temperature and oxygen partial pressure. Oxidation testing at 1540 deg C suggested that a 20-wt percent Re concentration at the inner wall surface should be established as the failure criterion. The present study was performed to better define Ir-oxidation behavior as a function of Re concentration and to supplement the data base for the life model. Samples ranging from pure Ir to Ir-40 wt percent Re (Ir-40Re) were tested at 1500 deg C, in two different oxygen environments. There were indications that the oxidation rate of the Ir-Re alloy increased significantly when it went from a single-phase solid solution to a two-phase mixture, as was suggested in previous work. However, because of testing anomalies in this study, there were not enough dependable oxidation data to definitively raise the Ir/Re rocket failure criterion from 20-wt percent Re to a Re concentration corresponding to entry into the two-phase region. Author

N95-30706# Brookhaven National Lab., Upton, NY.
EFFECTS OF TEMPERATURE RAMP RATE DURING HEAT TREATMENT ON HYSTERESIS LOSS AND CRITICAL CURRENT DENSITY OF INTERNAL TIN PROCESSED WIRES
M. Suenaga and R. L. Sabatini 1995 4 p Presented at the 9th US/Japan Workshop on High-field Superconducting Materials, Kyoto, Japan, 11-16 Mar. 1995
(Contract DE-AC02-76CH-00016)
(DE95-009551; BNL-61242; CONF-9503127-1) Avail: CASI HC A01/MF A01

It has been shown that temperature ramp rates utilized in heat treatment schedules for internal tin processed Nb3Sn wires substantially influence both hysteresis loss and critical current density J(sub c) of the wires, i.e. a slow ramp rate (e.g. 6(degree)C/h) favors a higher J(sub c) while a fast ramp (e.g. 60(degree)C/h) results in a low hysteresis loss of the wire. DOE

N95-30733# Oak Ridge National Lab., TN.
DETERMINATION OF SITE-OCCUPANCIES IN ALUMINIDE INTERMETALLICS BY ALCHEMI
I. M. Anderson, J. Bentley, and A. J. Duncan (Florida Univ., Gainesville, FL.) 1995 7 p Presented at the 1994 Fall Meeting of the Materials Research Society, Boston, MA, 28 Nov.- 2 Dec. 1994
(Contract DE-AC05-84OR-21400)
(DE95-009179; CONF-941144-117) Avail: CASI HC A02/MF A01

The site-distributions of Fe in four B2-ordered NiAl-based alloys with Fe concentrations of 10%, 2%, and 0.5% have been determined by ALCHEMI (atom-location by channeling-enhanced microanalysis). Site-distributions have been extracted with standard errors between approximately 1.5% (10% Fe concentration) and approximately 6% (0.5% Fe concentration). The results show that Fe has no strong site-preference in NiAl and tends to reside on the site of the stoichiometrically deficient host element. An improved ALCHEMI analysis procedure is outlined. The analysis explicitly addresses the phenomenon of ionization delocalization, which previously complicated the determination of site-distributions in aluminide intermetallics, leading to inaccurate and oftentimes nonphysical results. The improved ALCHEMI analysis also addresses the presence of anti-site defects. The data acquisition conditions have been optimized to minimize the sources of statistical and systematic error. This optimized procedure should be suitable for all analyses of B2-ordered alloys. Several analyses at different channeling orientations show that the extracted site-occupancies are robust as long as the data are acquired at orientations that are remote from any major pole of the crystal. DOE

N95-30750 Department of the Navy, Washington, DC.
HIGH ASPECT RATIO METAL MICROSTRUCTURES AND METHOD FOR PREPARING THE SAME Patent
Jacque H. Georger, Jr., inventor (to Navy), Martin C. Peckerar, inventor (to Navy), Milton L. Rebbert, inventor (to Navy), Jeffrey M. Calvert, inventor (to Navy), and James J. Hickman, inventor (to Navy) 30 Aug. 1994 17 p Filed 27 Apr. 1992
(AD-D017463; US-Patent-5,342,737; US-Patent-Appl-SN-874403; US-Patent-Class-430-324) Avail: US Patent and Trademark Office

High aspect ratio metal microstructures may be prepared by a method involving: (1) forming a layer of a photoresistance on a substrate; (2) exposing the layer to actinic radiation in an image wise manner and developing the exposed layer to obtain a surface which contains regions having no remaining photoresist and regions covered with photoresist; (3) metallizing the surface to form a layer of metal on the region of the

surface having no remaining photoresist and on the sides of the regions of photoresist remaining on the surface; and (4) optionally, stripping the photoresist remaining on the surface. DTIC

N95-30757# Ames Lab., IA.
DISSOLUTION OF EUTECTIC MICROSTRUCTURES Ph.D. Thesis
C. Nordlund 10 Feb. 1995 74 p
(Contract W-7405-eng-82)
(DE95-010244; IS-T-1718) Avail: CASI HC A04/MF A01

Literature review of microstructural development during melting revealed comprehensive work on interface stability but only observations of two-phase melting, including eutectic systems, with no analytical work. Four analytical models were developed to establish the role of solute diffusion and surface energy on morphology of a directionally melted lamellar eutectic. First, a mass balance of solute provided solute profile equations for the cases of no diffusion and complete diffusion in the liquid. Second, an energy balance at the interface provided separate equations for the average mp of each phase vs velocity, lamellar spacing, and material constants. Third, the diffusion equation was solved for a planar melting interface (solving for the average temperature of interface and combining with solute profile allowed solution of interface shape). Finally, a balance of the normal solute flux at the interface was used to examine the relation between interface morphology and solute diffusion in the liquid and solid. Experiments were conducted using a transparent organic lamellar eutectic alloy in which the melting interface could be observed in-situ. Steady-state interface morphologies were compared with predictions of solution of diffusion equation. Most experiments fitted the predicted morphologies, with exceptions where diffusive coupling was not maintained and a nonisothermal, nonplanar interface resulted. Experiment also revealed interface instabilities, including brief periods of a single phase planar interface and a Rayleighian instability for the nonplanar morphologies. DOE

N95-30761# Japan Atomic Energy Research Inst., Tokyo (Japan).
EVALUATION ON MATERIALS PERFORMANCE OF HASTELLOY ALLOY XR FOR HTTR USES. 4: TENSILE PROPERTIES OF BASE METALS AND WELDED JOINTS
Katsutoshi Watanabe (Japan Atomic Energy Research Inst., Tokai, Japan.), Hajime Nakajima (Japan Atomic Energy Research Inst., Tokai, Japan.), Teiichiro Saitoh, Tamao Takatsu, Hajime Koikegami, and Makoto Higuchi Jun. 1994 29 p In JAPANESE
(DE95-721871; JAERI-M-94-081-4) Avail: CASI HC A03/MF A01

Tensile properties due to thermal aging on Hastelloy Alloy XR base metals and welded joints were investigated as a series of evaluation tests on the base metals and filler metals for the High Temperature Engineering Test Reactor (HTTR) components. Tensile test in air was performed at R.T. and then same temperatures as the thermal aging temperatures after the specimens were aged at 800, 900, and 1000 C for 1000 hrs. In comparison with the previous data, the present results had no significant difference on the strength characteristics, and were in the previous data band on the ductility. Therefore, it is concluded that these base metals and filler metals for the HTTR components have excellent tensile properties. DOE

N95-30776# Technische Univ., Delft (Netherlands).
HYDROGEN ABSORPTION IN IRON AND STEEL DURING GAS TUNGSTEN ARC WELDING Thesis
J. Hooijmans Nov. 1994 169 p
(PB95-197018; ISBN-90-407-1071-6) Copyright Avail: CASI HC A08/MF A02

This thesis deals with the process of hydrogen absorption during arc welding of iron and steel. Fundamental insight in this process is of vital importance as the hydrogen absorbed by the weld metal can result in serious problems, as described in the foregoing. Understanding of the absorption mechanism will make it possible to indicate in which ways hydrogen absorption can be reduced. NTIS

N95-30797# Oak Ridge National Lab., TN.
AMORPHIZATION THRESHOLD IN SI-IMPLANTED STRAINED SiGe ALLOY LAYERS
T. W. Simpson (University of Western Ontario, London, Ontario.), D. Love (University of Western Ontario, London, Ontario.), E. Endisch (University of Western Ontario, London, Ontario.), R. D. Goldberg (University of Western Ontario, London, Ontario.), I. V. Mitchell (University of Western Ontario, London, Ontario.), T. E. Haynes (Oak Ridge National Lab., TN.), and J. M. Baribeau (National Research Council of Canada, Ottawa, Ontario.) Dec. 1994 7 p Presented at the 1994 Fall Meeting of the Materials Research Society, Boston, MA, 28 Nov. - 2 Dec. 1994
(Contract DE-AC05-84OR-21400)
(DE95-008901; CONF-941144-105) Avail: CASI HC A02/MF A01

The authors have examined the damage produced by Si-ion implantation into strained Si(1-x) Ge(x) epilayers. Damage accumulation in the implanted layers was monitored in situ by time-resolved reflectivity and measured by ion channeling techniques to determine the amorphization threshold in strained Si(1-x)Ge(x) (x = 0.16 and 0.29) over the temperature range 30-110 C. The results are compared with previously reported measurements on unstrained Si(1-x)Ge(x), and with the simple model used to describe those results. They report here data which lend support to this model and which indicate that pre-existing strain does not enhance damage accumulation in the alloy layer. DOE

N95-30945# Army Armament Research, Development and Engineering Center, Watervliet, NY. Benet Lab.
THE ELECTRODEPOSITION OF LOW CONTRACTION CHROMIUM/MOLYBDENUM ALLOYS USING PULSE-REVERSE PLATING Final Report
Mark D. Miller and Stephen Langston Dec. 1994 18 p
(AD-A292727; ARCCB-TR-94049) Avail: CASI HC A03/MF A01

The use of modulated pulse periodic reverse (pulse-reverse) current to electrodeposit a low contraction (LC) chromium/molybdenum alloy has been evaluated. When using one full pulse-reverse plating cycle, the percent molybdenum in the deposit increased almost 400 percent (from 1 to 4 percent) as the current in the reverse cycle was increased from 0 to 10 amps. However, when the pulse reverse current was carried to six full plating cycles, the percent molybdenum in the deposit was not dependent upon the current and remained constant at about 1 percent. This is about the same percent molybdenum that could be expected in direct current-plated LC chromium/molybdenum alloy and about half the percent molybdenum that could be expected in an on/off pulse-plated LC chromium/molybdenum alloy. DTIC

N95-30977# Johns Hopkins Univ., Baltimore, MD.
LOCALIZATION IN TUNGSTEN HEAVY ALLOYS SUBJECTED TO SHEARING DEFORMATIONS UNDER SUPERIMPOSED HIGH PRESSURES Final Report, Sep. 1991 - Nov. 1994
K. T. Ramesh 27 Feb. 1995 20 p
(Contract DAAL03-91-G-0079)
(AD-A293177; ARO-28272.10-MS) Avail: CASI HC A03/MF A01

This report presents the results of investigations into the deformation and failure of tungsten-based composites (tungsten heavy alloys) at very high strain rates. Several new experimental techniques developed during the course of the work include pressure-shear recovery, allowing the recovery of samples subjected to high-rate shearing deformations; the dynamic measurement of radial strains, and the continuous measurement of projectile velocities. The experimental results showed that the development of adiabatic shear localization in tungsten heavy alloys is influenced by a superimposed hydrostatic pressure. Experimental characterizations have been performed of the very high-rate response of tungsten composites with tungsten-nickel-iron and hafnium matrices. It has been shown that these materials must be treated as dual-phase composites. The addition of a hard particulate reinforcement is shown to result in a substantial increase in matrix rate-sensitivity in a model metal-matrix composite. A simple modeling approach has been developed that allows one to predict the dynamic mechanical properties of a particle-reinforced metal-matrix composite given only the properties of the matrix phase. DTIC

N95-31052 Selskapet for Industriell og Teknisk Forskning, Trondheim (Norway). Div. of Production Engineering.
EFFECT OF LOCAL MELTING ON TRIBOLOGY IN METAL CUTTING
N. Tomac, K. Toennessen, and F. O. Rasch 8 Aug. 1994 14 p Prepared in cooperation with Technical Univ. of Norway, Trondheim; and Narvik Inst. of Tech., Narvik, Norway
(PB95-195392; STF30-S94003) Avail: Issuing Activity (National Technical Information Service (NTIS))

A feature when cutting many types of metals is that workpiece material

adheres to the cutting tool at the sliding contact surfaces between the work material and the tool. The built-up material formed during cutting is of fundamental importance in machining. The paper especially concerns the material build-up at the side flanks of the tool. This type of build-up differs from the more familiar built-up edge (BUE) and is termed 'flank build-up' (FBU). The FBU appears at high cutting speeds in materials like magnesium alloys, nodular cast iron, particle reinforced and cast aluminum alloys with a high content of silicon. Comprehensive machining tests of various magnesium alloys have shown that the presence of the intermetallic Beta-phase is associated with the FBU-formation. In the present paper, a close relationship between the critical cutting speed (temperature) and the amount of Beta-phase in the workpiece material is diagrammatically presented. NTIS

N95-31053 Selskapet for Industriell og Teknisk Forskning, Trondheim (Norway). Dept. for Materials Technology.
PHYSICAL MODELLING OF MICROSTRUCTURAL EVOLUTION DURING THERMOMECHANICAL PROCESSING OF ALUMINIUM ALLOYS
E. Nes, H. E. Vatne, O. Daaland, T. Furu, and R. Oersund 1994 35 p Prepared in cooperation with Technical Univ. of N orway, Trondheim; and Hydro Aluminum A/S, Karmoy, Norway
(PB95-196341; STF24-S94003) Avail: Issuing Activity (National Technical Information Service (NTIS))

New physically based models for substructure evolution, recrystallization kinetics, grain size and texture after single and multipass hot deformation of aluminum are presented. The approach taken differs from similar models developed for steels. The models discussed here rely on the calculation of the stored energy during deformation and the subsequent recrystallization kinetics and related reaction products such as grain size and texture. Much effort has been directed towards identifying the nature of the nucleation sites for recrystallized grains of different crystallographic orientations. This is essential in order to elevate the model from an empirical to a physical level, the latter being necessary for a good insight into, as well as control of, the rolling process. Particle stimulated nucleation, nucleation from cube bands and grain boundary areas have been incorporated in the model. These concepts are then applied to some examples from commercial production of aluminum sheets. NTIS

N95-31105# Oak Ridge National Lab., TN.
MICROSTRUCTURAL AND MECHANICAL PROPERTY CHANGES IN MODEL Fe-Cu ALLOYS
P. M. Rice, R. E. Stoller, B. N. Lucas, and W. C. Oliver (Nano Instruments, Inc., Knoxville, TN.) 1994 7 p Presented at the 1994 Fall Meeting of the Materials Research Society (MRS), Boston, MA, 28 Nov. - 2 Dec. 1994
(Contract DE-AC05-84OR-21400)
(DE95-010117; CONF-941144-130) Avail: CASI HC A02/MF A01

This paper describes a technique developed to determine values for the dislocation barrier strength of the defects believed to be responsible for the embrittlement of light water reactor (LWR) pressure vessel steels. Microstructures consisting of a single defect type were introduced by ion irradiation or thermal annealing, and the defect distributions were determined by TEM. Hardness changes were measured using a nano indenter and the dislocation barrier strengths for the defects involved were computed based on a dispersed barrier hardening model. DOE

N95-31106# Oak Ridge National Lab., TN.
REVIEW OF ENVIRONMENTAL EFFECTS IN INTERMETALLICS
E. P. George and C. T. Liu 1994 16 p Presented at the 1994 Fall Meeting of the Materials Research Society (MRS), Boston, MA, 28 Nov. - 2 Dec. 1994
(Contract DE-AC05-84OR-21400)
(DE95-010120; CONF-941144-131) Avail: CASI HC A03/MF A01

The phenomenology and mechanisms of environmental embrittlement in ordered intermetallics is reviewed by considering two model alloy systems of the L1(sub 2) and B2 crystal classes (Ni3Al and FeAl). Both H2O and H2, at levels found in ordinary ambient air, are found to cause environmental embrittlement, with the former usually more deleterious. In the case of H2O, the micromechanism involves reaction with the intermetallic to form an oxide (or hydroxide) and simultaneous generation of atomic hydrogen which then enters the metal and causes embrittlement. In the case of H2, on the other hand, atomic hydrogen is generated as a result of the dissociation of physisorbed hydrogen molecules on the intermetallic surfaces. Consistent with the proposed embrittlement mechanism, ductility is found to increase with decreasing amounts of H2O (or H2) in the test environment, increasing strain rate, and decreasing (or increasing) temperature. Environmental embrittlement in Ni3Al (and other L1(sub 2) alloys) occurs predominantly intergranularly, whereas in FeAl (and other B2 alloys) it can also occur transgranularly, presumably because diffusion of hydrogen is fast enough through the bulk in the more open B2 structure but only so along grain boundaries in the L1(sub 2) structure. Microalloying with B, which segregates strongly to the grain boundaries, can overcome environmental embrittlement in L1(sub 2) alloys, but not in B2 alloys; in the latter, alloying additions probably have to be added at significantly higher (macroalloy) levels to affect the bulk properties. In neither alloy is environmental embrittlement the sole source of brittleness: depending on the alloy stoichiometry, and grain boundary character, a given grain boundary may be intrinsically weaker (or stronger) than the bulk, thereby influencing overall ductility. DOE

N95-31107# Oak Ridge National Lab., TN.
THE EFFECT OF GRAIN REFINEMENT ON THE ROOM-TEMPERATURE DUCTILITY OF AS-CAST Fe3Al-BASED ALLOYS
S. Viswanathan, V. K. Andleigh, and C. G. McKamey 1994 6 p Presented at the 1994 Fall Meeting of the Materials Research Society (MRS), Boston, MA, 28 Nov. - 2 Dec. 1994
(Contract DE-AC05-84OR-21400)
(DE95-010121; CONF-941144-132) Avail: CASI HC A02/MF A01

Fe3Al-based alloys exhibit poor room temperature ductility in the as-cast condition. The effect of grain refinement of the as-cast alloy on room-temperature ductility was investigated. Small melts of Fe-28 at. % Al-5 at. % Cr were inoculated with various alloying additions and cast into a 50 x 30 x 30-mm graphite mold. The resulting ingots were examined metallographically for evidence of grain refinement, and three-point bend tests were conducted on samples to assess the effect on room-temperature ductility. Ductility was assumed to correlate with the strain corresponding to the maximum stress obtained in the bend test. The results showed that titanium was extremely effective in grain refinement, although it severely embrittled the alloy in contents exceeding 1%. Boron additions strengthened the alloy significantly, while carbon additions reduced both the strength and ductility. The best ductility was found in an alloy containing titanium, boron, and carbon. DOE

N95-31111# Oak Ridge National Lab., TN.
SHAPE MEMORY PROPERTIES OF AN IRON MODIFIED NICKEL ALUMINIDE ALLOY
J. A. Horton, C. T. Liu, and E. P. George 1994 6 p Presented at the 1994 Fall Meeting of the Materials Research Society (MRS), Boston, MA, 28 Nov. - 2 Dec. 1994
(Contract DE-AC05-84OR-21400)
(DE95-010223; CONF-941144-128) Avail: CASI HC A02/MF A01

The ordered intermetallic NiAl with aluminum levels near 36% undergoes a B2 to martensite transformation. Shape memory alloys based on NiAl + Fe have the potential for transition temperatures of greater than 150 C. While binary alloys appear inherently brittle, alloying with iron and boron results in two phase alloys with L1(sub 2) and B2 phases and with about 7% room temperature tensile ductility. These alloys show a two-way shape memory effect over a range of transition temperatures with austenite peak temperature, Ap, between 100 to 200 C based on composition. Unfortunately, the B2 phase and its low temperature body centered tetragonal martensitic form are not stable and both can transform to Ni5Al3 with a loss in ductility. These alloys with a constant tensile load show a two way shape recovery of up to 0.6% during temperature cycling between 100 and 200 C. A thorough survey of the shape memory properties of one such alloy with a composition of Ni-25.5 Al-16 Fe-0.12 B (at.%) as a function of prior cold work, tensile loading, and other training steps is presented. Nanoindentation was used to independently measure the mechanical properties of the two phases. DOE

N95-31121# Los Alamos National Lab., NM.
HYDROSTATIC EXTRUSION OF BSCCO/Ag COMPOSITE WIRE
John F. Bingert, Barry L. Bingham, Robert J. Sebring, and Ann M. Kelly 1995 11 p Presented at the Annual Meeting and Exhibition of the Minerals, Metals and Materials Society, Las Vegas, NV, 12-16 Feb. 1995

(Contract W-7405-eng-36)
(DE95-007862; LA-UR-95-654; CONF-950201-9) Avail: CASI HC A03/MF A01

The application of hydrostatic extrusion processing to composite wire fabrication offers several advantages over conventional reduction techniques. These include enhanced uniformity, increased reduction capability, and successful extrusion of normally brittle materials. Specifically, this work involved an experiment to screen the effects of seven extrusion process parameters on the uniformity and density of as-extruded BSCCO-core wire, and the required extrusion pressure. Results suggest the following factors to be potentially significant: (1) back pressure, extrusion ratio, and die angle on core uniformity, (2) packing method, extrusion ratio, silver powder additions, and temperature on density, and (3) extrusion ratio and temperature on extrusion pressure. DOE

N95-31150# Sandia National Labs., Albuquerque, NM.
HYDROGEN DIFFUSION AND PASSIVATION IN InGaAlN ALLOYS
S. J. Pearton (Florida Univ., Gainesville, FL.), C. R. Abernathy (Florida Univ., Gainesville, FL.), J. D. MacKenzie (Florida Univ., Gainesville, FL.), C. B. Vartuli (Florida Univ., Gainesville, FL.), R. G. Wilson (Hughes Research Labs., Malibu, CA.), J. M. Zavada (Army Research Office, Research Triangle Park, NC.), and R. J. Shul 1995 6 p Presented at the Spring Meeting of the Materials Research Society, San Francisco, CA, 17-21 Apr. 1995 Sponsored in part by an NSF grant from the Division of Materials Research, an AFOSR University Research Initiative, an AASERT grant through USARO, and a US Army Research Office grant
(Contract DE-AC04-94AL-85000)
(DE95-010889; SAND-95-0856C; CONF-950412-3) Avail: CASI HC A02/MF A01

Hydrogen is found to readily diffuse into InGaN, InAlN and InGaAlN epitaxial layers during plasma exposures at 170-250 C for 40 sec-30 min. The diffusivity of hydrogen is greater than 10(exp -11) sq cm (center dot)/s at 170 C, and the native donor species are passivated by association with the hydrogen. Reactivation of these species occurs at 450-500 C, but the hydrogen remains in the material until greater than or equal to 800 C. DOE

N95-31154# Japan Atomic Energy Research Inst., Tokyo (Japan).
EFFECT OF COLD WORK ON CREEP PROPERTIES OF HASTELLOY XR
Yuji Kurata (Japan Atomic Energy Research Inst., Tokai, Japan.) and Hajime Nakajima Aug. 1994 37 p In JAPANESE
(DE95-722056; JAERI-Research-94-004) Avail: CASI HC A03/MF A01

Creep tests of Hastelloy XR, in 10%, 20% cold worked or solution treated condition, were made at 800 to 1000 C for times up to about 2000 ks in order to investigate the effect of cold work on creep properties. The results obtained are as follows: (1) Below 950 C, creep rupture strength of 10% cold worked Hastelloy XR is beyond the value of solution treated one within this experimental condition. 950 C and cold work of 10% are the highest values experienced in an intermediate heat exchanger of the High Temperature Engineering Test Reactor (HTTR) under normal condition, respectively. (2) At 800 and 850 C, creep rupture time of 20% cold worked Hastelloy XR is longer than that of solution treated one. However, the effect disappears above 900 C. At 950 and 1000 C, it becomes shorter than that of solution treated Hastelloy XR. (3) Rupture elongation and reduction of area of cold worked Hastelloy XR are smaller than those of solution treated one. While these values of 10% or 20% cold worked material are lowest at 900 C, they recover considerably at 1000 C. (4) Minimum creep rate, epsilon-dot (sub m), of 10% or 20% cold worked Hastelloy XR is decreased by as much as a factor of 20 to 50 at 800 to 900 C. On the other hand, epsilon-dot (sub m) of 10% or 20% cold worked material is increased at 1000 C. (5) From the results of microstructure observation of ruptured specimens, decrease in creep rupture strength of cold worked Hastelloy XR is interpreted in terms of extensive recrystallization which occurs during creep at 1000 C. DOE

N95-31188# Oak Ridge National Lab., TN.
EFFECT OF IRRADIATION SPECTRUM ON THE MICROSTRUCTURE OF ION-IRRADIATED Al2O3
S. J. Zinkle 1994 6 p Presented at the 1994 Fall Meeting of the Materials Research Society (MRS), Boston, MA, 28 Nov. - 2 Dec. 1994
(Contract DE-AC05-84OR-21400)
(DE95-010225; CONF-941144-126) Avail: CASI HC A02/MF A01

Polycrystalline samples of alpha-alumina have been irradiated with various ions ranging from 3.6 MeV Fe(+) to 1 MeV H(+) ions at 650 C. Cross-section transmission electron microscopy was used to investigate the depth-dependent microstructure of the irradiated specimens. The microstructure following irradiation was observed to be dependent on the irradiation spectrum. In particular, defect cluster nucleation was effectively suppressed in specimens irradiated with light ions such as 1 MeV H(+) ions. On the other hand, light ion irradiation tended to accelerate the growth rate of dislocation loops. The microstructural observations are discussed in terms of ionization enhanced diffusion processes. DOE

N95-31220# Comision Nacional de Energia Atomica, Buenos Aires (Argentina). Dept. de Materiales.
A PROPOSED PHASE EQUILIBRIUM DIAGRAM FOR Pt-Zr SYSTEM [PROPUESTA DE DIAGRAMA DE EQUILIBRIO DE FASES DEL SISTEMA PT-ZR]
D. E. Arias and L. Gribaudo 1993 10 p In SPANISH Presented at the 78th National Meeting of the Argentine Physics Association, Rosario, Argentina, 12-15 Oct. 1993
(DE95-620904; INIS-AR-089; CONF-9310347) Avail: CASI HC A02/MF A01 (US Sales Only)

A revision of the phase diagram of the Pt-Zr system is presented using up to date information from recent publications. The proposed change concerning the invariant transformation in the Pt-rich zone is supported by simplified thermodynamic evaluations. DOE

N95-31344 Defence Science and Technology Organisation, Melbourne (Australia). Ship Structures and Material Div.
OBSERVATIONS OF STAR FRACTURE AND LONGITUDINAL SPLITTING IN BIS 812 EMA AND Q1N SUBMARINE CONSTRUCTION STEELS
I. A. Burch and David S. Saunders Mar. 1995 31 p
(DSTO-RR-0014; AR-008-963) Avail: Issuing Activity (DSTO Aeronautical and Maritime Research Lab., GPO Box 4331, Melbourne, Victoria 3001, Australia)

The tensile properties and fracture behavior of two submarine construction steels, BIS 812 EMA and Q1N, have been studied. Their properties and fracture behavior were measured over a wide range of test temperatures utilizing plain and notched tensile specimens. The yield strength of both materials was found to increase with decreasing temperature and the fracture surface appearance of these steels was also temperature dependent. Under certain conditions 'star fracture' was exhibited, rather than the usual cup-and-cone type fracture. The predominance of the 'star type fracture' increased with decreasing temperature in both plain and notched tensile specimens, however, it was suppressed by notching. This paper describes in detail the fractographic features of the surfaces and proposes that a range of conditions exist under which 'star fracture' occurs in these materials. Author

N95-31406# Sandia National Labs., Albuquerque, NM.
SOLDERABILITY ENHANCEMENT OF COPPER THROUGH CHEMICAL ETCHING
Joel O. Stevenson, Terry R. Guilinger, F. Michael Hosking, Fred G. Yost, and N. Robert Sorensen 1995 16 p Presented at the Institute for Interconnecting and Packaging Electronic Circuits (IPC) Printed Circuits Expo 1995, San Diego, CA, 30 Apr. - 4 May 1995
(Contract DE-AC04-94AL-85000)
(DE95-010514; SAND-95-0734C; CONF-9504142-1) Avail: CASI HC A03/MF A01

Sandia National Laboratories has established a Cooperative Research and Development Agreement with consortium members of the National Center for Manufacturing Sciences (NCMS) to develop fundamental generic technology in the area of printed wiring board materials and surface finishes. Improved solderability of copper substrates is an important component of the Sandia-NCMS program. The authors are investigating the effects of surface roughness on the wettability and solderability behavior of several different types of copper board finishes. In this paper, the authors present roughness and solderability characterizations for a variety of chemically-etched copper substrates. Initial testing on six chemical etches demonstrate that surface roughness can be greatly enhanced through

chemical etching. Noticeable improvements in solder wettability were observed to accompany increases in roughness. A number of different algorithms and measures of roughness were used to gain insight into surface morphologies that lead to improved solderability. DOE

N95-31407# Comision Nacional de Energia Atomica, Buenos Aires (Argentina). Dept. Quimica Analitica.

VOLUMETRIC AND ELECTRO ANALYTICAL TECHNIQUES FOR CHEMICAL CHARACTERIZATION OF NUCLEAR GRADE Ag-In-Cd ALLOYS [TECNICAS VOLUMETRICAS Y ELECTROANALITICAS PARA LA CARACTERIZACION QUIMICA DE ALEACIONES AG-IN-CD GRADO NUCLEAR]

Norberto Bandin, Hector Laspina, Ricardo Crubellati, and Jorge Magallanes 1993 3 p In SPANISH Presented at the 21st Meeting of the Argentine Association of Nuclear Technology, Mar del Plata, Argentina, 8-12 Nov. 1993

(DE95-620664; INIS-AR-093; CONF-9311167) Avail: CASI HC A01/MF A01 (US Sales Only)

Silver-Indium-Cadmium alloys of nuclear grade are chemically characterized by volumetric and electrical analytical techniques. DOE

N95-31409# Comision Nacional de Energia Atomica, San Carlos de Bariloche (Argentina).

NEUTRONIC METHODS FOR DETERMINATION OF VERY LOW CONCENTRATIONS OF HYDROGEN IN METALS [METODOS NEUTRONICOS PARA LA DETERMINACION DE MUY BAJAS CONCENTRACIONES DE HIDROGENO EN METALES]

J. R. Granada and J. R. Santisteban 1993 3 p In SPANISH Presented at the 21st Meeting of the Argentine Association of Nuclear Technology, Mar del Plata, Argentina, 8-12 Nov. 1993

(DE95-623967; INIS-AR-105; CONF-9311167) Avail: CASI HC A01/MF A01 (US Sales Only)

Neutronic measuring methods for determining low hydrogen concentrations in metals is presented. DOE

N95-31464# Carnegie-Mellon Univ., Pittsburgh, PA.

METALLURGICAL AND MATERIALS TRANSACTIONS

Dec. 1994 331 p Repr. from Metallurgical and Materials Transactions A (Pittsburgh, PA), v. 25A, no. 12, Dec. 1994 p 2549-2844 plus index

(Contract N00014-93-1-0026)

(AD-A293617) Avail: CASI HC A15/MF A03

Metallurgical and Materials Transactions publishes contributions on all aspects of research and significant engineering advances in materials science and metallurgy. Approved manuscripts will be published according to subject matter in Section A or B. Metallurgical and Materials Transactions A publishes contributions on all aspects of physical metallurgy and materials science, with a special emphasis on relationships among the processing, structure, and properties of materials. DTIC

N95-31561# Naval Surface Warfare Center, Bethesda, MD.

COMPARISON OF CATHODIC PROTECTION CURRENTS ON 70/30 COPPER-NICKEL AND ALLOY 625 PIPING SYSTEMS Final Report

Harvey P. Hack and Walter L. Wheatfall Mar. 1995 25 p Limited Reproducibility: Document partially illegible

(AD-A292953; CARDIVNSWC-TR-61-94/14) Avail: CASI HC A03/MF A01

The objective of this study was to determine whether the demand on a cathodic protection system changes when the protected pipe material is changed from copper-nickel to alloy 625. Two piping mockups were designed to simulate a probable geometry for a cathodically protected piping system. Each mockup consisted of a 20-ft (610-cm) length of nominal 2-in.- (5-cm-) diameter piping with a zinc anode for cathodic protection inserted in the discharge end of each. One mockup was made with 70/30 copper-nickel pipe and the other with alloy 625 pipe. Protection currents and potential profiles inside the pipes were measured over a 6-month exposure period in natural seawater flowing at 7 ft/s (210 cm/s). The total protection current and sacrificial anode consumption for alloy 625 pipe were half that for copper-nickel pipe. Thus, replacing copper-nickel pipe with alloy 625 pipe in areas close to cathodically protected heat exchangers or hulls will result in less demand on the cathodic protection system, as opposed to the original copper-nickel piping. DTIC

N95-31599# Naval Surface Warfare Center, Bethesda, MD. Carderock Div.

HOT COMPRESSION TESTING OF TUNGSTEN

M. G. Vassilaros Mar. 1995 67 p

(AD-A293683; CARDIVNSWC-TR-61-94/17) Avail: CASI HC A04/MF A01

A study of the high temperature deformation behavior of tungsten was performed. The cylindrical specimen dimensions were 0.4 inch diameter and 0.6 inch long (10.2 x 15.2 mm) as machined from a tungsten forging. The compression tests were performed in a thermal-mechanical simulator 'Gleeble 1500' at temperatures of 600 to 3000 F (315 to 1650 C). The specimens were deformed to a strain of approximately 0.3 with lubricated test fixtures that suppressed any specimen barreling. Compressive stress - strain curves were produced for all specimens and analyzed for 0.2% offset strength as well as 1.0, 2.0 and 5.0% offset strengths. The strengths were observed to decrease with higher temperatures, but appeared to be on a plateau at 50 ksi (345 MPa) in the temperature range of 1200 to 2200 F (650 to 1200 C) . The compression specimens tested at or below 10000 F (538 C) experienced cracking. The fracture mode appeared to be intergranular in a single phase microstructure with an elongated grain shape. DTIC

N95-31615# Lawrence Livermore National Lab., Livermore, CA. Applied Superconductivity Group.

INDUSTRY PARTICIPATION WORKSHOP: CHROMIUM ELECTROPLATING OF SUPERCONDUCTOR STRAND. PROCEEDINGS

13 Dec. 1994 66 p Presented at the Industrial Participate Workshop: Chromium Electroplating of Superconductor Strand, Livermore, CA, 13 Dec. 1994

(Contract W-7405-eng-48)

(DE95-009629; CONF-941242) Avail: CASI HC A04/MF A01

The primary objective of the workshop was to inform US plating vendors about the opportunity to participate in the effort on Cr plating of large quantities of superconducting wires required for the ITER and the TPX projects and DOE's interest in developing several reliable and high quality suppliers of Chromium plating services for the superconducting strand industry. The objective was also to inform plating vendors about the Cr plating technology developed in LLNL and invite interested plating vendors to get the technology. Finally the workshop was intended to inform the plating vendors about the plan to get verification of capability of two to four vendors for Cr plating of superconducting strands. DOE

N95-31632# Oak Ridge National Lab., TN.

MODELING OF STRESS DISTRIBUTIONS ON THE MICROSTRUCTURAL LEVEL IN ALLOY 600

K. J. Kozaczek, B. G. Petrovic (Pennsylvania State Univ., University Park, PA.), C. O. Ruud (Pennsylvania State Univ., University Park, PA.), and A. R. McIlree (Electric Power Research Inst., Palo Alto, CA.) 1995 10 p Presented at the Joint ASME/JSME Pressure Vessels and Piping Conference, Honolulu, HI, 23-27 Jul. 1995

(Contract DE-AC05-84OR-21400)

(DE95-009135; CONF-950740-18) Avail: CASI HC A02/MF A01

Stress distribution in a random polycrystalline material (Alloy 600) was studied using a topologically correct microstructural model. Distributions of von Mises and hydrostatic stresses at the grain vertices, which could be important in intergranular stress corrosion cracking, were analyzed as functions of microstructure, grain orientations and loading conditions. Grain size, shape, and orientation had a more pronounced effect on stress distribution than loading conditions. At grain vertices the stress concentration factor was higher for hydrostatic stress (1.7) than for von Mises stress (1.5). The stress/strain distribution in the volume (grain interiors) is a normal distribution and does not depend on the location of the studied material volume i.e., surface vs/bulk. The analysis of stress distribution in the volume showed the von Mises stress concentration of 1.75 and stress concentration of 2.2 for the hydrostatic pressure. The observed stress concentration is high enough to cause localized plastic microdeformation, even when the polycrystalline aggregate is in the macroscopic elastic regime. Modeling of stresses and strains in polycrystalline materials can identify the microstructures (grain size distributions, texture) intrinsically susceptible to stress/strain concentrations and justify the correctness of applied stress state during the stress corrosion cracking tests. Also, it supplies the

information necessary to formulate the local failure criteria and interpret of nondestructive stress measurements. DOE

N95-31636# Los Alamos National Lab., NM.
INFLUENCE OF STRAIN RATE AND TEMPERATURE ON THE MECHANICAL BEHAVIOR OF IRON ALUMINIDE-BASED ALLOYS
G. T. Gray 1995 5 p Presented at the Plasticity and Its Current Applications Symposium, Osaka, Japan, 17-21 Jul. 1995
(Contract W-7405-eng-36)
(DE95-009426; LA-UR-95-918; CONF-9507100-1) Avail: CASI HC A01/MF A01

Iron aluminides are receiving increasing attention as potential high temperature structural materials due to their excellent oxidation and sulfidation resistance. Although the influence of strain rate on the microstructure/property relationships of pure iron and a variety of iron alloys and steels has been extensively studied, the effect of strain rate on the stress-strain and deformation response of iron aluminides remains poorly understood. In this paper the influence of strain rate, varied between 0.001 and 10(exp 4)/ sec, and temperature, between 77 & 1073 K, on the mechanical behavior of Fe-40Al-0.1B and Fe-16.12Al-5.44-Cr-0.11Zr-0.13C-1.07Mo-006Y, called FAP-Y, (both in at. percent) is presented. The rate sensitivity and work hardening of Fe-40Al and the disordered alloy based on Fe-16 percent Al are discussed as a function of strain rate and temperature. DOE

N95-31643# Oak Ridge National Lab., TN. Metals and Ceramics Div.
INITIAL SURVEY ON FRACTURE TOUGHNESS OF COMMERCIAL Nd2Fe14B
J. A. Horton and J. H. Schneibel 1994 4 p Presented at the 1994 Fall Meeting of the Materials Research Society (MRS), Boston, MA, 28 Nov. - 2 Dec. 1994
(Contract DE-AC05-84OR-21400)
(DE95-009813; CONF-941144-138) Avail: CASI HC A01/MF A01

Nd2Fe14B is currently the best (highest energy product) hard magnet available. Like most magnetic materials, it is rather brittle. The fracture toughness of specimens of commercially available Nd2Fe14B magnets were measured us ing a chevron notch three point bend test. Values ranged from nearly 2 to 5.5 MPa(radical)m. Consistent differences were found between the five different types of materials tested. In this initial survey, insufficient tests were done for good statistics to be obtained. However, it appears that this test will allow differences in fracture toughness between alloys with different compositions and fabricated by different production methods to be measured and tracked as improvements are made. DOE

N95-31689# Sandia National Labs., Albuquerque, NM.
A STUDY OF SWITCHING BEHAVIOR IN Pb(Zr,Ti)O3 THIN FILMS USING X-RAY DIFFRACTION
M. O. Eatough, D. Dimos, B. A. Tuttle, W. L. Warren, and R. Ramesh (Bell Communications Research, Inc., Red Bank, NJ.) 1995 6 p Presented at the 1994 Fall Meeting of the Materials Research Society (MRS), Boston, MA, 28 Nov. - 2 Dec. 1994
(Contract DE-AC04-94AL-85000)
(DE95-010859; SAND-95-0761C; CONF-941144-145) Avail: CASI HC A02/MF A01

Pb(Zr,Ti)O3 (PZT) thin films are being developed for use in optical and electronic memory devices. To study ferroelectric switching behavior, the authors have produced relatively untextured PZT thin films on Si substrates. They have developed a method for using x-ray diffraction to observe domain switching in situ. This study involved the use of a micro-diffractometer to monitor the switching behavior in relatively small (0.7 mm diameter) electroded areas. Diffraction analyses were done while DC voltages were applied and removed, representing several places in the hysteresis loop. In particular, the authors were looking for relative intensity changes in the (h00),(001) diffraction peaks as a function of position in the hysteresis loop. This study indicates that the 90 deg domain switching exhibited by bulk ferroelectrics is very limited in films on Si when grain sizes are less than about 1 micron. DOE

N95-31825# Oak Ridge National Lab., TN.
MODELING OF GRAIN BOUNDARY STRESSES IN ALLOY 600
K. J. Kozaczek, A. Sinharoy (Pennsylvania State Univ., University Park, PA.), C. O. Ruud (Pennsylvania State Univ., University Park, PA.), and A. R. McIlree (Electric Research and Management, Inc., State College, PA.) 1995 9 p Presented at the Joint ASME/JSME Pressure Vessels and Piping Conference, Honolulu, HI, 23-27 Jul. 1995
(Contract DE-AC05-84OR-21400)
(DE95-009033; CONF-950740-19) Avail: CASI HC A02/MF A01

Corrosive environments combined with high stress levels and susceptible microstructures can cause intergranular stress corrosion cracking (IGSCC) of Alloy 600 components on both primary and secondary sides of pressurized water reactors. One factor affecting the IGSCC is intergranular carbide precipitation controlled by heat treatment of Alloy 600. This study is concerned with analysis of elastic stress fields in vicinity of M7C3 and M23C6 carbides precipitated in the matrix and at a grain boundary triple point. The local stress concentration which can lead to IGSCC initiation was studied using a two-dimensional finite element model. The intergranular precipitates are more effective stress raisers than the intragranular precipitates. The combination of the elastic property mismatch and the precipitate shape can result in a local stress field substantially different than the macroscopic stress. The maximum local stresses in the vicinity of the intergranular precipitate were almost twice as high as the applied stress. DOE

N95-31974 Michigan Univ., Ann Arbor, MI.
THE INFLUENCE OF MATRIX MICROSTRUCTURE AND TEMPERATURE ON CYCLIC DEFORMATION AND FATIGUE OF PARTICLE-REINFORCED 2219 ALUMINUM Ph.D. Thesis
Gregory Michael Vyletel 1994 171 p
Avail: Univ. Microfilms Order No. DA9423338

Room temperature and elevated temperature (150 C) fatigue studies were conducted on naturally aged, peak-aged, and overaged 2219/TiC/ISp and 2219 Al. In addition, the grain size of 2219/TiC/15p was altered from 35 micrometers to 276 micrometers in an attempt to understand how grain size influences the room temperature and elevated temperature cyclic deformation and fatigue life behavior. Plastic strain-controlled testing was used to study the low-cycle fatigue and cyclic response behaviors while stress-controlled testing was used to investigate the high cycle fatigue behavior. The cyclic response and dislocation microstructures of both reinforced and unreinforced materials were very similar for comparable microstructures. Naturally aged materials showed evidence of cyclic hardening, and in some cases, cyclic softening, while the cyclic response of peak-aged and overaged materials showed no evidence of cyclic hardening or softening (except for overaged 2219 Al at high plastic strain amplitudes). Decreasing grain size was found to modestly increase the cyclic flow stress of 2219/TiC/15p while providing very little improvement in the fatigue-life behavior. The addition of TiC reinforcement was found to improve the stress-controlled fatigue life provided processing defects (i.e., intermetallics and particle clusters) were kept low; however, the plastic strain-controlled fatigue life of the composite was inferior to that of the unreinforced material. At 150 C, cyclic softening was observed at all plastic strain amplitudes for the composite materials and at plastic strain amplitudes greater than approximately 2.5 x 10(exp -3) for the unreinforced materials. This softening was attributed to the decomposition of the theta' strengthening precipitates to the equilibrium theta precipitates. This (theta') decomposition occurred in all materials; however, the combination of cyclic deformation and the presence of reinforcing TiC particles appeared to greatly increase the kinetics, or rate of decomposition. Grain size did not appear to have any significant effect on the extent of the decomposition or the degree of cyclic softening. Dissert. Abstr.

N95-31975 Michigan Univ., Ann Arbor, MI.
THE INFLUENCE OF MICROSTRUCTURE ON CREEP DEFORMATION IN NEAR-GAMMA TiAl ALLOYS Ph.D. Thesis
Brian Daly Worth 1994 151 p
Avail: Univ. Microfilms Order No. DA9423350

The influence of microstructure on creep deformation has been examined in the near-gamma TiAl alloys Ti-49Al-1V and Ti-48Al-1V-0.3C between 760 C and 870 C in the stress range of 50 MPa to 200 MPa. A systematic approach was made to develop methods to control microstructural morphologies and alpha(sub 2) volume fraction has been conducted. By carefully controlling thermo-mechanical processing parameters, the influence of solution temperature, cooling rate, and secondary heat treatment on volume fraction and morphology of alpha(sub 2) has been determined. Microstructure was shown to have a significant influence on the creep

behavior of the near-gamma TiAl alloy Ti-49Al-1V, with a fully lamellar having the highest creep resistance. Overall creep resistance was by the volume fraction of lamellar constituent, with the lowest creep resistance observed at intermediate lamellar volume fractions. The decrease in creep resistance of the duplex microstructure, compared to the near-gamma microstructure can be explained by an increase in dislocation mobility within the equiaxed gamma constituent. The high creep resistance of the fully lamellar microstructure is attributed to the fine spacing of the lamellar structure, which results in a decreased effective slip length for dislocation motion. The influence of interstitial strengthening and microstructure on creep deformation has been examined in the near-gamma TiAl alloy Ti-48Al-1V-0.3C. Significant improvement in creep resistance was observed in this alloy compared with the Ti-49Al-1V alloy containing low levels of carbon (0.07 at percent). The degree of strengthening resulting from the addition of carbon was greater in the near-gamma and duplex microstructures than in the fully lamellar microstructure. A decrease in stress exponent from 4 to 3 occurs and the formation of sub-boundaries is inhibited with the addition of carbon in both the duplex microstructure and near-gamma microstructures. These findings suggest that solute/dislocation interaction mechanisms are responsible for the significant increase in creep resistance observed in this alloy with the addition of carbon. Dissert. Abstr.

N95-32023# Ames Lab., IA.
A STUDY OF DAMASCUS STEEL Ph.D. Thesis
P. Berge 16 Feb. 1995 77 p
(Contract W-7405-eng-82)
(DE95-010127; IS-T-1703) Avail: CASI HC A05/MF A01

The Damascus sword has been an article of fascination for many years to blade collectors and metallurgists alike. The blades were given their name by Europeans who encountered these blades which originated from Damascus, Syria. They are best known for the appearance of the blade face. Genuine Damascus blades show swirling patterns of alternating light and dark regions which are due to the microstructure of the steel. The microstructure consists of arrays of well rounded cementite patterns in a matrix of either pearlite, bainite, or martensite. When this structure is etched the matrix will turn dark leaving the cementite particles light. Although many blades were produced over the centuries, while some of the process is known the making of a genuine Damascus blade today is generally considered a lost art. Many scientists have studied the subject in an attempt to understand the complex process by which the clustered arrays of cementite particles develop in the steel blades. The most prominent theories to date are presented in the General Introduction to this thesis. The thesis is divided into four main parts. In the first part, four proposed mechanisms of cementite cluster sheet formation as they relate to the banding theory are introduced. Experiments to investigate these mechanisms are presented. In Part 2, collaborative research focused on the methodology of the reconstructed process for making Damascus steel is presented. In the third part, a study into the graphitization of the reconstructed blades is presented. In Part 4, experimental attempts at producing Damascus steel ingots in the laboratory are presented. DOE

N95-32051# Lawrence Livermore National Lab., Livermore, CA. Dept. of Chemistry and Materials Science.
SYNTHESIS AND CHARACTERIZATION OF NANOPHASE FACE-CENTERED-CUBIC TITANIUM
Alan F. Jankowski and Mark A. Wall Feb. 1995 6 p Presented at the Annual Meeting and Exhibition of the Minerals, Metals and Materials Society (TMS), Las Vegas, NV, 12-16 Feb. 1995
(Contract W-7405-eng-48)
(DE95-009533; UCRL-JC-119682; CONF-950201-10) Avail: CASI HC A02/MF A01

Unalloyed Ti is sputter deposited in the formation of two trilayer films. Each layer within the combinations of Ni-Ti-Ni and Ti-Ni-Ti is less than 0.1 micro m thick. High resolution imaging and electron diffraction results are presented for the microstructural characterization of both trilayer films. Nanophase fcc Ti is initially found in crystalline layers grown on Ni whereas hcp Ti is found in layers grown without a Ni epilayer. Conditions are further examined under which the fcc to hcp transition occurs for Ti deposited on Ni. DOE

N95-32052# Pacific Northwest Lab., Richland, WA.
INTERFACIAL SEGREGATION AND DEFORMATION OF SUPERPLASTICALLY DEFORMED Al-Mg-Mn ALLOYS
John S. Vetrano, Curt A. Lavender, and Stephen M. Bruemmer Mar. 1995 9 p Presented at the Annual Meeting and Exhibition of the Minerals, Metals and Materials Society (TMS), Las Vegas, NV, 12-16 Feb. 1995
(Contract DE-AC06-76RL-01830)
(DE95-009572; PNL-SA-26013; CONF-950201-13) Avail: CASI HC A02/MF A01

Microstructural and microchemical studies have been carried out on superplastically deformed Al-Mg-Mn (AA5083-type) alloys. Grain boundary composition was measured using a Scanning Auger Microprobe (SAM) and an Analytical Transmission Electron Microscope (ATEM), while conventional TEM was used for microstructural evaluation. Non-equilibrium segregation of Si to grain boundaries following deformation was measured by both techniques. Significant interfacial Si enrichment was only detected in gage sections of tensile specimens after uniaxial strains from 50 to 200%. Grip regions which experience identical thermal histories, but without plastic deformation, did not reveal Si segregation. Selected samples also showed a slight depletion of Mg at grain boundaries after deformation. The only reproducible observation of equilibrium segregation was in Zr-modified alloys, where Sn was detected by SAM in both the deformed and undeformed sections of the sample. Microstructural analysis documented subgrain formation and subgrain-precipitate interactions during superplastic deformation. In addition, many grain boundaries and precipitate interfaces contained small (5 to 20 nm) voids. Compositional analysis of these nano-voids revealed that they were enriched in Mg with the adjacent boundary regions correspondingly depleted. DOE

N95-32098# Lehigh Univ., Bethlehem, PA.
ROBOTIC WELD OVERLAY COATINGS FOR EROSION CONTROL Quarterly Technical Progress Report, Oct. 1994 - Dec. 1994
B. F. Levin, J. N. Dupont, and A. R. Marder 25 Jan. 1995 17 p
(Contract DE-FG22-92PC-92542)
(DE95-009643; DOE/PC-92542/T9) Avail: CASI HC A03/MF A01

Research is presently being conducted to develop a criteria for selecting weld overlay coatings for erosion mitigation in Circulated Fluidized Beds. Initially, eleven weld overlay alloys were selected for erosion testing based upon a literature review. All eleven coatings were deposited on 1018 steel substrates using the plasma arc welding process. Ten samples from each coating were prepared for erosion testing. The coating deposition and sample preparation procedures were described in the second quarterly report. All selected coatings were erosion tested at 400 C and their erosion resistance was evaluated by determining the steady state erosion rate. In addition, the microstructure of each coating was characterized before and after the erosion tests. The results of the tests are discussed in the third quarterly report. No correlations were found between room temperature hardness of the weld overlay coatings and their erosion resistance at elevated temperature. During the last quarter tensile tests were performed at 400 C for the Ultimet, Inconel-625, 316L SS, C-22, and Stellite-6 wrought alloys. The erosion tests for these materials at 400 C are in progress. The results of mechanical and erosion tests will be used to correlate mechanical properties of selected wrought alloys such as tensile toughness, ductility, strain hardening coefficient and yield strength to their erosion resistance at 400 C. Also, the erosion behavior of the wrought alloys compared with similar weld alloys will be analyzed. The experimental procedure and results of the tensile tests are presented in this progress report. DOE

N95-32104# Illinois Univ., Urbana, IL.
CASCADE DAMAGE IN THE ORDERED ALLOY Ni3Al
T. X. Bui, I. M. Robertson, and M. A. Kirk (Argonne National Lab., IL.) Jan. 1995 6 p Presented at the 1994 Fall Meeting of the Materials Research Society (MRS), Boston, MA, 28 Nov. - 2 Dec. 1994
(Contracts DE-FG02-91ER-45439; W-31-109-eng-38)
(DE95-009893; ANL/MSD/CP-85468; CONF-941144-134) Avail: CASI HC A02/MF A01

The damage (disordered zones and vacancy loops) produced in the ordered alloy Ni3Al by irradiation with different ions (Ar(+), Kr(+), Xe(+)), ion energies (30 and 50 keV), and at 30 and 300 K has been investigated by using transmission electron microscopy. At room temperature and at constant ion energy, the average size of the disordered zones increases

as the ion mass increases from Ar(+) to Kr(+) and to Xe(+) ions. This trend is opposite to that of the collisional volume which decreases with increasing ion mass and highlights the importance of the thermal spike in causing disorder. At room temperature and at constant ion mass, the zone size increases with increasing ion energy. At 30 K, for the same ion mass and ion energy, the size of the disordered zones is smaller than at room temperature. At both irradiation temperatures, the dislocation loop yield increases with increasing ion energy and ion mass. The loop yield was lower for irradiations at 30 K compared to at 300 K. Comparison of the dislocation loop yield and the size of the disordered zones indicates that the probability for forming a loop increases with the size of the disordered zone. DOE

N95-32154# National Renewable Energy Lab., Golden, CO.
COMPREHENSIVE RESEARCH ON THE STABILITY AND ELECTRONIC PROPERTIES OF a-Si:H AND a-SiGe:H ALLOYS AND DEVICES Final Subcontract Report, 10 Mar. 1991 - 30 Aug. 1994
V. Dalal (Iowa State Univ. of Science and Technology, Ames, IA.) Apr. 1995 108 p
(Contract DE-AC36-83CH-10093)
(DE95-004088; NREL/TP-411-7695) Avail: CASI HC A06/MF A02

This report describes work on the growth of a-Si:H and a-(Si,Ge):H materials and devices using well-controlled growth techniques. The a-Si:H materials were grown at higher temperatures (300-375 C) using electron-cyclotron-resonance (ECR) plasma techniques with a remote H beam. These films have excellent electronic quality and show significant improvements in stability compared with glow-discharge-produced a-Si:H materials. Several problems were encountered during the fabrication of devices in these materials, and we were able to overcome them by a systematic work on buffer layers in these cells. We also studied alternative designs for improving the stability of a-Si:H cells and produced graded-gap a-Si:H cells using glow-discharge that are more stable than comparable standard, ungraded glow discharge devices. Finally, systematic work was done to produce good-quality a-(Si,Ge):H films, using triode radio frequency (RF) glow-discharge with ion bombardment during growth. Diagnostic devices were made using these films, and the properties of the material, such as Urbach energies and hole mobility-lifetime products, were measured in these devices. We found a systematic increase in the Urbach energies, and a corresponding decrease in the hole and electron mu tau products, as the Ge content of the alloys increases. DOE

N95-32183*# National Aeronautics and Space Administration. Lyndon B. Johnson Space Center, Houston, TX.
SPACE SHUTTLE ORBITER CORROSION HISTORY, 1981-1993: A REVIEW AND ANALYSIS OF ISSUES INVOLVING STRUCTURES AND SUBSYSTEMS
May 1995 37 p Original contains color illustrations
(NASA-TM-104810; S-796; NAS 1.15:104810; JSC-27031) Avail: CASI HC A01/MF A01; 5 functional color pages

This report summarizes past corrosion issues experienced by the NASA space shuttle orbiter fleet. Design considerations for corrosion prevention and inspection methods are reviewed. Significant corrosion issues involving structures and subsystems are analyzed, including corrective actions taken. Notable successes and failures of corrosion mitigation systems and procedures are discussed. The projected operating environment used for design is contrasted with current conditions in flight and conditions during ground processing. Author

N95-32241# Sandia National Labs., Albuquerque, NM.
MINUTES OF THE FOURTH ANNUAL WORKSHOP ON CHROMATE REPLACEMENTS IN LIGHT METAL FINISHING
T. R. Guilinger, R. G. Buchheit, C. Drewien, L. M. Maestas, K. R. Zavadil, G. Bierwagen (North Dakota State Univ., Fargo, ND.), M. Kendig (Rockwell International Science Center, Palo Alto, CA.), R. Rungta (General Motors Corp., Anderson, IN.), and L. Vega (Aluminum Co. of America, Alcoa Center, PA.) Apr. 1995 160 p Presented at the 4th Annual Workshop on Chromate Replacements in Light Metal Finishing, Albuquerque, NM, 18-19 Aug. 1994
(Contract DE-AC04-94AL-85000)
(DE95-010937; SAND-94-3010; CONF-9408156) Avail: CASI HC A08/MF A02

The purpose of publishing the minutes of this workshop is to document the content of the presentations and the direction of the discussions at the workshop as a means of fostering collaborative research and development on chromate replacements throughout the defense, automotive, aerospace, and packaging industries. The goal of the workshop was to bring together coating researchers, developers, and users from a variety of industries to discuss new coating ideas, testing methods, and coating preparation techniques from the perspective not only of end user, but also from the perspective of coating supplier, developer, and researcher. To this end, we succeeded because of the wide-ranging interests of attendees present in the more than 60 workshop registrants. It is our hope that future workshops, not only this one but others like it throughout government and industry, can benefit from the recorded minutes of our meeting and use them as a starting point for future discussions of the directions for chromate replacements in light metal finishing. DOE

N95-32265# Arizona Univ., Tucson, AZ.
INFLUENCE OF LAYER ORDER AND COMPOSITION ON THE MAGNETIC ANISOTROPY OF ULTRA-THIN Co SANDWICHES
B. N. Engel, C. Marliere, and C. M. Falco 1994 3 p Presented at the 14th International Colloquium on Magnetic Films and Surfaces, Duesseldorf, Germany, 29 Aug. - 2 Sep. 1994
(Contract DE-FG03-93ER-45488)
(DE95-010608; DOE/ER-45488/1; CONF-940829-2) Avail: CASI HC A01/MF A01

In situ polar Kerr effect measurements have been used to study the magnetic anisotropy of molecular beam epitaxially (MBE)-grown X/Co/Y sandwich structures, where X and Y are each one of the nonmagnetic metals Ag, Au, Cu, or Pd. This lead to the discovery, reported earlier, that the magnitude of the X/Co/Y perpendicular anisotropy is strongly peaked at approximately 1 atomic layer overlayer coverage. Reported here are extensions of this work to investigate the influence of layering order and overlayer composition on this anomalous anisotropy behavior. Measurements to date indicate that the peak in perpendicular anisotropy is present regardless of layer order, i.e. X/Co/Y or Y/Co/X. However, layer-order-dependent behavior is found when the overlayer material is changed after initial coverage, i.e. X/Co/Y/X. Derived from text

N95-32272# Lawrence Livermore National Lab., Livermore, CA.
CREEP OF A FINE-GRAINED, FULLY-LAMELLAR, TWO-PHASE TiAl ALLOY AT 760 C
J. N. Wang, A. J. Schwartz, T. G. Nieh, C. T. Liu, V. K. Sikka, and D. Clemens (Pratt and Whitney Aircraft, Jupiter, FL.) Feb. 1995 9 p Presented at the Annual Meeting and Exhibition of the Minerals, Metals and Materials Society (TMS), Las Vegas, NV, 12-16 Feb. 1995
(Contracts W-7405-eng-48; DE-AC05-84OR-21400)
(DE95-009531; UCRL-JC-119681; CONF-950201-11) Avail: CASI HC A02/MF A01

Creep of a TiAl alloy, having a composition of Ti-47Al-2Cr-2Nb (in atom %) and a fine-grained, fully-lamellar structure, was carried out at 760 C and stresses between 69-723 MPa. It was found that, in addition to having good room temperature properties, the alloy exhibits higher creep resistance than other TiAl alloys with a similar composition. Both the creep data and microstructures of the alloy suggest that there exists a change in deformation mechanism from a glide-controlled process at high stresses to a recovery-controlled process at low stresses. Also, microstructural evidence indicates that the rate-controlling recovery mechanism is the climb of dislocation segments pinned by ledges at gamma/alpha(sub 2) interfacial boundaries. DOE

N95-32283# Lawrence Livermore National Lab., Livermore, CA.
FIRST-PRINCIPLES APPROACHES TO MATERIALS STABILITY
Patrice E. A. Turchi Dec. 1994 18 p Presented at the Metallurgical Society (TMC) Conference on High Performance Composites, Rosemont, IL, 10-15 Oct. 1994
(Contract W-7405-eng-48)
(DE95-011533; UCRL-JC-116447; CONF-9410184-7) Avail: CASI HC A03/MF A01

Parameter-free electronic structure approaches are now being used to predict chemical order and, to a lesser extent, structural transformations in multicomponent alloys, as a function of temperature, concentration, and pressure. The underlying state-of-the-art framework is briefly reviewed, and applications to specific aspects of the statics and kinetics of alloy

transformations are discussed. Finally special emphasis is put on the relations between stability and mechanical properties in substitutional alloys with examples pertaining to the energetics of antiphase boundaries and interfaces. DOE

27 NONMETALLIC MATERIALS

Includes physical, chemical, and mechanical properties of plastics, elastomers, lubricants, polymers, textiles, adhesives, and ceramic materials.

For composite materials see *24 Composite Materials*.

N95-30362# Sandia National Labs., Albuquerque, NM.
SYNTHESIS OF NOVEL PRECURSORS FOR PMN POWDERS AND THE THIN FILMS OBTAINED FROM THEM
T. J. Boyle, D. B. Dimos, and G. J. Moore 1995 7 p Presented at the International Symposium on Advanced Synthesis and Processing, College Station, TX, 11-15 Mar. 1995
(Contract DE-AC04-94AL-85000)
(DE95-008543; SAND-95-0322C; CONF-9503115-1) Avail: CASI HC A02/MF A01

Sol-gel processing has been widely used in the preparation of lead zirconate titanate (PZT) thin films. The authors have applied this methodology to the formation of lead magnesium niobate (PMN) spin-cast deposited thin films. Since there is a limited number of soluble, commercially available compounds, the authors have recently synthesized a series of novel metal alkoxides for use as precursors for generation of PMN thin films and powders. The process for generation of the perovskite phase of these PMN powders and films are reported. DOE

N95-30389# Sandia National Labs., Albuquerque, NM.
EPOXY AND ACRYLATE STEREOLITHOGRAPHY RESINS: IN-SITU MEASUREMENTS OF CURE SHRINKAGE AND STRESS RELAXATION
T. R. Guess, R. S. Chambers, T. D. Hinnerichs, G. D. McCarty, and R. N. Shagam 1995 14 p Presented at the 6th International Conference on Rapid Prototyping, Dayton, OH, 4-6 Jun. 1995
(Contract DE-AC04-94AL-85000)
(DE95-008506; SAND-94-2569C; CONF-9506149-1) Avail: CASI HC A03/MF A01

Techniques were developed to make in situ measurements of gelled resin to determine linear shrinkage, stress-strain response and stress relaxation of single strands of SL 5170 epoxy and SL 5149 photocurable resins. Epoxy strands shrank approximately 1.4% and the acrylate strands about 1.0% after a single exposure. No forces were measured during cure shrinkage of strands following the first laser exposure. In multiple laser exposures, the acrylate continues to shrink; whereas (University of Dayton data) no additional shrinkage is observed in epoxy strands on a second hit. In force relaxation tests, a strand is drawn and then a 0.5% step strain is applied after different elapsed times. The epoxy initial modulus evolves (increases) with elapsed time following draw of the strand, and this evolution in modulus occurs after linear shrinkage has stopped. On the other hand, acrylates show no evolution of modulus with elapsed time following a single laser draw; i.e., once shrinkage stops after one laser hit, the initial modulus remains stable with elapsed time. Finally, relaxation response times of epoxy strands get larger with increasing elapsed time after laser draw. In acrylate strands there was no evolution in initial modulus with elapsed time after a single draw so relaxation times are not a function of elapsed time after a single hit with the laser. DOE

N95-30405# Arizona Univ., Tucson, AZ. Dept. of Materials Sciences and Engineering.
CERAMICS DERIVED FROM METAL-ORGANIC PRECURSORS Final Report, 1 May 1991 - 31 Jul. 1994
Donald R. Uhlmann 6 Jun. 1994 162 p
(Contract F49620-91-C-0033)
(AD-A290791; AFOSR-95-0070TR) Avail: CASI HC A08/MF A02

Research carried out under the present grant has during the past year been directed to four principal areas: (1) Ferroelectric Films; (2) Organic-Inorganic Hybrid Materials (POLYCERAMS); (3) Nonlinear Optic Dyes in POLYCERAM Hosts; and (4) Gradient Refractive Index Lenses. In all cases, the research was based upon developing novel combinations of chemistry and processing to produce novel materials and structures with exceptional properties and characteristics. Also carried out have been systematic investigations of important phenomena and modeling of observed behavior. DTIC

N95-30415 Department of the Navy, Washington, DC.
PROCESS FOR PRODUCING HYDROPHILIC POLYMER MEMBRANES Patent
Barbara F. Howell, inventor (to Navy), Ravanasamudram S. Venkatachalam, inventor (to Navy), and John P. Wehrle, inventor (to Navy) 18 Oct. 1994 5 p Filed 28 Sep. 1993
(AD-D017355; US-Patent-5,356,936; US-Patent-Appl-SN-128289) Avail: US Patent and Trademark Office

Hydrophilicity of hydrophilic polymers, in the form of heat-crosslinked coatings on porous membranes, is increased by exposure to an oxygen plasma, preferable for about 60 seconds. The plasma is generated at an oxygen gas pressure of about 1.5 Torrs in a chamber subjected to radio frequency electromagnetic radiation with a power of 25-100 watts. Such highly hydrophilic membranes have increased efficiency and durability when used as ultrafiltration membranes for separating hydrophobic and hydrophilic materials, such as smoke-air and oil-water mixtures. DTIC

N95-30422# Melbourne Univ., Parkville (Australia).
ORIENTATION OF RAPID THERMALLY ANNEALED LEAD ZIRCONATE TITANATE THIN FILMS ON (111) Pt SUBSTRATE
K. G. Brooks, I. M. Reaney, R. Klissurska, Y. Huang, L. A. Bursill, and N. Setter 1994 45 p
(DE95-615232; UM-P-94/39) Avail: CASI HC A03/MF A01 (US Sales Only)

The nucleation, growth and orientation of lead zirconate titanate thin films prepared from organometallic precursor solutions by spin coating on (111) oriented platinum substrates and crystallized by rapid thermal annealing was investigated. The effects of pyrolysis temperature, post-pyrolysis thermal treatments, excess lead addition, and Nb dopant substitution are reported. The use of post pyrolysis oxygen anneals at temperatures in the regime of 350-450 C was found to strongly effect the kinetics of subsequent amorphous-pyrochlore perovskite crystallization by rapid thermal annealing. It has also allowed films of reproducible microstructure and textures (both (100) and (111)) to be prepared by rapid thermal annealing. It is suggested that such anneals and pyrolysis temperature affect the oxygen concentration/average Pb valence in the amorphous films prior to annealing. The changes in Pb valence state then affect the stability of the transient pyrochlore phase and thus the kinetics of perovskite crystallization. Nb dopant was also found to influence the crystallization kinetics. DOE

N95-30450# Melbourne Univ., Parkville (Australia).
SYNTHESIS OF CARBO-NITRIDE FILMS USING HIGH-ENERGY SHOCK PLASMA DEPOSITION
V. N. Gurarie, A. V. Orlov, K. W. Nugent, P. Weiser, and S. Prawer 1994 6 p
(DE95-615231; UM-P-94/27) Avail: CASI HC A02/MF A01 (US Sales Only)

Recent investigations shows that an enhanced nitrogen content of carbo-nitride films improves wear resistance, hardness, tribological and other properties of these films. The present work reports on the properties of nitrogen rich carbon films produced by an intense gas discharge between carbon electrodes in a nitrogen atmosphere. The energy of the discharge, initial nitrogen pressure, number of discharges and geometry are varied to establish their effect on the nitrogen content and the mechanical, structural and morphological characteristics of the deposited carbon-nitride films. The structural diagnostics include optical and scanning electron microscopy, as well as Auger and Raman Spectroscopes and Rutherford Backscattering. The C-N films formed fell into two categories, differing in morphology and mechanical properties. Type I are C-N films, containing up to 35 at. % nitrogen, and which have an amorphous structure. These films are formed at relatively low plasma shock pressure and exhibit relatively low microhardness, approximately 2 GPa. In a relatively narrow range of the plasma shock pressure and temperature the second type of C-N deposition is observed consisting of high density, closely-packed crystal-like grains growing perpendicular to the substrate surface and displaying a cauliflower-like morphology. The microhardness of these films reaches 15 GPa, as measured by the Vickers method. DOE

N95-30451# Melbourne Univ., Parkville (Australia).
ION IMPLANTATION AND THERMAL STRESS RESISTANCE OF CERAMICS
V. N. Gurarie, J. S. Wiliams, and A. J. Watt 1994 15 p
(DE95-615349; UM-P-93/93) Avail: CASI HC A03/MF A01 (US Sales Only)

Monocrystals of sapphire and magnesia together with glass samples have been subjected to ion implantation prior to thermal shock testing in a plasma of continuously varied intensity. Measurements of the gap between adjacent fragments have been used to estimate the surface temperature. Fracture and deformation characteristics of the surface layer are measured in ion implanted and unimplanted samples using optical and scanning electron microscopy. Ion implantation is shown to modify the near-surface structure of ceramic samples by introducing damage, which makes crack initiation easier under thermal stresses in sapphire and magnesia crystals. The fracture threshold and maximum crack density are shifted towards the lower temperature range. Ion implanted MgO crystals show a ten fold increase in surface crack density. An increased crack density results in a decreased degree of damage characterized by the depth of crack penetration. The thermal stress resistance parameter of glass samples is increased at relatively small doses and decreased at higher doses. The results suggest that crack density and the degree of fracture damage in brittle ceramics operating under thermal shock conditions can be effectively controlled by ion implantation which provides crack initiating defects in the near-surface region. DOE

N95-30459# Technische Univ., Delft (Netherlands).
ELECTROCHEMICAL VAPOUR DEPOSITION OF SOFC INTERCONNECTION MATERIALS Ph.D. Thesis
V. vanDieten 23 Jan. 1995 206 p
(PB95-197844; ISBN-90-407-1075-9) Avail: CASI HC A10/MF A03

The aim of this thesis is to investigate the synthesis of the SOFC (Solid Oxide Fuel Cells) interconnection material Mg-doped LaCrO3 by means of EVD (electrochemical vapor deposition). Although the EVD process is the key technology for the fabrication of the interconnect of the Westinghouse tubular concept SOFC, very little has been published on this subject. Nearly all publications on EVD are dealing with the synthesis of the electrolyte material YSZ. In Chapter 2 the principle of the EVD process is described, as well as the experimental setups used for the synthesis experiments. In Chapter 3 a thermodynamic analysis of the La-Cr-Mg-O-H-Cl-Ar system is made in order to determine how the EVD process conditions may affect the incorporation of magnesium in LaCrO3, and to predict the range of experimental conditions for the synthesis of Mg-doped LaCrO3 by means of CVD (chemical vapor deposition)/EVD. In Chapter 4 the EVD stage of the growth process is modeled. The experimental results of the synthesis of Mg-doped LaCrO3 on porous and gastight substrates are described in Chapter 5. In Chapter 6 the first results on the synthesis of the perovskite oxide YCrO3, a material resembling LaCrO3, by means of particle-precipitation-aided CVD(PP-CVD) are described, as well as the principles of the process. NTIS

N95-30487 National Physical Lab., Teddington (England).
ROUND-ROBIN VALIDATION EXERCISE FOR PLATE TWIST TEST METHOD
W. Nimmo and G. D. Sims Feb. 1995 25 p
(PB95-208088; NPL-DMM(A)156) Copyright Avail: Issuing Activity (National Technical Information Service (NTIS))

A round-robin validation exercise has been undertaken to obtain precision data for the plate twist test method for determination of in-plane shear modulus. Six fiber-reinforced, polymer matrix composite materials representing a range of composite materials and shear moduli (1-6 GPa) were tested. The tests were undertaken by eight laboratories, seven of which had not previously used the method, according to the draft test procedure developed by National Physical Laboratory (NPL). The exercise was organized and the results were analyzed according to ISO 5275 using 95% confidence limits. The detailed results are given in Appendix 1. The test method has been studied and the improved analysis validated as part of the NPL program on test methods for composites. NTIS

N95-30543# Oak Ridge National Lab., TN.
INTERFACE DEGRADATION IN CAS/NICALON DURING ELEVATED TEMPERATURE AGING
K. P. Plucknett, R. L. Cain (Warwick Univ., Coventry, England.), and M. H. Lewis (Warwick Univ., Coventry, England.) 1995 7 p Presented at the 1994 Fall Meeting of the Materials Research Society (MRS), Boston, MA, 28 Nov. - 2 Dec. 1994
(Contract DE-AC05-84OR-21400)
(DE95-008843; CONF-941144-115) Avail: CASI HC A02/MF A01

A CaO-Al2O3-SiO2 (CAS)/Nicalon glass-ceramic matrix composite has been subjected to elevated temperature oxidation heat-treatments between 375 and 1200 C, for up to 100 hours. Micro- and macro-mechanical properties have been determined by fiber push-down, using a mechanical properties microprobe, and flexure testing, respectively. Aging between 450 and 800 C results in significant property degradation, with reduced bending modulus and flexure strength, increased fiber sliding stress, and a transition to a purely brittle failure mode. Aging degradation is due to oxidative removal of the carbon interlayer, with the subsequent formation of a silica bond between fiber and matrix. At higher temperatures, carbon is retained due to the formation of a protective silica plug at exposed fiber ends, with the subsequent retention of composite properties. Short duration pre-treatment schedules, at 1000 or 1100 C, were developed to prevent intermediate temperature property degradation. DOE

N95-30545# Oak Ridge National Lab., TN.
IONIC CONDUCTIVITIES OF LITHIUM PHOSPHORUS OXYNITRIDE GLASSES, POLYCRYSTALS, AND THIN FILMS
B. Wang, J. B. Bates, B. C. Chakoumakos, B. C. Sales, B. S. Kwak, R. A. Zuhr, and J. D. Robertson (Kentucky Univ., Lexington, KY.) Nov. 1994 13 p Presented at the 1994 Fall Meeting of the Materials Research Society (MRS), Boston, MA, 28 Nov. - 2 Dec. 1994
(Contract DE-AC05-84OR-21400)
(DE95-008898; CONF-941144-103) Avail: CASI HC A03/MF A01

Various lithium phosphorus oxynitrides have been prepared in the form of glasses, polycrystals, and thin films. The structures of these compounds were investigated by x-ray and neutron diffraction, x-ray photoelectron spectroscopy (XPS), and high-performance liquid chromatography (HPLC). The ac impedance measurements indicate a significant improvement of ionic conductivity as the result of incorporation of nitrogen into the structure. In the case of polycrystalline Li(2.88)PO(3.73)N(0.14) with the (gamma)-Li3PO4 structure, the conductivity increased by several orders of magnitude on small addition of nitrogen. The highest conductivities in the bulk glasses and thin films were found to be 3.0 x 10(exp -7) and 8.9 x 10(exp -7) S(center dot)/cm at 25 C, respectively. DOE

N95-30548# Oak Ridge National Lab., TN.
AN EXPLANATION FOR THE SHAPE OF NANOINDENTATION UNLOADING CURVES BASED ON FINITE ELEMENT SIMULATION
A. Bolshakov, G. M. Pharr (Rice Univ., Houston, TX.), and W. C. Oliver (Nano Instruments, Inc., Knoxville, TN.) 1995 6 p Presented at the 1994 Fall Meeting of the Materials Research Society (MRS), Boston, MA, 28 Nov. - 2 Dec. 1994
(Contracts DE-AC05-84OR-21400; DE-AC05-76OR-00033)
(DE95-008905; CONF-941144-99) Avail: CASI HC A02/MF A01

Current methods for measuring hardness and modulus from nanoindentation load-displacement data are based on Sneddon's equations for the indentation of an elastic half-space by an axially symmetric rigid punch. Recent experiments have shown that nanoindentation unloading data are distinctly curved in a manner which is not consistent with either the flat punch or the conical indenter geometries frequently used in modeling, but are more closely approximated by a parabola of revolution. Finite element simulations for conical indentation of an elastic-plastic material are presented which corroborate the experimental observations, and from which a simple explanation for the shape of the unloading curve is derived. The explanation is based on the concept of an effective indenter shape whose geometry is determined by the shape of the plastic hardness impression formed during indentation. DOE

N95-30558# Army Construction Engineering Research Lab., Champaign, IL. Engineering and Materials Div.
OFF-POTENTIAL MEASUREMENT SYSTEMS FOR IMPRESSED CURRENT CATHODIC PROTECTION Final Report
Vincent F. Hock, Lewis F. Setliff, Wesley A. Houtz, Michael Noble, and Brad J. Lewis Sep. 1994 74 p

(DA Proj. 4A1-62784A-T41)
(AD-A290876; CERL-TR-FM-94/16) Avail: CASI HC A04/MF A01

The Army currently maintains more than 20,000 underground storage tanks, over 3000 miles of buried pipeline, and more than 3000 elevated water storage tanks, all requiring some form of corrosion control. Impressed current, cathodic protection (CP) systems are a widely used form of corrosion control for these structures. These CP systems contain numerous components that are susceptible to failure if not installed or maintained correctly. To ensure corrosion protection for a structure, the performance of a CP system must be determined in the field. This study investigated off-potential measurement systems-for impressed current CP systems in the laboratory and in the field. Commercially available off-potential measurement devices were investigated to test their reliability in recording off-potentials, which define the effectiveness of a CP system. Off-potential measurement devices were found to provide accurate system performance data. DTIC

N95-30580# Naval Undersea Warfare Center, New London, CT. Submarine Sonar Dept.

MOLECULAR MODELING OF PMN CERAMICS Final Report

George J. Kavarnos Newport, IL 23 Jan. 1995 42 p
(NUWC Proj. A10016)
(AD-A290879; NUWC-NL-TR-10797) Avail: CASI HC A03/MF A01

Extended HOeckel theory was used to analyze the orbital interactions in PbNbO3(+) and LaNbO3(2+) model structures representative of lead magnesium niobate (PMN)ceramic. These structures were chosen to determine the orbital effects, if any, that an A-site substitutional such as Pb(2+) has on bond stability in the crystal lattice structure. It was determined that the A-site ion does not directly influence bonding between the A-site ion and atoms in the neighboring crystal lattice but does change the position of the Fermi level, which in PbNbO3(+) is -10.1 eV and in LaNbO3(2+) is -14.5eV. In PbNbO3(+), the Fermi level is so positioned that the bonds linking Nb and O are destabilized. In contrast, there is no antibonding character in LaNbO3(+). The shifting of the Fermi level as a function of the A-site ion is used to rationalize the experimental observation that pure PMN does not coarsen or undergo additional crystallization during annealing, but La-substituted PMN does in fact favor ordering of the crystal structure. DTIC

N95-30572# Oak Ridge National Lab., TN.

MODELING OF THERMAL, ELECTRONIC, HYDRODYNAMIC, AND DYNAMIC DEPOSITION PROCESSES FOR PULSED-LASER DEPOSITION OF THIN FILMS

C. L. Liu, J. N. LeBoeuf, R. F. Wood, D. B. Geohegan, J. M. Donato, K. R. Chen, and A. A. Puretzky Nov. 1994 8 p Presented at the 1994 Fall Meeting of the Materials Research Society (MRS), Boston, MA, 28 Nov. - 2 Dec. 1994
(Contract DE-AC05-84OR-21400)
(DE95-008906; CONF-941144-100) Avail: CASI HC A02/MF A01

Various physical processes during laser ablation of solids for pulsed-laser deposition (PLD) are studied using a variety of computational techniques. In the course of the authors combined theoretical and experimental effort, they have been trying to work on as many aspects of PLD processes as possible, but with special focus on the following areas: (1) the effects of collisional interactions between the particles in the plume and in the background on the evolving flow field and on thin film growth; (2) interactions between the energetic particles and the growing thin films and their effects on film quality; (3) rapid phase transformations through the liquid and vapor phases under possibly nonequilibrium thermodynamic conditions induced by laser-solid interactions; (4) breakdown of the vapor into a plasma in the early stages of ablation through both electronic and photoionization processes; and (5) hydrodynamic behavior of the vapor/plasma during and after ablation. The computational techniques used include finite difference (FD) methods, particle-in-cell model, and atomistic simulations using molecular dynamics (MD) techniques. DOE

N95-30599# Swedish Inst. for Materials Testing, Boras (Sweden).

INFLUENCE OF ADHESIVES AND BONDING TECHNIQUES ON THE PROPERTIES OF GLUED TIMBER-STEELPLATE JOINTS

1994 89 p
(PB95-211470; SP-RAPP-1994:39) Avail: CASI HC A05/MF A01

This research has been carried out as the first part of a project, whose aim is to develop a safe, simple, cost-effective frame joint for glulam constructions with large spans. Today traditional glulam frames are limited to a maximum span of about 60 m mainly due to transportation limitations. To facilitate the transportation of the structure, smaller glulam beams with glued-in steelplates could be prefabricated and sent to the building site. The joint could be mounted at the building site by means of welding or screwing. The influence of glues and glueing techniques on the joints' strength have been analyzed. NTIS

N95-30621*# National Aeronautics and Space Administration. Lewis Research Center, Cleveland, OH.

ENHANCEMENT OF PERFLUOROPOLYETHER BOUNDARY LUBRICATION PERFORMANCE: I. PRELIMINARY RESULTS

W. R. Jones, Jr., O. O. Ajayi (Wedeven Associates, Inc., Edgmont, PA.), A. J. Goodell (Wedeven Associates, Inc., Edgmont, PA.), L. D. Wedeven (Wedeven Associates, Inc., Edgmont, PA.), E. Devine (Swales and Associates, Beltsville, MD.), and R. E. Premore (National Aeronautics and Space Administration. Goddard Space Flight Center, Greenbelt, MD.) Jun. 1995 12 p Presented at the 207th National Meeting, San Deigo, CA, 13-18 Mar. 1994; sponsored the American Chemical Society
(RTOP 233-02-0D)
(NASA-TM-106937; E-9665; NAS 1.15:106937) Avail: CASI HC A03/MF A01

A ball bearing simulator operating under starved conditions was used to evaluate the boundary lubrication performance of a perfluoropolyether (PFPE) Krytox 143 AB. Several approaches to enhance boundary lubrication were studied. These included: (1) soluble boundary additives, (2) bearing surface modifications, (3) 'run-in' surface films, and (4) ceramic bearing components. In addition, results were compared with two non-perfluorinated liquid lubricant formulations. Based on these preliminary tests, the following tentative conclusions can be made: (1) substantial improvements in boundary lubrication performance were observed with a beta-diketone boundary additive and a tricresyl phosphate (TCP) liquid surface pretreatment; (2) the use of rough Si3N4 balls (Ra = 40 micro-in) also provided substantial improvement but with concomitant abrasive wear; (3) marginal improvements were seen with two boundary additives (a phosphine and a phosphatriazine) and a neat (100%) fluid (a carboxylic acid terminated PFPE); and surface pretreatments with a synthetic hydrocarbon, a PTFE coating, and TiC coated 440C and smooth Si3N4 balls (R(sub a) less than 1 micro-in); and (4) two non-PFPE lubricant formulations (a PAO and a synthetic hydrocarbon) yielded substantial improvements. Author

N95-30645# International Centre for Theoretical Physics, Trieste (Italy).

ELECTRICAL CONDUCTIVITY STUDY ON POLYTHIOPHENES FILMS

I. Youm, M. Cadene (Montpellier-2 Univ., France), and D. Laplaze (Montpellier-2 Univ., France) Oct. 1994 8 p
(DE95-614309; IC-94/315) Avail: CASI HC A02/MF A01 (US Sales Only)

The electrical conduction mechanism of two classes of polythiophenes: polythiophene (PT) and poly(3-methylthiophene) (PMT) films containing various levels of doping counter-ions was investigated. The temperature dependence of electrical conductivity obeys the Mott equation based on variable range hopping. The dimension of the variable range hopping is correlated with the structure of the conducting polymer. It seems for these polymers that carrier transport via mobile conjugational defects does not play a detectable role. DOE

N95-30664 Selskapet for Industriell og Teknisk Forskning, Trondheim (Norway). Dept. for Materials Technology.

TEM-EXAMINATION OF CERAMIC-METAL INTERFACES

T. Torvund, O. M. Akselsen, O. Grong, and J. H. Ulvensoen 2 Jun. 1994 10 p
(PB95-196531; STF24-S94002) Avail: Issuing Activity (National Technical Information Service (NTIS))

In the present investigation, a novel approach to the examination of ceramic-metal interfaces by means of transmission electron microscopy (TEM) is described. A special composite material containing a SiC powder (50 micrometers) in a matrix of a Ag-4wt%Ti filler metal has been made for this purpose. The SiC-powder, mixed with the alloy, was held at 1,000 C for 20 minutes under high vacuum conditions. Thin foils were subsequently extruded from the sample. By combining EDS (energy dispersive spectrometry) and TEM examinations, both Ti5Si3 and TiC were disclosed

as reaction products. These are presumably the same constituent phases that form during brazing of SiC with Ag-4wt%Ti filler metals under similar conditions. NTIS

N95-30715 Department of the Navy, Washington, DC.
ENERGY ABSORPTION APPARATUS Patent
James M. Powers, inventor (to Navy), Mark B. Moffett, inventor (to Navy), and Stephen S. Gilardi, inventor (to Navy) 6 Dec. 1994 11 p Filed 4 Jan. 1993
(AD-D017361; US-Patent-5,371,801; US-Patent-Appl-SN-000031; US-Patent-Class-381-71) Avail: US Patent and Trademark Office

Apparatus for absorbing acoustic energy directed toward a wall is presented. The apparatus includes a piezoelectric layer intermediate the wall and the source of the acoustic energy. Circuitry attached to the output of the transducer compensates blocked and motional capacitances of the transducer so that the output signal generates real current for dissipation in a resistor thereby to minimize any echo reflected from the piezoelectric layer. DTIC

N95-30730# Oak Ridge National Lab., TN. Solid State Div.
MECHANISMS OF ENHANCED IONIC CONDUCTION AT INTERFACES IN CERAMICS
D. Lubben and F. A. Modine Nov. 1994 13 p Presented at the 1994 Fall Meeting of the Materials Research Society, Boston, MA, 28 Nov. - 2 Dec. 1994
(Contract DE-AC05-84OR-21400)
(DE95-009125; CONF-941144-108) Avail: CASI HC A03/MF A01

A large enhancement in the ionic conductivity of certain compounds occurs when the compound is produced as a composite material containing a finely-dispersed non-conductor such as SiO2 or Al2O3. This paper describes recent experiments which proposes that extended defects such as dislocations and grain boundaries, either resulting from or stabilized by the interface, are responsible for the enhancement. The ionic conductivities of LiI and CaF2 thin films grown on sapphire(0001) substrates were monitored in-situ during deposition as a function of film thickness and deposition conditions. LiI films grown at 27 C exhibited a region of enhanced conduction within 100 nm of the substrate and a lesser enhancement as the film thickness was increased further. This conduction enhancement was not stable but annealed out with a characteristic log(time) dependence. The observed annealing behavior was fit with a model based on dislocation motion which implies that the increase in conduction near the interface is due to extended defects generated during the growth process. CaF2 films grown at 200 C showed a behavior similar to the 27 C LiI films, with a region of thermally unstable enhanced conduction that occurs within 10 nm of the substrate. Amorphous Al2O3 films deposited over the CaF2 layers created no additional enhancement but did increase the stability of the conduction, consistent with an extended defect model. Simultaneous deposition of CaF2 and Al2O3 produced films consisting of very-fine -grained CaF2 and particles of amorphous Al2O3 (5-10 nm grain and particle size) a nd a high defect density which was stable even well above the growth temperature. Measured conduction in the composite at 200 C was approximately 360 times that of bulk CaF2. DOE

N95-30732# Oak Ridge National Lab., TN. High Temperature Materials Lab.
STRESS RELAXATION OF SILICON NITRIDE AT ELEVATED TEMPERATURES
A. A. Wereszczak, M. K. Ferber, T. P. Kirkland, E. Lara-Curzio, V. Parthasarathy (Solar Turbines, Inc. San Diego, CA.), and T. T. Gribb (Wisconsin Univ., Madison, WI.) 1995 10 p Presented at the 19th Annual Conference on Advanced Ceramics, Materials and Structures, Cocoa Beach, FL, 9-12 Jan. 1995
(Contract DE-AC05-84OR-21400)
(DE95-009177; CONF-950129-4) Avail: CASI HC A02/MF A01

The stress relaxation behavior of SN88, SN253, and NCX-5102 silicon nitride materials was experimentally determined in tension at 1300 C using buttonhead specimens. Specimens were held at constant strain after being loaded at 10 MPa/s to an initial stress of 276 MPa (40 ksi) or 414 MPa (60 ksi). The subsequent decay in tensile stress was measured as a function of time. A non-negative least squares algorithm used in conjunction with a generalized Maxwell model proved to be an efficient means to define characteristic relaxation modulus spectra and stress relaxation behavior. In the last part of this study, the utility of using short-term stress relaxation testing to predict long-term creep performance was examined. DOE

N95-30738# Nevada Univ. System, Reno, NV. Dept. of Chemical and Metallurgical Engineering.
ANODICALLY ENHANCED DIFFUSION IN Cu/Ag THIN FILM COUPLES
Denny A. Jones and Alan F. Jankowski (Lawrence Livermore National Lab., Livermore, CA.) 1995 13 p Presented at the Alloy 600 Experts Meeting, Warrenton, VA, 5-9 Apr. 1993; sponsored by the Electric Power Research Inst.
(Contract DE-FC08-90NV-10891)
(DE95-009198; CONF-9304146-4) Avail: CASI HC A03/MF A01

Thin, 100-nm films of first silver and then copper were deposited consecutively onto pure single-crystal (111) silicon substrates by magneton sputter deposition. Controlled anodic current density was applied at room temperature to dissolve the outer copper film to varying depths approaching the copper/silver interface. Profiles of copper and silver concentration vs. depth below the anodically dissolved surfaces were subsequently obtained by argon ion sputtering and simultaneous Auger Electron Spectroscopy. Despite some intrinsic mixing during the profile analysis, there is clear evidence that diffusion of copper and silver into one another is enhanced by anodic currents at the outer copper surface. Preliminary interpretation leads the authors to believe that the effect is caused by surface formation of vacancies during anodic dissolution. The anodically generated vacancies can migrate as divacancies to the copper/silver interface where they enhance diffusion by the usual vacancy exchange mechanism. DOE

N95-30765# Fermi National Accelerator Lab., Batavia, IL.
REDUCING PROCESS NOISE IN SUPERCONDUCTING HELIUM LIQUID LEVEL PROBES
J. Brubaker Mar. 1995 7 p
(Contract DE-AC02-76CH-03000)
(DE95-008956; FNAL-TM-1929) Avail: CASI HC A02/MF A01

This memo presents methods to reduce the process noise accompanying the use of superconducting helium liquid level probes in a splashing environment. The development of these methods followed unsatisfactory operation of unmodified, commercially available, level probes used in each of the 24 valve box dewars of Tevatron refrigerators. The dewars function both as reservoirs of refrigeration and as phase separators at the inlet of the cold compressors used in subatmospheric magnet cooling operation. DOE

N95-30767# Trane Co., LaCrosse, WI.
COMPATIBILITY OF REFRIGERANTS AND LUBRICANTS WITH MOTOR MATERIALS UNDER RETROFIT CONDITIONS Quarterly Technical Progress Report, 1 Oct. - 31 Dec. 1994
Robert Doerr and Todd Waite 12 Jan. 1995 83 p Prepared for Air-Conditioning and Refrigeration Technology Inst., Inc., Arlington, VA
(Contract DE-FG02-91CE-23810)
(DE95-010185; DOE/CE-23810/51B) Avail: CASI HC A05/MF A01

Motor materials were exposed to original refrigerants R-11, R-12, R-22, and R-502 in the presence of mineral oil for 500 hours. These same materials were then exposed to alternative refrigerants R-123, R-134a, R-407C (R-32/R-125/R-134a), and R-404A (R-125/R-143a/R-134a), respectively, in the presence of the appropriate lubricant for 500 hours. As a control, some samples were exposed to the original refrigerant/mineral oil for a total of 1,000 hours. These tests were conducted to determine whether exposure to the original refrigerant/mineral oil would affect compatibility of the motor materials with the alternative refrigerant/lubricant after retrofit. Motor materials exposed to the alternative refrigerant and lubricant (after an initial exposure to the original refrigerant and mineral oil) appeared to be compatible with the alternative refrigerant and lubricant. The only concerns were embrittlement of the polyethylene terephthalate (PET) sheet and sleeving insulations, and delamination and blistering of the Nomex sheet insulation in the R-22, R-502, and R-12. Embrittlement of the PET materials was attributed to moisture present during the exposure. Separation of the 475 varnish from metal surfaces in the R-123 was also a concern. The sheet and sleeving insulations were affected by the original refrigerant/mineral oil to a greater extent than by the alternative refrigerant and lubricant. DOE

N95-30791# Melbourne Univ., Parkville (Australia). School of Physics.
POLARIZED RAMAN SPECTROSCOPY OF CHEMICALLY VAPOUR DEPOSITED DIAMOND FILMS
S. Prawer, K. W. Nugent, and P. S. Weiser 1994 11 p
(DE95-616776; UM-P-94/45) Avail: CASI HC A03/MF A01 (US Sales Only)

Polarized micro-Raman spectra of chemical vapor deposited diamond films are presented. It is shown that important parameters often extracted from the Raman spectra such as the ratio of the diamond to non-diamond component of the films and the estimation of the level of residual stress depend on the orientation of the diamond crystallites with respect to the polarization of the incident laser beam. The dependence originates from the fact that the Raman scattering from the non-diamond components in the films is almost completely depolarized while the scattering from the diamond components is strongly polarized. The results demonstrate the importance of taking polarization into account when attempting to use Raman spectroscopy in even a semi-quantitative fashion for the assessment of the purity, perfection and stress in CVD diamond films. DOE

N95-30798# Allied-Signal Aerospace Co., Kansas City, MO.
URETHANE FOAM PROCESS IMPROVEMENTS Final Report
D. R. Watson Mar. 1995 51 p
(Contract DE-AC04-76DP-00613)
(DE95-008957; KCP-613-5539) Avail: CASI HC A04/MF A01

A study was completed to evaluate the foam molding process for environmental and technical improvements. The investigation led to a replacement for chlorinated solvent usage, a potential permanent mold release coating, improved tooling design, and shrinkage characterization of foams filled with varying levels of aluminum oxide. DOE

N95-30799# Oak Ridge National Lab., TN.
POROUS SPHERICAL SHELLS AND MICROSPHERES BY ELECTRODISPERSION PRECIPITATION
Michael T. Harris, Warren G. Sisson, Osman A. Basaran, Susan M. Hayes, and Sophie J. Bobrowski 1994 6 p Presented at the 1994 Fall Meeting of the Materials Research Society, Boston, MA, 28 Nov. - 2 Dec. 1994
(Contract DE-AC05-84OR-21400)
(DE95-009073; CONF-941144-116) Avail: CASI HC A02/MF A01

The ability to reproduce the synthesis of dense- and porous-microspheres and micron-sized spherical shells is very important in (1) the development of ceramics for structural, electronic, catalyst and thermal applications; and (2) the encapsulation of products for controlled-release of drugs, flavors and perfumes, and inks and dyes, and the protection of light-sensitive components and mechanical support of fragile materials. Larger metallic- and ceramic-spherical shells have been used in inertial confinement fusion (ICF) experiments and as catalyst supports. The current paper will focus on a recent technique that has been developed for synthesizing ceramic microspheres and micro-shells. Pulsed electric fields have been used to enhance the dispersion of aqueous metal (Zr and Al) salt solutions from a nozzle and into a nonconducting liquid continuous phase that is immiscible with the aqueous phase. The diameter of the resulting microdroplets ranged in size from approximately 0.1 to 10 micrometers. Precipitation of hydrous metal oxides occurred as ammonia, which was dissolved in varying amounts in the continuous phase, diffused into the aqueous microdroplets. Spherical shells were formed at higher ammonia concentrations and microspheres were produced at lower ammonia concentrations. Upon drying, dimples appeared in the particles that were synthesized at higher ammonia concentrations. The latter result accords with the well known fact that under certain conditions spherical shells collapse when a fluid is extracted from the core of the particle. No dimples were observed in the microspheres that were produced at lower ammonia concentrations. Analog x-ray dot maps for aluminum and zirconium were done to determine the spatial distribution of each metal in the particles. DOE

N95-30871 Selskapet for Industriell og Teknisk Forskning, Trondheim (Norway). Div. of Refrigeration Engineering.
CFC-REPLACEMENT BY NATURAL WORKING FLUIDS: R&D AND INDUSTRIAL CHALLENGES WITHIN THE REFRIGERATION, AIR CONDITIONING AMD HEAT PUMP AREAS
P. E. Frivik 6 Apr. 1994 34 p Presented at the Seminar on Heat Transfer, Thermophysical Properties and Cycle Performance of Alternative Refrigerants, Kitakyushu, Japan, 6-8 Dec. 1993 Prepared in cooperation with Norges Tekniske Hoegskole, Trondheim
(PB95-195756; STF11-A94037) Avail: Issuing Activity (National Technical Information Service (NTIS))

The chlorofluorocarbon (CFC) phase-out appears to be much slower in refrigeration, air conditioning and heat pump applications than in other areas. In addition to technical challenges and dependence on end-user decisions, the task is much bigger than most people outside of our industry are aware of. Although it is evident that the replacement will have to be done mainly with hydrochlorofluorocarbons (HCFC's) and hydrofluorocarbons (HFC's), there are questions about their long term use. The alternative can be natural working fluids, such as ammonia, CO2, and hydrocarbons, or water, air and noble gases. Such fluids are inherently safe for the global environment, due to their long term presence in the biosphere, but some of them pose challenges with respect to safety as well as to the need for improved or new processes, components and systems. NTIS

N95-30894# Naval Research Lab., Washington, DC.
COMPUTATIONAL MODELING OF COATING INTEGRITY EFFECTS ON IMPRESSED CURRENT CATHODIC PROTECTION SYSTEM Final Report, Aug. 1993 - Dec. 1994
Virginia G. DeGiorgi and C. P. Hamilton 28 Mar. 1995 16 p
(AD-A293256; NRL/MR/6380-95/7424) Avail: CASI HC A03/MF A01

Coatings are often used in conjunction with impressed current cathodic protection (ICCP) systems to minimize the effect of corrosion on marine structures. The presence of a coating reduces the current required by an ICCP system. The integrity and efficiency of the coating determines the level of current reduction achieved over the bare metal condition. One of the difficulties is designing a combined coating and ICCP system is that coatings deteriorate with time in service due to a variety of factors including mechanical wear and organic attack. Computational modeling is used to determine the variation in current demand required for corrosion protection for increased levels of damage to the protective coating applied to the propellers of a surface ship. DTIC

N95-30897# Ames Lab., IA.
ROOM TEMPERATURE FRACTURE AND HIGH TEMPERATURE CREEP DEFORMATION PROPERTIES OF ALUMINA REINFORCED WITH 20 VOL% PARTICULATE NIOBIUM Ph.D. Thesis
S. Lane 20 Oct. 1994 98 p
(Contract W-7405-eng-82)
(DE95-010234; IS-T-1716) Avail: CASI HC A05/MF A02

For this material, an increase in RT crack growth resistance of greater than or equal to 300% was achieved; this property increases with increasing Nb particle size. SEM and in-situ crack growth observations show that crack bridging is the primary toughening mechanism for the increased crack growth resistance. A model was presented which uses existing models to determine the steady state bridging length given a stress intensity due to crack bridging. This model showed that the specimen size used for determining the RT fracture toughness was too small. It was also determined that the creep strain rate is in the same range as and comparable to existing studies of Al2O3 and Al2O3 systems. The creep mechanism of the composite material was found to be similar to that of unreinforced Al2O3 with a stress redistribution to the particle/matrix interface. DOE

N95-30955# Pennsylvania Univ., Philadelphia, PA.
NONLINEAR OPTICAL PROCESSES IN POLYMER FILMS Final Technical Report, 30 Sep. 1991 - 29 Sep. 1994
Anthony F. Garito 29 Sep. 1994 13 p
(Contract F49620-91-C-0100; DARPA Order 8103)
(AD-A293384) Avail: CASI HC A03/MF A01

Electrooptic organic polymer thin films show great promise for applications in integrated optoelectronic devices. These materials are usually formed as guest-host polymer systems that exhibit large second order nonlinear optical coefficients, low DC and microwave dielectric constants, and broad optical transparency ranges. The major obstacle to the development of practical polymer optoelectronic devices has been the thermal stability of the electrooptic coefficients of the guest-host polymer films. Current research has focused on finding new guest dye chromophores that possess large nonlinear optical coefficients and thermal stabilities greater than 300 degrees. We summarize our recent development of a new class of high thermal stability fused-ring chromophores, 1,8-naphthoylene

benzimidazoles, based on computer aided molecular design and experimental measurements of microscopic second order optical coefficients. The new chromophores were designed for their structural similarity to polyimide repeat units and consequent easy incorporation into high temperature host polyimides. They are highly colored, comparatively soluble in common organic solvents, and very stable in polyamic acid solutions. They possess relatively large second order optical coefficients and thermal stabilities exceeding 340 degrees. DTIC

N95-30974# Case Western Reserve Univ., Cleveland, OH. Dept. of Macromolecular Science.
FROM MOLECULAR TO MACROMOLECULAR LIQUID CRYSTALS
V. Percec 3 Apr. 1995 248 p
(Contract N00014-89-J-1828)
(AD-A293170) Avail: CASI HC A11/MF A03

The goal of this chapter is to discuss the dependence between various molecular parameters including structure, molecular weight, architecture, etc., and phase behavior. An attempt will be made to follow this trend on passing from a molecular to a macromolecular liquid crystal. The main goal is to provide the reader with the presently available tools which can be used to tailor-make liquid crystalline polymers. A brief and general introduction to low molar mass and polymeric liquid crystals which is required for this purpose will also be made. DTIC

N95-30997# University of Southern California, Los Angeles, CA.
THE IMPACT OF MICROBIOLOGICALLY INFLUENCED CORROSION ON PROTECTIVE POLYMER COATINGS Technical Report, 1 Oct. 1993 - 30 Sep. 1994
F. Mansfeld, H. Xiao, L. T. Han, C. C. Lee, and J. Jones-Meehan Dec. 1994 16 p
(Contract N00014-94-1-0026)
(AD-A288896; TR-1) Avail: CASI HC A03/MF A01

Thirteen polymer coating systems on steel have been exposed to Pacific ocean water (NS) and artificial seawater (AS). Impedance data and electrochemical noise data have been obtained for two-electrode systems on a weekly basis. For comparison, three-electrode impedance measurements have been performed on a monthly basis. Noise data were obtained several times each week. The impedance and noise data at the Port Hueneme, CA test site (NS) were collected by an on-site computer system with a multiplexer which is controlled via modem by a computer system at CEEL/USC. In the laboratory a more traditional approach was used. Experimental data for two coating systems exposed to NS and AS for three months show that the experimental approach developed for data collection at a remote test site produced reliable results which were in general agreement with results obtained in the laboratory. DTIC

N95-31010# Department of the Navy, Washington, DC.
GLASS MATRIX DOPED WITH ACTIVATED LUMINESCENT NANOCRYSTALLINE PARTICLES Patent Application
Alan L. Huston, inventor (to Navy) and Brian C. Justus, inventor (to Navy) 11 Jan. 1995 30 p
(AD-D017416; US-Patent-Appl-SN-371306) Avail: CASI HC A03/MF A01

A luminescent glass includes nanocrystalline semiconductor particles, such as ZnS nanocrystals, and an activator, such as copper, for the particles. The glass is made by depositing the nanocrystalline semiconductor particles and the activator within a porous glass matrix, such as 7930 Vycor and then thermally activating the glass. The porous glass matrix may be at least partially consolidated or may be allowed to remain porous. The nanometer particle size permits the luminescent glasses of the present invention to be transparent to its luminescent emissions. DTIC

N95-31011# Department of the Navy, Washington, DC.
GERMANATE GLASS CERAMIC Patent Application
John M. Jewell, inventor (to Navy), Barry B. Harbison, inventor (to Navy), and Ishwar D. Aggarwal, inventor (to Navy) 23 Dec. 1994 17 p
(AD-D017418; US-Patent-Appl-SN-367074) Avail: CASI HC A03/MF A01

A germanate glass ceramic article which has better thermal and physical properties than the competing materials of zinc sulfide, spinel, and sapphire is made by mixing germanate ceramic glass components; melting the components to form a molten mass; cooling the molten mass to form a solid glass article; nucleating the solid article by heating it in the range of about 630-790 C for about 1-16 hours to develop nuclei in the article; and crystallizing the nucleated article by heating it, after nucleation, in the range of about 1/2 minute to about 8 hours to grow the nuclei to crystallites having an average diameter of less then about 1000 nanometer (nm); and cooling to form the glass ceramic. DTIC

N95-31057# Air-Conditioning and Refrigeration Technology Inst.,. Inc., Arlington, VA.
ARTI REFRIGERANT DATABASE
James M. Calm Feb. 1995 282 p
(Contract DE-FG02-91CE-23810)
(DE95-008336; DOE/CE-23810/51E) Avail: CASI HC A13/MF A03

The Refrigerant Database consolidates and facilitates access to information to assist industry in developing equipment using alternative refrigerants. The underlying purpose is to accelerate phase-out of chemical compounds of environmental concern. DOE

N95-31058# Sandia National Labs., Albuquerque, NM.
HIGH STRAIN RATE PROPERTIES AND CONSTITUTIVE MODELING OF GLASS
T. J. Holmquist (Alliant Techsystems, Inc., Hopkins, MN.), G. R. Johnson (Alliant Techsystems, Inc., Hopkins, MN.), C. M. Lopatin (Alliant Techsystems, Inc., Hopkins, MN.), Dennis E. Grady, and E. S. Hertel, Jr. 1995 14 p Presented at the 15th International Symposium on Ballistics, Haifa, Israel, 21-24 May 1995
(Contract DE-AC04-94AL-85000)
(DE95-008434; SAND-95-0379C; CONF-950537-2) Avail: CASI HC A03/MF A01

This paper presents experimental data and computational modeling for a well-defined glass material. The experimental data cover a wide range of strains, strain rates, and pressures that are obtained from quasi-static compression and tension tests, split Hopkinson pressure bar compression tests, explosively driven flyer plate impact tests, and depth of penetration ballistic tests. The test data are used to obtain constitutive model constants for the improved Johnson-Holmquist (JH-2) brittle material model. The model and constants are then used to perform computations of the various tests. DOE

N95-31103# Oak Ridge National Lab., TN.
AN ASSESSMENT OF THE COST OF MICROWAVE SINTERING CERAMIC TILES FOR ARMOR APPLICATIONS. PHASE 2 REPORT
S. Das and T. R. Curlee Mar. 1995 56 p
(DE95-010000; ORNL/TM-12896) Avail: CASI HC A04/MF A01

This report documents work to assess the costs of microwave sintering ceramic tiles for armor applications. In the previous phase of work, the cost of microwave sintering and preliminary estimates of the total cost of microwave-sintered tiles under two microwave frequencies (i.e., 2.45 GHz and 28 GHz) for alumina and silicon carbide materials were reported. The second phase of work extends the previous work to include all pre- and post-sintering manufacturing steps and considers process and cost variations in these steps that may result from the adoption of microwave sintering. Two separate models were developed for two different materials. As before, a process-cost approach was utilized within a spreadsheet environment. When compared to conventional sintering, the manufacturing of microwave-sintered alumina armor tiles will require an additional binder removal step prior to microwave sintering. The base-case cost of microwave-sintered alumina tiles is estimated to be $46.80/part and $50.50/part, given the use of 2.45 GHz and 28 GHz microwave power sources, respectively. In the case of microwave sintering of silicon carbide armor tiles, the material preparation step will be significantly different from conventional sintering. Instead of a binder removal step, there will be a green machining step. The base-case cost of microwave-sintered silicon carbide tiles is estimated to be $324.50/part and $327.50/part for 2.45 GHz and 28 GHz microwave power sources, respectively, compared to $235/part for conventionally-sintered tiles. Several sensitivity analyses of the impacts of variations in key economic and technical parameters on the costs of microwave-sintered tiles were conducted. Those analyses indicate that costs are quite sensitive to changes in the quantity of energy required during sintering. DOE

N95-31108# Ames Lab., IA.
MAGNETIC RESONANCE SPECTROSCOPY OF FULLERENES AND (PI)-CONJUGATED POLYMERS Ph.D. Thesis
P. A. Lane 20 Oct. 1994 120 p
(Contract W-7405-eng-82)
(DE95-010131; IS-T-1717) Avail: CASI HC A06/MF A02

Photophysics of two pi-conjugated systems, buckminsterfullerene and pi-conjugated polymers, were studied using photoluminescence-detected magnetic resonance (PLDMR). PLDMR of C60 and C70 dissolved in toluene/polystyrene glasses and of fullerene films is described. PLDMR of the glasses is due to a triplet exciton delocalized over the entire molecule; that of (sup 3)C70 differs from (sup 3)C60 due to its longer triplet lifetime. In the films, the delocalized triplet, distorted by intermolecular interactions, reveals a half-field resonance due to triplet-triplet fusion; a second triplet localized on a pentagon or hexagon face next to a neighbor molecule is also detected. Narrow PL-enhancing resonances at g = 2.0017 and 2.0029 for C60 and C70 are observed; these are attributed to recombination of long-lived charged polarons. PLDMR of photooxidized and photopolymerized C60 and C70 reveals a third triplet exciton delocalized across several molecules. The PLDMR of a number of pi-conjugated polymer systems showed three features: (1) a narrow PL-enhancing polaron resonance, and (2) broad full- and (3) half-field triplet exciton powder patterns. PLDMR on fullerene-doped polymers indicate that polarons and triplet excitons quench the PL and are stabilized by defects which break the conjugation. Results on conjugated polymers incorporating noncarbon atoms suggest that these sites trap both polarons and triplet excitons, increasing their lifetimes and populations. This and other results on electroluminescent devices implies that the energy levels of the polarons are distributed over a significant range. DOE

N95-31115# SRA Technologies, Inc., Falls Church, VA.
SERVICES TO DEVELOP, STANDARDIZE, AND VALIDATE POLYMERASE CHAIN REACTION (PCR) PROTOCOLS FOR THE DETECTION OF LEISHMANIASIS IN CLINICAL SAMPLES Final Report, Sep. 1992 - Sep. 1994
Frank A. White, III and Kalachar Suryanaarayana 17 Oct. 1994 126 p
(Contract DAMD17-92-C-2097)
(AD-A290155) Avail: CASI HC A07/MF A02

The disease Leishmaniasis, endemic in Africa, South West Asia, and South America, is caused by transmission of a parasite of the Leishmania species via the bite of an infected sandfly. The severity of the disease ranges from cutaneous lesions to a frequently fatal visceralization of the internal organs unless treated at an early stage. Detection of the parasite is difficult because only low numbers of infected cells are found in peripheral blood. Existing tests for Leishmania parasites are time consuming and have high (50%) false negative rates. We report the development of a rapid polymerase chain reaction (PCR) based diagnostic capable of detecting 1-10 infected cells in 1.5 x 10(exp 6) PBMC's or 2-5 mls of peripheral blood. The test has an accuracy greater than 92%, and a false negative rate of less than 8%, when validated against known clinical samples. Author

N95-31124# Naval Air Warfare Center, Warminster, PA.
A COMPARISON OF COATING ALTERNATIVES FOR US COAST GUARD AIRCRAFT Final Report, for Apr. 1993 - Aug. 1994
Donald J. Hirst and Stephen J. Spadafora 12 Dec. 1994 21 p
(AD-A293270; NAWCADWAR-95014-43) Avail: CASI HC A03/MF A01

Current coatings used on U.S. Coast Guard aircraft contain high volatile organic compound (VOC) contents. Federal, state and local environmental agencies restrict the amount of VOC's from the use of these materials through legislation such as the Clean Air Act and local Air Quality Management District Rules. At the request of the Coast Guard, the Naval Air Warfare Center Aircraft Division Warminster investigated several low VOC candidate replacements to the current paint scheme. The physical performance properties of these materials (i.e. corrosion resistance, adhesion, etc.) were characterized using standard coatings tests. The results of this program show that there are several acceptable alternatives. Replacement of current coating systems would reduce the total amount of hazardous materials emitted from Coast Guard painting operations and eliminate the need for expensive control equipment which will be required by the Clean Air Act (resulting in substantial future cost savings). DTIC

N95-31126# Massachusetts Univ., Lowell, MA.
POLARIZED LASER INDUCED HOLOGRAPHIC SURFACE RELIEF GRATINGS ON POLYMER FILMS Technical Report, 1 Oct. 1994 - 30 Sep. 1995
D. Y. Kim, Lian Li, V. Shivshankar, J. Kumar, and S. K. Tripathy 4 Apr. 1995 27 p
(Contract N00014-90-J-1148)
(AD-A293275; Rept-1148-95-04) Avail: CASI HC A03/MF A01

Large amplitude holographic surface relief gratings on azobenzene containing polymer films were optically induced without any subsequent processing steps. The surface relief structures were observed upon exposure to an interference pattern of polarized Ar+ laser beams. The surface relief structures were investigated using atomic force microscopy. Very regularly spaced surface grating with a surface modulation depth of over 1000 A was obtained. The gratings were stable at ambient conditions and the samples were reusable after erasing the gratings by heating the film above the glass transition temperature. The orientation of the azobenzene groups were induced first and followed by the surface deformation process. The polarization of the writing beam had significant effect on the surface modulation process. The relation between the surface change and optically induced orientation of the azobenzene groups was discussed. Thermal effects were also investigated by studying the dependence of writing intensity and grating spacing on the grating formation process. DTIC

N95-31135# Oak Ridge National Lab., TN.
LIFE PREDICTION METHODOLOGY FOR CERAMIC COMPONENTS OF ADVANCED HEAT ENGINES: PHASE 1. VOLUME 1 Final Report
J. C. Cuccio, P. Brehm, H. T. Fang, J. Hartman, W. Meade, M. N. Menon, A. Peralta, J. Z. Song, T. Strangman, and J. Wade et al Mar. 1995 369 p Prepared in cooperation with Allied-Signal Corp., Phoenix, AZ
(Contract DE-AC05-84OR-21400)
(DE95-010805; ORNL/SUB/89-SC674/1/V1) Avail: CASI HC A16/MF A03

Emphasis of this program is to develop and demonstrate ceramics life prediction methods, including fast fracture, stress rupture, creep, oxidation, and nondestructive evaluation. Significant advancements were made in these methods and their predictive capabilities successfully demonstrated. DOE

N95-31136# Oak Ridge National Lab., TN.
LIFE PREDICTION METHODOLOGY FOR CERAMIC COMPONENTS OF ADVANCED HEAT ENGINES. PHASE 1: VOLUME 2. APPENDICES
J. C. Cuccio, P. Brehm, H. T. Fang, J. Hartman, W. Meade, M. N. Menon, A. Peralta, J. Z. Song, T. Strangman, and J. Wade et al Mar. 1995 306 p Prepared in cooperation with Allied-Signal Corp., Phoenix, AZ
(Contract DE-AC05-84OR-21400)
(DE95-010806; ORNL/SUB/89-SC674/1/V2) Avail: CASI HC A14/MF A03

This volume presents the following appendices: ceramic test specimen drawings and schematics; mixed-mode and biaxial stress fracture of structural ceramics for advanced vehicular heat engines (U. Utah); mode I/mode II fracture toughness and tension/torsion fracture strength of NT154 Si nitride (Brown U.); summary of strength test results and fractography; fractography photographs; derivations of statistical models; and Weibull strength plots for fast fracture test specimens, and size functions. DOE

N95-31152# Los Alamos National Lab., NM.
USE OF A VARIABLE FREQUENCY SOURCE WITH A SINGLE-MODE CAVITY TO PROCESS CERAMIC FILAMENTS
Gerald J. Vogt, Amy H. Regan, Anton S. Rohlev, and Michael T. Curtin 1995 9 p Presented at the 97th Annual Meeting of the American Ceramic Society, Cincinnati, OH, 30 Apr. - 1 May 1995
(Contract W-7405-eng-36)
(DE95-010992; LA-UR-95-1440; CONF-950401-2) Avail: CASI HC A02/MF A01

Rapid feedback control is needed for practical microwave processing of continuous ceramic oxide filaments to regulate the process temperature where the dielectric properties of the filaments change rapidly with temperature. A broadband traveling wave tube (TWT) amplifier provides a highly versatile process control platform for filament processing. By comparing a RF signal from the cavity to a reference signal from the TWT, phase information can be used in a negative feedback loop to allow the oscillator to track the cavity frequency as it shifts due to the changing

dielectric constant in the filaments being heated. By sampling the field level in the cavity with a detector, amplitude control can be done to maintain a consistent electric field level in the cavity, which is important for controlling the filament heating and temperature. The system design will be discussed along with application data for commercial ceramic samples. DOE

N95-31153# Oak Ridge National Lab., TN.
LOW TEMPERATURE FABRICATION FROM NANO-SIZE CERAMIC POWDERS Final Report
Edward J. Gonzalez, Gasper J. Piermarini, Bernard Hockey, Subhas G. Malghan, Stephen C. Danforth (Rutgers Univ., Piscataway, NJ.), and Alexander Pechenik (Department of the Air Force, Washington, DC.) 28 Apr. 1995 83 p Prepared in cooperation with National Inst. of Standards and Technology, Gaithersburg, MD
(Contract DE-AC05-84OR-21400)
(DE95-010995; ORNL/SUB-92-22041/02) Avail: CASI HC A05/MF A01

Understanding of compaction and rheology of ceramic powders is needed for production of defect-free greenware. High pressure and lubricating media (liq. N2, pentane) were used for increased green body density. High green densities could be achieved with nanosize Si nitride and (gamma) alumina. A pressure/temperature system was built which uses an Instron screw-driven press and a piston/cylinder die. Max random packing density of 57 +/- 2% theoretical was achieved for dry compaction of Si nitride at 2.5 GPa and RT; compaction under liq. N2 gave 64 +/- 2%. Dry compaction of alumina was 64% theoretical at 2.5 GPa. Pressureless sintering of Si nitride green compacts did not result in further densification. Hot pressing increased the hardness. In alumina, increased compaction pressure enhances the (gamma)-(alpha) transition and increases the densification upon heat treatment. It is difficult to obtain dense material without coarsened pore/grain microstructure. SANS showed alumina results similar to those found for materials made by inert-gas-condensation. Theoretical studies were also made to model the compaction process. Future studies are outlined. DOE

N95-31175# Oak Ridge National Lab., TN.
CRACKING DURING NANOINDENTATION AND ITS USE IN THE MEASUREMENT OF FRACTURE TOUGHNESS
D. S. Harding, G. M. Pharr (Rice Univ., Houston, TX.), and W. C. Oliver (Nano Instruments, Inc., Knoxville, TN.) 1994 6 p Presented at the 1994 Fall Meeting of the Materials Research Society (MRS), Boston, MA, 28 Nov. - 2 Dec. 1994
(Contract DE-AC05-84OR-21400)
(DE95-008839; CONF-941144-106) Avail: CASI HC A02/MF A01

Results of an investigation aimed at developing a technique by which the fracture toughness of a thin film or small volume can be determined in nanoindentation experiments are reported. The method is based on the radial cracking which occurs when brittle materials are deformed by a sharp indenter such as a Vickers or Berkovich diamond. In microindentation experiments, the lengths of radial cracks have been found to correlate reasonably well with fracture toughness, and a simple semi-empirical method has been developed to compute the toughness from the crack lengths. However, a problem is encountered in extending this method into the nanoindentation regime with the standard Berkovich indenter in that there are well defined loads, called cracking thresholds, below which indentation cracking does not occur in most brittle materials. We have recently found that the problems imposed by the cracking threshold can be largely overcome by using an indenter with the geometry of the corner of a cube. For the cube-corner indenter, cracking thresholds in most brittle materials are as small as 1 micron (approximately 0.1 grams). In addition, the simple, well-developed relation between toughness and crack length used for the Vickers indenter in the microindentation regime can be used for the cube-corner indenter in the nanoindentation regime provided a different empirical constant is used. DOE

N95-31187# Oak Ridge National Lab., TN.
SYNTHESIS AND SELECTED MICRO-MECHANICAL PROPERTIES OF TITANIUM NITRIDE THIN FILMS BY THE PYROLYSIS OF TETRAKIS TITANIUM IN AMMONIA
Y. W. Bae, W. Y. Lee, T. M. Besmann, P. J. Blau, and L. Riester 1994 6 p Presented at the 1994 Fall Meeting of the Materials Research Society (MRS), Boston, MA, 28 Nov. - 2 Dec. 1994
(Contract DE-AC05-84OR-21400)
(DE95-010224; CONF-941144-127) Avail: CASI HC A02/MF A01

Thin films of titanium nitride were chemical vapor deposited on (100)-oriented single-crystal silicon substrates from tetrakis (dimethylamino) titanium, Ti((CH3)2N)4, and ammonia gas mixtures in a cold-wall reactor at 623 K and 655 Pa. The films were characterized by Auger electron spectroscopy, X-ray diffraction, and transmission electron spectroscopy. The nano-scale hardness of the film, measured by nanoindentation, was 12.7 +/- 0.6 GPa. The average kinetic friction coefficient against unlubricated, type 440 C stainless steel was determined using a computer-controlled friction microprobe to be approximately 0.43. DOE

N95-31221# Comision Nacional de Energia Atomica, Buenos Aires (Argentina).
BEHAVIOUR OF POLYMERS IN RADIOACTIVE ENVIRONMENTS: EFFECTS OF DOSE SPEED [COMPORTAMIENTO DE POLIMEROS EN AMBIENTES RADIACTIVOS: EFECTOS DE LA VELOCIDAD DE DOSIS]
A. S. Docters and M. E. Gonzalez 1993 3 p In SPANISH Presented at the 21st Meeting of the Argentine Association of Nuclear Technology, Mar del Plata, Argentina, 8-12 Nov. 1993
(DE95-621008; INIS-AR-091; CONF-9311167) Avail: CASI HC A01/MF A01 (US Sales Only)

The scope of this research is to determine the degradation of mechanical properties of cable insulating PVC after irradiation in air at a Cobalt-60 ((gamma)-ray) facility. Amongst the mechanical properties elongation at break and tensile strength were chosen as they are the most sensible to radiation. The samples were exposed to combined radiation-thermal environments with constant airflow in order to obtain accelerated aging data at doses up to 50-300 kGy, with dose rates ranging between 1.3 and 5.6 kGy/h at temperatures from 60 C to 100 C. At lower dose rates the degradation of mechanical properties increased after the same total dose: elongation at break decreases sharply while tensile strength decreases to a less extent, showing dose rate effects. A strong synergy between irradiation and thermal processes was also observed. DOE

N95-31272 Department of the Navy, Washington, DC.
PHTHALONITRILE PREPOLYMER AS HIGH TEMPERATURE SIZING MATERIAL FOR COMPOSITE FIBERS Patent
Teddy M. Keller, inventor (to Navy) 14 Feb. 1995 6 p Filed 28 Jun. 1993
(AD-D017447; US-Patent-5,389,441; US-Patent-Appl-SN-082645; US-Patent-Class-428-395) Avail: US Patent and Trademark Office

Sized fibers, for use as reinforcements in high temperature polymeric composites, are prepared by coating the outside surface of the fibers with an amorphous, B-stage bisphthalonitrile prepolymer. The prepolymer may be prepared by curing a bisphthalonitrile monomer with an organic amine, an aromatic organic acid, a mineral acid, a Lewis acid or a salt of any of the above. Then, the fibers are coated by passage through an organic solution of the prepolymer. Either before or after completely curing the prepolymer coating on the fibers, the coated fibers are covered with a resin, for example, by passage through a solution or melt of a polyimide or bisphthalonitrile resin. If the phthalonitrile coating was incompletely cured prior to covering the phthalonitrile-coated fiber with the resin, the heat during the subsequent cure of the resin also completely cures the phthalonitrile coating. The resulting composite has excellent high temperature properties. In a preferred embodiment, the coated fibers are used to form a prepreg for usage in composite fabrication. DTIC

N95-31377# Los Alamos National Lab., NM.
SUBSTRATE HEATING MEASUREMENTS IN PULSED ION BEAM FILM DEPOSITION
J. C. Olson, H. A. Davis, D. J. Rej, W. J. Waganaar, D. R. Tallant (Sandia National Labs., Albuquerque, NM.), and M. O. Thompson (Cornell Univ., Ithaca, NY.) 1995 7 p Presented at the Spring Meeting of the Materials Research Society, San Francisco, CA, 17-21 Apr. 1995
(Contract W-7405-eng-36)
(DE95-010862; LA-UR-95-1281; CONF-950412-4) Avail: CASI HC A02/MF A01

Diamond-like Carbon (DLC) films have been deposited at Los Alamos National Laboratory by pulsed ion beam ablation of graphite targets. The targets were illuminated by an intense beam of hydrogen, carbon, and

oxygen ions at a fluence of 15-45 J/sq cm. Ion energies were on the order of 350 keV, with beam current rising to 35 kA over a 400 ns ion current pulse. Raman spectra of the deposited films indicate an increasing ratio of sp(sup 3) to sp(sup 2) bonding as the substrate is moved further away from the target and further off the target normal. Using a thin film platinum resistor at varying positions, we have measured the heating of the substrate surface due to the kinetic energy and heat of condensation of the ablated material. This information is used to determine if substrate heating is responsible for the lack of DLC in positions close to the target and near the target normal. Latest data and analysis will be presented.
DOE

N95-31395# Arizona Univ., Tucson, AZ.
INTELLIGENT SYNTHETIC POLYMERS Final Report, Jun. 1991 - Dec. 1994
Paul D. Calvert and H. K. Hall, Jr. 1 Mar. 1995 10 p
(Contract DAAL03-91-G-0169)
(AD-A292905; ARO-28900.13-MS) Avail: CASI HC A02/MF A01

Block copolymers of hydrophobic and hydrophilic acrylates were to be made and tested for control of mineralization by calcium oxalate. Acrylate copolymers in solution inhibited crystal growth to an extent dependent on their acid content but not dependent on the architecture. Solid films of acrylate polymers became mineralized when exposed to oxalate solutions. This effect was very dependent on the structure of the polymer. Methods were also developed for forming inorganic layers on polymer films by overlaying two polymers, each containing solubilized precipitants. Reaction and precipitation would occur at the film/film interface. Cross-linked methacrylic acid films could be templated with rigid molecules such as caffeine, and then would be absorb the templated molecule selectively from solution. Methods were also developed for coupling short protein chains to acrylate polymers as a route to combining biochemical specificity with localization on inorganic surfaces.
DTIC

N95-31410# California Univ., Los Angeles, CA. Dept. of Chemistry.
PROCESSING OF POLYMERS USING SUPERCRITICAL FLUIDS Final Technical Report, 1 Jul. 1989 - 31 Dec. 1992
John J. Aklonis and Eric J. Amis 27 Mar. 1995 19 p
(Contract N00014-89-J-3063)
(AD-A292880) Avail: CASI HC A03/MF A01

In this project we seek to use this variability of solvating power to dissolve high molecular weight polymers, provide solution processing capacity for polymers which are typically difficult to process, and produce blends of normally incompatible polymers from cosolvated mixtures. This last area, polymer blends, this one of great potential and interest because traditional polymer blends are often phase separate into large domains. For example, we expect that by molecularly blending a liquid crystallize polymer with long chain, fiber forming, crystalline polymers, we will reduce the macroscopic phase separation that now limits effective utilization of both the LCP (liquid crystal polymers) reinforcement and the matrix polymer processibility.
DTIC

N95-31417# University of Northern Illinois, De Kalb, IL. Dept. of Chemistry.
DEPOSITION AND CHARACTERIZATION OF PHOTOCONDUCTIVE PZT THIN FILMS
C. T. Lin, L. Li, J. S. Webb, M. S. Leung (Aerospace Corp., El Segundo, CA.), and R. A. Lipeles (Aerospace Corp., El Segundo, CA.) El Segundo, CA Aerospace Corp. 1 Sep. 1994 17 p
(Grant NSF CTS-93-12875)
(ATR-93(8308)-7) Avail: CASI HC A03/MF A01

Deposition by Aqueous Acetate Solution (DAAS) technique was used to synthesize highly crystalline thin films of undoped and 2 percent iron-doped Pb(Zr(0.53)Ti(0.47))O3 (PZT) perovskites on sapphire and Pt-coated silicon substrates at 600 C. Iron ions were added either at the precursor stage or by thermal diffusion. The crystallinity of the film was measured by X-ray diffraction. The ferroelectric activity was examined by polarization-voltage (P-E) hysteresis loops. The electro-optical properties of ferroelectric/photoconductive PZT thin films were investigated by photocurrent action and 77K emission spectroscopies. The photoconductivity measured at visible wavelengths was enhanced for the thermally diffused, but not the precursor-processed doped materials. This, together with lattice parameters obtained from X-ray data and P-E hysteresis loop measurements, suggested that the precursor-processed doped ions are strongly bonded in the perovskite lattice, whereas the thermally diffused ions are more weakly bound in the grain boundaries.
Author

N95-31461# Rochester Univ., NY. Dept. of Chemical Engineering.
CONJUGATED AROMATIC POLYIMINES. 2. SYNTHESIS, STRUCTURE, AND PROPERTIES OF NEW AROMATIC POLYAZOMETHINES
Chen-Jen Yang and Samson A. Jenekhe 20 Mar. 1995 68 p
(Contract N00014-94-1-0540)
(AD-A292955; TR-5) Avail: CASI HC A04/MF A01

A series of 20 conjugated aromatic Polyimines, containing p-phenylene, p-biphenylene, p-terphenylene, 4,4'- stilbene, and 1,5-naphthalene linkages in the backbone and various electron-donating and electron-withdrawing side-group substitutions, have been synthesized, characterized, and used to investigate the effects of molecular structure on the electronic structure and properties of conjugated polymers. Soluble gallium trichloride or diarylphosphate complexes of the aromatic polyimines in organic solvents facilitated their solution spectroscopic characterization and their processing into thin film and coatings. Electrochemical reduction of the aromatic polyimines was reversible with formal potential of -1.93 to -1.52 V (SCE) and 0.22 to 0.86 charge transferred whereas oxidation was irreversible. The electron affinity and ionization potentials of the series of polymers varied from 2.46 to 2.94 eV and from 4.80 to 5.38 eV, respectively. The associated LUMO and HOMO energy levels are thus tunable by up to 0.48 eV and 0.58 eV, respectively. The electrochemically and optically determined LUMO-HOMO energy gaps of thin films were very close and in the range of 2.08-2.77 eV. The results of this study show that aromatic polyimines are an interesting class of pi-conjugated polymers whose structure and properties can be regulated over a wide range by variation in backbone structure, side group substitution, and through intramolecular hydrogen bonding or complexation, backbone planarity.
DTIC

N95-31462# Rochester Univ., NY. Dept. of Chemical Engineering.
EXCITED-STATE COMPLEXES OF CONJUGATED POLYMERS: NOVEL PHOTOPHYSICAL PROCESSES AND OPTOELECTRONIC MATERIALS
Samson A. Jenekhe 20 Mar. 1995 5 p
(Contract N00014-94-1-0540)
(AD-A292958; TR-7) Avail: CASI HC A01/MF A01

Although the ground-state charge transfer complexes of pi-conjugated polymers have been widely investigated in the past two decades, the corresponding excited-state complexes were only recently discovered. The results of our extensive studies of intermolecular excimers and exciplexes of many conjugated polymers will be presented in the talk. The observation of excimer and excimer emission of many conjugated polymers provides a new model of the photophysics of the materials. It will be shown that the modified Birks' mechanism of intermolecular excimers can explain all the essential features of the luminescence of conjugated polymers. The luminescence and charge photogeneration in exciplexes of conjugated polymers with donor triarylamines will also be presented.
DTIC

N95-31466# Rochester Univ., NY. Dept. of Chemical Engineering.
EXCITED-STATE COMPLEXES OF CONJUGATED POLYMERS
Samson A. Jenekhe 20 Mar. 1995 13 p
(Contract N00014-94-1-0540)
(AD-A292960; TR-8) Avail: CASI HC A03/MF A01

Recent research on the role of supramolecular structure and morphology on the photophysics of conjugated polymers has resulted in the discovery of their excited-state complexes. Intermolecular excimers are found to play a central role in the photophysics of conjugated polymers. Exciplexes of conjugated polymers are suggested to hold potential for more efficient optoelectronic devices through the ready regulation of luminescence, charge transport, and charge photogeneration.
DTIC

N95-31467# Rochester Univ., NY. Dept. of Chemical Engineering.
EFFECTS OF MOLECULAR STRUCTURE ON THE ELECTROACTIVE AND OPTICAL PROPERTIES OF CONJUGATED RIGID-ROD POLYBENZOBISAZOLES
John A. Osaheni and Samson A. Jenekhe 20 Mar. 1995 55 p
(Contract N00014-94-1-0540)
(AD-A292968; TR-6) Avail: CASI HC A04/MF A01

The effects of molecular structure on the electronic structure and electrochemical and linear optical properties of a series of pi-conjugated

rigid-rod polybenzobisazoles, including three new polymers, were explored by cyclic voltammetry and measurement of the optical dispersion of the refractive index. The electrochemical reduction of the polymers was reversible whereas oxidation was not reversible in accord with the electron deficient nature of the benzobisazole ring. The observed variation of the reduction and oxidation potentials, electron affinity, and ionization potential of the series of polymers was related to the variation in backbone structure. The electron affinity of the polymers was 2.4 to 3.0 eV which indicated that the LUMO energy level was tunable by up to 0.6 eV. The ionization potential (5.2 to 5.7 eV) and associated HOMO level of the polymers was tunable by up to 0.5 eV. The measured wavelength dispersion of the refractive index of the polybenzobisazoles showed that n(lambda = 1064 nm) and n(lambda = 2500 run) were 1.74-2.03 and 1.55-1.95 respectively. The large refractive index variation with molecular structure was satisfactorily accounted for by the competing effects of polarizability and molar volume. These results provide a basis for understanding the electronic, optoelectronic, and optical properties of the conjugated polybenzobisazoles in terms of the underlying molecular and electronic structures. DTIC

N95-31471# Illinois Univ., Chicago, IL. Dept. of Civil Engineering Mechanics and Metallurgy.

FAILURE ANALYSIS FOR POLYCARBONATE TRANSPARENCIES Final Report, 1 May 1992 - 1 Sep. 1993

A. Chudnovsky, T. J. Chen, Z. Zhou, C. P. Bosnyak, and K. Sehanobish May 1994 45 p

(Contract F33615-92-C-3405)

(AD-A292992; WL-TR-94-3064) Avail: CASI HC A03/MF A01

Today polymers are increasingly used in advanced structural applications such as aircraft canopies. However, there are no well established models which could be used by design engineers for predicting time to failure for these materials. Development of adequate criteria for three basic stages of fracture (crack initiation, stable crack growth and dynamic crack propagation) is necessary for the accurate prediction of service lifetime. Part 1 of this report reflects a recent progress in understanding of various failure initiation mechanisms in transparency-grade Polycarbonate (PC). A new fatigue crack initiation map for PC is proposed. Another important stage of the fracture process which may strongly influence the total lifetime is crack propagation. Propagation of a crack surrounded by the process zone is a well-known phenomenon for the PC. The properties of the material in the process zone may strongly influence such critical fracture parameters as lifetime, fracture toughness, etc. The deformation of PC by shear banding at a notch-tip was found very similar to that obtained by cold-drawing of PC. In Part 2 of this report the tensile cold-drawing (necking) behavior of PC is further examined using simple tensile extension coupled with temperature measurements via an infrared camera. DTIC

N95-31514# Army Research Lab., Fort Monmouth, NJ.

COMPOSITE POLYMER ELECTROLYTE FOR LITHIUM BATTERIES Technical Report, Jul. 1994 - Feb. 1995

Steve Slane and Mark Salomon Mar. 1995 17 p

(AD-A293924; ARL-TR-426) Avail: CASI HC A03/MF A01

Composite polymer electrolyte films consisting of zeolite powders dispersed in poly(acrylonitrile)(PAN) based gels with lithium hexafluoroarsenate have been prepared and their electrochemical properties studied. Gel electrolytes prepared by adding lithium hexafluoroarsenate in propylene carbonate (PC) and ethylene carbonate (EC) mixtures with PAN have demonstrated ionic conductivities greater than 0.001 siemens per cm at room temperature and above. The addition of zeolite powders increased ionic conductivity at low temperatures due to the highly amorphous nature of the composite film. Impedance spectroscopy was performed to study the lithium electrode/electrolyte interface, and a reduction of the passivation kinetics was observed. Cyclic voltammetry showed that addition of PAN and zeolite powder to liquid electrolyte mixtures with EC/PC did not change the stable electrochemical potential window. In Li/lithium cobalt dioxide cells, at 25 C, these composite electrolytes demonstrated current densities as high as 0.5 milliamps per sq cm, with little voltage or capacity loss compared to cells with liquid electrolytes. DTIC

N95-31559# Washington Univ., Seattle, WA.

DESIGN AND PROCESSING OF MATERIALS BY BIOMIMICKING. SECTIONS 1. PUBLICATIONS Final 3rd Year Report, 1 Jun. 1991 - Sep. 1994

Mehmet Sarikaya and James T. Staley Sep. 1994 88 p

(Grant AF-AFOSR-0281-91)

(AD-A293852; AFOSR-95-0325TR) Avail: CASI HC A05/MF A01

The goal of this research has been to find dispersants for ceramic processing applications. The polyelectrolytes currently in use in the industry are synthesized from toxic precursors which present health hazards to workers. We have investigated polyelectrolytes produced from natural sources such as bacteria and kelp, as well as some polymers which have been produced synthetically. The polyelectrolytes which we have investigated include polysaccharides (alginate and dextran) and polypeptides (polyglutamic acid and polyaspartic acid). Some have been obtained from cultures of bacteria grown in our laboratories, others have been obtained from chemical supply houses. In addition, we have investigated the feasibility of using an in situ process by which we incubate the polymer-producing bacteria in the presence of ceramic powders. In this system, polymer adsorbs to the powder in a high affinity state, allowing subsequent washing to remove the bacterial cells, while retaining the adsorbed polymer. DTIC

N95-31617# Army Research Lab., Watertown, MA. Materials Directorate.

MODE I LARGE STRAIN VISCOELASTIC CRACK BEHAVIOR IN NITRILE RUBBER SHEETS Final Report

Claudia J. Quigley and Joey L. Mead Oct. 1994 41 p

(AD-A289984; ARL-TR-513) Avail: CASI HC A03/MF A01

A finite element analysis of a Mode I crack in a viscoelastic, hyperelastic, and incompressible material was performed under relaxation conditions. Loading of the finite element model was applied until the far field strain reached 50%; the viscoelastic material was then allowed to relax for 15 minutes. The numerical results were compared to experimental material behavior. The applied load and stretch ratio histories obtained from the finite element analysis agreed closely with experimental results. The S22 stress component was the dominant stress and possessed a singularity of o(r(sub -1)), similar to the asymptotic solution for a mechanical crack tip stress field, which does not include viscoelasticity, in a hyperelatic material. The order of the singularity did not change with relaxation. Examination of the crack tip stress field showed that maximum stresses were found close to the crack surface suggesting that crack propagation should initiate above and below the deformed crack tip. DTIC

N95-31623# Melbourne Univ., Parkville (Australia). School of Physics.

CHARACTERIZATION OF /11'01/ TWIN DISLOCATION STRUCTURES IN EVAPORATED TITANIUM THIN FILMS BY HREM

Y. Kasukabe (Tohoku Univ., Sendai, Japan.), Y. Yamada (Tohoku Univ., Sendai, Japan.), Pengju Lin, and L. A. Bursill 1994 16 p

(DE95-615391; UM-P-92/86) Avail: CASI HC A03/MF A01 (US Sales Only)

The structure of /11'01/ twin dislocations in Ti films evaporated on NaCl substrates at 250 C has been examined and characterized by high-resolution electron microscopy. The results have revealed that a twin dislocation structure with step height 4 x d(K(sub 1)), where d(K(sub 1)) is the spacing of the /11'01/ twin planes, actually dissociates into two /11'01/ twin dislocations with step heights of d(K(sub 1)) and 3 x d(K(sub 1)). The twin dislocation with a step height of 3 x d(K(sub 1)) contains an edge dislocation in the core while that with a step height of d(K(sub 1)) is a simple classical twin dislocation structure. Twin dislocations with step height of 2 x d(K(sub 1)), including an edge dislocation in the core, also occur. The atomic-scale core structures of /11'01/ twin dislocations may be derived by analysis of the high-resolution images. The relative mobilities of the three types of twin dislocations is then discussed. DOE

N95-31629# Los Alamos National Lab., NM.

SOLUTION BASED TEMPERATURE OF PEROVSKITE-TYPE OXIDE FILMS AND POWDERS Ph.D. Thesis

J. M. McHale, Jr. Apr. 1995 210 p

(Contract W-7405-eng-36)

(DE95-009089; LA-12825-T) Avail: CASI HC A10/MF A03

Conventional solid state reactions are diffusion limited processes that require high temperatures and long reaction times to reach completion. In this work, several solution based methods were utilized to circumvent this diffusion limited reaction and achieve product formation at lower temperatures. The solution methods studied all have the common goal of trapping the homogeneity inherent in a solution and transferring this

homogeneity to the solid state, thereby creating a solid atomic mixture of reactants. These atomic mixtures can yield solid state products through 'diffusionless' mechanisms. The effectiveness of atomic mixtures in solid state synthesis was tested on three classes of materials, varying in complexity. A procedure was invented for obtaining the highly water soluble salt, titanyl nitrate, TiO(NO3)2, in crystalline form, which allowed the production of titanate materials by freeze drying. The freeze drying procedures yielded phase pure, nanocrystalline BaTiO3 and the complete SYNROC-B phase assemblage after ten minute heat treatments at 600 C and 1100 C, respectively. Two novel methods were developed for the solution based synthesis of Ba2YCu3O(7-x) and Bi2Sr2Ca2Cu3O10. Thin and thick films of Ba2YCu3O(7-x) and Bi2Sr2Ca2Cu3O10 were synthesizedby an atmospheric pressure, chemical vapor deposition technique. Liquid ammonia solutions of metal nitrates were atomized with a stream of N2O and ignited with a hydrogen/oxygen torch. The resulting flame was used to coat a substrate with superconducting material. Bulk powders of Ba2YCu3O(7-x) and Bi2Sr2Ca2Cu3O10 were synthesized through a novel acetate glass method. The materials prepared were characterized by XRD, TEM, SEM, TGA, DTA, magnetic susceptibility and electrical resistivity measurements. DOE

N95-31663# Army Tank-Automotive Research and Development Command, Warren, MI.

COMPATIBILITY OF SINGLE HYDRAULIC FLUID WITH MILITARY SPECIFICATION FLUIDS, SEALS AND METALLURGY

Ellen M. Purdy and Donna M. Rutkowski Mar. 1995 18 p

(AD-A292954; TRDEC-TR-13620) Avail: CASI HC A03/MF A01

This report documents the results of compatibility studies designed to determine the compatibility of Single Hydraulic Fluid (SHF) with currently used military specification hydraulic fluids (MIL-H- 6083, MIL-H-46170), elastomer seals, and hydraulic system metallurgy. The evaluations consisted of subjecting various elastomer samples including nitrile, polyacrylate, and fluorocarbon to SHF by itself and SHF mixed at various percentages with MIL-H-6083 and MIL-H-46170, determining their volume and hardness change, then immediately subjecting them to immersion in SHF. The elastomers were again examined for any net change in hardness and volume after the sequential immersion. Finally, SHF compatibility was tested with the elastomers and the metallurgy in each other's presence to determine if any decomposition in elastomers or fluid or metallurgy occurs. It was found that SHF is fully compatible with MIL-H-6083 and MIL-H-46170 and the existing metallurgy. SHF was also found to be completely compatible with 5 of the 6 elastomers tested. The only exception was fluorosilicone which exhibited anomalous behavior in the sequential fluid testing. It performs well in SHF by itself and when immersed in fluid mixtures of SHF and MIL-H-6083 or MIL-H-46170, yet it exhibited significant shrinkage when subjected to SHF after immersion in the other fluids. This behavior cannot be explained in the scope of this evaluation. Further examination will be required to determine if fluorosilicone seals can be used successfully with SHF. DTIC

N95-31664# Army Tank-Automotive Research and Development Command, Warren, MI.

RECYCLING MIL-H-46170 HYDRAULIC FLUID TO EXTEND FLUID SERVICE LIFE Final Report, 1 Oct. 1993 - 31 Aug. 1994

Ellen M. Purdy, Donna M. Rutkowski, and Franklyn D. Sterling Mar. 1995 19 p

(AD-A293035; TARDEC-TR-13619) Avail: CASI HC A03/MF A01

This report documents the laboratory efforts in proving that used hydraulic fluid could be recycled by removing contaminants and mixing with new fluid. Once the used fluid has been filtered to remove solid particulate contamination and dehumidified to bring the moisture content below 500 ppm water, it can be mixed with new fluid in a 75:25 ratio to bring the fluid mixture up to specification performance. The recycled used fluid by itself could not pass the foaming characteristic requirement thus requiring re-inhibition. Instead of adding more antifoaming agent to the fluid, the decision was made to mix recycled fluid with new fluid to provide the re-inhibition effect. Mixing in new fluid results in an enhancement of all additive performance and eliminated any possible problems with adding too much or too little anti-foaming agent. These efforts set the standards for evaluating commercial recycling units that can recycle hydraulic fluid on a large scale and also establish doctrine for successfully extending the service life of used hydraulic fluid. DTIC

N95-31666# Army Tank-Automotive Research and Development Command, Warren, MI.

EVALUATION OF ENVIRONMENTALLY ACCEPTABLE HYDRAULIC FLUIDS Final Report, Oct. 1993 - Sep. 1994

In-Sek Rhee, Carlos Velez, and Karen VonBernewitz Mar. 1995 23 p

(AD-A293037; TARDEC-TR-13640) Avail: CASI HC A03/MF A01

This describes the laboratory evaluation of environmentally acceptable (EA) commercial hydraulic fluids formulated with vegetable oils and synthetic esters. Evaluations included viscosity, flammability, corrosion and wear protection, thermal and oxidation stability, low temperature capability, elastomer compatibility, and storage stability. Results showed the vegetable based products were limited in operational temperature ranges (-10 to 90 C) due to poor thermal and low temperature stabilities. On the other hand, synthetic ester based fluids showed a wide operational capability (-40 to 150 C) which can meet the requirements of military mobile hydraulic fluids. Although EA hydraulic fluids did not meet the current military specification requirements they are potentially good candidate fluids for the replacement of some current petroleum based military hydraulic fluids. DTIC

N95-31699# Massachusetts Univ., Lowell, MA.

AN INTERPENETRATING POLYMER NETWORK FOR SECOND-ORDER NONLINEAR OPTICS Technical Report, 1 Oct 1994 - 30 Sep. 1995

L. Li, J. I. Chen, S. Marturunkakul, J. Kumar, and S. K. Tripathy 23 Mar. 1995 18 p

(Contract N00014-90-J-1148)

(AD-A293019; TR-95-01) Avail: CASI HC A03/MF A01

The linear optical and second order nonlinear optical (NLO) properties of an interpenetrating polymer network (IPN) have been investigated. For the poled and cured IPN samples, large second order NLO coefficients, d(sub 33), were measured at 1.064 and 1.542 micron. The linear electrooptic coefficients, r(sub 33), were determined at various wavelengths. The poled and cured IPN samples showed no measurable decay of the second-order optical nonlinearity after being treated at 110 C for more than 1000 hours. This excellent long-term stability of the NLO property is ascribed to the novel interpenetrating crosslinked molecular structure of the IPN system. DTIC

N95-31705# Los Alamos National Lab., NM.

DIELECTRIC PROPERTY MEASUREMENT OF ZIRCONIA FIBERS AT HIGH TEMPERATURES

Gerald J. Vogt, Wayne R. Tinga (Alberta Univ., Edmonton, Alberta.), and Ross H. Plovnick (Minnesota Mining and Mfg. Co., Saint Paul, MN.) 1995 14 p Presented at the 97th Annual Meeting of the American Ceramic Society, Cincinnati, OH, 30 Apr. - 1 May 1995

(Contract W-7405-eng-36)

(DE95-010991; LA-UR-95-1459; CONF-950401-1) Avail: CASI HC A03/MF A01

Using a self-heating, electronically tunable microwave dielectrometer, the complex dielectric constant of zirconia-based filaments was measured at 915 MHz from 350 to 1100 C. This fibrous material cools rapidly to near room temperature within several seconds due to a large surface area to volume ratio. Such rapid sample cooling necessitates the use of a self-heating technique to measure the complex dielectric constant at temperatures up to 1100 C. Sample temperature was measured with optical fiber thermometry. The effect of sample temperature measurement on data accuracy is discussed. DOE

N95-32025# Oak Ridge National Lab., TN.

PREDICTIONS OF TENSILE BEHAVIOR AND STRENGTHS OF A SI3N4 CERAMIC AT HIGH TEMPERATURES BASED ON A VISCOPLASTIC MODEL

K. C. Liu, R. Brinkman, Jow-Lian Ding, and Shenghin Lin 1995 7 p Presented at the ASME International Gas Turbine and Aeroengine Congress and Exposition: Land, Sea and Air, Houston, TX, 5-8 Jun. 1995

(Contract DE-AC05-84OR-21400)

(DE95-010220; CONF-950629-5) Avail: CASI HC A02/MF A01

Tensile deformation and rupture behavior were simulated using a viscoplastic model developed recently. The model was formulated based on the state variable approach, which provides flexibility and versatility for characterizing the time-dependent behavior of ceramic materials under general thermomechanical loading conditions. Simulations portrayed by the model were compared with experimental tensile data obtained under two

different tensile stressing rates. Results showed that the model was capable of simulating deformation behavior for all practical engineering purposes, but estimated high-temperature fracture strengths somewhat conservatively. DOE

N95-32043# Oak Ridge National Lab., TN.
MICROSTRUCTURE OF Al2O3 IRRADIATED WITH AN APPLIED ELECTRIC FIELD
S. J. Zinkle, J. D. Hunn, and R. E. Stoller 1994 6 p Presented at the 1994 Fall Meeting of the Materials Research Society (MRS), Boston, MA, 28 Nov. - 2 Dec. 1994
(Contract DE-AC05-84OR-21400)
(DE95-010278; CONF-941144-133) Avail: CASI HC A02/MF A01

A thin amorphous film of alumina was irradiated with 2-MeV He(sup +) ions at (approximately) 400 C up to a damage level of about 0.01 displacements per atom (dpa). The alumina films were sufficiently thin ((approximately) 1.8 (mu)m) to allow the ion beam to be completely transmitted through the specimen. An electric field of (approximately) 280 V/mm (dc) was applied continuously during the irradiation. Radiation induced electrical degradation (RIED), i.e. a permanent increase in the conductance of the film, was observed in specimens irradiated at temperatures near 400 to 450 C but did not occur in a specimen irradiated above 500 C. Transmission electron microscopy found no evidence for colloid formation. The observed increase in the conductance of the alumina film may be due to radiation-induced microcracking. DOE

N95-32075# Texas Univ. at Dallas, Richardson, TX. Dept. of Chemistry.
TUNABLE COMPOSITE MEMBRANES FOR GAS SEPARATIONS Progress Report, Sep. 1994 - Jan. 1995
J. P. Ferraris, K. J. Balkus, Jr., and I. H. Musselman Jan. 1995 3 p
(Contract DE-FG22-94PC-94222)
(DE95-010602; DOE/PC-94222/1) Avail: CASI HC A01/MF A01

Progress is briefly summarized on three fronts: instrument construction (membrane gas permeameter), polymer synthesis (poly(3- octylthiophene), poly(3-dodecylthiophene)), and membrane fabrication and microscopy. DOE

N95-32085# Oak Ridge National Lab., TN.
GELCASTING OF SINTERED REACTION-BONDED SILICON NITRIDE FOR IMPROVED MECHANICAL PROPERTIES
J. P. Maria, J. O. Kiggans, T. N. Tiegs, and S. D. Nunn 1995 7 p Presented at the 19th Annual Conference on Advanced Ceramics, Materials and Structures, Cocoa Beach,FL, 9-12 Jan. 1995
(Contract DE-AC05-84OR-21400)
(DE95-010282; CONF-950129-6) Avail: CASI HC A02/MF A01

Gelcasting of silicon metal for the production of sintered reaction bonded silicon nitride (SRBSN), was investigated in order to identify associated advantages over conventional forming techniques; i.e., die and isostatic pressing. Compacts were formed from identical powder mixtures by both gelcasting and pressing, and were nitrided and sintered to produce SRBSN ceramics. Characterization of the samples included measurement of green density, green and nitrided pore structure, weight gain during nitridation, final density, microstructure, toughness, and flexural strength. It was found that a more uniform pore structure existed in the green gelcast samples. It is believed that this pore configuration aided in nitridation, and manifested itself in a more uniform final microstructure. In addition, improved mechanical properties were achieved in the gelcast samples. This improvement can be attributed to green microstructure homogeneity. DOE

N95-32101# Sandia National Labs., Albuquerque, NM.
MODELS OF TRANSPORT, GAS-PHASE AND SURFACE CHEMISTRY IN DIAMOND CHEMICAL VAPOR DEPOSITION
D. S. Dandy and M. E. Coltrin 1995 7 p Presented at the 187th Meeting of the Electrochemical Society, Reno, NV, 21-26 May 1995
(Contract DE-AC04-94AL-85000)
(DE95-009861; SAND-95-0583C; CONF-950518-4) Avail: CASI HC A02/MF A01

This paper presents an analysis of the Chemical Vapor Deposition of diamond thin films in a direct-current (dc) arc-jet reactor. The analysis discussed here includes a model of the performance of the arc-jet hydrogen excitation source, chemistry in the free-stream region, diffusive transport and chemistry in the boundary layer and at the surface. The surface chemistry model includes pathways for deposition of diamond, as well as creation of defects in the diamond lattice. DOE

N95-32161# Sandia National Labs., Albuquerque, NM.
THE PYROCHLORE-TO-PEROVSKITE TRANSFORMATION IN SOLUTION-DERIVED LEAD ZIRCONATE TITANATE THIN FILMS
James A. Voigt, B. A. Tuttle, T. J. Headley, and D. L. Lamppa 1995 7 p Presented at the 4th Material Research Society-Ferroelectric Thin Films Conference, Boston, MA, 5-9 Dec. 1994
(Contract DE-AC04-94AL-85000)
(DE95-010453; SAND-95-0735C; CONF-941267-1) Avail: CASI HC A02/MF A01

The authors have characterized the pyrochlore-to-perovskite crystallization process in solution-derived Pb(Zr(0.20)Ti(0.80))O3 thin films on (100)MgO single crystal substrates. It has been determined that the perovskite phase nucleated preferentially at the film/MgC interface out of a nanocrystalline (approx. 100 angstrom grains) pyrochlore matrix. During the early stages of the pyrochlore-to-perovskite conversion process, perovskite growth proceeded nearly isotropically from the substrate to form hemispherically shaped grains. Deviations from isotropic growth were shown to result from a growth dependence based on the crystallographic orientation of a growing perovskite grain relative to the orientations of pyrochlore grains being transformed. The volume change that occurs during the pyrochlore-to-perovskite transformation along with two-dimensional grain growth has been used to develop a mechanism for formation of porosity that commonly is concentrated in grain boundary regions. DOE

N95-32208*# National Aeronautics and Space Administration. Lewis Research Center, Cleveland, OH.
LOW COST FABRICATION OF SILICON CARBIDE BASED CERAMICS AND FIBER REINFORCED COMPOSITES
M. Singh and S. R. Levine Jul. 1995 15 p
(Contract NAS3-27186; RTOP 537-04-10)
(NASA-TM-107001; E-9216-1; NAS 1.15:107001) Avail: CASI HC A03/MF A01

A low cost processing technique called reaction forming for the fabrication of near-net and complex shaped components of silicon carbide based ceramics and composites is presented. This process consists of the production of a microporous carb/ ı preform and subsequent infiltration with liquid silicon or silicon-refractory metal alloys. The microporous preforms are made by the pyrolysis of a polymerized resin mixture with very good control of pore volume and pore size thereby yielding materials with tailorable microstructure and composition. Mechanical properties (elastic modulus, flexural strength, and fracture toughness) of reaction-formed silicon carbide ceramics are presented. This processing approach is suitable for various kinds of reinforcements such as whiskers, particulates, fibers (tows, weaves, and filaments), and 3-D architectures. This approach has also been used to fabricate continuous silicon carbide fiber reinforced ceramic composites (CFCC's) with silicon carbide based matrices. Strong and tough composites with tailorable matrix microstructure and composition have been obtained. Microstructure and thermomechanical properties of a silicon carbide (SCS-6) fiber reinforced reaction-formed silicon carbide matrix composites are discussed. Author

N95-32253 National Defence Research Establishment, Stockholm (Sweden).
INFLUENCE OF STORAGE ON THE MAXIMAL PULL-OUT FORCE OF THREE DIFFERENT OPTICAL FIBERS FROM THREE EPOXIDES [INVERKAN AV LAGRING PA MAXIMALA UTDRAGSKRAFTEN AV TRE OLIKA OPTISKA FIBRER FRAN TRE EPOXIDER]
T. Karlsson Dec. 1994 17 p In SWAHILI
(PB95-211777; FOA-R-94-00075-2.5-SE) Avail: Issuing Activity (National Technical Information Service (NTIS))

Three different optical fibers were embedded in three different epoxies. After 1.5 to 12 months storage, either in room atmosphere or at 40 C and 80% relative humidity, the maximum force for fiber pull-out was measured. Storage in moisture increased the maximum pull-out force by the swelling of the matrices. The thermal shrinking during cooling of the matrices crosslinked at elevated temperatures also increased the pull-out force. After storage for a month, in ambient air or moisture, the shrinkage had

relaxed. However the bond between the quartz fiber and its plastic cover did not seem to be changed by the storage. NTIS

N95-32298# Tennessee Univ., Knoxville, TN. Dept. of Chemistry.
STUDY OF THE SURFACE PROPERTIES OF CERAMIC MATERIALS BY CHROMATOGRAPHY Final Report
Georges Guiochon Apr. 1995 16 p
(Contract DE-FG05-88ER-13859)
(DE95-011578; DOE/ER-13859/T1) Avail: CASI HC A03/MF A01

This report summarizes the progress made on the subject project from its beginning up to near the end of the last project year and describes their plans for the end of the year. During the grant period, the authors have (1) developed a theoretical model permitting the calculation of the adsorption energy distribution from the isotherm without making any assumptions regarding the experimental isotherm, by contrast with what current methods do; (2) coded, tested, and validated the calculation procedures developed, which involved solving serious computational difficulties; (3) carried out a systematic investigation of the propagation of the experimental and model errors made in the chromatographic measurements to the energy distribution derived from these data; (4) prepared series of columns with silica particles of various origins, virgin or bonded with different groups; and (5) determined the adsorption energy distributions of diethylether, methanol, ethanol, n-heptane, pyridine, and tetrahydrofuran on the surfaces of several of these adsorbents. DOE

N95-32305# Materials Technologies of Virginia, Blacksburg, VA.
WHISKER REINFORCED GLASS CERAMIC Quarterly Progress Report No. 2, 27 Dec. 1994 - 27 Mar. 1995
G. R. Pickrell and J. J. Brown, Jr. 25 Apr. 1995 7 p
(Contract DE-FG01-94CE-15599)
(DE95-010542; DOE/CE-15599/T2) Avail: CASI HC A02/MF A01

The goal of this project is to investigate the physical properties of an in-situ whisker reinforced glass ceramic material and to produce prototype heat exchanger tubes for testing in a coal combustion environment. The in-situ whisker reinforced glass ceramic process was developed and patented at Virginia Tech and licensed to MATVA. Successful completion of this project will demonstrate the potential for this new material to replace existing heat exchanger materials due to its superior chemical and physical properties. This report covers the progress made during this period. Topics covered here are glass melting and sample preparation. Density and microstructure results are given for samples. DOE

N95-32352# Oak Ridge National Lab., TN.
NONDESTRUCTIVE TESTING OF CERAMIC COMPONENTS: COOPERATIVE RESEARCH AND DEVELOPMENT AGREEMENT COMPLETION REPORT
D. A. Carpenter, T. W. Dews, M. W. Moyer, and R. E. Oakes 22 Dec. 1994 34 p
(Contract DE-AC05-84OR-21400)
(DE95-009510; Y/DW-1352) Avail: CASI HC A03/MF A01

In a joint Cooperative Research and Development Agreement (CRADA) between Martin Marietta Energy Systems (MMES) and an industrial partner, Y-12 has been evaluating nondestructive evaluation (NDE) techniques to identify the quality of high strength aluminum oxide tubes used in laser applications. In Phase 1, several NDE techniques were developed to inspect the tubes. In Phase 2 a correlation between detected defects, actual failure mode and strength of the tubes was developed. In Phase 2 the industrial partner supplied tubes manufactured under a variety of conditions and containing material defects expected from process control variations. The tubes were inspected at MMES utilizing a variety of available acoustic techniques. After inspection, ring tensile specimens were fabricated to determine the tensile strength. The data were evaluated utilizing Weibull statistics to determine the statistical impact of the defects upon strength and correlate the data with the nondestructive evaluations of the tubes and observed defect distribution. DOE

N95-32361# University of Southern Mississippi, Hattiesburg, MS. Dept. of Polymer Science.
RESPONSIVE COPOLYMERS FOR ENHANCED PETROLEUM RECOVERY Quarterly Technical Progress Report, 21 Dec. 1994 - 22 Mar. 1995
Charles McCormick and Roger Hester 22 Mar. 1995 23 p
(Contract DE-AC22-92BC-14882)
(DE95-011857; DOE/BC-14882/12) Avail: CASI HC A03/MF A01

The purpose of this study is to extend the concept of micellar polymerization to more complex systems, and to explore the responsive nature of hydrophobically modified polyelectrolytes by tailoring the microstructure. The synthesis of hydrophobically modified acrylamide/acrylic acid copolymer is described. These types of polymers are of interest as thickening agents utilized in enhanced oil recovery. DOE

N95-31760*# Electronics Mfg. Productivity Facility, Indianapolis, IN.
THE SEARCH FOR CFC ALTERNATIVES IS OVER?
Tim Crawford *In* NASA. Marshall Space Flight Center, Aerospace Environmental Technology Conference Mar. 1995 p 157-161 (For primary document see N95-31746 11-23)
Avail: CASI HC A01/MF A06

N95-31763*# Martin Marietta Energy Systems, Inc., Oak Ridge, TN.
THE OAK RIDGE REFRIGERANT MANAGEMENT PROGRAM
Thomas H. Kevil *In* NASA. Marshall Space Flight Center, Aerospace Environmental Technology Conference Mar. 1995 p 179-186 (For primary document see N95-31746 11-23)
(Contract DE-AC05-84OR-21400)
Avail: CASI HC A02/MF A06

N95-31764*# Glidco Organics Corp., Jacksonville, FL.
Prepsolv (TM): THE OPTIMUM ALTERNATIVE TO 1,1,1-TRICHLOROETHANE AND METHYL ETHYL KETONE FOR HAND-WIPE CLEANING OF AEROSPACE MATERIALS
R. Scott Gallagher, John A. Purvis (Hercules Aerospace Co., Magna, UT.), and Wade W. Moran (Hercules Aerospace Co., Magna, UT.) *In* NASA. Marshall Space Flight Center, Aerospace Environmental Technology Conference Mar. 1995 p 187-197 (For primary document see N95-31746 11-23)
Avail: CASI HC A03/MF A06

N95-31765*# Martin Marietta Corp., Huntsville, AL.
A WATER BLOWN URETHANE INSULATION FOR USE IN CRYOGENIC ENVIRONMENTS
Elana Blevins and Jon Sharpe *In* NASA. Marshall Space Flight Center, Aerospace Environmental Technology Conference Mar. 1995 p 201-206 (For primary document see N95-31746 11-23)
(Contract NAS8-36200)
Avail: CASI HC A02/MF A06

N95-31766*# Martin Marietta Corp., Huntsville, AL. Manned Space Systems.
EVALUATION OF HFC 245ca AND HFC 236ea AS FOAM BLOWING AGENTS
Jon Sharpe, Doug MacArthur, Tom Kollie (Oak Ridge National Lab., TN.), Ron Graves (Oak Ridge National Lab., TN.), Matthew Liu (Martin Marietta Corp., New Orleans, LA.), and Robert V. Hendriks (Environmental Protection Agency, Research Triangle Park, NC.) *In* NASA. Marshall Space Flight Center, Aerospace Environmental Technology Conference Mar. 1995 p 207-224 (For primary document see N95-31746 11-23)
(Contracts NAS8-36200; DE-AC05-84OR-21400; EPA-DW-899349-75)
Avail: CASI HC A03/MF A06

N95-31767*# Battelle Memorial Inst., Columbus, OH.
ALTERNATIVES TO OZONE DEPLETING REFRIGERANTS IN TEST EQUIPMENT
Richard L. Hall and Madeleine R. Johnson (Aerospace Guidance and Metrology Center, Newark Air Force Station, OH.) *In* NASA. Marshall Space Flight Center, Aerospace Environmental Technology Conference Mar. 1995 p 225-232 (For primary document see N95-31746 11-23)
Avail: CASI HC A02/MF A06

N95-31769*# Spectrex, Inc., Cedar Gove, NJ.
NEXT GENERATION FIRE SUPPRESSANTS
Jerry A. Brown *In* NASA. Marshall Space Flight Center, Aerospace Environmental Technology Conference Mar. 1995 p 239-243 (For

primary document see N95-31746 11-23)
Avail: CASI HC A01/MF A06

N95-31770*# Great Lakes Chemical Corp., West Lafayette, IN.
F-200(TM): THE NEW SOLUTION FOR FIRE PROTECTION
Alfred J. Thornton and Gerald J. Walter *In* NASA. Marshall Space Flight Center, Aerospace Environmental Technology Conference Mar. 1995 p 245-248 (For primary document see N95-31746 11-23)
Avail: CASI HC A01/MF A06

N95-31771*# National Center for Mfg. Sciences, Ann Arbor, MI.
ASSESSMENT OF POLLUTION PREVENTION AND CONTROL TECHNOLOGY FOR PLATING OPERATIONS
Paul D. Chalmer, William A. Sonntag (National Association of Metal Finishers, Chicago, IL.), and George C. Cushnie, Jr. (Chrome Application, Inc., Oakton, VA.) *In* NASA. Marshall Space Flight Center, Aerospace Environmental Technology Conference Mar. 1995 p 251-266 (For primary document see N95-31746 11-23)
Avail: CASI HC A03/MF A06

N95-31772*# Rockwell International Corp., Canoga Park, CA. Rocketdyne Div.
THIN-FILM SULFURIC ACID ANODIZING AS A REPLACEMENT FOR CHROMIC ACID ANODIZING
K. J. Kallenborn and J. R. Emmons *In* NASA. Marshall Space Flight Center, Aerospace Environmental Technology Conference Mar. 1995 p 267-276 (For primary document see N95-31746 11-23)
Avail: CASI HC A02/MF A06

N95-31773*# Boeing Defense and Space Group, Seattle, WA.
CADMIUM PLATING REPLACEMENTS
Mary J. Nelson and Earl C. Groshart *In* NASA. Marshall Space Flight Center, Aerospace Environmental Technology Conference Mar. 1995 p 277-284 (For primary document see N95-31746 11-23)
Avail: CASI HC A02/MF A06

N95-31774*# National Aeronautics and Space Administration. Marshall Space Flight Center, Huntsville, AL.
REPLACEMENT OF CORROSION PROTECTION CHROMATE PRIMERS AND PAINTS USED IN CRYOGENIC APPLICATIONS ON THE SPACE SHUTTLE WITH WIRE ARC SPRAYED ALUMINUM COATINGS
R. L. Daniel (Rockwell International Corp., Huntsville, AL.), H. L. Sanders (Rockwell International Corp., Huntsville, AL.), and F. R. Zimmerman *In its* Aerospace Environmental Technology Conference Mar. 1995 p 285-291 (For primary document see N95-31746 11-23)
(Contract NAS8-40000)
Avail: CASI HC A02/MF A06

N95-31775*# Northrop Grumman Corp., Pico Rivera, CA. Environmentally Technology Development.
ENVIRONMENTALLY REGULATED AEROSPACE COATINGS
Virginia L. Morris *In* NASA. Marshall Space Flight Center, Aerospace Environmental Technology Conference Mar. 1995 p 295-305 (For primary document see N95-31746 11-23)
Avail: CASI HC A03/MF A06

N95-31776*# United Space Boosters, Inc., Huntsville, AL. Materials and Processes Lab.
CONVERGENT SPRAY PROCESS FOR ENVIRONMENTALLY FRIENDLY COATINGS
Jack Scarpa *In* NASA. Marshall Space Flight Center, Aerospace Environmental Technology Conference Mar. 1995 p 307-313 (For primary document see N95-31746 11-23)
Avail: CASI HC A02/MF A06

N95-31777*# Rockwell International Corp., Canoga Park, CA. Rocketdyne Div.
SSME MAIN COMBUSTION CHAMBER (MCC) HOT OIL DEWAXING
Anthony U. Akpati *In* NASA. Marshall Space Flight Center, Aerospace Environmental Technology Conference Mar. 1995 p 315-323 (For primary document see N95-31746 11-23)
Avail: CASI HC A02/MF A06

N95-31778*# San Antonio Air Logistics Center, Kelly AFB, TX. Aircraft Production Div.
BICARBONATE OF SODA PAINT STRIPPING PROCESS VALIDATION AND MATERIAL CHARACTERIZATION
Michael N. Haas *In* NASA. Marshall Space Flight Center, Aerospace Environmental Technology Conference Mar. 1995 p 325-329 (For primary document see N95-31746 11-23)
Avail: CASI HC A01/MF A06

N95-31779*# National Aeronautics and Space Administration. Marshall Space Flight Center, Huntsville, AL.
WATERJET PROCESSES FOR COATING REMOVAL
Fletcher Burgess (United Space Boosters, Inc., Huntsville, AL.), Steve Cosby (United Space Boosters, Inc., Huntsville, AL.), and David Hoppe *In its* Aerospace Environmental Technology Conference Mar. 1995 p 331-336 (For primary document see N95-31746 11-23)
Avail: CASI HC A02/MF A06

N95-31780*# Jet Edge, Inc., Minneapolis, MN.
ULTRA-HIGH PRESSURE WATER JETTING FOR COATING REMOVAL AND SURFACE PREPARATION
Spencer T. Johnson *In* NASA. Marshall Space Flight Center, Aerospace Environmental Technology Conference Mar. 1995 p 337-347 (For primary document see N95-31746 11-23)
Avail: CASI HC A03/MF A06

N95-31781*# Forward Technology Industries, Inc., Minneapolis, MN.
AQUEOUS CLEANING DESIGN PRESENTATION
Peter F. Maltby *In* NASA. Marshall Space Flight Center, Aerospace Environmental Technology Conference Mar. 1995 p 351-363 (For primary document see N95-31746 11-23)
Avail: CASI HC A03/MF A06

N95-31782*# National Aeronautics and Space Administration. Marshall Space Flight Center, Huntsville, AL.
EVALUATION OF PRESSURIZED WATER CLEANING SYSTEMS FOR HARDWARE REFURBISHMENT
Terry W. Dillard (Thiokol Corp., Huntsville, AL.), Charles D. DeWeese, David T. Hoppe, John H. Vickers, Gary J. Swenson (Thiokol Corp., Brigham City, UT.), and Dale E. Hutchens (Thiokol Corp., Huntsville, AL.) *In its* Aerospace Environmental Technology Conference Mar. 1995 p 365-368 (For primary document see N95-31746 11-23)
Avail: CASI HC A01/MF A06

N95-31789*# Thiokol Corp., Brigham City, UT.
QFD ANALYSIS OF RSRM AQUEOUS CLEANERS
Roy D. Marrs and Randy K. Jones *In* NASA. Marshall Space Flight Center, Aerospace Environmental Technology Conference Mar. 1995 p 431-437 (For primary document see N95-31746 11-23)
Avail: CASI HC A02/MF A06

N95-31790*# National Aeronautics and Space Administration. Marshall Space Flight Center, Huntsville, AL.
A DESIGN OF EXPERIMENTS TEST TO DEFINE CRITICAL SPRAY CLEANING PARAMETERS FOR BRULIN 815 GD AND JETTACIN CLEANERS
Jill M. Keen (Thiokol Corp., Huntsville, AL.), Kurt B. Evans (Thiokol Corp., Brigham City, UT.), Robert L. Schiffman (Thiokol Corp., Brigham City, UT.), C. Darrell DeWeese, and Michael E. Prince *In its* Aerospace Environmental Technology Conference Mar. 1995 p 439-448 (For primary document see N95-31746 11-23)
Avail: CASI HC A02/MF A06

N95-31792*# Martin Marietta Energy Systems, Inc., Oak Ridge, TN.
CLEANING WITHOUT CHLORINATED SOLVENTS
L. M. Thompson and R. F. Simandl *In* NASA. Marshall Space Flight Center, Aerospace Environmental Technology Conference Mar. 1995 p 461-470 (For primary document see N95-31746 11-23)
(Contract DE-AC05-84OR-21400)
Avail: CASI HC A02/MF A06

N95-31793*# Aerospace Corp., El Segundo, CA. Mechanics and Materials Technology Center.
REPLACEMENT OF OZONE DEPLETING AND TOXIC CHEMICALS IN GRAVIMETRIC ANALYSIS OF NON-VOLATILE RESIDUE
G. S. Arnold, J. C. Uht, and F. B. Sinsheimer *In* NASA. Marshall Space Flight Center, Aerospace Environmental Technology Conference Mar. 1995 p 471-480 (For primary document see N95-31746 11-23)
(Contract F04701-92-C-0021)
Avail: CASI HC A02/MF A06

N95-31795*# United Space Boosters, Inc., Huntsville, AL. Materials and Processes Dept.
ENVIRONMENTALLY COMPATIBLE HAND WIPE CLEANING SOLVENTS
Catherine P. Clayton and Michael P. Kovach *In* NASA. Marshall Space Flight Center, Aerospace Environmental Technology Conference Mar. 1995 p 491-497 (For primary document see N95-31746 11-23)
Avail: CASI HC A02/MF A06

N95-31796*# National Aeronautics and Space Administration. Marshall Space Flight Center, Huntsville, AL.
IMPLEMENTATION OF ENVIRONMENTALLY COMPLIANT CLEANING AND INSULATION BONDING FOR MNASA
Dale E. Hutchens (Thiokol Corp., Huntsville, AL.), Jill M. Keen (Thiokol Corp., Huntsville, AL.), Gary M. Smith (Thiokol Corp., Huntsville, AL.), Terry W. Dillard (Thiokol Corp., Huntsville, AL.), C. Darrell DeWeese, and Seth W. Lawson *In its* Aerospace Environmental Technology Conference Mar. 1995 p 499-506 (For primary document see N95-31746 11-23)
(Contract NAS8-38100)
Avail: CASI HC A02/MF A06

28 PROPELLANTS AND FUELS

Includes rocket propellants, igniters, and oxidizers; their storage and handling procedures; and aircraft fuels.

For related information see also *07 Aircraft Propulsion and Power, 20 Spacecraft Propulsion and Power,* and *44 Energy Production and Conversion.*

N95-30626 National Defence Research Establishment, Stockholm (Sweden).
AGEING CONTROL NO. 3 OF PROPELLANTS FOR ROCKET MOTORS RB 27 AND RB 28 [ALDRINGSKONTROLL NR 3 AV KRUT 1 RAKETMOTORER FOER RB 27 OCH RB 28]
A. Pettersson and R. Sanden Sep. 1994 63 p
(PB95-210357; FOA-R-94-00029-2.1-SE) Copyright Avail: Issuing Activity (National Technical Information Service (NTIS))

Measurements of aging properties of composite propellants with polysulfide as fuel-binder have been made. Tensile strength, adhesion of liner, thermal expansion, glass transition temperature, hardness and burning rate have been measured. The results have been compared with measurements on propellants from the same sort of motors in USA and with earlier measurements at Forsvarets Forskningsanstalt (FOA). The results now obtained correspond well with earlier results. No indications of deterioration of properties since the last test at FOA can be seen. NTIS

N95-31149# National Hellenic Research Foundation, Athens (Greece).
PROPERTIES OF NEW MATERIALS RELEVANT TO ENERGY AND FUEL RESEARCH Final Report, 30 Sep. 1991 - 29 Jun. 1994
Cleanthes A. Nicolaides 1 Dec. 1994 8 p
(Grant AF-AFOSR-0405-91)
(AD-A289734; EOARD-TR-95-01) Avail: CASI HC A02/MF A01

The work represents a contribution toward the quantitative understanding of certain energy trapping and release processes of the molecular level for novel compounds. In particular, it has dealt via advanced computations with questions of formation, properties as equilibrium and at transition states, and of spontaneous or laser-induced fragmentation of unusual molecules existing because of local minima on repulsive surfaces. Such molecules are a number of new nonclassical hydrogen complexes (e.g. OBeH2, F3AlH2, F4Mg2 H2). For diatomic volcanic and excimer states, newly developed ab initio computational methods were applied for obtaining the time-dependent probabilities for a number of multiphoton dissociation and excitation processes. DTIC

N95-31194 Johns Hopkins Univ., Columbia, MD. Chemical Propulsion Information Agency.
THE 31ST JANNAF COMBUSTION SUBCOMMITTEE MEETING, VOLUME 1
Mary T. Gannaway, ed. Oct. 1994 454 p Meeting held in Sunnyvale, CA, 17-21 Oct. 1994; sponsored by the Joint NASA, Army, Navy, Air Force Interagency Propulsion Committee
(Contract N00014-91-C-0001)
Avail: CPIA, 10630 Little Patuxent Pkwy., Suite 202, Columbia, MD 21044-3200 HC

This volume, the first of our volumes, is a collection of 32 unclassified/unlimited papers which were presented at the 31st Joint Army-Navy-NASA-Air Force (JANNAF) Combustion Subcommittee Meeting in conjunction with the Exhaust Plume Technology Subcommittee and SPIRITS User Group Meeting held 17-21 October 1994 at the Lockheed Missiles and Space Company, Sunnyvale, California. Specific subjects discussed include: combustion characteristics of metallized solids in nozzles and plumes; airbreathing propulsion; advanced and electrothermal-chemical guns; gun propellant ignition and interior ballistics; liquid propellant guns; liquid propellant combustion and combustion oscillation and liquid rocket engine combustion. For individual titles, see N95-31195 through N95-31212.

N95-31195 Analytical Methods, Inc., Bellevue, WA.
SURVEY OF RECENT Al2O3 DROPLET SIZE DATA IN SOLID ROCKET CHAMBERS, NOZZLES, AND PLUMES c20
Mark Salita *In* Johns Hopkins Univ., The 31st JANNAF Combustion Subcommittee Meeting, Volume 1 Oct. 1994 p 1-18 (For primary document see N95-31194 11-28)
Avail: CPIA, 10630 Little Patuxent Pkwy., Suite 202, Columbia, MD 21044-3200 HC

The size distribution of Al2O3 droplets in a solid propellant rocket is very different in the chamber, nozzle, and plume, primarily due to breakup and collision/coalescence in the nozzle. This paper attempts to summarize, evaluate, and relate the results of 19 recent experimental and analytical studies of droplet size in order to construct a unified model of droplet size evolution from the chamber through the nozzle and into the plume. It is believed that the distribution of droplet mass in the chamber is bimodal log-normal, with 1 micron smoke comprising about 80% of the mass and 50-100 micron caps comprising the remaining 20%. During passage through the nozzle, the caps shatter to product droplets whose diameters are about 10% of the caps but still 10 times those of smoke, while all but 1-2% of the smoke mass collides and coalesces with the shatter products to generate an essentially monomodal mass distribution at the nozzle exit whose D43 agrees with Hermsen's correlation and whose standard deviation alpha approximately or equal to 0.13 is smaller than both the chamber smoke (alpha approximately or equal to 0.40) or caps (alpha approximately or equal to 0.20). Author

N95-31196 Georgia Inst. of Tech., Atlanta, GA.
THE Al AND Al2O3 DROPLET CLOUD IN SOLID ROCKET MOTORS c20
E. W. Price and R. K. Sigman *In* Johns Hopkins Univ., The 31st JANNAF CombustionSubcommittee Meeting, Volume 1 Oct. 1994 p 19-28 (For primary document see N95-31194 11-28)
(Contract N00014-89-J-1293)
Avail: CPIA, 10630 Little Patuxent Pkwy., Suite 202, Columbia, MD 21044-3200 HC

A discussion is presented of the current state of understanding and prediction of size and spatial distribution of aluminum and Al2O3 droplets in a motor. It is noted that available theory and experimental results are inadequate for prediction of two phase flow effects (e.g., slag formation, damping of oscillations), especially with propellants other than those based on AP and hydrocarbon binder. Potentially important phenomena that have received almost no attention include fragmentation of Al droplets near burnout, and growth of larger oxide droplets by accretion of fine 'smoke' droplets. Author

N95-31197* Naval Air Warfare Center, China Lake, CA.
SHUTTLE REDESIGNED SOLID ROCKET MOTOR ALUMINUM OXIDE INVESTIGATIONS **c20**
Fred S. Blomshield, Karl J. Kraeutle, and Richard A. Stalnaker *In* Johns Hopkins Univ., The 31st JANNAF Combustion Subcommittee Meeting, Volume 1 Oct. 1994 p 29-40 (For primary document see N95-31194 11-28)
Avail: CPIA, 10630 Little Patuxent Pkwy., Suite 202, Columbia, MD 21044-3200 HC

During the launch of STS-54, a 15 psi pressure blip was observed in the ballistic pressure trace of one of the two Space Shuttle Redesigned Solid Rocket Motors (RSRM). One possible scenario for the observed pressure increase deals with aluminum oxide slag formation in the RSRM. The purpose of this investigation was to examine changes which may have occurred in the aluminum oxide formation in shuttle solid propellant due to changes in the ammonium perchlorate. Aluminum oxide formation from three propellants, all having the same formulation, but containing ammonium perchlorate from different manufacturers, will be compared. Three methods have been used to look for possible differences among the propellants. The first method was to examine window bomb movies of the propellants burning at 100, 300 and 600 psia. The motor operating pressure during the pressure blip was around 600 psia. The second method used small samples of propellant which were fired in a combustion bomb which quenched the burning aluminum particles soon after they left the propellant surface. The bomb was fired in both argon and Nitrogen atmospheres at various pressures. Products from this device were examined by optical microscopy. The third method used larger propellant samples fired into a particle collection device which allowed the aluminum to react and combust more completely. This device was pressurized with Nitrogen to motor operating pressures. The collected products were subdivided into size fractions by screening and sedimentation and analyzed optically with an optical microscope. the results from all three methods indicate very small changes in the size distribution of combustion products. Author

N95-31198 Brigham Young Univ., Provo, UT.
BURN TIME MEASUREMENTS OF SINGLE ALUMINUM PARTICLES IN STEAM AND CARBON DIOXIDE MIXTURES **c25**
S. E. Olsen and M. W. Beckstead *In* Johns Hopkins Univ., The 31st JANNAF Combustion Subcommittee Meeting, Volume 1 Oct. 1994 p 41-58 (For primary document see N95-31194 11-28)
(Grant AF-AFOSR-0152-91)
Avail: CPIA, 10630 Little Patuxent Pkwy., Suite 202, Columbia, MD 21044-3200 HC

In this study, single aluminum particles (40 to 80 micron) were burned in H2O/CO2 mixtures. Burn times were measured electronically using a PMT (photomultiplier). In addition, the effect of oxidizer composition was determined. Burn times were also measured for single particles, quenched at various stages of combustion. SEM (scanning electron microscopy) micrographs of quenched specimens were obtained. The results were used in determining particle burn times. Study of quenched particles revealed the formation of large hollow aluminum oxide spheres nearly the size of the original aluminum particles. These spheres have been reported by other investigators at both atmospheric and high pressure conditions. It was found that burn time measurements are very sensitive to the method of analysis used. Using the results of an aluminum combustion model by Brooks, effective oxygen concentrations were calculated for this work and other data. A relationship exists between the effective oxygen concentration and burn times reported for a given diameter. The particle burn times measured in this work compare well with other data if the effective oxygen concentration is properly accounted for. Author

N95-31199 Naval Postgraduate School, Monterey, CA.
AN INVESTIGATION OF THE SIDE-DUMP DUAL IN-LINE RAMJET COMBUSTOR **c07**
M. W. Deppe, R. F. Salyer, and D. W. Netzer *In* Johns Hopkins Univ., The 31st JANNAF Combustion Subcommittee Meeting, Volume 1 Oct. 1994 p 59-74 (For primary document see N95-31194 11-28)
Avail: CPIA, 10630 Little Patuxent Pkwy., Suite 202, Columbia, MD 21044-3200 HC

Three inlet-side-dump ramjet-combustor geometric configurations were investigated using non-intrusive water-tunnel flow visualization techniques to qualitatively determine optimum flame-stablization dome lengths and fuel-injection locations and to investigate whether new configurations may be more capable of providing high combustion efficiencies under wide operating limits. The optimum dome lengths which provided good fuel distribution and steady mixing all had lengths between 0.31 and 1.4 combustor diameters. Fuel injection in a narrow region on the upstream side of the dump inlet was the only location found capable of distributing fuel into the flame-holding region. Multiple injection locations in the inlet were required to distribute fuel uniformly into the main combustion region. Based upon the flow visualization results a dual, axially-inline, side-dump, liquid-fueled ramjet combustor was designed and tested. Particle size distributions from the fuel atomizers were measured both in ambient conditions and under hot-air, contra-flow engine conditions. Data obtained under ambient conditions were found to have little value for the engine flow environment. This geometry provided improved flammability limits and combustion efficiency at lean fuel-air ratios. Direct fuel injection into the recirculation was required for sustained combustion at lean equivalence ratios for the single side-dump configuration, but not for the dual in-line configuration. The fuel distribution in the inlet duct that is required for good flammability limits and combustion efficiency was opposite to that required to prevent pressure oscillations. A dump angle of 45 deg resulted in lower than desired combustion efficiencies, apparently due to poor mixing from the aft inlet. Author

N95-31200 Naval Air Warfare Center, China Lake, CA.
ENHANCED ENERGY RELEASE AND SOOT REDUCTION IN ACTIVELY CONTROLLED FLAMES **c25**
E. J. Gutmark, T. P. Parr, D. M. Hanson-Parr, and K. C. Schadow *In* Johns Hopkins Univ., The 31st JANNAF Combustion Subcommittee Meeting, Volume 1 Oct. 1994 p 75-84 (For primary document see N95-31194 11-28)
(Contract N00014-93-WX-24268)
Avail: CPIA, 10630 Little Patuxent Pkwy., Suite 202, Columbia, MD 21044-3200 HC

An active control system designed to reduce soot formation and increase energy release was demonstrated in open and enclosed flames. The control is based on synchronized periodic injection of fuel (ethylene) into air vortices at a timing which ensures energizing of the vortices and homogeneous mixing. It was shown that dual fuel injection during a single air vortex period can reduce the soot formation by several orders of magnitude relative to an unforced flame and doubles the flame temperature. Laser diagnostics were utilized to obtain planar simultaneous visualizations of the mixing process between the fuel and air flows as well as the combustion zone, indicated by OH, and soot production regions. It was shown that a proper timing of fuel injection results in homogeneous fuel/air mixing within the vortices, while injection which is out of phase with the proper one results in interference with the vortex formation and islands of unmixed fuel, leading to poor combustion and a sooty flame. The interaction of the flame with the external air was studied using particle Imaging Velocimetry (PIV). It was determined that the entrained air is crucial to maintain control authority on the flame. Blockage of the entrained external air resulted in the loss of control. A method for substitution for the external air by direct injection of air into the flame base was developed. Its efficacy was demonstrated in open and enclosed systems. The latter is especially significant due to the lack of air rich flow in the ambient of such systems. The secondary air injection doubled the flame temperature near the flame holder of an enclosed flame. Author

N95-31201 Naval Air Warfare Center, China Lake, CA.
A PULSED LIQUID FUEL RAMJET **c07**
K. J. Wilson, E. J. Gutmark, R. A. Smith, and K. C. Schadow *In* Johns Hopkins Univ., The 31st JANNAF Combustion Subcommittee Meeting, Volume 1 Oct. 1994 p 85-99 (For primary document see N95-31194 11-28)
Avail: CPIA, 10630 Little Patuxent Pkwy., Suite 202, Columbia, MD 21044-3200 HC

A new design concept for a liquid-fueled-ramjet with increased efficiency is presented. The concept utilizes vortex combustion, a method which is based on the idea that by confining the combustion process to occur within vortices it is possible to use several advantageous features of vortical flow: combined bulk mixing of the reactants with intense fine-scale mixing leading to enhanced molecular mixing, long residence time to achieve complete combustion, localized high temperature regions, and an easily

controllable environment. The concept was initially tested in laboratory scale ethylene diffusion flames. Air vortices were stabilized by acoustically forcing a turbulent air jet at its most unstable mode. Fuel was injected into the air vortices synchronously with the vortex formation sequence. The proper timing of the process was determined to be critical; when the vortex formation, the ambient air entrainment induced by the vortices and fuel injection occurred in a certain sequence the fuel burning was more complete and the energy release increased significantly. The pulsed ramjet design is based on these basic principles. The liquid fueled ramjet is a coaxial dump combustor with an axial air inlet. A pulser located in the air inlet conduit produces pressure pulses in the inlet flow using spark ignition of premixed fuel/air which generates a train of flame kernels. These growing kernels interact with the jet flow to stabilize air vortices within the combustor. Liquid fuel injectors at the dump plane inject fuel into the vortices at a controlled frequency and timing. The pulser also supplies a periodic ignition source which stabilizes the flame and extends the lean flammability limit. This design ensures that the energy release occurs close to the dump plane and that the fuel is consumed in the region of highest local temperature to obtain maximum heat release within minimal combustion chamber length. Author

N95-31202 Army Research Lab., Aberdeen Proving Ground, MD. Propulsion and Flight Div.

EXPERIMENTS IN A 120-mm RAM ACCELERATOR INCLUDING FLOW VISUALIZATION **c25**

David L. Kruczynski *In* Johns Hopkins Univ., The 31st JANNAF Combustion Subcommittee Meeting, Volume 1 Oct. 1994 p 101-114 (For primary document see N95-31194 11-28)

Avail: CPIA, 10630 Little Patuxent Pkwy., Suite 202, Columbia, MD 21044-3200 HC

A technique to visualize transient and steady combustion phenomena in ram accelerators using sacrificial transparent acrylic chambers is demonstrated. This technique allows the normal operating environment of ram accelerators to be very closely approximated. Using this technique, details of the environment during the transient starting phase as the projectile enters the accelerator and the obturator is discarded are seen for the first time. In addition, steady or running combustion around the projectile after the obturator has been shed is captured. These flow visualizations are shown to be useful in validating computational fluid dynamics codes and in providing guidance in reducing projectile unstarts while increasing initial accelerator performance. Author

N95-31203 Army Research Lab., Aberdeen Proving Ground, MD. Propulsion and Flight Div.

NUMERICAL SIMULATION OF RAM ACCELERATOR PERFORMANCE INCLUDING TRANSIENT EFFECTS DURING INITIATION OF COMBUSTION AND SENSITIVITY STUDIES **c25**

Michael J. Nusca *In* Johns Hopkins Univ., The 31st JANNAF Combustion Subcommittee Meeting, Volume 1 Oct. 1994 p 115-128 (For primary document see N95-31194 11-28)

Avail: CPIA, 10630 Little Patuxent Pkwy., Suite 202, Columbia, MD 21044-3200 HC

Computational fluid dynamics solutions of the full Navier-Stokes equations have been used to numerically simulate the reacting in-bore flowfield for the ram accelerator projectile propulsion system. In this system a projectile and obturator are injected at supersonic velocity into a stationary tube filled with a pressurized mixture of hydrocarbon, oxidizer and inert gases. Flow stagnation on the obturator initiates combustion of the mixture. A system of shock waves generated on the projectile, in conjunction with viscous heating, sustains combustion. The resulting energy release, which travels with the projectile, also generates high pressures that impart thrust to the projectile. Numerical simulations utilizing finite-rate chemical kinetics have been used to investigate this flowfield. Numerical results are used to visualize the flowfield, predict effects of variation in system parameters, and predict projectile in-bore velocity. Author

N95-31204 Washington Univ., Seattle, WA. Aerospace and Energetics Research Program.

INVESTIGATION OF RAM ACCELERATOR PERFORMANCE CAPABILITIES **c25**

A. J. Higgins, C. Knowlen, and A. P. Bruckner *In* Johns Hopkins Univ., The 31st JANNAF Combustion Subcommittee Meeting, Volume 1 Oct. 1994 p 165-176 (For primary document see N95-31194 11-28)

(Contracts F49620-92-J-0375; DAAL03-92-G-0110)

Avail: CPIA, 10630 Little Patuxent Pkwy., Suite 202, Columbia, MD 21044-3200 HC

Systematic experimental investigations of the regimes of heat release and Mach number in which the ram accelerator will operate have been carried out at the University of Washington in methane/oxygen/nitrogen and hydrogen/oxygen/methane propellant mixtures. Several distinct mechanisms have been identified which limit the peak velocity that can be reached in a particular propellant mixture for the projectile configurations used in the investigations. Maximum and minimum propellant energetics were determined by decreasing and increasing the diluent concentration until the immediate cessation of thrust was observed as the projectile entered the test mixture. Within these energetic limits there is a relatively wide range of diluent concentrations that will accelerate the projectile beyond the Chapman-Jouguet (CJ) detonation speed of the propellant mixture. These effects are readily seen by plotting the experimental results in the heat release-Mach number plane. The projectile acceleration was almost always terminated by an unstart. the most energetic mixtures unstarted immediately with no observed projectile acceleration. The Mach number obtained in the test section increased to a maximum as the propellant energetics were reduced. After reaching the optimal mixture, the unstart Mach number steadily decreased as the energetics were further reduced until combustion could no longer be supported. The phenomena which determine how the unstart Mach number depends on propellant energetics are the topics of this study. Propellant mixtures with less heat release than the optimum for peak Mach number consistently unstart at velocities approximately 30% above the CJ speed. Variations in projectile geometry and materials are used to experimentally investigate the unstart mechanisms in this chemistry regime. Preliminary results indicate that the nose cone material has a significant effect on the unstart Mach number. Comparison of experiments in the two different types of propellant mixture confirm that Mach number and heat release are the primary variables that determine ram accelerator performance. The analytical and experimental results of these investigations are discussed in this paper. Author

N95-31205 Army Research Lab., Aberdeen Proving Ground, MD. Weapons Technology Directorate.

PULSE FORMING NETWORK IN THE ETC COMBUSTION CHARACTERIZATION OF PLASMA AUGMENTED SOLID PROPELLANTS **c25**

M. DelGuercio, H. Burden, I. Stobie, K. White, G. Katulka, and S. Driesen *In* Johns Hopkins Univ., The 31st JANNAF Combustion Subcommittee Meeting, Volume 1 Oct. 1994 p 177-188 (For primary document see N95-31194 11-28)

Avail: CPIA, 10630 Little Patuxent Pkwy., Suite 202, Columbia, MD 21044-3200 HC

The combustion of solid propellants, subjected to plasma augmentation, has been studied with a 300 kJ maximum stored energy pulse forming network (PFN) in the range of 1 kJ/g of electrical energy over a 1.2-ms pulse length. The need to characterize the effects of such plasma augmentation on propellant combustion over a longer pulse length is the motivation for the upgrading of the aforementioned PFN to a maximum stored energy output of 400 kJ with a 2.4-ms pulse length. In this report the theoretical calculations, PFN upgrade design and fabrication details, will be provided. Also discussed are the modifications to a plasma generator resulting from test firings. Author

N95-31206 Johns Hopkins Univ., Baltimore, MD. Dept. of Mechanical Engineering.

VISCOUS HEATING OF LIQUID LAYERS UNDER INTENSE SHEAR

H. Yuan and A. Prosperetti *In its* The 31st JANNAF Combustion Subcommittee Meeting, Volume 1 Oct. 1994 p 325-334 (For primary document see N95-31194 11-28)

(Contract DAAL04-93-G-0409)

Avail: CPIA, 10630 Little Patuxent Pkwy., Suite 202, Columbia, MD 21044-3200 HC

Viscous heating under high shear has been proposed as a possible cause for the accidental ignition of liquid monopropellants. A typical experiment consists in the rapid compression of a drop of liquid between two parallel nearly-rigid planes. This process is simulated numerically by solving the full Navier-Stokes equations. It is found that allowing for the

decrease of viscosity with increasing temperature leads to a peak temperature reduction of nearly an order of magnitude. On the basis of these results it would seem that accidental ignition by viscous heating is an unlikely event. Author

N95-31207 Johns Hopkins Univ., Baltimore, MD. Dept. of Mechanical Engineering.
NUMERICAL STUDY OF SHEAR-INDUCED HEATING IN HIGH-SPEED NOZZLE FLOW OF LIQUID MONOPROPELLANT
J. Katz, X. Shi, and O. M. Knio *In its* The 31st JANNAF Combustion Subcommittee Meeting, Volume 1 Oct. 1994 p 335-344 (For primary document see N95-31194 11-28)
(Contract DAAH04-93-G-0413)
Avail: CPIA, 10630 Little Patuxent Pkwy., Suite 202, Columbia, MD 21044-3200 HC

A numerical study is performed which focuses on peak temperatures experienced by a liquid monopropellant during high-speed injection in a small-diameter nozzle. Attention is focused on short-duration injection during which the nozzle wall boundary layer is predominantly laminar. An unsteady 1D analysis of the temperature distribution associated with sudden fluid acceleration over a flat insulated boundary is first conducted. Expressions are provided which relate the normalized peak wall temperature to the prevailing Eckert, and Prandtl numbers. Results reveal a quadratic dependence of the normalized wall temperature on impulse velocity, and a nonlinear variation with Prandtl number. Next, simulation of high-speed flow in an axisymmetric nozzle is performed. The numerical schemes are based on finite-difference discretization of a vorticity-based formulation of the mass, momentum and energy conservation equations. Implementation of the numerical schemes to flow of LP 1846 in a 4mm-diameter nozzle indicates that preignition is likely to occur for velocities higher than 200 m/s. The effects of wall heat transfer and temperature-dependent properties are also discussed. Author

N95-31208 Army Research Lab., Aberdeen Proving Ground, MD.
WORKSHOP REPORT: MEASUREMENT TECHNIQUES IN HIGHLY TRANSIENT, SPECTRALLY RICH COMBUSTION ENVIRONMENTS c25
Todd E. Rosenberger *In* Johns Hopkins Univ., The 31st JANNAF Combustion Subcommittee Meeting, Volume 1 Oct. 1994 p 345-354 (For primary document see N95-31194 11-28)
Avail: CPIA, 10630 Little Patuxent Pkwy., Suite 202, Columbia, MD 21044-3200 HC

With the emergence of advanced propulsion systems such as liquid propellant (LP), electrothermal-chemical (ETC), electromagnetic (EM), conventional hypervelocity, and in-bore ramjet, the measurement of combustion phenomena has become more complex. the data associated with these systems can be rich in high-frequency components, and share similar transient behavior. Measurement techniques associated with conventional solid propellant systems are not always capable of accurately recording these phenomena. The accuracy of pressure and acceleration measurements in combustion chambers, barrels, and on-board projectiles has been compromised by the lack of a fundamental understanding of the effects of the mounting configuration and the mechanical and electrical components of the transducer on the integrity of the measurement. Consequently, the system development and technical understanding of the physical processes involved in the ignition and combustion of such advanced propulsion systems have been compromised. A workshop was needed to bring together experts from the aforementioned and related communities to disseminate knowledge of lessons learned and to discuss the techniques necessary to make high-fidelity pressure measurements in these environments. This paper states the objectives, identifies the participants who met to address them, provides a list of the technical presentations made, presents highlights from these presentations and the discussions that they prompted, and ends with conclusions and recommendations which came out of the workshop. Author

N95-31209 Army Research Lab., Aberdeen Proving Ground, MD. Weapons Technology Directorate.
PRESSURE TRANSDUCER PERFORMANCE AND MEASUREMENT TRADE-OFFS IN A TRANSIENT, HIGH TEMPERATURE, COMBUSTION ENVIRONMENT c25
Todd E. Rosenberger, Joseph W. Colburn, Carl R. Ruth, John R. Hewitt, Melvin B. Ridgley, James F. Tuerk, and Arthur A. Koszoru *In* Johns Hopkins Univ., The 31st JANNAF Combustion Subcommittee Meeting, Volume 1 Oct. 1994 p 355-374 (For primary document see N95-31194 11-28)
Avail: CPIA, 10630 Little Patuxent Pkwy., Suite 202, Columbia, MD 21044-3200 HC

At the U.S. Army Research Laboratory (ARL), a series of tests were performed in a 120-mm cannon to characterize the effects of transducer type, transducer port configuration, thermal protection media, and severe mechanical forces on the amplitude and frequency response of the pressure measurement. A ring of five pressure transducer ports (82 deg apart) was machined 2.6 m from the rear face of a 120-mm gun tube. The physical configuration of the transducer ports consisted of three single-diameter ports with varying stand-off distances, a conventional two-diameter port, and a blind port. As the projectile passed the longitudinal position the pressure transducers were exposed to a transient, high temperature environment which allowed the investigators to study the fidelity of the pressure measurement under transient, high temperature, mechanically adverse gun conditions. These tests demonstrated that the use of single-diameter pressure ports with cavity depths of 0.254 mm (0.010 in) and 0.711 mm (0.030 in) will more accurately characterize the oscillatory nature of the pressure measurement than would the use of a single-diameter port with a cavity depth of 1.600 mm (0.060 in). It was determined that thermal protection filling materials have a notable effect on the measurement. In addition, the combustion chamber of the weapon was also highly instrumented with pressure transducers in an attempt to evaluate the effects of various transducer types and thermal protection greases on the magnitude of the pressure measurement. This study showed that the Kistler 6211 pressure transducer (quartz) reads about 5% higher than the E30MA pressure transducer (tourmaline) in both the forward and rear of the chamber. No conclusion could be reached as to which gage gives the more correct quasi-steady-state pressure level. In addition, the results of these tests have established this test configuration as a viable diagnostic tool that can be used for future pressure measurement phenomenology studies. Author

N95-31210* Engineering-Science, Inc., Huntsville, AL.
ATOMIZATION SIMULATIONS USING AN EULERIAN-VOF-LAGRANGIAN METHOD c34
Yen-Sen Chen, Huan-Min Shang, Paul Liaw, and C. P. Chen (Alabama Univ., Huntsville, AL.) *In* Johns Hopkins Univ., The 31st JANNAF Combustion Subcommittee Meeting, Volume 1 Oct. 1994 p 375-386 (For primary document see N95-31194 11-28)
(Contract NAS8-40148)
Avail: CPIA, 10630 Little Patuxent Pkwy., Suite 202, Columbia, MD 21044-3200 HC

This paper summarizes the technical development and validation of a multiphase computational fluid dynamics (CFD) numerical method using the volume-of-fluid (VOF) model and a Lagrangian tracking model which can be employed to analyze general multiphase flow problems with free surface mechanism. The gas-liquid interface mass, momentum and energy conservations are modeled by continuum surface mechanisms. A new solution method is developed such that the present VOF model can be applied for all-speed flow regimes. The objectives of the present study are to develop and verify the fractional volume-of-fluid cell partitioning approach into a predictor-corrector algorithm and to demonstrate the effectiveness of the present innovative approach by simulating benchmark problems including the coaxial jet atomization. Author

N95-31211* Spectral Sciences, Inc., Burlington, MA.
DEVELOPMENT OF A NEW INSTRUMENT FOR ROCKET ENGINE COMBUSTION DIAGNOSTICS c25
M. Gersh, N. Goldstein, L. Bernstein, and J. Lee *In* Johns Hopkins Univ., The 31st JANNAF Combustion Subcommittee Meeting, Volume 1 Oct. 1994 p 387-400 (For primary document see N95-31194 11-28)
(Contract NAS8-40162)
Avail: CPIA, 10630 Little Patuxent Pkwy., Suite 202, Columbia, MD 21044-3200 HC

In order to develop more efficient rocket engines, it is necessary to have a technique to measure their mixing and combustion efficiency, both for assessing the efficiency of specific engines and for evaluating computer models of propellant mixing and combustion. This paper describes the development of an instrument that can quantitatively measure the results of incomplete mixing in rocket engines. This is done by using a novel

diode laser absorption spectroscopy technique to measure the spatial distribution of acetylene, CO, CO2, O2, or other species at the rocket nozzle exit plane. These species are characteristic of the low and high oxidizer to fuel ratio regions of the plume flowfield that result from incomplete mixing and combustion. Such spatial mapping of the nozzle exit plane has not previously been achieved for minor plume species such as acetylene that are sensitive to incomplete combustion. This instrument could be used to monitor combustion inefficiency for a wide variety of propellant types, including amine/N2O4, hydrocarbon/LOX, and LH2/LOX. The instrument development effort is currently in Phase 2 of a NASA SBIR contract. The key experimental results achieved during Phase 1 were: (1) use of a laboratory breadboard sensor to demonstrate C2H2 detection under simulated plume conditions; (2) selection and demonstration of a C2H2 absorption line that is free from significant interference by major plume species absorption lines; and (3) demonstration of C2H2 detection in an atmospheric pressure laboratory hydrocarbon/air flame. These and more recent data will be discussed in the papers, along with a description of the Phase 2 instrument that will be delivered to NASA for installation on an engine test stand. Author

N95-31212 Rockwell International Corp., Canoga Park, CA. Rocketdyne Div.

DESIGN AND TESTING OF AN OXIDIZER-RICH PREBURNER **c25**

S. Farhangi, K. Hunt, L. Tuegel, and D. Matthews *In* Johns Hopkins Univ., The 31st JANNAF Combustion Subcommittee Meeting, Volume 1 Oct. 1994 p 401-408 (For primary document see N95-31194 11-28)

Avail: CPIA, 10630 Little Patuxent Pkwy., Suite 202, Columbia, MD 21044-3200 HC

A full-scale oxidizer-rich liquid oxygen/gaseous hydrogen preburner article has been successfully designed, fabricated and hot-fire tested by Rocketdyne over an operating range of approximately 2000-3100 psia chamber pressure, 117-174 mass mixture ratio (MIR), and 30-50 lb/sec total propellant flow rate. Designed to minimize cost, weight, and operational complexity, the advanced oxidizer-rich preburner features direct propellant injection at a single (injector face) plane, with uniform combustion achieved in a straight length of uncooled chamber. In a series of eight mainstage tests ranging from approximately 1-5 sec in duration, the 3.5-in. diameter oxidizer-rich preburner injector repeatedly demonstrated successful ignition, flame propagation, and flameholding characteristics while achieving measured c* efficiencies of 99% with no evidence of combustion instability. Measured near wall product gas temperatures averaged from 500F (at MR = 174) to 1000F (at MR = 117), with individual thermocouple measurements falling within a 75F temperature band for each test. Through the successful hot-fire testing of a full-scale oxidizer-rich O2/H2 preburner article, a key technology enabling low-cost turbopump and full-flow staged combustion cycle (FFSC) engine design has been demonstrated. This paper describes the hardware design, fabrication, and hot-fire test results obtained in the Rocketdyne ox-rich preburner demonstration program. Author

N95-31282 Johns Hopkins Univ., Columbia, MD. Chemical Propulsion Informaiton Agency.

THE 31ST JANNAF COMBUSTION SUBCOMMITTEE MEETING, VOLUME 2

Mary T. Gannaway, ed. Oct. 1994 479 p Meeting held in Sunnyvale, CA, 17-21 Oct. 1994; sponsored by the Joint NASA, Army, Navy, Air Force Interagency Propulsion Committee

(Contract N00014-91-C-0001)

(CPIA-Publ-620) Avail: CPIA, 10630 Little Patuxent Pkwy., Suite 202, Columbia, MD 21044-3200 HC

This volume, the second of four volumes, is a collection of 36 unclassified/unlimited papers which were presented at the 31st Joint Army-Navy-NASA-Air Force (JANNAF) Combustion Subcommittee Meeting in conjunction with the Exhaust Plume Technology Subcommittee and SPIRITS User Group Meeting held 17-21 October 1994 at the Lockheed Missiles and Space Company, Sunnyvale, California. Specific subjects discussed include solid propellant combustion instability and unsteady combustion, rocket motors, guns and marine combustion characteristics, solid propellant formulation and solid and gas phase combustion kinetics. For individual titles, see N95-31283 through N95-31315.

N95-31283 Tennessee Univ., Tullahoma, TN. Space Inst.

STABILITY PREDICTION WITH ROTATIONAL FLOW EFFECTS **c25**

G. A. Flandro *In* JHU, The 31st JANNAF Combustion Subcommittee Meeting, Volume 2 Oct. 1994 p 1-26 (For primary document see N95-31282 11-28)

Avail: CPIA, 10630 Little Patuxent Pkwy., Suite 202, Columbia, MD 21044-3200 HC

Time-dependent vorticity effects are incorporated in a three-dimensional combustion instability theory in this paper. Gas oscillations parallel to a burning propellant surface create waves of vorticity that modify the acoustic wave structure. The Crocco-Vazsonyi theorem shows that this oscillatory rotational flow is a consequence of the axial unsteady pressure gradient across the mean flow streamlines at the injection boundary. Viscous stresses are not important unless the ratio of frequency to injection Mach number is very high. Nevertheless, the no-slip boundary condition must be satisfied. The unsteady, rotational, closed-form flowfield solutions are in excellent agreement with cold-flow experimental data. Stability calculations with vorticity effects included yield a damping effect that is identical to Culick's one-dimensional flow-turning correction. This validates the incorporation of the one-dimensional flow-turning result in the three-dimensional, irrotational stability algorithm. However, another consequence of the no-slip requirement is a fluctuating radial flow that arises from the axial momentum defect at the injection surface. It gives rise to a flow-driving gain that cancels the flowturning loss for a full-length cylindrical propellant grain. Application of the new theory in predictive mode demonstrates much improved agreement with experimental stability data. Author

N95-31284 Illinois Univ. at Urbana-Champaign, Savoy, IL. Dept. of Mechanical and Industrial Enineering.

UNSTEADY LASER AUGMENTED COMBUSTION OF PURE OXIDIZERS AP AND RDX **c25**

T. B. Schroeder and M. Q. Brewster *In* JHU, The 31st JANNAF Combustion Subcommittee Meeting, Volume 2 Oct. 1994 p 27-34 (For primary document see N95-31282 11-28)

(Contract N00014-91-J-1977)

Avail: CPIA, 10630 Little Patuxent Pkwy., Suite 202, Columbia, MD 21044-3200 HC

Unsteady laser augmented combustion of AP and RDX was investigated. A CO2 laser was used as an external radiant energy source to sustain AP combustion at 1 atm and to perturb the burning rate which was measured by a force transducer. Steady burning was modeled by a one-step, zeroth order decomposition process in the condensed phase. Linearized quasi-steady theory was used to model the unsteady combustion response. Both the steady and unsteady burning rate data (below 70 Hz) were reasonably well fit using E(sub c) = 2E(sub s) = 35 kcal/mole and Q(sub c) = 60 cal/g. Application of the model to RDX is also discussed.

Author

N95-31285 Illinois Univ., Urbana, IL.

THEORY OF UNSTEADY COMBUSTION OF SOLIDS: INVESTIGATION OF QUASI-STEADY ASSUMPTION **c25**

M. A. Zebrowski and M. Q. Brewster *In* JHU, The 31st JANNAF Combustion Subcommittee Meeting, Volume 2 Oct. 1994 p 35-50 (For primary document see N95-31282 11-28)

(Contract N00014-91-J-1977)

Avail: CPIA, 10630 Little Patuxent Pkwy., Suite 202, Columbia, MD 21044-3200 HC

A numerical model was developed to predict the linear and non-linear combustion response of energetic materials with condensed phase controlled burning to time-dependent incident radiation. Both surface (quasisteady) and distributed condensed phase reactions were considered. Code validation was accomplished by comparing the linear surface reaction response with the predictions of analysis (ZN or QSHOD theory). Numerical results indicated that for realistic dimensionless activation energies (greater than 5), the error in the linear response due to the quasi-steady condensed phase reaction assumption can be significant. A significant difference was also observed in the linear surface reaction response for intermediate reaction layer opacities between a constant reaction layer transmissivity, f(sub r), and a variable f(sub r). An interesting multiple-peaked non-linear response was also discovered. This multiple-peaked response was easily triggered by a pulse input. The response peaks at frequencies above that of the condensed phase thermal relaxation response appear to be caused by higher harmonics of the lower frequency components of the pulse input.

Author

N95-31286 Illinois Univ., Urbana, IL.
OSCILLATORY COMBUSTION OF ALUMINIZED AP/HTPB PROPELLANTS **c25**
S. R. Hickman and M. Q. Brewster *In* JHU, The 31st JANNAF Combusrion Subcommittee Meeting, Volume 2 Oct. 1994 p 51-61 (For primary document see N95-31282 11-28)
(Contract N00014-91-C-1977)
Avail: CPIA, 10630 Little Patuxent Pkwy., Suite 202, Columbia, MD 21044-3200 HC

The unsteady combustion of metalized propellants was studied using the laser recoil technique. A pulsed Nd:YAG laser and a CO2 laser were used to perturb the dynamic burning rate which was measured by a force transducer. It was found that at 1 atm, certain Al/AP/HTPB propellants exhibited strong oscillatory burning between 30 and 80 Hz. This effect did not correspond to the classical solid thermal conduction-relaxation response, or QSHOD theory. These oscillations in the propellant burn rate appeared to be related to the processes of unsteady accumulation, agglomeration, ignition, and departure of aluminum at the burning surface of the propellant. The results with the CO2 laser were generally in agreement with the YAG results. A variety of AP/HTPB propellants and ingredients were tested, including aluminum, magnesium, boron, zirconium carbide, and variations in AP and Al particle size and binder concentration. Of these formulations, the ones that showed the strongest oscillatory combustion behavior were those that contained at least 15 percent aluminum and an aluminum particle size below 15 m. Flame luminosity measurements showed periodic departure of aluminum at the propellant surface at the same frequency and in phase with the burning rate oscillations. The luminosity measurements were confirmed by the use of a high speed video camera Preliminary results for the laser-driven combustion response at pressures above 1 atm were also obtained. These results, combined with the results of many control propellants, confirm that aluminum can have a much stronger influence on the combustion of AP/HTPB propellants than that indicated by the normally small changes observed in the macroscopically steady burning rate or the mean burning rate during macroscopically unsteady combustion. Scaling arguments were used to predict the frequency of the oscillations in the burn rate. Experiments showed that the frequency of the oscillations was proportional to the mean burn rate which agrees with a model based on the assumption of periodic accumulation and departure of aluminum at the surface. Author

N95-31287 Brigham Young Univ., Provo, UT.
CHARACTERIZATION OF AN IMPROVED RIJKE BURNER AS PRELUDE TO MEASUREMENTS OF ALUMINUM DISTRIBUTED COMBUSTION **c25**
B. R. Newbold, M. W. Beckstead, W. Erikson, and S. Olsen *In* JHU, The 31st JANNAF Combustion Subcommittee Meeting, Volume 2 Oct. 1994 p 63-77 (For primary document see N95-31282 11-28)
(Grant AF-AFOSR-91-0152)
Avail: CPIA, 10630 Little Patuxent Pkwy., Suite 202, Columbia, MD 21044-3200 HC

As prelude to the quantitative study of aluminum distributed combustion, the current work has characterized the acoustic growth, frequency, and temperature of an improved Rijke burner as a function of mass flow rate, gas composition, and geometry. Previous researchers have qualitatively studied the distributed combustion of metals in Rijke burners, but none of them have conducted a detailed investigation of their burner without particle combustion which would strengthen the relevance of their efforts. Before characterization, the burner was redesigned with an increased flow velocity of over 70 cm/s so particles will entrain. Also the flame temperature was raised to over 2400 K so aluminum particles will ignite. The burner was fitted with multiple ports for thermocouple insertion so the radial and axial temperature profiles could be quantified which is crucial for parallel efforts to model the Rijke burner. The flame's position relative to the burner's acoustic driving regions along with the temperature profile primarily determined which mode would be driven and the magnitude of that acoustic driving. By varying the exhaust temperature profile, the acoustic growth rate can be as much as tripled from the baseline value of approximately 120 s(exp -1). At baseline, the burner operated in the third harmonic mode at a frequency of 1300 Hz, but geometry or temperature changes could shift operation to a second mode. During oscillatory combustion, centerline temperatures in the exhaust rose by as much as 80 K when compared to the non-oscillating case. With oscillations, the mean flow of gases in the boundary slowed with a consequent decrease in heat transfer to the walls. The information gained in this study will aid in refining burner modeling efforts and allow interpretation of planned aluminum combustion studies in hopes of gaining a greater understanding of distributed combustion as a driving mechanism in the combustion instability of solid propellant rocket motors. Author

N95-31288 Naval Air Warfare Center, China Lake, CA. Research and Technology Div.
ACTIVE CONTROL OF COMBUSTION INSTABILITY USING INJECTION TECHNIQUES **c25**
C. J. Bicker, Fred S. Blomshield, and Richard Stalnaker *In* JHU, The 31st JANNAF Combustion Subcommittee Meeting, Volume 2 Oct. 1994 p 79-88 (For primary document see N95-31282 11-28)
Avail: CPIA, 10630 Little Patuxent Pkwy., Suite 202, Columbia, MD 21044-3200 HC

Active control of solid propellant combustion oscillations in a T-burner by properly timed, pulsed chemical injection was investigated. The principal purpose was to demonstrate a realistic active control mechanism that could be applied to solid rocket motors. Active injection control would be especially applicable to large booster systems and motors where conventional methods of suppressing instabilities cannot be used. This paper describes the experimental strategy, the results obtained and future plans. Author

N95-31289* National Aeronautics and Space Administration. Lewis Research Center, Cleveland, OH.
CENTRIFUGAL AND AXIAL PUMP DESIGN AND OFF-DESIGN PERFORMANCE PREDICTION **c37**
Joseph P. Veres *In* JHU, The 31st JANNAF Combustion Subcommittee Meeting, Volume 2 Oct. 1994 p 109-122 (For primary document see N95-31282 11-28)
Avail: CPIA, 10630 Little Patuxent Pkwy., Suite 202, Columbia, MD 21044-3200 HC

A meanline pump flow modeling method has been developed to provide a fast capability for modeling pumps of cryogenic rocket engines. Based on this method, a meanline pump flow code PUMPA has been written that can predict the performance of pumps at off-design operating conditions, given the loss of the diffusion system at the design point. The design point rotor efficiency and slip factor are obtained from empirical correlations to rotor specific speed and geometry. The pump code can model axial or inducer, mixed-flow and centrifugal pumps. The code can model multi-stage pumps in series. The rapid input setup and computer run time for the meanline pump flow code makes it an effective analysis and conceptual design tool. The map generation capabilities of the code provides the information needed for interfacing with a rocket engine system modeling code. The off-design and multi-stage modeling capabilities of the code permit the user to do parametric design space exploration of candidate pump configurations and provide head-flow maps for engine system evaluation. Author

N95-31290 United Technologies Corp., San Jose, CA.
MODEL FOR DEFINING PROPELLANT BURN RATE PERFORMANCE BOUNDARIES **c25**
W. M. Fisher and R. R. Miller *In* JHU, The 31st JANNAF Combustion Subcommittee Meeting, Volume 2 Oct. 1994 p 123-131 (For primary document see N95-31282 11-28)
Avail: CPIA, 10630 Little Patuxent Pkwy., Suite 202, Columbia, MD 21044-3200 HC

A method for formulating solid rocket propellants with a constant burn rate has been developed. The method uses a model, which predicts burn rate for a particular ammonium perchlorate size distribution, to search the particle size space to identify the region which gives the desired burn rate. The model used to predict the burn rate was put forward by Kerstein. It defines burn rate in terms of an ideal rate for a binder-ammonium perchlorate system, that is modified to account for over or under oxidation. The ideal burn rate was expressed in terms of a modified Springfield relationship. The modifier is a scaling function which equals one at the optimum fuel/oxidizer ratio and decays as the ratio deviates from the optimum. The procedure has been used to develop an applied propellant formulation, by

defining ammonium perchlorate size distributions which possessed a constant burn rate. The candidate formulations then were optimized for processibility. Author

N95-31291 Johns Hopkins Univ., Columbia, MD. Chemical Propulsion Information Agency.

SURVEY OF US BURNING RATE MEASUREMENT METHODS FOR SOLID PROPULSION APPLICATIONS c25

Ronald S. Fry *In* JHU, The 31st JANNAF Combustion Subcommittee Meeting, Volume 2 Oct. 1994 p 123-131 (For primary document see N95-31282 11-28)

Avail: CPIA, 10630 Little Patuxent Pkwy., Suite 202, Columbia, MD 21044-3200 HC

The continuing need for advanced solid propellants during these times of great change within the propulsion industry is creating a need for improved developmental methods. The Johns Hopkins University, Chemical Propulsion Information Agency is acting as a catalyst to document common practices and standardized methods used within the U.S. propulsion industry to measure solid propellant burning rate. This work has guided the early planning stages for a working group of the Advisory Group for Aerospace Research and Development (AGARD), Propulsion and Energetics Panel (PEP). The scope of the AGARD/PEP working group is to arrive at a consensus on consistent burning rate measurement methods for the participating NATO nations. The experience base of years of solid propellant development and advances in non-intrusive diagnostics applied to burning rate measurement technology are thought to provide opportunities to contribute to the affordability, accuracy, and reliability of the future solid propellant data base. A review is presented of standardized methods and current experience base within the U.S. gun and solid rocket propulsion industry for measuring propellant burning rate. Industry trends in methods used and the degree of uniformity and standardization are identified. Results indicate how facilities are responding to the changing state of the propulsion industry. These results also served to guide the focus of the AGARD/PEP working group toward (1) solid propellant burning rate measurement by small/subscale motor methods, and (2) solid propellant burning rate measurement by non-intrusive techniques. Future activities include the updating and expanding of JHU/CPIA's national reference manuals on propulsion to include facilities to measure solid propellant burning rate; planning and conducting a JANNAF workshop in 1995 on the current state and advances in U.S. solid propellant burning rate measurement methods; and initiating the AGARD/PEP working group in late 1995. Author

N95-31292 Brigham Young Univ., Provo, UT.

AN IGNITION MODEL FOR MODERN DOUBLE BASE PROPELLANTS c25

M. W. Beckstead *In* JHU, The 31st JANNAF Combustion Subcommittee Meeting, Volume 2 Oct. 1994 p 163-180 Sponsored in cooperation with LMSC (For primary document see N95-31282 11-28)

Avail: CPIA, 10630 Little Patuxent Pkwy., Suite 202, Columbia, MD 21044-3200 HC

A computer code has been developed for predicting the ignition characteristics of modern double base propellants in a motor environment. The code is based on the NWC ignition code developed by Price of the NAWC. The physical model is based on the characteristics of the combined ingredients of typical energetic propellants: HMX, AP, a nitroglycerin based binder, and aluminum. The fundamental equation in the model is the transient heat conduction equation for the solid. It is assumed that a single averaged equation adequately describes the propellant. Each ingredient (HMX, AP, and NG based binder) is assumed to react through two condensed phase reactions and a gas phase or flame reaction. From these equations the model predicts a time to ignition and a steady burning rate. Care was taken to ensure that the ignition process transitions smoothly to the combustion process. A disadvantage of previous ignition codes has been the determination of the various combustion parameters in a model. Various schemes have been used to arrive at realistic values. In the current approach, activation energies are taken from the literature wherever possible. This ensures the use of realistic kinetic parameters in the calculations. The computer code has most of the required physical, thermochemical and kinetic parameters built into it and uses rational techniques to average these properties to correspond to an input propellant formulation. Using this approach, all of the propellant properties, including physical, chemical and kinetic, are inherent to the code. This greatly simplifies the input task for a typical user. Validation of the computer code was achieved by making calculations for each of the three principal ingredients and comparing those calculations to available data. The primary comparisons were made between calculated and experimentally measured burning rates and ignition times. Comparisons were also made between calculated and experimentally measured surface temperatures. The agreement between the calculations for HMX, AP and double base binder and the available data was very reasonable. Calculations have also been made for a typical propellant containing 51% HMX, 19% aluminum, 5% AP and 25% binder. Ignition times of approximately 10 msec were calculated for flux levels of approximately 100 cal. The model predicts that the ignition time should decrease with increasing heat flux and should increase with decreasing pressure, which are the observed trends. Author

N95-31293 Army Research Lab., Aberdeen Proving Ground, MD. Weapons Technology Directorate.

MOLECULAR MODELS FOR NITRO COMPOUNDS

George F. Adams, Betsy M. Rice, and Cary F. Chabalowski *In* JHU, The 31st JANNAF Combustion Subcommittee Meeting, Volume 2 Oct. 1994 p 181-184 (For primary document see N95-31282 11-28)

Avail: CPIA, 10630 Little Patuxent Pkwy., Suite 202, Columbia, MD 21044-3200 HC

This paper summarizes our recent research to extend the applicability of molecular modeling and molecular dynamics computational methods in the area of energetic materials chemistry and physics. We describe progress in the extension of a molecular forcefield that includes parameters that enable the researcher to include nitro compounds of several types. The evolution of methods for deriving the forcefield is briefly discussed, and we suggest a variety of molecular modeling applications that may benefit from this approach to forcefield derivation. In addition, we describe the classical simulation of the decomposition paths accessible to methylene nitramine. The chemical rates and mechanisms of the two primary decomposition channels are presented. The classical barrier heights for the two dominant decomposition channels: (a) N-N bond scission to form CH2N and NO2, and (b) concerted dissociation via a five-center transition state, differ by 2 kcal/mol. Author

N95-31294 Hercules, Inc., Magna, UT.

ESTIMATING HEAT OF FORMATION OF ENERGETIC COMPOUNDS USING CORRECTED SEMIEMPIRICAL MOLECULAR ORBITAL THEORY c25

R. L. Raun and A. G. Butcher *In* JHU, The 31st JANNAF Combustion Subcommittee Meeting, Volume 2 Oct. 1994 p 185-196 (For primary document see N95-31282 11-28)

(Contract DAAH01-90-C-0833)

Avail: CPIA, 10630 Little Patuxent Pkwy., Suite 202, Columbia, MD 21044-3200 HC

A new method for estimating heat of formation (HF) of energetic compounds has been developed. This method is based on the AM1 semiempirical molecular orbital method. The AM1 method generally does well at predicting HF for organic compounds. However, this method does poorly at estimating HF for energetic compounds containing nitro groups. Using statistical methods, a systematic correction to the AM1 method has been developed for nitro compounds. This correction brings AM1 HF predictions for energetic compounds into agreement with experimental data. This method offers an independent check on HF predicted using other methods. The method should be particularly useful in predicting HF for caged compounds. Author

N95-31295 Army Research Lab., Aberdeen Proving Ground, MD.

CONDENSED-PHASE PROCESSES DURING SOLID PROPELLANT COMBUSTION. 5: FURTHER OBSERVATIONS ON DEPTH PROFILING OF BURNED SURFACES OF XM39 AND M43 PROPELLANTS c25

M. A. Schroeder, R. A. Fifer, M. S. Miller, R. A. Pesce-Rodriguez, and J. M. Widder *In* JHU, The 31st JANNAF Combustion Subcommittee Meeting, Volume 2 Oct. 1994 p 211-220 (For primary document see N95-31282 11-28)

Avail: CPIA, 10630 Little Patuxent Pkwy., Suite 202, Columbia, MD 21044-3200 HC

Samples of gun propellants that have been self-extinguished at low pressures have been examined under a scanning electron microscope; the results suggest that the surface Layers consist of a thin layer of binder

and decomposition product, above a thicker layer of crystalline material that is presumably mostly solidified (liquefied during combustion) RDX oxidizer. Photoacoustic FTIR spectra of some burned/extinguished samples of XM39, JA2 and RDX are also reported and discussed. Author

N95-31296 Pennsylvania State Univ., University Park, PA.
OBSERVATION AND CHARACTERIZATION OF BURNING SURFACE REACTION ZONES OF SOLID PROPELLANTS c25
Ericefan T. Boyer, Yeu-Cherng Lu, Kevin Desmarais, and Kenneth K. Kuo *In* JHU, The 31st JANNAF Combustion Subcommittee Meeting, Volume 2 Oct. 1994 p 211-220 (For primary document see N95-31282 11-28)
(Contracts DAAL04-93-G-0364; DAAL03-92-G-0118)
Avail: CPIA, 10630 Little Patuxent Pkwy., Suite 202, Columbia, MD 21044-3200 HC

It is generally known that a surface reaction zone exists on the burning surface of nitramine propellants at pressures less than 6.87 MPa (1000 psia). Although this layer is acknowledged to play an important role in the combustion process, the detailed structure remains relatively uncharacterized due to variations with propellant formulation and operating conditions and the difficulty of instrumentation under combustion conditions. Using a high-magnification imaging system, in situ surface phenomena were observed on 0.64 cm (0.25 in) diameter samples of RDX, the nitramine composite propellants XM39 and M43, and a triplebased propellant JA-2 over a pressure range of 0.10 MPa (0 psig) to 3.55 MPa (500 psig). At atmospheric pressure, RDX formed a thick bubbling foam layer up to 650 mu m thick. The thickness of the layer quickly decreased with increase in pressure, but the layer was present at all conditions tested. Liquid layers of XM39 and M43 were similar in appearance with small mobile carbonaceous particles in the liquid layer that agglomerated into flame-holding sites at higher pressures. The pressure at which the liquid layer disappeared was lower for M43 than that for XM39. Carbonaceous residues were important as sites for flame attachment to the surface on all propellants tested. Author

N95-31297 Pennsylvania State Univ., University Park, PA. Dept. of Mechanical Engineering.
MODELING OF THERMAL RESPONSE OF FILAMENT USED IN T-JUMP EXPERIMENT c25
Stefan T. Thynell, Polly E. Gongwer (Delaware Univ., Newark, DE.), and Thomas B. Brill (Delaware Univ., Newark, DE.) *In* JHU, The 31st JANNAF Combustion Subcommittee Meeting, Volume 2 Oct. 1994 p 221-232 (For primary document see N95-31282 11-28)
(Contract DAAL03-92-G-0118)
Avail: CPIA, 10630 Little Patuxent Pkwy., Suite 202, Columbia, MD 21044-3200 HC

During the combustion of solid propellants, explosives or pyrotechnics, the condensed phase experiences heating rates that may exceed 20,000 K/s. At such high heating rates, the thermal decomposition behavior of the energetic material could be affected by its rate of decomposition. To simulate the high heating rate environment, the T-jump experiment was developed for use with FT-IR spectroscopy. The T-jump experiment utilizes electrical resistance heating of a thin Pt filament on which a small amount of the energetic test sample is placed. This work describes a heat transfer model of the filament and sample, a model of the current's control circuit, and global decomposition and heat release mechanisms of RDX, which is an energetic ingredient used in propellants and explosives. Comparisons of model calculations with experimental data reveal an excellent agreement. Similarly, the predicted time to rapid heat release for the highly energetic RDX sample also show a good agreement with experimental results. Thus the use of the developed model in conjunction of with experiments should be a useful tool in studying the thermal decomposition behavior of energetic materials under combustion-like conditions. Author

N95-31298 Illinois Univ., Urbana, IL.
LASER PYROLYSIS OF HTPB c25
D. R. Esker and M. Q. Brewster *In* JHU, The 31st JANNAF Combustion Subcommittee Meeting, Volume 2 Oct. 1994 p 235-245 (For primary document see N95-31282 11-28)
(Contract N00014-91-J-1977; NSF CTS-91-13151)
Avail: CPIA, 10630 Little Patuxent Pkwy., Suite 202, Columbia, MD 21044-3200 HC

A method was developed for measuring the dynamic mass loss rate during laser pyrolysis of polymeric binder materials. This method was applied to an investigation of the thermal decomposition of hydroxyl-terminated polybutadiene (HTPB). A technique was developed for measuring the laser plume transmission loss during laser pyrolysis. Microthermocouple measurements of the surface temperature were also performed. The effective sample heating rate ranged from 10(exp 2) to 10(exp 4) K/s. A zeroth order global condensed phase decomposition model was used to fit the measured data and extract kinetic and thermochemical parameters. The kinetic parameters agreed well with Chen and Brill's SMATCH/FTIR results measured at 250 to 350 K/s while the heat of decomposition agreed with that of Cohen, et al. It was also found that the presence of one percent carbon black in HTPB lowered the regression rate by at least 30 percent. Author

N95-31299 Pennsylvania State Univ., University Park, PA. Dept. of Mechanical Engineering.
ASSESSMENT OF DYNAMIC BURNING BEHAVIOR FOR JA-2 PROPELLANT RODS c25
T. J. Watson, K. K. Kuo, and S. T. Thynell *In* JHU, The 31st JANNAF Combustion Subcommittee Meeting, Volume 2 Oct. 1994 p 247-257 (For primary document see N95-31282 11-28)
(Contract DAAL03-92-G-0020)
Avail: CPIA, 10630 Little Patuxent Pkwy., Suite 202, Columbia, MD 21044-3200 HC

Under transient conditions, the instantaneous burn rate of solid propellants may differ significantly from the steady-state value. Any instantaneous burn rate difference caused by rapid pressurization may introduce in the performance prediction of gun propulsion systems. With this as motivation, research has been performed on a commonly used triple-base gun propellant, JA-2, to determine the effect of large pressure excursions on instantaneous burning rate. Transient burning rate tests were conducted using an interrupted burner with x-ray translucent windows that permit observation of the propellant samples during the transient event. The interrupted burner also allows the propellant samples to be recovered from within the chamber after rapid depressurization terminates combustion. The instantaneous burning rates of JA-2 propellant rods were determined using two techniques. The first technique utilized real-time x-ray radiography images to deduce the instantaneous change in diameter for each propellant rod. The second technique utilized a modified interior ballistic burn rate analysis code that took advantage of the propellant sample recovery feature of the interrupted burner. The instantaneous burning rates deduced from both of the analysis techniques were compared to the steady-state burning rate values, obtained using an optical strand burner, in order to assess the degree of dynamic burning. For JA-2 propellant rods subjected to high pressurization rates (dp/dt less than 11,000 MPa/s), departure from the steady-state burning rate was found to be small. This observation was explained using the stability theory of Novozhilov with measured temperature sensitivity and best estimated surface temperature variation with chamber pressure. Author

N95-31300 Princeton Scientific Enterprises, NJ.
PROGRESS IN DEVELOPING PROPELLANT IGNITION SYSTEMS BASED UPON ELECTRICALLY CONDUCTIVE POLYMERS c25
David W. Blair *In* JHU, The 31st JANNAF Combustion Subcommittee Meeting, Volume 2 Oct. 1994 p 259-268 (For primary document see N95-31282 11-28)
(Contract DAAL01-94-C-0073)
Avail: CPIA, 10630 Little Patuxent Pkwy., Suite 202, Columbia, MD 21044-3200 HC

This is a report on a Phase 2 SBIR contract to develop a system of ignitors for propellants and pyrotechnics based upon electrically conductive organic polymers. The feasibility of developing such ignitors was demonstrated under a Phase 1 contract. The Phase 2 contract was signed August 15, 1994, and this paper reports on the status of the program at this time. Author

N95-31301 Picatinny Arsenal, Dover, NJ. Armament Engineering Directorate.
ACIDITY AND BASICITY OF NITRO SUBSTITUTED IMIDAZOLES
T. Vladimiroff *In* JHU, The 31st JANNAF Combustion Subcommittee Meeting, Volume 2 Oct. 1994 p 269-276 (For primary document see

N95-31282 11-28)
Avail: CPIA, 10630 Little Patuxent Pkwy., Suite 202, Columbia, MD 21044-3200 HC

The antibiotic azomycin is 2-nitroimidazole. 2,4-dinitroimidazole has recently been found to be a fairly powerful yet stable explosive. The family of all nitro substituted imidazoles constitute an interesting series of molecules from both the biological and the energetic material points of view. Imidazole is a heterocyclic five membered ring with two nitrogen atoms in the ring. One of these nitrogens is bound to a hydrogen atom so that it can act as a proton donor. The other nitrogen can act as a proton acceptor. The molecule can therefore act as both an acid and a base. In this work the protonation and deprotonation energies for all the nitro substituted imidazoles are computed with several basis sets. The GAUSSIAN 92 set of programs is used and all computations are performed at the SCF level of theory. The geometry of all the structures are determined using gradient techniques and compared to experimentally obtained geometries when available. It is found that these materials become more acidic and less basic as the degree of nitration increases. Author

N95-31302 Pennsylvania State Univ., University Park, PA. Dept. of Mechanical Engineering.

MEASUREMENT OF TEMPERATURES AND OH CONCENTRATIONS OF SOLID PROPELLANT FLAMES USING ABSORPTION SPECTROSCOPY c25

Yeu-Cherng Lu, Todd Freyman, and Kenneth K. Kuo *In* JHU, The 31st JANNAF Combustion Subcommittee Meeting, Volume 2 Oct. 1994 p 277-290 (For primary document see N95-31282 11-28)
(Contract DAAL03-92-G-0118)
Avail: CPIA, 10630 Little Patuxent Pkwy., Suite 202, Columbia, MD 21044-3200 HC

Multi-parameters least-squares analysis of rotationally resolved absorption spectroscopy in the Alpha(sup 2)Sigma(sup 2)-Chi(sup 2)Pi (0,0) vibrational band system of OH from 307 to 311 nm was performed to determine the flame temperatures and OH concentrations of JA-2 double base propellant under steady-state burning at elevated pressures with a spatial resolution of 50-100 micrometers. Deduced flame temperatures were 2754 +/- 124 K, 2836 +/- 147 K, 2852 +/- 179 K, and 2873 +/- 188 K at pressures of 1.60, 3.55, 5.62, and 6.99 MPa, respectively; the corresponding OH number densities were (1.09 +/- 0.34) x 10(exp 17), (2.31 +/- 0.48) x 10(exp 17), (3.31 +/- 0.27) x 10(exp 17), and (3.44 +/- 0.30) x 10(exp 17) molecules/c.c., respectively. The results at 1.60 MPa agree well with data in the literature, and deduced flame temperatures at high pressures agree well with chemical equilibrium calculations. OH mole fractions are about 40 percent lower than the equilibrium analysis. This work represents the first set of optical absorption measurements performed on solid propellants at pressures above 2.0 MPa. Author

N95-31303 Pennsylvania State Univ., University Park, PA. Dept. of Mechanical Engineering.

SPECIES AND TEMPERATURE PROFILES OF PROPELLANT FLAMES OBTAINED FROM FTIR ABSORPTION SPECTROSCOPY c25

C. F. Mallery and S. T. Thynell *In* JHU, The 31st JANNAF Combustion Subcommittee Meeting, Volume 2 Oct. 1994 p 291-305 (For primary document see N95-31282 11-28)
(Contract DAAL03-92-G-0118)
Avail: CPIA, 10630 Little Patuxent Pkwy., Suite 202, Columbia, MD 21044-3200 HC

The use of Fourier transform infrared (FTIR) absorption spectroscopy to obtain species and temperature profiles within solid-propellants flames is described in this paper. Measurements were performed at a spectral resolution of 4 cm(exp -1) and a spatial resolution of 1 mm within the flame-zone of two nitramine composite propellants. A nonlinear, least-squares routine fitted the experimentally acquired absorption spectra to theoretical spectra which yielded a prediction of the absolute species concentrations of CO, NO, H20 and CO2 as well as the rotational temperature. Line-of-sight deduced temperature profiles for XM39 and M43 propellants showed dark-zone/luminous flame-zone structures for both propellants. The mole fraction of CO increased while the mole fraction of NO decreased from the beginning of the dark-zone to the luminous flame zone. Data on the spatial variation of species concentration and temperature within the flame zone are important for the development and validation of chemical kinetic mechanisms of these solid propellants. Author

N95-31304 Pennsylvania State Univ., University Park, PA.

A STUDY OF GAS-PHASE PROCESSES DURING THE DEFLAGRATION OF RDX COMPOSITE PROPELLANTS USING A TRIPLE QUADRUPOLE MASS SPECTROMETER c25

Ching-Jen Tang, Young Joo Lee, and Thomas A. Litzinger *In* JHU, The 31st JANNAF Combustion Subcommittee Meeting, Volume 2 Oct. 1994 p 307-316 (For primary document see N95-31282 11-28)
(Contract DAAL03-92-G-0118)
Avail: CPIA, 10630 Little Patuxent Pkwy., Suite 202, Columbia, MD 21044-3200 HC

Measurements of chemical species were obtained in a study of RDX composite propellants, XM39 and M43 as well as binders, Cellulose Acetate Butyrate (CAB) and Acetyl Triethyl Citrate (ATEC). Experiments were conducted in an argon environment and a CO2 laser was used to initiate and sustain reaction of the propellants. Measurements of species were conducted at a pressure of one atm, with heat fluxes of 100 and 400 W/cu cm, cc. Gas samples were extracted using a quartz microprobe and analyzed using a triple quadrupole mass spectrometer (TQMS). The TQMS is capable of resolving species which could contribute on the same masses: CO, C2H4 and N2 to mass 28, and CO2, CH3CHO and N2O to mass 44. Using the parent and daughter modes of the TQMS and careful calibration, it was possible to identify and quantify these species. Both materials exhibited similar gas phase reaction chemistry at one atm and heat fluxes of 100 and 400 W/cm. The major species at the surface were NO2, CO2, CH2O, NO, N2O, HCN and H2O for XM39 and M43. Species at 44 amu were mainly N2O and CO2, while species at 28 amu were composed primarily of CO and N2. The measurements also also revealed that the primary flame zone was 3.5 mm for XM39 and 2 mm for M43. The results indicated that the reaction zones for both materials were significantly stretched out in comparison to that for RDX mono-propellant. The most notable difference between RDX mono-propellant and both RDX composite propellants was in the absence of CH2O observed by Lee. These results indicated that the primary flame of both propellants formed by the reaction of CH2O and NO2 was different from that of RDX. CAB and ATEC were studied at one atm and a heat flux of 100 W/cu cm, cc. Species at molecular weights of 60, 44, 43, 42, 28, 29, 73 and 41 for CAB and 57, 56, 43, 91, 92, 45, 41 and 31 for ATEC were detected by TQMS. The daughter spectra revealed that the major contributors for CAB were large hydrocarbons, CO2 and CO. Author

N95-31305 Aerodyne Research, Inc., Billerica, MA. Center for Chemical and Environmental Physics.

EMBEDDED INFRARED FIBER OPTIC ABSORPTION STUDIES OF NITRAMINE PROPELLANT STRAND BURNING c25

J. Wormhoudt and P Kebabian, L. *In* JHU, The 31st JANNAF Combustion Subcommittee Meeting, Volume 2 Oct. 1994 p 317-324 (For primary document see N95-31282 11-28)
(Contract DAAH04-93-C-0053)
Avail: CPIA, 10630 Little Patuxent Pkwy., Suite 202, Columbia, MD 21044-3200 HC

This paper reports on continued work to develop and demonstrate the use of infrared fiber optics to probe the decomposition processes in burning gun propellant strands. Our experiments involve measuring the absorption across an open gap between two embedded fibers as it fills with gaseous decomposition products. Several improvements have been made to the experimental technique. In the most significant, a visible detection system for NO2 based on differential absorption by red and green HeNe lasers has been added to the N2O detection system using two infrared bandpass filters described previously. As with N2O, we have observed NO2 evolving into the observation volume during the burning of an RDX-based composite propellant. Observations to date indicate that NO2 appears simultaneously with N2O, that is, while the observation region is relatively cool and far from the burning surface. More observations will be required before we can be sure there are no significant differences in the time history of the evolution of the two gases. These data will provide additional information on the physical and chemical processes in the condensed phases of this composite propellant, including the development of pressurized voids or matrix-trapped bubbles which can release decomposition gases into unburned propellant through suddenly opening cracks. Author

N95-31306 Army Research Lab., Aberdeen Proving Ground, MD.
IMPROVEMENTS IN INFRARED ABSORPTION OF SOLID PROPELLANT FLAMES c25
S. H. Modiano and J. A. Vanderhoff *In* JHU, The 31st JANNAF Combustion Subcommittee Meeting, Volume 2 Oct. 1994 p 325-332 (For primary document see N95-31282 11-28)
Avail: CPIA, 10630 Little Patuxent Pkwy., Suite 202, Columbia, MD 21044-3200 HC

Last year we reported the first application of a multichannel infrared absorption technique for the study of the dark zone of solid propellant flames. This year we report improvements in the technique which include an increase in the data acquisition rate by a factor of five, the ability to sequentially acquire an emission spectrum for each absorption spectrum during the acquisition cycle, the ability to correct for any emission background which may distort the absorption spectrum, and better compensation for the underlying broadband absorption feature thought to be due to soot formation. The improved instrument has been used to obtain dark zone measurements for two nitramine propellants (M43 and XM39). From these measurements and the HITRAN database concentration and temperature estimates for HCN, H2O, CO, CH4, H2CO, and N2O have been determined. It is shown that a single temperature model may be inadequate for simulating the H2O features in the observed spectra. Author

N95-31307 Naval Air Warfare Center, China Lake, CA. Combustion Diagnostics Lab.
ADVANCED OXIDIZERS DIFFUSION FLAMES STRUCTURE c25
Tim Parr and Donna Hanson-Parr *In* JHU, The 31st JANNAF Combustion Subcommittee Meeting, Volume 2 Oct. 1994 p 333-344 (For primary document see N95-31282 11-28)
(Contract N00014-92-WX-24097)
Avail: CPIA, 10630 Little Patuxent Pkwy., Suite 202, Columbia, MD 21044-3200 HC

The diffusion flame structure of sandwich geometry propellants made from HMX, TNAZ, AP, ADN (Ammonium Dinitramide), and a variety of polymers including wax, HTPB, N5, and various high energy binders including some based on GAP and BAMO/NMMO, was studied using Planar Laser Induced Fluorescence (PLIF) and Mie scatter imaging for sandwiches deflagrating at pressures between 1 and 20 atm. Flame species imaged as two dimensional profiles included CN, OH, and NO (v=0 and v=1). Two dimensional gas temperature profiles were obtained from OH rotational and NO vibrational population distributions. Various lamina thicknesses were studied down to a binder layer thickness of 50 mu m. Neat TNAZ was found to be much harder to ignite than HMX or RDX and to self deflagrate with a visible flame only at pressures above 8 atm. Under these conditions the hot flame is very close to the surface. The combination of either HMX or TNAZ with HTPB, N5, or energetic binders produced no evidence of a diffusion flame: the binder decomposition products slowed the nitramine dark zone kinetics in the diffusion mixing fan coming from the interface and caused the nitramine secondary flame to standoff higher from the surface than normal. In sharp contrast, the combination of HMX or TNAZ with either AP or ADN lead to obvious diffusion flame interactions: the AP or ADN decomposition products accelerated the nitramine dark zone kinetics and caused the secondary flame height to drop significantly from it's normal height. This lead to higher heat feedback in the interface region and a somewhat faster nitramine regression rate. The ammonia (and other amine) products from the AP or ADN decomposition probably speed the reduction of NO thereby accelerating the nitramine dark zone reactions. Author

N95-31308 Army Research Lab., Aberdeen Proving Ground, MD.
AN ab Initio STUDY OF THE REACTION HNO+NO YIELDS OH+N2O: PRELIMINARY RESULTS c25
Steven W. Bunte, Cary F. Chabalowski, and Betsy M. Rice *In* JHU, The 31st JANNAF Combustion Subcommittee Meeting, Volume 2 Oct. 1994 p 345-354 (For primary document see N95-31282 11-28)
Avail: CPIA, 10630 Little Patuxent Pkwy., Suite 202, Columbia, MD 21044-3200 HC

The reaction of HNO with NO to produce N20 and OH has been studied by ab initio molecular orbital calculations. Preliminary results indicate that there are two distinct pathways that lead to products, however, only one is energetically favorable. The first reaction path begins with N-N association and forms a cis ONNO intermediate before encountering a 66 kcal/mole barrier, thus effectively halting the reaction. The second pathway also begins with N-N attack, this time however in a trans ONNO arrangement. While not complete at this writing, this pathway appears to be the first substantiation of an energetically viable pathway for this reaction. Author

N95-31309 Princeton Univ., NJ. Dept. of Mechanical and Aerospace Engineering.
THE OXIDATION OF CARBON MONOXIDE BY NITROUS OXIDE c25
M. T. Allen, R. A. Yetter, and F. L. Dryer *In* JHU, The 31st JANNAF Combustion Subcommittee Meeting, Volume 2 Oct. 1994 p 355-365 (For primary document see N95-31282 11-28)
(Contract N00014-90-J-4062)
Avail: CPIA, 10630 Little Patuxent Pkwy., Suite 202, Columbia, MD 21044-3200 HC

Kinetics experiments on mixtures of CO/N2O/H2O/N2 were performed in a variable pressure flow reactor at three atmospheres and temperatures near 1100 K. Experimentally measured profiles of CO, CO2. O2, H2O, N2O, NO and temperature were compared with modeling predictions obtained from a detailed chemical kinetic mechanism. At these conditions, the direct reaction of carbon monoxide with nitrous oxide results in at most 10 percent of the observed CO2 formation. The overall reaction rate is strongly affected by background water concentrations. Refinements in the current C/H/N/O kinetic mechanism are still incapable of precisely predicting these experimental data. Reaction flux and sensitivity analyses were used to identify the rate controlling reactions. For the first time, the individual catalytic effect of water vapor is clearly evident and a quantitative treatment of its influence is now possible. Author

N95-31310 Princeton Univ., NJ. Dept. of Mechanical and Aerospace Engineering.
THE OXIDATION OF CARBON MONOXIDE BY NITROGEN DIOXIDE c25
J. L. Gatto, R. A. Yetter, and F. L. Dryer *In* JHU, The 31st JANNAF Combustion Subcommittee Meeting, Volume 2 Oct. 1994 p 367-375 (For primary document see N95-31282 11-28)
(Contract N00014-90-J-4062)
Avail: CPIA, 10630 Little Patuxent Pkwy., Suite 202, Columbia, MD 21044-3200 HC

The kinetics of dilute CO/NO2/H2O mixtures have been studied in a flow reactor at temperatures of 773 K and 873 K, equivalence ratios near 10, and a pressure of 9 atm. Concentrations of NO2, NO, CO, CO2, and H2O were measured, providing a highly constrained set of reactant and product profiles as a function of time. These were compared to profiles from an evolving detailed kinetic model, using reaction flux and sensitivity analyses to identify rate controlling reactions. These first experiments, detailing the effects of water on the NO2/CO system, show a strong rate dependence on the water concentration. In direct contrast to the experimental results, the model predicts very little effect from water, and a reaction rate significantly slower than the experimental rate, even in experiments with low background water concentrations. Author

N95-31311 Naval Research Lab., Washington, DC. Chemistry Div.
DETAILED CHEMICAL KINETIC MODELING OF PREMIXED HYDROCARBON FLAMES SUPPORTED BY NO2 c25
Bradley A. Williams and James W. Fleming *In* JHU, The 31st JANNAF Combustion Subcommittee Meeting, Volume 2 Oct. 1994 p 377-386 (For primary document see N95-31282 11-28)
(Contract N00014-94-WX-2D001)
Avail: CPIA, 10630 Little Patuxent Pkwy., Suite 202, Columbia, MD 21044-3200 HC

Efforts to model the chemical structure of premixed flames of various hydrocarbon fuels supported by NO2 are presented and compared to available experimental data. The flames investigated include CH2O/NO2/O2, CH4/NO2/O2, HCN/NO2, C2N2/NO2, and C2H2/NO2. Structures of flames of C fuels are generally well predicted by current reaction sets, but the acetylene/nitrogen dioxide flame cannot be accurately modeled. The principle cause of this is postulated reactions of NO and NO2 with various species containing two carbon atoms whose rates are either completely unknown or have only been measured for a very limited set of conditions. Flame systems and individual reactions for which further study is needed are discussed. Author

N95-31312 Army Research Lab., Aberdeen Proving Ground, MD.
STUDIES OF REACTIONS PERTAINING TO AND DEVELOPMENT OF A REDUCED MECHANISM FOR THE DOUBLE BASE PROPELLANT DARK ZONE **c25**
W. R Anderson, N. Ilincic (California Univ., La Jolla, CA.), and K. Seshadri (California Univ., La Jolla, CA.) *In* JHU, The 31st JANNAF Combustion Subcommittee Meeting, Volume 2 Oct. 1994 p 387-397 (For primary document see N95-31282 11-28)
(Contract DAAL03-90-G-0084)
Avail: CPIA, 10630 Little Patuxent Pkwy., Suite 202, Columbia, MD 21044-3200 HC

Efforts to develop a detailed mechanism describing the chemical kinetics and structure of the dark zone of double base propellants are discussed. The detailed mechanism has been developed and first reduced in several steps to a skeletal mechanism of elementary steps consisting of 43 reactions amongst 16 species. It is then discussed how this mechanism has been further reduced by four species using steady state assumptions. This reduction involves usage on a homogeneous ignition delay type of problem and is the first of its kind, demonstrating that viable reduced mechanisms indeed can be produced for such ignition delay applications. In the development of the detailed mechanism, a very important consideration was the proper rate coefficient to use for N2O + O = NO + NO. Detailed modeling calculations of the shock tube experiments which have led to very high values in the literature for the rate coefficient of this reaction are shown to have been seriously affected by an incorrect assumption that the reaction H + N2O = NO + NH may be neglected. This and other key reactions in the development of the detailed mechanism are discussed. Author

N95-31313 Army Research Lab., Aberdeen Proving Ground, MD.
FLAME STRUCTURE STUDIES OF NEAT AND NH3 DOPED H2/N2O FLAMES EMPLOYING MOLECULAR BEAM MASS SPECTROMETRY AND MODELING **c25**
R. C. Sausa, G. Singh, G. W. Lemire, and W. R. Anderson *In* JHU, The 31st JANNAF Combustion Subcommittee Meeting, Volume 2 Oct. 1994 p 399-406 Sponsored in cooperation with NRC/NAS (For primary document see N95-31282 11-28)
Avail: CPIA, 10630 Little Patuxent Pkwy., Suite 202, Columbia, MD 21044-3200 HC

State-of-the-art combustion diagnostics and advanced computational tools, developed at the Army Research Laboratory, have been applied to studies of the detailed flame chemistry relevant to the gaseous flames of burning energetic materials. The experimental results provide the necessary validation for combustion models that are being developed to simulate energetic material combustion for increased system performance. In this paper, we report a combined experimental and detailed kinetic modeling study on neat and NH3-doped H2/N2O burner stabilized flames in order to understand the fundamental mechanism for NO formation and destruction, and to determine and predict the efficacy of NH(x) additives on rate of conversion of NO to the final product N2. NO is an environmental pollutant and a product of incomplete combustion (PIC). In many systems, including propellants and explosives, it acts as a chemical inhibiter, thus preventing full energy release. This system was chosen because it has important implications in understanding nitramine propellant combustion and decomposition, and NO(x) pollutant formation during demilitarization operations. Species concentration and temperature profiles were obtained using molecular beam mass spectrometry and thin-wire thermocouples, respectively. Species profiled include H2, N2O, NH3, Ar, H2O, N2, O2 and NO. These profiles are compared to calculated profiles generated using PREMIX, a one dimensional premixed laminar flame code. The detailed chemical mechanism employed in the code consists of 88 reactions and 20 species, and was derived from preliminary calculations using a more comprehensive set of reactions (greater than 200) obtained from a critical literature review. Our experimental results show that the addition of small amounts of NH3 reduces significantly the NO concentration, e.g. a 50 percent reduction for a 4 percent NH3 addition. This result is also borne out in our model calculations. Rate and sensitivity analyses were performed on the PREMIX results using an interactive postprocessing code we have written so that the details of the chemistry may be understood. Applications of these results for better propellant formulation and increased performance are also discussed. Author

N95-31314 Naval Air Warfare Center, China Lake, CA. Research and Technology Div.
RDX LASER-ASSISTED FLAME STRUCTURE **c25**
Donna Hanson-Parr and Tim Parr *In* JHU, The 31st JANNAF Combustion Subcommittee Meeting, Volume 2 Oct. 1994 p 407-423 (For primary document see N95-31282 11-28)
(Contract N00014-92-WX-24097)
Avail: CPIA, 10630 Little Patuxent Pkwy., Suite 202, Columbia, MD 21044-3200 HC

UV-Visible absorption measurements have been done in RDX flames to obtain concentrations of NO, NO2, CN, OH, and RDX using different laser fluxes and then compared with those obtained for the steady state (no laser) case. For the CO2 laser fluxes used, it was found that the NO and NO2 species profiles, scaled to the CN radical flame height, were very nearly the same, except that both were low if the flux was not high enough. This showed that a laser could be used to stretch out the flame to improve spatial resolution of measurements and validate the results obtained. The (OH) concentration in the burnt gas region appeared to be the same for all laser fluxes, but the (CN) apparently increased. Burning rates as a function of laser flux were also obtained and were linear with flux except at the low end where the heat feedback produced under steady state conditions became comparable to the external laser flux, as evidenced by the similar CN flame standoff distance. Other results showed that the mole fraction of H2CO coming off the surface is below 1 percent even at heating rates very much lower than what the RDX would see in a deflagrating rocket propellant, but may be as high as 7 percent in the 'melt' layer. It was observed that RDX smoke is formed prior to ignition and an interesting, but as yet unassigned, structured absorption band in the 320 - 400 nm region, not due to formaldehyde, HONO, NO2, or atomic absorption, is clearly visible and was not seen in HMX smoke. Particle imaging velocimetry was used to obtain a velocity vector field of a laser-assisted flame and showed that the centerline velocity was essentially constant at 5.5 m/s through the dark zone and secondary flame. Author

N95-31315 Pennsylvania State Univ., University Park, PA.
A STUDY OF THE GAS-PHASE PROCESSES OF RDX COMBUSTION USING A TRIPLE QUADRUPOLE MASS-SPECTROMETER **c25**
Young Joo Lee, Ching-Jen Tang, and Thomas A. Litzinger *In* JHU, The 31st JANNAF Combustion Subcommittee Meeting, Volume 2 Oct. 1994 p 425-437 (For primary document see N95-31282 11-28)
(Contract N00014-93-1-0080)
Avail: CPIA, 10630 Little Patuxent Pkwy., Suite 202, Columbia, MD 21044-3200 HC

Measurements of gas-phase chemical species were obtained in an RDX mono-propellant flame to study key chemical processes. Experiments were conducted in an argon environment and a high-power CO2 laser was used to initiate and sustain combustion. Measurements of species were conducted over a pressure range of 0.1 to 3 atm, and at several heat fluxes over the range of 50 to 600 W/cm (exp 2). Gas samples were extracted using a quartz microprobe and analyzed using a triple quadrupole mass spectrometer (TQMS). The TQMS is capable of resolving species which could contribute on the same mass: N2 and CO to mass 28; N2O and CO2 to mass 44. This capability was also applied to differentiate NO and CH2O at mass 30, and to identify species other than CHO present at mass 29. Using parent and daughter modes of the TQMS and careful calibration, it was possible to differentiate and quantify many of these species. For the experimental conditions selected, the major species at the surface were NO, HCN, H2O, N2O, CO, NO2 and mass 29. The ratio of (N2)/(CO) is approximately 1.5 at the surface, and decreased to about 1.0 at the end of the luminous flame zone at mass 28. Mass 44 totally consisted of N2O at the surface without CO2, and the portion of N2O decreased exponentially to 0 at the end of reaction zones, while the reverse trend was true for CO2. At 1 atm and a heat flux of 100 W/cm (exp 2), near the surface, NO turned out to constitute the majority of mass 30, and only small amount of CH2O was identified. As identified by the species profiles of HCN, NO and N2O, the reaction zones expanded as heat flux increased and pressure decreased. Even with the expansion of reaction zones, no evidence of the near surface-reaction zone was found. Author

N95-31470# Phillips Lab., Edwards AFB, CA.
PROCEEDINGS OF THE HIGH ENERGY DENSITY MATTER (HEDM) CONTRACTOR'S CONFERENCE Special Report
T. L. Thompson and S. L. Rogers Dec. 1994 308 p Conference held in Crystal Bay, NV, 5-7 Jun. 1994
(AD-A292988; PL-TR-94-3036) Avail: CASI HC A14/MF A03

This report documents the information presented at the eighth annual High Energy Density Matter (HEDM) Contractors' Conference held 5-7 June 1994 in Crystal Bay, NV. This report contains the extended abstracts of the oral, workshop, and poster presentations given by the Air Force funded contractors and by the in-house researchers from the Phillips Laboratory. The main purpose of the High Energy Density Matter (HEDM) program is to research and develop advanced high energy compounds containing increased energy densities (energy to mass ratios) to produce greater specific impulses (thrust per weight flow rate of propellant) which will enable spacecraft to carry larger payloads. With these advanced propellants, future space-bound payloads could be possibly four times greater that they are today. DTIC

N95-31526# Army Armament Research, Development and Engineering Center, Picatinny Arsenal, NJ.
ACIDITY AND BASICIDITY OF NITRO SUBSTITUTED IMIDAZOLES
T. Vladimiroff Apr. 1995 16 p
(AD-A293969; ARAED-TR-94-021) Avail: CASI HC A03/MF A01

The antibiotic azomycin is 2-nitroimidazole. 2,4-dinitroimidazole has recently been found to be a fairly powerful yet stable explosive. The family of all nitro substituted imidazoles constitute an interesting series of molecules from both the biological and the energetic material points of view. Imidazole is a heterocyclic five membered ring with two nitrogen atoms in the ring. One of these nitrogens is bound to a hydrogen atom so that it can act as a proton donor. The other nitrogen can act as a proton acceptor. The molecule can therefore act as both an acid and a base. In this work the protonation and deprotonation energies for all the nitro substituted imidazoles are computed with several basis sets. The GAUSSIAN 92 set of programs is used and all computations are performed at the SCF level of theory. The geometry of all the structures are determined using gradient techniques and compared to experimentally obtained geometries when available. It is found that these materials become more acidic and less basic as the degree of nitration increases. DTIC

N95-31531 Pennsylvania Univ., Philadelphia, PA.
THE PHYSICAL AND CHEMICAL PROCESSES GOVERNING CO2 LASER-INDUCED PYROLYSIS AND COMBUSTION OF THE SOLID PROPELLANTS RDX, ADN, XM39, AND M43 Ph.D. Thesis
Barry Lynn Fetherolf 1993 238 p
Avail: Univ. Microfilms Order No. DA9414276

CO2 laser-induced pyrolysis and combustion of RDX, XM39, M43, and ammonium dinitramide (ADN) were investigated experimentally and by kinetic modelling. Gas species and temperature profiles as a function of measuring height, laser heat flux, and pressure were measured with a microprobe/mass spectrometer system and fine-wire thermocouples. Gas phase processes for RDX and ADN were modelled with CHEMKIN as a 1-D, premixed flame. Three distinct categories of laser-induced behavior were observed: laser-induced pyrolysis (LIP) characterized by decomposition without stable surface regression, laser-induced regression (LIR), and laser-assisted combustion (LAC), the latter two categories characterized by stable regression of the surface but with a luminous flame only observed for LAC. Under LIP conditions, RDX exhibited a thick melt layer with considerable bubbling. Gas species within a bubble were measured with the most abundant species being CH2O, H2O, NO2, and N2O. Species profiles for RDX at 0.5 and 1.0 atmospheres under LAC conditions were measured. Reaction of CH2O and NO2 occurred directly above the surface followed by a final luminous flame due to reaction of HCN, NO, and N2O. The kinetic model for RDX produced excellent agreement between model and experimental species profiles. Both XM39 and M43 exhibited the same overall reaction chemistry as pure RDX but displayed distinctly different laser-induced behavior. M43 exhibited a higher surface temperature and less CH2O and NO2 at the surface than XM39, possibly due to increased condensed phase reaction. XM39 did not exhibit LAC until five atmospheres whereas M43 required a pressure of only three atmospheres to achieve LAC. ADN pyrolyzed and burned roughly an order of magnitude faster than the other propellants. Under LIR conditions, ADN evolved N2O, H2O, N2, NO2, and NH3 in order of decreasing mole fraction, and numerous particles of ammonium nitrate. LAC was observed for ADN at three atmospheres with an unstable flame whereas tests at five atmospheres produced a more stable flame with individual flamelets just above the surface. The flame produced significant amounts of NO and H2O and a gas temperature of about 1350 K. Dissert. Abstr.

N95-31564# Southwest Research Inst., San Antonio, TX. Belvoir Fuels and Lubricants Research Facility.
NATURAL GAS LIQUEFIER FOR VEHICLE FUEL Interim Report, Jan. - Dec. 1994
E. C. Owens and K. Randall Kohuth (General Pneumatics Corp., Scottsdale, AZ.) Mar. 1995 86 p
(Contract DAAK70-92-C-0059)
(AD-A293619; TFLRF-310) Avail: CASI HC A05/MF A01

This project was a continuation and refinement of a feasibility prototype natural gas liquefier that had been designed, fabricated, and tested under a U.S. Department of Energy (DoE) Small Business Innovation Research (SBIR) contract. Extensive performance testing was conducted to characterize the natural gas liquefier refrigeration capability and to collect data for diagnostic purposes. Analysis of the effectiveness of the regenerator concluded that the current design would require substantial empirical iterations. The final prototype with a design target of 1,000 Watts (W) refrigeration was able to achieve only 400 W of refrigeration, projected to 550 W at a higher charge pressure. Recommendations are made for further testing, analysis, and correlation to achieve a better optimized regenerator design for a second generation prototype natural gas liquefier. DTIC

N95-31638# National Renewable Energy Lab., Golden, CO.
BIOFACTS: FUELING A STRONGER ECONOMY. METHANOL FROM BIOMASS, REVISION 2
1995 4 p
(Contract DE-AC36-83CH-10093)
(DE95-010302; NREL/SP-420-5570-Rev-2) Avail: CASI HC A01/MF A01

This informational pamphlet written by the National Renewable Energy Laboratory discusses obtaining methanol, a liquid transportation fuel, from biomass, defined as crop residues, grasses, forest residues, short-rotation tree crops, and more than half of the municipal solid waste and industrial waste streams. The biomass resource is proposed in place of fossil domestic resources such as natural gas, coal and residual oil. Advances in production, processing and pilot plant design, as well as utilization concerns and environmental advantages, are addressed. DOE

N95-31639# National Renewable Energy Lab., Golden, CO.
BIOFACTS: FUELING A STRONGER ECONOMY. ETHANOL FROM BIOMASS, REVISION 2
Jan. 1995 4 p
(Contract DE-AC36-83CH-10093)
(DE95-010304; NREL/SP-420-5572-Rev-2) Avail: CASI HC A01/MF A01

Ethanol from biomass is a domestically produced liquid fuel from renewable, virtually inexhaustible domestic resources. It is a nonfossil transportation fuel that contributes little, if any, net carbon dioxide to the atmosphere during production and use. It is a high-octane fuel that can contribute substantially to the US automotive fuel supply. It is a fuel that can be used as a blend, a component of ethyl tertiary butyl ether (ETBE), or as a pure fuel, with excellent efficiency and performance. It is a potentially clean-burning fuel that reduces smog and emissions of carbon monoxide. This overview presents the resource potential, processing techniques, DOE program highlights, utilization potential and environmental effects of ethanol from biomass. DOE

N95-32048# Los Alamos National Lab., NM.
BASE HYDROLYSIS AND HYDROTHERMAL PROCESSING OF PBX-9404 EXPLOSIVE
J. A. Sanchez, R. L. Flesner, T. Spontarelli, P. C. DellOrco, and J. F. Kramer 26 Feb. 1995 13 p Presented at the Maes National Symposium and Career Fair, Los Angeles, CA, 26-29 Mar. 1995
(Contract W-7405-eng-36)
(DE95-009437; LA-UR-95-795; CONF-9503123-1) Avail: CASI HC A03/MF A01

Base hydrolysis in combination with hydrothermal processing has been proposed as an environmentally acceptable alternative to open burning/open detonation for degradation and destruction of high explosives. In this report, the authors examine gaseous and aqueous products of base hydrolysis of the HMX-based plastic bonded explosive, PBX-9404. The authors also examine products from the subsequent hydrothermal treatment of the base hydrolysate. The gases produced from hydrolysis of PBX-9404 are ammonia, nitrous oxide, and nitrogen. Major aqueous products are sodium formate, acetate, nitrate, and nitrite, but not all carbon products have been identified. Hydrothermal processing of base hydrolysate destroyed up to 98% of the organic carbon in solution, and higher destruction efficiencies are possible. Major gas products detected from hydrothermal processing were nitrogen and nitrous oxide. DOE

N95-32158# Oklahoma Univ., Norman, OK.
LIQUID NATURAL GAS AS A TRANSPORTATION FUEL IN THE HEAVY TRUCKING INDUSTRY Second Quarterly Progress Report, 1 Oct. 1994 - 30 Dec. 1994
W. H. Sutton 1995 8 p
(DE95-010376; DOE/BC-14971/2) Avail: CASI HC A02/MF A01

Studies aimed at using liquefied natural gas as a diesel fuel replacement are presented. Research concerning short and long term storage is discussed. DOE

N95-32249 National Defence Research Establishment, Stockholm (Sweden). Dept. of Weapon Systems, Effects and Protection.
THERMOPLASTIC ELASTOMERS AS A BINDER IN COMPOSITE PROPELLANTS [TERMOELASTER SOM BINDEMEDEL I KOMPOSITKRUT]
M. Ekeberg, B. Stenberg, and R. Sanden Nov. 1994 35 p In SWAHILI Prepared in cooperation with Royal Inst. of Tech.
(PB95-211553; FOA-R-94-00061-2.1-SE) Avail: Issuing Activity (National Technical Information Service (NTIS))

Several commercial thermoplastic elastomers have been studied in order to investigate whether they can be used as a binder for composite propellants. A literature survey is presented and some interesting commercial thermoplastic elastomers of SBS, EVA and polyester type are described. Thermochemical calculations using ammonium perchlorate as an oxidant give a slightly lower impulse than an equivalent HTPB propellant. Without oxidizer, as fuel in air-breathing motors, the two polymers give almost the same impulse. The results suggest that this EVA material is an interesting alternative to HTPB as a binding material in composite propellants. It is also likely to work as a binder for fuel-rich propellants for air-breathing motors such as ducted rocket and solid fuel ramjet engines. NTIS

N95-32355# Los Alamos National Lab., NM.
BASE HYDROLYSIS AND HYDROTHERMAL PROCESSING OF PBX-9404 EXPLOSIVE
J. A. Sanchez, R. L. Flesner, T. Spontarelli, P. C. DellOrco, and J. F. Kramer 1994 14 p Presented at the Life Cycles of Energetic Materials, Del Mar, CA, 11-16 Dec. 1994
(Contract W-7405-eng-36)
(DE95-009497; LA-UR-95-1074; CONF-941255-3) Avail: CASI HC A03/MF A01

Base hydrolysis in combination with hydrothermal processing has been proposed as an environmentally acceptable alternative to open burning/open detonation for degradation and destruction of high explosives. In this report, we examine gaseous and aqueous products of base hydrolysis of the HMX-based plastic bonded explosive, PBX-9404. We also examine products from the subsequent hydrothermal treatment of the base hydrolysate. The gases produced from hydrolysis of PBX-9404 are ammonia, nitrous oxide, and nitrogen. Major aqueous products are sodium formate, acetate, nitrate, and nitrite, but not all carbon products have been identified. Hydrothermal processing of base hydrolysate destroyed up to 98% of the organic carbon in solution, and higher destruction efficiencies are possible. Major gas products detected from hydrothermal processing were nitrogen and nitrous oxide. DOE

N95-31751*# Thiokol Corp., Brigham City, UT.
AP RECLAMATION AND REUSE IN RSRM PROPELLANT
Kathryn F. Miks and Stacey A. Harris (Phillips Lab., Edwards AFB, CA.) *In* NASA. Marshall Space Flight Center, Aerospace Environmental Technology Conference Mar. 1995 p 67-86 (For primary document see N95-31746 11-23)
Avail: CASI HC A03/MF A06

N95-31752*# Stevens Inst. of Tech., Hoboken, NJ. Center for Environmental Engineering.
ENHANCED ALKALINE HYDROLYSIS AND BIODEGRADABILITY STUDIES OF NITROCELLULOSE-BEARING MISSILE PROPELLANT
Mohammed Sidhoum, Christos Christodoulatos, Tsan-Liang Su, and Mercurios Redis *In* NASA. Marshall Space Flight Center, Aerospace Environmental Technology Conference Mar. 1995 p 87-98 Sponsored by US Army Construction Research Lab. (For primary document see N95-31746 11-23)
Avail: CASI HC A03/MF A06

N95-31753*# Hercules Aerospace Co., Magna, UT.
ENVIRONMENTALLY COMPATIBLE SOLID ROCKET PROPELLANTS
James L. Jacox and Daniel J. Bradford *In* NASA. Marshall Space Flight Center, Aerospace Environmental Technology Conference Mar. 1995 p 99-104 (For primary document see N95-31746 11-23)
Avail: CASI HC A02/MF A06

N95-31754*# Thiokol Corp., Brigham City, UT.
LOW ACID PRODUCING SOLID PROPELLANTS
Robert R. Bennett *In* NASA. Marshall Space Flight Center, Aerospace Environmental Technology Conference Mar. 1995 p 105-114 (For primary document see N95-31746 11-23)
Avail: CASI HC A02/MF A06

N95-31755*# McDonnell-Douglas Aerospace, Huntsville, AL.
IMPROVED HYBRID ROCKET FUEL
David L. Dean *In* NASA. Marshall Space Flight Center, Aerospace Environmental Technology Conference Mar. 1995 p 115-121 Sponsored by MDA-HSV-IRAD (For primary document see N95-31746 11-23)
Avail: CASI HC A02/MF A06

N95-31768*# Department of the Air Force, Wright-Patterson AFB, OH.
ENVIRONMENTALLY SAFE AVIATION FUELS
Patricia D. Liberio *In* NASA. Marshall Space Flight Center, Aerospace Environmental Technology Conference Mar. 1995 p 233-237 (For primary document see N95-31746 11-23)
Avail: CASI HC A01/MF A06

29 MATERIALS PROCESSING

Includes space-based development of products and processes for commercial applications.

For biological materials see *55 Space Biology*.

N95-31359*# National Aeronautics and Space Administration. Lewis Research Center, Cleveland, OH.
NUMERICAL MODELING OF BRIDGMAN GROWTH OF PbSnTe IN A MAGNETIC FIELD
Minwu Yao (Ohio Aerospace Inst., Brook Park, OH.), Arnon Chait, Archibald L. Fripp (National Aeronautics and Space Administration. Langley Research Center, Hampton, VA.), and William J. Debnam (National Aeronautics and Space Administration. Langley Research Center, Hampton, VA.) Jul. 1995 54 p Presented at the Sixth FIDAP Users Conference, Chicago, IL, 30 Apr. - 2 May 1995; sponsored by Fluid Dynamics International
(Contract NCC3-208; NAG3-1096; RTOP 963-35-08)
(NASA-TM-106996; E-9773; NAS 1.15:106996) Avail: CASI HC A04/MF A01

In this work we study heat and mass transport, fluid motion, and solid/liquid phase change in the process of steady Bridgman growth of Pb(.8)Sn(.2)Te (LTT) in an axially-imposed uniform magnetic field under terrestrial and microgravity conditions. In particular, this research is concerned with the interrelationships among segregation, buoyancy-driven convection, and magnetic damping in the LTT melt. The main objectives are to provide a quantitative understanding of the complex transport phenomena during solidification of the nondilute binary of LTT, to provide estimates of the strength of magnetic field required to achieve the desired

diffusion-dominated growth, and to assess the role of magnetic damping for space and earth based control of the buoyancy-induced convection. The problem was solved by using FIDAP and numerical results for both vertical and horizontal growth configurations with respect to the acceleration of gravity vector are presented. Author

N95-31472# Maryland Univ., College Park, MD.
THE EFFECT OF GRAVITY ON THE DEPOSITION OF THIN FILMS: THE PHYSICAL VAPOR TRANSPORT OF COPPER PHTHALOCYANINE Final Technical Report, 1 Aug. 1991 - 31 Jul. 1994
T. L. Einstein, M. E. Fisher, J. D. Weeks, and J. A. Yorke 31 Jul. 1994 99 p Limited Reproducibility: Document partially illegible
(Grant AF-AFOSR-0297-91)
(AD-A292997; AFOSR-95-0226TR) Avail: CASI HC A05/MF A02

We describe our progress and final conclusions in our theoretical analysis of the growth of thin films of Copper Phthalocyanine (CuPc) via physical vapor transport using a closed cell ampoule. Three projects are discussed. The first is an analysis of the possibility of convection in the ampoule. This provides the most natural explanation for the experimental differences seen in thin films grown on earth and on the Space Shuttle. However we conclude that convection alone is unlikely to be able to explain these differences. The other two projects examined general features of CuPc crystal growth arising from its very anisotropic shape. The second project modeled the CuPc molecule as a hard square shaped object and examined detailed features of the packing of such objects by a physically motivated deposition algorithm. The third project developed a more realistic intermolecular potential for CuPc involving attractive as well as repulsive intermolecular forces. Crystal structures and diffusion barriers were examined. These considerations have more general applicability to the crystal growth of anisotropic molecules on earth, and we believe further work along these lines is called for. DTIC

N95-31983*# National Academy of Sciences - National Research Council, Washington, DC.
MICROGRAVITY RESEARCH OPPORTUNITIES FOR THE 1990S
1995 159 p
(Contract NASw-4627)
(NASA-CR-199109; LC-94-74623; NAS 1.26:199109) Avail: CASI HC A08/MF A02

The Committee on Microgravity Research (CMGR) was made a standing committee of the Space Studies Board (SSB) and charged with developing a long-range research strategy. The scientific disciplines contained within the microgravity program, and covered in this report, include fluid mechanics and transport phenomena, combustion, biological sciences and biotechnology, materials science, and microgravity physics. The purpose of this report is to recommend means to accomplish the goal of advancing science and technology in each of the component disciplines. Microgravity research should be aimed at making significant impacts in each discipline emphasized. The conclusions and recommendations presented in this report fall into five categories: (1) overall goals for the microgravity research program; (2) general priorities among the major scientific disciplines affected by gravity; (3) identification of the more promising experimental challenges and opportunities within each discipline; (4) general scientific recommendations that apply to all microgravity-related disciplines; and (5) recommendations concerning administrative policies and procedures that are essential to the conduct of excellent laboratory science.
Derived from text

31 ENGINEERING (GENERAL)

Includes vacuum technology; control engineering; display engineering; cryogenics; and fire prevention.

N95-30455# Technische Univ., Twente (Netherlands). Dept. of Computer Science.
METRICS IN METHOD ENGINEERING
S. Brinkkemper and M. Rossi Dec. 1994 29 p
(PB95-197687; Memo-INF-94-79) Copyright Avail: CASI HC A03/MF A01

As customizable computer aided software engineering (CASE) tools, or CASE shells, have been introduced in academia and industry, there has been a growing interest into the systematic construction of methods and their support environments, i.e. method engineering. To aid the method developers and method selectors in their tasks, we propose two sets of metrics, which measure the complexity of diagrammatic specification techniques on the one hand, and of complete systems development methods on the other hand. Proposed metrics provide a relatively fast and simple way to analyze the technique (or method) properties, and when accompanied with other selection criteria, can be used for estimating the cost of learning the technique and the relative complexity of a technique compared to others. To demonstrate the applicability of the proposed metrics, we have applied them to 34 techniques and 15 methods. NTIS

N95-30521 Selskapet for Industriell og Teknisk Forskning, Trondheim (Norway). Div. of Safety and Reliability.
METASCIENTIFIC PROBLEMS IN SAFETY SCIENCE
R. Rosness 31 Dec. 1993 18 p
(PB95-196408; STF75-S93041) Avail: Issuing Activity (National Technical Information Service (NTIS))

This paper is an introduction to a workshop on safety science and the theory of science. The paper examines a study of helicopter safety in order to identify some of the metascientific problems in safety science. It then considers the nature of safety science in more general terms. Finally, it argues that a considerable part of safety science cannot be expected to conform to orthodox falsified criteria of science. This leads to the conclusion that safety scientists should take the responsibility of proposing and justifying norms for empirical and theoretical work in the area. NTIS

N95-30630# Swedish Inst. for Materials Testing, Boras (Sweden).
SIMPLE MODEL OF FOAM SPREADING ON LIQUID SURFACES
B. Persson and M. Dahlberg 1994 31 p
(PB95-211207; SP-RAPP-94:27) Avail: CASI HC A03/MF A01

An approximate theoretical model of foam spreading on liquids has been formulated. The model is analogous to the spreading of oil slicks on water surfaces. Viscous friction is assumed to be the dominating mechanism in opposing the foam spread. The spreading process is decoupled from the mass transport due to evaporation and drainage of water contained in the foam. The evaporation is assumed to be caused by external radiation, thus simulating the important case of foam spreading on a burning surface. The reduction of the foam layer thickness is accounted for by including a prescribed rate of decrease fixed by the radiation intensity. The decrease rate has been determined in a separate experiment. In the present formulation it is assumed that the foam layer has a triangular shape which presumably is a poor approximation for the initial phase of the spread. More work is needed to find out if this assumption needs to be modified. NTIS

N95-30684# Oak Ridge National Lab., TN.
ADVANCED COMPUTATIONAL RESEARCH IN MATERIALS PROCESSING FOR DESIGN AND MANUFACTURING
T. Zacharia 1995 8 p Presented at the 1994 Review of Progress in Quantitative Nondestructive Evaluation Conference, Snowmass, CO, 31 Jul. - 5 Aug. 1994
(Contract DE-AC05-84OR-21400)
(DE95-009130; CONF-9407123-6) Avail: CASI HC A02/MF A01

Advanced mathematical techniques and computer simulation play a major role in providing enhanced understanding of conventional and advanced materials processing operations. Development and application of mathematical models and computer simulation techniques can provide a quantitative understanding of materials processes and will minimize the need for expensive and time consuming trial- and error-based product development. As computer simulations and materials databases grow in complexity, high performance computing and simulation are expected to play a key role in supporting the improvements required in advanced material syntheses and processing by lessening the dependence on expensive prototyping and re-tooling. Many of these numerical models are highly compute-intensive. It is not unusual for an analysis to require several hours of computational time on current supercomputers despite the simplicity of the models being studied. For example, to accurately simulate the heat transfer in a 1-cu m block using a simple computational method requires 10(exp 12) arithmetic operations per second of simulated time. For a computer to do the simulation in real time would require a sustained computation rate 1000 times faster than that achievable by current

supercomputers. Massively parallel computer systems, which combine several thousand processors able to operate concurrently on a problem are expected to provide orders of magnitude increase in performance. This paper briefly describes advanced computational research in materials processing at ORNL. Continued development of computational techniques and algorithms utilizing the massively parallel computers will allow the simulation of conventional and advanced materials processes in sufficient generality. DOE

N95-30777# Technische Univ., Delft (Netherlands). Dept. of Mechanical Engineering and Marine Technology.
SYSTEM IDENTIFICATION FOR ROBUST PROCESS CONTROL. NOMINAL MODELS AND ERROR BOUNDS Ph.D. Thesis
R. G. Hakvoort 29 Nov. 1994 292 p
(PB95-197026; ISBN-90-370-0114-9) Avail: CASI HC A13/MF A03

The main contribution of this thesis is the development of a robust-control-oriented identification procedure. The identification procedure delivers a nominal model and an explicit model error bound suited for use in high-performance robust process control. The basic steps of the procedure are outlined. After the development of new identification tools, a more detailed description of the entire identification procedure is given in Chapter 8. An essential step in the identification procedure is the identification of a system uncertainty set. This set specifies explicit bounds on the frequency response or weighted pulse response of the system to be identified. The system uncertainty set is constructed on the basis of measurement data and a priori information about the system and the noise which corrupts the data. On the basis of this set both the nominal model and the model error bound are constructed. NTIS

N95-31122# Naval Postgraduate School, Monterey, CA.
CONSTRUCTION AND PERFORMANCE MEASUREMENT OF A PORTABLE THERMOACOUSTIC REFRIGERATOR DEMONSTRATION APPARATUS M.S. Thesis
Todd J. Berhow Dec. 1994 96 p
(AD-A293265) Avail: CASI HC A05/MF A01

This thesis documents the construction and performance measurement of a portable thermoacoustic refrigerator demonstration apparatus. The objective of the portable refrigerator is to graphically display, as a demonstration during lectures, a substantial thermoacoustic cooling power. Within minutes of start up, the apparatus develops frost on a small metal portion of the device. The refrigerator is small and compact and fits into a portable carrying case along with all ancillary equipment. The construction of the device had been started in a previous thesis project. This thesis describes the remaining construction steps required to complete the refrigerator and the subsequent performance evaluation of the unit in laboratory test trials. DTIC

N95-31690*# National Aeronautics and Space Administration. Goddard Space Flight Center, Greenbelt, MD.
PREVENTING CRACKING OF ANODIZED COATINGS
Charles C. He (Unisys Corp., Greenbelt, MD.) and Thomas M. Heslin Aug. 1995 13 p
(NASA-TM-104622; Rept-95B00106; NAS 1.15:104622) Avail: CASI HC A03/MF A01

Anodized coatings have been used as optical and thermal surfaces in spacecraft. Particulate contamination from cracked coatings is a concern for many applications. The major cause for the cracking is the difference in the coefficient of thermal expansion between the oxide coatings and the aluminum substrate. The loss of water when the coating is exposed to a vacuum also could induce cracking of the coating. Hot-water sealing was identified as the major cause for the cracking of the coatings because of the large temperature change when the parts were immersed in boiling water and the water was absorbed in the coating. when the hot-water sealing process was eliminated, the cracking resistance of the anodized coatings was greatly improved. Also, it was found that dyed black coatings were more susceptible than clear coatings to cracking during thermo-vacuum cyclings. Author

N95-31727# Foreign Broadcasting Information Service, Washington, DC.
FBIS REPORT: SCIENCE AND TECHNOLOGY. CENTRAL EURASIA
6 Jul. 1995 83 p Transl. into ENGLISH from various Central Eurasian articles
(FBIS-UST-95-027) Avail: CASI HC A05/MF A01

Translated articles cover the following topics: Dissension Among Space Specialists Viewed; and Status of Space Industry Discussed. CASI

N95-31729# Foreign Broadcasting Information Service, Washington, DC.
FBIS REPORT: SCIENCE AND TECHNOLOGY. CENTRAL EURASIA
10 Jul. 1995 115 p Transl. into ENGLISH from various Central Eurasian articles
(FBIS-UST-95-028) Avail: CASI HC A06/MF A02

Translated articles cover the following topics: numerical solution of the three-dimensional problem of high-speed interaction of a cylinder with an undeformable barrier considering temperature effects; review of methods for suppressing rocket engine instability; numerical modeling of deflagration-detonation transition in rocket fuels; and interaction of vestibular inputs with different orientation of otoliths in gravity field. Author

N95-32082# Sandia National Labs., Albuquerque, NM.
VIBRATION CONTROL FOR PRECISION MANUFACTURING AT SANDIA NATIONAL LABORATORIES
Terry Hinnerichs and David Martinez 1995 16 p Presented at the North American Conference on Smart Structures and Materials, San Diego, CA, 26 Feb. - 3 Mar. 1995
(Contract DE-AC04-94AL-85000)
(DE95-009582; SAND-95-0609C; CONF-950228-5) Avail: CASI HC A03/MF A01

Sandia National Laboratories performs R&D in structural dynamics and vibration suppression for precision applications in weapon systems, space, underwater, transportation and civil structures. Over the last decade these efforts have expanded into the areas of active vibration control and 'smart' structures and material systems. In addition, Sandia has focused major resources towards technology to support weapon product development and agile manufacturing capability for defense and industrial applications. This paper will briefly describe the structural dynamics modeling and verification process currently in place at Sandia that supports vibration control and some specific applications of these techniques to manufacturing in the areas of lithography, machine tools and flexible robotics. DOE

N95-32123# Advisory Group for Aerospace Research and Development, Neuilly-Sur-Seine (France). Mission Systems Panel.
GUIDANCE AND CONTROL FOR FUTURE AIR-DEFENCE SYSTEMS [TECHNIQUES DE GUIDAGE/PILOTAGE POUR LES SYSTEMES FUTURS DE DEFENCE ANTI-AERIENNE]
Jan. 1995 202 p ENGLISH and FRENCH Presented at the Mission Systems Panel 1st Symposium, Copenhagen, Denmark, 17-20 May 1994
(AGARD-CP-555; ISBN-92-836-0008-8) Copyright Avail: CASI HC A10/MF A03

This volume contains the Technical Evaluation Report and the 18 unclassified papers, presented at the Mission Systems Panel Symposium held in Copenhagen, Denmark from 17th to 20th May 1994. The papers presented covered the following headings: (1) Ballistic Missile Defense Architecture and Air Defense Simulation; (2) Advanced Sensors Technology and Techniques; (3) Acquisition, Pointing, Fire Control and System Integration (4) Data Fusion, Tracking and Identification; (5) Threat Detection, Suppression and Situation Assessment; (6) Missile Guidance and Control; and (7) C3I Aspects. For individual titles, see N95-32124 through N95-32141.

N95-32124# North Atlantic Treaty Organization, Brussels (Belgium). NATO Industrial Advisory Group.
STUDY OF EXTENDED AIR DEFENCE POST 2000
Peter J. Mantle *In* AGARD, Guidance and Control for Future Air-Defence Systems Jan. 1995 16 p (For primary document see N95-32123 11-31)
Copyright Avail: CASI HC A03/MF A03

This invited paper, which was the second oral presentation at the conference, covered the conclusions found by NIAG SG-37 during a one year research of the issues and solutions to furnishing extended air defense capability to NATO and its forces. Key issues diagnosed included: (1) the requirement of a multi-layered defense system that includes space-based defense, aircraft, missiles, and other hardware; (2) the electronics needed

for this support; and (3) the materials, propulsion devices, and lethality of the systems. A technological forecast of funding recommendations is included. CASI

N95-32125# GIE Cosyde, Velizy-Villacoublay (France).
DEFINITION OF AN ANTI-MISSILE BALLISTIC DEFENSE ARCHITECTURE FOR EUROPE [DEFINITION D'UNE ARCHITECTURE DE DEFENSE ANTI-MISSILE BALISTIQUE POUR L'EUROPE]
M. Deas and A. Tanter *In* AGARD, Guidance and Control for Future Air-Defence Systems Jan. 1995 7 p In FRENCH (For primary document see N95-32123 11-31)
Copyright Avail: CASI HC A02/MF A03

The end of the Seventies and beginning of the Eighties showed significant technological developments in ballistic missiles, in particular,impact precision. These improvements caused Western strategists to be concerned with use of ballistic missiles equipped with conventional loads against military objectives (the Pact of Varsovie). The concept of ballistic missile tactical had been born. The ballistic vector, which until this time was marked with a 'strategic' label, was then 'standardized' and has interested a number of countries in the process of its development. The world has just entered the era of the ballistic proliferation. From the very start of the Eighties, the United States and, to a lesser degree, NATO lead studies and reflections concerned with defense against tactical ballistic missiles within a East West framework. From these studies the ATBM (Anti Tactical Ballistic Missile) made its appearance. In spite of the attempts at control, missile proliferation has accelerated and led, towards the end of the Eighties and the beginning of the Nineties, to the awakening of a new risk known as proliferating. The 1991 Gulf War was accelerated in this manner. This conflict also clarified the fact that the ballistic weapon constituted a formidable means of pressure for countries which had it, in spite of the PATRIOT, which demonstrated the feasibility of an active defense against ballistic missiles, in spite of their limited performances. This present presentation proposes an overall analysis of the ballistic risk and the possible threat which could result from it and examines the means available for protection against this risk by looking further into all the defensive means. This will constitute the main part of the speech. Lastly, we will endeavor to evaluate the difficulties faced by the architects of the DAMB. CASI

N95-32126# MATRA Defense Espace, Velizy-Villacoublay (France).
POSSIBLE ALLIED BALLISTIC MISSILE DEFENSE SYSTEMS: RELATED GUIDANCE AND CONTROL REQUIREMENTS
C. Roche and C. Cotillard *In* AGARD, Guidance and Control for Future Air-Defence Systems Jan. 1995 5 p (For primary document see N95-32123 11-31)
Copyright Avail: CASI HC A01/MF A03

This document discusses several different types of Ballistic Missile Defense Systems for NATO for both medium and long range attacks. The feasibility, technological assessment and forecasting, and defense architecture is presented, along with each system's capabilities. CASI

N95-32127# GIE Cosyde, Velizy-Villacoublay (France).
SOSIE: A PRAGMATIC APPROACH TO THE SIMULATION OF BROAD AIR DEFENSE APPLIED TO THE THEATER LEVEL [SOSIE: UNE APPROCHE PRAGMATIQUE DE LA SIMULATION EN DEFENSE AERIENNE ELARGIE APPLIQUEE AU NIVEAU DU THEATRE]
A. Tanter and M. Deas *In* AGARD, Guidance and Control for Future Air-Defence Systems Jan. 1995 8 p In FRENCH (For primary document see N95-32123 11-31)
Copyright Avail: CASI HC A02/MF A03

The SOSIE concept rests on an approach consisting of using existing simulation models of various systems and subsystems and automatically integrating them with minimum modifications within a center of simulation. The defense simulation against ballistic missiles on the theater level calls upon three levels of simulation: DIAMS; TACSIT, and SPOOK. DIAMS presents a fine level system simulation of weapon ground-to-air average carry, TACSIT presents a level of site defense (base air for example), and SPOOK deals with the theater level itself. SOSIE enables users to use the same detailed simulators, developed by an originator of weapon systems or information and communications, without having to know in detail the models of the simulation. Envisioned in the future is the integration of other models of simulations relating to the air-to-air combat, in particular, the networks of command, controls and communications. CASI

N95-32128# Ballistic Missile Defense Organization, Washington, DC. Advanced Capabilities Div.
TMD DETECTION AND TRACKING USING IMPROVED AWACS SENSORS **c32**
Steve Petersen, Yasuhiro Kinashi (Nichols Research Corp., Vienna, VA.), and Daniel Leslie (Schafer, W. J. Associates, Inc., Arlington, VA.) *In* AGARD, Guidance and Control for Future Air-Defence Systems Jan. 1995 10 p (For primary document see N95-32123 11-31)
Copyright Avail: CASI HC A02/MF A03

This paper identifies an UOES (User Operational Evaluation Systems) version of an airborne surveillance sensor funded by the BMDO (Ballistic Missile Defense Organization). The sensors will be integrated into an operational AWACS E-3 upgrade program. This BMDO program initiative is called Extended Airborne Global Launch Evaluator, or EAGLE. Initial Operational Capability (IOC) of the EAGLE system will be ready in time to support the THAAD/GBR UOES capability. This airborne system, when developed, will consist of a passive infrared surveillance sensor (IRSS) with an active laser-ranger, on board an upgraded AWACS E3 aircraft to operate effectively in the TMD (theater missile defense) mission. The objective for the EAGLE is to field, in a reasonably short time and at a relatively low cost, a cueing sensor capability in regional conflicts to augment the existing space-based surveillance systems. With autonomous surveillance capability to search a wide-sector field, the EAGLE can detect and track boosting TBM's shortly after launch or as they break the clouds. Its passive IR sensor can also detect and track warm hardbody targets. Together with its laser-ranger, it is able to determine, immediately after the booster burn-out, very precise target state vectors that are accurate enough to predict their eventual impact points, to cue fire control radars, and to engage the weapons, if needed. Its primary TMD mission is to provide precise cueing of fire control radars to initiate the active defense weapon systems. Accurate cues from the EAGLE will off load radar resources to enable earlier detection of the targets at longer extended ranges, thereby increasing the interceptor battlespace for potentially more effective defense engagements and opportunities. It can also provide a precise early warning message to enable immediate TBM attack assessment and appropriate selection of defense engagement options by the battle manager. The functions of the sensor suite can be distributed, such that it can be tasked independently to observe the threat intercept, while providing continuous surveillance of new TBM launches, to support the kill assessment function for shoot-look-shoot opportunities. Another potential function that can be performed by the EAGLE is the estimation of TMD launch points (LPE) for counterforce support. This technical paper provides an expanded discussion of the EAGLE's mission roles, specific system functions, and its detection and tracking performance capability. The paper also addresses the sensor and the laser subsystem design characteristics and operational modes required to accomplish all its functions. Initial analyses indicate that the impact of scattering and absorption of the IR signatures and laser signals will be minimal on the performance of the system. Recent satellite data provides measurement of atmospheric extinction. Propagation statistics, based on satellite observations are presented for global regions of interest to TMD. Derived from text

N95-32129# Defence Research Establishment Valcartier, Courcellette (Quebec).
INFRARED AND MILLIMETER WAVE DETECTION USING THIN FILMS OF Pb DOPED BiSrCaCuO SUPERCONDUCTOR **c35**
L. Ngo Phong *In* AGARD, Guidance and Control for Future Air-Defence Systems Jan. 1995 10 p (For primary document see N95-32123 11-31)
Copyright Avail: CASI HC A02/MF A03

Thin film detectors made of CuO superconductors were developed in our laboratory. This article reports details of the fabrication and testing of Pb doped BiSrCaCuO detectors. The detector comprises a film sensor housed in a small cryostat with built-in bias supply and temperature control circuitry. The film sensor was first deposited by magnetron rf sputtering and then crystallized under a rapid thermal annealing process. The characteristics of the response of the detector under millimeter wave and infrared illumination were investigated. The millimeter wave response exhibited a Josephson component with a D(*) approximately 10(exp 8) -

10(exp 9) cm.Hz(exp (1/2))/W in the wavelength range of 3 - 8 mm. The transient response to short pulses indicated a time constant tau less than or equal to 10 ns for this component. The response to laser pulses was thermal in origin and inherently compressible, preventing saturation of the detector electronics to intense beams. The wide band characteristic of the responses at both infrared and millimeter wavelengths could be confirmed. The damage threshold of the film sensor was shown to exceed 10 mJ / sq cm per 3 ns pulse. The possible use of these detectors for threat detection and the optimization of their figure of merit are discussed.

Author

N95-32130# Officine Galileo S.p.A., Florence (Italy).

OPTIMAL INFRARED DETECTOR CONFIGURATIONS FOR AIR TARGET DETECTION **c74**

G. Uda and G. Barani *In* AGARD, Guidance and Control for Future Air-Defence Systems Jan. 1995 10 p (For primary document see N95-32123 11-31)

Copyright Avail: CASI HC A02/MF A03

The airtarget detection by a thermal camera is a typical problem of 'hot spot detection' and the knowledge of the available energy on the infrared sensor becomes a critical item to analyse. In order to evaluate the performances of an infrared system in search and track threat warning or passive surveillance, it is necessary to compute the Signal to Noise Ratio (SNR) of the system. The maximization of the SNR is an important goal to assure long detection ranges against stealth threats or cruise missiles with very low emissivities. The large number of detectors is just one of the requirements for this kind of application and some energetic considerations lead up to consider particular geometrical array configurations. Usually, in the SNR evaluation it is assumed that all the energy from a target is focused by the optical system on a single detector element of the array. However, the image of a point source on the focal plane has a finite extent (spot) and its energy distribution is given by the Point Spread Function (PSF) of the optics. The interaction of the finite spot size with the array gives rise to a spreading of the energy impinging on the individual detectors, which causes a decrease of performances. In this paper a statistical evaluation of the loss of energy impinging on the detector due to the finite image size of point targets was performed through a Monte Carlo simulation. By considering the maximum of the energy integrated by a single detector, it is possible to compute the effective SNR of the system. A new figure of merit, called Spreading Factor (SF), defined as the ratio between the maximum of the energy integrated by the single detector of the array and the total energy subtended by the PSF, permits to evaluate the capability of a detector array to detect point sources. Some typical detector and system configurations with their technological impacts have been examined.

Author

N95-32131# Department of the Air Force, Washington, DC.

ACQUISITION, TRACKING, POINTING AND FIRE CONTROL FOR BALLISTIC MISSILE DEFENSE

Thomas W. Humpherys and Gary Gurski (GRC, Vienna, VA.) *In* AGARD, Guidance and Control for Future Air-Defence Systems Jan. 1995 10 p (For primary document see N95-32123 11-31)

Copyright Avail: CASI HC A02/MF A03

The benefits of the ATP (Acquisition Tracking and Pointing) assets to TMD (Theater Missile Defense) are that the platform provides high resolution standoff sensors at low cost and can provide sub micro radian tracking and imaging of dynamic targets, active and passive multispectral data and non-cooperative fire control algorithms. The platform is relatively low cost and can be flown from 4-6 times a year for either sensor performance or phenomenology data collection. The process for collecting and certifying the data are in place and available today. During the past decade we have made significant advances in ATP-FC technologies for ballistic missile defense. The current BMDO ATP assets in general and the HABE testbed in particular can be a key asset in developing TMD weapon systems by providing a means to collect key phenomenology data, test sensor and guidance components, or view and collect data to score test or exercises.

Derived from text

N95-32132# Phillips Lab., Kirtland AFB, NM.

THE HIGH ALTITUDE BALLOON EXPERIMENT DEMONSTRATION OF ACQUISITION, TRACKING, AND POINTING TECHNOLOGIES (HABE-ATP)

D. Dimiduk, M. Caylor, D. Williamson, and L. Larson *In* AGARD, Guidance and Control for Future Air-Defence Systems Jan. 1995 11 p (For primary document see N95-32123 11-31)

Copyright Avail: CASI HC A03/MF A03

The High Altitude Balloon Experiment demonstration of Acquisition, Tracking, and Pointing (HABE-ATP) is a system built around balloon-borne payload which is carried to a nominal 26-km altitude. The goal is laser tracking thrusting theater and strategic missiles, and then pointing a surrogate laser weapon beam, with performance levels end a timeline traceable to operational laser weapon system requirements. This goal leads to an experiment system design which combines hardware from many technology areas: an optical telescope and IR sensors; an advanced angular inertial reference; a flexible multi-level of actuation digital control system; digital tracking processors which incorporate real-time image analysis and a pulsed, diode-pumped solid state tracking laser. The system components have been selected to meet the overall experiment goals of tracking unmodified boosters at 50- 200 km range. The ATP system on HABE must stabilize and control a relative line of sight between the platform and the unmodified target booster to a 1 microrad accuracy. The angular pointing reference system supports both open loop and closed loop track modes; GPS provides absolute position reference. The control system which positions the line of sight for the ATP system must sequence through accepting a state vector handoff, closed-loop passive IR acquisition, passive IR intermediate fine track, active fine track, and then finally aimpoint determination and maintenance modes. Line of sight stabilization to fine accuracy levels is accomplished by actuating wide bandwidth fast steering mirrors (FSM's). These control loops off-load large-amplitude errors to the outer gimbal in order to remain within the limited angular throw of the FSM's. The SWIR acquisition and MWIR intermediate fine track sensors (both PtSi focal planes) image the signature of the rocket plume. After Hard Body Handover (HBHO), active fine tracking is conducted with a visible focal plane viewing the laser-illuminated target rocket body. The track and fire control performance must be developed to the point that an aimpoint can be selected, maintained, and then track performance scored with a low-power 'surrogate' weapon beam. Extensive instrumentation monitors not only the optical sensors and the video data, but all aspects of each of the experiment subsystems such as the control system, the experiment flight vehicle, and the tracker. Because the system is balloon-borne and recoverable, it is expected to fly many times during its development program.

Derived from text

N95-32133# British Aerospace Defence Ltd., Preston (England).

INTEGRATION ISSUES IN MODULAR MISSION MANAGEMENT AID DEVELOPMENT

F. M. Watkins, C. A. Noonan, K. Roberts, and N. K. Upton (British Aerospace Defence Ltd., Farnborough, England.) *In* AGARD, Guidance and Control for Future Air-Defence Systems Jan. 1995 10 p (For primary document see N95-32123 11-31)

Copyright Avail: CASI HC A02/MF A03

The Mission Management Aid (MMA) program at British Aerospace Defence includes research in the areas of Sensor Data Fusion, Sensor Management, Tactical Situation Assessment and Tactical Decision Aids. Each project has developed and continues to refine workstation prototypes. As the technology in these prototypes matures it is used to update and improve an integrated MMA system prototype. This paper is concerned with the integration process and the issues surrounding it. The factors which influenced progress during integration include the use of compatible development platforms and programming languages for the prototypes, and the choice of a host architecture which allows a flexible approach to the MMA architecture. The benefits gained from the integration framework include the ability to develop integrated displays and controls, to evaluate performance and effectiveness metrics, and to investigate the boundaries and interactions between the subsystems.

Derived from text

N95-32134# Office National d'Etudes et de Recherches Aeronautiques, Paris (France). Ingenieurs de Recherche.

DESIGN OF SURVEILLANCE AND MULTISENSOR ANTI-AERIAL SYSTEMS [CONCEPTION DE SYSTEMES DE SURVEILLANCE ET DE DEFENSE ANTI-AERIENNE MULTI-SENSEURS] **c35**

C. Nahum and H. Cantalloube *In* AGARD, Guidance and Control for Future Air-Defence Systems Jan. 1995 9 p In FRENCH (For

primary document see N95-32123 11-31)
Copyright Avail: CASI HC A02/MF A03

Software ROSACE (Optimization of Realistic Systems, Contributes to the Design and the Evaluation), is developed within the framework of the study methodology of multisensors for anti-aircraft defense and is financed by the DRET (contract n 91-34-846). This document concerns a interactive tool, that is evolutionary, portable and of assistance to the definition, the qualification, and the optimization of multisensor systems for anti-aircraft monitoring and defense. This product constitutes a support for the expertise and search for new treatments which utilize the fusion of information and are likely to improve the performance of the system. These algorithms primarily ensure (but not exclusively) the tasks of detection and continuation or classification of air machines and make it possible to analyze the reliability of the system confronted with different scenarios. CASI

N95-32135# Raytheon Canada Ltd., Waterloo (Ontario).
MULTISENSOR DATA FUSION FOR INTEGRATED MARITIME SURVEILLANCE **c32**
A. Premji and A. M. Ponsford *In* AGARD, Guidance and Control for Future Air-Defence Systems Jan. 1995 12 p (For primary document see N95-32123 11-31)
Copyright Avail: CASI HC A03/MF A03

A prototype Integrated Coastal Surveillance system has been developed on Canada's East Coast to provide effective surveillance out to and beyond the 200 nautical mile Exclusive Economic Zone. The system has been designed to protect Canada's natural resources, and to monitor and control the coastline for smuggling, drug trafficking, and similar illegal activity. This paper describes the Multiple Sensor - Multiple Target data fusion system that has been developed. The fusion processor has been developed around the celebrated Multiple Hypothesis Tracking algorithm which accommodates multiple targets, new targets, false alarms, and missed detections. This processor performs four major functions: plot-to-track association to form individual radar tracks; fusion of radar tracks with secondary sensor reports; track identification and tagging using secondary reports; and track level fusion to form common tracks. Radar data from coherent and non-coherent radars has been used to evaluate the performance of the processor. This paper presents preliminary results. Derived from text

N95-32136# Waterloo Univ. (Ontario). Dept. of System Design.
MULTIPLE TARGET TRACKING BASED ON CONSTELLATION MATCHING AND KALMAN FILTER **c32**
Andrew K. C. Wong and Henry Leung (Defence Research Establishment Ottawa, Ottawa, Ontario.) *In* AGARD, Guidance and Control for Future Air-Defence Systems Jan. 1995 22 p (For primary document see N95-32123 11-31)
Copyright Avail: CASI HC A03/MF A03

A new approach to multiple target tracking (MTT) problem is developed. The data association (DA) problem is solved by an attributed subgraph isomorphism approach called constellation matching (CM). The CM method exploits, in the most direct way, the spatial configuration of the collection of targets which are subject to temporal and spatial constraints. The CM-based tracking system combines the CM technique with the Kalman filter to track and confirm the trajectories of multiple targets. The efficiency of this new approach is demonstrated using real-life multiple target radar tracking data and the results are compared to those obtained by a multiple hypothesis tracking (MHT) system. Author

N95-32137# National Aerospace Lab., Amsterdam (Netherlands).
MULTI-SENSOR DATA FUSION IN COMMAND AND CONTROL AND THE MERIT OF ARTIFICIAL INTELLIGENCE **c63**
Rene G. Zuidgeest *In* AGARD, Guidance and Control for Future Air-Defence Systems Jan. 1995 12 p (For primary document see N95-32123 11-31)
Copyright Avail: CASI HC A03/MF A03

The human operator observing the real world is confronted with a huge amount of data from multiple sensor systems observing that world. Multi-sensor data fusion (MSDF) is one of the emerging fields in advanced information processing, concerned with fusing sensor data from these multiple sensor systems. Automated multi-sensor data fusion can help the operator by processing sensor data into concise and surveyable information that is more useful than each sensor system separately can provide. The merit of MSDF can be increased by employing the knowledge of the human operator about the real world, the sensor systems and the fusion process. With the aid of this knowledge, automated MSDF can assign meaning to sensor data and is able to reason about the observed world at a high level, comparable to what humans do. Artificial intelligence provides techniques to represent this knowledge and to reason with it. These techniques are discussed in the context of a generic framework comprising a world model and fusion processes. These techniques can contribute to an effective updating of the world model and can support its fusion processes. In addition, a global distributed fusion architecture based on the framework is proposed. As specific domain of fusion, battlefield surveillance is considered. This paper shows the potential use of artificial intelligence in multi-sensor data fusion. Derived from text

N95-32138# Siemens A.G., Unterschleissheim (Germany). Defence Electronics.
AIDEX: AN EXPERT SYSTEM FOR AIRCRAFT IDENTIFICATION **c63**
J. Ebmeyer and H. Freyler *In* AGARD, Guidance and Control for Future Air-Defence Systems Jan. 1995 4 p (For primary document see N95-32123 11-31)
Copyright Avail: CASI HC A01/MF A03

The AIDEX (Advanced Identification Expert System) is the first expert system developed for aircraft identification providing a knowledge-based fusion of identification data from various sensors and identification sources. Derived from text

N95-32139# UNISYS GSG Canada, Inc., Montreal (Quebec).
ARCHITECTURE AND IMPLEMENTATION OF A MULTI-SENSOR DATA FUSION DEMONSTRATION MODEL WITHIN THE REAL-TIME COMBAT SYSTEM OF THE CANADIAN PATROL FRIGATE **c63**
F. Begin, E. Boily, T. Mignacca, E. Shahbazian, and P. Valin *In* AGARD, Guidance and Control for Future Air-Defence Systems Jan. 1995 8 p (For primary document see N95-32123 11-31)
Copyright Avail: CASI HC A02/MF A03

The research and development (R&D) group at UNISYS Government Systems Group (GSG) Canada is working on a demonstration model of a multi-sensor data fusion (MSDF) implementation for the Canadian Patrol Frigate (CPF). The conditions are made very realistic by the use of the Software Test and Development Facility (STDF) situated on the premises in Montreal. The paper describes the implementation design of the system. More emphasis is put on the architecture of both the simulation and the fusion systems. The fusion system is divided into four processes: Information Management (IM), Multi-Sensor Data Fusion (MSDF), Performance Evaluation (PE) and Display Management (DM). Each process within the fusion system is outlined. Derived from text

N95-32140# Department of the Air Force, Eglin AFB, FL.
ELECTRONIC COMBAT AND LETHAL DEFENSE SUPPRESSION **c32**
Leo. J. Rose *In* AGARD, Guidance and Control for Future Air-Defence Systems Jan. 1995 3 p (For primary document see N95-32123 11-31)
Copyright Avail: CASI HC A01/MF A03

Air forces across the world strive to protect their valuable resources from both the air and ground threats. Over the past few years, the surface-to-air missile threat has become more sophisticated and more deadly. It is far cheaper and less technical for a country to own and operate a ground missile system than to maintain a credible air force. It is for this reason that the attention to the ground threat has grown over the past few years. This paper discusses the approach the U.S. Air Force has taken in protecting its aircraft from these ground threats and how the mission of Lethal Defense Suppression has evolved into the complimentary tasks of Reactive Suppression and Pre-emptive Destruction.
Derived from text

N95-32141# Ballistic Missile Defense Organization, Washington, DC.
USING A RED TEAM TO DEVISE COUNTERMEASURES **c32**
R. L. Swedenburg *In* AGARD, Guidance and Control for Future Air-Defence Systems Jan. 1995 12 p (For primary document see N95-32123 11-31)
Copyright Avail: CASI HC A03/MF A03

The ability of a defense system to operate effectively when deployed in battle is dependent on designs able to deal with countermeasures against the defense. The formation of a technical Red Team to stress the preliminary

designs of the defensive system with technologically feasible and effective potential countermeasures provides a means to identify such potential countermeasures. This paper describes the experience of the U.S. Ballistic Missile Defense Organization's (BMDO) Theater Missile Defense Red Team since the Gulf War in 1991, the Red-Blue Exchange process, and the value it has provided to the designers of the U.S. Theater Missile Defense systems for developing robust systems. A wide-range of technologically feasible countermeasures has been devised, analyzed, tested for feasibility, and provided to the system developers for mitigation design. The process for independently analyzing possible susceptibilities of preliminary designs and exploiting the susceptibilities to identify possible countermeasures is explained. Designing and characterizing the Red Team's countermeasures, determining their feasibility, and analyzing their potential effectiveness against the defense are explained. A technique for the Blue Team's designers to deal with a wide range of potential countermeasures is explained.

Derived from text

N95-32165# Advisory Group for Aerospace Research and Development, Neuilly-Sur-Seine (France). Structures and Materials Panel.

ENVIRONMENTALLY SAFE AND EFFECTIVE PROCESSES FOR PAINT REMOVAL [PROCEDES EFFICACES ET ECOLOGIQUES POUR L'ENLEVEMENT DES PEINTURES]

Apr. 1995 91 p Lecture series held in Lisbon, Portugal 27-28 Apr. 1995, in Eskisehir, Turkey 1-2 May 1995 and in Ottobrunn, Germany 4-5 May 1995

(AGARD-LS-201; ISBN-92-836-1017-2) Copyright Avail: CASI HC A05/MF A01

Paint stripping and repainting of aircraft surfaces are required periodically during the operating lifetime of an aircraft. Historically, paint removal has been achieved using chemical strippers, involving materials which contain toxic components and which create hazardous working conditions. The process generates large amounts of hazardous waste from the chemicals used. Alternative methods for aircraft paint removal are now being investigated within the NATO nations with regard to their environmental safety and effective application. These processes include: Plastic Media Blasting, Wheat Starch Dry Media Blasting, Carbon Dioxide Pellet Blasting, Sodium Bicarbonate Blasting and Thermal Decomposition Methods (Laser, Flash Lamps/Carbon Dioxide). The Lecture Series will review these current state-of-the-art alternative methods with environmental effects and related health hazards, costs, process controls, and more. For individual titles, see N95-32166 through N95-32181.

N95-32166# Esquimalt Defence Research Detachment, Victoria (British Columbia).

OVERVIEW OF PAINT REMOVAL METHODS

Terry Foster *In* AGARD, Environmentally Safe and Effective Processes for Paint Removal Apr. 1995 7 p (For primary document see N95-32165 11-31)

Copyright Avail: CASI HC A02/MF A01

With the introduction of strict environmental regulations governing the use and disposal of methylene chloride and phenols, major components of chemical paint strippers, there have been many new environmentally safe and effective methods of paint removal developed. The new methods developed for removing coatings from aircraft and aircraft components include: mechanical methods using abrasive media such as plastic, wheat starch, walnut shells, ice and dry ice, environmentally safe chemical strippers and paint softeners, and optical methods such as lasers and flash lamps. Each method has its advantages and disadvantages, and some have unique applications. For example, mechanical and abrasive methods can damage sensitive surfaces such as composite materials and strict control of blast parameters and conditions are required. Optical methods can be slow, leaving paint residues, and chemical methods may not remove all of the coating or require special coating formulations to be effective. As an introduction to environmentally safe and effective methods of paint removal, this paper is an overview of the various methods available. The purpose of this overview is to introduce the various paint removal methods available. Derived from text

N95-32167# Aerospatiale, Toulouse (France). Direction des Estudes.

PAINT REMOVAL PRINCIPLES

Olivier Malavallon *In* AGARD, Environmentally Safe and Effective Processes for Paint Removal Apr. 1995 4 p (For primary document see N95-32165 11-31)

Copyright Avail: CASI HC A01/MF A01

An attempt is made to group the various processes of paint removal into families. The classifications are distinguished by chemical, mechanical, and thermal phenomena. For each of these phenomena, it is possible to identify the main mechanisms brought into play in material removal leading to paint stripping. The chemical strippers used are methylene chloride, phenolic compounds, and activated acids or activated bases free from phenols, chromates or methylene chloride. However, the methylene chloride and phenolic compounds are being replaced by a new generation of chemical strippers which are less active and their solvent power is lower. To improve the chemical kinetics, 'active' elements are introduced into the composition of these products. Mechanical stripping includes technologies using mechanical phenomena based on erosion, achieved by friction or blasting particles. Thermal stripping, the last classification, makes use of electronics and automation. CASI

N95-32168# Esquimalt Defence Research Detachment, Victoria (British Columbia).

BACKGROUND TO PLASTIC MEDIA BLASTING

Terry Foster *In* AGARD, Environmentally Safe and Effective Processes for Paint Removal Apr. 1995 3 p (For primary document see N95-32165 11-31)

Copyright Avail: CASI HC A01/MF A01

Chemical strippers based on active phenolic components in a chlorinated solvent have been the traditional method for removing of paints and coatings from aircraft. With the recent recognition of the environmental and health concerns of chlorinated solvents and the problem disposing of phenols there have been some major developments in paint removal technology. One of the first techniques developed to replace chemical strippers and now one of the most widely used techniques for paint removal from aircraft was plastic media blasting (PMB). The PMB technique is similar to traditional grit blasting (slag, sand alumina or carborundum) techniques used on steel and other metals (based on grits) but using polymer based media that are softer and less aggressive. Plastic media are ranked by hardness and density as well as chemical composition. Derived from text

N95-32169# Esquimalt Defence Research Detachment, Victoria (British Columbia).

DRY MEDIA BLASTING WITH WHEAT STARCH

Terry Foster *In* AGARD, Environmentally Safe and Effective Processes for Paint Removal Apr. 1995 11 p (For primary document see N95-32165 11-31)

Copyright Avail: CASI HC A03/MF A01

The brand name TECHNOSTRIP covers several types of installations and facilities. These were developed mainly to meet the requirements of customers in the aeronautic field. The range of products includes: complete self-supporting and semi-automated system for aircraft stripping; large-size blasting booth for semi-automatic stripping; manual blasting booth; and sealed and portable manual stripping head. Wheat starch media was developed for particle blasting stripping and is used in TECHNOSTRIP. This paper reviews its origins and use as well as use of automated facilities, reliability, effects on materials, effects on environment, and utilization examples. Derived from text

N95-32170# Esquimalt Defence Research Detachment, Victoria (British Columbia).

WATER BLASTING PAINT REMOVAL METHODS

Terry Foster *In* AGARD, Environmentally Safe and Effective Processes for Paint Removal Apr. 1995 3 p (For primary document see N95-32165 11-31)

Copyright Avail: CASI HC A01/MF A01

Water blasting is a paint removal technique that has been used for cleaning and paint removal for many years. The major disadvantages until recently were the slow rate of paint removal and the possibility of damage to the substrate from the high pressures used. With the improvement in nozzle design that allows for higher operating pressures and the use of environmentally compliant paint softeners or strippers, water blasting is becoming a recognized technique for paint removal in the aircraft industry. Author

N95-32171# Esquimalt Defence Research Detachment, Victoria (British Columbia).
PAINT REMOVAL AND SURFACE CLEANING USING ICE PARTICLES
Terry Foster and S. Visaisouk (Ice Blast International Corp., Victoria, British Columbia.) *In* AGARD, Environmentally Safe and Effective Processes for Paint Removal Apr. 1995 9 p (For primary document see N95-32165 11-31)
Copyright Avail: CASI HC A02/MF A01

Research into the possibility of using ice particles as a blast medium was first initiated at Defence Research Establishment Pacific (DREP) in an effort to develop a more environmentally acceptable paint removal method. A paint removal process was also required that could be used in areas where normal grit blasting could not be used due to the possibility of the residual blasting grit contaminating machinery and other equipment. As a result of this research a commercial ice blasting system was developed by RETECH. This system is now being used to remove paint from substrates that cannot be easily blasted by conventional techniques and also to clean soiled or contaminated surfaces. The problems involved in the development of an ice blast system and its components and their functions are described. Due to the complexity of paint removal using ice blasting, parameters such as air pressure, ice particle size and ice particle flow rate were studied and adjusted to suit the nature of the particular coating and substrate of interest. The mechanism of paint removal by ice particles has also been investigated. A theoretical model has been developed to explain the different paint removal mechanisms such as erosion by abrasion and erosion by fracture as they relate to ice blasting. Finally, the use of ice blasting to removal paint from a variety of substrates is presented as well as examples of surface cleaning and surface decontamination. Author

N95-32172# Aerospatiale, Toulouse (France). Direction des Estudes.
STRIPPING WITH DRY ICE
Olivier Malavallon *In* AGARD, Environmentally Safe and Effective Processes for Paint Removal Apr. 1995 2 p (For primary document see N95-32165 11-31)
Copyright Avail: CASI HC A01/MF A01

Mechanical-type stripping using dry ice (solid CO2) consists in blasting particles of dry ice onto the painted surface. This surface can be used alone or in duplex according to type of substrate to be treated. According to operating conditions, three physical mechanisms may be involved when blasting dry ice particles onto a paint system: thermal shock, differential thermal contraction, and mechanical shock. The blast nozzle, nozzle travel speed, blast angle, stripping distance, and compressed air pressure and media flow rate influence the stripping quality and the uniformity and efficiency obtained. Derived from text

N95-32173# Aerospatiale, Toulouse (France). Direction des Etudes.
AQUASTRIP
Olivier Malavallon *In* AGARD, Environmentally Safe and Effective Processes for Paint Removal Apr. 1995 3 p (For primary document see N95-32165 11-31)
Copyright Avail: CASI HC A01/MF A01

The Aquastrip stripping process is a mechanical process. It consists of applying a high-pressure water jet by means of a rotating stripping head with two water jets. The efficiency of these water jets is improved in certain cases by using a paint softener before applying the water jet process. Derived from text

N95-32174# Aerospatiale, Toulouse (France). Direction des Estudes.
STRIPPING BY LASER **c36**
Olivier Malavallon *In* AGARD, Environmentally Safe and Effective Processes for Paint Removal Apr. 1995 4 p (For primary document see N95-32165 11-31)
Copyright Avail: CASI HC A01/MF A01

Laser beam stripping can be achieved using several active materials: YAG, CO2 Tea, or Excimer. The YAG laser appears to be the most efficient laser assessed in this report. However, the results obtained for productivity, quality, and type of stripping were very poor. Also, for stripping and on account of its specifications, the laser beam can only be used in an automated manner. In spite of these results, it seems that certain companies in Europe have recently developed technical solutions allowing better results to be obtained. Derived from text

N95-32175# Aerospatiale, Toulouse (France). Direction des Estudes.
SELECTIVE CHEMICAL STRIPPING
Olivier Malavallon *In* AGARD, Environmentally Safe and Effective Processes for Paint Removal Apr. 1995 3 p (For primary document see N95-32165 11-31)
Copyright Avail: CASI HC A01/MF A01

At the end of the 80's, some of the large European airlines expressed a wish for paint systems with improved strippability on their aircraft, allowing the possibility to strip down to the primer without altering it, using 'mild' chemical strippers based on methylene chloride. These improvements were initially intended to reduce costs and stripping cycle times while facilitating rapid repainting, and this without the need to change the conventionally used industrial facilities. The level of in-service performance of these paint systems was to be the same as the previous ones. Requirements related to hygiene safety and the environment were added to these initial requirements. To meet customers' expectations, Aerospatiale, within the Airbus Industry GIE, formed a work group. This group was given the task of specifying, following up the elaboration and qualifying the paint systems allowing requirements to be met, in relation with the paint suppliers and the airlines. The analysis made in this report showed the interest of transferring as far upstream as possible (to paint conception level) most of the technical constraints related to stripping. Thus, the concept retained for the paint system, allowing selective chemical stripping, is a 3-coat system with characteristics as near as possible to the previously used paints. Derived from text

N95-32176# Esquimalt Defence Research Detachment, Victoria (British Columbia).
FACILITIES USED FOR PLASTIC MEDIA BLASTING **c09**
Terry Foster *In* AGARD, Environmentally Safe and Effective Processes for Paint Removal Apr. 1995 4 p (For primary document see N95-32165 11-31)
Copyright Avail: CASI HC A01/MF A01

The equipment used for plastic media blasting (PMB) is generally independent of the media and is similar to equipment used in traditional abrasive blasting. PMB equipment is usually modified to enable the close control of the media flow and the operation at low pressures (30 - 40 psi). Because of the delicate nature of some of the stripping procedures, the nozzles used for PMB have been redesigned to improve cleaning rates, give an even distribution of particles and reduce the variation in particle velocity across the blast stream. This results in a more equal distribution of particles and impact energies at the substrate. There are three types of blast facilities available: blast cabinets for small components; blast booths which will accommodate larger components but may be used for purposes other than blasting, and blast rooms which are designed for complete vehicles or aircraft and are generally not used for other purposes. Derived from text

N95-32177# Esquimalt Defence Research Detachment, Victoria (British Columbia).
TREATMENT OF PLASTIC MEDIA WASTE **c45**
Terry Foster *In* AGARD, Environmentally Safe and Effective Processes for Paint Removal Apr. 1995 1 p (For primary document see N95-32165 11-31)
Copyright Avail: CASI HC A01/MF A01

Although plastic media itself is not generally considered a hazardous waste, the paint particles containing chromate pigments contaminating the spent media are considered a hazardous waste product. There are currently four approaches under investigation aiming to reduce the volume of hazardous waste produced during paint stripping: elimination of the chromate containing pigments or other hazardous pigments from primers and coatings; separation of the paint or hazardous materials from the plastic or other media; encapsulation or recycling of the contaminated media to make it safe for disposal or reuse; and produce a biodegradable media. Research to develop new pigments and primers that will result in the elimination of hazardous pigments such as strontium chromate and in developing alternative anti-corrosive surface treatments to replace cadmium plating is continuing. Contamination of the spent media will remain a problem because the hazardous pigments and surface treatments will still be used on aircraft and their components for the foreseeable future. Therefore, the only realistic alternatives at the moment to reduce the volume of hazardous waste

produced by PMB (plastic media blasting) are to recycle or re-use the media in some form or remove the hazardous materials from the media. Derived from text

N95-32178# Aerospatiale, Toulouse (France). Direction des Etudes.
BIOREMEDIATION OF WHEAT STARCH MEDIA WASTE c45
Olivier Malavallon and John Oestreich (CAE Electronics Ltd., Montreal, Quebec.) *In* AGARD, Environmentally Safe and Effective Processes for Paint Removal Apr. 1995 2 p (For primary document see N95-32165 11-31)
Copyright Avail: CASI HC A01/MF A01

The development of a bioremediation process is designed to minimize most of the waste generated with dry media paint removal. The bioremediation method was developed by DOT Technologies in Canada. When paint is removed with wheat starch media, a dust waste is produced containing both starch and paint. The waste will also contain a percentage of inorganic materials from the starch, the paint waste and contaminants from the aircraft (sealants, tapes, ...). This disposal method first uses enzymes to render the starch component soluble in water, converting the starch to various sugars. Specially bred bacteria then digest the sugars, and some of the hydrocarbons in the paint. At this stage, the primary end products are carbon dioxide and water. This bioremediation method reduces the waste generated by dry paint removal by approximately 95 percent. The bacteria, bred by natural selection, tolerates high levels of heavy metals, and toxic hydrocarbons. The basic chemistry of bioremediation, as well as the management of bacteria in this application are summarized hereafter. Derived from text

N95-32179# Esquimalt Defence Research Detachment, Victoria (British Columbia).
OPERATIONAL PARAMETERS AND MATERIAL EFFECTS
Terry Foster *In* AGARD, Environmentally Safe and Effective Processes for Paint Removal Apr. 1995 6 p (For primary document see N95-32165 11-31)
Copyright Avail: CASI HC A02/MF A01

Although there are six types of plastic media, the focus on operational parameters and materials effects of PMB (plastic media blasting) will be on the Type 5 acrylic media with some reference and comparisons to Type 2 media. The other four plastic media are not used extensively in general aircraft stripping and will not be discussed in this paper. There are several military and commercial documents available with detailed procedures for plastic media stripping of aircraft. The actual choice of blasting parameters will, to a great extent, depend on the media chosen and the substrate to be stripped. The effects of various blasting conditions on materials can be evaluated using visual, optical microscopy, scanning electron microscopy (SEM) and mechanical and corrosion test methods. In some test methods up to twelve specimens are required to give meaningful results, therefore statistical analysis tools are also required to interpret the results due to the scatter in some of the data. Derived from text

N95-32180# Aerospatiale, Toulouse (France). Direction des Etudes.
PROCESS EVALUATION
Olivier Malavallon *In* AGARD, Environmentally Safe and Effective Processes for Paint Removal Apr. 1995 3 p (For primary document see N95-32165 11-31)
Copyright Avail: CASI HC A01/MF A01

It is not always easy to conduct a study and implement a systematic policy in the aeronautical paint stripping field. The situations to be studied are complicated by extensive technical data, material conditions and financial unknowns. To these are added demands both in the civil and military fields to increase the performance obtained, optimize cycles, reduce recurrent costs, quickly amortize investments and now increasing respect for the environment. To reply correctly, the various possibilities must be assessed using, if possible, identical criteria and reference systems. The only criterion which applies to all the processes and methods is the overall stripping cost. It is not sufficient for a process to meet the related technical requirements (for example 'IATA guidelines'), it must also be economically justifiable. The overall costs take into account therefore the costs and materials, labor and also the downtime of the aircraft, amortization and maintenance of the installations and processing of waste, etc. For many years now, AEROSPATIALE has undertaken research and development programs to find and evaluate alternatives to the conventional chemical stripping process. This work has led it to carry out comparative analyses from technical elements enhanced as the work progressed. Derived from text

N95-32181# Aerospatiale, Toulouse (France). Direction des Etudes.
STANDARDIZATION WORK
Olivier Malavallon *In* AGARD, Environmentally Safe and Effective Processes for Paint Removal Apr. 1995 1 p (For primary document see N95-32165 11-31)
Copyright Avail: CASI HC A01/MF A01

For several years now, the main civil aircraft manufacturers (Airbus and its partners, Boeing, Fokker, McDonnell Douglas) have been working jointly on the writing of technical recommendations and the drawing up of an international standard. This work concerns the evaluation of the processes and products used to strip aeronautical paint systems. This procedure was initiated on request from the main airlines. In effect, the airlines are faced with situations in which the financial and operational objectives are becoming increasingly important. The need was felt to rationalize and, if possible, harmonize the criteria and technical requirements of the various civil aircraft manufacturers in order to facilitate in-service maintenance of the fleets of airlines operating Airbus, Boeing, Douglas aircraft, etc. Derived from text

32 COMMUNICATIONS AND RADAR

Includes radar; land and global communications; communications theory; and optical communications.

For related information see also *04 Aircraft Communications and Navigation* and *17 Space Communications, Spacecraft Communications, Command and Tracking.* For search and rescue see *03 Air Transportation and Safety,* and *16 Space Transportation.*

N95-30368# Joint Inst. for Nuclear Research, Dubna (USSR).
THE INTERACTION OF MAGNETIZATIONS WITH AN EXTERNAL ELECTROMAGNETIC FIELD AND A TIME-DEPENDENT MAGNETIC AHARONOV-BOHM EFFECT
G. N. Afanasev, M. Nelhiebel (Technische Univ., Vienna, Austria.), and Yu. P. Stepanovskij (Academy of Sciences of the Ukraine, Kharkov, Ukraine.) 1994 20 p
(DE95-613463; JINR-E-2-94-297) Avail: CASI HC A03/MF A01 (US Sales Only)

We investigate how the choice of the magnetization distribution inside the sample affects its interaction with the external electromagnetic field. The strong selectivity to the time dependence of the external electromagnetic field arises for the particular magnetizations. This can be used for the storage and ciphering of information. We propose a time-dependent Aharonov-Bohm-like experiment in which the phase of the wave function is changed by the time-dependent vector magnetic potential. The arising time-dependent interference picture may be viewed as a new channel for the information transfer. DOE

N95-30370# Joint Inst. for Nuclear Research, Dubna (USSR).
NEW TENSOR INTERACTION AND THE K(SUB L) - K(SUB S)MASS DIFFERENCE
M. V. Chizhov (Sofia Univ., Bulgaria.) 1994 8 p
(DE95-613597; JINR-E-2-94-253) Avail: CASI HC A02/MF A01 (US Sales Only)

The minimal standard electroweak model yields approximately half the observed value of the K(sub L) - K(sub S) mass difference. Antisymmetric tensor fields incorporated into the standard model can provide the rest 0.5 x (Delta m(sub LS))(sub exp). The effective lepton-lepton, quark-lepton and quark-quark tensor interactions induced by the charged tensor particles are presented. DOE

N95-30398# Zwillinger and Associates, Newton, MA.
VISUALIZATION OF CIRCUIT CARD ELECTROMAGNETIC FIELDS Final Report
Daniel Zwillinger 20 Jan. 1995 86 p
(Contract F41608-94-C-1126)
(AD-A291491; AF95-1) Avail: CASI HC A05/MF A01

Circuit boards are used in nearly every electrical appliance. Most

board failures cause differing currents in the circuit board traces and components. This causes the circuit board to radiate a differing electromagnetic field. Imaging this radiated field, which is equivalent to measuring the field, could be used for error detection. Using estimates of the fields radiated by a low power digital circuit board, properties of known materials, and available equipment, we determined how well the following technologies could be used to visualize circuit board electromagnetic fields (prioritized by promise): electrooptical techniques, magnetooptical techniques, piezoelectric techniques, thermal techniques, and electrodynamic force technique. We have determined that sensors using the electrooptical effect (Pockels effect) appear to be sufficiently sensitive for use in a circuit board imaging system. Sensors utilizing the magnetooptical effect may also be adequate for this purpose, when using research materials. These sensors appear to be capable of achieving direct broadband measurements. We also reviewed existing electromagnetic field sensors. Only one of the sensors (recently patented) was specifically designed for circuit board measurements. DTIC

N95-30417 Department of the Navy, Washington, DC.
MICROWAVE REPEATER WITH BROADBAND ACTIVE AND/OR PASSIVE ISOLATION CONTROL Patent
Emanuel Briguglio, inventor (to Navy) 13 Dec. 1994 6 p Filed 31 Dec. 1990
(AD-D017358; US-Patent-5,373,297; US-Patent-Appl-SN-638114; US-Patent-Class-342-15) Avail: US Patent and Trademark Office

A microwave repeater with antenna isolation comprises a first receiving antenna for receiving an input signal from a distant source; an amplifier section for amplifying and modulating the input signal to produce an output signal; a transmitting antenna coupled to the amplifier section; and an isolation control means including a second receiving antenna for isolating the first receiving antenna from the transmitting antenna. In one preferred embodiment, the second receiving antenna is aligned so as to match the gain and phase from the transmitting antenna to the first receiving antenna. The isolation control means comprises a phase shifter coupled to the second receiving antenna; and a power combiner having inputs coupled to the first receiving antenna and the phase shifter and an output coupled to the amplifier section. The power combiner receives the input signal from the first receiving antenna and a 1 SO phased shifted signal from the phase shifter. DTIC

N95-30479 National Defence Research Establishment, Linkoeping (Sweden).
INTERFERENCE REJECTION TECHNIQUES IN A DS SPREAD-SPECTRUM HF RADIO SYSTEM [INTERFERENSUNDERTRYCKNING I ETT DS-RADIOSYSTEM FOER KORTVAGSKOMMUNIKATION]
N. Hallqwist and B. Lagerquist Dec. 1994 63 p In SWAHILI
(PB95-211660; FOA-R-94-00066-3.5-SE) Avail: Issuing Activity (National Technical Information Service (NTIS))

The report presents results from research and simulations of different algorithms for interference rejection in a direct-sequence spread-spectrum high frequency (HF) radio system. The overall purpose of the efforts was to propose a practical working method and to investigate possible gains, using the BER (bit error rate) as performance measure. The simulations have been performed using the simulation program SPW. The interference environment is assumed to consist of white Gaussian noise, and/or narrowband interfering signals, distributed according to the Laycock-Gott model. The proposed algorithm transforms the signals, excludes the largest 10 percent of the components and finally performs an inverse transform. The results predict that considerable gains can be expected using this interference rejection method. NTIS

N95-30516 Selskapet for Industriell og Teknisk Forskning, Trondheim (Norway).
EMAIL: WHY AND HOW
S. Haug 26 Sep. 1994 90 p Presented at the NORUG Conference, 25-27 May 1993
(PB95-195327; STF13-S94001) Avail: Issuing Activity (National Technical Information Service (NTIS))

The document is a collection of transparencies from a presentation on electronic mail at the NORUG conference held 25-27 May 1993. NTIS

N95-30562# Environmental Research Inst. of Michigan, Ann Arbor, MI. Electro-Optics Lab.
UNCONVENTIONAL IMAGING FIELD EXPERIMENT PLAN Final Report, Jun. 1993 - May 1994
James R. Fienup, Jack N. Cederquist, Joseph C. Marron, and Richard G. Paxman Dec. 1994 145 p
(Contract N00014-93-C-0093)
(AD-A291492; Rept-253200-7-F) Avail: CASI HC A07/MF A02

We investigated the feasibility of conducting experiments at the Innovative Science and Technology Experimental Facility (ISTEF). The experiments are to test unconventional imaging concepts that use laser illumination and pupil-plane detection. We show the trade-off between the sparsity of the number of sub-apertures and the number of speckle realizations collected. We invented and demonstrated two new algorithms for phasing heterodyne arrays that work for sparse arrays of detectors. We performed analysis showing that near-ground turbulence makes the isoplanatic patch size for a 10 km horizontal path impractically small, but for a 1 km path it can be accommodated by using a small target. We invented a new imaging modality involving collection of intensity data at multiple wavelengths from which we can reconstruct a 3-D image using an opacity constraint. We invented a new sparse-array pattern design in the shape of an arrow that fills a square OTF with a smaller number of sub-aperture than computer-optimized patterns. We showed that we can trade off background suppression for the ability to measure multiple speckles over a sub-aperture by placing the detector array in a plane beyond the focal plane. DTIC

N95-30567# Helsinki Univ. of Technology, Espoo (Finland).
SIX-VECTOR FORMALISM IN ELECTROMAGNETICS OF BIANISOTROPIC MEDIA
I. V. Lindell, K. Sihvola, and K. Suchy Jul. 1994 16 p
(PB95-207130; ISBN-951-22-2218-3) Avail: CASI HC A03/MF A01

Notation applying six-vectors and six-dyadics appears very applicable for describing electromagnetic problems in general bianisotropic media because, with normal three-vector notation, the analytic expressions often tend to be very complicated. Power of the notation is increased by introducing some operations with which recourse to the three-vector and three-dyadic notation during the analysis can be avoided. A number of theorems and concepts of electromagnetic fields in bianisotropic media are given as examples of applying the six-vector and six-dyadic notation. NTIS

N95-30581*# Jet Propulsion Lab., California Inst. of Tech., Pasadena, CA.
SIGNAL-PROCESSING THEORY FOR THE TurboRogue RECEIVER
J. B. Thomas 1 Apr. 1995 97 p
(Contract NAS7-1260)
(NASA-CR-198882; JPL-Publ-95-06; NAS 1.26:198882) Avail: CASI HC A05/MF A02

Signal-processing theory for the TurboRogue receiver is presented. The signal form is traced from its formation at the GPS satellite, to the receiver antenna, and then through the various stages of the receiver, including extraction of phase and delay. The analysis treats the effects of ionosphere, troposphere, signal quantization, receiver components, and system noise, covering processing in both the 'code mode' when the P code is not encrypted and in the 'P-codeless mode' when the P code is encrypted. As a possible future improvement to the current analog front end, an example of a highly digital front end is analyzed. Author

N95-30605# Joint Inst. for Nuclear Research, Dubna (USSR).
THE RADIATION CONDITIONED BY THE 'VELOCITY PART' OF THE ELECTROMAGNETIC FIELD OF A MOVING CHARGE
V. N. Streltsov 1994 4 p
(DE95-613366; JINR-D-2-94-244) Avail: CASI HC A01/MF A01 (US Sales Only)

The Cherenkov radiation, the transition radiation and the radiation in gas below the Cherenkov threshold are considered as varieties of one phenomenon. This (non breaking) radiation is conditioned by the velocity part of the electromagnetic field of a relativistic charge. The forward direction of the radiation reflects the corresponding direction of the field (its retarded strengths). DOE

N95-30629# National Defence Research Establishment, Linkoeping (Sweden).
MICROWAVE COUPLING INTO A SLOTTED CAVITY. ADDITIONAL RESULTS
M. Baeckstroem and J. Loren Dec. 1994 56 p
(PB95-210381; FOA-R-94-00042-3.2-SE) Avail: CASI HC A04/MF A01

Further evaluation of simple formulas for shielding effectiveness and for absorption cross section of a wire inside a shielded structure have been made. The results give further support to the expressions, derived earlier in FOA report C 30712-8.3,3.2 (PB94-123742). The main objective of the work has been to find and evaluate simple expressions for microwave coupling into electronic compartments. The expressions are intended to be used for bounding calculations in design and analysis of system hardness against intense microwave radiation, e.g. HPM (High Power Microwaves). It is shown that introduction of microwave absorbing material into the cavity gives an expected increase in shielding effectiveness. It is also shown that shielding effectiveness depends only to a little extent on the position and length of the wire. The total transmission area for multiple apertures can be expressed as the sum of the areas of the individual apertures. The absorption cross section for a wire inside the cavity is shown to depend only slightly on wire position and length, even when the wire is located very close to a wall. The results lead to further improvement of the methodology for analysis of system hardness against HPM radiation. It also lays a foundation for a more scientific approach in the design of shielded structures. Such an approach would result in an increased reliability and also in a reduction of costs due to a reduced need for (large) safety margins and fewer late design modifications. The report also proposes a new method to measure shielding effectiveness of apertures. NTIS

N95-30660 Department of the Navy, Washington, DC.
WAVEFRONT SIMULATOR FOR EVALUATING RF COMMUNICATION ARRAY SIGNAL PROCESSORS Patent
Steven B. Minarik, inventor (to Navy) 16 Aug. 1994 15 p Filed 27 Oct. 1993
(AD-D017372; US-Patent-5,339,087; US-Patent-Appl-SN-145352; US-Patent-Class-342-375) Avail: US Patent and Trademark Office

A wavefront simulator that emulates plane wave propagation from multiple transmitting antennas is used to evaluate, in both a static and a dynamic manner, an array processor used in RF communications to determine the location of transmitting antennas and possibly to perform beamforming for cancelling the energy of an interfering transmitter. The wavefront simulator generates time delay signals, giving the appearance of being emitted from different transmitters or sources, and simulates those signals as being received by an antenna array associated with the array processor. The array processor utilizes the time delay signals to calculate, e.g., the angle of arrival of the signals from the emitting antennas. DTIC

N95-30669 Michigan Univ., Ann Arbor, MI.
SCATTERING AND RADIATION FROM CYLINDRICALLY CONFORMAL ANTENNAS Ph.D. Thesis
Leo Charles Kempel 1994 180 p
Avail: Univ. Microfilms Order No. DA9423227

Microstrip patch antennas offer considerable advantages in terms of weight, aerodynamic drag, cost, flexibility, and observability over more conventional protruding antennas. Two hybrid finite element methods are presented and are used to examine the scattering and radiation behavior of cylindrically conformal patches. In conjunction with a new divergence-free cylindrical shell element, the finite element-boundary integral method is shown to have low computational and memory requirements when compared with competing approaches. This method uses an efficient creeping wave series for the computation of the dyadic Green's function and a uniform surface mesh so that a fast Fourier transform may be used to reduce the computational and memory burden of the method. An alternative finite element-absorbing boundary condition approach incorporates a new conformal vector condition which minimizes the computational domain. The latter method is more flexible than the former because it can incorporate surface coatings and protruding antennas. Guidelines are established for minimal ABC displacement from the aperture. These two hybrid finite element methods are used to study the scattering, radiation, and input impedance of typical conformal antenna arrays. In particular, the effect of curvature and cavity size is examined for both discrete and wraparound antenna arrays. Dissert. Abstr.

N95-30727 Department of the Navy, Washington, DC.
APPARATUS AND METHOD FOR PRODUCING THREE-DIMENSIONAL IMAGES Patent
Kenneth K. Knaell, inventor (to Navy) and Glen R. Heidbreder, inventor (to Navy) 28 Feb. 1995 13 p Filed 30 Sep. 1993
(AD-D017455; US-Patent-5,394,151; US-Patent-Appl-SN-129499; US-Patent-Class-342-25) Avail: US Patent and Trademark Office

An apparatus and method is capable of acquiring useful three-dimensional radar images from an aircraft which travels in a curvilinear path to generate only a sparsely filled synthetic array. A motion measurement unit outputs position measurements as the aircraft travels in the curvilinear path. The system includes a motion compensation and timing unit and a wave transmitter which outputs chirped radar signals. An antenna coupled to the wave generator sends the chirped radar signals to a region to be imaged and receives scattered chirped radar return signals from scatterers in the region. DTIC

N95-30743 Department of the Navy, Washington, DC.
COHERENT INTEGRATOR Patent
Aldo G. DiLoreto, inventor (to Navy) 14 Feb. 1995 7 p Filed 14 Jul. 1983
(AD-D017422; US-Patent-5,390,154; US-Patent-Appl-SN-510976; US-Patent-Class-367-98) Avail: US Patent and Trademark Office

A method and circuit for performing coherent integration on a signal output from a conventional signal processing circuit's detector/averager is presented. The post-processing coherent integrator is designed to be inserted in a conventional signal processing circuit between the detector/averager circuit and the threshold detector circuit. A digital form of the post processing coherent integrator comprises a sample-and-hold circuit to receive a signal output from the detector averager of the conventional signal processing circuit, an analog to digital converter, a delay and multiplier circuit, a memory circuit for storing weighting constants, a Summer circuit, and an output to a conventional signal processing system's threshold detector and display. DTIC

N95-30746 Department of the Navy, Washington, DC.
REPLY-FREQUENCY INTERFERENCE/JAMMING DETECTOR Patent
Walton B. Bishop, inventor (to Navy) 3 Jan. 1995 6 p Filed 26 Sep. 1975
(AD-D017428; US-Patent-5,379,043; US-Patent-Appl-SN-617470; US-Patent-Class-342-45) Avail: US Patent and Trademark Office

Received IFF reply-frequency signals are examined to determine whether they are being interfered with by enemy sources and indication of the extent of detected interference is provided. The number of correct replies received from selected range bins surrounding and including the center one in which a target leading edge is first declared is counted and compared with the count of the number of friend-accept decisions made based on replies from the selected range bins. The level of interference is then indicated by the ratio between the two counts. DTIC

N95-30812# Technische Univ., Eindhoven (Netherlands).
DYNAMIC ROUTATION IN DISTRIBUTED ENVIRONMENTS
L. J. N. Franken, P. Janssen, B. R. Haverkort, and G. vanLiempd 7 Sep. 1994 36 p Prepared in cooperation with PTT Research
(PB95-197968; Memo-INF-94-62) Copyright Avail: CASI HC A03/MF A01

In this paper, we address the issues of communication routing and process allocation in an integrated way, the so-called routations. After the definition of a formal framework for distributed systems and their applications, routations can be defined. Existing routing and allocation algorithms are discussed in a unified way, using this framework. This facilitates the basis for a proper comparison of algorithms. We then propose a routation algorithm based on the A* intelligent tree-search algorithm. Although this algorithm yields optimal routations, it is too slow to be used in practice. We therefore developed three heuristics, each again in three variants, that accomplish the same task, however, with far reduced computational effort. We then propose to use the A* algorithm in combination with one of the heuristics in a real distributed environment. In the appendices we describe the pseudo-codes of the introduced algorithms, as well as an experimental, ANSAware-based, distributed system in which the routations take place using the heuristics we developed. NTIS

N95-30828 Manitoba Univ., Winnipeg, Manitoba (Canada).
PROPAGATION AND SCATTERING OF ELASTIC WAVES IN LAMINATED CIRCULAR CYLINDERS Ph.D. Thesis
Nipon Rattanawangcharoen 1993 134 p
(ISBN-0-315-85957-1) Avail: Univ. Microfilms Order No. DANN85957

Propagation and scattering of guided elastic waves in circular cylinders are investigated. An analytical method is formulated to study wave propagation in laminated isotropic cylinders while Rayleigh-Ritz type approximations are developed for laminated composite cylinder where the analytical solutions are unattainable. The effects of circumferential wavenumber, thickness to radius ratio, ply lay-up configuration, and layering on dispersion characteristics of free guided waves are investigated through these techniques. The problem of reflection of waves normally incident upon the free end of cylinders is studied as a special case of wave scattering problems. A wave functions expansion procedure is employed in developing least square and variational methods for the investigation. Numerical results demonstrate the successful application of the Rayleigh Ritz type approximation and the variational technique for the free end reflection problem in laminated composite cylinders. A hybrid method is presented to analyze the scattering of plan strain waves by load or flaw in cylindrical cross-section. The domain of the cross-section is divided into two regions, an interior region and an exterior region. The interior region which contains the load or flaw is modeled by finite elements while a wave functions expansion is employed for the exterior region. The numerical results for the scattered amplitudes from the load and from flaw are presented for Zr-Nb pressure tube. Dissert. Abstr.

N95-30869# Fast Mathematical Algorithms and Hardware Corp., Hamden, CT.
FAST MULTIPOLE METHODS FOR SCATTERING COMPUTATIONS Final Technical Report, 1 Sep. 1991 - 31 Aug. 1994
Vladimir Rokhlin, Ronald R. Coifman, and Victor Wickerhauser Oct. 1994 208 p
(Contracts F49620-91-C-0084; DARPA Order 7894; N00014-89-J-1527)
(AD-A291093; AFOSR-95-0102TR) Avail: CASI HC A10/MF A03

The purpose of this phase of the project was to develop fast algorithms for computations of electromagnetic scattering (radar), and assist in the implementation and development of fast engineering software using these algorithms by the team at Hughes Research Laboratories. Present methods for computing radar cross sections and other scattering crossections are severely limited by prohibitive processing and memory requirements. New fundamental Fast Multipole Methods developed over the last few years by Rokhlin (for 2-D scattering) held the promise for breaking this computational bottleneck, the goal set out in this project was to extend the work to higher dimensions and to complete the computational infrastructure needed for converting these algorithms to engineering tools. The codes and algorithms obtained in this joint effort between HRL and FMAH have already changed the state of the art in this area of electromagnetics simulations and promise to revolutionize computational design technology. We have verified that these algorithms provide the expected improvements and scaling. DTIC

N95-30895# Rome Lab., Hanscom AFB, MA.
PROCEEDINGS OF THE ANTENNA APPLICATIONS SYMPOSIUM, VOLUME 1
Daniel H. Schaubert Feb. 1995 265 p Symposium held in Griffiss AFB, NY
(AF Proj. 4600)
(AD-A293258; RL-TR-95-47-Vol-1) Avail: CASI HC A12/MF A03

The Proceedings of the 1994 Antenna Applications Symposium is a collection of state-of-the-art papers relating to phased array antennas, multibeam antennas, satellite antennas, microstrip antennas, reflector antennas, HF, VHF, UHF, and various other antennas. DTIC

N95-30902# Federal Aviation Administration, Atlantic City, NJ.
OFFSHORE NEXT GENERATION WEATHER RADAR (NEXRAD) OT&E INTEGRATION AND OT&E OPERATIONAL TEST Final Report
Radame Martinez, Baxter Stretcher, John Porcello, Peter Guthlein, and William Diviney Mar. 1995 83 p
(AD-A293223; DOT/FAA/CT-TN95/10) Avail: CASI HC A05/MF A01

This document is the Final Report for Phase 1 limited Operational Test and Evaluation (OT&E) Integration and OT&E Operational testing of the first Federal Aviation Administration (FAA) redundant configuration Next Generation Weather Radar (NEXRAD) installed in Kauai, Hawaii, and provides an account of the results of OT&E testing, including recommendations for future considerations. This report provides background information on the Offshore NEXRAD system. In addition, the report contains a description of testing and evaluation including information about the test schedule and location test participants, specialized test equipment used during testing, test objectives/criteria, test descriptions, test results, and methods used for data collection and analysis. The report continues with a comprehensive discussion of overall test results, including Critical Operational Issues (C 01) and their resolution. Finally, the report ends with test conclusions and recommendations to improve system performance. DTIC

N95-30904# Pacific-Sierra Research Corp., Santa Monica, CA.
AIRBORNE OCEAN WATER LIDAR (OWL) REAL TIME PROCESSOR (RTP)
M. Hryszko Mar. 1995 51 p
(Contract N66269-90-C-0551)
(AD-A293226; PSR-2531) Avail: CASI HC A04/MF A01

The Hyperflo Real Time Processor (RTP) was developed by Pacific-Sierra Research Corporation as a part of the Naval Air Warfare Center's Ocean Water Lidar (OWL) system. The RTP was used for real time support of open ocean field tests at Barbers Point, Hawaii, in March 1993 (EMERALD I field test), and Jacksonville, Florida, in July 1994 (EMERALD I field test). This report describes the system configuration, and accomplishments associated with the preparation and execution of these exercises. This document is intended to supplement the overall test reports and provide insight into the development and use of the PTP. A secondary objective is to provide basic information on the capabilities, versatility and expandability of the Hyperflo RTP for possible future projects. It is assumed herein that the reader has knowledge of the OWL system, field test operations, general lidar processing methods, and basic computer architecture. DTIC

N95-30910# Federal Aviation Administration, Atlantic City, NJ.
TERMINAL DOPPLER WEATHER RADAR (TDWR) BUILD 5B OPERATIONAL TEST AND EVALUATION (OT&E) INTEGRATION AND OT&E OPERATIONAL TEST PLAN
Radame Martinez, Steven Viveiros, Donne Wedge, and Peter Guthlein Mar. 1995 61 p
(AD-A293251; DOT/FAA/CT-TN94/59) Avail: CASI HC A04/MF A01

The Terminal Doppler Weather Radar (TDWR) Build 5B Enhancement Operational Test and Evaluation (OT&E) Integration and OT&E Operational Test Plan provides the overall philosophy and approach to Build 5B OT&E testing, and identifies OT&E objectives, responsibilities, and resources. The TDWR Build 5B Enhancement provides connectivity to the Low Level Wind Shear Alert System (LLWAS) III to display LLWAS III data along with TDWR hazardous weather data on TDWR Geographic Situation Displays (GSD) and Ribbon Display Terminals (RDT). The TDWR Build 5B OT&E is scheduled to occur at the TDWR sites in Denver, CO, November and December 1994, and in Orlando, FL, spring 1995. DTIC

N95-30917# Department of the Navy, Washington, DC.
ADVANCED SIGNAL PROCESSING FILTER Patent Application
Ronald A. Wagstaff, inventor (to Navy) 30 Sep. 1994 22 p
(AD-D017324; US-Patent-Appl-SN-314281) Avail: CASI HC A03/MF A01

A filter, and method of the filtering, for increasing the signal to noise ratio of relatively small and constant amplitude signals in the presence of relatively large and varying amplitude signals. The filter produces a filtered power level az proportional to az = (Sum of xi(-z) from i = 1 to N)(-1/z) where x1 are power realizations of the signal in a selected frequency bin, and i = 1, 2, . . ., N, and z is a non-zero real number not equal to -1, 0, or 1, and is preferably positive. For positive z, because filtered power level a2 depends on a sum of xi(-z), sum az disproportionately favors smaller, more stable, signals. DTIC

N95-30932# Rhode Island Univ., Kingston, RI.
STATISTICAL INTERFACE FOR CHAOTIC SIGNAL IN NOISE Final Report, 1 Sep. 1992 - 30 Sep. 1994
Steven Kay 30 Sep. 1994 14 p
(Contract F49620-93-1-0006)
(AD-A290271; AFOSR-95-0039TR) Avail: CASI HC A03/MF A01

A method for determining the frequency of a real sinusoid is proposed. Based on exponential sampling of the waveform, the approach requires virtually no computation. It can be easily implemented in digital hardware. A dynamic programming algorithm and a suboptical kit computationally efficient method for estimation of a chaotic signal in white Gaussian noise are proposed. The nonlinear map is assumed known so that only the initial condition need be estimated. Computer simulations confirm that both approaches produces efficient estimates at high signal-to-noise ratios. DTIC

N95-30935# Science and Engineering Services, Inc., Burtonsville, MD.
DEVELOPMENT OF A NOVEL WIND LIDAR, PHASE 1 Final Report, 13 May - 13 Nov. 1994
H. S. Lee 8 Feb. 1995 35 p
(Contract F49620-94-C-0052)
(AD-A292703; AF-94-1; AFOSR-95-0177TR) Avail: CASI HC A03/MF A01

A prototype new incoherent Doppler lidar system was designed for atmospheric wind measurements with a high accuracy up to a 5 kilometer slant path range in Phase 1. This sensor is based on the pseudo-random modulation CW lidar technique in conjunction with a new incoherent Doppler lidar method, in which the return PRM laser signal is passed through a Doppler filter before being digitally processed to determine range resolved wind velocity in real time. Extensive simulation study shows, in the baseline system configuration with a 50 cm receiver and one watt transmitter power, a 200 seconds signal integration will provide the required signal to noise ratio for a few percent accuracy measurement which corresponds to 1 m/s accuracy over a 50 m/sec dynamic range. Our Phase 1 experiment provided a unique technology basis for the construction of a high power narrow linewidth SLM diode laser system for cost effective and robust PRM laser transmitter. Consisting of the transmitter module, solid etalon based Doppler filter module, PRM data module and a receiver module, the sensor will be compact and lightweight with low power consumption and low cost. The sensor will be intrinsically insensitive to noise, background radiation, and other system bias. DTIC

N95-30954# Naval Postgraduate School, Monterey, CA.
ANALOG PREPROCESSING IN A SNS 2 MICROMETERS LOW-NOISE CMOS FOLDING ADC M.S. Thesis
Richard D. Carr Dec. 1994 120 p
(AD-A293356) Avail: CASI HC A06/MF A02

Significant research in high performance analog-to-digital converters (ADC's) has been directed at retaining part of the high-speed flash ADC architecture, while reducing the total number of comparators in the circuit. The symmetrical number system (SNS) can be used to preprocess the analog input signal, reducing the number of comparators and thus reducing the chip area and power consumption of the ADC. This thesis examines a Very Large Scale Integrated (VLSI) design for a folding circuit for a SNS analog preprocessing architecture in a 9-bit folding ADC with a total of 23 comparators. The analog folding circuit layout uses the Orbit 2 micrometers CMOS N-well double-metal, double-poly low-noise analog process. The effects of Spice level 2 parameter tolerances during fabrication on the operation of the folding circuit are investigated numerically. The frequency response of the circuit is also quantified. An Application Specific Integrated Circuit (ASIC) is designed. DTIC

N95-30962 Delaware Univ., Newark, DE.
INVERSE AND CONTROL PROBLEMS IN ELECTROMAGNETICS Final Report, 1 Jul. 1991 - 30 Jun. 1994
T. S. Angell and R. E. Kleinman 30 Jun. 1994 236 p Limited Reproducibility: More than 20% of this document may be affected by poor print
(Grant AF-AFOSR-0277-91)
(AD-A292993; AFOSR-95-0199TR) Avail: Issuing Activity (Defense Technical Information Center (DTIC))

This report summarizes work carried out in a number of specific areas of investigation in inverse scattering and optimal control problems in electromagnetics. The progress is briefly described and detailed results are included in an appendix. The major accomplishments include: the application of multi-criteria optimization techniques to problems in antenna design; the development of inverse scattering algorithms which use scattered field data in the frequency domain to reconstruct the well posedness of electromagnetic scattering problems with resistive or conductive boundary conditions; and derivation of new boundary integral equations for electromagnetic scattering from local distributions of a plane screen. In addition some new results on low frequency scattering have been found which establish the exact nature of the asymptotic expansion in two dimensions. DTIC

N95-31142# Cornell Univ., Ithaca, NY.
HIGH ENERGY PULSED MICROWAVE SOURCES Final Report, 1 Feb. 1993 - 31 Oct. 1994
John A. Nation 26 Jan. 1995 31 p
(Contract F49620-93-1-0103)
(AD-A293334; AFOSR-95-0232TR) Avail: CASI HC A03/MF A01

The work summarized in this report covers research carried out at Cornell University during the period 2/01/93 to 10/31/94. During this period our research focused on the generation of ultra high power microwave signals, especially on the elimination of sidebands from the amplifiers used, and in the latter period on the possibility of developing a tuneable high power amplifier. In this report we summarize both aspects of our program. Details of the results obtained may be found in the published papers, copies of which are appended to this report. DTIC

N95-31158# Helsinki Univ. of Technology, Espoo (Finland).
NORDIC SYMPOSIUM ON ANALYSIS OF ELECTROMAGNETIC TRANSIENT PHENOMENA USING EMTP, PART 3
T. Jokinen 1994 135 p Conference held in Espoo, Finland, 22-26 Aug. 1994
(PB95-206504) Avail: CASI HC A07/MF A02

The Electromagnetic Transients Program (EMTP) is a computer program used to simulate electromagnetic, electromechanical, and control system transients on multiphase electric power systems. Section headings in this volume include the following: Ideal Sources in EMTP; Three Phase Dynamic Synchronous Machine Model in EMTP (TYPE-59); Universal Machine Modeling in EMTP; and Transient Analysis of Control Systems (TACS) - Fundamental Concepts. NTIS

N95-31159# Helsinki Univ. of Technology, Espoo (Finland).
PLANE WAVE REFLECTION FROM A UNIAXIAL CHIRAL QUARTER-WAVE POLARIZATION TRANSFORMER
A. J. Viitanen Jun. 1994 14 p
(PB95-206512; ISBN-951-22-2210-8) Avail: CASI HC A03/MF A01

A uniaxial chiral slab is shown to have applications as a polarization transformer by choosing the thickness of the slab and the material parameters properly. The slab transforms linear polarization to any elliptic polarization by rotating the slab. The reflection coefficients for the slab are calculated numerically and the results show us that by choosing the material parameters properly the reflection from the slab can be minimized. This is very important for practical applications of the chiral quarter-wave polarization transformer. NTIS

N95-31160# Helsinki Univ. of Technology, Espoo (Finland). Electromagnetics Lab.
NORDIC SYMPOSIUM ON ANALYSIS OF ELECTROMAGNETIC TRANSIENT PHENOMENA USING EMTP, PART 2
Tapani Jokinen, ed. 1994 230 p Symposium held in Espoo, Finland 22-26 Aug. 1994 See also Part 1, PB95-206595 and Part 3, PB95-206504
(PB95-206579) Avail: CASI HC A11/MF A03

The Electromagnetic Transients Program (EMTP) is a computer program used to simulate electromagnetic, electromechanical, and control system transients on multiphase electric power systems. Section headings in this volume include the following: Case Studies for Electromagnetic Transients; Transformers - Section 6 from EMTP Theory Book, Second Edition; What Is Needed In Transformer Representations; and Transformer Inrush Current, Test Case 1. NTIS

N95-31161# Helsinki Univ. of Technology, Espoo (Finland). Electromagnetics Lab.
NORDIC SYMPOSIUM ON ANALYSIS OF ELECTROMAGNETIC TRANSIENT PHENOMENA USING EMTP, PART 4
Tapani Jokinen, ed. 1994 163 p Symposium held in Espoo, Finland,

22-26 Aug. 1994 See also Part 3, PB95-206504
(PB95-206587) Avail: CASI HC A08/MF A02

The Electromagnetic Transients Program (EMTP) is a computer program used to simulate electromagnetic, electromechanical, and control system transients on multiphase electric power systems. Section headings in this volume include the following: HVDC Model Applications; Frequency Dependent Network Equivalents (FDNE); Steady-State Analysis in EMTP; Some System Studies Using the EMTP; and EMTP Computer Lab Notebook - The Windows and OS/2 Personal Computer Versions. NTIS

N95-31182# Helsinki Univ. of Technology, Espoo (Finland). Electromagnetics Lab.

NORDIC SYMPOSIUM ON ANALYSIS OF ELECTROMAGNETIC TRANSIENT PHENOMENA USING EMTP, PART 1

Tapani Jokinen, ed. 1994 133 p Symposium held in Espoo, Finland, 22-26 Aug. 1994 See also Part 2, PB95-206579
(PB95-206595) Avail: CASI HC A07/MF A02

The Electromagnetic Transients Program (EMTP) is a computer program used to simulate electromagnetic, electromechanical, and control system transients on multiphase electric power systems. Section headings in this volume include the following: Power Systems Analysis Using Electromagnetic Transients Programs; EMTP Applications; EMTP Simulation of Simple Switching Transients Trapezoidal Integration; EMTP Theory; Line Models in the EMTP; and Frequency Dependent Cable Models. NTIS

N95-31280 New York Univ., New York, NY. Courant Inst. of Mathematical Sciences.

DIRECT AND INVERSE PROBLEMS IN RANDOM MEDIA Final Report, 1 Dec. 1991 - 31 Oct. 1994

George Papanicolaou 30 Dec. 1994 5 p Limited Reproducibility: More than 20% of this document may be affected by poor print
(Contract F49620-92-J-0098)
(AD-A293033; AFOSR-95-0181TR) Avail: Issuing Activity (Defense Technical Information Center (DTIC))

During this period of the grant I worked in the following three general areas: (1) Direct and inverse problem for waves in random media. This is the principal focus of the work funded; (2) Convection enhanced diffusion; (3) The effect of normal time dispersion on laser beam self-focusing. DTIC

N95-31357# Polish Academy of Sciences, Warsaw (Poland). Acoustic Phonetics Workshop.

AUTOMATION OF THE CONTROL OF ACOUSTIC PARAMETERS IN A DIGITAL SPEECH SYNTHESIZER [AUTOMATYZACJA STEROWANIA PARAMETRAMI AKUSTYCZNYMI W CYFROWYM SYNTEZATORZE MOWY]

Ignacy Nowak, Mariusz Owsianny, and Janusz Imoilczyk Feb. 1995 31 p In POLISH
(ISSN 0208-5658)
(IFTR-2/1995) Avail: CASI HC A03/MF A01

The authors describe the results of their modifications of the implementation of a formant model for a serial-parallel speech synthesizer which operates according to D. H. Klatt's system. The basic version of the implementation was developed at the Acoustic Phonetics Workshop of the Institute of Basic Problems of Technology of the Polish Academy of Sciences in Poznan by M. Owsianny. The modifications proceeded in several directions, including: (1) adaptation of the control of the model to synthesize complex sequences of Polish vowels; (2) improvements in the speed of the programmed synthesis model; and (3) modification of the user interface for the software. The accomplishment of the most important part of the work (item 1 above) made it possible to: (1) switch between different synthesis modes without conflict (within a single synthetic utterance); (2) simplify the synthesis mode switching system; and (3) provide precise control of parameters in extending the synthesis process to subsequent time frames. All of these improvements made it possible to speed up the synthesis process without adversely affecting the quality of the synthesized speech and make the synthesizer software much more comfortable for users. The new synthesizer software requires better hardware than the old software, with the minimum requirements being an IBM PC 386 with a math co-processor. Author

N95-31367# Mitre Corp., Bedford, MA.

HIGH FREQUENCY (HF) UPGRADE STUDY FOR THE CANADIAN REGIONAL OPERATIONS CONTROL CENTER (ROCC) AWACS DIGITAL INFORMATION LINK (RADIL) PROJECT Final Report

Kenneth Wickwire Apr. 1995 78 p
(Contract F19628-89-C-0001)
(AD-A293435; MTR-93B0000141; ESC-TR-95-104) Avail: CASI HC A05/MF A01

The Regional Operations Control Center AWACS Digital Information Link/Rapidly Deployable Integrated Command and Control System (RADIL/RADIC) System Program Office, Canadian RADIL Program, has acquired high-frequency (HF) radio equipment for two Canadian ground stations under the RADIL Project. This equipment will allow those stations to carry out Tactical Digital Information Link (TADIL) A data transmissions assisted by MIL-STD-188-141A automatic link establishment (ALE). The MITRE Corporation has been tasked to study whether U.S. TADIL stations should be equipped with similar HF-ALE modems. This report analyzes the improvements in performance over northern links that can be expected from the addition of ALE to the TADIL A system. Since there is only a small amount of data on ALE-assisted digital communications in northern regions, the analysis combines a probabilistic approach to comparison of ALE and conventional linking techniques with actual HF propagation data from links in Canada, Iceland, and Norway. The report also assesses the risks to effective communications of using an ALE-TADIL A system in the north and recommends several improvements in hardware and software that can lower those risks. DTIC

N95-31387# Rome Lab., Griffiss AFB, NY.

PROCEEDINGS OF THE ANTENNA APPLICATIONS SYMPOSIUM. VOLUME 2

Daniel H. Schaubert Feb. 1995 249 p Symposium held jn Griffiss AFB, NY
(AF Proj. 4600)
(AD-A293259; RL-TR-95-47-Vol-2) Avail: CASI HC A11/MF A03

The Proceedings of the 1994 Antenna Applications Symposium is presented. This volume, volume 2, contains a collection of state-of-the-art papers relating to phased array antennas, multibeam antennas, satellite antennas, microstrip antennas, reflector antennas, HF, VHF, UHF and various other antennas. DTIC

N95-31392 Department of the Navy, Washington, DC.

DETECTION OF RADAR TARGETS USING HIGHER-ORDER STATISTICS Patent

Robert D. Pierce, inventor (to Navy) 28 Mar. 1995 18 p Filed 28 Sep. 1993
(AD-D017442; US-Patent-5,402,131; US-Patent-Appl-SN-127619; US-Patent-Class-342-194) Avail: US Patent and Trademark Office

A signal detection system, preferably for use with a coherent radar system selects certain combination of input signal samples in a block of signal samples to derive a test statistic which is unbiased by Gaussian noise. Products of pairs of sample values are stored in a data sample look-up table. An index look-up table is created by scanning through possible combinations of addresses and excluding those combinations of sample values which would be redundant over other combination and would result in a contribution to biasing by noise. DTIC

N95-31426# Stanford Univ., CA. Dept. of Electrical Engineering.

MULTI-DIMENSIONAL DATA COMPRESSION FOR PORTABLE COMMUNICATION Final Report, 1 Aug. 1991 - 31 Dec. 1994

Teresa H. Meng 1995 44 p
(Contract DABT63-91-K-0002)
(AD-A292751) Avail: CASI HC A03/MF A01

This project provides an integrated design approach of a portable video on demand system capable of delivering high quality image and video in a wireless communication environment. The research focuses on both the algorithm and circuit design techniques developed for implementing a low power video compression/decompression system at power levels that are two orders of magnitude below existing solutions. The three main technological challenges in realizing such a system are high compression efficiency for transmission bandwidth reduction, error resiliency to minimize the effects of channel error, and low power implementation for portability. DTIC

N95-31430# Massachusetts Inst. of Tech., Cambridge, MA.
MULTIRESOLUTION SIGNAL AND SYSTEM ANALYSIS AND THE ANALYSIS AND CONTROL OF DISCRETE-EVENT DYNAMIC SYSTEMS Final Report, 1 Oct. 1991 - 30 Sep. 1994
Alan S. Willsky 1 Oct. 1994 24 p
(Contract F49620-92-J-0002)
(AD-A292775; AFOSR-95-0227TR) Avail: CASI HC A03/MF A01

This final report summarizes research accomplishments supported by AFOSR Grant F49620-92-J-0002. Over the three-year period of support under this grant we have had considerable success in each of the several components of our research program, namely the development of multiresolution statistical approaches to problems of image analysis, the analysis of singular systems with applications in efficient processing of multidimensional data, large-scale estimation and computation in remote sensing and space-time data assimilation, multiresolution and wavelet-based methods for the detection and classification of abrupt changes in signals, and data fusion and inversion using multiresolution and wavelet-based methods. In this report we outline our accomplishments in each of these areas and also include a complete list of reports and publications describing this work. DTIC

N95-31448# Logistics Management Inst., Bethesda, MD.
THE QUAD-SERVICE SATELLITE TRANSMITTING AND RECEIVING SYSTEM FOR MEDICAL SUPPLY SUPPORT: A BATTLEFIELD INTEROPERABILITY AND COMMUNICATIONS SYSTEM PROTOTYPE, VOLUME 2. USER DOCUMENTATION Final Report
John Lycas and Roger E. Miller Aug. 1994 202 p
(Contract MDA903-90-C-0006)
(AD-A292835; LMI-DL205-01R1) Avail: CASI HC A10/MF A03

This report documents the design and development of a prototype information communications system for quad-service use in a theater of operations. The prototype was designed to allow seamless integration of legacy information systems operated by each of the four services, and is based on a combination of software interfaces and commercial satellite communications hardware. The QSTARS-MS prototype has been tested in a variety of garrison and deployment settings including extensive use in Somalia and the former Yugoslav republics. The prototype demonstrates the feasibility of achieving joint interoperability through rapidly designed interfaces between legacy information systems. The prototype also offers world-wide, portable, and affordable satellite communications capability through the use of the International Maritime Satellite network. DTIC

N95-31449# Logistics Management Inst., Bethesda, MD.
THE QUAD-SERVICE SATELLITE TRANSMITTING AND RECEIVING SYSTEM FOR MEDICAL SUPPLY SUPPORT: A BATTLEFIELD INTEROPERABILITY AND COMMUNICATIONS SYSTEM PROTOTYPE, VOLUME 1 Final Report
John Lycas and Roger E. Miller Jul. 1994 33 p
(Contract MDA903-90-C-0006)
(AD-A292836; LMI-DL205-01R1) Avail: CASI HC A03/MF A01

This report documents the design and development of a prototype information communications system for quad-service use in a theater of operations. The prototype was designed to allow seamless integration of legacy information systems operated by each of the four services, and is based on a combination of software interfaces and commercial satellite communications hardware. The QSTARS-MS prototype has been tested in a variety of garrison and deployment settings, including extensive use in Somalia and the former Yugoslav republics. The prototype demonstrates the feasibility of achieving joint interoperability through rapidly designed interfaces between legacy information systems. The prototype also offers world-wide, portable, and affordable satellite communications capability through the use of the International Maritime Satellite network. DTIC

N95-31457*# Massachusetts Univ., Amherst, MA. Dept. of Electrical and Computer Engineering.
INVESTIGATION OF MICROWAVE BACKSCATTER FROM THE AIR-SEA INTERFACE Final Report
Robert E. McIntosh and James R. Carswell [1995] 22 p
(Grant NAGw-1112)
(NASA-CR-198854; NAS 1.26:198854) Avail: CASI HC A03/MF A01

Monitoring the ocean surface winds and mean ocean surface level is essential for improving our knowledge of the climate. Two instruments that may provide us with this information are satellite-based scatterometers and altimeters. However, these instruments measure the backscatter characteristics of the ocean surface from which other physical parameters, such as the wind speed or ocean surface height, are derived. To improve the algorithms or models that relate the electromagnetic backscatter to the desired physical parameters, the University of Massachusetts (UMass) Microwave Remote Sensing Laboratory (MIRSL) designed and fabricated three airborne scatterometers: a C-band scatterometer (CSCAT), Ku-band scatterometer (KUSCAT) and C/Ku-band scatterometer (EMBR). One or more of these instruments participated in the Electromagnetic Bias experiment (EM Bias), Shelf Edge Exchange Processes experiment (SEEP), Surface Wave Dynamics Experiment (SWADE), Southern Ocean Wave Experiment (SOWEX), Hurricane Tina research flights, Tropical Ocean Global Atmosphere Coupled Ocean-Atmosphere Response Experiment (TOGA COARE), and Ladir In-space Technology Experiment (LITE). This document describes the three scatterometers, summarizes our measurement campaigns and major contributions to the scientific and engineering communities, lists the publications that resulted, and presents the degrees earned under the support of this NASA grant. Derived from text

N95-31510# Defence Science and Technology Organisation, Canberra (Australia).
FUNCTIONS FOR PROCESSING SYNTHETIC APERTURE RADAR IMAGERY
Robert Whatmough and Paul Whitbread Jan. 1995 47 p
(AD-A293895; DSTO-TR-0146; DODA-AR-008-799) Avail: CASI HC A03/MF A01

The INGARA synthetic aperture radar system can potentially benefit from higher level algorithms and software to enhance its basic imagery so that important features are obvious to human operators. These could include filters for removing speckle, zooming functions for correcting the aspect ratio of the imagery and classifiers for distinguishing ground cover types. The system could also make use of a development environment in which such functions can be easily developed and trialled. This Note describes the Khoros image processing system and functions added to that system by researchers in ITD that could be of use in processing INGARA data. It also includes results of tests of the effectiveness of these functions in enhancing sample INGARA data. DTIC

N95-31513# Air Force Inst. of Tech., Wright-Patterson AFB, OH. School of Engineering.
INVESTIGATION OF GROUND TARGET DETECTION METHODS IN FULLY POLARIMETRIC WIDE ANGLE SYNTHETIC APERTURE RADAR IMAGES M.S. Thesis
Wayne B. Laggan Mar. 1995 177 p
(AD-A293922; AFIT/GE/ENG/95M-02) Avail: CASI HC A09/MF A02

Target detection is a high priority of the Air Force for the purpose of reconnaissance and bombardment. This research investigates and develops methods to distinguish ground targets from clutter (i.e. foliage, landscape etc.) in Wide Angle Synthetic Aperture Radar (WASAR) images. WASAR uses multiple aspect angle SAR images of the same target scene. The WASAR data was generated from a pre-release software package (XPATCH-ES) provided by the sponsor (WL-AARA). A statistical analysis and feature extraction is performed on the XPATCH-ES data. Polarimetric and wide angle covariance matrices are estimated and analyzed. From an analysis of the wide angle covariance matrix it is shown that natural clutter has in general a uniform radar return for changing aspect angles, whereas the radar return for a target varies. Based on this analysis, two new wide angle algorithms, the WASAR Whitening Filter and the Adaptive WASAR Whitening Filter (AWWF) are developed. The target detection performance of polarimetric and multi aspect angle image combining algorithms are quantified using Receiver Operating Characteristic curves and target to clutter ratios. It is shown that wide angle processing provides superior target detection performance over polarimetric processing. Combinations of wide angle and polarimetric algorithms were used to achieve a 13.7 dB processing gain in target to clutter ratio when compared to unprocessed images of the target scene. This represents a significant improvement in target detection capabilities. DTIC

N95-31537# Michigan Univ., Ann Arbor, MI. Dept. of Electrical Engineering and Computer Science.
FAST ALGORITHMS FOR THREE-DIMENSIONAL INVERSE SCATTERING PROBLEMS Final Technical Report
Andrew E. Yagle 30 Sep. 1994 450 p
(Contract N00014-90-J-1897)
(AD-A293510) Avail: CASI HC A19/MF A04

This report is the final report for grant N00014-90-J-1897. This project develops fast algorithms for multidimensional inverse scattering problems. DTIC

N95-31551# Pennsylvania Univ., Philadelphia, PA. Valley Forge Research Center.
RESEARCH IN GROUND-TO-AIR MICROWAVE IMAGING Final Report
Bernard D. Steinberg and Donald Carlson Mar. 1995 29 p
(Contract DAAL03-89-K-0066)
(AD-A292907; UP-VFRC-11-95; ARO-25350.15-EL) Avail: CASI HC A03/MF A01

Many potential applications exist for high resolution radar such as direction finding, high accuracy tracking, target counting, and high resolution radar imaging. All of these applications require the use of large, thinned, random or periodic antenna arrays. Many uncertainties exist in such large antenna systems. For example, exact element positions are generally not known because of surveying problems or flexing of the large antenna structure. Adaptive beamforming (ABF) is the solution to the unusual design that achieves these objectives. It deduces the errors in the locations of the receivers that are distributed around the airport or on the air frame and automatically compensates for them in the image processing. This year's work concentrated on three tasks. The first was to develop a generalized ABF theory for the class of spatial correlation algorithms. The second was to extend the resolution of a microwave imaging radar to 15 cm, and the third was to study enhanced target detection sensitivity and target recognition. DTIC

N95-31555# Air Force Inst. of Tech., Wright-Patterson AFB, OH. School of Engineering.
DYNAMIC MAINTENANCE SCHEDULING FOR A STOCHASTIC TELECOMMUNICATION NETWORK: DETERMINATION OF PERFORMANCE FACTORS
Todd S. Patterson Mar. 1995 133 p
(AD-A293829; AFIT/GOR/ENS/95M-14) Avail: CASI HC A07/MF A02

This research proposes an analytical approach to access the relationship between maintenance facility location and communication network performance measurement using a selected dynamic maintenance scheduling protocol. There were three objectives established for this effort. The first objective was the determination of an upper-bound upon the level of performance for a telecommunication network using dynamically scheduled maintenance to evaluate maintenance depot location. This was achieved by using a two-stage algorithm, first locate a maintenance depot by using stochastic algorithms, and then to measure the resulting impact upon performance with a multi-commodity network flow model. The second objective was to develop the metrics by which network performance should be measured. This was accomplished by comparing multiple criteria using a constraint conversion technique. The third objective created the mathematical models necessary to evaluate network operations. The models were created within a least-cost multi-commodity network flow environment. The approaches used in this research are offered as initial investigations toward the long-term goal of automated maintenance scheduling for a stochastic communication network. DTIC

N95-31574# Army Test and Evaluation Command, Aberdeen Proving Ground, MD.
TEST OPERATIONS PROCEDURE (TOP) 1-2-512 ELECTROMAGNETIC COMPATIBILITY TESTS Final Report
15 May 1995 16 p
(AD-A293758; TOP-1-2-512) Avail: CASI HC A03/MF A01

This TOP provides guidance for the planning, execution, and reporting of grounding and bonding and electromagnetic compatibility (EMC) tests of electrical, electronic, and electrochemical equipment, subsystems, and systems. DTIC

N95-31588# Range Commanders Council, White Sands Missile Range, NM.
USING SATELLITES FOR RADAR PERFORMANCE MONITORING AND CALIBRATION
Mar. 1995 89 p
(AD-A293809; RCC-296860) Avail: CASI HC A05/MF A01

This document describes the process by which satellites may be used to calibrate and to maintain the performance of metric tracking radar systems. Historical background is included to show why an aggressive radar performance monitoring program became necessary. DTIC

N95-31590# Naval Research Lab., Washington, DC.
MILLIMETER WAVE RADIOMETER UTILITY STUDY Final Report, May 1993 - Oct. 1994
Peter W. Gaiser, James P. Hollinger, Steven R. Highley, and Glenn D. Sandlin 27 Mar. 1995 105 p
(AD-A293811; NRL/MR/7220-95-7652) Avail: CASI HC A06/MF A02

Many military and environmental applications require wide area surveillance on a timely and global basis. Passive microwave and millimeter wave imaging has the advantage over visual and infrared systems of being a near all-weather surveillance system with the ability to see through clouds and most adverse weather conditions with equal day and night sensitivity. The major disadvantage of microwave and millimeter wave radiometric systems is that the relatively long wavelengths require aperture several orders of magnitude larger than at infrared to obtain comparable spatial resolution. However, even low resolution microwave and millimeter wave radiometers can contribute significantly to intelligence gathering and environmental remote sensing. This document presents a study of the capabilities of microwave and millimeter wave imaging from space with systems which provide resolutions of 100-400 m at observation frequencies of 1.4-140 GHz. Possible radiometer architectures and their space development are examined the surveillance and environmental remote sensing benefits of multifrequency high resolution microwave and millimeter wave radiometry are discussed in depth. DTIC

N95-31601# Army Research Lab., Aberdeen Proving Ground, MD.
TWO-DIMENSIONAL FINITE DIFFERENCE TIME DOMAIN (FD-TD) MODEL OF ELECTROMAGNETIC (EM) SCATTERING FROM A BURIED RECTANGULAR OBJECT Final Report, Jun. 1993 - Jun. 1994
Thomas A. Korjack Feb. 1995 36 p
(AD-A293685; ARL-TR-713) Avail: CASI HC A03/MF A01

A two-dimensional transverse-magnetic (TM) electromagnetic (EM) scattering problem from buried dielectric objects due to a Gaussian pulse is numerically solved using the Finite Difference Time Domain (FD-TD) method with absorbing boundary conditions via Maxwell's equations. The scatterers are rectangular cross sections in a multilayer media; the Gaussian pulse is reflected into a lossy earth by a finite, 450 plate that is part of the detector that receives the EM signal. Spatial distributions of electric field components are calculated over time for single and multiple land scatterers (mines). The scattered fields gradually diminish with time and are then eventually dissipated. Carpet plots are illustrated to depict the spatial distributions of the scattered field component at comparative time steps for one, two, and three distinct scatterers or land mines within the lossy media. Results clearly illustrate the typical wave patterns expected under the simulated conditions as presented in this report - i.e., conductivity (s) for the air is 0, conductivity for the earth is 0.01, conductivity for the grass is 0.005, and conductivity for the mines are 0, 0.02, and 0.008; permeability values ranged from 1 for air, 9 for earth, 5.5 for grass, and 2.3, 5.6, and 23.0 for the mines, respectively. Numerical analysis indicates that the difference of scattered signals between single and multiple scatterers are considerably obvious from the point of view of both time domain and frequency domain. DTIC

N95-31606# Naval Command, Control and Ocean Surveillance Center, Kailua, HI.
COMPARISONS OF TARGET DETECTION CLUTTER USING DATA FROM THE 1993 FOPEN EXPERIMENTS
E. M. Winter, M. J. Schlangen, and C. R. Hendrickson Oct. 1994 13 p
(AD-A293052) Avail: CASI HC A03/MF A01

During 1993, a series of experiments were performed under the Advanced Research Projects Agency (ARPA) sponsorship using the SRI Ultra-Wide Band UHF Synthetic Aperture Radar (SAR). These experiments

were performed over a variety of clutter backgrounds to assess the foliage penetration capability of the technology and to investigate target detection in clutter. Experiments were conducted observing tropical rain forest backgrounds in Panama, several different desert backgrounds in the Yuma vicinity, and the mid-latitude temperate forest of Maine. SAR images were formed from the raw data using Differential GPS to aid in the focusing. The three locations represent different levels of foliage cover, ranging from the sparsely vegetated desert sites to the triple canopied rain forest. The characteristics of each site are discussed first through a presentation of photography and SAR imagery. The clutter characteristics are studied through a comparison of the cumulative distributions, which are plotted using a variety of conventions (e.g., log-normal, normal, Weibull). For each case, at least one reference target is included in the test scene. The signal of that target as processed by a common algorithm will be compared to the processed clutter distribution. DTIC

N95-31628# Sandia National Labs., Albuquerque, NM.
FOLDED COMPACT RANGE DEVELOPMENT AND COHERENT CHANGE DETECTION MEASUREMENT PROJECT
K. W. Sorensen Mar. 1995 82 p
(Contract DE-AC04-94AL-85000)
(DE95-009082; SAND-95-0389) Avail: CASI HC A05/MF A01

A novel, folded compact range configuration has been developed at the Sandia National Laboratories compact range antenna and radar cross section measurement facility, operated by the Radar/Antenna Department 2343, as a means of performing indoor, environmentally-controlled, far-field simulations of synthetic aperture radar (SAR) coherent change detection (CCD) measurements. This report describes the development of the folded compact range configuration, as well as the initial set of coherent change detection measurements made with the system. These measurements have been highly successful, and have demonstrated the viability of the folded compact range concept in simulating SAR CCD measurements. It is felt that follow-on measurements have the potential of contributing significantly to the body of knowledge available to the scientific community involved in CCD image generation and processing, and that this tool will be a significant aid in the research and development of change detection methodologies. DOE

N95-31649# Helsinki Univ. of Technology, Espoo (Finland).
REFLECTION AND TRANSMISSION OF ELECTROMAGNETIC PLANE WAVES FROM A UNIAXIAL CHIRO-OMEGA SLAB
P. K. Koivisto Jun. 1994 21 p
(PB95-206629; ISBN-951-22-2215-9) Avail: CASI HC A03/MF A01

Chiro-omega medium is a combination of the reciprocal chiral and omega media, and can be obtained by mixing helical and Omega-shaped wire elements in the host medium. In this article the most general uniaxial chiro-omega medium is studied. The solutions for the dispersion equations and corresponding eigenwaves are derived. Transmission and reflection properties of a chiro-omega slab at a normal incidence are studied, and the polarization, direction of the polarization ellipse, and relative powers of transmitted and reflected waves are given. The results are applied to find suitable parameters for designing a polarization transformer. These results are compared with those obtained in earlier studies on wave propagation in a free uniaxial chiral space, where the effect of the boundaries of a proposed polarization transforming device have been neglected. NTIS

N95-31673# Naval Postgraduate School, Monterey, CA.
AUTOMATIC TARGET RECOGNITION (ATR): BACKGROUND STATISTICS AND THE DETECTION OF TARGETS IN CLUTTER M.S. Thesis
Nicholas Wager Dec. 1994 153 p
(AD-A293062) Avail: CASI HC A08/MF A02

This research investigated signal processing of two dimensional signals for the detection of targets in noise, particularly in complex background pattern noise. The researchers hypothesized that this type of noise was vulnerable to nonlinear processing. They investigated whether the human eye/brain acting as a surrogate for a nonlinear processor could outperform an optimum linear processor in a quantitative sense. The researchers did this by conducting computer experiments to determine the ability of an operator and an optimum linear filter to determine a known pattern's presence or absence in a noisy image. The performance of both the operator and optimum linear filter are recorded as probability of detection, probability of false alarm pairs, which the researchers use to determine effective signal-to-noise ratio. The performance of man versus machine (optimum linear filter) is compared quantitatively using the effective signal-to-noise ratio. Operator and machine/filter are tested against circular targets in random white gaussian noise and in satellite images. The researchers report that the machine filter outperforms the man when the details of both target and background are known in advance, but the man outperforms the machine/filter when the details are known only in a statistical sense. DTIC

N95-31744 Japan Broadcasting Corp., Tokyo (Japan). Lightwave and Radio Engineering Research Div.
PORTABLE DIGITAL SATELLITE NEWS GATHERING (SNG) RF TERMINAL USING A FLAT ANTENNA
Takao Murata, Hideo Mitsumoto, Masaru Fujita, Shoji Tanaka, Kouichi Takano, Kazuo Imai, and Noboru Toyama May 1995 19 p
(ISSN 0027-657X)
(NHK-Labs-Note-436) Copyright Avail: Issuing Activity (Japan Broadcasting Corp., 1-10-11, Kinuta, Setagaya-ku, Tokyo 157, Japan)

In this paper, a Ku-band portable SNG RF terminal using a flat antenna is proposed for making the best use of digital SNG systems. This portable terminal uses 16 planar microstrip subarray antennas, each with a solid-state power amplifier (SSPA) mounted on its rear. The proposed RF terminal is different from a conventional portable RF terminal with parabolic antenna in that it has electronic tracking capability. Electronic antenna tracking reduces time it takes to set up the terminal because precise alignment of the antenna is not required. The flat antenna meets the design objectives specified by the ITU-R Recommendations. The SSPA's have an efficiency of 21 percent and a power output of 5 W. The tracking performance of the feedback system which uses four subarrays, is also presented. Author

N95-31839 Iowa State Univ. of Science and Technology, Ames, IA.
A BOUNDARY INTEGRAL EQUATION APPROACH TO THREE DIMENSIONAL ELECTROMAGNETIC WAVE SCATTERING PROBLEMS Ph.D. Thesis
Joseph Chiu Chao 1994 121 p
Avail: Univ. Microfilms Order No. DA9424201

Electromagnetic scattering models are finding increasing interest in many applications ranging from nondestructive evaluation (NDE) to design of optical systems. The availability of a computational scattering model characterizing the underlying system serves several purposes. First, it serves as an inexpensive test bed to simulate a variety of test situations. For instance, the forward model can be used to evaluate various polarizations and incidence angles of the incident source fields and the corresponding spatial distribution of the scattered fields which in turn provides information useful for optimizing the measurement of scattered fields. By preserving some of the realism that is usually possible in purely analytical methods, it provides valuable insight into the physics of actual problems. Second, forward scattering models are important in solving the inverse problem where the scattered fields are used for characterizing the size, the shape, and the constitution of the scatterer. The development of theoretical models largely relies on the use of numerical techniques such as boundary element method (BEM), finite element method (FEM), or finite difference method (FDM). However, no single numerical method has emerged as the optimal method for solving all electromagnetic scattering problems. One numerical method might be preferred over others, depending on the nature of the problem. For instance, problems which involve homogeneous scatterers and propagation of waves in an infinite medium are typically solved using the BEM whereas problems which involve a naturally truncated region are modeled using FEM and FDM. This dissertation presents a boundary integral equation (BIE) formulation for the problem of electromagnetic scattering due to homogeneous dielectric scatterers. The governing BIE's are then evaluated numerically using the BEM. Several fundamental electromagnetic scattering geometries are considered. The first problem involves solving for the scattered fields in the presence of a single, three dimensional, arbitrarily shaped, dielectric scatterer suspended in an infinite medium. The formulation is then extended to modeling the scattered fields in the presence of multiple dielectric scatterers as well as a dielectric scatterer in the proximity of an infinite perfect conducting plane. Lastly, the problem of a dielectric scatterer situated close to a dielectric half-space is discussed. The geometries are chosen so that the work presented in this dissertation

will serve as a basic model and solutions to a large range of problems can be obtained by modifying one or more of the configurations presented. Dissert. Abstr.

N95-32045# Sandia National Labs., Livermore, CA.
VIDEO CONFERENCING USING DAVE USER'S GUIDE
J. A. Frieson Mar. 1995 34 p
(Contract DE-AC04-94AL-85000)
(DE95-010341; SAND-95-8211) Avail: CASI HC A03/MF A01

This guide is intended to provide information to new users of Sandia National Laboratories Distributed Audio Video Environment (DAVE) applications. DOE

N95-32050# Los Alamos National Lab., NM. Theoretical Div.
BASIC SCIENCE WITH PULSED POWER AND SOME OFF-THE-WALL IDEAS
Johndale C. Solem 1995 13 p Presented at the Spring Workshop on Basic Science Using Pulsed Power, Santa Barbara, CA, 5-7 Apr. 1995
(Contract W-7405-eng-36)
(DE95-009486; LA-UR-95-1110; CONF-9504132-1) Avail: CASI HC A03/MF A01

This paper discusses aspects of pulsed power for use in basic research, with a principal emphasis on ATLAS, a planned 36-MJ pulsed-power machine with a circular architecture designed primarily for z-pinch implosion of cylindrical foils. The objective of the paper is to give an overview and touch on subjects which might test the limits of this technology. DOE

N95-32114 Xidian Univ., Xian (China). Inst. of Electronic Engineering.
ADAPTIVE SPACE-TIME PROCESSING FOR AIRBORNE RADARS BASED ON DOPPLER PRE-PROCESSING
G. S. Liao, Z. Bao, and Y. Zhang 1994 9 p Sponsored by Institute of Scientific and Technical Information of China
(PB95-205464; ISTIC-TR-94245) Avail: Issuing Activity (National Technical Information Service (NTIS))

A new partial joint-domain spatial-temporal adaptive processing approach to airborne radars based on a pre-processing with a multi-channel Doppler filtering operation is proposed, assuming that the antenna is a rectangular planar array, in which the elements in each column are combined into a subarray. The principle and performance of the proposed processor are analyzed in detail, compared with those of two other processors. The excellent performance of the processor in the presence of large random amplitude and phase errors between the array elements is shown by theoretical analysis and computer simulation, particularly when targets are close to the mainlobe clutter. NTIS

N95-32145# Sandia National Labs., Albuquerque, NM. Electronic Fuzing and Sensors Dept.
SCANNERLESS RANGE IMAGING WITH A SQUARE WAVE
Maritza R. Muguira, John T. Sackos, and Bart D. Bradley 1995 8 p Presented at the SPIE International Symposium on Aerospace/Defense Sensing and Dual-use Photonics, Orlando, FL, 17-21 Apr. 1995
(Contract DE-AC04-94AL-85000)
(DE95-009840; SAND-95-0721C; CONF-950472-6) Avail: CASI HC A02/MF A01

Scannerless range imaging (SRI) is a unique approach to three dimensional imaging without scanners. SRI does, however, allow a more powerful light source to be used as compared to conventional Laser Radar (LADAR) systems due to the speed of operation associated with this staring system. As a result, a more efficient method of operation was investigated. As originally conceived, SRI transmits a continuous intensity modulated sinusoidal signal; however, a square wave driver is more energy efficient than a sinusoidal driver. In order to take advantage of this efficiency, a square wave operational methodology was investigated. As a result, four image frames are required for the extraction of range using a square wave to unambiguously resolve all time delays within one time period compared to a minimum of three frames for the sinusoidal wave. DOE

N95-32192# Polish Academy of Sciences, Warsaw (Poland). Acoustic Phonetics Workshop.
THE CONTEXTUAL VARIANCE OF DEVOICED FRICATIVES IN POLISH [WARIANTYWNOSC KONTEKSTOWA SPOLGLOSEK TRACYCH BEZDZWIECZNYCH JEZYKA POLSKIEGO]
Lutoslawa Richter and Piotr Domagala Jul. 1995 32 p In POLISH
(Contract KBN-3-P401-002-05) (ISSN 0208-5658)
(IFTR-7/1995) Avail: CASI HC A03/MF A01

This article describes a study of the changes which occur in the spectra of voiceless fricative consonants as a result of the proximity of a vowel and a consonant. The authors adopted spectrum level values sensed at different intervals and expressed as a 25-element vector as their basis for parameterization. Measurement results were subjected to discriminant analysis, which made it possible to determine the degree of similarity between the mean vectors representing different contexts. The authors discovered that neighboring vowels, especially /u/ and /i/, cause major changes in the spectra of fricatives, but this statement does not apply to all consonants. Among the fricatives they studied, /x/ exhibited the greatest proclivity for allophonization in a vowel context and the least proclivity for allophonization in a consonant context. Transl. by Schreiber

N95-32221*# Jet Propulsion Lab., California Inst. of Tech., Pasadena, CA.
THE TELECOMMUNICATIONS AND DATA ACQUISITION REPORT Progress Report, Jan. - Mar. 1995
Joseph H. Yuen, ed. 15 May 1995 296 p
(NASA-CR-198911; JPL-TDA-42-121; NAS 1.26:198911) Avail: CASI HC A13/MF A03

This quarterly publication provides archival reports on developments in programs managed by JPL's Telecommunications and Mission Operations Directorate (TMOD), which now includes the former Telecommunications and Data Acquisition (TDA) Office. In space communications, radio navigation, radio science, and ground-based radio and radar astronomy, it reports on activities of the Deep Space Network (DSN) in planning, supporting research and technology, implementation, and operations. Also included are standards activity at JPL for space data and information systems and reimbursable DSN work performed for other space agencies through NASA. The preceding work is all performed for NASA's Office of Space Communications (OSC). For individual titles, see N95-32222 through N95-32240.

N95-32222*# Jet Propulsion Lab., California Inst. of Tech., Pasadena, CA.
DETERMINATION OF THE POSITION OF JUPITER FROM RADIO METRIC TRACKING OF VOYAGER 1 **c91**
W. M. Folkner and R. J. Haw *In its* The Telecommunications and Data Acquisition Report 15 May 1995 p 1-8 (For primary document see N95-32221 11-32)
Avail: CASI HC A02/MF A03

The Voyager 1 spacecraft flew by Jupiter on March 5, 1979. Spacecraft navigation was performed with radio tracking data from NASA's Deep Space Network. In the years since then, there has been a great deal of progress in the definition of celestial reference frames and in determining the orbit and orientation of the Earth. Using these improvements, the radio metric range and Doppler data acquired from the Voyager 1 spacecraft near its encounter with Jupiter have been reanalyzed to determine the plane-of-sky position of Jupiter with much greater accuracy than was possible at the time of the encounter. The position of Jupiter at the time of encounter has been determined with an accuracy of 40 nrad in right ascension and 140 nrad in declination with respect to the celestial reference frame defined by the International Earth Rotation Service. This position estimate has been done to improve the ephemeris of Jupiter prior to the upcoming encounter of the Galileo spacecraft with Jupiter. Author

N95-32223*# Jet Propulsion Lab., California Inst. of Tech., Pasadena, CA.
RATE CONSIDERATIONS IN DEEP SPACE TELEMETRY **c17**
M. Costa, M. Belongie, and F. Pollara *In its* The Telecommunications and Data Acquisition Report 15 May 1995 p 9-15 (For primary document see N95-32221 11-32)
Avail: CASI HC A02/MF A03

The relationship between transmission rate and source and channel signal-to-noise ratios (SNR's) is discussed for the transmission of a Gaussian source over a binary input, additive Gaussian channel, with a mean-squared distortion criterion. We point out that for any finite rate, and sufficiently high channel SNR, the fidelity criterion (reproduction SNR) is upper bounded by a function of the transmission rate. Thus, the performance becomes

rate limited rather than power limited. This effect is not observed with the binary symmetric source, the binary-input Gaussian channel combination, or the Gaussian source, unconstrained-input Gaussian channel combination. Author

N95-32224*# Jet Propulsion Lab., California Inst. of Tech., Pasadena, CA.

AN EFFICIENT IMPLEMENTATION OF FORWARD-BACKWARD LEAST-MEAN-SQUARE ADAPTIVE LINE ENHANCERS **c33**

H.-G. Yeh and T. M. Nguyen *In its* The Telecommunications and Data Acquisition Report 15 May 1995 p 16-26 (For primary document see N95-32221 11-32)

Avail: CASI HC A03/MF A03

An efficient implementation of the forward-backward least-mean-square (FBLMS) adaptive line enhancer is presented in this article. Without changing the characteristics of the FBLMS adaptive line enhancer, the proposed implementation technique reduces multiplications by 25% and additions by 12.5% in two successive time samples in comparison with those operations of direct implementation in both prediction and weight control. The proposed FBLMS architecture and algorithm can be applied to digital receivers for enhancing signal-to-noise ratio to allow fast carrier acquisition and tracking in both stationary and nonstationary environments. Author

N95-32225*# Jet Propulsion Lab., California Inst. of Tech., Pasadena, CA.

COMPUTER SIMULATION RESULTS FOR PCM/PM/NRZ RECEIVERS IN NONIDEAL CHANNELS **c17**

A. Anabtawi, T. M. Nguyen, and S. Million *In its* The Telecommunications and Data Acquisition Report 15 May 1995 p 27-53 (For primary document see N95-32221 11-32)

Avail: CASI HC A03/MF A03

This article studies, by computer simulations, the performance of deep-space telemetry signals that employ the pulse code modulation/phase modulation (PCM/PM) technique, using nonreturn-to-zero data, under the separate and combined effects of unbalanced data, data asymmetry, and a band-limited channel. The study is based on measuring the symbol error rate performance and comparing the results to the theoretical results presented in previous articles. Only the effects of imperfect carrier tracking due to an imperfect data stream are considered. The presence of an imperfect data stream (unbalanced and/or asymmetric) produces undesirable spectral components at the carrier frequency, creating an imperfect carrier reference that will degrade the performance of the telemetry system. Further disturbance to the carrier reference is caused by the intersymbol interference created by the band-limited channel. Author

N95-32226*# Jet Propulsion Lab., California Inst. of Tech., Pasadena, CA.

THE APPLICATION OF NONCOHERENT DOPPLER DATA TYPES FOR DEEP SPACE NAVIGATION **c17**

S. Bhaskaran *In its* The Telecommunications and Data Acquisition Report 15 May 1995 p 54-65 (For primary document see N95-32221 11-32)

Avail: CASI HC A03/MF A03

Recent improvements in computational capability and DSN technology have renewed interest in examining the possibility of using one-way Doppler data alone to navigate interplanetary spacecraft. The one-way data can be formulated as the standard differenced-count Doppler or as phase measurements, and the data can be received at a single station or differenced if obtained simultaneously at two stations. A covariance analysis, which analyzes the accuracy obtainable by combinations of one-way Doppler data, is performed and compared with similar results using standard two-way Doppler and range. The sample interplanetary trajectory used was that of the Mars Pathfinder mission to Mars. It is shown that differenced one-way data are capable of determining the angular position of the spacecraft to fairly high accuracy, but have relatively poor sensitivity to the range. When combined with single-station data, the position dispersions are roughly an order of magnitude larger in range and comparable in angular position as compared to dispersions obtained with standard two-way data types. It was also found that the phase formulation is less sensitive to data weight variations and data coverage than the differenced-count Doppler formulation. Author

N95-32227*# Jet Propulsion Lab., California Inst. of Tech., Pasadena, CA.

MULTIPLE TURBO CODES FOR DEEP-SPACE COMMUNICATIONS

D. Divsalar and F. Pollara *In its* The Telecommunications and Data Acquisition Report 15 May 1995 p 66-77 (For primary document see N95-32221 11-32)

Avail: CASI HC A03/MF A03

In this article, we introduce multiple turbo codes and a suitable decoder structure derived from an approximation to the maximum a posteriori probability (MAP) decision rule, which is substantially different from the decoder for two-code-based encoders. We analyze the effect of interleaver choice on the weight distribution of the code, and we describe simulation results on the improved performance of these new codes. Author

N95-32228*# Jet Propulsion Lab., California Inst. of Tech., Pasadena, CA.

DEGRADATION IN FINITE-HARMONIC SUBCARRIER DEMODULATION

Y. Feria, S. Townes, and T. Pham *In its* The Telecommunications and Data Acquisition Report 15 May 1995 p 78-86 (For primary document see N95-32221 11-32)

Avail: CASI HC A02/MF A03

Previous estimates on the degradations due to a subcarrier loop assume a square-wave subcarrier. This article provides a closed-form expression for the degradations due to the subcarrier loop when a finite number of harmonics are used to demodulate the subcarrier, as in the case of the buffered telemetry demodulator. We compared the degradations using a square wave and using finite harmonics in the subcarrier demodulation and found that, for a low loop signal-to-noise ratio, using finite harmonics leads to a lower degradation. The analysis is under the assumption that the phase noise in the subcarrier (SC) loop has a Tikhonov distribution. This assumption is valid for first-order loops. Author

N95-32229*# Jet Propulsion Lab., California Inst. of Tech., Pasadena, CA.

TOWARDS OPTIMUM DEMODULATION OF BANDWIDTH-LIMITED AND LOW SNR SQUARE-WAVE SUBCARRIER SIGNALS

Y. Feria and W. Hurd *In its* The Telecommunications and Data Acquisition Report 15 May 1995 p 87-95 (For primary document see N95-32221 11-32)

Avail: CASI HC A02/MF A03

The optimum phase detector is presented for tracking square-wave subcarriers that have been bandwidth limited to a finite number of harmonics. The phase detector is optimum in the sense that the loop signal-to-noise ratio (SNR) is maximized and, hence, the rms phase tracking error is minimized. The optimum phase detector is easy to implement and achieves substantial improvement. Also presented are the optimum weights to combine the signals demodulated from each of the harmonics. The optimum weighting provides SNR improvement of 0.1 to 0.15 dB when the subcarrier loop SNR is low (15 dB) and the number of harmonics is high (8 to 16).

Author

N95-32230*# Jet Propulsion Lab., California Inst. of Tech., Pasadena, CA.

ENHANCED DECODING FOR THE GALILEO LOW-GAIN ANTENNA MISSION: VITERBI REDECODING WITH FOUR DECODING STAGES

S. Dolinar and M. Belongie *In its* The Telecommunications and Data Acquisition Report 15 May 1995 p 96-109 (For primary document see N95-32221 11-32)

Avail: CASI HC A03/MF A03

The Galileo low-gain antenna mission will be supported by a coding system that uses a (14,1/4) inner convolutional code concatenated with Reed-Solomon codes of four different redundancies. Decoding for this code is designed to proceed in four distinct stages of Viterbi decoding followed by Reed-Solomon decoding. In each successive stage, the Reed-Solomon decoder only tries to decode the highest redundancy codewords not yet decoded in previous stages, and the Viterbi decoder redecodes its data utilizing the known symbols from previously decoded Reed-Solomon codewords. A previous article analyzed a two-stage decoding option that was not selected by Galileo. The present article analyzes the four-stage decoding scheme and derives the near-optimum set of redundancies selected for use by Galileo. The performance improvements relative to one- and two-stage decoding systems are evaluated. Author

N95-32231*# Jet Propulsion Lab., California Inst. of Tech., Pasadena, CA.

TESTING THE PERFORMANCE OF FEEDBACK CONCATENATED DECODER WITH A NONIDEAL RECEIVER

Y. Feria and S. Dolinar *In its* The Telecommunications and Data Acquisition Report 15 May 1995 p 110-130 (For primary document see N95-32221 11-32)

Avail: CASI HC A03/MF A03

One of the inherent problems in testing the feedback concatenated decoder (FCD) at our operating symbol signal-to-noise ratio (SSNR) is that the bit-error rate is so low that we cannot measure it directly through simulations in a reasonable time period. This article proposes a test procedure that will give a reasonable estimate of the expected losses even though the number of frames tested is much smaller than needed for a direct measurement. This test procedure provides an organized robust methodology for extrapolating small amounts of test data to give reasonable estimates of FCD loss increments at unmeasurable miniscule error rates. Using this test procedure, we have run some preliminary tests on the FCD to quantify the losses due to the fact that the input signal contains multiplicative non-white non-Gaussian noises resulting from the buffered telemetry demodulator (BTD). Besides the losses in the BTD, we have observed additional loss increments of 0.3 to 0.4 dB at the output of the FCD for several test cases with loop signal-to-noise ratios (SNR's) lower than 20 dB. In contrast, these loss increments were less than 0.1 dB for a test case with the subcarrier loop SNR at about 28 dB. This test procedure can be applied to more extensive test data to determine thresholds on the loop SNRs above which the FCD will not suffer substantial loss increments. Author

N95-32232*# Jet Propulsion Lab., California Inst. of Tech., Pasadena, CA.

PERFORMANCE OF RESIDUAL CARRIER ARRAY-FEED COMBINING IN CORRELATED NOISE

H. H. Tan *In its* The Telecommunications and Data Acquisition Report 15 May 1995 p 131-147 (For primary document see N95-32221 11-32)

Avail: CASI HC A03/MF A03

An array feed combining system for the recovery of signal-to-noise ratio (SNR) loss due to antenna reflector deformation has been implemented and is currently being evaluated on the Jet Propulsion Laboratory's 34-meter DSS-13 antenna. In this system, the defocused signal field captured by a focal plane array feed is recovered using real-time signal-processing and signal-combining techniques. The current signal-processing and signal-combining algorithms are optimum under the assumption that the white Gaussian noise processes in the received signals from different array elements are mutually uncorrelated. Experimental data at DSS 13 indicate that these noise processes are indeed mutually correlated. The main result of this article is an analytical derivation of the actual SNR performance of the current suboptimal signal-combining algorithm in this correlated-noise environment. The analysis here shows that the combined signal SNR can either be improved or degraded depending on the relation between the array signal and noise correlation coefficient phases. Further performance improvement will require the development of signal-combining methods that take into account the correlated noises. Author

N95-32233*# Jet Propulsion Lab., California Inst. of Tech., Pasadena, CA.

MINIMAL TRELLISES FOR LINEAR BLOCK CODES AND THEIR DUALS

A. B. Kiely, S. Dolinar, L. Ekroot, R. J. McEliece (California Inst. of Tech., Pasadena, CA.), and W. Lin (California Inst. of Tech., Pasadena, CA.) *In its* The Telecommunications and Data Acquisition Report 15 May 1995 p 148-158 (For primary document see N95-32221 11-32)

Avail: CASI HC A03/MF A03

We consider the problem of finding a trellis for a linear block code that minimizes one or more measures of trellis complexity for a fixed permutation of the code. We examine constraints on trellises, including relationships between the minimal trellis of a code and that of the dual code. We identify the primitive structures that can appear in a minimal trellis and relate this to those for the minimal trellis of the dual code. Author

N95-32234*# Jet Propulsion Lab., California Inst. of Tech., Pasadena, CA.

TRELLIS COMPLEXITY BOUNDS FOR DECODING LINEAR BLOCK CODES

A. B. Kiely, S. Dolinar, L. Ekroot, R. J. McEliece (California Inst. of Tech., Pasadena, CA.), and W. Lin (California Inst. of Tech., Pasadena, CA.) *In its* The Telecommunications and Data Acquisition Report 15 May 1995 p 159-172 (For primary document see N95-32221 11-32)

Avail: CASI HC A03/MF A03

We consider the problem of finding a trellis for a linear block code that minimizes one or more measures of trellis complexity. The domain of optimization may be different permutations of the same code or different codes with the same parameters. Constraints on trellises, including relationships between the minimal trellis of a code and that of the dual code, are used to derive bounds on complexity. We define a partial ordering on trellises: If a trellis is optimum with respect to this partial ordering, if has the desirable property that it simultaneously minimizes all of the complexity measures examined. We examine properties of such optimal trellises and give examples of optimal permutations of codes, most notably the (48,24,12) quadratic residue code. Author

N95-32235*# Jet Propulsion Lab., California Inst. of Tech., Pasadena, CA.

RESIDUAL AND SUPPRESSED-CARRIER ARRAYING TECHNIQUES FOR DEEP-SPACE COMMUNICATIONS

M. Shihabi, B. Shah, S. Hinedi, and S. Million *In its* The Telecommunications and Data Acquisition Report 15 May 1995 p 173-201 (For primary document see N95-32221 11-32)

Avail: CASI HC A03/MF A03

Three techniques that use carrier information from multiple antennas to enhance carrier acquisition and tracking are presented. These techniques in combination with baseband combining are analyzed and simulated for residual and suppressed-carrier modulation. It is shown that the carrier arraying using a single carrier loop technique can acquire and track the carrier even when any single antenna in the array cannot do so by itself. The carrier aiding and carrier arraying using multiple carrier loop techniques, on the other hand, are shown to lock on the carrier only when one of the array elements has sufficient margin to acquire the carrier on its own. Author

N95-32236*# Jet Propulsion Lab., California Inst. of Tech., Pasadena, CA.

A HIGH-SPEED PHOTONIC CLOCK AND CARRIER REGENERATOR **c35**

X. S. Yao and G. Lutes *In its* The Telecommunications and Data Acquisition Report 15 May 1995 p 202-210 (For primary document see N95-32221 11-32)

Avail: CASI HC A02/MF A03

As data communications rates climb toward 10 Gbits/s, clock recovery and synchronization become more difficult, if not impossible, using conventional electronic circuits. The high-speed photonic clock regenerator described in this article may be more suitable for such use. This photonic regenerator is based on a previously reported photonic oscillator capable of fast acquisition and synchronization. With both electrical and optical clock inputs and outputs, the device is easily interfaced with fiber-optic systems. The recovered electrical clock can be used locally and the optical clock can be used anywhere within a several kilometer radius of the clock/carrier regenerator. Author

N95-32237*# Jet Propulsion Lab., California Inst. of Tech., Pasadena, CA.

EFFECTS OF CORRELATED NOISE ON THE FULL-SPECTRUM COMBINING AND COMPLEX-SYMBOL COMBINING ARRAYING TECHNIQUES

P. Vazirani *In its* The Telecommunications and Data Acquisition Report 15 May 1995 p 211-241 (For primary document see N95-32221 11-32)

Avail: CASI HC A03/MF A03

The process of combining telemetry signals received at multiple antennas, commonly referred to as arraying, can be used to improve communication link performance in the Deep Space Network (DSN). By coherently adding telemetry from multiple receiving sites, arraying produces

an enhancement in signal-to-noise ratio (SNR) over that achievable with any single antenna in the array. A number of different techniques for arraying have been proposed and their performances analyzed in past literature. These analyses have compared different arraying schemes under the assumption that the signals contain additive white Gaussian noise (AWGN) and that the noise observed at distinct antennas is independent. In situations where an unwanted background body is visible to multiple antennas in the array, however, the assumption of independent noises is no longer applicable. A planet with significant radiation emissions in the frequency band of interest can be one such source of correlated noise. For example, during much of Galileo's tour of Jupiter, the planet will contribute significantly to the total system noise at various ground stations. This article analyzes the effects of correlated noise on two arraying schemes currently being considered for DSN applications: full-spectrum combining (FSC) and complex-symbol combining (CSC). A framework is presented for characterizing the correlated noise based on physical parameters, and the impact of the noise correlation on the array performance is assessed for each scheme. Author

N95-32238*# Jet Propulsion Lab., California Inst. of Tech., Pasadena, CA.

A SEISMIC DATA COMPRESSION SYSTEM USING SUBBAND CODING

A. B. Kiely and F. Pollara *In its* The Telecommunications and Data Acquisition Report 15 May 1995 p 242-251 (For primary document see N95-32221 11-32)

Avail: CASI HC A02/MF A03

This article presents a study of seismic data compression techniques and a compression algorithm based on subband coding. The algorithm includes three stages: a decorrelation stage, a quantization stage that introduces a controlled amount of distortion to allow for high compression ratios, and a lossless entropy coding stage based on a simple but efficient arithmetic coding method. Subband coding methods are particularly suited to the decorrelation of nonstationary processes such as seismic events. Adaptivity to the nonstationary behavior of the waveform is achieved by dividing the data into separate blocks that are encoded separately with an adaptive arithmetic encoder. This is done with high efficiency due to the low overhead introduced by the arithmetic encoder in specifying its parameters. The technique could be used as a progressive transmission system, where successive refinements of the data can be requested by the user. This allows seismologists to first examine a coarse version of waveforms with minimal usage of the channel and then decide where refinements are required. Rate-distortion performance results are presented and comparisons are made with two block transform methods. Author

N95-32239*# Jet Propulsion Lab., California Inst. of Tech., Pasadena, CA.

DSS-24 MICROWAVE HOLOGRAPHY MEASUREMENTS **c35**

D. J. Rochblatt, P. M. Withington, and H. J. Jackson *In its* The Telecommunications and Data Acquisition Report 15 May 1995 p 252-270 (For primary document see N95-32221 11-32)

Avail: CASI HC A03/MF A03

The JPL DSN Microwave Antenna Holography System (MAHST) was applied to the newly constructed DSS-24 34-m beam-waveguide antenna at Goldstone, California. The application of MAHST measurements and corrections at DSS 24 provided the critical RF performance necessary to not only meet the project requirements and goals, but to surpass them. A performance increase of 0.35 dB at X-band (8.45 GHz) and 4.9 dB at Ka-band (32 GHz) was provided by MAHST, resulting in peak efficiencies of 75.25 percent at X-band and 60.6 percent at Ka-band (measured from the Cassegrain focus at f1). The MAHST enabled setting the main reflector panels of DSS 24 to 0.25-mm rms, making DSS 24 the highest precision antenna in the NASA/JPL DSN. The precision of the DSS-24 antenna (diameter/rms) is 1.36 x 10(exp 5), and its gain limit is at 95 GHz. Author

N95-32240*# Jet Propulsion Lab., California Inst. of Tech., Pasadena, CA.

DIGITAL SIGNAL PROCESSING IN THE RADIO SCIENCE STABILITY ANALYZER

C. A. Greenhall *In its* The Telecommunications and Data Acquisition Report 15 May 1995 p 271-288 (For primary document see N95-32221 11-32)

Avail: CASI HC A03/MF A03

The Telecommunications Division has built a stability analyzer for testing Deep Space Network installations during flight radio science experiments. The low-frequency part of the analyzer operates by digitizing wave signals with bandwidths between 80 Hz and 45 kHz. Processed outputs include spectra of signal, phase, amplitude, and differential phase; time series of the same quantities; and Allan deviation of phase and differential phase. This article documents the digital signal-processing methods programmed into the analyzer. Author

N95-32247 National Defence Research Establishment, Linkoeping (Sweden).

FAST IDENTIFICATION OF SOME TYPICAL DIGITAL MODULATION SCHEMES [SNABB IDENTIFIERING AV NAGRA TYPISKA DIGITALA MODULATIONSFORMER]

M. Johansson Dec. 1994 57 p In SWAHILI

(PB95-211454; FOA-R-94-00051-3.6-SE) Avail: Issuing Activity (National Technical Information Service (NTIS))

Two algorithms have been developed to make a fast determination as to whether a signal is a burst transmission or not. The result shows that it is possible to make an identification within 0.2 to 0.3 seconds. A better performance will be obtained when the algorithms are implemented in the dedicated system. NTIS

N95-32259# Phase Four Systems, Inc., Huntsville, AL.

THE DYNAMIC RANGE OF RADAR SIGNAL GENERATION IN THE MSS-2 SIMULATION FACILITY Final Report

Chris Bishop Mar. 1995 79 p

(AD-A293856; AMSMI/RD-TR-CR-SS-95-10) Avail: CASI HC A05/MF A01

The dynamic range of radar signal generation in the MSS-2 affects the types of targets and environments which the MSS-2 facility can simulate. Only the power handling capability of the facility limits the maximum size of large targets; however, assessing the ability of the MSS-2 to produce very small targets is quite difficult and depends on the characteristics of the device under test. This report addresses the issues which limit minimum target size and calculations the dynamic range of the radar signal generation equipment in the MSS-2 given a typical seeker. DTIC

N95-32313 National Defence Research Establishment, Stockholm (Sweden).

MATERIALS WITH CONTROLLABLE SIGNATURE PROPERTIES [MATERIAL MED STYRBARA SIGNATUREGENSKAPER]

O. Dickman, B. Holmberg, T. Karlsson, and S. Savage Feb. 1995 28 p In SWAHILI

(PB95-222964; FOA-R-95-00093-2.4-SE) Avail: Issuing Activity (National Technical Information Service (NTIS))

We have in this report considered some types of material with potential for use in signature control of structures. The material types selected for inclusion in this study were electrically conductive polymers, fullerenes, nanostructured materials and Langmuir-Blodgett films. To control the signature of a structure in real time it must be possible to vary the material emissivity, structural transmission, and reflection or absorption of electromagnetic radiation in the relevant wavelength region. This may be achieved by changes in temperature, pressure, electrical or magnetic field or by the concentration of a chemical substance within the material. It is concluded that it is feasible to develop electrically conductive polymeric materials with controllable properties for practical signature control application within 5 to 10 years. NTIS

N95-32314 National Defence Research Establishment, Linkoeping (Sweden).

POINT REFLECTOR MODEL FOR THE SIMULATION OF RADAR TARGET GLINT AND DOPPLER PHENOMENA [PUNKTREFLEKTORMODELL FOER SIMULERING AV RADARMALS GLINT- OCH DOPPLEREGENSKAPER]

H. Grubeck Feb. 1995 44 p In SWAHILI

(PB95-222980; FOA-R-94-00025-3.3-SE) Avail: Issuing Activity (National Technical Information Service (NTIS))

This report describes the mathematics of a radar model for the simulation of glint and Doppler phenomena. Glint is an unwanted phenomenon, which

deteriorates radar tracking performance. The term denotes a fluctuation of the target direction, experienced by a radar, tracking a complex target. Doppler shift refers to the frequency change of a radar wave, due to the reflection against a moving target. It can be used by modern so-called coherent radar systems for velocity determination. A three-dimensional space is modeled, containing a rigid body of point scattering reflectors (the target) and a point of measuring (the radar). The target and the radar can move freely and independently in the space. The movement of the target and the radar is described with a number of coordinate systems, which are presented in this report. Some simple simulations are also presented in this report. A simulation tool is available for interested users and the purpose of this report is to announce its existence. The program is written in MATLAB Simulink. NTIS

N95-32128# Ballistic Missile Defense Organization, Washington, DC. Advanced Capabilities Div.
TMD DETECTION AND TRACKING USING IMPROVED AWACS SENSORS
Steve Petersen, Yasuhiro Kinashi (Nichols Research Corp., Vienna, VA.), and Daniel Leslie (Schafer, W. J. Associates, Inc., Arlington, VA.) *In* AGARD, Guidance and Control for Future Air-Defence Systems Jan. 1995 10 p (For primary document see N95-32123 11-31)
Copyright Avail: CASI HC A02/MF A03

N95-32135# Raytheon Canada Ltd., Waterloo (Ontario).
MULTISENSOR DATA FUSION FOR INTEGRATED MARITIME SURVEILLANCE
A. Premji and A. M. Ponsford *In* AGARD, Guidance and Control for Future Air-Defence Systems Jan. 1995 12 p (For primary document see N95-32123 11-31)
Copyright Avail: CASI HC A03/MF A03

N95-32136# Waterloo Univ. (Ontario). Dept. of System Design.
MULTIPLE TARGET TRACKING BASED ON CONSTELLATION MATCHING AND KALMAN FILTER
Andrew K. C. Wong and Henry Leung (Defence Research Establishment Ottawa, Ottawa, Ontario.) *In* AGARD, Guidance and Control for Future Air-Defence Systems Jan. 1995 22 p (For primary document see N95-32123 11-31)
Copyright Avail: CASI HC A03/MF A03

N95-32140# Department of the Air Force, Eglin AFB, FL.
ELECTRONIC COMBAT AND LETHAL DEFENSE SUPPRESSION
Leo. J. Rose *In* AGARD, Guidance and Control for Future Air-Defence Systems Jan. 1995 3 p (For primary document see N95-32123 11-31)
Copyright Avail: CASI HC A01/MF A03

N95-32141# Ballistic Missile Defense Organization, Washington, DC.
USING A RED TEAM TO DEVISE COUNTERMEASURES
R. L. Swedenburg *In* AGARD, Guidance and Control for Future Air-Defence Systems Jan. 1995 12 p (For primary document see N95-32123 11-31)
Copyright Avail: CASI HC A03/MF A03

N95-32320*# Naval Observatory, Washington, DC. Time Service Dept.
THE 1994 INTERNATIONAL TRANSATLANTIC TWO-WAY SATELLITE TIME AND FREQUENCY TRANSFER EXPERIMENT: PRELIMINARY RESULTS
James A. DeYoung, William J. Klepczynski, Angela Davis McKinley, William M. Powell, Phu V. Mai, P. Hetzel (Physikalisch-Technische Bundesanstalt, Brunswick, Germany.), A. Bauch (Physikalisch-Technische Bundesanstalt, Brunswick, Germany.), J. A. Davis (National Physical Lab., Teddington, England.), P. R. Pearce (National Physical Lab., Teddington, England.), and Francoise S. Baumont (Observatoire de la Cote d'Azur, Grasse, France.) et al *In* NASA. Goddard Space Flight Center, The 26th Annual Precise Time and Time Interval (PTTI) Applications and Planning Meeting May 1995 p 39-49 (For primary document see N95-32319 11-70)
Avail: CASI HC A03/MF A04

N95-32334*# Jet Propulsion Lab., California Inst. of Tech., Pasadena, CA.
THE DEEP SPACE NETWORK STABILITY ANALYZER
Julian C. Breidenthal, Charles A. Greenhall, Robert L. Hamell, and Paul F. Kuhnle *In* NASA. Goddard Space Flight Center, The 26th Annual Precise Time and Time Interval (PTTI) Applications and Planning Meeting May 1995 p 221-233 (For primary document see N95-32319 11-70)
Avail: CASI HC A03/MF A04

33 ELECTRONICS AND ELECTRICAL ENGINEERING

Includes test equipment and maintainability; components, e.g., tunnel diodes and transistors; microminiaturization; and integrated circuitry.

For related information see also *60 Computer Operations and Hardware* and *76 Solid-State Physics.*

N95-30374# Argonne National Lab., IL.
HIGH-TEMPERATURE SUPERCONDUCTING CURRENT LEADS
R. C. Niemann 1995 2 p Presented at the Power Generation Conference, Orlando, FL, 7-9 Dec. 1994
(Contract W-31-109-eng-38)
(DE95-008404; ANL/ES/PP-85380; CONF-941210-12) Avail: CASI HC A01/MF A01

Use of high-temperature superconductors (HTS's) for current leads to deliver power to devices at liquid helium temperature can reduce refrigeration requirements to values significantly below those achievable with conventional leads. HTS leads are now near commercial realization. Argonne National Laboratory (ANL) has developed a sinter-forge process to fabricate current leads from bismuth-based superconductors. The current-carrying capacity of these leads is five times better than that of HTS leads made by a conventional fabrication process. ANL along with Superconductivity, Inc., has developed a 1500 ampere current lead for an existing superconducting magnetic energy storage (SMES) device. With Babcock & Wilcox Company, Argonne is creating 16-kiloampere leads for use in a 0.5 MWh SMES. In a third project Argonne performed characterization testing of a existing, proprietary conduction-cooled lead being developed by Zer Res Corp. DOE

N95-30480 National Defence Research Establishment, Stockholm (Sweden).
SEMI-ITERATIVE METHOD FOR ESTIMATION OF THE DIPOLE PARAMETERS USING THE KNOWLEDGE OF THE DIPOLE ORIENTATION [SEMIITERATIV METOD FOER SKATTNING AV DIPOLPARAMETRAR UTIFRAN KAENNEDOMEN OM DIPOLENS ORIENTERING]
P. Huotila Dec. 1994 54 p In SWAHILI
(PB95-211736; FOA-R-94-00056-2.2-SE) Avail: Issuing Activity (National Technical Information Service (NTIS))

This report suggests how to geometrically determine the position vector to and the strength of an arbitrary dipole source by using the knowledge of its orientation in space and if the dipole field is measured by a three-axial sensor. An iterative model for estimation of the direction vector of the dipole moment is also described. NTIS

N95-30538# Helsinki Univ. of Technology, Espoo (Finland). High Voltage Lab.
WORLDWIDE INTERCOMPARISON OF IMPULSE VOLTAGE MEASURING SYSTEMS AT 600 kV LEVEL
M. Aro, J. Haellstroem, and M. L. Pykaelae 30 Nov. 1994 105 p
(PB95-195574; TKK-SJT-16) Avail: CASI HC A06/MF A02

Nine laboratories participated the intercomparison. Laboratories compared their impulse voltage measuring systems (one or several) to the circulating measuring system at voltage levels of 300 and 600 kV and with different impulse shapes, i.e. with full smooth, front-chopped (0.5 micro sec), sliced (MOA load) and oscillating impulse at both positive and negative polarities. The circulating measuring system was a complete system consisting of 10 kiloohm 700 kV resistive voltage divider, h.v. lead, damping resistor, measuring cable, terminator and peak voltmeter. For the first time

in intercomparisons with impulse voltages, together with similar parallel intercomparison in Europe, the circulating system was a complete system including also the l.v. cable and instrument. Both peak values and time parameters were compared. However, the former has larger significance, because the circulating system was complete for that measurement only. At the time it was not feasible to circulate any digital recorder. The measurements were performed during two years between October 1991 and January 1993. The results are generally good both in peak value and time parameter comparisons with all of the used impulse shapes. NTIS

N95-30561# University Coll. of North Wales, Bangor (United Kingdom). School of Electronic Engineering and Computer Systems.
LARGE AREA SMART PIEZOELECTRIC AND PYROELECTRIC SENSORS
D. K. Das-Gupta and M. P. Wenger Jan. 1995 7 p
(Contract DAJA45-93-C-0017)
(AD-A291487; R/D-6980-EE-01) Avail: CASI HC A02/MF A01

The present report provides an account of the embedding of a composite material transducer within an E-glass reinforced epoxy laminate structure for use as an in-situ AE sensor, strain gauge, or ultrasonic detector 1 transmitter for NDT (nondestructive testing) techniques. It is envisaged that by embedding a transducer within a structure it may be used as an 'early warning' device, which would warn against potential failure of the structure. Another way of thinking is that the transducer while being used in a sensing mode can then be used in an actuating mode by use of a feedback circuit thus for example being used to damp out any unwanted vibrations of the structure. DTIC

N95-30596# Swedish Inst. for Materials Testing, Boras (Sweden).
EMC REQUIREMENTS FOR TYPE APPROVAL OF MARINE ELECTRONICS. NORDTEST PROJECT 1157-94
L. Bergsten and P. Guldbrandsen 1994 40 p
(PB95-211330; SP-RAPP-1994:50) Avail: CASI HC A03/MF A01

Marine electronic equipment is tested according to the requirements of several ship classification societies. Testing is also carried out as specified in military standards. The ship classification requirements are similar to each other but not identical, while the military requirements often significantly differ from the commercial ones and will not be treated in this report. The European Union (EU) directive on electromagnetic compatibility (EMC) is applicable to marine electronics but no EN standard is available and there are no plans to come up with one. A manufacturer who wants to have his equipment approved according to the requirements as mentioned above will have difficulties in writing a test program that covers all relevant requirements. An overview is therefore needed of a common test specification that is accepted by all classification societies. NTIS

N95-30633 Swedish Inst. for Materials Testing, Boras (Sweden).
DEVELOPMENT OF A METHOD FOR MEASUREMENT OF TRIBOELECTRIC CHARGING
A. Boerjesson and S. Byheden 1994 46 p Limited Reproducibility: More than 20% of this document may be affected by microfiche quality
(PB95-211322; SP-RAPP-1994:34) Avail: CASI HC A03

A method for measurement of triboelectric charging has been defined. The principle of the method is measurement by an electrostatic voltmeter of the voltage developed on a test piece after a roll has rolled over it. The roll materials used are quartz and teflon respectively. Other materials can be used but are not verified in this work. The method is evaluated to give a repeatability when measuring electrostatic conductive foils to better than +/- 10%. This figure includes spread in the test item itself. Before being proposed as a standard, the method has to be further evaluated. Comparative measurements (Round Robin tests) should be performed by other laboratories to evaluate the reproducibility of the method. NTIS

N95-30649# International Centre for Theoretical Physics, Trieste (Italy).
A SIMPLE MODEL FOR THE DC FLUX TRANSFORMER IN LAYERED SUPERCONDUCTORS WITH JOSEPHSON COUPLING
K. K. Uprety and D. Dominguez (Los Alamos National Lab., NM.) Sep. 1994 30 p
(DE95-614468; IC-94/291) Avail: CASI HC A03/MF A01 (US Sales Only)

We present a model for the dc flux transformer configuration in layered superconductors with Josephson coupling. It consists of a simple extension of a model introduced by Clem for the traditional dc flux transformer, but including Josephson coupling and dissipation between planes. We calculate the non-linear current-voltage characteristics for different cases. We find two kinds of behaviour. For weak pinning or strong interplane coupling (both due to magnetic forces and Josephson effect) there is an onset of dissipation with the same voltages in both the top and the bottom faces of the sample, at a given critical current. At a higher current there is a decoupling of the two faces where they have different voltages. This corresponds to a cutting of the vortices that occurs between the first (top) and the second planes. The decoupling current is independent of pinning and vanishes linearly with temperature close to T(c). For strong pinning or weak interplane coupling, each face behaves independently with corresponding different critical currents for the onset of dissipation and different voltages. DOE

N95-30651*# Jet Propulsion Lab., California Inst. of Tech., Pasadena, CA.
A THEORETICAL ANALYSIS OF STEADY-STATE PHOTOCURRENTS IN SIMPLE SILICON DIODES
L. Edmonds Mar. 1995 151 p
(Contract NAS7-1260)
(NASA-CR-198885; JPL-Publ-95-10; NAS 1.26:198885) Avail: CASI HC A08/MF A02

A theoretical analysis solves for the steady-state photocurrents produced by a given photo-generation rate function with negligible recombination in simple silicon diodes, consisting of a uniformly doped quasi-neutral region (called 'substrate' below) adjacent to a p-n junction depletion region (DR). Special attention is given to conditions that produce 'funneling' (a term used by the single-eventeffects community) under steady-state conditions. Funneling occurs when carriers are generated so fast that the DR becomes flooded and partially or completely collapses. Some or nearly all of the applied voltage, plus built-in potential normally across the DR, is now across the substrate. This substrate voltage drop affects substrate currents. The steady-state problem can provide some qualitative insights into the more difficult transient problem. First, it was found that funneling can be induced from a distance, i.e., from carriers generated at locations outside of the DR. Secondly, it was found that the substrate can divide into two subregions, with one controlling substrate resistance and the other characterized by ambipolar diffusion. Finally, funneling was found to be more difficult to induce in the p(sup +)/n diode than in the n(sup +)/p diode. The carrier density exceeding the doping density in the substrate and at the DR boundary is not a sufficient condition to collapse a DR. Author

N95-30659 Department of the Navy, Washington, DC.
PRE-AMPLIFIER WITH MULTI-STAGE FEEDBACK Patent
James D. Hagerty, inventor (to Navy) 6 Dec. 1994 7 p Filed 22 Mar. 1994
(AD-D017371; US-Patent-5,371,479; US-Patent-Appl-SN-215879; US-Patent-Class-330-294) Avail: US Patent and Trademark Office

A circuit for amplifying an input signal comprises an operational amplifier, a dual operational amplifier, and a buffering operational amplifier all cascaded in the afore-mentioned order. The first operational amplifier amplifies the input signal with minimum noise degradation, is set up as a non-inverting amplifier stage, and has a local negative feedback loop comprising a resistor and capacitor in parallel. The dual operational amplifier has two amplifying devices. One device forms a second amplifying stage which increases the gain of the pre-amplified input signal and has a local negative feedback loop comprising a resistor. The other device is a third operational amplifier which combines with the buffering operational amplifier to form an amplifying and buffering stage. The third operational amplifier connects in series to the output of the second amplifying stage. The buffering operational amplifier connects in series to the output of the third operational amplifier and buffers the amplified signal at this output. The amplifying and buffering stage has a two-stage feedback loop comprising a resistor connected between the output of the buffering operational amplifier and the inventing input of the third operational amplifier. A four-stage feedback loop includes a resistor and capacitor in parallel and connects between the output of the buffering operational amplifier and the inverting input of the first operational amplifier. DTIC

N95-30707# Sandia National Labs., Albuquerque, NM.
FRACTAL QUANTUM WELL HETEROSTRUCTURES FOR BROADBAND LIGHT EMITTERS
M. H. Crawford, P. L. Gourley, K. E. Meissner, M. B. Sinclair, E. D. Jones, W. W. Chow, and R. P. Schneider, Jr. 1994 11 p Presented at the SPIE 1995 Conference on Optics, Electro-optics, and Laser Application in Science, Engineering and Medicine, San Jose, CA, 5-10 Feb. 1995
(Contract DE-AC04-94AL-85000)
(DE95-009579; SAND-94-2169C; CONF-950226-31) Avail: CASI HC A03/MF A01

We examine carrier relaxation and radiative recombination in AlGaAs based near IR and AlGaInP based visible fractal quantum well heterostructures. Through temperature dependent photoluminescence, we demonstrate that enhanced population of higher lying energy levels can be achieved by varying the thickness of the layers in the fractal heterostructure. This distribution of carriers results in room temperature emission over a relatively broad range of wavelengths: approximately 700-855 nm for AlGaAs structures and 575-650 nm for AlGaInP structures. Spectra are compared to theoretical calculations to evaluate the non-equilibrium nature of the carrier distributions. Time resolved photoluminescence measurements demonstrate an approximately linear relationship between the radiative decay time and the layer thickness of the structure. Correspondingly, integrated luminescence measurements at room temperature reveal a factor of four increase in the light output efficiency of the structure as the fractal layer thickness is increased from 50 to 400 angstrom. The applicability of these heterostructures to broadband LED's is discussed. DOE

N95-30726 Department of the Navy, Washington, DC.
VOLTAGE SURGE SUPPRESSION POWER CIRCUITS Patent
George J. Stahl, inventor (to Navy) 7 Feb. 1995 16 p Filed 18 Sep. 1992
(AD-D017454; US-Patent-5,388,021; US-Patent-Appl-SN-946716; US-Patent-Class-361-56) Avail: US Patent and Trademark Office

The utilization of clusters of two or more metal oxide varistors (MOV's) connected in parallel for suppressing surges and transients. Particular embodiments are disclosed for both grounded and ungrounded power systems. Also disclosed are two-stage and multi-stage uni-directional and bi-directional suppressors. Uni-directional means that the suppressor is intended to be placed between a source and a load for the purpose-of preventing voltage surges and transients from being propagated from the source into the load. DTIC

N95-30748 Department of the Navy, Washington, DC.
CASCADING SYNCHRONIZED CHAOTIC SYSTEMS Patent
Louis M. Pecora, inventor (to Navy) and Thomas L. Carroll, inventor (to Navy) 3 Jan. 1995 40 p Filed 30 Sep. 1993
(AD-D017458; US-Patent-5,379,346; US-Patent-Appl-SN-129495; US-Patent-Class-380-48) Avail: US Patent and Trademark Office

A cascaded synchronized nonlinear system includes a nonlinear transmitter having stable first and second subparts. The first subpart produces a first transmitter signal for driving the second subpart and the second subpart produces a second transmitter signal for driving the first subpart. The nonlinear transmitter transmits the second transmitter signal to a nonlinear cascaded receiver. The receiver, being for producing an output signal in synchronization with the second transmitter signal, includes a first stage (a duplicate of the first subpart) responsive to the second transmitter signal for -producing a first receiver signal. DTIC

N95-30886# Raytheon Co., Tewksbury, MA. Missile Systems Div.
NEURAL NETWORK FALSE ALARM FILTER, VOLUME 2 Final Report, Sep. 1992 - Sep. 1994
F. Aylstock, L. Elerin, J. Hintz, C. Learoyd, and R. Press Dec. 1994 91 p
(Contract F30602-92-C-0065)
(AD-A293114; RL-TR-94-216-Vol-2) Avail: CASI HC A05/MF A01

This effort identified, developed, and demonstrated a set of approaches for applying neural network learning techniques to the development of a real-time built-in test (BIT) capability to filter out false-alarms from the BIT output. Following a state-of-the-art assessment, a decision space of 19 neural network models, 9 fault report causes, and 12 common groups of BIT techniques was identified. From this space, four unique, high-potential combinations were selected for further investigation. These techniques were subsequently simulated for application to a MILSATCOM system. Detailed analyses of their strengths and weaknesses were performed along with cost/benefit analyses. This study concluded that the best candidates for neural network insertion are new systems where neural network requirements can be included in the initial system design and that a major challenge is the availability of real data for training of the networks. Volume 1 of this report documents the activities and findings of the effort, including an extensive, annotated bibliography. Volume 2 contains a tutorial overview of the neural networks, BIT techniques, and false alarm causes utilized in the final phases of this study. DTIC

N95-30900# Naval Postgraduate School, Monterey, CA.
DECIMATION OF ENCODING ERRORS IN AN OPTIMUM SNS 2 MICRON LOW-NOISE CMOS ADC M.S. Thesis
Jeffrey L. Schafer Mar. 1995 202 p
(AD-A293208) Avail: CASI HC A10/MF A03

Significant research in high performance analog-to-digital converters (ADC's) has been directed at retaining part of the high-speed flash ADC architecture, while reducing the total number of comparators in the circuit. The symmetrical number system (SNS) can he used to preprocess the analog input signal, reducing the number of comparators and thus reducing the chip area and power consumption of the ADC. This thesis examines the issue of encoding errors that result when the separate channels m sub i are brought together to derive the input analog voltage. The Very Large Scale Integrated (VLSI) design for the comparators, error checking circuits and Programmable Logic Arrays (PLA's) use the Orbit 2 Micron CMOS N-well double-metal, double-poly fabrication process. Steady state transfer functions are shown which detail encoding errors that occur when the folded input samples lie at one of the code transition points. To discard the encoding errors that occur, a decimation band is constructed at each transition Point The effectiveness of the decimation band in eliminating the encoding errors and the linearity error is quantified. An Application Specific Integrated Circuit (ASIC) is designed. DTIC

N95-30922# Federal Aviation Administration, Atlantic City, NJ.
ELECTRICAL SHORT CIRCUIT AND CURRENT OVERLOAD TESTS ON AIRCRAFT WIRING
Patricia Cahill Mar. 1995 13 p
(AD-A293308; DOT/FAA/CT-TN94/55) Avail: CASI HC A03/MF A01

This document describes the electrical short circuit and current overload tests that were conducted on wires used in commercial transport category aircraft. This testing was conducted to evaluate the fire potential that may result from electrical faults. Results of this testing showed that circuit breakers provide reliable overcurrent protection and that circuit breakers may not protect wire from ticking faults but can protect wire from direct shorts. It also showed that circuit breakers may not safeguard against the ignition of flammable materials by ticking faults. Preliminary testing also indicated that direct short circuits are not likely to start a fire and that direct short circuits do not erode insulation and conductors to the same degree that ticking faults do. Current overload testing that resulted in complete thermal degradation of the wire was also conducted to compare it with a fire-exposed wire. No differences were seen; however, the conductor of the wire subjected to the fire was more brittle than the current overloaded wire. Further testing along with metallurgical evaluation would be necessary to substantiate this finding fully. DTIC

N95-30940# Analytic Power Corp., Boston, MA.
MOBILE ELECTRIC POWER Final Report
David P. Bloomfield, Valerie J. Bloomfield, Paul D. Grosjean, and James W. Kelland 28 Feb. 1995 46 p
(Contract DAAL03-92-C-0041)
(AD-A292721; ARO-30066.1-CH-SB2) Avail: CASI HC A03/MF A01

The objective of this program was to develop a mobile fuel cell power supply for use by soldiers. The Century Series of 100 through 500 watt fuel cell power supplies was developed. The Century Series fuel cell power supplies are made up of a fuel cell stack, chemical hydride hydrogen supply, a fan and a controller. The FC-200, the 200 watt Century Series power supply, weighs 8.8 lb. and has a volume of 322 cu in. The operating point is 0.7 volt/cell at 125 ASF; a power density of 22.7 watts/cu in. or 0.62 watts/cu in. and an energy density of 110 whr/lb. The prototype 750 whr hydrogen supply weighs 7 lbs. and has a volume of 193 cu in. The

fuel elements weigh 0.45 lb. and require 0.79 lbs. of water. The FC-200 has powered a scooter requiring a starting current of three times the rated current of the stack. It has also powered a microclimate cooler. DTIC

N95-30942# Argonne National Lab., IL.
OPTIMIZATION OF HIGH-TEMPERATURE SUPERCONDUCTOR CURRENT LEADS
S. Y. Seol (Chonnam National Univ., Kwangju, Republic of Korea.), J. R. Hull, and M. C. Chyu (Texas Technological Univ., Lubbock, TX.) 1995 5 p Presented at the Applied Superconductivity Conference, Boston, MA, 16-21 Oct. 1994
(Contract W-31-109-eng-38)
(DE95-005838; ANL/ET/CP-82190; CONF-941013-31) Avail: CASI HC A01/MF A01

Methods to improve the performance of high-temperature superconducting current leads are analyzed. Designs are considered that are inherently safe from burnup, even if the lead enters the normal state. The effect of a tapered lead that takes advantage of the increase in critical current density with decreasing temperature will decrease helium boiloff by about a factor of two for an area ratio of four. A new concept, in which Ag powder is distributed in increasing concentration from the cold end to the hot end of the lead in sintered YBCO, is shown to have comparable performance to that of leads made with Ag-alloy sheaths. Performance of the best inherently safe designs is about one order of magnitude better than that of optimized nonsuperconducting leads. BSCCO leads with Ag-alloy sheaths show improved performance for Au fractions up to about 3%, after which increases in Au fraction yield negligible performance improvement. DOE

N95-30943# Argonne National Lab., IL.
PERFORMANCE EVALUATION OF HIGH-TEMPERATURE SUPERCONDUCTING CURRENT LEADS FOR MICRO-SMES SYSTEMS
R. C. Niemann, Y. S. Cha, J. R. Hull, W. E. Buckles (Superconductivity, Inc., Madison, WI.), B. R. Weber (Superconductivity, Inc., Madison, WI.), and S. T. Yang (Wisconsin Univ., Madison, WI.) 1995 5 p Presented at the Applied Superconductivity Conference, Boston, MA, 16-21 Oct. 1994
(Contract W-31-109-eng-38)
(DE95-005843; ANL/ET/CP-84477; CONF-941013-32) Avail: CASI HC A01/MF A01

As part of the U.S. Department of Energy's Superconductivity Technology Program, Argonne National Laboratory and Superconductivity, Inc., are developing high-temperature superconductor (HTS) current leads for application to micro-SMES systems. Two 1500-A HTS leads have been designed and constructed. A component performance evaluation program was conducted to confirm performance predictions and/or to qualify the design features for construction. The evaluations included HTS characteristics, demountable electrical connections, and heat intercept effectiveness. The performance of current lead assemblies is being evaluated in a zero-magnetic-field test program that included assembly procedures, tooling, and quality assurance; thermal and electrical performance; and flow and mechanical characteristics. The leads were installed in a liquid helium test cryostat and connected at their cold ends by a current jumper. The leads were heat intercepted with a cryocooler. DOE

N95-30950# Naval Postgraduate School, Monterey, CA.
EXPERIMENTAL INVESTIGATION OF THE EFFECTIVENESS OF FLOW-THROUGH MODULES FOR ELECTRONICS COOLING M.S. Thesis
William G. Plott Dec. 1994 118 p
(AD-A293284) Avail: CASI HC A06/MF A02

The heat transfer characteristics and performance capabilities of a liquid flow-through module for electronics cooling were investigated experimentally using the Standard Electronics Module, format 'E' (SEM-E) size module. Brayco Micronic 889, a dielectric polyalphaolefin, was tested as the coolant. One surface of the flow-through module was populated with six etched foil heaters placed on the module over the fluid flow path. With thermocouples affixed to the surface and placed in the inlet and outlet tubing, data was gathered and analyzed to quantity module effectiveness in dissipating heat over a variety of power input settings and coolant flow rates. DTIC

N95-30979# Maryland Univ., College Park, MD.
HARMONIC GYROTRON AMPLIFIERS AND PHASE-LOCKED OSCILLATORS Final Report, 30 Sep. 1991 - 29 Sep. 1994
Victor L. Granatstein and Robert J. Barker 29 Dec. 1994 49 p
(Grant AF-AFOSR-0390-91)
(AD-A293185; AFOSR-95-0250TR) Avail: CASI HC A03/MF A01

The research area for this project is the mode competition and multi-frequency effects on high power fast wave devices. Specifically: (1) high power gyrotrons for plasma heating; (2) parametric mode interactions in harmonic gyrotrons; (3) multi-frequency effects in fel oscillators; and (4) modeling of harmonic gyroklystrons, phase locked gyro oscillators, and gyro-twystrons. The time dependent multi-mode simulation code, MAGY, is being used for the nonlinear simulation of high power gyrotrons.
Derived from text

N95-31059# California Univ., Berkeley. Lawrence Berkeley Lab, CA.
THE ART AND SCIENCE OF MAGNET DESIGN: SELECTED NOTES OF KLAUS HALBACH, VOLUME 2
Feb. 1995 262 p
(Contract DE-AC03-76SF-00098)
(DE95-008450; LBL-PUB-755) Avail: CASI HC A12/MF A03

This volume contains a compilation of 57 notes written by Dr. Klaus Halbach selected from his collection of over 1650 such documents. It provides an historic snapshot of the evolution of magnet technology and related fields as the notes range from as early as 1965 to the present, and is intended to show the breadth of Dr. Halbach's interest and ability that have long been an inspiration to his many friends and colleagues. As Halbach is an experimental physicist whose scientific interests span many areas, and who does his most innovative work with pencil and paper rather than at the workbench or with a computer, the vast majority of the notes in this volume were handwritten and their content varies greatly--some reflect original work or work for a specific project, while others are mere clarifications of mathematical calculations or design specifications. As the authors converted the notes to electronic form, some were superficially edited and corrected, while others were extensively re-written to reflect current knowledge and notation. The notes are organized under five categories which reflect their primary content: Beam Position Monitors, (bpm), Current Sheet Electron Magnets (csem), Magnet Theory, (thry), Undulators and Wigglers (u-w), and Miscellaneous (misc). Within the category, they are presented chronologically starting from the most recent note and working backwards in time. DOE

N95-31133# Lawrence Livermore National Lab., Livermore, CA.
SELF-CONSISTENT, 2D SIMULATIONS OF FILAMENT PROPAGATION IN PHOTOCONDUCTING SWITCHES
P. W. Rambo, W. S. Lawson, C. D. Capps (Boeing Defense and Space Group, Seattle, WA.), and R. A. Falk (Boeing Defense and Space Group, Seattle, WA.) Sep. 1994 10 p Presented at the SPIE Annual Conference of the Optical Society of America and Exhibit, Boston, MA, 30 Oct. - 4 Nov. 1994
(Contract W-7405-eng-48)
(DE95-010794; UCRL-JC-116955; CONF-941006-5) Avail: CASI HC A02/MF A01

The authors present simulations of time-dependent filament propagation in laser-triggered GaAs photoswitches. Unlike previous modeling, the calculations are self-consistent in 2-D axisymmetric (r-z) geometry. Realistic electron and hole mobilities as well as field dependent impact ionization are included. The authors report filament propagation with speeds U(sub f) approx. 10(exp 8)--10(exp 9) cm/s, much larger than the saturated carrier drift velocity, u(sup sat) approx. 10(exp 7) cm/s. The self-consistently determined filament radius and carrier number density are typically R(sub f) approx. 20--60 micro m and n(sub f) approx. 10(exp 17)--10(exp 18) cm(sup -3) respectively. Results are presented for filament propagation in systems with both uniform and nonuniform profiles of background carrier density and electric field. DOE

N95-31147# Advanced Fuel Research, Inc., East Hartford, CT.
HTS JOSEPHSON TECHNOLOGY ON SILICON WITH APPLICATION TO HIGH SPEED DIGITAL MICROELECTRONICS Monthly Progress Report, 30 Oct. - 28 Nov. 1994
Peter Rosenthal 28 Nov. 1994 3 p

(Contract N00014-94-C-0261)
(AD-A288627) Avail: CASI HC A01/MF A01

We have identified parasitic inductance as a critical parameter governing the margins and performance of HTS RSFQ devices. Thermal expansion mismatch induced stress limits the overall thickness of HTS films on silicon substrates to under 70 nm. Because this thickness is less than the london penetration depth, typically 150 nm - 400 nm, we expect a substantial kinetic inductance to be associated with wiring and transmission lines. The kinetic inductance associated with the Josephson junctions themselves is still poorly understood. Because of the importance of inductance to overall circuit performance, we have fabricated and measured (Task 3) some dc SQUID's and RSFQ flip flops incorporating SQUID's. The estimated sheet parasitic kinetic inductance is given by the formula L sub sq = lambda sub L(2)/d, where lambda sub L is the London penetration depth, d is the film thickness (d much less than lambda sub L) and the current distribution is assumed to be uniform. The total loop inductance in a dc squid can be extracted from the magnitude of the magnetic field induced critical current modulation. We have performed measurements on a SQUID fabricated from a 25 nm thick film grown on an LaAlO3 substrate by the barium fluoride process. The inductance calculated over a wide temperature range are plotted in Figure 1. Similar results for a much smaller SQUID imbedded in an RSFQ flip flop are also shown in the figure. The temperature dependence to the sheet inductance is a signature of substantial kinetic inductance. Since kinetic inductance negatively impacts circuit performance, it is essential that careful quantitative account of all sources of inductance be included in circuit design efforts. DTIC

N95-31179# Department of the Navy, Washington, DC.
MICROWAVE ELECTRO-OPTIC MIXER Patent Application
G. K. Gopalakrishnan, inventor (to Navy) and W. K. Burns, inventor (to Navy) 10 Jun. 1994 71 p
(AD-D017328; US-Patent-Appl-SN-258028) Avail: CASI HC A04/MF A01

An electro-optic mixer includes means for providing first and second microwave signals having first and second frequencies, respectively, a device for providing a source light, a first modulator responsive to the source light and to the first microwave signal for producing a first modulated optical signal, a second modulator cascade coupled to the first modulator and being responsive to the first modulated signal and to the second microwave signal for producing a second modulated optical signal having a frequency component at the sum or difference or both of the first and second frequencies, and means coupled between the first and second modulators for transmitting the first modulated signal to the second modulator. DTIC

N95-31185# Technische Univ., Twente (Netherlands).
EFFECTIVE BANDWIDTH TECHNIQUES IN BUFFERLESS AND BUFFERED ATM MULTIPLEXERS
B. G. Kim and I. G. Niemegeers Oct. 1994 16 p
(PB95-207072; Memo-INF-94-47) Copyright Avail: CASI HC A03/MF A01

In order to aid the connection admission control, it is necessary to estimate the bandwidth required for a connection. The effective bandwidth techniques derives the estimated bandwidth for a source solely on the basis of the traffic characteristics of the source. Since it is not affected by the status of resource availability and the characteristics if other connections sharing resources, it is computationally efficient. The effective bandwidth can be derived in a multiplexer without a buffer by using the large deviations theory. The one in a buffered multiplexer can be derived by considering an asymptotic behavior with a large buffer size. Usually, the dominant eigenvalue plays a major role in the asymptotic behavior. Several bandwidth estimation techniques are summarized and compared with the results from the effective bandwidth techniques. NTIS

N95-31275 Department of the Navy, Washington, DC.
THIN-FILM EDGE FIELD EMITTER DEVICE AND METHOD OF MANUFACTURE THEREFOR Patent
Henry F. Gray, inventor (to Navy) and David S. Hsu, inventor (to Navy) 17 Jan. 1995 16 p Filed 31 Mar. 1993
(AD-D017453; US-Patent-5,382,185; US-Patent-Appl-SN-040944) Avail: US Patent and Trademark Office

Thin-film edge field emitter devices are provided which are capable of low voltage operation. The method of manufacture of the devices takes advantage of chemical beams deposition and other thin-film fabrication techniques. Both gated and ungated devices are provided and all of the devices include a plurality of thin-films deposited on the side-wall of a non-flat substrate. The gated emitter devices include alternating conductive and electrically insulating layers, and upper parts of the latter are removed to expose the upper edges of the conductive layers, with a central one of these conductive layers comprising an emitter for emitting electrons. The emitter devices can be inexpensively produced with a high degree of precision and reproducibility without the need for expensive lithographic machines. The devices can be used in field emitter arrays employed as vacuum transistors, vacuum microelectronic analog and digital devices, and modulated or cold electron sources. DTIC

N95-31342 Department of the Navy, Washington, DC.
METHOD AND APPARATUS FOR A HIGH RESOLUTION, FLAT PANEL CATHODOLUMINESCENT DISPLAY DEVICE Patent
Henry F. Gray, inventor (to Navy) and Ronald R. Price, inventor (to Navy) 3 Jan. 1995 11 p Filed 29 May 1992
(AD-D017434; US-Patent-5,378,962; US-Patent-Appl-SN-889885; US-Patent-Class-313-495) Avail: US Patent and Trademark Office

A high resolution, cathodoluminescent display screen or device and a method of producing such a display device is disclosed. The display screen includes a plurality of channel structures having longitudinal ends, a transparent medium formed in a plane to which the channel structures are fixed with one longitudinal end thereof oriented toward the plane of the transparent medium, and a cathodoluminescent material deposited on the channel structures whereby incident electrons and light generated by the incident electrons are directed along the channel structures. Preferably, the display screen also includes a mechanism for removing built up charge from the display screen, such as conductive channel structures and/or a conductive transparent medium. The cathodoluminescent material can include phosphors, and for producing a color display, different materials producing different colors would be used. In one preferred embodiment, the channel structures are tubules. Alternately, the channel structures can be channel plates or other structures providing channeling structures. In the preferred embodiment, the transparent medium is glass. However, the transparent medium could be quartz or some other equivalent material. In order to provide a display device the display screen is then mated with an addressable electron source for generating electrons incident on the cathodoluminescent material of selected channel structures. Preferably, the electron source means includes a field emitter array with a reflecting surface. DTIC

N95-31343 Department of the Navy, Washington, DC.
METHOD AND APPARATUS FOR NON-DESTRUCTIVELY MEASURING LOCAL RESISTIVITY OF SEMICONDUCTORS Patent
D. K. Gaskill, inventor (to Navy), Nicholas Bottka, inventor (to Navy), and Alok K. Berry, inventor (to Navy) 3 Jan. 1995 14 p Filed 17 Jun. 1992
(AD-D017436; US-Patent-5,379,109; US-Patent-Appl-SN-899977; US-Patent-Class-356-445) Avail: US Patent and Trademark Office

An apparatus for non-destructively measuring resistivity of a semiconductor, such as InP, comprises light sources for illuminating a preselected portion of the semiconductor with first and second light beams, each of a preselected single wavelength, the first light beam operating to excite the semiconductor by photo injecting carriers, and the second light beam bombarding the local portion of the semiconductor with a preselected photon energy. The apparatus measures a fractional change in reflectance of the second light beam responsive to the first light beam, and records this fractional change in reflectance for various values of photon energy of the second light beam, to generate a photoreflectance line-shape. The photoreflectance line-shape is used to calculate a photoreflectance line-shape phase angle, which is used to determine the resistivity of the preselected portion of the semiconductor. DTIC

N95-31442# Missouri Univ., Saint Louis, MO.
QUANTUM 1/f NOISE IN HIGH TECHNOLOGY APPLICATIONS INCLUDING ULTRASMALL STRUCTURES AND DEVICES Final Technical Report, 15 Jun. 1989 - 14 Feb. 1994
Peter H. Handel 14 May 1994 76 p
(Grant AF-AFOSR-0416-89)
(AD-A292812) Avail: CASI HC A05/MF A01

The present report brings a final answer to the question on the nature of fundamental 1/f noise and its ubiquity. A sufficient criterion for a 1/f spectrum in arbitrary chaotic nonlinear systems is derived for the first time. This criterion guarantees a 1/f spectrum for nonlinear systems which also satisfy a condition of mathematical homogeneity. Briefly stated, nonlinearity + homogeneity = 1/f noise. The criterion results because the 1/f spectrum reproduces itself in a self-convolution. Among the five examples to which the criterion is applied is also quantum electrodynamics (QED), resulting in quantum 1/f noise as a fundamental form of quantum chaos. Nonlinearity of the system of a charged particle and its field, plus the basic homogeneity of physical equations causes the criterion to predict the quantum 1/f effect. The simple universal quantum 1/f formula is applied to infrared detectors and yields quantum 1/f noise in the dark current, but not in the photogenerated current. The fractal dimension of quantum 1/f noise is determined on the basis of its quantum chaos definition and is obtained theoretically as a function of bandwidth in a simple model by applying the Grassberger-Procaccia-Takens algorithm to the quantum 1/f theory. The quantum 1/f effect is successfully applied to quartz resonators and bipolar junction transistors. Finally, the quantum 1/f mobility fluctuations are calculated in silicon and the coherent quantum 1/f effect is derived for the first time from a new QED propagator with branch-point singularity. This opens the way to better bridging the gap between coherent and conventional quantum 1/f noise in small and ultrasmall devices. DTIC

N95-31607# Army Communications-Electronics Command, Fort Monmouth, NJ.

MAGNESIUM BATTERY DISPOSAL CHARACTERISTICS

Louis Soffer and Terrill Atwater Dec. 1994 10 p

(AD-A293053; CECOM-TR-94-7) Avail: CASI HC A02/MF A01

This study assesses the disposal characteristics of U.S. Army procured military magnesium batteries under current Resource Conservation and Recovery Act (RCRA) hazardous waste identification regulations administered by the U.S. Environmental Protection Agency. Magnesium batteries were tested at 100, 50, 10 and 0 percent remaining state of charge. Present findings indicate that magnesium batteries with less than 50 percent remaining charge do not exceed the federal regulatory limit of 5.0 mg/L for chromium. All other RCRA contaminates were below regulatory limits at all levels of remaining charge. Assay methods, findings, disposal requirements and design implications are discussed. DTIC

N95-31611# Sandia National Labs., Albuquerque, NM.

DEGRADATION OF BLUE AlGaN/InGaN/GaN LEDs SUBJECTED TO HIGH CURRENT PULSES

Daniel L. Barton, Joachim Zeller (New Mexico Univ., Albuquerque, NM.), B. Scott Phillips (New Mexico Univ., Albuquerque, NM.), Pei-Chih Chiu (New Mexico Univ., Albuquerque, NM.), Sabrina Askar (New Mexico Univ., Albuquerque, NM.), Dong-Seung Lee (New Mexico Univ., Albuquerque, NM.), Lee Marek Osinski (New Mexico Univ., Albuquerque, NM.), and Kevin J. Malloy (New Mexico Univ., Albuquerque, NM.) 1994 9 p Presented at the International Reliability Physics Symposium, Las Vegas, NV, 3-6 Apr. 1995

(Contract DE-AC04-94AL-85000)

(DE95-008824; SAND-95-0504C; CONF-950432-2) Avail: CASI HC A02/MF A01

Short-wavelength, visible-light emitting optoelectronic devices are needed for a wide range of commercial applications, including high-density optical data storage, full-color displays, and underwater communications. In 1994, high-brightness blue LED's based on gallium nitride and related compounds (InGaN/AlGaN) were introduced by Nichia Chemical Industries. The Nichia diodes are 100 times brighter than the previously available SiC blue LED's. Group-3 nitrides combine a wide, direct bandgap with refractory properties and high physical strength. So far, no studies of degradation of GaN based LED's have been reported. The authors study, reported in this paper, focuses on the performance of GaN LED's under high electrical stress conditions. Their observations indicate that, in spite of a high defect density, which normally would have been fatal to other 3-5 devices, defects in group-3 nitrides are not mobile even under high electrical stress. Defect tubes, however, can offer a preferential path for contact metals to electromigrate towards the p-n junction, eventually resulting in a short. The proposed mechanism of GaN diode degradation raises concern for prospects of reliable lasers in the group-3 nitrides grown on sapphire. DOE

N95-31669# David Sarnoff Research Center, Princeton, NJ.

HIGH PERFORMANCE YBCO FILMS R/D Final Report, 25 Mar. 1991 - 31 Mar. 1995

Edgar J. Denlinger 31 Mar. 1995 16 p

(Contract N00014-91-C-0216; ARPA Order 8100)

(AD-A293045) Avail: CASI HC A03/MF A01

A suitable low loss, low dielectric constant substrate for HTS circuitry has been identified and shown to permit the deposition of high quality YBCO films that are comparable to that achieved with lanthanum aluminate substrates. The substrate is magnesium fluoride which has a dielectric constant of 5.3 and a loss tangent of 0.0001 at 77 K. The benefits of this technology are higher speed interconnects for multichip module (MCM) assemblies applied to digital processing, higher power handling at microwave frequencies applied to multiplexers and other passive components, and lower frequency dispersion and lower loss at millimeter wave frequencies applied to antenna feed networks, T/R modules, and delay lines. We have developed a novel fabrication technique for MCM structures that features an ultra-thin YBCO-covered magnesium fluoride substrate glass bonded to a metal handle, which provides excellent mechanical support and good heat sinking characteristics. For a sample demonstration of this technology, an MCM structure with a YBCO signal plane that is suitable for microwave/millimeter wave circuitry was fabricated and tested to have excellent electrical characteristics with a YBCO film surface resistance of 1 mohm. DTIC

N95-31674# Naval Air Warfare Center, China Lake, CA. Weapons Div.

THE 19TH ANNUAL ELECTRONICS MANUFACTURING SEMINAR

Feb. 1995 148 p Seminar held in Ridgecrest, CA, 22-24 Feb. 1995; sponsored by the Manufacturing Engineering Div., the Systems Engineering Dept., and Comarco, Inc.

(AD-A293067; NAWC-WPNS-TP-8242) Avail: CASI HC A07/MF A02

Presented are the proceedings of the 19th Annual Electronics Manufacturing Seminar held on 22-24 February 1995. The proceedings include the papers presented at the seminar and cover all aspects of soldering technology and electronics manufacturing. The proceedings are a compilation of information provided by both nongovernment and government sources. The proceedings are published in the interest of furthering communication and broadening awareness of current activities among soldering technology and electronics manufacturing specialists. DTIC

N95-31725# Army Armament Research, Development and Engineering Center, Watervliet, NY. Benet Labs.

CONTACTLESS CHARACTERIZATION OF SEMICONDUCTORS USING LASER-INDUCED SURFACE PHOTO-CHARGE VOLTAGE MEASUREMENTS Final Report

A. Abbate, P. Rencibia, O. Ivanov, G. Masini, F. Palma, and P. Das Jan. 1995 16 p Presented at the 1st International Symposium on Semiconductor Processing and Characterization with Lasers, Stuttgard, Germany

(AD-A293618; ARCCB-TR-95004) Avail: CASI HC A03/MF A01

A new technique to evaluate the electrical properties of semiconductor wafers and devices using surface photo-charge voltage (SPCV) measurements is presented. SPCV measures the change in the surface electrical charge induced by a chopped laser light whose photon energy exceeds the band gap energy of the semiconductor sample. This charge is measured capacitatively, thus SPCV measurements do not require the fabrication of metal contacts. In photocharge voltage spectroscopy measurements, the SPCV is measured as a function of the energy of a subband gap monochromatic steady-state illumination, and its derivative spectrum is associated with the density of surface states. A qualitative analysis of the proposed measurement is presented along with experimental results performed on gallium arsenide samples passivated with a thin zinc selenide film of variable thickness. The proposed technique is completely contactless, and it can be used as an in-line nondestructive characterization of semiconductor wafers during the various stages of integrated circuits fabrication. DTIC

N95-31728# Foreign Broadcasting Information Service, Washington, DC.

FBIS REPORT: SCIENCE AND TECHNOLOGY. CENTRAL EURASIA

18 Jul. 1995 81 p Transl. into ENGLISH from various Central Eurasian articles

(FBIS-UST-95-029) Avail: CASI HC A05/MF A01

Translated articles cover the following topics: Use of Radar Set With Synthesized Antenna for Estimating Effectiveness of Active Masking and Simulating Interference Signals; Simulation of Echo Signals Picked From Sea Surface by Grazing Radar Beam at Low Grazing Angle; Methods and Algorithms of Sea Surface Radar Image Processing and Identification; Aircraft Optimum Control Synthesis Based on Group Analysis of Motion Equations; On Issue of Maximizing Aircraft Glide Range Planning; Effect of Amplitude and Phase Noise on Quality of Radar Image Formation; Narrow-Band Infrared (1.0-1.2 micron) Photodiodes on Stressed Selective Epitaxial GaAs/InGaAs Structures; Selection of Transverse Modes in InGaAsP Lasers with Dielectric Coating on Mirrors; Single-Mode Strip-Geometry lambda = 1.55 micron Stripe-Geometry InGaAsP/InP Lasers; and Effect of Hydrogen on Cracking of Metals and Testing Them for Indication of Cracking Processes by Acoustic Emission. CASI

N95-31742*# National Aeronautics and Space Administration. Lewis Research Center, Cleveland, OH.

OPERATIONAL CHARACTERISTICS OF A 200 C LC PARALLEL RESONANT CIRCUIT

Eric D. Baumann and Ahmad N. Hammoud Jun. 1995 6 p Presented at the 1995 Conference on Electrical Insulation and Dielectric Phenomena, Virginia Beach, VA, 22-25 Oct. 1995; sponsored by IEEE Dielectrics and Electrical Insulation Society

(Contract NAS3-27186; RTOP 233-01-0C)

(NASA-TM-106983; E-9752; NAS 1.15:106983) Avail: CASI HC A02/MF A01

Research efforts are currently underway at the NASA Lewis Research Center to design and demonstrate an inverter capable of operating with a baseplate temperature of 200 C. In support of this project, various electrical components including capacitors, inductors, transformers, cables, and semiconductor switches are being developed or evaluated for integration into the inverter. In this work, a parallel LC resonant circuit was constructed and evaluated under simultaneous electrical and thermal stressing. The tests were performed in the temperature range of 25 to 200 C with an applied voltage of up to 90 V, 20 kHz. The individual components were comprised of high temperature film capacitors and powder core inductors developed in-house. The circuit was characterized in terms of the component currents and case temperatures as well as frequency of resonance as a function of applied bias and temperature. The results obtained, which have indicated good functional stability up to 200 C, are presented and discussed. Author

N95-31842# Army Aeromedical Research Lab., Fort Rucker, AL.

DESIGN OF DIGITAL LOW-PASS FILTERS FOR TIME-DOMAIN RECURSIVE FILTERING OF IMPACT ACCELERATION SIGNALS Final Report

Nabih Alem and Matthew Perry Jan. 1995 42 p

(DA Proj. 3O1-62787-A8-78)

(AD-A293086; USAARL-95-13) Avail: CASI HC A03/MF A01

Simplified and portable computer programs are presented to design and implement recursive digital Butterworth filters. The design method described uses the bilinear transformation to convert the well established analog design to digital formulation. Fortran codes for the design and implementation of the filter are included. The resulting design is compared to another filter proposed in SAE J211 guideline for filtering impact acceleration signals. Although both design methods produced filters which are within corridors prescribed in the J211 guideline, the standard design produces a Butterworth-like response whereas the J211 design does not. Additionally, the standard design methods and the implementation algorithms allow the design of any even order filter which may be required for filtering other long duration signals. DTIC

N95-31844# Research Triangle Inst., Research Triangle Park, NC. Center for Systems Engineering.

MISSION CRITICAL FAILURE EFFECTS ANALYSIS USING QUANTITATIVE TECHNIQUES Final Report, Feb. 1993 - Feb. 1994

Mark Royale, Rahul Kapoor, and Nick Kanopoulos Dec. 1994 104 p

(Contract F30602-93-C-0009)

(AD-A293098; RL-TR-94-212) Avail: CASI HC A06/MF A02

This report addresses the problem of assessing the criticality of faults in a large digital system. In particular, it addresses simulation-based methods for determining the effectiveness of built-in-test. The approach is based on automated fault injection in a VHDL model of the system, and statistical analysis of the resulting behavior of the system. The behavioral entities of the VHDL model would correspond to Line Replaceable Units (LRU's) or Line Replaceable Modules (LRM's). This report provides the top level design requirements and rationale for the detailed design of this capability. DTIC

N95-31847*# National Aeronautics and Space Administration. Lewis Research Center, Cleveland, OH.

AN ACTIVE MAGNETIC BEARING WITH HIGH T(SUB c) SUPERCONDUCTING COILS AND FERROMAGNETIC CORES

G. V. Brown, E. DiRusso, and A. J. Provenza Jul. 1995 11 p Presented at the 1995 Cryogenic Engineering Conference, Columbus, OH, 16-20 Jul. 1995; sponsored by Centennial Conferences

(RTOP 505-63-5B)

(NASA-TM-106995; E-9772; NAS 1.15:106995) Avail: CASI HC A03/MF A01

A proof-of-feasibility demonstration showed that high-T(sub c) superconductor (HTS) coils can be used in a high-load, active magnetic bearing in LN2. A homopolar radial bearing with commercially wound HTS (Bi 2223) bias and control coils produced over 890 N (200 lb) radial load capacity (measured non-rotatings) and supported a shaft to 14,000 rpm. The goal was to show that HTS coils can operate stably with ferromagnetic cores in a feedback controlled system at a current density similar to that for Cu in LN2. The bias coil, wound with non-twisted, multifilament HTS conductor, dissipated negligible power for its direct current. The control coils, wound with monofilament HTS sheathed in Ag, dissipated negligible power for direct current. AC losses increased rapidly with frequency and quadratically with AC amplitude. Above about 2 Hz, the effective resistance of the control coils exceeds that of the silver which is in electrical parallel with the oxide superconductor. These results show that twisted multifilament conductor is not needed for stable levitation but may be desired to reduce control power for sizable dynamic loads. Author

N95-31948 Clarkson Univ., Potsdam, NY.

A TIME STEPPING COUPLED FINITE ELEMENT-STATE SPACE MODELING ENVIRONMENT FOR SYNCHRONOUS MACHINE PERFORMANCE AND DESIGN ANALYSIS IN THE ABC FRAME OF REFERENCE Ph.D. Thesis

Fang Deng 1994 290 p

Avail: Univ. Microfilms Order No. DA9422824

This dissertation centers on the development of a modeling environment to predict the performance and operating characteristics of salient-pole synchronous generators. The model basically consists of an algorithm consisting of two sections, a time stepping two-dimensional (2D) magnetostatic field finite element (FE) computation algorithm coupled to a state-space (SS) time-domain model of the winding circuits. Hence the term time stepping Coupled Finite Element-State Space (CFE-SS) modeling environment is adopted for this approach. In the FE section, magnetic vector potential (MVP) based finite element (FE) formulations and computation of two-dimensional (2D) magnetostatic fields are used to get the magnetic field solutions throughout a machine's cross-section at a sequence (samplings) of rotor positions covering a complete (360 deg e) ac cycle. These field solutions yield the winding inductances by means of an energy and current perturbation method. The output of the FE section is the magnetic field solutions and the entire set of phase, field, damper, and sleeve winding inductance profiles versus rotor position, including all space harmonics due to rotor saliency, damper bar slotting, sleeve segmentation, stator slotting, and magnetic saturation. These inductance profiles are decomposed into their harmonic components by Fourier analysis. The magnetic field solutions and resulting winding inductances represent the key input data to the SS portion of the CFE-SS modeling environment. Laminated machine iron core loss calculations, which include the losses in the stator and rotor as well as pole face are subsequently performed using the magnetic field solution data. Conversely, the output of the SS portion is the entire set of phase, field, damper winding (circuit), and sleeve segment currents, which also include all the resulting time harmonics. These winding current results form in turn the key input data to the FE portion of the modeling environment which is iteratively used in obtaining inductance parameters prior to another round of SS computation of the steady-state current profiles. Again, the model is iterative in nature, in which the user continues cycling through the two sections, namely the FE

and SS sections of the CFE-SS modeling environment, until the desired degree of convergence is achieved. The CFE-SS approach uses only design data such as physical dimensions, magnetic circuit geometry, magnetic material characteristics, winding particulars and layouts, and hence does not depend on the existence of actual hardware. The modeling environment is totally within the ABC frame of reference, therefore no approximating assumptions such as sinusoidally distributed mmf's or current sheets were made. Dissert. Abstr.

N95-32077# Pacific Northwest Lab., Richland, WA.
THE POTENTIAL FOR MICROTECHNOLOGY APPLICATIONS IN ENERGY SYSTEMS: RESULTS OF AN EXPERTS WORKSHOP
Feb. 1995 50 p
(Contract DE-AC06-76RL-01830)
(DE95-009103; PNL-10478) Avail: CASI HC A03/MF A01

Microscale technologies, or microelectromechanical systems (MEMS), are currently under development in the United States and abroad. Examples include microsensors, microactuators (including micromotors), and microscale heat exchangers. Typically, microscale devices have features ranging in size from a few microns to several millimeters, with fabrication methods adapted from those developed for the semiconductor industry. Microtechnologies are already being commercialized; initial markets include the biomedical and transportation industries. Applications are being developed in other industries as well. Researchers at the Pacific Northwest Laboratory (PNL) hypothesize that a significant number of energy applications are possible. These applications range from environmental sensors that support enhanced control of building (or room) temperature and ventilation to microscale heat pumps and microscale heat engines that could collectively provide for kilowatt quantities of energy conversion. If efficient versions of these devices are developed, they could significantly advance the commercialization of distributed energy conversion systems, thereby reducing the energy losses associated with energy distribution. Based upon the potential for energy savings, the U.S. Department of Energy (DOE) Office of Building Technologies (OBT) has proposed a new initiative in energy systems miniaturization. The program would focus on the development of microtechnologies for the manufactured housing sector and would begin in either FY 1997 or FY 1998, ramping up to $5 million per year investment by FY 2001. DOE

N95-32084# Ames Lab., IA.
AN EXPERIMENTAL SEARCH FOR HIGH ZT SEMICONDUCTORS: A SURVEY OF THE PREPARATION AND PROPERTIES OF SEVERAL ALLOY SYSTEMS
S. H. Han and B. A. Cook 1994 5 p Presented at the 13th International Conference on Thermoelectrics, Kansas City, MO, 30 Aug. - 1 Sep. 1994
(Contract W-7405-eng-82)
(DE95-010232; IS-M-810; CONF-940830-4) Avail: CASI HC A01/MF A01

A survey was conducted of several alloy systems identified as having certain properties thought to be desirable in high figure-of-merit thermoelectric materials. The systems examined include the cerium and lanthanum borocarbides, yttrium nitrides, osmium silicides, and titanium sulfides. Various approaches to the preparation of these alloy systems were explored including vapor transport, arc melting, and mechanical alloying. Among these systems, the borocarbides were found to exhibit p-type conductivity but generally suffered from relatively high carrier concentrations (on the order of 10(exp 21)/cu cm and low mobilities (less than or equal to 10 sq cm/V-s). Both carbon and sulfur dopants produced the highest figure of merit (0.13 x 10(exp -3)/deg C in the yttrium nitride system at room temperature. Excess silicon was observed to increase carrier concentration and Hall mobility in osmium disilicide while additions of chromium were observed to stabilize the OsSi2 crystal structure. Electrical power factors comparable to state of the art silicon-germanium alloys were achieved in titanium disulfide, however, the electrical transport properties were found to be critically dependent upon the amount of excess Ti in Ti(1+x)S2. DOE

N95-32100# Lawrence Livermore National Lab., Livermore, CA.
STABILITY ANALYSIS OF THE TPX TOROIDAL FIELD COIL
R. L. Wong 13 Oct. 1994 6 p Presented at the Applied Superconductivity Conference, Boston, MA, 16-21 Oct. 1994
(Contract W-7405-eng-48)
(DE95-009666; UCRL-JC-116966; CONF-941013-33) Avail: CASI HC A02/MF A01

The energy stability margin of the TPX/TF conductor has been calculated as a response to heat pulses with short initial quench zones and with long initial quench zones. The short IQZ's approximate ramp-rate induced heating, and the long IQZ's approximate heating from a plasma disruption. These IQZ's are centered in the bore inner leg of the double pancake, where the operating field and temperature are maximum. Energy margin stability curves are plotted as a function of current. At the 33.5 kA design current, the minimum calculated stability margin with short IQZ's is 390 mJ/cc. The minimum calculated stability margin with long IQZ's is 205 mJ/cc. A comparison the stability margin with the available enthalpy (short IQZ's) and with the available internal energy (long IQZ's) shows that the conductor utilizes the available helium energy well. The energy margin stability curve is generally divided into two regions. The regions can be characterized on the basis of a decrease or an increase in heating after the initiating heat pulse during a marginal quench. The low current well-cooled region exists when the heating rate during the pulse is greater than the Joule heating after the pulse. Since the heating rate decreases, the energy margin is high. The high current ill-cooled region exists when the heating rate during the pulse is less than the Joule heating after the pulse. Since the heating rate increases, the energy margin is low. In the evaluation of a well-cooled or an ill-cooled condition, this Joule heating should be included in the strength of the initiating pulse. When this is done for the TPX/TF conductor, the limiting current approaches the critical current, explaining why the stability curves are entirely in the well-cooled region. The important result is that the conductor does not exhibit a large decrease in energy margin to an ill-cooled region until the current approaches the critical current. DOE

N95-32207*# National Aeronautics and Space Administration. Lewis Research Center, Cleveland, OH.
EFFECTS OF TEMPERATURE, FREQUENCY, FLUX DENSITY, AND EXCITATION WAVEFORM ON THE CORE LOSS AND DYNAMIC B-H LOOPS OF SUPERMALLOY
Gene E. Schwarze, William R. Wieserman (Pittsburgh Univ., Johnstown, PA.), and Janis M. Niedra (NYMA, Inc., Brook Park, OH.) Jul. 1995 8 p Presented at the 30th Intersocieyty Energy Conversion Engineering Conference, Orlando, FL, 31 Jul. - 4 Aug. 1995; sponsored by ASME, IEEE, AIChE, ANS, SAE, ACS, and AIAA
(Contract NAS3-27186; RTOP 233-01-0C)
(NASA-TM-106982; E-9751; NAS 1.15:106982; IECEC-95-329) Avail: CASI HC A02/MF A01

The availability of experimental data which characterize the performance of soft magnetic materials for the combined conditions of temperature and frequency over a wide flux density range for different types of excitation is almost nonexistent. An experimental investigation of an 80-20 Ni-Fe alloy (Supermalloy) was conducted over the temperature (T) range of 23 to 300 C, frequency (f) range of 1 to 50 kHz, and maximum flux densities (B(sub M)) from 0.1 T up to 0.7 T for both sine and square wave voltage excitation. The investigation focused on the effects of (B(sub M)), f, T, and excitation waveform on the specific core loss (SCL) and dynamic B-H loops. The results show that the ratio (R) of sine to square wave excitation specific core loss was always greater than unity for a given f and T and identical values of B(sub M). The values of R ranged from 1.07 to 1.34. The classical theory of core loss separation into a hysteresis and eddy current loss component was used to theoretically determine the lower and upper bounds on R, against which the experimental R-values were compared. The experimental R-values were also used to make a comparison of the core loss of a sine and square wave voltage driven transformer. Author

N95-32300# Lawrence Livermore National Lab., Livermore, CA.
VOLTAGE CONTROLLED MESFET PULSE SHAPE GENERATOR
Scott C. Burkhart 26 Oct. 1994 7 p
(Contract W-7405-eng-48)
(DE95-011656; UCRL-ID-116054) Avail: CASI HC A02/MF A01

A programmable pulse shape generator capable of producing pulse shapes for Nova and Beamlet has been designed and simulated using the circuit code SPICE. The design utilizes power MESFETS, which are commonly used in microwave amplifiers. The pulse shape is varied by setting a bias voltage on each in a chain of MESFETS with a 200 ps temporal resolution. The electrical pulse then drives an integrated

electro-optic modulator similar to what is on Beamlet. Pulse shapes 22 and 25, used on Nova, have been generated by this design. There is no fundamental barrier to making such a pulse generator for use on the National Ignition Facility (NIF). In fact, the longer time scales on the NIF pulse will ease the high speed requirements of the pulse shape generator allowing the use of less expensive components. DOE

N95-32369 Direction des Recherches, Etudes et Techniques, Paris (France). Centre de Documentation de l'Armement.
HYPERFREQUENCY COMPONENTS [COMPOSANTS HYPERFREQUENCES]
29 Sep. 1994 168 p In FRENCH Symposium held on Sep. 29, 1994
(PB95-208302) Avail: Issuing Activity (National Technical Information Service (NTIS))

The document has a collection of 19 papers (11 on technologies, 8 on applications) by 26 authors and coauthors. Technological topics include: evolution from conventional HEMT's double heterojunction and planar types of pseudomorphic HEMT's; MMIC R&D and production aspects for very-low-noise, low-power, and very-low-noise, high-power applications; hyperfrequency CAD tools; parametric measurements of hyperfrequency components on plug-in cards for design and in-process testing uses; design of Class B power amplifiers and millimetric-wave, bigrid-transistor mixers, exemplifying combined use of three major types of physical simulation in electrical modeling of microwave components; FET's for power amplification at up to 110 GHz; production, characterization, and nonlinear applications of resonant tunnel diodes. Applications topics include: development of active modules for major European programs; tubes versus solid-state components in hyperfrequency applications; status and potentialities of national and international cooperative R&D on MMIC's and CAD of hyperfrequency circuitry; attainable performance levels in multifunction MMIC applications; state of the art relative of MESFET power amplifiers (Bands S, C, X, Ku); creating a hyperfrequency functions library, of parametrizable reference cells or macrocells; and design of a single-stage, low-noise, band-W amplifier toward development of a three-stage amplifier. NTIS

N95-32224*# Jet Propulsion Lab., California Inst. of Tech., Pasadena, CA.
AN EFFICIENT IMPLEMENTATION OF FORWARD-BACKWARD LEAST-MEAN-SQUARE ADAPTIVE LINE ENHANCERS
H.-G. Yeh and T. M. Nguyen *In its* The Telecommunications and Data Acquisition Report 15 May 1995 p 16-26 (For primary document see N95-32221 11-32)
Avail: CASI HC A03/MF A03

34 FLUID MECHANICS AND HEAT TRANSFER

Includes boundary layers; hydrodynamics; fluidics; mass transfer; and ablation cooling.

For related information see also *02 Aerodynamics* and *77 Thermodynamics and Statistical Physics.*

N95-30383# Sandia National Labs., Albuquerque, NM.
VISCOUS DIFFUSION OF VORTICITY IN UNSTEADY WALL LAYERS USING THE DIFFUSION VELOCITY CONCEPT
J. H. Strickland, S. N. Kempka, and W. P. Wolfe 1995 14 p Presented at the Application of Vortex Methods to Engineering Problems Forum, Albuquerque, NM, 22-24 Feb. 1995
(Contract DE-AC04-94AL-85000)
(DE95-008537; SAND-95-0278C; CONF-950283-2) Avail: CASI HC A03/MF A01

The primary purpose of this paper is to provide a careful evaluation of the diffusion velocity concept with regard to its ability to predict the diffusion of vorticity near a moving wall. A computer code BDIF has been written which simulates the evolution of the vorticity field near a wall of infinite length which is moving in an arbitrary fashion. The simulations generated by this code are found to give excellent results when compared to several exact solutions. We also outline a two-dimensional unsteady viscous boundary layer model which utilizes the diffusion velocity concept and is compatible with vortex methods. A primary goal of this boundary layer model is to minimize the number of vortices generated on the surface at each time step while achieving good resolution of the vorticity field near the wall. Preliminary results have been obtained for simulating a simple two-dimensional laminar boundary layer. DOE

N95-30412 Department of the Navy, Washington, DC.
ELECTROMAGNETICALLY ACTIVATED COMPLIANT WAVY-WALL Patent
Richard H. Nadolink, inventor (to Navy) 25 Oct. 1994 9 p Filed 27 Aug. 1993
(AD-D017340; US-Patent-5,359,574; US-Patent-Appl-SN-113378; US-Patent-Class-367-1) Avail: US Patent and Trademark Office

Electromagnets are disposed in an elastomeric coating affixed to a body exposed to a fluid. Controllable magnetic forces created by the electromagnets produce a wavy-wall configuration in the surface of the coating which may be static, dynamic, or static in part and dynamic in part, and which interfaces with the fluid to controllably alter noise, turbulence and drag characteristics of the body mechanically. Electrodes may be fixed on the surface of the coating to produce electric force fields for interacting with the magnetic fields and the wavy-wall, to produce magnetohydrodynamically generated Lorentz forces which controllably further alter noise, turbulence and drag characteristics of the body. DTIC

N95-30449 University of Southern California, Los Angeles, CA.
SMALL SCALE TURBULENCE IN A PLANE MIXING LAYER Ph.D. Thesis
Judith Kathleen Foss 1994
Avail: Issuing Activity (Univ. of Southern California, Doheny Library, Micrographics Dept., Los Angeles, CA 90089-0182)

Two measures of small scale turbulence, viscous dissipation and a direct count of the random fine eddies which dissipate energy, were correlated to the large scale coherent motions in a plane mixing layer. Experiments were conducted in a low speed wind tunnel at moderate Reynolds number with laminar boundary layers separating from both the high and low speed sides. Extensive x- and parallel-wire measurements yielded three-component velocity data taken point by point in a plane normal to the freestream. The location of the large scale coherent motions was determined by spatially differentiating the long-time averages of these data. The primary spanwise vortex was identified from Delta U/Delta y while the secondary streamwise ribs were obtained from Delta V/Delta z, where Delta y and Delta z represent the spacing between data points in the cross-stream and spanwise directions, respectively. It will be demonstrated how Delta U/Delta z identifies the rib locations, as well. The data, moreover, were taken so that the fine-scale eddies, those whose length scale corresponds exactly to the peak in the 3-D dissipation spectrum, were resolved both spatially and temporally. These 'dissipative' eddies were identified by a novel technique, the peak-valley-counting (PVC) method. Several of the viscous dissipation terms were also calculated. The fine-scale eddy population distributions and the measures of viscous dissipation correlated extremely well. Indeed, the 'dissipative' eddies dissipate the energy, and the PVC method identifies them. Both sets of distributions peak in the core of the spanwise vortex, and are independent of the streamwise ribs at this downstream location. Dissert. Abstr.

N95-30464# Sandia National Labs., Albuquerque, NM.
VELOCITY BOUNDARY CONDITIONS FOR VORTICITY FORMULATIONS OF THE INCOMPRESSIBLE NAVIER-STOKES EQUATIONS
S. N. Kempka, J. H. Strickland, M. W. Glass, J. S. Peery, and M. S. Ingber (New Mexico Univ., Albuquerque, NM.) 1995 20 p Presented at the Application of Vortex Methods to Engineering Problems Forum, Albuquerque, NM, 22-24 Feb. 1995
(Contract DE-AC04-94AL-85000)
(DE95-008715; SAND-94-1735C; CONF-950283-1) Avail: CASI HC A03/MF A01

Velocity boundary conditions for the vorticity form of the incompressible, viscous fluid momentum equations are presented. Vorticity is created on boundaries to simultaneously satisfy the tangential and normal components of the velocity boundary condition. The newly created vorticity is specified by a kinematical formulation which is a generalization of Helmholtz decomposition of a vector field. Related forms of the decomposition were developed by Bykhovskiy and Smirnov in 1983, and Wu and Thompson in 1973. Though it has not been generally recognized as such, these formulations resolve the over-specification issues associated with determining

a velocity field from velocity boundary conditions and a vorticity field. The generalized decomposition has not been widely used, however, apparently due to a general lack of a useful physical interpretation. An analysis is presented which shows that the generalized decomposition has a relatively simple physical interpretation which facilitates its numerical implementation. The implementation of the generalized decomposition for the normal and tangential velocity boundary conditions is discussed in detail. As an example of the use of this boundary condition, the flow in a lid-driven cavity is simulated. The solution technique is based on a Lagrangian transport algorithm in the hydrocode ALEGRE. ALEGRE's Lagrangian transport algorithm has been modified to solve the vorticity transport equation, thus providing a new, accurate method to simulate incompressible flows. This numerical implementation and the new boundary condition formulation allow vorticity-based formulations to be used in a wider range of engineering problems. DOE

N95-30524*# National Aeronautics and Space Administration. Lewis Research Center, Cleveland, OH.

THE EFFECT OF ADDING ROUGHNESS AND THICKNESS TO A TRANSONIC AXIAL COMPRESSOR ROTOR

Kenneth L. Suder, Rodrick V. Chima, Anthony J. Strazisar, and William B. Roberts (Flow Application Research, Fremont, CA.) Jun. 1995 22 p Presented at the 39th International Gas Turbine and Aeroengine Congress and Exposition, The Hague, Neatherlands, 13-16 Jun. 1994; sponsored by ASME

(RTOP 505-62-52)

(NASA-TM-106958; E-9709; NAS 1.15:106958) Avail: CASI HC A03/MF A01

The performance deterioration of a high speed axial compressor rotor due to surface roughness and airfoil thickness variations is reported. A 0.025 mm (0.001 in.) thick rough coating with a surface finish of 2.54-3.18 RMS microns (100-125 RMS microinches) is applied to the pressure and suction surface of the rotor blades. Coating both surfaces increases the leading edge thickness by 10% at the hub and 20% at the tip. Application of this coating results in a loss in efficiency of 6 points and a 9% reduction in the pressure ratio across the rotor at an operating condition near the design point. To separate the effect of thickness and roughness, a smooth coating of equal thickness is also applied to the blade. The smooth coating surface finish is 0.254-0.508 RMS microns (10-20 RMS microinches), compared to the bare metal blade surface finish of 0.508 RMS microns (20 RMS microinches). The smooth coating results in approximately half of the performance deterioration found from the rough coating. Both coatings are then applied to different portions of the blade surface to determine which portions of the airfoil are most sensitive to thickness/roughness variations. Aerodynamic performance measurements are presented for a number of coating configurations at 60%, 80%, and 100% of design speed. The results indicate that thickness/roughness over the first 10% of blade chord accounts for virtually all of the observed performance degradation for the smooth coating, compared to about 70% of the observed performance degradation for the rough coating. The performance deterioration is investigated in more detail at design speed using laser anemometer measurements as well as predictions generated by a quasi-3D Navier-Stokes flow solver which includes a surface roughness model. Measurements and analysis are performed on the baseline blade and the full-coverage smooth and rough coatings. The results indicate that coating the blade causes a thickening of the blade boundary layers. The interaction between the rotor passage shock and the thickened suction surface boundary layer then results in an increase in blockage which reduces the diffusion level in the rear half of the blade passage, thus reducing the aerodynamic performance of the rotor. Author

N95-30553 Department of the Navy, Washington, DC.

ACTIVE TURBULENCE CONTROL USING MICROELECTRODES, PERMANENT MAGNETS IN MICROGROOVES Patent

James C. Meng, inventor (to Navy) 1 Nov. 1994 4 p Filed 11 Feb. 1993

(AD-D017351; US-Patent-5,359,951; US-Patent-Appl-SN-016326; US-Patent-Class-114-67R) Avail: US Patent and Trademark Office

Electrodes and magnets are disposed in alternating on confronting surfaces of microgrooves respectively produce electric and magnetic fields cooperative to provide a force that acts along direction defined between a vessel and a relatively moving medium to controllably diminish turbulence generation in seawater. DTIC

N95-30557# Air Force Inst. of Tech., Wright-Patterson AFB, OH.

AN EXPERIMENTAL STUDY OF PLANAR HETEROGENEOUS SUPERSONIC CONFINED JETS Ph.D. Thesis

Frederick J. Tanis, Jr. Dec. 1994 184 p

(AD-A290859; AFIT/DS/AA/94-6) Avail: CASI HC A09/MF A02

The effects of varying the exit pressure of a supersonic helium jet exhausting coaxially with two parallel supersonic air streams into a constant area duct were investigated. The method used to evaluate the mass entrainment rate was to measure helium molar concentration profiles and mass flux across the duct using a binary gas probe then calculate the mass entrainment into the helium jet. In order to conduct this study a novel binary gas probe was developed which allowed helium concentration and mass flux data to be obtained during continuous traverses across the supersonic flowfield. High exit pressure ratio (EPR) led to improved overall mixing compared to the baseline case with an EPR near unity. The high EPR caused low mass entrainment along the jet shear layers due to high convective Mach numbers and velocity ratios, but the high EPR caused oblique shocks to form which reflected off the duct walls and intersected with the helium jet several times causing significant mass entrainment due to numerous shock-shear layer interactions (SSLI's). A correlation between the vorticity generated during a SSLI and the mass entrainment into the jet was developed. DTIC

N95-30672 Department of the Navy, Washington, DC.

METHOD AND SYSTEM FOR REDUCING DRAG ON A BODY MOVING THROUGH A FLUID MEDIUM Patent

Richard A. Katz, inventor (to Navy) 15 Nov. 1994 18 p Filed 2 Sep. 1993

(AD-D017336; US-Patent-5,365,490; US-Patent-Appl-SN-117512; US-Patent-Class-367-1) Avail: US Patent and Trademark Office

A method of detecting the onset of turbulence in connection with a body moving through a fluid medium and of reducing body drag and as well reducing the amount of drag noise radiated from the body. First, the body is supplied with sensors each for generating a signal suitable for measuring amplitude of pressures fluctuations of the of this medium proximate a region of said sidewall of the body in at least a region of the body in which turbulence is expected to occur. During a reference stage during which the body moves through the fluid medium when it is known that turbulence is occurring around at least a portion of said body, the sensors each generate reference temporal pressure data representing fluctuations in pressure of the fluid medium around said body. In response to reference temporal pressure data generated by sensors in a turbulence zone at which turbulence is occurring and sensors in a transition zone between the turbulence zone and a laminar flow zone, method-of-delay phase portraits are generated for a progression of selected delay intervals. DTIC

N95-30710*# National Aeronautics and Space Administration. Lewis Research Center, Cleveland, OH.

NUMERICAL SIMULATION OF FLOW IN A WHIRLING ANNULAR SEAL AND COMPARISON WITH EXPERIMENTS

M. M. Athavale (CFD Research Corp., Huntsville, AL.), R. C. Hendricks, and B. M. Steinetz Jun. 1995 22 p Presented at the 31st Joint Portpulsion Conference and Exhibit, San Diego, CA, 10-12 Jul. 1995; sponsored by AIAA, ASME, SAE, and ASEE Original contains color illustrations

(Contract NAS3-25644; RTOP 242-70-02)

(NASA-TM-106961; NAS 1.15:106961) Avail: CASI HC A03/MF A01; 2 functional color pages

The turbulent flow field in a simulated annular seal with a large clearance/radius ratio (0.015) and a whirling rotor was simulated using an advanced 3D CFD code SCISEAL. A circular whirl orbit with synchronous whirl was imposed on the rotor center. The flow field was rendered quasi-steady by making a transformation to a totaling frame. Standard k-epsilon model with wall functions was used to treat the turbulence. Experimentally measured values of flow parameters were used to specify the seal inlet and exit boundary conditions. The computed flow-field in terms of the velocity and pressure is compared with the experimental measurements inside the seal. The agreement between the numerical results

and experimental data with correction is fair to good. The capability of current advanced CFD methodology to analyze this complex flow field is demonstrated. The methodology can also be extended to other whirl frequencies. Half- (or sub-) synchronous (fluid film unstable motion) and synchronous (rotor centrifugal force unbalance) whirls are the most unstable whirl modes in turbomachinery seals, and the flow code capability of simulating the flows in steady as well as whirling seals will prove to be extremely useful in the design, analyses, and performance predictions of annular as well as other types of seals. Author

N95-30763# Texas Univ., Austin, TX. Inst. for Fusion Studies.
SINGULAR EIGENFUNCTIONS FOR SHEARING FLUIDS I
N. J. Balmforth and P. J. Morrison Feb. 1995 79 p
(Contract DE-FG05-80ET-53088)
(DE95-008952; DOE/ET-53088/692; IFSR-692) Avail: CASI HC A05/MF A01

The authors construct singular eigenfunctions corresponding to the continuous spectrum of eigenvalues for shear flow in a channel. These modes are irregular as a result of a singularity in the eigenvalue problem at the critical layer of each mode. They consider flows with monotonic shear, so there is only a single critical layer for each mode. They then solve the initial-value problem to establish that these continuum modes, together with any discrete, growing/decaying pairs of modes, comprise a complete basis. They also view the problem within the framework of Hamiltonian theory. In that context, the singular solutions can be viewed as the kernel of an integral, canonical transformation that allows us to write the fluid system, an infinite-dimensional Hamiltonian system, in action-angle form. This yields an expression for the energy in terms of the continuum modes and provides a means for attaching a characteristic signature (sign) to the energy associate with each eigenfunction. They follow on to consider shear-flow stability within the Hamiltonian framework. Next, the authors show the equivalence of integral superpositions of the singular eigenfunctions with the solution derived with Laplace transform techniques. In the long-time limit, such superpositions have decaying integral averages across the channel, revealing phase mixing or continuum damping. Under some conditions, this decay is exponential and is then the fluid analogue of Landau damping. Finally, the authors discuss the energetics of continuum damping. DOE

N95-30810# Technische Univ., Eindhoven (Netherlands). Dept. of Mathematics and Computing Science.
EXISTENCE OF SOLUTIONS IN PLANE QUASISTATIONARY STOKES FLOW DRIVEN BY SURFACE TENSION
G. Prokert Nov. 1994 26 p
(PB95-197935; RANA-94-23) Avail: CASI HC A03/MF A01

Recently, the free boundary problem of quasistationary Stokes flow of a mass of viscous liquid under the action of surface tension forces has been considered by R.W. Hopper, L.K. Antanovskii, and others. The solution of the Stokes equations is represented by analytic functions, and a time dependent conformal mapping onto the flow domain is applied for the transformation of the problem to the unit disk. Two coupled Hilbert problems have to be solved there which leads to a Fredholm boundary integral equation. The solution of this equation determines the time evolution of the conformal mapping. The question of existence of a solution to this evolution problem for arbitrary (smooth) initial data has not yet been answered completely. In this paper, local existence in time is proved using a theorem of Ovsiannikov on Cauchy problems in an appropriate scale of Banach spaces. The necessary estimates are obtained in a way that is oriented at the a priori estimates for the solution given by Antanovskii. In the case of small deviations from the stationary solution represented by a circle, these a priori estimates together with the local results are used to prove even global existence of the solution in time. NTIS

N95-30811# Technische Univ., Eindhoven (Netherlands).
NUMERICAL COMPUTATION OF ONE-DIMENSIONAL DETONATION WAVES
A. C. Berkenbosch, E. F. Kaasschieter, and J. H. M. tenThijeBoonkkamp Oct. 1994 29 p
(PB95-197950; RANA-94-21) Avail: CASI HC A03/MF A01

In this paper we consider the numerical computation of one-dimensional detonation waves. Detonation waves are travelling wave solutions of the reactive Euler equations. An essential numerical difficulty in the numerical computation of detonation waves is the occurrence of completely wrong wave speeds, corresponding with non-physical solutions of the reactive Euler equations. The numerical propagation speed is strongly influenced by the choice of the ignition temperature. In this paper it is proved that non-physical solutions are always weak detonation waves. Furthermore, we present theoretical insights assessing why a correct ignition temperature will exclude non-physical weak detonation waves, just like the entropy condition excludes non-physical expansion shocks in the non-reacting case. This is illustrated by numerical computations quite well. NTIS

N95-30836# Technische Univ., Eindhoven (Netherlands). Dept. of Mathematics and Computing Science.
SIMULATION OF VISCOUS SINTERING
G. A. L. vandeVorst and R. M. M. Mattheij Oct. 1994 50 p Sponsored by the Technology Foundation
(PB95-197109; RANA-94-19) Avail: CASI HC A03/MF A01

The objective of this research is to develop reliable numerical methods to predict the deformation of an incompressible Newtonian viscous fluid region (Stokes Flow) driven by surface tension. In particular this mathematical model describes the physical processes that appear when a compact of glassy particles is heated to such a high temperature that the glass becomes a viscous creeping fluid. As a result, the particles are joining together so that the cohesion of the compact is increasing with time. This phenomenon is usually called viscous sintering and, e.g., appears in the production of high-quality glasses. From the methods developed, theoretical insights can be obtained about the densification kinetics of such a compact. Therefore, a numerical simulation program is developed that calculates the deformation of a representative two-dimensional or an axisymmetric unit cell of the compact. A Boundary Element Method is applied to solve the involved integral equations of Stokes flow and the time integration is carried out by a variable step, variable order Backward Differences Formulae method. NTIS

N95-30840 Virginia Polytechnic Inst. and State Univ., Blacksburg, VA.
A TURBULENCE MODEL FOR STEADY AND UNSTEADY BOUNDARY LAYERS IN STRONG PRESSURE GRADIENTS Ph.D. Thesis
Evangelos Hytopoulos 1994 234 p
Avail: Univ. Microfilms Order No. DA9422527

A new turbulence model designed for two-dimensional, steady and unsteady boundary layers in strong adverse pressure gradients is described. The model is developed in a rational way based on an understanding of the flow physics obtained from recent experimental observations. The turbulent shear stress is given by a mixing length model, but the variation of the mixing length in the outer region is not constant; it varies according to an integral form of the turbulence kinetic-energy equation. This approach allows for the history effects of the turbulence to be taken into account in an approximate but rational way. The form of the near-wall mixing length model is derived based on the rigorous distribution of the shear stress near the wall, and it takes into account the pressure and convection terms which become important in strong adverse pressure gradients. Since the significance of the normal stresses in turbulent kinetic-energy production is increasing as separation is approached, a model accounting for this contribution is incorporated. The model is calibrated using available experimental data. These data also indicate a change in turbulence structure near and through separation. Such a change can be significant and is accounted for here using an empirical function. The complete model was tested against steady and unsteady, two-dimensional experimental cases with adverse pressure gradient up to separation. Improved predictions compared to those obtained with other turbulence models were demonstrated. The general and rational approach that led to the derivation of the model allows the straightforward extension of the model in the region of separation. The further extension to steady and unsteady, three-dimensional cases is indicated. Dissert. Abstr.

N95-30862*# National Aeronautics and Space Administration. Marshall Space Flight Center, Huntsville, AL.
NAVIER-STOKES FLOW FIELD ANALYSIS OF COMPRESSIBLE FLOW IN A HIGH PRESSURE SAFETY RELIEF VALVE
Bruce Vu, Ten-See Wang, Ming-Hsin Shih (Mississippi State Univ., Mississippi State, MS.), and Bharat Soni (Mississippi State Univ., Mississippi State, MS.) [1993] 9 p
(NASA-TM-110640; NAS 1.15:110640) Avail: CASI HC A02/MF A01

The objective of this study is to investigate the complex three-dimensional flowfield of an oxygen safety pressure relieve valve during an incident, with a computational fluid dynamic (CFD) analysis. Specifically, the analysis will provide a flow pattern that would lead to the expansion of the eventual erosion pattern of the hardware, so as to combine it with other findings to piece together a most likely scenario for the investigation. The CFD model is a pressure based solver. An adaptive upwind difference scheme is employed for the spatial discretization, and a predictor, multiple corrector method is used for the velocity-pressure coupling. The computational result indicated vortices formation near the opening of the valve which matched the erosion pattern of the damaged hardware. Author

N95-30863*# National Aeronautics and Space Administration. Marshall Space Flight Center, Huntsville, AL.

NEARLY STEADY FLOWS IN GONG PROTOTYPE DATA

David H. Hathaway 1993 4 p Sponsored by the National Science Foundation

(RTOP 170-38-53-56)

(NASA-CR-198935; NAS 1.26:198935) Avail: CASI HC A01/MF A01

Doppler velocity images obtained with the GONG prototype instrument were analyzed to measure the nearly steady photospheric flows. The data consists of 88 images each of velocity, intensity, and modulation obtained at 20:00 UT on 88 days from July 1992 to February 1994. Each velocity image was temporally filtered to remove the p-mode oscillations, masked to exclude active regions, and then analyzed using spherical harmonics and orthogonal functions as described by Hathaway (1992). The spectral coefficients show very consistent results for the entire time interval with some evidence of year-to-year variations. The rotation profile agrees well with previous results and exhibits a north-south asymmetry that reverses sign during the 20 month interval. The residual rotation velocities exhibit structures with amplitudes of approximately 5 m/s that may be related to torsional oscillations. The meridional circulation is directed from the equator toward the poles with a peak velocity in the photosphere of approximately 50 m/s. The higher order components are very weak but indicate a divergent flow from the mid-latitudes (opposite that found for the June 1989 data). The convective limb shift is well fit by a 3rd order polynomial. The convection spectrum has a prominent peak at spherical harmonic degrees of l approximately 150 with very little signal in the low degree modes. Analysis of this signal shows that there is no evidence for giant cell convection at the level of approximately 10 m/s for all modes up to l = 32. Author

N95-30872# Technische Univ., Delft (Netherlands). Dept. of Mechanical Engineering and Marine Technology.

SIMULTANEOUS HEAT AND MASS TRANSFER IN A HORIZONTAL TUBE ABSORBER: NUMERICAL TOOLS FOR PRESENT AND FUTURE ABSORBER DESIGNS Ph.D. Thesis

Reinder Hette Wassenaar 7 Nov. 1994 245 p

(PB95-196978; ISBN-90-370-0109-3) Copyright Avail: CASI HC A11/MF A03

Absorption cycles like the absorption heat pump or the absorption heat transformer can contribute to savings on one of the earth's resources, energy. Because of the high initial expenses, application of an conventional absorption apparatus is only economical in the MW range at today's prices. In this project numerical tools were developed for the design of heat and mass exchangers with a better price-performance ratio, that open a wider field of application for absorption cycles. The tools are mathematical formulations of the conservation of energy and mass for absorption in a falling film flow along a cooled wall. The resulting set of partial differential equations with appropriate boundary conditions is made dimensionless to make them applicable to any mixture or geometry and to summarize the model parameters in a few dimensionless groups. The numerical tools developed give, in contrast to the existing finite difference descriptions, accurate outcomes at very low computational costs and apply also on a flow field of arbitrary geometry. NTIS

N95-30889# Army Research Lab., Aberdeen Proving Ground, MD.

THREE-DIMENSIONAL (3D) LARGE FLUID FLOW COMPUTATIONS FOR US ARMY APPLICATIONS ON KSR-1, CM-200, CM-5, AND CRAY C-90 Final Report, Jul. 1992 - Jul. 1994

Nisheeth Patel, Harris Edge, and Jerry Clarke Feb. 1995 31 p

(AD-A293125; ARL-TR-712) Avail: CASI HC A03/MF A01

The thrust of this research is to investigate the use of emerging massively parallel computer architectures for production type fluid flow applications. Typical flow computations in a ballistic simulation have reached a stage where a grid set involving a couple of million points are needed for adequate understanding of the flow behavior and computing the resulting forces acting on a projectile with a complex geometrical shape. For acceptable turnaround time, the simulation requires a system with large memory and high performance. Because of the hardware scalability and availability of large in-core memory, the emerging massively parallel processors (MPP) architectures such as Connection Machine's CM-5 and Kendall Square Research KSR-1 have become attractive for ballistic computations. Thus, this research is focused on implementation of complex real-world applications (not simple scaled down problems) on MPP's with the goal of sustainable performance. Because performance measurements obtained using the kernel of the full application and/or scaled down application size or 2-D cases could lead to considerably higher performance estimates, these factors are discussed in light of results from full 3-D applications obtained on MPP's. DTIC

N95-30946# Naval Undersea Warfare Center, New London, CT. New London Detachment.

WAVE PROPAGATION IN A FLUID-LOADED HOMOGENEOUS, TRANSVERSELY ISOTROPIC, ELASTIC CYLINDER OF ARBITRARY THICKNESS Ph.D. Thesis

Marilyn J. Berliner 15 Mar. 1995 140 p

(AD-A292728; NUWC-NL-TR-10845) Avail: CASI HC A07/MF A02

The problem of wave propagation in an infinite, fluid-loaded, homogeneous, transversely isotropic cylinder is studied within the framework of the linearized, three-dimensional theory of elasticity. The equations of motion of the cylinder are formulated using the constitutive equations of a transversely isotropic material with a preferred material direction collinear with the longitudinal axis of the cylinder. The equations of motion of the internal and external fluids are formulated using the constitutive equations of an inviscid fluid. Displacement potentials are used to solve the equations of motion of the cylinder and the fluids. The frequency equation of the coupled system, consisting of the cylinder and the internal and external fluids, is developed under the assumption of perfect-slip boundary conditions at the fluid-solid interfaces. This frequency equation is general in axial wavenumber k, circumferential wavenumber n, cylinder wall thickness h, and radial frequency. Cut-off frequencies and frequency spectra are computed for the n=1 modes in hollow cylinders, hypothetical fluid columns, fluid-filled cylinders, and cylinders that are fluid filled and immersed in fluid. Numerical results are obtained for two isotropic cylinders (composed of steel and soft (linear) and for a highly anisotropic, fiber-reinforced cylinder. DTIC

N95-30956 Technische Univ., Delft (Netherlands).

DYNAMICAL SYSTEMS AS MODELS FOR FLOW-INDUCED VIBRATIONS

A. H. P. vanderBurgh 1994 34 p Limited Reproducibility: More than 20% of this document may be affected by microfiche quality

(PB95-206991) Copyright Avail: Issuing Activity (National Technical Information Service (NTIS))

In this paper a number of oscillators with two degrees of freedom is considered. Attention is paid to the case in which only one degree of freedom interacts with a flowing medium. For the modeling of the flow-induced vibrations use is made of a quasi-steady theory. Model equations systems of non-linearly coupled harmonic oscillators are obtained. The analysis of these equations is restricted to special periodic and quasi-periodic solutions. The physical interpretation may be of relevance for the understanding of a number of technical problems. NTIS

N95-30957# Technische Univ., Delft (Netherlands).

ACCELERATION POTENTIAL MODELS PREDICHAT/PREDICDYN APPLIED FOR CALCULATION OF AXISYMMETRIC DYNAMIC INFLOW CASES

G. J. W. vanBussel Dec. 1993 32 p

(PB95-207015; IW-93071R) Avail: CASI HC A03/MF A01

Under the assumption of incompressible, inviscid and irrotational flow, it can be shown that the pressure perturbation in the complete flow field is given by a Laplace equation and acts as an acceleration potential function. The rotor blades are represented in the model as discrete surfaces on which a pressure discontinuity is present. The model implies the presence

of spanwise and chordwise pressure distributions, which are composed of analytical asymptotic solutions for the Laplace equation. This model is implemented in the PREDICHAT and PREDICDYN computer code series, for steady and axisymmetric dynamic inflow cases respectively. Dynamic inflow concerns with large scale unsteady rotor aerodynamics, such as coherent wind gusts, collective blade pitch and rotor speed variations. The basic equations implemented in the codes are presented, as well as some results from uniform flow, blade pitching and a safety stop. Comparisons with other calculations and with measurements are presented and show a good agreement. NTIS

N95-30985# Air Force Systems Command, Wright-Patterson AFB, OH. National Air Intelligence Center.

10 kW HEAT PIPE-HEAT SINK DEVELOPMENT

Chengti Qiu and Deren Xie 27 Mar. 1995 21 p Transl. into ENGLISH from Nanjing Gongxueyuan Xuebao, China, v. 16, no. 4, 1986 p 76-85 (AD-A293167; NAIC-ID(RS)T-0495-94) Avail: CASI HC A03/MF A01

A design of heat pipe with heat sink for cooling 10 kW klystron is presented. The radial heat pipe with heat sink is adopted and the later is optimized by computer for its minimum weight. In order to find its performance and life, the life testing is made and lasted for 1154 hours under the dissipated 5kW condition in addition to the traditional performance testing. The results obtained show that this heat pipe with heat sink is reliable, and with which the calculation results are consistent. DTIC

N95-30986 Johns Hopkins Univ., Columbia, MD. Chemical Propulsion Information Agency.

THE 21ST JANNAF EXHAUST PLUME TECHNOLOGY MEETING, VOLUME 1

Mary T. Gannaway, ed. Oct. 1994 170 p Meeting held in Sunnyvale, CA, 19-21 Oct. 1994; sponsored by the Joint NASA, Army, Navy, Air Force Interagency Propulsion Committee

(Contract N00014-91-C-0001)

(CPIA-Publ-621-Vol-1) Avail: CPIA, 10630 Little Patuxent Pkwy., Suite 202, Columbia, MD 21044-3200 HC

This volume, the first of three volumes, is a collection of 10 unclassified/unlimited papers which were presented at the 21st Joint Army-Navy-NASA-Air Force (JANNAF) Exhaust Plume Technology Subcommittee Meeting in conjunction with the Combustion Subcommittee and SPIRITS User Group Meeting held 19-21 October 1994 at the Lockheed Missiles and Space Company, Sunnyvale, California. Specific subjects discussed include behavior of aluminum and aluminum oxide in solid rocket plumes, exhaust plume flowfield characterization and plume phenomena at high altitudes. For individual titles, see N95-30987 through N95-30996.

N95-30987 Analytical Methods, Inc., Ogden, UT.

SURVEY OF RECENT Al2O3 DROPLET SIZE DATA IN SOLID ROCKET CHAMBERS, NOZZLES, AND PLUMES c20

Mark Salita *In* JHU, The 21st JANNAF Exhaust Plume Technology Meeting, Volume 1 Oct. 1994 p 1-17 (For primary document see N95-30986 11-34)

Avail: CPIA, 10630 Little Patuxent Pkwy., Suite 202, Columbia, MD 21044-3200 HC

The size distribution of Al2O3 droplets in a solid propellant rocket is very different in the chamber, nozzle, and plume, primarily due to breakup and collision/coalescence in the nozzle. This paper attempts to summarize, evaluate, and relate the results of 19 recent experimental and analytical studies of droplet size in order to construct a unified model of droplet size evolution from the chamber through the nozzle and into the plume. It is believed that the distribution of droplet mass in the chamber is bimodal lognormal, with 1 micrometer smoke comprising about 80 percent of the mass and 50-100 micrometer caps comprising the remaining 20 percent. During passage through the nozzle, the caps shatter to product droplets whose diameters are about 10 percent of the caps but still 10 times those of smoke, while all but 1-2 percent of the smoke mass collides and coalesces with the shatter products to generate an essentially monomodal mass distribution at the nozzle exit whose D(sub 43) agrees with Hermsen's correlation and whose standard deviation sigma approximately equals 0.13 is smaller than both the chamber smoke (sigma approximately equals 0.40) or caps (sigma approximately equals 0.20). Author

N95-30988 Georgia Inst. of Tech., Atlanta, GA.

THE Al AND A(LC)L2O3 DROPLET CLOUD IN SOLID ROCKET MOTORS c20

Ed W. Price and R. K. Sigman *In* JHU, The 21st JANNAF Exhaust Plume Technology Meeting, Volume 1 Oct. 1994 p 19-28 (For primary document see N95-30986 11-34)

(Contract N00014-89-J-1293)

Avail: CPIA, 10630 Little Patuxent Pkwy., Suite 202, Columbia, MD 21044-3200 HC

A discussion is presented of the current state of understanding and prediction of size and spatial distribution of aluminum and Al2O3 droplets in a motor. It is noted that available theory and experimental results are inadequate for prediction of two phase flow effects (e.g., slag formation, damping of oscillations), especially with propellants other than those based on AP and hydrocarbon binder. Potentially important phenomena that have received almost no attention include fragmentation of Al droplets near burnout, and growth of larger oxide droplets by accretion of fine 'smoke' droplets. Author

N95-30989*# Naval Air Warfare Center, China Lake, CA.

SHUTTLE REDESIGNED SOLID ROCKET MOTOR ALUMINUM OXIDE INVESTIGATIONS c20

Fred S. Blomshield, Karl J. Kraeutle, and Richard A. Stalnaker *In* JHU, The 21st JANNAF Exhaust Plume Technology Meeting, Volume 1 Oct. 1994 p 29-39 Sponsored by NASA. Marshall Space Flight Center (For primary document see N95-30986 11-34)

Avail: CPIA, 10630 Little Patuxent Pkwy., Suite 202, Columbia, MD 21044-3200 HC

During the launch of STS-54, a 15 psi pressure blip was observed in the ballistic pressure trace of one of the two Space Shuttle Redesigned Solid Rocket Motors (RSRM). One possible scenario for the observed pressure increase deals with aluminum oxide slag formation in the RSRM. The purpose of this investigation was to examine changes which may have occurred in the aluminum oxide formation in shuttle solid propellant due to changes in the ammonium perchlorate. Aluminum oxide formation from three propellants, all having the same formulation, but containing ammonium perchlorate from different manufacturers, will be compared. Three methods have been used to look for possible differences among the propellants. The first method was to examine window bomb movies of the propellants burning at 100, 300 and 600 psia. The motor operating pressure during the pressure blip was around 600 psia. The second method used small samples of propellant which were fired in a combustion bomb which quenched the burning aluminum particles soon after they left the propellant surface. The bomb was fired in both argon and Nitrogen atmospheres at various pressures. Products from this device were examined by optical microscopy. The third method used larger propellant samples fired into a particle collection device which allowed the aluminum to react and combust more completely. This device was pressurized with Nitrogen to motor operating pressures. The collected products were subdivided into size fractions by screening and sedimentation and analyzed optically with an optical microscope. The results from all three methods indicate very small changes in the size distribution of combustion products. Author

N95-30990 Brigham Young Univ., Provo, UT.

BURN TIME MEASUREMENTS OF SINGLE ALUMINUM PARTICLES IN STEAM AND CARBON DIOXIDE MIXTURES c25

Shane E. Olsen and Merrill W. Beckstead *In* JHU, The 21st JANNAF Exhaust Plume Technology Meeting, Volume 1 Oct. 1994 p 41-58 (For primary document see N95-30986 11-34)

(Grant AF-AFOSR-0152-91)

Avail: CPIA, 10630 Little Patuxent Pkwy., Suite 202, Columbia, MD 21044-3200 HC

In this study, single aluminum particles (40 to 80 micrometers) were burned in H2O/CO2 mixtures. Burn times were measured electronically using a PMT. In addition, the effect of oxidizer composition was determined. Burn times were also measured for single particles, quenched at various stages of combustion. SEM micrographs of quenched specimens were obtained. The results were used in determining particle burn times. Study of quenched particles revealed the formation of large hollow aluminum oxide spheres nearly the size of the original aluminum particle. These spheres have been reported by other investigators at both atmospheric and high pressure conditions. It was found that burn time measurements

are very sensitive to the method of analysis used. Using the results of an aluminum combustion model by Brooks (1993), effective oxygen concentrations were calculated for this work and other data. A relationship exists between the effective oxygen concentration and burn times reported for a given diameter. The particle burn times measured in this work compare well with other data if the effective oxygen concentration is properly accounted for. Author

N95-30991 Science Applications International Corp., Fort Washington, PA. Propulsive Sciences Div.

HOT JET/WAKE TURBULENT STRUCTURE AND LASER PROPAGAION. PART 1: JET/WAKE TURBULENCE MODELING

Sandy M. Dash and D. C. Kenzakowski *In* JHU, The 21st JANNAF Exhaust Plume Technology Meeting, Volume 1 Oct. 1994 p 59-78 (For primary document see N95-30986 11-34)

(Contract PSR-92-1028-01)

Avail: CPIA, 10630 Little Patuxent Pkwy., Suite 202, Columbia, MD 21044-3200 HC

The prediction of laser propagation through the hot turbulent exhaust of an aircraft (or missile) requires knowledge of the detailed turbulent structure, and in particular, density/temperature fluctuations and inner/outer turbulent scales. The ability to predict the mean flow structure of round turbulent jets in an isolated environment has now become well established including hot jets and supersonic jets. However, the ability to predict density or temperature fluctuations and inner scales is poorly established, as is the ability to predict jet interactions with the aerodynamic vorticity (e.g. with the wing-tip vortex). A three-tier program of work has been in progress to enhance our understanding of the turbulent structure in hot jets and its influence on laser propagation. In Part 1 of this paper, the turbulence modeling activities will be described whose basis is the new data being generated at NASA LaRC, to be described in Part 2 of this paper. The kappa epsilon turbulence model and 'g' scalar-fluctuation extension have been implemented in this work. The coefficients of the g-equation have been revised in accordance with new temperature fluctuation data for hot, subsonic jets into still air. Data is now being gathered for hot jets in a co-flow which interact with wing-tip vortices. The inclusion of the g-equation into a Navier-Stokes framework and its analysis of this complex jet data for which detailed turbulence statistics will be available will comprise the main part of this paper. The utility of direct numerical simulation (LES approach to be described in paper by Sinha and Dash) to provide additional insight into this complex problem will also be discussed. Part 2 of this paper discusses the new data, the measurement techniques, and the complexities entailed in data reduction. Part 3 discusses the military applications (laser countermeasures), new laser propagation data through hot jets (as well as new atmospheric turbulence data), and predictive methodology. Author

N95-30992 Pacific-Sierra Research Corp., Santa Monica, CA.

HOT JET/WAKE TURBULENT STRUCTURE AND LASER PROPAGATION. PART 3: LASER PROPAGATION MEASUREMENTS AND MODELING

Alan R. Shapiro and J. H. Churnside (National Oceanic and Atmospheric Administration, Boulder, CO.) *In* JHU, The 21st JANNAF Exhaust Plume Technology Meeting, Volume 1 Oct. 1994 p 79-95 (For primary document see N95-30986 11-34)

(Contract F33615-92-C-1028)

Avail: CPIA, 10630 Little Patuxent Pkwy., Suite 202, Columbia, MD 21044-3200 HC

The use of lasers aboard aircraft is affected by the perturbed airflow in its vicinity. Therefore, an ability to predict the structure of aircraft-induced turbulence would be useful in system and performance analysis. Pacific-Sierra Research Corp. performed temperature and velocity fluctuation measurements in the wakes of an NRA-3B and a B-1B at trail distances of 50 to 5500 m, at two Mach numbers (0.5 and 0.75) and at two altitudes (0.9 and 6 km). Analysis of the data suggested significant differences with the predictions of the computational fluid dynamics code (CFD) WAKE developed for this application by ARAP for the U.S. Air Force. The magnitude and scales of the temperature fluctuations suggest that first order laser propagation models would not apply. The principal difference between the data and the CFD predictions is that the temperature fluctuations which determine C(n)-2 are not isotropic-and exhibit spectra and correlation scales which differ greatly from those of velocity. This paper reports wind tunnel measurements to determine the source of this temperature structure in aircraft wakes and laser propagation measurements in this regime. Modifications to CFD and to propagation models are suggested. Author

N95-30993*# Science Applications International Corp., Fort Washington, PA. Propulsive Sciences Div.

LARGE EDDY SIMULATION OF JETS USING STRUCTURED UPWIND NUMERICS

N. Sinha and Sandy M. Dash *In* JHU, The 21st JANNAF Exhaust Plume Technology Meeting, Volume 1 Oct. 1994 p 97-115 (For primary document see N95-30986 11-34)

(Contract NAS1-19570)

Avail: CPIA, 10630 Little Patuxent Pkwy., Suite 202, Columbia, MD 21044-3200 HC

This paper discusses the analysis of unsteady jets/free shear flows using large eddy simulation (LES) methodology which directly calculates the turbulence large-scale structure and models the higher frequency, finer scales, using subgrid stress (SGS) terms. Fundamental shear layer studies had exhibited the ability of this approach to yield accurate rms values of density/temperature fluctuations (of interest in optical propagation studies), not readily calculable by conventional time-averaged turbulence models. Unsteady phenomena associated with acoustic/turbulence interactions such as vortex shedding are calculable using LES methodology and provide solutions to many complex problems where acoustic waves change the jet structure significantly (e.g. jet passing over a cavity). This paper presents in detail the analysis of a planar, underexpanded Mach 2 jet mixing with quiescent, ambient air. The paper presented the transient features of the rapidly oscillating jets as well as the 'time-averaged' mean flow pattern. Turbulent statistics have been derived by sampling the instantaneous data and spectral characteristics identified. Author

N95-30994 Spectral Sciences, Inc., Burlington, MA.

THE PASSAGE FROM TRANSITIONAL TO FREE MOLECULAR PLUMES

James B. Elgin, Edmond Murad (Phillips Lab., Hanscom AFB, MA.), and Charles Pike (Phillips Lab., Hanscom AFB, MA.) *In* JHU, The 21st JANNAF Exhaust Plume Technology Meeting, Volume 1 Oct. 1994 p 117-127 (For primary document see N95-30986 11-34)

(Contract F19628-91-C-0145)

Avail: CPIA, 10630 Little Patuxent Pkwy., Suite 202, Columbia, MD 21044-3200 HC

As DSMC (Direct Simulation Monte Carlo) transition flow plume codes (e.g., SOCRATES or the Monte Carlo modules of CHARM) are applied at increasing altitudes (or decreasing thrusts), the calculations do not always get progressively easier; rather, they tend to reach a 'plateau' of computational difficulty. Unfortunately, this plateau is frequently still a substantial burden for current computers. To address this problem, simplified free molecular models (for example the HAPAIR module of CHARM) have been devised. These models usually consider only first collisions and ignore quenching and molecular motion between the points of excitation and emission. In the case of HAPAIR, there is also an additional simplification made of constant gas-kinetic cross sections. Under the above assumptions, the free molecular models never agree with the Monte Carlo transition flow modules, and the discontinuity between the two predictions has been the source of vexation in the past. The present paper introduces a new free molecular flow model called NOMAD (an acronym for Nonequilibrium Original Monte-Carlo with Approximate Dynamics), which runs two to three orders of magnitude faster than the transition flow Monte Carlo modules, yet agrees with them when applied in the free molecular flow regime. The theory behind this new approach is discussed and sample comparisons are given. Author

N95-30995 Aero Optics, Inc., Rolling Hills Estates, CA.

VACUUM PLUME BACKFLOW AND RAREFACTION

Gordon R. Scriven and G. N. Freeman *In* JHU, The 21st JANNAF Exhaust Plume Technology Meeting, Volume 1 Oct. 1994 p 129-136 (For primary document see N95-30986 11-34)

Avail: CPIA, 10630 Little Patuxent Pkwy., Suite 202, Columbia, MD 21044-3200 HC

Spacecraft surface contamination and sensor interference can result from nozzle-exhaust molecules, droplets, and/or condensate-clusters which expand and scatter to fill the space volume at large angles from the nozzle thrust axis. Only a small fraction of the exhaust products expands

to large angles; however, the amount is sufficient to influence the design and performance of spacecraft sensor platforms which are subject to contamination/interference effects. The large-angle plume mass/species distribution functions depend on (1) the interacting effects of pressure/shear forces and diffusion/rarefaction effects during the rapid angular expansion at the nozzle lip, and (2) the nozzle boundary layer characteristics upstream of the lip expansion. Prediction methods include Euler or Navier-Stokes for continuum regions and direct simulation Monte Carlo (DSMC) for transitional regions. A new formulation was developed which extends the viscous-flow equations (in flow-conformal curvilinear coordinates) to account for flow rarefaction effects. The formulation provides a unified continuous prediction capability which bridges from the continuum region of the nozzle interior to the rarefied region of the plume backflow. Predictions are shown which illustrate the impact of viscous/rarefaction effects on the near-field plume expansion and far-field angular mass flux distribution. Author

N95-30996 Hughes STX, Inc., Edwards AFB, CA.
COMPARISON OF DSMC PREDICTIONS WITH TEMPORALLY RESOLVED VIBRATIONAL STATE MEASUREMENTS IN NO
Ingrid J. Wysong and David H. Campbell *In* JHU, The 21st JANNAF Exhaust Plume Technology Meeting, Volume 1 Oct. 1994 p 137-142
(For primary document see N95-30986 11-34)
Avail: CPIA, 10630 Little Patuxent Pkwy., Suite 202, Columbia, MD 21044-3200 HC

A laser pump-probe experimental technique has been used to obtain temporally resolved vibrational population distributions in the lower vibrational levels of NO under non-equilibrium conditions. These vibrational population time histories have been compared to direct simulation Monte Carlo predictions in which the vibrational levels are treated as individual chemical species in the calculation. The effects of using species weighting factors in the calculation have also been investigated. Weighting factors will be needed when minor species must be tracked (such as for UV radiation) if large, realistic calculations are to be feasible. However, it appears that the present implementation of weighting factors is seriously flawed. Author

N95-31100 California Univ., Santa Barbara, CA.
STUDY OF EFFECT OF BUBBLES ON A FREE-SHEAR LAYER Ph.D. Thesis
Sanjeev Kumar 1993 240 p
Avail: Univ. Microfilms Order No. DA9419083

An experimental study of the effect of bubbles on a free shear flow - a mixing layer - has been carried out. The problem of dispersion of particles in a mixing layer has been a topic of extensive research, both experimental and numerical, in the past. Numerical schemes assume a one way coupling between the two phases for dilute solutions i.e., the dynamics of the particles in the shear layer is assumed to be governed by the underlying flow field, but the fluid flow pattern is not modified due to the presence of particles. The objective of these experiments was to investigate whether the presence of particles in the shear layer modifies the flow field in terms of the growth of the mixing layer and the characteristics of the flow field therein. Experiments were performed in a closed loop water tunnel. Quantitative information was obtained using optical flow measurement and visualization techniques. The results show that for a void fraction of 0.5 percent the growth rate of the shear layer is modified in the initial as well as the turbulent region of the shear layer. In the initial region a change in the vortex merging pattern is observed and in the far downstream region the growth rate is observed to increase by as much as 25 percent for certain flow conditions. Different factors which could influence the flow field are discussed. These include the change in density, compressibility, and viscosity of the fluid due to the presence of particles in the flow as well as the change in initial conditions, and the dynamics of bubbles inside the shear layer. No attempt has been made to describe the relative importance of the factors which can be considered significant, because in the experiments it was not possible to isolate the influence of one factor from another. Dissert. Abstr.

N95-31132# Oak Ridge National Lab., TN.
QMR METHODS IN COMPUTATIONAL FLUID DYNAMICS
N. M. Nachtigal and B. D. Semeraro 1995 10 p Presented at the 12th AIAA Computational Fluid Dynamics Conference, San Diego, CA, 19-22 Jun. 1995
(Contract DE-AC05-84OR-21400)
(DE95-010293; CONF-950634-2) Avail: CASI HC A02/MF A01

The authors examine the application of QMR (Quasi-Minimal Residual) methods to the solution of linear systems of equations arising from the use of implicit solution methods in computational fluid dynamics. They will deal with implicit finite difference schemes for solving the Euler equations. These schemes may arise from the implicit treatment of the time dependent equations or from the use of Newton's method for the solution of the steady state equations. In both situations it is necessary to solve a large sparse nonsymmetric linear system of equations at each iteration. They will examine the effectiveness of QMR in the solution of these systems. They compare the resulting methods to methods which rely on some other simplifying technique to solve the linear systems. The goal is to show that the QMR method is a viable alternative to the more ad-hoc schemes for solving implicit computational fluid dynamics problems. DOE

N95-31317 Iowa Univ., Iowa City, IA.
ROLE OF FREE-SURFACE BOUNDARY CONDITIONS AND NONLINEARITIES IN WAVE/BOUNDARY-LAYER AND WAKE INTERACTION Ph.D. Thesis
Jung-Eun Choi 1993 344 p
Avail: Univ. Microfilms Order No. DA9421109

In Part One of this two-part thesis, laminar and turbulent solutions are presented for the Stokes-wave/flat-plate boundary-layer and wake for small - large wave steepness, including exact and approximate treatments of the viscous free-surface boundary conditions. The macro-scale flow exhibits the wave-induced pressure-gradient effects described in a precursory work. For laminar flow, the micro-scale flow indicates that the free-surface boundary conditions have a profound influence over the boundary layer and near and intermediate wake: the wave elevation and slopes correlate with the depthwise velocity; the streamwise and transverse velocities and vorticity display large variations, including islands of maximum/minimum values, whereas the depthwise velocity and pressure indicate small variations; significant free-surface vorticity flux and complex vorticity transport are displayed; wave-induced effects normalized by wave steepness are larger for small steepness with the exception of wave-induced separation; order-of-magnitude estimates are confirmed; and appreciable errors are introduced through approximations to the free-surface boundary conditions. For turbulent flow, the results are similar, but preliminary due to the present uncertainty in appropriate treatment of the free-surface boundary conditions and meniscus boundary layer. In Part Two, Navier-Stokes, boundary-layer, and perturbation expansion solutions are presented for the model problem of a flat-plate boundary layer and wake with temporal, spatial, and traveling horizontal-wave external flows, which are characterized by Stokes-layer overshoots, phase angles, and streaming and nonlinearities. The temporal wave displays close agreement with previous studies and is useful for validation and placing the current work in technical perspective. The spatial wave indicates significantly increased magnitudes and complex nature (e.g., wake bias), which is attributed to nonlinearities associated with large convective acceleration, i.e., nonlinear interaction between the steady and first-harmonic solutions. The traveling wave shows limiting behavior for small and large wave speed of the spatial and temporal waves, respectively, and smooth transition between the two for intermediate values, and extreme wake response for small wave speeds and short wave lengths. In both Parts, implications with regard to practical applications are discussed.
Dissert. Abstr.

N95-31341*# Colorado Univ., Boulder, CO. Dept. of Aerospace Engineering Sciences.
NUMERICAL SIMULATION OF SHOCK/TURBULENT BOUNDARY LAYER INTERACTION Final Year Report
Sedat Biringen and Ferhat F. Hatay [1993] 47 p
(Grant NAG1-1472)
(NASA-CR-198846; NAS 1.26:198846) Avail: CASI HC A03/MF A01

Most flows of aerodynamic interest are compressible and turbulent. However, our present knowledge on the structures and mechanisms of turbulence is mostly based on incompressible flows. In the present work, compressibility effects in turbulent, high-speed, boundary layer flows are systematically investigated using the Direct Numerical Simulation (DNS) approach. Three-dimensional, time-dependent, fully nonlinear, compressible Navier-Stokes equations were numerically integrated by high-order finite-difference methods; no modeling for turbulence is used during the

solution because the available resolution is sufficient to capture the relevant scales. The boundary layer problem deals with fully-turbulent compressible flows over flat geometries. Apart from its practical relevance to technological flows, turbulent compressible boundary layer flow is the simplest experimentally realizable turbulent compressible flow. Still, measuring difficulties prohibit a detailed experimental description of the flow, especially in the near-wall region. DNS studies provide a viable means to probe the physics of compressible turbulence in this region. The focus of this work is to explore the paths of energy transfer through which compressible turbulence is sustained. The structural similarities and differences between the incompressible and compressible turbulence are also investigated. The energy flow patterns or energy cascades are found to be directly related to the evolution of vortical structures which are generated in the near-wall region. Near-wall structures, and mechanisms which are not readily accessible through physical experiments are analyzed and their critical role on the evolution and the behavior of the flow is documented extensively.

Author

N95-31349 Stanford Univ., CA.
SHEAR-FREE TURBULENT BOUNDARY LAYERS Ph.D. Thesis
James Blair Perot 1994 189 p
Avail: Univ. Microfilms Order No. DA9414637

Walls affect turbulence through a number of different mechanisms. The most prominent and well understood mechanism is that due to mean shear. But other, more subtle mechanisms also exist and can be isolated through the study of shear-free boundary layers where the influence of mean shear has been eliminated. In this work, direct numerical simulation on a massively parallel supercomputer (the Connection Machine) is used to investigate the shear-free turbulent boundary layer. The physics of the near wall region and the wall/turbulence interaction is fully investigated and the resulting physical insights are then used to improve near wall turbulence models. Performance comparisons between the Cray Y-MP and the Connection Machine are presented and massively parallel programming issues are discussed. The viscous and kinematic mechanisms of the wall/turbulence interaction are isolated, and a physical model of near wall behavior that is consistent with simulation data is presented. Improved near wall models for the dissipation, pressure-strain, and turbulent transport terms of the Reynolds stress evolution equations are discussed.

Dissert. Abstr.

N95-31355# Deutsche Forschungsanstalt fuer Luft- und Raumfahrt, Cologne (Germany). Inst. fuer Antriebstechnik.
EXPERIMENTAL INVESTIGATION OF TURBULENT PARTICLE DISPERSION IN SWIRLING FLOWS Ph.D. Thesis - Ruhr Univ. Bochum [EXPERIMENTELLE UNTERSUCHUNG DER TURBULENTEN PARTIKELDISPERSION IN DRALLSTROEMUNGEN]
Christoph Hassa [1994] 155 p In GERMAN
(ISSN 0939-2963)
(DLR-FB-94-20) Avail: CASI HC A08/MF A02

The turbulent particle dispersion is investigated with regard to the two-phase flow of fuel spray and combustion air in gas turbine combustion chambers. For that purpose, an atmospheric isothermal experiment is presented, that allows the verification of mathematical models for the calculation of turbulent two-phase flows by virtue of the application of nonintrusive measuring techniques and the similarity of its flow configuration to the practical flow. The basic configuration of the gas flow is an axisymmetric, expanding swirl flow with a practical swirl strength and expansion ratio. By using a monodisperse droplet generator, the investigation of turbulent dispersion was separated from atomization. For the gaseous phase, mean and fluctuating velocities as well as Eulerian integral time scales have been measured. The droplet-phase is documented by the measurement of droplet-flux density, velocity, and ensemble rms velocity.

Author

N95-31412 Clarkson Univ., Potsdam, NY.
SELF-ADAPTIVE MULTILEVEL METHODS FOR FLUID FLOW PROBLEMS Ph.D. Thesis
Anwar M. Saleh 1994 122 p
Avail: Univ. Microfilms Order No. DA9416309

A computational study of self-adaptive multilevel methods for complex fluid flow problems is made to test the efficiency of these methods. The model problem is time-dependent, nonlinear, convective dominated, and diffusion-limited. Numerical solutions exist, although not multilevel or adaptive ones. A comparison of two adaptive multilevel methods, the multilevel adaptive technique (MLAT) and the fast adaptive composite grid method (FAC), is given to show the possible advantages of the FAC method over the MLAT method by applying them to solve a Poisson equation with an analytical solution. The model problem consists of the quasi-compressible system of the anelastic equations with an initial condition representing a negatively buoyant blob of cold air, which descends to the ground and spreads laterally forming a cold front. A multilevel solution is first obtained on a staggered grid using finite differencing both in time and space. Then the two self-adaptive multilevel methods (MLAT ant FAC) are applied. Numerical results are discussed and compared to numerical solution obtained by Fulton (18) using a Fourier-Chebyshev spectral method with a semi-implicit Runge-Kutta scheme for time integration. Numerical results, as expected, show the FAC is more accurate (at interface) than the MLAT when applied to a Poisson equation. When the self-adaptive versions of the FAC and the MLAT are applied to the complex anelastic equations, computational results show little difference between the two methods and a saving of up to 70 percent in execution time (compared to uniform grid methods of the same accuracy), and when compared to a Fourier-Chebyshev spectral model of the same problem, they are faster for modest accuracy, while the spectral method is faster for higher accuracy.

Dissert. Abstr.

N95-31414# Royal Inst. of Tech., Stockholm (Sweden). Dept. of Numerical Analysis and Computing Science.
NUMERICAL SIMULATION OF TIME DEPENDENT VISCOELASTIC FLUID FLOW
Fredrik Olsson [1993] 7 p Prepared in cooperation with Stockholm Univ., Sweden
(TRITA-NA-9311) Avail: CASI HC A02/MF A01

In the last decade, the numerical methods for solving stationary viscoelastic flows have developed rapidly. Many flows with strong viscoelastic or non-Newtonian behavior can be predicted quite accurately. There are however some basic problems remaining to be solved. One is to calculate the flow in irregular geometries, such as the flow around convex corners. Another problems is to predict flow instabilities, which are different from those seen for a Newtonian fluid. Depending on the flow, the introduction of elasticity can both stabilize and destabilize it. Several of the existing methods rely on constitutive equations on differential form, most of which are based on the upper convected Maxwell (UCM) model. The UCM model can be derived from basic assumptions using simple molecular models, continuum mechanical arguments, or physical considerations. However, this constitutive equation is more often used in modified forms which comply better with experiments and behave better numerically. The Giesekus and the PTT model are two popular models which differ from the constitutive equation only in lower order terms, i.e. in terms with no derivatives. Since lower order terms generally do not change the well-posedness properties of a partial differential equation, we will study the UCM model. It enables us to see that this model gives a well-posed system of partial differential equations. We also see why the modified models behave better in numerical computations.

Derived from text

N95-31415# Royal Inst. of Tech., Stockholm (Sweden). Dept. of Numerical Analysis and Computing Science.
SOME ASPECTS ON THE MODELLING OF NON-NEWTONIAN FLUID FLOW
Jacob Ystroem [1993] 6 p Prepared in cooperation with Stockholm Univ., Sweden
(TRITA-NA-9317) Avail: CASI HC A02/MF A01

Several of the existing models describing viscoelastic fluid flow rely on constitutive equations on differential form. The essential difference of these constitutive equations to the equations describing a Non-Newtonian fluid with a generalized Newtonian constitutive equation, is that a time derivative of the stress tensor is included. This term mimics memory effects for the material, and gives a relaxation model for the stresses. The larger the coefficient is for the time derivative the larger the 'memory' effect is. One of the simplest constitutive equations of this type is the Upper Convected Maxwell (UCM) model. If Newtonian viscosity is also included one obtains the Oldroyd-B model, the up till now mostly used model for viscoelastic fluid flow simulations. The UCM model can be derived from basic assumptions using simple molecular models or continuum mechanics arguments. There is a family of models often used to comply better with

experiments and rheological behavior that are mathematically obtained by adding lower order terms to the UCM model. In this paper we consider a viscoelastic fluid with artificial compressibility and assume a linear relationship between the pressure and the density, where rho(*), and p(*) are constants. Derived from text

N95-31423*# Allison Engine Co., Indianapolis, IN.
ADVANCED k-EPSILON MODELING OF HEAT TRANSFER Final Report
Okey Kwon and Forrest E. Ames Jul. 1995 153 p
(Contract NAS3-25950; RTOP 505-62-10)
(NASA-CR-4679; E-9748; NAS 1.26:4679) Avail: CASI HC A08/MF A02

This report describes two approaches to low Reynolds-number k-epsilon turbulence modeling which formulate the eddy viscosity on the wall-normal component of turbulence and a length scale. The wall-normal component of turbulence is computed via integration of the energy spectrum based on the local dissipation rate and is bounded by the isotropic condition. The models account for the anisotropy of the dissipation and the reduced mixing length due to the high strain rates present in the near-wall region. The turbulent kinetic energy and its dissipation rate were computed from the k and epsilon transport equations of Durbin. The models were tested for a wide range of turbulent flows and proved to be superior to other k-epsilon models, especially for nonequilibrium anisotropic flows. For the prediction of airfoil heat transfer, the models included a set of empirical correlations for predicting laminar-turbulent transition and laminar heat transfer augmentation due to the presence of freestream turbulence. The predictions of surface heat transfer were generally satisfactory. Author

N95-31432# Christian Brothers Coll., Memphis, TN.
IMPROVED MODELING OF UNSTEADY HEAT TRANSFER (THE FIRST STEP) Final Report, 1 Jun. - 31 Jul. 1994
Mark A. Driver 28 Feb. 1995 69 p
(Contract F49620-94-1-0292)
(AD-A292777; AFOSR-95-0192TR) Avail: CASI HC A04/MF A01

Application of Total Variation Diminishing (TVD) schemes to turbulent flows is considered. The mathematical and physical basis of TVD schemes is discussed. TVD methodology is extended to the solution of turbulent flow problems. A first-order time accurate, second-order space accurate algorithm is used to compute solutions to the problems of shock-boundary-layer interaction, turbine rotor cascade flow, and unsteady, shock-induced heat transfer using the TVD algorithm. This algorithm provides the capability to accurately predict separation, reattachment and pressure and skin friction profiles for shock-boundary-layer inter action. Improved accuracy is demonstrated in computing surface pressures for a turbine rotor cascade. Heat transfer for the cascade is predicted with fair accuracy, showing all the significant features of the experimental Stanton number profile. Fairly accurate comparison with theory and experiment is evident in the unsteady solutions. DTIC

N95-31443# Mississippi Univ., University, MS.
INVESTIGATING THE USE OF SMART ACOUSTICALLY ACTIVE SURFACES FOR FLOW SEPARATION CONTROL IN TURBOMACHINERY Final Report, 1 Sep. 1991 - 31 Aug. 1994
Sumon K. Sinha 21 Feb. 1995 60 p
(Grant AF-AFOSR-0410-91)
(AD-A292819; SKS/95/1; AFOSR-95-0191TR) Avail: CASI HC A04/MF A01

In order to develop a mechanically simple and robust actuator for active flow separation control on axial compressor blades, three different types of acoustic transducers were tested in a wind tunnel. Flow separation on a cylinder in cross flow was used. The first transducer had an internally mounted acoustic speaker blowing through a slot. It could control flow separation only for low Reynolds number laminar flows. A flush mounted high-frequency circular piezo-electric transducer was tried next. It was marginally effective only around the laminar-turbulent transition regime. Since it could not focus the perturbations over a small area, the Acoustosurf was developed next. It consisted of an array of flush mounted narrow strip shaped acoustic transducers capable of detecting surface pressure fluctuations prior to separation. When the appropriate strips were excited at the predominant fluctuation frequency, separation was delayed for transitional and tripped flows. It is believed that the Acoustosurf produces a synergistic interaction between roughness, surface compliance and acoustic radiation to redirect the kinetic energy of the flow by exploiting flow instabilities. Negligible power is therefore needed to operate the Acoustosurf. This has attracted the attention of several aircraft manufacturers. DTIC

N95-31475# Hampton Univ., VA.
APPLICATION OF MULTIGRID COMPUTATIONAL FLUID DYNAMICS (CFD) METHODS TO ROTOR ANALYSIS Final Report, 1 Sep. 1993 - 31 Aug. 1994
Hong Hu Mar. 1995 158 p
(Contract DAAJ02-93-C-0021)
(AD-A293012; USAATCOM-TR-94-D-22) Avail: CASI HC A08/MF A02

The TLNS3DR code is applied to various advanced rotor blades to study tip vortex and to investigate the general capabilities of the code. For nonrotating flows, the solutions in terms of the tip vortex and surface pressure coefficients are obtained for realistic helicopter rotor-tip configurations to study effects of blade planforms on the tip vortex under incompressible flow condition. Calculated results are compared with experimentally obtained data at NASA-Langley's Basic Aerodynamic Research Wind Tunnel (BART). A Berp-type tip, a swept-type tip and its equivalent taper-type tip configurations are investigated. For both nonrotating and rotating flows, the Berp-type blade, the swept-type blade, and its equivalent taper-type and rectangle-type blades with zero twist are considered under compressible flow condition. Solutions are presented. DTIC

N95-31516# Air Force Inst. of Tech., Wright-Patterson AFB, OH. School of Engineering.
COMPRESSIBLE TURBULENCE MEASUREMENT IN LOW-ANGLE INJECTION INTO A SUPERSONIC FLOW M.S. Thesis
Gregory J. McCann Mar. 1995 119 p
(AD-A293836; AFIT/GAE/ENY/95M-03) Avail: CASI HC A06/MF A02

Mean flow and compressible turbulence measurements have been obtained at two stations downstream of low-angle supersonic injection into a Mach 3.0 flow (Re/m = 15 x 10(exp 6)). Data were collected using conventional Pitot and cone-static probes, single and multiple overheat cross-wire anemometry, and flow visualization techniques (shadowgraphs and schlierens). A direct measure of total Reynolds shear stress was accomplished using a turbulence transformation of the Reynolds-averaged Navier-Stokes equations. Results show compressibility effects, indicated by density fluctuations, to be large relative to the velocity fluctuations and on the same order in all three components. Compressibility appears to account for as much as 75% of the total Reynolds shear. The results of the present study suggest turbulent compressibility effects are very important for this class of flows. DTIC

N95-31532 Duke Univ., Durham, NC.
FUNDAMENTAL TOPICS IN HEAT TRANSFER THROUGH DEFORMABLE TWO-PHASE MEDIA Ph.D. Thesis
Alex Jackson Fowler 1993 217 p
Avail: Univ. Microfilms Order No. DA9414128

The reported research focuses on fundamental aspects of convection in a wide variety of media. Chapter 1 investigates the effect of shrinkage during the cooking of meat. Results are reported in the form of dimensionless charts. Comparing these charts with the Heisler charts indicates that shrinkage can have a significant effect on predicted cooking times. Chapter 2 applies contact melting theory to the analysis of sliding on ice. Both pressure melting and viscous heating are taken into account. The results compare favorably with experimental measurements. A method is also proposed to account for ice asperities in the melting model. Chapter 3 is a numerical analysis of natural convection in a porous medium composed of fibers coated with a phase-change material. The results present the time for complete melting of the fiber coatings. It is also shown that these results can be used to predict the solidification time of the fiber coatings. Chapter 4 focuses on trying to develop a universal curve for determining the optimal size of a body with a specified heat transfer duty parameter. The body's optimal size is based either on entropy minimization or cost. Chapter 5 numerically and experimentally investigates the pressure drop and heat transfer in forced convection through tube bundles at low Reynolds numbers, in the fully developed regime, and if the tube bundles are not necessarily perpendicular to the flow direction. It is shown that extrapolation of the available heat exchanger data to this regime results in significant

error. Chapter 6 is a numerical investigation of the effect of a flexible fiber coating on forced convection from a plate in stagnation flow. It is shown that simple relationships exist for predicting the heat transfer coefficient from a surface coated with inflexible fibers; and that fiber bending does not have a large impact on the heat transfer coefficient for the cases studied. Dissert. Abstr.

N95-31586# Catholic Univ. of America, Washington, DC. Dept. of Mechanical Engineering.

APPLICATION OF WAVELET-FILTERING TECHNIQUES TO INTERMITTENT TURBULENT AND WALL PRESSURE EVENTS. PART 2. DETECTION OF CLUSTER PATTERNS Progress Report, Nov. 1994 - Nov. 1995

Mario J. Casarella, Pablo B. Penafiel, and Mark E. Kammeyer 26 Apr. 1995 62 p

(Contract N00014-88-K-0141)

(AD-A293805) Avail: CASI HC A04/MF A01

Large amplitude wall-pressure events, observed beneath a turbulent boundary layer, appear to be signatures of intermittent organized motions within the turbulent flow. Experimental studies were made investigating this relationship. Part 1 presented the first phase of this investigation and reported on the results of utilizing time-frequency localization techniques (wavelet transforms) for the detection of these events. The application of wavelet filtering for the analyses of turbulent data was introduced. This report presents the results of the second phase of the investigation. A wavelet filter was selected based on maintaining the integrity of intermittent near wall burst events. The correlations between individual turbulent flow and wall-pressure events were confirmed using both the original time records and the generated VITA function time records. A localized windowed peak detection algorithm was developed that detects the groupings of these events. The algorithm detects the temporal locations and durations of the clusters. Correlation and conditional sampling methods were then used to postulate the sequential burst events contained within the individual clusters. Conditional sampling showed a bidirectional relationship between positive wall-pressure events and burst ejections in the near-wall region. DTIC

N95-31591# Lawrence Livermore National Lab., Livermore, CA.

LARGE-EDDY SIMULATION OF TURBULENT FLOW USING THE FINITE ELEMENT METHOD Ph.D. Thesis

R. C. McCallen 15 Feb. 1995 346 p

(Contract W-7405-eng-48)

(DE95-009464; UCRL-LR-114962) Avail: CASI HC A15/MF A03

The equations of motion describing turbulent flows (in both the low and high Reynolds-number regimes) are well established. However, present day computers cannot meet the enormous computational requirement for numerically solving the governing equations for common engineering flows in the high Reynolds number turbulent regime. The characteristics that make turbulent, high Reynolds number flows difficult to simulate is the extreme range of time and space scales of motion. Most current engineering calculations are performed using semi-empirical equations, developed in terms of the flow mean (average) properties. These turbulence 'models' (semi-empirical/analytical approximations) do not explicitly account for the eddy structures and thus, the temporal and spatial flow fluctuations are not resolved. In these averaging approaches, it is necessary to approximate all the turbulent structures using semi-empirical relations, and as a result, the turbulence models must be tailored for specific flow conditions and geometries with parameters obtained (usually) from physical experiments. The motivation for this research is the development of a finite element turbulence modeling approach which will ultimately be used to predict the wind flow around buildings. Accurate turbulence models of building flow are needed to predict the dispersion of airborne pollutants. The building flow turbulence models used today are not capable of predicting the three-dimensional separating and reattaching flows without the manipulation of many empirical parameters. These empirical parameters must be set by experimental data and they may vary unpredictably with building geometry, building orientation, and upstream flow conditions. DOE

N95-31592# California Univ., Davis, CA. Dept. of Chemical Engineering.

PARTICLE FILTRATION: AN ANALYSIS USING THE METHOD OF VOLUME AVERAGING

M. Quintard and S. Whitaker Dec. 1994 53 p

(Contract W-7405-eng-48)

(DE95-009467; UCRL-CR-119484) Avail: CASI HC A04/MF A01

The process of filtration of non-charged, submicron particles is analyzed using the method of volume averaging. The particle continuity equation is represented in terms of the first correction to the Smoluchowski equation that takes into account particle inertia effects for small Stokes numbers. This leads to a cellular efficiency that contains a minimum in the efficiency as a function of the particle size, and this allows us to identify the most penetrating particle size. Comparison of the theory with results from Brownian dynamics indicates that the first correction to the Smoluchowski equation gives reasonable results in terms of both the cellular efficiency and the most penetrating particle size. However, the results for larger particles clearly indicate the need to extend the Smoluchowski equation to include higher order corrections. Comparison of the theory with laboratory experiments, in the absence of adjustable parameters, provides interesting agreement for particle diameters that are equal to or less than the diameter of the most penetrating particle. DOE

N95-31637# California Univ., Davis, CA. Dept. of Chemical Engineering and Materials Science.

PARTICLE FILTRATION: A COMPARISON BETWEEN THEORY AND EXPERIMENT

M. Quintard and S. Whitaker Dec. 1994 35 p Presented at the Encontro Sobre Escoamento Em Meios Porosos, Floriaopolis, Brazil, 19-21 Oct. 1994

(Contract W-7405-eng-48)

(DE95-009442; UCRL-JC-119485; CONF-9410330-1) Avail: CASI HC A03/MF A01

The process of filtration of non-charged, submicron particles represents an example of transport in homogeneous and heterogeneous porous media that can be analyzed using the method of volume averaging. In this article the authors develop the local volume averaged particle transport equation for a homogeneous filter and compare the results with experimental data. The particle continuity equation is represented in terms of the first correction to the Smoluchowski equation that takes into account particle inertia effects for small Stokes numbers. This leads to a cellular efficiency that contains a minimum in the efficiency as a function of the particle size, and this allows them to identify the most penetrating particle size. Comparison of the theory with experimental results indicates that the first correction to the Smoluchowski equation gives reasonable results for the most penetrating particle size and for smaller particles; however, results for larger particles clearly indicate the need to extend the Smoluchowski equation to include higher order corrections. The influence of local heterogeneities on the measured filter efficiency may account for some of the observed differences between theory and experiment. DOE

N95-31707 Stanford Univ., CA.

ON THE INTERACTIONS BETWEEN PARTICLES AND TURBULENCE IN A FULLY-DEVELOPED CHANNEL FLOW IN AIR Ph.D. Thesis

Johathan D. Kulick 1994 215 p

Avail: Univ. Microfilms Order No. DA9414602

The interactions between small, dense particles and fluid turbulence have been investigated in a downflow, fully-developed channel in air. The particles were selected to respond to some but not all of the scales of turbulent motions. Particle velocities and concentration fields were examined to determine particle response to turbulence. Gas-phase velocities were measured to investigate turbulence modification by particles; particle relaxation time and mass loading were varied. The channel flow was at Reynolds number 13,800. Three classes of narrowly sized spherical beads were used: 50 micron and 90 micron diameter glass beads and 70 micron diameter copper shot. The particles were smaller than the Kolmogorov scale of turbulence; particle relaxation times ranged from 18 ms to 95 ms. Particle mass loadings ranged up to 0.8 yet particle volume fractions remained under 0.02 percent. Particle and gas-phase velocities were measured by LDA, with pedestal amplitude discrimination. Particle concentration fields were determined from computer processed laser flow visualization (these experiments also used 25 micron glass beads and Lycopodium powder). Particle mean velocity profiles were flatter than air velocity profiles. Streamwise particle velocity fluctuation intensities were larger than the corresponding fluid turbulence intensities, while the opposite behavior was observed in the transverse direction. Particle number density distributions furnished evidence of preferential concentration of particles by

turbulence, previously observed in the computational studies of Squires and Eaton. Gas-phase mean velocity profiles exhibited no effects of particle loading, with the air mass flow-rate held constant. Turbulence attenuation increased with both particle mass loading and particle relaxation time, with reductions in turbulence kinetic energy of up to 80 percent. Particles at low mass loadings attenuated turbulence more strongly in the transverse than in the streamwise direction, which is attributed to the different turbulence spectra seen by the particle in the two directions. Turbulence attenuation increased with distance from the wall. Estimates of the contribution of particles to the dissipation of turbulence kinetic energy, based on k-epsilon models, showed that smaller relative increases in dissipation in channel flow, compared with those in forced isotropic turbulence, corresponded to larger reductions of turbulence intensity. Dissert. Abstr.

N95-31708 Stanford Univ., CA.
HEAT TRANSFER IN SHEAR-FREE TURBULENT BOUNDARY LAYERS Ph.D. Thesis
Paul Malan 1994 256 p
Avail: Univ. Microfilms Order No. DA9414613

Shear-free turbulent boundary layers are idealized near-surface flows without gradients in mean velocity. Direct numerical simulation was used to investigate passive-scalar (temperature) transport in these flows. The configuration corresponds to the sudden insertion of infinite, impermeable surfaces into turbulence that was previously isotropic, homogeneous, and at a different, uniform temperature. The study is relevant to: (1) effects of ultra-high free-stream turbulence intensities on surface heat-transfer and (2) scalar transport at the free surfaces of turbulent liquids. It is an important limiting case for turbulent heat transfer models, since the Reynolds analogy fails totally and there is no production of turbulence. Two hydrodynamic boundary conditions were considered: a simulated solid surface and an idealization of a clean, undisturbed, free surface. Statistics are presented for an initial turbulent Reynolds number (Re(sub t) is identical with k(exp 2)/(epsilon nu)) of approximately 150; Prandtl numbers of 0.1, 0.71, and 2; and a constant-temperature thermal boundary condition. Additional data are included for initial turbulent Reynolds numbers of 60 and 380. Visualizations of the instantaneous fields illustrate the turbulent structures that augment the heat transfer. At least one eddy-turnover time after the surfaces are introduced, the heat transfer is governed by turbulent transport (if the turbulent Peclet number is high enough). The heat-transfer coefficient is related to the inverse of the far-field Kolmogorov length-scale for a given fluid Prandtl number and initial turbulence spectrum. Previously reported studies on scalar transport at free surfaces support this finding. A generalized gradient-diffusion model for the turbulent heat-flux was tested. The model appears adequate for the turbulent Peclet numbers considered. Detailed budgets of the terms in the transport equation for the turbulent heat-flux were used to investigate near-surface heat-flux closure hypotheses. New suggestions were made for modeling the diffusive and dissipative correlations. Current models for the turbulent-transport terms do not work well in this situation. The simulation data enable the scalar-pressure gradient correlation to be examined in the absence of any contribution from mean strain. Dissert. Abstr.

N95-31733 Stanford Univ., CA.
CONTROL OF HIGH REYNOLDS NUMBER ROUND JETS Ph.D. Thesis
Philippe Jean-Daniel Juvet 1994 216 p
Avail: Univ. Microfilms Order No. DA9414588

The entrainment and mixing ability of jets are of particular interest in propulsion and combustion systems. The present work concentrates on the experimental investigation of active and passive techniques for control of high Reynolds number jets. Three control techniques were considered; (1) dual-mode dual-frequency acoustic excitation, (2) tangential blowing along an axisymmetric curved wall, and (3) self-excitation. The basic flow was an air jet, with an exit diameter of 20 mm, at Reynolds numbers between 20,000 and 120,000. The flow was studied by hot-wire anemometry and flow visualization. The development of a round jet can be altered significantly by a combined axial-helical acoustic forcing. Entrainment was estimated, using a shroud placed around the jet, at a Reynolds number of 100,000 and for various levels of axial and helical forcing. Dual-mode excitation was shown to increase entrainment by a factor of up to 2.4, which could not be achieved by axial excitation only. Exit shear-layer manipulation did not ease the forcing requirements. The flow produced by tangential blowing along an axisymmetric curved wall placed around the jet exhibits two regimes, depending on the blowing ratio. For a subcritical blowing ratio, the flow is jet-like, whereas for a supercritical blowing ratio, the jet is entirely diverted radially and develops further as a radial wall jet. The key mechanism for this dramatic change of topology was shown to be entrainment. The critical blowing ratio is almost independent of the Reynolds number and lies around 10 percent. A family of exit geometries was found to induce jet self-excitation, which appears attractive as a replacement to external axial acoustic forcing. The main characteristics of these geometries are a sudden cross-section increase (backstep) at the contraction termination, followed by a curved-wall diffuser, and an axisymmetric cavity connected to the backstep. The axial oscillation of the flow separation on the curved wall causes the regular production of vortex rings, as in an axially-excited jet. The oscillation dominant frequency is proportional to the jet throughflow velocity leading to a constant Strouhal number (between 0.2 and 0.4). This Strouhal number depends mainly on the wall radius of curvature. Dissert. Abstr.

N95-31738*# National Aeronautics and Space Administration. Lewis Research Center, Cleveland, OH.
EXPERIMENTAL AND COMPUTATIONAL INVESTIGATION OF THE TIP CLEARANCE FLOW IN A TRANSONIC AXIAL COMPRESSOR ROTOR
Kenneth L. Suder and Mark L. Celestina (Sverdrup Technology, Inc., Brook Park, OH.) Jun. 1995 17 p Presented at the 39th International Gas Turbine and Aeroengine Congress and Exposition, The Hague, Netherlands, 13-16 Jun. 1994, sponsored by ASME
(Contract NAS3-25266; RTOP 505-62-52)
(NASA-TM-106711; E-9076; NAS 1.15:106711) Avail: CASI HC A03/MF A01

Experimental and computational techniques are used to investigate tip clearance flows in a transonic axial compressor rotor at design and part speed conditions. Laser anemometer data acquired in the endwall region are presented for operating conditions near peak efficiency and near stall at 100% design speed and at near peak efficiency at 60% design speed. The role of the passage shock/leakage vortex interaction in generating endwall blockage is discussed. As a result of the shock/vortex interaction at design speed, the radial influence of the tip clearance flow extends to 20 times the physical tip clearance height. At part speed, in the absence of the shock, the radial extent is only 5 times the tip clearance height. Both measurements and analysis indicate that under part-speed operating conditions a second vortex, which does not originate from the tip leakage flow, forms in the endwall region within the blade passage and exits the passage near midpitch. Mixing of the leakage vortex with primary flow downstream of the rotor at both design and part speed conditions is also discussed. Author

N95-31817# Polish Academy of Sciences, Warsaw (Poland). Mechanics Center.
SELECTED FLOWS WITH FREE SURFACES: STREAMS AND DROPS [WYBRANE PRZEPLYWY ZE SWOBODNA POWIERZCHNIA: STRUGI I KROPLE]
Tomasz A. Kowalewski Mar. 1995 96 p In POLISH
(ISSN 0208-5658)
(IFTR-3/1995) Avail: CASI HC A05/MF A01

The basic purpose of the research described in this article was to develop a non contact method for diagnosing the physical parameters of the free surface of a liquid using drop oscillation analysis. In particular, the purpose is to measure the temperature of an evaporating surface. The realization of this goal has led to the development of new experimental techniques which make it possible to record fast processes using video and digital imaging equipment. Experimental studies of the process of the formation of drops as a result of the controlled breakup of a stream revealed the existence of an additional phase in the process based on the formation of microstreams and microsatellites with micrometer-like dimensions. A comparison of measurement results with Eggers' asymptotic model (23) confirmed the model's basic assumption of the local nature of the final phase in the disintegration of the stream, which at the same time points to the existence of a number of discrepancies which provide evidence of the limitations of this approximation. The next part of the article presents the results of observations of the instability of streams of liquid caused by its evaporation. In an attempt to analyze the mechanisms which initiate the turbulence of the evaporating surface, the author focused on surface tension gradients as an essential factor in the destabilization of

small-diameter streams. The author also described the occurrence of a number of new phenomena in the destabilization of a stream, including the separation of surface fragments, their stabilization by the flow of vapor, and a quasistable change in the trajectory of the stream. The author also developed an experimental method which makes it possible to detect and produce a precise description of the deformation of drops. Measurements of the oscillations of small drops in the air led to the development of a complete non-linear model of the oscillations of a viscous drop and made it possible to verify simplified models. The author presents examples which demonstrate the possibility of using the oscillating drop method to study the physical properties of the liquid and determine the temperature and composition of the surfaces of evaporating drops. Author

N95-31837 Old Dominion Univ., Norfolk, VA.
UNSTEADY FLOW SIMULATIONS ABOUT MOVING BOUNDARY CONFIGURATIONS USING DYNAMIC DOMAIN DECOMPOSITION TECHNIQUES Ph.D. Thesis
Guan-Wei Yen 1994 155 p
Avail: Univ. Microfilms Order No. DA9423440

A computational method is developed to solve the coupled governing equations of an unsteady flowfield and those of rigid-body dynamics in six degrees-of-freedom (6-DOF). This method is capable of simulating the unsteady flowfields around multiple component configurations with at least one of the components in relative motion with respect to the others. Two of the important phenomena that such analyses can help us to understand are the unsteady aerodynamic interference and the boundary-induced component of such a flowfield. By hybridizing two dynamic domain decomposition techniques, the grid generation task is simplified, the computer memory requirement is reduced, and the governing equations of the rigid-body dynamics are simplified with certain assumptions. Three dimensional, unsteady Navier-Stokes equations are solved on each of the subdomains by a fully-vectorized, finite-volume, upwind-biased, and approximately-factored method. These equations are solved on the composite meshes of hybrid subdomain grids that can move with respect to each other. Hence, the present method combines the advantages of an efficient, geometrically conservative, minimally and automatically dissipative algorithm with the advantages and flexibility of the domain decomposition techniques. Several measures that reduce the numerical error are studied and compared with the exact solution of a moving normal shock in a tube. This solution compares very well with the analytic solution of the isentropic equations. It is concluded, that as a minimum measure, the connectivity of nonconservative overlapped scheme needs to be second-order accurate for spatial and temporal discretizations, as well as for the moving subdomain interpolations. Furthermore, the CFL numbers should be restricted to below unity, if affordable, for flows with high flow gradients. The method is further scrutinized by simulating the flow past a sinusoidally pitching airfoil, and the flow past a sinusoidally pitching and plunging airfoil. The results of the former case are successfully compared with the experimental data. The final two-dimensional case is the separation of a store from an airfoil along a prescribed path. As the first three dimensional case, the flowfield past an oscillating cylinder near a vertical wall is simulated. Prior to coupling it with the flowfield equations, the 6-DOF trajectory method is validated by successfully comparing the path it predicts with the one used in a captive trajectory testing. Finally, a rigid-body dynamics method is used to predict the aerodynamically determined trajectory of a store dropped from its initial position under a wing. The results of the present investigation contribute to the understanding of the unsteady aerodynamic interference and the boundary-induced component of such a flowfield. However, its main contribution is the newly proposed computational method for flows involving relative boundary motions. Dissert. Abstr.

N95-31978*# Institute for Computer Applications in Science and Engineering, Hampton, VA.
ANALYSIS AND MODELING OF SUBGRID SCALAR MIXING USING NUMERICAL DATA Final Report
Sharath S. Girimaji and Ye Zhou May 1995 32 p Submitted for publication in Physics of Fluids
(Contract NAS1-19480; RTOP 505-90-52-01)
(NASA-CR-198169; NAS 1.26:198169; ICASE-95-44) Avail: CASI HC A03/MF A01

Direct numerical simulations (DNS) of passive scalar mixing in isotropic turbulence is used to study, analyze and, subsequently, model the role of small (subgrid) scales in the mixing process. In particular, we attempt to model the dissipation of the large scale (supergrid) scalar fluctuations caused by the subgrid scales by decomposing it into two parts: (1) the effect due to the interaction among the subgrid scales; and (2) the effect due to interaction between the supergrid and the subgrid scales. Model comparisons with DNS data show good agreement. This model is expected to be useful in the large eddy simulations of scalar mixing and reaction. Author

N95-32033# Oak Ridge National Lab., TN.
MPI IMPLEMENTATION OF PHOENICS: A GENERAL PURPOSE COMPUTATIONAL FLUID DYNAMICS CODE
S. Simunovic, T. Zacharia, N. Baltas (Combustion, Heat and Mass Transfer Ltd., Wimbleton, England.), and D. B. Spalding (Combustion, Heat and Mass Transfer Ltd., Wimbleton, England.) 1995 6 p Presented at the High Performance Computing 1995 Conference, Tucson, AZ, 9-13 Apr. 1995
(Contract DE-AC05-84OR-21400)
(DE95-009810; CONF-950431-1) Avail: CASI HC A02/MF A01

PHOENICS is a suite of computational analysis programs that are used for simulation of fluid flow, heat transfer, and dynamical reaction processes. The parallel version of the solver EARTH for the Computational Fluid Dynamics (CFD) program PHOENICS has been implemented using Message Passing Interface (MPI) standard. Implementation of MPI version of PHOENICS makes this computational tool portable to a wide range of parallel machines and enables the use of high performance computing for large scale computational simulations. MPI libraries are available on several parallel architectures making the program usable across different architectures as well as on heterogeneous computer networks. The Intel Paragon NX and MPI versions of the program have been developed and tested on massively parallel supercomputers Intel Paragon XP/S 5, XP/S 35, and Kendall Square Research, and on the multiprocessor SGI Onyx computer at Oak Ridge National Laboratory. The preliminary testing results of the developed program have shown scalable performance for reasonably sized computational domains. DOE

N95-32049# Lawrence Livermore National Lab., Livermore, CA.
NUMERICAL SIMULATION OF THE LANGEVIN EQUATION FOR SKEWED TURBULENCE
Donald L. Ermak and John S. Nasstrom Dec. 1994 8 p Presented at the 11th Symposium on Boundary Layers and Turbulence, Charlotte, NC, 27-31 Mar. 1995 Prepared in cooperation with EG and G Energy Measurements, Inc., Pleasanton, CA
(Contracts DE-AC08-93NV-11265; W-7405-eng-48)
(DE95-009477; UCRL-JC-118404; CONF-950381-1) Avail: CASI HC A02/MF A01

In this paper the authors present a numerical method for the generalized Langevin equation of motion with skewed random forcing for the case of homogeneous, skewed turbulence. The authors begin by showing how the analytic solution to the Langevin equation for this case can be used to determine the relationship between the particle velocity moments and the properties of the skewed random force. They then present a numerical method that uses simple probability distribution functions to simulate the effect of the random force. The numerical solution is shown to be exact in the limit of infinitesimal time steps, and to be within acceptable error limits when practical time steps are used. DOE

N95-32109 Virginia Univ., Charlottesville, VA.
SPATIALLY-RESOLVED VELOCITY MEASUREMENTS IN STEADY, HIGH-SPEED, REACTING FLOWS USING LASER-INDUCED OH FLUORESCENCE Ph.D. Thesis
Kurt G. Klavuhn 1994 180 p
Avail: Univ. Microfilms Order No. DA9424479

The theoretical development and calibration of a nonintrusive, high-resolution, optical flowfield-diagnostic technique utilizing OH laser-induced fluorescence (OH LIF) for the measurement of velocity in steady, high-speed, reacting flows is reported. The particular high-speed, reacting flows of interest are those occurring in supersonic combustors for proposed hypersonic flight vehicles. The theory of the OH LIF strategy employed is described, with emphasis on the optimization of the strategy for quantitative velocity measurements. A simplified model is derived for the calculation of expected signal levels from pulsed, narrow-linewidth,

(1,0) band excitation of OH in flames when collecting filtered (1,1) and (0,0) band fluorescence with a gated detector. Several illumination techniques are presented for measuring the Doppler shift of the OH LIF while eliminating systematic errors. A unique reacting underexpanded jet was constructed for the calibration of the OH LIF velocity measurement technique over a wide range of flow conditions. A complete analysis of the distribution of flow properties in the jet flowfield is presented, including results from a full Navier-Stokes calculation with finite-rate chemistry. Comparisons of results from pointwise OH LIF velocity measurements along the centerline and planar OH LIF velocity measurements along the central plane of the reacting underexpanded jet with the numerical solution demonstrate the resolution, range, and accuracy of the technique. Measured and calculated velocities in the supersonic jet core agree on average to within +/- 1.3 percent for the pointwise measurements and +/- 2.2 percent for the planar measurements. The uncertainty (2 sigma) in the pointwise velocity measurements in the jet core was on average +/- 6.0 percent for a single measurement and +/- 3.5 percent for the average value of three scans. For the planar velocity measurements in the jet core, the uncertainty (2 sigma) was on average +/- 4.9 percent for a single measurement and +/- 2.2 percent for the average value of five scans. Dissert. Abstr.

N95-32210*# Toledo Univ., OH.
AN EFFICIENT NUMERICAL PROCEDURE FOR THERMOHYDRODYNAMIC ANALYSIS OF CAVITATING BEARINGS Final Contractor Report
D. Vijayaraghavan Jul. 1995 26 p Presented at the 1995 Tribology Conference, Kissimmee, FL, 8-11 Oct. 1995; sponsored by the Society of Tribologists and Lubrication Engineers and the ASME
(Contract NCC3-291; RTOP 505-62-10; DA Proj. 1L1-61102-AH-45)
(NASA-CR-195476; E-9692; NAS 1.26:195476; ARL-CR-237) Avail: CASI HC A03/MF A01

An efficient and accurate numerical procedure to determine the thermo-hydrodynamic performance of cavitating bearings is described. This procedure is based on the earlier development of Elrod for lubricating films, in which the properties across the film thickness are determined at Lobatto points and their distributions are expressed by collocated polynomials. The cavitated regions and their boundaries are rigorously treated. Thermal boundary conditions at the surfaces, including heat dissipation through the metal to the ambient, are incorporated. Numerical examples are presented comparing the predictions using this procedure with earlier theoretical predictions and experimental data. With a few points across the film thickness and across the journal and the bearing in the radial direction, the temperature profile is very well predicted. Author

N95-32216*# Columbia Univ., Old Saybrook, CT.
FILM TEMPERATURES IN THE PRESENCE OF CAVITATION Final Contractor Report
Harold G. Elrod and D. Vijayaraghavan (Toledo Univ., OH.) Jun. 1995 16 p
(Contract NCC3-291; NASA Order C-78749-C; RTOP 505-62-10; DA Proj. 1L1-62211-A-47-A)
(NASA-CR-195481; E-9713; NAS 1.26:195481; ARL-CR-231) Avail: CASI HC A03/MF A01

Numerical algorithms are developed and implemented for the treatment of laminar lubricating-film temperatures associated with cavitated regions. The reformation front, with its film-content discontinuity and flow reversal, is given special attention. Computational economy is achieved through the use of Lobatto-point locations for flow-property determinations. Author

N95-32219*# State Univ. of New York, Buffalo, NY. Dept. of Mechanical and Aerospace Engineering.
LES, DNS AND RANS FOR THE ANALYSIS OF HIGH-SPEED TURBULENT REACTING FLOWS Annual Report, 1 Aug. 1994 - 31 Jul. 1995
V. Adumitroaie, P. J. Colucci, D. B. Taulbee, and P. Givi 31 Jul. 1995 67 p
(Grant NAG1-1122)
(NASA-CR-199075; NAS 1.26:199075) Avail: CASI HC A04/MF A01

The purpose of this research is to continue our efforts in advancing the state of knowledge in large eddy simulation (LES), direct numerical simulation (DNS), and Reynolds averaged Navier Stokes (RANS) methods for the computational analysis of high-speed reacting turbulent flows. In the second phase of this work, covering the period 1 Aug. 1994 - 31 Jul. 1995, we have focused our efforts on two programs: (1) developments of explicit algebraic moment closures for statistical descriptions of compressible reacting flows and (2) development of Monte Carlo numerical methods for LES of chemically reacting flows. Author

N95-32309# Sandia National Labs., Livermore, CA.
OPTIMAL HEAT TRANSFER DESIGN OF CHEMICAL VAPOR DEPOSITION REACTORS
Christopher D. Moen, Paul A. Spence, and Juan C. Meza Apr. 1995 29 p
(Contract DE-AC04-94AL-85000)
(DE95-010997; SAND-95-8223) Avail: CASI HC A03/MF A01

A new tool for optimal heat transfer design has been constructed by coupling the OPT++ optimization library to the TAC02D finite element heat transfer code. The optimization heat transfer code can be used to quickly and efficiently find optimal operating parameters required for target design criteria. This tool has been applied to the heat transfer design of a rotating disk chemical vapor deposition reactor. The results from two reactor design problems indicate that optimal solutions can be found quickly and efficiently. DOE

N95-31210* Engineering-Science, Inc., Huntsville, AL.
ATOMIZATION SIMULATIONS USING AN EULERIAN-VOF-LAGRANGIAN METHOD
Yen-Sen Chen, Huan-Min Shang, Paul Liaw, and C. P. Chen (Alabama Univ., Huntsville, AL.) *In* Johns Hopkins Univ., The 31st JANNAF Combustion Subcommittee Meeting, Volume 1 Oct. 1994 p 375-386
(For primary document see N95-31194 11-28)
(Contract NAS8-40148)
Avail: CPIA, 10630 Little Patuxent Pkwy., Suite 202, Columbia, MD 21044-3200 HC

35 INSTRUMENTATION AND PHOTOGRAPHY

Includes remote sensors; measuring instruments and gages; detectors; cameras and photographic supplies; and holography.

For aerial photography see *43 Earth Resources and Remote Sensing.* For related information see also *06 Aircraft Instrumentation,* and *19 Spacecraft Instrumentation.*

N95-30378 California Univ., Berkeley. Lawrence Berkeley Lab, CA.
A ROOM TEMPERATURE LSO/PIN PHOTODIODE PET DETECTOR MODULE THAT MEASURES DEPTH OF INTERACTION
W. W. Moses, S. E. Derenzo, C. L. Melcher (Schlumberger-Doll Research, Ridgefield, CT.), and R. A. Manente (Schlumberger-Doll Research, Ridgefield, CT.) Nov. 1994 6 p Presented at the IEEE Nuclear Science Symposium, Norfolk, VA, 1-5 Nov. 1994 Limited Reproducibility: More than 20% of this document may be affected by microfiche quality
(Contract DE-AC03-76SF-00098)
(DE95-008447; LBL-36274; CONF-9411173-6) Avail: CASI HC A02

We present measurements of a 4 element PET detector module that uses a 2 x 2 array of 3 mm square PIN photodiodes to both measure the depth of interaction (DOI) and identify the crystal of interaction. Each photodiode is coupled to one end of a 3 x 3 x 25 mm LSO crystal, with the opposite ends of all 4 crystals attached to a single PMT that provides a timing signal and initial energy discrimination. Each LSO crystal is coated with a 'lossy' reflector, so the ratio of light detected in the photodiode and PMT depends on the position of interaction in the crystal, and is used to determine this position on an event by event basis. This module is operated at +25 C photodiode amplifier peaking time of 2 micro s. micro s. When excited by a collimated beam of 511 photons at the photodiode end of the module (i.e. closest to the patient), the DOI resolution is 4 mm fwhm and the crystal of interaction is identified correctly 95% of the time. When excited at the opposite end of the module, the DOI resolution is 13 mm fwhm and the crystal of interaction is identified correctly 73% of the time. The channel to channel variations in performance are minimal. DOE

N95-30384# Sandia National Labs., Albuquerque, NM.
MICROMACHINED SENSOR AND ACTUATOR RESEARCH AT THE MICROELECTRONICS DEVELOPMENT LABORATORY

J. H. Smith, C. C. Barron, J. G. Fleming, S. Montague, J. L. Rodriguez, B. K. Smith, and J. J. Sniegowski 1994 6 p Presented at the North American Conference on Smart Structures and Materials, San Diego, CA, 26 Feb. - 3 Mar. 1995
(Contract DE-AC04-94AL-85000)
(DE95-008540; SAND-94-2193C; CONF-950228-4) Avail: CASI HC A02/MF A01

An overview of the major sensor and actuator projects using the micromachining capabilities of the Microelectronics Development Laboratory at Sandia National Laboratories is presented. Development efforts are underway for a variety of micromechanical devices and control electronics for those devices. Surface micromachining is the predominant technology under development. Pressure sensors based on silicon nitride diaphragms have been developed. Hot polysilicon filaments for calorimetric gas sensing have been developed. Accelerometers based upon high-aspect ratio surface micromachining are under development. Actuation mechanisms employing either electrostatic or steam power are being combined with a three-level active (plus an additional passive level) polysilicon surface micromachining process to couple these actuators to external devices. Results of efforts toward integration of micromechanics with the driving electronics for actuators or the amplification/signal processing electronics for sensors is also described. This effort includes a tungsten metallization process to allow the CMOS electronics to withstand high-temperature micromechanical processing. DOE

N95-30502# Norwegian Defence Research Establishment, Kjeller (Norway).
RESULTS FROM TESTS OF THE KEARFOTT T16-B INERTIAL MEASUREMENT UNIT
B. Jalving 6 Jan. 1995 87 p
(PB95-212031) Avail: CASI HC A05/MF A01

The Norwegian Defense Research Establishment (NDRE) has tested Kearfott Guidance & Navigation Corporation's T16-B Inertial Measurement Unit (IMU) as part of a program for investigating alternative technologies and vendors for the new antiship missile for the Royal Norwegian Navy. Two different IMU's were tested. Among the tests carried out were static navigation, gyro compassing, dynamic navigation, performance during vibrations and determination of gyro random walk coefficients, accelerometer biases and gyro biases. Additionally the applicability of the IMU navigation data for seeker stabilization has been investigated. Significant difference in performance between the two tested units and dependence on the flight profile were observed. The results obtained indicate that the Kearfott T16-B IMU is well suited for the new antiship missile. NTIS

N95-30507# Lawrence Livermore National Lab., Livermore, CA.
INTEGRATED X-RAY TESTING OF THE ELECTRO-OPTICAL BREADBOARD MODEL FOR THE XMM REFLECTION GRATING SPECTROMETER
J. V. Bixler, W. Craig, T. Decker, H. Aarts (Space Research Organization Netherlands, Utrecht, Netherlands.), T. denBoggende (Space Research Organization Netherlands, Utrecht, Netherlands.), A. C. Brinkman (Space Research Organization Netherlands, Utrecht, Netherlands.), W. Burkert (Max-Planck-Inst. fuer Extraterrestrische Physik, Munich, Germany.), and H. Brauninger (Max-Planck-Inst. fuer Extraterrestrische Physik, Munich, Germany.) 12 Jul. 1994 12 p Presented at the Annual Meeting of the Society of Photo-Optical Instrumentation Engineers, San Diego, CA, 24-29 Jul. 1994
(Contract W-7405-eng-48)
(DE95-008829; UCRL-JC-118213; CONF-940723-36) Avail: CASI HC A03/MF A01

X-ray calibration of the Electro-Optical Breadboard Model (EOBB) of the XXM Reflection Grating Spectrometer has been carried out at the Panter test facility in Germany. The EOBB prototype optics consisted of a four-shell grazing incidence mirror module followed by an array of eight reflection gratings. The dispersed x-rays were detected by an array of three CCD's. Line profile and efficiency measurements where made at several energies, orders, and geometric configurations for individual gratings and for the grating array as a whole. The x-ray measurements verified that the grating mounting method would meet the stringent tolerances necessary for the flight instrument. Post EOBB metrology of the individual gratings and their mountings confirmed the precision of the grating boxes fabrication. Examination of the individual grating surface's at micron resolution revealed the cause of anomalously wide line profiles to be scattering due to the crazing of the replica's surface. DOE

N95-30587*# National Aeronautics and Space Administration. Lewis Research Center, Cleveland, OH.
FABRY-PEROT INTERFEROMETER MEASUREMENT OF STATIC TEMPERATURE AND VELOCITY FOR ASTOVL MODEL TESTS
Helen E. Kourous and Richard G. Seacholtz Jul. 1995 8 p Presented at the Symposium on Laser Anemometry: Advances and Applications, Lake Tahoe, NV, 19-23 Jun. 1994; sponsored by ASME
(RTOP 505-62-50)
(NASA-TM-107014; E-9799; NAS 1.15:107014) Avail: CASI HC A02/MF A01

A spectrally resolved Rayleigh/Mie scattering diagnostic was developed to measure temperature and wing-spanwise velocity in the vicinity of an ASTOVL aircraft model in the Lewis 9 x 15 Low Speed Wind Tunnel. The spectrum of argon-ion laser light scattered by the air molecules and particles in the flow was resolved with a Fabry-Perot interferometer. Temperature was extracted from the spectral width of the Rayleigh scattering component, and spanwise gas velocity from the gross spectral shift. Nozzle temperature approached 800 K, and the velocity component approached 30 m/s. The measurement uncertainty was about 5 percent for the gas temperature, and about 10 m/s for the velocity. The large difference in the spectral width of the Mie scattering from particles and the Rayleigh scattering from gas molecules allowed the gas temperature to be measured in flow containing both naturally occurring dust and LDV seed (both were present). Author

N95-30600 National Defence Research Establishment, Stockholm (Sweden).
FOG [MAETNINGAR PA FIBEROPTISKT GYRO]
S. Arnzen and U. Ekstroem Nov. 1994 42 p In SWAHILI
(PB95-211546; FOA-R-94-00055-8.4-SE) Avail: Issuing Activity (National Technical Information Service (NTIS))

The report gives an account of results from an evaluation test of a fiber optic gyroscope (FOG) with the use of a recently modified gyro rate table of one-axis design. The gyro of single axis rate type is an Alcatel Standard Electrik Loren (SEL) design with designation PM1DE 90/00079. It is a first generation FOG from the German company SEL with all electronics collected on a separate so called European standard PCB card. The purpose of the test is to enhance our competence of knowledge within the field of modern gyros, where FOG's are of special interest as future sensors in weapon systems of different kinds. The results seem to be in good agreement with the SEL specifications for the most important parameters of bias uncertainty, scale factor, linearity, input range, and noise. Only concerning the variation of the scale factor with temperature, disagreement was noticeable at the high temperature end. NTIS

N95-30658 Department of the Navy, Washington, DC.
FIBER OPTIC ACCELEROMETER WITH CENTRALLY SUPPORTED FLEXURAL DISK Patent
Thomas J. Hofler, inventor (to Navy), David A. Brown, inventor (to Navy), and Steven L. Garrett, inventor (to Navy) 29 Nov. 1994 8 p Filed 9 Dec. 1993
(AD-D017369; US-Patent-5,369,485; US-Patent-Appl-SN-163789; US-Patent-Class-356-345) Avail: US Patent and Trademark Office

An accelerometer or seismometer has an elastic disk bearing a mass distributed peripherally around the disk. The disk is supported for flexure and for isolation from mounting strain by a stob centrally through the disk. The accelerometer or seismometer has a pair of flat spirals of optical fiber, each spiral being fixedly attached to a corresponding disk side so that disk flexure lengthens a spiral on one disk side and shortens a spiral on an oppositely facing disk side and so that temperature differences between the spirals are minimized. The pair of spirals are connected as legs of a fiber optic interferometer so that the interferometer provides an output corresponding to the flexure. Several of the disks and associated pairs of spirals may be coaxially mounted to provide increased sensitivity. DTIC

N95-30687 Mississippi State Univ., Mississippi State, MS.
MULTI-COLOR PYROMETER TEMPERATURE MEASUREMENT SYSTEM Topical Report No. 10

R. A. Green and T. Philip 1995 40 p Limited Reproducibility: More than 20% of this document may be affected by microfiche quality
(Contract DE-AC02-80ET-15601)
(DE95-009825; DOE/ET-15601/T69) Avail: CASI HC A03

The Multi-Color Pyrometer System is one of the advanced optical diagnostic instruments developed at DIAL to measure temperatures in the coal combustion environments of large scale facilities. The principles of operation, a description of the system and its capabilities, and the operational details of this instrument are presented in this report. DOE

N95-30691 Rutherford Appleton Lab., Oxford (England).
EXPERIMENTAL CHARACTERISATION OF GAS MICROSTRIP DETECTORS. PART 3: LIFETIME CHARACTERISTICS
J. E. Bateman, J. F. Connolly, Y. N. Pestov, L. I. Shekhtman, and R. Mutikainen Nov. 1994 27 p Prepared in cooperation with Academy of Sciences (USSR), Novosibirsk, USSR, and Tehcnical Research Centre of Finland, Oulu, Finland
(PB95-192845; RAL-94-114-Pt-3) Avail: Issuing Activity (National Technical Information Service (NTIS))

The results of a program of research into the experimental properties of gas microstrip detectors are reported. In this report, information on the lifetime characteristics of the devices is presented. NTIS

N95-30693 Rutherford Appleton Lab., Oxford (England).
METROLOGY OF CHROME ON QUARTZ PHOTOMASKS USING LOW VOLTAGE SCANNING ELECTRON MICROSCOPY. PART 1: PHYSICAL SEM PARAMETERS
B. H. Bracher and R. Jonckheere Jan. 1995 29 p Prepared in cooperation with Interuniversity Micro-Electronics Center, Leuven, Belgium
(PB95-195780; RAL-95-011-Pt-1) Avail: Issuing Activity (National Technical Information Service (NTIS))

This report is the first of two, describing work done under the JESSI T8 Project on scanning electron microscopy (SEM) metrology of Cr/quartz photomasks. It outlines the T8 Project itself and describes in detail the determination of optimum physical parameters for low voltage SEM inspection. In addition, correlation with optical measurements is described. A second report deals with further optimization of SEM usage in photomask metrology. NTIS

N95-30752*# Karlsruhe Univ. (Germany). Inst. fuer Angewandte Physik.
OPTIMIZATION OF A THERMOELECTRIC IR-DETECTOR FOR LOW WORKING TEMPERATURE
R. Fettig, H. J. Lerchenmueller, and E. Mueller 1993 5 p
(Contract NASw-4685)
(NASA-CR-198933; NAS 1.26:198933) Avail: CASI HC A01/MF A01

Thermoelectric IR-detectors have been developed for working at a temperature of 170 K in the CIRS experiment of the designated interplanetary CASSINI mission. Thermoelectric legs of p- and n-type are soldered isolated one from another to a metallized ceramic substrate. Pyramidal legs are formed by electric discharge machining (EDM). A thin gold foil is welded to the cones and blackened for high absorption of radiation. Characterization measurements are carried out to correlate detector properties with the influence of preparation process and material used. Thermoelectric behaviour is described by measuring the current-voltagecharacteristics from liquid nitrogen up to room temperature. Material of various composition within the pseudobinary systems Bi2Te3-Sb2Te3 (for p-type) and Bi2Te3-Bi2Se3 (for n-type) has been used for detector preparation. By choosing material of proper doping the maximum of the figure of merit could be shifted towards lower temperatures. Author

N95-30851*# National Aeronautics and Space Administration. Lewis Research Center, Cleveland, OH.
A LASER-BASED ICE SHAPE PROFILOMETER FOR USE IN ICING WIND TUNNELS
Edward A. Hovenac (NYMA, Inc., Brook Park, OH.) and Mario Vargas Jun. 1995 25 p Original contains color illustrations
(Contract NAS3-27186)
(NASA-TM-106936; E-9864; NAS 1.15:106936) Avail: CASI HC A03/MF A01; 1 functional color page

A laser-based profilometer was developed to measure the thickness and shape of ice accretions on the leading edge of airfoils and other models in icing wind tunnels. The instrument is a hand held device that is connected to a desk top computer with a 10 meter cable. It projects a laser line onto an ice shape and used solid state cameras to detect the light scattered by the ice. The instrument corrects the image for camera angle distortions, displays an outline of the ice shape on the computer screen, saves the data on a disk, and can print a full scale drawing of the ice shape. The profilometer has undergone extensive testing in the laboratory and in the NASA Lewis Icing Research Tunnel. Results of the tests show very good agreement between profilometer measurements and known simulated ice shapes and fair agreement between profilometer measurements and hand tracing techniques. Author

N95-30921# Air Force Systems Command, Wright-Patterson AFB, OH. National Air Intelligence Center.
APPLICATION OF COMPUTER GENERATED HOLOGRAMS TO OPTICAL TRANSFORMATIONS
Shanfeng Zheng and Tianji Wang 8 Mar. 1995 13 p
(AD-A293146; NAIC-ID(RS)T-0393-94) Avail: CASI HC A03/MF A01

This paper discusses how to use computer-generated holograms as a holographic lens to realize optical transformations of ring-to-line, line-to-point and ring-to-point, etc. By use of liquid crystal Television spatial light modulating devices one can fabricate computer generated holograms in quasi-real time. DTIC

N95-30941# Argonne National Lab., IL. Materials Science Div.
ON THE USE OF ELECTRONIC TILT SENSORS AS ANGLE ENCODERS FOR SYNCHROTRON APPLICATIONS
G. S. Knapp, H. You, and Gary R. Holzhausen (Applied Geomechanics, Inc., Santa Cruz, CA.) Sep. 1994 12 p Presented at the International Meeting on Synchrotron Radiation Instrumentation, Stony Brook, NY, 18-22 Jul. 1994 Submitted for publication in Review of Scientific Instruments
(Contract W-31-109-eng-38)
(DE95-005836; ANL/MSD/CP-82825; CONF-940714-53) Avail: CASI HC A03/MF A01

The authors have tested several electrolytic tilt sensors produced by Applied Geomechanics Inc. A pair of sensors were tested by mounting them on the Chi circle of a Huber 4 circle diffractometer. The angles were scanned in 1 degree intervals over a range of +/- 35 degrees. In these tests the resolution was about +/- 5 (mu)rad but the repeatability depended on angle and varied from 70 (mu)rad (one standard deviation) at large angles to 7 (mu)rad at small angles. This type of tilt sensor may be too slow (2-10 second settling time) as a primary angle encoder for a monochromator or diffractometer, but for a system run by stepping motors, they would prove quite useful as secondary angle encoders. Other models which have a narrower angular range would be useful in setting and tuning focusing mirrors. DOE

N95-30980# Air Force Systems Command, Wright-Patterson AFB, OH. National Air Intelligence Center.
A REAL TIME METHOD FOR FOURIER TRANSFORM HOLOGRAPHIC INFORMATION STORAGE
Tiequan Cai, Hui Wan, and Zhiwei Tian 27 Mar. 1995 8 p Transl. into ENGLISH from Zhongguo Jigung, China, v. 18, no. 5, 1991
(AD-A293186; NAIC-ID(RS)T-0394-94) Avail: CASI HC A02/MF A01

In a designed experiment, S is the white light source and is recorded as O(x0,y0). The LCLV is a light crystal light valve in a mixed field effect. The lens L1 forms the image I(x,y) on a CdS membrane of the light conducting layer of the light valve. When the voltage of the liquid crystal layer is greater than the threshold of the liquid crystal, a voltage image can be formed on the CdS membrane and the liquid crystal which corresponds to the input light image. DTIC

N95-31167# International Centre for Theoretical Physics, Trieste (Italy).
THEORETICAL ASPECTS OF ELECTRON EMISSION HOLOGRAPHY
L. Fonda (Trieste Univ., Italy.) Nov. 1994 28 p
(DE95-614371; IC-94/342) Avail: CASI HC A03/MF A01 (US Sales Only)

A new surface structure determination approach, called either photoelectron or Auger electron holography depending on the process under consideration, to get three-dimensional images of the close vicinity of a given near-surface atom emitter, has recently been developed. The great advantage of this holographic method lies in the knowledge of the reference wave, a point which is not shared by structure determination

approaches using an external beam of particles, such as e.g. x-ray and neutron diffractions, where the reference wave is lost into some direction which is not observed, and the experimenter is therefore faced with the so-called 'phase problem.' DOE

N95-31385# Colorado Univ., Boulder, CO. Dept. of Physics and Astrophysics.

TEMPORAL FEATURE EXTRACTION IN PHOTOREFRACTIVE RESONATORS Final Report

Dana Z. Anderson, Gan Zhou, and Germano Montemezzani 1 Dec. 1994 18 p

(Contract DAAL03-91-G-0312)

(AD-A292908; ARO-28592.4-PH) Avail: CASI HC A03/MF A01

A holographic optical system listens to an incoming signal and extracts the most common repetitive temporal features of that signal. An example might be to extract the features of Morse code, which consists of two tone lengths and two pause lengths. This optical system is self-organizing, in that very little a priori information is imbeded in the system to indicate what form the temporal signals take. The primary constraints imposed on the signal is: (1) finite bandwidth; (2) limited feature duration; and (3) rates of reoccurrence. The optical apparatus uses a photorefractively pumped multimode optical oscillator having a delay line in the feedback loop. The delay line serves to translate the temporal dimension into a spatial one, and it also builds into the system a notion of the direction of time. Temporal feature extraction takes place as a competitive interaction among sets of modes, which are termed chronomodes. Experiments illustrate the principles of such a system by extracting the two most probable temporal features from a signal imposed on a laser beam. DTIC

N95-31456*# Jet Propulsion Lab., California Inst. of Tech., Pasadena, CA.

THE WIDE FIELD/PLANETARY CAMERA 2 (WFPC-2) MOLECULAR ADSORBER

Jack Barengoltz, Sonya Moore, David Soules, and Gerald Voecks 15 Jan. 1995 49 p

(Contract NAS7-1260; RTOP 485-15-00-03)

(NASA-CR-198866; JPL-Publ-94-001; NAS 1.26:198866) Avail: CASI HC A03/MF A01

A device has been developed at the Jet Propulsion Laboratory, California Institute of Technology, for the adsorption of contaminants inside a space instrument during flight. The molecular adsorber was developed for use on the Wide Field Planetary Camera 2, and it has been shown to perform at its design specifications in the WFPC-2. The basic principle of the molecular adsorber is a zeolite-coated ceramic honeycomb. The arrangement is efficient for adsorption and also provides the needed rigidity to retain the special zeolite coating during the launch vibrational environment. The adsorber, on other forms, is expected to be useful for all flight instruments sensitive to internal sources of contamination. Typically, some internal contamination is unavoidable. A common design solution is to increase the venting to the exterior. However, for truly sensitive instruments, the external contamination environment is more severe. The molecular adsorber acts as a one-way vent to solve this problem. Continued development is planned for this device. Author

N95-31694# SRI International Corp., Menlo Park, CA.

NOVEL MASS SPECTROMETRIC INSTRUMENT FOR GASEOUS AND PARTICULATE CHARACTERIZATION AND MONITORING Final Report, Sep. 1992 - - Aug. 1994

M. J. Coggiola, C. H. Becker, and C. L. Witham Oct. 1994 62 p

(Contract DE-AC21-92MC-29116)

(DE95-000047; DOE/MC-29116/3956) Avail: CASI HC A04/MF A01

An instrument is being developed that will be capable of providing real-time (less than 1 minute), quantitative, chemical analysis of gaseous and particulate pollutants generated from DOE waste cleanup activities. The instrument can detect and identify volatile organic compounds, polynuclear aromatic hydrocarbons, heavy metals, and transuranic species released during waste cleanup. It consists of an isokinetic sampler operable up to 500 K and wide flow rate range, a high- to low-pressure transition and sampling region separating particles from vapors for separate analysis, two small mass spectrometers (one for organic analysis by field ionization and one for particulate analysis by thermal pyrolysis and electron-impact ionization), and a powerful PC for control/data acquisition. Initially, the instrument will used with the K-1435 Toxic Substances Control Act (TSCA) incinerator at K-25; other applications are also possible, e.g., vitrification monitoring, storage tank offgassing analysis, etc. It will be easily transportable. DOE

N95-31828# California Univ., Los Angeles, CA.

STABLE HIGH-POWER HARMONIC GYRO-AMPLIFIERS Final Report

N. C. Luhmann, Jr. 30 Sep. 1994 26 p

(Grant AF-AFOSR-0382-91)

(AD-A293697; AFOSR-95-0327TR) Avail: CASI HC A03/MF A01

The focus of our Tri-Service University Research Program in Vacuum Electronics has been on basic research issues associated with operating harmonic gyrotron devices as high-power, coherent millimeter-wave amplifiers. Substantial theoretical and experimental progress has been achieved. We introduced the marginal stability design (MSD) procedure for achieving stability in high-performance gyro-TWT's. We also concluded the initial tests of the high power, second-armonic TE21 gyro-TWT amplifier which is based on the MSD procedure and the novel concept that harmonic operation is capable of significantly increasing the output power because the start-oscillation beam current is much higher for the relatively weak harmonic interaction. Indeed, the second-harmonic gyro-TWT amplifier's unprecedented output power of 207 kW exceeded the previous record-level of 120 kW, which was produced by a first-harmonic gyro-TWT. Our amplifier yielded an efficiency of 13%, a saturated gain of 16 dB with a bandwidth of 2% and was stable for zero RF input power. DTIC

N95-31836 Michigan Univ., Ann Arbor, MI.

GLOBAL STABILIZATION OF NONLINEAR GYROSCOPIC SYSTEMS Ph.D. Thesis

Chih-Jian Wan 1994 191 p

Avail: Univ. Microfilms Order No. DA9423340

We concentrate on the problems of stability and stabilization of equilibrium points for certain nonlinear dynamical systems, primarily rigid body systems with gyroscopic effects. We analyze stability of the equilibrium points of these systems, and, in the presence of control inputs, we synthesize control laws that globally asymptotically stabilize these systems to the equilibrium points. The control law synthesis method developed here is based on the Hamilton-Jacobi-Bellman theorem which guarantees stability and also provides an optimality interpretation for the control law. In particular, we attempt to achieve both the objectives of stability and optimality for the nonlinear control system by finding solutions to the Hamilton-Jacobi-Bellman equation. It is shown that the performance index obtained is not prescribed a priori, rather, there is a relationship between the nonlinear system, the stabilizing control law and the Lyapunov function for the closed-loop system through the Hamilton-Jacobi-Bellman equation. These results are then specialized to nonlinear affine control systems, Jurdjevic-Quinn type systems and minimum phase system with relative degree (1,...,1). The dynamical systems considered in this dissertation are primarily gyroscopic systems which include, in general, nonlinear coupling, centrifugal forces and trigonometric functions in the equations of motion. These inherent nonlinearities can help stabilize the nonlinear system as shown in examples in which the interplay between dynamics and control plays an important role. Hence, we connect modern nonlinear control theory and classical optimal control theory in the framework of the Hamilton-Jacobi-Bellman theorem and apply this to several nonlinear gyroscopic systems. We show that by taking advantage of the inherent nonlinearities embedded in the nonlinear system, we derive elegant and powerful results which are useful for practical applications. Dissert. Abstr.

N95-32047# Lawrence Livermore National Lab., Livermore, CA.

HIGH-RESOLUTION SUPERCONDUCTING X-RAY SPECTROMETERS WITH ALUMINUM TRAPPING LAYERS OF DIFFERENT THICKNESSES

C. A. Mears, S. E. Labov, L. H. Miller, M. Frank, H. Netel, F. Azgui, and A. T. Barfknecht Oct. 1994 6 p Presented at the Applied Superconductivity Conference, Boston, MA, 16-21 Oct. 1994

(Contract W-7405-eng-48)

(DE95-010253; UCRL-JC-119292; CONF-941013-35) Avail: CASI HC A02/MF A01

Superconducting tunnel junctions coupled to superconducting absorbers may be used as high-resolution, high-efficiency x-ray spectrometers. We have tested devices with niobium x-ray absorbing layers coupled to aluminum layers that serve as quasiparticle traps. We present a study of device

performance as a function of thickness of the trapping layers. We measured the best energy resolution using a device with a high-quality barrier and 200 nm-thick trapping layers on both sides of the tunnel barrier. This energy resolution was 36 eV full width at half maximum at 6 keV, about 4 times better than that obtainable using semiconductor ionization detectors.
DOE

N95-32159# Brookhaven National Lab., Upton, NY.
THE SUPERCONDUCTING KAON SPECTROMETER
A. Pascolini, ed. (Padua Univ., Italy.), S. Ajimura (Osaka Univ., Osaka, Japan.), K. Aoki (National Lab. for High Energy Physics, Tsukuba, Japan.), H. Bhang (Seoul National Univ., Republic of Korea.), Y. Doi (National Lab. for High Energy Physics, Tsukuba, Japan.), T. Fukuda (Tokyo Univ., Tanashi, Japan.), Y. Gavrilov (Tokyo Univ., Tanashi, Japan.), T. Hasegawa (Tokyo Univ., Tanashi, Japan.), O. Hashimoto (Tokyo Univ., Tanashi, Japan.), and A. Higashi (Tokyo Univ., Tanashi, Japan.) et al 1995 6 p Presented at the 13th International Conference on Particles and Nuclei, Perugia, Italy, 27 Jun. - 3 Jul. 1993
(Contract DE-AC02-76CH-00016)
(DE95-010436; BNL-61653; CONF-930637-16) Avail: CASI HC A02/MF A01

A new superconducting kaon spectrometer has been installed in the north experimental hall of KEK 12-GeV proton synchrotron and has started its operation. It was designed to have a good momentum resolution of 0.1% FWHM and a large acceptance of 100 msr. Through preliminary analyses, a good energy resolution better than 2 MeV has been confirmed in pion-nucleus elastic scatterings and the (pi(+), K(+)) reaction on C-12.
DOE

N95-32245 National Defence Research Establishment, Linkoeping (Sweden).
FEASIBILITY STUDY CONCERNING AN ACTIVE MILLIMETERWAVE SENSOR. PROJECT PHASE MMS2.1 [REALISERBARHETSSTUDIE AVSEENDE EN AKTIV MILLIMETERVAGSSENSOR. PROJEKTFAS MMS2.1]
J. Svedin, U. Dahlgren, H. Johansson, O. J. Hagel, and H. Zirath Oct. 1994 32 p In SWAHILI; Test in SWEDISH; summary in ENGLISH Prepared in cooperation with Chalmers Univ. and the Industrial Microelectronics Center
(PB95-210399; FOA-R-94-00007-3.2-SE) Avail: Issuing Activity (National Technical Information Service (NTIS))

This report gives a summary of activities and results attained in the project during the project phase MMS2.1. It is mainly intended for the sponsors of the project, and for those who are familiar with the project's activities. A number of millimeter wave (35 and 94 GHz) 1X4 integrated receiver arrays aimed at anti-collision radar and target seeker applications have been designed, manufactured and characterized. The circuits, which are patterned on a BCB substrate using a uniplanar hybrid technology (MMS1.2b) presented earlier, comprise integrated microstrip patch antennas, resistive InP HEMT mixers, and microstrip distribution, matching and diplexer networks. To facilitate an accurate characterization using our probe station, circuit breakouts including via holes have been manufactured. At 35 GHz we have measured antenna diagrams for separate receivers in an array, conversion loss, various bandwidths and linearity for a mixer breakout, and s-parameters for some of the passive microstrip circuit breakouts. A performance comparison with the GaAs based HEMT mixer presented earlier has also been carried out.
NTIS

N95-32129# Defence Research Establishment Valcartier, Courcellette (Quebec).
INFRARED AND MILLIMETER WAVE DETECTION USING THIN FILMS OF Pb DOPED BiSrCaCuO SUPERCONDUCTOR
L. Ngo Phong *In* AGARD, Guidance and Control for Future Air-Defence Systems Jan. 1995 10 p (For primary document see N95-32123 11-31)
Copyright Avail: CASI HC A02/MF A03

N95-32134# Office National d'Etudes et de Recherches Aeronautiques, Paris (France). Ingenieurs de Recherche.
DESIGN OF SURVEILLANCE AND MULTISENSOR ANTI-AERIAL SYSTEMS [CONCEPTION DE SYSTEMES DE SURVEILLANCE ET DE DEFENSE ANTI-AERIENNE MULTI-SENSEURS]
C. Nahum and H. Cantalloube *In* AGARD, Guidance and Control for Future Air-Defence Systems Jan. 1995 9 p In FRENCH (For primary document see N95-32123 11-31)
Copyright Avail: CASI HC A02/MF A03

N95-32236*# Jet Propulsion Lab., California Inst. of Tech., Pasadena, CA.
A HIGH-SPEED PHOTONIC CLOCK AND CARRIER REGENERATOR
X. S. Yao and G. Lutes *In its* The Telecommunications and Data Acquisition Report 15 May 1995 p 202-210 (For primary document see N95-32221 11-32)
Avail: CASI HC A02/MF A03

N95-32239*# Jet Propulsion Lab., California Inst. of Tech., Pasadena, CA.
DSS-24 MICROWAVE HOLOGRAPHY MEASUREMENTS
D. J. Rochblatt, P. M. Withington, and H. J. Jackson *In its* The Telecommunications and Data Acquisition Report 15 May 1995 p 252-270 (For primary document see N95-32221 11-32)
Avail: CASI HC A03/MF A03

36 LASERS AND MASERS

Includes parametric amplifiers.
For related information see also *76 Solid-State Physics*.

N95-30379# Sandia National Labs., Albuquerque, NM.
LASER TRACKER 3: SANDIA NATIONAL LABORATORIES' THIRD GENERATION LASER TRACKING SYSTEM
D. L. Patrick 1995 5 p Presented at the SPIE International Symposium on Aerospace/Defense Sensing and Dual-use Photonics, Orlando, FL, 17-21 Apr. 1995
(Contract DE-AC04-94AL-85000)
(DE95-008525; SAND-95-0472C; CONF-950472-2) Avail: CASI HC A01/MF A01

At Sandia Labs' Coyote Canyon Test Complex, it became necessary to develop a precision single station solution to provide time space position information (tspi) when tracking airborne test vehicles. Sandia's first laser tracker came on line in 1968, replacing the fixed camera technique for producing trajectory data. This system shortened data reduction time from weeks to minutes. Laser Tracker 2 began operations in 1982, replacing the original tracker. It incorporated improved optics and electronics, with the addition of a microprocessor-based real-time control (rtc) system within the main servo loop. The rtc added trajectory prediction with the loss of adequate tracking signal and automatic control of laser beam divergence according to target range. Laser Tracker 3, an even more advanced version of the systems, came on line in 1990. Unlike LT 2, which is mounted in a trailer and must by moved by a tractor, LT 3 is mounted on its own four-wheel drive carrier. This allows the system to be used at even the most remote locations. It also incorporated improved optics and electronics with the addition of absolute ranging, acquisition on the fly, and automatic transition from manual Joystick tracking to laser tracking for aircraft tests. LT 3 provides a unique state of the art tracking capability for missile, rocket sled, aircraft, submunition, and parachute testing. Used in conjunction with LT 2, the systems together can provide either simultaneous or extended range tracking. Mobility, accuracy, reliability, and cost effectiveness enable these systems to support a variety of testing at Department of Energy and Department of Defense ranges.
DOE

N95-30380# Sandia National Labs., Albuquerque, NM. Photonics Research Dept.
POLARIZATION CHARACTERISTICS, CONTROL, AND MODULATION OF VERTICAL-CAVITY SURFACE EMITTING LASERS
K. D. Choquette, K. L. Lear, R. P. Schneider, Jr., J. J. Figiel, S. P. Kilcoyne, M. Hagerott-Crawford, J. C. Zolper, R. E. Leibenguth (Bell Telephone Labs., Inc., Breiningsville, PA.), J. J. Figiel, and S. P. Kilcoyne et al 1995 12 p Presented at the SPIE 1995: SPIE Conference on Optics, Electro-Optics, and Laser Application in Science, Engineering and Medicine, San Jose, CA, 5-10 Feb. 1995
(Contract DE-AC04-94AL-85000)

(DE95-008526; SAND-95-0482C; CONF-950226-26) Avail: CASI HC A03/MF A01

The gain-dependent polarization properties of vertical-cavity surface emitting lasers and methods for polarization control and modulation are discussed. The partitioning of power between the two orthogonal eigen polarizations is shown to depend upon the relative spectral alignment of the nondegenerate polarization cavity resonances with the laser gain spectrum. A dominant polarization can thus be maintained by employing a blue-shifted offset of the peak laser gain relative to the cavity resonance wavelength. Alternatively, the polarization can be controlled through use of anisotropic transverse cavity geometries. The orthogonal eigen polarizations are also shown to enable polarization modulation. By exploiting polarization switching transitions in cruciform lasers, polarization modulation of the fundamental mode up to 50 MHz is demonstrated. At lower modulation frequencies, complementary digital polarized output or frequency doubling of the polarized output is obtained. Control and manipulation of vertical-cavity laser polarization may prove valuable for present and future applications. DOE

N95-30390# Sandia National Labs., Albuquerque, NM.
MANY-BODY EFFECTS IN SEMICONDUCTOR LASERS
W. W. Chow 1995 9 p Presented at the SPIE 1995: SPIE Conference on Optics, Electro-optics, and Laser Application in Science, Engineering and Medicine, San Jose, CA, 5-10 Feb. 1995
(Contract DE-AC04-94AL-85000)
(DE95-008534; SAND-95-0455C; CONF-950226-27) Avail: CASI HC A02/MF A01

A microscopic theory, that is based on the coupled Maxwell-semiconductor-Bloch equations, is used to investigate the effects of many-body Coulomb interactions in semiconductor laser devices. This paper describes two examples where the many-body effects play important roles. Experimental data supporting the theoretical results are presented. DOE

N95-30394# Aerospace Corp., El Segundo, CA. Technology Operations.
OPTIMUM TRUNCATION OF A GAUSSIAN BEAM FOR PROPAGATION THROUGH ATMOSPHERIC TURBULENCE
H. T. Yura 15 Nov. 1994 20 p
(Contract F04701-93-C-0094)
(AD-A291156; TR-94(4925)-2; SMC-TR-95-7) Avail: CASI HC A03/MF A01

We consider the mean on-axis far-field (or focal-plane) irradiance of a Gaussian beam truncated by a circular aperture in the presence of atmospheric turbulence. In the absence of turbulence, we present an accurate analytic approximation for the irradiance distribution that is valid within the main central lobe of the beam. Based on this approximation, we then obtain the mean on-axis far-field irradiance and corresponding turbulence Strehl ratio for the truncated Gaussian beam. By maximizing the on-axis irradiance, we obtain the optimum ratio of the beam diameter to the aperture diameter in the presence of turbulence and present results for the corresponding maximum on-axis irradiance as a function of the strength of turbulence. In particular, for D/r sub 0 greater than 1, where D is the aperture diameter, and r sub 0 is Fried's coherence length, optimum truncation of a Gaussian beam and uniform illumination of a circular aperture (where the same total power is uniformly distributed over the aperture) result in the same on-axis irradiance in the presence of uncompensated turbulence. DTIC

N95-30498 California Univ., Santa Barbara, CA.
EXTENDED TUNING RANGE SEMICONDUCTOR LASERS WITH SAMPLED GRATINGS Ph.D. Thesis
Vijaysekhar Jayaraman 1994 211 p
Avail: Univ. Microfilms Order No. DA9423867

Prior to 1991, the most advanced tunable semiconductor laser was the 'Distributed Bragg Reflector' or DBR laser. The tuning limitation in DBR lasers is a cavity design which constrains the fractional wavelength tuning Delta lambda/lambda to be no more than the achievable refractive index change Delta mu/mu in a semiconductor waveguide. The maximum index shift is approximately 0.7 percent. As a result, the best DBR lasers have a tuning range of 10 nanometers (nm) around their nominal operating wavelength of 1.5 microns. This dissertation describes a new type of tunable semiconductor laser, which can have a tuning range Delta lambda/lambda which is much larger than Delta mu/mu. This new laser relies on reflection gratings like DBR lasers, and therefore relies on a similar fabrication technology. In contrast to DBR lasers, however, the 'sampled grating' DBR of this dissertation uses gratings which are periodically turned on and off, generating a reflection spectrum with periodic maxima. This spectrum allows tunability over much wider ranges than the single reflection maximum associated with DBR mirrors. The first chapter of this dissertation is devoted to describing the history of tunable semiconductor lasers. The next two chapters describe the theory of sampled gratings and the tuning properties of lasers employing them. The following two chapters describe fabrication and device results. In particular, in Chapter 5, we describe tunable lasers with 10 mW output power, tuning ranges over 70 nm, and single-frequency operation with very large suppression of spurious laser cavity modes. Chapter 6 summarizes, and concludes with some suggestions for improving device performance and exploring new geometries. Dissert. Abstr.

N95-30609# International Centre for Theoretical Physics, Trieste (Italy).
ELECTRON-OPTICAL NONLINEAR INTERACTION IN ASYMMETRIC QUANTUM-WELL LASER HETEROSTRUCTURES
V. K. Kononenko, A. A. Afonenko (Belarussian State Univ., Minsk, Belarus.), and I. S. Manak (Belarussian State Univ., Minsk, Belarus.) Sep. 1994 10 p Sponsored by Fundamental Research Foundation of the Republic of Belarus
(DE95-613443; IC-94/284) Avail: CASI HC A02/MF A01 (US Sales Only)

The effects of nonlinear electron-optical interaction between two quantum wells in the active region of low-dimensional lasers with inhomogeneous excitation are discussed. The conditions for realizing bistable behaviour of optical output and self-sustained pulsations of radiation at two optical wavelengths are determined. The influence of current carrier leakage on the hard regime of lasing is considered. The synchronization effect of coupled well modulation of injection on pulse generation has been predicted. Analysis based on rate equations has been performed for the GaAs - Al(x)Ga(1-x)As system. DOE

N95-30744 Department of the Navy, Washington, DC.
METHOD FOR LASER-ASSISTED SILICON ETCHING USING HALOCARBON AMBIENTS Patent
Stephen D. Russell, inventor (to Navy), Douglas A. Sexton, inventor (to Navy), and Richard J. Orazi, inventor (to Navy) 31 Jan. 1995 23 p Filed 29 Mar. 1990
(AD-D017426; US-Patent-5,385,633; US-Patent-Appl-SN-501707; US-Patent-Class-156-693) Avail: US Patent and Trademark Office

An etching process allows a selective single-step patterning of silicon devices in a noncorrosive environment. The etching of silicon relies on a maskless laser-assisted technique in a gaseous halocarbon ambient, such as the gaseous chlorofluorocarbons, dichlorodifluoromethane and chloropentafluoroethane. Laser-assisted photothermal chemical etching reactions on silicon occur in these ambients when the incident fluence from an excimer laser at 248 nm exceeds the melt threshold (approximately 0.75 J/sq cm). When incident fluence exceeds the ablation threshold (approximately 2.2 J/sq cm) an undesirable increased surface roughness is observed. Etch rates as large as approximately 15 angstroms per pulse are attained within predetermined processing windows. This provides a means for thin membrane formation in silicon, rapid etches and processing of packaged devices or partially fabricated dies. The reduction in processing steps as compared to conventional wet chemical etches provides improvements in yield, reliability and cost. DTIC

N95-30805 Oklahoma Univ., Norman, OK.
TV-VI SEMICONDUCTOR QUANTUM WELL LASERS, PHYSICS AND ENGINEERING Ph.D. Thesis
Majed Fouad Khodr 1994 253 p
Avail: Univ. Microfilms Order No. DA9422557

In this work, a theoretical model that calculates the gain-current density relationship for IV-VI semiconductor quantum well lasers was developed. The model, based on Kane's two band model, solves for the anisotropy in the constant energy surfaces and for the strong nonparabolicity of the bands. The system investigated was the EuSePbSe(0.78)Te(0.22) quantum well structure at 77 K. The nonparabolicity of the bands in the growth direction was found to shift the energy levels in the PbSe(0.78)Te(0.22)

quantum well to lower energies as compared to a quantum well with parabolic bands. Nonparabolicity of the bands also resulted in an energy dependent density of states in the junction plane of the structure. These two effects cause the gain-current density relation for the parabolic system to be altered. The single quantum well (SQW) design was optimized by investigating three quantum well structures: the multiple quantum well (MQW), the modified multiple quantum well (MMQW) and the separate confinement heterostructure-single quantum well (SCH-SQW) structures. The effects of nonparabolicity on the confinement factor and threshold current values were also calculated. Nonparabolicity lowers the confinement factor values and thus, the modal gain. Also, it increases the threshold current values for short cavity lasers. For moderate and long cavity lasers, these effects are negligible. Studies were performed on BaF2 films because of their importance as intermediate layers that lattice match the IV-VI semiconductor devices to silicon. BaF2 films were grown in a vacuum system with a base pressure of 10(exp -6) Torr on Si(111) substrates at four substrate temperatures: room temperature, 250 C, 450 C and 650 C. The fluoride films were characterized using ellipsometry, X-ray diffraction, scanning electron microscopy (SEM) and capacitance versus voltage techniques. At a growth temperature of 650 C, the BaF2 films were epitaxial with a (111) preferred growth direction. At this temperature, the surface was partially smooth with some cracking apparent. Prolonged heating of a chemically uncleaned substrate before deposition resulted in smooth and crack-free CaF2 films. The electrical properties of the films correlated with the thermal history of the sample rather than with the crystalline quality.

Dissert. Abstr.

N95-30906# Arnold Engineering Development Center, Arnold AFS, TN.
ANALYSIS OF PLANAR LASER-INDUCED FLUORESCENCE IMAGES OBTAINED DURING SHAKEDOWN TESTING OF THE AEDC IMPULSE FACILITY Final Report, Oct. 1993 - Sep. 1994
W. M. Ruyten, W. D. Williams, and F. L. Heltsley Mar. 1995 62 p
(AD-A293237; AEDC-TR-94-14) Avail: CASI HC A04/MF A01

Following a proof-of-principle demonstration of Planar Laser-Induced Fluorescence (PLIF) in the AEDC Impulse Facility in FY93, a set of four PLIF images was obtained during FY94 runs of the facility. The images were obtained away from the nose region of a spherically blunt cone, using excitation of nitric oxide in the flow. Two laser sheet geometries were employed and two excitation wavelengths were used. A procedure was developed whereby calibration images allow the remapping of the PLIF images to test article coordinates. Using this technique, it was shown that the bow shock positions determined by PLIF agree well with the shock positions measured using schlieren photography. More importantly, the set of PLIF images constitutes an initial database against which Computational Fluid Dynamics calculations of high enthalpy flows can be compared. Initial results of such a comparison, obtained through Computational Flow Imaging, are reported. Recommendations are given for future PLIF applications at the Impulse Facility. DTIC

N95-30914# Joint Inst. for Nuclear Research, Dubna (USSR).
FREE ELECTRON LASER AS ENERGY DRIVER FOR INERTIAL CONFINEMENT FUSION
E. L. Saldin, E. A. Shnejdmiller, Yu. N. Ulyanov, V. P. Sarantsev, and M. V. Yurkov 1994 42 p
(DE95-614252; JINR-E-9-94-237) Avail: CASI HC A03/MF A01 (US Sales Only)

A FEL based energy driver for Inertial Confinement Fusion (ICF) is proposed. The key element of the scheme is free electron laser system. Novel technical solutions reveal a possibility to construct the FEL system operating at radiation wavelength lambda = 0.5 micro m and providing flash energy E = 1 MJ and brightness 4 x 10(exp 22) W/sq cm.sr within steering pulse duration 0.1-2 ns. Total energy efficiency of the proposed ICF energy driver is about of 11% and repetition rate is 40 Hz. Dimensions of such an ICF driver are comparable with those of heavy-ion ICF driver, while the problem of technical realization seems to be more realistic. It is shown that the FEL based ICF energy driver may be constructed at the present level of accelerator technique R&D. DOE

N95-31139# Sandia National Labs., Albuquerque, NM. Physical and Joining Metallurgy Dept.
SPOTSIZE MEASUREMENTS OF A FOCUSED CW Nd: YAG LASER
Marcelino Essien, L. Paul Schanwald, and Phillip W. Fuerschbach 1995 7 p Presented at the SPIE 1995 Conference: SPIE Conference on Optics, Electro-optics, and Laser Application in Science, Engineering and Medicine, San Jose, CA, 5-10 Feb. 1995
(Contract DE-AC04-94AL-85000)
(DE95-007746; SAND-94-0252C; CONF-950226-20) Avail: CASI HC A02/MF A01

The minimum spotsize, beam quality or M(sup 2), and Strehl ratio of a focused laser beam provide different measures of the performance of the laser/optic system. Focusing lenses typically used to provide irradiances sufficient to cause melting and/or vaporization of metals or ceramics typically exhibit considerable spherical aberration, and thus limit the minimum spotsize attainable for a given lens at a specific laser power. The purpose of this work is to quantify the increase in the minimum spotsize and decrease in Strehl ratio of a focused materials processing CW Nd:YAG laser caused by laser cavity heating and spherical aberration introduced by the focusing lens. Minimum spotsize was determined by making several measurements of spotsize along the propagation direction using a scanning aperture system, and fitting the data to the laser propagation equation. These measurements were performed for 6 plano-convex lenses of different focal lengths, using laser powers ranging from 500 to 1500 watts. A nonlinear variation of spotsize with laser power and with focal length was observed for the lenses and power levels tested. DOE

N95-31145# University of Central Florida, Orlando, FL. Center for Research in Electro-optics and Lasers.
EXPERIMENTAL INVESTIGATION OF OPTICAL NONLINEARITIES IN CONJUGATED POLYMERS Annual Report, 1 Sep. 1993 - 31 Aug. 1994
George Stegeman 31 Aug. 1994 6 p
(Contract F49620-93-1-0554)
(AD-A288353; AFOSR-94-0093TR) Avail: CASI HC A02/MF A01

The nonlinear optics of sublimated films of 2-dimensional conjugated planar molecules has been investigated by third harmonic generation. Two were planar phthalocyanines, metal-free and copper substituted, and the third was an asymmetric (non-planar) phthalocyanine (subphthalocyanine), employed as a precursors in the synthesis of certain phtalocyanines. A very rich spectrum has been observed in each case and the analysis is currently underway. In the future this work will be expanded to include other materials. DTIC

N95-31190# Naval Research Lab., Washington, DC.
DESIGN CONSIDERATIONS FOR A DENSITY-CHANNEL-GUIDED LASER WAKE-FIELD ACCELERATOR Interim Report
Jonathan Krall and Arie Zigler 14 Apr. 1995 22 p Prepared in cooperation with Hebrew Univ. of Jerusalem, Rehovot, Israel
(AD-A292876; NRL/MR/6790-95-7651) Avail: CASI HC A03/MF A01

A self-modulated laser wake-field accelerator configuration in which the laser pulse is optically guided by a plasma density channel is considered. Preliminary experiments on the generation of a plasma channel by a slow capillary discharge are described. It is shown that homogeneous channels with length L sub channel much greater than lambda p can be produced, where lambda sub p is the plasma wavelength. Key issues are addressed, including phase detuning between the accelerated electron bunch and the wake field, beam-plasma and laser-plasma instabilities, and the effect of density variations that might occur over the length of the plasma channel. Numerical simulations, using present experimental parameters, show accelerating gradients in excess of 50 GV/m. DTIC

N95-31213 Department of the Navy, Washington, DC.
A 1.94 MICROMETER LASER APPARATUS, SYSTEM AND METHOD USING A THULIUM-DOPED YTTRIUM-LITHIUM-FLUORIDE LASER CRYSTAL PUMPED WITH A DIODE LASER Patent
Leon Esterowitz, inventor (to Navy) and Robert C. Stoneman, inventor (to Navy) 10 Jan. 1995 8 p Filed 28 Jan. 1993
(AD-D017435; US-Patent-5,381,433; US-Patent-Appl-SN-010253; US-Patent-Class-372-41) Avail: US Patent and Trademark Office

A laser apparatus, system and method include a laser crystal formed of thulium-doped yttrium-lithium-fluoride, and a laser diode arranged in proximity to the laser crystal. The laser diode is capable of emitting a first laser light which is suitable for use as a pump beam for causing lasing to occur in the laser crystal. In response to the first laser light from the laser diode, the laser crystal emits a second laser light at a wavelength which

is relatively highly-absorbed by organic tissue and/or water. The second laser light is therefore well-suited to medical applications, for example, and can be used to irradiate organic tissue for medical treatment. DTIC

N95-31230 Lawrence Livermore National Lab., Livermore, CA.
FUTURE SCIENTIFIC APPLICATIONS FOR HIGH-ENERGY LASERS
R. W. Lee, comp. 1 Aug. 1994 78 p Limited Reproducibility: More than 20% of this document may be affected by microfiche quality
(Contract W-7405-eng-48)
(DE95-009380; UCRL-ID-118223) Avail: CASI HC A05/MF A01

This report discusses future applications for high-energy lasers in the areas of astrophysics and space physics; hydrodynamics; material properties; plasma physics; radiation sources; and radiative properties. DOE

N95-31273 Department of the Navy, Washington, DC.
DIODE-PUMPED, CONTINUOUSLY TUNABLE, 2.3 MICRON CW LASER Patent
Leon Esterowitz, inventor (to Navy), Robert C. Stoneman, inventor (to Navy), and Joseph F. Pinto, inventor (to Navy) 7 Feb. 1995 9 p Filed 29 Apr. 1994
(AD-D017448; US-Patent-5,388,112; US-Patent-Appl-SN-235844; US-Patent-Class-372-20) Avail: US Patent and Trademark Office

A room-temperature solid state laser for producing an output laser emission at any wavelength within a preselected range of wavelengths is disclosed. In a preferred embodiment, the laser comprises; a pump laser for emitting a CW pump beam at a preselected wavelength; a laser cavity defined by a first reflective element, an output coupler reflective element and a folded mirror disposed between the first reflective element and the output coupler reflective element to form a reflective path there among in the laser cavity; a laser crystal disposed in the laser cavity, the laser crystal being responsive to the CW pump beam at the preselected wavelength for producing a CW laser emission within a preselected range of wavelengths when the laser crystal is pumped the the CW pump beam at the preselected wavelength, the folded mirror operating to collimate the CW laser emission in the optical path between the folded mirror and the output coupler reflective element; and a tuning element disposed in the laser cavity between the folded mirror and the output coupler reflective element for tuning the collimated CW laser emission to any wavelength within the preselected range of wavelengths. DTIC

N95-31274 Department of the Navy, Washington, DC.
TUNABLE YTTERBIUM-DOPED SOLID STATE LASER Patent
John M. McMahon, inventor (to Navy), Robert C. Stoneman, inventor (to Navy), and Leon Esterowitz, inventor (to Navy) 10 Jan. 1995 8 p Filed 30 Jul. 1993
(AD-D017449; US-Patent-5,381,428; US-Patent-Appl-SN-099638; US-Patent-Class-372-20) Avail: US Patent and Trademark Office

A tunable ytterbium-doped solid-state laser has a laser cavity defined a pair of mirrors, a laser medium positioned in this cavity, means for pumping the laser medium, and means for tuning the output of this laser medium to a selected wavelength within a wavelength range. The laser medium has a host material doped with enough ytterbium ions to produce a longitudinal mode laser emission when the laser medium is pumped. In a most preferred embodiment, the laser emission is frequency-doubled and tuned to a wavelength corresponding to a Fraunhoffer line in the solar spectrum. DTIC

N95-31389# Department of the Air Force, Wright-Patterson AFB, OH. National Air Intelligence Center.
ADVANCES IN HIGH-POWER CHEMICAL LASERS
Sha Guoha (Academia Sinica, Guiyang, China.) 15 Dec. 1994 15 p Transl. into ENGLISH from Zhongguo Jiguang, v. A21, no. 5, May 1994 p 387-390 Prepared by Leo Kanner Associates
(Contract F33657-88-D-2188)
(AD-A289737; NAIC-IS(RS)T-0703-94) Avail: CASI HC A03/MF A01

Chemical laser is characteristically energized by an exoergic chemical reaction which produces the necessary population inversion of lasing species. Based on the enormous chemical energy deposit, several kinds of chemical laser now deliver the cw power outputs of megawatt magnitude, far higher than any other lasers. Accordingly, along with the improvement of gas medium homogeneity and mode-selectivity of the optical cavity chemical laser has also attained high beam quality of a near diffraction-limited divergence angle. Recent efforts in developing new chemical laser have focused on the short wavelength chemical laser system, e.g. from the early DF (iota = 3.8 micrometer) and HF (lambda = 2.7 micrometer) to late O2(1) Delta)-1 (lambda = 1.315 micrometer) and HF overtone transition laser (approx. 13 micrometer). At present the community of chemical physics are much interested in the visible chemical laser which may be realized by stimulated emission of an electronic excited state. DTIC

N95-31394# Sandia National Labs., Albuquerque, NM.
ION-ASSISTED PULSED LASER DEPOSITION OF AMORPHOUS TETRAHEDRAL-COORDINATED CARBON FILMS
T. A. Friedmann, D. R. Tallant, J. P. Sullivan, M. P. Siegal, and R. L. Simpson 1994 6 p Presented at the 1994 Fall Meeting of the Materials Research Society (MRS), Boston, MA, 28 Nov. - 2 Dec. 1994
(Contract DE-AC04-94AL-85000)
(DE95-010861; SAND-95-0166C; CONF-941144-143) Avail: CASI HC A02/MF A01

A parametric study has been performed of amorphous tetrahedral carbon (a-tC) films produced by ion-assisted pulsed laser deposition (IAPLD). The ion voltage, current density, and feed gas composition (nitrogen in argon) have been varied. The resultant films were characterized by thickness, residual stress, Raman spectroscopy, and electrical resistivity. The Raman spectra have been fit to two gaussian peaks, the so called graphitic (G) peak and the disorder (D) peak. It has been found that the magnitude of the D peak and the residual compressive stress are inversely correlated. At low beam voltages and currents, the magnitude of the D peak is low, increasing as the ion beam voltage and current are raised. The ion beam voltage has the most dramatic effect on the magnitude of the D peak. At low voltages (200-500 V) the magnitude of the D peak is greater for ion beams with high percentages of nitrogen possibly indicative of C-N bonding in the films. At higher voltages (500-1500 V) the D peak intensity is less sensitive to the nitrogen content of the beam. DOE

N95-31434# Lightwave Electronics Corp., Mountain View, CA.
A COMPACT AND EFFICIENT VIOLET LASER SOURCE Final Report, 15 Jun. - 15 Dec. 1994
D. C. Gerstenberger Feb. 1995 15 p
(Contract F49620-94-C-0036)
(AD-A292782) Avail: CASI HC A03/MF A01

The purpose of this Phase 1 program was to investigate a compact and efficient laser source in the 430nm violet spectral range using frequency-doubling of a cw single-mode AlGaAs diode laser in an external resonant doubler constructed of potassium niobate. The primary objective of the Phase 1 program was to develop and evaluate a novel monolithic frequency-doubler design. Another goal was to eliminate the need for an optical isolator. Several monolithic potassium niobate resonant doublers were constructed and tested with Fabry-Perot (F-P) and distributed-Bragg-reflector (DBR) diode lasers. Approximately 9mW of cw 430nm violet light was generated with the best doubler. The DBR laser was found to be more than 100 times less sensitive to feedback than the F-P diode laser, but neither laser provided stable frequency-doubled output in Phase 1 experiments. DTIC

N95-31528# Illinois Univ., Urbana, IL. Dept. of Electrical and Computer Engineering.
ULTRAVIOLET AND VISIBLE LASERS: RARE EARTH-DOPED WAVEGUIDE DEVICES AND NON-LINEAR OPTICAL EXTRACTION TECHNIQUES Final Report, 1 Dec. 1991 - 30 Nov. 1994
J. G. Eden Dec. 1994 37 p
(Contract F49620-92-J-0089)
(AD-A293976; AFOSR-95-0321TR) Avail: CASI HC A03/MF A01

Over the past three years, AFOSR has supported a combined experiment at the University of Illinois that has focused on the demonstration and development of new coherent sources operating in the ultraviolet and short wavelength portion of the visible (green to violet). This research effort has two thrusts. Emphasis is being placed on the demonstration of fiber and planar waveguide lasers based upon upconversion processes in rare earth doped glasses. These devices have several attractive features for applications in communications, reprographics and medicine (in particular), including: (1) wide tunability (several nm); (2) broad absorption spectra suitable for diode laser pumping; (3) overall efficiencies exceeding 10% despite the required absorption of at least two pump photons; (4) pump-gain

medium interaction lengths not normally available with bulk crystals; (5) the ability to integrate planar waveguide glass-based lasers with other devices such as EO-modulators and laser diodes; and (6) multiple wavelengths and high quantum efficiencies (greater than 50%). DTIC

N95-31563# Texas Univ. at Dallas, Richardson, TX. Richardson Center for Quantum Electronics.

BASIC STUDY OF THE PUMPING OF A GAMMA-RAY LASER Annual Report, 15 Mar. 1994 - 14 Mar. 1995

C. B. Collins and J. J. Carroll 15 Apr. 1995 116 p

(Contract N00014-93-K-2005)

(AD-A293561; GRL/9501) Avail: CASI HC A06/MF A02

The most productive approaches to the problem of the gamma ray laser have focused upon upconversion techniques in which metastable nuclei are pumped with long wavelength radiation. At the nuclear level the storage of energy can approach tera-Joules (10(exp 12)J) per liter for thousands of years. However, any plan to use such a resource for a gamma ray laser poses problems of a broad interdisciplinary nature requiring the fusion of concepts taken from relatively unrelated fields of physics. Our research group has described several means through which this energy might be coupled to radiation field with cross sections for stimulated emission that could reach 10(exp -17) sq cm. Such a stimulated release could lead to output powers as great as 3 x 102 Watts/liter. Since 1978 we have pursued an approach for the upconversion of longer wavelength radiation incident upon isomeric nuclear populations that can avoid many of the difficulties encountered with traditional concepts of single-photon pumping. Experiments have confirmed the general theory and have indicated that a gamma-ray laser is feasible if the right combination of energy levels and branching ratios exists in some real material. Of the 1,886 distinguishable nuclear materials, the present state-of-the-art has been adequate to identify 29 first-class candidates, but further evaluation cannot proceed without remeasurements of nuclear. A laser-grade database of nuclear properties does not yet exist but the techniques for constructing one have been developed and utilize under this contract. DTIC

N95-31833# Naval Postgraduate School, Monterey, CA.

PRIME POWER FOR SHIPBOARD HIGH-AVERAGE POWER FELs M.S. Thesis

Robert A. Lyon, Jr. Dec. 1994 97 p Limited Reproducibility: Document partially illegible

(AD-A293718) Avail: CASI HC A05/MF A02

High-power free electron lasers (FEL's), capable of deployment aboard naval combatants, would place a unique and significant demand upon the ship's electrical distribution system. A shipboard FEL must be power efficient, relatively compact, and present a minimum radiation hazard to nearby personnel. The feasibility of deploying an FEL aboard a ship is analyzed from a power system perspective. To produce 1 MW of laser power, it is determined that 6.6 MW of high-voltage dc power is required to drive the FEL when superconductor accelerator technology is employed and 9 MW is required when conventional room temperature accelerator technology is used. The required prime power electrical distribution is easily compatible with the gas turbine engineering plants of modern surface combatants. This distribution will add 22 tons to the ship's displacement and require 22 m3 of the ship's volume to implement. Simulation results show that the FEL would require an undulator with only 16 periods to produce 1 MW for the electron beam parameters developed during the power analysis. This FEL exhibits a large tolerance to electron beam quality. From a power analysis viewpoint, FEL's may become a competitive technology for a prospective naval laser weapon. DTIC

N95-31848 Michigan Univ., Ann Arbor, MI.

CARRIER DYNAMICS AND OPTICAL PROPERTIES OF GaAs- AND InP-BASED STRAINED QUANTUM WELL LASERS Ph.D. Thesis

Lawrence John Davis, IV 1994 161 p

Avail: Univ. Microfilms Order No. DA9423171

As material quality and processing techniques continue to improve over the years, the performance of optoelectronic devices using multiple quantum wells has reached the point where intrinsic material characteristics, such as carrier transport, recombination lifetime, etc., are expected to be important issues. These intrinsic characteristics have been investigated with respect to laser and modulator structures. Carrier transport was investigated in AlGaAs/GaAs and InGaAs/InAlAs modulator structures using an all-optical time-of-flight technique, allowing temporal resolution of approximately 1 ps. The observed fast transport times can only be explained by a field-dependent carrier emission out of the quantum well, after which transport through the continuum states can occur. The carrier relaxation processes to the quantum well, including the carrier diffusion, capture into the quantum well and relaxation in the well, have been studied. If the electron-hole (e-h) recombination time by stimulated emission for a laser at high injection approaches these relaxation times, the carrier distribution in the quantum well can be 'hot' and is not described by a quasi Fermi distribution. This creates serious limitations for the laser performance by introducing gain-compression enhanced Auger rates and other hot-carrier related effects. These Auger recombination rates have been measured in compressively strained In(x)Ga(1-x)As/InGaAsP/InP quantum wells for the first time. The Auger recombination rates were derived from the measured turn-on delay times during large-signal modulation of single mode lasers. A new device concept has been demonstrated to overcome these intrinsic processes. In this device, termed the tunneling injection quantum well laser, carriers are transported to the active lasing subband by resonant and sequential tunneling. Record performance compared to other single quantum well lasers has been demonstrated in terms of differential gain and modulation bandwidth, showing the potential for this new device. Dissert. Abstr.

N95-32029# Lawrence Livermore National Lab., Livermore, CA.

ENHANCED BRIGHTNESS X-RAY LASERS

A. S. Wan, R. C. Cauble, L. B. DaSilva, J. C. Moreno, and J. Nilsen Sep. 1994 6 p Presented at the ECLIM 23: Laser Interaction With Matter, Oxford (England), 19-23 Sep. 1994

(Contract W-7405-eng-48)

(DE95-010735; UCRL-JC-116841; CONF-9409226-6) Avail: CASI HC A02/MF A01

We are developing short-pulsed, enhanced-brightness, and coherent x-ray lasers (XRL's) for applications in areas such as plasma imaging. In a traveling wave pump setup the optical laser creating the XRL plasma sweeps along the lasant axis at the same speed as the x-rays. This technique becomes increasingly important as the target length increases and the gain duration shortens. An order of magnitude increase in output energy was measured with vs without traveling wave pump. Using multiple pulse techniques and multilayer mirrors to inject the output of one pulse back into the plasma formed by a later pulse we have begun to develop the x-ray analog of a multi-pass amplifier. The use of multiple pulses separated by as much as 1.6 ns reduces multilayer mirror damage. This injection technique is demonstrated by imaging the near-field emission profiles of the XRL. The addition of multilayer beamsplitter will allow us to effectively produce a soft XRL cavity. DOE

N95-32143# Sandia National Labs., Albuquerque, NM. Energetic and Environmental Test Dept.

SANDIA NATIONAL LAB'S PRECISION LASER TRACKING SYSTEMS

D. Patrick 1995 5 p Presented at the Test Facility Working Group Conference, Las Vegas, NV, 12-16 Jun. 1995

(Contract DE-AC04-94AL-85000)

(DE95-009837; SAND-95-0670C; CONF-9506174-1) Avail: CASI HC A01/MF A01

Sandia Labs' mobile tracking systems have only one moving part. The double gimballed 18 inch diameter beryllium mirror is capable of constant tracking velocities up to 5 rads/sec in both axes, and accelerations to 150 rads/sec(exp 2) in both axes. Orthogonality is less than 10 microradians. The mirror directs the 488 and 514 nm wavelength CW laser beams to adhesive-backed reflective material applied to the test unit. The mirror catches the return beam and visual image, directing the visual image to three camera bays, and the return beam to an image dissector behind an 80 inch gathering telescope. The image dissector or image position sensor is a photomultiplier with amplifying drift tube and electron aperture and its associated electronics. During the test, the image dissector scan senses the change in position of the reflective material and produces signals to operate the azimuth and elevation torque motors in the gimbal assembly. With the help of 1 1/8 in. diameter azimuth and elevation galvonometer steering mirrors in the optical path, the laser beam is kept on the target at extremely high velocities. To maintain a constant return signal strength, the outgoing beam is run through a microprocessor controlled beam focusing telescope. DOE

N95-32152# Department of the Air Force, Wright-Patterson AFB, OH. National Air Intelligence Center.
LUMINESCENCE PROPERTIES OF ZnWO4:Cr(3+) LASER CRYSTALS
Zang Jingcun (Beijing Polytechnic Univ., China.), Wu Shanhua (Beijing Polytechnic Univ., China.), and Ma Yue (Beijing Polytechnic Univ., China.) 30 Mar. 1995 11 p Transl. into ENGLISH from Zhongguo Jiguang (China), v. 18, no. 6, Jun. 1991 p 446-449
(AD-A293065; NAIC-ID(RS)T-0496-94) Avail: CASI HC A02/MF A01

Luminescence properties of ZnWO4:Cr(3+) laser crystals were investigated. (4)T2 energy level of Cr(3+) split into three levels, 13550, 14205 and 14706/cm, and the Stokes shift of luminescence spectra is 236 nm. The best intensity peak of emission is at 912nm. If the excitation wavelength was selected as 608 nm and doping concentration was 0.01 wt%, a broad emission band would be observed at 532 nm excitation. DTIC

N95-32155# Lawrence Livermore National Lab., Livermore, CA.
FEMTOSECOND, Cr(4+):YAG LASER
H. Nathel, A. Sennaroglu, and C. R. Pollock Aug. 1994 2 p Presented at the 9th Ultra Short Phenomenon, Heidelberg, Germany, 2-5 May 1994 (Contract W-7405-eng-48)
(DE95-004964; UCRL-JC-118408; CONF-9405308-1) Avail: CASI HC A01/MF A01

Results from both a regeneratively-initiated and self-initiated, mode-locked Cr:YAG laser which is tunable from 1.51 to 1.53 micro m are reported. One hundred and twenty femtosecond, nearly transform-limited pulses have been generated with peak output powers of 45 kW. The stable, high peak power pulses and room temperature operation of this laser make it a very suitable alternative to the cumbersome, cryogenic mode-locked NaCl laser commonly used in both narrow bandgap semiconductor and optical communications research. DOE

N95-32280# Sandia National Labs., Albuquerque, NM.
THE DEVELOPMENT OF A PULSED LASER IMAGING SYSTEM FOR NATURAL GAS LEAK DETECTION Abstract Only
Thomas J. Kulp 1995 2 p Presented at the Natural Gas Research, Development and Demonstration Contractors Review Meeting, Baton Rouge, LA, 4-6 Apr. 1995
(Contract DE-AC04-94AL-85000)
(DE95-011407; SAND-95-8561A; CONF-950494) Avail: CASI HC A01/MF A01

The detection of gas leaks represents a critical operation performed regularly by the gas industry to maintain the integrity and safety of its vast network of piping, both above and below the ground. We are developing a technology that allows the real-time imaging of gas plumes in a television format. Termed backscatter absorption gas imaging (BAGI), the technique operates by illuminating a scene with infrared laser radiation having a wavelength that is absorbed by the gas to be detected (in this case, methane). Backscattered laser radiation is used to create a video image of the scene. If a leak of the target gas is present in the field-of-view of the camera, it attenuates a portion of the backscatter and creates a dark cloud in the video picture. The specific purpose of this project is to investigate a new method of accomplishing BAGI using a pulsed laser source. The pulsed laser imager under development in this project is expected to have a range (greater than or equal to 40 m) and sensitivity (less than 10 ppm-m) that will surpass the respective attributes of a scanned continuous wave laser imager. The pulsed system will operate by flooding (rather than scanning) the imaged scene with pulses of laser radiation. Imaging will be accomplished using a focal-plane array camera that operates in a snapshot format. The higher power of the pulsed laser source and the more effective collection optics of the focal-plane array-based receiver will allow the performance enhancements to be achieved. DOE

N95-32174# Aerospatiale, Toulouse (France). Direction des Estudes.
STRIPPING BY LASER
Olivier Malavallon *In* AGARD, Environmentally Safe and Effective Processes for Paint Removal Apr. 1995 4 p (For primary document see N95-32165 11-31)
Copyright Avail: CASI HC A01/MF A01

N95-32347*# National Aeronautics and Space Administration. Goddard Space Flight Center, Greenbelt, MD.
LASER RETROREFLECTOR EXPERIMENT ON NAVSTAR 35 AND 36
E. C. Pavlis and Ronald L. Beard (Naval Research Lab., Washington, DC.) *In its* The 26th Annual Precise Time and Time Interval (PTTI) Applications and Planning Meeting May 1995 p 427-441 (For primary document see N95-32319 11-70)
Avail: CASI HC A03/MF A04

N95-32348*# Observatoire de la Cote d'Azur, Grasse (France).
(T2L2) TIME TRANSFER BY LASER LINK
Christian Veillet and Patricia Fridelance *In* NASA. Goddard Space Flight Center, The 26th Annual Precise Time and Time Interval (PTTI) Applications and Planning Meeting May 1995 p 443-453 (For primary document see N95-32319 11-70)
Avail: CASI HC A03/MF A04

37 MECHANICAL ENGINEERING

Includes auxiliary systems (nonpower); machine elements and processes; and mechanical equipment.

N95-30386 Department of the Navy, Washington, DC.
LOW VIBRATION POLYMERIC COMPOSITE ENGINE Patent
David P. Guimond, inventor (to Navy) and Rolf K. Muench, inventor (to Navy) 6 Dec. 1994 6 p Filed 28 Sep. 1993
(AD-D017332; US-Patent-5-370,087; US-Patent-Appl-SN-127546; US-Patent-Class-123-546) Avail: US Patent and Trademark Office

An internal combustion engine is constructed with metallic parts in its regions which are subjected to high stress (temperature, pressure) during combustion and polymeric materials in its regions which are subjected to relatively lower stresses. The integrated construction helps realize increased power densities and reductions on engine noise without compromising engine performance. V-configuration Diesel engines particularly benefit from this construction. DTIC

N95-30387 Department of the Navy, Washington, DC.
COUPLING STUD ASSEMBLY Patent
Gus F. Plangetis, inventor (to Navy) 29 Nov. 1994 12 p Filed 24 Sep. 1993
(AD-D017335; US-Patent-5,368,344; US-Patent-Appl-SN-125712; US-Patent-Class-285-412) Avail: US Patent and Trademark Office

A coupling stud assembly for coupling together a pair of flanges is discussed. A stud having a tapered surface is inserted into respective overlapping through-holes provided in the flanges so that a space is defined between the stud and inner walls of the holes. A wedge is fitted into the space and is pressed by a wedge spacer so as to tighten contact between the stud and the inner walls of the through holes. Nuts are provided on threaded ends of the stud to securely couple the flanges together. This arrangement provides a tight, vibration-free coupling between the flanges. DTIC

N95-30399 Department of the Navy, Washington, DC.
GEAR PUMP WITH REDUCED FLUID-BORNE NOISE Patent
John W. Henry, inventor (to Navy), William F. Flickinger, inventor (to Navy), Joseph F. Dolinar, Jr., inventor (to Navy), Francisco A. Rodriguez, inventor (to Navy), and James W. Smith, inventor (to Navy) 1 Nov. 1994 9 p Filed 30 Sep. 1993
(AD-D017362; US-Patent-5,360,325; US-Patent-Appl-SN-129501; US-Patent-Class-418-126) Avail: US Patent and Trademark Office

A crescent internal gear pump achieves greatly improved sealing against counter flow of fluid and greatly reduced noise by increase of the number of teeth of each of the ring and pinion gears which form discrete volumes of pumped fluid against a crescent-shaped member or insert. Reduction of the size of the teeth ring and pinion gears allows an increase in the angular extent of the crescent-shaped insert in order to increase the number of discrete volumes to be increased to a minimum of nineteen for each of the ring and pinion gears. The reduction in noise is accompanied by an increase in the fundamental frequency of the remaining noise, which can be more readily attenuated by acoustic filtering and isolation. Perfecting features of the invention include shaping of the crescent shaped member

to equalize the number of discrete volumes formed by each of the ring and pinion gears and shaping the teeth of the pinion gear to equalize the volumes of the discrete volumes formed by each gear. DTIC

N95-30414 Department of the Navy, Washington, DC.
LOCKING DEVICE FOR FLUID COUPLING Patent
Kenneth J. Beatrice, inventor (to Navy) and George M. Christie, inventor (to Navy) 20 Dec. 1994 4 p Filed 22 Feb. 1993
(AD-D017354; US-Patent-5,374,085; US-Patent-Appl-SN-020939; US-Patent-Class-385-81) Avail: US Patent and Trademark Office

A mechanical locking device for use with conventional quick disconnect fluid coupling having a release collar on the female component spaced from a flange or nut also on the female component. Upper and lower half shells of the locking device fit between the release collar and flange to prevent inadvertent movement of the release collar. The half shells are assembled by two threaded fasteners which must be unthreaded to remove the device from the fluid coupling. DTIC

N95-30416 Department of the Navy, Washington, DC.
FAST-ACTING VALVE FOR PROJECTIVE LAUNCHING SYSTEMS Patent
Nicholas Bitsakis, inventor (to Navy) 27 Dec. 1994 10 p Filed 20 Dec. 1993
(AD-D017357; US-Patent-5,375,502; US-Patent-Appl-SN-169277; US-Patent-Class-891-810) Avail: US Patent and Trademark Office

A fast acting valve for use in a stored energy projectile launching system. The valve has an inlet port for connection to a storage energy device, an outlet port for connection to a launching tube and an intermediate chamber. The interior of the valve seat communicates with one of the ports through a plurality of apertures that permit liquid to transfer between the ports. A cylindrical valve lies inside the cylindrical valve seat and sealingly, slidingly engages the interior of the cylindrical valve seat. A microprocessor-based control system provides a controlled velocity profile transfer of the valve between a first position in which the valve seals the ports and a second position in which the valve clears the ports. DTIC

N95-30532 Department of the Navy, Washington, DC.
VIBRATION ISOLATION MOUNT WITH LOCKING MEANS Patent
Stuart C. Dickinson, inventor (to Navy) 22 Nov. 1994 5 p Filed 29 Mar. 1993
(AD-D017367; US-Patent-5,366,198; US-Patent-Appl-SN-037878; US-Patent-Class-248-550) Avail: US Patent and Trademark Office

A vibration isolation mount is described. It comprises: (1) a frame adapted for attachment to a support member; (2) a spring device mounted on the frame and adapted for attachment to a protected device, the spring device being movable on the frame to permit movement of the protected device relative to the support member; and (3) a locking mechanism for limiting movement of the spring device on the frame, thereby to limit movement of the protected device relative to the support member. DTIC

N95-30701# Royal Inst. of Tech., Stockholm (Sweden). Dept. of Mathematics.
SPEED CONTROL OF AN ELASTIC TWO-MASS SYSTEM: OPTIMIZATION AND SYSTEMS THEORY
C. G. Baril and J. Galic 1994 37 p Sponsored by Swedish National Board for Industrial and Technical Development
(PB95-212106; TRITA-MAT-1994-29) Avail: CASI HC A03/MF A01

The speed control problem of an elastic two-mass system is studied in this work. This simple and basic system is often found in mechanical devices where a load inertia is driven by an electrical motor through an elastic coupling. Different linear controllers are checked and the applicability of each of them is established. We show some frequency domain constraints that must be satisfied by the controller in order to avoid low damped oscillations. These constraints are very difficult to satisfy for systems where the load inertia is small compared with the motor inertia. For this case we also show that with a minimum phase controller the peak shaft torque will be considerably high when a disturbance is applied on the load side. We finally present a cascaded linear controller, where the measured signals are both the motor speed and the shaft torque, or alternatively the motor speed and the load speed. In the first case the shaft torque measurement is used to estimate the load speed. This simple controller is able to damp the oscillations and to reduce the maximum shaft torque. NTIS

N95-30716 Department of the Navy, Washington, DC.
SMART MATERIAL JOINT BAND Patent
Michael A. Tucchio, inventor (to Navy), Robert A. Stoodt, inventor (to Navy), and Robert A. Livsey, inventor (to Navy) 22 Nov. 1994 6 p Filed 30 Dec. 1993
(AD-D017374; US-Patent-5,366,254; US-Patent-Appl-SN-176373; US-Patent-Class-285-23) Avail: US Patent and Trademark Office

The present invention relates to an improved connector for joining two tubular members together. The connector is formed by a plurality of longitudinally extending fingers extending from an end of one of tubular members and at least one locking groove in the other of the tubular members for receiving the fingers. The connector further includes a circumferentially extending wire member which is received in a notch in a head portion of each of the plurality of fingers. The wire member is preferably formed from a shape memory alloy and has an original circumference less than the circumference of a circle formed by the notches in a head portions of the fingers. The connector includes apertures through which electric wires may be connected to the shape memory alloy ring member so as to cause the shape memory alloy ring member to return to its original shape and allow release of the joint connection. DTIC

N95-30829 Columbia Univ., New York, NY.
PRECISION MANIPULATION WITH A DEXTROUS ROBOT HAND Ph.D. Thesis
Paul Michelman 1994 195 p
Avail: Univ. Microfilms Order No. DA9421381

In this thesis, we discuss a framework for describing and synthesizing precision manipulation tasks with a robot hand. Precision manipulations are those in which the motions of grasped objects are caused by finger motions alone (as distinct from arm or wrist motion). Experiments demonstrating the capabilities of the Utah-MIT hand are presented. This work begins by examining current research on biological motor control to raise a number of questions. For example, is the control centralized and organized by a central processor? Or is the control distributed throughout the nervous system? Motor control research on manipulation has focused on developing classifications of hand motions, concentrating solely on finger motions, while neglecting grasp stability and interaction forces that occur in manipulation. In addition, these taxonomies have not been explicitly functional. This thesis defines and analyzes a basic set of manipulation strategies that includes both position and force trajectories. The fundamental purposes of the manipulations are: (1) rectilinear and rotational motion of grasped objects of different geometries; and (2) the application of forces and moments against the environment by the grasped objects. First, task partitioning is described to allocate the fingers their roles in the task. Second, for each strategy, the mechanics and workspace of the tasks are analyzed geometrically to determine the gross finger trajectories required to achieve the tasks. Techniques illustrating the combination of simple manipulations into complex, multiple degree-of-freedom tasks are presented. There is a discussion of several tasks that use multiple elementary strategies. The tasks described are removing the top of a childproof medicine bottle, putting the top back on, rotating and regrasping a block and a cylinder within the grasp. Finally, experimental results are presented. The experimental setup at Columbia University's Center for Research in Intelligent Systems and experiments with a Utah-MIT hand is discussed. First, the overall system design is described. Two hybrid position/force controllers were designed and built. After a discussion of the entire system, experimental results are presented describing each of the basic manipulation and complex manipulation strategies. Dissert. Abstr.

N95-30830 Iowa Univ., Iowa City, IA.
ROBUST POSITION AND FORCE TRACKING CONTROL FOR A ROBOT IN CONTRACT Ph.D. Thesis
Sang-moo Lee 1993 166 p
Avail: Univ. Microfilms Order No. DA9421158

This thesis presents a robust position and force tracking control approach for a robot in contact. When a robot involves in a task of changing between free and contact motion, tracking contact position or force is a difficult problem in control. The approach uses the computed torque linearization to cancel the nonlinear dynamics of the robot. A target dynamics is then applied to the linearized system. The target dynamics relates position errors and force errors through force error compensators. Using the high-order compensators, the target dynamics guarantees smooth transition

between free and contact maneuvers, position or force tracking, and robust performance to environmental uncertainty. In case of single degree-of-freedom robots, tracking in steady states can be achieved by designing compensators, placing zeros or poles at the origin for position or force tracking control, respectively. To improve tracking performance in transient states, the H(sub infinity) control synthesis is adopted to design a compensator that minimizes H(sub infinity) optimality. The optimality is augmented to trade off between mixed sensitivities and joint loads. The designed compensator for the multi-input and multioutput system shows that the tracking performance meets the design specifications. When the environmental uncertainty is structured as a simple inertia-damper-stiffness system with unbounded coefficients, robustly stable compensators exist for all variations of the coefficients. When the uncertainty is unstructured and bounded, the H(sub infinity) robust performance condition is employed to design a compensator robust to the uncertainty. A reduced-order compensator is obtained by iteratively applying optimization to a fixed-order compensator with unknown coefficients. The computed torque linearization is subject to modeling errors in sensing, measurements, and estimations, which degrade the stability of the controlled system. A sufficient condition for stability robust to the modeling errors is derived by combining the operator theory and the small gain theorem. The condition determines the allowable limits of the modeling errors. Author

N95-30949# Naval Postgraduate School, Monterey, CA.
FAILURE ANALYSIS OF A REPAIRABLE SYSTEM: THE CASE STUDY OF A CAM-DRIVEN RECIPROCATING PUMP M.S. Thesis
Donald D. Dudenhoeffer Sep. 1994 100 p
(AD-A293144) Avail: CASI HC A05/MF A02

This thesis supplies a statistical and economic tool for analysis of the failure characteristics of one typical piece of equipment under evaluation: a cam-driven reciprocating pump used in the submarine's distillation system. Comprehensive statistical techniques and parametric modeling are employed to identify and quantify pump failure characteristics. Specific areas of attention include: the derivation of an optimal maximum replacement interval based on costs, an evaluation of the mission reliability for the pump as a function of pump age, and a calculation of the expected times between failures. The purpose of this analysis is to evaluate current maintenance practices of time-based replacement and examine the consequences of different replacement intervals in terms of costs and mission reliability. Tradeoffs exist between cost savings and system reliability that must be fully understood prior to making any policy decisions. DTIC

N95-31332 Pennsylvania Univ., Philadelphia, PA.
CONTROL OF MECHANICAL SYSTEMS WITH ROLLING CONTACTS: APPLICATIONS TO ROBOTICS Ph.D. Thesis
Nilanjan Sarkar 1993 165 p
Avail: Univ. Microfilms Order No. DA9413904

The problems of modeling and control of mechanical dynamic systems subject to rolling contacts are investigated. There are two important theoretical contributions in this dissertation. First, contact kinematic relationships up to second order are developed for two rigid bodies in point contact. These equations relate gross rigid body motion to the changes in the positions of the points of contact. Second, a unified approach to the control of mechanical systems subject to both holonomic and nonholonomic constraints is proposed. The basic approach is to extend the state-space to include, in the addition to the generalized coordinates and velocities, contact coordinates which describe the displacements of the contact points and their derivatives. This redundant state-space formulation provides a convenient way to specify output equations to control contact motion. The control problem is formulated as an affine nonlinear problem and a differential-geometric, control-theoretic approach is used to decouple and linearize such systems. It is shown that such a system, even though not input-state linearizable, is input-output linearizable. Further, the zero dynamics of such a system is shown to be Lagrange stable. The proposed methodology is applied to three different robotic systems: (1) wheeled mobile robots; (2) two arms manipulating an object with rolling contact between each arm and the object; and (3) a single robot arm maintaining controlled contact against a moving environment. In each case, a nonlinear controller is designed to achieve the desired performances. For mobile robots, a new control algorithm called dynamic path following is proposed and shown to be quite effective and robust. In the context of two arm manipulation, grasp adaptation through the control of contact motion is demonstrated. Maintaining rolling contact with a moving surface is formulated as an acatastatic system. The proposed scheme involves simultaneously controlling interaction forces as well as the relative (rolling) motion. In all cases, computer simulations results are presented to demonstrate the efficacy of the control schemes. Dissert. Abstr.

N95-31374# Analytic Power Corp., Boston, MA.
LINEAR MOTOR FREE PISTON COMPRESSOR Final Report
David P. Bloomfield 17 Feb. 1995 30 p
(Contract DAAL03-92-C-0016)
(AD-A293452; ARO-30443.1-CH-5) Avail: CASI HC A03/MF A01

A Linear Motor Free Piston Compressor (LMFPC), a free piston pressure recovery system for fuel cell powerplants was developed. The LMFPC consists of a reciprocating compressor and a reciprocating expander which are separated by a piston. In the past energy efficient turbochargers have been used for pressure large (over 50 kW) fuel cell powerplants by recovering pressure energy from the powerplant exhaust. A free piston compressor allows pressurizing 3 - 5 kW sized fuel cell powerplants. The motivation for pressurizing PEM fuel cell powerplants is to improve fuel cell performance. Pressurization of direct methanol fuel cells will be required if PEM membranes are to be used Direct methanol oxidation anode catalysts require high temperatures to operate at reasonable power densities. The elevated temperatures above 80 C will cause high water loss from conventional PEM membranes unless pressurization is employed. Because pressurization is an energy intensive process, recovery of the pressure energy is required to permit high efficiency in fuel cell powerplants. A complete LMFPC which can pressurize a 3 kW fuel cell stack was built. This unit is one of several that were constructed during the course of the program. DTIC

N95-31382*# Technetics, Inc., DeLand, FL.
BRUSH SEAL SHAFT WEAR RESISTANT COATINGS Final Report, May 1994 - Mar. 1995
Harold Howe 28 Mar. 1995 38 p
(Contract NAS3-27383)
(NASA-CR-198950; NAS 1.26:198950; AD-A292886) Avail: CASI HC A03/MF A01

Brush seals suffer from high wear, which reduces their effectiveness. This work sought to reduce brush seal wear by identifying and testing several industry standard coatings. One of the coatings was developed for this work. It was a co-sprayed PSZ with boron-nitride added for a high temperature dry lubricant. Other coatings tested were a PSZ, chrome carbide and a bare rotor. Testing of these coatings included thermal shocking, tensile testing and wear/coefficient of friction testing. Wear testing consisted of applying a coating to a rotor and then running a sample tuft of SiC ceramic fiber against the coating. Surface speeds at point of contact were slightly over 1000 ft/sec. Rotor wear was noted, as well as coefficient of friction data. Results from the testing indicates that the oxide ceramic coatings cannot withstand the given set of conditions. Carbide coatings will not work because of the need for a metallic binder, which oxidizes in the high heat produced by friction. All work indicated a need for a coating that has a lubricant contained within itself and the coating must be resistant to an oxidizing environment. DTIC

N95-31566# Naval Postgraduate School, Monterey, CA.
ANALYTIC AND EXPERIMENTAL INVESTIGATION OF ROTORDYNAMIC RESPONSE AND BACKWARD WHIRL INDUCED BY SPLIT RESONANCE M.S. Thesis
Curtis E. Vejvoda Dec. 1994 135 p
(AD-A293639) Avail: CASI HC A07/MF A02

Rotordynamic response phenomena, including backward whirl, were investigated both analytically and experimentally. A two degrees-of-freedom rotor model was developed to simulate the steady state, lateral vibration characteristics of a simply supported, single disk rotor. This model includes the effects of direct and cross-coupled, linear damping and stiffness coefficients. The computer model was used to quantify the influence of bearing characteristics on rotordynamic response. The presence of split resonance, which appears to be due to separate and distinct natural frequencies in the two orthogonal lateral directions and the occurrence of backward whirl between these two frequencies was studied. The effects of geometric imperfections in the bearing sleeve, gravitational forces and bearing support stiffnesses were isolated using the experimental apparatus. It was determined that the split resonance induced backward whirl and the

different natural frequencies were caused by asymmetric stiffness of the bearing support structure as well as gravitational forces. Bearing imperfections did not create the backward whirl phenomena. The bearing support characteristics necessary to create the observed rotor orbits were determined. DTIC

N95-31576# Naval Postgraduate School, Monterey, CA.
FINITE ELEMENT ANALYSIS OF SMART STRUCTURES AND MODAL TESTING OF A FLEXIBLE SPACECRAFT ARM M.S. Thesis
James C. Trump Dec. 1994 58 p
(AD-A293761) Avail: CASI HC A04/MF A01

This thesis deals with analytical predictions and experimental determination of the modal frequencies and shapes associated with the arm portion of the Naval Postgraduate School's Flexible Spacecraft Simulator (FSS). A description of how piezoceramic sensors and actuators are incorporated in finite element modeling is presented. A MATLAB (tm) code conducting the finite element modeling of the arm is used to verify the modal frequencies generated via Structural Dynamic Research Corporation's I-DEAS (tm) software. Modal testing is conducted with the I-DEAS test package to determine the first four physical modal frequencies and shapes so that we may compare them with the analytical results. The results of the testing indicated that finite element analysis predicted modes one and three within an average of 23.1%, and modes two and four within an average of 4.4%. DTIC

N95-31710 University of Southern California, Los Angeles, CA.
ON THE KINEMATIC PERFORMANCE OF MECHANICAL MANIPULATORS OPERATING IN THE PRESENCE OF AN OBSTRUCTION Ph.D. Thesis
Victor Charles Rogers 1993
Avail: Issuing Activity (Univ. of Southern California, Doheny Library, Micrographics Dept., Los Angeles, CA 90089-0182)

Mechanical manipulators constitute an essential element of such technological systems as teleoperators, prosthesis, telecherics, locomotion devices, and robots. The earliest systems tended to be kinematically nonredundant and incorporated planar regional substructures. As technology advanced, systems incorporating redundant joint axes were developed. Their advantages have been categorized in terms of such criteria as slenderness, dexterity, and range of motion. Particular emphasis is placed on redundancy for avoiding workspace singularities and when the manipulator must operate in obstructed environments. The advantages provided by kinematic redundancy are offset by practical considerations including increased complexity in both basic design and control strategy. Questions remain unanswered regarding the number, type, and order of joints which a redundant system should have. No consensus exists regarding the most advantageous proportioning of link lengths. This dissertation provides a quantitative assessment of the obstruction effects in an effort to answer some of these questions. Value is placed on the size of the reachable workspace, and it is used as a figure of merit to assess kinematic performance. Kinematic performance is evaluated for a specific class of manipulator operating in the presence of a single circular or spherical obstruction. Planar and spatial designs, constructed from rigid links and incorporating planar 2R and 3R regional structures, are studied in detail. The limiting case of an infinitely redundant manipulator is established. The effects of kinematic redundancy, joint motion limitations, and the use of prismatic pairs are considered. Traditional kinematic concepts of equivalent mechanisms, mobility, and displacement analysis are used to map the boundary of the obstructed workspace for the regional structure of the manipulator. Within the workspace, parametric variations of obstacle size and location are made. Numerical integration is used to quantify the size of the region which is lost due to the obstruction. Using workspace size as a performance measure, topics of optimal link length selection and obstacle placement within the workspace are addressed. Upper bounds are established for performance improvement through joint addition or link length adjustment. Design guidelines, applicable to manipulator synthesis and workcell arrangement, are presented. Dissert. Abstr.

N95-32119 Ohio State Univ., Columbus, OH.
FLUID-FILM LUBRICATION WITH AN APPLICATION TO PISTON RINGS Ph.D. Thesis
Mohsen Esfahanian 1994 250 p
Avail: Univ. Microfilms Order No. DA9420949

This dissertation consists of four related studies. The first part provides dimensionless film thickness equations for four fluid-film lubrication regimes found for nonconformal surfaces while considering side-leakage effects. These regimes are isoviscous rigid, piezoviscous rigid, isoviscous elastic, and piezoviscous elastic. The influence or lack of influence of elastic effects from the solid surfaces and pressure-viscosity effects from the lubricant is a factor that distinguishes these regimes. Results are presented as a map of the lubrication regimes for four values of the ellipticity parameter. The second part deals with integrating artificial intelligence and conventional numerical design techniques to aid in tribological design. The study concentrates on the application of contact stresses. The result is a computer code, the Design Expert for Contact Stress, which incorporates and combines an expert system with numerical analysis techniques to aid the user in designing machine elements. This menu-driven program also performs a design compatibility analysis, which evaluates the compatibility between the specifications and the design, provides a rating on the overall design, lists reasons for the evaluation, and gives suggestions for improvements. The third part investigates the rheological effects in elastohydrodynamic lubrication. In this study the effects on fluid viscosity of pressure, temperature, shear strain rate, shear stress, and time are examined. A number of non-Newtonian models are introduced. The effects of pressure on fluid density are described. The role of solidification pressure on the density of the lubricants is also examined. The possible influence of a lubricant's viscoelastic behavior on its viscosity is considered. Finally, the influence of rheological effects on elastohydrodynamic lubrication is explained. The last part describes fundamental research into the basic mechanisms involved in piston ring lubrication. A recently developed system numerical approach is used for obtaining the lubrication characteristics of the piston ring-cylinder liner conjunction. A complete hydrodynamic and elastohydrodynamic lubrication analysis considering lubricant film shapes and pressure profiles is performed. This requires the simulation of both squeeze and entraining motion of the piston ring throughout an engine cycle. Existence of fluid-film lubrication throughout the engine cycle is examined. Dissert. Abstr.

N95-32163# Allison Engine Co., Indianapolis, IN.
ADVANCED TURBINE SYSTEMS PROGRAM CONCEPTUAL DESIGN AND PRODUCT DEVELOPMENT Quarterly Report, Nov. 1993 - Jan. 1994
Jan. 1995 16 p
(Contract DE-AC21-93MC-29257)
(DE95-000088; DOE/MC-29257/4018) Avail: CASI HC A03/MF A01

This report describes progress made in the advanced turbine systems program conceptual design and product development. The topics of the report include selection of the Allison GFATS, castcool technology development for industrial engines test plan and schedule, code development and background gathering phase for the ultra low NOx combustion technology task, active turbine clearance task, and water vapor/air mixture cooling of turbine vanes task. DOE

N95-32367# Westinghouse Savannah River Co., Aiken, SC.
WELDING ISOTOPIC HEAT SOURCES FOR THE CASSINI MISSION TO SATURN
E. A. Franco-Ferreira and T. G. George (Los Alamos National Lab., NM.)
28 Feb. 1995 35 p Presented at the 75th American Welding Society (AWS) Annual Meeting, Philadelphia, PA, 10-15 Apr. 1994
(Contract DE-AC09-89SR-18035)
(DE95-060104; WSRC-MS-93-316P; CONF-9404233-1) Avail: CASI HC A03/MF A01

In 1997 NASA will launch the Cassini scientific probe to the planet Saturn. Electric power for this probe will be provided by Radioisotope Thermoelectric Generators thermally driven by General Purpose Heat Source modules. RTGs convert the decay heat of a radioisotope, plutonium 238, into electrical energy. The radioisotope is in the form of sintered pellets of (238)PuO2 which are encapsulated in cylindrical shells of iridium alloy to guard against release to the environment in the event of launch or re-entry accident. DOE

N95-31289* National Aeronautics and Space Administration. Lewis Research Center, Cleveland, OH.
CENTRIFUGAL AND AXIAL PUMP DESIGN AND OFF-DESIGN PERFORMANCE PREDICTION
Joseph P. Veres *In* JHU, The 31st JANNAF Combustion Subcommittee

Meeting, Volume 2 Oct. 1994 p 109-122 (For primary document see N95-31282 11-28)
Avail: CPIA, 10630 Little Patuxent Pkwy., Suite 202, Columbia, MD 21044-3200 HC

N95-31784*# Oak Ridge National Lab., TN.
A CENTRIFUGE CO2 PELLET CLEANING SYSTEM
C. A. Foster, P. W. Fisher, W. D. Nelson, and D. E. Schechter *In* NASA. Marshall Space Flight Center, Aerospace Environmental Technology Conference Mar. 1995 p 379-389 (For primary document see N95-31746 11-23)
(Contract DE-AC05-84OR-21400)
Avail: CASI HC A03/MF A06

N95-31785*# Tomco Equipment Co., Loganville, GA.
CO2 (DRY ICE) CLEANING SYSTEM
Donald M. Barnett *In* NASA. Marshall Space Flight Center, Aerospace Environmental Technology Conference 391-398 (SEE N95-31746 11-23) Mar. 1995 (For primary document see N95-31746 11-23)
Avail: CASI HC A02/MF A06

N95-31787*# National Aeronautics and Space Administration. John F. Kennedy Space Center, Cocoa Beach, FL.
AQUEOUS CLEANING AND VERIFICATION PROCESSES FOR PRECISION CLEANING OF SMALL PARTS
Gale J. Allen and Kenneth A. Fishell (Wiltech Corp. of Florida, Inc., Cocoa Beach, FL.) *In* NASA. Marshall Space Flight Center, Aerospace Environmental Technology Conference Mar. 1995 p 411-419 (For primary document see N95-31746 11-23)
Avail: CASI HC A02/MF A06

N95-31791*# Jet Propulsion Lab., California Inst. of Tech., Pasadena, CA.
DEGRADATION OF TCE USING SEQUENTIAL ANAEROBIC BIOFILM AND AEROBIC IMMOBILIZED BED REACTOR
Kirit D. Chapatwala (Selma Univ., AL.), G. R. V. Babu (Selma Univ., AL.), Larry Baresi, and Richard M. Trunzo *In* NASA. Marshall Space Flight Center, Aerospace Environmental Technology Conference Mar. 1995 p 449-457 (For primary document see N95-31746 11-23)
(Grant NAGw-3969)
Avail: CASI HC A02/MF A06

N95-31794*# National Aeronautics and Space Administration. Marshall Space Flight Center, Huntsville, AL.
EVALUATION OF CONTROL PARAMETERS FOR SPRAY-IN-AIR (SIA) AQUEOUS CLEANING FOR SHUTTLE RSRM HARDWARE
S. J. Davis (Micro Craft, Inc., Huntsville, AL.) and C. D. DeWeese *In its* Aerospace Environmental Technology Conference Mar. 1995 p 481-490 (For primary document see N95-31746 11-23)
Avail: CASI HC A02/MF A06

N95-31805*# National Aeronautics and Space Administration. John F. Kennedy Space Center, Cocoa Beach, FL.
CLEANING VERIFICATION BY AIR/WATER IMPINGEMENT
Lisa L. Jones, Maria D. Littlefield, Gregory S. Melton, Raoul E. B. Caimi, and Eric A. Thaxton *In* NASA. Marshall Space Flight Center, Aerospace Environmental Technology Conference Mar. 1995 p 583-591 (For primary document see N95-31746 11-23)
Avail: CASI HC A02/MF A06

N95-31809*# Thiokol Corp., Brigham City, UT. Science and Engineering Analytical Labs. Dept.
THE ROLE OF SURFACE CHEMICAL ANALYSIS IN A STUDY TO SELECT REPLACEMENT PROCESSES FOR TCA VAPOR DEGREASING
Michael W. Lesley, Lawrence E. Davis (Physical Electronics Labs., Eden Prairie, MN.), John F. Moulder (Physical Electronics Labs., Eden Prairie, MN.), and Brad A. Carlson (Physical Electronics Labs., Eden Prairie, MN.) *In* NASA. Marshall Space Flight Center, Aerospace Environmental Technology Conference Mar. 1995 p 619-630 (For primary document see N95-31746 11-23)
Avail: CASI HC A03/MF A06

38 QUALITY ASSURANCE AND RELIABILITY

Includes product sampling procedures and techniques; and quality control.

N95-30510 Selskapet for Industriell og Teknisk Forskning, Trondheim (Norway). Div. of Safety and Reliability.
MEASURES OF RELIABILITY AND RCM
S. Lydersen 31 Dec. 1993 15 p Prepared in cooperation with Technical Univ. of Norway, Trondheim
(PB95-192985; STF75-S93005) Avail: Issuing Activity (National Technical Information Service (NTIS))

This paper presents some new measures of reliability importance: reliability importance for component classes, cut set structural importance. Practical interpretations are given, with application to design improvement and reliability centered maintenance (RCM). The suggested measures are compared to existing measures. NTIS

N95-30520 Selskapet for Industriell og Teknisk Forskning, Trondheim (Norway). Div. of Safety and Reliability.
QUALITY IN APPLIED SCIENCE
T. Sten 31 Dec. 1993 11 p
(PB95-196390; STF75-S93040) Avail: Issuing Activity (National Technical Information Service (NTIS))

Science is in many senses a special kind of craft and only skilled craftsmen are able to distinguish good work from bad. Due to the variation in approaches, methods and even philosophical basis, it is nearly impossible to derive a general set of quality criteria for scientific work outside specific research traditions. Applied science introduces a new set of quality criteria having to do with the application of results in practical situations and policy making. A scientist doing basic research relates mainly to the scientific community of which he is a member, while in applied contract research the scientist has to consider the impact of his results both for the immediate users and upon interest groups possibly being affected. Application thus raises a whole new set of requirements having to do with business ethics, policy consequences and societal ethics in general. NTIS

N95-30783*# National Aeronautics and Space Administration. Langley Research Center, Hampton, VA.
ORBITER RAREFIED-FLOW REENTRY MEASUREMENTS FROM THE OARE ON STS-62
R. C. Blanchard and J. Y. Nicholson (Vigyan Research Associates, Inc., Hampton, VA.) Jun. 1995 36 p
(RTOP 242-80-01-01)
(NASA-TM-110182; NAS 1.15:110182) Avail: CASI HC A03/MF A01

Acceleration data taken from the Orbital Acceleration Research Experiment (OARE) during reentry on STS-62 has been analyzed using calibration factors taken on-orbit. The data includes the flight regime from orbital altitudes down to about 100 km which covers the free-molecule-flow regime and some of the flow-transition into the hypersonic continuum. Ancillary data on orbiter position, orientation, velocity, and rotation rates have been used in models to transform the measured accelerations to the orbiter center-of-gravity, from which aerodynamic accelerations along the orbiter body axes have been calculated. Additional steps are discussed which remove residual offsets introduced in the measurements by unmodeled orbiter forces. The resulting aerodynamic accelerations and their ratios, A(sub z)/A(sub x), are discussed and compared with free-molecule-flow predictions of the aerodynamic coefficient ratios C(sub N)/C(sub A).
Author

N95-31362 Centrum voor Regeleving en Onderzoek, Ede (Netherlands)
QUALITY ASSURANCE TENDERING AND AWARDING CONTRACTS [KWALITEITSBORGING, AANBESTEDING EN GUNNING]
Dec. 1994 54 p In DUTCH
(PB95-197760; ISBN-90-6628-186-3) Avail: Issuing Activity (National Technical Information Service (NTIS))

Standards relating to quality control can be significantly useful when tendering for and awarding contracts. However, because it is sometimes difficult to express these standards in palpable economic terms, they can (practically) never be applied as criteria for awarding contracts in accordance with U.A.R. (Uniform General Standards) 1986. Therefore it would be advisable in the future to regard the availability of a (certified) system of

quality control as being a standard requirement. To this end, a paragraph setting requirements for a quality control plan should be included in the specification. A quality control plan will be required on awarding a contract. This envisaged scenario can best achieved through a transitional phase. During this period there will be opportunity enough for removing any shortcomings in the wording and for considering standards to be required and assessment procedures. NTIS

N95-31530*# National Aeronautics and Space Administration, Washington, DC.
RECOMMENDED TECHNIQUES FOR EFFECTIVE MAINTAINABILITY. A CONTINUOUS IMPROVEMENT INITIATIVE OF THE NASA RELIABILITY AND MAINTAINABILITY STEERING COMMITTEE
Dec. 1994 105 p
(NASA-TM-4628; NAS 1.15:4628) Avail: CASI HC A06/MF A02

This manual presents a series of recommended techniques that can increase overall operational effectiveness of both flight and ground based NASA systems. It provides a set of tools that minimizes risk associated with: (1) restoring failed functions (both ground and flight based); (2) conducting complex and highly visible maintenance operations; and (3) sustaining a technical capability to support the NASA mission using aging equipment or facilities. It considers (1) program management - key elements of an effective maintainability effort; (2) design and development - techniques that have benefited previous programs; (3) analysis and test - quantitative and qualitative analysis processes and testing techniques; and (4) operations and operational design techniques that address NASA field experience. This document is a valuable resource for continuous improvement ideas in executing the systems development process in accordance with the NASA 'better, faster, smaller, and cheaper' goal without compromising safety.
Author

N95-31799*# Thiokol Corp., Huntsville, AL. Space Operations.
CLEANLINESS INSPECTION TOOL FOR RSRM BOND SURFACES
Robert A. Mattes *In* NASA. Marshall Space Flight Center, Aerospace Environmental Technology Conference Mar. 1995 p 525-531 (For primary document see N95-31746 11-23)
Avail: CASI HC A02/MF A06

N95-31802*# Physical Sciences, Inc., Andover, MA.
CONTAMINATION DETECTION NDE FOR CLEANING PROCESS INSPECTION
W. J. Marinelli, V. DiCristina, D. Sonnenfroh, and D. Blair *In* NASA. Marshall Space Flight Center, Aerospace Environmental Technology Conference Mar. 1995 p 551-560 Sponsored by NASA. Langley Research Center (For primary document see N95-31746 11-23)
Avail: CASI HC A02/MF A06

39 STRUCTURAL MECHANICS

Includes structural element design and weight analysis; fatigue; and thermal stress.

For applications see *05 Aircraft Design, Testing and Performance* and *18 Spacecraft Design, Testing and Performance.*

N95-30458# Technische Univ., Delft (Netherlands).
ACOUSTOELASTIC STRESS EVALUATION IN METAL PLATE USING ABSOLUTE SHEAR AND LONGITUDINAL TIME-OF-FLIGHT DATA Ph.D. Thesis
M. Janssen 5 Dec. 1994 220 p
(PB95-197810; ISBN-90-507-1055-4) Copyright Avail: CASI HC A10/MF A03

Stress evaluation in solids plays an important role in engineering. Many experimental techniques have therefore been developed, ranging from the destructive holedrilling method to a large number of non-destructive methods based on x-ray or neutron diffraction, photoelasticity, the determination of magnetic properties and ultrasonic measurements. The subject of this thesis is stress evaluation in metal using ultrasonic waves. The measurements are based on a phenomenon known as acoustoelasticity, i.e. the dependence of wave propagation on the state of deformation or stress in the material.
NTIS

N95-30492# Technische Univ., Delft (Netherlands).
STRESS AND STRAIN CONCENTRATION FACTORS OF WELDED MULTIPLANAR JOINTS BETWEEN SQUARE HOLLOW SECTIONS Ph.D. Thesis
E. PanjehShahi 1994 232 p Sponsored by Stichting voor de Technische Wetenschappen
(PB95-208260; ISBN-90-407-1084-8) Copyright Avail: CASI HC A11/MF A03

The results of an experimental and numerical investigation on the fatigue behavior of uniplanar and multiplanar joints made of square hollow sections are presented in this work. This work has been carried out within the framework of the research program DCT80-1457 sponsored by the Netherlands Technical Foundation (STW). After calibration of the numerical models of the joints with the experimental results, a numerical investigation for the joint parameters for the determination of stress concentration factors (SCF's) and strain concentration factors (SNCF's) was conducted. The software 'HOTSHS' is developed which uses the data base of this parameter study to calculate the hot spot stresses at the weld toes in the various joint types investigated for a given load combination, within the range of the parameters studied. The aim of this research program is to provide stress concentration factors for the fatigue design of uniplanar and multiplanar joints in square hollow sections.
NTIS

N95-30559# RE/SPEC, Inc., Rapid City, SD.
EXPERIMENTAL DETERMINATION OF PROBABILITY DISTRIBUTIONS FOR PARAMETERS OF A SALEM LIMESTONE CAP PLASTICITY MODEL Technical Report, 31 Jan. 1992 - 30 Jun. 1994
Arlo F. Fossum, Tom W. Pfeifle, and Kirby D. Mellegard 1 Jan. 1995 63 p
(Contract DNA001-92-C-0030)
(AD-A290878; RSI-0502; DNA-TR-94-39) Avail: CASI HC A04/MF A01

Marginal probability density functions and a correlation matrix are determined for parameters of the Weidlinger cap plasticity model for Salem limestone specimens originating from Bedford, Indiana. The report describes a program comprising precision laboratory testing, parameter estimation, and probability distribution model fitting. A novel testing scheme allows a complete set of material parameters to be determined from a single test specimen. Statistical properties and distributions are determined by replication. The fitted model is validated by predicting loading histories not included in the fitting database. The testing program includes uniaxial strain tests in axial strain control, unconfined compression tests in all strain control (-1 x 10(exp 6/8)), hydrostatic compression tests in load control (-0.02 MPa/s), and triaxial compression tests in axial strain control (-1 x 10(exp 5/8)), during loading and load control during unloading (-0.02 MPa/s). All specimens are tested at a constant temperature of 20 C and at a water saturation level of 50%. The validation study clearly demonstrates that the parameter estimation procedure produces high quality parameter values, and that the fitted model can not only reproduce measured data included in the fitting database, but also predicts responses from tests conducted under loading histories different from those found in the fitting database.
DTIC

N95-30585 Technische Hogeschool, Delft (Netherlands).
STATIC BEHAVIOUR OF AXIALLY LOADED UNIPLANAR AND MULTIPLANAR TUBULAR X-JOINTS
G. J. vanderVegte 1994 99 p Prepared in cooperation with Instituut TNO voor Bouwmaterialen en Bouwconstructies Limited Reproducibility: More than 20% of this document may be affected by microfiche quality
(PB95-207866) Avail: CASI HC A05

In nature, many applications of hollow sections as a structural element can be observed. Besides excellent properties with regard to resisting compression, tension, bending and torsion forces, hollow sections offer the possibility for architecturally attractive designs. In particular, circular hollow sections have proved to be suitable structural elements. Due to their shape, circular hollow sections have relatively low drag coefficients and are therefore the most favorite choice for elements subjected to wind and wave loading. In addition, the surface area of structures made of circular hollow sections, is much smaller than for comparable structures made of open structures. This, in combination with the smooth circular shape, requires lower costs for protection against corrosion and maintenance of circular members. Therefore, circular hollow sections are applied in a wide range of onshore and offshore structures, e.g. buildings, barriers, towers, bridges, offshore

platforms, etc. Since all of these structures are three dimensional, it is obvious that in many cases multiplanar connections are present at the intersection of several circular members. NTIS

N95-30586# Technische Univ., Delft (Netherlands).
FATIGUE BEHAVIOUR OF MULTIPLANAR TUBULAR JOINTS
A. Romeijn 1994 84 p Sponsored by Stichting voor de Technische Wetenschappen
(PB95-207874) Avail: CASI HC A05/MF A01

Circular hollow sections are frequently used in structures subjected to fatigue loading such as bridges, offshore structures and cranes. These sections are generally connected by direct welding of the sections to each other. For the design of these welded connections, information is required on the fatigue behavior. Especially for multiplanar connections, insufficient data is available regarding stress concentration factors (SCF's) which affect the fatigue life. Also, there is no standard for determining the fatigue strength of welded tubular joints. This has led to a divergence in the methods being used both experimentally as well as numerically. This publication presents the results of experimental and numerical research on the fatigue strength of welded tubular joints. The research projects aim to provide guidelines and design recommendations on the fatigue strength of welded tubular joints, to be proposed for inclusion in international codes of practice such as Eurocode 3. NTIS

N95-30613*# National Aeronautics and Space Administration. Marshall Space Flight Center, Huntsville, AL.
ANALYSIS OF STRESS CONCENTRATION AT HOLES IN COMPONENTS MADE OF 2195 ALUMINUM-LITHIUM
R. Ahmed Washington May 1995 33 p Original contains color illustrations
(NASA-TP-3554; M-781; NAS 1.60:3554) Avail: CASI HC A03/MF A01; 2 functional color pages

Because the 2195 aluminum-lithium of the super lightweight external tank (SLWT ET) has a lower toughness than the 2219 aluminum used in previous ET's, careful attention must be paid to stress concentration in the SLWT ET. This report details the initial analysis performed by NASA to determine the material properties required to ensure structural integrity in these critical areas. Author

N95-30634# Technische Univ., Delft (Netherlands).
DIFFRACTION-LINE BROADENING ANALYSIS AND STRESS RELAXATION IN THIN METAL LAYERS Thesis [ANALYSE VAN DIFFRACTIE-LIJNVERBREDING EN SPANNINGSRELAXATIE IN DUNNE METAALLAGEN]
A. C. Vermeulen 1995 147 p Sponsored by Stichting voor Fundamenteel Onderzoek der Materie, Amsterdam (Netherlands), and Nederlandse Organisatie voor Wetenschappelijk Onderzoek, The Hague
(PB95-213898; ISBN-90-9007530-5) Avail: CASI HC A07/MF A02

This thesis has been subdivided into three parts, which have diffraction-line broadening analysis in common. In Part 1 a correction for the inevitable problem of truncation has been developed. In Part 2 the separation of size and strain broadening has been investigated. In Part 3 a method for determination of the orientation distribution of dislocations have been developed and applied to the analysis of the mechanism of stress relaxation in thin metal layers. NTIS

N95-30682*# National Aeronautics and Space Administration. Langley Research Center, Hampton, VA.
STRUCTURAL DESIGN USING EQUILIBRIUM PROGRAMMING FORMULATIONS
Stephen J. Scotti Jun. 1995 116 p
(RTOP 537-06-21-09)
(NASA-TM-110175; NAS 1.15:110175) Avail: CASI HC A06/MF A02

Solutions to increasingly larger structural optimization problems are desired. However, computational resources are strained to meet this need. New methods will be required to solve increasingly larger problems. The present approaches to solving large-scale problems involve approximations for the constraints of structural optimization problems and/or decomposition of the problem into multiple subproblems that can be solved in parallel. An area of game theory, equilibrium programming (also known as noncooperative game theory), can be used to unify these existing approaches from a theoretical point of view (considering the existence and optimality of solutions), and be used as a framework for the development of new methods for solving large-scale optimization problems. Equilibrium programming theory is described, and existing design techniques such as fully stressed design and constraint approximations are shown to fit within its framework. Two new structural design formulations are also derived. The first new formulation is another approximation technique which is a general updating scheme for the sensitivity derivatives of design constraints. The second new formulation uses a substructure-based decomposition of the structure for analysis and sensitivity calculations. Significant computational benefits of the new formulations compared with a conventional method are demonstrated. Author

N95-30786*# Convolve, Inc., Armonk, NY.
MINIMIZING STRUCTURAL VIBRATIONS WITH INPUT SHAPING (TM) Final Report
Bill Singhose and Neil Singer Jan. 1995 170 p Sponsored by NASA, Washington
(Contract NAS5-32034)
(NASA-CR-189439; NAS 1.26:189439) Avail: CASI HC A08/MF A02

A new method for commanding machines to move with increased dynamic performance was developed. This method is an enhanced version of input shaping, a patented vibration suppression algorithm. This technique intercepts a command input to a system command that moves the mechanical system with increased performance and reduced residual vibration. This document describes many advanced methods for generating highly optimized shaping sequences which are tuned to particular systems. The shaping sequence is important because it determines the trade off between move/settle time of the system and the insensitivity of the input shaping algorithm to variations or uncertainties in the machine which can be controlled. For example, a system with a 5 Hz resonance that takes 1 second to settle can be improved to settle instantaneously using a 0.2 shaping sequence (thus improving settle time by a factor of 5). This system could vary by plus or minus 15% in its natural frequency and still have no apparent vibration. However, the same system shaped with a 0.3 second shaping sequence could tolerate plus or minus 40% or more variation in natural frequency. This document describes how to generate sequences that maximize performance, sequences that maximize insensitivity, and sequences that trade off between the two. Several software tools are documented and included. Author

N95-30825 Stanford Univ., CA.
FOURIER SERIES METHODS FOR CRACKS IN POLYGONAL PLATES AND SHELLS OF REVOLUTION Ph.D. Thesis
Frankie Man Wai Kwok 1994 145 p
Avail: Univ. Microfilms Order No. DA9422098

The objective of the study is to develop efficient numerical methods of solving fracture mechanics problems. In addition to computational efficiency, these methods must require minimal user set-up times. A final criterion is the avoidance of special crack-tip elements to capture the singular behavior. The first part of the study focuses on cracked polygonal plates under anti-plane loading. The basis of this work is the Fourier series method, which transforms a problem with a complicated geometry into a summation of half-plane problems. Through this method, the problem takes the form of a matrix equation, solution of which gives the out-of-plane displacement at any point in the plate. With this solution, the J-integral is found to be an accurate and efficient method of obtaining the stress intensity factor. A number of examples are given to illustrate the versatility of this Fourier series method. The second part of the study continues onward to shells of revolution with circumferential through cracks. The shell problem is formulated as a state vector equation. With an asymptotic-numeric procedure, the edge stiffness matrix for each Fourier circumferential harmonic is obtained. The next step involves constructing the expansion and contraction matrices, which relate the Fourier harmonics of the crack domain to those of the whole circumferential domain. By combining the edge stiffness matrices with the expansion and contraction matrices, a matrix equation is formed. Solution of this equation yields the crack-face displacements satisfying the traction free condition in the crack domain. Numerous examples are presented, which include cracks at the middle sections or fixed ends of cylindrical shells under tensile, bending, or torsional loads. With the above methods, various fracture mechanics parameters can be obtained. These include the crack driving force, the stress intensity factor, the crack opening displacement and area. For the

anti-plane problem, stress intensity factor results compare well with an analytical solution. For shells of revolution, comparisons are made with analytical results from the shallow shell and thin shell theories, and the finite element method. These comparisons highlight the limitations of the different approaches. Dissert. Abstr.

N95-31007# Army Armament Research, Development and Engineering Center, Watervliet, NY. Benet Lab.

A SIMPLE AND ACCURATE TECHNIQUE FOR MONITORING CRACK GROWTH BEHAVIOR USING A WAVE FORM ANALYZER Final Report

D. E. Leighton and Ronald T. Abbott Jan. 1995 16 p

(AD-A293161; ARCCB-TR-95001) Avail: CASI HC A03/MF A01

A technique for monitoring the change in compliance of a standard three-point bend specimen during fatigue cycling has been developed. This method allows for accurate measurement of the load-line displacement it changes that occur as a crack grows from the notch. The significance of this technique is that it allows accurate determination of crack grows behavior throughout the life cycle of the specimen when a clip gage is impractical or impossible to use. DTIC

N95-31054# General Electric Co., Schenectady, NY.

RESIDUAL STRESSES AND STRESS CORROSION CRACKING IN PIPE FITTINGS

Ronald J. Parrington, James J. Scott, and Freddie Torres Jun. 1994 8 p Presented at the Fontevraud 3 Conference, Chinon, France, 12-16 Sep. 1994

(Contract DE-AC12-76SN-00052)

(DE95-009332; KAPL-4798; CONF-9409321-1) Avail: CASI HC A02/MF A01

Residual stresses can play a key role in the SCC performance of susceptible materials in PWR primary water applications. Residual stresses are stresses stored within the metal that develop during deformation and persist in the absence of external forces or temperature gradients. Sources of residual stresses in pipe fittings include fabrication processes, installation and welding. There are a number of methods to characterize the magnitude and orientation of residual stresses. These include numerical analysis, chemical cracking tests, and measurement (e.g., X-ray diffraction, neutron diffraction, strain gage/hole drilling, strain gage/trepanning, strain gage/section and layer removal, and acoustics). This paper presents 400 C steam SCC test results demonstrating that residual stresses in as-fabricated Alloy 600 pipe fittings are sufficient to induce SCC. Residual stresses present in as-fabricated pipe fittings are characterized by chemical cracking tests (stainless steel fittings tested in boiling magnesium chloride solution) and by the sectioning and layer removal (SLR) technique. DOE

N95-31098 Ecole Polytechnique, Montreal (Quebec).

THERMAL-MECHANICAL FATIGUE CRACK GROWTH IN AIRCRAFT ENGINE MATERIALS Ph.D. Thesis

Yi Dai 1993 353 p

(ISBN-0-315-86543-1) Avail: Univ. Microfilms Order No. DANN86543

This thesis summarizes the major technical achievements obtained as a part of a collaborative research and development project between Ecole Polytechnique and Pratt & Whitney Canada. These achievements include: (1) a thermal-mechanical fatigue (TMF) testing rig which is capable of studying the fatigue behaviors of gas turbine materials under simultaneous changes of temperatures and strains or stress; (2) an advanced alternative current potential drop (ACPD) measurement system which is capable of performing on-line monitoring of fatigue crack initiation and growth in specimen testing under isothermal and TMF conditions; (3) fatigue crack initiation and short crack growth data for the titanium specimens designed with notch features associated with bolt holes of compressor discs; (4) thermal-mechanical fatigue crack growth data for two titanium alloys being used in PWC engine components, which explained the material fatigue behavior encountered in full-scale component testing; (5) a complete fractographic analysis for the tested specimens which enhanced the understanding of the fatigue crack growth mechanisms and helped to establish an analytical crack growth model; and (6) application of the ACPD fatigue crack monitoring technique to single tooth firtree specimen (STFT) LCF testing of PWA 1480 single crystal alloy. Finally, a comprehensive discussion concerning the results pertaining to this research project is presented. Dissert. Abstr.

N95-31131# Oak Ridge National Lab., TN.

EFFECT OF CYCLIC LOADING ON THE CREEP PERFORMANCE OF SILICON NITRIDE

A. A. Wereszczak, M. K. Ferber, T. P. Kirkland, and C. K. J. Lin (National Central Univ., Chung-Li, Taiwan.) 1995 8 p Presented at the ASME International Gas Turbine and Aeroengine Congress and Exposition: Land, Sea and Air, Houston, TX, 5-8 Jun. 1995

(Contract DE-AC05-84OR-21400)

(DE95-010289; CONF-950629-6) Avail: CASI HC A02/MF A01

Tension-tension cyclic fatigue tests (triangular waveform, sigma(sub max) = 100 MPa, R = 0.1) were conducted on hot isostatically pressed (HIPed) silicon nitride at frequencies spanning several orders of magnitude (5.6 x 10(exp-6) to 0.1 Hz or 10(exp -3) MPa/s to 18 MPa/s) at 1,370 C in air. The amount of cyclic creep strain was found to be a function of the frequency or stressing rate with greater strains to failure observed as the frequency or stressing rate decreased. The total strain was viewed as the sum of elastic, anelastic (or transient recoverable), and plastic (viscous or non-recoverable) strain contributions, after the empirical Pao and Marin model. The plastic strain was found to be the dominant component of the total creep and was unsatisfactorily represented by the Pao and Marin model. To circumvent this, a time exponent was introduced in the plastic strain term in the Pao and Marin model. This modification resulted in good correlation between model and experiment at the slower frequencies examined but over-predicted the cyclic creep strain at the faster frequencies. The utility of using the modified Pao and Marin model to predict cyclic creep response from static creep and strain relaxation tests is described. DOE

N95-31254# Illinois Univ., Urbana, IL.

DAMAGE DOSIMETRY AND EMBRITTLEMENT MONITORING OF NUCLEAR PRESSURE VESSELS IN REAL TIME BY MAGNETIC PROPERTIES MEASUREMENT Final Report

A. M. Ougouag, J. F. Stubbins, J. F. Williams, and Wei-Ja Shong Apr. 1995 35 p

(Contract DE-FG02-90ER-13030)

(DE95-011454; DOE/ER-13030/T1) Avail: CASI HC A03/MF A01

This program developed a nondestructive technique for gauging the progress of embrittlement of nuclear pressure vessel steels (PVS) by means of monitoring radiation-induced changes in magnetic properties. The technique was developed by running a series of experiments in reactor on typical nuclear pressure vessel steels and weldment material. Following irradiation, changes in magnetic properties were measured and correlated with irradiation dose and with mechanical properties changes, where possible. The changes in magnetic properties were unique to the irradiation environment, and were much larger than those produce by thermal aging in the absence of irradiation. Special techniques for magnetic properties change measurement were developed and complimented by more standard magnetic properties measurement techniques including SQUID measurements. The results of the experiments revealed that magnetic properties were very sensitive to irradiation. Changes in microstructurally-related magnetic properties of as much as 40% were noted after irradiation exposure of as little as 10(exp 17) n/sq cm (E greater than 0.1 MeV). The magnetic properties changes plateaued out after doses of around as 10(exp 18) n/cm(sup 2) (E greater than 0.1 MeV). It is unclear whether further changes would be noted at higher doses which would also be useful for tracking the embrittlement phenomenon. This is recommended for further study. The work supported here resulted in several publications in the open scientific literature. DOE

N95-31263# Asian Office of Aerospace Research and Development, APO San Francisco, CA. Air Force Office of Scientific Research.

THE 10TH INTERNATIONAL CONFERENCE ON THE STRENGTH OF MATERIALS

P. McQuay 26 Aug. 1994 4 p Conference held in Sendai, Japan, 21-26 Aug. 1994

(AD-A292335; AOARD-TR-94-24) Avail: CASI HC A01/MF A01

The ICSMA 10 conference provided an excellent snapshot of our current understanding of the fundamental mechanisms of the deformation and failure of crystalline materials. One of the more provocative papers was presented by Prof Vitek who presented a model linking brittle intergranular fracture caused by the structure of segregated grain boundaries in alloys, and the grain boundary structures in intermetallics. Several interesting papers

of an empirical nature were also presented, including reviews of nano-laminated materials, high strength, ductility and stiffness quasicrystalline Al-based alloys, and a comprehensive review of superplastically formable fine-grained ceramics. DTIC

N95-31316 Purdue Univ., West Lafayette, IN.
ENERGY FLOW ANALYSIS OF COUPLED STRUCTURES Ph.D. Thesis
Phillip Eung-Ho Cho 1993 336 p
Avail: Univ. Microfilms Order No. DA9420802

Energy flow analysis (EFA) is an analytical tool for prediction of the frequency-averaged vibrational response of built-up structures at high audible frequencies. The procedure is based on two developments; firstly, the derivation of the partial differential equations that govern the propagation of energy-related quantities in simple structural elements such as rods, beams, plates, and acoustic cavities; secondly, the derivation of coupling relationships in terms of energy-related quantities that describe the transfer of energy for various joints (e.g., beam-to-beam, plate-to-plate, and structure-to acoustic field couplings). In this investigation, EFA is used to predict the vibrational response of various coupled structures. In the process of predicting the vibrational response of the coupled structures, the energy flow coupling relationships at the joints of these structures are derived. In addition, the finite element formulation of the governing energy equations are developed. Because the energy density is discontinuous at the joint, a special global assembly procedure is developed to assemble the finite element matrix equations into global matrix equations. The global matrix assembly procedure is predicated on the development of joint element matrix equations using energy flow coupling relationships for various structural joints. The results predicted by EFA for a frame structure with a three-dimensional joint, where four wave types propagate in the structure, are shown to be a reasonable approximation of the frequency-averaged 'exact' energetics, which are computed from classical displacement solutions. The accuracy of the results predicted by EFA increased with high mode count and modal overlap factor or high non-dimensional wavenumber band and non-dimensional damped wavenumber band in the frequency band of interest. An experimental investigation of vibrational response of a light truck frame structure was performed to verify the results of EFA when applied to structures of complicated geometry. The predicted frequency-averaged (one-third octave band) vibrational response of the truck frame structure were in good agreement with the experimental results even with a crude simulation model. The EFA results also showed the important energy transmission mechanisms in these applications to built-up structures. Dissert. Abstr.

N95-31318 Georgia Inst. of Tech., Atlanta, GA.
A FINITE ELEMENT FORMULATION FOR THE TIME DOMAIN VIBRATION ANALYSIS OF AN ELASTIC-VISCOELASTIC STRUCTURE Ph.D. Thesis
Richard Gerard Szumski 1993 216 p
Avail: Univ. Microfilms Order No. DA9415670

The equations of motion for the vibration study of a partially elastic and partially linearly viscoelastic structure are developed in the time domain. The unique feature of these equations is that they contain both differential and integral terms. The integral terms are convolution integrals whose convolution is made between the time derivative of the viscoelastic relaxation modulus and the displacement history. They account for viscoelastic damping of the structure. The equations are simplified through the solution of a real eigenvalue problem which is subsequently used to decouple all but the damping term. A numerical solution procedure is presented using the finite element method for the spatial domain and a Runge Kutta-Verner numerical integration routine for temporal domain of the problem. Partial decoupling of the equations of motion reduces computation time and saves storage space. The convolution integrals are evaluated at each time step using the trapezoidal rule. Two new viscoelastic constitutive laws are introduced that are shown to characterize material properties over a broad frequency spectrum with few material parameters. They are convenient to work with because they have simple rational forms in both the time and frequency domains and also unconditionally obey the second law of thermodynamics. To verify the theory, computer program, and new viscoelastic constitutive laws, a simple elastic-viscoelastic structure known as a constrained layer damper was constructed and tested. The displacement history of the constrained layer damper was measured as an initial static displacement was suddenly released. Good agreement was obtained between the measurements and the numerical simulation of the same event using the theory developed here with the new constitutive laws. The solution procedure is a viable method for solving for the vibratory response of viscoelastically damped structures and is suitable for large-scale finite element analysis through a modified form of Guyan reduction. The new viscoelastic constitutive laws appear to be robust in characterizing the viscoelastic materials used in the study. Dissert. Abstr.

N95-31331 Purdue Univ., West Lafayette, IN.
STUDIES IN NON-LINEAR MULTI-MODE RESPONSES OF HARMONICALLY EXCITED RECTANGULAR PLATES WITH INTERNAL RESONANCES Ph.D. Thesis
Seo Il Chang 1993 186 p
Avail: Univ. Microfilms Order No. DA9420796

Nonlinear flexural vibrations of a rectangular plate with uniform stretching are studied for the case when it is harmonically excited with forces acting normal to the midplane of the plate. Through the Galerkin procedure, the von Karman equations of motion are reduced to a coupled set of nonlinear ordinary differential equations governing the motions of the N-modes. The physical phenomena of interest here arise when the plate has two distinct linear modes of vibration with nearly the same natural frequency. When the two modes are in primary or secondary resonance with the external excitation, the response of the plate can be approximated by two coupled modal equations governing the motions of the two modes in internal resonance. The method of averaging is utilized in the two resonance cases to transform the two nonlinear modal equations into sets of four dimensional dynamical systems which govern the amplitudes and phases of the two modes. The averaged systems are studied in detail by using local bifurcation theory and it is shown that, depending on the spatial distribution of the external forces, the plate can undergo harmonic motions either in one of the two individual modes or in a mixed-mode. The mixed-mode motion can be in the form of either a standing wave or a traveling wave. Stable single-mode and mixed-mode solutions can also coexist over a wide range in the amplitudes and frequency of excitation. For low damping levels, the presence of Hopf bifurcations in the mixed-mode response leads to complicated amplitude-modulated dynamics including period-doubling bifurcations, chaos, coexistence of multiple chaotic motions, and crisis, whereby the chaotic attractors suddenly disappear and the plate resumes small amplitude harmonic motions in a single-mode. The averaged equations for the case of subharmonic motions of order-three are also found to exhibit complicated dynamics including periodic and chaotic solutions. The conservative limit of the two-mode approximation of the plate equations is then studied by using the canonical averaging technique. The integrable autonomous system is found to have homoclinic and heteroclinic orbits that are destroyed by external forcing into chaotic motions. Dissert. Abstr.

N95-31338# Polish Academy of Sciences, Warsaw (Poland). Mechanics Center.
AN ANALYSIS OF THE COVER OF A LIQUID-FILLED CIRCULAR CONTAINER [ANALIZA POKRYWY ZAMYKAJACEJ KOLOWY ZBIORNIK WYPELNIONY CIECZA]
Joanna Sokol-Supel Jan. 1995 34 p In POLISH
(ISSN 0208-5658)
(IFTR-1/1995) Avail: CASI HC A03/MF A01

Up to this point in time, either an elastic plate or a rigid-plastic plate have been used as computer models for the cover. In this study the author uses a model of an elastic-ideally plastic plate as a model which most resembles reality and makes it possible to estimate the deformation of the cover during the entire loading process, i.e. until the moment its ultimate load-bearing strength is reached. The purpose of this study was to provide a complete analytical description of the deformation of the plate as its load increases to a point of partial or complete plasticization. The author examines an elastic-plastic plate with rotational geometric and loading symmetry which covers a container filled with an ideal liquid. The plate is subjected to quasistatic loading. Transl. by Schreiber

N95-31346 California Univ., Los Angeles, CA.
MODELING MULTI-BEAM STRUCTURES FOR CONTROL Ph.D. Thesis
Hanching Grant Wang 1994 108 p
Avail: Univ. Microfilms Order No. DA9420511

A new approach to find the 1-D homogeneous beam model for a

beam-like repetitive structure is proposed. The displacement field of the repetitive structure is approximated by polynomials; the periodic cross-sectional mass and stiffness matrices are obtained by energy equivalence; then the 1-D periodic beam model is formed by Hamiltonian formulation. The 1-D periodic beam model is further homogenized into an equivalent 1-D homogeneous beam model using the additive property of flexibility. A new tabulated mode calculation for chained multibeam structures is also presented. The characteristic matrices (CM's) of a simple beam with various boundary conditions are derived via functional analysis. This derivation reveals a simple rule to write down these matrices by inspection. A multibeam structure is a collection of homogenized beam models coupled through boundary conditions. The CM of the multibeam structure is derived to show that it is a binary composition of the CM's of the simple beam. The CM of a multibeam structure then can be obtained in a tabulated scheme. This greatly simplifies the formation of CM's for multibeam structures. The major contribution is the new systematic modeling approach, the observation of additivity property in homogenization, the resulted homogenized beam model operators, the formation of simple beam's CM's by inspection, and the novel demonstration that the CM of a multibeam structure is composed from the CM of a simple beam. Dissert. Abstr.

N95-31418*# Virginia Polytechnic Inst. and State Univ., Blacksburg, VA. Dept. of Engineering Science and Mechanics.

AN EVALUATION OF THE IOSIPESCU SPECIMEN FOR COMPOSITE MATERIALS SHEAR PROPERTY MEASUREMENT Ph.D. Thesis

Henjen Ho Jul. 1991 203 p Sponsored by Virginia Tech NSF Center for High Performance Polymeric Adhesives and Composites

(Grant NAG1-1053)

(NASA-CR-198755; NAS 1.26:198755) Avail: CASI HC A10/MF A03

A detailed evaluation of the suitability of the Iosipescu specimen tested in the modified Wyoming fixture is presented. An experimental investigation using conventional strain gage instrumentation and moire interferometry is performed. A finite element analysis of the Iosipescu shear test for unidirectional and cross-ply composites is used to assess the uniformity of the shear stress field in the vicinity of the notch, and demonstrate the effect of the nonuniform stress field upon the strain gage measurements used for the determination of composite shear moduli. From the test results for graphite-epoxy laminates, it is shown that the proximity of the load introduction point to the test section greatly influences the individual gage readings for certain fiber orientations but the effect upon shear modulus measurement is relatively unimportant. A numerical study of the load contact effect shows the sensitivity of some fiber configurations to the specimen/fixture contact mechanism and may account for the variations in the measured shear moduli. A comparison of the strain gage readings from one surface of a specimen with corresponding data from moire interferometry on the opposite face documented an extreme sensitivity of some fiber orientations to eccentric loading which induced twisting and yielded spurious shear stress-strain curves. In the numerical analysis, it is shown that the Iosipescu specimens for different fiber orientations have to be modeled differently in order to closely approximate the true loading conditions. Correction factors are needed to allow for the nonuniformity of the strain field and the use of the average shear stress in the shear modulus evaluation. The correction factors, which are determined for the region occupied by the strain gage rosette, are found to be dependent upon the material orthotropic ratio and the finite element models. Based upon the experimental and numerical results, recommendations for improving the reliability and accuracy of the shear modulus values are made, and the implications for shear strength measurement discussed. Further application of the Iosipescu shear test to woven fabric composites is presented. The limitations of the traditional strain gage instrumentation on the satin weave and high tow plain weave fabrics is discussed. Test results of a epoxy based aluminum particulate composite is also presented. A modification of the Iosipescu specimen is proposed and investigated experimentally and numerically. It is shown that the proposed new specimen design provides a more uniform shear stress field in the test section and greatly reduces the normal and shear stress concentrations in the vicinity of the notches. While the fabrication and the material cost of the proposed specimen is tremendously reduced, it is shown the accuracy of the shear modulus measurement is not sacrificed. Author

N95-31419*# National Aeronautics and Space Administration. Langley Research Center, Hampton, VA.

POST-IMPACT FATIGUE OF CROSS-PLIED, THROUGH-THE-THICKNESS REINFORCED CARBON/EPOXY COMPOSITES M.S. Thesis - Clemson Univ.

Thomas E. Serdinak May 1994 176 p

(NASA-TM-110625; NAS 1.15:110625) Avail: CASI HC A09/MF A02

An experimental investigation of the post-impact fatigue response of integrally woven carbon/epoxy composites was conducted. Five different through-the-thickness (TTT) reinforcing fibers were used in an experimental textile process that produced an integrally woven (0/90/0/90/0/90/0/90/0)(sub T) ply layup with 21K AS4 carbon tow fiber. The resin was Hercules 3501-6, and the five TTT reinforcing fibers were Kevlar, Toray carbon, AS4 carbon, glass, and IM6 carbon. The purpose of this investigation was to study the post-impact fatigue response of these material systems and to identify the optimum TTT fiber. Samples were impacted with one half inch diameter aluminum balls with an average velocity of 543 ft/sec. Post-impact static compression and constant amplitude tension-compression fatigue tests were conducted. Fatigue tests were conducted with a loading ratio of R=-5, and frequency of 4 Hz. Damage growth was monitored using x-radiographic and sectioning techniques and by examining the stress-strain response (across the impact site) throughout the fatigue tests. The static compressive stress versus far-field strain response was nearly linear for all material groups. All the samples had a transverse shear failure mode. The average compressive modulus (from far-field strain) was about 10 Msi. The average post-impact static compressive strength was about 35.5 Ksi. The IM6 carbon sample had a strength of over 40 Ksi, more than 16 percent stronger than average. There was considerable scatter in the S-N data. However, the IM6 carbon samples clearly had the best fatigue response. The response of the other materials, while worse than IM6 carbon, could not be ranked definitively. The initial damage zones caused by the impact loading and damage growth from fatigue loading were similar for all five TTT reinforcing materials. The initial damage zones were circular and consisted of delaminations, matrix cracks and ply cracks. Post-impact fatigue loading caused delamination growth, ply cracking and fiber bundle failures, typically 45 deg from impact load direction. During the initial 97 percent of fatigue life, delaminations, ply cracks and fiber bundle failures primarily grew at and near the impact site. During the final 3 percent of life, damage grew rapidly transverse to the loading direction as a through-the-thickness transverse shear failure. The stress-strain response was typically linear during the initial 50 percent of life, and stiffness dropped about 20 percent during this period. During the next 47 percent of life, stiffness dropped about 34 percent, and the stress-strain response was no longer linear. The stiffness decreased about 23 percent during the final 3 percent of life. These trends were typical of all the materials tested. Therefore, by monitoring stiffness loss, fatigue failure could be accurately anticipated. Author

N95-31474# Virginia Univ., Charlottesville, VA.

LARGE DEFORMATION FAILURE MECHANISMS IN NONLINEAR SOLIDS Annual Technical Report, 1 Jan. 1992 - 31 Dec. 1994

Cornelius O. Horgan 30 Jan. 1995 17 p

(Contract F49620-92-J-0112)

(AD-A293010; AFOSR-95-0182TR) Avail: CASI HC A03/MF A01

This work was concerned with research on fundamental mechanics and mathematics of large deformation induced failures in nonlinear solids. The specific area investigated was that of void nucleation and growth due to large deformations in nonlinear solids. Research on cavitation phenomena, which serve as a precursor to fracture, is crucial to the understanding of failure mechanisms in rubber-like solids (e.g. polymers, solid rocket propellants) and of ductile fracture processes in metals. Mathematically, the work involves investigation of singular solutions of the second-order quasilinear system of partial differential equations describing equilibrium states of nonlinearly elastic bodies. For radially symmetric deformations, the basic problem reduces to a bifurcation problem for a single second-order nonlinear ordinary differential equation. Particular emphasis was placed on the effect of material inhomogeneity, compressibility and anisotropy on void nucleation and growth. DTIC

N95-31568# Naval Postgraduate School, Monterey, CA.

RESPONSE OF DUAL-LAYERED STRUCTURES SUBJECTED TO

SHOCK PRESSURE WAVE M.S. Thesis
Thomas P. Brasek Dec. 1994 85 p
(AD-A293731) Avail: CASI HC A05/MF A01

The response of coated, metallic structures subjected to shock pressure waves is studied. The coating is either an elastic material or nearly incompressible rubber of variable stiffness separating the structure from an air or water medium. The stress, nodal velocity, and internal energy of the coated structure are compared to a system without a coating (homogeneous system) to examine the effect of various coating types and configurations on the response of the structure to shock conditions. The results show that a mismatch of impedance, rho c sub o, between the coating and structure governs the degree of energy exchange between the coating and structure at the interface. The impedance mismatch between the structure and a rubber coating at the threshold value is termed the critical difference. If the impedance mismatch exceeds the critical difference, the dynamic response will be more adverse. A softer coating generally has a smaller impedance and tends to concentrate stress wave energy in the underlying structure. DTIC

N95-31614# Sandia National Labs., Albuquerque, NM.
HIGH STRAIN-RATE TESTING OF PARACHUTE MATERIALS
Kenneth W. Gwinn, John J. Totten, and Donald E. Waye 1994 8 p Presented at the 13th Aerodynamics Decelerator Systems Technology Conference, Clearwater, FL, 15-19 May 1995
(Contract DE-AC04-94AL-85000)
(DE95-009577; SAND-94-2302C; CONF-950550-2) Avail: CASI HC A02/MF A01

Research at Sandia National Laboratories has shown a strain rate dependence of many materials used in the production of parachutes. Differences in strength of 30% have been found between strain rates of 12/s and slow rates normally used to define material properties for lightweight nylon cloth. These structures are sometimes deployed in a rapid fashion and the loading is experienced in milliseconds; the production of material data in the same loading regime is required for full understanding of material response. Also, material behavior suitable for structural analysis of these structures is required for successful analysis. This is especially important when different materials are used in the same fabric structure. Determining the distribution of load to various portions of a nylon and Kevlar parachute requires the correct moduli and material behavior in the analytical model. The effect of strain rate on the material properties of nylon and Kevlar components commonly used in parachute construction are reported in this paper. These properties are suitable for use in analytical models of these fabric structures. DOE

N95-31706 Purdue Univ., West Lafayette, IN.
NONLINEAR DYNAMICS AND CHAOTIC MOTIONS OF A SINGULARLY PERTURBED NONLINEAR VISCOELASTIC BEAM Ph.D. Thesis
Ioannis Theodorou Georgiou 1993 338 p
Avail: Univ. Microfilms Order No. DA9420829

The dynamics of one- or two-dimensional structures such as rods, beams, plates, etc., is usually described by one- or two-dimensional nonlinear partial or integro-partial differential equations (PDE's). The equations of motion of such structural systems, with the associated boundary conditions, are amenable to numerical study and to some extent to analytical study. In practice there are many complex structural systems composed of simpler structural members or subsystems with well diverse flexibilities. A simple example is that of a frame comprised of a flexible beam mounted on two relatively stiff columns. The objective of this investigation is to relate the dynamics of a given structure to the dynamics of a simpler structure which is obtained in the limit when the much stiffer substructure of the system is assumed to be perfectly rigid. Without loss of generality, we study both analytically and numerically the dynamics of a representative complex structure, the frame. More precisely, it consists of a nonlinear viscoelastic beam hinged at its ends to two linear viscoelastic columns (supports). We view the equations of motion of the frame structure with sufficiently stiff supports as a singular perturbation of the simpler structure: the nonlinear beam pinned on rigid supports. By applying the Galerkin reduction method, we approximate the equations of motion (coupled PDEs) by a system of a finite number of coupled nonlinear oscillators interacting with a finite number of linear oscillators. Under certain conditions on system parameters, this finite system of ordinary differential equations (ODE's) constitutes the core or 'backbone' of the coupled integro-partial differential equations of motion, an infinite dimensional nonlinear dynamical system. By applying the singular perturbation methodology and the theory of invariant manifolds, we show that for sufficiently stiff linear oscillators (stiff supports) the steady state behavior including nonlinear vibrations and chaotic motions of the above finite dynamical system (full order system) is described by a system of lower dimensions. This reduced system is defined on a nonlinear invariant manifold of the full order system and it possesses symmetry properties that are exactly the same as those of the degenerate reduced system, i.e., the system obtained in the limit when the linear oscillators are assumed to be perfectly rigid. Dissert. Abstr.

N95-31730*# Colorado Univ., Boulder, CO. Dept. of Aerospace Engineering Sciences.
A COMPUTATIONAL PROCEDURE FOR MULTIBODY SYSTEMS INCLUDING FLEXIBLE BEAM DYNAMICS
J. D. Downer, K. C. Park, and J. C. Chiou Apr. 1990 42 p
(Grant NAG1-756)
(NASA-CR-199035; NAS 1.26:199035; CU-CSSC-90-08) Avail: CASI HC A03/MF A01

A computational procedure suitable for the solution of equations of motions for flexible multibody systems has been developed. The flexible beams are modeled using a fully nonlinear theory which accounts for both finite rotations and large deformations. The present formulation incorporates physical measures of conjugate Cauchy stress and covariant strain increments. As a consequence, the beam model can easily be interfaced with real-time strain measurements and feedback control systems. A distinct feature of the present work is the computational preservation of total energy for undamped systems; this is obtained via an objective strain increment/stress update procedure combined with an energy-conserving time integration algorithm which contains an accurate update of angular orientations. The procedure is demonstrated via several example problems. Author

N95-31734 Stanford Univ., CA.
APPLICATION OF SHALLOW SHELL STABILITY TO PLANT MORPHOGENESIS BY FOURIER SERIES Ph.D. Thesis
Cheng-Hsiu Wu 1994 175 p
Avail: Univ. Microfilms Order No. DA9414679

A Fourier series method of solution is presented for shallow shell buckling problems. The shallow shell equations are generally referred to as the von Karman equations, or the Marguerre equations if initial displacement exists. These equations were first solved by the Navier type solutions for a rectangular plate with simply supported boundaries. The method takes full advantage of the fast Fourier transform and a straightforward direct iteration is employed. An edge function method using Fourier series was later developed to handle shallow shells in polygonal platforms. Fundamental solutions that satisfy the homogeneous parts of the Marguerre equations are superimposed to match the prescribed boundary conditions for both the plate bending and in-plane problems, while the two-dimensional Fourier transform handles the inhomogeneity. For a convex polygon, the whole shallow shell is considered as one element, therefore, the set-up time is minimum. In the effort to explain plant morphogenesis by the principle of minimum potential energy, the method was used to solve several examples that emulate plant growth. Preliminary results show that the buckling pattern of a shallow shell experiencing upward pressure and thermal expansion is sensitive to the boundary conditions and the initial shape of the surface. Dissert. Abstr.

N95-32024# Ames Lab., IA.
A NUMERICAL ANALYSIS OF CRACK GROWTH IN MICROCRACKING CERAMIC AND CERAMIC COMPOSITES
S. B. Biner 1994 6 p Presented at the 1994 Fall Meeting of the Materials Research Society (MRS), Boston, MA, 28 Nov. - 2 Dec. 1994
(Contract W-7405-eng-82)
(DE95-010132; IS-M-820; CONF-941144-140) Avail: CASI HC A02/MF A01

A set of numerical analyses of crack growth was performed to elucidate the influence of microcracking on the fracture behavior of microcracking ceramic and ceramic composites. The random nucleation, orientation and size effects of discrete nucleating microcracks and resulting interactions are fully accounted for in a hybrid finite element model. The results obtained from the finite element analysis are compared with the continuum description

of the microcracking. Although continuum description can provide a reasonable estimation of shielding, it fails to resolve the details of micromechanism of toughening resulting from microcracking, since not every shielding event during the course of crack extension corresponds to an increase in the Rcurve. Moreover, as seen in the composite cases, the local events leading to toughening behavior may not be associated with the microcracking even in the presence of large population of microcracks. DOE

N95-32102# Lawrence Livermore National Lab., Livermore, CA.
SIMULATION OF FRACTURE IN COMPRESSION USING A FIELD-THEORY MODEL
S. C. Blair and N. G. W. Cook (California Univ., Berkeley, CA.) 23 Feb. 1995 7 p Presented at the 35th US Symposium on Rock Mechanics, South Lake Tahoe, NV, 4-7 Jun. 1995
(Contract W-7405-eng-48)
(DE95-009874; UCRL-JC-118417; CONF-950655-6) Avail: CASI HC A02/MF A01

Compressive fracture in rock is simulated and analyzed in terms of crack patterns and crack strain energy. Results indicate that initially cracks are randomly located and non-interesting. When approximately 10% of the sites are cracked, crack interaction becomes important and cluster of cracked sites form and extend. Finally, a few critical connecting cracks form and link the clusters to cause failure. DOE

N95-32112 Michigan Univ., Ann Arbor, MI.
AN EXTREMUM PRINCIPLE FOR THE ANALYSIS AND DESIGN OF CONSTITUTIVELY NONLINEAR SYSTEMS Ph.D. Thesis
Sheldon Kent Plaxton 1994 157 p
Avail: Univ. Microfilms Order No. DA9423292

The actual nonlinear constitutive character of most elastic materials is often approximated in engineering analysis by a linear relation-generalized Hooke's law. This approximation may introduce significant error into an analysis problem. This dissertation presents and demonstrates an approach for equilibrium analysis of a class of constitutively nonlinear systems within the context of small deformation (kinematically linear) elasticity. The approach is given in the form of an extremum principle stated in terms of mixed stress and displacement field variables. Such fields represent a pointwise additive decomposition of the total stress field throughout the material domain. Nonlinear constitutive behavior is achieved through functional bounds on the individual stress component fields, in combination with a set of constraints which assure satisfaction of equilibrium and boundary conditions. A finite-dimensional approximation of the extremum problem statement is obtained through the introduction of discrete representations of the problem fields. Numerical solutions for the resulting convex constrained minimization problem are obtained using an established minimization routine. Examples are presented which demonstrate the substantial flexibility available in specifying constitutive behavior within the model. Applications of the described modeling approach within the context of nonconservative (inelastic) systems are also discussed. In addition, extensions of the established framework to problems of optimal design are presented. Specifically, a methodology for predicting the optimal distribution of nonlinear material properties, as defined for the additive representation, is described and demonstrated. Dissert. Abstr.

N95-32118 Minnesota Univ., Minneapolis, MN.
A MODE DECOMPOSITION BASED FINITE ELEMENT FORMULATION FOR THE NONLINEAR DYNAMICS OF FLEXIBLE SPATIAL STRUCTURES AND MECHANISMS Ph.D. Thesis
Joseph Francis DCosta 1994 146 p
Avail: Univ. Microfilms Order No. DA9422294

A mode decomposition based finite element formulation is presented for the nonlinear dynamics of spatial structures. The formulation admits finite deformation, including finite extension, shear and torsion and incorporates all inertial effects that significantly effect the dynamics of a multibody system. In addition, the present development eliminates the shear and membrane locking phenomena that arise due to the inability of a finite element to capture pure bending without the introduction of shear and membrane modes. In this regard the finite element is very well suited to the modeling of the components of a multibody system where finite deformation is expected and could cause a component to curve significantly. Since the locking phenomena manifests itself through the introduction of spurious high frequency components to the system response, its elimination mitigates computational difficulties in the solution of the equations of a dynamical system. An inertia operator, which is consistent with the mode decomposition based formulation of the stiffness operator, is derived. This operator, besides contributing to the accuracy with which the kinematics of the beam is captured, also leads to a better approximation of the total kinetic energy content of a multibody system in a finite dimensional approximation setting. A time integration algorithm, based on a singularity free representation of finite rotations, is presented. However, unlike similar representations in the literature, the present time stepping procedure is totally free of the numerical singularities introduced due to computer round-off errors. A rigid body formulation, employing kinematic variables identical to those used in the flexible beam, is presented to enable the unified modeling of interconnected rigid and flexible components in a multibody system if desired. Several examples are presented to verify the formulations. Dissert. Abstr.

N95-32157# Oak Ridge National Lab., TN.
VALIDATION OF FAVOR CODE LINEAR ELASTIC FRACTURE SOLUTIONS FOR FINITE-LENGTH FLAW GEOMETRIES
T. L. Dickson, J. A. Keeney, and J. W. Bryson 1995 9 p Presented at the Joint ASME/JSME Pressure Vessels and Piping Conference, Honolulu, HI, 23-27 Jul. 1995
(Contract DE-AC05-84OR-21400)
(DE95-009034; CONF-950740-16) Avail: CASI HC A02/MF A01

One of the current tasks within the U.S. Nuclear Regulatory Commission (NRC)-funded Heavy Section Steel Technology Program (HSST) at Oak Ridge National Laboratory (ORNL) is the continuing development of the FAVOR (Fracture, analysis of Vessels: Oak Ridge) computer code. FAVOR performs structural integrity analyses of embrittled nuclear reactor pressure vessels (RPVs) with stainless steel cladding, to evaluate compliance with the applicable regulatory criteria. Since the initial release of FAVOR, the HSST program has continued to enhance the capabilities of the FAVOR code. ABAQUS, a nuclear quality assurance certified (NQA-1) general multidimensional finite element code with fracture mechanics capabilities, was used to generate a database of stress-intensity-factor influence coefficients (SIFIC's) for a range of axially and circumferentially oriented semieliptical inner-surface flaw geometries applicable to RPV's with an internal radius (Ri) to wall thickness (w) ratio of 10. This database of SIRC's has been incorporated into a development version of FAVOR, providing it with the capability to perform deterministic and probabilistic fracture analyses of RPVs subjected to transients, such as pressurized thermal shock (PTS), for various flaw geometries. This paper discusses the SIFIC database, comparisons with other investigators, and some of the benchmark verification problem specifications and solutions. DOE

N95-32191 Columbia Univ., New York, NY.
NUMERICAL EVALUATION OF THREE-DIMENSIONAL CRACK-TIP INTEGRALS FOR LAYERED ANISOTROPIC SOLIDS Ph.D. Thesis
Albert John DiNicola 1993 162 p
Avail: Univ. Microfilms Order No. DA9412745

A general purpose three-dimensional boundary element analysis computer code was developed to solve the boundary integral equations (BIE's) of anisotropic elasticity. The code is a significant advancement in that it can treat full material anisotropy. Fundamental integral kernels used for the numerical solution, previously defined improperly in the literature, were correctly developed. The computer program directly computes all singular integrals arising from the BIEs, including the strongly singular Cauchy Principal Value (CPV) integrals. In this way, conventional indirect techniques were avoided and significant insight into the nature of the CPV integral was gained. Benchmark stress analyses for both isotropic and anisotropic material behavior showed the program results to be highly accurate. A multizone substructuring algorithm was incorporated into the program and demonstrated comparable accuracy. The program was applied in conjunction with the crack tip J-integral in order to compute the interface crack fracture mechanics parameters for several bodies. The J-integral was decomposed into pure Mode 1, 2, and 3 components to yield physically meaningful fracture parameters. Using the decomposed components the near tip J-integral was rigorously equated to a remote contour integral plus an area integral. Results proved to be accurate for both isotropic and anisotropic materials. Using a relatively coarse mesh of nonsingular elements, the difference between closed-form fracture mechanics and boundary

element solutions were 6 percent or less. Mixed mode results for interface cracks between dissimilar anisotropic solids were generated; these results have direct application in the study of delamination cracks between plies of fiber reinforced polymer composites. Dissert. Abstr.

N95-32202*# Colorado Univ., Boulder, CO. Center for Space Structures and Controls.

STAGGERED SOLUTION PROCEDURES FOR MULTIBODY DYNAMICS SIMULATION

K. C. Park, J. C. Chiou, and J. D. Downer Apr. 1990 32 p
(Grant NAG1-756)
(NASA-CR-199034; NAS 1.26:199034; CU-CSSC-90-07) Avail: CASI HC A03/MF A01

The numerical solution procedure for multibody dynamics (MBD) systems is termed a staggered MBD solution procedure that solves the generalized coordinates in a separate module from that for the constraint force. This requires a reformulation of the constraint conditions so that the constraint forces can also be integrated in time. A major advantage of such a partitioned solution procedure is that additional analysis capabilities such as active controller and design optimization modules can be easily interfaced without embedding them into a monolithic program. After introducing the basic equations of motion for MBD system in the second section, Section 3 briefly reviews some constraint handling techniques and introduces the staggered stabilized technique for the solution of the constraint forces as independent variables. The numerical direct time integration of the equations of motion is described in Section 4. As accurate damping treatment is important for the dynamics of space structures, we have employed the central difference method and the mid-point form of the trapezoidal rule since they engender no numerical damping. This is in contrast to the current practice in dynamic simulations of ground vehicles by employing a set of backward difference formulas. First, the equations of motion are partitioned according to the translational and the rotational coordinates. This sets the stage for an efficient treatment of the rotational motions via the singularity-free Euler parameters. The resulting partitioned equations of motion are then integrated via a two-stage explicit stabilized algorithm for updating both the translational coordinates and angular velocities. Once the angular velocities are obtained, the angular orientations are updated via the mid-point implicit formula employing the Euler parameters. When the two algorithms, namely, the two-stage explicit algorithm for the generalized coordinates and the implicit staggered procedure for the constraint Lagrange multipliers, are brought together in a staggered manner, they constitute a staggered explicit-implicit procedure which is summarized in Section 5. Section 6 presents some example problems and discussions concerning several salient features of the staggered MBD solution procedure are offered in Section 7. Derived from text

N95-32205*# Toledo Univ., OH.

FPCAS3D USER'S GUIDE: A THREE DIMENSIONAL FULL POTENTIAL AEROELASTIC PROGRAM, VERSION 1 Final Contractor Report

Milind A. Bakhle Jul. 1995 46 p
(Grant NAG3-1234; RTOP 538-06-14)
(NASA-CR-198367; E-9796; NAS 1.26:198367) Avail: CASI HC A03/MF A01

The FPCAS3D computer code has been developed for aeroelastic stability analysis of bladed disks such as those in fans, compressors, turbines, propellers, or propfans. The aerodynamic analysis used in this code is based on the unsteady three-dimensional full potential equation which is solved for a blade row. The structural analysis is based on a finite-element model for each blade. Detailed explanations of the aerodynamic analysis, the numerical algorithms, and the aeroelastic analysis are not given in this report. This guide can be used to assist in the preparation of the input data required by the FPCAS3D code. A complete description of the input data is provided in this report. In addition, six examples, including inputs and outputs, are provided. Author

N95-32206*# National Aeronautics and Space Administration. Lewis Research Center, Cleveland, OH.

A PROBABILISTIC DESIGN METHOD APPLIED TO SMART COMPOSITE STRUCTURES

Michael C. Shiao and Christos C. Chamis (NYMA, Inc., Brook Park, OH.) Aug. 1995 18 p Presented ath the 39th International Symposium and Exhibition, Anaheim, CA, 11-14 Apr. 1994; sponsored by the Society for the Advancement of Materials, and Process Engineering
(Contract NAS3-27186; RTOP 505-62-10)
(NASA-TM-106715; E-9081; NAS 1.15:106715) Avail: CASI HC A03/MF A01

A probabilistic design method is described and demonstrated using a smart composite wing. Probabilistic structural design incorporates naturally occurring uncertainties including those in constituent (fiber/matrix) material properties, fabrication variables, structure geometry and control-related parameters. Probabilistic sensitivity factors are computed to identify those parameters that have a great influence on a specific structural reliability. Two performance criteria are used to demonstrate this design methodology. The first criterion requires that the actuated angle at the wing tip be bounded by upper and lower limits at a specified reliability. The second criterion requires that the probability of ply damage due to random impact load be smaller than an assigned value. When the relationship between reliability improvement and the sensitivity factors is assessed, the results show that a reduction in the scatter of the random variable with the largest sensitivity factor (absolute value) provides the lowest failure probability. An increase in the mean of the random variable with a negative sensitivity factor will reduce the failure probability. Therefore, the design can be improved by controlling or selecting distribution parameters associated with random variables. This can be implemented during the manufacturing process to obtain maximum benefit with minimum alterations. Author

N95-32317# Oak Ridge National Lab., TN.

RESIDUAL STRESS DISTRIBUTION IN FeAl WELD OVERLAY ON STEEL

X. L. Wang, S. Spooner, C. R. Hubbard, P. J. Maziasz, G. M. Goodwin, Z. Feng, and T. Zacharia 1994 6 p Presented at the 1994 Fall Meeting of the Materials Research Society (MRS), Boston, MA, 28 Nov. - 2 Dec. 1994
(Contract DE-AC05-84OR-21400)
(DE95-009178; CONF-941144-118) Avail: CASI HC A02/MF A01

Neutron diffraction was used to measure the residual stress distribution in an FeAl weld overlay on steel. It was found that the residual stresses accumulated during welding were essentially removed by the post-weld heat treatment that was applied to the specimen; most residual stresses in the specimen developed during cooling following the post-weld heat treatment. The experimental data were compared with a plasto-elastic finite element analysis. While some disagreement exists in absolute strain values, there is satisfactory agreement in strain spatial distribution between the experimental data and the finite element analysis. DOE

42 GEOSCIENCES (GENERAL)

N95-31413# Japan Information Center of Science and Technology, Tokyo (Japan).

DIRECTORY OF GLOBAL ENVIRONMENTAL SCIENCES IN JAPAN

1994 517 p
Avail: CASI HC A22/MF A04

The Japan Information Center of Science and Technology (JICST) has compiled this directory in which information is collected and arranged for an improved understanding of scientific activities on global environmental problems in Japan. Entries are grouped into government research organizations, regional public research organizations, national and private universities and colleges, and other organizations. Data sets are structured based on the Directory Interchange Format (DIF) created by NASA and adopted by the Committee on Earth Observation Satellites (CEOS) as its International Directory Network (IDN). CASI

43 EARTH RESOURCES AND REMOTE SENSING

Includes remote sensing of earth resources by aircraft and spacecraft; photogrammetry; and aerial photography.

For instrumentation see *35 Instrumentation and Photography.*

N95-30363# Sandia National Labs., Albuquerque, NM.

SIMULATION OF AIRBORNE ELECTROMAGNETIC MEASUREMENTS IN THREE DIMENSIONAL ENVIRONMENTS

D. L. Alumbaugh and G. A. Newman 1994 11 p Presented at the 8th Annual Symposium on the Application of Geophysics to Environmental and Engineering Problems, Orlando, FL, 23-27 Apr. 1995

(Contract DE-AC04-94AL-85000)

(DE95-008546; SAND-94-2546C; CONF-950450-4) Avail: CASI HC A03/MF A01

A 3-D frequency domain EM modeling code has been implemented for helicopter electromagnetic (HEM) simulations. A vector Helmholtz formulation for the electric fields is employed to avoid problems associated with the first order Maxwell's equations numerically decoupling in the air. Additional stability is introduced by formulating the problem in terms of the scattered electric fields which replaces an impressed dipole source with an equivalent source that possesses a much smoother spatial dependence and is easier to model. In older to compute this equivalent source, a primary field arising from dipole sources in a whole space must be calculated where ever the conductivity is different than that of the background. The Helmholtz equation is approximated using finite differences on a staggered grid. After finite differencing, a complex-symmetric matrix system of equations is assembled and preconditioned using Jacobi scaling before it is solved using the quasi-minimum residual (QMR) method. In order to both speed up the solution and allow for larger, more realistic models to be simulated, the scheme has been modified to run on massively parallel architectures. The solution has been compared against other 1-D and 3-D numerical models and is found to produce results in good agreement. The versatility of the scheme is demonstrated by simulating a survey over a salt water intrusion zone in the Florida Everglades. DOE

N95-30472# Lawrence Livermore National Lab., Livermore, CA.

COMPUTER VISION FOR DETECTING AND QUANTIFYING GAMMA-RAY SOURCES IN CODED-APERTURE IMAGES

P. C. Schaich, G. A. Clark, S. K. Sengupta, and K. P. Ziock 2 Nov. 1994 10 p Presented at the 28d Annual Asilomar Conference on Signals, Systems, and Computers, Pacific Grove, CA, 31 Oct. - 2 Nov. 1994 Submitted for publication

(Contract W-7405-eng-48)

(DE95-008810; UCRL-JC-117476; CONF-9410156-4) Avail: CASI HC A02/MF A01

The authors report the development of an automatic image analysis system that detects gamma-ray source regions in images obtained from a coded aperture, gamma-ray imager. The number of gamma sources in the image is not known prior to analysis. The system counts the number (K) of gamma sources detected in the image and estimates the lower bound for the probability that the number of sources in the image is K. The system consists of a two-stage pattern classification scheme in which the probabilistic neural network is used in the supervised learning mode. The algorithms were developed and tested using real gamma-ray images from controlled experiments in which the number and location of depleted uranium source disks in the scene are known. DOE

N95-30536 Selskapet for Industriell og Teknisk Forskning, Trondheim (Norway).

WEATHER INFLUENCE ON PASSIVE MICROWAVE BRIGHTNESS TEMPERATURES

S. M. Loevas, I. Rubinstein, and C. Ulstad Aug. 1994 17 p Prepared in cooperation with Norwegian Hydrodynamic Labs., Trondheim, Norway

(PB95-195384; STF60-S94005) Avail: Issuing Activity (National Technical Information Service (NTIS))

Sea ice charts produced using spaceborne passive microwave observations are used on routine basis at several ice forecasting centers and during sea ice research campaigns. The capability of passive microwave sensors to monitor the earth, regardless of cloud cover or daylight, and the 1400 km swath width (SSM/I) make these sensors well suited not only for ice forecasting but also for providing information needed for planning northern oceanic routes. The retrieval of sea ice parameters is carried out by utilizing 37 and 19 GHz brightness temperatures measured by Special Sensor Microwave Imager (SSM/I) on the Defense Meteorological Satellite Program (DMSP) platform. The ice type identification uses a priori established signature brightness temperatures for each ice type. The algorithm generating the sea ice information contains some climatological information on the weather dependence of the observed brightness temperature. A comparison between passive microwave (SSM/I) retrieved ice parameters and ice maps from the Norwegian Meteorological Institute (DNMI) indicates that the weather correcting procedure within the algorithm may need regionalized input. The correlation of variability of the observed brightness temperatures with the weather changes has to be derived prior to introducing any corrections to the existing algorithms. NTIS

N95-30718# Helsinki Univ. of Technology, Espoo (Finland).

RADIOMETER MEASUREMENTS OF SEA ICE IN THE GULF OF BOTHNIA 1992

L. Kurvonen Sep. 1994 72 p

(PB95-206611; ISBN-951-22-2275-2) Avail: CASI HC A04/MF A01

A helicopter-borne multifrequency radiometer (24, 34, 48 and 94 GHz, vertical polarization) was used to investigate the behavior of the brightness temperature of different sea ice types in the Gulf of Bothnia. The radiometer measurements and their analyses are presented. The measurements were made in dry and wet conditions (air temperature above and below 0 C). The angle of incidence was 45 deg in all measurements. The aim of the study is to determine: (1) frequency dependency of the brightness temperature of different ice types, (2) the capability of the multifrequency radiometer to classify ice types; and (3) the optimum measurement frequencies for mapping sea ice. NTIS

N95-30818# Technische Univ., Delft (Netherlands). Faculty of Civil Engineering.

GEOSTATISTICS AND HYDROLOGY. PART 3. HYDRO-METEOROLOGICAL NETWORK DESIGN

M. J. vanDijk and T. H. M. Rientjes May 1994 37 p

(ISSN 0169-6246)

(PB95-206462; Rept-59-Pt-3) Avail: CASI HC A03/MF A01

At present, the collection of environmental information is increasing in importance. Environmental modeling and defining measures relating to environmental protection policies are usually taken on the basis of the collected information. Hydrological information like precipitation data, runoff data, groundwater table data, piezometric data, etc., is gathered and stored throughout the years by monitoring gaging stations of a (well designed) network. In developing countries, however, gaging stations are often badly spatially distributed, not well managed and often not included in a network. Many water resources management projects are (still) designed with inadequate and incorrect data or even with virtually no data at all. As a consequence of this, it is likely that wrong water management decisions will be taken, the wrong design criteria will be applied, and the inappropriate and uneconomic designs will be developed and operated. The designing of efficient and economic networks is therefore an important issue for hydrologists and civil engineers. The system or network of hydrological gauging stations provides the necessary information to be able to understand and to describe the hydrological phenomena and processes under study. NTIS

N95-30819 Technische Univ., Delft (Netherlands). Faculty of Civil Engineering.

GEOSTATISTICS AND HYDROLOGY. PART 1: SPATIAL AND TEMPORAL VARIABILITY. COMMUNICATIONS OF THE SANITARY ENGINEERING AND WATER MANAGEMENT DIVISION

M. J. vanDijk and T. H. M. Rientjes Sep. 1993 39 p Limited Reproducibility: More than 20% of this document may be affected by microfiche quality

(ISSN 0169-6246)

(PB95-206470; Rept-56-Pt-1) Avail: CASI HC A03

The various phenomena that are important in hydrology have two important characteristics: they take place in physical space (they manifest themselves in a regionalized form), and each phenomena is known to be unique (i.e. rainfall distribution, soil-moisture content). Those phenomena are all functions of time and space and very often highly variable. A rational framework dealing with spatial variability and uncertainty on the

behavior of phenomena is provided by the theory of random functions. However, the spatial variability is, in general, not random; measured values at two different locations become similar at decreasing distance. In other words, there is some kind of relation in the spatial distribution of these phenomena. Quantities of these phenomena are called 'regionalized variables': they are variables typical of a phenomenon developing in space and possessing a certain structure (here, spatial correlation). The theory of REgionalized Variables (REV's) is based on the theory of random functions, which expresses simultaneously the structured and random character of REV's, as well as mathematical tools necessary for application. The random functions theory covers all possible variabilities, from very low to very high. Its aim is twofold: to establish the theoretical grounds for expressing the structural properties of natural phenomena in a useful mathematical form, and to provide a practical means for solving various problems of estimation. NTIS

N95-31125# Naval Postgraduate School, Monterey, CA.
SHIPTRACKS IN THE CALIFORNIAN STRATUS REGION: DEPENDENCY ON MARINE ATMOSPHERIC BOUNDARY LAYER DEPTH M.S. Thesis
Eric J. Trehubenko Dec. 1994 99 p
(AD-A293272) Avail: CASI HC A05/MF A02

Analysis of AVHRR (Advanced Very High Resolution Radiometer) satellite image/atmospheric sounding pairs reveals that the development and persistence of shiptracks is dependent on Marine Atmospheric Boundary Layer Depth (MABL). 65 image/sounding pairs were analyzed with eight cases featured. The data was collected from the SEAHUNT (July 1991) and MAST (June 1994) field experiments off the western coast of the United States. A distribution of cloud-topped MABL's for the dataset reveals that shiptracks developed in boundary layers of depth less than 750 meters. A mean number of shiptracks versus MABL depth reveals that shiptracks decrease in number with increasing boundary layer depth, supporting MAST hypotheses. Several mechanisms are proposed to explain the decrease in track development with increasing MABL depth and these present several avenues for future data analyses. Additionally, a composite track environment is also presented to document other environmental variables encountered during the analysis deemed pertinent to shiptrack formation. DTIC

N95-31148# Naval Research Lab., Bay Saint Louis, MS.
SATELLITE MULTISENSOR DATA TECHNIQUES FOR SEA ICE MAPPING Final Report
Denise J. Gineris, Douglas A. May, and Jeffrey D. Hawkins 8 Dec. 1994 54 p Limited Reproducibility: Document partially illegible
(AD-A289729; NRL/MR/7240-94-7556) Avail: CASI HC A04/MF A01

Operational sea ice mapping capabilities utilizing ground truth data are extremely limited due to the remote proximity and harsh environment of the polar regions. Satellite remote sensing offers a sufficient quantity of accurate, high resolution environmental parameters that satisfy many ice mapping requirements. This study explores the application of multiple satellite sensor data combination techniques for sea ice analysis. Sea ice information from visible, infrared, passive microwave, and active radar sensors are examined and open water from other ice types in all regions. DTIC

N95-31156 Environmental Research Office of the US Army, London (England).
BRIEF REVIEW OF REMOTE SENSING LITERATURE PERTAINING TO CLASSIFICATION AND GEOSTATISTICS Interim Report No. 1, Oct. 1994 - Jan. 1995
Margaret A. Oliver and Richard Webster 19 Jan. 1995 7 p Limited Reproducibility: More than 20% of this document may be affected by poor print
(Contract N68171-95-C-9007)
(AD-A290932; RSS-USA-1; R/D-7493-EN-01) Avail: Issuing Activity (Defense Technical Information Center (DTIC))

This report summarizes the most relevant information for the project from among the wide range of literature on remote sensing. The facilities offered by IMAGINE have been examined. IMAGINE is a digital image processing package that can store, manipulate, and analyze georeferenced data. It is the most widely used software for remote sensing applications. The other literature cited relates specifically to the aim of the project, i.e. to optimize field sampling from remote images using geostatistics. It includes applications of kriging and spatial filtering to classify remotely sensed date and to enhance the image, the neural net approach, fuzzy classification, sampling images effectively and economically, the use of training data, confidence levels for classification, and the redundancy of information. DTIC

N95-31265# Asian Office of Aerospace Research and Development, APO San Francisco, CA. Air Force Office of Scientific Research.
VISIT TO IONOSPHERIC MODELING AND REMOTE SENSING BRANCH, PHILLIPS LABORATORY IN HANSCOM AFB, MA
Gary Tuck (Queensland Univ., Brisbane, Australia.) 2 Nov. 1994 8 p
(AD-A292339; AOARD-TR-94-34) Avail: CASI HC A02/MF A01

With financial support provided under the AFOSR sponsored Window-on-Science program, Dr Gary Tuck of the University of Queensland, Australia spent a two week tour at Ionospheric Modeling and Remote Sensing Branch, Phillips Laboratory in Hanscom AFB, MA for the purpose of carrying out preliminary discussions with Phillips Lab's gravity group personnel on use of the terrain correction methods. The report provides a scope of Dr Tuck's research in which he is intended to work together with Phillips Lab personnel during his continuing stay at Phillips laboratory this year and part of the next year. The two research areas discussed by Dr Tuck in this report are (1) detailed gravimetric surveying to locate underground structures and (2) the use of air-borne gravity gradiometry to avoid oncoming terrain. DTIC

N95-31390# Naval Research Lab., Bay Saint Louis, MS.
DIGITAL MAPPING CHARTING AND GEODESY ANALYSIS PROGRAM TECHNICAL REVIEW OF VECTOR PRODUCT FORMAT (VPF) Final Report
H. Vincent Miller (Mississippi State Univ., Bay Saint Louis, MS.), S. Danette Coughlan, Kevin B. Shaw, and Susan V. Carter 29 Nov. 1994 19 p
(AD-A289766; NRL/MR/7441-94-7539) Avail: CASI HC A03/MF A01

The Vector Product Format has been instrumental in providing the Defense Mapping Agency (DMA) with a standard format in which to store port and effectively maintain vector databases. As with practically any standard however, current advances necessitate changes. NRL's Digital Mapping, Charting, and Geodesy Analysis Program (DMAP) has been given the opportunity to suggest changes which would enhance the Navy's use of VPF. DMAP's comments range from specific essential/suggested changes to more broad issues of data quality and topology. Suggested figures are given to clarify sections of text. DTIC

N95-31603# Naval Postgraduate School, Monterey, CA.
COMPARISON OF SATELLITE-DERIVED MSU BRIGHTNESS TEMPERATURES AND CONVENTIONALLY-DERIVED FIELDS M.S. Thesis
Matthew C. Parke Dec. 1994 111 p
(AD-A293692) Avail: CASI HC A06/MF A02

A statistical analysis is performed on a six-month global data set consisting of satellite-derived channel 3 Microwave Sounding Unit (MSU) brightness-temperatures from the Marshall Space Flight Center and various conventionally-derived fields obtained from the National Meteorological Center Global Data Assimilation System (GDAS) to quantify the potential usefulness of MSU analyses in the nowcasting and forecasting of baroclinic waves especially over data sparse regions. High positive spatial and temporal correlations are obtained between the MSU and the 400-100 mb thickness over all wavelengths in the data. Slightly lesser positive correlations are found between the MSU and the 200-mb temperature. The MSU-500-mb and MSU-50-mb height correlations indicate a scale dependence in the hydrostatic spreading of thickness anomalies in the vertical. Most significantly, relatively high negative MSU-500-mb height correlations for the short (less than synoptic scale) wavelength portion of the data suggest that upper-level thermal anomalies are reflected downwards and that the MSU can be used to track mid-level synoptic-scale baroclinic waves. This conclusion is also suggested in MSU-500-mb vorticity and MSU-dynamic tropopause correlations. A MSU collection and analysis procedure is also described that demonstrates the practicality and usefulness of generating MSU analyses from locally obtained polar-orbiter data. DTIC

N95-32027# Lawrence Livermore National Lab., Livermore, CA.
DESIGN OF AN IMMERSION ECHELLE-PRISM MID-IR SPECTROGRAPH FOR CHEMICAL REMOTE SENSING
N. L. Thomas, S. A. Johnson, and C. G. Stevens Jul. 1994 14 p Presented at the Annual Meeting of the Society of Photo-Optical

Instrumentation Engineers, San Diego, CA, 24-29 Jul. 1994
(Contract W-7405-eng-48)
(DE95-010729; UCRL-JC-118224; CONF-940723-38) Avail: CASI HC A03/MF A01

We have designed an immersion echelle-prism spectrograph for the remote detection of chemicals in the atmosphere. The instrument operates in the 2 and 3 micron atmospheric windows and provides maximum throughput at 0.1 cm-1 resolution. Crossed dispersers consisting of a high order silicon immersion echelle (13.5 grooves/mm) and 43 degree immersion prism (Rutherford prism) are combined in a Littrow configuration to generate a two-dimensional spectrum in the image plane. DOE

N95-32115# Swedish Polar Research Secretariat, Stockholm (Sweden).
SWEDISH POLAR BIBLIOGRAPHY: A GUIDE TO SWEDISH LITERATURE ON POLAR RESEARCH, 1945-1988 WITH SUPPLEMENT, 1989-1992
1993 201 p
(PB95-208161; ISBN-91-970769-1-0) Avail: CASI HC A10/MF A03

The aim of the Bibliography is to list publications: (1) by Swedish authors active during the period 1945-1988 in Sweden or abroad; and (2) by foreign authors active in Swedish projects or working at Swedish institutions. Efforts have also been made to list the works of foreign authors who have written on the subject of Swedish polar research and Swedish polar scientists. The Swedish Polar Bibliography includes monographs, conference reports, articles in journals, and reports from government authorities and private companies. NTIS

N95-32316 Selskapet for Industriell og Teknisk Forskning, Trondheim (Norway). Div. of Industrial Mathematics.
INVERSION OF ERS-1 WAVEMODE SPECTRA. USER'S AND PROGRAMMER'S GUIDE
O. Samset and H. E. Krogstad 1 Dec. 1994 113 p
(PB95-223582; STF10-A94014) Avail: Issuing Activity (National Technical Information Service (NTIS))

The Ocean-SAR Inversion System (OSIS) is a set of FORTRAN subroutines and programs for analyzing the ERS-1 Wavemode product and carrying out an Ocean-SAR spectral inversion based on the quasi-linear Ocean-SAR forward transform and a simplified inversion procedure. This User's Guide gives a general description of the system, and how to install and run the programs. NTIS

44 ENERGY PRODUCTION AND CONVERSION

Includes specific energy conversion systems, e.g., fuel cells; global sources of energy; geophysical conversion; and windpower.

For related information see also *07 Aircraft Propulsion and Power, 20 Spacecraft Propulsion and Power,* and *28 Propellants and Fuels.*

N95-30375# Argonne National Lab., IL.
PRODUCING USABLE FUEL FROM MUNICIPAL SOLID WASTE
O. O. Ohlsson 1995 2 p Presented at the Power Generation Conference, Orlando, FL, 7-9 Dec. 1994
(Contract W-31-109-eng-38)
(DE95-008405; ANL/ES/CP-85392; CONF-941210-13) Avail: CASI HC A01/MF A01

Refuse disposal is a matter of increasing concern for municipalities and state governments. As existing land-fills become filled to capacity, and new landfills become more costly to site, it has become critical to develop alternative disposal methods. Some of the refuse that is presently being landfilled has the potential to provide considerable quantities of energy and thereby replace conventional fossil fuels. Another environmental concern is the problem of the emissions associated with combustion of traditional fossil fuels. The Clean Air Act Amendments of 1990 significantly restrict the level of sulfur dioxide (SO2) and nitrogen oxides (NO(x)) emissions permissible as effluent from combustion facilities. To address both of these concerns, Argonne National Laboratory, under sponsorship of the U.S. Department of Energy (DOE), has developed a means of producing fuel from municipal solid waste that can be co-fired with coal to supplement coal supplies and reduce problematic emissions. DOE

N95-30408# Air Force Inst. of Tech., Wright-Patterson AFB, OH. School of Engineering.
THE JUNCTION CHARACTERISTICS AND CURRENT CONDUCTION MECHANISMS OF GaInP2 n(+)p DIODES AND SOLAR CELLS Ph.D. Thesis
Kitt C. Reinhardt Dec. 1994 256 p
(AD-A290857; AFIT/WSF/ENP/94-05) Avail: CASI HC A12/MF A03

This work involves an investigation of GaInP2 n+p diode and solar cell dark current mechanisms, the defect centers that affect these mechanisms, and the response of dark current and solar cell photovoltaic parameters to I MeV electron irradiation and thermal annealing. Dark current due to carrier diffusion, recombination, and tunneling were identified, and recombination current was found to dominate at the maximum power-point voltage of the GaInP2 solar cells. Carrier recombination was found to occur via defect centers at the perimeter and within the bulk of the junction. Two deep majority-hole trap centers were found at E(a1) = E(t) - E(v) approximately 0.45 eV and E(a2) = E(t) - E(v) approximately 0.05 eV. Dark current due to carrier tunneling was dominant in 'leaky' diodes and solar cells that contained line-like morphological defects believed to be due to lattice mismatch between GaInP2 and GaAs. The effects of 1 MeV electron irradiation and thermal annealing on solar cell and diode dark current mechanisms and efficiency were also studied. DTIC

N95-30505# National Renewable Energy Lab., Golden, CO.
ADVANCED SYSTEM IDENTIFICATION TECHNIQUES FOR WIND TURBINE STRUCTURES
J. T. Bialasiewicz and R. M. Osgood Mar. 1995 9 p Presented at the 1995 Society for Experimental Mechanics Spring Conference, Grand Rapids, MI, 12-14 Jun. 1995
(Contract DE-AC36-83CH-10093)
(DE95-004049; NREL/TP-442-6930; CONF-9506145-2) Avail: CASI HC A02/MF A01

The new approach to modal parameter identification, presented in this paper, uses an asymptotically stable observer to form a discrete state-space model for a wind turbine structure. The identification is performed using input-output time-series. A special software package developed in this research has been tested using the data generated by the ADAMS(trademark) model of the Micon 65/13 wind turbine structure. Numerical and graphical presentation of some of the results, generated by the programs developed, illustrates the range of their applicability. DOE

N95-30519 Selskapet for Industriell og Teknisk Forskning, Trondheim (Norway). Div. of Applied Thermodynamics.
OVERVIEW OF IEA BIOMASS COMBUSTION ACTIVITIES
J. E. Hustad 12 Jul. 1994 13 p Presented at the Seminar on Small-Scale Combustion Technology and Emissions, Jyvaekylae, Finland, May 1994
(PB95-196374; STF15-S94007) Avail: Issuing Activity (National Technical Information Service (NTIS))

The objectives of the International Energy Agency (IEA) bioenergy program are: (1) to encourage cooperative research, development and use of energy and the increased utilization of alternatives to oil; and (2) to establish increased program and project cooperation between participants in the whole field of bioenergy. There are four Task Annexes to the Implementing Agreement during the period 1992-1994: Efficient and Environmentally Sound Biomass Production Systems; Harvesting and Supply of Woody Biomass for Energy; Biomass Utilization; and Conversion of Municipal Solid Waste Feedstock to Energy. The report describes the following biomass combustion activities during the period 1992-1994: Round robin test of a wood stove; Emissions from biomass combustion; A pilot project cofiring biomass with oil to reduce SO2 emissions; Small scale biomass chip handling; Energy from contaminated wood waste combustion; Modeling of biomass combustion; Wood chip cogeneration; Combustion of wet biomass feedstocks, ash reinjection and carbon burnout; Oxidation of wet biomass; Catalytic combustion in small wood burning appliances; Characterization of biomass fuels and ashes; Measurement techniques (FTIR). NTIS

N95-30526# National Renewable Energy Lab., Golden, CO.
STATE-OF-THE-ART LOW-COST SOLAR REFLECTOR MATERIALS
C. Kennedy and G. Jorgensen Nov. 1994 14 p Presented at the 8th International Vacuum Web Coating Conference, Las Vegas, NV, 6-8 Nov.

1994
(Contract DE-AC36-83CH-10093)
(DE95-000260; NREL/TP-471-7022; CONF-9411174-1) Avail: CASI HC A03/MF A01

Solar thermal technologies generate power by concentrating sunlight with large mirrors. The National Renewable Energy Laboratory (NREL) is working with industrial partners to develop the optical reflector materials needed for the successful deployment of this technology. The reflector materials must be low in cost and maintain high specular reflectance for extended lifetimes in severe outdoor environments. Currently, the best candidate materials for solar mirrors are silver-coated low-iron glass and silvered polymer films. Polymer reflectors are lighter in weight, offer greater flexibility in system design, and have the potential for lower cost than glass mirrors. In parallel with collaborative activities, several innovative candidate reflector-material constructions were investigated at NREL. The low-cost material requirement necessitates manufacturing compatible with mass-production techniques. Future cooperative efforts with the web-coating industry offers the promise of exciting new alternative materials and the potential for dramatic cost savings in developing advanced solar reflector materials. DOE

N95-30640# Stockholm Environment Inst., Stockholm (Sweden).
SLEEPING RENEWABLE BEAUTY: WILL THE PRINCE EVER COME
L. Kristoferson 1993 12 p
(PB95-214573; ISBN-91-88116-54-9) Copyright Avail: CASI HC A03/MF A01

The report describes a presentation the author made at a workshop on renewable energy sources (RES). He describes the various types of RES, their possible environmental impacts, skepticism about the usefulness of RES, cost effectiveness, and necessary institutional changes that will have to accompany the development of RES. NTIS

N95-30723# International Centre for Theoretical Physics, Trieste (Italy).
SPECTRAL RESPONSE OF A POLYCRYSTALLINE SILICON SOLAR CELL
B. Ba and M. Kane (Dakar Univ., Senegal.) Oct. 1994 12 p
(DE95-614370; IC-94/337) Avail: CASI HC A03/MF A01 (US Sales Only)

A theoretical study of the spectral response of a polycrystalline silicon n-p junction solar cell is presented. The case of a fibrously oriented grain structure, involving grain boundary recombination velocity and grain size effects is discussed. The contribution of the base region on the internal quantum efficiency Q(sub int) is computed for different grain sizes and grain boundary recombination velocities in order to examine their influence. Suggestions are also made for the determination of base diffusion length in polycrystalline silicon solar cells using the spectral response method. DOE

N95-30745# Oak Ridge National Lab., TN.
PUBLICATIONS OF THE FOSSIL ENERGY ADVANCED RESEARCH AND TECHNOLOGY DEVELOPMENT MATERIALS PROGRAM: APRIL 1, 1993-MARCH 31, 1995
Paul T. Carlson, comp. Apr. 1995 34 p
(Contract DE-AC05-84OR-21400)
(DE95-009200; ORNL/FMP-95/2) Avail: CASI HC A03/MF A01

The objective of the Fossil Energy Advanced Research and Technology Development (AR and TD) Materials Program is to conduct research and development on materials for fossil energy applications, with a focus on the longer-term needs for materials with general applicability to the various fossil fuel technologies. The Program includes research aimed at a better understanding of materials behavior in fossil energy environments and on the development of new materials capable of substantial improvement in plant operations and reliability. The scope of the Program addresses materials requirements for all fossil energy systems, including materials for coal preparation, coal liquefaction, coal gasification, heat engines and heat recovery, combustion systems, and fuel cells. Work on the Program is conducted at national and government laboratories, universities, and industrial research facilities. This bibliography covers the period of April 1, 1993, through March 31, 1995, and is a supplement to previous bibliographies in this series. It is the intent of this series of bibliographies to list only those publications that can be conveniently obtained by a researcher through relatively normal channels. The publications listed in this document have been limited to topical reports, open literature publications in referred journals, full-length papers in published proceedings of conferences, full-length papers in unreferred journals, and books and book articles. DOE

N95-30887# National Renewable Energy Lab., Golden, CO.
VALIDATION OF THE FLAGSOL PARABOLIC TROUGH SOLAR POWER PLANT PERFORMANCE MODEL
H. W. Price, P. Svoboda (Flachglas Solartechnick G.m.b.H., Cologne, Germany.), and D. Kearney (Kearney and Associates, Del Mar, CA.) Oct. 1994 6 p Presented at the American Society of Mechanical Engineers/Japanese Society of Mechanical Engineers/Japan Solar Energy Society International Solar Energy Conference, Lahaina, HI, 19-24 Mar. 1995
(Contract DE-AC36-83CH-10093)
(DE95-000263; NREL/TP-471-7297; CONF-950336-19) Avail: CASI HC A02/MF A01

This paper describes the results of a validation of the FLAGSOL parabolic trough solar power plant performance model. The validation was accomplished by simulating an operating solar electric generating system (SEGS) parabolic trough solar thermal power plant and comparing the model output results with actual plant operating data. This comparison includes instantaneous, daily, and annual total solar thermal electric output, gross solar electric generation, and solar mode parasitic electric consumption. The results indicate that the FLAGSOL model adequately predicts the gross solar electric output of an operating plant, both on a daily and an annual basis. DOE

N95-30893# Spire Corp., Bedford, MA.
InP SOLAR CELL DEVELOPMENT ON INEXPENSIVE SI SUBSTRATES Report, 22 Feb. 1994 - 22 Feb. 1995
22 Feb. 1995 3 p
(Contract N00014-94-C-2030)
(AD-A293255) Avail: CASI HC A01/MF A01

Emitter designs have been roughly optimized for both P/N and N/P cells. For P/N cells, the emitter formation and cell junction depth are determined by zinc diffusion from the InGaAs contact cap. Zinc is a P-type dopant in InP. When we attempted to define epitaxially grown emitters, these emitters, which had thickness on the order of 1000 A, were dominated by zinc diffusing out of the InGaAs contact cap, which effectively set the emitter depth at about 3000 A. It therefore made little difference whether the epitaxially grown emitter layer was 100 or 1000 A, since the junction depth was fixed by the zinc diffusing out of the InGaAs to 3000 A. We were able to improve the P/N cell performance by controlling the thickness of the InGaAs cap layer, the solid state diffusion source for the zinc, as well as the growth temperature. Best cell performance was with a 1000 A InGaAs cap thickness with the entire cell grown at 650 C. DTIC

N95-30896# National Renewable Energy Lab., Golden, CO.
A MANUAL FOR THE ECONOMIC EVALUATION OF ENERGY EFFICIENCY AND RENEWABLE ENERGY TECHNOLOGIES
W. Short, D. J. Packey, and T. Holt Mar. 1995 119 p
(Contract DE-AC36-83CH-10093)
(DE95-000211; NREL/TP-462-5173) Avail: CASI HC A06/MF A02

This manual is a guide for analyzing the economics of energy efficiency and renewable energy (EE) technologies and projects. It is intended: (1) to help analysts determine the appropriate approach or type of analysis and the appropriate level of detail, and (2) to assist EE analysts in completing consistent analyses using standard assumptions and bases, when appropriate. Included are analytical techniques that are commonly required for the economic analysis of EE technologies and projects. The manual consists of six sections: Introduction, Fundamentals, Selection Criteria Guide, Economic Measures, Special Considerations for Conservation and Renewable Energy Systems, and References. A glossary and eight appendices are also included. Each section has a brief introductory statement, a presentation of necessary formulae, a discussion, and when appropriate, examples and descriptions of data and data availability. The objective of an economic analysis is to provide the information needed to make a judgment or a decision. The most complete analysis of an investment in a technology or a project requires the analysis of each year of the life of the investment, taking into account relevant direct costs, indirect and overhead costs, taxes, and returns on investment, plus any externalities, such as environmental impacts, that are relevant to the decision to be

made. However, it is important to consider the purpose and scope of a particular analysis at the outset because this will prescribe the course to follow. The perspective of the analysis is important, often dictating the approach to be used. Also, the ultimate use of the results of an analysis will influence the level of detail undertaken. The decision-making criteria of the potential investor must also be considered. DOE

N95-30947# Auburn Univ., AL.
PROSPECTOR 7: SMALL FUEL CELLS FOR PORTABLE POWER WORKSHOP Final Report, 16 Sep. 1994 - 15 Apr. 1995
Calvin R. Johnson and M. F. Rose 3 Nov. 1994 516 p Workshop held in Durham, NC, 31 Oct. - 3 Nov. 1994
(Contract DAAH04-94-G-0422)
(AD-A292729; ARO-33865.1-CH-CF) Avail: CASI HC A22/MF A04

Papers are presented at the Small Fuel Cells for Portable Power Workshop, October 31 - November 3, 1994. The focus of this workshop, Prospector 7, is on the options available to potential users in applications of small, portable fuel cell systems for man-portable military systems and commercial devices. The intent of this workshop is to incorporate the many advances in fuel cell design, power production techniques, chemistry and chemical engineering issues, fuels, and manufacturing opportunities into a concise strategy for significant advancements over the next decade. DTIC

N95-31138# Helsinki Univ. of Technology, Otaniemi (Finland). Dept. of Technical Physics.
CALORSTOCK 1994: THERMAL ENERGY STORAGE. BETTER ECONOMY, ENVIRONMENT, TECHNOLOGY
M. T. Kangas, ed. and P. D. Lund, ed. 1994 432 p Presented at the 6th International Conference on Thermal Energy Storage, Espoo, Finland, 22-25 Aug. 1994 Sponsored by the Polish Committee of Scientific Research
(DE95-772422; NEI-FI-261-Vol-2; CONF-940801-Vol-2) Avail: CASI HC A19/MF A04

This publication is the second volume of the Proceedings of CALORSTOCK'94, the Sixth International Conference on Thermal Energy Storage held in Espoo, Finland on 22-25 Aug. 1994. This volume contains 51 presentations from the following six sessions: Chemical storage; Heat storage and environment; Central solar heating plants with seasonal storage; Water storage pits and tanks; Cooling; and National activities. DOE

N95-31155 New Energy and Industrial Technology Development Organization, Tokyo (Japan).
DATA ON DEVELOPMENT OF NEW ENERGY TECHNOLOGIES
Mar. 1994 296 p In JAPANESE Limited Reproducibility: More than 20% of this document may be affected by microfiche quality
(DE95-764135; NEDO-P-9320) Avail: Issuing Activity (Department of Energy (DOE))

The paper compiles data on the trend of development of new energy technologies into a book. By category, renewable energy is solar energy, wind power generation, geothermal power generation, ocean energy, and biomass. As a category of fuel form conversion, cited are coal liquefaction/gasification, coal gasification combined cycle power generation, and natural gas liquefaction/decarbonization. The other categories are cogeneration by fuel cell and ceramic gas turbine, district heat supply system, power load leveling technology, transportation-use substitution-fuel vehicle, and others (Stirling engine, superconducting power generator, etc.). The data are systematically compiled on essential principles, transition of introduction, objectives of introduction, status of production, cost, development schedule, performance, etc. The paper also deals with the related legislation system, developmental organizations, and a menu for power companies' buying surplus power. DOE

N95-31157# Technische Univ., Delft (Netherlands).
DIGITAL SIMULATION OF WIND VELOCITIES FOR WIND TURBINE ROTORS: GENERAL CONSIDERATIONS
J. B. Dragt Dec. 1993 18 p
(PB95-206447; IW-93070R) Avail: CASI HC A03/MF A01

One of the methods to reliably predict the dynamic loads of a wind turbine rotor due to the turbulence of the atmosphere is to simulate the stochastic wind field over the rotor area in a digital way, in order to generate the wind input for a rotor dynamical code. As many points in the rotor area are involved and many time steps, a rather time consuming computation is required. A number of different approaches can be followed, some of which have been realized in practical computer programs, others still have to be explored. This report gives a general overview of simulation methods based on the inverse fast Fourier transform. NTIS

N95-31162# National Renewable Energy Lab., Golden, CO.
PHOTOVOLTAIC CZOCHRALSKI SILICON MANUFACTURING TECHNOLOGY IMPROVEMENTS Annual Subcontract Report, 1 Apr. 1993 - 31 Mar. 1994
T. Jester (Siemens Solar Industries, Camarillo, CA.) Mar. 1995 19 p Prepared in cooperation with Siemens Solar Industries, Camarillo, CA
(Contract DE-AC36-83CH-10093)
(DE95-004066; NREL/TP-411-7498) Avail: CASI HC A03/MF A01

This report describes work performed under a three-year, three-phase, cost-share contract to demonstrate significant cost reductions and improvements in manufacturing technology. The objective of the program is to reduce costs in photovoltaic manufacturing by approximately 10% per year. The work was focused in three main areas: (1) silicon crystal growth and thin wafer technology; (2) silicon cell processing; and (3) silicon module fabrication and environmental, safety, and health issues. During this reporting period, several significant improvements were achieved. The crystal growing operation improved significantly with an increase in growth capacity due to larger crucibles, higher polysilicon packing density, and high pull speeds. Wafer processing with wire saws progressed rapidly, and the operation is completely converted to wire saw wafer processing. The wire saws yield almost 50% more wafers per inch in production, thus improving manufacturing volume by 50% without any additional expense in crystal growth. Cell processing improvements focused on better understanding the contact paste and firing processes. Module designs for lower material and labor costs began with the focus on a new junction box, larger modules with larger cells, and a less costly framing technique. In addition, chlorofluorocarbon (CFC) usage was completely eliminated in the Siemens manufacturing facility during this period, resulting in significant reductions in the cost of caustic waste treatment. DOE

N95-31163# National Renewable Energy Lab., Golden, CO.
LARGE-AREA, TRIPLE-JUNCTION a-Si ALLOY PRODUCTION SCALE-UP Semiannual Subcontract Report, 17 Mar. - 18 Sep. 1994
R. Oswald and J. Morris Mar. 1995 22 p Prepared in cooperation with Solarex Corp., Newtown, PA
(Contract DE-AC36-83CH-10093)
(DE95-004067; NREL/TP-411-7682) Avail: CASI HC A03/MF A01

This report describes work performed under a three-year subcontract to advance Solarex's photovoltaic (PV) manufacturing technologies, reduce its hydrogenated amorphous silicon (a-Si:H) module production costs, increase module performance, and expand the Solarex commercial production capacity. During the period covered by this report, Solarex focused on (1) improving deposition of the front contact, (2) investigating alternate feed stocks for the front contact, (3) maximizing throughput and area utilization for all laser scribes, (4) optimizing a-Si:H deposition equipment to achieve uniform deposition over large areas, (5) optimizing the triple-junction module fabrication process, (6) evaluating the materials to deposit the rear contact, and (7) optimizing the combination of isolation scribe and encapsulant to pass the wet high-potential test. DOE

N95-31164# Washington State Univ., Richland, WA.
INVESTIGATION OF POLYCRYSTALLINE THIN FILM CuInSe2 SOLAR CELLS BASED ON ZnSe WINDOWS Annual Subcontract Report, 15 Feb. 1993 - 14 Feb. 1994
L. C. Olsen Mar. 1995 19 p
(Contract DE-AC36-83CH-10093)
(DE95-004068; NREL/TP-413-7684) Avail: CASI HC A03/MF A01

This report concerns studies of CIS solar cells based on ZnSe window layers. ZnSe/CIS devices are fabricated by growing ZnSe films by MOCVD onto Siemens CIS and graded absorber substrates. ZnSe films are grown by reacting H2Se with a zinc adduct. ZnSe/CIS heterojunctions have been studied by depositing transparent aluminum contacts onto ZnSe. These studies indicate that ZnSe/CIS solar cells can be fabricated with an efficiency greater than 14%. Open circuit voltages are typically larger than 500 mV and the optimum range of ZnSe film thickness for maximum efficiency is between 100 Angstrom and 250 Angstrom. Photocurrents are significantly

reduced as the film thickness exceeds 250 Angstrom. Photoluminescence spectroscopy has been utilized to characterize the physical nature of CIS substrate surfaces, and ZnSe-CIS interfaces. These studies indicate that a segregated phase(s) exists at the surface of as received Siemens substrates. Additionally, it is determined that the segregated phase(s) still exist after the ZnSe growth process. To date, sputtered ZnO top contact layers have caused degradation of the photovoltaic properties of the ZnSe/CIS structure. Investigations of the effects of MOCVD grown ZnO upon ZnSe/CIS structures will soon be initiated. To establish the feasibility of ZnSe as a window layer, cells have been fabricated by incorporating a protective layer of CdS between the ZnSe and ZnO. A total area efficiency of 11% was obtained with such a structure. DOE

N95-31381# National Renewable Energy Lab., Golden, CO.
PHOTOVOLTAIC MODULE CERTIFICATION/LABORATORY ACCREDITATION CRITERIA DEVELOPMENT
C. R. Osterwald, R. L. Hammond (Arizona State Univ., Tempe, AZ.), B. D. Wood (Arizona State Univ., Tempe, AZ.), C. E. Backus (Arizona State Univ., Tempe, AZ.), R. L. Sears (Arizona State Univ., Tempe, AZ.), G. A. Zerlaut (SC International, Inc., Phoenix, AZ.), and R. V. DAiello (SC International, Inc., Phoenix, AZ.) Apr. 1995 181 p
(Contract DE-AC36-83CH-10093)
(DE95-004063; NREL/TP-412-7680) Avail: CASI HC A09/MF A02

This document provides an overview of the structure and function of typical product certification/laboratory accreditation programs. The overview is followed by a model program which could serve as the basis for a photovoltaic (PV) module certification/laboratory accreditation program. The model covers quality assurance procedures for the testing laboratory and manufacturer, third-party certification and labeling, and testing requirements (performance and reliability). A 30-member Criteria Development Committee was established to guide, review, and reach a majority consensus regarding criteria for a PV certification/laboratory accreditation program. Committee members represented PV manufacturers, end users, standards and codes organizations, and testing laboratories. DOE

N95-31554# Army Research Lab., Fort Monmouth, NJ.
LITHIUM ION AQUEOUS CELLS Technical Report, Jul. - Dec. 1994
Edward J. Plichta and Wishvender K. Behl Feb. 1995 19 p
(AD-A293828; ARL-TR-422) Avail: CASI HC A03/MF A01

Lithium ion aqueous cells were investigated using lithium intercalating compounds as anodes and cathodes. The aqueous electrolyte consisted of 4 to 5 molar solutions of either lithium perchlorate or lithium nitrate which contained lithium hydroxide in millimolar amounts to make the solutions slightly basic with a pH of about 8.5. Several electrode combinations were evaluated using lithium intercalating compounds such as lithium cobalt oxide and lithium manganese oxide as cathodes and lithium vanadium oxide, lithium manganese oxide, titanium disulfide, and molybdenum dioxide as the anodes. The cell employing manganese oxide as both the anode and cathode exhibited good charge-discharge characteristics with an open circuit potential of about one volt. DTIC

N95-31640# Sandia National Labs., Livermore, CA.
NaK POOL-BOILER SOLAR RECEIVER DURABILITY BENCH TEST. VOLUME 2: METALLURGICAL ANALYSIS
S. H. Goods and R. W. Bradshaw Jan. 1995 60 p
(Contract DE-AC04-94AL-85000)
(DE95-010338; SAND-94-8235) Avail: CASI HC A04/MF A01

The principal materials used in the construction of a NaK based pool-boiler were analyzed. The device, operated for 7500 hours, accumulated 1000 thermal cycles to a peak temperature of 750 C. Haynes 230, used to fabricate the pool-boiler vessel, was found to perform satisfactorily. Air-side corrosion of the pool-boiler vessel was insignificant. Internal surface of the alloy exhibited some NaK-induced elemental dissolution; this dissolution was somewhat more extensive where the alloy was exposed to the liquid metal compared to regions exposed only to NaK vapor; however, the corresponding metal loss in all regions was inconsequential, never exceeding more than a few microns. Autogenous seam welds of the alloy responded in a similar fashion, exhibiting only minimal metal loss over the course of the experiment. While there was 50% loss in ductility of the alloy there remained adequate ductility for the anticipated operating environment. An enhanced boiling nucleation surface comprised of stainless steel powder brazed to the vessel ID showed no change in its structure. It remained intact, showing no cracking after repeated thermal cycling. Other materials used in the experiment showed more extensive degradation after exposure to the NaK. IN 600, used to fabricate thermowells, exhibited extensive surface and intergranular dissolution. Grain boundary dissolution was sufficiently severe in one of the thermowells to cause an air leak, resulting in experiment termination. BNi-3, a brazing alloy used to join the pool-boiler vessel, endcaps and thermowells, showed some dissolution where it was exposed to the NaK as well as thermal aging effects. However, all brazes remained structurally sound. A nickel metal ribbon showed catastrophic dissolution, resulting in the formation of deep (greater than 30 (mu)m) pits and cavities. A zirconium metal foil used to getter oxygen from the NaK became extremely brittle. DOE

N95-31661# National Renewable Energy Lab., Golden, CO.
PHOTOVOLTAIC ENERGY PROGRAM OVERVIEW: FISCAL YEAR 1994
Mar. 1995 25 p
(Contract DE-AC36-83CH-10093)
(DE94-011871; DOE/GO-10095-082) Avail: CASI HC A03/MF A01

This is the 1994 overview for the Photovoltaic (PV) Energy Program. The topics of this overview include cooperative research projects to improve PV systems and develop precommercial prototypes of new PV products, expanding understanding of the fundamental mechanisms governing the formation and performance of PV materials, and helping US industry enhance its leadership position in the PV market. DOE

N95-31735 Iowa State Univ. of Science and Technology, Ames, IA.
STUDY OF MELTING AND FREEZING PROCESSES OF WATER FOR APPLICATION TO ICE THERMAL ENERGY STORAGE SYSTEM Ph.D. Thesis
Liang Yong 1993 150 p
Avail: Univ. Microfilms Order No. DA9414040

This thesis presents the results of a study of the solid-liquid phase change process of water in a rectangular enclosure for application to thermal energy storage systems. The work performed combined experimental results with analytical and numerical methods to develop computer models of the system. Experiments were performed to obtain data to verify the models under various melting and freezing conditions. A connective heat transfer correlation, for melting of ice in a container confined by two horizontal plates, was obtained based on the experimental work. An analytical model based on heat conduction was developed to predict ice formation in an enclosure which was cooled isothermally. A model incorporating the effects of convection, conduction, and buoyancy was developed to predict the solid-liquid interface position and melting rate for the melting of unfixed ice in the enclosure which was heated isothermally. Comparisons were made between the models and the experiment data. The results demonstrated satisfactory agreement. Finally, a preliminary model was developed to predict the overall performance of melting in a cool thermal energy storage system. The results of the model were used to produce design criteria for thermal energy storage systems. Dissert. Abstr.

N95-31822# National Renewable Energy Lab., Golden, CO.
BIOFACTS: FUELING A STRONGER ECONOMY, THERMOCHEMICAL CONVERSION OF BIOMASS
Dec. 1994 4 p
(Contract DE-AC36-83CH-10093)
(DE94-006866; NREL/SP-420-6379) Avail: CASI HC A01/MF A01

A primary mission of the US DOE is to stimulate the development, acceptance, and use of transportation fuels made from plants and wastes called biomass. Through the National Renewable Energy Laboratory (NREL), DOE is developing and array of biomass conversion technologies that can be easily integrated into existing fuel production and distribution systems. The variety of technology options being developed should enable individual fuel producers to select and implement the most cost-effective biomass conversion process suited to their individual needs. Current DOE biofuels research focuses on the separate and tandem uses of biochemical and thermochemical conversion processes. This overview specifically addresses NREL's thermochemical conversion technologies, which are largely based on existing refining processes. DOE

N95-31952 Clarkson Univ., Potsdam, NY.
SILICON CARBIDE-SILICON HETEROSTRUCTURE SOLAR CELLS Ph.D.

Thesis
Attaullah Solangi 1994 104 p
Avail: Univ. Microfilms Order No. DA9422827

Silicon Carbide/Silicon/Silicon (SiC/Si/Si) (N-n-p) heteroface solar cells are designed, fabricated, and evaluated. In these solar cells the top SiC layer, which is transparent to most of the solar spectrum, yields a low lateral resistance and passivates the surface of the n-Si layer. Processes are developed to fabricate SiC/Si heterostructure solar cells. SiC films are grown on (100) Si substrates using an Atmospheric Pressure Chemical Vapor Deposition (APCVD) technique. Hydrogen, Silane (SiH4), and Propane (C3H8) serve as a carrier gas, Silicon and Carbon source gases, respectively. A process is developed to in situ dope single crystal Silicon Carbide (beta-SiC) films using phosphine (PH3). The beta-SiC films are characterized using x-ray Diffractometer and four-point probe. Optical studies show that the absorption coefficient of ,19-SiC films increases with increase in doping level and ranges from 10 to 6 x 10(exp 4) cm(exp -1) in the energy range between 2.42 and 4.4 eV. The bandgap of beta-SiC films ranges between 2.13 and 2.32 eV. APCVD grown films in the 1150 deg C and 1200 deg C temperature range are single crystal beta-SiC and show the doping effect. The sheet resistance (r(sub s)) value of the in situ doped beta-SiC films ranges from 90 to 500 Omega/(square). The r(sub s) becomes smaller at higher growth temperature and higher PH3 flow rate. The lowest r(sub s) value achieved is 90 Omega/(square). A computer analysis of the heterostructure and homojunction Si solar cells, based on the drift-diffusion model, is carried out. It is noted that employing a SiC layer as a top window material in Si-based solar cells reduces the series resistance of the cell and increases the efficiency. Also, the light generated current in the SiC/Si cells does not decrease appreciably with increasing thickness of the top SiC layer. In contrast, in Si/Si cells the current reduces significantly with increasing thickness of the top Si layer. The Si-based heterostructure solar cells (with beta-SiC as the top window material) are designed and fabricated. At AM 1.5 solar radiation these cells exhibit the following typical characteristics: V(sub oc) = 540 mV, J(sub sc) = 27.66 mA/sq cm, FF = 76 percent, Efficiency = 11.36 percent, while similar Si homojunction solar cells made from the same Si substrate show inferior characteristics. This study shows that the SiC/Si is a potentially useful system for fabricating high efficiency Si-based solar cells. Dissert. Abstr.

N95-32057# Astropower, Inc., Newark, DE.
DEVELOPMENT OF LARGE-AREA MONOLITHICALLY INTEGRATED SILICON-FILM(TRADEMARK) PHOTOVOLTAIC MODULES Final Subcontract Report, 1 May 1991 - 31 Dec. 1994
R. B. Hall, J. A. Rand, and J. E. Cotter Apr. 1995 27 p
(Contract DE-AC36-83CH-10093)
(DE95-004089; NREL/TP-413-7702) Avail: CASI HC A03/MF A01

The objective of this program is to develop Silicon Film(trademark) Product-3 into a low-cost, stable solar cell for large-scale terrestrial power applications. The Product-3 structure is a thin (less than 100 micro m) polycrystalline layer of silicon on a durable, insulating, ceramic substrate. The insulating substrate allows the silicon layer to be isolated and metallized to form a monolithically interconnected array of solar cells. High efficiency is achieved by the use of light trapping and passivated surfaces. This project focused on the development of five key technologies associated with the monolithic sub-module device structure: (1) development of the film deposition and growth processes; (2) development of the low-cost ceramic substrate; (3) development of a metallurgical barrier technology; (4) development of sub-element solar cell processing techniques; and (5) development of sub-module (isolation and interconnection) processes. This report covers the development approaches and results relating to these technologies. Significant progress has been made in the development of all of the related technologies. This is evidenced by the fabrication of a working 12.0 sq cm prototype sub-module consisting of 7 elements and testing with an open circuit voltage of 3.9 volts, a short circuit current of 35.2 mA and a fill factor of 63% and an overall efficiency of 7.3%. Another significant result achieved is a 13.4% (NREL verified), 1.0 sq cm solar cell fabricated from material deposited and grown on a graphite cloth substrate. The significant technological hurdle of the program was and remains the low quality of the photovoltaic layer which is caused by contamination of the photovoltaic layer from the low-cost ceramic substrate by trace impurities found in the substrate precursor materials. The ceramic substrate and metallurgical barrier are being developed specifically to solve this problem. DOE

N95-32058# National Renewable Energy Lab., Golden, CO.
SOLAR THERMAL ELECTRIC: PROGRAM OVERVIEW, FISCAL YEARS 1993-1994
Mar. 1995 23 p
(Contract DE-AC36-83CH-10093)
(DE94-000240; DOE/GO-10095-085) Avail: CASI HC A03/MF A01

The Solar Thermal Electric Program Overview and Accomplishments for Fiscal Years 1993-1994 are documented. DOE

N95-32072# New Energy and Industrial Technology Development Organization, Tokyo (Japan).
EVALUATION AND ANALYSIS SURVEY ON NEW ENERGY INTRODUCTION, PART 3
Mar. 1994 235 p In JAPANESE
(DE95-769806; NEDO-P-9327) Avail: CASI HC A11/MF A03

A detailed study is made on introduction of the photovoltaic power generation system to Japan. The paper analyzes influences of production learning of the equipment, fund subsidies and overseas export production on wide spread of the photovoltaic power generation system, and clarifies the potential amount of the future introduction. The analysis is conducted by converting learning coefficients of battery cell and inverter to 0.7, 0.8 (standard), and 0.9. The cumulative spread of the system by 2040 will amount to 14,911MW, 819MW (standard), 117MW, respectively. The future introduction amount is analyzed by changing exports of the photovoltaic power generation. The cumulative spread of the system by 2040 will increase up to 2,015MW in case of 6% as against 819MW in standard case of 3%. If changing the rate of fund subsidies to 50% (standard), 67% and 75%, the cumulative spread amount will be 819MW (standard), 6,257MW and 10,173MW, and reduction of CO2 emissions will be 1 million t-c/yr, 2 million t-c/yr and 3 million t-c/yr, respectively. DOE

N95-32090# Sandia National Labs., Albuquerque, NM.
ENERGY STORAGE AND ALTERNATIVES TO IMPROVE TRAIN VOLTAGE ON A MASS TRANSIT SYSTEM
S. P. Gordon and W. S. Rorke Apr. 1995 66 p
(Contract DE-AC04-94AL-85000)
(DE95-010344; SAND-95-8222) Avail: CASI HC A04/MF A01

The wide separation of substations in the Bay Area Rapid Transit system's transbay tunnel contributes to voltage sag when power demand is high. In the future, expansions to the system will exacerbate this problem by increasing traffic density. Typically, this situation is remedied through the installation of additional substations to increase the system's power capacity. We have evaluated the efficacy of several alternatives to this approach - specifically, installation of an 8 megajoule energy storage system, modification of the existing substations, or reduction of the resistance of the running rails or the third rail. To support this analysis, we have developed a simple model of the traction power system in the tunnel. We have concluded that the storage system does not have sufficient capacity to deal with the expected voltage sags; in this application, the alternatives present more effective solutions. We have also investigated the potential impact of these system upgrades on expected future capital outlays by BART for traction power infrastructure additions. We have found that rail or substation upgrades may reduce the need for additional substations. These upgrades may also be effective on other parts of the BART system and on other traction power systems. DOE

N95-32212*# City Coll. of the City Univ. of New York, NY.
INVESTIGATION OF THE BASIC PHYSICS OF HIGH EFFICIENCY SEMICONDUCTOR HOT CARRIER SOLAR CELL Annual Status Report, 31 May 1994 - 30 May 1995
R. R. Alfano, W. B. Wang, J. M. Mohaidat, M. A. Cavicchia, and O. Y. Raisky 30 May 1995 17 p
(Grant NAG3-1490)
(NASA-CR-198945; NAS 1.26:198945) Avail: CASI HC A03/MF A01

The main purpose of this research program is to investigate potential semiconductor materials and their multi-band-gap MQW (multiple quantum wells) structures for high efficiency solar cells for aerospace and commercial applications. The absorption and PL (photoluminescence) spectra, the carrier dynamics, and band structures have been investigated for semiconductors

of InP, GaP, GaInP, and InGaAsP/InP MQW structures, and for semiconductors of GaAs and AlGaAs by previous measurements. The barrier potential design criteria for achieving maximum energy conversion efficiency, and the resonant tunneling time as a function of barrier width in high efficiency MQW solar cell structures have also been investigated in the first two years. Based on previous carrier dynamics measurements and the time-dependent short circuit current density calculations, an InAs/InGaAs - InGaAs/GaAs - GaAs/AlGaAs MQW solar cell structure with 15 bandgaps has been designed. The absorption and PL spectra in InGaAsP/InP bulk and MQW structures were measured at room temperature and 77 K with different pump wavelength and intensity, to search for resonant states that may affect the solar cell activities. Time-resolved IR absorption for InGaAsP/InP bulk and MQW structures has been measured by femtosecond visible-pump and IR-probe absorption spectroscopy. This, with the absorption and PL measurements, will be helpful to understand the basic physics and device performance in multi-bandgap InAs/InGaAs - InGaAs/InP - InP/InGaP MQW solar cells. In particular, the lifetime of the photoexcited hot electrons is an important parameter for the device operation of InGaAsP/InP MQW solar cells working in the resonant tunneling conditions. Lastly, time evolution of the hot electron relaxation in GaAs has been measured in the temperature range of 4 K through 288 K using femtosecond pump-IR-probe absorption technique. The temperature dependence of the hot electron relaxation time in the X valley has been measured. Derived from text

N95-32286 Selskapet for Industriell og Teknisk Forskning, Trondheim (Norway). Norwegian Hydrotechnical Lab.
PRODUCTION SIMULATOR FOR WAVE POWER PLANTS
K. Torsethaugen 7 Jul. 1994 25 p
(PB95-212262; STF60-A94094) Avail: Issuing Activity (National Technical Information Service (NTIS))

The report gives plans and specifications for a wave power production simulator. The simulator is a computer program that computes how much of the energy in the open ocean that can be converted to usable energy at a site off or onshore. The production of wave power from sea waves is not an easy task. Efforts have been made in several countries to develop devices that can extract energy from the ocean, but very few have so far been successful. During the last 15 years a considerable know-how has been established in Norway on wave energy utilization. Part of this know-how will be included in the proposed production simulator. Evaluation of new devices and new sites can be done in a more comparative and efficient way by this tool. It will contribute to interdisciplinary activity in the field of wave power utilization, and should be applicable for the nonexpert. The simulator consists of several modules, joined together by computer software. The plans so far include purpose, needs and background for the development of a wave power plant simulator and a high level specification of the software and scope of work. NTIS

N95-32288# American Sun Co., Blue Hill, ME.
EXTRA FOCAL CONVECTIVE SUPPRESSING SOLAR COLLECTOR Second Quarterly Technical Progress Report
1995 4 p
(Contract DE-FG01-94CE-15601)
(DE95-010170; DOE/CE-15601/T1) Avail: CASI HC A01/MF A01

Second quarter efforts have focused on completing Task 1, refining and improving tracking electronics, and working on Tasks 2 and 3, optics and absorber/fluid system, respectively. Calculated collector performance for various configurations based on collector component manufacturers product data lead to the following conclusions: (1) all loss mechanisms are proportional to the absorber area; (2) for sufficiently high concentration ratios, at the temperatures that are significant for residential applications, the reduced convective losses at the absorber associated with a transparent cover are partially offset by the reduced transmission, and therefore energy input, of the cover; (3) radiative losses are most effectively reduced by use of a spectrally-selective absorber and minimizing the absorber area; (4) for a concentrating system operating at a temperature useful for residential applications (above 60 C, probably around 100 C), the ambient temperature (range: -30 C to +30 C) makes relatively little difference in the collectible power; and (5) on account of the first conclusion, the most cost-effective system will have a concentration ratio as high as cost-effectively possible. Derived from text

N95-32302# Sandia National Labs., Albuquerque, NM.
OUTLOOK FOR RENEWABLE ENERGY TECHNOLOGIES: ASSESSMENT OF INTERNATIONAL PROGRAMS AND POLICIES
Linda J. Branstetter, Richard C. Vidal, Vicki L. Bruch, and Rena Zurn Feb. 1995 112 p
(Contract DE-AC04-94AL-85000)
(DE95-009084; SAND-94-0854) Avail: CASI HC A06/MF A02

The report presents an evaluation of worldwide research efforts in three specific renewable energy technologies, with a view towards future United States (US) energy security, environmental factors, and industrial competitiveness. The overall energy technology priorities of foreign governments and industry leaders, as well as the motivating factors for these priorities, are identified and evaluated from both technological and policy perspectives. The specific technologies of interest are wind, solar thermal, and solar photovoltaics (PV). These program areas, as well as the overall energy policies of Denmark, France, Germany, Italy, the United Kingdom (UK), Japan, Russia, and the European Community as a whole are described. The present and likely future picture for worldwide technological leadership in these technologies is portrayed. The report is meant to help in forecasting challenges to US preeminence in the various technology areas, particularly over the next ten years, and to help guide US policy-makers as they try to identify specific actions which would help to retain and/or expand the US leadership position. DOE

N95-32368# Helsinki Univ. of Technology, Otaniemi (Finland).
CALORSTOCK'94. THERMAL ENERGY STORAGE. BETTER ECONOMY, ENVIRONMENT, TECHNOLOGY
M. T. Kangas, ed. and P. D. Lund, ed. 1994 490 p Presented at the 6th International Conference on Thermal Energy Storage, Espoo, Finland, 15-17 Aug. 1994
(DE95-772421; NEI-FI-261-Vol-1; CONF-940801-Vol-1) Avail: CASI HC A21/MF A04

This publication is the first volume of the proceedings of CALORSTOCK'94, the sixth international conference on thermal energy storage held in Espoo, Finland on August 22-25, 1994. This volume contains 58 presentations from the following six sessions: Aquifer storage, Integration into energy systems, Simulation models and design tools, IEA energy conservation through energy storage programme workshop, Earth coupled storage, and District heating and utilities. DOE

45 ENVIRONMENT POLLUTION

Includes atmospheric, noise, thermal, and water pollution.

N95-30358 Colorado State Univ., Fort Collins, CO.
NATIONAL INSTITUTE FOR GLOBAL ENVIRONMENTAL CHANGE Final Report
W. R. Cotton, B. Stevens, D. Duda, W. Richardson, and G. Feingold Mar. 1995 44 p Prepared in cooperation with National Inst. for Global Environmental Change Limited Reproducibility: More than 20% of this document may be affected by microfiche quality
(Contract DE-FC03-90ER-61010)
(DE95-008333; DOE/ER-61010/T27) Avail: CASI HC A03

Over the past decade or so the evolution and equilibria of persistent decks of stratocumulus climatologically clinging to the edge of summertime subtropical highs has been an issue of increased scientific inquiry. The particular interest in the microphysical structure of these clouds stems from a variety of hypotheses which suggest that anthropogenic influences or biogenic feedbacks may alter the structure of these clouds in a manner which may be climatically significant. Most hypotheses regarding boundary layer influences on climate have been formulated by an examination of the solution space of simple models. The earliest hypothesis of this sort (and the one on the most solid footing) is due to Twomey (1974), who posited that enhanced concentrations of CCN could lead to enhanced droplet reflectivity and enhanced albedos in clouds of modest optical depths. In low lying clouds where the albedo effect dominates, the climate sensitivity to a robust perturbation in cloud albedo may be significant. One of the primary objectives of this current research has been to explore the hypothesis of Twomey. The basic approach was to couple radiative calculations with detailed representations of the droplet spectra. The detailed representation of the droplet spectra was generated by the Large Eddy Simulation-Explicit

Microphysics (LES-EM) model coupled to a simple mixed emissivity radiation scheme in order to drive the dynamics. Several simulations were carried out and the resultant microphysical fields were taken from the stationary regime of the turbulent simulation and used to drive a two dimensional radiative model. By comparing the radiative properties of the simulated clouds formed in environments with different CCN concentrations we were able to more accurately quantify the albedo susceptibility of stratocumulus taken to be typical of the FIRE experimental area. DOE

N95-30677# Institute of Energy Economics of Japan, (Japan).
ECONOMICAL ANALYSIS RELATING TO THE GLOBAL WARMING ISSUE
Aug. 1994 220 p
(DE95-764072; IEE-SR-257) Avail: CASI HC A10/MF A03

An analysis using global macro economic models is conducted on how to think and cope with the global warming issue from political and economic aspects. As viewpoints of evaluation, cited are cost estimation for the CO2 emission control, damage caused by the global warming and its economic evaluation, and the catastrophic effects on the ecosystem except the economic evaluation. Cline says that maximum efforts should be exerted to suppress CO2 emission to the level of 1990 by the year of 2000. It is said that to confirm how serious greenhouse effects will be in 2000, it is necessary to concentrate on scientific researches, and that the international society should make its second-stage determination in terms of freezing or reducing the level of 2000, or admitting that the level will go upward. For this, the economic distortion should be removed by removing assistance to fossil fuels step by step. Assistance to developing countries and economical efficiency should be raised by introducing the carbon tax. Improvement of efficiency and arrangement of incentives are required for individual technologies. Measures for forest preservation are necessary under the financial assistance program, etc. DOE

N95-30686 Arizona Univ., Phoenix, AZ.
THE LAND COMPONENT OF THE GLOBAL CLIMATE SYSTEM WITH ADEQUATE SPATIAL RESOLUTION Final Report, 1 Sep. 1991 - - 31 Aug. 1994
R. E. Dickinson, A. N. Hahmann, X. Zeng, M. Chen, J. Vaughan, and B. A. Auvine 30 Nov. 1994 58 p Limited Reproducibility: More than 20% of this document may be affected by microfiche quality
(Contract DE-FG02-91ER-61216)
(DE95-009323; DOE/ER-61216/3) Avail: CASI HC A04

The focus of the work done under this grant has been to couple global circulation models (in particular, the National Center for Atmospheric Research (NCAR) Community Climate Model Version 2 (CCM2)) to a land-surface model at a much finer mesh than that used for the atmospheric processes. The end objective has been to incorporate into the CHAMMP modeling system a state-of-the-art land model on a mesh independent of the atmospheric model resolution. Efforts have emphasized the following: development and graphical displays of the fine-mesh land surface boundary conditions; the data structures required to carry out integrations on the land fine-mesh; the physical parameterization required to diaggregate model precipitation; analyses of the NCAR 10-year control simulation of the frozen version of CM2/BATS; implementation of changes in the cloud optical properties to mitgate excess incident solar radiation and temperatures over middle latitudes in the Northern Hemisphere summer; prototype development of the CCM2/BASTS fine-mesh treatment. DOE

N95-30755 Department of Energy, Washington, DC. Office of Energy Research.
GLOBAL CHANGE RESEARCH: SUMMARIES OF RESEARCH IN FY 1994
Apr. 1994 236 p Limited Reproducibility: More than 20% of this document may be affected by microfiche quality
(DE95-009660; DOE/ER-0641T) Avail: Issuing Activity (Department of Energy (DOE))

Global climate change is a significant issue for DOE because energy production and use now contributes more than half of the total human emissions of greenhouse gases on a global basis. Within the DOE Global Change Research Program, we are proceeding with the transition from the carbon-cycle and vegetation-research programs to a reconfigured and integrated program on terrestrial carbon processes. The overall objective is to increase our knowledge and understanding of the role of terrestrial components in the global carbon cycle with special reference to biological controls on atmospheric carbon dioxide concentration. The primary objective of DOE's global-change program remains the improved prediction of global change as a basis for sustainable development. This publication describes all of the projects funded by the Environmental Sciences Division of DOE in FY 1994. Each description contains the project's title; its 3-year funding history; the period over which the funding applies; the name of the principal investigator(s); the institution(s) conducting the projects; and the project's objectives, products, approach, and results to date. DOE

N95-30793# Oak Ridge National Lab., TN. Environmental Sciences Div.
FIELD PERFORMANCE OF THE WALKER BRANCH THROUGHFALL DISPLACEMENT EXPERIMENT
P. J. Hanson, D. E. Todd, N. T. Edwards, and M. A. Huston Oct. 1994 12 p Presented at the International Symposium On Ecosystem Manipulation, Bowness-on-Windermere, UK, 19-21 Oct. 1994
(Contract DE-AC05-84OR-21400)
(DE95-008677; CONF-9410327-1) Avail: CASI HC A03/MF A01

The authors are conducting a large-scale manipulative field experiment in an upland oak forest on the Walker Branch Watershed in eastern Tennessee USA to identify important ecosystem responses that might result from future precipitation changes. The manipulation of soil moisture is being implemented by a gravity-driven transfer of throughfall precipitation from one treatment plot to another. Throughfall is intercepted in (approx) 2,000 subcanopy troughs (0.3 x 5 m) suspended above the forest floor of the dry plots ((approx) 33% of the ground area is covered) and transferred by gravity flow across an ambient plot for subsequent distribution onto the wet treatment plot. Percent soil water is being monitored with time domain reflectometers at 310 sampling locations across the site. The experimental system is able to produce statistically significant differences in soil water content in years having both extremely dry and extremely wet conditions. Furthermore, comparisons of pre- and post-installation soil temperature measurements have documented the ability of the experimental design to produce these changes without changing the microclimate of the forest understory. DOE

N95-30802 Department of Energy, Washington, DC.
HISTORY AND STATUS OF THE ATMOSPHERIC RADIATION MEASUREMENT PROGRAM
P. Lunn, T. Cress (Pacific Northwest Lab., Richland, WA.), and G. Stokes (Pacific Northwest Lab., Richland, WA.) Apr. 1995 373 p Presented at the Atmospheric Radiation Measurement Science Team Meeting, Charleston, SC, 28 Feb. - 3 Mar. 1994 Limited Reproducibility: More than 20% of this document may be affected by microfiche quality
(DE95-009951; CONF-940277) Avail: CASI HC A16

This document contains the summaries of papers presented at the 1994 Atmospheric Radiation Measurement (ARM) Science Team meeting held in Charleston, South Carolina. To put these papers in context, it is useful to consider the history and status of the ARM Program at the time of the meeting. The history of the project has several themes. First, the program has from its very beginning attempted to respond to most critical scientific issues facing the United States Global Change Research Program. Second, the program has been strongly coupled to other agency and international programs. The program reflects an unprecedented collaboration among the various elements of the national research community, including a significant level of cooperation among the U.S. Department of Energy's (DOE) national laboratories. Next, ARM has always attempted to make the most judicious use of its resources by collaborating and leveraging existing assets and has managed to maintain an aggressive schedule despite budgets that have been much smaller than planned. Finally, the program has attracted some of the very best scientific talent in the climate research community and has, as a result, been very productive scientifically. An introduction covers the first three points; the papers themselves speak to the last point. DOE

N95-31447# Stevens Inst. of Tech., Hoboken, NJ. Center for Environmental Engineering.
ANALYTICAL INSTRUMENTATION FOR ENVIRONMENTAL RESEARCH Final Report, 30 Sep. 1993 - 29 Sep. 1994
George P. Korfistis 25 Feb. 1995 12 p
(Contract F49620-93-1-0596)
(AD-A292832; AFOSR-95-0169TR) Avail: CASI HC A03/MF A01

The Bioflo reactor and the respirometer are used to carry out degradation experiments for various environmental pollutants present in propellants as well as degradation of energetic materials. The HPLC, and GC/MS, Capillary Electrophoresis, and the LC/Ms/Ms are used for quantification and identification of Dinitrotoluene, Nitroglycerin, Diphenylamine, Nitroglycerine and their intermediates. The purchased equipment are utilized in various phases of the projects described below. In particular, these instruments are used for propellant components, intermediate biodegradation products, and enzymes. DTIC

N95-31556# Air Force Inst. of Tech., Wright-Patterson AFB, OH. School of Engineering.

SPATIAL TIME-SERIES: POLLUTION PATTERN RECOGNITION UNDER IRREGULAR INTERVENTIONS M.S. Thesis

Samuel A. Wright Mar. 1995 191 p

(AD-A293830; AFIT/GOR/ENS/95M-19) Avail: CASI HC A09/MF A02

The Fernald Environmental Restoration Management Corporation (FERMCO) has noted the introduction of arsenic contamination to groundwater around the area of the groundwater recovery system, which captures uranium contaminated groundwater. The introduction of arsenic occurs during high levels of pumping and is particularly sensitive to the western two of the five pumps. Auto-Regressive Moving Average (ARMA) and Spatial-Temporal ARMA (STARMA) empirical analyses are used to model the level of arsenic contamination found through time. The intervention of varied levels of pumping is modeled with a transfer function using analytic techniques to create a causal intervention transfer function input series to give physical meaning to the impulse response weights found. Spatial weights employed in the STARMA modeling are also created using analytic, causal methods. Results suggest a physical interpretation of the relationship between a particular level of pumping and the amount of arsenic to be found at the site in the temporal case, while including the effect of the pumping on a site of interest's neighbors in the spatial-temporal case. Models presented may be employed in the forecasting of arsenic levels at monitoring well sites due to a given change in the operation level of the groundwater recovery system. DTIC

N95-31612# Oak Ridge National Lab., TN. Biofuels Feedstock Development Program.

BIOMASS PRODUCTION BY FESCUE AND SWITCHGRASS ALONE AND IN MIXED SWARDS WITH LEGUMES Final Project Report

Michael Collins Jun. 1994 101 p Prepared in cooperation with Kentucky Univ., Lexington, KY

(Contract DE-AC05-84OR-21400)

(DE95-009137; ORNL/Sub-88-SC617) Avail: CASI HC A06/MF A02

In assessing the role of biomass in alleviating potential global warming, the absence of information on the sustainability of biomass production on soils of limited agricultural potential is cited as a major constraint to the assessment of the role of biomass. Research on the sustainability of yields, recycling of nutrients, and emphasis on reduced inputs of agricultural chemicals in the production of biomass are among the critical research needs to clarify optimum cropping practice in biomass production. Two field experiments were conducted between 1989 and 1993. One study evaluated biomass production and composition of switchgrass (Panicum virgatum L.) grown alone and with bigflower vetch (Vicia grandiflora L.) and the other assessed biomass productivity and composition of tall fescue (Festuca arundinacea Schreb.) grown alone and with perennial legumes. Switchgrass received 0, 75 or 150 kg/ha of N annually as NH4NO3 or was interseeded with vetch. Tall fescue received 0, 75, 150 or 225 kg/ha of N annually or was interseeded with alfalfa (Medicago L.) or birdsfoot trefoil (Lotus corniculatus L.). It is hoped that production systems can be designed to produce high yields of biomass with minimal inputs of fertilizer N. Achievement of this goal would reduce the potential for movement of NO3 and other undesirable N forms outside t he biomass production system into the environment. In addition, management systems involving legumes could reduce the cost of biomass production. DOE

N95-31651*# Jet Propulsion Lab., California Inst. of Tech., Pasadena, CA.

ENVIRONMENTAL PROJECTS. VOLUME 16: WASTE MINIMIZATION ASSESSMENT

15 Dec. 1994 73 p

(Contract NAS7-1260; RTOP 314-40-32-10-23)

(NASA-CR-198861; JPL-Publ-87-4-Vol-16; NAS 1.26:198861) Avail: CASI HC A04/MF A01

The Goldstone Deep Space Communications Complex (GDSCC), located in the MoJave Desert, is part of the National Aeronautics and Space Administration's (NASA's) Deep Space Network (DSN), the world's largest and most sensitive scientific telecommunications and radio navigation network. The Goldstone Complex is operated for NASA by the Jet Propulsion Laboratory. At present, activities at the GDSCC support the operation of nine parabolic dish antennas situated at five separate locations known as 'sites.' Each of the five sites at the GDSCC has one or more antennas, called 'Deep Space Stations' (DSS's). In the course of operation of these DSS's, various hazardous and non-hazardous wastes are generated. In 1992, JPL retained Kleinfelder, Inc., San Diego, California, to quantify the various streams of hazardous and non-hazardous wastes generated at the GDSCC. In June 1992, Kleinfelder, Inc., submitted a report to JPL entitled 'Waste Minimization Assessment.' This present volume is a JPL-expanded version of the Kleinfelder, Inc. report. The 'Waste Minimization Assessment' report did not find any deficiencies in the various waste-management programs now practiced at the GDSCC, and it found that these programs are being carried out in accordance with environmental rules and regulations. Author

N95-31695# National Renewable Energy Lab., Golden, CO.

SUSTAINABILITY PROTECTS RESOURCES FOR FUTURE GENERATIONS

Apr. 1995 6 p

(Contract DE-AC36-83CH-10093)

(DE95-000285; DOE/GO-10095-041) Avail: CASI HC A02/MF A01

This publication by the National Renewable Energy Laboratory addresses the steps necessary to provide livable urban centers for future generations through sustainable development, or sustainability. To illustrate this concept, nonsustainable cities and sustainable cities are compared. Sustainable city projects for several major US cites are reviewed. DOE

N95-31703# Lovelace Biomedical and Environmental Research Inst., Albuquerque, NM.

PARTICULATE AIR POLLUTION AND INCREASED MORTALITY: BIOLOGICAL PLAUSIBILITY FOR CAUSAL RELATIONSHIP

R. F. Henderson 1995 8 p Presented at the Air and Waste Management Association Meeting, San Antonio, TX, 18-23 Jun. 1995

(Contract DE-AC04-76EV-01013)

(DE95-006161; CONF-950646-1) Avail: CASI HC A02/MF A01

Recently, a number of epidemiological studies have concluded that ambient particulate exposure is associated with increased mortality and morbidity at PM concentrations well below those previously thought to affect human health. These studies have been conducted in several different geographical locations and have involved a range of populations. While the consistency of the findings and the presence of an apparent concentration response relationship provide a strong argument for causality, epidemiological studies can only conclude this based upon inference from statistical associations. The biological plausibility of a causal relationship between low concentrations of PM and daily mortality and morbidity rates is neither intuitively obvious nor expected based on past experimental studies on the toxicity of inhaled particles. Chronic toxicity from inhaled, poorly soluble particles has been observed based on the slow accumulation of large lung burdens of particles, not on small daily fluctuations in PM levels. Acute toxicity from inhaled particles is associated mainly with acidic particles and is observed at much higher concentrations than those observed in the epidemiology studies reporting an association between PM concentrations and morbidity/mortality. To approach the difficult problem of determining if the association between PM concentrations and daily morbidity and mortality is biologically plausible and causal, one must consider (1) the chemical and physical characteristics of the particles in the inhaled atmospheres, (2) the characteristics of the morbidity/mortality observed and the people who are affected, and (3) potential mechanisms that might link the two. DOE

N95-31720 Northwestern Univ., Chicago, IL.

THE ROLE OF THE HYDROLOGICAL CYCLE AND THE OCEAN'S THERMOHALINE CIRCULATION IN CLIMATE CHANGE: A

MULTICOMPONENT CLIMATE MODEL STUDY Ph.D. Thesis
Huaxiao Wang 1993 132 p
Avail: Univ. Microfilms Order No. DA9415831

Global ocean-atmosphere and ocean-atmosphere-continental ice sheet models are developed to address the question of feedbacks between the hydrological cycle and the global thermohaline circulation capable of explaining the climate changes seen in paleoclimate records of the late Pleistocene and the last deglaciation. The ocean-atmosphere model climate system displays two distinct stable equilibria controlled by latitudinal water vapor transport and the net flux of water vapor from the Atlantic to the Pacific Ocean. If the inter-basin transport is sufficiently large, small changes in water vapor transport over the North Atlantic can effect bifurcation; maximum difference between the modes occurs in the North Atlantic. If the inter-basin transport is from the Pacific to the Atlantic and sufficiently large, latitudinal vapor transport in the North Pacific controls the bifurcations, with maximum changes occurring in the North Pacific. For intermediate values of inter-basin transport, no rapid transitions occur in either basin. In the regime with vapor flux from the Atlantic to the Pacific, one mode has strong production of deep water in the North Atlantic and a large flux of heat to the atmosphere from the high latitude North Atlantic. The other has strong deep water production in the Southern Ocean and weak production in the North Pacific and small heat transport to high-latitude North Atlantic. The ocean-atmosphere-ice sheet system displays feedbacks which produce century/millennium time scale oscillations. The thermohaline circulation plays a central role in these feedbacks because of its transport of both heat and salt. The feedbacks could potentially play a causal role in the century/milliennium climate change seen in the paleoclimate record. Dissert. Abstr.

N95-31821# National Renewable Energy Lab., Golden, CO.
BIOFACTS: FUELING A STRONGER ECONOMY, GLOBAL WARMING AND BIOFUELS EMISSIONS
Dec. 1994 4 p
(Contract DE-AC36-83CH-10093)
(DE94-006864; NREL/SP-420-6365) Avail: CASI HC A01/MF A01

The focus of numerous federal and state regulations being proposed and approved today is the reduction of automobile emissions, particularly carbon dioxide (CO2), which is the greenhouse gas considered responsible for global warming. Studies conducted by the US DOE through the National Renewable Energy Laboratory (NREL) indicate that the production and use of biofuels such as biodiesel, ethanol, and methanol could nearly eliminate the contribution of net CO2 from automobiles. This fact sheet provides an overview of global warming, followed by a summary of NREL's study results. DOE

N95-31851 Oregon Graduate Inst. of Science and Technology, Beaverton, OR.
THE GCRC TWO-DIMENSIONAL ZONALLY AVERAGED STATISTICAL DYNAMICAL CLIMATE MODEL: DEVELOPMENT, MODEL PERFORMANCE, AND CLIMATE SENSITIVITY Ph.D. Thesis
Robert Malcolm MacKay 1994 273 p
Avail: Univ. Microfilms Order No. DA9415946

The two-dimensional statistical dynamical climate model that has recently been developed at the Global Change Research Center and the Oregon Graduate Institute of Science & Technology (GCRC 2D climate model) is presented and several new results obtained using the model are discussed. The model solves the 2-D primitive equations in finite difference form (mass continuity, Newton's second law, and the first law of thermodynamics) for the prognostic variables zonal mean density, zonal mean zonal velocity, zonal mean meridional velocity, and zonal mean temperature on a grid that has 18 nodes in latitude and 9 vertical nodes (plus the surface). The equation of state, p = (rho RT) and an assumed hydrostatic atmosphere, Delta(p) = -(rho g Delta z) are used to diagnostically calculate the zonal mean pressure and vertical velocity for each grid node, and the moisture balance equation is used to estimate the precipitation rate. The performance of the model at simulating the two-dimensional temperature, zonal winds, and mass stream function is explored. The strengths and weaknesses of the model are highlighted and suggestions for future model improvements are given. The parameterization of the transient eddy fluxes of heat and momentum developed by Stone and Yao (1987 and 1990) are used with small modifications. These modifications are shown to help the performance of the model at simulating the observed climate system as well as increase the model's computational stability. Following earlier world that analyzed the response of the zonal wind fields predicted by three GCM simulations for a doubling of atmospheric CO2, the response of the GCRC 2D model's zonal wind fields is also explored for the same experiment. Unlike the GCM simulations, our 2D model results in distinct patterns of change. It is suggested that the observed changes in zonal winds for the 2xCO2 experiment are related to the increase in the upper level temperature gradients predicted by our model and most climate models of adequate sophistication and resolution. We thus suggest that the same mechanism controlling the changes in zonal winds for the 2xCO2 experiment in our model also contributes to the simulated changes in zonal winds of the more complex GCM's. Dissert. Abstr.

N95-31981*# University of Southern California, Los Angeles, CA. Dept. of Biological Sciences.
GLOBAL CLIMATOLOGY AND VARIABILITY OF POTENTIAL NEW PRODUCTION ESTIMATED FROM REMOTE SENSING OF SEA-SURFACE TEMPERATURE Final Report, 1 May 1992 - 30 Apr. 1995
Richard C. Dugdale and Frances P. Wilkerson 30 Apr. 1995 13 p
(Grant NAGw-3149)
(NASA-CR-198840; NAS 1.26:198840; NRA-91-OSSA-07) Avail: CASI HC A03/MF A01

During this project we have collected numerous shipboard data-bases of oceanic nitrate and silicate versus temperature for both equatorial and coastal upwelling regions. These cruises all have accompanying N-15 measurements of new production. The inverse relationships between nutrients and temperatures have been determined and are being used to obtain surface nutrient fields from sea surface temperatures measured remotely by satellite borne sensors- i.e. AVHRR data from NOAA satellites contained in the MCSST data set for the world ocean provided by the University of Miami. The images and data derived from space in this way show the strong seasonal fluctuations and interannual el Nino fluctuations of the nitrate field. the nitrate data has been used to make estimates of new production for the equatorial pacific which are compared with shipboard measurements when available. The importance of silicate as a nutrient driving new production and the ratio of nitrate to silicate has been discovered to be crucial to better understand the causes of new production variability, so we have added these parameters to our study and have begun to make estimates of these for the equatorial Pacific, derived from the weekly averaged sea surface temperatures (SSTs). Derived from text

N95-32099# Oak Ridge National Lab., TN.
CARBON DIOXIDE CONCENTRATIONS IN SURFACE WATER AND THE ATMOSPHERE DURING 1986-1989 NOAA/PMEL CRUISES IN THE PACIFIC AND INDIAN OCEANS
P. P. Murphy, K. C. Kelly, R. A. Feely, and R. H. Gammon Jan. 1995 197 p
(Contract DE-AC05-84OR-21400)
(DE95-009659; ORNL/CDIAC-75; NDP-047) Avail: CASI HC A09/MF A03

The carbonate system in seawater is one of the most complex and important topics in oceanography. The system has long interested many oceanographers from various fields because it plays a major role in all three subspheres of the earth (biosphere, lithosphere, and hydrosphere). Carbon dioxide is a soluble gas that dissolves in sea water. As a result, the oceans are a potential sink for the CO2, produced by the burning of fossil fuels, and we seek to understand the role of the World Ocean in regulating atmospheric levels of CO2. With refined determinations for the various dissociation constants of carbonic and boric acids in seawater and the advances in sophisticated instrumentation for measuring the carbonate parameters, our knowledge of the CO2-carbonate system of the ocean has rapidly increased. Extensive oceanographic investigations have been carried out in the World Ocean. Those extensive studies, especially in physical oceanography, have provided an excellent foundation for other types of study, such as that of the CO2-carbonate system. This document presents the results of quasi-continuously measured CO2 concentrations in surface water and the atmosphere during 5 Pacific Marine Environmental Laboratory cruises in the Pacific and Indian Oceans. DOE

N95-32156# Argonne National Lab., IL.
COMBATTING URBAN AIR POLLUTION THROUGH NATURAL GAS VEHICLE (NGV) ANALYSIS, TESTING, AND DEMONSTRATION
1995 12 p Presented at the CNG Conference, Cairo, Egypt, 20-21 Nov. 1994
(Contract W-31-109-eng-38)
(DE95-008300; ANL/ES/CP-85156; CONF-9411214-Summ) Avail: CASI HC A03/MF A01

Deteriorating urban air quality ranks as a top concern worldwide, since air pollution adversely affects both public health and the environment. The outlook for improving air quality in the world's megacities need not be bleak, however. The use of natural gas as a transportation fuel can measurably reduce urban pollution levels, mitigating chronic threats to health and the environment. Besides being clean burning, natural gas vehicles (NGV's) are economical to operate and maintain. The current cost of natural gas is lower than that of gasoline. Natural gas also reduces the vehicle's engine wear and noise level, extends engine life, and decreases engine maintenance. Today, about 700,000 NGV's operate worldwide, the majority of them converted from gasoline or diesel fuel. This article discusses the economic, regulatory and technological issues of concern to the NGV industry. DOE

N95-32276# Los Alamos National Lab., NM.
SIMULATION OF KATABATIC FLOW AND MOUNTAIN WAVES
G. S. Poulos 1995 3 p Presented at the Mountain Meteorology, Breckenridge, CO, 17-21 Jul. 1995
(Contract W-7405-eng-36)
(DE95-010863; LA-UR-95-1280; CONF-9507120-2) Avail: CASI HC A01/MF A01

It is well-known that both mountain waves and katabatic flows frequently form in the severe relief of the Front Range of the Rocky Mountains. Occasionally these phenomena have been found to occur simultaneously. Generally, however, the large body of literature regarding them has treated each individually, seldom venturing into the regime of their potential interaction. The simulations overviewed here attempt to reproduce both atmospheric features simultaneously for two case days during the 1993 ASCOT observational program near Rocky Flats, Colorado. DOE

N95-32281# Lawrence Livermore National Lab., Livermore, CA.
NO-THERMAL PLASMA PROCESSING OF VOCs AND NO(x) AT LLNL
Bernard T. Merritt, M. C. Hsiao, B. M. Penetrante, G. E. Vogtlin, and P. H. Wallman 15 Feb. 1995 23 p Presented at the Air and Waste Management Association Meeting, San Antonio, TX, 18-23 Jun. 1995
(Contract W-7405-eng-48)
(DE95-011445; UCRL-JC-120503; CONF-950646-17) Avail: CASI HC A03/MF A01

For the past few years, Lawrence Livermore National Laboratory has been conducting a comprehensive research program on the application of non-thermal plasmas for air pollution control and abatement. This program combines an extensive modeling effort with an experimental facility and test program. We believe that there are two major issues to be addressed in order to apply non-thermal plasma processing to air pollution control; these are electrical energy consumption and byproduct identification. The thrust of our work has been to understand the scalability of the non-thermal process by focusing on the energy efficiency of the non-thermal process and to identify the byproducts to ensure that effluent gases from a non-thermal processor are benign. We have compared different types of electrical discharge reactors both theoretically and experimentally. Our interests in the application of non-thermal plasmas vary from the destruction of volatile organic compounds (VOC's) to NO(x) reduction for mobile applications. This paper discusses the processing of both NO(x) and VOC's by non-thermal plasmas at LLNL. DOE

N95-32350# Lawrence Livermore National Lab., Livermore, CA. Global Climate Research Div.
CALCULATION OF A RESIDUAL MEAN MERIDIONAL CIRCULATION FOR A ZONAL-MEAN TRACER TRANSPORT MODEL
Woo Kap Choi, Douglas A. Rotman, and Donald J. Wuebbles 1995 30 p
(Contract W-7405-eng-48)
(DE95-009474; UCRL-ID-119565) Avail: CASI HC A03/MF A01

Because of their computational advantages, zonally-averaged chemical-radiative-transport models are widely used to investigate the distribution of chemical species and their change due to the anthropogenic chemicals in the lower and middle atmosphere. In general, the Lagrangian-mean formulation would be ideal to treat transport due to the zonal mean circulation and eddies. However, the Lagrangian formulation is difficult to use in practical applications. The most widely-used formulation for treating global atmospheric dynamics in two-dimensional models is the transformed Eulerian mean (TEM) equations. The residual mean meridional circulation (RMMC) in the TEM system is used to advect tracers. In this study, the authors describe possible solution techniques for obtaining the RMMC in the LLNL two-dimensional chemical-radiative-transport model. In the first section, the formulation will be described. In sections 3 and 4, possible solution procedures will be described for a diagnostic and prognostic case, respectively. DOE

N95-32364# Air-Conditioning and Refrigeration Technology Inst., Inc., Arlington, VA.
COMPATIBILITY OF MANUFACTURING PROCESS FLUIDS WITH HFC REFRIGERANTS AND ESTER LUBRICANTS Final Report, 3 Jan. 1994 - 30 Nov. 1994
R. C. Cavestri (Imagination Resources, Inc., Dublin, OH.) Nov. 1994 36 p
(Contract DE-FG02-91CE-23810)
(DE95-012152; DOE/CE-23810/43) Avail: CASI HC A03/MF A01

Included in this report is a compiled partial list of presently used processing materials in the air-conditioning and refrigeration industry and the manufacturers, intended uses, and applications of each. Also listed are the processing materials that have received final acceptance for this contracted study. An analytical methodology discussion is presented, including the final decision and the limitations of said methodology, as well as how to establish a level of confidence in observed immiscible material components in two 32 ISO VG polyolesters: (1) Mobil EAL Arctic 32; and (2) ICI Emkarate RL32H, both with HFC 134a refrigerant solutions. DOE

N95-31747*# Thiokol Corp., Brigham City, UT. Space Operations.
ATMOSPHERIC ENVIRONMENTAL IMPLICATIONS OF PROPULSION SYSTEMS
Allan J. McDonald and Robert R. Bennett *In* NASA. Marshall Space Flight Center, Aerospace Environmental Technology Conference Mar. 1995 p 3-14 (For primary document see N95-31746 11-23)
Avail: CASI HC A03/MF A06

N95-31748*# National Aeronautics and Space Administration. Marshall Space Flight Center, Huntsville, AL.
MANUFACTURING WASTE DISPOSAL PRACTICES OF THE CHEMICAL PROPULSION INDUSTRY
Benjamin E. Goldberg, Daniel E. Adams, and Scott A. Schutzenhofer *In its* Aerospace Environmental Technology Conference Mar. 1995 p 15-24 (For primary document see N95-31746 11-23)
Avail: CASI HC A02/MF A06

N95-31749*# National Aeronautics and Space Administration. Marshall Space Flight Center, Huntsville, AL.
CFD ASSESSMENT OF THE POLLUTANT ENVIRONMENT FROM RD-170 PROPULSION SYSTEM TESTING
Terl-See Wang, Paul McConnaughey, Saif Warsi (Sverdrup Technology, Inc., Huntsville, AL.), and Yen-Sen Chen (Engineering-Science, Inc., Huntsville, AL.) *In its* Aerospace Environmental Technology Conference Mar. 1995 p 25-47 (For primary document see N95-31746 11-23)
Avail: CASI HC A03/MF A06

N95-31750*# National Aeronautics and Space Administration. Marshall Space Flight Center, Huntsville, AL.
ENVIRONMENTAL BENEFITS OF CHEMICAL PROPULSION
Joyce A. Hayes, Benjamin E. Goldberg, and David M. Anderson *In its* Aerospace Environmental Technology Conference Mar. 1995 p 49-63 (For primary document see N95-31746 11-23)
Avail: CASI HC A03/MF A06

N95-31757*# National Aeronautics and Space Administration. Marshall Space Flight Center, Huntsville, AL.
PRIORITIZATION METHODOLOGY FOR CHEMICAL REPLACEMENT

Wendy Cruit, Ben Goldberg, and Scott Schutzenhofer *In its* Aerospace Environmental Technology Conference Mar. 1995 p 131-141 (For primary document see N95-31746 11-23)
Avail: CASI HC A03/MF A06

N95-31758*# National Center for Mfg. Sciences, Ann Arbor, MI.
NATIONAL CENTER FOR MANUFACTURING SCIENCES: ENVIRONMENTALLY CONSCIOUS MANUFACTURING
Clare Vinton *In* NASA. Marshall Space Flight Center, Aerospace Environmental Technology Conference Mar. 1995 p 145-147 (For primary document see N95-31746 11-23)
Avail: CASI HC A01/MF A06

N95-31759*# Pennsylvania State Univ., State College, PA. Applied Research Lab.
AIR POLLUTION CONTROL SYSTEM RESEARCH: AN ITERATIVE APPROACH TO DEVELOPING AFFORDABLE SYSTEMS
Lewis C. Watt, Fred S. Cannon, Robert J. Heinsohn, and Timothy A. Spaeder *In* NASA. Marshall Space Flight Center, Aerospace Environmental Technology Conference Mar. 1995 p 149-156 (For primary document see N95-31746 11-23)
Avail: CASI HC A02/MF A06

N95-31761*# Air Force Civil Engineering Center, Tyndall AFB, FL. Directorate of Construction Cost Management.
MAJOR WEAPON SYSTEM ENVIRONMENTAL LIFE-CYCLE COST ESTIMATING FOR CONSERVATION, CLEANUP, COMPLIANCE AND POLLUTION PREVENTION (C3P2)
Wesley Hammond, Marland Thurston (Delta Research Corp., Niceville, FL.), and Christopher Hood (Delta Research Corp., Niceville, FL.) *In* NASA. Marshall Space Flight Center, Aerospace Environmental Technology Conference Mar. 1995 p 163-168 (For primary document see N95-31746 11-23)
Avail: CASI HC A02/MF A06

N95-31762*# United Technologies Corp., Huntsville, AL.
EVALUATING THE COST EFFECTIVENESS OF ENVIRONMENTAL PROJECTS: CASE STUDIES IN AEROSPACE AND DEFENSE
James F. Shunk *In* NASA. Marshall Space Flight Center, Aerospace Environmental Technology Conference Mar. 1995 p 169-177 (For primary document see N95-31746 11-23)
Avail: CASI HC A02/MF A06

N95-31812*# National Aeronautics and Space Administration. Marshall Space Flight Center, Huntsville, AL.
THE EFFECT OF ENVIRONMENTAL INITIATIVES ON NASA SPECIFICATIONS AND STANDARDS ACTIVITIES
Dennis Griffin, David Webb, and Beth Cook *In its* Aerospace Environmental Technology Conference Mar. 1995 p 649-659 (For primary document see N95-31746 11-23)
Avail: CASI HC A03/MF A06

N95-31814*# Athens State Coll., AL. Dept. of Management of Technology.
DEVELOPMENT OF A CFC CRITICAL AREA RESPONSE (CAR) PACKAGE
J. Wayne McCain *In* NASA. Marshall Space Flight Center, Aerospace Environmental Technology Conference Mar. 1995 p 667-671 (For primary document see N95-31746 11-23)
Avail: CASI HC A01/MF A06

N95-32177# Esquimalt Defence Research Detachment, Victoria (British Columbia).
TREATMENT OF PLASTIC MEDIA WASTE
Terry Foster *In* AGARD, Environmentally Safe and Effective Processes for Paint Removal Apr. 1995 1 p (For primary document see N95-32165 11-31)
Copyright Avail: CASI HC A01/MF A01

N95-32178# Aerospatiale, Toulouse (France). Direction des Etudes.
BIOREMEDIATION OF WHEAT STARCH MEDIA WASTE
Olivier Malavallon and John Oestreich (CAE Electronics Ltd., Montreal, Quebec.) *In* AGARD, Environmentally Safe and Effective Processes for Paint Removal Apr. 1995 2 p (For primary document see N95-32165 11-31)
Copyright Avail: CASI HC A01/MF A01

46 GEOPHYSICS

Includes aeronomy; upper and lower atmosphere studies; ionospheric and magnetospheric physics; and geomagnetism.
For space radiation see *93 Space Radiation.*

N95-30373# Lawrence Livermore National Lab., Livermore, CA.
IR DIAL PERFORMANCE MODELING
E. T. Sharlemann Jul. 1994 4 p Presented at the 1994 Chemical Analysis By Laser Interrogation of Proliferation Effluents (CALIOPE ITR) Interim Technical Review, Livermore, CA, 26-28 Apr. 1994
(Contract W-7405-eng-48)
(DE95-008377; UCRL-JC-118285; CONF-9404162-18) Avail: CASI HC A01/MF A01

We are developing a DIAL performance model for CALIOPE at LLNL. The intent of the model is to provide quick and interactive parameter sensitivity calculations with immediate graphical output. A brief overview of the features of the performance model is given, along with an example of performance calculations for a non-CALIOPE application. DOE

N95-30525*# Jet Propulsion Lab., California Inst. of Tech., Pasadena, CA.
CHEMICAL KINETICS AND PHOTOCHEMICAL DATA FOR USE IN STRATOSPHERIC MODELING: EVALUATION NUMBER 11
W. B. DeMore, S. P. Sander, D. M. Golden (SRI International Corp., Menlo Park, CA.), R. F. Hampson (National Inst. of Standards and Technology, Gaithersburg, MD.), M. J. Kurylo (National Inst. of Standards and Technology, Gaithersburg, MD.), C. J. Howard (National Oceanic and Atmospheric Administration, Boulder, CO.), A. R. Ravishankara (National Oceanic and Atmospheric Administration, Boulder, CO.), C. E. Kolb (Aerodyne Research, Inc., Billerica, MA.), and M. J. Molina (Massachusetts Inst. of Tech., Cambridge, MA.) 15 Dec. 1994 284 p
(Contract NAS7-1260; RTOP 464-41-04-01-00)
(NASA-CR-198863; JPL-Publ-94-26; NAS 1.26:198863) Avail: CASI HC A13/MF A03

This is the eleventh in a series of evaluated sets of rate constants and photochemical cross sections compiled by the NASA Panel for Data Evaluation. The primary application of the data is in the modeling of stratospheric processes, with special emphasis on the ozone layer and its possible perturbation by anthropogenic and natural phenomena.
Author (revised)

N95-30588 Institut des Hautes Etudes Scientifiques, Bures-sur-Yvette (France).
GRAVITATIONAL-RADIATION DAMPING OF COMPACT BINARY SYSTEMS TO SECOND POST-NEWTONIAN ORDER
L. Blanchet, T. Damour, B. R. Iyer, C. M. Will, and A. G. Wiseman Jan. 1995 13 p Prepared in cooperation with Observatoire de Paris, Washington Univ., and Northwestern Univ. Limited Reproducibility: More than 20% of this document may be affected by microfiche quality
(PB95-207882; IHES/P/95/4) Avail: CASI HC A03

The rate of gravitational-wave energy loss from inspiralling binary systems of compact objects of arbitrary mass is derived through second post-Newtonian (2PN) order O((Gm/r(c squared))squared) beyond the quadrupole approximation. The result has been derived by two independent calculations of the (source) multipole moments. The 2PN terms, and in particular the finite mass contribution therein (which cannot be obtained in perturbation calculations of black hole spacetimes), are shown to make a significant contribution to the accumulated phase of theoretical templates to be used in matched filtering of the data from future gravitational-wave detectors. NTIS

N95-30590# Institut des Hautes Etudes Scientifiques, Bures-sur-Yvette (France).
GRAVITATIONAL WAVES FROM INSPIRALLING COMPACT BINARIES: ENERGY LOSS AND WAVEFORM TO SECOND-POST-NEWTONIAN ORDER
L. Blanchet, T. Damour, and B. R. Iyer Jan. 1995 45 p Prepared in cooperation with Raman Research Inst.
(PB95-207890; IHES/P/95/8) Avail: CASI HC A03/MF A01

Gravitational waves generated by inspiralling compact binaries are investigated to the second-post-Newtonian (2PN) approximation of general relativity. Using a recently developed 2PN-accurate wave generation formalism, we compute the gravitational waveform and associated energy loss rate from a binary system of point-masses moving on a quasi-circular orbit. The crucial new input is our computation of the 2PN-accurate 'source' quadrupole moment of the binary. Tails in both the waveform and energy loss rate at infinity are explicitly computed. Gravitational radiation reaction effects on the orbital frequency and phase of the binary are deduced from the energy loss. In the limiting case of a very small mass ratio between the two bodies, we recover the results obtained by black hole perturbation methods. We find that finite mass ratio effects are very significant as they increase the 2PN contribution to the phase by up to 52%. The results of this paper should be of use when deciphering the signals observed by the future LIGO/VIRGO network of gravitational-wave detectors. NTIS

N95-30627# Swedish Inst. of Space Physics, Kiruna (Sweden).
KIRUNA GEOPHYSICAL DATA. DATA SUMMARY 94/4-6, APRIL-JUNE 1994
S. Kirkwood 1994 59 p
(PB95-210365) Avail: CASI HC A04/MF A01

The table of contents for this Kiruna geophysical data summary include: (1) Geomagnetic data; (2) All-sky camera data; (3) Ionospheric absorption data; (4) Tables of April-June 1994 - Geomagnetic K-indices; (5) All-sky camera; (6) Reproductions of April-June 1994 - Magnetogram plots; and (7) Riometer recordings. NTIS

N95-30628# Swedish Inst. of Space Physics, Kiruna (Sweden).
KIRUNA GEOPHYSICAL DATA. DATA SUMMARY 94/1-3, JANUARY-MARCH 1994
S. Kirkwood 1994 62 p
(PB95-210373) Avail: CASI HC A04/MF A01

The table of contents for this Kiruna geophysical data summary from the Swedish Institute of Space Physics includes: Legend - Geomagnetic data; All-sky camera data; Ionospheric absorption data; Tables of January-March 1994 - Geomagnetic K-indices; All-sky camera; Reproductions for January-March 1994 - Magnetogram plots; and Riometer recordings. NTIS

N95-30631# Swedish Inst. for Materials Testing, Boras (Sweden).
GENERATION OF EARTHQUAKE SIGNALS
G. Kjell Feb. 1995 27 p
(PB95-211223; SP-RAPP-1994:59) Avail: CASI HC A03/MF A01

Seismic verification can be performed either as a full scale test on a shaker table or as numerical calculations. In both cases it is necessary to have an earthquake acceleration time history. The report describes generation of such time histories by filtering white noise. Analogue and digital filtering methods are compared. Different methods of predicting the response spectrum of a white noise signal filtered by a band-pass filter are discussed. Prediction of both the average response level and the statistical variation around this level are considered. Examples with both the IEEE 301 standard response spectrum and a ground spectrum suggested for Swedish nuclear power stations are included in the report. NTIS

N95-30643# National Oceanic and Atmospheric Administration, Washington, DC.
SUPRIOIUS SEMI-DIURNAL VARIATION IN THE E.R.B.E. OUTGOING LONGWAVE RADIATION
Chandrasekhara R. Kondragunta (Maryland Univ., College Park, MD.) and Arnold Gruber (National Environmental Satellite Service, Washington, DC.) Jun. 1995 29 p
(NOAA-TR-NESDIS-84) Avail: CASI HC A03/MF A01

The Outgoing Longwave Radiation (OLR) data from the Earth Radiation Budget Experiment (ERBE) were analyzed for the period during which all three ERBE satellites were operating, i.e., December 6, 1986 to January 19, 1987, to study the diurnal variation. A cubic spline interpolation technique was used to fill the gaps between the sampled hours of OLR. The interpolated data was composited to obtain mean diurnal time series of OLR. In order to extract the diurnally varying dominant modes, an Empirical Orthogonal Function (EOF) analysis technique was applied to the normalized anomalies of the composite daily OLR. The first EOF mode explains 53.2% of the total normalized variance. Its spatial pattern is dominated by positive loadings located over the oceanic cloudy regions and its temporal variation indicates a strong semi-diurnal cycle with maxima and minima coinciding with the equator crossing times of the NOAA-9 and NOAA-10 satellites. It is argued that the semi-diurnal cycle noticed in this mode is not realistic and is caused by biases in retrieving OLR from different instruments on board NOAA-9 and NOAA-10. The temporal variation of the second EOF model indicates a true diurnal signal with most of the spatial variation occurring over the dry continental regions. In the third EOF mode, most of the variation is over cloudy regions, whose temporal variation indicates a semi-diurnal variation modulated by a large amplitude diurnal cycle. The effect of this instrumental bias is clearly evident in the global averages of the OLR. Author

N95-30675# International Centre for Theoretical Physics, Trieste (Italy).
ESAA: ENVIRONMENT FOR SEISMIC ACTIVITY ANALYSIS
Shu-Yu Zhang and Bai-Lin Hao Sep. 1994 9 p
(DE95-612416; IC-94/283) Avail: CASI HC A02/MF A01 (US Sales Only)

ESAA is an X-window based, graphical and interactive, software system for analyzing seismic activity, using the earthquake catalogs of a given region as input. Basic design idea and structure of this system, as well as the progress in its implementation are reported. DOE

N95-30683# Oak Ridge National Lab., TN.
ALGORITHM COMPARISON AND BENCHMARKING USING A PARALLEL SPECTRA TRANSFORM SHALLOW WATER MODEL
P. H. Worley, I. T. Foster (Argonne National Lab., IL.), and B. Toonen (Argonne National Lab., IL.) 1995 13 p Presented at the 6th Workshop on Use of Parallel Processors in Meterology, Reading, England, 24 Nov. 1994
(Contract DE-AC05-84OR-21400)
(DE95-009124; CONF-9411178-2) Avail: CASI HC A03/MF A01

In recent years, a number of computer vendors have produced supercomputers based on a massively parallel processing (MPP) architecture. These computers have been shown to be competitive in performance with conventional vector supercomputers for some applications. As spectral weather and climate models are heavy users of vector supercomputers, it is interesting to determine how these models perform on MPP's, and which MPPs are best suited to the execution of spectral models. The benchmarking of MPP's is complicated by the fact that different algorithms may be more efficient on different architectures. Hence, a comprehensive benchmarking effort must answer two related questions: which algorithm is most efficient on each computer and how do the most efficient algorithms compare on different computers. In general, these are difficult questions to answer because of the high cost associated with implementing and evaluating a range of different parallel algorithms on each MPP platform. DOE

N95-30758# Japan Atomic Energy Research Inst., Tokyo (Japan).
SHEAT: A COMPUTER CODE FOR PROBABILISTIC SEISMIC HAZARD ANALYSIS, USER'S MANUAL
Katsumi Ebisawa (Japan Atomic Energy Research Inst., Tokai, Japan.), Masaaki Kondo (Japan Atomic Energy Research Inst., Tokai, Japan.), Kiyoharu Abe (Japan Atomic Energy Research Inst., Tokai, Japan.), Toshiaki Tanaka, and Michio Takani Aug. 1994 143 p In JAPANESE
(DE95-717874; JAERI-Data/Code-94-009) Avail: CASI HC A07/MF A02

The SHEAT code developed at Japan Atomic Energy Research Institute is for probabilistic seismic hazard analysis which is one of the tasks needed for seismic Probabilistic Safety Assessment (PSA) of a nuclear power plant. Seismic hazard is defined as an annual exceedance frequency of occurrence of earthquake ground motions at various levels of intensity at a given site. With the SHEAT code, seismic hazard is calculated by the following two steps. (1) Modeling of earthquake generation around a site: Future earthquake generation (locations, magnitudes and frequencies of postulated earthquakes) is modeled based on the historical earthquake records, active

fault data, and expert judgement. (2) Calculation of probabilistic seismic hazard at the site: An earthquake ground motion is calculated for each postulated earthquake using an attenuation model taking into account its standard deviation. Then the seismic hazard at the site is calculated by summing the frequencies of ground motions by all the earthquakes. This document is the user's manual of the SHEAT code. It includes: (1) outlines of the code, which include overall concept, logical process, code structure, data file used, and special characteristics of the code; (2) functions of subprograms and analytical models in them; (3) guidance of input and output data; and (4) sample run results. The code has been widely used at JAERI to analyze seismic hazard at various nuclear power plant sites in Japan. DOE

N95-30773# Aerospace Corp., Los Angeles, CA. Engineering and Technology Group.

LOW-LATITUDE BOUNDARY LAYER NEAR NOON: AN OPEN FIELD LINE MODEL

L. R. Lyons, M. Schulz, D. C. Pridmore-Brown, and J. L. Roeder El Segundo, CA 15 Oct. 1994 16 p Repr. from Journal of Geophysical Research, v. 99, no. A9, Sep. 1994 p 17,367-17,377

(Grant NSF ATM-91-20072)

(ATR-93(7270)-1) Avail: CASI HC A03/MF A01

We propose that many features of the cusp and low-latitude boundary layer (LLBL) observed near noon MLT can be explained by interpreting the LLBL as being on open lines with an inner boundary at the separatrix between open and closed magnetic field lines. This interpretation places the poleward boundary of the LLBL and equatorward boundary of the cusp along the field line that bifurcates at the cusp neutral point. The interpretation accounts for the abrupt boundary and magnetosheath particles at the inner edge of the LLBL, a feature that is inconsistent with LLBL formation by diffusion onto closed field lines, and for the distribution of magnetosheath particles appearing more as one continuous region than as two distinct regions across the noon cusp/LLBL boundary. Furthermore, we can explain the existence of energetic radiation belt electrons and protons with differing pitch angle distributions within the LLBL and their abrupt cutoff at the poleward boundary of the LLBL. By modeling the LLBL and cusp region quantitatively, we can account for a hemispherical difference in the location of the equatorial boundary of the cusp that is observed to be dependent on the dipole tilt angle but not on the interplanetary magnetic field (IMF) x component. We also find important variations and hemispherical differences in that the size of the LLBL should depend strongly upon the x component of the IMF. This prediction is observationally testable. Finally, we find that when the IMF is strongly northward, the LLBL may include a narrow region adjacent to the magnetopause where field lines are detached (i.e., have both ends connected to the IMF). Author

N95-30848*# Iowa Univ., Iowa City, IA. Dept. of Physics and Astronomy.

PERPENDICULAR ELECTRON HEATING BY ABSORPTION OF AURORAL KILOMETRIC RADIATION

D. D. Morgan, J. D. Menietti, R. M. Winglee (Washington Univ., Seattle, WA.), and H. K. Wong (Southwest Research Inst., San Antonio, TX.) Sep. 1994 31 p Revised

(Grant NAG5-2102)

(NASA-198815; NAS 1.26:198815) Avail: CASI HC A03/MF A01

We investigate the possibility of perpendicular heating of electrons and the generation of '90 deg -electron conics' by particle diffusion in velocity space due to wave-particle interaction with intense auroral kilometric radiation. This interaction is made possible by the downward shift in the R-X cutoff below the electron cyclotron frequency that occurs in the presence of warm plasma. We stimulate this condition and solve the diffusion equation using a finite difference algorithm. The results show strong perpendicular electron heating and indicate that the main characteristics of an electron conic distribution can be reproduced under these conditions. Author

N95-30865*# Oregon State Univ., Corvallis, OR.

LABORATORY SIMULATED HYDROTHERMAL ALTERATION OF SEDIMENTARY ORGANIC MATTER FROM GUAYMAS BASIN, GULF OF CALIFORNIA Ph.D. Thesis

Roald N. Leif 23 Jul. 1993 291 p Sponsored by Donors of the Petroleum Research Fund

(Grants NAGw-2833; NSF OCE-90-02366; NSF OCE-86-01316)

(NASA-CR-198951; NAS 1.26:198951) Copyright Avail: CASI HC A13/MF A03

High temperature alteration of sedimentary organic matter associated with marine hydrothermal systems involves complex physical and chemical processes that are not easily measured in most natural systems. Many of these processes can be evaluated indirectly by examining the geochemistry of the hydrothermal system in the laboratory. In this investigation, an experimental organic geochemical approach to studying pyrolysis of sedimentary organic matter is applied to the hydrothermal system in the Guaymas Basin, Gulf of California. A general survey of hydrothermal oils and extractable organic matter (bitumen) in hydrothermally altered sediments identified several homologous series of alkanones associated with a high temperature hydrothermal origin. The alkanones range in carbon number from C11 to C30 with no carbon number preference. Alkan-2-ones are in highest concentrations, with lower amounts of 3-, 4-, 5- (and higher) homologs. The alkanones appear to be pyrolysis products synthesized under extreme hydrothermal conditions. Hydrous pyrolysis and confinement pyrolysis experiments were performed to simulate thermally enhanced diagenetic and catagenetic changes in the immature sedimentary organic matter. The extent of alteration was measured by monitoring the n-alkanes, acyclic isoprenoids, steroid and triterpenoid biomarkers, polycyclic aromatic hydrocarbons and alkanones. The results were compared to bitumen extracts from sediments which have been naturally altered by a sill intrusion and accompanied hydrothermal fluid flow. These pyrolysis experiments duplicated many of the organic matter transformations observed in the natural system. Full hopane and sterane maturation occurred after 48 hr in experiments at 330 deg C with low water/rock mass ratios (0.29). A variety of radical and ionic reactions are responsible for the organic compound conversions which occur under extreme hydrothermal conditions. Short duration pyrolysis experiments revealed that a portion of the hydrocarbons generated from kerogen was observed to go through alkene intermediates, and the rate of alkene isomerization was influenced by the ionic strength and catalytic mineral phases. Confinement of the organic pyrolysate to the bulk sediment accelerated the rates of the biomarker epimerization reactions, suggesting that these reactions are influenced strongly by the association of the inorganic matrix, and that the relative rates of some ionic and radical reactions can be influenced by the water/rock ratio during the pyrolysis experiments. Author

N95-31012# Computational Physics, Inc., Waltham, MA.

SSUSI SINGLE SENSOR AURORAL E-LAYER ALGORITHM: FUNCTIONAL DESCRIPTION

Robert E. Daniell, Jr., William G. Whartenby, and Lincoln D. Brown 6 Jul. 1994 39 p

(Contract F19628-91-C-0103)

(AD-A288630; PL-TR-94-2195) Avail: CASI HC A03/MF A01

This report describes the SSUSI single sensor Auroral E-layer algorithm developed by Computational Physics, Inc. for Phillips Laboratory and provided to the Johns Hopkins University Applied Physics Laboratory for incorporation into the operational software for SSUSI. SSUSI is an Ultraviolet Disk and Limb Imager to be flown aboard DMSP satellites for ionospheric and thermospheric remote sensing purposes. The algorithm described here uses the Lyman-alpha intensity and the intensities in two wavelength bands dominated by the Lyman-Birge-Hopfield band system from molecular nitrogen to estimate the characteristic energy and energy flux of electrons and protons in the auroral region. A simple auroral chemistry model is then used to estimate the peak density and height of the auroral E-layer. Uncertainties in the measured intensities and the algorithm parameters are estimated at each stage of the calculation and an estimate of the uncertainty in the calculated quantities is provided along with the quantities themselves. DTIC

N95-31278# Colorado Univ., Boulder, CO.

MODELING AND PARAMETERIZATION OF GRAVITY WAVE BREAKING, INTERACTIONS, AND INSTABILITY PROCESSES IN THE LOWER AND MIDDLE ATMOSPHERE Final Report, 1 Jan. 1992 - 31 Dec. 1993

David Fritts 8 Jul. 1994 5 p

(Contract F49620-92-J-0138)

(AD-A292740; AFOSR-95-0217TR) Avail: CASI HC A01/MF A01

The goal of this research were to address two sets of problems relating

to gravity wave effects in the lower and middle atmosphere. One approach was intended to apply analytic and pseudo-spectral collocation techniques for studies of wave excitation, instability, dissipation, and interaction processes thought to play important role in the circulation, structure, and variability throughout the atmosphere. A second effort was intended to apply our current understanding of the spectral character of the atmosphere motion field to the development of a parametrization scheme for the most important wave effects in large-scale models of the atmosphere.

Derived from text

N95-31335 Illinois Univ., Urbana-Champaign, IL.
SEISMIC STUDIES OF SUBDUCTED LITHOSPHERE Ph.D. Thesis
Mary Ann Glennon 1994 233 p
Avail: Univ. Microfilms Order No. DA9416362

This dissertation investigates dynamic processes in the mantle using source parameters, waveforms, and travel times associated with deep-focus earthquakes. First, I systematically determined the focal mechanisms and depths of all large-to-moderate sized earthquakes that occurred along the Kuril-Kamchatka in the past 30 years. My results show that the configuration of the subducting slab and the state of strain within the subducted lithosphere are,highly variable along both the strike and dip. In particular, I observed down-dip compressional strain in the northern and central portions of the arc between depths of 200 and 650 km. In these regions, deformation of the subducted slab near the base of the upper mantle is delineated by seismicity, probably in response to resistance encountered near the 670-km discontinuity. Second, I analyzed P and SH waveforms from eight deep-focus earthquakes in subduction zones of the northwestern Pacific to investigate whether complexities in broadband waveforms can be adequately explained by simple source models. Both sub-horizontal and sub-vertical ruptures are found within the same subducting system. At a depth of approximately 480 km, the length of one such rupture constrains the seismogenic thickness of the subducted slab to be approximately 40 km. Finally, using both digital and analog seismograms, I precisely measured approximately 400 arrival times of teleseismic P phases for seven earthquakes, most of which occurred since 1987 in the Kuril region, In this region, fast P azimuths residuals of deep-focus earthquakes at azimuths to the north-northeast and south-southwest are often interpreted as evidence for a deep penetrating slab. Along these azimuths, I also observed that P residuals of a deep focus earthquake in the northern Kuril-Kamchatka are significantly faster than those of both deep and shallow-focus earthquakes located beneath the Sakhalin Island near southern Kuril. My observations suggest that seismic wave speeds below depths of approximately 650 km vary along the arc. A synthesis of my results shows a correlation between the state of strain within subducted lithosphere in the upper mantle, as determined from source parameters, and the extent of slab penetration into the lower mantle, as inferred from travel-time analysis. Dissert. Abstr.

N95-31386# Texas Univ., El Paso, TX. Center for Geotechnical and Highway Materials Research.
IMPACT BEHAVIOR OF THE ACTIVE ZONE WITHIN A FROZEN SOIL PROFILE Final Report, Sep. 1990 - Aug. 1994
Niguel Picornell and Soheil Nazarian Feb. 1995 148 p
(Contract DAAL03-90-G-0196)
(AD-A292909; ARO-28201.1-GS-SAH) Avail: CASI HC A07/MF A02

The report describes a lab experiment with a pavement profile subject to a freeze/thaw cycle. The 5 x 5 x 5 ft lab specimen was instrumented with thermocouples, resistivity sensors, and 48 embedded geophones. The records of these sensors were used to delineate the progress of a freezing front through the soil profile and to implement a tomographic survey. At selected intervals, a 550-lb impulse, lasting 15 milliseconds, was imparted on a circular plate placed on the surficial asphalt layer, and the records at all geophone locations were recorded. The surface deflection bowl was used to backcalculate the moduli of all pavement layers present using a computer code: WESDEF. Then, the two sets of moduli from WESDEF and those found from the tomographic survey were used to predict the deflections at all geophone locations. The report describes the comparison of the measured with the predicted deflections to evaluate the capabilities of the backcalculation procedure in the presence of frozen and thawed soil layers. DTIC

N95-31535# Naval Command, Control and Ocean Surveillance Center, San Diego, CA. RDT and E Div.
MEASUREMENTS OF IONOSPHERIC VARIABILITY Final Report
R. A. Sprague Oct. 1994 34 p
(AD-A293495; NRAD-TD-2730) Avail: CASI HC A03/MF A01

This document reports on FY 94 progress in the ongoing measurement of ionospheric variability. Two measurement campaigns are described and results-to-date are presented. Comparisons of measured signal power are made to predictions from the PROPHET ionospheric propagation model. Examples of a new variability index for several ionospheric F-region parameters (foF2, MUF(3000), hmF2, and ymF2) are presented. DTIC

N95-31536# Aerospace Corp., El Segundo, CA. Technology Operations.
OXYGEN CHARGE STATE ABUNDANCE IN THE INNER MAGNETOSPHERE
J. F. Fennell, J. L. Roeder, M. Grande (Rutherford Appleton Lab., Chilton, England.), and B. Wilken (Max-Planck-Inst. fuer Aeronomie, Hanover, Germany.) 30 Jan. 1995 10 p
(Contract F04701-93-C-0094)
(AD-A293497; TR-95(5940)-4; SMC-TR-95-11) Avail: CASI HC A02/MF A01

The CRRES Magnetospheric Ion Composition Sensor (MICS) was used to obtain the relative oxygen charge state abundances in the earth's inner magnetosphere (3 less than L less than 7.5). These abundances were obtained for average and quiet (Kp less than or equal to 2+, absolute value of DST less than 11) conditions. They are presented as normalized spectra and compared to the predictions of Spjeldvik and Fritz (1978). These comparisons show that the observed spectra agree best with the Spjeldvik and Fritz predictions that assume an O+ source, at the high L boundary in their model, for oxygen with Q less than or equal to +3 but agree better with their predictions for a solar wind source, O(+6), for oxygen with Q greater than +3 on average. As expected, O(+) is the dominant oxygen ion at all times in the inner magnetosphere for energies greate r than 60 keV/Q. During average conditions the Q greater than or equal to +4 ions have fluxes comparable to O(+3) in the L = 4.5 - 7.5 region and are about 50% of the O(+3) fluxes in the L = 3 - 5 regions. Thus, the average O(+3) fluxes appear to represent a transition state between ionospheric and solar wind source oxygen. DTIC

N95-31560# Battelle Memorial Inst., Columbus, OH.
MONTE CARLO CODE FOR EVALUATING THE BOUNDARY LAYER ILLUMINATION AND RADIATION BALANCE MODEL (BLIRB)
Michael B. Wells Jan. 1995 92 p
(Contract DAAL03-91-C-0034)
(AD-A293963) Avail: CASI HC A05/MF A01

The AGGIE Monte Carlo code was modified by providing an output file giving information on the location and direction of motion for each source photon and collided photon during a run. The CUBCLD1 code was developed to analyze the collision file to determine the polar and azimuthal angle distribution of the photons escaping from each side of a box-shaped cloud. The AGGIE code was modified to evaluate hemispheric emission from a box-shaped cloud. The modified code was used to provide calculational data for both a sunlight source and ground and cloud emission. The results were compared to data reported by McKee and Cox; Harshvardhan, Weinmann, and Davies; and Zardecki. The comparison shows that AGGIE is capable of providing accurate radiation transport data used for validating the BLIRB code. DTIC

N95-31575# Phillips Lab., Hanscom AFB, MA.
PROCEEDINGS OF THE 16TH ANNUAL CONFERENCE ON ATMOSPHERIC TRANSMISSION MODELS, VOLUME 1
Gail P. Anderson and James H. Chetwynd 7 Apr. 1995 392 p Conference held in Hanscomb AFB, MA, 8-9 Jun. 1993 Limited Reproducibility: Document partially illegible
(AF Proj. 3054)
(AD-A293807; PL-TR-95-2042; ERP-1168-Vol-1) Avail: CASI HC A17/MF A04

This report contains the viewgraphs and other materials for the 37 papers presented at the 16th Annual Review Conference on Atmospheric Transmission Models held at the Geophysics Directorate, Phillips Laboratory (AFMC), Hanscom AFB, MA on 8-9 June 1993. DTIC

N95-31589# Army Research Lab., White Sands Missle Range, NM.
VALIDATION OF THE ATMOSPHERIC TRANSMISSION LARGE-AREA ANALYSIS SYSTEM (ATLAS) Final Report
Max P. Bleiweiss Feb. 1995 44 p
(AD-A293810; ARL-TR-544) Avail: CASI HC A03/MF A01

The Atmospheric Transmission Large-Area Analysis System (ATLAS) is a unique tool that has been under development at the U.S. Army Research Laboratory since the mid-1980's. ATLAS is a nonintrusive, passive technique capable of producing two-dimensional transmittance maps of a smoke cloud in a plane perpendicular to the main-optical-axis line of sight (LOS). (Off-axis LOS's are not perpendicular but are in a fan with an angular intersect determined by the overall field of view of the imager.) The accuracy and precision of the transmission values depends on the test conditions during which the measurements are made but can be defined through the error analyses discussed in this report. The spatial resolution of the resulting transmission maps is also test specific, but, typically, is of the order of a few tens of centimeters. The temporal resolution is determined by the video rates of the imaging system, which, after preliminary low-pass filtering, yields maps at 10 Hz. ATLAS is at the stage of development that it is used on a regular basis to support smoke/obscurant field tests. For this reason, a validation process was defined and implemented in 1989. This report documents the completion of that effort as a major milestone for the laboratory during FY92. In addition, the capabilities and limitations of the ATLAS technique are discussed in detail. DTIC

N95-31604# Phillips Lab., Hanscom AFB, MA.
PROCEEDINGS OF THE 16TH ANNUAL CONFERENCE ON ATMOSPHERIC TRANSMISSION MODELS, VOLUME 2
Gail P. Anderson and James H. Chetwynd 7 Apr. 1995 411 p Conference held in Hanscom AFB, MA, 8-9 Jun. 1993
(AF Proj. 3054)
(AD-A293806; PL-TR-95-2042; ERP-1168-Vol-2) Avail: CASI HC A18/MF A04

This report contains the viewgraphs and other materials for the 37 papers presented at the 16th Annual Review Conference on Atmospheric Transmission Models held on 8-9 June 1993. Topics include spectroscopy applications, non-LTE spectroscopy applications, structure algorithms, climatologies, and lidar applications. DTIC

N95-31610# Sandia National Labs., Albuquerque, NM.
DEVELOPMENT OF THE MULTI-LEVEL SEISMIC RECEIVER (MLSR)
G. E. Sleefe, B. P. Engler, P. M. Drozda, R. J. Franco, and Jeff Morgan Feb. 1995 231 p
(Contract DE-AC04-94AL-85000)
(DE95-008823; SAND-94-2162) Avail: CASI HC A11/MF A03

The Advanced Geophysical Technology Department (6114) and the Telemetry Technology Development Department (2664) have, in conjunction with the Oil Recovery Technology Partnership, developed a Multi-Level Seismic Receiver (MLSR) for use in crosswell seismic surveys. The MLSR was designed and evaluated with the significant support of many industry partners in the oil exploration industry. The unit was designed to record and process superior quality seismic data operating in severe borehole environments, including high temperature (up to 200 C) and static pressure (10,000 psi). This development has utilized state-of-the-art technology in transducers, data acquisition, and real-time data communication and data processing. The mechanical design of the receiver has been carefully modeled and evaluated to insure excellent signal coupling into the receiver. DOE

N95-31698# Northwest Research Associates, Inc., Bellevue, WA.
A PROTOTYPE IONOSPHERIC TOMOGRAPHY SYSTEM (ITS) Final Report, 30 Jul. 1991 - 30 Apr. 1994
E. J. Fremouw and J. A. Secan 15 Jun. 1994 32 p
(Contract F19628-90-C-0116)
(AD-A293015; NWRA-CR-94-R117; PL-TR-94-2190) Avail: CASI HC A03/MF A01

Northwest Research Associates has developed a prototype ionospheric tomography system (ITS) for use with the 'Transit' satellites of the U.S. Navy Navigation Satellite System (NNSS). The NNSS satellites transmit coherent signals at 150 and 400 MHz. The ITS consists of a data-collection subsystem made up of five newly designed, largely digital ITS 105 coherent radio receivers for recording dispersive phase between the two NNSS signals, a data retrieval subsystem, and a central processor. In addition to dispersive phase, the receivers measure the signal intensities, all at 50 samples per sec (sps), for recording signal scintillation due to scattering in medium-scale (of order km) plasma-density irregularities. The dispersive phase is smoothed to one sps for use as a measure of the path-integral of plasma density (the 'total electron content,' or TEC). Data may be retrieved from on-line personal computers associated with each receiver either on diskettes or by means of modems that constitute the primary data retrieval subsystem. The data retrieval subsystem also includes one 'data collection platform' for satellite relay of data from a remote station to CONUS for subsequent modem retrieval. The central processor consists of six FORTRAN programs developed for tomographic inversion of TEC data by means of a weighted, damped, least squares formulation of discrete inverse theory. This report describes application of that theory to the central processor and briefly describes the data collection and data retrieval subsystems. DTIC

N95-31718 Stanford Univ., CA.
ASPECTS OF THE MAGNETOSPHERIC AMPLIFICATION PHENOMENON IN DUCTED WHISTLER-MODE WAVES Ph.D. Thesis
Thomas A. Mielke 1994 88 p
Avail: Univ. Microfilms Order No. DA9414621

Interactions between ducted whistler-mode waves and energetic particles in the magnetosphere often lead to strong wave amplification, characteristically associated with such non-linear effects as the appearance of sidebands and triggering of free-running emissions. Experiments at Siple Station, Antarctica, were conducted to study the growth process. Data from the experiment on antenna polarization effects on coupling of wave energy into the whistler-mode agree well with theory. Results of experiments aimed at determining the wave-particle interaction underlying the observed wave growth were consistent with a gyroresonance interaction but not with a Landau resonance interaction. Experiments using pulses with parabolic rather than linear frequency chirps also produced wave growth, providing the capability to test theories of the effects of spatial variations on the wave growth process. A further observed phenomenon, that of a wave power threshold below which the growth and emissions effect does not occur, was also investigated. While very suggestive, data from an experiment on the effects of artificial noise on the threshold level fail to conclusively discriminate between competing theories of wave growth (involving trapped versus non-trapped electrons interacting with the whistler-mode wave).
Dissert. Abstr.

N95-31736 Illinois Univ., Urbana-Champaign, IL.
MIDDLE ATMOSPHERE STRUCTURE AND DYNAMICS: LIDAR STUDIES AT THE SOUTH POLE, SYOWA AND URBANA Ph.D. Thesis
Richard Laurence Collins 1994 158 p
Avail: Univ. Microfilms Order No. DA9416352

We present lidar observations of the middle atmosphere at the South Pole (90 deg S), Syowa (69 deg S, 39 deg E), and Urbana (88 deg W, 40 deg N). The South Pole stratospheric observations yield a high resolution data set of stratospheric temperature and polar stratospheric cloud (PSC) backscatter ratio profiles during the austral winter and spring of 1990. The observations show that the seasonal development of the clouds is primarily determined by the behavior of the temperature field. The PSC's are composed predominantly of nitric acid trihydrate particles. Correlation with frost-point measurements shows that nitric acid mixing ratios are depressed in the spring. The small-scale structure of the clouds appears to be controlled by gravity waves propagating upward through the clouds. Lidar measurements of the mesospheric Na layer at the South Pole in 1990 and Syowa in 1985 are used to characterize mesopause region gravity wave activity over Antarctica. The structure of the Na layer reflects the general circulation of the high-latitude mesopause. The monochromatic waves observed over Antarctica show the same general characteristics as those reported from other sites. The mean density variance of the gravity wave perturbations at the South Pole is similar to that observed at a variety of lower latitude sites. A distinct feature of the South Pole observations is the presence of strong coherent oscillations in the bottomside density contours of the Na layer close to the inertial frequency. Na Doppler/temperature lidar measurements of Na density and temperature at Urbana yield a high resolution seasonal data set of gravity wave activity. The direct measurement of the Brunt-Vaisala period allows accurate calculation of the horizontal velocity and vertical displacement from the density measurements. The

horizontal velocity and vertical displacement m-spectrum magnitudes and indices show considerable seasonal and nightly variability, behaviors which contradict the predictions of Linear Instability Theory and Scale-Dependent Diffusion Theory. We present a detailed comparison of the observations with the predictions of the Scale-Independent Diffusive Filtering Theory. The magnitudes of the m-spectrum, the form of the joint (m, omega) spectrum, the systematic relationships between the monochromatic gravity wave periods, wavelengths, and amplitudes agree remarkably well with those predicted for Scale-Independent Diffusive Filtering Theory. This observational study suggests that the complex nonlinear interactions of the gravity wave field can be modeled successfully as a diffusion process, where the diffusivity is a function of the total wave variance.

Dissert. Abstr.

N95-31743*# National Aeronautics and Space Administration. Marshall Space Flight Center, Huntsville, AL.

DE-1 OBSERVATIONS OF POLAR O(+) STREAM BULK PARAMETERS AND COMPARISON WITH A MODEL OF THE CENTRIFUGALLY-ACCELERATED POLAR WIND

C. Wing Ho and J. L. Horwitz 1995 14 p

(Grants NAG8-134; NAG8-822; NAG1-554; RTOP 432-20-00)

(NASA-CR-198930; NAS 1.26:198930) Avail: CASI HC A03/MF A01

A survey of bulk parameters of analyzable O(+) outward streams in the mid-altitude (3-4.7 R(sub E) geocentric distance) polar cap magnetosphere is obtained from measurements by the Retarding Ion Mass Spectrometer (RIMS) aboard the Dynamics Explorer-1 (DE-1) spacecraft. There is wide scatter in the obtained densities, but they do display discernible trends: the average O(+) density in these streams decreases from about 60 ions/cc at 3.5 R(sub E) to about 1 ion/cc at 4.6 R(sub E). The streaming velocities are somewhat more defined, and their average increases from about 8 km/s at 3.5 R(sub E) to about 12 km/s at 4.6 R(sub E). The densities and bulk velocities are inversely correlated. We have further compared these observational trends with model profiles for the centrifugally-accelerated polar wind as recently described by Horwitz et al. (1994). The large outflow velocities observed can be understood in part as centrifugally-driven by convection with ionospheric electric field magnitudes of the order 50-70 mV/m, perhaps including plasma expansion effects.

Author

N95-31820*# Aerospace Corp., Los Angeles, CA.

GLOBAL ULTRAVIOLET IMAGER (GUVI) INVESTIGATION Final Report, 8 Nov. 1993 - 7 Dec. 1994

Andrew B. Christensen Jan. 1995 106 p

(Contract NAS5-32572)

(NASA-CR-189430; NAS 1.26:189430) Avail: CASI HC A06/MF A02

This report covers the activities performed under NAS5-32572. The results of those activities are included in this Final Report. TIMED Science Objectives: (1) To determine the temperature, density, and wind structure of the MLTI (mixed layer thermal inertia), including the seasonal and latitudinal variations; and (2) To determine the relative importance of the various radiative, chemical, electrodynamical, and dynamical sources and sinks of energy for the thermal structure of the MLTI. GUVI Science Goals: (1) Determine the spatial and temporal variations of temperature and constituent densities in the lower thermosphere; and (2) Determine the importance of auroral energy sources and solar EUV (extreme ultraviolet) to the energy balance of the region.

Author

N95-31951 Massachusetts Univ., Lowell, MA.

UNDERDENSE HEATING OF THE IONOSPHERE USING OBLIQUE HIGH POWER HF RADIOWAVES Ph.D. Thesis

Yuming Huang 1994 126 p

Avail: Univ. Microfilms Order No. DA9423783

This paper presents a systematic analysis of changes in ionosphere caused by underdense heating using oblique incidence high power radiowave considering the influence of earth's magnetic field. The generalized definition of the plasma field and the differential equation of electron temperature considering the earth magnetic field are presented. The field strength, electron temperature, collision frequency and the heater-induced absorption in the lower ionosphere under different heating modes (X-Mode and O-Mode) in nighttime are investigated on a self-consistent basis. The behavior of sporadic-E layers under the interaction of high power radiowaves is also reviewed and the conditions of possible F-region heating is qualitatively analyzed. Numerical calculations are carried out to investigate how the incident electric field and plasma field change the electron temperature, collision frequency and heater-induced absorption for different heating powers, frequencies and elevation angles. The data and results from a Voice of America (VOA) high power heating experiments are presented. An explanation based on primary heating and secondary heating effects is presented to explain the observed results for both a series of former Soviet Union ionospheric modification experiments and our VOA experiments. The primary heating effect is produced in the lower ionosphere, resulting in additional absorption and leading to an instantaneous decrease of amplitude of the received signal. The secondary heating effect relates to the perturbation of electron density which is quite different at different altitudes for daytime and nighttime. The analysis of these effects considers both the magnitude of the change in the steady state and the time constant for these changes.

Dissert. Abstr.

N95-32080# Sandia National Labs., Albuquerque, NM.

PRELIMINARY DESIGN FOR ARCTIC ATMOSPHERIC RADIATIVE TRANSFER EXPERIMENTS

B. D. Zak, H. W. Church, K. Stamnes (Alaska Univ., Fairbanks, AK.), G. Shaw (Alaska Univ., Fairbanks, AK.), V. Filyushkin (Alaska Univ., Fairbanks, AK.), Z. Jin (Alaska Univ., Fairbanks, AK.), R. G. Ellingson (Maryland Univ., College Park, MD.), and S. C. Tsay (National Aeronautics and Space Administration. Goddard Space Flight Center, Greenbelt, MD.) 1995 3 p Presented at the 4th Conference on Polar Meteorology and Oceanography, Dallas, TX, 15-20 Jan. 1995

(Contract DE-AC04-94AL-85000)

(DE95-009580; SAND-95-0571C; CONF-950153-3) Avail: CASI HC A01/MF A01

If current plans are realized, within the next few years, an extraordinary set of coordinated research efforts focusing on energy flows in the Arctic will be implemented. All are motivated by the prospect of global climate change. SHEBA (Surface Energy Budget of the Arctic Ocean), led by the National Science Foundation (NSF) and the Office of Naval Research (ONR), involves instrumenting an ice camp in the perennial Arctic ice pack, and taking data for 12-18 months. The ARM (Atmospheric Radiation Measurement) North Slope of Alaska and Adjacent Arctic Ocean (NSA/AAO) Cloud and Radiation Testbed (CART) focuses on atmospheric radiative transport, especially in the presence of clouds. The NSA/AAO CART involves instrumenting a sizeable area on the North Slope of Alaska and adjacent waters in the vicinity of Barrow, and acquiring data over a period of about 10 years. FIRE (First ISCCP (International Satellite Cloud Climatology Program) Regional Experiment) Phase 3 is a program led by the National Aeronautics and Space Administration (NASA) which focuses on Arctic clouds, and which is coordinated with SHEBA and ARM. FIRE has historically emphasized data from airborne and satellite platforms. All three program anticipate initiating Arctic data acquisition during spring, 1997. In light of his historic opportunity, the authors discuss a strawman atmospheric radiative transfer experimental plan that identifies which features of the radiative transport models they think should be tested, what experimental data are required for each type of test, the platforms and instrumentation necessary to acquire those data, and in general terms, how the experiments could be conducted. Aspects of the plan are applicable to all three programs.

DOE

N95-32142# National Oceanic and Atmospheric Administration, Boulder, CO. Environmental Technology Lab.

FEASIBILITY OF TROPOSPHERIC WATER VAPOR PROFILING USING INFRARED HETERODYNE DIFFERENTIAL ABSORPTION LIDAR

Christian J. Grund, R. Michael Hardesty, and Barry J. Rye (Colorado Univ., Boulder, CO.) 3 Apr. 1995 61 p

(Contract DE-AI03-94ER-61761)

(DE95-009647; DOE/ER-61761/1) Avail: CASI HC A04/MF A01

Continuous, high quality profiles of water vapor, free of systematic bias, and of moderate temporal and spatial resolution, acquired over long periods at low operational and maintenance cost, are fundamental to the success of the ARM CART program. The development and verification of realistic climate model parameterizations for clouds and net radiation balance, and the correction of other CART site sensor observations for interferences due to the presence of water vapor are critically dependent on water vapor profile measurements. Application of profiles acquired with current techniques, have, to date, been limited by vertical resolution and uniqueness

of solution (e.g. high resolution infrared (IR) Fourier transform radiometry), poor spatial and temporal coverage and high operating cost (e.g. radiosondes), or diminished daytime performance, lack of eye-safety, and high maintenance cost (e.g. Raman lidar). Recent developments in infrared laser and detector technology make possible compact IR differential absorption lidar (DIAL) systems at eye-safe wavelengths. In the study reported here, we develop DIAL system performance models and examine the potential to solve some of the shortcomings of previous methods using parameterizations representative of current technologies. These models are also applied to diagnose and evaluate other strengths and weaknesses unique to the DIAL method for this application. This work is to continue in the direction of evaluating yet smaller and lower-cost laser diode-based systems for routine monitoring of the lower altitudes using photon counting detection methods. We regard the present report as interim in nature and will update and extend it as a final report at the end of the term of the contract. DOE

47 METEOROLOGY AND CLIMATOLOGY

Includes weather forecasting and modification.

N95-30403# Pennsylvania State Univ., University Park, PA.
MULTIPARAMETER RADAR MEASUREMENTS OF PRECIPITATION IN COMPLEX TERRAIN: METEOROLOGICAL AND HYDROLOGICAL APPLICATIONS Final Technical Report
Kultegin Aydin 9 Sep. 1994 18 p
(Contract DAAL03-89-K-0158)
(AD-A290786; ARO-26982.10-GS) Avail: CASI HC A03/MF A01

The primary objective of this research program was to investigate problems related to the use of a C-band polarimetric radar for estimating the rainfall in a region with complex terrain and where storm development and structure are highly variable and poorly understood. The anticipated experimental opportunities or conclusive testing of whether dual polarization C-band reflectivity factor measurements are adequate for quantitative estimation of rainfall under these conditions did not materialize. A number of associated problems were identified and subsequently investigated. Methods for reduction of clutter and noise in rainfall fields were developed. Techniques for translating radar-derived rainfall parameters to the ground were introduced. Storm runoff simulation studies were performed based on radar measurements in rainstorms. Tomographic imaging techniques, which use microwave propagation links, were studied for rainfall measurements in complex terrain. The effects of vertical reflectivity gradients and attenuation on radar measurements in rainfall were investigated and correction algorithms were tested for the latter. Attenuation in rainfall was observed as a major problem for C-band dual-polarization reflectivity factor measurements in rain. For operational purposes there are presently no demonstrated reliable attenuation correction methods. This indicates: that S-band frequencies, which suffer little or negligible rainfall attenuation, should be the choice for operational rainfall measuring radars at this time. DTIC

N95-30782*# Miami Univ., FL. Div. of Marine and Atmospheric Chemistry.
AEROSOL MEASUREMENTS OVER THE PACIFIC OCEAN IN SUPPORT OF THE IR AEROSOL BACKSCATTER PROGRAM Final Technical Report, 13 Aug. 1990 - 12 Feb. 1992
Joseph M. Prospero and Dennis L. Savoie [1995] 43 p
(Grant NAG8-841)
(NASA-CR-198925; NAS 1.26:198925) Avail: CASI HC A03/MF A01

The major efforts under NASA contract NAG8-841 included: (1) final analyses of the samples collected during the first GLOBE survey flight that occurred in November 1989 and collections and analysis of aerosol samples during the second GLOBE survey flight in May and June 1990. During the first GLOBE survey flight, daily samples were collected at four stations (Midway, Rarotonga, American Samoa, and Norfolk Island) throughout the month of November 1989. Weekly samples were collected at Shemya, Alaska, and at Karamea, New Zealand. During the second GLOBE survey flight, daily samples were collected at Midway, Oahu, American Samoa, Rarotonga, and Norfolk Island; weekly samples were collected at Shemya. These samples were all analyzed for sodium (sea-salt), chloride, nitrate, sulfate, and methanesulfonate at the University of Miami and for aluminum at the University of Rhode Island (under a subcontract). (2) Samples continued to be collected on a weekly basis at all stations during the periods between and after the survey flights. These weekly samples were also analyzed at the University of Miami for the suite of water-soluble species. (3) In August 1990, the results obtained from the above studies were submitted to the appropriate personnel at NASA Marshall Space Flight Center to become part of the GLOBE data base for comparison with data from instruments used aboard the aircraft. In addition, the data will be compared with data previously obtained at these stations as part of the Sea-Air Exchange (SEAREX) Program. This comparison will provide valuable information on the representativeness of the periods in terms of the longer term aerosol climatology over the Pacific Ocean. (4) Several publications have been written using data from this grant. The data will continue to be used in the future as part of a continuing investigation of the long-term trends and interannual variations in aerosol species concentrations over the Pacific Ocean. Author

N95-30832# Colorado State Univ., Fort Collins, CO. Dept. of Atmospheric Science.
FORECAST OF ATLANTIC SEASONAL HURRICANE ACTIVITY FOR 1994
William M. Gray 7 Jun. 1994 22 p Sponsored by NSF, and NOAA National Weather Service and Climate Analysis Center
Avail: CASI HC A03/MF A01

This paper presents details of the author's forecast for the amount of tropical cyclone activity expected to occur in the Atlantic Ocean region including the Caribbean Sea and the Gulf of Mexico during 1994. This forecast is based on the author and colleague's ongoing research relating the amount of seasonal Atlantic tropical cyclone activity to five basic physical parameters. These are: (1) the Quasi-Biennial Oscillation (QBO) of equatorial stratospheric wind; (2) the El Nino Southern Oscillation (ENSO); (3) West African Rainfall (AR) anomalies during the previous year; (4) anomalous west to east gradients of surface pressure and surface temperature (delta PT) in West Africa during February through May; and (5) Caribbean Basin Sea Level Pressure and Upper level Zonal Winds Anomalies (SLPA and ZWA respectively). Information received by the author up to 6 June 1994 indicates that the overall 1994 hurricane season should be a below average with about 5 hurricanes (average is 5.7), 9 named storms (average is 9.3) of at least tropical storm intensity, a total of about 15 hurricane days (average is 23), 35 named storm days (average is 48) and total Hurricane Destruction Potential (HDP) of 40 (average is 68). It is also expected that there should be only one intense or major hurricane of Saffir/Simpson intensity category 3, 4, or 5 this season (average is 2.2) and only about 1 major hurricane day (average is 4.5). These parameters represent an overall measure of total hurricane and tropical cyclone activity which is only about 70% of the last 44-year average. The amount of hurricane activity in this forecast has been reduced from that in the author's 19 November 1993 forecast and update discussion of 11 March 1994 at the New Orleans National Hurricane Conference. This forecast reduction is due to the slower than anticipated dissipation of the current El Nino, new estimates of West African February through May surface east-west pressure and temperature gradients, and to above average values of April-May Caribbean basin SLPA and ZWA values. This forecast will be updated on 5 August 1994, just before the beginning of the climatologically most active part of the hurricane season. The updated August forecast will make use of June and July data and should provide a more reliable forecast, particularly with regard to the African rainfall as it related to prospects for intense hurricane activity. The updated forecast will also provide a much better gage on the extent of expected dissipation of the current El Nino event. Author

N95-30842# Colorado State Univ., Fort Collins, CO. Dept. of Atmospheric Science.
SUMMARY OF 1993 ATLANTIC TROPICAL CYCLONE ACTIVITY AND VERIFICATION OF AUTHOR'S FORECAST. A YEAR OF UNANTICIPATED LIGHT HURRICANE ACTIVITY AND A POOR FORECAST: THE EXPECTED DISSIPATION OF THE EL NINO DID NOT TAKE PLACE AND CARIBBEAN BASIN SURFACE PRESSURE BECAME QUITE HIGH
William M. Gray 19 Nov. 1993 19 p Sponsored by NSF and NOAA
Avail: CASI HC A03/MF A01

This paper summarized the tropical cyclone (TC) activity which occurred in the Atlantic Basin during 1993, and verifies the author's seasonal forecast of this activity which were issued on 24 November of last year and updated

on 5 June and 4 August of this year. The 1993 hurricane season was relatively inactive with eight named storms (average 9.3) and four hurricanes (average 5.7). There was only one major (or intense) Saffir/Simpson category 3-4-5 hurricane (average is 2.2) and this storm (Emily) was only a marginal category 3 intensity for slightly less than one day. The seasonal total of hurricane days was only 10 (average is 23) and the seasonal total of named storm days was just 30 (average is 46). Only two systems (tropical cyclone Arlene in south Texas and Hurricane Emily near Cape Hatteras) affected the U.S. mainland. The author had forecast a substantially more active hurricane season. This forecast failure was primarily the result of the misjudgment of the remarkably persistent El Nino conditions which occurred this year and of the high Caribbean basin surface pressure which became established in August. The Caribbean pressure changes are believed to be unrelated to the El Nino and are a result of the intertropical covergence line being shifted southward over the South American continent. Additional unfavorable hurricane conditions included a continuing West Sahel drought. It is quite unusual for an El Nino to last through three consecutive seasons as the current El Nino event has. Actually, warm water has persisted in the equatorial Pacific through the last four hurricane seasons. The El Nino is the most dominant of the climate influences affecting Atlantic hurricane activity, tending to strongly suppress the activity. The long lasting (1991-1993) El Nino conditions had finally started weakening in June and July and this weakening was expected to continue. But, beginning in late August, a surprising resurgence of warming SST conditions occurred in the eastern Pacific. This warming led to a stronger upper tropospheric trough over the western Atlantic and Caribbean sea, and with it, enhanced vertical wind shear. All tropical cyclone activity ended after the 21st of September, a date which is normally only 60% of the way through the Atlantic cyclone season. Author

N95-30844# Colorado State Univ., Fort Collins, CO. Dept. of Atmospheric Science.

EARLY AUGUST UPDATED FORECAST OF ATLANTIC SEASONAL HURRICANE ACTIVITY FOR 1994

William M. Gray 5 Aug. 1994 24 p Sponsored by NSF and Climate Analysis Center

Avail: CASI HC A03/MF A01

This paper presents details of the author's forecast for the amount of tropical cyclone activity expected to occur in the Atlantic Ocean region including the Caribbean Sea and the Gulf of Mexico during 1994. This forecast is based on the author and colleague's ongoing research relating the amount of seasonal Atlantic tropical cyclone activity to five basic physical parameters. These are: (1) the quasi-Biennial Oscillation (QBO) of equatorial stratospheric wind; (2) the El Nino Southern Oscillation (ENSO); (3) West African Rainfall (AR) anomalies; (4) anomalous west to east gradients of surface pressure and surface temperature (delta PT) in West Africa during February through May; and (5) Caribbean Basin Sea Level Pressure and Upper Level Zonal Wind Anomalies (SLPA and ZWA respectively). Information received by the author through 4 August 1994 indicates that the overall 1994 hurricane season should be below average with about 4 hurricanes (average is 5.7), 7 named storms (average is 9.2) of at least tropical storm intensity, a total of about 12 hurricane days (average is 23), 30 named storm days (average is 46) and total Hurricane Destruction Potential (HDP) of 35 (average is 69). It is also expected that there should be only one intense or major hurricane of Saffir/Simpson intensity category 3, 4 or 5 this season (average is 2.1) and only about 1 major hurricane day (average is 4.5). These parameters represent an overall measure of total hurricane and tropical cyclone activity which is only about 55% of the last 44-year average. The amount of hurricane activity in this forecast has been reduced from that in the author's 19 November 1993 forecast and update 7 June 1994 forecast. This forecast reduction is due to the slower than anticipated dissipation of the current El Nino, new estimates of below average West African rainfall, and much above average values of June-July Caribbean basin sea level pressure. Author

N95-30951# Nevada Univ., Reno, NV.

CLOUD CONDENSATION NUCLEI MEASUREMENTS IN SHIPTRAILS Annual Report, 1 Feb. 1994 - 31 Jan. 1995

James G. Hudson 13 Apr. 1995 3 p

(Contract N00014-94-1-0339)

(AD-A293302) Avail: CASI HC A01/MF A01

At the end of May the CCN spectrometer and calibration equipment were transported to Monterey for the field project. The equipment operated successfully for most of the time on 11 of the 12 research flights. For most of the time the CCN spectrometer directly monitored the ambient CCN spectrum. Occasionally, the sample aerosol was heated to obtain particle volatility. Sometimes the aerosol was size classified to obtain the relative solubility of the CCN. During some of the in-cloud passes the CCN spectrometer monitored the residue from the cloud droplets from the counterflow virtual impactor (CVI) which allows a precise determination of the CCN that are actually within the cloud droplets. DTIC

N95-30976# Army Engineer Waterways Experiment Station, Vicksburg, MS.

QTSAW (QUICK TYPHOON SURGE AND WAVES). WAVE INFORMATION STUDIES OF US COASTLINES Final Report

Barbara A. Tracy Jan. 1995 42 p

(AD-A293172; WES-WIS-31) Avail: CASI HC A03/MF A01

This report is a user's guide for the personal-computer (PC)-based system called QTSAW (Quick Typhoon Surge and Waves). The programs and data to operate this system were developed on a 386 (33-MHz) PC and are included on two computer diskettes. The data set is the storm parameter data for all the typhoons in the Guam area (10 deg by 17 deg N latitude and 141.5 by 148.5 deg E longitude) from 1945-1991. The programs in the system create wind and pressure fields from the input storm data. These wind and pressure fields are then used as input to programs that calculate the wave and surge conditions for the Island of Guam. Several graphical display programs are available for the output results. This system was set up as part of the Wave Information Studies to help meet the needs of the Pacific Ocean Division, U.S. Army Corps of Engineers. DTIC

N95-31123*# Science Applications, Inc., Bellevue, WA.

NASA TROPICAL RAINFALL MEASUREMENT MISSION (TRMM): EFFECTS OF TROPICAL RAINFALL ON UPPER OCEAN DYNAMICS, AIR-SEA COUPLING AND HYDROLOGIC CYCLE Final Report

Gary Lagerloef, Antonio J. Busalacchi (National Aeronautics and Space Administration. Goddard Space Flight Center, Greenbelt, MD.), W. Timothy Liu (Jet Propulsion Lab., California Inst. of Tech., Pasadena, CA.), Roger B. Lukas (Hawaii Univ., Hilo, HI.), Pern P. Niiler (California Univ., San Diego, CA.), and Calvin T. Swift (Massachusetts Univ., Amherst, MA.) Jan. 1995 9 p

(Contract NAS5-31358)

(NASA-CR-189437; NAS 1.26:189437) Avail: CASI HC A02/MF A01

This was a Tropical Rainfall Measurement Mission (TRMM) modeling, analysis and applications research project. Our broad scientific goals addressed three of the seven TRMM Priority Science Questions, specifically: What is the monthly average rainfall over the tropical ocean areas of about 10(exp 5) sq km, and how does this rain and its variability affect the structure and circulation of the tropical oceans? What is the relationship between precipitation and changes in the boundary conditions at the Earth's surface (e.g., sea surface temperature, soil properties, vegetation)? How can improved documentation of rainfall improve understanding of the hydrological cycle in the tropics? Author

N95-31128*# Albany Univ., Albany, NY. The Research Foundation.

LAWS HURRICANE STUDIES Final Report, 21 Sep. 1993 - 20 Sep. 1994

John Molinari Feb. 1995 5 p

(NASA Order S-12870-F)

(NASA-CR-189438; Rept-320-6597B; NAS 1.26:189438) Avail: CASI HC A01/MF A01

The Laser Atmospheric Wind Sounder (LAWS) has recently been deselected from the Earth Observing System (EOS). A broad range of orbital altitudes and laser power are being considered for future wind lidar missions. As a result, as was anticipated in the proposed work, it may be impossible to meaningfully study tropical cyclones with lidar wind data because data coverage (i.e., swath width) is insufficient. Research on this grant has focused on how to maximize the benefits of a wind lidar regardless of the choice of platform or laser. Our studies have shown that major unsolved problems in tropical meteorology relate to the structure, dynamics, and role in tropical cyclogenesis of 'easterly waves'. These disturbances exist almost everywhere in the global subtropics. Results are described that focus upon easterly wave impacts on eastern Pacific tropical

cyclogenesis. The availability of wind lidar data would create tremendous opportunities for the study of these waves and their role in the general circulation. Author

N95-31453# Colorado State Univ., Fort Collins, CO.
CLOUDS: THEIR PREDICTION AND SIMULATION Final Report, 1 Jun. 1991 - 31 Dec. 1994
W. R. Cotton 24 Feb. 1995 14 p
(Grant AF-AFOSR-0269-91)
(AD-A292864) Avail: CASI HC A03/MF A01

Physically-based cloud forecasting algorithms have been developed in support of the long range goal of developing a comprehensive mesoscale numerical prediction cloud forecast system. Algorithms for forecasting cirrus clouds include development of both heterogeneous and homogeneous ice nucleation schemes, a double-moment ice crystal distribution parameterization, liquid and ice saturation calculations at very cold temperatures, and of radiative properties of cirrus. The impact of these algorithms on mesoscale prediction of cirrus has been evaluated for a number of FIRE 1 and 2 cirrus data sets. One of the FIRE stratus cases was simulated to evaluate various boundary layer cloud fractional coverage schemes. The best performing schemes have been interfaced with the RAMS radiation codes for forecasting boundary layer stratus. A convective cloud parameterization scheme designed for use in mesoscale models has been tested against data observed during the Cape over South Florida. Improvements to the cumulus parameterization scheme are now being made and tested. A new two-moment microphysics scheme has been developed, implemented and tested in RAMS. The additional degrees of freedom in this scheme allow a more realistic prediction of cloud microstructure and corresponding radar reflectivities and optical depths. DTIC

N95-31465# Massachusetts Inst. of Tech., Lexington, MA.
INITIAL EVALUATION OF THE OREGON STATE UNIVERSITY PLANETARY BOUNDARY LAYER COLUMN MODEL FOR ITWS APPLICATIONS
J. L. Keller, F. W. Wilson, and C. B. Smith 13 Apr. 1995 28 p
(Contracts DTFA01-91-Z-02036; F19628-95-C-0002)
(AD-A293775; ATC-233) Avail: CASI HC A03/MF A01

The Federal Aviation Administration (FAA) Integrated Terminal Weather System (ITWS) is supporting the development of products important for air traffic control in the terminal area. Some ITWS products will allow air traffic managers to anticipate operationally significant short-term (0-30 min) changes in ceiling and visibility (C&V) and aircraft separations necessary to avoid encounters with wake vortices. Development of such products exploits data that will by available from new FAA terminal area sensor systems. These sensor systems include Terminal Doppler Weather Radar (TDWR), Next Generation Weather Radar (NEXRAD), the Meteorological Data Collection and Reporting System (MDCRS), and the Automated Surface Observing System (ASOS). A Dynamic Atmospheric Vertical Structure Nowcast System (DAVS-NS) is being developed that will add value to ITWS by providing current analyses and short-term forecasts of the vertical atmospheric structure focused at specific sites within the terminal domain. This report summarizes the initial evaluation of the Oregon State University one-dimensional boundary layer model for its potential role within a DAVS-NS. DTIC

N95-31522# Atmospheric and Environmental Research, Inc., Cambridge, MA.
SUPPORT OF ENVIRONMENTAL REQUIREMENTS FOR CLOUD ANALYSIS AND ARCHIVE (SERCAA): DATABASE MANAGEMENT FACILITY Final Report, 28 Dec. 1990 - 30 Sep. 1994
Charles F. Ivaldi, Joseph Doherty, Courtney C. Scott, and Gary B. Gustafson 20 Nov. 1994 83 p
(Contract F19628-91-C-0011)
(AD-A293938; PL-TR-94-2290) Avail: CASI HC A05/MF A01

A satellite database management facility was developed to support implementation and real-data testing of new multisource, multi spectral satellite-based cloud analysis algorithms. Cloud algorithms were produced separately under Phase 1 of the Support of Environmental Requirements for Cloud Analysis and Archive (SERCAA) research and development project. The objective of the database project was to develop a unified capability to store, update, retrieve and catalog satellite and supporting data plus derived algorithm products. Data processing and storage requirements dictated a centralized database management facility capable of operating over a network of processing and mass storage systems. Based on these requirements, specifications were generated for a suitable database management facility. This was followed by development and implementation of software and hardware on the Air Force Interactive Meteorological System (AIMS) used by the Atmospheric Sciences Division at the Air Force Phillips Laboratory for SERCAA algorithm testing. Key features of the database management facility include simultaneous access to the database by multiple users, support for interactive and programmed queries, easy access to satellite and ancillary data from within application programs, network access to the database from multiple-vendor computers, and support for both on-line and removable data storage media. DTIC

N95-31524# Air Force Environmental Technical Applications Center, Scott AFB, IL.
EQUATORIAL AFRICA: A CLIMATOLOGICAL STUDY
Christopher A. Donahue, Kathleen M. Traxler, Kenneth R. Walters, Sr., John W. Louer, III, and Michael T. Gilford Mar. 1995 276 p
(AD-A293956; USAFETAC/TN-95/001) Avail: CASI HC A13/MF A03

A climatological study of Equatorial Africa, a region that comprises Senegal, Gambia, Guinea-Bissau, Guinea, Sierra Leone, Liberia, Ivory Coast, Ghana, Togo, Benin, Nigeria, Cameroon, Equatorial Guinea, Gabon, Congo, Central African Republic, Rwanda, Burundi, Uganda, Tanzania, Kenya, Malawi, the southern parts of Mauritania, Mali, and Niger, and the northern parts of Angola, Mozambique, Zaire, and Zambia is presented. After describing the geography and major meteorological features of the entire region, the study discusses the climatic controls of each of Equatorial Africa's eight 'zones of climatic commonality' in detail. Each 'season' is defined and discussed in considerable detail, to include general weather, clouds, visibility, winds, precipitation, temperature, and other hazards. DTIC

N95-31541# City Coll. of the City Univ. of New York, NY.
MODERN METHODS IN METEOROLOGICAL AND OCEANOGRAPHIC DATA ACQUISITION AND ANALYSES
Ward Hindman 25 Apr. 1995 15 p
(Contract N00014-93-1-0486)
(AD-A293884) Avail: CASI HC A03/MF A01

The objectives of this contract are to educate and train students to collect and analyze meteorological and oceanographic data using the developing CCNY (City College of New York) weather station computer system; to purchase the necessary software and hardware to keep the system up-to-date; and to teach students scientific programming. DTIC

N95-31571# Naval Postgraduate School, Monterey, CA.
VALIDATION OF SPECIAL SENSOR MICROWAVE/IMAGER OCEAN SURFACE WIND RETRIEVALS IN EQUATORIAL REGIONS M.S. Thesis
Elton G. Sayward Dec. 1994 77 p
(AD-A293750) Avail: CASI HC A05/MF A01

The Fleet Numerical Meteorology and Oceanography Center (FNMOC) has the charter to provide Special Sensor Microwave/Imager (SSM/I) data to DOD and NOAA users. This tasking has led to new methods for processing SSM/I data being developed to improve NAVY SSM/I products, in particular the ability to remotely sense ocean surface winds. Currently, alternative SSM/I ocean surface wind speed algorithms include 'physical' or 'statistical' methods. Typically physical retrievals require additional data, e.g., cloud liquid water, along with SSM/I brightness temperatures while statistical methods are stand alone algorithms based on brightness temperature only. In this study four candidate wind retrieval methods proposed at the SSM/I Algorithm Symposium (June 1993) for implementation at FNMOC are examined. Limitations of the SSM/I calibration/validation data set to the midlatitude region prompted the requirement to develop a tropical data set for evaluation of alternative algorithms. Comparison of SSM/I wind retrieval methods reveal neural networks display a high wind speed bias for winds above 11 m/s and a low wind speed bias for winds below 3 m/s. The current FNMOC operational algorithm may overestimates wind speeds when water vapor is greater than 50 kg/m(exp 2). Partitioning of SSM/I retrieved wind speeds according to accuracy is by accomplished when using brightness temperature received at 37 GHz. DTIC

N95-31577# Naval Research Lab., Washington, DC.
A NUMERICAL STUDY OF THE EFFECT OF THE GULF STREAM AND THE APPALACHIAN MOUNTAINS ON CAROLINA COASTAL FRONTOGENESIS
Liang Xu, Sethu Raman, and Rangarao V. Madala 27 Apr. 1995 21 p
(NR Proj. RR0-3303)
(AD-A293765; NRL/FR/7220-95-9774) Avail: CASI HC A03/MF A01

Three numerical experiments were conducted to understand the role of the Gulf Stream and the Appalachian Mountains on the formation of coastal frontogenesis along the mid-Atlantic coast during the winter months. A 3-dimensional, 10-layer, 1-way interactive, triple-nested hydrostatic model was used. The model physics includes dry convective adjustment, explicit large-scale precipitation, parameterized convective-scale circulations, and parameterized boundary layer physics using a similarity theory formulation. Initial conditions for the numerical model are obtained from the Second Intensive Observation Period (IOP-2) of the Genesis of Atlantic Lows Experiment (GALE). Results of the numerical experiments show that the Gulf Stream plays a significant role in developing coastal frontogenesis through transfer of large amounts of sensible and latent heats to the cold, dry atmospheric air of Arctic origin. The Gulf Stream is also found to be crucial in producing convective precipitation along the Carolina coast. On the other hand, the Appalachian Mountains, which are responsible for cold air damming, are found to play only a minor role in the coastal frontogenesis. DTIC

N95-31587# Federal Aviation Administration, Atlantic City, NJ.
THE ATC OPERATIONAL EVALUATION OF THE PROTOTYPE INTEGRATED TERMINAL WEATHER SYSTEM (ITWS) AT DALLAS/FORT WORTH AND ORLANDO AIRPORTS (MAY-SEPTEMBER 1993) Final Technical Note
Thomas M. Weiss Mar. 1995 119 p
(AD-A293808; DOT/FAA/CT-TN95/1) Avail: CASI HC A06/MF A02

The Integrated Terminal Weather System (ITWS) was developed by Massachusetts Institute of Technology/Lincoln Laboratory (MITILL). The ITWS processor acquires data from Federal Aviation Administration (FAA) and National Weather Service (NWS) weather sensors in the terminal area and provides an integrated set of safety and planning weather products to air traffic personnel. An operational evaluation of the ITWS functional prototype was performed from May through September, 1993 at Dallas/Fort Worth (DFW) and Orlando (MCO) airports. ITWS geographical situation displays (6 SD) were located both at DFW and MCO as well as the Fort Worth Air Route Control Center (ARTCCXZFW) and Jacksonville ARTCC (ZJX). The purpose of testing ITWS at these sites was to evaluate various technical and operational issues of IIWS weather products and their display and usability on the GSD. DTIC

N95-31675# State Univ. of New York, Albany, NY. Dept. of Atmospheric Science.
DIAGNOSIS OF THE KINEMATICS AND DYNAMICS OF RAPIDLY DEVELOPING MARITIME CYCLONES Progress Report, 1 Apr. 1994 - 31 Mar. 1995
31 Mar. 1995 6 p
(Contract N00014-92-J-1532)
(AD-A293919) Avail: CASI HC A02/MF A01

The following tasks have been completed: (1) identification of planetary-scale flow signatures preceding and coincident with explosive western North Atlantic cyclogenesis; (2) examination of the relationship between the large-scale flow, the evolution of upper troughs, and the degree of surface development during ERICA; (3) investigation of the life cycles of upper-tropospheric troughs during ERICA; (4) analysis of factors modulating surface development; (5) application of high-resolution diagnostics illustrating upper-tropospheric trough genesis and evolution.
Derived from text

N95-31721 Florida State Univ., Tallahassee, FL.
BRIGHTNESS TEMPERATURE SIMULATIONS FOR THE PHYSICAL AND SYNOPTIC INTERPRETATION OF ADVANCED MICROWAVE SOUNDING UNIT MOISTURE CHANNELS Ph.D. Thesis
Bradley Moore Muller 1993 206 p
Avail: Univ. Microfilms Order No. DA9416153

Radiative transfer simulations are performed in three phases to determine how water vapor and clouds affect passive brightness temperatures (T(sub B)s) of moisture sounding channels on the Advanced Microwave Sounding Unit (AMSU). Phase 1 employs idealized profiles of water vapor, cloud liquid water, and cloud ice as input to the radiative transfer model to investigate how AMSU frequencies at 23.8, 89, 157, 176, 180 and 182 GHz respond to clear and cloudy non-precipitating atmospheres. Phase 2 represents an effort to verify the microwave radiative transfer approach using observed data from an aircraft-mounted prototype radiometer. Phase 3 of the research employs output from a mesoscale model simulation of the ERICA IOP4 cyclone in an effort to gain insight about the synoptic interpretation of microwave water vapor image signatures. Model soundings are used in the radiative transfer code to generate synthetic 182 GHz imagery, as if a satellite were viewing the model atmosphere. In Phase 1, T(sub B)s at 23.8 GHz and 89 GHz are more strongly affected by 'altostratus' liquid clouds than by 'cirrus' clouds for equivalent water paths. Channels near 157 and 183 GHz are more strongly affected by ice clouds. Phase 2 results indicate that the radiative transfer approach is adequate for simulating observed TBS, and that TBS at the relatively high microwave frequencies considered here are very sensitive to the ice particle size distribution. Phase 3 results show that 50 percent of the radiance contribution at 182 GHs for clear atmospheres emanates from the upper 0.35 mm of precipitable water, that is, above 380-400 mb, while 90 percent comes from the top 1.5 mm. A warm radiometric feature occurs near a tropopause fold. Dry upper and middle tropospheric air over the extremely dry formerly stratospheric air brought down by the tropopause fold allow the simulated 182 GHz channel to sense the strong vertical moisture gradient below 700 mb, at the bottom edge of the upper level frontal zone. Dissert. Abstr.

N95-31726# National Renewable Energy Lab., Golden, CO.
MEXICO WIND RESOURCE ASSESSMENT PROJECT
Marc N. Schwartz and Dennis L. Elliott May 1995 12 p Presented at the 25th Annual Conference and Exhibition on Wind Power, Washington, DC, 26-30 Mar. 1995
(Contract DE-AC36-83CH-10093)
(DE95-009202; NREL/TP-441-7809; CONF-950309-5) Avail: CASI HC A03/MF A01

A preliminary wind energy resource assessment of Mexico that produced wind resource maps for both utility-scale and rural applications was undertaken as part of the Mexico-U.S. Renewable Energy Cooperation Program. This activity has provided valuable information needed to facilitate the commercialization of small wind turbines and windfarms in Mexico and to lay the groundwork for subsequent wind resource activities. A surface meteorological data set of hourly data in digital form was utilized to prepare a more detailed and accurate wind resource assessment of Mexico than otherwise would have been possible. Software was developed to perform the first ever detailed analysis of the wind characteristics data for over 150 stations in Mexico. The hourly data set was augmented with information from weather balloons (upper-air data), ship wind data from coastal areas, and summarized wind data from sources in Mexico. The various data were carefully evaluated for their usefulness in preparing the wind resource assessment. The preliminary assessment has identified many areas of good-to-excellent wind resource potential and shows that the wind resource in Mexico is considerably greater than shown in previous surveys. DOE

N95-32184*# National Aeronautics and Space Administration. Ames Research Center, Moffett Field, CA.
USE OF ARM MEASUREMENTS TO IMPROVE RADIATIVE TRANSFER MODELS USED IN CLIMATE MODELS
Robert W. Bergstrom, S. Kinne, O. B. Toon, Doug Westphal, Tony Clough, and Eli Mlawer (Atmospheric and Environmental Research, Inc., Cambridge, MA.) 31 Jul. 1995 4 p Prepared in cooperation with Bay Area Environmental Research Inst., San Francisco, CA
(Contract NCC2-817)
(NASA-CR-199014; NAS 1.26:199014) Avail: CASI HC A01/MF A01

The demands of accurate predictions of radiative transfer for climate applications are well-documented. While much effort is being devoted to evaluating the accuracy of the GCM radiative transfer schemes, the problem of developing accurate, computationally efficient schemes for climate models still remains. This paper discusses our efforts in developing accurate and fast computational methods for global and regional climate models.
Author

N95-32315 National Defence Research Establishment, Linkoeping (Sweden).
SPECTRAL SKY BACKGROUND IN THE IR: MEASUREMENTS WITH FTIR [SPEKTRAL HIMMELSBAKGRUND I IR-OMRADET: MAETNINGAR MED FTIR]
P. Nilsson Sep. 1994 95 p In SWAHILI
(PB95-222998; FOA-R-94-00026-3.1-SE) Avail: Issuing Activity (National Technical Information Service (NTIS))

Measurements of the sky spectral background in the region 750-2500/cm (4-13 micrometers) have been performed with an FTIR spectrometer. The measurements were made at different weather conditions and at different elevations over the horizon. In order to investigate the correlation between the sky radiance and the different weather parameters, a weather station was used at all measurements. The most apparent thing in the results is the considerable influence of the clouds on the sky radiance. Clouds generally act like greybodies but when they increase in thickness they emit like blackbodies. For a clear sky the radiance is high just over the horizon and then drops as the elevation increases towards zenith. This is because the aerosol concentration is higher at the ground and because the path through the atmosphere is longer for small elevations. The measurement results show a good agreement with results from calculations with the atmospheric program Modtran. NTIS

48 OCEANOGRAPHY

Includes biological, dynamic, and physical oceanography; and marine resources.

For related information see also *43 Earth Resources and Remote Sensing.*

N95-30396# Naval Postgraduate School, Monterey, CA.
YELLOW SEA THERMAL STRUCTURE M.S. Thesis
Charles R. Fralick, Jr. Sep. 1994 95 p
(AD-A291159) Avail: CASI HC A05/MF A01

There exists a need in the oceanography community to be able to produce climatologies of remote or poorly sampled shallow water areas through remote sensing techniques. Our goal was to construct a three-dimensional thermal structure of the Yellow Sea based primarily upon sea surface temperature data. The ability to do this successfully could lead the way to applying these techniques elsewhere using remotely sensed SST. The shallow water and dynamic conditions of the Yellow Sea made it an ideal study area. The large MOODS observational data set for the area provided us with 15,000 observations from 1929 to 1991. For the winter months we used regression techniques on the predominantly well-mixed, vertically isothermal profiles with excellent results. For the summer we applied a feature model which extracted physically significant depths and gradients from the observations. These modeled data were statistically compared with mixed results indicating little link between SST and mixed-layer depth but good correlation between SST and thermocline gradient. We believe interannual variability and significant sampling errors in our data contributed to our mixed results. Overall, we feel our approach is robust and has potential for further applications providing data quality issues are addressed. DTIC

N95-30457# Technische Univ., Delft (Netherlands).
REMOVAL OF SCATTERED SURFACE WAVES FROM SEISMIC DATA Ph.D. Thesis
B. Blonk 16 Jan. 1995 141 p
(PB95-197802; ISBN-90-9007865-7) Avail: CASI HC A07/MF A02

Exploration seismology aims at the detection of oil- and gas-reservoirs. Therefore, detailed knowledge about the structure and rock properties of the sub-surface layers is required, especially about the deep layers. This knowledge is often obtained from seismic waves that have been reflected at the deep layers. The properties of the shallow subsurface often vary significantly. Those strong variations can give rise to complex near-surface scattered waves that depreciate the quality of land seismic data; these waves contain no information about the deep subsurface and can mask the reflections from the deep layers. In this thesis, a 3D elastodynamic inverse scattering method is presented for eliminating these near-surface scattered waves. The method is based on the estimation of a suitable shallow scattering model by a data-fitting procedure, using as much seismic data as possible. NTIS

N95-30711 Defence Science and Technology Organisation, Melbourne (Australia). Aeronautical and Maritime Research Lab.
OCEAN MASS DENSITY CALCULATIONS FROM TEMPERATURE AND SALINITY DATA
Graham D. Furnell Jun. 1994 38 p
(DSTO-TR-0023; AR-008-538) Copyright Avail: Issuing Activity

A knowledge of the mass density stratification of ocean waters is a fundamental requirement when performing calculations in the field of dynamical oceanography. Experimentally, ocean temperature and salinity stratifications can be conveniently measured. In this report, details are given of a computational procedure which uses the International Equation of State of Sea Water (IES 80) to calculate an ocean mass density stratification from temperature and salinity data. The results of calculations are presented which yield mass density stratifications at a number of locations in waters to the West and NorthWest of Australia. Author

N95-30857*# National Aeronautics and Space Administration. Goddard Space Flight Center, Greenbelt, MD.
SeaWiFS TECHNICAL REPORT SERIES. VOLUME 29: SeaWiFS CZCS-TYPE PIGMENT ALGORITHM
Stanford B. Hooker, ed., Elaine R. Firestone, ed. (General Sciences Corp., Laurel, MD.), James Aiken (Plymouth Marine Lab., England.), Gerald F. Moore (Plymouth Marine Lab., England.), Charles C. Trees (San Diego State Univ., San Diego, CA.), and Dennis K. Clark (National Oceanic and Atmospheric Administration, Camp Springs, MD.) Apr. 1995 37 p
(NASA-TM-104566; Rept-95B00096; NAS 1.15:104566) Avail: CASI HC A03/MF A01

The Sea-viewing Wide Field-of-view Sensor (SeaWiFS) mission will provide operational ocean color that will be superior to the previous Coastal Zone Color Sensor (CZCS) proof-of-concept mission. an algorithm is needed that exploits the full functionality of SeaWiFS whilst remaining compatible in concept with algorithms used for the CZCS. This document describes the theoretical rationale of radiance band-radio methods for determining chlorophyll alpha and other important biogeochemical parameters, and their implementation for the SeaWiFS mission. Pigment interrelationships are examined to explain the success of the CZCS algorithms. In the context where chlorophyll alpha absorbs only weakly at 520 nm, the success of the 520 nm to 550 nm CZCS band ratio needs to be explained. This is explained by showing that in pigment data from a range of oceanic provinces chlorophyll alpha (absorbing at less than 490 nm), carotenoids (absorbing at greater than 460 nm), and total pigment are highly correlated. Correlations within pigment groups particularly photoprotectant and photosynthetic carotenoids are less robust. The sources of variability in optical data re examined using the NIMBUS Experiment Team (NET) bio-optical data set and bio-optical model. In both the model and NET data, the majority of the variance in the optical data is attributed to variability in pigment (chlorophyll alpha, and total particulates, with less than 5% of the variability resulting from pigment assemblage. The relationships between band ratios and chlorophyll is examined analytically, and a new formulation based on a dual hyperbolic model is suggested which gives a better calibration curve than the conventional log-log linear regression fit. The new calibration curve shows that 490:555 ratio is the best single-band ratio and is the recommended CZCS-type pigment algorithm. Using both the model and NET data, a number of multiband algorithms are developed; the best of which is an algorithm based on the 443:555 and 490:555 ratios. From model data, the form of potential algorithms for other products, such as total particulates and dissolved organic matter (DOM), are suggested. Author

N95-30859*# Jet Propulsion Lab., California Inst. of Tech., Pasadena, CA.
JPL PHYSICAL OCEANOGRAPHY DISTRIBUTED ACTIVE ARCHIVE CENTER (PO.DAAC) DATA AVAILABILITY, VERSION 1-94
21 Feb. 1994 57 p Revised
(Contract NAS7-918; RTOP 428-33-07-06-86)
(NASA-CR-198871; JPL-Publ-90-49-Rev-5; NAS 1.26:198871) Avail: CASI HC A04/MF A01

The Physical Oceanography Distributed Active Archive Center (PO.DAAC) archive at the Jet Propulsion Laboratory (JPL) includes satellite data sets

for the ocean sciences and global-change research to facilitate multidisciplinary use of satellite ocean data. Parameters include sea-surface height, surface-wind vector, sea-surface temperature, atmospheric liquid water, and integrated water vapor. The JPL PO.DAAC is an element of the Earth Observing System Data and Information System (EOSDIS) and is the United States distribution site for Ocean Topography Experiment (TOPEX)/POSEIDON data and metadata. Author

N95-30918# Woods Hole Oceanographic Inst., MA.
BIBLIOGRAPHY OF TECHNICAL REPORTS, 1993
Susan S. Berteaux Oct. 1994 16 p
(AD-A292741; WHOI-94-31) Avail: CASI HC A03/MF A01

The technical reports prepared by the Woods Hole Oceanographic Institution in 1993 are listed in this bibliography. DTIC

N95-30964# Northwest Research Associates, Inc., Bellevue, WA.
SEA ICE STRESS RESEARCH Annual Report, 18 Feb. 1994 - 17 Feb. 1995
Max D. Coon 3 Apr. 1995 58 p
(Contract N00014-92-C-0027)
(AD-A293164; NWRA-CR-95-R135) Avail: CASI HC A04/MF A01

During last year, the Northwest Research Associates Arctic team completed the Spring SIMI field program in the Beaufort Sea. We have subsequently conducted data analysis and written papers on that data. In addition, we organized the Ice Mechanics and Arctic Modeling Workshop to be held in Anchorage, AK, April 25-28, 1995, which will report on the research findings of SIMI and will also address future research needs. During this year, we presented a paper on Sea Ice Mechanics Initiative (SIMI) at the Offshore Technology Conference in Houston, TX, in May 1994. The presentation was an attempt to foster communication between the Arctic research being done at the Office of Naval Research and the Arctic offshore-work of the oil industry. The findings of our SIMI field work are reported in our paper entitled 'Sea Ice Mechanics Research,' which appears in Volume I of the Sea Ice Mechanics and Arctic Modeling Workshop proceedings. We have written a paper entitled 'Forced-Displacement Measurements of a First-year Pressure Ridge and Keel' to be presented at Sea Ice Mechanics '95 Symposium as part of the ASME Joint Applied Mechanics and Materials summer meeting at UCLA in June 1995. The results from this data analysis show that the strength of partially consolidated ridges changes in a period of two weeks from an active component in sea ice dynamics to an inactive component, because of its strength. We participated in the preparation of a second paper for the Ice Mechanics '95 Symposium with Dr. R. S. Pritchard of IceCasting and with Drs. D. M. Farmer and Y. Xie of Institute of Ocean Sciences. This paper, entitled 'Acoustic Signatures of Falling Ice Blocks,' examines the acoustic signature from small-scale processes associated with ridging. DTIC

N95-31523# Texas Univ., Austin, TX. Applied Research Lab.
MULTIPLE SCATTER THEORY OF OCEAN SEDIMENTS Semiannual Report, 1 Aug. 1994 - 31 Jan. 1995
Nicholas P. Chotiros and Dennis Yelton 25 Apr. 1995 6 p
(Contract N00014-94-1-0438)
(AD-A293951; TL-AS-95-94) Avail: CASI HC A02/MF A01

To develop a new model of acoustic bottom backscatter from sandy sediments, based on a multiple scattering theory approach, and hence, properly explain observed phenomena, including Lambert's rule and frequency dependence of backscattering strength, particularly at shallow grazing angels, for which current theories are at a loss. The idea underlying our current approach to this problem is that real sediments are granular. The hypothesis we are trying to prove isthat physical mechanisms for both attenuation and scattering may be found in the interaction of acoustic waves with the granular structure. DTIC

N95-31600# Woods Hole Oceanographic Inst., MA.
ARABIAN SEA MIXED LAYER DYNAMICS EXPERIMENT: MOORING DEPLOYMENT CRUISE REPORT
Richard P. Trask, Bryan S. Way, William M. Ostrom, Geoffrey P. Allsup, and Robert A. Weller Jan. 1995 66 p
(Contract N00014-94-1-0161)
(AD-A293684; WHOI-95-01) Avail: CASI HC A04/MF A01

An array of surface and subsurface moorings were deployed in the Arabian Sea to provide high quality time series of local forcing and upper ocean currents, temperature, and conductivity in order to investigate the dynamics of the ocean 5 response to the monsoonal forcing characteristic of the area. The moored array was deployed during R/V Thomas Thompson cruise number 40. One Woods Hole Oceanographic Institution (WHOI) surface mooring, two Scripps Institution of Oceanography (SIO) surface moorings and two University of Washington (UW) Profiling Current Meter moorings were deployed. The moorings were deployed for a period of one year beginning in October 1994 as part of the Office of Naval Research (ONR) funded Arabian Sea experiment. Two six month deployments were planned. The moorings were deployed at 15.5N 61.5E (WHOI), 15.7N 61.30E (SIO), 15.31 61.31 (SIO), 15.7N 61.7E (UW), and 15.3N 61.7E (UW). The WHOI surface mooring was outfitted with two meteorological data collection systems. A Vector Averaging Wind Recorder (VAWR) and an IMET system made measurements of wind speed and direction, sea surface temperature, air temperature, short wave radiation, long wave radiation, barometric pressure, relative humidity and precipitation. Subsurface instrumentation included Vector Measuring Current Meters (VMCM's), Multi-Variable Moored Systems (MVMS); conductivity and temperature recorders and single point temperature recorders. Expendable bathythermograph (XBT) data and CTD data were collected while in transit to the site and between mooring locations. This report describes in a general manner the work that took place during R/V Thomas Thompson cruise number 40 which was the initial deployment cruise for this moored array. DTIC

N95-31701# Washington Univ., Seattle, WA.
THE TEVA EXPERIMENT CRUISE REPORT
Peter H. Dahl, Darrell R. Jackson, and Kevin L. Williams Mar. 1995 22 p Prepared in cooperation with Pennsylvania State Univ.
(Contract N00039-92-C-0100)
(AD-A293025; APL-UW-TM1-95) Avail: CASI HC A03/MF A01

A team from APL-UW made monostatic reverberation and bistatic forward scattering measurements in a shallow water channel (depth 25.6 m) located within the Dry Tortugus collection of islands (24 deg 36.7 min N 82 deg 50.7 min W) during the period 9-17 Feb. 1995. Accompanying the acoustic measurements were continuous measurements of wind speed and surface wave spectra, including wave directional information. The data will be used for sonar model development and model/data comparisons and in underwater system design, development, and performance predictions. The experiment, called the Torpedo Environmental Acoustic (TEVA) experiment, was conducted in conjunction with the Coastal Benthic Boundary Layer (CBBL) experiment organized by the Naval Research Laboratory, whose focus included measuring the geoacoustic and acoustic properties of the sea bed. The detailed environmental characterization afforded by combining assets of both the TEVA and CBBL experiments will also allow rigorous comparisons of acoustic models and measurements. DTIC

N95-31719 Northwestern Univ., Chicago, IL.
STUDIES IN MARINE TECTONICS: PROPAGATING RIFTS, DEPTH ANOMALIES AND SUBDUCTION ZONE ANISOTROPY Ph.D. Thesis
Thomas G. Shoberg 1993 125 p
Avail: Univ. Microfilms Order No. DA9415619

The tectonics of oceanic lithosphere is applied in four studies. The first two investigate how kinematic models of propagating rifts are constrained using seafloor fabric and magnetic anomaly data. The case study area is the Cobb Offset, along the Juan de Fuca ridge in the northeast Pacific Ocean basin. First I develop a method to constrain the kinematic history along this 'dueling propagator' with fabric data. Then I develop a technique that fits the rift propagation model predictions jointly to digital magnetic anomaly and seafloor fabric data. The results show that the propagation history of this region is best fit for fast rift propagation rates. The geometry is constrained most strongly by the magnetic anomaly data and the propagation rates by the fabric data. The third study constructs seafloor age relations for the Indian Ocean basin which are combined with bathymetric, sediment isopach and heat flow data to derive curves for depth and heat flow versus age. These curves are then compared with predictions from three thermal models of oceanic lithosphere evolution. They show a better fit with the GDH1 model which is characterized by a hotter, thinner lithosphere than the other models. The fourth and last study considers the observed velocity contrast between the descending lithosphere and the overlying mantle wedge in subduction zones. I quantify how much of this velocity contrast might be explained by the seismic

anisotropic behavior of constituent mineral assemblages in this region. Specifically I consider the 'remanent' anisotropy in the subducting lithosphere and the 'dynamically induced' anisotropy in the overlying mantle wedge. Three models of mantle wedge flow are considered, with parameters representative of the Japan Trench region. The results imply that seismic anisotropy can only play a strong role in explaining this velocity contrast if there is a large component of dip-axis parallel flow in the mantle above the subducting slab, but if no such flow occurs in the overlying mantle wedge, then the seismic anisotropy makes it even more difficult to explain the observed velocity contrasts. Dissert. Abstr.

N95-31829# Oregon State Univ., Corvallis, OR.
THE DETERMINATION OF WAVE GROUP PARAMETERS FROM THE RESOLUTION OF INCIDENT AND REFLECTED WAVES M.S. Thesis
Gregory E. Selfridge 9 Mar. 1995 64 p
(Contract N00123-89-G-0508)
(AD-A293703) Avail: CASI HC A04/MF A01

Laboratory tests conducted to determine the effects of wave groups on rubble mound breakwater stability are analyzed. A literature review outlining the controversy regarding whether or not wave groups effect breakwater stability is given. Resolution of this controversy is proposed using two independent parameters that characterize wave groups. The two parameters are an envelope exceedance coefficient a and spectral shape gamma. The incident time series must be known to compute alpha, and an algorithm is given that will resolve incident and reflected wave time series from closely spaced wave gauges. The digital to analog simulation of laboratory waves with specified wave group characteristics is reviewed. It is recommended that further studies be conducted to parameterize the envelope exceedance coefficient alpha with a non-biased groupiness factor. DTIC

N95-31850*# National Aeronautics and Space Administration. Goddard Space Flight Center, Greenbelt, MD.
SeaWiFS TECHNICAL REPORT SERIES. VOLUME 28: SeaWiFS ALGORITHMS, PART 1
Stanford B. Hooker, ed., Elaine R. Firestone, ed. (General Sciences Corp., Laurel, MD.), James G. Acker, ed. (Hughes STX, Inc., Lanham, MD.), Charles R. McClain, Kevin Arrigo, Wayne E. Esaias, Michael Darzi (General Sciences Corp., Laurel, MD.), Frederick S. Patt (General Sciences Corp., Laurel, MD.), Robert H. Evans (Miami Univ., FL.), and James W. Brown (Miami Univ., FL.) et al Jun. 1995 50 p Original contains color illustrations
(NASA-TM-104566-Vol-28; Rept-95B00091-Vol-28; NAS 1.15:104566-Vol-28) Avail: CASI HC A03/MF A01; 6 functional color pages

This document provides five brief reports that address several algorithm investigations sponsored by the Calibration and Validation Team (CVT) within the Sea-viewing Wide Field-of-view Sensor (SeaWiFS) Project. This volume, therefore, has been designated as the first in a series of algorithm volumes. Chapter 1 describes the initial suite of masks, used to prevent further processing of contaminated radiometric data, and flags, which are employed to mark data whose quality (due to a variety of factors) may be suspect. In addition to providing the mask and flag algorithms, this chapter also describes the initial strategy for their implementation. Chapter 2 evaluates various strategies for the detection of clouds and ice in high latitude (polar and sub-polar regions) using Coastal Zone Color Scanner (CZCS) data. Chapter 3 presents an algorithm designed for detecting and masking coccolithosphore blooms in the open ocean. Chapter 4 outlines a proposed scheme for correcting the out-of-band response when SeaWiFS is in orbit. Chapter 5 gives a detailed description of the algorithm designed to apply sensor calibration data during the processing of level-1b data. Author

N95-32122*# National Aeronautics and Space Administration. Goddard Space Flight Center, Greenbelt, MD.
SeaWiFS TECHNICAL REPORT SERIES. VOLUME 24: SeaWiFS TECHNICAL REPORT SERIES CUMULATIVE INDEX, VOLUMES 1-23
Stanford B. Hooker, ed. and Elaine R. Firestone, ed. (General Sciences Corp., Laurel, MD.) Jun. 1995 40 p
(NASA-TM-104566-Vol-24; Rept-95B00092-Vol-24; NAS 1.15:104566-Vol-24) Avail: CASI HC A03/MF A01

The Sea-viewing Wide Field-of-view Sensor (SeaWiFS) is the follow-on ocean color instrument to the Coastal Zone Color Scanner (CZCS), which ceased operations in 1986, after an eight-year mission. SeaWiFS is expected to be launched in 1995, on the SeaStar satellite, being built by Orbital Sciences Corporation (OSC). The SeaWiFS Project at the National Aeronautics and Space Administration's (NASA) Goddard Space Flight Center (GSFC), has undertaken the responsibility of documenting all aspects of this mission, which is critical to the ocean color and marine science communities. This documentation, entitled the SeaWiFS Technical Report Series, is the form of NASA Technical Memorandum Number 104566. All reports published are volumes within the series. This particular volume serves as a reference, or guidebook, to the previous 23 volumes and consists of 6 sections including: an errata, an addendum (summaries of various SeaWiFS Working Group Bio-optical Algorithm and Protocols Subgroups Workshops, and other auxiliary information), an index to key words and phrases, a list of all references cited, and lists of acronyms and symbols used. It is the editors' intention to publish a cumulative index of this type after every five volumes in the series. Each index covers the topics published in all previous editions, that is, each new index will include all of the information contained in the preceeding indices. Author

N95-32220*# National Aeronautics and Space Administration. Goddard Space Flight Center, Greenbelt, MD.
SeaWiFS TECHNICAL REPORT SERIES. VOLUME 13: CASE STUDIES FOR SeaWiFS CALIBRATION AND VALIDATION, PART 1
Stanford B. Hooker, ed., Elaine R. Firestone, ed. (General Sciences Corp., Laurel, MD.), Charles R. McClain, Josefino C. Comiso, Robert S. Fraser, James K. Firestone (General Sciences Corp., Laurel, MD.), Brian D. Schieber (General Sciences Corp., Laurel, MD.), Eueng-nan Yeh (General Sciences Corp., Laurel, MD.), Kevin R. Arrigo (Oak Ridge Inst. for Science and Education, TN.), and Cornelius W. Sullivan (University of Southern California, Los Angeles, CA.) Jan. 1994 79 p Original contains color illustrations
(NASA-TM-104566-Vol-13; Rept-94B00042; NAS 1.15:104566-Vol-13)
Avail: CASI HC A05/MF A01; 20 functional color pages

Although the Sea-viewing Wide Field-of-view Sensor (SeaWiFS) Calibration and Validation Program relies on the scientific community for the collection of bio-optical and atmospheric correction data as well as for algorithm development, it does have the responsibility for evaluating and comparing the algorithms and for ensuring that the algorithms are properly implemented within the SeaWiFS Data Processing System. This report consists of a series of sensitivity and algorithm (bio-optical, atmospheric correction, and quality control) studies based on Coastal Zone Color Scanner (CZCS) and historical ancillary data undertaken to assist in the development of SeaWiFS specific applications needed for the proper execution of that responsibility. The topics presented are as follows: (1) CZCS bio-optical algorithm comparison, (2) SeaWiFS ozone data analysis study, (3) SeaWiFS pressure and oxygen absorption study, (4) pixel-by-pixel pressure and ozone correction study for ocean color imagery, (5) CZCS overlapping scenes study, (6) a comparison of CZCS and in situ pigment concentrations in the Southern Ocean, (7) the generation of ancillary data climatologies, (8) CZCS sensor ringing mask comparison, and (9) sun glint flag sensitivity study. Author

N95-32363# Applied Mathematics, Inc., Gales Ferry, CT.
OBJECTIVE ANALYSIS OF OCEANIC DATA FOR COAST GUARD TRAJECTORY MODELS Final Report
Mar. 1994 93 p
(Contract DTRS57-93-C-00133)
(AD-A292864; USCG-D-05-95) Avail: CASI HC A05/MF A01

The Coast Guard uses ocean surface velocity fields as input to trajectory models in search planning to determine search area movement. Statistical techniques, called objective analysis, are used by meteorologists and oceanographers to combine observed data, which are irregularly distributed in space and time, to make conclusions about the total variation of the variables within a region of interest. The purpose of the Phase 1 research was to study the feasibility of adapting objective analysis techniques for use with Coast Guard data. The following research was completed. Objective analysis techniques were used to combine irregularly spaced and temporally observed ocean current velocity data in order to determine an optimally estimated velocity field and associated error field. The technique was applied to a drifting buoy data set collected by the Coast Guard. A numerical experiment was also conducted to examine the number of buoys required to determine the velocity field in a typical Search and Rescue domain.

Techniques for combining two velocity fields were also investigated. The research findings were that objective analysis techniques can be used to provide the Coast Guard with accurate estimates, in real time, of ocean surface velocity and associated error. Potential applications of this research are in support of Coast Guard Search and Rescue, Ice Patrol and Environmental Protection missions. DTIC

51 LIFE SCIENCES (GENERAL)

N95-30452 Texas Univ., Austin, TX. Dept. of Chemical Engineering.
BIOSENSORS BASED ON CROSS-LINKING OF BIOTINYLATED GLUCOSE OXIDASE BY AVIDIN Technical Report, 1 Jan. 1994 - 25 Jan. 1995
Mark S. Vreeke and Patrick Rocca (Institut National des Sciences Appliquees de Rouen, Mont Saint Aignan, France.) 19 Jan. 1995 20 p Limited Reproducibility: More than 20% of this document may be affected by poor print
(AD-A290439; TR-014-1995) Avail: Issuing Activity (Defense Technical Information Center (DTIC))

Avidin, having four biotin binding units, cross-links and immobilizes glucose oxidase (GOX) labeled with multiple biotins (B-GOX) when solutions of B-GOX and avidin are mixed on an electrode. The H2O2 flux generated in the B-GOX catalyzed oxidation of glucose by dissolved O2 is measured as an electroreduction current at a horseradish peroxidase (HRP) redox conducting hydrogel electrode poised at +100 mV (Ag/AgCl). The sensitivity of the resulting glucose sensor is 0.14A/sq cm/M with a linear range up to 2mM glucose. DTIC

N95-30512 Selskapet for Industriell og Teknisk Forskning, Trondheim (Norway). Section for Extreme Work Environment.
EFFECTS OF AIR BUBBLES ON RABBIT BLOOD BRAIN BARRIER
G. Bolstad, A. Hjelde, and A. O. Brubakk 1993 4 p
(PB95-195293) Avail: Issuing Activity (National Technical Information Service (NTIS))

In the present investigation three groups of six animals were infused with an isoosmotic solution of NaCl w/Macrodex and 1 percent Tween. The solution was saturated with air bubbles. Infusion of degassed NaCl solution alone affected white, but not grey matter of both hemispheres. This indicates that the infusion of NaCl, as such, at least partly may explain the formation of edema, in white matter, while this does not seem to be the case in grey matter. It is thus suggested that factors connected to infusion procedures may affect the Blood Brain Barrier (BBB) of rabbits. NTIS

N95-30515 Selskapet for Industriell og Teknisk Forskning, Trondheim (Norway). Section for Extreme Work Environment.
ARTERIAL GAS BUBBLES AFTER DECOMPRESSION IN PIGS WITH PATENT FORAMEN OVALE
A. Vik, B. M. Jenssen, and A. O. Brubakk 1993 13 p Prepared in cooperation with Trondheim Univ., Norway
(PB95-195319) Avail: Issuing Activity (National Technical Information Service (NTIS))

With patent foramen ovale (PFO), thought to be a risk factor for some forms of decompression sickness (DCS), venous bubbles may pass through the patent opening to become arterial bubbles. We exposed 14 anesthetized, spontaneously breathing pigs to air at 5 bar (500 kPa, absolute pressure) for 30 min and then rapidly decompressed at 2 bar/min to 1 bar. We measured intravascular pressures, blood gases, and with transesophageal echocardiology, bubbles in the pulmonary artery and ascending aorta. Autopsy showed that six of the pigs had a PFO. Arterial bubbles occurred more frequently in the PFO group (in six out of six) than in the non-PFO group (in two out of eight, P less than 0.01). When arterial bubbles were detected, the venous bubble count and the pulmonary artery pressure tended to be lower in pigs with PFO than in pigs without a PFO. We conclude that a PFO increases the risk of arterial bubbles after decompression. NTIS

N95-30665 Selskapet for Industriell og Teknisk Forskning, Trondheim (Norway). Section for Extreme Work Environment.
EFFECT OF OXYGEN AND DECOMPRESSION BUBBLES ON INERT GAS WASHOUT
V. Flook, A. O. Brubakk, O. Eftedal, I. M. Holmen, and A. L. Ustad 13 Sep. 1994 109 p
(PB95-196556; STF23-A94031) Avail: Issuing Activity (National Technical Information Service (NTIS))

This report describes experiments designed to answer two questions: How does the use of increased oxygen in the breathing gas affect inert gas washout and How does the presence of decompression bubbles affect the washout of inert gas. The experiments were carried out on pigs, were designed in such a way that the influence of oxygen was studied separately from the influence of decompression bubbles, and involved direct measurement of blood nitrogen concentrations. The conclusions are: Increased partial pressure of oxygen slows down the rate of nitrogen washout to a degree which relates to the level of inspired oxygen; The presence of decompression bubbles slows the removal of inert gas from the body and this slowing relates to the number of mixed venous nitrogen concentration; The pressure of large numbers of decompression bubbles causes further uptake of nitrogen following return to normobaric conditions. NTIS

N95-31144# Illinois Univ., Urbana, IL. Dept. of Cell and Structural Biology.
AASERT-92 AUGMENTATION OF RESEARCH TRAINING IN CHRONOBIOLOGY: REGULATION OF THE MAMMALIAN CIRCADIAN CLOCK BY NEUROTRANSMITTERS Annual Report, 1 Jun. 1993 - 31 May 1994
Martha Gillette 31 May 1994 2 p
(Contract F49620-93-1-0413)
(AD-A288243; AFOSR-94-0681TR) Avail: CASI HC A01/MF A01

Our research program aims to understand the mechanisms by which major neurotransmitter pathways regulate the biological clock in the suprachiasmatic nucleus (SCN) of the mammalian brain. Our model species is the rat. The specific progress made by each of the three students supported by the AASERT award in FY1 is summarized below. Each of these students has maintained satisfactory grades and progress toward their degree requirements during the funding period. DTIC

N95-32040# Department of Energy, Washington, DC. Medical Applications and Biophysical Research Div.
SUMMARIES OF FISCAL YEAR 1994 PROJECTS IN MEDICAL APPLICATIONS AND BIOPHYSICAL RESEARCH
Apr. 1995 123 p
(DE95-010405; DOE/ER-0645) Avail: CASI HC A06/MF A02

This report provides information on the research supported in Fiscal Year 1994 by the Medical Applications and Biophysical Research Division of the Office of Health and Environmental Research. A brief statement of the scope of the following areas is presented: dosimetry; measurement science; radiological and chemical physics; structural biology; human genome; and medical applications. Summaries of the research projects in these categories are presented. DOE

N95-32358# Lawrence Livermore National Lab., Livermore, CA.
IMPLEMENTATION AND PERFORMANCE OF THE PSEUDOKNOT PROBLEM IN SISAL
J. Feo and M. Ivory Dec. 1994 15 p Presented at the High Performance Functional Computing, Denver, CO, 9-11 Apr. 1995
(Contract W-7405-eng-48)
(DE95-009573; UCRL-JC-119529; CONF-9504126-1) Avail: CASI HC A03/MF A01

The Pseudoknot Problem is an application from molecular biology that computes all possible three-dimensional structures of one section of a nucleic acid molecule. The problem spans two important application domains: it includes a deterministic, backtracking search algorithm and floating-point intensive computations. Recently, the application has been used to compare and to contrast functional languages. In this paper, we describe a sequential and parallel implementation of the problem in Sisal. We present a method for writing recursive, floating-point intensive applications in Sisal that preserves performance and parallelism. We discuss compiler optimizations,

runtime execution, and performance on several multiprocessor systems. DOE

52 AEROSPACE MEDICINE

Includes physiological factors; biological effects of radiation; and effects of weightlessness on man and animals.

N95-30494 Direction des Recherches, Etudes et Techniques, Paris (France).
PHYSIOLOGY AND PHYSIOPATHOLOGY OF EQUILIBRATION Final Report [PHYSIOLOGIE ET PHYSIOPATHOLOGIE DE L'EQUILIBRATION]
Feb. 1994 80 p In FRENCH
(PB95-208328) Avail: Issuing Activity (National Technical Information Service (NTIS))

The study analyzes the transduction, transmission, and modulation of the vestibular sensorial message. It focuses on the role of calcium in the acquisition of the vestibular information and its control, and on the ion exchanges involved in these mechanisms. NTIS

N95-30511 Selskapet for Industriell og Teknisk Forskning, Trondheim (Norway). Section for Extreme Work Environment.
DECOMPRESSION ILLNESS, OBSERVABLE BUBBLES. (SESSION K)
O. Eftedal, S. Koteng, and A. O. Brubakk 1993 4 p Prepared in cooperation with Trondheim Univ., Norway
(PB95-195285) Avail: Issuing Activity (National Technical Information Service (NTIS))

A long period of training is required for Doppler raters to reach a standard where they can work independently grading Doppler recordings for intravascular gas bubbles. The aim of this study was to evaluate Transesophageal Echocardiography (TEE) imaging and a grading system with 6 levels as a method for quantifying bubbles. A video tape with 20 1-minute TEE recordings was shown individually to 20 persons. None of the raters had any previous experience with bubble grading. A total of 400 gradings were performed. 293 gradings were consistent with what had been protocolled, 100 differed by 1 grade, 6 differed by 2 grades and 1 differed by 3 grades. We conclude that TEE imaging is well suited for quantitative evaluation of intravascular gas bubbles, even by persons with little previous experience. The grading scale used in the experiments can probably be improved by altering the definitions of grade 1 and 2. NTIS

N95-30513 Selskapet for Industriell og Teknisk Forskning, Trondheim (Norway). Section for Extreme Work Environment.
DETECTING INTRAVASCULAR GAS BUBBLES IN ULTRASONIC IMAGES
O. Eftedal and A. O. Brubakk Nov. 1993 9 p Prepared in cooperation with Trondheim Univ., Norway
(PB95-195301) Copyright Avail: Issuing Activity (National Technical Information Service (NTIS))

To study the effects of decompression on the human body, a reliable system for determining the presence and number of intravascular gas bubbles is required. Detection methods involving ultrasound enable portable, non-invasive systems that can be used in many different situations to be developed. A system capable of identifying single bubbles, even when the number of bubbles is high, would give a linear measure of the total number of intravascular gas bubbles. In scanned two-dimensional ultrasonic images, the grey scale value of each pixel is obtained through a logarithmic amplification of the amplitude of the reflected ultrasound from the corresponding sample volume. Gas bubbles appear as bright 'blobs' in the images. By digitizing the images, simple computer programs for automatic identification of such blobs are feasible. Systems for digitizing and transferring ultrasonic images to computers are commercially available. We present a computer program, EchoBubble, that performs automatic identification and quantification of intravascular gas bubbles in digitized images. NTIS

N95-30563# Naval Health Research Center, San Diego, CA.
CONTROL OF SKIN BLOOD FLOW IN THE NEUTRAL ZONE OF HUMAN BODY TEMPERATURE REGULATION Final Report
Margaret V. Savage, George L. Brengelmann, Donald E. Roberts, and Robert S. Pozos 4 Nov. 1994 37 p
(AD-A291499; NHRC-94-27) Avail: CASI HC A03/MF A01

In humans, matching of heat loss and heat production in the 'neutral' zone, defined operationally in terms of a range of skin temperatures (Tsk), is accomplished by regulation of skin blood flow (SkBF). In four men and four women, we investigated the control of SkBF in this range by setting Tsk at 33 and 35 C in a square wave pattern (15 min at each temperature) or a step pattern (60 min at 33 C separating short periods at 35 C) by means of water sprayed over the entire body except the head, neck, and one forearm. Forearm blood flow (FBF) followed the pattern of Tsk, both in the forearm in which Tsk followed that of the rest of the body and in the arm exposed to room air (average local Tsk 31.22 C). Esophageal temperature (Tes) rose after Tsk fell and vice versa. This inverse relationship is predicted by a simple one-compartment thermal model in which control of SkBF is simulated as a linear combination of skin and core temperature (Tc). Similar patterns of Tsk applied to only one arm had little influence on FBF. We conclude that the feedforward reflex influence of Tsk on SkBF overcompensates for the effect of Tsk on thermal balance in the neutral zone so that equilibrium Tc has an inverse relationship to Tsk. DTIC

N95-30846*# National Aeronautics and Space Administration. John F. Kennedy Space Center, Cocoa Beach, FL.
ELECTROMYOSTIMULATION, CIRCUITS AND MONITORING
Donald F. Doerr [1994] 5 p
(NASA-TM-110741; NAS 1.15:110741) Avail: CASI HC A01/MF A01

One method to determine the benefit of electromyostimulation (EMS) requires an accurate strength assessment of the muscle of interest using a muscle force testing device. Several commercial devices are available. After a pre-EMS muscle assessment, a protocol with accurately controlled stimulation parameters must be applied and monitored. both the actual current and the resultant muscle force must be measured throughout the study. At the conclusion of the study, a reassessment of the muscle strength must be gathered. In our laboratory, electromyostimulation is being studied as a possible countermeasure to the muscle atrophy (degeneration) experienced in space. This muscle loss not only weakens the astronaut, but adversely affects his/her readaptation to 1-g upon return from space. Muscle atrophy is expected to have a more significant effect in long term space flight as anticipated in our space station. Our studies have concentrated on stimulating the four major muscle groups in the leg. These muscles were stimulated sequentially to allow individual muscle force quantification above the knee and ankle. The leg must be restrained in an instrumented brace to allow this measurement and preclude muscle cramping. Derived from text

N95-30870# Lovelace Scientific Resources, Inc., Albuquerque, NM. Inst. for Basic and Applied Medical Research.
CONFERENCE PERSPECTIVE. NEUROIMMUNOMODULATION: STRESS AND IMMUNE FUNCTION
Michael C. Powanda (M/P Biomedical Consultants, Mill Valley, CA.) and Matthew J. Kluger 9 Feb. 1995 11 p Conference held in Albuquerque, NM, 7-9 Oct. 1994
(Contract N00014-95-1-0124)
(AD-A291351) Avail: CASI HC A03/MF A01

The bidirectional communication and interaction between the brain and the immune system is one of the most exciting areas of biomedical research. Although many symposia contain sessions relating to the above topic (e.g. Experimental Biology 1994, Neurosciences), there are few meeting devoted exclusively to this topic. Most of these have been in foreign countries, which limits the participation of American scientists. Some 25 distinguished scientists lectured in the workshop/symposium, and another 50-60 scientists were participants. The symposium was held in a state-of-the-art conference facility, and there was ample opportunities for one-on-one discussion of science. A more detailed description of the symposium is provided. DTIC

N95-30924# Georgia Univ., Athens, GA.
MEMBRANE TRANSPORT: A CELLULAR PROBE OF HEAT STROKE Midterm Report
John S. Willis 2 Feb. 1995 37 p
(Contract DAMD17-93-J-3031)
(AD-A293327; Rept-10-21-RR194-207) Avail: CASI HC A03/MF A01

Red blood cells of guinea pig were used to explore the effects of

temperatures above 37 C on membrane permeability to Na+ and K+ as part of an effort to evaluate the Energy Depletion Hypothesis of heat stroke. Cell Na+ and K+ does not change at 41 C and 45 C for up to 2 hours of incubation in simple saline medium. Na-K pump activity measured as ouabain-sensitive K+ influx increases with warming, as do Na+ influx and K influx. The rise in the pump activity matches the rise in Na+ influx quantitatively, accounting for the lack of change in Na+ cell. The rise in Na+ influx is in the face of a decrease in activity of Na-H exchange transport capacity. The rise in K+ influx consists largely of activation of a single, carrier-mediated path, K-C1 cotransport and corresponds to an apparent activation of this path in the reverse direction (K+ efflux), leading to dumping of K+ at elevated temperature. Na-K-C1, a third passive carrier pathway, shows a temperature optimum between 30 C and 37 C. A new hypothesis proposes that these diverse responses to temperature change contribute to the maintenance of ion balance. DTIC

N95-30981# Naval Surface Warfare Center, Silver Spring, MD.
ELECTROMAGNETIC FIELD EXPOSURE DOSIMETER Final Report, Sep. 1992 - May 1993
A. C. Feaga, M. P. Hilliard, and R. Link 28 Jul. 1994 32 p
(AD-A293191; NSWCDD/TR-94/76) Avail: CASI HC A03/MF A01

The growing concern about adverse health effects caused by electromagnetic radiation prompted the ideas for this dosimeter. Data have been presented that link prolonged exposure to electromagnetic radiation from power lines to leukemia and some types of cancer. At present, though, there is a lack of recording instrumentation to measure the prolonged exposure of an individual; thus, it is not possible to correlate properly the amount of exposure or dose to health effects. With the recent advances in small, low-power devices, a small measuring device can be developed. Once this is built, a large data base can be obtained to help correlate electromagnetic field exposure to health conditions. The objective of this project is to develop an instrument which can measure electromagnetic fields over a prolonged period of time. The instrument would be small, say about the size of a radio Walkman, and would be worn throughout the day while taking data, as the individual goes about normal activities. A PC would be used to retrieve the data from the instrument at the end of the day. The dosimeter comprises a triaxial ferrite-loaded coil sensor, a set of amplifiers and filters, analog-to-digital converters, a microcontroller, and random access data memory. The signals from the sensor are filtered into three frequency ranges: one to measure 60-Hz exposure and two harmonics, another to measure high-energy pulsed energy, and a third frequency range to record the activity level of the individual. The signals from the filters are digitized and read into a microcontroller. The microcontroller performs a few calculations and controls the flow of the data to either random access memory or to a computer. A computer is used to retrieve the data from the dosimeter, and can store and display the measured data. DTIC

N95-30998# Air Force Inst. of Tech., Wright-Patterson AFB, OH.
EVALUATION OF CALIBRATION PARAMETERS AND PERFORMANCE OF THE VIDEO IMAGING TECHNIQUE OF ASSESSING EXPOSURE (VITAE SYSTEM) M.S. Thesis
Keith M. Groth Aug. 1994 128 p
(AD-A289023; AFIT/CI/CIA-94-130) Avail: CASI HC A07/MF A02

Assessing exposures to chemicals that can be absorbed through the skin presents the industrial hygienist with a perplexing and sometimes frustrating dilemma. The fact that three of the articles appearing in the February 1993 AIHA Journal addressed surface wipe sampling is a testament to an increasing concern over the impact of dermally absorbed chemicals. In addition to increased awareness of percutaneous absorption as a potentially major factor in total body burden, this concern probably is fueled by frequent reductions in the allowable levels of many airborne contaminants for the workplace. As allowable workplace levels drop, the percentage of total body burden that is a result of dermal absorption may increase. This is especially true if dermal exposures are not controlled as rigorously as inhalation exposures. In fact, in many instances where the chemical has a low vapor pressure and is not aerosolized, dermal absorption is the primary route of exposure. DTIC

N95-31373# Armstrong Lab., Brooks AFB, TX. Crew Systems Directorate.
FORWARD RAPID ROTATION SHIFTWORK IN USAF AIR TRAFFIC CONTROLLERS: SLEEP, ACTIVITY, FATIGUE AND MOOD ANALYSES Interim Technical Report, 10 Aug. - 3 Sep. 1992
Thomas D. Luna, Jonathan French, Jennifer L. Mitcha, and Kelly J. Neville 9 Dec. 1994 33 p
(AF Proj. 7930)
(AD-A293448; AL/CF-TR-1994-0156) Avail: CASI HC A03/MF A01

The purpose of this study was to evaluate the shift-specific sleep, general activity levels, mood and cognitive performance of air traffic controllers (ATC's) working a forward 2-2-2 rapid rotation shift schedule. ATC's recorded their sleep, oral temperature and subjective fatigue levels, took a computerized cognitive performance battery (N=13) and completed the Profile of Mood States questionnaire (POMS) (N=12). Actigraphs were used to objectively monitor general activity levels and score sleep and the restlessness of scored sleep (N=9). Analyses were made on the basis of duty shift, post-shift, day of shift, and duty location. There was significantly more actigraph scored sleep, subjectively reported sleep and subjectively measured fatigue and confusion for the ATC's while they were on duty on the night-shift. The night-shift was also associated with decreased vigor and general activity levels. Significantly more sleep was reported following the first day on each of the three shifts than following the second. Significantly more sleep was reported and scored by actigraph following the swing-shift than following the day-shift. A comparison group of non ATC day-workers reported more post-shift sleep than the ATC's. The radar approach ATC's reported greater confusion and less vigor than the tower ATC's. Insufficient trials were available for direct performance analysis. DTIC

N95-31446# Madigan Army Medical Center, Takoma, WA. Dept. of Clinical Investigation.
USE OF BODY SURFACE HEAT PATTERNS FOR PREDICTING AND EVALUATING ACUTE LOWER EXTREMITY PAIN AMONG SOLDIERS Final Report, 15 Dec. 1989 - 30 Sep. 1994
Richard A. Sherman 12 Dec. 1994 53 p
(Contract MIPR-90MM052D)
(AD-A292829) Avail: CASI HC A04/MF A01

This project determined (1) that neither thermographs or podoscopes can be used to predict which basic trainees are likely to develop significant lower limb pain during training, (2) that thermography is not clinically useful in tracking changes in training related lower limb pain, (3) that contact thermographs are not useful in the TMC environment due to their inaccuracy, that videothermographs are too cumbersome and expensive to use relative to the information provided in the TMC environment, but that infrared beam thermometers are valuable adjuncts to assessment and tracking, (4) that having trainees wear shock absorbing inserts throughout basic training does not reduce the incidence and severity of lower limb pain, and (5) that training related stress fractures probably do heal faster when exposed to pulsing electromagnetic fields. DTIC

N95-31552# Armstrong Lab., Brooks AFB, TX. Aerospace Medicine Directorate.
SIMULATION OF OCULOMOTOR POST-INHIBITORY REBOUND BURST FIRING USING A HODGKIN-HUXLEY MODEL OF A NEURON
John D. Enderle and Edward J. Engelken 13 Feb. 1995 7 p
(AF Proj. 7755)
(AD-A293821; AL/AO-PC-1995-0012) Avail: CASI HC A02/MF A01

A number of theories have been reported on post saccade phenomenon describing dynamic overshoot, glissadic overshoot and undershoot, and undershoot, all naturally and frequency occurring saccadic eye movements. Electrophysiological evidence for post-inhibitory rebound burst firing activity during saccadic eye movements is prevalent in the literature. However, the cause for the phenomenon is not known. Marked inhibition of neurons within the Paramedian Pontine Reticular Formation often results in post-inhibitory rebound burst firing activity at the beginning and end of a saccade. In this paper, post-inhibitory rebound burst firing activity after marked hyperpolarization is postulated to occur in the Paramedian Pontine Reticular Formation due to a low membrane threshold voltage. With this biophysical property, a single neuron is capable of firing at high rates automatically and without stimulation when released from inhibition.

Simulations using the Hodgkin-Huxley model of a neuron demonstrate that a single neuron is capable of firing at high. rates automatically without stimulation when released from inhibition. DTIC

N95-31570# Tel-Aviv Univ., Ramat-Aviv, Tel-Aviv (Israel).
LASER INDUCED VITREORETINAL SCARRING. EVALUATION OF CAUSATIVE FACTORS AND A THERAPEUTIC APPROACH Final Report, 1 Sep. 1991 - 30 Sep. 1994
Nava Naveh and Naphthali Savion 10 Mar. 1995 50 p
(Contract DAMD17-91-Z-1031)
(AD-A293742) Avail: CASI HC A03/MF A01

Eyes subjected to laser exposure develop an inflammatory reaction, leading to scarring and bleeding, ensuing in visual impairment. This study demonstrated two main findings. (1) The angiogenic (neovascularization) activity of vitreous from lasered eye in rats cornea: The DPI an NADPH inhibitor curtailed significantly angiogenesis, as well as the initial vascular response. (2) Vitreous of lasered eyes enhances cell proliferation of retinal pigment epithelium, vascular endothel: This unique finding explains the development of visual impairment weeks and months post laser of subjects unaware of being hit by laser. Therefore subjects exposed to laser should be screened regularly to find laser lesions and a therapeutic regimen of antioxidants and/or steroidal should be initiated. DTIC

N95-31714# National Aerospace Lab., Tokyo (Japan).
DYNAMICAL ANALYSIS OF THE CORIOLIS EFFECT WHICH CAUSES SPACE DISORIENTATION
Takao Suzuki, Jiro Koo (Tokai Univ., Hiratsuka, Japan.), and Masaki Kume (Mukaino-oka Technical High School, Japan.) Oct. 1994 10 p In JAPANESE
(ISSN 0389-4010)
(NAL-TR-1258) Avail: CASI HC A02/MF A01

The coriolis effect or illusion is a sensation of angular motion in response to an inclination of the head when the head is undergoing a passive rotation. A dummy head including three gyros and three accelerometers was assembled, and was supported with a pivot and four springs to simulate human neck mechanisms. The dummy head was tilted on a rotating table and the data obtained by the inertial sensors were analyzed to explain the cause of the Coriolis effect responsible for the illusion. In conclusion, the force acting on the dummy head is proportional to the angular velocity of the rotating table as well as to the linear velocity of the tilting motion. The force is found to be well described mainly by the principle of the coriolis acceleration. Author

N95-32097# Lawrence Livermore National Lab., Livermore, CA.
AUTOMATED VOLUMETRIC GRID GENERATION FOR FINITE ELEMENT MODELING OF HUMAN HAND JOINTS
K. Hollerbach, K. Underhill, and R. Rainsberger Feb. 1995 4 p Presented at the 1995 ASME Summer Bioengineering Conference, Beaver Creek, CO, 28 Jun. - 2 Jul. 1995
(Contract W-7405-eng-48)
(DE95-009575; UCRL-JC-119773; CONF-9506173-1) Avail: CASI HC A01/MF A01

We are developing techniques for finite element analysis of human joints. These techniques need to provide high quality results rapidly in order to be useful to a physician. The research presented here increases model quality and decreases user input time by automating the volumetric mesh generation step. DOE

53 BEHAVIORAL SCIENCES

Includes psychological factors; individual and group behavior; crew training and evaluation; and psychiatric research.

N95-30905# Armstrong Lab., Brooks AFB, TX. Aerospace Medicine Directorate.
USING COMPUTERIZED NEUROPSYCHOLOGICAL TESTING TO ASSESS AVIATOR SKILLS Final Technical Report
Christopher F. Flynn and Raymond B. King Dec. 1994 21 p
(AF Proj. 7755; AF Proj. ILIR)
(AD-A293227; AL/AO-TR-1994-0174) Avail: CASI HC A03/MF A01

Successful pilots must be cognitively and psychologically 'fit' to preserve cockpit situational awareness while executing complex job demands in an unforgiving environment. The neuropsychological attributes of successful U.S. Air Force (USAF) aircrew, however, are largely unstudied. To conveniently collect a large sample of aviators data for comparison to mission performance, an easy-to-use and reliable test delivery system is required. The Neuropsychiatrically Enhanced Flight Screening (N-EFS) program is one product of an effort by Armstrong Laboratory's (AL) Neuropsychiatry Branch (AOCN). N-EFS measures the cognitive functioning (using the Multidimensional Aptitude Battery, MAB; and CogScreen) and psychological attributes and crew resource management potential (using the Personal Characteristics Inventory PCI; and the Revised NEO-Personality Inventory, NEO-PI-R) of all USAF pilot candidates. This data will establish a range of cognitive attributes of pilot applicants, and will provide MAB CogScreen baseline data for future reference. The N-EFS program also seeks to validate the MAB, CogScreen, NEO-PI-R. and PCI as future tools for pilot selection and understanding situational awareness. N-EFS builds on earlier AL/AOCN efforts to develop a 'field-friendly,' self-administered, computerized psychometric testing battery to define attributes of successful pilots. DTIC

N95-31140# Army Aeromedical Research Lab., Fort Rucker, AL.
LUMINANCE EFFECTS ON VISUAL ACUITY AND SMALL LETTER CONTRAST SENSITIVITY Final Report
Jeff Rabin Feb. 1995 15 p
(AD-A293310; USAARL-95-14) Avail: CASI HC A03/MF A01

The purpose of this study was to evaluate the effects of luminance on visual acuity (VA) and small letter contrast sensitivity (SLCS). Computer-generated letter charts were used to measure VA and SLCS (6/7.5 (20/25) Snellen equivalent) as a function of stimulus luminance. Letter size (VA) and contrast (SLCS) were varied in equal logarithmic steps, making the task and scoring procedure comparable for the two types of measurement. Both VA and SLCS decreased with decreasing luminance, but the effect was far greater in the contrast domain. Reducing luminance from 116 cd/rn2 to 0.23 cd/sq m produced a 3 x reduction in VA, but a 17 x reduction in SLCS. The greater sensitivity of SLCS to luminance endured even after correction for greater measurement variability. SLCS is a sensitive approach for detecting resolution loss undisclosed by standard measures of VA. It may be useful for monitoring visual loss from light attenuation in early cataracts, and for detecting subtle resolution loss from neural or pathologic factors in ocular and neuroophthalmologic disease. DTIC

N95-31376# Armstrong Lab., Brooks AFB, TX. Aerospace Medicine Directorate.
PSYCHOLOGICAL PILOT SELECTION IN THE US AIR FORCE, THE LUFTWAFFE, AND THE GERMAN AEROSPACE RESEARCH ESTABLISHMENT Final Technical Report
Monika Gnan, Christopher F. Flynn, and Raymond E. King Feb. 1995 33 p
(AD-A293779; AL/AO-TR-1995-0003) Avail: CASI HC A03/MF A01

As financial resources for the U.S. Air Force (USAF) and the German Luftwaffe (LW) dwindle, reducing attrition from military aviation training becomes vital. Finding the optimal mixture of applicant personality, stamina, and psychomotor skills for aviation is a goal as complicated as it is elusive. This paper compares the USAF, LW and German Aerospace Research Establishment (DLR) pilot selection programs. The LW and DLR utilize a sequential psychological selection system including apparatus tests, psychological interviews and behavioral observations, while in the USAF psychological selection does not play an important role. Instead, medical standards, flight screening, and training attrition are used as USAF selection criteria. However, a new USAF program, Neuropsychiatrically Enhanced Flight Screening (N-EFS) will examine the personality characteristics of pilot applicants for further study. The USAF and LW could learn from the strengths and weaknesses of their respective selection programs. The opportunity for cooperative research is even greater, considering that the USAF and LW pilot students share common jet pilot training. DTIC

N95-31383# Carnegie-Mellon Univ., Pittsburgh, PA. School of Computer Science.
VISUAL TRACKING OF SELF-OCCLUDING ARTICULATED OBJECTS
James R. Rehg and Takeo Kanade 31 Dec. 1994 42 p Presented at the International Conference on Computer Vision, Boston, MA, Jun. 1995

Sponsored in part by NASA George Marshall Space Flight Center
(Grant NGT-50559)
(AD-A292894; CMU-CS-94-224) Avail: CASI HC A03/MF A01

Computer sensing of hand and limb motion is an important problem for applications in human-computer interaction, virtual reality, and athletic performance measurement. We describe a framework for local tracking of self-occluding motion, in which parts of the mechanism obstruct each others visibility to the camera. Our approach uses a kinematic model to predict occlusion and windowed templates to track partially occluded objects. We analyze our model of self-occlusion, discuss the implementation of our algorithm, and give experimental results for 3D hand tracking under significant amounts of self-occlusion. These results extend the DigitEyes system for articulated tracking described in 22, 21 to handle self-occluding motions. DTIC

N95-31436# Smith-Kettlewell Inst. of Visual Sciences, San Francisco, CA.
VISUAL PROCESSING OF OBJECT VELOCITY AND ACCELERATION Final Technical Report, 15 Jan. 1992 - 14 Jan. 1995
Suzanne McKee 6 Mar. 1995 17 p
(Contract F49620-92-J-0156)
(AD-A292789; AFOSR-95-0243TR) Avail: CASI HC A03/MF A01

The main objective of this project was the analysis of the detection of trajectory signals in random motion noise. Results from experiments demonstrated that detection was limited by the probability of mismatch, not noise density per se; detection was based on a motion signal, not a form or position signal; detection was limited by higher-order aspects of motion processing, not the ratio of signal to noise in the primary motion detectors. The Yuille-Grzywacz 'Motion Coherence' model was modified to provide a computational model for these findings. Computer simulations showed that this model was adequate to reproduce our results. In addition, three other projects were supported by this grant: motion transparency from speed signals alone; speed discrimination for targets moving in depth; trajectory motion detection in three-dimensional noise. Nine papers from this project have been accepted in referred journals; one additional paper has been submitted. Four chapters were also supported by this grant. DTIC

N95-31583# Galaxy Scientific Corp., Lackland AFB, TX.
CONTEXTUAL INTERFERENCE EFFECTS ON ACQUISITION AND TRANSFER OF A COMPLEX MOTOR TASK Interim Report, Oct. 1993 - Mar. 1994
Barry P. Goettl Feb. 1995 15 p
(Contract F41622-92-D-0006)
(AD-A293788; AL/HR-TP-1994-0034) Avail: CASI HC A03/MF A01

Research in motor skill and verbal memory suggests that random sequencing of trials results in retention and transfer that is superior to blocked presentation of trials. The contextual interference effect is based largely on relatively simple motor and verbal tasks. The present study explores the generalizability of the contextual interference effect to a complex flight simulator task. Subjects were assigned to three groups: whole-task training, low contextual interference, and high contextual interference. Results indicated that whole task subjects showed the best retention and that the two contextual interference groups did not differ. Additionally, all three groups showed equivalent performance on the transfer task. These results suggest that the contextual interference effect may not generalize to complex tasks. DTIC

N95-31585# Colorado Univ., Boulder, CO.
OPTIMIZING THE LONG-TERM RETENTION OF SKILLS: STRUCTURAL AND ANALYTIC APPROACHES TO SKILL MAINTENANCE Final Report, May 1990 - Oct. 1993
Alice F. Healey Jan. 1995 46 p
(Contract MDA903-90-K-0066; DA Proj. 201-61102-B-74-F)
(AD-A293798; ARI-RN-95-16) Avail: CASI HC A03/MF A01

Progress has been made in determining guidelines for optimizing the long-term retention of skills. Studies on learning and retention of color-word interference, schedule components, list components, mental arithmetic, and vocabulary acquisition suggest that optimal retention will result from using procedures during training, relating information to previous experience, making the information distinctive, promoting direct retrieval of the information, and providing refresher or practice tests. DTIC

N95-31685# Carnegie-Mellon Univ., Pittsburgh, PA. Robotics Inst.
FORCE AND VISION RESOLVABILITY FOR ASSIMILATING DISPARATE SENSORY FEEDBACK
Bradley J. Nelson and Pradeep K. Khosla Feb. 1995 48 p
(Contract DAAL03-91-G-0272)
(AD-A293581; CMU-RI-TR-95-11) Avail: CASI HC A03/MF A01

Force and vision sensors provide complementary information, yet they are fundamentally different sensing modalities. This implies that traditional sensor integration techniques that require common data representations are not appropriate for combining the feedback from these two disparate sensor. In this paper, we introduce the concept of vision and force sensor resolvability as a means of comparing the ability of the two sensing modes to provide useful information during robotic manipulation tasks. By monitoring the resolvability of the two sensing modes with respect to the task, the information provided by the disparate sensors can be seamlessly assimilated during task execution. A nonlinear force/vision serving algorithm that uses force and vision resolvability to switch between sensing modes is proposed. The advantages of the assimilation technique is demonstrated during contact transitions between a stiff manipulator and rigid environment, a system configuration that easily becomes unstable when force control alone is used. Experimental results show that robust contact transitions are made by the proposed nonlinear controller while simultaneously satisfying the conflicting task requirements of fast approach velocities, maintaining stability, minimizing impact forces, and suppressing bounce between contact surfaces. DTIC

N95-31686# California Univ., Los Angeles, CA. Dept. of Psychology.
A COGNITIVE ARCHITECTURE FOR SOLVING ILL-DEFINED PROBLEMS Interim Report, Sep. 1986 - Aug. 1987
Keith J. Holyoak and Paul R. Thagard (Princeton Univ., NJ.) Feb. 1995 59 p
(Contract MDA903-86-K-0297)
(AD-A293582; ARI-RN-95-24) Avail: CASI HC A04/MF A01

A computational theory of analogical mapping is described, based on a small set of constraints. The theory is embodied in a computer simulation that is applied to several examples, including psychological data on the mapping process. DTIC

54 MAN/SYSTEM TECHNOLOGY AND LIFE SUPPORT

Includes human engineering; biotechnology; and space suits and protective clothing.

For related information see also *16 Space Transportation.*

N95-30522 Selskapet for Industriell og Teknisk Forskning, Trondheim (Norway). Div. of Safety and Reliability.
SPECIFIC METHOD FOR TASK-BASED INTERACTION DESIGN
E. Hollnagel, P. Hougaard, R. Rosness, T. Paulsen, and O. Oegard 1994 20 p Prepared in cooperation with Computer Resources International A/S, Denmark), and ESA. ESTEC, Noordwijk, Netherlands
(PB95-196440; STF75-S93007) Avail: Issuing Activity (National Technical Information Service (NTIS))

The developments in computers and information technology have led to a growing dependence on the proper functioning of human-machine interaction (HMI). It is therefore important that the design of HMI is addressed as a specific problem and that proper concepts and methods are developed. The design process serves to increase the constraints governing the situation so that only one option or alternative is left for each requirement. HMI design must therefore be supported by methods that can elicit the requirements, determine the constraints and options, and finally assist in achieving the proper combination of requirements and options that constitutes the desired solution. The paper describes such a method, based on a systematic task analysis. The design is developed based on a definition of the functional requirements which then are combined with information about presentation styles and standards and dialog design principles. The Task Based Interaction Design method is illustrated by an example from a space application. NTIS

N95-30552 Department of the Navy, Washington, DC.
RELEASEABLE UNCONSTRAINED INFLATABLE BODY PROTECTOR Patent
Frederick C. Guill, inventor (to Navy) 6 Nov. 1994 8 p Filed 11 Aug. 1993
(AD-D017350; US-Patent-5,362,098; US-Patent-Appl-SN-104682; US-Patent-Class-280) Avail: US Patent and Trademark Office

A device for providing crash protection to people aboard a land, air, sea or space vehicle is described. A crash sensor mounted on the vehicle is used to sense a crash, impact or jarring motion. Data from the crash sensor is then transmitted via wireless communication by a signal transmitter to a signal receiver mounted on a harness worn by a crew member or passenger. When a crash signal is received, inflation mechanisms inflate inflatable bladders mounted on the harness, thereby protection the person wearing the harness. DTIC

N95-30888# Air Force Systems Command, Wright-Patterson AFB, OH. National Air Intelligence Center.
WIDE FIELD OF VIEW HELMET DISPLAY SYSTEMS MOUNTED FOR HELICOPTER SIMULATION
Lin Yi Zhong 23 Mar. 1995 11 p Transl. into ENGLISH from Guoji Hangkong, China, no. 4, 6 p Apr. 1993
(AD-A293123; NAIC-ID(RS)T-0414-94) Avail: CASI HC A03/MF A01

The wide field of view helmet mounted display system with a broad detection span will have significant impact on future reconnaissance and military helicopter simulation. This paper briefly discusses its application with emphasis on visualization of extremely close objects/terrain during low-level flight, target display, and head aiming. CASI

N95-30907# Michigan State Univ., East Lansing, MI. Dept. of Biomechanics.
ERECT, NEUTRAL AND SLUMP SITTING POSTURES: A STUDY OF THE TORSO LINKAGE SYSTEM FROM SHOULDER TO HIP JOINT Final Report, Dec. 1983 - Dec. 1985
Herbert M. Reynolds Oct. 1994 175 p
(Contract F33615-84-C-0507)
(AD-A293239; AL/CF-TR-1994-0151) Avail: CASI HC A08/MF A02

Sitting postures representative of a maximum erect, neutral and maximum slumped spinal curvature were defined by comparable anatomical pointmarks in three dimensional space. Nine, male, unembalmed cadavers were measured with a roentgen stereophotogrammetric system. The results describe thoracic and lumbar curvatures in three postures and the locations of specific landmarks representing the shoulder joint, spinal column, and hip joint in a three dimensional seat reference system. In addition to the three dimensional analysis of sitting posture, the range of notion for each motion segment measured in the spine was calculated. These data were used to evaluate the contribution of specific lumbar motion segments in the change of sitting posture from maximum erect to maximum slump. To evaluate the condition of each subject's musculoskeletal system, osteological, morphological and physiological procedures were used to describe the sample. DTIC

N95-31134*# Cleveland State Univ., OH.
DEVELOPMENT AND COMPUTER IMPLEMENTATION OF DESIGN/ANALYSIS TECHNIQUES FOR MULTILAYERED COMPOSITE STRUCTURES. PROBABILISTIC FIBER COMPOSITE MICROMECHANICS M.S. Thesis, Mar. 1987 Final Report, 1 Sep. 1984 - 1 Oct. 1990
Thomas A. Stock 19 Jun. 1995 193 p
(Grant NAG3-550)
(NASA-CR-198979; NAS 1.26:198979) Avail: CASI HC A09/MF A03

Probabilistic composite micromechanics methods are developed that simulate expected uncertainties in unidirectional fiber composite properties. These methods are in the form of computational procedures using Monte Carlo simulation. The variables in which uncertainties are accounted for include constituent and void volume ratios, constituent elastic properties and strengths, and fiber misalignment. A graphite/epoxy unidirectional composite (ply) is studied to demonstrate fiber composite material property variations induced by random changes expected at the material micro level. Regression results are presented to show the relative correlation between predictor and response variables in the study. These computational procedures make possible a formal description of anticipated random processes at the intraply level, and the related effects of these on composite properties. Author

N95-31267# Korea Cancer Center Hospital, Seoul (Republic of Korea).
THE DEVELOPMENT OF HUMAN BEHAVIOUR ANALYSIS TECHNIQUES AND THE DEVELOPMENT OF HUMAN FACTORS TECHNOLOGIES
Jung Woon Lee (Korean Atomic Energy Research Inst., Seoul, Republic of Korea.), Se Woo Cheon (Korean Atomic Energy Research Inst., Seoul, Republic of Korea.), Sang Moon Shu (Korean Atomic Energy Research Inst., Seoul, Republic of Korea.), Geun Ok Park (Korean Atomic Energy Research Inst., Seoul, Republic of Korea.), Yong Hee Lee (Korean Atomic Energy Research Inst., Seoul, Republic of Korea.), Han Yeong Lee (Korean Atomic Energy Research Inst., Seoul, Republic of Korea.), Jae Chang Park (Korean Atomic Energy Research Inst., Seoul, Republic of Korea.), Eu Jin Lee (Korean Atomic Energy Research Inst., Seoul, Republic of Korea.), and Seung Hee Lee (Korean Atomic Energy Research Inst., Seoul, Republic of Korea.) Apr. 1994 250 p In KOREAN
(DE95-613356; KAERI/RR-1339/93) Avail: CASI HC A11/MF A03

This project has two major areas; one is the development of an operator task simulation software and another is the development of human error analysis and application technologies. In this year project, the second year, for the development of an operator task simulation software, we studied the following: - analysis of the characteristics of operator tasks, - development of operator task structures: Macro Structures, - development of an operator task simulation analyzes, - analysis of performance measures. And the following for the development of human error analysis and application technologies: - analysis of human error mechanisms, - analysis of human error characteristics in tasks, - analysis of human error occurrence in Korean Nuclear Power Plants, - establishment of an experimental environment for human error data collection with Compact Nuclear Simulator, - basic design of a Multimedia-based Human Error Representing System. DOE

N95-31399 Federal Aviation Administration, Atlantic City, NJ.
HUMAN FACTORS AT THE FAA TECHNICAL CENTER: BIBLIOGRAPHY Technical Note, Dec. 1993 - Dec. 1994
Earl S. Stein, ed., Edward Buckley, ed., and Kathy Mann, ed. (Princeton Economic Research, Inc., NJ.) Dec. 1994 47 p Limited Reproducibility: More than 20% of this document may be affected by microfiche quality
(AD-A288638; DOT/FAA/CT-TN94/50) Avail: Issuing Activity (Defense Technical Information Center (DTIC))

Since the Federal Aviation Administration (FAA) arrived in Atlantic City in 1958, there have been ongoing efforts in aviation human factors. These efforts have taken many forms and have focused on both the ground and air sides of the airspace system. Psychologists, engineers, systems analysts, computer scientists, and others have participated in the studies that have led to the numerous reports and papers cited in this bibliography. While the listing is probably not all inclusive, it covers virtually all work that is referenced in automated data bases plus publications that were identified by current and past researchers, but which never made it to the computerized listings. This bibliography is meant to highlight the work that has gone on over the years. While many of the documents cited are still available from the Technical Center library, or from the authors themselves, the editors do not suggest that everything is retrievable, and, in fact, much of the older work has been superseded by more modern technology and thinking. The research of 30 years ago has served as a foundation for the human factors engineering that that is being done today. The references are provided in alphabetical order and indexed by numbers associated with subject matter categories. Human factors research is alive and continues to progress in the FAA and at the Technical Center. Author

N95-31401# Carnegie-Mellon Univ., Pittsburgh, PA. School of Computer Science.
HUMAN-COMPUTER INTERACTION (HCI) SPECIALIZATION TRACK MASTERS OF SOFTWARE ENGINEERING (MSE) PROGRAM
Carol L. Hoover 1 Mar. 1995 13 p
(AD-A292895; CMU-CS-95-123) Avail: CASI HC A03/MF A01

There is an increasing demand for software to implement human-computer interfaces. Software engineers who develop these interfaces need an understanding of the interactions between the human, the available computer technology, and human tasks. They should also

understand empirical methods used to evaluate the usability of existing human-computer interfaces. The Human-Computer Interaction Specialization Track, which is an option within the Masters of Software Engineering (MSE) Program at Carnegie Mellon University, enables graduate software engineering students to obtain knowledge and skills related to the design, implementation, and evaluation of interactive computing systems. Students can acquire hands-on experience in the design of computer technology to support individual users as well as group interactions. The track is flexible in that it allows students to choose their own set of track courses from a list of approved HCI courses. This report describes the track rationale and requirements and presents educational guidelines to help students select courses. The report includes a list of approved courses and brief course synopses. The report is based on the author's work in developing specialization tracks for the MSE program. The author started this work during the spring of 1993. DTIC

N95-31538# Department of the Air Force, Wright-Patterson AFB, OH. Crew Systems Directorate.
DESIGN AND INTEGRATION ISSUES OF VISUALLY-COUPLED EVALUATION Interim Report, Jul. 1991 - Oct. 1994
H. L. Task and Dean F. Kocian Mar. 1995 139 p
(AF Proj. 7184)
(AD-A293521; AL/CF-SR-1995-0004) Avail: CASI HC A07/MF A02

This document is the text of a short course presented at SPIE in 1992 and 1994 dealing with design and integration issues of visually-coupled systems (VCS). The VCS described are composed of a helmet-mounted display, a display image source, and a head helmet tracker. DTIC

N95-31671# Department of the Air Force, Wright-Patterson AFB, OH. Crew Systems Directorate.
VERTICAL IMPACT TESTING OF TWO HELMET-MOUNTED NIGHT VISION SYSTEMS Interim Report, Jun. 1993 - Dec. 1993
Chris E. Perry Jun. 1994 25 p
(AD-A293055; AL/CF-SR-1994-0013) Avail: CASI HC A03/MF A01

The Air Force is investigating the use of helmet-mounted technology to improve pilot performance. One potential draw-back to the new helmet systems is the potential for increased neck injuries during emergency ejection due to the helmet's weight and center-of-gravity. A recent test program evaluated the risk of neck injury of two helmet-mounted night vision systems by subjecting an instrumented manikin (ADAM) to +Gz impacts using a vertical deceleration tower. The helmets were the Concept 6 from Night Vision Corporation and the ANVIS 49/49 from ITT. Results indicate that both helmets were lighter than previous helmets, and met the Interim Head and Neck Criteria. They also produced neck loads in an ACES 2 seat that are less than what a standard helmet produces in a B-52 seat, and produced neck loads in a B-52 seat that are less than the maximum (400 lbs) required for major neck injury (fracture, etc.). DTIC

55 SPACE BIOLOGY

Includes exobiology; planetary biology; and extraterrestrial life.

No abstracts in this category.

59 MATHEMATICAL AND COMPUTER SCIENCES (GENERAL)

N95-30857*# Institute for Computer Applications in Science and Engineering, Hampton, VA.
SEMIANNUAL REPORT Final Report, 1 Oct. 1994 - 31 Mar. 1995
Jun. 1995 81 p
(Contracts NAS1-19480; NAS1-18605; NAS1-18107; NAS1-17070; NAS1-17130; NAS1-15810; NAS1-16394; NAS1-14101; NAS1-14472; RTOP 505-90-52-01)
(NASA-CR-198172; NAS 1.26:198172) Avail: CASI HC A05/MF A01

This report summarizes research conducted at the Institute for Computer Applications in Science and Engineering in applied mathematics, fluid mechanics, and computer science during the period 1 Oct. 1994 - 31 Mar. 1995. Author (revised)

60 COMPUTER OPERATIONS AND HARDWARE

Includes hardware for computer graphics, firmware, and data processing.

For components see *33 Electronics and Electrical Engineering.*

N95-30892# Stanford Univ., CA. Dept. of Electrical Engineering.
FOUNDATIONS OF TECHNOLOGY FOR CONSTRUCTING HIGHLY RELIABLE DISTRIBUTED REALTIME SYSTEMS Final Report, 1 Aug. 1991 - 30 Sep. 1994
David C. Luckham 30 Sep. 1994 12 p
(Grant AF-AFOSR-0354-91)
(AD-A293254; AFOSR-95-0235TR) Avail: CASI HC A03/MF A01

We have investigated event-based specification and constraint language extensions of our Rapide prototyping language. We have also investigated testing methods and tools for detecting constraint violations in simulations of distributed time-sensitive avionics systems and control systems. Rapide models the behavior of a distributed system by generating causal event simulations. A causal event simulation is a timed poset (partially ordered set of events with timing). Dependencies between events as well as their timing are captured in the poset execution model, thus providing a more detailed and precise picture of the behavior of a realtime, distributed system than current simulation technology based upon sequential traces of events. Posets allow more powerful constraint specifications than traces, e.g., asynchronous behavior. This work has developed (1) basic algorithms for implementing poset computations, (2) a constraint language for specifying behavior in terms of posets, and (3) automatable algorithms and tool-set for detecting constraint violations in posets. To establish the feasibility of scaling this simulation technology to practical avionics examples, we have applied the technology to developing high level systems architectures of avionics systems. We have also applied constraint monitoring of the avionics simulations to detect design errors. The avionics systems studied include the IBM ADAGE helicopter avionics system architecture, and a high level architecture of the Boeing DARTS system for building flight simulators. DTIC

N95-30967# Syracuse Univ., NY. Center for Molecular Electronics.
HIGH SPEED RANDOM ACCESS, FOURIER TRANSFORM HOLOGRAPHIC ASSOCIATIVE AND HIGH DENSITY TWO-PHOTON THREE-DIMENSIONAL OPTICAL MEMORIES BASED ON BACTERIORHODOPSIN Final Report
Robert R. Birge Jan. 1995 36 p
(Contract F30602-91-C-0084)
(AD-A293389; RL-TR-95-6) Avail: CASI HC A03/MF A01

The goals were to optimize bacteriorhodopsin based photochromic and photorefractive materials for use in optical memories. Two spatial light modulators (SLM's) based on bacteriorhodopsin were developed, one that could be controlled via applied voltage and the other controlled by light. The former performed below target specification; whereas the latter achieved diffraction efficiencies two-fold above target. Preliminary results on the three-dimensional data cube were sufficiently exciting to adjust the first year statement of work to also include the optimization of the bacteriorhodopsin data cube. DTIC

N95-31130# Oak Ridge National Lab., TN.
IMPLEMENTATION OF KIVA-3 ON DISTRIBUTED MEMORY MIMD COMPUTERS
O. Yasar, T. Zacharia, R. Aggarwal, A. A. Amsden, and J. R. Baumgardner 1995 7 p Presented at the High Performance Computing 1995, Tucson, AZ, 9-13 Apr. 1995
(Contract DE-AC05-84OR-21400)
(DE95-010288; CONF-950431-2) Avail: CASI HC A02/MF A01

KIVA-3 is the latest version of a 3-D Finite Difference CFD code developed by Amsden for combustion engine simulations. A distributed-memory implementation has many advantages for problems that hardly fit affordable existing memory banks. Previous attempts to parallelize

KIVA-2 by Yasar, et al. were focused mostly on diffusion solvers because of their heavy time consumption during execution. The study suggested a complete parallelization of the code, including advection and spray dynamics, along with the use of a block-wise decomposition scheme to assure an efficient load balancing and a low communication/computation ratio. Here, the authors report rather a general analysis of the issues involved in such a distributed implementation for the latest version of the code, KIVA-3, on MIMD parallel systems. A more detailed analysis of the code and corresponding algorithms have already been implemented by Yasar and will be published soon. DOE

N95-31645# Los Alamos National Lab., NM.
AN ASSESSMENT OF WORLDWIDE SUPERCOMPUTER USAGE
H. J. Wasserman, M. L. Simmons, and A. H. Hayes Jan. 1995 121 p
(Contract W-7405-eng-36)
(DE95-009879; LA-UR-95-375) Avail: CASI HC A06/MF A02

This report provides a comparative study of advanced supercomputing usage in Japan and the United States as of Spring 1994. It is based on the findings of a group of US scientists whose careers have centered on programming, evaluating, and designing high-performance supercomputers for over ten years. The report is a follow-on to an assessment of supercomputing technology in Europe and Japan that was published in 1993. Whereas the previous study focused on supercomputer manufacturing capabilities, the primary focus of the current work was to compare where and how supercomputers are used. Research for this report was conducted through both literature studies and field research in Japan. DOE

N95-31704# Lawrence Livermore National Lab., Livermore, CA.
CLASS OF SERVICE IN THE HIGH PERFORMANCE STORAGE SYSTEM
S. Louis and D. Teaff (IBM Federal Systems Div., Houston, TX.) 10 Jan. 1995 14 p Presented at the International Federation of Information Processing International Conference on Open Distributedd Processing, Brisbane, Australia, 21-24 Feb. 1995
(Contract W-7405-eng-48)
(DE95-007959; UCRL-JC-119754; CONF-950286-1) Avail: CASI HC A03/MF A01

Quality of service capabilities are commonly deployed in archival mass storage systems as one or more client-specified parameters to influence physical location of data in multilevel device hierarchies for performance or cost reasons. The capabilities of new high-performance storage architectures and the needs of data-intensive applications require better quality of service models for modern storage systems. HPSS, a new distributed, high-performance, scalable, storage system, uses a Class of Service (COS) structure to influence system behavior. The authors summarize the design objectives and functionality of HPSS and describes how COS defines a set of performance, media, and residency attributes assigned to storage objects managed by HPSS servers. COS definitions are used to provide appropriate behavior and service levels as requested (or demanded) by storage system clients. They compare the HPSS COS approach with other quality of service concepts and discuss alignment possibilities. DOE

N95-31988*# Institute for Computer Applications in Science and Engineering, Hampton, VA.
THE LINUX OPERATING SYSTEM: AN INTRODUCTION
Shahid H. Bokhari Jun. 1995 21 p Sponsored by University of Engineering and Technology, Lahore, Pakistan
(Contract NAS1-19480; RTOP 505-90-52-01)
(NASA-CR-198178; NAS 1.26:198178; ICASE-95-49) Avail: CASI HC A03/MF A01

Linux is a Unix-like operating system for Intel 386/486/Pentium based IBM-PCs and compatibles. The kernel of this operating system was written from scratch by Linus Torvalds and, although copyrighted by the author, may be freely distributed. A world-wide group has collaborated in developing Linux on the Internet. Linux can run the powerful set of compilers and programming tools of the Free Software Foundation, and XFree86, a port of the X Window System from MIT. Most capabilities associated with high performance workstations, such as networking, shared file systems, electronic mail, TeX, LaTeX, etc. are freely available for Linux. It can thus transform cheap IBM-PC compatible machines into Unix workstations with considerable capabilities. The author explains how Linux may be obtained, installed and networked. He also describes some interesting applications for Linux that are freely available. The enormous consumer market for IBM-PC compatible machines continually drives down prices of CPU chips, memory, hard disks, CDROMs, etc. Linux can convert such machines into powerful workstations that can be used for teaching, research and software development. For professionals who use Unix based workstations at work, Linux permits virtually identical working environments on their personal home machines. For cost conscious educational institutions Linux can create world-class computing environments from cheap, easily maintained, PC clones. Finally, for university students, it provides an essentially cost-free path away from DOS into the world of Unix and X Windows. Author

N95-32046*# Institute for Computer Applications in Science and Engineering, Hampton, VA.
A MICROECONOMIC SCHEDULER FOR PARALLEL COMPUTERS Final Report
Ion Stoica, Hussein Abdel-Wahab, and Alex Pothen May 1995 21 p Presented at the Workshop on Job Scheduling Strategies for Parallel Processing
(Contracts NAS1-19480; RTOP 505-90-52-01; DE-FG05-94ER-25216; NSF CCR-90-24954)
(NASA-CR-198153; NAS 1.26:198153; ICASE-95-33) Avail: CASI HC A03/MF A01

We describe a scheduler based on the microeconomic paradigm for scheduling on-line a set of parallel jobs in a multiprocessor system. In addition to the classical objectives of increasing the system throughput and reducing the response time, we consider fairness in allocating system resources among the users, and providing the user with control over the relative performances of his jobs. We associate with every user a savings account in which he receives money at a constant rate. When a user wants to run a job, he creates an expense account for that job to which he transfers money from his savings account. The job uses the funds in its expense account to obtain the system resources it needs for execution. The share of the system resources allocated to the user is directly related to the rate at which the user receives money; the rate at which the user transfers money into a job expense account controls the job's performance. We prove that starvation is not possible in our model. Simulation results show that our scheduler improves both system and user performances in comparison with two different variable partitioning policies. It is also shown to be effective in guaranteeing fairness and providing control over the performance of jobs. Author

N95-32257# Primal Solutions, Inc., Palo Alto, CA.
USER-FRIENDLY MICROCOMPUTER INTERFACE WITH OPTIMIZATION LANGUAGES AF94-007 Final Report, 15 Jun. - 15 Dec. 1994
Sam Savage 15 Dec. 1994 15 p
(Contract F49620-94-C-0045)
(AD-A293184; AFOSR-95-0225TR) Avail: CASI HC A03/MF A01

All Phase 1 goals were met. Add-in command for IMPROV were developed that allowed specification of variables and constraints, translation, optimization, and display of results. DTIC

61 COMPUTER PROGRAMMING AND SOFTWARE

Includes computer programs, routines, alogorithms, and specific applications, e.g., CAD/CAM.

N95-30376# Sandia National Labs., Albuquerque, NM.
A PHENOMENOLOGICAL FINITE ELEMENT MODEL OF PART BUILDING IN THE STEREOLITHOGRAPHY PROCESS
R. S. Chambers, T. R. Guess, and T. D. Hinnerichs 1995 10 p Presented at the 6th International Conference on Rapid Prototyping, Dayton, OH, 4-8 Jun. 1995
(Contract DE-AC04-94AL-85000)
(DE95-008437; SAND-94-2565C; CONF-9506149-2) Avail: CASI HC A02/MF A01

The finite element method has been used to develop the framework for a tool that can be used to model the structural deformation arising from the stereolithography build process. Such a tool when fully developed can facilitate numerical studies aimed at evaluating build parameters and

build styles. Although the current software makes no attempt to capture all the physics of the process, provisions for three important build features have been made: (1) laser path history including scanning rate and depth of cure, (2) structural linkage, and (3) time varying material behavior. For demonstration purposes, a three dimensional finite element code was modified to include a phenomenological material model of solidification. The model was based on cure shrinkage and stress relaxation data collected from in-situ tests on individual strands drawn using 3D Systems' stereolithography apparatus (SLA-250). To depict the directed path of solidification within layers, a finite element birthing scheme was conceived to activate elements along the predetermined coordinate path of the laser. Structural linkage was enforced by joining element strands of layers when laser paths connect or overlap, respectively. A limited number of analyses have been performed to contrast simple build styles. DOE

N95-30397# Army Research Lab., White Sands Missle Range, NM. Battlefield Environment Directorate.
USER'S MANUAL FOR THE SCANNING FAST FIELD PROGRAM (SCAFFIP) EOSAEL VERSION 1.0
John M. Noble and Dave Marlin Jan. 1995 115 p
(AD-A291445; ARL-TR-282) Avail: CASI HC A06/MF A02

The Scanning Fast Field Program (SCAFFIP) is an atmospheric acoustic propagation model incorporating many of the effects on the environment on the sound field such as geometrical spreading, refraction, diffraction, molecular absorption, and complex ground impedance. SCAFFIP provides range estimations from the sensor or target for signal-noise of -10, -5, 0, 5, and 10 dB (re: 20 micro-Pa) with azimuth for a given geometry, sound level of target at a given frequency, and meteorological profile. The meteorological profile and the geometry provides the model the ability to calculate the sound speed profile. The geometry profile is required because the angular dependence of the sound speed on the wind direction is relative to the direction of propagation. This model works over a flat-earth and a nonturbulent atmosphere. Even with these restrictions, the model performs very well for many scenarios. The model contains a friendly user interface requiring a minimum amount of information to run the model. There are also flags that can be set to obtain more detailed information. DTIC

N95-30454# Technische Univ., Twente (Netherlands). Dept. of Computer Science.
EXPERIMENTAL RESEARCH INTO USABILITY AND ORGANIZATION IMPACT OF WORKFLOW SOFTWARE
P. Boersma, S. Joosten, and G. vanderVeer Dec. 1994 25 p
(PB95-197679; Memo-INF-94-77) Copyright Avail: CASI HC A03/MF A01

The University of Twente has started an Open Workflow Laboratory (OWL) to facilitate experimental research in the area of workflow software. This article reports the setup, adopted method and results of the first two experiments conducted in this laboratory. In a simulated office environment two groups of 4 and 5 subjects both used a non-workflow and a workflow application to deal with instances of a loan application process. The results show an increase in productivity and waiting times, and mixed effects on consultation times. Recommendations regarding future experiments and the Open Workflow Laboratory are given and a scenario for future workflow experiments is proposed. NTIS

N95-30501# Norwegian Defence Research Establishment, Kjeller (Norway).
BASIS IMAGE PROCESSOR PR5200: MODULE COMMON PART
K. Tvete 11 Jan. 1995 154 p
(PB95-212023) Avail: CASI HC A08/MF A02

Features which are common for Coprocessor modules are implemented in the hardware design Module Common Part. The Module Common Part can roughly be divided into three sections: the Image Bus Interface, the Coprocessor Service Bus Interface, and the Board Transputer. The Module Common Part design will be included in a Coprocessor board design. NTIS

N95-30539 Newcastle-upon-Tyne Univ., Newcastle (England). Dept. of Computing Science.
C++ AS AN INTRODUCTORY PROGRAMMING LANGUAGE
P. A. Lee and R. J. Stroud Oct. 1994 22 p
(PB95-195715; TRS-496) Copyright Avail: Issuing Activity (National Technical Information Service (NTIS))

The paper discusses some of the factors that led to the University of Newcastle upon Tyne deciding to change to C++ as its introductory teaching language. NTIS

N95-30568# Helsinki Univ. of Technology, Espoo (Finland).
FEATURE-BASED MODELING OF PRODUCT FAMILIES
T. Laakko and M. Maentylae 1994 22 p
(PB95-207148; TKK-TKO-B117) Avail: CASI HC A03/MF A01

A feature-based product modeling system is introduced where the user can incrementally create and modify product families. Product family and feature descriptions are coded in a special definition language and can be easily added and modified by the user. The descriptions include dynamically maintained constraints. The definition language description of a new family can be automatically created on the basis of a recognized prototypical instance. A stored design history can be used for generating the geometry definition of the family. NTIS

N95-30584*# Institute for Computer Applications in Science and Engineering, Hampton, VA.
AN EXECUTABLE SPECIFICATION FOR THE MESSAGE PROCESSOR IN A SIMPLE COMBINING NETWORK Final Report
David Middleton Jun. 1995 39 p
(Contract NAS1-19480; RTOP 505-90-52-01)
(NASA-CR-198174; ICASE-95-47; NAS 1.26:198174) Avail: CASI HC A03/MF A01

While the primary function of the network in a parallel computer is to communicate data between processors, it is often useful if the network can also perform rudimentary calculations. That is, some simple processing ability in the network itself, particularly for performing parallel prefix computations, can reduce both the volume of data being communicated and the computational load on the processors proper. Unfortunately, typical implementations of such networks require a large fraction of the hardware budget, and so combining networks are viewed as being impractical. The FFP Machine has such a combining network, and various characteristics of the machine allow a good deal of simplification in the network design. Despite being simple in construction however, the network relies on many subtle details to work correctly. This paper describes an executable model of the network which will serve several purposes. It provides a complete and detailed description of the network which can substantiate its ability to support necessary functions. It provides an environment in which algorithms to be run on the network can be designed and debugged more easily than they would on physical hardware. Finally, it provides the foundation for exploring the design of the message receiving facility which connects the network to the individual processors. Author

N95-30598 Norwegian Inst. for Air Research, Kjeller (Norway).
CESAR3 MALU LIBRARY
H. Bjordal 1994 80 p
(Proj. FFIE/654/170)
(PB95-211363; FFI/RAPPORT-94/5417) Avail: Issuing Activity (National Technical Information Service (NTIS))

All the available programs for Microprogrammable Arithmetic Logic Unit (MALU), the computational unit in the Computer for Experimental Synthetic Aperture Radar-3 (Cesar3) vector processor system, are described. The report also includes a very short overview of the MALU programming tools. NTIS

N95-30602# Los Alamos National Lab., NM.
SENSOR FUSION AND NONLINEAR PREDICTION FOR ANOMALOUS EVENT DETECTION
Jose V. Hernandez, Kurt R. Moore, and Richard C. Elphic Mar. 1995 15 p Presented at the SPIE International Symposium on Aerospace/Defense Sensing and Dual-use Photonics, Orlando, FL, 17-21 Apr. 1995
(Contract W-7405-eng-36)
(DE95-009429; LA-UR-95-883; CONF-950472-4) Avail: CASI HC A03/MF A01

The authors consider the problem of using the information from various time series, each one characterizing a different physical quantity, to predict

the future state of the system and, based on that information, to detect and classify anomalous events. They stress the application of principal components analysis (PCA) to analyze and combine data from different sensors. They construct both linear and nonlinear predictors. In particular, for linear prediction the authors use the least-mean-square (LMS) algorithm and for nonlinear prediction they use both backpropagation (BP) networks and fuzzy predictors (FP). As an application, they consider the prediction of gamma counts from past values of electron and gamma counts recorded by the instruments of a high altitude satellite. DOE

N95-30603# Los Alamos National Lab., NM.
PERIODICALLY SPECIFIED PROBLEMS: AN EXPONENTIAL COMPLEXITY GAP BETWEEN EXACT AND APPROXIMATE SOLUTIONS
H. B. Hunt, III (Albany Univ., Albany, NY.), D. J. Rosenkrantz (Albany Univ., Albany, NY.), R. E. Stearns (Albany Univ., Albany, NY.), M. V. Marathe (Albany Univ., Albany, NY.), and V. Radhakrishnan (Hewlett-Packard Co., Cupertino, CA.) 28 Nov. 1994 19 p Presented at the 27th ACM Annual Symposium on Theory of Computing, Livermore, CA, Mar. 1995
(Contract W-7405-eng-36; NSF CCR-89-03319; NSF CCR-89-05296; NSF CCR-90-06396; NSF CCR-94-06611)
(DE95-009435; LA-UR-95-20; CONF-9503122-1) Avail: CASI HC A03/MF A01

We study both the complexity and approximability of various graph and combinatorial problems specified using two dimensional narrow periodic specifications. The following two general kinds of results are presented. (1) We prove that a number of natural graph and combinatorial problems are NEXPTIME- or EXPSPACE-complete when instances are so specified. (2) In contrast, we prove that the optimization versions of several of these NEXPTIME-, EXPSPACE-complete problems have polynomial time approximation algorithms with constant performance guarantees. Moreover, some of these problems even have polynomial time approximation schemes. We also sketch how our NEXPTIME-hardness results can be used to prove analogous NEXPTIME-hardness results for problems specified using other kinds of succinct specification languages. Our results provide the first natural problems for which there is a proven exponential (and possibly doubly exponential) gap between the complexities of finding exact and approximate solutions. DOE

N95-30625 Selskapet for Industriell og Teknisk Forskning, Oslo (Norway).
REFINEMENT TECHNIQUES IN COMPUTER GRAPHICS
M. Daehlen and T. Lyche 30 Aug. 1994 37 p Prepared in cooperation with Oslo Univ.
(PB95-208526; STF33-A94043) Avail: Issuing Activity (National Technical Information Service (NTIS))

With the emphasis on applications within computer graphics, this paper gives an introduction to refinement techniques, including knot insertion for splines, 'corner cutting' methods and some interpolatory subdivision schemes for curves and surfaces. NTIS

N95-30662 Selskapet for Industriell og Teknisk Forskning, Trondheim (Norway).
UNIX AND PC SECURITY IN A NETWORK ENVIRONMENT. UNINETT
S. Haug 26 Sep. 1994 33 p
(PB95-196291; STF13-S94002) Avail: Issuing Activity (National Technical Information Service (NTIS))

The document is a collection of transparencies from a presentation on computer security issues when converting to UNIX, in a mixed personal computer (PC)/UNIX environment, or when connecting to an external network. The talk was given at the Uninett Bo conference held October 4-6, 1993. NTIS

N95-30663 Selskapet for Industriell og Teknisk Forskning, Trondheim (Norway). Dept. of Instrumentation.
DEVELOPMENT OF FLEXIBLE FEEDER TECHNIQUES
K. Aamold and B. Langbeck 19 Jul. 1994 13 p
(PB95-196317; STF31-A94033) Avail: Issuing Activity (National Technical Information Service (NTIS))

The FAMOS Flexfeed project has been established to focus feeding of small parts in assembly systems. The project aims at finding more flexible feeder solutions for small parts. Modularity, standard units and cost effective use of sensors are keywords for more flexible feeders that will be included in a new 'tool-box concept'. In addition to new feeding methods and solutions, the project partners expect knowledge gained in the area of feeding technology as an important result from the project. Intermediate results in the project will be applied and tested in the end-user facilities during the project. Practical use of new technology or new use of old technology are keywords for success. NTIS

N95-30697 Selskapet for Industriell og Teknisk Forskning, Trondheim (Norway).
UNIX AND PC SECURITY IN A NETWORK ENVIRONMENT. LOKALNETT 1993
S. Haug 26 Sep. 1994 34 p
(PB95-196309; STF13-S94003) Avail: Issuing Activity (National Technical Information Service (NTIS))

The document is a collection of transparencies from a presentation on computer security issues when converting to UNIX, in a mixed personal computer (PC)/UNIX environment, or when connecting to an external network. The talk was given at the Lokalnett conference held October 13-15, 1993. NTIS

N95-30759# Japan Atomic Energy Research Inst., Tokyo (Japan).
DEVELOPMENT OF BERMUDA: A RADIATION TRANSPORT CODE SYSTEM. PART 3: A ONE-DIMENSIONAL ADJOINT NEUTRON TRANSPORT CODE
Tomoo Suzuki (Nuclear Energy Data Center, Japan.), Akira Hasegawa, Shun-ichi Tanaka, and Hiroshi Nakashima Jul. 1994 29 p
(DE95-717875; JAERI-Data/Code-94-002-Pt-3) Avail: CASI HC A03/MF A01

A radiation transport code system BERMUDA has been developed for one-, two-, and three-dimensional geometry. The purpose of the development is to establish a basis of an accurate shielding calculation method for general use. The time-independent transport equation is numerically solved using a direct spatial integration method in a multigroup model, to obtain spatial, angular, and energy distribution of neutron, gamma rays, or adjoint neutron flux. Reported is the deveiopment of an adjoint neutron transport code for one-dimensional spherical geometry. Adjoint neutron flux is used in a sensitivity analysis or in a perturbation calculation. Use of the spherical harmonics expansion is avoided in representing anisotropy of both angular flux and scattering cross section. A group-angle transfer matrix is obtained by integrating double-differential cross sections numerically, taking energy-angle correlation into account. A first collision source method is utilized for a case of point source. Angular flux distribution is obtained by integrating the transport equation over a line segment along each angular discrete ordinate toward each spatial mesh point. A fine energy grid method is used, with a rebalancing scheme concerning the number of gain and loss of particles over each spatial region and also in each energy grid. Validity of the present code BERMUDA-1DNA has been tested for five sample problems by comparing the calculated results with those from the forward neutron transport code BERMUDA-1DN. The tests have shown that accurate results are obtainable with BERMUDA-1DNA. The derivation of the adjoint equation, the calculational method, and the validity tests are described. Job control languages, input data specifications, and output data are also described so that the present report is available as a user's manual. DOE

N95-30792# Royal Inst. of Tech., Stockholm (Sweden). Dept. of Mathematics.
SIMPLEX METHOD FOR SEMI-DEFINITE PROGRAMMING: OPTIMIZATION AND SYSTEMS THEORY
U. Braennlund 1994 7 p
(PB95-212122; TRITA/MAT-94-47) Avail: CASI HC A02/MF A01

We present a simplex method for semi-definite programming. The method is based on standard column generation. NTIS

N95-30796# Sandia National Labs., Albuquerque, NM.
THE ROLE OF ADVANCED ENGINEERING SIMULATION IN MODEL-BASED DESIGN
P. J. Hommert and J. H. Biffle 1995 6 p Presented at the Agile Manufacturing Conference, Albuquerque, NM, 16-17 Mar. 1995
(Contract DE-AC04-94AL-85000)

(DE95-008815; SAND-95-0492C; CONF-9503112-2) Avail: CASI HC A02/MF A01

The agile manufacturing paradigm engenders many new concepts and work approaches for manufacturing operations. A technology often invoked in the concept of agility is modeling and simulation. Few would disagree that modeling and simulation holds the potential to substantially reduce the product development cycle and lead to improve product reliability and performance. Advanced engineering simulation can impact manufacturing in three areas: process design, product design, and process control. However, despite that promise, the routine utilization of modeling and simulation by industry within the design process is very limited. Advanced simulation is still used primarily in a troubleshooting mode examining design or process problems after the fact. Sandia National Laboratories has been engaged in the development of advanced engineering simulation tools for many years and more recently has begun to focus on the application of such models to manufacturing processes important for the defense industry. These efforts involve considerable interaction and cooperative research with US industry. Based upon this experience, this presentation examines the elements that are necessary for advanced engineering simulation to become an integral part of the design process. DOE

N95-30831 Stanford Univ., CA.

A GRAPHICAL PROGRAMMING LANGUAGE FOR SERVICE ROBOTS IN SEMI-STRUCTURED ENVIRONMENTS Ph.D. Thesis

David Spencer Lees 1994 154 p

Avail: Univ. Microfilms Order No. DA9422101

One of the main obstacles to programming a robot to do useful work is the difficulty of establishing effective, efficient communication between the programmer and the robot. In many environments we cannot depend on CAD drawings or a pre-existing assembly sequence to specify the motions that the robot must execute. However, in most cases the programmer can envision the task that the robot is to accomplish. The difficulty lies in creating a user interface that effectively communicate the programmer's wishes to the robot. To address this problem, an environment for programming robot manipulations with graphical symbols (RoboGlyph) was developed, and experiments were conducted to evaluate its performance. Programs are assembled by dragging symbols representing robot positions and actions onto a 'story-board' that stores the sequence of motions needed to perform a task. Also, force-sensing is used to detect and control interactions with the environment, so the user is not responsible for fine-positioning tasks. The RoboGlyph system is being used to program a service robot for severely disabled (high-level quadriplegic) users. In service applications, it is valuable if the users of a robot can modify its manipulation programs themselves. RoboGlyph was designed to be easier to use and more reliable than traditional text-based programming languages and to be accessible to a wider user population. Experiments with RoboGlyph have shown that, after only one or two hours of training, computer literate health care professionals with no robotics experience can write working robot programs as quickly as expert robot programmers. Expert programmers who use RoboGlyph can program at least as fast as they can with textual robot programming languages, after only one hour of training. The programs written by all RoboGlyph users were much easier to read and maintain than those written in text-based languages. Dissert. Abstr.

N95-30903# Carnegie-Mellon Univ., Pittsburgh, PA. Software Engineering Inst.

SUMMARY OF TECHNICAL OPERATIONS

1994 55 p

(AD-A293224) Avail: CASI HC A04/MF A01

The Software Process Program focuses on improving the process of software development. Projects within the program are appraising and teaching others to appraise the actual practice of software engineering in the software community, training organizations to gain management control over their software development processes, supporting the use of quantitative methods and measures as a basis for process improvement, and developing improved methods for software process management. DTIC

N95-30931# Massachusetts Inst. of Tech., Lexington, MA.

RASSP BENCHMARK 1 EXECUTABLE REQUIREMENTS USER'S MANUAL Project Report

Allan H. Anderson and Gary A. Shaw 20 Dec. 1994 48 p

(Contract F19628-95-C-0002)

(AD-A290060; RASSP-2; ESC-TR-94-114) Avail: CASI HC A03/MF A01

This User's Manual describes the installation and use of a set of computer programs and data files which comprise the Executable Requirement for the first benchmark in the RASSP program. The VHDL programs provide a simulation of a Synthetic Aperture Radar processor and a test bench for the simulation. Several C-language utility programs and an image display program are provided. Two sets of data, one from an airborne radar and one synthetic, and images created from the data by a C-language implementation of the SAR algorithm are described. Example scripts for execution of the simulation on Vantage and Mentor simulators are presented along with performance data from example runs. DTIC

N95-30968# Naval Research Lab., Bay Saint Louis, MS.

FISHFINDE: INTERACTIVE SOFTWARE PACKAGE TO PREDICT FISH LOCATIONS USING SATELLITE IMAGE DATA AND FISH SPECIES BEHAVIOR RULES Final Report

Robert A. Arnone, R. A. Oriol, R. Crout, and Paul M. Martinolich 10 Feb. 1995 31 p

(AF Proj. R03-5-B)

(AD-A293394; NRL/MR/7420-94-7566) Avail: CASI HC A03/MF A01

A software program has been developed to aid in the prediction of fish location. Satellite and geophysical oceanographic databases have been assembled for the west coast of the U.S. which are used to predict the locations of fish. A user interactive graphical interface written in Interactive Data Language visually displays the databases and connects a series of fish rules by performing logical operations. The resultant bitmap displays the intersection of the rules which are the locations of possible fish locations. The fish rules are still under development. The software provides a real time interactive display for testing and developing an understanding of fish behavior. DTIC

N95-30999# Air Force Inst. of Tech., Wright-Patterson AFB, OH. School of Engineering.

UNIFICATION OF LARCH AND Z-BASED OBJECT MODELS TO SUPPORT ALGEBRAICALLY-BASED DESIGN REFINEMENT: THE LARCH PERSPECTIVE M.S. Thesis

Catherine J. Lin Dec. 1994 165 p

(AD-A289235; AFIT/GSC/ENG/94D-15) Avail: CASI HC A08/MF A02

This research describes the feasibility of developing object-oriented LARCH specifications, part of a dual approach for formally extending object-oriented analysis models using LARCH and Z. The first phase consisted of two steps: establishing a set of transformation heuristics for algebraically representing object models and implementing a robust LARCH parser. The LARCH parser produced abstract syntax trees (AST's) of objects forming the basis for analyzing the similarities and differences between Z-based and LARCH-based object representations. The second phase used the analysis of LARCH and Z to identify fundamental core constructs in the languages and abstract syntax trees. These core constructs consisted of similar syntactic and semantic notions of signatures and axioms for describing a problem domain, thereby forming a canonical framework for formal object representations. This canonical framework provides a front-end for producing design refinement artifacts such as interface languages theorem proving sentences, and synthesis diagrams. The final phase demonstrated the feasibility of interface language generation by establishing an executable framework. This executable framework mapped LARCH into the SOFTWARE REFINERY(TM) Programming Environment to rapidly prototype object-oriented LARCH specifications. DTIC

N95-31001# Naval Air Warfare Center, Arlington, VA.

OPERATOR'S HANDBOOK: NAWC SOFTWARE PRODUCTION FACILITY

Jan. 1995 28 p

(AD-A290216) Avail: CASI HC A03/MF A01

The Software Production Facility (SPF) was developed as a state-of-the-art replacement for the VP's Program Generation Center (PGC). The PGC, created in the 1960's, was established as a support center for the development and maintenance of the P3 mission software for the CP-901 military computer. The SPF allows user generated databases and media to be developed utilizing the NAWC Ethernet Bridge thus eliminating the outdated use of program decks, and thereby providing improved utility and user interface processing. DTIC

N95-31050# Mitre Corp., McLean, VA.
CONFEDERATION VERIFICATION, VALIDATION, AND ACCREDITATION MASTER PLAN (CVVAMP). TECHNICAL TEST PLAN Final Report
Apr. 1994 15 p
(AD-A289717) Avail: CASI HC A03/MF A01

The 1994 Confederation of Models is a set of DOD training simulations from each branch of the service which utilize the Aggregate Level Simulation Protocol (ALSP) to interact The Confederation Verification, Validation, and Accreditation Master Plan (CVVAMP) consists of a several test plans and reports which include the: (1) Confederation of Models Verification, Validation, and Accreditation Master Plan; (2) Technical Test Plan; (3) Integrated Test Plan; (4) Load Test Plan; (5) Verification Test Plan. Related reports include the: (1) Accreditation Report for the Confederation of Models in General Headquarters 94; (2) Recommendations on the Use ofthe Seven Member Confederation of Models. The Technical Test Plan outlines test steps and test verification procedures for areas to include test setup, join/refresh/resign, time synchronization, filter operations, confederation save and restore, and ghosting objects. DTIC

N95-31056# Lawrence Livermore National Lab., Livermore, CA.
IMAGE ENHANCEMENT BY EDGE-PRESERVING FILTERING
Yiu-fai Wong Nov. 1994 5 p Presented at the Institute of Electrical and Electronics Engineers (IEEE) International Conference on Image Processing, Austin, TX, 13-16 Nov. 1994
(Contract W-7405-eng-48)
(DE95-008077; UCRL-JC-116695; CONF-9411104-3) Avail: CASI HC A01/MF A01

Image enhancement is useful when the details in an image are lost due to various reasons. It is common to subtract a mask from a given image to enhance the details. The trick is how to obtain a good mask. We describe here how an edge-preserving filter can be used to generate a mask which is smooth over areas with fine details, yet preserving most of the edges. Experiments with real images show that our scheme is very effective. DOE

N95-31109# Oak Ridge National Lab., TN.
A SCALABLE PARALLEL STRASSEN'S MATRIX MULTIPLY ALGORITHM FOR DISTRIBUTED MEMORY COMPUTERS
Q. Luo and J. B. Drake 1995 7 p Presented at the Symposium on Applied Computing (SAC '95), Nashville, TN, 26-28 Feb. 1995
(Contract DE-AC05-84OR-21400)
(DE95-010213; CONF-950242-2) Avail: CASI HC A02/MF A01

The authors present a scalable parallel Strassen's matrix multiply algorithm for distributed memory, message passing computers. Strassen's algorithm to multiply two N x N matrices reduces the asymptotic operation count from O(N(exp 3)) of the traditional algorithm to O(N(exp 2.81)). In a sequential implementation the Strassen's algorithm offers better performance even for relatively low order matrices. However, due to its complexity, the parallel Strassen's algorithm is less than straight forward. Here a scalable parallel Strassen's algorithm is presented and compared with several other parallel algorithms. Performances of these algorithms are tested on a 128-processor Intel iPSC/860. DOE

N95-31228# Defence Science and Technology Organisation, Canberra (Australia).
AN APPROACH TO AUTOMATED REASONING ABOUT OPERATIONAL SEMANTICS Research Report
A. Cant and M. A. Ozols Aug. 1994 58 p
(AD-A291127; DSTO-RR-0008; DODA-AR-008-926) Avail: CASI HC A04/MF A01

The assurance of the safety or security of critical software rests on a clear understanding of the formal semantics of the programming language used. Operational semantics is the most widely used means of formally defining a language. The need for high levels of assurance, along with the complexity of these definitions for real programming languages, means that tool support is essential for carrying out reasoning about code with respect to the language definition. In this paper, we describe a generic approach to automated reasoning about the operational semantics of programming languages. As an application of this approach, we describe the construction of an environment for reasoning about programs written in a functional subset of ML. The system we describe (called Elle) captures the formal operational semantics definition of a large subset of Standard ML within the theorem prover Isabelle, and provides some support for the verification of ML programs. DTIC

N95-31234*# National Aeronautics and Space Administration. Goddard Space Flight Center, Greenbelt, MD.
PROCEEDINGS OF THE 19TH ANNUAL SOFTWARE ENGINEERING WORKSHOP
Dec. 1994 364 p Workshop held in Greenbelt, MD, 30 Nov. - 1 Dec. 1994
(NASA-CR-189411; NAS 1.26:189411; SEL-94-006) Avail: CASI HC A16/MF A03

The Software Engineering Laboratory (SEL) is an organization sponsored by NASA/GSFC and created to investigate the effectiveness of software engineering technologies when applied to the development of applications software. The goals of the SEL are: (1) to understand the software development process in the GSFC environment; (2) to measure the effects of various methodologies, tools, and models on this process; and (3) to identify and then to apply successful development practices. The activities, findings, and recommendations of the SEL are recorded in the Software Engineering Laboratory Series, a continuing series of reports that include this document. For individual titles, see N95-31235 through N95-31252.

N95-31235*# National Aeronautics and Space Administration. Goddard Space Flight Center, Greenbelt, MD.
CHANGES AND CHALLENGES IN THE SOFTWARE ENGINEERING LABORATORY
Rose Pajerski *In its* Proceedings of the 19th Annual Software Engineering Workshop Dec. 1994 p 3-10 (For primary document see N95-31234 11-61)
Avail: CASI HC A02/MF A03

Since 1976, the Software Engineering Laboratory (SEL) has been dedicated to understanding and improving the way in which one NASA organization, the Flight Dynamics Division (FDD), develops, maintains, and manages complex flight dynamics systems. The SEL is composed of three member organizations: NASA/GSFC, the University of Maryland, and Computer Sciences Corporation. During the past 18 years, the SEL's overall goal has remained the same: to improve the FDD's software products and processes in a measured manner. This requires that each development and maintenance effort be viewed, in part, as a SEL experiment which examines a specific technology or builds a model of interest for use on subsequent efforts. The SEL has undertaken many technology studies while developing operational support systems for numerous NASA spacecraft missions. Derived from text

N95-31236*# Maryland Univ., College Park, MD. Dept. of Computer Science.
DOMAIN ANALYSIS FOR THE REUSE OF SOFTWARE DEVELOPMENT EXPERIENCES
V. R. Basili, L. C. Briand (CRIM, Montreal, Quebec.), and W. M. Thomas *In* NASA. Goddard Space Flight Center, Proceedings of the 19th Annual Software Engineering Workshop Dec. 1994 p 11-34 Sponsored in part by the National Science Foundation and CRIM (For primary document see N95-31234 11-61)
(Grant NAG5-123)
Avail: CASI HC A03/MF A03

We need to be able to learn from past experiences so we can improve our software processes and products. The Experience Factory is an organizational structure designed to support and encourage the effective reuse of software experiences. This structure consists of two organizations which separates project development concerns from organizational concerns of experience packaging and learning. The experience factory provides the processes and support for analyzing, packaging, and improving the organization's stored experience. The project organization is structured to reuse this stored experience in its development efforts. However, a number of questions arise: What past experiences are relevant? Can they all be used (reused) on our current project? How do we take advantage of what has been learned in other parts of the organization? How do we take advantage of experience in the world-at-large? Can someone else's best practices be used in our organization with confidence? This paper describes approaches to help answer these questions. We propose both quantitative

and qualitative approaches for effectively reusing software development experiences. Derived from text

N95-31237*# National Aeronautics and Space Administration. Goddard Space Flight Center, Greenbelt, MD.

BUILDING AN EXPERIENCE FACTORY FOR MAINTENANCE

Jon D. Valett, Steven E. Condon (Computer Sciences Corp., Lanham, MD.), Lionel Briand (Maryland Univ., College Park, MD.), Yong-Mi Kim (Maryland Univ., College Park, MD.), and Victor R. Basili (Maryland Univ., College Park, MD.) *In its* Proceedings of the 19th Annual Software Engineering Workshop Dec. 1994 p 35-54 (For primary document see N95-31234 11-61)

Avail: CASI HC A03/MF A03

This paper reports the preliminary results of a study of the software maintenance process in the Flight Dynamics Division (FDD) of the National Aeronautics and Space Administration/Goddard Space Flight Center (NASA/GSFC). This study is being conducted by the Software Engineering Laboratory (SEL), a research organization sponsored by the Software Engineering Branch of the FDD, which investigates the effectiveness of software engineering technologies when applied to the development of applications software. This software maintenance study began in October 1993 and is being conducted using the Quality Improvement Paradigm (QIP), a process improvement strategy based on three iterative steps: understanding, assessing, and packaging. The preliminary results represent the outcome of the understanding phase, during which SEL researchers characterized the maintenance environment, product, and process. Findings indicate that a combination of quantitative and qualitative analysis is effective for studying the software maintenance process, that additional measures should be collected for maintenance (as opposed to new development), and that characteristics such as effort, error rate, and productivity are best considered on a 'release' basis rather than on a project basis. The research thus far has documented some basic differences between new development and software maintenance. It lays the foundation for further application of the QIP to investigate means of improving the maintenance process and product in the FDD. Author

N95-31238*# Computer Sciences Corp., Lanham, MD.

CLOSING THE LOOP ON IMPROVEMENT: PACKAGING EXPERIENCE IN THE SOFTWARE ENGINEERING LABORATORY

Sharon R. Waligora, Linda C. Landis, and Jerry T. Doland *In* NASA. Goddard Space Flight Center, Proceedings of the 19th Annual Software Engineering Workshop Dec. 1994 p 55-76 (For primary document see N95-31234 11-61)

Avail: CASI HC A03/MF A03

As part of its award-winning software process improvement program, the Software Engineering Laboratory (SEL) has developed an effective method for packaging organizational best practices based on real project experience into useful handbooks and training courses. This paper shares the SEL's experience over the past 12 years creating and updating software process handbooks and training courses. It provides cost models and guidelines for successful experience packaging derived from SEL experience. Author

N95-31239*# Motorola, Inc., Arlington Heights, IL.

PROCESS MATURITY PROGRESS AT MOTOROLA CELLULAR SYSTEMS DIVISION

Ron Borgstahl, Mark Criscione, Kim Dobson, and Allan Willey *In* NASA. Goddard Space Flight Center, Proceedings of the 19th Annual Software Engineering Workshop Dec. 1994 p 79-90 (For primary document see N95-31234 11-61)

Avail: CASI HC A03/MF A03

We believe that the key success elements are related to our recognition that Software Process Improvement (SPI) can and should be organized, planned, managed, and measured as if it were a project to develop a new process, analogous to a software product. We believe that our process improvements have come as the result of these key elements: use of a rigorous, detailed requirements set (Capability Maturity Model, CMM); use of a robust, yet flexible architecture (IEEE 1074); use of a SPI project, resourced and managed like other work, to produce the specifications and implement them; and development of both internal and external goals, with metrics to support them. Derived from text

N95-31240*# Software Technology, Process and People, Bradford Woods, PA.

THE PERSONAL SOFTWARE PROCESS: DOWNSCALING THE FACTORY

Daniel M. Roy *In* NASA. Goddard Space Flight Center, Proceedings of the 19th Annual Software Engineering Workshop Dec. 1994 p 91-112 (For primary document see N95-31234 11-61)

Avail: CASI HC A03/MF A03

It is argued that the next wave of software process improvement (SPI) activities will be based on a people-centered paradigm. The most promising such paradigm, Watts Humphrey's personal software process (PSP), is summarized and its advantages are listed. The concepts of the PSP are shown also to fit a down-scaled version of Basili's experience factory. The author's data and lessons learned while practicing the PSP are presented along with personal experience, observations, and advice from the perspective of a consultant and teacher for the personal software process. Author

N95-31241*# Master Systems, Inc., McLean, VA.

APPLYING PROGRAM COMPREHENSION TECHNIQUES TO IMPROVE SOFTWARE INSPECTIONS

Stan Rifkin and Lionel Deimel (Deimel, Lionel, Pittsburgh, PA.) *In* NASA. Goddard Space Flight Center, Proceedings of the 19th Annual Software Engineering Workshop Dec. 1994 p 115-126 (For primary document see N95-31234 11-61)

Avail: CASI HC A03/MF A03

Software inspections are widely regarded as a cost-effective mechanism for removing defects in software, though performing them does not always reduce the number of customer-discovered defects. We present a case study in which an attempt was made to reduce such defects through inspection training that introduced program comprehension ideas. The training was designed to address the problem of understanding the artifact being reviewed, as well as other perceived deficiencies of the inspection process itself. Measures, both formal and informal, suggest that explicit training in program understanding may improve inspection effectiveness. Author

N95-31242*# Maryland Univ., College Park, MD. Dept. of Computer Science.

AN EXPERIMENT TO ASSESS THE COST-BENEFITS OF CODE INSPECTIONS IN LARGE SCALE SOFTWARE DEVELOPMENT

A. Porter, H. Siy, C. A. Toman (Bell Telephone Labs., Inc., Naperville, IL.), and L. G. Votta (Bell Telephone Labs., Inc., Naperville, IL.) *In* NASA. Goddard Space Flight Center, Proceedings of the 19th Annual Software Engineering Workshop Dec. 1994 p 127-150 (For primary document see N95-31234 11-61)

(Grant NAG5-123)

Avail: CASI HC A01/MF A03

This experiment (currently in progress) is designed to measure costs and benefits of different code inspection methods. It is being performed with a real development team writing software for a commercial product. The dependent variables for each code unit's inspection are the elapsed time and the number of defects detected. We manipulate the method of inspection by randomly assigning reviewers, varying the number of reviewers and the number of teams, and, when using more than one team, randomly assigning author repair and non-repair of detected defects between code inspections. After collecting and analyzing the first 17 percent of the data, we have discovered several interesting facts about reviewers, about the defects recorded during reviewer preparation and during the inspection collection meeting, and about the repairs that are eventually made. (1) Only 17 percent of the defects that reviewers record in their preparations are true defects that are later repaired. (2) Defects recorded at the inspection meetings fall into three categories: 18 percent false positives requiring no author repair, 57 percent soft maintenance where the author makes changes only for readability or code standard enforcement, and 25 percent true defects requiring repair. (3) The median elapsed calendar time for code inspections is 10 working days - 8 working days before the collection meeting and 2 after. (4) In the collection meetings, 31 percent of the defects discovered by reviewers during preparation are suppressed. (5) Finally, 33 percent of the true defects recorded are discovered at the collection meetings and not during any reviewer's preparation. The results to date suggest that inspections with two sessions (two different teams) of

two reviewers per session (2sX2p) are the most effective. These two-session inspections may be performed with author repair or with no author repair between the two sessions. We are finding that the two-session, two-person with repair (2sX2pR) inspections are the most expensive, taking 15 working days of calendar time from the time the code is ready for review until author repair is complete, whereas two-session, two-person with no repair (2sX2pN) inspections take only 10 working days, but find about 10 percent fewer defects. Author

N95-31243*# West Virginia Univ., Fairmont, WV. NASA Software Independent Verification and Validation Facility.

A PROCESS IMPROVEMENT MODEL FOR SOFTWARE VERIFICATION AND VALIDATION

John Callahan and George Sabolish *In* NASA. Goddard Space Flight Center, Proceedings of the 19th Annual Software Engineering Workshop Dec. 1994 p 151-170 (For primary document see N95-31234 11-61)
(Contract NCCw-0040)
Avail: CASI HC A03/MF A03

We describe ongoing work at the NASA Independent Verification and Validation (IV&V) Facility to establish a process improvement model for software verification and validation (V&V) organizations. This model, similar to those used by some software development organizations, uses measurement-based techniques to identify problem areas and introduce incremental improvements. We seek to replicate this model for organizations involved in V&V on large-scale software development projects such as EOS and space station. At the IV&V Facility, a university research group and V&V contractors are working together to collect metrics across projects in order to determine the effectiveness of V&V and improve its application. Since V&V processes are intimately tied to development processes, this paper also examines the repercussions for development organizations in large-scale efforts. Author

N95-31244*# National Aeronautics and Space Administration. Ames Research Center, Moffett Field, CA.

LEVERAGING OBJECT-ORIENTED DEVELOPMENT AT AMES

Greg Wenneson and John Connell *In* NASA. Goddard Space Flight Center, Proceedings of the 19th Annual Software Engineering Workshop Dec. 1994 p 173-190 (For primary document see N95-31234 11-61)
Avail: CASI HC A03/MF A03

This paper presents lessons learned by the Software Engineering Process Group (SEPG) from results of supporting two projects at NASA Ames using an Object Oriented Rapid Prototyping (OORP) approach supported by a full featured visual development environment. Supplemental lessons learned from a large project in progress and a requirements definition are also incorporated. The paper demonstrates how productivity gains can be made by leveraging the developer with a rich development environment, correct and early requirements definition using rapid prototyping, and earlier and better effort estimation and software sizing through object-oriented methods and metrics. Although the individual elements of OO methods, RP approach and OO metrics had been used on other separate projects, the reported projects were the first integrated usage supported by a rich development environment. Overall the approach used was twice as productive (measured by hours per OO Unit) as a C++ development. Author

N95-31245*# Computer Sciences Corp., Lanham, MD.

LESSONS LEARNED IN TRANSITIONING TO AN OPEN SYSTEMS ENVIRONMENT

Dillard E. Boland, David S. Green, and Warren L. Steger *In* NASA. Goddard Space Flight Center, Proceedings of the 19th Annual Software Engineering Workshop Dec. 1994 p 191-210 (For primary document see N95-31234 11-61)
Avail: CASI HC A03/MF A03

Software development organizations, both commercial and governmental, are undergoing rapid change spurred by developments in the computing industry. To stay competitive, these organizations must adopt new technologies, skills, and practices quickly. Yet even for an organization with a well-developed set of software engineering models and processes, transitioning to a new technology can be expensive and risky. Current industry trends are leading away from traditional mainframe environments and toward the workstation-based, open systems world. This paper presents the experiences of software engineers on three recent projects that pioneered open systems development for NASA's Flight Dynamics Division of the Goddard Space Flight Center (GSFC). Author

N95-31246*# IBM Canada Lab., North York (Ontario).

LESSONS LEARNED IN DEPLOYING SOFTWARE ESTIMATION TECHNOLOGY AND TOOLS

Nikki Panlilio-Yap and Danny Ho *In* NASA. Goddard Space Flight Center, Proceedings of the 19th Annual Software Engineering Workshop Dec. 1994 p 211-228 (For primary document see N95-31234 11-61)
Avail: CASI HC A03/MF A03

Developing a software product involves estimating various project parameters. This is typically done in the planning stages of the project when there is much uncertainty and very little information. Coming up with accurate estimates of effort, cost, schedule, and reliability is a critical problem faced by all software project managers. The use of estimation models and commercially available tools in conjunction with the best bottom-up estimates of software-development experts enhances the ability of a product development group to derive reasonable estimates of important project parameters. This paper describes the experience of the IBM Software Solutions (SWS) Toronto Laboratory in selecting software estimation models and tools and deploying their use to the laboratory's product development groups. It introduces the SLIM and COSTAR products, the software estimation tools selected for deployment to the product areas, and discusses the rationale for their selection. The paper also describes the mechanisms used for technology injection and tool deployment, and concludes with a discussion of important lessons learned in the technology and tool insertion process. Author

N95-31247*# Jet Propulsion Lab., California Inst. of Tech., Pasadena, CA.

EXPERIENCE REPORT: USING FORMAL METHODS FOR REQUIREMENTS ANALYSIS OF CRITICAL SPACECRAFT SOFTWARE

Robyn R. Lutz and Yoko Ampo (Nippon Electric Co. Ltd., Tokyo, Japan.) *In* NASA. Goddard Space Flight Center, Proceedings of the 19th Annual Software Engineering Workshop Dec. 1994 p 231-248 (For primary document see N95-31234 11-61)
Avail: CASI HC A03/MF A03

Formal specification and analysis of requirements continues to gain support as a method for producing more reliable software. However, the introduction of formal methods to a large software project is difficult, due in part to the unfamiliarity of the specification languages and the lack of graphics. This paper reports results of an investigation into the effectiveness of formal methods as an aid to the requirements analysis of critical, system-level fault-protection software on a spacecraft currently under development. Our experience indicates that formal specification and analysis can enhance the accuracy of the requirements and add assurance prior to design development in this domain. The work described here is part of a larger, NASA-funded research project whose purpose is to use formal-methods techniques to improve the quality of software in space applications. The demonstration project described here is part of the effort to evaluate experimentally the effectiveness of supplementing traditional engineering approaches to requirements specification with the more rigorous specification and analysis available with formal methods.
Derived from text

N95-31248*# Tennessee Univ., Chattanooga, TN. Software Quality Research Lab.

EXPERIMENTAL CONTROL IN SOFTWARE RELIABILITY CERTIFICATION

Carmen J. Trammell and Jesse H. Poore *In* NASA. Goddard Space Flight Center, Proceedings of the 19th Annual Software Engineering Workshop Dec. 1994 p 249-264 (For primary document see N95-31234 11-61)
Avail: CASI HC A03/MF A03

There is growing interest in software 'certification', i.e., confirmation that software has performed satisfactorily under a defined certification protocol. Regulatory agencies, customers, and prospective reusers all want assurance that a defined product standard has been met. In other industries, products are typically certified under protocols in which random samples of the product are drawn, tests characteristic of operational use are applied, analytical or statistical inferences are made, and products meeting a standard

are 'certified' as fit for use. A warranty statement is often issued upon satisfactory completion of a certification protocol. This paper outlines specific engineering practices that must be used to preserve the validity of the statistical certification testing protocol. The assumptions associated with a statistical experiment are given, and their implications for statistical testing of software are described. Derived from text

N95-31249*# Virginia Univ., Charlottesville, VA. Dept. of Computer Science.
GENERALIZED IMPLEMENTATION OF SOFTWARE SAFETY POLICIES
John C. Knight and Kevin G. Wika *In* NASA. Goddard Space Flight Center, Proceedings of the 19th Annual Software Engineering Workshop Dec. 1994 p 265-280 (For primary document see N95-31234 11-61)
(Grants NAG1-1123; NSF CCR-92-13427)
Avail: CASI HC A03/MF A03

As part of a research program in the engineering of software for safety-critical systems, we are performing two case studies. The first case study, which is well underway, is a safety-critical medical application. The second, which is just starting, is a digital control system for a nuclear research reactor. Our goal is to use these case studies to permit us to obtain a better understanding of the issues facing developers of safety-critical systems, and to provide a vehicle for the assessment of research ideas. The case studies are not based on the analysis of existing software development by others. Instead, we are attempting to create software for new and novel systems in a process that ultimately will involve all phases of the software lifecycle. In this abstract, we summarize our results to date in a small part of this project, namely the determination and classification of policies related to software safety that must be enforced to ensure safe operation. We hypothesize that this classification will permit a general approach to the implementation of a policy enforcement mechanism.
Derived from text

N95-31250*# Tennessee State Univ., Nashville, TN. Dept. of Computer and Information Sciences.
A QUANTITATIVE COMPARISON OF CORRECTIVE AND PERFECTIVE MAINTENANCE
Joel Henry and James Cain *In* NASA. Goddard Space Flight Center, Proceedings of the 19th Annual Software Engineering Workshop Dec. 1994 p 283-296 (For primary document see N95-31234 11-61)
Avail: CASI HC A03/MF A03

This paper presents a quantitative comparison of corrective and perfective software maintenance activities. The comparison utilizes basic data collected throughout the maintenance process. The data collected are extensive and allow the impact of both types of maintenance to be quantitatively evaluated and compared. Basic statistical techniques test relationships between and among process and product data. The results show interesting similarities and important differences in both process and product characteristics. Author

N95-31251*# Coopers and Lybrand, Hamburg (Germany).
DOES SOFTWARE DESIGN COMPLEXITY AFFECT MAINTENANCE EFFORT?
Andreas Epping and Christopher M. Lott (Kaiserslautern Univ., Germany.) *In* NASA. Goddard Space Flight Center, Proceedings of the 19th Annual Software Engineering Workshop Dec. 1994 p 297-313 (For primary document see N95-31234 11-61)
Avail: CASI HC A03/MF A03

The design complexity of a software system may be characterized within a refinement level (e.g., data flow among modules), or between refinement levels (e.g., traceability between the specification and the design). We analyzed an existing set of data from NASA's Software Engineering Laboratory to test whether changing software modules with high design complexity requires more personnel effort than changing modules with low design complexity. By analyzing variables singly, we identified strong correlations between software design complexity and change effort for error corrections performed during the maintenance phase. By analyzing variables in combination, we found patterns which identify modules in which error corrections were costly to perform during the acceptance test phase. Author

N95-31252*# National Aeronautics and Space Administration. Goddard Space Flight Center, Greenbelt, MD.
PROFILE OF SOFTWARE ENGINEERING WITHIN THE NATIONAL AERONAUTICS AND SPACE ADMINISTRATION (NASA)
Craig C. Sinclair and Kellyann F. Jeletic *In its* Proceedings of the 19th Annual Software Engineering Workshop Dec. 1994 p 315-324 (For primary document see N95-31234 11-61)
Avail: CASI HC A03/MF A03

This paper presents findings of baselining activities being performed to characterize software practices within the National Aeronautics and Space Administration. It describes how such baseline findings might be used to focus software process improvement activities. Finally, based on the findings to date, it presents specific recommendations in focusing future NASA software process improvement efforts. The findings presented in this paper are based on data gathered and analyzed to date. As such, the quantitative data presented in this paper are preliminary in nature. Author

N95-31257# Gosudarstvennyi Komitet po Ispolzovaniyu Atomnoi Energii, Leningrad (USSR).
ON DRAWING COMPLICATED 3D SURFACES
L. N. Nikitin and V. V. Talanov 1994 10 p
(DE95-619199; IHEP-94-23) Avail: CASI HC A02/MF A01 (US Sales Only)

The problem of constructing images of complicated 3D surfaces - world sheets of string is considered. The world sheet representation in the form of a frame of points determined with a specified supporting curve is described. The pictures of the world sheets of free string are constructed using various graphical technologies. DOE

N95-31262# Asian Office of Aerospace Research and Development, APO San Francisco, CA. Air Force Office of Scientific Research.
VIRTUAL REALITY SOFTWARE AND TECHNOLOGY '94
Juan Motiwalla and Steve Feiner 23 Aug. 1994 26 p Conference held in Singapore, 22-26 Aug. 1994
(AD-A292334; AOARD-TR-94-30) Avail: CASI HC A03/MF A01

A summary of the Virtual Reality Software and Technology 94 conference, conducted August 22-26, 1994 at the National Institute of Science and Technology of Singapore is presented. Abstracts of all presented papers are included, as is a complete list of conference registrants. This report is based upon information collected via conference attendance, review of the proceedings, and conversations with other attendees. DTIC

N95-31277# Massachusetts Inst. of Tech., Cambridge, MA.
Sodabot: A SOFTWARE AGENT ENVIRONMENT AND CONSTRUCTION SYSTEM M.S. Thesis
Michael H. Coen Jun. 1994 80 p
(Contract N00014-91-J-4038; NSF IRI-93-57761)
(AD-A290056; AI-TR-1493) Avail: CASI HC A05/MF A01

This thesis presents SodaBot, a general-purpose software agent user-environment and construction system. Its primary component is the basic software agent - a computational framework for building agents which is essentially an agent operating system. We also present a new language for programming the basic software agent whose primitives are designed around human-level descriptions of agent ac tivity. Via this programming language, users can easily implement a wide-range of typical software agent applications, e.g. personal on-line assistants and meeting scheduling agents. The SodaBot system has been implemented and tested, and its description comprises the bulk of this thesis. DTIC

N95-31391# Naval Postgraduate School, Monterey, CA.
DEVELOPMENT OF A STRUCTURED DESIGN AND PROGRAMMING METHODOLOGY FOR EXPERT SYSTEMS SHELLS UTILIZING A VISUAL PROGRAMMING LANGUAGE: APPLICATION OF STRUCTURED METHODOLOGY TO THE MK92 MAINTENANCE ADVISOR EXPERT SYSTEM, PERFORMANCE MODULE PROTOTYPE M.S. Thesis
Lucy Michelle Smith Sep. 1994 156 p
(AD-A289897) Avail: CASI HC A08/MF A02

This thesis was initiated as part of a continuing effort to design and implement a diagnostic expert system for the MK92 MOD 2 Fire Control System (FCS) undertaken by the Naval Postgraduate School (NPS) faculty and graduate students. The focus of this thesis is the development of a structured methodology for the design and implementation of an expert

system in an expert system shell utilizing a visual programming language. Guidelines for the application of the structured methodology in the Adept expert system shell were develop and these guidelines applied to the Performance module prototype of the MK92 MOD 2 FCS Maintenance Advisor Export System. DTIC

N95-31404# Allied-Signal Aerospace Co., Kansas City, MO.
COMPUTER-AIDED INSPECTION PROCESS DEFINITION: DEVELOPMENT OF AN EXPERT PLANNING AND PROGRAMMING SYSTEM FOR COORDINATE METROLOGY Final Report
C. W. Brown Apr. 1995 29 p
(Contract DE-AC04-76DP-00613)
(DE95-010411; KCP-613-5528) Avail: CASI HC A03/MF A01

This work discusses accomplishments obtained from the design and prototype development of a computer-aided inspection process planning system for the dimensional measurement of manufactured parts. The system, IPPEX (Inspection Planning and Programming EXpert), is a knowledge-based system. This prototype system applies intelligence techniques and implements an advanced product definition modeling system. The IPPEX framework is based on a functional architecture designed for the purpose of producing inspection process plans, CMM part programs, and support information. The IPPEX conceptual prototype system selects the appropriate CMM, identifies the measurable surfaces, suggests probing point determination, performs inspection work element planning, and creates an initial Dimensional Measurement Interface Specification part program, all for a specific workpiece. This work describes the IPPEX system, its functional architecture, system architecture, system approach, product modeling environment, inspection features, inspection knowledge, hierarchical planning strategy, user interface formats, and other fundamental issues related to inspection planning and part programming for CMMs. Finally, this document describes research that will contribute toward furthering the development of automated inspection planning, advancing product modelling systems with application accessible tolerances, and defining standard dimensional inspection techniques and methodologies. DOE

N95-31408# Comision Nacional de Energia Atomica, San Carlos de Bariloche (Argentina).
DEVELOPMENT AND IMPLEMENTATION OF A COMPUTER FACILITY FOR NUCLEAR DATA UPDATING AND REACTOR CALCULATIONS USING PERSONAL COMPUTERS [DESARROLLO E IMPLEMENTACION DE FACILIDADES COMPUTACIONALES PARA LA ACTUALIZACION DE DATOS NUCLEARES Y CALCULOS DE REACTORES EN COMPUTADORAS PERSONALES]
Francisco Leszczynski and Osvaldo Calzetta 1993 3 p In SPANISH Presented at the 21st Meeting of the Argentine Association of Nuclear Technology, Mar del Plata, Argentina, 8-12 Nov. 1993
(DE95-623577; INIS-AR-103; CONF-9311167) Avail: CASI HC A01/MF A01 (US Sales Only)

A computer systems design and development for a nuclear reactor facility is the focus of this short communication. Personal computers are used to provide for the updating of nuclear data and for reactor calculations. DOE

N95-31420*# National Aeronautics and Space Administration. Langley Research Center, Hampton, VA.
SOLID MODELING AEROSPACE RESEARCH TOOL (SMART) USER'S GUIDE, VERSION 2.0
Mark L. McMillin, Jan L. Spangler (Vigyan Research Associates, Inc., Hampton, VA.), Stephen M. Dahmen (Vigyan Research Associates, Inc., Hampton, VA.), and John J. Rehder Jul. 1993 97 p
(RTOP 506-49-11-01)
(NASA-TM-4431; L-17007; NAS 1.15:4431) Avail: CASI HC A05/MF A02

The Solid Modeling Aerospace Research Tool (SMART) software package is used in the conceptual design of aerospace vehicles. It provides a highly interactive and dynamic capability for generating geometries with Bezier cubic patches. Features include automatic generation of commonly used aerospace constructs (e.g., wings and multilobed tanks); cross-section skinning; wireframe and shaded presentation; area, volume, inertia, and center-of-gravity calculations; and interfaces to various aerodynamic and structural analysis programs. A comprehensive description of SMART and how to use it is provided. Author (revised)

N95-31431# Utah State Univ., Logan, UT.
QUASI-NEWTON UPDATING FOR LARGE SCALE NONLINEAR SYSTEMS Final Report, 1 Jul. 1991 - 30 Jun. 1994
H. F. Walker 1994 10 p
(Grant AF-AFOSR-0294-91)
(AD-A292776; AFOSR-95-0209TR) Avail: CASI HC A02/MF A01

Research was directed toward developing robust and efficient iterative methods for large-scale systems of nonlinear algebraic equations, especially discretizations of continuous problems such as partial differential and integral equations. The specific goal was to develop effective Newton iterative methods (implementations of Newton's method using iterative linear algebra methods) and improved iterative linear solvers for use in them. A theoretically sound abstract framework was formulated. Significant progress was made toward a well-developed software implementation. Useful advances were made in the development and understanding of iterative linear solvers. DTIC

N95-31452# New York Univ., New York, NY. Dept. of Computer Science.
TOWARDS INCREASED PRODUCTIVITY OF ALGORITHM IMPLEMENTATION Final Technical Report, 1 Aug. 1993 - 30 Sep. 1994
Robert Paige 20 Dec. 1994 8 p
(Grant AF-AFOSR-0308-91)
(AD-A292862; AFOSR-95-0223TR) Avail: CASI HC A02/MF A01

Last year we reported experimental results in productivity of nonnumerical algorithm implementation using transformational programming. Comparative benchmarks suggest that productivity can be increased by our approach over conventional hand crafted programming by factors ranging from 5.1 to 9.9. Preliminary results also showed that the running time of C code produced by this new approach can be as fast as 1.5 times that of tightly coded high quality Fortran. DTIC

N95-31455# Massachusetts Univ., Amherst, MA. Dept. of Mechanical Engineering.
INTELLIGENT FINITE ELEMENT SUBMODELING OF MULTICHIP MODULES FOR RELIABILITY ANALYSIS Final Technical Report, Jan. 1993 - Jan. 1994
Ian R. Grosse, Michael Sheehy, Prasanna Katragadda, and Shankar Raman Dec. 1994 122 p
(Contract F30602-93-C-0040)
(AD-A292911; RL-TR-94-218) Avail: CASI HC A06/MF A02

Modeling methodologies were developed, implemented, and tested for both rapid thermal finite element analysis of small-scale integrated circuit features in MCM's, and for thermal stress finite element analysis of chip-to-substrate interconnects. A three-step sequential analysis methodology was developed that is initiated with a macroscope thermal analysis of the entire MCM package. The macroscope finite element thermal analysis is then followed by two successive finite element thermal submodels of the hottest die first and then of the hottest die microfeature. In this manner, the thermal analysis process mathematically zooms into the hottest IC microfeature without resorting to supercomputer-size finite element models of the MCM. A two-step sequential thermal-stress finite element submodeling analysis procedure was also developed for thermally induced stress analysis of the most highly stressed wirebond or TAB interconnect in an MCM package. For automation purposes, both the IC thermal submodeling and the interconnect elastostatic submodeling methodologies were implemented into an existing blackboard-based, object-oriented MCM software design tool called the Intelligent MCM Analysis (IMCMA). DTIC

N95-31459# Pittsburgh Univ., Pittsburgh, PA. Learning Research and Development Center.
ANALYSIS OF SYMBOLIC PARAMETER MODELS Final Technical Report, 15 Feb. 1991 - 14 Feb. 1993
Herbert A. Simon, Thad Polk, and Kurt Vanlehn 16 Mar. 1995 34 p
(Contract N00014-91-J-1529)
(AD-A292916) Avail: CASI HC A03/MF A01

Model-fitting, the problem of finding parameter settings that cause a model to fit given data as closely as possible, is a hard but important problem in cognitive science in general, and in cognitive diagnosis in particular. Efficient solutions have been found for certain types of model-fitting problems (e.g., linear and integer programming) that involve specific types of parameters (usually continuous) and models (usually linear).

But these techniques usually do not apply to computational cognitive models whose parameters are often discrete and symbolic and whose internal workings must be treated as a black box for the purposes of fitting. We have constructed ASPM (Analysis of Symbolic Parameter Models), a suite of computational tools for fitting and analyzing such symbolic parameter models. We have shown how it can be used to fit and analyze computational models with well over 10 billion combinations of parameter settings. We have made a good start towards making ASPM robust and user friendly in preparation for releasing it for public use. DTIC

N95-31460# Carnegie-Mellon Univ., Pittsburgh, PA. Dept. of Computer Science.
THE OCCURRENCE OF CONTINUATION PARAMETERS IN CPS TERMS
Olivier Danvy and Frank Pfenning Feb. 1995 24 p
(Grant NSF CCR-93-33383)
(AD-A292952; CMU-CS-95-121) Avail: CASI HC A03/MF A01

We prove an occurrence property about formal parameters of continuations in Continuation-Passing Style (CPS) terms that have been automatically produced by CPS transformation of pure, call-by-value lamda-terms. Essentially, parameters of continuations obey a stack-like discipline. This property was introduced, but not formally proven, in an earlier work on the Direct-Style transformation (the inverse of the CPS transformation). The proof has been implemented in Elf, a constraint logic programming language based on the logical framework LF. In fact, it was the implementation that inspired the proof. Thus this note also presents a case study of machine-assisted proof discovery. DTIC

N95-31533 Rutgers - The State Univ., New Brunswick, NJ.
THE REMAINDER FORM AND THE CORD-SLOPE FORM IN GLOBAL OPTIMIZATION WITH INTERVAL METHODS Ph.D. Thesis
Junjie Xiong 1993 124 p
Avail: Univ. Microfilms Order No. DA9412704

The dissertation is devoted to the study of algorithms for global optimization using interval methods. It consists of two parts. In part one, global optimization of a univariate function on an interval is studied. This function is assumed to be three times differentiable. The cord-slope form of a function is introduced and is used to eliminate parts of the initial interval which cannot contain the global optimum. Twelve test problems are solved and computational results are compared with those of Eldon Hansen's algorithm. The algorithm is further extended locate all the global optima of the function on the interval as well as to the case where the problem is constrained. Then, the cord-slope form has a special structure which leads to a more efficient algorithm. It is proved also that when natural extension form is used for evaluating the bounds of the slope, the interval arithmetic algorithm is equivalent to a decomposition-based global optimization algorithm (GOP) proposed by Floudas and Visweswaran. Finally, an exact version of the Alienor method is developed. In the original version of Alienor method proposed by Cherruault and Guillez, Alienor transformation is used to approximate an n-dimensional function by a univariate function; then the globally optimal solution of the univariate problem can be used as an approximate solution of the original problem. We explore what conditions have to be imposed on the parameters to make the algorithm exact, i.e. to guarantee that the globally optimal value found is at most epsilon away from the true globally optimal value and apply the cord-slope form algorithm to solve the resulting univariate problem. In part two the multivariate global optimization problem is studied. The first case considered is where the objective function is an indefinite quadratic function and only range constraints are present. The algorithm is of branch-and-bound type and branching is done according to the sign of the derivatives. Comparison is made with an interval arithmetic implementation. The algorithm is then applied to find the range of general functions (three times differentiable) using the remainder form proposed by Cornelius and Lohner and comparison is made with the bounds found by using natural extension directly. An algorithm is also proposed for the general case when the objective function is a nonlinear differentiable function and nonlinear constraints are present. Dissert. Abstr.

N95-31573# Army Construction Engineering Research Lab., Champaign, IL.
EFFECTIVENESS OF AN ELECTRONIC PERFORMANCE SUPPORT SYSTEM FOR USE WITH COMPUTER-AIDED DESIGN SOFTWARE Final Report
Doris S. Shaw, Thomas Mack, Julie L. Webster, Daniel J. Nix, and Donald K. Hicks Jan. 1995 70 p
(DA Proj. 4A1-62784-AT-41)
(AD-A293757; CERL-FF-95/06) Avail: CASI HC A04/MF A01

Although Bentley Systems, Inc. (BSI) CAD, a computer-aided design program used in many U.S. Army Corps of Engineers offices, can produce the detailed documents necessary for planning, review, construction, and management of a facility, such software requires extensive training. Allocating the time and resources to learn such computer-based technology is a pressing productivity concern in both government and commercial settings. The U.S. Army Construction Engineering Research Laboratories (USACERL) has studied the use of Computer-Aided Instruction (CAI) to train architects and engineers to use many types of automated systems. Development of the Mentor Hypertext Electronic Performance Support System can help meet this need for cost-effective CAD training done within the context of current working projects, by incorporating embedded online instruction into MicroStation CAD software. This study enhanced the Mentor CAI system for use with MicroStation software and tested the system with users representing a range of disciplines and CAD expertise. At the end of the test period, a survey was administered to determine their use of the system, attitudes, learning preferences, and reactions to the program. DTIC

N95-31594 Army Research Lab., Adelphi, MD.
A TWO-DIMENSIONAL FINITE DIFFERENCE ALGORITHM ON THE KSR1 Final Report, Jul. 1993 - Sep. 1994
Christopher S. Kenyon Apr. 1995 21 p Limited Reproducibility: More than 20% of this document may be affected by poor print
(AD-A293576; ARL-MR-213) Avail: Issuing Activity (Defense Technical Information Center (DTIC))

Executing electromagnetic pulse (EMP) codes on the fastest possible computers has been a goal of research in recent years, because it would allow new classes of EMP problems to be solved. A new kind of supercomputer architecture has emerged in recent years, called a massively parallel processor (MPP). This study examines the performance of a two-dimensional finite difference algorithm, a Yee algorithm, which is a major part of some EMP codes, on an MPP computer, the KSR1. Performance of the Yee algorithm, using a mesh of 2000 x 2000, scales roughly in proportion to the number of processors, up to about 32. The maximum performance of the Yee algorithm on the KSR1 was 161 Mflops using 50 processors, or 5.8 times faster than on a 50-MHz IBM RS/6000 workstation. For a 2000 x 2000 matrix multiply test, representative of an important algorithm in moment methods for solving electromagnetic problems, the peak performance on the KSR1 was 279 Mflops with 32 processors. This matrix multiply ran about three times faster than on the IBM workstation. It was concluded that the modest gains found here were insufficient to warrant a full port of a large EMP code to the KSR1. DTIC

N95-31630# Michigan Univ., Ann Arbor, MI.
SPECTRAL METHODS AND SUM ACCELERATION ALGORITHMS Final Report, May 1991 - Aug. 1994
John Boyd Mar. 1995 5 p
(Contract DE-FG02-91ER-25109)
(DE95-009689; DOE/ER-25109/T1) Avail: CASI HC A01/MF A01

The principle investigator pursued his investigation of numerical algorithms during the period of the grant. The attached list of publications is so lengthy that it is impossible to describe them in detail. However, the author calls attention to the four articles on sequence acceleration and fourteen more on spectral methods, which fulfill the goals of the original proposal. He also continued his research on nonlinear waves, and wrote a dozen papers on this, too. DOE

N95-31631# Oak Ridge National Lab., TN.
FINITE-SAMPLE BASED LEARNING ALGORITHMS FOR FEEDFORWARD NETWORKS
N. S. V. Rao, V. Protopopescu, R. C. Mann, E. M. Oblow, and S. S. Iyengar (Louisiana State Univ., Baton Rouge, LA.) 1995 12 p Presented at the Symposium on Theory of Computing, Las Vegas, NV, 29 May - 1 Jun. 1995
(Contract DE-AC05-84OR-21400)
(DE95-009123; CONF-9505145-2) Avail: CASI HC A03/MF A01

We discuss two classes of convergent algorithms for learning continuous

functions (and also regression functions) that are represented by FeedForward Networks (FFN). The first class of algorithms, applicable to networks with unknown weights located only in the output layer, is obtained by utilizing the potential function methods of Aizerman et al. The second class, applicable to general feedforward networks, is obtained by utilizing the classical Robbins-Monro style stochastic approximation methods. Conditions relating the sample sizes to the error bounds are derived for both classes of algorithms using martingale-type inequalities. For concreteness, the discussion is presented in terms of neural networks, but the results are applicable to general feedforward networks, in particular to wavelet networks. The algorithms can also be directly applied to concept learning problems. A main distinguishing feature of the this work is that the sample sizes are based on explicit algorithms rather than information-based methods. DOE

N95-31634# Oak Ridge National Lab., TN.
NETWORK USER'S GUIDE
P. W. McGrady Dec. 1994 135 p
(Contract DE-AC05-84OR-21400)
(DE95-009185; ORNL/TM-12867) Avail: CASI HC A07/MF A02

NETWORK is a FORTRAN code used to model process flow systems in the gaseous diffusion plants at Portsmouth, Ohio and Paducah, Kentucky, operated by the United States Enrichment Corporation. It can handle a wide range of components and several different types of controllers. NETWORK can be run in either a steady-state mode or a transient mode. In the transient mode many different types of perturbations may be modeled. It is currently being used to model taking a cell off-stream in a gaseous diffusion plant. A brief description of the code is given, and process equipment models and input data are discussed. DOE

N95-31644# Sandia National Labs., Albuquerque, NM.
A SIMPLE AND EFFICIENT PROCEDURE FOR POLYHEDRAL ASSEMBLY PARTITIONING UNDER INFINITESIMAL MOTIONS
L. J. Guibas, D. Halperin, J. C. Latombe (Stanford Univ., CA.), Hirohisa Hirukawa (Ministry of International Trade and Industry, Tsukuba, Japan.), and R. H. Wilson 1994 8 p Presented at the 1995 International Conference on Robotics and Automation, Nagoya, Japan, 21-27 May 1995
(Contract DE-AC04-94AL-85000)
(DE95-009838; SAND-94-3129C; CONF-9505193-4) Avail: CASI HC A02/MF A01

The authors study the following problem: given a collection A of polyhedral parts in 3D, determine whether there exists a subset S of the parts that can be moved as a rigid body by an infinitesimal translation and rotation, without colliding with the rest of the parts, A/S. A negative result implies that the object whose constituent parts are the collection A cannot be taken apart with two hands. A positive result, together with the list of movable parts in S and a direction of motion for S, can be used by an assembly sequence planner. This problem has attracted considerable attention within and outside the robotics community. They devise an efficient algorithm to solve this problem. The solution is based on the ability to focus on selected portions of the tangent space of rigid motions and efficiently access these portions. The algorithm is complete (in the sense that it is guaranteed to find a solution if one exists), simple, and improves significantly over the best previously known solutions. The authors report experimental results with an implementation of their algorithm. DOE

N95-31657 Rochester Univ., NY. Dept. of Computer Science.
AN ANALYSIS OF HIERARCHICAL GENETIC PROGRAMMING
Justinian P. Rosca Mar. 1995 27 p Limited Reproducibility: More than 20% of this document may be affected by poor print
(Contract MDA972-92-J-1012; NSF IRI-94-06481)
(AD-A293964; TR-566) Avail: Issuing Activity (Defense Technical Information Center (DTIC))

Hierarchical genetic programming (HGP) approaches rely on the discovery, modification, and use of new functions to accelerate evolution. This paper provides a qualitative explanation of the improved behavior of HGP, based on an analysis of the evolution process from the dual perspective of diversity and causality. From a static point of view, the use of an HGP approach enables the manipulation of a population of higher diversity programs. Higher diversity increases the exploratory ability of the genetic search process, as demonstrated by theoretical and experimental fitness distributions and expanded structural complexity of individuals. From a dynamic point of view, this report analyzes the causality of the crossover operator. Causality relates changes in the structure of an object with the effect of such changes, i.e. changes in the properties or behavior of the object. The analyses of crossover causality suggests that HGP discovers and exploits useful structures in a bottom-up, hierarchical manner. Diversity and causality are complementary, affecting exploration and exploitation in genetic search. Unlike other machine learning techniques that need extra machinery to control the tradeoff between them, HGP automatically trades off exploration and exploitation. DTIC

N95-31683# Unisys Corp., Reston, VA. Reston Technology Center.
PENELOPE REFERENCE MANUAL: VERSION 3-3 (C001). INCLUDES LARCH/Ada SPECIFICATION MANUAL FOR SEQUENTIAL Ada (C002)
Carla Marceau 2 Sep. 1994 155 p
(Contract F19628-93-C-0130)
(AD-A289828; STARS-AC-C001/001/00) Avail: CASI HC A08/MF A02

Penelope is an interactive environment that helps its user to develop and verify programs written in a rich subset of sequential Ada. Penelope is well-suited to developing programs in the goal-directed style advocated by Gries and Dijkstra. In this style the programmer develops a program from a specification in a way that ensures the program will meet the specification. Of course, Penelope can also be used to verify previously written programs. With Penelope, it is often possible to modify a verified program and verify the modified version with minimal effort by replaying and modifying the original program's proof. DTIC

N95-31684# Dayton Univ., OH. Research Inst.
IMAGE REPRESENTATION USING FAST ALGORITHMS BASED ON THE ZAK TRANSFORM Final Technical Report, Oct. 1990 - Mar. 1994
George A. Geri and Izidor C. Gertner Dec. 1994 124 p Prepared in cooperation with City College of the City Univ. of New York, NY
(Contract F33615-90-C-0006)
(AD-A293416; AL/HR-TR-1994-0106) Avail: CASI HC A06/MF A01

Flight simulator imagery is often made up of natural scenes whose characteristics are not constant across the image. This property suggests that such imagery can be most efficiently represented by spectral techniques that use spatially localized basis functions. This report describes techniques for decomposing full gray-scale images into a joint position/spatial-frequency domain using bases derived from various window functions. The first set of window functions consists of the hermite functions which are related to gaussian derivatives. The second set is based on a new window function that is obtained from a weighted ZAK transform and that provides good localization properties and stable computation. The third set is based on a localized cosine function and allows images to be decomposed using real numbers only. All of the techniques described provide a framework for filtering images in a position-varying manner. For all the basis functions described here, image generation from combined position and spatial-frequency information involves a computationally intensive four-dimensional summation. By an application of the Zak Transform, we are able to replace this summation with a fast Fourier transform, significantly reducing the complexity of the computation. DTIC

N95-31688# Carnegie-Mellon Univ., Pittsburgh, PA. Robotics Inst.
PORK OBJECT SYSTEM PROGRAMMER'S GUIDE
Ora Lassila Apr. 1995 68 p
(Contract F30602-90-C-0119)
(AD-A293596; CMU-RI-TR-95-12) Avail: CASI HC A04/MF A01

Pork is an object system which brings a conventional object-oriented language closer to the requirements of frame-based programming. It only provides a very limited set of features (on top of the base object system itself), and aims to achieve seamless integration with conventional programming. PORK is implemented as a portable metalevel extension of the Common Lisp Object System (CLOS). It extends CLOS by adding the following concepts: (1) Named objects - These simplify debugging and linked frame model construction. Collections of named objects (called 'namespaces') can also be used as a low-level implementation vehicle for knowledge bases; (2) References to nonexisting named objects - Programs can manipulate objects that have not yet been created. This greatly simplifies definition of complex linked frame models with circular references; (3) Slots with multiple values, and a mechanism for defining an access interface; (4) Automatic updating of inverse slots. DTIC

N95-31834# Carnegie-Mellon Univ., Pittsburgh, PA. Software Engineering Inst.

PROCEEDINGS OF THE 1ST ANNUAL SOFTWARE ENGINEERING TECHNIQUES WORKSHOP ON SOFTWARE REENGINEERING Final Report

Leonard Green, John Bergey, Walter Lamia, and Dennis Smith Nov. 1994 133 p

(Contract F19628-90-C-0003)

(AD-A293724; CMU/SEI-94-SR-008) Avail: CASI HC A07/MF A02

This is a report of the proceedings of the May 1994 Software Engineering Institute's Software Engineering Techniques Workshop on Software Reengineering. The report includes brief biographies of the workshop speakers and authors, and detailed accounts of nine working group session discussions on the following topics: reengineering architecture, decision, analysis, system evolution and design records, reengineering economics analysis, understanding legacy systems, using lessons learned from other software reengineering projects, reengineering process models, software reuse, and reengineering technology and tools. The workshop established a foundation for capturing the best practices within reengineering and resulted in a detailed outline for a reengineering best practices handbook. DTIC

N95-31835# Naval Postgraduate School, Monterey, CA.

APPLICATION OF A GENETIC ALGORITHM TO OPTIMIZE STAFFING LEVELS IN SOFTWARE DEVELOPMENT M.S. Thesis

Donald C. Johnson Dec. 1994 72 p

(AD-A293725) Avail: CASI HC A04/MF A01

Human resource management is gaining recognition as being one of the core attributes of effective software project management. With the great dependency the Department of Defense (DOD) has on systems software, the development of an optimal staffing policy that minimizes overall software project costs will be very valuable. This research aims at developing such a system using a dynamic simulation model that incorporates data collected during an actual software development project. A genetic algorithm is used to arrive at a solution to this nonlinear optimization problem. The simulation model accepts varying staffing schemes supplied from the genetic algorithm allowing for the examination of the effects of the staffing schemes on total project cost. The results indicate that the system was able to obtain a solution reducing overall project costs, but at the cost of additional workdays. DTIC

N95-31843# Carnegie-Mellon Univ., Pittsburgh, PA. Dept. of Computer Science.

EXPERIENCE WITH A COURSE ON ARCHITECTURES FOR SOFTWARE SYSTEMS. PART 2: EDUCATIONAL MATERIALS

David Garlan, Mary Shaw, and Jose Galmes Aug. 1994 474 p

(Contract MDA972-92-J-1002)

(AD-A293090; CMU-CS-94-178) Avail: CASI HC A20/MF A04

This report contains the materials used by the instructors to teach the course CS 15-775: Architectures for Software Systems in Spring 1994 in the School of Computer Science at Carnegie Mellon University. The materials include the lecture slides, questions (with answers) on readings, and homework assignments (with sample solutions). DTIC

N95-31982*# Old Dominion Univ., Norfolk, VA. Dept. of Computer Science.

GEOMETRIC MODELING FOR COMPUTER AIDED DESIGN Final Report, period ended 30 Jun. 1995

James L. Schwing and Stephen Olariu Jul. 1995 28 p

(Contract NCC1-99)

(NASA-CR-198828; NAS 1.26:198828) Avail: CASI HC A03/MF A01

The primary goal of this grant has been the design and implementation of software to be used in the conceptual design of aerospace vehicles particularly focused on the elements of geometric design, graphical user interfaces, and the interaction of the multitude of software typically used in this engineering environment. This has resulted in the development of several analysis packages and design studies. These include two major software systems currently used in the conceptual level design of aerospace vehicles. These tools are SMART, the Solid Modeling Aerospace Research Tool, and EASIE, the Environment for Software Integration and Execution. Additional software tools were designed and implemented to address the needs of the engineer working in the conceptual design environment. SMART provides conceptual designers with a rapid prototyping capability and several engineering analysis capabilities. In addition, SMART has a carefully engineered user interface that makes it easy to learn and use. Finally, a number of specialty characteristics have been built into SMART which allow it to be used efficiently as a front end geometry processor for other analysis packages. EASIE provides a set of interactive utilities that simplify the task of building and executing computer aided design systems consisting of diverse, stand-alone, analysis codes. Resulting in a streamlining of the exchange of data between programs reducing errors and improving the efficiency. EASIE provides both a methodology and a collection of software tools to ease the task of coordinating engineering design and analysis codes. Derived from text

N95-32019# Carnegie-Mellon Univ., Pittsburgh, PA. Dept. of Computer Science.

A PROGRAMMING INTERFACE FOR APPLICATION-AWARE ADAPTATION IN MOBILE COMPUTING

Brian D. Noble, Morgan Price, and M. Satyanarayanan Feb. 1995 14 p Presented at the 2nd USENIX Symposium on Mobile and Location-Independent Computing, Ann Arbor, MI, Apr. 1995

(Contract F19628-93-C-0193)

(AD-A293107; CMU-SC-95-119) Avail: CASI HC A03/MF A01

Mobile clients face wide variations in network conditions and local resource availability when accessing remote data. Coping with this uncertainty requires the ability to retrieve and present data at varying degrees of fidelity. In this paper we present application-aware adaptation as a solution to this problem. The essence of our solution is a collaborative partnership between applications and the operating system. We describe the Odyssey API for application-aware adaptation and demonstrate its use in accessing two types of data: video and maps. DTIC

N95-32020# Carnegie-Mellon Univ., Pittsburgh, PA. Dept. of Computer Science.

PADO: LEARNING TREE STRUCTURED ALGORITHMS FOR ORCHESTRATION INTO AN OBJECT RECOGNITION SYSTEM

Astro Teller and Manuela Veloso 10 Feb. 1995 34 p

(AD-A293109; CMU-CS-95-101) Avail: CASI HC A03/MF A01

Most artificial intelligence systems today work on simple problems and artificial domains because they rely on the accurate sensing of the task world. Object recognition is a crucial part of the sensing challenge and machine learning stands in a position to catapult object recognition into real world domains. Given that, to date, machine learning has not delivered general object recognition, we propose a different point of attack: the learning architectures themselves. We have developed a method for directly learning and combining algorithms in a new way that imposes little burden on or bias from the humans involved. This learning architecture, PADO, and the new results it brings to the problem of natural image object recognition is the focus of this report. DTIC

N95-32030# Oak Ridge National Lab., TN.

MONTE CARLO TESTS OF THE ELIPGRID-PC ALGORITHM

J. R. Davidson Apr. 1995 113 p

(Contract DE-AC05-84OR-21400)

(DE95-010811; ORNL/TM-12899) Avail: CASI HC A06/MF A02

The standard tool for calculating the probability of detecting pockets of contamination called hot spots has been the ELIPGRID computer code of Singer and Wickman. The ELIPGRID-PC program has recently made this algorithm available for an IBM(reg sign) PC. However, no known independent validation of the ELIPGRID algorithm exists. This document describes a Monte Carlo simulation-based validation of a modified version of the ELIPGRID-PC code. The modified ELIPGRID-PC code is shown to match Monte Carlo-calculated hot-spot detection probabilities to within +/- 5% for 319 out of 320 test cases. The one exception, a very thin elliptical hot spot located within a rectangular sampling grid, differed from the Monte Carlo-calculated probability by about 1%. These results provide confidence in the ability of the modified ELIPGRID-PC code to accurately predict hot-spot detection probabilities within an acceptable range of error. DOE

N95-32044# Sandia National Labs., Livermore, CA.

A STOCHASTIC EM ALGORITHM FOR APPROXIMATING THE MAXIMUM LIKELIHOOD ESTIMATE

J. Diebolt and E. H. S. Ip Mar. 1995 26 p
(Contract DE-AC04-94AL-85000)
(DE95-010328; SAND-95-8102) Avail: CASI HC A03/MF A01

Stochastic EM is an algorithm designed to handle missing data in statistical applications. Instead of performing the expectation step in the Expectation-Maximization (EM) algorithm, Stochastic EM impute a sample value drawn from the conditional distribution of the missing data given the parameter. This paper explains how the algorithm can be applied in statistical inference to avoid numerical integrations and presents two examples using the Stochastic EM algorithm. The first example deals with censored Weibull data and the second example deals with an empirical Bayes model that arises in educational testing. Some variants of the algorithm are also discussed. This report only treats the theory underlying the Stochastic EM briefly. The properties of the Stochastic EM estimates are dealt with in depth in a sequel of this report. DOE

N95-32073 Air Force Inst. of Tech., Wright-Patterson AFB, OH. School of Engineering.
ANALYSIS AND EXTENSION OF MODEL-BASED SOFTWARE EXECUTIVES M.S. Thesis, 1994
Keith E. Lewis Jan. 1995 100 p Limited Reproducibility: More than 20% of this document may be affected by poor print
(AD-A293834; AFIT/GE/ENG/95M-01) Avail: Issuing Activity (Defense Technical Information Center (DTIC))

This research developed a comprehensive description of the simulation environment of Architect, a domain-oriented application composition system being developed at the Air Force Institute of Technology to explore new software engineering technologies. The description combines information from several previous research efforts and Architect's source code into a single, comprehensive document. A critical evaluation of the simulation environment was also performed, identifying improvements and modifications that enhance Architecture's application execution capabilities by reducing complexity and execution time. The analysis was then taken one step further and presented extensions to the current simulation environment. The extensions included investigating the feasibility of mixed-mode execution and integrating the composition of application executives with the visual system interface. DTIC

N95-32087# Sandia National Labs., Albuquerque, NM.
ESTIMATION IN SECOND ORDER DEPENDENCY MODEL FOR MULTIVARIATE BINARY DATA
Eddie H. S. Ip (Stanford Univ., CA.) Apr. 1995 18 p
(Contract DE-AC04-94AL-85000)
(DE95-010326; SAND-95-8100; UC-405) Avail: CASI HC A03/MF A01

This paper proposes a normal model for multivariate binary data. The normal model is an extension to the bivariate normal model for 2 x 2 contingency table proposed by Pearson. A stochastic algorithm using Gibbs sampler is developed to estimate the parameters for high dimensional binary data. The method is compared to the second order dependency Bahadur-Lazarsfeld representation of binary density. Two examples, one from psychological testing and one from medical science, are used to substantiate the above ideas. DOE

N95-32088# Sandia National Labs., Albuquerque, NM.
A STOCHASTIC DIFFERENCE EQUATION APPROACH TO INFERENCE WITH MISSING DATA: SOME NEW RESULTS
Eddie H. S. Ip and Jean Diebolt (Stanford Univ., CA.) Apr. 1995 25 p
(Contract DE-AC04-94AL-85000)
(DE95-010327; SAND-95-8101; UC-405) Avail: CASI HC A03/MF A01

This paper is concerned with the study of the properties of the Stochastic EM estimator. The Stochastic EM estimator is an estimator derived from an iterative algorithm which handles statistical model with missing data. The first result we obtain is on the decomposition of a general stochastic difference equation underlying the Stochastic EM iterates into an additive form. Such decomposition allows a further analysis of the Markov chain underlying the Stochastic EM algorithm. The second result indicates that the Stochastic EM estimator differs from the maximum likelihood estimate by O (1/n) where n is the sample size. It also shows that iterates derived from the additive stochastic difference equation converges to a normal distribution which is centered at the true value of the parameter as n (yields) (infinity). DOE

N95-32089# Sandia National Labs., Albuquerque, NM.
A STOCHASTIC EM ESTIMATOR IN THE PRESENCE OF MISSING DATA: THEORY AND APPLICATIONS
E. H. S. Ip (Stanford Univ., CA.) Apr. 1995 116 p
(Contract DE-AC04-94AL-85000)
(DE95-010329; SAND-95-8103) Avail: CASI HC A06/MF A02

This thesis provides a study of a Monte Carlo version of the EM (for Expectation-Maximization) algorithm for handling complex missing-data structure in which high-dimensional integrations may be involved. Assuming a parametric model for the complete data, we propose a method for imputing values for missing data and then iteratively perform direct parametric inference based on the pseudo-complete data. If the iteration converges, the result of the procedure is a sample from a stationary distribution derived from the Markov chain formed by the iterations of the parameter. This algorithm is called Stochastic EM and the estimator we propose is the mean of the stationary distribution. We provide new theoretical results on the Stochastic EM estimator. First, under an exponential family setting, we show that asymptotically the Markov chain kernel of Stochastic EM can be decomposed into an additive stochastic difference equation. This decomposition allows us to provide useful results for the asymptotic behavior of the stationary distribution under specific conditions. The next result we obtain is that the Stochastic EM estimator is close to the maximum likelihood estimate. Another result shows that asymptotically the Stochastic EM iterations converge to a normal distribution with the true parameter as its mean. Bounds are obtained for the norm of the covariance matrix. There are two examples, one from medical science and one from education to substantiate the theory. In the education example, the use of straightforward EM would require performing an overwhelmingly large number of high-dimensional numerical integrations even for a moderate sample of a thousand multivariate binary observations. DOE

N95-32190*# Colorado Univ., Boulder, CO. Dept. of Aerospace Engineering Sciences.
EVALUATION OF DISCRETIZATION PROCEDURES FOR TRANSITION ELEMENTS IN ADAPTIVE MESH REFINEMENT
K. C. Park, Itzak Levit (Lockheed Missiles and Space Co., Palo Alto, CA.), and Gary M. Stanley (Lockheed Missiles and Space Co., Palo Alto, CA.) May 1991 16 p
(Grant NAG1-756)
(NASA-CR-199037; NAS 1.26:199037; CU-CSSC-91-15) Avail: CASI HC A03/MF A01

Three transition interpolation schemes for use in h-or r-refinement have been analyzed in terms of accuracy, implementation ease and extendability. They include blending-function interpolation, displacement averaging, and strain matching at discrete points along the transition edge lines. The results suggest that the choice of matching depends strongly on the element formulations, (viz. displacement or assumed strain, etc.) and mesh refinement criteria employed, and to a lesser extent the choice of computer architecture (serial vs. parallel) and the equation solution procedures. A recommended pairing of some of the elements with the choice factors is suggested.
Author

N95-32203*# Colorado Univ., Boulder, CO. Center for Aerospace Structures.
A SURVEY OF THE CORE-CONGRUENTIAL FORMULATION FOR GEOMETRICALLY NONLINEAR TL FINITE ELEMENTS
Carlos A. Felippa, Luis A. Crivelli, and Bjorn Haugen May 1994 58 p
Submitted for publication in Archives of Computational Methods in Engineering
(Contract NAG1-756; NAG3-1273; F49620-87-C-0074; NSF ASC-92-17394)
(NASA-CR-199044; NAS 1.26:199044; CU-CAS-94-08) Avail: CASI HC A04/MF A01

This article presents a survey of the core-congruential formulation (CCF) for geometrically nonlinear mechanical finite elements based on the total Lagrangian (TL) kinematic description. Although the key ideas behind the CCF can be traced back to Rajasekaran and Murray in 1973, it has not subsequently received serious attention. The CCF is distinguished by a two-phase development of the finite element stiffness equations. The initial phase developed equations for individual particles. These equations are expressed in terms of displacement gradients as degrees of freedom. The second phase involves congruential-type transformations that eventually binds the element particles of an individual element in terms of its

node-displacement degrees of freedom. Two versions of the CCF, labeled direct and generalized, are distinguished. The direct CCF (DCCF) is first described in general form and then applied to the derivation of geometrically nonlinear bar, and plane stress elements using the Green-Lagrange strain measure. The more complex generalized CCF (GCCF) is described and applied to the derivation of 2D and 3D Timoshenko beam elements. Several advantages of the CCF, notably the physically clean separation of material and geometric stiffnesses, and its independence with respect to the ultimate choice of shape functions and element degrees of freedom, are noted. Application examples involving very large motions solved with the 3D beam element display the range of applicability of this formulation, which transcends the kinematic limitations commonly attributed to the TL description. Author

N95-32214*# Colorado Univ., Boulder, CO. Center for Space Structures and Controls.

A TRANSIENT FETI METHODOLOGY FOR LARGE-SCALE PARALLEL IMPLICIT COMPUTATIONS IN STRUCTURAL MECHANICS

Charbel Farhat, Luis Crivelli, and Francois-Xavier Roux (Office National d'Etudes et de Recherches Aerospatiales, Chatillon, France.) Nov. 1992 45 p

(Grant NAG1-756)

(NASA-CR-199040; NAS 1.26:199040; CU-CSSC-92-15) Avail: CASI HC A03/MF A01

Explicit codes are often used to simulate the nonlinear dynamics of large-scale structural systems, even for low frequency response, because the storage and CPU requirements entailed by the repeated factorizations traditionally found in implicit codes rapidly overwhelm the available computing resources. With the advent of parallel processing, this trend is accelerating because explicit schemes are also easier to parallelize than implicit ones. However, the time step restriction imposed by the Courant stability condition on all explicit schemes cannot yet -- and perhaps will never -- be offset by the speed of parallel hardware. Therefore, it is essential to develop efficient and robust alternatives to direct methods that are also amenable to massively parallel processing because implicit codes using unconditionally stable time-integration algorithms are computationally more efficient when simulating low-frequency dynamics. Here we present a domain decomposition method for implicit schemes that requires significantly less storage than factorization algorithms, that is several times faster than other popular direct and iterative methods, that can be easily implemented on both shared and local memory parallel processors, and that is both computationally and communication-wise efficient. The proposed transient domain decomposition method is an extension of the method of Finite Element Tearing and Interconnecting (FETI) developed by Farhat and Roux for the solution of static problems. Serial and parallel performance results on the CRAY Y-MP/8 and the iPSC-860/128 systems are reported and analyzed for realistic structural dynamics problems. These results establish the superiority of the FETI method over both the serial/parallel conjugate gradient algorithm with diagonal scaling and the serial/parallel direct method, and contrast the computational power of the iPSC-860/128 parallel processor with that of the CRAY Y-MP/8 system. Author

N95-32215*# Colorado Univ., Boulder, CO. Dept. of Aerospace Engineering Sciences.

THE INDIVIDUAL ELEMENT TEST REVISITED

Carmelo Militello and Carlos A. Felippa Aug. 1991 13 p Submitted for publication in The Finite Element Method in the 1990's

(Grant NAG1-756)

(NASA-CR-199039; NAS 1.26:199039; CU-CSSC-91-25) Avail: CASI HC A03/MF A01

The subject of the patch test for finite elements retains several unsettled aspects. In particular, the issue of one-element versus multielement tests needs clarification. Following a brief historical review, we present the individual element test (IET) of Bergan and Hanssen in an expanded context that encompasses several important classes of new elements. The relationship of the IET to the multielement forms A, B, and C of the patch test and to the single element test are clarified. Author

N95-32246 National Defence Research Establishment, Linkoeping (Sweden).

BRUTUS: A PROGRAM FOR CONVERSION BETWEEN IMAGE FORMATS [BRUTUS: ETT BILDKONVERTERINGSPROGRAM]

M. Karlsson Oct. 1994 38 p In SWAHILI

(PB95-211421; FOA-R-00047-3.6-SE) Avail: Issuing Activity (National Technical Information Service (NTIS))

This report describes a computer program, BRUTUS, for conversion of images. The program converts image data formats generated by AGEMA Thermovision (R) Burst Recording Unit, software version 4.2 to Teragon image data format. The program also handles some related tasks, such as extraction and presentation of data stored together with the image content. The report serves both as documentation and a users guide. NTIS

N95-32248 National Defence Research Establishment, Stockholm (Sweden).

ASSESSMENT OF COMPUTER AIDS DURING COMMUNICATION EXERCISE 1991 [UTVAERDERING AV DATORSTOED UNDER SOE 1991 IAKTTAGEL SER AV DATORSTOEDETS ANVAENDNING OCH FUNKTION]

I. Alm, T. Naeslund, and T. Nordqvist Oct. 1994 22 p In SWAHILI

(PB95-211462; FOA-R-94-00065-5.5-SE) Avail: Issuing Activity (National Technical Information Service (NTIS))

This study describes functions and applications of three computer systems used during Communication exercise '91, and summarizes an account of two inquiries about the computer systems. The observations, interviews, and the inquiries indicate that the users of the computer system were insufficiently educated and trained with respect to pragmatic use of the systems. The use of the systems was both cautious and fumbling. Moreover, the integration of the different applications was insufficient, and hence, the ability to utilize the systems efficiently was reduced during these circumstances. It seems that expectations about what the system can do were somewhat optimistic. NTIS

N95-32251 National Defence Research Establishment, Linkoeping (Sweden).

TEXTURE BASED METHODS FOR IMAGE ANALYSIS: A REVIEW [TEXTURBASERADE METODER FOER BILDANALYS: EN OEVERSIKT]

M. Uppsaell Oct. 1994 23 p In SWAHILI

(PB95-211595; FOA-R-94-00006-3.1-SE) Avail: Issuing Activity (National Technical Information Service (NTIS))

In the report, a review of recent scientific papers concerning different aspects of texture analysis has been made. The most common methods of texture analysis are different kinds of cooccurrence matrices, filter and transform based methods and texture models based on the theory of stochastic processes. The report is primarily intended for persons with knowledge in signal theory and mathematics on the university level. NTIS

N95-32252 Norwegian Defence Research Establishment, Kjeller (Norway).

[THE COPROCESSOR MANAGER IN THE BASIS PROCESSOR SYSTEM]

P. Sornes Jul. 1994 81 p

(Proj. FFIE/566/139)

(PB95-211611) Avail: Issuing Activity (National Technical Information Service (NTIS))

This report describes the Coprocessor Manager (CPM) in the BASIS processor system. The CPM is the master controller of the BASIS image coprocessor. It manages the image flow, configures and performs run-time control of all boards in the coprocessor rack including the mother board. NTIS

N95-32270# California Univ., Berkeley, CA.

GIGABIT TESTBED RESEARCH PROJECT Final Report, 1 Aug. 1992 - 31 Dec. 1994

D. Ferrari, R. Katz, and J. Ousterhout 1995 11 p

(Contract DE-FG03-92ER-25135)

(DE95-010728; DOE/ER-25135/T1) Avail: CASI HC A03/MF A01

This project was aimed at investigating some of the computer and communication technologies on which imaging applications are being and will be built (high-speed networks, quality-preserving continuous-media protocols, large and fast storage servers), and demonstrating the use of those technologies in some energy-related applications. It complemented and provided useful technological underpinnings to several Lawrence Berkeley Laboratory research efforts supported by DOE, in particular to

High Speed Distributing of Network-based Video Microscopy and Supercomputer Access Techniques. DOE

N95-32289# Loral Federal Systems, Gaithersburg, MD.
SOFTWARE PROCESS FRAMEWORK. TOOL TO DETERMINE CONSISTENCY WITH THE CMM (SOFTWARE TECHNOLOGY FOR ADAPTABLE, RELIABLE SYSTEMS (STARS) PROGRAM)
Paul G. Arnold, William H. Ett, and S. Wayne Sherer 16 Jan. 1995 45 p
(Contract F19628-93-C-0129)
(AD-A292815) Avail: CASI HC A03/MF A01

This paper presents the results and lessons learned from trial usage of the Software Engineering Institute's (SEI) Software Process Framework (SPF). The SPF was used to check consistency of the Cleanroom Software Engineering (CSE) process against the SEI Capability Maturity Model (CMM) for software. The trial usage was done for a STARS (Software Technology for Adaptable, Reliable Systems) supported software development project, Improved Mortar Ballistic Computer (IMBC), at the US Army's Picatinny Arsenal Life Cycle Software Engineering Center (LCSEC). DTIC

N95-32290# Loral Federal Systems, Gaithersburg, MD.
USING PROCESS TO INTEGRATE SOFTWARE ENGINEERING ENVIRONMENTS (SOFTWARE TECHNOLOGY FOR ADAPTABLE, RELIABLE SYSTEMS (STARS) PROGRAM)
Richard L. Randall and William H. Ett 16 Jan. 1995 65 p
(Contract F19628-93-C-0129)
(AD-A292816) Avail: CASI HC A04/MF A01

A layered architecture is fundamental to the megaprogramming approach being followed by the Air Force/STARS Demonstration Project, as engineers develop the Space Command and Control Architectural Infrastructure application for NORAD and USSPACECOM. This layering strategy also applies to the Software Engineering Environment (SEE) being used to support the application development. This paper focuses on one particular SEE layer: a layer that leverages one of an organization's most valued assets - its process - and uses it as a basis for SEE integration. The activity to produce and use the PSE has yielded useful lessons learned which can guide other organizations as they pursue their own process-driven SEE's. DTIC

N95-32291# Loral Federal Systems, Gaithersburg, MD.
SWSC DOMAIN ENGINEERING EXPERIENCE (SOFTWARE TECHNOLOGY FOR ADAPTABLE, RELIABLE SYSTEMS (STARS) PROGRAM)
Brian Bulet 15 Jan. 1995 51 p
(Contract F19628-93-C-0129)
(AD-A292817) Avail: CASI HC A04/MF A01

The Space and Warning Systems Center (SWSC) in Colorado Springs maintains and develops Command and Control Systems for NORAD, USSPACECOM, and AFSPC. Twenty-seven 'stovepipe' systems imbedding twenty-four languages and ten millions lines of code make for a maintenance nightmare and for a fertile ground for megaprogramming, or product line software reuse. At the SWSC, the SCAI (Space Command and Control Architectural Infrastructure) project has been instituting architecture-based, product line software reuse for the past two years. The SCAI project is the STARS/Loral/Air Force Megaprogramming Demonstration Project out of ARPA. This paper presents the lessons learned in developing and using a domain architecture, a domain architecture framework, and a domain engineering process, while developing a SCAI space surveillance application. DTIC

N95-32292# Loral Federal Systems, Gaithersburg, MD.
INTEGRATING A SEE FOR MEGAPROGRAMMING: LESSONS LEARNED (SOFTWARE TECHNOLOGY FOR ADAPTABLE, RELIABLE SYSTEMS (STARS) PROGRAM)
Richard L. Randall, Robert K. Ekman, Gary S. Turner, and Scott Kent 17 Jan. 1995 59 p
(Contract F19628-93-C-0129)
(AD-A292838) Avail: CASI HC A04/MF A01

The objective of megaprogramming technology is to make possible a software product-line organization - one that can produce related systems cheaper, better, and faster by using a methodical process based on a common architectural approach. To apply such state-of-the-art technology, a product-line organization needs a common software engineering environment (SEE) that is itself a result of product-line engineering. This paper describes how megaprogramming principles are being applied to assemble and integrate the SEE for one of the three STARS demonstration projects. It provides practical lesson learned, some hard-won, that should be useful to organizations planning their own SEE integration efforts, particularly for organizations considering a transition to megaprogramming. DTIC

N95-32293# Loral Federal Systems, Gaithersburg, MD.
DEFINING MANUALLY ENACTABLE PROCESSES USING THE PROCESS DEFINITION INFORMATION ORGANIZER TEMPLATES (SOFTWARE TECHNOLOGY FOR ADAPTABLE, RELIABLE SYSTEMS (STARS) PROGRAM)
William H. Ett, Dick Phillips, Jim Over, and Marc Kellner 6 Mar. 1995 80 p
(Contract F19628-93-C-0129)
(AD-A292854) Avail: CASI HC A05/MF A01

This document consists of the presentation slides to be used as a tutorial at the 1995 SEPG Conference to be held in Boston, MA on May 22-25, 1995. This tutorial will cover planning for the definition of a project's processes, an approach for defining manually enactable processes, and an approach for evaluating process definition results. DTIC

N95-32294# Loral Federal Systems, Gaithersburg, MD.
THE SOCIOLOGY OF MEGAPROGRAMMING: EXPERIENCES IN GENERATING AN ORGANIZATIONAL LEARNING ENTERPRISE (SOFTWARE TECHNOLOGY FOR ADAPTABLE, RELIABLE SYSTEMS(STARS) PROGRAM)
Lynn B. Underhill 27 Jan. 1995 35 p
(Contract F19628-93-C-0129)
(AD-A292998) Avail: CASI HC A03/MF A01

The STARS Program is currently involved in transitioning advanced software engineering technologies into practice within the DOD under the aegis of 'megaprogramming.' Megaprogramming, which integrates the notions of process-driven, domain specific, reuse based, and supporting automation via a software engineering environment, is intended to enable the formation of product-line organizations with the objective of producing systems 'cheaper, better, faster.' Transitioning to megaprogramming can involve significant changes to existing ways of doing business, and to an organization's underlying paradigms. Given the degree of change, sociological forces come into play. The project that forms the basis of this experience is the SCAT demonstration project, performed by the AF SWSC at Peterson AFB. As a vehicle for organizing the analysis of our project's experience, we will relate it to the disciplines distinguished by Peter Senge in 'The Fifth Discipline, the Art and Practice of the Learning Organization.' For each discipline, we present our interpretation of our experience, and our recommendations based on our lessons. DTIC

N95-32311 National Defence Research Establishment, Stockholm (Sweden).
ANALYSIS OF THE FINAL RESULT FROM THE IMAGE TEMPLATE MATCHING METHOD WITH FUZZY LOGIC [ANALYS AV SLUTRESULTATET VID MODELLBASERAD BILDMATCHNING MED OSKARP LOGIK]
A. Malmros Aug. 1994 108 p In SWAHILI
(PB95-222915; FOA-R-94-00011-3.4-SE) Avail: Issuing Activity (National Technical Information Service (NTIS))

This report presents an algorithm used to mark the quality of an image template matching and a literature study concerning fuzzy logic and fuzzy sets. When using an image template matching method, for instance the Hierarchical Chamfer Matching Algorithm, the result is a list of measurements. The measurements describe, pixel by pixel, the distance between a point on the template and nearest edge from the original picture. The algorithm, called Malmros' algorithm, constructs fuzzy sets on the measurements using statistics and weights them using fuzzy logic. Finally, defuzzification is used to get a per cent value as a measurement of the quality of the image template matching. The algorithm has been tested on available material and no greater disadvantage of the method has been noticed. The algorithm gives a good, but not optimal, solution of the problem. NTIS

62 COMPUTER SYSTEMS

Includes computer networks and special application computer systems.

N95-30577# Oak Ridge National Lab., TN.
AN OVERVIEW OF HIGH-SPEED NETWORKING FOR WORKSTATIONS
K. Hake 1995 15 p Presented at the Geographic Information System (GIS), Vancouver, Canada, 27-30 Mar. 1995
(Contract DE-AC05-84OR-21400)
(DE95-009076; CONF-9503121-1) Avail: CASI HC A03/MF A01

The telecommunications industry provides new technologies for GIS (Geographic Information System) workstation upgrades: Fast Ethernet, 100VG-AnyLAN, and Asynchronous Transfer Mode (ATM). These network technologies are based on approved standards and have industry backing (alliance for Fast Ethernet). This paper briefly examines these technologies. Fast Ethernet is an extension to its predecessor 10 Mbps Ethernet, providing a 10x increase in transmission rate. 100VG-AnyLAN offers extensions to Ethernet but embraces the Token Ring technology, allowing internetworking and better performance for networked video. ATM takes a radial approach by simplifying the information quantum to a 53-byte cell, resulting in rapid data handling for telecommunications equipment and allowing efficient transport of data, video, and voice communications. Switched Ethernet and Full Duplexing are among the other technologies competing for this market. The ultimate test of usefulness for any technology lies in how they handle the GIS environment requirements; working demonstration systems will help clarify marketing rhetoric and determine which vendor best implemented the standard. DOE

N95-30578# Lawrence Livermore National Lab., Livermore, CA.
RECOMMENDATIONS FOR DEVELOPING PORTABLE PARALLEL I/O FACILITIES FOR SCIENTIFIC APPLICATIONS
R. K. Yates 1 Dec. 1994 8 p
(Contract W-7405-eng-48)
(DE95-009384; UCRL-ID-119528) Avail: CASI HC A02/MF A01

We outline a plan to develop portable parallel I/O facilities for scientific applications on parallel computers. We recommend that efforts be focussed on three areas: a new standard I/O library for message passing environments, efficient parallel I/O implementations for data parallel programming in Fortran 90 and High Performance Fortran (which may require new parallel I/O commands), and the promotion of high performance parallel I/O facilities in high-level scientific toolkits. In the next year we will concentrate primarily on the first area, designing and implementing a portable parallel I/O library to work with the new MPI standard Message Passing Interface. DOE

N95-30721# Technische Univ., Twente (Netherlands).
WORKFLOW LITERATURE GUIDE, VERSION 1
S. Joosten, E. Mulder, and J. McCrory Sep. 1994 76 p
(PB95-207080; Memo-INF-94-51) Copyright Avail: CASI HC A05/MF A01

Administrative organizations in the financial, government and service sectors are introducing workflow technology as a method of integrating office procedures. Until now, such organizations have had difficulty obtaining workflow literature. The main aim of this guide is to provide a summary of all consequential workflow articles and how they have been located. Subsidiary aims include a listing of associations, conferences and internet sources. This guide will not only be useful to large organizations but to anyone embarking upon a study of workflow. NTIS

N95-30868# NYSERNET, Inc., Liverpool, NY.
WIDE AREA NETWORKING R&D Final Report, 3 Jan. 1989 - 3 May 1993
Richard Mandelbaum and James D. Luckatt Dec. 1994 134 p
(Contract F30602-89-C-0016; ARPA Order 6474; ARPA Order 6797)
(AD-A291057; NYSERNET-01; RL-TR-94-2113) Avail: CASI HC A07/MF A02

This was a joint Rome Laboratory/ARPA advanced development effort that: (1) provided wide area high speed networking services for the New York State (NYS) Arpanet; (2) created the National Networking Testbed (NNET); and (3) developed Simple Network Management Protocol (SNMP) software tools. Under the first task, existing NYS Arpanet users were provided Transmission Control Protocol/Internet Protocol (TCP/IP) network service and support, access to the Defense Research Internet (DRI) with connectivity to the Internet, and upgraded service from 56 kbps to 1.544 mbps. The second task involved the installation and operation of the NNT, a nationwide, high-speed computer data network dedicated to ARPA's use to support domestic military and NASA sites, with access provided to the U.S. Dept. of Energy. The NNT provided a non-production network environment to field test a variety of network infrastructure devices and management control software tools. The third task involved the development of network management software technology to operate and maintain reliable end-to-end NNT connectivity. In addition to SNMP software tools, some software development work involved applications related to the International Standards Organization Development Environment (ISODE) and X.500 Directory areas. DTIC

N95-30930# Rochester Univ., NY. Dept. of Computer Science.
ALGORITHMS FOR CATEGORIZING MULTIPROCESSOR COMMUNICATION UNDER INVALIDATE AND UPDATE-BASED COHERENCE PROTOCOLS
Ricardo Bianchini and Leonidas Kontothanassis Sep. 1994 24 p
(Contract N00014-92-J-1801; ARPA Order 8930)
(AD-A290022; TR-533) Avail: CASI HC A03/MF A01

In this paper, we present algorithms that characterize the main sources of communication generated by parallel applications under both invalidate and update based cache coherence protocols. The algorithms provide insight into the reference and sharing patterns of parallel programs and into the amount of useless traffic entailed by each coherence protocol. Under an invalidate based protocol, our algorithms classify the data traffic caused by the different types of cache misses. Under an update based protocol, our algorithms not only categorize the data traffic, but also classify update transactions with respect to the sharing patterns that caused them. Although our algorithms deal with numerous hardware features such as finite sized caches and coalescing write buffers, our categorization is widely applicable and can be easily simplified for use in less detailed environments. Our work extends previous categorizations of cache misses in write invalidate protocols, while introducing a new categorization of the coherence traffic in update based protocols. DTIC

N95-31051 Rutherford Appleton Lab., Oxford (England).
CLIENT SERVER ARCHITECTURE FOR MULTIDATABASE ACCESS. INGRES SQL SERVER
M. Dixon Nov. 1994 29 p Prepared in cooperation with Leeds Metropolitan Univ., Leeds, England
(PB95-192852; RAL-94-118) Avail: Issuing Activity (National Technical Information Service (NTIS))

The interoperating of multiple database systems requires a client application which acts as a mediating agent for database server processes; these server processes must be accessed using network procedure calls. This report addresses the problems and associated design options that arise in constructing a dynamic Structured Query Language (SQL) server process for the Ingres Relational Database Management System. The Ingres SQL server has been constructed in C on a Unix platform and accessed across a SunOS network. It is intended that the narrative in this report together with the source code for both the SQL Server and the primitive Client would act as a starting template for a writer of application code that required dynamic SQL access to an Ingres database. The choice of a network protocol is discussed. NTIS

N95-31445# BBN Systems and Technologies Corp., Cambridge, MA.
INTEGRATED HIGH PERFORMANCE DISTRIBUTED SYSTEM Final Technical Report, Aug. 1992 - Feb. 1994
Dec. 1994 52 p
(Contract F30602-92-C-0102)
(AD-A292821; BBN-7987; RL-TR-94-237) Avail: CASI HC A04/MF A01

The objective of the Integrated High Performance Distributed System (IHPDS) project is to design, implement, and demonstrate a distributed programming environment that will integrate and support very high bandwidth networks with heterogeneous computer architectures, including parallel and specialized processors, and that will support multiple programming models. The IHPDS project is developing the Photon distributed programming environment to meet the emerging needs of distributed application programmers. Photon provides an object-oriented programming model. This

provides users with a consistent view of all services while insulating the user from the implementation details of those services. This enforcement of modularity and the separation of policy and mechanism make the object model a powerful way to build large-scale, distributed applications. Photon is a distributed computing environment that supports distributed application development across heterogeneous machine architectures and programming languages. It is particularly targeted to support the needs of high performance applications. Photon not only supports applications whose components are located within a single local area network, but also supports applications whose components are widely dispersed geographically. DTIC

N95-31605# Sandia National Labs., Albuquerque, NM.
REQUIREMENTS FOR SECURITY SIGNALLING
Lyndon G. Pierson and Thomas D. Tarman Feb. 1995 8 p Presented at the ATM Forum Technical Committee Meeting, Denver, CO, 10 Apr. 1995
(Contract DE-AC04-94AL-85000)
(DE95-008714; SAND-95-0486C; CONF-9504139-3) Avail: CASI HC A02/MF A01

There has been some interest lately in the need for 'authenticated signalling', and the development of signalling specifications by the ATM Forum that support this need. The purpose of this contribution is to show that if authenticated signalling is required, then supporting signalling facilities for directory services (i.e. key management) are also required. Furthermore, this contribution identifies other security related mechanisms that may also benefit from ATM-level signalling accommodations. For each of these mechanisms outlined here, an overview of the signalling issues and a rough cut at the required fields for supporting Information Elements are provided. Finally, since each of these security mechanisms are specified by a number of different standards, issues pertaining to the selection of a particular security mechanism at connection setup time (i.e. specification of a required 'Security Quality of Service') are also discussed. DOE

N95-32021# Carnegie-Mellon Univ., Pittsburgh, PA. Dept. of Computer Science.
IMPROVING DATA CONSISTENCY IN MOBILE COMPUTING USING ISOLATION-ONLY TRANSACTIONS
Qi Lu and M. Satyanarayanan Mar. 1995 10 p Presented at the 5th Workshop on Hot Topics in Operating Systems, Orcas Island, WA, 4-5 May 1995
(Contract F19628-93-C-0193)
(AD-A293110; CMU-CS-95-126) Avail: CASI HC A02/MF A01

Disconnected operation is an important technique for providing mobile access to shared data in distributed file systems. However, data inconsistency resulting from partitioned sharing remains a serious concern. This paper presents a new mechanism called isolation-only transaction (IOT) that uses serializability constraints to automatically detect read/write conflicts. The IOT consistency model provides a set of options for automatic and manual conflict resolution. In addition, application specific knowledge can be incorporated to detect and resolve conflicts. To preserve upward Unix compatibility, the IOT mechanism is provided as an optional file system facility and its flexible interfaces allow any existing Unix application to be executed as an IOT. This paper describes high level system design and implementation and concludes with related work and current status. DTIC

N95-32065# Sandia National Labs., Albuquerque, NM.
SCALABLE ATM ENCRYPTION
1995 19 p Presented at the Cray User Group Spring Conference, Denver, CO, 15 Mar. 1995
(Contract DE-AC04-94AL-85000)
(DE95-009868; SAND-95-0661C; CONF-9503129-1) Avail: CASI HC A03/MF A01

In order to provide needed security assurances for traffic carried in Asynchronous Transfer Mode (ATM) networks, methods of protecting the integrity and privacy of traffic must be employed. Cryptographic methods can be used to assure authenticity and privacy, but are hard to scale and the incorporation of these methods into computer networks can severely impact functionality, reliability, and performance. To study these trade-offs, a research prototype encryptor/decryptor is under development. This prototype is to demonstrate the viability of implementing certain encryption techniques in high speed networks by processing Asynchronous Transfer Mode (ATM) cells in a SONET OC-3 payload. This paper describes the objectives and design trade-offs intended to be investigated with the prototype. User requirements for high performance computing and communication have driven Sandia to do work in the areas of functionality, reliability, security, and performance of high speed communication networks. Adherence to standards (including emerging standards) achieves greater functionality of high speed computer networks by providing wide interoperability of applications, network hardware, and network software. DOE

N95-32146# Sandia National Labs., Albuquerque, NM.
A PROPOSED GENERIC AUTHENTICATION INFORMATION ELEMENT
Thomas D. Tarman 10 Apr. 1995 5 p Presented at the ATM Forum Technical Committee Meeting, Denver, CO, 10 Apr. 1995
(Contract DE-AC04-94AL-85000)
(DE95-009862; SAND-95-0665C; CONF-9504139-2) Avail: CASI HC A01/MF A01

This contribution describes a proposed information element that can convey authentication information within an ATM signaling message. The design of this information element provides a large amount of flexibility to the user because it does not specify a particular signature algorithm, and it does not specify which information elements must accompany the Authentication IE in a signaling message. This allows the user to implement authenticated signaling based on her site's security policies and performance requirements. DOE

N95-32250*# National Aeronautics and Space Administration. Langley Research Center, Hampton, VA.
ASSIST USER MANUAL
Sally C. Johnson and David P. Boerschlein Aug. 1995 103 p Sponsored by NASA, Washington
(RTOP 505-64-10-07)
(NASA-TM-4592; L-17407; NAS 1.15:4592) Avail: CASI HC A06/MF A02

Semi-Markov models can be used to analyze the reliability of virtually any fault-tolerant system. However, the process of delineating all the states and transitions in a complex system model can be devastatingly tedious and error prone. The Abstract Semi-Markov Specification Interface to the SURE Tool (ASSIST) computer program allows the user to describe the semi-Markov model in a high-level language. Instead of listing the individual model states, the user specifies the rules governing the behavior of the system, and these are used to generate the model automatically. A few statements in the abstract language can describe a very large, complex model. Because no assumptions are made about the system being modeled, ASSIST can be used to generate models describing the behavior of any system. The ASSIST program and its input language are described and illustrated by examples. Author

N95-32255 Montpellier-2 Univ. (France)
UNIVERSAL MESSAGE PASSING LIBRARY, OR HOW TO WRITEA TRULY PORTABLE CODE FOR PARALLEL COMPUTERS Final Report [LIBRAIRIE DE PASSAGE DE MESSAGES UNIVERSELLE OU COMMENT ECRIRE UN CODE VRAIMENT PORTABLE POUR CALCULATEURS PARALLELES]
B. Meltz 1994 33 p In FRENCH Prepared in cooperation with Los Alamos National Lab., NM; sponsored by Direction des Recherches, Etudes et Techniques, Paris, France. Centre de Docu mentation de l'Armement
(Contract DRET-921438)
(PB95-212221; IEP-87/822) Avail: Issuing Activity (National Technical Information Service (NTIS))

Universal Communication Library (UNCOL) is a message passing library, intended for the painless parallelization of numerical simulation codes. Originally aimed at a finite difference, domain decomposition computational fluid dynamics (CFD) code, it has since been successfully applied to several other cases. We show how we achieved our initial goal, and what are the pros and cons of the portability-oriented strategy. NTIS

N95-32277# Los Alamos National Lab., NM.
COMPACT LOCATION PROBLEMS WITH BUDGET AND COMMUNICATION CONSTRAINTS
S. O. Krumke, H. Noltemeier (Wuerzburg Univ., Germany.), S. S. Ravi, and M. V. Marathe 1995 24 p Presented at the 1st Annual International Computing and Combinatorics Conference, Xian, China, 24 Aug. 1995

(Contract W-7405-eng-36)
(DE95-010876; LA-UR-95-1293; CONF-9508113-1) Avail: CASI HC A03/MF A01

We consider the problem of placing a specified number p of facilities on the nodes of a given network with two nonnegative edge-weight functions so as to minimize the diameter of the placement with respect to the first distance function under diameter or sum-constraints with respect to the second weight function. Define an (alpha, beta)-approximation algorithm as a polynomial-time algorithm that produces a solution within alpha times the optimal function value, violating the constraint with respect to the second distance function by a factor of at most beta. We observe that in general obtaining an (alpha, beta)-approximation for any fixed alpha, beta greater than or equal to 1 is NP-hard for any of these problems. We present efficient approximation algorithms for the case when both edge-weight functions obey the triangle inequality. For the problem of minimizing the diameter under a diameter constraint with respect to the second weight-function, we provide a (2,2)-approximation algorithm. We also show that no polynomial time algorithm can provide an (alpha, 2 minus epsilon) or (2 - epsilon, beta) approximation for any fixed epsilon greater than 0 and alpha, beta greater than or equal to 1, unless P = NP. This result is proved to remain true, even if one fixes epsilon' greater than 0 and allows the algorithm to place only 2p/(absolute value of V)(sup 1/(6 - epsilon')) facilities. Our techniques can be extended to the case when either the objective or the constraint is of sum-type and also to handle additional weights on the nodes of the graph. Here our heuristics provide performance guarantees of (2 - 2/p, 2) and (2, 2 - 2/p) respectively. DOE

N95-32371 Ecole Centrale de Nantes (France). Lab. d'Automatique de Nantes.
FRANCE
A. Arnold, J. Beauquier, and O. Roux 1994 294 p In FRENCH Conference held in Nantes, France, 21-24 Jun. 1991 Sponsored by Direction des Recherches, Etudes et Techniques, Paris, France. Centre de Documentation de l'Armement
(Contract DRET-C-94-1021/A000)
(PB95-208385) Avail: Issuing Activity (National Technical Information Service (NTIS))

The document is a collection of 13 papers (9 in French, 4 in English) on the general theme of modeling and verification of parallel computer systems for the control of industrial processes. Topics addressed include: theory and implementation of control of discrete-event systems (in English); applications of the theory of (max,+) automata to discrete-event systems (English); finite dimensional pseudomodules (English); modeling problems in automated industrial production systems; event structures and flow nets (part in French, part in English); automata and transition systems; temporal extensions of Basic LOTOS, including RT-LOTOS; verification of timed automata; cellular asynchronous and distributed automata; timed logics and verification; and on-the-fly verification of finite transition systems (English). NTIS

63 CYBERNETICS

Includes feedback and control theory, artificial intelligence, robotics and expert systems.

For related information see also *54 Man/System Technology and Life Support.*

N95-30377# Sandia National Labs., Albuquerque, NM.
A HEURISTIC AND COMPLETE PLANNER FOR THE CLASSICAL MOVER'S PROBLEM
Yong K. Hwang and Pang C. Chen 1995 8 p Presented at the 1995 International Conference on Robotics and Automation, Nagoya, Japan, 21-27 May 1995
(Contract DE-AC04-94AL-85000)
(DE95-008440; SAND-95-0242C; CONF-9505193-1) Avail: CASI HC A02/MF A01

We present a motion planner for the classical mover's problem in three dimensions that is both resolution-complete and efficient in that it has performance commensurate with task difficulty. It is based on the SANDROS search strategy, which uses a hierarchical, multi-resolution representation of the configuration space along with a generate-and-test paradigm for solution paths. This planner can control the trade-offs between the computation resource and algorithmic completeness/solution path quality, and thus can fully utilize the available computing power. It is useful for navigation of mobile robots, submarines and spacecraft, or part motion feasibility in assembly planning. DOE

N95-30395# Northwestern Univ., Evanston, IL. Inst. for the Learning Sciences.
LEARNING IN AN INTENTIONAL SYSTEM Final Report, 1 Aug. 1991 - 31 Jul. 1994
Lawerence Birnbaum and Gregg Collins Dec. 1994 27 p
(Grant AF-AFOSR-0341-91)
(AD-A291158; AFOSR-95-0087TR) Avail: CASI HC A03/MF A01

The goal of the project, as outlined in the original proposal, was to carry out research aimed at the construction of adaptive planning systems that can learn in response to planning failures, i.e., modeling learning to plan as a process of debugging. Previous approaches to failure-driven learning have been based on a traditional models of planning, in which the planner generates a monolithic, self-contained plan to be passed on to another module for execution. Such approaches have thus focused on the process of debugging a plan that has proven to be faulty during execution. However, such traditional models of planning have increasingly come under attack, as it has come to be recognized that planners operating in the real world must be reactive, changing plans on the fly to cope with unexpected circumstances. In such a model, there may be no single, monolithic plan that governs the systems behavior during execution. DTIC

N95-30400# Technische Univ., Eindhoven (Netherlands). Dept. of Mathematics and Computing Science.
ANALYZING GI/ERLANG-R/1 QUEUES
I. J. B. F. Adan and Yiqiang Zhao Nov. 1994 17 p Prepared in cooperation with Winnipeg Univ., Manitoba Sponsored by the Natural Sciences and Engineering Research Council of Canada
(ISSN 0926-4493)
(PB95-197034; MEMO-COSOR-94-37) Avail: CASI HC A03/MF A01

In this paper we study a single-server system with Erlang-r distributed service times and arbitrarily distributed interarrival times. It is shown that the waiting-time distribution can be expressed as a finite sum of exponentials, the exponents of which are the roots of an equation. Under certain conditions for the interarrival-time distribution, this equation can be transformed to r contraction equations, the roots which can be easily found by successive substitutions. The conditions are satisfied for several practically relevant arrival processes. The resulting numerical procedures are easy to implement and efficient and appear to be remarkably stable, even for extreme high value of r and for values of the traffic load close to 1. Numerical results are presented. NTIS

N95-30406# Air Force Inst. of Tech., Wright-Patterson AFB, OH.
SELECTING OPTIMAL EXPERIMENTS FOR FEEDFORWARD MULTILAYER PERCEPTRONS Ph.D. Thesis
Lisa M. Belue Mar. 1995 187 p
(AD-A290856; AFIT/DS/ENS/95-01) Avail: CASI HC A09/MF A02

Where should a researcher conduct experiments to provide training data for a multilayer perceptron? This question is investigated and a statistically-based method for optimally selecting experimental design points for multilayer perceptrons is introduced. Specifically, a criterion is developed based on the size of an estimated confidence ellipsoid for the weights in the multilayer perceptron. This criterion is minimized over a set of exemplars to find optimal design points. Initially, single output networks are examined. An example is used to demonstrate the superiority of optimally selected design points over randomly chosen points and points chosen in a grid pattern. Also, two measures are successfully used to rank the design points in terms of their importance. Two methods are presented to significantly reduce complexity-a distributed linear feedthrough network structure and a weight subset method. Next, multiple output networks are examined. The criterion in this framework becomes more complex and a simplifying technique is employed to judiciously choose desired outputs of the network to produce uncorrelated actual outputs. Finally, the methods described above are integrated and tested on two applications dealing with aircraft survivability. In both cases, simulating the indicated experiments produced a superior multilayer perceptron. DTIC

N95-30462# Technische Univ., Eindhoven (Netherlands). Dept. of Mathematics and Computing Science.
FITTING DISCRETE DISTRIBUTIONS ON THE FIRST TWO MOMENTS
I. J. B. F. Adan, M. J. A. vanEenige, and J. A. C. Resing Nov. 1994 15 p
(PB95-197885; MEMO-COSOR-94-36) Avail: CASI HC A03/MF A01

In this paper we present a simple method to fit a discrete distribution on the first two moments of a given distribution. With the fitted distribution we solve approximately Lindley's equation for the discrete-time D/G/1 queue using a moment-iteration method. Numerical results show excellent performance of the method. NTIS

N95-30463# Sandia National Labs., Albuquerque, NM.
ADAPTIVE PATH PLANNING: ALGORITHM AND ANALYSIS
Pang C. Chen 1995 8 p Presented at the 1995 International Conference on Robotics and Automation, Nagoya, Japan, 21-27 May 1995
(Contract DE-AC04-94AL-85000)
(DE95-008549; SAND-95-0241C; CONF-9505193-3) Avail: CASI HC A02/MF A01

To address the need for a fast path planner, we present a learning algorithm that improves path planning by using past experience to enhance future performance. The algorithm relies on an existing path planner to provide solutions to difficult tasks. From these solutions, an evolving sparse network of useful robot configurations is learned to support faster planning. More generally, the algorithm provides a framework in which a slow but effective planner may be improved both cost-wise and capability-wise by a faster but less effective planner coupled with experience. We analyze the algorithm by formalizing the concept of improvability and deriving conditions under which a planner can be improved within the framework. The analysis is based on two stochastic models, one pessimistic (on task complexity), the other randomized (on experience utility). Using these models, we derive quantitative bounds to predict the learning behavior. We use these estimation tools to characterize the situations in which the algorithm is useful and to provide bounds on the training time. In particular, we show how to predict the maximum achievable speedup. Additionally, our analysis techniques are elementary and should be useful for studying other types of probabilistic learning as well. DOE

N95-30478 National Defence Research Establishment, Linkoeping (Sweden).
NONLINEAR DYNAMICAL SYSTEMS: ELEMENTS OF A COMPLEX SYSTEM ANALYSIS [OLINJAERA DYNAMISKA SYSTEM: EN KOMPLEX SYSTEMANALYS I VARDANDE]
S. Palmgren Nov. 1994 25 p In SWAHILI
(PB95-211652; FOA-R-94-00060-3.4-SE) Avail: Issuing Activity (National Technical Information Service (NTIS))

This report describes in very general terms some trends in the development of methods for dealing with nonlinear dynamical systems. This description serves as an environment for the discussion of the basis for a modern system analysis--a Complex System Analysis. NTIS

N95-30564# Technische Univ., Eindhoven (Netherlands).
FIXED MODES IN QUASI-STATIC STATE FEEDBACK DECOUPLING
R. Andiarti, C. H. Moog, and H. J. C. Huijberts Sep. 1994 15 p Prepared in cooperation with Nantes Univ.
(PB95-206850; MEMO-COSOR-94-30) Avail: CASI HC A03/MF A01

We consider the problem of noninteracting control with stability for a square affine nonlinear system, where its decoupling matrix is not necessarily invertible. The recent notion of quasi-static state feedback is used. The results of this paper show that the dimension of the fixed dynamics with respect to any quasi-static state feedback may be determined by using the so-called accessibility cospaces. NTIS

N95-30655*# Ohio Univ., Athens, OH. Dept. of Electrical and Computer Engineering.
COMPUTERIZED DESIGN OF CONTROLLERS USING DATA MODELS Final Report
Dennis Irwin, Jerrel Mitchell, Enrique Medina, Dan Allwine, Garth Frazier, and Mark Duncan Jul. 1995 242 p
(Grant NAG8-217)
(NASA-CR-198921; NAS 1.26:198921) Avail: CASI HC A11/MF A03

The major contributions of the grant effort have been the enhancement of the Compensator Improvement Program (CIP), which resulted in the Ohio University CIP (OUCIP) package, and the development of the Model and Data-Oriented Computer Aided Design System (MADCADS). Incorporation of direct z-domain designs into CIP was tested and determined to be numerically ill-conditioned for the type of lightly damped problems for which the development was intended. Therefore, it was decided to pursue the development of z-plane designs in the w-plane, and to make this conversion transparent to the user. The analytical development needed for this feature, as well as that needed for including compensator damping ratios and DC gain specifications, closed loop stability requirements, and closed loop disturbance rejection specifications into OUCIP are all contained in Section 3. OUCIP was successfully tested with several example systems to verify proper operation of existing and new features. The extension of the CIP philosophy and algorithmic approach to handle modern multivariable controller design criteria was implemented and tested. Several new algorithms for implementing the search approach to modern multivariable control system design were developed and tested. This analytical development, most of which was incorporated into the MADCADS software package, is described in Section 4, which also includes results of the application of MADCADS to the MSFC ACES facility and the Hubble Space Telescope. Derived from text

N95-30784*# Charles River Analytics, Inc., Cambridge, MA.
APPLICATION OF GENETIC ALGORITHMS AND MACHINE LEARNING TO SCHEDULING Final Report
Sherif M. Botros and Alper K. Caglayan 14 Jun. 1995 41 p
(Contract NAS9-19263)
(NASA-CR-198965; R94281; NAS 1.26:198965) Avail: CASI HC A03/MF A01

While there exists a number of successful heuristic scheduling rules, these rules usually suffer from limited applicability and unpredicted performance. The main objective of this Phase 1 effort is to demonstrate the feasibility of applying the emerging optimization and machine learning technology in scheduling. The incorporation of machine learning capability in scheduling provides generality and wide applicability in addition to improved schedule quality. In Phase 1, we explored the application of recurrent neural networks, genetic algorithms (GA) and reinforcement learning (RL) to resource constrained scheduling and tested their feasibility in realistic scheduling problems. The specific tasks performed during the Phase 1 effort are: (1) the specification and design of a machine-learning-based intelligent scheduler which combines scheduling heuristic rules and machine learning techniques to improve scheduling performance; (2) testing the feasibility of applying GA and RL techniques to scheduling, and demonstrating how these techniques result in good performance when applied to realistic complex scheduling problems; (3) implementing many of the supporting scheduling tools in the form of C++ class libraries; and (4) specifying the requirements for a Phase 2 full-scope implementation. The results obtained in Phase 1 demonstrate the feasibility and advantages of developing a machine-learning-based scheduler. Author

N95-30807# Technische Univ., Eindhoven (Netherlands). Dept. of Mathematics and Computing Science.
GENERALIZED CONTROLLED INVARIANCE FOR NONLINEAR SYSTEMS
H. J. C. Huijberts, C. H. Moog, and R. Andiarti Nov. 1994 35 p
(PB95-197901; MEMO-COSOR-94-34) Avail: CASI HC A03/MF A01

A general setting is developed which describes controlled invariance for nonlinear control systems and which incorporates the previous approaches dealing with controlled invariant (co-) distributions. A special class of controlled invariant subspaces, called controllability cospaces, is introduced. These geometric notions are shown to be useful for deriving a (geometric) solution to the dynamic disturbance decoupling problem and for characterizing the so-called fixed dynamics for the general input-ouput noninteracting control problem via dynamic compensation. These fixed dynamics are a major issue for studying noninteracting control with stability. The class of quasi-static state feedbacks is used. NTIS

N95-30808# Technische Univ., Eindhoven (Netherlands).
SYMMETRIC LONGEST QUEUE SYSTEM
I. J. B. F. Adan, C. J. vanHoutum, and J. vanderWal Oct. 1994 20 p
(PB95-197919; MEMO-COSOR-94-33) Avail: CASI HC A03/MF A01

In this paper we derive the performance of the exponential symmetric

longest queue system from two variants: a longest queue system with Threshold Rejection of jobs and one with Threshold Addition of jobs. It is shown that these two systems provide lower and upper bounds for the performance on the longest queue system. Both variants can be analyzed efficiently. Numerical experiments demonstrate the power of the approach. NTIS

N95-30813# Technische Univ., Eindhoven (Netherlands).
NOISY-NETWORK ACCEPTORS
M. F. J. Drossaers Oct. 1994 119 p
(PB95-197976; Memo-INF-94-63) Copyright Avail: CASI HC A06/MF A02

In this paper a number of neural networks for sequence recognition is reviewed, and a noisy version of the neural-network acceptor, the noisy-network acceptor, is introduced and analyzed. The paper starts off exposing the computational weakness of attractor neural networks in sequence recognition tasks. This shows very explicitly to what problem the neural-network acceptor provides an answer. The theory of noisy-network acceptors introduced in this paper provides a framework for the examination of sequence recognition if the acceptor is subjected to noise. Analyses of the noisy-network acceptor's performance show that the noisy-network acceptor is a robust recognition device. Also a great agreement between analytical and simulation results was found. NTIS

N95-30833# Technische Univ., Eindhoven (Netherlands). Dept. of Mathematics and Computing Science.
H(SUB 2) OPTIMAL CONTROLLERS WITH OBSERVER BASED ARCHITECTURE FOR CONTINUOUS-TIME SYSTEMS: SEPARATION PRINCIPLE
Ali Saberi, Peddapullaiah Sannuti, and A. A. Stoorvogel 9 Dec. 1994 30 p Prepared in cooperation with Washington State Univ., Pullman and Rutgers State Univ., Piscataway, NJ
(PB95-197067; MEMO-COSOR-94-41) Avail: CASI HC A03/MF A01

For a general H(sub 2) optimal control problem, at first all H(sub 2) optimal measurement feedback controllers are characterized and parameterized, and then attention is focused on controllers with observer based architecture. Both full order as well as reduced order observer based H(sub 2) optimal controllers are characterized and parameterized. Also, systematic methods of designing them are presented. An important problem that can be coined as an H(sub 2) optimal control problem with simultaneous pole placement, is formulated and solved. That is, since in general there exist many H(sub 2) optimal measurement feedback controllers, utilizing such flexibility and freedom, we can solve the problem of simultaneously placing the closed-loop poles at desirable locations whenever possible while still preserving H(sub 2) optimality. All the design algorithms developed here are easily computer implementable. NTIS

N95-30884# Pennsylvania Univ., Philadelphia, PA.
NEURODYNAMICAL SYSTEMS FOR COGNITION AND TARGET IDENTIFICATION Final Technical Report, 1 Jul. 1991 - 30 Jun. 1994
N. H. Farhat Oct. 1994 83 p
(Contract DAAL03-91-G-0209)
(AD-A293111; ARO-28125.9-MA) Avail: CASI HC A05/MF A01

Our study of cognitive automated target recognition (ATR) based on the neural paradigm for information processing reveals that inclusion of bifurcation and synchronicity (phase-locking) in network dynamics can markedly improve the performance of ATR systems. This gave impetus to our study of how synchronicity could arise in cortical networks when it is known the brain has no central clock. Raising this question has led us, through analysis of models of biological neurons employing the tools of nonlinear dynamics, to the development of the bifurcating neuron concept and model. This spiking neuron model combines functional complexity comparable to that of biological neurons with structural simplicity and low power consumption when implemented electronically or optoelectronically. These attributes make the bifurcating neuron ideally suited for use as building block of a new generation of spiking neural networks that employ phase-locking, bifurcation, and chaos, on the single processing element level, to emulate higher-level cortical functions such as feature-binding and cognition that are essential for advanced ATR systems, and other operations like separation of object from background, inferencing, and rudimentary reasoning. DTIC

N95-30890# Massachusetts Inst. of Tech., Lexington, MA.
MACHINE LEARNING FOR A TOOLKIT FOR IMAGE MINING
Richard L. Delaney and Richard J. Sasiela 6 Mar. 1995 27 p
(Contract F19628-95-C-0002)
(AD-A293137; TR-1017; ESC-TR-94-112) Avail: CASI HC A03/MF A01

Given the exponential growth in the number of images stored in databases around the world, there is a clear need for computer-assisted means of searching images. Keywords and computed indices, referred to as metadata, can be used to tag images for subsequent retrieval. Most potential applications, however, will require searching for images on the basis of image content, but existing techniques for content-based search are either too slow, customized at great expense for a single application, or simply do not work well. An environment has been created enabling a user with limited computer skills to interactively train a computer algorithm to recognize patterns of spectral or textural features in imagery. The trained algorithm can then be exported as an independent agent to search large databases for matching image patterns. Following their retrieval, a user can further refine agent performance by indicating mistakes. The final product is a search tool capable of prescreening and highlighting images, significantly reducing the workload of analysts attempting to detect regions or objects in imagery. An approach to interactive learning has been developed as part of this environment. Based on techniques of knowledge-based image processing, this approach uses interest images to provide a means of continuous feedback of algorithm performance to the user, who in turn responds by indicating where the algorithm is making mistakes. The set of user-indicated examples and counterexamples form the inputs to a new machine learning algorithm called functional template learning. This algorithm is competitive with other machine learning techniques in terms of classification accuracy and exhibits several advantages in terms of speed and understandability that make it particularly well suited to interactive, supervised machine learning and autonomous searching of databases. DTIC

N95-30891# Air Force Systems Command, Wright-Patterson AFB, OH. National Air Intelligence Center.
MULTI-VALUED NEURAL NETWORK MODIFIED MODEL AND ITS OPTICAL REALIZATION.
Weili Zhu and Yansong Chen 7 Mar. 1995 14 p Transl. into ENGLISH from Guangxue Xuebao, China, v. 12, no. 5, May 1992 p 457
(AD-A293140; NAIC-ID(RS)T-0379-94) Avail: CASI HC A03/MF A01

This paper presents a modified optical neural network model, and the optical system, constructed with spatial light modulator PROM, can materialize the associative memory computation of such kinds of models. From the computer simulation and experimental results, it is clarified that the modified model improves cognitive ability of an optical neural network and also improves the storage capacity to a certain extent. DTIC

N95-30925*# National Aeronautics and Space Administration. Lyndon B. Johnson Space Center, Houston, TX.
MAKING INTELLIGENT SYSTEMS TEAM PLAYERS. A GUIDE TO DEVELOPING INTELLIGENT MONITORING SYSTEMS
Sherry A. Land, Jane T. Malin, Carroll Thronesberry (Metrica, Inc., Houston, TX.), and Debra L. Schreckenghost (Metrica, Inc., Houston, TX.) Jul. 1995 100 p
(NASA-TM-104807; S-790; NAS 1.15:104807) Avail: CASI HC A05/MF A02

This reference guide for developers of intelligent monitoring systems is based on lessons learned by developers of the DEcision Support SYstem (DESSY), an expert system that monitors Space Shuttle telemetry data in real time. DESSY makes inferences about commands, state transitions, and simple failures. It performs failure detection rather than in-depth failure diagnostics. A listing of rules from DESSY and cue cards from DESSY subsystems are included to give the development community a better understanding of the selected model system. The G-2 programming tool used in developing DESSY provides an object-oriented, rule-based environment, but many of the principles in use here can be applied to any type of monitoring intelligent system. The step-by-step instructions and examples given for each stage of development are in G-2, but can be used with other development tools. This guide first defines the authors' concept of real-time monitoring systems, then tells prospective developers how to determine system requirements, how to build the system through a combined design/development process, and how to solve problems involved

in working with real-time data. It explains the relationships among operational prototyping, software evolution, and the user interface. It also explains methods of testing, verification, and validation. It includes suggestions for preparing reference documentation and training users. Author

N95-30961 Michigan Univ., Ann Arbor, MI.
ROBUST FIXED-STRUCTURE CONTROL Final Report, 1 Feb. 1992 - 30 Sep. 1994
Dennis S. Bernstein 30 Oct. 1994 28 p Limited Reproducibility: More than 20% of this document may be affected by poor print
(Contract F49620-92-J-0127)
(AD-A292883; AFOSR-95-0202TR) Avail: Issuing Activity (Defense Technical Information Center (DTIC))

This final report for AFOSR Grant F49620-92-J-0127 summarizes results obtained in five areas, namely, robust control, linear control, sampled-data control, tracking and disturbance rejection, and nonlinear control. Principal results include new bounds for the structured singular value, implementation of structured singular value synthesis using fixed-structure optimization techniques, a more rigorous foundation for the Maximum Entropy control technique, extensions of linear-quadratic control to stable stabilizing controllers, determination of the achievable performance of sampled-data controllers in the presence of sample-rate constraints, control of noise in an acoustic duct, stability theory for second-order systems, a rigorous treatment of Guyan reduction, a deterministic foundation for energy flow theory, a unified treatment of quadratic optimality and servocompensation, nonlinear control of the spinning top and rotating bodies with known and unknown mass imbalance, global stabilization of the oscillating eccentric rotor using integrator backstepping, and Lyapunov theory for finite-time convergence. DTIC

N95-31055 Brown Univ., Providence, RI. Div. of Applied Mathematics.
WORKSHOP ON DIFFUSION APPROXIMATION IN COMMUNICATION AND STOCHASTIC SYSTEMS THEORY Final Technical Report, 1 Jun. 1993 - 31 May 1994
Paul Dupuis 11 Oct. 1994 11 p Limited Reproducibility: More than 20% of this document may be affected by poor print
(Contract F49620-91-1-0279)
(AD-A292872; AFOSR-95-0190TR) Avail: Issuing Activity (Defense Technical Information Center (DTIC))

The workshop Stochastic Systems and Their Applications was held in Newport, RI on April 15 & 16, 1994. The main topics of the conference were asymptotic methods in stochastic systems theory, and related applications. The goal of the conference was to review recent advances in asymptotic methods and expose some important new application areas where those methods might be useful. DTIC

N95-31161# Los Alamos National Lab., NM.
A TWO-TIMESCALE APPROACH TO NONLINEAR MODEL PREDICTIVE CONTROL
Kevin L. Buescher and Christopher C. Baum 1994 18 p Presented at the 1995 American Control Conference, Seattle, WA, Jun. 1995
(Contract W-7405-eng-36)
(DE95-000943; LA-UR-94-3256; CONF-950653-1) Avail: CASI HC A03/MF A01

Model predictive control (MPC) schemes generate controls by using a model to predict the plant's response to various control strategies. A problem arises when the underlying model is obtained by fitting a general nonlinear function, such as a neural network, to data: an exorbitant amount of data may be required to obtain accurate enough predictions. We describe a means of avoiding this problem that involves a simplified plant model which bases its predictions on averages of past control inputs. This model operates on a timescale slower than the rate at which the controls are updated and the plant outputs are sampled. Not only does this technique give better closed-loop performance from the same amount of open-loop data, but it requires far less on-line computation as well. We illustrate the usefulness of this two-timescale approach by applying it to a simulated exothermic continuously stirred tank reactor with jacket dynamics. DOE

N95-31255# Department of Energy, Pittsburgh, PA. Energy Technology Center.
HIGH-TECH CONTROLS FOR ENERGY AND ENVIRONMENT
S. J. Biondo, ed. and C. J. Drummond, ed. 1994 287 p Presented at the Adaptive Control Systems Technology Symposium, Pittsburgh, PA, 24-25 Oct. 1994
(DE95-011702; CONF-9410335) Avail: CASI HC A13/MF A03

The Department of Energy, in cooperation with the IEEE Neural Networks Council, Naval Research Laboratory, Electric Power Research Institute, and U.S. Bureau of Mines, sponsored the Adaptive Control Systems Technology Symposium in Pittsburgh, Pennsylvania from October 24 to 25, 1994. The theme of the Symposium was High-Tech Controls for Energy and Environment. This extraordinary gathering was designed to bring together individuals from the control systems and computational intelligence communities to focus attention on potential benefits to be derived from the application of adaptive controls to energy and environmental systems. Leading authorities from industry, academic, and government institutions presented tutorial overviews on each of three computational intelligence paradigms -- viz., neural networks, fuzzy logic, genetic algorithms -- identified useful hybrid forms, and introduced intelligent and adaptive control systems concepts and applications. There were also papers presented that focussed on specific applications of intelligent control and adaptive control in energy and environmental control systems. Individual papers have been cataloged separately. DOE

N95-31266# Honeywell, Inc., Minneapolis, MN.
ADVANCES IN ROBUST CONTROL Final Technical Report, Nov. 1991 - Feb. 1995
Blaise Morton Feb. 1995 58 p
(Contract F49620-92-C-0007)
(AD-A291126; C950028; AFOSR-95-0089TR) Avail: CASI HC A04/MF A01

This report describes recent developments in the algebraic theory of structured singular values. The algebric theory presented in this report is a product of an effort to compute the value of the mu-function exactly (for special structure) and to construct worst-case parameter sets. DTIC

N95-31279 Brown Univ., Providence, RI. Div. of Applied Mathematics.
THEORY & NUMERICAL METHODS FOR PROBLEMS IN SHAPE RECONSTRUCTION AND LARGE DEVIATIONS Final Technical Report, 1 Jun. 1993 - 31 May 1994
Paul Dupuis 26 Jul. 1994 5 p Limited Reproducibility: More than 20% of this document may be affected by poor print
(Contract F49620-93-1-0264)
(AD-A292874; AFOSR-95-0189TR) Avail: Issuing Activity (Defense Technical Information Center (DTIC))

This report describes work on problems from stochastic systems theory where the noise effects are small. The work has addressed two current needs: extension of the theory to cover practically interesting problems (such as design of data networks), and the development of computational methods for large deviation problems. Problems of particular interest that were dealt with are approximation of rare events in queueing systems and the control of reliable systems. We also discuss a recently developed method for obtaining rate of convergence estimates for a variety of approximations in deterministic and stochastic optimal control. DTIC

N95-31517# Air Force Inst. of Tech., Wright-Patterson AFB, OH. School of Engineering.
ACQUIRING CONSISTENT KNOWLEDGE FOR BAYESIAN FORESTS M.S. Thesis
Darwyn O. Banks Mar. 1995 101 p
(AD-A293858; AFIT/GSO/ENG/95M-01) Avail: CASI HC A06/MF A02

This thesis develops a methodology and a tool for knowledge acquisition with the new probabilistic knowledge representation-the Bayesian Forest. It establishes the structure of the Knowledge Acquisition and Maintenance module of the Probabilities, Expert Systems, Knowledge and Inference (PESKI) architecture. The tool, MACK, is designed to be used directly by the domain expert(s) rather than by knowledge engineer(s), and thus supports automated knowledge acquisition. This research determines and implements the constraints necessary to ensure the consistency of Bayesian Forest knowledge bases as data is both acquired and subsequently maintained. The impact to the PESKI architecture of time-dependent information and default assumptions during reasoning is also explored. The tool has been applied to NASA's Post-Test Diagnostics System which locates anomalies aboard the Space Shuttles' Main Engines. DTIC

N95-31540# Carnegie-Mellon Univ., Pittsburgh, PA. Robotics Inst.
NEURAL NETWORKS FOR REAL-TIME TERRAIN TYPING
Ian Lane Davis Jan. 1995 16 p
(Contracts DACA76-89-C-0014; DAAE07-90-C-R059)
(AD-A293569; CMU-RI-TR-95-06) Avail: CASI HC A03/MF A01

Many robotics tasks require an ability to determine quickly the nature of the terrain surrounding the robot. In cross country navigation in particular, the robot needs to know where the vegetation is and where the hard obstacles are. I have developed a general system which has successfully allowed real-time terrain typing in the NavLab II autonomous vehicle. This system and training paradigm are based on standard neural network technology and allow the robot to learn arbitrary non-linear mappings from color and texture space to terrain space. DTIC

N95-31562# Raytheon Co., Bedford, MA.
NEURAL NETWORK FALSE ALARM FILTER, VOLUME 1 Report, Sep. 1992 - 1994
F. Ayistock, L. Elerin, J. Hintz, C. Learoyd, and R. Press Dec. 1994 186 p
(AD-A293097; RL-TR-94-216) Avail: CASI HC A09/MF A02

This effort identified, developed and demonstrated a set of approaches for applying neural network learning techniques to the development of a real-time built-in test (BIT) capability to filter out false-alarms from the BIT output. Following a state-of-the-art assessment, a decision space of 19 neural network models, 9 fault report causes and 12 common groups of BIT techniques was identified. From this space, 4 unique, high-potential combinations were selected for further investigation. These techniques were subsequently simulated for application to a MILSATCOM system. Detailed analyses of their strengths and weaknesses were performed along with cost/benefit analyses. This study concluded that the best candidates for neural network insertion are new systems where neural network requirements can be included in the initial system design and that a major challenge is the availability or real data for training of the networks. Volume 1 of this report documents the activities and findings of the effort, including an extensive, annotated bibliography. Volume 2 contains a tutorial overview of the neural networks, BIT techniques and false alarm causes utilized in the final phases of this study. DTIC

N95-31582# Air Force Inst. of Tech., Wright-Patterson AFB, OH. School of Engineering.
THE EFFECT OF REPEATEDLY SAMPLING AN EMBEDDED METAMODEL ON THE SIMULATION RESPONSE M.S. Thesis
J. K. Patterson Mar. 1995 49 p
(AD-A293783; AFIT/GOA/ENS/95M-6) Avail: CASI HC A03/MF A01

This study investigated the effect on simulation output of repeatedly sampling an embedded metamodel. A metamodel is said to be embedded within a simulation if it is used to replace a submodule of that simulation. Replacing a deterministic module with an embedded deterministic metamodel poses no apparent mathematical problems. However, using a deterministic metamodel to replace a stochastic simulation component could require additional corrective actions. This research was performed in two phases. The first phase dealt with a set of tandem queues. It was shown that as each queue was sequentially replaced with a metamodel, the total system variance was inappropriately diminished. A theoretical model of the error components was postulated and used to compensate for this missing variation, restoring the parent simulation's variance to approximately its original level. In the second phase, the problem was extended to the case of repeatedly sampling an embedded metamodel with similar results. In addition, guidelines for metamodel use were presented. In some situations, sampling from a probability distribution is more appropriate than the use of metamodel. DTIC

N95-31654# Carnegie-Mellon Univ., Pittsburgh, PA. Robotics Inst.
USING CASE-BASED REASONING AS A REINFORCEMENT LEARNING FRAMEWORK FOR OPTIMIZATION WITH CHANGING CRITERIA
Dajun Zeng and Katia Sycara Mar. 1995 17 p
(Contract F30602-91-C-0016)
(AD-A293602; CMU-RI-TR-95-13) Avail: CASI HC A03/MF A01

Practical optimization problems such as job-shop scheduling of-ten involve optimization criteria that change over time. Repair-based frameworks have been identified as flexible computational paradigms for difficult combinatorial optimization problems. Since the control problem of repair-based optimization is severe, Reinforcement Learning (RL) techniques can be potentially helpful. However, some of the fundamental assumptions made by traditional RL algorithms are not valid for repair-based optimization. Case-Based Reasoning (CBR) compensates for some of the limitations of traditional RL approaches. In this paper, we present a Case-Based Reasoning RL approach, implemented in the CABINS system, for repair-based optimization. We chose job-shop scheduling as the testbed for our approach. Our experimental results show that CABINS is able to effectively solve problems with changing optimization criteria which are not known to the system and only exist implicitly in a extensional manner in the case base. DTIC

N95-31692# Department of the Navy, Washington, DC.
NEURAL NETWORK BASED DATA FUSION SYSTEM Patent Application
Chris DeAngelis, inventor (to Navy) and Robert Green, inventor (to Navy) 18 Oct. 1994 30 p
(AD-D017440; US-Patent-Appl-SN-324641) Avail: CASI HC A03/MF A01

A method is described for providing an estimate of the state of a moving contact. The method comprises providing a device for estimating the state of the contact; inputting information about a location of an observer platform at particular time intervals and information from at least one sensor about a position of the moving contact relative to the observer platform at each time interval into the device; transforming the inputted information into a series of geographical grids with one grid being formed for each reading of the at least one sensor; combining grids corresponding to similar time intervals into a series of consolidated grid representations; and analyzing the series of consolidated grid representations to produce an estimate of the state of the contact at a final point in time where an observation was made. The device of the present invention includes a grid stimulation block for forming the geographical grids, a fusion block for forming the consolidated grid representations, a correlation block for providing a path likelihood vector, and an estimation block for providing the desired estimate. DTIC

N95-31693# Department of the Navy, Washington, DC.
NEURAL NETWORK BASED THREE DIMENSIONAL OCEAN MODELER Patent Application
Chris M. DeAngelis, inventor (to Navy) 11 Oct. 1994 26 p
(AD-D017441; US-Patent-Appl-SN-324640) Avail: CASI HC A03/MF A01

A method is described for providing an estimate of the state of a moving contact in a three dimensional ocean. The method comprises the steps of providing a device for estimating the state of the contact, inputting into the device information about a location of an observer during a sequence of time, information from at least one sensor about a position of the contact relative to the observer during the time sequence, and a knowledge vector, transforming the inputted information into a series of three dimensional geographical grids, and analyzing the geographical grids to produce an estimate of the state of the contact with respect to the location of the observer. The device for providing the estimate of the state of the moving contact is a neurally inspired contact estimation device. The device includes a grid stimulation block for transforming the inputted information into the three dimensional geographical grids, a fusion block where grids corresponding to similar time intervals are combined or fused, a correlation block for providing constraints such as constant speed and heading and for producing a path likelihood vector, and an estimation block for providing the estimate of the state of the moving contact. The device further includes a controller for providing knowledge to the aforementioned blocks. DTIC

N95-31827# Carnegie-Mellon Univ., Pittsburgh, PA. Dept. of Computer Science.
PRODUCTION MATCHING FOR LARGE LEARNING SYSTEMS Ph.D. Thesis
Robert B. Doorenbos 31 Jan. 1995 208 p Sponsored by the National Science Foundation, Wright Lab., Aeronautical Systems Center, Air Force Materiel Command, USAF, and the Advanced Research Projects Agency
(Contract F33615-98-1-1330)
(AD-A293105; CMU-CS-95-113) Avail: CASI HC A10/MF A03

One of the central results of AI research in the 1970's was that to

achieve good performance, AI systems must have large amounts of knowledge. Machine learning techniques have been developed to automatically acquire knowledge, often in the form of if-then rules (productions). Unfortunately, this often leads to a utility problem - the 'learning' ends up causing an overall slowdown in the system. This is because the more rules a system has, the longer it takes to match them against the current situation in order to determine which ones are applicable. To address this problem, this thesis is aimed at enabling the scaling up of the number of rules in production systems. We examine a diverse set of testbed systems, each of which learns at least 100,000 rules. We show that with the best existing match algorithms, the match cost increases linearly in the number of rules in these systems. This is inadequate for large learning systems, because it leads to a utility problem. We then examine the causes of this linear increase, and develop techniques which eliminate the major causes. The end result is an improved match algorithm, Rete/UL, which is a general extension of the existing state-of-the-art Rete match algorithm. Rete/UL's performance scales well on a significantly broader class of systems than existing match algorithms. The use of Rete/UL rather than Rete significantly reduces or eliminates the utility problem in all the testbed systems. DTIC

N95-31838 Cincinnati Univ., OH.
ARTIFICIAL NEURAL NETWORKS AND MODEL-BASED RECOGNITION OF 3-D OBJECTS FROM 2-D IMAGES Ph.D. Thesis
Chih-ho Chao 1994 190 p
Avail: Univ. Microfilms Order No. DA9424550

A computer vision system is developed for 3-D object recognition from a 2-D gray-scale image with the application of artificial neural networks in both low-level and high-level process and with the usage of a model-based top-down feedback analysis approach. This vision system can adequately address the problems caused by using an incomplete edge map which is provided by the low-level processor for 3-D representation and recognition. This system uses the key patterns which are assigned with priorities by the intermediate-level organizer. The highest priority is given to a key pattern with the most connected node and associated features including the space invariant structure and the information of orientation of edge primitives. The labeled key features are mapped to real space and provided as input to an artificial neural network for the purpose of matching. Hopfield-Tank neural networks have been applied to low-level edge detection and to high-level matching. In the intermediate level, the edges extracted by the low-level processor are reprocessed and organized into various edge key patterns with priorities assigned. The features of the connected edge primitives are mapped to computable real numbers. A candidate with the highest priority is selected and sent to the high level for matching through the model base. The first match is to choose the class of possible model, the second match is to find the model closest to the candidate. In the end, the closest model is rotated in 3-D space to achieve the best match with the candidate. The result of such match is utilized in generating the model-driven top-down feedback analysis to verify the recognition and to provide the inherent 3-D features of objects. In the case of multiple objects, this matching strategy is very active and powerful in its ability to recognize objects using one pattern at a time. It is also suitable to recognize partially occluded objects. Dissert. Abstr.

N95-31949 Case Western Reserve Univ., Cleveland, OH.
STABILITY ANALYSIS OF LINEAR CONTROL SYSTEMS WITH UNCERTAIN PARAMETERS Ph.D. Thesis
Yuguang Fang 1994 326 p
Avail: Univ. Microfilms Order No. DA9425520

In this dissertation, we study stochastic stability of linear systems whose parameters are randomly varying in a certain sense. In particular, we present a new approach to stochastic stability analysis of systems whose system structure is randomly changing among a finite set of possibilities which capture the abrupt changes in systems parameters or sudden failures of system components. These types of systems are referred to as jump linear systems with a finite state Markov chain form process. We first investigate the properties of various types of moment stability for stochastic jump linear systems, and use large deviation theory to study the relationship between 'lower moment' stability and almost sure stability. In particular, we have proved that the region for delta-moment stability is monotonically increasing as delta is decreasing to zero and asymptotically converges to the region for almost sure stability. Roughly speaking, this is equivalent to saying that almost sure stability is equivalent to delta-moment stability for sufficiently small delta greater than 0. Furthermore, we prove that although the top delta-moment Lyapunov exponent is, in general, not differentiable at zero, it is differentiable at zero from the right and its right derivative at zero is equal to the top Lyapunov exponent. This answers a long standing question in this area. Based on this analysis, a new Lyapunov function is constructed to obtain a very general sufficient condition for almost sure stability, and this condition is also conjectured to be a necessary condition for almost sure stability. Moreover, a few new approaches for the study of almost sure stability are proposed and some easily-testable conditions for both moment stability and almost sure stability are obtained. Based on the results on almost sure stability and moment stability, the stochastic stabilization problem is also considered and a few future research topics are identified. This dissertation is the first research work in the current literature to use large deviation theory to study stochastic stability and further represents a systematic study of almost sure stability of jump linear systems with a finite state Markov chain form process. It is our high hope that this work will pave the way for further studies on the almost sure (sample path) stability for stochastic systems. Dissert. Abstr.

N95-32137# National Aerospace Lab., Amsterdam (Netherlands).
MULTI-SENSOR DATA FUSION IN COMMAND AND CONTROL AND THE MERIT OF ARTIFICIAL INTELLIGENCE
Rene G. Zuidgeest *In* AGARD, Guidance and Control for Future Air-Defence Systems Jan. 1995 12 p (For primary document see N95-32123 11-31)
Copyright Avail: CASI HC A03/MF A03

N95-32138# Siemens A.G., Unterschleissheim (Germany). Defence Electronics.
AIDEX: AN EXPERT SYSTEM FOR AIRCRAFT IDENTIFICATION
J. Ebmeyer and H. Freyler *In* AGARD, Guidance and Control for Future Air-Defence Systems Jan. 1995 4 p (For primary document see N95-32123 11-31)
Copyright Avail: CASI HC A01/MF A03

N95-32139# UNISYS GSG Canada, Inc., Montreal (Quebec).
ARCHITECTURE AND IMPLEMENTATION OF A MULTI-SENSOR DATA FUSION DEMONSTRATION MODEL WITHIN THE REAL-TIME COMBAT SYSTEM OF THE CANADIAN PATROL FRIGATE
F. Begin, E. Boily, T. Mignacca, E. Shahbazian, and P. Valin *In* AGARD, Guidance and Control for Future Air-Defence Systems Jan. 1995 8 p (For primary document see N95-32123 11-31)
Copyright Avail: CASI HC A02/MF A03

64 NUMERICAL ANALYSIS

Includes iteration, difference equations, and numerical approximation.

N95-30401# Technische Univ., Eindhoven (Netherlands). Dept. of Mathematics and Computing Science.
ALBUM OF SIMPLE PERFECT SQUARED SQUARES OF ORDER 26
C. J. Bouwkamp and A. J. W. Duijvestijn Dec. 1994 472 p
(PB95-197398; EUT-94-WSK-02) Avail: CASI HC A20/MF A04

A Perfect Squared Square (PSS) of order n is a square dissected into n smaller squares all differing in size. If the PSS contains a rectangle (or a square) that itself is dissected into squares, the PSS is called Compound (CPSS), otherwise it is called Simple (SPSS). The Album contains 441 squares of order 26, numbered from 1 to 441. NTIS

N95-30425# Melbourne Univ., Parkville (Australia). School of Physics.
EXTENSIONS AND RESULTS FROM A METHOD FOR EVALUATING FRACTIONAL INTEGRALS
Victor Kowalenko and M. L. Glasser (Clarkson Univ., Potsdam, NY.) 1994 50 p
(DE95-616272; UM-P-94/76) Avail: CASI HC A03/MF A01 (US Sales Only)

A method has been derived from the Laplace transform that enables the evaluation of Weyl fractional integrals by transforming them into known integrals. This method is adapted and extended in a variety of ways to

demonstrate the utility of the method in deriving alternative representations for other classes of integrals. The authors utilized the Feynman integral of quantum electrodynamics and found that they could develop more sophisticated results from this integral, which are given in Appendix C. A list of various fractional integrals evaluated by this technique is presented in Appendix A. DOE

N95-30445# Melbourne Univ., Parkville (Australia). School of Physics.
SIMULATION WITH COMPLEX MEASURES
T. D. Kieu and C. J. Griffin 1994 3 p
(DE95-616333; UM-P-93/108) Avail: CASI HC A01/MF A01 (US Sales Only)

The simulation of statistical and quantum systems suffers from the sign problem when the generating function measures are indefinite or are complex, such as lattice quantum chromodynamics with finite temperature and density and chiral gauge theory. A new approach is proposed which yields statistical errors smaller than the crude Monte Carlo using absolute values of the original measures. The one-dimensional complex-coupling Ising model is employed as an illustration. DOE

N95-30470# Lawrence Livermore National Lab., Livermore, CA.
MULTIDIMENSIONAL DISCRETIZATION OF CONSERVATION LAWS FOR UNSTRUCTURED POLYHEDRAL GRIDS
D. E. Burton 22 Aug. 1994 26 p Presented at the SAMGOP-1994: 2d International Workshop on Analytical Methods and Process Optimization in Fluid and Gas Mechanics, Arzamas, Russia, 10-16 Sep. 1994 Submitted for publication
(Contract W-7405-eng-48)
(DE95-008796; UCRL-JC-118306; CONF-9409314-1) Avail: CASI HC A03/MF A01

To the extent possible, a discretized system should satisfy the same conservation laws as the physical system. The author considers the conservation properties of a staggered-grid Lagrange formulation of the hydrodynamics equations (SGH) which is an extension of a 1D scheme due to von Neumann and Richtmyer (VNR). The term staggered refers to spatial centering in which position, velocity, and kinetic energy are centered at nodes, while density, pressure, and internal energy are at cell centers. Traditional SGH formulations consider mass, volume, and momentum conservation, but tend to ignore conservation of total energy, conservation of angular momentum, and requirements for thermodynamic reversibility. The author shows that, once the mass and momentum discretizations have been specified, discretization for other quantities are dictated by the conservation laws and cannot be independently defined. The spatial discretization method employs a finite volume procedure that replaces differential operators with surface integrals. The method is appropriate for multidimensional formulations (1D, 2D, 3D) on unstructured grids formed from polygonal (2D) or polyhedral (3D) cells. Conservation equations can then be expressed in conservation form in which conserved currents are exchanged between control volumes. In addition to the surface integrals, the conservation equations include source terms derived from physical sources or geometrical considerations. In Cartesian geometry, mass and momentum are conserved identically. Discussion of volume conservation will be temporarily deferred. The author shows that the momentum equation leads to a form-preserving definition for kinetic energy and to an exactly conservative evolution equation for internal energy. Similarly, the author derives a form-preserving definition and corresponding conservation equation for a zone-centered angular momentum. DOE

N95-30471# Lawrence Livermore National Lab., Livermore, CA.
THREE-D MESH OPTIMIZATION METHODS FOR UNSTRUCTURED POLYHEDRA Progress Report
Douglas S. Miller and Donald E. Burton 22 Nov. 1994 6 p Presented at the Nuclear Explosives Code Developers Conference (NECDC), Las Vegas, NV, 25-28 Oct. 1994 Submitted for publication
(Contract W-7405-eng-48)
(DE95-008808; UCRL-JC-119206; CONF-9410254-5) Avail: CASI HC A02/MF A01

A mesh optimization scheme allows a Lagrangian code to run problems with extreme mesh distortion by reconfiguring node and zone connectivity as the problem evolves. We have developed some 3D mesh optimization operations and criteria for applying them. These are demonstrated in a 3D Free Lagrange code being developed at LLNL. In the simplest case of a mesh or mesh subregion composed purely of tetrahedra we can maintain a Delaunay tetrahedralization. For more interesting meshes, made up of general polyhedra, a suite of optimization operations and their respective application criteria have been developed. DOE

N95-30477# Royal Inst. of Tech., Stockholm (Sweden).
SIZE OF FULTON'S ESSENTIAL SET
K. Eriksson and S. Linusson Jan. 1995 18 p
(PB95-211645; TRITA-MAT-1995-0002) Avail: CASI HC A03/MF A01

The essential set of a permutation was defined by Fulton as the set of southeast corners of the diagram of the permutation. In this paper we determine explicit formulas for the average size of the essential set in the two cases of arbitrary permutations in S(sub n) and 321-avoiding permutations in S(sub n). Vexillary permutations are discussed too. We also prove that the generalized Catalan numbers count r x k-matrices dotted with n dots that are extendable to 321-avoiding permutation matrices. NTIS

N95-30488# Institut des Hautes Etudes Scientifiques, Bures-sur-Yvette (France).
CANONICAL SYMMETRIC INVARIANT PAIRINGS IN VERTEX OPERATOR SUPER ALGEBRAS AND GRAMIANS
H. Tamanoi Feb. 1995 49 p
(PB95-208112; IHES/M/95/14) Avail: CASI HC A03/MF A01

Any connected vertex operator super algebra canonically admits a symmetric bilinear pairing with various operator invariance properties including the translation invariance. The notion of quasi-primary vectors lead to an orthogonal double grading of the algebra. The canonical Hermitian pairings associated to certain conjugate linear involutions are shown to be positive definite and integral for algebras generated by vectors of weight one half. No Hilbert space structure is assumed. We deduce it. Our construction can be carried out over the ring of integers. The canonical pairings of basis vectors can be expressed in terms of the Gramian determinants of matrices of binomial coefficients. The proof of positive definiteness of the Hermitian pairings uses the integral representation of the Gramian determinants. NTIS

N95-30490# Institut des Hautes Etudes Scientifiques, Bures-sur-Yvette (France).
LOCAL INDEX FORMULA IN NONCOMMUTATIVE GEOMETRY
A. Connes and H. Moscovici Mar. 1995 86 p
(PB95-208146; IHES/M/95/19) Avail: CASI HC A05/MF A01

In noncommutative geometry, a geometric space is described from a spectral point of view, as a triple (A, H, D) consisting of a *-algebra A represented in a Hilbert space H together with an unbounded self-adjoint operator D, with compact resolvent, which interacts with the algebra in a bounded fashion. This paper contributes to the advancement of this point of view in two significant ways: (1) by showing that any pseudogroup of transformations of a manifold gives rise to such a spectral triple of finite summability degree, and (2) by proving a general, in some sense universal, local index formula for an arbitrary spectral triple of finite summability degree, in terms of the Dixmier trace and its residue-type extension. NTIS

N95-30495 Direction des Recherches, Etudes et Techniques, Paris (France).
SPECTRAL METHODS IN COMPLEX GEOMETRIES [METHODES SPECTRALES EN GEOMETRIES COMPLEXES]
Y. Maday 21 Jun. 1994 26 p In FRENCH
(PB95-208336) Avail: Issuing Activity (National Technical Information Service (NTIS))

The document is a study of the problem of compatibility between the discrete representation of geometry, order of quadrature methods, and degree of polynomial approximation, with a view of preserving optimal approximation of the solution. The author discusses the method used, then proceeds to a numerical analysis of the spectral method applied to a curved domain, taking into account the parameters introduced in the foregoing discussion, then to a numerical illustration of the theoretical conclusions thus derived, and finally a study of the case of decomposition in a subdomain. NTIS

N95-30499# Royal Inst. of Tech., Stockholm (Sweden).
NEWTON METHODS FOR LARGE-SCALE LINEAR INEQUALITY-CONSTRAINED MINIMIZATION: OPTIMIZATION AND SYSTEMS THEORY
A. Forsgren and W. Murray Dec. 1994 20 p
(PB95-210332; TRITA-MAT-1994-44) Copyright Avail: CASI HC A03/MF A01

Newton methods of the linesearch type for large-scale minimization subject to linear inequality constraints are discussed. The purpose of the paper is twofold: (1) to give an active-set type method with the ability to delete multiple constraints simultaneously and (2) to give a relatively short general convergence proof for such a method. It is also discussed how multiple constraints can be added simultaneously. The approach is an extension of previous work by the same authors for equality-constrained problems. It is shown how the search directions can be computed without the need to compute the reduced Hessian of the objective function. The convergence analysis states that every limit point of a sequence of iterates satisfies the second-order necessary optimality conditions. NTIS

N95-30500# Royal Inst. of Tech., Stockholm (Sweden).
COMBINATION OF FULTON'S ESSENTIAL SET
K. Eriksson and S. Linusson Jan. 1995 22 p
(PB95-211637; TRITA-MAT-1995-0001) Avail: CASI HC A03/MF A01

Fulton introduced the ranked essential set of a permutation. We give a new elementary proof of the fact that the ranked essential set of a permutation w determines w. We then characterize the class of ranked sets that arise as ranked essential sets of permutations by giving necessary and sufficient conditions. Several classes of permutations are characterized in terms of their essential set. NTIS

N95-30506# Institut des Hautes Etudes Scientifiques, Bures-sur-Yvette (France).
GIBBS MEASURES AND QUASI-PERIODIC SOLUTIONS FOR NONLINEAR HAMILTONIAN PARTIAL DIFFERENTIAL EQUATIONS
J. Bourgain Feb. 1995 21 p
(PB95-207932; IHES/M/95/13) Avail: CASI HC A03/MF A01

The purpose of this expose is to present a summary of some new developments in the theory of Hamiltonian nonlinear evolution equations, more specifically, nonlinear Schrodinger equations. The themes and methods discussed are closely related to classical mechanics. The first topic is the existence of an invariant measure for the flow. This invariant measure is the (properly normalized) Gibbs measure from statistical mechanics and we establish wellposedness of the equation on its support. Results are obtained in 1D (in the focusing and defocusing case) and in the 2D defocusing case. The second topic concerns the persistency of time periodic and quasi-periodic solutions for Hamiltonian perturbations of linear and integrable equations. We follow a method, the so-called Liapounov-Schmidt decomposition. The main advantage of this technique is the fact that it overcomes certain limitations of the KAM scheme, which is necessary to deal in particular with the problems in space-dimension D = or greater than 2. This work is a new approach to KAM problems, also in finite dimensional phase space. NTIS

N95-30540 Rutherford Appleton Lab., Oxford (England).
HERA AND THE ASYMPTOTIC BEHAVIOUR OF F2(SUP RHO)
J. R. Forshaw and R. G. Roberts Jan. 1995 12 p
(PB95-195764; RAL-95-008) Avail: Issuing Activity (National Technical Information Service (NTIS))

We examine the recent HERA data on the deep inelastic structure function, F(sub 2, sup rho). The data are analyzed in terms of the 'double scaling' variables, square root of (ln(1/x) ln(ln Q(sup 2))) and square root of (ln(1/x)/ln(ln Q(sup2))). Although the data can be well describedby the 'double asymptotic scaling' prediction of perturbative QCD, we find that this is not the only possible scenario and hence conclude that, as yet, the HERA data is unable to identify the essential physics driving the small x rise in F(sub 2, sup rho). NTIS

N95-30556# Institut des Hautes Etudes Scientifiques, Bures-sur-Yvette (France).
ANALYSIS ON FRACTALS, LAPLACIANS ON SELF-SIMILAR SETS, NONCOMMUTATIVE GEOMETRY AND SPECTRAL DIMENSIONS
M. L. Lapidus Feb. 1995 78 p Prepared in cooperation with California Univ.
(PB95-208005; IHES/M/95/9) Avail: CASI HC A05/MF A01

This paper addresses the question of finding a suitable analogue of Weyl's asymptotic formula for the eigenvalue distribution of Laplacians on (certain classes of self-similar) fractals. We propose, in particular, an analogue of the notion of 'Riemannian volume' on fractals and establish, in the process, some connections between analysis on 'fractals', spectral geometry, and aspects of Connes' noncommutative geometry. NTIS

N95-30570 Defense Advanced Research Projects Agency, Arlington, VA.
CONVERGENCE PROPERTIES OF AN AUGMENTED LAGRANGIAN ALGORITHM FOR OPTIMIZATION WITH A COMBINATION OF GENERAL EQUALITY AND LINEAR CONSTRAINTS
A. R. Conn, N. I. M. Gould, A. Sartenaer, and P. L. Toint Jan. 1995 34 p Prepared in cooperation with IBM Thomas J.
(PB95-208039; RAL-95-009) Avail: Issuing Activity (National Technical Information Service (NTIS))

We consider the global and local convergence properties of a class of augmented Lagrangian methods for solving nonlinear programming problems. In these methods, linear and more general constraints are handled in different ways. The general constraints are combined with the objective function in an augmented Lagrangian. The iteration consists of solving a sequence of subproblems; in each subproblem the augmented Lagrangian is approximately minimized in the region defined by the linear constraints. A subproblem is terminated as soon as a stopping condition is satisfied. The stopping rules that we consider here encompass practical tests used in several existing packages for linearly constrained optimization. Our algorithm also allows different penalty parameters to be associated with disjoint subsets of the general constraints. In this paper, we analyze the convergence of the sequence of iterates generated by such an algorithm and prove global and fast linear convergence as well as showing that potentially troublesome penalty parameters remain bounded away from zero. NTIS

N95-30601# Royal Inst. of Tech., Stockholm (Sweden).
COMPLEX MEAN VALUE INTERPOLATION
L. Filipsson Jan. 1995 14 p
(PB95-211629; TRITA-MAT-1995-0003) Avail: CASI HC A03/MF A01

We show that complex mean value interpolation may be defined in any domain that is C-convex whereas the original definition required ordinary, real convexity. We also show that C-convex domains are the natural ones in which to perform mean value interpolation, in the sense that any Runge domain which admits mean value interpolation must in fact be C-convex. NTIS

N95-30607# International Centre for Theoretical Physics, Trieste (Italy).
DRESSING SYMMETRY OF THE UNIFORMIZATION SOLUTION OF LIOUVILLE EQUATION
Jian-Min Shen Oct. 1994 15 p Sponsored by NNSF Grant of China
(DE95-613380; IC-94/324) Avail: CASI HC A03/MF A01 (US Sales Only)

In this paper, the relations between monodromy group and dressing group for Liouville equation in uniformization theorem are discussed. The representation of monodromy transformation, acting on the chiral components of the solution of Liouville equation, is obtained. The non-trivial exchange algebra for monodromy transformation is calculated. DOE

N95-30608# International Centre for Theoretical Physics, Trieste (Italy).
GENERALIZED KUMMER SURFACES AND DIFFERENTIABLE INVARIANTS OF NOETHER-HORIKAWA SURFACES 1
Fabrizio Catanese Nov. 1994 55 p
(DE95-613382; IC-94/341) Avail: CASI HC A04/MF A01 (US Sales Only)

The moduli spaces M of surfaces of general type with a fixed topological type are known to have several connected components: there is a map (pi)(sub 0) (M) (yields) Diff, where Diff is the set of differentiable types of 4-manifolds. The unsolved question is whether this map is injective or not. The simplest surfaces of general type for which the moduli space is known to be disconnected are the so called Noether-Horikawa surfaces, for which one should try to calculate the Donaldson differentiable invariants. DOE

N95-30622 Institut des Hautes Etudes Scientifiques, Bures-sur-Yvette (France).
GOOD METRIC SPACES WITHOUT GOOD PARAMETERIZATIONS
S. Semmes Jan. 1995 68 p Sponsored by National Science Foundation Limited Reproducibility: More than 20% of this document may be affected by microfiche quality
(PB95-208427; IHES/M/95/2) Avail: CASI HC A04

A classical problem in geometric topology is to recognize when a topological space is a topological manifold. This paper addresses the question of when a metric space admits a quasisymmetric parameterization by providing counterexamples to the obvious optimistic conjectures, or, in other words, by providing examples of spaces with many Euclidean-like properties which are nonetheless substantially different from Euclidean geometry. These examples are geometrically self-similar versions of classical topologically self-similar examples from geometric topology, and they can be realized as codimension 1 subsets of Euclidean spaces. Unlike earlier examples going back to Rickman, these sets enjoy good bounds on their geodesic distance functions and good mass bounds (Ahlfors regularity). They are also smooth except for reasonably tame degenerations near small sets, they are uniformly rectifiable, and they have good properties in terms of analysis (like Sobolev and Poincare' inequalities). The construction also produces uniform domains which have many nice properties but which are not quasiconformally equivalent to balls. NTIS

N95-30623 Institut des Hautes Etudes Scientifiques, Bures-sur-Yvette (France).
HIGHER SCHWARZIAN OPERATORS AND COMBINATORICS OF SCHWARZIAN DERIVATIVE
H. Tamanoi Dec. 1994 26 p Limited Reproducibility: More than 20% of this document may be affected by microfiche quality
(PB95-208435; IHES/M/94/67) Avail: CASI HC A03

A family of Mobius invariant nonlinear differential operators (higher Schwarzian operators) is constructed in the context of the best Mobius approximations of analytic functions in one complex variable. Viewing the Schwarzian equation purely algebraically, we obtain a sequence of polynomials (Schwarzian polynomials) with positive integral coefficients expressing the higher Schwarzian operators in terms of derivatives of the classical Schwarzian derivative, and vice versa. These Schwarzian polynomials can be expressed in terms of the partial Bell polynomials. Integrality, positivity, and negativity properties of the Taylor coefficients of solutions to the Schwarzian equation are shown. The higher Schwarzian operators allow us to prove that any Mobius invariant differential operators can be derived from the classical Schwarzian derivative. In the Appendix, we give examples of Schwarzian polynomials. NTIS

N95-30624# Institut des Hautes Etudes Scientifiques, Bures-sur-Yvette (France).
QUASI-PERIODIC SOLUTIONS OF HAMILTONIAN PERTURBATIONS OF 2D LINEAR SCHROEDINGER EQUATIONS
J. Bourgain Jan. 1995 36 p
(PB95-208443; IHES/M/95/1) Avail: CASI HC A03/MF A01

This paper is a continuation of the author's work on constructing periodic and quasi-periodic solutions of Hamiltonian perturbations of linear PDE's (with periodic boundary conditions). The method used for this purpose was initiated in the work of Craig and Wayne for 1D-equations and time periodic solutions. It is an infinite dimensional phase space version of the Liapunov-Schmidt argument for the construction of periodic solutions. The basic idea of the Liapunov-Schmidt scheme consists in splitting the problem in a resonant finite dimensional piece given by the Q-equation and the remainder of the problem, the P-equation, which is infinite dimensional and contains the small divisors issues. To achieve frequency variation, we will rely on outer parameters contained in the equation rather than amplitude-frequency modulation depending on the nonlinear term. The model equation considered here is the nonlinear Schrodinger equation. NTIS

N95-30642# International Centre for Theoretical Physics, Trieste (Italy).
EQUIVALENCE OF TWO NON-COMMUTATIVE GEOMETRY APPROACHES
Han-Ying Guo (China Center for Advanced Science and Technology, Beijing, China.), Ke Wu (China Center for Advanced Science and Technology, Beijing, China.), and Jian-Ming Li Oct. 1994 12 p
(DE95-613469; IC-94/322) Avail: CASI HC A03/MF A01 (US Sales Only)

We show that differential calculus on discrete group Z(2) is equivalent to A. Connes' approach in the case of two discrete points. They are the same theory in terms of different basis and the discrete group Z(2) is the permutation group of two discrete point. DOE

N95-30676# International Centre for Theoretical Physics, Trieste (Italy).
THE ITERATION FORMULA OF THE MASLOV-TYPE INDEX THEORY WITH APPLICATIONS TO NONLINEAR HAMILTONIAN SYSTEMS
Dong Di (Nankai Univ., Tiangjin, China.) and Yiming Long Oct. 1994 81 p Sponsored by YTF of Education Comm.; and NNSF of China
(DE95-613379; IC-94/318) Avail: CASI HC A05/MF A01 (US Sales Only)

In this paper, the iteration formula of the Maslov-type index theory for linear Hamiltonian systems with continuous periodic and symmetric coefficients is established. This formula yields a new method to determine the minimality of the period for solutions of nonlinear autonomous Hamiltonian systems via their Maslov-type indices. Applications of this formula give new results on the existence of periodic solutions with prescribed minimal period for such systems. DOE

N95-30688# Melbourne Univ., Parkville (Australia). Dept. of Physics.
ASSOCIATORS IN GENERALIZED OCTONIONIC MAPS
C. J. Griffin and G. C. Joshi 10 Sep. 1992 13 p
(DE95-616243; UM-P-92/84) Avail: CASI HC A03/MF A01 (US Sales Only)

Generalizing previous work, it is shown that structural transitions are a general property of a large class of octonionic maps. They can thus be used as an indicator of non-associativity in an octonionic map. DOE

N95-30692 Rutherford Appleton Lab., Oxford (England). Central Computing Dept.
USE OF ELEMENT-BY-ELEMENT PRECONDITIONERS TO SOLVE LARGE SCALE PARTIALLY SEPARABLE OPTIMIZATION PROBLEMS
M. J. Dayde, J. Y. LExcellent, and N. I. M. Gould Jan. 1995 33 p Prepared in cooperation with Centre Europeen Recherche et de Formation Advanceen Calcul Scientific, and CNRS, Toulouse, France
(PB95-195772; RAL-95-010) Avail: Issuing Activity (National Technical Information Service (NTIS))

We study the solution of large-scale nonlinear optimization problems by methods which aim to exploit their inherent structure. In particular, we consider the all-pervasive property of partial separability, first studied by Griewank and Toint (1982b). A typical minimization method for nonlinear optimization problems approximately solves a sequence of simplified linearized subproblems. In this paper, we explore how partial separability may be exploited by iterative methods for solving these subproblems. We particularly address the issue of computing effective preconditioners for such iterative methods. Numerical experiments indicate the effectiveness of these preconditioners on large-scale examples. NTIS

N95-30696# Institut des Hautes Etudes Scientifiques, Bures-sur-Yvette (France).
PI1(SUP INFINITY) AND INFINITE SIMPLE HOMOTOPY TYPE IN DIMENSION THREE: A RESEARCH ANNOUNCEMENT
Valentin Poenaru Jan. 1995 36 p
(PB95-196283; IHES/M/95/6) Avail: CASI HC A03/MF A01

In this note we announce several results which, in some way or another, are all related to the following well-known main conjecture. 'If M(sup 3) is a closed 3-manifold with infinite pi(sub 1), then the universal covering space M tilde (sup 3) is simply connected at infinity. NTIS

N95-30713# Royal Inst. of Tech., Stockholm (Sweden). Dept. of Numerical Analysis and Computing Science.
POTENTIAL INTEGRAL EQUATIONS OF THE 2D LAPLACE OPERATOR IN WAVELET BASIS
Mihai Dorobantu [1994] 34 p Prepared in cooperation with Stockholm Univ., Sweden
(TRITA-NA-9401) Avail: CASI HC A03/MF A01

In this paper we solve the Laplace equation by solving a boundary integral equation in a wavelet basis. The idea of solving integral equations using a hierarchical approach is used in the Multipole method and

Wavelet-Galerkin methods in the non-standard form. Due to the orthogonality of the wavelet transform, the discrete linear systems preserve their good conditioning while their sparse structures speed up iterative solvers. We investigate the link between the two multi-scale methods and the convergence of Wavelet Galerkin discretizations. The behaviour of GCR algorithms under wavelet transformations and in non-standard form is investigated. Finally we analyze the optimal choice of Daubechies filters in the non-standard form and describe some numerical experiments. Author

N95-30754*# Ohio Univ., Athens, OH. Dept. of Electrical and Computer Engineering.
ENHANCEMENTS TO THE SSME TRANSFER FUNCTION MODELING CODE Interim Report
R. Dennis Irwin, Jerrel R. Mitchell, David L. Bartholomew, and Russell D. Glenn Jul. 1995 59 p
(Grant NAG8-1041)
(NASA-CR-198957; NAS 1.26:198957) Avail: CASI HC A04/MF A01

This report details the results of a one year effort by Ohio University to apply the transfer function modeling and analysis tools developed under NASA Grant NAG8-167 (Irwin, 1992), (Bartholomew, 1992) to attempt the generation of Space Shuttle Main Engine High Pressure Turbopump transfer functions from time domain data. In addition, new enhancements to the transfer function modeling codes which enhance the code functionality are presented, along with some ideas for improved modeling methods and future work. Section 2 contains a review of the analytical background used to generate transfer functions with the SSME transfer function modeling software. Section 2.1 presents the 'ratio method' developed for obtaining models of systems that are subject to single unmeasured excitation sources and have two or more measured output signals. Since most of the models developed during the investigation use the Eigensystem Realization Algorithm (ERA) for model generation, Section 2.2 presents an introduction of ERA, and Section 2.3 describes how it can be used to model spectral quantities. Section 2.4 details the Residue Identification Algorithm (RID) including the use of Constrained Least Squares (CLS) and Total Least Squares (TLS). Most of this information can be found in the report (and is repeated for convenience). Section 3 chronicles the effort of applying the SSME transfer function modeling codes to the a51p394.dat and a51p1294.dat time data files to generate transfer functions from the unmeasured input to the 129.4 degree sensor output. Included are transfer function modeling attempts using five methods. The first method is a direct application of the SSME codes to the data files and the second method uses the underlying trends in the spectral density estimates to form transfer function models with less clustering of poles and zeros than the models obtained by the direct method. In the third approach, the time data is low pass filtered prior to the modeling process in an effort to filter out high frequency characteristics. The fourth method removes the presumed system excitation and its harmonics in order to investigate the effects of the excitation on the modeling process. The fifth method is an attempt to apply constrained RID to obtain better transfer functions through more accurate modeling over certain frequency ranges. Section 4 presents some new C main files which were created to round out the functionality of the existing SSME transfer function modeling code. It is now possible to go from time data to transfer function models using only the C codes; it is not necessary to rely on external software. The new C main files and instructions for their use are included. Section 5 presents current and future enhancements to the XPLOT graphics program which was delivered with the initial software. Several new features which have been added to the program are detailed in the first part of this section. The remainder of Section 5 then lists some possible features which may be added in the future. Section 6 contains the conclusion section of this report. Section 6.1 is an overview of the work including a summary and observations relating to finding transfer functions with the SSME code. Section 6.2 contains information relating to future work on the project. Author (revised)

N95-30770# International Centre for Theoretical Physics, Trieste (Italy).
AROUND RATNER
A. N. Starkov Oct. 1994 17 p
(DE95-613377; IC-94/300) Avail: CASI HC A03/MF A01 (US Sales Only)

We demonstrate how Ratner's fundamental results on unipotent homogeneous actions can be applied to the study of general homogeneous actions. We consider such questions as the structure of orbits and minimal sets, multiple mixing, and measure isomorphisms of one parameter homogeneous flows. DOE

N95-30778# Technische Univ., Eindhoven (Netherlands). Dept. of Mathematics and Computing Science.
REDUCED HEAT KERNELS ON NILPOTENT LIE GROUPS
A. F. M. terElst and D. W. Robinson Aug. 1994 42 p
(PB95-206926; RANA-94-16) Avail: CASI HC A03/MF A01

Let U be a basis representation of an irreducible unitary representation of a nilpotent Lie group G in L(sub 2)(R(sub k)) and let dU denote the representation of the Lie algebra g obtained by differentiation. If b(sub 1), ..., b(sub d) is a basis of g and B(sub i) = dU (b(sub i)) we consider the operators H = - Summation from i,j = 1 to d, of (C(sub ij)B(sub i)B(sub j)) + Summation, i = 1 to d, of (C(sub i)B(sub i)) where C = (C(sub ij)) is a real symmetric strictly positive matrix and C(sub i) is included in C. Then H generates a continuous semigroup S, holomorphic in the open right half-plane, with a reduced kernel Kappa defined by (S(sub z)Phi)(x) = integral over R(sup k) of dy Kappa(sub z)(x;y) Phi(y). We prove Gaussian off-diagonal bounds and 'exponential' on-diagonal bounds for Kappa. NTIS

N95-30803# International Centre for Theoretical Physics, Trieste (Italy).
EXACT SMOOTH CLASSIFICATION OF HAMILTONIAN VECTOR FIELDS ON SYMPLECTIC 2-MANIFOLDS
B. S. Krouglikov Oct. 1994 20 p
(DE95-613378; IC-94/314) Avail: CASI HC A03/MF A01 (US Sales Only)

Complete exact classification of Hamiltonian systems with one degree of freedom and Morse Hamiltonian is carried out. As it is a main part of trajectory classification of integrable Hamiltonian systems with two degrees of freedom, the corresponding generalization is considered. The dual problem of classification of symplectic form together with Morse foliation is carried out as well. DOE

N95-30820# International Centre for Theoretical Physics, Trieste (Italy).
STUDY OF THE GENERALIZED SOLUTIONS OF n-BODY TYPE PROBLEMS WITH WEAK FORCES
Hasna Riahi Oct. 1994 15 p
(DE95-613381; IC-94/332) Avail: CASI HC A03/MF A01 (US Sales Only)

We show that the generalized solutions of n-body type problems with weak forces, in R(sup l), obtained as limits of classical solutions of problems with strong force potentials, have at most a finite number of collisions if l greater orequal (2(n-2) + 1). We also estimate the number of collisions using the Morse index of the approximated solutions when l greater than or equal (2(n - 1) + 1) and in particular, we show the existence of a non-collision solution in the case of a symmetrical potential and l greater than or equal (2(n - 1) + 1). DOE

N95-30821# International Centre for Theoretical Physics, Trieste (Italy).
ON THE DEGREE OF APPROXIMATION BY JACKSON TYPE OPERATORS
Huzoor H. Khan Oct. 1994 4 p
(DE95-613383; IC-94/344) Avail: CASI HC A01/MF A01 (US Sales Only)

In the present paper we obtained the degree of approximation of functions belonging to newly defined class Lip (psi(u,v);p), p greater than 1 using the Jackson type operators of the double Fourier series of f(x,y). DOE

N95-30835# Technische Univ., Eindhoven (Netherlands). Dept. of Mathematics and Computing Science.
FOURIER ANALYSIS OF A ROBUST MULTIGRID METHOD FOR CONVECTION-DIFFUSION EQUATIONS
A. A. Reusken Sep. 1994 38 p
(PB95-197091; RANA-94-17) Avail: CASI HC A03/MF A01

We consider a two-grid method for solving 2D convection-diffusion problems. The coarse grid correction is based on approximation of the Schur complement. As a preconditioner of the Schur complement, we use the exact Schur complement of modified fine grid equations. We assume constant coefficients and periodic boundary conditions and apply Fourier analysis. We prove an upper bound for the spectral radius of the two-grid

iteration matrix that is smaller than one and independent of the mesh size, the convection/diffusion ratio and the flow direction; i.e. we have a (strong) robustness result. Numerical results illustrating the robustness of the corresponding multigrid W-cycle are given. NTIS

N95-30855*# National Aeronautics and Space Administration. Lewis Research Center, Cleveland, OH.
A TURBULENCE MODULE FOR THE NPARC CODE
J. Zhu and T.-H. Shih Jun. 1995 12 p Presented at the 31st Joint Propulsion Conference and Exhibit, San Diego, CA, 10-12 Jul. 1995; sponsored by AIAA, ASME, SAE, and ASEE
(Contract NCC3-370; RTOP 505-90-5K)
(NASA-CR-198358; E-9745; NAS 1.26:198358; ICOMP-95-12; CMOTT-95-1; AIAA Paper 95-2612) Avail: CASI HC A03/MF A01

A turbulence module is developed for the 2D version of the NPARC code which is currently restricted to planar or axisymmetric flows without swirling. Four turbulence models have been built into the module: Baldwin-Lomax, Chien, Shih-Lumley and CMOTT models. The first is a mixing-length eddy-viscosity model which is mainly used for initialization of computational fields and the last three are the low Reynolds number two-equation models. Unlike chien's model, both the Shih-Lumley and CMOTT models do not involve the dimensionless wall distance y(sup +), an advantage for separated flow calculations. Contrary to the NPARC and most other compressible codes, the non-delta form of transport equations is used which leads to a simpler linearization and is more effective than using the delta form in ensuring the positiveness of the turbulent kinetic energy and its dissipation rate. To reduce numerical diffusion while maintaining necessary stability, a second-order accurate and bounded scheme is used for the convective terms of the turbulent transport equations. This scheme is implemented in a deferred correction manner so that the main coefficients of the resulting difference equations are always positive, thus making the numerical solutions process unconditionally stable. The system of equations is solved via a decoupled method and by the alternating direction TDMA of Thomas. The module can be easily linked to the NPARC code for turbulent flow calculations. Author

N95-30953# Army Research Lab., Adelphi, MD.
LOCAL FRACTAL DIMENSION ESTIMATION Final Report, FY93 - FY94
Mark C. Wellman Feb. 1995 23 p
(AD-A293354; ARL-TR-517) Avail: CASI HC A03/MF A01

This study focused on developing a fractal dimension estimator which will be accurate over the limited range of fractal dimensions characteristic of the earth's natural relief. The estimator presented will have the advantage of reduced complexity and processing over the more optimal techniques. Local window estimates will be investigated as well as synthetic fractal surfaces produced from two different synthesis techniques. DTIC

N95-31002# Advanced Scientific Concepts, Inc., Pittsburgh, PA.
TRAINING METACOGNITIVE SKILLS FOR PROBLEM SOLVING Final Report, Jun. - Dec. 1993
James Geiwitz Nov. 1994 51 p
(Contract MDA903-93-C-0109)
(AD-A290310; ASC-TR-051-3; ARI-RN-95-03) Avail: CASI HC A04/MF A01

Metacognitive skills that involve monitoring and control of cognitive skills like problem solving develop in expert executives and lead to great improvement in the problem-solving process. In this report, we review theory and research on metacognition to construct a conceptual model that has three characteristics: (1) it shows the interrelationship of metacognitive skills and cognitive task performances, (2) it suggests the most valid assessment techniques for the measurement of metacognitive skills, and (3) it shows the development of metacognitive skills. From the third characteristic, we designed a training program to accelerate the acquisition of metacognitive skills in officers in the U.S. Armed Forces. From the second characteristic, we will construct proficiency tests of metacognitive skills for measuring these skills in commanders at various levels of professional development; the tests will also be used to evaluate the effectiveness of the training. DTIC

N95-31120*# Institute for Computer Applications in Science and Engineering, Hampton, VA.
PSEUDO-TIME METHODS FOR CONSTRAINED OPTIMIZATION PROBLEMS GOVERNED BY PDE Final Report
Shlomo Taasan May 1995 16 p Submitted for publication in SIAM Journal on Optimization
(Contract NAS1-19480; RTOP 505-90-52-01)
(NASA-CR-195081; ICASE-95-32; NAS 1.26:195081) Avail: CASI HC A03/MF A01

In this paper we present a novel method for solving optimization problems governed by partial differential equations. Existing methods are gradient information in marching toward the minimum, where the constrained PDE is solved once (sometimes only approximately) per each optimization step. Such methods can be viewed as a marching techniques on the intersection of the state and costate hypersurfaces while improving the residuals of the design equations per each iteration. In contrast, the method presented here march on the design hypersurface and at each iteration improve the residuals of the state and costate equations. The new method is usually much less expensive per iteration step since, in most problems of practical interest, the design equation involves much less unknowns that that of either the state or costate equations. Convergence is shown using energy estimates for the evolution equations governing the iterative process. Numerical tests show that the new method allows the solution of the optimization problem in a cost of solving the analysis problems just a few times, independent of the number of design parameters. The method can be applied using single grid iterations as well as with multigrid solvers. Author

N95-31137# Academy of Sciences (USSR), Novosibirsk (USSR).
RECOIL CORRECTION IN THE DIRAC-COULOMB PROBLEM
A. S. Elkhovskij 1994 8 p
(DE95-619241; BUDKERINP-94-27; IYaF-94-27) Avail: CASI HC A02/MF A01 (US Sales Only)

The expression for the first recoil correction to the Dirac-Coulomb spectrum is obtained in terms of gauge invariant quantum electrodynamics. DOE

N95-31183# Leiden Univ. (Netherlands).
NUMERICAL STABILITY INVESTIGATIONS OF PROCESSES FOR SOLVING LINEAR INITIAL VALUE PROBLEMS
J. L. M. vanDorsselaer Oct. 1994 35 p Sponsored by Nederlandse Organisatie voor Wetenschappelijk Onderzoek, The Hague
(PB95-207023) Avail: CASI HC A03/MF A01

An algorithm is presented which can be used to verify a priori whether a given numerical process for solving a linear initial value problem will behave stably or not. This algorithm, which is based on so-called M-numerical ranges and resolvent conditions, can give reliable results in cases where the classical eigenvalue criterion fails. The algorithm will be applied to investigate the stability of numerical schemes for solving an evolution problem for a convection-diffusion equation. The spatial discretization of the convection-diffusion equation is based on a spectral collocation method. For different types of collocation points the stability will be investigated. A theoretical result concerning stability in case of the Legendre-Gauss-Lobatto points is also given. NTIS

N95-31184# Leiden Univ. (Netherlands).
EFFECT OF THE STOPPING OF THE NEWTON ITERATION IN IMPLICIT LINEAR MULTISTEP METHODS
M. N. Spijker Aug. 1994 26 p
(PB95-207056) Avail: CASI HC A03/MF A01

This paper concerns the application of implicit, linear multistep methods in the numerical solution of stiff, nonlinear initial value problems. Previously the (modified) Newton iteration for coping with the nonlinear equations connected with the implicitness of the multistep methods was studied. Formulas were found for the order of the corresponding Newton stopping errors. It was later shown that for a class of strongly nonlinear initial value problems, estimates for the Newton stopping errors are in force with an order that is even lower. In the present paper the authors find that the actual effect of the stopping of the Newton iteration differs remarkably from what one might expect. The effect turns out to be of a higher order. The authors find that the original order is reliable for stiff problems that

are mildly nonlinear. Moreover, for stiff problems that are strongly nonlinear, the order of the accumulated effect of all Newton stopping errors turns out to be greater (by one) than the order which one may expect. NTIS

N95-31229# Royal Inst. of Tech., Stockholm (Sweden). Dept. of Mathematics.
FROBENIUS ALGEBRAS AND QUANTUM YANG-BAXTER EQUATION 2
K. I. Beidar, Y. Fong, and A. A. Stolin Feb. 1995 25 p Prepared in cooperation with Moscow State Univ.
(PB95-212130; TRITA-MAT-1995-0006) Avail: CASI HC A03/MF A01

It is shown that every Frobenius algebra over a commutative ring determines a class of solutions of the quantum Yang-Baxter equation, which forms a subbimodule of its tensor square. Moreover, this subbimodule is free of rank one as a left (right) submodule. An explicit form of a generator in terms of Frobenius homomorphism is given. It turns out that the generator is invertable in the tensor square if and only if the algebra is Azumaya. NTIS

N95-31253# Los Alamos National Lab., NM.
MCNP ANALYSES OF CRITICALITY CALCULATION RESULTS
R. A. Forster and T. E. Booth 1995 13 p Presented at the Nuclear Criticality Technology and Safety Project (NCTSP) Annual Meeting, San Diego, CA, 17 May 1995
(Contract W-7405-eng-36)
(DE95-010886; LA-UR-95-1159; CONF-9505195-3) Avail: CASI HC A03/MF A01

Careful assessment of the results of a calculation by the code itself can reduce mistakes in the problem setup and execution. MCNP has over four hundred error messages that inform the user of FATAL or WARNING errors that have been discovered during the processing of just the input file. The latest version, MCNP4A, now performs a self assessment of the calculated results to aid the user in determining the quality of the Monte Carlo results. MCNP4A, which was released to RSIC in October 1993, contains new analyses of the MCNP Monte Carlo calculation that provide simple user WARNING's for both criticality and fixed source calculations. The goal of the new analyses is to provide the MCNP criticality practitioner with enough information in the output to assess the validity of the k(sub eff) calculation and any associated tallies. The results of these checks are presented in the k(sub eff) results summary page, several k(sub eff) tables and graphs, and tally tables and graphs. Plots of k(sub eff) at the workstation are also available as the problem is running or in a postprocessing mode to assess problem performance and results. DOE

N95-31258# Gosudarstvennyi Komitet po Ispolzovaniyu Atomnoi Energii, Leningrad (USSR).
A COMPACT EXPRESSION FOR BILINEAR COMBINATION OF DIRAC SPINORS VIA WORLD TENSORS
R. N. Rogalev 1994 8 p
(DE95-619200; IHEP-94-4) Avail: CASI HC A02/MF A01 (US Sales Only)

A compact expression for a product of two Dirac spinors is obtained as a linear combination of 16 Dirac gamma-matrices. The result is presented in a convenient from, which can give rise to using it for analytical calculations of multiparticle amplitudes. It has been shown that a bilinear combination of Dirac spinors can be expressed by momentum and spin vectors of the corresponding particles up to a phase factor. DOE

N95-31264# Asian Office of Aerospace Research and Development, APO San Francisco, CA. Air Force Office of Scientific Research.
THE 2ND JAPAN-US SYMPOSIUM ON FINITE ELEMENT METHODS IN LARGE SCALE COMPUTATIONAL FLUID DYNAMICS
T. Davis 16 Mar. 1994 35 p Symposium held in Tokyo, Japan, 14-16 Mar. 1994
(AD-A292337; AOARD-TR-94-06) Avail: CASI HC A03/MF A01

A summary of the 2nd Japan-US Symposium on Finite Element Methods in Large Scale Computational Fluid Dynamics, conducted Mar. 14-16, 1994 at Chuo University in Tokyo, Japan is presented. Abstracts of all symposium presentations are included. This report is based upon information collected via symposium attendance, review of the symposium proceedings, and a post symposium conversation with Professor Mutsuto Kawahara, Department of Civil Engineering, Chuo University, who served as the Japanese co-chair of the symposium organizing committee. DTIC

N95-31319*# Institute for Computer Applications in Science and Engineering, Hampton, VA.
REPRESENTATION OF FEEDBACK OPERATORS FOR HYPERBOLIC SYSTEMS Final Report
John A. Burns (Virginia Polytechnic Inst., Blacksburg, VA.) and Belinda B. King (Oregon State Univ., Corvallis, OR.) May 1995 14 p
(Contract NAS1-19480; RTOP 505-90-52-01)
(NASA-CR-198171; NAS 1.26:198171; ICASE-95-45) Avail: CASI HC A03/MF A01

We consider the problem of obtaining integral representation of feedback operators for damped hyperbolic control systems. We show that for the wave equation with Kelvin-Voigt damping and non-compact input operator, the feedback gain operator is Hilbert-Schmidt. This result is then used to provide an explicit integral representation for the feedback operator in terms of functional gains. Numerical results are given to illustrate the role that damping plays in the smoothness of these gains. Author

N95-31337# Polish Academy of Sciences, Warsaw (Poland). Independent Plasma Dynamics Lab.
A SIMPLIFIED TECHNIQUE FOR DETERMINING THE SYMMETRY GROUPS OF NON-LINEAR PLASMA KINETIC EQUATIONS [UPROSZCZONA TECHNIKA WYZNACZANIA GRUP SYMETRII NIELINIOWYCH ROWNAN KINETYCZNYCH PLAZMY]
B. Atamaniuk and A. J. Turski Aug. 1995 13 p In POLISH
(ISSN 0208-5658)
(IFTR-8/1995) Avail: CASI HC A03/MF A01

The authors use an example of plasma kinetic equations to describe a simplified technique for determining the symmetry groups of differential-integral equations with 'simple' integral terms.
Transl. by Schreiber

N95-31339# Polish Academy of Sciences, Warsaw (Poland). Independent Plasma Dynamics Lab.
DETERMINATION OF THE SYMMETRY OF A NON-LINEAR SCHROEDINGER EQUATION [WYZNACZENIE SYMETRII NIELINIOWEGO ROWNANIA SCHROEDINGERA]
Jacek Zawistowski Oct. 1995 17 p In POLISH
(ISSN 0208-5658)
(IFTR-10/1995) Avail: CASI HC A03/MF A01

The author uses a complex generalization of the Ovsyannikov method to determine the generators of the symmetry group of a Schroedinger equation. The author performs a detailed analysis of this equation. The author determines the commutation relations between the generators of the symmetry group and the uniparametric groups of transformations which correspond to specific generators. The author provides an explanation for the fact that the coefficient in a nonlinear term has no effect on the symmetry group. Transl. by Schreiber

N95-31361# Royal Inst. of Tech., Stockholm (Sweden). Dept. of Numerical Analysis and Computing Science.
A STUDY OF NUMERICAL SOLUTIONS OF CONSERVATION LAWS
Gunilla Johansson [1993] 60 p Prepared in cooperation with Stockholm Univ., Sweden
(TRITA-NA-9315) Avail: CASI HC A04/MF A01

We analyze the influence of artificial viscosity introduced by first order methods for nonlinear hyperbolic problems with solutions containing shocks. Numerical computations of two different scalar equations and the gasdynamic equations are presented. We introduce a method, constructed such that numerical solutions of the wave equation are well behaved also when the solutions contain discontinuities. The wave equation serves as a model problem for the Euler equations when the solution contain a contact discontinuity. Numerical results imply that the method gives well behaved solutions both for discontinuous and smooth initial data. Author

N95-31363# Helsinki Univ. of Technology, Espoo (Finland). Inst. of Mathematics.
DiffEqlab: A MATLAB BASED PACKAGE FOR STUDYING ORDINARY DIFFERENTIAL EQUATIONS Research Report
S. K. Kivelae Aug. 1994 15 p
(PB95-207197; ISBN-951-22-2263-9) Avail: CASI HC A03/MF A01

DiffEqLab is a software package based on the interactive mathematical program Matlab and intended to study ordinary differential equations at the

level of basic mathematics courses in universities. The background in the computer aided mathematics teaching is discussed, the main structure and use of the package is represented, and some general remarks on the teaching of differential equations are made. NTIS

N95-31397# Royal Inst. of Tech., Stockholm (Sweden). Dept. of Mathematics.
ANTIPODES AND INTEGRALS IN HOPF ALGEBRAS OVER RINGS AND QUANTUM YANG-BAXTER EQUATION
K. I. Beidar, Y. Fong, and A. A. Stolin Feb. 1995 24 p Prepared in cooperation with Moscow State Univ.
(PB95-212155; TRITA-MAT-95/MA-07) Copyright Avail: CASI HC A03/MF A01

In another paper we showed that every Frobenius algebra over a commutative ring determined a solution of the quantum Yang-Baxter equation. Applying this result to Hopf algebras over commutative rings which are finitely generated and projective as modules, we obtain an explicit formula for this solution. It turns out that this solution plays an important role in the structure theory of Hopf algebras over commutative rings. Making use of its properties, we characterize separable Hopf algebras. As a corollary it is shown that the dimension of a simple module over a semisimple Hopf algebra over an algebraically closed field is not divisible by its characteristic. Some results on order of antipode are also obtained. NTIS

N95-31398# Royal Inst. of Tech., Stockholm (Sweden). Dept. of Mathematics.
POISSON APPROXIMATION USING THE STEIN-CHEN METHOD AND COUPLING: NUMBER OF EXCEEDANCES OF A DISCRETE-TIME-CHI-SQUARED PROCESS
M. Raab 1995 46 p
(PB95-212205; TRITA-MAT-1995/MS-1) Avail: CASI HC A03/MF A01

Consider a discrete-time-chi-squared process, i.e. a process defined as the sum of squares of independent and identically distributed normal processes. Count the number of values that exceeds a certain level. Let this level grow together with the number of time-points considered so that the expected number of points above the level remains fixed. It is shown that the number of exceeding points converges in distribution to a Poisson distribution, if the dependence in the underlying normal processes is not too strong. By using the coupling approach of the Stein-Chen method, both limit theorems and rates of convergence can be obtained. Finally the convergence is illustrated by numerical examples on ARMA-processes. NTIS

N95-31422# Technische Univ., Eindhoven (Netherlands).
FORMALIZATION OF THE RAMIFIED TYPE THEORY
T. Laan 1 Sep. 1994 49 p
(PB95-206785) Avail: CASI HC A03/MF A01

We give a formalization of the ramified type theory as described in the Principia Mathematica, trying to keep it as close as possible to the ideas of the Principia. As an alternative, distancing ourselves from the Principia, we express notions from the ramified type theory in a lambda calculus style, thus clarifying the type system in a contemporary setting. Both formalizations are inspired by current developments in research on type theory and typed lambda calculus. In these formalizations, and also when defining 'truth', we will need the notion of substitution. As substitution is not formally defined in the Principia, we have to define it ourselves. NTIS

N95-31518# Air Force Inst. of Tech., Wright-Patterson AFB, OH. School of Engineering.
A NEW GOODNESS-OF-FIT TEST FOR THE GAMMA DISTRIBUTION BASED ON SAMPLE SPACINGS FROM COMPLETE AND CENSORED SAMPLES M.S. Thesis
Huseyin Duman Mar. 1995 168 p
(AD-A293875; AFIT/GOR/ENC/ENS/95M-08) Avail: CASI HC A08/MF A02

This thesis studies a new goodness-of-fit test for the gamma distribution with known shape parameter. This test statistic, Z^*, is based on spacings from complete or censored samples. The size of samples varied between 5 and 35. The critical value tables were generated for the Z^* test statistic for complete and censored samples. The critical values were obtained for five different significance levels: 0.20 0.15, 0.10, 0.05, and 0.01. An extensive power study, containing 50,000 Monte Carlo runs was conducted using nine alternative distributions, H(a). It was observed that the Z^* test statistic was more powerful against certain alternatives which are less skewed than the gamma distribution with a given shape parameter. A regression between the critical values and the sample size, shape parameter, significance levels and degree of censoring was established. The power of the Z^* test statistic is compared to the powers of the competing test statistics (K-S, W sub 2, and A-D). This thesis reveals that the Z^* test statistic is a directional test. This feature may be utilized to attain higher power values by coupling the Z^* and the A-D test statistics in a sequential test. DTIC

N95-31557# Air Force Inst. of Tech., Wright-Patterson AFB, OH. School of Engineering.
MULTIPOINT QUADRATIC APPROXIMATION FOR NUMERICAL OPTIMIZATION M.S. Thesis
Michael A. Blaylock 21 Mar. 1995 111 p
(AD-A293837; AFIT/GA/ENY/95M-1) Avail: CASI HC A06/MF A02

A quadratic approximation for nonlinear functions is developed in order to realize computational savings in solving numerical optimization problems. Function and gradient information accumulated from multiple design points during the iteration history is used in estimating the Hessian matrix. The approximate Hessian matrix is the available for a second order Taylor series approximation to the functions of interest. Several truss and frame models will be used to demonstrate the effectiveness of the new Multipoint Quadratic Approximation (MQA) in solving structural optimization problems. DTIC

N95-31619# Joint Inst. for Nuclear Research, Dubna (USSR).
REMOVAL OF THE ENERGY DEPENDENCE FROM THE RESOLVENT LIKE ENERGY DEPENDENT INTERACTIONS
A. K. Motovilov 1994 20 p
(DE95-613385; JINR-E-5-94-259) Avail: CASI HC A03/MF A01 (US Sales Only)

The spectral problem $(A + V(z))psi = z\ psi$ is considered where main Hamiltonian A is a self-adjoint operator of sufficiently arbitrary nature. The perturbation $V(z) = -B(A'-z)(sup\ -1)\ B(sup\ *)$ depends on the energy z as resolvent of another self-adjoint operator A'. The latter is usually interpreted as Hamiltonian describing an internal structure of physical system. The operator B is assumed to have a finite Hilbert-Schmidt norm. The conditions are formulated when one can replace the perturbation V(z) with an energy independent 'potential' W such that the Hamiltonian $H = A + W$ has the same spectrum (more exactly a part of spectrum) and the same eigenfunctions as the initial spectral problem. The Hamiltonian H is constructed as a solution of the non-linear operator equation $H = A + V(H)$. It is established that this equation is closely connected with the problem of searching for invariant subspaces for the Hamiltonian $H = A(sub\ B)(sup\ *)\ B(sub\ A)'$. The orthogonality and expansion theorems are proved for eigenfunction systems of the Hamiltonian $H = A+W$. Scattering theory is developed for this Hamiltonian in the case when operator A has continuous spectrum. DOE

N95-31648# Royal Inst. of Tech., Stockholm (Sweden). Dept. of Numerical Analysis and Computing Science.
THE COMPLEXITY AND APPROXIMABILITY OF FINDING MAXIMUM FEASIBLE SUBSYSTEMS OF LINEAR RELATIONS
Edoardo Amaldi (Eidgenoessische Technische Hochschule, Lausanne, Switzerland.) and Viggo Kann [1993] 31 p Prepared in cooperation with Stockholm Univ., Sweden
(TRITA-NA-9313) Avail: CASI HC A03/MF A01

We study the combinatorial problem which consists, given a system of linear relations, of finding a maximum feasible subsystem, that is a solution satisfying as many relations as possible. The computational complexity of this general problem, named MAX FLS, is investigated for the four types of relations =, greater than or equal to, greater than, and does not equal. Various constrained versions of MAX FLS, where a subset of relations must be satisfied or where the variables take bounded discrete values, are also considered. We establish the complexity of solving these problems optimally and, whenever they are intractable, we determine their degree of approximability. MAX FLS with =, greater than or equal to, or greater than relations is NP-hard even when restricted to homogeneous systems with bipolar coefficients, whereas it can be solved in polynomial time for nonequivalent relations with real coefficients. The various NP-hard versions

of MAX FLS belong to different approximability classes depending on the type of relations and the additional constraints. We show that the range of approximability stretches from MAX SNP-hard problems which can be approximated within a constant but not within every constant unless P=NP, to MAX PB-complete ones that are as hard to approximate as all maximization problems with polynomially bounded objective functions. While MAX FLS with equations and integer coefficients cannot be approximated within rho(exp epsilon) for some epsilon greater than 0 where rho is the number of relations, the same problem over GF(q) for a prime q can be approximated within q but not within q(exp epsilon) for some epsilon greater than 0. MAX FLS with strict or nonstrict inequalities can be approximated within 2 but not within every constant factor. Our results also provide strong bounds on the approximability of two variants of MAX FLS with greater than and greater than relations that arise when training perceptrons, which are the building blocks of artificial neural networks. Dissert. Abstr.

N95-31947 Toronto Univ. (Ontario).
A UNIFIED INTERPRETATION OF SINGULAR AND NEAR-SINGULAR INTEGRALS IN THE BOUNDARY ELEMENT METHOD Ph.D. Thesis
Dan Rosen 1993 207 p
(ISBN-0-315-86297-1) Avail: Univ. Microfilms Order No. DANN86297

The computation of element integrals is of major importance to the Boundary Element Method (BEM). This thesis provides a unified framework for understanding and computing a large class of singular and near-singular integrals. In the continuation approach, the singular surface integrals, of the type which arise in the BEM, are viewed merely as 'continuations' of non-singular (but perhaps near-singular) ones. Thus, in this approach, singular integrals are obtained from a limiting process in which the singularity of the integrand originally lies outside the integration domain and is gradually moved towards it. The analysis presents a clear and intuitive picture of the behavior of these integrals, which leads to general efficient formulae for singular and near-singular integral evaluation, the former being a special case of the latter. In addition, we obtain necessary and sufficient conditions, herein referred to as 'gauge conditions', that guarantee the boundedness of the continuation singular integrals. It is further shown that, when these conditions are met, the continuation singular integral encompasses the classical cases of Cauchy principal value integrals, jump terms, and Hadamard finite part. Numerical examples, which illustrate the computational advantages of the continuation formulae, are presented. For flat integration surfaces, the continuation approach exploits the functional homogeneity of many Green's functions. The analysis is expanded to more general integrands and to curved integration domains by using the series expansion/subtraction ideas, popular in the BEM literature. It is shown that this expansion is greatly simplified by first mapping the integral to the tangent plane at the (near-)singularity, instead of to the parametric element. The continuation approach is also presented for the case when the singularity lies on, or close to, a corner (or non-smooth part) of the domain. This analysis is of considerable practical importance since it overcomes the difficulties and limitations of strictly analytical techniques. Moreover, it is shown that the gauge conditions of the singular integrals impose some constraints on the functional approximation of the source's densities, in BEM discretizations. A systematic method to obtain these constraints and to incorporate them into the formulation of general problems is presented. Dissert. Abstr.

N95-32067# International Centre for Theoretical Physics, Trieste (Italy).
PRESERVATION THEOREMS ON FINITE STRUCTURES
Michel Hebert (American Univ., Cairo, Egypt.) Sep. 1994 7 p
(DE95-613442; IC-94/273) Avail: CASI HC A02/MF A01 (US Sales Only)

This paper concerns classical preservation results applied to finite structures. We consider binary relations for which a strong form of preservation theorem (called strong interpolation) exists in the usual case. This includes most classical cases: embeddings, extensions, homomorphisms into and onto, sandwiches, etc. We establish necessary and sufficient syntactic conditions for the preservation theorems for sentences and for theories to hold in the restricted context of finite structures. We deduce that for all relations above, the restricted theorem for theories hold provided the language is finite. For the sentences the restricted version fails in most cases; in fact the 'homomorphism into' case seems to be the only possible one, but the efforts to show that have failed. We hope our results may help to solve this frustrating problem; in the meantime, they are used to put a lower bound on the level of complexity of potential counterexamples. DOE

N95-32068# International Centre for Theoretical Physics, Trieste (Italy).
RICCI-FLAT KAEHLER METRICS ON SYMMETRIC VARIETIES
Hassan Azad (Quaid-i-Azam Univ., Islamabad, Pakistan.) and Ryoichi Kobayashi Aug. 1994 53 p
(DE95-613459; IC-94/240) Avail: CASI HC A04/MF A01 (US Sales Only)

We prove the existence of a complete Ricci-flat Kaehler metric on symmetric varieties and describe its asymptotic behaviour at infinity. DOE

N95-32076# Sandia National Labs., Albuquerque, NM.
A MODIFICATION TO THE GMRES METHOD FOR ILL-CONDITIONED LINEAR SYSTEMS
J. C. Meza Apr. 1995 21 p
(Contract DE-AC04-94AL-85000)
(DE95-010661; SAND-95-8220) Avail: CASI HC A03/MF A01

This paper concerns the use of a method for the solution of ill-conditioned linear systems. We show that the Generalized Minimum Residual Method (GMRES) in conjunction with a truncated singular value decomposition can be used to solve large nonsymmetric linear systems of equations which are nearly singular. Error bounds are given for the right singular vectors and singular values computed. A consequence of the error bounds results in a method for computing some of the singular values and right singular vectors for large matrices. DOE

N95-32095# International Centre for Theoretical Physics, Trieste (Italy).
NEWTON RAPHSON METHOD, SCALING AT FRACTAL BOUNDARIES AND MATHEMATICA
Ajay Kumar Bisoi Sep. 1994 19 p
(DE95-613374; IC-94/268) Avail: CASI HC A03/MF A01 (US Sales Only)

The basins of convergence of cubic polynomials having real roots are studied using Newton Raphson iterative method. The limiting value for the ratio of basin segments for equispaced roots is explained. An algorithm is presented for computing the basin boundaries on the real axis which obviates the necessity of taking recourse to extensive search. Mathematica programs have been developed to help in the above study and also to depict the basins in the complex plane. DOE

N95-32117# International Centre for Theoretical Physics, Trieste (Italy).
BIFURCATIONS OF CONTRACTING SINGULAR CYCLES
Rafael Labarca Aug. 1994 44 p
(DE95-613371; IC/93/366) Avail: CASI HC A03/MF A01 (US Sales Only)

The aim of this work is to continue the analysis of a new mechanism, the singular cycles, through which a vector field, depending on parameters, may evolve when the parameter varies from a vector field exhibiting simple dynamics into one having non-trivial dynamics. DOE

N95-32256 Selskapet for Industriell og Teknisk Forskning, Oslo (Norway). Dept. of Informatics.
DATA REDUCTION OF PIECEWISE LINEAR CURVES
E. Arge and M. Daehlen 31 Aug. 1994 26 p Prepared in cooperation with Oslo Univ. and the Royal Norwegian Council for Scientific and Industrial Research
(PB95-212270; STF33-A94042) Avail: Issuing Activity (National Technical Information Service (NTIS))

The authors present and study two new algorithms for data reduction or simplification of piecewise linear plane curves. Given a curve P and a tolerance epsilon greater than or equal to 0, both methods determine a new curve Q, with few vertices, which is at most epsilon in Hausdorff distance from P. The methods differ from most existing methods in that they do not require a vertex in Q to be a vertex in P. Several examples are given where the authors show that the methods presented here compare favorably to other methods found in the literature. The authors also show how the vertices of a curve can be reordered so that the first, say n, vertices of the reordered sequence form an approximation to the curve itself. NTIS

65 STATISTICS AND PROBABILITY

Includes data sampling and smoothing; Monte Carlo method; and stochastic processes.

N95-30610# International Centre for Theoretical Physics, Trieste (Italy).
GENERALIZED DEFORMED PARA-BOSE OSCILLATOR AND ITS COHERENT STATES
Ha Huy Bang Sep. 1994 11 p Sponsored by National Basic Research Programme on Natural Sciences of Government of Vietnam
(DE95-613444; IC-94/296) Avail: CASI HC A03/MF A01 (US Sales Only)

Generalized deformed commutation relations for a single mode para-Bose oscillator are constructed. The connection of generalized deformed para-Bose oscillators with para-Bose oscillators is determined. From these, the energy spectrum of generalized deformed para-Bose oscillators and the coherent states of the annihilation operators are discussed. DOE

N95-30680 Technische Univ., Delft (Netherlands). Dept. of Civil Engineering.
ANALYSIS OF VARIATION EMBEDDING TESTS WITH 17 MM DOWEL: DENSIFIED VENEER WOOD FOREST PROJECT, PART 7
A. J. M. Leijten Jan. 1994 215 p Limited Reproducibility: More than 20% of this document may be affected by microfiche quality
(PB95-206876) Avail: CASI HC A10

The aim of the research was to determine some physical and mechanical properties of densified veneer wood for structural purposes. Preliminary tests with densified veneer wood (dvw) locally glued to the surface of the timber members of joints showed an appreciable improvement of the joint strength stiffness and ductility capacity. As the improvement proved to be interesting for industry further research was initiated. The joints fit for this reinforcement are mainly build-up joints as applied in trusses and portal frames. The joint members are connected by means of mechanical fasteners like dowel type fasteners. Densified veneer wood (dvw) for this application is cross-wise layered. This report is part of a set with the statistical analysis of all test data. It deals with the analysis of embedding test data on 8 mm thick dvw. NTIS

N95-31375# Armstrong Lab., Brooks AFB, TX. Aerospace Medicine Directorate.
NUMERICAL SOLUTION OF A SINGULAR INTEGRAL EQUATION ARISING FROM A SEQUENTIAL PROBABILITY RATIO TEST Final Report
Sherwood Samn Mar. 1995 14 p
(AD-A293463; AL/AO-TR-1995-0020) Avail: CASI HC A03/MF A01

Integral equations arise naturally in problem's in engineering and physics, and their numerical solutions can be obtained directly using popular commercial software packages. The same cannot be said of singular integral equations. This report proposes two numerical methods for solving a singular integral equation that arises in the computation of critical values for a sequential probability ratio test. DTIC

N95-31396# Royal Inst. of Tech., Stockholm (Sweden). Dept. of Mathematics.
ASPECTS OF THE SEARCH TIME IN BINARY SEARCH TREES MODIFIED ACCORDING TO THE MOVE-TO-ROOT HEURISTIC
J. Bodell 1994 52 p
(PB95-212148; TRITA-MAT-1994-48) Avail: CASI HC A04/MF A01

The search time in a binary search tree organized according to the self-organizing move-to-root heuristic is considered. Supposing that the records in the tree are requested independently with constant probabilities, the mean, variance and two different (but equivalent) expressions for the generating function for the search time in stationarity are derived by embedding in Poisson processes. We look for the 'worst' request probabilities, i.e., those that maximize the search time, and rearrange them into a 'best' permutation that minimizes the search time. Mean, variance and probability functions are computed numerically for some illustrating request probability distributions and their 'best' and 'worst' permutations. Finally, an approximating distribution is found for the search time in the special case arising when all of the request probabilities are equal. NTIS

N95-31429# California Univ., Davis, CA.
NONPARAMETRIC METHODS FOR INCOMPLETE DATA IN RELIABILITY AND FOR CHANGEPOINTS IN SMOOTH FUNCTIONS Final Report, 1 Jul. 1991 - 30 Jun. 1994
Hans-Georg Mueller and Jane-Ling Wang 16 Dec. 1994 17 p
(Grant AF-AFOSR-0386-89)
(AD-A292773; AFOSR-95-0229TR) Avail: CASI HC A03/MF A01

The research funded during this period led to more than 30 accepted or published papers in refereed statistical journals. Several graduate students were involved in the research during this period who contributed significantly to the success of the project as well as benefited form opportunities for educational and research achievements leading to the PhD degree (Sam Hawala, Kathryn Prewitt and Kai-Sheng Song). The research achievements for this project roughly fall into five areas of research, all of which are in nonparametric statistics. They cover a wide range of topics from the applied to the theoretical and have important implications for data analysis, as well as for the theory of Statistics. DTIC

N95-31543# Alabama Univ., Huntsville, AL. Aerophysics Research Center.
AEROPHYSICS TEST PROGRAM 1 Final Report, 19 Sep. 1989 - 31 Dec. 1994
Richard A. Hayami Dec. 1994 50 p
(Contract DASG60-89-C-0129)
(AD-A293890; UAH/ARC-TR-94-07) Avail: CASI HC A03/MF A01

This report summarizes the efforts performed in this contract which involved two major line items - the disassembly, transportation, reassembly on Redstone Arsenal, Huntsville, AL, proofing of the gun system and validation of instrumentation functionality of a major ballistic range facility; and the performance of Task Assignments primarily involving the use of this facility for test and analyses. The test activities started in early 1992 and 19 Task Assignments were performed in this program. Tests performed were primarily in Kinetic Energy Lethality. DTIC

N95-31558# Air Force Inst. of Tech., Wright-Patterson AFB, OH. School of Engineering.
NONLINEAR TIME SERIES ANALYSIS M.S. Thesis
James A. Stewart Mar. 1995 91 p
(AD-A293841; AFIT/GOA/ENG/95M-01) Avail: CASI HC A05/MF A01

This thesis applies neural network feature selection techniques to multivariate time series data to improve prediction of a target time series. Two approaches to feature selection are used. First, a subset enumeration method is used to determine which financial indicators are most useful for aiding in prediction of the S&P 500 futures daily price. The candidate indicators evaluated include RSI, Stochastics and several moving averages. Results indicate that the Stochastics and RSI indicators result in better prediction results than the moving averages. The second approach to feature selection is calculation of individual saliency metrics. A new decision boundary-based individual saliency metric, and a classifier independent saliency metric are developed and tested. Ruck's saliency metric, the decision boundary based saliency metric, and the classifier independent saliency metric are compared for a data set consisting of the RSI and Stochastics indicators as well as delayed closing price values. The decision based metric and the Ruck metric results are similar, but the classifier independent metric agrees with neither of the other metrics. The nine most salient features, determined by the decision boundary based metric, are used to train a neural network and the results are presented and compared to other published results. DTIC

N95-31565 Rochester Univ., NY. Dept. of Computer Science.
NONPARAMETRIC RECOGNITION OF NONRIGID MOTION
Ramprasad B. Polana and Randal C. Nelson Mar. 1995 31 p Sponsored in part by an ARPA subcontract from the University of Maryland Limited Reproducibility: More than 20% of this document may be affected by poor print
(Contract N00014-93-1-0221)
(AD-A293630; TR-575) Avail: Issuing Activity (Defense Technical Information Center (DTIC))

The recognition of nonrigid motion, particularly that arising from human movement (and by extension from the locomotory activity of animals) has typically made use of high-level parametric models representing the various body parts (legs, arms, trunk, head etc.) and their connections to each

other. Such model-based recognition has been successful in some cases; however, the methods are often difficult to apply to real-world scenes, and are severely limited in their generalizability. The first problem arises from the difficulty of acquiring and tracking the requisite model parts, usually specific joints such as knees, elbows or ankles. This generally requires some prior high-level understanding and segmentation of the scene, or initialization by a human operator. The second problem, with generalization, is due to the fact that the human model is not much good for dogs or birds, and for each new type of motion, a new model must be hand-crafted. In this paper, we show that the recognition of human or animal locomotion, and, in fact, any repetitive activity can be done using low-level, non-parametric representations. Such an approach has the advantage that the same underlying representation is used for all examples, and no individual tailoring of models or prior scene understanding is required. We show in particular, that repetitive motion is such a strong cue. That the moving actor can be segmented, normalized spatially and temporally, and recognized by matching against a spatio-temporal template of motion features. DTIC

N95-31831# Southern Methodist Univ., Dallas, TX. Dept. of Statistical Science.
A HYPOTHESIS-TESTING APPROACH TO DISCRIMINANT ANALYSIS WITH MIXED CATEGORICAL AND CONTINUOUS VARIABLES WHEN DATA ARE MISSING
J. W. Miller, W. A. Woodward, H. L. Gray, and G. D. McCartor Jul. 1994 41 p
(Contract F19628-93-C-0199; ARPA Order A128)
(AD-A293714; SMU-DS-TR273; PL-TR-94-2241; SR-1) Avail: CASI HC A03/MF A01

In this report we consider the problem of discriminant analysis with discrete (categorical) and continuous variables with data missing at random. We use a hypothesis-testing approach based on the generalized likelihood ratio as proposed by Baek, et al. We use bootstrapping to determine critical values in order to control the Type 1 error rate. We present three algorithms for dealing with this case, each assuming a different model for the data: the INDICATOR algorithm replaces categorical variables with indicator variables, and treats these as if they were continuous, the FULL algorithm assumes a multinomial distribution for the discrete part, and a multivariate normal distribution (with mean and covariances depending on the discrete part) as the conditional distribution of the continuous part given the discrete part, and the COMMON algorithm assumes a multinomial distribution for the discrete part, and a multivariate normal distribution (with only the means depending on the discrete part) as the conditional distribution of the continuous part given the discrete part. (That is, a common covariance matrix is assumed across all multinomial cells.) The performance of these algorithms is compared through a simulation study. While the INDICATOR algorithm seems to have highest power, it also tends to display a higher Type 1 error rate than desired. The FULL and the COMMON algorithms have very similar power, but the COMMON algorithm appears to control the Type 1 error rate most effectively, and is least susceptible to problems occurring when some multinomial cells are sparsely represented. DTIC

66 SYSTEMS ANALYSIS

Includes mathematical modeling; network analysis; and operations research.

N95-30565# Technische Univ., Twente (Netherlands).
OPERATING SYSTEM SUPPORT FOR DISTRIBUTED MULTIMEDIA APPLICATIONS: A SURVEY OF CURRENT RESEARCH
T. M. Burkow Sep. 1994 43 p
(PB95-207096; Memo-INF-94-49) Copyright Avail: CASI HC A03/MF A01

The report examines current research, and general design characteristics in operating system support for multimedia. Generally, conventional operating systems do not provide adequate support for distributed multimedia applications. Important design aspects are: reducing the amount of data copying; lowering the number of kernel boundary crossings; and implementing efficient context switches between threads. Quality of Service (QoS) management is also an important aspect in the design, and furthermore, mechanisms for synchronization are needed. There are several projects working with operating system support for multimedia applications, some addressing file system design, some addressing kernel design and some both. NTIS

N95-31987# General Accounting Office, Washington, DC. National Security and International Affairs Div.
REPORT TO THE CHAIRMAN, LEGISLATION AND NATIONAL SECURITY SUBCOMMITTEE, COMMITTEE ON GOVERNMENT OPERATIONS, HOUSE OF REPRESENTATIVES. TACTICAL AIRCRAFT: F-15 REPLACEMENT IS PREMATURE AS CURRENTLY PLANNED
25 Mar. 1994 10 p
(GAO/NSIAD-94-118; B-253662) Avail: CASI HC A02/MF A01; GAO, PO Box 6015, Gaithersburg, MD 20877 HC

The F-22 program was initiated in 1981 to meet the evolving threat in the mid-1990's. This threat revolved around a fighter threat that had a significant quantitative advantage and was becoming more capable with the introduction of two new high performance fighters. Since the F-22 program entered full-scale development in 1991, the severity of the projected military threat in terms of quantities and capabilities has declined. Instead of confronting thousands of modern Soviet fighters, U.S. air forces are expected to confront potential adversary air forces that include few fighters that have the capability to challenge the F-15 - the U.S. front line fighter. The F-15 exceeds the most advanced threat system expected to exist. And no improvements will be made to the F-15 but the capability of the 'most advanced threat' assumes certain modifications. Further, analysis shows that the current inventory of F-15's can be economically maintained in a structurally sound condition until 2015 or later. Thus, the F-22's initial operational capability can be delayed 7 years and its planned production start date of 1996 can be postponed to a future date deemed appropriate by DOD to meet the new initial operational capability date.
Derived from text

N95-32287# Stanford Univ., CA. Dept. of Computer Science.
AUTOMATIC VERIFICATION AND SYNTHESIS OF FINITE-STATE HARD REAL-TIME SYSTEMS Final Technical Report
David Dill 31 May 1994 8 p
(Contract N00014-91-J-1901)
(AD-A291279) Avail: CASI HC A02/MF A01

The goal is to develop computationally feasible automatic methods for the formal verification and synthesis of hard real-time systems. The current year's focus has been on making approximation methods work for more realistic system designs. Considerable effort has been invested in generalizing the approximation techniques in the hope that they can be used in other domains. The current algorithm works by successive approximation. It proceeds in a sequence of forward and backwards passes. It is consistently able to handle all of the examples attempted, including the difficult ethernet example of Weinberg and Zuck. In addition, an algorithm has been developed for handling 'skewed clock automata,' which allow timers that increase at variable rates, where only upper and lower bounds on the rates are known. CASI

67 THEORETICAL MATHEMATICS

Includes topology and number theory.

N95-30369# Joint Inst. for Nuclear Research, Dubna (USSR).
A QUEER REDUCTION OF DEGREES OF FREEDOM
L. V. Avdeev and M. V. Chizhov (Sofia Univ., Bulgaria.) 1994 6 p
(DE95-613471; JINR-E-2-94-263) Avail: CASI HC A02/MF A01 (US Sales Only)

The classical dynamics of antisymmetric second-rank tensor matter fields is analyzed. The conformally invariant action for the tensor field leads to a positive-definite Hamiltonian on the class of the solutions that are bounded at the time infinity (plane waves). Only the longitudinal waves contribute to the energy and momentum. The helicity proves to be equal to zero. DOE

N95-30428# Melbourne Univ., Parkville (Australia). School of Physics.
COVARIANT PHASE SPACE FORMULATIONS OF SUPERPARTICLES AND SUPERSYMMETRIC WZW MODELS
G. Au and B. Spence Feb. 1994 15 p

(DE95-616278; UM-P-93/107) Avail: CASI HC A03/MF A01 (US Sales Only)

The Wess-Zumino-Witten (WZW) models are fundamental rational conformal field theories, and have a rich structure which has occasioned much interest. With regard to the further development of the formulation of this approach, as well as to the various applications of supersymmetric WZW models in superstring theories, the authors consider the question of whether one can generalize this covariant phase space formulation to the supersymmetric WZW models and discuss superparticles moving upon group manifolds. These systems share many of the important features of the supersymmetric WZW models. The WZW models are then discussed. It is shown that the full current algebras arise naturally for these models and the topological issues which arose in the bosonic case are found here with the same resolution. DOE

N95-30430# Hamburg Univ. (Germany). Inst. for Theoretical Physics.
THE SOLUTIONS OF AFFINE AND CONFORMAL AFFINE TODA FIELD THEORY
G. Papadopoulos and B. Spence (Melbourne Univ., Parkville, Australia.) Feb. 1994 10 p
(DE95-616280; UM-P-93/75) Avail: CASI HC A02/MF A01 (US Sales Only)

We give new formulations of the solutions of the field equations of the affine Toda and conformal affine Toda theories on a cylinder and two-dimensional Minkowski space-time. These solutions are parameterized in terms of initial data and the resulting covariant phase spaces are diffeomorphic to the Hamiltonian ones. We derive the fundamental Poisson brackets of the parameters of the solutions and give the general static solutions for the affine theory. DOE

N95-30432# Melbourne Univ., Parkville (Australia). School of Physics.
PLAQUETTE EXPANSION PROOF AND INTERPRETATION
N. S. Witte and Lloyd C. L. Hollenberg 2 Sep. 1993 19 p Submitted for publication in the Journal of Mathematical Physics
(DE95-616282; UM-P-93/87) Avail: CASI HC A03/MF A01 (US Sales Only)

The plaquette expansion, a general non-perturbative method for calculating the properties of lattice Hamiltonian systems, is established up to the first two orders for an arbitrary system. This method employs an expansion of the Lanczos coefficients, the tridiagonal Hamiltonian matrix elements or equivalently the continued fraction coefficients of the resolvent, in a descending series in the size of the system. The coefficients of this series are formed from the low order cumulants or connected Hamiltonian moments. The lowest order approximation in the plaquette expansion corresponds to a Gaussian model which is a consequence of the control limit theorem. DOE

N95-30435# Melbourne Univ., Parkville (Australia). School of Physics.
A GENERAL NON-PERTURBATIVE ESTIMATE OF THE ENERGY DENSITY OF LATTICE HAMILTONIANS
Lloyd C. L. Hollenberg and N. S. Witte 1994 14 p
(DE95-616283; UM-P-93/90) Avail: CASI HC A03/MF A01 (US Sales Only)

Employing a theorem on lower bounds on the zeros of orthogonal polynomials, the plaquette expansion to order 1/N(sub p) of the tri-diagonal Lanczos matrix elements is solved for the ground state energy density in the infinite lattice limit. The resulting non-perturbative expression for the estimate of the energy density in terms of the connected coefficients to order (H(sup 4))(sub c) is completely general. This expression is applied to various Hamiltonian systems - the Heisenberg model in D dimensions and SU(2) and SU(3) lattice gauge theory in 3 + 1 dimensions. In all cases the analytic estimate to the energy density is not only a significant improvement on the trial state, but is typically accurate to a few percent. The energy density of the D-dimensional Heisenberg model is predicted to approach (epsilon)(sub 0)(Neel) - 1/8 for large D. In the case of SU(2) and SU(3) the specific heat derived from the energy density peaks at the correct strong to weak coupling transition. DOE

N95-30439# Melbourne Univ., Parkville (Australia). School of Physics.
ELECTROWEAK INTERACTIONS ON THE LATTICE
Tien Dung Kieu Jul. 1994 6 p
(DE95-616287; UM-P-94/74; RCHEP-94/22) Avail: CASI HC A02/MF A01 (US Sales Only)

It is shown that the lattice fermion doubling phenomenon is connected to the chiral anomaly which is unique to the electroweak interactions. The chiral anomaly is the breaking of chiral gauge symmetry at the quantum level due to the quantum fluctuations. Such breaking, however, is undesirable and to be avoided. The preservation of gauge symmetry imposes stringent constraints on acceptable chiral gauge theory. It is argued that the constraints are unnecessary because the conventional quantization of chiral gauge theory has missed out some crucial contributions of the chiral interactions. The corrected quantization yields consistent theory in which there is no gauge anomaly and in which various mass terms can be introduced with neither the loss of gauge invariance nor the need for the Higgs mechaniam. The new quantization also provides a solution to the difficulty of how to model the electroweak interactions on the lattice. DOE

N95-30489# Institut des Hautes Etudes Scientifiques, Bures-sur-Yvette (France).
TORUS BUNDLES AND THE GROUP COHOMOLOGY OF GL(N,Z)
J. M. Bismut and J. Lott Feb. 1995 54 p Prepared in cooperation with Michigan Univ.
(PB95-208120; IHES/M/95/16) Avail: CASI HC A04/MF A01

We prove the vanishing of a certain characteristic class of flat vector bundles when the structure groups of the bundles are contained in GL(N,Z). We do so by explicitly writing the characteristic class as an exact form on the base of the bundle. NTIS

N95-30504# Institut des Hautes Etudes Scientifiques, Bures-sur-Yvette (France).
STRANGE COMPACTIFICATION THEOREM: INFINITE PROCESSES AND THE 3-DIMENSIONAL POINCARE CONJECTURE 6. PART A
V. Poenaru Feb. 1995 75 p
(PB95-207924; IHES/M/95/15) Avail: CASI HC A04/MF A01

The present paper is the sixth and last one from the sequence of reports beginning in 1992. We finally get here to the proof of THEOREM 1.0. (THE POINCARE CONJECTURE): Any homotopy 3-sphere Sigma(sup 3) is homeomorphic to S(sup 3), i.e. Sigma(sup 3) = S(sup 3). NTIS

N95-30509# Institut des Hautes Etudes Scientifiques, Bures-sur-Yvette (France).
4-MANIFOLD TOPOLOGY 2: DWYER'S FILTRATION AND SURGERY KERNELS
M. H. Freedman and P. Teichner Feb. 1995 27 p Sponsored by National Science Foundation
(PB95-207940; IHES/M/95/12) Avail: CASI HC A03/MF A01

Even when the fundamental group is intractable (i.e. not 'good') many interesting 4-dimensional surgery problems have topological solutions. We unify and extend the known examples and show how they compare to the (presumed) counter examples by reference to Dwyer's filtration on second homology. The development brings together many basic results on the nilpotent theory of links. As a special case, a class of links only slightly smaller than 'homotopically trivial links' is shown to have (free) slices on their Whitehead doubles. NTIS

N95-30523# Technische Univ., Eindhoven (Netherlands). Dept. of Mathematics and Computing Science.
EXTENSION TO HIGHER DIMENSIONS OF THE JAESCHKE-EICKER RESULT ON THE STANDARDIZED EMPIRICAL PROCESS
J. H. J. Einmahl Sep. 1994 16 p
(PB95-206868; MEMO-COSOR-94-31) Avail: CASI HC A03/MF A01

The asymptotic distribution of the sup-norm of the heavily weighted empirical process is established in the multidimensional case. This theorem extends in particular the famous result in Jaeschke (1975, 1979) to higher dimensions. There is a striking difference between the behavior for higher dimensions and that for dimension one, especially the limiting distribution is now a simple transformation of a standard exponential random variable. NTIS

N95-30555# Institut des Hautes Etudes Scientifiques, Bures-sur-Yvette (France).
THE 4-MANIFOLD TOPOLOGY 1: SUBEXPONENTIAL GROUPS

M. H. Freedman and P. Teichner Feb. 1995 21 p
(PB95-207957; IHES/M/95/11) Avail: CASI HC A03/MF A01

The technical lemma underlying the 5-dimensional topological s-cobordism conjecture and the 4-dimensional topological surgery conjecture is a purely smooth category statement about locating pi(sub 1)-null immersions of disks. These conjectures are theorems precisely for those fundamental groups ('good groups') where the pi(sub 1)-null disk lemma (NDL) is known. We expand the class of good groups to all groups of subexponential growth and those that can be formed from these by a finite number of application of two operations: (1) extension and (2) direct limit. Good finitely generated groups are amenable and as far as is known these may be all the amenable groups. NTIS

N95-30501# Institut des Hautes Etudes Scientifiques, Bures-sur-Yvette (France).
ARITHMETIC FEATURES OF RATIONAL CONFORMAL FIELD THEORY
I. T. Todorov Feb. 1995 29 p Prepared in cooperation with Bulgarian Academy of Sciences
(PB95-207908; IHES/P/95/10) Avail: CASI HC A03/MF A01

Rational conformal field theory (RCFT) gradually opened the way to an intrusion of number theoretic methods into mathematical physics. Intriguing parallels between V. Jones theory of subfactors and patterns of 2-dimensional (2D) critical behavior led to the introduction of lattice models labeled by Dynkin diagrams and to the A-D-E classification of A(1) current algebra and minimal conformal models. This work used number theoretic tools and triggered an interaction between the two fields. The trend continues in recent work on the role of Galois symmetry in the search for modular invariants and in applying the representation theory of affine superalgebras to number theoretic problems. The present paper displays (and makes use of) some number theoretic features of braid matrices and structure constants in RCFT models, that have remained unnoticed in otherwise comprehensive studies in the past. NTIS

N95-30635# International Centre for Theoretical Physics, Trieste (Italy).
SOME FUNCTIONAL SOLUTIONS OF THE YANG-BAXTER EQUATION
D. Ts. Stoyanov Sep. 1994 8 p
(DE95-613584; IC-94/289; INRNE-Th-02/94) Avail: CASI HC A02/MF A01 (US Sales Only)

A general functional definition of the infinite dimensional quantum R-matrix satisfying the Yang-Baxter equation is given. A procedure for extracting a finite dimensional R-matrix from the general definition is demonstrated in a particular case when the group SU(2) takes place. DOE

N95-30681# Technische Univ., Eindhoven (Netherlands). Dept. of Mathematics and Computing Science.
CO-GROUPS ON SEQUENTIALLY COMPLETE, LOCALLY CONVEX, TOPOLOGICAL VECTOR SPACES IN PARTICULAR ON STRICT LF-SPACES
S. J. L. vanEijndhoven Aug. 1994 42 p
(PB95-206918; RANA-94-15) Avail: CASI HC A03/MF A01

In this report we develop the theory of C(sub 0)-groups (Pi(sub t)), t a member of R, on locally convex, sequentially complete, topological vector spaces V. We prove that under mild conditions on the locally convex topology of V the infinitesimal generator delta (sub pi) of the C(sub 0)-group is closed as well as the operators q (delta (sub pi)) with their natural domain where q denotes any polynomial. NTIS

N95-30719# Technische Univ., Eindhoven (Netherlands).
BARENDREGT CUBE WITH DEFINITIONS AND GENERALIZED REDUCTION
R. Bloo, F. Kamareddine, and R. Nederpelt 2 Sep. 1994 40 p Prepared in cooperation with Glasgow Univ.
(PB95-206793) Avail: CASI HC A03/MF A01

In this paper, we propose to extend the Barendregt Cube by generalizing reduction and by adding definition mechanisms. We show that this extension satisfies all the original properties of the Cube including Church Rosser, Subject Reduction and Strong Normalization. NTIS

N95-31259# Academy of Sciences (USSR), Novosibirsk (USSR).
INSTANTON - ANTIINSTANTON INTERACTION AND ASYMPTOTICS OF PERTURBATION THEORY EXPANSION OF IN DOUBLE WELL OSCILLATOR
S. V. Faleev and P. G. Silvestrov 1994 15 p
(DE95-619245; BUDKERINP-94-24; IYaF-94-24) Avail: CASI HC A03/MF A01 (US Sales Only)

Instanton - antiinstanton pair is considered as a source of singularity at the Borel plane for the ground state energy of anharmonic oscillator. The problem of defining the short range instanton - antiinstanton interaction reduces to calculation of a smooth part of the Borel function. The one - loop quantum contribution to instanton - antiinstanton interaction and the second quantum correction to a single instanton density were considered. DOE

N95-31379# Gosudarstvennyi Komitet po Ispolzovaniyu Atomnoi Energii, Serpukhov (USSR). Inst. for High Energy Physics.
LOCAL SOLUTIONS OF HARMONICAL AND BI-HARMONICAL EQUATIONS, UNIVERSAL FIELD EQUATION AND SELF-DUAL CONFIGURATIONS OF YANG-MILLS FIELDS IN FOUR DIMENSIONS
A. N. Leznov 1994 6 p Submitted for publication in the Journal Lett. Math. Phys.
(DE95-620521; IHEP-94-21) Avail: CASI HC A02/MF A01 (US Sales Only)

A general method for the construction of solutions of the d'Alamberian and double d'Alamberian (harmonic and bi-harmonic) equations with local dependence of arbitrary functions upon two independent arguments is proposed. The connection between solutions of this kind and self-dual configurations of gauge fields having no singularities is established. DOE

N95-32066# Academy of Sciences (USSR), Novosibirsk (USSR). Inst. of Nuclear Physics.
INSTABILITY OF WEAKLY NONLINEAR CHAOTIC STRUCTURES
V. V. Vecheslavov 1994 9 p
(DE95-613441; BudkerINP-94-53; IYaF-94-53) Avail: CASI HC A02/MF A01 (US Sales Only)

A linear oscillator driven by periodic perturbation is considered. The infinite connected chaotic structures in phase plane emerge when the perturbation is of the form of the periodic (delta)-function and the exact resonance condition is fulfilled. These structures are shown to be unstable and completely destroyed if the duration of the perturbation kick is arbitrarily short but finite. DOE

70 PHYSICS (GENERAL)

For precision time and time interval (PTTI) see *35 Instrumentation and Photography;* for geophysics, astrophysics or solar physics see *46 Geophysics, 90 Astrophysics,* or *92 Solar Physics.*

N95-30668# Ames Lab., IA.
A METALLURGICAL APPROACH TOWARD ALLOYING IN RARE EARTH PERMANENT MAGNET SYSTEMS Ph.D. Thesis
Daniel James Branagan 23 Feb. 1995 274 p
(Contract W-7405-eng-82)
(DE95-010242; IS-T-1719) Avail: CASI HC A12/MF A03

The approach was developed to allow microstructural enhancement and control during solidification and processing. Compound additions of Group IVA, VA, or VIA transition metals (TM) and carbon were added to Nd2Fe14B (2-14-1). Transition metal carbides formed in IVA (TiC, ZrC, HfC) and Group VA (VC, NbC, TaC) systems, but not in the VIA system. The alloying ability of each TM carbide was graded using phase stability, liquid and equilibrium solid solubility, and high temperature carbide stability. Ti with C additions was chosen as the best system. The practically zero equilibrium solid solubility means that the Ti and C additions will ultimately form TiC after heat treatment which allows the development of a composite microstructure consisting of the 2-14-1 phase and TiC. Thus, the excellent intrinsic magnetic properties of the 2-14-1 phase remain unaltered and the extrinsic properties relating to the microstructure are enhanced due to the TiC stabilized microstructure which is much more resistant to grain growth. When Ti + C are dissolved in the liquid melt or solid phases, such as the glass or 2-14-1 phase, the intrinsic properties are changed; favorable changes include increased glass forming ability, reduced optimum cooling rate, increased optimum energy product, and enhanced nucleation kinetics of crystallization. DOE

N95-30739# International Centre for Theoretical Physics, Trieste (Italy).
NEW FERMI-LIQUID APPROACH FOR THE THEORY OF DISORDERED MAGNETICS
M. Yu. Kovalevsky and A. A. Rozhkov (Academy of Sciences of the Ukraine, Kharkov, Ukraine.) Oct. 1994 17 p
(DE95-613448; IC-94/330) Avail: CASI HC A03/MF A01 (US Sales Only)

Hydro- and thermodynamics of disordered magnetics are derived in the framework of Fermi-liquid approach. The spectra of free oscillations with and without external magnetic field are obtained and analyzed. Low-frequency asymptotics of the Green function are calculated with a homogeneous magnetic field applied. The singularities of the basic Green functions are considered. DOE

N95-30809# Technische Univ., Eindhoven (Netherlands). Dept. of Mathematics and Computing Science.
GOLDEN TEN EQUATIONS OF MOTION
J. C. deVos and A. A. F. vandeVen Nov. 1994 28 p
(PB95-197927; RANA-94-24) Avail: CASI HC A03/MF A01

This paper employs a mechanical model to describe the motion of the ball in the drum during a game of Golden Ten. The result of this model is a set of differential equations. Provided that the values of the physical constants in the model are known, this set of equations can be solved numerically. The friction coefficients generate a problem here, because they have to be estimated by means of complementary experiments. After the numerical solution has been presented, the paper proceeds with a quest for an analytical solution. The system of equations is rewritten in terms of a set of small parameters--implicitly representing the friction coefficients and the drum's angle of inclination--and an analytical method is employed to express the solution as an asymptotic power series. A part of the solution is even determined exactly. At the end of the paper, the attained results are utilized to predict the outcome of the game. The paper concludes with some suggestions and directives for further research. NTIS

N95-30939# Stanford Univ., CA. Edward L Ginzton Lab. of Physics.
NEW MATERIAL FOR HIGH AVERAGE POWER INFRARED GENERATION: QPM-DB GaAs Final Technical Report
Robert L. Byer, Ropbert S. Feigelson, Robert C. Eckardt, Roger K. Route, and Leslie A. Gordon 3 Mar. 1995 30 p
(Contract DAAL03-92-G-0400)
(AD-A292714; GL-5256; ARO-30708.3-PH) Avail: CASI HC A03/MF A01

We have demonstrated diffusion-bonded-stacked GaAs to have good potential for high average power infrared generation. Diffusion bonding is the formation of a crystalline bond between two single-crystal wafers. Quasi phasematching is achieved in a stack of wafers of alternating orientation with the goal of retaining the low loss and high damage threshold of bulk single-crystal material. In this program we have substantially reduced loss per interface from 2% to 0.5% at 2 micrometers. This is adequate for single-pass applications in harmonic, sum and difference frequency generation, but further reduction of loss is required for resonant cavity applications such as optical parametric oscillation. We have performed studies of bonding techniques, surface preparation, optical damage thresholds, and numerical modeling of nonlinear frequency conversion. We are continuing this investigation with new characterization facilities and bonding apparatus and techniques developed in this program. DTIC

N95-31177# Melbourne Univ., Parkville (Australia). School of Physics.
RELATIVISTIC NON-INTERACTING ELECTRON GAS IN A MAGNETIC FIELD
M. L. Glasser and N. E. Frankel 1994 9 p
(DE95-616903; UM-P-94/89) Avail: CASI HC A02/MF A01 (US Sales Only)

The ground state properties of a noninteracting relativistic electron gas are investigated as a function of the strength of a uniform applied magnetic field for two and three dimensions. The calculation of the de Haas-van Alphen terms in the density is also presented. DOE

N95-31625# Sandia National Labs., Albuquerque, NM.
EVALUATION OF NONLINEAR STRUCTURAL DYNAMIC RESPONSES USING A FAST-RUNNING SPRING-MASS FORMULATION
A. S. Benjamin, B. S. Altman, and J. D. Gruda 1995 9 p Presented at the International Conference on Computational Engineering Science, Mauna Lani, HI, 30 Jul. - 3 Aug. 1995
(Contract DE-AC04-94AL-85000)
(DE95-008503; SAND-95-0349C; CONF-950788-2) Avail: CASI HC A02/MF A01

In today's world, accurate finite-element simulations of large nonlinear systems may require meshes composed of hundreds of thousands of degrees of freedom. Even with today's fast computers and the promise of ever-faster ones in the future, central processing unit (CPU) expenditures for such problems could be measured in days. Many contemporary engineering problems, such as those found in risk assessment, probabilistic structural analysis, and structural design optimization, cannot tolerate the cost or turnaround time for such CPU-intensive analyses, because these applications require a large number of cases to be run with different inputs. For many risk assessment applications, analysts would prefer running times to be measurable in minutes. There is therefore a need for approximation methods which can solve such problems far more efficiently than the very detailed methods and yet maintain an acceptable degree of accuracy. For this purpose, we have been working on two methods of approximation: neural networks and spring-mass models. This paper presents our work and results to date for spring-mass modeling and analysis, since we are further along in this area than in the neural network formulation. It describes the physical and numerical models contained in a code we developed called STRESS, which stands for 'Spring-mass Transient Response Evaluation for structural Systems'. The paper also presents results for a demonstration problem, and compares these with results obtained for the same problem using PRONTO3D, a state-of-the-art finite element code which was also developed at Sandia. DOE

N95-32319*# National Aeronautics and Space Administration. Goddard Space Flight Center, Greenbelt, MD.
THE 26TH ANNUAL PRECISE TIME AND TIME INTERVAL (PTTI) APPLICATIONS AND PLANNING MEETING
Richard Sydnor, ed. (Jet Propulsion Lab., California Inst. of Tech., Pasadena, CA.) May 1995 473 p Meeting held in Reston, VA, 6-8 Dec. 1994; sponsored by NASA, Washington, JPL, Naval Observatory, Space and Naval Warfare Systems Command, NRL, ARL, and AFOSR
(Contract NAS5-31000)
(NASA-CP-3302; Rept-95B00083; NAS 1.55:3302) Avail: CASI HC A20/MF A04

This document is a compilation of technical papers presented at the 26th Annual PTTI Applications and Planning Meeting. Papers are in the following categories: (1) Recent developments in rubidium, cesium, and hydrogen-based frequency standards, and in cryogenic and trapped-ion technology; (2) International and transnational applications of Precise Time and Time Interval technology with emphasis on satellite laser tracking, GLONASS timing, intercomparison of national time scales and international telecommunications; (3) Applications of Precise Time and Time Interval technology to the telecommunications, power distribution, platform positioning, and geophysical survey industries; (4) Applications of PTTI technology to evolving military communications and navigation systems; and (5) Dissemination of precise time and frequency by means of GPS, GLONASS, MILSTAR, LORAN, and synchronous communications satellites. For individual titles, see N95-32320 through N95-32349.

N95-32320*# Naval Observatory, Washington, DC. Time Service Dept.
THE 1994 INTERNATIONAL TRANSATLANTIC TWO-WAY SATELLITE TIME AND FREQUENCY TRANSFER EXPERIMENT: PRELIMINARY RESULTS c32
James A. DeYoung, William J. Klepczynski, Angela Davis McKinley, William M. Powell, Phu V. Mai, P. Hetzel (Physikalisch-Technische Bundesanstalt, Brunswick, Germany.), A. Bauch (Physikalisch-Technische Bundesanstalt, Brunswick, Germany.), J. A. Davis (National Physical Lab., Teddington, England.), P. R. Pearce (National Physical Lab., Teddington, England.), and Francoise S. Baumont (Observatoire de la Cote d'Azur, Grasse, France.) et al *In* NASA. Goddard Space Flight Center, The 26th Annual Precise Time and Time Interval (PTTI) Applications and Planning Meeting May 1995 p 39-49 (For primary document see N95-32319 11-70)
Avail: CASI HC A03/MF A04

The international transatlantic time and frequency transfer experiment was designed by participating laboratories and has been implemented during

1994 to test the international communications path involving a large number of transmitting stations. This paper will present empirically determined clock and time scale differences, time and frequency domain instabilities, and a representative power spectral density analysis. The experiments by the method of co-location which will allow absolute calibration of the participating laboratories have been performed. Absolute time differences and accuracy levels of this experiment will be assessed in the near future. Author

N95-32321*# Naval Observatory, Washington, DC.
HIGH ACCURACY TIME TRANSFER SYNCHRONIZATION
Paul J. Wheeler, Paul A. Koppang, David Chalmers, Angela Davis, Anthony Kubik, and William M. Powell *In* NASA. Goddard Space Flight Center, The 26th Annual Precise Time and Time Interval (PTTI) Applications and Planning Meeting May 1995 p 51-61 (For primary document see N95-32319 11-70)
Avail: CASI HC A03/MF A04

In July 1994, the U.S. Naval Observatory (USNO) Time Service System Engineering Division conducted a field test to establish a baseline accuracy for two-way satellite time transfer synchronization. Three Hewlett-Packard model 5071 high performance cesium frequency standards were transported from the USNO in Washington, DC to Los Angeles, California in the USNO's mobile earth station. Two-Way Satellite Time Transfer links between the mobile earth station and the USNO were conducted each day of the trip, using the Naval Research Laboratory(NRL) designed spread spectrum modem, built by Allen Osborne Associates(AOA). A Motorola six channel GPS receiver was used to track the location and altitude of the mobile earth station and to provide coordinates for calculating Sagnac corrections for the two-way measurements, and relativistic corrections for the cesium clocks. This paper will discuss the trip, the measurement systems used and the results from the data collected. We will show the accuracy of using two-way satellite time transfer for synchronization and the performance of the three HP 5071 cesium clocks in an operational environment.
Author

N95-32322*# Space Operations Squadron (2nd), Falcon AFB, CO.
FINE TUNING GPS CLOCK ESTIMATION IN THE MCS
Steven T. Hutsell *In* NASA. Goddard Space Flight Center, The 26th Annual Precise Time and Time Interval (PTTI) Applications and Planning Meeting May 1995 p 63-74 (For primary document see N95-32319 11-70)
Avail: CASI HC A03/MF A04

With the completion of a 24 operational satellite constellation, GPS is fast approaching the critical milestone, Full Operational Capability (FOC). Although GPS is well capable of providing the timing accuracy and stability figures required by system specifications, the GPS community will continue to strive for further improvements in performance. The GPS Master Control Station (MCS) recently demonstrated that timing improvements are always composite Clock, and hence, Kalman Filter state estimation, providing a small improvement to user accuracy. Author

N95-32323*# National Inst. of Standards and Technology, Boulder, CO. Time and Frequency Div.
IMPLEMENTATION OF A STANDARD FORMAT FOR GPS COMMON VIEW DATA
Marc A. Weiss and Claudine Thomas (Bureau International des Poids et Mesures, Sevres, France.) *In* NASA. Goddard Space Flight Center, The 26th Annual Precise Time and Time Interval (PTTI) Applications and Planning Meeting May 1995 p 75-88 (For primary document see N95-32319 11-70)
Avail: CASI HC A03/MF A04

A new format for standardizing common view time transfer data, recommended by the Consultative Committee for the Definition of the Second, is being implemented in receivers commonly used for contributing data for the generation of International Atomic Time. We discuss three aspects of this new format that potentially improve GPS common-view time transfer: (1) the standard specifies the method for treating short term data, (2) it presents data in consistent formats including needed terms not previously available, and (3) the standard includes a header of parameters important for the GPS common-view process. In coordination with the release of firmware conforming to this new format the Bureau International des Poids et Mesures will release future international track schedules consistent with the new standard. Author

N95-32324*# Istituto Elettrotecnico Nazionale, Turin (Italy).
EUROPEAN PLANS FOR NEW CLOCKS IN SPACE
Sigfrido M. Leschiutta and Patrizia Tavella *In* NASA. Goddard Space Flight Center, The 26th Annual Precise Time and Time Interval (PTTI) Applications and Planning Meeting May 1995 p 101-110 (For primary document see N95-32319 11-70)
Avail: CASI HC A02/MF A04

An outline of the future European space research program where precise clocks are necessary is presented, pointing out how space applications are posing impressive requirements as regards clock mass, power, ruggedness, long life, accuracy and, in some cases, spectral purity. The material presented was gathered in some laboratories; useful information was obtained from the Space Agencies of France (CNES), Germany (DARA) and Italy (ASI), but the bulk is coming from a recent exercise promoted inside ESA (the European Space Agency) and aimed to prefigure space research activities at the beginning of the next millennium. This exercise was called Horizon 2000 plus; the outcomings were summarized in two reports, presented by ESA in may 1994. Precise clocks and time measurements are needed not only for deep-space or out-ward space missions, but are essential tools also for Earth oriented activities. In this latter field, the European views and needs were discussed in October 1994, in a meeting organized by ESA and devoted to Earth Observation problems. By a scrutiny of these reports, an analysis was performed on the missions requiring a precise clock on board and the driving requirements were pointed out, leading to a survey of the necessary PTTI developments that, to some extent, are in the realm of possibility but that pose serious challenges. In this report the use of frequency standards in the satellite navigation systems is not considered. Author

N95-32325*# Bureau International des Poids et Mesures, Sevres (France).
TIME ACTIVITIES AT THE BIPM
Claudine Thomas *In* NASA. Goddard Space Flight Center, The 26th Annual Precise Time and Time Interval (PTTI) Applications and Planning Meeting May 1995 p 111-125 (For primary document see N95-32319 11-70)
Avail: CASI HC A03/MF A04

The generation and dissemination of International Atomic Time, TAI, and of Coordinated Universal Time, UTC, are explicitly mentioned in the list of the principal tasks of the BIPM, recalled in the Comptes Rendus of the 18th Conference Generale des Poids et Mesures, in 1987. These tasks are fulfilled by the BIPM Time Section, thanks to international cooperation with national timing centers, which maintain, under metrological conditions, the clocks used to generate TAI. Besides the current work of data collection and processing, research activities are carried out in order to adapt the computation of TAI to the most recent improvements occurring in the time and frequency domains. Studies concerning the application of general relativity and pulsar timing to time metrology are also actively pursued. This paper summarizes the work done in all these fields and outlines future projects. Author

N95-32326*# Bureau International des Poids et Mesures, Sevres (France).
ANTICIPATED UNCERTAINTY BUDGETS OF PRARETIME AND T2L2 TECHNIQUES AS APPLIED TO ExTRAS
Claudine Thomas, Peter Wolf, Pierre J. M. Uhrich (Laboratoire Primaire du Temps et des Frequences, Paris, France.), W. Schaefer (Stuttgart Univ., Germany.), H. Nau (Deutsche Forschungsanstalt fuer Luft- und Raumfahrt, Oberpfaffenhofen, Germany.), and Christian Veillet (Geomatics Canada, Ottawa, Ontario.) *In* NASA. Goddard Space Flight Center, The 26th Annual Precise Time and Time Interval (PTTI) Applications and Planning Meeting May 1995 p 127-139 (For primary document see N95-32319 11-70)
Avail: CASI HC A03/MF A04

The Experiment on Timing Ranging and Atmospheric Soundings, ExTRAS, was conceived jointly by the European Space Agency, ESA, and the Russian Space Agency, RSA. It is also designated the 'Hydrogen-maser in Space/Meteor-3M project'. The launch of the satellite is scheduled for early 1997. The package, to be flown on board a Russian meteorological satellite includes ultra-stable frequency and time sources, namely two active and auto-tuned hydrogen masers. Communication between the on-board hydrogen masers and the ground station clocks is effected by means of a

microwave link using the modified version for time transfer of the Precise Range And Range-rate Equipment, PRARETIME, technique, and an optical link which uses the Time Transfer by Laser Link, T2L2, method. Both the PRARETIME and T2L2 techniques operate in a two-directional mode, which makes it possible to carry out accurate transmissions without precise knowledge of the satellite and station positions. Due to the exceptional quality of the on-board clocks and to the high performance of the communication techniques with the satellite, satellite clock monitoring and ground clocks synchronization are anticipated to be performed with uncertainties below 0.5 ns (1 sigma). Uncertainty budgets and related comments are presented. Author

N95-32327*# National Research Council of Canada, Ottawa (Ontario). Time and Frequency Standards Group.

PTTI APPLICATIONS AT THE LIMITS OF GPS

Rob J. Douglas and J. Popelar (Geomatics Canada, Ottawa, Ontario.) *In* NASA. Goddard Space Flight Center, The 26th Annual Precise Time and Time Interval (PTTI) Applications and Planning Meeting May 1995 p 141-151 (For primary document see N95-32319 11-70)

Avail: CASI HC A03/MF A04

Canadian plans for precise time and time interval services are examined in the light of GPS capabilities developed for geodesy. We present our experience in establishing and operating a geodetic type GPS station in a time laboratory setting, and show sub-nanosecond residuals for time transfer between geodetic sites. We present our approach to establishing realistic standard uncertainties for short-term frequency calibration services over time intervals of hours, and for longer-term frequency dissemination at better than the 10(exp -15) level of accuracy. Author

N95-32328*# Laboratoire Primaire du Temps et des Frequences, Paris (France).

TIME ASPECTS OF THE EUROPEAN COMPLEMENT TO GPS: CONTINENTAL AND TRANSATLANTIC EXPERIMENTAL PHASES

Pierre J. M. Uhrich, B. Juompan, R. Tourde, M. Brunet (Centre National d'Etudes Spatiales, Toulouse, France.), and J.-F. Dutrey (Centre National d'Etudes Spatiales, Toulouse, France.) *In* NASA. Goddard Space Flight Center, The 26th Annual Precise Time and Time Interval (PTTI) Applications and Planning Meeting May 1995 p 153-166 (For primary document see N95-32319 11-70)

Avail: CASI HC A03/MF A04

The CNES project of a European Complement to GPS (CE-GPS) is conceived to fulfill the needs of Civil Aviation for a non-precise approach phase with GPS as sole navigation means. This generates two missions: a monitoring mission - alarm of failure - ,and a navigation mission - generating a GPS-like signal on board the geostationary satellites. The host satellites will be the Inmarsat constellation. The CE-GPS missions lead to some time requirements, mainly the accuracy of GPS time restitution and of monitoring clock synchronization. To demonstrate that the requirements of the CE-GPS could be achieved, including the time aspects, an experiment has been scheduled over the Last two years, using a part of the Inmarsat II F-2 payload and specially designed ground stations based on 10 channels GPS receivers. This paper presents a review of the results obtained during the continental phase of the CE-GPS experiment with two stations in France, along with some experimental results obtained during the transatlantic phase (three stations in France. French Guyana, and South Africa). It describes the synchronization of the monitoring clocks using the GPS Common-view or the C- to L-Band transponder of the Inmarsat satellite, with an estimated accuracy better than 10 ns (1 sigma). Author

N95-32329*# Naval Observatory, Washington, DC. Directorate of Time.

NETWORK TIME SYNCHRONIZATION SERVERS AT THE US NAVAL OBSERVATORY

Richard E. Schmidt *In* NASA. Goddard Space Flight Center, The 26th Annual Precise Time and Time Interval (PTTI) Applications and Planning Meeting May 1995 p 175-183 (For primary document see N95-32319 11-70)

Avail: CASI HC A02/MF A04

Responding to an increased demand for reliable, accurate time on the Internet and Milnet, the U.S. Naval Observatory Time Service has established the network time servers, tick.usno.navy.mil and tock.usno.navy.mil. The system clocks of these HP9000/747i industrial work stations are synchronized to within a few tens of microseconds of USNO Master Clock 2 using VMEbus IRIG-B interfaces. Redundant time code is available from a VMEbus GPS receiver. UTC(USNO) is provided over the network via a number of protocols, including the Network Time Protocol (NTP) (DARPA Network Working Group Report RFC-1305), the Daytime Protocol (RFC-867), and the Time protocol (RFC-868). Access to USNO network time services is presently open and unrestricted. An overview of USNO time services and results of LAN and WAN time synchronization tests will be presented. Author

N95-32330*# Radiocode Clocks Ltd., Penryn (England).

CUSTOM TURNKEY TIME AND FREQUENCY SYSTEMS: A STRUCTURED, EXPANDABLE APPROACH

David F. Wright *In* NASA. Goddard Space Flight Center, The 26th Annual Precise Time and Time Interval (PTTI) Applications and Planning Meeting May 1995 p 185-190 (For primary document see N95-32319 11-70)

Avail: CASI HC A02/MF A04

Radiocode Clocks Ltd. have developed a Turnkey Time and Frequency Generation and Distribution, System strategy based upon a bus of three, 'core' signals from which any Time code, Pulse rate or Frequency can be produced. The heart of the system is a ruggedized 19 inch, 3U Single Eurocard chassis constructed from machined 10mm aluminum alloy plate and designed to meet stringent Military, Security and Telecommunications specifications. The chassis is fitted with an advanced multilayer backplane with separate ground planes for analog and digital signals ensuring no degradation of low noise frequency references in the proximity of high speed digital pulse transmissions. The system has been designed to be used in three possible configurations: 1) As a stand alone generation and distribution instrument; 2) As a primary distribution unit in a turnkey Time and Frequency system; and 3) As a secondary distribution unit at a remote location from the Turnkey Time and Frequency System providing regeneration of core signals and correction for transmission delays. When configured as a secondary distribution unit the system will continue to provide usable outputs when one, two or even all three of the 'core' signals are lost. The instrument's placement within a system as a possible single point of system failure has required the development of very high reliability translator, synthesizer, phase locked loop and distribution modules together with a comprehensive alarm and monitoring strategy. Author

N95-32331*# National Physical Lab., Teddington (England). Time and Frequency Div.

HIGH RESOLUTION TIME INTERVAL COUNTER

Victor S. Zhang, Dick D. Davis, and Michael A. Lombardi *In* NASA. Goddard Space Flight Center, The 26th Annual Precise Time and Time Interval (PTTI) Applications and Planning Meeting May 1995 p 191-200 (For primary document see N95-32319 11-70)

Avail: CASI HC A02/MF A04

In recent years, we have developed two types of high resolution, multi-channel time interval counters. In the NIST two-way time transfer MODEM application, the counter is designed for operating primarily in the interrupt-driven mode, with 3 start channels and 3 stop channels. The intended start and stop signals are 1 PPS, although other frequencies can also be applied to start and stop the count. The time interval counters used in the NIST Frequency Measurement and Analysis System are implemented with 7 start channels and 7 stop channels. Four of the 7 start channels are devoted to the frequencies of 1 MHz, 5 MHz or 10 MHz, while triggering signals to all other start and stop channels can range from 1 PPS to 100 kHz. Time interval interpolation plays a key role in achieving the high resolution time interval measurements for both counters. With a 10 MHz time base, both counters demonstrate a single-shot resolution of better than 40 ps, and a stability of better than 5 x 10(exp -12) (sigma(sub chi)(tau)) after self test of 1000 seconds). The maximum rate of time interval measurements (with no dead time) is 1.0 kHz for the counter used in the MODEM application and is 2.0 kHz for the counter used in the Frequency Measurement and Analysis System. The counters are implemented as plug-in units for an AT-compatible personal computer. This configuration provides an efficient way of using a computer not only to control and operate the counters, but also to store and process measured data. Author

N95-32332*# Naval Observatory, Washington, DC.
INVESTIGATION INTO THE EFFECTS OF VHF AND UHF BAND RADIATION ON HEWLETT-PACKARD (HP) CESIUM BEAM FREQUENCY STANDARDS
Andrew Dickens *In* NASA. Goddard Space Flight Center, The 26th Annual Precise Time and Time Interval (PTTI) Applications and Planning Meeting May 1995 p 201-208 (For primary document see N95-32319 11-70)
Avail: CASI HC A02/MF A04

This paper documents an investigation into reports which have indicated that exposure to VHF and UHF band radiation has adverse effects on the frequency stability of HP cesium beam frequency standards. Tests carried out on the basis of these reports show that sources of VHF and UHF radiation such as two-way hand held police communications devices do cause reproducible adverse effects. This investigation examines reproducible effects and explores possible causes. Author

N95-32333*# Rockwell International Corp., Cedar Rapids, IA. Avionics and Communications Div.
RELATIVISTIC TIMESCALE ANALYSIS SUGGESTS LUNAR THEORY REVISION
Steven D. Deines and Carol A. Williams (University of South Florida, Tampa, FL.) *In* NASA. Goddard Space Flight Center, The 26th Annual Precise Time and Time Interval (PTTI) Applications and Planning Meeting May 1995 p 209-219 (For primary document see N95-32319 11-70)
Avail: CASI HC A03/MF A04

The SI second of the atomic clock was calibrated to match the Ephemeris Time (ET) second in a mutual four year effort between the National Physical Laboratory (NPL) and the United States Naval Observatory (USNO). The ephemeris time is 'clocked' by observing the elapsed time it takes the Moon to cross two positions (usually occultation of stars relative to a position on Earth) and dividing that time span into the predicted seconds according to the lunar equations of motion. The last revision of the equations of motion was the Improved Lunar Ephemeris (ILE), which was based on E. W. Brown's lunar theory. Brown classically derived the lunar equations from a purely Newtonian gravity with no relativistic compensations. However, ET is very theory dependent and is affected by relativity, which was not included in the ILE. To investigate the relativistic effects, a new, noninertial metric for a gravitated, translationally accelerated and rotating reference frame has three sets of contributions, namely (1) Earth's velocity, (2) the static solar gravity field and (3) the centripetal acceleration from Earth's orbit. This last term can be characterized as a pseudogravitational acceleration. This metric predicts a time dilation calculated to be -0.787481 seconds in one year. The effect of this dilation would make the ET timescale run slower than had been originally determined. Interestingly, this value is within 2 percent of the average leap second insertion rate, which is the result of the divergence between International Atomic Time (TAI) and Earth's rotational time called Universal Time (UT or UTI). Because the predictions themselves are significant, regardless of the comparison to TAI and UT, the authors will be rederiving the lunar ephemeris model in the manner of Brown with the relativistic time dilation effects from the new metric to determine a revised, relativistic ephemeris timescale that could be used to determine UT free of leap second adjustments. Author

N95-32334*# Jet Propulsion Lab., California Inst. of Tech., Pasadena, CA.
THE DEEP SPACE NETWORK STABILITY ANALYZER c32
Julian C. Breidenthal, Charles A. Greenhall, Robert L. Hamell, and Paul F. Kuhnle *In* NASA. Goddard Space Flight Center, The 26th Annual Precise Time and Time Interval (PTTI) Applications and Planning Meeting May 1995 p 221-233 (For primary document see N95-32319 11-70)
Avail: CASI HC A03/MF A04

A stability analyzer for testing NASA Deep Space Network installations during flight radio science experiments is described. The stability analyzer provides realtime measurements of signal properties of general experimental interest: power, phase, and amplitude spectra; Allan deviation; and time series of amplitude, phase shift, and differential phase shift. Input ports are provided for up to four 100 MHz frequency standards and eight baseband analog (greater than 100 kHz bandwidth) signals. Test results indicate the following upper bounds to noise floors when operating on 100 MHz signals: -145 dBc/Hz for phase noise spectrum further than 200 Hz from carrier, 2.5 x 10(exp -15) (tau =1 second) and 1.5 x 10(exp -17) (tau =1000 seconds) for Allan deviation, and 1 x 10(exp -4) degrees for 1-second averages of phase deviation. Four copies of the stability analyzer have been produced, plus one transportable unit for use at non-NASA observatories. Author

N95-32335*# Hewlett-Packard Co., Santa Clara, CA.
A GLOBALLY EFFICIENT MEANS OF DISTRIBUTING UTC TIME AND FREQUENCY THROUGH GPS
John A. Kusters, Robin P. Giffard (Hewlett-Packard Co., Palo Alto, CA.), Leonard S. Cutler (Hewlett-Packard Co., Palo Alto, CA.), David W. Allan (Allan's Time, Fountain Green, UT.), and Mihran Miranian (Naval Observatory, Washington, DC.) *In* NASA. Goddard Space Flight Center, The 26th Annual Precise Time and Time Interval (PTTI) Applications and Planning Meeting May 1995 p 235-254 (For primary document see N95-32319 11-70)
Avail: CASI HC A03/MF A04

Time and frequency outputs comparable in quality to the best laboratories have been demonstrated on an integrated system suitable for field application on a global basis. The system measures the time difference between 1 pulse-per-second (pps) signals derived from local primary frequency standards and from a multi-channel GPS C/A receiver. The measured data is processed through optimal SA Filter algorithms that enhance both the stability and accuracy of GPS timing signals. Experiments were run simultaneously at four different sites. Even with large distances between sites, the overall results show a high degree of cross-correlation of the SA noise. With sufficiently long simultaneous measurement sequences, the data shows that determination of the difference in local frequency from an accepted remote standard to better than 1 x 10(exp -14) is possible. This method yields frequency accuracy, stability, and timing stability comparable to that obtained with more conventional common-view experiments. In addition, this approach provides UTC(USNO MC) in real time to an accuracy better than 20 ns without the problems normally associated with conventional common-view techniques. An experimental tracking loop was also set up to demonstrate the use of enhanced GPS for dissemination of UTC(USNO MC) over a wide geographic area. Properly disciplining a cesium standard with a multi-channel GPS receiver, with additional input from USNO, has been found to permit maintaining a timing precision of better than 10 ns between Palo Alto, CA and Washington, DC. Author

N95-32336*# Aerospace Corp., Los Angeles, CA. Electronics Technology Center.
MONTE CARLO SIMULATIONS OF PRECISE TIMEKEEPING IN THE MILSTAR COMMUNICATION SATELLITE SYSTEM
James C. Camparo and R. P. Frueholz *In* NASA. Goddard Space Flight Center, The 26th Annual Precise Time and Time Interval (PTTI) Applications and Planning Meeting May 1995 p 291-303 (For primary document see N95-32319 11-70)
Avail: CASI HC A03/MF A04

The Milstar communications satellite system will provide secure antijam communication capabilities for DOD operations into the next century. In order to accomplish this task, the Milstar system will employ precise timekeeping on its satellites and at its ground control stations. The constellation will consist of four satellites in geosynchronous orbit, each carrying a set of four rubidium (Rb) atomic clocks. Several times a day, during normal operation, the Mission Control Element (MCE) will collect timing information from the constellation, and after several days use this information to update the time and frequency of the satellite clocks. The MCE will maintain precise time with a cesium (Cs) atomic clock, synchronized to UTC(USNO) via a GPS receiver. We have developed a Monte Carlo simulation of Milstar's space segment timekeeping. The simulation includes the effects of: uplink/downlink time transfer noise; satellite crosslink time transfer noise; satellite diurnal temperature variations; satellite and ground station atomic clock noise; and also quantization limits regarding satellite time and frequency corrections. The Monte Carlo simulation capability has proven to be an invaluable tool in assessing the performance characteristics of various timekeeping algorithms proposed for Milstar, and also in highlighting the timekeeping capabilities of the system. Here, we provide a brief overview of the basic Milstar timekeeping architecture as it is presently envisioned. We then describe the Monte Carlo simulation of space segment timekeeping, and provide examples of the simulation's efficacy in resolving timekeeping issues. Author

N95-32337*# National Service of Metrology, Delft (Netherlands).
AUTOMATED DELAY MEASUREMENT SYSTEM FOR AN EARTH STATION FOR TWO-WAY SATELLITE TIME AND FREQUENCY TRANSFER
Gerrit deJong and Michel C. Polderman *In* NASA. Goddard Space Flight Center, The 26th Annual Precise Time and Time Interval (PTTI) Applications and Planning Meeting May 1995 p 305-317 (For primary document see N95-32319 11-70)
Avail: CASI HC A03/MF A04

The measurement of the difference of the transmit and receive delays of the signals in a Two-Way Satellite Time and Frequency Transfer (TWSTFT) Earth station is crucial for its nanosecond time transfer capability. Also, the monitoring of the change of this delay difference with time, temperature, humidity, or barometric pressure is important for improving the TWSTFT capabilities. An automated system for this purpose has been developed from the initial design at NMi-VSL. It calibrates separately the transmit and receive delays in cables, amplifiers, upconverters and downconverters, and antenna feeds. The obtained results can be applied as corrections to the TWSTFT measurement when, before and after a measurement session, a calibration session is performed. Preliminary results obtained at NMi-VSL will be shown. Also, if available, the results of a manual version of the system that is planned to be circulated in Sept. 1994 together with a USNO portable station on a calibration trip to European TWSTFT Earth stations. Author

N95-32338*# Bureau International des Poids et Mesures, Sevres (France).
STUDY OF TROPOSPHERIC CORRECTION FOR INTERCONTINENTAL GPS COMMON-VIEW TIME TRANSFER
Wlodzimierz W. Lewandowski, William J. Klepczynski (National Physical Lab., Teddington, England.), Mihran Miranian (National Physical Lab., Teddington, England.), P. Gruedler (Observatoire de la Cote d'Azur, Grasse, France.), Francoise S. Baumont (Observatoire de la Cote d'Azur, Grasse, France.), and M. Imae (Communications Research Lab., Tokyo, Japan.) *In* NASA. Goddard Space Flight Center, The 26th Annual Precise Time and Time Interval (PTTI) Applications and Planning Meeting May 1995 p 319-332 (For primary document see N95-32319 11-70)
Avail: CASI HC A03/MF A04

Current practice is to incorporate general empirical models of the troposphere, which depend only on the station height and the elevation of the satellite, in GPS time receivers used for common-view time transfer. Comparisons of these models with a semi-empirical model based on weather measurements show differences of several nanoseconds. This paper reports on a study of tropospheric correction during GPS common-view time transfer over a short baseline of about 700 km, and three long baselines of 6400 km, 9000 km and 9600 km. It is shown that the use of a general empirical model of the troposphere within a region where the climate is similar does not affect time transfer by more than a few hundreds of picoseconds. For the long distance links, differences between the use of a general empirical model and the use of a semi-empirical model reach several nanoseconds. Author

N95-32339*# Fiat Research Center, Orbassano, Turin (Italy).
PROSPECTS FOR HIGH ACCURACY TIME DISSEMINATION AND SYNCHRONIZATION USING CODED RADAR PULSES FROM A LOW-EARTH ORBITING SPACECRAFT
Edoardo V. Detoma and C. Dionisio *In* NASA. Goddard Space Flight Center, The 26th Annual Precise Time and Time Interval (PTTI) Applications and Planning Meeting May 1995 p 333-345 (For primary document see N95-32319 11-70)
Avail: CASI HC A03/MF A04

The radar (an acronym for radio detection and ranging) is an instrument developed just before the WW-II to precisely measure the position of an object (target) in space. This is done by emitting a narrow pulse of electromagnetic energy in the RF spectrum, receiving the return echo and measuring the time of flight in the two-way path from the emitter to the target. The propagation delay provides a measure of the range to the target, which is not in itself sufficient to uniquely locate the position of the same in space. However, if a directional antenna is used, the direction of the echo can be assessed by the antenna pointing angles. In this way the position of the target can be uniquely determined in space. How well this can be done is a function of the resolution of the measurements performed (range and direction, i.e.: angles); in turn, the resolution will dictate the time and frequency requirements of the reference oscillator. Author

N95-32340*# National Research Council of Canada, Ottawa (Ontario). Time and Frequency Standards Group.
METAFITTING: WEIGHT OPTIMIZATION FOR LEAST-SQUARES FITTING OF PTTI DATA
Rob J. Douglas and J.-S. Boulanger *In* NASA. Goddard Space Flight Center, The 26th Annual Precise Time and Time Interval (PTTI) Applications and Planning Meeting May 1995 p 347-360 (For primary document see N95-32319 11-70)
Avail: CASI HC A03/MF A04

For precise time intercomparisons between a master frequency standard and a slave time scale, we have found it useful to quantitatively compare different fitting strategies by examining the standard uncertainty in time or average frequency. It is particularly useful when designing procedures which use intermittent intercomparisons, with some parameterized fit used to interpolate or extrapolate from the calibrating intercomparisons. We use the term 'metafitting' for the choices that are made before a fitting procedure is operationally adopted. We present methods for calculating the standard uncertainty for general, weighted least-squares fits and a method for optimizing these weights for a general noise model suitable for many PTTI applications. We present the results of the metafitting of procedures for the use of a regular schedule of (hypothetical) high-accuracy frequency calibration of a maser time scale. We have identified a cumulative series of improvements that give a significant reduction of the expected standard uncertainty, compared to the simplest procedure of resetting the maser synthesizer after each calibration. The metafitting improvements presented include the optimum choice of weights for the calibration runs, optimized over a period of a week or 10 days. Author

N95-32341*# Naval Observatory, Washington, DC.
METHODOLOGIES FOR STEERING CLOCKS
Harold Chadsey *In* NASA. Goddard Space Flight Center, The 26th Annual Precise Time and Time Interval (PTTI) Applications and Planning Meeting May 1995 p 361-368 (For primary document see N95-32319 11-70)
Avail: CASI HC A02/MF A04

One of the concerns of the PTTI community is the coordination of one time scale with another. This is accomplished through steering one clock system to another, with a goal of a zero or constant offset in time and frequency. In order to attain this goal, rate differences are calculated and allowed for by the steering algorithm. This paper will present several of these different methods of determining rate differences. Ideally, any change in rate should not cause the offset to change sign (overshoot) by any amount, but certainly not by as much as its previous absolute value. The advantages and disadvantages of each depend on the user's situation. Author

N95-32342*# Naval Observatory, Washington, DC. Directorate of Time.
THE EFFECTS OF CLOCK ERRORS ON TIMESCALE STABILITY
Lee A. Breakiron *In* NASA. Goddard Space Flight Center, The 26th Annual Precise Time and Time Interval (PTTI) Applications and Planning Meeting May 1995 p 369-380 (For primary document see N95-32319 11-70)
Avail: CASI HC A03/MF A04

The weighting scheme for the cesium clocks and hydrogen masers constituting the USNO timing ensemble is reexamined from an empirical standpoint of maximizing both frequency accuracy and timescale uniformity. The utility of a sliding-weight relation between the masers and the cesiums is reaffirmed, but improvement is found if one incorporates inverse Allan variances for sampling times of 12 and 6 hours for the cesiums and masers, respectively, with some dependence on clock model. Author

N95-32343*# Bureau International des Poids et Mesures, Sevres (France).
RELATIVISTIC THEORY FOR SYNTONIZATION OF CLOCKS IN THE VICINITY OF THE EARTH
Peter Wolf and G. Petit *In* NASA. Goddard Space Flight Center, The 26th Annual Precise Time and Time Interval (PTTI) Applications and Planning

Meeting May 1995 p 381-391 (For primary document see N95-32319 11-70)
Avail: CASI HC A02/MF A04

A well known prediction of Einstein's general theory of relativity states that two ideal clocks that move with a relative velocity, and are submitted to different gravitational fields will, in general, be observed to run at different rates. Similarly the rate of a clock with respect to the coordinate time of some spacetime reference system is dependent on the velocity of the clock in that reference system and on the gravitational fields it is submitted to. For the syntonization of clocks and the realization of coordinate times (like TAI) this rate shift has to be taken into account at an accuracy level which should be below the frequency stability of the clocks in question, i.e. all terms that are larger than the instability of the clocks should be corrected for. We present a theory for the calculation of the relativistic rate shift for clocks in the vicinity of the Earth, including all terms larger than one part in 10(exp 18). This, together with previous work on clock synchronization (Petit & Wolf 1993, 1994), amounts to a complete relativistic theory for the realization of coordinate time scales at picosecond synchronization and 10(exp -18) syntonization accuracy, which should be sufficient to accommodate future developments in time transfer and clock technology. Author

N95-32344*# Aerospace Corp., El Segundo, CA.
ALLAN DEVIATION COMPUTATIONS OF A LINEAR FREQUENCY SYNTHESIZER SYSTEM USING FREQUENCY DOMAIN TECHNIQUES
Andy Wu *In* NASA. Goddard Space Flight Center, The 26th Annual Precise Time and Time Interval (PTTI) Applications and Planning Meeting May 1995 p 393-404 (For primary document see N95-32319 11-70)
Avail: CASI HC A03/MF A04

Allan Deviation computations of linear frequency synthesizer systems have been reported previously using real-time simulations. Even though it takes less time compared with the actual measurement, it is still very time consuming to compute the Allan Deviation for long sample times with the desired confidence level. Also noises, such as flicker phase noise and flicker frequency noise, can not be simulated precisely. The use of frequency domain techniques can overcome these drawbacks. In this paper the system error model of a fictitious linear frequency synthesizer is developed and its performance using a Cesium (Cs) atomic frequency standard (AFS) as a reference is evaluated using frequency domain techniques. For a linear timing system, the power spectral density at the system output can be computed with known system transfer functions and known power spectral densities from the input noise sources. The resulting power spectral density can then be used to compute the Allan Variance at the system output. Sensitivities of the Allan Variance at the system output to each of its independent input noises are obtained, and they are valuable for design trade-off and trouble-shooting. Author

N95-32345*# Space Operations Squadron (2nd), Falcon AFB, CO.
SVN 9 END-OF-LIFE TESTING **c18**
Gregory E. Hatten *In* NASA. Goddard Space Flight Center, The 26th Annual Precise Time and Time Interval (PTTI) Applications and Planning Meeting May 1995 p 405-413 (For primary document see N95-32319 11-70)
Avail: CASI HC A02/MF A04

SVN 9 was a GPS Block I research and development satellite. When it was launched in Jun. 1984, questions regarding the future performance of atomic frequency standards in orbit remained to be answered. In Mar. 1994, after performing for twice its designed life span, SVN 9 was deactivated as a member of the operational GPS satellite constellation. During the next two months, U.S. Air Force and Rockwell personnel performed various tests to determine just how well the atomic frequency standards had withstood ten years in the space environment. The results of these tests are encouraging. With a full constellation of Block II/IIA satellites on orbit, as well as the anticipated launch of the Block IIR satellites, results from the end of life testing will be helpful in assuring the continued success of the GPS program. Author

N95-32346*# Jet Propulsion Lab., California Inst. of Tech., Pasadena, CA.
FIBER OPTIC REFERENCE FREQUENCY DISTRIBUTION TO REMOTE BEAM WAVEGUIDE ANTENNAS **c74**
Malcolm Calhoun, Paul Kuhnle, and Julius Law *In* NASA. Goddard Space Flight Center, The 26th Annual Precise Time and Time Interval (PTTI) Applications and Planning Meeting May 1995 p 415-426 (For primary document see N95-32319 11-70)
Avail: CASI HC A03/MF A04

In the NASA/JPL Deep Space Network (DSN), radio science experiments (probing outer planet atmospheres, rings, gravitational waves, etc.) and very long-base interferometry (VLBI) require ultra-stable, low phase noise reference frequency signals at the user locations. Typical locations for radio science/VLBI exciters and down-converters are the cone areas of the 34 m high efficiency antennas or the 70 m antennas, located several hundred meters from the reference frequency standards. Over the past three years, fiber optic distribution links have replaced coaxial cable distribution for reference frequencies to these antenna sites. Optical fibers are the preferred medium for distribution because of their low attenuation, immunity to EMI/IWI, and temperature stability. A new network of Beam Waveguide (BWG) antennas presently under construction in the DSN requires hydrogen maser stability at tens of kilometers distance from the frequency standards central location. The topic of this paper is the design and implementation of an optical fiber distribution link which provides ultra-stable reference frequencies to users at a remote BWG antenna. The temperature profile from the earth's surface to a depth of six feet over a time period of six months was used to optimize the placement of the fiber optic cables. In-situ evaluation of the fiber optic link performance indicates Allan deviation on the order of parts in 10(exp -15) at 1000 and 10,000 seconds averaging time; thus, the link stability degradation due to environmental conditions still preserves hydrogen maser stability at the user locations. This paper reports on the implementation of optical fibers and electro-optic devices for distributing very stable, low phase noise reference signals to remote BWG antenna locations. Allan deviation and phase noise test results for a 16 km fiber optic distribution link are presented in the paper. Author

N95-32347*# National Aeronautics and Space Administration. Goddard Space Flight Center, Greenbelt, MD.
LASER RETROREFLECTOR EXPERIMENT ON NAVSTAR 35 AND 36 **c36**
E. C. Pavlis and Ronald L. Beard (Naval Research Lab., Washington, DC.) *In its* The 26th Annual Precise Time and Time Interval (PTTI) Applications and Planning Meeting May 1995 p 427-441 (For primary document see N95-32319 11-70)
Avail: CASI HC A03/MF A04

In GPS one of the primary errors contributing to positioning inaccuracy is the performance of the on-board atomic clock. To determine and predict the performance of this atomic clock has been a problem due to the ambiguity of the orbital position error and clock uncertainty in the Radio Frequency (RF) tracking of the navigation signals. The Laser Retroreflector Experiment (LRE) on-board NAVSTAR 35 and 36 provides a means of separating these ambiguous errors by enabling highly precise and accurate satellite positions to be determined independently of the RF signals. The results of examining onboard clock behavior after removing the orbital position signatures will be discussed. GPS RF tracking data from various DOD and other sites are used to reconstruct the onboard clock data and examine the clock behavior. From these data, the effects of clock performance on GPS positioning performance can examined. Author

N95-32348*# Observatoire de la Cote d'Azur, Grasse (France).
(T2L2) TIME TRANSFER BY LASER LINK **c36**
Christian Veillet and Patricia Fridelance *In* NASA. Goddard Space Flight Center, The 26th Annual Precise Time and Time Interval (PTTI) Applications and Planning Meeting May 1995 p 443-453 (For primary document see N95-32319 11-70)
Avail: CASI HC A03/MF A04

T2L2 (Time Transfer by Laser Link) is a new generation time transfer experiment based on the principles of LASSO (Laser Synchronization from Synchronous Orbit) and used with an operational procedure developed at OCA (Observatoire de la Cote d'Azur) during the active intercontinental phase of LASSO. The hardware improvements could lead to a precision better than 10 ps for time transfer (flying clock monitoring or ground based clock comparison). Such a package could fly on any spacecraft with a stable clock. It has been developed in France in the frame of the PHARAO project (cooled atom clock in orbit) involving CNES and different laboratories. But T2L2 could fly on any spacecraft carrying a stable oscillator. A GPS satellite would be a good candidate, as T2L2 could allow to link

the flying clock directly to ground clocks using light, aiming to important accuracy checks, both for time and for geodesy. Radioastron (a flying VLBI antenna with a H-maser) is also envisioned, waiting for a PHARAO flight. The ultimate goal of T2L2 is to be part of more ambitious missions, as SORT (Solar Orbit Relativity Test), aiming to examine aspects of the gravitation in the vicinity of the Sun. Author

N95-32349*# Bureau International des Poids et Mesures, Sevres (France).
SATELLITE TEST OF THE ISOTROPY OF THE ONE-WAY SPE ED OF LIGHT USING ExTRAS
Peter Wolf *In* NASA. Goddard Space Flight Center, The 26th Annual Precise Time and Time Interval (PTTI) Applications and Planning Meeting May 1995 p 455-463 (For primary document see N95-32319 11-70)
Avail: CASI HC A02/MF A04

A test of the second postulate of special relativity, the universality of the speed of light, using the ExTRAS (Experiment on Timing Ranging and Atmospheric Sounding) payload to be flown on board a Russian Meteor-3M satellite (launch date January 1997) is proposed. The propagation time of a light signal transmitted from one point to another without reflection would be measured directly by comparing the phases of two hydrogen maser clocks, one on board and one on the ground, using laser or microwave time transfer systems. An estimated uncertainty budget of the proposed measurements is given, resulting in an expected sensitivity of the experiment of delta c/c is less than 8xl0(exp -10) which would be an improvement by a factor of approximately 430 over previous direct measurements and by a factor of approximately 4 over the best indirect measurement. The proposed test would require no equipment additional to what is already planned and so is of inherently low-cost. It could be carried out by anyone having access to a laser or microwave ground station and a hydrogen maser. Author

71 ACOUSTICS

Includes sound generation, transmission and attenuation.
For noise pollution see *45 Environmental Pollution.*

N95-30411 Department of the Navy, Washington, DC.
METHOD AND SYSTEM FOR SUPPRESSING NOISE INDUCED IN A FLUID MEDIUM BY A BODY MOVING THERETHROUGH Patent
Richard A. Katz, inventor (to Navy) 25 Oct. 1994 18 p Filed 2 Sep. 1993
(AD-D017339; US-Patent-5,359,663; US-Patent-Appl-SN-117513; US-Patent-Class-381-71) Avail: US Patent and Trademark Office

A method of detecting the onset of turbulence in connection with a body moving through a fluid medium and reducing turbulence noise acoustic sensor systems carried thereby. First, the body is supplied with sensors each for generating a signal suitable for measuring amplitude of pressure fluctuations of the medium proximate a region of said sidewall of the body in at least a region of the body in which turbulence is expected to occur. During a reference stage during which the body moves through the fluid medium when it is known that turbulence is occurring around at least a portion of said body the sensors each generate reference temporal pressure data representing fluctuations in pressure of the fluid medium around said body. In response to reference temporal pressure data representing by sensors in a turbulence zone at which turbulence is occurring and sensors in a transition zone at which turbulence zone and a laminar flow zone, method-of-delay phase portraits are generated for a progression selected delay intervals. During an operational stage, the signals from the sensors are filtered to generate a portion representing the turbulence due to motion of the body through a portion representing signals from external acoustic signal sources, and the turbulence signal portion is used to generate signals of appropriate phase which are injected into the medium to reduce the turbulence noise signals. DTIC

N95-30413 Department of the Navy, Washington, DC.
THERMOACOUSTIC SOUND GENERATOR Patent
Thomas B. Gabrielson, inventor (to Navy) 29 Nov. 1994 10 p Filed 31 May 1991
(AD-D017342; US-Patent-5,369,625; US-Patent-Appl-SN-709901; US-Patent-Class-367-140) Avail: US Patent and Trademark Office

A submersible acoustic generator for projection of sound waves into a body of water comprises a tubular resonator, open at its lower end and closed at its upper end, and having a multiple-plate thermoacoustic stack located near the upper end between a pair of heat exchangers which set up a temperature gradient in the stack. The upper heat exchanger is heated by a chemical fuel, and the lower heat exchanger is cooled by the surrounding water. The resonator is gas-filled, and the wavelength of the oscillations produced is approximately twice the length of the resonator. A portion of the resonator tube can be surrounded by a coaxial tube which serves as an impedance matching stub. The stack plates can be made anisotropic by means of embedded copper wires. In alternative versions of the apparatus, the resonator can have two stacks, one near the open end and the other near the closed end, and the temperature gradient in the stack can be established cryogenically. DTIC

N95-30461# Technische Univ., Delft (Netherlands). Inst. of Applied Physics.
DESIGN OF SYSTEMS FOR ACTIVE SOUND CONTROL Ph.D. Thesis
N. J. Doelman 2 Dec. 1993 228 p Sponsored by Stichting voor de Technische Wetenschappen
(PB95-197869; ISBN-90-9006731-0) Copyright Avail: CASI HC A11/MF A03

In this thesis the complete trajectory of designing a control system for active sound reduction is described. Starting with the fundamental acoustical theory, the design deals with discrete source and sensor distributions, discrete acoustic processes, control strategies and, finally, a large number of practical experiments. The acoustical essence of active sound reduction is based on a distribution of Huygens' sources, that has the potential to reconstruct a primary sound field with equal strength but opposite phase. A continuous distribution of monopoles and dipoles on a closed surface is shown to be the ideal anti-sound source distribution. It is capable of completely attenuating a sound field inside the closed surface. The acoustic part of the design is completed by addressing the distribution of a limited number of sensors. Two types of sensors are required. First, a distribution of detection sensors measures the incident primary sound field. Second, a distribution of error sensors measures the residual sound field. Given a source-sensor distribution, a digital control strategy has to be designed. A first step in this is to model the discrete acoustic processes or transfer functions. It is demonstrated that a discrete acoustic process is likely to have a non-minimum phase behavior. This has to be accounted for in the design of the controller. NTIS

N95-30481# National Defence Research Establishment, Stockholm (Sweden).
RAY TRACE MODEL OF SOUND PROPAGATION IN RANGE DEPENDENT MEDIA
T. Serenander Jun. 1994 63 p
(PB95-211751; FOA-C-20982-2.2) Avail: CASI HC A04/MF A01

This report treats numerical calculation of sound propagation in range dependent media when the frequency is sufficiently high for classical ray theory to be applicable. The sound field is then described by ray paths, that can be computed numerically by solving a system of ordinary differential equations (ODE's). The ODE's are formulated in terms of the sound speed c(r) of the medium as function of position r. Two methods are studied for constructing smooth approximations c tilde(r) of functions c(r) that vary in two dimensions (range and depth). In both methods, c tilde(r) is represented by B-splines and is computed from given sparsely located observed values of c(r). This representation of c(r) is implemented as an extension of a ray-tracing program which previously could handle range-independent cases only. The program solves the ODE's of the ray paths by an implicit linear multistep method with adaptively chosen stepsize and order. The program is written in FORTRAN and IS-Lab. Examples of ray trace calculations are presented. Ray patterns produced with realistic range dependent velocity files are compared with those obtained using range independent approximations. As a last example we study the propagation of a ray fan in a channel with sinusoidal bottom depth. NTIS

N95-30530 Department of the Navy, Washington, DC.
APPARATUS FOR PRODUCING IMAGES ACOUSTICALLY Patent
Michael J. Sullivan, inventor (to Navy), Douglas G. Dussault, inventor (to Navy), Rick H. Charette, inventor (to Navy), and Ray E. DAddio, inventor

(to Navy) 22 Nov. 1994 9 p Filed 29 Mar. 1993
(AD-D017365; US-Patent-5,367,496; US-Patent-Appl-SN-038364;
US-Patent-Class-367-7) Avail: US Patent and Trademark Office

A detector array of operationally independent transducers is deployed in a medium such as water is described. Each transducer generates an electrical signal across independent first and second electrodes corresponding to impinging acoustic energy. Each of the positions in the detector array is identified in sequence along with the identification of a corresponding pixel position or display position in a display structure. A first multiplexer connects to all the first electrodes and a second multiplexer connects to all the second electrodes to enable the identification circuit to select corresponding electrodes for each detector position. A single amplifier circuit couples the signals front the multiplexer to a circuit for controlling the illumination of a selected display position. DTIC

N95-30549 Department of the Navy, Washington, DC.
METHOD AND APPARATUS FOR LOCATING AN ACOUSTIC SOURCE Patent
Bruce J. Bates, inventor (to Navy) and Susan M. Bates, inventor (to Navy) 18 Oct. 1994 15 p Filed 22 Oct. 1993
(AD-D017347; US-Patent-5,357,484; US-Patent-Appl-SN-147237;
US-Patent-Class-367-116) Avail: US Patent and Trademark Office

An apparatus and method for determining the range and depth to an acoustic source from a sampling site in a medium are described. A linear array of pressure transducers monitors the acoustic field produced by the acoustic source. A measurement processor utilizes the measured acoustic field to produce an initial field condition for each member of the array. An environmental model include environmental data in the form of acoustically pertinent field condition and the acoustically pertinent variables to produce, for each incremental range and depth, an amplitude function. An index processor normalizes the amplitude functions for each incremental range and depth, and an index extreme value processor selects the amplitude function with the maximum amplitude. The range and depth of that extreme value amplitude function is used to determine the range and depth for the acoustic source. DTIC

N95-30550 Department of the Navy, Washington, DC.
EXPERT SYSTEM FOR ASSESSING ACCURACY OF MODELS OF PHYSICAL PHENOMENA AND FOR SELECTING ALTERNATE MODELS IN THE PRESENCE OF NOISE Patent
David J. Ferkinhoff, inventor (to Navy), Kai F. Gong, inventor (to Navy), Kathleen D. Keay, inventor (to Navy), and Steven C. Nardone, inventor (to Navy) 13 Dec. 1994 13 p Filed 2 Nov. 1992
(AD-D017348; US-Patent-5,373,456; US-Patent-Appl-SN-976349;
US-Patent-Class-364-574) Avail: US Patent and Trademark Office

A system for providing an iterative method of assessing accuracy of selected models of physical phenomena and for determining selection of alternate models in response to a data sequence in the presence of noise is described. Initially, a residual sequence is generated reflecting difference values between in response to said data sequence and an expected data sequence as would be represented by a selected model. Feature estimate values of a plurality of predetermined data features in the residual sequence are then generated. In response to the feature estimate values, a threshold value is generated for each feature at an estimated ratio of data to noise. Probability values are generated in response to the threshold value, representing the likelihood that the feature exists in the data sequence, does not exist in the data sequence, and that the existence or non-existence in the data sequence is not determinable. Finally, a model is selected in response to the probability values for use during a subsequent iteration. DTIC

N95-30725 Department of the Navy, Washington, DC.
FAR FIELD ACOUSTIC RADIATION REDUCTION Patent
Michael A. Sartori, inventor (to Navy) and Joseph A. Clark, inventor (to Navy) 10 Jan. 1995 6 p Filed 30 Sep. 1993
(AD-D017452; US-Patent-5,381,381; US-Patent-Appl-SN-128411;
US-Patent-Class-367-1) Avail: US Patent and Trademark Office

A system and method are provided to reduce a structure's far field acoustic radiation signature. A plurality of acoustic sensors are positioned in the acoustic near field of the structure for measuring the near field acoustic radiation of the structure. A programmable controller generates a prediction of the structure's far field acoustic radiation signature using the near field acoustic radiation. The prediction is then used to generate a noise control signal applied to a plurality of acoustic radiators suspended within the structure. The radiators convert substantially all of the noise control signal to airborne acoustic energy within the structure. DTIC

N95-30747 Department of the Navy, Washington, DC.
NOISE SIGNAL PROCESSOR Patent
Lawrence C. Pharo, Jr., inventor (to Navy) and John J. Portelli, inventor (to Navy) 4 Oct. 1994 11 p Filed 13 May 1982
(AD-D017430; US-Patent-5,353,260; US-Patent-Appl-SN-378444;
US-Patent-Class-367-135) Avail: US Patent and Trademark Office

This patent discloses an apparatus for providing a direct quantitative readout of the amplitudes of various frequency lines that constitute the envelope of an amplitude-modulated broadband noise signal. A selected band of carrier frequencies is fed to an AGC circuit that provides a constant-input signal amplitude to a demodulator for a period of time that is greater than the period of the lowest frequency of the modulating signal for detection. The detected signal is fed to a spectrum analyzer for the direct reading of the percent modulation. DTIC

N95-30850*# National Aeronautics and Space Administration. Langley Research Center, Hampton, VA.
SOLUTION OF THE THREE-DIMENSIONAL HELMHOLTZ EQUATION WITH NONLOCAL BOUNDARY CONDITIONS
Steve L. Hodge (Virginia Consortium for Engineering and Science, Hampton, VA.), William E. Zorumski, and Willie R. Watson May 1995 40 p
(RTOP 505-63-50-25)
(NASA-TM-110174; NAS 1.15:110174) Avail: CASI HC A03/MF A01

The Helmholtz equation is solved within a three-dimensional rectangular duct with a nonlocal radiation boundary condition at the duct exit plane. This condition accurately models the acoustic admittance at an arbitrarily-located computational boundary plane. A linear system of equations is constructed with second-order central differences for the Helmholtz operator and second-order backward differences for both local admittance conditions and the gradient term in the nonlocal radiation boundary condition. The resulting matrix equation is large, sparse, and non-Hermitian. The size and structure of the matrix makes direct solution techniques impractical; as a result, a nonstationary iterative technique is used for its solution. The theory behind the nonstationary technique is reviewed, and numerical results are presented for radiation from both a point source and a planar acoustic source. The solutions with the nonlocal boundary conditions are invariant to the location of the computational boundary, and the same nonlocal conditions are valid for all solutions. The nonlocal conditions thus provide a means of minimizing the size of three-dimensional computational domains. Author

N95-31365 Defence Science and Technology Organisation, Melbourne (Australia). Maritime Operations Div.
CALCULATIONS OF THE SOUND SCATTERING FROM FLUID-FILLED SPHERICAL SHELL SONAR TARGETS
Mark Readhead Jan. 1995 71 p Original contains color illustrations
(DSTO-RR-0020; AR-008-995) Avail: Issuing Activity (DSTO Aeronautical and Maritime Research Lab., GPO Box 4331, Melbourne, Victoria 3001, Australia)

The theory of the sound pressure scattered from a fluid-filled spherical shell immersed in a second fluid is developed. An arbitrary combination of fluids may be used to fill the shell, and both the sound source and the receiver may be in the near field. The theory is used to calculate the pressure field in both the interior and exterior fluids and is extended to determine the time-dependence of the reflected signal and the target strength. The dependence of these quantities as a function of frequency and pulse type; shell material, diameter and wall thickness; fluid combination; temperature; and distance of the receiver from the sphere is examined, and is shown to be sensitive to most of these parameters. The performance of spheres filled with a Freon-113(tm)-ethanol or Fluorinert FC-72(tm)-n-hexane mixture is considered. Author

N95-31527# Rockwell International Corp., Albuquerque, NM. Power Systems Group.
ADAPTIVE OPTICS DESIGN FOR THE ADVANCED ELECTRO-OPTICAL SYSTEM (AEOS) Final Report, Mar. 1993 - Mar. 1994
David W. Tyler and Amy E. Prochko Nov. 1994 60 p Prepared in

cooperation with Schafer Associates, Inc.
(Contract F29601-90-C-0068)
(AD-A293972; PL-TR-94-1043) Avail: CASI HC A04/MF A01

We develop an algorithm to guide the use of computer simulations in the design of application-specific adaptive optics (AO) systems. We then use this method to specify the number of deformable-mirror actuators and closed-loop bandwidth for the Advanced Electro-Optical System (AEOS) telescope AO system. To develop the algorithm we present analysis to show the normalized on-axis intensity can be minimized for a given AO configuration by selecting an optimum imaging wavelength. This wavelength minimizes the combined effects of diffraction, which increases with wavelength, and residual (post-compensation) phase aberration, which decreases as wavelength increases. We also show that the closed-loop AO bandwidth minimizing the sum of wavefront sensor noise error and control loop lag error is independent of wavelength. This allows the optimum bandwidth-wavelength combination for any AO configuration to be calculated non-iteratively in two steps. We describe a high-fidelity computer simulation and measures of merit used to select from among four candidate configurations. Finally, we present simulation results used to select the AEOS adaptive optics configuration and recommend the AEOS system use approximately 700 actuators with a maximum closed-loop bandwidth of at least 400 Hz. DTIC

N95-31608# Army Research Lab., White Sands Missle Range, NM. Battlefield Environment Directorate.
THE EFFECTS OF LARGE AND SMALL SCALE TURBULENCE ON SOUND PROPAGATION IN THE ATMOSPHERE
John M. Noble and Harry J. Auvermann Mar. 1995 64 p
(AD-A293657; ARL-TR-565) Avail: CASI HC A04/MF A01

Propagation of acoustic waves in the atmosphere is affected by several mechanisms. Two of the effects are the scattering of sound by small-scale atmospheric turbulence and fluctuation of the speed of sound gradients by the passage of large-scale atmospheric turbulence. Small- and large-scale atmospheric turbulence causes the acoustic waves to be altered by different mechanisms. Until recently, the majority of work in turbulence effect on acoustics has concentrated on the small-scale turbulence regime of the inertial subrange of the Kolmogorov spectrum. Earlier small-scale turbulence models have concentrated on the statistical-based work of Tatarski. Current turbulence models deal more with the structural nature of the turbulence because the statistical approach does not account for all of the turbulence effects being measured during acoustic propagation experiments. The large-scale turbulence problem cannot be handled very well with a statistical approach to atmospheric turbulence because the regime of the large-scale turbulence extends into the energy containing subrange or sometimes referred to as the source region. This report discusses the current and past turbulence models used to treat the effect of small- and large-scale turbulence on atmospheric acoustic propagation. DTIC

N95-31650# Helsinki Univ. of Technology, Espoo (Finland).
FRACTIONAL DELAY WAVEGUIDE MODELING OF ACOUSTIC TUBES
V. Vaelimaeki 1994 135 p
(PB95-206637; ISBN-951-22-2158-6) Avail: CASI HC A07/MF A02

The theme of this work is computational modeling of acoustic tubes. The models are intended to be used in a sound synthesizer based on physical modeling. Such a synthesizer could be used producing realistic sounds of, e.g., woodwind instruments or the human voice. This work deals with digital waveguide modeling of acoustic tubes, such as bores of musical woodwind instruments or the human vocal tract. The acoustic tube systems considered in this work are those consisting of a straight cylindrical or conical tube or of concatenated cylindrical or conical tube sections. Also, the joint of three tube sections is studied. Of special interest for our application is a junction where a side branch is connected to a cylindrical tube as it is needed in the simulation of finger holes of wood-wind instruments. All of the cylindrical tube models are described for both pressure and volume velocity. In the case of conical bores, only pressure waves are considered as models for volume velocity waves are more complicated. The basic waveguide models are extended by employing the concept of fractional delay, which means a delay smaller than a unit delay. The fractional delays are implemented using bandlimited interpolation. Applying fractional delay filtering techniques, a spatially discretized waveguide model is turned into a spatially continuous one. This implies that the length of the digital waveguide can be adjusted as accurately as required, and a change of the impedance of a waveguide may occur at any desired point between sampling points. The authors call this kind of system a fractional delay waveguide filter (FDWF). It is a discrete-time structure but a spatially continuous model of a physical system. NTIS

N95-31783*# Blackstone Corp., Jamestown, NY.
ULTRASONIC CLEANING: FUNDAMENTAL THEORY AND APPLICATION
F. John Fuchs *In* NASA. Marshall Space Flight Center, Aerospace Environmental Technology Conference Mar. 1995 p 369-378 (For primary document see N95-31746 11-23)
Avail: CASI HC A02/MF A06

N95-31788*# Rockwell International Corp., Canoga Park, CA. Rocketdyne Div.
ULTRASONIC FREQUENCY SELECTION FOR AQUEOUS FINE CLEANING
Joann F. Becker *In* NASA. Marshall Space Flight Center, Aerospace Environmental Technology Conference Mar. 1995 p 421-430 (For primary document see N95-31746 11-23)
Avail: CASI HC A02/MF A06

72 ATOMIC AND MOLECULAR PHYSICS

Includes atomic structure, electron properties, and molecular spectra.

N95-30367# Joint Inst. for Nuclear Research, Dubna (USSR).
DYNAMICAL ANALOGY OF CABIBBO-KOBAYASHI-MASKAWA MATRICES
Kh. M. Beshtoev 1994 6 p
(DE95-613462; JINR-E-2-94-293) Avail: CASI HC A02/MF A01 (US Sales Only)

The dynamical analogy of Cabibbo-Kobayashi-Maskawa matrices is built, i.e. the expansion of the weak interaction theory with the inclusion of three doublets of the vector bosons B(sup (+-)), C(sup (+-)), D(sup (+-)), leading to the quarks mixing is suggested. Estimation of the bosons masses is performed. The quasielastic processes proceeding through exchange of the bosons are given. DOE

N95-30372# Joint Inst. for Nuclear Research, Dubna (USSR).
THE MECHANISM OF PARTICLE PRODUCTION PROCESS IN HADRON-NUCLEON COLLISIONS
Z. Strugalski 1994 10 p
(DE95-613727; JINR-E-1-94-294) Avail: CASI HC A02/MF A01 (US Sales Only)

The mechanism of particle production process in hadron-nucleon collisions has been studied experimentally, using intranuclear detector. Particles are created via intermediate objects decaying into commonly observed resonances and particles after the lifetime more than about 10(sup 22) s. The appearance of the well-collimated spurts of particles, or jets, in the final state, and of the large transverse momenta are therefore naturally a simple and indispensable consequence of such mechanism of the particle production. DOE

N95-30388# California Univ., Berkeley. Lawrence Berkeley Lab, CA.
CURRENT ISSUES IN PERTURBATIVE QCD
I. Hinchliffe Dec. 1994 28 p Presented at the Meeting of the Division of Particles and Fields of the American Physical Society, Albuquerque, NM, 2-6 Aug. 1994
(Contract DE-AC03-76SF-00098)
(DE95-008448; LBL-36374; CONF-940816-92) Avail: CASI HC A03/MF A01

This review talk discusses some issues of active research in perturbative QCD. The following topics are discussed: (1) current value of alpha(sub s); (2) heavy quark production in hadron collisions; (3) production of Psi and Upsilon in p anti-p collisions; (4) prompt photon production; (5) small-x and related phenomena; and (6) particle multiplicity in heavy quark jets. DOE

N95-30393# Melbourne Univ., Parkville (Australia). School of Physics.
THE SEARCH FOR THE DECAY OF Z BOSON INTO TWO GAMMA AS A TEST OF BOSE STATISTICS
A. Y. Ignatiev, G. C. Joshi, and M. Matsuda (Aichi Univ. of Education, Japan.) 1994 9 p
(DE95-616373; UM-P-94/63; RCHEP-94/17) Avail: CASI HC A02/MF A01 (US Sales Only)

It is suggested that Bose statistics for photons can be tested by looking for decays of spin-1 bosons into two photons. The experimental upper limit on the decay Z (yields) (gamma)(gamma) is used to establish for the first time the quantitative measure of the validity of Bose symmetry for photons. DOE

N95-30410# Colorado Univ., Boulder, CO.
STATE RESOLVED DYNAMICS OF ION-MOLECULE COLLISIONS IN A FLOWING AFTERGLOW Final Report, 1 Nov. 1991 - 31 Oct. 1994
31 Dec. 1994 40 p
(Contract F49620-92-J-0072)
(AD-A290895; AFOSR-95-0068TR) Avail: CASI HC A03/MF A01

Flowing afterglow, flow-drift, and selected ion flow tube techniques have been coupled with laser-induced fluorescence detection to explore the chemistry and dynamics of gas phase ion-molecule interactions. The vibrational product state distributions of proton transfer and charge transfer reactions have been characterized. The competition between reaction and quenching has been probed for the interactions of vibrationally excited molecular nitrogen cation with ten neutral reagents. These reactions exhibit a rich and diverse chemistry; for example, reaction with molecular hydrogen is independent of the vibrational state of the nitrogen cation, whereas the exothermic reaction with krypton shows increasing reactivity as the excitation is systematically increased over the five lowest vibrational levels. Single frequency laser probing has been employed to characterize of the potential parameters and velocity correlations for barium cation drifted in argon, to measure the mobility of vibrationally and rotationally excited molecular ions, to intercompare mobilities measured by laser-induced fluorescence with those from standard ion shutter techniques and to probe the velocity dependence of ion alignment. DTIC

N95-30423# Melbourne Univ., Parkville (Australia). School of Physics.
MAGNETO-OPTICAL TRANSMISSION-REFLECTION BEAM SPLITTER FOR MULTI-LEVEL ATOMS
John E. Murphy, Peter Goodman, and Andrei I. Sidorov (Academy of Sciences, USSR, Moscow, USSR.) 1994 18 p
(DE95-616267; UM-P-94/60) Avail: CASI HC A03/MF A01 (US Sales Only)

An atomic de Broglie wave beam splitter is proposed. The interaction of multi-level atoms (J(g) = 1 - J(e) = 0) with a laser beam in the presence of a static magnetic field leads to the partial transmission and reflection of the atomic beam. The coherent splitting of the atomic beam occurs due to non-adiabatic transitions between different dressed states in the vicinity of avoided crossings. The transition probabilities and populations of split beams are dependent on the value of the magnetic field, laser detuning, and the ratio between different polarization components in the laser beam. For optimal conditions the population of each of the two transmitted and two reflected beams is 25%. For cooled atoms it is possible to obtain splitting angles of 80 mrad. The effect of spontaneous emission during the atom-light interaction was estimated and for a reasonable detuning losses were reduced to less than 10%. DOE

N95-30427# Melbourne Univ., Parkville (Australia).
THE FOLDY-WOUTHUYSEN TRANSFORMATION
John P. Costella and Bruce H. J. McKellar 1994 9 p Sponsored in part by the Australian Research Council, an Australian Postgraduate Research Allowance,and a Dixson Research Scholarship
(DE95-616277; UM-P-94/78; RCHEP-94/23) Avail: CASI HC A02/MF A01 (US Sales Only)

The Foldy-Wouthuysen transformation of Dirac Hamiltonian is generally taught as a mathematical trick that allows one to obtain a two-component theory in the low-energy limit. It is not often emphasized that the transformed representation is the only one in which one can take meaningful classical limit, in terms of particles and antiparticles. The history and physics of this transformation are briefly revised. DOE

N95-30429# Padua Univ. (Italy).
COMPLEX CONJUGATE PAIRS IN STATIONARY STURMIANS
P. J. Dortmans, L. Canton, G. Pisent, and K. Amos (Melbourne Univ., Parkville, Australia.) 1994 8 p
(DE95-616279; UM-P-93/112) Avail: CASI HC A02/MF A01 (US Sales Only)

Sturmian expansions enable a simply accurate separable specification of two nucleon matrices based upon realistic two nucleon interactions. Sturmian eigenstates specified by stationary scattering boundary conditions are particularly useful in that context, and they can be calculated by solving a generalized eigenvalue equation using real and symmetric matrices. In general, the spectrum of such an equation may contain complex eigenvalues. But to each complex eigenvalues there is a corresponding conjugate partner. In studies using realistic two nucleon potentials, and in certain positive energy intervals, these complex conjugated pairs indeed appear in the Sturmian spectrum. However, it is demonstrated that it is possible to recombine the complex conjugate pairs and corresponding states into a new, (and useful) pair of real eigenvalues and eigenstates with which of effect separable expansions of the (real) two nucleon reactance matrices. DOE

N95-30441# Melbourne Univ., Parkville (Australia). School of Physics.
CP VIOLATING EFFECTS IN e(+) e(-) YIELDS ZH AND THEIR OPTIMIZATION
J. P. Ma and B. H. J. McKellar 1994 12 p Sponsored in part by the Australian Research Council
(DE95-616302; UM-P-94/50; RCHEP-94/13) Avail: CASI HC A03/MF A01 (US Sales Only)

The authors consider the possibilities of testing CP conservation in the process e(+) e(-) yields ZH. The easiest is to measure the forward-backward asymmetry of the Z boson, a nonzero value of which signals CP violation. The effects of CP violation are predicted in the two Higgs doublet model. Although the number of events is not large, useful information about CP violating parameters can be extracted. DOE

N95-30442# Melbourne Univ., Parkville (Australia). School of Physics.
REAL HIGGS SINGLET AND ELECTROWEAK PHASE TRANSITION IN THE STANDARD MODEL
J. Choi and R. R. Volkas 1994 16 p
(DE95-616315; UM-P-93/80; OZ-93/20) Avail: CASI HC A03/MF A01 (US Sales Only)

The effective potential at finite temperature is constructed within the minimal standard model when a real Higgs singlet is added on. It was found that a region of parameter space exists for which one can find a first order transition strong enough to prevent the erasure due to sphalerons of baryon asymmetry, while keeping the mass of the smallest Higgs boson above the experimental lower bound of about 60 GeV. DOE

N95-30443# Melbourne Univ., Parkville (Australia). School of Physics.
EFFECTIVE LAGRANGIAN APPROACH TO THE FERMION MASS PROBLEM
D. S. Shaw and R. R. Volkas 1994 22 p
(DE95-616316; UM-P-93/81; OZ-93/21) Avail: CASI HC A03/MF A01 (US Sales Only)

An effective theory is proposed, combining the standard gauge group SU(3)(sub C) direct-product SU(2)(sub L) direct-product U(1)(sub Y) with a horizontal discrete symmetry. By assigning appropriate charges under this discrete symmetry to the various fermion fields and to (at least) two Higgs doublets, the broad spread of the fermion mass and mixing angle spectrum can be explained as a result of suppressed, non-renormalizable terms. A particular model is constructed which achieves the above while simultaneously suppressing neutral Higgs-induced flavor-changing processes. DOE

N95-30446# Melbourne Univ., Parkville (Australia). School of Physics.
PHENOMENOLOGY OF THE TWO HIGGS DOUBLET SECTOR OF A QUARK-LEPTON SYMMETRIC MODEL
C. C. Lassig and R. R. Volkas Mar. 1994 19 p
(DE95-616337; UM-P-94/21; OZ-94/8) Avail: CASI HC A03/MF A01 (US Sales Only)

In the simplest examples of models with a discrete quark-lepton symmetry, an electroweak symmetry braking sector with more than one

Higgs doublet is necessary to obtain the correct mass relations between quarks and leptons. A two Higgs doublet model version has flavor-nonconserving Yukawa couplings, which are proportional to the masses of the quark-lepton symmetric partners of the fermions. The main focus of this paper will be on flavor-changing leptonic decays, in particular those of muons since these give the most opportunity for experimental investigation. The neutral Higgs mediated decay mu(sup -) yields e(sup -) e(sup +)e(sup -) will be investigated at tree-level, as will the charged-Higgs contribution to the decay mu(sup -) yields upsilon(sub mu) e(sup -) upsilon (sup -)bar (sub e). A one-loop calculation of the process mu yields e gamma will be performed. This will lead on to an examination of the effect on the muon anomalous magnetic moment. Finally, the effect of the quark-lepton symmetric 2HDM contribution to b yields s gamma will briefly be considered. DOE

N95-30447# Melbourne Univ., Parkville (Australia). School of Physics.
DENSITY DEPENDENT EFFECTIVE INTERACTIONS
P. J. Dortmans and K. Amos 1994 21 p
(DE95-616348; UM-P-93/84) Avail: CASI HC A03/MF A01 (US Sales Only)

An effective nucleon-nucleon interaction is defined by an optimal fit to select on and half-off of the energy shell t- and g-matrices determined by solutions of the Lippmann-Schwinger and Brueckner-Bethe-Goldstone equations with the Paris nucleon-nucleon interaction as input. As such, it is seen to better reproduce the interaction on which it is based than other commonly used density dependent effective interactions. The new (medium modified) effective interaction, when folded with appropriate density matrices, has been used to define proton-(sup 12)C and proton-(sup 16)O optical potentials. With them elastic scattering data are well fit and the medium effects identifiable. DOE

N95-30465# Texas Univ., Austin, TX. Center for Particle Physics.
HADRONIC PRODUCTION OF S-WAVE AND P-WAVE CHARMED BEAUTY MESONS VIA HEAVY QUARK FRAGMENTATION
K. Cheung and Tzu Chiang Yuan (California Univ., Davis, CA.) Feb. 1995 29 p
(Contract DE-FG03-93ER-40757)
(DE95-008737; DOE/ER-40757/060; UCD-95-4) Avail: CASI HC A03/MF A01

At hadron colliders the dominant production mechanism of (bar-b c) mesons with large transverse momentum is due to parton fragmentation. The authors compute in a model-independent way the production rates and transverse momentum spectra for S-wave and P-wave (bar-b c) mesons at the Tevatron via the direct fragmentation of the bottom antiquark as well as the Altarelli-Parisi induced gluon fragmentation. Since all the radially and orbitally excited (bar-b c) mesons below the BD flavor threshold will cascade into the pseudoscalar ground state B(sub c) through electromagnetic and/or hadronic transitions, they all contribute to the inclusive production of B(sub c). The contributions of the excited S-wave and P-wave states to the inclusive production of B(sub c) are 58 and 23%, respectively, and hence significant. DOE

N95-30474# Melbourne Univ., Parkville (Australia). School of Physics.
STRUCTURAL INVESTIGATION OF XENON ION-BEAM-IRRADIATED GLASSY CARBON
D. G. McCulloch (Monash Univ., Clayton, Australia.), S. Prawer, and A. Hoffman (Technion - Israel Inst. of Tech., Haifa, Israel.) 1994 38 p
(DE95-616777; UM-P-94/52) Avail: CASI HC A03/MF A01 (US Sales Only)

Raman spectroscopy, cross-sectional transmission microscopy, and electron energy loss spectroscopy have been used to monitor the ion beam induced transformation in glassy carbon irradiated with 320 keV xenon ions to doses between 5 x 10(exp 12) and 6 x 10(exp 16) ions/cm(exp 2). It was found that the ion beam amorphizes the glassy carbon structure, the amorphization is accompanied by a compaction of the glassy carbon from an initial density of 1.55 to 2.2 +/- 0.2 g/cm(exp 3) and that approximately 15% of the graphite-like bonds in glassy carbon are converted to diamond-like bonds in the amorphization process. The transformation occurs in two distinct stages as a function of ion dose. For damage levels up to 0.2 dpa the effect of ion beam is to decrease the average graphitic crystallite size. Above 0.2 dpa, disorder in bond length and bond angle away from ideal graphitic threefold coordination occurs leading to complete amorphization at high doses. The amorphization, compaction and presence of approximative 15% sp(exp 3) bonds in the implanted layer of glassy carbon results in surface layer which is significantly more resistant to abrasion than as-grown glassy carbon. DOE

N95-30475# Melbourne Univ., Parkville (Australia). School of Physics.
INELASTIC PLASMON AND INTER-BAND ELECTRON-SCATTERING POTENTIALS FOR SI FROM DIELECTRIC MATRIX CALCULATIONS
T. W. Josefsson and A. E. Smith (Monash Univ., Clayton, Australia.) 1994 24 p
(DE95-616778; UM-P-94/55) Avail: CASI HC A03/MF A01 (US Sales Only)

Inelastic scattering of electrons in a crystalline environment may be represented by a complex non-Hermitian potential. Complete generalized expressions for this inelastic electron scattering potential matrix, including virtual inelastic scattering, are derived for outer-shell electron and plasmon excitations. The relationship between these expressions and the general anisotropic dielectric response matrix of the solid is discussed. These generalized expressions necessarily include the off-diagonal terms representing effects due to departure from translational invariance in the interaction. Results are presented for the diagonal back structure dependent inelastic and virtual inelastic scattering potentials for Si, from a calculation of the inverse dielectric matrix in the random phase approximation. Good agreement is found with experiment as a function of incident energies from 10 eV to 100 keV. Anisotropy effects and hence the interaction delocalization represented by the off-diagonal scattering potential terms are found to be significant below 1 keV. DOE

N95-30476# Melbourne Univ., Parkville (Australia). School of Physics.
THE EFFECT OF A NON-HERMITIAN CRYSTAL POTENTIAL ON THE SCATTERING MATRIX IN REFLECTION ELECTRON DIFFRACTION
A. E. Smith (Monash Univ., Clayton, Australia.) and T. W. Josefsson 1994 13 p
(DE95-616779; UM-P-94/56) Avail: CASI HC A03/MF A01 (US Sales Only)

An extension to include general inelastic scattering effects is developed for the case of reflection electron diffraction scattering from surfaces. In this extension of work by Lynch and Moodie, it is shown how the resultant non-Hermitian matrix problem can be recast in a form that is suitable for computation. In particular, a computational method is outlined based on techniques developed by Eberlein for matrix diagonalization using complex rotations and shears. The resultant methods are applied to the problem of convergent beam RHEED. DOE

N95-30484 Rutherford Appleton Lab., Oxford (England).
CONFRONTING LEFT-RIGHT SYMMETRIC MODELS WITH ELECTROWEAK PRECISION DATA AT THE Z PEAK
A. Pilaftsis Jan. 1995 26 p
(PB95-208054; RAL-95-014) Avail: Issuing Activity (National Technical Information Service (NTIS))

In view of the recent and future electroweak precision data accumulated at LEP and SLC, we systematically analyze possible new physics effects that may occur in the leptonic sector within the context of SU(2)(sub R) x SU(2)(sub L) x U(1)(sub B-L) theories. It is shown that nonobservation of flavor-violating Z-boson decays, lepton universality in the decays Z to l(l bar), and universality of lepton asymmetries at the Z peak form a set of complementary observables, yielding severe constraints on the parameter space of these theories. Contributions of new-physics effects to R(sub b) = Gamma(Z to b(b bar))/Gamma(Z to hadrons) are found to give interesting mass relations for the flavor-changing Higgs scalars present in these models. NTIS

N95-30508# Joint Inst. for Nuclear Research, Dubna (USSR).
ON EXPLANATION OF PROTON ELECTROMAGNETIC FORM FACTOR NEAR p (ANTI p)-THRESHOLD FROM THE PS-170 EXPERIMENT
V. A. Meshcheryakov and G. V. Meshcheryakov 1994 18 p In RUSSIAN
(DE95-613766; JINR-R-4-94-280) Avail: CASI HC A03/MF A01 (US Sales Only)

A review is given for studies on the data of experiment PS-170. Model-dependence of the approach based on the assumption of the existence of a quasi nuclear state in a p anti-p -system is discussed. A

previous conclusion on a low binding energy E and small width Gamma of the quasi nuclear bound state is confirmed: E equivalent to Gamma equivalent to 2 MeV. DOE

N95-30528# Joint Inst. for Nuclear Research, Dubna (USSR).
NEW TENSOR INTERACTIONS IN MICRON-DECAY
M. V. Chizhov (Sofia Univ., Bulgaria.) 1994 6 p
(DE95-613760; JINR-E-2-94-254) Avail: CASI HC A02/MF A01 (US Sales Only)

The most general form of the Hamiltonian for the muon decay is presented. We assume that it arises as a result of the exchange of intermediate bosons with a momentum q and naturally should depend on this momentum. This allows us to introduce two additional coupling constants for the tensor interactions which give rise to new parameters in the energy spectrum of positrons. The experimental consequences of such a generalization are discussed. DOE

N95-30546# Oak Ridge National Lab., TN.
SEMICONDUCTOR NANOCRYSTALS FORMED IN SiO2 BY ION IMPLANTATION
J. G. Zhu, C. W. White, J. D. Budai, S. P. Withrow, and Y. Chen Nov. 1994 8 p Presented at the 1994 Fall Meeting of the Materials Research Society (MRS), Boston, MA, 28 Nov. - 2 Dec. 1994
(Contracts DE-AC05-84OR-21400; DE-AC05-76OR-00033)
(DE95-008900; CONF-941144-98) Avail: CASI HC A02/MF A01

Nanocrystals of group 4 (Si, Ge and SiGe), 3-4 (GaAs), and 2-6 (CdSe) semiconductor materials have been fabricated inside SiO2 by ion implantation and subsequent thermal annealing. The microstructure of these nanocrystalline semiconductor materials has been studied by transmission electron microscopy (TEM). The nanocrystals form in near-spherical shape with random crystal orientations in amorphous SiO2. Extensive studies on the nanocrystal size distributions have been carried out for the Ge nanocrystals by changing the implantation doses and the annealing temperatures. Remarkable roughening of the nanocrystals occurs when the annealing temperature is raised over the melting temperature of the implanted semiconductor material. Strong red photoluminescence peaked around 1.67 eV has been achieved in samples with Si nanocrystals in SiO2. DOE

N95-30573 Pacific Northwest Lab., Richland, WA.
SCALING OF CROSS SECTIONS IN ION-ATOM COLLISIONS
R. D. DuBois Nov. 1994 12 p Presented at the 13th International Conference on the Application of Accelerators in Research and Industry, Denton, TX, 7-10 Nov. 1994 Limited Reproducibility: More than 20% of this document may be affected by microfiche quality
(Contract DE-AC06-76RL-01830)
(DE95-008938; PNL-SA-24529; CONF-941129-21) Avail: CASI HC A03

Differential electron emission at 15 deg is investigated for 50-500 keV/amu hydrogen impactingon He and H targets. From hydrogen particles (H, H(+), H2(+), H3(+)) ratios of cross sections relative to proton impact data, it is shown how bound projectile electrons influence the differential electron emission and where different ionization mechanisms are important. It is demonstrated that the H2(+) and H3(+) molecular ions interact as though they are composed of independent nuclei with the appropriate number of bound electrons, the electronic structure of the components appearing to be unimportant. DOE

N95-30574 State Univ. of New York, Binghamton, NY.
PHOTOCHEMISTRY OF INTERMOLECULAR C-H BOND ACTIVATION REACTIONS Progress Report, 15 Sep. 1994 - 15 Mar. 1995
A. J. Lees 15 Dec. 1994 5 p Limited Reproducibility: More than 20% of this document may be affected by microfiche quality
(Contract DE-FG02-89ER-14039)
(DE95-008991; DOE/ER-14039/4) Avail: CASI HC A01

Since the last progress report (March 15, 1994), attention was paid to the solution photochemistry of (HBPz*3)Rh(CO2) (Pz* = 3,5-dimethylpyrazolyl) at different excitation wavelengths and in various hydrocarbon solvents (n-pentane). Absolute quantum efficiencies were obtained for the intermolecular C-H bond activation at different wavelengths and temperatures. Results indicate that there are two excited states with different reactivities and two reaction channels. The intermediate that is highly reactive toward hydrocarbon C-H bonds is probably the monocarbonyl (HBPz*3)Rh(CO) species. Related studies are being carried out on tungsten(4) eight-coordinate-chelate complexes. DOE

N95-30579# Melbourne Univ., Parkville (Australia). School of Physics.
POSSIBLE REASON WHY LEPTONS ARE LIGHTER THAN QUARKS
R. R. Volkas 1994 9 p Sponsored in part by the Australian Research Council
(DE95-616383; UM-P-94/19; OZ-94/6) Avail: CASI HC A02/MF A01 (US Sales Only)

The minimal model of spontaneously broken leptonic color and discrete quark-lepton symmetry predicts that charged leptons have the same masses as their partner charge +2/3 quarks up to small radiative corrections. By invoking a different pattern of symmetry breaking, a similar model can be constructed with the structural feature that charged leptons have to be lighter than their partner quarks because of fermion mixing effects. As well as furnishing a new model-building tool, this is phenomenologically interesting because the scale of the new physics responsible for the quark-lepton mass hierarchy could be as low as several hundred GeV. DOE

N95-30580# Melbourne Univ., Parkville (Australia). School of Physics.
TOP QUARK AND HIGGS BOSON MASSES FROM WORMHOLE PHYSICS
B. A. Harris and G. C. Joshi 1994 29 p
(DE95-616384; UM-P-93/117) Avail: CASI HC A03/MF A01 (US Sales Only)

This paper, brings together quantum field theory on S(sub 4) with the Coleman wormhole hypothesis, which imposes constraints on terms in the gravitational Lagrangian. In particular, it investigates the effect of matter fields on the trace anomaly, which is related to the curvature terms, by the use of the renormalization group equations. A toy model of a non-conformally coupled Higgs boson to a single top quark is considered. By numerically solving the renormalization group equations for the couplings of the model, preferred values of the particle masses were found for various values of the bare non-conformal coupling. By making the ad-hoc assumption that the tree-level, Higgs boson trace anomaly, vanishes on shell, a unique prediction can be made within this model for the masses of both the Higgs and the Top. DOE

N95-30583# Melbourne Univ., Parkville (Australia). School of Physics.
INVERSION OF THE TOTAL CROSS SECTIONS FOR ELECTRON-MOLECULE AND ELECTRON-ATOM SCATTERING
D. R. Lun, K. Amos, and L. J. Allen 1994 14 p
(DE95-616466; UM-P-94/93) Avail: CASI HC A03/MF A01 (US Sales Only)

Inverse scattering theory has been applied to construct the interaction potentials from total cross sections as a function of energy for electrons scattered off of atoms and molecules. The underlying potentials are assumed to be real and energy independent and are evaluated using the Eikonal approximation and with real phase shifts determined from the total cross sections. The inversion potentials have been determined using either a high energy limit approximation or by using a fixed energy inversion method at select energies. These procedures have been used to analyse e(-) - CH4, e(-) - SiH4, e(-) - Kr and e(-) - Xe scattering data in particular. DOE

N95-30616# Louisiana State Univ., Baton Rouge, LA. Intermediate Energy Physics Group.
THE DESIGN AND CONSTRUCTION OF THE MUON ARM IN PHENIX Progress Report, 15 Dec. 1993 - 1 Dec. 1994
P. N. Kirk 15 Dec. 1994 89 p
(Contract DE-FG05-88ER-40445)
(DE95-010156; DOE/ER-40445/46) Avail: CASI HC A05/MF A01

This report describes activities performed by the Intermediate Energy Nuclear Physics Group (IENPG) at the Louisiana State University (LSU). The report covers the period of time between approximately December 15, 1993, and the present. The principal focus of the activities is the muon subgroup of the PHENIX Collaboration. During the preceding year the authors have contributed substantially to the development of hardware for the muon arm of PHENIX and have undertaken an important simulation. The authors are, however, in the process of concluding other activities, most notably their membership in the Di-Lepton Spectrometer (DLS) Collaboration at LBL. During the preceding year the authors have undertaken a major calculation on behalf of the DLS Collaboration. Because of its

fundamental nature, its importance to the DLS Collaboration, and its applicability to any other spectrometer, they discuss this calculation in considerable detail. DOE

N95-30637# International Centre for Theoretical Physics, Trieste (Italy).
ELECTROMAGNETIC-GRAVITATIONAL CONVERSION CROSS SECTIONS IN EXTERNAL ELECTROMAGNETIC FIELDS
Hoang Ngoc Long, Dang Van Soa, and Tuan A. Tran Sep. 1994 11 p
(DE95-613589; IC-94/285) Avail: CASI HC A03/MF A01 (US Sales Only)

The classical processes: the conversion of photons into gravitons in the static electromagnetic fields are considered by using Feynman perturbation techniques. The differential cross sections are presented for the conversion in the electric field of the flat condenser and the magnetic field of the solenoid. A numerical evaluation shows that the cross sections may have the observable value in the present technical scenario. DOE

N95-30639# Technische Univ., Delft (Netherlands). Interfaculty Reactor Inst.
HOLISTIC ANALYSIS OF GAMMA-RAY SPECTRA IN INSTRUMENTAL NEUTRON ACTIVATION ANALYSIS Ph.D. Thesis
M. Blaauw 15 Nov. 1993 176 p
(PB95-214458; ISBN-90-73861-16-0) Copyright Avail: CASI HC A09/MF A02

This thesis describes the scientific aspects of the analysis software written for the new automated system for INAA at IRI. Its scope is limited to the computerized analysis of gamma-ray spectra as obtained with Ge detectors in INAA with a research reactor as a source of neutrons. The analysis of gamma-ray spectra is considered to consist of reduction, standardization and interpretation. The standardization comprises the theoretical modelling of the processes occurring during activation and measurement. INAA has on many occasions proven to be a potentially accurate technique for trace element analysis because of the simplicity of the sample preparation and the physical basis of the techniques. Intercomparisons however reveal large discrepancies between the results obtained by different laboratories. Several possible causes for these discrepancies are examined and remedies looked for this work. One of the causes may be the treatment of spectral interferences (two elements contributing to the same peak in the gamma-ray spectrum). Most INAA protocols are based on activity and subsequent concentration calculations from pairs of characteristic peak areas (the 'characteristic peak method'): One peak from the gamma-ray spectrum of the sample, one from the spectrum of the comparator. Interferences may go unnoticed because the presence or absence of other peaks in the spectrum is disregarded. In the present study, an attempt is made to interpret all peaks in the spectra obtained from a sample at once. NTIS

N95-30652# International Centre for Theoretical Physics, Trieste (Italy).
PROPERTIES OF A MULTICHANNEL RESONANT-LEVEL MODEL
Yu-Mei Zhang (Tongji Univ., Shanghai, China.), Hong Chen (China Center for Advanced Science and Technology, Beijing, China.), and Xiang Wu Oct. 1994 7 p
(DE95-614482; IC-94/304) Avail: CASI HC A02/MF A01 (US Sales Only)

By use of Tomonaga-Luttinger bosonization we find that a multichannel resonant-level model can be transformed into a single-channel Kondo model with antiferro- or ferromagnetic interaction depending on the parameter gamma given in terms of the phase shifts. The specific heat and the dynamics of the local impurity have been studied which show a Fermi-liquid vs non-Fermi-liquid transition at gamma(c) = 1. DOE

N95-30654# Japan Atomic Energy Research Inst., Tokyo (Japan).
ANALYTIC CROSS SECTIONS FOR COLLISIONS OF H, H2, He AND LI ATOMS AND IONS WITH ATOMS AND MOLECULES
Rinsuke Ito (Osaka Prefecture Univ., Sakai, Japan.), Tatsuo Tabata (Osaka Prefecture Univ., Sakai, Japan.), Toshizo Shirai, and R. A. Phaneuf Jul. 1994 99 p
(DE95-722055; JAERI-Data/Code-94-005) Avail: CASI HC A05/MF A02

Analytic expressions fitted to Barnett's recommended data are given for the cross sections of excitation and spectral line emission by H, H(+), He(+), He, and He(2+) colliding with atoms and molecules. The expressions use the semiempirical functional forms proposed by Green and McNeal and some modified forms to make it possible not only to interpolate but also to extrapolate the recommended data. DOE

N95-30656# Japan Atomic Energy Research Inst., Tokyo (Japan).
MVP/GMVP: GENERAL PURPOSE MONTE CARLO CODES FOR NEUTRON AND PHOTON TRANSPORT CALCULATIONS BASED ON CONTINUOUS ENERGY AND MULTIGROUP METHODS
Takamasa Mori and Masayuki Nakagawa Aug. 1994 160 p
(DE95-722072; JAERI-Data/Code-94-007) Avail: CASI HC A08/MF A02

In order to realize fast and accurate Monte Carlo simulation of neutron and photon transport problems, new algorithms have been studied, and two fully vectorized Monte Carlo codes MVP and GMVP have been developed for FACOM VP series vector supercomputers. The former and latter codes use the continuous energy model and the multi-group model, respectively. Compared with conventional scalar codes, these codes achieve higher computation speed by a factor of 10 or more on FACOM VP-2600. Both codes have functions for production use including accurate physics model, geometry description capability and variance reduction technique. In addition to the execution on the vector supercomputers, these codes can be used on vector-parallel supercomputers with parallel calculation capability and on workstations with an OS of UNIX. For the continuous energy method, many nuclear data libraries have been prepared based on mainly JENDL 3. This report describes the physics model, geometry description method used in the codes and how to use them. DOE

N95-30666 Selskapet for Industriell og Teknisk Forskning, Trondheim (Norway). Materials Technology.
TEXTURE DEVELOPMENT IN ALUMINIUM EXTRUSION
T. Aukrust and H. E. Vatne 28 Jun. 1994 65 p
(PB95-196598; STF24-A94044) Avail: Issuing Activity (National Technical Information Service (NTIS))

In this report, a study of texture, anisotropy and constitutive relations in a metal forming process has been performed. In Norway, extruded aluminum represents a large volume of products and the crystallographical texture is an important governing factor for product properties such as surface appearance (streaks and shading), anisotropic strength and formability. Thus, to study the evolution of texture and anisotropy, extrusion of a flat profile was chosen as the metal forming process. A careful characterization of the texture has been done and the crystallographical texture as a function of the deformation history has been simulated and compared with the observed texture. NTIS

N95-30689# Melbourne Univ., Parkville (Australia). School of Physics.
INTERFEROMETRY WITH PARTICLES OF NON-ZERO REST MASS: TOPOLOGICAL EXPERIMENTS
Geoffrey I. Opat 1994 27 p
(DE95-616244; UM-P-94/09) Avail: CASI HC A03/MF A01 (US Sales Only)

Interferometry as a space-time process is described, together with its topology. Starting from this viewpoint, a convenient unified formalism for the phase shifts which arise in particle interferometry is developed. This formalism is based on a covariant form of Hamilton's action principle and Lagrange's equations of motion. It will be shown that this Lorentz invariant formalism yields a simple perturbation theoretic expression for the general phase shift that arises in matter-wave interferometry. The Lagrangian formalism is compared with the more usual formalism based on the wave propagation vector and frequency. The resulting formalism will be used to analyse the Sagnac effect, gravitational field measurements, and several Aharonov-Bohm-like topological phase shifts. Several topological interferometric experiments using particles of non-zero rest mass are discussed. These experiments involve the use of electrons, neutrons and neutral atoms. Neutron experiments will be emphasized. DOE

N95-30695 Rutherford Appleton Lab., Oxford (England).
MINIJET VETO: A TOOL FOR THE HEAVY HIGGS SEARCH AT THE LHC
V. Barger, R. J. N. Phillips, and D. Zeppenfeld Jan. 1995 23 p
Prepared in cooperation with Wisconsin Univ., Madison, WI, and DOE, Washington, DC
(Contract DE-AC02-76ER-00881)

(PB95-196234; RAL-94-120) Avail: Issuing Activity (National Technical Information Service (NTIS))

The distinct color flow of the qq yields qqH, H yields W(+)W(-) process leads to suppressed radiation of soft gluons in the central region, a feature which is not shared by major background processes like t(bar-t) production of q(bar-q) yields W(+)W(-). For the leptonic decay of a heavy Higgs boson, H yields W(+)(W-) yields l(+)(nu)l(-)(bar-nu), it is shown that these backgrounds are typically accompanied by minijet emission in the 20-40 GeV range. A central minijet veto thus constitutes a powerful background rejection tool. It may be regarded as a rapidity gap trigger at the semihard parton level which should work even at high luminosities. NTIS

N95-30705# Los Alamos National Lab., NM.
LOW-DENSITY IONIZATION BEHAVIOR
G. A. Baker, Jr. 1995 12 p Presented at the Condensed Matter Theories, Caracas, Venezuela, 12-17 Jun. 1995
(Contract W-7405-eng-36)
(DE95-009495; LA-UR-95-1082; CONF-9506170-1) Avail: CASI HC A03/MF A01

As part of a continuing study of the physics of matter under extreme conditions, we give some results on matter at extremely low density. In particular we compare a quantum mechanical calculation of the pressure for atomic hydrogen with the corresponding pressure given by Thomas-Fermi theory. (This calculation differs from the 'confined atom' approximation in a physically significant way.) Since Thomas-Fermi theory in some sense, represents the case of infinite nuclear charge, these cases should represent extremes. Comparison is also made with Saha theory, which considers ionization from a chemical point of view, but is weak on excited-state effects. In this theory, the pressure undergoes rapid variation as electron ionization levels are passed. This effect is in contrast to the smooth behavior of the Thomas-Fermi fixed temperature, complete ionization occurs in the low density limit, we study the case where the temperature goes appropriately to zero with the density. Although considerable modification is required, Saha theory is closer to the actual results for this case than is Thomas-Fermi theory. DOE

N95-30706# Sandia National Labs., Albuquerque, NM.
FORMATION OF CAVITIES IN SI AND THEIR CHEMISORPTION OF MATERIALS
D. M. Follstaedt and S. M. Myers 1994 7 p Presented at the 9th International Conference on Microscopy of Semiconducting Materials, Oxford, England, 20-23 Mar. 1995
(Contract DE-AC04-94AL-85000)
(DE95-009586; SAND-94-3247C; CONF-9503125-1) Avail: CASI HC A02/MF A01

Nanometer-size cavities formed in Si by He(+) implantation and annealing are examined with cross-section TEM. During annealing at 700 C or above, He degasses from the specimens, leaving uhv cavities with reactive Si bonds on their walls. Cavity microstructures have been characterized in detail for an implanted fluence of 1 x 10(exp 17) He/sq cm: cavity volume remains approximately constant (0.75 lattice sites/He) for anneals from 700 to approximately 1000 C, while surface area (3 to 7 times the wafer area) decreases with temperature as the cavities coarsen. The cavities are found to getter up to approximately 1 monolayer of Cu or Au from solution in Si without second-phase formation, thus identifying the trapping mechanism as chemisorption on the cavity walls. DOE

N95-30740# International Centre for Theoretical Physics, Trieste (Italy).
INTRODUCTION TO THE THEORY OF GOYAKS: OPERATOR MANIFOLD APPROACH TO GEOMETRY AND PARTICLE PHYSICS
G. T. Ter-Kazarian Sep. 1994 76 p
(DE95-613460; IC-94/290) Avail: CASI HC A05/MF A01 (US Sales Only)

The main purpose of the theory of goyaks is the generalization and the further expansion of the basic ideas of the theory of distortion of space-time continuum, in order to find out the basic deeper structures, that underlay both geometry G(223) and particles. It will be appropriate to turn to them as the primordial deeper structures. Suggested theory will address itself to the question of the origin of fundamental concepts of particle physics, such as the quarks, their spins, internal symmetries and associated with them different charges. Within its context the prime-cause of origin of mentioned above fundamental principles, especially of the most challenging ones, just such as Gauge and Color Confinement principles, will be cleared up. DOE

N95-30760# Japan Atomic Energy Research Inst., Tokyo (Japan).
NEUTRON SHIELDING POINT KERNEL INTEGRAL CALCULATION CODE FOR PERSONAL COMPUTER: PKN-pc
Hiroshi Kotegawa (Japan Atomic Energy Research Inst., Tokai, Japan.), Yukio Sakamoto (Japan Atomic Energy Research Inst., Tokai, Japan.), Yoshihiro Nakane (Japan Atomic Energy Research Inst., Tokai, Japan.), Ken-ichi Tomita, and Naohiro Kurosawa Jul. 1994 83 p In JAPANESE
(DE95-717876; JAERI-Data/Code-94-004) Avail: CASI HC A05/MF A01

A personal computer version of PKN code, PKN-pc, has been developed to calculate neutron and secondary gamma-ray 1 cm depth dose equivalents in water, ordinary concrete, and iron for neutron source. Characteristics of PKN code are to be able to calculate dose equivalents in multilayer three-dimensional system, which are described with two-dimensional surface, for monoenergetic neutron source from 0.01 to 14.9 MeV, Cf-252 fission and (sup 241)Am-Be neutron source quick and easily. In addition to these features, the PKN-pc is possible to process interactive input and to get graphical system configuration and graphical results easily. DOE

N95-30774# Technische Univ., Delft (Netherlands). Interfaculty Reactor Inst.
PHOTOPHYSICAL PROPERTIES OF OPTO-ELECTRIC MOLECULES STUDIED BY TIME-RESOLVED MICROWAVE CONDUCTIVITY Ph.D. Thesis
Wouter Schuddeboom 17 Nov. 1994 253 p
(PB95-196994; ISBN-90-73861-21-7) Avail: CASI HC A12/MF A03

In this thesis the photophysical properties of various donor-acceptor (DA) and symmetrical organic compounds were investigated using the Time-Resolved Microwave Conductivity (TRMC) technique in combination with steady-state and time-resolved fluorescence techniques. On flash-photolysis of the molecules charge separated states are formed whose properties depend on aspects such as the nature of the donor and acceptor group, the length and the nature of the bridging unit, geometrical aspects such as flexibility and rotation, orbital symmetry and the dielectric properties of the bulk medium. With the TRMC technique the changes in dielectric loss, on formation of the dipolar transients can be detected with nanosecond time-resolution, by measuring the decrease in power of X-band microwaves at the resonance frequency of a cavity. If measurements are made at the half-power resonance frequencies of the cavity, additional information can be gained on the change in dielectric constant, or molecular polarizability. NTIS

N95-30790# Melbourne Univ., Parkville (Australia). School of Physics.
ZONE AXIS BACKSCATTERED ELECTRON CONTRAST FOR FAST ELECTRONS
C. J. Rossouw (Commonwealth Scientific and Industrial Research Organization, Clayton, Australia.), P. R. Miller (Commonwealth Scientific and Industrial Research Organization, Clayton, Australia.), T. W. Josefsson, and L. J. Allen 1994 25 p
(DE95-616775; UM-P-94/34) Avail: CASI HC A03/MF A01 (US Sales Only)

A dependent Bloch wave theory for inelastic scattering is adapted to predict backscattered electron (BSE) contrast from perfect crystals. This is correlated with 300 keV data from a number of zone axes from spinal, chromia, silicon, aluminium and gallium arsenide. This theory is shown to supersede an independent Bloch wave theory for BSE contrast which is incapable of accounting for asymmetry across polar axes. Orientation dependence of thermal dechanneling of fast electrons is shown to be important. The BSE scattering potential is shown to approximate to a delta function scaled by the atomic number squared on each atom. DOE

N95-30911# Joint Inst. for Nuclear Research, Dubna (USSR).
INSTANTANEOUS CHIRAL QUARK MODEL FOR RELATIVISTIC MESONS IN A HOT AND DENSE MEDIUM
D. Blaschke (Rostock Univ., German D.R.), Yu. L. Kalinovskij (Rostock Univ., German D.R.), G. Roepke (Rostock Univ., German D.R.), S. Schmidt (Rostock Univ., German D.R.), L. Muenchow, and V. N. Pervushin 1994

27 p
(DE95-613782; JINR-E-2-94-307) Avail: CASI HC A03/MF A01 (US Sales Only)

A chiral quark model with covariant instantaneous interactions is formulated using relativistic thermodynamic Green functions. The approach is applied to the description of mesons as relativistic bound state in hot and dense quark matter. The Schwinger-Dyson equation for the quark mass operator is obtained for a covariant four-point interaction kernel. The Salpeter equations for quark-antiquark bound states in a two-component relativistic quark plasma are given in the scalar-pseudoscalar as well as vector-axial-vector channels. The case of nonvanishing total momentum of bound state relative to the medium is considered. Numerical results for the meson mass spectrum and the pion decay constant at finite temperature are presented for the special case of a separable interaction which can be applied to the case of more realistic potentials. DOE

N95-30912# Joint Inst. for Nuclear Research, Dubna (USSR).
MULTICHANNEL RESONANCES IN COUPLED CHANNELS OF MESON SCATTERING: SCALAR SECTOR
D. Krupa, V. A. Meshcheryakov, and Yu. S. Surovtsev 1994 22 p
(DE95-613783; JINR-R-2-94-243) Avail: CASI HC A03/MF A01 (US Sales Only)

The method to obtain the model-independent values of multichannel-resonance parameters is formulated for determining their QCD nature. The approach is based on the immediate application of such general principles, as analyticity and unitarity, to the analysis of experimental data on the coupled processes of particle scattering. The resonance representation by pairs of complex conjugate clusters of poles and zeros on the Riemann surfaces of the 2- and 3-channel S-matrices are discussed. The multi sheet structure of the Riemann surfaces is taken into account through the choice of proper uniformizing variables. The method permits, on the basis of the analysis on one process, to predict the remaining coupled-process amplitudes. This can be made in two manners: using the analytical continuations of S-matrix to all the unphysical sheets of the Riemann surface and the formulae of the Le Couteur-Newton type. The role of closed channels in forming the resonances is investigated in both the K- and S-matrix approaches. The method is concretized with the isoscalar s-wave channel of coupled processes pi pi yields pi pi, anti-K K, eta eta and of scalar resonances. DOE

N95-30913# Joint Inst. for Nuclear Research, Dubna (USSR).
EXPERIMENTAL RESULTS ON CHARGE EXCHANGE REACTIONS WITH DELTA EXCITATIONS AND POLARIZATION STUDIES OF DELTA AND N(SUP *) (1440) RESONANCES
E. A. Strokovsky and F. A. Gareev 1994 15 p
(DE95-614022; JINR-E-1-94-241) Avail: CASI HC A03/MF A01 (US Sales Only)

Main results of inclusive and exclusive experimental studies of (He-3, t), (t, He-3), (p, n), (p, p') reactions on protons and nuclei with Delta excitation are discussed and summarized. New possibilities for investigation of coherent pion production are discussed. We point out that experiments at various energies with different projectiles offer a possibility to separate partial contributions of mechanisms of charge-exchange reactions with excitation of broad baryonic resonances (Delta and N(sup *) (1440)) in nuclei. The importance of interference effects in this class of reactions is stressed. We discuss the (d, d') reaction on protons and nuclei, which gives a possibility to study polarization effects in reactions with resonance excitations. Such information in the Delta, Roper and overlapping region, where interference between these resonances might be essential, can help much in understanding their properties and underlying mechanisms of the reactions considered. It is particularly important for the theory of charge-exchange reactions at intermediate energies which cannot at present provide quantitative description of these reactions with nuclei. DOE

N95-30915# Joint Inst. for Nuclear Research, Dubna (USSR).
INVESTIGATION OF Fe3O4 COLLOID BEHAVIOUR IN A MAGNETIC FIELD BY POLARIZED NEUTRON TRANSMISSION
E. B. Dokukin, S. V. Kozhevnikov, Yu. V. Nikitenko, and A. V. Petrenko 1994 3 p
(DE95-614351; JINR-E-3-94-291) Avail: CASI HC A01/MF A01 (US Sales Only)

Experiments were conducted to measure the dependence of neutron polarization following their transmission through a magnetic colloid on the concentration of magnetic particles, magnetic field strength and wavelength of neutrons. In a magnetic field up to 500 Oe the precession of the neutron polarization is seen. Comparison of the experimental data and theory is made and colloid magnetization is determined. The measurement was carried out with the SPN-1 polarized neutron spectrometer at the high-flux pulsed reactor IBR-2 in Dubna. DOE

N95-30916# Melbourne Univ., Parkville (Australia). School of Physics.
K-SHELL IONIZATION UNDER ZONE AXIS ELECTRON DIFFRACTION CONDITIONS
T. W. Josefsson, L. J. Allen, P. R. Miller (Commonwealth Scientific and Industrial Research Organization, Clayton, Australia.), and C. J. Rossouw (Commonwealth Scientific and Industrial Research Organization, Clayton, Australia.) 1994 35 p
(DE95-616780; UM-P-94/57) Avail: CASI HC A03/MF A01 (US Sales Only)

A comprehensive theoretical treatment for the inelastic scattering of fast electrons in a crystalline environment is applied to account for variations in characteristic x-ray emission rates from spinel and chromia under zone axis diffraction conditions for 300 keV electrons. X-ray counts as well as backscattered electron contrast are recorded as the beam is tilted by about 70 mrad on a two-dimensional scan raster. Calculated K-shell ionization and backscattering cross sections, based on a model which takes into account interaction delocalization, thermal diffuse scattering and the consequent thickness dependent channelling effects in a realistic way, are in good agreement with experiment. DOE

N95-30952# Wisconsin Univ., Madison, WI.
ENERGY TRANSFER DYNAMICS IN ISOLATED AND COLLIDING HIGHLY VIBRATIONALLY EXCITED MOLECULES Technical Report, Nov. 1991 - Oct. 1994
F. F. Crim, M. B. Randunsky, Jon A. Booze, D. B. Govoni, and M. D. Fritz 15 Mar. 1995 30 p
(Contract F49620-92-J-0040)
(AD-A293304; AFOSR-95-0251TR) Avail: CASI HC A03/MF A01

The flow of energy in molecules, either isolated or colliding, is fundamental to complex phenomena occurring in atmospheric chemistry, combustion, molecular lasers, plasmas, and a host of other environments containing energetic species. We have developed, proven, and applied a technique that combines vibrational overtone excitation, to prepare highly vibrationally excited initial states, and time-resolved spectroscopic detection, to probe the evolution of the prepared state, for studying energy transfer in vibrationally energized molecules. Our experiments on acetylene have demonstrated the power of this approach for learning about otherwise inaccessible vibrations in electronically excited molecules, for determining the pathways of intramolecular energy transfer in isolated molecules, and for measuring fully state-resolved rotational and vibrational energy transfer rates in collisions. DTIC

N95-30970# Fermi National Accelerator Lab., Batavia, IL.
WW AND WZ PRODUCTION AT THE TEVATRON
Theresa A. Fuess (Argonne National Lab., IL.) Apr. 1995 14 p Presented at the International Symposium on Vector Boson Interactions, Los Angeles, CA, 1-3 Feb. 1995
(Contract DE-AC02-76CH-03000)
(DE95-011014; FNAL/C-95/072-E; CONF-950287-2) Avail: CASI HC A03/MF A01

Direct limits are set on WWZ and WW gamma three-boson couplings in a search for WW and WZ production in p bar-p collisions at square root of s = 1.8 TeV using the D0 and CDF detectors at the Fermilab Tevatron. DOE

N95-31003# International Centre for Theoretical Physics, Trieste (Italy).
INNER- AND OUTER-SHELL EXCITATION IN LITHIUM ISOELECTRONIC SEQUENCE
S. N. Tiwary and P. Kumar (Langat Singh Coll., Muzaffarpur, India.) Sep. 1994 13 p
(DE95-614107; IC-94/295) Avail: CASI HC A03/MF A01 (US Sales Only)

The inner-shell excitation 1s(sup 2)2s(sup 2)S(sup e) yields 1s2s(sup 2)(sup 2)S(sup e), which leads to autoionization (Auger transition), as well as

the outer-shell excitation 1s(sup 2)2s (sup 2)S(sup e) yields 1s(sup 2)2p (sup 2)P(sup 0) transitions have been investigated in Li, Be(+), B(2+) and C(3+) ions of the lithium isoelectronic sequence employing the configuration interaction wave functions for both the initial and final states involved in the transition matrix element. Results are compared with other available theoretical predictions and experimental observations. Comparison shows that our present theoretical results are encouraging. DOE

N95-31060# International Centre for Theoretical Physics, Trieste (Italy).
SIGNATURES OF VIRTUAL LSP'S AT THE TEVATRON
A. Datta, S. Chakravarti (Maharaja Manindra Chandra Coll., Calcutta, India.), and M. Guchait (Jadavpur Univ., Calcutta, India.) Oct. 1994 9 p
(DE95-613798; IC-94/303; HEPPH-9410331) Avail: CASI HC A02/MF A01 (US Sales Only)

Relatively light sneutrinos which are experimentally allowed and are not theoretically disfavored may significantly affect the currently popular search strategies for supersymmetric particles by decaying dominantly into an invisible channel. In certain cases the second lightest neutralino may also decay invisibly leading to two extra carriers of missing energy (in addition to the lightest supersymmetric particle (LSP)) - the virtual LSP's (VLSP's). The lighter charginos which would be produced in pairs with reasonably large cross-sections at TEVATRON energies, decay dominantly into the hadronically quiet lepton + sneutrino (E(sub T)) modes with large branching ratios leading to interesting unlike sign dilepton events which are not swamped by the standard model background. The kinematical cuts required to eliminate the backgrounds from WW, Drell-Yan and (tau) pair production are discussed in detail. With 100 pb(sup -1) luminosity 10-35 background free events can be found in a large region of the SUSY parameter space. DOE

N95-31104# Oak Ridge National Lab., TN.
MOLECULAR DYNAMICS SIMULATIONS OF HIGH ENERGY CASCADES IN IRON
R. E. Stoller 1994 6 p Presented at the 1994 Fall Meeting of the Materials Research Society (MRS), Boston, MA, 28 Nov. - 2 Dec. 1994
(Contract DE-AC05-84OR-21400)
(DE95-010116; CONF-941144-129) Avail: CASI HC A02/MF A01

A series of high-energy, up to 20 keV, displacement cascades in iron have been investigated for times up to 200 ps at 100 K using the method of molecular dynamics simulation. The simulations were carried out using the MOLDY code and a modified version of the many-body interatomic potential developed by Finnis and Sinclair. The paper focuses on those results obtained at the highest energies, 10 and 20 keV. The results indicate that the fraction of the Frenkel pairs surviving in-cascade recombination remains fairly high in iron and that the fraction of the surviving point defects that cluster is lower than in materials such as copper. In particular, vacancy clustering appears to be inhibited in iron. Some of the interstitial clusters were observed to exhibit an unexpectedly complex, three-dimensional morphology. The observations are discussed in terms of their relevance to microstructural evolution and mechanical property changes in irradiated iron-based alloys. DOE

N95-31168# International Centre for Theoretical Physics, Trieste (Italy).
EFFECTIVE CHIRAL-SPIN HAMILTONIAN FOR ODD-NUMBERED COUPLED HEISENBERG CHAINS
V. Subrahmanyam Sep. 1994 8 p
(DE95-614445; IC-94/288) Avail: CASI HC A02/MF A01 (US Sales Only)

An L x infinity system of odd number of coupled Heisenberg spin chains is studied using a degenerate perturbation theory, where L is the number of coupled chains. An effective chain Hamiltonian is derived explicitly in terms of two spin half degrees of freedom of a closed chain of L sites, valid in the regime the inter-chain coupling is stronger than the intra-chain coupling. The spin gap has been calculated numerically using the effective Hamiltonian for L = 3,5,7,9 for a finite chain up to ten sites. It is suggested that the ground state of the effective Hamiltonian is correlated, by examining various variational trial states for the effective-spin chain Hamiltonian. DOE

N95-31174# Lawrence Livermore National Lab., Livermore, CA.
EXPERIMENTS WITH HIGHLY CHARGED IONS UP TO BARE U(SUP 92+) ON THE ELECTRON BEAM ION TRAP
P. Beiersdorfer Jul. 1994 25 p Presented at the 14th International Conference on Atomic Physics, Boulder, CO, 31 Jul. - 5 Aug. 1994
(Contract W-7405-eng-48)
(DE95-008827; UCRL-JC-118297; CONF-940707-1) Avail: CASI HC A03/MF A01

An overview is given of the current experimental effort to investigate the level structure of highly charged ions with the Livermore electron beam ion trap (EBIT) facility. The facility allows the production and study of virtually any ionization state of any element up to bare U(sup 92+). Precision spectroscopic measurements have been performed for a range of (Delta)n = 0 and (Delta)n = 1 transitions. Examples involving 3-4 and 2-3 as well as 3-3 and 2-2 transitions in uranium ions are discussed that illustrated some of the measurement and analysis techniques employed. The measurements have allowed tests of calculations of the the quantum electrodynamical contributions to the transitions energies at the 0.4 percent level in a regime where (Z(alpha)) (approx) 1. DOE

N95-31176# Melbourne Univ., Parkville (Australia). School of Physics.
COULOMB CORRECTION CALCULATIONS OF pp BREMSSTRAHLUNG
A. Katsogiannis, K. Amos, M. Jetter (Hamburg Univ., Germany.), and H. V. vonGeramb (Hamburg Univ., Germany.) 1994 38 p
(DE95-616349; UM-P-93/88) Avail: CASI HC A03/MF A01 (US Sales Only)

The effects of the Coulomb interaction upon the photon cross section and analyzing power from pp Bremsstrahlung have been studied in detail. Off-shell properties of the Coulomb T matrices have been considered but the associated, Coulomb modified, hadronic T matrices are important elements in any analyses of low energy, forward proton scattering data. At the lowest energy considered (5 MeV), the full calculations gave cross sections that were half the size of those found without Coulomb effects or with a simple model approximation to them. With increasing energy, the cross sections varied to those characteristic of magnetic interaction dominance and the specific differences due to Coulomb effects diminished. DOE

N95-31178# Tokyo Univ., Tanashi (Japan). Inst. for Nuclear Study.
THE 10TH INS SCIENTIFIC COMPUTATIONAL PROGRAMS
Jun. 1994 57 p In JAPANESE Programs held in Japan, 1 Jun. 1993 - 30 Mar. 1994
(DE95-717864; INS-T-528) Avail: CASI HC A04/MF A01 (US Sales Only)

Nine groups were accepted as the 10-th INS Scientific Computational Programs (ISCP). This ISCP can use full resources of the INS central computer without an operational limitation. The 10-th ISCP started 1 Jun. 1993 and ended 30 Mar. 1994. Some results were already published in journals or appeared in physical meetings. This is a sum of the used statistics of the 10-th ISCP and reports presented by groups performed the 10-th ISCP. DOE

N95-31214# Gosudarstvennyi Komitet po Ispolzovaniyu Atomnoi Energii, Serpukhov (USSR). Inst. for High Energy Physics.
TESTING VECTOR BOSON DOMINANCE OF ELECTROWEAK INTERACTIONS VIA e(+)e(-) (YIELDS) f-BAR f
V. V. Kabachenko (Moscow Inst. of Physics and Technology, Moscow, Russia.) and Y. F. Pirogov 1994 21 p Submitted for publication in Int. J. Mat. Phys.
(DE95-620528; IHEP-94-52) Avail: CASI HC A03/MF A01 (US Sales Only)

In the framework of the Vector Boson Dominance (VBD) of electroweak interactions for composite leptons, quarks and Higgs bosons, restrictions on the universal four-fermion contact interactions are investigated. Manifestations of the VBD via these interactions at the 2 TeV e(+)e(-) linear collider are studied. Definite signatures of the VBD are exposed. It is shown that the VBD could be tested at the collider for the unified substructure scale up to O(50 TeV), which lies well in naturally preferred Deca-TeV region. DOE

N95-31215# Gosudarstvennyi Komitet po Ispolzovaniyu Atomnoi Energii, Serpukhov (USSR). Inst. for High Energy Physics.
PERIOD DOUBLING DYNAMICS IN HADRON PHYSICS: EXACT CALCULATIONS

A. V. Batunin 1994 11 p
(DE95-620535; IHEP-94-20) Avail: CASI HC A03/MF A01 (US Sales Only)

Some characteristics of the limit 2(sup m)-cycles and Feigenbaum attractor and their agreement with corresponding (in the framework of a bifurcation model) experimental values are obtained. DOE

N95-31216# Gosudarstvennyi Komitet po Ispolzovaniyu Atomnoi Energii, Serpukhov (USSR). Inst. for High Energy Physics.
HADRONIC PRODUCTION OF B(SUB c)-MESONS
A. V. Berezhnoj, M. V. Shevlyagin, and A. K. Likhoded 1994 23 p Submitted for publication in Yad. Fiz.
(DE95-620536; IHEP-94-48) Avail: CASI HC A03/MF A01 (US Sales Only)

On the basis of the exact formulas of QCD perturbation theory and parton model the hadronic production cross-sections for B(sub c)(B(sub c)(sup *))-mesons (1(sup 1)S(sub 0), 1(sup 3)S(sub 1), 2(sup 1)S(sub 0), 2(sup 3)S(sub 1)-states) are calculated. The method used is the direct calculation of appropriate amplitudes with the help of a FORTRAN program and subsequent Monte-Carlo integration over the phase space and convolution with the structure functions. DOE

N95-31217# Gosudarstvennyi Komitet po Ispolzovaniyu Atomnoi Energii, Serpukhov (USSR). Inst. for High Energy Physics.
B(SUB c)-MESON PRODUCTION IN HADRON-HADRON COLLISIONS
S. R. Slabospitskij 1994 21 p Submitted for publication in Phys. Rev. D.
(DE95-620537; IHEP-94-53) Avail: CASI HC A03/MF A01 (US Sales Only)

The B(sub c)-meson production cross section was calculated in the perturbative QCD. Various distributions of the charged leptons from the B(sub c) (yields) l(nu)J/(psi)((yields)l(sup +)l(sup -)) decay were obtained. The B(sub c)-meson mass measurement from such decays is also discussed. DOE

N95-31218# Gosudarstvennyi Komitet po Ispolzovaniyu Atomnoi Energii, Serpukhov (USSR). Inst. for High Energy Physics.
SCALING BEHAVIOUR OF LEPTONIC DECAY CONSTANTS FOR HEAVY QUARKONIA AND HEAVY MESONS
V. V. Kiselev 1994 15 p
(DE95-620539; IHEP-94-63) Avail: CASI HC A03/MF A01 (US Sales Only)

In the framework of QCD sum rules one uses a scheme, allowing one to apply the conditions of both nonrelativistic heavy quark motion inside mesons and the heavy quark flavour independence of nonsplitting nS-state density. In the leading order an analytic expression is derived for leptonic constants of both heavy quarkonia and heavy mesons with a single heavy quark. The expression allows one explicitly to determine scaling properties of the constants. DOE

N95-31219# Gosudarstvennyi Komitet po Ispolzovaniyu Atomnoi Energii, Serpukhov (USSR). Inst. for High Energy Physics.
DOUBLE CHARMED BARYONS PRODUCTION AT B-FACTORY
V. V. Kiselev, A. K. Likhoded, and M. V. Shevlyagin 1994 6 p
(DE95-620540; IHEP-94-56) Avail: CASI HC A02/MF A01 (US Sales Only)

The cross-section for the double charmed baryon production at a B-factory is estimated on the basis of the perturbative QCD calculations as well as of the quark-hadron duality for the cc-diquark production. DOE

N95-31223# Tokyo Univ., Tanashi (Japan). Inst. for Nuclear Study.
PION-PAIR PRODUCTION BY TWO PHOTONS
Hidezumi Terazawa Jul. 1994 12 p
(DE95-737162; INS-1045) Avail: CASI HC A03/MF A01

The cross section for pion-pair production by two photons is calculated approximately by using the low energy theorem previously derived from partially-conserved-axial-vector-current hypothesis and current algebra, and found to agree very well with the experimental data recently obtained by the Mark 2, TPC/Two-Gamma and CLEO Collaborations. DOE

N95-31224# Tokyo Univ., Tanashi (Japan). Inst. for Nuclear Study.
QUANTIZATION OF A RELATIVISTIC PARTICLE ON THE SL(2,R) MANIFOLD BASED ON HAMILTONIAN REDUCTION
G. Jorjadze (Tbilisi State Univ., USSR.), L. ORaifeartaigh (Dublin Inst. for Advanced Studies, Ireland.), and I. Tsutsui Jul. 1994 13 p
(DE95-737163; INS-1042; DIAS-STP-94-22) Avail: CASI HC A03/MF A01

A quantum theory is constructed for the system of a relativistic particle with mass m moving freely on the SL(2,R) group manifold. Applied to the cotangent bundle of SL(2,R), the method of Hamiltonian reduction allows us to split the reduced system into two coadjoint orbits of the group. We find that the Hilbert space consists of states given by the discrete series of the unitary irreducible representations of SL(2,R), and with a positive-definite, discrete spectrum. DOE

N95-31225# Tokyo Univ., Tanashi (Japan). Inst. for Nuclear Study.
THE TOPOLOGICAL STRING ASSOCIATED WITH A SIMPLE SINGULARITY OF TYPE D
Toshio Nakatsu Aug. 1994 15 p
(DE95-737229; INS-1047) Avail: CASI HC A03/MF A01

The partition function of D(sub N+1) topological string, the coupled system of topological gravity and D(sub N+1) topological minimal matter, is proposed in the framework of KP hierarchy. It is specified by the elements of GL((infinity)) which constitute the deformed family from the A(sub 2N-1) topological string. Its dispersionless limit is investigated from the view of both dispersionless KP hierarchy and singularity theory. In particular the free energy restricted on the small phase space coincides with that for the topological Landau-Ginzburg model of type D(sub N+1). DOE

N95-31227# Tokyo Univ., Tanashi (Japan). Inst. for Nuclear Study.
PION-NUCLEON AND KAON-NUCLEON SCATTERING LENGTHS IN QCD SUM RULES
Y. Kondo, O. Morimatsu, and Y. Nishino (Osaka Univ., Ibaraki, Japan.) Sep. 1994 15 p
(DE95-737278; INS-1059) Avail: CASI HC A03/MF A01

The pion-nucleon and kaon-nucleon scattering lengths are studied in the QCD sum rule. We show that the leading and next-to-leading order terms of OPE give rise to the Tomozawa-Weinberg and sigma terms, respectively. We also show that in the kaon-nucleon system the (Lambda)(1405) contribution has to be subtracted from the OPE side in order to obtain the scattering length. The odd components of the T-matrices are in agreement with the experimental values not only in the pion-nucleon channel but also in the kaon-nucleon channel after the (Lambda)(1405) contribution subtracted. The even components disagree with the experimental values in the pion-nucleon channel, which is similar to the situation in the PCAC-plus-current-algebra approach at the Weinberg point. We speculate that this discrepancy should be explained by the continuum contribution in the spectral function above the pion-nucleon threshold. DOE

N95-31260# Gosudarstvennyi Komitet po Ispolzovaniyu Atomnoi Energii, Leningrad (USSR).
STUDY OF DIFFERENT TYPE NEUTRINO OSCILLATIONS BASED ON NEUTRINO BEAMS FROM 600 GeV
A. S. Arefev and L. B. Bezrukov (Academy of Sciences, USSR, Moscow, USSR.) 1994 24 p
(DE95-619267; IFVE-ONF-94-36) Avail: CASI HC A03/MF A01 (US Sales Only)

The problems of the different type neutrino oscillations based on a wide-band and narrow-band neutrino beam from the 600 GeV UNK-1 machine using the Baical Neutrino Telescope (4200 km from a accelerator) are discussed. The main parameters of the neutrino channel are presented. DOE

N95-31261# Gosudarstvennyi Komitet po Ispolzovaniyu Atomnoi Energii, Leningrad (USSR).
ON POSSIBILITY TO STUDY NEUTRINO OSCILLATIONS BY DETECTORS LOCATED AT GRAN SASSO (ITALY) USING BEAMS FROM 600 GeV UNK-1 MACHINE
Yu. S. Fedotov, V. I. Garkusha, and S. S. Gershctejn 1994 8 p
(DE95-619268; IHEP-94-34) Avail: CASI HC A02/MF A01 (US Sales Only)

The paper presents the results of a preliminary consideration of the

possibility to form beams from the 600 GeV UNK-1 machine toward Gran Sasso (Italy) laboratory as well as to study neutrino oscillations using the ICARUS facility. Depending on the experiment conditions the expected range for the study of the oscillation parameters is Delta m(exp 2) up to 10(exp -3) eV(exp 2) under complete mixing and sin(exp 2)(2 theta) up to 6x10(exp -3) at Delta m(sup 2) approx. 2x10(exp -2) eV(exp 2). DOE

N95-31378# Gosudarstvennyi Komitet po Ispolzovaniyu Atomnoi Energii, Serpukhov (USSR). Inst. for High Energy Physics.
DO THE NARROW CRYPTOEXOTIC BARYON RESONANCES EXIST?
L. G. Landsberg 1993 11 p
(DE95-619291; IHEP-93-149) Avail: CASI HC A03/MF A01 (US Sales Only)

The possibility of the existence of the cryptoexotic baryons with hidden charm and with mass, smaller than approximately 4 GeV, is discussed. Only OZI suppressed baryon decays can occur in this case. These baryons would have anomalously narrow decay widths. Possible production and decay mechanism for exotic baryons of this kind are considered as well as the perspectives of their experimental searches. DOE

N95-31402# Oak Ridge National Lab., TN.
CONVOY ELECTRON EMISSION FROM SURFACES
Carlos O. Reinhold, Joachim Burgdoerfer (Tennessee Univ., Knoxville, TN.), Kenji Kimura, and Michihiko Mannami (Kyoto Univ., Japan.) 1994 14 p Presented at the 13th International Conference on the Application of Accelerators in Research and Industry, Denton, TX, 7-10 Nov. 1994 Sponsored in part by NSF and the Japan-US Cooperative Scientific Program
(Contract DE-AC05-84OR-21400)
(DE95-010298; CONF-941129-23) Avail: CASI HC A03/MF A01

The authors present results of a microscopic simulation of fast electron emission in glancing-angle ion-surface collisions. The model accounts for both dynamic image interactions and multiple scattering near the surface and predicts a pronounced convoy electron peak for small emission angles. Good agreement is found with their recent coincidence experiments for 0.2-0.5 MeV/u Li ions interacting with SnTe(001) surfaces. They find that convoy electrons principally originate from target core states and are emitted while the ion is in very close proximity to the topmost layer of target atoms. Because of the rapid charge changing cycle that the ions undergo during emission, almost no correlation is found between the convoy peak position and the final charge state of the ions. DOE

N95-31427# North Carolina Univ., Chapel Hill, NC. Dept. of Chemistry.
ELECTRON TRANSFER KINETICS OF SELF-ASSEMBLED FERROCENE C(12) ALKANETHIOL MONOLAYERS ON GOLD ELECTRODES FROM 125K TO 175K Interim Report
John N. Richardson, Gary K. Rowe, Michael T. Carter, Leonard M. Tender, and Larry S. Curtin 23 Mar. 1995 34 p
(Contract N00014-90-J-11230)
(AD-A292754; TR-63) Avail: CASI HC A03/MF A01

The electron transfer kinetics of monolayers of CpFeCpCO2(CH2)12SH and CH3(Ch2)11SH co-chemisorbed on gold electrodes have been measured in 2:1 (v:v) chloroethane/butyronitrile solvent at temperatures ranging from 125K to 175K with potential steps and cyclic voltammetry. Rate constants, k deg, measured using cyclic voltammetry range from 3 x 10(exp -4) to 10(exp -1)/s over these temperatures; an activation plot of log K DEG/K(SUB BETA)T(1/2) vs. 1/T gave Lambda= 0.89 eV for the reorganization energy for the Cp2Fe(+/0) reaction and a pre-factor of 6.5 x 10(exp 6) eV(-1)/s. The rate constants were obtained by comparison of experimental delta E PEAK values with those of cyclic voltammograms digitally simulated with Marcus-DOS theory. A value of Lambda = 0.76 eV is predicted from dielectric continuum theory. The CpFeCpCO2(CH2)12SH monolayers are kinetically inhomogeneous (disperse) as shown by nonlinear 1nl vs. time plots in potential step experiments. The kinetic dispersity has adverse effects on determinations of Lambda values from cyclic voltammetric waveshapes and from plots of potential step-derived rate constants, k(sub app,tau), against overpotential (eta), producing depressed values for Lambda. DTIC

N95-31546# International Centre for Theoretical Physics, Trieste (Italy).
STRUCTURE FORMATION WITH MAJORON SUPERMULTIPLET
E. J. Chun Oct. 1994 8 p
(DE95-613596; IC-94/306) Avail: CASI HC A02/MF A01 (US Sales Only)

We show that the late-decaying particle scenario may be realized in the supersymmetric singlet majoron model with the majoron scale 10-200 TeV. The majoron decaying into two neutrinos is the late-decaying particle with the mass 0.1 - 1 TeV and the life-time 2 x 10(exp 3) - 8 x 10(exp 4) seconds. The lower limit of the majorino mass is 4 - 40 TeV in order to avoid the overclosure of the universe due to the decay-produced LSP. The muon neutrino and the tau neutrino can be used to explain the atmospheric and the solar neutrino deficit. DOE

N95-31547# International Centre for Theoretical Physics, Trieste (Italy).
SEARCH FOR NEW PHYSICS INDIRECT EFFECTS IN e(+)e(-) YIELDS W(+)W(-) AT LINEAR COLLIDERS WITH POLARIZED BEAMS
A. A. Babich, A. A. Pankov, and N. Paver (Trieste Univ., Italy.) Oct. 1994 19 p
(DE95-613688; IC-94/327; UTS-DFT-94-15) Avail: CASI HC A03/MF A01 (US Sales Only)

We discuss the potential of a 0.5-TeV linear collider to explore manifestations of extended (or alternative) electroweak models of current interest, through measurements of the reaction e(+)e(-) yields W(+)W(-) with both initial and final states polarization. Specifically, we consider the possibility to put stringent constraints on lepton mixing (or extended lepton couplings) and Z - Z' mixing, showing in particular the usefulness of polarization in order to disentangle these effects. DOE

N95-31548# International Centre for Theoretical Physics, Trieste (Italy).
UNITARIZATION OF KOERNER-KURODA MODEL OF ELECTROMAGNETIC STRUCTURE OF OCTET 1/2(+) BARYONS
S. Dubnicka, A. Z. Dubnickova (Comenius Univ., Bratislava, Czechoslovakia.), J. Kraskiewicz (International School for Advanced Studies, Trieste, Italy.), and R. Raczka (International School for Advanced Studies, Trieste, Italy.) Oct. 1994 23 p
(DE95-613765; IC-94/333) Avail: CASI HC A03/MF A01 (US Sales Only)

The Koerner-Kuroda model of the electromagnetic structure of octet 1/2(+) baryons is restored on a more topical physical basis. Electromagnetic radii of baryons under consideration are calculated and compared with other model predictions. By an incorporation of a two-cut approximation of correct form factor analytic properties and nonzero vector-meson widths, the Koerner-Kuroda model is unitarized, providing in this manner imaginary parts of the octet 1/2(+) baryon form factors to be nonzero just starting from a branch point corresponding to the lowest threshold. DOE

N95-31549# Gosudarstvennyi Komitet po Ispolzovaniyu Atomnoi Energii, Serpukhov (USSR).
SEARCH FOR EXOTIC BARYONS WITH THE SPHINX FACILITY
L. G. Landsberg 1993 12 p
(DE95-613774; IHEP-93-100; IFVE-93-100) Avail: CASI HC A03/MF A01

In the experiments at the SPHINX facility in the proton beam of the IHEP accelerator (E(sub p) = 70 GeV) a number of diffractive production reactions were studied. Among them are p + N yields (K(+)K(-)p) + N; p + N yields (phi p) + N; p + N yields (Lambda(1520)K(+)) + N; p + N yields (Sigma(1385)(sup 0)K(+)) + N, as well as some other processes. The results of the search for narrow heavy baryon states, candidates for the cryptoexotic hadrons with hidden strangeness, are presented. DOE

N95-31550# Academy of Sciences (USSR), Novosibirsk (USSR). Inst. Yadernoj Fiziki.
REMOVAL OF IMPURITY IONS FROM A MAGNETIC TRAP WITH A TWO-COMPONENT PLASMA ON THEIR COLLISION WITH FAST COMPONENT IONS
Yu. A. Tsidulko 1993 21 p
(DE95-614171; IYaF-93-44) Avail: CASI HC A03/MF A01 (US Sales Only)

It is shown that at the sufficient energy and intensity of fast particle injection in a gas-dynamic trap the collisions of the particles with impurity ions prevent storage of the impurity ions, which is connected with availability of potential barriers in the points of fast ion stops. Formulae for the

cleaning rate and efficiency are obtained. Results of calculations for a concrete variant of trap parameters are presented. DOE

N95-31597# Naval Postgraduate School, Monterey, CA.
EFFECTS OF MOSAICITY ON PARAMETRIC X-RADIATION PRODUCTION M.S. Thesis
William M. Buckingham and Lisa R. Ivey Dec. 1994 88 p
(AD-A293677) Avail: CASI HC A05/MF A01

Previous measurements of parametric x-radiation (PXR) spectra from mosaic graphite observed yields that greatly exceeded theoretical predictions. At the Bragg scattering condition, the interaction of relativistically charged particles and the atomic planes of a crystal produces scattering of virtual photons. This is known as PXR. The discrepancies between actual yields and theoretical predictions might possibly have been caused by the mosaic spread of the atomic planes of the crystal. Re-analysis of previous data has shown a miscalculation of the effective target thickness used in earlier work. There was also an error in the calculation of the theory that was used for comparison. Correction of the two errors brought the data and theory in closer agreement, but the mosaic spread does change the intensity of the PXR. In this thesis, three samples of thick mosaic carbon graphite crystal with differing mosaic spreads are compared to determine the effect of the mosaicity on PXR yield. By obtaining 'rocking curves' where the target orientation angle is changed with respect to the incident electron beam and observation angle, it was found that the mosaic spread does have an effect on the PXR spectral distribution. This effect is quite significant and can be seen when viewing the 'rocking curves' of the samples. As the mosaicity is increased, the angular distribution was spread out and the coherence condition was relaxed. DTIC

N95-31609# Florida Univ., Gainesville, FL. Quantum Theory Project.
ELECTRONIC STRUCTURE OF DONOR-SPACER-ACCEPTOR MOLECULES OF POTENTIAL INTEREST FOR MOLECULAR ELECTRONICS III: GEOMETRY AND ABSORPTION SPECTRUM OF CH3-ALPHA P3CNQ
Anders Broo and Michael C. Zerner 18 Apr. 1995 30 p
(Contract N00014-90-J-1608)
(AD-A293662; TR-26) Avail: CASI HC A03/MF A01

The geometry of Z-Beta-(1-methyl-2-pyridinium) - alpha-cyano-4-styryldicyanomethanide was optimized using semi-empirical and ab initio quantum chemical methods. The predicted geometries using a one determinant description do not compare well with the observed geometry. A better description of the geometry is obtained with a multi-determinant approach. Good agreement with experiment is obtained only when consideration of the media is taken into account. Absorption spectra in the solid state and in solution were calculated and the results compare very well with the experimental spectra. The solvatochromic shift of the absorption spectrum was calculated using a self-consistent reaction field approach. We also discuss the question of whether the title molecule is best described as a zwitterion. DTIC

N95-31616# Argonne National Lab., IL. Intense Pulsed Neutron Source Div.
IPNS NEUTRON SCATTERING INSTRUMENTATION. A: EXISTING AND PLANNED. B: POSSIBILITIES FOR IPNS UPGRADE, A 1-MW SPALLATION SOURCE
Bruce Brown and Kent Crawford 1994 12 p Presented at the 1994 Fall Meeting of the Materials Research Society (MRS), Boston, MA, 28 Nov. - 2 Dec. 1994
(Contract W-31-109-eng-38)
(DE95-004119; ANL/IPNS/CP-84859) Avail: CASI HC A03/MF A01

The Intense Pulsed Neutron Source (IPNS) is a pulsed spallation neutron source located at Argonne National laboratory near Chicago, Illinois in the US. This facility is the outgrowth of a long line of pioneering work on pulsed spallation neutron sources begun at Argonne in the early 1970s. IPNS uses protons accelerated in the Rapid Cycling Synchrotron to produce neutron via the spallation process (effectively a nuclear evaporation in which 10-50 neutrons are released per incident proton) in heavy element target. These neutrons are then moderated to produce spectra peaked at thermal or subthermal energies, and directed into beam which serve a variety of instruments. This paper discusses the diffractometers, various spectrometers, and reflectometers in existence and those planned for the upgrade of the IPNS. DOE

N95-31620# Joint Inst. for Nuclear Research, Dubna (USSR).
INSTABILITY OF WEAK VACUUM
G. A. Kozlov 1994 11 p
(DE95-613590; JINR-E-2-94-303) Avail: CASI HC A03/MF A01 (US Sales Only)

We study the characteristic features of a hypothetical candidate for new scalar field chi. The mass constraint under which such a chi-boson occurs is presented. The instability of weak vacuum is investigated. By considering the approximate breaking symmetry, we find that the mass m(sub chi) less than 15 GeV of the chi-particle is unnatural. In the case of heavy top quark mass, m(sub top) approx. 170 GeV (the recent CDF collaboration has reported m(sub top, sup exp) = 174 +/- 16 GeV), we have carried out that the physically acceptable chi-boson upper bound will not exceed the 1 TeV level. For certain values of m(sub top) and m(sub chi), the one-loop approximation consideration leads to the fact that the physical (our) vacuum cannot be absolutely stable. DOE

N95-31621# Joint Inst. for Nuclear Research, Dubna (USSR).
ELECTROMAGNETIC HADRON MASS DIFFERENCES AND ESTIMATION OF ISOTOPIC SYMMETRY VIOLATION PARAMETERS OF QCD VACUUM FROM QUARK MODEL
A. E. Dorokhov 1994 15 p
(DE95-613628; JINR-E-2-94-231) Avail: CASI HC A03/MF A01 (US Sales Only)

The estimations of the light quark mass differences, m(sub d) - m(sub u), and the light quark condensate differences, (D(bar-D))- (U(bar-U)), are obtained in the framework of the quark model with QCD vacuum induced quark interaction. We consider long-wave condensate and short wave instanton contributions to the electromagnetic hadron mass differences and show that the latter significantly improve the results on baryon octet. The results are: m(sub d) - m(sub u) approx. equal to 3.5 MeV and (D(bar-D)) - (U(bar-U)) approx. equal to -(0 approx. 3) (centerdot)10(exp -3) (U(bar-U)). DOE

N95-31622# Joint Inst. for Nuclear Research, Dubna (USSR).
RENORMCHARGES IN V-A THEORIES
Kh. M. Beshtoev 1994 6 p
(DE95-613689; JINR-E-2-94-221) Avail: CASI HC A02/MF A01 (US Sales Only)

It is shown that in the theory of weak interaction there may not exist any group of the renormtransformation of charge (i.e., the charge-g(sub L) remains constant) because this theory can be characterized as a 'left' one, or if such a group exists it is then realized for the charge g(sub L), and it is not related to the charge g in the vector theory. In connection with the above said there arises a problem of relating the charges g(sub L) and g when constructing the unified theory of interaction. DOE

N95-31642# Oak Ridge National Lab., TN.
AMORPHIZATION AND THE EFFECT OF IMPLANTED IONS IN SiC
L. L. Snead and S. J. Zinkle 1994 7 p Presented at the 1994 Fall Meeting of the Materials Research Society (MRS), Boston, MA, 28 Nov. - 2 Dec. 1994
(Contract DE-AC05-84OR-21400)
(DE95-009699; CONF-941144-139) Avail: CASI HC A02/MF A01

The effects of implanted ion chemistry and displacement damage on the amorphization threshold dose of SiC were studied using cross-section transmission electron microscopy. Room temperature as well as 200 and 400 C irradiations were carried out with 3.6 MeV Fe, 1.8 MeV Cl, 1 MeV He or 0.56 MeV Si ions. The room temperature amorphization threshold dose in irradiated regions well separated from the implanted ions was found to range from 0.3 to 0.5 dpa for the four different ion species. The threshold dose for amorphization in the He, Si and Fe ion-implanted regions was also (approximately)0.3 to 0.5 dpa. On the other hand, the amorphization threshold in the Cl-implanted region was only about 0.1 dpa. The volume change associated with amorphization was (approximately)17%. No evidence for amorphization was obtained in specimens irradiated at 200 or 400 C. An understanding of the microstructural evolution of SiC under irradiation is critical to the application of these materials in fusion energy systems. DOE

N95-31658# Tokyo Univ., Tanashi (Japan). Inst. for Nuclear Study.
ATOMIC APPROACHES IN METASTABLE ANTIPROTONIC HELIUM ATOMS. REPLY TO ANALYSIS OF THE LIFETIMES AND FRACTIONS OF ANTIPROTONS TRAPPED IN METASTABLE ANTIPROTONIC HELIUM STATES BY I. SHIMAMHURA AND M. KIMURA
Toshimitsu Yamazaki and Kazumasa Ohtsuki (University of Electro-Communications, Chofu, Japan.) Aug. 1994 13 p
(DE95-737228; INS-1050) Avail: CASI HC A03/MF A01

In the present note the authors clarify the purpose of YO and complement its essential points, thus showing that the criticisms of SK are inappropriate. The paper YO was aimed at discussing some new aspects related to the metastability of hadronic helium atoms which had been discovered when negative kaons, negative pions and antiprotons were stopped in liquid helium. The delayed fraction, time spectrum shape and lifetimes were the observables. Further experimental studies are in progress, and as of today there is no successful explanation for these interesting phenomena. So, YO tried to give brief and rather qualitative estimates for the observations in an intuitive way, considering only the leading terms. The following problems are discussed in as simple a manner as possible, starting from the exotic-atom viewpoints of Condo and Russell: (1) the atomic core polarization effect; (2) the structure and radiative lifetimes; (3) the non-statistical distribution of the angular momentum and an estimate of the delayed fraction; and (4) the isotope effect, though the title represents only (1). To respond to the comments of SK, it is important to consider the correspondence between the atomic approach and the molecular approach for the metastable antiprotonic helium atom of Condo-Russell. We therefore begin this note with a discussion of this aspect. DOE

N95-31682# Stanford Linear Accelerator Center, Menlo Park, CA
STUDIES OF THE STRONG AND ELECTROWEAK INTERACTIONS AT THE Z(SUB 0) POLE Ph.D. Thesis
M. D. Hildreth Mar. 1995 186 p
(Contract DE-AC03-76SF-00515)
(DE95-010353; SU-SLAC-R-95-458) Avail: CASI HC A09/MF A02

This thesis presents studies of the strong and electroweak forces, two of the fundamental interactions that govern the behavior of matter at high energies. The authors have used the hadronic decays of Z(sup 0) bosons produced with the unique experimental apparatus of the e(+)e(-) Linear Collider at the Stanford Linear Accelerator Center (SLAC) and the SLAC Large Detector (SLD) for these measurements. Employing the precision tracking capabilities of the SLD, they isolated samples of Z(sup 0) events containing primarily the decays of the Z(sup 0) to a chosen quark type. With an inclusive selection technique, they have tested the flavor independence of the strong coupling, alpha(sub s) by measuring the rates of multi-jet production in isolated samples of light (uds), c, and b quark events. They find: alpha(sub s, sup uds)/alpha(sub s, sup all) 0.987 +/- 0.027(stat) +/- 0.022(syst) +/- 0.022(theory), alpha(sub s, sup c)/alpha(sub s, sup all) = 1.012 +/- 0.104(stat) +/- 0.102(syst) +/- 0.096(theory), alpha(sub s, sup b)/alpha(sub s, sup all) = 1.026 +/- 0.041(stat) +/- 0.030(theory), which implies that the strong interaction is independent of quark flavor within the present experimental sensitivity. They have also measured the extent of parity-violation in the Z(sup 0) c(bar-c) coupling, given by the parameter A(sub c, sup 0), using a sample of fully and partially reconstructed D* and D(+) meson decays and the longitudinal polarization of the SLC electron beam. This sample of charm quark events was derived with selection techniques based on their kinematic properties and decay topologies. They find A(sub c, sup 0) = 0.73 +/- 0.22(stat) +/- 0.10(syst). This value is consistent with that expected in the electroweak standard model of particle interactions. DOE

N95-31702# Brookhaven National Lab., Upton, NY.
LONG BASELINE NEUTRINO OSCILLATION EXPERIMENT AT THE AGS Physics Design Report
D. Beavis, A. Carroll, and I. Chiang Apr. 1995 270 p
(Contract DE-AC02-76CH-00016)
(DE95-004378; BNL-52459) Avail: CASI HC A12/MF A03

The authors present a design for a multidetector long baseline neutrino oscillation experiment at the BNL AGS. It has been approved by the BNL-HENP-PAC as AGS Experiment 889. The experiment will search for oscillations in the nu(sub mu) disappearance channel and the nu(sub mu) reversible reaction nu(sub e) appearance channel by means of four identical neutrino detectors located 1, 3, 24, and 68 km from the AGS neutrino source. Observed depletion of the nu(sub mu) flux (via quasi-elastic muon neutrino events, nu(sub mu)n yields mu(-)p) in the far detectors not attended by an observed proportional increase of the nu(sub e) flux (via quasi-elastic electron neutrino events, nu(sub e)n yields e(-)p) in those detectors will be prima facie evidence for the oscillation channel nu(sub mu) reversible reaction nu(sub tau). The experiment is directed toward exploration of the region of the neutrino oscillation parameters Delta m(exp 2) and sin(exp 2) 2 theta, suggested by the Kamiokande and IMB deep underground detectors but it will also explore a region more than two orders of magnitude larger than that of previous accelerator experiments. The experiment will run in a mode new to BNL. It will receive the fast extracted proton beam on the neutrino target approximately 20 hours per day when the AGS is not filling RHIC. A key aspect of the experimental design involves placing the detectors 1.5 degrees off the center line of the neutrino beam, which has the important advantage that the central value of the neutrino energy (approximately 1 GeV) and the beam spectral shape are, to a good approximation, the same in all four detectors. The proposed detectors are massive, imaging, water Cherenkov detectors similar in large part to the Kamiokande and IMB detectors. The design has profited from their decade-long experience, and from the detector designs of the forthcoming SNO and SuperKamiokande detectors. DOE

N95-31818# Polish Academy of Sciences, Warsaw (Poland). Atomic Frequency Standards Lab.
DETECTION OF THE PHASE SHIFT WHICH ACCOMPANIES THE EXCITATION OF AN ATOMIC BEAM BY N. F. RAMSEY'S METHOD [DETEKCJA PRZESUNIECIA FAZOWEGO WYSTEPUJACEGO PRYZ POBUDZANIU WIAZKI ATOMOWEJ METODA N. F. RAMSEY'A]
Andrzej Chachulski and Krystyna Drogon May 1995 19 p In POLISH
(ISSN 0208-5658)
(IFTR-5/1995) Avail: CASI HC A03/MF A01

This article contains a description of a new method for measuring the phase shift which occurs in an apparatus. This method seems to be quite accurate. The authors found that there is a close relationship between the asymmetry of two adjacent resonance frequencies of the main interference line (which accompanies the use of N. F. Ramsey's excitation method) and the resultant phase shift. Calculations were performed using an example of a system with a beam of cesium atoms. The authors studied the asymmetry of frequency relative to the phase difference for an example of phase detection on the constant component of detector current, as they did for a case of the analysis of the resonance curve of a phase-modulated signal and synchronic detection. The authors describe the physical conditions and the hardware implementations of the principle. Author

N95-31832# Florida Univ., Gainesville, FL.
ELECTRONIC STRUCTURE OF DONOR-SPACER-ACCEPTOR MOLECULES OF POTENTIAL INTEREST FOR MOLECULAR ELECTRONICS 4. GEOMETRY AND DEVICE PROPERTIES OF P3CNQ AND Q3CNQ Interim Report
Anders Broo and Michael C. Zerner 18 Apr. 1995 30 p
(Contract N00014-90-J-1608)
(AD-A293717; TR-28) Avail: CASI HC A03/MF A01

Z-Beta (1-hexadecyl 4 quinolinium) alpha-cyano 4-styryldicyano methanide (C16H33-Q3CNQ) and the pyridinium analogue yryldicyanomethanide (C16H33P3CNQ) are two very promising candidates for molecular device design. We obtain the geometry of the ground and excited state of these systems using the PM3 quantum mechanical model. The absorption spectra in vacuum and in solution are calculated using the INDO/CI model, and compared to experimental spectra. The solvatochromic shift of the absorption spectra was calculated using a self-consistent reaction field approach. The observed bleaching of Langmuir-Blodgett films and solutions of C16H33-Q3CNQ and C16H33-P3CNQ is explained as resulting from a twisted configuration formed without barrier upon absorption into a twisted intramolecular charge transfer state. The observed rectification is explained from a ground state potential energy surface with two minima, one of which is characterized by a very large dipole moment. The relative energy of these minima is easily shifted by an electric field. The overall electron transport rate is found to be very small due to the small electronic coupling between the mono-layers of the L-B film. Thus, the electron transport through the sample is likely through defects of the L-B film. A way to increase the electronic coupling between the monolayers is also discussed. DTIC

N95-32026# Stanford Linear Accelerator Center, Stanford, CA.
A SEARCH FOR MILLICHARGED PARTICLES AT SLAC
J. A. Jaros 1995 6 p Presented at the 30th Recontres De Moriond: Dark Matter in Cosmology, Clocks, and Tests of Fundamental Laws, Villar-sur-Ollon, Switzerland, 21-28 Jan. 1995
(Contract DE-AC03-76SF-00515)
(DE95-010694; SU-SLAC-PUB-95-6810; CONF-950183-1) Avail: CASI HC A02/MF A01

Particles with electric charge q/e less than or equal to 10(exp -3) and masses in the range 1-1000 MeV/c(sup 2) are not excluded by present experiments or by astrophysical or cosmological arguments. Such millicharged particles may be a form of shadow matter that couples to ordinary matter by virtue of shadow photon/photon mixing. This paper describes a search for millicharged particles in a dedicated beam-dump experiment at SLAC. A preliminary analysis of part of this data excludes particles of mass (approximately) 1 MeV/c(sup 2) with q/e greater than 6 x 10(exp -5). DOE

N95-32031# Brookhaven National Lab., Upton, NY.
POLARIZED PROTON BEAMS
T. Roser 1995 6 p Presented at the Particle Accelerator Conference, Dallas, TX, 1-5 May 1995
(Contract DE-AC02-76CH-00016)
(DE95-010843; BNL-61022; CONF-950512-12) Avail: CASI HC A02/MF A01

The acceleration of polarized proton beams in circular accelerators is complicated by the presence of numerous depolarizing spin resonances. Careful and tedious minimization of polarization loss at each of these resonances allowed acceleration of polarized proton beams up to 22 GeV. It has been the hope that Siberian Snakes, which are local spin rotators inserted into ring accelerators, would eliminate these resonances and allow acceleration of polarized beams with the same ease and efficiency that is now routine for unpolarized beams. First tests at IUCF with a full Siberian Snake showed that the spin dynamics with a Snake can be understood in detail. The author now has results of the first tests of a partial Siberian Snake at the AGS, accelerating polarized protons to an energy of about 25 GeV. These successful tests of storage and acceleration of polarized proton beams open up new possibilities such as stored polarized beams for internal target experiments and high energy polarized proton colliders. DOE

N95-32032# Brookhaven National Lab., Upton, NY.
OBSERVATION OF INTENSITY DEPENDENT LOSSES IN Au(15+) BEAMS
M. Blakiewicz, L. A. Ahrens, H. C. Hseuh, T. Roser, Y. Shoji, and K. Zeno 1995 3 p Presented at the Particle Accelerator Conference, Dallas, TX, 1-5 May 1995
(Contract DE-AC02-76CH-00016)
(DE95-010845; BNL-61092; CONF-950512-14) Avail: CASI HC A01/MF A01

During the 1994 heavy ion run at Brookhaven a strongly intensity dependent loss for the Au(15+) beam in the AGS Booster was encountered. Coherent instabilities or space charge induced stopband losses were neither expected nor consistent with the data. It was found that the beam lifetime was an order of magnitude shorter for normal operating conditions than in the low intensity limit with the inverse lifetime increasing monotonically with the injected number of particles. Studies data are presented and the Au(15+) situation is compared with that for Au(33+). Various hypothetical mechanisms are considered. DOE

N95-32038# Lawrence Livermore National Lab., Livermore, CA.
STUDIES OF HIGHLY CHARGED IONS WITH EBIT AND SUPER-EBIT
S. R. Elliott 14 Sep. 1994 25 p Presented at the 7th International Conference on Physics of Highly Charged Ions, Vienna, 19-23 Sep. 1994
(Contract W-7405-eng-48)
(DE95-010251; UCRL-JC-117182; CONF-940922-5) Avail: CASI HC A03/MF A01

The LLNL electron beam ion traps provide cold highly charged ions up to bare U. These machines have provided a wealth of atomic physics data using a compact, relatively inexpensive, device. The physics program has studied electron-ion collisions, QED, ion-surface interactions, and plasmas physics among many other topics. The prospects for the study of the highest charge states in the highest Z ions led to the beam energy upgrade of the first EBIT into Super-EBIT. The desire to use ions as a research probe in themselves led to an ion extraction program on EBIT-2. Finally, a Penning trap (referred to as the RETRAP) has been constructed to catch extracted ions where they can be further cooled and studied. Results of several experiments at the LLNL EBIT facility are described. The program's capabilities are discussed. DOE

N95-32039# Lawrence Livermore National Lab., Livermore, CA.
THE ANTIPROTON-HYDROGEN ATOM INTERACTION
D. L. Morgan, Jr. Jul. 1994 12 p Presented at the 6th Workshop on Exotic Atoms, Molecules and Their Interactions, Erice, Italy, 21-30 Mar. 1994
(Contract W-7405-eng-48)
(DE95-010252; UCRL-JC-118216; CONF-9403221-1) Avail: CASI HC A03/MF A01

The (bar p)-H interaction is the most important aspect of the (bar p)pe system. While this interaction is worthy of study in itself, it is also relevant to a number of (bar p) applications, both practical and in the area of fundamental physics. Theoretical study of p-H commenced more than 20 years ago and has continued with growing interest through the present. Experimental study has been limited, but recently measurements have been made of (bar p)'s slowing in hydrogen at KeV energies, which shed light on their interaction with hydrogen atoms. Theoretical work involving various kinds and levels of approximation has now been carried out for a variety of (bar p) energy domains. Particular attention has been given to (bar p) capture at low and sub eV energies, in which a bound (bar p)-p state is formed, and to H excitation and ionization at KeV energies. Such calculations now extend into the sub Kelvin domain of energies. It is beginning to be possible to make comparisons between experiment and calculation and to compare calculations to one another. These comparisons suggest that theoretical work needs to be carried out in some intermediate energy domains and that some past calculations have to be repeated with more accurate methods. DOE

N95-32041# Lawrence Livermore National Lab., Livermore, CA.
WAVELENGTHS MEASUREMENTS OF THE He-LIKE KRYPTON K-SHELL SPECTRUM
K. Widmann, P. Beiersdorfer, and V. Decaux 13 Sep. 1994 11 p Presented at the 7th International Conference on Physics of Highly Charged Ions, Vienna, Austria, 19-23 Sep. 1994
(Contract W-7405-eng-48)
(DE95-010264; UCRL-JC-118364; CONF-940922-6) Avail: CASI HC A03/MF A01

We present accurate measurements of the 1s2s, Is2p (yields) 1s(sup 2) transitions of He-like krypton. The measurements were performed on the EBIT facility using a high-resolution crystal spectrometer and a precision of 50 ppM was achieved. Unlike earlier measurements from the GANIL accelerator, our results are in good agreement with recent theoretical predictions. DOE

N95-32053# Academy of Sciences (USSR), Novosibirsk (USSR). Inst. Yadernoj Fiziki.
CALIBRATION OF MULTICHANNEL ANALYZER OF CHARGE-EXCHANGE ATOMS
D. V. Antipin and I. N. Churkin 1994 11 p
(DE95-614178; IYaF-94-36) Avail: CASI HC A03/MF A01 (US Sales Only)

The aim of the paper is calibration of units of a multichannel analyzer of charge-exchange neutrals intended for hot plasma diagnostics. A dependence is obtained between the microchannel-plate detector output current and fast H(sup 0) current at the analyzer input in the 5-80 keV range. Operation modes of a gas target and the amplification coefficient of the microchannel-plate detector are determined. DOE

N95-32055# Academy of Sciences (USSR), Novosibirsk (USSR). Inst. Yadernoj Fiziki.
LONGITUDINAL LOSSES OF CHARGED PARTICLES FROM AN OPEN CONFIGURATION WITH ARBITRARY BETA RATIO
V. N. Khudik 1994 17 p
(DE95-614187; IYaF-94-33) Avail: CASI HC A03/MF A01 (US Sales Only)

On the base of the Fokker-Planck linearized equation are calculated classical longitudinal losses of charged particles' from an open trap with arbitrary mirror ratio. It is shown that at all physically interested mirror ratios the mean energy, taken away by one charge particle from a trap, equals epsilon(sub 0)+T where epsilon(sub 0) = -e(Phi) (Phi is the ambipolar trapping potential and T is temperature of charged particles). DOE

N95-32063# Brookhaven National Lab., Upton, NY.
MONTE CARLO SIMULATIONS OF MUON PRODUCTION
Robert B. Palmer, Juan C. Gallardo, Richard C. Fernow, Yagmur Torun, David Neuffer (Continuous Electron Beam Accelerator Facility, Newport New, VA.), and David Winn (Fairfield Univ., CT.) Mar. 1995 19 p Presented at the 2nd Workshop on Physics Potential and Development of Mu(+) Mu(-) Colliders, Sausalito, CA, 17-19 Nov. 1994
(Contracts DE-AC02-76CH-00016; DE-AC03-76SF-00515)
(DE95-009554; BNL-61581; CONF-9411210-3) Avail: CASI HC A03/MF A01

Muon production requirements for a muon collider are presented. Production of muons from pion decay is studied. Lithium lenses and solenoids are considered for focusing pions from a target, and for matching the pions into a decay channel. Pion decay channels of alternating quadrupoles and long solenoids are compared. Monte Carlo simulations are presented for production of pi yields mu by protons over a wide energy range, and criteria for choosing the best proton energy are discussed. DOE

N95-32069# Academy of Sciences (USSR), Novosibirsk (USSR). Inst. of Nuclear Physics.
SO(8) COLOR AS POSSIBLE ORIGIN OF GENERATIONS
Z. K. Silagadze 1993 42 p
(DE95-613560; BudkerINP-93-93; IYaF-93-93) Avail: CASI HC A03/MF A01 (US Sales Only)

A possible connection between the existence of three quark-lepton generations and the triality property of SO(8) group (the equality between 8-dimensional vectors and spinors) is investigated. SO(8) appears to be a natural one-flavor unification group. Family formation due to weak interactions results in SO(10) group and a broken triality symmetry. Further speculations about how to restore this symmetry lead finally to E(sub 6) exceptional group and three quark-lepton families. DOE

N95-32070# International Centre for Theoretical Physics, Trieste (Italy).
RENORMALIZATION GROUP ANALYSES OF PARTICLE MASSES IN FULL FOUR-GENERATION FERMION CONDENSATE SCHEME
Bangrong Zhou Sep. 1994 28 p
(DE95-613595; IC-94/277) Avail: CASI HC A03/MF A01 (US Sales Only)

The renormalization group analyses of the masses of the heavy fermions and the Higgs boson, including the discussions of possible fixed points and applicability of perturbation theory, are expounded in the full four-generation quark-lepton condensate scheme of the minimal electroweak symmetry breaking. The results also indicate that the model could accommodate itself to the top-quark mass m(sub t) = 160 - 180 GeV. The predicted Higgs boson mass is in fact not too sensitive to the above change of m(sub t). It is also found that for a model without the fourth generation of leptons, the limitation to Lambda imposed by the requirement that the masses of the fourth generation of extra quarks are bigger than m(sub t) = 174 GeV could be greatly relaxed up to (less than or equal) 10(exp 11) GeV. DOE

N95-32078# Joint Inst. for Nuclear Research, Dubna (USSR). Lab. of Theoretical Physics.
FORM FACTOR OF THE PROCESS GAMMA(*) GAMMA(*) YIELDS PI(SUP 0) FOR SMALL VIRTUALITY OF ONE OF THE PHOTONS AND QCD SUM RULES (2): SUM RULE
A. V. Radyushkin and R. Ruskov 1994 20 p
(DE95-613629; JINR-E-2-94-248) Avail: CASI HC A03/MF A01 (US Sales Only)

We extend the QCD sum rule analysis of the F(sub gamma(*) gamma(*)) yields pi(sup 0) (q(sup 2, sub 1), q(sup 2, sub 2)) form factor into the region where one of the photons has small virtuality: absolute value of(q(sup 2, sub 1)) much less than absolute value of (q(sup 2, sub 2)) greater than or equal to 1 GeV(sup 2). In this kinematics one should perform an additional factorization of short- and long-distance contributions. The extra long distance sensitivity of the three-point amplitude is described by two-point correlators (bilocals), and the low-momentum dependence of the correlators involving composite operators of two lowest twists is extracted from auxiliary QCD sum rules. The sum rule obtained is regular in the limit q(sup 2, sub 1) yields 0. Our estimates for F(sub gamma(*), gamma(*)) yields pi(sup 0) (q(sup 2, sub 1) = 0, Q(sup 2, sub 2)) are in good agreement with existing experimental data. DOE

N95-32079# Brookhaven National Lab., Upton, NY. Physics Dept.
APPLICATIONS OF CHIRAL SYMMETRY
Robert D. Pisarski Mar. 1995 48 p Presented at the Workshop on Finite Temperature QCD and Quark-Gluon Transport Theory, Wuhan, China, 18-21 Apr. 1994
(Contract DE-AC02-76CH-00016)
(DE95-009552; BNL-61547; CONF-9404253-1) Avail: CASI HC A03/MF A01

The author discusses several topics in the applications of chiral symmetry at nonzero temperature. First, where does the rho go? The answer: up. The restoration of chiral symmetry at a temperature T(sub chi) implies that the rho and a(sub 1) vector mesons are degenerate in mass. In a gauged linear sigma model the rho mass increases with temperature, m(sub rho)(T(sub chi)) greater than m(sub (rho))(0). The author conjectures that at T(sub chi) the thermal rho - a(sub 1), peak is relatively high, at about approximately 1 GeV, with a width approximately that at zero temperature (up to standard kinematic factors). The omega-meson also increases in mass, nearly degenerate with the rho, but its width grows dramatically with temperature, increasing to at least approximately 100 MeV by T(sub chi). The author also stresses how utterly remarkable the principle of vector meson dominance is, when viewed from the modern perspective of the renormalization group. Secondly, he discusses the possible appearance of disoriented chiral condensates from 'quenched' heavy ion collisions. It appears difficult to obtain large domains of disoriented chiral condensates in the standard two flavor model. This leads to the last topic, which is the phase diagram for QCD with three flavors, and its proximity to the chiral critical point. QCD may be very near this chiral critical point, and one might there by generated large domains of disoriented chiral condensates. DOE

N95-32083# Stanford Linear Accelerator Center, Menlo Park, CA
A SEARCH FOR JET HANDEDNESS IN HADRONIC Z-0 DECAYS
Yoji Hasegawa Mar. 1995 134 p
(Contract DE-AC03-76SF-00515)
(DE95-010099; SU-SLAC-R-95-459; TOHOKU-HEP-95-02; TOHOKU-HEP-NOTE-95-07; UC-414) Avail: CASI HC A07/MF A02

Transport of polarization through hadronization process is one of the fundamental interest in Quantum Chromodynamics which is a theory of strong interactions. In the low energy region where the hadronization occurs, QCD calculations are difficult, therefore at present the transport can be investigated experimentally. In this study the authors have searched for signatures of polarization of quarks and antiquarks in hadronic jets from Z(sup 0) (yields) q(bar q) decays. The polarization of quarks and antiquark produced by Z(sup 0) decays are predicted by the Standard Model of elementary particle physics. The authors defined several quantities depending on 'jet handedness' methods and studied the correlation between the predicted polarization and the quantities. The signal was estimated by analyzing power which represents degree of the polarization transport through the hadronization process. The Z(sup 0) decays were measured by SLC Large Detector and the polarized electron beam provided by SLAC Linear Collider was useful for this study. The data from the 1993 run showed no signature of the transport of quark and antiquark polarization. Upper limits on magnitude of the analyzing power were set in the range 0.05-0.15 depending on the methods. DOE

N95-32093# Joint Inst. for Nuclear Research, Dubna (USSR).
SPIN MOMENTUM CORRELATION (HANDEDNESS) IN THE PROCESS OF FOUR PION PRODUCTION IN THE ELECTRON-POSITRON COLLISIONS
E. L. Bratkovskaya, E. A. Kuraev, Z. K. Silagadze, and O. V. Teryaev 1994 10 p
(DE95-613690; JINR-E-4-94-234) Avail: CASI HC A02/MF A01 (US Sales Only)

We discuss a special type of polarization asymmetry ('handedness') in

the process e(+)e(-) yields 4 pi, when one of the initial particles is longitudinally polarized. The asymmetry is proportional to the degree of polarization and to the width of mass ratio of rho-meson. It can reach 4-5% in some kinematic region. Both channels 2pi(+)2pi(-) and 2pi(0)pi(+)pi(-) are considered in the framework of the effective chiral Lagrangian with vector mesons, in the energy range approx. 1.2 GeV. The corresponding total cross sections are also calculated. DOE

N95-32096# International Centre for Theoretical Physics, Trieste (Italy).
SUPERSYMMETRIC MAGNETIC MOMENTS SUM RULES AND SPONTANEOUS SUPERSYMMETRY BREAKING
S. S. Khalil Sep. 1994 12 p
(DE95-613771; IC-94/280) Avail: CASI HC A03/MF A01 (US Sales Only)

In supersymmetry the anomalous magnetic moment of particles belonging to the same supermultiplet is related by simple sum rules. We study the modification of these sum rules in the case of the spontaneously broken N=1 global supersymmetry. DOE

N95-32120# Kansas State Univ., Manhattan, KS. Dept. of Physics.
GENERALIZED RAMSAUER-TOWNSEND MINIMA IN HEAVY-ION INDUCED ELECTRON CONTINUA
C. Liao, S. Hagmann, S. R. Grabbe, C. P. Bhalla, P. Richard, and T. Zaepfel 1995 2 p Presented at the 19th International Conference on the Physics of Electronic and the Atomic Collisions, Whistler, Canada, 26 Jul. - 1 Aug. 1995
(Contract DE-FG02-86ER-13491)
(DE95-010913; DOE/ER-13491/767; CONF-950706-7) Avail: CASI HC A01/MF A01

We have measured doubly differential cross sections (DDCS) for electron emission in ion-atom collisions for F, Cl, Br, I, and Au projectiles impinging on H2 targets for collision energies between 0.18 MeV/u and 0.62 MeV/u and electron emission angles between 0 and 70 degres. We relate the observed diffraction phenomena in the binary encounter region to diffraction structures previously established in elastic scattering of electrons in the finite range potentials of atoms and partially ionized ions. Whereas for swift light ions the binary encounter energy follows simple 2-body kinematics and the cross section is derived from the first order Born approximation for scattering of an electron in the field of a point projectile core charge, for heavy projectiles energy and cross section of the binary encounter show a very complex behavior. DOE

N95-32151# Academy of Sciences (USSR), Novosibirsk (USSR). Budker Inst. of Nuclear Physics.
MIXING PHASES OF UNSTABLE TWO-LEVEL SYSTEMS
V. V. Sokolov and P. vonBrentano (Cologne Univ., Germany.) 1993 15 p
(DE95-613844; BudkerINP-93-95; IYaF-93-95) Avail: CASI HC A03/MF A01

An unstable two-level system decaying into an arbitrary number of channels is considered. It is shown that the mixing phases of the two overlapping resonances can be expressed in the terms of their partial widths and one additional universal mixing parameter. Some applications to a doublet of 2(sup +) resonances in Be-8 and to the rho - omega systems are considered. The mixing phases in the 2(pi) and 3(pi) channels are found. The mixing energy shifts are also calculated for both systems considered. DOE

N95-32160# Brookhaven National Lab., Upton, NY.
VALIDITY OF THE DIFFERENTIAL EQUATIONS FOR IONIZATION COOLING
R. C. Fernow and J. C. Gallardo Mar. 1995 10 p Presented at the 2nd Workshop on Physics Potential and Development of Mu+ Mu- Colliders, Sausalito, CA, 17-19 Nov. 1994
(Contract DE-AC02-76CH-00016)
(DE95-010438; BNL-61579; CONF-9411210-4) Avail: CASI HC A02/MF A01

The authors examine the validity of the differential equations used to describe ionization cooling. They find that the simple heating term due to multiple scattering given by D. Neuffer is a good approximation to the expression obtained from a more rigorous derivation. DOE

N95-32162# Fermi National Accelerator Lab., Batavia, IL.
SEARCH FOR ANOMALOUS ZZ(SUB GAMMA) AND Z(SUB (GAMMA, GAMMA)) COUPLINGS WITH D0
Gregg Landsberg 1995 6 p Presented at the International Symposium on Vector Boson Interactions, Los Angeles, CA, 1-3 Feb. 1995
(Contract DE-AC02-76CH-03000)
(DE95-010457; FNAL/C-95/061-E; CONF-950287-1) Avail: CASI HC A02/MF A01

A direct test of the Standard Model by searching for anomalous ZZ(sub gamma) and Z(sub(gamma, gamma))couplings is presented. The authors analyze p(bar p) yields ll(sub gamma) + X, (l = e,mu) events at radical s = 1.8 TeV with the D0 detector at the Fermilab Tevatron Collider. A fit to the transverse energy spectrum of the photon in the signal events, based on the data set corresponding to an integrated luminosity of 13.9 pb(sup -1) (13.3 pb(sup -1)) for the electron muon channel, yields the following 95% CL limits on the anomalous CP-conserving ZZ(sub gamma) couplings: -1.9 less than h(sub 30, sup Z) less than 1.8 (h(sub 40, sup Z) = 0), and -0.5 less than h(sub 40, sup Z) less than 0.5 (h(sub 30, supZ) = 0), for a form-factor scale Lambda = 500 GeV. Limits on the Z(sub (gamma, gamma)) couplings and CP-violating couplings are also discussed. DOE

N95-32261# Gosudarstvennyi Komitet po Ispolzovaniyu Atomnoi Energii, Serpukhov (USSR).
ON THE SEARCH FOR EXOTIC HADRONS IN THE EXPERIMENTS WITH HIGH ENERGY HYPERON BEAM
L. G. Landsberg (Gosudarstvennyi Komitet po Ispolzovaniyu Atomnoi Energii, Protvino, USSR.), M. A. Kubantsev (Gosudarstvennyi Komitet po Ispolzovaniyu Atomnoi Energii, Moscow, USSR.), and M. A. Moinester (Tel-Aviv Univ., Ramat-Aviv, Tel-Aviv, Israel.) 1994 43 p
(DE95-620534; IHEP-94-19) Avail: CASI HC A03/MF A01 (US Sales Only)

The possibilities to search for exotic mesons, baryons and dibaryons in the framework of E781 Fermilab experiment with high energy hyperon and meson beams with momenta of approximately 600 GeV are analyzed. It is shown that there are good possibilities for the observation of different types of exotic hadrons in E781 experiment. DOE

N95-32266# Stanford Linear Accelerator Center, Menlo Park, CA
A MEASUREMENT OF QUARK AND GLUON JET DIFFERENCES AT THE Z(SUP 0) RESONANCE Ph.D. Thesis
Yoshihito Iwasaki Mar. 1995 70 p
(Contract DE-AC03-76SF-00515)
(DE95-010666; SU-SLAC-R-95-460; TOHOKU-HEP-95-01; TOHOKU-HEP-NOTE-95-06) Avail: CASI HC A04/MF A01

The authors have studied the differences in properties between quark and gluon jets using three-jet events in hadronic decays of Z(sup 0) bosons collected by the SLD experiment at SLAC. Gluon jets were identified in three-jet events containing one jet tagged as a heavy quark jet. The tagged gluon jets were compared with a mixed sample of light quark (u, d and s) and gluon jets, and also with a mixed sample of heavy quark (c and b) and gluon jets. The study shows that the particle multiplicity of gluon jets is higher than that of light quark or heavy quark jets. The ratios of average charged multiplicities of gluon and quark jets are measured and results are given. These results are in quantitative agreement with QCD model expectations. Differences are also observed in particle energy spectra and jet widths, consistent with naive QCD expectations. The experimental results are compared to Monte Carlo models of the hadronization process. DOE

N95-32267# Stanford Linear Accelerator Center, Menlo Park, CA
AN EXPERIMENTAL STUDY OF QCD AND JETS IN e(+)e(-) ANNIHILATION Ph.D. Thesis
Yukiyoshi Ohnishi Mar. 1995 78 p
(Contract DE-AC03-76SF-00515)
(DE95-010667; SU-SLAC-R-95-461) Avail: CASI HC A05/MF A01

This thesis is concerned with an experimental study of QCD and jets using hadronic decays of Z(sup 0) bosons by the SLD experiment at the SLAC Linear Collider. The strong coupling alpha(sub s)(M(sub Z)(sup 2)) has been measured, which is an important test of perturbative QCD theory. This comprehensive study comprised fifteen observables that describe hadronic final states; six event shapes, differential two-jet rates defined by six different jet resolution/recombination schemes, energy-energy

correlations and their asymmetry, and the jet cone energy fraction. The data were compared with QCD predictions both at fixed order, O(alpha(sub s)(sup 2)), and including resummed analytic formula based on the leading and next-to-leading logarithmic approximation. The consistency was checked between alpha(sub s)(M(sub Z)(sup 2)) values extracted from these different measures. A final average of alpha(sub s)(M(sub Z)(sup 2)) = 0.1200 +/- 0.0025 (exp.) +/- 0.0078 (theor.), corresponding to Lambda(sub (bar MS)) = 253(sub -96)(sup +130) MeV, was obtained by combining all results. The dominant uncertainty is from uncalculated higher order contributions. DOE

N95-32271# Kansas State Univ., Manhattan, KS.
KINEMATICAL THRESHOLD OF RECOIL-ION LONGITUDINAL MOMENTUM DISTRIBUTION IN SINGLE IONIZATION OF HELIUM BY PROTONS AND ALPHA PARTICLES
V. D. Rodrigues (Buenos Aires Univ., Argentina.), Y. D. Wang, and C. D. Lin 1995 2 p Presented at the 19th International Conference on the Physics of Electronic and the Atomic Collisions, Whistler, Canada, 26 Jul. - 1 Aug. 1995
(Contract DE-FG02-86ER-13491)
(DE95-010803; DOE/ER-13491/777; CONF-950706-6) Avail: CASI HC A01/MF A01

The study of recoil-ion momentum spectroscopy can help better understand ionization dynamics in ion-atom scattering. We analyze recent experiment of the collisions of helium by fast protons and alpha particles where the longitudinal momentum distributions for recoil ions are measured for impact energies between 250 keV/u to 1 MeV/u. We apply the CDW-EIS and the first Born approximations within the independent electron model to analyze the experimental results. Derived from text

N95-32273# Kansas State Univ., Manhattan, KS.
IONIZATION OF He BY HIGHLY CHARGED IONS AT LOW VELOCITY
Y. D. Wang, C. D. Lin, and N. Toshima (Tsukuba Univ., Ibaraki, Japan.) 1995 2 p Presented at the 19th International Conference on the Physics of Electronic and the Atomic Collisions, Whistler, Canada, 26 Jul. - 1 Aug. 1995
(Contract DE-FG02-86ER-13491)
(DE95-010815; DOE/ER-13491/775; CONF-950706-2) Avail: CASI HC A01/MF A01

A close-coupling calculation has been completed for ionization of He by highly charged bare ions at low velocity within the independent electron model. The main results for ionization by C(6+) ions are summarized. The ratio of single ionization cross section to single capture cross section and the impact parameter dependence of ionization and capture probabilities are given. Derived from text

N95-32274# Kansas State Univ., Manhattan, KS.
RECOIL LONGITUDINAL MOMENTUM SPECTROSCOPY OF ELECTRON CAPTURE FROM He BY O(7+) AND F(8+)
W. Wu, K. L. Wong, C. L. Cocke, J. P. Giese, and E. C. Montenegro 1995 2 p Presented at the 19th International Conference on the Physics of Electronic and the Atomic Collisions, Whistler, Canada, 26 Jul. - 1 Aug. 1995 Ilisions, Whistler, Canada, 26 Jul. - 1 Aug. 1995
(Contract DE-FG02-86ER-13491)
(DE95-010823; DOE/ER-13491/764; CONF-950706-10) Avail: CASI HC A01/MF A01

Recoil momentum spectroscopy is used to study final state distributions for single capture and for transfer ionization for hydrogenlike O and F projectiles on He. Beams of O(7+) and F(8+) were directed to a He gas jet. The recoil ions were extracted by an electric field and projected onto the face of a position sensitive channel plate detector. The time of flight of the recoil, measured in coincidence with the charge-state-analyzed projectile, and its position were used to reconstruct its vector momentum. Spectra of the longitudinal momentum transfer to the recoil ion, p(sub x), are shown in three channels: (1) single ionization, target ionization without any change in projectile charge-state; (2) single capture, for which the recoils are thrown backwards; and (3) transfer ionization. CASI

N95-32275# Kansas State Univ., Manhattan, KS.
STUDY OF ALIGNED STATES IN ION-ATOM COLLISIONS
P. Richard, G. Toth, S. Hagmann, S. R. Grabbe, C. P. Bhalla, E. C. Montenegro, and T. Zouros 1995 2 p Presented at the 19th International Conference on the Physics of Electronic and the Atomic Collisions, Whistler, Canada, 26 Jul. - 1 Aug. 1995
(Contract DE-FG02-86ER-13491)
(DE95-010825; DOE/ER-13491/762; CONF-950706-8) Avail: CASI HC A01/MF A01

The excitation of 1s2s2p (sup 4)P aligned states in ion-atom collisions by measuring the differential cross sections for Auger electron emission at zero-degrees is investigated. These states are formed by one-electron excitation from the ground state of three electron projectile ions. It is proposed that the relative excitation of the aligned three electron (sup 4)P state to the (sup 2)P states can be used to determine the importance of electron-electron interaction relative to electron-nucleus interactions in ion-atom collisions for heavy atom targets. The differential cross sections for exciting the (sup 4)P state for Ne, Ar, Kr, and Xe targets are measured. CASI

N95-32278# Brookhaven National Lab., Upton, NY.
REVIEW OF LONGITUDINAL PERTURBATION FORMALISM
S. Y. Zhang 1995 4 p Presented at the Particle Accelerator Conference, Dallas, TX, 1-5 May 1995
(Contract DE-AC02-76CH-00016)
(DE95-010894; BNL-61071; CONF-950512-41) Avail: CASI HC A01/MF A01

The foundation of the beam perturbation formalism was established on the Sacherer integral equation. The original solution was obtained by using simplified radial functions, and the results can be used to explain several important beam instability problems. To solve the instabilities caused by high beam intensities calls for more complete solution and the extension to the formalism as well. For the noncoupled perturbation problem without frequency spread, two different eigenvalue type solutions were proposed. The formalism is also modified to solve the azimuthal mode coupling instability and the beam instability with synchrotron frequency spread, where both dispersion type and eigenvalue type solutions were proposed. In this article, a brief review of longitudinal perturbation formalism based on Sacherer integral equation is given. Some perspectives will also be discussed. DOE

N95-32303# Fermi National Accelerator Lab., Batavia, IL.
CHARM PHOTOPRODUCTION DYNAMICS
Peter H. Garbincius Mar. 1995 13 p Presented at the LAFEX International School in High Energy Physics, Rio de Janeiro, Brazil, 20 Feb. 1995
(Contract DE-AC02-76CH-03000)
(DE95-009106; FNAL/C-95/041; CONF-950285-1) Avail: CASI HC A03/MF A01

Photoproduction of open charm is reviewed, both as a tool for studying the properties of charm particles such as spectroscopy, decays, and lifetimes, and as a testing ground for theoretical calculations of production dynamics. Many characteristics of charm photoproduction are described in terms of the leading order (LO) (alpha(sub EM))(alpha(sub S)) Photon-Gluon Fusion (PGF) model. The next-to-leading order (NLO) corrections of strength (alpha(sub EM))(alpha(sub S)(sup 2)) due to radiation of additional gluons are then added. The sensitivities of the NLO calculations on the mass of the charm quark, m(sub c), and on the choice of the gluon structure function of the nucleon are illustrated for the energy dependence of the cross section for charm photoproduction. These are compared with fixed target data and new HERA data. The single charm particle inclusive distributions in x(sub f) and p(sup 2)(perpendicular), along with sigma(gamma N yields c(anti-c)X) give good estimates of m(sub c) and n(sub g), the shape parameter for the gluon distribution within the nucleon. As in hadroproduction, some disagreements between prediction and observation begin to appear in trying to simultaneously match the distributions in both p(sup 2)(perpendicular) for single charm particles and in the Delta Phi acoplanarity angle between pairs of charm particles. These can be partially remedied by modifying the fragmentation function for c-quarks into charm particles, and by including extra k(sup2)(perpendicular) transverse smearing of the gluon distributions within the target nucleon. Initial studies of the relative production between charm particles and anti-particles indicate disagreement with the predictions of the independent string fragmentation model. DOE

N95-32304# International Centre for Theoretical Physics, Trieste (Italy).
ON HADRONIC PRODUCTION OF THE B(SUB c) MESON
Chaohsi Chang, Yuqi Chen, Guoping Han, and Hongtao Jiang Aug. 1994 18 p
(DE95-613726; IC-94/225; AS-ITP-94-24) Avail: CASI HC A03/MF A01 (US Sales Only)

Various approaches to the hadronic productions of the double heavy meson B(sub c) are investigated in this paper. The resultant cross sections obtained by the approaches are compared with in several aspects. One may see that the differences are quite substantial. The advantages and shortcomings of the approaches are discussed. DOE

N95-32353# International Centre for Theoretical Physics, Trieste (Italy).
SPIN PUZZLE IN NUCLEON
R. Ramachandran Sep. 1994 12 p
(DE95-613654; IC-94/261) Avail: CASI HC A03/MF A01 (US Sales Only)

The object of this brief review is to reconcile different points of view on how the spin of proton is made up from its constituents. On the basis of naive quark model with flavor symmetry such as isospin or SU(3) one finds a static description. On the contrary the local SU(3) colour symmetry gives a dynamical view. Both these views are contrasted and the role of U(1) axial anomaly and the ambiguity for the measurable spin content is discussed. DOE

N95-32354# Academy of Sciences (USSR), Novosibirsk (USSR).
NUCLEAR-SPIN-DEPENDENT PARITY-NONCONSERVING EFFECTS IN THALLIUM, LEAD AND BISMUTH ATOMS
I. B. Khriplovich 1994 17 p
(DE95-614120; BUDKERINP-94-56; IYaF-94-56) Avail: CASI HC A03/MF A01 (US Sales Only)

Nuclear-spin-dependent P-odd optical activity in atomic Tl, Pb and Bi is calculated. Its magnitude is expressed analytically through the main contribution to the optical rotation, which is independent of nuclear spin. The accuracy of results is discussed. DOE

N95-32365# Washington Univ., Bellingham, WA.
ELECTROWEAK BARYOGENESIS
D. B. Kaplan 1995 11 p
(Contract DE-FG06-90ER-40561)
(DE95-012169; DOE/ER-40561/189) Avail: CASI HC A03/MF A01

Baryogenesis during the electroweak phase transition is a plausible scenario for the origin of matter in the Universe. Furthermore, it has the advantage over other scenarios in that one can imagine the much of the physics involved may be experimentally probed before long. In the past year a consensus has developed about the major mechanisms involved. In this talk I give an overview of the standard picture, and discuss briefly the advances over the past year that suggest electroweak baryogenesis is a robust phenomenon. DOE

73 NUCLEAR AND HIGH-ENERGY PHYSICS

Includes elementary and nuclear particles; and reactor theory. For space radiation see *93 Space Radiation.*

N95-30360 California Univ., Berkeley. Lawrence Berkeley Lab, CA.
BEAM-BEAM EFFECTS
A. Zholents Dec. 1994 10 p Presented at the Workshop on Nonlinear Dynamics in Particle Accelerators: Theory and Experiments, Arcidosso, Italy, 4-9 Sep. 1994 Limited Reproducibility: More than 20% of this document may be affected by microfiche quality
(Contract DE-AC03-76SF-00098)
(DE95-008443; LBL-36572; CBP-131; CONF-9409258-7) Avail: CASI HC A02

The term beam-beam effects is usually used to designate different phenomena associated with interactions of counter-rotating beams in storage rings. Typically, the authors speak about beam-beam effects when such interactions lead to an increase of the beam core size or to a reduction of the beam lifetime or to a growth of particle's population in the beam halo and a correspondent increase of the background. Although observations of beam-beam effects are very similar in most storage rings, it is very likely that every particular case is largely unique and machine-dependent. This constitutes one of the problems in studying the beam-beam effects, because the experimental results are often obtained without characterizing a machine at the time of the experiment. Such machine parameters as a dynamic aperture, tune dependencies on amplitude of particle oscillations and energy, betatron phase advance between the interaction points and some others are not well known, thus making later analysis uncertain. The authors begin their discussion with demonstrations that beam-beam effects are closely related to non linear resonances. Then, they will show that a non linearity of the space charge field is responsible for the excitation of these resonances. After that, they will consider how beam-beam effects could be intensified by machine imperfections. Then, they will discuss a leading mechanism for the formation of the beam halo and will describe a new technique for beam tails and lifetime simulations. They will finish with a brief discussion of the coherent beam-beam effects. DOE

N95-30527 Columbia Univ., New York, NY.
THEORETICAL HIGH ENERGY PHYSICS
T. D. Lee 1994 33 p Limited Reproducibility: More than 20% of this document may be affected by microfiche quality
(Contract DE-FG02-92ER-40699)
(DE95-003107; DOE/ER-40699/3) Avail: CASI HC A03

This report is a progress report for the period 1 May 1993 - 30 Apr. 1994 from the Theory Group at Columbia University, headed by T. D. Lee. The report summarizes work by nine researchers from this institution. This work touches on phase transitions in QCD, calculated on massive parallel processors, weak matrix element calculations in lattice QCD, extensions of lattice QCD calculations, heavy ion inelastic scattering, quark-gluon plasmas, string theories, black holes, and field theory. DOE

N95-30604# Joint Inst. for Nuclear Research, Dubna (USSR).
BACKGROUND EVENT DISCRIMINATION IN NEUTRON TIME-OF-FLIGHT MEASUREMENTS AT BEAMS OF RELATIVISTIC NUCLEI OF THE JINR SYNCHROTRON
I. O. Tsvetkov, V. I. Yurevich, and V. G. Lyapin 1994 10 p
(DE95-613006; JINR-R-1-94-239) Avail: CASI HC A02/MF A01 (US Sales Only)

The sources of background events and background discrimination methods have been investigated for time-of-flight neutron spectrometry with nuclear beam of the JINR synchrotron. DOE

N95-30615# Texas A&M Univ., College Station, TX. Dept. of Physics.
[THE ACTIVITIES OF THE HIGH ENERGY PHYSICS PROGRAM] Annual Report, 1 Oct. 1993 - 30 Sept. 1994
Oct. 1994 150 p
(Contract DE-FG05-91ER-40633)
(DE95-010155; DOE/ER-40633/3) Avail: CASI HC A07/MF A02

The experimental and theoretical high energy physics programs at Texas A and M University have continued their ambitious research activities over the past year. On the experimental side, the authors have continued their participation in two major operating experiments, CDF and MACRO, and each of these programs have attained significant milestones during this period. Especially noteworthy is the CDF Collaborations paper on the 'evidence' for the top quark and MACRO's completion of the construction of the 'Attico.' In CDF, the Texas A and M group continues to play a leading role in the plans for upgrading the silicon vertex detector, as well as supporting the ongoing running of this experiment during its current data taking run. In addition, the group has focused its analysis efforts on studies of trilepton events as well as searching for supersymmetric particles. In MACRO, the authors have continued their work on the development of the final version of the waveform digitizing system. Within the past month the final production circuits have been assembled and they are currently testing these units at Texas A and M. The authors plan to complete this testing and commission the waveform digitizing system on the MACRO detector by the end of 1994. The theoretical high energy physics program has also continued to develop during the past funding cycle. Investigators have continued the study of the successful string-derived model that unifies all known interactions: flipped SU(5), which is the leading candidate for a theory of everything. Work has continued on generalizations of the symmetries of string theory, known as W algebras. DOE

N95-30717 Selskapet for Industriell og Teknisk Forskning, Trondheim (Norway). Div. of Applied Physics.
MAY MULTIPLE INELASTIC SCATTERING IN CBED PATTERNS BE REMOVED ANALYTICALLY
R. Hoeier, K. Marthinsen, and R. Holmestad 21 Apr. 1994 4 p Prepared in cooperation with Trondheim Univ., Norway
(PB95-196333; STF19-S94001) Avail: Issuing Activity (National Technical Information Service (NTIS))

Quantitative convergent beam electron diffraction (CBED) has developed considerably over the last years. One can today determine individual structure factors with high accuracy and some charge density maps with focus on bonding effects have recently been published. This does not mean that the method in its present stage of development is fully established and can be routinely applied. Experimentally the method is both demanding and expensive as both energy filtering for partly removing the background and digital recording is on its way in. The mathematics is based on multiparameter least square fitting between theory and experiment. Here central problems, as for example the number of beams to be included and how to include the Debye-Waller factors even in simple, isotropic, monoatomic specimens, is still disputed. In the present studies, the focus is on the general background formed by inelastic scattering. We shall especially discuss multiple plasmon scattering and the possibility of numerical filtering of the plasmon contributions in the observed CBED intensity.
NTIS

N95-30800# Fermi National Accelerator Lab., Batavia, IL.
BACKGROUNDS AND DETECTOR PERFORMANCE AT A 2 X 2 TeV (MU)(+)(MU)(-) COLLIDER
G. William Foster and Nikolai V. Mokhov Mar. 1995 13 p Presented at the 2nd Workshop on Physics Potential and Development of Mu(+) Mu(-) Colliders, Sausalito, CA, 17-19 Nov. 1994
(Contract DE-AC02-76CH-03000)
(DE95-009107; FNAL/C-95/037; CONF-9411210-1) Avail: CASI HC A03/MF A01

The rich physics potential of a high-energy high-luminosity (mu)(+)(mu)(-) collider and the surprising feasibility of a design attract the attention of many people these days. A few issues define the practicality of such a project, with the enormous particle background levels in a detector due to unavoidable reasons holding first place. In contrast to hadron colliders where particle backgrounds come both from interaction point (IP) and accelerator, almost all the backgrounds in the muon collider detectors arise in the machine. The decay length for 2 TeV muons is (lambda)(sub D)(sup -1) approximately 10(exp -7)/m. With 10(exp 12) muons in a bunch one has 10(exp 5) decays per meter in a single pass through an interaction region, and 10(exp 8) decays per meter per 12 msec store. This paper examines two major classes of detector backgrounds presented in the muon collider: beam halo backgrounds, and the 'direct' backgrounds from electrons from (mu)(yields)e(nu)(bar (nu)) decay occurring in the beam channel. The authors describe the nature of both of these backgrounds, provide results of first realistic calculations for both sources and discuss their effects on plausible detectors. Various shielding and collimation geometries have been simulated, and their efficacy and the nature of the surviving background discussed. DOE

N95-30960# Melbourne Univ., Parkville (Australia). School of Physics.
REFLECTION AND DIFFRACTION OF ATOMIC DE BROGLIE WAVES BY EVANESCENT LASER WAVES. BARE-STATE METHOD
Xiaoping Feng, N. S. Witte, C. L. Hollenberg, and G. Opat 1994 17 p
(DE95-616458; UM-P-94/17) Avail: CASI HC A03/MF A01 (US Sales Only)

Two methods are presented for the investigation of the reflection and diffraction of atoms by gratings formed either by standing or travelling evanescent laser waves. Both methods use the bare-state rather than dressed-state picture. One method is based on the Born series, whereas the other is based on the Laplace transformation of the coupled differential equations. The two methods yield the same theoretical expressions for the reflected and diffracted atomic waves in the whole space including the interaction and the asymptotic regions. DOE

N95-31127# Lawrence Livermore National Lab., Livermore, CA.
HOLLOW CATHODE ELECTRON GUN RESEARCH AND DEVELOPMENT
M. A. Gundersen Aug. 1994 8 p
(Contract W-7405-eng-48)
(DE95-010262; UCRL-CR-118231) Avail: CASI HC A02/MF A01

This work was in support of the development of a high-perveance, low-emittance, high-current hollow-cathode electron beam gun for applications including the Lawrence Livermore National Laboratory's Electron Beam Ion Trap (EBIT). The motivation for developing the hollow-cathode electron beam gun was described in the proposal by B.M. Penetrante, 'Superemissive hollow-cathode electron gun', (LDRD Project No. 92-LW-42). The work at the University of Southern California provided technical support in production and testing of prototypes. DOE

N95-31151# Los Alamos National Lab., NM.
THE LOS ALAMOS ACCELERATOR CODE GROUP
Frank L. Krawczyk, James H. Billen, Robert D. Ryne, Harunori Takeda, and Lloyd M. Young 1995 4 p Presented at the Particle Accelerator Conference and International Conference on High-Energy Accelerators, Dallas, TX, 1-5 May 1995
(Contract W-7405-eng-36)
(DE95-010989; LA-UR-95-1452; CONF-950512-26) Avail: CASI HC A01/MF A01

The Los Alamos Accelerator Code Group (LAACG) is a national resource for members of the accelerator community who use and/or develop software for the design and analysis of particle accelerators, beam transport systems, light sources, storage rings, and components of these systems. Below the authors describe the LAACG's activities in high performance computing, maintenance and enhancement of POISSON/SUPERFISH and related codes and the dissemination of information on the INTERNET. DOE

N95-31165# Fermi National Accelerator Lab., Batavia, IL.
IMPLEMENTATION OF THE SHOWER MAX ELECTRON TRIGGER AT CDF
K. Byrum, J. Dawson, L. Nodulman, A. B. Wicklund, D. Amidei, K. Burkett, D. Gerdes, C. Miao, and D. Wolinski Jun. 1994 18 p Presented at the 27th International Conference on High Energy Physics, Glasgow, Scotland, 20-27 Jul.1994
(Contract DE-AC02-76CH-03000)
(DE95-006684; FNAL/C-94/150-E; CONF-940722-44) Avail: CASI HC A03/MF A01

The authors have built and installed new electronics which brings the central shower max detector into the CDF Level-2 trigger. By matching a stiff track from the central fast track processor to an associated shower max cluster, this trigger improvement reduces the electron Level-2 cross section by approximately 50% while retaining greater than 85% of real electrons and allows the authors to lower their electron trigger threshold.
DOE

N95-31166# Sandia National Labs., Albuquerque, NM.
WORKSHOP ON TRANSPORT FOR A COMMON ION DRIVER
C. C. Olson, E. Lee (California Univ., Berkeley. Lawrence Berkeley Lab, CA.), and B. Langdon (Lawrence Livermore National Lab., Livermore, CA.) 1994 447 p Presented at the Workshop on Transport for a Common Ion Driver, Albuquerque, NM, 20-21 Sep. 1994
(Contract DE-AC04-94AL-85000)
(DE95-007298; SAND-95-0116; CONF-9409304) Avail: CASI HC A19/MF A04

This report contains research in the following areas related to beam transport for a common ion driver: multi-gap acceleration; neutralization with electrons; gas neutralization; self-pinched transport; HIF and LIF transport, and relevance to common ion driver; LIF and HIF reactor concepts and relevance to common ion driver; atomic physics for common ion driver; code capabilities and needed improvement. DOE

N95-31232# Los Alamos National Lab., NM.
PULSE POWER FOR HIGH ENERGY DENSITY PHYSICS EXPERIMENTS
Robert E. Reinovsky 1995 9 p Presented at the Spring Workshop on Basic Science Using Pulsed Power, Santa Barbara, CA, 5-7 Apr. 1995
(Contract W-7405-eng-36)
(DE95-010868; LA-UR-95-1208; CONF-9504132-3) Avail: CASI HC A02/MF A01

Pulse power technology has been supported and developed in the U.S. over the last 4 decades by the Department of Energy in support of the

nuclear weapons and energy research programs, and by the Department of Defense for advanced weapons technology and nuclear weapons effects research. Recent changes in the priorities and orientation of these programs have made the planning and conduct of basic science experiments possible using facilities heretofore completely dedicated to a more narrow range of experimental activities. The purpose of the 'Spring Workshop on Basic Science Using Pulsed Power' is to introduce high performance pulse power technology to a broader cross-section of the community and to discuss, with the community, experiments which can be planned now using currently operating systems and to begin to consider experiments which can be planned for the systems of the future. DOE

N95-31256# Stanford Linear Accelerator Center, Menlo Park, CA
MEASUREMENT OF THE EFFECT OF COLLIMATOR GENERATED WAKEFIELDS ON THE BEAMS IN THE SLC
K. L. F. Bane, C. Adolphsen, F. J. Decker, P. Emma, P. Krejcik, and F. Zimmermann 1995 3 p Presented at the Particle Accelerator Conference, Dallas, TX, 1-5 May 1995
(Contract DE-AC03-76SF-00515)
(DE95-012101; SU-SLAC-PUB-95-6865; CONF-950512-30) Avail: CASI HC A01/MF A01

Collimators with adjustable jaws are used in the SLC linac, arcs, and final focus to eliminate the tails of the beams that produce backgrounds in the SLD detectors. However, if the beams are not centered within the jaws of the collimators, transverse wakefields are generated which act to increase the beam emittances. The sensitivity to the beam offset is largest in the vertical collimators in the linac where the small beam sizes (less than 100 micro m) require that the gap between the jaws be reduced to about a millimeter for effective background reduction. To study the wakefield effect of the collimators, measurements of the induced mean angular kick were made as function of the beam offset in one of the SLC collimators. The authors are interested in both the linear (dipole) behavior near the axis of the collimator and the non-linear behavior near the jaws of the collimator. In this paper they present the results together with a comparison to theoretical predictions. Besides helping them to quantify the effect of the collimators in the SLC these results are also useful in understanding their effect in future linear colliders, in which collimators will also be important components. DOE

N95-31336# Polish Academy of Sciences, Warsaw (Poland). Atomic Frequency Standards Lab.
RESONANCE CHARACTERISTICS IN THE CASE OF THE EXCITATION OF A MONOENERGETIC BEAM OF FREE ATOMS BY MEANS OF N. F. RAMSEY'S METHOD [WLASNOSCI REZONANSOWE W PRZYPADKU POBUDZANIA MONOENERGETYCZNEJ WIAZKI WOLNYCH ATOMOW PRZY ZASTOSOWANIU METODY N. F. RAMSEY'A]
Andrzej Chachulski and Krystyna Drogon Jun. 1995 15 p In POLISH
(ISSN 0208-5658)
(IFTR-6/1995) Avail: CASI HC A03/MF A01

This article contains an analysis of the resonance characteristics of a system with a beam of cesium atoms as a function of the decrease (relative to natural conditions) of the velocity of the atoms and the narrowing of the distribution band of this velocity. In particular, the authors examine the effect of amplitude and phase differences on the probability of a quantum state change for the above examples. Transl. by Schreiber

N95-31405# Brookhaven National Lab., Upton, NY.
THE COUPLING IMPEDANCE OF A TOROIDAL BEAM PIPE WITH CIRCULAR CROSS SECTION
H. Hahn 1995 3 p Presented at the Particle Accelerator Conference, Dallas, TX, 1-5 May 1995
(Contract DE-AC02-76CH-00016)
(DE95-010442; BNL-61223; CONF-950512-9) Avail: CASI HC A01/MF A01

In this paper, the topic of coupling impedances and beam-induced forces in a toroidal beam pipe is revisited. In straight, smooth accelerator beam pipe configurations, the space charge forces on a charged test particle due to beam-induced electric and magnetic fields are subject to a near perfect cancellation in the ultra-relativistic limit. It is well known that in toroidal geometries the cancellation is imperfect, resulting in residual, 'energy-independent' longitudinal and transverse forces which can impact the accelerator performance. Whereas the present-day designs of high-energy hadron accelerators/colliders are based on beam pipes with circular cross section, essentially all theoretical studies assume rectangular geometries, the notable exception being the report by Zotter. The expressions here presented are intended to amend this deficiency. An analytic expression for the non-resonant longitudinal coupling impedance in a toroidal beam pipe with circular cross section is derived using a perturbation treatment carried out in a local orthogonal coordinate system. DOE

N95-31627# Stanford Linear Accelerator Center, Menlo Park, CA
SPIN STRUCTURE IN HIGH ENERGY PROCESSES
L. DePorcel, ed. and C. Dunwoodie, ed. Dec. 1994 593 p Presented at the 21st Annual SLAC Summer Institute on Particle Physics: Spin Structure in High-energy Processes, Stanford, CA, 26 Jul. - 6 Aug. 1993
(Contract DE-AC03-76SF-00515)
(DE95-008628; SU-SLAC-444; CONF-930767) Avail: CASI HC A25/MF A06

This report contains papers of the following topics: Spin, Mass, and Symmetry; physics with polarized Z(sup 0)s; spin and precision electroweak physics; polarized electron sources; polarization phenomena in quantum chromodynamics; polarized lepton-nucleon scattering; polarized targets in high energy physics; spin dynamics in storage rings and linear accelerators; spin formalism and applications to new physics searches; precision electroweak physics at LEP; recent results on heavy flavor physics from LEP experiments using 1990--1992 data; precise measurement of the left-right cross section asymmetry in Z boson production by electron-positron collisions; preliminary results on heavy flavor physics at SLD; QCD tests with SLD and polarized beams; recent results from TRISTAN at KEK; recent B physics results from CLEO; searching for the H dibaryon at Brookhaven; recent results from the compton observatory; the spin structure of the deuteron; spin structure of the neutron ((sup 3)HE) and the Bjoerken sum rule; a consumer's guide to lattice QCD results; top ten models constrained by b yields sy; a review of the Fermilab fixed target program; results from the D0 experiment; results from CDF at FNAL; quantum-mechanical suppression of bremsstrahlung; report from the ZEUS collaboration at HERA; physics from the first year of H1 at HERA, and hard diffraction. These papers have been cataloged separately elsewhere. DOE

N95-31647 Northwestern Univ., Chicago, IL.
A STUDY OF ION TRAPPING AND INSTABILITY IN THE FERMILAB ANTIPROTON ACCUMULATOR Ph.D. Thesis
Ping Zhou 1993 149 p
Avail: Univ. Microfilms Order No. DA9415841

In particle accelerators, electron-ion pairs are constantly created by beam particle collision with residual gas molecules. The beam may trap opposite charged ions. If uncorrected, trapped ions may cause beam instability and beam loss, and limit accelerator performance. The ion trapping problem especially related to the Fermi-lab antiproton accumulator, where the beam is unbunched and negatively charged, is studied here. The old clearing electrode system is found to be insufficient for complete ion clearing. The proposed upgrade to the clearing electrode system greatly improved the performance of the machine. Incomplete ion clearing is found to directly contribute to beam coherent oscillation and therefore beam coherent instability. A model has been developed which includes the effect of trapped ions in the normal beam coherent instability treatment with conventional machine impedance. It is found that the effect of trapped ions on the beam coherent instability can be described as a form of impedance. Together with physical arguments, it can be used to explain some of the behavior of the beam coherent instability observed in the accumulator. An Ion Detector and Energy Analyzer system was developed which provides the ability to directly monitor the ions coming out of the beam and measure their energy spectrum. Ions are observed to interact with explosive coherent oscillations that lead to emittance blowups. The ion energy distribution extends to much higher energy than expected. The flux of ions escaping with cool, stable beam is also higher than previously thought. The main subject of the study is related only to ion trapping in a DC beam, although a few issues are illustrated with a case study on the Tevatron with separated orbits of proton and antiproton beams. Dissert. Abstr.

N95-32042# Lawrence Livermore National Lab., Livermore, CA.
EXCITATION MECHANISMS OF 2s(SUB 1/2)-2p(SUB 3/2) AND 2p(SUB 1/2)-2p(SUB 3/2)IN U(82+) THROUGH U(89+)

V. Decaux, P. Beiersdorfer, and A. Osterheld 14 Sep. 1994 10 p Presented at the 7th International Conference on Physics of Highly Charged Ions, Vienna, Austria, 19-23 Sep. 1994
(Contract W-7405-eng-48)
(DE95-010265; UCRL-JC-118363; CONF-940922-7) Avail: CASI HC A02/MF A01

A model based on detailed calculations of the electron-impact excitation of n = 2 electrons in the Li- to Ne-like uranium ions was developed to interpret and explain measurements on EBIT (Electron Beam Ion Trap). While only considering the direct excitation process provided a good model for the electric dipole (El) transitions, it was necessary for the magnetic dipole (Ml) spectrum to include various additional excitation processes in the model. In particular, the model was expanded to include electron-impact excitation of n = 3 levels followed by radiative cascades. Moreover, excitation by the ionization of 2s(sub 1/2), 2p(sub 1/2), and 2p(sub 3/2) electrons and by radiative capture of beam electrons into excited levels was added. The new model demonstrates that the dipole-forbidden lines are almost exclusively produced by indirect excitation processes. DOE

N95-32059# Brookhaven National Lab., Upton, NY.
PHYSICS GOALS OF A MU(+) MU(-) COLLIDER
V. Barger, M. S. Berger (Indiana Univ., Bloomington, IN.), K. Fujii (National Lab. for High Energy Physics, Ibaraki, Japan.), J. F. Gunion (California Univ., Davis, CA.), T. Han (California Univ., Davis, CA.), C. Heusch (California Univ., Santa Cruz, CA.), W. Hong (California Univ., Los Angeles, CA.), S. K. Oh, Z. Parsa, and S. Rajpoot (California State Univ., Stanislaus, CA.) et al Mar. 1995 16 p Presented at the 2nd Workshop on Physics Potential and Development of Mu(+) Mu(-) Colliders, Sausalito, CA, 17-19 Nov. 1994
(Contracts DE-AC02-76CH-00016; DE-FG02-95ER-40896; DE-FG03-91ER-40674)
(DE95-009546; BNL-61593; CONF-9411210-2) Avail: CASI HC A03/MF A01

This working group report focuses on the physics potential of mu(+) mu(-) colliders beyond what can be accomplished at linear e(+)e(-) colliders and the LHC. Particularly interesting possibilities include: (1) s-channel resonance production to discover and study heavy Higgs bosons with ZZ and WW couplings that are suppressed or absent at tree-level (such as the H and A Higgs bosons of supersymmetric models); (2) study of the strongly interacting electroweak sector, where higher energies give larger signals; and (3) measurements of the masses and properties of heavy supersymmetric particles. DOE

N95-32074# Lawrence Livermore National Lab., Livermore, CA.
THE HYLIFE-2 INERTIAL FUSION ENERGY POWER PLANT CONCEPT AND IMPLICATIONS FOR IFE
Ralph W. Moir Nov. 1994 9 p Presented at the Meeting of the Division of Plasma Physics of the American Physical Society, Minneapolis, MN, 7-11 Nov. 1994
(Contract W-7405-eng-48)
(DE95-010561; UCRL-JC-119070; CONF-941101-10) Avail: CASI HC A02/MF A01

HYLIFE-II is based on nonflammable, renewable-liquid-wall fusion target chambers formed with Li2BeF4 molten-salt jets, a heavy-ion driver, and single-sided illumination of indirect-drive targets. Building fusion chambers from existing materials with life-of-plant structural walls behind the liquid walls, while still meeting non-nuclear grade construction and low-level waste requirements, has profound implications for IFE development. Fluid-flow work and computational fluid dynamics predict chamber clearing adequate for 6-Hz pulse rates. Predicted electricity cost is reduced about 30% to 4.4 cents/kWh at 1 GWe. Development can be foreshortened and cost reduced by obviating expensive neutron sources to develop first-wall materials. The driver and chamber can be upgraded in stages, avoiding separate and sequential facilities. The most important features of a practical inertial fusion power plant are sufficient ignition and gain in targets; a low-cost, efficient, rep-ratable driver; and low-cost targets. DOE

N95-32092# Brookhaven National Lab., Upton, NY.
RADIAL MODE EVOLUTION IN LONGITUDINAL BUNCHED BEAM INSTABILITY
S. Y. Zhang and W. T. Weng 1995 4 p Presented at the Particle Accelerator Conference, Dallas, TX, 1-5 May 1995
(Contract DE-AC02-76CH-00016)
(DE95-010895; BNL-61070; CONF-950512-40) Avail: CASI HC A01/MF A01

An indispensable aspect of the bunched beam instability mechanism is the variation of the particle distribution with respect to the beam intensity. This density variation can be shown as the evolution of radial modes. The radial modes, which are determined by the stationary particle distribution and the impedance, represent the coherence of the particle density variation governed by the Vlasov equation. Using this coherence in the beam instability analysis gives rise to not only the computational efficiency but also the physical insight into the instability mechanism. The evolution of the radial modes displays several interesting properties for the cases without and with synchrotron frequency spread. If the azimuthal mode coupling cannot be neglected, then corresponding to each coherent frequency shift there exists an extended radial mode which includes the interactions from other azimuthal modes. In this article, the radial mode evolution and the related physical implications will be discussed, which are useful for the understanding of the beam instabilities, and also useful for the beam diagnostics. DOE

N95-32242# Brookhaven National Lab., Upton, NY.
KRAKEN, A NUMERICAL MODEL OF RHIC IMPEDANCES
S. Peggs and V. Mane 1995 4 p Presented at the Particle Accelerator Conference, Dallas, TX, 1-5 May 1995
(Contract DE-AC02-76CH-00016)
(DE95-011563; BNL-61166; CONF-950512-59) Avail: CASI HC A01/MF A01

The simulation code KRAKEN confirms analytical predictions of head-tail stability criteria, in the presence of momentum dependent linear coupling. It also confirms that resistive wall transverse wake fields are not a serious threat to strong head-tail stability in RHIC, at the vulnerable stage of proton injection. Equation 10, derived from the perspective of two macroparticles, potentially offers a very convenient seminumerical evaluation of the effects of arbitrary transverse wake potentials. It remains to be seen how well the two macroparticle results correlate with simulations using, say, 100 macroparticles. KRAKEN is still under rapid development. Future plans are to include resonant wakefields, multiple bunches, space charge wakefields, betatron detuning, and a connection to the detailed RHIC impedance database. DOE

N95-32243# Brookhaven National Lab., Upton, NY.
SKEW CHROMATICITY IN LARGE ACCELERATORS
S. Peggs and G. F. Dell 1995 4 p Presented at the Particle Accelerator Conference, Dallas, TX, 1-5 May 1995
(Contract DE-AC02-76CH-00016)
(DE95-011564; BNL-61167; CONF-950512-60) Avail: CASI HC A01/MF A01

The 2-D 'skew chromaticity' vector k is introduced when the standard on-momentum description of linear coupling is extended to include off-momentum particles. A lattice that is well decoupled on-momentum may be badly decoupled off-momentum, inside the natural momentum spread of the beam. There are two general areas of concern: (1) the free space in the tune plane is decreased; (2) collective phenomena may be destabilized. Two strong new criteria for head-tail stability in the presence of off-momentum coupling are derived, which are consistent with experimental and operational observations at the Tevatron, and with tracking data from RHIC. DOE

N95-32244# Brookhaven National Lab., Upton, NY.
NORMAL MODE TUNES FOR LINEAR COUPLED MOTION IN SIX DIMENSIONAL PHASE SPACE
G. Parzen 1995 3 p Presented at the Particle Accelerator Conference, Dallas, TX, 1-5 May 1995
(Contract DE-AC02-76CH-00016)
(DE95-011565; BNL-61168; CONF-950512-61) Avail: CASI HC A01/MF A01

The motion of a particle in 6-dimensional phase space in the presence of linear coupling can be written as the sum of 3 normal modes. A cubic equation is found for the tune of the normal modes, which allows the normal mode tunes to be computed from the 6 x 6 one turn transfer matrix. This result is similar to the quadratic equation found for the normal mode tunes for the motion of a particle in 4-dimensional phase space. These results are useful in tracking programs where the one turn transfer

matrix can be computed by multiplying the transfer matrices of each element of the lattice. The tunes of the 3 normal modes for motion in 6-dimensional phase space can then be found by solving the cubic equation. Explicit solutions of the cubic equation for the tune are given in terms of the elements of the 6 x 6 one turn transfer matrix. DOE

N95-32260# Brookhaven National Lab., Upton, NY.
BEAM STABILITY AT SRRC STORAGE RING
W. T. Weng (Synchrotron Radiation Research Center, Hsinchu, Taiwan.), H. P. Chang (Synchrotron Radiation Research Center, Hsinchu, Taiwan.), J. R. Chen (Synchrotron Radiation Research Center, Hsinchu, Taiwan.), Y. Cheng (Synchrotron Radiation Research Center, Hsinchu, Taiwan.), K. T. Hsu (Synchrotron Radiation Research Center, Hsinchu, Taiwan.), C. C. Kuo (Synchrotron Radiation Research Center, Hsinchu, Taiwan.), J. C. Lee (Synchrotron Radiation Research Center, Hsinchu, Taiwan.), K. K. Lin (Synchrotron Radiation Research Center, Hsinchu, Taiwan.), Y. C. Liu (Synchrotron Radiation Research Center, Hsinchu, Taiwan.), and G. H. Luo (Synchrotron Radiation Research Center, Hsinchu, Taiwan.) et al 1995 4 p Presented at the Particle Accelerator Conference, Dallas, TX, 1-5 May 1995
(Contract DE-AC02-76CH-00016)
(DE95-010842; BNL-61719; CONF-950512-21) Avail: CASI HC A01/MF A01

To satisfy the need of users of the synchrotron radiation at SRRC, the photon flux at the end station has to be kept at a constant with minimum fluctuation. The sources of flux variation attributable to the electron beam in the storage ring have been carefully studied and the effects on the flux have been investigated. The sources include floor vibration, power supply ripples, cooling water, ion trapping and transverse instability. The cures attempted or in plan include removal of vibration sources, reduction of ripple, local orbit feedback, ion cleaning and damping. A special diagnostic beamline has been constructed and used solely for accelerator studies and improvements. DOE

N95-32262# Japan Atomic Energy Research Inst., Tokyo (Japan).
DESIGN STUDY OF PROTOTYPE ACCELERATOR AND MeV TEST FACILITY FOR DEMONSTRATION OF 1 MeV, 1 A NEGATIVE ION BEAM PRODUCTION
Takashi Inoue, Masaya Hanada, Kenji Miyamoto, Yoshihiro Ohara, Yoshikazu Okumura, Kazuhiro Watanabe (Japan Atomic Energy Research Inst., Ibaraki, Japan.), and Shuichi Maeno (Nissin Electric Mfg. Co. Ltd., Tokyo, Tokyo, Japan.) Aug. 1994 95 p
(DE95-737208; JAERI-Tech-94-007) Avail: CASI HC A05/MF A01

In fusion reactors such as ITER, a neutral beam injector of MeV class beam energy and several tens MW class power is required as one of candidates of heating and current drive systems. However, the beam energy of existing high power accelerators are one order of magnitude lower than the required value. In order to realize a neutral beam injector for the fusion reactor, 'Proof-of-Principle' of such high energy acceleration is a critical issue at a reactor relevant beam current and pulse length. An accelerator and an accelerator facility which are necessary to demonstrate the Proof-of-Principle acceleration of negative ion beams up to 1 MeV, have been designed in the present study. The accelerator is composed of a cesium-volume type ion source and a multi-stage electrostatic acceleration system 'Prototype Accelerator'. A negative hydrogen ion beam with the current of about one ampere (1 A) can be accelerated up to 1 MeV at a low operating pressure. Two types of acceleration systems, a multi-multi type and a multi-single type, have been studied. The test facility has sufficient capability for the test of the Prototype Accelerator (MeV Test Facility). The dc high voltage generator for negative ion acceleration is a Cockcroft-Walton type and capable of delivering 1 A at 1 MV (=1 MW) for 60 s. High voltage components including Prototype Accelerator are installed in a SF(sub 6) vessel pressurized at 6 kg/cm(exp 2) to overcome high voltage gradients. The vessel and the beamline are installed in a X-ray shield. DOE

N95-32296# Joint Inst. for Nuclear Research, Dubna (USSR). Lab. of Theoretical Physics.
RADIATIVE CORRECTIONS TO THE THREE QUANTUM ANNIHILATION CROSS SECTION IN HIGH ENERGY ELECTRON-POSITRON COLLISIONS
E. A. Kuraev and Z. K. Silagadze (Academy of Sciences, USSR, Novosibirsk, USSR.) 1994 7 p In RUSSIAN Submitted for publication in Yadernaya Fizika
(DE95-623675; JINR-R-2-94-324) Avail: CASI HC A02/MF A01 (US Sales Only)

The radiative corrections to the large-angle three photon annihilation differential cross section in high energy electron-positron collisions are calculated in logarithmic approximation. We show that the result can be written in the form of Drell-Yan process cross section. The accuracy of logarithmic approximation is estimated to be 4-6%. DOE

N95-32297# Brookhaven National Lab., Upton, NY.
TUNE MODULATION DUE TO SYNCHROTRON OSCILLATIONS AND CHROMATICITY, AND THE DYNAMIC APERTURE
G. Parzen 1995 3 p Presented at the Particle Accelerator Conference, Dallas, TX, 1-5 May 1995
(Contract DE-AC02-76CH-00016)
(DE95-011566; BNL-61169; CONF-950512-62) Avail: CASI HC A01/MF A01

A tracking study was done of the effects of a tune modulations, due to synchrotron oscillations and the tune dependence on momentum (chromaticity), on the dynamic aperture. The studies were done using several RHIC lattices and tracking runs of about 1 x 10(exp 6) turns. The dynamic aperture was found to decrease roughly linearly with the amplitude of the tune modulation. Lower order nonlinear resonances, like the 1/3 and 1/4 resonance, are not crossed because of the tune modulation. Three different cases were studied, corresponding to RHIC lattices with different beta*, and with different synchrotron oscillation amplitudes. In each case, the tune modulation amplitude was varied by changing the chromaticity. In each case, roughly the same result was found. The result found here for the effect of a tune modulation due to chromaticity may be compared with the result found for the effect of a tune modulation due to a gradient ripple in the quadrupoles. The effect of a tune modulation due to a gradient ripple appears to be about four times stronger than the effect of a tune modulation due to chromaticity and synchrotron oscillations. DOE

N95-32306# Brookhaven National Lab., Upton, NY.
RFQ-DTL MATCHING SOLUTIONS FOR DIFFERENT REQUIREMENTS
D. Raparia 1995 4 p Presented at the Particle Accelerator Conference, Dallas, TX, 1-5 May 1995
(Contract DE-AC02-76CH-00016)
(DE95-010897; BNL-61181; CONF-950512-42) Avail: CASI HC A01/MF A01

The Radio-Frequency Quadrupole (RFQ) has a FODO lattice and Drift-Tube-Linacs (DTL) in general also have FODO lattices. Therefore the natural solution for the matching between these is a FODO lattice. For matching in all three planes one then needs sixteen degrees of freedom. However different requirements, depending on the applications, may change this solution. For example, in the production environment (like medical and industrial applications), one needs fixed current and fixed beam quality. On the other hand, in the research environment one not only needs all degrees of freedom, but may also want the chopping of beam pulse length. This paper discusses matching solutions for these different requirements. DOE

74 OPTICS

Includes light phenomena; and optical devices.
For lasers see *36 Lasers and Masers.*

N95-30402 Department of the Navy, Washington, DC.
DEMODULATORS FOR OPTICAL FIBER INTERFEROMETERS WITH (3 X 3) OUTPUTS Patent
Robert M. Keolian, inventor (to Navy), Steven L. Garrett, inventor (to Navy), and Charles B. Cameron, inventor (to Navy) 17 May 1994 41 p Filed 17 Aug. 1992
(AD-D017415; US-Patent-5,313,266; US-Patent-Appl-SN-931228; US-Patent-Class-356-345) Avail: US Patent and Trademark Office

A highly sensitive optical fiber interferometer sensor comprising a laser light source, a (2 x 2) optical fiber coupler to split the beam in two, a differential transducer which converts a signal of interest into optical phase shift in the laser light transmitted through the two optical fibers in the interferometer and a (3 x 3) optical fiber complex which recombines the

two beams, producing interference which can be electronically detected. The use of the (3 x 3) coupler permits Passive Homodyne demodulation of the phase-modulated signals provided by the interferometer without feedback control or modulation of the laser itself and without requiring the use of electronics within the interferometer. DTIC

N95-30529 Department of the Navy, Washington, DC.
PASSIVE, MULTI-CHANNEL FIBER OPTIC ROTARY JOINT ASSEMBLY Patent
Gregory H. Ames, inventor (to Navy) and Roger L. Morency, inventor (to Navy) 6 Dec. 1994 14 p Filed 8 Nov. 1993
(AD-D017353; US-Patent-5,371,814; US-Patent-Appl-SN-151396; US-Patent-Class-385-25) Avail: US Patent and Trademark Office

A passive multi-channel optical fiber rotary joint couples optical fiber communication channels via axially bilaterally symmetrically disposed lens housings, or array pieces, for receiving miniature-collimation-lenses to one and the other sides of an image-derotation-prism and prism-rotational-drive-subassembly including an image derotation prism which rotates at a predetermined ratio of the relative rotation of the array pieces. This establishes transverse pseudo-planar rotary interfaces respectively between the one and another array piece and the confronting sides of the prism-and-prism- drive-subassembly. Each channel, at the axially outward side of each of one and the other array pieces, includes a fiber and lens junction in which the fiber is attached to the axially outward side of the collimation lens at a predetermined axially bilaterally symmetrical position chosen for maximum coupling of signal power through the joint, and individual lateral positions relative to the lens chosen to provide coupling with a path of beam propagation perpendicular to the rotary interface at the other side of the collimation lens. Each array piece forms a precision tolerance locality of axial engagement with the confronting side of the prism-and -prism -drive-subassembly, which in turn defines the respective rotary interfaces. DTIC

N95-30678 Department of the Navy, Washington, DC.
PASSIVE RANGE MEASUREMENT SYSTEM Patent
Walter L. Harriman, inventor (to Navy) 22 Nov. 1994 6 p Filed 27 Jul. 1992
(AD-D017344; US-Patent-5,367,333; US-Patent-Appl-SN-921863; US-Patent-Class-348-117) Avail: US Patent and Trademark Office

A method and apparatus provides instantaneous passive range measurement onboard an aircraft for determining the range between the aircraft and a target. The target may either be stationary and on the Earth's surface, or a slower moving vehicle. Calculation of the desired range is achieved using the formula: Range = Sin a/Sin b V; where a = angle from aircraft heading to target, b = turning rate; and V = ground velocity. The apparatus consists of an automatic video tracker, a video camera, and a servo controlled aiming platform. A resolver on the aiming platform is utilized to determine the angle from the aircraft axis to the target. This angle is added to the aircraft drift angle to determine the total angle from the aircraft heading to the target. The video tracker is utilized to determine the turning rate of the aiming platform. Using the difference in contrast between the target and the background of the video scene, the tracker provides error signals (azimuth and elevation) to keep the aiming platform pointed at the target. The azimuth error signal determines the turning rate of the aiming platform. The total turning rate is determined by adding the aiming platform turning rate to the aircraft turning rate obtained from the aircraft inertial system. DTIC

N95-30679 Department of the Navy, Washington, DC.
OPTICAL FIBER PRESSURE SENSOR FOR LIQUID LEVEL MONITORING Patent
Frank W. Cuomo, inventor (to Navy) 6 Dec. 1994 7 p Filed 22 Feb. 1994
(AD-D017346; US-Patent-5,371,720; US-Patent-Appl-SN-199868; US-Patent-Class-367-149) Avail: US Patent and Trademark Office

An apparatus for continuously monitoring changes in a liquid level in accordance with a differential pressure is provided. A sensor body immersed in the liquid supports two thin-filmed metallic diaphragms that are independently axially responsive to pressure of the liquid. Each diaphragm has a different modulus of elasticity. Two fiber optic pressure sensors are mounted within an air space encased by the sensor body in combination with the two diaphragms. Each of the two fiber optic pressure sensors detects the axial response of one of the two diaphragms. The displacement difference between the two diaphragms is an indication of differential pressure related to the liquid level. DTIC

N95-30724 Department of the Navy, Washington, DC.
ULTRASONIC TWO PROBE SYSTEM FOR LOCATING AND SIZING Patent
Errol E. Wallingford, inventor (to Navy) and Robert DeNale, inventor (to Navy) 24 Jan. 1995 21 p Filed 26 Oct. 1992
(AD-D017438; US-Patent-5,383,366; US-Patent-Appl-SN-966825; US-Patent-Class-73-602) Avail: US Patent and Trademark Office

A two probe time-of-flight system has a transmit probe emitting a diverging beam into a test material at a certain beam-center angle, and a receive probe with its main beam extending into the test material at that same angle, with the two probes being arranged symmetrical about a centerline normal to the test face. The transmit probe generates a pulse wherein a portion of the pulse reflects at the incident angle back to the receive probe, which detects the reflections and marks the reception time as a reference. A sampling unit captures subsequent echo energy returning from a region within the test material. The sampled energy above a given threshold is processed to identify the sample times relative to the marked reference time. The identified sample times are used to determine the depth that the echo energy originated from. Consecutive identified samples in the depth direction are used to detect the height of a flaw within the test material. By scanning the probes in an x-y pattern, the planar dimensions of the flaw are determinad. DTIC

N95-30753 Department of the Navy, Washington, DC.
FIBER OPTIC INTERFEROMETRIC ELECTRIC FIELD AND VOLTAGE SENSOR UTILIZING AND ELECTROSTRICTIVE TRANSDUCER Patent
Sandeep T. Vohra, inventor (to Navy), Frank Bucholtz, inventor (to Navy), and Alan D. Kersey, inventor (to Navy) 7 Mar. 1995 11 p Filed 27 Aug. 1992
(AD-D017433; US-Patent-5,396,166; US-Patent-Appl-SN-936986; US-Patent-Class-324-96) Avail: US Patent and Trademark Office

A fiber optic interferometer sensor system utilizing a fiber optic interferometer with an elecrostrictive transducer bonded to one of first and second optical fiber arms of the interferometer for obtaining excellent low frequency voltage detectors and electric field sensors. The non-linear characteristics of the electrostrictive transducer allows for detecting low frequency or dc signals at sidebands of a high frequency carrier, resolving extremely small voltages at low frequencies, or sensing low frequency electric fields. Examples of electrostrictive material include Ba:PZT, PLZT, PMN+PT, and other doped ferroelectric relaxors. DTIC

N95-30772*# Transition Research, Inc., Danbury, CT.
LOG-POLAR BINOCULAR VISION SYSTEM Final Report
Carl F. R. Weinman Dec. 1994 91 p
(Contract NAS9-18637; SBIR-09.05-8988A)
(NASA-CR-188375; NAS 1.26:188375) Avail: CASI HC A05/MF A01

The objective of this research is to develop and implement new techniques for real time stereo vision for robots, based on active binocular vision using log-polar pixel layout and novel Gabor filter processing. The active vision platform is a high performance servo controlled binocular mount designed and built under this project. It emulates the articulation and speed of the human eye-head system. High performance processing is based on local Gabor filters embedded in global log-polar image plane geometry. This choice of geometry and processing, developed from first principles, closely resembles the structure and function of the primate retina and visual cortex. Binocular stereo vision is demonstrated on an autonomous mobile robot equipped with active binocular vision. Using real time visual guidance, the robot can perceive 3D environments and maneuver according to its perceptions. The new approach to vision relieves the computational bottlenecks of conventional machine vision, and provides robust sensory information which is well suited to real time maneuvering and manipulation. Space applications include eye-hand coordination for manipulators and high precision passive sensing for docking. Commercial applications include 3D visual telepresence for remote inspection and repair in nuclear and hazardous environments, visual autopilot for autonomous vehicles, and real time vision for robot arms in unstructured manipulation environments. The latter includes semi-autonomous aides for the elderly and handicapped. Author

N95-30849*# National Aeronautics and Space Administration. Lewis Research Center, Cleveland, OH.

CALCULATED COUPLING EFFICIENCY BETWEEN AN ELLIPTICAL-CORE OPTICAL FIBER AND AN OPTICAL WAVEGUIDE OVER TEMPERATURE

Margaret L. Tuma, Andreas Weisshaar, Jian Li, and Glenn Beheim Jul. 1995 14 p Presented at the International Symposium on Optical Science, Engineering, and Instrumentation, San Diego, CA, 8-14 Jul. 1995; Sponsored by Society of Photo-Optical Instrumentation Engineers

(RTOP 505-62-50)

(NASA-TM-107005; E-9787; NAS 1.15:107005) Avail: CASI HC A03/MF A01

To determine the feasibility of coupling the output of a single-mode optical fiber into a single-mode rib waveguide in a temperature varying environment, a theoretical calculation of the coupling efficiency between the two was investigated. Due to the complex geometry of the rib guide, there is no analytical solution to the wave equation for the guided modes, thus, approximation and/or numerical techniques must be utilized to determine the field patterns of the guide. In this study, three solution methods were used for both the fiber and guide fields; the effective-index method (EIM), Marcatili's approximation, and a Fourier method. These methods were utilized independently to calculate the electric field profile of each component at two temperatures, 20 C and 300 C, representing a nominal and high temperature. Using the electric field profile calculated from each method, the theoretical coupling efficiency between an elliptical-core optical fiber and a rib waveguide was calculated using the overlap integral and the results were compared. It was determined that a high coupling efficiency can be achieved when the two components are aligned. The coupling efficiency was more sensitive to alignment offsets in the y direction than the x, due to the elliptical modal field profile of both components. Changes in the coupling efficiency over temperature were found to be minimal. Author

N95-30901# Air Force Systems Command, Wright-Patterson AFB, OH. National Air Intelligence Center.

REAL TIME CORRELATING OPERATION ON DIFFUSE OBJECTS

Wang Tianji, Yang Shining, Li Y. Tang, and Zhang S. Chao 1995 11 p

(AD-A293220; NAIC-ID(RS)T-0373-94) Avail: CASI HC A03/MF A01

Real time correlating operations on diffuse objects are an expansion and outgrowth on 2-D transparent objects. A real time optical correlator with two transparent pieces is made using photorefractive crystal Bi12SiO20 (BSO) and noncrystal membrane As2S3 as recording media (1-3). Due to the absence of wave filter that is associated with the typical real time optical correlator, this enables the two transparent pieces to have real time correlation and have potential applications in feature recognition. However, test object and reference object have to be in transparent state. In reality, most objects that need to be recognized tend to be diffuse objects, or they have to rely on natural light (incoherent light) for lightening. The realization of real time correlation on two diffuse objects or incoherent light images remains to be fulfilled. DTIC

N95-30908# Air Force Systems Command, Wright-Patterson AFB, OH. National Air Intelligence Center.

OPTICAL LOGIC AND SIGNAL PROCESSING USING A SEMICONDUCTOR LASER DIODE-BASED OPTICAL BISTABILITY DEVICE

Yuancheng Zhang, Qian Song, and Shaowei He 23 Feb. 1995 13 p Transl. into ENGLISH from Jiguang Zazhi, China, v. 13, no. 1, Feb. 1992

(AD-A293248; NAIC-ID(RS)T-0411-94) Avail: CASI HC A03/MF A01

Using an optical fibre-coupled semiconductor laser diode OBD with output feedback pumping operation in 5 modes (differential gain, bistability, zero-bias, inverted differential gain, and inverted bistability) has been realized respectively, and 5 elementary optical logic functions (AND, OR, NOT, NAND, and NOR) and some optical signal processing such as limiting, reshaping, and triggering have been implemented. DTIC

N95-30909# Air Force Systems Command, Wright-Patterson AFB, OH. National Air Intelligence Center.

A STUDY OF END-FIRE COUPLING OF SINGLE-MODE FIBER TO TI: LINBO3-SINGLE-MODE PLANAR WAVEGUIDE

Zhao Qinghua, Gai Junjie, Fan Junqing, and Xu Chengjie 6 Mar. 1995 15 p Transl. into ENGLISH from Faguang Xue Bao, China, v. 12, no. 3, Sep. 1991 p 1

(AD-A293249; NAIC-ID(RS)T-0420-94) Avail: CASI HC A03/MF A01

Most of the widely studied modulator, switch, spectrum analyzer in integrated optics use Ti-diffused LiNbO3 waveguides. Improving single-mode fiber to waveguide coupling efficiency and realizing the fixed connection between them is one of the most fundamental problems. In our experiment, a direct coupling of single-mode fiber to waveguide is used. The major limiting factor in coupling is the uneven profile of mode field of the single-mode fiber and waveguide, and the accuracy in transverse realignment between them. By using single-mode fiber microlens, the transverse field can be evenly adjusted. By using 2-D etched silicone V groove as a micromodulator, the alignment accuracy between them can be fine tuned. The maximum value for the coupling is measured at 64%, and the coupling has also been found very stable. DTIC

N95-30966# Air Force Systems Command, Wright-Patterson AFB, OH. National Air Intelligence Center.

OPTICAL FEATURE RECOGNITION

Song F. Jun 6 Mar. 1995 21 p Transl. into ENGLISH from Wuli, China, v. 20, no. 12, Dec. 1991

(AD-A293168; NAIC-ID(RS)T-0366-94) Avail: CASI HC A03/MF A01

Compared with digital image recognition technology optical feature recognition has faster speed and larger capacity for information processing, therefore it lies at the cutting edge of real time recognition technology trends. Here I will summarize the development of optical feature recognition and discuss physical models on Vander Lugt pairwise wave filter and joint interchangeable correlation recognition method, and introduce an optical-electrical real time correlation recognition system which utilizes spatial light modulator. DTIC

N95-30973# Massachusetts Univ., Lowell, MA.

LASER-INDUCED HOLOGRAPHIC SURFACE RELIEF GRATINGS ON NONLINEAR OPTICAL POLYMER FILMS Technical Report, 1 Oct. 1994 - 30 Sep. 1995

D. Y. Kim, L. Li, J. Kumar, and S. K. Tripathy 30 Mar. 1995 13 p

(Contract N00014-90-J-1148)

(AD-A293169; TR-95-02) Avail: CASI HC A03/MF A01

We report observation of holographic surface relief gratings with relatively large amplitude on a second order nonlinear optical polymeric material. Surface relief gratings on these polymer films were created upon exposure to polarized Ar+ laser beams at 488 nm without any subsequent processing steps. The surface structure of the relief gratings was investigated by atomic force microscopy. The depth of the surface relief in a typical case was 140 nm which is approximately 25% of the original film thickness. Diffraction efficiency of gold-coated gratings were investigated as a function of wavelength and capability of recording orthogonal gratings on the same film was demonstrated. DTIC

N95-31005 Louisville Univ., KY. Dept. of Physics.

DEPSCOR92-WIDE FIELD SPECTRAL IMAGER Final Report, 30 Sep. 1993 - 29 Sep. 1994

John A. Kielkopf 29 Sep. 1994 20 p Limited Reproducibility: More than 20% of this document may be affected by poor print

(Contract F49620-93-1-0559)

(AD-A293079; AFOSR-95-0220TR) Avail: Issuing Activity (Defense Technical Information Center (DTIC))

The Wide Field Spectral Imager (WISPI) project was designed to provide a new capability for measuring the spectrum of the sky across fields of view much larger than the full moon. The instrument which we proposed would use a high speed optical system to form an image on the entrance slit of a matching stigmatic spectrometer, which would then disperse a spectrum of a strip of the sky onto a sensitive two-dimensional detector. A separate imaging system would be used for pointing and tracking, and both instruments would be on a computer controlled mounting that would permit automated data acquisition. Data from the instrument could be acquired remotely and then stored and analyzed on a high speed workstation. DTIC

N95-31006# Air Force Systems Command, Wright-Patterson AFB, OH. National Air Intelligence Center.
PHASE OBJECT DISPLAY BY USING ACOUSTO-OPTICAL BRAGG DIFFRACTION
Xie Yongchang 23 Feb. 1995 14 p Transl. into ENGLISH from Guangxue Xuebao, China, v. 10, no. 10, Oct. 1990 p 9
(AD-A293153; NAIC-ID(RS)T-0410-94) Avail: CASI HC A03/MF A01

Based on the method of phase object display, this article proposes the possibility of showing the phase gradient of an object that can be realized by the acousto-optical Bragg diffraction. Mathematical formulas are derived and a discussion is presented. DTIC

N95-31114# Harvard Univ., Cambridge, MA.
X-RAY STANDING WAVE INTERFEROMETRY-OPTICS AT 1 ANGSTROM WITH APPLICATIONS TO SURFACE AND MATERIAL SCIENCES Final Report
1995 10 p
(Contract DE-FG02-89ER-45399)
(DE95-011453; DOE/ER-45399/T2) Avail: CASI HC A02/MF A01

The goal of this proposal was to advance basic knowledge in x-ray optics by continuing to apply and refine x-ray standing wave interferometric methods of studying crystal surfaces and by developing new x-ray optical methods to probe matter. This report is divided into two sections outlining the accomplishments made first in the area of applying crystal optics to the study of crystal surfaces, and secondly in the more general area of developing new crystal optics. DOE

N95-31141# SRI International Corp., Menlo Park, CA.
IR MATERIALS PRODUCIBILITY Quarterly Technical Report, Sep. - Nov. 1994
M. A. Berding, Sr., A. Sher, and S. Krishnamurthy, Sr. 13 Apr. 1995 47 p
(Contract MDA972-92-C-0053; ARPA Order 8557)
(AD-A293330; SRI-3820) Avail: CASI HC A03/MF A01

The work summarized in this report covers the ninth quarter of a program with a goal that is threefold: first, to study the properties of native point defects in infrared focal-plane array (IRFPA) active and substrate materials; second, to study the properties of native point defects in two classes of photonic materials, the wide-gap 2-6 compounds (ZnSe as the prototype for which impurity properties will also be calculated) and the nonlinear optical materials (LiNbO3 as the prototype); the third, to study the properties of HgZnTe as a very-long-wave infrared (VLWIR) detector material. During the ninth quarter: Completed the calculation of the Hall coefficient in HgCdTe and related materials. Completed two papers for presentation at the MCT workshop. DTIC

N95-31192# Research Sciences Corp., Lexington, MA.
MEASUREMENT AND ANALYSIS RELATED TO INFRARED EMISSIONS Final Report, 6 Jun. 1991 - 30 Sep. 1994
R. E. Murphy, M. H. Bruce, B. D. Green, and G. A. Vanasse 30 Sep. 1994 256 p
(Contract F19628-91-C-0042)
(AD-A293296; PL-TR-94-2268) Avail: CASI HC A12/MF A03

PL/GPO field programs, CIRRIS-IA, EXCEDE III, FISTA and others have collected interferometer data i.e., interferograms, which were Fourier transformed to recover spectral information. Specific analysis has been performed to ascertain fundamental properties regarding the nature of the earth/atmosphere emissions. For the CIRRIS-1A nadir viewing interferometer data, fundamental relations regarding resolution limitations imposed by the finite character of the data are presented. Chromatic and achromatic sources are considered with conclusions on increasing spatial resolution. An extensive documentation on the earth/atmosphere ultraviolet radiation backgrounds is provided. Transformed EXCEDE III interferograms yielding high resolution spectra of electron (18 amp, 2.5 keV) irradiated air over 85 to 115 km are presented. The emission characteristics of many species are reveled including NO(+) (Delta v =1) with over 40 vibration-rotation lines isolated. Energy efficiency of NO(+) (Delta v= 1) photon production is derived. A computer model of electron impacting air was generated to follow radiation history of NO+. Detailed reaction rates have been derived for the nacient distribution of N(+) + O2 yields NO(+)(v). DTIC

N95-31270 Department of the Navy, Washington, DC.
TECHNIQUE TO PREPARE HIGH-REFLECTANCE OPTICAL FIBER BRAGG GRATINGS WITH SINGLE EXPOSURE IN-LINE OR FIBER DRAW TOWER Patent
Charles G. Askins, inventor (to Navy) and Edward J. Friebele, inventor (to Navy) 21 Mar. 1995 11 p Filed 21 Jan. 1993
(AD-D017445; US-Patent-5,400,422; US-Patent-Appl-SN-006544; US-Patent-Class-385-37) Avail: US Patent and Trademark Office

A process for making an optical reflection grating in a glass fiber includes exposing all unjacketed optic fiber to a single writing pulse from a pair of interfering light beams that form an interference pattern in the fiber. A novel optical fiber has at least one optical grating with a preselected Bragg spacing in at least one region of the fiber, with a periodic modulation in its index of refraction, with high thermal stability and narrow linewidth. A process for making an array of optical reflection gratings in a glass fiber includes exposing a fiber to a plurality of writing pulse from a pair of interfering light beams that form an interference pattern in the fiber, where these pulses are applied sequentially as the fiber is drawn from a draw furnace. A novel optical fiber has a plurality of unspliced gratings with high thermal stability and narrow linewidth. DTIC

N95-31411 Northwestern Univ., Chicago, IL.
NUMERICAL STUDIES OF NONLINEAR OPTICAL PULSE PROPAGATION Ph.D. Thesis
Cheryl Vaught Hile 1993 100 p
Avail: Univ. Microfilms Order No. DA9415740

A one-dimensional mathematical model and numerical solution of Maxwell's equations describing the propagation of soliton-like pulses in nonlinear dispersive optical media is presented. The model includes linear dispersion, expressed in the time-domain, and a Kerr nonlinearity. The model is written in a coordinate system moving with the group velocity of the pulse, which allows significant reduction of the size of the computational grid. When the electromagnetic fields are assumed to be circularly polarized, an asymptotic analysis of Maxwell's equations is used to reduce them to the nonlinear Schrodinger (NLS) equation. This reduction provides approximate initial conditions for Maxwell's equations which generate soliton-like pulse solutions. These solutions are then compared to corresponding solutions of the NLS equation. Several specific cases of this comparison are presented and show good agreement. When the electromagnetic fields are assumed to be linearly polarized, the propagation of 'daughter' pulses, small amplitude pulses which propagate at three times the frequency of the soliton pulse, are observed. These daughter pulses are found to be the direct result of third harmonics generated by the soliton. Initial conditions which include both waves propagating at the same frequency as the soliton pulse and waves propagating at three times the frequency of the soliton pulse are derived. These initial conditions are used to solve the linearly polarized equations and result in the elimination of the daughter pulses. In addition, numerical solutions of an averaged envelope equation describing pulse propagation in a nonlinear optical fiber where loss in the fiber is balanced by a chain of periodically spaced, phase-sensitive amplifiers are presented. Pulse solutions are found to be stable, even when propagating for very long distances. Comparisons are made with similar solutions describing pulse propagation in a nonlinear optical fiber with erbium-doped amplifiers and indicate that phase-sensitive amplifiers effectively attenuate linear dispersive radiation while erbium doped amplifiers do not. Dissert. Abstr.

N95-31435# Quantum Magnetics, Inc., San Diego, CA.
INDUCTIVELY COUPLED IR STARING ARRAY BASED ON PHOTOFLUXONIC PIXELS Final Report, 15 Jul. 1994 - 14 Jan. 1995
Andrew D. Hibbs, Alan L. Singsaas, and Douglas A. Taussig 14 Mar. 1995 29 p
(Contract F49620-94-C-0058)
(AD-A292784; CM1198F; AFOSR-95-0241TR) Avail: CASI HC A03/MF A01

The goal of this study was to investigate the feasibility of fabricating a new type of monolithic focal plane multipixel staring array for infrared (IR) radiation detection. This sensor works by the recently postulated process of photofluxonic conversion in which an infrared photon creates a vortex-antivortex pair in a superconducting material. The novelty of the new sensor lies in the detection mechanism itself, and in the way the vortex (or antivortex) is trapped in the device allowing individual sensing

pixels to be readout without direct electrical connections. The overall objective of Phase 1 was to determine the feasibility of building an inductively coupled, non-contact staring array based on the new photofluxonic detection elements. To this end, we have performed a series of experiments on a single array element, a 2 mm diameter loop of YBa2Cu307, and considered pixel requirements for constructing an array. The new system offers tremendous potential for improvement over current infrared detection devices via both the enhanced detection sensitivity and the greatly reduced system complexity. DTIC

N95-31441# University of Central Florida, Orlando, FL.
NONLINEAR ORGANIZED MATERIALS FOR OPTICAL DEVICES Final Report
G. I. Stegeman 1995 15 p
(AF Proj. 2305)
(AD-A292809; AFOSR-95-0167TR) Avail: CASI HC A03/MF A01

Although polymers have been under development for nonlinear optics applications for about two decades, it is only in the last 5-7 years that serious efforts have been made towards device applications. Their unique properties in terms of electron conjugation and efficient charge transfer have led to very large nonlinearities. However, the challenges to using these materials are very different from the more standard nonlinear materials, for example semiconductors, and these challenges have to be overcome before organics will truly be used in devices. This research program dealt with supplying some of the necessary knowledge base and developing new device concepts, for both second and third order nonlinear optics in polymers. DTIC

N95-31458# Tufts Univ., Medford, MA. Electro-Optics Technology Center.
PHOTOREFRACTIVE NONLINEAR OPTICS Final Report
Mark Cronin-Golomb 2 Mar. 1995 24 p
(Contract DAAL03-91-G-0243)
(AD-A292913; ARO-28526.16-PH) Avail: CASI HC A03/MF A01

This research program resulted in the development of several new photorefractive devices, and an increase in basic understanding of photorefractive nonlinear interactions. We developed an interferometric phase conjugating ellipsometer which also led to a new highly accurate class of interferometer applicable to polarimetry and distance measurement. The effectiveness of photorefractive beam cleanup was investigated, and found to be most useful for highly aberrated beams. We investigated the feasibility of efficient self aligning coupling of multiple beams simultaneously into a single single mode fiber. This has applications to fiber optic communications. We studied methods of broadening the spectral bandwidth of volume holographic devices by using achromatic techniques. Applications are in self-pumped phase conjugation of trains of femtosecond pulses, and high data rate transmission in optical fibers. The photorefractive beam propagation method was developed as a tool to analyze photorefractive devices and effects involving large bandwidth signals. It was also applied to model amplified photorefractive scattering (fanning) and the double phase conjugate mirror. A successful statistical model of fanning was developed and tested. We have also begun to study photorefractive waveguides, both epitaxially grown and self induced. High resolution X-ray topography was used to investigate photorefractive crystals and waveguides. A new method for nonvolatile data storage in photorefractive crystals was discovered and theoretically analyzed. DTIC

N95-31515# Colorado Univ., Boulder, CO.
OPTICAL FREQUENCY STANDARDS: HERTZ-LEVEL WORKING STANDARDS AND THEIR ABSOLUTE FREQUENCY MEASUREMENT Final Report
Leo Hollberg and John Hall 26 Aug. 1994 6 p
(Grant AF-AFOSR-0283-91)
(AD-A293930; AFOSR-95-0332TR) Avail: CASI HC A02/MF A01

Promising optical frequency/wavelength standards in the visible based on neutral atoms and precise laser sources are studied. In particular we have developed high accuracy systems using diode-lasers with calcium atoms and also diode-pumped Yag-lasers with Iodine molecules. An actual frequency measurement of the Iodine transition at 532 nm is made with the frequency doubled Yag system. On the calcium transition at 657 nm in the red, optical Ramsey-fringes as narrow as 10 kHz have been observed with a high signal-to-noise ratio using diode lasers. High resolution multi-photon spectroscopy on laser cooled and trapped atoms (Na and Ca) have also been explored. In these pursuits, significant new diode-laser and frequency- measurement technology has been developed, including; highly stabilized diode and Yag lasers, the ability to coherently measure the frequency difference between two lasers to as high as approx. 700GHz, and the extension of the spectral coverage of diode laser sources to the blue (for laser cooling of calcium) and IR spectral regions by using nonlinear optical techniques. DTIC

N95-31519# Johns Hopkins Univ., Baltimore, MD. Dept. of Electrical and Computer Engineering.
QUANTUM AND NONLINEAR OPTICS RESEARCH Final Technical Report, 1 Mar. 1990 - 28 Feb. 1993
Alexander E. Kaplan Jun. 1994 40 p
(Grant AF-AFOSR-0180-90)
(AD-A293879; AFOSR-95-0329TR) Avail: CASI HC A03/MF A01

Since the research on this AFOSR grant started on March 1, 1990, a number of new results were obtained by this principal investigator and his group in the field of nonlinear optics and quantum electronics. The research progressed basically in these directions: Pilot theoretical research on X-ray nonlinear optics, including resonant saturation related effects in plasmas (nonlinear absorption and nonlinear refractive index), and proposals for X-ray third harmonics generation, X-ray laser with noncoherent pumping, and X-ray four-wave mixing; Experimental discovery and experimental and theoretical research on dark spatial solitons; Theoretical investigation of previously discovered by this PI and his group dispersion related multimode amplification, instabilities, oscillations and chaos in nonlinear counterpropagating waves; Theoretical research on the fundamental problem of gradient-field-induced second-order nonlinear optical processing vacuum due to the photon-photon scattering of intense laser radiation in a dc magnetic field. DTIC

N95-31529# Southampton Univ. (England).
ACOUSTO-OPTICAL FREQUENCY SHIFTERS IN DUAL-CORE OPTICAL FIBRES Final Report, 30 Sep. 1993 - 29 Mar. 1995
T. A. Birks, P. J. Russell, D. O. Culverhouse, S. G. Farwell, and C. N. Pannell Mar. 1995 97 p
(Grant AF-AFOSR-0387-91)
(AD-A293979; EOARD-TR-95-09) Avail: CASI HC A05/MF A02

The aim of this project is the design and implementation of a practical acousto-optic frequency-shifter compatible with single-mode optical fibre. The frequency shifter was originally to be based on a special fibre with two dissimilar cores. Normally, little light couples between the cores, but in the presence of an appropriate flexural acoustic wave a large transfer of optical power, with a frequency shift, takes place. This interaction has been analyzed theoretically, a dual-core fibre frequency shifter designed, and its component parts assembled. Progress towards this initial experiment was hampered by fiber fabrication problems. In the meantime, an alternative type of frequency shifter was pursued. Here the acousto-optic interaction takes place between two modes in the narrow uniform waist of a special 'null' fused taper coupler. This has so many compelling advantages that the earlier dual-core work was put to one side. A prototype null coupler device was built and tested, and immediately satisfied some of the project's goals. The design promises to be able to satisfy the remainder also. DTIC

N95-31542# Brown Univ., Providence, RI.
NONLINEAR OPTICS IN NOVEL COMPOSITE MEDIA
Nabil M. Lawandy 6 Jun. 1994 38 p
(Grant AF-AFOSR-0107-91)
(AD-A293886; AFOSR-95-0331TR) Avail: CASI HC A03/MF A01

During this period of funding the research group has covered a variety of areas of nonlinear optical phenomena in composite materials as well as several new spin-off areas. An update is given for the following: Pyroelectric Detection Using Molecular Guest-Host Complexes; Optical Limiter Action and Oxidation Chemistry of C60 in Organic Polymers; High Density Optical Information Storage in Glasses; Second-Harmonic Generation in Semiconductor Doped Glass Waveguides; Improved Conversion Efficiencies and New Frequency Doubling Fibers; Discovery of Thermally Driven Spontaneous Damage in Germanosilicate Fibers and the Optical Fuse; Simultaneous Self-Starting Additive Pulse Mode-Locking and Second Harmonic Generation of an Nd:YAG Laser using Self-Organized

Germanosilicate Optical Fibers; Nonlinear Propagation in Anisotropic Crystals: Beam Fission and Optically Induced Bending in Ruby; High Efficiency Stimulated Raman Scattering in Gases using External Seeding Processes; Kinematic Modelocking of a Ring Dye Laser; Development of a Picoliter Viscometer; Theory of Nonlinear Optical Properties of Crystalline Guest Host Complexes; Second Harmonic and Sum Frequency Generation in Silica Based Glass; Carrier Screening Effects in Semiconductor Microcrystallite-doped Glass Second Harmonic Generation; Saturation of Near Resonant xi(3) in Quantum Confined Semiconductors; Cerenkov Emission in a Photonic Bandgap Crystal; Dispersion Interactions Between Excited Atoms; Superradiance Effects on the Vibrational Fluorescence of Optically Pumped Molecules; and Light Driven Complex Structures in Colloidal Media. DTIC

N95-31635# California Univ., Berkeley. Lawrence Berkeley Lab, CA.
ANNUAL MEETING OF THE ADVANCED LIGHT SOURCE USERS' ASSOCIATION
Feb. 1995 102 p Presented at the 7th Annual Meeting of the Advanced Light Source Users Association, Berkeley, CA, 20-21 Oct. 1994
(Contract DE-AC03-76SF-00098)
(DE95-009373; LBL-36500; CONF-9410246) Avail: CASI HC A06/MF A02

This report contains papers on the following topics: ALS Director's Report; ALS Operations Update; Recent Results in Machine Physics; Progress in Beamline Commissioning and Overview of New Projects; The ALS Scientific Program; First Results from the SpectroMicroscopy Beamline; Soft X-ray Fluorescence Spectroscopy of Solids; Soft X-Ray Fluorescence Spectroscopy of Molecules; Microstructures and Micromachining at the ALS; High-Resolution Photoemission from Simple Atoms and Molecules; X-Ray Diffraction at the ALS; Utilizing Synchrotron Radiation in Advanced Materials Industries; Polymer Microscopy: About Balls, Rocks and Other 'Stuff'; Infrared Research and Applications; and ALS User Program. DOE

N95-31652 Naval Postgraduate School, Monterey, CA.
DESIGN AND TESTING OF AN OPTIMAL DIGITAL LINK CAPABLE OF 14-CHANNEL TRANSMISSION M.S. Thesis Final Report
Nejat Polat Sep. 1994 68 p Limited Reproducibility: More than 20% of this document may be affected by microfiche quality
(AD-A288505) Avail: Issuing Activity (Defense Technical Information Center (DTIC))

This thesis presents the design, implementation, and evaluation of a communication system, capable of serializing 14-channel digital parallel data, transmission, and reception of the serial data over a high speed fiber link at 39 Mbps and converting the serial data back to its 14-channel parallel form. A time division multiplexing technique was used to transmit the data. The high-speed Emitter-Coupled Logic devices were employed to construct the design. Author

N95-31665# Massachusetts Inst. of Tech., Lexington, MA.
PHYSICAL OPTICS POLARIZATION SCATTERING MATRIX FOR A RIGHT-ANGLE DIHEDRAL
J. G. Verly 7 Feb. 1995 60 p
(Contract F19628-95-C-0002)
(AD-A293036; TR-1008; ESC-TR-94-092) Avail: CASI HC A04/MF A01

Using the geometrical optics (GO) and physical optics (PO) approximations, a correct, complete, ready-to-use formula is derived for the backscatter (monostatic) polarization scattering matrix (PSM) of the perfectly conducting right dihedral at arbitrary incidence angle. The absence of such a result from the literature is surprising given that the dihedral's PSM is needed in many applications, such as in the calibration of polarimetric radars, including synthetic aperture radars (SAR), in the generation of simulated polarimetric radar imagery, and in automatic target recognition (ATR). Because the new results provided are important to many researchers who may not be experts in electromagnetic theory (as is often the case for the computer-vision researchers working on ATR), the report is relatively self-contained and takes the reader from the definitions of PSMs and complex radar cross-sections, through the mathematical formulation of Huygen's Principle, the combined use of GO and PO, and changes of polarization bases, to the derivation, discussion, and simplification of the dihedral's PSM. DTIC

N95-31672# Office of Naval Research, Arlington, VA.
DATA COLLECTION AT THE LOCKHEED SANTA CRUZ FACILITY USING MIDWAVE HYPERSPECTRAL IMAGERS
William A. Shaffer, Alan P. Schaum, Michelle Hinnrichs, Mark A. Massie, and David Fields 8 Feb. 1995 16 p Prepared in cooperation with Pacific Advanced Technology, Solvang, CA and Lawrence Livermore National Lab., Livermore, CA
(AD-A293057; NRL/MR/5620-95-7648) Avail: CASI HC A03/MF A01

From September 12-15, 1994, two midwave hyperspectral imagers (the Infrared Multispectral Sensor (IMSS) of Pacific Advanced Technology and the Livermore Imaging Fourier Transform Infrared Spectrometer (LIFTIRS) of Lawrence Livermore National Laboratory) made measurements of particular patches of forest background and a Lockheed Santa Cruz Facility test stand at various times of day and observed the firing of the rocket engine from a sensitive piece of hardware mounted in the Lockheed test stand. The hyperspectral image cubes of the same patch of background observed at various times will be used to investigate the temporal nature of the constituent-temperature interaction. The data of the rocket firing was collected as part of a classified program of the U.S. Army Missile Command. Two sets of data cubes taken of the same background region by IMSS and LIFTIRS simultaneously will be used both to compare the two instruments and to aid in instrument characterization. This paper describes the instruments used in this data collection, the types of backgrounds observed and the experiments performed, and the data collected. DTIC

N95-31681# Sandia National Labs., Livermore, CA.
AN INVESTIGATION OF A NOVEL APPROACH TO ELEMENTAL IMAGING IN THREE DIMENSIONS
M. C. Nichols, R. P. Goehner (Sandia National Labs., Albuquerque, NM.), and R. G. Tissot, Jr. (Sandia National Labs., Albuquerque, NM.) Apr. 1995 19 p
(Contract DE-AC04-94AL-85000)
(DE95-010340; SAND-95-8210) Avail: CASI HC A03/MF A01

Feasibility of a radically different method of using X-ray excited X-ray fluorescence to perform two- and three-dimensional elemental imaging at the micrometer size scale was examined. The proposed new approach was investigated using both laboratory and synchrotron X-ray sources. The project was funded as a high-risk venture by the Laboratory Directed Research & Development (LDRD) program at Sandia National Laboratories. Investigations centered around the use of two different types of monochromators and a CCD detector to allow the imaging of characteristic excited X-radiation in two dimensions, one element at a time. The goal of this approach was to be able to obtain three-dimensional images in a similar way as is now possible using X-ray tomographic microscopy methods. Unfortunately, it was not possible to obtain sufficient signal using either X-ray source to warrant further study in this area, and the project was terminated. It is possible that the advent of more intense synchrotron X-ray sources could allow this technique to be used for certain restricted applications, but the results obtained here indicate that, without some further breakthrough, it is unlikely that a practical instrument could result using this approach. DOE

N95-31697# Rome Lab., Griffiss AFB, NY.
OPTICAL CORRELATOR OPTIMIZATIONS AND EXTENSIONS FOR AUTOMATED OPTICAL TARGET RECOGNITION Report, Oct. 1990 - Oct. 1993
Wesley E. Foor, Harold G. Andrews, II, and Mark A. Getbehead Dec. 1994 41 p
(AF Proj. 4600)
(AD-A293013; RL-TR-94-220) Avail: CASI HC A03/MF A01

This report presents a detailed overview of the research performed by the analog optical signal processing group at the Photonics Center of Rome Laboratory in the area of automated optical target recognition. This research encompasses phase-only filter optical correlator filter development, optical image remapping, optical image segmentation, and optical neural networks. While the focus of the work is directed toward military applications we also present potential commercial uses for many of these systems. DTIC

N95-31700# Massachusetts Univ., Lowell, MA.
NOVEL UNSYMMETRICAL POLYDIACETYLENES AS MATERIALS FOR SECOND AND THIRD ORDER NONLINEAR OPTICS Technical Report, 1 Oct. 1994 - 30 Sep. 1995
C. E. Masse, K. VandeWiede, W. H. Kim, X. L. Jiang, and J. Kumar 30 Mar. 1995 22 p
(Contract N00014-90-J-1148)
(AD-A293020; TR-95-03) Avail: CASI HC A03/MF A01

The objective of this investigation was to develop stable nonlinear optical (NLO) materials which possess both second and third order NLO properties. These materials were envisioned as having a polydiacetylene (PDA) backbone with a second order active NLO chromophoric substituent. The choice of a PDA backbone in this investigation was twofold. In terms of third order NLO properties, the extensive p-conjugation of the PDA backbone leads to large ultrafast third order effects. In terms of second order NLO properties, the high thermal stability and rigidity of the PDA matrix in a 'perfect' polymeric single crystal is expected to prevent the randomization of the NLO chromophores in the noncentrosymmetric environment. This paper focuses on the synthesis, structural analysis, and NLO properties of the unsymmetrical diacetylene monomers, ((9-Butoxy carbonyl) methyl urethanyl)- 1-(4-urethanyl- 4'-nitrobiphenyl)- nona-2,4-diyne, and ((9-Butoxy carbonyl) methyl urethanyl)- 1-(4-urethanyl- 4'-nitroazobenzene)-nona-2,4-diyne. DTIC

N95-31745 Defence Science and Technology Organisation, Melbourne (Australia). Aeronautical and Maritime Research Lab.
THE EFFECT OF RAY CURVATURE ON LLOYD'S MIRROR FRINGE ESTIMATES AND SOURCE LOCALISATION
Paul R. Lewis Sep. 1994 31 p
(DSTO-TR-0064; AR-008-927) Avail: Issuing Activity (DSTO Aeronautical and Maritime Lab., GPO Box 4331, Melbourne, Victoria 3001, Australia)

A knowledge of the interference between direct, surface and bottom reflected rays emanating from a moving underwater source can be used to determine the source-detector relative positions. Using simple ray tracing, the frequency-time interference patterns for a broadband frequency source arising when the propagating medium has a piecewise linear sound speed profile are considered, and are compared with those for a constant sound speed. It is found that even small deviations from a constant sound speed can lead to a noticeably different interference fringe placement and shape, and consequently to the inferred source-detector geometry. Further, comparisons of model calculations to experimentally observed fringe systems demonstrate the inadequacy of the constant sound speed model, whereas the use of the simple segmented profile is capable of replicating the observed patterns. Author

N95-31841# Naval Postgraduate School, Monterey, CA.
ANALYSIS OF TARGET CONTRAST IMPROVEMENT USING POLARIZATION FILTERING IN THE INFRARED REGION M.S. Thesis
David Gavin Moretz Dec. 1994 123 p
(AD-A293085) Avail: CASI HC A06/MF A02

Computer analysis with Interactive Data Language (IDL) was performed on polarized infrared image data obtained during the MAPTIP coastal experiment. Analysis of contrast enhancement of the oceanographic ship Hr. Ms. Tydeman and a Lynx helicopter using polarization filters is presented. Contrast of vertical and horizontal polarized images was determined by two methods. Unpolarized image contrast was developed from polarization data and used to calculate contrast improvement factors for vertical and horizontal polarizations. Background effects upon contrast were explored. Dependence of projected ship area on contrast improvement was analyzed. Vertical and horizontal polarized images were compared to verify preliminary observations of negligible predominant polarization of man-made targets. Results of this analysis confirm that vertically polarized sea background radiance can be reduced by polarization filtering to enhance ship-to-background contrast. Man-made targets appear to present negligible polarization. Sky background immediately above the horizon also appears unpolarized. Combining radiance from both sky background above the horizon and sea background to form an average background reference radiance reduces overall contrast improvement. Ship-to-background contrast should be calculated with respect to the horizon location. DTIC

N95-31950 California Univ., San Diego, CA.
IMPROVED LINEAR DYNAMIC RANGE IN EXTERNALLY MODULATED FIBER-OPTIC LINKS Ph.D. Thesis
Mark Lalon Farwell 1994 240 p
Avail: Univ. Microfilms Order No. DA9424917

This dissertation proposes two different methods for increasing the linear dynamic range of a fiber-optic link past the fundamental limits imposed by (1) the power handling capability of the detector and (2) the sinusoidal response of a conventional electro-optic modulator. The first method requires using a novel, linearized modulator called the linearized directional coupler in order to reduce the nonlinear distortion. This modulator utilizes an all-optical nonlinear compensation process that is unique in that it requires only a single electro-optic interaction. Because of this, the linearized directional coupler is the most promising design for achieving linearized modulation over a significant bandwidth. An algorithm for a computer simulation program is presented whereby the nonlinear distortion of any coupled waveguide modulator design can be calculated. The algorithm also provides a way in which the electro-optic phase mismatch can be accounted for and thus enables the nonlinearities to be determined as a function of frequency. Using computer simulation, the theoretical performance and the optimal design for the new modulator are determined. Theoretical performance calculations indicate that significant, broadband third-order nonlinear suppression is possible below 1 GHz with a simple electrode structure. Significant nonlinear suppression for an upper bandwidth limit larger than 1 GHz can be achieved by fabricating a traveling-wave electrode structure. The requirements on the traveling-wave electrodes as a function of frequency and required nonlinear suppression are determined in this work as well. Experimental results of both two-tone and forty-tone tests with prototype modulators at KHz, MHz and 1 GHz frequencies are reported. Significant, broadband third-order suppression is demonstrated up to approximately 200 MHz. Third-order compensation is also demonstrated at 1 GHz using a traveling-wave prototype. The second method, is a simple operational method called low biasing. This method allows linearized modulation to be achieved with a conventional modulator at the expense of an increase in optical source power. Increased even-order distortion, however, limits this method to single-octave transmission bandwidths. The nonlinear suppression possible with this method is particularly attractive since it is independent of frequency. This method is also shown to result in a significant increase in modulation efficiency without a trade-off in bandwidth. Using this method, a high fidelity fiber-optical transmission of forty CATV carriers is experimentally demonstrated. Dissert. Abstr.

N95-32064# Sandia National Labs., Albuquerque, NM.
CURRENT TRENDS IN THE PACKAGING OF PHOTONIC DEVICES
Richard F. Carson 1995 66 p Presented at the Spring Meeting on Optoelectronic and Photonic Devices, Tucson, AZ, 6 Apr. 1995
(Contract DE-AC04-94AL-85000)
(DE95-009583; SAND-95-0588C; CONF-9504140-1) Avail: CASI HC A04/MF A01

Optoelectronic and photonic devices hold great promise for high data-rate communication and computing. Their wide implementation was limited first by the device technologies and now suffers due to the need for high-precision packaging that is mass-produced. The use of photons as a medium of communication and control implies a unique set of packaging constraints that are highly driven by the need for micron and even sub-micron alignments between photonic devices and their transmission media. Current trends in optoelectronic device packaging are reviewed and future directions are identified both for free-space (3-dimensional) and guided-wave (2-dimensional) photonics. Emphasis will be placed on the special needs generated by increasing levels of device integration. DOE

N95-32153# Department of the Air Force, Wright-Patterson AFB, OH. National Air Intelligence Center.
PHOTO-REFRACTIVE Bi12SiO20: SPATIAL LIGHT MODULATOR
Zhao Mingjun, Li Yulin, and Wang Zhao (Xian Inst. of Optics and Precision Mechanics, China.) 27 Mar. 1995 13 p Transl. into ENGLISH from Guangxue Xuebao (China), v. 11, no. 9, Sep. 1991 p 810-814
(AD-A293084; NAIC-ID(RS)T-0396-94) Avail: CASI HC A03/MF A01

This paper uses non-degenerate and degenerate multi-wave mixing frequencies of the photo-refractive Bi12SiO20 crystal to create incoherent - coherent conversions; wavelength conversion and image subtraction

between coherent and incoherent images, and thus experimental results are so given. DTIC

N95-32187*# National Aeronautics and Space Administration. Ames Research Center, Moffett Field, CA.
STRATOSPHERIC OBSERVATORY FOR INFRARED ASTRONOMY (SOFIA). PHASE A: SYSTEM CONCEPT DESCRIPTION
1995 439 p
(Proj. SOFIA)
(NASA-TM-110669; NAS 1.15:110669) Avail: CASI HC A19/MF A04

Infrared astronomers have made significant discoveries using the NASA/Ames Research Center C-141 Kuiper airborne Observatory (KAO) with its 0.91-meter telescope. The need for a 3-meter class airborne observatory has been established to improve astronomy data gathering capability. The new system envisioned by NASA and the international community of astronomers will be known as the Stratospheric Observatory for Infrared Astronomy (SOFIA). The platform of choice for SOFIA is a modified Boeing 747SP. SOFIA is viewed as a logical progression from the KAO. Potentially, a 3-meter telescope operating at the altitude achievable by the 747SP aircraft can be 11 times more sensitive than the KAO, can have 3.3 times better angular resolution, and will allow observations of compact sources in a volume of space up to 36 times that of the KAO. The KAO has enabled detection of about 15 percent of the far infrared IRAS survey point-sources; SOFIA should be able to detect them all. This document presents the results of in-house ARC and contracted concept definition studies for SOFIA. Using the ARC-based Kuiper Airborne Observatory as a basis for both SOFIA design and operations concepts, the SOFIA system concept has been developed with a view toward demonstrating mission and technical feasibility, and preparing preliminary cost estimates. The reference concept developed is not intended to represent final design, and should be treated accordingly. The most important products of this study, other than demonstration of system feasibility, are the understanding of system trade-offs and the development of confidence in the technology base that exists to move forward with a program leading to implementation of the Stratospheric Observatory for Infrared Astronomy (SOFIA). Derived from text

N95-32312 National Defence Research Establishment, Linkoeping (Sweden).
Z-SCAN USING A DYE LASER [Z-SCAN MED FAERGAEMNESLASER]
S. Svensson, M. Lindgren, and B. Ericson Sep. 1994 27 p In SWAHILI
(PB95-222923; F0A-R-94-00021-3.1-SE) Avail: Issuing Activity (National Technical Information Service (NTIS))

The continuing development of laser technology increases the risk of harmful laser exposure of eyes and/or electro-optical sensors. Materials which spontaneously alter their optical properties when subjected to intense optical radiation might be utilized in protective devices. The research in this area of non-linear optics is therefore urgent and demanding. We have chosen to employ the z-scan method in our experimental work on non-linear optical protection of sensors. After a limited number of tests, we have noticed non-linear optical phenomena. Due to the dye-laser's poor beam profile, too long pulse duration, and frequent malfunctions, the laser does not suit our purposes. NTIS

N95-32356# Stanford Linear Accelerator Center, Menlo Park, CA
NOTES ON LIE ALGEBRAIC ANALYSIS OF ACHROMATS
Chunxi Wang and A. Chao Jan. 1995 31 p
(Contract DE-AC03-76SF-00515)
(DE95-009524; SU-SLAC/AP-100) Avail: CASI HC A03/MF A01

Normal form technique is a powerful method to analyze the achromat problem. Assume the one cell map M(sub cell) = AR e(sup :h(sub 3)):(sub e)(sup :h(sub 4)): A(sup -1), where h(sub 3),h(sub 4) are the normal forms of the generators of the unit cell map, and A is the nonlinear transformation that brings M(sub cell) into its normal form (and :h: represents the classical Poisson bracket operation); then the map of the whole system is M(sub N) = M(sub cell)(sup N) = AR(sup N) A(sup -1) = I, provided that we can set e(sup :h(sub 3)):, e(sup :h(sub 4)), and R(sup N) to the identity (or only (delta) dependent) maps. Therefore, the conditions to form an achromat are h(sub 3) and h(sub 4) equal to zero (or delta dependent only) and the total linear map is identity. In this report, we will apply these conditions to a FODO array (a simple model system) to make it an achromat. We will start from Hamiltonians and work all the way up to obtain the analytical expressions of the required sextupole and octupole strengths. DOE

N95-31800*# National Aeronautics and Space Administration. Langley Research Center, Hampton, VA.
THE DESIGN AND DEVELOPMENT OF A THIRD GENERATION OSEE INSTRUMENT
D. F. Perey, W. T. Yost, F. D. Stone, C. S. Welch (College of William and Mary, Williamsburg, VA.), E. Scales (Analytical Services and Materials, Inc., Hampton, VA.), E. S. Gasser (Analytical Services and Materials, Inc., Hampton, VA.), E. Joe (Analytical Services and Materials, Inc., Hampton, VA.), T. Goodman (Analytical Services and Materials, Inc., Hampton, VA.), X. Pascual (Analytical Services and Materials, Inc., Hampton, VA.), and B. Hefner (Analytical Services and Materials, Inc., Hampton, VA.) et al *In* NASA. Marshall Space Flight Center, Aerospace Environmental Technology Conference Mar. 1995 p 533-540 (For primary document see N95-31746 11-23)
Avail: CASI HC A02/MF A06

N95-31801*# Alabama Univ., Huntsville, AL.
STUDY OF SURFACES USING NEAR INFRARED OPTICAL FIBER SPECTROMETRY
G. L. Workman, W. A. Arendale, and C. Hughes *In* NASA. Marshall Space Flight Center, Aerospace Environmental Technology Conference Mar. 1995 p 541-549 Sponsored by Thiokol (For primary document see N95-31746 11-23)
(Contract NAS8-38609)
Avail: CASI HC A02/MF A06

N95-31803*# Martin Marietta Energy Systems, Inc., Oak Ridge, TN.
SURFACE INSPECTION USING FTIR SPECTROSCOPY
G. L. Powell, N. R. Smyrl, D. M. Williams, H. M. Meyers, III, T. E. Barber (Oak Ridge Inst. for Science and Education, TN.), and M. Marrero-Rivera (Oak Ridge Inst. for Science and Education, TN.) *In* NASA. Marshall Space Flight Center, Aerospace Environmental Technology Conference Mar. 1995 p 563-571 (For primary document see N95-31746 11-23)
(Contract DE-AC05-84OR-21400)
Avail: CASI HC A02/MF A06

N95-31804*# Thiokol Corp., Brigham City, UT.
CLEANLINESS EVALUATION OF ROUGH SURFACES WITH DIFFUSE IR REFLECTANCE
L. H. Pearson *In* NASA. Marshall Space Flight Center, Aerospace Environmental Technology Conference Mar. 1995 p 573-581 (For primary document see N95-31746 11-23)
Avail: CASI HC A02/MF A06

N95-32130# Officine Galileo S.p.A., Florence (Italy).
OPTIMAL INFRARED DETECTOR CONFIGURATIONS FOR AIR TARGET DETECTION
G. Uda and G. Barani *In* AGARD, Guidance and Control for Future Air-Defence Systems Jan. 1995 10 p (For primary document see N95-32123 11-31)
Copyright Avail: CASI HC A02/MF A03

N95-32346*# Jet Propulsion Lab., California Inst. of Tech., Pasadena, CA.
FIBER OPTIC REFERENCE FREQUENCY DISTRIBUTION TO REMOTE BEAM WAVEGUIDE ANTENNAS
Malcolm Calhoun, Paul Kuhnle, and Julius Law *In* NASA. Goddard Space Flight Center, The 26th Annual Precise Time and Time Interval (PTTI) Applications and Planning Meeting May 1995 p 415-426 (For primary document see N95-32319 11-70)
Avail: CASI HC A03/MF A04

75 PLASMA PHYSICS

Includes magnetohydrodynamics and plasma fusion.
For ionospheric plasmas see *46 Geophysics*. For space plasmas see *90 Astrophysics*.

N95-30359# General Atomics Co., San Diego, CA.
ADVANCES IN THE SIMULATION OF TOROIDAL GYRO LANDAU FLUID MODEL TURBULENCE
R. E. Waltz, G. D. Kerbel (Lawrence Livermore National Lab., Livermore, CA.), J. Milovich (Lawrence Livermore National Lab., Livermore, CA.), and G. W. Hammett (Princeton Univ., NJ.) Dec. 1994 33 p Presented at the Meeting of the Division of Plasma Physics of the American Physical Society, Minneapolis, MN, 7-11 Nov. 1994 Prepared in cooperation with Princeton Univ.
(Contracts DE-AC02-76CH-03073; DE-FG03-92ER-54150; W-7405-eng-48) (DE95-008387; GA-A-21871; CONF-941101-5) Avail: CASI HC A03/MF A01

The gyro-Landau fluid (GLF) model equations for toroidal geometry have been recently applied to the study ion temperature gradient (ITG) mode turbulence using the 3D nonlinear ballooning mode representation (BMR). The present paper extends this work by treating some unresolved issues concerning ITG turbulence with adiabatic electrons. Although eddies are highly elongated in the radial direction long time radial correlation lengths are short and comparable to poloidal lengths. Although transport at vanishing shear is not particularly large, transport at reverse global shear, is significantly less. Electrostatic transport at moderate shear is not much effected by inclusion of local shear and average favorable curvature. Transport is suppressed when critical E x B rotational shear is comparable to the maximum linear growth rate with only a weak dependence on magnetic shear. Self consistent turbulent transport of toroidal momentum can result in a transport bifurcation at sufficiently large r/(Rq). However the main thrust of the new formulation in the paper deals with advances in the development of finite beta GLF models with trapped electron and BMR numerical methods for treating the fast parallel field motion of the untrapped electrons. DOE

N95-30468*# National Aeronautics and Space Administration. Marshall Space Flight Center, Huntsville, AL.
OPERATING IN THE SPACE PLASMA ENVIRONMENT: A SPACECRAFT CHARGING STUDY OF THE SOLAR X-RAY IMAGER
Joel L. Herr (Sverdrup Technology, Inc., Huntsville, AL.), Matthew B. McCollum, and Bonnie F. James [1994] 6 p
(NASA-TM-110644; NAS 1.15:110644) Avail: CASI HC A02/MF A01

This study presents the results of a spacecraft charging effects protection study conducted on the Solar X-ray Imager (SXI). The SXI is being developed by NASA Marshall Space Flight Center for NOAA's Space Environment Laboratory, and will be used to aid in forecasting energetic particle events and geomagnetic storms. Images will provide information on the intensity and location of solar flares, coronal mass ejections, and high speed solar streams. The SXI will be flown on a next-generation GOES sometime in the mid to late 1990's. Charging due to the encounter with a worst-case magnetic substorm environment is modeled using the NASCAP/GEO computer code. Charging levels of exterior surfaces and the floating potential of the spacecraft relative to plasma are determined as a function of spacecraft design, operational configuration, and orbital conditions. Areas where large surface voltage gradients exist on or near the SXI are identified as possible arc-discharge sites. Results of the charging analysis are then used to develop design recommendations that will limit the effects of spacecraft charging on the SXI operation. Derived from text

N95-30473# Instituto Politecnico Nacional, Mexico City (Mexico). Escuela Superior de Ingenieria Mecanica y Electrica.
POWER OSCILLATOR IN THE TOKAMAKS TRAINING Ph.D. Thesis [USO DE UN OSCILADOR DE POTENCIA PARA EL ACONDICIONAMIENTO DE TOKAMAKS]
Raul ValenciaAlvarado 1994 147 p In SPANISH
(DE95-616538; INIS-mf-14453) Avail: CASI HC A07/MF A02 (US Sales Only)

This work reports the results obtained from the cleaning of the Novillo Tokamak Chamber, using an A.F. Taylor Discharge Cleaning (TDC) in H2 with a power oscillator of 20 kW and 17.5 kHz. The plasma temperature in the discharge was of one electron-volt (Te approximately equal 1 eV) with a moderate electron density n(sub e) approximately equal 4 x 10(exp 11) cm(exp -3). This discharge cleaning was found helpful in the removal of C and O via the formation of pumping compounds such as CH4 and H2O. A residual gas analyzer was used to monitor the partial pressure of these and other compounds, indicating removal rates as high as two monolayers/hour at the beginning of the discharge. A value of Z(sub eff) = 3 was estimated for a discharge of 7 kA after conditioning. DOE

N95-30612# General Atomics Co., San Diego, CA.
EFFECTS OF PARTICLE FUELING AND PLASMA WALL INTERACTIONS ON D3-D DISCHARGES
G. L. Jackson, D. R. Baker, K. L. Holtrop, G. M. Staebler, W. P. West, R. Maingi (Oak Ridge National Lab., TN.), and S. Konoshima (Japan Atomic Energy Research Inst., Tokyo, Japan.) Nov. 1994 55 p Presented at the 11th International Conference on Plasma Surface Interactions in Controlled Fusion Devices, Mito, Japan, 23-27 May 1994
(Contract DE-AC03-89ER-51114)
(DE95-009608; GA-A-21716; CONF-940580-26) Avail: CASI HC A04/MF A01

D3-D has successfully operated with an all-graphite first wall, including the first observations of VH-mode without boronization. A major goal of this, and other recent upgrades, was to control impurity influxes and hydrogenic fueling. Graphite tiles were carefully preconditioned, first by ex situ preparation and then by baking and helium glow conditioning. No deuterium or hydrogen was used until tokamak operation commenced. With the all graphite wall, both impurity and deuterium influxes during tokamak discharges were lower than previous boronized discharges; central nickel impurity line radiation, NiXXV and NiXXVI, was an order of magnitude lower than previous discharges during the ELM free beam heated phase. The effect of reduced particle fueling on plasma performance, particularly H- and VH-mode discharges, will be presented. DOE

N95-30641# General Atomics Technologies Corp., San Diego, CA.
DEVELOPMENT OF A TOKAMAK PLASMA OPTIMIZED FOR STABILITY AND CONFINEMENT
P. A. Politzer Feb. 1995 11 p Presented at the 6th International Toki Conference on Plasma Physics and Controlled Nuclear Fusion: Research for Advanced Concepts in Magnetic Fusion, Toki-city, Japan, 29 Nov. - 2 Dec. 1994 Submitted for publication in the Proceedings of the 6th International Conference on Plasma Physics and Controlled Nuclear Fusion
(Contracts DE-AC03-89ER-51114; DE-AC05-84OR-21400; W-7405-eng-48) (DE95-009609; GA-A-21926; CONF-941182-3) Avail: CASI HC A03/MF A01

Design of an economically attractive tokamak fusion reactor depends on producing steady-state plasma operation with simultaneous high energy density (beta) and high energy confinement (tau(E)); either of these, by itself, is insufficient. In operation of the DIII-D tokamak, both high confinement enhancement (H equivalent to tau(E)/tau(ITER - 89P) = 4) and high normalized beta(beta(N) equivalent to beta/(I/aB) = 6%-m-T/MA) have been obtained. For the present, these conditions have been produced separately and in transient discharges. The DIII-D advanced tokamak development program is directed toward developing an understanding of the characteristics which lead to high stability and confinement, and to use that understanding to demonstrate stationary, high performance operation through active control of the plasma shape and profiles. The authors have identified some of the features of the operating modes in DIII-D that contribute to better performance. These are control of the plasma shape, control of both bulk plasma rotation and shear in the rotation and Er profiles, and particularly control of the toroidal current profiles. In order to guide their future experiments, they are developing optimized scenarios based on their anticipated plasma control capabilities, particularly using fast wave current drive (on-axis) and electron cyclotron current drive (off-axis). The most highly developed model is the second-stable core VH-mode, which has a reversed magnetic shear safety factor profile (q(0) = 3.9, q(min) = 2.6, and q(95) = 6). This model plasma uses profiles which the authors expect to be realizable. At (beta)(N) is greater than or equal to 6, it is stable to n = 1 kink modes and ideal ballooning modes, and is expected to reach H greater than or equal to 3 with VH-mode-like confinement. DOE

N95-30671# National Inst. for Fusion Science, Nagoya (Japan).
PHYSICS AND APPLICATION OF HIGH DENSITY Z-PINCHES
T. Miyamoto, ed. and K. Takasugi, ed. Jul. 1993 106 p Conference held in Nagoya, Japan, 11-12 Dec., 1992
(ISSN 0915-6348)
(NIFS-PROC-14) Avail: CASI HC A06/MF A02

This publication is a collection of papers presented at the research meeting on 'Physics and Application of Z-pinches' held at the National Institute for Fusion Science on December 11-12, 1992, in which thirty-seven persons attended from eighteen organizations, and eighteen lectures were given. The Z-pinch is an old subject that has been studied since the 1950's, but recently is noticed again in a new point of view. The classical Z-pinch is characterized by discharging in a dilute gas filled in the glass tube and by applying the relatively low discharge voltage of a few 10's of kV. On the other hand, the modern Z-pinch is characterized by puffing a gas into a vacuum vessel or using a solid fiber, and also by applying the relatively high discharge voltage, i.e., more than several hundred kV. Hence, the pulse power device is often used instead of the capacitor bank, and permits the generation of the Z-pinch using a solid narrow wire for which the discharge is explosive in a few 10's of kV. The modern Z-pinch researchers give a prospect in the important field, i.e., the discharge excitation of short wave length lasers, the production of a fusion plasma, etc. Nevertheless, it is regrettable that there is no Z-pinch research group in Japan that equips the pulse power device. One of the purposes of this meeting was to stimulate the researchers on Z-pinches and related subjects. This report includes the macroscopic behaviors and radiation measurements on gas-puff and metal-vapor Z-pinches which were presented by Nihon University and Tokyo Institute of Technology, soft x-ray measuring methods and data processing by Gunma University, the related technical problems on voltage amplification and closing switch by Himeji Institute of Technology and Kumamoto University, and unstable motion of toroidal Z-discharge plasma by Utsunomiya University. In the meeting several review talks (on pulsed power technology and x-ray laser) and other problems were given besides the above papers. Derived from text

N95-30685# General Atomics Co., San Diego, CA.
HELIUM TRANSPORT AND EXHAUST STUDIES IN ENHANCED CONFINEMENT REGIMES IN DIII-D
M. R. Wade, D. L. Hillis, J. T. Hogan, M. A. Mahdavi, R. Maingi, W. P. West, K. H. Burrell, D. F. Finkenthal, P. Gohil, and R. J. Groebner et al Feb. 1995 29 p Presented at the Meeting of the Division of Plasma Physics of the American Physical Society, Minneapolis, MN, 7-11 Nov. 1994
(Contracts DE-AC03-89ER-51114; W-7405-eng-48; DE-AC05-84OR-21400; DE-AC04-76DP-00789)
(DE95-009134; GA-A-21905; CONF-941101-7) Avail: CASI HC A03/MF A01

A better understanding of helium transport in the plasma core and edge in enhanced confinement regimes is now emerging from recent experimental studies on DIII-D. Overall, the results are encouraging. Significant helium exhaust (tau(sup *, sub He)/tau(sub E) approximately 11) has been obtained in a diverted, H-mode plasmas with edge-localized modes (ELM's) simultaneous with a central source of helium. Detailed analysis of the helium profile evolution indicates that the exhaust rate is limited by the exhaust efficiency of the pump (approximately 5%) and not by the intrinsic helium transport properties of the plasma. Perturbative helium transport studies using gas puffing have shown that D(sub He)/X(sub eff) approximately 1 in all confinement regimes studied to date (including H-mode and VH-mode). Furthermore, there is no evidence of preferential accumulation of helium in any of these regimes. However, measurements in the core and pumping plenum show a significant dilution of helium as it flows from the plasma core to the pumping plenum. Such dilution could be the limiting factor in the overall removal rate of helium in a reactor system. DOE

N95-30742# Lawrence Livermore National Lab., Livermore, CA.
REFLECTIVITY OF PLASMAS CREATED BY HIGH-INTENSITY, ULTRA-SHORT LASER PULSES Ph.D. Thesis
David Michael Gold Jun. 1994 225 p
(Contract W-7405-eng-48)
(DE95-009536; UCRL-LR-117512) Avail: CASI HC A10/MF A03

Experiments were performed to characterize the creation and evolution of high-temperature (T(sub e)(approximately)100eV), high-density (n(sub e) greater than 10(exp 22)/cu cm plasmas created with intense approximately 10(exp 12)-10(exp 16)W/sq cm, ultra-short (130fs) laser pulses. The principle diagnostic was plasma reflectivity at optical wavelengths (614nm). An array of target materials (Al, Au, Si, SiO2) with widely differing electronic properties tested plasma behavior over a large set of initial states. Time-integrated plasma reflectivity was measured as a function of laser intensity. Space- and time-resolved reflectivity, transmission and scatter were measured with a spatial resolution of approximately 3 micrometers and a temporal resolution of 130fs. An amplified, mode-locked dye laser system was designed to produce approximately 3.5mJ, approximately 130fs laser pulses to create and nonintrusively probe the plasmas. Laser prepulse was carefully controlled to suppress preionization and give unambiguous, high-density plasma results. In metals (Al and Au), it is shown analytically that linear and nonlinear inverse Bremsstrahlung absorption, resonance absorption, and vacuum heating explain time-integrated reflectivity at intensities near 10(exp 16)W/sq cm. In the insulator, SiO2, a non-equilibrium plasma reflectivity model using tunneling ionization, Helmholtz equations, and Drude conductivity agrees with time-integrated reflectivity measurements. Moreover, a comparison of ionization and Saha equilibration rates shows that plasma formed by intense, ultra-short pulses can exist with a transient, non-equilibrium distribution of ionization states. All targets are shown to approach a common reflectivity at intensities approximately 10(exp 16)W/sq cm, indicating a material-independent state insensitive to atomic or solid-state details. DOE

N95-30769# Lawrence Livermore National Lab., Livermore, CA. High Temperature Physics Div.
EBIT: ELECTRON BEAM ION TRAP V-DIVISION EXPERIMENTAL PHYSICS Annual Report 1993
Dieter Schneider, ed. Aug. 1994 112 p
(Contract W-7405-eng-48)
(DE95-010207; UCRL-ID-118274) Avail: CASI HC A06/MF A02

This report discusses research being conducted using the electron beam ion trap. The areas of this research are: atomic structure measurements; diagnostics for fusion and astrophysics; ion/surface interaction studies; electron-ion interaction studies; electron, positron, and ion collisions; and instrumental developments. DOE

N95-30794# Texas Univ., Austin, TX. Inst. for Fusion Studies.
STABILIZATION OF THE RESISTIVE SHELL MODE IN TOKAMAKS
Richard Fitzpatrick and Ahmet Aydemir Feb. 1995 56 p
(Contract DE-FG05-80ET-53088)
(DE95-008748; DOE/ET-53088/694; IFSR-694) Avail: CASI HC A04/MF A01

The stability of current-driven external-kink modes is investigated in a tokamak plasma surrounded by an external shell of finite electrical conductivity. According to conventional theory, the ideal mode can be stabilized by placing the shell sufficiently close to the plasma, but the non-rotating 'resistive shell mode,' which grows on the characteristic L/R time of the shell, always persists. It is demonstrated, using both analytic and numerical techniques, that a combination of strong edge plasma rotation and dissipation somewhere inside the plasma is capable of stabilizing the resistive shell mode. This stabilization mechanism does not necessarily depend on toroidicity or presence of resonant surfaces inside the plasma. DOE

N95-30795# Texas Univ., Austin, TX. Inst. for Fusion Studies.
REYNOLDS STRESS OF LOCALIZED TOROIDAL MODES
Y. Z. Zhang (International Centre for Theoretical Physics, Trieste, Italy.) and S. M. Mahajan Feb. 1995 27 p
(Contract DE-FG05-80ET-53088)
(DE95-008750; DOE/ET-53088/691; IFSR-691) Avail: CASI HC A03/MF A01

An investigation of the 2D toroidal eigenmode problem reveals the possibility of a new consistent 2D structure, the dissipative BM-2 mode. In contrast to the conventional ballooning mode, the new mode is poloidally localized at (pi)/2 (or -(pi)/2), and possesses significant radial asymmetry. The radial asymmetry, in turn, allows the dissipative BM-2 to generate considerably larger Reynolds stress as compared to the standard slab drift type modes. It is also shown that a wide class of localized dissipative

toroidal modes are likely to be of the dissipative BM-II nature, suggesting that at the tokamak edge, the fluctuation generated Reynolds stress (a possible source of poloidal flow) can be significant. DOE

N95-30801# Texas Univ., Austin, TX. Inst. for Fusion Studies.
SHEAR FLOW EFFECTS ON ION THERMAL TRANSPORT IN TOKAMAKS
T. Tajima, W. Horton, J. Q. Dong, and Y. Kishimoto (Japan Atomic Energy Research Inst., Naka, Japan.) Mar. 1995 41 p
(Contract DE-FG05-80ET-53088)
(DE95-009115; DOE/ET-53088/697; IFSR-697) Avail: CASI HC A03/MF A01

From various laboratory and numerical experiments, there is clear evidence that under certain conditions the presence of sheared flows in a tokamak plasma can significantly reduce the ion thermal transport. In the presence of plasma fluctuations driven by the ion temperature gradient, the flows of energy and momentum parallel and perpendicular to the magnetic field are coupled with each other. This coupling manifests itself as significant off-diagonal coupling coefficients that give rise to new terms for anomalous transport. The authors derive from the gyrokinetic equation a set of velocity moment equations that describe the interaction among plasma turbulent fluctuations, the temperature gradient, the toroidal velocity shear, and the poloidal flow in a tokamak plasma. Four coupled equations for the amplitudes of the state variables radially extended over the transport region by toroidicity induced coupling are derived. The equations show bifurcations from the low confinement mode without sheared flows to high confinement mode with substantially reduced transport due to strong shear flows. Also discussed is the reduced version with three state variables. In the presence of sheared flows, the radially extended coupled toroidal modes driven by the ion temperature gradient disintegrate into smaller, less elongated vortices. Such a transition to smaller spatial correlation lengths changes the transport from Bohm-like to gyrobohm-like. The properties of these equations are analyzed. The conditions for the improved confined regime are obtained as a function of the momentum-energy deposition rates and profiles. The appearance of a transport barrier is a consequence of the present theory. DOE

N95-30804 New Hampshire Univ., Durham, NH.
STUDY OF CROSS-TAIL CURRENT CARRIERS IN MAGNETOTAIL Ph.D. Thesis
Chen Lu 1993 137 p
Avail: Univ. Microfilms Order No. DA9420565

The purpose of this study is to gain physical insight into how charged particles, which violate the guiding center approximations, contribute to cross-tail current in a self-consistent plasma sheet. A technique to generate self-consistent one-dimensional (1-D) current sheets is described. Groups of monoenergetic protons are followed in a model magnetic field. The sample current sheets are characterized by resonant quasiadiabatic and stochastic orbits. The magnetic moment of a quasiadiabatic ion which is injected from outside a current sheet changes substantially during an interaction with the current sheet, but returns to almost its initial value by the time the ion leaves. The resonant nature of the interaction is associated with a strong energy dependence. The magnetic moment of a stochastic ion changes substantially during an interaction with the current sheet. Several ion and electron groups are combined to produce a plasma sheet in which the charged particles carry the currents needed to generate the magnetic field in which the orbits are traced. An electric field also is required to maintain charge neutrality. Three distinct orbit types, one involving untrapped and two composed of trapped ions, are identified. Each class of ions carries a qualitatively different current distribution. Contributions from all three groups are needed when resonant ions are used to generate a typical quiet-time self-consistent current sheet. It was found that self-consistent current sheets can not be generated using only stochastic ions. A relatively small density of resonant protons must be added to a current sheet in which stochastic ions dominate. Distribution functions are evaluated so that the expected count rates and several fluid parameters could be plotted. Limitations associated with the use of a 1-D model also are investigated. It is found that the model can provide a good physical picture of an important component of the cross tail current. However, we conclude that 1-D models cannot adequately describe any region of the magnetotail in which the principal current sheet is separated from the plasma sheet boundary layer by a nearly isotropic outer portion of the central plasma sheet. Dissert. Abstr.

N95-31004# Korea Cancer Center Hospital, Seoul (Republic of Korea).
DEVELOPMENT OF PLASMA DIAGNOSTICS TECHNOLOGIES: A STUDY ON NUCLEAR FUSION REACTOR
Churl Kew Hwang, Seong Kyu Kim, Kwang Won Lee, Sang Ryeol In, Byeong Ho Choi, Bong Geun Hong, Seung Ho Chung, Byeong Hoon Oh, Jae Seong Yoon, and Byeong Joo Yoon et al Jul. 1994 139 p
(DE95-614180; KAERI/RR-1365/93) Avail: CASI HC A07/MF A02 (US Sales Only)

Plasma diagnostics systems are studied and designed in detail for tokamak KAERIT. The systems for the electron cyclotron emission (ECE) receiver, the soft X-ray spectroscopy, visible light spectroscopy, static electric probes and data acquisition to process the diagnostic data are planned to develop. Also studied for detail design in the next year are the systems for mm wave interferometry, vacumm-UV light spectroscopy and neutral beam detection. The ECE receiver is designed in single channel at 93 GHz aimming to get high sensitivity. The soft X-ray spectroscopy system consists of a carbon target which emits electrons by X-ray and an energy analyser for the electrons. The electric probe is designed in tripple electrodes and capable of detection in real time mode. DOE

N95-31366# Korea Cancer Center Hospital, Seoul (Republic of Korea).
THE DEVELOPMENT OF THE TOKAMAK SYSTEM TECHNOLOGY: A STUDY ON THE FUSION REACTOR
Sang Ryul In, Chul Kew Hwang, Kwang Won Lee, Sung Kyu Kim, Byung Hoon Oh, Seung Ho Jeong, Bong Guen Hong, Jae Sung Yoon, Byung Joo Yoon, and Woo Sup Song et al Jul. 1994 170 p
(DE95-614256; KAERI/RR-1364/93) Avail: CASI HC A08/MF A02

The object of this project was the completion of a KT-2 tokamak device concept definition, completion of preliminary conceptual design, and assurance of technical feasibility. The content and scope of the study included identification of the research goal and program -- derivation of basic specifications of the plasma and the tokamak, and preliminary conceptual design of core components (magnets, power sources, vacuum system, and auxiliary heating system). The results of the research included a definition of the KT-2 tokamak concept: a medium-sized, large-aspect-ratio bootstrap tokamak with fast-wave current-drive; numerical scoping for performance and identification of KT-2 operation regimes (general specification from zero-dimensional analysis using TETRA and magnetic configuration and MHD equilibrium properties with FBT and basic specification of the PF system and derivation of basic operation scenario); basic specification of the magnet-power supply system and the vacuum system for detailed engineering study in the next step; and general specification for auxiliary system necessary for research goal and subsequent device concept. DOE

N95-31534# Massachusetts Inst. of Tech., Cambridge, MA. Dept. of Aeronautics and Astronautics.
THEORY AND SIMULATION OF ELECTROSTATIC WAVE TURBULENCE IN THE SPACE SHUTTLE-INDUCED PLASMA ENVIRONMENT Final Report, 3 Jan. 1990 - 30 Sep. 1994
David R. Rivas and Daniel E. Hastings 30 Sep. 1994 313 p
(Contract F19628-90-K-0021)
(AD-A293467; PL-TR-95-2021) Avail: CASI HC A14/MF A03

One of the important observations of the Plasma Diagnostic Package (PDP) experiments that were designed to probe the environment around the shuttle was the high degree of electrostatic turbulence in the ambient plasma compared to what has been observed from similar instruments flown on unmanned spacecraft. It is shown that the turbulence is caused by a process which involves the outgassing of water vapor from the shuttle orbiter, the subsequent collisional charge exchange of these water neutral molecules with ionospheric oxygen ions for form pick-up water ions, and the excitation of the beam-arc plasma instability. This is a new instability which is driven by the interaction of the beam-arc (i.e., asymmetric ring) velocity distribution function of the contaminating water ions with the background ionospheric plasma. DTIC

N95-31613# Los Alamos National Lab., NM.
PLASMA SOURCE ION IMPLANTATION OF METAL IONS: SYNCHRONIZATION OF CATHODIC-ARC PLASMA PRODUCTION AND TARGET BIAS PULSES
Blake P. Wood, William A. Reass, and Ivars Henins 1995 21 p
(Contract W-7405-eng-36)
(DE95-009431; LA-UR-95-872) Avail: CASI HC A03/MF A01

An erbium cathodic-arc has been installed on a Plasma Source Ion Implantation (PS2) experiment to allow the implantation of erbium metal and the growth of adherent erbia (erbium oxide) films on a variety of substrates. Operation of the PS2 pulser and the cathodic-arc are synchronized to achieve pure implantation, rather than the hybrid implantation/deposition being investigated in other laboratories. The relative phase of the 20 (mu)s PS2 and cathodic-arc pulses can to adjusted to tailor the energy distribution of implanted ions and suppress the initial high-current drain on the pulse modulator. The authors present experimental data on this effect and make a comparison to results from particle-in-cell simulations. DOE

N95-31624# General Atomics Co., San Diego, CA.
STABILIZATION OF BALLOONING MODES WITH SHEARED TOROIDAL ROTATION
R. L. Miller, F. W. Waelbroeck, L. L. Lao, and T. S. Taylor Nov. 1994 7 p Presented at the 15th International Conference on Plasma Physics and Controlled Nuclear Fusion Research, Madrid, Spain, 26 Sep. - 1 Oct. 1994
(Contract DE-FG03-92ER-54150)
(DE95-008388; GA-A-21793; CONF-940933-36) Avail: CASI HC A02/MF A01

A new code demonstrates the stabilization of MHD ballooning modes by sheared toroidal rotation. A shifted-circle model is used to elucidate the physics and numerically reconstructed equilibria are used to analyze DIII-D discharges. In the ballooning representation, the modes shift periodically along the field line to the next point of unfavorable curvature. The shift frequency (d(Omega)/dq where Omega is the angular toroidal velocity and q is the safety factor) is proportional to the rotation shear and inversely proportional to the magnetic shear. Stability improves with increasing shift frequency and, in the shifted circle model, direct stable access to the second stability regime occurs when this frequency is a fraction of the Alfven frequency omega(sub A) = V(sub A)/qR. Shear stabilization is also demonstrated for an equilibrium reconstruction of a DIII-D VH-mode. DOE

N95-31626# Sandia National Labs., Albuquerque, NM.
TARGET DIAGNOSTICS FOR INTENSE LITHIUM ION HOHLRAUM EXPERIMENTS ON PBFA 2
R. J. Leeper, J. E. Bailey, and A. L. Carlson 1994 16 p Presented at the 10th Topical Conference on High-temperature Plasma Diagnostics, Rochester, NY, 8-12 May 1994
(Contract DE-AC04-94AL-85000)
(DE95-008517; SAND-94-0282C; CONF-940552-35) Avail: CASI HC A03/MF A01

A review of the diagnostics used at Sandia National Laboratories to measure the parameters of intense lithium ion-beam hohlraum target experiments on PBFA 2 will be presented. This diagnostic package contains an extensive suite of x-ray spectral and imaging diagnostics that enable measurements of target temperature and x-ray output. The x-ray diagnostics include time-integrated and time-resolved pinhole cameras, energy-resolved 1-D streaked imaging, diagnostics, time-integrated and time-resolved grazing, incidence spectrographs, a transmission grating spectrograph, an elliptical crystal spectrograph, a bolometer array, an eleven-element x-ray diode (XRD) array, and an eleven-element PIN diode detector array. The incident Li beam symmetry and an estimate of incident Li beam power density can be measured from ion beam-induced characteristic x-ray line emission and neutron emission. DOE

N95-31679# Academy of Sciences (USSR), Novosibirsk (USSR). Inst. Yadernoj Fiziki.
OPTIMIZATION OF AN EXPANDER OF A GAS-DYNAMIC TRAP
I. A. Kotelnikov 1994 9 p
(DE95-614172; IYaF-94-63) Avail: CASI HC A02/MF A01 (US Sales Only)

A problem of the gas-dynamic trap expander optimization is solved. The equation is obtained for the line of force, providing the maximal safety factor in a trap. DOE

N95-31680# Academy of Sciences (USSR), Novosibirsk (USSR).
DETERMINATION OF ELECTRIC AND MAGNETIC FIELDS IN OPEN TRAP PLASMAS BY MEANS OF ATOMIC-MOLECULAR BEAM HYDROGEN ISOTOPES
A. A. Kabantsev 1994 20 p
(DE95-614177; IYaF-94-35) Avail: CASI HC A03/MF A01 (US Sales Only)

This paper describes a method for simultaneous measurement of electric and magnetic fields and their fluctuations in open trap plasmas with beta less than 1. The method is based on radial injections of a 15-60 keV atomic/molecular beam of hydrogen isotopes. The time resolution is expected to be of the order of 1 microsecond. DOE

N95-31737# Polish Academy of Sciences, Warsaw (Poland). Mechanics Center.
SELECTED PROBLEMS OF THE IDENTIFICATION OF WEAK DOUBLE LAYERS IN PLASMA ON A BACKGROUND OF DIFFERENT APERIODIC NON-COLLISION STRUCTURES [WYBRANE ZAGADNIENIA IDENTYFIKACJI SLABYCH WARSTW PODWOJNYCH W PLAZMIE NA TLE INNYCH NIEPERIODYCZNYCH STRUKTUR BEZZDERZENIOWYCH]
Krzysztof Zuchowski Apr. 1995 36 p In POLISH
(ISSN 0208-5658)
(IFTR-4/1995) Avail: CASI HC A03/MF A01

The authors compare weak ion-acoustic type double layers with other non-collision aperiodic structures in an equilibrial plasma. These non-collision structures include strong double layers, soliton waves, and non-monotonic and monotonic non-collision shock waves. The authors assume that a definite temperature is associated with the free electrons. Free ions, with the exception of strong double layers, are interpreted as cold ions. Author

N95-32028# Lawrence Livermore National Lab., Livermore, CA.
DIAGNOSING HIGH DENSITY, FAST-EVOLVING PLASMAS USING X-RAY LASERS
R. Cauble, L. B. DaSilva, T. W. Barbee, Jr., P. Celliers, S. Libby, J. C. Moreno, S. Mrowka, D. Ress, J. E. Trebes, and A. S. Wan et al Sep. 1994 6 p Presented at the ECLIM 23: Laser Interaction With Matter, Oxford (England), 19-23 Sep. 1994
(Contract W-7405-eng-48)
(DE95-010734; UCRL-JC-116843; CONF-9409226-7) Avail: CASI HC A02/MF A01

As x-ray laser (XRL) research has matured, it has become possible to reliably utilize XRL's for applications in the laboratory. Laser coherence, high brightness and short pulse duration all make the XRL a unique tool for the diagnosis of laboratory plasmas. The high brightness of XRL's makes them well-suited for imaging and for interferometry when used in conjunction with multilayer mirrors and beamsplitters. We have utilized a soft x-ray laser in such an imaging system to examine laser-produced plasmas using radiography, moire deflectometry, and interferometry. Radiography experiments yield 100-200 ps snapshots of laser driven foils at a resolution of 1-2 micrometers. Moire deflectometry with an XRL has been used to probe plasmas at higher density than by optical means. Interferograms, which allow direct measurement of electron density in laser plasmas, have been obtained with this system. DOE

N95-32054# Academy of Sciences (USSR), Novosibirsk (USSR). Inst. Yadernoj Fiziki.
ENERGY SPECTRA OF CHARGE-EXCHANGE ATOMS FROM A ROTATING PLASMA
V. I. Volosov and I. N. Churkin 1994 12 p
(DE95-614179; IYaF-94-67) Avail: CASI HC A03/MF A01 (US Sales Only)

For determining the real spectrum of ions in a rotating plasma are considered the problems in the ion spectra for cases with the ion distribution function in velocity in the form of the delta function, a shifted delta function and for an arbitrary ion spectrum. DOE

N95-32056# Academy of Sciences (USSR), Novosibirsk (USSR). Inst. Yadernoj Fiziki.

BERNSTEIN-GREEN-KRUSKAL WAVE

N. S. Buchelnikova and B. N. Lazeev 1993 18 p

(DE95-614201; IYaF-93-97) Avail: CASI HC A03/MF A01 (US Sales Only)

The simulation model (PIC method) of the Bernstein-Green-Kruskal wave (BGK wave) with the trapping region filled by the trapped electrons is described. The parameters of the BGK wave (phase velocity, amplitude, energy, density and velocity distribution) in homogeneous collisionless plasma with the fixed ions are shown to be constant at the time interval approx. 100(sub oe). DOE

N95-32116# General Atomics Co., San Diego, CA.

WALL STABILIZATION OF HIGH BETA PLASMAS IN D3-D

T. S. Taylor, E. J. Strait, L. L. Lao, M. Mauel (Columbia Univ., Dobbs Ferry, NY.), K. H. Burrell, M. S. Chu, J. R. Ferron, R. J. Groebner, R. J. LaHaye, and B. W. Rice et al Feb. 1995 29 p Presented at the Meeting of the Division of Plasma Physics of the American Physical Society, Minneapolis, MN, 7-11 Nov. 1994 Prepared in cooperation with Oak Ridge National Lab., TN and Lawrence Livermore National Lab., Livermore, CA

(Contracts DE-AC03-89ER-51114; DE-AC05-84OR-21400; W-7405-eng-48) (DE95-009607; GA-A-21914; CONF-941101-9) Avail: CASI HC A03/MF A01

Detailed analysis of recent high beta discharges in the D3-D tokamak demonstrates that the resistive vacuum vessel can provide stabilization of low-n magnetohydrodynamic (MHD) modes. The experimental beta values reaching up to beta(sub T) = 12.6% are more than 30% larger than the maximum stable beta calculated with no wall stabilization. Plasma rotation is essential for stabilization. When the plasma rotation slows sufficiently, unstable modes with the characteristics of the predicted 'resistive wall' mode are observed. Through slowing of the plasma rotation between the q = 2 and q = 3 surfaces with the application of a non-axisymmetric field, the authors have determined that the rotation at the outer rational surfaces is most important, and that the critical rotation frequency is of the order of Omega/2(pi) = 1 kHz. DOE

N95-32148# Lawrence Livermore National Lab., Livermore, CA. Applied Superconductivity Group.

MEASUREMENTS OF STABILITY MARGINS AND CURRENT DISTRIBUTION IN LARGE-SCALE Nb3Sn CABLE-IN-CONDUIT CONDUCTORS

Stewart S. Shen and Takaaki Isono 7 Mar. 1995 8 p Presented at the 9th US/Japan Workshop on High-field Superconducting Materials, Kyoto, Japan, 11-16 Mar. 1995

(Contract W-7405-eng-48)

(DE95-009869; UCRL-JC-120076; CONF-9503127-2) Avail: CASI HC A02/MF A01

The main goal of the ITER Conductor Testing Program is to validate the design and the fabrication process of the CICC (Cable-In-Conduit Conductor) and its joints, in full-size samples. For testing large-scale cable-in-conduit conductors, several practical experimental techniques have been developed to specifically address the issues of conductor stability. The following described techniques enable experimentalists to quantify the effects and thus provide useful tools to improve the conductor performance in magnet applications. In this paper, the authors, present two experimental techniques: (a) stability margin calibration, and (b) current distribution. Both are much needed in the laboratory for testing the conductor stability. DOE

N95-32263# Japan Atomic Energy Research Inst., Tokyo (Japan).

ONSET OF ELMs IN JT-60U

Yutaka Kamada, Masayasu Sato, Mitsuru Kikuchi, and Masahiro Mori (Japan Atomic Energy Research Inst., Ibaraki, Japan.) Aug. 1994 22 p

(DE95-737209; JAERI-Research-94-011) Avail: CASI HC A03/MF A01

The ELM's limiting the energy confinement in JT-60U appear when the heating power is high enough compared to the threshold power for the L-H transition. The ELM-free phase is observed when n-bar(sub e) is lower than the threshold density n-bar(sub e, sup th). The threshold density n-bar(sub e, sup th) increases with (B(sub t, sup 2)/(Rq(sub eff, sup 2)))I(sub i) which is a measure parameter for the ballooning stability, where q(sub eff) is the effective safety factor at the edge. The edge pressure gradient estimated by n-bar(sub e, sup th) T(sub i) (95%)/(T(sub i) (95%)(sup 0.5)/B(sub p) (a)) is proportional to (B(sub t, sup 2)/(Rq(sub eff, sup 2)))I(sub i) which allows us to understand that the ELM's are related to the ballooning instability. A time dependent analysis of the evolution of pressure and current profiles including the boot-strap current shows that the steep edge pressure gradient is close to the marginal value for the high-n ideal ballooning instability at the onset of ELM's. DOE

N95-32264# Japan Atomic Energy Research Inst., Tokyo (Japan). Dept. of Fusion Engineering Research.

DEVELOPMENT OF INTEGRATED INSULATION JOINT FOR COOLING PIPE IN TOKAMAK REACTOR

Satoshi Nishio, Tetsuya Abe (Japan Atomic Energy Research Inst., Ibaraki, Japan.), Masashi Kawamura, and Seiichiro Yamazaki Aug. 1994 23 p

(DE95-737220; JAERI-Tech-94-006) Avail: CASI HC A03/MF A01

In a tokamak fusion reactor, an electrically insulated part is needed for an in-vessel piping system in order to break an electric circuit loop. When a closed loop is formed in the piping system, large induced electromagnetic forces during a plasma disruption (rapid plasma current quench) could give damages on the piping system. Ceramic brazing joint is a conventional method for the electric circuit break, but an application to the fusion reactor is not feasible due to its brittleness. Here, a stainless steel / ceramics / stainless steel functionally gradient material (FGM) has been proposed and developed as an integrated insulation joint of the piping system. Both sides of the joint can be welded to the main pipes, and expected to be reliable even in the fusion reactor environment. When the FGM joint is manufactured by way of a sintering process, a residual thermal stress is the key issue. Through detailed computations of the residual thermal stress and several trial productions, tubular elements of FGM joints have been successfully manufactured. DOE

N95-32299# National Inst. of Standards and Technology, Gaithersburg, MD.

MEASUREMENTS OF QUANTUM ELECTRODYNAMIC SENSITIVE TRANSITIONS IN Na-LIKE AND Cu-LIKE IONS Final Report, 1 Oct. 1993 - 29 Sep. 1994

Joseph Reader 1994 7 p

(Contract DE-FG03-93SF-20143)

(DE95-011593; DOE/SF-20143/T2) Avail: CASI HC A02/MF A01

The object was to use the GDL laser at the Laboratory for Laser Energetics at the University of Rochester to measure the energies of spectral transitions that would be of importance for testing the accuracy of calculations used to predict properties of plasmas found in inertial fusion experiments as well as in tokamaks and x-ray lasers. The general method to be used for this experiment was to focus the beam from the GDL laser to a small point so as to create a laser-produced plasma of the material of interest. Light from the plasma was to be photographed with a 2.2-m grazing incidence spectrograph transported to Rochester from NIST. The region of observation was 10-300 angstrom. In the initial phase of the work a series of spectrograms were made of highly ionized iron. For this a special target chamber was fabricated at NIST and interfaced to the light beam from the GDL laser. The results for iron provided valuable data for Li-like iron, Fe(23+). An example of the spectrum obtained in the region of 30-40 angstrom is shown. The lower spectrum shows intense lines of Fe(23+), obtained by focusing the GDL beam tightly onto the target surface. For the upper spectrum the GDL beam was focused slightly in front of the target, producing lines of Fe(23+) that are much reduced in intensity. Measurement of their wavelengths provided a comparison with ab initio values calculated with the Dirac-Fock quantum mechanics computer code of Desclaux. After completing the observations for Li-like iron, the GDL laser was shut down for the planned upgrade to much higher energy. The 2.2-m spectrograph was shipped back to NIST. Extensive work was undertaken to interface the NIST target chamber to the 30-cm-diameter beam of the upgraded GDL laser. The NIST system is now ready for use with the upgraded GDL laser. DOE

N95-32310# Wisconsin Univ., Madison, WI. Dept. of Plasma Physics Research.

LOWER HYBRID ACCESSIBILITY IN A LARGE, HOT REVERSED FIELD PINCH M.S. Thesis

Robin Ann Dziubek Feb. 1995 48 p
(Contract DE-FG02-85ER-53212)
(DE95-011001; DOE/ER-53212/256) Avail: CASI HC A03/MF A01

Recent theoretical and experimental results indicate that driving a current in the outer radius of an RPF suppresses sawtooth activity and increases particle and energy confinement times. One candidate for a form of steady state current drive is the slow wave at the lower hybrid frequency. Here, the accessibility of such a wave in an RFP plasma is investigated theoretically, with focus on the RFX machine of Padua, Italy. To drive current, the slow wave with frequency between 1.0-1.5 GHz is considered where optimal Landau damping is desired at r/a approximately 0.7. By numerically determining the values of the wave's perpendicular index of refraction which satisfy the hot plasma dispersion relation, regions of propagation and evanescence can be found. The path of the wave can then be traced over a contour map of these regions so that accessibility can be clearly seen. The possibility of mode conversion events can be ascertained by plotting the values of the perpendicular index of refraction for the fast and slow wave and observing convergence points. To locate regions of maximum Landau damping, a technique developed by Stix was adapted for use with the slow wave in an RFP plasma. Results show that the slow wave is accessible to the target region without mode conversion so long as the value of the parallel index of refraction is correctly chosen at the edge of the plasma. Landau damping can also be optimized with this method. In an RFP, 2-20% of the electron population consists of fast electrons. Because this species alters the total electron distribution function and raises the effective temperature in the outer regions of the plasma, its presence is expected to shift the location of ideal Landau damping. DOE

N95-32351# Los Alamos National Lab., NM.
A COLLISIONLESS SHOCK WAVE EXPERIMENT
Dan Winske, Michael E. Jones, Anthony G. Sgro, and Vincent A. Thomas 1995 10 p Presented at the Spring Workshop on Basic Science Using Pulsed Power, Santa Barbara, CA, 5-7 Apr. 1995
(Contract W-7405-eng-36)
(DE95-009489; LA-UR-95-1097; CONF-9504132-2) Avail: CASI HC A02/MF A01

Collisionless shock waves are a very important heating mechanism for plasmas and are commonly found in space and astrophysical environments. Collisionless shocks were studied in the laboratory more than 20 years ago, and more recently in space via in situ satellite measurements. The authors propose a new laboratory shock wave experiment to address unresolved issues related to the differences in the partition of plasma heating between electrons and ions in space and laboratory plasmas, which can have important implications for a number of physical systems. DOE

N95-32357# Brookhaven National Lab., Upton, NY.
THERMAL RHO'S IN THE QUARK-GLUON PLASMA
R. D. Pisarski Mar. 1995 5 p Presented at the 11th International Conference on Ultra-Relativistic Nucleus-Nucleus Collisions, Monterey, CA, 9-13 Jan. 1995
(Contract DE-AC02-76CH-00016)
(DE95-009543; BNL-61549; CONF-950127-2) Avail: CASI HC A01/MF A01

Models which predict changes in the mass of the thermal rho field are disscussed. I emphasize that while the predictions are strongly model dependent, nevertheless substantial shifts in the thermal rho mass are expected to occur at the point of phase transition. As long as the thermal rho peak does not become too broad, this should provide a striking signature of the existence of a phase transition. DOE

N95-31786*# Oak Ridge National Lab., TN.
A MICROWAVE PLASMA CLEANING APPARATUS
C. C. Tsai, W. D. Nelson, D. E. Schechter, L. M. Thompson, and A. L. Glover *In* NASA. Marshall Space Flight Center, Aerospace Environmental Technology Conference Mar. 1995 p 399-408 (For primary document see N95-31746 11-23)
Avail: CASI HC A02/MF A06

76 SOLID-STATE PHYSICS

Includes superconductivity.

For related information, see also *33 Electronics and Electrical Engineering* and *36 Lasers and Masers.*

N95-30381# Sandia National Labs., Albuquerque, NM.
MAGNETOLUMINESCENCE CHARACTERIZATION OF QUANTUM WELL STRUCTURES
E. D. Jones and S. R. Kurtz 1995 8 p Presented at the Workshop on Semiconductor Characterization, Gaithersburg, MD, 30 Jan. - 2 Feb. 1995
(Contract DE-AC04-94AL-85000)
(DE95-008527; SAND-95-0085C; CONF-950117-3) Avail: CASI HC A02/MF A01

Three applications of magnetic field effects upon the photoluminescence spectrum which provide unique information about semiconductor quantum well structures are presented. The first example shows data which provide a quantitative measure of both the conduction and valence-band the energy dispersion curves for an InGaAs/GaAs single-strained-quantum well and a GaAs/AlGaAs lattice-matched single quantum well. The second subject discusses magnetoluminescence data which provides a clear demonstration for the existence of spectral shifts related to ionized-impurity scattering and the third study involves infrared magnetoluminescence measurements on narrow bandgap semiconductor alloys and heterostructures. DOE

N95-30382# Sandia National Labs., Albuquerque, NM.
LOW-VOLTAGE CATHODOLUMINESCENCE OF EUROPIUM-ACTIVATED YTTRIUM ORTHOVANADATE
M. L. F. Phillips 1995 8 p Presented at the SPIE 1995: SPIE Conference on Optics, Electro-Optics, and Laser Application in Science, Engineering and Medicine, San Jose, CA, 5-10 Feb. 1995
(Contract DE-AC04-94AL-85000)
(DE95-008536; SAND-95-0393C; CONF-950226-29) Avail: CASI HC A02/MF A01

Emissive flat panel display systems operating in full color demand higher performance at low voltages (ca. 501000 V) from cathodoluminescent (CL) phosphors than cathode ray tubes require. Hydrothermal synthesis has been suggested as a route to phosphors with improved efficiencies, lower voltage thresholds, and increased saturation power. This hypothesis was tested in europium-doped yttrium orthovanadate (YVO4:Eu), an efficient, red emitting CL phosphor. The CL efficiency of YVO4:Eu crystallized from aqueous solution at 200 C is relatively low until it is annealed. The distribution of particle sizes in the low-temperature phosphor is similar to that in material made via a solid-state route, but crystallites remain much smaller (ca. 400 Angstrom) until they are annealed. These observations, along with the anomalously strong dependence of CL intensity on europium concentration, support a model in which efficiency principally depends on crystallite size. CL efficiency of both solid state and hydrothermal YVO4:Eu increases with voltage at constant power. Surface-bound electrons are likely the dominant influence on efficiency at voltages near threshold. Saturation power is independent of synthetic route. It is apparent that the CL properties of hydrothermally synthesized YVO4:Eu are essentially the same as those of YVO4:Eu produced via conventional, high-temperature routes. DOE

N95-30391# Sandia National Labs., Albuquerque, NM.
NIR HIGH-EFFICIENCY SUBWAVELENGTH DIFFRACTIVE STRUCTURES IN SEMICONDUCTORS
R. E. Smith, M. E. Warren, J. R. Wendt, and G. A. Vawter 1995 7 p Presented at the SPIE 1995: SPIE Conference on Optice, Electro-optics, and Laser Application in Science, Engineering and Medicine, San Jose, CA, 5-10 Feb. 1995
(Contract DE-AC04-94AL-85000)
(DE95-008535; SAND-95-0446C; CONF-950226-28) Avail: CASI HC A02/MF A01

We have fabricated sub-wavelength diffractive optical elements with binary phase profiles for operation at 975 nm. Blazed transmission gratings with minimum features 63 nm wide were designed by using rigorous coupled-wave analysis and fabricated by direct-write e-beam lithography and reactive ion beam etching in gallium arsenide. Transmission

measurements show 85% diffraction efficiency into the first order. Anti-reflection surfaces, with features 42 nm wide were also designed and fabricated. DOE

N95-30419# Joint Inst. for Nuclear Research, Dubna (USSR).
THE NEUTRON POWDER DIFFRACTION AND ACOUSTIC INVESTIGATIONS OF THE NH4SCN PHASE DIAGRAM
L. S. Smirnov, I. Natkaniec, S. I. Bragin, A. I. Solovev, J. Brankowski, V. A. Goncharova, and Gromnitskay 1994 10 p
(DE95-614372; JINR-E-14-94-266) Avail: CASI HC A02/MF A01 (US Sales Only)

The phase diagram of NH4SCN was investigated by neutron powder diffraction and acoustic methods, in order to search for a possible triple point and to reveal possible peculiarities near 200 K, observed by other authors, by Raman light scattering. The transition from the monoclinic to the orthorhombic phase was determined on the p-T phase plane in the range of 193-323 K and up to 1.6 GPa by the acoustic method. The temperature dependences of the unit cell parameters and volume and of the transversal wave velocity reveal some anomalies in the monoclinic NH4SCN phase near 200 K. It is possible that these observed anomalies are due to a freezing of the reorientation processes of NH4(+) ions. DOE

N95-30421# Melbourne Univ., Parkville (Australia).
CRYSTALLIZATION OF SOL-GEL DERIVED LEAD ZIRCONATE TITANATE THIN FILMS IN ARGON AND OXYGEN ATMOSPHERES
L. A. Bursill and K. G. Brooks (Ecole Polytechnique Federale de Lausanne, Switzerland.) 1994 27 p
(DE95-615230; UM-P-93/98) Avail: CASI HC A03/MF A01 (US Sales Only)

Electron diffraction and high-resolution electron microscopic techniques are applied to reveal the mechanisms of crystallization of 75 nm thin films of ferroelectric lead-zirconate-titanate (PZT). Sol-gel methods, followed by pyrolysis at 350 C, were used to provide a common starting point after which a variety of rapid-thermal annealing (RTA) experiments in the temperature range 400-700 C were made in argon, oxygen and nitrogen/hydrogen atmospheres. The results are interpreted in terms of the crystal chemical analysis, which points out that partial pressure of oxygen and heating rate are important experimental parameters which must be controlled if ferroelectric perovskite-type Pb2ZrTiO6, rather than pyrochlore-type Pb2ZrTiO(6 + x), where 0 less than X less than 1 or -1 less than X less than 0, is to be obtained after the RTA step. Thus significant improvements in the crystallization of perovskite-type PZT were clearly demonstrated by using argon atmospheres for the RTA step. The results have significance for the production of high-quality ferroelectric thin films, with improved switching and fatigue characteristics, since even small amounts of the pyrochlore phase prove detrimental for these properties. DOE

N95-30485 Rutherford Appleton Lab., Oxford (England).
FINITE ELEMENT SIMULATION OF GaAs MESFET'S
A. Baric, P. McNally, R. F. Fowler, and C. Greenough Jan. 1995 16 p
(PB95-208062; RAL-95-015) Avail: Issuing Activity (National Technical Information Service (NTIS))

The modifications required to convert the Silicon version of a three-dimensional semiconductor device simulator into a simulator suitable for the simulation of GaAs devices have been described. These modifications include GaAs specific parameters, mobility models, and the Schottky barrier boundary conditions. The simulations of an epitaxial and an ion-implanted MESFET have shown that the robustness of the original package has not been deteriorated. NTIS

N95-30503 Institut des Hautes Etudes Scientifiques, Bures-sur-Yvette (France).
BRAVAIS CLASSES, VORONOIE CELLS, DELONE SYMBOLS
L. Michel Dec. 1994 41 p Prepared in cooperation with Technion - Israel Inst. of Tech. Limited Reproducibility: More than 20% of this document may be affected by microfiche quality
(PB95-207916; IHES/P/94/63) Avail: CASI HC A03

We give the most refined intrinsic classification of three dimensional Euclidean lattices by combining the 14 Bravais classes, the 5 combinatorial types of Voronoi cells and the 24 Delone symbols. After recalling the fundamental concepts of group actions, we define Bravais classes and Voronoi cells in arbitrary dimension. We are quite explicit for the application to two and three dimensions. NTIS

N95-30533 Department of the Navy, Washington, DC.
LOW TEMPERATURE SYNTHESIS OF YBa2Cu3O(8-x) AND OTHER CRYSTALLINE OXIDES Patent
Josephine Covino-Hrbacek, inventor (to Navy) 27 Dec. 1994 4 p Filed 2 Aug. 1993
(AD-D017370; US-Patent-5,376,594; US-Patent-Appl-SN-104955; US-Patent-Class-501-12) Avail: US Patent and Trademark Office

Process for preparing a high temperature superconductor such as yttrium barium copper oxides is discussed. Suitable proportions of hydrolyzable salts, oxides, or organometallic compounds of yttrium, barium and copper are dissolved in an acid pH-controlled water-containing organic solvent such as methanol, and subjecting the resulting solution to ultrasonic energy or to an oxidation reduction reaction, preferably while passing oxygen under a positive pressure through the solution, and precipitating a hydrolyzed precursor material. Such precursor material is then heated or annealed at temperatures between about 300 C and about 600 C, also preferably in the presence of flowing oxygen, to produce the desired high temperature superconductor material. DTIC

N95-30535 Selskapet for Industriell og Teknisk Forskning, Trondheim (Norway).
STM STUDIES OF CLEAN, CO- AND O2-EXPOSED Pt(100)-HEX-R0.7 DEG
A. Borg, A. M. Hilmen, and E. Bergene 19 May 1994 13 p Prepared in cooperation with Technical Univ. of Norway, Trondheim
(PB95-195376; STF19-S94002) Copyright Avail: Issuing Activity (National Technical Information Service (NTIS))

The structure of the Pt(100)-hex-R0.7 deg reconstructed phase has been studied by scanning tunneling microscopy (STM). The hexagonal first layer superstructure of this surface was imaged with atomic resolution. The fivefold periodicity of this reconstruction was confirmed. The coexistence of differently oriented hexagonal domains on a single terrace was observed. Steps along the longer corrugation length of the surface reconstruction were found, on the average, to follow the (N 1) direction of the hexagonal Pt overlayer rather than any low-index direction of the square substrate. Upon exposure to various adsorbates, such as CO and O2, the hexagonal reconstructions at the Pt(100) surface are lifted. At room temperature an adsorbate-covered (1 x 1) surface remains. This structural transformation was investigated. NTIS

N95-30542# Oak Ridge National Lab., TN.
MORPHOLOGY AND MICROSTRUCTURE OF (111) CRYSTALLINE CeO2 FILMS GROWN ON AMORPHOUS SiO2 SUBSTRATES BY PULSED-LASER ABLATION
S. Zhu, D. H. Lowndes, J. D. Budai, T. Thundat, D. P. Norton, and R. J. Warmack Nov. 1994 6 p Presented at the 1994 Fall Meeting of the Materials Research Society (MRS), Boston, MA, 28 Nov. - 2 Dec. 1994
(Contract DE-AC05-84OR-21400)
(DE95-008842; CONF-941144-110) Avail: CASI HC A02/MF A01

The surface morphology and microstructure of (111)-oriented CeO2 thin films, grown on amorphous fused silica (SiO2) substrates by low-energy-ion-beam assisted pulsed laser ablation, have been studied by atomic force microscopy (AFM) and x-ray diffraction (XRD). These CeO2 films are aligned with respect to a single in-plane axis despite being deposited on an amorphous substrate. There is a honeycomb-like growth morphology to the films and island-growth can be observed in thicker films. These islands, inside of which are high density of honeycomb-like clusters, are separated by a void network with approximately 700 nm width. However, on the surface of the thinnest film approximately 3 nm, only very small clusters (diameter less than 60 nm) appear, and the boundaries of the void network are undefined, which implies that the film is just beginning to coalesce into clusters (grains). The combined AFM images and XRD pattern suggest these clusters probably are the initial seeds for the subsequent island growth. Based on these results, the growth mechanism of oriented CeO2 films on amorphous fused silica substrates is discussed. DOE

N95-30544# Oak Ridge National Lab., TN.
DIRECT DETERMINATION OF GRAIN BOUNDARY ATOMIC STRUCTURE IN SrTiO3
M. M. McGibbon, N. D. Browning, A. J. McGibbon, M. F. Chisholm, and S. J. Pennycook Dec. 1994 6 p Presented at the 1994 Fall Meeting of the Materials Research Society (MRS), Boston, MA, 28 Nov. - 2 Dec. 1994
(Contract DE-AC05-84OR-21400)
(DE95-008847; CONF-941144-102) Avail: CASI HC A02/MF A01

In the electroceramic SrTiO3 the grain boundary atomic structure governs a variety of electrical properties such as non-linear 1-5 characteristics. An understanding of this atomic structure-property relationship for individual grain boundaries requires a technique which probes both composition and chemical bonding on an atomic scale. Atomic structure models for tilt boundaries in SrTiO3 bicrystals have been determined directly from experimental data, by combining high-resolution Z-contrast imaging to locate the cation columns at the boundary, with simultaneous electron energy loss spectroscopy to examine light element coordination at atomic resolution. In this paper we compare and contrast the grain boundary structure models of symmetric and asymmetric boundaries in SrTiO3. DOE

N95-30571# Los Alamos National Lab., NM.
A VALENCE-FLUCTUATION MECHANISM WITH HIGHLY ANISOTROPIC S-WAVE PAIRING
B. H. Brandow 1995 3 p Presented at the Stanford Conference on Spectroscopies in Novel Superconductors, Stanford, CA, 15-18Mar. 1995 Submitted for publication in Journal of Physics and Chemistry of Solids
(Contract W-7405-eng-36)
(DE95-009419; LA-UR-95-972; CONF-950356-1) Avail: CASI HC A01/MF A01

The author has developed a fairly ab initio theory of cuprate superconductivity, based on the concept that the above-T(sub c) state is a normal Fermi liquid with strong electronic correlations of the type found in valence-fluctuation (VF) and heavy-fermion materials. The ground-state-correlation aspect is found to provide a satisfactory source or mechanism for the pairing. In addition to the high T(sub c)'s this explains many of the unusual features of cuprate superconductivity. DOE

N95-30576# Oak Ridge National Lab., TN.
DIRECT SUBLATTICE IMAGING OF INTERFACE DISLOCATION STRUCTURES IN CdTe/GaAs(001)
A. J. McGibbon, S. J. Pennycook, J. E. Angelo (Sandia National Labs., Livermore, CA.), and M. J. Mills (Sandia National Labs., Livermore, CA.) Jan. 1995 7 p Presented at the 1994 Fall Meeting of the Materials Research Society (MRS), Boston, MA, 28 Nov. - 2 Dec. 1994
(Contracts DE-AC05-84OR-21400; DE-AC04-94AL-85000)
(DE95-009031; CONF-941144-113) Avail: CASI HC A02/MF A01

This paper presents directly interpretable atomic resolution images of dislocation structures at interfaces in CdTe/GaAs(001) systems. This is achieved using the technique of Z-contrast imaging in a 300 kV scanning transmission electron microscope in conjunction with maximum entropy image analysis. In addition to being used to further the understanding of the relation between growth conditions and exhibited properties, the data presented provides direct information on the atomic arrangements at dislocation cores. DOE

N95-30644# International Centre for Theoretical Physics, Trieste (Italy).
ALLOYING EFFECTS OF KONDO INSULATORS
Cheng-Chung Lee, Wang Xu (Nanjing Univ., China.), Chun Chen (Nanjing Univ., China.), and Ming-Wen Xiao (Nanjing Univ., China.) Sep. 1994 28 p
(DE95-614308; IC-94/286) Avail: CASI HC A03/MF A01 (US Sales Only)

The effects of nonmagnetic impurities (Kondo holes) in Kondo insulators (KI) are studied which is based on the U = (infinity) Anderson model in the framework of a slave-boson mean-field theory under the coherent-potential approximation (CPA). The density of states for f-electrons and its variation with the concentration of Kondo holes are calculated self-consistently. The specific-heat coefficient, residual resistivity, and the T = 0 static susceptibility in the alloying system are obtained. The results show that the insulating gap in KI can easily be smeared out by Kondo holes, and the system changes gradually from an insulator to a heavy-fermion metal with increasing concentration, which is in qualitative agreement with experiments. Furthermore, the appearance of an impurity band in the gap comes out naturally in the dilute limit of our CPA calculations. DOE

N95-30647# International Centre for Theoretical Physics, Trieste (Italy).
THE ONE-DIMENSIONAL MODEL OF THE OFF-CENTRE POTENTIAL OF THE FLUORINE ION IN THE NaBr LATTICE
F. Despa Oct. 1994 11 p
(DE95-614310; IC-94/316) Avail: CASI HC A03/MF A01 (US Sales Only)

Fluorine ions in NaBr have associated large dipole moments with low-lying energy levels. It is well known that the dipoles were found to have equilibrium orientations in the (110) direction. A one-dimensional, double-well harmonic oscillator potential model is assumed for the relaxation rate calculation of this off-center system. It is possible by superimposing an asymmetric potential which localizes the particle in one potential well and assuming that, the coupling between the particle and the lattice vibrations can lead to the relaxation of the system. These preliminaries theoretical studies are used to determine the height of the potential barrier between the two minima of the off-center potential in the one-dimensional case approximation. DOE

N95-30648# International Centre for Theoretical Physics, Trieste (Italy).
HAMILTONIAN DYNAMICS OF THE CONDENSED MEDIA WITH SPONTANEOUSLY BROKEN SYMMETRY
M. Yu. Kovalevsky, A. A. Isayev (Academy of Sciences of the Ukraine, Kharkov, Ukraine.), and S. V. Peletminsky (Academy of Sciences of the Ukraine, Kharkov, Ukraine.) Oct. 1994 35 p
(DE95-614448; IC-94/329) Avail: CASI HC A03/MF A01 (US Sales Only)

In this work it is shown how the PB (Poisson Bracket) for different physical systems can be obtained proceeding from transformations that leaves invariant the kinematic part of the action. Outside integral terms in the action variation are interpreted as generators of these transformations. Equations for the determination of the admitted variations are found. On the base of the developed approach, we have considered the classical continuum, the theory of elasticity, hydrodynamics, the number of liquid crystal phases as well as the magnetically ordering and superfluid systems. DOE

N95-30650# International Centre for Theoretical Physics, Trieste (Italy).
ON THE THEORY OF HOLE PROPAGATION IN AN ANTIFERROMAGNETIC BACKGROUND
A. L. Kuzemsky Oct. 1994 15 p
(DE95-614469; IC-94/297) Avail: CASI HC A03/MF A01 (US Sales Only)

The spectrum of hole quasiparticles and the role of magnetic correlations has been considered in the self-consistent Irreducible Green Functions formalism, motivated from Strongly Correlated Electron systems for correlated electron models of high-Tc superconductivity. The hole quasiparticle dynamics has been discussed for t-J model and compared with that of the spin-fermion model. For this Kondo-Heisenberg-type model it was clearly pointed out on the self-energy level, beyond Hartree-Fock approximation, how the one-and two magnon processes define the true nature of carriers in HTSC. DOE

N95-30653# International Centre for Theoretical Physics, Trieste (Italy).
THE QUANTUM INTERFERENCE EFFECT IN SEMICONDUCTOR SPACE CHARGE LAYERS STUDIED BY FEYNMAN PATH INTEGRALS: GENERAL FORMALISM AND ILLUSTRATIVE EXAMPLES
I. Nachev Oct. 1994 20 p
(DE95-614483; IC-94/334) Avail: CASI HC A03/MF A01 (US Sales Only)

The subband energy states in low-dimensional structures, quantum wells, and heterostructures are computed by a new method, which directly accounts for the quantum interference effect. It is based on the sum of Feynman paths in real space and time. The basis of this method is a special procedure, which sums a huge number of Feynman paths - to of order of 10(exp 663), as shown in one of the presented examples. The method has a wider applicability range as compared to conventional techniques based on the Schroedinger equation, and can be applied to modelling the following two cases: (1) resonant tunneling structures or space charge layers in which one discrete energy level interacts with quasi-continuum of

states; and (2) compounds with negative energy gaps. Several illustrative examples are given and possible modifications and applications to other problems are outlined. DOE

N95-30667# Ames Lab., IA.
PHASE TRANSFORMATIONS IN MELT-SPUN Y-Ba-Cu-O BULK SUPERCONDUCTOR
H. Wu, M. J. Kramer, K. W. Dennis, and R. W. McCallum 1994 4 p Presented at the Applied Superconductivity Conference, Boston, MA, 16-21 Oct. 1994
(Contract W-7405-eng-82)
(DE95-010237; IS-M-814; CONF-941013-34) Avail: CASI HC A01/MF A01

Powders of YBa2Cu3O7 (Y123) and compositions around Y123 were heated by a containerless process and melt-spun in 21 percent oxygen atmosphere at temperatures of 1400 to 1650 C. Homogeneous materials were obtained with micron and submicron crystalline phases uniformly dispersed in an amorphous matrix. For Y123, the crystalline phases are identified by x-ray absorbsion diffraction (XRD) as BaCu2O2 and Y2O3 when the melt-spinning temperature is below 1600 C. At 1650 C, the crystalline phases are Y4Ba3O9, BaCu2O2 and Y2O3. The phase composition of the solidified melt is directly related to the oxygen content of the melt and can be related to the equilibrium phase diagrams at lower oxygen partial pressures. Isothermal annealing in oxygen at temperatures 500 to 950 C reveals that the crystallization sequence is: Y123 begins to form at 500 C, Y123 with minor amount of Y2BaCuO5 at 800 C, Y123 with very minor amount of CuO at 900 C, and single phase Y123 at 950 C. DOE

N95-30673 Department of the Navy, Washington, DC.
JOSEPHSON BREAK JUNCTION THIN FILM DEVICE Patent
Ignacio M. Perez, inventor (to Navy) and William R. Scott, inventor (to Navy) 27 Dec. 1994 9 p Filed 10 Oct. 1991
(AD-D017343; US-Patent-5,376,624; US-Patent-Appl-SN-777773; US-Patent-Class-505-190) Avail: US Patent and Trademark Office

A Josephson break junction device suitable for highly sensitive electronic detecting systems. A superconductor film such as YBa2Al3O7 is deposited on a substrate such as a single-crystal MgO. The film is fractured across a narrow strip by at least one indentation in the substrate juxtaposed from the strip to form a break junction. A transducer is affixed to the substrate for applying a bending movement to the substrate to regulate the distance across the gap formed at the fracture to produce a Josephson turned junction effect. Alternatively or in addition to the transducer, a bridge of a nobel metal is applied across the gap to produce a weak- link junction. DTIC

N95-30703*# National Aeronautics and Space Administration. Lewis Research Center, Cleveland, OH.
SPACE QUALIFIED HYBRID SUPERCONDUCTOR/SEMICONDUCTOR PLANAR OSCILLATOR CIRCUIT
F. A. Miranda, C. M. Chorey, R. R. Romanofsky, and K. B. Bhasin Jun. 1995 12 p Presented at the Low Temperature Electronics and High Temperature Superconductivity Symposium, Reno, NV, 21-26 May 1995; sponsored by the Electrochemical Society
(RTOP 235-01-0A)
(NASA-TM-106978; E-9541; NAS 1.15:106978) Avail: CASI HC A03/MF A01

We report on the space qualification of a hybrid superconductor/semiconductor planar local oscillator (LO) at 8.4 GHz. This oscillator was designed, fabricated, and tested as a component for the High Temperature Superconductivity Space Experiment 2 (HTSSE-2). The LO consisted of a GaAs MESFET and microstrip circuitry patterned onto a YBa2Cu3O(7-delta) high temperature superconducting (HTS) thin film on a 1.0 x 1.0 sq cm lanthanum aluminate (LaAlO3) substrate. At 77 K, this oscillator achieved power output levels up to 10 dBm into a 50 Ohm load. When incorporated into a full cryogenic receiver, the LO provided output powers within 0.0-3.0 dBm with less than 50 mW of dc power dissipation. Space qualification data on the sensitivity of the HTS films to the processing steps involved in the fabrication of HTS-based components are presented. Data on ohmic contacts, strength of wire bonds made to such contacts, and aging effects as well as vibration test results are discussed. Author

N95-30720# Technische Univ., Delft (Netherlands).
SOLVABILITY OF A CLASS OF HYPERSINGULAR NONLINEAR INTEGRAL EQUATIONS
S. A. Vavilov, A. B. Movchan, and V. V. Zalipaev 1994 18 p Prepared in cooperation with Bath Univ.
(PB95-207031) Avail: CASI HC A03/MF A01

The nonhomogeneous hypersingular integral equation of the Peierls type is analyzed. The method, based on the theory of branching of solutions to nonlinear equations, is used to prove the solvability of the problem. Applications to the theory of dislocations are considered. NTIS

N95-30722# International Centre for Theoretical Physics, Trieste (Italy).
MULTISITE ANTIFERROMAGNETIC ISING SPIN MODEL: PHASE TRANSITION THROUGH DOUBLING BIFURCATION
N. S. Ananikian and K. A. Oganessyan Oct. 1994 10 p
(DE95-614311; IC-94/326) Avail: CASI HC A02/MF A01 (US Sales Only)

The three-site antiferromagnetic Ising spin model on Husimi tree in external magnetic field is investigated and the line of the second order phase transitions is obtained. The upper bound of the temperature at which period doubling bifurcation and hence second order phase transition appeared is also obtained. DOE

N95-30728 Department of the Navy, Washington, DC.
DEVICE FOR LOW ELECTRIC-FIELD INDUCED SWITCHING OF LANGMUIR-BLODGETT FERROELECTRIC LIQUID CRYSTAL POLYMER FILMS Patent
Jawad Naciri, inventor (to Navy), Ranganathan Shashidar, inventor (to Navy), Sebastian Pfeiffer, inventor (to Navy), and Thomas L. Fare, inventor (to Navy) 8 Mar. 1994 22 p Filed 31 Dec. 1992
(AD-D017457; US-Patent-5,293,261; US-Patent-Appl-SN-999619; US-Patent-Class-359-087) Avail: US Patent and Trademark Office

Devices in which a Langmuir-Blodgett film of a liquid crystal polymer is disposed between electrodes on the surface of a substrate exhibit fast ferroelectric switching in response to an electric field generated by the electrodes, and Langmuir-Blodgett films of a liquid crystal polymer exhibit pyroelectric properties even at thicknesses below 10-15 microns. DTIC

N95-30736# International Centre for Theoretical Physics, Trieste (Italy).
ACOUSTOMAGNETOELECTRIC EFFECT IN A SUPERLATTICE
S. Y. Mensah, F. K. A. Allotey, and S. K. Adjepong (Cape Coast Univ., Ghana.) Sep. 1994 9 p
(DE95-613445; IC-94/298) Avail: CASI HC A02/MF A01 (US Sales Only)

The acoustomagnetoelectric effect (AME) in a semiconductor superlattice (SL) has been studied for an acoustic wave in the region ql much greater than 1. The expression for the acoustomagnetoelectric current j(sup AME) was calculated in the (tau) = constant approximation. The result indicates that the existence of j(sup AME) in SL may be due to the finite gap band and the periodicity of the electron spectrum. It is shown, in particular, that when (omega)(sub q) greater than (Delta) and (Delta) much greater than T ((omega)(sub q) is the frequency of the acoustic phonons; 2(Delta) is the miniband width of SL and T is the temperature measured in energy unit) the SL behaves as a monopolar semiconductor bulk material and in that case j(sup AME) (yields) 0. DOE

N95-30737# International Centre for Theoretical Physics, Trieste (Italy).
A MONTE-CARLO MODEL OF IONIC TRANSPORT ACROSS A SOLID INTERFACE
Ivo. S. Nachev Oct. 1994 17 p
(DE95-613447; IC-94/320) Avail: CASI HC A03/MF A01 (US Sales Only)

An improved Monte-Carlo model of ionic transport across a solid interface in two-dimensional triangular lattice is presented. The new features of the model are: (1) more-realistic form of the microscopic potential of the ion-ion interaction; and (2) accounting of the mutual ion interactions up to second nearest neighbors. This way it is possible to simulate more flexible the ionic transport across the real interface between a fast-ion conducting glass and the intercalate in the cathode of a Lithium thin-film battery. Numerical results computed with this model are presented by emphasizing on the influence of the internal interface on the ion distribution, the site energies and the open circuit voltage. DOE

N95-30756# Ames Lab., IA.
PROCESSING AND CHARACTERIZATION OF NANOCRYSTALLINE MOLYBDENUM DISILICIDE (MoSi2) CONSOLIDATED BY HOT ISOSTATIC PRESSING (HIP) Ph.D. Thesis
M. S. Haji-Mahmood 10 Feb. 1995 97 p
(Contract W-7405-eng-82)
(DE95-010243; IS-T-1729) Avail: CASI HC A05/MF A02

This work studied the effect nanocrystalline processing may have on mechanical properties of MoSi2 and the ease with which MoSi2 powder can be processed into a bulk shape. MoSi2 presently is limited by poor strength above 1000 C and brittleness below DBTT. This work studied cold and hot isostatic pressing (CIP, HIP). The attrited, CIPed, and HIPed samples were characterized by chemical analysis, XRD, SEM, microhardness, optical microscopy, and quantitative metallography (porosity, density). Fracture toughness of the nanocrystalline MoSi2 was found to be a factor of two higher than conventional MoSi2 and the hardness of 1500 C-HIPed compacts were higher, as well. Modulus test showed the calculated elastic constants to be higher than the original Cerac material. DOE

N95-30789# Melbourne Univ., Parkville (Australia). School of Physics.
POLARISATION RESONANCE IN X-RAY DIFFRACTION
P. Goodman, D. Paterson, and S. Matheson 1994 15 p
(DE95-616727; UM-P-94/44) Avail: CASI HC A03/MF A01 (US Sales Only)

The study of crystal structures by means of dynamic X-ray diffraction has placed a challenge to theoreticians to revise the X-ray diffraction theory based on Maxwell's equation. In this paper the feasibility of using 'polarization resonance' as a tool in the determination of absolute configuration for asymmetric structures is investigated. Two (left- and right-handed), sigma(+) and sigma(-), circular polarization states for 3-beam conditions are considered. Moreover, extending interaction into the 3rd dimension (normal to the beam) opens the possibility of absolute configuration determination of asymmetric structures in 3 dimensions. The computational scheme used is shown in terms of scattering diagrams.
DOE

N95-30822 California Univ., Los Angeles, CA.
VERTICAL TRANSPORT IN GaAs/AlGaAs SUPERLATTICES Ph.D. Thesis
Shahla Khorram 1993 115 p
Avail: Univ. Microfilms Order No. DA9420496

An improved experimental method has been developed to study perpendicular carrier transport in heterostructures by a microwave time of flight technique. Transport properties of three samples, one with bulk GaAs, one with a AlGaAs barrier and one with a AlGaAs/GaAs superlattice have been measured and analyzed in a comparative manner. A direct measurement of miniband conduction in superlattices is presented. The carrier velocity-field characteristic of GaAs/AlGaAs superlattice is measured in the field range of 10-40 kV/cm at 77 K. Perpendicular transport of electrons in a series of GaAs/AlGaAs superlattices is investigated by a microwave time of flight technique. Hot carrier transient effects are studied by analyzing the phase versus bias data in two GaAs/Al(0.2)Ga(0.8)As superlattices. The effect of hot carrier transient behavior on the phase data is found to be more pronounced at fields below 30 kV/cm. Barrier height dependence of the carrier transport in GaAs/AlGaAs superlattices is also investigated, and the velocity-field characteristics of a GaAs/Al(0.4)Ga(0.6)As superlattice at 77 K is obtained. It is found that the electron velocity in superlattices has a strong dependence on the barrier height. We observe an oscillatory behavior in the velocity-field characteristics of all the superlattices. A simple scattering limited transport model which is closely related to Bloch oscillations is invoked to explain the data.
Dissert. Abstr.

N95-30847*# Michigan State Univ., East Lansing, MI. Dept. of Electrical Engineering.
DIAMOND THIN FILM TEMPERATURE AND HEAT-FLUX SENSORS Final Report
M. Aslam, G. S. Yang, A. Masood, and R. Fredricks 3 Jul. 1995 20 p
(Grant NAG1-1328)
(NASA-CR-198859; NAS 1.26:198859) Avail: CASI HC A03/MF A01

Diamond film temperature and heat-flux sensors are developed using a technology compatible with silicon integrated circuit processing. The technology involves diamond nucleation, patterning, doping, and metallization. Multi-sensor test chips were designed and fabricated to study the thermistor behavior. The minimum feature size (device width) for 1st and 2nd generation chips are 160 and 5 micron, respectively. The p-type diamond thermistors on the 1st generation test chip show temperature and response time ranges of 80-1270 K and 0.29-25 microseconds, respectively. An array of diamond thermistors, acting as heat flux sensors, was successfully fabricated on an oxidized Si rod with a diameter of 1 cm. Some problems were encountered in the patterning of the Pt/Ti ohmic contacts on the rod, due mainly to the surface roughness of the diamond film. The use of thermistors with a minimum width of 5 micron (to improve the spatial resolution of measurement) resulted in lithographic problems related to surface roughness of diamond films. We improved the mean surface roughness from 124 nm to 30 nm by using an ultra high nucleation density of 10(exp 11)/sq cm. To deposit thermistors with such small dimensions on a curved surface, a new 3-D diamond patterning technique is currently under development. This involves writing a diamond seed pattern directly on the curved surface by a computer-controlled nozzle.
Author

N95-30933# Carnegie-Mellon Univ., Pittsburgh, PA. Dept. of Materials Science and Engineering.
STRUCTURAL, CHEMICAL AND ELECTRONIC PROPERTIES OF SUPERCONDUCTING THIN FILMS AND JUNCTIONS Final Report
Michael E. McHenry May 1994 183 p
(Contracts F49620-92-J-0415; F49620-91-C-0034)
(AD-A292700; AFOSR-95-0162TR) Avail: CASI HC A09/MF A02

Ba(1-x)K(x)BiO3 (BKBO) has a transition temperature, T(sub c), of 34 K and is unique among the high-temperature oxide superconductors because it is isotropic. It has been little studied and it is desirable to understand its behavior from the perspectives of both potential electronic applications and fundamental understanding of superconductivity. This study has involved a determination of the structural, electronic, and chemical properties of BKBO films and junctions deposited by RF magnetron sputtering. It was found that films with the highest T(sub c) and lowest rocking curve widths were consistently grown on SrTiO3. This material was therefore used as a buffer layer for growing high-quality BKBO films on the more practical substrates LaAlO3 and NdGaO3. SrTiO3 was also used as a barrier to fabricate BKBO/SrTiO3/BKBO SIS junctions for the first time. These junctions exhibited tunneling behavior. Modelling based on electrical measurements and electron diffraction observations of surface structure indicated island-type growth of the barrier material. The thickness variation in the tunnel barrier as a result of island formation limits the practical potential of such junctions in most applications where tunneling current uniformity and junction reproducibility are required.
DTIC

N95-30944# Army Foreign Science and Technology Center, Charlottesville, VA.
STUDIES OF C(60) AND C(70) AND OTHER FULLURENES: SYNTHESIS, DERIVATION, ELECTROCHEMISTRY, LUBRICANT PROPERTIES AND NEW COMPOSITION MATERIALS Final Report
R. E. Smalley, J. L. Margrave, R. H. Hauge, L. J. Wilson, and W. E. Billups Feb. 1995 37 p
(Contract DAAL03-92-G-0186)
(AD-A292726; ARO-30446.1-CH) Avail: CASI HC A03/MF A01

New designs for fullerene generators have been developed, including systems for producing endohedral species with metals inside the C60 or C70 cages. Also, focussed solar energy has been utilized for fullerene production. Electrochemical studies have led to the identification of C60(-1), C60(-2), C60(-6) ions and utilized for preparation of superconducting K3C60. Birch reductions of C60 and C70 led to C60H30 and C70H30 respectively. Adducts of C60 with tetraphenylcyclopentadienone and with cyclopropananaphthalene are described, and low-temperature reactions of C60 with H2 and with energetic nitrogen ion beams are reported. C60 does not appear to enhance the lubricity of motor oil formulations. The vapor pressure has been measured and it is estimated that the total pressure reaches one atmosphere at c.a. 1523K.
DTIC

N95-30958# International Centre for Theoretical Physics, Trieste (Italy).
FERROMAGNETIC POTTS MODEL IN A MAGNETIC FIELD: FINITE LATTICE EXTRAPOLATION OF THE (1 + 1)-DIMENSIONAL HAMILTONIAN
A. Bassir and A. Benyoussef (Laboratoire de Magnetisme et Physique des

Hautes E Energies, Rabat, Morocco.) Sep. 1994 6 p
(DE95-614447; IC-94/294) Avail: CASI HC A02/MF A01 (US Sales Only)

The (1 + 1)-dimensional Hamiltonian q-state ferromagnetic Potts model in an external magnetic field H is studied using finite lattice extrapolation techniques. The possible phases and their boundaries are determined from the ground state energy and the gap in the excitation energy, for arbitrary values of q and both for positive and negative field. We found that, for H positive, there is a critical value q(c), where a first order transition line appears for q greater than q(c), starting at the zero field transition point and terminating at a critical point in (h/lambda, H/lambda) plane, which separates the disordered phase and the ordered phase in the direction of H. For h negative a critical transition line separating the disordered phase and the others (q - 1) ordered phases becomes first order for q greater than q(c). DOE

N95-30959# International Centre for Theoretical Physics, Trieste (Italy).
DYNAMICS OF AN INHOMOGENEOUS ANISOTROPIC ANTIFERROMAGNETIC SPIN CHAIN
M. Daniel and R. Amuda (Bharathidasan Univ., Tamil Nadu, India.) Nov. 1994 15 p
(DE95-614449; IC-94/340) Avail: CASI HC A03/MF A01 (US Sales Only)

We investigate the nonlinear spin excitations in the two sublattice model of a one dimensional classical continuum Heisenberg inhomogeneous antiferromagnetic spin chain. The dynamics of the inhomogeneous chain reduces to that of its homogeneous counterpart when the inhomogeneity assumes a particular form. Apart from the usual twists and pulses, we obtain some planar configurations representing the nonlinear dynamics of spins. DOE

N95-30969# Lantan, Moscow (Russia).
LANGASITE CRYSTALS GROWTH WITH QUALITY FACTOR Q, THAT EXCEEDS THE Q OF QUARTZ, AND WHICH ARE SUITABLE FOR HIGH-PRECISION RESONATORS Final Report, 16 Dec. 1994 - 31 Mar. 1995
A. N. Gotalskaja, D. I. Dresin, S. N. Schegolkova, N. I. Saveleva, and V. V. Bezdelkin 31 Mar. 1995 24 p
(Contract N68171-94-C-9004)
(AD-A293397; R/D-7152-EE-01) Avail: CASI HC A03/MF A01

Processes of langasite crystal growth are considered. Distribution of temperature fields, heat assembly design, pulling and rotation rates are optimized. Composition of charge, impurity content, and technology of its manufacture have been studied. Influence of annealing regimes and gaseous medium on crystal quality are discussed. The main defect types encountering in crystals are identified. Langasite resonator at 5 MHz, 3rd overtone has been developed. DTIC

N95-30982# University of Southern California, Los Angeles, CA.
PICOSECOND PHASE CONJUGATION: NEW APPLICATIONS, DEVICES, AND MATERIALS Final Report, 1 Oct. 1991 - 31 Dec. 1994
Jack Feinberg 31 Dec. 1994 65 p
(Contract F49620-92-J-0022)
(AD-A293195; AFOSR-95-0238TR) Avail: CASI HC A04/MF A01

In this project we investigated four main areas: (1) Temporal shaping of picosecond laser pulses using beam coupling in a photorefractive crystal. We showed both theoretically and experimentally that one can add or subtract picosecond light pulses onto existing light pulses to create arbitrary temporal waveforms; (2) The physics of the photorefractive effect in barium titanate crystals. We showed that photovoltaic currents play an important role in the formation of photorefractive gratings in barium titanate. We also derived a theory to explain the curved beam paths observed in photorefractive phase conjugators; (3) Frequency doubling in infrared light in glass. We proved decisively that second harmonic generation in optically prepared glass is caused by a dc electric field imprisoned in the glass. We mapped the spatial profile of this dc field to a resolution of one micron; and (4) Injecting diode laser arrays using phase conjugation. We demonstrated that injecting broad-area diode laser with light causes the laser array to emit a spatially and spectrally narrow output beam. We use a double phase conjugator to guide light from an injecting laser into the lasing regions of the laser array. DTIC

N95-30983# Carnegie-Mellon Univ., Pittsburgh, PA. Dept. of Electrical and Computer Engineering.
DEVELOPMENT OF GERMANIUM-SILICON GROWTH TECHNOLOGY Final Report, 1 Feb. 1992 - 31 Jan. 1995
D. W. Greve 15 Mar. 1995 24 p
(Contract F49620-92-J-0155)
(AD-A293199) Avail: CASI HC A03/MF A01

Germanium-silicon epitaxial heterostructures have been grown and evaluated for possible use in far-infrared detectors. Growth was performed by ultra-high vacuum chemical vapor deposition at temperatures of 550-600 C. Multiple quantum well structures were grown and evaluated by X-ray diffraction, secondary ion mass spectrometry, and photoluminescence. Infrared absorption measurements showed that free-carrier absorption was dominant for normal-incidence illumination. Heterojunction internal photoemission structures have also been grown and characterized. The results show that both structures can be successfully fabricated using this technique when growth parameters are correctly chosen. DTIC

N95-30984# Naval Research Lab., Washington, DC.
X-BAND MAGNICON AMPLIFIER RESEARCH AT THE NAVAL RESEARCH LABORATORY Interim Report
Steven H. Gold, Bahman Hafizi, and Arne W. Fliflet 19 Apr. 1995 10 p
(AD-A293203; NRL/MR/6793-95-7666) Avail: CASI HC A02/MF A01

We present a progress report on a program to develop a high-power second harmonic magnicon amplifier at 11.4 GHz for linear accelerator applications. The experiments are being carried out on the NRL Long-Pulse Accelerator Facility using a plasma cathode to create the electron beam. Typical beam parameters are 500 kV, 200 A, 5.5 mm diameter, with a approximately 300 nsec voltage flattop and a approximately 10(exp -2) Hz repetition rate. An initial deflection cavity experiment demonstrated two-cavity gain of approximately 15 dB at a frequency ship of 0.18%, in good agreement with theory and simulation. A complete five cavity magnicon circuit was designed via computer simulation, fabricated, and cold tested. This circuit is now undergoing experimental tests. In preliminary experiments, a low power saturation effect was observed in the deflection cavities, apparently due to plasma formation caused by the diode x-ray flux and by inadequate vacuum conditions. Following a major effort to improve the vacuum and surface conditions, very recent experiments have shown that is possible to 'burn through' this low power saturation effect, and achieve high fields in the deflection cavities. However, high power emission from the output cavity has not yet been observed. We are also evaluating new fourth magnicon designs via time-dependent multimode simulations. DTIC

N95-30985# Scientific Research Associates, Inc., Glastonbury, CT.
OPTO-ELECTRONIC COMPONENTS FROM NON-STOICHIOMETRIC 3-5 MATERIALS Final Report, 15 Jun. - 15 Dec. 1994
H. L. Grubin and J. P. Kreskovsky 28 Feb. 1995 31 p
(Contract F49620-94-C-0032)
(AD-A293206; R9139-F; AFOSR-95-0236TR) Avail: CASI HC A03/MF A01

An investigation was undertaken to determine the feasibility of integrating low temperature growth GaAs:As and silicon for the development of optoelectronic devices. These devices attempt to exploit the optoelectronic properties of LT GaAs while integrating the structure on silicon substrates. Numerical models of LT GaAs are developed and implemented to aid in the design of such devices. An integrated MSM-LED structure was successfully fabricated on a silicon substrate. The results of the study show that it is feasible to integrate LT GaAs devices and silicon technology. Further development of the design software and a variety of structures, including a high voltage switch, a transceiver and a GHz tunable filter are proposed for a Phase 2 effort. DTIC

N95-31008# Wayne State Univ., Detroit, MI. Dept. of Physics.
INVESTIGATIONS OF YBaCuO MATERIALS WITH NEAR-ROOM-TEMPERATURE RESISTIVITY TRANSITIONS Final Report, 15 Jun. 1991 - 14 Oct. 1994
Lowell E. Wenger and J. T. Chen 14 Dec. 1994 506 p
(Grant AF-AFOSR-0319-91)
(AD-A293405; AFOSR-95-0170TR) Avail: CASI HC A22/MF A04

This final technical report describes the continual superconductivity research on the materials and structural phases responsible for the above 200-K superconducting transitions, their synthesis conditions, and the study

of the physical properties associated with these transitions. Resistive transitions having superconducting-like character have been observed in multi-phase ceramic YBaCuO samples and on surfaces of nominal YBa2Cu3O7 single crystals in the temperature range of 260 K to 340 K. The appearance of these transitions appears to require certain experimental measuring conditions including an oxygen atmosphere during measurements. Magnetization studies on these materials show a flux-trapping hysteretic behavior at similar temperatures, i.e., a more diamagnetic behavior in the zero-field-cooled-magnetization than the field-cooled-magnetization characteristic of a weak superconducting phase being present. The synthesis conditions and structural information on multi-phase YBaCuO samples exhibiting reproducible flux-trapping phenomenon at 336 K is also detailed. In addition, studies of the paramagnetic Meissner effect on a niobium disk and of Josephson properties in YBa2Cu3O7 single crystals and YBaCuO thin films are reported. DTIC

N95-31112# Sandia National Labs., Albuquerque, NM.
BAND GAP MEASUREMENT OF Si(1-x)C(x)/Si (0 LESS THAN OR EQUAL TO X LESS THAN OR EQUAL TO 0.014) ALLOYS USING PHOTOLUMINESCENCE AND SPECTROSCOPIC ELLIPSOMETRY
H. Lee, S. R. Kurtz, J. A. Floro, J. Strane, C. H. Seager, S. R. Lee, E. D. Jones, J. F. Nelson, T. Mayer, and S. T. Picraux 1995 6 p Presented at the Spring Meeting of the Materials Research Society, San Francisco, CA, 17-21 Apr. 1995
(Contract DE-AC04-94AL-85000)
(DE95-011020; SAND-94-2718C; CONF-950412-8) Avail: CASI HC A02/MF A01

The authors have characterized the optical properties of heteroepitaxial Si(1-x)C(x)/Si (0 less than or equal to x less than or equal to 0.014) alloys grown on Si substrates by solid phase epitaxy using spectroscopic ellipsometry and photoluminescence. The measured dielectric function confirms that the samples are of good crystalline quality. The 14-K photoluminescence spectra of Si(1-x)C(x)/Si show several defect peaks. After hydrogen passivation, the authors observed a new peak near 1.15-1.17 eV which increases in energy with the incorporation of carbon. The authors tentatively assign this peak as the no-phonon peak of the Si(1-x)C(x) epilayer. They discuss the alloy shift of the observed spectroscopic features in terms of the C-induced change in the Si indirect band gap. DOE

N95-31189# Minnesota Univ., Minneapolis, MN. Dept. of Chemical Engineering and Materials Science.
MOLECULAR NANOCLUSTERS AS PRECURSORS TO CONDUCTIVE THIN FILMS AND CRYSTALS Technical Report, 1 May 1994 - 30 Jun. 1995
Andrew C. Hillier, Joachim H. Schott, and Michael D. Ward 20 Jan. 1995 17 p
(Contract N00014-93-1-0563)
(AD-A290278; TR-8) Avail: CASI HC A03/MF A01

The fabrication of electrically conductive organic thin films and crystals is of both fundamental and technological interest. However, the mechanisms that control crystal structure and morphology during crystallization are not yet completely understood. In order to address these issues, we have employed scanning tunneling and atomic force microscopies to view the formation of molecular conductors on single crystal substrates. We have observed that these materials form ordered molecular nanoclusters, in which at least one dimension has molecular length scale. These nanoclusters evolve into thin films, and eventually, bulk crystals. The role of interactions between the substrate and organic overlayers, as well as the influence of intermolecular interactions within the molecular clusters, has been revealed. DTIC

N95-31222# Tokyo Univ., Tanashi (Japan). Inst. for Nuclear Study.
ON THE STRING EQUATION AT c=1
Toshio Nakatsu Jul. 1994 18 p
(DE95-737161; INS-1043) Avail: CASI HC A03/MF A01

The analogue of the string equation which specifies the partition function of c=1 string with a compactification radius (beta) is an element of Z(sub (greater than or equal to 1) is described in the framework of Toda lattice hierarchy. DOE

N95-31231# Los Alamos National Lab., NM.
DYNAMICS OF CURRENT DRIVEN DISORDERED JOSEPHSON JUNCTION ARRAYS
Daniel Dominguez, Niels Gronbech-Jensen, and Alan R. Bishop 1995 13 p Presented at the Workshop on Macroscopic Quantum Phenomena and Coherence in Superconducting Networks, Frascati, France, 1-5 Mar. 1995
(Contract W-7405-eng-36)
(DE95-009418; LA-UR-95-967; CONF-9503124-1) Avail: CASI HC A03/MF A01

We present dynamical simulations of disordered Josephson junction arrays with a bias current. We study the 4 characteristics and vortex dynamics as a function of integer frustration f = n, weak frustration f = n + delta (delta much less than 1) and full frustration pairs close to the critical current i(sub c). We focus on the study of the plastic flow of vortices (f = n + delta), of vortex-antivortex pairs (f = n), and the dynamics of domain walls (f = n + 1/2) close to i(sub c). We analyze the voltage noise and vortex fluctuations in the plastic flow regimes. We obtain the phase diagram for the different dynamical regimes as a function of disorder and applied current. We also study the dynamical critical behavior of depinning close to i(sub c) in the gauge glass limit of the model, f approaches infinity, calculating critical exponents for the voltage onset and voltage fluctuations. We discuss our results within the context of present theories of the non-linear dynamics of disordered media. DOE

N95-31233# Sandia National Labs., Albuquerque, NM.
MINORITY AND MAJORITY CARRIER TRANSPORT CHARACTERIZATION IN COMPOUND SEMICONDUCTORS
Michael L. Lovejoy 1995 15 p Presented at the Workshop on Semiconductor Characterization, Gaithersburg, MD, 30 Jan. - 2 Feb. 1995
(Contract DE-AC04-94AL-85000)
(DE95-010873; SAND-95-0054C; CONF-950117-4) Avail: CASI HC A03/MF A01

A review of minority and majority carrier transport characterization techniques is presented. Minority transport is discussed in the context of base transport in HBTs where the base transit time can be an important component of the total transit time through the transistor. Characterization techniques to measure minority carrier mobilities in heavily-doped compound semiconductors and theoretical results are reviewed. Majority carrier transport in high-performance PHEMT structures is discussed. Parallel conduction of the heavily-doped contact layer and the 2-D electron gas makes measurements of the 2-D electron concentration difficult. Techniques to measure the 2-D concentration are reviewed. Recent application of these techniques have yielded new data for GaAs that has important implications for device design and shows the need for measurements of other CS-materials and devices to realize accurate device design and optimization. DOE

N95-31269 Department of the Navy, Washington, DC.
METHOD OF SYNTHESIZING HIGH QUALITY, DOPED DIAMOND AND DIAMONDS AND DEVICES OBTAINED THEREFROM Patent
John W. Glesener, inventor (to Navy), Arthur A. Merrish, inventor (to Navy), and Keith A. Snail, inventor (to Navy) 17 Jan. 1995 14 p Filed 20 Aug. 1991
(AD-D017432; US-Patent-5,381,755; US-Patent-Appl-SN-747321; US-Patent-Class-117-88) Avail: US Patent and Trademark Office

Diamond crystals and films having a well-controlled amount of dopant therein are synthesized by incorporating a dopant into a deposition species formed from a gaseous source of carbon and a gaseous source of hydrogen. Flame and/or plasma deposition may be used. Various apparatuses for carrying out the growth of the doped diamond are also disclosed. DTIC

N95-31438# Minnesota Univ., Minneapolis, MN.
TRANSITIONS, DEFECTS, AND WHISKERED MICROSTRUCTURES Final Technical Report, 1 Jul. 1991 - 31 Dec. 1994
Richard James, David Kinderlehrer, and Mitchell Luskin 15 Feb. 1995 10 p
(Grant AF-AFOSR-0301-91)
(AD-A292796; AFOSR-95-0178TR) Avail: CASI HC A02/MF A01

James and Kinderlehrer have given a new theory of magnetostriction. The theory shows excellent agreement with experiment and has motivated new experiments on the relation between domain structure and behavior

by Lord and by DeGraef. The theory implies a new mechanism for magnetostriction in Tb(x)Dy(1-x)Fe2 (x near 0.3). It also strongly suggests the existence of materials (termed 'magnetomemory' materials by the authors) that would have magnetostrictive strain that is two orders of magnitude larger than the largest produced by current giant magnetostrictive materials. Luskin and his research group have developed an advanced computational model for the dynamics of crystals which undergo a martensitic transformation. They have used this model to compute the development of martensitic microstructure and the propagation of the interface separating the austenitic phase from the martensitic phase, and they have obtained results for the influence of the surface energy and the viscosity on the dynamics. James, Kinderlehrer, Luskin and their collaborators have studied new mechanisms for hysteresis, and have clarified the role of elastic incompatibility, shuffling, kinetics, and microstructure. DTIC

N95-31444# Cornell Univ., Ithaca, NY. Dept. of Chemistry.
SDIO: DISCOVERING SUPERCONDUCTING MATERIALS AT HIGH TEMPERATURES Final Technical Report, Jun. 1993 - 31 May 1994
Francis J. DiSalvo 25 Aug. 1994 3 p
(Contract F49620-93-1-0328)
(AD-A292820; AFOSR-95-0139TR) Avail: CASI HC A01/MF A01

The research funded under this grant focused on the layered structure compounds BaNIS2 and BaCoS2. The former is a metallic conductor while the latter is a magnetic Mott insulator. We planned doping studies to study the effects of both disorder and the crossover to the metallic state. It is hoped that doping a Mott insulator to the metallic state might produce a high temperature superconductor. Unfortunately, due to the termination of the SDIO program, this research was supported for only one year (instead of the planned three years), so the project is not complete. DTIC

N95-31539# Army Research Lab., Fort Monmouth, NJ.
POISSON'S RATIO FOR HEXAGONAL CRYSTALS
Arthur Ballato Mar. 1995 13 p
(AD-A293556; ARL-TR-424) Avail: CASI HC A03/MF A01

General expressions for Poisson's ratio are derived for hexagonal crystals; simplified forms are given for cases involving symmetry directions. Crystals of hexagonal symmetry include a number of the binary semiconductor systems with the piezoelectric wurtzite structure, such as GaN and AlN. These are becoming increasingly important for high technology applications. One of the most important representatives of this class is the family of poled electroceramics, including BaTiO3, PZT, and related alloys. All hexagonal classes have the same elastic matrix scheme, so for our purposes it is not necessary to distinguish between the different point groups; the presence of piezoelectricity is neglected. DTIC

N95-31641# Oak Ridge National Lab., TN. Metals and Ceramics Div.
PHASE STABILITY, POINT DEFECTS AND SITE PREFERENCE OF FeAl AND NiAl WITH TERNARY ADDITIONS
C. L. Fu and J. Zou 1994 7 p Presented at the 1994 Fall Meeting of the Materials Research Society (MRS), Boston, MA, 28 Nov. - 2 Dec. 1994
(Contract DE-AC05-84OR-21400)
(DE95-009694; CONF-941144-141) Avail: CASI HC A02/MF A01

First-principles calculations have been used to investigate the defect properties and the site preference of FeAl and NiAl with ternary additions. It is found that a 'triple-defect' structure model becomes invalid in describing the defect structure of FeAl (which is weakly ordered). The calculated mono-vacancy concentration on the Fe sites is lower than available experimental values by an order of magnitude, which may suggest the formation of defect complexes or the need of sufficiently long annealing time to anneal out quenched-in vacancies. For the site preference of ternary additions in FeAl, Cr and Ti are found to occupy Al sublattices, whereas Ni has a distinct preference for the Fe sites. The substitutional behavior of ternary elements in FeAl is consistent with the trend in the calculated heat-of-formation. For Fe addition in Al-rich NiAl, Fe atoms occupy Ni sublattices exclusively. The site preference of Fe addition in Ni-rich NiAl is dependent on alloy composition and temperature. At low temperatures, Fe atoms are found to preferentially occupy Al sublattices in Ni-rich alloys. DOE

N95-31826# Massachusetts Inst. of Tech., Lexington, MA. Lincoln Lab.
SOLID STATE RESEARCH Quarterly Technical Report, 1 May - 31 Jul. 1994
Alan L. McWhorter 17 Feb. 1995 58 p
(Contract F19628-95-C-0002)
(AD-A293083; Rept-1994-3; ESC-TR-94-106) Avail: CASI HC A04/MF A01

This report covers in detail the research work of the Solid State Division at Lincoln Laboratory for the period 1 May through 31 July 1994. The topics covered are Electrooptical Devices, Quantum Electronics, Materials Research, Submicrometer Technology, High Speed Electronics, Microelectronics, and Analog Device Technology. Funding is provided primarily by the Air Force, with additional support provided by the Army, ARPA, Navy, BMDO, NASA, and NIST. DTIC

N95-32018# North Carolina State Univ., Raleigh, NC. Dept. of Materials Science and Engineering.
GROWTH, CHARACTERIZATION AND DEVICE DEVELOPMENT IN MONOCRYSTALLINE DIAMOND FILMS Quarterly Technical Report, 1 Jan. - 31 Mar. 1995
Robert F. Davis, J. T. Glass, R. J. Nemanich, K. S. Ailey, F. R. Sivazlian, and S. D. Wolter Mar. 1995 55 p
(Contract N00014-93-I-0437)
(AD-A293106) Avail: CASI HC A04/MF A01

Research continued in the growth of boron nitride films on various substrates including Si(100), diamond (100), Cu(100) and Ni(100) via ion beam assisted electron beam evaporation. Fourier transform infrared spectroscopy and high resolution transmission electron microscopy showed that the total films on Si and diamond consisted of the sequence from the substrate: a-BN, h-BN, c-BN. The c-BN layers formed as a function of deposition temperature, ion current and thickness. The occurrence of this layer is attributed to increasing intrinsic biaxial compressive stress generated during deposition. The interface and surface structure of highly oriented diamond films were examined by low resolution transmission electron microscopy (LRTEM), high resolution transmission electron microscopy (HRTEM) and using a transmission electron microscope with in situ cathodoluminescence. Interface studies by HRTEM indicated that SiC formation may have assisted in the formation of highly oriented diamond. Additionally, in some areas diamond appeared to be in direct contact with the silicon substrate; no indication of an amorphous or crystalline interlayer was observed. The grain boundaries of the highly oriented (100) diamond particles observed by LRTEM showed that the misorientation between these particles was compensated by a series of parallel dislocations. Finally, TEM/CL results showed that the majority of luminescence in the plan view was from misoriented or highly defective diamond grains. DTIC

N95-32037# Iowa State Univ. of Science and Technology, Ames, IA.
TERAHERTZ SPECTROSCOPY OF SILICON MICROMACHINED THREE-DIMENSIONAL PHOTONIC BANDGAP CRYSTAL
E. Oezbay, E. Michel, G. Tuttle, R. Biswas, K. M. Ho, J. Bostak, and D. M. Bloom 1995 2 p Presented at the 9th International Conference on Ultrafast Phenomena, Dana Point, CA, 1-5 May 1994
(Contract W-7405-eng-82)
(DE95-010233; IS-M-791; CONF-940593-15) Avail: CASI HC A01/MF A01

Using micromachined silicon wafers, the authors have fabricated three-dimensional photonic bandgap crystals. Terahertz spectroscopy techniques have been used to measure bandgap frequencies over 500 GHz. DOE

N95-32062# Argonne National Lab., IL.
ON THE POSSIBILITY OF A TWO-STATE MAGNETIC STRUCTURE FOR NANOCRYSTALLINE CHROMIUM
M. R. Fitzsimmons, R. A. Robinson, J. A. Eastman, and J. W. Lynn (National Inst. of Standards and Technology, Gaithersburg, MD.) Mar. 1995 6 p Presented at the Annual Meeting and Exhibition of the Minerals, Metals and Materials Society (TMS), Las Vegas, NV, 12-16 Feb. 1995 Prepared in cooperation with Los Alamos National Lab., NM
(Contracts W-31-109-eng-38; W-7405-eng-36)
(DE95-009914; ANL/MSD/CP-84769; CONF-950201-12) Avail: CASI HC A02/MF A01

Wide-angle neutron diffraction measurements taken at temperatures from

6 to 250 K indicate that the portion of a chromium sample with a mean grain size of 73 nm is antiferromagnetically ordered at temperatures below 100 K. The Neel temperature (about 120 +/- 10 K) for this nanocrystalline sample is suppressed considerably below that of strain-free single-crystal chromium (311 K). Similar measurements of other samples indicate that the amount of antiferromagnetic order decreases with decreasing grain size. The grain size dependence of antiferromagnetic order is discussed in the context of a two-state model. DOE

N95-32071# International Centre for Theoretical Physics, Trieste (Italy).
SCHWINGER-BOSON STUDIES OF THE SINGLE HOLE MOTION IN A 2D QUANTUM ANTIFERROMAGNET
C. Q. Wu, L. Yu, and Z. B. Su (Academia Sinica, Beijing, China.) Sep. 1994 17 p
(DE95-614444; IC-94/272) Avail: CASI HC A03/MF A01 (US Sales Only)

Within the Schwinger-boson approach for the t-J model, the single hole problem in a two-dimensional quantum antiferromagnet is studied by using the quantum Bogoliubov-de Gennes formalism which treats the distortion of the spin background and quantum spin fluctuations on an equal footing. Several self-trapped localized hole states are found in the distorted spin-background as in the case of an anisotropic Heisenberg model. These localized hole states survive at finite temperatures when the antiferromagnetic order becomes short-ranged. The energy separation between the two lowest states is reduced by considering the spin-background distortion, but it remains finite. DOE

N95-32103# Illinois Univ., Urbana, IL.
EVIDENCE FOR ELECTRONIC ENERGY LOSS PROCESSES STIMULATING SOLID PHASE EPITAXIAL REGROWTH OF SPATIALLY ISOLATED AMORPHOUS REGIONS IN SEMICONDUCTOR SYSTEMS
I. Jencic, I. M. Robertson, M. W. Bench (Minnesota Univ., Minneapolis, MN.), and M. A. Kirk (Argonne National Lab., IL.) Jan. 1995 6 p Presented at the 1994 Fall Meeting of the Materials Research Society (MRS), Boston, MA, 28 Nov. - 2 Dec. 1994
(Contracts DE-FG02-91ER-45439; W-31-109-eng-38)
(DE95-009892; ANL/MSD/CP-85469; CONF-941144-135) Avail: CASI HC A02/MF A01

Solid phase epitaxial regrowth of spatially isolated amorphous regions in Si, Ge and GaP has been stimulated by using an electron beam with energies in the range of 50 to 300 keV. In all materials, the rate at which the amorphous zones disappear decreases as the energy of the electron beam increases from 50 keV reaching a minimum below the threshold displacement voltage before it again increases with increasing electron energy. The experimental results are interpreted in terms of creation and motion of defects (dangling bonds, charged defects) along the amorphous-crystalline interface. DOE

N95-32105# Argonne National Lab., IL.
DEFECT CONFIGURATIONS IN NEUTRON-IRRADIATED U3Si2
S. K. Chan, R. C. Birtcher, M. H. Mueller, and J. W. Richardson, Jr. Dec. 1994 7 p Presented at the 1994 Fall Meeting of the Materials Research Society (MRS), Boston, MA, 28 Nov. - 2 Dec. 1994
(Contract W-31-109-eng-38)
(DE95-009896; ANL/MSD/CP-83382; CONF-941144-136) Avail: CASI HC A02/MF A01

Investigations of the nature of defects in neutron-irradiated intermetallic U3Si2 as a function of dose have been carried out. Defect categories of vacancies and interstitials, their clusters and dislocation loops have been considered. The effects of the displacement field from each on the neutron scattering intensity profiles are presented. The theoretical predictions are compared with experimentally determined intensity profiles from time-of-flight data using the General Purpose Powder Diffractometer at the Intense Pulse Neutron Source of Argonne National Laboratory. The results are illustrated for a particular peak at various doses and the physical implications discussed. DOE

N95-32147# Sandia National Labs., Albuquerque, NM. Chemical Processing Science Dept.
GCMS AND FTIR STUDIES OF BY-PRODUCT INHIBITED GROWTH AND THE RATE-LIMITING STEP IN TEOS-BASED SiO2 CVD
Michael E. Bartram and Harry K. Moffat 1995 8 p Presented at the 187th Meeting of the Electrochemical Society, Reno, NV, 21-26 May 1995
(Contracts DE-AC04-94AL-85000; DE-AC04-76DP-00789)
(DE95-009863; SAND-95-0664C; CONF-950518-3) Avail: CASI HC A02/MF A01

To improve process reliability and deposition methods, it is essential to identify the rate-limiting step in TEOS-based SiO2 CVD and its dependence on process conditions. For this purpose, experiments designed to evaluate by-product inhibition effects and to identify the rate-limiting step in TEOS decomposition have been carried out in a research reactor using GCMS and FTIR. By repetitively sampling a series of reactions in which TEOS was first mixed with ethylene, ethanol, and water in the gas-phase, GCMS was used to show clearly that these reaction by-products do not inhibit the heterogeneous reaction step on SiO2 at 1,000 K. FTIR was used to determine that ethoxy groups from TEOS dissociative chemisorption have a significant lifetime on the SiO2 surface at CVD temperatures and have an activation energy for decomposition of 16 kcal/mol +/- 4 kcal/mol. This is much higher than the activation energy of 6 kcal/mol reported for the initial chemisorption step and is near the 22 kcal/mol reported for the overall activation energy for SiO2 deposition in a cold-wall reactor. These results suggest that, whether or not surface ethoxy groups inhibit TEOS reactions, their decomposition may be directly related to the rate-limiting step in SiO2 deposition. DOE

N95-32268# Lawrence Livermore National Lab., Livermore, CA.
LASER PROPERTIES OF Yb(3+)-DOPED Sr5(PO4)3F CRYSTALS
C. D. Marshall, S. A. Payne, L. K. Smith, K. I. Schaffers, R. Beach, M. Emanuel, H. T. Powell, W. F. Krupke, and B. H.T. Chai Jun. 1994 5 p Presented at the Lasers and Electro-Optics Society Annual Meeting, Boston, MA, 31 Oct. - 3 Nov. 1994
(Contract W-7405-eng-48)
(DE95-010686; UCRL-JC-117359; CONF-9410192-2) Avail: CASI HC A01/MF A01

Yb(3+) based lasers have received substantial attention over the past several years. Yb-based materials, which typically lase around 1 micron, are aided by the simple electronic structure of Yb(3+) in that it has only two accessible electronic states eliminating the detrimental impact of upconversion or excited state absorption. In addition, the inherently small quantum defect of approximately 10-15% has led to relatively large intrinsic laser slope efficiencies. The pumping and extraction dynamics of Yb:Sr5(PO4)3F crystals will be discussed. A diode array and a free running Cr:LiSAF laser are utilized as pump sources for both Yb-oscillators and amplifiers. DOE

N95-32284# Lawrence Livermore National Lab., Livermore, CA. Dept. of Chemistry and Materials Science.
METALLIC MULTILAYERS AT THE NANOSCALE
Alan F. Jankowski Nov. 1994 16 p Presented at the 2nd International Conference on Nanostructured Materials, Stuttgart, Germany, 2-7 Oct. 1994
(Contract W-7405-eng-48)
(DE95-011534; UCRL-JC-118972; CONF-941039-5) Avail: CASI HC A03/MF A01

The development of multilayer structures has been driven by a wide range of commercial applications requiring enhanced material behaviors. Innovations in physical vapor deposition technologies, in particular magnetron sputtering, have enabled the synthesis of metallic-based structures with nanoscaled layer dimensions as small as one-to-two monolayers. Parameters used in the deposition process are paramount to the formation of these small layer dimensions and the stability of the structure. Therefore, optimization of the desired material properties must be related to assessment of the actual microstructure. Characterization techniques such as x-ray diffraction and high resolution microscopy are useful to reveal the interface and layer structure - whether ordered or disordered crystalline, amorphous, compositionally abrupt or graded, and/or lattice strained. Techniques for the synthesis of metallic multilayers with subnanometric layers are reviewed with applications based on enhancing material behaviors as reflectivity and magnetic anisotropy but with emphasis on experimental studies of mechanical properties. DOE

N95-32301# Oak Ridge National Lab., TN.
SUPPRESSION OF SELF-INTERSTITIALS IN SILICON DURING ION IMPLANTATION VIA IN-SITU PHOTOEXCITATION

J. Ravi (North Carolina State Univ., Raleigh, NC.), Yu Erokhin (North Carolina State Univ., Raleigh, NC.), K. Christensen (North Carolina State Univ., Raleigh, NC.), G. A. Rozgonyi (North Carolina State Univ., Raleigh, NC.), B. K. Patnaik (North Carolina Univ., Chapel Hill, NC.), and C. W. White Feb. 1995 7 p Presented at the 1994 Fall Meeting of the Materials Research Society (MRS), Boston, MA, 28 Nov. - 2 Dec. 1994 Sponsored in part by the National Science Foundation
(Contract DE-AC05-84OR-21400)
(DE95-009173; CONF-941144-119) Avail: CASI HC A02/MF A01

The influence of in-situ photoexcitation during low temperature implantation on self-interstitial agglomeration following annealing has been investigated using transmission electron microscopy (TEM). A reduction in the level of as-implanted damage determined by RBS and TEM occurs athermally during 150 keV self-ion implantation. The damage reduction following a 300 C anneal suggests that it is mostly divacancy related. Subsequent thermal annealing at 800 C resulted in the formation of (311) rod like defects or dislocation loops for samples with and without in-situ photoexcitation, respectively. Estimation of the number of self-interstitials bound by these defects in the sample without in-situ photoexcitation corresponds to the implanted dose; whereas for the in-situ photoexcitation sample a suppression of approx. 2 orders in magnitude is found. The kinetics of the athermal annealing process are discussed within the framework of either a recombination enhanced defect reaction mechanism, or a charge state enhanced defect migration and Coulomb interaction. DOE

N95-32307# Sandia National Labs., Albuquerque, NM.
ENERGETICS OF Pt ADSORPTION ON Pt(111)
P. J. Feibelman, J. S. Nelson, and G. L. Kellogg Apr. 1995 35 p
(Contract DE-AC04-94AL-85000)
(DE95-010933; SAND-93-2577) Avail: CASI HC A03/MF A01

First-principles Local Density Functional (FP-LDF) and Embedded Atom Method (EAM) total energies, for a single Pt atom adsorbed on Pt(111), are compared to each other and to Field Ion Microscope (FIM) observations. Our EAM calculations predict a small barrier to diffusion and only a slight energy difference between adsorption in the fcc and hcp three-fold hollows (both smaller than 1 meV). They correspond poorly to the results of the FP-LDF calculations, which imply a diffusion barrier of 0.38 eV for passage over a bridge, and a preference of 0.18 eV for the fcc as against the hcp site. FIM measurements yield a diffusion barrier of (0.25 +/- 0.02) eV, and imply that binding in the fcc site is preferred. DOE

N95-32308# Sandia National Labs., Albuquerque, NM. Surface and Interface Science.
STM MEASUREMENTS OF THE INTERACTION OF VACANCIES AND STEPS DURING LOW-ENERGY-ION BOMBARDMENT OF Si(001)
B. S. Swartzentruber Apr. 1995 10 p
(Contract DE-AC04-94AL-85000)
(DE95-010935; SAND-95-0594) Avail: CASI HC A02/MF A01

We create mobile surface vacancies on vicinal Si(001) by bombarding the surface with 300 eV Xe ions at a substrate temperature of 465 C. The vacancies preferentially annihilate at the rough steps retracting them with respect to their smooth neighbors. This process leads to a bimodal terrace width distribution. The retraction of the rough steps due to the vacancy annihilation is in competition with the healing process by which the surface tries to maintain its equilibrium configuration of equally spaced steps. As the two competing processes balance, the surface reaches steady state and subsequent removal of surface atoms is manifest as simple step flow. DOE

N95-32366# California Univ., Berkeley. Lawrence Berkeley Lab, CA.
SUPERCONDUCTING AND NORMAL-STATE PROPERTIES OF NOVEL MATERIALS Ph.D. Thesis
V. H. Crespi Sep. 1994 195 p
(Contract DE-AC03-76SF-00098)
(DE95-012368; LBL-36770) Avail: CASI HC A09/MF A03

Interest in solid state physics naturally gravitates towards novel systems such as the copper oxide superconductors or the alkali-doped fullerenes. This paper tackles high temperature superconductivity by extension of the BCS theory for ordinary superconductors, in particular, incorporation of anharmonicity in phonon dynamics and anisotropy in electron-phonon coupling. These refinements can account for many anomalous properties of the cuprates. Phonon anharmonicity is consistent with a small isotope effect at optimal doping and a larger isotope effect in suboptimal systems. Anisotropy in the interaction, a plausible consequence of certain anharmonic models, can circumvent objections to electron-phonon coupling based on transport measurements. Such anisotropy is consistent with gap anisotropy and strong temperature dependence of Hall coefficient. In contrast to cuprates, the doped fullerenes appear understandable within the standard model of single electron band theory and BCS theory. Microscopic parameters derivable from transport and critical field measurements yield a self-consistent picture of a disordered Type-2 BCS superconductor. Isotope effects imply that superconductivity is mediated by carbon phonons opposed to alkali atom vibrations. The novel properties of the fullerenes are generally traceable to their microscopic heterogeneity, being a collection of tightly bound but weakly overlapping molecules. Separation of electronic regimes into weak intermolecular overlap and strong carbon-carbon on-ball bonds yields a superconductor with both a large density of states and a high phonon frequency, properties consistent with a relatively high (Tc). Disordered nature of intermolecular overlap produces a large residual resistivity and a universal dependence to the Hall coefficient. This disorder is also consistent with the anomalously large carbon isotope effect for heterogeneous isotopic substitution. DOE

77 THERMODYNAMICS AND STATISTICAL PHYSICS

Includes quantum mechanics; theoretical physics; and Bose and Fermi statistics.

For related information see also *25 Inorganic and Physical Chemistry* and *34 Fluid Mechanics and Heat Transfer.*

N95-30364# Joint Inst. for Nuclear Research, Dubna (USSR).
SIMULTANEITY AND LENGTH OF THE MOVING ROD
M. S. Khvastunov 1994 7 p
(DE95-613369; JINR-R-2-94-223) Avail: CASI HC A02/MF A01 (US Sales Only)

Einstein's length measuring procedure of a rod moving with velocity upsilon (0 less than or equal (absolute value of upsilon) less c) is discussed.The part of this procedure, namely measuring the length of the resting (upsilon = 0) rod, leads to the elongation of the moving rod and agrees with Einstein's simultaneity concept. The other part of Einstein's procedure measuring the length of the moving (upsilon different than 0) rod leads to thecontraction of the moving rod and is at variance with the simultaneity concept. DOE

N95-30365# Joint Inst. for Nuclear Research, Dubna (USSR).
ELLIPTIC DEFORMED CLASSICAL MECHANICS IN THREE-DIMENSIONAL PHASE SPACE
R. M. Yamaleev 1994 10 p
(DE95-613384; JINR-E-2-94-249) Avail: CASI HC A02/MF A01 (US Sales Only)

We suggest the new way of introduction into three-dimensional phase space. Our approach is based on the elliptic deformation of two-dimensional phase space. This kind of deformation we call 'elliptic' because oscillator of deformed mechanics is described by the Jacobi elliptic functions. The theory contains a parameter mu of energy dimensionality, so that for mu approaches infinity the deformed dynamics is reduced to the Newton equations. The quasiclassical way of quantization is considered. DOE

N95-30371# Joint Inst. for Nuclear Research, Dubna (USSR).
ON THE COMPTON TWIST-3 ASYMMETRIES
V. M. Korotkiyan and O. V. Teryaev 1994 16 p
(DE95-613627; JINR-E-2-94-200) Avail: CASI HC A03/MF A01 (US Sales Only)

The 'fermionic poles' contribution to the twist-3 single asymmetry in the gluon Compton process is calculated. The 'gluonic poles' existence seems to contradict the density matrix positivity. Qualitative predictions for the direct photon and jets asymmetries are presented. DOE

N95-30424# Melbourne Univ., Parkville (Australia). School of Physics.
MULTI-PARTICLE CORRELATIONS IN QUATERNIONIC QUANTUM SYSTEMS
S. P. Brumby, G. C. Joshi, and R. Anderson (Massachusetts Inst. of Tech., Cambridge, MA.) 1994 16 p
(DE95-616271; UM-P-94/54; RCHEP-94/15) Avail: CASI HC A03/MF A01 (US Sales Only)

The authors investigated the outcomes of measurements on correlated, few-body quantum systems described by a quaternionic quantum mechanics that allows for regions of quaternionic curvature. It was found that a multi particles interferometry experiment using a correlated system of four nonrelativistic, spin-half particles has the potential to detect the presence of quaternionic curvature. Two-body systems, however, are shown to give predictions identical to those of standard quantum mechanics when relative angles are used in the construction of the operators corresponding to measurements of particle spin components. DOE

N95-30426# Melbourne Univ., Parkville (Australia). School of Physics.
QUANTUM DYNAMICS IN REGIONS OF QUATERNIONIC CURVATURE
S. P. Brumby and G. Joshi 1994 11 p
(DE95-616276; UM-P-94/24; OZ-94/11) Avail: CASI HC A03/MF A01 (US Sales Only)

The complex unit appearing in the equations of quantum mechanics is generalized to a quaternionic structure on spacetime, leading to the consideration of complex quantum mechanical particles whose dynamical behavior is governed by inhomogeneous Dirac and Schroedinger equations. Mixing of hyper-complex components of wavefunctions occurs through their interaction with potentials dissipative into the extra quaternionic degrees of freedom. An interferometric experiment is analyzed to illustrate the effect. DOE

N95-30431# Melbourne Univ., Parkville (Australia). School of Physics.
INTEGRALS OF MOTION IN THE TWO KILLING VECTOR REDUCTION OF GENERAL RELATIVITY
Nenad Manojlovic (Syracuse Univ., NY.) and Bill Spence Aug. 1993 19 p
(DE95-616281; UM-P-93/77; SU-GP-93/7-8) Avail: CASI HC A03/MF A01 (US Sales Only)

We apply the inverse scattering method to the midi-superspace models that are characterized by a two-parameter Abelian group of motions with two spacelike Killing vectors. We present a formulation that simplifies the construction of the soliton solutions of Belinskii and Zakharov. Furthermore, it enables us to obtain the zero curvature formulation for these models. Using this, and imposing periodic boundary conditions corresponding to the Gowdy models when the spatial topology is a three torus T(3), we show that the equation of motion for the monodromy matrix is an evolution equation of the Heisenberg type. Consequently, the eigenvalues of the monodromy matrix are the generating functionals for the integrals of motion. Furthermore, we utilize a suitable formulation of the transition matrix to obtain explicit expressions for the integrals of motion. This involves recursion relations which arise in solving an equation of Riccati type. In the case when the two Killing vectors are hypersurface orthogonal the integrals of motion have a particularly simple form. DOE

N95-30436# Melbourne Univ., Parkville (Australia). School of Physics.
TWO-LOOP VACUUM AMPLITUDES IN A NON-ABELIAN GAUGE THEORY ON S(SUB 4)
B. A. Harris and G. C. Joshi 1994 35 p
(DE95-616284; UM-P-93/91) Avail: CASI HC A03/MF A01 (US Sales Only)

The authors have developed a matrix element approach to quantum field theory on S(sub 4), and used a complex l-plane method of performing the resulting angular momentum sums. The methods have been used to reproduce previous results for both one-loop and two-loop vacuum amplitudes for an Abelian gauge theory, including Dirac fermions and scalar bosons. In this paper they extend the formalism to non-Abelian gauge theory and show how the new complex l-plane methods allow the calculation of two-loop vacuum amplitudes involving ghost and gauge fields. It is shown how it is possible to overcome previous calculational limitations, resulting from the form of the ghost and gauge propagators, by performing the entire calculation in angular momentum space without reference to any particular configuration space form of the propagators. The two-loop interacting vacuum amplitude is derived in a non-Abelian gauge theory on a curved background and the required counterterm to renormalize the background gravitational action on S(sub 4) is given. DOE

N95-30437# Melbourne Univ., Parkville (Australia). School of Physics.
WHAT'S WRONG WITH ANOMALOUS CHIRAL GAUGE THEORY?
T. D. Kieu May 1994 9 p Presented at the First International Symposium on Symmetries in Subatomic Physics, Taipei, Taiwan, 16-18 May, 1994 Sponsored in part by the Australian Research Council
(DE95-616285; UM-P-94/58; RCHEP-94/16) Avail: CASI HC A02/MF A01 (US Sales Only)

It is argued on general ground and demonstrated in the particular example of the Chiral Schwinger Model that there is nothing wrong with apparently anomalous chiral gauge theory. If quantized correctly, there should be no gauge anomaly and chiral gauge theory should be renormalizable and unitary, even in higher dimensions and with non-Abelian gauge groups. Furthermore, it is claimed that mass terms for gauge bosons and chiral fermions can be generated without spoiling the gauge invariance. DOE

N95-30438# Melbourne Univ., Parkville (Australia). School of Physics.
BEYOND THE VARIATIONAL PRINCIPLE IN QUANTUM FIELD THEORY
Lloyd C. L. Hollenberg 1994 8 p Sponsored in part by the Australian Research Council
(DE95-616286; UM-P-94/64; RCHEP-94/18) Avail: CASI HC A02/MF A01 (US Sales Only)

A method of summing diagrams in quantum field theory beyond the variational Gaussian approximation is proposed using the continuum form of the recently developed plaquette expansion. In the context of (lambda)(phi)(sup 4) theory the Hamiltonian, H(phi), of Schroedinger functional equation H(phi) Psi(phi) = E Psi (phi) can be written down in tri-diagonal form as a cluster expansion in terms of connected moment coefficients derived from Hamiltonian moments with respect to a trial state V(sub 1)(phi). The usual variational procedure corresponds to minimizing the zeroth order of this cluster expansion. At first order in the expansion the Hamiltonian in this form can be diagonalized analytically. The subsequent expression for the vacuum energy E contains Hamiltonian moments up to fourth order and hence is a summation over multi-loop diagrams laying the foundation for the calculation of the effective potential beyond the Gaussian approximation. DOE

N95-30440# Melbourne Univ., Parkville (Australia). School of Physics.
CHIRAL GAUGE THEORY IN FOUR DIMENSIONS
Tien D. Kieu Sep. 1994 9 p Sponsored in part by the Australian Research Council
(DE95-616288; UM-P-94/96; IASSNS-HEP-94/70; RCHEP-94/26) Avail: CASI HC A02/MF A01 (US Sales Only)

A formulation of Abelian and non-Abelian chiral gauge theories is presented together with arguments for the unitarity and renormalizability in four dimensions. DOE

N95-30444# Melbourne Univ., Parkville (Australia). School of Physics.
APPROXIMATE ANALYTIC DIAGONALIZATION OF LATTICE QCD
Lloyd C. L. Hollenberg 1994 12 p
(DE95-616332; UM-P-93/106; OZ-93/25) Avail: CASI HC A03/MF A01 (US Sales Only)

The first order plaquette expansion of lattice Hamiltonians is applied to quantum chromodynamics with two massless quarks. Analytic expressions are obtained for the vacuum energy density, epsilon(sub 0)(g), and lowest vector and nucleon masses, M(sub V)(g) and M(sub N)(g). The vacuum energy density is valid into the weak coupling region down to about g(sup 2) approximately 0.8, demonstrating the genuine non-perturbative nature of these approximates. The 'specific heat' derived from epsilon(sub 0)(g) agrees well with numerical calculations in the t-expansion. The ratio R = M(sub N)/M(sub V) increases from the strong coupling limit of zero to a more realistic value of R approximately = 1.2 approaches 1.3 at the transition from strong to weak coupling. DOE

N95-30636# International Centre for Theoretical Physics, Trieste (Italy).
ON PERTURBATIVE ASYMPTOTIC OF REGGE TRAJECTORIES
M. N. Sergeenko Oct. 1994 10 p

(DE95-613585; IC-94/338) Avail: CASI HC A02/MF A01 (US Sales Only)

The perturbative asymptotic of the Regge trajectories, alpha(t), at -t yields infinity is deduced on the basis of a known solution of a relativistic wave equation with the Coulomb-like potential. We obtain the perturbative asymptotic at -t yields infinity of the leading S = 1 quarkonium Regge trajectories of the form alpha(sub R)(t) = 0, and leading S = 1/2 nucleon Regge trajectories of the form alpha(sub N)(t) = -1/2. DOE

N95-30741# International Centre for Theoretical Physics, Trieste (Italy).
LIGHT-FRONT DYNAMICS OF CHERN-SIMONS SYSTEMS
Prem P. Srivastava Oct. 1994 17 p
(DE95-613467; IC-94/305) Avail: CASI HC A03/MF A01 (US Sales Only)

The Chern-Simons theory coupled to complex scalars is quantized on the light-front in the local light-cone gauge by constructing the self-consistent Hamiltonian theory. It is shown that no inconsistency arises on using two local gauge-fixing conditions in the Dirac procedure. The light-front Hamiltonian turns out to be simple and the framework may be useful to construct renormalized field theory of particles with fractional statistics (anyons). The theory is shown to be relativistic and the extra term in the transformation of the matter field under space rotations, interpreted in previous works as anomaly, is argued to be gauge artefact. DOE

N95-30771# International Centre for Theoretical Physics, Trieste (Italy).
A BRST CHARGE FOR NON-CRITICAL W2(s) STRINGS
L. Palacios Oct. 1994 11 p
(DE95-613470; IC-94/336) Avail: CASI HC A03/MF A01 (US Sales Only)

We present a general argument for the construction of BRST charges of the 'non-critical' W(sub 2,4), W(sub 2,5) W(sub 2,6), and W(sub 2,8) strings. This evidences the existence of BRST charges for a kind of soft-type algebras which can be constructed from two copies of quantum W(sub 2,s) algebras, (s = 3,4,5,6,8). DOE

N95-30775# Technische Univ., Delft (Netherlands).
LANTHANIDE(III) CATALYZED REACTIONS: STRUCTURE AN D THERMODYNAMICS OF INTERMEDIATE COMPLEXES, AND IMPLICATIONS FOR REACTIVITY Ph.D. Thesis
Jurriaan Huskens 21 Nov. 1994 230 p Sponsored by Netherlands Foundation for Chemical Research. and Nederlandse Organisatie voor Wetenschappelijk Onderzoek, The Hague
(PB95-197000; ISBN-90-9007656-5) Avail: CASI HC A11/MF A03

This thesis is devoted to homogeneous lanthanide(III) catalyzed reactions. The structure and thermodynamics of intermediate complexes are investigated with the use of multinuclear magnetic resonance, potentiometry, and calorimetry. Attention is paid to reaction mechanisms and the activating role of Ln(III). NTIS

N95-30781*# National Academy of Sciences - National Research Council, Washington, DC. Space Studies Board.
REVIEW OF GRAVITY PROBE B
1995 35 p
(Contract NASw-4627)
(NASA-CR-198959; NAS 1.26:198959) Avail: CASI HC A03/MF A01

In response to a request by the NASA Administrator, the National Research Council (NRC) has conducted an accelerated scientific review of NASA's Gravity Probe B (GP-B) mission. The review was carried out by the Task Group on Gravity Probe B, under the auspices of the NRC's Space Studies Board and Board on Physics and Astronomy. The specific charge to the task group was to review the GP-B mission with respect to the following terms of reference: (1) scientific importance - including a current assessment of the value of the project in the context of recent progress in gravitational physics and relevant technology; (2) technical feasibility - the technical approach will be evaluated for likelihood of success, both in terms of achievement of flight mission objectives but also in terms of scientific conclusiveness of the various possible outcomes for the measurements to be made; and (3) competitive value - if possible, GP-B science will be assessed qualitatively against the objectives and accomplishments of one or more fundamental physics projects of similar cost (e.g., the Cosmic Background Explorer, COBE). Derived from text

N95-30972# Joint Inst. for Nuclear Research, Dubna (USSR).
EINSTEIN'S LENGTH CONCEPT
M. S. Khvastunov 1994 7 p
(DE95-613368; JINR-R-2-94-222) Avail: CASI HC A02/MF A01 (US Sales Only)

Einstein's length measuring procedure of a rod moving with velocity upsilon (0 less than or equal upsilon less than c) is discussed. The part of this procedure, namely measuring the length of the resting (upsilon = 0) rod, is realizable and leads to the elongation of the moving rod. The other part of Einstein's procedure, measuring the length of the moving (upsilon not equal to 0) rod, is not realizable and leads to the contraction of the moving rod. As the result of this procedure the moving rod contraction concept is supposed physically unfounded. DOE

N95-31186# International Centre for Theoretical Physics, Trieste (Italy).
IRREDUCIBLE GREEN'S FUNCTIONS METHOD IN THE THEORY OF HIGHLY CORRELATED SYSTEMS
A. L. Kuzemsky Sep. 1994 27 p
(DE95-614446; IC-94/292) Avail: CASI HC A03/MF A01 (US Sales Only)

The self-consistent theory of the correlation effects in highly correlated systems (HCS) is presented. The novel irreducible Green's function (IGF) method is discussed in detail for the Hubbard model and random Hubbard model. The interpolation solution for the quasiparticle spectrum, which is valid for both the atomic and band limit, is obtained. The IGF method permits calculation of the quasiparticle spectra of many-particle systems with the complicated spectra and strong interaction in a very natural and compact way. The essence of the method is deeply related to the notion of the generalized mean fields (GMF), which determine the elastic scattering corrections. The inelastic scattering corrections leads to the damping of the quasiparticles and are the main topic of the present consideration. The calculation of the damping has been done in a self-consistent way for both limits. For the random Hubbard model the weak coupling case has been considered and the self-energy operator has been calculated using the combination of the IGF method and coherent potential approximation (CPA). The other applications of the method to the s-f model, Anderson model, Heisenberg antiferromagnet, electron-phonon interaction models, and quasiparticle tunneling are discussed briefly. DOE

N95-31193# Gosudarstvennyi Komitet po Ispolzovaniyu Atomnoi Energii, Serpukhov (USSR). Inst. for High Energy Physics.
HAMILTONIAN FORMULATION OF TWO BODY PROBLEM IN WHEELER-FEYNMAN ELECTRODYNAMICS
I. N. Nikitin 1994 25 p
(DE95-620526; IHEP-94-13) Avail: CASI HC A03/MF A01 (US Sales Only)

A Hamiltonian formulation for the classical problem of electromagnetic interaction of two charged relativistic particles is found. DOE

N95-31226# Tokyo Univ., Tanashi (Japan). Inst. for Nuclear Study.
GLOBAL ASPECTS OF THE WZNW REDUCTION TO TODA THEORIES
I. Tsutsui and L. Feher (Ecole Normale Superieure, Lyon, France.) Aug. 1994 23 p
(DE95-737230; INS-1048) Avail: CASI HC A03/MF A01

It is well-known that the Toda Theories can be obtained by reduction from the Wess-Zumino-Novikov-Witten (WZNW) model, but it is less known that this WZNW (yields) Toda reduction is 'incomplete'. The reason for this incompleteness being that the Gauss decomposition used to define the Toda fields from the WZNW field is valid locally but not globally over the WZNW group manifold, which implies that actually the reduced system is not just the Toda theory but has much richer structures. In this note we furnish a framework which allows us to study the reduced system globally, and thereby present some preliminary results on the global aspects. For simplicity, we analyze primarily 0+1 dimensional toy models for G=SL(n,R), but we also discuss the 1+1 dimensional model for G=SL(2,R) which corresponds to the WZNW (yields) Liouville reduction. DOE

N95-31276# Novosibirsk State Univ. (USSR). Budker Inst. of Nuclear Physics.
SHNIRELMAN PEAK IN THE LEVEL SPACING STATISTICS
B. V. Chirikov and D. L. Shepelyansky 1994 11 p

(DE95-623599; BUDKERINP-94-26; IYaF-94-26) Avail: CASI HC A03/MF A01 (US Sales Only)

The first results on the statistical properties of the quantum quasidegeneracy are presented. A physical interpretation of the Shnirelman theorem predicted the bulk quasidegeneracy is given. The conditions for the strong impact of the degeneracy on the quantum level statistics are formulated which allows to extend the application of the Shnirelman theorem into a broad class of quantum systems. DOE

N95-31281# Tokyo Univ., Tanashi (Japan). Inst. for Nuclear Study.
NON-CRITICAL STRING FIELD THEORY WITH NON-ORIENTABLE STRING INTERACTIONS
Yoshiyuki Watabiki Jun. 1994 16 p
(DE95-737160; INS-1038) Avail: CASI HC A03/MF A01 (US Sales Only)

We study the non-critical string field theory with non-orientable string interactions by using the transfer matrix formalism in the dynamical triangulation. For any value of c (total central charge of matter), we have constructed the non-orientable string field theory at the discrete level. Two coupling constants G and G' which satisfy the relation (G')(sup 3)=GG' are introduced, where G counts the number of untwisted handles of the world-sheet while G' counts the number of cross-caps. In the case of the non-critical string theory which correspond to multicritical one matrix models (including c=0 case), we have succeeded in taking the continuum limit, and then have obtained the continuous string field theory. DOE

N95-31511# Army Research Lab., Aberdeen Proving Ground, MD.
DERIVATION OF TWO-DIMENSIONAL (2-D) CONDUCTION EQUATION IN GENERALIZED COORDINATES WITH CONSTANT AND ANISOTROPIC PHYSICAL PROPERTIES Final Report, Jan. - Aug. 1993
Paul J. Conroy May 1995 31 p
(DA Proj. 1L1-62618-A-1-FL)
(AD-A293896; ARL-MR-219) Avail: CASI HC A03/MF A01

The purpose of this paper is to provide a working report for potential future modifications to existing heat conduction codes. A generalized form of the two-dimensional (2-D) arbitrary geometry axisymetric heat conduction equation has been derived from first principles. This has been further generalized by allowing nonidealized anisotropic behavior of the material properties. DTIC

N95-31545# Northwestern Univ., Evanston, IL.
CHAOS-ENHANCED TRANSPORT AND AGGREGATION IN CHAOTIC FLOWS Final Technical Report, 15 Nov. 1993 - 14 Nov. 1994
Julio M. Ottino 7 Apr. 1995 6 p
(Contract F49620-92-J-0060)
(AD-A293892; AFOSR-95-0319TR) Avail: CASI HC A02/MF A01

Chaos-enhanced transport in cellular flows - such as those generated within cavities by a top free-flowing stream - are studied with the long term objective of devising means to increase the rate of transport between surfaces and bulk flows. In several experimental cavities chaotic advection is generated by periodic modulation of the free stream velocity. We find that transport occurs only near reattachment points of wall-attached streamlines. Detailed local measurements of transport in these regions places upper bounds on global transport rates in the cavity. The buildup of mixed area is measured and exit manifolds for lower cells are identified. DTIC

N95-31646 Rice Univ., Houston, TX.
VARIATIONAL OPTIMIZATION IN QUANTUM FIELD THEORY Ph.D. Thesis
Alan Charles Mattingly 1993 90 p
Avail: Univ. Microfilms Order No. DA9408646

We examine two different techniques for studying quantum field theories in which a 'variational' optimization of parameters plays a crucial role. In the context of the O(N)-symmetric lambda phi(exp 4) theory we discuss variational calculations of the effective potential that go beyond the Gaussian approximation. Trial wavefunctionals are constructed by applying a unitary operator to a Gaussian state. We calculate the expectation value of the Hamiltonian using the nonGaussian trial states generated, and thus obtain optimization equations for the variational-parameter functions of the ansatz. At the origin, phi(sub c) = O, these equations can be solved explicitly and lead to a nontrivial correction to the mass renormalization, with respect to the Gaussian case. Numerical results are obtained for the (O + 1)-dimensional case and show a worthwhile quantitative improvement over the Gaussian approximation. We also discuss the use of optimized perturbation theory (OPT) as applied to the third-order quantum chromodynamics (QCD) corrections to R(sub e(+)e(-)). The OPT method, based on the principle of minimal sensitivity, finds an effective coupling constant that remains finite down to zero energy. This allows us to apply the Poggio-Quinn-Weinberg smearing method down to energies below 1 GeV, where we find good agreement between theory and experiment. The couplant freezes to a zero-energy value ofalpha(sub s)/pi = 0.26, which is in remarkable concordance with values obtained phenomenologically. Dissert. Abstr.

N95-32094# International Centre for Theoretical Physics, Trieste (Italy).
METHOD OF NORMAL COORDINATES IN THE FORMULATION OF A SYSTEM WITH DISSIPATION: THE HARMONIC OSCILLATOR
E. D. Mshelia Jul. 1994 13 p
(DE95-613372; IC-94/188) Avail: CASI HC A03/MF A01 (US Sales Only)

The method of normal coordinates of the theory of vibrations is used in decoupling the motion of n oscillators (1 less than or equal to n less than or equal to 4) representing intrinsic degrees of freedom coupled to collective motion in a quantum mechanical model that allows the determination of the probability for energy transfer from collective to intrinsic excitations in a dissipative system. DOE

N95-32106# Florida Univ., Gainesville, FL.
ELECTROWEAK FLAVOR-CONSERVING GAUGE PROCESSES: VIRTUAL EFFECTS
D. C. Kennedy Nov. 1994 14 p Presented at the 27th International Conference on High Energy Physics, Glasgow, 21-27 Jul. 1994
(Contract DE-FG05-86ER-40272)
(DE95-009922; DOE/ER-40272/212; UFIFT-HEP-9416; CONF-940722-45) Avail: CASI HC A03/MF A01

The electroweak Standard Model is summarized at the classical and quantum levels, including its gauge symmetry and symmetry-breaking aspects. The full implications of precise measurements of electroweak gauge forces are presented in terms of electroweak parameters and quantum corrections. The minimal Standard Model (SM) (including the top quark) satisfies the data well, up to one-loop accuracy. Possible non-Standard states subject to electroweak forces in quantum corrections is highly restricted by the present data. The status of exact and approximate symmetries of the electroweak Standard Model is summarized. DOE

N95-32150# Academy of Sciences (USSR), Novosibirsk (USSR). Budker Inst. of Nuclear Physics.
STATISTICAL PROPERTIES OF CHAOTIC SCATTERING WITH ONE OPEN CHANNEL
F. M. Izrailev (Gesamthochschule, Essen, Germany.), D. Saher (Gesamthochschule, Essen, Germany.), and V. V. Sokolov 1993 23 p
(DE95-613370; BudkerINP-93-94; IYaF-93-94) Avail: CASI HC A03/MF A01 (US Sales Only)

The correspondence between statistical properties of decaying states and fluctuations in resonance scattering is studied in a statistical model with one open channel. The model is described by an ensemble of random nonhermitian matrices. The dependence of the correlation length on the coupling parameter both for the S-matrix and the cross-section is studied numerically. DOE

N95-32295# Joint Inst. for Nuclear Research, Dubna (USSR). Lab. of Theoretical Physics.
HARMONIC COORDINATES IN THE PROBLEM ON STATIC GRAVITATIONAL AND MASSLESS SCALAR FIELDS WITH A POINT SOURCE
R. A. Asanov 1994 6 p Presented at the International Scholl-Seminar on Multidimensional Gravity and Cosmology, Yaroslavl, 1994
(DE95-623632; JINR-E-2-94-341) Avail: CASI HC A02/MF A01 (US Sales Only)

Here approximate expressions for the De Donder-Fock harmonic coordinates are given in the case when kG(exp 2)is much greater than k(exp 2)m(exp 2) and in the case kG(exp 2) is much less than k(exp 2)m(exp 2), where k is the Newton gravitational constant, G is a scalar

constant, m is the mass of a system. Harmonic coordinates appear, in particular, in the Rosen bimetric general relativity and in the Chernikov theory with two connections but one metric if one passes to the Einstein theory. They both contain a generalized condition, which tends to the De Donder harmonic condition in the limiting case. DOE

N95-32359# Lawrence Livermore National Lab., Livermore, CA.
PHASE TRANSITIONS AND GRAVITATIONAL COLLAPSE Ph.D. Thesis
N. A. Gentile Sep. 1994 142 p
(Contract W-7405-eng-48)
(DE95-011732; UCRL-LR-118331) Avail: CASI HC A07/MF A02

Results are presented for numerical calculations of gravitational collapses and explosions. Two effects are studied. The first involves aspects of the numerical models used in almost all current gravitational collapse calculations. The second involves phase transitions in the equation of state of dense matter. A (1 + 1) dimensional general relativistic hydrodynamics code was constructed to investigate both effects. A modification of standard artificial viscosity methods was developed. This extended both the tensor artificial viscosity formulation and the artificial heat conduction formulation to the general relativistic regime. This method shows better results for collapse calculations than the standard scalar artificial viscosity. Numerical collapse calculations were also examined with respect to the number of zones used in the model. These calculations suggest that the number of zones used in current supernova calculations may be insufficient, and that the more sophisticated artificial viscosity methods used may be useful in future core collapse investigations. The second effect studied by this thesis is the impact of phase transitions in dense matter on the results of core collapse in Type 2 supernovae. Two different phase transitions were investigated. The QCD phase transition embodies the prediction of quantum chromodynamics that at high density the constituents of baryonic matter will be free quarks and gluons. The effects on the shock wave formed by core collapse and bounce is studied for various phase transitions. We find that some of the phase transitions modeled significantly increase the shock strength. DOE

80 SOCIAL SCIENCES (GENERAL)

Includes educational matters.

N95-30699# Goeteborg Univ. (Sweden). Dept. of Education and Educational Research.
SELECTION OF SWEDISH SCHOLASTIC APTITUDE TEST TAKERS AS A FUNCTION OF SOCIOECONOMIC BACKGROUND AND ABILITY: EVALUATION THROUGH FOLLOW-UP
S. E. Reuterberg 1994 40 p
(PB95-212072) Avail: CASI HC A03/MF A01

The present study is part of project which aims at studying recruitment to higher education in Sweden. The Swedish Scholastic Aptitude Test (SweSAT) plays an important part in the admission to this educational level and therefore it is natural to start the project by examining the function of this test. In the present study we will confine ourselves to the process of self-selection to the SweSAT among individuals from different socioeconomic groups. The strength of the self-selection is measured by the difference between the SweSAT takers and the others within each socioeconomic group on grades from compulsory school, achievement tests and intelligence tests. According to all variables studied, the test takers constitute a positively selected group within all socioeconomic groups. The strongest selection effects are found within group 3 and the weakest ones in group 1. However, due to great social differences in the total sample, the test takers from group 3 still obtain lower means on all variables studied than do the test takers from group 1. NTIS

N95-30700# Goeteborg Univ. (Sweden). Dept. of Education and Educational Research.
NON-COMPARABILITY OF FEMALE AND MALE ADMISSION TEST TAKERS: EVALUATION THROUGH FOLLOW-UP
A. Maekitalo 1994 26 p
(PB95-212080) Avail: CASI HC A03/MF A01

The purpose of the study is to investigate the possible differential selection to the Swedish Scholastic Aptitude Test (SweSAT) to see whether the gender differences in results on the SweSAT may, to some extent, be explained by initial differences in achievement between the male and female SweSAT takers. The empirical results consistently showed that male SweSAT takers constituted a more strongly selected group with respect to ability and previous school achievement than did female SweSaT takers. Thus, within the areas where females excelled initially, the selection effect decreased their advantage among the SweSAT takers. Within the areas where males excelled, the selection effect increased their advantage among the SweSAT takers. These results show that we cannot assume that selected and self-selected groups are comparable. Thereby, it is argued that it is essential to take the differential selection effects into account. NTIS

81 ADMINISTRATION AND MANAGEMENT

Includes management planning and research.

N95-30834# Technische Univ., Eindhoven (Netherlands). Dept. of Mathematics and Computing Science.
PLANNING BOARD GENERATOR. PART 1: PROBLEM INSTANCES AND TYPES
M. Wennink and M. W. P. Savelsbergh Dec. 1994 49 p
(PB95-197075; MEMO-COSOR-94-42) Avail: CASI HC A03/MF A01

A planning board is a planning tool that use the Gantt chart as its main representation mechanism. A planning board generator aims at facilitating the development of planning boards; using a description of the problem type for which a planning board is to be developed and the desired representations and manipulations, the generator automatically creates a prototype of the planning board. In this paper we discuss our view of a planning board generator and introduce a method to describe problem instances and types. NTIS

N95-31380*# National Aeronautics and Space Administration, Washington, DC.
MANAGEMENT OF MAJOR SYSTEM PROGRAMS AND PROJECTS. HANDBOOK
8 Nov. 1993 218 p
(NHB-7120.5; NAS 1.18:7120.5) Avail: CASI HC A10/MF A03

This Handbook establishes the detailed policies and processes for implementing NMI 7120.4, 'Management of Major System Programs and Projects'. It constitutes a comprehensive source of the specific policies and processes governing management of major development programs/projects and is intended as a resource to the entire program/project management (PPM) community. Derived from text

N95-31659# General Accounting Office, Washington, DC. National Security and International Affairs Div.
REPORT TO THE SECRETARY OF DEFENSE. ACQUISITION REFORM: COMPARISON OF ARMY'S COMMERICAL HELICOPTER BUY AND PRIVATE SECTOR BUYS
17 Mar. 1995 31 p
(GAO/NSIAD-95-54; B-260371) Avail: CASI HC A03/MF A01; GAO, PO Box 6015, Gaithersburg, MD 20884-6015 HC

Army officials have cited the acquisition of the Army's New Training Helicopter (NTH) as an early example of success in streamlining its acquisition process to buy a commercial item. In this report, as a 'case study,' we (1) compare this Army acquisition with acquisitions by two of the largest private sector purchases of similar helicopters to determine key differences between these buys and the reasons for such differences, (2) identify successes the Army achieved in streamlining the NTH acquisition, and (3) discuss potential improvements that could be achieved from acquisition reform efforts. Our comparison is not intended to suggest that the identified private sector processes would be appropriate for a government procurement. However, as the government moves to greater use of commercial practices to procure commercial items, a comparative analysis can be a helpful tool in gauging status and progress. Author

N95-31986# Comptroller General of the United States, Washington, DC.
ANNUAL REPORT TO THE CHAIRMAN AND RANKING MINORITY MEMBERS, HOUSE AND SENATE COMMITTEES ON APPROPRIATIONS. STATUS OF OPEN RECOMMENDATIONS: IMPROVING OPERATIONS OF FEDERAL DEPARTMENTS AND AGENCIES (Diskette Supplement)
30 Jan. 1995 268 p Diskette supplement: 3.5 diskette Contains pamplet as supplement
(GAO/OP-95-1; B-205879) Avail: CASI HC A12/MF A03/DK A02; GAO, PO Box 6015, Gaithersburg, MD 20877 HC

Each year, GAO's work contributes to many legislative and executive branch actions that result in significant financial savings and other improvements in government operations. Some, but not all, are identified through GAO's system for periodically following up to determine the status of actions taken on the recommendations made in its audit and evaluation reports. In fiscal year 1994, GAO made 1,450 recommendations, but, more importantly, about 4,400 GAO recommendations made over the past 5 years have been implemented. This report includes summary information on the status of all GAO recommendations that have not been fully implemented and highlights some of the key ones. This information should help congressional and agency leaders prepare for upcoming appropriations and oversight activities and stimulate further actions to achieve the desired improvements in government operations. In addition to including printed issue area summaries highlighting the ipact of GAO's work and the key open recommendations, this volume includes a set of computer diskettes with details on all open recommendations. Author

N95-32195# General Accounting Office, Washington, DC. Resources, Community, and Economic Development Div.
REPORT TO CONGRESSIONAL COMMITTEES. FEDERAL RESEARCH: INTERIM REPORT ON THE PILOT TECHNOLOGY ACCESS PROGRAM
7 Mar. 1994 27 p
(GAO/RCED-94-75; B-255654) Avail: CASI HC A03/MF A01; GAO, PO Box 6015, Gaithersburg, MD 20877 HC

This interim report provides information on the status, implementation, and evaluation of the Pilot Technology Access Program (TAPP). In addition, this report includes the judgements of the participating centers' directors on TAPP's effect on small businesses' productivity and innovation. TAPP provides small businesses with access to (1) computerized data bases containing technical and business information that they typically are not aware of, or cannot afford, and (2) experts knowledgeable in a wide range of technical fields. Derived from text

N95-32200# General Accounting Office, Washington, DC. Resources, Community, and Economic Development Div.
REPORT TO CONGRESSIONAL COMMITTEES. FEDERAL RESEARCH: INTERIM REPORT ON THE SMALL BUSINESS INNOVATION RESEARCH PROGRAM
8 Mar. 1995 35 p
(GAO/RCED-95-59; B-259333) Avail: CASI HC A03/MF A01; GAO, PO Box 6015, Gaithersburg, MD 20877 HC

This report, authorized by the Small Business Research and Development Enhancement Act of 1992, focuses on the quality of small businesses' research proposals for technological innovation, the implementation of a provision for technical assistance by agencies participating in the program, and duplicate funding of similar research by more than one agency. To improve interagency coordination and to reduce the risk of funding duplicate research, GAO recommends that steps be taken to (1) determine whether the certification form that accompanies SBIR proposals needs to be improved and, if so, take the necessary steps to revise it; (2) develop substantive definitions and guidelines for agencies and companies regarding 'duplicate' research; and (3) provide interagency access to current information regarding recent SBIR awards. Derived from text

N95-32213# General Accounting Office, Washington, DC. National Security and International Affairs Div.
FEDERALLY FUNDED R AND D CENTERS: EXECUTIVE COMPENSATION AT THE AEROSPACE CORPORATION. REPORT TO CONGRESSIONAL REQUESTORS
7 Feb. 1995 18 p
(GAO/NSIAD-95-75; B-259373) Avail: CASI HC A03/MF A01; GAO, PO Box 6015, Gaithersburg, MD 20877 HC

The financial and management practices of The Aerospace Corporation, which operates a federally funded research and development center (FFRDC) sponsored by the Air Force, is reviewed. This report discusses the salary and other benefits provided to Aerospace's corporate officers and other senior management personnel and includes information on Defence Contract Audit Agency (DCAA) audits on Aerospace compensation costs and congressional actions regarding FFRDC compensation. This report does not draw conclusions about the comparability or reasonableness of Aerospace executive compensation. Derived from text

82 DOCUMENTATION AND INFORMATION SCIENCE

Includes information management; information storage and retrieval technology; technical writing; graphic arts; and micrography.

For computer documentation see *61 Computer Programming and Software.*

N95-30392# Idaho National Engineering Lab., Idaho Falls, ID.
DATA MANAGEMENT SYSTEM: USER'S GUIDE
15 Nov. 1994 29 p
(Contract DE-AC07-94ID-13223)
(DE95-008692; INEL-94/0121) Avail: CASI HC A03/MF A01

Data Management System (DMS) is a menu-driven, user-friendly system that allows you to manipulate software and data files as follows: Download files and software from the network to your personal computer; Compress files into a single archive file; Decompress files from an archive file; Remove files from your PC; Copy files from the source directory to the destination directory; and Configure DMS for your specific PC and network configuration. This user's guide provides instructions for operating the system and setup configuration. DOE

N95-30453# Technische Univ., Twente (Netherlands). Dept. of Computer Science.
CONTRIBUTION OF GROUPWARE TO CORPORATE COMMUNICATION: TOWARDS THE HORIZONTAL ORGANIZATION
S. Joosten, E. Ploeger, and S. Brinkkemper Dec. 1994 22 p
(PB95-197661; Memo-INF-94-76) Copyright Avail: CASI HC A03/MF A01

Groupware is a name for computer-based systems supporting groups of people engaged in a common task. Groupware systems are used in the corporate communication architecture to facilitate a shift towards a horizontal organization. This paper reports about empirical comparative research which was done to find out whether groupware actually facilitates the horizontal organization, and how. Twenty-two applications in five organizations with groupware experience have been studied with respect to the communication type, the application type and the supported business function. This research shows which contributions are made to the horizontal organization and what difficulties are encountered. NTIS

N95-30456# Technische Univ., Twente (Netherlands). Dept. of Computer Science.
PROTOCOLS FOR INTEGRITY CONSTRAINT CHECKING IN FEDERATED DATABASES
P. Grefen and J. Widom (Stanford Univ., CA.) Dec. 1994 47 p
(PB95-197695; Memo-INF-94-80) Copyright Avail: CASI HC A03/MF A01

In this report, we describe a family of integrity constraint checking protocols that do not require global control and are thus fit for federated database systems. The various protocols in the family differ with respect to consistency guarantees, system requirements, and execution costs. Thereby, the presented approach allows fitting constraint checking to specific situations in federated systems. NTIS

N95-30483 Syracuse Univ., NY.
DATA STORAGE MODELING AND MANAGEMENT FOR MULTIMEDIA INFORMATION SYSTEMS Ph.D. Thesis
Kingsley Chukwudum Nwosu 1993 184 p
Avail: Univ. Microfilms Order No. DA9422257

In spite of the tremendous technological advances, there is a paramount

hindrance to the full realization of real-time multimedia information processing. The bandwidths of the secondary storage devices have not improved relative to other technological advances. For real-time information retrieval and presentation, it is imperative that data, for a given medium, be retrievable at a given rate. For some media, these rates exceed the capability of current storage devices. As a result of these and other related problems in multimedia information processing, this research (1) captures the different storage allocation and retrieval requirements of various multimedia objects through a multimedia object model that incorporates different classifications of multimedia objects based on their I/O requirements; (2) presents some decomposition strategies necessary for generating the storage allocation units of multimedia objects in order to achieve their I/O requirements; (3) describes the necessary and sufficient conditions and criteria for an object's allocatability to a storage device; (4) presents efficient allocation criteria and techniques for multimedia object storage and distribution; (5) describes the bipartite graph model for mapping objects to storage devices as a precondition for determining optimal allocation of objects; (6) presents the optimal matching of objects to storage devices via the bipartite graph using the Hungarian Method; (7) presents techniques for exploiting the configuration of storage devices as a means of achieving efficient multimedia object allocations; (8) develops the extensions of the allocation strategies discussed for object allocations in a distributed computing environment; (9) presents simulation results based on the decomposition and allocation strategies developed that achieve the retrieval requirements of multimedia objects and also efficiently distribute the objects on the storage devices; (10) presents the designs of the storage and retrieval schemes for a multimedia object manager which are necessary for implementing the allocation strategies in a computing system; and (11) develops the design of the integrated data management system that describes the resolutions of the critical issues of distributed computing with respect to the multimedia object allocation strategies presented and also details the system functionalities and management interfaces and processes. This research develops a multimedia object model that classifies every multimedia object based on its I/O requirements; and using the decomposition techniques, and allocation parameters and criteria developed that take cognizance of the various characteristics of the objects, it shows that by optimizing the allocation of multimedia objects, we can achieve efficient object storage. The necessary storage and retrieval schemes are also developed that demonstrate the implementability of the proposed strategies. Dissert. Abstr.

N95-30496# Gesellschaft fuer Mathematik und Datenverarbeitung, Saint Augustin (Germany).

PROCEEDINGS OF THE CSCW 1994 WORKSHOP COLLABORATIVE HYPERMEDIA SYSTEMS

J. M. Haake Sep. 1994 68 p Conference held in Chapel Hill, NC, 22 Oct. 1994

(PB95-208393; GMD-239) Copyright Avail: CASI HC A04/MF A01

Contents: Open Issues in Collaborative Hypermedia Systems; Palimpsest: A Data Model for Revision Control; Hypermedia as an Enabling Technology for Computer Supported Cooperative Work (CSCW) Systems Development; Extending the World Wide Web for Writing and Viewing Collaborative Hypermedia; VIEW Media: A Multiuser Hypermedia System for Interactive Distance Presentation; Hypermedia and Collaboration in the On-line Design Journal; The Support for Emergence of Collaboration in a Hypertext Document System; Collaborative Hypermedia for the Classroom and Beyond: A Year's Experience with the Collaboratory Notebook; Collaborative Hypermedia for Engineers; Organizational Characteristics as Indicators for the Uptake CSCW Systems; The Human Element in Collaborative Hypertext/Hypermedia. NTIS

N95-30566# Technische Univ., Twente (Netherlands).

EXTENDING A MULTI-SET RELATIONAL ALGEBRA TO A PARALLEL ENVIRONMENT

P. W. P. J. Grefen and J. Flokstra Sep. 1994 21 p

(PB95-207106; Memo-INF-94-50) Copyright Avail: CASI HC A03/MF A01

The report proposes an extended relational algebra for use with parallel database systems. The language has a close connection to the standard relational algebra and thus has a well-known and widely accepted background. The language is formally defined and has clear semantics. Further, the language has complete DML expressiveness, so it can either be used as a full-blown database manipulation language on its own, or as a formal background for other languages. Section 2 describes the extended relational algebra in a sequential (centralized) database environment. Section 3 extends the sequential language to a parallel language by adding concepts for data distribution and process allocation. It is shown that these concepts nicely fit into the formal character of the language. Section 4 discusses expression rewriting in the extended algebra, as performed in query optimization and query parallelization. Finally, Section 5 describes experience with the language in the PRISMA parallel database system project. NTIS

N95-30619# Virginia Univ. Hospital, Charlottesville, VA. Dept. of Computer Science.

SUPPORTING DATA INTENSIVE APPLICATIONS WITH MEDIUM GRAINED PARALLELISM Final Report, Jul. 1991 - - Jun. 1994

John L. Pfaltz, James C. French, Andrew S. Grimshaw, and Sang H. Son Jul. 1994 39 p

(Contract DE-FG05-88ER-25063)

(DE95-010164; DOE/ER-25063/T14; UVA-527437/CS95/101) Avail: CASI HC A03/MF A01

The purpose of this second three year grant was to investigate opportunities for medium grained parallelism in data intensive applications; or more succinctly, can one create effective parallel database systems? It should be noted that the last three years have not been kind to parallel object-oriented database systems: to our knowledge none of those that have been implemented has been particularly effective. A second, implicit goal was to complete the innovative functional, object-oriented database language and system, called ADAMS, and to demonstrate its performance in a parallel environment. Thus the overall agenda was (1) to create new mechanisms that exploit parallel computing power, (2) install it in ADAMS, and (3) analyze its behavior. It will be seen that, while we did come up with several new innovative ideas which we thoroughly tested, we did not always have time to install them into the run-time ADAMS library. Although we proposed rewriting our storage manager to take advantage of the Concurrent File System (CFS) on the Intel iPSC/2, we did not. During the grant period, the Computer Science Department acquired a dedicated cluster of 8 SPARC 10's. Gradually the hypercube implementation has been phased out, and replaced by that on the SPARC cluster. DOE

N95-30620# Nevada Univ., Las Vegas, NV. Dept. of Electrical and Computer Engineering.

ADAPTIVE IMAGE ENHANCEMENT OF TEXT IMAGES THAT CONTAIN TOUCHING OR BROKEN CHARACTERS

P. Stubberud, V. Kalluri, and J. Kanai 29 Nov. 1994 20 p

(Contract DE-FC08-90NV-10872)

(DE95-010173; DOE/NV-10872/T176) Avail: CASI HC A03/MF A01

Text images that contain touching or broken characters can significantly degrade the accuracy of optical character recognition (OCR) systems. This paper proposes an adaptive image restoration technique that can improve OCR accuracy by enhancing touching or broken character images. The technique begins by processing a distorted text image with an OCR system. Using the distorted text image and output information from the OCR system, an inverse model of the distortion that caused the touching or broken character problem is generated. After generating the inverse model, the unrecognized distorted characters are filtered by the inverse model and then processes by the OCR system. To demonstrate its feasibility, six distorted text images were processed using this technique. Four of the text images, two with touching characters and two with broken characters, were synthesized using mathematical distortion models. The remaining two distorted text images, one with touching characters and one with broken characters, were distorted using a photocopier. The performance of the adaptive image restoration technique was measured using pixel accuracy and OCR improvement. The examples demonstrate that this technique can improve both the pixel and OCR accuracy of text images containing touching or broken characters. DOE

N95-30764 State Univ. of New York, Buffalo, NY.

JOIN PROCESSING IN RELATIONAL DATABASE SYSTEMS Ph.D. Thesis

Ram Danturti Gopal 1993 216 p

Avail: Univ. Microfilms Order No. DA9420149

An extremely important issue in the efficient implementation of a relational database system is query optimization. Query optimization is

concerned with the minimization of the amount of information that must be accessed from a database in order to respond to a user's query. In this research, we address the issue of join processing in relational database systems. Join is an important query which arises frequently, both in traditional and in emerging database applications. The need for efficient join processing algorithms is strongly underscored in the literature as it is an expensive query operation which directly limits the wide spread use of database systems in real world application. The central premise of this research is that optimization of the sequence in which the data pages of the underlying relations are accessed can lead to a significant improvement in the join execution cost over the current methods. Accordingly, we develop three approaches for join processing. In the first two approaches, we develop a tree representation consisting of the data pages of the relations. The tree representation reveals the structural properties of the join and provides a framework to identify the optimal page access sequence that minimizes the join execution cost. We formulate the join as a tree traversal process and accordingly develop efficient tree traversal algorithms. The third approach draws its inspiration from the hybrid hash algorithm, which is considered the state-of-the-art join processing method. In this approach, we segment the relations into zones. The join is materialized by processing the zones sequentially. We theoretically show that the proposed approach is guaranteed to outperform the hybrid hash method. The proposed approaches utilize indices on the participating relations to accelerate the join. The algorithms developed in this research are proceduraly straight forward and are easily transportable to any database management system. The data structures needed for the algorithms are simple, and easy to create and manage. Our computational experience suggests that the proposed approaches can lead to an order of magnitude improvement over current approaches to join processing, and thus constitute an important contribution to the theory and practice of relational database management. Dissert. Abstr.

N95-30780*# National Aeronautics and Space Administration. Marshall Space Flight Center, Huntsville, AL.

SPACE SCIENCES LABORATORY PUBLICATIONS AND PRESENTATIONS Annual Report, 1 Jan. - 31 Dec. 1994

T. W. Moorehead, compl Washington Apr. 1995 74 p

(NASA-TM-108484; NAS 1.15:108484) Avail: CASI HC A04/MF A01

This document lists the significant publications and presentations of the Space Sciences Laboratory during the period Jan. 1 - Dec. 31, 1994. Entries in the main part of the document are categorized according to NASA Reports (arranged by report number), Open Literature, and Presentations (arranged alphabetically by title). Also included for completeness is an appendix (arranged by report number) listing preprints issued by the laboratory during this reporting period. Some of the preprints have not been published; those already published are so indicated. Most of the articles listed under Open Literature have appeared in referenced professional journals, books, monographs, or conference proceedings. Although many published abstracts are eventually expanded into full papers for publications in scientific and technical journals, they are often sufficiently comprehensive to include the significant results of the research reported. Therefore, published abstracts are listed separately in a subsection under Open Literature. The organizational code of the cognizant SSL branch or office is given at the end of each entry. Author

N95-30858*# Jet Propulsion Lab., California Inst. of Tech., Pasadena, CA.

SYSTEM CONSIDERATIONS FOR EFFICIENT COMMUNICATION AND STORAGE OF MSTI IMAGE DATA

Robert F. Rice Oct. 1994 84 p Prepared for Ballistic Missile Defense Organization, Washington, DC

(Contract NAS7-1260; RTOP 889-54-49-10-20)

(NASA-CR-198869; JPL-Publ-94-16; NAS 1.26:198869) Avail: CASI HC A05/MF A01

The Ballistic Missile Defense Organization has been developing the capability to evaluate one or more high-rate sensor/hardware combinations by incorporating them as payloads on a series of Miniature Seeker Technology Insertion (MSTI) flights. This publication represents the final report of a 1993 study to analyze the potential impact f data compression and of related communication system technologies on post-MSTI 3 flights. Lossless compression is considered alone and in conjunction with various spatial editing modes. Additionally, JPEG and Fractal algorithms are examined in order to bound the potential gains from the use of lossy compression. but lossless compression is clearly shown to better fit the goals of the MSTI investigations. Lossless compression factors of between 2:1 and 6:1 would provide significant benefits to both on-board mass memory and the downlink. for on-board mass memory, the savings could range from $5 million to $9 million. Such benefits should be possible by direct application of recently developed NASA VLSI microcircuits. It is shown that further downlink enhancements of 2:1 to 3:1 should be feasible thorough use of practical modifications to the existing modulation system and incorporation of Reed-Solomon channel coding. The latter enhancement could also be achieved by applying recently developed VLSI microcircuits. Author

N95-30882# Korea Cancer Center Hospital, Seoul (Republic of Korea).

DEVELOPMENT OF TECHNICAL INFORMATION PROCESSING SYSTEMS

Ji Ho Lee, Tae Whan Kim, Sun Ja Kim, Young Min Kim, Kwang Choi, Joung Hun Oh, Hyun Suk Choung, Jong Yong Keum, An Na Yoo, and Deuck Haing Harn et al Dec. 1993 52 p In KOREAN

(DE95-613311; KAERI/RR-1269/93) Avail: CASI HC A04/MF A01

The major goal is to develop a more efficient information management system by connecting the KAREI serials database, which enables the users to access the database from their own laboratory facilities through KAREI-NET. The importance of this project is to make the serials information of KAERI easily accessible to users as valuable resources for research and development activities. The results of the project are as follows. (1) Development of the serials database and retrieval system enabled us to access the serials holding information through KAERI-NET. (2) The database construction establishes a foundation for the management of 1600 serials held in KAERI. (3) The system can be applied not only to KAERI but also to similar medium-level libraries. DOE

N95-30883# Korea Cancer Center Hospital, Seoul (Republic of Korea).

THE DEVELOPMENT OF KAERI MANAGEMENT INFORMATION SYSTEM 2: THE DEVELOPMENT OF TIME SHEET MANAGEMENT SYSTEM

Sin Bok Kang, Yeong Taek Kim, Soo Jin Park, Yeong Cheol Ko, Jong Bok Lee, Eun Sook Han, and Hyeon Jeong Kim Jan. 1994 104 p In KOREAN

(DE95-613355; KAERI/RR-1300/93) Avail: CASI HC A06/MF A02

The work done for the development, operation, and maintenance of Time Sheet Management System is described. This work is a part of the development of KAERI management information system. Manpower management is essential to cope with the external circumstances promptly and to maximize the productivity of the organization. This work aims at setting up a basis for the manpower management system. It is widely recognized that neither timely decision making nor competitive edge can be secured with the traditional management technology in a so rapidly changing situation at home and abroad, which can be characterized by openness and informality. The necessity of efficient and scientific man-power management by time-study has emerged on the reorganization of KAERI by expanding matrix system in order to enhance the research and development productivity. DOE

N95-30928# Naval Postgraduate School, Monterey, CA.

AN ARCHITECTURAL APPROACH TO STRATEGIC INFORMATION SYSTEMS PLANNING FOR THE OFFICE OF NAVAL INTELLIGENCE M.S. Thesis

Bruce F. Loveless Sep. 1994 166 p

(AD-A289930) Avail: CASI HC A08/MF A02

Strategic information systems (IS) planning aligns an organization's information systems with its critical strategic goals and supporting mission-specific functions. This thesis demonstrates a structured approach to strategic IS planning and provides a guide for developing an information systems architecture to support the organizational goals of the Office of Naval Intelligence (ONI). By first examining established information systems planning practices, architectural design methodologies. Department of Defense (DOD) guidelines, and published ONI organizational objectives, this thesis guides the reader through the decision-making process involved in strategic IS planning. The methodology is structured on guidance provided by the DOD's Technical Architecture Framework for Information Management (TAFIM) Standards-Based Architecture (SBA) Planning Guide. This thesis

demonstrates the validity of using the structured architectural approach, presented by the TAFIM and other strategic IS planning concepts, in concert with intelligence-specific IS planning guidance to systematically address the issues, problems, and critical decisions faced by organizations attempting the strategic IS planning process. DTIC

N95-31334 Houston Univ., TX.
IMPACT OF TASK PROPERTIES, DATA DISPLAY FORMAT AND COGNITIVE CHARACTERISTICS ON RECALL PERFORMANCE: A CUMULATIVE RESEARCH INVESTIGATION Ph.D. Thesis
Narayan S. Umanath 1987 345 p
Avail: Univ. Microfilms Order No. DA9411842

This research evaluates individual performance in an information recall context examining the effects due to MIS variables, task environment, and individual cognitive characteristics. The principal MIS variables manipulated here are data display format and order of presentation. Task-related variables are claimed to be capable of explaining a substantial amount of variance in the response variable of interest. To date, the rich and potentially significant factor, task properties, has not been sufficiently harnessed for use as a treatment variable(s) in MIS-oriented research. Three basic elements, content, structure, and complexity, may, in combination, provide a reasonable description of 'task.' Experiments in this research attempt to measure task characteristics by manipulating one or more of these three task elements simultaneously. Individual differences, especially individual cognitive style/skill, have been used as moderator(s) in several studies/experiments that assess the impact of IS on managerial performance. Though the value of cognitive style as an explanatory variable in MIS-related inquiries is questioned by some, this research attempts to examine the merits/demerits of cognitive factors (cognitive style and skill) in an information recall context. A framework reflecting the theme of the inquiry was developed to guide the research effort. A research strategy based on the concept of the cumulative research paradigm (a series of studies/experiments that are conducted such that every study/experiment in the program is firmly anchored to and builds on the findings of its predecessor(s)) was adopted. In all, five experiments and a field survey were conducted. The cumulative findings of this research clearly demarcate recall performance into two operational categories, viz., point value and pattern recall. Point value recall performance was repeatedly found to be significantly better with the use of tabular displays rather than graphics and was also relatively indifferent to all other effects examined. Pattern recollection, on the other hand, was found to be vulnerable to task characteristics, display format, order of presentation as well as imagery-oriented individual cognitive style. The chief contributions of this research are, it is hoped, (1) the reinstatement of 'recall' as a context of evaluation in the problem solving/decision making scenario, (2) the operationalization of attributes of task environment in the context of information recall, and (3) the demonstration of the cumulative research approach in empirical investigations. Dissert. Abstr.

N95-31348 Rensselaer Polytechnic Inst., Troy, NY.
ADAPTIVENESS IN INFORMATION SYSTEMS INTEGRATION Ph.D. Thesis
Gilbert Babin 1993 253 p
Avail: Univ. Microfilms Order No. DA9420307

Interoperability, local autonomy, and concurrent processing are major problems facing the integration of multiple data and knowledge systems, such as those found in today's manufacturing enterprises. Their solution, however, requires new analyses and insights beyond the previous understanding and formulation of these issues. We submit that the key to solving these problems is adaptiveness. The objective of this research, therefore, is to develop the new capabilities of adaptiveness needed to enable the enterprise to grow (i.e., incorporating new or legacy systems into the environment) and change its integrated information system while avoiding the well-known performance problems caused by the traditional approaches to global control and management. The solution utilizes (1) a metadatabase serving as the knowledge base for enterprise integration, (2) a concurrent architecture using the metadatabase for integration, and (3) a rule-oriented programming environment (ROPE) for implementing and managing the concurrent architecture. The technical nature of the research problem is concerned with concurrent knowledge representation and processing. This knowledge method must be able to (1) control the application logic of local systems without the use of a central controller, (2) enhance the local applications with a distributed knowledge capability for global behavior, and (3) transfer the needed knowledge both between the metadatabase and the local applications, and among the local applications themselves. The new ROPE method contributes not only to the metadatabase solutions to the problem of adaptiveness, making the metadatabase an active heterogeneous distributed database management systems, but also to the general concepts of local autonomy, open system architecture, interoperability, and systems evolution. Together, the research extends the current information integration technology and results in a particular method effecting adaptiveness in managing multiple systems environments. Moreover, its specific generic results provide the architecture, algorithms, and languages to further the state-of-the-art of current knowledge representation and processing, as well as the shells design which affords an efficient model for application program interface systems in general. Dissert. Abstr.

N95-31618# Rice Univ., Houston, TX. Dept. of Statistics.
TOPICS IN EXPLORATORY AND SPECULATIVE DATA ANALYSIS Final Report, 1 Jul. 1991 - 30 Sep. 1994
James R. Thompson Oct. 1994 7 p
(Contract DAAL03-91-G-0210)
(AD-A290505; ARO-28686.3-MA) Avail: CASI HC A02/MF A01

Synopses are presented for nine published papers generated by this research. Technological areas covered include: data analysis, tumor metastases, stochastic processes, structure failure, design analysis, data sets, multivariate control, quality control and sampling. Personnel supported by this research and doctoral degrees are listed. DTIC

N95-31662# Sandia National Labs., Albuquerque, NM.
TOWARD A RISK-BASED APPROACH TO THE ASSESSMENT OF THE SURETY OF INFORMATION SYSTEMS
G. D. Wyss, S. K. Fletcher, R. D. Halbgewachs, R. M. Jansma, J. J. Lim, M. Murphy, and P. D. Sands 1995 8 p Presented at the Joint ASME/JSME Pressure Vessels and Piping Conference, Honolulu, HI, 23-27 Jul. 1995
(Contract DE-AC04-94AL-85000)
(DE95-008821; SAND-95-0501C; CONF-950740-14) Avail: CASI HC A02/MF A01

Traditional approaches to the assessment of information systems have treated system security, system reliability, data integrity, and application functionality as separate disciplines. However, each area's requirements and solutions have a profound impact on the successful implementation of the other areas. A better approach is to assess the 'surety' of an information system, which is defined as ensuring the 'correct' operation of an information system by incorporating appropriate levels of safety, functionality, confidentiality, availability, and integrity. Information surety examines the combined impact of design alternatives on all of these areas. We propose a modeling approach that combines aspects of fault trees and influence diagrams for assessing information surety requirements under a risk assessment framework. This approach allows tradeoffs to be based on quantitative importance measures such as risk reduction while maintaining the modeling flexibility of the influence diagram paradigm. This paper presents an overview of the modeling method and a sample application problem. DOE

N95-31713*# Jet Propulsion Lab., California Inst. of Tech., Pasadena, CA.
GUIDELINES FOR CREATING AND USING ABBREVIATIONS AND ACRONYMS
Diane F. Miller Apr. 1995 34 p
(Contract NAS7-1260; RTOP 889-21-32)
(NASA-CR-198884; JPL-Publ-95-9; NAS 1.26:198884) Avail: CASI HC A03/MF A01

The unchecked use of acronyms and initialisms in technical writing presents a huge obstacle to clarity and readability. Although technical communicators are certainly more aware of this problem than are the engineers, scientists, and managers with whom they work, they need concrete guidelines and at least a small degree of self-righteousness on this subject to help them cope with the onslaught. That acronyms frustrate communication is well founded in linguistic theory, not to mention common sense. Suggestions for mitigating their destructiveness include issues of

audience, term selectivity, frequency and occasion of use, and aesthetics.
Author

N95-31823# West Virginia Univ., Morgantown, VA.
MANAGEMENT, VISUALIZATION, AND ANALYSIS OF ENVIRONMENTAL AND GEOTECHNICAL DATA
Sep. 1994 74 p
(Contract DE-FC21-92MC-29467)
(DE95-000063; DOE/MC-29467/3986) Avail: CASI HC A04/MF A01

This topical report evaluates current technology on the management, visualization, and analysis of engineering and environmental data. This report gives an overview and assessment of the Integrated Computer Assisted Site Evaluation/Graphical Remedial Assessment and Cost Evaluation (ICASE/GRACE) system and includes brief descriptions of the Environmental Technology '94: Computing and Information Conference and the National Conference on Environmental Problem Solving with Geographic Information Systems (GIS). DOE

N95-32107# Westinghouse Hanford Co., Richland, WA.
WESTINGHOUSE HANFORD COMPANY DATA MANAGEMENT PLAN TEMPLATE, REVISION 1
K. K. Friday 1 Mar. 1995 36 p
(Contract DE-AC06-87RL-10930)
(DE95-010046; WHC-SD-GN-UM-30008-Rev-1) Avail: CASI HC A03/MF A01

The Data Management Plan Template provides guidelines for the content and writing of data management plans. These plans discuss how data management is being implemented within the scope of any given project, program, or business function. The entire document was revised and changed to reflect a simplified outline and clarification of required information.
DOE

N95-32144# Sandia National Labs., Albuquerque, NM.
PROPOSED DDS-SPECIFIC FIELDS FOR THE GENERIC AUTHENTICATION INFORMATION ELEMENT
Thomas D. Tarman 10 Apr. 1995 6 p Presented at the ATM Forum Technical Committee Meeting, Denver, CO, 10 Apr. 1995
(Contract DE-AC04-94AL-85000)
(DE95-009839; SAND-95-0666C; CONF-9504139-1) Avail: CASI HC A02/MF A01

This contribution proposes the format of the 'Algorithm-Specific Information' and 'Signature' fields within the 'Proposed Generic Authentication Information Element' for authentication IE's based on the Digital Signature Standard (DSS). These fields are designed to allow various levels of authentication 'strength' (or robustness), and many of these fields may be omitted in systems that optimize authentication performance by sharing common (public) Digital Signature Algorithm (DSA) parameters. This allows users and site security officers to design their authenticated signaling according to site security and performance requirements. DOE

N95-32149# Nevada Univ., Las Vegas, NV. Information Science Research Inst.
AN EVALUATION OF AN AUTOMATIC MARKUP SYSTEM
Kazem Taghva, Allen Condit, and Julie Borsack 1995 11 p Presented at the SPIE 1995: SPIE Conference on Optics, Electro-optics, and Laser Application in Science, Engineering and Medicine, San Jose, CA, 5-10 Feb. 1995
(Contract DE-FC08-90NV-10672)
(DE95-009885; CONF-950226-33) Avail: CASI HC A03/MF A01

One predominant application of OCR (Optical Character Recognition) is the recognition of full text documents for information retrieval. Modern retrieval systems exploit both the textual content of the document as well as its structure. The relationship between textual content and character accuracy has been the focus of recent studies. It has been shown that, due to the redundancies in text, average precision and recall is not heavily affected by OCR character errors. What is not fully known is to what extent OCR devices can provide reliable information that can be used to capture the structure of the document. In this paper, the authors present a preliminary report on the design and evaluation of a system to automatically markup technical documents, based on information provided by an OCR device. The device the authors use differs from traditional OCR devices in that it not only performs optical character recognition, but also provides detailed information about page layout, word geometry, and font usage. Their automatic markup program, which they call Autotag, uses this information, combined with dictionary, lookup and content analysis, to identify structural components of the text. These include the document title, author information, abstract, sections, section titles, paragraphs, sentences, and de-hyphenated words. A visual examination of the hardcopy will be compared to the output of their markup system to determine its correctness. DOE

N95-32182 Japan Broadcasting Corp., Tokyo (Japan). Program Production Technology Research Div.
TRANSLATION WORKBENCH FOR GENERATING SUBTITLES FOR ENGLISH TV NEWS
Hideki Sumiyoshi, Hideki Tanaka, Nobuko Hatada, and Terumasa Ehara Apr. 1995 8 p
(ISSN 0027-657X)
(NHK-435) Copyright Avail: Issuing Activity (Japan Broadcasting Corp., 1-10-11, Kinuta, Setagaya-ku, Tokyo 157, Japan)

An English-Japanese machine translation (MT) system has been used for the subtitles of a part of the World News program on NHK's satellite Channel 1 since August, 1989. The MT system does not merely translate English. Starting with the input of the original news script, it translates the text, converts it into subtitles, and specifies which subtitles are overlaid and when on the video signal. This procedure is inefficient, however, because each task is processed separately. We have now developed a prototype subtitle generation system that integrates all tasks efficiently. It is called the translation workbench. We describe its configuration and the operating procedure. Author

N95-32254 Selskapet for Industriell og Teknisk Forskning, Trondheim (Norway). Div. of Safety and Reliability.
DATA ANALYSIS: NAIVE INDUCTIVISM
J. Vatn 31 Dec. 1993 11 p
(PB95-212213; STF75-S93039) Avail: Issuing Activity (National Technical Information Service (NTIS))

The objectives of collecting and analyzing data is discussed. It is claimed that it is not always possible to control all relevant factors, and this may lead to biased results. In its nature, prediction of future parameters based on events in the past is inductive. A Bayesian approach, however, stimulates deductive reasoning. A situation where important explanatory variables are missing is discussed at the end of the article. It is claimed that in its nature, the assessment of hardware reliability and human reliability is identical. NTIS

N95-32285# Lawrence Livermore National Lab., Livermore, CA. Computer Security Technology Center.
RECOMMENDATIONS FOR PROTECTING NATIONAL LIBRARY OF MEDICINE COMPUTING AND NETWORKING RESOURCES
Richard Feingold Nov. 1994 23 p
(Contract W-7405-eng-48)
(DE95-011554; UCRL-ID-118894) Avail: CASI HC A03/MF A01

Protecting information technology (IT) involves a number of interrelated factors. These include mission, available resources, technologies, existing policies and procedures, internal culture, contemporary threats, and strategic enterprise direction. In the face of this formidable list, a structured approach provides cost effective actions that allow the organization to manage its risks. We face fundamental challenges that will persist for at least the next several years. It is difficult if not impossible to precisely quantify risk. IT threats and vulnerabilities change rapidly and continually. Limited organizational resources combined with mission restraints, such as availability and connectivity requirements, will insure that most systems will not be absolutely secure (if such security were even possible). In short, there is no technical (or administrative) 'silver bullet.' Protection is employing a stratified series of recommendations, matching protection levels against information sensitivities. Adaptive and flexible risk management is the key to effective protection of IT resources. The cost of the protection must be kept less than the expected loss, and one must take into account that an adversary will not expend more to attack a resource than the value of its compromise to that adversary. Notwithstanding the difficulty if not impossibility to precisely quantify risk, the aforementioned allows us to avoid the trap of choosing a course of action simply because 'it's safer' or ignoring an area because no one had explored its potential risk. Recommendations for protecting IT resources begins with discussing

contemporary threats and vulnerabilities, and then procedures from general to specific preventive measures. From a risk management perspective, it is imperative to understand that today, the vast majority of threats are against UNIX hosts connected to the Internet. DOE

N95-32362# Nevada Univ., Las Vegas, NV.
UNLV: INFORMATION SCIENCE RESEARCH INSTITUTE Quarterly Progress Report
T. A. Nartker 31 Mar. 1995 8 p
(Contract DE-FC08-90NV-10872)
(DE95-011941; DOE/NV-10872/T187) Avail: CASI HC A02/MF A01

Research programs from the Information Science research Institute are briefly described in the areas of document analysis and text retrieval. DOE

N95-32370 Centre National de la Recherche Scientifique, Marseilles (France). Lab. de Neurosciences Cognitives.
TEMPORAL INFORMATION PROCESSING MECHANISMS Final Report [MECANISMES DE TRAITEMENT DE L'INFORMATION TEMPORELLE]
F. Macar Oct. 1993 40 p In FRENCH Sponsored by Direction des Recherches, Etudes et Techniques, Paris, France. Centre de Documentation de l'Armement
(Contract DRET-91/1200A)
(PB95-208344) Avail: Issuing Activity (National Technical Information Service (NTIS))

The author details a series of experiments and results obtained in behavioral and electrophysiological studies to show the existence of specific temporal processing mechanisms in man and animals that come into play, mobilizing a part of the subject's available attention resources, when a prospective temporal judgment and a precise estimation of times of short duration are called for. NTIS

N95-31810*# National Aeronautics and Space Administration. Marshall Space Flight Center, Huntsville, AL.
ENVIRONMENTAL DATABASES AND OTHER COMPUTERIZED INFORMATION TOOLS
Marceia Clark-Ingram *In its* Aerospace Environmental Technology Conference Mar. 1995 p 633-641 (For primary document see N95-31746 11-23)
Avail: CASI HC A02/MF A06

N95-31811*# National Aeronautics and Space Administration. Marshall Space Flight Center, Huntsville, AL.
NEIS (NASA ENVIRONMENTAL INFORMATION SYSTEM)
Beth Cook *In its* Aerospace Environmental Technology Conference Mar. 1995 p 643-647 (For primary document see N95-31746 11-23)
Avail: CASI HC A01/MF A06

83 ECONOMICS AND COST ANALYSIS

Includes cost effectiveness studies.

No abstracts in this category.

84 LAW, POLITICAL SCIENCE AND SPACE POLICY

Includes NASA appropriation hearings; aviation law; space law and policy; international law; international cooperation; and patent policy.

No abstracts in this category.

85 URBAN TECHNOLOGY AND TRANSPORTATION

Includes applications of space technology to urban problems; technology transfer; technology assessment; and surface and mass transportation.

For related information see also *03 Air Transportation and Safety, 16 Space Transportation,* and *44 Energy Production and Conversion.*

N95-30385# Sandia National Labs., Albuquerque, NM.
THE TECHNOLOGY INFORMATION ENVIRONMENT WITH INDUSTRY (TIE-In): A MECHANISM FOR ACCESSING LABORATORY SOLUTIONS
J. A. Ang, G. D. Machin, and E. L. Marek 1994 13 p Presented at the Agile Manufacturing Enterprise Forum, Atlanta, GA, 7-8 Mar. 1995
(Contract DE-AC04-94AL-85000)
(DE95-008542; SAND-94-3279C; CONF-9503109-2) Avail: CASI HC A03/MF A01

The Technology Information Environment with Industry (TIE-In) is a system that helps users obtain laboratory-developed technical solutions without requiring that they duplicate the technical resources (in people, hardware and software) at the national laboratories. TIE-In is based on providing users with controlled access to distributed laboratory resources that are packaged in intelligent user interfaces. These interfaces help users obtain technical solutions without requiring that the user have specialized technical and computer expertise. As a designated DOE Technology Deployment Center/User Facility, industry users can access a broad range of laboratory-developed technologies on a cost-recovery basis. TIE-In will also be used to share laboratory resources with partners in US industry that help the DOE meet future manufacturing needs for the stewardship of our nation's nuclear weapons stockpile. DOE

N95-31345# General Accounting Office, Washington, DC. Program Evaluation and Methodology Div.
NATIONAL LABORATORIES: ARE THEIR R AND D ACTIVITIES RELATED TO COMMERCIAL PRODUCT DEVELOPMENT? REPORT TO CONGRESSIONAL REQUESTERS
25 Nov. 1994 99 p
(GAO/PEMD-95-2; B-256574) Avail: CASI HC A05/MF A02; GAO, PO Box 6015, Gaithersburg, MD 20884-6015 HC

The current balance of the research effort in the DOE 10 laboratories' research programs is addressed. The extent to which the national laboratories are engaged in basic and applied research or in research related to commercial product development is examined. Derived from text

N95-32201# General Accounting Office, Washington, DC. Resources, Community, and Economic Development Div.
REPORT TO THE VICE CHAIRMAN, JOINT ECONOMIC COMMITTEE, US CONGRESS. TECHNOLOGY TRANSFERS: BENEFITS OF COOPERATIVE R AND D AGREEMENTS
16 Dec. 1994 28 p
(GAO/RCED-95-52; B-253616) Avail: CASI HC A03/MF A01; GAO, PO Box 6015, Gaithersburg, MD 20877 HC

Cooperative Research and Development Agreements (CRADAS) are one of several mechanisms whereby federal laboratories and private industry collaborate on research and development. CRADAS define the terms and conditions of the collaboration. This report points out the benefit CRADAS have given federal agencies and private companies. The CRADAS offered opportunities for federal laboratories and industry to collaborate on research while meeting their missions. Technology from federal laboratories was transferred to the private sector, resulting in commercial products. Research and Development programs were advanced. The sharing of resources aided federal laboratories and private companies in accomplishing the CRADAS' objectives. In addition, some of the CRADAS demonstrated a potential for long-term improvements to our nation's economy, health, and environment. Derived from text

88 SPACE SCIENCES (GENERAL)

N95-31979*# National Aeronautics and Space Administration, Washington, DC.
AERONAUTICS AND SPACE REPORT OF THE PRESIDENT Activities Report, Fiscal Year 1994
1995 147 p Original contains color illustrations
(NASA-TM-110743; NAS 1.15:110743) Avail: CASI HC A07/MF A02; 1 functional color page

This report describes the activities and accomplishments of all agencies of the United States in the fields of aeronautics and space science during FY 1994. Activity summaries are presented for the following areas: space launch activities, space science, space flight and space technology, space communications, aeronautics, and studies of the planet Earth. Several appendices providing data on U.S. launch activities, the Federal budget for space and aeronautics, remote sensing capabilities, and space policy are included. CASI

89 ASTRONOMY

Includes radio, gamma-ray, and infrared astronomy, and astrometry.

N95-30469*# National Aeronautics and Space Administration. Marshall Space Flight Center, Huntsville, AL. Div. of Physics, Mathematics, and Astronomy.
OBSERVATIONS OF ACCRETING PULSARS
Thomas A. Prince (California Inst. of Tech., Pasadena, CA.), Lars Bildsten (California Inst. of Tech., Pasadena, CA.), Deepto Chakrabarty (California Inst. of Tech., Pasadena, CA.), Robert B. Wilson, and Mark H. Finger 1994 10 p
(Grants NAGw-1919; NAG5-1458; NGT-51184)
(NASA-CR-198931; NAS 1.26:198931) Avail: CASI HC A02/MF A01

We discuss recent observations of accreting binary pulsars with the all-sky BATSE instrument on the Compton Gamma Ray Observatory. BATSE has detected and studied nearly half of the known accreting pulsar systems. Continuous timing studies over a two-year period have yielded accurate orbital parameters for 9 of these systems, as well as new insights into long-term accretion torque histories. Author

N95-31099* Interface, Inc., Fort Collins, CO.
NASA SPACE ASTRONOMY UPDATE 6 (Videotape)
1 Oct. 1992 Videotape: 6 min. 30 sec. playing time, in color, with sound
(NASA-CR-197664; NONP-NASA-VT-95-46007) Avail: CASI VHS A02/BETA A22

Professor Stu Bowyer (University of California at Berkeley) explains the Extreme Ultraviolet Explorer and its telescope in this video. Both instrument and satellite are kept in perfect working condition. The satellite picks up extra galactic objects outside our galaxy. CASI

N95-31129# Lawrence Livermore National Lab., Livermore, CA.
X-RAY PERFORMANCE OF THE ENGINEERING PROTOTYPE STELLAR X-RAY POLARIMETER
E. Silver, K. Ziock, and J. Dwyer 1994 10 p Presented at the Annual Meeting of the Society of Photo-Optical Instrumentation Engineers, San Diego, CA, 24-29 Jul. 1994
(Contract W-7405-eng-48)
(DE95-010268; UCRL-JC-118726; CONF-940723-37) Avail: CASI HC A02/MF A01

The performance of the engineering prototype Stellar X-Ray Polarimeter (SXRP) has been evaluated. Hundred percent polarized monochromatic x-rays at 2.6 keV and 9.7 keV were used to measure the response of the instrument in the energy bands of the graphite and lithium polarizing elements, respectively. On-line analysis showed that the respective depths of modulation are 96% and 70% as expected. Irradiating SXRP with broadband unpolarized x-rays in the energy band 2--17 keV demonstrated that the level of spurious modulation inherent in the instrument is less than 3%. Up-to-date results are presented and compared to the predictions of Monte Carlo simulations. DOE

N95-31364*# Space Telescope Science Inst., Baltimore, MD.
THE FUTURE OF SPACE IMAGING. REPORT OF A COMMUNITY-BASED STUDY OF AN ADVANCED CAMERA FOR THE HUBBLE SPACE TELESCOPE Final Technical Report
Robert A. Brown, ed. Oct. 1993 150 p
(Contract NAGw-3135; NAS5-26555)
(NASA-CR-198818; NAS 1.26:198818) Avail: CASI HC A07/MF A02

The scientific and technical basis for an Advanced Camera (AC) for the Hubble Space Telescope (HST) is discussed. In March 1992, the NASA Program Scientist for HST invited the Space Telescope Science Institute to conduct a community-based study of an AC, which would be installed on a scheduled HST servicing mission in 1999. The study had three phases: a broad community survey of views on candidate science program and required performance of the AC, an analysis of technical issues relating to its implementation, and a panel of experts to formulate conclusions and prioritize recommendations. From the assessment of the imaging tasks astronomers have proposed for or desired from HST, we believe the most valuable 1999 instrument would be a camera with both near ultraviolet/optical (NUVO) and far ultraviolet (FUV) sensitivity, and with both wide field and high resolution options. CASI

90 ASTROPHYSICS

Includes cosmology; celestial mechanics; space plasmas; and interstellar and interplanetary gases and dust.

For related information see also *75 Plasma Physics*.

N95-30361# California Univ., Berkeley. Lawrence Berkeley Lab, CA.
STRANGE-MATTER STARS
F. Weber, C. Kettner, and M. K. Weigel Dec. 1994 10 p Presented at the Symposium on Strangeness and Quark Matter, Crete, Greece, 1-5 Sep. 1994
(Contract DE-AC03-76SF-00098)
(DE95-008446; LBL-36210; CONF-9409310-2) Avail: CASI HC A02/MF A01

This paper gives an overview of the properties of all possible equilibrium sequences of compact strange-matter stars with nuclear crusts, which range from strange stars to strange dwarfs. In contrast to their non-strange counterparts--neutron stars and white dwarfs--their properties are determined by two (rather than one) parameters, the central star density and the density at the base of the nuclear crust. This leads to stellar strange-matter configurations whose properties are much more complex than those of the conventional sequence. As an example, two generically different categories of stable strange dwarfs are found, which could be the observed white dwarfs. Furthermore the authors find very-low-mass strange stellar objects, with masses as small as those of Jupiter or even lighter planets. Such objects, if abundant enough, should be seen by the presently performed gravitational microlensing searches. DOE

N95-30366# Joint Inst. for Nuclear Research, Dubna (USSR).
LARGE SCALE PERIODICITY OF THE UNIVERSE AND BARYOGENESIS
M. V. Chizhov (Sofia Univ., Bulgaria.) and D. P. Kirilova (Bulgarian Academy of Sciences, Sofia, Bulgaria.) 1994 7 p
(DE95-613461; JINR-E-2-94-258) Avail: CASI HC A02/MF A01 (US Sales Only)

A mechanism for generating baryon perturbations in the scalar field condensate baryogenesis scenario is proposed. This mechanism may naturally explain the observed periodic distribution of the luminous matter in the Universe with the characteristic scale of 128 h(sup -1) M pc. It is found that both the observed baryon asymmetry and the periodicity in the large structure of the Universe can be explained through the behaviour of a complex scalar field condensate formed at the inflationary stage. DOE

N95-30466*# National Aeronautics and Space Administration. Marshall Space Flight Center, Huntsville, AL.
CHROMOSPHERICALLY ACTIVE STARS. 6: GIANTS WITH COMPACT HOT COMPANIONS AND THE BARIUM STAR SCENARIO
Francis C. Fekel, Gregory W. Henry (Tennessee Univ., Nashville, TN.), Michael R. Busby (Tennessee Univ., Nashville, TN.), and Joseph J. Eitter (Iowa State Univ. of Science and Technology, Ames, IA.) [1993] 42 p

(Grants NAG5-397; NAG8-111; NSF HRD-91-04484; NSF AST-82-05956; NSF AST-86-04324; NSF AST-88-19696)
(NASA-TM-110641; NAS 1.26:110641) Avail: CASI HC A03/MF A01

We have determined spectroscopic orbits for three chromospherically active giants that have hot compact companions. They are HD 160538 (K0 III + wd, P = 904 days), HD 165141 (G8 III + wd, P approximately 5200 days), and HD 185510 (K0 III + sdB, P = 20.6619 days). By fitting an IUE spectrum with theoretical models, we find the white dwarf companion of HD 165141 has a temperature of about 35000 K. Spectral types and rotational velocities have been determined for the three giants and distances have been estimated. These three systems and 39 Ceti are compared with the barium star mass-transfer scenario. The long-period mild barium giant HD 165141 as well as HD 185510 and 39 Ceti, which have relatively short periods and normal abundance giants, appear to be consistent with this scenario. The last binary, HD 160538, a system with apparently near solar abundances, a white dwarf companion, and orbital characteristics similar to many barium stars, demonstrates that the existence of a white-dwarf companion is insufficient to produce a barium star. The paucity of systems with confirmed white-dwarf companions makes abundance analyses of HD 160538 and HD 165141 of great value in examining the role of metallicity in barium star formation. Author

N95-30569# Chalmers Univ. of Technology, Goeteborg (Sweden).
MOLECULAR GAS IN STARBURST GALAXIES: LINE INTENSITIES AND PHYSICAL CONDITIONS
S. Aalto, R. S. Booth, J. H. Black, and L. E. B. Johansson Mar. 1995 16 p Prepared in cooperation with Steward Observatory
(PB95-208021) Avail: CASI HC A03/MF A01

We present an extended study of molecular excitation for a selection of starburst galaxies. It extends a study of the (12)CO/(13)CO 1-0 intensity ratio of these galaxies, with an additional goal to investigate the notion of a two-type molecular medium in the inner regions of bright IR galaxies. NTIS

N95-30606# Joint Inst. for Nuclear Research, Dubna (USSR).
THE CONICAL SINGULARITY AND QUANTUM CORRECTIONS TO ENTROPY OF BLACK HOLE
S. N. Solodukhin 1994 22 p
(DE95-613367; JINR-E-2-94-246) Avail: CASI HC A03/MF A01 (US Sales Only)

It is well known that at the temperature different from the Hawking temperature there appears a conical singularity in the Euclidean classical solution of gravitational equations. The method of regularizing the cone by regular surface is used to determine the curvature tensors for such metrics. It allows to calculate the one-loop matter effective action and the corresponding one-loop quantum corrections to the entropy in the framework of the path integral approach of Gibbons and Hawking. The two-dimensional and four-dimensional cases are considered. The entropy of the Rindler space is shown to be divergent logarithmically in two dimensions and quadratically in four dimensions. It corresponds to the results obtained earlier. For the eternal 2D black hole we observe finite, dependent on the mass, correction to the entropy. The entropy of the 4D Schwarzschild black hole is shown to possess an additional (in comparison to the 4D Rindler space) logarithmically divergent correction which does not vanish in the limit of infinite mass of the black hole. We argue that infinities of the entropy in four dimensions are renormalized with the renormalization of the gravitational coupling. DOE

N95-30729# Texas Univ., Austin, TX. Inst. for Fusion Studies.
ON THE QUASIHYDROSTATIC FLOWS OF RADIATIVELY COOLING SELF-GRAVITATING GAS CLOUDS
B. Meerson (Hebrew Univ. of Jerusalem, Rehovot, Israel.), E. Megged (Hebrew Univ. of Jerusalem, Rehovot, Israel.), and T. Tajima Mar. 1995 39 p
(Contract DE-FG05-80ET-53088)
(DE95-009116; DOE/ET-53088/698; IFSR-698) Avail: CASI HC A03/MF A01

Two model problems are considered, illustrating the dynamics of quasihydrostatic flows of radiatively cooling, optically thin self-gravitating gas clouds. In the first problem, spherically symmetric flows in an unmagnetized plasma are considered. For a power-law dependence of the radiative loss function on the temperature, a one-parameter family of self-similar solutions is found. The authors concentrate on a constant-mass cloud, one of the cases, when the self-similarity indices are uniquely selected. In this case, the self-similar flow problem can be formally reduced to the classical Lane-Emden equation and therefore solved analytically. The cloud is shown to undergo radiative condensation, if the gas specific heat ratio (gamma) greater than 4/3. The condensation proceeds either gradually, or in the form of (quasihydrostatic) collapse. For (gamma) less than 4/3, the cloud is shown to expand. The second problem addresses a magnetized plasma slab that undergoes quasihydrostatic radiative cooling and condensation. The problem is solved analytically, employing the Lagrangian mass coordinate. DOE

N95-30751*# Pennsylvania State Univ., Erie, PA. Div. of Science.
A SEARCH FOR INTERSTELLAR CH3D: LIMITS TO THE METHANE ABUNDANCE IN ORION-KL
Maria Womack, L. M. Ziurys (Arizona State Univ., Tempe, AZ.), and A. J. Apponi (Arizona State Univ., Tempe, AZ.) 30 Jun. 1995 18 p Sponsored in part by the Margaret Cullinan Wray Charitable Lead Annuity Trust
(Grant NAGw-3065)
(NASA-CR-198932; NAS 1.26:198932) Avail: CASI HC A03/MF A01

A search has been performed for interstellar CH3D via its J(K) = 1(0) - 0(0) transition at 230 GHz and its J(K) = 2(0) - 1(0) and J(K) = 2(1) - 1(1) lines at 465 GHz using the NRAO 12 m and CSO 10 m telescopes towards Orion-KL. This search was done in conjunction with laboratory measurements of all three transitions of CH3D using mm/sub-mm direct absorption spectroscopy. The molecule was not detected down to a 3 sigma level of T(A) less than 0.05 K towards Orion, which suggests an upper limit to the CH3D column density of N less than 6 x 10(exp 18)/sq cm in the hot core region and a fractional abundance (with respect to H2) of less than 6 x 10(exp -6). These measurements suggest that the methane abundance in the Orion hot core is f less than 6 x 10-4, assuming D/H approximately 0.01. Such findings are in agreement with recent hot core chemical models, which suggest CH4/H2 approximately 10(exp -4). Author

N95-31102# Florida Univ., Gainesville, FL.
PARTONS AND BLACK HOLES
L. Susskind (Stanford Univ., CA.) and P. Griffin 1994 23 p Presented at the Theory of Hadrons and Light-front QCD Workshop, Polona Zgorzelisko, Poland, Aug. 1994
(Contract DE-FG05-86ER-40272)
(DE95-009921; DOE/ER-40272/209; UFIFT-HEP-9413; HEP-PH-9410306; CONF-9408188-2) Avail: CASI HC A03/MF A01

A light-front renormalization group analysis is applied to study matter which falls into massive black holes, and the related problem of matter with transplankian energies. One finds that the rate of matter spreading over the black hole's horizon unexpectedly saturates the causality bound. This is related to the transverse growth behavior of transplankian particles as their longitudinal momentum increases. This growth behavior suggests a natural mechanism to implement 't Hooft's scenario that the universe is an image of data stored on a 2 + 1 dimensional hologram-like projection. DOE

N95-31424*# Computer Sciences Corp., Calverton, MD.
VOYAGER GO PROGRAM Final Report
Myron Smith Mar. 1995 32 p
(NASA Order S-97229-E)
(NASA-CR-189435; NAS 1.26:189435; RHPU-0428) Avail: CASI HC A03/MF A01

This contract pertained to the investigation of the time variability of the ultraviolet continuum flux of three stars: lambda Eri, 53 Persei, and gamma Cas. The Voyager observations of 53 Persei were conducted simultaneously with a global ground-based campaign of visual-wavelength photometry. The optical campaign established beyond doubt the existence of two nonradial pulsation modes with periods near two days. The second part of the program concerned the ultraviolet continuum modulations of the B2E star lambda Eri. Voyager observations of lambda Eri showed that the ultraviolet light curve of lambda Eri shows no variations over a timescale of a day, but may show excursions on the order of an hour. There was little actual overlap between the Voyager and the IUE datasets in time so we could not determine whether the short-term variations from Voyager are instrumental or from the star. The third and final part of the program

concerned the ultraviolet continuum variations of the B0.53 star gamma Cas. The Voyager observations of gamma Cas show that 10-20% variations occur on a timescale of 1-2 hours and are commonplace.

Derived from text

N95-31819*# Computer Sciences Corp., Calverton, MD.
CEPHEID TEMPERATURE AND THE BLAZHKO EFFECT
Terry Teays Mar. 1995 52 p
(Contract NAS5-31845)
(NASA-CR-189433; NAS 1.26:189433; RHPU-0456) Avail: CASI HC A04/MF A01

Two separate research projects were covered under this contract. The first project was to study the temperatures of Cepheid variable stars, while the second was a study of the Blazhko effect in RR Larae, both of them using IUE data. They will be reported on separately, in what follows.

Author

N95-32269# California Univ., Berkeley, CA.
RESEARCH PROGRESS REPORT
1995 14 p
(Contract DE-FG05-90ER-40559)
(DE95-010726; DOE/ER-40559/T1) Avail: CASI HC A03/MF A01

A brief summary is given for the progress made by the 11 different researchers. The research covered is as follows: (1) phenomenological problems caused by moduli in string theory; (2) formulating nonperturbative critical string theory, constructing noncritical string theory in medium spacetime dimensions, and constructing the space of conformal boundary conditions for conformal field theory; (3) regularization of chiral gauge theories and random matrix model for localization and quantum chaos; (4) dynamics of four dimensional supersymmetric field theories; (5) four dimensional field theory with dynamic supersymmetry breaking, stringy inflation, and black hole entropy; (6) extension of Thermodynamic Bethe Ansatz in integrable quantum field theory; (7) nonperturbative dynamics of the supersymmetric gauge theories and post-inflation gravitino production; and (8) string theory and quantum chromodynamics. DOE

91 LUNAR AND PLANETARY EXPLORATION

Includes planetology; and manned and unmanned flights.
For spacecraft design or space stations see *18 Spacecraft Design, Testing and Performance.*

N95-30806# Liege Univ. (Belgium). Lab. de Physique Atmospherique et Planetaire.
HST-FOC OBSERVATIONS OF A REMARKABLE UV AURORAL EVENT ON JUPITER
J. C. Gerard, D. Grodent, R. Range (Institut d'Astrophysique, Paris, France.), J. H. Waite (Southwest Research Inst., San Antonio, TX.), G. R. Gladstone (Southwest Research Inst., San Antonio, TX.), V. Dols, F. Paresce (Space Telescope Science Inst., Baltimore, MD.), A. Storrs (Space Telescope Science Inst., Baltimore, MD.), G. Ballester (Michigan Univ., Ann Arbor, MI.), and L. BenJaffel (Institut d'Astrophysique, Paris, France.) et al Jun. 1994 22 p Original contains color illustrations
Avail: CASI HC A03/MF A01

Two sets of UV (ultraviolet) images of the Jovian north aurora were obtained with the Faint Object Camera (FOC) on Hubble. The first series shows a very intense discrete arc in corotation with the planet. The maximum apparent H2 emission rate corresponds to an electron precipitation of approximately 1/sq Wm, a very large flux in comparison with the solar EUV (extreme ultraviolet) heating. The hugh particle heating rate of the auroral upper atmosphere of Jupiter is expected to cause a large transient temperature increase and generate strong thermospheric winds. Twenty hours later, the discrete arc had considerably decreased in brightness. The timescale and magnitude of the change in the UV aurora strongly suggests that the discrete Jovian auroral precipitation is related to large scale current system variations as are the Earth's discrete aurorae.

Author

N95-30845*# Jet Propulsion Lab., California Inst. of Tech., Pasadena, CA.
MARS TOGETHER AND FIRE AND ICE: REPORT OF THE JOINT US/RUSSIAN TECHNICAL WORKING GROUPS
Oct. 1994 116 p Sponsored by Russian Space Agency; and Russian Academy of Sciences Original contains color illustrations
(Contract NAS7-1260)
(NASA-CR-198864; JPL-Publ-94-29; NAS 1.26:198864) Avail: CASI HC A06/MF A02; 1 functional color page

The Cold War's end opened an opportunity for greater cooperation in planetary exploration for the United States and Russia. Two study groups were formed, Mars Together and FIRE and ICE. The Mars Together team developed a concept for a flight in 1998 that merged one U.S. Mars Surveyor 98 mission with the former Russian Mars 96 mission to further understanding of the Mars surface and atmosphere. The FIRE and ICE team developed concepts for a dual-spacecraft mission to the solar corona and for a mission to Pluto. The missions, scientific potential, and open issues are described.

Author

N95-32222*# Jet Propulsion Lab., California Inst. of Tech., Pasadena, CA.
DETERMINATION OF THE POSITION OF JUPITER FROM RADIO METRIC TRACKING OF VOYAGER 1
W. M. Folkner and R. J. Haw *In its* The Telecommunications and Data Acquisition Report 15 May 1995 p 1-8 (For primary document see N95-32221 11-32)
Avail: CASI HC A02/MF A03

92 SOLAR PHYSICS

Includes solar activity, solar flares, solar radiation and sunspots.
For related information see *93 Space Radiation.*

N95-30467*# National Aeronautics and Space Administration. Marshall Space Flight Center, Huntsville, AL.
ON THE RELATIONSHIP BETWEEN SUNSPOTS NUMBER AND THE FLARE INDEX
Robert M. Wilson [1994] 12 p
(NASA-TM-110643; NAS 1.15:110643) Avail: CASI HC A03/MF A01

During the years 1976-1991, sunspot number and the Kleczek flare index have displayed a strong linear correlation ($r = 0.94$), one that can be described by the equation $y = -0.15 + 0.10\ x$, where x denotes annual sunspot number. While true, the temporal behaviors of the two parameters have differed, with sunspot number peaking first in 1979 and the flare index peaking much later in 1982 during cycle 21 and with more contemporaneous behavior in cycle 22 (both peaking in 1989, with a secondary peak in 1991). The difference appears to be directly attributable to the way in which the Kleczek flare index has been defined; namely, the annual flare index is the sum of the product of each flare's intensity (importance) times its duration (in minutes) divided by the total number of flares during the year. Because the number of 'major' flares (those of importance greater than or equal to 2) and flares of very long duration (duration greater than or equal to 100 min) both peaked after sunspot maximum (1982/81, respectively) in cycle 21, one should have expected the flare index to also peak (which it did). Likewise, because the number of major flares and flares of very long duration peaked simultaneously with sunspot number (1989) in cycle 22, one should have expected the flare index to also peak (which it did).

Author

N95-30482# Asian Office of Aerospace Research and Development, APO San Francisco, CA. Air Force Office of Scientific Research.
XV NSO/SAC PEAK SOLAR WORKSHOP
Y. Suematsu (National Astronomical Observatory, Tokyo, Japan.) 23 Sep. 1994 10 p Workshop held in Sunspot, NM, 19-23 Sep. 1994
(AD-A292319; AOARD-TR-94-35) Avail: CASI HC A02/MF A01

We present some results on studies of line profile fitting analysis of He I 1083-nm line spectra which were obtained with a 25-cm aperture coronagraph at the Norikura Solar Observatory.

DTIC

N95-30582*# National Aeronautics and Space Administration. Marshall Space Flight Center, Huntsville, AL.

ON REFLECTION OF ALFVEN WAVES IN THE SOLAR WIND

M. Krogulec (Alabama Univ., Huntsville, AL.), Z. E. Musielak (Alabama Univ., Huntsville, AL.), S. T. Suess, R. L. Moore, and S. F. Nerney [1993] 36 p Sponsored by Polish Academy of Sciences

(Grants NAGw-2933; NAG8-839; NSF INT-90-16514; NSF ATM-91-19580) (NASA-TM-110642; NAS 1.15:110642) Avail: CASI HC A03/MF A01

We have revisited the problem of propagation of toroidal and linear Alfven waves formulated by Heinemann and Olbert (1980) to compare WKB and non-WKB waves and their effects on the solar wind. They considered two solar wind models and showed that reflection is important for Alfven waves with periods of the order of one day and longer, and that non-WKB Alfven waves are no more effective in accelerating the solar wind than WKB waves. There are several recently published papers which seem to indicate that Alfven waves with periods of the order of several minutes should be treated as non-WKB waves and that these non-WKB waves exert a stronger acceleration force than WKB waves. The purpose of this paper is to study the origin of these discrepancies by performing parametric studies of the behavior of the waves under a variety of different conditions. In addition, we want to investigate two problems that have not been addressed by Heinemann and Olbert, namely, calculate the efficiency of Alfven wave reflection by using the reflection coefficient and identify the region of strongest wave reflection in different wind models. To achieve these goals, we investigated the influence of temperature, electron density distribution, wind velocity and magnetic field strength on the waves. The obtained results clearly demonstrate that Alfven wave reflection is strongly model dependent and that the strongest reflection can be expected in models with the base temperatures higher than 10(exp 6) K and with the base densities lower than 7 x 10(exp 7) cm(exp -3). In these models as well as in the models with lower temperatures and higher densities, Alfven waves with periods as short as several minutes have negligible reflection so that they can be treated as WKB waves; however, for Alfven waves with periods of the order of one hour or longer reflection is significant, requiring a non-WKB treatment. We also show that non-WKB, linear Alfven waves are always less effective in accelerating the plasma than WKB Alfven waves. Finally, it is evident from our results that the region of strongest wave reflection is usually located at the base of the models, and hence that interpretation of wave reflection based solely on the reflection coefficient can be misleading. Author

N95-30618# Louisiana State Univ., Baton Rouge, LA.

LOW ENERGY SOLAR NEUTRINO EXPERIMENTS: THE SOVIET AMERICAN GALLIUM EXPERIMENT (SAGE) Final Report, 12 Aug. 1988 - 31 Oct. 1994

1995 31 p

(Contract DE-FG05-88ER-40481)

(DE95-010159; DOE/ER-40481/T1) Avail: CASI HC A03/MF A01

Two Ga-71 experiments are currently in operation. The first is the 60 ton Soviet American Gallium Experiment (SAGE) at Baksan, which has recently reported a signal level of 73 +18/-16 (stat) +5/-7 (syst) solar neutrino units (SNU); the second is the 30 ton GALLEX experiment at Gran Sasso, which sees 87 +/-14 +/-7 SNU. Both results are consistent, and both suggest a neutrino flux level low compared to the total expected from standard solar model calculations. It is not possible, however, to make a case for flux levels lower than the p-p prediction. Assuming the experiments are correct, it is not at all clear yet whether the answer lies with the neutrino physics, solar physics, or a combination of both. Nevertheless, though solar model effects cannot be ruled out, if the Homestake and Kamiokande results are taken at face value, then these two experiments alone imply that neutrino oscillations or some similar particle physics result must be present to some degree. This report reviews the SAGE experiment and recent results. Nonradiochemical experiments are also discussed, with an emphasis on the Kamiokande water Cerenkov results. DOE

N95-30690# National Geophysical Data Center, Boulder, CO.

SOLAR-GEOPHYSICAL DATA NUMBER 604, DECEMBER 1994. PART 2: (COMPREHENSIVE REPORTS). DATA FOR JUNE 1994, AND MISCELLANEOUS

Helen E. Coffey Dec. 1994 32 p Repr. from Solar-Geophysical Data Comprehensive Reports (Boulder, CO), no. 604, pt. 2, Dec. 1994 See also Part 1, PB95-181848

(PB95-191995; SGD-604-Pt-2) Avail: CASI HC A03/MF A01

Solar geophysical data is intended to keep research workers informed on a timely schedule of the major events of solar activity and the associated interplanetary, ionospheric, radio propagation, and other geophysical effects. This report contains a detailed index for 1994 and comprehensive reports for June 1994 on: Solar Flares, Solar Radio Bursts at Fixed Frequencies; Solar X-ray Radiation from GOES Satellite, Active Prominences and Filaments. NTIS

N95-30785*# Hughes STX, Inc., Lanham, MD.

STUDYING THE THERMAL/NON-THERMAL CROSSOVER IN SOLAR FLARES Contractor Report, 1 Nov. 1993 - 1 Nov. 1994

R. A. Schwartz Dec. 1994 36 p

(Contract NAS5-32584)

(NASA-CR-189436; NAS 1.26:189436; IHK-341-03) Avail: CASI HC A03/MF A01

This report describes work performed under contract NAS5-32584 for Phase 3 of the Compton Gamma Ray Observatory (CGRO) from 1 November 1993 through 1 November 1994. We have made spectral observations of the hard x-ray and gamma-ray bremsstrahlung emissions from solar flares using the Burst and Transit Source Experiment (BASTE) on CGRO. These measurements of their spectrum and time profile provided valuable information on the fundamental flare processes of energy release, particle acceleration, and energy transport. Our scientific objective was to study both the thermal and non-thermal sources of solar flare hard x-ray and gamma-ray emission. Author (revised)

N95-30816# National Geophysical Data Center, Boulder, CO.

SOLAR-GEOPHYSICAL DATA NUMBER 606, FEBRUARY 1995. PART 1: (PROMPT REPORTS). DATA FOR DECEMBER 1994, JANUARY 1995, AND LATE DATA

Helen E. Coffey, ed. Feb. 1995 138 p

(ISSN 0038-0911)

(PB95-200853; SGD-606-Pt-1; LC-79-640375) Avail: CASI HC A07/MF A02

This report contains a detailed Index solar-geophysical data for 1994-1995. The data for January 1995 include: Solar-Terrestrial Environment; IUWDS Alert Periods (Advance and Worldwide); Solar Activity Indices; Solar Flares; Solar Radio Emission; Stanford Mean Solar Magnetic Field; and GOES-7 Daily Electron Fluence. While the data for December 1994 are on: Solar Active Regions; Sudden Ionospheric Disturbances; Solar Radio Spectral Observations; Solar Radioheliograph - 164 MHz - Nancay; Cosmic Ray Measurements by Neutron Monitor; Geomagnetic Indices; Principal Magnetic Storms; and Sudden Commencements/Solar Flare Effects. In addition, late data for January-December 1993 on Geomagnetic Indices and Sudden Commencements/Solar Flare effects are included. NTIS

N95-30817# National Geophysical Data Center, Boulder, CO.

SOLAR-GEOPHYSICAL DATA NUMBER 606, FEBRUARY 1995. PART 2: (COMPREHENSIVE REPORTS). DATA FOR AUGUST 1994, AND MISCELLANEOUS

Helen E. Coffey, ed. Feb. 1995 64 p

(ISSN 0038-0911)

(PB95-200861; SGD-606-Pt-2; LC-79-640375) Avail: CASI HC A04/MF A01

Detailed Index of solar-geophysical data for 1994-1995 are provided. Data for August 1994 include: Solar Flares; Solar Radio Bursts at Fixed Frequencies; Solar X-Ray Radiation from GOES Satellite; and Active Prominences and Filaments. Miscellaneous Data on Interplanetary Energetic Particles and Flux from SAMPEX Satellite (Descriptive Text, January-June 1993 -- Revised Plots, July-December 1993) are also included. NTIS

N95-31450# Stanford Univ., CA. Center for Space Science and Astrophysics.

ENVIRONMENTAL CONDITIONS RESPONSIBLE FOR SOLAR ACTIVITY Final Technical Report, 1 Oct. 1991 - 30 Sep. 1994

Peter A. Sturrock 28 Feb. 1995 18 p

(Contract F49620-92-J-0015)

(AD-A292859; AFOSR-95-0221TR) Avail: CASI HC A03/MF A01

Solar coronal activity is of concern to the Air Force primarily because

of the terrestrial effects of coronal mass ejections and solar flares. Coronal mass ejections can lead to geomagnetic disturbances that in turn cause magnetospheric substorms. This geomagnetic activity disturbs the ionosphere, especially in the polar regions, interfering with radio propagation. Ionizing radiation (UV and X-ray) and particle events from solar flares can also lead to ionospheric disturbances. Furthermore, major flares pose serious hazards to astronauts. During the past three years, the Stanford group has obtained significant theoretical insights into the driving mechanism of eruptive events in the solar corona. The question of what causes coronal eruptions inevitably leads to questions concerning the plasma conditions and magnetic field configurations in which eruptions occur. In particular, we have grappled with the long-standing issue of how the coronal plasma is maintained at a temperature of several million degrees, while the underlying surface of the sun that is visible in white light has a temperature of only a few thousand degrees. Our work over the past three years has taken us closer to the goal of being able to predict the imminent onset of solar flares and coronal mass ejections. DTIC

N95-32218*# Iowa Univ., Iowa City, IA. Dept. of Physics and Astronomy.
ANALYSIS OF PLASMA MEASUREMENTS FOR THE GEOTAIL MISSION Annual Performance Report, 1 Oct. 1994 - 30 Sep. 1995
Louis A. Frank 30 Sep. 1995 11 p
(Grant NAG5-2371)
(NASA-CR-199074; NAS 1.26:199074) Avail: CASI HC A03/MF A01

The first phase of the Geotail mission, an exploration of the distant magnetotail, was successfully concluded in October 1994. Geotail is currently engaged in a survey of plasmas at distances from Earth approximately 10 to 30 R(sub E). Throughout the mission the Comprehensive Plasma Instrumentation has functioned well with successful return of data. The analysis of the CPI measurements has resulted in a series of publications, and research efforts are ongoing. Research topics include interaction of the magnetotail with the fields and plasmas of the solar wind, steady-state magnetic reconnection in the distant magnetotail at a neutral line bounded by a pair of slow-mode magnetohydrodynamic shocks, development and evolution of plasmoids in magnetotail and magnetospheric substorms, and cold ion beams coexisting as distinct components in the presence of hot plasma-sheet plasmas. Derived from text

93 SPACE RADIATION

Includes cosmic radiation; and inner and outer earth's radiation belts.

For biological effects of radiation see *52 Aerospace Medicine*. For theory see *73 Nuclear and High-Energy Physics*.

N95-32282# Lawrence Livermore National Lab., Livermore, CA.
RADIATION EFFECTS IN SPACE: THE CLEMENTINE 1 MISSION
T. Gregory Guzik (Louisiana State Univ., Baton Rouge, LA.), Edmund Clayton (Louisiana State Univ., Baton Rouge, LA.), and John P. Wefel (Louisiana State Univ., Baton Rouge, LA.) 20 Dec. 1994 106 p
(Contract W-7405-eng-36)
(DE95-011513; UCRL-CR-119438) Avail: CASI HC A06/MF A02

The space radiation environment for the Clementine 1 mission was investigated using a new calculational model, CHIME, which includes the effects of galactic cosmic rays (GCR), anomalous component (AC) species and solar energetic particle (SEP) events and their variations as a function of time. Unlike most previous radiation environment models, CHIME is based upon physical theory and is 'calibrated' with energetic particle measurements made over the last two decades. Thus, CHIME provides an advance in the accuracy of estimating the interplanetary radiation environment. Using this model we have calculated particle energy spectra, fluences and linear energy transfer (LET) spectra for all three major components of the Clementine 1 mission during 1994: (1) the spacecraft in lunar orbit, (2) the spacecraft during asteroid flyby, and (3) the interstage adapter (ISA) in earth orbit. Our investigations indicate that during 1994 the level of solar modulation, which dominates the variation in the GCR and AC flux as a function of time, will be decreasing toward solar minimum levels. Consequently the GCR and AC flux will be increasing during the year and, potentially, will rise to levels seen during previous solar minimums. The estimated radiation environment also indicates that the AC will dominate the energetic particle spectra for energies below 30-50 MeV/nucleon, while the GCR have a peak flux at approximately 300 MeV/nucleon and maintain a relatively high flux level up to greater than 1000 MeV/nucleon. The AC significantly enhances the integrated flux for LET in the range 1 to 10 MeV/(mg/sq cm), but due to the steep energy spectra of the AC a relatively small amount of material (approximately 50 mils of Al) can effectively shield against this component. The GCR are seen to be highly penetrating and require massive amounts of shielding before there is any appreciable decrease in the LET flux. DOE

99 GENERAL

N95-30899# Air Force Office of Scientific Research, Bolling AFB, Washington, DC.
RESEARCH PROPOSAL Quarterly Status Report, Oct. - Dec. 1994
1994 67 p
(AD-A293207; AFOSR-95-0256TR) Avail: CASI HC A04/MF A01

This research proposal status report is published quarterly as of March, June, September and December of each year. It lists all the research proposals received by the Air Force Office of Scientific Research (AFOSR) in the six month period prior to the date of this report. Normally, decision and actions are made within six months after receving a research proposal. The action taken (i.e. initiated, declined, or withdraw) will be listed in this report. The report is divided into two parts: Part 1 is the institution index which lists the proposals received, alphabetically by institution. Part 2 is the AFOSR Directorate index in which the proposal received are listed alphabetically by directorate and alphabetically by AFOSR Program Manager within the directorate. The purpose of the quarterly report is to inform other government sponsoring agencies of the proposals received by the AFOSR and the action taken on these proposals. DTIC

N95-32279# Westinghouse Hanford Co., Richland, WA.
LABORATORY DIRECTED RESEARCH AND DEVELOPMENT REPORT Annual Report, FY 1994
Feb. 1995 284 p Prepared in cooperation with Pacific Northwest Lab., Richland, WA
(Contract DE-AC06-87RL-10930)
(DE95-011405; PNL-10458) Avail: CASI HC A13/MF A03

The Department of Energy Order DOE 5000.4A establishes DOE's policy and guidelines regarding Laboratory Directed Research and Development (LDRD) at its multiprogram laboratories. This report represents Pacific Northwest Laboratory's (PNL's) LDRD report for FY 1994. During FY 1994, 161 LDRD projects were selected for support through PNL's LDRD project selection process. Consistent with the Mission Statement and Strategic Plan provided in PNL's Institutional Plan, the LDRD investments are focused on developing new and innovative approaches in research related to our 'core competencies.' Currently, PNL's core competencies have been identified as integrated environmental research, process science and engineering, and energy systems development. Individual summaries of LDRD projects are organized according to these core competencies. The largest proportion of laboratory-level LDRD funds is allocated to the core competency of integrated environmental research. Projects within the three core competency areas were approximately 91.4 % of total LDRD project funding at PNL in FY 1994. A significant proportion of PNL's LDRD funds are also allocated to projects within the various research centers that are proposed by individual researchers or small research teams. The report provides an overview of PNL's LDRD program, the management process used for the program, and project summaries for each LDRD project. DOE

Typical Subject Index Listing

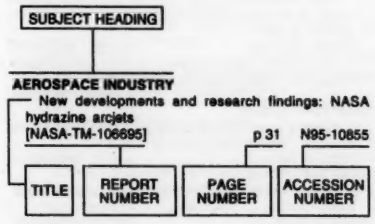

The subject heading is a key to the subject content of the document. Titles, report numbers, and accession numbers of pertinent documents are provided under each subject heading. When the title is insufficiently descriptive of the document content, a title extension is added, separated from the title by three hyphens. The report number helps to indicate the type of document cited (e.g., NASA report, NASA translation, NASA contractor report). The accession number is the number by which the document abstracts are arranged in this journal and by which the document is sold or requested. The page number helps you locate the citation in the abstract section. The titles, with title extensions if present, are arranged under each subject heading in ascending accession number order. The subject headings have been selected from the latest revision of the *NASA Thesaurus*.

A

A-10 AIRCRAFT
Improved altimeter settings for A-10 aircraft
[AD-A293142] p 2753 N95-30920

A-320 AIRCRAFT
Flying qualities of civil transport aircraft with electrical flight control p 2761 N95-32016

A-340 AIRCRAFT
Flying qualities of civil transport aircraft with electrical flight control p 2761 N95-32016

ABBREVIATIONS
Guidelines for creating and using abbreviations and acronyms
[NASA-CR-198884] p 3025 N95-31713

ABERRATION
Skew chromaticity in large accelerators
[DE95-011564] p 2994 N95-32243
Notes on lie algebraic analysis of achromats
[DE95-009524] p 3002 N95-32356

ABLATION
Morphology and microstructure of (111) crystalline CeO2 films grown on amorphous SiO2 substrates by pulsed-laser ablation
[DE95-008842] p 3009 N95-30542

ABLATIVE MATERIALS
Waterjet processes for coating removal
p 2777 N95-31779

ABRASIVES
Overview of paint removal methods
p 2843 N95-32166

ABSORBERS (EQUIPMENT)
Simultaneous heat and mass transfer in a horizontal tube absorber: Numerical tools for present and future absorber designs
[PB95-196978] p 2869 N95-30872

ABSORBERS (MATERIALS)
Energy absorption apparatus
[AD-D017361] p 2814 N95-30715
Extension of the pore tree model to describe pore interconnectivity
[AD-A290366] p 2793 N95-30971

ABSORPTION
Hydrogen absorption in iron and steel during gas tungsten arc welding
[PB95-197018] p 2804 N95-30776

ABSORPTION COOLING
Simultaneous heat and mass transfer in a horizontal tube absorber: Numerical tools for present and future absorber designs
[PB95-196978] p 2869 N95-30872

ABSORPTION CROSS SECTIONS
Chemical kinetics and photochemical data for use in stratospheric modeling: Evaluation number 11
[NASA-CR-198863] p 2912 N95-30525
Ionization of He by highly charged ions at low velocity
[DE95-010815] p 2990 N95-32273

ABSORPTION SPECTRA
Theoretical absorption spectroscopy of high-temperature metal vapors: Model and experiment compared
[AD-A290872] p 2791 N95-30409
A search for interstellar CH3D: Limits to the methane abundance in Orion-KL
[NASA-CR-198932] p 3029 N95-30751
Measurement of temperatures and OH concentrations of solid propellant flames using absorption spectroscopy
p 2801 N95-31302
Improvements in infrared absorption of solid propellant flames p 2801 N95-31306
Electronic structure of Donor-Spacer-Acceptor molecules of potential interest for molecular electronics III: Geometry and absorption spectrum of CH3-Alpha P3CNQ
[AD-A293662] p 2985 N95-31609
Absorption and ionization spectra of model rubredoxins
[AD-A293668] p 2796 N95-31691
Electronic structure of Donor-Spacer-Acceptor molecules of potential interest for molecular electronics 4. Geometry and device properties of P3CNQ and Q3CNQ
[AD-A293717] p 2986 N95-31832
Investigation of the basic physics of high efficiency semiconductor hot carrier solar cell
[NASA-CR-198945] p 2906 N95-32212

ABSORPTION SPECTROSCOPY
Theoretical absorption spectroscopy of high-temperature metal vapors: Model and experiment compared
[AD-A290872] p 2791 N95-30409
Smart active multiwave sensing with zero background amplitude modulated probes
[DE95-008813] p 2792 N95-30714
Measurement of temperatures and OH concentrations of solid propellant flames using absorption spectroscopy
p 2801 N95-31302
Species and temperature profiles of propellant flames obtained from FTIR absorption spectroscopy
p 2801 N95-31303
Calculated structures and electronic absorption spectroscopy for magnesium phthalocyanine and its anion radical
[AD-A293672] p 2796 N95-31596
GCMS and FTIR studies of by-product inhibited growth and the rate-limiting step in TEOS-based SiO2 CVD
[DE95-009863] p 3016 N95-32147

ABSTRACTS
Proceedings of the high energy density matter (HEDM) contractor's conference
[AD-A292988] p 2836 N95-31470

ABUNDANCE
Chromospherically active stars. 6: Giants with compact hot companions and the barium star scenario
[NASA-TM-110641] p 3028 N95-30466
A search for interstellar CH3D: Limits to the methane abundance in Orion-KL
[NASA-CR-198932] p 3029 N95-30751
Oxygen charge state abundance in the inner magnetosphere
[AD-A293497] p 2915 N95-31536

ACCELERATION
Spectral methods and sum acceleration algorithms
[DE95-009689] p 2941 N95-31630

ACCELERATION (PHYSICS)
Generation of earthquake signals
[PB95-211223] p 2913 N95-30631
Orbiter rarefied-flow reentry measurements from the OARE on STS-62
[NASA-TM-110182] p 2891 N95-30783

ACCELERATORS
The Los Alamos accelerator code group
[DE95-010989] p 2992 N95-31151
Physics goals of a mu(+) mu(-) collider
[DE95-009546] p 2994 N95-32059
Monte Carlo simulations of muon production
[DE95-009554] p 2988 N95-32063

ACCELEROMETERS
Micromachined sensor and actuator research at the Microelectronics Development Laboratory
[DE95-008540] p 2878 N95-30384
Results from tests of the Honeywell integrated flight management unit
[PB95-211355] p 2748 N95-30597
Fiber optic accelerometer with centrally supported flexural disk
[AD-D017369] p 2879 N95-30858
Orbiter rarefied-flow reentry measurements from the OARE on STS-62
[NASA-TM-110182] p 2891 N95-30783
A novel instrumentation system for measurement of helicopter rotor motions and loads data, phase 1
[AD-A293309] p 2751 N95-30923

ACCEPTABILITY
Evaluation of alternative pavement marking materials
[AD-A292973] p 2763 N95-31468

ACCEPTOR MATERIALS
Photophysical properties of opto-electric molecules studied by time-resolved microwave conductivity
[PB95-196994] p 2980 N95-30774
Noisy-network acceptors
[PB95-197976] p 2951 N95-30813

ACCESS CONTROL
UNIX and PC security in a network environment. UNINETT
[PB95-196291] p 2934 N95-30662
UNIX and PC security in a network environment. LOKALNETT 1993
[PB95-196309] p 2934 N95-30697
Effective bandwidth techniques in bufferless and buffered ATM multiplexers
[PB95-207072] p 2862 N95-31185

ACCIDENT PREVENTION
Metascientific problems in safety science
[PB95-196408] p 2838 N95-30521
SCARLET: DLR rate saturation flight experiment
p 2746 N95-31068

ACCUMULATORS
A study of Damascus steel
[DE95-010127] p 2809 N95-32023

ACCURACY
Flight test evaluation of the Stanford University/United Airlines differential GPS Category 3 automatic landing system
[NASA-TM-110354] p 2743 N95-30788
Improved altimeter settings for A-10 aircraft
[AD-A293142] p 2753 N95-30920

ACETYLENE
Development of a new instrument for rocket engine combustion diagnostics p 2799 N95-31211

ACHIEVEMENT
Selection of Swedish scholastic aptitude test takers as a function of socioeconomic background and ability: Evaluation through follow-up
[PB95-212072] p 3021 N95-30699

ACID RAIN
Atmospheric environmental implications of propulsion systems p 2771 N95-31747

ACIDITY
Acidity and basicity of nitro substituted imidazoles
p 2832 N95-31301
Acidity and basicidity of nitro substituted imidazoles
[AD-A293969] p 2836 N95-31526

ACOUSTIC ATTENUATION
Gear pump with reduced fluid-borne noise
[AD-D017362] p 2887 N95-30399
Advanced signal processing filter
[AD-D017324] p 2848 N95-30917
Materials for adaptive structural acoustic control, volume 1
[AD-A293444] p 2788 N95-31369
Materials for adaptive structural acoustic control, volume 2
[AD-A293445] p 2788 N95-31370
Materials for adaptive structural acoustic control, volume 3
[AD-A293446] p 2788 N95-31371
Materials for adaptive structural acoustic control, volume 4
[AD-A293447] p 2788 N95-31372
ACOUSTIC COUPLING
Energy flow analysis of coupled structures
p 2895 N95-31316
ACOUSTIC DUCTS
Robust fixed-structure control
[AD-A292883] p 2952 N95-30961
ACOUSTIC EMISSION
Apparatus for producing images acoustically
[AD-D017365] p 2973 N95-30530
ACOUSTIC EXCITATION
Control of high Reynolds number round jets
p 2876 N95-31733
Combustion response to acoustic perturbation in liquid rocket engines p 2770 N95-31972
ACOUSTIC FREQUENCIES
Ultrasonic frequency selection for aqueous fine cleaning p 2779 N95-31788
ACOUSTIC MEASUREMENT
Method for extracting forward acoustic wave components from rotating microphone measurements in the inlets of turbofan engines
[NASA-CR-195457] p 2755 N95-30779
The TEVA experiment cruise report
[AD-A293025] p 2923 N95-31701
ACOUSTIC PROPAGATION
User's manual for the Scanning Fast Field Program (SCAFFIP) EOSAEL version 1.0
[AD-A291445] p 2933 N95-30397
ACOUSTIC PROPERTIES
Sea ice stress research
[AD-A293164] p 2923 N95-30964
Rationale and summary of methods for determining ultrasonic properties of materials at Lawrence Livermore National Laboratory
[DE95-009475] p 2795 N95-31593
ACOUSTIC SCATTERING
Sonic apparatus for degassing liquids
[AD-D017352] p 2791 N95-30554
Calculations of the sound scattering from fluid-filled spherical shell sonar targets
[DSTO-RR-0020] p 2974 N95-31365
Multiple scatter theory of ocean sediments
[AD-A293951] p 2923 N95-31523
The effects of large and small scale turbulence on sound propagation in the atmosphere
[AD-A293657] p 2975 N95-31608
ACOUSTIC VELOCITY
User's manual for the Scanning Fast Field Program (SCAFFIP) EOSAEL version 1.0
[AD-A291445] p 2933 N95-30397
The effects of large and small scale turbulence on sound propagation in the atmosphere
[AD-A293657] p 2975 N95-31608
The effect of ray curvature on Lloyd's mirror fringe estimates and source localisation
[DSTO-TR-0064] p 3001 N95-31745
ACOUSTICS
Far field acoustic radiation reduction
[AD-D017452] p 2974 N95-30725
The effects of large and small scale turbulence on sound propagation in the atmosphere
[AD-A293657] p 2975 N95-31608
Combustion response to acoustic perturbation in liquid rocket engines p 2770 N95-31972
The contextual variance of devoiced fricatives in polish
[IFTR-7/1995] p 2854 N95-32192
ACOUSTO-OPTICS
Phase object display by using acousto-optical Bragg diffraction
[AD-A293153] p 2998 N95-31006
Temporal feature extraction in photorefractive resonators
[AD-A292906] p 2881 N95-31365
Acousto-optical frequency shifters in dual-core optical fibres
[AD-A293979] p 2999 N95-31529
ACRYLATES
Epoxy and acrylate stereolithography resins: In-situ measurements of cure shrinkage and stress relaxation
[DE95-008506] p 2811 N95-30389
Intelligent synthetic polymers
[AD-A292905] p 2819 N95-31395
ACRYLIC ACID
Responsive copolymers for enhanced petroleum recovery
[DE95-011857] p 2823 N95-32361
ACRYLIC RESINS
Experiments in a 120-mm ram accelerator including flow visualization p 2799 N95-31202
Intelligent synthetic polymers
[AD-A292905] p 2819 N95-31395
Compatibility of Single Hydraulic Fluid with military specification fluids, seals and metallurgy
[AD-A292954] p 2821 N95-31663
Operational parameters and material effects
p 2845 N95-32179
Responsive copolymers for enhanced petroleum recovery
[DE95-011857] p 2823 N95-32361
ACTINIDE SERIES
Faster, cheaper radioanalytical methods
[DE95-009913] p 2797 N95-32061
ACTIVATION
Glass matrix doped with activated luminescent nanocrystalline particles
[AD-D017416] p 2816 N95-31010
ACTIVE CONTROL
Microwave repeater with broadband active and/or passive isolation control
[AD-D017358] p 2846 N95-30417
Design of systems for active sound control
[PB95-197869] p 2973 N95-30461
Active turbulence control using microelectrodes, permanent magnets in microgrooves
[AD-D017351] p 2867 N95-30553
Flight Vehicle Integration Panel Workshop on Pilot Induced Oscillations
[AGARD-AR-335] p 2745 N95-31061
Enhanced energy release and soot reduction in actively controlled flames p 2799 N95-31200
Active control of combustion instability using injection techniques p 2800 N95-31288
Investigating the use of smart acoustically active surfaces for flow separation control in turbomachinery
[AD-A292819] p 2874 N95-31443
Active control technology: Applications and lessons learned
[AGARD-CP-560] p 2757 N95-31989
The role of handling qualities specifications in flight control system design p 2757 N95-31990
The importance of flying qualities design specifications for active control systems p 2757 N95-31992
Experiences with ADS-33 helicopter specification testing and contributions to refinement research
p 2757 N95-31993
Model following control for tailoring handling qualities: ACT experience with ATTHeS p 2758 N95-32000
Structural aspects of active control technology
p 2760 N95-32006
Flight test results of the F-16 aircraft modified with axisymmetric vectoring exhaust nozzle
p 2752 N95-32007
Experimental Aircraft Programme (EAP): Flight control system design and test p 2760 N95-32010
Pilot Induced Oscillation: A report on the AGARD Workshop on PIO p 2761 N95-32017
Vibration control of spacecrafts and space structures from lift-off to on-orbit environments
p 2767 N95-32110
Vibration reduction in helicopter rotors using an actively controlled partial span trailing edge flap located on the blade p 2762 N95-32111
ACTUATORS
Micromachined sensor and actuator research at the Microelectronics Development Laboratory
[DE95-008540] p 2878 N95-30384
New adaptive methods for reconfigurable flight control systems, appendix 1
[AD-A292711] p 2756 N95-30937
Materials for adaptive structural acoustic control, volume 3
[AD-A293446] p 2788 N95-31371
Investigating the use of smart acoustically active surfaces for flow separation control in turbomachinery
[AD-A292819] p 2874 N95-31443
ADA (PROGRAMMING LANGUAGE)
Penelope reference manual: Version 3-3 (C001). Includes Larch/Ada specification manual for sequential Ada (C002)
[AD-A289828] p 2942 N95-31683
ADAPTIVE CONTROL
High-tech controls for energy and environment
[DE95-011702] p 2952 N95-31255
Materials for adaptive structural acoustic control, volume 1
[AD-A293444] p 2788 N95-31369
Materials for adaptive structural acoustic control, volume 2
[AD-A293445] p 2788 N95-31370
Materials for adaptive structural acoustic control, volume 3
[AD-A293446] p 2788 N95-31371
Materials for adaptive structural acoustic control, volume 4
[AD-A293447] p 2788 N95-31372
Flight assessment of the onboard propulsion system model for the Performance Seeking Control algorithm on an F-15 aircraft
[NASA-TM-4705] p 2756 N95-31425
An efficient implementation of Forward-Backward Least-Mean-Square Adaptive Line Enhancers
p 2855 N95-32224
ADAPTIVE FILTERS
Adaptive space-time processing for airborne radars based on Doppler pre-processing
[PB95-205464] p 2854 N95-32114
ADAPTIVE OPTICS
Adaptive optics design for the advanced electro-optical system (AEOS)
[AD-A293972] p 2974 N95-31527
ADDITIVES
Diamond thin film temperature and heat-flux sensors
[NASA-CR-198859] p 3012 N95-30847
Environmentally safe aviation fuels
p 2775 N95-31768
Silicon carbide-silicon heterostructure solar cells
p 2905 N95-31952
A stochastic EM estimator in the presence of missing data: Theory and applications
[DE95-010329] p 2944 N95-32089
ADDUCTS
Studies of C(60) and C(70) and other fullurenes: Synthesis, derivation, electrochemistry, lubricant properties and new composition materials
[AD-A292726] p 3012 N95-30944
ADHESION TESTS
Verification of surface preparation for adhesive bonding p 2782 N95-31807
ADHESIVE BONDING
Influence of adhesives and bonding techniques on the properties of glued timber-steelplate joints
[PB95-211470] p 2813 N95-30599
Implementation of environmentally compliant cleaning and insulation bonding for MNASA p 2780 N95-31796
Cleanliness inspection tool for RSRM bond surfaces
p 2781 N95-31799
Verification of surface preparation for adhesive bonding p 2782 N95-31807
ADSORBENTS
Extension of the pore tree model to describe pore interconnectivity
[AD-A290366] p 2793 N95-30971
The Wide Field/Planetary Camera 2 (WFPC-2) molecular adsorber
[NASA-CR-198866] p 2881 N95-31456
ADSORPTION
Applications of SXPS for studying surface structure, reaction mechanisms and kinetics
[DE95-008903] p 2803 N95-30547
Consequences of kinetic dispersion on the electrochemistry of an adsorbed redox-active monolayer
[AD-A292794] p 2795 N95-31437
Study of the surface properties of ceramic materials by chromatography
[DE95-011578] p 2823 N95-32298
Energetics of Pt adsorption on Pt(111)
[DE95-010933] p 3017 N95-32307
ADVANCED SOLID ROCKET MOTOR (STS)
Shuttle Redesigned Solid Rocket Motor aluminum oxide investigations p 2770 N95-31197
ADVANCED VERY HIGH RESOLUTION RADIOMETER
Shiptracks in the Californian stratus region: Dependency on marine atmospheric boundary layer depth
[AD-A293272] p 2901 N95-31125
ADVECTION
Calculation of a residual mean meridional circulation for a zonal-mean tracer transport model
[DE95-009474] p 2911 N95-32350
AERIAL PHOTOGRAPHY
Optical feature recognition
[AD-A293168] p 2997 N95-30966
AEROACOUSTICS
Method for extracting forward acoustic wave components from rotating microphone measurements in the inlets of turbofan engines
[NASA-CR-195457] p 2755 N95-30779

AEROBES
Degradation of TCE using sequential anaerobic biofilm and aerobic immobilized bed reactor
p 2780 N95-31791
AERODYNAMIC CHARACTERISTICS
Transonic aerodynamic characteristics of a proposed wing-body reusable launch vehicle concept
[NASA-TM-108489] p 2742 N95-30712
Hypervelocity wind tunnel number 9, high Mach number development program
[AD-A289934] p 2743 N95-30929
Unified criteria for ACT aircraft longitudinal dynamics
p 2745 N95-31065
Effects of cavity bleed and its configuration on aerodynamic characteristics of supersonic internal flow
[NAL-TR-1247] p 2744 N95-31715
AERODYNAMIC COEFFICIENTS
Static behaviour of axially loaded uniplanar and multiplanar tubular x-joints
[PB95-207866] p 2892 N95-30585
Side force acting on blunted circular cylinder bodies at high angles of attack in supersonic flow
[NAL-TR-1255] p 2744 N95-31741
AERODYNAMIC CONFIGURATIONS
A general inverse design procedure for aerodynamic bodies p 2750 N95-30497
Numerical investigation into vortical flow about a delta-wing configuration up to incidences at which vortex breakdown occurs in experiment
[PB95-198024] p 2743 N95-30837
Application of multigrid computational fluid dynamics (CFD) methods to rotor analysis
[AD-A293012] p 2874 N95-31475
Afterbody/nozzle pressure distributions of a twin-tail twin-engine fighter with axisymmetric nozzles at Mach numbers from 0.6 to 1.2
[NASA-TP-3509] p 2744 N95-31984
AERODYNAMIC DRAG
Static behaviour of axially loaded uniplanar and multiplanar tubular x-joints
[PB95-207866] p 2892 N95-30585
AERODYNAMIC FORCES
Transonic aerodynamic characteristics of a proposed wing-body reusable launch vehicle concept
[NASA-TM-108489] p 2742 N95-30712
Side force acting on blunted circular cylinder bodies at high angles of attack in supersonic flow
[NAL-TR-1255] p 2744 N95-31741
Advanced gust management systems: Lessons learned and perspectives p 2759 N95-32002
AERODYNAMIC HEAT TRANSFER
Advanced k-epsilon modeling of heat transfer
[NASA-CR-4679] p 2874 N95-31423
AERODYNAMIC INTERFERENCE
Unsteady flow simulations about moving boundary configurations using dynamic domain decomposition techniques p 2877 N95-31837
AERODYNAMIC LOADS
A novel instrumentation system for measurement of helicopter rotor motions and loads data, phase 1
[AD-A293309] p 2751 N95-30923
Probabilistic reliability modeling of fatigue on the H-46 tie bar
[AD-A289926] p 2751 N95-30927
Digital simulation of wind velocities for wind turbine rotors: General considerations
[PB95-206447] p 2904 N95-31157
AERODYNAMIC STABILITY
Transonic aerodynamic characteristics of a proposed wing-body reusable launch vehicle concept
[NASA-TM-108489] p 2742 N95-30712
Looking for the simple PIO model
p 2745 N95-31066
FPCAS3D User's guide: A three dimensional full potential aeroelastic program, version 1
[NASA-CR-198367] p 2899 N95-32205
AERODYNAMIC STALLING
Validation of the helicopter rotor code HERO
[PB95-198040] p 2751 N95-30838
Vorticity dynamics and control of dynamic stall
[AD-A286658] p 2756 N95-31400
X-31: A program overview and flight test status
p 2753 N95-32013
Control of unsteady separated flow associated with the dynamic stall of airfoils
[NASA-CR-198972] p 2744 N95-32193
AEROELASTICITY
Aeroelastic pilot-in-the-loop oscillations
p 2746 N95-31070
Performance improvement of composite wings through aeroelastic tailoring and modern control
[AD-A293689] p 2752 N95-31602
Vibration reduction in helicopter rotors using an actively controlled partial span trailing edge flap located on the blade p 2762 N95-32111
FPCAS3D User's guide: A three dimensional full potential aeroelastic program, version 1
[NASA-CR-198367] p 2899 N95-32205
AEROEMBOLISM
Arterial gas bubbles after decompression in pigs with Patent Foramen Ovale
[PB95-195319] p 2925 N95-30515
AERONAUTICS
Aeronautics and space report of the President
[NASA-TM-110743] p 3028 N95-31979
AEROSOLS
Aerosol measurements over the Pacific Ocean in support of the IR aerosol backscatter program
[NASA-CR-198925] p 2918 N95-30782
Cloud condensation nuclei measurements in shiptrails
[AD-A293302] p 2919 N95-30951
AEROSPACE ENGINEERING
Design of fibre reinforced composite panels for aerospace applications
[PB95-197851] p 2784 N95-30460
Effects of thermal and electrical stressing on the breakdown behavior of space wiring
[NASA-CR-198360] p 2768 N95-30860
Flight Vehicle Integration Panel Workshop on Pilot Induced Oscillations
[AGARD-AR-335] p 2745 N95-31061
Advanced small rocket chambers. Option 3: 110 lbf Ir-Re rocket, volume 1
[NASA-CR-195435-VOL-1] p 2768 N95-31169
AEROSPACE ENVIRONMENTS
Operating in the space plasma environment: A spacecraft charging study of the Solar X-ray Imager
[NASA-TM-110644] p 3003 N95-30468
Aerospace Environmental Technology Conference
[NASA-CP-3298] p 2771 N95-31746
Radiation effects in space: The Clementine 1 mission
[DE95-011513] p 3032 N95-32282
SVN 9 End-Of-Life testing p 2767 N95-32345
AEROSPACE INDUSTRY
Aerospace Environmental Technology Conference: Exectutive summary
[NASA-CP-3297] p 2771 N95-31350
AEROSPACE MEDICINE
Electromyostimulation, circuits and monitoring
[NASA-TM-110741] p 2926 N95-30846
Psychological pilot selection in the US Air Force, the Luftwaffe, and the German Aerospace Research Establishment
[AD-A293779] p 2928 N95-31376
AEROSPACE SAFETY
GPHS-RTGs in support of the Cassini RTG Program
[DE95-010306] p 2768 N95-30674
AEROSPACE SCIENCES
Space Sciences Laboratory Publications and Presentations
[NASA-TM-108484] p 3024 N95-30780
Aeronautics and space report of the President
[NASA-TM-110743] p 3028 N95-31979
AEROSPACE SYSTEMS
A manual for pyrotechnic design, development and qualification
[NASA-TM-110172] p 2766 N95-31358
Computational methods for control and optimal design of aerospace systems
[AD-A292861] p 2751 N95-31451
Space systems environmental interaction studies
[AD-A293826] p 2766 N95-31553
The Telecommunications and Data Acquisition Report
[NASA-CR-198911] p 2854 N95-32221
AEROSPACE VEHICLES
Solid Modeling Aerospace Research Tool (SMART) user's guide, version 2.0
[NASA-TM-4431] p 2940 N95-31420
Preventing cracking of anodized coatings
[NASA-TM-104622] p 2839 N95-31690
Environmentally regulated aerospace coatings
p 2777 N95-31775
AFRICA
Equatorial Africa: A climatological study
[AD-A293956] p 2920 N95-31524
AFTERBODIES
Validation of the NPARC code for nozzle afterbody flows at transonic speeds
[NASA-TM-106971] p 2742 N95-30704
Afterbody/nozzle pressure distributions of a twin-tail twin-engine fighter with axisymmetric nozzles at Mach numbers from 0.6 to 1.2
[NASA-TP-3509] p 2744 N95-31984
AGGLOMERATION
Oscillatory combustion of aluminized AP/HTPB propellants p 2800 N95-31286
AGGREGATES
Confederation Verification, Validation, and Accreditation Master Plan (CVVAMP). Technical test plan
[AD-A289717] p 2936 N95-31050
AGING (MATERIALS)
Ageing control no. 3 of propellants for rocket motors RB 27 and RB 28
[PB95-210357] p 2825 N95-30626
Evaluation on materials performance of Hastelloy Alloy XR for HTTR uses. 4: Tensile properties of base metals and welded joints
[DE95-721871] p 2804 N95-30761
NaK pool-boiler solar receiver durability bench test. Volume 2: Metallurgical analysis
[DE95-010338] p 2905 N95-31640
AGING (METALLURGY)
Interface degradation in CAS/Nicalon during elevated temperature aging
[DE95-008843] p 2812 N95-30543
The influence of matrix microstructure and temperature on cyclic deformation and fatigue of particle-reinforced 2219 aluminum p 2808 N95-31974
AGRICULTURE
Biomass production by fescue and switchgrass alone and in mixed swards with legumes
[DE95-009137] p 2909 N95-31612
AIR
Differences in creep performance of a HIPed silicon nitride in ambient air and inert environments
[DE95-009172] p 2796 N95-31633
AIR BREATHING ENGINES
The 31st JANNAF Combustion Subcommittee Meeting, volume 1 p 2825 N95-31194
AIR CONDITIONING EQUIPMENT
Compatibility of refrigerants and lubricants with motor materials under retrofit conditions
[DE95-010185] p 2814 N95-30767
Simultaneous heat and mass transfer in a horizontal tube absorber: Numerical tools for present and future absorber designs
[PB95-196978] p 2869 N95-30872
AIR COOLING
10 kW heat pipe-heat sink development
[AD-A293167] p 2870 N95-30965
AIR DEFENSE
Guidance and Control for Future Air-Defence Systems
[AGARD-CP-555] p 2839 N95-32123
Study of Extended Air Defence Post 2000
p 2839 N95-32124
SOSIE: A pragmatic approach to the simulation of Broad Air Defense applied to the theater level
p 2840 N95-32127
Electronic combat and lethal defense suppression
p 2842 N95-32140
AIR DUCTS
An investigation of the side-dump dual in-line ramjet combustor p 2756 N95-31199
AIR FLOW
An experimental study of planar heterogeneous supersonic confined jets
[AD-A290859] p 2867 N95-30557
10 kW heat pipe-heat sink development
[AD-A293167] p 2870 N95-30965
Enhanced energy release and soot reduction in actively controlled flames p 2799 N95-31200
On the interactions between particles and turbulence in a fully-developed channel flow in air
p 2875 N95-31707
AIR INTAKES
A pulsed liquid fuel ramjet p 2756 N95-31201
AIR JETS
A pulsed liquid fuel ramjet p 2756 N95-31201
Control of high Reynolds number round jets
p 2876 N95-31733
Cleaning verification by air/water impingement
p 2782 N95-31805
AIR LAND INTERACTIONS
A numerical study of the effect of the Gulf Stream and the Appalachian Mountains on Carolina coastal frontogenesis
[AD-A293765] p 2921 N95-31577
Simulation of katabatic flow and mountain waves
[DE95-010863] p 2911 N95-32276
AIR POLLUTION
Overview of IEA biomass combustion activities
[PB95-196374] p 2902 N95-30519
Demonstration of split-flow ventilation and recirculation as flow-reduction methods in an Air Force paint spray booth, volume 2
[AD-A286808] p 2762 N95-30926
Cloud condensation nuclei measurements in shiptrails
[AD-A293302] p 2919 N95-30951
Demonstration of split-flow ventilation and recirculation as flow-reduction methods in an Air Force paint spray booth, volume 1
[AD-A286807] p 2763 N95-31101
Environmental projects. Volume 16: Waste minimization assessment
[NASA-CR-198861] p 2909 N95-31651

Particulate air pollution and increased mortality: Biological plausibility for causal relationship
[DE95-006161] p 2909 N95-31703
Air pollution control system research: An iterative approach to developing affordable systems
p 2773 N95-31759
Combatting urban air pollution through Natural Gas Vehicle (NGV) analysis, testing, and demonstration
[DE95-008300] p 2911 N95-32156
No-thermal plasma processing of VOCs and NO(x) at LLNL
[DE95-011445] p 2911 N95-32281
Calculation of a residual mean meridional circulation for a zonal-mean tracer transport model
[DE95-009474] p 2911 N95-32350

AIR QUALITY
Producing usable fuel from municipal solid waste
[DE95-008405] p 2902 N95-30375
Combatting urban air pollution through Natural Gas Vehicle (NGV) analysis, testing, and demonstration
[DE95-008300] p 2911 N95-32156
Compatibility of manufacturing process fluids with HFC refrigerants and ester lubricants
[DE95-012152] p 2911 N95-32364

AIR SAMPLING
Aerosol measurements over the Pacific Ocean in support of the IR aerosol backscatter program
[NASA-CR-198925] p 2918 N95-30782
Novel mass spectrometric instrument for gaseous and particulate characterization and monitoring
[DE95-000047] p 2881 N95-31694

AIR SEA ICE INTERACTIONS
The role of the hydrological cycle and the ocean's thermohaline circulation in climate change: A multicomponent climate model study
p 2909 N95-31720

AIR TRAFFIC
A NASPAC-Based analysis of the delay and cost effects of the western-pacific region preliminary resectorization effort of 1993
[AD-A288696] p 2748 N95-31013
Effects of civil tiltrotor service in the northeast corridor on en route airspace loads
[AD-A293586] p 2747 N95-31687
Integration of air traffic databases: A case study
[AD-A293691] p 2749 N95-32022

AIR TRAFFIC CONTROL
Human factors at the FAA Technical Center: Bibliography
[AD-A288638] p 2930 N95-31399
Emerging applications in probability (Sensor management)
[AD-A292781] p 2749 N95-31433
Initial evaluation of the Oregon State University planetary boundary layer column model for ITWS applications
[AD-A293775] p 2920 N95-31465
Integrated terminal weather system (ITWS) demonstration and validation operational test and evaluation
[AD-A293932] p 2749 N95-31521
The ATC operational evaluation of the prototype integrated terminal weather system (ITWS) at Dallas/Fort Worth and Orlando airports (May-September 1993)
[AD-A293808] p 2921 N95-31587
FAA aviation forecasts: Fiscal year 1995-2006
[AD-A293682] p 2741 N95-31598
Controller resource management: What can we learn from aircrews?
[DOT/FAA/AM-95/21] p 2750 N95-32186
Fact sheet for Congressional Committees. Air traffic control: Status of FAA's modernization program
[GAO/RCED-94-167FS] p 2750 N95-32197
Report to the Chairman, Subcommittee on Transportation and Related Agencies, Committee on Appropriations, House of Representatives. Air traffic control: Status of FAA's plans to close and contract out low-activity towers
[GAO/RCED-94-265] p 2750 N95-32199

AIR TRAFFIC CONTROLLERS (PERSONNEL)
Forward rapid rotation shiftwork in USAF air traffic controllers: Sleep, activity, fatigue and mood analyses
[AD-A293448] p 2927 N95-31373
The ATC operational evaluation of the prototype integrated terminal weather system (ITWS) at Dallas/Fort Worth and Orlando airports (May-September 1993)
[AD-A293808] p 2921 N95-31587
Controller resource management: What can we learn from aircrews?
[DOT/FAA/AM-95/21] p 2750 N95-32186

AIR TRANSPORTATION
Aviation capacity enhancement plan 1994
[AD-A292758] p 2747 N95-31428
Patient/aircraft forecasting for the strategic aeromedical evacuation lift-bed process
[AD-A293902] p 2747 N95-31512
Effects of civil tiltrotor service in the northeast corridor on en route airspace loads
[AD-A293586] p 2747 N95-31687
Special investigation report: Safety of the air tour industry in the United States
[PB95-917004] p 2748 N95-32185

AIR WATER INTERACTIONS
NASA Tropical Rainfall Measurement Mission (TRMM): Effects of tropical rainfall on upper ocean dynamics, air-sea coupling and hydrologic cycle
[NASA-CR-189437] p 2919 N95-31123
Shiptracks in the Californian stratus region: Dependency on marine atmospheric boundary layer depth
[AD-A293272] p 2901 N95-31125
Investigation of microwave backscatter from the air-sea interface
[NASA-CR-198854] p 2851 N95-31457
A numerical study of the effect of the Gulf Stream and the Appalachian Mountains on Carolina coastal frontogenesis
[AD-A293765] p 2921 N95-31577
The role of the hydrological cycle and the ocean's thermohaline circulation in climate change: A multicomponent climate model study
p 2909 N95-31720
Carbon dioxide concentrations in surface water and the atmosphere during 1986-1989 NOAA/PMEL cruises in the Pacific and Indian Oceans
[DE95-009659] p 2910 N95-32099

AIRBORNE EQUIPMENT
Simulation of airborne electromagnetic measurements in three dimensional environments
[DE95-008546] p 2900 N95-30363
Radiometer measurements of sea ice in the Gulf of Bothnia 1992
[PB95-206611] p 2900 N95-30718
Airborne ocean water lidar (OWL) real time processor (RTP)
[AD-A293226] p 2848 N95-30904
Stratospheric Observatory For Infrared Astronomy (SOFIA). Phase A: System concept description
[NASA-TM-110669] p 3002 N95-32187

AIRBORNE RADAR
Adaptive space-time processing for airborne radars based on Doppler pre-processing
[PB95-205464] p 2854 N95-32114

AIRBORNE SURVEILLANCE RADAR
Multisensor data fusion for integrated maritime surveillance p 2842 N95-32135

AIRBORNE/SPACEBORNE COMPUTERS
Model following control for tailoring handling qualities: ACT experience with ATTHeS p 2758 N95-32000

AIRCRAFT ACCIDENTS
The relation of handling qualities ratings to aircraft safety p 2746 N95-31067
SAAB experience with PIO p 2746 N95-31069
Annual review of aircraft accident data: US general aviation calendar year 1993
[PB95-215828] p 2747 N95-31712
Special investigation report: Safety of the air tour industry in the United States
[PB95-917004] p 2748 N95-32185

AIRCRAFT COMPARTMENTS
Aircraft evacuations through Type-3 exits I: Effects of seat placement at the exit
[DOT/FAA/AM-95/22] p 2748 N95-31845

AIRCRAFT CONFIGURATIONS
A general inverse design procedure for aerodynamic bodies p 2750 N95-30497
Numerical investigation into vortical flow about a delta-wing configuration up to incidences at which vortex breakdown occurs in experiment
[PB95-198024] p 2743 N95-30837
Application of multigrid computational fluid dynamics (CFD) methods to rotor analysis
[AD-A293012] p 2874 N95-31475

AIRCRAFT CONSTRUCTION MATERIALS
Thermal-mechanical fatigue crack growth in aircraft engine materials
[ISBN-0-315-86543-1] p 2894 N95-31098
Development of stitched/RTM primary structures for transport aircraft
[NASA-CR-191441] p 2789 N95-31421
Aerospace Environmental Technology Conference
[NASA-CP-3298] p 2771 N95-31746

AIRCRAFT CONTROL
Moving base simulation of an integrated flight and propulsion control system for an ejector-augmentor STOVL aircraft in hover
[NASA-TM-108867] p 2750 N95-30646
Flight Vehicle Integration Panel Workshop on Pilot Induced Oscillations
[AGARD-AR-335] p 2745 N95-31061
The process for addressing the challenges of aircraft pilot coupling p 2745 N95-31063
Observations on PIO p 2745 N95-31064
Unified criteria for ACT aircraft longitudinal dynamics p 2745 N95-31065
Looking for the simple PIO model p 2745 N95-31066
SAAB experience with PIO p 2746 N95-31069
Aeroelastic pilot-in-the-loop oscillations p 2746 N95-31070
Handling qualities analysis on rate limiting elements in flight control systems p 2746 N95-31071
Calspan experience of PIO and the effects of rate limiting p 2746 N95-31072
Computational methods for control and optimal design of aerospace systems
[AD-A292861] p 2751 N95-31451
Flight test validation of a frequency-based system identification method on an F-15 aircraft
[NASA-TM-4704] p 2757 N95-31846
The prevention of PIO by design p 2757 N95-31991
Robust control: A structured approach to solve aircraft flight control problems p 2758 N95-31995
Evaluation of the techniques of fuzzy control for the piloting an aircraft p 2758 N95-31997
Control law design using H-infinity and mu-synthesis short-period controller for a tail-airplane p 2758 N95-31999
Flight demonstration of an advanced pitch control law in the VAAC Harrier aircraft p 2760 N95-32012
X-31: A program overview and flight test status p 2753 N95-32013
Flying qualities of civil transport aircraft with electrical flight control p 2761 N95-32016
Pilot Induced Oscillation: A report on the AGARD Workshop on PIO p 2761 N95-32017

AIRCRAFT DESIGN
A general inverse design procedure for aerodynamic bodies p 2750 N95-30497
The process for addressing the challenges of aircraft pilot coupling p 2745 N95-31063
The relation of handling qualities ratings to aircraft safety p 2746 N95-31067
Handling qualities analysis on rate limiting elements in flight control systems p 2746 N95-31071
Development of stitched/RTM primary structures for transport aircraft
[NASA-CR-191441] p 2789 N95-31421
Geometric modeling for computer aided design
[NASA-CR-198828] p 2943 N95-31982
Catapult-launching of the RAFALE design and experimentation p 2752 N95-32008

AIRCRAFT DETECTION
AIDEX: An expert system for aircraft identification p 2842 N95-32138

AIRCRAFT ENGINES
Thermal-mechanical fatigue crack growth in aircraft engine materials
[ISBN-0-315-86543-1] p 2894 N95-31098
Icing simulation in the aeropropulsion systems test facility propulsion development test cell C-2
[AD-A293039] p 2747 N95-31667

AIRCRAFT EQUIPMENT
Apparent size passive range method
[AD-D017360] p 2753 N95-31180

AIRCRAFT FUELS
Environmentally safe aviation fuels p 2775 N95-31768

AIRCRAFT ICING
Icing simulation in the aeropropulsion systems test facility propulsion development test cell C-2
[AD-A293039] p 2747 N95-31667

AIRCRAFT INSTRUMENTS
Guidelines for the design of GPS and LORAN receiver controls and displays
[AD-A293753] p 2749 N95-31572

AIRCRAFT LANDING
Flight test evaluation of the Stanford University/United Airlines differential GPS Category 3 automatic landing system
[NASA-TM-110354] p 2743 N95-30788

AIRCRAFT MAINTENANCE
Bicarbonate of soda paint stripping process validation and material characterization p 2777 N95-31778
Environmentally Safe and Effective Processes for Paint Removal
[AGARD-LS-201] p 2843 N95-32165
Process evaluation p 2845 N95-32180
Standardization work p 2845 N95-32181

AIRCRAFT PARTS
Bicarbonate of soda paint stripping process validation and material characterization p 2777 N95-31778

AIRCRAFT PERFORMANCE
Flight assessment of the onboard propulsion system model for the Performance Seeking Control algorithm on an F-15 aircraft
[NASA-TM-4705] p 2756 N95-31425

Performance improvement of composite wings through aeroelastic tailoring and modern control
[AD-A293689] p 2752 N95-31602
Flight test validation of a frequency-based system identification method on an F-15 aircraft
[NASA-TM-4704] p 2757 N95-31846
Report to the Chairman, Legislation and National Security Subcommittee, Committee on Government Operations, House of Representatives. Tactical aircraft: F-15 replacement is premature as currently planned
[GAO/NSIAD-94-118] p 2964 N95-31987
Lavi flight control system: Design requirements, development and flight test results p 2758 N95-31994
Report to the Chairman, Legislation and National Security Subcommittee, Committee on Government Operations, House of Representatives. Unmanned aerial vehicles: Performance of short-range system still in question
[GAO/NSIAD-94-65] p 2752 N95-32196

AIRCRAFT PILOTS
Using computerized neuropsychological testing to assess aviator skills
[AD-A293227] p 2928 N95-30905
Psychological pilot selection in the US Air Force, the Luftwaffe, and the German Aerospace Research Establishment
[AD-A293779] p 2928 N95-31376

AIRCRAFT PRODUCTION
Report to the Chairman, Legislation and National Security Subcommittee, Committee on Government Operations, House of Representatives. Tactical aircraft: F-15 replacement is premature as currently planned
[GAO/NSIAD-94-118] p 2964 N95-31987

AIRCRAFT SAFETY
Electrical short circuit and current overload tests on aircraft wiring
[AD-A293308] p 2860 N95-30922
The relation of handling qualities ratings to aircraft safety p 2746 N95-31067
Chemical options to halons for aircraft use
[AD-A293741] p 2747 N95-31569
Aircraft evacuations through Type-3 exits I: Effects of seat placement at the exit
[DOT/FAA/AM-95/22] p 2748 N95-31845
Special investigation report: Safety of the air tour industry in the United States
[PB95-917004] p 2748 N95-32185

AIRCRAFT SPECIFICATIONS
Experiences with ADS-33 helicopter specification testing and contributions to refinement research p 2757 N95-31993
Lavi flight control system: Design requirements, development and flight test results p 2758 N95-31994
The control system design methodology of the STOL and maneuver technology demonstrator p 2758 N95-31998
Control law design using H-infinity and mu-synthesis short-period controller for a tail-airplane p 2758 N95-31999

AIRCRAFT STABILITY
Flight Vehicle Integration Panel Workshop on Pilot Induced Oscillations
[AGARD-AR-335] p 2745 N95-31051
Unified criteria for ACT aircraft longitudinal dynamics p 2745 N95-31065
Looking for the simple PIO model p 2745 N95-31066
Aeroelastic pilot-in-the-loop oscillations p 2746 N95-31070
The prevention of PIO by design p 2757 N95-31991
Pilot Induced Oscillation: A report on the AGARD Workshop on PIO p 2761 N95-32017

AIRCRAFT STRUCTURES
A comparison of coating alternatives for US Coast Guard aircraft
[AD-A293270] p 2817 N95-31124
Failure analysis for polycarbonate transparencies
[AD-A292992] p 2820 N95-31471
Performance improvement of composite wings through aeroelastic tailoring and modern control
[AD-A293689] p 2752 N95-31602
The FCS-structural coupling problem and its solution p 2759 N95-32005
Mapping hidden aircraft defects with dual-band infrared computed tomography
[DE95-011531] p 2741 N95-32164
Selective chemical stripping p 2844 N95-32175

AIRCRAFT WAKES
Hot jet/wake turbulent structure and laser propagation. Part 3: Laser propagation measurements and modeling p 2871 N95-30992

AIRFOIL OSCILLATIONS
Control of unsteady separated flow associated with the dynamic stall of airfoils
[NASA-CR-198972] p 2744 N95-32193

AIRFOIL PROFILES
Control of unsteady separated flow associated with the dynamic stall of airfoils
[NASA-CR-198972] p 2744 N95-32193

AIRFOILS
Axial loads on yawed rotors
[PB95-214193] p 2742 N95-30638
Multigrid convergence acceleration for the 2D Euler equations applied to high-lift systems
[PB95-198081] p 2743 N95-30814
A laser-based ice shape profilometer for use in icing wind tunnels
[NASA-TM-106936] p 2880 N95-30851

AIRFRAMES
Development of stitched/RTM primary structures for transport aircraft
[NASA-CR-191441] p 2789 N95-31421
The FCS-structural coupling problem and its solution p 2759 N95-32005

AIRLINE OPERATIONS
Development of advanced approach and departure procedures. Failure scenarios
[PB95-198123] p 2748 N95-30815
A NASPAC-Based analysis of the delay and cost effects of the western-pacific region preliminary resectorization effort of 1993
[AD-A288696] p 2748 N95-31013
Integrated terminal weather system (ITWS) demonstration and validation operational test and evaluation
[AD-A293932] p 2749 N95-31521
Analysis and modeling of an airport departure process
[AD-A293782] p 2749 N95-31581

AIRPORT TOWERS
FAA aviation forecasts: Fiscal year 1995-2006
[AD-A293682] p 2741 N95-31598
Report to the Chairman, Subcommittee on Transportation and Related Agencies, Committee on Appropriations, House of Representatives. Air traffic control: Status of FAA's plans to close and contract out low-activity towers
[GAO/RCED-94-265] p 2750 N95-32199

AIRPORTS
Development of advanced approach and departure procedures. Failure scenarios
[PB95-198123] p 2748 N95-30815
A NASPAC-Based analysis of the delay and cost effects of the western-pacific region preliminary resectorization effort of 1993
[AD-A288696] p 2748 N95-31013
Aviation capacity enhancement plan 1994
[AD-A292758] p 2747 N95-31428
Evaluation of alternative pavement marking materials
[AD-A292973] p 2763 N95-31468
Integrated terminal weather system (ITWS) demonstration and validation operational test and evaluation
[AD-A293932] p 2749 N95-31521
Analysis and modeling of an airport departure process
[AD-A293782] p 2749 N95-31581
The ATC operational evaluation of the prototype integrated terminal weather system (ITWS) at Dallas/Fort Worth and Orlando airports (May-September 1993)
[AD-A293808] p 2921 N95-31587
FAA aviation forecasts: Fiscal year 1995-2006
[AD-A293682] p 2741 N95-31598
Integration of air traffic databases: A case study
[AD-A293691] p 2749 N95-32022
Fact sheet for Congressional Committees. Air traffic control: Status of FAA's modernization program
[GAO/RCED-94-167FS] p 2750 N95-32197

AIRSPACE
Effects of civil tiltrotor service in the northeast corridor on en route airspace loads
[AD-A293586] p 2747 N95-31687

AIRSPEED
Experimental and computational investigation of the tip clearance flow in a transonic axial compressor rotor
[NASA-TM-106711] p 2876 N95-31738

ALBEDO
National Institute for Global Environmental Change
[DE95-008333] p 2907 N95-30358

ALCOHOLS
Enantioselectivity of quinoprotein alcohol dehydrogenases: Production of enantiomerically pure C3-alcohol synthons
[PB95-196960] p 2771 N95-30734

ALGEBRA
Canonical symmetric invariant pairings in vertex operator super algebras and gramians
[PB95-208112] p 2955 N95-30488
Strange compactification theorem: Infinite processes and the 3-dimensional poincare conjecture 6. Part A
[PB95-207924] p 2965 N95-30504
Extending a multi-set relational algebra to a parallel environment
[PB95-207106] p 3023 N95-30566
Dressing symmetry of the uniformization solution of Liouville equation
[DE95-613380] p 2956 N95-30607
Associators in generalized octonionic maps
[DE95-616243] p 2957 N95-30688
A BRST charge for non-critical W2(s) strings
[DE95-613470] p 3019 N95-30771
Advances in robust control
[AD-A291126] p 2952 N95-31266
Antipodes and integrals in Hopf algebras over rings and quantum Yang-Baxter equation
[PB95-212155] p 2961 N95-31397
Quasi-Newton updating for large scale nonlinear systems
[AD-A292776] p 2940 N95-31431
Notes on lie algebraic analysis of achromats
[DE95-009524] p 3002 N95-32356

ALGORITHMS
A Heuristic and complete planner for the classical mover's problem
[DE95-008440] p 2949 N95-30377
Adaptive path planning: Algorithm and analysis
[DE95-008549] p 2950 N95-30463
Convergence properties of an augmented lagrangian algorithm for optimization with a combination of general equality and linear constraints
[PB95-208039] p 2956 N95-30570
Refinement techniques in computer graphics
[PB95-208526] p 2934 N95-30625
MVP/GMVP: General purpose Monte Carlo codes for neutron and photon transport calculations based on continuous energy and multigroup methods
[DE95-722072] p 2979 N95-30656
ESAA: Environment for Seismic Activity Analysis
[DE95-612416] p 2913 N95-30675
Algorithm comparison and benchmarking using a parallel spectra transform shallow water model
[DE95-009124] p 2913 N95-30683
Join processing in relational database systems p 3023 N95-30764
Simplex method for semi-definite programming: Optimization and systems theory
[PB95-212122] p 2934 N95-30792
Dynamic routation in distributed environments
[PB95-197968] p 2847 N95-30812
SeaWiFS Technical Report Series. Volume 29: SeaWiFS CZCS-type pigment algorithm
[NASA-TM-104566] p 2922 N95-30857
Fast multipole methods for scattering computations
[AD-A291093] p 2848 N95-30869
Terminal doppler weather radar (TDWR) build 5B operational test and evaluation (OT&E) integration and OT&E operational test plan
[AD-A293251] p 2848 N95-30910
Algorithms for categorizing multiprocessor communication under invalidate and update-based coherence protocols
[AD-A290022] p 2947 N95-30930
Statistical interface for chaotic signal in noise
[AD-A290271] p 2848 N95-30932
New adaptive methods for reconfigurable flight control systems, appendix 1
[AD-A292711] p 2756 N95-30937
Inverse and control problems in electromagnetics
[AD-A292993] p 2849 N95-30962
SSUSI single sensor auroral E-layer algorithm: Functional description
[AD-A288630] p 2914 N95-31012
Workshop on diffusion approximation in communication and stochastic systems theory
[AD-A292872] p 2952 N95-31055
A scalable parallel Strassen's matrix multiply algorithm for distributed memory computers
[DE95-010213] p 2936 N95-31109
Numerical stability investigations of processes for solving linear initial value problems
[PB95-207023] p 2959 N95-31183
Effective bandwidth techniques in bufferless and buffered ATM multiplexers
[PB95-207072] p 2862 N95-31185
Control of mechanical systems with rolling contacts: Applications to robotics p 2889 N95-31332
Flight assessment of the onboard propulsion system model for the Performance Seeking Control algorithm on an F-15 aircraft
[NASA-TM-4705] p 2756 N95-31425
Multi-dimensional data compression for portable communication
[AD-A292751] p 2850 N95-31426
Improved modeling of unsteady heat transfer (The first step)
[AD-A292777] p 2874 N95-31432

Towards increased productivity of algorithm implementation
[AD-A292862] p 2940 N95-31452
Clouds: Their prediction and simulation
[AD-A292864] p 2920 N95-31453
Functions for processing synthetic aperture radar imagery
[AD-A293895] p 2851 N95-31510
Integrated terminal weather system (ITWS) demonstration and validation operational test and evaluation
[AD-A293932] p 2749 N95-31521
Adaptive optics design for the advanced electro-optical system (AEOS)
[AD-A293972] p 2974 N95-31527
The remainder form and the cord-slope form in global optimization with interval methods p 2941 N95-31533
Fast algorithms for three-dimensional inverse scattering problems
[AD-A293510] p 2852 N95-31537
Spectral methods and sum acceleration algorithms
[DE95-009689] p 2941 N95-31630
Finite-sample based learning algorithms for feedforward networks
[DE95-009123] p 2941 N95-31631
A simple and efficient procedure for polyhedral assembly partitioning under infinitesimal motions
[DE95-009838] p 2942 N95-31644
Using case-based reasoning as a Reinforcement Learning framework for optimization with changing criteria
[AD-A293602] p 2953 N95-31654
Image representation using fast algorithms based on the Zak transform
[AD-A293416] p 2942 N95-31684
Production matching for large learning systems
[AD-A293105] p 2953 N95-31827
SeaWiFS technical report series. Volume 28: SeaWiFS algorithms, part 1
[NASA-TM-104566-VOL-28] p 2924 N95-31850
PADO: Learning tree structured algorithms for orchestration into an object recognition system
[AD-A293109] p 2943 N95-32020
Monte Carlo tests of the ELIPGRID-PC algorithm
[DE95-010811] p 2943 N95-32030
A Stochastic EM algorithm for approximating the maximum likelihood estimate
[DE95-010328] p 2943 N95-32044
A stochastic difference equation approach to inference with missing data: Some new results
[DE95-010327] p 2944 N95-32088
A stochastic EM estimator in the presence of missing data: Theory and applications
[DE95-010329] p 2944 N95-32089
Proposed DDS-specific fields for the Generic Authentication Information Element
[DE95-009839] p 3026 N95-32144
A proposed Generic Authentication Information Element
[DE95-009862] p 2948 N95-32146
An efficient implementation of Forward-Backward Least-Mean-Square Adaptive Line Enhancers p 2855 N95-32224
A seismic data compression system using subband coding p 2857 N95-32238
Fast identification of some typical digital modulation schemes
[PB95-211454] p 2857 N95-32247
Data reduction of piecewise linear curves
[PB95-212270] p 2962 N95-32256
Compact location problems with budget and communication constraints
[DE95-010876] p 2948 N95-32277
Metafitting: Weight optimization for least-squares fitting of PTTI data p 2971 N95-32340

ALLOCATIONS
Report to Congressional Committees. Federal Research: Interim report on the small business innovation research program
[GAO/RCED-95-59] p 3022 N95-32200

ALLOYING
Mechanical alloying processing with application to structural materials
[AD-A290788] p 2802 N95-30404
Alloying effects of Kondo insulators
[DE95-614306] p 3010 N95-30644
A metallurgical approach toward alloying in rare earth permanent magnet systems
[DE95-010242] p 2966 N95-30668
The effect of grain refinement on the room-temperature ductility of as-cast Fe3Al-based alloys
[DE95-010121] p 2805 N95-31107
Shape memory properties of an iron modified nickel aluminide alloy
[DE95-010223] p 2805 N95-31111

ALLOYS
Mechanical alloying processing with application to structural materials
[AD-A290788] p 2802 N95-30404
Wettability of boron carbide
[PB95-196358] p 2802 N95-30518
First-principles approaches to materials stability
[DE95-011533] p 2810 N95-32283

ALTERNATIVES
A comparison of coating alternatives for US Coast Guard aircraft
[AD-A293270] p 2817 N95-31124
The search for CFC alternatives is over? p 2774 N95-31760
Evaluating the cost effectiveness of environmental projects: Case studies in aerospace and defense p 2774 N95-31762
The Oak Ridge Refrigerant Management Program p 2774 N95-31763
Prepsolv (TM): The optimum alternative to 1,1,1-trichloroethane and methyl ethyl ketone for hand-wipe cleaning of aerospace materials p 2774 N95-31764
Evaluation of HFC 245ca and HFC 236ea as foam blowing agents p 2775 N95-31766
Alternatives to ozone depleting refrigerants in test equipment p 2775 N95-31767
F-200(TM): The new solution for fire protection p 2776 N95-31770
Aqueous cleaning design presentation p 2778 N95-31781
An overview of NASA testing requirements for alternate cleaning solvents used in liquid and gaseous oxygen environments p 2783 N95-31813
Development of a CFC Critical Area Response (CAR) package p 2783 N95-31814
Energy storage and alternatives to improve train voltage on a mass transit system
[DE95-010344] p 2906 N95-32090
Treatment of plastic media waste p 2844 N95-32177
Process evaluation p 2845 N95-32180

ALTIMETERS
Improved altimeter settings for A-10 aircraft
[AD-A293142] p 2753 N95-30920

ALTIMETRY
Improved altimeter settings for A-10 aircraft
[AD-A293142] p 2753 N95-30920
Investigation of microwave backscatter from the air-sea interface
[NASA-CR-198854] p 2851 N95-31457

ALTITUDE SIMULATION
Icing simulation in the aeropropulsion systems test facility propulsion development test cell C-2
[AD-A293039] p 2747 N95-31667

ALUMINIDES
Reaction synthesis of intermetallics
[DE95-009029] p 2803 N95-30575
Determination of site-occupancies in aluminide intermetallics by ALCHEMI
[DE95-009179] p 2803 N95-30733
The effect of interface properties on nickel base alloy composites
[NASA-CR-198363] p 2785 N95-30787
Shape memory properties of an iron modified nickel aluminide alloy
[DE95-010223] p 2805 N95-31111
Influence of strain rate and temperature on the mechanical behavior of iron aluminide-based alloys
[DE95-009426] p 2808 N95-31636
Creep of a fine-grained, fully-lamellar, two-phase TiAl alloy at 760 C
[DE95-009531] p 2810 N95-32272

ALUMINUM
Trivalent chromium solutions for sealing anodized aluminum
[AD-D017349] p 2803 N95-30551
Texture development in aluminium extrusion
[PB95-196598] p 2979 N95-30666
The 21st JANNAF Exhaust Plume Technology Meeting, volume 1
[CPIA-PUBL-621-VOL-1] p 2870 N95-30986
The Al and A(lc)l2O3 droplet cloud in solid rocket motors p 2770 N95-30988
Burn time measurements of single aluminum particles in steam and carbon dioxide mixtures p 2799 N95-30990
The Al and Al2O3 droplet cloud in solid rocket motors p 2770 N95-31196
Burn time measurements of single aluminum particles in steam and carbon dioxide mixtures p 2799 N95-31198
Oscillatory combustion of aluminized AP/HTPB propellants p 2800 N95-31286
Characterization of an improved Rijke burner as prelude to measurements of aluminum distributed combustion p 2800 N95-31287
In situ composites in the aluminum nitride-alumina system
[AD-A293776] p 2789 N95-31509
Response of dual-layered structures subjected to shock pressure wave
[AD-A293731] p 2896 N95-31568
Thin-film sulfuric acid anodizing as a replacement for chromic acid anodizing p 2776 N95-31772
A microwave plasma cleaning apparatus p 2779 N95-31786
The influence of matrix microstructure and temperature on cyclic deformation and fatigue of particle-reinforced 2219 aluminum p 2808 N95-31974
High-resolution superconducting x-ray spectrometers with aluminum trapping layers of different thicknesses
[DE95-010253] p 2881 N95-32047

ALUMINUM ALLOYS
Physical modelling of microstructural evolution during thermomechanical processing of aluminium alloys
[PB95-196341] p 2805 N95-31053
Review of environmental effects in intermetallics
[DE95-010120] p 2805 N95-31106
The effect of grain refinement on the room-temperature ductility of as-cast Fe3Al-based alloys
[DE95-010121] p 2805 N95-31107
The 10th International Conference on the Strength of Materials
[AD-A292335] p 2894 N95-31263
Surface inspection using FTIR spectroscopy p 2782 N95-31803
Processing and microstructural evolution of alumina/aluminum alloy and aluminum nitride/aluminum alloy composites by directed melt oxidation p 2789 N95-31973
The influence of microstructure on creep deformation in near-gamma TiAl alloys p 2808 N95-31975
Control of interfacial chemistry and mechanical properties in metal/ceramic composites p 2790 N95-31976
Interfacial segregation and deformation of superplastically deformed Al-Mg-Mn alloys
[DE95-009572] p 2809 N95-32052
Cascade damage in the ordered alloy Ni3Al
[DE95-009893] p 2809 N95-32104
Residual stress distribution in FeAl weld overlay on steel
[DE95-009178] p 2899 N95-32317

ALUMINUM COATINGS
Replacement of corrosion protection chromate primers and paints used in cryogenic applications on the Space Shuttle with wire arc sprayed aluminum coatings p 2776 N95-31774

ALUMINUM GALLIUM ARSENIDES
Magnetoluminescence characterization of quantum well structures
[DE95-008527] p 3008 N95-30381
Fractal quantum well heterostructures for broadband light emitters
[DE95-009579] p 2860 N95-30707
Vertical transport in GaAs/AlGaAs superlattices p 3012 N95-30822
Optical logic and signal processing using a semiconductor laser diode-based optical bistability device
[AD-A293248] p 2997 N95-30908
A compact and efficient violet laser source
[AD-A292782] p 2885 N95-31434

ALUMINUM NITRIDES
Hydrogen diffusion and passivation in InGaAlN alloys
[DE95-010889] p 2806 N95-31150
Pseudomorphic heterostructure materials for high performance devices
[AD-A292906] p 2788 N95-31384

ALUMINUM OXIDES
Observation of a low-binding-energy peak in the 2p core-level photoemission from oxidized Al(111)
[PB95-195350] p 2802 N95-30534
Mechanisms of enhanced ionic conduction at interfaces in ceramics
[DE95-009125] p 2814 N95-30730
Urethane foam process improvements
[DE95-008957] p 2815 N95-30798
Innovative processing of composites for ultra-high temperature applications, book 3
[AD-A290891] p 2786 N95-30866
Innovative processing of composites for ultra-high temperature applications, book 4
[AD-A290892] p 2786 N95-30867
Room temperature fracture and high temperature creep deformation properties of alumina reinforced with 20 vol% particulate niobium
[DE95-010234] p 2815 N95-30897

The 21st JANNAF Exhaust Plume Technology Meeting, volume 1
[CPIA-PUBL-621-VOL-1] p 2870 N95-30986
Survey of recent Al2O3 droplet size data in solid rocket chambers, nozzles, and plumes p 2770 N95-30987
The Al and A(lc)l2O3 droplet cloud in solid rocket motors p 2770 N95-30988
Shuttle redesigned solid rocket motor aluminum oxide investigations p 2770 N95-30989
An assessment of the cost of microwave sintering ceramic tiles for armor applications. Phase 2 report
[DE95-010000] p 2816 N95-31103
Low temperature fabrication from nano-size ceramic powders
[DE95-010995] p 2818 N95-31153
Effect of irradiation spectrum on the microstructure of ion-irradiated Al2O3
[DE95-010225] p 2806 N95-31188
Survey of recent Al2O3 droplet size data in solid rocket chambers, nozzles, and plumes p 2770 N95-31195
The Al and Al2O3 droplet cloud in solid rocket motors p 2770 N95-31196
Shuttle Redesigned Solid Rocket Motor aluminum oxide investigations p 2770 N95-31197
Processing and microstructural evolution of alumina/aluminum alloy and aluminum nitride/aluminum alloy composites by directed melt oxidation p 2789 N95-31973
Control of interfacial chemistry and mechanical properties in metal/ceramic composites p 2790 N95-31976
Microstructure of Al2O3 irradiated with an applied electric field
[DE95-010278] p 2822 N95-32043
Nondestructive testing of ceramic components: Cooperative Research and Development Agreement completion report
[DE95-009510] p 2823 N95-32352

ALUMINUM-LITHIUM ALLOYS
Analysis of stress concentration at holes in components made of 2195 aluminum-lithium
[NASA-TP-3554] p 2893 N95-30613

AMBIENT TEMPERATURE
Differences in creep performance of a HIPed silicon nitride in ambient air and inert environments
[DE95-009172] p 2796 N95-31633

AMBIPOLAR DIFFUSION
A theoretical analysis of steady-state photocurrents in simple silicon diodes
[NASA-CR-198885] p 2859 N95-30651

AMMONIA
Porous spherical shells and microspheres by electrodispersion precipitation
[DE95-009073] p 2815 N95-30799
Flame structure studies of neat and NH3 doped H2/N2O flames employing molecular beam mass spectrometry and modeling p 2801 N95-31313
Self-lubricating, TiN-MoS2 composite coatings produced by simultaneous deposition from Ti((CH3))2N4/NH3/MoF6H2S gas mixture
[DE95-010359] p 2788 N95-31403

AMMONIUM COMPOUNDS
The neutron powder diffraction and acoustic investigations of the NH4SCN phase diagram
[DE95-614372] p 3009 N95-30419

AMMONIUM PERCHLORATES
Shuttle redesigned solid rocket motor aluminum oxide investigations p 2770 N95-30989
Shuttle Redesigned Solid Rocket Motor aluminum oxide investigations p 2770 N95-31197
Unsteady laser augmented combustion of pure oxidizers AP and RDX p 2799 N95-31284
Oscillatory combustion of aluminized AP/HTPB propellants p 2800 N95-31286
Model for defining propellant burn rate performance boundaries p 2800 N95-31290
AP reclamation and reuse in RSRM propellant p 2772 N95-31751

AMORPHOUS MATERIALS
Orientation of rapid thermally annealed lead zirconate titanate thin films on (111) Pt substrate
[DE95-615232] p 2811 N95-30422
Synthesis of carbo-nitride films using high-energy shock plasma deposition
[DE95-615231] p 2811 N95-30450
Morphology and microstructure of (111) crystalline CeO2 films grown on amorphous SiO2 substrates by pulsed-laser ablation
[DE95-006842] p 3009 N95-30542
Phthalonitrile prepolymer as high temperature sizing material for composite fibers
[AD-D017447] p 2818 N95-31272
Microstructure of Al2O3 irradiated with an applied electric field
[DE95-010278] p 2822 N95-32043
Comprehensive research on the stability and electronic properties of a-Si:H and a-SiGe:H alloys and devices
[DE95-004088] p 2810 N95-32154

AMORPHOUS SEMICONDUCTORS
Evidence for electronic energy loss processes stimulating solid phase epitaxial regrowth of spatially isolated amorphous regions in semiconductor systems
[DE95-009892] p 3016 N95-32103

AMORPHOUS SILICON
Large-area, triple-junction a-Si alloy production scale-up
[DE95-004067] p 2904 N95-31163
Evidence for electronic energy loss processes stimulating solid phase epitaxial regrowth of spatially isolated amorphous regions in semiconductor systems
[DE95-009892] p 3016 N95-32103

AMPLIFICATION
Pre-amplifier with multi-stage feedback
[AD-D017371] p 2859 N95-30659

AMPLITUDE MODULATION
Smart active multiwave sensing with zero background amplitude modulated probes
[DE95-008813] p 2792 N95-30714

AMPLITUDES
Handling qualities analysis on rate limiting elements in flight control systems p 2746 N95-31071

AMPOULES
The effect of gravity on the deposition of thin films: The physical vapor transport of copper phthalocyanine
[AD-A292997] p 2838 N95-31472

ANAEROBES
Degradation of TCE using sequential anaerobic biofilm and aerobic immobilized bed reactor p 2780 N95-31791

ANALOG SIMULATION
Generation of earthquake signals
[PB95-211223] p 2913 N95-30631

ANALOG TO DIGITAL CONVERTERS
Coherent integrator
[AD-D017422] p 2847 N95-30743
Decimation of encoding errors in an optimum SNS 2 micron low-noise CMOS ADC
[AD-A293208] p 2860 N95-30900
Analog preprocessing in a SNS 2 micrometers low-noise CMOS folding ADC
[AD-A293356] p 2849 N95-30954
Electromagnetic field exposure dosimeter
[AD-A293191] p 2927 N95-30981

ANALOGIES
Unification of LARCH and Z-based object models to support algebraically-based design refinement: The LARCH perspective
[AD-A289235] p 2935 N95-30999
A cognitive architecture for solving ill-defined problems
[AD-A293582] p 2929 N95-31686

ANALOGS
On the string equation at c=1
[DE95-737161] p 3014 N95-31222

ANALYSIS (MATHEMATICS)
MPI implementation of PHOENICS: A general purpose computational fluid dynamics code
[DE95-009810] p 2877 N95-32033

ANALYSIS OF VARIANCE
Modeling F/A-18 flight hour program costs using regression analysis
[AD-A293771] p 2752 N95-31579

ANALYTIC FUNCTIONS
Higher Schwarzian operators and combinatorics of Schwarzian derivative
[PB95-208435] p 2957 N95-30623
Existence of solutions in plane quasistationary stokes flow driven by surface tension
[PB95-197935] p 2868 N95-30810

ANGLE OF ATTACK
Transonic aerodynamic characteristics of a proposed wing-body reusable launch vehicle concept
[NASA-TM-108489] p 2742 N95-30712
Multigrid convergence acceleration for the 2D Euler equations applied to high-lift systems
[PB95-198081] p 2743 N95-30814
Unsteady transonic wind tunnel test on a semispan straked delta wing, oscillating in pitch. Part 1: Description of the model, test setup, data acquisition, and data processing
[AD-A293113] p 2743 N95-30885
Side force acting on blunted circular cylinder bodies at high angles of attack in supersonic flow
[NAL-TR-1255] p 2744 N95-31741
X-31: A program overview and flight test status p 2753 N95-32013

ANGULAR MOMENTUM
Two-loop vacuum amplitudes in a non-Abelian gauge theory on S(sub 4)
[DE95-616284] p 3018 N95-30436
Nuclear-spin-dependent parity-nonconserving effects in thallium, lead and bismuth atoms
[DE95-614120] p 2991 N95-32354

ANGULAR RESOLUTION
Beam-centroid tracking instrument for ion thrusters
[AD-A293654] p 2769 N95-31567

ANGULAR VELOCITY
Dynamical analysis of the coriolis effect which causes space disorientation
[NAL-TR-1258] p 2928 N95-31714

ANIMALS
Temporal information processing mechanisms
[PB95-208344] p 3027 N95-32370

ANIONS
The one-dimensional model of the off-centre potential of the fluorine ion in the NaBr lattice
[DE95-614310] p 3010 N95-30647
Calculated structures and electronic absorption spectroscopy for magnesium phthalocyanine and its anion radical
[AD-A293672] p 2796 N95-31596

ANISOTROPIC MEDIA
Numerical evaluation of three-dimensional crack-tip integrals for layered anisotropic solids p 2898 N95-32191

ANISOTROPY
Texture development in aluminium extrusion
[PB95-196598] p 2979 N95-30666
TV-VI semiconductor quantum well lasers, physics and engineering p 2883 N95-30805
A viscoelastic anisotropic wave propagation model for composite cure evaluation p 2786 N95-30839
Dynamics of an inhomogeneous anisotropic antiferromagnetic spin chain
[DE95-614449] p 3013 N95-30959
The effect of gravity on the deposition of thin films: The physical vapor transport of copper phthalocyanine
[AD-A292997] p 2838 N95-31472
Derivation of two-dimensional (2-D) conduction equation in generalized coordinates with constant and anisotropic physical properties
[AD-A293896] p 3020 N95-31511
Rationale and summary of methods for determining ultrasonic properties of materials at Lawrence Livermore National Laboratory
[DE95-009475] p 2795 N95-31593
Influence of layer order and composition on the magnetic anisotropy of ultra-thin Co sandwiches
[DE95-010608] p 2810 N95-32265

ANNEALING
Orientation of rapid thermally annealed lead zirconate titanate thin films on (111) Pt substrate
[DE95-615232] p 2811 N95-30422
Phase transformations in melt-spun Y-Ba-Cu-O bulk superconductor
[DE95-010237] p 3011 N95-30667
Formation of cavities in Si and their chemisorption of materials
[DE95-009586] p 2980 N95-30708
Phase stability, point defects and site preference of FeAl and NiAl with ternary additions
[DE95-009694] p 3015 N95-31641

ANNIHILATION REACTIONS
Generalized deformed para-Bose oscillator and its coherent states
[DE95-613444] p 2963 N95-30610
WW and WZ production at the tevatron
[DE95-011014] p 2981 N95-30970
Radiative corrections to the three quantum annihilation cross section in high energy electron-positron collisions
[DE95-623675] p 2995 N95-32296
STM measurements of the interaction of vacancies and steps during low-energy-ion bombardment of Si(001)
[DE95-010935] p 3017 N95-32308

ANNUAL VARIATIONS
Middle atmosphere structure and dynamics: Lidar studies at the South Pole, Syowa and Urbana p 2916 N95-31736
Global climatology and variability of potential new production estimated from remote sensing of sea-surface temperature
[NASA-CR-198840] p 2910 N95-31961

ANODES
Anodically enhanced diffusion in Cu/Ag thin film couples
[DE95-009198] p 2814 N95-30738

ANODIC COATINGS
Trivalent chromium solutions for sealing anodized aluminum
[AD-D017349] p 2803 N95-30551
Preventing cracking of anodized coatings
[NASA-TM-104622] p 2839 N95-31690

ANODIZING
Preventing cracking of anodized coatings
[NASA-TM-104622] p 2839 N95-31690

Thin-film sulfuric acid anodizing as a replacement for chromic acid anodizing p 2776 N95-31772

ANOMALIES

Forecast of Atlantic seasonal hurricane activity for 1994 p 2918 N95-30832

A RASCAL in-bore dynamic analysis of the task B and task C electromagnetic railguns
[AD-A292742] p 2764 N95-30948

Comparison of satellite-derived MSU brightness temperatures and conventionally-derived fields
[AD-A293692] p 2901 N95-31603

ANTARCTIC REGIONS

Middle atmosphere structure and dynamics: Lidar studies at the South Pole, Syowa and Urbana p 2916 N95-31736

Swedish polar bibliography: A guide to Swedish literature on polar research, 1945-1988 with supplement, 1989-1992
[PB95-208161] p 2902 N95-32115

ANTENNA ARRAYS

Scattering and radiation from cylindrically conformal antennas p 2847 N95-30669

Proceedings of the antenna applications symposium, volume 1
[AD-A293258] p 2848 N95-30895

Proceedings of the antenna applications symposium, volume 2
[AD-A293259] p 2850 N95-31387

Research in ground-to-air microwave imaging
[AD-A292907] p 2852 N95-31551

Portable digital Satellite News Gathering (SNG) RF terminal using a flat antenna
[NHK-LABS-NOTE-436] p 2853 N95-31744

Adaptive space-time processing for airborne radars based on Doppler pre-processing
[PB95-205464] p 2854 N95-32114

Performance of residual carrier array-feed combining in correlated noise p 2856 N95-32232

Residual and suppressed-carrier arraying techniques for deep-space communications p 2856 N95-32235

Effects of correlated noise on the full-spectrum combining and complex-symbol combining arraying techniques p 2856 N95-32237

ANTENNA COMPONENTS

Portable digital Satellite News Gathering (SNG) RF terminal using a flat antenna
[NHK-LABS-NOTE-436] p 2853 N95-31744

ANTENNA DESIGN

Proceedings of the antenna applications symposium, volume 1
[AD-A293258] p 2848 N95-30895

Inverse and control problems in electromagnetics
[AD-A292993] p 2849 N95-30962

Research in ground-to-air microwave imaging
[AD-A292907] p 2852 N95-31551

Portable digital Satellite News Gathering (SNG) RF terminal using a flat antenna
[NHK-LABS-NOTE-436] p 2853 N95-31744

ANTENNA FEEDS

Proceedings of the antenna applications symposium, volume 1
[AD-A293258] p 2848 N95-30895

Proceedings of the antenna applications symposium, volume 2
[AD-A293259] p 2850 N95-31387

ANTENNA RADIATION PATTERNS

Scattering and radiation from cylindrically conformal antennas p 2847 N95-30669

ANTHROPOMETRY

Erect, neutral and slump sitting postures: A study of the torso linkage system from shoulder to hip joint
[AD-A293239] p 2930 N95-30907

ANTIBIOTICS

Acidity and basicity of nitro substituted imidazoles p 2832 N95-31301

Acidity and basicidity of nitro substituted imidazoles
[AD-A293969] p 2836 N95-31526

ANTIFERROMAGNETISM

On the theory of hole propagation in an antiferromagnetic background
[DE95-614469] p 3010 N95-30650

Properties of a multichannel resonant-level model
[DE95-614482] p 2979 N95-30652

Multisite antiferromagnetic Ising spin model: Phase transition through doubling bifurcation
[DE95-614311] p 3011 N95-30722

Dynamics of an inhomogeneous anisotropic antiferromagnetic spin chain
[DE95-614449] p 3013 N95-30959

On the possibility of a two-state magnetic structure for nanocrystalline chromium
[DE95-009914] p 3015 N95-32062

Schwinger-boson studies of the single hole motion in a 2D quantum antiferromagnet
[DE95-614444] p 3016 N95-32071

ANTIMISSILE DEFENSE

Definition of an anti-missile ballistic defense architecture for Europe p 2840 N95-32125

Design of surveillance and multisensor anti-aerial systems p 2841 N95-32134

ANTIMONY

Preparation of diisopropyl stibines and use thereof
[AD-D017419] p 2771 N95-30418

ANTIPARTICLES

The Foldy-Wouthuysen transformation
[DE95-616277] p 2976 N95-30427

Instanton - antiinstanton interaction and asymptotics of perturbation theory expansion of in double well oscillator
[DE95-619245] p 2966 N95-31259

ANTIPODES

Antipodes and integrals in Hopf algebras over rings and quantum Yang-Baxter equation
[PB95-212155] p 2961 N95-31397

ANTIPROTONS

On explanation of proton electromagnetic form Factor near p (anti p)-threshold from the PS-170 experiment
[DE95-613766] p 2977 N95-30508

Atomic approaches in metastable antiprotonic helium atoms. Reply to Analysis of the lifetimes and fractions of antiprotons trapped in metastable antiprotonic helium states by I. Shimamhura and M. Kimura --- mura
[DE95-737228] p 2986 N95-31658

The antiproton-hydrogen atom interaction
[DE95-010252] p 2987 N95-32039

ANTISHIP MISSILES

Results from tests of the Kearfott T16-B Inertial Measurement Unit
[PB95-212031] p 2879 N95-30502

Results from tests of the Honeywell integrated flight management unit
[PB95-211355] p 2748 N95-30597

APERTURES

Tune modulation due to synchrotron oscillations and chromaticity, and the dynamic aperture
[DE95-011566] p 2995 N95-32297

APPALACHIAN MOUNTAINS (NORTH AMERICA)

A numerical study of the effect of the Gulf Stream and the Appalachian Mountains on Carolina coastal frontogenesis
[AD-A293765] p 2921 N95-31577

APPLICATION SPECIFIC INTEGRATED CIRCUITS

Decimation of encoding errors in an optimum SNS 2 micron low-noise CMOS ADC
[AD-A293208] p 2860 N95-30900

APPLICATIONS OF MATHEMATICS

Semiannual report
[NASA-CR-198172] p 2931 N95-30657

APPLICATIONS PROGRAMS (COMPUTERS)

User's manual for the Scanning Fast Field Program (SCAFFIP) EOSAEL version 1.0
[AD-A291445] p 2933 N95-30397

Advanced system identification techniques for wind turbine structures
[DE95-004049] p 2902 N95-30505

Detecting intravascular gas bubbles in ultrasonic images
[PB95-195301] p 2926 N95-30513

Object-oriented approach for gas turbine engine simulation
[NASA-TM-106970] p 2754 N95-30594

Computerized design of controllers using data models
[NASA-CR-198921] p 2950 N95-30655

MVP/GMVP: General purpose Monte Carlo codes for neutron and photon transport calculations based on continuous energy and multigroup methods
[DE95-722072] p 2979 N95-30656

ESAA: Environment for Seismic Activity Analysis
[DE95-612416] p 2913 N95-30675

Validation of the NPARC code for nozzle afterbody flows at transonic speeds
[NASA-TM-106971] p 2742 N95-30704

Enhancements to the SSME transfer function modeling code
[NASA-CR-198957] p 2958 N95-30754

SHEAT: A computer code for probabilistic seismic hazard analysis, user's manual
[DE95-717874] p 2913 N95-30758

Development of BERMUDA: A radiation transport code system. Part 3: A one-dimensional adjoint neutron transport code
[DE95-717875] p 2934 N95-30759

Neutron shielding point kernel integral calculation code for personal computer: PKN-pc
[DE95-717876] p 2980 N95-30760

Wide area networking R&D
[AD-A291057] p 2947 N95-30868

Improved altimeter settings for A-10 aircraft
[AD-A293142] p 2753 N95-30920

Acceleration potential models PREDICHAT/PREDICDYN applied for calculation of axisymmetric dynamic inflow cases
[PB95-207015] p 2869 N95-30957

FISHFINDE: Interactive software package to predict fish locations using satellite image data and fish species behavior rules
[AD-A293394] p 2935 N95-30968

QTSAW (Quick Typhoon Surge and Waves). Wave information studies of US coastlines
[AD-A293172] p 2919 N95-30976

Implementation of KIVA-3 on distributed memory MIMD computers
[DE95-010288] p 2931 N95-31130

Nordic symposium on analysis of electromagnetic transient phenomena using EMTP, part 3
[PB95-206504] p 2849 N95-31158

Nordic Symposium on Analysis of Electromagnetic Transient Phenomena Using EMTP, part 2
[PB95-206579] p 2849 N95-31160

Nordic Symposium on Analysis of Electromagnetic Transient Phenomena Using EMTP, part 4
[PB95-206587] p 2849 N95-31181

Nordic Symposium on Analysis of Electromagnetic Transient Phenomena Using EMTP, part 1
[PB95-206595] p 2850 N95-31182

Hadronic production of B(sub c)-mesons
[DE95-620536] p 2983 N95-31216

An ignition model for modern double base propellants p 2800 N95-31292

Automation of the control of acoustic parameters in a digital speech synthesizer
[IFTR-2/1995] p 2850 N95-31357

Numerical solution of a singular integral equation arising from a sequential probability ratio test
[AD-A293463] p 2963 N95-31375

Aspects of the search time in binary search trees modified according to the move-to-root heuristic
[PB95-212148] p 2963 N95-31396

Solid Modeling Aerospace Research Tool (SMART) user's guide, version 2.0
[NASA-TM-4431] p 2940 N95-31420

Investigation of ground target detection methods in fully polarimetric wide angle synthetic aperture radar images
[AD-A293922] p 2851 N95-31513

Modern methods in meteorological and oceanographic data acquisition and analyses
[AD-A293884] p 2920 N95-31541

Space systems environmental interaction studies
[AD-A293826] p 2766 N95-31553

Monte Carlo code for evaluating the Boundary Layer Illumination and Radiation Balance model (BLIRB)
[AD-A293963] p 2915 N95-31560

Network user's guide
[DE95-009185] p 2942 N95-31634

Experimental and computational investigation of the tip clearance flow in a transonic axial compressor rotor
[NASA-TM-106711] p 2876 N95-31738

Environmental databases and other computerized information tools p 2783 N95-31810

NEIS (NASA Environmental Information System) p 2783 N95-31811

Geometric modeling for computer aided design
[NASA-CR-198828] p 2943 N95-31982

Practical experiences in control systems design using the NCR Bell 205 Airborne Simulator p 2761 N95-32015

TMD detection and tracking using improved AWACS sensors p 2840 N95-32128

Operation of the computer model for direct atomic oxygen exposure of Earth satellites
[NASA-CR-198188] p 2767 N95-32189

Numerical evaluation of three-dimensional crack-tip integrals for layered anisotropic solids p 2898 N95-32191

FPCAS3D User's guide: A three dimensional full potential aeroelastic program, version 1
[NASA-CR-198367] p 2899 N95-32205

BRUTUS: A program for conversion between image formats
[PB95-211421] p 2945 N95-32246

ASSIST user manual
[NASA-TM-4592] p 2948 N95-32250

Production simulator for wave power plants
[PB95-212262] p 2907 N95-32286

Inversion of ERS-1 wavemode spectra. User's and programmer's guide
[PB95-223582] p 2902 N95-32316

APPROACH INDICATORS

Flight test evaluation of the Stanford University/United Airlines differential GPS Category 3 automatic landing system
[NASA-TM-110354] p 2743 N95-30788

APPROPRIATIONS
Annual report to the Chairman and Ranking Minority Members, House and Senate Committees on Appropriations. Status of open recommendations: Improving operations of federal departments and agencies
| GAO/OP-95-1 | p 3022 N95-31986
APPROXIMATION
Spectral methods in complex geometries
| PB95-208336 | p 2955 N95-30495
Periodically Specified Problems: An Exponential Complexity Gap Between Exact and Approximate Solutions
| DE95-009435 | p 2934 N95-30603
Higher Schwarzian operators and combinatorics of Schwarzian derivative
| PB95-208435 | p 2957 N95-30623
Calculated coupling efficiency between an elliptical-core optical fiber and an optical waveguide over temperature
| NASA-TM-107005 | p 2997 N95-30849
Workshop on diffusion approximation in communication and stochastic systems theory
| AD-A292872 | p 2952 N95-31055
Direct and inverse problems in random media
| AD-A293033 | p 2850 N95-31280
Poisson approximation using the Stein-Chen method and coupling: Number of exceedances of a discrete-time-chi-squared process
| PB95-212205 | p 2961 N95-31398
Multipoint quadratic approximation for numerical optimization
| AD-A293837 | p 2961 N95-31557
Evaluation of nonlinear structural dynamic responses using a fast-running spring-mass formulation
| DE95-008503 | p 2967 N95-31625
The complexity and approximability of finding maximum feasible subsystems of linear relations
| TRITA-NA-9313 | p 2961 N95-31648
Compact location problems with budget and communication constraints
| DE95-010876 | p 2948 N95-32277
APTITUDE
Selection of Swedish scholastic aptitude test takers as a function of socioeconomic background and ability: Evaluation through follow-up
| PB95-212072 | p 3021 N95-30699
Non-comparability of female and male admission test takers: Evaluation through follow-up
| PB95-212080 | p 3021 N95-30700
AQUEOUS SOLUTIONS
On-line surfactant monitoring
| DE95-009417 | p 2792 N95-30735
Burn time measurements of single aluminum particles in steam and carbon dioxide mixtures
p 2799 N95-30990
Lithium ion aqueous cells
| AD-A293828 | p 2905 N95-31554
Aqueous cleaning design presentation
p 2778 N95-31781
Aqueous cleaning and verification processes for precision cleaning of small parts p 2779 N95-31787
QFD analysis of RSRM aqueous cleaners
p 2779 N95-31789
Cleaning without chlorinated solvents
p 2780 N95-31792
Evaluation of control parameters for Spray-In-Air (SIA) aqueous cleaning for shuttle RSRM hardware
p 2780 N95-31794
Laboratory robotics: An automated tool for preparing Ion Chromatography calibration standards
| DE95-009441 | p 2798 N95-32318
Base hydrolysis and hydrothermal processing of PBX-9404 explosive
| DE95-009497 | p 2837 N95-32355
AQUIFERS
CALORSTOCK 1994: Thermal energy storage. Better economy, environment, technology
| DE95-772422 | p 2904 N95-31138
CALORSTOCK'94. Thermal energy storage. Better economy, environment, technology
| DE95-772421 | p 2907 N95-32368
ARABIAN SEA
Arabian Sea mixed layer dynamics experiment: Mooring deployment cruise report
| AD-A293684 | p 2923 N95-31600
ARC DISCHARGES
Operating in the space plasma environment: A spacecraft charging study of the Solar X-ray Imager
| NASA-TM-110644 | p 3003 N95-30468
ARCHITECTURE
Definition of an anti-missile ballistic defense architecture for Europe p 2840 N95-32125
ARCHITECTURE (COMPUTERS)
Workflow literature guide, version 1
| PB95-207080 | p 2947 N95-30721
Foundations of technology for constructing highly reliable distributed realtime systems
| AD-A293254 | p 2931 N95-30892
An architectural approach to strategic information systems planning for the Office of Naval Intelligence
| AD-A289930 | p 3024 N95-30928
Implementation of KIVA-3 on distributed memory MIMD computers
| DE95-010288 | p 2931 N95-31130
Integrated high performance distributed system
| AD-A292821 | p 2947 N95-31445
Acquiring consistent knowledge for Bayesian Forests
| AD-A293858 | p 2952 N95-31517
Analysis and extension of model-based software executives
| AD-A293834 | p 2944 N95-32073
Integration issues in modular mission management aid development p 2841 N95-32133
Architecture and implementation of a multi-sensor data fusion demonstration model within the real-time combat system of the Canadian Patrol Frigate
p 2842 N95-32139
ARCTIC REGIONS
Sea ice stress research
| AD-A293164 | p 2923 N95-30964
Preliminary design for Arctic atmospheric radiative transfer experiments
| DE95-009580 | p 2917 N95-32080
Swedish polar bibliography: A guide to Swedish literature on polar research, 1945-1988 with supplement, 1989-1992
| PB95-208161 | p 2902 N95-32115
ARGON
Differences in creep performance of a HIPed silicon nitride in ambient air and inert environments
| DE95-009172 | p 2796 N95-31633
A microwave plasma cleaning apparatus
p 2779 N95-31786
ARITHMETIC
Arithmetic features of rational conformal field theory
| PB95-207908 | p 2966 N95-30591
ARITHMETIC AND LOGIC UNITS
Cesar3 MALU library
| PB95-211363 | p 2933 N95-30598
ARMED FORCES (UNITED STATES)
Research proposal
| AD-A293207 | p 3032 N95-30899
Psychological pilot selection in the US Air Force, the Luftwaffe, and the German Aerospace Research Establishment
| AD-A293779 | p 2928 N95-31376
ARMOR
An assessment of the cost of microwave sintering ceramic tiles for armor applications. Phase 2 report
| DE95-010000 | p 2816 N95-31103
ARPA COMPUTER NETWORK
Comparisons of target detection clutter using data from the 1993 FOPEN experiments
| AD-A293052 | p 2852 N95-31606
ARSENIC
Spatial time-series: Pollution pattern recognition under irregular interventions
| AD-A293830 | p 2909 N95-31556
ARTERIES
Arterial gas bubbles after decompression in pigs with Patent Foramen Ovale
| PB95-195319 | p 2925 N95-30515
ARTIFICIAL INTELLIGENCE
A Heuristic and complete planner for the classical mover's problem
| DE95-008440 | p 2949 N95-30377
Precision manipulation with a dextrous robot hand
p 2888 N95-30829
Making intelligent systems team players. A guide to developing intelligent monitoring systems
| NASA-TM-104807 | p 2951 N95-30925
High-tech controls for energy and environment
| DE95-011702 | p 2952 N95-31255
Artificial intelligence techniques for flight test planning, phase 1
| AD-A293962 | p 2751 N95-31525
A cognitive architecture for solving ill-defined problems
| AD-A293582 | p 2929 N95-31686
Production matching for large learning systems
| AD-A293105 | p 2953 N95-31827
PADO: Learning tree structured algorithms for orchestration into an object recognition system
| AD-A293109 | p 2943 N95-32020
Multi-sensor data fusion in command and control and the merit of artificial intelligence p 2842 N95-32137
AIDEX: An expert system for aircraft identification
p 2842 N95-32138
ARTIFICIAL SATELLITES
Computer interface development for the petite amateur navy satellite (PANSAT) simulator
| AD-A293263 | p 2766 N95-31388
ASSEMBLING
Development of flexible feeder techniques
| PB95-196317 | p 2934 N95-30663
ASSIMILATION
Comparison of satellite-derived MSU brightness temperatures and conventionally-derived fields
| AD-A293692 | p 2901 N95-31603
ASTRONAUTS
Electromyostimulation, circuits and monitoring
| NASA-TM-110741 | p 2926 N95-30846
Mir 18 post flight presentation
| NASA-TM-110657 | p 2766 N95-30854
STS-70 flight: Day 8
| NASA-TM-110666 | p 2764 N95-30873
ASTRONOMICAL POLARIMETRY
X-ray performance of the engineering prototype Stellar x-ray polarimeter
| DE95-010268 | p 3028 N95-31129
ASTRONOMICAL SPECTROSCOPY
Chromospherically active stars. 6: Giants with compact hot companions and the barium star scenario
| NASA-TM-110641 | p 3028 N95-30466
ASTROPHYSICS
Abstracts of Annual Physics Conference of Iran
| DE95-611717 | p 2768 N95-30881
Future scientific applications for high-energy lasers
| DE95-009380 | p 2885 N95-31230
A search for millicharged particles at SLAC
| DE95-010094 | p 2987 N95-32026
ASYMMETRY
On the Compton twist-3 asymmetries
| DE95-613627 | p 3017 N95-30371
Electron-optical nonlinear interaction in asymmetric quantum-well laser heterostructures
| DE95-613443 | p 2883 N95-30609
Experimental investigation of optical nonlinearities in conjugated polymers
| AD-A288353 | p 2884 N95-31145
Detection of the phase shift which accompanies the excitation of an atomic beam by N. F. Ramsey's method
| IFTR-5/1995 | p 2986 N95-31818
ASYMPTOTIC METHODS
Workshop on diffusion approximation in communication and stochastic systems theory
| AD-A292872 | p 2952 N95-31055
ASYMPTOTIC PROPERTIES
HERA and the asymptotic behaviour of F2(sup rho)
| PB95-195764 | p 2956 N95-30540
ASYMPTOTIC SERIES
Extension to higher dimensions of the Jaeschke-Eicker result on the standardized empirical process
| PB95-206868 | p 2965 N95-30523
Golden ten equations of motion
| PB95-197927 | p 2967 N95-30809
Instanton - antiinstanton interaction and asymptotics of perturbation theory expansion of in double well oscillator
| DE95-619245 | p 2966 N95-31259
Numerical studies of nonlinear optical pulse propagation p 2998 N95-31411
Ricci-flat Kaehler metrics on symmetric varieties
| DE95-613459 | p 2962 N95-32068
ATLANTIC OCEAN
Forecast of Atlantic seasonal hurricane activity for 1994 p 2918 N95-30832
Early August updated forecast of Atlantic seasonal hurricane activity for 1994 p 2919 N95-30844
ATMOSPHERIC ATTENUATION
User's manual for the Scanning Fast Field Program (SCAFFIP) EOSAEL version 1.0
| AD-A291445 | p 2933 N95-30397
ATMOSPHERIC BOUNDARY LAYER
Study of cross-tail current carriers in magnetotail
p 3005 N95-30804
Shiptracks in the Californian stratus region: Dependency on marine atmospheric boundary layer depth
| AD-A293272 | p 2901 N95-31125
Global Ultraviolet Imager (GUVI) investigation
| NASA-CR-189430 | p 2917 N95-31820
ATMOSPHERIC CHEMISTRY
Measurement and analysis related to infrared emissions
| AD-A293296 | p 2998 N95-31192
Global Ultraviolet Imager (GUVI) investigation
| NASA-CR-189430 | p 2917 N95-31820
ATMOSPHERIC CIRCULATION
IR DIAL performance modeling
| DE95-008377 | p 2912 N95-30373
Development of a novel wind lidar, phase 1
| AD-A292703 | p 2849 N95-30935
Adaptive optics design for the advanced electro-optical system (AEOS)
| AD-A293972 | p 2974 N95-31527

Diagnosis of the kinematics and dynamics of rapidly developing maritime cyclones
[AD-A293919] p 2921 N95-31675
Global Ultraviolet Imager (GUVI) investigation
[NASA-CR-189430] p 2917 N95-31820
The GCRC two-dimensional zonally averaged statistical dynamical climate model: Development, model performance, and climate sensitivity
p 2910 N95-31851
Simulation of katabatic flow and mountain waves
[DE95-010863] p 2911 N95-32276

ATMOSPHERIC COMPOSITION
Global change research: Summaries of research in FY 1994
[DE95-009660] p 2908 N95-30755
Aerosol measurements over the Pacific Ocean in support of the IR aerosol backscatter program
[NASA-CR-198925] p 2916 N95-30782
The GCRC two-dimensional zonally averaged statistical dynamical climate model: Development, model performance, and climate sensitivity
p 2910 N95-31851
Carbon dioxide concentrations in surface water and the atmosphere during 1986-1989 NOAA/PMEL cruises in the Pacific and Indian Oceans
[DE95-009659] p 2910 N95-32099

ATMOSPHERIC CORRECTION
SeaWiFS technical report series. Volume 13: Case studies for SeaWiFS calibration and validation, part 1
[NASA-TM-104566-VOL-13] p 2924 N95-32220

ATMOSPHERIC EFFECTS
Atmospheric environmental implications of propulsion systems p 2771 N95-31747

ATMOSPHERIC GENERAL CIRCULATION MODELS
The land component of the global climate system with adequate spatial resolution
[DE95-009323] p 2908 N95-30686

ATMOSPHERIC HEATING
HST-FOC observations of a remarkable UV auroral event on Jupiter p 3030 N95-30806
Underdense heating of the ionosphere using oblique high power HF radiowaves p 2917 N95-31951

ATMOSPHERIC MODELS
IR DIAL performance modeling
[DE95-008377] p 2912 N95-30373
User's manual for the Scanning Fast Field Program (SCAFFIP) EOSAEL version 1.0
[AD-A291445] p 2933 N95-30397
Chemical kinetics and photochemical data for use in stratospheric modeling: Evaluation number 11
[NASA-CR-198863] p 2912 N95-30525
Algorithm comparison and benchmarking using a parallel spectra transform shallow water model
[DE95-009124] p 2913 N95-30683
Modeling and parameterization of gravity wave breaking, interactions, and instability processes in the lower and middle atmosphere
[AD-A292740] p 2914 N95-31278
Initial evaluation of the Oregon State University planetary boundary layer column model for ITWS applications
[AD-A293775] p 2920 N95-31465
Measurements of ionospheric variability
[AD-A293495] p 2915 N95-31535
Proceedings of the 16th Annual Conference on Atmospheric Transmission Models, volume 1
[AD-A293807] p 2915 N95-31575
A numerical study of the effect of the Gulf Stream and the Appalachian Mountains on Carolina coastal frontogenesis
[AD-A293765] p 2921 N95-31577
Validation of the atmospheric transmission large-area analysis system (ATLAS)
[AD-A293810] p 2916 N95-31589
Proceedings of the 16th Annual Conference on Atmospheric Transmission Models, volume 2
[AD-A293806] p 2916 N95-31604
DE-1 observations of polar O(+) stream bulk parameters and comparison with a model of the centrifugally-accelerated polar wind
[NASA-CR-198930] p 2917 N95-31743
Calculation of a residual mean meridional circulation for a zonal-mean tracer transport model
[DE95-009474] p 2911 N95-32350

ATMOSPHERIC MOISTURE
Brightness temperature simulations for the physical and synoptic interpretation of advanced microwave sounding unit moisture channels p 2921 N95-31721

ATMOSPHERIC OPTICS
Optimum truncation of a Gaussian beam for propagation through atmospheric turbulence
[AD-A291156] p 2883 N95-30394

ATMOSPHERIC PHYSICS
Kiruna geophysical data. Data summary 94/1-3, January-March 1994
[PB95-210373] p 2913 N95-30628
Future scientific applications for high-energy lasers
[DE95-009380] p 2885 N95-31230

ATMOSPHERIC PRESSURE
Summary of 1993 Atlantic tropical cyclone activity and verification of author's forecast. A year of unanticipated light hurricane activity and a poor forecast: The expected dissipation of the El Nino did not take place and Caribbean basin surface pressure became quite high
p 2918 N95-30842
Early August updated forecast of Atlantic seasonal hurricane activity for 1994 p 2919 N95-30844

ATMOSPHERIC RADIATION
History and status of the atmospheric radiation measurement program
[DE95-009951] p 2908 N95-30802
Monte Carlo code for evaluating the Boundary Layer Illumination and Radiation Balance model (BLIRB)
[AD-A293963] p 2915 N95-31560
Preliminary design for Arctic atmospheric radiative transfer experiments
[DE95-009580] p 2917 N95-32080
Feasibility of tropospheric water vapor profiling using infrared heterodyne differential absorption lidar
[DE95-009647] p 2917 N95-32142
Use of arm measurements to improve radiative transfer models used in climate models
[NASA-CR-199014] p 2921 N95-32184
Spectral sky background in the IR: Measurements with FTIR
[PB95-222998] p 2922 N95-32315

ATMOSPHERIC REFRACTION
Measurements of ionospheric variability
[AD-A293495] p 2915 N95-31535

ATMOSPHERIC SOUNDING
Anticipated uncertainty budgets of PRARETIME and T2L2 techniques as applied to ExTRAS
p 2968 N95-32326

ATMOSPHERIC TEMPERATURE
Middle atmosphere structure and dynamics: Lidar studies at the South Pole, Syowa and Urbana
p 2916 N95-31736
Global Ultraviolet Imager (GUVI) investigation
[NASA-CR-189430] p 2917 N95-31820
The GCRC two-dimensional zonally averaged statistical dynamical climate model: Development, model performance, and climate sensitivity
p 2910 N95-31851

ATMOSPHERIC TURBULENCE
Optimum truncation of a Gaussian beam for propagation through atmospheric turbulence
[AD-A291156] p 2883 N95-30394
Digital simulation of wind velocities for wind turbine rotors: General considerations
[PB95-206447] p 2904 N95-31157
The effects of large and small scale turbulence on sound propagation in the atmosphere
[AD-A293657] p 2975 N95-31608

ATMOSPHERIC WINDOWS
Design of an immersion echelle-prism mid-IR spectrograph for chemical remote sensing
[DE95-010729] p 2901 N95-32027

ATMOSPHERICS
Validation of the atmospheric transmission large-area analysis system (ATLAS)
[AD-A293810] p 2916 N95-31589

ATOMIC BEAMS
Magneto-optical transmission-reflection beam splitter for multi-level atoms
[DE95-616267] p 2976 N95-30423
Reflection and diffraction of atomic de Broglie waves by evanescent laser waves. Bare-state method
[DE95-616458] p 2992 N95-30960
Resonance characteristics in the case of the excitation of a monoenergetic beam of free atoms by means of N. F. Ramsey's method
[IFTR-6/1995] p 2993 N95-31336
Determination of electric and magnetic fields in open trap plasmas by means of atomic-molecular beam hydrogen isotopes
[DE95-614177] p 3006 N95-31680
Detection of the phase shift which accompanies the excitation of an atomic beam by N. F. Ramsey's method
[IFTR-5/1995] p 2986 N95-31818

ATOMIC CLOCKS
Time activities at the BIPM p 2968 N95-32325
Relativistic timescale analysis suggests lunar theory revision p 2970 N95-32333
Monte Carlo simulations of precise timekeeping in the Milstar communication satellite system
p 2970 N95-32336
Metafitting: Weight optimization for least-squares fitting of PTTI data p 2971 N95-32340
Methodologies for steering clocks
p 2971 N95-32341
The effects of clock errors on timescale stability
p 2971 N95-32342
Relativistic theory for syntonization of clocks in the vicinity of the Earth p 2971 N95-32343
Allan deviation computations of a linear frequency synthesizer system using frequency domain techniques
p 2972 N95-32344
SVN 9 End-Of-Life testing p 2767 N95-32345
Laser retroreflector experiment on NAVSTAR 35 and 36 p 2887 N95-32347
(T2L2) Time Transfer by Laser Link
p 2887 N95-32348
Satellite test of the isotropy of the one-way spe ed of light using ExTRAS p 2973 N95-32349

ATOMIC COLLISIONS
Inversion of the total cross sections for electron-molecule and electron-atom scattering
[DE95-616466] p 2978 N95-30583
Analytic cross sections for collisions of H, H2, He and Li atoms and ions with atoms and molecules
[DE95-722055] p 2979 N95-30654
Operation of the computer model for direct atomic oxygen exposure of Earth satellites
[NASA-CR-198188] p 2767 N95-32189
Study of aligned states in ion-atom collisions
[DE95-010825] p 2990 N95-32275

ATOMIC ENERGY LEVELS
Magnetic resonance spectroscopy of fullerenes and (pi)-conjugated polymers
[DE95-010131] p 2817 N95-31108

ATOMIC EXCITATIONS
Inner- and outer-shell excitation in lithium isoelectronic sequence
[DE95-614107] p 2981 N95-31003
Resonance characteristics in the case of the excitation of a monoenergetic beam of free atoms by means of N. F. Ramsey's method
[IFTR-6/1995] p 2993 N95-31336
On the Jahn-Teller effect of Mn(2+) in zinc-blende ZnS crystal
[AD-A293711] p 2797 N95-31830
Study of aligned states in ion-atom collisions
[DE95-010825] p 2990 N95-32275

ATOMIC PHYSICS
Analytic cross sections for collisions of H, H2, He and Li atoms and ions with atoms and molecules
[DE95-722055] p 2979 N95-30654
Abstracts of Annual Physics Conference of Iran
[DE95-611717] p 2768 N95-30881
Atomic approaches in metastable antiprotonic helium atoms. Reply to Analysis of the lifetimes and fractions of antiprotons trapped in metastable antiprotonic helium states by I. Shimamhura and M. Kimura --- mura
[DE95-737228] p 2986 N95-31658
Studies of highly charged ions with EBIT and Super-EBIT
[DE95-010251] p 2987 N95-32038

ATOMIC SPECTRA
Analytic cross sections for collisions of H, H2, He and Li atoms and ions with atoms and molecules
[DE95-722055] p 2979 N95-30654

ATOMIC STRUCTURE
Direct determination of grain boundary atomic structure in SrTiO3
[DE95-008847] p 3010 N95-30544
EBIT: Electron Beam Ion Trap V-division experimental physics
[DE95-010207] p 3004 N95-30769
Theoretical aspects of electron emission holography
[DE95-614371] p 2880 N95-31167
Experiments with highly charged ions up to bare U(sup 92+) on the electron beam ion trap
[DE95-008827] p 2982 N95-31174
Acidity and basicity of nitro substituted imidazoles
p 2832 N95-31301
Conjugated aromatic polyimines. 2. Synthesis, structure, and properties of new aromatic polyazomethines
[AD-A292955] p 2819 N95-31461
Effects of molecular structure on the electroactive and optical properties of conjugated rigid-rod polybenzobisazoles
[AD-A292968] p 2819 N95-31467
Electronic structure of Donor-Spacer-Acceptor molecules of potential interest for molecular electronics III: Geometry and absorption spectrum of CH3-Alpha P3CNQ
[AD-A293662] p 2985 N95-31609
Electronic structure of Donor-Spacer-Acceptor molecules of potential interest for molecular electronics 4. Geometry and device properties of P3CNQ and Q3CNQ
[AD-A293717] p 2986 N95-31832
First-principles approaches to materials stability
[DE95-011533] p 2810 N95-32283

ATOMIZING
Atomization simulations using an Eulerian-VOF-Lagrangian method p 2828 N95-31210

Primary atomization of liquid jets issuing from rocket engine coaxial injectors p 2769 N95-31716

ATOMS

Theoretical absorption spectroscopy of high-temperature metal vapors: Model and experiment compared
[AD-A290872] p 2791 N95-30409

Low-density ionization behavior
[DE95-009495] p 2980 N95-30705

Effects of mosaicity on Parametric X-Radiation production
[AD-A293677] p 2985 N95-31597

Nuclear-spin-dependent parity-nonconserving effects in thallium, lead and bismuth atoms
[DE95-614120] p 2991 N95-32354

ATROPHY

Electromyostimulation, circuits and monitoring
[NASA-TM-110741] p 2926 N95-30846

ATTENUATION

Design of systems for active sound control
[PB95-197869] p 2973 N95-30461

ATTITUDE (INCLINATION)

Direct determination of grain boundary atomic structure in SrTiO3
[DE95-008847] p 3010 N95-30544

On the use of electronic tilt sensors as angle encoders for synchrotron applications
[DE95-005836] p 2880 N95-30941

Synthetic Terrain Imagery for Helmet-Mounted Display, volume 1
[AD-A293612] p 2753 N95-31656

ATTITUDE CONTROL

Practical experiences in control systems design using the NCR Bell 205 Airborne Simulator p 2761 N95-32015

AUDIO EQUIPMENT

Fractional delay waveguide modeling of acoustic tubes
[PB95-206637] p 2975 N95-31650

AUDIO FREQUENCIES

Characterization of an improved Rijke burner as prelude to measurements of aluminum distributed combustion p 2800 N95-31287

AUGER EFFECT

Inner- and outer-shell excitation in lithium isoelectronic sequence
[DE95-614107] p 2981 N95-31003

Theoretical aspects of electron emission holography
[DE95-614371] p 2880 N95-31167

AUGMENTATION

Mechanisms of enhanced ionic conduction at interfaces in ceramics
[DE95-009125] p 2814 N95-30730

Enhancements to the SSME transfer function modeling code
[NASA-CR-198957] p 2958 N95-30754

AASERT-92 augmentation of research training in chronobiology: Regulation of the mammalian circadian clock by neurotransmitters
[AD-A288243] p 2925 N95-31144

The 25th International Symposium on Combustion
[AD-A286825] p 2794 N95-31268

Aviation capacity enhancement plan 1994
[AD-A292758] p 2747 N95-31428

AURORAS

HST-FOC observations of a remarkable UV auroral event on Jupiter p 3030 N95-30806

Perpendicular electron heating by absorption of auroral kilometric radiation
[NASA-198815] p 2914 N95-30848

SSUSI single sensor auroral E-layer algorithm: Functional description
[AD-A288630] p 2914 N95-31012

Global Ultraviolet Imager (GUVI) investigation
[NASA-CR-189430] p 2917 N95-31820

AUSTENITE

Transitions, defects, and whiskered microstructures
[AD-A292796] p 3014 N95-31438

AUTOIONIZATION

Inner- and outer-shell excitation in lithium isoelectronic sequence
[DE95-614107] p 2981 N95-31003

AUTOMATA THEORY

France --- modeling and verification of parallel computer systems
[PB95-206385] p 2949 N95-32371

AUTOMATIC CONTROL

Laser Tracker 3: Sandia National Laboratories' third generation laser tracking system
[DE95-008525] p 2882 N95-30379

Passive range measurement system
[AD-D017344] p 2996 N95-30678

New adaptive methods for reconfigurable flight control systems, appendix 1
[AD-A292711] p 2756 N95-30937

Inversion of ERS-1 wavemode spectra. User's and programmer's guide
[PB95-223582] p 2902 N95-32316

France --- modeling and verification of parallel computer systems
[PB95-206385] p 2949 N95-32371

AUTOMATIC FLIGHT CONTROL

Automatic flight control system for an unmanned helicopter system design and flight test results p 2759 N95-32004

AUTOMATIC GAIN CONTROL

Noise signal processor
[AD-D017430] p 2974 N95-30747

AUTOMATIC LANDING CONTROL

Flight test evaluation of the Stanford University/United Airlines differential GPS Category 3 automatic landing system
[NASA-TM-110354] p 2743 N95-30788

AUTOMATIC PILOTS

Digital autopilot design for combat aircraft in ALENIA p 2760 N95-32009

AUTOMOBILE FUELS

BioFacts: Fueling a stronger economy. Methanol from biomass, revision 2
[DE95-010302] p 2836 N95-31638

BioFacts: Fueling a stronger economy. Ethanol from biomass, revision 2
[DE95-010304] p 2836 N95-31639

BioFacts: Fueling a stronger economy, global warming and biofuels emissions
[DE94-006864] p 2910 N95-31821

BioFacts: Fueling a stronger economy, thermochemical conversion of biomass
[DE94-006866] p 2905 N95-31822

Combatting urban air pollution through Natural Gas Vehicle (NGV) analysis, testing, and demonstration
[DE95-008300] p 2911 N95-32156

Liquid natural gas as a transportation fuel in the heavy trucking industry
[DE95-010376] p 2837 N95-32158

AUTONOMOUS NAVIGATION

Adaptive path planning: Algorithm and analysis
[DE95-008549] p 2950 N95-30463

Neural networks for real-time terrain typing
[AD-A293569] p 2953 N95-31540

AVERAGE

Particle filtration: An analysis using the method of volume averaging
[DE95-009467] p 2875 N95-31592

AVIATION PSYCHOLOGY

Human factors at the FAA Technical Center: Bibliography
[AD-A288638] p 2930 N95-31399

Controller resource management: What can we learn from aircrews?
[DOT/FAA/AM-95/21] p 2750 N95-32186

AVIONICS

Foundations of technology for constructing highly reliable distributed realtime systems
[AD-A293254] p 2931 N95-30892

Experimental Aircraft Programme (EAP): Flight control system design and test p 2760 N95-32010

AWARDS

Quality assurance tendering and awarding contracts
[PB95-197760] p 2891 N95-31362

AXIAL FLOW

Development of a linearized unsteady Euler analysis for turbomachinery blade rows
[NASA-CR-4677] p 2742 N95-30611

AXIAL FLOW PUMPS

Centrifugal and axial pump design and off-design performance prediction p 2830 N95-31289

AXIAL LOADS

Experimental determination of probability distributions for parameters of a Salem limestone cap plasticity model
[AD-A290878] p 2892 N95-30559

Axial loads on yawed rotors
[PB95-214193] p 2742 N95-30638

An inverse method to measure the axial modulus of composite materials under tension
[AD-A293042] p 2789 N95-31668

AXIAL STRAIN

Interfacial segregation and deformation of superplastically deformed Al-Mg-Mn alloys
[DE95-009572] p 2809 N95-32052

AXIOMS

Unification of LARCH and Z-based object models to support algebraically-based design refinement: The LARCH perspective
[AD-A289235] p 2935 N95-30999

Inductively coupled IR staring array based on photofluxonic pixels
[AD-A292784] p 2998 N95-31435

AXISYMMETRIC FLOW

An explanation for the shape of nanoindentation unloading curves based on finite element simulation
[DE95-008905] p 2812 N95-30548

A turbulence module for the NPARC code
[NASA-CR-198358] p 2959 N95-30855

Acceleration potential models PREDICHAT/PREDICDYN applied for calculation of axisymmetric dynamic inflow cases
[PB95-207015] p 2869 N95-30957

AZIMUTH

Apparent size passive range method
[AD-D017360] p 2753 N95-31180

AZOLES

Acidity and basicity of nitro substituted imidazoles p 2832 N95-31301

B

BACKGROUND NOISE

Background event discrimination in neutron time-of-flight measurements at beams of relativistic nuclei of the JINR synchrotron
[DE95-613006] p 2991 N95-30604

Automatic Target Recognition (ATR): Background statistics and the detection of targets in clutter
[AD-A293062] p 2853 N95-31673

Effects of correlated noise on the full-spectrum combining and complex-symbol combining arraying techniques p 2856 N95-32237

BACKGROUND RADIATION

Spectral sky background in the IR: Measurements with FTIR
[PB95-222998] p 2922 N95-32315

BACKSCATTERING

Zone axis backscattered electron contrast for fast electrons
[DE95-616775] p 2980 N95-30790

K-shell ionization under zone axis electron diffraction conditions
[DE95-616780] p 2981 N95-30916

Investigation of microwave backscatter from the air-sea interface
[NASA-CR-198854] p 2851 N95-31457

Physical optics polarization scattering matrix for a right-angle dihedral
[AD-A293036] p 3000 N95-31665

Middle atmosphere structure and dynamics: Lidar studies at the South Pole, Syowa and Urbana p 2916 N95-31736

The development of a pulsed laser imaging system for natural gas leak detection
[DE95-011407] p 2887 N95-32260

BACKUPS

An overview of high-speed networking for workstations
[DE95-009076] p 2947 N95-30577

BACKWARD WAVES

Harmonic gyrotron amplifiers and phase-locked oscillators
[AD-A293185] p 2861 N95-30979

BACTERIA

Design and processing of materials by biomimicking. Sections 1. Publications
[AD-A293852] p 2820 N95-31559

BAINITE

A study of Damascus steel
[DE95-010127] p 2809 N95-32023

BALL BEARINGS

Enhancement of perfluoropolyether boundary lubrication performance: I. Preliminary results
[NASA-TM-106937] p 2813 N95-30621

BALLISTIC MISSILES

Definition of an anti-missile ballistic defense architecture for Europe p 2840 N95-32125

Possible allied ballistic missile defense systems: Related guidance and control requirements p 2840 N95-32126

SOSIE: A pragmatic approach to the simulation of Broad Air Defense applied to the theater level p 2840 N95-32127

TMD detection and tracking using improved AWACS sensors p 2840 N95-32128

Acquisition, tracking, pointing and fire control for Ballistic Missile Defense p 2841 N95-32131

Using a Red Team to devise countermeasures p 2842 N95-32141

BALLISTIC RANGES

Aerophysics test program 1
[AD-A293890] p 2963 N95-31543

BALLISTICS

Three-dimensional (3D) large fluid flow computations for US Army applications on KSR-1, CM-200, CM-5, and Cray C-90
[AD-A293125] p 2869 N95-30889

BALLOONING MODES
Advances in the simulation of toroidal gyro Landau fluid model turbulence
[DE95-008387] p 3003 N95-30359
Reynolds stress of localized toroidal modes
[DE95-008750] p 3004 N95-30795
Stabilization of ballooning modes with sheared toroidal rotation
[DE95-008388] p 3006 N95-31624
Onset of ELMs in JT-60U
[DE95-737209] p 3007 N95-32263
BALTIC SEA
Radiometer measurements of sea ice in the Gulf of Bothnia 1992
[PB95-206611] p 2900 N95-30718
BANACH SPACE
Solvability of a class of hypersingular nonlinear integral equations
[PB95-207031] p 3011 N95-30720
BAND RATIOING
SeaWiFS Technical Report Series. Volume 29: SeaWiFS CZCS-type pigment algorithm
[NASA-TM-104566] p 2922 N95-30857
BAND STRUCTURE OF SOLIDS
The quantum interference effect in semiconductor space charge layers studied by Feynman path integrals: General formalism and illustrative examples
[DE95-614483] p 3010 N95-30653
BANDPASS FILTERS
Advanced signal processing filter
[AD-D017324] p 2848 N95-30917
BANDWIDTH
Diffraction-line broadening analysis and stress relaxation in thin metal layers
[PB95-213886] p 2893 N95-30634
Effective bandwidth techniques in bufferless and buffered ATM multiplexers
[PB95-207072] p 2862 N95-31185
Quantum 1/f noise in high technology applications including ultrasmall structures and devices
[AD-A292812] p 2862 N95-31442
Integrated high performance distributed system
[AD-A292821] p 2947 N95-31445
Towards optimum demodulation of bandwidth-limited and low SNR square-wave subcarrier signals
p 2855 N95-32229
BARIUM FLUORIDES
TV-VI semiconductor quantum well lasers, physics and engineering p 2883 N95-30805
BARIUM OXIDES
Innovative processing of composites for ultra-high temperature applications, book 3
[AD-A290891] p 2786 N95-30866
BARIUM TITANATES
Picosecond phase conjugation: New applications, devices, and materials
[AD-A293195] p 3013 N95-30982
BARS
An inverse method to measure the axial modulus of composite materials under tension
[AD-A293042] p 2789 N95-31668
BARYON RESONANCE
Do the narrow cryptoexotic baryon resonances exist?
[DE95-619291] p 2984 N95-31378
Search for exotic baryons with the SPHINX facility
[DE95-613774] p 2984 N95-31549
BARYONS
Strange-matter stars
[DE95-008446] p 3028 N95-30361
Large scale periodicity of the universe and baryogenesis
[DE95-613461] p 3028 N95-30366
Real Higgs singlet and electroweak phase transition in the standard model
[DE95-616315] p 2976 N95-30442
The 10th INS Scientific Computational Programs
[DE95-717864] p 2982 N95-31178
Double charmed baryons production at B-factory
[DE95-620540] p 2983 N95-31219
Do the narrow cryptoexotic baryon resonances exist?
[DE95-619291] p 2984 N95-31378
Unitarization of Koerner-Kuroda model of electromagnetic structure of octet 1/2(+) baryons
[DE95-613765] p 2984 N95-31548
Search for exotic baryons with the SPHINX facility
[DE95-613774] p 2984 N95-31549
Electroweak baryogenesis
[DE95-012169] p 2991 N95-32365
BASES (CHEMICAL)
Acidity and basicidity of nitro substituted imidazoles
[AD-A293969] p 2836 N95-31526
BAYES THEOREM
Acquiring consistent knowledge for Bayesian Forests
[AD-A293858] p 2952 N95-31517
Data analysis: Naive inductivism
[PB95-212213] p 3026 N95-32254
BAYS (TOPOGRAPHIC FEATURES)
Energy storage and alternatives to improve train voltage on a mass transit system
[DE95-010344] p 2906 N95-32090
BCS THEORY
Superconducting and normal-state properties of novel materials
[DE95-012368] p 3017 N95-32366
BEAM CURRENTS
The coupling impedance of a toroidal beam pipe with circular cross section
[DE95-010442] p 2993 N95-31405
BEAM INJECTION
Measurement of the effect of collimator generated wakefields on the beams in the SLC
[DE95-012101] p 2993 N95-31256
Determination of electric and magnetic fields in open trap plasmas by means of atomic-molecular beam hydrogen isotopes
[DE95-614177] p 3006 N95-31680
KRAKEN, a numerical model of RHIC impedances
[DE95-011563] p 2994 N95-32242
Design study of prototype accelerator and MeV test facility for demonstration of 1 MeV, 1 A negative ion beam production
[DE95-737208] p 2995 N95-32262
RFQ-DTL matching solutions for different requirements
[DE95-010897] p 2995 N95-32306
BEAM INTERACTIONS
Beam-beam effects
[DE95-008443] p 2991 N95-30360
A study of ion trapping and instability in the Fermilab antiproton accumulator p 2993 N95-31647
BEAM SPLITTERS
Magneto-optical transmission-reflection beam splitter for multi-level atoms
[DE95-616267] p 2976 N95-30423
BEAM WAVEGUIDES
Fiber optic reference frequency distribution to remote beam waveguide antennas p 2972 N95-32346
BEAMFORMING
Beam-beam effects
[DE95-008443] p 2991 N95-30360
Wavefront simulator for evaluating RF communication array signal processors
[AD-D017372] p 2847 N95-30660
Phase object display by using acousto-optical Bragg diffraction
[AD-A293153] p 2998 N95-31006
RFQ-DTL matching solutions for different requirements
[DE95-010897] p 2995 N95-32306
BEAMS (RADIATION)
Beam-beam effects
[DE95-008443] p 2991 N95-30360
The art and science of magnet design: Selected notes of Klaus Halbach, volume 2
[DE95-008450] p 2861 N95-31059
Advances in high-power chemical lasers
[AD-A289737] p 2885 N95-31389
On the search for exotic hadrons in the experiments with high energy hyperon beam
[DE95-620534] p 2989 N95-32261
RFQ-DTL matching solutions for different requirements
[DE95-010897] p 2995 N95-32306
BEAMS (SUPPORTS)
Modeling multi-beam structures for control
p 2895 N95-31346
Nonlinear dynamics and chaotic motions of a singularly perturbed nonlinear viscoelastic beam
p 2897 N95-31706
BEAUFORT SEA (NORTH AMERICA)
Sea ice stress research
[AD-A293164] p 2923 N95-30964
BELL AIRCRAFT
Practical experiences in control systems design using the NCR Bell 205 Airborne Simulator
p 2761 N95-32015
BEND TESTS
The effect of grain refinement on the room-temperature ductility of as-cast Fe3Al-based alloys
[DE95-010121] p 2805 N95-31107
Control of interfacial chemistry and mechanical properties in metal/ceramic composites
p 2790 N95-31976
BENDING
Interface degradation in CAS/Nicalon during elevated temperature aging
[DE95-008843] p 2812 N95-30543
Static behaviour of axially loaded uniplanar and multiplanar tubular x-joints
[PB95-207866] p 2892 N95-30585
BERYLLIUM ISOTOPES
Mixing phases of unstable two-level systems
[DE95-613844] p 2989 N95-32151
BETATRONS
Beam-beam effects
[DE95-008443] p 2991 N95-30360
BIAS
Plasma source ion implantation of metal ions: Synchronization of cathodic-arc plasma production and target bias pulses
[DE95-009431] p 3006 N95-31613
BIBLIOGRAPHIES
Workflow literature guide, version 1
[PB95-207080] p 2947 N95-30721
Space Sciences Laboratory Publications and Presentations
[NASA-TM-108484] p 3024 N95-30780
Bibliography of technical reports, 1993
[AD-A292741] p 2923 N95-30918
Human factors at the FAA Technical Center: Bibliography
[AD-A288638] p 2930 N95-31399
Swedish polar bibliography: A guide to Swedish literature on polar research, 1945-1988 with supplement, 1989-1992
[PB95-208161] p 2902 N95-32115
BICRYSTALS
Direct determination of grain boundary atomic structure in SrTiO3
[DE95-008847] p 3010 N95-30544
BIMETRIC THEORIES
Harmonic coordinates in the problem on static gravitational and massless scalar fields with a point source
[DE95-623632] p 3020 N95-32295
BINARY DATA
Gravitational-radiation damping of compact binary systems to second post-Newtonian order
[PB95-207882] p 2912 N95-30588
Gravitational waves from inspiralling compact binaries: Energy loss and waveform to second-post-Newtonian order
[PB95-207890] p 2913 N95-30590
Aspects of the search time in binary search trees modified according to the move-to-root heuristic
[PB95-212148] p 2963 N95-31396
Estimation in second order dependency model for multivariate binary data
[DE95-010326] p 2944 N95-32087
BINARY FLUIDS
Calculations of the sound scattering from fluid-filled spherical shell sonar targets
[DSTO-RR-0020] p 2974 N95-31365
BINARY SYSTEMS (MATERIALS)
Poisson's ratio for hexagonal crystals
[AD-A293556] p 3015 N95-31539
BINDING ENERGY
On explanation of proton electromagnetic form Factor near p (anti p)-threshold from the PS-170 experiment
[DE95-613766] p 2977 N95-30508
Observation of a low-binding-energy peak in the 2p core-level photoemission from oxidized Al(111)
[PB95-195350] p 2802 N95-30534
Applications of SXPS for studying surface structure, reaction mechanisms and kinetics
[DE95-008903] p 2803 N95-30547
Energetics of Pt adsorption on Pt(111)
[DE95-010933] p 3017 N95-32307
BINOCULAR VISION
Log-polar binocular vision system
[NASA-CR-188375] p 2996 N95-30772
BINOMIAL COEFFICIENTS
Canonical symmetric invariant pairings in vertex operator super algebras and gramians
[PB95-208112] p 2955 N95-30488
BIOCONVERSION
BioFacts: Fueling a stronger economy. Methanol from biomass, revision 2
[DE95-010302] p 2836 N95-31638
BioFacts: Fueling a stronger economy, thermochemical conversion of biomass
[DE94-006866] p 2905 N95-31822
BIODEGRADABILITY
Enhanced alkaline hydrolysis and biodegradability studies of nitrocellulose-bearing missile propellant
p 2772 N95-31752
BIODEGRADATION
Degradation of TCE using sequential anaerobic biofilm and aerobic immobilized bed reactor
p 2780 N95-31791
BIODYNAMICS
Vertical impact testing of two helmet-mounted night vision systems
[AD-A293055] p 2931 N95-31671

BIOINSTRUMENTATION
Biosensors based on cross-linking of biotinylated Glucose Oxidase by avidin
[AD-A290439] p 2925 N95-30452
BIOLOGICAL EFFECTS
Particulate air pollution and increased mortality: Biological plausibility for causal relationship
[DE95-006161] p 2909 N95-31703
BIOLOGICAL MODELS (MATHEMATICS)
SeaWiFS Technical Report Series. Volume 29: SeaWiFS CZCS-type pigment algorithm
[NASA-TM-104566] p 2922 N95-30857
Neurodynamical systems for cognition and target identification
[AD-A293111] p 2951 N95-30884
BIOMASS
Overview of IEA biomass combustion activities
[PB95-196374] p 2902 N95-30519
Biomass production by fescue and switchgrass alone and in mixed swards with legumes
[DE95-009137] p 2909 N95-31612
BioFacts: Fueling a stronger economy. Methanol from biomass, revision 2
[DE95-010302] p 2836 N95-31638
BioFacts: Fueling a stronger economy. Ethanol from biomass, revision 2
[DE95-010304] p 2836 N95-31639
BIOMASS ENERGY PRODUCTION
Overview of IEA biomass combustion activities
[PB95-196374] p 2902 N95-30519
Sleeping renewable beauty: Will the prince ever come
[PB95-214573] p 2903 N95-30640
Data on development of new energy technologies
[DE95-764135] p 2904 N95-31155
BioFacts: Fueling a stronger economy. Methanol from biomass, revision 2
[DE95-010302] p 2836 N95-31638
BioFacts: Fueling a stronger economy, global warming and biofuels emissions
[DE94-006864] p 2910 N95-31821
BioFacts: Fueling a stronger economy, thermochemical conversion of biomass
[DE94-006866] p 2905 N95-31822
BIOPHYSICS
Simulation of oculomotor post-inhibitory rebound burst firing using a Hodgkin-Huxley model of a neuron
[AD-A293821] p 2927 N95-31552
Summaries of fiscal year 1994 projects in medical applications and biophysical research
[DE95-010405] p 2925 N95-32040
BIOPOLYMER DENATURATION
Services to develop, standardize, and validate Polymerase Chain Reaction (PCR) protocols for the detection of leishmaniasis in clinical samples
[AD-A290155] p 2817 N95-31115
BIOREACTORS
STS-70 flight: Day 7
[NASA-TM-110665] p 2764 N95-30874
Degradation of TCE using sequential anaerobic biofilm and aerobic immobilized bed reactor
p 2780 N95-31791
BIOTIN
Biosensors based on cross-linking of biotinylated Glucose Oxidase by avidin
[AD-A290439] p 2925 N95-30452
BIPOLAR TRANSISTORS
Minority and majority carrier transport characterization in compound semiconductors
[DE95-010873] p 3014 N95-31233
BISMUTH
Nuclear-spin-dependent parity-nonconserving effects in thallium, lead and bismuth atoms
[DE95-614120] p 2991 N95-32354
BISMUTH COMPOUNDS
Photo-refractive Bi12SiO20: Spatial light modulator
[AD-A293084] p 3001 N95-32153
BIT ERROR RATE
Testing the performance of feedback concatenated decoder with a nonideal receiver p 2856 N95-32231
BIT SYNCHRONIZATION
Methodologies for steering clocks
p 2971 N95-32341
BITUMENS
Laboratory simulated hydrothermal alteration of sedimentary organic matter from Guaymas Basin, Gulf of California
[NASA-CR-198951] p 2914 N95-30865
BIVARIATE ANALYSIS
Estimation in second order dependency model for multivariate binary data
[DE95-010326] p 2944 N95-32087
BLACK HOLES (ASTRONOMY)
Theoretical high energy physics
[DE95-003107] p 2991 N95-30527
Gravitational-radiation damping of compact binary systems to second post-Newtonian order
[PB95-207882] p 2912 N95-30588
The conical singularity and quantum corrections to entropy of black hole
[DE95-613367] p 3029 N95-30606
Partons and black holes
[DE95-009921] p 3029 N95-31102
BLADE TIPS
Application of multigrid computational fluid dynamics (CFD) methods to rotor analysis
[AD-A293012] p 2874 N95-31475
Experimental and computational investigation of the tip clearance flow in a transonic axial compressor rotor
[NASA-TM-106711] p 2876 N95-31738
BLADE-VORTEX INTERACTION
Experimental and computational investigation of the tip clearance flow in a transonic axial compressor rotor
[NASA-TM-106711] p 2876 N95-31738
BLAST LOADS
Dry media blasting with wheat starch
p 2843 N95-32169
Paint removal and surface cleaning using ice particles
p 2844 N95-32171
Stripping with dry ice p 2844 N95-32172
Facilities used for plastic media blasting
p 2763 N95-32176
Operational parameters and material effects
p 2845 N95-32179
BLOCK COPOLYMERS
Intelligent synthetic polymers
[AD-A292905] p 2819 N95-31395
BLOOD CIRCULATION
Effects of air bubbles on rabbit blood brain barrier
[PB95-195293] p 2925 N95-30512
Arterial gas bubbles after decompression in pigs with Patent Foramen Ovale
[PB95-195319] p 2925 N95-30515
BLOOD FLOW
Control of skin blood flow in the neutral zone of human body temperature regulation
[AD-A291499] p 2926 N95-30563
BLOOD-BRAIN BARRIER
Effects of air bubbles on rabbit blood brain barrier
[PB95-195293] p 2925 N95-30512
BLOWING
Control of high Reynolds number round jets
p 2876 N95-31733
BLUNT BODIES
Analysis of planar laser-induced fluorescence images obtained during shakedown testing of the AEDC impulse facility
[AD-A293237] p 2884 N95-30906
The 25th International Symposium on Combustion
[AD-A286825] p 2794 N95-31268
Side force acting on blunted circular cylinder bodies at high angles of attack in supersonic flow
[NAL-TR-1255] p 2744 N95-31741
BODY CENTERED CUBIC LATTICES
Energetics of Pt adsorption on Pt(111)
[DE95-010933] p 3017 N95-32307
BODY TEMPERATURE
Control of skin blood flow in the neutral zone of human body temperature regulation
[AD-A291499] p 2926 N95-30563
BODY-WING CONFIGURATIONS
Transonic aerodynamic characteristics of a proposed wing-body reusable launch vehicle concept
[NASA-TM-108489] p 2742 N95-30712
Numerical investigation into vortical flow about a delta-wing configuration up to incidences at which vortex breakdown occurs in experiment
[PB95-198024] p 2743 N95-30837
BOEING AIRCRAFT
Development of advanced approach and departure procedures. Failure scenarios
[PB95-198123] p 2748 N95-30815
BOLTZMANN-VLASOV EQUATION
Dressing symmetry of the uniformization solution of Liouville equation
[DE95-613380] p 2956 N95-30607
Radial mode evolution in longitudinal bunched beam instability
[DE95-010895] p 2994 N95-32092
BOMBARDMENT
STM measurements of the interaction of vacancies and steps during low-energy-ion bombardment of Si(001)
[DE95-010935] p 3017 N95-32308
BONDED JOINTS
Cleanliness evaluation of rough surfaces with diffuse IR reflectance p 2782 N95-31804
The role of surface chemical analysis in a study to select replacement processes for TCA vapor degreasing
p 2782 N95-31809
BONDING
Formation of cavities in Si and their chemisorption of materials
[DE95-009586] p 2960 N95-30706
The effect of interface properties on nickel base alloy composites
[NASA-CR-198363] p 2785 N95-30787
BOOSTER ROCKET ENGINES
Environmentally compatible solid rocket propellants
p 2772 N95-31753
BOREHOLES
Development of the Multi-Level Seismic Receiver (MLSR)
[DE95-008823] p 2916 N95-31610
BORN APPROXIMATION
Reflection and diffraction of atomic de Broglie waves by evanescent laser waves. Bare-state method
[DE95-616458] p 2992 N95-30960
Radiative corrections to the three quantum annihilation cross section in high energy electron-positron collisions
[DE95-623675] p 2995 N95-32296
BORON
The structure and reactivity of boron and carbon surfaces
[AD-A292804] p 2795 N95-31440
BORON CARBIDES
Wettability of boron carbide
[PB95-196358] p 2802 N95-30518
BORON NITRIDES
Growth, characterization and device development in monocrystalline diamond films
[AD-A293106] p 3015 N95-32018
BOSONS
Dynamical analogy of Cabibbo-Kobayashi-Maskawa matrices
[DE95-613462] p 2975 N95-30367
Current issues in perturbative QCD
[DE95-008448] p 2975 N95-30388
The search for the decay of Z boson into two gamma as a test of Bose statistics
[DE95-616373] p 2976 N95-30393
CP violating effects in e(+) e(-) yields ZH and their optimization
[DE95-616302] p 2976 N95-30441
Confronting left-right symmetric models with electroweak precision data at the Z peak
[PB95-208054] p 2977 N95-30484
Properties of a multichannel resonant-level model
[DE95-614482] p 2979 N95-30652
Minijet veto: A tool for the heavy Higgs search at the LHC
[PB95-196234] p 2979 N95-30695
WW and WZ production at the tevatron
[DE95-011014] p 2981 N95-30970
Testing vector boson dominance of electroweak interactions via e(+)e(-) (yields) f-bar f
[DE95-620528] p 2982 N95-31214
Search for new physics indirect effects in e(+)e(-) yields W(+)W(-) at linear colliders with polarized beams
[DE95-613688] p 2984 N95-31547
Studies of the strong and electroweak interactions at the Z(sub 0) pole
[DE95-010353] p 2986 N95-31682
Search for anomalous ZZ(sub gamma) and Z(sub (gamma, gamma)) couplings with D0
[DE95-010457] p 2989 N95-32162
A measurement of quark and gluon jet differences at the Z(sup 0) resonance
[DE95-010666] p 2989 N95-32266
An experimental study of QCD and jets in e(+)e(-) annihilation
[DE95-010667] p 2989 N95-32267
BOUNDARIES
Operating system support for distributed multimedia applications: A survey of current research
[PB95-207098] p 2964 N95-30565
BOUNDARY CONDITIONS
Velocity boundary conditions for vorticity formulations of the incompressible Navier-Stokes equations
[DE95-008715] p 2966 N95-30464
On perturbative asymptotic of Regge trajectories
[DE95-613585] p 3018 N95-30636
The land component of the global climate system with adequate spatial resolution
[DE95-009323] p 2908 N95-30686
Solution of the three-dimensional Helmholtz equation with nonlocal boundary conditions
[NASA-TM-110174] p 2974 N95-30850
Probabilistic reliability modeling of fatigue on the H-46 tie bar
[AD-A289926] p 2751 N95-30927
Inverse and control problems in electromagnetics
[AD-A292993] p 2849 N95-30962
Stability prediction with rotational flow effects
p 2799 N95-31283

Role of free-surface boundary conditions and nonlinearities in wave/boundary-layer and wake interaction p 2872 N95-31317
Two-dimensional Finite Difference Time Domain (FD-TD) model of electromagnetic (EM) scattering from a buried rectangular object
[AD-A293685] p 2852 N95-31601

BOUNDARY ELEMENT METHOD
Simulation of viscous sintering
[PB95-197109] p 2868 N95-30636
A unified interpretation of singular and near-singular integrals in the boundary element method
[ISBN-0-315-86297-1] p 2962 N95-31947
Numerical evaluation of three-dimensional crack-tip integrals for layered anisotropic solids p 2898 N95-32191

BOUNDARY INTEGRAL METHOD
Inverse and control problems in electromagnetics
[AD-A292993] p 2849 N95-30962
A boundary integral equation approach to three dimensional electromagnetic wave scattering problems p 2853 N95-31839
Numerical evaluation of three-dimensional crack-tip integrals for layered anisotropic solids p 2898 N95-32191

BOUNDARY LAYER CONTROL
Active turbulence control using microelectrodes, permanent magnets in microgrooves
[AD-D017351] p 2867 N95-30553
Effects of cavity bleed and its configuration on aerodynamic characteristics of supersonic internal flow
[NAL-TR-1247] p 2744 N95-31715
Control of unsteady separated flow associated with the dynamic stall of airfoils
[NASA-CR-198972] p 2744 N95-32193

BOUNDARY LAYER FLOW
An experimental study of planar heterogeneous supersonic confined jets
[AD-A290859] p 2867 N95-30557
Shear-free turbulent boundary layers p 2873 N95-31349
Advanced k-epsilon modeling of heat transfer
[NASA-CR-4679] p 2874 N95-31423
Compressible turbulence measurement in low-angle injection into a supersonic flow
[AD-A293836] p 2874 N95-31516
Application of wavelet-filtering techniques to intermittent turbulent and wall pressure events. Part 2. Detection of cluster patterns
[AD-A293805] p 2875 N95-31586

BOUNDARY LAYER SEPARATION
Vorticity dynamics and control of dynamic stall
[AD-A288658] p 2756 N95-31400
Investigating the use of smart acoustically active surfaces for flow separation control in turbomachinery
[AD-A292819] p 2874 N95-31443
Control of unsteady separated flow associated with the dynamic stall of airfoils
[NASA-CR-198972] p 2744 N95-32193

BOUNDARY LAYERS
A numerical study of the starting process in a hypersonic shock tunnel p 2762 N95-30493
Low-latitude boundary layer near noon: An open field line model
[ATR-93(7270)-1] p 2914 N95-30773
A turbulence model for steady and unsteady boundary layers in strong pressure gradients p 2868 N95-30840
Role of free-surface boundary conditions and nonlinearities in wave/boundary-layer and wake interaction p 2872 N95-31317
Monte Carlo code for evaluating the Boundary Layer Illumination and Radiation Balance model (BLIRB)
[AD-A293963] p 2915 N95-31560
Numerical simulation of the Langevin equation for skewed turbulence
[DE95-009477] p 2877 N95-32049

BOUNDARY LUBRICATION
Enhancement of perfluoropolyether boundary lubrication performance: I. Preliminary results
[NASA-TM-106937] p 2813 N95-30621

BOUNDARY VALUE PROBLEMS
Singular eigenfunctions for shearing fluids I
[DE95-008952] p 2868 N95-30763
Existence of solutions in plane quasistationary stokes flow driven by surface tension
[PB95-197935] p 2868 N95-30810
A viscoelastic anisotropic wave propagation model for composite cure evaluation p 2786 N95-30839
A feedback linearization approach to orbital maneuvers p 2765 N95-30841
Numerical stability investigations of processes for solving linear initial value problems
[PB95-207023] p 2959 N95-31183
Effect of the stopping of the Newton iteration in implicit linear multistep methods
[PB95-207056] p 2959 N95-31184

BOW WAVES
Analysis of planar laser-induced fluorescence images obtained during shakedown testing of the AEDC impulse facility
[AD-A293237] p 2884 N95-30906

BRACKETS
Hamiltonian dynamics of the condensed media with spontaneously broken symmetry
[DE95-614448] p 3010 N95-30648

BRAGG ANGLE
May multiple inelastic scattering in CBED patterns be removed analytically
[PB95-196333] p 2992 N95-30717
Phase object display by using acousto-optical Bragg diffraction
[AD-A293153] p 2998 N95-31006
Technique to prepare high-reflectance optical fiber Bragg gratings with single exposure in-line or fiber draw tower
[AD-D017445] p 2998 N95-31270
Effects of mosaicity on Parametric X-Radiation production
[AD-A293677] p 2985 N95-31597

BRAIN
Effects of air bubbles on rabbit blood brain barrier
[PB95-195293] p 2925 N95-30512

BRANCHING (MATHEMATICS)
Bifurcations of contracting singular cycles
[DE95-613371] p 2962 N95-32117

BRAVAIS CRYSTALS
Bravais classes, Voronoie cells, Delone symbols
[PB95-207916] p 3009 N95-30503

BREADBOARD MODELS
Integrated X-ray testing of the electro-optical breadboard model for the XMM reflection grating spectrometer
[DE95-008829] p 2879 N95-30507
Development of a new instrument for rocket engine combustion diagnostics p 2799 N95-31211

BREAKWATERS
The determination of wave group parameters from the resolution of incident and reflected waves
[AD-A293703] p 2924 N95-31829

BREATHING APPARATUS
Effect of oxygen and decompression bubbles on inert gas washout
[PB95-196556] p 2925 N95-30665

BREMSSTRAHLUNG
Studying the thermal/non-thermal crossover in solar flares
[NASA-CR-189436] p 3031 N95-30785
Coulomb correction calculations of pp Bremsstrahlung
[DE95-616349] p 2982 N95-31176

BRIDGES (STRUCTURES)
Fatigue behaviour of multiplanar tubular joints
[PB95-207874] p 2893 N95-30586

BRIDGMAN METHOD
Numerical modeling of Bridgman growth of PbSnTe in a magnetic field
[NASA-TM-106996] p 2837 N95-31359

BRIGHTNESS
Diagnosing high density, fast-evolving plasmas using x-ray lasers
[DE95-010734] p 3006 N95-32028
Enhanced brightness x-ray lasers
[DE95-010735] p 2886 N95-32029

BRIGHTNESS TEMPERATURE
Weather influence on passive microwave brightness temperatures
[PB95-195384] p 2900 N95-30536
Radiometer measurements of sea ice in the Gulf of Bothnia 1992
[PB95-206611] p 2900 N95-30718
Comparison of satellite-derived MSU brightness temperatures and conventionally-derived fields
[AD-A293692] p 2901 N95-31603
Brightness temperature simulations for the physical and synoptic interpretation of advanced microwave sounding unit moisture channels p 2921 N95-31721

BRITTLE MATERIALS
High strain rate properties and constitutive modeling of glass
[DE95-008434] p 2816 N95-31058
Cracking during nanoindentation and its use in the measurement of fracture toughness
[DE95-008839] p 2818 N95-31175

BRITTLENESS
Interface degradation in CAS/Nicalon during elevated temperature aging
[DE95-006843] p 2812 N95-30543
Processing and characterization of nanocrystalline molybdenum disilicide (MoSi2) consolidated by hot isostatic pressing (HIP)
[DE95-010243] p 3012 N95-30756
The 10th International Conference on the Strength of Materials
[AD-A292335] p 2894 N95-31263
Initial survey on fracture toughness of commercial Nd2Fe14B
[DE95-009813] p 2808 N95-31643

BROADBAND
Microwave repeater with broadband active and/or passive isolation control
[AD-D017358] p 2846 N95-30417
Fractal quantum well heterostructures for broadband light emitters
[DE95-009579] p 2860 N95-30707
Noise signal processor
[AD-D017430] p 2974 N95-30747
Use of a variable frequency source with a single-mode cavity to process ceramic filaments
[DE95-010992] p 2817 N95-31152
Infrared and millimeter wave detection using thin films of Pb doped BiSrCaCuO superconductor p 2840 N95-32129

BROKEN SYMMETRY
Possible reason why leptons are lighter than quarks
[DE95-616383] p 2978 N95-30579
Hamiltonian dynamics of the condensed media with spontaneously broken symmetry
[DE95-614448] p 3010 N95-30648
Electromagnetic hadron mass differences and estimation of isotopic symmetry violation parameters of QCD vacuum from quark model
[DE95-613628] p 2985 N95-31621
SO(8) color as possible origin of generations
[DE95-613560] p 2988 N95-32069
Supersymmetric magnetic moments sum rules and spontaneous supersymmetry breaking
[DE95-613771] p 2989 N95-32096
Research progress report
[DE95-010726] p 3030 N95-32269

BROWNIAN MOVEMENTS
Particle filtration: An analysis using the method of volume averaging
[DE95-009467] p 2875 N95-31592

BRUSH SEALS
Brush seal shaft wear resistant coatings
[NASA-CR-198950] p 2889 N95-31382

BSCCO SUPERCONDUCTORS
Hydrostatic extrusion of BSCCO/Ag composite wire
[DE95-007862] p 2805 N95-31121
Solution based temperature of Perovskite-type oxide films and powders
[DE95-009089] p 2820 N95-31629
Infrared and millimeter wave detection using thin films of Pb doped BiSrCaCuO superconductor p 2840 N95-32129

BUBBLES
Decompression illness, observable bubbles. (Session K)
[PB95-195285] p 2926 N95-30511
Effects of air bubbles on rabbit blood brain barrier
[PB95-195293] p 2925 N95-30512
Detecting intravascular gas bubbles in ultrasonic images
[PB95-195301] p 2926 N95-30513
Arterial gas bubbles after decompression in pigs with Patent Foramen Ovale
[PB95-195319] p 2925 N95-30515
Effect of oxygen and decompression bubbles on inert gas washout
[PB95-196556] p 2925 N95-30665
Study of effect of bubbles on a free-shear layer p 2872 N95-31100

BUCKLING
Application of shallow shell stability to plant morphogenesis by Fourier series p 2897 N95-31734

BUCKMINSTERFULLERENE
Magnetic resonance spectroscopy of fullerenes and (pi)-conjugated polymers
[DE95-010131] p 2817 N95-31108

BUFFERS
Effective bandwidth techniques in bufferless and buffered ATM multiplexers
[PB95-207072] p 2862 N95-31185

BUNCHING
Radial mode evolution in longitudinal bunched beam instability
[DE95-010895] p 2994 N95-32092

BURNERS
Characterization of an improved Rijke burner as prelude to measurements of aluminum distributed combustion p 2800 N95-31287

BURNING RATE
Unsteady laser augmented combustion of pure oxidizers AP and RDX p 2799 N95-31284
Oscillatory combustion of aluminized AP/HTPB propellants p 2800 N95-31286
Model for defining propellant burn rate performance boundaries p 2800 N95-31290
Survey of US burning rate measurement methods for solid propulsion applications p 2800 N95-31291

Assessment of dynamic burning behavior for JA-2 propellant rods p 2800 N95-31299

BURNING TIME

Burn time measurements of single aluminum particles in steam and carbon dioxide mixtures p 2799 N95-30990

Burn time measurements of single aluminum particles in steam and carbon dioxide mixtures p 2799 N95-31198

BUTANES

Evaluation of halon alternatives in inerting experiments [AD-A293774] p 2795 N95-31580

BY-PRODUCTS

GCMS and FTIR studies of by-product inhibited growth and the rate-limiting step in TEOS-based SiO2 CVD [DE95-009863] p 3016 N95-32147

BYPASS RATIO

Wave rotor-enhanced gas turbine engines [NASA-TM-106998] p 2754 N95-30517

BYPASSES

Response of mechanically fastened composite joints under multiple bypass loads p 2785 N95-30824

C

C BAND

Multiparameter radar measurements of precipitation in complex terrain: Meteorological and hydrological applications [AD-A290786] p 2918 N95-30403

C++ (PROGRAMMING LANGUAGE)

C++ as an introductory programming language [PB95-195715] p 2933 N95-30539

CADMIUM

Cadmium plating replacements p 2776 N95-31773

CADMIUM ALLOYS

Volumetric and electro analytical techniques for chemical characterization of nuclear grade Ag-In-Cd alloys [DE95-620664] p 2807 N95-31407

CADMIUM SELENIDES

Semiconductor nanocrystals formed in SiO2 by ion implantation [DE95-008900] p 2978 N95-30546

CADMIUM TELLURIDES

Direct sublattice imaging of interface dislocation structures in CdTe/GaAs(001) [DE95-009031] p 3010 N95-30576

CALCIUM

Physiology and physiopathology of equilibration [PB95-208328] p 2926 N95-30494

Optical frequency standards: Hertz-level working standards and their absolute frequency measurement [AD-A293930] p 2999 N95-31515

CALCIUM FLUORIDES

Mechanisms of enhanced ionic conduction at interfaces in ceramics [DE95-009125] p 2814 N95-30730

CALCULUS

Barendregt cube with definitions and generalized reduction [PB95-206793] p 2966 N95-30719

Formalization of the ramified type theory [PB95-206785] p 2961 N95-31422

CALIBRATING

Standardization of (13)CO2 production procedure from organic matter for mass spectrometric analysis [DE95-614629] p 2791 N95-30420

Integrated X-ray testing of the electro-optical breadboard model for the XMM reflection grating spectrometer [DE95-008829] p 2879 N95-30507

FOG --- evaluation test of a fiber optic gyroscope (FOG) [PB95-211546] p 2879 N95-30600

Evaluation of calibration parameters and performance of the video imaging technique of assessing exposure (VITAE system) [AD-A289023] p 2927 N95-30998

Using satellites for radar performance monitoring and calibration [AD-A293809] p 2852 N95-31588

Standardization of surface contamination analysis systems p 2781 N95-31798

Calibration of multichannel analyzer of charge-exchange atoms [DE95-614178] p 2987 N95-32053

SeaWiFS technical report series. Volume 13: Case studies for SeaWiFS calibration and validation, part 1 [NASA-TM-104566-VOL-13] p 2924 N95-32220

Laboratory robotics: An automated tool for preparing Ion Chromatography calibration standards [DE95-009441] p 2798 N95-32318

High accuracy time transfer synchronization p 2968 N95-32321

Relativistic timescale analysis suggests lunar theory revision p 2970 N95-32333

Automated delay measurement system for an Earth station for Two-Way Satellite Time and Frequency Transfer p 2971 N95-32337

Metafitting: Weight optimization for least-squares fitting of PTTI data p 2971 N95-32340

CAMERAS

Passive range measurement system [AD-D017344] p 2996 N95-30678

STS-70 flight: Day 7 [NASA-TM-110665] p 2764 N95-30874

The future of space imaging. Report of a community-based study of an advanced camera for the Hubble Space Telescope [NASA-CR-198818] p 3028 N95-31364

The Wide Field/Planetary Camera 2 (WFPC-2) molecular adsorber [NASA-CR-198866] p 2881 N95-31456

Optimal infrared detector configurations for air target detection p 2841 N95-32130

CANADA

Architecture and implementation of a multi-sensor data fusion demonstration model within the real-time combat system of the Canadian Patrol Frigate p 2842 N95-32139

CANARD CONFIGURATIONS

Catapult-launching of the RAFALE design and experimentation p 2752 N95-32008

CANONICAL FORMS

Canonical symmetric invariant pairings in vertex operator super algebras and gramians [PB95-208112] p 2955 N95-30488

CANOPIES

Failure analysis for polycarbonate transparencies [AD-A292992] p 2820 N95-31471

CAPACITANCE

TV-VI semiconductor quantum well lasers, physics and engineering p 2883 N95-30805

Contactless characterization of semiconductors using laser-induced surface photo-charge voltage measurements [AD-A293618] p 2863 N95-31725

CAPACITANCE SWITCHES

Operational characteristics of a 200 C LC parallel resonant circuit [NASA-TM-106983] p 2864 N95-31742

CAPACITORS

Pre-amplifier with multi-stage feedback [AD-D017371] p 2859 N95-30659

Operational characteristics of a 200 C LC parallel resonant circuit [NASA-TM-106983] p 2864 N95-31742

CARBIDES

Modeling of grain boundary stresses in Alloy 600 [DE95-009033] p 2808 N95-31825

CARBON

Synthesis of carbo-nitride films using high-energy shock plasma deposition [DE95-615231] p 2811 N95-30450

Power oscillator in the tokamaks training [DE95-616538] p 3003 N95-30473

A metallurgical approach toward alloying in rare earth permanent magnet systems [DE95-010242] p 2966 N95-30668

Ultrasonic characterization of fiber-matrix interphasial properties and damage in high-temperature composites p 2785 N95-30823

Method of synthesizing high quality, doped diamond and diamonds and devices obtained therefrom [AD-D017432] p 3014 N95-31269

X-ray diffraction study of clusters in a-tC films [DE95-010860] p 2794 N95-31393

Ion-Assisted Pulsed Laser Deposition of amorphous tetrahedral-coordinated carbon films [DE95-010861] p 2885 N95-31394

The structure and reactivity of boron and carbon surfaces [AD-A292804] p 2795 N95-31440

Ionization of He by highly charged ions at low velocity [DE95-010815] p 2990 N95-32273

CARBON CYCLE

Global change research: Summaries of research in FY 1994 [DE95-009660] p 2908 N95-30755

Carbon dioxide concentrations in surface water and the atmosphere during 1986-1989 NOAA/PMEL cruises in the Pacific and Indian Oceans [DE95-009659] p 2910 N95-32099

CARBON DIOXIDE

Standardization of (13)CO2 production procedure from organic matter for mass spectrometric analysis [DE95-614629] p 2791 N95-30420

Development of a new instrument for rocket engine combustion diagnostics p 2799 N95-31211

A centrifuge CO2 pellet cleaning system p 2778 N95-31784

CO2 (dry ice) cleaning system p 2778 N95-31785

BioFacts: Fueling a stronger economy, global warming and biofuels emissions [DE94-006864] p 2910 N95-31821

Stripping with dry ice p 2844 N95-32172

CARBON DIOXIDE CONCENTRATION

Economical analysis relating to the global warming issue [DE95-764072] p 2908 N95-30677

Global change research: Summaries of research in FY 1994 [DE95-009660] p 2908 N95-30755

Carbon dioxide concentrations in surface water and the atmosphere during 1986-1989 NOAA/PMEL cruises in the Pacific and Indian Oceans [DE95-009659] p 2910 N95-32099

CARBON DIOXIDE LASERS

RDX laser-assisted flame structure p 2801 N95-31314

The physical and chemical processes governing CO2 laser-induced pyrolysis and combustion of the solid propellants RDX, ADN, XM39, and M43 p 2836 N95-31531

CARBON DIOXIDE REMOVAL

Standardization of (13)CO2 production procedure from organic matter for mass spectrometric analysis [DE95-614629] p 2791 N95-30420

CARBON FIBER REINFORCED PLASTICS

A study of elevated temperature testing techniques for the fatigue behavior of PMCS: Application to T650-35/AMB21 [NASA-TM-106927] p 2791 N95-32209

CARBON FIBERS

Intermodulation Interference (IMI) testing of composite materials [AD-A288621] p 2787 N95-31146

CARBON MONOXIDE

STM studies of clean, CO- and O2-exposed Pt(100)-hex-R0.7 deg [PB95-195376] p 3009 N95-30535

Molecular gas in starburst galaxies: Line intensities and physical conditions [PB95-208021] p 3029 N95-30569

The oxidation of carbon monoxide by nitrous oxide p 2801 N95-31309

The oxidation of carbon monoxide by nitrogen dioxide p 2801 N95-31310

An analysis of gas phase ethanol/water chemistry for diamond CVD [AD-A293009] p 2795 N95-31473

CARBONATES

Composite polymer electrolyte for lithium batteries [AD-A293924] p 2820 N95-31514

Bicarbonate of soda paint stripping process validation and material characterization p 2777 N95-31778

Carbon dioxide concentrations in surface water and the atmosphere during 1986-1989 NOAA/PMEL cruises in the Pacific and Indian Oceans [DE95-009659] p 2910 N95-32099

CARGO AIRCRAFT

Report to Congressional Committees. Military airlift: C-17 settlement is not a good deal [GAO/NSIAD-94-141] p 2741 N95-32198

CARIBBEAN REGION

Summary of 1993 Atlantic tropical cyclone activity and verification of author's forecast. A year of unanticipated light hurricane activity and a poor forecast: The expected dissipation of the El Nino did not take place and Caribbean basin surface pressure became quite high p 2918 N95-30842

CARRIER FREQUENCIES

Noise signal processor [AD-D017430] p 2974 N95-30747

Degradation in finite-harmonic subcarrier demodulation p 2855 N95-32228

CARRIER INJECTION

Method and apparatus for non-destructively measuring local resistivity of semiconductors [AD-D017436] p 2862 N95-31343

CARRIER MOBILITY

Electrical conductivity study on polythiophenes films [DE95-614309] p 2813 N95-30645

Minority and majority carrier transport characterization in compound semiconductors [DE95-010873] p 3014 N95-31233

Carrier dynamics and optical properties of GaAs- and InP-based strained quantum well lasers p 2886 N95-31848

CASCADE CONTROL

Pre-amplifier with multi-stage feedback [AD-D017371] p 2859 N95-30659

CASCADE FLOW
Improved modeling of unsteady heat transfer (The first step)
| AD-A292777 | p 2874 N95-31432
CASCADES
Microwave electro-optic mixer
| AD-D017328 | p 2862 N95-31179
CASSINI MISSION
GPHS-RTGs in support of the Cassini RTG Program
| DE95-010306 | p 2768 N95-30674
Welding isotopic heat sources for the cassini mission to Saturn
| DE95-060104 | p 2890 N95-32367
CAST ALLOYS
Effect of local melting on tribology in metal cutting
| PB95-195392 | p 2804 N95-31052
The effect of grain refinement on the room-temperature ductility of as-cast Fe3Al-based alloys
| DE95-010121 | p 2805 N95-31107
CASTING
Urethane foam process improvements
| DE95-008957 | p 2815 N95-30798
CATALOGS (PUBLICATIONS)
Album of simole perfect squared squares of order 26
| PB95-197398 | p 2954 N95-30401
CATALYSIS
Biosensors based on cross-linking of biotinylated Glucose Oxidase by avidin
| AD-A290439 | p 2925 N95-30452
Lanthanide(III) catalyzed reactions: Structure an d thermodynamics of intermediate complexes, and implications for reactivity
| PB95-197000 | p 3019 N95-30775
Extension of the pore tree model to describe pore interconnectivity
| AD-A290366 | p 2793 N95-30971
Electrified microheterogeneous catalysis
| AD-D017446 | p 2794 N95-31271
CATALYSTS
Catalytic reactions of synthesis gas. Part 4: Heterogeneous hydroformylation
| PB95-195558 | p 2791 N95-30537
Fischer-tropsch synthesis in supercritical fluids
| DE95-009631 | p 2792 N95-30709
Enantioselectivity of quinoprotein alcohol dehydrogenases: Production of enantiomerically pure C3-alcohol synthons
| PB95-196960 | p 2771 N95-30734
A study of catalysts and mechanisms in synthesis reactions
| DE95-010177 | p 2793 N95-30766
Porous spherical shells and microspheres by electrodispersion precipitation
| DE95-009073 | p 2815 N95-30799
Aqueous TiO2 photocatalysis of metal-EDTA complexes
| DE95-011058 | p 2793 N95-31113
CATALYTIC ACTIVITY
The oxidation of carbon monoxide by nitrous oxide
p 2801 N95-31309
CATAPULTS
Catapult-launching of the RAFALE design and experimentation p 2752 N95-32008
CATHODE RAY TUBES
Low-voltage cathodoluminescence of europium-activated yttrium orthovanadate
| DE95-008536 | p 3008 N95-30382
CATHODES
A Monte-Carlo model of ionic transport across a solid interface
| DE95-613447 | p 3011 N95-30737
X-band magnicon amplifier research at the Naval Research Laboratory
| AD-A293203 | p 3013 N95-30984
CATHODIC COATINGS
Off-potential measurement systems for impressed current cathodic protection
| AD-A290876 | p 2812 N95-30558
Comparison of cathodic protection currents on 70/30 copper-nickel and alloy 625 piping systems
| AD-A292953 | p 2807 N95-31561
CATHODOLUMINESCENCE
Low-voltage cathodoluminescence of europium-activated yttrium orthovanadate
| DE95-008536 | p 3008 N95-30382
Method and apparatus for a high resolution, flat panel cathodoluminescent display device
| AD-D017434 | p 2862 N95-31342
CATIONS
Measurements of quantum electrodynamic sensitive transitions in Na-like and Cu-like ions
| DE95-011593 | p 3007 N95-32299
CAVITATION FLOW
Large deformation failure mechanisms in nonlinear solids
| AD-A293010 | p 2898 N95-31474
Chaos-enhanced transport and aggregation in chaotic flows
| AD-A293892 | p 3020 N95-31545
Ultrasonic cleaning: Fundamental theory and application p 2778 N95-31783
An efficient numerical procedure for thermohydrodynamic analysis of cavitating bearings
| NASA-CR-195476 | p 2878 N95-32210
Film temperatures in the presence of cavitation
| NASA-CR-195481 | p 2878 N95-32216
CAVITIES
Microwave coupling into a slotted cavity. Additional results
| PB95-210381 | p 2847 N95-30629
Formation of cavities in Si and their chemisorption of materials
| DE95-009586 | p 2980 N95-30708
Use of a variable frequency source with a single-mode cavity to process ceramic filaments
| DE95-010992 | p 2817 N95-31152
Tunable ytterbium-doped solid state laser
| AD-D017449 | p 2885 N95-31274
Effects of cavity bleed and its configuration on aerodynamic characteristics of supersonic internal flow
| NAL-TR-1247 | p 2744 N95-31715
CAVITY RESONATORS
New material for high average power infrared generation: QPM-DB GaAs
| AD-A292714 | p 2967 N95-30939
X-band magnicon amplifier research at the Naval Research Laboratory
| AD-A293203 | p 3013 N95-30984
CELL MEMBRANES (BIOLOGY)
Membrane transport: A cellular probe of heat stroke
| AD-A293327 | p 2926 N95-30924
CEMENTITE
A study of Damascus steel
| DE95-010127 | p 2809 N95-32023
CEMENTS
LLW solidification in cement: Effect of dilution
| DE95-010108 | p 2798 N95-32091
CENSORED DATA (MATHEMATICS)
A Stochastic EM algorithm for approximating the maximum likelihood estimate
| DE95-010328 | p 2943 N95-32044
CENTRIFUGAL COMPRESSORS
Laser anemometer measurements of the three-dimensional rotor flow field in the NASA low-speed centrifugal compressor
| NASA-TP-3527 | p 2756 N95-31985
CENTRIFUGAL PUMPS
Centrifugal and axial pump design and off-design performance prediction p 2830 N95-31289
CENTRIFUGES
A centrifuge CO2 pellet cleaning system
p 2778 N95-31784
CEPHEID VARIABLES
Cepheid temperature and the Blazhko effect
| NASA-CR-189433 | p 3030 N95-31819
CERAMIC COATINGS
Off-potential measurement systems for impressed current cathodic protection
| AD-A290876 | p 2812 N95-30558
Brush seal shaft wear resistant coatings
| NASA-CR-198950 | p 2889 N95-31382
CERAMIC FIBERS
Innovative processing of composites for ultra-high temperature applications, book 3
| AD-A290891 | p 2786 N95-30866
Dielectric property measurement of zirconia fibers at high temperatures
| DE95-010991 | p 2821 N95-31705
CERAMIC HONEYCOMBS
The Wide Field/Planetary Camera 2 (WFPC-2) molecular adsorber
| NASA-CR-198866 | p 2881 N95-31456
CERAMIC MATRIX COMPOSITES
Interfacial studies of coated fiber reinforced glass-ceramic matrix composites
| AD-A290780 | p 2783 N95-30433
Innovative processing of composites for ultra-high temperature applications, book 3
| AD-A290891 | p 2786 N95-30866
Characterization of compressive damage mechanisms in ceramic and polymeric matrix composite materials
| AD-A293171 | p 2787 N95-30975
A numerical analysis of crack growth in microcracking ceramic and ceramic composites
| DE95-010132 | p 2897 N95-32024
Low cost fabrication of silicon carbide based ceramics and fiber reinforced composites
| NASA-TM-107001 | p 2822 N95-32208
CERAMICS
Ceramics derived from metal-organic precursors
| AD-A290791 | p 2811 N95-30405
Ion implantation and thermal stress resistance of ceramics
| DE95-615349 | p 2812 N95-30451
Molecular modeling of PMN ceramics
| AD-A290879 | p 2813 N95-30560
TEM-examination of ceramic-metal interfaces
| PB95-196531 | p 2813 N95-30664
Advanced computational research in materials processing for design and manufacturing
| DE95-009130 | p 2838 N95-30684
Mechanisms of enhanced ionic conduction at interfaces in ceramics
| DE95-009125 | p 2814 N95-30730
Porous spherical shells and microspheres by electrodispersion precipitation
| DE95-009073 | p 2815 N95-30799
Ultrasonic characterization of fiber-matrix interphasial properties and damage in high-temperature composites
p 2785 N95-30823
Ceramic/Metal Composite Circuit-Board-Level Technology for Application Specific Electronic Modules (ASEM's)
| AD-A293183 | p 2787 N95-30978
Investigations of YBaCuO materials with near-room-temperature resistivity transitions
| AD-A293405 | p 3013 N95-31008
Germanate glass ceramic
| AD-D017418 | p 2816 N95-31011
An assessment of the cost of microwave sintering ceramic tiles for armor applications. Phase 2 report
| DE95-010000 | p 2816 N95-31103
Life prediction methodology for ceramic components of advanced heat engines: Phase 1. Volume 1
| DE95-010805 | p 2817 N95-31135
Life prediction methodology for ceramic components of advanced heat engines. Phase 1: Volume 2. Appendices
| DE95-010806 | p 2817 N95-31136
Use of a variable frequency source with a single-mode cavity to process ceramic filaments
| DE95-010992 | p 2817 N95-31152
Low temperature fabrication from nano-size ceramic powders
| DE95-010995 | p 2818 N95-31153
Cracking during nanoindentation and its use in the measurement of fracture toughness
| DE95-008839 | p 2818 N95-31175
The 10th International Conference on the Strength of Materials
| AD-A292335 | p 2894 N95-31263
Design and processing of materials by biomimicking. Sections 1. Publications
| AD-A293852 | p 2820 N95-31559
Differences in creep performance of a HIPed silicon nitride in ambient air and inert environments
| DE95-009172 | p 2796 N95-31633
Control of interfacial chemistry and mechanical properties in metal/ceramic composites
p 2790 N95-31976
A numerical analysis of crack growth in microcracking ceramic and ceramic composites
| DE95-010132 | p 2897 N95-32024
Predictions of tensile behavior and strengths of a Si3N4 ceramic at high temperatures based on a viscoplastic model
| DE95-010220 | p 2821 N95-32025
Development of large-area monolithically integrated Silicon-Film(trademark) photovoltaic modules
| DE95-004089 | p 2906 N95-32057
Low cost fabrication of silicon carbide based ceramics and fiber reinforced composites
| NASA-TM-107001 | p 2822 N95-32208
Study of the surface properties of ceramic materials by chromatography
| DE95-011578 | p 2823 N95-32298
Whisker reinforced glass ceramic
| DE95-010542 | p 2823 N95-32305
Nondestructive testing of ceramic components: Cooperative Research and Development Agreement completion report
| DE95-009510 | p 2823 N95-32352
CERENKOV COUNTERS
Long baseline neutrino oscillation experiment at the AGS
| DE95-004378 | p 2986 N95-31702
CERENKOV RADIATION
The radiation conditioned by the 'velocity part' of the electromagnetic field of a moving charge
| DE95-613366 | p 2846 N95-30605
CERIUM
An experimental search for high ZT semiconductors: A survey of the preparation and properties of several alloy systems
| DE95-010232 | p 2865 N95-32084

CERIUM OXIDES
Morphology and microstructure of (111) crystalline CeO2 films grown on amorphous SiO2 substrates by pulsed-laser ablation
| DE95-008842 | p 3009 N95-30542
CERTIFICATION
Flight test evaluation of the Stanford University/United Airlines differential GPS Category 3 automatic landing system
| NASA-TM-110354 | p 2743 N95-30788
Experimental control in software reliability certification p 2938 N95-31248
Photovoltaic module certification/laboratory accreditation criteria development
| DE95-004063 | p 2905 N95-31381
CESIUM
Resonance characteristics in the case of the excitation of a monoenergetic beam of free atoms by means of N. F. Ramsey's method
| IFTR-6/1995 | p 2993 N95-31336
The 26th Annual Precise Time and Time Interval (PTTI) Applications and Planning Meeting
| NASA-CP-3302 | p 2967 N95-32319
High accuracy time transfer synchronization p 2968 N95-32321
Investigation into the effects of VHF and UHF band radiation on Hewlett-Packard (HP) Cesium Beam Frequency Standards p 2970 N95-32332
The effects of clock errors on timescale stability p 2971 N95-32342
Allan deviation computations of a linear frequency synthesizer system using frequency domain techniques p 2972 N95-32344
CHANGE DETECTION
Surface inspection using FTIR spectroscopy p 2782 N95-31803
CHANNEL FLOW
K-shell ionization under zone axis electron diffraction conditions
| DE95-616780 | p 2981 N95-30916
On the interactions between particles and turbulence in a fully-developed channel flow in air p 2875 N95-31707
CHANNEL NOISE
Noisy-network acceptors
| PB95-197976 | p 2951 N95-30813
CHANNELS (DATA TRANSMISSION)
Design and testing of an optimal digital link capable of 14-channel transmission
| AD-A288505 | p 3000 N95-31652
Rate considerations in deep space telemetry p 2765 N95-32223
Computer simulation results for PCM/PM/NRZ receivers in nonideal channels p 2765 N95-32225
CHAOS
Chaos-enhanced transport and aggregation in chaotic flows
| AD-A293892 | p 3020 N95-31545
Nonlinear dynamics and chaotic motions of a singularly perturbed nonlinear viscoelastic beam p 2897 N95-31706
CHARACTER RECOGNITION
Adaptive image enhancement of text images that contain touching or broken characters
| DE95-010173 | p 3023 N95-30620
Optical feature recognition
| AD-A293168 | p 2997 N95-30966
An evaluation of an automatic markup system
| DE95-009885 | p 3026 N95-32149
CHARACTERIZATION
Characterization of an improved Rijke burner as prelude to measurements of aluminum distributed combustion p 2800 N95-31287
Conjugated aromatic polyimines. 2. Synthesis, structure, and properties of new aromatic polyazomethines
| AD-A292955 | p 2819 N95-31461
Growth, characterization and device development in monocrystalline diamond films
| AD-A293106 | p 3015 N95-32018
CHARGE COUPLED DEVICES
The future of space imaging. Report of a community-based study of an advanced camera for the Hubble Space Telescope
| NASA-CR-198818 | p 3028 N95-31364
Folded compact range development and coherent change detection measurement project
| DE95-009082 | p 2853 N95-31628
CHARGE EXCHANGE
Experimental results on charge exchange reactions with delta excitations and polarization studies of delta and N(sup *) (1440) resonances
| DE95-614022 | p 2981 N95-30913
CHARGE TRANSFER
Excited-state complexes of conjugated polymers: Novel photophysical processes and optoelectronic materials
| AD-A292958 | p 2819 N95-31462
Excited-state complexes of conjugated polymers
| AD-A292960 | p 2819 N95-31466
Theory and simulation of electrostatic wave turbulence in the space shuttle-induced plasma environment
| AD-A293467 | p 3005 N95-31534
Electronic structure of Donor-Spacer-Acceptor molecules of potential interest for molecular electronics 4. Geometry and device properties of P3CNQ and Q3CNQ
| AD-A293717 | p 2986 N95-31832
CHARGED PARTICLES
Hamiltonian formulation of two body problem in Wheeler-Feynman electrodynamics
| DE95-620526 | p 3019 N95-31193
The coupling impedance of a toroidal beam pipe with circular cross section
| DE95-010442 | p 2993 N95-31405
Quantum 1/f noise in high technology applications including ultrasmall structures and devices
| AD-A292812 | p 2862 N95-31442
Oxygen charge state abundance in the inner magnetosphere
| AD-A293497 | p 2915 N95-31536
Effects of mosaicity on Parametric X-Radiation production
| AD-A293677 | p 2985 N95-31597
Renormcharges in V-A theories
| DE95-613689 | p 2985 N95-31622
Longitudinal losses of charged particles from an open configuration with arbitrary beta ratio
| DE95-614187 | p 2987 N95-32055
CHARM (PARTICLE PHYSICS)
Hadronic production of S-wave and P-wave charmed beauty mesons via heavy quark fragmentation
| DE95-008737 | p 2977 N95-30465
Do the narrow cryptoexotic baryon resonances exist?
| DE95-619291 | p 2984 N95-31378
Charm photoproduction dynamics
| DE95-009106 | p 2990 N95-32303
CHARTS
Luminance effects on visual acuity and small letter contrast sensitivity
| AD-A293310 | p 2928 N95-31140
An exploratory survey of information requirements for instrument approach charts
| AD-A293882 | p 2749 N95-31520
CHECKOUT
Applying program comprehension techniques to improve software inspections p 2937 N95-31241
CHELATION
A theoretical treatment of the absorption and emission properties of Cu(2) porphyrin
| AD-A293669 | p 2795 N95-31595
CHEMICAL ANALYSIS
Processing and characterization of nanocrystalline molybdenum disilicide (MoSi2) consolidated by hot isostatic pressing (HIP)
| DE95-010243 | p 3012 N95-30756
Shuttle Redesigned Solid Rocket Motor aluminum oxide investigations p 2770 N95-31197
Surface contamination analysis technology team overview p 2781 N95-31797
Standardization of surface contamination analysis systems p 2781 N95-31798
The role of surface chemical analysis in a study to select replacement processes for TCA vapor degreasing p 2782 N95-31809
Waste minimization via preparative scale high performance gel permeation chromatography
| DE95-011797 | p 2798 N95-32360
CHEMICAL BONDS
Direct determination of grain boundary atomic structure in SrTiO3
| DE95-008847 | p 3010 N95-30544
Molecular modeling of PMN ceramics
| AD-A290879 | p 2813 N95-30560
CHEMICAL CLEANING
The 19th Annual Electronics Manufacturing Seminar
| AD-A293067 | p 2863 N95-31674
Aqueous cleaning design presentation p 2778 N95-31781
CO2 (dry ice) cleaning system p 2778 N95-31785
Aqueous cleaning and verification processes for precision cleaning of small parts p 2779 N95-31787
QFD analysis of RSRM aqueous cleaners p 2779 N95-31789
A design of experiments test to define critical spray cleaning parameters for Brulin 815 GD and Jettacin cleaners p 2779 N95-31790
Cleaning without chlorinated solvents p 2780 N95-31792
Evaluation of control parameters for Spray-In-Air (SIA) aqueous cleaning for shuttle RSRM hardware p 2780 N95-31794
Environmentally compatible hand wipe cleaning solvents p 2780 N95-31795
Implementation of environmentally compliant cleaning and insulation bonding for MNASA p 2780 N95-31796
CHEMICAL COMPOSITION
ARTI Refrigerant Database
| DE95-008336 | p 2816 N95-31057
Self-lubricating, TiN-MoS2 composite coatings produced by simultaneous deposition from Ti((CH3))2N4/NH3/MoF6H2S gas mixture
| DE95-010359 | p 2788 N95-31403
CHEMICAL ENGINEERING
Prospector 7: Small fuel cells for portable power workshop
| AD-A292729 | p 2904 N95-30947
Aerospace Environmental Technology Conference: Exectutive summary
| NASA-CP-3297 | p 2771 N95-31350
JPRS report: Science and technology. Central Eurasia
| JPRS-UST-95-025 | p 2771 N95-31360
CHEMICAL EXPLOSIONS
Base hydrolysis and hydrothermal processing of PBX-9404 explosive
| DE95-009437 | p 2836 N95-32048
Base hydrolysis and hydrothermal processing of PBX-9404 explosive
| DE95-009497 | p 2837 N95-32355
CHEMICAL LASERS
The 25th International Symposium on Combustion
| AD-A286825 | p 2794 N95-31268
Advances in high-power chemical lasers
| AD-A289737 | p 2885 N95-31389
CHEMICAL PROPERTIES
Structural, chemical and electronic properties of superconducting thin films and junctions
| AD-A292700 | p 3012 N95-30933
ARTI Refrigerant Database
| DE95-008336 | p 2816 N95-31057
Volumetric and electro analytical techniques for chemical characterization of nuclear grade Ag-In-Cd alloys
| DE95-620664 | p 2807 N95-31407
CHEMICAL PROPULSION
Survey of US burning rate measurement methods for solid propulsion applications p 2800 N95-31291
Manufacturing waste disposal practices of the chemical propulsion industry p 2771 N95-31748
Environmental benefits of chemical propulsion p 2772 N95-31750
CHEMICAL REACTIONS
Preparation of diisopropyl stibines and use thereof
| AD-D017419 | p 2771 N95-30418
Catalytic reactions of synthesis gas. Part 4: Heterogeneous hydroformylation
| PB95-195558 | p 2791 N95-30537
Method for laser-assisted silicon etching using halocarbon ambients
| AD-D017426 | p 2883 N95-30744
Lanthanide(III) catalyzed reactions: Structure an d thermodynamics of intermediate complexes, and implications for reactivity
| PB95-197000 | p 3019 N95-30775
Electrified microheterogeneous catalysis
| AD-D017446 | p 2794 N95-31271
An ab initio study of the reaction HNO + NO yields OH + N2O: Preliminary results p 2801 N95-31308
Studies of reactions pertaining to and development of a reduced mechanism for the double base propellant dark zone p 2801 N95-31312
The physical and chemical processes governing CO2 laser-induced pyrolysis and combustion of the solid propellants RDX, ADN, XM39, and M43 p 2836 N95-31531
Prioritization methodology for chemical replacement p 2773 N95-31757
CHEMICAL REACTORS
No-thermal plasma processing of VOCs and NO(x) at LLNL
| DE95-011445 | p 2911 N95-32281
Optimal heat transfer design of chemical vapor deposition reactors
| DE95-010997 | p 2878 N95-32309
CHEMICAL TESTS
Residual stresses and stress corrosion cracking in pipe fittings
| DE95-009332 | p 2894 N95-31054
CHEMISORPTION
Formation of cavities in Si and their chemisorption of materials
| DE95-009586 | p 2980 N95-30708
CHEMOTHERAPY
Laser induced vitreoretinal scarring. Evaluation of causative factors and a therapeutic approach
| AD-A293742 | p 2928 N95-31570
CHIPS
Overview of IEA biomass combustion activities
| PB95-196374 | p 2902 N95-30519

CHIPS (ELECTRONICS)
Diamond thin film temperature and heat-flux sensors
[NASA-CR-198659] p 3012 N95-30847
Decimation of encoding errors in an optimum SNS 2 micron low-noise CMOS ADC
[AD-A293208] p 2860 N95-30900
Intelligent finite element submodeling of multichip modules for reliability analysis
[AD-A292911] p 2940 N95-31455
CHIRAL DYNAMICS
Reflection and transmission of electromagnetic plane waves from a uniaxial chiro-omega slab
[PB95-206629] p 2853 N95-31649
CHIRALITY
What's wrong with anomalous chiral gauge theory?
[DE95-616285] p 3018 N95-30437
Electroweak interactions on the lattice
[DE95-616287] p 2965 N95-30439
Chiral gauge theory in four dimensions
[DE95-616288] p 3018 N95-30440
Instantaneous chiral quark model for relativistic mesons in a hot and dense medium
[DE95-613782] p 2960 N95-30911
Plane wave reflection from a uniaxial chiral quarter-wave polarization transformer
[PB95-206512] p 2849 N95-31159
Effective chiral-spin Hamiltonian for odd-numbered coupled Heisenberg chains
[DE95-614445] p 2982 N95-31168
Global aspects of the WZNW reduction to Toda theories
[DE95-737230] p 3019 N95-31226
Applications of chiral symmetry
[DE95-009552] p 2988 N95-32079
CHLORIDES
Conjugated aromatic polyimines. 2. Synthesis, structure, and properties of new aromatic polyazomethines
[AD-A292955] p 2819 N95-31461
CHLORINATION
Urethane foam process improvements
[DE95-008957] p 2815 N95-30798
CHLOROETHYLENE
Degradation of TCE using sequential anaerobic biofilm and aerobic immobilized bed reactor
p 2780 N95-31791
CHLOROFLUOROCARBONS
Method for laser-assisted silicon etching using halocarbon ambients
[AD-D017426] p 2883 N95-30744
Compatibility of refrigerants and lubricants with motor materials under retrofit conditions
[DE95-010185] p 2814 N95-30767
CFC-replacement by natural working fluids: R&D and industrial challenges within the refrigeration, air conditioning amd heat pump areas
[PB95-195756] p 2815 N95-30871
Aerospace Environmental Technology Conference: Exectutive summary
[NASA-CP-3297] p 2771 N95-31350
Aerospace Environmental Technology Conference
[NASA-CP-3298] p 2771 N95-31746
The search for CFC alternatives is over?
p 2774 N95-31760
The Oak Ridge Refrigerant Management Program
p 2774 N95-31763
Evaluation of HFC 245ca and HFC 236ea as foam blowing agents p 2775 N95-31766
Aqueous cleaning design presentation
p 2778 N95-31781
Aqueous cleaning and verification processes for precision cleaning of small parts p 2779 N95-31787
Development of a CFC Critical Area Response (CAR) package p 2783 N95-31814
CHLOROPHYLLS
SeaWiFS Technical Report Series. Volume 29: SeaWiFS CZCS-type pigment algorithm
[NASA-TM-104566] p 2922 N95-30857
CHROMATES
Replacement of corrosion protection chromate primers and paints used in cryogenic applications on the Space Shuttle with wire arc sprayed aluminum coatings
p 2776 N95-31774
Treatment of plastic media waste
p 2844 N95-32177
Minutes of the fourth annual workshop on chromate replacements in light metal finishing
[DE95-010937] p 2810 N95-32241
CHROMATOGRAPHY
Determination of halogens in a petroleum product by ion chromatography
[DE95-002056] p 2797 N95-31840
Study of the surface properties of ceramic materials by chromatography
[DE95-011578] p 2823 N95-32298
Laboratory robotics: An automated tool for preparing Ion Chromatography calibration standards
[DE95-009441] p 2798 N95-32318
CHROMIC ACID
Thin-film sulfuric acid anodizing as a replacement for chromic acid anodizing p 2776 N95-31772
CHROMIUM
Metrology of chrome on quartz photomasks using low voltage scanning electron microscopy. Part 1: Physical SEM parameters
[PB95-195780] p 2880 N95-30693
Magnesium battery disposal characteristics
[AD-A293053] p 2863 N95-31607
Industry participation workshop: Chromium electroplating of superconductor strand. Proceedings
[DE95-009629] p 2807 N95-31615
On the possibility of a two-state magnetic structure for nanocrystalline chromium
[DE95-009914] p 3015 N95-32062
Luminescence properties of ZnWO4:Cr(3+) laser crystals
[AD-A293065] p 2887 N95-32152
Femtosecond, Cr(4+):YAG laser
[DE95-004964] p 2887 N95-32155
CHROMIUM ALLOYS
The electrodeposition of low contraction chromium/molybdenum alloys using pulse-reverse plating
[AD-A292727] p 2804 N95-30945
Comparison of cathodic protection currents on 70/30 copper-nickel and alloy 625 piping systems
[AD-A292953] p 2807 N95-31561
CHROMIUM COMPOUNDS
Trivalent chromium solutions for sealing anodized aluminum
[AD-D017349] p 2803 N95-30551
CHROMIUM OXIDES
K-shell ionization under zone axis electron diffraction conditions
[DE95-616780] p 2981 N95-30916
CHROMOPHORES
Nonlinear optical processes in polymer films
[AD-A293384] p 2815 N95-30955
CHROMOSPHERE
Studying the thermal/non-thermal crossover in solar flares
[NASA-CR-189436] p 3031 N95-30785
CIRCADIAN RHYTHMS
AASERT-92 augmentation of research training in chronobiology: Regulation of the mammalian circadian clock by neurotransmitters
[AD-A288243] p 2925 N95-31144
CIRCUIT BOARDS
Visualization of circuit card electromagnetic fields
[AD-A291491] p 2845 N95-30398
BASIS image processor PR5200: Module Common Part
[PB95-212023] p 2933 N95-30501
Ceramic/Metal Composite Circuit-Board-Level Technology for Application Specific Electronic Modules (ASEM's)
[AD-A293183] p 2787 N95-30978
CIRCUIT BREAKERS
Electrical short circuit and current overload tests on aircraft wiring
[AD-A293308] p 2860 N95-30922
CIRCUITS
Voltage surge suppression power circuits
[AD-D017454] p 2860 N95-30726
Coherent integrator
[AD-D017422] p 2847 N95-30743
Noise signal processor
[AD-D017430] p 2974 N95-30747
X-band magnicon amplifier research at the Naval Research Laboratory
[AD-A293208] p 3013 N95-30984
HTS Josephson technology on silicon with application to high speed digital microelectronics
[AD-A288627] p 2861 N95-31147
Multi-dimensional data compression for portable communication
[AD-A292751] p 2850 N95-31426
The 19th Annual Electronics Manufacturing Seminar
[AD-A293067] p 2863 N95-31674
A time stepping coupled finite element-state space modeling environment for synchronous machine performance and design analysis in the ABC frame of reference p 2864 N95-31948
CIRCULAR CYLINDERS
Propagation and scattering of elastic waves in laminated circular cylinders
[ISBN-0-315-85957-1] p 2848 N95-30828
CIRCULAR POLARIZATION
Polarisation resonance in X-ray diffraction
[DE95-616727] p 3012 N95-30789
CIRCULAR TUBES
Electrically heated tube investigation of cooling channel geometry effects
[NASA-TM-106985] p 2768 N95-30856
The coupling impedance of a toroidal beam pipe with circular cross section
[DE95-010442] p 2993 N95-31405
CIRCULATION
Demonstration of split-flow ventilation and recirculation as flow-reduction methods in an Air Force paint spray booth, volume 2
[AD-A286808] p 2762 N95-30926
CIRRUS CLOUDS
Clouds: Their prediction and simulation
[AD-A292864] p 2920 N95-31453
CIVIL AVIATION
Development of advanced approach and departure procedures. Failure scenarios
[PB95-198123] p 2748 N95-30815
Human factors at the FAA Technical Center: Bibliography
[AD-A288638] p 2930 N95-31399
Effects of civil tiltrotor service in the northeast corridor on en route airspace loads
[AD-A293586] p 2747 N95-31687
Integration of air traffic databases: A case study
[AD-A293691] p 2749 N95-32022
Special investigation report: Safety of the air tour industry in the United States
[PB95-917004] p 2748 N95-32185
CLASSICAL MECHANICS
Elliptic deformed classical mechanics in three-dimensional phase space
[DE95-613384] p 3017 N95-30365
Gibbs measures and quasi-periodic solutions for nonlinear Hamiltonian partial differential equations
[PB95-207932] p 2956 N95-30506
CLASSIFICATIONS
Bravais classes, Voronoie cells, Delone symbols
[PB95-207916] p 3009 N95-30503
Arithmetic features of rational conformal field theory
[PB95-207908] p 2966 N95-30591
Exact smooth classification of Hamiltonian vector fields on symplectic 2-manifolds
[DE95-613378] p 2958 N95-30803
Fuel-type classification and parameters prediction by Gas Liquid Chromatography analysis
[AD-A293442] p 2794 N95-31368
Paint removal principles p 2843 N95-32167
CLAYS
LLW solidification in cement: Effect of dilution
[DE95-010108] p 2798 N95-32091
CLEAN FUELS
BioFacts: Fueling a stronger economy. Ethanol from biomass, revision 2
[DE95-010304] p 2836 N95-31639
CLEANERS
The search for CFC alternatives is over?
p 2774 N95-31760
Prepsolv (TM): The optimum alternative to 1,1,1-trichloroethane and methyl ethyl ketone for hand-wipe cleaning of aerospace materials
p 2774 N95-31764
Ultrasonic frequency selection for aqueous fine cleaning p 2779 N95-31788
QFD analysis of RSRM aqueous cleaners
p 2779 N95-31789
A design of experiments test to define critical spray cleaning parameters for Brulin 815 GD and Jettacin cleaners p 2779 N95-31790
Environmentally compatible hand wipe cleaning solvents p 2780 N95-31795
The role of surface chemical analysis in a study to select replacement processes for TCA vapor degreasing
p 2782 N95-31809
The effect of environmental initiatives on NASA specifications and standards activities
p 2783 N95-31812
An overview of NASA testing requirements for alternate cleaning solvents used in liquid and gaseous oxygen environments p 2783 N95-31813
CLEANING
Power oscillator in the tokamaks training
[DE95-616538] p 3003 N95-30473
Major weapon system environmental life-cycle cost estimating for Conservation, Cleanup, Compliance and Pollution Prevention (C3P2) p 2774 N95-31761
Prepsolv (TM): The optimum alternative to 1,1,1-trichloroethane and methyl ethyl ketone for hand-wipe cleaning of aerospace materials
p 2774 N95-31764
Bicarbonate of soda paint stripping process validation and material characterization p 2777 N95-31778
Ultra-high pressure water jetting for coating removal and surface preparation p 2778 N95-31780

Evaluation of pressurized water cleaning systems for hardware refurbishment p 2778 N95-31782
A centrifuge CO2 pellet cleaning system p 2778 N95-31784
A microwave plasma cleaning apparatus p 2779 N95-31786
Contamination detection NDE for cleaning process inspection p 2781 N95-31802
Cleaning verification by air/water impingement p 2782 N95-31805
Investigation of cleanliness verification techniques for rocket engine hardware p 2770 N95-31806
The role of surface chemical analysis in a study to select replacement processes for TCA vapor degreasing p 2782 N95-31809
The effect of environmental initiatives on NASA specifications and standards activities p 2783 N95-31812
An overview of NASA testing requirements for alternate cleaning solvents used in liquid and gaseous oxygen environments p 2783 N95-31813
Environmentally Safe and Effective Processes for Paint Removal
[AGARD-LS-201] p 2843 N95-32165
Dry media blasting with wheat starch p 2843 N95-32169
Water blasting paint removal methods p 2843 N95-32170
Paint removal and surface cleaning using ice particles p 2844 N95-32171
Aquastrip p 2844 N95-32173
Selective chemical stripping p 2844 N95-32175
Facilities used for plastic media blasting p 2763 N95-32176
Operational parameters and material effects p 2845 N95-32179
Standardization work p 2845 N95-32181

CLEANLINESS
Cleaning without chlorinated solvents p 2780 N95-31792
Surface contamination analysis technology team overview p 2781 N95-31797
Cleanliness inspection tool for RSRM bond surfaces p 2781 N95-31799
Study of surfaces using near infrared optical fiber spectrometry p 2781 N95-31801
Contamination detection NDE for cleaning process inspection p 2781 N95-31802
Cleanliness evaluation of rough surfaces with diffuse IR reflectance p 2782 N95-31804
Investigation of cleanliness verification techniques for rocket engine hardware p 2770 N95-31806

CLEAR AIR TURBULENCE
Modeling and parameterization of gravity wave breaking, interactions, and instability processes in the lower and middle atmosphere
[AD-A292740] p 2914 N95-31278

CLIMATE
National Institute for Global Environmental Change
[DE95-008333] p 2907 N95-30358
The land component of the global climate system with adequate spatial resolution
[DE95-009323] p 2908 N95-30686
The GCRC two-dimensional zonally averaged statistical dynamical climate model: Development, model performance, and climate sensitivity p 2910 N95-31851

CLIMATE CHANGE
National Institute for Global Environmental Change
[DE95-008333] p 2907 N95-30358
Global change research: Summaries of research in FY 1994
[DE95-009660] p 2908 N95-30755
Equatorial Africa: A climatological study
[AD-A293956] p 2920 N95-31524
The role of the hydrological cycle and the ocean's thermohaline circulation in climate change: A multicomponent climate model study p 2909 N95-31720
The GCRC two-dimensional zonally averaged statistical dynamical climate model: Development, model performance, and climate sensitivity p 2910 N95-31851
Preliminary design for Arctic atmospheric radiative transfer experiments
[DE95-009580] p 2917 N95-32080

CLIMATE MODELS
National Institute for Global Environmental Change
[DE95-008333] p 2907 N95-30358
The land component of the global climate system with adequate spatial resolution
[DE95-009323] p 2908 N95-30686
History and status of the atmospheric radiation measurement program
[DE95-009951] p 2908 N95-30802
The role of the hydrological cycle and the ocean's thermohaline circulation in climate change: A multicomponent climate model study p 2909 N95-31720
The GCRC two-dimensional zonally averaged statistical dynamical climate model: Development, model performance, and climate sensitivity p 2910 N95-31851
Feasibility of tropospheric water vapor profiling using infrared heterodyne differential absorption lidar
[DE95-009647] p 2917 N95-32142
Use of arm measurements to improve radiative transfer models used in climate models
[NASA-CR-199014] p 2921 N95-32184

CLIMATOLOGY
Global change research: Summaries of research in FY 1994
[DE95-009660] p 2908 N95-30755
Aerosol measurements over the Pacific Ocean in support of the IR aerosol backscatter program
[NASA-CR-198925] p 2918 N95-30782
History and status of the atmospheric radiation measurement program
[DE95-009951] p 2908 N95-30802
JPL Physical Oceanography Distributed Active Archive Center (PO.DAAC) data availability, version 1-94
[NASA-CR-198871] p 2922 N95-30859
Directory of global environmental sciences in Japan p 2899 N95-31413
Evaluation of alternative pavement marking materials
[AD-A292973] p 2763 N95-31468
Equatorial Africa: A climatological study
[AD-A293956] p 2920 N95-31524
Global climatology and variability of potential new production estimated from remote sensing of sea-surface temperature
[NASA-CR-198840] p 2910 N95-31981
Use of arm measurements to improve radiative transfer models used in climate models
[NASA-CR-199014] p 2921 N95-32184

CLINICAL MEDICINE
Services to develop, standardize, and validate Polymerase Chain Reaction (PCR) protocols for the detection of leishmaniasis in clinical samples
[AD-A290155] p 2817 N95-31115

CLOCKS
AASERT-92 augmentation of research training in chronobiology: Regulation of the mammalian circadian clock by neurotransmitters
[AD-A288243] p 2925 N95-31144
A high-speed photonic clock and carrier regenerator p 2856 N95-32236
Fine tuning GPS clock estimation in the MCS p 2968 N95-32322
European plans for new clocks in space p 2968 N95-32324
Anticipated uncertainty budgets of PRARETIME and T2L2 techniques as applied to ExTRAS p 2968 N95-32326
Time aspects of the European Complement to GPS: Continental and transatlantic experimental phases p 2969 N95-32328
Network time synchronization servers at the US Naval Observatory p 2969 N95-32329
Custom Turnkey Time and Frequency Systems: A structured, expandable approach p 2969 N95-32330

CLOUD COVER
History and status of the atmospheric radiation measurement program
[DE95-009951] p 2908 N95-30802

CLOUDS (METEOROLOGY)
Support of environmental requirements for cloud analysis and archive (SERCAA): Database management facility
[AD-A293938] p 2920 N95-31522
Proceedings of the 16th Annual Conference on Atmospheric Transmission Models, volume 1
[AD-A293807] p 2915 N95-31575
Spectral sky background in the IR: Measurements with FTIR
[PB95-222998] p 2922 N95-32315

CLUTTER
Investigation of ground target detection methods in fully polarimetric wide angle synthetic aperture radar images
[AD-A293922] p 2851 N95-31513
Comparisons of target detection clutter using data from the 1993 FOPEN experiments
[AD-A293052] p 2852 N95-31606
Automatic Target Recognition (ATR): Background statistics and the detection of targets in clutter
[AD-A293062] p 2853 N95-31673

CMOS
Decimation of encoding errors in an optimum SNS 2 micron low-noise CMOS ADC
[AD-A293208] p 2860 N95-30900
Analog preprocessing in a SNS 2 micrometers low-noise CMOS folding ADC
[AD-A293356] p 2849 N95-30954

COAL
Multi-color pyrometer temperature measurement system
[DE95-009825] p 2879 N95-30687
Whisker reinforced glass ceramic
[DE95-010542] p 2823 N95-32305

COAL GASIFICATION
Publications of the Fossil Energy Advanced Research and Technology Development Materials Program: April 1, 1993-March 31, 1995
[DE95-009200] p 2903 N95-30745

COAL LIQUEFACTION
Publications of the Fossil Energy Advanced Research and Technology Development Materials Program: April 1, 1993-March 31, 1995
[DE95-009200] p 2903 N95-30745

COASTAL PLAINS
QTSAW (Quick Typhoon Surge and Waves). Wave information studies of US coastlines
[AD-A293172] p 2919 N95-30978

COASTAL ZONE COLOR SCANNER
SeaWiFS Technical Report Series. Volume 29: SeaWiFS CZCS-type pigment algorithm
[NASA-TM-104566] p 2922 N95-30857
SeaWiFS technical report series. Volume 24: SeaWiFS technical report series cumulative index, volumes 1-23
[NASA-TM-104566-VOL-24] p 2924 N95-32122

COASTS
A numerical study of the effect of the Gulf Stream and the Appalachian Mountains on Carolina coastal frontogenesis
[AD-A293765] p 2921 N95-31577

COATING
Electromagnetically activated compliant wavy-wall
[AD-D017340] p 2866 N95-30412
The impact of microbiologically influenced corrosion on protective polymer coatings
[AD-A288896] p 2816 N95-30997
A comparison of coating alternatives for US Coast Guard aircraft
[AD-A293270] p 2817 N95-31124
Phthalonitrile prepolymer as high temperature sizing material for composite fibers
[AD-D017447] p 2818 N95-31272
Ultra-high pressure water jetting for coating removal and surface preparation p 2778 N95-31780

COATINGS
Process for producing hydrophilic polymer membranes
[AD-D017355] p 2811 N95-30415
The effect of adding roughness and thickness to a transonic axial compressor rotor
[NASA-TM-106958] p 2867 N95-30524
State-of-the-art low-cost solar reflector materials
[DE95-000260] p 2902 N95-30526
Ion-Assisted Pulsed Laser Deposition of amorphous tetrahedral-coordinated carbon films
[DE95-010861] p 2865 N95-31394
Waterjet processes for coating removal p 2777 N95-31779
A microwave plasma cleaning apparatus p 2779 N95-31786

COBALT
Catalytic reactions of synthesis gas. Part 4: Heterogeneous hydroformylation
[PB95-195558] p 2791 N95-30537
Reaction synthesis of intermetallics
[DE95-009029] p 2803 N95-30575
Influence of layer order and composition on the magnetic anisotropy of ultra-thin Co sandwiches
[DE95-010608] p 2810 N95-32265

COBALT 60
Behaviour of polymers in radioactive environments: Effects of dose speed
[DE95-821008] p 2818 N95-31221

CODERS
On the use of electronic tilt sensors as angle encoders for synchrotron applications
[DE95-005836] p 2880 N95-30941

CODING
Feature-based modeling of product families
[PB95-207148] p 2933 N95-30568
Decimation of encoding errors in an optimum SNS 2 micron low-noise CMOS ADC
[AD-A293208] p 2860 N95-30900
Towards increased productivity of algorithm implementation
[AD-A292862] p 2940 N95-31452
Multiple turbo codes for deep-space communications p 2855 N95-32227
Enhanced decoding for the Galileo low-gain antenna mission: Viterbi redecoding with four decoding stages p 2855 N95-32230

COEFFICIENT OF FRICTION
Golden ten equations of motion
[PB95-197927] p 2967 N95-30809
COEFFICIENTS
Specific rate coefficients from vibrational overtone activation of 1-methylcyclopropene
[AD-A288755] p 2793 N95-31014
COGENERATION
Overview of IEA biomass combustion activities
[PB95-196374] p 2902 N95-30519
COGNITION
Neurodynamical systems for cognition and target identification
[AD-A293111] p 2951 N95-30884
Using computerized neuropsychological testing to assess aviator skills
[AD-A293227] p 2928 N95-30905
Training metacognitive skills for problem solving
[AD-A290310] p 2959 N95-31002
Analysis of symbolic parameter models
[AD-A292916] p 2940 N95-31459
A cognitive architecture for solving ill-defined problems
[AD-A293582] p 2929 N95-31686
COGNITIVE PSYCHOLOGY
Impact of task properties, data display format and cognitive characteristics on recall performance: A cumulative research investigation p 3025 N95-31334
Optimizing the long-term retention of skills: Structural and analytic approaches to skill maintenance
[AD-A293798] p 2929 N95-31585
A cognitive architecture for solving ill-defined problems
[AD-A293582] p 2929 N95-31686
COHERENT RADAR
Multisensor data fusion for integrated maritime surveillance p 2842 N95-32135
Point reflector model for the simulation of radar target glint and Doppler phenomena
[PB95-222960] p 2857 N95-32314
COHERENT RADIATION
Stable high-power harmonic gyro-amplifiers
[AD-A293697] p 2881 N95-31828
COLD FLOW TESTS
Combustion response to acoustic perturbation in liquid rocket engines p 2770 N95-31972
COLD PLASMAS
Selected problems of the identification of weak double layers in plasma on a background of different aperiodic non-collision structures
[IFTR-4/1995] p 3006 N95-31737
Studies of highly charged ions with EBIT and Super-EBIT
[DE95-010251] p 2987 N95-32038
COLD PRESSING
Processing and characterization of nanocrystalline molybdenum disilicide (MoSi2) consolidated by hot isostatic pressing (HIP)
[DE95-010243] p 3012 N95-30756
COLD WEATHER TESTS
Impact behavior of the active zone within a frozen soil profile
[AD-A292909] p 2915 N95-31386
COLD WORKING
Effect of cold work on creep properties of Hastelloy XR
[DE95-722056] p 2806 N95-31154
COLLIMATORS
Measurement of the effect of collimator generated wakefields on the beams in the SLC
[DE95-012101] p 2993 N95-31256
COLLINEARITY
Wave propagation in a fluid-loaded homogeneous, transversely isotropic, elastic cylinder of arbitrary thickness
[AD-A292728] p 2869 N95-30948
COLLISIONLESS PLASMAS
Bernstein-Green-Kruskal wave
[DE95-614201] p 3007 N95-32056
A collisionless shock wave experiment
[DE95-009489] p 3008 N95-32351
COLLISIONS
Scaling of cross sections in ion-atom collisions
[DE95-008938] p 2978 N95-30573
B(sub c)-meson production in hadron-hadron collisions
[DE95-620537] p 2983 N95-31217
Monte Carlo code for evaluating the Boundary Layer Illumination and Radiation Balance model (BLIRB)
[AD-A293963] p 2915 N95-31560
COLLOIDS
Investigation of Fe3O4 colloid behaviour in a magnetic field by polarized neutron transmission
[DE95-614351] p 2961 N95-30915
On convective effects in sedimentation of concentrated suspensions with high effective gravity
[TRITA-NA-9316] p 2794 N95-31356
COLOR
Method and apparatus for a high resolution, flat panel cathodoluminescent display device
[AD-D017434] p 2862 N95-31342
Evaluation of alternative pavement marking materials
[AD-A292973] p 2763 N95-31468
Degradation of blue AlGaN/InGaN/GaN LEDs subjected to high current pulses
[DE95-008824] p 2863 N95-31611
Skew chromaticity in large accelerators
[DE95-011564] p 2994 N95-32243
COLORIMETRY
Hydrogen sulfide analyzer with protective barrier
[AD-D017412] p 2793 N95-31009
COLUMNS
Simplex method for semi-definite programming: Optimization and systems theory
[PB95-212122] p 2934 N95-30792
COMBAT
SOSIE: A pragmatic approach to the simulation of Broad Air Defense applied to the theater level p 2840 N95-32127
Electronic combat and lethal defense suppression p 2842 N95-32140
COMBINATORIAL ANALYSIS
Size of Fulton's essential set
[PB95-211645] p 2955 N95-30477
Combination of Fulton's essential set
[PB95-211637] p 2956 N95-30500
Bravais classes, Voronoie cells, Delone symbols
[PB95-207916] p 3009 N95-30503
Periodically Specified Problems: An Exponential Complexity Gap Between Exact and Approximate Solutions
[DE95-009435] p 2934 N95-30603
The complexity and approximability of finding maximum feasible subsystems of linear relations
[TRITA-NA-9313] p 2961 N95-31648
Using case-based reasoning as a Reinforcement Learning framework for optimization with changing criteria
[AD-A293602] p 2953 N95-31654
COMBUSTIBLE FLOW
An investigation of the side-dump dual in-line ramjet combustor p 2756 N95-31199
A pulsed liquid fuel ramjet p 2756 N95-31201
Spectral element method for numerical simulation of unsteady laminar diffusion flames p 2794 N95-31333
COMBUSTION
Overview of IEA biomass combustion activities
[PB95-196374] p 2902 N95-30519
Simulation of chemical kinetics in turbulent natural gas combustion. Volume 2: Experimental studies of nitric oxide production in gas flames
[PB95-196721] p 2791 N95-30541
NASA Lewis Research Center's preheated combustor and materials test facility
[NASA-TM-106676] p 2762 N95-30592
Multi-color pyrometer temperature measurement system
[DE95-009825] p 2879 N95-30687
Achieving improved cycle efficiency via pressure gain combustors
[DE95-008945] p 2792 N95-30762
The 49th International Symposium on Molecular Spectroscopy
[AD-A292708] p 2793 N95-30936
Pressure transducer performance and measurement trade-offs in a transient, high temperature, combustion environment p 2799 N95-31209
The 25th International Symposium on Combustion
[AD-A286825] p 2794 N95-31268
The 31st JANNAF Combustion Subcommittee Meeting, volume 2
[CPIA-PUBL-620] p 2829 N95-31282
Whisker reinforced glass ceramic
[DE95-010542] p 2823 N95-32305
COMBUSTION CHAMBERS
NASA Lewis Research Center's preheated combustor and materials test facility
[NASA-TM-106676] p 2762 N95-30592
Jet mixing and emission characteristics of transverse jets in annular and cylindrical confined crossflow
[NASA-TM-106976] p 2755 N95-30698
Achieving improved cycle efficiency via pressure gain combustors
[DE95-008945] p 2792 N95-30762
Jet mixing in a reacting cylindrical crossflow
[NASA-TM-106975] p 2755 N95-30853
Advanced small rocket chambers. Option 3: 110 1bf Ir-Re rocket, volume 1
[NASA-CR-195435-VOL-1] p 2768 N95-31169
Advanced small rocket chambers. Option 3: 110 1bf Ir-Re rocket, volume 2
[NASA-CR-195435-VOL-2] p 2769 N95-31170
Experimental investigation of turbulent particle dispersion in swirling flows
[DLR-FB-94-20] p 2873 N95-31355
Experiment of rocket-ram combined combustor
[NAL-TR-1249] p 2769 N95-31739
SSME Main Combustion Chamber (MCC) hot oil dewaxing p 2777 N95-31777
COMBUSTION CHEMISTRY
Overview of IEA biomass combustion activities
[PB95-196374] p 2902 N95-30519
Burn time measurements of single aluminum particles in steam and carbon dioxide mixtures p 2799 N95-30990
The 25th International Symposium on Combustion
[AD-A286825] p 2794 N95-31268
An ignition model for modern double base propellants p 2800 N95-31292
The oxidation of carbon monoxide by nitrous oxide p 2801 N95-31309
Detailed chemical kinetic modeling of premixed hydrocarbon flames supported by NO2 p 2801 N95-31311
Studies of reactions pertaining to and development of a reduced mechanism for the double base propellant dark zone p 2801 N95-31312
RDX laser-assisted flame structure p 2801 N95-31314
COMBUSTION CONTROL
Active control of combustion instability using injection techniques p 2800 N95-31288
COMBUSTION EFFICIENCY
Overview of IEA biomass combustion activities
[PB95-196374] p 2902 N95-30519
COMBUSTION PHYSICS
Burn time measurements of single aluminum particles in steam and carbon dioxide mixtures p 2799 N95-31198
Experiments in a 120-mm ram accelerator including flow visualization p 2799 N95-31202
Investigation of ram accelerator performance capabilities p 2799 N95-31204
Pulse forming network in the ETC combustion characterization of plasma augmented solid propellants p 2799 N95-31205
Workshop report: Measurement techniques in highly transient, spectrally rich combustion environments p 2799 N95-31208
Development of a new instrument for rocket engine combustion diagnostics p 2799 N95-31211
The 25th International Symposium on Combustion
[AD-A286825] p 2794 N95-31268
The 31st JANNAF Combustion Subcommittee Meeting, volume 2
[CPIA-PUBL-620] p 2829 N95-31282
Assessment of dynamic burning behavior for JA-2 propellant rods p 2800 N95-31299
Flame structure studies of neat and NH3 doped H2/N2O flames employing molecular beam mass spectrometry and modeling p 2801 N95-31313
Primary atomization of liquid jets issuing from rocket engine coaxial injectors p 2769 N95-31716
COMBUSTION PRODUCTS
The 21st JANNAF Exhaust Plume Technology Meeting, volume 1
[CPIA-PUBL-621-VOL-1] p 2870 N95-30986
The Al and A(lc)l2O3 droplet cloud in solid rocket motors p 2770 N95-30988
Shuttle redesigned solid rocket motor aluminum oxide investigations p 2770 N95-30989
Burn time measurements of single aluminum particles in steam and carbon dioxide mixtures p 2799 N95-30990
Vacuum plume backflow and rarefaction p 2871 N95-30995
Shuttle Redesigned Solid Rocket Motor aluminum oxide investigations p 2770 N95-31197
Burn time measurements of single aluminum particles in steam and carbon dioxide mixtures p 2799 N95-31198
A study of the gas-phase processes of RDX combustion using a triple quadrupole mass-spectrometer p 2801 N95-31315
Low acid producing solid propellants p 2773 N95-31754
Improved hybrid rocket fuel p 2773 N95-31755
COMBUSTION STABILITY
Design and testing of an oxidizer-rich preburner p 2799 N95-31212
The 31st JANNAF Combustion Subcommittee Meeting, volume 2
[CPIA-PUBL-620] p 2829 N95-31282
Stability prediction with rotational flow effects p 2799 N95-31283
Theory of unsteady combustion of solids: Investigation of Quasi-steady assumption p 2800 N95-31285

Active control of combustion instability using injection techniques p 2800 N95-31288
Effects of gas-phase thermal expansion on the stability of deflagration through a porous energetic material
[DE95-004382] p 2797 N95-31824
Combustion response to acoustic perturbation in liquid rocket engines p 2770 N95-31972

COMBUSTION SYNTHESIS
Reaction synthesis of intermetallics
[DE95-009029] p 2803 N95-30575

COMBUSTION TEMPERATURE
NASA Lewis Research Center's preheated combustor and materials test facility
[NASA-TM-106676] p 2762 N95-30592
Characterization of an improved Rijke burner as prelude to measurements of aluminum distributed combustion p 2800 N95-31287

COMMAND AND CONTROL
Guidance and Control for Future Air-Defence Systems
[AGARD-CP-555] p 2839 N95-32123
Study of Extended Air Defence Post 2000 p 2839 N95-32124
Multi-sensor data fusion in command and control and the merit of artificial intelligence p 2842 N95-32137

COMMAND GUIDANCE
Guidance and Control for Future Air-Defence Systems
[AGARD-CP-555] p 2839 N95-32123

COMMERCIAL AIRCRAFT
Electrical short circuit and current overload tests on aircraft wiring
[AD-A293308] p 2860 N95-30922
Integration of air traffic databases: A case study
[AD-A293691] p 2749 N95-32022
Standardization work p 2845 N95-32181
Special investigation report: Safety of the air tour industry in the United States
[PB95-917004] p 2748 N95-32185

COMMONWEALTH OF INDEPENDENT STATES
JPRS report: Science and technology. Central Eurasia
[JPRS-UST-95-025] p 2771 N95-31360

COMMUNICATION
Multiple turbo codes for deep-space communications p 2855 N95-32227

COMMUNICATION CABLES
Fiber optic reference frequency distribution to remote beam waveguide antennas p 2972 N95-32346

COMMUNICATION EQUIPMENT
The quad-service satellite transmitting and receiving system for medical supply support: A battlefield interoperability and communications system prototype, volume 2. User documentation
[AD-A292835] p 2851 N95-31448
The quad-service satellite transmitting and receiving system for medical supply support: A battlefield interoperability and communications system prototype, volume 1
[AD-A292836] p 2851 N95-31449

COMMUNICATION NETWORKS
Contribution of groupware to corporate communication: Towards the horizontal organization
[PB95-197661] p 3022 N95-30453
Dynamic routation in distributed environments
[PB95-197968] p 2847 N95-30812
System considerations for efficient communication and storage of MSTI image data
[NASA-CR-198869] p 3024 N95-30858
Wide area networking R&D
[AD-A291057] p 2947 N95-30868
Effective bandwidth techniques in bufferless and buffered ATM multiplexers
[PB95-207072] p 2862 N95-31185
Support of environmental requirements for cloud analysis and archive (SERCAA): Database management facility
[AD-A293938] p 2920 N95-31522
Dynamic maintenance scheduling for a stochastic telecommunication network: Determination of performance factors
[AD-A293829] p 2852 N95-31555
Scalable ATM encryption
[DE95-009868] p 2948 N95-32065
The 1994 international transatlantic two-way satellite time and frequency transfer experiment: Preliminary results p 2858 N95-32320
Network time synchronization servers at the US Naval Observatory p 2969 N95-32329

COMMUNICATION SATELLITES
High accuracy time transfer synchronization p 2968 N95-32321
Monte Carlo simulations of precise timekeeping in the Milstar communication satellite system p 2970 N95-32336
Automated delay measurement system for an Earth station for Two-Way Satellite Time and Frequency Transfer p 2971 N95-32337

COMPACTING
Low temperature fabrication from nano-size ceramic powders
[DE95-010995] p 2818 N95-31153
Gelcasting of sintered reaction-bonded silicon nitride for improved mechanical properties
[DE95-010282] p 2822 N95-32085

COMPANION STARS
Chromospherically active stars. 6: Giants with compact hot companions and the barium star scenario
[NASA-TM-110641] p 3028 N95-30466
Cepheid temperature and the Blazhko effect
[NASA-CR-189433] p 3030 N95-31819

COMPARATORS
Analog preprocessing in a SNS 2 micrometers low-noise CMOS folding ADC
[AD-A293356] p 2849 N95-30954

COMPARISON
Psychological pilot selection in the US Air Force, the Luftwaffe, and the German Aerospace Research Establishment
[AD-A293779] p 2928 N95-31376

COMPARTMENTS
Facilities used for plastic media blasting p 2763 N95-32176

COMPATIBILITY
Compatibility of refrigerants and lubricants with motor materials under retrofit conditions
[DE95-010185] p 2814 N95-30767
Compatibility of Single Hydraulic Fluid with military specification fluids, seals and metallurgy
[AD-A292954] p 2821 N95-31663
Evaluation of Environmentally Acceptable hydraulic fluids
[AD-A293037] p 2821 N95-31666

COMPENSATORS
Computerized design of controllers using data models
[NASA-CR-198921] p 2950 N95-30655
Robust position and force tracking control for a robot in contract p 2888 N95-30830

COMPETITION
Specific rate coefficients from vibrational overtone activation of 1-methylcyclopropene
[AD-A288755] p 2793 N95-31014

COMPILERS
The Linux operating system: An introduction
[NASA-CR-198178] p 2932 N95-31988

COMPLEX COMPOUNDS
Aqueous TiO2 photocatalysis of metal-EDTA complexes
[DE95-011058] p 2793 N95-31113

COMPLEX SYSTEMS
Nonlinear dynamical systems: Elements of a complex system analysis
[PB95-211652] p 2950 N95-30478
ASSIST user manual
[NASA-TM-4592] p 2948 N95-32250

COMPLEX VARIABLES
Complex mean value interpolation
[PB95-211629] p 2956 N95-30601

COMPLEXITY
Simulation with complex measures
[DE95-616333] p 2955 N95-30445
Does software design complexity affect maintenance effort? p 2939 N95-31251

COMPONENT RELIABILITY
Measures of reliability and RCM
[PB95-192985] p 2891 N95-30510
Performance evaluation of high-temperature superconducting current leads for micro-SMES systems
[DE95-005843] p 2861 N95-30943
Failure analysis of a repairable system: The case study of a cam-driven reciprocating pump
[AD-A293144] p 2889 N95-30949
Dynamic maintenance scheduling for a stochastic telecommunication network: Determination of performance factors
[AD-A293829] p 2852 N95-31555

COMPOSITE MATERIALS
Theoretical absorption spectroscopy of high-temperature metal vapors: Model and experiment compared
[AD-A290872] p 2791 N95-30409
Large area smart piezoelectric and pyroelectric sensors
[AD-A291487] p 2859 N95-30561
Thermoviscoelastic behaviour of solids
[PB95-196226] p 2784 N95-30694
Mechanisms of enhanced ionic conduction at interfaces in ceramics
[DE95-009125] p 2814 N95-30730
A theory for predicting and minimizing the effects of matrix degradation on the thermomechanical properties of general laminates p 2785 N95-30768
The effect of interface properties on nickel base alloy composites
[NASA-CR-198363] p 2785 N95-30787
A viscoelastic anisotropic wave propagation model for composite cure evaluation p 2786 N95-30839
Innovative processing of composites for ultra-high temperature applications, book 4
[AD-A290892] p 2786 N95-30867
Room temperature fracture and high temperature creep deformation properties of alumina reinforced with 20 vol% particulate niobium
[DE95-010234] p 2815 N95-30897
Metal nanotubule membranes with electrochemically switchable ion-transport selectivity
[AD-A292712] p 2793 N95-30938
Opto-electronic components from non-stoichiometric 3-5 materials
[AD-A293206] p 3013 N95-30985
Intermodulation Interference (IMI) testing of composite materials
[AD-A288621] p 2787 N95-31146
Elastic and inelastic micromechanical analysis of functionally graded materials and laminated structures using transformation fields p 2787 N95-31347
Materials for adaptive structural acoustic control, volume 1
[AD-A293444] p 2788 N95-31369
Materials for adaptive structural acoustic control, volume 2
[AD-A293445] p 2788 N95-31370
Materials for adaptive structural acoustic control, volume 4
[AD-A293447] p 2788 N95-31372
Self-lubricating, TiN-MoS2 composite coatings produced by simultaneous deposition from Ti((CH3))2N4/NH3/MoF6H2S gas mixture
[DE95-010359] p 2788 N95-31403
Development of stitched/RTM primary structures for transport aircraft
[NASA-CR-191441] p 2789 N95-31421
Metallurgical and Materials Transactions
[AD-A293617] p 2807 N95-31464
An inverse method to measure the axial modulus of composite materials under tension
[AD-A293042] p 2789 N95-31668

COMPOSITE PROPELLANTS
Ageing control no. 3 of propellants for rocket motors RB 27 and RB 28
[PB95-210357] p 2825 N95-30626
A study of gas-phase processes during the deflagration of RDX composite propellants using a triple quadrupole mass spectrometer p 2801 N95-31304
Thermoplastic elastomers as a binder in composite propellants
[PB95-211553] p 2837 N95-32249

COMPOSITE STRUCTURES
Low vibration polymeric composite engine
[AD-D017332] p 2887 N95-30386
Design of fibre reinforced composite panels for aerospace applications
[PB95-197851] p 2784 N95-30460
Composite structure forming a wear surface
[AD-D017462] p 2785 N95-30749
Response of mechanically fastened composite joints under multiple bypass loads p 2785 N95-30824
Effects of hydrostatic pressure on the mechanical behavior of composite materials
[AD-A293162] p 2787 N95-30963
Intermodulation Interference (IMI) testing of composite materials
[AD-A288621] p 2787 N95-31146
Materials for adaptive structural acoustic control, volume 2
[AD-A293445] p 2788 N95-31370
Materials for adaptive structural acoustic control, volume 4
[AD-A293447] p 2788 N95-31372
Development of stitched/RTM primary structures for transport aircraft
[NASA-CR-191441] p 2789 N95-31421
Performance improvement of composite wings through aeroelastic tailoring and modern control
[AD-A293689] p 2752 N95-31602
Mapping hidden aircraft defects with dual-band infrared computed tomography
[DE95-011531] p 2741 N95-32164
A probabilistic design method applied to smart composite structures
[NASA-TM-106715] p 2899 N95-32206

COMPRESSIBILITY
Some aspects on the modelling of non-Newtonian fluid flow
[TRITA-NA-9317] p 2873 N95-31415
Simulation of fracture in compression using a field-theory model
[DE95-009874] p 2898 N95-32102

COMPRESSIBILITY EFFECTS
Numerical simulation of shock/turbulent boundary layer interaction
[NASA-CR-198846] p 2872 N95-31341
Compressible turbulence measurement in low-angle injection into a supersonic flow
[AD-A293836] p 2874 N95-31516
COMPRESSIBLE BOUNDARY LAYER
Numerical simulation of shock/turbulent boundary layer interaction
[NASA-CR-198846] p 2872 N95-31341
COMPRESSIBLE FLOW
Navier-Stokes flow field analysis of compressible flow in a high pressure safety relief valve
[NASA-TM-110640] p 2868 N95-30862
Numerical simulation of shock/turbulent boundary layer interaction
[NASA-CR-198846] p 2872 N95-31341
Compressible turbulence measurement in low-angle injection into a supersonic flow
[AD-A293836] p 2874 N95-31516
LES, DNS and RANS for the analysis of high-speed turbulent reacting flows
[NASA-CR-199075] p 2878 N95-32219
COMPRESSION LOADS
Failure mechanisms in composite plates subjected to in-plane compressive loading p 2790 N95-32108
COMPRESSION TESTS
Characterization and prediction of post-impact fatigue damage in stitched composites p 2785 N95-30826
High strain rate properties and constitutive modeling of glass
[DE95-008434] p 2816 N95-31058
Hot compression testing of tungsten
[AD-A293683] p 2807 N95-31599
COMPRESSIVE STRENGTH
LLW solidification in cement: Effect of dilution
[DE95-010108] p 2798 N95-32091
COMPRESSOR BLADES
The effect of adding roughness and thickness to a transonic axial compressor rotor
[NASA-TM-106958] p 2867 N95-30524
Investigating the use of smart acoustically active surfaces for flow separation control in turbomachinery
[AD-A292819] p 2874 N95-31443
COMPRESSOR EFFICIENCY
The effect of adding roughness and thickness to a transonic axial compressor rotor
[NASA-TM-106958] p 2867 N95-30524
COMPRESSOR ROTORS
The effect of adding roughness and thickness to a transonic axial compressor rotor
[NASA-TM-106958] p 2867 N95-30524
Experimental and computational investigation of the tip clearance flow in a transonic axial compressor rotor
[NASA-TM-106711] p 2876 N95-31738
COMPRESSORS
Composite structure forming a wear surface
[AD-D017462] p 2785 N95-30749
Reducing process noise in superconducting helium liquid level probes
[DE95-008956] p 2814 N95-30765
Linear Motor Free Piston Compressor
[AD-A293452] p 2889 N95-31374
COMPTON EFFECT
On the Compton twist-3 asymmetries
[DE95-613627] p 3017 N95-30371
COMPUTATION
Statistical interface for chaotic signal in noise
[AD-A290271] p 2848 N95-30932
MCNP analyses of criticality calculation results
[DE95-010886] p 2960 N95-31253
Multiresolution signal and system analysis and the analysis and control of discrete-event dynamic systems
[AD-A292775] p 2851 N95-31430
COMPUTATIONAL ELECTROMAGNETICS
Scattering and radiation from cylindrically conformal antennas p 2847 N95-30669
A two-dimensional finite difference algorithm on the KSR1
[AD-A293576] p 2941 N95-31594
A boundary integral equation approach to three dimensional electromagnetic wave scattering problems p 2853 N95-31839
COMPUTATIONAL FLUID DYNAMICS
Velocity boundary conditions for vorticity formulations of the incompressible Navier-Stokes equations
[DE95-008715] p 2866 N95-30464
Multidimensional discretization of conservation laws for unstructured polyhedral grids
[DE95-008796] p 2955 N95-30470
Three-D mesh optimization methods for unstructured polyhedra
[DE95-008808] p 2955 N95-30471
A numerical study of the starting process in a hypersonic shock tunnel p 2762 N95-30493
Simulation of chemical kinetics in turbulent natural gas combustion. Volume 2: Experimental studies of nitric oxide production in gas flames
[PB95-196721] p 2791 N95-30541
Development of a linearized unsteady Euler analysis for turbomachinery blade rows
[NASA-CR-4677] p 2742 N95-30611
A numerical model for dynamic wave rotor analysis
[NASA-TM-106997] p 2754 N95-30617
Validation of the NPARC code for nozzle afterbody flows at transonic speeds
[NASA-TM-106971] p 2742 N95-30704
Numerical simulation of flow in a whirling annular seal and comparison with experiments
[NASA-TM-106961] p 2867 N95-30710
Computation of high-altitude hypersonic flow-field radiation p 2743 N95-30843
Parametrics on 2D Navier-Stokes analysis of a Mach 2.68 bifurcated rectangular mixed-compression inlet
[NASA-TM-107003] p 2755 N95-30861
Three-dimensional (3D) large fluid flow computations for US Army applications on KSR-1, CM-200, CM-5, and Cray C-90
[AD-A293125] p 2869 N95-30889
Acceleration potential models PREDICHAT/PREDICDYN applied for calculation of axisymmetric dynamic inflow cases
[PB95-207015] p 2869 N95-30957
QMR methods in computational fluid dynamics
[DE95-010293] p 2872 N95-31132
Atomization simulations using an Eulerian-VOF-Lagrangian method p 2828 N95-31210
The 2nd Japan-US Symposium on Finite Element Methods in Large Scale Computational Fluid Dynamics
[AD-A292337] p 2960 N95-31264
Role of free-surface boundary conditions and nonlinearities in wave/boundary-layer and wake interaction p 2872 N95-31317
Spectral element method for numerical simulation of unsteady laminar diffusion flames p 2794 N95-31333
Numerical simulation of shock/turbulent boundary layer interaction
[NASA-CR-198846] p 2872 N95-31341
Shear-free turbulent boundary layers p 2873 N95-31349
A study of numerical solutions of conservation laws
[TRITA-NA-9315] p 2960 N95-31361
Advanced k-epsilon modeling of heat transfer
[NASA-CR-4679] p 2874 N95-31423
Application of multigrid computational fluid dynamics (CFD) methods to rotor analysis
[AD-A293012] p 2874 N95-31475
Unsteady flow simulations about moving boundary configurations using dynamic domain decomposition techniques p 2877 N95-31837
Analysis and modeling of subgrid scalar mixing using numerical data
[NASA-CR-198169] p 2877 N95-31978
MPI implementation of PHOENICS: A general purpose computational fluid dynamics code
[DE95-009810] p 2877 N95-32033
The HYLIFE-2 inertial fusion energy power plant concept and implications for IFE
[DE95-010561] p 2994 N95-32074
Numerical solution of the full potential equation using a chimera grid approach
[NASA-TM-110360] p 2744 N95-32188
An efficient numerical procedure for thermohydrodynamic analysis of cavitating bearings
[NASA-CR-195476] p 2878 N95-32210
Film temperatures in the presence of cavitation
[NASA-CR-195481] p 2878 N95-32216
LES, DNS and RANS for the analysis of high-speed turbulent reacting flows
[NASA-CR-199075] p 2878 N95-32219
COMPUTATIONAL GEOMETRY
Equivalence of two non-commutative geometry approaches
[DE95-613469] p 2957 N95-30642
Geometric modeling for computer aided design
[NASA-CR-198828] p 2943 N95-31982
COMPUTATIONAL GRIDS
Fourier analysis of a robust multigrid method for convection-diffusion equations
[PB95-197091] p 2958 N95-30835
Parametrics on 2D Navier-Stokes analysis of a Mach 2.68 bifurcated rectangular mixed-compression inlet
[NASA-TM-107003] p 2755 N95-30861
Self-adaptive multilevel methods for fluid flow problems p 2873 N95-31412
Evaluation of discretization procedures for transition elements in adaptive mesh refinement
[NASA-CR-199037] p 2944 N95-32190
COMPUTER AIDED DESIGN
Metrics in method engineering
[PB95-197687] p 2838 N95-30455
A general inverse design procedure for aerodynamic bodies p 2750 N95-30497
Feature-based modeling of product families
[PB95-207148] p 2933 N95-30568
Refinement techniques in computer graphics
[PB95-208526] p 2934 N95-30625
Computerized design of controllers using data models
[NASA-CR-198921] p 2950 N95-30655
Structural design using equilibrium programming formulations
[NASA-TM-110175] p 2893 N95-30682
Advanced small rocket chambers. Option 3: 110 lbf Ir-Re rocket, volume 2
[NASA-CR-195435-VOL-2] p 2769 N95-31170
Virtual Reality Software and Technology '94
[AD-A292334] p 2939 N95-31262
Development and implementation of a computer facility for nuclear data updating and reactor calculations using personal computers
[DE95-623577] p 2940 N95-31408
Solid Modeling Aerospace Research Tool (SMART) user's guide, version 2.0
[NASA-TM-4431] p 2940 N95-31420
Effectiveness of an electronic performance support system for use with computer-aided design software
[AD-A293757] p 2941 N95-31573
Design of digital low-pass filters for time-domain recursive filtering of impact acceleration signals
[AD-A293086] p 2864 N95-31842
Geometric modeling for computer aided design
[NASA-CR-198828] p 2943 N95-31982
Data reduction of piecewise linear curves
[PB95-212270] p 2962 N95-32256
COMPUTER AIDED MANUFACTURING
Development of flexible feeder techniques
[PB95-196317] p 2934 N95-30663
Advanced computational research in materials processing for design and manufacturing
[DE95-009130] p 2838 N95-30684
Computer-aided inspection process definition: Development of an expert planning and programming system for coordinate metrology
[DE95-010411] p 2940 N95-31404
COMPUTER AIDED MAPPING
Digital Mapping Charting and Geodesy Analysis Program technical review of Vector Product Format (VPF)
[AD-A289766] p 2901 N95-31390
COMPUTER AIDED TOMOGRAPHY
A room temperature LSO/PIN photodiode PET detector module that measures depth of interaction
[DE95-008447] p 2878 N95-30378
Mapping hidden aircraft defects with dual-band infrared computed tomography
[DE95-011531] p 2741 N95-32164
COMPUTER ASSISTED INSTRUCTION
DiffEqlab: A MATLAB based package for studying ordinary differential equations
[PB95-207197] p 2960 N95-31363
Effectiveness of an electronic performance support system for use with computer-aided design software
[AD-A293757] p 2941 N95-31573
COMPUTER COMPONENTS
BASIS image processor PR5200: Module Common Part
[PB95-212023] p 2933 N95-30501
COMPUTER GRAPHICS
Refinement techniques in computer graphics
[PB95-208526] p 2934 N95-30625
ESAA: Environment for Seismic Activity Analysis
[DE95-612416] p 2913 N95-30675
Application of computer generated holograms to optical transformations
[AD-A293146] p 2880 N95-30921
QTSAW (Quick Typhoon Surge and Waves). Wave information studies of US coastlines
[AD-A293172] p 2919 N95-30978
Computer interface development for the petite amateur navy satellite (PANSAT) simulator
[AD-A293263] p 2766 N95-31388
COMPUTER INFORMATION SECURITY
UNIX and PC security in a network environment. UNINETT
[PB95-196291] p 2934 N95-30662
UNIX and PC security in a network environment. LOKALNETT 1993
[PB95-196309] p 2934 N95-30697
An approach to automated reasoning about operational semantics
[AD-A291127] p 2936 N95-31228
Toward a risk-based approach to the assessment of the surety of information systems
[DE95-008821] p 3025 N95-31682
Scalable ATM encryption
[DE95-009868] p 2948 N95-32065

Proposed DDS-specific fields for the Generic Authentication Information Element
[DE95-009839] p 3026 N95-32144
A proposed Generic Authentication Information Element
[DE95-009862] p 2948 N95-32146
Recommendations for protecting National Library of Medicine Computing and Networking Resources
[DE95-011554] p 3026 N95-32285
COMPUTER NETWORKS
Contribution of groupware to corporate communication: Towards the horizontal organization
[PB95-197661] p 3022 N95-30453
An overview of high-speed networking for workstations
[DE95-009076] p 2947 N95-30577
An executable specification for the message processor in a simple combining network
[NASA-CR-198174] p 2933 N95-30584
UNIX and PC security in a network environment. UNINETT
[PB95-196291] p 2934 N95-30662
UNIX and PC security in a network environment. LOKALNETT 1993
[PB95-196309] p 2934 N95-30697
Wide area networking R&D
[AD-A291057] p 2947 N95-30868
Operator's handbook: NAWC Software Production Facility
[AD-A290216] p 2935 N95-31001
A programming interface for application-aware adaptation in mobile computing
[AD-A293107] p 2943 N95-32019
MPI implementation of PHOENICS: A general purpose computational fluid dynamics code
[DE95-009810] p 2877 N95-32033
Scalable ATM encryption
[DE95-009868] p 2948 N95-32065
A proposed Generic Authentication Information Element
[DE95-009862] p 2948 N95-32146
COMPUTER PROGRAM INTEGRITY
Protocols for integrity constraint checking in federated databases
[PB95-197695] p 3022 N95-30456
Toward a risk-based approach to the assessment of the surety of information systems
[DE95-008821] p 3025 N95-31662
COMPUTER PROGRAMMING
Metrics in method engineering
[PB95-197687] p 2838 N95-30455
C++ as an introductory programming language
[PB95-195715] p 2933 N95-30539
Semiannual report
[NASA-CR-198172] p 2931 N95-30657
A graphical programming language for service robots in semi-structured environments p 2935 N95-30831
Changes and challenges in the Software Engineering Laboratory p 2936 N95-31235
Automation of the control of acoustic parameters in a digital speech synthesizer
[IFTR-2/1995] p 2850 N95-31357
Human-computer interaction (HCI) specialization track Masters of Software Engineering (MSE) program
[AD-A292895] p 2930 N95-31401
Computer-aided inspection process definition: Development of an expert planning and programming system for coordinate metrology
[DE95-010411] p 2940 N95-31404
Integrated high performance distributed system
[AD-A292821] p 2947 N95-31445
Computational methods for control and optimal design of aerospace systems
[AD-A292861] p 2751 N95-31451
Towards increased productivity of algorithm implementation
[AD-A292862] p 2940 N95-31452
The occurrence of continuation parameters in CPS terms
[AD-A292952] p 2941 N95-31460
Proceedings of the 1st Annual Software Engineering Techniques Workshop on Software Reengineering
[AD-A293724] p 2943 N95-31834
Experience with a course on architectures for software systems. Part 2: Educational materials
[AD-A293090] p 2943 N95-31843
The Linux operating system: An introduction
[NASA-CR-198178] p 2932 N95-31988
A programming interface for application-aware adaptation in mobile computing
[AD-A293107] p 2943 N95-32019
COMPUTER PROGRAMS
IR DIAL performance modeling
[DE95-008377] p 2912 N95-30373
Workflow literature guide, version 1
[PB95-207080] p 2947 N95-30721
A turbulence module for the NPARC code
[NASA-CR-198358] p 2959 N95-30855
Summary of technical operations
[AD-A293224] p 2935 N95-30903
RASSP benchmark 1 executable requirements user's manual
[AD-A290060] p 2935 N95-30931
The Los Alamos accelerator code group
[DE95-010989] p 2992 N95-31151
MCNP analyses of criticality calculation results
[DE95-010886] p 2960 N95-31253
SodaBot: A software agent environment and construction system
[AD-A290056] p 2939 N95-31277
Fuel-type classification and parameters prediction by Gas Liquid Chromatography analysis
[AD-A293442] p 2794 N95-31368
Impact behavior of the active zone within a frozen soil profile
[AD-A292909] p 2915 N95-31386
Computer interface development for the petite amateur navy satellite (PANSAT) simulator
[AD-A293263] p 2766 N95-31388
Proceedings of the 1st Annual Software Engineering Techniques Workshop on Software Reengineering
[AD-A293724] p 2943 N95-31834
Application of a genetic algorithm to optimize staffing levels in software development
[AD-A293725] p 2943 N95-31835
Monte Carlo tests of the ELIPGRID-PC algorithm
[DE95-010811] p 2943 N95-32030
Video conferencing using DAVE user's guide
[DE95-010341] p 2854 N95-32045
Analysis and extension of model-based software executives
[AD-A293834] p 2944 N95-32073
Validation of favor code linear elastic fracture solutions for finite-length flaw geometries
[DE95-009034] p 2898 N95-32157
Optimal heat transfer design of chemical vapor deposition reactors
[DE95-010997] p 2878 N95-32309
COMPUTER STORAGE DEVICES
Class of service in the high performance storage system
[DE95-007959] p 2932 N95-31704
COMPUTER SYSTEMS DESIGN
Data storage modeling and management for multimedia information systems p 3022 N95-30483
Semiannual report
[NASA-CR-198172] p 2931 N95-30657
Foundations of technology for constructing highly reliable distributed realtime systems
[AD-A293254] p 2931 N95-30892
Making intelligent systems team players. A guide to developing intelligent monitoring systems
[NASA-TM-104807] p 2951 N95-30925
Lessons learned in transitioning to an open systems environment p 2938 N95-31245
Human-computer interaction (HCI) specialization track Masters of Software Engineering (MSE) program
[AD-A292895] p 2930 N95-31401
Development and implementation of a computer facility for nuclear data updating and reactor calculations using personal computers
[DE95-623577] p 2940 N95-31408
Experience with a course on architectures for software systems. Part 2: Educational materials
[AD-A293090] p 2943 N95-31843
Possible allied ballistic missile defense systems: Related guidance and control requirements p 2840 N95-32126
SOSIE: A pragmatic approach to the simulation of Broad Air Defense applied to the theater level p 2840 N95-32127
Integration issues in modular mission management aid development p 2841 N95-32133
Design of surveillance and multisensor anti-aerial systems p 2841 N95-32134
Architecture and implementation of a multi-sensor data fusion demonstration model within the real-time combat system of the Canadian Patrol Frigate p 2842 N95-32139
COMPUTER SYSTEMS PERFORMANCE
Data storage modeling and management for multimedia information systems p 3022 N95-30483
A scalable parallel Strassen's matrix multiply algorithm for distributed memory computers
[DE95-010213] p 2936 N95-31109
A two-dimensional finite difference algorithm on the KSR1
[AD-A293576] p 2941 N95-31594
Class of service in the high performance storage system
[DE95-007959] p 2932 N95-31704
A microeconomic scheduler for parallel computers
[NASA-CR-198153] p 2932 N95-32046
The application of noncoherent Doppler data types for Deep Space Navigation p 2765 N95-32226
Assessment of computer aids during communication exercise 1991
[PB95-211462] p 2945 N95-32248
COMPUTER SYSTEMS PROGRAMS
Experience report: Using formal methods for requirements analysis of critical spacecraft software p 2938 N95-31247
The Linux operating system: An introduction
[NASA-CR-198178] p 2932 N95-31988
The Coprocessor Manager in the BASIS processor system
[PB95-211611] p 2945 N95-32252
Universal message passing library, or how to writea truly portable code for parallel computers
[PB95-212221] p 2948 N95-32255
Automatic verification and synthesis of finite-state hard real-time systems
[AD-A291279] p 2964 N95-32287
COMPUTER SYSTEMS SIMULATION
Testing the performance of feedback concatenated decoder with a nonideal receiver p 2856 N95-32231
COMPUTER TECHNIQUES
Contribution of groupware to corporate communication: Towards the horizontal organization
[PB95-197661] p 3022 N95-30453
Holistic analysis of gamma-ray spectra in instrumental neutron activation analysis
[PB95-214458] p 2979 N95-30639
Semiannual report
[NASA-CR-198172] p 2931 N95-30657
Machine learning for a toolkit for image mining
[AD-A293137] p 2951 N95-30890
Using computerized neuropsychological testing to assess aviator skills
[AD-A293227] p 2928 N95-30905
Development of a structured design and programming methodology for expert systems shells utilizing a visual programming language: Application of structured methodology to the MK92 maintenance advisor expert system, performance module prototype
[AD-A289897] p 2939 N95-31391
Computer-aided inspection process definition: Development of an expert planning and programming system for coordinate metrology
[DE95-010411] p 2940 N95-31404
Modern methods in meteorological and oceanographic data acquisition and analyses
[AD-A293884] p 2920 N95-31541
Management, visualization, and analysis of environmental and geotechnical data
[DE95-000063] p 3026 N95-31823
Translation workbench for generating subtitles for English TV news
[NHK-435] p 3026 N95-32182
A transient FETI methodology for large-scale parallel implicit computations in structural mechanics
[NASA-CR-199040] p 2945 N95-32214
Assessment of computer aids during communication exercise 1991
[PB95-211462] p 2945 N95-32248
Gigabit testbed research project
[DE95-010728] p 2945 N95-32270
COMPUTER VISION
Log-polar binocular vision system
[NASA-CR-188375] p 2996 N95-30772
Nonparametric recognition of nonrigid motion
[AD-A293630] p 2963 N95-31565
Force and vision resolvability for assimilating disparate sensory feedback
[AD-A293581] p 2929 N95-31685
Artificial neural networks and model-based recognition of 3-D objects from 2-D images p 2954 N95-31838
COMPUTERIZED SIMULATION
Simulation of airborne electromagnetic measurements in three dimensional environments
[DE95-008546] p 2900 N95-30363
IR DIAL performance modeling
[DE95-008377] p 2912 N95-30373
Simulation with complex measures
[DE95-616333] p 2955 N95-30445
Object-oriented approach for gas turbine engine simulation
[NASA-TM-106970] p 2754 N95-30594
Algorithm comparison and benchmarking using a parallel spectra transform shallow water model
[DE95-009124] p 2913 N95-30683
Advanced computational research in materials processing for design and manufacturing
[DE95-009130] p 2838 N95-30684
Spectral response of a polycrystalline silicon solar cell
[DE95-614370] p 2903 N95-30723

Control of flexible spacecraft structures using H-infinity wave absorbing control
| AD-A293141 | p 2766 N95-30919
A novel instrumentation system for measurement of helicopter rotor motions and loads data, phase 1
| AD-A293309 | p 2751 N95-30923
Algorithms for categorizing multiprocessor communication under invalidate and update-based coherence protocols
| AD-A290022 | p 2947 N95-30930
Large eddy simulation of jets using structured upwind numerics p 2871 N95-30993
The passage from transitional to free molecular plumes p 2871 N95-30994
Comparison of DSMC predictions with temporally resolved vibrational state measurements in NO p 2872 N95-30996
Confederation Verification, Validation, and Accreditation Master Plan (CVVAMP). Technical test plan
| AD-A289717 | p 2936 N95-31050
Calspan experience of PIO and the effects of rate limiting p 2746 N95-31072
Nordic symposium on analysis of electromagnetic transient phenomena using EMTP, part 3
| PB95-206504 | p 2849 N95-31158
Nordic Symposium on Analysis of Electromagnetic Transient Phenomena Using EMTP, part 2
| PB95-206579 | p 2849 N95-31160
Nordic Symposium on Analysis of Electromagnetic Transient Phenomena Using EMTP, part 4
| PB95-206587 | p 2849 N95-31181
Nordic Symposium on Analysis of Electromagnetic Transient Phenomena Using EMTP, part 1
| PB95-206595 | p 2850 N95-31182
Virtual Reality Software and Technology '94
| AD-A292334 | p 2939 N95-31262
The 2nd Japan-US Symposium on Finite Element Methods in Large Scale Computational Fluid Dynamics
| AD-A292337 | p 2960 N95-31264
The development of human behaviour analysis techniques and the development of human factors technologies
| DE95-613356 | p 2930 N95-31267
Centrifugal and axial pump design and off-design performance prediction p 2830 N95-31289
An ignition model for modern double base propellants p 2800 N95-31292
Control of mechanical systems with rolling contacts: Applications to robotics p 2889 N95-31332
Numerical simulation of shock/turbulent boundary layer interaction
| NASA-CR-198846 | p 2872 N95-31341
Numerical simulation of time dependent viscoelastic fluid flow
| TRITA-NA-9311 | p 2873 N95-31414
Visual processing of object velocity and acceleration
| AD-A292789 | p 2929 N95-31436
Adaptive optics design for the advanced electro-optical system (AEOS)
| AD-A293972 | p 2974 N95-31527
Theory and simulation of electrostatic wave turbulence in the space shuttle-induced plasma environment
| AD-A293467 | p 3005 N95-31534
Analytic and experimental investigation of rotordynamic response and backward whirl induced by split resonance
| AD-A293639 | p 2889 N95-31566
The effect of repeatedly sampling an embedded metamodel on the simulation response
| AD-A293783 | p 2953 N95-31582
Network user's guide
| DE95-009185 | p 2942 N95-31634
Brightness temperature simulations for the physical and synoptic interpretation of advanced microwave sounding unit moisture channels p 2921 N95-31721
Application of a genetic algorithm to optimize staffing levels in software development
| AD-A293725 | p 2943 N95-31835
Numerical simulation of the Langevin equation for skewed turbulence
| DE95-009477 | p 2877 N95-32049
Instability of weakly nonlinear chaotic structures
| DE95-613441 | p 2966 N95-32066
Automated volumetric grid generation for finite element modeling of human hand joints
| DE95-009575 | p 2928 N95-32097
SOSIE: A pragmatic approach to the simulation of Broad Air Defense applied to the theater level p 2840 N95-32127
Staggered solution procedures for multibody dynamics simulation
| NASA-CR-199034 | p 2899 N95-32202
Computational methods and software systems for dynamics and control of large space structures
| NASA-CR-199036 | p 2767 N95-32204
Computer model to simulate testing at the National Transonic Facility
| NASA-TM-4664 | p 2763 N95-32217
Computer simulation results for PCM/PM/NRZ receivers in nonideal channels p 2765 N95-32225
Residual and suppressed-carrier arraying techniques for deep-space communications p 2856 N95-32235
KRAKEN, a numerical model of RHIC impedances
| DE95-011563 | p 2994 N95-32242
Universal message passing library, or how to writea truly portable code for parallel computers
| PB95-212221 | p 2948 N95-32255
Simulation of katabatic flow and mountain waves
| DE95-010863 | p 2911 N95-32276
Production simulator for wave power plants
| PB95-212262 | p 2907 N95-32286
Point reflector model for the simulation of radar target glint and Doppler phenomena
| PB95-222980 | p 2857 N95-32314
Monte Carlo simulations of precise timekeeping in the Milstar communication satellite system p 2970 N95-32336

COMPUTERS
The Technology Information Environment with industry (TIE-In): A mechanism for accessing laboratory solutions
| DE95-008542 | p 3027 N95-30385

CONCENTRATION (COMPOSITION)
Measurement of temperatures and OH concentrations of solid propellant flames using absorption spectroscopy p 2801 N95-31302

CONCURRENT ENGINEERING
QFD analysis of RSRM aqueous cleaners p 2779 N95-31789

CONDENSATION NUCLEI
Cloud condensation nuclei measurements in shiptrails
| AD-A293302 | p 2919 N95-30951

CONDENSED MATTER PHYSICS
Abstracts of Annual Physics Conference of Iran
| DE95-611717 | p 2768 N95-30881

CONDUCTING POLYMERS
Electrical conductivity study on polythiophenes films
| DE95-614309 | p 2813 N95-30645
Magnetic resonance spectroscopy of fullerenes and (pi)-conjugated polymers
| DE95-010131 | p 2817 N95-31108
Materials with controllable signature properties
| PB95-222964 | p 2857 N95-32313

CONDUCTIVE HEAT TRANSFER
An ignition model for modern double base propellants p 2800 N95-31292
Derivation of two-dimensional (2-D) conduction equation in generalized coordinates with constant and anisotropic physical properties
| AD-A293896 | p 3020 N95-31511

CONDUCTIVITY
Ionic conductivities of lithium phosphorus oxynitride glasses, polycrystals, and thin films
| DE95-008898 | p 2812 N95-30545
Mechanisms of enhanced ionic conduction at interfaces in ceramics
| DE95-009125 | p 2814 N95-30730
Composite polymer electrolyte for lithium batteries
| AD-A293924 | p 2820 N95-31514

CONDUCTORS
Measurements of stability margins and current distribution in large-scale Nb3Sn cable-in-conduit conductors
| DE95-009869 | p 3007 N95-32148

CONFERENCES
XV NSO/Sac Peak Solar workshop
| AD-A292319 | p 3030 N95-30482
Proceedings of the CSCW 1994 workshop collaborative hypermedia systems
| PB95-208393 | p 3023 N95-30496
Email: Why and how
| PB95-195327 | p 2846 N95-30516
History and status of the atmospheric radiation measurement program
| DE95-009951 | p 2908 N95-30802
Conference perspective. Neuroimmunomodulation: Stress and immune function
| AD-A291351 | p 2926 N95-30870
Abstracts of Annual Physics Conference of Iran
| DE95-611717 | p 2768 N95-30881
Proceedings of the antenna applications symposium, volume 1
| AD-A293258 | p 2848 N95-30895
The 49th International Symposium on Molecular Spectroscopy
| AD-A292708 | p 2793 N95-30936
The 21st JANNAF Exhaust Plume Technology Meeting, volume 1
| CPIA-PUBL-621-VOL-1 | p 2870 N95-30986
Workshop on diffusion approximation in communication and stochastic systems theory
| AD-A292872 | p 2952 N95-31055
Flight Vehicle Integration Panel Workshop on Pilot Induced Oscillations
| AGARD-AR-335 | p 2745 N95-31061
CALORSTOCK 1994: Thermal energy storage. Better economy, environment, technology
| DE95-772422 | p 2904 N95-31138
Nordic symposium on analysis of electromagnetic transient phenomena using EMTP, part 3
| PB95-206504 | p 2849 N95-31158
Nordic Symposium on Analysis of Electromagnetic Transient Phenomena Using EMTP, part 2
| PB95-206579 | p 2849 N95-31160
Nordic Symposium on Analysis of Electromagnetic Transient Phenomena Using EMTP, part 4
| PB95-206587 | p 2849 N95-31181
Nordic Symposium on Analysis of Electromagnetic Transient Phenomena Using EMTP, part 1
| PB95-206595 | p 2850 N95-31182
The 31st JANNAF Combustion Subcommittee Meeting, volume 1 p 2825 N95-31194
Proceedings of the 19th Annual Software Engineering Workshop
| NASA-CR-189411 | p 2936 N95-31234
The 25th International Symposium on Combustion
| AD-A286825 | p 2794 N95-31268
The 31st JANNAF Combustion Subcommittee Meeting, volume 2
| CPIA-PUBL-620 | p 2829 N95-31282
Aerospace Environmental Technology Conference: Exectutive summary
| NASA-CP-3297 | p 2771 N95-31350
Proceedings of the antenna applications symposium. volume 2
| AD-A293259 | p 2850 N95-31387
Proceedings of the high energy density matter (HEDM) contractor's conference
| AD-A292988 | p 2836 N95-31470
Proceedings of the 16th Annual Conference on Atmospheric Transmission Models, volume 1
| AD-A293807 | p 2915 N95-31575
Proceedings of the 16th Annual Conference on Atmospheric Transmission Models, volume 2
| AD-A293806 | p 2916 N95-31604
Industry participation workshop: Chromium electroplating of superconductor strand. Proceedings
| DE95-009629 | p 2807 N95-31615
Annual meeting of the Advanced Light Source Users' Association
| DE95-009373 | p 3000 N95-31635
The 19th Annual Electronics Manufacturing Seminar
| AD-A293067 | p 2863 N95-31674
Aerospace Environmental Technology Conference
| NASA-CP-3298 | p 2771 N95-31746
Proceedings of the 1st Annual Software Engineering Techniques Workshop on Software Reengineering
| AD-A293724 | p 2943 N95-31834
Active control technology: Applications and lessons learned
| AGARD-CP-560 | p 2757 N95-31989
Guidance and Control for Future Air-Defence Systems
| AGARD-CP-555 | p 2839 N95-32123
Environmentally Safe and Effective Processes for Paint Removal
| AGARD-LS-201 | p 2843 N95-32165
The 26th Annual Precise Time and Time Interval (PTTI) Applications and Planning Meeting
| NASA-CP-3302 | p 2967 N95-32319
CALORSTOCK'94. Thermal energy storage. Better economy, environment, technology
| DE95-772421 | p 2907 N95-32368

CONFIGURATION INTERACTION
Inner- and outer-shell excitation in lithium isoelectronic sequence
| DE95-614107 | p 2981 N95-31003
A theoretical treatment of the absorption and emission properties of Cu(2) porphyrin
| AD-A293669 | p 2795 N95-31595

CONFORMAL MAPPING
Existence of solutions in plane quasistationary stokes flow driven by surface tension
| PB95-197935 | p 2868 N95-30810

CONGENITAL ANOMALIES
Arterial gas bubbles after decompression in pigs with Patent Foramen Ovale
| PB95-195319 | p 2925 N95-30515

CONGRESSIONAL REPORTS
National Laboratories: Are their R and D activities related to commercial product development? Report to Congressional Requesters
| GAO/PEMD-95-2 | p 3027 N95-31345
Annual report to the Chairman and Ranking Minority Members, House and Senate Committees on Appropriations. Status of open recommendations: Improving operations of federal departments and agencies
| GAO/OP-95-1 | p 3022 N95-31986

Report to the Chairman, Legislation and National Security Subcommittee, Committee on Government Operations, House of Representatives. Tactical aircraft: F-15 replacement is premature as currently planned
| GAO/NSIAD-94-118 | p 2964 N95-31987
Report to the Chairman, Legislation and National Security Subcommittee, Committee on Government Operations, House of Representatives. Unmanned aerial vehicles: Performance of short-range system still in question
| GAO/NSIAD-94-65 | p 2752 N95-32196
Report to Congressional Committees. Military airlift: C-17 settlement is not a good deal
| GAO/NSIAD-94-141 | p 2741 N95-32198
Report to the Chairman, Subcommittee on Transportation and Related Agencies, Committee on Appropriations, House of Representatives. Air traffic control: Status of FAA's plans to close and contract out low-activity towers
| GAO/RCED-94-265 | p 2750 N95-32199

CONICAL BODIES
The 25th International Symposium on Combustion
| AD-A286825 | p 2794 N95-31268
Fractional delay waveguide modeling of acoustic tubes
| PB95-206637 | p 2975 N95-31650

CONICS
Perpendicular electron heating by absorption of auroral kilometric radiation
| NASA-198815 | p 2914 N95-30848

CONIFERS
Unification of LARCH and Z-based object models to support algebraically-based design refinement: The LARCH perspective
| AD-A289235 | p 2935 N95-30999

CONJUGATE GRADIENT METHOD
Use of element-by-element preconditioners to solve large scale partially separable optimization problems
| PB95-195772 | p 2957 N95-30692

CONJUGATES
Complex conjugate pairs in stationary Sturmians
| DE95-616279 | p 2976 N95-30429

CONJUGATION
Experimental investigation of optical nonlinearities in conjugated polymers
| AD-A288353 | p 2884 N95-31145
Nonlinear organized materials for optical devices
| AD-A292809 | p 2999 N95-31441
Photorefractive nonlinear optics
| AD-A292913 | p 2999 N95-31458
Conjugated aromatic polyimines. 2. Synthesis, structure, and properties of new aromatic polyazomethines
| AD-A292955 | p 2819 N95-31461
Excited-state complexes of conjugated polymers: Novel photophysical processes and optoelectronic materials
| AD-A292958 | p 2819 N95-31462
Excited-state complexes of conjugated polymers
| AD-A292960 | p 2819 N95-31466
Effects of molecular structure on the electroactive and optical properties of conjugated rigid-rod polybenzobisazoles
| AD-A292968 | p 2819 N95-31467

CONNECTORS
Smart material joint band
| AD-D017374 | p 2888 N95-30716

CONSERVATION
CP violating effects in e(+) e(-) yields ZH and their optimization
| DE95-616302 | p 2976 N95-30441
Major weapon system environmental life-cycle cost estimating for Conservation, Cleanup, Compliance and Pollution Prevention (C3P2) p 2774 N95-31761

CONSERVATION EQUATIONS
Some aspects on the modelling of non-Newtonian fluid flow
| TRITA-NA-9317 | p 2873 N95-31415

CONSERVATION LAWS
Multidimensional discretization of conservation laws for unstructured polyhedral grids
| DE95-008796 | p 2955 N95-30470
A study of numerical solutions of conservation laws
| TRITA-NA-9315 | p 2960 N95-31361
Computational methods for control and optimal design of aerospace systems
| AD-A292861 | p 2751 N95-31451

CONSISTENCY
Improving data consistency in mobile computing using Isolation-Only Transactions
| AD-A293110 | p 2948 N95-32021

CONSONANTS (SPEECH)
The contextual variance of devoiced fricatives in polish
| IFTR-7/1995 | p 2854 N95-32192

CONSTANTS
Electron transfer kinetics of self-assembled ferrocene C(12) alkanethiol monolayers on gold electrodes from 125K to 175K
| AD-A292754 | p 2984 N95-31427

CONSTELLATIONS
Multiple Target Tracking based on constellation matching and Kalman filter p 2842 N95-32136

CONSTITUTIVE EQUATIONS
Wave propagation in a fluid-loaded homogeneous, transversely isotropic, elastic cylinder of arbitrary thickness
| AD-A292728 | p 2869 N95-30946
Some aspects on the modelling of non-Newtonian fluid flow
| TRITA-NA-9317 | p 2873 N95-31415

CONSTRAINTS
Pseudo-time methods for constrained optimization problems governed by PDE
| NASA-CR-195081 | p 2959 N95-31120
Control of mechanical systems with rolling contacts: Applications to robotics p 2889 N95-31332

CONSTRUCTION
Low vibration polymeric composite engine
| AD-D017332 | p 2887 N95-30386
Influence of adhesives and bonding techniques on the properties of glued timber-steelplate joints
| PB95-211470 | p 2813 N95-30599
The HYLIFE-2 inertial fusion energy power plant concept and implications for IFE
| DE95-010561 | p 2994 N95-32074

CONSTRUCTION MATERIALS
Mechanical alloying processing with application to structural materials
| AD-A290788 | p 2802 N95-30404
Observations of star fracture and longitudinal splitting in BIS 812 EMA and Q1N submarine construction steels
| DSTO-RR-0014 | p 2806 N95-31344

CONTAMINANTS
Achieving improved cycle efficiency via pressure gain combustors
| DE95-008945 | p 2792 N95-30762
The 49th International Symposium on Molecular Spectroscopy
| AD-A292708 | p 2793 N95-30936
Evaluation of calibration parameters and performance of the video imaging technique of assessing exposure (VITAE system)
| AD-A289023 | p 2927 N95-30998
Analytical instrumentation for environmental research
| AD-A292832 | p 2908 N95-31447
Magnesium battery disposal characteristics
| AD-A293053 | p 2863 N95-31607
CFD assessment of the pollutant environment from RD-170 propulsion system testing p 2772 N95-31749
Verification of surface preparation for adhesive bonding p 2782 N95-31807
Spectroscopic ellipsometry as a sensitive monitor of materials contamination p 2782 N95-31808
Bioremediation of wheat starch media waste p 2845 N95-32178
Calculation of a residual mean meridional circulation for a zonal-mean tracer transport model
| DE95-009474 | p 2911 N95-32350

CONTAMINATION
Vacuum plume backflow and rarefaction p 2871 N95-30995
Spatial time-series: Pollution pattern recognition under irregular interventions
| AD-A293830 | p 2909 N95-31556
Preventing cracking of anodized coatings
| NASA-TM-104622 | p 2839 N95-31690
Surface contamination analysis technology team overview p 2781 N95-31797
Standardization of surface contamination analysis systems p 2781 N95-31798
Cleanliness inspection tool for RSRM bond surfaces p 2781 N95-31799
The design and development of a third generation OSEE instrument p 2781 N95-31800
Study of surfaces using near infrared optical fiber spectrometry p 2781 N95-31801
Contamination detection NDE for cleaning process inspection p 2781 N95-31802
Surface inspection using FTIR spectroscopy p 2782 N95-31803
Cleanliness evaluation of rough surfaces with diffuse IR reflectance p 2782 N95-31804
Spectroscopic ellipsometry as a sensitive monitor of materials contamination p 2782 N95-31808
The role of surface chemical analysis in a study to select replacement processes for TCA vapor degreasing p 2782 N95-31809
Monte Carlo tests of the ELIPGRID-PC algorithm
| DE95-010811 | p 2943 N95-32030
Treatment of plastic media waste p 2844 N95-32177

CONTINGENCY
Patient/aircraft forecasting for the strategic aeromedical evacuation lift-bed process
| AD-A293902 | p 2747 N95-31512
Estimation in second order dependency model for multivariate binary data
| DE95-010326 | p 2944 N95-32087

CONTINUITY (MATHEMATICS)
A unified interpretation of singular and near-singular integrals in the boundary element method
| ISBN-0-315-86297-1 | p 2962 N95-31947

CONTINUITY EQUATION
Particle filtration: An analysis using the method of volume averaging
| DE95-009467 | p 2875 N95-31592

CONTINUOUS RADIATION
Development of a novel wind lidar, phase 1
| AD-A292703 | p 2849 N95-30935
Diode-pumped, continuously tunable, 2.3 micron CW laser
| AD-D017448 | p 2885 N95-31273
Advances in high-power chemical lasers
| AD-A289737 | p 2885 N95-31389

CONTINUOUS SPECTRA
Singular eigenfunctions for shearing fluids I
| DE95-008952 | p 2868 N95-30763

CONTINUOUS WAVE LASERS
Spotsize measurements of a focused CW Nd: YAG laser
| DE95-007746 | p 2884 N95-31139
The 25th International Symposium on Combustion
| AD-A286825 | p 2794 N95-31268
Diode-pumped, continuously tunable, 2.3 micron CW laser
| AD-D017448 | p 2885 N95-31273
A compact and efficient violet laser source
| AD-A292782 | p 2885 N95-31434
Sandia National Lab's precision laser tracking systems
| DE95-009837 | p 2886 N95-32143

CONTINUUM FLOW
Numerical simulation of time dependent viscoelastic fluid flow
| TRITA-NA-9311 | p 2873 N95-31414

CONTINUUM MECHANICS
Numerical simulation of time dependent viscoelastic fluid flow
| TRITA-NA-9311 | p 2873 N95-31414
Some aspects on the modelling of non-Newtonian fluid flow
| TRITA-NA-9317 | p 2873 N95-31415

CONTINUUM MODELING
Dynamics of an inhomogeneous anisotropic antiferromagnetic spin chain
| DE95-614449 | p 3013 N95-30959
Modeling of fiber-reinforced composites incorporating distinct interface properties p 2787 N95-31110
A computational procedure for multibody systems including flexible beam dynamics
| NASA-CR-199035 | p 2897 N95-31730

CONTINUUMS
Beyond the variational principle in quantum field theory
| DE95-616286 | p 3018 N95-30438
Singular eigenfunctions for shearing fluids I
| DE95-008952 | p 2868 N95-30763

CONTRACT MANAGEMENT
Quality assurance tendering and awarding contracts
| PB95-197760 | p 2891 N95-31362
Report to Congressional Committees. Military airlift: C-17 settlement is not a good deal
| GAO/NSIAD-94-141 | p 2741 N95-32198

CONTRACT NEGOTIATION
Quality assurance tendering and awarding contracts
| PB95-197760 | p 2891 N95-31362
Report to Congressional Committees. Military airlift: C-17 settlement is not a good deal
| GAO/NSIAD-94-141 | p 2741 N95-32198

CONTRACTION
The electrodeposition of low contraction chromium/molybdenum alloys using pulse-reverse plating
| AD-A292727 | p 2804 N95-30945

CONTRACTORS
Proceedings of the high energy density matter (HEDM) contractor's conference
| AD-A292988 | p 2836 N95-31470

CONTRAILS
Cloud condensation nuclei measurements in shiptrails
| AD-A293302 | p 2919 N95-30951

CONTRAST
Luminance effects on visual acuity and small letter contrast sensitivity
| AD-A293310 | p 2928 N95-31140

CONTROL STABILITY
Stability analysis of linear control systems with uncertain parameters p 2954 N95-31949
An investigation of pilot induced oscillation phenomena in digital-flight control systems p 2760 N95-32011

CONTROL SURFACES
Transonic aerodynamic characteristics of a proposed wing-body reusable launch vehicle concept [NASA-TM-108489] p 2742 N95-30712
The FCS-structural coupling problem and its solution p 2759 N95-32005
Structural aspects of active control technology p 2760 N95-32006

CONTROL SYSTEMS DESIGN
Computerized design of controllers using data models [NASA-CR-198921] p 2950 N95-30655
System identification for robust process control. Nominal models and error bounds [PB95-197026] p 2839 N95-30777
Generalized controlled invariance for nonlinear systems [PB95-197901] p 2950 N95-30807
Control of flexible spacecraft structures using H-infinity wave absorbing control [AD-A293141] p 2766 N95-30919
Flight Vehicle Integration Panel Workshop on Pilot Induced Oscillations [AGARD-AR-335] p 2745 N95-31061
SCARLET: DLR rate saturation flight experiment p 2746 N95-31068
Handling qualities analysis on rate limiting elements in flight control systems p 2746 N95-31071
Calspan experience of PIO and the effects of rate limiting p 2746 N95-31072
High-tech controls for energy and environment [DE95-011702] p 2952 N95-31255
Representation of feedback operators for hyperbolic systems [NASA-CR-198171] p 2960 N95-31319
The role of handling qualities specifications in flight control system design p 2757 N95-31990
The importance of flying qualities design specifications for active control systems p 2757 N95-31992
Lavi flight control system: Design requirements, development and flight test results p 2758 N95-31994
Robust control: A structured approach to solve aircraft flight control problems p 2758 N95-31995
Dynamic inversion: An evolving methodology for flight control design p 2758 N95-31996
Evaluation of the techniques of fuzzy control for the piloting an aircraft p 2758 N95-31997
The control system design methodology of the STOL and maneuver technology demonstrator p 2758 N95-31998
Control law design using H-infinity and mu-synthesis short-period controller for a tail-airplane p 2758 N95-31999
Model following control for tailoring handling qualities: ACT experience with ATTHeS p 2758 N95-32000
X-29 flight control system: Lessons learned p 2759 N95-32001
The FCS-structural coupling problem and its solution p 2759 N95-32005
Structural aspects of active control technology p 2760 N95-32006
Flight test results of the F-16 aircraft modified with axisymmetric vectoring exhaust nozzle p 2752 N95-32007
Digital autopilot design for combat aircraft in ALENIA p 2760 N95-32009
Experimental Aircraft Programme (EAP): Flight control system design and test p 2760 N95-32010
An investigation of pilot induced oscillation phenomena in digital-flight control systems p 2760 N95-32011
Advanced flight control technology achievements at Boeing Helicopters p 2761 N95-32014
Practical experiences in control systems design using the NCR Bell 205 Airborne Simulator p 2761 N95-32015
Integration issues in modular mission management aid development p 2841 N95-32133
Using a Red Team to devise countermeasures p 2842 N95-32141

CONTROL THEORY
Fixed modes in quasi-static state feedback decoupling [PB95-206850] p 2950 N95-30564
System identification for robust process control. Nominal models and error bounds [PB95-197026] p 2839 N95-30777
H(sub 2) optimal controllers with observer based architecture for continuous-time systems: Separation principle [PB95-197067] p 2951 N95-30833
SCARLET: DLR rate saturation flight experiment p 2746 N95-31068
A two-timescale approach to nonlinear Model Predictive Control [DE95-000943] p 2952 N95-31161
Advances in robust control [AD-A291126] p 2952 N95-31266
Global stabilization of nonlinear gyroscopic systems p 2881 N95-31836
Flight demonstration of an advanced pitch control law in the VAAC Harrier aircraft p 2760 N95-32012
Advanced flight control technology achievements at Boeing Helicopters p 2761 N95-32014
Practical experiences in control systems design using the NCR Bell 205 Airborne Simulator p 2761 N95-32015
Methodologies for steering clocks p 2971 N95-32341

CONTROLLABILITY
Generalized controlled invariance for nonlinear systems [PB95-197901] p 2950 N95-30807
The process for addressing the challenges of aircraft pilot coupling p 2745 N95-31063
Observations on PIO p 2745 N95-31064
The relation of handling qualities ratings to aircraft safety p 2746 N95-31067
SAAB experience with PIO p 2746 N95-31069
Aeroelastic pilot-in-the-loop oscillations p 2746 N95-31070
Analysis of heads-up display quickening versus handling qualities [AD-A293797] p 2753 N95-31584
The role of handling qualities specifications in flight control system design p 2757 N95-31990
Experiences with ADS-33 helicopter specification testing and contributions to refinement research p 2757 N95-31993
Control law design using H-infinity and mu-synthesis short-period controller for a tail-airplane p 2758 N95-31999
Model following control for tailoring handling qualities: ACT experience with ATTHeS p 2758 N95-32000

CONTROLLERS
Computerized design of controllers using data models [NASA-CR-198921] p 2950 N95-30655
Speed control of an elastic two-mass system: Optimization and systems theory [PB95-212106] p 2888 N95-30701
Precision manipulation with a dextrous robot hand p 2888 N95-30829
H(sub 2) optimal controllers with observer based architecture for continuous-time systems: Separation principle [PB95-197067] p 2951 N95-30833
Mobile electric power [AD-A292721] p 2860 N95-30940
Robust fixed-structure control [AD-A292883] p 2952 N95-30961
Robust control: A structured approach to solve aircraft flight control problems p 2758 N95-31995
Evaluation of the techniques of fuzzy control for the piloting an aircraft p 2758 N95-31997
Control law design using H-infinity and mu-synthesis short-period controller for a tail-airplane p 2758 N95-31999

CONVECTION
Direct and inverse problems in random media [AD-A293033] p 2850 N95-31280
On convective effects in sedimentation of concentrated suspensions with high effective gravity [TRITA-NA-9316] p 2794 N95-31356
Numerical modeling of Bridgman growth of PbSnTe in a magnetic field [NASA-TM-106996] p 2837 N95-31359
Fundamental topics in heat transfer through deformable two-phase media p 2874 N95-31532
Numerical simulation of the Langevin equation for skewed turbulence [DE95-009477] p 2877 N95-32049

CONVECTION-DIFFUSION EQUATION
Fourier analysis of a robust multigrid method for convection-diffusion equations [PB95-197091] p 2958 N95-30835
Numerical stability investigations of processes for solving linear initial value problems [PB95-207023] p 2959 N95-31183

CONVECTIVE FLOW
A turbulence model for steady and unsteady boundary layers in strong pressure gradients p 2868 N95-30840

CONVERGENCE
Convergence properties of an augmented lagrangian algorithm for optimization with a combination of general equality and linear constraints [PB95-208039] p 2956 N95-30570
Multigrid convergence acceleration for the 2D Euler equations applied to high-lift systems [PB95-198081] p 2743 N95-30814
Theory & numerical methods for problems in shape reconstruction and large deviations [AD-A292874] p 2952 N95-31279
Convergent spray process for environmentally friendly coatings p 2777 N95-31776
Newton Raphson method, scaling at fractal boundaries and mathematica [DE95-613374] p 2962 N95-32095
The individual element test revisited [NASA-CR-199039] p 2945 N95-32215

CONVEXITY
Complex mean value interpolation [PB95-211629] p 2956 N95-30601
Co-groups on sequentially complete, locally convex, topological vector spaces in particular on strict LF-spaces [PB95-206918] p 2966 N95-30681

CONVOLUTION INTEGRALS
A finite element formulation for the time domain vibration analysis of an elastic-viscoelastic structure p 2895 N95-31318

COOLANTS
Experimental investigation of the effectiveness of flow-through modules for electronics cooling [AD-A293284] p 2861 N95-30950

COOLING
On the quasihydrostatic flows of radiatively cooling self-gravitating gas clouds [DE95-009116] p 3029 N95-30729
Electrically heated tube investigation of cooling channel geometry effects [NASA-TM-106985] p 2768 N95-30856
Construction and performance measurement of a portable thermoacoustic refrigerator demonstration apparatus [AD-A293265] p 2839 N95-31122

COOPERATION
A system simulation development project: Leveraging resources through partnerships [NASA-TM-106962] p 2753 N95-30514

COORDINATES
Computer-aided inspection process definition: Development of an expert planning and programming system for coordinate metrology [DE95-010411] p 2940 N95-31404
Derivation of two-dimensional (2-D) conduction equation in generalized coordinates with constant and anisotropic physical properties [AD-A293896] p 3020 N95-31511
Method of normal coordinates in the formulation of a system with dissipation: The harmonic oscillator [DE95-613372] p 3020 N95-32094
Harmonic coordinates in the problem on static gravitational and massless scalar fields with a point source [DE95-623632] p 3020 N95-32295

COPOLYMERS
Thermoplastic elastomers as a binder in composite propellants [PB95-211553] p 2837 N95-32249
Responsive copolymers for enhanced petroleum recovery [DE95-011857] p 2823 N95-32361

COPPER
Anodically enhanced diffusion in Cu/Ag thin film couples [DE95-009198] p 2814 N95-30738
Glass matrix doped with activated luminescent nanocrystalline particles [AD-D017416] p 2816 N95-31010
Experimental investigation of optical nonlinearities in conjugated polymers [AD-A288353] p 2884 N95-31145
Solderability enhancement of copper through chemical etching [DE95-010514] p 2806 N95-31406
The effect of gravity on the deposition of thin films: The physical vapor transport of copper phthalocyanine [AD-A292997] p 2838 N95-31472

COPPER ALLOYS
Metallurgical and Materials Transactions [AD-A293617] p 2807 N95-31464
Comparison of cathodic protection currents on 70/30 copper-nickel and alloy 625 piping systems [AD-A292953] p 2807 N95-31561

COPPER OXIDES
A valence-fluctuation mechanism with highly anisotropic S-wave pairing [DE95-009419] p 3010 N95-30571
Superconducting and normal-state properties of novel materials [DE95-012368] p 3017 N95-32366

COPPER SELENIDES
Investigation of polycrystalline thin film CuInSe2 solar cells based on ZnSe windows [DE95-004068] p 2904 N95-31164

CORIOLIS EFFECT
Dynamical analysis of the coriolis effect which causes space disorientation
[NAL-TR-1258] p 2928 N95-31714
COROTATION
HST-FOC observations of a remarkable UV auroral event on Jupiter p 3030 N95-30806
CORPUSCULAR RADIATION
Particle filtration: An analysis using the method of volume averaging
[DE95-009467] p 2875 N95-31592
CORRECTION
The conical singularity and quantum corrections to entropy of black hole
[DE95-613367] p 3029 N95-30606
Functions for processing synthetic aperture radar imagery
[AD-A293895] p 2851 N95-31510
SeaWiFS technical report series. Volume 28: SeaWiFS algorithms, part 1
[NASA-TM-104566-VOL-28] p 2924 N95-31850
Radiative corrections to the three quantum annihilation cross section in high energy electron-positron collisions
[DE95-623675] p 2995 N95-32296
CORRELATION
Multi-particle correlations in quaternionic quantum systems
[DE95-616271] p 3018 N95-30424
SeaWiFS Technical Report Series. Volume 29: SeaWiFS CZCS-type pigment algorithm
[NASA-TM-104566] p 2922 N95-30857
Patterns in the sky: Natural visualization of aircraft flow fields
[NASA-SP-514] p 2741 N95-31000
Statistical properties of chaotic scattering with one open channel
[DE95-613370] p 3020 N95-32150
CORROSION
Off-potential measurement systems for impressed current cathodic protection
[AD-A290876] p 2812 N95-30558
The impact of microbiologically influenced corrosion on protective polymer coatings
[AD-A288896] p 2816 N95-30997
Space Shuttle Orbiter corrosion history, 1981-1993: A review and analysis of issues involving structures and subsystems
[NASA-TM-104810] p 2810 N95-32183
CORROSION PREVENTION
Off-potential measurement systems for impressed current cathodic protection
[AD-A290876] p 2812 N95-30558
Computational modeling of coating integrity effects on impressed current cathodic protection system
[AD-A293256] p 2815 N95-30894
Assessment of pollution prevention and control technology for plating operations p 2776 N95-31771
Replacement of corrosion protection chromate primers and paints used in cryogenic applications on the Space Shuttle with wire arc sprayed aluminum coatings p 2776 N95-31774
Space Shuttle Orbiter corrosion history, 1981-1993: A review and analysis of issues involving structures and subsystems
[NASA-TM-104810] p 2810 N95-32183
Minutes of the fourth annual workshop on chromate replacements in light metal finishing
[DE95-010937] p 2810 N95-32241
CORROSION RESISTANCE
Trivalent chromium solutions for sealing anodized aluminum
[AD-D017349] p 2803 N95-30551
Evaluation of Environmentally Acceptable hydraulic fluids
[AD-A293037] p 2821 N95-31666
Thin-film sulfuric acid anodizing as a replacement for chromic acid anodizing p 2776 N95-31772
Cadmium plating replacements p 2776 N95-31773
Environmentally regulated aerospace coatings p 2777 N95-31775
Robotic weld overlay coatings for erosion control
[DE95-009643] p 2809 N95-32098
CORROSION TESTS
NaK pool-boiler solar receiver durability bench test. Volume 2: Metallurgical analysis
[DE95-010338] p 2905 N95-31640
COSMIC GASES
Molecular gas in starburst galaxies: Line intensities and physical conditions
[PB95-208021] p 3029 N95-30569
COSMIC RAYS
Solar-geophysical data number 606, February 1995. Part 1: (Prompt reports). Data for December 1994, January 1995, and late data
[PB95-200853] p 3031 N95-30816
COSMOLOGY
Large scale periodicity of the universe and baryogenesis
[DE95-613461] p 3028 N95-30366
COSMONAUTS
STS-71 post flight presentation
[NASA-TM-110658] p 2764 N95-30852
Mir 18 post flight presentation
[NASA-TM-110657] p 2766 N95-30854
COST ANALYSIS
An assessment of the cost of microwave sintering ceramic tiles for armor applications. Phase 2 report
[DE95-010000] p 2816 N95-31103
Neural network false alarm filter, volume 1
[AD-A293097] p 2953 N95-31562
Modeling F/A-18 flight hour program costs using regression analysis
[AD-A293771] p 2752 N95-31579
Study of Extended Air Defence Post 2000 p 2839 N95-32124
COST EFFECTIVENESS
Evaluating the cost effectiveness of environmental projects: Case studies in aerospace and defense p 2774 N95-31762
COST ESTIMATES
Lessons learned in deploying software estimation technology and tools p 2938 N95-31246
Major weapon system environmental life-cycle cost estimating for Conservation, Cleanup, Compliance and Pollution Prevention (C3P2) p 2774 N95-31761
COST REDUCTION
Photovoltaic Czochralski silicon manufacturing technology improvements
[DE95-004066] p 2904 N95-31162
Large-area, triple-junction a-Si alloy production scale-up
[DE95-004067] p 2904 N95-31163
Photovoltaic Energy Program overview: Fiscal year 1994
[DE94-011871] p 2905 N95-31661
Report to the Chairman, Subcommittee on Transportation and Related Agencies, Committee on Appropriations, House of Representatives. Air traffic control: Status of FAA's plans to close and contract out low-activity towers
[GAO/RCED-94-265] p 2750 N95-32199
COSTS
Failure analysis of a repairable system: The case study of a cam-driven reciprocating pump
[AD-A293144] p 2889 N95-30949
A NASPAC-Based analysis of the delay and cost effects of the western-pacific region preliminary resectorization effort of 1993
[AD-A288696] p 2748 N95-31013
Integration of air traffic databases: A case study
[AD-A293691] p 2749 N95-32022
COULOMB POTENTIAL
Coulomb correction calculations of pp Bremsstrahlung
[DE95-616349] p 2982 N95-31176
COUNTING
Reply-frequency interference/jamming detector
[AD-D017428] p 2847 N95-30746
COUPLED MODES
Normal mode tunes for linear coupled motion in six dimensional phase space
[DE95-011565] p 2994 N95-32244
Review of longitudinal perturbation formalism
[DE95-010894] p 2990 N95-32278
COUPLERS
Demodulators for optical fiber interferometers with (3 x 3) outputs
[AD-D017415] p 2995 N95-30402
Diode-pumped, continuously tunable, 2.3 micron CW laser
[AD-D017448] p 2885 N95-31273
Improved linear dynamic range in externally modulated fiber-optic links p 3001 N95-31950
COUPLES
Passive, multi-channel fiber optic rotary joint assembly
[AD-D017353] p 2996 N95-30529
Anodically enhanced diffusion in Cu/Ag thin film couples
[DE95-009198] p 2814 N95-30738
COUPLING
Locking device for fluid coupling
[AD-D017354] p 2888 N95-30414
A theory for predicting and minimizing the effects of matrix degradation on the thermomechanical properties of general laminates p 2785 N95-30768
Physics goals of a mu(+) mu(-) collider
[DE95-009546] p 2994 N95-32059
Search for anomalous ZZ(sub gamma) and Z(sub (gamma, gamma)) couplings with D0
[DE95-010457] p 2989 N95-32162
Normal mode tunes for linear coupled motion in six dimensional phase space
[DE95-011565] p 2994 N95-32244
COUPLING CIRCUITS
Pre-amplifier with multi-stage feedback
[AD-D017371] p 2859 N95-30659
COUPLING COEFFICIENTS
Shear flow effects on ion thermal transport in tokamaks
[DE95-009115] p 3005 N95-30601
COUPLINGS
Coupling stud assembly
[AD-D017335] p 2887 N95-30387
CRACK BRIDGING
Fatigue crack growth behavior of a titanium matrix composite under thermomechanical loading p 2784 N95-30491
CRACK GEOMETRY
Cracking during nanoindentation and its use in the measurement of fracture toughness
[DE95-008839] p 2818 N95-31175
CRACK INITIATION
Failure analysis for polycarbonate transparencies
[AD-A292992] p 2820 N95-31471
CRACK PROPAGATION
Fatigue crack growth behavior of a titanium matrix composite under thermomechanical loading p 2784 N95-30491
Room temperature fracture and high temperature creep deformation properties of alumina reinforced with 20 vol% particulate niobium
[DE95-010234] p 2815 N95-30897
A simple and accurate technique for monitoring crack growth behavior using a wave form analyzer
[AD-A293161] p 2894 N95-31007
Thermal-mechanical fatigue crack growth in aircraft engine materials
[ISBN-0-315-86543-1] p 2894 N95-31098
Cracking during nanoindentation and its use in the measurement of fracture toughness
[DE95-008839] p 2818 N95-31175
Failure analysis for polycarbonate transparencies
[AD-A292992] p 2820 N95-31471
Mode I large strain viscoelastic crack behavior in nitrile rubber sheets
[AD-A289984] p 2820 N95-31617
A numerical analysis of crack growth in microcracking ceramic and ceramic composites
[DE95-010132] p 2897 N95-32024
Simulation of fracture in compression using a field-theory model
[DE95-009874] p 2898 N95-32102
CRACK TIPS
Numerical evaluation of three-dimensional crack-tip integrals for layered anisotropic solids p 2898 N95-32191
CRACKING (FRACTURING)
Ion implantation and thermal stress resistance of ceramics
[DE95-615349] p 2812 N95-30451
Fourier series methods for cracks in polygonal plates and shells of revolution p 2893 N95-30825
The 10th International Conference on the Strength of Materials
[AD-A292335] p 2894 N95-31263
Preparation of S-70A-9 Black Hawk helicopter for flight tests to investigate cause of cracking of inner fuselage panel
[AD-A293891] p 2752 N95-31544
Mode I large strain viscoelastic crack behavior in nitrile rubber sheets
[AD-A289984] p 2820 N95-31617
Numerical evaluation of three-dimensional crack-tip integrals for layered anisotropic solids p 2898 N95-32191
CRACKS
Fourier series methods for cracks in polygonal plates and shells of revolution p 2893 N95-30825
A simple and accurate technique for monitoring crack growth behavior using a wave form analyzer
[AD-A293161] p 2894 N95-31007
Preventing cracking of anodized coatings
[NASA-TM-104622] p 2839 N95-31690
Simulation of fracture in compression using a field-theory model
[DE95-009874] p 2898 N95-32102
CRANES
Fatigue behaviour of multiplanar tubular joints
[PB95-207874] p 2893 N95-30586
CRASHES
Releaseable unconstrained inflatable body protector
[AD-D017350] p 2930 N95-30552

CREEP PROPERTIES
Room temperature fracture and high temperature creep deformation properties of alumina reinforced with 20 vol% particulate niobium
[DE95-010234] p 2815 N95-30897
Effect of cyclic loading on the creep performance of silicon nitride
[DE95-010289] p 2894 N95-31131
Effect of cold work on creep properties of Hastelloy XR
[DE95-722056] p 2806 N95-31154
The influence of microstructure on creep deformation in near-gamma TiAl alloys p 2808 N95-31975
Creep of a fine-grained, fully-lamellar, two-phase TiAl alloy at 760 C
[DE95-009531] p 2810 N95-32272

CREEP RUPTURE STRENGTH
Effect of cold work on creep properties of Hastelloy XR
[DE95-722056] p 2806 N95-31154

CREEP STRENGTH
Creep of a fine-grained, fully-lamellar, two-phase TiAl alloy at 760 C
[DE95-009531] p 2810 N95-32272

CREEP TESTS
Interfacial studies of coated fiber reinforced glass-ceramic matrix composites
[AD-A290780] p 2783 N95-30433
Effect of cyclic loading on the creep performance of silicon nitride
[DE95-010289] p 2894 N95-31131
Effect of cold work on creep properties of Hastelloy XR
[DE95-722056] p 2806 N95-31154
Creep of a fine-grained, fully-lamellar, two-phase TiAl alloy at 760 C
[DE95-009531] p 2810 N95-32272

CRITERIA
Quantum 1/f noise in high technology applications including ultrasmall structures and devices
[AD-A292812] p 2862 N95-31442

CRITICAL TEMPERATURE
Multisite antiferromagnetic Ising spin model: Phase transition through doubling bifurcation
[DE95-614311] p 3011 N95-30722

CROSS FLOW
Simulation of chemical kinetics in turbulent natural gas combustion. Volume 2: Experimental studies of nitric oxide production in gas flames
[PB95-196721] p 2791 N95-30541
Effects of initial conditions on a single jet in crossflow
[NASA-TM-107002] p 2754 N95-30589
Jet mixing and emission characteristics of transverse jets in annular and cylindrical confined crossflow
[NASA-TM-106976] p 2755 N95-30698
Jet mixing in a reacting cylindrical crossflow
[NASA-TM-106975] p 2755 N95-30853

CROSS SECTIONS
Pion-pair production by two photons
[DE95-737162] p 2983 N95-31223

CROSSLINKING
Process for producing hydrophilic polymer membranes
[AD-D017355] p 2811 N95-30415
Biosensors based on cross-linking of biotinylated Glucose Oxidase by avidin
[AD-A290439] p 2925 N95-30452
An interpenetrating polymer network for second-order nonlinear optics
[AD-A293019] p 2821 N95-31699
Influence of storage on the maximal pull-out force of three different optical fibers from three epoxides
[PB95-211777] p 2822 N95-32253

CRUDE OIL
Responsive copolymers for enhanced petroleum recovery
[DE95-011857] p 2823 N95-32361

CRYOGENIC EQUIPMENT
Supplemental multilayer insulation research facility
[NASA-TM-106991] p 2768 N95-30595
Reducing process noise in superconducting helium liquid level probes
[DE95-008956] p 2814 N95-30765
Replacement of corrosion protection chromate primers and paints used in cryogenic applications on the Space Shuttle with wire arc sprayed aluminum coatings p 2776 N95-31774

CRYOGENIC FLUIDS
Optimization of high-temperature superconductor current leads
[DE95-005836] p 2861 N95-30942
Performance evaluation of high-temperature superconducting current leads for micro-SMES systems
[DE95-005843] p 2861 N95-30943

CRYOGENIC ROCKET PROPELLANTS
Combustion of LOX with H2(sub g) under subcritical and supercritical conditions p 2797 N95-31717

CRYOGENIC TEMPERATURE
A water blown urethane insulation for use in cryogenic environments p 2775 N95-31765

CRYOGENIC WIND TUNNELS
Computer model to simulate testing at the National Transonic Facility
[NASA-TM-4664] p 2763 N95-32217

CRYOGENICS
Supplemental multilayer insulation research facility
[NASA-TM-106991] p 2768 N95-30595
The 26th Annual Precise Time and Time Interval (PTTI) Applications and Planning Meeting
[NASA-CP-3302] p 2967 N95-32319

CRYOSTATS
Free electron laser as energy driver for inertial confinement fusion
[DE95-614252] p 2884 N95-30914

CRYPTOGRAPHY
Requirements for security signalling
[DE95-008714] p 2948 N95-31605
Scalable ATM encryption
[DE95-009868] p 2948 N95-32065
Proposed DDS-specific fields for the Generic Authentication Information Element
[DE95-009839] p 3026 N95-32144
A proposed Generic Authentication Information Element
[DE95-009862] p 2948 N95-32146

CRYSTAL DEFECTS
Microstructural and mechanical property changes in model Fe-Cu alloys
[DE95-010117] p 2805 N95-31105
Effect of irradiation spectrum on the microstructure of ion-irradiated Al2O3
[DE95-010225] p 2806 N95-31188
Evidence for electronic energy loss processes stimulating solid phase epitaxial regrowth of spatially isolated amorphous regions in semiconductor systems
[DE95-009892] p 3016 N95-32103
Defect configurations in neutron-irradiated U3Si2
[DE95-009896] p 3016 N95-32105
Suppression of self-interstitials in silicon during ion implantation via in-situ photoexcitation
[DE95-009173] p 3016 N95-32301

CRYSTAL DISLOCATIONS
Diffraction-line broadening analysis and stress relaxation in thin metal layers
[PB95-213898] p 2893 N95-30634
Characterization of /11'01/ twin dislocation structures in evaporated titanium thin films by HREM
[DE95-615391] p 2820 N95-31623

CRYSTAL GROWTH
Orientation of rapid thermally annealed lead zirconate titanate thin films on (111) Pt substrate
[DE95-615232] p 2811 N95-30422
Synthesis of carbo-nitride films using high-energy shock plasma deposition
[DE95-615231] p 2811 N95-30450
Langasite crystals growth with quality factor Q, that exceeds the Q of quartz, and which are suitable for high-precision resonators
[AD-A293397] p 3013 N95-30969
Intelligent synthetic polymers
[AD-A292905] p 2819 N95-31395
Metallurgical and Materials Transactions
[AD-A293617] p 2807 N95-31464
The effect of gravity on the deposition of thin films: The physical vapor transport of copper phthalocyanine
[AD-A292997] p 2838 N95-31472
Characterization of /11'01/ twin dislocation structures in evaporated titanium thin films by HREM
[DE95-615391] p 2820 N95-31623
Silicon carbide-silicon heterostructure solar cells p 2905 N95-31952
Processing and microstructural evolution of alumina/aluminum alloy and aluminum nitride/aluminum alloy composites by directed melt oxidation p 2789 N95-31973

CRYSTAL LATTICES
The neutron powder diffraction and acoustic investigations of the NH4SCN phase diagram
[DE95-614372] p 3009 N95-30419
Electroweak interactions on the lattice
[DE95-616287] p 2965 N95-30439
Molecular modeling of PMN ceramics
[AD-A290879] p 2813 N95-30560
The one-dimensional model of the off-centre potential of the fluorine ion in the NaBr lattice
[DE95-614310] p 3010 N95-30647
Zone axis backscattered electron contrast for fast electrons
[DE95-616775] p 2980 N95-30790
TV-VI semiconductor quantum well lasers, physics and engineering p 2883 N95-30805
Ferromagnetic Potts model in a magnetic field: Finite lattice extrapolation of the (1 + 1)-dimensional Hamiltonian
[DE95-614447] p 3012 N95-30958
Dynamics of an inhomogeneous anisotropic antiferromagnetic spin chain
[DE95-614449] p 3013 N95-30959
Pseudomorphic heterostructure materials for high performance devices
[AD-A292906] p 2788 N95-31384
Metallurgical and Materials Transactions
[AD-A293617] p 2807 N95-31464
Characterization of /11'01/ twin dislocation structures in evaporated titanium thin films by HREM
[DE95-615391] p 2820 N95-31623
Synthesis and characterization of nanophase face-centered-cubic titanium
[DE95-009533] p 2809 N95-32051

CRYSTAL OPTICS
X-ray standing wave interferometry-optics at 1 angstrom with applications to surface and material sciences
[DE95-011453] p 2998 N95-31114

CRYSTAL STRUCTURE
Crystallization of sol-gel derived lead zirconate titanate thin films in argon and oxygen atmospheres
[DE95-615230] p 3009 N95-30421
Structural investigation of xenon ion-beam-irradiated glassy carbon
[DE95-616777] p 2977 N95-30474
STM studies of clean, CO- and O2-exposed Pt(100)-hex-R0.7 deg
[PB95-195376] p 3009 N95-30535
Molecular modeling of PMN ceramics
[AD-A290879] p 2813 N95-30560
Diffraction-line broadening analysis and stress relaxation in thin metal layers
[PB95-213898] p 2893 N95-30634
A theoretical analysis of steady-state photocurrents in simple silicon diodes
[NASA-CR-198885] p 2859 N95-30651
Phase transformations in melt-spun Y-Ba-Cu-O bulk superconductor
[DE95-010237] p 3011 N95-30667
Polarisation resonance in X-ray diffraction
[DE95-616727] p 3012 N95-30789
Zone axis backscattered electron contrast for fast electrons
[DE95-616775] p 2980 N95-30790
Molecular nanoclusters as precursors to conductive thin films and crystals
[AD-A290278] p 3014 N95-31189
Poisson's ratio for hexagonal crystals
[AD-A293556] p 3015 N95-31539

CRYSTAL SURFACES
X-ray standing wave interferometry-optics at 1 angstrom with applications to surface and material sciences
[DE95-011453] p 2998 N95-31114

CRYSTALLINITY
Morphology and microstructure of (111) crystalline CeO2 films grown on amorphous SiO2 substrates by pulsed-laser ablation
[DE95-008842] p 3009 N95-30542
Fabrication and modification of metal nanocluster composites using ion and laser beams
[DE95-009131] p 2784 N95-30731
New material for high average power infrared generation: QPM-DB GaAs
[AD-A292714] p 2967 N95-30939

CRYSTALLIZATION
Crystallization of sol-gel derived lead zirconate titanate thin films in argon and oxygen atmospheres
[DE95-615230] p 3009 N95-30421
The pyrochlore-to-perovskite transformation in solution-derived lead zirconate titanate thin films
[DE95-010453] p 2822 N95-32161

CRYSTALLOGRAPHY
Orientation of rapid thermally annealed lead zirconate titanate thin films on (111) Pt substrate
[DE95-615232] p 2811 N95-30422
Characterization of /11'01/ twin dislocation structures in evaporated titanium thin films by HREM
[DE95-615391] p 2820 N95-31623

CRYSTALS
A room temperature LSO/PIN photodiode PET detector module that measures depth of interaction
[DE95-008447] p 2878 N95-30378
The neutron powder diffraction and acoustic investigations of the NH4SCN phase diagram
[DE95-614372] p 3009 N95-30419
Crystallization of sol-gel derived lead zirconate titanate thin films in argon and oxygen atmospheres
[DE95-615230] p 3009 N95-30421
Low temperature synthesis of YBa2Cu3O(8-x) and other crystalline oxides
[AD-D017370] p 3009 N95-30533

Semiconductor nanocrystals formed in SiO2 by ion implantation
[DE95-008900] p 2978 N95-30546
Molecular nanoclusters as precursors to conductive thin films and crystals
[AD-A290278] p 3014 N95-31189
Method of synthesizing high quality, doped diamond and diamonds and devices obtained therefrom
[AD-D017432] p 3014 N95-31269
Transitions, defects, and whiskered microstructures
[AD-A292796] p 3014 N95-31438
Proceedings of the high energy density matter (HEDM) contractor's conference
[AD-A292988] p 2836 N95-31470
Poisson's ratio for hexagonal crystals
[AD-A293556] p 3015 N95-31539
Effects of mosaicity on Parametric X-Radiation production
[AD-A293677] p 2985 N95-31597
Wavelengths measurements of the He-like krypton K-shell spectrum
[DE95-010264] p 2987 N95-32041
Luminescence properties of ZnWO4:Cr(3+) laser crystals
[AD-A293065] p 2887 N95-32152
Photo-refractive Bi12SiO20: Spatial light modulator
[AD-A293084] p 3001 N95-32153

CUBES (MATHEMATICS)
Barendregt cube with definitions and generalized reduction
[PB95-206793] p 2966 N95-30719

CUBIC LATTICES
Crystallization of sol-gel derived lead zirconate titanate thin films in argon and oxygen atmospheres
[DE95-615230] p 3009 N95-30421

CUMULATIVE DAMAGE
Robust Rocket Engine Concept
[NASA-TM-107010] p 2770 N95-32121

CURING
Epoxy and acrylate stereolithography resins: In-situ measurements of cure shrinkage and stress relaxation
[DE95-008506] p 2811 N95-30389
A viscoelastic anisotropic wave propagation model for composite cure evaluation p 2786 N95-30839
Phthalonitrile prepolymer as high temperature sizing material for composite fibers
[AD-D017447] p 2818 N95-31272

CURRENT ALGEBRA
Arithmetic features of rational conformal field theory
[PB95-207908] p 2966 N95-30591
Pion-pair production by two photons
[DE95-737162] p 2983 N95-31223

CURRENT DENSITY
Effects of temperature ramp rate during heat treatment on hysteresis loss and critical current density of internal tin processed wires
[DE95-009551] p 2803 N95-30706
Anodically enhanced diffusion in Cu/Ag thin film couples
[DE95-009198] p 2814 N95-30738
Optimization of high-temperature superconductor current leads
[DE95-005838] p 2861 N95-30942
Lower hybrid accessibility in a large, hot reversed field pinch
[DE95-011001] p 3007 N95-32310

CURRENT DISTRIBUTION
Optimization of a thermoelectric IR-detector for low working temperature
[NASA-CR-198933] p 2880 N95-30752
Measurements of stability margins and current distribution in large-scale Nb3Sn cable-in-conduit conductors
[DE95-009869] p 3007 N95-32148

CURRENT SHEETS
Study of cross-tail current carriers in magnetotail p 3005 N95-30804
The art and science of magnet design: Selected notes of Klaus Halbach, volume 2
[DE95-008450] p 2861 N95-31059

CURVATURE
Multi-particle correlations in quaternionic quantum systems
[DE95-616271] p 3018 N95-30424
Quantum dynamics in regions of quaternionic curvature
[DE95-616276] p 3018 N95-30426
The conical singularity and quantum corrections to entropy of black hole
[DE95-613367] p 3029 N95-30606
The effect of ray curvature on Lloyd's mirror fringe estimates and source localisation
[DSTO-TR-0064] p 3001 N95-31745

CURVE FITTING
Assessment of the NASA orbital debris engineering model
[AD-A293350] p 2766 N95-31143

CURVED BEAMS
Picosecond phase conjugation: New applications, devices, and materials
[AD-A293195] p 3013 N95-30982

CURVES (GEOMETRY)
Data reduction of piecewise linear curves
[PB95-212270] p 2962 N95-32256

CUTTERS
Effect of local melting on tribology in metal cutting
[PB95-195392] p 2804 N95-31052

CYANATES
The neutron powder diffraction and acoustic investigations of the NH4SCN phase diagram
[DE95-614372] p 3009 N95-30419

CYBERNETICS
Emerging applications in probability (Sensor management)
[AD-A292781] p 2749 N95-31433

CYCLES
A simple and accurate technique for monitoring crack growth behavior using a wave form analyzer
[AD-A293161] p 2894 N95-31007

CYCLIC LOADS
A simple and accurate technique for monitoring crack growth behavior using a wave form analyzer
[AD-A293161] p 2894 N95-31007
Effect of cyclic loading on the creep performance of silicon nitride
[DE95-010289] p 2894 N95-31131

CYCLOGENESIS
LAWS hurricane studies
[NASA-CR-189438] p 2919 N95-31128
Diagnosis of the kinematics and dynamics of rapidly developing maritime cyclones
[AD-A293919] p 2921 N95-31675

CYCLONES
Forecast of Atlantic seasonal hurricane activity for 1994 p 2918 N95-30832
Summary of 1993 Atlantic tropical cyclone activity and verification of author's forecast. A year of unanticipated light hurricane activity and a poor forecast: The expected dissipation of the El Nino did not take place and Caribbean basin surface pressure became quite high p 2918 N95-30842
Early August updated forecast of Atlantic seasonal hurricane activity for 1994 p 2919 N95-30844
Diagnosis of the kinematics and dynamics of rapidly developing maritime cyclones
[AD-A293919] p 2921 N95-31675

CYCLOTRON RADIATION
Perpendicular electron heating by absorption of auroral kilometric radiation
[NASA-198815] p 2914 N95-30848
Development of plasma diagnostics technologies: A study on nuclear fusion reactor
[DE95-614180] p 3005 N95-31004

CYCLOTRON RESONANCE DEVICES
Harmonic gyrotron amplifiers and phase-locked oscillators
[AD-A293185] p 2861 N95-30979
Stable high-power harmonic gyro-amplifiers
[AD-A293697] p 2881 N95-31828

CYLINDRICAL BODIES
Fast-acting valve for projective launching systems
[AD-D017357] p 2888 N95-30416
Metal nanotubule membranes with electrochemically switchable ion-transport selectivity
[AD-A292712] p 2793 N95-30938
Hot compression testing of tungsten
[AD-A293683] p 2807 N95-31599
Fractional delay waveguide modeling of acoustic tubes
[PB95-206637] p 2975 N95-31650
Side force acting on blunted circular cylinder bodies at high angles of attack in supersonic flow
[NAL-TR-1255] p 2744 N95-31741

CZOCHRALSKI METHOD
Photovoltaic Czochralski silicon manufacturing technology improvements
[DE95-004066] p 2904 N95-31162

D

DAMAGE
Amorphization threshold in Si-implanted strained SiGe alloy layers
[DE95-008901] p 2804 N95-30797
Response of mechanically fastened composite joints under multiple bypass loads p 2785 N95-30824

Computational modeling of coating integrity effects on impressed current cathodic protection system
[AD-A293256] p 2815 N95-30894
Probabilistic reliability modeling of fatigue on the H-46 tie bar
[AD-A289926] p 2751 N95-30927
New adaptive methods for reconfigurable flight control systems, appendix 1
[AD-A292711] p 2756 N95-30937
Microstructure of Al2O3 irradiated with an applied electric field
[DE95-010278] p 2822 N95-32043
Suppression of self-interstitials in silicon during ion implantation via in-situ photoexcitation
[DE95-009173] p 3016 N95-32301

DAMAGE ASSESSMENT
Economical analysis relating to the global warming issue
[DE95-764072] p 2908 N95-30677
Ultrasonic characterization of fiber-matrix interphasial properties and damage in high-temperature composites p 2785 N95-30823
Navier-Stokes flow field analysis of compressible flow in a high pressure safety relief valve
[NASA-TM-110640] p 2868 N95-30862
Damage dosimetry and embrittlement monitoring of nuclear pressure vessels in real time by magnetic properties measurement
[DE95-011454] p 2894 N95-31254
The determination of wave group parameters from the resolution of incident and reflected waves
[AD-A293703] p 2924 N95-31829
Mapping hidden aircraft defects with dual-band infrared computed tomography
[DE95-011531] p 2741 N95-32164

DAMPING
Gravitational-radiation damping of compact binary systems to second post-Newtonian order
[PB95-207882] p 2912 N95-30588

DATA ACQUISITION
Smart active multiwave sensing with zero background amplitude modulated probes
[DE95-008813] p 2792 N95-30714
Offshore next generation weather radar (NEXRAD) OT&E integration and OT&E operational test
[AD-A293223] p 2848 N95-30902
Impact behavior of the active zone within a frozen soil profile
[AD-A292909] p 2915 N95-31386
Acquiring consistent knowledge for Bayesian Forests
[AD-A293858] p 2952 N95-31517
Modern methods in meteorological and oceanographic data acquisition and analyses
[AD-A293884] p 2920 N95-31541
Arabian Sea mixed layer dynamics experiment: Mooring deployment cruise report
[AD-A293684] p 2923 N95-31600
Data collection at the Lockheed Santa Cruz facility using midwave hyperspectral imagers
[AD-A293057] p 3000 N95-31672
A programming interface for application-aware adaptation in mobile computing
[AD-A293107] p 2943 N95-32019
Acquisition, tracking, pointing and fire control for Ballistic Missile Defense p 2841 N95-32131
The Telecommunications and Data Acquisition Report
[NASA-CR-198911] p 2854 N95-32221

DATA BASE MANAGEMENT SYSTEMS
Data management system: User's guide
[DE95-008692] p 3022 N95-30392
Extending a multi-set relational algebra to a parallel environment
[PB95-207106] p 3023 N95-30566
Recommendations for developing portable parallel I/O facilities for scientific applications
[DE95-009384] p 2947 N95-30578
Supporting data intensive applications with medium grained parallelism
[DE95-010164] p 3023 N95-30619
Workflow literature guide, version 1
[PB95-207080] p 2947 N95-30721
Join processing in relational database systems p 3023 N95-30764
Development of technical information processing systems
[DE95-613311] p 3024 N95-30882
The development of KAERI management information system 2: The development of Time Sheet Management System
[DE95-613355] p 3024 N95-30883
Client server architecture for multidatabase access. Ingres SQL server
[PB95-192852] p 2947 N95-31051
Adaptiveness in information systems integration p 3025 N95-31348

Support of environmental requirements for cloud analysis and archive (SERCAA): Database management facility
[AD-A293938] p 2920 N95-31522
UNLV: Information Science Research Institute
[DE95-011941] p 3027 N95-32362

DATA BASES
Protocols for integrity constraint checking in federated databases
[PB95-197695] p 3022 N95-30456
Extending a multi-set relational algebra to a parallel environment
[PB95-207106] p 3023 N95-30566
Supporting data intensive applications with medium grained parallelism
[DE95-010164] p 3023 N95-30619
Geostatistics and hydrology. Part 3. Hydro-meteorological network design
[PB95-206462] p 2900 N95-30818
QTSAW (Quick Typhoon Surge and Waves). Wave information studies of US coastlines
[AD-A293172] p 2919 N95-30976
Operator's handbook: NAWC Software Production Facility
[AD-A290216] p 2935 N95-31001
Client server architecture for multidatabase access. Ingres SQL server
[PB95-192852] p 2947 N95-31051
ARTI Refrigerant Database
[DE95-008336] p 2816 N95-31057
Assessment of the NASA orbital debris engineering model
[AD-A293350] p 2766 N95-31143
Digital Mapping Charting and Geodesy Analysis Program technical review of Vector Product Format (VPF)
[AD-A289766] p 2901 N95-31390
Human factors at the FAA Technical Center: Bibliography
[AD-A288638] p 2930 N95-31399
Synthetic Terrain Imagery for Helmet-Mounted Display. Volume 3: Software user's manual
[AD-A293613] p 2753 N95-31463
Acquiring consistent knowledge for Bayesian Forests
[AD-A293858] p 2952 N95-31517
Support of environmental requirements for cloud analysis and archive (SERCAA): Database management facility
[AD-A293938] p 2920 N95-31522
Class of service in the high performance storage system
[DE95-007959] p 2932 N95-31704
Prioritization methodology for chemical replacement p 2773 N95-31757
Environmental databases and other computerized information tools p 2783 N95-31810
NEIS (NASA Environmental Information System) p 2783 N95-31811
Integration of air traffic databases: A case study
[AD-A293691] p 2749 N95-32022
Report to Congressional Committees. Federal research: Interim report on the pilot technology access program
[GAO/RCED-94-75] p 3022 N95-32195

DATA COLLECTION PLATFORMS
Development and implementation of a computer facility for nuclear data updating and reactor calculations using personal computers
[DE95-623577] p 2940 N95-31408

DATA COMPRESSION
System considerations for efficient communication and storage of MSTI image data
[NASA-CR-198869] p 3024 N95-30858
Multi-dimensional data compression for portable communication
[AD-A292751] p 2850 N95-31426
A seismic data compression system using subband coding p 2857 N95-32238

DATA CONVERSION ROUTINES
BRUTUS: A program for conversion between image formats
[PB95-211421] p 2945 N95-32246

DATA FLOW ANALYSIS
Computer simulation results for PCM/PM/NRZ receivers in nonideal channels p 2765 N95-32225

DATA LINKS
High Frequency (HF) upgrade study for the Canadian Regional Operations Control Center (ROCC) AWACS Digital Information Link (RADIL) project
[AD-A293435] p 2850 N95-31367
High accuracy time transfer synchronization p 2968 N95-32321

DATA MANAGEMENT
Expert system for assessing accuracy of models of physical phenomena and for selecting alternate models in the presence of noise
[AD-D017348] p 2974 N95-30550
Supporting data intensive applications with medium grained parallelism
[DE95-010164] p 3023 N95-30619
JPL Physical Oceanography Distributed Active Archive Center (PO.DAAC) data availability, version 1-94
[NASA-CR-198871] p 2922 N95-30859
Acquiring consistent knowledge for Bayesian Forests
[AD-A293858] p 2952 N95-31517
Class of service in the high performance storage system
[DE95-007959] p 2932 N95-31704
Management, visualization, and analysis of environmental and geotechnical data
[DE95-000063] p 3026 N95-31823
Westinghouse Hanford Company Data Management Plan Template, revision 1
[DE95-010046] p 3026 N95-32107

DATA PROCESSING
Expert system for assessing accuracy of models of physical phenomena and for selecting alternate models in the presence of noise
[AD-D017348] p 2974 N95-30550
ESAA: Environment for Seismic Activity Analysis
[DE95-612416] p 2913 N95-30675
Theory & numerical methods for problems in shape reconstruction and large deviations
[AD-A292874] p 2952 N95-31279
Development and implementation of a computer facility for nuclear data updating and reactor calculations using personal computers
[DE95-623577] p 2940 N95-31408
Support of environmental requirements for cloud analysis and archive (SERCAA): Database management facility
[AD-A293938] p 2920 N95-31522
Using satellites for radar performance monitoring and calibration
[AD-A293809] p 2852 N95-31588
Development of the Multi-Level Seismic Receiver (MLSR)
[DE95-008823] p 2916 N95-31610
Topics in exploratory and speculative data analysis
[AD-A290505] p 3025 N95-31618
Implementation of a standard format for GPS common view data p 2968 N95-32323
Time activities at the BIPM p 2968 N95-32325
High resolution time interval counter p 2969 N95-32331

DATA REDUCTION
Laser Tracker 3: Sandia National Laboratories' third generation laser tracking system
[DE95-008525] p 2882 N95-30379
Operating system support for distributed multimedia applications: A survey of current research
[PB95-207098] p 2964 N95-30565
Artificial intelligence techniques for flight test planning, phase 1
[AD-A293962] p 2751 N95-31525
Validation of special sensor microwave/imager ocean surface wind retrievals in equatorial regions
[AD-A293750] p 2920 N95-31571
Data reduction of piecewise linear curves
[PB95-212270] p 2962 N95-32256

DATA RETRIEVAL
Machine learning for a toolkit for image mining
[AD-A293137] p 2951 N95-30890

DATA SAMPLING
A two-timescale appróach to nonlinear Model Predictive Control
[DE95-000943] p 2952 N95-31161

DATA STORAGE
Data storage modeling and management for multimedia information systems p 3022 N95-30483
System considerations for efficient communication and storage of MSTI image data
[NASA-CR-198869] p 3024 N95-30858
A real time method for Fourier transform holographic information storage
[AD-A293186] p 2880 N95-30980
Degradation of blue AlGaN/InGaN/GaN LEDs subjected to high current pulses
[DE95-008824] p 2863 N95-31611
Class of service in the high performance storage system
[DE95-007959] p 2932 N95-31704
Gigabit testbed research project
[DE95-010728] p 2945 N95-32270

DATA STRUCTURES
Join processing in relational database systems p 3023 N95-30764

DATA SYSTEMS
JPL Physical Oceanography Distributed Active Archive Center (PO.DAAC) data availability, version 1-94
[NASA-CR-198871] p 2922 N95-30859
Comparison of satellite-derived MSU brightness temperatures and conventionally-derived fields
[AD-A293692] p 2901 N95-31603
Improving data consistency in mobile computing using Isolation-Only Transactions
[AD-A293110] p 2948 N95-32021
The application of noncoherent Doppler data types for Deep Space Navigation p 2765 N95-32226

DATA TRANSFER (COMPUTERS)
Effective bandwidth techniques in bufferless and buffered ATM multiplexers
[PB95-207072] p 2862 N95-31185

DATA TRANSMISSION
High Frequency (HF) upgrade study for the Canadian Regional Operations Control Center (ROCC) AWACS Digital Information Link (RADIL) project
[AD-A293435] p 2850 N95-31367
Requirements for security signalling
[DE95-008714] p 2948 N95-31605
Design and testing of an optimal digital link capable of 14-channel transmission
[AD-A288505] p 3000 N95-31652
Scalable ATM encryption
[DE95-009868] p 2948 N95-32065
Proposed DDS-specific fields for the Generic Authentication Information Element
[DE95-009839] p 3026 N95-32144
A proposed Generic Authentication Information Element
[DE95-009862] p 2948 N95-32146
Degradation in finite-harmonic subcarrier demodulation p 2855 N95-32228
Fast identification of some typical digital modulation schemes
[PB95-211454] p 2857 N95-32247
Gigabit testbed research project
[DE95-010728] p 2945 N95-32270

DBR LASERS
A compact and efficient violet laser source
[AD-A292782] p 2885 N95-31434

DE BROGLIE WAVELENGTHS
Magneto-optical transmission-reflection beam splitter for multi-level atoms
[DE95-616267] p 2976 N95-30423
Reflection and diffraction of atomic de Broglie waves by evanescent laser waves. Bare-state method
[DE95-616458] p 2992 N95-30960

DECISION MAKING
Dynamic maintenance scheduling for a stochastic telecommunication network: Determination of performance factors
[AD-A293829] p 2852 N95-31555

DECODERS
Enhanced decoding for the Galileo low-gain antenna mission: Viterbi redecoding with four decoding stages p 2855 N95-32230
Testing the performance of feedback concatenated decoder with a nonideal receiver p 2856 N95-32231

DECODING
Enhanced decoding for the Galileo low-gain antenna mission: Viterbi redecoding with four decoding stages p 2855 N95-32230
Trellis complexity bounds for decoding linear block codes p 2856 N95-32234

DECOMPOSITION
Applications of SXPS for studying surface structure, reaction mechanisms and kinetics
[DE95-008903] p 2803 N95-30547
Global aspects of the WZNW reduction to Toda theories
[DE95-737230] p 3019 N95-31226
Base hydrolysis and hydrothermal processing of PBX-9404 explosive
[DE95-009437] p 2836 N95-32048
A modification to the GMRES method for ill-conditioned linear systems
[DE95-010661] p 2962 N95-32076
A stochastic difference equation approach to inference with missing data: Some new results
[DE95-010327] p 2944 N95-32088
GCMS and FTIR studies of by-product inhibited growth and the rate-limiting step in TEOS-based SiO2 CVD
[DE95-009863] p 3016 N95-32147

DECOMPRESSION SICKNESS
Decompression illness, observable bubbles. (Session K)
[PB95-195285] p 2926 N95-30511
Effects of air bubbles on rabbit blood brain barrier
[PB95-195293] p 2925 N95-30512
Detecting intravascular gas bubbles in ultrasonic images
[PB95-195301] p 2926 N95-30513
Arterial gas bubbles after decompression in pigs with Patent Foramen Ovale
[PB95-195319] p 2925 N95-30515

DECONTAMINATION
Aqueous TiO2 photocatalysis of metal-EDTA complexes
[DE95-011058] p 2793 N95-31113
The Wide Field/Planetary Camera 2 (WFPC-2) molecular adsorber
[NASA-CR-196866] p 2881 N95-31456
Recycling MIL-H-46170 hydraulic fluid to extend fluid service life
[AD-A293035] p 2821 N95-31664
Replacement of ozone depleting and toxic chemicals in gravimetric analysis of non-volatile residue
p 2780 N95-31793

DECOUPLING
Fixed modes in quasi-static state feedback decoupling
[PB95-206850] p 2950 N95-30564
A simple model for the dc flux transformer in layered superconductors with Josephson coupling
[DE95-614468] p 2859 N95-30649
Generalized controlled invariance for nonlinear systems
[PB95-197901] p 2950 N95-30807
New adaptive methods for reconfigurable flight control systems, appendix 1
[AD-A292711] p 2756 N95-30937
Method of normal coordinates in the formulation of a system with dissipation: The harmonic oscillator
[DE95-613372] p 3020 N95-32094

DEDUCTION
Barendregt cube with definitions and generalized reduction
[PB95-206793] p 2966 N95-30719

DEEP SPACE
Rate considerations in deep space telemetry
p 2765 N95-32223
Multiple turbo codes for deep-space communications
p 2855 N95-32227
Residual and suppressed-carrier arraying techniques for deep-space communications p 2856 N95-32235
European plans for new clocks in space
p 2968 N95-32324

DEEP SPACE NETWORK
The Telecommunications and Data Acquisition Report
[NASA-CR-198911] p 2854 N95-32221
Determination of the position of Jupiter from radio metric tracking of Voyager 1 p 2854 N95-32222
Computer simulation results for PCM/PM/NRZ receivers in nonideal channels p 2765 N95-32225
The application of noncoherent Doppler data types for Deep Space Navigation p 2765 N95-32226
Effects of correlated noise on the full-spectrum combining and complex-symbol combining arraying techniques p 2856 N95-32237
DSS-24 microwave holography measurements
p 2857 N95-32239
Digital signal processing in the radio science stability analyzer p 2857 N95-32240
The Deep Space Network stability analyzer
p 2858 N95-32334
Fiber optic reference frequency distribution to remote beam waveguide antennas p 2972 N95-32346

DEFECTS
Ultrasonic two probe system for locating and sizing
[AD-D017438] p 2996 N95-30724
Mechanisms of enhanced ionic conduction at interfaces in ceramics
[DE95-009125] p 2814 N95-30730
Transitions, defects, and whiskered microstructures
[AD-A292796] p 3014 N95-31438
Phase stability, point defects and site preference of FeAl and NiAl with ternary additions
[DE95-009694] p 3015 N95-31641
The 19th Annual Electronics Manufacturing Seminar
[AD-A293067] p 2863 N95-31674
Validation of favor code linear elastic fracture solutions for finite-length flaw geometries
[DE95-009034] p 2898 N95-32157
Nondestructive testing of ceramic components: Cooperative Research and Development Agreement completion report
[DE95-009510] p 2823 N95-32352

DEFENSE INDUSTRY
Federally funded R and D centers: Executive compensation at the Aerospace Corporation. Report to Congressional requestors
[GAO/NSIAD-95-75] p 3022 N95-32213

DEFENSE PROGRAM
Unmanned aerial vehicles. 1994 master plan
p 2751 N95-31416
Definition of an anti-missile ballistic defense architecture for Europe p 2840 N95-32125

DEFLAGRATION
Preliminary assessment of combustion modes for internal combustion wave rotors
[NASA-TM-107000] p 2754 N95-30632
A study of gas-phase processes during the deflagration of RDX composite propellants using a triple quadrupole mass spectrometer p 2801 N95-31304
Effects of gas-phase thermal expansion on the stability of deflagration through a porous energetic material
[DE95-004382] p 2797 N95-31824

DEFLECTION
Impact behavior of the active zone within a frozen soil profile
[AD-A292909] p 2915 N95-31386

DEFORMATION
Generalized deformed para-Bose oscillator and its coherent states
[DE95-613444] p 2963 N95-30610
Simulation of viscous sintering
[PB95-197109] p 2868 N95-30836
Physical modelling of microstructural evolution during thermomechanical processing of aluminium alloys
[PB95-196341] p 2805 N95-31053
Residual stresses and stress corrosion cracking in pipe fittings
[DE95-009332] p 2894 N95-31054
The topological string associated with a simple singularity of type D
[DE95-737229] p 2983 N95-31225
Large deformation failure mechanisms in nonlinear solids
[AD-A293010] p 2896 N95-31474
Fundamental topics in heat transfer through deformable two-phase media p 2874 N95-31532
Hot compression testing of tungsten
[AD-A293683] p 2807 N95-31599
A computational procedure for multibody systems including flexible beam dynamics
[NASA-CR-199035] p 2897 N95-31730
The influence of matrix microstructure and temperature on cyclic deformation and fatigue of particle-reinforced 2219 aluminum p 2808 N95-31974
The influence of microstructure on creep deformation in near-gamma TiAl alloys p 2808 N95-31975
Structural analyses of the JPL Mars Pathfinder impact
[DE95-009581] p 2767 N95-32081

DEGASSING
Sonic apparatus for degassing liquids
[AD-D017352] p 2791 N95-30554

DEGRADATION
Interface degradation in CAS/Nicalon during elevated temperature aging
[DE95-008843] p 2812 N95-30543
A theory for predicting and minimizing the effects of matrix degradation on the thermomechanical properties of general laminates p 2785 N95-30768
The effect of interface properties on nickel base alloy composites
[NASA-CR-198363] p 2785 N95-30787
Behaviour of polymers in radioactive environments: Effects of dose speed
[DE95-621008] p 2818 N95-31221
Analytical instrumentation for environmental research
[AD-A292832] p 2908 N95-31447
Degradation of blue AlGaN/InGaN/GaN LEDs subjected to high current pulses
[DE95-008824] p 2863 N95-31611
Environmentally regulated aerospace coatings
p 2777 N95-31775
Base hydrolysis and hydrothermal processing of PBX-9404 explosive
[DE95-009437] p 2836 N95-32048
Residual and suppressed-carrier arraying techniques for deep-space communications p 2856 N95-32235

DEGREES OF FREEDOM
A queer reduction of degrees of freedom
[DE95-613471] p 2964 N95-30369
Robust position and force tracking control for a robot in contract p 2888 N95-30830
Dynamical systems as models for flow-induced vibrations
[PB95-206991] p 2869 N95-30956
Analytic and experimental investigation of rotordynamic response and backward whirl induced by split resonance
[AD-A293639] p 2889 N95-31566
A survey of the core-congruential formulation for geometrically nonlinear TL finite elements
[NASA-CR-199044] p 2944 N95-32203

DEHUMIDIFICATION
Recycling MIL-H-46170 hydraulic fluid to extend fluid service life
[AD-A293035] p 2821 N95-31664

DELAY
Analysis and modeling of an airport departure process
[AD-A293782] p 2749 N95-31581
Fractional delay waveguide modeling of acoustic tubes
[PB95-206637] p 2975 N95-31650

DELAY CIRCUITS
Coherent integrator
[AD-D017422] p 2847 N95-30743

DELTA WINGS
Numerical investigation into vortical flow about a delta-wing configuration up to incidences at which vortex breakdown occurs in experiment
[PB95-198024] p 2743 N95-30837
Unsteady transonic wind tunnel test on a semispan straked delta wing, oscillating in pitch. Part 1: Description of the model, test setup, data acquisition, and data processing
[AD-A293113] p 2743 N95-30885

DEMODULATION
Degradation in finite-harmonic subcarrier demodulation
p 2855 N95-32228
Towards optimum demodulation of bandwidth-limited and low SNR square-wave subcarrier signals
p 2855 N95-32229

DEMODULATORS
Demodulators for optical fiber interferometers with (3 x 3) outputs
[AD-D017415] p 2995 N95-30402
Noise signal processor
[AD-D017430] p 2974 N95-30747

DENSE PLASMAS
Development of a tokamak plasma optimized for stability and confinement
[DE95-009609] p 3003 N95-30641
Relativistic non-interacting electron gas in a magnetic field
[DE95-616903] p 2967 N95-31177

DENSITY (MASS/VOLUME)
Ocean mass density calculations from temperature and salinity data
[DSTO-TR-0023] p 2922 N95-30711

DENSITY (NUMBER/VOLUME)
Metal nanotubule membranes with electrochemically switchable ion-transport selectivity
[AD-A292712] p 2793 N95-30938

DENSITY DISTRIBUTION
Ocean mass density calculations from temperature and salinity data
[DSTO-TR-0023] p 2922 N95-30711

DENSITY MEASUREMENT
A prototype ionospheric tomography system (ITS)
[AD-A293015] p 2916 N95-31698

DEOXYRIBONUCLEIC ACID
Services to develop, standardize, and validate Polymerase Chain Reaction (PCR) protocols for the detection of leishmaniasis in clinical samples
[AD-A290155] p 2817 N95-31115

DEPENDENCE
From molecular to macromolecular liquid crystals
[AD-A293170] p 2816 N95-30974
Estimation in second order dependency model for multivariate binary data
[DE95-010326] p 2944 N95-32087

DEPLOYMENT
The quad-service satellite transmitting and receiving system for medical supply support: A battlefield interoperability and communications system prototype, volume 2. User documentation
[AD-A292835] p 2851 N95-31448
The quad-service satellite transmitting and receiving system for medical supply support: A battlefield interoperability and communications system prototype, volume 1
[AD-A292836] p 2851 N95-31449
Arabian Sea mixed layer dynamics experiment: Mooring deployment cruise report
[AD-A293684] p 2923 N95-31600
High strain-rate testing of parachute materials
[DE95-009577] p 2897 N95-31614

DEPOLARIZATION
Polarized proton beams
[DE95-010843] p 2967 N95-32031

DEPOSITION
Synthesis of carbo-nitride films using high-energy shock plasma deposition
[DE95-615231] p 2811 N95-30450
High temperature barrier coatings for refractory metals
[NASA-CR-195475] p 2802 N95-30531
Modeling of thermal, electronic, hydrodynamic, and dynamic deposition processes for pulsed-laser deposition of thin films
[DE95-008906] p 2813 N95-30572
Mechanisms of enhanced ionic conduction at interfaces in ceramics
[DE95-009125] p 2814 N95-30730
Glass matrix doped with activated luminescent nanocrystalline particles
[AD-D017416] p 2816 N95-31010
Method of synthesizing high quality, doped diamond and diamonds and devices obtained therefrom
[AD-D017432] p 3014 N95-31269

Thin-film edge field emitter device and method of manufacture therefor
| AD-D017453 | p 2862 N95-31275
Deposition and characterization of photoconductive PZT thin films
| ATR-93(8308)-7 | p 2819 N95-31417
Advanced thin-film deposition and physical properties of high-temperature and other novel superconducting materials
| AD-A292798 | p 2795 N95-31439
The effect of gravity on the deposition of thin films: The physical vapor transport of copper phthalocyanine
| AD-A292997 | p 2838 N95-31472
High performance YBCO films
| AD-A293045 | p 2863 N95-31669
Synthesis and characterization of nanophase face-centered-cubic titanium
| DE95-009533 | p 2809 N95-32051
Development of large-area monolithically integrated Silicon-Film(trademark) photovoltaic modules
| DE95-004089 | p 2906 N95-32057
Comprehensive research on the stability and electronic properties of a-Si:H and a-SiGe:H alloys and devices
| DE95-004088 | p 2810 N95-32154

DEPOSITS
Spectroscopic ellipsometry as a sensitive monitor of materials contamination p 2782 N95-31808

DEPRECIATION
Removal of scattered surface waves from seismic data
| PB95-197802 | p 2922 N95-30457

DEPTH
A room temperature LSO/PIN photodiode PET detector module that measures depth of interaction
| DE95-008447 | p 2878 N95-30378
Ultrasonic two probe system for locating and sizing
| AD-D017438 | p 2996 N95-30724
Shiptracks in the Californian stratus region: Dependency on marine atmospheric boundary layer depth
| AD-A293272 | p 2901 N95-31125

DEPTH MEASUREMENT
Seismic studies of subducted lithosphere p 2915 N95-31335

DERIVATION
Higher Schwarzian operators and combinatorics of Schwarzian derivative
| PB95-208435 | p 2957 N95-30623

DESIGN ANALYSIS
Specific method for task-based interaction design
| PB95-196440 | p 2929 N95-30522
Operating system support for distributed multimedia applications: A survey of current research
| PB95-207098 | p 2964 N95-30565
Effects of thermal and electrical stressing on the breakdown behavior of space wiring
| NASA-CR-198360 | p 2768 N95-30860
A novel instrumentation system for measurement of helicopter rotor motions and loads data, phase 1
| AD-A293309 | p 2751 N95-30923
Client server architecture for multidatabase access. Ingres SQL server
| PB95-192852 | p 2947 N95-31051
The art and science of magnet design: Selected notes of Klaus Halbach, volume 2
| DE95-008450 | p 2861 N95-31059
Advanced small rocket chambers. Option 3: 110 1bf Ir-Re rocket, volume 1
| NASA-CR-195435-VOL-1 | p 2768 N95-31169
Advanced small rocket chambers. Option 3: 110 1bf Ir-Re rocket, volume 2
| NASA-CR-195435-VOL-2 | p 2769 N95-31170
Management of major system programs and projects. Handbook
| NHB-7120.5 | p 3021 N95-31380
A time stepping coupled finite element-state space modeling environment for synchronous machine performance and design analysis in the ABC frame of reference p 2864 N95-31948
Underdense heating of the ionosphere using oblique high power HF radiowaves p 2917 N95-31951
Control law design using H-infinity and mu-synthesis short-period controller for a tail-airplane p 2758 N95-31999

DESTRUCTION
Acoustoelastic stress evaluation in metal plate using absolute shear and longitudinal time-of-flight data
| PB95-197810 | p 2892 N95-30458
Base hydrolysis and hydrothermal processing of PBX-9404 explosive
| DE95-009437 | p 2836 N95-32048
Base hydrolysis and hydrothermal processing of PBX-9404 explosive
| DE95-009497 | p 2837 N95-32355

DESTRUCTIVE TESTS
Round-robin validation exercise for plate twist test method
| PB95-208088 | p 2812 N95-30487

DETECTION
A room temperature LSO/PIN photodiode PET detector module that measures depth of interaction
| DE95-008447 | p 2878 N95-30378
Detecting intravascular gas bubbles in ultrasonic images
| PB95-195301 | p 2926 N95-30513
Method and system for reducing drag on a body moving through a fluid medium
| AD-D017336 | p 2867 N95-30672
Josephson break junction thin film device
| AD-D017343 | p 3011 N95-30673
Terminal doppler weather radar (TDWR) build 5B operational test and evaluation (OT&E) integration and OT&E operational test plan
| AD-A293251 | p 2848 N95-30910
Luminance effects on visual acuity and small letter contrast sensitivity
| AD-A293310 | p 2928 N95-31140
Study of different type neutrino oscillations based on neutrino beams from 600 GeV
| DE95-619267 | p 2983 N95-31260
On possibility to study neutrino oscillations by detectors located at Gran Sasso (Italy) using beams from 600 GeV UNK-1 machine
| DE95-619268 | p 2983 N95-31261
Inductively coupled IR staring array based on photofluxonic pixels
| AD-A292784 | p 2998 N95-31435
Investigation of ground target detection methods in fully polarimetric wide angle synthetic aperture radar images
| AD-A293922 | p 2851 N95-31513
Comparisons of target detection clutter using data from the 1993 FOPEN experiments
| AD-A293052 | p 2852 N95-31606
Folded compact range development and coherent change detection measurement project
| DE95-009082 | p 2853 N95-31628
Next generation fire suppressants p 2775 N95-31769
PADO: Learning tree structured algorithms for orchestration into an object recognition system
| AD-A293109 | p 2943 N95-32020
Design of an immersion echelle-prism mid-IR spectrograph for chemical remote sensing
| DE95-010729 | p 2901 N95-32027
Monte Carlo tests of the ELIPGRID-PC algorithm
| DE95-010811 | p 2943 N95-32030

DETERGENTS
Cleaning without chlorinated solvents p 2780 N95-31792

DETERMINANTS
Canonical symmetric invariant pairings in vertex operator super algebras and gramians
| PB95-208112 | p 2955 N95-30488
Electronic structure of Donor-Spacer-Acceptor molecules of potential interest for molecular electronics III: Geometry and absorption spectrum of CH3-Alpha P3CNQ
| AD-A293662 | p 2985 N95-31609

DETONATION
Base hydrolysis and hydrothermal processing of PBX-9404 explosive
| DE95-009437 | p 2836 N95-32048
Base hydrolysis and hydrothermal processing of PBX-9404 explosive
| DE95-009497 | p 2837 N95-32355

DETONATION WAVES
Numerical computation of one-dimensional detonation waves
| PB95-197950 | p 2868 N95-30811

DEUTERIDES
Preparation of diisopropyl stibines and use thereof
| AD-D017419 | p 2771 N95-30418

DEUTERIUM COMPOUNDS
A search for interstellar CH3D: Limits to the methane abundance in Orion-KL
| NASA-CR-198932 | p 3029 N95-30751

DEUTERIUM FLUORIDES
Advances in high-power chemical lasers
| AD-A289737 | p 2885 N95-31389

DEVELOPING NATIONS
Economical analysis relating to the global warming issue
| DE95-764072 | p 2908 N95-30677

DEWAXING
SSME Main Combustion Chamber (MCC) hot oil dewaxing p 2777 N95-31777

DIAGNOSIS
Services to develop, standardize, and validate Polymerase Chain Reaction (PCR) protocols for the detection of leishmaniasis in clinical samples
| AD-A290155 | p 2817 N95-31115
Development of a new instrument for rocket engine combustion diagnostics p 2799 N95-31211
Development of a structured design and programming methodology for expert systems shells utilizing a visual programming language: Application of structured methodology to the MK92 maintenance advisor expert system, performance module prototype
| AD-A289897 | p 2939 N95-31391
Analysis of symbolic parameter models
| AD-A292916 | p 2940 N95-31459
Diagnosing high density, fast-evolving plasmas using x-ray lasers
| DE95-010734 | p 3006 N95-32028

DIAMOND FILMS
Polarized Raman spectroscopy of chemically vapour deposited diamond films
| DE95-616776 | p 2815 N95-30791
Diamond thin film temperature and heat-flux sensors
| NASA-CR-198859 | p 3012 N95-30847
Method of synthesizing high quality, doped diamond and diamonds and devices obtained therefrom
| AD-D017432 | p 3014 N95-31269
Growth, characterization and device development in monocrystalline diamond films
| AD-A293106 | p 3015 N95-32018
Models of transport, gas-phase and surface chemistry in diamond chemical vapor deposition
| DE95-009861 | p 2822 N95-32101

DIAMONDS
Method of synthesizing high quality, doped diamond and diamonds and devices obtained therefrom
| AD-D017432 | p 3014 N95-31269
Substrate heating measurements in pulsed ion beam film deposition
| DE95-010862 | p 2818 N95-31377
An analysis of gas phase ethanol/water chemistry for diamond CVD
| AD-A293009 | p 2795 N95-31473
Growth, characterization and device development in monocrystalline diamond films
| AD-A293106 | p 3015 N95-32018
Models of transport, gas-phase and surface chemistry in diamond chemical vapor deposition
| DE95-009861 | p 2822 N95-32101

DIATOMIC MOLECULES
Properties of new materials relevant to energy and fuel research
| AD-A289734 | p 2825 N95-31149

DIBORANE
The structure and reactivity of boron and carbon surfaces
| AD-A292804 | p 2795 N95-31440

DICHROISM
The theoretical calculation of vibrational circular dichroism spectra
| AD-A293614 | p 2798 N95-32258

DIELECTRIC PROPERTIES
Band gap measurement of Si(1-x)C(x)/Si (0 less than or equal to x less than or equal to 0.014) alloys using photoluminescence and spectroscopic ellipsometry
| DE95-011020 | p 3014 N95-31112
Intermodulation Interference (IMI) testing of composite materials
| AD-A288621 | p 2787 N95-31146
Use of a variable frequency source with a single-mode cavity to process ceramic filaments
| DE95-010992 | p 2817 N95-31152
Materials for adaptive structural acoustic control, volume 2
| AD-A293445 | p 2788 N95-31370

DIELECTRICS
Ceramics derived from metal-organic precursors
| AD-A290791 | p 2811 N95-30405
Two-dimensional Finite Difference Time Domain (FD-TD) model of electromagnetic (EM) scattering from a buried rectangular object
| AD-A293685 | p 2852 N95-31601

DIESEL ENGINES
Low vibration polymeric composite engine
| AD-D017332 | p 2887 N95-30386

DIESEL FUELS
BioFacts: Fueling a stronger economy, global warming and biofuels emissions
| DE94-006864 | p 2910 N95-31821

DIFFERENCE EQUATIONS
A stochastic difference equation approach to inference with missing data: Some new results
| DE95-010327 | p 2944 N95-32088
A stochastic EM estimator in the presence of missing data: Theory and applications
| DE95-010329 | p 2944 N95-32089

DIFFERENTIAL ABSORPTION LIDAR
Feasibility of tropospheric water vapor profiling using infrared heterodyne differential absorption lidar
| DE95-009647 | p 2917 N95-32142
DIFFERENTIAL ANALYZERS
Demodulators for optical fiber interferometers with (3 x 3) outputs
| AD-D017415 | p 2995 N95-30402
DIFFERENTIAL CALCULUS
Equivalence of two non-commutative geometry approaches
| DE95-613469 | p 2957 N95-30642
DIFFERENTIAL EQUATIONS
Ray trace model of sound propagation in range dependent media
| PB95-211751 | p 2973 N95-30481
Development of a linearized unsteady Euler analysis for turbomachinery blade rows
| NASA-CR-4677 | p 2742 N95-30611
Higher Schwarzian operators and combinatorics of Schwarzian derivative
| PB95-208435 | p 2957 N95-30623
Golden ten equations of motion
| PB95-197927 | p 2967 N95-30809
Numerical computation of one-dimensional detonation waves
| PB95-197950 | p 2868 N95-30811
Multigrid convergence acceleration for the 2D Euler equations applied to high-lift systems
| PB95-198081 | p 2743 N95-30814
A finite element formulation for the time domain vibration analysis of an elastic-viscoelastic structure
p 2895 N95-31318
DiffEqlab: A MATLAB based package for studying ordinary differential equations
| PB95-207197 | p 2960 N95-31363
The remainder form and the cord-slope form in global optimization with interval methods p 2941 N95-31533
Validity of the differential equations for ionization cooling
| DE95-010438 | p 2989 N95-32160
DIFFERENTIAL PRESSURE
Optical fiber pressure sensor for liquid level monitoring
| AD-D017346 | p 2996 N95-30679
DIFFRACTION
NIR High-efficiency subwavelength diffractive structures in semiconductors
| DE95-008535 | p 3008 N95-30391
Phase object display by using acousto-optical Bragg diffraction
| AD-A293153 | p 2998 N95-31006
DIFFRACTOMETERS
IPNS neutron scattering instrumentation. A: Existing and planned. B: Possibilities for IPNS upgrade, a 1-MW spallation source
| DE95-004119 | p 2985 N95-31616
DIFFUSE RADIATION
Real time correlating operation on diffuse objects
| AD-A293220 | p 2997 N95-30901
Cleanliness evaluation of rough surfaces with diffuse IR reflectance p 2782 N95-31804
DIFFUSION
Viscous diffusion of vorticity in unsteady wall layers using the diffusion velocity concept
| DE95-008537 | p 2866 N95-30383
Anodically enhanced diffusion in Cu/Ag thin film couples
| DE95-009198 | p 2814 N95-30738
Simultaneous heat and mass transfer in a horizontal tube absorber: Numerical tools for present and future absorber designs
| PB95-196978 | p 2869 N95-30872
Extension of the pore tree model to describe pore interconnectivity
| AD-A290366 | p 2793 N95-30971
Solution based temperature of Perovskite-type oxide films and powders
| DE95-009089 | p 2820 N95-31629
Numerical simulation of the Langevin equation for skewed turbulence
| DE95-009477 | p 2877 N95-32049
Ultrasensitive fluorescence detection and photophysics in microdroplets
| DE95-010283 | p 2798 N95-32086
Energetics of Pt adsorption on Pt(111)
| DE95-010933 | p 3017 N95-32307
DIFFUSION COEFFICIENT
Fischer-tropsch synthesis in supercritical fluids
| DE95-009631 | p 2792 N95-30709
DIFFUSION FLAMES
Enhanced energy release and soot reduction in actively controlled flames p 2799 N95-31200
Advanced oxidizers diffusion flames structure
p 2801 N95-31307
Spectral element method for numerical simulation of unsteady laminar diffusion flames p 2794 N95-31333
DIFFUSION WELDING
New material for high average power infrared generation: QPM-DB GaAs
| AD-A292714 | p 2967 N95-30939
DIFFUSIVITY
Hydrogen diffusion and passivation in InGaAlN alloys
| DE95-010889 | p 2806 N95-31150
DIGITAL DATA
Detecting intravascular gas bubbles in ultrasonic images
| PB95-195301 | p 2926 N95-30513
High Frequency (HF) upgrade study for the Canadian Regional Operations Control Center (ROCC) AWACS Digital Information Link (RADIL) project
| AD-A293435 | p 2850 N95-31367
Digital Mapping Charting and Geodesy Analysis Program technical review of Vector Product Format (VPF)
| AD-A289766 | p 2901 N95-31390
Synthetic Terrain Imagery for Helmet-Mounted Display. Volume 3: Software user's manual
| AD-A293613 | p 2753 N95-31463
Design and testing of an optimal digital link capable of 14-channel transmission
| AD-A288505 | p 3000 N95-31652
DIGITAL ELECTRONICS
Visualization of circuit card electromagnetic fields
| AD-A291491 | p 2845 N95-30398
DIGITAL FILTERS
Design of digital low-pass filters for time-domain recursive filtering of impact acceleration signals
| AD-A293086 | p 2864 N95-31842
DIGITAL SIMULATION
Digital simulation of wind velocities for wind turbine rotors: General considerations
| PB95-206447 | p 2904 N95-31157
Atomization simulations using an Eulerian-VOF-Lagrangian method p 2828 N95-31210
DIGITAL SYSTEMS
Computer interface development for the petite amateur navy satellite (PANSAT) simulator
| AD-A293263 | p 2766 N95-31388
Portable digital Satellite News Gathering (SNG) RF terminal using a flat antenna
| NHK-LABS-NOTE-436 | p 2853 N95-31744
Mission critical failure effects analysis using quantitative techniques
| AD-A293098 | p 2864 N95-31844
Digital autopilot design for combat aircraft in ALENIA p 2760 N95-32009
An investigation of pilot induced oscillation phenomena in digital-flight control systems p 2760 N95-32011
Advanced flight control technology achievements at Boeing Helicopters p 2761 N95-32014
The High Altitude Balloon Experiment demonstration of acquisition, tracking, and pointing technologies (HABE-ATP) p 2841 N95-32132
Digital signal processing in the radio science stability analyzer p 2857 N95-32240
DILUTION
Jet mixing in a reacting cylindrical crossflow
| NASA-TM-106975 | p 2755 N95-30853
LLW solidification in cement: Effect of dilution
| DE95-010108 | p 2798 N95-32091
DIMENSIONAL ANALYSIS
Chiral gauge theory in four dimensions
| DE95-616288 | p 3018 N95-30440
DIMENSIONAL MEASUREMENT
Simultaneity and length of the moving rod
| DE95-613369 | p 3017 N95-30364
Einstein's length concept
| DE95-613368 | p 3019 N95-30972
DIMENSIONS
Local fractal dimension estimation
| AD-A293354 | p 2959 N95-30953
DIODES
The junction characteristics and current conduction mechanisms of GaInP2 n(+)p diodes and solar cells
| AD-A290857 | p 2902 N95-30408
A theoretical analysis of steady-state photocurrents in simple silicon diodes
| NASA-CR-198885 | p 2859 N95-30651
X-band magnicon amplifier research at the Naval Research Laboratory
| AD-A293203 | p 3013 N95-30984
A compact and efficient violet laser source
| AD-A292782 | p 2885 N95-31434
Degradation of blue AlGaN/InGaN/GaN LEDs subjected to high current pulses
| DE95-008824 | p 2863 N95-31611
DIPOLE MOMENTS
Semi-iterative method for estimation of the dipole parameters using the knowledge of the dipole orientation
| PB95-211736 | p 2858 N95-30480
DIRAC EQUATION
Quantum dynamics in regions of quaternionic curvature
| DE95-616276 | p 3018 N95-30426
The Foldy-Wouthuysen transformation
| DE95-616277 | p 2976 N95-30427
Light-front dynamics of Chern-Simons systems
| DE95-613467 | p 3019 N95-30741
Recoil correction in the Dirac-Coulomb problem
| DE95-619241 | p 2959 N95-31137
A compact expression for bilinear combination of Dirac spinors via world tensors
| DE95-619200 | p 2960 N95-31258
DIRECT CURRENT
A simple model for the dc flux transformer in layered superconductors with Josephson coupling
| DE95-614468 | p 2859 N95-30649
DIRECTIONAL SOLIDIFICATION (CRYSTALS)
Numerical modeling of Bridgman growth of PbSnTe in a magnetic field
| NASA-TM-106996 | p 2837 N95-31359
DIRECTIONAL STABILITY
Flight evaluation of forebody vortex control in post-stall flight p 2752 N95-32003
DIRECTORIES
Directory of global environmental sciences in Japan
p 2899 N95-31413
Requirements for security signalling
| DE95-008714 | p 2948 N95-31605
DISABILITIES
A graphical programming language for service robots in semi-structured environments p 2935 N95-30831
DISCONNECT DEVICES
Smart material joint band
| AD-D017374 | p 2888 N95-30716
DISCOVERY (ORBITER)
STS-70 flight: Day 8
| NASA-TM-110666 | p 2764 N95-30873
STS-70 flight: Day 7
| NASA-TM-110665 | p 2764 N95-30874
STS-70 flight: Day 6
| NASA-TM-110664 | p 2764 N95-30875
STS-70 flight: Day 5
| NASA-TM-110663 | p 2764 N95-30876
STS-70 flight: Day 4
| NASA-TM-110662 | p 2764 N95-30877
STS-70 flight: Day 3
| NASA-TM-110661 | p 2765 N95-30878
STS-70 flight: Day 2
| NASA-TM-110660 | p 2765 N95-30879
STS-70 flight: Day 1
| NASA-TM-110659 | p 2765 N95-30880
DISCRETE COSINE TRANSFORM
Image representation using fast algorithms based on the Zak transform
| AD-A293416 | p 2942 N95-31684
DISCRETE FUNCTIONS
Design of systems for active sound control
| PB95-197869 | p 2973 N95-30461
Fitting discrete distributions on the first two moments
| PB95-197885 | p 2950 N95-30462
Poisson approximation using the Stein-Chen method and coupling: Number of exceedances of a discrete-time-chi-squared process
| PB95-212205 | p 2961 N95-31398
DISCRIMINANT ANALYSIS (STATISTICS)
Selecting optimal experiments for feedforward multilayer perceptrons
| AD-A290856 | p 2949 N95-30406
A hypothesis-testing approach to discriminant analysis with mixed categorical and continuous variables when data are missing
| AD-A293714 | p 2964 N95-31831
DISCRIMINATORS
Background event discrimination in neutron time-of-flight measurements at beams of relativistic nuclei of the JINR synchrotron
| DE95-613006 | p 2991 N95-30604
DISCUSSION
Workshop report: Measurement techniques in highly transient, spectrally rich combustion environments
p 2799 N95-31208
DISILICIDES
Processing and characterization of nanocrystalline molybdenum disilicide (MoSi2) consolidated by hot isostatic pressing (HIP)
| DE95-010243 | p 3012 N95-30756
DISKS
Fiber optic accelerometer with centrally supported flexural disk
| AD-D017369 | p 2879 N95-30658
DISLOCATIONS (MATERIALS)
Solvability of a class of hypersingular nonlinear integral equations
| PB95-207031 | p 3011 N95-30720

DISORIENTATION
Dynamical analysis of the coriolis effect which causes space disorientation
[NAL-TR-1258] p 2928 N95-31714
DISPERSING
Design and processing of materials by biomimicking. Sections 1. Publications
[AD-A293852] p 2820 N95-31559
DISPLACEMENT
Field performance of the Walker Branch throughfall displacement experiment
[DE95-008677] p 2908 N95-30793
Amorphization and the effect of implanted ions in SiC
[DE95-009699] p 2985 N95-31642
Microstructure of Al2O3 irradiated with an applied electric field
[DE95-010278] p 2822 N95-32043
Evaluation of discretization procedures for transition elements in adaptive mesh refinement
[NASA-CR-199037] p 2944 N95-32190
DISPLACEMENT MEASUREMENT
A simple and accurate technique for monitoring crack growth behavior using a wave form analyzer
[AD-A293161] p 2894 N95-31007
DISPLAY DEVICES
Arithmetic features of rational conformal field theory
[PB95-207908] p 2966 N95-30591
Terminal doppler weather radar (TDWR) build 5B operational test and evaluation (OT&E) integration and OT&E operational test plan
[AD-A293251] p 2848 N95-30910
Application of computer generated holograms to optical transformations
[AD-A293146] p 2880 N95-30921
Impact of task properties, data display format and cognitive characteristics on recall performance: A cumulative research investigation p 3025 N95-31334
Method and apparatus for a high resolution, flat panel cathodoluminescent display device
[AD-D017434] p 2862 N95-31342
Guidelines for the design of GPS and LORAN receiver controls and displays
[AD-A293753] p 2749 N95-31572
Degradation of blue AlGaN/InGaN/GaN LEDs subjected to high current pulses
[DE95-008824] p 2863 N95-31611
Integration issues in modular mission management aid development p 2841 N95-32133
DISSIPATION
Stabilization of the resistive shell mode in tokamaks
[DE95-008748] p 3004 N95-30794
Reynolds stress of localized toroidal modes
[DE95-008750] p 3004 N95-30795
Experimental investigation of the effectiveness of flow-through modules for electronics cooling
[AD-A293284] p 2861 N95-30950
Method of normal coordinates in the formulation of a system with dissipation: The harmonic oscillator
[DE95-613372] p 3020 N95-32094
DISSOLVING
Dissolution of eutectic microstructures
[DE95-010244] p 2804 N95-30757
DISTILLATION
Synthesis of separation systems: Methods and applications in downstream gas processes
[PB95-208518] p 2798 N95-32372
DISTORTION
Adaptive image enhancement of text images that contain touching or broken characters
[DE95-010173] p 3023 N95-30620
Introduction to the theory of Goyaks: Operator manifold approach to geometry and particle physics
[DE95-613460] p 2980 N95-30740
Calculated structures and electronic absorption spectroscopy for magnesium phthalocyanine and its anion radical
[AD-A293672] p 2796 N95-31596
DISTRIBUTED PARAMETER SYSTEMS
Dynamic routation in distributed environments
[PB95-197968] p 2847 N95-30812
Representation of feedback operators for hyperbolic systems
[NASA-CR-198171] p 2960 N95-31319
DISTRIBUTED PROCESSING
Selecting optimal experiments for feedforward multilayer perceptrons
[AD-A290856] p 2949 N95-30406
Expert system for assessing accuracy of models of physical phenomena and for selecting alternate models in the presence of noise
[AD-D017348] p 2974 N95-30550
Foundations of technology for constructing highly reliable distributed realtime systems
[AD-A293254] p 2931 N95-30892
Implementation of KIVA-3 on distributed memory MIMD computers
[DE95-010288] p 2931 N95-31130
Requirements for security signalling
[DE95-008714] p 2948 N95-31605
DISTRIBUTION FUNCTIONS
Extension to higher dimensions of the Jaeschke-Eicker result on the standardized empirical process
[PB95-206868] p 2965 N95-30523
DISTRIBUTION MOMENTS
Fitting discrete distributions on the first two moments
[PB95-197885] p 2950 N95-30462
DIURNAL VARIATIONS
Suprioius semi-diurnal variation in the E.R.B.E. outgoing longwave radiation
[NOAA-TR-NESDIS-84] p 2913 N95-30643
Middle atmosphere structure and dynamics: Lidar studies at the South Pole, Syowa and Urbana p 2916 N95-31736
DIVERGENCE
An analysis of gas phase ethanol/water chemistry for diamond CVD
[AD-A293009] p 2795 N95-31473
DIVING (UNDERWATER)
Effect of oxygen and decompression bubbles on inert gas washout
[PB95-196556] p 2925 N95-30665
DMSP SATELLITES
SSUSI single sensor auroral E-layer algorithm: Functional description
[AD-A288630] p 2914 N95-31012
DOMAINS
PADO: Learning tree structured algorithms for orchestration into an object recognition system
[AD-A293109] p 2943 N95-32020
DOMINANCE
Testing vector boson dominance of electroweak interactions via e(+)e(-) (yields) f-bar f
[DE95-620528] p 2982 N95-31214
DONOR MATERIALS
Photophysical properties of opto-electric molecules studied by time-resolved microwave conductivity
[PB95-196994] p 2980 N95-30774
DOORS
Aircraft evacuations through Type-3 exits I: Effects of seat placement at the exit
[DOT/FAA/AM-95/22] p 2748 N95-31845
DOPED CRYSTALS
Orientation of rapid thermally annealed lead zirconate titanate thin films on (111) Pt substrate
[DE95-615232] p 2811 N95-30422
Alloying effects of Kondo insulators
[DE95-614308] p 3010 N95-30644
Electrical conductivity study on polythiophenes films
[DE95-614309] p 2813 N95-30645
A theoretical analysis of steady-state photocurrents in simple silicon diodes
[NASA-CR-198885] p 2859 N95-30651
Glass matrix doped with activated luminescent nanocrystalline particles
[AD-D017416] p 2816 N95-31010
A 1.94 micrometer laser apparatus, system and method using a thulium-doped yttrium-lithium-fluoride laser crystal pumped with a diode laser
[AD-D017435] p 2884 N95-31213
Method of synthesizing high quality, doped diamond and diamonds and devices obtained therefrom
[AD-D017432] p 3014 N95-31269
Deposition and characterization of photoconductive PZT thin films
[ATR-93(8308)-7] p 2819 N95-31417
Nonlinear optics in novel composite media
[AD-A293866] p 2999 N95-31542
Silicon carbide-silicon heterostructure solar cells p 2905 N95-31952
Infrared and millimeter wave detection using thin films of Pb doped BiSrCaCuO superconductor p 2840 N95-32129
Laser properties of Yb(3+)-doped Sr5(PO4)3F crystals
[DE95-010686] p 3016 N95-32268
Superconducting and normal-state properties of novel materials
[DE95-012368] p 3017 N95-32366
DOPPLER EFFECT
Point reflector model for the simulation of radar target glint and Doppler phenomena
[PB95-222980] p 2857 N95-32314
DOPPLER RADAR
Offshore next generation weather radar (NEXRAD) OT&E integration and OT&E operational test
[AD-A293223] p 2848 N95-30902
Terminal doppler weather radar (TDWR) build 5B operational test and evaluation (OT&E) integration and OT&E operational test plan
[AD-A293251] p 2848 N95-30910
Development of a novel wind lidar, phase 1
[AD-A292703] p 2849 N95-30935
LAWS hurricane studies
[NASA-CR-189438] p 2919 N95-31128
Initial evaluation of the Oregon State University planetary boundary layer column model for ITWS applications
[AD-A293775] p 2920 N95-31465
Using satellites for radar performance monitoring and calibration
[AD-A293809] p 2852 N95-31588
Adaptive space-time processing for airborne radars based on Doppler pre-processing
[PB95-205464] p 2854 N95-32114
The Telecommunications and Data Acquisition Report
[NASA-CR-198911] p 2854 N95-32221
Determination of the position of Jupiter from radio metric tracking of Voyager 1 p 2854 N95-32222
The application of noncoherent Doppler data types for Deep Space Navigation p 2765 N95-32226
The dynamic range of radar signal generation in the MSS-2 simulation facility
[AD-A293856] p 2857 N95-32259
DOSAGE
Behaviour of polymers in radioactive environments: Effects of dose speed
[DE95-621008] p 2818 N95-31221
Amorphization and the effect of implanted ions in SiC
[DE95-009699] p 2985 N95-31642
DOSIMETERS
Electromagnetic field exposure dosimeter
[AD-A293191] p 2927 N95-30981
Summaries of fiscal year 1994 projects in medical applications and biophysical research
[DE95-010405] p 2925 N95-32040
DOUBLE BASE PROPELLANTS
An ignition model for modern double base propellants p 2800 N95-31292
Measurement of temperatures and OH concentrations of solid propellant flames using absorption spectroscopy p 2801 N95-31302
Studies of reactions pertaining to and development of a reduced mechanism for the double base propellant dark zone p 2801 N95-31312
DOUBLE BASE ROCKET PROPELLANTS
Enhanced alkaline hydrolysis and biodegradability studies of nitrocellulose-bearing missile propellant p 2772 N95-31752
DRAG
Electromagnetically activated compliant wavy-wall
[AD-D017340] p 2866 N95-30412
DRAG REDUCTION
Method and system for reducing drag on a body moving through a fluid medium
[AD-D017336] p 2867 N95-30672
DROP SIZE
Survey of recent Al2O3 droplet size data in solid rocket chambers, nozzles, and plumes p 2770 N95-30987
The Al and A(lc)l2O3 droplet cloud in solid rocket motors p 2770 N95-30988
Survey of recent Al2O3 droplet size data in solid rocket chambers, nozzles, and plumes p 2770 N95-31195
DROPS (LIQUIDS)
National Institute for Global Environmental Change
[DE95-008333] p 2907 N95-30358
Survey of recent Al2O3 droplet size data in solid rocket chambers, nozzles, and plumes p 2770 N95-31195
The Al and Al2O3 droplet cloud in solid rocket motors p 2770 N95-31196
Selected flows with free surfaces: Streams and drops
[IFTR-3/1995] p 2876 N95-31817
Ultrasensitive fluorescence detection and photophysics in microdroplets
[DE95-010283] p 2798 N95-32086
DRUGS
Porous spherical shells and microspheres by electrodispersion precipitation
[DE95-009073] p 2815 N95-30799
DUALITY PRINCIPLE
Double charmed baryons production at B-factory
[DE95-620540] p 2983 N95-31219
DUCT GEOMETRY
An investigation of the side-dump dual in-line ramjet combustor p 2756 N95-31199
DUCTED FLOW
Solution of the three-dimensional Helmholtz equation with nonlocal boundary conditions
[NASA-TM-110174] p 2974 N95-30850
DUCTILITY
Analysis of variation embedding tests with 17 MM dowel: Densified veneer wood FOREST project, part 7
[PB95-206876] p 2963 N95-30680
The effect of grain refinement on the room-temperature ductility of as-cast Fe3Al-based alloys
[DE95-010121] p 2805 N95-31107

Shape memory properties of an iron modified nickel aluminide alloy
[DE95-010223] p 2805 N95-31111
Large deformation failure mechanisms in nonlinear solids
[AD-A293010] p 2896 N95-31474

DUMP COMBUSTORS
An investigation of the side-dump dual in-line ramjet combustor p 2756 N95-31199
A pulsed liquid fuel ramjet p 2756 N95-31201

DURABILITY
State-of-the-art low-cost solar reflector materials
[DE95-000260] p 2902 N95-30526
Evaluation of alternative pavement marking materials
[AD-A292973] p 2763 N95-31468
NaK pool-boiler solar receiver durability bench test. Volume 2: Metallurgical analysis
[DE95-010338] p 2905 N95-31640
Robust Rocket Engine Concept
[NASA-TM-107010] p 2770 N95-32121

DYE LASERS
Reflectivity of plasmas created by high-intensity, ultra-short laser pulses
[DE95-009536] p 3004 N95-30742
Z-scan using a dye laser
[PB95-222923] p 3002 N95-32312

DYNAMIC CHARACTERISTICS
Localization in tungsten heavy alloys subjected to shearing deformations under superimposed high pressures
[AD-A293177] p 2804 N95-30977
Assessment of dynamic burning behavior for JA-2 propellant rods p 2800 N95-31299
Normal mode tunes for linear coupled motion in six dimensional phase space
[DE95-011565] p 2994 N95-32244

DYNAMIC CONTROL
Control of mechanical systems with rolling contacts: Applications to robotics p 2889 N95-31332
Vorticity dynamics and control of dynamic stall
[AD-A288658] p 2756 N95-31400
Global stabilization of nonlinear gyroscopic systems p 2881 N95-31836

DYNAMIC LOADS
Sea ice stress research
[AD-A293164] p 2923 N95-30964

DYNAMIC MODELS
Control of flexible spacecraft structures using H-infinity wave absorbing control
[AD-A293141] p 2766 N95-30919

DYNAMIC PROGRAMMING
Statistical interface for chaotic signal in noise
[AD-A290271] p 2848 N95-30932
Fast algorithms for three-dimensional inverse scattering problems
[AD-A293510] p 2852 N95-31537
An analysis of hierarchical genetic programming
[AD-A293964] p 2942 N95-31657

DYNAMIC RANGE
Improved linear dynamic range in externally modulated fiber-optic links p 3001 N95-31950
The dynamic range of radar signal generation in the MSS-2 simulation facility
[AD-A293856] p 2857 N95-32259

DYNAMIC RESPONSE
Generation of earthquake signals
[PB95-211223] p 2913 N95-30631
Minimizing structural vibrations with Input Shaping (TM)
[NASA-CR-189439] p 2893 N95-30786
Response of mechanically fastened composite joints under multiple bypass loads p 2785 N95-30824
Dynamical systems as models for flow-induced vibrations
[PB95-206991] p 2869 N95-30956
Energy flow analysis of coupled structures p 2895 N95-31316
Studies in non-linear multi-mode responses of harmonically excited rectangular plates with internal resonances p 2895 N95-31331
Impact behavior of the active zone within a frozen soil profile
[AD-A292909] p 2915 N95-31386
Analytic and experimental investigation of rotordynamic response and backward whirl induced by split resonance
[AD-A293639] p 2889 N95-31566
Response of dual-layered structures subjected to shock pressure wave
[AD-A293731] p 2896 N95-31568
Evaluation of nonlinear structural dynamic responses using a fast-running spring-mass formulation
[DE95-008503] p 2967 N95-31625
A mode decomposition based finite element formulation for the nonlinear dynamics of flexible spatial structures and mechanisms p 2898 N95-32118

DYNAMIC STABILITY
Results from tests of the Kearfott T16-B Inertial Measurement Unit
[PB95-212031] p 2879 N95-30502
Beam stability at SRRC storage ring
[DE95-010842] p 2995 N95-32260

DYNAMIC STRUCTURAL ANALYSIS
Generation of earthquake signals
[PB95-211223] p 2913 N95-30631
Advanced small rocket chambers. Option 3: 110 lbf Ir-Re rocket, volume 2
[NASA-CR-195435-VOL-2] p 2769 N95-31170
Energy flow analysis of coupled structures p 2895 N95-31316
A finite element formulation for the time domain vibration analysis of an elastic-viscoelastic structure p 2895 N95-31318
Response of dual-layered structures subjected to shock pressure wave
[AD-A293731] p 2896 N95-31568
Finite element analysis of smart structures and modal testing of a flexible spacecraft arm
[AD-A293761] p 2890 N95-31576
Nonlinear dynamics and chaotic motions of a singularly perturbed nonlinear viscoelastic beam p 2897 N95-31706
A computational procedure for multibody systems including flexible beam dynamics
[NASA-CR-199035] p 2897 N95-31730
Finite element analysis of damped vibrations of laminated composite plates
[ISBN-0-315-84928-2] p 2789 N95-31731
Vibration control for precision manufacturing at Sandia National Laboratories
[DE95-009582] p 2839 N95-32082
A mode decomposition based finite element formulation for the nonlinear dynamics of flexible spatial structures and mechanisms p 2898 N95-32118
Staggered solution procedures for multibody dynamics simulation
[NASA-CR-199034] p 2899 N95-32202
Computational methods and software systems for dynamics and control of large space structures
[NASA-CR-199036] p 2767 N95-32204
A transient FETI methodology for large-scale parallel implicit computations in structural mechanics
[NASA-CR-199040] p 2945 N95-32214

DYNAMIC TESTS
Influence of strain rate and temperature on the mechanical behavior of iron aluminide-based alloys
[DE95-009426] p 2808 N95-31636

DYNAMICAL SYSTEMS
Nonlinear dynamical systems: Elements of a complex system analysis
[PB95-211652] p 2950 N95-30478
Around Ratner --- applications of Ratner's measure and topological theorems on unipotent homogeneous actions
[DE95-613377] p 2958 N95-30770
Dynamical systems as models for flow-induced vibrations
[PB95-206991] p 2869 N95-30956
Global stabilization of nonlinear gyroscopic systems p 2881 N95-31836

E

E GLASS
Large area smart piezoelectric and pyroelectric sensors
[AD-A291487] p 2859 N95-30561

E REGION
SSUSI single sensor auroral E-layer algorithm: Functional description
[AD-A288630] p 2914 N95-31012

EARTH ATMOSPHERE
IR DIAL performance modeling
[DE95-008377] p 2912 N95-30373
Atmospheric environmental implications of propulsion systems p 2771 N95-31747
Numerical simulation of the Langevin equation for skewed turbulence
[DE95-009477] p 2877 N95-32049
Preliminary design for Arctic atmospheric radiative transfer experiments
[DE95-009580] p 2917 N95-32080

EARTH IONOSPHERE
Kiruna geophysical data. Data summary 94/4-6, April-June 1994
[PB95-210365] p 2913 N95-30627
Kiruna geophysical data. Data summary 94/1-3, January-March 1994
[PB95-210373] p 2913 N95-30628
Holistic analysis of gamma-ray spectra in instrumental neutron activation analysis
[PB95-214458] p 2979 N95-30639
A prototype ionospheric tomography system (ITS)
[AD-A293015] p 2916 N95-31698
Underdense heating of the ionosphere using oblique high power HF radiowaves p 2917 N95-31951

EARTH MAGNETOSPHERE
Oxygen charge state abundance in the inner magnetosphere
[AD-A293497] p 2915 N95-31536
Aspects of the magnetospheric amplification phenomenon in ducted whistler-mode waves p 2916 N95-31718
DE-1 observations of polar O(+) stream bulk parameters and comparison with a model of the centrifugally-accelerated polar wind
[NASA-CR-198930] p 2917 N95-31743
A collisionless shock wave experiment
[DE95-009489] p 3008 N95-32351

EARTH MANTLE
Seismic studies of subducted lithosphere p 2915 N95-31335

EARTH OBSERVATIONS (FROM SPACE)
STS-70 flight: Day 6
[NASA-TM-110664] p 2764 N95-30875
STS-70 flight: Day 3
[NASA-TM-110661] p 2765 N95-30878
STS-70 flight: Day 2
[NASA-TM-110660] p 2765 N95-30879
European plans for new clocks in space p 2968 N95-32324

EARTH OBSERVING SYSTEM (EOS)
LAWS hurricane studies
[NASA-CR 189438] p 2919 N95-31128

EARTH ORBITAL ENVIRONMENTS
The NASA/JPL Evaluation of Oxygen Interactions with Materials-3 (EOIM-3)
[NASA-CR-198865] p 2796 N95-31660
Operation of the computer model for direct atomic oxygen exposure of Earth satellites
[NASA-CR-198188] p 2767 N95-32189

EARTH ORBITAL RENDEZVOUS
STS-71 post flight presentation
[NASA-TM-110658] p 2764 N95-30852
Mir 18 post flight presentation
[NASA-TM-110657] p 2766 N95-30854

EARTH ORBITS
Mir 18 post flight presentation
[NASA-TM-110657] p 2766 N95-30854
Radiation effects in space: The Clementine 1 mission
[DE95-011513] p 3032 N95-32282

EARTH RADIATION BUDGET
Suprioius semi-diurnal variation in the E.R.B.E. outgoing longwave radiation
[NOAA-TR-NESDIS-84] p 2913 N95-30643

EARTH RADIATION BUDGET EXPERIMENT
Suprioius semi-diurnal variation in the E.R.B.E. outgoing longwave radiation
[NOAA-TR-NESDIS-84] p 2913 N95-30643

EARTH SCIENCES
Directory of global environmental sciences in Japan p 2899 N95-31413

EARTH SURFACE
The land component of the global climate system with adequate spatial resolution
[DE95-009323] p 2908 N95-30686

EARTHQUAKES
Generation of earthquake signals
[PB95-211223] p 2913 N95-30631
ESAA: Environment for Seismic Activity Analysis
[DE95-612416] p 2913 N95-30675
SHEAT: A computer code for probabilistic seismic hazard analysis, user's manual
[DE95-717874] p 2913 N95-30758
Seismic studies of subducted lithosphere p 2915 N95-31335

ECCENTRIC ORBITS
A feedback linearization approach to orbital maneuvers p 2765 N95-30841

ECHO SUPPRESSORS
Energy absorption apparatus
[AD-D017361] p 2814 N95-30715

ECHOCARDIOGRAPHY
Decompression illness, observable bubbles. (Session K)
[PB95-195285] p 2926 N95-30511

ECOLOGY
Carbon dioxide concentrations in surface water and the atmosphere during 1986-1989 NOAA/PMEL cruises in the Pacific and Indian Oceans
[DE95-009659] p 2910 N95-32099

ECONOMIC ANALYSIS
Economical analysis relating to the global warming issue
[DE95-764072] p 2908 N95-30677
A manual for the economic evaluation of energy efficiency and renewable energy technologies
[DE95-000211] p 2903 N95-30896

ECONOMIC FACTORS
Evaluating the cost effectiveness of environmental projects: Case studies in aerospace and defense p 2774 N95-31762
ECOSYSTEMS
Field performance of the Walker Branch throughfall displacement experiment
[DE95-008677] p 2908 N95-30793
EDDY VISCOSITY
Advanced k-epsilon modeling of heat transfer
[NASA-CR-4679] p 2874 N95-31423
EDEMA
Effects of air bubbles on rabbit blood brain barrier
[PB95-195293] p 2925 N95-30512
EDGE DETECTION
Artificial neural networks and model-based recognition of 3-D objects from 2-D images p 2954 N95-31838
EDGE DISLOCATIONS
Characterization of /11'01/ twin dislocation structures in evaporated titanium thin films by HREM
[DE95-615391] p 2820 N95-31623
EDGES
Image enhancement by edge-preserving filtering
[DE95-008077] p 2936 N95-31056
Thin-film edge field emitter device and method of manufacture therefor
[AD-D017453] p 2862 N95-31275
EDUCATION
C++ as an introductory programming language
[PB95-195715] p 2933 N95-30539
Non-comparability of female and male admission test takers: Evaluation through follow-up
[PB95-212080] p 3021 N95-30700
Training metacognitive skills for problem solving
[AD-A290310] p 2959 N95-31002
Confederation Verification, Validation, and Accreditation Master Plan (CVVAMP). Technical test plan
[AD-A289717] p 2936 N95-31050
AASERT-92 augmentation of research training in chronobiology: Regulation of the mammalian circadian clock by neurotransmitters
[AD-A288243] p 2925 N95-31144
Human-computer interaction (HCI) specialization track Masters of Software Engineering (MSE) program
[AD-A292895] p 2930 N95-31401
Nonparametric methods for incomplete data in reliability and for changepoints in smooth functions
[AD-A292773] p 2963 N95-31429
Use of body surface heat patterns for predicting and evaluating acute lower extremity pain among soldiers
[AD-A292829] p 2927 N95-31446
EGRESS
Aircraft evacuations through Type-3 exits I: Effects of seat placement at the exit
[DOT/FAA/AM-95/22] p 2748 N95-31845
EIGENVALUES
Complex conjugate pairs in stationary Sturmians
[DE95-616279] p 2976 N95-30429
Analysis on fractals, laplacians on self-similar sets, noncommutative geometry and spectral dimensions
[PB95-208005] p 2956 N95-30556
The iteration formula of the Maslov-type index theory with applications to nonlinear Hamiltonian systems
[DE95-613379] p 2957 N95-30676
Singular eigenfunctions for shearing fluids I
[DE95-008952] p 2868 N95-30763
Around Ratner — applications of Ratner's measure and topological theorems on unipotent homogeneous actions
[DE95-613377] p 2958 N95-30770
A finite element formulation for the time domain vibration analysis of an elastic-viscoelastic structure p 2895 N95-31318
A modification to the GMRES method for ill-conditioned linear systems
[DE95-010661] p 2962 N95-32076
EIGENVECTORS
Complex conjugate pairs in stationary Sturmians
[DE95-616279] p 2976 N95-30429
Generalized deformed para-Bose oscillator and its coherent states
[DE95-613444] p 2963 N95-30610
Singular eigenfunctions for shearing fluids I
[DE95-008952] p 2868 N95-30763
EJECTION INJURIES
Vertical impact testing of two helmet-mounted night vision systems
[AD-A293055] p 2931 N95-31671
EL NINO
Forecast of Atlantic seasonal hurricane activity for 1994 p 2918 N95-30832
Summary of 1993 Atlantic tropical cyclone activity and verification of author's forecast. A year of unanticipated light hurricane activity and a poor forecast: The expected dissipation of the El Nino did not take place and Caribbean basin surface pressure became quite high p 2918 N95-30842
Early August updated forecast of Atlantic seasonal hurricane activity for 1994 p 2919 N95-30844
ELASTIC CYLINDERS
Wave propagation in a fluid-loaded homogeneous, transversely isotropic, elastic cylinder of arbitrary thickness
[AD-A292728] p 2869 N95-30946
ELASTIC DEFORMATION
An extremum principle for the analysis and design of constitutively nonlinear systems p 2898 N95-32112
ELASTIC PLATES
An analysis of the cover of a liquid-filled circular container
[IFTR-1/1995] p 2895 N95-31338
ELASTIC PROPERTIES
An explanation for the shape of nanoindentation unloading curves based on finite element simulation
[DE95-008905] p 2812 N95-30548
Wave propagation in a fluid-loaded homogeneous, transversely isotropic, elastic cylinder of arbitrary thickness
[AD-A292728] p 2869 N95-30946
Elastic and inelastic micromechanical analysis of functionally graded materials and laminated structures using transformation fields p 2787 N95-31347
An extremum principle for the analysis and design of constitutively nonlinear systems p 2898 N95-32112
Numerical evaluation of three-dimensional crack-tip integrals for layered anisotropic solids p 2898 N95-32191
ELASTIC SCATTERING
Density dependent effective interactions
[DE95-616348] p 2977 N95-30447
Inversion of the total cross sections for electron-molecule and electron-atom scattering
[DE95-616466] p 2978 N95-30583
ELASTIC WAVES
Propagation and scattering of elastic waves in laminated circular cylinders
[ISBN-0-315-85957-1] p 2848 N95-30828
Control of flexible spacecraft structures using H-infinity wave absorbing control
[AD-A293141] p 2766 N95-30919
Fractional delay waveguide modeling of acoustic tubes
[PB95-206637] p 2975 N95-31650
ELASTOHYDRODYNAMICS
Fluid-film lubrication with an application to piston rings p 2890 N95-32119
ELASTOMERS
Electromagnetically activated compliant wavy-wall
[AD-D017340] p 2866 N95-30412
Compatibility of Single Hydraulic Fluid with military specification fluids, seals and metallurgy
[AD-A292954] p 2821 N95-31663
Thermoplastic elastomers as a binder in composite propellants
[PB95-211553] p 2837 N95-32249
ELASTOPLASTICITY
An analysis of the cover of a liquid-filled circular container
[IFTR-1/1995] p 2895 N95-31338
ELECTRIC ARCS
Effects of thermal and electrical stressing on the breakdown behavior of space wiring
[NASA-CR-198360] p 2768 N95-30860
ELECTRIC BATTERIES
A Monte-Carlo model of ionic transport across a solid interface
[DE95-613447] p 3011 N95-30737
Composite polymer electrolyte for lithium batteries
[AD-A293924] p 2820 N95-31514
Evaluation and analysis survey on new energy introduction, part 3
[DE95-769806] p 2906 N95-32072
ELECTRIC CHARGE
The radiation conditioned by the 'velocity part' of the electromagnetic field of a moving charge
[DE95-613366] p 2846 N95-30605
Metal nanotubule membranes with electrochemically switchable ion-transport selectivity
[AD-A292712] p 2793 N95-30938
Contactless characterization of semiconductors using laser-induced surface photo-charge voltage measurements
[AD-A293618] p 2863 N95-31725
A search for millicharged particles at SLAC
[DE95-010694] p 2987 N95-32026
ELECTRIC CONDUCTORS
Molecular nanoclusters as precursors to conductive thin films and crystals
[AD-A290278] p 3014 N95-31189
ELECTRIC CONNECTORS
Performance evaluation of high-temperature superconducting current leads for micro-SMES systems
[DE95-005843] p 2861 N95-30943
Ceramic/Metal Composite Circuit-Board-Level Technology for Application Specific Electronic Modules (ASEM's)
[AD-A293183] p 2787 N95-30978
ELECTRIC CONTROL
Flying qualities of civil transport aircraft with electrical flight control p 2761 N95-32016
ELECTRIC CURRENT
A theoretical analysis of steady-state photocurrents in simple silicon diodes
[NASA-CR-198885] p 2859 N95-30651
Stability analysis of the TPX toroidal field coil
[DE95-009666] p 2865 N95-32100
ELECTRIC DIPOLES
Semi-iterative method for estimation of the dipole parameters using the knowledge of the dipole orientation
[PB95-211736] p 2858 N95-30480
Excitation mechanisms of 2s(sub 1/2)-2p(sub 3/2) and 2p(sub 1/2)-2p(sub 3/2)in U(82+) through U(89+)
[DE95-010265] p 2993 N95-32042
ELECTRIC DISCHARGES
Development of a method for measurement of triboelectric charging
[PB95-211322] p 2859 N95-30633
Optimization of a thermoelectric IR-detector for low working temperature
[NASA-CR-198933] p 2880 N95-30752
No-thermal plasma processing of VOCs and NO(x) at LLNL
[DE95-011445] p 2911 N95-32281
ELECTRIC EQUIPMENT TESTS
Test operations procedure (TOP) 1-2-512 electromagnetic compatibility tests
[AD-A293758] p 2852 N95-31574
ELECTRIC FIELDS
Electromagnetically activated compliant wavy-wall
[AD-D017340] p 2866 N95-30412
Device for low electric-field induced switching of Langmuir-Blodgett ferroelectric liquid crystal polymer films
[AD-D017457] p 3011 N95-30728
Fiber optic interferometric electric field and voltage sensor utilizing and electrostrictive transducer
[AD-D017433] p 2996 N95-30753
Porous spherical shells and microspheres by electrodispersion precipitation
[DE95-009073] p 2815 N95-30799
Electrified microheterogeneous catalysis
[AD-D017446] p 2794 N95-31271
Two-dimensional Finite Difference Time Domain (FD-TD) model of electromagnetic (EM) scattering from a buried rectangular object
[AD-A293685] p 2852 N95-31601
Determination of electric and magnetic fields in open trap plasmas by means of atomic-molecular beam hydrogen isotopes
[DE95-614177] p 3006 N95-31680
Microstructure of Al2O3 irradiated with an applied electric field
[DE95-010278] p 2822 N95-32043
ELECTRIC GENERATORS
A time stepping coupled finite element-state space modeling environment for synchronous machine performance and design analysis in the ABC frame of reference p 2864 N95-31948
ELECTRIC IGNITION
Progress in developing propellant ignition systems based upon electrically conductive polymers p 2800 N95-31300
ELECTRIC MOTORS
Compatibility of refrigerants and lubricants with motor materials under retrofit conditions
[DE95-010185] p 2814 N95-30767
ELECTRIC NETWORKS
Nordic symposium on analysis of electromagnetic transient phenomena using EMTP, part 3
[PB95-206504] p 2849 N95-31158
Nordic Symposium on Analysis of Electromagnetic Transient Phenomena Using EMTP, part 2
[PB95-206579] p 2849 N95-31160
Nordic Symposium on Analysis of Electromagnetic Transient Phenomena Using EMTP, part 4
[PB95-206587] p 2849 N95-31181
Nordic Symposium on Analysis of Electromagnetic Transient Phenomena Using EMTP, part 1
[PB95-206595] p 2850 N95-31182
ELECTRIC POTENTIAL
Low-voltage cathodoluminescence of europium-activated yttrium orthovanadate
[DE95-008536] p 3008 N95-30382
Density dependent effective interactions
[DE95-616348] p 2977 N95-30447
Worldwide intercomparison of impulse voltage measuring systems at 600 kV level
[PB95-195574] p 2858 N95-30538

Off-potential measurement systems for impressed current cathodic protection
[AD-A290876] p 2812 N95-30558
Development of a method for measurement of triboelectric charging
[PB95-211322] p 2859 N95-30633
A theoretical analysis of steady-state photocurrents in simple silicon diodes
[NASA-CR-198865] p 2859 N95-30651
Voltage surge suppression power circuits
[AD-D017454] p 2860 N95-30726
Fiber optic interferometric electric field and voltage sensor utilizing and electrostrictive transducer
[AD-D017433] p 2996 N95-30753
Decimation of encoding errors in an optimum SNS 2 micron low-noise CMOS ADC
[AD-A293208] p 2860 N95-30900
Energy storage and alternatives to improve train voltage on a mass transit system
[DE95-010344] p 2906 N95-32090
Voltage controlled MESFET pulse shape generator
[DE95-011656] p 2865 N95-32300

ELECTRIC POWER PLANTS

Production simulator for wave power plants
[PB95-212262] p 2907 N95-32286

ELECTRIC POWER TRANSMISSION

Nordic symposium on analysis of electromagnetic transient phenomena using EMTP, part 3
[PB95-206504] p 2849 N95-31158
Nordic Symposium on Analysis of Electromagnetic Transient Phenomena Using EMTP, part 2
[PB95-206579] p 2849 N95-31160
Nordic Symposium on Analysis of Electromagnetic Transient Phenomena Using EMTP, part 4
[PB95-206587] p 2849 N95-31181
Nordic Symposium on Analysis of Electromagnetic Transient Phenomena Using EMTP, part 1
[PB95-206595] p 2850 N95-31182
Prime power for shipboard high-average power FELs
[AD-A293718] p 2886 N95-31833

ELECTRIC PULSES

Electromyostimulation, circuits and monitoring
[NASA-TM-110741] p 2926 N95-30846

ELECTRIC STIMULI

Electromyostimulation, circuits and monitoring
[NASA-TM-110741] p 2926 N95-30846

ELECTRIC WIRE

Effects of thermal and electrical stressing on the breakdown behavior of space wiring
[NASA-CR-198360] p 2768 N95-30860
Electrical short circuit and current overload tests on aircraft wiring
[AD-A293308] p 2860 N95-30922

ELECTRICAL ENGINEERING

Effects of thermal and electrical stressing on the breakdown behavior of space wiring
[NASA-CR-198360] p 2768 N95-30860
JPRS report: Science and technology. Central Eurasia
[JPRS-UST-95-025] p 2771 N95-31360
FBIS report: Science and technology. Central Eurasia
[FBIS-UST-95-029] p 2863 N95-31728
FBIS report: Science and technology. Central Eurasia
[FBIS-UST-95-028] p 2839 N95-31729

ELECTRICAL FAULTS

Effects of thermal and electrical stressing on the breakdown behavior of space wiring
[NASA-CR-198360] p 2768 N95-30860

ELECTRICAL GROUNDING

Test operations procedure (TOP) 1-2-512 electromagnetic compatibility tests
[AD-A293758] p 2852 N95-31574

ELECTRICAL IMPEDANCE

Scattering and radiation from cylindrically conformal antennas p 2847 N95-30669

ELECTRICAL INSULATION

Alloying effects of Kondo insulators
[DE95-614308] p 3010 N95-30644
Effects of thermal and electrical stressing on the breakdown behavior of space wiring
[NASA-CR-198360] p 2768 N95-30860

ELECTRICAL MEASUREMENT

Visualization of circuit card electromagnetic fields
[AD-A291491] p 2845 N95-30398
Worldwide intercomparison of impulse voltage measuring systems at 600 kV level
[PB95-195574] p 2858 N95-30538
Off-potential measurement systems for impressed current cathodic protection
[AD-A290876] p 2812 N95-30558
Development of a method for measurement of triboelectric charging
[PB95-211322] p 2859 N95-30633
Optimization of a thermoelectric IR-detector for low working temperature
[NASA-CR-198933] p 2880 N95-30752
Electromyostimulation, circuits and monitoring
[NASA-TM-110741] p 2926 N95-30846
Volumetric and electro analytical techniques for chemical characterization of nuclear grade Ag-In-Cd alloys
[DE95-620664] p 2807 N95-31407
Dielectric property measurement of zirconia fibers at high temperatures
[DE95-010991] p 2821 N95-31705
Contactless characterization of semiconductors using laser-induced surface photo-charge voltage measurements
[AD-A293618] p 2863 N95-31725

ELECTRICAL PROPERTIES

Direct determination of grain boundary atomic structure in SrTiO3
[DE95-008847] p 3010 N95-30544
Development of a method for measurement of triboelectric charging
[PB95-211322] p 2859 N95-30633

ELECTRICAL RESISTANCE

Modeling of thermal response of filament used in T-jump experiment p 2800 N95-31297
Method and apparatus for non-destructively measuring local resistivity of semiconductors
[AD-D017436] p 2862 N95-31343

ELECTRICAL RESISTIVITY

Electrical conductivity study on polythiophenes films
[DE95-614309] p 2813 N95-30645
A simple model for the dc flux transformer in layered superconductors with Josephson coupling
[DE95-614468] p 2859 N95-30649
Stabilization of the resistive shell mode in tokamaks
[DE95-008748] p 3004 N95-30794
Investigations of YBaCuO materials with near-room-temperature resistivity transitions
[AD-A293405] p 3013 N95-31008
Progress in developing propellant ignition systems based upon electrically conductive polymers p 2800 N95-31300
Method and apparatus for non-destructively measuring local resistivity of semiconductors
[AD-D017436] p 2862 N95-31343

ELECTRICITY

Electromagnetic field exposure dosimeter
[AD-A293191] p 2927 N95-30981

ELECTRO-OPTICAL EFFECT

Z-scan using a dye laser
[PB95-222923] p 3002 N95-32312

ELECTRO-OPTICS

Integrated X-ray testing of the electro-optical breadboard model for the XMM reflection grating spectrometer
[DE95-008829] p 2879 N95-30507
Photophysical properties of opto-electric molecules studied by time-resolved microwave conductivity
[PB95-196994] p 2980 N95-30774
Nonlinear optical processes in polymer films
[AD-A293384] p 2815 N95-30955
Optical feature recognition
[AD-A293168] p 2997 N95-30966
Microwave electro-optic mixer
[AD-D017328] p 2862 N95-31179
Materials for adaptive structural acoustic control, volume 3
[AD-A293446] p 2788 N95-31371
Adaptive optics design for the advanced electro-optical system (AEOS)
[AD-A293972] p 2974 N95-31527
Ultraviolet and visible lasers: Rare earth-doped waveguide devices and non-linear optical extraction techniques
[AD-A293976] p 2885 N95-31528
Solid state research
[AD-A293083] p 3015 N95-31826
Improved linear dynamic range in externally modulated fiber-optic links p 3001 N95-31950

ELECTROACOUSTIC TRANSDUCERS

Investigating the use of smart acoustically active surfaces for flow separation control in turbomachinery
[AD-A292819] p 2874 N95-31443

ELECTROCHEMISTRY

Metal nanotubule membranes with electrochemically switchable ion-transport selectivity
[AD-A292712] p 2793 N95-30938
Studies of C(60) and C(70) and other fullurenes: Synthesis, derivation, electrochemistry, lubricant properties and new composition materials
[AD-A292726] p 3012 N95-30944
Consequences of kinetic dispersion on the electrochemistry of an adsorbed redox-active monolayer
[AD-A292794] p 2795 N95-31437

ELECTRODEPOSITION

High temperature barrier coatings for refractory metals
[NASA-CR-195475] p 2802 N95-30531
The electrodeposition of low contraction chromium/molybdenum alloys using pulse-reverse plating
[AD-A292727] p 2804 N95-30945

ELECTRODES

Biosensors based on cross-linking of biotinylated Glucose Oxidase by avidin
[AD-A290439] p 2925 N95-30452
Active turbulence control using microelectrodes, permanent magnets in microgrooves
[AD-D017351] p 2867 N95-30553
Device for low electric-field induced switching of Langmuir-Blodgett ferroelectric liquid crystal polymer films
[AD-D017457] p 3011 N95-30728
Electron transfer kinetics of self-assembled ferrocene C(12) alkanethiol monolayers on gold electrodes from 125K to 175K
[AD-A292754] p 2984 N95-31427
Lithium ion aqueous cells
[AD-A293828] p 2905 N95-31554

ELECTRODYNAMICS

Global Ultraviolet Imager (GUVI) investigation
[NASA-CR-189430] p 2917 N95-31820

ELECTROLYTES

Electrochemical vapour deposition of SOFC interconnection materials
[PB95-197844] p 2812 N95-30459
Composite polymer electrolyte for lithium batteries
[AD-A293924] p 2820 N95-31514
Lithium ion aqueous cells
[AD-A293828] p 2905 N95-31554
Design and processing of materials by biomimicking. Sections 1. Publications
[AD-A293852] p 2820 N95-31559

ELECTROLYTIC CELLS

Lithium ion aqueous cells
[AD-A293828] p 2905 N95-31554

ELECTROMAGNETIC ABSORPTION

Kiruna geophysical data. Data summary 94/4-6, April-June 1994
[PB95-210365] p 2913 N95-30627
Kiruna geophysical data. Data summary 94/1-3, January-March 1994
[PB95-210373] p 2913 N95-30628

ELECTROMAGNETIC COMPATIBILITY

EMC requirements for type approval of marine electronics. Nordtest project 1157-94
[PB95-211330] p 2859 N95-30596
Test operations procedure (TOP) 1-2-512 electromagnetic compatibility tests
[AD-A293758] p 2852 N95-31574

ELECTROMAGNETIC COUPLING

A simple model for the dc flux transformer in layered superconductors with Josephson coupling
[DE95-614468] p 2859 N95-30649

ELECTROMAGNETIC FIELDS

The interaction of magnetizations with an external electromagnetic field and a time-dependent magnetic Aharonov-Bohm effect
[DE95-613463] p 2845 N95-30368
Visualization of circuit card electromagnetic fields
[AD-A291491] p 2845 N95-30398
Six-vector formalism in electromagnetics of bianisotropic media
[PB95-207130] p 2846 N95-30567
The radiation conditioned by the 'velocity part' of the electromagnetic field of a moving charge
[DE95-613366] p 2846 N95-30605
Electromagnetic-gravitational conversion cross sections in external electromagnetic fields
[DE95-613589] p 2979 N95-30637
Electromagnetic field exposure dosimeter
[AD-A293191] p 2927 N95-30981
Direct and inverse problems in random media
[AD-A293033] p 2850 N95-31280
Numerical studies of nonlinear optical pulse propagation p 2998 N95-31411
Materials with controllable signature properties
[PB95-222964] p 2857 N95-32313

ELECTROMAGNETIC INTERACTIONS

New tensor interaction and the K(sub L) - K(sub S)mass difference
[DE95-613597] p 2845 N95-30370
Electromagnetic-gravitational conversion cross sections in external electromagnetic fields
[DE95-613589] p 2979 N95-30637
Introduction to the theory of Goyaks: Operator manifold approach to geometry and particle physics
[DE95-613460] p 2980 N95-30740
Hamiltonian formulation of two body problem in Wheeler-Feynman electrodynamics
[DE95-620526] p 3019 N95-31193

Electromagnetic hadron mass differences and estimation of isotopic symmetry violation parameters of QCD vacuum from quark model
[DE95-613628] p 2985 N95-31621
ELECTROMAGNETIC INTERFERENCE
The effect of ray curvature on Lloyd's mirror fringe estimates and source localisation
[DSTO-TR-0064] p 3001 N95-31745
ELECTROMAGNETIC MEASUREMENT
Simulation of airborne electromagnetic measurements in three dimensional environments
[DE95-008546] p 2900 N95-30363
ELECTROMAGNETIC PULSES
Nordic symposium on analysis of electromagnetic transient phenomena using EMTP, part 3
[PB95-206504] p 2849 N95-31158
Nordic Symposium on Analysis of Electromagnetic Transient Phenomena Using EMTP, part 2
[PB95-206579] p 2849 N95-31160
Nordic Symposium on Analysis of Electromagnetic Transient Phenomena Using EMTP, part 4
[PB95-206587] p 2849 N95-31161
Nordic Symposium on Analysis of Electromagnetic Transient Phenomena Using EMTP, part 1
[PB95-206595] p 2850 N95-31162
A two-dimensional finite difference algorithm on the KSR1
[AD-A293576] p 2941 N95-31594
Basic science with pulsed power and some off-the-wall ideas
[DE95-009486] p 2854 N95-32050
ELECTROMAGNETIC RADIATION
On explanation of proton electromagnetic form Factor near- p (anti p)-threshold from the PS-170 experiment
[DE95-613766] p 2977 N95-30508
The 49th International Symposium on Molecular Spectroscopy
[AD-A292706] p 2793 N95-30936
Electromagnetic field exposure dosimeter
[AD-A293191] p 2927 N95-30981
Reflection and transmission of electromagnetic plane waves from a uniaxial chiro-omega slab
[PB95-206629] p 2853 N95-31649
Materials with controllable signature properties
[PB95-222964] p 2857 N95-32313
ELECTROMAGNETIC SCATTERING
Scattering and radiation from cylindrically conformal antennas p 2847 N95-30669
Fast multipole methods for scattering computations
[AD-A291093] p 2848 N95-30869
Inverse and control problems in electromagnetics
[AD-A292993] p 2849 N95-30962
Two-dimensional Finite Difference Time Domain (FD-TD) model of electromagnetic (EM) scattering from a buried rectangular object
[AD-A293685] p 2852 N95-31601
A boundary integral equation approach to three dimensional electromagnetic wave scattering problems p 2853 N95-31639
ELECTROMAGNETIC SHIELDING
Microwave coupling into a slotted cavity. Additional results
[PB95-210381] p 2847 N95-30629
ELECTROMAGNETIC WAVE TRANSMISSION
Proceedings of the 16th Annual Conference on Atmospheric Transmission Models, volume 2
[AD-A293806] p 2916 N95-31604
Reflection and transmission of electromagnetic plane waves from a uniaxial chiro-omega slab
[PB95-206629] p 2853 N95-31649
ELECTROMAGNETISM
Six-vector formalism in electromagnetics of bianisotropic media
[PB95-207130] p 2846 N95-30567
Inverse and control problems in electromagnetics
[AD-A292993] p 2849 N95-30962
ELECTROMAGNETS
Electromagnetically activated compliant wavy-wall
[AD-D017340] p 2866 N95-30412
ELECTRON ACCELERATORS
Implementation of the shower max electron trigger at CDF
[DE95-006684] p 2992 N95-31165
ELECTRON BEAMS
EBIT: Electron Beam Ion Trap V-division experimental physics
[DE95-010207] p 3004 N95-30769
X-band magnicon amplifier research at the Naval Research Laboratory
[AD-A293203] p 3013 N95-30984
Hollow cathode electron gun research and development
[DE95-010262] p 2992 N95-31127
Experiments with highly charged ions up to bare U(sup 92+) on the electron beam ion trap
[DE95-006827] p 2982 N95-31174
Measurement of the effect of collimator generated wakefields on the beams in the SLC
[DE95-012101] p 2993 N95-31256
Method and apparatus for a high resolution, flat panel cathodoluminescent display device
[AD-D017434] p 2862 N95-31342
A microwave plasma cleaning apparatus p 2779 N95-31786
Growth, characterization and device development in monocrystalline diamond films
[AD-A293106] p 3015 N95-32018
Studies of highly charged ions with EBIT and Super-EBIT
[DE95-010251] p 2987 N95-32038
Wavelengths measurements of the He-like krypton K-shell spectrum
[DE95-010264] p 2987 N95-32041
Excitation mechanisms of 2s(sub 1/2)-2p(sub 3/2) and 2p(sub 1/2)-2p(sub 3/2)in U(82+) through U(89+)
[DE95-010265] p 2993 N95-32042
Beam stability at SRRC storage ring
[DE95-010842] p 2995 N95-32260
ELECTRON BUNCHING
Design considerations for a Density-Channel-Guided laser wake-field accelerator
[AD-A292876] p 2884 N95-31190
ELECTRON CAPTURE
Recoil longitudinal momentum spectroscopy of electron capture from He by O(7+) and F(8+)
[DE95-010823] p 2990 N95-32274
ELECTRON DENSITY (CONCENTRATION)
Determination of electric and magnetic fields in open trap plasmas by means of atomic-molecular beam hydrogen isotopes
[DE95-614177] p 3006 N95-31680
ELECTRON DIFFRACTION
The effect of a non-Hermitian crystal potential on the scattering matrix in reflection electron diffraction
[DE95-616779] p 2977 N95-30476
Application of spin-sensitive electron spectroscopies to investigations of electronic and magnetic properties of solid surfaces and epitaxial systems
[DE95-010154] p 2792 N95-30614
May multiple inelastic scattering in CBED patterns be removed analytically
[PB95-196333] p 2992 N95-30717
K-shell ionization under zone axis electron diffraction conditions
[DE95-616780] p 2981 N95-30916
ELECTRON EMISSION
Scaling of cross sections in ion-atom collisions
[DE95-008938] p 2978 N95-30573
Convoy electron emission from surfaces
[DE95-010298] p 2984 N95-31402
Surface contamination analysis technology team overview p 2781 N95-31797
The design and development of a third generation OSEE instrument p 2781 N95-31800
Study of surfaces using near infrared optical fiber spectrometry p 2781 N95-31801
Generalized Ramsauer-Townsend minima in heavy-ion induced electron continua
[DE95-010913] p 2989 N95-32120
Study of aligned states in ion-atom collisions
[DE95-010825] p 2990 N95-32275
ELECTRON ENERGY
Direct determination of grain boundary atomic structure in SrTiO3
[DE95-008847] p 3010 N95-30544
Relativistic non-interacting electron gas in a magnetic field
[DE95-616903] p 2967 N95-31177
ELECTRON GAS
Relativistic non-interacting electron gas in a magnetic field
[DE95-616903] p 2967 N95-31177
ELECTRON GUNS
Hollow cathode electron gun research and development
[DE95-010262] p 2992 N95-31127
ELECTRON IMPACT
Excitation mechanisms of 2s(sub 1/2)-2p(sub 3/2) and 2p(sub 1/2)-2p(sub 3/2)in U(82+) through U(89+)
[DE95-010265] p 2993 N95-32042
ELECTRON IRRADIATION
The junction characteristics and current conduction mechanisms of GaInP2 n(+)p diodes and solar cells
[AD-A290857] p 2902 N95-30408
ELECTRON MICROSCOPY
Annual meeting of the Advanced Light Source Users' Association
[DE95-009373] p 3000 N95-31635
Standardization of surface contamination analysis systems p 2781 N95-31798
ELECTRON MOBILITY
Self-consistent, 2D simulations of filament propagation in photoconducting switches
[DE95-010794] p 2861 N95-31133
ELECTRON OSCILLATIONS
Vertical transport in GaAs/AlGaAs superlattices p 3012 N95-30822
ELECTRON PLASMA
Perpendicular electron heating by absorption of auroral kilometric radiation
[NASA-198815] p 2914 N95-30848
Relativistic non-interacting electron gas in a magnetic field
[DE95-616903] p 2967 N95-31177
ELECTRON SCATTERING
Inelastic plasmon and inter-band electron-scattering potentials for Si from dielectric matrix calculations
[DE95-616778] p 2977 N95-30475
The effect of a non-Hermitian crystal potential on the scattering matrix in reflection electron diffraction
[DE95-616779] p 2977 N95-30476
Inversion of the total cross sections for electron-molecule and electron-atom scattering
[DE95-616466] p 2978 N95-30583
Zone axis backscattered electron contrast for fast electrons
[DE95-616775] p 2980 N95-30790
Convoy electron emission from surfaces
[DE95-010298] p 2984 N95-31402
The design and development of a third generation OSEE instrument p 2781 N95-31800
Contamination detection NDE for cleaning process inspection p 2781 N95-31802
ELECTRON SOURCES
Spin structure in high energy processes
[DE95-008628] p 2993 N95-31627
ELECTRON SPECTROSCOPY
Application of spin-sensitive electron spectroscopies to investigations of electronic and magnetic properties of solid surfaces and epitaxial systems
[DE95-010154] p 2792 N95-30614
Acoustomagnetoelectric effect in a superlattice
[DE95-613445] p 3011 N95-30736
ELECTRON SPIN
Dynamics of an inhomogeneous anisotropic antiferromagnetic spin chain
[DE95-614449] p 3013 N95-30959
ELECTRON STATES
Study of aligned states in ion-atom collisions
[DE95-010825] p 2990 N95-32275
Measurements of quantum electrodynamic sensitive transitions in Na-like and Cu-like ions
[DE95-011593] p 3007 N95-32299
ELECTRON TRANSFER
Electron transfer kinetics of self-assembled ferrocene C(12) alkanethiol monolayers on gold electrodes from 125K to 175K
[AD-A292754] p 2984 N95-31427
Consequences of kinetic dispersion on the electrochemistry of an adsorbed redox-active monolayer
[AD-A292794] p 2795 N95-31437
ELECTRON TRANSITIONS
Measurements of quantum electrodynamic sensitive transitions in Na-like and Cu-like ions
[DE95-011593] p 3007 N95-32299
ELECTRON-POSITRON PAIRS
Spin momentum correlation (handedness) in the process of four pion production in the electron-positron collisions
[DE95-613690] p 2988 N95-32093
ELECTRONIC CONTROL
Guidance and Control for Future Air-Defence Systems
[AGARD-CP-555] p 2839 N95-32123
Using a Red Team to devise countermeasures p 2842 N95-32141
ELECTRONIC COUNTERMEASURES
Electronic combat and lethal defense suppression p 2842 N95-32140
Using a Red Team to devise countermeasures p 2842 N95-32141
ELECTRONIC EQUIPMENT
EMC requirements for type approval of marine electronics. Nordtest project 1157-94
[PB95-211330] p 2859 N95-30596
Experimental investigation of the effectiveness of flow-through modules for electronics cooling
[AD-A293284] p 2861 N95-30850
Analysis of symbolic parameter models
[AD-A292916] p 2940 N95-31459
Dynamic maintenance scheduling for a stochastic telecommunication network: Determination of performance factors
[AD-A293629] p 2852 N95-31555
The 19th Annual Electronics Manufacturing Seminar
[AD-A293067] p 2863 N95-31674

ELECTRONIC EQUIPMENT TESTS
EMC requirements for type approval of marine electronics. Nordtest project 1157-94
[PB95-211330] p 2859 N95-30596
Test operations procedure (TOP) 1-2-512 electromagnetic compatibility tests
[AD-A293758] p 2852 N95-31574
Mission critical failure effects analysis using quantitative techniques
[AD-A293098] p 2864 N95-31844
ELECTRONIC MAIL
Email: Why and how
[PB95-195327] p 2846 N95-30516
Workflow literature guide, version 1
[PB95-207080] p 2947 N95-30721
ELECTRONIC MODULES
Ceramic/Metal Composite Circuit-Board-Level Technology for Application Specific Electronic Modules (ASEM's)
[AD-A293183] p 2787 N95-30978
ELECTRONIC WARFARE
Guidance and Control for Future Air-Defence Systems
[AGARD-CP-555] p 2839 N95-32123
Electronic combat and lethal defense suppression
p 2842 N95-32140
Using a Red Team to devise countermeasures
p 2842 N95-32141
ELECTRONS
Scaling of cross sections in ion-atom collisions
[DE95-008938] p 2978 N95-30573
Backgrounds and detector performance at a 2 x 2 TeV (mu)(+)(mu)(-) collider
[DE95-009107] p 2992 N95-30800
Perpendicular electron heating by absorption of auroral kilometric radiation
[NASA-198815] p 2914 N95-30848
K-shell ionization under zone axis electron diffraction conditions
[DE95-616780] p 2981 N95-30916
Irreducible Green's Functions method in the theory of highly correlated systems
[DE95-614446] p 3019 N95-31186
Thin-film edge field emitter device and method of manufacture therefor
[AD-D017453] p 2862 N95-31275
Search for anomalous ZZ(sub gamma) and Z(sub (gamma, gamma)) couplings with D0
[DE95-010457] p 2989 N95-32162
Radiative corrections to the three quantum annihilation cross section in high energy electron-positron collisions
[DE95-623675] p 2995 N95-32296
ELECTROPHORESIS
Analytical instrumentation for environmental research
[AD-A292832] p 2908 N95-31447
ELECTROPHOTOMETERS
The design and development of a third generation OSEE instrument p 2781 N95-31800
ELECTROPHYSIOLOGY
Simulation of oculomotor post-inhibitory rebound burst firing using a Hodgkin-Huxley model of a neuron
[AD-A293821] p 2927 N95-31552
Temporal information processing mechanisms
[PB95-208344] p 3027 N95-32370
ELECTROPLATING
Industry participation workshop: Chromium electroplating of superconductor strand. Proceedings
[DE95-009629] p 2807 N95-31615
ELECTROSTATIC CHARGE
Development of a method for measurement of triboelectric charging
[PB95-211322] p 2859 N95-30633
Theory and simulation of electrostatic wave turbulence in the space shuttle-induced plasma environment
[AD-A293467] p 3005 N95-31534
ELECTROSTATIC ENGINES
Beam-centroid tracking instrument for ion thrusters
[AD-A293654] p 2769 N95-31567
ELECTROSTATIC PROBES
Development of plasma diagnostics technologies: A study on nuclear fusion reactor
[DE95-614180] p 3005 N95-31004
Beam-centroid tracking instrument for ion thrusters
[AD-A293654] p 2769 N95-31567
Calibration of multichannel analyzer of charge-exchange atoms
[DE95-614178] p 2987 N95-32053
ELECTROSTATIC WAVES
Theory and simulation of electrostatic wave turbulence in the space shuttle-induced plasma environment
[AD-A293467] p 3005 N95-31534
ELECTROSTATICS
Development of a method for measurement of triboelectric charging
[PB95-211322] p 2859 N95-30633
Theory and simulation of electrostatic wave turbulence in the space shuttle-induced plasma environment
[AD-A293467] p 3005 N95-31534
ELECTROSTRICTION
Fiber optic interferometric electric field and voltage sensor utilizing and electrostrictive transducer
[AD-D017433] p 2996 N95-30753
Materials for adaptive structural acoustic control, volume 1
[AD-A293444] p 2788 N95-31369
Materials for adaptive structural acoustic control, volume 2
[AD-A293445] p 2788 N95-31370
Materials for adaptive structural acoustic control, volume 3
[AD-A293446] p 2788 N95-31371
Materials for adaptive structural acoustic control, volume 4
[AD-A293447] p 2788 N95-31372
ELECTROTHERMAL ENGINES
The 31st JANNAF Combustion Subcommittee Meeting, volume 1 p 2825 N95-31194
ELECTROWEAK INTERACTIONS (FIELD THEORY)
Electroweak interactions on the lattice
[DE95-616287] p 2965 N95-30439
Real Higgs singlet and electroweak phase transition in the standard model
[DE95-616315] p 2976 N95-30442
Phenomenology of the two Higgs doublet sector of a quark-lepton symmetric model
[DE95-616337] p 2976 N95-30446
Confronting left-right symmetric models with electroweak precision data at the Z peak
[PB95-208054] p 2977 N95-30484
WW and WZ production at the tevatron
[DE95-011014] p 2981 N95-30970
Testing vector boson dominance of electroweak interactions via e(+)e(-) (yields) f-bar f
[DE95-620528] p 2982 N95-31214
Renormcharges in V-A theories
[DE95-613689] p 2985 N95-31622
Spin structure in high energy processes
[DE95-008628] p 2993 N95-31627
Studies of the strong and electroweak interactions at the Z(sub 0) pole
[DE95-010353] p 2986 N95-31682
Physics goals of a mu(+) mu(-) collider
[DE95-009546] p 2994 N95-32059
Renormalization group analyses of particle masses in full four-generation fermion condensate scheme
[DE95-613595] p 2988 N95-32070
Electroweak flavor-conserving gauge processes: Virtual effects
[DE95-009922] p 3020 N95-32106
Electroweak baryogenesis
[DE95-012169] p 2991 N95-32365
ELECTROWEAK MODEL
New tensor interaction and the K(sub L) - K(sub S)mass difference
[DE95-613597] p 2845 N95-30370
Search for new physics indirect effects in e(+)e(-) yields W(+)W(-) at linear colliders with polarized beams
[DE95-613688] p 2984 N95-31547
ELEMENTARY EXCITATIONS
On the theory of hole propagation in an antiferromagnetic background
[DE95-614469] p 3010 N95-30650
ELEMENTARY PARTICLE INTERACTIONS
The mechanism of particle production process in hadron-nucleon collisions
[DE95-613727] p 2975 N95-30372
Current issues in perturbative QCD
[DE95-008448] p 2975 N95-30388
On explanation of proton electromagnetic form Factor near p (anti p)-threshold from the PS-170 experiment
[DE95-613766] p 2977 N95-30508
SO(8) color as possible origin of generations
[DE95-613560] p 2988 N95-32069
Form factor of the process gamma(*) gamma(*) yields pi(sup 0) for small virtuality of one of the photons and QCD sum rules (2): Sum rule
[DE95-613629] p 2988 N95-32078
Search for anomalous ZZ(sub gamma) and Z(sub (gamma, gamma)) couplings with D0
[DE95-010457] p 2989 N95-32162
ELEMENTARY PARTICLES
The Foldy-Wouthuysen transformation
[DE95-616277] p 2976 N95-30427
Covariant phase space formulations of superparticles and supersymmetric WZW models
[DE95-616278] p 2964 N95-30428
Interferometry with particles of non-zero rest mass: Topological experiments
[DE95-616244] p 2979 N95-30689
Introduction to the theory of Goyaks: Operator manifold approach to geometry and particle physics
[DE95-613460] p 2980 N95-30740
ELEVATION
Synthetic Terrain Imagery for Helmet-Mounted Display. Volume 3: Software user's manual
[AD-A293613] p 2753 N95-31463
Synthetic Terrain Imagery for Helmet-Mounted Display, volume 1
[AD-A293612] p 2753 N95-31656
ELEVATION ANGLE
Apparent size passive range method
[AD-D017360] p 2753 N95-31180
ELLIPSOMETERS
Photorefractive nonlinear optics
[AD-A292913] p 2999 N95-31458
ELLIPSOMETRY
Standardization of surface contamination analysis systems p 2781 N95-31798
Spectroscopic ellipsometry as a sensitive monitor of materials contamination p 2782 N95-31808
ELLIPTIC DIFFERENTIAL EQUATIONS
Reduced heat kernels on nilpotent lie groups
[PB95-206926] p 2958 N95-30778
ELLIPTIC FUNCTIONS
Elliptic deformed classical mechanics in three-dimensional phase space
[DE95-613384] p 3017 N95-30365
ELLIPTICAL ORBITS
A feedback linearization approach to orbital maneuvers p 2765 N95-30841
ELLIPTICAL POLARIZATION
Plane wave reflection from a uniaxial chiral quarter-wave polarization transformer
[PB95-206512] p 2849 N95-31159
ELONGATION
Einstein's length concept
[DE95-613368] p 3019 N95-30972
Behaviour of polymers in radioactive environments: Effects of dose speed
[DE95-621008] p 2818 N95-31221
EMBEDDING
Large area smart piezoelectric and pyroelectric sensors
[AD-A291487] p 2859 N95-30561
Analysis of variation embedding tests with 17 MM dowel: Densified veneer wood FOREST project, part 7
[PB95-206876] p 2963 N95-30680
Embedded infrared fiber optic absorption studies of nitramine propellant strand burning
p 2801 N95-31305
Aspects of the search time in binary search trees modified according to the move-to-root heuristic
[PB95-212148] p 2963 N95-31396
Influence of storage on the maximal pull-out force of three different optical fibers from three epoxides
[PB95-211777] p 2822 N95-32253
EMBRITTLEMENT
Microstructural and mechanical property changes in model Fe-Cu alloys
[DE95-010117] p 2805 N95-31105
Damage dosimetry and embrittlement monitoring of nuclear pressure vessels in real time by magnetic properties measurement
[DE95-011454] p 2894 N95-31254
EMISSION SPECTRA
Observations of accreting pulsars
[NASA-CR-198931] p 3028 N95-30469
Shiptracks in the Californian stratus region: Dependency on marine atmospheric boundary layer depth
[AD-A293272] p 2901 N95-31125
Measurement and analysis related to infrared emissions
[AD-A293296] p 2998 N95-31192
Luminescence properties of ZnWO4:Cr(3+) laser crystals
[AD-A293065] p 2887 N95-32152
EMITTANCE
Measurement of the effect of collimator generated wakefields on the beams in the SLC
[DE95-012101] p 2993 N95-31256
RFQ-DTL matching solutions for different requirements
[DE95-010897] p 2995 N95-32306
EMITTERS
Fractal quantum well heterostructures for broadband light emitters
[DE95-009579] p 2860 N95-30707
InP solar cell development on inexpensive Si substrates
[AD-A293255] p 2903 N95-30693
Thin-film edge field emitter device and method of manufacture therefor
[AD-D017453] p 2862 N95-31275

ENCAPSULATING
Porous spherical shells and microspheres by electrodispersion precipitation
[DE95-009073] p 2815 N95-30799
ENCLOSURES
Facilities used for plastic media blasting
p 2763 N95-32176
END EFFECTORS
Precision manipulation with a dextrous robot hand
p 2888 N95-30829
ENERGETIC PARTICLES
Modeling of thermal, electronic, hydrodynamic, and dynamic deposition processes for pulsed-laser deposition of thin films
[DE95-008906] p 2813 N95-30572
Radiation effects in space: The Clementine 1 mission
[DE95-011513] p 3032 N95-32282
ENERGY ABSORPTION
Energy absorption apparatus
[AD-D017361] p 2814 N95-30715
ENERGY BUDGETS
Global Ultraviolet Imager (GUVI) investigation
[NASA-CR-189430] p 2917 N95-31820
ENERGY CONSERVATION
A manual for the economic evaluation of energy efficiency and renewable energy technologies
[DE95-000211] p 2903 N95-30896
Free electron laser as energy driver for inertial confinement fusion
[DE95-614252] p 2884 N95-30914
The potential for microtechnology applications in energy systems: Results of an experts workshop
[DE95-009103] p 2865 N95-32077
CALORSTOCK'94. Thermal energy storage. Better economy, environment, technology
[DE95-772421] p 2907 N95-32368
ENERGY DISSIPATION
Direct determination of grain boundary atomic structure in SrTiO3
[DE95-008847] p 3010 N95-30544
Gravitational-radiation damping of compact binary systems to second post-Newtonian order
[PB95-207882] p 2912 N95-30588
Gravitational waves from inspiralling compact binaries: Energy loss and waveform to second-post-Newtonian order
[PB95-207890] p 2913 N95-30590
Observation of intensity dependent losses in Au(15+) beams
[DE95-010845] p 2987 N95-32032
The potential for microtechnology applications in energy systems: Results of an experts workshop
[DE95-009103] p 2865 N95-32077
Evidence for electronic energy loss processes stimulating solid phase epitaxial regrowth of spatially isolated amorphous regions in semiconductor systems
[DE95-009892] p 3016 N95-32103
ENERGY DISTRIBUTION
Study of the surface properties of ceramic materials by chromatography
[DE95-011578] p 2823 N95-32298
ENERGY GAPS (SOLID STATE)
The quantum interference effect in semiconductor space charge layers studied by Feynman path integrals: General formalism and illustrative examples
[DE95-614483] p 3010 N95-30653
Band gap measurement of Si(1-x)C(x)/Si (0 less than or equal to x less than or equal to 0.014) alloys using photoluminescence and spectroscopic ellipsometry
[DE95-011020] p 3014 N95-31112
Degradation of blue AlGaN/InGaN/GaN LEDs subjected to high current pulses
[DE95-006824] p 2863 N95-31611
Terahertz spectroscopy of silicon micromachined three-dimensional photonic bandgap crystal
[DE95-010233] p 3015 N95-32037
Investigation of the basic physics of high efficiency semiconductor hot carrier solar cell
[NASA-CR-198945] p 2906 N95-32212
ENERGY LEVELS
The quantum interference effect in semiconductor space charge layers studied by Feynman path integrals: General formalism and illustrative examples
[DE95-614483] p 3010 N95-30653
Inner- and outer-shell excitation in lithium isoelectronic sequence
[DE95-614107] p 2981 N95-31003
Experiments with highly charged ions up to bare U(sup 92+) on the electron beam ion trap
[DE95-008627] p 2982 N95-31174
Shnirelman peak in the level spacing statistics
[DE95-623599] p 3019 N95-31276
ENERGY METHODS
MVP/GMVP: General purpose Monte Carlo codes for neutron and photon transport calculations based on continuous energy and multigroup methods
[DE95-722072] p 2979 N95-30656
ENERGY POLICY
Outlook for renewable energy technologies: Assessment of international programs and policies
[DE95-009084] p 2907 N95-32302
ENERGY SPECTRA
Energy spectra of charge-exchange atoms from a rotating plasma
[DE95-614179] p 3006 N95-32054
Search for anomalous ZZ(sub gamma) and Z(sub (gamma, gamma)) couplings with D0
[DE95-010457] p 2989 N95-32162
ENERGY STORAGE
Data on development of new energy technologies
[DE95-764135] p 2904 N95-31155
Energy storage and alternatives to improve train voltage on a mass transit system
[DE95-010344] p 2906 N95-32090
CALORSTOCK'94. Thermal energy storage. Better economy, environment, technology
[DE95-772421] p 2907 N95-32368
ENERGY TECHNOLOGY
Overview of IEA biomass combustion activities
[PB95-196374] p 2902 N95-30519
Sleeping renewable beauty: Will the prince ever come
[PB95-214573] p 2903 N95-30640
Publications of the Fossil Energy Advanced Research and Technology Development Materials Program: April 1, 1993-March 31, 1995
[DE95-009200] p 2903 N95-30745
A manual for the economic evaluation of energy efficiency and renewable energy technologies
[DE95-000211] p 2903 N95-30896
CALORSTOCK 1994: Thermal energy storage. Better economy, environment, technology
[DE95-772422] p 2904 N95-31138
Properties of new materials relevant to energy and fuel research
[AD-A289734] p 2825 N95-31149
Data on development of new energy technologies
[DE95-764135] p 2904 N95-31155
High-tech controls for energy and environment
[DE95-011702] p 2952 N95-31255
Laboratory directed research and development report
[DE95-011405] p 3032 N95-32279
Outlook for renewable energy technologies: Assessment of international programs and policies
[DE95-009084] p 2907 N95-32302
CALORSTOCK'94. Thermal energy storage. Better economy, environment, technology
[DE95-772421] p 2907 N95-32368
ENERGY TRANSFER
Theoretical absorption spectroscopy of high-temperature metal vapors: Model and experiment compared
[AD-A290872] p 2791 N95-30409
Studying the thermal/non-thermal crossover in solar flares
[NASA-CR-189436] p 3031 N95-30785
Energy transfer dynamics in isolated and colliding highly vibrationally excited molecules
[AD-A293304] p 2981 N95-30952
Energy flow analysis of coupled structures
p 2895 N95-31316
Numerical simulation of shock/turbulent boundary layer interaction
[NASA-CR-198846] p 2872 N95-31341
Preliminary design for Arctic atmospheric radiative transfer experiments
[DE95-009580] p 2917 N95-32080
ENGINE ANALYZERS
Development of a new instrument for rocket engine combustion diagnostics p 2799 N95-31211
ENGINE CONTROL
Flight test validation of a frequency-based system identification method on an F-15 aircraft
[NASA-TM-4704] p 2757 N95-31846
Robust Rocket Engine Concept
[NASA-TM-107010] p 2770 N95-32121
ENGINE DESIGN
Wave rotor-enhanced gas turbine engines
[NASA-TM-106998] p 2754 N95-30517
Advanced small rocket chambers. Option 3: 110 1bf Ir-Re rocket, volume 1
[NASA-CR-195435-VOL-1] p 2768 N95-31169
Advanced small rocket chambers. Option 3: 110 1bf Ir-Re rocket, volume 2
[NASA-CR-195435-VOL-2] p 2769 N95-31170
An investigation of the side-dump dual in-line ramjet combustor p 2756 N95-31199
A pulsed liquid fuel ramjet p 2756 N95-31201
Design and testing of an oxidizer-rich preburner
p 2799 N95-31212
Experiment of rocket-ram combined combustor
[NAL-TR-1249] p 2769 N95-31739
ENGINE INLETS
Effects of initial conditions on a single jet in crossflow
[NASA-TM-107002] p 2754 N95-30589
Method for extracting forward acoustic wave components from rotating microphone measurements in the inlets of turbofan engines
[NASA-CR-195457] p 2755 N95-30779
ENGINE MONITORING INSTRUMENTS
Method for extracting forward acoustic wave components from rotating microphone measurements in the inlets of turbofan engines
[NASA-CR-195457] p 2755 N95-30779
ENGINE NOISE
An active liner system for jet engine exhaust silencers, phase 1
[AD-A293277] p 2756 N95-31191
ENGINE PARTS
Low vibration polymeric composite engine
[AD-D017332] p 2887 N95-30386
Bicarbonate of soda paint stripping process validation and material characterization p 2777 N95-31778
ENGINE TESTS
Advanced small rocket chambers. Option 3: 110 1bf Ir-Re rocket, volume 1
[NASA-CR-195435-VOL-1] p 2768 N95-31169
Advanced small rocket chambers. Option 3: 110 1bf Ir-Re rocket, volume 2
[NASA-CR-195435-VOL-2] p 2769 N95-31170
An active liner system for jet engine exhaust silencers, phase 1
[AD-A293277] p 2756 N95-31191
A pulsed liquid fuel ramjet p 2756 N95-31201
Investigation of ram accelerator performance capabilities p 2799 N95-31204
Development of a new instrument for rocket engine combustion diagnostics p 2799 N95-31211
Design and testing of an oxidizer-rich preburner
p 2799 N95-31212
Icing simulation in the aeropropulsion systems test facility propulsion development test cell C-2
[AD-A293039] p 2747 N95-31667
CFD assessment of the pollutant environment from RD-170 propulsion system testing p 2772 N95-31749
ENGINEERING
FBIS report: Science and technology. Central Eurasia
[FBIS-UST-95-028] p 2839 N95-31729
ENGINEERING MANAGEMENT
Geostatistics and hydrology. Part 1: Spatial and temporal variability. Communications of the Sanitary Engineering and Water Management Division
[PB95-206470] p 2900 N95-30819
ENGLISH LANGUAGE
Translation workbench for generating subtitles for English TV news
[NHK-435] p 3026 N95-32182
ENTRAINMENT
An experimental study of planar heterogeneous supersonic confined jets
[AD-A290659] p 2867 N95-30557
ENTROPY
The conical singularity and quantum corrections to entropy of black hole
[DE95-613367] p 3029 N95-30606
Numerical computation of one-dimensional detonation waves
[PB95-197950] p 2868 N95-30811
Period doubling dynamics in hadron physics: Exact calculations
[DE95-620535] p 2982 N95-31215
ENVIRONMENT EFFECTS
National Institute for Global Environmental Change
[DE95-008333] p 2907 N95-30358
BioFacts: Fueling a stronger economy. Ethanol from biomass, revision 2
[DE95-010304] p 2836 N95-31639
Environmental projects. Volume 16: Waste minimization assessment
[NASA-CR-198861] p 2909 N95-31651
Aerospace Environmental Technology Conference
[NASA-CP-3298] p 2771 N95-31746
Atmospheric environmental implications of propulsion systems p 2771 N95-31747
Low acid producing solid propellants
p 2773 N95-31754
Aqueous cleaning design presentation
p 2778 N95-31781
Environmental databases and other computerized information tools p 2783 N95-31810
The effect of environmental initiatives on NASA specifications and standards activities
p 2783 N95-31812

BioFacts: Fueling a stronger economy, global warming and biofuels emissions
[DE94-006864] p 2910 N95-31821
Environmentally Safe and Effective Processes for Paint Removal
[AGARD-LS-201] p 2843 N95-32165
Base hydrolysis and hydrothermal processing of PBX-9404 explosive
[DE95-009497] p 2837 N95-32355

ENVIRONMENT MANAGEMENT
Sleeping renewable beauty: Will the prince ever come
[PB95-214573] p 2903 N95-30640
Spatial time-series: Pollution pattern recognition under irregular interventions
[AD-A293830] p 2909 N95-31556
Sustainability protects resources for future generations
[DE95-000285] p 2909 N95-31695
Laboratory directed research and development report
[DE95-011405] p 3032 N95-32279

ENVIRONMENT MODELS
Geostatistics and hydrology. Part 3. Hydro-meteorological network design
[PB95-206462] p 2900 N95-30818

ENVIRONMENT POLLUTION
Chemical kinetics and photochemical data for use in stratospheric modeling: Evaluation number 11
[NASA-CR-198863] p 2912 N95-30525

ENVIRONMENT PROTECTION
Economical analysis relating to the global warming issue
[DE95-764072] p 2908 N95-30677
CFC-replacement by natural working fluids: R&D and industrial challenges within the refrigeration, air conditioning amd heat pump areas
[PB95-195756] p 2815 N95-30871
Aerospace Environmental Technology Conference: Exectutive summary
[NASA-CP-3297] p 2771 N95-31350
Magnesium battery disposal characteristics
[AD-A293053] p 2863 N95-31607
Evaluation of Environmentally Acceptable hydraulic fluids
[AD-A293037] p 2821 N95-31666
Manufacturing waste disposal practices of the chemical propulsion industry p 2771 N95-31748
Enhanced alkaline hydrolysis and biodegradability studies of nitrocellulose-bearing missile propellant p 2772 N95-31752
Environmentally compatible solid rocket propellants p 2772 N95-31753
Prioritization methodology for chemical replacement p 2773 N95-31757
National Center for Manufacturing Sciences: Environmentally conscious manufacturing p 2773 N95-31758
Major weapon system environmental life-cycle cost estimating for Conservation, Cleanup, Compliance and Pollution Prevention (C3P2) p 2774 N95-31761
The Oak Ridge Refrigerant Management Program p 2774 N95-31763
A water blown urethane insulation for use in cryogenic environments p 2775 N95-31765
Evaluation of HFC 245ca and HFC 236ea as foam blowing agents p 2775 N95-31766
Environmentally safe aviation fuels p 2775 N95-31768
F-200(TM): The new solution for fire protection p 2776 N95-31770
Replacement of corrosion protection chromate primers and paints used in cryogenic applications on the Space Shuttle with wire arc sprayed aluminum coatings p 2776 N95-31774
Environmentally regulated aerospace coatings p 2777 N95-31775
Convergent spray process for environmentally friendly coatings p 2777 N95-31776
SSME Main Combustion Chamber (MCC) hot oil dewaxing p 2777 N95-31777
Evaluation of pressurized water cleaning systems for hardware refurbishment p 2778 N95-31782
Implementation of environmentally compliant cleaning and insulation bonding for MNASA p 2780 N95-31796
Environmental databases and other computerized information tools p 2783 N95-31810
NEIS (NASA Environmental Information System) p 2783 N95-31811
Combatting urban air pollution through Natural Gas Vehicle (NGV) analysis, testing, and demonstration
[DE95-008300] p 2911 N95-32156
Overview of paint removal methods p 2843 N95-32166

ENVIRONMENTAL MONITORING
Directory of global environmental sciences in Japan p 2899 N95-31413
Environmental benefits of chemical propulsion p 2772 N95-31750

ENVIRONMENTAL SURVEYS
The effect of environmental initiatives on NASA specifications and standards activities p 2783 N95-31812

ENVIRONMENTS
High-tech controls for energy and environment
[DE95-011702] p 2952 N95-31255

ENZYMES
Enantioselectivity of quinoprotein alcohol dehydrogenases: Production of enantiomerically pure C3-alcohol synthons
[PB95-196960] p 2771 N95-30734
Bioremediation of wheat starch media waste p 2845 N95-32178

EPHEMERIS TIME
Relativistic timescale analysis suggests lunar theory revision p 2970 N95-32333

EPIDEMIOLOGY
Particulate air pollution and increased mortality: Biological plausibility for causal relationship
[DE95-006161] p 2909 N95-31703

EPITAXY
InP solar cell development on inexpensive Si substrates
[AD-A293255] p 2903 N95-30893
Development of germanium-silicon growth technology
[AD-A293199] p 3013 N95-30983
Band gap measurement of Si(1-x)C(x)/Si (0 less than or equal to x less than or equal to 0.014) alloys using photoluminescence and spectroscopic ellipsometry
[DE95-011020] p 3014 N95-31112
Evidence for electronic energy loss processes stimulating solid phase epitaxial regrowth of spatially isolated amorphous regions in semiconductor systems
[DE95-009892] p 3016 N95-32103

EPOXY COMPOUNDS
Effects of hydrostatic pressure on the mechanical behavior of composite materials
[AD-A293162] p 2787 N95-30963
An interpenetrating polymer network for second-order nonlinear optics
[AD-A293019] p 2821 N95-31699

EPOXY MATRIX COMPOSITES
Characterization and prediction of post-impact fatigue damage in stitched composites p 2785 N95-30826
Post-impact fatigue of cross-plied, through-the-thickness reinforced carbon/epoxy composites
[NASA-TM-110625] p 2896 N95-31419
Influence of storage on the maximal pull-out force of three different optical fibers from three epoxides
[PB95-211777] p 2822 N95-32253

EPOXY RESINS
Epoxy and acrylate stereolithography resins: In-situ measurements of cure shrinkage and stress relaxation
[DE95-008506] p 2811 N95-30389
Large area smart piezoelectric and pyroelectric sensors
[AD-A291487] p 2859 N95-30561
Evaluation of alternative pavement marking materials
[AD-A292973] p 2763 N95-31468
Influence of storage on the maximal pull-out force of three different optical fibers from three epoxides
[PB95-211777] p 2822 N95-32253

EQUATIONS OF MOTION
Elliptic deformed classical mechanics in three-dimensional phase space
[DE95-613384] p 3017 N95-30365
Integrals of motion in the two Killing vector reduction of general relativity
[DE95-616281] p 3018 N95-30431
Interferometry with particles of non-zero rest mass: Topological experiments
[DE95-616244] p 2979 N95-30689
Golden ten equations of motion
[PB95-197927] p 2967 N95-30809
Wave propagation in a fluid-loaded homogeneous, transversely isotropic, elastic cylinder of arbitrary thickness
[AD-A292728] p 2869 N95-30946
A finite element formulation for the time domain vibration analysis of an elastic-viscoelastic structure p 2895 N95-31318
Studies in non-linear multi-mode responses of harmonically excited rectangular plates with internal resonances p 2895 N95-31331
Large-eddy simulation of turbulent flow using the finite element method
[DE95-009464] p 2875 N95-31591
A computational procedure for multibody systems including flexible beam dynamics
[NASA-CR-199035] p 2897 N95-31730
Instability of weakly nonlinear chaotic structures
[DE95-613441] p 2966 N95-32066
Staggered solution procedures for multibody dynamics simulation
[NASA-CR-199034] p 2899 N95-32202

EQUATIONS OF STATE
Ocean mass density calculations from temperature and salinity data
[DSTO-TR-0023] p 2922 N95-30711
Phase transitions and gravitational collapse
[DE95-011732] p 3021 N95-32359

EQUATORIAL REGIONS
Equatorial Africa: A climatological study
[AD-A293956] p 2920 N95-31524
Validation of special sensor microwave/imager ocean surface wind retrievals in equatorial regions
[AD-A293750] p 2920 N95-31571

EQUILIBRIUM EQUATIONS
Analyzing GI/Erlang-r/1 queues
[PB95-197034] p 2949 N95-30400

EQUIPMENT SPECIFICATIONS
EMC requirements for type approval of marine electronics. Nordtest project 1157-94
[PB95-211330] p 2859 N95-30596

EQUIVALENCE
Equivalence of two non-commutative geometry approaches
[DE95-613469] p 2957 N95-30642

ERBIUM
Plasma source ion implantation of metal ions: Synchronization of cathodic-arc plasma production and target bias pulses
[DE95-009431] p 3006 N95-31613

ERGODIC PROCESS
Around Ratner --- applications of Ratner's measure and topological theorems on unipotent homogeneous actions
[DE95-613377] p 2958 N95-30770

EROSION
Navier-Stokes flow field analysis of compressible flow in a high pressure safety relief valve
[NASA-TM-110640] p 2868 N95-30862
Robotic weld overlay coatings for erosion control
[DE95-009643] p 2809 N95-32098

ERROR ANALYSIS
Effect of the stopping of the Newton iteration in implicit linear multistep methods
[PB95-207056] p 2959 N95-31184
MCNP analyses of criticality calculation results
[DE95-010886] p 2960 N95-31253
The development of human behaviour analysis techniques and the development of human factors technologies
[DE95-613356] p 2930 N95-31267
Using satellites for radar performance monitoring and calibration
[AD-A293809] p 2852 N95-31588
Allan deviation computations of a linear frequency synthesizer system using frequency domain techniques p 2972 N95-32344

ERROR CORRECTING CODES
Neural network false alarm filter, volume 2
[AD-A293114] p 2860 N95-30886

ERROR DETECTION CODES
Neural network false alarm filter, volume 2
[AD-A293114] p 2860 N95-30886

ERRORS
Determination of site-occupancies in aluminide intermetallics by ALCHEMI
[DE95-009179] p 2803 N95-30733
A hypothesis-testing approach to discriminant analysis with mixed categorical and continuous variables when data are missing
[AD-A293714] p 2964 N95-31831

ERYTHROCYTES
Membrane transport: A cellular probe of heat stroke
[AD-A293327] p 2926 N95-30924

ESTERS
Evaluation of Environmentally Acceptable hydraulic fluids
[AD-A293037] p 2821 N95-31666
Compatibility of manufacturing process fluids with HFC refrigerants and ester lubricants
[DE95-012152] p 2911 N95-32364

ESTIMATES
Theory & numerical methods for problems in shape reconstruction and large deviations
[AD-A292874] p 2952 N95-31279

ESTIMATING
Experimental determination of probability distributions for parameters of a Salem limestone cap plasticity model
[AD-A290878] p 2892 N95-30559
Golden ten equations of motion
[PB95-197927] p 2967 N95-30809
Local fractal dimension estimation
[AD-A293354] p 2959 N95-30953
Estimating heat of formation of energetic compounds using corrected semiempirical molecular orbital theory p 2800 N95-31294

A stochastic difference equation approach to inference with missing data: Some new results
[DE95-010327] p 2944 N95-32088
A stochastic EM estimator in the presence of missing data: Theory and applications
[DE95-010329] p 2944 N95-32089
ETCHING
Method for laser-assisted silicon etching using halocarbon ambients
[AD-D017426] p 2883 N95-30744
Solderability enhancement of copper through chemical etching
[DE95-010514] p 2806 N95-31406
ETHYL ALCOHOL
An analysis of gas phase ethanol/water chemistry for diamond CVD
[AD-A293009] p 2795 N95-31473
BioFacts: Fueling a stronger economy. Ethanol from biomass, revision 2
[DE95-010304] p 2836 N95-31639
BioFacts: Fueling a stronger economy, global warming and biofuels emissions
[DE94-006864] p 2910 N95-31821
ETHYLENE
Enhanced energy release and soot reduction in actively controlled flames p 2799 N95-31200
Composite polymer electrolyte for lithium batteries
[AD-A293924] p 2820 N95-31514
ETHYLENEDIAMINETETRAACETIC ACIDS
Aqueous TiO2 photocatalysis of metal-EDTA complexes
[DE95-011058] p 2793 N95-31113
EUCLIDEAN GEOMETRY
Bravais classes, Voronoie cells, Delone symbols
[PB95-207916] p 3009 N95-30503
The conical singularity and quantum corrections to entropy of black hole
[DE95-613367] p 3029 N95-30606
Good metric spaces without good parameterizations
[PB95-208427] p 2957 N95-30622
EULER EQUATIONS OF MOTION
Development of a linearized unsteady Euler analysis for turbomachinery blade rows
[NASA-CR-4677] p 2742 N95-30611
Multigrid convergence acceleration for the 2D Euler equations applied to high-lift systems
[PB95-198081] p 2743 N95-30814
QMR methods in computational fluid dynamics
[DE95-010293] p 2872 N95-31132
Atomization simulations using an Eulerian-VOF-Lagrangian method p 2828 N95-31210
EUROPE
Definition of an anti-missile ballistic defense architecture for Europe p 2840 N95-32125
EUROPEAN SPACE AGENCY
Integrated X-ray testing of the electro-optical breadboard model for the XMM reflection grating spectrometer
[DE95-008829] p 2879 N95-30507
EUROPEAN SPACE PROGRAMS
(T2L2) Time Transfer by Laser Link
p 2887 N95-32348
Satellite test of the isotropy of the one-way spe ed of light using ExTRAS p 2973 N95-32349
EUROPIUM
Low-voltage cathodoluminescence of europium-activated yttrium orthovanadate
[DE95-008536] p 3008 N95-30382
EUROPIUM ISOTOPES
Waste minimization via preparative scale high performance gel permeation chromatography
[DE95-011797] p 2798 N95-32360
EUTECTICS
Dissolution of eutectic microstructures
[DE95-010244] p 2804 N95-30757
EVACUATING (TRANSPORTATION)
Patient/aircraft forecasting for the strategic aeromedical evacuation lift-bed process
[AD-A293902] p 2747 N95-31512
Aircraft evacuations through Type-3 exits I: Effects of seat placement at the exit
[DOT/FAA/AM-95/22] p 2748 N95-31845
EVALUATION
Assessment of computer aids during communication exercise 1991
[PB95-211462] p 2945 N95-32248
EVAPORATION
Combustion of LOX with H2(sub g) under subcritical and supercritical conditions p 2797 N95-31717
Selected flows with free surfaces: Streams and drops
[IFTR-3/1995] p 2876 N95-31817
EVAPORATION RATE
Combustion of LOX with H2(sub g) under subcritical and supercritical conditions p 2797 N95-31717
EVENT HORIZON
Partons and black holes
[DE95-009921] p 3029 N95-31102
EXCIMER LASERS
Method for laser-assisted silicon etching using halocarbon ambients
[AD-D017426] p 2883 N95-30744
EXCIMERS
Properties of new materials relevant to energy and fuel research
[AD-A289734] p 2825 N95-31149
Excited-state complexes of conjugated polymers: Novel photophysical processes and optoelectronic materials
[AD-A292958] p 2819 N95-31462
Excited-state complexes of conjugated polymers
[AD-A292960] p 2819 N95-31466
EXCITATION
Photochemistry of intermolecular C-H bond activation reactions
[DE95-008991] p 2978 N95-30574
Electron-optical nonlinear interaction in asymmetric quantum-well laser heterostructures
[DE95-613443] p 2883 N95-30609
Experimental results on charge exchange reactions with delta excitations and polarization studies of delta and N(sup *) (1440) resonances
[DE95-614022] p 2981 N95-30913
Excited-state complexes of conjugated polymers
[AD-A292960] p 2819 N95-31466
Excitation mechanisms of 2s(sub 1/2)-2p(sub 3/2) and 2p(sub 1/2)-2p(sub 3/2)in U(82+) through U(89+)
[DE95-010265] p 2993 N95-32042
Method of normal coordinates in the formulation of a system with dissipation: The harmonic oscillator
[DE95-613372] p 3020 N95-32094
Mixing phases of unstable two-level systems
[DE95-613844] p 2989 N95-32151
EXHAUST CLOUDS
The Al and Al2O3 droplet cloud in solid rocket motors
p 2770 N95-31196
EXHAUST EMISSION
Jet mixing and emission characteristics of transverse jets in annular and cylindrical confined crossflow
[NASA-TM-106976] p 2755 N95-30698
Vacuum plume backflow and rarefaction
p 2871 N95-30995
CFD assessment of the pollutant environment from RD-170 propulsion system testing p 2772 N95-31749
Environmental benefits of chemical propulsion
p 2772 N95-31750
Environmentally compatible solid rocket propellants
p 2772 N95-31753
Low acid producing solid propellants
p 2773 N95-31754
Air pollution control system research: An iterative approach to developing affordable systems
p 2773 N95-31759
BioFacts: Fueling a stronger economy, global warming and biofuels emissions
[DE94-006864] p 2910 N95-31821
EXHAUST FLOW SIMULATION
Hot jet/wake turbulent structure and laser propagaion. Part 1: Jet/wake turbulence modeling
p 2871 N95-30991
EXHAUST GASES
The 21st JANNAF Exhaust Plume Technology Meeting, volume 1
[CPIA-PUBL-621-VOL-1] p 2870 N95-30986
Hot jet/wake turbulent structure and laser propagaion. Part 1: Jet/wake turbulence modeling
p 2871 N95-30991
Beam-centroid tracking instrument for ion thrusters
[AD-A293654] p 2769 N95-31567
CFD assessment of the pollutant environment from RD-170 propulsion system testing p 2772 N95-31749
EXHAUST NOZZLES
Vacuum plume backflow and rarefaction
p 2871 N95-30995
Flight test results of the F-16 aircraft modified with axisymmetric vectoring exhaust nozzle
p 2752 N95-32007
EXHAUST SYSTEMS
Demonstration of split-flow ventilation and recirculation as flow-reduction methods in an Air Force paint spray booth, volume 1
[AD-A286807] p 2763 N95-31101
EXISTENCE THEOREMS
Solvability of a class of hypersingular nonlinear integral equations
[PB95-207031] p 3011 N95-30720
EXPECTATION
A Stochastic EM algorithm for approximating the maximum likelihood estimate
[DE95-010328] p 2943 N95-32044
EXPERIMENT DESIGN
Selecting optimal experiments for feedforward multilayer perceptrons
[AD-A290856] p 2949 N95-30406
Experiments in a 120-mm ram accelerator including flow visualization p 2799 N95-31202
Long baseline neutrino oscillation experiment at the AGS
[DE95-004378] p 2986 N95-31702
A collisionless shock wave experiment
[DE95-009489] p 3008 N95-32351
EXPERIMENTATION
Pulse power for high energy density physics experiments
[DE95-010868] p 2992 N95-31232
EXPERT SYSTEMS
Expert system for assessing accuracy of models of physical phenomena and for selecting alternate models in the presence of noise
[AD-D017348] p 2974 N95-30550
Workflow literature guide, version 1
[PB95-207080] p 2947 N95-30721
Making intelligent systems team players. A guide to developing intelligent monitoring systems
[NASA-TM-104807] p 2951 N95-30925
Development of a structured design and programming methodology for expert systems shells utilizing a visual programming language: Application of structured methodology to the MK92 maintenance advisor expert system, performance module prototype
[AD-A289897] p 2939 N95-31391
Computer-aided inspection process definition: Development of an expert planning and programming system for coordinate metrology
[DE95-010411] p 2940 N95-31404
Acquiring consistent knowledge for Bayesian Forests
[AD-A293858] p 2952 N95-31517
An analysis of hierarchical genetic programming
[AD-A293964] p 2942 N95-31657
Multi-sensor data fusion in command and control and the merit of artificial intelligence p 2842 N95-32137
AIDEX: An expert system for aircraft identification
p 2842 N95-32138
EXPLORATION
SDIO: Discovering superconducting materials at high temperatures
[AD-A292820] p 3015 N95-31444
EXPLOSIVE DEVICES
A manual for pyrotechnic design, development and qualification
[NASA-TM-110172] p 2766 N95-31358
EXPLOSIVES
Base hydrolysis and hydrothermal processing of PBX-9404 explosive
[DE95-009497] p 2837 N95-32355
EXPOSURE
Evaluation of calibration parameters and performance of the video imaging technique of assessing exposure (VITAE system)
[AD-A289023] p 2927 N95-30998
Technique to prepare high-reflectance optical fiber Bragg gratings with single exposure in-line or fiber draw tower
[AD-D017445] p 2998 N95-31270
Operation of the computer model for direct atomic oxygen exposure of Earth satellites
[NASA-CR-198188] p 2767 N95-32189
EXTERNAL TANKS
Analysis of stress concentration at holes in components made of 2195 aluminum-lithium
[NASA-TP-3554] p 2893 N95-30613
EXTINGUISHING
An experimental and numerical study on the structure and extinction of laminar premixed flames
p 2792 N95-30670
EXTRACTION
On-line surfactant monitoring
[DE95-009417] p 2792 N95-30735
Ultraviolet and visible lasers: Rare earth-doped waveguide devices and non-linear optical extraction techniques
[AD-A293976] p 2885 N95-31528
EXTRAPOLATION
Analytic cross sections for collisions of H, H2, He and Li atoms and ions with atoms and molecules
[DE95-722055] p 2979 N95-30654
Ferromagnetic Potts model in a magnetic field: Finite lattice extrapolation of the (1 + 1)-dimensional Hamiltonian
[DE95-614447] p 3012 N95-30958
EXTREME ULTRAVIOLET EXPLORER SATELLITE
NASA space astronomy update 6
[NASA-CR-197664] p 3028 N95-31099
EXTREME ULTRAVIOLET RADIATION
HST-FOC observations of a remarkable UV auroral event on Jupiter p 3030 N95-30806
EXTREMELY HIGH FREQUENCIES
A theoretical treatment of the absorption and emission properties of Cu(2) porphyrin
[AD-A293869] p 2795 N95-31595

EXTREMELY LOW FREQUENCIES
The occurrence of continuation parameters in CPS terms
[AD-A292952] p 2941 N95-31480
EXTRUDING
Texture development in aluminium extrusion
[PB95-196598] p 2979 N95-30666
Hydrostatic extrusion of BSCCO/Ag composite wire
[DE95-007862] p 2805 N95-31121
EYE MOVEMENTS
Design and integration issues of visually-coupled evaluation
[AD-A293521] p 2931 N95-31538

F

F REGION
Measurements of ionospheric variability
[AD-A293495] p 2915 N95-31535
F-15 AIRCRAFT
Flight assessment of the onboard propulsion system model for the Performance Seeking Control algorithm on an F-15 aircraft
[NASA-TM-4705] p 2756 N95-31425
Flight test validation of a frequency-based system identification method on an F-15 aircraft
[NASA-TM-4704] p 2757 N95-31846
Report to the Chairman, Legislation and National Security Subcommittee, Committee on Government Operations, House of Representatives. Tactical aircraft: F-15 replacement is premature as currently planned
[GAO/NSIAD-94-118] p 2964 N95-31987
F-16 AIRCRAFT
Looking for the simple PIO model
p 2745 N95-31066
Flight test results of the F-16 aircraft modified with axisymmetric vectoring exhaust nozzle
p 2752 N95-32007
F-18 AIRCRAFT
Modeling F/A-18 flight hour program costs using regression analysis
[AD-A293771] p 2752 N95-31579
F-22 AIRCRAFT
Report to the Chairman, Legislation and National Security Subcommittee, Committee on Government Operations, House of Representatives. Tactical aircraft: F-15 replacement is premature as currently planned
[GAO/NSIAD-94-118] p 2964 N95-31987
FABRICATION
High-temperature superconducting current leads
[DE95-008404] p 2858 N95-30374
A phenomenological finite element model of part building in the stereolithography process
[DE95-008437] p 2932 N95-30376
NIR High-efficiency subwavelength diffractive structures in semiconductors
[DE95-008535] p 3008 N95-30391
Electrochemical vapour deposition of SOFC interconnection materials
[PB95-197844] p 2812 N95-30459
GPHS-RTGs in support of the Cassini RTG Program
[DE95-010306] p 2768 N95-30674
Fabrication and modification of metal nanocluster composites using ion and laser beams
[DE95-009131] p 2784 N95-30731
Low temperature fabrication from nano-size ceramic powders
[DE95-010995] p 2818 N95-31153
Investigation of polycrystalline thin film CuInSe2 solar cells based on ZnSe windows
[DE95-004068] p 2904 N95-31164
Thin-film edge field emitter device and method of manufacture therefor
[AD-D017453] p 2862 N95-31275
Inductively coupled IR staring array based on photofluxonic pixels
[AD-A292784] p 2998 N95-31435
Microstructure and aging response of SiCp reinforced A356 Al metal matrix composite subject to post fabrication thermomechanical processing
[AD-A292975] p 2789 N95-31469
Development of large-area monolithically integrated Silicon-Film(trademark) photovoltaic modules
[DE95-004089] p 2906 N95-32057
The potential for microtechnology applications in energy systems: Results of an experts workshop
[DE95-009103] p 2865 N95-32077
Comprehensive research on the stability and electronic properties of a-Si:H and a-SiGe:H alloys and devices
[DE95-004088] p 2810 N95-32154
Low cost fabrication of silicon carbide based ceramics and fiber reinforced composites
[NASA-TM-107001] p 2822 N95-32208
Whisker reinforced glass ceramic
[DE95-010542] p 2823 N95-32305
FABRICS
High strain-rate testing of parachute materials
[DE95-009577] p 2897 N95-31614
Structural analyses of the JPL Mars Pathfinder impact
[DE95-009581] p 2767 N95-32081
FABRY-PEROT INTERFEROMETERS
Fabry-Perot interferometer measurement of static temperature and velocity for ASTOVL model tests
[NASA-TM-107014] p 2879 N95-30587
FACE CENTERED CUBIC LATTICES
Diffraction-line broadening analysis and stress relaxation in thin metal layers
[PB95-213898] p 2893 N95-30634
Synthesis and characterization of nanophase face-centered-cubic titanium
[DE95-009533] p 2809 N95-32051
Energetics of Pt adsorption on Pt(111)
[DE95-010933] p 3017 N95-32307
FACTORIZATION
Newton methods for large-scale linear inequality-constrained minimization: Optimization and systems theory
[PB95-210332] p 2956 N95-30499
FADDEEV EQUATIONS
The 10th INS Scientific Computational Programs
[DE95-717864] p 2982 N95-31178
FAILURE
Development of advanced approach and departure procedures. Failure scenarios
[PB95-198123] p 2748 N95-30815
New adaptive methods for reconfigurable flight control systems, appendix 1
[AD-A292711] p 2756 N95-30937
The 10th International Conference on the Strength of Materials
[AD-A292335] p 2894 N95-31263
Large deformation failure mechanisms in nonlinear solids
[AD-A293010] p 2896 N95-31474
FAILURE ANALYSIS
Learning in an intentional system
[AD-A291158] p 2949 N95-30395
Response of mechanically fastened composite joints under multiple bypass loads p 2785 N95-30824
Summary of 1993 Atlantic tropical cyclone activity and verification of author's forecast. A year of unanticipated light hurricane activity and a poor forecast: The expected dissipation of the El Nino did not take place and Caribbean basin surface pressure became quite high
p 2918 N95-30842
Effects of thermal and electrical stressing on the breakdown behavior of space wiring
[NASA-CR-198360] p 2768 N95-30860
Failure analysis of a repairable system: The case study of a cam-driven reciprocating pump
[AD-A293144] p 2889 N95-30949
Sea ice stress research
[AD-A293164] p 2923 N95-30964
Characterization of compressive damage mechanisms in ceramic and polymeric matrix composite materials
[AD-A293171] p 2787 N95-30975
Localization in tungsten heavy alloys subjected to shearing deformations under superimposed high pressures
[AD-A293177] p 2804 N95-30977
Failure analysis for polycarbonate transparencies
[AD-A292992] p 2820 N95-31471
Mission critical failure effects analysis using quantitative techniques
[AD-A293098] p 2864 N95-31844
Failure mechanisms in composite plates subjected to in-plane compressive loading p 2790 N95-32108
FAILURE MODES
Interface degradation in CAS/Nicalon during elevated temperature aging
[DE95-008843] p 2812 N95-30543
Failure mechanisms in composite plates subjected to in-plane compressive loading p 2790 N95-32108
FAINT OBJECT CAMERA
HST-FOC observations of a remarkable UV auroral event on Jupiter p 3030 N95-30806
FALSE ALARMS
Neural network false alarm filter, volume 2
[AD-A293114] p 2860 N95-30886
Neural network false alarm filter, volume 1
[AD-A293097] p 2953 N95-31562
FAR FIELDS
Optimum truncation of a Gaussian beam for propagation through atmospheric turbulence
[AD-A291156] p 2883 N95-30394
Far field acoustic radiation reduction
[AD-D017452] p 2974 N95-30725
FAR INFRARED RADIATION
Molecular gas in starburst galaxies: Line intensities and physical conditions
[PB95-208021] p 3029 N95-30569
FAST FOURIER TRANSFORMATIONS
Image representation using fast algorithms based on the Zak transform
[AD-A293416] p 2942 N95-31684
FASTENERS
Coupling stud assembly
[AD-D017335] p 2887 N95-30387
Smart material joint band
[AD-D017374] p 2888 N95-30716
Response of mechanically fastened composite joints under multiple bypass loads p 2785 N95-30824
FATIGUE (BIOLOGY)
Forward rapid rotation shiftwork in USAF air traffic controllers: Sleep, activity, fatigue and mood analyses
[AD-A293448] p 2927 N95-31373
FATIGUE (MATERIALS)
Interfacial studies of coated fiber reinforced glass-ceramic matrix composites
[AD-A290780] p 2783 N95-30433
Fatigue crack growth behavior of a titanium matrix composite under thermomechanical loading
p 2784 N95-30491
TV-VI semiconductor quantum well lasers, physics and engineering p 2883 N95-30805
Characterization and prediction of post-impact fatigue damage in stitched composites p 2785 N95-30826
Probabilistic reliability modeling of fatigue on the H-46 tie bar
[AD-A289926] p 2751 N95-30927
A simple and accurate technique for monitoring crack growth behavior using a wave form analyzer
[AD-A293161] p 2894 N95-31007
Post-impact fatigue of cross-plied, through-the-thickness reinforced carbon/epoxy composites
[NASA-TM-110625] p 2896 N95-31419
Failure analysis for polycarbonate transparencies
[AD-A292992] p 2820 N95-31471
FATIGUE LIFE
Stress and strain concentration factors of welded multiplanar joints between square hollow sections
[PB95-208260] p 2892 N95-30492
Fatigue behaviour of multiplanar tubular joints
[PB95-207874] p 2893 N95-30586
The influence of matrix microstructure and temperature on cyclic deformation and fatigue of particle-reinforced 2219 aluminum p 2808 N95-31974
FATIGUE TESTS
Interfacial studies of coated fiber reinforced glass-ceramic matrix composites
[AD-A290780] p 2783 N95-30433
Thermal-mechanical fatigue crack growth in aircraft engine materials
[ISBN-0-315-86543-1] p 2894 N95-31098
Post-impact fatigue of cross-plied, through-the-thickness reinforced carbon/epoxy composites
[NASA-TM-110625] p 2896 N95-31419
A new goodness-of-fit test for the gamma distribution based on sample spacings from complete and censored samples
[AD-A293875] p 2961 N95-31518
A study of elevated temperature testing techniques for the fatigue behavior of PMCS: Application to T650-35/AMB21
[NASA-TM-106927] p 2791 N95-32209
FAULT DETECTION
Visualization of circuit card electromagnetic fields
[AD-A291491] p 2845 N95-30398
Neural network false alarm filter, volume 2
[AD-A293114] p 2860 N95-30886
FAULT TOLERANCE
Mission critical failure effects analysis using quantitative techniques
[AD-A293098] p 2864 N95-31844
ASSIST user manual
[NASA-TM-4592] p 2948 N95-32250
FEASIBILITY
An investigation of a novel approach to elemental imaging in three dimensions
[DE95-010340] p 3000 N95-31681
FEASIBILITY ANALYSIS
Unconventional imaging field experiment plan
[AD-A291492] p 2846 N95-30562
Calculated coupling efficiency between an elliptical-core optical fiber and an optical waveguide over temperature
[NASA-TM-107005] p 2997 N95-30649
System considerations for efficient communication and storage of MSTI image data
[NASA-CR-198869] p 3024 N95-30858
Neural network false alarm filter, volume 1
[AD-A293097] p 2953 N95-31562
Basic study of the pumping of a gamma-ray laser
[AD-A293561] p 2886 N95-31563
Possible allied ballistic missile defense systems: Related guidance and control requirements
p 2840 N95-32126

FEDERAL BUDGETS
Report to the Chairman, Subcommittee on Transportation and Related Agencies, Committee on Appropriations, House of Representatives. Air traffic control: Status of FAA's plans to close and contract out low-activity towers
[GAO/RCED-94-265] p 2750 N95-32199
FEED SYSTEMS
Performance of residual carrier array-feed combining in correlated noise p 2856 N95-32232
FEEDBACK
Fixed modes in quasi-static state feedback decoupling
[PB95-206850] p 2950 N95-30564
Testing the performance of feedback concatenated decoder with a nonideal receiver p 2856 N95-32231
FEEDBACK CONTROL
Computerized design of controllers using data models
[NASA-CR-198921] p 2950 N95-30655
H(sub 2) optimal controllers with observer based architecture for continuous-time systems: Separation principle
[PB95-197067] p 2951 N95-30833
A feedback linearization approach to orbital maneuvers p 2765 N95-30841
A novel instrumentation system for measurement of helicopter rotor motions and loads data, phase 1
[AD-A293309] p 2751 N95-30923
Use of a variable frequency source with a single-mode cavity to process ceramic filaments
[DE95-010992] p 2817 N95-31152
A two-timescale approach to nonlinear Model Predictive Control
[DE95-000943] p 2952 N95-31161
Representation of feedback operators for hyperbolic systems
[NASA-CR-198171] p 2960 N95-31319
Structural aspects of active control technology p 2760 N95-32006
FEEDERS
Development of flexible feeder techniques
[PB95-196317] p 2934 N95-30663
FEEDFORWARD CONTROL
Selecting optimal experiments for feedforward multilayer perceptrons
[AD-A290856] p 2949 N95-30406
Control of skin blood flow in the neutral zone of human body temperature regulation
[AD-A291499] p 2926 N95-30563
Finite-sample based learning algorithms for feedforward networks
[DE95-009123] p 2941 N95-31631
FEMALES
Non-comparability of female and male admission test takers: Evaluation through follow-up
[PB95-212060] p 3021 N95-30700
FERMI LIQUIDS
A valence-fluctuation mechanism with highly anisotropic S-wave pairing
[DE95-009419] p 3010 N95-30571
Properties of a multichannel resonant-level model
[DE95-614482] p 2979 N95-30652
New Fermi-liquid approach for the theory of disordered magnetics
[DE95-613448] p 2967 N95-30739
FERMI SURFACES
Molecular modeling of PMN ceramics
[AD-A290879] p 2813 N95-30560
FERMIONS
Electroweak interactions on the lattice
[DE95-616287] p 2965 N95-30439
Effective Lagrangian approach to the fermion mass problem
[DE95-616316] p 2976 N95-30443
Renormalization group analyses of particle masses in full four-generation fermion condensate scheme
[DE95-613595] p 2988 N95-32070
FERROCENES
Electron transfer kinetics of self-assembled ferrocene C(12) alkanethiol monolayers on gold electrodes from 125K to 175K
[AD-A292754] p 2984 N95-31427
Consequences of kinetic dispersion on the electrochemistry of an adsorbed redox-active monolayer
[AD-A292794] p 2795 N95-31437
FERROELECTRICITY
Ceramics derived from metal-organic precursors
[AD-A290791] p 2811 N95-30405
Crystallization of sol-gel derived lead zirconate titanate thin films in argon and oxygen atmospheres
[DE95-615230] p 3009 N95-30421
Device for low electric-field induced switching of Langmuir-Blodgett ferroelectric liquid crystal polymer films
[AD-D017457] p 3011 N95-30728
Materials for adaptive structural acoustic control, volume 1
[AD-A293444] p 2788 N95-31369
Materials for adaptive structural acoustic control, volume 2
[AD-A293445] p 2788 N95-31370
Materials for adaptive structural acoustic control, volume 3
[AD-A293446] p 2788 N95-31371
Materials for adaptive structural acoustic control, volume 4
[AD-A293447] p 2788 N95-31372
A study of switching behavior in Pb(Zr,Ti)O3 thin films using x-ray diffraction
[DE95-010859] p 2808 N95-31689
FERROMAGNETIC MATERIALS
Properties of a multichannel resonant-level model
[DE95-614482] p 2979 N95-30652
Ferromagnetic Potts model in a magnetic field: Finite lattice extrapolation of the (1 + 1)-dimensional Hamiltonian
[DE95-614447] p 3012 N95-30958
Dynamics of an inhomogeneous anisotropic antiferromagnetic spin chain
[DE95-614449] p 3013 N95-30959
FEYNMAN DIAGRAMS
On the Compton twist-3 asymmetries
[DE95-613627] p 3017 N95-30371
The quantum interference effect in semiconductor space charge layers studied by Feynman path integrals: General formalism and illustrative examples
[DE95-614483] p 3010 N95-30653
FIBER COMPOSITES
Interfacial studies of coated fiber reinforced glass-ceramic matrix composites
[AD-A290780] p 2783 N95-30433
Design of fibre reinforced composite panels for aerospace applications
[PB95-197851] p 2784 N95-30460
Round-robin validation exercise for plate twist test method
[PB95-208088] p 2812 N95-30487
Fatigue crack growth behavior of a titanium matrix composite under thermomechanical loading p 2784 N95-30491
Innovative processing of composites for ultra-high temperature applications, book 3
[AD-A290891] p 2786 N95-30866
Effects of hydrostatic pressure on the mechanical behavior of composite materials
[AD-A293162] p 2787 N95-30963
Characterization of compressive damage mechanisms in ceramic and polymeric matrix composite materials
[AD-A293171] p 2787 N95-30975
Modeling of fiber-reinforced composites incorporating distinct interface properties p 2787 N95-31110
Development and computer implementation of design/analysis techniques for multilayered composite structures. Probabilistic fiber composite micromechanics
[NASA-CR-198979] p 2930 N95-31134
Intermodulation Interference (IMI) testing of composite materials
[AD-A288621] p 2787 N95-31146
An evaluation of the Iosipescu specimen for composite materials shear property measurement
[NASA-CR-198755] p 2896 N95-31418
Control of interfacial chemistry and mechanical properties in metal/ceramic composites p 2790 N95-31976
Failure mechanisms in composite plates subjected to in-plane compressive loading p 2790 N95-32108
Low cost fabrication of silicon carbide based ceramics and fiber reinforced composites
[NASA-TM-107001] p 2822 N95-32208
FIBER OPTICS
Passive, multi-channel fiber optic rotary joint assembly
[AD-D017353] p 2996 N95-30529
FOG --- evaluation test of a fiber optic gyroscope (FOG)
[PB95-211546] p 2879 N95-30600
Fiber optic accelerometer with centrally supported flexural disk
[AD-D017369] p 2879 N95-30658
Optical fiber pressure sensor for liquid level monitoring
[AD-D017346] p 2996 N95-30679
Fiber optic interferometric electric field and voltage sensor utilizing and electrostrictive transducer
[AD-D017433] p 2996 N95-30753
Optical logic and signal processing using a semiconductor laser diode-based optical bistability device
[AD-A293248] p 2997 N95-30908
A study of end-fire coupling of single-mode fiber to Ti: LiNbO3-single-mode planar waveguide
[AD-A293249] p 2997 N95-30909
Embedded infrared fiber optic absorption studies of nitramine propellant strand burning p 2801 N95-31305
Photorefractive nonlinear optics
[AD-A292913] p 2999 N95-31458
Acousto-optical frequency shifters in dual-core optical fibres
[AD-A293979] p 2999 N95-31529
Improved linear dynamic range in externally modulated fiber-optic links p 3001 N95-31950
Current trends in the packaging of photonic devices
[DE95-009583] p 3001 N95-32064
Fiber optic reference frequency distribution to remote beam waveguide antennas p 2972 N95-32346
FIBER PULLOUT
Influence of storage on the maximal pull-out force of three different optical fibers from three epoxides
[PB95-211777] p 2822 N95-32253
FIBER STRENGTH
The effect of interface properties on nickel base alloy composites
[NASA-CR-198363] p 2785 N95-30787
FIBER-MATRIX INTERFACES
The effect of interface properties on nickel base alloy composites
[NASA-CR-198363] p 2785 N95-30787
Modeling of fiber-reinforced composites incorporating distinct interface properties p 2787 N95-31110
FIELD COILS
Stability analysis of the TPX toroidal field coil
[DE95-009666] p 2865 N95-32100
FIELD EFFECT TRANSISTORS
Finite element simulation of GaAs MESFET's
[PB95-208062] p 3009 N95-30485
Space qualified hybrid superconductor/semiconductor planar oscillator circuit
[NASA-TM-106978] p 3011 N95-30703
Pseudomorphic heterostructure materials for high performance devices
[AD-A292906] p 2788 N95-31384
Voltage controlled MESFET pulse shape generator
[DE95-011656] p 2865 N95-32300
Hyperfrequency components
[PB95-208302] p 2866 N95-32369
FIELD OF VIEW
SeaWiFS Technical Report Series. Volume 29: SeaWiFS CZCS-type pigment algorithm
[NASA-TM-104566] p 2922 N95-30857
Wide field of view helmet display systems mounted for helicopter simulation
[AD-A293123] p 2930 N95-30888
SeaWiFS technical report series. Volume 28: SeaWiFS algorithms, part 1
[NASA-TM-104566-VOL-28] p 2924 N95-31850
FIELD THEORY (PHYSICS)
Large scale periodicity of the universe and baryogenesis
[DE95-613461] p 3028 N95-30366
Covariant phase space formulations of superparticles and supersymmetric WZW models
[DE95-616278] p 2964 N95-30428
The solutions of affine and conformal affine Toda field theory
[DE95-616280] p 2965 N95-30430
Plaquette expansion proof and interpretation
[DE95-616282] p 2965 N95-30432
Theoretical high energy physics
[DE95-003107] p 2991 N95-30527
Equivalence of two non-commutative geometry approaches
[DE95-613469] p 2957 N95-30642
Alloying effects of Kondo insulators
[DE95-614308] p 3010 N95-30644
Irreducible Green's Functions method in the theory of highly correlated systems
[DE95-614446] p 3019 N95-31186
Molecular models for nitro compounds p 2831 N95-31293
Variational optimization in quantum field theory p 3020 N95-31646
FIGHTER AIRCRAFT
Numerical investigation into vortical flow about a delta-wing configuration up to incidences at which vortex breakdown occurs in experiment
[PB95-198024] p 2743 N95-30837
New adaptive methods for reconfigurable flight control systems, appendix 1
[AD-A292711] p 2756 N95-30937
Lavi flight control system: Design requirements, development and flight test results p 2758 N95-31994
Digital autopilot design for combat aircraft in ALENIA p 2760 N95-32009
Experimental Aircraft Programme (EAP): Flight control system design and test p 2760 N95-32010

FIGURE OF MERIT
An experimental search for high ZT semiconductors: A survey of the preparation and properties of several alloy systems
[DE95-010232] p 2865 N95-32084
FILE MAINTENANCE (COMPUTERS)
Building an experience factory for maintenance
p 2937 N95-31237
Applying program comprehension techniques to improve software inspections p 2937 N95-31241
An experiment to assess the cost-benefits of code inspections in large scale software development
p 2937 N95-31242
A quantitative comparison of corrective and perfective maintenance p 2939 N95-31250
Does software design complexity affect maintenance effort? p 2939 N95-31251
FILM COOLING
Effect of velocity and temperature distribution at the hole exit on film cooling of turbine blades
[NASA-TM-106954] p 2755 N95-30702
FILM THICKNESS
Mechanisms of enhanced ionic conduction at interfaces in ceramics
[DE95-009125] p 2814 N95-30730
Fluid-film lubrication with an application to piston rings
p 2890 N95-32119
FILMS
Substrate heating measurements in pulsed ion beam film deposition
[DE95-010862] p 2818 N95-31377
FILTRATION
4-manifold topology 2: Dwyer's filtration and surgery kernels
[PB95-207940] p 2965 N95-30509
Particle filtration: An analysis using the method of volume averaging
[DE95-009467] p 2875 N95-31592
Particle filtration: A comparison between theory and experiment
[DE95-009442] p 2875 N95-31637
FINANCE
Workflow literature guide, version 1
[PB95-207080] p 2947 N95-30721
FINANCIAL MANAGEMENT
Federally funded R and D centers: Executive compensation at the Aerospace Corporation. Report to Congressional requestors
[GAO/NSIAD-95-75] p 3022 N95-32213
FINGERS
Smart material joint band
[AD-D017374] p 2888 N95-30716
Precision manipulation with a dextrous robot hand
p 2888 N95-30829
FINISHES
Solderability enhancement of copper through chemical etching
[DE95-010514] p 2806 N95-31406
FINITE DIFFERENCE THEORY
Simulation of airborne electromagnetic measurements in three dimensional environments
[DE95-008546] p 2900 N95-30363
Method and apparatus for locating an acoustic source
[AD-D017347] p 2974 N95-30549
Fourier analysis of a robust multigrid method for convection-diffusion equations
[PB95-197091] p 2958 N95-30835
Simultaneous heat and mass transfer in a horizontal tube absorber: Numerical tools for present and future absorber designs
[PB95-196978] p 2869 N95-30872
Implementation of KIVA-3 on distributed memory MIMD computers
[DE95-010288] p 2931 N95-31130
QMR methods in computational fluid dynamics
[DE95-010293] p 2872 N95-31132
The 2nd Japan-US Symposium on Finite Element Methods in Large Scale Computational Fluid Dynamics
[AD-A292337] p 2960 N95-31264
Theory & numerical methods for problems in shape reconstruction and large deviations
[AD-A292874] p 2952 N95-31279
Numerical simulation of shock/turbulent boundary layer interaction
[NASA-CR-198846] p 2872 N95-31341
Self-adaptive multilevel methods for fluid flow problems p 2873 N95-31412
A two-dimensional finite difference algorithm on the KSR1
[AD-A293576] p 2941 N95-31594
Two-dimensional Finite Difference Time Domain (FD-TD) model of electromagnetic (EM) scattering from a buried rectangular object
[AD-A293685] p 2852 N95-31601
Staggered solution procedures for multibody dynamics simulation
[NASA-CR-199034] p 2899 N95-32202
FINITE ELEMENT METHOD
A phenomenological finite element model of part building in the stereolithography process
[DE95-008437] p 2932 N95-30376
Finite element simulation of GaAs MESFET's
[PB95-208062] p 3009 N95-30485
An explanation for the shape of nanoindentation unloading curves based on finite element simulation
[DE95-008905] p 2812 N95-30548
Scattering and radiation from cylindrically conformal antennas p 2847 N95-30669
Use of element-by-element preconditioners to solve large scale partially separable optimization problems
[PB95-195772] p 2957 N95-30692
Control of flexible spacecraft structures using H-infinity wave absorbing control
[AD-A293141] p 2766 N95-30919
The 2nd Japan-US Symposium on Finite Element Methods in Large Scale Computational Fluid Dynamics
[AD-A292337] p 2960 N95-31264
A finite element formulation for the time domain vibration analysis of an elastic-viscoelastic structure
p 2895 N95-31318
An evaluation of the Iosipescu specimen for composite materials shear property measurement
[NASA-CR-198755] p 2896 N95-31418
Intelligent finite element submodeling of multichip modules for reliability analysis
[AD-A292911] p 2940 N95-31455
Finite element analysis of smart structures and modal testing of a flexible spacecraft arm
[AD-A293761] p 2890 N95-31576
Large-eddy simulation of turbulent flow using the finite element method
[DE95-009464] p 2875 N95-31591
Mode I large strain viscoelastic crack behavior in nitrile rubber sheets
[AD-A289984] p 2820 N95-31617
Evaluation of nonlinear structural dynamic responses using a fast-running spring-mass formulation
[DE95-008503] p 2967 N95-31625
Finite element analysis of damped vibrations of laminated composite plates
[ISBN-0-315-84928-2] p 2789 N95-31731
A time stepping coupled finite element-state space modeling environment for synchronous machine performance and design analysis in the ABC frame of reference p 2864 N95-31948
A numerical analysis of crack growth in microcracking ceramic and ceramic composites
[DE95-010132] p 2897 N95-32024
Structural analyses of the JPL Mars Pathfinder impact
[DE95-009581] p 2767 N95-32081
Automated volumetric grid generation for finite element modeling of human hand joints
[DE95-009575] p 2928 N95-32097
A mode decomposition based finite element formulation for the nonlinear dynamics of flexible spatial structures and mechanisms p 2898 N95-32118
Validation of favor code linear elastic fracture solutions for finite-length flaw geometries
[DE95-009034] p 2898 N95-32157
Evaluation of discretization procedures for transition elements in adaptive mesh refinement
[NASA-CR-199037] p 2944 N95-32190
A survey of the core-congruential formulation for geometrically nonlinear TL finite elements
[NASA-CR-199044] p 2944 N95-32203
Computational methods and software systems for dynamics and control of large space structures
[NASA-CR-199036] p 2767 N95-32204
FPCAS3D User's guide: A three dimensional full potential aeroelastic program, version 1
[NASA-CR-198367] p 2899 N95-32205
A transient FETI methodology for large-scale parallel implicit computations in structural mechanics
[NASA-CR-199040] p 2945 N95-32214
The individual element test revisited
[NASA-CR-199039] p 2945 N95-32215
Residual stress distribution in FeAl weld overlay on steel
[DE95-009178] p 2899 N95-32317
FIRE CONTROL
Development of a structured design and programming methodology for expert systems shells utilizing a visual programming language: Application of structured methodology to the MK92 maintenance advisor expert system, performance module prototype
[AD-A289897] p 2939 N95-31391
Next generation fire suppressants
p 2775 N95-31769
Guidance and Control for Future Air-Defence Systems
[AGARD-CP-555] p 2839 N95-32123
Acquisition, tracking, pointing and fire control for Ballistic Missile Defense p 2841 N95-32131
FIRE EXTINGUISHERS
Simple model of foam spreading on liquid surfaces
[PB95-211207] p 2838 N95-30630
Next generation fire suppressants
p 2775 N95-31769
F-200(TM): The new solution for fire protection
p 2776 N95-31770
FIRE FIGHTING
Simple model of foam spreading on liquid surfaces
[PB95-211207] p 2838 N95-30630
Chemical options to halons for aircraft use
[AD-A293741] p 2747 N95-31569
Evaluation of halon alternatives in inerting experiments
[AD-A293774] p 2795 N95-31580
Next generation fire suppressants
p 2775 N95-31769
FIRE PREVENTION
F-200(TM): The new solution for fire protection
p 2776 N95-31770
Convergent spray process for environmentally friendly coatings p 2777 N95-31776
FIRES
Navier-Stokes flow field analysis of compressible flow in a high pressure safety relief valve
[NASA-TM-110640] p 2868 N95-30862
Electrical short circuit and current overload tests on aircraft wiring
[AD-A293308] p 2860 N95-30922
Next generation fire suppressants
p 2775 N95-31769
FISCHER-TROPSCH PROCESS
Catalytic reactions of synthesis gas. Part 4: Heterogeneous hydroformylation
[PB95-195558] p 2791 N95-30537
Fischer-tropsch synthesis in supercritical fluids
[DE95-009631] p 2792 N95-30709
FISHES
FISHFINDE: Interactive software package to predict fish locations using satellite image data and fish species behavior rules
[AD-A293394] p 2935 N95-30968
FITTING
Fitting discrete distributions on the first two moments
[PB95-197885] p 2950 N95-30462
Analysis of symbolic parameter models
[AD-A292916] p 2940 N95-31459
FITTINGS
Residual stresses and stress corrosion cracking in pipe fittings
[DE95-009332] p 2894 N95-31054
FIXTURES
Hot compression testing of tungsten
[AD-A293683] p 2807 N95-31599
FLAME PROPAGATION
An experimental and numerical study on the structure and extinction of laminar premixed flames
p 2792 N95-30670
The study of flame-vortex interactions using a particle image velocimeter p 2796 N95-31709
Effects of gas-phase thermal expansion on the stability of deflagration through a porous energetic material
[DE95-004382] p 2797 N95-31824
FLAME RETARDANTS
Chemical options to halons for aircraft use
[AD-A293741] p 2747 N95-31569
Evaluation of halon alternatives in inerting experiments
[AD-A293774] p 2795 N95-31580
FLAME TEMPERATURE
Measurement of temperatures and OH concentrations of solid propellant flames using absorption spectroscopy
p 2801 N95-31302
FLAMES
Simulation of chemical kinetics in turbulent natural gas combustion. Volume 2: Experimental studies of nitric oxide production in gas flames
[PB95-196721] p 2791 N95-30541
Species and temperature profiles of propellant flames obtained from FTIR absorption spectroscopy
p 2801 N95-31303
Improvements in infrared absorption of solid propellant flames p 2801 N95-31306
RDX laser-assisted flame structure
p 2801 N95-31314
A study of the gas-phase processes of RDX combustion using a triple quadrupole mass-spectrometer
p 2801 N95-31315
Next generation fire suppressants
p 2775 N95-31769
FLAMMABILITY
Evaluation of Environmentally Acceptable hydraulic fluids
[AD-A293037] p 2821 N95-31666

FLANGES
Coupling stud assembly
[AD-D017335] p 2887 N95-30387
FLAT PANEL DISPLAYS
Low-voltage cathodoluminescence of europium-activated yttrium orthovanadate
[DE95-008536] p 3008 N95-30382
Method and apparatus for a high resolution, flat panel cathodoluminescent display device
[AD-D017434] p 2862 N95-31342
FLAVOR (PARTICLE PHYSICS)
Phenomenology of the two Higgs doublet sector of a quark-lepton symmetric model
[DE95-616337] p 2976 N95-30446
On hadronic production of the B(sub c) meson
[DE95-613726] p 2991 N95-32304
Spin puzzle in nucleon
[DE95-613654] p 2991 N95-32353
FLEXIBILITY
Predictions of tensile behavior and strengths of a Si3N4 ceramic at high temperatures based on a viscoplastic model
[DE95-010220] p 2821 N95-32025
FLEXIBLE BODIES
Control of flexible spacecraft structures using H-infinity wave absorbing control
[AD-A293141] p 2766 N95-30919
A computational procedure for multibody systems including flexible beam dynamics
[NASA-CR-199035] p 2897 N95-31730
A mode decomposition based finite element formulation for the nonlinear dynamics of flexible spatial structures and mechanisms p 2898 N95-32118
FLEXIBLE SPACECRAFT
Finite element analysis of smart structures and modal testing of a flexible spacecraft arm
[AD-A293761] p 2890 N95-31576
Vibration control of spacecrafts and space structures from lift-off to on-orbit environments
p 2767 N95-32110
Computational methods and software systems for dynamics and control of large space structures
[NASA-CR-199036] p 2767 N95-32204
FLEXING
Interface degradation in CAS/Nicalon during elevated temperature aging
[DE95-008843] p 2812 N95-30543
Fiber optic accelerometer with centrally supported flexural disk
[AD-D017369] p 2879 N95-30658
Vibration-damping structural component
[AD-D017376] p 2784 N95-30661
Influence of fiber content on mechanical performance of SiC-fiber-reinforced reaction-bonded silicon nitride composites
[NASA-TM-110639] p 2790 N95-32060
FLIGHT CHARACTERISTICS
Aeroelastic pilot-in-the-loop oscillations
p 2746 N95-31070
FLIGHT CONDITIONS
Integrated terminal weather system (ITWS) demonstration and validation operational test and evaluation
[AD-A293932] p 2749 N95-31521
Icing simulation in the aeropropulsion systems test facility propulsion development test cell C-2
[AD-A293039] p 2747 N95-31667
FLIGHT CONTROL
Moving base simulation of an integrated flight and propulsion control system for an ejector-augmentor STOVL aircraft in hover
[NASA-TM-108867] p 2750 N95-30646
New adaptive methods for reconfigurable flight control systems, appendix 1
[AD-A292711] p 2756 N95-30937
Flight Vehicle Integration Panel Workshop on Pilot Induced Oscillations
[AGARD-AR-335] p 2745 N95-31061
The process for addressing the challenges of aircraft pilot coupling p 2745 N95-31063
Observations on PIO p 2745 N95-31064
SAAB experience with PIO p 2746 N95-31069
Handling qualities analysis on rate limiting elements in flight control systems p 2746 N95-31071
Calspan experience of PIO and the effects of rate limiting p 2746 N95-31072
Active control technology: Applications and lessons learned
[AGARD-CP-560] p 2757 N95-31989
The role of handling qualities specifications in flight control system design p 2757 N95-31990
The prevention of PIO by design
p 2757 N95-31991
The importance of flying qualities design specifications for active control systems p 2757 N95-31992
Experiences with ADS-33 helicopter specification testing and contributions to refinement research
p 2757 N95-31993
Lavi flight control system: Design requirements, development and flight test results p 2758 N95-31994
Robust control: A structured approach to solve aircraft flight control problems p 2758 N95-31995
Dynamic inversion: An evolving methodology for flight control design p 2758 N95-31996
Evaluation of the techniques of fuzzy control for the piloting an aircraft p 2758 N95-31997
The control system design methodology of the STOL and maneuver technology demonstrator
p 2758 N95-31998
Control law design using H-infinity and mu-synthesis short-period controller for a tail-airplane
p 2758 N95-31999
Model following control for tailoring handling qualities: ACT experience with ATTHeS p 2758 N95-32000
X-29 flight control system: Lessons learned
p 2759 N95-32001
The FCS-structural coupling problem and its solution
p 2759 N95-32005
Flight test results of the F-16 aircraft modified with axisymmetric vectoring exhaust nozzle
p 2752 N95-32007
Catapult-launching of the RAFALE design and experimentation p 2752 N95-32008
Digital autopilot design for combat aircraft in ALENIA
p 2760 N95-32009
Experimental Aircraft Programme (EAP): Flight control system design and test p 2760 N95-32010
An investigation of pilot induced oscillation phenomena in digital-flight control systems p 2760 N95-32011
Flight demonstration of an advanced pitch control law in the VAAC Harrier aircraft p 2760 N95-32012
Advanced flight control technology achievements at Boeing Helicopters p 2761 N95-32014
Flying qualities of civil transport aircraft with electrical flight control p 2761 N95-32016
Pilot Induced Oscillation: A report on the AGARD Workshop on PIO p 2761 N95-32017
FLIGHT CREWS
STS-70 flight: Day 5
[NASA-TM-110663] p 2764 N95-30876
Controller resource management: What can we learn from aircrews?
[DOT/FAA/AM-95/21] p 2750 N95-32186
FLIGHT MANAGEMENT SYSTEMS
Results from tests of the Honeywell integrated flight management unit
[PB95-211355] p 2748 N95-30597
FLIGHT MECHANICS
Flight Vehicle Integration Panel Workshop on Pilot Induced Oscillations
[AGARD-AR-335] p 2745 N95-31061
FLIGHT OPERATIONS
Advanced gust management systems: Lessons learned and perspectives p 2759 N95-32002
FLIGHT PATHS
Apparatus and method for producing three-dimensional images
[AD-D017455] p 2847 N95-30727
Analysis of heads-up display quickening versus handling qualities
[AD-A293797] p 2753 N95-31584
FLIGHT SAFETY
The relation of handling qualities ratings to aircraft safety p 2746 N95-31067
Human factors at the FAA Technical Center: Bibliography
[AD-A288638] p 2930 N95-31399
Environmental support of naval aviation
[AD-A292873] p 2747 N95-31454
Special investigation report: Safety of the air tour industry in the United States
[PB95-917004] p 2748 N95-32185
FLIGHT SIMULATION
Moving base simulation of an integrated flight and propulsion control system for an ejector-augmentor STOVL aircraft in hover
[NASA-TM-108867] p 2750 N95-30646
Wide field of view helmet display systems mounted for helicopter simulation
[AD-A293123] p 2930 N95-30888
SCARLET: DLR rate saturation flight experiment
p 2746 N95-31068
Model following control for tailoring handling qualities: ACT experience with ATTHeS p 2758 N95-32000
FLIGHT SIMULATORS
Moving base simulation of an integrated flight and propulsion control system for an ejector-augmentor STOVL aircraft in hover
[NASA-TM-108867] p 2750 N95-30646
Development of advanced approach and departure procedures. Failure scenarios
[PB95-198123] p 2748 N95-30815
Human factors at the FAA Technical Center: Bibliography
[AD-A288638] p 2930 N95-31399
Contextual interference effects on acquisition and transfer of a complex motor task
[AD-A293788] p 2929 N95-31583
Image representation using fast algorithms based on the Zak transform
[AD-A293416] p 2942 N95-31684
Experiences with ADS-33 helicopter specification testing and contributions to refinement research
p 2757 N95-31993
Model following control for tailoring handling qualities: ACT experience with ATTHeS p 2758 N95-32000
Practical experiences in control systems design using the NCR Bell 205 Airborne Simulator
p 2761 N95-32015
FLIGHT STABILITY TESTS
Practical experiences in control systems design using the NCR Bell 205 Airborne Simulator
p 2761 N95-32015
FLIGHT TEST INSTRUMENTS
Preparation of S-70A-9 Black Hawk helicopter for flight tests to investigate cause of cracking of inner fuselage panel
[AD-A293891] p 2752 N95-31544
FLIGHT TESTS
Flight test evaluation of the Stanford University/United Airlines differential GPS Category 3 automatic landing system
[NASA-TM-110354] p 2743 N95-30788
SCARLET: DLR rate saturation flight experiment
p 2746 N95-31068
Flight assessment of the onboard propulsion system model for the Performance Seeking Control algorithm on an F-15 aircraft
[NASA-TM-4705] p 2756 N95-31425
Artificial intelligence techniques for flight test planning, phase 1
[AD-A293962] p 2751 N95-31525
Preparation of S-70A-9 Black Hawk helicopter for flight tests to investigate cause of cracking of inner fuselage panel
[AD-A293891] p 2752 N95-31544
Flight test validation of a frequency-based system identification method on an F-15 aircraft
[NASA-TM-4704] p 2757 N95-31848
Lavi flight control system: Design requirements, development and flight test results p 2758 N95-31994
The control system design methodology of the STOL and maneuver technology demonstrator
p 2758 N95-31998
X-29 flight control system: Lessons learned
p 2759 N95-32001
Advanced gust management systems: Lessons learned and perspectives p 2759 N95-32002
Flight evaluation of forebody vortex control in post-stall flight p 2752 N95-32003
Automatic flight control system for an unmanned helicopter system design and flight test results
p 2759 N95-32004
Flight test results of the F-16 aircraft modified with axisymmetric vectoring exhaust nozzle
p 2752 N95-32007
Experimental Aircraft Programme (EAP): Flight control system design and test p 2760 N95-32010
Flight demonstration of an advanced pitch control law in the VAAC Harrier aircraft p 2760 N95-32012
X-31: A program overview and flight test status
p 2753 N95-32013
Report to the Chairman, Legislation and National Security Subcommittee, Committee on Government Operations, House of Representatives. Unmanned aerial vehicles: Performance of short-range system still in question
[GAO/NSIAD-94-65] p 2752 N95-32196
FLIGHT TIME
Modeling F/A-18 flight hour program costs using regression analysis
[AD-A293771] p 2752 N95-31579
FLIGHT TRAINING
Contextual interference effects on acquisition and transfer of a complex motor task
[AD-A293788] p 2929 N95-31583
Controller resource management: What can we learn from aircrews?
[DOT/FAA/AM-95/21] p 2750 N95-32186
FLOATING POINT ARITHMETIC
Implementation and performance of the pseudoknot problem in Sisal
[DE95-009573] p 2925 N95-32358

FLOW CHARACTERISTICS
Large-eddy simulation of turbulent flow using the finite element method
[DE95-009464] p 2875 N95-31591
Flow quality improvements in the NASA Lewis Research Center 9- by 15-foot Low Speed Wind Tunnel
[NASA-CR-195439] p 2763 N95-31653

FLOW DISTORTION
The study of flame-vortex interactions using a particle image velocimeter p 2796 N95-31709

FLOW DISTRIBUTION
An experimental study of planar heterogeneous supersonic confined jets
[AD-A290859] p 2867 N95-30557
Control of skin blood flow in the neutral zone of human body temperature regulation
[AD-A291499] p 2926 N95-30563
Modeling of thermal, electronic, hydrodynamic, and dynamic deposition processes for pulsed-laser deposition of thin films
[DE95-008906] p 2813 N95-30572
Axial loads on yawed rotors
[PB95-214193] p 2742 N95-30638
Computation of high-altitude hypersonic flow-field radiation p 2743 N95-30843
Navier-Stokes flow field analysis of compressible flow in a high pressure safety relief valve
[NASA-TM-110640] p 2868 N95-30862
Acceleration potential models PREDICHAT/PREDICDYN applied for calculation of axisymmetric dynamic inflow cases
[PB95-207015] p 2869 N95-30957
Patterns in the sky: Natural visualization of aircraft flow fields
[NASA-SP-514] p 2741 N95-31000
Numerical simulation of ram accelerator performance including transient effects during initiation of combustion and sensitivity studies p 2799 N95-31203
Investigating the use of smart acoustically active surfaces for flow separation control in turbomachinery
[AD-A292819] p 2874 N95-31443
Side force acting on blunted circular cylinder bodies at high angles of attack in supersonic flow
[NAL-TR-1255] p 2744 N95-31741
Laser anemometer measurements of the three-dimensional rotor flow field in the NASA low-speed centrifugal compressor
[NASA-TP-3527] p 2756 N95-31985

FLOW EQUATIONS
Simulation of viscous sintering
[PB95-197109] p 2868 N95-30836
A study of numerical solutions of conservation laws
[TRITA-NA-9315] p 2960 N95-31361

FLOW GEOMETRY
Large-eddy simulation of turbulent flow using the finite element method
[DE95-009464] p 2875 N95-31591

FLOW MEASUREMENT
Nearly steady flows in GONG prototype data
[NASA-CR-198935] p 2869 N95-30863
Compressible turbulence measurement in low-angle injection into a supersonic flow
[AD-A293836] p 2874 N95-31516
Spatially-resolved velocity measurements in steady, high-speed, reacting flows using laser-induced OH fluorescence p 2877 N95-32109

FLOW NETS
France --- modeling and verification of parallel computer systems
[PB95-208385] p 2949 N95-32371

FLOW STABILITY
Numerical simulation of time dependent viscoelastic fluid flow
[TRITA-NA-9311] p 2873 N95-31414

FLOW THEORY
Robust fixed-structure control
[AD-A292883] p 2952 N95-30961

FLOW VELOCITY
Numerical study of shear-induced heating in high-speed nozzle flow of liquid monopropellant p 2828 N95-31207
Design and testing of an oxidizer-rich preburner p 2799 N95-31212
Chaos-enhanced transport and aggregation in chaotic flows
[AD-A293892] p 3020 N95-31545
Laser anemometer measurements of the three-dimensional rotor flow field in the NASA low-speed centrifugal compressor
[NASA-TP-3527] p 2756 N95-31985

FLOW VISUALIZATION
Nearly steady flows in GONG prototype data
[NASA-CR-198935] p 2869 N95-30863
Analysis of planar laser-induced fluorescence images obtained during shakedown testing of the AEDC impulse facility
[AD-A293237] p 2884 N95-30906
Patterns in the sky: Natural visualization of aircraft flow fields
[NASA-SP-514] p 2741 N95-31000
An investigation of the side-dump dual in-line ramjet combustor p 2756 N95-31199
Enhanced energy release and soot reduction in actively controlled flames p 2799 N95-31200
Experiments in a 120-mm ram accelerator including flow visualization p 2799 N95-31202
Chaos-enhanced transport and aggregation in chaotic flows
[AD-A293892] p 3020 N95-31545

FLUENCE
Formation of cavities in Si and their chemisorption of materials
[DE95-009586] p 2980 N95-30708
Method for laser-assisted silicon etching using halocarbon ambients
[AD-D017426] p 2883 N95-30744

FLUID FILLED SHELLS
Calculations of the sound scattering from fluid-filled spherical shell sonar targets
[DSTO-RR-0020] p 2974 N95-31365

FLUID FILMS
Fluid-film lubrication with an application to piston rings p 2890 N95-32119
An efficient numerical procedure for thermohydrodynamic analysis of cavitating bearings
[NASA-CR-195476] p 2878 N95-32210
Film temperatures in the presence of cavitation
[NASA-CR-195481] p 2878 N95-32216

FLUID FLOW
Gear pump with reduced fluid-borne noise
[AD-D017362] p 2887 N95-30399
Self-adaptive multilevel methods for fluid flow problems p 2873 N95-31412
Computational methods for control and optimal design of aerospace systems
[AD-A292861] p 2751 N95-31451
Chaos-enhanced transport and aggregation in chaotic flows
[AD-A293892] p 3020 N95-31545
MPI implementation of PHOENICS: A general purpose computational fluid dynamics code
[DE95-009810] p 2877 N95-32033
The HYLIFE-2 inertial fusion energy power plant concept and implications for IFE
[DE95-010561] p 2994 N95-32074

FLUID JETS
Jet mixing in a reacting cylindrical crossflow
[NASA-TM-106975] p 2755 N95-30853
Primary atomization of liquid jets issuing from rocket engine coaxial injectors p 2769 N95-31716

FLUID MECHANICS
Electromagnetically activated compliant wavy-wall
[AD-D017340] p 2866 N95-30412
Semiannual report
[NASA-CR-198172] p 2931 N95-30657
Method and system for reducing drag on a body moving through a fluid medium
[AD-D017336] p 2867 N95-30672

FLUIDICS
Electrified microheterogeneous catalysis
[AD-D017446] p 2794 N95-31271

FLUIDIZED BED PROCESSORS
Robotic weld overlay coatings for erosion control
[DE95-009643] p 2809 N95-32098

FLUORESCENCE
Ultrasensitive fluorescence detection and photophysics in microdroplets
[DE95-010283] p 2798 N95-32086

FLUORIDES
Self-lubricating, TiN-MoS2 composite coatings produced by simultaneous deposition from Ti((CH3))2N4/NH3/MoF6H2S gas mixture
[DE95-010359] p 2788 N95-31403

FLUORINE
The one-dimensional model of the off-centre potential of the fluorine ion in the NaBr lattice
[DE95-614310] p 3010 N95-30647
Recoil longitudinal momentum spectroscopy of electron capture from He by O(7+) and F(8+)
[DE95-010823] p 2990 N95-32274

FLUORINE COMPOUNDS
Method for laser-assisted silicon etching using halocarbon ambients
[AD-D017426] p 2883 N95-30744
Laser properties of Yb(3+)-doped Sr5(PO4)3F crystals
[DE95-010686] p 3016 N95-32268

FLUOROCARBONS
Compatibility of Single Hydraulic Fluid with military specification fluids, seals and metallurgy
[AD-A292954] p 2821 N95-31683

FLUTTER
FPCAS3D User's guide: A three dimensional full potential aeroelastic program, version 1
[NASA-CR-198367] p 2899 N95-32205

FLUTTER ANALYSIS
FPCAS3D User's guide: A three dimensional full potential aeroelastic program, version 1
[NASA-CR-198367] p 2899 N95-32205

FLUX DENSITY
A general non-perturbative estimate of the energy density of lattice Hamiltonians
[DE95-616283] p 2965 N95-30435
Approximate analytic diagonalization of lattice QCD
[DE95-616332] p 3018 N95-30444
Synthesis of carbo-nitride films using high-energy shock plasma deposition
[DE95-615231] p 2811 N95-30450
TV-VI semiconductor quantum well lasers, physics and engineering p 2883 N95-30805
Mobile electric power
[AD-A292721] p 2860 N95-30940
Pulse power for high energy density physics experiments
[DE95-010888] p 2992 N95-31232
Proceedings of the high energy density matter (HEDM) contractor's conference
[AD-A292988] p 2836 N95-31470
Effects of temperature, frequency, flux density, and excitation waveform on the core loss and dynamic B-H loops of supermalloy
[NASA-TM-106982] p 2865 N95-32207

FLUXES
The 19th Annual Electronics Manufacturing Seminar
[AD-A293067] p 2863 N95-31674

FLY BY WIRE CONTROL
SCARLET: DLR rate saturation flight experiment p 2746 N95-31068
Model following control for tailoring handling qualities: ACT experience with ATTHeS p 2758 N95-32000
Digital autopilot design for combat aircraft in ALENIA p 2760 N95-32009
Advanced flight control technology achievements at Boeing Helicopters p 2761 N95-32014

FLYBY MISSIONS
Radiation effects in space: The Clementine 1 mission
[DE95-011513] p 3032 N95-32282

FOAMS
Simple model of foam spreading on liquid surfaces
[PB95-211207] p 2838 N95-30630
Urethane foam process improvements
[DE95-008957] p 2815 N95-30798
A water blown urethane insulation for use in cryogenic environments p 2775 N95-31765
Evaluation of HFC 245ca and HFC 236ea as foam blowing agents p 2775 N95-31766

FOCAL PLANE DEVICES
Inductively coupled IR staring array based on photofluxonic pixels
[AD-A292784] p 2998 N95-31435
Performance of residual carrier array-feed combining in correlated noise p 2856 N95-32232

FOCUSING
Spotsize measurements of a focused CW Nd: YAG laser
[DE95-007746] p 2884 N95-31139
IR materials producibility
[AD-A293330] p 2998 N95-31141

FOKKER-PLANCK EQUATION
Longitudinal losses of charged particles from an open configuration with arbitrary beta ratio
[DE95-614187] p 2987 N95-32055

FOLIAGE
Comparisons of target detection clutter using data from the 1993 FOPEN experiments
[AD-A293052] p 2852 N95-31606

FORCED CONVECTION
Fundamental topics in heat transfer through deformable two-phase media p 2874 N95-31532

FORCED VIBRATION
Dynamical systems as models for flow-induced vibrations
[PB95-206991] p 2869 N95-30956

FOREBODIES
Computational methods for control and optimal design of aerospace systems
[AD-A292861] p 2751 N95-31451
Flight evaluation of forebody vortex control in post-stall flight p 2752 N95-32003

FORECASTING
Clouds: Their prediction and simulation
[AD-A292864] p 2920 N95-31453

Patient/aircraft forecasting for the strategic aeromedical evacuation lift-bed process
[AD-A293902] p 2747 N95-31512
FAA aviation forecasts: Fiscal year 1995-2006
[AD-A293682] p 2741 N95-31598

FORESTS
Analysis of variation embedding tests with 17 MM dowel: Densified veneer wood FOREST project, part 7
[PB95-206876] p 2963 N95-30680
Field performance of the Walker Branch throughfall displacement experiment
[DE95-008677] p 2908 N95-30793

FORGING
Hot compression testing of tungsten
[AD-A293683] p 2807 N95-31599

FORM FACTORS
On explanation of proton electromagnetic form Factor near p (anti p)-threshold from the PS-170 experiment
[DE95-613766] p 2977 N95-30508
Unitarization of Koerner-Kuroda model of electromagnetic structure of octet 1/2(+) baryons
[DE95-613765] p 2984 N95-31548
Form factor of the process gamma(*) gamma(*) yields pi(sup 0) for small virtuality of one of the photons and QCD sum rules (2): Sum rule
[DE95-613629] p 2988 N95-32078
Search for anomalous ZZ(sub gamma) and Z(sub (gamma, gamma)) couplings with D0
[DE95-010457] p 2989 N95-32162

FORMALISM
Six-vector formalism in electromagnetics of bianisotropic media
[PB95-207130] p 2846 N95-30567
Gravitational waves from inspiralling compact binaries: Energy loss and waveform to second-post-Newtonian order
[PB95-207890] p 2913 N95-30590
On the theory of hole propagation in an antiferromagnetic background
[DE95-614469] p 3010 N95-30650
Properties of a multichannel resonant-level model
[DE95-614482] p 2979 N95-30652
The quantum interference effect in semiconductor space charge layers studied by Feynman path integrals: General formalism and illustrative examples
[DE95-614483] p 3010 N95-30653
Non-critical string field theory with non-orientable string interactions
[DE95-737160] p 3020 N95-31281
Formalization of the ramified type theory
[PB95-206785] p 2961 N95-31422

FORMING TECHNIQUES
Texture development in aluminium extrusion
[PB95-196598] p 2979 N95-30666
Gelcasting of sintered reaction-bonded silicon nitride for improved mechanical properties
[DE95-010282] p 2822 N95-32085

FORTRAN
Recommendations for developing portable parallel I/O facilities for scientific applications
[DE95-009384] p 2947 N95-30578
Hadronic production of B(sub c)-mesons
[DE95-620536] p 2983 N95-31216
Towards increased productivity of algorithm implementation
[AD-A292662] p 2940 N95-31452

FORWARD SCATTERING
The TEVA experiment cruise report
[AD-A293025] p 2923 N95-31701
A boundary integral equation approach to three dimensional electromagnetic wave scattering problems
p 2853 N95-31839

FOSSIL FUELS
Producing usable fuel from municipal solid waste
[DE95-008405] p 2902 N95-30375
Publications of the Fossil Energy Advanced Research and Technology Development Materials Program: April 1, 1993-March 31, 1995
[DE95-009200] p 2903 N95-30745

FOSSILS
Publications of the Fossil Energy Advanced Research and Technology Development Materials Program: April 1, 1993-March 31, 1995
[DE95-009200] p 2903 N95-30745

FOUR-WAVE MIXING
Photo-refractive Bi12SiO20: Spatial light modulator
[AD-A293084] p 3001 N95-32153

FOURIER ANALYSIS
Torus bundles and the group cohomology of GL(N,Z)
[PB95-208120] p 2965 N95-30489
On the degree of approximation by Jackson type operators
[DE95-613383] p 2958 N95-30821
Fourier analysis of a robust multigrid method for convection-diffusion equations
[PB95-197091] p 2958 N95-30835

FOURIER SERIES
On the degree of approximation by Jackson type operators
[DE95-613383] p 2958 N95-30821
Fourier series methods for cracks in polygonal plates and shells of revolution p 2893 N95-30825
Application of shallow shell stability to plant morphogenesis by Fourier series p 2897 N95-31734

FOURIER TRANSFORMATION
A real time method for Fourier transform holographic information storage
[AD-A293186] p 2880 N95-30980
Derivation of two-dimensional (2-D) conduction equation in generalized coordinates with constant and anisotropic physical properties
[AD-A293896] p 3020 N95-31511
Standardization of surface contamination analysis systems p 2781 N95-31798
Surface inspection using FTIR spectroscopy p 2782 N95-31803
Cleanliness evaluation of rough surfaces with diffuse IR reflectance p 2782 N95-31804
Statistical properties of chaotic scattering with one open channel
[DE95-613370] p 3020 N95-32150

FOURIER-BESSEL TRANSFORMATIONS
Apparatus and method for producing three-dimensional images
[AD-D017455] p 2847 N95-30727

FRACTALS
Analysis on fractals, laplacians on self-similar sets, noncommutative geometry and spectral dimensions
[PB95-208005] p 2956 N95-30556
Fractal quantum well heterostructures for broadband light emitters
[DE95-009579] p 2860 N95-30707
Local fractal dimension estimation
[AD-A293354] p 2959 N95-30953
Optical correlator optimizations and extensions for automated optical target recognition
[AD-A293013] p 3000 N95-31697
Newton Raphson method, scaling at fractal boundaries and mathematica
[DE95-613374] p 2962 N95-32095

FRACTOGRAPHY
Thermal-mechanical fatigue crack growth in aircraft engine materials
[ISBN-0-315-86543-1] p 2894 N95-31098
Life prediction methodology for ceramic components of advanced heat engines. Phase 1: Volume 2. Appendices
[DE95-010806] p 2817 N95-31136

FRACTURE MECHANICS
Fourier series methods for cracks in polygonal plates and shells of revolution p 2893 N95-30825
Effects of hydrostatic pressure on the mechanical behavior of composite materials
[AD-A293162] p 2787 N95-30963
Sea ice stress research
[AD-A293164] p 2923 N95-30964
Control of interfacial chemistry and mechanical properties in metal/ceramic composites p 2790 N95-31976
A numerical analysis of crack growth in microcracking ceramic and ceramic composites
[DE95-010132] p 2897 N95-32024
Simulation of fracture in compression using a field-theory model
[DE95-009874] p 2898 N95-32102
Validation of favor code linear elastic fracture solutions for finite-length flaw geometries
[DE95-009034] p 2898 N95-32157
Numerical evaluation of three-dimensional crack-tip integrals for layered anisotropic solids p 2898 N95-32191

FRACTURE STRENGTH
Room temperature fracture and high temperature creep deformation properties of alumina reinforced with 20 vol% particulate niobium
[DE95-010234] p 2815 N95-30897
Sea ice stress research
[AD-A293164] p 2923 N95-30964
Life prediction methodology for ceramic components of advanced heat engines. Phase 1: Volume 2. Appendices
[DE95-010806] p 2817 N95-31136
Cracking during nanoindentation and its use in the measurement of fracture toughness
[DE95-008839] p 2818 N95-31175
Initial survey on fracture toughness of commercial Nd2Fe14B
[DE95-009813] p 2808 N95-31643
Influence of fiber content on mechanical performance of SiC-fiber-reinforced reaction-bonded silicon nitride composites
[NASA-TM-110639] p 2790 N95-32060

FRACTURING
Life prediction methodology for ceramic components of advanced heat engines. Phase 1: Volume 2. Appendices
[DE95-010806] p 2817 N95-31136
Observations of star fracture and longitudinal splitting in BIS 812 EMA and Q1N submarine construction steels
[DSTO-RR-0014] p 2806 N95-31344
Failure analysis for polycarbonate transparencies
[AD-A292992] p 2820 N95-31471
Large deformation failure mechanisms in nonlinear solids
[AD-A293010] p 2896 N95-31474

FRAGMENTATION
Properties of new materials relevant to energy and fuel research
[AD-A289734] p 2825 N95-31149

FRAMES
Influence of adhesives and bonding techniques on the properties of glued timber-steelplate joints
[PB95-211470] p 2813 N95-30599
Nonlinear dynamics and chaotic motions of a singularly perturbed nonlinear viscoelastic beam p 2897 N95-31706

FREDHOLM EQUATIONS
Existence of solutions in plane quasistationary stokes flow driven by surface tension
[PB95-197935] p 2868 N95-30810

FREE BOUNDARIES
Existence of solutions in plane quasistationary stokes flow driven by surface tension
[PB95-197935] p 2868 N95-30810
Selected flows with free surfaces: Streams and drops
[IFTR-3/1995] p 2876 N95-31817

FREE CONVECTION
Fundamental topics in heat transfer through deformable two-phase media p 2874 N95-31532

FREE ELECTRON LASERS
Free electron laser as energy driver for inertial confinement fusion
[DE95-614252] p 2884 N95-30914
Harmonic gyrotron amplifiers and phase-locked oscillators
[AD-A293185] p 2861 N95-30979
Prime power for shipboard high-average power FELs
[AD-A293718] p 2886 N95-31833

FREE ELECTRONS
Selected problems of the identification of weak double layers in plasma on a background of different aperiodic non-collision structures
[IFTR-4/1995] p 3006 N95-31737

FREE ENERGY
The topological string associated with a simple singularity of type D
[DE95-737229] p 2983 N95-31225

FREE MOLECULAR FLOW
The passage from transitional to free molecular plumes p 2871 N95-30994

FREE VIBRATION
New Fermi-liquid approach for the theory of disordered magnetics
[DE95-613448] p 2967 N95-30739
Finite element analysis of damped vibrations of laminated composite plates
[ISBN-0-315-84928-2] p 2789 N95-31731

FREEZING
Study of melting and freezing processes of water for application to ice thermal energy storage system p 2905 N95-31735

FREQUENCIES
Noise signal processor
[AD-D017430] p 2974 N95-30747
Statistical interface for chaotic signal in noise
[AD-A290271] p 2848 N95-30932
Inverse and control problems in electromagnetics
[AD-A292993] p 2849 N95-30962
PIO: A historical perspective p 2745 N95-31062
Use of a variable frequency source with a single-mode cavity to process ceramic filaments
[DE95-010992] p 2817 N95-31152
Effects of temperature, frequency, flux density, and excitation waveform on the core loss and dynamic B-H loops of supermalloy
[NASA-TM-106982] p 2865 N95-32207
Custom Turnkey Time and Frequency Systems: A structured, expandable approach p 2969 N95-32330

FREQUENCY DISTRIBUTION
Fiber optic reference frequency distribution to remote beam waveguide antennas p 2972 N95-32346

FREQUENCY MEASUREMENT
Optical frequency standards: Hertz-level working standards and their absolute frequency measurement
[AD-A293930] p 2999 N95-31515

FREQUENCY MODULATION
Degradation in finite-harmonic subcarrier demodulation p 2855 N95-32228

FREQUENCY RANGES
Handling qualities analysis on rate limiting elements in flight control systems p 2746 N95-31071
FREQUENCY RESPONSE
Advanced system identification techniques for wind turbine structures
[DE95-004049] p 2902 N95-30505
Radiometer measurements of sea ice in the Gulf of Bothnia 1992
[PB95-206611] p 2900 N95-30718
Handling qualities analysis on rate limiting elements in flight control systems p 2746 N95-31071
Calspan experience of PIO and the effects of rate limiting p 2746 N95-31072
FREQUENCY SHIFT
Acousto-optical frequency shifters in dual-core optical fibres
[AD-A293979] p 2999 N95-31529
FREQUENCY STABILITY
Digital signal processing in the radio science stability analyzer p 2857 N95-32240
Review of longitudinal perturbation formalism
[DE95-010894] p 2990 N95-32278
A globally efficient means of distributing UTC time and frequency through GPS p 2970 N95-32335
Monte Carlo simulations of precise timekeeping in the Milstar communication satellite system p 2970 N95-32336
Automated delay measurement system for an Earth station for Two-Way Satellite Time and Frequency Transfer p 2971 N95-32337
Prospects for high accuracy time dissemination and synchronization using coded radar pulses from a low-earth orbiting spacecraft p 2971 N95-32339
Metafitting: Weight optimization for least-squares fitting of PTTI data p 2971 N95-32340
Methodologies for steering clocks p 2971 N95-32341
The effects of clock errors on timescale stability p 2971 N95-32342
Relativistic theory for syntonization of clocks in the vicinity of the Earth p 2971 N95-32343
FREQUENCY STANDARDS
Optical frequency standards: Hertz-level working standards and their absolute frequency measurement
[AD-A293930] p 2999 N95-31515
The 26th Annual Precise Time and Time Interval (PTTI) Applications and Planning Meeting
[NASA-CP-3302] p 2967 N95-32319
The 1994 international transatlantic two-way satellite time and frequency transfer experiment: Preliminary results p 2858 N95-32320
High accuracy time transfer synchronization p 2968 N95-32321
European plans for new clocks in space p 2968 N95-32324
High resolution time interval counter p 2969 N95-32331
Investigation into the effects of VHF and UHF band radiation on Hewlett-Packard (HP) Cesium Beam Frequency Standards p 2970 N95-32332
The Deep Space Network stability analyzer p 2858 N95-32334
A globally efficient means of distributing UTC time and frequency through GPS p 2970 N95-32335
Metafitting: Weight optimization for least-squares fitting of PTTI data p 2971 N95-32340
Methodologies for steering clocks p 2971 N95-32341
Allan deviation computations of a linear frequency synthesizer system using frequency domain techniques p 2972 N95-32344
SVN 9 End-Of-Life testing p 2767 N95-32345
Fiber optic reference frequency distribution to remote beam waveguide antennas p 2972 N95-32346
FREQUENCY SYNCHRONIZATION
Relativistic theory for syntonization of clocks in the vicinity of the Earth p 2971 N95-32343
FREQUENCY SYNTHESIZERS
Allan deviation computations of a linear frequency synthesizer system using frequency domain techniques p 2972 N95-32344
FRICTION
Simple model of foam spreading on liquid surfaces
[PB95-211207] p 2838 N95-30630
Evaluation of alternative pavement marking materials
[AD-A292973] p 2763 N95-31468
FRONTS (METEOROLOGY)
A numerical study of the effect of the Gulf Stream and the Appalachian Mountains on Carolina coastal frontogenesis
[AD-A293765] p 2921 N95-31577
FRUSTRATION
Evaluation of calibration parameters and performance of the video imaging technique of assessing exposure (VITAE system)
[AD-A289023] p 2927 N95-30998
FUEL CELLS
Electrochemical vapour deposition of SOFC interconnection materials
[PB95-197844] p 2812 N95-30459
Mobile electric power
[AD-A292721] p 2860 N95-30940
Prospector 7: Small fuel cells for portable power workshop
[AD-A292729] p 2904 N95-30947
FUEL COMBUSTION
Preliminary assessment of combustion modes for internal combustion wave rotors
[NASA-TM-107000] p 2754 N95-30632
An investigation of the side-dump dual in-line ramjet combustor p 2756 N95-31199
Enhanced energy release and soot reduction in actively controlled flames p 2799 N95-31200
A pulsed liquid fuel ramjet p 2756 N95-31201
Experiments in a 120-mm ram accelerator including flow visualization p 2799 N95-31202
Numerical simulation of ram accelerator performance including transient effects during initiation of combustion and sensitivity studies p 2799 N95-31203
Spectral element method for numerical simulation of unsteady laminar diffusion flames p 2794 N95-31333
FUEL CONSUMPTION
Wave rotor-enhanced gas turbine engines
[NASA-TM-106998] p 2754 N95-30517
FUEL INJECTION
An investigation of the side-dump dual in-line ramjet combustor p 2756 N95-31199
Enhanced energy release and soot reduction in actively controlled flames p 2799 N95-31200
A pulsed liquid fuel ramjet p 2756 N95-31201
Numerical simulation of ram accelerator performance including transient effects during initiation of combustion and sensitivity studies p 2799 N95-31203
Numerical study of shear-induced heating in high-speed nozzle flow of liquid monopropellant p 2828 N95-31207
Atomization simulations using an Eulerian-VOF-Lagrangian method p 2828 N95-31210
Design and testing of an oxidizer-rich preburner p 2799 N95-31212
Primary atomization of liquid jets issuing from rocket engine coaxial injectors p 2769 N95-31716
Combustion response to acoustic perturbation in liquid rocket engines p 2770 N95-31972
FUEL PRODUCTION
BioFacts: Fueling a stronger economy, thermochemical conversion of biomass
[DE94-006866] p 2905 N95-31822
FUEL SPRAYS
Experimental investigation of turbulent particle dispersion in swirling flows
[DLR-FB-94-20] p 2873 N95-31355
FUEL SYSTEMS
Prospector 7: Small fuel cells for portable power workshop
[AD-A292729] p 2904 N95-30947
FUELS
Prospector 7: Small fuel cells for portable power workshop
[AD-A292729] p 2904 N95-30947
Fuel-type classification and parameters prediction by Gas Liquid Chromatography analysis
[AD-A293442] p 2794 N95-31368
Natural gas liquefier for vehicle fuel
[AD-A293619] p 2836 N95-31564
FULL SCALE TESTS
Generation of earthquake signals
[PB95-211223] p 2913 N95-30631
FULLERENES
Studies of C(60) and C(70) and other fullurenes: Synthesis, derivation, electrochemistry, lubricant properties and new composition materials
[AD-A292726] p 3012 N95-30944
Materials with controllable signature properties
[PB95-222964] p 2857 N95-32313
Superconducting and normal-state properties of novel materials
[DE95-012368] p 3017 N95-32366
FUNCTION GENERATORS
Voltage controlled MESFET pulse shape generator
[DE95-011656] p 2865 N95-32300
FUNCTION SPACE
Local index formula in noncommutative geometry
[PB95-208146] p 2955 N95-30490
FUNCTIONAL ANALYSIS
Enhancements to the SSME transfer function modeling code
[NASA-CR-198957] p 2958 N95-30754
FUNCTIONALS
Some functional solutions of the Yang-Baxter equation
[DE95-613584] p 2966 N95-30635
FUNCTIONS (MATHEMATICS)
On the degree of approximation by Jackson type operators
[DE95-613383] p 2958 N95-30821
FUSELAGES
Development of stitched/RTM primary structures for transport aircraft
[NASA-CR-191441] p 2789 N95-31421
Preparation of S-70A-9 Black Hawk helicopter for flight tests to investigate cause of cracking of inner fuselage panel
[AD-A293891] p 2752 N95-31544
FUSION REACTORS
Development of a tokamak plasma optimized for stability and confinement
[DE95-009609] p 3003 N95-30641
Development of plasma diagnostics technologies: A study on nuclear fusion reactor
[DE95-614180] p 3005 N95-31004
Workshop on transport for a common ion driver
[DE95-007298] p 2992 N95-31166
The development of the tokamak system technology: A study on the fusion reactor
[DE95-614256] p 3005 N95-31366
Design study of prototype accelerator and MeV test facility for demonstration of 1 MeV, 1 A negative ion beam production
[DE95-737208] p 2995 N95-32262
Development of integrated insulation joint for cooling pipe in tokamak reactor
[DE95-737220] p 3007 N95-32264
FUZZY SETS
Analysis of the final result from the image template matching method with fuzzy logic
[PB95-222915] p 2946 N95-32311
FUZZY SYSTEMS
Evaluation of the techniques of fuzzy control for the piloting an aircraft p 2758 N95-31997
Analysis of the final result from the image template matching method with fuzzy logic
[PB95-222915] p 2946 N95-32311

G

GALACTIC COSMIC RAYS
Radiation effects in space: The Clementine 1 mission
[DE95-011513] p 3032 N95-32282
GALACTIC EVOLUTION
Large scale periodicity of the universe and baryogenesis
[DE95-613461] p 3028 N95-30366
GALERKIN METHOD
Potential integral equations of the 2D Laplace operator in wavelet basis
[TRITA-NA-9401] p 2957 N95-30713
GALLIUM
Conjugated aromatic polyimines. 2. Synthesis, structure, and properties of new aromatic polyazomethines
[AD-A292955] p 2819 N95-31461
GALLIUM ARSENIDES
Magnetoluminescence characterization of quantum well structures
[DE95-008527] p 3008 N95-30381
NIR High-efficiency subwavelength diffractive structures in semiconductors
[DE95-008535] p 3008 N95-30391
The junction characteristics and current conduction mechanisms of GaInP2 n(+)p diodes and solar cells
[AD-A290857] p 2902 N95-30408
Finite element simulation of GaAs MESFET's
[PB95-208062] p 3009 N95-30485
Semiconductor nanocrystals formed in SiO2 by ion implantation
[DE95-008900] p 2978 N95-30546
Direct sublattice imaging of interface dislocation structures in CdTe/GaAs(001)
[DE95-009031] p 3010 N95-30576
Vertical transport in GaAs/AlGaAs superlattices p 3012 N95-30822
New material for high average power infrared generation: QPM-DB GaAs
[AD-A292714] p 2967 N95-30939
Opto-electronic components from non-stoichiometric 3-5 materials
[AD-A293206] p 3013 N95-30985
Self-consistent, 2D simulations of filament propagation in photoconducting switches
[DE95-010794] p 2961 N95-31133

Carrier dynamics and optical properties of GaAs- and InP-based strained quantum well lasers
p 2886 N95-31848
Investigation of the basic physics of high efficiency semiconductor hot carrier solar cell
[NASA-CR-198945] p 2906 N95-32212

GALLIUM COMPOUNDS
Langasite crystals growth with quality factor Q, that exceeds the Q of quartz, and which are suitable for high-precision resonators
[AD-A293397] p 3013 N95-30969

GALLIUM NITRIDES
Hydrogen diffusion and passivation in InGaAlN alloys
[DE95-010689] p 2806 N95-31150
Pseudomorphic heterostructure materials for high performance devices
[AD-A292906] p 2788 N95-31384
Degradation of blue AlGaN/InGaN/GaN LEDs subjected to high current pulses
[DE95-008824] p 2863 N95-31611

GALLIUM PHOSPHIDES
The junction characteristics and current conduction mechanisms of GaInP2 n(+)p diodes and solar cells
[AD-A290857] p 2902 N95-30408

GAME THEORY
Structural design using equilibrium programming formulations
[NASA-TM-110175] p 2893 N95-30682

GAMMA RAY ASTRONOMY
Observations of accreting pulsars
[NASA-CR-198931] p 3028 N95-30469

GAMMA RAY BURSTS
Studying the thermal/non-thermal crossover in solar flares
[NASA-CR-189436] p 3031 N95-30785

GAMMA RAY LASERS
Basic study of the pumping of a gamma-ray laser
[AD-A293561] p 2886 N95-31563

GAMMA RAY OBSERVATORY
Studying the thermal/non-thermal crossover in solar flares
[NASA-CR-189436] p 3031 N95-30785

GAMMA RAY SPECTRA
Observations of accreting pulsars
[NASA-CR-198931] p 3028 N95-30469
Holistic analysis of gamma-ray spectra in instrumental neutron activation analysis
[PB95-214458] p 2979 N95-30639

GAMMA RAYS
Computer vision for detecting and quantifying gamma-ray sources in coded-aperture images
[DE95-008810] p 2900 N95-30472
Studying the thermal/non-thermal crossover in solar flares
[NASA-CR-189436] p 3031 N95-30785
Basic study of the pumping of a gamma-ray laser
[AD-A293561] p 2886 N95-31563
Search for anomalous ZZ(sub gamma) and Z(sub (gamma, gamma)) couplings with D0
[DE95-010457] p 2989 N95-32162

GAS ANALYSIS
Micromachined sensor and actuator research at the Microelectronics Development Laboratory
[DE95-008540] p 2878 N95-30384
Hydrogen sulfide analyzer with protective barrier
[AD-D017412] p 2793 N95-31009
Experiments in a 120-mm ram accelerator including flow visualization p 2799 N95-31202
Fuel-type classification and parameters prediction by Gas Liquid Chromatography analysis
[AD-A293442] p 2794 N95-31368
Novel mass spectrometric instrument for gaseous and particulate characterization and monitoring
[DE95-000047] p 2881 N95-31694

GAS CHROMATOGRAPHY
Specific rate coefficients from vibrational overtone activation of 1-methylcyclopropene
[AD-A288755] p 2793 N95-31014
Fuel-type classification and parameters prediction by Gas Liquid Chromatography analysis
[AD-A293442] p 2794 N95-31368
Analytical instrumentation for environmental research
[AD-A292832] p 2908 N95-31447

GAS DETECTORS
Experimental characterisation of gas microstrip detectors. Part 3: Lifetime characteristics
[PB95-192845] p 2880 N95-30691
Development of a new instrument for rocket engine combustion diagnostics p 2799 N95-31211
The development of a pulsed laser imaging system for natural gas leak detection
[DE95-011407] p 2887 N95-32280

GAS DISCHARGES
Synthesis of carbo-nitride films using high-energy shock plasma deposition
[DE95-615231] p 2811 N95-30450

GAS DYNAMICS
Numerical simulation of ram accelerator performance including transient effects during initiation of combustion and sensitivity studies p 2799 N95-31203
Atomization simulations using an Eulerian-VOF-Lagrangian method p 2828 N95-31210

GAS EXPANSION
Properties of a multichannel resonant-level model
[DE95-614482] p 2979 N95-30652

GAS FLOW
State resolved dynamics of ion-molecule collisions in a flowing afterglow
[AD-A290895] p 2976 N95-30410
Kinetic theory model predictions compared with low-thrust axisymmetric nozzle plume data
[NASA-CR-198934] p 2768 N95-30864

GAS GENERATORS
A numerical model for dynamic wave rotor analysis
[NASA-TM-106997] p 2754 N95-30617
Preliminary assessment of combustion modes for internal combustion wave rotors
[NASA-TM-107000] p 2754 N95-30632

GAS INJECTION
Enhanced energy release and soot reduction in actively controlled flames p 2799 N95-31200

GAS IONIZATION
Kinematical threshold of recoil-ion longitudinal momentum distribution in single ionization of helium by protons and alpha particles
[DE95-010803] p 2990 N95-32271
Ionization of He by highly charged ions at low velocity
[DE95-010815] p 2990 N95-32273
Recoil longitudinal momentum spectroscopy of electron capture from He by O(7+) and F(8+)
[DE95-010823] p 2990 N95-32274

GAS JETS
An experimental study of planar heterogeneous supersonic confined jets
[AD-A290859] p 2867 N95-30557
Hot jet/wake turbulent structure and laser propagaion. Part 1: Jet/wake turbulence modeling
p 2871 N95-30991

GAS MIXTURES
Investigation of ram accelerator performance capabilities p 2799 N95-31204
Evaluation of halon alternatives in inerting experiments
[AD-A293774] p 2795 N95-31580

GAS PRESSURE
Shuttle redesigned solid rocket motor aluminum oxide investigations p 2770 N95-30989
Shuttle Redesigned Solid Rocket Motor aluminum oxide investigations p 2770 N95-31197
Fourier Transform (FT) Raman spectroscopy of nitrogen at high pressure
[AD-A293051] p 2796 N95-31670

GAS STREAMS
CO2 (dry ice) cleaning system p 2778 N95-31785

GAS TEMPERATURE
Advanced oxidizers diffusion flames structure
p 2801 N95-31307

GAS TUNGSTEN ARC WELDING
Hydrogen absorption in iron and steel during gas tungsten arc welding
[PB95-197018] p 2804 N95-30776
Residual stress distribution in FeAl weld overlay on steel
[DE95-009178] p 2899 N95-32317

GAS TURBINE ENGINES
Wave rotor-enhanced gas turbine engines
[NASA-TM-106998] p 2754 N95-30517
Object-oriented approach for gas turbine engine simulation
[NASA-TM-106970] p 2754 N95-30594
A numerical model for dynamic wave rotor analysis
[NASA-TM-106997] p 2754 N95-30617
Preliminary assessment of combustion modes for internal combustion wave rotors
[NASA-TM-107000] p 2754 N95-30632
Jet mixing and emission characteristics of transverse jets in annular and cylindrical confined crossflow
[NASA-TM-106976] p 2755 N95-30698
Thermal-mechanical fatigue crack growth in aircraft engine materials
[ISBN-0-315-86543-1] p 2894 N95-31098
Advanced turbine systems program conceptual design and product development
[DE95-000088] p 2890 N95-32163

GAS TURBINES
Achieving improved cycle efficiency via pressure gain combustors
[DE95-008945] p 2792 N95-30762
Jet mixing in a reacting cylindrical crossflow
[NASA-TM-106975] p 2755 N95-30853
Prime power for shipboard high-average power FELs
[AD-A293718] p 2686 N95-31833

GAS-ION INTERACTIONS
State resolved dynamics of ion-molecule collisions in a flowing afterglow
[AD-A290895] p 2976 N95-30410

GAS-LIQUID INTERACTIONS
Atomization simulations using an Eulerian-VOF-Lagrangian method p 2828 N95-31210

GASEOUS DIFFUSION
Network user's guide
[DE95-009185] p 2942 N95-31634

GASES
Tunable composite membranes for gas separations
[DE95-010602] p 2822 N95-32075

GASIFICATION
BioFacts: Fueling a stronger economy, thermochemical conversion of biomass
[DE94-006866] p 2905 N95-31822

GAUGE INVARIANCE
What's wrong with anomalous chiral gauge theory?
[DE95-616285] p 3018 N95-30437
Chiral gauge theory in four dimensions
[DE95-616288] p 3018 N95-30440
Equivalence of two non-commutative geometry approaches
[DE95-613469] p 2957 N95-30642
Recoil correction in the Dirac-Coulomb problem
[DE95-619241] p 2959 N95-31137
Instability of weak vacuum
[DE95-613590] p 2985 N95-31620
Electroweak flavor-conserving gauge processes: Virtual effects
[DE95-009922] p 3020 N95-32106

GAUGE THEORY
A general non-perturbative estimate of the energy density of lattice Hamiltonians
[DE95-616283] p 2965 N95-30435
Two-loop vacuum amplitudes in a non-Abelian gauge theory on S(sub 4)
[DE95-616284] p 3018 N95-30436
What's wrong with anomalous chiral gauge theory?
[DE95-616285] p 3018 N95-30437
Chiral gauge theory in four dimensions
[DE95-616288] p 3018 N95-30440
Research progress report
[DE95-010726] p 3030 N95-32269

GEAR TEETH
Gear pump with reduced fluid-borne noise
[AD-D017362] p 2887 N95-30399

GEARS
Gear pump with reduced fluid-borne noise
[AD-D017362] p 2887 N95-30399

GELS
Composite polymer electrolyte for lithium batteries
[AD-A293924] p 2820 N95-31514

GENERAL AVIATION AIRCRAFT
Annual review of aircraft accident data: US general aviation calendar year 1993
[PB95-215828] p 2747 N95-31712
Special investigation report: Safety of the air tour industry in the United States
[PB95-917004] p 2748 N95-32185

GENETIC ALGORITHMS
Application of a genetic algorithm to optimize staffing levels in software development
[AD-A293725] p 2943 N95-31835

GEOCENTRIC COORDINATES
A feedback linearization approach to orbital maneuvers p 2765 N95-30841

GEOCHEMISTRY
Laboratory simulated hydrothermal alteration of sedimentary organic matter from Guaymas Basin, Gulf of California
[NASA-CR-198951] p 2914 N95-30865

GEODESIC LINES
On drawing complicated 3D surfaces
[DE95-619199] p 2939 N95-31257

GEODESY
Digital Mapping Charting and Geodesy Analysis Program technical review of Vector Product Format (VPF)
[AD-A289766] p 2901 N95-31390
PTTI applications at the limits of GPS
p 2969 N95-32327

GEODETIC SURVEYS
Visit to Ionospheric Modeling and Remote Sensing Branch, Phillips Laboratory in Hanscom AFB, MA
[AD-A292339] p 2901 N95-31265
Digital Mapping Charting and Geodesy Analysis Program technical review of Vector Product Format (VPF)
[AD-A289766] p 2901 N95-31390

GEOGRAPHIC DISTRIBUTION
FISHFINDE: Interactive software package to predict fish locations using satellite image data and fish species behavior rules
[AD-A293394] p 2935 N95-30968

GEOGRAPHIC INFORMATION SYSTEMS
An overview of high-speed networking for workstations
[DE95-009076] p 2947 N95-30577
FISHFINDE: Interactive software package to predict fish locations using satellite image data and fish species behavior rules
[AD-A293394] p 2935 N95-30968
Brief review of remote sensing literature pertaining to classification and geostatistics
[AD-A290932] p 2901 N95-31156
Management, visualization, and analysis of environmental and geotechnical data
[DE95-000063] p 3026 N95-31823

GEOLOGICAL FAULTS
Studies in marine tectonics: Propagating rifts, depth anomalies and subduction zone anisotropy
p 2923 N95-31719

GEOLOGY
Directory of global environmental sciences in Japan
p 2899 N95-31413

GEOMAGNETIC TAIL
Study of cross-tail current carriers in magnetotail
p 3005 N95-30804
Analysis of plasma measurements for the Geotail mission
[NASA-CR-199074] p 3032 N95-32218

GEOMAGNETISM
Kiruna geophysical data. Data summary 94/4-6, April-June 1994
[PB95-210365] p 2913 N95-30627
Kiruna geophysical data. Data summary 94/1-3, January-March 1994
[PB95-210373] p 2913 N95-30628
Low-latitude boundary layer near noon: An open field line model
[ATR-93(7270)-1] p 2914 N95-30773
Study of cross-tail current carriers in magnetotail
p 3005 N95-30804
Environmental conditions responsible for solar activity
[AD-A292859] p 3031 N95-31450
Underdense heating of the ionosphere using oblique high power HF radiowaves p 2917 N95-31951

GEOMETRICAL OPTICS
Physical optics polarization scattering matrix for a right-angle dihedral
[AD-A293036] p 3000 N95-31665

GEOMETRY
Local index formula in noncommutative geometry
[PB95-208146] p 2955 N95-30490

GEOPHYSICS
Kiruna geophysical data. Data summary 94/4-6, April-June 1994
[PB95-210365] p 2913 N95-30627
Kiruna geophysical data. Data summary 94/1-3, January-March 1994
[PB95-210373] p 2913 N95-30628
Solar-geophysical data number 604, December 1994. Part 2: (Comprehensive reports). Data for June 1994, and miscellaneous
[PB95-191995] p 3031 N95-30690
Development of the Multi-Level Seismic Receiver (MLSR)
[DE95-008823] p 2916 N95-31610

GEOSYNCHRONOUS ORBITS
Time aspects of the European Complement to GPS: Continental and transatlantic experimental phases
p 2969 N95-32328

GEOTHERMAL ENERGY CONVERSION
Data on development of new energy technologies
[DE95-764135] p 2904 N95-31155

GEOTHERMAL RESOURCES
Sleeping renewable beauty: Will the prince ever come
[PB95-214573] p 2903 N95-30640

GEOTHERMAL TECHNOLOGY
Sleeping renewable beauty: Will the prince ever come
[PB95-214573] p 2903 N95-30640

GERMANATES
Germanate glass ceramic
[AD-D017418] p 2816 N95-31011

GERMANIUM
Development of germanium-silicon growth technology
[AD-A293199] p 3013 N95-30983

GERMANIUM ALLOYS
Amorphization threshold in Si-implanted strained SiGe alloy layers
[DE95-008901] p 2804 N95-30797
Comprehensive research on the stability and electronic properties of a-Si:H and a-SiGe:H alloys and devices
[DE95-004088] p 2810 N95-32154

GERMANY
Psychological pilot selection in the US Air Force, the Luftwaffe, and the German Aerospace Research Establishment
[AD-A293779] p 2928 N95-31376

GIANT STARS
Chromospherically active stars. 6: Giants with compact hot companions and the barium star scenario
[NASA-TM-110641] p 3028 N95-30466

GLASS
Ion implantation and thermal stress resistance of ceramics
[DE95-615349] p 2812 N95-30451
State-of-the-art low-cost solar reflector materials
[DE95-000260] p 2902 N95-30526
Ionic conductivities of lithium phosphorus oxynitride glasses, polycrystals, and thin films
[DE95-008898] p 2812 N95-30545
A Monte-Carlo model of ionic transport across a solid interface
[DE95-613447] p 3011 N95-30737
Simulation of viscous sintering
[PB95-197109] p 2868 N95-30836
Picosecond phase conjugation: New applications, devices, and materials
[AD-A293195] p 3013 N95-30982
Glass matrix doped with activated luminescent nanocrystalline particles
[AD-D017416] p 2816 N95-31010
Germanate glass ceramic
[AD-D017418] p 2816 N95-31011
High strain rate properties and constitutive modeling of glass
[DE95-008434] p 2816 N95-31058
Nonlinear optics in novel composite media
[AD-A293886] p 2999 N95-31542
Whisker reinforced glass ceramic
[DE95-010542] p 2823 N95-32305

GLASS FIBER REINFORCED PLASTICS
Interfacial studies of coated fiber reinforced glass-ceramic matrix composites
[AD-A290780] p 2783 N95-30433

GLASS FIBERS
Technique to prepare high-reflectance optical fiber Bragg gratings with single exposure in-line or fiber draw tower
[AD-D017445] p 2998 N95-31270

GLASSY CARBON
Structural investigation of xenon ion-beam-irradiated glassy carbon
[DE95-616777] p 2977 N95-30474

GLINT
Point reflector model for the simulation of radar target glint and Doppler phenomena
[PB95-222980] p 2857 N95-32314

GLOBAL POSITIONING SYSTEM
Signal-processing theory for the TurboRogue receiver
[NASA-CR-198882] p 2846 N95-30581
Flight test evaluation of the Stanford University/United Airlines differential GPS Category 3 automatic landing system
[NASA-TM-110354] p 2743 N95-30788
Guidelines for the design of GPS and LORAN receiver controls and displays
[AD-A293753] p 2749 N95-31572
Fine tuning GPS clock estimation in the MCS
p 2968 N95-32322
Implementation of a standard format for GPS common view data p 2968 N95-32323
Time activities at the BIPM p 2968 N95-32325
PTTI applications at the limits of GPS
p 2969 N95-32327
Time aspects of the European Complement to GPS: Continental and transatlantic experimental phases
p 2969 N95-32328
Network time synchronization servers at the US Naval Observatory p 2969 N95-32329
A globally efficient means of distributing UTC time and frequency through GPS p 2970 N95-32335
Study of tropospheric correction for intercontinental GPS common-view time transfer p 2971 N95-32338
SVN 9 End-Of-Life testing p 2767 N95-32345
Laser retroreflector experiment on NAVSTAR 35 and 36 p 2887 N95-32347
(T2L2) Time Transfer by Laser Link
p 2887 N95-32348

GLOBAL WARMING
Economical analysis relating to the global warming issue
[DE95-764072] p 2908 N95-30677
Biomass production by fescue and switchgrass alone and in mixed swards with legumes
[DE95-009137] p 2909 N95-31612
Atmospheric environmental implications of propulsion systems p 2771 N95-31747
BioFacts: Fueling a stronger economy, global warming and biofuels emissions
[DE94-006864] p 2910 N95-31821

GLONASS
The 26th Annual Precise Time and Time Interval (PTTI) Applications and Planning Meeting
[NASA-CP-3302] p 2967 N95-32319

GLUCOSE
Biosensors based on cross-linking of biotinylated Glucose Oxidase by avidin
[AD-A290439] p 2925 N95-30452

GLUES
Influence of adhesives and bonding techniques on the properties of glued timber-steelplate joints
[PB95-211470] p 2813 N95-30599

GLUONS
Theoretical high energy physics
[DE95-003107] p 2991 N95-30527
A measurement of quark and gluon jet differences at the Z(sup 0) resonance
[DE95-010666] p 2989 N95-32266
Charm photoproduction dynamics
[DE95-009106] p 2990 N95-32303
Thermal rho's in the quark-gluon plasma
[DE95-009543] p 3008 N95-32357

GOES SATELLITES
Solar-geophysical data number 606, February 1995. Part 2: (Comprehensive reports). Data for August 1994, and miscellaneous
[PB95-200861] p 3031 N95-30817

GOLD
Optimization of a thermoelectric IR-detector for low working temperature
[NASA-CR-198933] p 2880 N95-30752
Electron transfer kinetics of self-assembled ferrocene C(12) alkanethiol monolayers on gold electrodes from 125K to 175K
[AD-A292754] p 2984 N95-31427
Observation of intensity dependent losses in Au(15+) beams
[DE95-010845] p 2987 N95-32032

GOODNESS OF FIT
A new goodness-of-fit test for the gamma distribution based on sample spacings from complete and censored samples
[AD-A293875] p 2961 N95-31518

GOVERNMENT PROCUREMENT
Quality assurance tendering and awarding contracts
[PB95-197760] p 2891 N95-31362
A case study of the teaming concept in the procurement of the V-22 aircraft
[AD-A293770] p 2752 N95-31578
Report to the Secretary of Defense. Acquisition reform: Comparison of Army's commerical helicopter buy and private sector buys
[GAO/NSIAD-95-54] p 3021 N95-31659
Report to Congressional Committees. Military airlift: C-17 settlement is not a good deal
[GAO/NSIAD-94-141] p 2741 N95-32198

GOVERNMENT/INDUSTRY RELATIONS
A case study of the teaming concept in the procurement of the V-22 aircraft
[AD-A293770] p 2752 N95-31578
Development of a CFC Critical Area Response (CAR) package p 2783 N95-31814
Report to the Vice Chairman, Joint Economic Committee, US Congress. Technology transfers: Benefits of cooperative R and D agreements
[GAO/RCED-95-52] p 3027 N95-32201

GRADIENTS
Phase object display by using acousto-optical Bragg diffraction
[AD-A293153] p 2998 N95-31006

GRAIN BOUNDARIES
Direct determination of grain boundary atomic structure in SrTiO3
[DE95-008847] p 3010 N95-30544
Spectral response of a polycrystalline silicon solar cell
[DE95-614370] p 2903 N95-30723
Mechanisms of enhanced ionic conduction at interfaces in ceramics
[DE95-009125] p 2814 N95-30730
The 10th International Conference on the Strength of Materials
[AD-A292335] p 2994 N95-31263
Modeling of grain boundary stresses in Alloy 600
[DE95-009033] p 2808 N95-31825

GRAIN SIZE
Spectral response of a polycrystalline silicon solar cell
[DE95-614370] p 2903 N95-30723
Physical modelling of microstructural evolution during thermomechanical processing of aluminium alloys
[PB95-196341] p 2805 N95-31053
The effect of grain refinement on the room-temperature ductility of as-cast Fe3Al-based alloys
[DE95-010121] p 2805 N95-31107

Rationale and summary of methods for determining ultrasonic properties of materials at Lawrence Livermore National Laboratory
[DE95-009475] p 2795 N95-31593
Modeling of stress distributions on the microstructural level in Alloy 600
[DE95-009135] p 2807 N95-31632
A study of switching behavior in Pb(Zr,Ti)O3 thin films using x-ray diffraction
[DE95-010859] p 2808 N95-31689
The influence of matrix microstructure and temperature on cyclic deformation and fatigue of particle-reinforced 2219 aluminum p 2808 N95-31974
On the possibility of a two-state magnetic structure for nanocrystalline chromium
[DE95-009914] p 3015 N95-32062

GRAPH THEORY
Periodically Specified Problems: An Exponential Complexity Gap Between Exact and Approximate Solutions
[DE95-009435] p 2934 N95-30603
Compact location problems with budget and communication constraints
[DE95-010676] p 2948 N95-32277

GRAPHICAL USER INTERFACE
A graphical programming language for service robots in semi-structured environments p 2935 N95-30831
Planning board generator. Part 1: Problem instances and types
[PB95-197075] p 3021 N95-30834
Geometric modeling for computer aided design
[NASA-CR-198828] p 2943 N95-31982

GRAPHITE
Effects of particle fueling and plasma wall interactions on D3-D discharges
[DE95-009608] p 3003 N95-30612
Intermodulation Interference (IMI) testing of composite materials
[AD-A288621] p 2787 N95-31146
Self-lubricating, TiN-MoS2 composite coatings produced by simultaneous deposition from Ti((CH3))2N4/NH3/MoF6H2S gas mixture
[DE95-010359] p 2788 N95-31403
Effects of mosaicity on Parametric X-Radiation production
[AD-A293677] p 2985 N95-31597

GRAPHITE-EPOXY COMPOSITES
An evaluation of the Iosipescu specimen for composite materials shear property measurement
[NASA-CR-198755] p 2896 N95-31418

GRAPHITE-POLYIMIDE COMPOSITES
Evaluation of static strength of T800H/PMR-15 carbon/polyimide laminates at room temperature and 300 C
[NAL-TR-1254] p 2789 N95-31740

GRAPHS (CHARTS)
Periodically Specified Problems: An Exponential Complexity Gap Between Exact and Approximate Solutions
[DE95-009435] p 2934 N95-30603

GRATINGS (SPECTRA)
Extended tuning range semiconductor lasers with sampled gratings p 2883 N95-30498
Integrated X-ray testing of the electro-optical breadboard model for the XMM reflection grating spectrometer
[DE95-008829] p 2879 N95-30507
Laser-induced holographic surface relief gratings on nonlinear optical polymer films
[AD-A293169] p 2997 N95-30973
Polarized laser induced holographic surface relief gratings on polymer films
[AD-A293275] p 2817 N95-31126

GRAVIMETRY
Visit to Ionospheric Modeling and Remote Sensing Branch, Phillips Laboratory in Hanscom AFB, MA
[AD-A292339] p 2901 N95-31265
Investigation of cleanliness verification techniques for rocket engine hardware p 2770 N95-31806

GRAVITATION
Field performance of the Walker Branch throughfall displacement experiment
[DE95-008677] p 2908 N95-30793
The topological string associated with a simple singularity of type D
[DE95-737229] p 2983 N95-31225

GRAVITATION THEORY
Top quark and Higgs boson masses from wormhole physics
[DE95-616384] p 2978 N95-30580
Review of Gravity Probe B
[NASA-CR-198959] p 3019 N95-30781
Partons and black holes
[DE95-009921] p 3029 N95-31102

GRAVITATIONAL COLLAPSE
Phase transitions and gravitational collapse
[DE95-011732] p 3021 N95-32359

GRAVITATIONAL EFFECTS
On convective effects in sedimentation of concentrated suspensions with high effective gravity
[TRITA-NA-9316] p 2794 N95-31356
The effect of gravity on the deposition of thin films: The physical vapor transport of copper phthalocyanine
[AD-A292997] p 2838 N95-31472

GRAVITATIONAL FIELDS
Harmonic coordinates in the problem on static gravitational and massless scalar fields with a point source
[DE95-623632] p 3020 N95-32295
Relativistic theory for syntonization of clocks in the vicinity of the Earth p 2971 N95-32343

GRAVITATIONAL LENSES
Strange-matter stars
[DE95-008446] p 3028 N95-30361

GRAVITATIONAL WAVES
Gravitational-radiation damping of compact binary systems to second post-Newtonian order
[PB95-207882] p 2912 N95-30588
Gravitational waves from inspiralling compact binaries: Energy loss and waveform to second-post-Newtonian order
[PB95-207890] p 2913 N95-30590
Electromagnetic-gravitational conversion cross sections in external electromagnetic fields
[DE95-613589] p 2979 N95-30637

GRAVITONS
Electromagnetic-gravitational conversion cross sections in external electromagnetic fields
[DE95-613589] p 2979 N95-30637

GRAVITY PROBE B
Review of Gravity Probe B
[NASA-CR-198959] p 3019 N95-30781

GRAVITY WAVES
Modeling and parameterization of gravity wave breaking, interactions, and instability processes in the lower and middle atmosphere
[AD-A292740] p 2914 N95-31278
Middle atmosphere structure and dynamics: Lidar studies at the South Pole, Syowa and Urbana p 2916 N95-31736

GREEN'S FUNCTIONS
On the theory of hole propagation in an antiferromagnetic background
[DE95-614469] p 3010 N95-30650
Instantaneous chiral quark model for relativistic mesons in a hot and dense medium
[DE95-613782] p 2980 N95-30911
Irreducible Green's Functions method in the theory of highly correlated systems
[DE95-614446] p 3019 N95-31186

GREENHOUSE EFFECT
Economical analysis relating to the global warming issue
[DE95-764072] p 2908 N95-30677
Global change research: Summaries of research in FY 1994
[DE95-009660] p 2908 N95-30755

GRID GENERATION (MATHEMATICS)
Multidimensional discretization of conservation laws for unstructured polyhedral grids
[DE95-008796] p 2955 N95-30470
Three-D mesh optimization methods for unstructured polyhedra
[DE95-008808] p 2955 N95-30471
Self-adaptive multilevel methods for fluid flow problems p 2873 N95-31412
Automated volumetric grid generation for finite element modeling of human hand joints
[DE95-009575] p 2928 N95-32097
Numerical solution of the full potential equation using a chimera grid approach
[NASA-TM-110360] p 2744 N95-32188

GROUND BASED CONTROL
FAA aviation forecasts: Fiscal year 1995-2006
[AD-A293682] p 2741 N95-31598

GROUND EFFECT (COMMUNICATIONS)
Investigation of ground target detection methods in fully polarimetric wide angle synthetic aperture radar images
[AD-A293922] p 2851 N95-31513

GROUND SPEED
Apparent size passive range method
[AD-D017360] p 2753 N95-31180

GROUND STATE
Ferromagnetic Potts model in a magnetic field: Finite lattice extrapolation of the (1 + 1)-dimensional Hamiltonian
[DE95-614447] p 3012 N95-30958
Relativistic non-interacting electron gas in a magnetic field
[DE95-616903] p 2967 N95-31177
Excited-state complexes of conjugated polymers: Novel photophysical processes and optoelectronic materials
[AD-A292958] p 2819 N95-31462

GROUND STATIONS
High Frequency (HF) upgrade study for the Canadian Regional Operations Control Center (ROCC) AWACS Digital Information Link (RADIL) project
[AD-A293435] p 2850 N95-31367
Environmental projects. Volume 16: Waste minimization assessment
[NASA-CR-198861] p 2909 N95-31651
Portable digital Satellite News Gathering (SNG) RF terminal using a flat antenna
[NHK-LABS-NOTE-436] p 2853 N95-31744
Automated delay measurement system for an Earth station for Two-Way Satellite Time and Frequency Transfer p 2971 N95-32337

GROUND SUPPORT EQUIPMENT
Space systems environmental interaction studies
[AD-A293826] p 2766 N95-31553

GROUND TESTS
CFD assessment of the pollutant environment from RD-170 propulsion system testing p 2772 N95-31749

GROUND TRUTH
Flight test evaluation of the Stanford University/United Airlines differential GPS Category 3 automatic landing system
[NASA-TM-110354] p 2743 N95-30788
Satellite multisensor data techniques for sea ice mapping
[AD-A289729] p 2901 N95-31148

GROUND WATER
Spatial time-series: Pollution pattern recognition under irregular interventions
[AD-A293830] p 2909 N95-31556

GROUND WIND
Validation of special sensor microwave/imager ocean surface wind retrievals in equatorial regions
[AD-A293750] p 2920 N95-31571

GROUP THEORY
Generalized Kummer surfaces and differentiable invariants of Noether-Horikawa surfaces 1
[DE95-613382] p 2956 N95-30608
Co-groups on sequentially complete, locally convex, topological vector spaces in particular on strict LF-spaces
[PB95-206918] p 2966 N95-30681
Reduced heat kernels on nilpotent lie groups
[PB95-206926] p 2958 N95-30778
Frobenius algebras and quantum Yang-Baxter equation 2
[PB95-212130] p 2960 N95-31229
SO(8) color as possible origin of generations
[DE95-613560] p 2988 N95-32069

GUIDANCE SENSORS
Guidance and Control for Future Air-Defence Systems
[AGARD-CP-555] p 2839 N95-32123

GULF STREAM
A numerical study of the effect of the Gulf Stream and the Appalachian Mountains on Carolina coastal frontogenesis
[AD-A293765] p 2921 N95-31577

GUN PROPELLANTS
The 31st JANNAF Combustion Subcommittee Meeting, volume 1 p 2825 N95-31194
Investigation of ram accelerator performance capabilities p 2799 N95-31204
Condensed-phase processes during solid propellant combustion. 5: Further observations on depth profiling of burned surfaces of XM39 and M43 propellants p 2800 N95-31295
Assessment of dynamic burning behavior for JA-2 propellant rods p 2800 N95-31299
Embedded infrared fiber optic absorption studies of nitramine propellant strand burning p 2801 N95-31305

GUST LOADS
Advanced gust management systems: Lessons learned and perspectives p 2759 N95-32002

GYROCOMPASSES
Results from tests of the Honeywell integrated flight management unit
[PB95-211355] p 2748 N95-30597

GYROSCOPES
Harmonic gyrotron amplifiers and phase-locked oscillators
[AD-A293185] p 2861 N95-30979
Global stabilization of nonlinear gyroscopic systems p 2881 N95-31836

GYROSCOPIC STABILITY
Global stabilization of nonlinear gyroscopic systems p 2881 N95-31836

H

H LINES
Analytic cross sections for collisions of H, H2, He and Li atoms and ions with atoms and molecules
[DE95-722055] p 2979 N95-30654
HST-FOC observations of a remarkable UV auroral event on Jupiter p 3030 N95-30806

H-INFINITY CONTROL
System identification for robust process control. Nominal models and error bounds
[PB95-197026] p 2839 N95-30777
Control of flexible spacecraft structures using H-infinity wave absorbing control
[AD-A293141] p 2766 N95-30919

HADRONS
Current issues in perturbative QCD
[DE95-008448] p 2975 N95-30388
Backgrounds and detector performance at a 2 x 2 TeV (mu)(+)(mu)(-) collider
[DE95-009107] p 2992 N95-30800
Period doubling dynamics in hadron physics: Exact calculations
[DE95-620535] p 2982 N95-31215
Hadronic production of B(sub c)-mesons
[DE95-620536] p 2983 N95-31216
B(sub c)-meson production in hadron-hadron collisions
[DE95-620537] p 2983 N95-31217
The coupling impedance of a toroidal beam pipe with circular cross section
[DE95-010442] p 2993 N95-31405
Electromagnetic hadron mass differences and estimation of isotopic symmetry violation parameters of QCD vacuum from quark model
[DE95-613628] p 2985 N95-31621
Studies of the strong and electroweak interactions at the Z(sub 0) pole
[DE95-010353] p 2986 N95-31682
The antiproton-hydrogen atom interaction
[DE95-010252] p 2987 N95-32039
A search for jet handedness in hadronic Z-0 decays
[DE95-010099] p 2988 N95-32083
On the search for exotic hadrons in the experiments with high energy hyperon beam
[DE95-620534] p 2989 N95-32261
On hadronic production of the B(sub c) meson
[DE95-613726] p 2991 N95-32304

HAFNIUM
Localization in tungsten heavy alloys subjected to shearing deformations under superimposed high pressures
[AD-A293177] p 2804 N95-30977

HALF PLANES
Reduced heat kernels on nilpotent lie groups
[PB95-206926] p 2958 N95-30778

HALIDES
Preparation of diisopropyl stibines and use thereof
[AD-D017419] p 2771 N95-30418

HALOCARBONS
Chemical kinetics and photochemical data for use in stratospheric modeling: Evaluation number 11
[NASA-CR-198863] p 2912 N95-30525
Method for laser-assisted silicon etching using halocarbon ambients
[AD-D017426] p 2883 N95-30744
Chemical options to halons for aircraft use
[AD-A293741] p 2747 N95-31569

HALOGENS
Determination of halogens in a petroleum product by ion chromatography
[DE95-002056] p 2797 N95-31840

HALOS
Backgrounds and detector performance at a 2 x 2 TeV (mu)(+)(mu)(-) collider
[DE95-009107] p 2992 N95-30800

HAMILTONIAN FUNCTIONS
A queer reduction of degrees of freedom
[DE95-613471] p 2964 N95-30369
The Foldy-Wouthuysen transformation
[DE95-616277] p 2976 N95-30427
Integrals of motion in the two Killing vector reduction of general relativity
[DE95-616281] p 3018 N95-30431
Plaquette expansion proof and interpretation
[DE95-616282] p 2965 N95-30432
A general non-perturbative estimate of the energy density of lattice Hamiltonians
[DE95-616283] p 2965 N95-30435
Beyond the variational principle in quantum field theory
[DE95-616286] p 3018 N95-30438
Approximate analytic diagonalization of lattice QCD
[DE95-616332] p 3018 N95-30444
Gibbs measures and quasi-periodic solutions for nonlinear Hamiltonian partial differential equations
[PB95-207932] p 2956 N95-30506
New tensor interactions in micron-decay
[DE95-613760] p 2978 N95-30528
Quasi-periodic solutions of Hamiltonian perturbations of 2D linear Schroedinger equations
[PB95-208443] p 2957 N95-30624
Hamiltonian dynamics of the condensed media with spontaneously broken symmetry
[DE95-614448] p 3010 N95-30648
The iteration formula of the Maslov-type index theory with applications to nonlinear Hamiltonian systems
[DE95-613379] p 2957 N95-30676
Light-front dynamics of Chern-Simons systems
[DE95-613467] p 3019 N95-30741
Singular eigenfunctions for shearing fluids I
[DE95-008952] p 2868 N95-30763
Exact smooth classification of Hamiltonian vector fields on symplectic 2-manifolds
[DE95-613378] p 2958 N95-30803
Ferromagnetic Potts model in a magnetic field: Finite lattice extrapolation of the (1 + 1)-dimensional Hamiltonian
[DE95-614447] p 3012 N95-30958
Effective chiral-spin Hamiltonian for odd-numbered coupled Heisenberg chains
[DE95-614445] p 2982 N95-31168
Hamiltonian formulation of two body problem in Wheeler-Feynman electrodynamics
[DE95-620526] p 3019 N95-31193
Quantization of a relativistic particle on the SL(2,R) manifold based on Hamiltonian reduction
[DE95-737163] p 2983 N95-31224
Removal of the Energy Dependence from the Resolvent Like Energy Dependent Interactions
[DE95-613385] p 2961 N95-31619
Variational optimization in quantum field theory p 3020 N95-31646
Notes on lie algebraic analysis of achromats
[DE95-009524] p 3002 N95-32356

HANDBOOKS
Operator's handbook: NAWC Software Production Facility
[AD-A290216] p 2935 N95-31001
Management of major system programs and projects. Handbook
[NHB-7120.5] p 3021 N95-31380

HANDEDNESS
A search for jet handedness in hadronic Z-0 decays
[DE95-010099] p 2988 N95-32083

HANDLES
A stochastic difference equation approach to inference with missing data: Some new results
[DE95-010327] p 2944 N95-32088

HANDLING EQUIPMENT
An overview of high-speed networking for workstations
[DE95-009076] p 2947 N95-30577

HANKEL FUNCTIONS
Plaquette expansion proof and interpretation
[DE95-616282] p 2965 N95-30432

HARDNESS
An explanation for the shape of nanoindentation unloading curves based on finite element simulation
[DE95-008905] p 2812 N95-30548
Cracking during nanoindentation and its use in the measurement of fracture toughness
[DE95-008839] p 2818 N95-31175

HARDWARE DESCRIPTION LANGUAGES
RASSP benchmark 1 executable requirements user's manual
[AD-A290060] p 2935 N95-30931
Mission critical failure effects analysis using quantitative techniques
[AD-A293098] p 2864 N95-31844

HARMONIC ANALYSIS
Advanced small rocket chambers. Option 3: 110 1bf Ir-Re rocket, volume 2
[NASA-CR-195435-VOL-2] p 2769 N95-31170

HARMONIC EXCITATION
Studies in non-linear multi-mode responses of harmonically excited rectangular plates with internal resonances p 2895 N95-31331

HARMONIC GENERATIONS
Harmonic gyrotron amplifiers and phase-locked oscillators
[AD-A293185] p 2861 N95-30979
Experimental investigation of optical nonlinearities in conjugated polymers
[AD-A288353] p 2884 N95-31145
Nonlinear optics in novel composite media
[AD-A293886] p 2999 N95-31542
Towards optimum demodulation of bandwidth-limited and low SNR square-wave subcarrier signals p 2855 N95-32229

HARMONIC GENERATORS
Stable high-power harmonic gyro-amplifiers
[AD-A293697] p 2881 N95-31828

HARMONIC MOTION
Degradation in finite-harmonic subcarrier demodulation p 2855 N95-32228

HARMONIC OSCILLATORS
The one-dimensional model of the off-centre potential of the fluorine ion in the NaBr lattice
[DE95-614310] p 3010 N95-30647
Dynamical systems as models for flow-induced vibrations
[PB95-206991] p 2869 N95-30956
Harmonic gyrotron amplifiers and phase-locked oscillators
[AD-A293185] p 2861 N95-30979
Instanton - antiinstanton interaction and asymptotics of perturbation theory expansion of in double well oscillator
[DE95-619245] p 2966 N95-31259
Instability of weakly nonlinear chaotic structures
[DE95-613441] p 2966 N95-32066
Method of normal coordinates in the formulation of a system with dissipation: The harmonic oscillator
[DE95-613372] p 3020 N95-32094

HARNESSES
Releaseable unconstrained inflatable body protector
[AD-D017350] p 2930 N95-30552

HARRIER AIRCRAFT
Flight demonstration of an advanced pitch control law in the VAAC Harrier aircraft p 2760 N95-32012

HARTREE APPROXIMATION
On the theory of hole propagation in an antiferromagnetic background
[DE95-614469] p 3010 N95-30650

HASTELLOY (TRADEMARK)
Evaluation on materials performance of Hastelloy Alloy XR for HTTR uses. 4: Tensile properties of base metals and welded joints
[DE95-721871] p 2804 N95-30761
Effect of cold work on creep properties of Hastelloy XR
[DE95-722056] p 2806 N95-31154

HAZARDS
Environmental conditions responsible for solar activity
[AD-A292859] p 3031 N95-31450
Enhanced alkaline hydrolysis and biodegradability studies of nitrocellulose-bearing missile propellant p 2772 N95-31752
Environmentally Safe and Effective Processes for Paint Removal
[AGARD-LS-201] p 2843 N95-32165

HEAD-UP DISPLAYS
Analysis of heads-up display quickening versus handling qualities
[AD-A293797] p 2753 N95-31584

HEALTH
Summaries of fiscal year 1994 projects in medical applications and biophysical research
[DE95-010405] p 2925 N95-32040

HEALTH PHYSICS
Electromagnetic field exposure dosimeter
[AD-A293191] p 2927 N95-30981

HEAT BALANCE
Control of skin blood flow in the neutral zone of human body temperature regulation
[AD-A291499] p 2926 N95-30563
Global Ultraviolet Imager (GUVI) investigation
[NASA-CR-189430] p 2917 N95-31820

HEAT ENGINES
Publications of the Fossil Energy Advanced Research and Technology Development Materials Program: April 1, 1993-March 31, 1995
[DE95-009200] p 2903 N95-30745
Life prediction methodology for ceramic components of advanced heat engines: Phase 1. Volume 1
[DE95-010805] p 2817 N95-31135
Life prediction methodology for ceramic components of advanced heat engines. Phase 1: Volume 2. Appendices
[DE95-010806] p 2817 N95-31136

HEAT EXCHANGERS
Thermoacoustic sound generator
[AD-D017342] p 2973 N95-30413
Simultaneous heat and mass transfer in a horizontal tube absorber: Numerical tools for present and future absorber designs
[PB95-196978] p 2869 N95-30872
Experimental investigation of the effectiveness of flow-through modules for electronics cooling
[AD-A293284] p 2861 N95-30950
Comparison of cathodic protection currents on 70/30 copper-nickel and alloy 625 piping systems
[AD-A292953] p 2807 N95-31561
Whisker reinforced glass ceramic
[DE95-010542] p 2823 N95-32305

HEAT FLUX
Diamond thin film temperature and heat-flux sensors
[NASA-CR-198859] p 3012 N95-30847
HEAT OF FORMATION
Estimating heat of formation of energetic compounds using corrected semiempirical molecular orbital theory
p 2800 N95-31294
HEAT OF SOLUTION
The influence of microstructure on creep deformation in near-gamma TiAl alloys p 2808 N95-31975
HEAT PIPES
10 kW heat pipe-heat sink development
[AD-A293167] p 2870 N95-30965
HEAT RESISTANT ALLOYS
Influence of strain rate and temperature on the mechanical behavior of iron aluminide-based alloys
[DE95-009426] p 2808 N95-31636
HEAT SINKS
10 kW heat pipe-heat sink development
[AD-A293167] p 2870 N95-30965
Global Ultraviolet Imager (GUVI) investigation
[NASA-CR-189430] p 2917 N95-31820
HEAT SOURCES
GPHS-RTGs in support of the Cassini RTG Program
[DE95-010306] p 2768 N95-30674
Welding isotopic heat sources for the cassini mission to Saturn
[DE95-060104] p 2890 N95-32367
HEAT STORAGE
CALORSTOCK 1994: Thermal energy storage. Better economy, environment, technology
[DE95-772422] p 2904 N95-31138
Study of melting and freezing processes of water for application to ice thermal energy storage system
p 2905 N95-31735
HEAT STROKE
Membrane transport: A cellular probe of heat stroke
[AD-A293327] p 2926 N95-30924
HEAT TRANSFER
Jet mixing in a reacting cylindrical crossflow
[NASA-TM-106975] p 2755 N95-30853
Electrically heated tube investigation of cooling channel geometry effects
[NASA-TM-106985] p 2768 N95-30856
Simultaneous heat and mass transfer in a horizontal tube absorber: Numerical tools for present and future absorber designs
[PB95-196978] p 2869 N95-30872
Experimental investigation of the effectiveness of flow-through modules for electronics cooling
[AD-A293284] p 2861 N95-30950
10 kW heat pipe-heat sink development
[AD-A293167] p 2870 N95-30965
Investigation of ram accelerator performance capabilities p 2799 N95-31204
Fundamental topics in heat transfer through deformable two-phase media p 2874 N95-31532
MPI implementation of PHOENICS: A general purpose computational fluid dynamics code
[DE95-009810] p 2877 N95-32033
Optimal heat transfer design of chemical vapor deposition reactors
[DE95-010997] p 2878 N95-32309
HEAT TRANSFER COEFFICIENTS
Effect of velocity and temperature distribution at the hole exit on film cooling of turbine blades
[NASA-TM-106954] p 2755 N95-30702
HEAT TREATMENT
Process for producing hydrophilic polymer membranes
[AD-D017355] p 2811 N95-30415
Interface degradation in CAS/Nicalon during elevated temperature aging
[DE95-006843] p 2812 N95-30543
Phase transformations in melt-spun Y-Ba-Cu-O bulk superconductor
[DE95-010237] p 3011 N95-30667
A metallurgical approach toward alloying in rare earth permanent magnet systems
[DE95-010242] p 2966 N95-30668
Effects of temperature ramp rate during heat treatment on hysteresis loss and critical current density of internal tin processed wires
[DE95-009551] p 2803 N95-30706
HEATING
Substrate heating measurements in pulsed ion beam film deposition
[DE95-010862] p 2818 N95-31377
CALORSTOCK'94. Thermal energy storage. Better economy, environment, technology
[DE95-772421] p 2907 N95-32368
HEAVY ELEMENTS
Mechanical alloying processing with application to structural materials
[AD-A290788] p 2802 N95-30404
HEAVY IONS
Theoretical high energy physics
[DE95-003107] p 2991 N95-30527
Observation of intensity dependent losses in Au(15+) beams
[DE95-010845] p 2987 N95-32032
Generalized Ramsauer-Townsend minima in heavy-ion induced electron continua
[DE95-010913] p 2989 N95-32120
KRAKEN, a numerical model of RHIC impedances
[DE95-011563] p 2994 N95-32242
HEISENBERG THEORY
Integrals of motion in the two Killing vector reduction of general relativity
[DE95-616281] p 3018 N95-30431
A general non-perturbative estimate of the energy density of lattice Hamiltonians
[DE95-616283] p 2965 N95-30435
On the theory of hole propagation in an antiferromagnetic background
[DE95-614469] p 3010 N95-30650
Dynamics of an inhomogeneous anisotropic antiferromagnetic spin chain
[DE95-614449] p 3013 N95-30959
Effective chiral-spin Hamiltonian for odd-numbered coupled Heisenberg chains
[DE95-614445] p 2982 N95-31168
Schwinger-boson studies of the single hole motion in a 2D quantum antiferromagnet
[DE95-614444] p 3016 N95-32071
HELICOPTER CONTROL
Experiences with ADS-33 helicopter specification testing and contributions to refinement research
p 2757 N95-31993
Model following control for tailoring handling qualities: ACT experience with ATTHeS p 2758 N95-32000
Practical experiences in control systems design using the NCR Bell 205 Airborne Simulator
p 2761 N95-32015
HELICOPTER DESIGN
A novel instrumentation system for measurement of helicopter rotor motions and loads data, phase 1
[AD-A293309] p 2751 N95-30923
Automatic flight control system for an unmanned helicopter system design and flight test results
p 2759 N95-32004
HELICOPTER WAKES
Validation of the helicopter rotor code HERO
[PB95-198040] p 2751 N95-30838
HELICOPTERS
Simulation of airborne electromagnetic measurements in three dimensional environments
[DE95-008546] p 2900 N95-30363
Probabilistic reliability modeling of fatigue on the H-46 tie bar
[AD-A289926] p 2751 N95-30927
Application of multigrid computational fluid dynamics (CFD) methods to rotor analysis
[AD-A293012] p 2874 N95-31475
Report to the Secretary of Defense. Acquisition reform: Comparison of Army's commerical helicopter buy and private sector buys
[GAO/NSIAD-95-54] p 3021 N95-31659
Advanced flight control technology achievements at Boeing Helicopters p 2761 N95-32014
Vibration reduction in helicopter rotors using an actively controlled partial span trailing edge flap located on the blade p 2762 N95-32111
HELIUM
Reducing process noise in superconducting helium liquid level probes
[DE95-008956] p 2814 N95-30765
Kinematical threshold of recoil-ion longitudinal momentum distribution in single ionization of helium by protons and alpha particles
[DE95-010803] p 2990 N95-32271
Ionization of He by highly charged ions at low velocity
[DE95-010815] p 2990 N95-32273
Recoil longitudinal momentum spectroscopy of electron capture from He by O(7+) and F(8+)
[DE95-010823] p 2990 N95-32274
HELIUM ATOMS
Atomic approaches in metastable antiprotonic helium atoms. Reply to Analysis of the lifetimes and fractions of antiprotons trapped in metastable antiprotonic helium states by I. Shimamhura and M. Kimura --- mura
[DE95-737228] p 2986 N95-31658
HELIUM ISOTOPES
Hamiltonian dynamics of the condensed media with spontaneously broken symmetry
[DE95-614448] p 3010 N95-30648
HELIUM PLASMA
Helium transport and exhaust studies in enhanced confinement regimes in DIII-D
[DE95-009134] p 3004 N95-30685
HELMET MOUNTED DISPLAYS
Wide field of view helmet display systems mounted for helicopter simulation
[AD-A293123] p 2930 N95-30888
Synthetic Terrain Imagery for Helmet-Mounted Display. Volume 3: Software user's manual
[AD-A293613] p 2753 N95-31463
Design and integration issues of visually-coupled evaluation
[AD-A293521] p 2931 N95-31538
Synthetic Terrain Imagery for Helmet-Mounted Display. Volume 2: Software design document
[AD-A293611] p 2753 N95-31655
Synthetic Terrain Imagery for Helmet-Mounted Display, volume 1
[AD-A293612] p 2753 N95-31656
Vertical impact testing of two helmet-mounted night vision systems
[AD-A293055] p 2931 N95-31671
HELMETS
Vertical impact testing of two helmet-mounted night vision systems
[AD-A293055] p 2931 N95-31671
HELMHOLTZ EQUATIONS
Solution of the three-dimensional Helmholtz equation with nonlocal boundary conditions
[NASA-TM-110174] p 2974 N95-30850
HERCULES ENGINE
Environmentally compatible solid rocket propellants
p 2772 N95-31753
HERMITIAN POLYNOMIAL
Image representation using fast algorithms based on the Zak transform
[AD-A293416] p 2942 N95-31684
HESSIAN MATRICES
Multipoint quadratic approximation for numerical optimization
[AD-A293837] p 2961 N95-31557
HETEROCYCLIC COMPOUNDS
Acidity and basicidity of nitro substituted imidazoles
[AD-A293969] p 2836 N95-31526
HETEROGENEITY
Catalytic reactions of synthesis gas. Part 4: Heterogeneous hydroformylation
[PB95-195558] p 2791 N95-30537
An experimental study of planar heterogeneous supersonic confined jets
[AD-A290859] p 2867 N95-30557
Integrated high performance distributed system
[AD-A292821] p 2947 N95-31445
Clouds: Their prediction and simulation
[AD-A292864] p 2920 N95-31453
Particle filtration: A comparison between theory and experiment
[DE95-009442] p 2875 N95-31637
Processing and microstructural evolution of alumina/aluminum alloy and aluminum nitride/aluminum alloy composites by directed melt oxidation
p 2789 N95-31973
MPI implementation of PHOENICS: A general purpose computational fluid dynamics code
[DE95-009810] p 2877 N95-32033
HETEROJUNCTION DEVICES
Minority and majority carrier transport characterization in compound semiconductors
[DE95-010873] p 3014 N95-31233
HETEROJUNCTIONS
The quantum interference effect in semiconductor space charge layers studied by Feynman path integrals: General formalism and illustrative examples
[DE95-614483] p 3010 N95-30653
Development of germanium-silicon growth technology
[AD-A293199] p 3013 N95-30983
Investigation of polycrystalline thin film CuInSe2 solar cells based on ZnSe windows
[DE95-004068] p 2904 N95-31164
HEURISTIC METHODS
A Heuristic and complete planner for the classical mover's problem
[DE95-008440] p 2949 N95-30377
Dynamic routation in distributed environments
[PB95-197968] p 2847 N95-30812
Unification of LARCH and Z-based object models to support algebraically-based design refinement: The LARCH perspective
[AD-A289235] p 2935 N95-30999
Aspects of the search time in binary search trees modified according to the move-to-root heuristic
[PB95-212148] p 2963 N95-31396
Compact location problems with budget and communication constraints
[DE95-010876] p 2948 N95-32277
HF LASERS
Advances in high-power chemical lasers
[AD-A289737] p 2885 N95-31389

HIERARCHIES
The topological string associated with a simple singularity of type D
[DE95-737229] p 2983 N95-31225
HIGGS BOSONS
Real Higgs singlet and electroweak phase transition in the standard model
[DE95-616315] p 2976 N95-30442
Effective Lagrangian approach to the fermion mass problem
[DE95-616316] p 2976 N95-30443
Phenomenology of the two Higgs doublet sector of a quark-lepton symmetric model
[DE95-616337] p 2976 N95-30446
Top quark and Higgs boson masses from wormhole physics
[DE95-616384] p 2978 N95-30580
Minijet veto: A tool for the heavy Higgs search at the LHC
[PB95-196234] p 2979 N95-30695
Testing vector boson dominance of electroweak interactions via e(+)e(-) (yields) f-bar f
[DE95-620528] p 2982 N95-31214
Instability of weak vacuum
[DE95-613590] p 2985 N95-31620
Physics goals of a mu(+) mu(-) collider
[DE95-009546] p 2994 N95-32059
Renormalization group analyses of particle masses in full four-generation fermion condensate scheme
[DE95-613595] p 2988 N95-32070
HIGH ACCELERATION
A RASCAL in-bore dynamic analysis of the task B and task C electromagnetic railguns
[AD-A292742] p 2764 N95-30948
HIGH ALTITUDE
Computation of high-altitude hypersonic flow-field radiation p 2743 N95-30843
HIGH ALTITUDE BALLOONS
The High Altitude Balloon Experiment demonstration of acquisition, tracking, and pointing technologies (HABE-ATP) p 2841 N95-32132
HIGH ASPECT RATIO
High aspect ratio metal microstructures and method for preparing the same
[AD-D017463] p 2803 N95-30750
Electrically heated tube investigation of cooling channel geometry effects
[NASA-TM-106985] p 2768 N95-30856
HIGH CURRENT
Degradation of blue AlGaN/InGaN/GaN LEDs subjected to high current pulses
[DE95-008824] p 2863 N95-31611
HIGH ELECTRON MOBILITY TRANSISTORS
Hyperfrequency components
[PB95-208302] p 2866 N95-32369
HIGH ENERGY ELECTRONS
Convoy electron emission from surfaces
[DE95-010298] p 2984 N95-31402
HIGH ENERGY INTERACTIONS
The search for the decay of Z boson into two gamma as a test of Bose statistics
[DE95-616373] p 2976 N95-30393
Theoretical high energy physics
[DE95-003107] p 2991 N95-30527
The activities of the high energy physics program
[DE95-010155] p 2991 N95-30615
On perturbative asymptotic of Regge trajectories
[DE95-613585] p 3018 N95-30636
The 10th INS Scientific Computational Programs
[DE95-717864] p 2982 N95-31178
Spin structure in high energy processes
[DE95-008628] p 2993 N95-31627
Physics goals of a mu(+) mu(-) collider
[DE95-009546] p 2994 N95-32059
Research progress report
[DE95-010726] p 3030 N95-32269
Radiative corrections to the three quantum annihilation cross section in high energy electron-positron collisions
[DE95-623675] p 2995 N95-32296
HIGH FREQUENCIES
Interference rejection techniques in a DS spread-spectrum HF radio system
[PB95-211660] p 2846 N95-30479
HIGH LEVEL LANGUAGES
ASSIST user manual
[NASA-TM-4592] p 2948 N95-32250
HIGH POLYMERS
Processing of polymers using supercritical fluids
[AD-A292880] p 2819 N95-31410
HIGH POWER LASERS
Reflectivity of plasmas created by high-intensity, ultra-short laser pulses
[DE95-009536] p 3004 N95-30742
Future scientific applications for high-energy lasers
[DE95-009380] p 2885 N95-31230
Advances in high-power chemical lasers
[AD-A289737] p 2885 N95-31389
Prime power for shipboard high-average power FELs
[AD-A293718] p 2886 N95-31833
HIGH PRESSURE
Navier-Stokes flow field analysis of compressible flow in a high pressure safety relief valve
[NASA-TM-110640] p 2868 N95-30862
Localization in tungsten heavy alloys subjected to shearing deformations under superimposed high pressures
[AD-A293177] p 2804 N95-30977
Low temperature fabrication from nano-size ceramic powders
[DE95-010995] p 2818 N95-31153
Fourier Transform (FT) Raman spectroscopy of nitrogen at high pressure
[AD-A293051] p 2796 N95-31670
Evaluation of pressurized water cleaning systems for hardware refurbishment p 2778 N95-31782
HIGH PRESSURE OXYGEN
Investigation of cleanliness verification techniques for rocket engine hardware p 2770 N95-31806
HIGH RESOLUTION
Direct determination of grain boundary atomic structure in SrTiO3
[DE95-008847] p 3010 N95-30544
Satellite multisensor data techniques for sea ice mapping
[AD-A289729] p 2901 N95-31148
Method and apparatus for a high resolution, flat panel cathodoluminescent display device
[AD-D017434] p 2862 N95-31342
Middle atmosphere structure and dynamics: Lidar studies at the South Pole, Syowa and Urbana p 2916 N95-31736
Growth, characterization and device development in monocrystalline diamond films
[AD-A293106] p 3015 N95-32018
Wavelengths measurements of the He-like krypton K-shell spectrum
[DE95-010264] p 2987 N95-32041
High-resolution superconducting x-ray spectrometers with aluminum trapping layers of different thicknesses
[DE95-010253] p 2881 N95-32047
High resolution time interval counter p 2969 N95-32331
HIGH REYNOLDS NUMBER
Large-eddy simulation of turbulent flow using the finite element method
[DE95-009464] p 2875 N95-31591
Control of high Reynolds number round jets p 2876 N95-31733
HIGH SPEED
An overview of high-speed networking for workstations
[DE95-009076] p 2947 N95-30577
DEPSCOR92-Wide field spectral imager
[AD-A293079] p 2997 N95-31005
HTS Josephson technology on silicon with application to high speed digital microelectronics
[AD-A288627] p 2861 N95-31147
Numerical study of shear-induced heating in high-speed nozzle flow of liquid monopropellant p 2828 N95-31207
A high-speed photonic clock and carrier regenerator p 2856 N95-32236
HIGH STRENGTH STEELS
Observations of star fracture and longitudinal splitting in BIS 812 EMA and Q1N submarine construction steels
[DSTO-RR-0014] p 2806 N95-31344
HIGH TEMPERATURE
Theoretical absorption spectroscopy of high-temperature metal vapors: Model and experiment compared
[AD-A290872] p 2791 N95-30409
Interface degradation in CAS/Nicalon during elevated temperature aging
[DE95-008843] p 2812 N95-30543
NASA Lewis Research Center's preheated combustor and materials test facility
[NASA-TM-106676] p 2762 N95-30592
High-temperature oxidation behavior of iridium-rhenium alloys
[NASA-TM-106720] p 2803 N95-30593
Stress relaxation of silicon nitride at elevated temperatures
[DE95-009177] p 2814 N95-30732
Reflectivity of plasmas created by high-intensity, ultra-short laser pulses
[DE95-009536] p 3004 N95-30742
Innovative processing of composites for ultra-high temperature applications, book 2
[AD-A290890] p 2786 N95-30898
Phthalonitrile prepolymer as high temperature sizing material for composite fibers
[AD-D017447] p 2818 N95-31272
Advanced thin-film deposition and physical properties of high-temperature and other novel superconducting materials
[AD-A292798] p 2795 N95-31439
SDIO: Discovering superconducting materials at high temperatures
[AD-A292820] p 3015 N95-31444
Hot compression testing of tungsten
[AD-A293683] p 2807 N95-31599
Dielectric property measurement of zirconia fibers at high temperatures
[DE95-010991] p 2821 N95-31705
Predictions of tensile behavior and strengths of a Si3N4 ceramic at high temperatures based on a viscoplastic model
[DE95-010220] p 2821 N95-32025
HIGH TEMPERATURE ENVIRONMENTS
Effects of thermal and electrical stressing on the breakdown behavior of space wiring
[NASA-CR-198360] p 2768 N95-30860
Pressure transducer performance and measurement trade-offs in a transient, high temperature, combustion environment p 2799 N95-31209
HIGH TEMPERATURE GASES
Computation of high-altitude hypersonic flow-field radiation p 2743 N95-30843
HIGH TEMPERATURE PLASMAS
Synthesis of carbo-nitride films using high-energy shock plasma deposition
[DE95-615231] p 2811 N95-30450
Calibration of multichannel analyzer of charge-exchange atoms
[DE95-614178] p 2987 N95-32053
Lower hybrid accessibility in a large, hot reversed field pinch
[DE95-011001] p 3007 N95-32310
HIGH TEMPERATURE SUPERCONDUCTORS
High-temperature superconducting current leads
[DE95-008404] p 2858 N95-30374
On the theory of hole propagation in an antiferromagnetic background
[DE95-614469] p 3010 N95-30650
Structural, chemical and electronic properties of superconducting thin films and junctions
[AD-A292700] p 3012 N95-30933
Optimization of high-temperature superconductor current leads
[DE95-005838] p 2861 N95-30942
Performance evaluation of high-temperature superconducting current leads for micro-SMES systems
[DE95-005843] p 2861 N95-30943
SDIO: Discovering superconducting materials at high temperatures
[AD-A292820] p 3015 N95-31444
An active magnetic bearing with high T(sub c) superconducting coils and ferromagnetic cores
[NASA-TM-106995] p 2864 N95-31847
Schwinger-boson studies of the single hole motion in a 2D quantum antiferromagnet
[DE95-614444] p 3016 N95-32071
Superconducting and normal-state properties of novel materials
[DE95-012368] p 3017 N95-32366
HIGH TEMPERATURE TESTS
Fatigue crack growth behavior of a titanium matrix composite under thermomechanical loading p 2784 N95-30491
Pressure transducer performance and measurement trade-offs in a transient, high temperature, combustion environment p 2799 N95-31209
Differences in creep performance of a HIPed silicon nitride in ambient air and inert environments
[DE95-009172] p 2796 N95-31633
Influence of strain rate and temperature on the mechanical behavior of iron aluminide-based alloys
[DE95-009426] p 2806 N95-31636
Evaluation of static strength of T800H/PMR-15 carbon/polyimide laminates at room temperature and 300 C
[NAL-TR-1254] p 2789 N95-31740
A study of elevated temperature testing techniques for the fatigue behavior of PMCS: Application to T650-35/AMB21
[NASA-TM-106927] p 2791 N95-32209
HIGHLY MANEUVERABLE AIRCRAFT
Computational methods for control and optimal design of aerospace systems
[AD-A292861] p 2751 N95-31451
HILBERT SPACE
Local index formula in noncommutative geometry
[PB95-208146] p 2955 N95-30490

Quantization of a relativistic particle on the SL(2,R) manifold based on Hamiltonian reduction
[DE95-737163] p 2983 N95-31224
HISTORIES
The art and science of magnet design: Selected notes of Klaus Halbach, volume 2
[DE95-008450] p 2861 N95-31059
PIO: A historical perspective p 2745 N95-31062
Space Shuttle Orbiter corrosion history, 1981-1993: A review and analysis of issues involving structures and subsystems
[NASA-TM-104810] p 2810 N95-32183
HOHLRAUMS
Target diagnostics for intense lithium ion hohlraum experiments on PBFA 2
[DE95-008517] p 3006 N95-31626
HOLES (ELECTRON DEFICIENCIES)
Alloying effects of Kondo insulators
[DE95-614308] p 3010 N95-30644
Schwinger-boson studies of the single hole motion in a 2D quantum antiferromagnet
[DE95-614444] p 3016 N95-32071
HOLES (MECHANICS)
Analysis of stress concentration at holes in components made of 2195 aluminum-lithium
[NASA-TP-3554] p 2893 N95-30613
Failure mechanisms in composite plates subjected to in-plane compressive loading p 2790 N95-32108
Contributions to the design of neutral cutouts in laminated plates and shells p 2790 N95-32113
HOLLOW CATHODES
Hollow cathode electron gun research and development
[DE95-010262] p 2992 N95-31127
HOLOGRAPHY
Application of computer generated holograms to optical transformations
[AD-A293146] p 2880 N95-30921
Optical feature recognition
[AD-A293168] p 2997 N95-30966
High speed random access, Fourier transform holographic associative and high density two-photon three-dimensional optical memories based on bacteriorhodopsin
[AD-A293389] p 2931 N95-30967
Laser-induced holographic surface relief gratings on nonlinear optical polymer films
[AD-A293169] p 2997 N95-30973
Polarized laser induced holographic surface relief gratings on polymer films
[AD-A293275] p 2817 N95-31126
Theoretical aspects of electron emission holography
[DE95-614371] p 2880 N95-31167
Temporal feature extraction in photorefractive resonators
[AD-A292908] p 2881 N95-31385
Photorefractive nonlinear optics
[AD-A292913] p 2999 N95-31458
HOMING DEVICES
System considerations for efficient communication and storage of MSTI image data
[NASA-CR-198869] p 3024 N95-30858
Feasibility study concerning an active millimeterwave sensor. Project phase MMS2.1
[PB95-210399] p 2882 N95-32245
The dynamic range of radar signal generation in the MSS-2 simulation facility
[AD-A293856] p 2857 N95-32259
HOMODYNE RECEPTION
Demodulators for optical fiber interferometers with (3 x 3) outputs
[AD-D017415] p 2995 N95-30402
HOMOGENEITY
Quantum 1/f noise in high technology applications including ultrasmall structures and devices
[AD-A292812] p 2862 N95-31442
A unified interpretation of singular and near-singular integrals in the boundary element method
[ISBN-0-315-86297-1] p 2962 N95-31947
HOMOGENEOUS TURBULENCE
Numerical simulation of the Langevin equation for skewed turbulence
[DE95-009477] p 2877 N95-32049
HOMOLOGY
Torus bundles and the group cohomology of GL(N,Z)
[PB95-208120] p 2965 N95-30489
4-manifold topology 2: Dwyer's filtration and surgery kernels
[PB95-207940] p 2965 N95-30509
HOMOTOPY THEORY
Strange compactification theorem: Infinite processes and the 3-dimensional poincare conjecture 6. Part A
[PB95-207924] p 2965 N95-30504
The iteration formula of the Maslov-type index theory with applications to nonlinear Hamiltonian systems
[DE95-613379] p 2957 N95-30676
Pi1(sup infinity) and infinite simple homotopy type in dimension three: A research announcement
[PB95-196283] p 2957 N95-30696
HOT ELECTRONS
Vertical transport in GaAs/AlGaAs superlattices p 3012 N95-30822
HOT ISOSTATIC PRESSING
Processing and characterization of nanocrystalline molybdenum disilicide (MoSi2) consolidated by hot isostatic pressing (HIP)
[DE95-010243] p 3012 N95-30756
Differences in creep performance of a HIPed silicon nitride in ambient air and inert environments
[DE95-009172] p 2796 N95-31633
HOVERING
Moving base simulation of an integrated flight and propulsion control system for an ejector-augmentor STOVL aircraft in hover
[NASA-TM-108867] p 2750 N95-30646
HTPB PROPELLANTS
Oscillatory combustion of aluminized AP/HTPB propellants p 2800 N95-31286
Laser pyrolysis of HTPB p 2800 N95-31298
HUBBLE SPACE TELESCOPE
The future of space imaging. Report of a community-based study of an advanced camera for the Hubble Space Telescope
[NASA-CR-198818] p 3028 N95-31364
The Wide Field/Planetary Camera 2 (WFPC-2) molecular adsorber
[NASA-CR-198866] p 2881 N95-31456
HUMAN BEHAVIOR
Temporal information processing mechanisms
[PB95-208344] p 3027 N95-32370
HUMAN BODY
Control of skin blood flow in the neutral zone of human body temperature regulation
[AD-A291499] p 2926 N95-30563
HUMAN FACTORS ENGINEERING
Specific method for task-based interaction design
[PB95-196440] p 2929 N95-30522
Precision manipulation with a dextrous robot hand p 2888 N95-30829
Virtual Reality Software and Technology '94
[AD-A292334] p 2939 N95-31262
The development of human behaviour analysis techniques and the development of human factors technologies
[DE95-613356] p 2930 N95-31267
Impact of task properties, data display format and cognitive characteristics on recall performance: A cumulative research investigation p 3025 N95-31334
Human factors at the FAA Technical Center: Bibliography
[AD-A288638] p 2930 N95-31399
Design and integration issues of visually-coupled evaluation
[AD-A293521] p 2931 N95-31538
Guidelines for the design of GPS and LORAN receiver controls and displays
[AD-A293753] p 2749 N95-31572
Analysis of heads-up display quickening versus handling qualities
[AD-A293797] p 2753 N95-31584
Dynamical analysis of the coriolis effect which causes space disorientation
[NAL-TR-1258] p 2928 N95-31714
Aircraft evacuations through Type-3 exits I: Effects of seat placement at the exit
[DOT/FAA/AM-95/22] p 2748 N95-31845
HUMAN PERFORMANCE
Training metacognitive skills for problem solving
[AD-A290310] p 2959 N95-31002
The development of human behaviour analysis techniques and the development of human factors technologies
[DE95-613356] p 2930 N95-31267
Impact of task properties, data display format and cognitive characteristics on recall performance: A cumulative research investigation p 3025 N95-31334
Forward rapid rotation shiftwork in USAF air traffic controllers: Sleep, activity, fatigue and mood analyses
[AD-A293448] p 2927 N95-31373
Contextual interference effects on acquisition and transfer of a complex motor task
[AD-A293788] p 2929 N95-31583
HUMAN RESOURCES
Application of a genetic algorithm to optimize staffing levels in software development
[AD-A293725] p 2943 N95-31835
HUMAN-COMPUTER INTERFACE
The Technology Information Environment with Industry (TIE-In): A mechanism for accessing laboratory solutions
[DE95-008542] p 3027 N95-30385
Specific method for task-based interaction design
[PB95-196440] p 2929 N95-30522
Automation of the control of acoustic parameters in a digital speech synthesizer
[IFTR-2/1995] p 2850 N95-31357
Visual tracking of self-occluding articulated objects
[AD-A292894] p 2928 N95-31383
Human-computer interaction (HCI) specialization track Masters of Software Engineering (MSE) program
[AD-A292895] p 2930 N95-31401
Guidelines for the design of GPS and LORAN receiver controls and displays
[AD-A293753] p 2749 N95-31572
User-friendly microcomputer interface with optimization languages AF94-007
[AD-A293184] p 2932 N95-32257
HUMIDITY
Patterns in the sky: Natural visualization of aircraft flow fields
[NASA-SP-514] p 2741 N95-31000
HURRICANES
Forecast of Atlantic seasonal hurricane activity for 1994 p 2918 N95-30832
Summary of 1993 Atlantic tropical cyclone activity and verification of author's forecast. A year of unanticipated light hurricane activity and a poor forecast: The expected dissipation of the El Nino did not take place and Caribbean basin surface pressure became quite high p 2918 N95-30842
Early August updated forecast of Atlantic seasonal hurricane activity for 1994 p 2919 N95-30844
LAWS hurricane studies
[NASA-CR-189438] p 2919 N95-31128
HYBRID CIRCUITS
Space qualified hybrid superconductor/semiconductor planar oscillator circuit
[NASA-TM-106978] p 3011 N95-30703
HYBRID PROPELLANTS
Improved hybrid rocket fuel p 2773 N95-31755
HYDRAULIC FLUIDS
Compatibility of Single Hydraulic Fluid with military specification fluids, seals and metallurgy
[AD-A292954] p 2821 N95-31663
Recycling MIL-H-46170 hydraulic fluid to extend fluid service life
[AD-A293035] p 2821 N95-31664
Evaluation of Environmentally Acceptable hydraulic fluids
[AD-A293037] p 2821 N95-31666
HYDRAULIC JETS
Evaluating the cost effectiveness of environmental projects: Case studies in aerospace and defense p 2774 N95-31762
Waterjet processes for coating removal p 2777 N95-31779
Ultra-high pressure water jetting for coating removal and surface preparation p 2778 N95-31780
Evaluation of pressurized water cleaning systems for hardware refurbishment p 2778 N95-31782
Cleaning verification by air/water impingement p 2782 N95-31805
Aquastrip p 2844 N95-32173
HYDRIDES
Preparation of diisopropyl stibines and use thereof
[AD-D017419] p 2771 N95-30418
Mobile electric power
[AD-A292721] p 2860 N95-30940
HYDROCARBON COMBUSTION
Non-intrusive combustion diagnostics of premixed hydrocarbon flames using FT-IR spectrometry p 2797 N95-31732
HYDROCARBON FUELS
Detailed chemical kinetic modeling of premixed hydrocarbon flames supported by NO2 p 2801 N95-31311
CFD assessment of the pollutant environment from RD-170 propulsion system testing p 2772 N95-31749
HYDROCARBONS
Photochemistry of intermolecular C-H bond activation reactions
[DE95-008991] p 2978 N95-30574
Evaluation of HFC 245ca and HFC 236ea as foam blowing agents p 2775 N95-31766
HYDROCHLORIC ACID
Environmentally compatible solid rocket propellants p 2772 N95-31753
Low acid producing solid propellants p 2773 N95-31754
HYDRODYNAMIC EQUATIONS
Particle filtration: A comparison between theory and experiment
[DE95-009442] p 2875 N95-31637
An efficient numerical procedure for thermohydrodynamic analysis of cavitating bearings
[NASA-CR-195476] p 2878 N95-32210
Film temperatures in the presence of cavitation
[NASA-CR-195481] p 2878 N95-32216

HYDRODYNAMICS
Multidimensional discretization of conservation laws for unstructured polyhedral grids
[DE95-008796] p 2955 N95-30470
Modeling of thermal, electronic, hydrodynamic, and dynamic deposition processes for pulsed-laser deposition of thin films
[DE95-008906] p 2813 N95-30572
Hamiltonian dynamics of the condensed media with spontaneously broken symmetry
[DE95-614448] p 3010 N95-30648
Future scientific applications for high-energy lasers
[DE95-009380] p 2885 N95-31230
Phase transitions and gravitational collapse
[DE95-011732] p 3021 N95-32359

HYDROELECTRICITY
Sleeping renewable beauty: Will the prince ever come
[PB95-214573] p 2903 N95-30640

HYDROFLUORIC ACID
Evaluation of halon alternatives in inerting experiments
[AD-A293774] p 2795 N95-31580

HYDROGEN
Scaling of cross sections in ion-atom collisions
[DE95-008938] p 2978 N95-30573
Low-density ionization behavior
[DE95-009495] p 2980 N95-30705
A search for interstellar CH3D: Limits to the methane abundance in Orion-KL
[NASA-CR-198932] p 3029 N95-30751
Hydrogen absorption in iron and steel during gas tungsten arc welding
[PB95-197018] p 2804 N95-30776
Mobile electric power
[AD-A292721] p 2860 N95-30940
Properties of new materials relevant to energy and fuel research
[AD-A289734] p 2825 N95-31149
Hydrogen diffusion and passivation in InGaAlN alloys
[DE95-010889] p 2806 N95-31150
Neutronic methods for determination of very low concentrations of hydrogen in metals
[DE95-623967] p 2807 N95-31409
An analysis of gas phase ethanol/water chemistry for diamond CVD
[AD-A293009] p 2795 N95-31473
The antiproton-hydrogen atom interaction
[DE95-010252] p 2987 N95-32039
The 26th Annual Precise Time and Time Interval (PTTI) Applications and Planning Meeting
[NASA-CP-3302] p 2967 N95-32319

HYDROGEN ATOMS
The antiproton-hydrogen atom interaction
[DE95-010252] p 2987 N95-32039

HYDROGEN EMBRITTLEMENT
Review of environmental effects in intermetallics
[DE95-010120] p 2805 N95-31106

HYDROGEN ISOTOPES
Mobile electric power
[AD-A292721] p 2860 N95-30940
Determination of electric and magnetic fields in open trap plasmas by means of atomic-molecular beam hydrogen isotopes
[DE95-614177] p 3006 N95-31680

HYDROGEN MASERS
Anticipated uncertainty budgets of PRARETIME and T2L2 techniques as applied to ExTRAS
p 2968 N95-32326
Metafitting: Weight optimization for least-squares fitting of PTTI data p 2971 N95-32340
The effects of clock errors on timescale stability
p 2971 N95-32342
Satellite test of the isotropy of the one-way spe ed of light using ExTRAS p 2973 N95-32349

HYDROGEN SULFIDE
Hydrogen sulfide analyzer with protective barrier
[AD-D017412] p 2793 N95-31009
Self-lubricating, TiN-MoS2 composite coatings produced by simultaneous deposition from Ti(((CH3))2N4/NH3/MoF6H2S gas mixture
[DE95-010359] p 2788 N95-31403

HYDROLOGICAL CYCLE
NASA Tropical Rainfall Measurement Mission (TRMM): Effects of tropical rainfall on upper ocean dynamics, air-sea coupling and hydrologic cycle
[NASA-CR-189437] p 2919 N95-31123
The role of the hydrological cycle and the ocean's thermohaline circulation in climate change: A multicomponent climate model study
p 2909 N95-31720

HYDROLOGY
Multiparameter radar measurements of precipitation in complex terrain: Meteorological and hydrological applications
[AD-A290786] p 2918 N95-30403
Geostatistics and hydrology. Part 3. Hydro-meteorological network design
[PB95-206462] p 2900 N95-30818
Geostatistics and hydrology. Part 1: Spatial and temporal variability. Communications of the Sanitary Engineering and Water Management Division
[PB95-206470] p 2900 N95-30819

HYDROLYSIS
Enhanced alkaline hydrolysis and biodegradability studies of nitrocellulose-bearing missile propellant
p 2772 N95-31752
Base hydrolysis and hydrothermal processing of PBX-9404 explosive
[DE95-009437] p 2836 N95-32048
Base hydrolysis and hydrothermal processing of PBX-9404 explosive
[DE95-009497] p 2837 N95-32355

HYDROSTATIC PRESSURE
Effects of hydrostatic pressure on the mechanical behavior of composite materials
[AD-A293162] p 2787 N95-30963
Localization in tungsten heavy alloys subjected to shearing deformations under superimposed high pressures
[AD-A293177] p 2804 N95-30977

HYDROSTATICS
Experimental determination of probability distributions for parameters of a Salem limestone cap plasticity model
[AD-A290878] p 2892 N95-30559
Hydrostatic extrusion of BSCCO/Ag composite wire
[DE95-007862] p 2805 N95-31121

HYDROTHERMAL SYSTEMS
Laboratory simulated hydrothermal alteration of sedimentary organic matter from Guaymas Basin, Gulf of California
[NASA-CR-198951] p 2914 N95-30865

HYDROXIDES
An ab initio study of the reaction HNO + NO yields OH + N2O: Preliminary results p 2801 N95-31308

HYDROXYL RADICALS
A study of catalysts and mechanisms in synthesis reactions
[DE95-010177] p 2793 N95-30766
Spatially-resolved velocity measurements in steady, high-speed, reacting flows using laser-induced OH fluorescence p 2877 N95-32109

HYGRAL PROPERTIES
A theory for predicting and minimizing the effects of matrix degradation on the thermomechanical properties of general laminates p 2785 N95-30768

HYPERBOLIC DIFFERENTIAL EQUATIONS
Representation of feedback operators for hyperbolic systems
[NASA-CR-198171] p 2960 N95-31319

HYPERONS
On the search for exotic hadrons in the experiments with high energy hyperon beam
[DE95-620534] p 2989 N95-32261

HYPERSONIC FLIGHT
Computation of high-altitude hypersonic flow-field radiation p 2743 N95-30843

HYPERSONIC FLOW
Flow models for the design of a hypersonic iodine vapor wind tunnel nozzle with chemical and vibrational nonequilibrium effects p 2742 N95-30448
A numerical study of the starting process in a hypersonic shock tunnel p 2762 N95-30493
Computation of high-altitude hypersonic flow-field radiation p 2743 N95-30843
Analysis of planar laser-induced fluorescence images obtained during shakedown testing of the AEDC impulse facility
[AD-A293237] p 2884 N95-30906

HYPERSONIC WIND TUNNELS
Flow models for the design of a hypersonic iodine vapor wind tunnel nozzle with chemical and vibrational nonequilibrium effects p 2742 N95-30448

HYPERTEXT
Effectiveness of an electronic performance support system for use with computer-aided design software
[AD-A293757] p 2941 N95-31573

HYPERVELOCITY GUNS
The 31st JANNAF Combustion Subcommittee Meeting, volume 1 p 2825 N95-31194
Pressure transducer performance and measurement trade-offs in a transient, high temperature, combustion environment p 2799 N95-31209

HYPERVELOCITY IMPACT
Hypervelocity wind tunnel number 9, high Mach number development program
[AD-A289934] p 2743 N95-30929
Aerophysics test program 1
[AD-A293890] p 2963 N95-31543

HYPERVELOCITY LAUNCHERS
Experiments in a 120-mm ram accelerator including flow visualization p 2799 N95-31202

HYPERVELOCITY PROJECTILES
Experiments in a 120-mm ram accelerator including flow visualization p 2799 N95-31202
Numerical simulation of ram accelerator performance including transient effects during initiation of combustion and sensitivity studies p 2799 N95-31203
Investigation of ram accelerator performance capabilities p 2799 N95-31204
Pressure transducer performance and measurement trade-offs in a transient, high temperature, combustion environment p 2799 N95-31209

HYPERVELOCITY WIND TUNNELS
Hypervelocity wind tunnel number 9, high Mach number development program
[AD-A289934] p 2743 N95-30929

HYPOTHESES
A hypothesis-testing approach to discriminant analysis with mixed categorical and continuous variables when data are missing
[AD-A293714] p 2964 N95-31831

HYSTERESIS
Effects of temperature ramp rate during heat treatment on hysteresis loss and critical current density of internal tin processed wires
[DE95-009551] p 2803 N95-30706
Investigations of YBaCuO materials with near-room-temperature resistivity transitions
[AD-A293405] p 3013 N95-31008
Effects of temperature, frequency, flux density, and excitation waveform on the core loss and dynamic B-H loops of supermalloy
[NASA-TM-106982] p 2865 N95-32207

I

ICE
A laser-based ice shape profilometer for use in icing wind tunnels
[NASA-TM-106936] p 2880 N95-30851
Study of melting and freezing processes of water for application to ice thermal energy storage system
p 2905 N95-31735
Paint removal and surface cleaning using ice particles
p 2844 N95-32171
Stripping with dry ice p 2844 N95-32172

ICE CLOUDS
Icing simulation in the aeropropulsion systems test facility propulsion development test cell C-2
[AD-A293039] p 2747 N95-31667
Middle atmosphere structure and dynamics: Lidar studies at the South Pole, Syowa and Urbana
p 2916 N95-31736

ICE FORMATION
A laser-based ice shape profilometer for use in icing wind tunnels
[NASA-TM-106936] p 2880 N95-30851
Sea ice stress research
[AD-A293164] p 2923 N95-30964
Study of melting and freezing processes of water for application to ice thermal energy storage system
p 2905 N95-31735

ICE MAPPING
Weather influence on passive microwave brightness temperatures
[PB95-195384] p 2900 N95-30536
Sea ice stress research
[AD-A293164] p 2923 N95-30964
Satellite multisensor data techniques for sea ice mapping
[AD-A289729] p 2901 N95-31148

ICE REPORTING
Satellite multisensor data techniques for sea ice mapping
[AD-A289729] p 2901 N95-31148

IFF SYSTEMS (IDENTIFICATION)
Reply-frequency interference/jamming detector
[AD-D017428] p 2847 N95-30746
AIDEX: An expert system for aircraft identification
p 2842 N95-32138

IGNITION
Preliminary assessment of combustion modes for internal combustion wave rotors
[NASA-TM-107000] p 2754 N95-30632
Viscous heating of liquid layers under intense shear
p 2827 N95-31206
Design and testing of an oxidizer-rich preburner
p 2799 N95-31212
The 25th International Symposium on Combustion
[AD-A286825] p 2794 N95-31268
An ignition model for modern double base propellants
p 2800 N95-31292

Investigation of cleanliness verification techniques for rocket engine hardware p 2770 N95-31806

IGNITION LIMITS

Evaluation of halon alternatives in inerting experiments [AD-A293774] p 2795 N95-31580

IGNITION TEMPERATURE

Numerical computation of one-dimensional detonation waves [PB95-197950] p 2868 N95-30811

Viscous heating of liquid layers under intense shear p 2827 N95-31206

ILL-CONDITIONED PROBLEMS (MATHEMATICS)

A modification to the GMRES method for ill-conditioned linear systems [DE95-010661] p 2962 N95-32076

ILLUSIONS

Dynamical analysis of the coriolis effect which causes space disorientation [NAL-TR-1258] p 2928 N95-31714

IMAGE ANALYSIS

Direct sublattice imaging of interface dislocation structures in CdTe/GaAs(001) [DE95-009031] p 3010 N95-30576

Multiresolution signal and system analysis and the analysis and control of discrete-event dynamic systems [AD-A292775] p 2851 N95-31430

Artificial neural networks and model-based recognition of 3-D objects from 2-D images p 2954 N95-31838

Texture based methods for image analysis: A review [PB95-211595] p 2945 N95-32251

IMAGE CLASSIFICATION

Computer vision for detecting and quantifying gamma-ray sources in coded-aperture images [DE95-008810] p 2900 N95-30472

Brief review of remote sensing literature pertaining to classification and geostatistics [AD-A290932] p 2901 N95-31156

Texture based methods for image analysis: A review [PB95-211595] p 2945 N95-32251

IMAGE CONTRAST

Analysis of target contrast improvement using polarization filtering in the infrared region [AD-A293085] p 3001 N95-31841

IMAGE ENHANCEMENT

Adaptive image enhancement of text images that contain touching or broken characters [DE95-010173] p 3023 N95-30620

Image enhancement by edge-preserving filtering [DE95-008077] p 2936 N95-31056

IMAGE FILTERS

Analysis of target contrast improvement using polarization filtering in the infrared region [AD-A293085] p 3001 N95-31841

IMAGE PROCESSING

BASIS image processor PR5200: Module Common Part [PB95-212023] p 2933 N95-30501

Detecting intravascular gas bubbles in ultrasonic images [PB95-195301] p 2926 N95-30513

Unconventional imaging field experiment plan [AD-A291492] p 2846 N95-30562

Adaptive image enhancement of text images that contain touching or broken characters [DE95-010173] p 3023 N95-30620

Apparatus and method for producing three-dimensional images [AD-D017455] p 2847 N95-30727

Machine learning for a toolkit for image mining [AD-A293137] p 2951 N95-30890

Analysis of planar laser-induced fluorescence images obtained during shakedown testing of the AEDC impulse facility [AD-A293237] p 2884 N95-30906

Local fractal dimension estimation [AD-A293354] p 2959 N95-30953

Optical feature recognition [AD-A293168] p 2997 N95-30966

Image enhancement by edge-preserving filtering [DE95-008077] p 2936 N95-31056

Brief review of remote sensing literature pertaining to classification and geostatistics [AD-A290932] p 2901 N95-31156

Nonparametric recognition of nonrigid motion [AD-A293630] p 2963 N95-31565

Folded compact range development and coherent change detection measurement project [DE95-009082] p 2853 N95-31628

A simple and efficient procedure for polyhedral assembly partitioning under infinitesimal motions [DE95-009638] p 2942 N95-31644

Image representation using fast algorithms based on the Zak transform [AD-A293416] p 2942 N95-31684

Video conferencing using DAVE user's guide [DE95-010341] p 2854 N95-32045

Scannerless Range Imaging with a square wave [DE95-009840] p 2854 N95-32145

Photo-refractive Bi12SiO20: Spatial light modulator [AD-A293084] p 3001 N95-32153

BRUTUS: A program for conversion between image formats [PB95-211421] p 2945 N95-32246

Texture based methods for image analysis: A review [PB95-211595] p 2945 N95-32251

The Coprocessor Manager in the BASIS processor system [PB95-211611] p 2945 N95-32252

Gigabit testbed research project [DE95-010728] p 2945 N95-32270

Analysis of the final result from the image template matching method with fuzzy logic [PB95-222915] p 2946 N95-32311

IMAGE RECONSTRUCTION

Image representation using fast algorithms based on the Zak transform [AD-A293416] p 2942 N95-31684

IMAGE RESOLUTION

Multiresolution signal and system analysis and the analysis and control of discrete-event dynamic systems [AD-A292775] p 2851 N95-31430

IMAGERY

Synthetic Terrain Imagery for Helmet-Mounted Display. Volume 3: Software user's manual [AD-A293613] p 2753 N95-31463

Functions for processing synthetic aperture radar imagery [AD-A293895] p 2851 N95-31510

Synthetic Terrain Imagery for Helmet-Mounted Display, volume 1 [AD-A293612] p 2753 N95-31656

IMAGES

Analysis of the final result from the image template matching method with fuzzy logic [PB95-222915] p 2946 N95-32311

IMAGING RADAR

Unconventional imaging field experiment plan [AD-A291492] p 2846 N95-30562

Research in ground-to-air microwave imaging [AD-A292907] p 2852 N95-31551

Prospects for high accuracy time dissemination and synchronization using coded radar pulses from a low-earth orbiting spacecraft p 2971 N95-32339

IMAGING SPECTROMETERS

Data collection at the Lockheed Santa Cruz facility using midwave hyperspectral imagers [AD-A293057] p 3000 N95-31672

IMAGING TECHNIQUES

Visualization of circuit card electromagnetic fields [AD-A291491] p 2845 N95-30398

Multiparameter radar measurements of precipitation in complex terrain: Meteorological and hydrological applications [AD-A290786] p 2918 N95-30403

Computer vision for detecting and quantifying gamma-ray sources in coded-aperture images [DE95-008810] p 2900 N95-30472

Decompression illness, observable bubbles. (Session K) [PB95-195285] p 2926 N95-30511

Apparatus for producing images acoustically [AD-D017365] p 2973 N95-30530

Direct determination of grain boundary atomic structure in SrTiO3 [DE95-008847] p 3010 N95-30544

Unconventional imaging field experiment plan [AD-A291492] p 2846 N95-30562

Direct sublattice imaging of interface dislocation structures in CdTe/GaAs(001) [DE95-009031] p 3010 N95-30576

A laser-based ice shape profilometer for use in icing wind tunnels [NASA-TM-106936] p 2880 N95-30851

Nearly steady flows in GONG prototype data [NASA-CR-198935] p 2869 N95-30863

Analysis of planar laser-induced fluorescence images obtained during shakedown testing of the AEDC impulse facility [AD-A293237] p 2884 N95-30906

Evaluation of calibration parameters and performance of the video imaging technique of assessing exposure (VITAE system) [AD-A289023] p 2927 N95-30998

DEPSCOR92-Wide field spectral imager [AD-A293079] p 2997 N95-31005

Theoretical aspects of electron emission holography [DE95-614371] p 2880 N95-31167

The future of space imaging. Report of a community-based study of an advanced camera for the Hubble Space Telescope [NASA-CR-195818] p 3028 N95-31364

Adaptive optics design for the advanced electro-optical system (AEOS) [AD-A293972] p 2974 N95-31527

Research in ground-to-air microwave imaging [AD-A292907] p 2852 N95-31551

Validation of the atmospheric transmission large-area analysis system (ATLAS) [AD-A293810] p 2916 N95-31589

An investigation of a novel approach to elemental imaging in three dimensions [DE95-010340] p 3000 N95-31681

Contamination detection NDE for cleaning process inspection p 2781 N95-31802

Diagnosing high density, fast-evolving plasmas using x-ray lasers [DE95-010734] p 3006 N95-32028

Enhanced brightness x-ray lasers [DE95-010735] p 2886 N95-32029

Scannerless Range Imaging with a square wave [DE95-009840] p 2854 N95-32145

The development of a pulsed laser imaging system for natural gas leak detection [DE95-011407] p 2887 N95-32280

IMMUNOLOGY

Conference perspective. Neuroimmunomodulation: Stress and immune function [AD-A291351] p 2926 N95-30870

IMPACT ACCELERATION

Design of digital low-pass filters for time-domain recursive filtering of impact acceleration signals [AD-A293086] p 2864 N95-31842

Structural analyses of the JPL Mars Pathfinder impact [DE95-009581] p 2767 N95-32081

IMPACT DAMAGE

Characterization and prediction of post-impact fatigue damage in stitched composites p 2785 N95-30826

Characterization of compressive damage mechanisms in ceramic and polymeric matrix composite materials [AD-A293171] p 2787 N95-30975

Post-impact fatigue of cross-plied, through-the-thickness reinforced carbon/epoxy composites [NASA-TM-110625] p 2896 N95-31419

IMPACT TESTS

High strain rate properties and constitutive modeling of glass [DE95-008434] p 2816 N95-31058

Aerophysics test program 1 [AD-A293890] p 2963 N95-31543

Vertical impact testing of two helmet-mounted night vision systems [AD-A293055] p 2931 N95-31671

IMPEDANCE

KRAKEN, a numerical model of RHIC impedances [DE95-011563] p 2994 N95-32242

IMPEDANCE MATCHING

Response of dual-layered structures subjected to shock pressure wave [AD-A293731] p 2896 N95-31568

IMPEDANCE MEASUREMENT

The impact of microbiologically influenced corrosion on protective polymer coatings [AD-A288896] p 2816 N95-30997

IMPELLERS

Laser anemometer measurements of the three-dimensional rotor flow field in the NASA low-speed centrifugal compressor [NASA-TP-3527] p 2756 N95-31985

IMPLANTATION

Formation of cavities in Si and their chemisorption of materials [DE95-009586] p 2980 N95-30708

Plasma source ion implantation of metal ions: Synchronization of cathodic-arc plasma production and target bias pulses [DE95-009431] p 3006 N95-31613

IMPLOSIONS

Ultrasonic cleaning: Fundamental theory and application p 2778 N95-31783

Basic science with pulsed power and some off-the-wall ideas [DE95-009486] p 2854 N95-32050

IMPULSE GENERATORS

Minimizing structural vibrations with Input Shaping (TM) [NASA-CR-189439] p 2893 N95-30786

IMPULSES

Worldwide intercomparison of impulse voltage measuring systems at 600 kV level [PB95-195574] p 2858 N95-30538

IMPURITIES

Power oscillator in the tokamaks training [DE95-616538] p 3003 N95-30473

Effects of particle fueling and plasma wall interactions on D3-D discharges [DE95-009608] p 3003 N95-30612

Alloying effects of Kondo insulators
[DE95-614308] p 3010 N95-30644
IR materials producibility
[AD-A293330] p 2998 N95-31141
Removal of impurity ions from a magnetic trap with a two-component plasma on their collision with fast component ions
[DE95-614171] p 2984 N95-31550

IN SITU MEASUREMENT
Experiments in a 120-mm ram accelerator including flow visualization p 2799 N95-31202

INCIDENT RADIATION
Theory of unsteady combustion of solids: Investigation of Quasi-steady assumption p 2800 N95-31285

INCOMPRESSIBLE FLOW
Velocity boundary conditions for vorticity formulations of the incompressible Navier-Stokes equations
[DE95-008715] p 2866 N95-30464
Axial loads on yawed rotors
[PB95-214193] p 2742 N95-30638
Acceleration potential models PREDICHAT/PREDICDYN applied for calculation of axisymmetric dynamic inflow cases
[PB95-207015] p 2869 N95-30957

INCONEL (TRADEMARK)
Modeling of stress distributions on the microstructural level in Alloy 600
[DE95-009135] p 2807 N95-31632
Modeling of grain boundary stresses in Alloy 600
[DE95-009033] p 2808 N95-31825

INDENTATION
Cracking during nanoindentation and its use in the measurement of fracture toughness
[DE95-008839] p 2818 N95-31175

INDEXES (DOCUMENTATION)
Research proposal
[AD-A293207] p 3032 N95-30899
SeaWiFS technical report series. Volume 24: SeaWiFS technical report series cumulative index, volumes 1-23
[NASA-TM-104566-VOL-24] p 2924 N95-32122

INDIUM ALLOYS
Volumetric and electro analytical techniques for chemical characterization of nuclear grade Ag-In-Cd alloys
[DE95-620664] p 2807 N95-31407

INDIUM GALLIUM ARSENIDES
Pseudomorphic heterostructure materials for high performance devices
[AD-A292906] p 2788 N95-31384

INDIUM PHOSPHIDES
The junction characteristics and current conduction mechanisms of GaInP2 n(+)p diodes and solar cells
[AD-A290857] p 2902 N95-30408
InP solar cell development on inexpensive Si substrates
[AD-A293255] p 2903 N95-30893
Carrier dynamics and optical properties of GaAs- and InP-based strained quantum well lasers
p 2886 N95-31848
Investigation of the basic physics of high efficiency semiconductor hot carrier solar cell
[NASA-CR-198945] p 2906 N95-32212

INDIUM SELENIDES
Investigation of polycrystalline thin film CuInSe2 solar cells based on ZnSe windows
[DE95-004068] p 2904 N95-31164

INDUCTANCE
A time stepping coupled finite element-state space modeling environment for synchronous machine performance and design analysis in the ABC frame of reference p 2864 N95-31948

INDUCTION (MATHEMATICS)
Data analysis: Naive inductivism
[PB95-212213] p 3026 N95-32254

INDUCTORS
Operational characteristics of a 200 C LC parallel resonant circuit
[NASA-TM-106983] p 2864 N95-31742

INDUSTRIAL MANAGEMENT
Manufacturing waste disposal practices of the chemical propulsion industry p 2771 N95-31748

INDUSTRIAL PLANTS
Network user's guide
[DE95-009185] p 2942 N95-31634

INDUSTRIAL WASTES
Manufacturing waste disposal practices of the chemical propulsion industry p 2771 N95-31748
Enhanced alkaline hydrolysis and biodegradability studies of nitrocellulose-bearing missile propellant
p 2772 N95-31752
National Center for Manufacturing Sciences: Environmentally conscious manufacturing
p 2773 N95-31758

INDUSTRIES
The Technology Information Environment with Industry (TIE-In): A mechanism for accessing laboratory solutions
[DE95-008542] p 3027 N95-30385
Metrics in method engineering
[PB95-197687] p 2838 N95-30455
An overview of high-speed networking for workstations
[DE95-009076] p 2947 N95-30577
The role of advanced engineering simulation in model-based design
[DE95-008815] p 2934 N95-30796
National Laboratories: Are their R and D activities related to commercial product development? Report to Congressional Requesters
[GAO/PEMD-95-2] p 3027 N95-31345
Development of the Multi-Level Seismic Receiver (MLSR)
[DE95-008823] p 2916 N95-31610
Industry participation workshop: Chromium electroplating of superconductor strand. Proceedings
[DE95-009629] p 2807 N95-31615

INELASTIC SCATTERING
Inelastic plasmon and inter-band electron-scattering potentials for Si from dielectric matrix calculations
[DE95-616778] p 2977 N95-30475
The effect of a non-Hermitian crystal potential on the scattering matrix in reflection electron diffraction
[DE95-616779] p 2977 N95-30476
Theoretical high energy physics
[DE95-003107] p 2991 N95-30527
May multiple inelastic scattering in CBED patterns be removed analytically
[PB95-196333] p 2992 N95-30717
Zone axis backscattered electron contrast for fast electrons
[DE95-616775] p 2980 N95-30790
K-shell ionization under zone axis electron diffraction conditions
[DE95-616780] p 2981 N95-30916

INEQUALITIES
Newton methods for large-scale linear inequality-constrained minimization: Optimization and systems theory
[PB95-210332] p 2956 N95-30499
The complexity and approximability of finding maximum feasible subsystems of linear relations
[TRITA-NA-9313] p 2961 N95-31648

INERTIA
Speed control of an elastic two-mass system: Optimization and systems theory
[PB95-212106] p 2888 N95-30701
Particle filtration: An analysis using the method of volume averaging
[DE95-009467] p 2875 N95-31592

INERTIAL CONFINEMENT FUSION
Porous spherical shells and microspheres by electrodispersion precipitation
[DE95-009073] p 2815 N95-30799
Free electron laser as energy driver for inertial confinement fusion
[DE95-614252] p 2884 N95-30914

INERTIAL GUIDANCE
Results from tests of the Kearfott T16-B Inertial Measurement Unit
[PB95-212031] p 2879 N95-30502

INERTIAL NAVIGATION
Results from tests of the Honeywell integrated flight management unit
[PB95-211355] p 2748 N95-30597

INFERENCE
A Stochastic EM algorithm for approximating the maximum likelihood estimate
[DE95-010328] p 2943 N95-32044
A stochastic difference equation approach to inference with missing data: Some new results
[DE95-010327] p 2944 N95-32088
A stochastic EM estimator in the presence of missing data: Theory and applications
[DE95-010329] p 2944 N95-32089

INFLATABLE STRUCTURES
Releaseable unconstrained inflatable body protector
[AD-D017350] p 2930 N95-30552

INFORMATION DISSEMINATION
The Los Alamos accelerator code group
[DE95-010989] p 2992 N95-31151
Report to Congressional Committees. Federal research: Interim report on the pilot technology access program
[GAO/RCED-94-75] p 3022 N95-32195

INFORMATION FLOW
Development of a CFC Critical Area Response (CAR) package p 2783 N95-31814

INFORMATION MANAGEMENT
Development of technical information processing systems
[DE95-613311] p 3024 N95-30882
Adaptiveness in information systems integration
p 3025 N95-31348
Defining manually enactable processes using the process definition information organizer templates (Software Technology for Adaptable, Reliable Systems (STARS) program)
[AD-A292854] p 2946 N95-32293

INFORMATION PROCESSING (BIOLOGY)
Physiology and physiopathology of equilibration
[PB95-208328] p 2926 N95-30494
Neurodynamical systems for cognition and target identification
[AD-A293111] p 2951 N95-30884
Temporal information processing mechanisms
[PB95-208344] p 3027 N95-32370

INFORMATION RETRIEVAL
Development of technical information processing systems
[DE95-613311] p 3024 N95-30882
An evaluation of an automatic markup system
[DE95-009885] p 3026 N95-32149
UNLV: Information Science Research Institute
[DE95-011941] p 3027 N95-32362

INFORMATION SYSTEMS
Protocols for integrity constraint checking in federated databases
[PB95-197695] p 3022 N95-30456
Data storage modeling and management for multimedia information systems p 3022 N95-30483
Proceedings of the CSCW 1994 workshop collaborative hypermedia systems
[PB95-208393] p 3023 N95-30496
Supporting data intensive applications with medium grained parallelism
[DE95-010164] p 3023 N95-30619
JPL Physical Oceanography Distributed Active Archive Center (PO.DAAC) data availability, version 1-94
[NASA-CR-198871] p 2922 N95-30859
An architectural approach to strategic information systems planning for the Office of Naval Intelligence
[AD-A289930] p 3024 N95-30928
Adaptiveness in information systems integration
p 3025 N95-31348
The quad-service satellite transmitting and receiving system for medical supply support: A battlefield interoperability and communications system prototype, volume 2. User documentation
[AD-A292835] p 2851 N95-31448
The quad-service satellite transmitting and receiving system for medical supply support: A battlefield interoperability and communications system prototype, volume 1
[AD-A292836] p 2851 N95-31449
The ATC operational evaluation of the prototype integrated terminal weather system (ITWS) at Dallas/Fort Worth and Orlando airports (May-September 1993)
[AD-A293808] p 2921 N95-31587
Requirements for security signalling
[DE95-008714] p 2948 N95-31605
Toward a risk-based approach to the assessment of the surety of information systems
[DE95-008821] p 3025 N95-31662
NEIS (NASA Environmental Information System)
p 2783 N95-31811
Multi-sensor data fusion in command and control and the merit of artificial intelligence p 2842 N95-32137
AIDEX: An expert system for aircraft identification
p 2842 N95-32138
The Telecommunications and Data Acquisition Report
[NASA-CR-198911] p 2854 N95-32221
Recommendations for protecting National Library of Medicine Computing and Networking Resources
[DE95-011554] p 3026 N95-32285

INFRARED ABSORPTION
Species and temperature profiles of propellant flames obtained from FTIR absorption spectroscopy
p 2801 N95-31303
Embedded infrared fiber optic absorption studies of nitramine propellant strand burning
p 2801 N95-31305
Improvements in infrared absorption of solid propellant flames p 2801 N95-31306
The development of a pulsed laser imaging system for natural gas leak detection
[DE95-011407] p 2867 N95-32260

INFRARED ASTRONOMY
XV NSO/Sac Peak Solar workshop
[AD-A292319] p 3030 N95-30482
Stratospheric Observatory For Infrared Astronomy (SOFIA). Phase A: System concept description
[NASA-TM-110669] p 3002 N95-32187

INFRARED DETECTORS
Optimization of a thermoelectric IR-detector for low working temperature
[NASA-CR-198933] p 2880 N95-30752

Apparent size passive range method
[AD-D017360] p 2753 N95-31180
Pseudomorphic heterostructure materials for high performance devices
[AD-A292906] p 2788 N95-31384
Quantum 1/f noise in high technology applications including ultrasmall structures and devices
[AD-A292812] p 2862 N95-31442
Data collection at the Lockheed Santa Cruz facility using midwave hyperspectral imagers
[AD-A293057] p 3000 N95-31672
TMD detection and tracking using improved AWACS sensors p 2840 N95-32128
Infrared and millimeter wave detection using thin films of Pb doped BiSrCaCuO superconductor
p 2840 N95-32129
Optimal infrared detector configurations for air target detection p 2841 N95-32130
The High Altitude Balloon Experiment demonstration of acquisition, tracking, and pointing technologies (HABE-ATP) p 2841 N95-32132
Feasibility of tropospheric water vapor profiling using infrared heterodyne differential absorption lidar
[DE95-009647] p 2917 N95-32142

INFRARED IMAGERY
Data collection at the Lockheed Santa Cruz facility using midwave hyperspectral imagers
[AD-A293057] p 3000 N95-31672
Analysis of target contrast improvement using polarization filtering in the infrared region
[AD-A293085] p 3001 N95-31841

INFRARED INSPECTION
Surface contamination analysis technology team overview p 2781 N95-31797

INFRARED INSTRUMENTS
Millimeter wave radiometer utility study
[AD-A293811] p 2852 N95-31590

INFRARED RADIATION
Optimization of a thermoelectric IR-detector for low working temperature
[NASA-CR-198933] p 2880 N95-30752
New material for high average power infrared generation: QPM-DB GaAs
[AD-A292714] p 2967 N95-30939
IR materials producibility
[AD-A293330] p 2998 N95-31141
Measurement and analysis related to infrared emissions
[AD-A293296] p 2998 N95-31192
Inductively coupled IR staring array based on photofluxonic pixels
[AD-A292784] p 2998 N95-31435
Use of body surface heat patterns for predicting and evaluating acute lower extremity pain among soldiers
[AD-A292829] p 2927 N95-31446
Annual meeting of the Advanced Light Source Users' Association
[DE95-009373] p 3000 N95-31635
Cleanliness evaluation of rough surfaces with diffuse IR reflectance p 2782 N95-31804
Design of an immersion echelle-prism mid-IR spectrograph for chemical remote sensing
[DE95-010729] p 2901 N95-32027
Infrared and millimeter wave detection using thin films of Pb doped BiSrCaCuO superconductor
p 2840 N95-32129
The theoretical calculation of vibrational circular dichroism spectra
[AD-A293614] p 2798 N95-32258
Spectral sky background in the IR: Measurements with FTIR
[PB95-222998] p 2922 N95-32315

INFRARED REFLECTION
Cleanliness evaluation of rough surfaces with diffuse IR reflectance p 2782 N95-31804

INFRARED SCANNERS
Next generation fire suppressants
p 2775 N95-31769

INFRARED SIGNATURES
Shiptracks in the Californian stratus region: Dependency on marine atmospheric boundary layer depth
[AD-A293272] p 2901 N95-31125

INFRARED SPECTRA
XV NSO/Sac Peak Solar workshop
[AD-A292319] p 3030 N95-30482
Cepheid temperature and the Blazhko effect
[NASA-CR-189433] p 3030 N95-31819
Growth, characterization and device development in monocrystalline diamond films
[AD-A293106] p 3015 N95-32018
Infrared and millimeter wave detection using thin films of Pb doped BiSrCaCuO superconductor
p 2840 N95-32129
GCMS and FTIR studies of by-product inhibited growth and the rate-limiting step in TEOS-based SiO2 CVD
[DE95-009863] p 3016 N95-32147
The theoretical calculation of vibrational circular dichroism spectra
[AD-A293614] p 2798 N95-32258

INFRARED SPECTROMETERS
Data collection at the Lockheed Santa Cruz facility using midwave hyperspectral imagers
[AD-A293057] p 3000 N95-31672
Cleanliness evaluation of rough surfaces with diffuse IR reflectance p 2782 N95-31804

INFRARED SPECTROSCOPY
Overview of IEA biomass combustion activities
[PB95-196374] p 2902 N95-30519
Species and temperature profiles of propellant flames obtained from FTIR absorption spectroscopy
p 2801 N95-31303
Non-intrusive combustion diagnostics of premixed hydrocarbon flames using FT-IR spectrometry
p 2797 N95-31732
Surface contamination analysis technology team overview p 2781 N95-31797
Standardization of surface contamination analysis systems p 2781 N95-31798
Study of surfaces using near infrared optical fiber spectrometry p 2781 N95-31801
Surface inspection using FTIR spectroscopy
p 2782 N95-31803
Growth, characterization and device development in monocrystalline diamond films
[AD-A293106] p 3015 N95-32018

INFRARED TELESCOPES
Stratospheric Observatory For Infrared Astronomy (SOFIA). Phase A: System concept description
[NASA-TM-110669] p 3002 N95-32187

INFRARED TRACKING
Apparent size passive range method
[AD-D017360] p 2753 N95-31180

INHOMOGENEITY
Solvability of a class of hypersingular nonlinear integral equations
[PB95-207031] p 3011 N95-30720
Dynamics of an inhomogeneous anisotropic antiferromagnetic spin chain
[DE95-614449] p 3013 N95-30959

INJECTION
Visible light emitting materials and injection devices
[AD-A292701] p 2786 N95-30934
Active control of combustion instability using injection techniques p 2800 N95-31288
Compressible turbulence measurement in low-angle injection into a supersonic flow
[AD-A293836] p 2874 N95-31516

INJECTION LASERS
Carrier dynamics and optical properties of GaAs- and InP-based strained quantum well lasers
p 2886 N95-31848

INJECTORS
Design and testing of an oxidizer-rich preburner
p 2799 N95-31212

INLET FLOW
Effects of initial conditions on a single jet in crossflow
[NASA-TM-107002] p 2754 N95-30589
An investigation of the side-dump dual in-line ramjet combustor p 2756 N95-31199
A pulsed liquid fuel ramjet p 2756 N95-31201

INNER RADIATION BELT
Oxygen charge state abundance in the inner magnetosphere
[AD-A293497] p 2915 N95-31536

INPUT/OUTPUT ROUTINES
Selecting optimal experiments for feedforward multilayer perceptrons
[AD-A290856] p 2949 N95-30406
Operator's handbook: NAWC Software Production Facility
[AD-A290216] p 2935 N95-31001

INSERTS
Gear pump with reduced fluid-borne noise
[AD-D017362] p 2887 N95-30399

INSPECTION
Metrology of chrome on quartz photomasks using low voltage scanning electron microscopy. Part 1: Physical SEM parameters
[PB95-195780] p 2880 N95-30693
Applying program comprehension techniques to improve software inspections p 2937 N95-31241
An experiment to assess the cost-benefits of code inspections in large scale software development
p 2937 N95-31242
Computer-aided inspection process definition: Development of an expert planning and programming system for coordinate metrology
[DE95-010411] p 2940 N95-31404
Cleanliness inspection tool for RSRM bond surfaces
p 2781 N95-31799
Contamination detection NDE for cleaning process inspection p 2781 N95-31802
Surface inspection using FTIR spectroscopy
p 2782 N95-31803
Verification of surface preparation for adhesive bonding p 2782 N95-31807
Space Shuttle Orbiter corrosion history, 1981-1993: A review and analysis of issues involving structures and subsystems
[NASA-TM-104810] p 2810 N95-32183
Nondestructive testing of ceramic components: Cooperative Research and Development Agreement completion report
[DE95-009510] p 2823 N95-32352

INSPIRATION
The art and science of magnet design: Selected notes of Klaus Halbach, volume 2
[DE95-008450] p 2861 N95-31059

INSTALLING
RASSP benchmark 1 executable requirements user's manual
[AD-A290060] p 2935 N95-30931

INSTANTONS
Instanton - antiinstanton interaction and asymptotics of perturbation theory expansion of in double well oscillator
[DE95-619245] p 2966 N95-31259

INSTRUMENT APPROACH
Aviation capacity enhancement plan 1994
[AD-A292758] p 2747 N95-31428
An exploratory survey of information requirements for instrument approach charts
[AD-A293882] p 2749 N95-31520

INSTRUMENT ERRORS
The effects of clock errors on timescale stability
p 2971 N95-32342
Allan deviation computations of a linear frequency synthesizer system using frequency domain techniques
p 2972 N95-32344

INSTRUMENT LANDING SYSTEMS
An exploratory survey of information requirements for instrument approach charts
[AD-A293882] p 2749 N95-31520

INSTRUMENT TRANSFORMERS
Operational characteristics of a 200 C LC parallel resonant circuit
[NASA-TM-106983] p 2864 N95-31742

INSULATION
Behaviour of polymers in radioactive environments: Effects of dose speed
[DE95-621008] p 2818 N95-31221
Thin-film edge field emitter device and method of manufacture therefor
[AD-D017453] p 2862 N95-31275
Waterjet processes for coating removal
p 2777 N95-31779

INSURANCE (CONTRACTS)
Workflow literature guide, version 1
[PB95-207080] p 2947 N95-30721

INTEGERS
Analysis of symbolic parameter models
[AD-A292916] p 2940 N95-31459

INTEGRAL EQUATIONS
Extensions and results from a method for evaluating fractional integrals
[DE95-616272] p 2954 N95-30425
Potential integral equations of the 2D Laplace operator in wavelet basis
[TRITA-NA-9401] p 2957 N95-30713
Solvability of a class of hypersingular nonlinear integral equations
[PB95-207031] p 3011 N95-30720
Relativistic non-interacting electron gas in a magnetic field
[DE95-616903] p 2967 N95-31177
Quasi-Newton updating for large scale nonlinear systems
[AD-A292776] p 2940 N95-31431
Review of longitudinal perturbation formalism
[DE95-010894] p 2990 N95-32278

INTEGRAL TRANSFORMATIONS
Singular eigenfunctions for shearing fluids I
[DE95-008952] p 2868 N95-30763

INTEGRALS
Extensions and results from a method for evaluating fractional integrals
[DE95-616272] p 2954 N95-30425
Integrals of motion in the two Killing vector reduction of general relativity
[DE95-616281] p 3018 N95-30431
The quantum interference effect in semiconductor space charge layers studied by Feynman path integrals: General formalism and illustrative examples
[DE95-614483] p 3010 N95-30653
Antipodes and integrals in Hopf algebras over rings and quantum Yang-Baxter equation
[PB95-212155] p 2961 N95-31397

A unified interpretation of singular and near-singular integrals in the boundary element method
[ISBN-0-315-86297-1] p 2962 N95-31947

INTEGRATED CIRCUITS
Space qualified hybrid superconductor/semiconductor planar oscillator circuit
[NASA-TM-106978] p 3011 N95-30703
Coherent integrator
[AD-D017422] p 2847 N95-30743
Diamond thin film temperature and heat-flux sensors
[NASA-CR-198859] p 3012 N95-30847
Intelligent finite element submodeling of multichip modules for reliability analysis
[AD-A292911] p 2940 N95-31455
Feasibility study concerning an active millimeterwave sensor. Project phase MMS2.1
[PB95-210399] p 2882 N95-32245
Hyperfrequency components
[PB95-208302] p 2866 N95-32369

INTEGRATED LIBRARY SYSTEMS
Development of technical information processing systems
[DE95-613311] p 3024 N95-30882

INTEGRATED MISSION CONTROL CENTER
FAA aviation forecasts: Fiscal year 1995-2006
[AD-A293682] p 2741 N95-31598

INTEGRATED OPTICS
A study of end-fire coupling of single-mode fiber to Ti: LiNbO3-single-mode planar waveguide
[AD-A293249] p 2997 N95-30909

INTEGRATORS
Coherent integrator
[AD-D017422] p 2847 N95-30743

INTELLIGENCE
An architectural approach to strategic information systems planning for the Office of Naval Intelligence
[AD-A289930] p 3024 N95-30928

INTELLIGENCE TESTS
Selection of Swedish scholastic aptitude test takers as a function of socioeconomic background and ability: Evaluation through follow-up
[PB95-212072] p 3021 N95-30699
Non-comparability of female and male admission test takers: Evaluation through follow-up
[PB95-212080] p 3021 N95-30700

INTERATOMIC FORCES
Molecular dynamics simulations of high energy cascades in iron
[DE95-010116] p 2982 N95-31104

INTERCALATION
Lithium ion aqueous cells
[AD-A293828] p 2905 N95-31554

INTERFACE STABILITY
Dissolution of eutectic microstructures
[DE95-010244] p 2804 N95-30757

INTERFACES
TEM-examination of ceramic-metal interfaces
[PB95-196531] p 2813 N95-30664
Computer interface development for the petite amateur navy satellite (PANSAT) simulator
[AD-A293263] p 2766 N95-31388
A programming interface for application-aware adaptation in mobile computing
[AD-A293107] p 2943 N95-32019

INTERFACIAL ENERGY
Control of interfacial chemistry and mechanical properties in metal/ceramic composites
p 2790 N95-31976

INTERFACIAL TENSION
Existence of solutions in plane quasistationary stokes flow driven by surface tension
[PB95-197935] p 2868 N95-30810

INTERFERENCE IMMUNITY
Interference rejection techniques in a DS spread-spectrum HF radio system
[PB95-211660] p 2846 N95-30479

INTERFEROMETERS
Demodulators for optical fiber interferometers with (3 x 3) outputs
[AD-D017415] p 2995 N95-30402
Fiber optic accelerometer with centrally supported flexural disk
[AD-D017369] p 2879 N95-30658
Fiber optic interferometric electric field and voltage sensor utilizing and electrostrictive transducer
[AD-D017433] p 2996 N95-30753
Microwave electro-optic mixer
[AD-D017328] p 2862 N95-31179
Photorefractive nonlinear optics
[AD-A292913] p 2999 N95-31458

INTERFEROMETRY
Multi-particle correlations in quaternionic quantum systems
[DE95-616271] p 3018 N95-30424
Interferometry with particles of non-zero rest mass: Topological experiments
[DE95-616244] p 2979 N95-30689
Fiber optic interferometric electric field and voltage sensor utilizing and electrostrictive transducer
[AD-D017433] p 2996 N95-30753
X-ray standing wave interferometry-optics at 1 angstrom with applications to surface and material sciences
[DE95-011453] p 2998 N95-31114
Photorefractive nonlinear optics
[AD-A292913] p 2999 N95-31458
Diagnosing high density, fast-evolving plasmas using x-ray lasers
[DE95-010734] p 3006 N95-32028

INTERGRANULAR CORROSION
Modeling of stress distributions on the microstructural level in Alloy 600
[DE95-009135] p 2807 N95-31632
Modeling of grain boundary stresses in Alloy 600
[DE95-009033] p 2808 N95-31825

INTERIOR BALLISTICS
The 31st JANNAF Combustion Subcommittee Meeting, volume 1 p 2825 N95-31194

INTERLAYERS
Diffraction-line broadening analysis and stress relaxation in thin metal layers
[PB95-213898] p 2893 N95-30634
Ultrasonic characterization of fiber-matrix interphasial properties and damage in high-temperature composites
p 2785 N95-30823
Control of interfacial chemistry and mechanical properties in metal/ceramic composites
p 2790 N95-31976

INTERMETALLICS
Reaction synthesis of intermetallics
[DE95-009029] p 2803 N95-30575
Determination of site-occupancies in aluminide intermetallics by ALCHEMI
[DE95-009179] p 2803 N95-30733
Ultrasonic characterization of fiber-matrix interphasial properties and damage in high-temperature composites
p 2785 N95-30823
Innovative processing of composites for ultra-high temperature applications, book 2
[AD-A290890] p 2786 N95-30898
Review of environmental effects in intermetallics
[DE95-010120] p 2805 N95-31106
The 10th International Conference on the Strength of Materials
[AD-A292335] p 2894 N95-31263
Control of interfacial chemistry and mechanical properties in metal/ceramic composites
p 2790 N95-31976
Defect configurations in neutron-irradiated U3Si2
[DE95-009896] p 3016 N95-32105
Comprehensive research on the stability and electronic properties of a-Si:H and a-SiGe:H alloys and devices
[DE95-004088] p 2810 N95-32154

INTERMODULATION
Intermodulation Interference (IMI) testing of composite materials
[AD-A288621] p 2787 N95-31146

INTERNAL COMBUSTION ENGINES
Low vibration polymeric composite engine
[AD-D017332] p 2887 N95-30386
Implementation of KIVA-3 on distributed memory MIMD computers
[DE95-010288] p 2931 N95-31130

INTERNAL ENERGY
Computation of high-altitude hypersonic flow-field radiation p 2743 N95-30843

INTERNAL FLOW
Effects of cavity bleed and its configuration on aerodynamic characteristics of supersonic internal flow
[NAL-TR-1247] p 2744 N95-31715

INTERNATIONAL COOPERATION
Mars together and FIRE and ICE: Report of the joint US/Russian technical working groups
[NASA-CR-198864] p 3030 N95-30845
Mir 18 post flight presentation
[NASA-TM-110657] p 2766 N95-30854

INTERNETS
The Los Alamos accelerator code group
[DE95-010989] p 2992 N95-31151
Recommendations for protecting National Library of Medicine Computing and Networking Resources
[DE95-011554] p 3026 N95-32285

INTERORBITAL TRAJECTORIES
A feedback linearization approach to orbital maneuvers p 2765 N95-30841

INTERPLANETARY MAGNETIC FIELDS
Low-latitude boundary layer near noon: An open field line model
[ATR-93(7270)-1] p 2914 N95-30773

INTERPLANETARY SPACE
Radiation effects in space: The Clementine 1 mission
[DE95-011513] p 3032 N95-32282

INTERPLANETARY SPACECRAFT
The application of noncoherent Doppler data types for Deep Space Navigation p 2765 N95-32226

INTERPLANETARY TRAJECTORIES
The application of noncoherent Doppler data types for Deep Space Navigation p 2765 N95-32226

INTERPOLATION
Complex mean value interpolation
[PB95-211629] p 2956 N95-30601
Analytic cross sections for collisions of H, H2, He and Li atoms and ions with atoms and molecules
[DE95-722055] p 2979 N95-30654
Preservation theorems on finite structures
[DE95-613442] p 2962 N95-32067
Evaluation of discretization procedures for transition elements in adaptive mesh refinement
[NASA-CR-199037] p 2944 N95-32190

INTERPROCESSOR COMMUNICATION
Compact location problems with budget and communication constraints
[DE95-010876] p 2948 N95-32277

INTERSTELLAR GAS
A search for interstellar CH3D: Limits to the methane abundance in Orion-KL
[NASA-CR-198932] p 3029 N95-30751

INTERSTITIALS
Molecular dynamics simulations of high energy cascades in iron
[DE95-010116] p 2982 N95-31104
The influence of microstructure on creep deformation in near-gamma TiAl alloys p 2808 N95-31975

INTERVALS
The remainder form and the cord-slope form in global optimization with interval methods p 2941 N95-31533

INTRAVASCULAR SYSTEM
Decompression illness, observable bubbles. (Session K)
[PB95-195285] p 2926 N95-30511
Detecting intravascular gas bubbles in ultrasonic images
[PB95-195301] p 2926 N95-30513
Arterial gas bubbles after decompression in pigs with Patent Foramen Ovale
[PB95-195319] p 2925 N95-30515

INTRUSION
Arithmetic features of rational conformal field theory
[PB95-207908] p 2966 N95-30591

INVARIANCE
The search for the decay of Z boson into two gamma as a test of Bose statistics
[DE95-616373] p 2976 N95-30393
CP violating effects in e(+) e(-) yields ZH and their optimization
[DE95-616302] p 2976 N95-30441
Canonical symmetric invariant pairings in vertex operator super algebras and gramians
[PB95-208112] p 2955 N95-30488
Dressing symmetry of the uniformization solution of Liouville equation
[DE95-613380] p 2956 N95-30607
The iteration formula of the Maslov-type index theory with applications to nonlinear Hamiltonian systems
[DE95-613379] p 2957 N95-30676
Generalized controlled invariance for nonlinear systems
[PB95-197901] p 2950 N95-30807
Studies of the strong and electroweak interactions at the Z(sub 0) pole
[DE95-010353] p 2986 N95-31682

INVERSE SCATTERING
Inversion of the total cross sections for electron-molecule and electron-atom scattering
[DE95-616466] p 2978 N95-30583
Inverse and control problems in electromagnetics
[AD-A292993] p 2849 N95-30962
Fast algorithms for three-dimensional inverse scattering problems
[AD-A293510] p 2852 N95-31537

INVERSIONS
Dynamic inversion: An evolving methodology for flight control design p 2758 N95-31996

INVERTERS
Operational characteristics of a 200 C LC parallel resonant circuit
[NASA-TM-106963] p 2884 N95-31742

INVISCID FLOW
Development of a linearized unsteady Euler analysis for turbomachinery blade rows
[NASA-CR-4677] p 2742 N95-30611
Axial loads on yawed rotors
[PB95-214193] p 2742 N95-30638

Parametrics on 2D Navier-Stokes analysis of a Mach 2.68 bifurcated rectangular mixed-compression inlet
[NASA-TM-107003] p 2755 N95-30861
Wave propagation in a fluid-loaded homogeneous, transversely isotropic, elastic cylinder of arbitrary thickness
[AD-A292728] p 2869 N95-30946
Acceleration potential models PREDICHAT/PREDICDYN applied for calculation of axisymmetric dynamic inflow cases
[PB95-207015] p 2869 N95-30957

IODIDES
Evaluation of halon alternatives in inerting experiments
[AD-A293774] p 2795 N95-31580

IODINE
Flow models for the design of a hypersonic iodine vapor wind tunnel nozzle with chemical and vibrational nonequilibrium effects p 2742 N95-30448
Optical frequency standards: Hertz-level working standards and their absolute frequency measurement
[AD-A293930] p 2999 N95-31515

ION ACCELERATORS
Workshop on transport for a common ion driver
[DE95-007298] p 2992 N95-31166
Skew chromaticity in large accelerators
[DE95-011564] p 2994 N95-32243

ION BEAMS
Fabrication and modification of metal nanocluster composites using ion and laser beams
[DE95-009131] p 2784 N95-30731
Hollow cathode electron gun research and development
[DE95-010262] p 2992 N95-31127
Workshop on transport for a common ion driver
[DE95-007298] p 2992 N95-31166
Experiments with highly charged ions up to bare U(sup 92+) on the electron beam ion trap
[DE95-008827] p 2982 N95-31174
Substrate heating measurements in pulsed ion beam film deposition
[DE95-010862] p 2818 N95-31377
Ion-Assisted Pulsed Laser Deposition of amorphous tetrahedral-coordinated carbon films
[DE95-010861] p 2885 N95-31394
Target diagnostics for intense lithium ion hohlraum experiments on PBFA 2
[DE95-008517] p 3006 N95-31626
A study of ion trapping and instability in the Fermilab antiproton accumulator p 2993 N95-31647
Growth, characterization and device development in monocrystalline diamond films
[AD-A293106] p 3015 N95-32018
Studies of highly charged ions with EBIT and Super-EBIT
[DE95-010251] p 2987 N95-32038
Excitation mechanisms of 2s(sub 1/2)-2p(sub 3/2) and 2p(sub 1/2)-2p(sub 3/2)in U(82+) through U(89+)
[DE95-010265] p 2993 N95-32042
Microstructure of Al2O3 irradiated with an applied electric field
[DE95-010278] p 2822 N95-32043
Skew chromaticity in large accelerators
[DE95-011564] p 2994 N95-32243
Design study of prototype accelerator and MeV test facility for demonstration of 1 MeV, 1 A negative ion beam production
[DE95-737208] p 2995 N95-32262
STM measurements of the interaction of vacancies and steps during low-energy-ion bombardment of Si(001)
[DE95-010935] p 3017 N95-32308

ION CONCENTRATION
Membrane transport: A cellular probe of heat stroke
[AD-A293327] p 2926 N95-30924

ION CURRENTS
Mechanisms of enhanced ionic conduction at interfaces in ceramics
[DE95-009125] p 2814 N95-30730

ION DENSITY (CONCENTRATION)
Energy spectra of charge-exchange atoms from a rotating plasma
[DE95-614179] p 3006 N95-32054

ION ENGINES
Beam-centroid tracking instrument for ion thrusters
[AD-A293654] p 2769 N95-31567

ION EXCHANGING
Laboratory robotics: An automated tool for preparing Ion Chromatography calibration standards
[DE95-009441] p 2798 N95-32318

ION IMPLANTATION
Ion implantation and thermal stress resistance of ceramics
[DE95-615349] p 2812 N95-30451
Structural investigation of xenon ion-beam-irradiated glassy carbon
[DE95-616777] p 2977 N95-30474
Semiconductor nanocrystals formed in SiO2 by ion implantation
[DE95-008900] p 2978 N95-30546
Fabrication and modification of metal nanocluster composites using ion and laser beams
[DE95-009131] p 2784 N95-30731
Amorphization threshold in Si-implanted strained SiGe alloy layers
[DE95-008901] p 2804 N95-30797
Plasma source ion implantation of metal ions: Synchronization of cathodic-arc plasma production and target bias pulses
[DE95-009431] p 3006 N95-31613
Suppression of self-interstitials in silicon during ion implantation via in-situ photoexcitation
[DE95-009173] p 3016 N95-32301

ION IRRADIATION
Structural investigation of xenon ion-beam-irradiated glassy carbon
[DE95-616777] p 2977 N95-30474
Effect of irradiation spectrum on the microstructure of ion-irradiated Al2O3
[DE95-010225] p 2806 N95-31188
Cascade damage in the ordered alloy Ni3Al
[DE95-009893] p 2809 N95-32104

ION SCATTERING
Theoretical high energy physics
[DE95-003107] p 2991 N95-30527
Kinematical threshold of recoil-ion longitudinal momentum distribution in single ionization of helium by protons and alpha particles
[DE95-010803] p 2990 N95-32271

ION TEMPERATURE
Shear flow effects on ion thermal transport in tokamaks
[DE95-009115] p 3005 N95-30801

ION TRAPS (INSTRUMENTATION)
EBIT: Electron Beam Ion Trap V-division experimental physics
[DE95-010207] p 3004 N95-30769
Experiments with highly charged ions up to bare U(sup 92+) on the electron beam ion trap
[DE95-008827] p 2982 N95-31174

IONIC COLLISIONS
State resolved dynamics of ion-molecule collisions in a flowing afterglow
[AD-A290895] p 2976 N95-30410
Analytic cross sections for collisions of H, H2, He and Li atoms and ions with atoms and molecules
[DE95-722055] p 2979 N95-30654
EBIT: Electron Beam Ion Trap V-division experimental physics
[DE95-010207] p 3004 N95-30769
Convoy electron emission from surfaces
[DE95-010298] p 2984 N95-31402
Removal of impurity ions from a magnetic trap with a two-component plasma on their collision with fast component ions
[DE95-614171] p 2984 N95-31550
Applications of chiral symmetry
[DE95-009552] p 2988 N95-32079
Generalized Ramsauer-Townsend minima in heavy-ion induced electron continua
[DE95-010913] p 2989 N95-32120
Kinematical threshold of recoil-ion longitudinal momentum distribution in single ionization of helium by protons and alpha particles
[DE95-010803] p 2990 N95-32271
Study of aligned states in ion-atom collisions
[DE95-010825] p 2990 N95-32275

IONIC MOBILITY
State resolved dynamics of ion-molecule collisions in a flowing afterglow
[AD-A290895] p 2976 N95-30410

IONIC REACTIONS
Laboratory simulated hydrothermal alteration of sedimentary organic matter from Guaymas Basin, Gulf of California
[NASA-CR-198951] p 2914 N95-30865
Amorphization and the effect of implanted ions in SiC
[DE95-009699] p 2985 N95-31642

IONIZATION
Low-density ionization behavior
[DE95-009495] p 2980 N95-30705
Determination of site-occupancies in aluminide intermetallics by ALCHEMI
[DE95-009179] p 2803 N95-30733
K-shell ionization under zone axis electron diffraction conditions
[DE95-616780] p 2981 N95-30916
The antiproton-hydrogen atom interaction
[DE95-010252] p 2987 N95-32039
Validity of the differential equations for ionization cooling
[DE95-010438] p 2989 N95-32160

IONIZATION CROSS SECTIONS
Ionization of He by highly charged ions at low velocity
[DE95-010815] p 2990 N95-32273

IONIZATION POTENTIALS
Absorption and ionization spectra of model rubredoxins
[AD-A293668] p 2796 N95-31691

IONIZED GASES
Low-density ionization behavior
[DE95-009495] p 2980 N95-30705

IONOSPHERIC DISTURBANCES
Measurements of ionospheric variability
[AD-A293495] p 2915 N95-31535

IONOSPHERIC ELECTRON DENSITY
A prototype ionospheric tomography system (ITS)
[AD-A293015] p 2916 N95-31698

IONOSPHERIC PROPAGATION
Kiruna geophysical data. Data summary 94/4-6, April-June 1994
[PB95-210365] p 2913 N95-30627
Kiruna geophysical data. Data summary 94/1-3, January-March 1994
[PB95-210373] p 2913 N95-30628
Measurements of ionospheric variability
[AD-A293495] p 2915 N95-31535
Underdense heating of the ionosphere using oblique high power HF radiowaves p 2917 N95-31951

IONOSPHERIC SOUNDING
A prototype ionospheric tomography system (ITS)
[AD-A293015] p 2916 N95-31698

IONS
Study of cross-tail current carriers in magnetotail p 3005 N95-30804
Studies of C(60) and C(70) and other fullurenes: Synthesis, derivation, electrochemistry, lubricant properties and new composition materials
[AD-A292726] p 3012 N95-30944
Effect of irradiation spectrum on the microstructure of ion-irradiated Al2O3
[DE95-010225] p 2806 N95-31188
Convoy electron emission from surfaces
[DE95-010298] p 2984 N95-31402
Amorphization and the effect of implanted ions in SiC
[DE95-009699] p 2985 N95-31642
A study of ion trapping and instability in the Fermilab antiproton accumulator p 2993 N95-31647
Studies of highly charged ions with EBIT and Super-EBIT
[DE95-010251] p 2987 N95-32038
Microstructure of Al2O3 irradiated with an applied electric field
[DE95-010278] p 2822 N95-32043

IRIDIUM
Advanced small rocket chambers. Option 3: 110 1bf Ir-Re rocket, volume 1
[NASA-CR-195435-VOL-1] p 2768 N95-31169

IRIDIUM ALLOYS
High-temperature oxidation behavior of iridium-rhenium alloys
[NASA-TM-106720] p 2803 N95-30593

IRON
Reaction synthesis of intermetallics
[DE95-009029] p 2803 N95-30575
Hydrogen absorption in iron and steel during gas tungsten arc welding
[PB95-197018] p 2804 N95-30776
Localization in tungsten heavy alloys subjected to shearing deformations under superimposed high pressures
[AD-A293177] p 2804 N95-30977
Molecular dynamics simulations of high energy cascades in iron
[DE95-010116] p 2982 N95-31104
Measurements of quantum electrodynamic sensitive transitions in Na-like and Cu-like ions
[DE95-011593] p 3007 N95-32299

IRON ALLOYS
Effect of local melting on tribology in metal cutting
[PB95-195392] p 2804 N95-31052
Molecular dynamics simulations of high energy cascades in iron
[DE95-010116] p 2982 N95-31104
Review of environmental effects in intermetallics
[DE95-010120] p 2805 N95-31106
The effect of grain refinement on the room-temperature ductility of as-cast Fe3Al-based alloys
[DE95-010121] p 2805 N95-31107
Shape memory properties of an iron modified nickel aluminide alloy
[DE95-010223] p 2805 N95-31111
Influence of strain rate and temperature on the mechanical behavior of iron aluminide-based alloys
[DE95-009426] p 2808 N95-31836
Residual stress distribution in FeAl weld overlay on steel
[DE95-009178] p 2899 N95-32317

IRON OXIDES
Investigation of Fe3O4 colloid behaviour in a magnetic field by polarized neutron transmission
[DE95-614351] p 2981 N95-30915
IRRADIANCE
Optimum truncation of a Gaussian beam for propagation through atmospheric turbulence
[AD-A291156] p 2883 N95-30394
IRRADIATION
Behaviour of polymers in radioactive environments: Effects of dose speed
[DE95-621008] p 2818 N95-31221
Microstructure of Al2O3 irradiated with an applied electric field
[DE95-010278] p 2822 N95-32043
ISING MODEL
Simulation with complex measures
[DE95-616333] p 2955 N95-30445
Multisite antiferromagnetic Ising spin model: Phase transition through doubling bifurcation
[DE95-614311] p 3011 N95-30722
ISOELECTRONIC SEQUENCE
Inner- and outer-shell excitation in lithium isoelectronic sequence
[DE95-614107] p 2981 N95-31003
ISOLATION
Microwave repeater with broadband active and/or passive isolation control
[AD-D017358] p 2846 N95-30417
Faster, cheaper radioanalytical methods
[DE95-009913] p 2797 N95-32061
ISOMERIZATION
Specific rate coefficients from vibrational overtone activation of 1-methylcyclopropene
[AD-A288755] p 2793 N95-31014
ISOMERS
Enantioselectivity of quinoprotein alcohol dehydrogenases: Production of enantiomerically pure C3-alcohol synthons
[PB95-196960] p 2771 N95-30734
ISOMORPHISM
Around Ratner --- applications of Ratner's measure and topological theorems on unipotent homogeneous actions
[DE95-613377] p 2958 N95-30770
ISOSTATIC PRESSURE
Gelcasting of sintered reaction-bonded silicon nitride for improved mechanical properties
[DE95-010282] p 2822 N95-32085
ISOTOPIC SPIN
Electromagnetic hadron mass differences and estimation of isotopic symmetry violation parameters of QCD vacuum from quark model
[DE95-613628] p 2985 N95-31621
Spin puzzle in nucleon
[DE95-613654] p 2991 N95-32353
ISOTROPIC TURBULENCE
Analysis and modeling of subgrid scalar mixing using numerical data
[NASA-CR-198169] p 2877 N95-31978
ISOTROPY
Structural, chemical and electronic properties of superconducting thin films and junctions
[AD-A292700] p 3012 N95-30933
Wave propagation in a fluid-loaded homogeneous, transversely isotropic, elastic cylinder of arbitrary thickness
[AD-A292728] p 2869 N95-30946
Satellite test of the isotropy of the one-way spe ed of light using ExTRAS p 2973 N95-32349
ITERATION
Convergence properties of an augmented lagrangian algorithm for optimization with a combination of general equality and linear constraints
[PB95-208039] p 2956 N95-30570
Pseudo-time methods for constrained optimization problems governed by PDE
[NASA-CR-195081] p 2959 N95-31120
A stochastic EM estimator in the presence of missing data: Theory and applications
[DE95-010329] p 2944 N95-32089
ITERATIVE SOLUTION
Semi-iterative method for estimation of the dipole parameters using the knowledge of the dipole orientation
[PB95-211736] p 2858 N95-30480
Use of element-by-element preconditioners to solve large scale partially separable optimization problems
[PB95-195772] p 2957 N95-30692
Effect of the stopping of the Newton iteration in implicit linear multistep methods
[PB95-207056] p 2959 N95-31184
Quasi-Newton updating for large scale nonlinear systems
[AD-A292776] p 2940 N95-31431
Multipoint quadratic approximation for numerical optimization
[AD-A293837] p 2961 N95-31557

J

J INTEGRAL
Numerical evaluation of three-dimensional crack-tip integrals for layered anisotropic solids
p 2898 N95-32191
JAHN-TELLER EFFECT
Calculated structures and electronic absorption spectroscopy for magnesium phthalocyanine and its anion radical
[AD-A293672] p 2796 N95-31596
On the Jahn-Teller effect of Mn(2+) in zinc-blende ZnS crystal
[AD-A293711] p 2797 N95-31830
JAPAN
Directory of global environmental sciences in Japan
p 2899 N95-31413
An assessment of worldwide supercomputer usage
[DE95-009879] p 2932 N95-31645
Translation workbench for generating subtitles for English TV news
[NHK-435] p 3026 N95-32182
JAPANESE SPACECRAFT
Evaluation of static strength of T800H/PMR-15 carbon/polyimide laminates at room temperature and 300 C
[NAL-TR-1254] p 2789 N95-31740
JAS-39 AIRCRAFT
SAAB experience with PIO p 2746 N95-31069
JET CONTROL
Control of high Reynolds number round jets
p 2876 N95-31733
JET ENGINES
An active liner system for jet engine exhaust silencers, phase 1
[AD-A293277] p 2756 N95-31191
JET EXHAUST
Hot jet/wake turbulent structure and laser propagation. Part 3: Laser propagation measurements and modeling
p 2871 N95-30992
JET FLAPS
A wind tunnel investigation of the effects of micro-vortex generators and Gurney flaps on the high-lift characteristics of a business jet wing
[NASA-TM-110626] p 2750 N95-30827
JET FLOW
Simulation of chemical kinetics in turbulent natural gas combustion. Volume 2: Experimental studies of nitric oxide production in gas flames
[PB95-196721] p 2791 N95-30541
Effects of initial conditions on a single jet in crossflow
[NASA-TM-107002] p 2754 N95-30589
Hot jet/wake turbulent structure and laser propagaion. Part 1: Jet/wake turbulence modeling
p 2871 N95-30991
Hot jet/wake turbulent structure and laser propagation. Part 3: Laser propagation measurements and modeling
p 2871 N95-30992
Large eddy simulation of jets using structured upwind numerics p 2871 N95-30993
Control of high Reynolds number round jets
p 2876 N95-31733
JET IMPINGEMENT
Cleaning verification by air/water impingement
p 2782 N95-31805
JET MIXING FLOW
An experimental study of planar heterogeneous supersonic confined jets
[AD-A290859] p 2867 N95-30557
Effects of initial conditions on a single jet in crossflow
[NASA-TM-107002] p 2754 N95-30589
Jet mixing and emission characteristics of transverse jets in annular and cylindrical confined crossflow
[NASA-TM-106976] p 2755 N95-30698
Jet mixing in a reacting cylindrical crossflow
[NASA-TM-106975] p 2755 N95-30853
Large eddy simulation of jets using structured upwind numerics p 2871 N95-30993
JET NOZZLES
An experimental study of planar heterogeneous supersonic confined jets
[AD-A290859] p 2867 N95-30557
JOINTS (ANATOMY)
Automated volumetric grid generation for finite element modeling of human hand joints
[DE95-009575] p 2928 N95-32097
JOINTS (JUNCTIONS)
Photochemistry of intermolecular C-H bond activation reactions
[DE95-008991] p 2978 N95-30574
Response of mechanically fastened composite joints under multiple bypass loads p 2785 N95-30824
New material for high average power infrared generation: QPM-DB GaAs
[AD-A292714] p 2967 N95-30939
Development of integrated insulation joint for cooling pipe in tokamak reactor
[DE95-737220] p 3007 N95-32264
JOSEPHSON JUNCTIONS
A simple model for the dc flux transformer in layered superconductors with Josephson coupling
[DE95-614468] p 2859 N95-30649
Josephson break junction thin film device
[AD-D017343] p 3011 N95-30673
HTS Josephson technology on silicon with application to high speed digital microelectronics
[AD-A288627] p 2861 N95-31147
Dynamics of Current Driven Disordered Josephson Junction Arrays
[DE95-009418] p 3014 N95-31231
High-resolution superconducting x-ray spectrometers with aluminum trapping layers of different thicknesses
[DE95-010253] p 2881 N95-32047
JOURNAL BEARINGS
An efficient numerical procedure for thermohydrodynamic analysis of cavitating bearings
[NASA-CR-195476] p 2878 N95-32210
Film temperatures in the presence of cavitation
[NASA-CR-195481] p 2878 N95-32216
JUPITER (PLANET)
HST-FOC observations of a remarkable UV auroral event on Jupiter p 3030 N95-30806
Determination of the position of Jupiter from radio metric tracking of Voyager 1 p 2854 N95-32222
JUPITER ATMOSPHERE
HST-FOC observations of a remarkable UV auroral event on Jupiter p 3030 N95-30806

K

K-EPSILON TURBULENCE MODEL
Numerical simulation of flow in a whirling annular seal and comparison with experiments
[NASA-TM-106961] p 2867 N95-30710
Hot jet/wake turbulent structure and laser propagaion. Part 1: Jet/wake turbulence modeling
p 2871 N95-30991
Advanced k-epsilon modeling of heat transfer
[NASA-CR-4679] p 2874 N95-31423
KALMAN FILTERS
Multiple Target Tracking based on constellation matching and Kalman filter p 2842 N95-32136
KAONS
New tensor interaction and the K(sub L) - K(sub S)mass difference
[DE95-613597] p 2845 N95-30370
Pion-nucleon and kaon-nucleon scattering lengths in QCD sum rules
[DE95-737278] p 2983 N95-31227
Atomic approaches in metastable antiprotonic helium atoms. Reply to Analysis of the lifetimes and fractions of antiprotons trapped in metastable antiprotonic helium states by I. Shimamhura and M. Kimura --- mura
[DE95-737228] p 2986 N95-31658
The superconducting kaon spectrometer
[DE95-010436] p 2882 N95-32159
KARMAN VORTEX STREET
The study of flame-vortex interactions using a particle image velocimeter p 2796 N95-31709
KERNEL FUNCTIONS
Operating system support for distributed multimedia applications: A survey of current research
[PB95-207098] p 2964 N95-30565
Singular eigenfunctions for shearing fluids I
[DE95-008952] p 2868 N95-30763
Reduced heat kernels on nilpotent lie groups
[PB95-206926] p 2958 N95-30778
A stochastic EM estimator in the presence of missing data: Theory and applications
[DE95-010329] p 2944 N95-32089
KINEMATICS
Hamiltonian dynamics of the condensed media with spontaneously broken symmetry
[DE95-614448] p 3010 N95-30648
Control of mechanical systems with rolling contacts: Applications to robotics p 2889 N95-31332
On the kinematic performance of mechanical manipulators operating in the presence of an obstruction
p 2890 N95-31710
A computational procedure for multibody systems including flexible beam dynamics
[NASA-CR-199035] p 2897 N95-31730

KINETIC ENERGY
Numerical study of shear-induced heating in high-speed nozzle flow of liquid monopropellant p 2828 N95-31207
Aerophysics test program 1
[AD-A293890] p 2963 N95-31543
KINETIC EQUATIONS
Kinetic theory model predictions compared with low-thrust axisymmetric nozzle plume data
[NASA-CR-198934] p 2768 N95-30864
A simplified technique for determining the symmetry groups of non-linear plasma kinetic equations
[IFTR-8/1995] p 2960 N95-31337
KINETIC HEATING
Viscous heating of liquid layers under intense shear p 2827 N95-31206
Numerical study of shear-induced heating in high-speed nozzle flow of liquid monopropellant p 2828 N95-31207
KINETIC THEORY
Kinetic theory model predictions compared with low-thrust axisymmetric nozzle plume data
[NASA-CR-198934] p 2768 N95-30864
KINETICS
Fabrication and modification of metal nanocluster composites using ion and laser beams
[DE95-009131] p 2784 N95-30731
Enantioselectivity of quinoprotein alcohol dehydrogenases: Production of enantiomerically pure C3-alcohol synthons
[PB95-196960] p 2771 N95-30734
Physical modelling of microstructural evolution during thermomechanical processing of aluminium alloys
[PB95-196341] p 2805 N95-31053
Electron transfer kinetics of self-assembled ferrocene C(12) alkanethiol monolayers on gold electrodes from 125K to 175K
[AD-A292754] p 2984 N95-31427
KITS
Hydrogen sulfide analyzer with protective barrier
[AD-D017412] p 2793 N95-31009
KNOWLEDGE BASED SYSTEMS
Selecting optimal experiments for feedforward multilayer perceptrons
[AD-A290856] p 2949 N95-30406
Machine learning for a toolkit for image mining
[AD-A293137] p 2951 N95-30690
Acquiring consistent knowledge for Bayesian Forests
[AD-A293858] p 2952 N95-31517
Nonparametric recognition of nonrigid motion
[AD-A293630] p 2963 N95-31565
Production matching for large learning systems
[AD-A293105] p 2953 N95-31827
Evaluation of the techniques of fuzzy control for the piloting an aircraft p 2758 N95-31997
Using a Red Team to devise countermeasures p 2842 N95-32141
KNOWLEDGE BASES (ARTIFICIAL INTELLIGENCE)
Workflow literature guide, version 1
[PB95-207080] p 2947 N95-30721
Adaptiveness in information systems integration p 3025 N95-31348
AIDEX: An expert system for aircraft identification p 2842 N95-32138
KNOWLEDGE REPRESENTATION
Adaptiveness in information systems integration p 3025 N95-31348
PORK object system programmer's guide
[AD-A293596] p 2942 N95-31688
Evaluation of the techniques of fuzzy control for the piloting an aircraft p 2758 N95-31997
KONDO EFFECT
Alloying effects of Kondo insulators
[DE95-614306] p 3010 N95-30644
On the theory of hole propagation in an antiferromagnetic background
[DE95-614469] p 3010 N95-30650
Properties of a multichannel resonant-level model
[DE95-614482] p 2979 N95-30652
KROOK EQUATION
Kinetic theory model predictions compared with low-thrust axisymmetric nozzle plume data
[NASA-CR-198934] p 2768 N95-30864
KRYPTON
Wavelengths measurements of the He-like krypton K-shell spectrum
[DE95-010264] p 2987 N95-32041

L

LABORATORIES
Worldwide intercomparison of impulse voltage measuring systems at 600 kV level
[PB95-195574] p 2858 N95-30538
National Laboratories: Are their R and D activities related to commercial product development? Report to Congressional Requesters
[GAO/PEMD-95-2] p 3027 N95-31345
High strain-rate testing of parachute materials
[DE95-009577] p 2897 N95-31614
LAGRANGE COORDINATES
Multidimensional discretization of conservation laws for unstructured polyhedral grids
[DE95-008796] p 2955 N95-30470
Staggered solution procedures for multibody dynamics simulation
[NASA-CR-199034] p 2899 N95-32202
LAGRANGIAN FUNCTION
Effective Lagrangian approach to the fermion mass problem
[DE95-616316] p 2976 N95-30443
Convergence properties of an augmented lagrangian algorithm for optimization with a combination of general equality and linear constraints
[PB95-208039] p 2956 N95-30570
Hamiltonian dynamics of the condensed media with spontaneously broken symmetry
[DE95-614448] p 3010 N95-30648
Interferometry with particles of non-zero rest mass: Topological experiments
[DE95-616244] p 2979 N95-30689
On the quasihydrostatic flows of radiatively cooling self-gravitating gas clouds
[DE95-009116] p 3029 N95-30729
Light-front dynamics of Chern-Simons systems
[DE95-613467] p 3019 N95-30741
Atomization simulations using an Eulerian-VOF-Lagrangian method p 2828 N95-31210
Global aspects of the WZNW reduction to Toda theories
[DE95-737230] p 3019 N95-31226
A survey of the core-congruential formulation for geometrically nonlinear TL finite elements
[NASA-CR-199044] p 2944 N95-32203
LAMINAR FLOW
An experimental and numerical study on the structure and extinction of laminar premixed flames p 2792 N95-30670
Method and system for reducing drag on a body moving through a fluid medium
[AD-D017336] p 2867 N95-30672
Simultaneous heat and mass transfer in a horizontal tube absorber: Numerical tools for present and future absorber designs
[PB95-196978] p 2869 N95-30872
Numerical study of shear-induced heating in high-speed nozzle flow of liquid monopropellant p 2828 N95-31207
Role of free-surface boundary conditions and nonlinearities in wave/boundary-layer and wake interaction p 2872 N95-31317
Spectral element method for numerical simulation of unsteady laminar diffusion flames p 2794 N95-31333
Vorticity dynamics and control of dynamic stall
[AD-A288658] p 2756 N95-31400
The study of flame-vortex interactions using a particle image velocimeter p 2796 N95-31709
LAMINATES
Large area smart piezoelectric and pyroelectric sensors
[AD-A291487] p 2859 N95-30561
Influence of adhesives and bonding techniques on the properties of glued timber-steelplate joints
[PB95-211470] p 2813 N95-30599
Vibration-damping structural component
[AD-D017376] p 2784 N95-30661
A theory for predicting and minimizing the effects of matrix degradation on the thermomechanical properties of general laminates p 2785 N95-30768
Ultrasonic characterization of fiber-matrix interphasial properties and damage in high-temperature composites p 2785 N95-30823
Response of mechanically fastened composite joints under multiple bypass loads p 2785 N95-30824
Characterization and prediction of post-impact fatigue damage in stitched composites p 2785 N95-30826
Propagation and scattering of elastic waves in laminated circular cylinders
[ISBN-0-315-85957-1] p 2848 N95-30828
Innovative processing of composites for ultra-high temperature applications, book 4
[AD-A290892] p 2786 N95-30867
Development and computer implementation of design/analysis techniques for multilayered composite structures. Probabilistic fiber composite micromechanics
[NASA-CR-198979] p 2930 N95-31134
Advanced oxidizers diffusion flames structure p 2801 N95-31307
Elastic and inelastic micromechanical analysis of functionally graded materials and laminated structures using transformation fields p 2787 N95-31347
An evaluation of the Iosipescu specimen for composite materials shear property measurement
[NASA-CR-198755] p 2896 N95-31418
Finite element analysis of damped vibrations of laminated composite plates
[ISBN-0-315-84928-2] p 2789 N95-31731
Evaluation of static strength of T800H/PMR-15 carbon/polyimide laminates at room temperature and 300 C
[NAL-TR-1254] p 2789 N95-31740
Failure mechanisms in composite plates subjected to in-plane compressive loading p 2790 N95-32108
Contributions to the design of neutral cutouts in laminated plates and shells p 2790 N95-32113
Metallic multilayers at the nanoscale
[DE95-011534] p 3016 N95-32284
LANDAU DAMPING
Lower hybrid accessibility in a large, hot reversed field pinch
[DE95-011001] p 3007 N95-32310
LANDAU-GINZBURG EQUATIONS
The topological string associated with a simple singularity of type D
[DE95-737229] p 2983 N95-31225
LANDFILLS
Producing usable fuel from municipal solid waste
[DE95-008405] p 2902 N95-30375
LANDING AIDS
Automatic flight control system for an unmanned helicopter system design and flight test results p 2759 N95-32004
LANGEVIN FORMULA
Numerical simulation of the Langevin equation for skewed turbulence
[DE95-009477] p 2877 N95-32049
LANGMUIR-BLODGETT FILMS
Device for low electric-field induced switching of Langmuir-Blodgett ferroelectric liquid crystal polymer films
[AD-D017457] p 3011 N95-30728
Electronic structure of Donor-Spacer-Acceptor molecules of potential interest for molecular electronics 4. Geometry and device properties of P3CNQ and Q3CNQ
[AD-A293717] p 2986 N95-31832
Materials with controllable signature properties
[PB95-222964] p 2857 N95-32313
LANGUAGES
Extending a multi-set relational algebra to a parallel environment
[PB95-207106] p 3023 N95-30566
Unification of LARCH and Z-based object models to support algebraically-based design refinement: The LARCH perspective
[AD-A289235] p 2935 N95-30999
LANTHANUM
Lanthanide(III) catalyzed reactions: Structure an d thermodynamics of intermediate complexes, and implications for reactivity
[PB95-197000] p 3019 N95-30775
An experimental search for high ZT semiconductors: A survey of the preparation and properties of several alloy systems
[DE95-010232] p 2865 N95-32084
LANTHANUM COMPOUNDS
Fiber optic interferometric electric field and voltage sensor utilizing and electrostrictive transducer
[AD-D017433] p 2996 N95-30753
Langasite crystals growth with quality factor Q, that exceeds the Q of quartz, and which are suitable for high-precision resonators
[AD-A293397] p 3013 N95-30969
LAPLACE EQUATION
Analysis on fractals, laplacians on self-similar sets, noncommutative geometry and spectral dimensions
[PB95-208005] p 2956 N95-30556
Potential integral equations of the 2D Laplace operator in wavelet basis
[TRITA-NA-9401] p 2957 N95-30713
LAPLACE TRANSFORMATION
Extensions and results from a method for evaluating fractional integrals
[DE95-616272] p 2954 N95-30425
Relativistic non-interacting electron gas in a magnetic field
[DE95-616903] p 2967 N95-31177
LARGE SPACE STRUCTURES
Vibration control of spacecrafts and space structures from lift-off to on-orbit environments p 2767 N95-32110
Computational methods and software systems for dynamics and control of large space structures
[NASA-CR-199036] p 2767 N95-32204

LASER ABLATION
Modeling of thermal, electronic, hydrodynamic, and dynamic deposition processes for pulsed-laser deposition of thin films
[DE95-008906] p 2813 N95-30572
LASER ANEMOMETERS
Experimental and computational investigation of the tip clearance flow in a transonic axial compressor rotor
[NASA-TM-106711] p 2876 N95-31738
Laser anemometer measurements of the three-dimensional rotor flow field in the NASA low-speed centrifugal compressor
[NASA-TP-3527] p 2756 N95-31985
LASER APPLICATIONS
Unconventional imaging field experiment plan
[AD-A291492] p 2846 N95-30562
Smart active multiwave sensing with zero background amplitude modulated probes
[DE95-008813] p 2792 N95-30714
A laser-based ice shape profilometer for use in icing wind tunnels
[NASA-TM-106936] p 2880 N95-30851
Laser-induced holographic surface relief gratings on nonlinear optical polymer films
[AD-A293169] p 2997 N95-30973
Hot jet/wake turbulent structure and laser propagaion. Part 1: Jet/wake turbulence modeling
p 2871 N95-30991
Hot jet/wake turbulent structure and laser propagation. Part 3: Laser propagation measurements and modeling
p 2871 N95-30992
Comparison of DSMC predictions with temporally resolved vibrational state measurements in NO
p 2872 N95-30996
Polarized laser induced holographic surface relief gratings on polymer films
[AD-A293275] p 2817 N95-31126
Future scientific applications for high-energy lasers
[DE95-009380] p 2885 N95-31230
Unsteady laser augmented combustion of pure oxidizers AP and RDX p 2799 N95-31284
Oscillatory combustion of aluminized AP/HTPB propellants p 2800 N95-31286
Laser pyrolysis of HTPB p 2800 N95-31298
RDX laser-assisted flame structure
p 2801 N95-31314
A study of the gas-phase processes of RDX combustion using a triple quadrupole mass-spectrometer
p 2801 N95-31315
The physical and chemical processes governing CO2 laser-induced pyrolysis and combustion of the solid propellants RDX, ADN, XM39, and M43
p 2836 N95-31531
Nonlinear optics in novel composite media
[AD-A293886] p 2999 N95-31542
Contamination detection NDE for cleaning process inspection p 2781 N95-31802
TMD detection and tracking using improved AWACS sensors p 2840 N95-32128
Sandia National Lab's precision laser tracking systems
[DE95-009837] p 2886 N95-32143
Stripping by laser p 2844 N95-32174
The development of a pulsed laser imaging system for natural gas leak detection
[DE95-011407] p 2887 N95-32280
Nondestructive testing of ceramic components: Cooperative Research and Development Agreement completion report
[DE95-009510] p 2823 N95-32352
LASER ARRAYS
Picosecond phase conjugation: New applications, devices, and materials
[AD-A293195] p 3013 N95-30982
Laser retroreflector experiment on NAVSTAR 35 and 36 p 2887 N95-32347
LASER BEAMS
Laser Tracker 3: Sandia National Laboratories' third generation laser tracking system
[DE95-008525] p 2882 N95-30379
Optimum truncation of a Gaussian beam for propagation through atmospheric turbulence
[AD-A291156] p 2883 N95-30394
Demodulators for optical fiber interferometers with (3 x 3) outputs
[AD-D017415] p 2995 N95-30402
Magneto-optical transmission-reflection beam splitter for multi-level atoms
[DE95-616267] p 2976 N95-30423
Fabrication and modification of metal nanocluster composites using ion and laser beams
[DE95-009131] p 2784 N95-30731
Free electron laser as energy driver for inertial confinement fusion
[DE95-614252] p 2884 N95-30914
Reflection and diffraction of atomic de Broglie waves by evanescent laser waves. Bare-state method
[DE95-616458] p 2992 N95-30960
Laser-induced holographic surface relief gratings on nonlinear optical polymer films
[AD-A293169] p 2997 N95-30973
Picosecond phase conjugation: New applications, devices, and materials
[AD-A293195] p 3013 N95-30982
Polarized laser induced holographic surface relief gratings on polymer films
[AD-A293275] p 2817 N95-31126
Spotsize measurements of a focused CW Nd: YAG laser
[DE95-007746] p 2884 N95-31139
A 1.94 micrometer laser apparatus, system and method using a thulium-doped yttrium-lithium-fluoride laser crystal pumped with a diode laser
[AD-D017435] p 2884 N95-31213
Direct and inverse problems in random media
[AD-A293033] p 2850 N95-31280
Contactless characterization of semiconductors using laser-induced surface photo-charge voltage measurements
[AD-A293618] p 2863 N95-31725
Sandia National Lab's precision laser tracking systems
[DE95-009837] p 2886 N95-32143
Stripping by laser p 2844 N95-32174
LASER CAVITIES
Polarization characteristics, control, and modulation of vertical-cavity surface emitting lasers
[DE95-008526] p 2882 N95-30380
Many-body effects in semiconductor lasers
[DE95-008534] p 2883 N95-30390
TV-VI semiconductor quantum well lasers, physics and engineering p 2883 N95-30805
A 1.94 micrometer laser apparatus, system and method using a thulium-doped yttrium-lithium-fluoride laser crystal pumped with a diode laser
[AD-D017435] p 2884 N95-31213
Diode-pumped, continuously tunable, 2.3 micron CW laser
[AD-D017448] p 2885 N95-31273
Tunable ytterbium-doped solid state laser
[AD-D017449] p 2885 N95-31274
Advances in high-power chemical lasers
[AD-A289737] p 2885 N95-31389
LASER DAMAGE
Laser induced vitreoretinal scarring. Evaluation of causative factors and a therapeutic approach
[AD-A293742] p 2928 N95-31570
Z-scan using a dye laser
[PB95-222923] p 3002 N95-32312
LASER GYROSCOPES
Results from tests of the Honeywell integrated flight management unit
[PB95-211355] p 2748 N95-30597
LASER INDUCED FLUORESCENCE
State resolved dynamics of ion-molecule collisions in a flowing afterglow
[AD-A290895] p 2976 N95-30410
Analysis of planar laser-induced fluorescence images obtained during shakedown testing of the AEDC impulse facility
[AD-A293237] p 2884 N95-30906
Spatially-resolved velocity measurements in steady, high-speed, reacting flows using laser-induced OH fluorescence p 2877 N95-32109
LASER INTERFEROMETRY
Magneto-optical transmission-reflection beam splitter for multi-level atoms
[DE95-616267] p 2976 N95-30423
LASER MATERIALS
Solid state research
[AD-A293083] p 3015 N95-31826
Laser properties of Yb(3+)-doped Sr5(PO4)3F crystals
[DE95-010686] p 3016 N95-32268
LASER MODE LOCKING
Femtosecond, Cr(4+):YAG laser
[DE95-004964] p 2887 N95-32155
LASER OUTPUTS
Polarization characteristics, control, and modulation of vertical-cavity surface emitting lasers
[DE95-008526] p 2882 N95-30380
Spotsize measurements of a focused CW Nd: YAG laser
[DE95-007746] p 2884 N95-31139
Diode-pumped, continuously tunable, 2.3 micron CW laser
[AD-D017448] p 2885 N95-31273
A compact and efficient violet laser source
[AD-A292782] p 2885 N95-31434
Prime power for shipboard high-average power FELs
[AD-A293718] p 2886 N95-31833
Luminescence properties of ZnWO4:Cr(3+) laser crystals
[AD-A293065] p 2887 N95-32152
Femtosecond, Cr(4+):YAG laser
[DE95-004964] p 2887 N95-32155
Z-scan using a dye laser
[PB95-222923] p 3002 N95-32312
LASER PLASMAS
Enhanced brightness x-ray lasers
[DE95-010735] p 2886 N95-32029
LASER PUMPING
Free electron laser as energy driver for inertial confinement fusion
[DE95-614252] p 2884 N95-30914
A 1.94 micrometer laser apparatus, system and method using a thulium-doped yttrium-lithium-fluoride laser crystal pumped with a diode laser
[AD-D017435] p 2884 N95-31213
Ultraviolet and visible lasers: Rare earth-doped waveguide devices and non-linear optical extraction techniques
[AD-A293976] p 2885 N95-31528
Basic study of the pumping of a gamma-ray laser
[AD-A293561] p 2886 N95-31563
Laser properties of Yb(3+)-doped Sr5(PO4)3F crystals
[DE95-010686] p 3016 N95-32268
LASER RANGE FINDERS
(T2L2) Time Transfer by Laser Link
p 2887 N95-32348
LASER RANGER/TRACKER
Laser Tracker 3: Sandia National Laboratories' third generation laser tracking system
[DE95-008525] p 2882 N95-30379
TMD detection and tracking using improved AWACS sensors p 2840 N95-32128
Laser retroreflector experiment on NAVSTAR 35 and 36 p 2887 N95-32347
(T2L2) Time Transfer by Laser Link
p 2887 N95-32348
Satellite test of the isotropy of the one-way spe ed of light using ExTRAS p 2973 N95-32349
LASER SPECTROSCOPY
Fourier Transform (FT) Raman spectroscopy of nitrogen at high pressure
[AD-A293051] p 2796 N95-31670
LASER WEAPONS
The High Altitude Balloon Experiment demonstration of acquisition, tracking, and pointing technologies (HABE-ATP) p 2841 N95-32132
LASERS
A phenomenological finite element model of part building in the stereolithography process
[DE95-008437] p 2932 N95-30376
Electron-optical nonlinear interaction in asymmetric quantum-well laser heterostructures
[DE95-613443] p 2883 N95-30609
Method for laser-assisted silicon etching using halocarbon ambients
[AD-D017426] p 2883 N95-30744
A laser-based ice shape profilometer for use in icing wind tunnels
[NASA-TM-106936] p 2880 N95-30851
Airborne ocean water lidar (OWL) real time processor (RTP)
[AD-A293226] p 2848 N95-30904
Specific rate coefficients from vibrational overtone activation of 1-methylcyclopropene
[AD-A288755] p 2793 N95-31014
Diode-pumped, continuously tunable, 2.3 micron CW laser
[AD-D017448] p 2885 N95-31273
Tunable ytterbium-doped solid state laser
[AD-D017449] p 2885 N95-31274
Diagnosing high density, fast-evolving plasmas using x-ray lasers
[DE95-010734] p 3006 N95-32028
LATERAL STABILITY
Transonic aerodynamic characteristics of a proposed wing-body reusable launch vehicle concept
[NASA-TM-108489] p 2742 N95-30712
LATTICE PARAMETERS
Electroweak interactions on the lattice
[DE95-616287] p 2965 N95-30439
Approximate analytic diagonalization of lattice QCD
[DE95-616332] p 3018 N95-30444
Simulation with complex measures
[DE95-616333] p 2955 N95-30445
LATTICE VIBRATIONS
The one-dimensional model of the off-centre potential of the fluorine ion in the NaBr lattice
[DE95-614310] p 3010 N95-30647
LATTICES (MATHEMATICS)
Plaquette expansion proof and interpretation
[DE95-616282] p 2965 N95-30432

Theoretical high energy physics
[DE95-003107] p 2991 N95-30527
Direct sublattice imaging of interface dislocation structures in CdTe/GaAs(001)
[DE95-009031] p 3010 N95-30576
On the string equation at c=1
[DE95-737161] p 3014 N95-31222
Phase stability, point defects and site preference of FeAl and NiAl with ternary additions
[DE95-009694] p 3015 N95-31641

LAUNCHERS
Fast-acting valve for projective launching systems
[AD-D017357] p 2888 N95-30416

LAW (JURISPRUDENCE)
Prioritization methodology for chemical replacement
p 2773 N95-31757
Environmental databases and other computerized information tools p 2783 N95-31810

LAY-UP
Design of fibre reinforced composite panels for aerospace applications
[PB95-197851] p 2784 N95-30460

LAYERS
Impact behavior of the active zone within a frozen soil profile
[AD-A292909] p 2915 N95-31386

LC CIRCUITS
Operational characteristics of a 200 C LC parallel resonant circuit
[NASA-TM-106983] p 2864 N95-31742

LEAD (METAL)
Infrared and millimeter wave detection using thin films of Pb doped BiSrCaCuO superconductor
p 2840 N95-32129
Nuclear-spin-dependent parity-nonconserving effects in thallium, lead and bismuth atoms
[DE95-614120] p 2991 N95-32354

LEAD COMPOUNDS
Synthesis of novel precursors for PMN powders and the thin films obtained from them
[DE95-008543] p 2811 N95-30362
Molecular modeling of PMN ceramics
[AD-A290879] p 2813 N95-30560

LEAD TELLURIDES
Numerical modeling of Bridgman growth of PbSnTe in a magnetic field
[NASA-TM-106996] p 2837 N95-31359

LEAD TITANATES
Large area smart piezoelectric and pyroelectric sensors
[AD-A291487] p 2859 N95-30561

LEAD ZIRCONATE TITANATES
Crystallization of sol-gel derived lead zirconate titanate thin films in argon and oxygen atmospheres
[DE95-615230] p 3009 N95-30421
Orientation of rapid thermally annealed lead zirconate titanate thin films on (111) Pt substrate
[DE95-615232] p 2811 N95-30422
Deposition and characterization of photoconductive PZT thin films
[ATR-93(8308)-7] p 2819 N95-31417
A study of switching behavior in Pb(Zr,Ti)O3 thin films using x-ray diffraction
[DE95-010859] p 2808 N95-31689
The pyrochlore-to-perovskite transformation in solution-derived lead zirconate titanate thin films
[DE95-010453] p 2822 N95-32161

LEADING EDGES
Reply-frequency interference/jamming detector
[AD-D017426] p 2847 N95-30746
A laser-based ice shape profilometer for use in icing wind tunnels
[NASA-TM-106936] p 2880 N95-30851
Vorticity dynamics and control of dynamic stall
[AD-A286658] p 2756 N95-31400
Control of unsteady separated flow associated with the dynamic stall of airfoils
[NASA-CR-196972] p 2744 N95-32193

LEARNING
Optimizing the long-term retention of skills: Structural and analytic approaches to skill maintenance
[AD-A293798] p 2929 N95-31585
The sociology of megaprogramming: Experiences in generating an organizational learning enterprise (Software Technology for Adaptable, Reliable Systems(STARS) program)
[AD-A292998] p 2946 N95-32294

LEAST SQUARES METHOD
Apparatus and method for producing three-dimensional images
[AD-D017455] p 2847 N95-30727
Nonparametric methods for incomplete data in reliability and for changepoints in smooth functions
[AD-A292773] p 2963 N95-31429
The effect of repeatedly sampling an embedded metamodel on the simulation response
[AD-A293783] p 2953 N95-31582
An efficient implementation of Forward-Backward Least-Mean-Square Adaptive Line Enhancers
p 2855 N95-32224
Metafitting: Weight optimization for least-squares fitting of PTTI data p 2971 N95-32340

LECTURES
Experience with a course on architectures for software systems. Part 2: Educational materials
[AD-A293090] p 2943 N95-31843

LEG (ANATOMY)
Electromyostimulation, circuits and monitoring
[NASA-TM-110741] p 2926 N95-30846

LEGIBILITY
Adaptive image enhancement of text images that contain touching or broken characters
[DE95-010173] p 3023 N95-30620

LENGTH
Simultaneity and length of the moving rod
[DE95-613369] p 3017 N95-30364
Einstein's length concept
[DE95-613368] p 3019 N95-30972

LENSES
Ceramics derived from metal-organic precursors
[AD-A290791] p 2811 N95-30405
Spotsize measurements of a focused CW Nd: YAG laser
[DE95-007746] p 2884 N95-31139

LEPTONS
Phenomenology of the two Higgs doublet sector of a quark-lepton symmetric model
[DE95-616337] p 2976 N95-30446
Confronting left-right symmetric models with electroweak precision data at the Z peak
[PB95-208054] p 2977 N95-30484
Possible reason why leptons are lighter than quarks
[DE95-616383] p 2978 N95-30579
The design and construction of the muon arm in PHENIX
[DE95-010156] p 2978 N95-30616
Testing vector boson dominance of electroweak interactions via e(+)e(-) (yields) f-bar f
[DE95-620528] p 2982 N95-31214
B(sub c)-meson production in hadron-hadron collisions
[DE95-620537] p 2983 N95-31217
SO(8) color as possible origin of generations
[DE95-613560] p 2988 N95-32069

LESIONS
Laser induced vitreoretinal scarring. Evaluation of causative factors and a therapeutic approach
[AD-A293742] p 2928 N95-31570

LETHALITY
Aerophysics test program 1
[AD-A293890] p 2963 N95-31543

LEVITATION
An active magnetic bearing with high T(sub c) superconducting coils and ferromagnetic cores
[NASA-TM-106995] p 2864 N95-31847

LIBRARIES
MPI implementation of PHOENICS: A general purpose computational fluid dynamics code
[DE95-009810] p 2877 N95-32033

LIE GROUPS
Some functional solutions of the Yang-Baxter equation
[DE95-613584] p 2966 N95-30635
Around Ratner --- applications of Ratner's measure and topological theorems on unipotent homogeneous actions
[DE95-613377] p 2958 N95-30770
Reduced heat kernels on nilpotent lie groups
[PB95-206926] p 2958 N95-30778
Frobenius algebras and quantum Yang-Baxter equation 2
[PB95-212130] p 2960 N95-31229
Ricci-flat Kaehler metrics on symmetric varieties
[DE95-613459] p 2962 N95-32068
Notes on lie algebraic analysis of achromats
[DE95-009524] p 3002 N95-32356

LIFE (DURABILITY)
Ageing control no. 3 of propellants for rocket motors RB 27 and RB 28
[PB95-210357] p 2825 N95-30626
Experimental characterisation of gas microstrip detectors. Part 3: Lifetime characteristics
[PB95-192845] p 2880 N95-30691
A simple and accurate technique for monitoring crack growth behavior using a wave form analyzer
[AD-A293161] p 2894 N95-31007
Life prediction methodology for ceramic components of advanced heat engines: Phase 1. Volume 1
[DE95-010805] p 2817 N95-31135
Life prediction methodology for ceramic components of advanced heat engines. Phase 1: Volume 2. Appendices
[DE95-010806] p 2817 N95-31136

LIFE CYCLE COSTS
Major weapon system environmental life-cycle cost estimating for Conservation, Cleanup, Compliance and Pollution Prevention (C3P2) p 2774 N95-31761

LIFE SCIENCES
JPRS report: Science and technology. Central Eurasia
[JPRS-UST-95-025] p 2771 N95-31360
FBIS report: Science and technology. Central Eurasia
[FBIS-UST-95-026] p 2839 N95-31729

LIFE SPAN
SVN 9 End-Of-Life testing p 2767 N95-32345

LIFT
Multigrid convergence acceleration for the 2D Euler equations applied to high-lift systems
[PB95-196081] p 2743 N95-30814
A wind tunnel investigation of the effects of micro-vortex generators and Gurney flaps on the high-lift characteristics of a business jet wing
[NASA-TM-110626] p 2750 N95-30827
Validation of the helicopter rotor code HERO
[PB95-198040] p 2751 N95-30838

LIFT DEVICES
A wind tunnel investigation of the effects of micro-vortex generators and Gurney flaps on the high-lift characteristics of a business jet wing
[NASA-TM-110626] p 2750 N95-30827

LIGANDS
A theoretical treatment of the absorption and emission properties of Cu(2) porphyrin
[AD-A293669] p 2795 N95-31595
Absorption and ionization spectra of model rubredoxins
[AD-A293668] p 2796 N95-31691

LIGHT (VISIBLE RADIATION)
Degradation of blue AlGaN/InGaN/GaN LEDs subjected to high current pulses
[DE95-008824] p 2863 N95-31611

LIGHT BEAMS
Technique to prepare high-reflectance optical fiber Bragg gratings with single exposure in-line or fiber draw tower
[AD-D017445] p 2998 N95-31270

LIGHT EMISSION
Study of surfaces using near infrared optical fiber spectrometry p 2781 N95-31801

LIGHT EMITTING DIODES
Optical logic and signal processing using a semiconductor laser diode-based optical bistability device
[AD-A293248] p 2997 N95-30908
Opto-electronic components from non-stoichiometric 3-5 materials
[AD-A293206] p 3013 N95-30985
Degradation of blue AlGaN/InGaN/GaN LEDs subjected to high current pulses
[DE95-008824] p 2863 N95-31611

LIGHT MODULATION
Smart active multiwave sensing with zero background amplitude modulated probes
[DE95-008813] p 2792 N95-30714
Real time correlating operation on diffuse objects
[AD-A293220] p 2997 N95-30901
Application of computer generated holograms to optical transformations
[AD-A293146] p 2880 N95-30921
Improved linear dynamic range in externally modulated fiber-optic links p 3001 N95-31950
Photo-refractive Bi12SiO20: Spatial light modulator
[AD-A293084] p 3001 N95-32153

LIGHT SCATTERING
A 1.94 micrometer laser apparatus, system and method using a thulium-doped yttrium-lithium-fluoride laser crystal pumped with a diode laser
[AD-D017435] p 2884 N95-31213
Method and apparatus for a high resolution, flat panel cathodoluminescent display device
[AD-D017434] p 2862 N95-31342

LIGHT SOURCES
Demodulators for optical fiber interferometers with (3 x 3) outputs
[AD-D017415] p 2995 N95-30402
A real time method for Fourier transform holographic information storage
[AD-A293186] p 2880 N95-30980
The Los Alamos accelerator code group
[DE95-010989] p 2992 N95-31151
Method and apparatus for non-destructively measuring local resistivity of semiconductors
[AD-D017436] p 2862 N95-31343
Annual meeting of the Advanced Light Source Users' Association
[DE95-009373] p 3000 N95-31835
Scannerless Range Imaging with a square wave
[DE95-009840] p 2854 N95-32145

LIGHT TRANSMISSION
Optimum truncation of a Gaussian beam for propagation through atmospheric turbulence
[AD-A291156] p 2883 N95-30394
Passive, multi-channel fiber optic rotary joint assembly
[AD-D017353] p 2996 N95-30529
A study of end-fire coupling of single-mode fiber to Ti: LiNbO3-single-mode planar waveguide
[AD-A293249] p 2997 N95-30909
Satellite test of the isotropy of the one-way spe ed of light using ExTRAS p 2973 N95-32349

LIGHT VALVES
A real time method for Fourier transform holographic information storage
[AD-A293186] p 2880 N95-30980

LIGHT WATER REACTORS
Microstructural and mechanical property changes in model Fe-Cu alloys
[DE95-010117] p 2805 N95-31105

LIGHT-CONE EXPANSION
Light-front dynamics of Chern-Simons systems
[DE95-613467] p 3019 N95-30741

LIKELIHOOD RATIO
A hypothesis-testing approach to discriminant analysis with mixed categorical and continuous variables when data are missing
[AD-A293714] p 2964 N95-31831

LIMESTONE
Experimental determination of probability distributions for parameters of a Salem limestone cap plasticity model
[AD-A290878] p 2892 N95-30559

LINE OF SIGHT
Validation of the atmospheric transmission large-area analysis system (ATLAS)
[AD-A293810] p 2916 N95-31589

LINE SPECTRA
Molecular gas in starburst galaxies: Line intensities and physical conditions
[PB95-208021] p 3029 N95-30569
An efficient implementation of Forward-Backward Least-Mean-Square Adaptive Line Enhancers p 2855 N95-32224
Measurements of quantum electrodynamic sensitive transitions in Na-like and Cu-like ions
[DE95-011593] p 3007 N95-32299

LINEAR ACCELERATORS
X-band magnicon amplifier research at the Naval Research Laboratory
[AD-A293203] p 3013 N95-30984
Measurement of the effect of collimator generated wakefields on the beams in the SLC
[DE95-012101] p 2993 N95-31256
Spin structure in high energy processes
[DE95-008628] p 2993 N95-31627
RFQ-DTL matching solutions for different requirements
[DE95-010897] p 2995 N95-32306

LINEAR ARRAYS
Passive, multi-channel fiber optic rotary joint assembly
[AD-D017353] p 2996 N95-30529

LINEAR EQUATIONS
Quasi-periodic solutions of Hamiltonian perturbations of 2D linear Schroedinger equations
[PB95-208443] p 2957 N95-30624
Numerical stability investigations of processes for solving linear initial value problems
[PB95-207023] p 2959 N95-31183
The complexity and approximability of finding maximum feasible subsystems of linear relations
[TRITA-NA-9313] p 2961 N95-31648

LINEAR FILTERS
Automatic Target Recognition (ATR): Background statistics and the detection of targets in clutter
[AD-A293062] p 2853 N95-31673

LINEAR POLARIZATION
Plane wave reflection from a uniaxial chiral quarter-wave polarization transformer
[PB95-206512] p 2849 N95-31159

LINEAR PREDICTION
Sensor Fusion and Nonlinear Prediction for Anomalous Event Detection
[DE95-009429] p 2933 N95-30602

LINEAR PROGRAMMING
Simplex method for semi-definite programming: Optimization and systems theory
[PB95-212122] p 2934 N95-30792
Analysis of symbolic parameter models
[AD-A292916] p 2940 N95-31459
Minimal trellises for linear block codes and their duals p 2856 N95-32233

LINEAR QUADRATIC REGULATOR
Representation of feedback operators for hyperbolic systems
[NASA-CR-198171] p 2960 N95-31319

LINEAR SYSTEMS
Potential integral equations of the 2D Laplace operator in wavelet basis
[TRITA-NA-9401] p 2957 N95-30713
Apparatus and method for producing three-dimensional images
[AD-D017455] p 2847 N95-30727
Enhancements to the SSME transfer function modeling code
[NASA-CR-198957] p 2958 N95-30754
Solution of the three-dimensional Helmholtz equation with nonlocal boundary conditions
[NASA-TM-110174] p 2974 N95-30850
QMR methods in computational fluid dynamics
[DE95-010293] p 2872 N95-31132
Linear Motor Free Piston Compressor
[AD-A293452] p 2889 N95-31374
Stability analysis of linear control systems with uncertain parameters p 2954 N95-31949
A modification to the GMRES method for ill-conditioned linear systems
[DE95-010661] p 2962 N95-32076
Allan deviation computations of a linear frequency synthesizer system using frequency domain techniques p 2972 N95-32344

LINEAR TRANSFORMATIONS
Robust control: A structured approach to solve aircraft flight control problems p 2758 N95-31995

LINEARIZATION
Development of a linearized unsteady Euler analysis for turbomachinery blade rows
[NASA-CR-4677] p 2742 N95-30611
A feedback linearization approach to orbital maneuvers p 2765 N95-30841
Improved linear dynamic range in externally modulated fiber-optic links p 3001 N95-31950

LININGS
Ageing control no. 3 of propellants for rocket motors RB 27 and RB 28
[PB95-210357] p 2825 N95-30626
Composite structure forming a wear surface
[AD-D017462] p 2785 N95-30749
An active liner system for jet engine exhaust silencers, phase 1
[AD-A293277] p 2756 N95-31191

LINKAGES
Erect, neutral and slump sitting postures: A study of the torso linkage system from shoulder to hip joint
[AD-A293239] p 2930 N95-30907
Probabilistic reliability modeling of fatigue on the H-46 tie bar
[AD-A289926] p 2751 N95-30927
Conjugated aromatic polyimines. 2. Synthesis, structure, and properties of new aromatic polyazomethines
[AD-A292955] p 2819 N95-31461

LIOUVILLE EQUATIONS
Dressing symmetry of the uniformization solution of Liouville equation
[DE95-613380] p 2956 N95-30607

LIQUEFIED NATURAL GAS
Natural gas liquefier for vehicle fuel
[AD-A293619] p 2836 N95-31564
Liquid natural gas as a transportation fuel in the heavy trucking industry
[DE95-010376] p 2837 N95-32158

LIQUID CHROMATOGRAPHY
Fuel-type classification and parameters prediction by Gas Liquid Chromatography analysis
[AD-A293442] p 2794 N95-31368
Analytical instrumentation for environmental research
[AD-A292832] p 2908 N95-31447
Waste minimization via preparative scale high performance gel permeation chromatography
[DE95-011797] p 2798 N95-32360

LIQUID CRYSTALS
Hamiltonian dynamics of the condensed media with spontaneously broken symmetry
[DE95-614448] p 3010 N95-30648
Device for low electric-field induced switching of Langmuir-Blodgett ferroelectric liquid crystal polymer films
[AD-D017457] p 3011 N95-30728
Real time correlating operation on diffuse objects
[AD-A293220] p 2997 N95-30901
Application of computer generated holograms to optical transformations
[AD-A293146] p 2880 N95-30921
From molecular to macromolecular liquid crystals
[AD-A293170] p 2816 N95-30974
A real time method for Fourier transform holographic information storage
[AD-A293186] p 2880 N95-30980
Processing of polymers using supercritical fluids
[AD-A292880] p 2819 N95-31410

LIQUID FILLED SHELLS
An analysis of the cover of a liquid-filled circular container
[IFTR-1/1995] p 2895 N95-31338

LIQUID FUELS
A pulsed liquid fuel ramjet p 2756 N95-31201
Atomization simulations using an Eulerian-VOF-Lagrangian method p 2828 N95-31210

LIQUID HELIUM
High-temperature superconducting current leads
[DE95-008404] p 2858 N95-30374
Atomic approaches in metastable antiprotonic helium atoms. Reply to Analysis of the lifetimes and fractions of antiprotons trapped in metastable antiprotonic helium states by I. Shimamhura and M. Kimura --- mura
[DE95-737228] p 2986 N95-31658

LIQUID HYDROGEN
Design and testing of an oxidizer-rich preburner p 2799 N95-31212

LIQUID LEVELS
Optical fiber pressure sensor for liquid level monitoring
[AD-D017346] p 2996 N95-30679
Reducing process noise in superconducting helium liquid level probes
[DE95-008956] p 2814 N95-30765

LIQUID OXYGEN
Design and testing of an oxidizer-rich preburner p 2799 N95-31212
Primary atomization of liquid jets issuing from rocket engine coaxial injectors p 2769 N95-31716
Combustion of LOX with H2(sub g) under subcritical and supercritical conditions p 2797 N95-31717

LIQUID PHASES
Porous spherical shells and microspheres by electrodispersion precipitation
[DE95-009073] p 2815 N95-30799

LIQUID PROPELLANT ROCKET ENGINES
The 31st JANNAF Combustion Subcommittee Meeting, volume 1 p 2825 N95-31194
Primary atomization of liquid jets issuing from rocket engine coaxial injectors p 2769 N95-31716
Experiment of rocket-ram combined combustor
[NAL-TR-1249] p 2769 N95-31739
Combustion response to acoustic perturbation in liquid rocket engines p 2770 N95-31972

LIQUID ROCKET PROPELLANTS
The 31st JANNAF Combustion Subcommittee Meeting, volume 1 p 2825 N95-31194
Workshop report: Measurement techniques in highly transient, spectrally rich combustion environments p 2799 N95-31208
Design and testing of an oxidizer-rich preburner p 2799 N95-31212

LIQUID SURFACES
Simple model of foam spreading on liquid surfaces
[PB95-211207] p 2838 N95-30630

LIQUID WASTES
Determination of halogens in a petroleum product by ion chromatography
[DE95-002056] p 2797 N95-31840

LIQUID-SOLID INTERFACES
Study of melting and freezing processes of water for application to ice thermal energy storage system p 2905 N95-31735

LIQUIDS
Fast-acting valve for projective launching systems
[AD-D017357] p 2888 N95-30416
Sonic apparatus for degassing liquids
[AD-D017352] p 2791 N95-30554
Ultrasensitive fluorescence detection and photophysics in microdroplets
[DE95-010283] p 2798 N95-32086

LISP (PROGRAMMING LANGUAGE)
PORK object system programmer's guide
[AD-A293596] p 2942 N95-31668

LITHIUM
Ionic conductivities of lithium phosphorus oxynitride glasses, polycrystals, and thin films
[DE95-008898] p 2812 N95-30545
A Monte-Carlo model of ionic transport across a solid interface
[DE95-613447] p 3011 N95-30737
Inner- and outer-shell excitation in lithium isoelectronic sequence
[DE95-614107] p 2981 N95-31003
Convoy electron emission from surfaces
[DE95-010298] p 2984 N95-31402
Composite polymer electrolyte for lithium batteries
[AD-A293924] p 2820 N95-31514
Lithium ion aqueous cells
[AD-A293828] p 2905 N95-31554
Target diagnostics for intense lithium ion hohlraum experiments on PBFA 2
[DE95-008517] p 3006 N95-31626

LITHIUM COMPOUNDS
Lithium ion aqueous cells
[AD-A293828] p 2905 N95-31554
LITHIUM NIOBATES
A study of end-fire coupling of single-mode fiber to Ti: LiNbO3-single-mode planar waveguide
[AD-A293249] p 2997 N95-30909
LITHOGRAPHY
A phenomenological finite element model of part building in the stereolithography process
[DE95-008437] p 2932 N95-30376
Epoxy and acrylate stereolithography resins: In-situ measurements of cure shrinkage and stress relaxation
[DE95-008506] p 2811 N95-30389
NIR High-efficiency subwavelength diffractive structures in semiconductors
[DE95-008535] p 3008 N95-30391
LITHOSPHERE
Studies in marine tectonics: Propagating rifts, depth anomalies and subduction zone anisotropy
p 2923 N95-31719
LOAD CARRYING CAPACITY
Analysis of stress concentration at holes in components made of 2195 aluminum-lithium
[NASA-TP-3554] p 2893 N95-30613
LOAD DISTRIBUTION (FORCES)
Impact behavior of the active zone within a frozen soil profile
[AD-A292909] p 2915 N95-31386
LOAD TESTS
Round-robin validation exercise for plate twist test method
[PB95-208088] p 2812 N95-30487
Electrical short circuit and current overload tests on aircraft wiring
[AD-A293308] p 2860 N95-30922
Confederation Verification, Validation, and Accreditation Master Plan (CVVAMP). Technical test plan
[AD-A289717] p 2936 N95-31050
LOADING RATE
Rationale and summary of methods for determining ultrasonic properties of materials at Lawrence Livermore National Laboratory
[DE95-009475] p 2795 N95-31593
LOADS (FORCES)
Speed control of an elastic two-mass system: Optimization and systems theory
[PB95-212106] p 2888 N95-30701
A theory for predicting and minimizing the effects of matrix degradation on the thermomechanical properties of general laminates p 2785 N95-30768
Robust position and force tracking control for a robot in contract p 2888 N95-30830
LOCAL AREA NETWORKS
Email: Why and how
[PB95-195327] p 2846 N95-30516
Integrated high performance distributed system
[AD-A292821] p 2947 N95-31445
Gigabit testbed research project
[DE95-010728] p 2945 N95-32270
Recommendations for protecting National Library of Medicine Computing and Networking Resources
[DE95-011554] p 3026 N95-32285
LOCKING
Locking device for fluid coupling
[AD-D017354] p 2888 N95-30414
Vibration isolation mount with locking means
[AD-D017367] p 2888 N95-30532
LOCKS (FASTENERS)
Locking device for fluid coupling
[AD-D017354] p 2888 N95-30414
LOGIC PROGRAMMING
Barendregt cube with definitions and generalized reduction
[PB95-206793] p 2966 N95-30719
The occurrence of continuation parameters in CPS terms
[AD-A292952] p 2941 N95-31460
LOGISTICS MANAGEMENT
Fact sheet for Congressional Committees. Air traffic control: Status of FAA's modernization program
[GAO/RCED-94-167FS] p 2750 N95-32197
LONG WAVE RADIATION
Suprioius semi-diurnal variation in the E.R.B.E. outgoing longwave radiation
[NOAA-TR-NESDIS-84] p 2913 N95-30643
LONGITUDINAL CONTROL
Flight Vehicle Integration Panel Workshop on Pilot Induced Oscillations
[AGARD-AR-335] p 2745 N95-31061
LONGITUDINAL STABILITY
Transonic aerodynamic characteristics of a proposed wing-body reusable launch vehicle concept
[NASA-TM-108489] p 2742 N95-30712
Unified criteria for ACT aircraft longitudinal dynamics
p 2745 N95-31065
LORAN
Guidelines for the design of GPS and LORAN receiver controls and displays
[AD-A293753] p 2749 N95-31572
LORENTZ TRANSFORMATIONS
Simultaneity and length of the moving rod
[DE95-613369] p 3017 N95-30364
Einstein's length concept
[DE95-613368] p 3019 N95-30972
LOSSES
Effects of temperature ramp rate during heat treatment on hysteresis loss and critical current density of internal tin processed wires
[DE95-009551] p 2803 N95-30706
On the quasihydrostatic flows of radiatively cooling self-gravitating gas clouds
[DE95-009116] p 3029 N95-30729
Polarized proton beams
[DE95-010843] p 2987 N95-32031
Effects of temperature, frequency, flux density, and excitation waveform on the core loss and dynamic B-H loops of supermalloy
[NASA-TM-106982] p 2865 N95-32207
Testing the performance of feedback concatenated decoder with a nonideal receiver p 2856 N95-32231
LOW ALTITUDE
Improved altimeter settings for A-10 aircraft
[AD-A293142] p 2753 N95-30920
Synthetic Terrain Imagery for Helmet-Mounted Display, volume 1
[AD-A293612] p 2753 N95-31656
Advanced gust management systems: Lessons learned and perspectives p 2759 N95-32002
LOW CONCENTRATIONS
Neutronic methods for determination of very low concentrations of hydrogen in metals
[DE95-623967] p 2807 N95-31409
LOW COST
State-of-the-art low-cost solar reflector materials
[DE95-000260] p 2902 N95-30526
Rationale and summary of methods for determining ultrasonic properties of materials at Lawrence Livermore National Laboratory
[DE95-009475] p 2795 N95-31593
Low cost fabrication of silicon carbide based ceramics and fiber reinforced composites
[NASA-TM-107001] p 2822 N95-32208
LOW DENSITY MATERIALS
Simple model of foam spreading on liquid surfaces
[PB95-211207] p 2838 N95-30630
LOW EARTH ORBITS
Assessment of the NASA orbital debris engineering model
[AD-A293350] p 2766 N95-31143
The NASA/JPL Evaluation of Oxygen Interactions with Materials-3 (EOIM-3)
[NASA-CR-198865] p 2796 N95-31660
Operation of the computer model for direct atomic oxygen exposure of Earth satellites
[NASA-CR-198188] p 2767 N95-32189
LOW FREQUENCIES
Fiber optic interferometric electric field and voltage sensor utilizing and electrostrictive transducer
[AD-D017433] p 2996 N95-30753
LOW PASS FILTERS
Design of digital low-pass filters for time-domain recursive filtering of impact acceleration signals
[AD-A293086] p 2864 N95-31842
LOW REYNOLDS NUMBER
Advanced k-epsilon modeling of heat transfer
[NASA-CR-4679] p 2874 N95-31423
LOW SPEED WIND TUNNELS
Flow quality improvements in the NASA Lewis Research Center 9- by 15-foot Low Speed Wind Tunnel
[NASA-CR-195439] p 2763 N95-31653
LOW TEMPERATURE
Optimization of a thermoelectric IR-detector for low working temperature
[NASA-CR-198933] p 2880 N95-30752
Low temperature fabrication from nano-size ceramic powders
[DE95-010995] p 2818 N95-31153
LOW VOLTAGE
Thin-film edge field emitter device and method of manufacture therefor
[AD-D017453] p 2862 N95-31275
LOWER ATMOSPHERE
Modeling and parameterization of gravity wave breaking, interactions, and instability processes in the lower and middle atmosphere
[AD-A292740] p 2914 N95-31278
Calculation of a residual mean meridional circulation for a zonal-mean tracer transport model
[DE95-009474] p 2911 N95-32350
LUBRICANTS
Enhancement of perfluoropolyether boundary lubrication performance: I. Preliminary results
[NASA-TM-106937] p 2813 N95-30621
Compatibility of refrigerants and lubricants with motor materials under retrofit conditions
[DE95-010185] p 2814 N95-30767
Studies of C(60) and C(70) and other fullurenes: Synthesis, derivation, electrochemistry, lubricant properties and new composition materials
[AD-A292726] p 3012 N95-30944
Compatibility of manufacturing process fluids with HFC refrigerants and ester lubricants
[DE95-012152] p 2911 N95-32364
LUBRICATING OILS
Spectroscopic ellipsometry as a sensitive monitor of materials contamination p 2782 N95-31808
LUBRICATION
Fluid-film lubrication with an application to piston rings
p 2890 N95-32119
An efficient numerical procedure for thermohydrodynamic analysis of cavitating bearings
[NASA-CR-195476] p 2878 N95-32210
Film temperatures in the presence of cavitation
[NASA-CR-195481] p 2878 N95-32216
LUMINANCE
Luminance effects on visual acuity and small letter contrast sensitivity
[AD-A293310] p 2928 N95-31140
LUMINESCENCE
Glass matrix doped with activated luminescent nanocrystalline particles
[AD-D017416] p 2816 N95-31010
Excited-state complexes of conjugated polymers: Novel photophysical processes and optoelectronic materials
[AD-A292958] p 2819 N95-31462
Excited-state complexes of conjugated polymers
[AD-A292960] p 2819 N95-31466
Luminescence properties of ZnWO4:Cr(3+) laser crystals
[AD-A293065] p 2887 N95-32152
LUNAR ORBITS
Radiation effects in space: The Clementine 1 mission
[DE95-011513] p 3032 N95-32282
LYMAN ALPHA RADIATION
SSUSI single sensor auroral E-layer algorithm: Functional description
[AD-A288630] p 2914 N95-31012
LYRA CONSTELLATION
Cepheid temperature and the Blazhko effect
[NASA-CR-189433] p 3030 N95-31819

M

MACH NUMBER
Transonic aerodynamic characteristics of a proposed wing-body reusable launch vehicle concept
[NASA-TM-108489] p 2742 N95-30712
Unsteady transonic wind tunnel test on a semispan straked delta wing, oscillating in pitch. Part 1: Description of the model, test setup, data acquisition, and data processing
[AD-A293113] p 2743 N95-30885
Hypervelocity wind tunnel number 9, high Mach number development program
[AD-A289934] p 2743 N95-30929
Investigation of ram accelerator performance capabilities p 2799 N95-31204
Side force acting on blunted circular cylinder bodies at high angles of attack in supersonic flow
[NAL-TR-1255] p 2744 N95-31741
Control of unsteady separated flow associated with the dynamic stall of airfoils
[NASA-CR-198972] p 2744 N95-32193
MACHINE LEARNING
Learning in an intentional system
[AD-A291158] p 2949 N95-30395
Selecting optimal experiments for feedforward multilayer perceptrons
[AD-A290856] p 2949 N95-30406
Adaptive path planning: Algorithm and analysis
[DE95-008549] p 2950 N95-30463
Machine learning for a toolkit for image mining
[AD-A293137] p 2951 N95-30890
Neural networks for real-time terrain typing
[AD-A293569] p 2953 N95-31540
Neural network false alarm filter, volume 1
[AD-A293097] p 2953 N95-31562
Finite-sample based learning algorithms for feedforward networks
[DE95-009123] p 2941 N95-31631
An analysis of hierarchical genetic programming
[AD-A293964] p 2942 N95-31657
Production matching for large learning systems
[AD-A293105] p 2953 N95-31827

MACHINE TOOLS
Computer-aided inspection process definition: Development of an expert planning and programming system for coordinate metrology
[DE95-010411] p 2940 N95-31404
MACHINE TRANSLATION
Translation workbench for generating subtitles for English TV news
[NHK-435] p 3026 N95-32182
MACHINING
Effect of local melting on tribology in metal cutting
[PB95-195392] p 2804 N95-31052
MACROMOLECULES
From molecular to macromolecular liquid crystals
[AD-A293170] p 2816 N95-30974
MAGNESIUM
Electrochemical vapour deposition of SOFC interconnection materials
[PB95-197844] p 2812 N95-30459
Calculated structures and electronic absorption spectroscopy for magnesium phthalocyanine and its anion radical
[AD-A293672] p 2796 N95-31596
MAGNESIUM ALLOYS
Effect of local melting on tribology in metal cutting
[PB95-195392] p 2804 N95-31052
Interfacial segregation and deformation of superplastically deformed Al-Mg-Mn alloys
[DE95-009572] p 2809 N95-32052
MAGNESIUM CELLS
Magnesium battery disposal characteristics
[AD-A293053] p 2863 N95-31607
MAGNESIUM COMPOUNDS
Synthesis of novel precursors for PMN powders and the thin films obtained from them
[DE95-008543] p 2811 N95-30362
Molecular modeling of PMN ceramics
[AD-A290879] p 2813 N95-30560
MAGNESIUM FLUORIDES
High performance YBCO films
[AD-A293045] p 2863 N95-31669
MAGNESIUM OXIDES
The pyrochlore-to-perovskite transformation in solution-derived lead zirconate titanate thin films
[DE95-010453] p 2822 N95-32161
MAGNET COILS
An active magnetic bearing with high T(sub c) superconducting coils and ferromagnetic cores
[NASA-TM-106995] p 2864 N95-31847
MAGNETIC ANOMALIES
Studies in marine tectonics: Propagating rifts, depth anomalies and subduction zone anisotropy
p 2923 N95-31719
MAGNETIC BEARINGS
An active magnetic bearing with high T(sub c) superconducting coils and ferromagnetic cores
[NASA-TM-106995] p 2864 N95-31847
MAGNETIC CORES
Effects of temperature, frequency, flux density, and excitation waveform on the core loss and dynamic B-H loops of supermalloy
[NASA-TM-106982] p 2865 N95-32207
MAGNETIC DISTURBANCES
Environmental conditions responsible for solar activity
[AD-A292859] p 3031 N95-31450
MAGNETIC EFFECTS
The interaction of magnetizations with an external electromagnetic field and a time-dependent magnetic Aharonov-Bohm effect
[DE95-613463] p 2845 N95-30368
Magnetoluminescence characterization of quantum well structures
[DE95-008527] p 3008 N95-30381
Underdense heating of the ionosphere using oblique high power HF radiowaves p 2917 N95-31951
MAGNETIC ENERGY STORAGE
Performance evaluation of high-temperature superconducting current leads for micro-SMES systems
[DE95-005843] p 2861 N95-30943
MAGNETIC FIELD CONFIGURATIONS
On the possibility of a two-state magnetic structure for nanocrystalline chromium
[DE95-009914] p 3015 N95-32062
MAGNETIC FIELD RECONNECTION
Analysis of plasma measurements for the Geotail mission
[NASA-CR-199074] p 3032 N95-32218
MAGNETIC FIELDS
Electromagnetically activated compliant wavy-wall
[AD-D017340] p 2866 N95-30412
Magneto-optical transmission-reflection beam splitter for multi-level atoms
[DE95-616267] p 2976 N95-30423
Multisite antiferromagnetic Ising spin model: Phase transition through doubling bifurcation
[DE95-614311] p 3011 N95-30722
New Fermi-liquid approach for the theory of disordered magnetics
[DE95-613448] p 2967 N95-30739
Shear flow effects on ion thermal transport in tokamaks
[DE95-009115] p 3005 N95-30801
Ferromagnetic Potts model in a magnetic field: Finite lattice extrapolation of the (1 + 1)-dimensional Hamiltonian
[DE95-614447] p 3012 N95-30958
Relativistic non-interacting electron gas in a magnetic field
[DE95-616903] p 2967 N95-31177
Numerical modeling of Bridgman growth of PbSnTe in a magnetic field
[NASA-TM-106996] p 2837 N95-31359
Determination of electric and magnetic fields in open trap plasmas by means of atomic-molecular beam hydrogen isotopes
[DE95-614177] p 3006 N95-31680
MAGNETIC FLUX
A simple model for the dc flux transformer in layered superconductors with Josephson coupling
[DE95-614468] p 2859 N95-30649
MAGNETIC MATERIALS
New Fermi-liquid approach for the theory of disordered magnetics
[DE95-613448] p 2967 N95-30739
Initial survey on fracture toughness of commercial Nd2Fe14B
[DE95-009813] p 2808 N95-31643
Effects of temperature, frequency, flux density, and excitation waveform on the core loss and dynamic B-H loops of supermalloy
[NASA-TM-106982] p 2865 N95-32207
MAGNETIC MEASUREMENT
Damage dosimetry and embrittlement monitoring of nuclear pressure vessels in real time by magnetic properties measurement
[DE95-011454] p 2894 N95-31254
MAGNETIC MIRRORS
Removal of impurity ions from a magnetic trap with a two-component plasma on their collision with fast component ions
[DE95-614171] p 2984 N95-31550
Optimization of an expander of a gas-dynamic trap
[DE95-614172] p 3006 N95-31679
Longitudinal losses of charged particles from an open configuration with arbitrary beta ratio
[DE95-614187] p 2987 N95-32055
MAGNETIC MOMENTS
Supersymmetric magnetic moments sum rules and spontaneous supersymmetry breaking
[DE95-613771] p 2989 N95-32096
MAGNETIC PROPERTIES
Acoustoelastic stress evaluation in metal plate using absolute shear and longitudinal time-of-flight data
[PB95-197810] p 2892 N95-30458
A metallurgical approach toward alloying in rare earth permanent magnet systems
[DE95-010242] p 2966 N95-30668
Damage dosimetry and embrittlement monitoring of nuclear pressure vessels in real time by magnetic properties measurement
[DE95-011454] p 2894 N95-31254
Influence of layer order and composition on the magnetic anisotropy of ultra-thin Co sandwiches
[DE95-010608] p 2810 N95-32265
MAGNETIC RESONANCE
Lanthanide(III) catalyzed reactions: Structure an d thermodynamics of intermediate complexes, and implications for reactivity
[PB95-197000] p 3019 N95-30775
Magnetic resonance spectroscopy of fullerenes and (pi)-conjugated polymers
[DE95-010131] p 2817 N95-31108
MAGNETIC SIGNATURES
Kiruna geophysical data. Data summary 94/4-6, April-June 1994
[PB95-210365] p 2913 N95-30627
Kiruna geophysical data. Data summary 94/1-3, January-March 1994
[PB95-210373] p 2913 N95-30628
MAGNETIC STORMS
Environmental conditions responsible for solar activity
[AD-A292859] p 3031 N95-31450
Analysis of plasma measurements for the Geotail mission
[NASA-CR-199074] p 3032 N95-32218
MAGNETICALLY TRAPPED PARTICLES
Study of cross-tail current carriers in magnetotail
p 3005 N95-30804
MAGNETIZATION
The interaction of magnetizations with an external electromagnetic field and a time-dependent magnetic Aharonov-Bohm effect
[DE95-613463] p 2845 N95-30368
Multisite antiferromagnetic Ising spin model: Phase transition through doubling bifurcation
[DE95-614311] p 3011 N95-30722
Investigation of Fe3O4 colloid behaviour in a magnetic field by polarized neutron transmission
[DE95-614351] p 2981 N95-30915
Investigations of YBaCuO materials with near-room-temperature resistivity transitions
[AD-A293405] p 3013 N95-31008
MAGNETO-OPTICS
Magneto-optical transmission-reflection beam splitter for multi-level atoms
[DE95-616267] p 2976 N95-30423
MAGNETOHYDRODYNAMIC FLOW
Nearly steady flows in GONG prototype data
[NASA-CR-198935] p 2869 N95-30863
DE-1 observations of polar O(+) stream bulk parameters and comparison with a model of the centrifugally-accelerated polar wind
[NASA-CR-198930] p 2917 N95-31743
MAGNETOHYDRODYNAMIC STABILITY
Advances in the simulation of toroidal gyro Landau fluid model turbulence
[DE95-008387] p 3003 N95-30359
Development of a tokamak plasma optimized for stability and confinement
[DE95-009609] p 3003 N95-30641
Physics and application of high density Z-pinches
[NIFS-PROC-14] p 3004 N95-30671
Reynolds stress of localized toroidal modes
[DE95-008750] p 3004 N95-30795
Design considerations for a Density-Channel-Guided laser wake-field accelerator
[AD-A292876] p 2884 N95-31190
Stabilization of ballooning modes with sheared toroidal rotation
[DE95-008388] p 3006 N95-31624
A study of ion trapping and instability in the Fermilab antiproton accumulator p 2993 N95-31647
Optimization of an expander of a gas-dynamic trap
[DE95-614172] p 3006 N95-31679
Radial mode evolution in longitudinal bunched beam instability
[DE95-010895] p 2994 N95-32092
Wall stabilization of high beta plasmas in D3-D
[DE95-009607] p 3007 N95-32116
Skew chromaticity in large accelerators
[DE95-011564] p 2994 N95-32243
Onset of ELMs in JT-60U
[DE95-737209] p 3007 N95-32263
MAGNETOHYDRODYNAMIC TURBULENCE
Theory and simulation of electrostatic wave turbulence in the space shuttle-induced plasma environment
[AD-A293467] p 3005 N95-31534
MAGNETOHYDRODYNAMICS
Electromagnetically activated compliant wavy-wall
[AD-D017340] p 2866 N95-30412
Stabilization of ballooning modes with sheared toroidal rotation
[DE95-008388] p 3006 N95-31624
MAGNETOSHEATH
Low-latitude boundary layer near noon: An open field line model
[ATR-93(7270)-1] p 2914 N95-30773
MAGNETOSPHERIC INSTABILITY
Environmental conditions responsible for solar activity
[AD-A292859] p 3031 N95-31450
MAGNETOSTATIC FIELDS
A time stepping coupled finite element-state space modeling environment for synchronous machine performance and design analysis in the ABC frame of reference p 2864 N95-31948
MAGNETOSTRICTION
Transitions, defects, and whiskered microstructures
[AD-A292796] p 3014 N95-31438
MAGNETRON SPUTTERING
Structural, chemical and electronic properties of superconducting thin films and junctions
[AD-A292700] p 3012 N95-30933
MAGNETS
The art and science of magnet design: Selected notes of Klaus Halbach, volume 2
[DE95-008450] p 2861 N95-31059
Initial survey on fracture toughness of commercial Nd2Fe14B
[DE95-009813] p 2808 N95-31643
MAIN SEQUENCE STARS
Cepheid temperature and the Blazhko effect
[NASA-CR-189433] p 3030 N95-31819

MAINTAINABILITY
Recommended techniques for effective maintainability. A continuous improvement initiative of the NASA Reliability and Maintainability Steering Committee
[NASA-TM-4628] p 2892 N95-31530
MAINTENANCE
Design of fibre reinforced composite panels for aerospace applications
[PB95-197851] p 2784 N95-30460
Measures of reliability and RCM
[PB95-192985] p 2891 N95-30510
Dynamic maintenance scheduling for a stochastic telecommunication network: Determination of performance factors
[AD-A293829] p 2852 N95-31555
MAJORITY CARRIERS
Minority and majority carrier transport characterization in compound semiconductors
[DE95-010873] p 3014 N95-31233
MAMMALS
AASERT-92 augmentation of research training in chronobiology: Regulation of the mammalian circadian clock by neurotransmitters
[AD-A288243] p 2925 N95-31144
MAN ENVIRONMENT INTERACTIONS
National Institute for Global Environmental Change
[DE95-008333] p 2907 N95-30358
MAN MACHINE SYSTEMS
Human factors at the FAA Technical Center: Bibliography
[AD-A288638] p 2930 N95-31399
Guidance and Control for Future Air-Defence Systems
[AGARD-CP-555] p 2839 N95-32123
AIDEX: An expert system for aircraft identification
p 2842 N95-32138
MANAGEMENT
Planning board generator. Part 1: Problem instances and types
[PB95-197075] p 3021 N95-30834
MANAGEMENT ANALYSIS
Annual report to the Chairman and Ranking Minority Members, House and Senate Committees on Appropriations. Status of open recommendations: Improving operations of federal departments and agencies
[GAO/OP-95-1] p 3022 N95-31986
MANAGEMENT INFORMATION SYSTEMS
The development of KAERI management information system 2: The development of Time Sheet Management System
[DE95-613355] p 3024 N95-30883
MANAGEMENT METHODS
Domain analysis for the reuse of software development experiences p 2936 N95-31236
Building an experience factory for maintenance
p 2937 N95-31237
Closing the loop on improvement: Packaging experience in the Software Engineering Laboratory
p 2937 N95-31238
Process maturity progress at Motorola Cellular Systems Division p 2937 N95-31239
The Personal Software Process: Downscaling the factory p 2937 N95-31240
Management of major system programs and projects. Handbook
[NHB-7120.5] p 3021 N95-31380
Recommended techniques for effective maintainability. A continuous improvement initiative of the NASA Reliability and Maintainability Steering Committee
[NASA-TM-4628] p 2892 N95-31530
The Oak Ridge Refrigerant Management Program
p 2774 N95-31763
Application of a genetic algorithm to optimize staffing levels in software development
[AD-A293725] p 2943 N95-31835
MANAGEMENT PLANNING
An architectural approach to strategic information systems planning for the Office of Naval Intelligence
[AD-A289930] p 3024 N95-30928
Management of major system programs and projects. Handbook
[NHB-7120.5] p 3021 N95-31380
Unmanned aerial vehicles. 1994 master plan
p 2751 N95-31416
The Oak Ridge Refrigerant Management Program
p 2774 N95-31763
Westinghouse Hanford Company Data Management Plan Template, revision 1
[DE95-010046] p 3026 N95-32107
MANEUVERABILITY
Dynamic inversion: An evolving methodology for flight control design p 2758 N95-31996
X-31: A program overview and flight test status
p 2753 N95-32013
MANEUVERS
Synthetic Terrain Imagery for Helmet-Mounted Display, volume 1
[AD-A293612] p 2753 N95-31656
MANGANESE
On the Jahn-Teller effect of Mn(2+) in zinc-blende ZnS crystal
[AD-A293711] p 2797 N95-31830
MANGANESE ALLOYS
Interfacial segregation and deformation of superplastically deformed Al-Mg-Mn alloys
[DE95-009572] p 2809 N95-32052
MANIFOLDS (MATHEMATICS)
Local index formula in noncommutative geometry
[PB95-208146] p 2955 N95-30490
4-manifold topology 2: Dwyer's filtration and surgery kernels
[PB95-207940] p 2965 N95-30509
The 4-manifold topology 1: Subexponential groups
[PB95-207957] p 2965 N95-30555
Generalized Kummer surfaces and differentiable invariants of Noether-Horikawa surfaces 1
[DE95-613382] p 2956 N95-30608
Good metric spaces without good parameterizations
[PB95-208427] p 2957 N95-30622
Pi1(sup infinity) and infinite simple homotopy type in dimension three: A research announcement
[PB95-196283] p 2957 N95-30696
Introduction to the theory of Goyaks: Operator manifold approach to geometry and particle physics
[DE95-613460] p 2980 N95-30740
Exact smooth classification of Hamiltonian vector fields on symplectic 2-manifolds
[DE95-613378] p 2958 N95-30803
Quantization of a relativistic particle on the SL(2,R) manifold based on Hamiltonian reduction
[DE95-737163] p 2983 N95-31224
Global aspects of the WZNW reduction to Toda theories
[DE95-737230] p 3019 N95-31226
Bifurcations of contracting singular cycles
[DE95-613371] p 2962 N95-32117
MANIPULATORS
Force and vision resolvability for assimilating disparate sensory feedback
[AD-A293581] p 2929 N95-31685
On the kinematic performance of mechanical manipulators operating in the presence of an obstruction
p 2890 N95-31710
On-orbit truss structure tele-operation experiment by Engineering Test Satellite-7
[NAL-TR-1246] p 2767 N95-31980
MANNED SPACE FLIGHT
Aeronautics and space report of the President
[NASA-TM-110743] p 3028 N95-31979
MANUALS
A manual for the economic evaluation of energy efficiency and renewable energy technologies
[DE95-000211] p 2903 N95-30896
A manual for pyrotechnic design, development and qualification
[NASA-TM-110172] p 2766 N95-31358
Video conferencing using DAVE user's guide
[DE95-010341] p 2854 N95-32045
MANUFACTURING
The role of advanced engineering simulation in model-based design
[DE95-008815] p 2934 N95-30796
Photovoltaic Czochralski silicon manufacturing technology improvements
[DE95-004066] p 2904 N95-31162
Large-area, triple-junction a-Si alloy production scale-up
[DE95-004067] p 2904 N95-31163
Photovoltaic module certification/laboratory accreditation criteria development
[DE95-004063] p 2905 N95-31381
The 19th Annual Electronics Manufacturing Seminar
[AD-A293067] p 2863 N95-31674
Manufacturing waste disposal practices of the chemical propulsion industry p 2771 N95-31748
Technology transfer into the solid propulsion industry
p 2770 N95-31756
National Center for Manufacturing Sciences: Environmentally conscious manufacturing
p 2773 N95-31758
The search for CFC alternatives is over?
p 2774 N95-31760
Prepsolv (TM): The optimum alternative to 1,1,1-trichloroethane and methyl ethyl ketone for hand-wipe cleaning of aerospace materials
p 2774 N95-31764
Evaluation and analysis survey on new energy introduction, part 3
[DE95-769806] p 2906 N95-32072
Vibration control for precision manufacturing at Sandia National Laboratories
[DE95-009582] p 2839 N95-32082
MANY BODY PROBLEM
Many-body effects in semiconductor lasers
[DE95-008534] p 2883 N95-30390
Multi-particle correlations in quaternionic quantum systems
[DE95-616271] p 3018 N95-30424
Study of the generalized solutions of n-body type problems with weak forces
[DE95-613381] p 2958 N95-30820
Irreducible Green's Functions method in the theory of highly correlated systems
[DE95-614446] p 3019 N95-31186
Removal of the Energy Dependence from the Resolvent Like Energy Dependent Interactions
[DE95-613385] p 2961 N95-31619
MAPPING
Associators in generalized octonionic maps
[DE95-616243] p 2957 N95-30688
Synthetic Terrain Imagery for Helmet-Mounted Display. Volume 3: Software user's manual
[AD-A293613] p 2753 N95-31463
MAPS
Digital Mapping Charting and Geodesy Analysis Program technical review of Vector Product Format (VPF)
[AD-A289766] p 2901 N95-31390
MARINE ENVIRONMENTS
Analysis of target contrast improvement using polarization filtering in the infrared region
[AD-A293085] p 3001 N95-31841
Multisensor data fusion for integrated maritime surveillance p 2842 N95-32135
MARINE METEOROLOGY
Aerosol measurements over the Pacific Ocean in support of the IR aerosol backscatter program
[NASA-CR-198925] p 2918 N95-30782
QTSAW (Quick Typhoon Surge and Waves). Wave information studies of US coastlines
[AD-A293172] p 2919 N95-30976
Shiptracks in the Californian stratus region: Dependency on marine atmospheric boundary layer depth
[AD-A293272] p 2901 N95-31125
Modern methods in meteorological and oceanographic data acquisition and analyses
[AD-A293884] p 2920 N95-31541
Validation of special sensor microwave/imager ocean surface wind retrievals in equatorial regions
[AD-A293750] p 2920 N95-31571
A numerical study of the effect of the Gulf Stream and the Appalachian Mountains on Carolina coastal frontogenesis
[AD-A293765] p 2921 N95-31577
Diagnosis of the kinematics and dynamics of rapidly developing maritime cyclones
[AD-A293919] p 2921 N95-31675
MARINE TECHNOLOGY
Active turbulence control using microelectrodes, permanent magnets in microgrooves
[AD-D017351] p 2867 N95-30553
Static behaviour of axially loaded uniplanar and multiplanar tubular x-joints
[PB95-207866] p 2892 N95-30585
Fatigue behaviour of multiplanar tubular joints
[PB95-207874] p 2893 N95-30586
EMC requirements for type approval of marine electronics. Nordtest project 1157-94
[PB95-211330] p 2859 N95-30596
MARINER MARK 2 SPACECRAFT
Welding isotopic heat sources for the cassini mission to Saturn
[DE95-060104] p 2890 N95-32367
MARKET RESEARCH
Photovoltaic Energy Program overview: Fiscal year 1994
[DE94-011871] p 2905 N95-31661
MARKOV CHAINS
Analyzing GI/Erlang-r/1 queues
[PB95-197034] p 2949 N95-30400
A stochastic EM estimator in the presence of missing data: Theory and applications
[DE95-010329] p 2944 N95-32089
MARKOV PROCESSES
Analysis and modeling of an airport departure process
[AD-A293782] p 2749 N95-31581
MARS (PLANET)
Mars together and FIRE and ICE: Report of the joint US/Russian technical working groups
[NASA-CR-198864] p 3030 N95-30845
MARS EXPLORATION
Mars together and FIRE and ICE: Report of the joint US/Russian technical working groups
[NASA-CR-198864] p 3030 N95-30845

MARS SURFACE
Mars together and FIRE and ICE: Report of the joint US/Russian technical working groups
[NASA-CR-198864] p 3030 N95-30845
MARTENSITE
Transitions, defects, and whiskered microstructures
[AD-A292796] p 3014 N95-31438
MARTENSITIC TRANSFORMATION
Shape memory properties of an iron modified nickel aluminide alloy
[DE95-010223] p 2805 N95-31111
Transitions, defects, and whiskered microstructures
[AD-A292796] p 3014 N95-31438
MASERS
Enhanced brightness x-ray lasers
[DE95-010735] p 2886 N95-32029
MASS DISTRIBUTION
Dissolution of eutectic microstructures
[DE95-010244] p 2804 N95-30757
Assessment of the NASA orbital debris engineering model
[AD-A293350] p 2766 N95-31143
MASS FLOW
An experimental study of planar heterogeneous supersonic confined jets
[AD-A290859] p 2867 N95-30557
Existence of solutions in plane quasistationary stokes flow driven by surface tension
[PB95-197935] p 2868 N95-30810
MASS RATIOS
Proceedings of the high energy density matter (HEDM) contractor's conference
[AD-A292988] p 2836 N95-31470
MASS SPECTROMETERS
Novel mass spectrometric instrument for gaseous and particulate characterization and monitoring
[DE95-000047] p 2881 N95-31694
MASS SPECTROSCOPY
Standardization of (13)CO2 production procedure from organic matter for mass spectrometric analysis
[DE95-614629] p 2791 N95-30420
A study of gas-phase processes during the deflagration of RDX composite propellants using a triple quadrupole mass spectrometer p 2801 N95-31304
A study of the gas-phase processes of RDX combustion using a triple quadrupole mass-spectrometer p 2801 N95-31315
Analytical instrumentation for environmental research
[AD-A292832] p 2908 N95-31447
MASS TRANSFER
Simultaneous heat and mass transfer in a horizontal tube absorber: Numerical tools for present and future absorber designs
[PB95-196978] p 2869 N95-30872
MASSIVELY PARALLEL PROCESSORS
Algorithm comparison and benchmarking using a parallel spectra transform shallow water model
[DE95-009124] p 2913 N95-30683
Advanced computational research in materials processing for design and manufacturing
[DE95-009130] p 2838 N95-30684
Three-dimensional (3D) large fluid flow computations for US Army applications on KSR-1, CM-200, CM-5, and Cray C-90
[AD-A293125] p 2869 N95-30889
A two-dimensional finite difference algorithm on the KSR1
[AD-A293576] p 2941 N95-31594
MPI implementation of PHOENICS: A general purpose computational fluid dynamics code
[DE95-009810] p 2877 N95-32033
MATCHING
Production matching for large learning systems
[AD-A293105] p 2953 N95-31827
Multiple Target Tracking based on constellation matching and Kalman filter p 2842 N95-32136
MATERIALS RECOVERY
Recycling MIL-H-46170 hydraulic fluid to extend fluid service life
[AD-A293035] p 2821 N95-31664
Responsive copolymers for enhanced petroleum recovery
[DE95-011857] p 2823 N95-32361
MATERIALS SCIENCE
Metallurgical and Materials Transactions
[AD-A293617] p 2807 N95-31464
Laboratory directed research and development report
[DE95-011405] p 3032 N95-32279
MATERIALS TESTS
Localization in tungsten heavy alloys subjected to shearing deformations under superimposed high pressures
[AD-A293177] p 2804 N95-30977
MATHEMATICAL LOGIC
Preservation theorems on finite structures
[DE95-613442] p 2962 N95-32067
MATHEMATICAL MODELS
A phenomenological finite element model of part building in the stereolithography process
[DE95-008437] p 2932 N95-30376
Theoretical absorption spectroscopy of high-temperature metal vapors: Model and experiment compared
[AD-A290872] p 2791 N95-30409
Covariant phase space formulations of superparticles and supersymmetric WZW models
[DE95-616278] p 2964 N95-30428
Finite element simulation of GaAs MESFET's
[PB95-208062] p 3009 N95-30485
Advanced system identification techniques for wind turbine structures
[DE95-004049] p 2902 N95-30505
Overview of IEA biomass combustion activities
[PB95-196374] p 2902 N95-30519
Experimental determination of probability distributions for parameters of a Salem limestone cap plasticity model
[AD-A290878] p 2892 N95-30559
Molecular modeling of PMN ceramics
[AD-A290879] p 2813 N95-30560
Feature-based modeling of product families
[PB95-207148] p 2933 N95-30568
A numerical model for dynamic wave rotor analysis
[NASA-TM-106997] p 2754 N95-30617
Quasi-periodic solutions of Hamiltonian perturbations of 2D linear Schroedinger equations
[PB95-208443] p 2957 N95-30624
Simple model of foam spreading on liquid surfaces
[PB95-211207] p 2838 N95-30630
Axial loads on yawed rotors
[PB95-214193] p 2742 N95-30638
Alloying effects of Kondo insulators
[DE95-614306] p 3010 N95-30644
The one-dimensional model of the off-centre potential of the fluorine ion in the NaBr lattice
[DE95-614310] p 3010 N95-30647
A simple model for the dc flux transformer in layered superconductors with Josephson coupling
[DE95-614468] p 2859 N95-30649
On the theory of hole propagation in an antiferromagnetic background
[DE95-614469] p 3010 N95-30650
Properties of a multichannel resonant-level model
[DE95-614482] p 2979 N95-30652
Economical analysis relating to the global warming issue
[DE95-764072] p 2908 N95-30677
Advanced computational research in materials processing for design and manufacturing
[DE95-009130] p 2838 N95-30684
Associators in generalized octonionic maps
[DE95-616243] p 2957 N95-30688
Potential integral equations of the 2D Laplace operator in wavelet basis
[TRITA-NA-9401] p 2957 N95-30713
Enhancements to the SSME transfer function modeling code
[NASA-CR-198957] p 2958 N95-30754
A theory for predicting and minimizing the effects of matrix degradation on the thermomechanical properties of general laminates p 2785 N95-30768
TV-VI semiconductor quantum well lasers, physics and engineering p 2883 N95-30805
A viscoelastic anisotropic wave propagation model for composite cure evaluation p 2786 N95-30839
Computation of high-altitude hypersonic flow-field radiation p 2743 N95-30843
Calculated coupling efficiency between an elliptical-core optical fiber and an optical waveguide over temperature
[NASA-TM-107005] p 2997 N95-30849
Kinetic theory model predictions compared with low-thrust axisymmetric nozzle plume data
[NASA-CR-198934] p 2768 N95-30864
Validation of the FLAGSOL parabolic trough solar power plant performance model
[DE95-000263] p 2903 N95-30887
Multi-valued neural network modified model and its optical realization.
[AD-A293140] p 2951 N95-30891
Failure analysis of a repairable system: The case study of a cam-driven reciprocating pump
[AD-A293144] p 2889 N95-30949
Dynamical systems as models for flow-induced vibrations
[PB95-206991] p 2869 N95-30956
Acceleration potential models PREDICHAT/PREDICDYN applied for calculation of axisymmetric dynamic inflow cases
[PB95-207015] p 2869 N95-30957
Ferromagnetic Potts model in a magnetic field: Finite lattice extrapolation of the (1' + 1)-dimensional Hamiltonian
[DE95-614447] p 3012 N95-30958
Dynamics of an inhomogeneous anisotropic antiferromagnetic spin chain
[DE95-614449] p 3013 N95-30959
SSUSI single sensor auroral E-layer algorithm: Functional description
[AD-A288630] p 2914 N95-31012
Workshop on diffusion approximation in communication and stochastic systems theory
[AD-A292872] p 2952 N95-31055
High strain rate properties and constitutive modeling of glass
[DE95-008434] p 2816 N95-31058
Looking for the simple PIO model p 2745 N95-31066
Calspan experience of PIO and the effects of rate limiting p 2746 N95-31072
Effect of cyclic loading on the creep performance of silicon nitride
[DE95-010289] p 2894 N95-31131
Effective bandwidth techniques in bufferless and buffered ATM multiplexers
[PB95-207072] p 2862 N95-31185
Numerical simulation of ram accelerator performance including transient effects during initiation of combustion and sensitivity studies p 2799 N95-31203
Viscous heating of liquid layers under intense shear p 2827 N95-31206
Numerical study of shear-induced heating in high-speed nozzle flow of liquid monopropellant p 2828 N95-31207
Dynamics of Current Driven Disordered Josephson Junction Arrays
[DE95-009418] p 3014 N95-31231
The 2nd Japan-US Symposium on Finite Element Methods in Large Scale Computational Fluid Dynamics
[AD-A292337] p 2960 N95-31264
Advances in robust control
[AD-A291126] p 2952 N95-31266
The 25th International Symposium on Combustion
[AD-A286825] p 2794 N95-31268
Theory of unsteady combustion of solids: Investigation of Quasi-steady assumption p 2800 N95-31285
An ignition model for modern double base propellants p 2800 N95-31292
Control of mechanical systems with rolling contacts: Applications to robotics p 2889 N95-31332
Modeling multi-beam structures for control p 2895 N95-31346
Numerical modeling of Bridgman growth of PbSnTe in a magnetic field
[NASA-TM-106996] p 2837 N95-31359
Visual tracking of self-occluding articulated objects
[AD-A292894] p 2928 N95-31383
Numerical studies of nonlinear optical pulse propagation p 2998 N95-31411
Numerical simulation of time dependent viscoelastic fluid flow
[TRITA-NA-9311] p 2873 N95-31414
Some aspects on the modelling of non-Newtonian fluid flow
[TRITA-NA-9317] p 2873 N95-31415
Nonparametric methods for incomplete data in reliability and for changepoints in smooth functions
[AD-A292773] p 2963 N95-31429
Visual processing of object velocity and acceleration
[AD-A292789] p 2929 N95-31436
Clouds: Their prediction and simulation
[AD-A292864] p 2920 N95-31453
Analysis of symbolic parameter models
[AD-A292916] p 2940 N95-31459
Derivation of two-dimensional (2-D) conduction equation in generalized coordinates with constant and anisotropic physical properties
[AD-A293896] p 3020 N95-31511
A new goodness-of-fit test for the gamma distribution based on sample spacings from complete and censored samples
[AD-A293875] p 2961 N95-31518
Fast algorithms for three-dimensional inverse scattering problems
[AD-A293510] p 2852 N95-31537
Spatial time-series: Pollution pattern recognition under irregular interventions
[AD-A293830] p 2909 N95-31556
Multipoint quadratic approximation for numerical optimization
[AD-A293837] p 2961 N95-31557
Nonlinear time series analysis
[AD-A293841] p 2963 N95-31558
Nonparametric recognition of nonrigid motion
[AD-A293630] p 2963 N95-31565

Analytic and experimental investigation of rotordynamic response and backward whirl induced by split resonance
[AD-A293639] p 2889 N95-31566
Analysis and modeling of an airport departure process
[AD-A293782] p 2749 N95-31581
The effect of repeatedly sampling an embedded metamodel on the simulation response
[AD-A293783] p 2953 N95-31582
Large-eddy simulation of turbulent flow using the finite element method
[DE95-009464] p 2875 N95-31591
Network user's guide
[DE95-009185] p 2942 N95-31634
Fractional delay waveguide modeling of acoustic tubes
[PB95-206637] p 2975 N95-31650
Study of melting and freezing processes of water for application to ice thermal energy storage system
p 2905 N95-31735
Selected flows with free surfaces: Streams and drops
[IFTR-3/1995] p 2876 N95-31817
Modeling of grain boundary stresses in Alloy 600
[DE95-009033] p 2808 N95-31825
A hypothesis-testing approach to discriminant analysis with mixed categorical and continuous variables when data are missing
[AD-A293714] p 2964 N95-31831
The GCRC two-dimensional zonally averaged statistical dynamical climate model: Development, model performance, and climate sensitivity
p 2910 N95-31851
A time stepping coupled finite element-state space modeling environment for synchronous machine performance and design analysis in the ABC frame of reference p 2864 N95-31948
Preservation theorems on finite structures
[DE95-613442] p 2962 N95-32067
Vibration control for precision manufacturing at Sandia National Laboratories
[DE95-009582] p 2839 N95-32082
Estimation in second order dependency model for multivariate binary data
[DE95-010326] p 2944 N95-32087
A stochastic difference equation approach to inference with missing data: Some new results
[DE95-010327] p 2944 N95-32088
Automated volumetric grid generation for finite element modeling of human hand joints
[DE95-009575] p 2928 N95-32097
Models of transport, gas-phase and surface chemistry in diamond chemical vapor deposition
[DE95-009861] p 2822 N95-32101
Simulation of fracture in compression using a field-theory model
[DE95-009874] p 2898 N95-32102
A mode decomposition based finite element formulation for the nonlinear dynamics of flexible spatial structures and mechanisms p 2898 N95-32118
Optimal infrared detector configurations for air target detection p 2841 N95-32130
Architecture and implementation of a multi-sensor data fusion demonstration model within the real-time combat system of the Canadian Patrol Frigate
p 2842 N95-32139
Using a Red Team to devise countermeasures
p 2842 N95-32141
KRAKEN, a numerical model of RHIC impedances
[DE95-011563] p 2994 N95-32242
Study of tropospheric correction for intercontinental GPS common-view time transfer p 2971 N95-32338
Phase transitions and gravitational collapse
[DE95-011732] p 3021 N95-32359
Objective analysis of oceanic data for Coast Guard trajectory models
[AD-A292884] p 2924 N95-32363

MATHEMATICAL PROGRAMMING
Numerical solution of a singular integral equation arising from a sequential probability ratio test
[AD-A293463] p 2963 N95-31375

MATRICES (MATHEMATICS)
Density dependent effective interactions
[DE95-616348] p 2977 N95-30447
Control of flexible spacecraft structures using H-infinity wave absorbing control
[AD-A293141] p 2766 N95-30919
A scalable parallel Strassen's matrix multiply algorithm for distributed memory computers
[DE95-010213] p 2936 N95-31109
Advances in robust control
[AD-A291126] p 2952 N95-31266
Non-critical string field theory with non-orientable string interactions
[DE95-737160] p 3020 N95-31281
A modification to the GMRES method for ill-conditioned linear systems
[DE95-010661] p 2962 N95-32076
Normal mode tunes for linear coupled motion in six dimensional phase space
[DE95-011565] p 2994 N95-32244
Texture based methods for image analysis: A review
[PB95-211595] p 2945 N95-32251

MATRIX MATERIALS
A theory for predicting and minimizing the effects of matrix degradation on the thermomechanical properties of general laminates p 2785 N95-30768
Metallurgical and Materials Transactions
[AD-A293617] p 2807 N95-31464
Influence of fiber content on mechanical performance of SiC-fiber-reinforced reaction-bonded silicon nitride composites
[NASA-TM-110639] p 2790 N95-32060

MATRIX METHODS
Fourier series methods for cracks in polygonal plates and shells of revolution p 2893 N95-30825

MATRIX THEORY
Dynamical analogy of Cabibbo-Kobayashi-Maskawa matrices
[DE95-613462] p 2975 N95-30367

MAXIMUM ENTROPY METHOD
Direct sublattice imaging of interface dislocation structures in CdTe/GaAs(001)
[DE95-009031] p 3010 N95-30576
Robust fixed-structure control
[AD-A292883] p 2952 N95-30961

MAXIMUM LIKELIHOOD ESTIMATES
Expert system for assessing accuracy of models of physical phenomena and for selecting alternate models in the presence of noise
[AD-D017348] p 2974 N95-30550
Failure analysis of a repairable system: The case study of a cam-driven reciprocating pump
[AD-A293144] p 2889 N95-30949
Nonparametric methods for incomplete data in reliability and for changepoints in smooth functions
[AD-A292773] p 2963 N95-31429
A new goodness-of-fit test for the gamma distribution based on sample spacings from complete and censored samples
[AD-A293875] p 2961 N95-31518
A hypothesis-testing approach to discriminant analysis with mixed categorical and continuous variables when data are missing
[AD-A293714] p 2964 N95-31831
A Stochastic EM algorithm for approximating the maximum likelihood estimate
[DE95-010328] p 2943 N95-32044
Multiple turbo codes for deep-space communications
p 2855 N95-32227

MAXIMUM PRINCIPLE
An extremum principle for the analysis and design of constitutively nonlinear systems p 2898 N95-32112

MAXWELL EQUATION
Many-body effects in semiconductor lasers
[DE95-008534] p 2883 N95-30390
Six-vector formalism in electromagnetics of bianisotropic media
[PB95-207130] p 2846 N95-30567
Numerical studies of nonlinear optical pulse propagation p 2998 N95-31411
Two-dimensional Finite Difference Time Domain (FD-TD) model of electromagnetic (EM) scattering from a buried rectangular object
[AD-A293685] p 2852 N95-31601

MCDONNELL DOUGLAS AIRCRAFT
Report to Congressional Committees. Military airlift: C-17 settlement is not a good deal
[GAO/NSIAD-94-141] p 2741 N95-32198

MEAN
Complex mean value interpolation
[PB95-211629] p 2956 N95-30601

MEAN SQUARE VALUES
An efficient implementation of Forward-Backward Least-Mean-Square Adaptive Line Enhancers
p 2855 N95-32224

MEASUREMENT
Survey of US burning rate measurement methods for solid propulsion applications p 2800 N95-31291

MEASURING INSTRUMENTS
Light-front dynamics of Chern-Simons systems
[DE95-613467] p 3019 N95-30741
Tunable composite membranes for gas separations
[DE95-010602] p 2822 N95-32075

MECHANICAL DEVICES
Locking device for fluid coupling
[AD-D017354] p 2888 N95-30414
Speed control of an elastic two-mass system: Optimization and systems theory
[PB95-212106] p 2888 N95-30701

MECHANICAL ENGINEERING
Advanced small rocket chambers. Option 3: 110 1bf lr-Re rocket, volume 1
[NASA-CR-195435-VOL-1] p 2768 N95-31169
Advanced small rocket chambers. Option 3: 110 1bf lr-Re rocket, volume 2
[NASA-CR-195435-VOL-2] p 2769 N95-31170

MECHANICAL IMPEDANCE
The coupling impedance of a toroidal beam pipe with circular cross section
[DE95-010442] p 2993 N95-31405

MECHANICAL MEASUREMENT
An inverse method to measure the axial modulus of composite materials under tension
[AD-A293042] p 2789 N95-31668

MECHANICAL PROPERTIES
Interface degradation in CAS/Nicalon during elevated temperature aging
[DE95-008843] p 2812 N95-30543
Analysis of variation embedding tests with 17 MM dowel: Densified veneer wood FOREST project, part 7
[PB95-206876] p 2963 N95-30680
Processing and characterization of nanocrystalline molybdenum disilicide (MoSi2) consolidated by hot isostatic pressing (HIP)
[DE95-010243] p 3012 N95-30756
The effect of interface properties on nickel base alloy composites
[NASA-CR-198363] p 2785 N95-30787
Innovative processing of composites for ultra-high temperature applications, book 4
[AD-A290892] p 2786 N95-30867
Innovative processing of composites for ultra-high temperature applications, book 2
[AD-A290890] p 2786 N95-30898
Synthesis and selected micro-mechanical properties of titanium nitride thin films by the pyrolysis of tetrakis titanium in ammonia
[DE95-010224] p 2818 N95-31187
Behaviour of polymers in radioactive environments: Effects of dose speed
[DE95-621008] p 2818 N95-31221
Damage dosimetry and embrittlement monitoring of nuclear pressure vessels in real time by magnetic properties measurement
[DE95-011454] p 2894 N95-31254
The 10th International Conference on the Strength of Materials
[AD-A292335] p 2894 N95-31263
Metallurgical and Materials Transactions
[AD-A293617] p 2807 N95-31464
In situ composites in the aluminum nitride-alumina system
[AD-A293776] p 2789 N95-31509
High strain-rate testing of parachute materials
[DE95-009577] p 2897 N95-31614
Influence of fiber content on mechanical performance of SiC-fiber-reinforced reaction-bonded silicon nitride composites
[NASA-TM-110639] p 2790 N95-32060
Gelcasting of sintered reaction-bonded silicon nitride for improved mechanical properties
[DE95-010282] p 2822 N95-32085

MECHANICAL SHOCK
Releaseable unconstrained inflatable body protector
[AD-D017350] p 2930 N95-30552

MECHANICAL TWINNING
Characterization of /11'01/ twin dislocation structures in evaporated titanium thin films by HREM
[DE95-615391] p 2820 N95-31623

MECHANORECEPTORS
Physiology and physiopathology of equilibration
[PB95-208328] p 2926 N95-30494

MEDICAL SCIENCE
Summaries of fiscal year 1994 projects in medical applications and biophysical research
[DE95-010405] p 2925 N95-32040

MEDICAL SERVICES
Patient/aircraft forecasting for the strategic aeromedical evacuation lift-bed process
[AD-A293902] p 2747 N95-31512

MELT SPINNING
Phase transformations in melt-spun Y-Ba-Cu-O bulk superconductor
[DE95-010237] p 3011 N95-30667

MELTING
Dissolution of eutectic microstructures
[DE95-010244] p 2804 N95-30757
Effect of local melting on tribology in metal cutting
[PB95-195392] p 2804 N95-31052
Fundamental topics in heat transfer through deformable two-phase media p 2874 N95-31532
Study of melting and freezing processes of water for application to ice thermal energy storage system
p 2905 N95-31735

MEMBRANE STRUCTURES
Structural analyses of the JPL Mars Pathfinder impact
[DE95-009581] p 2767 N95-32081

MEMBRANES
Process for producing hydrophilic polymer membranes
[AD-D017355] p 2811 N95-30415
On-line surfactant monitoring
[DE95-009417] p 2792 N95-30735
Metal nanotubule membranes with electrochemically switchable ion-transport selectivity
[AD-A292712] p 2793 N95-30938
Faster, cheaper radioanalytical methods
[DE95-009913] p 2797 N95-32061
Tunable composite membranes for gas separations
[DE95-010602] p 2822 N95-32075

MEMORY
Contextual interference effects on acquisition and transfer of a complex motor task
[AD-A293788] p 2929 N95-31583

MEMORY (COMPUTERS)
Implementation of KIVA-3 on distributed memory MIMD computers
[DE95-010288] p 2931 N95-31130

MENTAL PERFORMANCE
Training metacognitive skills for problem solving
[AD-A290310] p 2959 N95-31002
Impact of task properties, data display format and cognitive characteristics on recall performance: A cumulative research investigation p 3025 N95-31334
Forward rapid rotation shiftwork in USAF air traffic controllers: Sleep, activity, fatigue and mood analyses
[AD-A293448] p 2927 N95-31373
Optimizing the long-term retention of skills: Structural and analytic approaches to skill maintenance
[AD-A293798] p 2929 N95-31585

MERIDIONAL FLOW
Global Ultraviolet Imager (GUVI) investigation
[NASA-CR-189430] p 2917 N95-31820

MESOMETEOROLOGY
Clouds: Their prediction and simulation
[AD-A292864] p 2920 N95-31453

MESON-NUCLEON INTERACTIONS
Pion-nucleon and kaon-nucleon scattering lengths in QCD sum rules
[DE95-737278] p 2983 N95-31227

MESONS
Hadronic production of S-wave and P-wave charmed beauty mesons via heavy quark fragmentation
[DE95-008737] p 2977 N95-30465
Instantaneous chiral quark model for relativistic mesons in a hot and dense medium
[DE95-613782] p 2980 N95-30911
Multichannel resonances in coupled channels of meson scattering: Scalar sector
[DE95-613783] p 2981 N95-30912
B(sub c)-meson production in hadron-hadron collisions
[DE95-620537] p 2983 N95-31217
Scaling behaviour of leptonic decay constants for heavy quarkonia and heavy mesons
[DE95-620539] p 2983 N95-31218
Mixing phases of unstable two-level systems
[DE95-613844] p 2989 N95-32151
Charm photoproduction dynamics
[DE95-009106] p 2990 N95-32303
On hadronic production of the B(sub c) meson
[DE95-613726] p 2991 N95-32304

MESOPAUSE
Middle atmosphere structure and dynamics: Lidar studies at the South Pole, Syowa and Urbana
p 2916 N95-31736

MESOSCALE PHENOMENA
Clouds: Their prediction and simulation
[AD-A292864] p 2920 N95-31453
A numerical study of the effect of the Gulf Stream and the Appalachian Mountains on Carolina coastal frontogenesis
[AD-A293765] p 2921 N95-31577
Brightness temperature simulations for the physical and synoptic interpretation of advanced microwave sounding unit moisture channels p 2921 N95-31721
Simulation of katabatic flow and mountain waves
[DE95-010863] p 2911 N95-32276

MESSAGE PROCESSING
An executable specification for the message processor in a simple combining network
[NASA-CR-198174] p 2933 N95-30584
Universal message passing library, or how to writea truly portable code for parallel computers
[PB95-212221] p 2948 N95-32255

MESSAGES
MPI implementation of PHOENICS: A general purpose computational fluid dynamics code
[DE95-009810] p 2877 N95-32033

METAL BONDING
Influence of adhesives and bonding techniques on the properties of glued timber-steelplate joints
[PB95-211470] p 2813 N95-30599
New material for high average power infrared generation: QPM-DB GaAs
[AD-A292714] p 2967 N95-30939
Cleanliness inspection tool for RSRM bond surfaces
p 2781 N95-31799

METAL COATINGS
High temperature barrier coatings for refractory metals
[NASA-CR-195475] p 2802 N95-30531
High aspect ratio metal microstructures and method for preparing the same
[AD-D017463] p 2803 N95-30750
Advanced small rocket chambers. Option 3: 110 1bf Ir-Re rocket, volume 1
[NASA-CR-195435-VOL-1] p 2768 N95-31169
Self-lubricating, TiN-MoS2 composite coatings produced by simultaneous deposition from Ti((CH3))2N4/NH3/MoF6H2S gas mixture
[DE95-010359] p 2788 N95-31403

METAL COMBUSTION
Burn time measurements of single aluminum particles in steam and carbon dioxide mixtures
p 2799 N95-30990
The Al and Al2O3 droplet cloud in solid rocket motors
p 2770 N95-31196
Shuttle Redesigned Solid Rocket Motor aluminum oxide investigations p 2770 N95-31197
Burn time measurements of single aluminum particles in steam and carbon dioxide mixtures
p 2799 N95-31198
Characterization of an improved Rijke burner as prelude to measurements of aluminum distributed combustion
p 2800 N95-31287

METAL CRYSTALS
Picosecond phase conjugation: New applications, devices, and materials
[AD-A293195] p 3013 N95-30982

METAL CUTTING
Effect of local melting on tribology in metal cutting
[PB95-195392] p 2804 N95-31052

METAL FATIGUE
Ultrasonic characterization of fiber-matrix interphasial properties and damage in high-temperature composites
p 2785 N95-30823
The influence of matrix microstructure and temperature on cyclic deformation and fatigue of particle-reinforced 2219 aluminum p 2808 N95-31974

METAL FILMS
Diffraction-line broadening analysis and stress relaxation in thin metal layers
[PB95-213898] p 2893 N95-30634
Synthesis and selected micro-mechanical properties of titanium nitride thin films by the pyrolysis of tetrakis titanium in ammonia
[DE95-010224] p 2818 N95-31187
Characterization of /11'01/ twin dislocation structures in evaporated titanium thin films by HREM
[DE95-615391] p 2820 N95-31623
Influence of layer order and composition on the magnetic anisotropy of ultra-thin Co sandwiches
[DE95-010608] p 2810 N95-32265
Metallic multilayers at the nanoscale
[DE95-011534] p 3016 N95-32284

METAL FINISHING
SSME Main Combustion Chamber (MCC) hot oil dewaxing p 2777 N95-31777
Minutes of the fourth annual workshop on chromate replacements in light metal finishing
[DE95-010937] p 2810 N95-32241

METAL FOILS
Optimization of a thermoelectric IR-detector for low working temperature
[NASA-CR-198933] p 2880 N95-30752
Surface inspection using FTIR spectroscopy
p 2782 N95-31803

METAL IONS
On-line surfactant monitoring
[DE95-009417] p 2792 N95-30735
Lithium ion aqueous cells
[AD-A293828] p 2905 N95-31554
Plasma source ion implantation of metal ions: Synchronization of cathodic-arc plasma production and target bias pulses
[DE95-009431] p 3006 N95-31613
Target diagnostics for intense lithium ion hohlraum experiments on PBFA 2
[DE95-008517] p 3006 N95-31626
Generalized Ramsauer-Townsend minima in heavy-ion induced electron continua
[DE95-010913] p 2989 N95-32120
Measurements of quantum electrodynamic sensitive transitions in Na-like and Cu-like ions
[DE95-011593] p 3007 N95-32299

METAL JOINTS
Cleanliness evaluation of rough surfaces with diffuse IR reflectance p 2782 N95-31804
Verification of surface preparation for adhesive bonding p 2782 N95-31807

METAL MATRIX COMPOSITES
Fatigue crack growth behavior of a titanium matrix composite under thermomechanical loading
p 2784 N95-30491
TEM-examination of ceramic-metal interfaces
[PB95-196531] p 2813 N95-30664
Ultrasonic characterization of fiber-matrix interphasial properties and damage in high-temperature composites
p 2785 N95-30823
Innovative processing of composites for ultra-high temperature applications, book 2
[AD-A290890] p 2786 N95-30898
Localization in tungsten heavy alloys subjected to shearing deformations under superimposed high pressures
[AD-A293177] p 2804 N95-30977
Ceramic/Metal Composite Circuit-Board-Level Technology for Application Specific Electronic Modules (ASEM's)
[AD-A293183] p 2787 N95-30978
Microstructure and aging response of SiCp reinforced A356 Al metal matrix composite subject to post fabrication thermomechanical processing
[AD-A292975] p 2789 N95-31469
Processing and microstructural evolution of alumina/aluminum alloy and aluminum nitride/aluminum alloy composites by directed melt oxidation
p 2789 N95-31973
The influence of matrix microstructure and temperature on cyclic deformation and fatigue of particle-reinforced 2219 aluminum p 2808 N95-31974
Control of interfacial chemistry and mechanical properties in metal/ceramic composites
p 2790 N95-31976

METAL OXIDES
Voltage surge suppression power circuits
[AD-D017454] p 2860 N95-30726
A study of catalysts and mechanisms in synthesis reactions
[DE95-010177] p 2793 N95-30766
Porous spherical shells and microspheres by electrodispersion precipitation
[DE95-009073] p 2815 N95-30799

METAL PARTICLES
Glass matrix doped with activated luminescent nanocrystalline particles
[AD-D017416] p 2816 N95-31010
Burn time measurements of single aluminum particles in steam and carbon dioxide mixtures
p 2799 N95-31198

METAL PLATES
Acoustoelastic stress evaluation in metal plate using absolute shear and longitudinal time-of-flight data
[PB95-197810] p 2892 N95-30458
Influence of adhesives and bonding techniques on the properties of glued timber-steelplate joints
[PB95-211470] p 2813 N95-30599

METAL POWDER
Mechanical alloying processing with application to structural materials
[AD-A290788] p 2802 N95-30404
Optimization of high-temperature superconductor current leads
[DE95-005838] p 2861 N95-30942
Burn time measurements of single aluminum particles in steam and carbon dioxide mixtures
p 2799 N95-30990
Operational characteristics of a 200 C LC parallel resonant circuit
[NASA-TM-106983] p 2864 N95-31742

METAL PROPELLANTS
The Al and Al2O3 droplet cloud in solid rocket motors
p 2770 N95-31196
Shuttle Redesigned Solid Rocket Motor aluminum oxide investigations p 2770 N95-31197
Burn time measurements of single aluminum particles in steam and carbon dioxide mixtures
p 2799 N95-31198

METAL SHEETS
Surface inspection using FTIR spectroscopy
p 2782 N95-31803

METAL SURFACES
Observation of a low-binding-energy peak in the 2p core-level photoemission from oxidized Al(111)
[PB95-195350] p 2802 N95-30534
STM studies of clean, CO- and O2-exposed Pt(100)-hex-R0.7 deg
[PB95-195376] p 3009 N95-30535
NaK pool-boiler solar receiver durability bench test. Volume 2: Metallurgical analysis
[DE95-010338] p 2905 N95-31640
Compatibility of Single Hydraulic Fluid with military specification fluids, seals and metallurgy
[AD-A292954] p 2821 N95-31663

A design of experiments test to define critical spray cleaning parameters for Brulin 815 GD and Jettacin cleaners p 2779 N95-31790
Standardization of surface contamination analysis systems p 2781 N95-31798
Cleanliness inspection tool for RSRM bond surfaces p 2781 N95-31799
Surface inspection using FTIR spectroscopy p 2782 N95-31803
Cleanliness evaluation of rough surfaces with diffuse IR reflectance p 2782 N95-31804
Verification of surface preparation for adhesive bonding p 2782 N95-31807
The role of surface chemical analysis in a study to select replacement processes for TCA vapor degreasing p 2782 N95-31809

METAL VAPORS
Theoretical absorption spectroscopy of high-temperature metal vapors: Model and experiment compared
[AD-A290872] p 2791 N95-30409

METAL WORKING
Texture development in aluminium extrusion
[PB95-196598] p 2979 N95-30666

METAL-GAS SYSTEMS
Neutronic methods for determination of very low concentrations of hydrogen in metals
[DE95-623967] p 2807 N95-31409

METALLIC STARS
Chromospherically active stars. 6: Giants with compact hot companions and the barium star scenario
[NASA-TM-110641] p 3028 N95-30466

METALLICITY
Chromospherically active stars. 6: Giants with compact hot companions and the barium star scenario
[NASA-TM-110641] p 3028 N95-30466

METALLIZING
High aspect ratio metal microstructures and method for preparing the same
[AD-D017463] p 2803 N95-30750

METALLURGY
Metallurgical and Materials Transactions
[AD-A293617] p 2807 N95-31464

METALORGANIC CHEMICAL VAPOR DEPOSITION
Investigation of polycrystalline thin film CuInSe2 solar cells based on ZnSe windows
[DE95-004068] p 2904 N95-31164

METALS
Mechanical alloying processing with application to structural materials
[AD-A290788] p 2802 N95-30404
Wettability of boron carbide
[PB95-196358] p 2802 N95-30518
TEM-examination of ceramic-metal interfaces
[PB95-196531] p 2813 N95-30664
On-line surfactant monitoring
[DE95-009417] p 2792 N95-30735
Studies of C(60) and C(70) and other fullurenes: Synthesis, derivation, electrochemistry, lubricant properties and new composition materials
[AD-A292726] p 3012 N95-30944
Aqueous TiO2 photocatalysis of metal-EDTA complexes
[DE95-011058] p 2793 N95-31113

METASTABLE ATOMS
Atomic approaches in metastable antiprotonic helium atoms. Reply to Analysis of the lifetimes and fractions of antiprotons trapped in metastable antiprotonic helium states by I. Shimamhura and M. Kimura --- mura
[DE95-737228] p 2986 N95-31658

METASTABLE STATE
Atomic approaches in metastable antiprotonic helium atoms. Reply to Analysis of the lifetimes and fractions of antiprotons trapped in metastable antiprotonic helium states by I. Shimamhura and M. Kimura --- mura
[DE95-737228] p 2986 N95-31658

METEOROLOGICAL BALLOONS
Mexico Wind Resource Assessment Project
[DE95-009202] p 2921 N95-31726

METEOROLOGICAL INSTRUMENTS
Modern methods in meteorological and oceanographic data acquisition and analyses
[AD-A293884] p 2920 N95-31541

METEOROLOGICAL PARAMETERS
Initial evaluation of the Oregon State University planetary boundary layer column model for ITWS applications
[AD-A293775] p 2920 N95-31465
Modern methods in meteorological and oceanographic data acquisition and analyses
[AD-A293884] p 2920 N95-31541
Arabian Sea mixed layer dynamics experiment: Mooring deployment cruise report
[AD-A293684] p 2923 N95-31600
Comparison of satellite-derived MSU brightness temperatures and conventionally-derived fields
[AD-A293692] p 2901 N95-31603
Mexico Wind Resource Assessment Project
[DE95-009202] p 2921 N95-31726

METEOROLOGICAL RADAR
Multiparameter radar measurements of precipitation in complex terrain: Meteorological and hydrological applications
[AD-A290786] p 2918 N95-30403
Offshore next generation weather radar (NEXRAD) OT&E integration and OT&E operational test
[AD-A293223] p 2848 N95-30902
Terminal doppler weather radar (TDWR) build 5B operational test and evaluation (OT&E) integration and OT&E operational test plan
[AD-A293251] p 2848 N95-30910
LAWS hurricane studies
[NASA-CR-189438] p 2919 N95-31128
Initial evaluation of the Oregon State University planetary boundary layer column model for ITWS applications
[AD-A293775] p 2920 N95-31465

METEOROLOGICAL SATELLITES
Support of environmental requirements for cloud analysis and archive (SERCAA): Database management facility
[AD-A293938] p 2920 N95-31522
Anticipated uncertainty budgets of PRARETIME and T2L2 techniques as applied to ExTRAS p 2968 N95-32326

METEOROLOGICAL SERVICES
Integrated terminal weather system (ITWS) demonstration and validation operational test and evaluation
[AD-A293932] p 2749 N95-31521
The ATC operational evaluation of the prototype integrated terminal weather system (ITWS) at Dallas/Fort Worth and Orlando airports (May-September 1993)
[AD-A293808] p 2921 N95-31587

METEOROLOGY
Geostatistics and hydrology. Part 3. Hydro-meteorological network design
[PB95-206462] p 2900 N95-30818
JPL Physical Oceanography Distributed Active Archive Center (PO.DAAC) data availability, version 1-94
[NASA-CR-198871] p 2922 N95-30859
Directory of global environmental sciences in Japan p 2899 N95-31413
Preliminary design for Arctic atmospheric radiative transfer experiments
[DE95-009580] p 2917 N95-32080

METHANE
A search for interstellar CH3D: Limits to the methane abundance in Orion-KL
[NASA-CR-198932] p 3029 N95-30751
Self-lubricating, TiN-MoS2 composite coatings produced by simultaneous deposition from Ti((CH3))2N4/NH3/MoF6H2S gas mixture
[DE95-010359] p 2788 N95-31403

METHOD OF CHARACTERISTICS
Holistic analysis of gamma-ray spectra in instrumental neutron activation analysis
[PB95-214458] p 2979 N95-30639

METHYL ALCOHOL
BioFacts: Fueling a stronger economy. Methanol from biomass, revision 2
[DE95-010302] p 2836 N95-31638
BioFacts: Fueling a stronger economy, global warming and biofuels emissions
[DE94-006864] p 2910 N95-31821

METHYL COMPOUNDS
A study of catalysts and mechanisms in synthesis reactions
[DE95-010177] p 2793 N95-30766
Specific rate coefficients from vibrational overtone activation of 1-methylcyclopropene
[AD-A288755] p 2793 N95-31014

METRIC SPACE
Generalized Kummer surfaces and differentiable invariants of Noether-Horikawa surfaces 1
[DE95-613382] p 2956 N95-30608
Good metric spaces without good parameterizations
[PB95-208427] p 2957 N95-30622
Determination of the position of Jupiter from radio metric tracking of Voyager 1 p 2854 N95-32222
Data reduction of piecewise linear curves
[PB95-212270] p 2962 N95-32256

METROLOGY
Metrology of chrome on quartz photomasks using low voltage scanning electron microscopy. Part 1: Physical SEM parameters
[PB95-195780] p 2880 N95-30693
Computer-aided inspection process definition: Development of an expert planning and programming system for coordinate metrology
[DE95-010411] p 2940 N95-31404

MICROANALYSIS
Crystallization of sol-gel derived lead zirconate titanate thin films in argon and oxygen atmospheres
[DE95-615230] p 3009 N95-30421
Orientation of rapid thermally annealed lead zirconate titanate thin films on (111) Pt substrate
[DE95-615232] p 2811 N95-30422
Synthesis of carbo-nitride films using high-energy shock plasma deposition
[DE95-615231] p 2811 N95-30450
Interface degradation in CAS/Nicalon during elevated temperature aging
[DE95-008843] p 2812 N95-30543
Determination of site-occupancies in aluminide intermetallics by ALCHEMI
[DE95-009179] p 2803 N95-30733
A study of the gas-phase processes of RDX combustion using a triple quadrupole mass-spectrometer p 2801 N95-31315
Interfacial segregation and deformation of superplastically deformed Al-Mg-Mn alloys
[DE95-009572] p 2809 N95-32052

MICROCHANNEL PLATES
Calibration of multichannel analyzer of charge-exchange atoms
[DE95-614178] p 2987 N95-32053

MICROCOMPUTERS
User-friendly microcomputer interface with optimization languages AF94-007
[AD-A293184] p 2932 N95-32257

MICROCRACKS
Characterization of compressive damage mechanisms in ceramic and polymeric matrix composite materials
[AD-A293171] p 2787 N95-30975
A numerical analysis of crack growth in microcracking ceramic and ceramic composites
[DE95-010132] p 2897 N95-32024

MICROELECTRONICS
Micromachined sensor and actuator research at the Microelectronics Development Laboratory
[DE95-008540] p 2878 N95-30384
System considerations for efficient communication and storage of MSTI image data
[NASA-CR-198869] p 3024 N95-30858
HTS Josephson technology on silicon with application to high speed digital microelectronics
[AD-A288627] p 2861 N95-31147
Solid state research
[AD-A293083] p 3015 N95-31826
The potential for microtechnology applications in energy systems: Results of an experts workshop
[DE95-009103] p 2865 N95-32077

MICROGRAVITY
Numerical modeling of Bridgman growth of PbSnTe in a magnetic field
[NASA-TM-106996] p 2837 N95-31359
Microgravity research opportunities for the 1990s
[NASA-CR-199109] p 2838 N95-31983

MICROGRAVITY APPLICATIONS
Microgravity research opportunities for the 1990s
[NASA-CR-199109] p 2838 N95-31983

MICROHARDNESS
Synthesis of carbo-nitride films using high-energy shock plasma deposition
[DE95-615231] p 2811 N95-30450
Microstructural and mechanical property changes in model Fe-Cu alloys
[DE95-010117] p 2805 N95-31105

MICROMACHINING
Micromachined sensor and actuator research at the Microelectronics Development Laboratory
[DE95-008540] p 2878 N95-30384
Annual meeting of the Advanced Light Source Users' Association
[DE95-009373] p 3000 N95-31635
Terahertz spectroscopy of silicon micromachined three-dimensional photonic bandgap crystal
[DE95-010233] p 3015 N95-32037

MICROMECHANICS
Micromachined sensor and actuator research at the Microelectronics Development Laboratory
[DE95-008540] p 2878 N95-30384
Review of environmental effects in intermetallics
[DE95-010120] p 2805 N95-31106
Modeling of fiber-reinforced composites incorporating distinct interface properties p 2787 N95-31110
Development and computer implementation of design/analysis techniques for multilayered composite structures. Probabilistic fiber composite micromechanics
[NASA-CR-198979] p 2930 N95-31134
Elastic and inelastic micromechanical analysis of functionally graded materials and laminated structures using transformation fields p 2787 N95-31347

MICROPARTICLES
Porous spherical shells and microspheres by electrodiapersion precipitation
[DE95-009073] p 2815 N95-30799
Particle filtration: An analysis using the method of volume averaging
[DE95-009467] p 2875 N95-31592
Particle filtration: A comparison between theory and experiment
[DE95-009442] p 2875 N95-31637

MICROPHONES
Method for extracting forward acoustic wave components from rotating microphone measurements in the inlets of turbofan engines
[NASA-CR-195457] p 2755 N95-30779

MICROSCOPY
Tunable composite membranes for gas separations
[DE95-010602] p 2822 N95-32075

MICROSTRIP ANTENNAS
Scattering and radiation from cylindrically conformal antennas p 2847 N95-30669
Proceedings of the antenna applications symposium. volume 2
[AD-A293259] p 2850 N95-31387
Portable digital Satellite News Gathering (SNG) RF terminal using a flat antenna
[NHK-LABS-NOTE-436] p 2853 N95-31744

MICROSTRIP DEVICES
Experimental characterisation of gas microstrip detectors. Part 3: Lifetime characteristics
[PB95-192845] p 2880 N95-30691

MICROSTRUCTURE
Interfacial studies of coated fiber reinforced glass-ceramic matrix composites
[AD-A290780] p 2783 N95-30433
Synthesis of carbo-nitride films using high-energy shock plasma deposition
[DE95-615231] p 2811 N95-30450
Morphology and microstructure of (111) crystalline CeO2 films grown on amorphous SiO2 substrates by pulsed-laser ablation
[DE95-008842] p 3009 N95-30542
Semiconductor nanocrystals formed in SiO2 by ion implantation
[DE95-008900] p 2978 N95-30546
Diffraction-line broadening analysis and stress relaxation in thin metal layers
[PB95-213898] p 2893 N95-30634
TEM-examination of ceramic-metal interfaces
[PB95-196531] p 2813 N95-30664
A metallurgical approach toward alloying in rare earth permanent magnet systems
[DE95-010242] p 2966 N95-30668
Formation of cavities in Si and their chemisorption of materials
[DE95-009586] p 2980 N95-30708
High aspect ratio metal microstructures and method for preparing the same
[AD-D017463] p 2803 N95-30750
Dissolution of eutectic microstructures
[DE95-010244] p 2804 N95-30757
TV-VI semiconductor quantum well lasers, physics and engineering p 2883 N95-30805
Physical modelling of microstructural evolution during thermomechanical processing of aluminium alloys
[PB95-196341] p 2805 N95-31053
Microstructural and mechanical property changes in model Fe-Cu alloys
[DE95-010117] p 2805 N95-31105
Effect of cyclic loading on the creep performance of silicon nitride
[DE95-010289] p 2894 N95-31131
Effect of irradiation spectrum on the microstructure of ion-irradiated Al2O3
[DE95-010225] p 2806 N95-31188
Burn time measurements of single aluminum particles in steam and carbon dioxide mixtures p 2799 N95-31198
Self-lubricating, TiN-MoS2 composite coatings produced by simultaneous deposition from Ti((CH3))2N4/NH3/MoF6H2S gas mixture
[DE95-010359] p 2788 N95-31403
Transitions, defects, and whiskered microstructures
[AD-A292796] p 3014 N95-31438
Microstructure and aging response of SiCp reinforced A356 Al metal matrix composite subject to post fabrication thermomechanical processing
[AD-A292975] p 2789 N95-31469
In situ composites in the aluminum nitride-alumina system
[AD-A293776] p 2789 N95-31509
Modeling of stress distributions on the microstructural level in Alloy 600
[DE95-009135] p 2807 N95-31632
Differences in creep performance of a HIPed silicon nitride in ambient air and inert environments
[DE95-009172] p 2796 N95-31633
Annual meeting of the Advanced Light Source Users' Association
[DE95-009373] p 3000 N95-31635
Influence of strain rate and temperature on the mechanical behavior of iron aluminide-based alloys
[DE95-009426] p 2808 N95-31636
Modeling of grain boundary stresses in Alloy 600
[DE95-009033] p 2808 N95-31825
Processing and microstructural evolution of alumina/aluminum alloy and aluminum nitride/aluminum alloy composites by directed melt oxidation p 2789 N95-31973
The influence of matrix microstructure and temperature on cyclic deformation and fatigue of particle-reinforced 2219 aluminum p 2808 N95-31974
The influence of microstructure on creep deformation in near-gamma TiAl alloys p 2808 N95-31975
A study of Damascus steel
[DE95-010127] p 2809 N95-32023
Microstructure of Al2O3 irradiated with an applied electric field
[DE95-010278] p 2822 N95-32043
Synthesis and characterization of nanophase face-centered-cubic titanium
[DE95-009533] p 2809 N95-32051
Interfacial segregation and deformation of superplastically deformed Al-Mg-Mn alloys
[DE95-009572] p 2809 N95-32052
Creep of a fine-grained, fully-lamellar, two-phase TiAl alloy at 760 C
[DE95-009531] p 2810 N95-32272

MICROWAVE ABSORPTION
Microwave coupling into a slotted cavity. Additional results
[PB95-210381] p 2847 N95-30629

MICROWAVE AMPLIFIERS
Microwave repeater with broadband active and/or passive isolation control
[AD-D017358] p 2846 N95-30417
X-band magnicon amplifier research at the Naval Research Laboratory
[AD-A293203] p 3013 N95-30984
High energy pulsed microwave sources
[AD-A293334] p 2849 N95-31142
Stable high-power harmonic gyro-amplifiers
[AD-A293697] p 2881 N95-31828

MICROWAVE ANTENNAS
Microwave repeater with broadband active and/or passive isolation control
[AD-D017358] p 2846 N95-30417
Proceedings of the antenna applications symposium. volume 2
[AD-A293259] p 2850 N95-31387
DSS-24 microwave holography measurements p 2857 N95-32239

MICROWAVE CIRCUITS
Space qualified hybrid superconductor/semiconductor planar oscillator circuit
[NASA-TM-106978] p 3011 N95-30703
High performance YBCO films
[AD-A293045] p 2863 N95-31669
Hyperfrequency components
[PB95-208302] p 2866 N95-32369

MICROWAVE COUPLING
Microwave coupling into a slotted cavity. Additional results
[PB95-210381] p 2847 N95-30629

MICROWAVE EQUIPMENT
Microwave electro-optic mixer
[AD-D017328] p 2862 N95-31179
Millimeter wave radiometer utility study
[AD-A293811] p 2852 N95-31590
Hyperfrequency components
[PB95-208302] p 2866 N95-32369

MICROWAVE FREQUENCIES
Microwave coupling into a slotted cavity. Additional results
[PB95-210381] p 2847 N95-30629
High energy pulsed microwave sources
[AD-A293334] p 2849 N95-31142

MICROWAVE HOLOGRAPHY
The Telecommunications and Data Acquisition Report
[NASA-CR-198911] p 2854 N95-32221
DSS-24 microwave holography measurements p 2857 N95-32239

MICROWAVE IMAGERY
Weather influence on passive microwave brightness temperatures
[PB95-195384] p 2900 N95-30536
Research in ground-to-air microwave imaging
[AD-A292907] p 2852 N95-31551
Validation of special sensor microwave/imager ocean surface wind retrievals in equatorial regions
[AD-A293750] p 2920 N95-31571
Millimeter wave radiometer utility study
[AD-A293811] p 2852 N95-31590

MICROWAVE LANDING SYSTEMS
Flight test evaluation of the Stanford University/United Airlines differential GPS Category 3 automatic landing system
[NASA-TM-110354] p 2743 N95-30788
Development of advanced approach and departure procedures. Failure scenarios
[PB95-198123] p 2748 N95-30815

MICROWAVE OSCILLATORS
Space qualified hybrid superconductor/semiconductor planar oscillator circuit
[NASA-TM-106978] p 3011 N95-30703

MICROWAVE RADIOMETERS
Radiometer measurements of sea ice in the Gulf of Bothnia 1992
[PB95-206611] p 2900 N95-30718
Millimeter wave radiometer utility study
[AD-A293811] p 2852 N95-31590

MICROWAVE SCATTERING
Investigation of microwave backscatter from the air-sea interface
[NASA-CR-198854] p 2851 N95-31457

MICROWAVE SENSORS
Feasibility study concerning an active millimeterwave sensor. Project phase MMS2.1
[PB95-210399] p 2882 N95-32245

MICROWAVE SIGNATURES
Weather influence on passive microwave brightness temperatures
[PB95-195384] p 2900 N95-30536

MICROWAVE SOUNDING
Comparison of satellite-derived MSU brightness temperatures and conventionally-derived fields
[AD-A293692] p 2901 N95-31603
Brightness temperature simulations for the physical and synoptic interpretation of advanced microwave sounding unit moisture channels p 2921 N95-31721

MICROWAVE TRANSMISSION
Microwave repeater with broadband active and/or passive isolation control
[AD-D017358] p 2846 N95-30417

MICROWAVES
Microwave coupling into a slotted cavity. Additional results
[PB95-210381] p 2847 N95-30629
High energy pulsed microwave sources
[AD-A293334] p 2849 N95-31142
Use of a variable frequency source with a single-mode cavity to process ceramic filaments
[DE95-010992] p 2817 N95-31152
A microwave plasma cleaning apparatus p 2779 N95-31786

MID-OCEAN RIDGES
Studies in marine tectonics: Propagating rifts, depth anomalies and subduction zone anisotropy p 2923 N95-31719

MIDDLE ATMOSPHERE
Modeling and parameterization of gravity wave breaking, interactions, and instability processes in the lower and middle atmosphere
[AD-A292740] p 2914 N95-31278
Calculation of a residual mean meridional circulation for a zonal-mean tracer transport model
[DE95-009474] p 2911 N95-32350

MILITARY AIRCRAFT
Catapult-launching of the RAFALE design and experimentation p 2752 N95-32008
Report to the Chairman, Legislation and National Security Subcommittee, Committee on Government Operations, House of Representatives. C-17 Aircraft program: Improvements in initial provisioning process
[GAO/NSIAD-94-63] p 2741 N95-32194

MILITARY AVIATION
Environmental support of naval aviation
[AD-A292873] p 2747 N95-31454

MILITARY HELICOPTERS
Wide field of view helmet display systems mounted for helicopter simulation
[AD-A293123] p 2930 N95-30688
Preparation of S-70A-9 Black Hawk helicopter for flight tests to investigate cause of cracking of inner fuselage panel
[AD-A293891] p 2752 N95-31544

MILITARY OPERATIONS
Unmanned aerial vehicles. 1994 master plan p 2751 N95-31416

MILITARY PSYCHOLOGY
Psychological pilot selection in the US Air Force, the Luftwaffe, and the German Aerospace Research Establishment
[AD-A293779] p 2928 N95-31376

MILLIMETER WAVES
Millimeter wave radiometer utility study
[AD-A293811] p 2852 N95-31590
Infrared and millimeter wave detection using thin films of Pb doped BiSrCaCuO superconductor
p 2840 N95-32129
Feasibility study concerning an active millimeterwave sensor. Project phase MMS2.1
[PB95-210399] p 2882 N95-32245
MIMD (COMPUTERS)
Implementation of KIVA-3 on distributed memory MIMD computers
[DE95-010288] p 2931 N95-31130
MINERAL OILS
Spectroscopic ellipsometry as a sensitive monitor of materials contamination p 2782 N95-31808
MINIATURIZATION
The potential for microtechnology applications in energy systems: Results of an experts workshop
[DE95-009103] p 2865 N95-32077
MINIMA
Properties of new materials relevant to energy and fuel research
[AD-A289734] p 2825 N95-31149
Generalized Ramsauer-Townsend minima in heavy-ion induced electron continua
[DE95-010913] p 2989 N95-32120
MINIMAX TECHNIQUE
Representation of feedback operators for hyperbolic systems
[NASA-CR-198171] p 2960 N95-31319
MINKOWSKI SPACE
The solutions of affine and conformal affine Toda field theory
[DE95-616280] p 2965 N95-30430
On drawing complicated 3D surfaces
[DE95-619199] p 2939 N95-31257
A compact expression for bilinear combination of Dirac spinors via world tensors
[DE95-619200] p 2960 N95-31258
MINORITY CARRIERS
Minority and majority carrier transport characterization in compound semiconductors
[DE95-010873] p 3014 N95-31233
MIR SPACE STATION
STS-71 post flight presentation
[NASA-TM-110658] p 2764 N95-30852
Mir 18 post flight presentation
[NASA-TM-110657] p 2766 N95-30854
MIRRORS
Tunable ytterbium-doped solid state laser
[AD-D017449] p 2885 N95-31274
The effect of ray curvature on Lloyd's mirror fringe estimates and source localisation
[DSTO-TR-0064] p 3001 N95-31745
Enhanced brightness x-ray lasers
[DE95-010735] p 2886 N95-32029
Sandia National Lab's precision laser tracking systems
[DE95-009837] p 2886 N95-32143
MISSILE CONTROL
Results from tests of the Kearfott T16-B Inertial Measurement Unit
[PB95-212031] p 2879 N95-30502
Results from tests of the Honeywell integrated flight management unit
[PB95-211355] p 2748 N95-30597
Guidance and Control for Future Air-Defence Systems
[AGARD-CP-555] p 2839 N95-32123
MISSILE DEFENSE
Guidance and Control for Future Air-Defence Systems
[AGARD-CP-555] p 2839 N95-32123
Possible allied ballistic missile defense systems: Related guidance and control requirements
p 2840 N95-32126
TMD detection and tracking using improved AWACS sensors p 2840 N95-32128
Acquisition, tracking, pointing and fire control for Ballistic Missile Defense p 2841 N95-32131
Using a Red Team to devise countermeasures
p 2842 N95-32141
MISSILE DETECTION
TMD detection and tracking using improved AWACS sensors p 2840 N95-32128
Optimal infrared detector configurations for air target detection p 2841 N95-32130
MISSILE SYSTEMS
Electronic combat and lethal defense suppression
p 2842 N95-32140
MISSILE TRACKING
TMD detection and tracking using improved AWACS sensors p 2840 N95-32128
Acquisition, tracking, pointing and fire control for Ballistic Missile Defense p 2841 N95-32131
The High Altitude Balloon Experiment demonstration of acquisition, tracking, and pointing technologies (HABE-ATP) p 2841 N95-32132
MISSION PLANNING
An architectural approach to strategic information systems planning for the Office of Naval Intelligence
[AD-A289930] p 3024 N95-30928
Integration issues in modular mission management aid development p 2841 N95-32133
Electronic combat and lethal defense suppression
p 2842 N95-32140
Stratospheric Observatory For Infrared Astronomy (SOFIA). Phase A: System concept description
[NASA-TM-110669] p 3002 N95-32187
MIXERS
Microwave electro-optic mixer
[AD-D017328] p 2862 N95-31179
MIXING
Effects of initial conditions on a single jet in crossflow
[NASA-TM-107002] p 2754 N95-30589
MIXING LAYERS (FLUIDS)
Small scale turbulence in a plane mixing layer
p 2866 N95-30449
Study of effect of bubbles on a free-shear layer
p 2872 N95-31100
Viscous heating of liquid layers under intense shear
p 2827 N95-31206
Chaos-enhanced transport and aggregation in chaotic flows
[AD-A293892] p 3020 N95-31545
Global Ultraviolet Imager (GUVI) investigation
[NASA-CR-189430] p 2917 N95-31820
MIXING LENGTH FLOW THEORY
A turbulence model for steady and unsteady boundary layers in strong pressure gradients p 2868 N95-30840
A turbulence module for the NPARC code
[NASA-CR-198358] p 2959 N95-30855
MOBILITY
In situ composites in the aluminum nitride-alumina system
[AD-A293776] p 2789 N95-31509
MODAL RESPONSE
Finite element analysis of smart structures and modal testing of a flexible spacecraft arm
[AD-A293761] p 2890 N95-31576
MODEL REFERENCE ADAPTIVE CONTROL
New adaptive methods for reconfigurable flight control systems, appendix 1
[AD-A292711] p 2756 N95-30937
MODELS
Expert system for assessing accuracy of models of physical phenomena and for selecting alternate models in the presence of noise
[AD-D017348] p 2974 N95-30550
The effect of interface properties on nickel base alloy composites
[NASA-CR-198363] p 2785 N95-30787
Unification of LARCH and Z-based object models to support algebraically-based design refinement: The LARCH perspective
[AD-A289235] p 2935 N95-30999
Solid Modeling Aerospace Research Tool (SMART) user's guide, version 2.0
[NASA-TM-4431] p 2940 N95-31420
Thermal rho's in the quark-gluon plasma
[DE95-009543] p 3008 N95-32357
MODEMS
High resolution time interval counter
p 2969 N95-32331
MODES (STANDING WAVES)
Harmonic gyrotron amplifiers and phase-locked oscillators
[AD-A293185] p 2861 N95-30979
MODULARITY
Development of flexible feeder techniques
[PB95-196317] p 2934 N95-30663
MODULATION
Development of a novel wind lidar, phase 1
[AD-A292703] p 2849 N95-30935
Tune modulation due to synchrotron oscillations and chromaticity, and the dynamic aperture
[DE95-011566] p 2995 N95-32297
MODULATORS
Microwave electro-optic mixer
[AD-D017328] p 2862 N95-31179
Improved linear dynamic range in externally modulated fiber-optic links p 3001 N95-31950
MODULES
Intelligent finite element submodeling of multichip modules for reliability analysis
[AD-A292911] p 2940 N95-31455
MODULUS OF ELASTICITY
Optical fiber pressure sensor for liquid level monitoring
[AD-D017346] p 2996 N95-30679
Rationale and summary of methods for determining ultrasonic properties of materials at Lawrence Livermore National Laboratory
[DE95-009475] p 2795 N95-31593
An inverse method to measure the axial modulus of composite materials under tension
[AD-A293042] p 2789 N95-31668
MOIRE INTERFEROMETRY
An evaluation of the Iosipescu specimen for composite materials shear property measurement
[NASA-CR-198755] p 2896 N95-31418
MOJAVE DESERT (CA)
Environmental projects. Volume 16: Waste minimization assessment
[NASA-CR-198861] p 2909 N95-31651
MOLECULAR BEAM EPITAXY
Visible light emitting materials and injection devices
[AD-A292701] p 2786 N95-30934
Pseudomorphic heterostructure materials for high performance devices
[AD-A292906] p 2788 N95-31384
MOLECULAR BEAMS
Determination of electric and magnetic fields in open trap plasmas by means of atomic-molecular beam hydrogen isotopes
[DE95-614177] p 3006 N95-31680
MOLECULAR BIOLOGY
Implementation and performance of the pseudoknot problem in Sisal
[DE95-009573] p 2925 N95-32358
MOLECULAR CLOUDS
Molecular gas in starburst galaxies: Line intensities and physical conditions
[PB95-208021] p 3029 N95-30569
A search for interstellar CH3D: Limits to the methane abundance in Orion-KL
[NASA-CR-198932] p 3029 N95-30751
MOLECULAR CLUSTERS
Molecular nanoclusters as precursors to conductive thin films and crystals
[AD-A290278] p 3014 N95-31189
X-ray diffraction study of clusters in a-tC films
[DE95-010860] p 2794 N95-31393
MOLECULAR COLLISIONS
State resolved dynamics of ion-molecule collisions in a flowing afterglow
[AD-A290895] p 2976 N95-30410
Inversion of the total cross sections for electron-molecule and electron-atom scattering
[DE95-616466] p 2978 N95-30583
Analytic cross sections for collisions of H, H2, He and Li atoms and ions with atoms and molecules
[DE95-722055] p 2979 N95-30654
Energy transfer dynamics in isolated and colliding highly vibrationally excited molecules
[AD-A293304] p 2981 N95-30952
The passage from transitional to free molecular plumes p 2871 N95-30994
MOLECULAR DIFFUSION
Fischer-tropsch synthesis in supercritical fluids
[DE95-009631] p 2792 N95-30709
MOLECULAR DYNAMICS
Energy transfer dynamics in isolated and colliding highly vibrationally excited molecules
[AD-A293304] p 2981 N95-30952
Molecular dynamics simulations of high energy cascades in iron
[DE95-010116] p 2982 N95-31104
Molecular models for nitro compounds
p 2831 N95-31293
MOLECULAR ELECTRONICS
Electronic structure of Donor-Spacer-Acceptor molecules of potential interest for molecular electronics III: Geometry and absorption spectrum of CH3-Alpha P3CNQ
[AD-A293662] p 2985 N95-31609
Electronic structure of Donor-Spacer-Acceptor molecules of potential interest for molecular electronics 4. Geometry and device properties of P3CNQ and Q3CNQ
[AD-A293717] p 2986 N95-31832
MOLECULAR ENERGY LEVELS
Electronic structure of Donor-Spacer-Acceptor molecules of potential interest for molecular electronics 4. Geometry and device properties of P3CNQ and Q3CNQ
[AD-A293717] p 2986 N95-31832
MOLECULAR EXCITATION
Molecular gas in starburst galaxies: Line intensities and physical conditions
[PB95-208021] p 3029 N95-30569
Energy transfer dynamics in isolated and colliding highly vibrationally excited molecules
[AD-A293304] p 2981 N95-30952
Ferromagnetic Potts model in a magnetic field: Finite lattice extrapolation of the (1 + 1)-dimensional Hamiltonian
[DE95-614447] p 3012 N95-30958

Dynamics of an inhomogeneous anisotropic antiferromagnetic spin chain
[DE95-614449] p 3013 N95-30959
Comparison of DSMC predictions with temporally resolved vibrational state measurements in NO
p 2872 N95-30996

MOLECULAR GASES
State resolved dynamics of ion-molecule collisions in a flowing afterglow
[AD-A290895] p 2976 N95-30410
Molecular gas in starburst galaxies: Line intensities and physical conditions
[PB95-208021] p 3029 N95-30589
A search for interstellar CH3D: Limits to the methane abundance in Orion-KL
[NASA-CR-198932] p 3029 N95-30751
SSUSI single sensor auroral E-layer algorithm: Functional description
[AD-A288630] p 2914 N95-31012
An analysis of gas phase ethanol/water chemistry for diamond CVD
[AD-A293009] p 2795 N95-31473

MOLECULAR INTERACTIONS
Photochemistry of intermolecular C-H bond activation reactions
[DE95-008991] p 2978 N95-30574
Excited-state complexes of conjugated polymers: Novel photophysical processes and optoelectronic materials
[AD-A292958] p 2819 N95-31462

MOLECULAR IONS
State resolved dynamics of ion-molecule collisions in a flowing afterglow
[AD-A290895] p 2976 N95-30410

MOLECULAR ORBITALS
Molecular modeling of PMN ceramics
[AD-A290879] p 2813 N95-30560
Estimating heat of formation of energetic compounds using corrected semiempirical molecular orbital theory
p 2800 N95-31294
An ab initio study of the reaction HNO+NO yields OH+N2O: Preliminary results p 2801 N95-31308

MOLECULAR PHYSICS
Analytic cross sections for collisions of H, H2, He and Li atoms and ions with atoms and molecules
[DE95-722055] p 2979 N95-30654
From molecular to macromolecular liquid crystals
[AD-A293170] p 2816 N95-30974

MOLECULAR SPECTROSCOPY
The 49th International Symposium on Molecular Spectroscopy
[AD-A292708] p 2793 N95-30936

MOLECULAR STRUCTURE
Lanthanide(III) catalyzed reactions: Structure an d thermodynamics of intermediate complexes, and implications for reactivity
[PB95-197000] p 3019 N95-30775
X-ray diffraction study of clusters in a-tC films
[DE95-010860] p 2794 N95-31393
Conjugated aromatic polyimines. 2. Synthesis, structure, and properties of new aromatic polyazomethines
[AD-A292955] p 2819 N95-31461
Effects of molecular structure on the electroactive and optical properties of conjugated rigid-rod polybenzobisazoles
[AD-A292968] p 2819 N95-31467
Absorption and ionization spectra of model rubredoxins
[AD-A293668] p 2796 N95-31691
Electronic structure of Donor-Spacer-Acceptor molecules of potential interest for molecular electronics 4. Geometry and device properties of P3CNQ and Q3CNQ
[AD-A293717] p 2986 N95-31832

MOLECULES
State resolved dynamics of ion-molecule collisions in a flowing afterglow
[AD-A290895] p 2976 N95-30410
Photophysical properties of opto-electric molecules studied by time-resolved microwave conductivity
[PB95-196994] p 2980 N95-30774
The 49th International Symposium on Molecular Spectroscopy
[AD-A292708] p 2793 N95-30936
Experimental investigation of optical nonlinearities in conjugated polymers
[AD-A288353] p 2884 N95-31145
Properties of new materials relevant to energy and fuel research
[AD-A289734] p 2825 N95-31149
Electronic structure of Donor-Spacer-Acceptor molecules of potential interest for molecular electronics III: Geometry and absorption spectrum of CH3-Alpha P3CNQ
[AD-A293662] p 2985 N95-31609
Ultrasensitive fluorescence detection and photophysics in microdroplets
[DE95-010283] p 2798 N95-32086

MOLYBDENUM
Processing and characterization of nanocrystalline molybdenum disilicide (MoSi2) consolidated by hot isostatic pressing (HIP)
[DE95-010243] p 3012 N95-30756
The electrodeposition of low contraction chromium/molybdenum alloys using pulse-reverse plating
[AD-A292727] p 2804 N95-30945

MOLYBDENUM COMPOUNDS
Processing and characterization of nanocrystalline molybdenum disilicide (MoSi2) consolidated by hot isostatic pressing (HIP)
[DE95-010243] p 3012 N95-30756

MOLYBDENUM DISULFIDES
Self-lubricating, TiN-MoS2 composite coatings produced by simultaneous deposition from Ti((CH3))2N4/NH3/MoF6H2S gas mixture
[DE95-010359] p 2788 N95-31403

MOLYBDENUM SULFIDES
Self-lubricating, TiN-MoS2 composite coatings produced by simultaneous deposition from Ti((CH3))2N4/NH3/MoF6H2S gas mixture
[DE95-010359] p 2788 N95-31403

MOMENTUM
Shear flow effects on ion thermal transport in tokamaks
[DE95-009115] p 3005 N95-30801
Instantaneous chiral quark model for relativistic mesons in a hot and dense medium
[DE95-613782] p 2980 N95-30911
Spin momentum correlation (handedness) in the process of four pion production in the electron-positron collisions
[DE95-613690] p 2988 N95-32093

MOMENTUM THEORY
Velocity boundary conditions for vorticity formulations of the incompressible Navier-Stokes equations
[DE95-008715] p 2866 N95-30464
On convective effects in sedimentation of concentrated suspensions with high effective gravity
[TRITA-NA-9316] p 2794 N95-31356

MOMENTUM TRANSFER
Renormcharges in V-A theories
[DE95-613689] p 2985 N95-31622
Recoil longitudinal momentum spectroscopy of electron capture from He by O(7+) and F(8+)
[DE95-010823] p 2990 N95-32274

MONOMERS
Phthalonitrile prepolymer as high temperature sizing material for composite fibers
[AD-D017447] p 2818 N95-31272
Novel unsymmetrical polydiacetylenes as materials for second and third order nonlinear optics
[AD-A293020] p 3001 N95-31700

MONOMOLECULAR FILMS
Metallic multilayers at the nanoscale
[DE95-011534] p 3016 N95-32284

MONOPOLES
Design of systems for active sound control
[PB95-197869] p 2973 N95-30461

MONOPROPELLANTS
Viscous heating of liquid layers under intense shear
p 2827 N95-31206
Numerical study of shear-induced heating in high-speed nozzle flow of liquid monopropellant
p 2828 N95-31207

MONTE CARLO METHOD
MVP/GMVP: General purpose Monte Carlo codes for neutron and photon transport calculations based on continuous energy and multigroup methods
[DE95-722072] p 2979 N95-30656
A Monte-Carlo model of ionic transport across a solid interface
[DE95-613447] p 3011 N95-30737
The passage from transitional to free molecular plumes p 2871 N95-30994
Comparison of DSMC predictions with temporally resolved vibrational state measurements in NO
p 2872 N95-30996
X-ray performance of the engineering prototype Stellar x-ray polarimeter
[DE95-010268] p 3028 N95-31129
Development and computer implementation of design/analysis techniques for multilayered composite structures. Probabilistic fiber composite micromechanics
[NASA-CR-198979] p 2930 N95-31134
MCNP analyses of criticality calculation results
[DE95-010886] p 2960 N95-31253
A new goodness-of-fit test for the gamma distribution based on sample spacings from complete and censored samples
[AD-A293875] p 2961 N95-31518
Monte Carlo code for evaluating the Boundary Layer Illumination and Radiation Balance model (BLIRB)
[AD-A293963] p 2915 N95-31560
Monte Carlo tests of the ELIPGRID-PC algorithm
[DE95-010811] p 2943 N95-32030
Monte Carlo simulations of muon production
[DE95-009554] p 2988 N95-32063
A stochastic EM estimator in the presence of missing data: Theory and applications
[DE95-010329] p 2944 N95-32089
Optimal infrared detector configurations for air target detection p 2841 N95-32130
LES, DNS and RANS for the analysis of high-speed turbulent reacting flows
[NASA-CR-199075] p 2878 N95-32219
Monte Carlo simulations of precise timekeeping in the Milstar communication satellite system
p 2970 N95-32336

MOODS
Forward rapid rotation shiftwork in USAF air traffic controllers: Sleep, activity, fatigue and mood analyses
[AD-A293448] p 2927 N95-31373

MOON
DEPSCOR92-Wide field spectral imager
[AD-A293079] p 2997 N95-31005
Relativistic timescale analysis suggests lunar theory revision p 2970 N95-32333

MOORING
Arabian Sea mixed layer dynamics experiment: Mooring deployment cruise report
[AD-A293684] p 2923 N95-31600

MORPHOLOGY
Morphology and microstructure of (111) crystalline CeO2 films grown on amorphous SiO2 substrates by pulsed-laser ablation
[DE95-008842] p 3009 N95-30542
Dissolution of eutectic microstructures
[DE95-010244] p 2804 N95-30757
Molecular nanoclusters as precursors to conductive thin films and crystals
[AD-A290278] p 3014 N95-31189
Excited-state complexes of conjugated polymers
[AD-A292960] p 2819 N95-31466

MORSE POTENTIAL
Study of the generalized solutions of n-body type problems with weak forces
[DE95-613381] p 2958 N95-30820

MORTALITY
Particulate air pollution and increased mortality: Biological plausibility for causal relationship
[DE95-006161] p 2909 N95-31703

MOSAICS
Effects of mosaicity on Parametric X-Radiation production
[AD-A293677] p 2985 N95-31597

MOTION
Nonparametric recognition of nonrigid motion
[AD-A293630] p 2963 N95-31565

MOTOR VEHICLES
Natural gas liquefier for vehicle fuel
[AD-A293619] p 2836 N95-31564

MSM (SEMICONDUCTORS)
Opto-electronic components from non-stoichiometric 3-5 materials
[AD-A293206] p 3013 N95-30985

MULTIBEAM ANTENNAS
Proceedings of the antenna applications symposium. volume 2
[AD-A293259] p 2850 N95-31387

MULTIBLOCK GRIDS
Numerical solution of the full potential equation using a chimera grid approach
[NASA-TM-110360] p 2744 N95-32188

MULTICHANNEL COMMUNICATION
Passive, multi-channel fiber optic rotary joint assembly
[AD-D017353] p 2996 N95-30529

MULTIDISCIPLINARY DESIGN OPTIMIZATION
Robust Rocket Engine Concept
[NASA-TM-107010] p 2770 N95-32121

MULTIDISCIPLINARY RESEARCH
Microgravity research opportunities for the 1990s
[NASA-CR-199109] p 2838 N95-31983

MULTIGRID METHODS
Multigrid convergence acceleration for the 2D Euler equations applied to high-lift systems
[PB95-196061] p 2743 N95-30614
Fourier analysis of a robust multigrid method for convection-diffusion equations
[PB95-197091] p 2958 N95-30835

MULTILAYER INSULATION
Supplemental multilayer insulation research facility
[NASA-TM-106991] p 2768 N95-30595

MULTIMEDIA
Data storage modeling and management for multimedia information systems p 3022 N95-30483

Proceedings of the CSCW 1994 workshop collaborative hypermedia systems
[PB96-206393] p 3023 N95-30496
Operating system support for distributed multimedia applications: A survey of current research
[PB95-207098] p 2964 N95-30565

MULTIPHASE FLOW
Atomization simulations using an Eulerian-VOF-Lagrangian method p 2828 N95-31210

MULTIPLE TARGET TRACKING
Multiple Target Tracking based on constellation matching and Kalman filter p 2842 N95-32136

MULTIPLEXING
Smart active multiwave sensing with zero background amplitude modulated probes
[DE95-008813] p 2792 N95-30714
Effective bandwidth techniques in bufferless and buffered ATM multiplexers
[PB95-207072] p 2862 N95-31185

MULTIPLICATION
A scalable parallel Strassen's matrix multiply algorithm for distributed memory computers
[DE95-010213] p 2936 N95-31109

MULTIPLIERS
Coherent integrator
[AD-D017422] p 2847 N95-30743

MULTIPOLES
Gravitational-radiation damping of compact binary systems to second post-Newtonian order
[PB95-207882] p 2912 N95-30588
Potential integral equations of the 2D Laplace operator in wavelet basis
[TRITA-NA-9401] p 2957 N95-30713
Fast multipole methods for scattering computations
[AD-A291093] p 2848 N95-30869

MULTIPROCESSING (COMPUTERS)
Algorithms for categorizing multiprocessor communication under invalidate and update-based coherence protocols
[AD-A290022] p 2947 N95-30930
Implementation and performance of the pseudoknot problem in Sisal
[DE95-009573] p 2925 N95-32358

MULTISENSOR APPLICATIONS
Diamond thin film temperature and heat-flux sensors
[NASA-CR-198858] p 3012 N95-30847
Force and vision resolvability for assimilating disparate sensory feedback
[AD-A293581] p 2929 N95-31685
Design of surveillance and multisensor anti-aerial systems p 2841 N95-32134
Multi-sensor data fusion in command and control and the merit of artificial intelligence p 2842 N95-32137
Architecture and implementation of a multi-sensor data fusion demonstration model within the real-time combat system of the Canadian Patrol Frigate p 2842 N95-32139

MULTISENSOR FUSION
Sensor Fusion and Nonlinear Prediction for Anomalous Event Detection
[DE95-009429] p 2933 N95-30602
Neural network based data fusion system
[AD-D017440] p 2953 N95-31692
Neural network based three dimensional ocean modeler
[AD-D017441] p 2953 N95-31693
Integration issues in modular mission management aid development p 2841 N95-32133
Multisensor data fusion for integrated maritime surveillance p 2842 N95-32135
Multi-sensor data fusion in command and control and the merit of artificial intelligence p 2842 N95-32137
AIDEX: An expert system for aircraft identification p 2842 N95-32138
Architecture and implementation of a multi-sensor data fusion demonstration model within the real-time combat system of the Canadian Patrol Frigate p 2842 N95-32139

MULTIVARIATE STATISTICAL ANALYSIS
The remainder form and the cord-slope form in global optimization with interval methods p 2941 N95-31533
Nonlinear time series analysis
[AD-A293841] p 2963 N95-31558
Topics in exploratory and speculative data analysis
[AD-A290505] p 3025 N95-31618
Estimation in second order dependency model for multivariate binary data
[DE95-010325] p 2944 N95-32087

MUONS
Phenomenology of the two Higgs doublet sector of a quark-lepton symmetric model
[DE95-616337] p 2976 N95-30446
New tensor interactions in micron-decay
[DE95-613760] p 2978 N95-30528
The design and construction of the muon arm in PHENIX
[DE95-010156] p 2978 N95-30616
Backgrounds and detector performance at a 2 x 2 TeV (mu)(+)(mu)(-) collider
[DE95-009107] p 2992 N95-30800
Physics goals of a mu(+) mu(-) collider
[DE95-009546] p 2994 N95-32059
Monte Carlo simulations of muon production
[DE95-009554] p 2988 N95-32063

MUSCLES
Electromyostimulation, circuits and monitoring
[NASA-TM-110741] p 2926 N95-30846

MUSCULOSKELETAL SYSTEM
Erect, neutral and slump sitting postures: A study of the torso linkage system from shoulder to hip joint
[AD-A293239] p 2930 N95-30907

MUSIC
Fractional delay waveguide modeling of acoustic tubes
[PB95-206637] p 2975 N95-31650

N

N ELECTRONS
Excitation mechanisms of 2s(sub 1/2)-2p(sub 3/2) and 2p(sub 1/2)-2p(sub 3/2)in U(82+) through U(89+)
[DE95-010265] p 2993 N95-32042

N-TYPE SEMICONDUCTORS
Optimization of a thermoelectric IR-detector for low working temperature
[NASA-CR-198933] p 2880 N95-30752

NARCOSIS
Effect of oxygen and decompression bubbles on inert gas washout
[PB95-196556] p 2925 N95-30865

NASA PROGRAMS
Changes and challenges in the Software Engineering Laboratory p 2936 N95-31235
Profile of software engineering within the National Aeronautics and Space Administration (NASA) p 2939 N95-31252
SeaWiFS technical report series. Volume 24: SeaWiFS technical report series cumulative index, volumes 1-23
[NASA-TM-104566-VOL-24] p 2924 N95-32122

NASA SPACE PROGRAMS
NASA space astronomy update 6
[NASA-CR-197664] p 3028 N95-31099

NATIONAL AIRSPACE SYSTEM
A NASPAC-Based analysis of the delay and cost effects of the western-pacific region preliminary resectorization effort of 1993
[AD-A288696] p 2748 N95-31013
Effects of civil tiltrotor service in the northeast corridor on en route airspace loads
[AD-A293586] p 2747 N95-31687

NATIONAL AVIATION SYSTEM
FAA aviation forecasts: Fiscal year 1995-2006
[AD-A293682] p 2741 N95-31598

NATURAL GAS
Simulation of chemical kinetics in turbulent natural gas combustion. Volume 2: Experimental studies of nitric oxide production in gas flames
[PB95-196721] p 2791 N95-30541
A study of catalysts and mechanisms in synthesis reactions
[DE95-010177] p 2793 N95-30766
Combatting urban air pollution through Natural Gas Vehicle (NGV) analysis, testing, and demonstration
[DE95-008300] p 2911 N95-32156
The development of a pulsed laser imaging system for natural gas leak detection
[DE95-011407] p 2887 N95-32280

NAVIER-STOKES EQUATION
Velocity boundary conditions for vorticity formulations of the incompressible Navier-Stokes equations
[DE95-008715] p 2866 N95-30464
Computation of high-altitude hypersonic flow-field radiation p 2743 N95-30843
Parametrics on 2D Navier-Stokes analysis of a Mach 2.68 bifurcated rectangular mixed-compression inlet
[NASA-TM-107003] p 2755 N95-30861
Navier-Stokes flow field analysis of compressible flow in a high pressure safety relief valve
[NASA-TM-110640] p 2868 N95-30862
Numerical simulation of ram accelerator performance including transient effects during initiation of combustion and sensitivity studies p 2799 N95-31203
The 2nd Japan-US Symposium on Finite Element Methods in Large Scale Computational Fluid Dynamics
[AD-A292337] p 2960 N95-31264
The 25th International Symposium on Combustion
[AD-A286825] p 2794 N95-31268
Numerical simulation of shock/turbulent boundary layer interaction
[NASA-CR-198846] p 2872 N95-31341
Compressible turbulence measurement in low-angle injection into a supersonic flow
[AD-A293836] p 2874 N95-31516
Unsteady flow simulations about moving boundary configurations using dynamic domain decomposition techniques p 2877 N95-31837
LES, DNS and RANS for the analysis of high-speed turbulent reacting flows
[NASA-CR-199075] p 2878 N95-32219

NAVIGATION
A Heuristic and complete planner for the classical mover's problem
[DE95-008440] p 2949 N95-30377
Qualitative environmental navigation: Theory and practice --- robot navigation p 2748 N95-30486
Time aspects of the European Complement to GPS: Continental and transatlantic experimental phases p 2969 N95-32328

NAVIGATION AIDS
An exploratory survey of information requirements for instrument approach charts
[AD-A293882] p 2749 N95-31520

NAVIGATION INSTRUMENTS
EMC requirements for type approval of marine electronics. Nordtest project 1157-94
[PB95-211330] p 2859 N95-30596
System considerations for efficient communication and storage of MSTI image data
[NASA-CR-198869] p 3024 N95-30858
Guidelines for the design of GPS and LORAN receiver controls and displays
[AD-A293753] p 2749 N95-31572

NAVIGATION SATELLITES
SVN 9 End-Of-Life testing p 2767 N95-32345
(T2L2) Time Transfer by Laser Link p 2887 N95-32348

NAVSTAR SATELLITES
Laser retroreflector experiment on NAVSTAR 35 and 36 p 2887 N95-32347

NAVY
Environmental support of naval aviation
[AD-A292873] p 2747 N95-31454

NEAR FIELDS
Far field acoustic radiation reduction
[AD-D017452] p 2974 N95-30725

NEAR INFRARED RADIATION
Fractal quantum well heterostructures for broadband light emitters
[DE95-009579] p 2860 N95-30707
Study of surfaces using near infrared optical fiber spectrometry p 2781 N95-31801

NECK (ANATOMY)
Vertical impact testing of two helmet-mounted night vision systems
[AD-A293055] p 2931 N95-31671

NEEL TEMPERATURE
On the possibility of a two-state magnetic structure for nanocrystalline chromium
[DE95-009914] p 3015 N95-32062

NEGATIVE FEEDBACK
Pre-amplifier with multi-stage feedback
[AD-D017371] p 2859 N95-30659

NEGATIVE IONS
Design study of prototype accelerator and MeV test facility for demonstration of 1 MeV, 1 A negative ion beam production
[DE95-737208] p 2995 N95-32262

NEODYMIUM COMPOUNDS
A metallurgical approach toward alloying in rare earth permanent magnet systems
[DE95-010242] p 2966 N95-30668

NEODYMIUM LASERS
Spotsize measurements of a focused CW Nd: YAG laser
[DE95-007746] p 2884 N95-31139

NERVOUS SYSTEM
Conference perspective. Neuroimmunomodulation: Stress and immune function
[AD-A291351] p 2926 N95-30870

NETHERLANDS
Development of advanced approach and departure procedures. Failure scenarios
[PB95-198123] p 2748 N95-30815

NETWORK ANALYSIS
Periodically Specified Problems: An Exponential Complexity Gap Between Exact and Approximate Solutions
[DE95-009435] p 2934 N95-30603
Noisy-network acceptors
[PB95-197976] p 2951 N95-30813
Nordic symposium on analysis of electromagnetic transient phenomena using EMTP, part 3
[PB95-206504] p 2849 N95-31158

Nordic Symposium on Analysis of Electromagnetic Transient Phenomena Using EMTP, part 2
[PB95-206579] p 2849 N95-31160
Nordic Symposium on Analysis of Electromagnetic Transient Phenomena Using EMTP, part 4
[PB95-206587] p 2849 N95-31181
Nordic Symposium on Analysis of Electromagnetic Transient Phenomena Using EMTP, part 1
[PB95-206595] p 2850 N95-31182
Dynamic maintenance scheduling for a stochastic telecommunication network: Determination of performance factors
[AD-A293829] p 2852 N95-31555
The Deep Space Network stability analyzer
p 2858 N95-32334

NETWORK SYNTHESIS
Compact location problems with budget and communication constraints
[DE95-010876] p 2948 N95-32277

NEURAL NETS
The Technology Information Environment with Industry (TIE-In): A mechanism for accessing laboratory solutions
[DE95-008542] p 3027 N95-30385
Selecting optimal experiments for feedforward multilayer perceptrons
[AD-A290856] p 2949 N95-30406
Noisy-network acceptors
[PB95-197976] p 2951 N95-30813
Neurodynamical systems for cognition and target identification
[AD-A293111] p 2951 N95-30884
Neural network false alarm filter, volume 2
[AD-A293114] p 2860 N95-30886
Multi-valued neural network modified model and its optical realization.
[AD-A293140] p 2951 N95-30891
High-tech controls for energy and environment
[DE95-011702] p 2952 N95-31255
Temporal feature extraction in photorefractive resonators
[AD-A292908] p 2881 N95-31385
Acquiring consistent knowledge for Bayesian Forests
[AD-A293858] p 2952 N95-31517
Neural networks for real-time terrain typing
[AD-A293569] p 2953 N95-31540
Simulation of oculomotor post-inhibitory rebound burst firing using a Hodgkin-Huxley model of a neuron
[AD-A293821] p 2927 N95-31552
Nonlinear time series analysis
[AD-A293841] p 2963 N95-31558
Neural network false alarm filter, volume 1
[AD-A293097] p 2953 N95-31562
Evaluation of nonlinear structural dynamic responses using a fast-running spring-mass formulation
[DE95-008503] p 2967 N95-31625
Finite-sample based learning algorithms for feedforward networks
[DE95-009123] p 2941 N95-31631
Neural network based data fusion system
[AD-D017440] p 2953 N95-31692
Neural network based three dimensional ocean modeler
[AD-D017441] p 2953 N95-31693
Artificial neural networks and model-based recognition of 3-D objects from 2-D images p 2954 N95-31838

NEUROLOGY
Conference perspective. Neuroimmunomodulation: Stress and immune function
[AD-A291351] p 2926 N95-30870

NEURONS
Simulation of oculomotor post-inhibitory rebound burst firing using a Hodgkin-Huxley model of a neuron
[AD-A293821] p 2927 N95-31552

NEUROPHYSIOLOGY
Physiology and physiopathology of equilibration
[PB95-208328] p 2926 N95-30494

NEUROPSYCHIATRY
Using computerized neuropsychological testing to assess aviator skills
[AD-A293227] p 2928 N95-30905

NEUTRAL ATOMS
Optical frequency standards: Hertz-level working standards and their absolute frequency measurement
[AD-A293930] p 2999 N95-31515

NEUTRAL BEAMS
Design study of prototype accelerator and MeV test facility for demonstration of 1 MeV, 1 A negative ion beam production
[DE95-737208] p 2995 N95-32262

NEUTRAL PARTICLES
Unitarization of Koerner-Kuroda model of electromagnetic structure of octet 1/2(+) baryons
[DE95-613765] p 2984 N95-31548

NEUTRALIZERS
Enhanced alkaline hydrolysis and biodegradability studies of nitrocellulose-bearing missile propellant
p 2772 N95-31752

NEUTRINO BEAMS
Study of different type neutrino oscillations based on neutrino beams from 600 GeV
[DE95-619267] p 2983 N95-31260
On possibility to study neutrino oscillations by detectors located at Gran Sasso (Italy) using beams from 600 GeV UNK-1 machine
[DE95-619268] p 2983 N95-31261

NEUTRINOS
Signatures of virtual LSP's at the TEVATRON
[DE95-613798] p 2982 N95-31060
Study of different type neutrino oscillations based on neutrino beams from 600 GeV
[DE95-619267] p 2983 N95-31260
On possibility to study neutrino oscillations by detectors located at Gran Sasso (Italy) using beams from 600 GeV UNK-1 machine
[DE95-619268] p 2983 N95-31261
Structure formation with majoron supermultiplet
[DE95-613596] p 2984 N95-31546
Long baseline neutrino oscillation experiment at the AGS
[DE95-004378] p 2986 N95-31702

NEUTRON ACTIVATION ANALYSIS
Holistic analysis of gamma-ray spectra in instrumental neutron activation analysis
[PB95-214458] p 2979 N95-30639

NEUTRON BEAMS
Background event discrimination in neutron time-of-flight measurements at beams of relativistic nuclei of the JINR synchrotron
[DE95-613006] p 2991 N95-30604
Investigation of Fe3O4 colloid behaviour in a magnetic field by polarized neutron transmission
[DE95-614351] p 2981 N95-30915
Neutronic methods for determination of very low concentrations of hydrogen in metals
[DE95-623967] p 2807 N95-31409

NEUTRON DIFFRACTION
The neutron powder diffraction and acoustic investigations of the NH4SCN phase diagram
[DE95-614372] p 3009 N95-30419
Acoustoelastic stress evaluation in metal plate using absolute shear and longitudinal time-of-flight data
[PB95-197810] p 2892 N95-30458
Ionic conductivities of lithium phosphorus oxynitride glasses, polycrystals, and thin films
[DE95-008898] p 2812 N95-30545
Residual stresses and stress corrosion cracking in pipe fittings
[DE95-009332] p 2894 N95-31054
On the possibility of a two-state magnetic structure for nanocrystalline chromium
[DE95-009914] p 3015 N95-32062
Residual stress distribution in FeAl weld overlay on steel
[DE95-009178] p 2899 N95-32317

NEUTRON IRRADIATION
Defect configurations in neutron-irradiated U3Si2
[DE95-009896] p 3016 N95-32105

NEUTRON SCATTERING
IPNS neutron scattering instrumentation. A: Existing and planned. B: Possibilities for IPNS upgrade, a 1-MW spallation source
[DE95-004119] p 2985 N95-31616
Defect configurations in neutron-irradiated U3Si2
[DE95-009896] p 3016 N95-32105

NEUTRON SOURCES
IPNS neutron scattering instrumentation. A: Existing and planned. B: Possibilities for IPNS upgrade, a 1-MW spallation source
[DE95-004119] p 2985 N95-31616
Defect configurations in neutron-irradiated U3Si2
[DE95-009896] p 3016 N95-32105

NEUTRON STARS
Observations of accreting pulsars
[NASA-CR-198931] p 3028 N95-30469

NEUTRONS
Background event discrimination in neutron time-of-flight measurements at beams of relativistic nuclei of the JINR synchrotron
[DE95-613006] p 2991 N95-30604
Development of BERMUDA: A radiation transport code system. Part 3: A one-dimensional adjoint neutron transport code
[DE95-717875] p 2934 N95-30759
Neutron shielding point kernel integral calculation code for personal computer: PKN-pc
[DE95-717876] p 2980 N95-30760
Investigation of Fe3O4 colloid behaviour in a magnetic field by polarized neutron transmission
[DE95-614351] p 2981 N95-30915
IPNS neutron scattering instrumentation. A: Existing and planned. B: Possibilities for IPNS upgrade, a 1-MW spallation source
[DE95-004119] p 2985 N95-31616

NEWTON METHODS
Elliptic deformed classical mechanics in three-dimensional phase space
[DE95-613384] p 3017 N95-30365
Newton methods for large-scale linear inequality-constrained minimization: Optimization and systems theory
[PB95-210332] p 2956 N95-30499
Effect of the stopping of the Newton iteration in implicit linear multistep methods
[PB95-207056] p 2959 N95-31184
Quasi-Newton updating for large scale nonlinear systems
[AD-A292778] p 2940 N95-31431

NEWTON-RAPHSON METHOD
Newton Raphson method, scaling at fractal boundaries and mathematica
[DE95-613374] p 2962 N95-32095

NEWTONIAN FLUIDS
Simulation of viscous sintering
[PB95-197109] p 2868 N95-30836
Numerical simulation of time dependent viscoelastic fluid flow
[TRITA-NA-9311] p 2873 N95-31414

NICKEL
Reaction synthesis of intermetallics
[DE95-009029] p 2803 N95-30575
Localization in tungsten heavy alloys subjected to shearing deformations under superimposed high pressures
[AD-A293177] p 2804 N95-30977

NICKEL ALLOYS
The effect of interface properties on nickel base alloy composites
[NASA-CR-198363] p 2785 N95-30787
Innovative processing of composites for ultra-high temperature applications, book 4
[AD-A290892] p 2786 N95-30867
Review of environmental effects in intermetallics
[DE95-010120] p 2805 N95-31106
Shape memory properties of an iron modified nickel aluminide alloy
[DE95-010223] p 2805 N95-31111
Comparison of cathodic protection currents on 70/30 copper-nickel and alloy 625 piping systems
[AD-A292953] p 2807 N95-31561
Cadmium plating replacements p 2776 N95-31773
Synthesis and characterization of nanophase face-centered-cubic titanium
[DE95-009533] p 2809 N95-32051
Cascade damage in the ordered alloy Ni3Al
[DE95-009893] p 2809 N95-32104

NIOBATES
Synthesis of novel precursors for PMN powders and the thin films obtained from them
[DE95-006543] p 2811 N95-30362
Molecular modeling of PMN ceramics
[AD-A290879] p 2813 N95-30560
A compact and efficient violet laser source
[AD-A292782] p 2885 N95-31434

NIOBIUM
Orientation of rapid thermally annealed lead zirconate titanate thin films on (111) Pt substrate
[DE95-615232] p 2811 N95-30422
High-resolution superconducting x-ray spectrometers with aluminum trapping layers of different thicknesses
[DE95-010253] p 2881 N95-32047

NIOBIUM ALLOYS
Room temperature fracture and high temperature creep deformation properties of alumina reinforced with 20 vol% particulate niobium
[DE95-010234] p 2815 N95-30897
Measurements of stability margins and current distribution in large-scale Nb3Sn cable-in-conduit conductors
[DE95-009869] p 3007 N95-32148

NITRAMINE PROPELLANTS
Molecular models for nitro compounds
p 2831 N95-31293
Embedded infrared fiber optic absorption studies of nitramine propellant strand burning
p 2801 N95-31305
Flame structure studies of neat and NH3 doped H2/N2O flames employing molecular beam mass spectrometry and modeling p 2801 N95-31313

NITRATES
Global climatology and variability of potential new production estimated from remote sensing of sea-surface temperature
[NASA-CR-198840] p 2910 N95-31981

NITRATION
Acidity and basicity of nitro substituted imidazoles
p 2832 N95-31301
Acidity and basicidity of nitro substituted imidazoles
[AD-A293969] p 2836 N95-31526
NITRIC OXIDE
Simulation of chemical kinetics in turbulent natural gas combustion. Volume 2: Experimental studies of nitric oxide production in gas flames
[PB95-196721] p 2791 N95-30541
An ab initio study of the reaction HNO + NO yields OH + N2O: Preliminary results p 2801 N95-31308
NITRIDES
The neutron powder diffraction and acoustic investigations of the NH4SCN phase diagram
[DE95-614372] p 3009 N95-30419
Low temperature fabrication from nano-size ceramic powders
[DE95-010995] p 2818 N95-31153
Degradation of blue AlGaN/InGaN/GaN LEDs subjected to high current pulses
[DE95-008824] p 2863 N95-31611
An experimental search for high ZT semiconductors: A survey of the preparation and properties of several alloy systems
[DE95-010232] p 2865 N95-32084
NITRIDING
Gelcasting of sintered reaction-bonded silicon nitride for improved mechanical properties
[DE95-010282] p 2822 N95-32085
NITRILES
Mode I large strain viscoelastic crack behavior in nitrile rubber sheets
[AD-A289984] p 2820 N95-31617
Compatibility of Single Hydraulic Fluid with military specification fluids, seals and metallurgy
[AD-A292954] p 2821 N95-31663
NITRO COMPOUNDS
Molecular models for nitro compounds
p 2831 N95-31293
Estimating heat of formation of energetic compounds using corrected semiempirical molecular orbital theory
p 2800 N95-31294
NITROGEN
State resolved dynamics of ion-molecule collisions in a flowing afterglow
[AD-A290895] p 2976 N95-30410
Synthesis of carbo-nitride films using high-energy shock plasma deposition
[DE95-615231] p 2811 N95-30450
Flame structure studies of neat and NH3 doped H2/N2O flames employing molecular beam mass spectrometry and modeling p 2801 N95-31313
Fourier Transform (FT) Raman spectroscopy of nitrogen at high pressure
[AD-A293051] p 2796 N95-31670
NITROGEN COMPOUNDS
Acidity and basicidity of nitro substituted imidazoles
[AD-A293969] p 2836 N95-31526
NITROGEN DIOXIDE
The oxidation of carbon monoxide by nitrogen dioxide
p 2801 N95-31310
NITROGEN HYDRIDES
The neutron powder diffraction and acoustic investigations of the NH4SCN phase diagram
[DE95-614372] p 3009 N95-30419
NITROGEN OXIDES
No-thermal plasma processing of VOCs and NO(x) at LLNL
[DE95-011445] p 2911 N95-32281
NITROUS OXIDES
Comparison of DSMC predictions with temporally resolved vibrational state measurements in NO
p 2872 N95-30996
An ab initio study of the reaction HNO + NO yields OH + N2O: Preliminary results p 2801 N95-31308
The oxidation of carbon monoxide by nitrous oxide
p 2801 N95-31309
Detailed chemical kinetic modeling of premixed hydrocarbon flames supported by NO2
p 2801 N95-31311
NOISE
Electromagnetically activated compliant wavy-wall
[AD-D017340] p 2866 N95-30412
NOISE GENERATORS
Gear pump with reduced fluid-borne noise
[AD-D017362] p 2887 N95-30399
NOISE MEASUREMENT
Advanced system identification techniques for wind turbine structures
[DE95-004049] p 2902 N95-30505
NOISE REDUCTION
Gear pump with reduced fluid-borne noise
[AD-D017362] p 2887 N95-30399
Method and system for suppressing noise induced in a fluid medium by a body moving therethrough
[AD-D017339] p 2973 N95-30411
Smart active multiwave sensing with zero background amplitude modulated probes
[DE95-008813] p 2792 N95-30714
Energy absorption apparatus
[AD-D017361] p 2814 N95-30715
Reducing process noise in superconducting helium liquid level probes
[DE95-008956] p 2814 N95-30765
An active liner system for jet engine exhaust silencers, phase 1
[AD-A293277] p 2756 N95-31191
An efficient implementation of Forward-Backward Least-Mean-Square Adaptive Line Enhancers
p 2855 N95-32224
NOISE SPECTRA
The contextual variance of devoiced fricatives in polish
[IFTR-7/1995] p 2854 N95-32192
NONDESTRUCTIVE TESTS
Method and apparatus for non-destructively measuring local resistivity of semiconductors
[AD-D017436] p 2862 N95-31343
An evaluation of the losipescu specimen for composite materials shear property measurement
[NASA-CR-198755] p 2896 N95-31418
Surface contamination analysis technology team overview p 2781 N95-31797
Study of surfaces using near infrared optical fiber spectrometry p 2781 N95-31801
Contamination detection NDE for cleaning process inspection p 2781 N95-31802
Mapping hidden aircraft defects with dual-band infrared computed tomography
[DE95-011531] p 2741 N95-32164
Metallic multilayers at the nanoscale
[DE95-011534] p 3016 N95-32284
Nondestructive testing of ceramic components: Cooperative Research and Development Agreement completion report
[DE95-009510] p 2823 N95-32352
NONEQUILIBRIUM CONDITIONS
Modeling of thermal, electronic, hydrodynamic, and dynamic deposition processes for pulsed-laser deposition of thin films
[DE95-008906] p 2813 N95-30572
NONEQUILIBRIUM FLOW
Flow models for the design of a hypersonic iodine vapor wind tunnel nozzle with chemical and vibrational nonequilibrium effects p 2742 N95-30448
NONFLAMMABLE MATERIALS
The HYLIFE-2 inertial fusion energy power plant concept and implications for IFE
[DE95-010561] p 2994 N95-32074
NONINTRUSIVE MEASUREMENT
An investigation of the side-dump dual in-line ramjet combustor p 2756 N95-31199
Non-intrusive combustion diagnostics of premixed hydrocarbon flames using FT-IR spectrometry
p 2797 N95-31732
Contamination detection NDE for cleaning process inspection p 2781 N95-31802
Spatially-resolved velocity measurements in steady, high-speed, reacting flows using laser-induced OH fluorescence p 2877 N95-32109
NONLINEAR EQUATIONS
Gibbs measures and quasi-periodic solutions for nonlinear Hamiltonian partial differential equations
[PB95-207932] p 2956 N95-30506
Higher Schwarzian operatörs and combinatorics of Schwarzian derivative
[PB95-208435] p 2957 N95-30623
Solvability of a class of hypersingular nonlinear integral equations
[PB95-207031] p 3011 N95-30720
Effect of the stopping of the Newton iteration in implicit linear multistep methods
[PB95-207056] p 2959 N95-31184
Determination of the symmetry of a non-linear Schroedinger equation
[IFTR-10/1995] p 2960 N95-31339
Numerical simulation of shock/turbulent boundary layer interaction
[NASA-CR-198846] p 2872 N95-31341
Numerical studies of nonlinear optical pulse propagation p 2998 N95-31411
Quasi-Newton updating for large scale nonlinear systems
[AD-A292776] p 2940 N95-31431
NONLINEAR EVOLUTION EQUATIONS
Gibbs measures and quasi-periodic solutions for nonlinear Hamiltonian partial differential equations
[PB95-207932] p 2956 N95-30506
NONLINEAR OPTICS
Ceramics derived from metal-organic precursors
[AD-A290791] p 2811 N95-30405
Fabrication and modification of metal nanocluster composites using ion and laser beams
[DE95-009131] p 2784 N95-30731
Nonlinear optical processes in polymer films
[AD-A293384] p 2815 N95-30955
Laser-induced holographic surface relief gratings on nonlinear optical polymer films
[AD-A293169] p 2997 N95-30973
Experimental investigation of optical nonlinearities in conjugated polymers
[AD-A288353] p 2884 N95-31145
Temporal feature extraction in photorefractive resonators
[AD-A292908] p 2881 N95-31385
Numerical studies of nonlinear optical pulse propagation p 2998 N95-31411
Nonlinear organized materials for optical devices
[AD-A292809] p 2999 N95-31441
Photorefractive nonlinear optics
[AD-A292913] p 2999 N95-31458
Quantum and nonlinear optics research
[AD-A293879] p 2999 N95-31519
Ultraviolet and visible lasers: Rare earth-doped waveguide devices and non-linear optical extraction techniques
[AD-A293976] p 2885 N95-31528
Nonlinear optics in novel composite media
[AD-A293886] p 2999 N95-31542
An interpenetrating polymer network for second-order nonlinear optics
[AD-A293019] p 2821 N95-31699
Novel unsymmetrical polydiacetylenes as materials for second and third order nonlinear optics
[AD-A293020] p 3001 N95-31700
Z-scan using a dye laser
[PB95-222923] p 3002 N95-32312
NONLINEAR PROGRAMMING
Convergence properties of an augmented lagrangian algorithm for optimization with a combination of general equality and linear constraints
[PB95-208039] p 2956 N95-30570
Structural design using equilibrium programming formulations
[NASA-TM-110175] p 2893 N95-30682
NONLINEAR SYSTEMS
Nonlinear dynamical systems: Elements of a complex system analysis
[PB95-211652] p 2950 N95-30478
Fixed modes in quasi-static state feedback decoupling
[PB95-206850] p 2950 N95-30564
The iteration formula of the Maslov-type index theory with applications to nonlinear Hamiltonian systems
[DE95-613379] p 2957 N95-30676
Cascading synchronized chaotic systems
[AD-D017458] p 2860 N95-30748
Generalized controlled invariance for nonlinear systems
[PB95-197901] p 2950 N95-30807
Workshop on diffusion approximation in communication and stochastic systems theory
[AD-A292872] p 2952 N95-31055
A two-timescale approach to nonlinear Model Predictive Control
[DE95-000943] p 2952 N95-31161
Role of free-surface boundary conditions and nonlinearities in wave/boundary-layer and wake interaction p 2872 N95-31317
Control of mechanical systems with rolling contacts: Applications to robotics p 2889 N95-31332
Quasi-Newton updating for large scale nonlinear systems
[AD-A292776] p 2940 N95-31431
Quantum 1/f noise in high technology applications including ultrasmall structures and devices
[AD-A292812] p 2862 N95-31442
Multipoint quadratic approximation for numerical optimization
[AD-A293837] p 2961 N95-31557
Evaluation of nonlinear structural dynamic responses using a fast-running spring-mass formulation
[DE95-008503] p 2967 N95-31625
Global stabilization of nonlinear gyroscopic systems
p 2881 N95-31836
An extremum principle for the analysis and design of constitutively nonlinear systems p 2898 N95-32112
A mode decomposition based finite element formulation for the nonlinear dynamics of flexible spatial structures and mechanisms p 2898 N95-32118
A survey of the core-congruential formulation for geometrically nonlinear TL finite elements
[NASA-CR-199044] p 2944 N95-32203

NONLINEARITY
Direct determination of grain boundary atomic structure in SrTiO3
[DE95-008847] p 3010 N95-30544
Electron-optical nonlinear interaction in asymmetric quantum-well laser heterostructures
[DE95-613443] p 2883 N95-30609
Cascading synchronized chaotic systems
[AD-D017458] p 2860 N95-30748
Fiber optic interferometric electric field and voltage sensor utilizing and electrostrictive transducer
[AD-D017433] p 2996 N95-30753
New adaptive methods for reconfigurable flight control systems, appendix 1
[AD-A292711] p 2756 N95-30937
Robust fixed-structure control
[AD-A292883] p 2952 N95-30961
IR materials producibility
[AD-A293330] p 2998 N95-31141
Self-adaptive multilevel methods for fluid flow problems p 2873 N95-31412
Nonlinear organized materials for optical devices
[AD-A292809] p 2999 N95-31441
Quantum 1/f noise in high technology applications including ultrasmall structures and devices
[AD-A292812] p 2862 N95-31442
Computational methods for control and optimal design of aerospace systems
[AD-A292861] p 2751 N95-31451
Photorefractive nonlinear optics
[AD-A292913] p 2999 N95-31458
Large deformation failure mechanisms in nonlinear solids
[AD-A293010] p 2896 N95-31474
Nonlinear time series analysis
[AD-A293841] p 2963 N95-31558
Removal of the Energy Dependence from the Resolvent Like Energy Dependent Interactions
[DE95-613385] p 2961 N95-31619
Spectral methods and sum acceleration algorithms
[DE95-009689] p 2941 N95-31630
Dynamic inversion: An evolving methodology for flight control design p 2758 N95-31996

NONNEWTONIAN FLOW
Numerical simulation of time dependent viscoelastic fluid flow
[TRITA-NA-9311] p 2873 N95-31414
Some aspects on the modelling of non-Newtonian fluid flow
[TRITA-NA-9317] p 2873 N95-31415

NONNEWTONIAN FLUIDS
Numerical simulation of time dependent viscoelastic fluid flow
[TRITA-NA-9311] p 2873 N95-31414
Some aspects on the modelling of non-Newtonian fluid flow
[TRITA-NA-9317] p 2873 N95-31415

NONPARAMETRIC STATISTICS
Nonparametric methods for incomplete data in reliability and for changepoints in smooth functions
[AD-A292773] p 2963 N95-31429
Nonparametric recognition of nonrigid motion
[AD-A293630] p 2963 N95-31565

NORMAL DENSITY FUNCTIONS
A stochastic EM estimator in the presence of missing data: Theory and applications
[DE95-010329] p 2944 N95-32089

NORMALIZING
Barendregt cube with definitions and generalized reduction
[PB95-206793] p 2966 N95-30719

NORTH ATLANTIC TREATY ORGANIZATION (NATO)
Study of Extended Air Defence Post 2000 p 2839 N95-32124

NOSES (FOREBODIES)
Side force acting on blunted circular cylinder bodies at high angles of attack in supersonic flow
[NAL-TR-1255] p 2744 N95-31741
Flight evaluation of forebody vortex control in post-stall flight p 2752 N95-32003

NOTCH TESTS
The effect of interface properties on nickel base alloy composites
[NASA-CR-198383] p 2785 N95-30787
Initial survey on fracture toughness of commercial Nd2Fe14B
[DE95-009813] p 2808 N95-31643

NOTCHES
A simple and accurate technique for monitoring crack growth behavior using a wave form analyzer
[AD-A293161] p 2894 N95-31007

NOWCASTING
Comparison of satellite-derived MSU brightness temperatures and conventionally-derived fields
[AD-A293692] p 2901 N95-31603

NOZZLE DESIGN
Flow models for the design of a hypersonic iodine vapor wind tunnel nozzle with chemical and vibrational nonequilibrium effects p 2742 N95-30448
Advanced small rocket chambers. Option 3: 110 lbf Ir-Re rocket, volume 2
[NASA-CR-195435-VOL-2] p 2769 N95-31170
Numerical study of shear-induced heating in high-speed nozzle flow of liquid monopropellant p 2828 N95-31207

NOZZLE FLOW
Flow models for the design of a hypersonic iodine vapor wind tunnel nozzle with chemical and vibrational nonequilibrium effects p 2742 N95-30448
Validation of the NPARC code for nozzle afterbody flows at transonic speeds
[NASA-TM-106971] p 2742 N95-30704
Kinetic theory model predictions compared with low-thrust axisymmetric nozzle plume data
[NASA-CR-198934] p 2768 N95-30864
Numerical study of shear-induced heating in high-speed nozzle flow of liquid monopropellant p 2828 N95-31207

NUCLEAR BINDING ENERGY
Applications of SXPS for studying surface structure, reaction mechanisms and kinetics
[DE95-008903] p 2803 N95-30547

NUCLEAR FUSION
Development of plasma diagnostics technologies: A study on nuclear fusion reactor
[DE95-614180] p 3005 N95-31004
The development of the tokamak system technology: A study on the fusion reactor
[DE95-614256] p 3005 N95-31366
Electroweak baryogenesis
[DE95-012169] p 2991 N95-32365

NUCLEAR INTERACTIONS
Experimental results on charge exchange reactions with delta excitations and polarization studies of delta and N(sup *) (1440) resonances
[DE95-614022] p 2981 N95-30913

NUCLEAR MEDICINE
Summaries of fiscal year 1994 projects in medical applications and biophysical research
[DE95-010405] p 2925 N95-32040

NUCLEAR PHYSICS
The design and construction of the muon arm in PHENIX
[DE95-010156] p 2978 N95-30616
Abstracts of Annual Physics Conference of Iran
[DE95-611717] p 2768 N95-30881

NUCLEAR POWER PLANTS
SHEAT: A computer code for probabilistic seismic hazard analysis, user's manual
[DE95-717874] p 2913 N95-30758
Damage dosimetry and embrittlement monitoring of nuclear pressure vessels in real time by magnetic properties measurement
[DE95-011454] p 2894 N95-31254
Development and implementation of a computer facility for nuclear data updating and reactor calculations using personal computers
[DE95-623577] p 2940 N95-31408
Validation of favor code linear elastic fracture solutions for finite-length flaw geometries
[DE95-009034] p 2898 N95-32157

NUCLEAR REACTORS
Development and implementation of a computer facility for nuclear data updating and reactor calculations using personal computers
[DE95-623577] p 2940 N95-31408
Validation of favor code linear elastic fracture solutions for finite-length flaw geometries
[DE95-009034] p 2898 N95-32157

NUCLEAR SPIN
Nuclear-spin-dependent parity-nonconserving effects in thallium, lead and bismuth atoms
[DE95-614120] p 2991 N95-32354

NUCLEAR WEAPONS
The Technology Information Environment with Industry (TIE-In): A mechanism for accessing laboratory solutions
[DE95-008542] p 3027 N95-30385

NUCLEATION
Orientation of rapid thermally annealed lead zirconate titanate thin films on (111) Pt substrate
[DE95-615232] p 2811 N95-30422
Molecular nanoclusters as precursors to conductive thin films and crystals
[AD-A290278] p 3014 N95-31189
Clouds: Their prediction and simulation
[AD-A292864] p 2920 N95-31453
Large deformation failure mechanisms in nonlinear solids
[AD-A293010] p 2896 N95-31474
NaK pool-boiler solar receiver durability bench test. Volume 2: Metallurgical analysis
[DE95-010338] p 2905 N95-31640
A numerical analysis of crack growth in microcracking ceramic and ceramic composites
[DE95-010132] p 2897 N95-32024

NUCLEIC ACIDS
Implementation and performance of the pseudoknot problem in Sisal
[DE95-009573] p 2925 N95-32358

NUCLEON-NUCLEON INTERACTIONS
Complex conjugate pairs in stationary Sturmians
[DE95-616279] p 2976 N95-30429
Density dependent effective interactions
[DE95-616348] p 2977 N95-30447
Coulomb correction calculations of pp Bremsstrahlung
[DE95-616349] p 2982 N95-31176
Search for exotic baryons with the SPHINX facility
[DE95-613774] p 2984 N95-31549

NUCLEONS
Complex conjugate pairs in stationary Sturmians
[DE95-616279] p 2976 N95-30429
Pion-nucleon and kaon-nucleon scattering lengths in QCD sum rules
[DE95-737278] p 2983 N95-31227
Spin puzzle in nucleon
[DE95-613654] p 2991 N95-32353

NUMERICAL ANALYSIS
Semiannual report
[NASA-CR-198172] p 2931 N95-30657
Achieving improved cycle efficiency via pressure gain combustors
[DE95-008945] p 2792 N95-30762
Residual stresses and stress corrosion cracking in pipe fittings
[DE95-009032] p 2894 N95-31054
Theory & numerical methods for problems in shape reconstruction and large deviations
[AD-A292874] p 2952 N95-31279
Numerical studies of nonlinear optical pulse propagation p 2998 N95-31411
Self-adaptive multilevel methods for fluid flow problems p 2873 N95-31412
A numerical analysis of crack growth in microcracking ceramic and ceramic composites
[DE95-010132] p 2897 N95-32024

NUMERICAL CONTROL
DEPSCOR92-Wide field spectral imager
[AD-A293079] p 2997 N95-31005
Catapult-launching of the RAFALE design and experimentation p 2752 N95-32008

NUMERICAL INTEGRATION
A finite element formulation for the time domain vibration analysis of an elastic-viscoelastic structure p 2895 N95-31318
Staggered solution procedures for multibody dynamics simulation
[NASA-CR-199034] p 2899 N95-32202

NUMERICAL STABILITY
Numerical stability investigations of processes for solving linear initial value problems
[PB95-207023] p 2959 N95-31183

NYLON (TRADEMARK)
High strain-rate testing of parachute materials
[DE95-009577] p 2897 N95-31614

O

OBJECT-ORIENTED PROGRAMMING
ESAA: Environment for Seismic Activity Analysis
[DE95-612416] p 2913 N95-30675
Leveraging object-oriented development at Ames p 2938 N95-31244
Nonparametric recognition of nonrigid motion
[AD-A293630] p 2963 N95-31565
PORK object system programmer's guide
[AD-A293596] p 2942 N95-31688

OBSERVATION AIRCRAFT
Special investigation report: Safety of the air tour industry in the United States
[PB95-917004] p 2748 N95-32185

OBSTACLE AVOIDANCE
On the kinematic performance of mechanical manipulators operating in the presence of an obstruction p 2890 N95-31710

OCCUPATION
An assessment of worldwide supercomputer usage
[DE95-009879] p 2932 N95-31645

OCEAN BOTTOM
Multiple scatter theory of ocean sediments
[AD-A293951] p 2923 N95-31523
Studies in marine tectonics: Propagating rifts, depth anomalies and subduction zone anisotropy p 2923 N95-31719

OCEAN CURRENTS
Arabian Sea mixed layer dynamics experiment: Mooring deployment cruise report
[AD-A293684] p 2923 N95-31600
The role of the hydrological cycle and the ocean's thermohaline circulation in climate change: A multicomponent climate model study
p 2909 N95-31720
Objective analysis of oceanic data for Coast Guard trajectory models
[AD-A292884] p 2924 N95-32363

OCEAN DATA ACQUISITIONS SYSTEMS
SeaWiFS technical report series. Volume 28: SeaWiFS algorithms, part 1
[NASA-TM-104566-VOL-28] p 2924 N95-31850
SeaWiFS technical report series. Volume 24: SeaWiFS technical report series cumulative index, volumes 1-23
[NASA-TM-104566-VOL-24] p 2924 N95-32122
SeaWiFS technical report series. Volume 13: Case studies for SeaWiFS calibration and validation, part 1
[NASA-TM-104566-VOL-13] p 2924 N95-32220

OCEAN DYNAMICS
NASA Tropical Rainfall Measurement Mission (TRMM): Effects of tropical rainfall on upper ocean dynamics, air-sea coupling and hydrologic cycle
[NASA-CR-189437] p 2919 N95-31123
Arabian Sea mixed layer dynamics experiment: Mooring deployment cruise report
[AD-A293684] p 2923 N95-31600
The role of the hydrological cycle and the ocean's thermohaline circulation in climate change: A multicomponent climate model study
p 2909 N95-31720

OCEAN MODELS
QTSAW (Quick Typhoon Surge and Waves). Wave information studies of US coastlines
[AD-A293172] p 2919 N95-30976
The role of the hydrological cycle and the ocean's thermohaline circulation in climate change: A multicomponent climate model study
p 2909 N95-31720
Objective analysis of oceanic data for Coast Guard trajectory models
[AD-A292884] p 2924 N95-32363

OCEAN SURFACE
NASA Tropical Rainfall Measurement Mission (TRMM): Effects of tropical rainfall on upper ocean dynamics, air-sea coupling and hydrologic cycle
[NASA-CR-189437] p 2919 N95-31123
Investigation of microwave backscatter from the air-sea interface
[NASA-CR-198854] p 2851 N95-31457
Validation of special sensor microwave/imager ocean surface wind retrievals in equatorial regions
[AD-A293750] p 2920 N95-31571
The determination of wave group parameters from the resolution of incident and reflected waves
[AD-A293703] p 2924 N95-31829
Objective analysis of oceanic data for Coast Guard trajectory models
[AD-A292884] p 2924 N95-32363

OCEAN TEMPERATURE
Ocean mass density calculations from temperature and salinity data
[DSTO-TR-0023] p 2922 N95-30711

OCEAN THERMAL ENERGY CONVERSION
Data on development of new energy technologies
[DE95-764135] p 2904 N95-31155

OCEANOGRAPHIC PARAMETERS
Ocean mass density calculations from temperature and salinity data
[DSTO-TR-0023] p 2922 N95-30711
Bibliography of technical reports, 1993
[AD-A292741] p 2923 N95-30918
NASA Tropical Rainfall Measurement Mission (TRMM): Effects of tropical rainfall on upper ocean dynamics, air-sea coupling and hydrologic cycle
[NASA-CR-189437] p 2919 N95-31123
Modern methods in meteorological and oceanographic data acquisition and analyses
[AD-A293884] p 2920 N95-31541
Objective analysis of oceanic data for Coast Guard trajectory models
[AD-A292884] p 2924 N95-32363

OCEANOGRAPHY
JPL Physical Oceanography Distributed Active Archive Center (PO.DAAC) data availability, version 1-94
[NASA-CR-198871] p 2922 N95-30859
Bibliography of technical reports, 1993
[AD-A292741] p 2923 N95-30918
Directory of global environmental sciences in Japan
p 2899 N95-31413
Arabian Sea mixed layer dynamics experiment: Mooring deployment cruise report
[AD-A293684] p 2923 N95-31600
SeaWiFS technical report series. Volume 28: SeaWiFS algorithms, part 1
[NASA-TM-104566-VOL-28] p 2924 N95-31850

OCEANS
Airborne ocean water lidar (OWL) real time processor (RTP)
[AD-A293226] p 2848 N95-30904
SeaWiFS technical report series. Volume 28: SeaWiFS algorithms, part 1
[NASA-TM-104566-VOL-28] p 2924 N95-31850
Inversion of ERS-1 wavemode spectra. User's and programmer's guide
[PB95-223582] p 2902 N95-32316

OCTETS
Unitarization of Koerner-Kuroda model of electromagnetic structure of octet 1/2(+) baryons
[DE95-613765] p 2984 N95-31548

OCULOMOTOR NERVES
Simulation of oculomotor post-inhibitory rebound burst firing using a Hodgkin-Huxley model of a neuron
[AD-A293821] p 2927 N95-31552

OFFSHORE PLATFORMS
Fatigue behaviour of multiplanar tubular joints
[PB95-207874] p 2893 N95-30586

OHMIC DISSIPATION
Energy absorption apparatus
[AD-D017361] p 2814 N95-30715

OIL EXPLORATION
Development of the Multi-Level Seismic Receiver (MLSR)
[DE95-008823] p 2916 N95-31610

OIL RECOVERY
Development of the Multi-Level Seismic Receiver (MLSR)
[DE95-008823] p 2916 N95-31610

OILS
Evaluation of Environmentally Acceptable hydraulic fluids
[AD-A293037] p 2821 N95-31666
Determination of halogens in a petroleum product by ion chromatography
[DE95-002056] p 2797 N95-31840

OMEGA-MESONS
Applications of chiral symmetry
[DE95-009552] p 2988 N95-32079

ON-LINE SYSTEMS
On-line surfactant monitoring
[DE95-009417] p 2792 N95-30735
Support of environmental requirements for cloud analysis and archive (SERCAA): Database management facility
[AD-A293938] p 2920 N95-31522
Laboratory robotics: An automated tool for preparing Ion Chromatography calibration standards
[DE95-009441] p 2798 N95-32318

ONBOARD DATA PROCESSING
Experience report: Using formal methods for requirements analysis of critical spacecraft software
p 2938 N95-31247
Information Switching Processor (ISP) contention analysis and control
[NASA-CR-195471] p 2765 N95-31849

ONBOARD EQUIPMENT
System considerations for efficient communication and storage of MSTI image data
[NASA-CR-198869] p 3024 N95-30858

ONE DIMENSIONAL FLOW
Simple model of foam spreading on liquid surfaces
[PB95-211207] p 2838 N95-30630
Study of cross-tail current carriers in magnetotail
p 3005 N95-30804

OPERATING COSTS
Modeling F/A-18 flight hour program costs using regression analysis
[AD-A293771] p 2752 N95-31579

OPERATING SYSTEMS (COMPUTERS)
SodaBot: A software agent environment and construction system
[AD-A290056] p 2939 N95-31277
The occurrence of continuation parameters in CPS terms
[AD-A292952] p 2941 N95-31460
The Linux operating system: An introduction
[NASA-CR-198178] p 2932 N95-31988

OPERATIONAL AMPLIFIERS
Pre-amplifier with multi-stage feedback
[AD-D017371] p 2859 N95-30659

OPERATIONS RESEARCH
Symmetric longest queue system
[PB95-197919] p 2950 N95-30808

OPERATOR PERFORMANCE
The development of human behaviour analysis techniques and the development of human factors technologies
[DE95-613356] p 2930 N95-31267
Automatic Target Recognition (ATR): Background statistics and the detection of targets in clutter
[AD-A293062] p 2853 N95-31673

OPERATORS (MATHEMATICS)
Generalized Kummer surfaces and differentiable invariants of Noether-Horikawa surfaces 1
[DE95-613382] p 2956 N95-30608
Higher Schwarzian operators and combinatorics of Schwarzian derivative
[PB95-208435] p 2957 N95-30623
Co-groups on sequentially complete, locally convex, topological vector spaces in particular on strict LF-spaces
[PB95-206918] p 2966 N95-30681
Potential integral equations of the 2D Laplace operator in wavelet basis
[TRITA-NA-9401] p 2957 N95-30713
On the degree of approximation by Jackson type operators
[DE95-613383] p 2958 N95-30821
Representation of feedback operators for hyperbolic systems
[NASA-CR-198171] p 2960 N95-31319

OPTICAL BISTABILITY
Optical logic and signal processing using a semiconductor laser diode-based optical bistability device
[AD-A293248] p 2997 N95-30908

OPTICAL COMMUNICATION
Passive, multi-channel fiber optic rotary joint assembly
[AD-D017353] p 2996 N95-30529
Design and testing of an optimal digital link capable of 14-channel transmission
[AD-A288505] p 3000 N95-31652
A high-speed photonic clock and carrier regenerator
p 2856 N95-32236

OPTICAL COMPUTERS
Optical logic and signal processing using a semiconductor laser diode-based optical bistability device
[AD-A293248] p 2997 N95-30908

OPTICAL CORRECTION PROCEDURE
SeaWiFS technical report series. Volume 13: Case studies for SeaWiFS calibration and validation, part 1
[NASA-TM-104566-VOL-13] p 2924 N95-32220

OPTICAL CORRELATORS
Real time correlating operation on diffuse objects
[AD-A293220] p 2997 N95-30901
Optical correlator optimizations and extensions for automated optical target recognition
[AD-A293013] p 3000 N95-31697

OPTICAL COUPLING
Calculated coupling efficiency between an elliptical-core optical fiber and an optical waveguide over temperature
[NASA-TM-107005] p 2997 N95-30849
The coupling impedance of a toroidal beam pipe with circular cross section
[DE95-010442] p 2993 N95-31405

OPTICAL DATA PROCESSING
SeaWiFS Technical Report Series. Volume 29: SeaWiFS CZCS-type pigment algorithm
[NASA-TM-104566] p 2922 N95-30857
Multi-valued neural network modified model and its optical realization.
[AD-A293140] p 2951 N95-30891
Optical logic and signal processing using a semiconductor laser diode-based optical bistability device
[AD-A293248] p 2997 N95-30908
Application of computer generated holograms to optical transformations
[AD-A293146] p 2880 N95-30921
Optical feature recognition
[AD-A293168] p 2997 N95-30966
Temporal feature extraction in photorefractive resonators
[AD-A292908] p 2881 N95-31385
Optical correlator optimizations and extensions for automated optical target recognition
[AD-A293013] p 3000 N95-31697

OPTICAL DATA STORAGE MATERIALS
High speed random access, Fourier transform holographic associative and high density two-photon three-dimensional optical memories based on bacteriorhodopsin
[AD-A293389] p 2931 N95-30967

OPTICAL EQUIPMENT
Multi-color pyrometer temperature measurement system
[DE95-009825] p 2879 N95-30687
Nonlinear organized materials for optical devices
[AD-A292809] p 2999 N95-31441
Scannerless Range Imaging with a square wave
[DE95-009840] p 2854 N95-32145

OPTICAL FIBERS
Demodulators for optical fiber interferometers with (3 x 3) outputs
| AD-D017415 | p 2995 N95-30402
Passive, multi-channel fiber optic rotary joint assembly
| AD-D017353 | p 2996 N95-30529
Fiber optic accelerometer with centrally supported flexural disk
| AD-D017369 | p 2879 N95-30658
Optical fiber pressure sensor for liquid level monitoring
| AD-D017346 | p 2996 N95-30679
Fiber optic interferometric electric field and voltage sensor utilizing and electrostrictive transducer
| AD-D017433 | p 2996 N95-30753
Calculated coupling efficiency between an elliptical-core optical fiber and an optical waveguide over temperature
| NASA-TM-107005 | p 2997 N95-30849
Technique to prepare high-reflectance optical fiber Bragg gratings with single exposure in-line or fiber draw tower
| AD-D017445 | p 2998 N95-31270
Numerical studies of nonlinear optical pulse propagation p 2998 N95-31411
Acousto-optical frequency shifters in dual-core optical fibres
| AD-A293979 | p 2999 N95-31529
Standardization of surface contamination analysis systems p 2781 N95-31798
Study of surfaces using near infrared optical fiber spectrometry p 2781 N95-31801
Influence of storage on the maximal pull-out force of three different optical fibers from three epoxides
| PB95-211777 | p 2822 N95-32253
Fiber optic reference frequency distribution to remote beam waveguide antennas p 2972 N95-32346

OPTICAL FILTERS
Optical correlator optimizations and extensions for automated optical target recognition
| AD-A293013 | p 3000 N95-31697

OPTICAL GYROSCOPES
FOG --- evaluation test of a fiber optic gyroscope (FOG)
| PB95-211546 | p 2879 N95-30600

OPTICAL MATERIALS
State-of-the-art low-cost solar reflector materials
| DE95-000260 | p 2902 N95-30526
Nonlinear optical processes in polymer films
| AD-A293384 | p 2815 N95-30955
Laser-induced holographic surface relief gratings on nonlinear optical polymer films
| AD-A293169 | p 2997 N95-30973
IR materials producibility
| AD-A293330 | p 2998 N95-31141
An interpenetrating polymer network for second-order nonlinear optics
| AD-A293019 | p 2821 N95-31699
Novel unsymmetrical polydiacetylenes as materials for second and third order nonlinear optics
| AD-A293020 | p 3001 N95-31700

OPTICAL MEASUREMENT
Effects of molecular structure on the electroactive and optical properties of conjugated rigid-rod polybenzobisazoles
| AD-A292968 | p 2819 N95-31467

OPTICAL MEASURING INSTRUMENTS
Fiber optic accelerometer with centrally supported flexural disk
| AD-D017369 | p 2879 N95-30658

OPTICAL MEMORY (DATA STORAGE)
High speed random access, Fourier transform holographic associative and high density two-photon three-dimensional optical memories based on bacteriorhodopsin
| AD-A293389 | p 2931 N95-30967

OPTICAL POLARIZATION
Polarization characteristics, control, and modulation of vertical-cavity surface emitting lasers
| DE95-008526 | p 2882 N95-30380

OPTICAL PROPERTIES
Effects of molecular structure on the electroactive and optical properties of conjugated rigid-rod polybenzobisazoles
| AD-A292968 | p 2819 N95-31467
An interpenetrating polymer network for second-order nonlinear optics
| AD-A293019 | p 2821 N95-31699
Novel unsymmetrical polydiacetylenes as materials for second and third order nonlinear optics
| AD-A293020 | p 3001 N95-31700
Carrier dynamics and optical properties of GaAs- and InP-based strained quantum well lasers p 2886 N95-31848

OPTICAL PYROMETERS
Multi-color pyrometer temperature measurement system
| DE95-009825 | p 2879 N95-30687

OPTICAL RADAR
Unconventional imaging field experiment plan
| AD-A291492 | p 2846 N95-30562
Airborne ocean water lidar (OWL) real time processor (RTP)
| AD-A293226 | p 2848 N95-30904
Development of a novel wind lidar, phase 1
| AD-A292703 | p 2849 N95-30935
LAWS hurricane studies
| NASA-CR-189438 | p 2919 N95-31128
Middle atmosphere structure and dynamics: Lidar studies at the South Pole, Syowa and Urbana p 2916 N95-31736
Scannerless Range Imaging with a square wave
| DE95-009840 | p 2854 N95-32145

OPTICAL REFLECTION
Technique to prepare high-reflectance optical fiber Bragg gratings with single exposure in-line or fiber draw tower
| AD-D017445 | p 2998 N95-31270

OPTICAL RESONATORS
Temporal feature extraction in photorefractive resonators
| AD-A292908 | p 2881 N95-31385

OPTICAL SCANNERS
An evaluation of an automatic markup system
| DE95-009885 | p 3026 N95-32149

OPTICAL SWITCHING
A study of end-fire coupling of single-mode fiber to Ti: LiNbO3-single-mode planar waveguide
| AD-A293249 | p 2997 N95-30909

OPTICAL TRACKING
Laser Tracker 3: Sandia National Laboratories' third generation laser tracking system
| DE95-008525 | p 2882 N95-30379
Visual tracking of self-occluding articulated objects
| AD-A292894 | p 2928 N95-31383
The High Altitude Balloon Experiment demonstration of acquisition, tracking, and pointing technologies (HABE-ATP) p 2841 N95-32132
Sandia National Lab's precision laser tracking systems
| DE95-009837 | p 2886 N95-32143

OPTICAL WAVEGUIDES
Ceramics derived from metal-organic precursors
| AD-A290791 | p 2811 N95-30405
Calculated coupling efficiency between an elliptical-core optical fiber and an optical waveguide over temperature
| NASA-TM-107005 | p 2997 N95-30849
A study of end-fire coupling of single-mode fiber to Ti: LiNbO3-single-mode planar waveguide
| AD-A293249 | p 2997 N95-30909
Ultraviolet and visible lasers: Rare earth-doped waveguide devices and non-linear optical extraction techniques
| AD-A293976 | p 2885 N95-31528

OPTIMAL CONTROL
H(sub 2) optimal controllers with observer based architecture for continuous-time systems: Separation principle
| PB95-197067 | p 2951 N95-30833
A feedback linearization approach to orbital maneuvers p 2765 N95-30841
Inverse and control problems in electromagnetics
| AD-A292993 | p 2849 N95-30962
SCARLET: DLR rate saturation flight experiment p 2746 N95-31068
A two-timescale approach to nonlinear Model Predictive Control
| DE95-000943 | p 2952 N95-31161
Theory & numerical methods for problems in shape reconstruction and large deviations
| AD-A292874 | p 2952 N95-31279
Global stabilization of nonlinear gyroscopic systems p 2881 N95-31836
Robust control: A structured approach to solve aircraft flight control problems p 2758 N95-31995
Model following control for tailoring handling qualities: ACT experience with ATTHeS p 2758 N95-32000

OPTIMIZATION
Three-D mesh optimization methods for unstructured polyhedra
| DE95-008808 | p 2955 N95-30471
A general inverse design procedure for aerodynamic bodies p 2750 N95-30497
Newton methods for large-scale linear inequality-constrained minimization: Optimization and systems theory
| PB95-210332 | p 2956 N95-30499
Speed control of an elastic two-mass system: Optimization and systems theory
| PB95-212106 | p 2888 N95-30701
Join processing in relational database systems p 3023 N95-30764
Robust position and force tracking control for a robot in contract p 2888 N95-30830
Robust fixed-structure control
| AD-A292883 | p 2952 N95-30961
Pseudo-time methods for constrained optimization problems governed by PDE
| NASA-CR-195081 | p 2959 N95-31120
Solderability enhancement of copper through chemical etching
| DE95-010514 | p 2806 N95-31406
The remainder form and the cord-slope form in global optimization with interval methods p 2941 N95-31533
Variational optimization in quantum field theory p 3020 N95-31646
Using case-based reasoning as a Reinforcement Learning framework for optimization with changing criteria
| AD-A293602 | p 2953 N95-31654
Optimization of an expander of a gas-dynamic trap
| DE95-614172 | p 3006 N95-31679
The design and development of a third generation OSEE instrument p 2781 N95-31800
Polarized proton beams
| DE95-010843 | p 2987 N95-32031
An efficient implementation of Forward-Backward Least-Mean-Square Adaptive Line Enhancers p 2855 N95-32224

OPTOELECTRONIC DEVICES
Opto-electronic components from non-stoichiometric 3-5 materials
| AD-A293206 | p 3013 N95-30985
Method and apparatus for non-destructively measuring local resistivity of semiconductors
| AD-D017436 | p 2862 N95-31343
Excited-state complexes of conjugated polymers
| AD-A292960 | p 2819 N95-31466
Degradation of blue AlGaN/InGaN/GaN LEDs subjected to high current pulses
| DE95-008824 | p 2863 N95-31611
Current trends in the packaging of photonic devices
| DE95-009583 | p 3001 N95-32064
A high-speed photonic clock and carrier regenerator p 2856 N95-32236
Fiber optic reference frequency distribution to remote beam waveguide antennas p 2972 N95-32346

ORBITAL ELEMENTS
Observations of accreting pulsars
| NASA-CR-198931 | p 3028 N95-30469
Assessment of the NASA orbital debris engineering model
| AD-A293350 | p 2766 N95-31143

ORBITAL MANEUVERS
A feedback linearization approach to orbital maneuvers p 2765 N95-30841

ORBITAL RENDEZVOUS
On-orbit truss structure tele-operation experiment by Engineering Test Satellite-7
| NAL-TR-1246 | p 2767 N95-31980

ORDER-DISORDER TRANSFORMATIONS
Structural investigation of xenon ion-beam-irradiated glassy carbon
| DE95-616777 | p 2977 N95-30474
New Fermi-liquid approach for the theory of disordered magnetics
| DE95-613448 | p 2967 N95-30739
Cascade damage in the ordered alloy Ni3Al
| DE95-009893 | p 2809 N95-32104
First-principles approaches to materials stability
| DE95-011533 | p 2810 N95-32283

ORDNANCE
Aerophysics test program 1
| AD-A293890 | p 2963 N95-31543

ORGANIC COMPOUNDS
Preparation of diisopropyl stibines and use thereof
| AD-D017419 | p 2771 N95-30418
Laboratory simulated hydrothermal alteration of sedimentary organic matter from Guaymas Basin, Gulf of California
| NASA-CR-198951 | p 2914 N95-30865
No-thermal plasma processing of VOCs and NO(x) at LLNL
| DE95-011445 | p 2911 N95-32281

ORGANIC MATERIALS
Standardization of (13)CO2 production procedure from organic matter for mass spectrometric analysis
| DE95-614629 | p 2791 N95-30420
Laboratory simulated hydrothermal alteration of sedimentary organic matter from Guaymas Basin, Gulf of California
| NASA-CR-198951 | p 2914 N95-30865
Molecular nanoclusters as precursors to conductive thin films and crystals
| AD-A290278 | p 3014 N95-31189

ORGANIC SEMICONDUCTORS
Magnetic resonance spectroscopy of fullerenes and (pi)-conjugated polymers
| DE95-010131 | p 2817 N95-31108

ORGANIZATIONS
Contribution of groupware to corporate communication: Towards the horizontal organization
| PB95-197661 | p 3022 N95-30453
An architectural approach to strategic information systems planning for the Office of Naval Intelligence
| AD-A289930 | p 3024 N95-30928
National Center for Manufacturing Sciences: Environmentally conscious manufacturing
p 2773 N95-31758
Federally funded R and D centers: Executive compensation at the Aerospace Corporation. Report to Congressional requestors
| GAO/NSIAD-95-75 | p 3022 N95-32213
The sociology of megaprogramming: Experiences in generating an organizational learning enterprise (Software Technology for Adaptable, Reliable Systems(STARS) program)
| AD-A292998 | p 2946 N95-32294
ORGANOMETALLIC COMPOUNDS
Ceramics derived from metal-organic precursors
| AD-A290791 | p 2811 N95-30405
ORIFICES
Investigation of cleanliness verification techniques for rocket engine hardware p 2770 N95-31806
ORION CONSTELLATION
A search for interstellar CH3D: Limits to the methane abundance in Orion-KL
| NASA-CR-198932 | p 3029 N95-30751
ORTHOGONAL FUNCTIONS
Nearly steady flows in GONG prototype data
| NASA-CR-198935 | p 2869 N95-30863
OSCILLATING FLOW
Dynamical systems as models for flow-induced vibrations
| PB95-206991 | p 2869 N95-30956
OSCILLATIONS
New material for high average power infrared generation: QPM-DB GaAs
| AD-A292714 | p 2967 N95-30939
Study of different type neutrino oscillations based on neutrino beams from 600 GeV
| DE95-619267 | p 2983 N95-31260
On possibility to study neutrino oscillations by detectors located at Gran Sasso (Italy) using beams from 600 GeV UNK-1 machine
| DE95-619268 | p 2983 N95-31261
Long baseline neutrino oscillation experiment at the AGS
| DE95-004378 | p 2986 N95-31702
OSCILLATORS
Elliptic deformed classical mechanics in three-dimensional phase space
| DE95-613384 | p 3017 N95-30365
Generalized deformed para-Bose oscillator and its coherent states
| DE95-613444 | p 2963 N95-30610
A high-speed photonic clock and carrier regenerator
p 2856 N95-32236
OSMIUM
An experimental search for high ZT semiconductors: A survey of the preparation and properties of several alloy systems
| DE95-010232 | p 2865 N95-32084
OUTGASSING
The Wide Field/Planetary Camera 2 (WFPC-2) molecular adsorber
| NASA-CR-198866 | p 2881 N95-31456
OXIDASE
Biosensors based on cross-linking of biotinylated Glucose Oxidase by avidin
| AD-A290439 | p 2925 N95-30452
OXIDATION
Observation of a low-binding-energy peak in the 2p core-level photoemission from oxidized Al(111)
| PB95-195350 | p 2802 N95-30534
Interface degradation in CAS/Nicalon during elevated temperature aging
| DE95-008843 | p 2812 N95-30543
High-temperature oxidation behavior of iridium-rhenium alloys
| NASA-TM-106720 | p 2803 N95-30593
A study of catalysts and mechanisms in synthesis reactions
| DE95-010177 | p 2793 N95-30766
The oxidation of carbon monoxide by nitrous oxide
p 2801 N95-31309
The oxidation of carbon monoxide by nitrogen dioxide
p 2801 N95-31310
Effects of molecular structure on the electroactive and optical properties of conjugated rigid-rod polybenzobisazoles
| AD-A292968 | p 2819 N95-31467
Processing and microstructural evolution of alumina/aluminum alloy and aluminum nitride/aluminum alloy composites by directed melt oxidation
p 2789 N95-31973
OXIDATION RESISTANCE
High temperature barrier coatings for refractory metals
| NASA-CR-195475 | p 2802 N95-30531
Evaluation of Environmentally Acceptable hydraulic fluids
| AD-A293037 | p 2821 N95-31666
OXIDE FILMS
Observation of a low-binding-energy peak in the 2p core-level photoemission from oxidized Al(111)
| PB95-195350 | p 2802 N95-30534
Plasma source ion implantation of metal ions: Synchronization of cathodic-arc plasma production and target bias pulses
| DE95-009431 | p 3006 N95-31613
Solution based temperature of Perovskite-type oxide films and powders
| DE95-009089 | p 2820 N95-31629
OXIDES
Electrochemical vapour deposition of SOFC interconnection materials
| PB95-197844 | p 2812 N95-30459
Chemical kinetics and photochemical data for use in stratospheric modeling: Evaluation number 11
| NASA-CR-198863 | p 2912 N95-30525
Low temperature synthesis of YBa2Cu3O(8-x) and other crystalline oxides
| AD-D017370 | p 3009 N95-30533
Structural, chemical and electronic properties of superconducting thin films and junctions
| AD-A292700 | p 3012 N95-30933
OXIDIZERS
Burn time measurements of single aluminum particles in steam and carbon dioxide mixtures
p 2799 N95-31198
Development of a new instrument for rocket engine combustion diagnostics p 2799 N95-31211
Advanced oxidizers diffusion flames structure
p 2801 N95-31307
OXYGEN
Power oscillator in the tokamaks training
| DE95-616538 | p 3003 N95-30473
STM studies of clean, CO- and O2-exposed Pt(100)-hex-R0.7 deg
| PB95-195376 | p 3009 N95-30535
Effect of oxygen and decompression bubbles on inert gas washout
| PB95-196556 | p 2925 N95-30665
Phase transformations in melt-spun Y-Ba-Cu-O bulk superconductor
| DE95-010237 | p 3011 N95-30667
Navier-Stokes flow field analysis of compressible flow in a high pressure safety relief valve
| NASA-TM-110640 | p 2868 N95-30862
Investigations of YBaCuO materials with near-room-temperature resistivity transitions
| AD-A293405 | p 3013 N95-31008
Burn time measurements of single aluminum particles in steam and carbon dioxide mixtures
p 2799 N95-31198
The structure and reactivity of boron and carbon surfaces
| AD-A292804 | p 2795 N95-31440
A microwave plasma cleaning apparatus
p 2779 N95-31786
OXYGEN ATOMS
The NASA/JPL Evaluation of Oxygen Interactions with Materials-3 (EOIM-3)
| NASA-CR-198865 | p 2796 N95-31660
Operation of the computer model for direct atomic oxygen exposure of Earth satellites
| NASA-CR-198188 | p 2767 N95-32189
OXYGEN IONS
Oxygen charge state abundance in the inner magnetosphere
| AD-A293497 | p 2915 N95-31536
DE-1 observations of polar O(+) stream bulk parameters and comparison with a model of the centrifugally-accelerated polar wind
| NASA-CR-198930 | p 2917 N95-31743
Recoil longitudinal momentum spectroscopy of electron capture from He by O(7+) and F(8+)
| DE95-010823 | p 2990 N95-32274
OXYGEN PLASMA
Process for producing hydrophilic polymer membranes
| AD-D017355 | p 2811 N95-30415
OXYGEN SUPPLY EQUIPMENT
Investigation of cleanliness verification techniques for rocket engine hardware p 2770 N95-31806
An overview of NASA testing requirements for alternate cleaning solvents used in liquid and gaseous oxygen environments p 2783 N95-31813
OXYNITRIDES
Ionic conductivities of lithium phosphorus oxynitride glasses, polycrystals, and thin films
| DE95-008898 | p 2812 N95-30545
OZONE DEPLETION
Aerospace Environmental Technology Conference: Exectutive summary
| NASA-CP-3297 | p 2771 N95-31350
Atmospheric environmental implications of propulsion systems p 2771 N95-31747
Manufacturing waste disposal practices of the chemical propulsion industry p 2771 N95-31748
Alternatives to ozone depleting refrigerants in test equipment p 2775 N95-31767
F-200(TM): The new solution for fire protection
p 2776 N95-31770
Aqueous cleaning design presentation
p 2778 N95-31781
The effect of environmental initiatives on NASA specifications and standards activities
p 2783 N95-31812
OZONOSPHERE
Chemical kinetics and photochemical data for use in stratospheric modeling: Evaluation number 11
| NASA-CR-198863 | p 2912 N95-30525

P

P WAVES
Hadronic production of S-wave and P-wave charmed beauty mesons via heavy quark fragmentation
| DE95-008737 | p 2977 N95-30465
P-N JUNCTIONS
The junction characteristics and current conduction mechanisms of GaInP2 n(+)p diodes and solar cells
| AD-A290857 | p 2902 N95-30408
Spectral response of a polycrystalline silicon solar cell
| DE95-614370 | p 2903 N95-30723
InP solar cell development on inexpensive Si substrates
| AD-A293255 | p 2903 N95-30893
P-TYPE SEMICONDUCTORS
Optimization of a thermoelectric IR-detector for low working temperature
| NASA-CR-198933 | p 2880 N95-30752
PACIFIC ISLANDS
Seismic studies of subducted lithosphere
p 2915 N95-31335
PACIFIC OCEAN
Aerosol measurements over the Pacific Ocean in support of the IR aerosol backscatter program
| NASA-CR-198925 | p 2918 N95-30782
QTSAW (Quick Typhoon Surge and Waves). Wave information studies of US coastlines
| AD-A293172 | p 2919 N95-30976
The impact of microbiologically influenced corrosion on protective polymer coatings
| AD-A288696 | p 2816 N95-30997
PACKAGING
Current trends in the packaging of photonic devices
| DE95-009583 | p 3001 N95-32064
PACKET SWITCHING
Information Switching Processor (ISP) contention analysis and control
| NASA-CR-195471 | p 2765 N95-31849
PACKETS (COMMUNICATION)
Information Switching Processor (ISP) contention analysis and control
| NASA-CR-195471 | p 2765 N95-31849
PAIN
Use of body surface heat patterns for predicting and evaluating acute lower extremity pain among soldiers
| AD-A292829 | p 2927 N95-31446
PAINTS
Demonstration of split-flow ventilation and recirculation as flow-reduction methods in an Air Force paint spray booth, volume 2
| AD-A286808 | p 2762 N95-30926
Demonstration of split-flow ventilation and recirculation as flow-reduction methods in an Air Force paint spray booth, volume 1
| AD-A286807 | p 2763 N95-31101
A comparison of coating alternatives for US Coast Guard aircraft
| AD-A293270 | p 2817 N95-31124
Air pollution control system research: An iterative approach to developing affordable systems
p 2773 N95-31759
Cadmium plating replacements p 2776 N95-31773
Replacement of corrosion protection chromate primers and paints used in cryogenic applications on the Space Shuttle with wire arc sprayed aluminum coatings
p 2776 N95-31774
Bicarbonate of soda paint stripping process validation and material characterization p 2777 N95-31778

Ultra-high pressure water jetting for coating removal and surface preparation p 2778 N95-31780
A centrifuge CO2 pellet cleaning system p 2778 N95-31784
Environmentally Safe and Effective Processes for Paint Removal
| AGARD-LS-201 | p 2843 N95-32165
Overview of paint removal methods p 2843 N95-32166
Paint removal principles p 2843 N95-32167
Background to plastic media blasting p 2843 N95-32168
Dry media blasting with wheat starch p 2843 N95-32169
Water blasting paint removal methods p 2843 N95-32170
Paint removal and surface cleaning using ice particles p 2844 N95-32171
Stripping with dry ice p 2844 N95-32172
Aquastrip p 2844 N95-32173
Stripping by laser p 2844 N95-32174
Selective chemical stripping p 2844 N95-32175
Treatment of plastic media waste p 2844 N95-32177
Bioremediation of wheat starch media waste p 2845 N95-32178
Operational parameters and material effects p 2845 N95-32179
Process evaluation p 2845 N95-32180
Standardization work p 2845 N95-32181

PAIR PRODUCTION
Complex conjugate pairs in stationary Sturmians
| DE95-616279 | p 2976 N95-30429
Signatures of virtual LSP's at the TEVATRON
| DE95-613798 | p 2982 N95-31060
Pion-pair production by two photons
| DE95-737162 | p 2983 N95-31223

PANELS
Design of fibre reinforced composite panels for aerospace applications
| PB95-197851 | p 2784 N95-30460
Verification of surface preparation for adhesive bonding p 2782 N95-31807

PAPER (MATERIAL)
Effect of local melting on tribology in metal cutting
| PB95-195392 | p 2804 N95-31052

PARABOLIC REFLECTORS
Validation of the FLAGSOL parabolic trough solar power plant performance model
| DE95-000263 | p 2903 N95-30887

PARACHUTE FABRICS
High strain-rate testing of parachute materials
| DE95-009577 | p 2897 N95-31614

PARACHUTES
High strain-rate testing of parachute materials
| DE95-009577 | p 2897 N95-31614

PARALLEL COMPUTERS
Recommendations for developing portable parallel I/O facilities for scientific applications
| DE95-009384 | p 2947 N95-30578
An executable specification for the message processor in a simple combining network
| NASA-CR-198174 | p 2933 N95-30584
France --- modeling and verification of parallel computer systems
| PB95-208385 | p 2949 N95-32371

PARALLEL PROCESSING (COMPUTERS)
Extending a multi-set relational algebra to a parallel environment
| PB95-207106 | p 3023 N95-30566
Supporting data intensive applications with medium grained parallelism
| DE95-010164 | p 3023 N95-30619
Algorithm comparison and benchmarking using a parallel spectra transform shallow water model
| DE95-009124 | p 2913 N95-30683
Advanced computational research in materials processing for design and manufacturing
| DE95-009130 | p 2838 N95-30684
Three-dimensional (3D) large fluid flow computations for US Army applications on KSR-1, CM-200, CM-5, and Cray C-90
| AD-A293125 | p 2869 N95-30689
Algorithms for categorizing multiprocessor communication under invalidate and update-based coherence protocols
| AD-A290022 | p 2947 N95-30930
A scalable parallel Strassen's matrix multiply algorithm for distributed memory computers
| DE95-010213 | p 2936 N95-31109
Shear-free turbulent boundary layers p 2873 N95-31349
Integrated high performance distributed system
| AD-A292821 | p 2947 N95-31445
A two-dimensional finite difference algorithm on the KSR1
| AD-A293576 | p 2941 N95-31594
A microeconomic scheduler for parallel computers
| NASA-CR-198153 | p 2932 N95-32046
Computational methods and software systems for dynamics and control of large space structures
| NASA-CR-199036 | p 2767 N95-32204
A transient FETI methodology for large-scale parallel implicit computations in structural mechanics
| NASA-CR-199040 | p 2945 N95-32214
Implementation and performance of the pseudoknot problem in Sisal
| DE95-009573 | p 2925 N95-32358
France --- modeling and verification of parallel computer systems
| PB95-208385 | p 2949 N95-32371

PARALLEL PROGRAMMING
Recommendations for developing portable parallel I/O facilities for scientific applications
| DE95-009384 | p 2947 N95-30578
Universal message passing library, or how to writea truly portable code for parallel computers
| PB95-212221 | p 2948 N95-32255

PARAMETER IDENTIFICATION
Advanced system identification techniques for wind turbine structures
| DE95-004049 | p 2902 N95-30505
New adaptive methods for reconfigurable flight control systems, appendix 1
| AD-A292711 | p 2756 N95-30937
Failure analysis of a repairable system: The case study of a cam-driven reciprocating pump
| AD-A293144 | p 2889 N95-30949
Handling qualities analysis on rate limiting elements in flight control systems p 2746 N95-31071

PARAMETERIZATION
Good metric spaces without good parameterizations
| PB95-208427 | p 2957 N95-30622

PARASITES
HTS Josephson technology on silicon with application to high speed digital microelectronics
| AD-A288627 | p 2861 N95-31147

PARASITIC DISEASES
Services to develop, standardize, and validate Polymerase Chain Reaction (PCR) protocols for the detection of leishmaniasis in clinical samples
| AD-A290155 | p 2817 N95-31115

PARSING ALGORITHMS
Unification of LARCH and Z-based object models to support algebraically-based design refinement: The LARCH perspective
| AD-A289235 | p 2935 N95-30999

PARTIAL DIFFERENTIAL EQUATIONS
Gibbs measures and quasi-periodic solutions for nonlinear Hamiltonian partial differential equations
| PB95-207932 | p 2956 N95-30506
Quasi-periodic solutions of Hamiltonian perturbations of 2D linear Schroedinger equations
| PB95-208443 | p 2957 N95-30624
Use of element-by-element preconditioners to solve large scale partially separable optimization problems
| PB95-195772 | p 2957 N95-30692
Pseudo-time methods for constrained optimization problems governed by PDE
| NASA-CR-195081 | p 2959 N95-31120
Numerical stability investigations of processes for solving linear initial value problems
| PB95-207023 | p 2959 N95-31183
Self-adaptive multilevel methods for fluid flow problems p 2873 N95-31412
Some aspects on the modelling of non-Newtonian fluid flow
| TRITA-NA-9317 | p 2873 N95-31415
Quasi-Newton updating for large scale nonlinear systems
| AD-A292776 | p 2940 N95-31431
Derivation of two-dimensional (2-D) conduction equation in generalized coordinates with constant and anisotropic physical properties
| AD-A293896 | p 3020 N95-31511

PARTICLE ACCELERATION
Studying the thermal/non-thermal crossover in solar flares
| NASA-CR-189436 | p 3031 N95-30785

PARTICLE ACCELERATOR TARGETS
Target diagnostics for intense lithium ion hohlraum experiments on PBFA 2
| DE95-008517 | p 3006 N95-31626

PARTICLE ACCELERATORS
Minijet veto: A tool for the heavy Higgs search at the LHC
| PB95-196234 | p 2979 N95-30695
The Los Alamos accelerator code group
| DE95-010989 | p 2992 N95-31151
The coupling impedance of a toroidal beam pipe with circular cross section
| DE95-010442 | p 2993 N95-31405
Target diagnostics for intense lithium ion hohlraum experiments on PBFA 2
| DE95-008517 | p 3006 N95-31626
A study of ion trapping and instability in the Fermilab antiproton accumulator p 2993 N95-31647
KRAKEN, a numerical model of RHIC impedances
| DE95-011563 | p 2994 N95-32242
Normal mode tunes for linear coupled motion in six dimensional phase space
| DE95-011565 | p 2994 N95-32244
Design study of prototype accelerator and MeV test facility for demonstration of 1 MeV, 1 A negative ion beam production
| DE95-737208 | p 2995 N95-32262

PARTICLE BEAMS
Target diagnostics for intense lithium ion hohlraum experiments on PBFA 2
| DE95-008517 | p 3006 N95-31626
Radial mode evolution in longitudinal bunched beam instability
| DE95-010895 | p 2994 N95-32092
Validity of the differential equations for ionization cooling
| DE95-010438 | p 2989 N95-32160
Review of longitudinal perturbation formalism
| DE95-010894 | p 2990 N95-32278
Tune modulation due to synchrotron oscillations and chromaticity, and the dynamic aperture
| DE95-011566 | p 2995 N95-32297

PARTICLE COLLISIONS
The mechanism of particle production process in hadron-nucleon collisions
| DE95-613727 | p 2975 N95-30372
On perturbative asymptotic of Regge trajectories
| DE95-613585 | p 3018 N95-30636
WW and WZ production at the tevatron
| DE95-011014 | p 2981 N95-30970
Spin momentum correlation (handedness) in the process of four pion production in the electron-positron collisions
| DE95-613690 | p 2988 N95-32093
Radiative corrections to the three quantum annihilation cross section in high energy electron-positron collisions
| DE95-623675 | p 2995 N95-32296

PARTICLE DECAY
The search for the decay of Z boson into two gamma as a test of Bose statistics
| DE95-616373 | p 2976 N95-30393
Confronting left-right symmetric models with electroweak precision data at the Z peak
| PB95-208054 | p 2977 N95-30484
New tensor interactions in micron-decay
| DE95-613760 | p 2978 N95-30528
Minijet veto: A tool for the heavy Higgs search at the LHC
| PB95-196234 | p 2979 N95-30695
Instantaneous chiral quark model for relativistic mesons in a hot and dense medium
| DE95-613782 | p 2980 N95-30911
Signatures of virtual LSP's at the TEVATRON
| DE95-613798 | p 2982 N95-31060
B(sub c)-meson production in hadron-hadron collisions
| DE95-620537 | p 2983 N95-31217
Do the narrow cryptoexotic baryon resonances exist?
| DE95-619291 | p 2984 N95-31378
Structure formation with majoron supermultiplet
| DE95-613596 | p 2984 N95-31546
Studies of the strong and electroweak interactions at the Z(sub 0) pole
| DE95-010353 | p 2986 N95-31682
Monte Carlo simulations of muon production
| DE95-009554 | p 2988 N95-32063
A search for jet handedness in hadronic Z-0 decays
| DE95-010099 | p 2988 N95-32083
A measurement of quark and gluon jet differences at the Z(sup 0) resonance
| DE95-010666 | p 2989 N95-32266
An experimental study of QCD and jets in e(+)e(-) annihilation
| DE95-010667 | p 2989 N95-32267

PARTICLE ENERGY
Beam-beam effects
| DE95-008443 | p 2991 N95-30360
Lower hybrid accessibility in a large, hot reversed field pinch
| DE95-011001 | p 3007 N95-32310

PARTICLE IMAGE VELOCIMETRY
The study of flame-vortex interactions using a particle image velocimeter p 2796 N95-31709

PARTICLE INTERACTIONS
On the string equation at c=1
| DE95-737161 | p 3014 N95-31222
Pion-pair production by two photons
| DE95-737162 | p 2983 N95-31223

The topological string associated with a simple singularity of type D
[DE95-737229] p 2983 N95-31225
Global aspects of the WZNW reduction to Toda theories
[DE95-737230] p 3019 N95-31226
Instanton - antiinstanton interaction and asymptotics of perturbation theory expansion of in double well oscillator
[DE95-619245] p 2986 N95-31259

PARTICLE MASS
Effective Lagrangian approach to the fermion mass problem
[DE95-616316] p 2976 N95-30443
Top quark and Higgs boson masses from wormhole physics
[DE95-616384] p 2978 N95-30580
Electromagnetic hadron mass differences and estimation of isotopic symmetry violation parameters of QCD vacuum from quark model
[DE95-613628] p 2985 N95-31621
Renormalization group analyses of particle masses in full four-generation fermion condensate scheme
[DE95-613595] p 2988 N95-32070
Applications of chiral symmetry
[DE95-009552] p 2988 N95-32079
Charm photoproduction dynamics
[DE95-009106] p 2990 N95-32303
Thermal rho's in the quark-gluon plasma
[DE95-009543] p 3008 N95-32357

PARTICLE MOTION
Particle filtration: A comparison between theory and experiment
[DE95-009442] p 2875 N95-31637

PARTICLE PRODUCTION
The mechanism of particle production process in hadron-nucleon collisions
[DE95-613727] p 2975 N95-30372
Current issues in perturbative QCD
[DE95-008448] p 2975 N95-30388
Hadronic production of S-wave and P-wave charmed beauty mesons via heavy quark fragmentation
[DE95-008737] p 2977 N95-30465
Experimental results on charge exchange reactions with delta excitations and polarization studies of delta and N(sup *) (1440) resonances
[DE95-614022] p 2981 N95-30913
WW and WZ production at the tevatron
[DE95-011014] p 2981 N95-30970
Signatures of virtual LSP's at the TEVATRON
[DE95-613798] p 2982 N95-31060
Period doubling dynamics in hadron physics: Exact calculations
[DE95-620535] p 2982 N95-31215
B(sub c)-meson production in hadron-hadron collisions
[DE95-620537] p 2983 N95-31217
Double charmed baryons production at B-factory
[DE95-620540] p 2983 N95-31219
Do the narrow cryptoexotic baryon resonances exist?
[DE95-619291] p 2984 N95-31378
Search for exotic baryons with the SPHINX facility
[DE95-613774] p 2984 N95-31549
A search for millicharged particles at SLAC
[DE95-010694] p 2987 N95-32026
Physics goals of a mu(+) mu(-) collider
[DE95-009546] p 2994 N95-32059
Monte Carlo simulations of muon production
[DE95-009554] p 2988 N95-32063
Spin momentum correlation (handedness) in the process of four pion production in the electron-positron collisions
[DE95-613690] p 2988 N95-32093
On the search for exotic hadrons in the experiments with high energy hyperon beam
[DE95-620534] p 2989 N95-32261
A measurement of quark and gluon jet differences at the Z(sup 0) resonance
[DE95-010666] p 2989 N95-32266
Charm photoproduction dynamics
[DE95-009106] p 2990 N95-32303
On hadronic production of the B(sub c) meson
[DE95-613726] p 2991 N95-32304

PARTICLE SIZE DISTRIBUTION
The Al and Al2O3 droplet cloud in solid rocket motors p 2770 N95-31196
Model for defining propellant burn rate performance boundaries p 2800 N95-31290
Particle filtration: A comparison between theory and experiment
[DE95-009442] p 2875 N95-31637

PARTICLE SPIN
The search for the decay of Z boson into two gamma as a test of Bose statistics
[DE95-616373] p 2976 N95-30393
Multi-particle correlations in quaternionic quantum systems
[DE95-616271] p 3018 N95-30424
Plaquette expansion proof and interpretation
[DE95-616282] p 2965 N95-30432
Application of spin-sensitive electron spectroscopies to investigations of electronic and magnetic properties of solid surfaces and epitaxial systems
[DE95-010154] p 2792 N95-30614
Effective chiral-spin Hamiltonian for odd-numbered coupled Heisenberg chains
[DE95-614445] p 2982 N95-31168

PARTICLE THEORY
Possible reason why leptons are lighter than quarks
[DE95-616383] p 2978 N95-30579
The activities of the high energy physics program
[DE95-010155] p 2991 N95-30615
Abstracts of Annual Physics Conference of Iran
[DE95-611717] p 2768 N95-30881
Structure formation with majoron supermultiplet
[DE95-613596] p 2984 N95-31546

PARTICLE TRAJECTORIES
On perturbative asymptotic of Regge trajectories
[DE95-613585] p 3018 N95-30636

PARTICLES
On the interactions between particles and turbulence in a fully-developed channel flow in air p 2875 N95-31707

PARTICULATE SAMPLING
Novel mass spectrometric instrument for gaseous and particulate characterization and monitoring
[DE95-000047] p 2881 N95-31694

PARTICULATES
Hydrogen sulfide analyzer with protective barrier
[AD-D017412] p 2793 N95-31009
Preventing cracking of anodized coatings
[NASA-TM-104622] p 2839 N95-31690
Particulate air pollution and increased mortality: Biological plausibility for causal relationship
[DE95-006161] p 2909 N95-31703

PARTONS
Minijet veto: A tool for the heavy Higgs search at the LHC
[PB95-196234] p 2979 N95-30695
Partons and black holes
[DE95-009921] p 3029 N95-31102
Hadronic production of B(sub c)-mesons
[DE95-620536] p 2983 N95-31216

PASSAGEWAYS
Aircraft evacuations through Type-3 exits I: Effects of seat placement at the exit
[DOT/FAA/AM-95/22] p 2748 N95-31845

PASSENGER AIRCRAFT
Special investigation report: Safety of the air tour industry in the United States
[PB95-917004] p 2748 N95-32185

PASSIVITY
Hydrogen diffusion and passivation in InGaAlN alloys
[DE95-010889] p 2806 N95-31150

PATCH TESTS
The individual element test revisited
[NASA-CR-199039] p 2945 N95-32215

PATIENTS
Patient/aircraft forecasting for the strategic aeromedical evacuation lift-bed process
[AD-A293902] p 2747 N95-31512

PATROLS
Objective analysis of oceanic data for Coast Guard trajectory models
[AD-A292884] p 2924 N95-32363

PATTERN RECOGNITION
Selecting optimal experiments for feedforward multilayer perceptrons
[AD-A290856] p 2949 N95-30406
Computer vision for detecting and quantifying gamma-ray sources in coded-aperture images
[DE95-008810] p 2900 N95-30472
Unconventional imaging field experiment plan
[AD-A291492] p 2846 N95-30562
Feature-based modeling of product families
[PB95-207148] p 2933 N95-30568
Noisy-network acceptors
[PB95-197976] p 2951 N95-30813
Neurodynamical systems for cognition and target identification
[AD-A293111] p 2951 N95-30884
Neural network false alarm filter, volume 2
[AD-A293114] p 2860 N95-30886
Machine learning for a toolkit for image mining
[AD-A293137] p 2951 N95-30890
Nonparametric recognition of nonrigid motion
[AD-A293630] p 2963 N95-31565
Optical correlator optimizations and extensions for automated optical target recognition
[AD-A293013] p 3000 N95-31697
Artificial neural networks and model-based recognition of 3-D objects from 2-D images p 2954 N95-31838
PADO: Learning tree structured algorithms for orchestration into an object recognition system
[AD-A293109] p 2943 N95-32020

PATTERN REGISTRATION
Navier-Stokes flow field analysis of compressible flow in a high pressure safety relief valve
[NASA-TM-110640] p 2868 N95-30862

PAVEMENTS
Impact behavior of the active zone within a frozen soil profile
[AD-A292909] p 2915 N95-31386
Evaluation of alternative pavement marking materials
[AD-A292973] p 2763 N95-31468

PAYLOAD DELIVERY (STS)
STS-70 flight: Day 1
[NASA-TM-110659] p 2765 N95-30880

PAYLOADS
The High Altitude Balloon Experiment demonstration of acquisition, tracking, and pointing technologies (HABE-ATP) p 2841 N95-32132

PEARLITE
A study of Damascus steel
[DE95-010127] p 2809 N95-32023

PECLET NUMBER
Heat transfer in shear-free turbulent boundary layers p 2876 N95-31708

PENDULUMS
Dynamical systems as models for flow-induced vibrations
[PB95-206991] p 2869 N95-30956

PENETRATION
HTS Josephson technology on silicon with application to high speed digital microelectronics
[AD-A288627] p 2861 N95-31147
Comparisons of target detection clutter using data from the 1993 FOPEN experiments
[AD-A293052] p 2852 N95-31606

PERFLUORO COMPOUNDS
Enhancement of perfluoropolyether boundary lubrication performance: I. Preliminary results
[NASA-TM-106937] p 2813 N95-30621
Evaluation of halon alternatives in inerting experiments
[AD-A293774] p 2795 N95-31580

PERFORMANCE PREDICTION
Generation of earthquake signals
[PB95-211223] p 2913 N95-30631
Validation of the FLAGSOL parabolic trough solar power plant performance model
[DE95-000263] p 2903 N95-30887
Probabilistic reliability modeling of fatigue on the H-46 tie bar
[AD-A289926] p 2751 N95-30927
Performance evaluation of high-temperature superconducting current leads for micro-SMES systems
[DE95-005843] p 2861 N95-30943
Hot jet/wake turbulent structure and laser propagation. Part 3: Laser propagation measurements and modeling p 2871 N95-30992
Life prediction methodology for ceramic components of advanced heat engines: Phase 1. Volume 1
[DE95-010805] p 2817 N95-31135
Life prediction methodology for ceramic components of advanced heat engines. Phase 1: Volume 2. Appendices
[DE95-010806] p 2817 N95-31136
Centrifugal and axial pump design and off-design performance prediction p 2830 N95-31289
Experiment of rocket-ram combined combustor
[NAL-TR-1249] p 2769 N95-31739
Evaluation of static strength of T800H/PMR-15 carbon/polyimide laminates at room temperature and 300 C
[NAL-TR-1254] p 2789 N95-31740
The application of noncoherent Doppler data types for Deep Space Navigation p 2765 N95-32226

PERFORMANCE TESTS
Integrated X-ray testing of the electro-optical breadboard model for the XMM reflection grating spectrometer
[DE95-008829] p 2879 N95-30507
Results from tests of the Honeywell integrated flight management unit
[PB95-211355] p 2748 N95-30597
FOG --- evaluation test of a fiber optic gyroscope (FOG)
[PB95-211546] p 2879 N95-30600
A novel instrumentation system for measurement of helicopter rotor motions and loads data, phase 1
[AD-A293309] p 2751 N95-30923
On the use of electronic tilt sensors as angle encoders for synchrotron applications
[DE95-005836] p 2880 N95-30941
10 kW heat pipe-heat sink development
[AD-A293167] p 2870 N95-30965
Construction and performance measurement of a portable thermoacoustic refrigerator demonstration apparatus
[AD-A293265] p 2839 N95-31122

Advanced small rocket chambers. Option 3: 110 1bf Ir-Re rocket, volume 1
| NASA-CR-195435-VOL-1 | p 2768 N95-31169
Advanced small rocket chambers. Option 3: 110 1bf Ir-Re rocket, volume 2
| NASA-CR-195435-VOL-2 | p 2769 N95-31170
Investigation of ram accelerator performance capabilities p 2799 N95-31204
Pressure transducer performance and measurement trade-offs in a transient, high temperature, combustion environment p 2799 N95-31209
Natural gas liquefier for vehicle fuel
| AD-A293619 | p 2836 N95-31564
Alternatives to ozone depleting refrigerants in test equipment p 2775 N95-31767
Environmentally safe aviation fuels p 2775 N95-31768
Cadmium plating replacements p 2776 N95-31773
Ultrasonic frequency selection for aqueous fine cleaning p 2779 N95-31788
A design of experiments test to define critical spray cleaning parameters for Brulin 815 GD and Jettacin cleaners p 2779 N95-31790
Environmentally compatible hand wipe cleaning solvents p 2780 N95-31795
Surface inspection using FTIR spectroscopy p 2782 N95-31803
Cleaning verification by air/water impingement p 2782 N95-31805
An overview of NASA testing requirements for alternate cleaning solvents used in liquid and gaseous oxygen environments p 2783 N95-31813
Report to the Chairman, Legislation and National Security Subcommittee, Committee on Government Operations, House of Representatives. Unmanned aerial vehicles: Performance of short-range system still in question
| GAO/NSIAD-94-65 | p 2752 N95-32196
Assessment of computer aids during communication exercise 1991
| PB95-211462 | p 2945 N95-32248
Thermoplastic elastomers as a binder in composite propellants
| PB95-211553 | p 2837 N95-32249
A globally efficient means of distributing UTC time and frequency through GPS p 2970 N95-32335
SVN 9 End-Of-Life testing p 2767 N95-32345
Fiber optic reference frequency distribution to remote beam waveguide antennas p 2972 N95-32346

PERIOD DOUBLING
Multisite antiferromagnetic Ising spin model: Phase transition through doubling bifurcation
| DE95-614311 | p 3011 N95-30722
Period doubling dynamics in hadron physics: Exact calculations
| DE95-620535 | p 2982 N95-31215

PERIODIC VARIATIONS
Large scale periodicity of the universe and baryogenesis
| DE95-613461 | p 3028 N95-30366
On reflection of Alfven waves in the solar wind
| NASA-TM-110642 | p 3031 N95-30582
Acoustomagnetoelectric effect in a superlattice
| DE95-613445 | p 3011 N95-30736

PERMAFROST
Impact behavior of the active zone within a frozen soil profile
| AD-A292909 | p 2915 N95-31386

PERMANENT MAGNETS
Active turbulence control using microelectrodes, permanent magnets in microgrooves
| AD-D017351 | p 2867 N95-30553
A metallurgical approach toward alloying in rare earth permanent magnet systems
| DE95-010242 | p 2966 N95-30668

PERMEABILITY
Membrane transport: A cellular probe of heat stroke
| AD-A293327 | p 2926 N95-30924
Extension of the pore tree model to describe pore interconnectivity
| AD-A290366 | p 2793 N95-30971

PERMITTIVITY
Dielectric property measurement of zirconia fibers at high temperatures
| DE95-010991 | p 2821 N95-31705

PERMUTATIONS
Size of Fulton's essential set
| PB95-211645 | p 2955 N95-30477
Combination of Fulton's essential set
| PB95-211637 | p 2956 N95-30500

PEROVSKITES
Orientation of rapid thermally annealed lead zirconate titanate thin films on (111) Pt substrate
| DE95-615232 | p 2811 N95-30422
Deposition and characterization of photoconductive PZT thin films
| ATR-93(8308)-7 | p 2819 N95-31417
The pyrochlore-to-perovskite transformation in solution-derived lead zirconate titanate thin films
| DE95-010453 | p 2822 N95-32161

PERSONAL COMPUTERS
UNIX and PC security in a network environment. UNINETT
| PB95-196291 | p 2934 N95-30662
UNIX and PC security in a network environment. LOKALNETT 1993
| PB95-196309 | p 2934 N95-30697

PERSONNEL MANAGEMENT
The development of KAERI management information system 2: The development of Time Sheet Management System
| DE95-613355 | p 3024 N95-30883
Application of a genetic algorithm to optimize staffing levels in software development
| AD-A293725 | p 2943 N95-31835

PERTURBATION
Large scale periodicity of the universe and baryogenesis
| DE95-613461 | p 3028 N95-30366
Gravitational-radiation damping of compact binary systems to second post-Newtonian order
| PB95-207882 | p 2912 N95-30588
Removal of the Energy Dependence from the Resolvent Like Energy Dependent Interactions
| DE95-613385 | p 2961 N95-31619
Combustion response to acoustic perturbation in liquid rocket engines p 2770 N95-31972

PERTURBATION THEORY
Current issues in perturbative QCD
| DE95-008448 | p 2975 N95-30388
Quasi-periodic solutions of Hamiltonian perturbations of 2D linear Schroedinger equations
| PB95-208443 | p 2957 N95-30624
The iteration formula of the Maslov-type index theory with applications to nonlinear Hamiltonian systems
| DE95-613379 | p 2957 N95-30676
Solvability of a class of hypersingular nonlinear integral equations
| PB95-207031 | p 3011 N95-30720
Effective chiral-spin Hamiltonian for odd-numbered coupled Heisenberg chains
| DE95-614445 | p 2982 N95-31168
Hadronic production of B(sub c)-mesons
| DE95-620536 | p 2983 N95-31216
Instanton - antiinstanton interaction and asymptotics of perturbation theory expansion of in double well oscillator
| DE95-619245 | p 2966 N95-31259
Instability of weakly nonlinear chaotic structures
| DE95-613441 | p 2966 N95-32066
Renormalization group analyses of particle masses in full four-generation fermion condensate scheme
| DE95-613595 | p 2988 N95-32070
Review of longitudinal perturbation formalism
| DE95-010894 | p 2990 N95-32278

PETROLEUM PRODUCTS
Determination of halogens in a petroleum product by ion chromatography
| DE95-002056 | p 2797 N95-31840

PH
On-line surfactant monitoring
| DE95-009417 | p 2792 N95-30735

PHASE CONJUGATION
Picosecond phase conjugation: New applications, devices, and materials
| AD-A293195 | p 3013 N95-30982
Photorefractive nonlinear optics
| AD-A292913 | p 2999 N95-31458

PHASE DIAGRAMS
The neutron powder diffraction and acoustic investigations of the NH4SCN phase diagram
| DE95-614372 | p 3009 N95-30419
Phase transformations in melt-spun Y-Ba-Cu-O bulk superconductor
| DE95-010237 | p 3011 N95-30667
A proposed phase equilibrium diagram for Pt-Zr system
| DE95-620904 | p 2806 N95-31220

PHASE LOCKED SYSTEMS
Harmonic gyrotron amplifiers and phase-locked oscillators
| AD-A293185 | p 2861 N95-30979

PHASE MODULATION
Demodulators for optical fiber interferometers with (3 x 3) outputs
| AD-D017415 | p 2995 N95-30402
Computer simulation results for PCM/PM/NRZ receivers in nonideal channels p 2765 N95-32225

PHASE SHIFT
Microwave repeater with broadband active and/or passive isolation control
| AD-D017358 | p 2846 N95-30417
Interferometry with particles of non-zero rest mass: Topological experiments
| DE95-616244 | p 2979 N95-30689
Detection of the phase shift which accompanies the excitation of an atomic beam by N. F. Ramsey's method
| IFTR-5/1995 | p 2986 N95-31818
Satellite test of the isotropy of the one-way spe ed of light using ExTRAS p 2973 N95-32349

PHASE SHIFT KEYING
Rate considerations in deep space telemetry p 2765 N95-32223
Fast identification of some typical digital modulation schemes
| PB95-211454 | p 2857 N95-32247

PHASE STABILITY (MATERIALS)
First-principles approaches to materials stability
| DE95-011533 | p 2810 N95-32283

PHASE TRANSFORMATIONS
The neutron powder diffraction and acoustic investigations of the NH4SCN phase diagram
| DE95-614372 | p 3009 N95-30419
Real Higgs singlet and electroweak phase transition in the standard model
| DE95-616315 | p 2976 N95-30442
Theoretical high energy physics
| DE95-003107 | p 2991 N95-30527
Modeling of thermal, electronic, hydrodynamic, and dynamic deposition processes for pulsed-laser deposition of thin films
| DE95-008906 | p 2813 N95-30572
Phase transformations in melt-spun Y-Ba-Cu-O bulk superconductor
| DE95-010237 | p 3011 N95-30667
Multisite antiferromagnetic Ising spin model: Phase transition through doubling bifurcation
| DE95-614311 | p 3011 N95-30722
Fundamental topics in heat transfer through deformable two-phase media p 2874 N95-31532
The pyrochlore-to-perovskite transformation in solution-derived lead zirconate titanate thin films
| DE95-010453 | p 2822 N95-32161
First-principles approaches to materials stability
| DE95-011533 | p 2810 N95-32283
Thermal rho's in the quark-gluon plasma
| DE95-009543 | p 3008 N95-32357
Phase transitions and gravitational collapse
| DE95-011732 | p 3021 N95-32359

PHASE VELOCITY
Dissolution of eutectic microstructures
| DE95-010244 | p 2804 N95-30757
Vertical transport in GaAs/AlGaAs superlattices p 3012 N95-30822
Ultrasonic characterization of fiber-matrix interphasial properties and damage in high-temperature composites p 2785 N95-30823

PHASE-SPACE INTEGRAL
Covariant phase space formulations of superparticles and supersymmetric WZW models
| DE95-616278 | p 2964 N95-30428

PHENOMENOLOGY
Phenomenology of the two Higgs doublet sector of a quark-lepton symmetric model
| DE95-616337 | p 2976 N95-30446

PHOSPHATES
Laser properties of Yb(3+)-doped Sr5(PO4)3F crystals
| DE95-010686 | p 3016 N95-32268

PHOSPHORS
Low-voltage cathodoluminescence of europium-activated yttrium orthovanadate
| DE95-008536 | p 3008 N95-30382

PHOSPHORUS
Ionic conductivities of lithium phosphorus oxynitride glasses, polycrystals, and thin films
| DE95-008898 | p 2812 N95-30545

PHOTOCHEMICAL REACTIONS
Chemical kinetics and photochemical data for use in stratospheric modeling: Evaluation number 11
| NASA-CR-198863 | p 2912 N95-30525
Photochemistry of intermolecular C-H bond activation reactions
| DE95-008991 | p 2978 N95-30574

PHOTOCONDUCTIVE CELLS
Self-consistent, 2D simulations of filament propagation in photoconducting switches
| DE95-010794 | p 2861 N95-31133

PHOTOCONDUCTIVITY
Photophysical properties of opto-electric molecules studied by time-resolved microwave conductivity
| PB95-196994 | p 2980 N95-30774

Self-consistent, 2D simulations of filament propagation in photoconducting switches
| DE95-010794 | p 2861 N95-31133
Deposition and characterization of photoconductive PZT thin films
| ATR-93(8308)-7 | p 2819 N95-31417
Contactless characterization of semiconductors using laser-induced surface photo-charge voltage measurements
| AD-A293618 | p 2863 N95-31725

PHOTOCONDUCTORS
High aspect ratio metal microstructures and method for preparing the same
| AD-D017463 | p 2803 N95-30750
Deposition and characterization of photoconductive PZT thin films
| ATR-93(8308)-7 | p 2819 N95-31417

PHOTODIODES
A room temperature LSO/PIN photodiode PET detector module that measures depth of interaction
| DE95-008447 | p 2878 N95-30378

PHOTOELASTICITY
Acoustoelastic stress evaluation in metal plate using absolute shear and longitudinal time-of-flight data
| PB95-197810 | p 2892 N95-30458

PHOTOELECTRIC EFFECT
Contactless characterization of semiconductors using laser-induced surface photo-charge voltage measurements
| AD-A293618 | p 2863 N95-31725

PHOTOELECTRIC EMISSION
A theoretical analysis of steady-state photocurrents in simple silicon diodes
| NASA-CR-198885 | p 2859 N95-30651
Development of germanium-silicon growth technology
| AD-A293199 | p 3013 N95-30983
Theoretical aspects of electron emission holography
| DE95-614371 | p 2880 N95-31167
Annual meeting of the Advanced Light Source Users' Association
| DE95-009373 | p 3000 N95-31635

PHOTOELECTRIC MATERIALS
Photophysical properties of opto-electric molecules studied by time-resolved microwave conductivity
| PB95-196994 | p 2980 N95-30774

PHOTOELECTRON SPECTROSCOPY
Observation of a low-binding-energy peak in the 2p core-level photoemission from oxidized Al(111)
| PB95-195350 | p 2802 N95-30534
Applications of SXPS for studying surface structure, reaction mechanisms and kinetics
| DE95-008903 | p 2803 N95-30547
The structure and reactivity of boron and carbon surfaces
| AD-A292804 | p 2795 N95-31440

PHOTOELECTRONS
Photophysical properties of opto-electric molecules studied by time-resolved microwave conductivity
| PB95-196994 | p 2980 N95-30774
Cleanliness inspection tool for RSRM bond surfaces p 2781 N95-31799

PHOTOEXCITATION
Magnetic resonance spectroscopy of fullerenes and (pi)-conjugated polymers
| DE95-010131 | p 2817 N95-31108
Suppression of self-interstitials in silicon during ion implantation via in-situ photoexcitation
| DE95-009173 | p 3016 N95-32301

PHOTOLUMINESCENCE
Magnetoluminescence characterization of quantum well structures
| DE95-008527 | p 3008 N95-30381
Fractal quantum well heterostructures for broadband light emitters
| DE95-009579 | p 2660 N95-30707
Magnetic resonance spectroscopy of fullerenes and (pi)-conjugated polymers
| DE95-010131 | p 2817 N95-31108
Investigation of polycrystalline thin film CuInSe2 solar cells based on ZnSe windows
| DE95-004068 | p 2904 N95-31164
Investigation of the basic physics of high efficiency semiconductor hot carrier solar cell
| NASA-CR-198945 | p 2906 N95-32212

PHOTOLYSIS
Aqueous TiO2 photocatalysis of metal-EDTA complexes
| DE95-011058 | p 2793 N95-31113

PHOTOMASKS
Metrology of chrome on quartz photomasks using low voltage scanning electron microscopy. Part 1: Physical SEM parameters
| PB95-195780 | p 2880 N95-30693

PHOTON BEAMS
A room temperature LSO/PIN photodiode PET detector module that measures depth of interaction
| DE95-008447 | p 2878 N95-30378

PHOTON DENSITY
Beam stability at SRRC storage ring
| DE95-010842 | p 2995 N95-32260

PHOTONICS
Current trends in the packaging of photonic devices
| DE95-009583 | p 3001 N95-32064
The Telecommunications and Data Acquisition Report
| NASA-CR-198911 | p 2854 N95-32221

PHOTONS
On the Compton twist-3 asymmetries
| DE95-613627 | p 3017 N95-30371
The search for the decay of Z boson into two gamma as a test of Bose statistics
| DE95-616373 | p 2976 N95-30393
Electromagnetic-gravitational conversion cross sections in external electromagnetic fields
| DE95-613589 | p 2979 N95-30637
Pion-pair production by two photons
| DE95-737162 | p 2983 N95-31223
Inductively coupled IR staring array based on photofluxonic pixels
| AD-A292784 | p 2998 N95-31435
Integrated high performance distributed system
| AD-A292821 | p 2947 N95-31445
Monte Carlo code for evaluating the Boundary Layer Illumination and Radiation Balance model (BLIRB)
| AD-A293963 | p 2915 N95-31560
Effects of mosaicity on Parametric X-Radiation production
| AD-A293677 | p 2985 N95-31597
Form factor of the process gamma(*) gamma(*) yields pi(sup 0) for small virtuality of one of the photons and QCD sum rules (2): Sum rule
| DE95-613629 | p 2988 N95-32078

PHOTOPRODUCTION
Electromagnetic-gravitational conversion cross sections in external electromagnetic fields
| DE95-613589 | p 2979 N95-30637
The 10th INS Scientific Computational Programs
| DE95-717864 | p 2982 N95-31178
Charm photoproduction dynamics
| DE95-009106 | p 2990 N95-32303

PHOTOREFRACTIVITY
Photo-refractive Bi12SiO20: Spatial light modulator
| AD-A293084 | p 3001 N95-32153

PHOTOSPHERE
Nearly steady flows in GONG prototype data
| NASA-CR-198935 | p 2869 N95-30863

PHOTOTHERMAL CONVERSION
Extra focal convective suppressing solar collector
| DE95-010170 | p 2907 N95-32288

PHOTOVOLTAIC CELLS
Photovoltaic module certification/laboratory accreditation criteria development
| DE95-004063 | p 2905 N95-31381
Space systems environmental interaction studies
| AD-A293826 | p 2766 N95-31553
Photovoltaic Energy Program overview: Fiscal year 1994
| DE94-011871 | p 2905 N95-31661
Development of large-area monolithically integrated Silicon-Film(trademark) photovoltaic modules
| DE95-004089 | p 2906 N95-32057
Evaluation and analysis survey on new energy introduction, part 3
| DE95-769806 | p 2906 N95-32072

PHOTOVOLTAIC CONVERSION
Photovoltaic Energy Program overview: Fiscal year 1994
| DE94-011871 | p 2905 N95-31661
Evaluation and analysis survey on new energy introduction, part 3
| DE95-769806 | p 2906 N95-32072
Outlook for renewable energy technologies: Assessment of international programs and policies
| DE95-009084 | p 2907 N95-32302

PHOTOVOLTAIC EFFECT
The junction characteristics and current conduction mechanisms of GaInP2 n(+)p diodes and solar cells
| AD-A290857 | p 2902 N95-30408

PHTHALOCYANIN
The effect of gravity on the deposition of thin films: The physical vapor transport of copper phthalocyanine
| AD-A292997 | p 2838 N95-31472
Calculated structures and electronic absorption spectroscopy for magnesium phthalocyanine and its anion radical
| AD-A293672 | p 2798 N95-31596

PHYSICAL OPTICS
Physical optics polarization scattering matrix for a right-angle dihedral
| AD-A293036 | p 3000 N95-31665

PHYSICAL PROPERTIES
Advanced thin-film deposition and physical properties of high-temperature and other novel superconducting materials
| AD-A292798 | p 2795 N95-31439
Excited-state complexes of conjugated polymers: Novel photophysical processes and optoelectronic materials
| AD-A292958 | p 2819 N95-31462
Whisker reinforced glass ceramic
| DE95-010542 | p 2823 N95-32305

PHYSIOLOGICAL RESPONSES
Electromyostimulation, circuits and monitoring
| NASA-TM-110741 | p 2926 N95-30846
Electromagnetic field exposure dosimeter
| AD-A293191 | p 2927 N95-30981

PIEZOELECTRIC CERAMICS
Large area smart piezoelectric and pyroelectric sensors
| AD-A291487 | p 2859 N95-30561
Materials for adaptive structural acoustic control, volume 1
| AD-A293444 | p 2788 N95-31369
Materials for adaptive structural acoustic control, volume 2
| AD-A293445 | p 2788 N95-31370
Materials for adaptive structural acoustic control, volume 3
| AD-A293446 | p 2788 N95-31371
Materials for adaptive structural acoustic control, volume 4
| AD-A293447 | p 2788 N95-31372
Poisson's ratio for hexagonal crystals
| AD-A293556 | p 3015 N95-31539

PIEZOELECTRIC CRYSTALS
Langasite crystals growth with quality-factor Q, that exceeds the Q of quartz, and which are suitable for high-precision resonators
| AD-A293397 | p 3013 N95-30969
Materials for adaptive structural acoustic control, volume 1
| AD-A293444 | p 2788 N95-31369

PIEZOELECTRIC TRANSDUCERS
Large area smart piezoelectric and pyroelectric sensors
| AD-A291487 | p 2859 N95-30561
Energy absorption apparatus
| AD-D017361 | p 2814 N95-30715
Finite element analysis of smart structures and modal testing of a flexible spacecraft arm
| AD-A293761 | p 2890 N95-31576

PIEZOELECTRICITY
Energy absorption apparatus
| AD-D017361 | p 2814 N95-30715
Materials for adaptive structural acoustic control, volume 2
| AD-A293445 | p 2788 N95-31370
Materials for adaptive structural acoustic control, volume 3
| AD-A293446 | p 2788 N95-31371
Materials for adaptive structural acoustic control, volume 4
| AD-A293447 | p 2788 N95-31372

PIGMENTS
Treatment of plastic media waste p 2844 N95-32177

PILOT INDUCED OSCILLATION
Flight Vehicle Integration Panel Workshop on Pilot Induced Oscillations
| AGARD-AR-335 | p 2745 N95-31061
PIO: A historical perspective p 2745 N95-31062
The process for addressing the challenges of aircraft pilot coupling p 2745 N95-31063
Observations on PIO p 2745 N95-31064
Unified criteria for ACT aircraft longitudinal dynamics p 2745 N95-31065
Looking for the simple PIO model p 2745 N95-31066
SCARLET: DLR rate saturation flight experiment p 2746 N95-31068
SAAB experience with PIO p 2746 N95-31069
Aeroelastic pilot-in-the-loop oscillations p 2746 N95-31070
Calspan experience of PIO and the effects of rate limiting p 2746 N95-31072
The role of handling qualities specifications in flight control system design p 2757 N95-31990
The prevention of PIO by design p 2757 N95-31991
An investigation of pilot induced oscillation phenomena in digital-flight control systems p 2760 N95-32011
Pilot Induced Oscillation: A report on the AGARD Workshop on PIO p 2761 N95-32017

PILOT PERFORMANCE
PIO: A historical perspective p 2745 N95-31062
Looking for the simple PIO model p 2745 N95-31066

PILOT SELECTION
Using computerized neuropsychological testing to assess aviator skills
| AD-A293227 | p 2928 N95-30905
Psychological pilot selection in the US Air Force, the Luftwaffe, and the German Aerospace Research Establishment
| AD-A293779 | p 2928 N95-31376
PILOTLESS AIRCRAFT
Unmanned aerial vehicles. 1994 master plan
p 2751 N95-31416
Automatic flight control system for an unmanned helicopter system design and flight test results
p 2759 N95-32004
Report to the Chairman, Legislation and National Security Subcommittee, Committee on Government Operations, House of Representatives. Unmanned aerial vehicles: Performance of short-range system still in question
| GAO/NSIAD-94-65 | p 2752 N95-32196
PIONS
Experimental results on charge exchange reactions with delta excitations and polarization studies of delta and N(sup *) (1440) resonances
| DE95-614022 | p 2981 N95-30913
Pion-nucleon and kaon-nucleon scattering lengths in QCD sum rules
| DE95-737278 | p 2983 N95-31227
Atomic approaches in metastable antiprotonic helium atoms. Reply to Analysis of the lifetimes and fractions of antiprotons trapped in metastable antiprotonic helium states by I. Shimamhura and M. Kimura --- mura
| DE95-737228 | p 2986 N95-31658
Monte Carlo simulations of muon production
| DE95-009554 | p 2988 N95-32063
Spin momentum correlation (handedness) in the process of four pion production in the electron-positron collisions
| DE95-613690 | p 2988 N95-32093
PIPES (TUBES)
Residual stresses and stress corrosion cracking in pipe fittings
| DE95-009332 | p 2894 N95-31054
Comparison of cathodic protection currents on 70/30 copper-nickel and alloy 625 piping systems
| AD-A292953 | p 2807 N95-31561
Development of integrated insulation joint for cooling pipe in tokamak reactor
| DE95-737220 | p 3007 N95-32264
Nondestructive testing of ceramic components: Cooperative Research and Development Agreement completion report
| DE95-009510 | p 2823 N95-32352
PISTON ENGINES
Linear Motor Free Piston Compressor
| AD-A293452 | p 2889 N95-31374
PISTONS
Fluid-film lubrication with an application to piston rings
p 2890 N95-32119
PITCH (INCLINATION)
Flight demonstration of an advanced pitch control law in the VAAC Harrier aircraft p 2760 N95-32012
PIXELS
Inductively coupled IR staring array based on photofluxonic pixels
| AD-A292784 | p 2998 N95-31435
PLANAR STRUCTURES
Analysis of planar laser-induced fluorescence images obtained during shakedown testing of the AEDC impulse facility
| AD-A293237 | p 2884 N95-30906
PLANE WAVES
Six-vector formalism in electromagnetics of bianisotropic media
| PB95-207130 | p 2846 N95-30567
Plane wave reflection from a uniaxial chiral quarter-wave polarization transformer
| PB95-206512 | p 2849 N95-31159
Fast algorithms for three-dimensional inverse scattering problems
| AD-A293510 | p 2852 N95-31537
Reflection and transmission of electromagnetic plane waves from a uniaxial chiro-omega slab
| PB95-206629 | p 2853 N95-31649
PLANETARY ATMOSPHERES
Mars together and FIRE and ICE: Report of the joint US/Russian technical working groups
| NASA-CR-198864 | p 3030 N95-30845
PLANETARY BOUNDARY LAYER
Initial evaluation of the Oregon State University planetary boundary layer column model for ITWS applications
| AD-A293775 | p 2920 N95-31465
PLANNING
Learning in an intentional system
| AD-A291158 | p 2949 N95-30395
Planning board generator. Part 1: Problem instances and types
| PB95-197075 | p 3021 N95-30834
PLASMA ARC WELDING
Robotic weld overlay coatings for erosion control
| DE95-009643 | p 2809 N95-32098
PLASMA COMPOSITION
Removal of impurity ions from a magnetic trap with a two-component plasma on their collision with fast component ions
| DE95-614171 | p 2984 N95-31550
PLASMA CONTROL
Advances in the simulation of toroidal gyro Landau fluid model turbulence
| DE95-008387 | p 3003 N95-30359
Effects of particle fueling and plasma wall interactions on D3-D discharges
| DE95-009608 | p 3003 N95-30612
Development of a tokamak plasma optimized for stability and confinement
| DE95-009609 | p 3003 N95-30641
Helium transport and exhaust studies in enhanced confinement regimes in DIII-D
| DE95-009134 | p 3004 N95-30685
Stabilization of ballooning modes with sheared toroidal rotation
| DE95-008388 | p 3006 N95-31624
Target diagnostics for intense lithium ion hohlraum experiments on PBFA 2
| DE95-008517 | p 3006 N95-31626
Optimization of an expander of a gas-dynamic trap
| DE95-614172 | p 3006 N95-31679
Onset of ELMs in JT-60U
| DE95-737209 | p 3007 N95-32263
PLASMA DENSITY
Design considerations for a Density-Channel-Guided laser wake-field accelerator
| AD-A292876 | p 2884 N95-31190
A prototype ionospheric tomography system (ITS)
| AD-A293015 | p 2916 N95-31698
PLASMA DIAGNOSTICS
Physics and application of high density Z-pinches
| NIFS-PROC-14 | p 3004 N95-30671
EBIT: Electron Beam Ion Trap V-division experimental physics
| DE95-010207 | p 3004 N95-30769
Development of plasma diagnostics technologies: A study on nuclear fusion reactor
| DE95-614180 | p 3005 N95-31004
Target diagnostics for intense lithium ion hohlraum experiments on PBFA 2
| DE95-008517 | p 3006 N95-31626
Determination of electric and magnetic fields in open trap plasmas by means of atomic-molecular beam hydrogen isotopes
| DE95-614177 | p 3006 N95-31680
A prototype ionospheric tomography system (ITS)
| AD-A293015 | p 2916 N95-31698
Calibration of multichannel analyzer of charge-exchange atoms
| DE95-614178 | p 2987 N95-32053
Energy spectra of charge-exchange atoms from a rotating plasma
| DE95-614179 | p 3006 N95-32054
Analysis of plasma measurements for the Geotail mission
| NASA-CR-199074 | p 3032 N95-32218
PLASMA DIFFUSION
Lower hybrid accessibility in a large, hot reversed field pinch
| DE95-011001 | p 3007 N95-32310
PLASMA HEATING
Perpendicular electron heating by absorption of auroral kilometric radiation
| NASA-198815 | p 2914 N95-30848
A collisionless shock wave experiment
| DE95-009489 | p 3008 N95-32351
PLASMA INTERACTIONS
Effects of particle fueling and plasma wall interactions on D3-D discharges
| DE95-009608 | p 3003 N95-30612
Pulse forming network in the ETC combustion characterization of plasma augmented solid propellants
p 2799 N95-31205
PLASMA LAYERS
Selected problems of the identification of weak double layers in plasma on a background of different aperiodic non-collision structures
| IFTR-4/1995 | p 3006 N95-31737
PLASMA PHYSICS
Physics and application of high density Z-pinches
| NIFS-PROC-14 | p 3004 N95-30671
A simplified technique for determining the symmetry groups of non-linear plasma kinetic equations
| IFTR-8/1995 | p 2960 N95-31337
Selected problems of the identification of weak double layers in plasma on a background of different aperiodic non-collision structures
| IFTR-4/1995 | p 3006 N95-31737
PLASMA RADIATION
Physics and application of high density Z-pinches
| NIFS-PROC-14 | p 3004 N95-30671
PLASMA SHEATHS
Study of cross-tail current carriers in magnetotail
p 3005 N95-30804
PLASMA SPRAYING
A microwave plasma cleaning apparatus
p 2779 N95-31786
PLASMA TEMPERATURE
Shear flow effects on ion thermal transport in tokamaks
| DE95-009115 | p 3005 N95-30801
PLASMA TURBULENCE
Advances in the simulation of toroidal gyro Landau fluid model turbulence
| DE95-008387 | p 3003 N95-30359
PLASMA WAVES
On reflection of Alfven waves in the solar wind
| NASA-TM-110642 | p 3031 N95-30582
Bernstein-Green-Kruskal wave
| DE95-614201 | p 3007 N95-32056
PLASMA-PARTICLE INTERACTIONS
Study of cross-tail current carriers in magnetotail
p 3005 N95-30804
Perpendicular electron heating by absorption of auroral kilometric radiation
| NASA-198815 | p 2914 N95-30848
No-thermal plasma processing of VOCs and NO(x) at LLNL
| DE95-011445 | p 2911 N95-32281
PLASMAS (PHYSICS)
Advances in the simulation of toroidal gyro Landau fluid model turbulence
| DE95-008387 | p 3003 N95-30359
Theoretical absorption spectroscopy of high-temperature metal vapors: Model and experiment compared
| AD-A290872 | p 2791 N95-30409
Helium transport and exhaust studies in enhanced confinement regimes in DIII-D
| DE95-009134 | p 3004 N95-30685
On the quasihydrostatic flows of radiatively cooling self-gravitating gas clouds
| DE95-009116 | p 3029 N95-30729
Reflectivity of plasmas created by high-intensity, ultra-short laser pulses
| DE95-009536 | p 3004 N95-30742
Stabilization of the resistive shell mode in tokamaks
| DE95-008748 | p 3004 N95-30794
Shear flow effects on ion thermal transport in tokamaks
| DE95-009115 | p 3005 N95-30801
X-band magnicon amplifier research at the Naval Research Laboratory
| AD-A293203 | p 3013 N95-30984
Design considerations for a Density-Channel-Guided laser wake-field accelerator
| AD-A292876 | p 2884 N95-31190
Pulse forming network in the ETC combustion characterization of plasma augmented solid propellants
p 2799 N95-31205
Future scientific applications for high-energy lasers
| DE95-009380 | p 2885 N95-31230
Pulse power for high energy density physics experiments
| DE95-010868 | p 2992 N95-31232
Plasma source ion implantation of metal ions: Synchronization of cathodic-arc plasma production and target bias pulses
| DE95-009431 | p 3006 N95-31613
Diagnosing high density, fast-evolving plasmas using x-ray lasers
| DE95-010734 | p 3006 N95-32028
Enhanced brightness x-ray lasers
| DE95-010735 | p 2886 N95-32029
Thermal rho's in the quark-gluon plasma
| DE95-009543 | p 3008 N95-32357
PLASMONS
Inelastic plasmon and inter-band electron-scattering potentials for Si from dielectric matrix calculations
| DE95-616778 | p 2977 N95-30475
May multiple inelastic scattering in CBED patterns be removed analytically
| PB95-196333 | p 2992 N95-30717
PLASTIC DEFORMATION
Characterization of compressive damage mechanisms in ceramic and polymeric matrix composite materials
| AD-A293171 | p 2787 N95-30975
The 10th International Conference on the Strength of Materials
| AD-A292335 | p 2894 N95-31263

Interfacial segregation and deformation of superplastically deformed Al-Mg-Mn alloys
| DE95-009572 | p 2809 N95-32052

PLASTIC FLOW

Dynamics of Current Driven Disordered Josephson Junction Arrays
| DE95-009418 | p 3014 N95-31231

PLASTIC PLATES

An analysis of the cover of a liquid-filled circular container
| IFTR-1/1995 | p 2895 N95-31338

PLASTICS

Background to plastic media blasting
p 2843 N95-32168

Facilities used for plastic media blasting
p 2763 N95-32176

Treatment of plastic media waste
p 2844 N95-32177

PLATE THEORY

A theory for predicting and minimizing the effects of matrix degradation on the thermomechanical properties of general laminates p 2785 N95-30768

Elastic and inelastic micromechanical analysis of functionally graded materials and laminated structures using transformation fields p 2787 N95-31347

Contributions to the design of neutral cutouts in laminated plates and shells p 2790 N95-32113

PLATES (STRUCTURAL MEMBERS)

Finite element analysis of damped vibrations of laminated composite plates
| ISBN-0-315-84928-2 | p 2789 N95-31731

Failure mechanisms in composite plates subjected to in-plane compressive loading p 2790 N95-32108

PLATING

High temperature barrier coatings for refractory metals
| NASA-CR-195475 | p 2802 N95-30531

The electrodeposition of low contraction chromium/molybdenum alloys using pulse-reverse plating
| AD-A292727 | p 2804 N95-30945

Assessment of pollution prevention and control technology for plating operations p 2776 N95-31771

Cadmium plating replacements p 2776 N95-31773

PLATINUM

Orientation of rapid thermally annealed lead zirconate titanate thin films on (111) Pt substrate
| DE95-615232 | p 2811 N95-30422

STM studies oi clean, CO- and O2-exposed Pt(100)-hex-R0.7 deg
| PB95-195376 | p 3009 N95-30535

Energetics of Pt adsorption on Pt(111)
| DE95-010933 | p 3017 N95-32307

PLATINUM ALLOYS

A proposed phase equilibrium diagram for Pt-Zr system
| DE95-620904 | p 2806 N95-31220

PLUMES

Modeling of thermal, electronic, hydrodynamic, and dynamic deposition processes for pulsed-laser deposition of thin films
| DE95-008906 | p 2813 N95-30572

Kinetic theory model predictions compared with low-thrust axisymmetric nozzle plume data
| NASA-CR-198934 | p 2768 N95-30864

Cloud condensation nuclei measurements in shiptrails
| AD-A293302 | p 2919 N95-30951

The passage from transitional to free molecular plumes p 2871 N95-30994

Vacuum plume backflow and rarefaction
p 2871 N95-30995

Survey of recent Al2O3 droplet size data in solid rocket chambers, nozzles, and plumes p 2770 N95-31195

Vorticity dynamics and control of dynamic stall
| AD-A288658 | p 2756 N95-31400

Beam-centroid tracking instrument for ion thrusters
| AD-A293654 | p 2769 N95-31567

PLUTO (PLANET)

Mars together and FIRE and ICE: Report of the joint US/Russian technical working groups
| NASA-CR-198864 | p 3030 N95-30845

POINCARE PROBLEM

Strange compactification theorem: Infinite processes and the 3-dimensional poincare conjecture 6. Part A
| PB95-207924 | p 2965 N95-30504

Good metric spaces without good parameterizations
| PB95-208427 | p 2957 N95-30622

POINCARE SPHERES

Strange compactification theorem: Infinite processes and the 3-dimensional poincare conjecture 6. Part A
| PB95-207924 | p 2965 N95-30504

POINT DEFECTS

Molecular dynamics simulations of high energy cascades in iron
| DE95-010116 | p 2982 N95-31104

IR materials producibility
| AD-A293330 | p 2998 N95-31141

Phase stability, point defects and site preference of FeAl and NiAl with ternary additions
| DE95-009694 | p 3015 N95-31641

POINT SOURCES

Solution of the three-dimensional Helmholtz equation with nonlocal boundary conditions
| NASA-TM-110174 | p 2974 N95-30850

Optimal infrared detector configurations for air target detection p 2841 N95-32130

Harmonic coordinates in the problem on static gravitational and massless scalar fields with a point source
| DE95-623632 | p 3020 N95-32295

POINT SPREAD FUNCTIONS

Optimal infrared detector configurations for air target detection p 2841 N95-32130

POINTING CONTROL SYSTEMS

Guidance and Control for Future Air-Defence Systems
| AGARD-CP-555 | p 2839 N95-32123

Acquisition, tracking, pointing and fire control for Ballistic Missile Defense p 2841 N95-32131

The High Altitude Balloon Experiment demonstration of acquisition, tracking, and pointing technologies (HABE-ATP) p 2841 N95-32132

POISSON DENSITY FUNCTIONS

Failure analysis of a repairable system: The case study of a cam-driven reciprocating pump
| AD-A293144 | p 2889 N95-30949

Poisson approximation using the Stein-Chen method and coupling: Number of exceedances of a discrete-time-chi-squared process
| PB95-212205 | p 2961 N95-31398

POISSON EQUATION

Hamiltonian dynamics of the condensed media with spontaneously broken symmetry
| DE95-614448 | p 3010 N95-30648

Self-adaptive multilevel methods for fluid flow problems p 2873 N95-31412

POISSON RATIO

Poisson's ratio for hexagonal crystals
| AD-A293556 | p 3015 N95-31539

POLAND

Automation of the control of acoustic parameters in a digital speech synthesizer
| IFTR-2/1995 | p 2850 N95-31357

POLAR CAPS

DE-1 observations of polar O(+) stream bulk parameters and comparison with a model of the centrifugally-accelerated polar wind
| NASA-CR-198930 | p 2917 N95-31743

POLAR METEOROLOGY

Kiruna geophysical data. Data summary 94/4-6, April-June 1994
| PB95-210365 | p 2913 N95-30627

Kiruna geophysical data. Data summary 94/1-3, January-March 1994
| PB95-210373 | p 2913 N95-30628

Middle atmosphere structure and dynamics: Lidar studies at the South Pole, Syowa and Urbana
p 2916 N95-31736

POLAR REGIONS

Kiruna geophysical data. Data summary 94/4-6, April-June 1994
| PB95-210365 | p 2913 N95-30627

Satellite multisensor data techniques for sea ice mapping
| AD-A289729 | p 2901 N95-31148

Environmental conditions responsible for solar activity
| AD-A292859 | p 3031 N95-31450

POLARIMETERS

X-ray performance of the engineering prototype Stellar x-ray polarimeter
| DE95-010268 | p 3028 N95-31129

POLARIMETRY

Photorefractive nonlinear optics
| AD-A292913 | p 2999 N95-31458

Investigation of ground target detection methods in fully polarimetric wide angle synthetic aperture radar images
| AD-A293922 | p 2851 N95-31513

POLARIZATION

Six-vector formalism in electromagnetics of bianisotropic media
| PB95-207130 | p 2846 N95-30567

POLARIZATION (CHARGE SEPARATION)

Experimental results on charge exchange reactions with delta excitations and polarization studies of delta and N(sup *) (1440) resonances
| DE95-614022 | p 2981 N95-30913

POLARIZATION (SPIN ALIGNMENT)

On the Compton twist-3 asymmetries
| DE95-613627 | p 3017 N95-30371

Application of spin-sensitive electron spectroscopies to investigations of electronic and magnetic properties of solid surfaces and epitaxial systems
| DE95-010154 | p 2792 N95-30614

Investigation of Fe3O4 colloid behaviour in a magnetic field by polarized neutron transmission
| DE95-614351 | p 2981 N95-30915

Spin momentum correlation (handedness) in the process of four pion production in the electron-positron collisions
| DE95-613690 | p 2988 N95-32093

POLARIZATION (WAVES)

Polarized Raman spectroscopy of chemically vapour deposited diamond films
| DE95-616776 | p 2815 N95-30791

Physical optics polarization scattering matrix for a right-angle dihedral
| AD-A293036 | p 3000 N95-31665

Analysis of target contrast improvement using polarization filtering in the infrared region
| AD-A293085 | p 3001 N95-31841

POLARIZATION CHARACTERISTICS

Polarization characteristics, control, and modulation of vertical-cavity surface emitting lasers
| DE95-008526 | p 2882 N95-30380

POLARIZATION MODULATION

Polarization characteristics, control, and modulation of vertical-cavity surface emitting lasers
| DE95-008526 | p 2882 N95-30380

POLARIZED RADIATION

Magneto-optical transmission-reflection beam splitter for multi-level atoms
| DE95-616267 | p 2976 N95-30423

Polarized laser induced holographic surface relief gratings on polymer films
| AD-A293275 | p 2817 N95-31126

POLARIZERS

Plane wave reflection from a uniaxial chiral quarter-wave polarization transformer
| PB95-206512 | p 2849 N95-31159

POLICIES

Economical analysis relating to the global warming issue
| DE95-764072 | p 2908 N95-30677

Management of major system programs and projects. Handbook
| NHB-7120.5 | p 3021 N95-31380

Environmental benefits of chemical propulsion
p 2772 N95-31750

Process evaluation p 2845 N95-32180

Report to the Chairman, Legislation and National Security Subcommittee, Committee on Government Operations, House of Representatives. C-17 Aircraft program: Improvements in initial provisioning process
| GAO/NSIAD-94-63 | p 2741 N95-32194

POLLUTION CONTROL

Economical analysis relating to the global warming issue
| DE95-764072 | p 2908 N95-30677

Demonstration of split-flow ventilation and recirculation as flow-reduction methods in an Air Force paint spray booth, volume 1
| AD-A286807 | p 2763 N95-31101

Enhanced alkaline hydrolysis and biodegradability studies of nitrocellulose-bearing missile propellant
p 2772 N95-31752

Technology transfer into the solid propulsion industry
p 2770 N95-31756

Air pollution control system research: An iterative approach to developing affordable systems
p 2773 N95-31759

Major weapon system environmental life-cycle cost estimating for Conservation, Cleanup, Compliance and Pollution Prevention (C3P2) p 2774 N95-31761

Assessment of pollution prevention and control technology for plating operations p 2776 N95-31771

Environmentally regulated aerospace coatings
p 2777 N95-31775

No-thermal plasma processing of VOCs and NO(x) at LLNL
| DE95-011445 | p 2911 N95-32281

POLLUTION MONITORING

Cloud condensation nuclei measurements in shiptrails
| AD-A293302 | p 2919 N95-30951

Novel mass spectrometric instrument for gaseous and particulate characterization and monitoring
| DE95-000047 | p 2881 N95-31694

POLLUTION TRANSPORT

Calculation of a residual mean meridional circulation for a zonal-mean tracer transport model
| DE95-009474 | p 2911 N95-32350

POLYBUTADIENE

Laser pyrolysis of HTPB p 2800 N95-31298

POLYCARBONATES

Failure analysis for polycarbonate transparencies
| AD-A292992 | p 2820 N95-31471

POLYCRYSTALS

Ionic conductivities of lithium phosphorus oxynitride glasses, polycrystals, and thin films
| DE95-008898 | p 2812 N95-30545

Spectral response of a polycrystalline silicon solar cell
| DE95-614370 | p 2903 N95-30723
Investigation of polycrystalline thin film CuInSe2 solar cells based on ZnSe windows
| DE95-004068 | p 2904 N95-31164
Effect of irradiation spectrum on the microstructure of ion-irradiated Al2O3
| DE95-010225 | p 2806 N95-31188
Development of large-area monolithically integrated Silicon-Film(trademark) photovoltaic modules
| DE95-004089 | p 2906 N95-32057

POLYIMIDE RESINS
A study of elevated temperature testing techniques for the fatigue behavior of PMCS: Application to T650-35/AMB21
| NASA-TM-106927 | p 2791 N95-32209

POLYMER BLENDS
Processing of polymers using supercritical fluids
| AD-A292880 | p 2819 N95-31410

POLYMER CHEMISTRY
Process for producing hydrophilic polymer membranes
| AD-D017355 | p 2811 N95-30415
Progress in developing propellant ignition systems based upon electrically conductive polymers
p 2800 N95-31300
Intelligent synthetic polymers
| AD-A292905 | p 2819 N95-31395

POLYMER MATRIX COMPOSITES
Low vibration polymeric composite engine
| AD-D017332 | p 2887 N95-30386
Round-robin validation exercise for plate twist test method
| PB95-208088 | p 2812 N95-30487
Characterization of compressive damage mechanisms in ceramic and polymeric matrix composite materials
| AD-A293171 | p 2787 N95-30975

POLYMERIC FILMS
State-of-the-art low-cost solar reflector materials
| DE95-000260 | p 2902 N95-30526
Electrical conductivity study on polythiophenes films
| DE95-614309 | p 2813 N95-30645
Nonlinear optical processes in polymer films
| AD-A293384 | p 2815 N95-30955
Laser-induced holographic surface relief gratings on nonlinear optical polymer films
| AD-A293169 | p 2997 N95-30973
Polarized laser induced holographic surface relief gratings on polymer films
| AD-A293275 | p 2817 N95-31126
Intelligent synthetic polymers
| AD-A292905 | p 2819 N95-31395
An interpenetrating polymer network for second-order nonlinear optics
| AD-A293019 | p 2821 N95-31699
Novel unsymmetrical polydiacetylenes as materials for second and third order nonlinear optics
| AD-A293020 | p 3001 N95-31700

POLYMERIZATION
Intelligent synthetic polymers
| AD-A292905 | p 2819 N95-31395
Responsive copolymers for enhanced petroleum recovery
| DE95-011857 | p 2823 N95-32361

POLYMERS
Process for producing hydrophilic polymer membranes
| AD-D017355 | p 2811 N95-30415
Effects of hydrostatic pressure on the mechanical behavior of composite materials
| AD-A293162 | p 2787 N95-30963
From molecular to macromolecular liquid crystals
| AD-A293170 | p 2816 N95-30974
Tunable composite membranes for gas separations
| DE95-010602 | p 2822 N95-32075

POLYNOMIALS
Size of Fulton's essential set
| PB95-211645 | p 2955 N95-30477
Spectral methods in complex geometries
| PB95-208336 | p 2955 N95-30495
Co-groups on sequentially complete, locally convex, topological vector spaces in particular on strict LF-spaces
| PB95-206918 | p 2966 N95-30681
The complexity and approximability of finding maximum feasible subsystems of linear relations
| TRITA-NA-9313 | p 2961 N95-31648
Newton Raphson method, scaling at fractal boundaries and mathematica
| DE95-613374 | p 2962 N95-32095

POLYPEPTIDES
Design and processing of materials by biomimicking. Sections 1. Publications
| AD-A293852 | p 2820 N95-31559

POLYSACCHARIDES
Design and processing of materials by biomimicking. Sections 1. Publications
| AD-A293852 | p 2820 N95-31559

POLYTETRAFLUOROETHYLENE
Enhancement of perfluoropolyether boundary lubrication performance: I. Preliminary results
| NASA-TM-106937 | p 2813 N95-30621

POLYURETHANE RESINS
Compatibility of Single Hydraulic Fluid with military specification fluids, seals and metallurgy
| AD-A292954 | p 2821 N95-31663

POPULATION INVERSION
Many-body effects in semiconductor lasers
| DE95-008534 | p 2883 N95-30390

POROSITY
Porous spherical shells and microspheres by electrodispersion precipitation
| DE95-009073 | p 2815 N95-30799
Electrified microheterogeneous catalysis
| AD-D017446 | p 2794 N95-31271
In situ composites in the aluminum nitride-alumina system
| AD-A293776 | p 2789 N95-31509
Effects of gas-phase thermal expansion on the stability of deflagration through a porous energetic material
| DE95-004382 | p 2797 N95-31824

POROUS MATERIALS
Process for producing hydrophilic polymer membranes
| AD-D017355 | p 2811 N95-30415
Extension of the pore tree model to describe pore interconnectivity
| AD-A290366 | p 2793 N95-30971
Particle filtration: A comparison between theory and experiment
| DE95-009442 | p 2875 N95-31637
Effects of gas-phase thermal expansion on the stability of deflagration through a porous energetic material
| DE95-004382 | p 2797 N95-31824

PORPHYRINS
A theoretical treatment of the absorption and emission properties of Cu(2) porphyrin
| AD-A293669 | p 2795 N95-31595

PORTABLE EQUIPMENT
Prospector 7: Small fuel cells for portable power workshop
| AD-A292729 | p 2904 N95-30947
Construction and performance measurement of a portable thermoacoustic refrigerator demonstration apparatus
| AD-A293265 | p 2839 N95-31122
Portable digital Satellite News Gathering (SNG) RF terminal using a flat antenna
| NHK-LABS-NOTE-436 | p 2853 N95-31744

PORTS (OPENINGS)
Fast-acting valve for projective launching systems
| AD-D017357 | p 2868 N95-30416

POSITION (LOCATION)
Ultrasonic two probe system for locating and sizing
| AD-D017438 | p 2996 N95-30724
Demonstration of split-flow ventilation and recirculation as flow-reduction methods in an Air Force paint spray booth, volume 2
| AD-A286808 | p 2762 N95-30926
FISHFINDE: Interactive software package to predict fish locations using satellite image data and fish species behavior rules
| AD-A293394 | p 2935 N95-30968
Dynamic maintenance scheduling for a stochastic telecommunication network: Determination of performance factors
| AD-A293829 | p 2852 N95-31555
Determination of the position of Jupiter from radio metric tracking of Voyager 1 p 2854 N95-32222

POSITION ERRORS
Robust position and force tracking control for a robot in contract p 2888 N95-30830
Laser retroreflector experiment on NAVSTAR 35 and 36 p 2887 N95-32347

POSITRON ANNIHILATION
CP violating effects in e(+) e(-) yields ZH and their optimization
| DE95-616302 | p 2976 N95-30441
Search for new physics indirect effects in e(+)e(-) yields W(+)W(-) at linear colliders with polarized beams
| DE95-613688 | p 2984 N95-31547
An experimental study of QCD and jets in e(+)e(-) annihilation
| DE95-010667 | p 2989 N95-32267

POSITRONS
A room temperature LSO/PIN photodiode PET detector module that measures depth of interaction
| DE95-008447 | p 2878 N95-30378
New tensor interactions in micron-decay
| DE95-613760 | p 2978 N95-30528
Radiative corrections to the three quantum annihilation cross section in high energy electron-positron collisions
| DE95-623675 | p 2995 N95-32296

POSTURE
Erect, neutral and slump sitting postures: A study of the torso linkage system from shoulder to hip joint
| AD-A293239 | p 2930 N95-30907

POTASSIUM
Membrane transport: A cellular probe of heat stroke
| AD-A293327 | p 2926 N95-30924
A compact and efficient violet laser source
| AD-A292782 | p 2885 N95-31434

POTASSIUM ALLOYS
NaK pool-boiler solar receiver durability bench test. Volume 2: Metallurgical analysis
| DE95-010338 | p 2905 N95-31640

POTENTIAL FLOW
Axial loads on yawed rotors
| PB95-214193 | p 2742 N95-30638
Acceleration potential models PREDICHAT/PREDICDYN applied for calculation of axisymmetric dynamic inflow cases
| PB95-207015 | p 2869 N95-30957
Numerical solution of the full potential equation using a chimera grid approach
| NASA-TM-110360 | p 2744 N95-32188

POWDER (PARTICLES)
The neutron powder diffraction and acoustic investigations of the NH4SCN phase diagram
| DE95-614372 | p 3009 N95-30419
Phase transformations in melt-spun Y-Ba-Cu-O bulk superconductor
| DE95-010237 | p 3011 N95-30667
Processing and characterization of nanocrystalline molybdenum disilicide (MoSi2) consolidated by hot isostatic pressing (HIP)
| DE95-010243 | p 3012 N95-30756
Low temperature fabrication from nano-size ceramic powders
| DE95-010995 | p 2818 N95-31153
Composite polymer electrolyte for lithium batteries
| AD-A293924 | p 2820 N95-31514
Gelcasting of sintered reaction-bonded silicon nitride for improved mechanical properties
| DE95-010282 | p 2822 N95-32085

POWDER METALLURGY
Mechanical alloying processing with application to structural materials
| AD-A290788 | p 2802 N95-30404

POWER AMPLIFIERS
High energy pulsed microwave sources
| AD-A293334 | p 2849 N95-31142
Stable high-power harmonic gyro-amplifiers
| AD-A293697 | p 2881 N95-31828

POWER LINES
Electromagnetic field exposure dosimeter
| AD-A293191 | p 2927 N95-30981
Nordic Symposium on Analysis of Electromagnetic Transient Phenomena Using EMTP, part 1
| PB95-206595 | p 2850 N95-31182

POWER SERIES
Golden ten equations of motion
| PB95-197927 | p 2967 N95-30809

POWER SPECTRA
Allan deviation computations of a linear frequency synthesizer system using frequency domain techniques
p 2972 N95-32344

POWER SUPPLY CIRCUITS
Operational characteristics of a 200 C LC parallel resonant circuit
| NASA-TM-106983 | p 2864 N95-31742

POWERED LIFT AIRCRAFT
Moving base simulation of an integrated flight and propulsion control system for an ejector-augmentor STOVL aircraft in hover
| NASA-TM-108867 | p 2750 N95-30646

PRANDTL NUMBER
Heat transfer in shear-free turbulent boundary layers
p 2876 N95-31708

PREAMPLIFIERS
Pre-amplifier with multi-stage feedback
| AD-D017371 | p 2859 N95-30659

PREBURNERS
Design and testing of an oxidizer-rich preburner
p 2799 N95-31212

PRECIPITATION (METEOROLOGY)
Multiparameter radar measurements of precipitation in complex terrain: Meteorological and hydrological applications
| AD-A290786 | p 2918 N95-30403
Forecast of Atlantic seasonal hurricane activity for 1994 p 2918 N95-30832

PRECIPITATION HARDENING
Microstructural and mechanical property changes in model Fe-Cu alloys
| DE95-010117 | p 2805 N95-31105
Modeling of grain boundary stresses in Alloy 600
| DE95-009033 | p 2808 N95-31825

PRECISION
Precision manipulation with a dextrous robot hand p 2888 N95-30829
Wavelengths measurements of the He-like krypton K-shell spectrum
|DE95-010264| p 2987 N95-32041
PRECONDITIONING
Use of element-by-element preconditioners to solve large scale partially separable optimization problems
|PB95-195772| p 2957 N95-30692
PREDICTION ANALYSIS TECHNIQUES
Experimental determination of probability distributions for parameters of a Salem limestone cap plasticity model
|AD-A290878| p 2892 N95-30559
A theory for predicting and minimizing the effects of matrix degradation on the thermomechanical properties of general laminates p 2785 N95-30768
Acceleration potential models PREDICHAT/PREDICDYN applied for calculation of axisymmetric dynamic inflow cases
|PB95-207015| p 2869 N95-30957
Hot jet/wake turbulent structure and laser propagation. Part 3: Laser propagation measurements and modeling p 2871 N95-30992
Vacuum plume backflow and rarefaction p 2871 N95-30995
Comparison of DSMC predictions with temporally resolved vibrational state measurements in NO p 2872 N95-30996
An ignition model for modern double base propellants p 2800 N95-31292
Clouds: Their prediction and simulation
|AD-A292864| p 2920 N95-31453
PREDICTIONS
SHEAT: A computer code for probabilistic seismic hazard analysis, user's manual
|DE95-717874| p 2913 N95-30758
Achieving improved cycle efficiency via pressure gain combustors
|DE95-008945| p 2792 N95-30762
Use of body surface heat patterns for predicting and evaluating acute lower extremity pain among soldiers
|AD-A292829| p 2927 N95-31446
Failure analysis for polycarbonate transparencies
|AD-A292992| p 2820 N95-31471
PREFORMS
Characterization and prediction of post-impact fatigue damage in stitched composites p 2785 N95-30826
PRELAUNCH SUMMARIES
STS-70 flight: Day 1
|NASA-TM-110659| p 2765 N95-30880
PRELAUNCH TESTS
STS-71 post flight presentation
|NASA-TM-110658| p 2764 N95-30852
PREMIXED FLAMES
An experimental and numerical study on the structure and extinction of laminar premixed flames p 2792 N95-30670
Detailed chemical kinetic modeling of premixed hydrocarbon flames supported by NO2 p 2801 N95-31311
Flame structure studies of neat and NH3 doped H2/N2O flames employing molecular beam mass spectrometry and modeling p 2801 N95-31313
The study of flame-vortex interactions using a particle image velocimeter p 2796 N95-31709
Non-intrusive combustion diagnostics of premixed hydrocarbon flames using FT-IR spectrometry p 2797 N95-31732
PREPARATION
Standardization of (13)CO2 production procedure from organic matter for mass spectrometric analysis
|DE95-614629| p 2791 N95-30420
PREPOLYMERS
Phthalonitrile prepolymer as high temperature sizing material for composite fibers
|AD-D017447| p 2818 N95-31272
PREPROCESSING
Analog preprocessing in a SNS 2 micrometers low-noise CMOS folding ADC
|AD-A293356| p 2849 N95-30954
PRESIDENTIAL REPORTS
Aeronautics and space report of the President
|NASA-TM-110743| p 3028 N95-31979
PRESSES
Low temperature fabrication from nano-size ceramic powders
|DE95-010995| p 2818 N95-31153
PRESSURE
Application of multigrid computational fluid dynamics (CFD) methods to rotor analysis
|AD-A293012| p 2874 N95-31475
PRESSURE DEPENDENCE
Low-density ionization behavior
|DE95-009495| p 2980 N95-30705
Hydrostatic extrusion of BSCCO/Ag composite wire
|DE95-007862| p 2805 N95-31121
PRESSURE DISTRIBUTION
Calculations of the sound scattering from fluid-filled spherical shell sonar targets
|DSTO-RR-0020| p 2974 N95-31365
Application of wavelet-filtering techniques to intermittent turbulent and wall pressure events. Part 2. Detection of cluster patterns
|AD-A293805| p 2875 N95-31586
Afterbody/nozzle pressure distributions of a twin-tail twin-engine fighter with axisymmetric nozzles at Mach numbers from 0.6 to 1.2
|NASA-TP-3509| p 2744 N95-31984
PRESSURE EFFECTS
Effects of hydrostatic pressure on the mechanical behavior of composite materials
|AD-A293162| p 2787 N95-30963
Assessment of dynamic burning behavior for JA-2 propellant rods p 2800 N95-31299
Combustion of LOX with H2(sub g) under subcritical and supercritical conditions p 2797 N95-31717
PRESSURE GRADIENTS
A turbulence model for steady and unsteady boundary layers in strong pressure gradients p 2868 N95-30840
PRESSURE ICE
Sea ice stress research
|AD-A293164| p 2923 N95-30964
PRESSURE MEASUREMENT
Method and system for reducing drag on a body moving through a fluid medium
|AD-D017336| p 2867 N95-30672
Workshop report: Measurement techniques in highly transient, spectrally rich combustion environments p 2799 N95-31208
Pressure transducer performance and measurement trade-offs in a transient, high temperature, combustion environment p 2799 N95-31209
PRESSURE OSCILLATIONS
Method and system for suppressing noise induced in a fluid medium by a body moving therethrough
|AD-D017339| p 2973 N95-30411
Forecast of Atlantic seasonal hurricane activity for 1994 p 2918 N95-30832
Early August updated forecast of Atlantic seasonal hurricane activity for 1994 p 2919 N95-30844
PRESSURE PULSES
A pulsed liquid fuel ramjet p 2756 N95-31201
Pulse forming network in the ETC combustion characterization of plasma augmented solid propellants p 2799 N95-31205
PRESSURE RATIO
Application of multigrid computational fluid dynamics (CFD) methods to rotor analysis
|AD-A293012| p 2874 N95-31475
PRESSURE RECOVERY
Linear Motor Free Piston Compressor
|AD-A293452| p 2889 N95-31374
PRESSURE REDUCTION
Effect of oxygen and decompression bubbles on inert gas washout
|PB95-196556| p 2925 N95-30665
Effects of cavity bleed and its configuration on aerodynamic characteristics of supersonic internal flow
|NAL-TR-1247| p 2744 N95-31715
PRESSURE SENSORS
Micromachined sensor and actuator research at the Microelectronics Development Laboratory
|DE95-008540| p 2878 N95-30384
Method and system for suppressing noise induced in a fluid medium by a body moving therethrough
|AD-D017339| p 2973 N95-30411
Method and system for reducing drag on a body moving through a fluid medium
|AD-D017336| p 2867 N95-30672
Optical fiber pressure sensor for liquid level monitoring
|AD-D017346| p 2996 N95-30679
Calculated coupling efficiency between an elliptical-core optical fiber and an optical waveguide over temperature
|NASA-TM-107005| p 2997 N95-30849
Workshop report: Measurement techniques in highly transient, spectrally rich combustion environments p 2799 N95-31208
Pressure transducer performance and measurement trade-offs in a transient, high temperature, combustion environment p 2799 N95-31209
PRESSURE VESSELS
Damage dosimetry and embrittlement monitoring of nuclear pressure vessels in real time by magnetic properties measurement
|DE95-011454| p 2894 N95-31254
Validation of favor code linear elastic fracture solutions for finite-length flaw geometries
|DE95-009034| p 2898 N95-32157
PRESSURIZING
Linear Motor Free Piston Compressor
|AD-A293452| p 2889 N95-31374
PREVENTION
The prevention of PIO by design p 2757 N95-31991
PRINCIPAL COMPONENTS ANALYSIS
Sensor Fusion and Nonlinear Prediction for Anomalous Event Detection
|DE95-009429| p 2933 N95-30602
PRIVACY
UNIX and PC security in a network environment. LOKALNETT 1993
|PB95-196309| p 2934 N95-30697
PROBABILITY DENSITY FUNCTIONS
Experimental determination of probability distributions for parameters of a Salem limestone cap plasticity model
|AD-A290878| p 2892 N95-30559
PROBABILITY DISTRIBUTION FUNCTIONS
Design of systems for active sound control
|PB95-197869| p 2973 N95-30461
Fitting discrete distributions on the first two moments
|PB95-197885| p 2950 N95-30462
Experimental determination of probability distributions for parameters of a Salem limestone cap plasticity model
|AD-A290878| p 2892 N95-30559
Equivalence of two non-commutative geometry approaches
|DE95-613469| p 2957 N95-30642
PROBABILITY THEORY
Probabilistic reliability modeling of fatigue on the H-46 tie bar
|AD-A289926| p 2751 N95-30927
Effective bandwidth techniques in bufferless and buffered ATM multiplexers
|PB95-207072| p 2862 N95-31185
Numerical solution of a singular integral equation arising from a sequential probability ratio test
|AD-A293463| p 2963 N95-31375
Emerging applications in probability (Sensor management)
|AD-A292781| p 2749 N95-31433
Visual processing of object velocity and acceleration
|AD-A292789| p 2929 N95-31436
Monte Carlo tests of the ELIPGRID-PC algorithm
|DE95-010811| p 2943 N95-32030
A probabilistic design method applied to smart composite structures
|NASA-TM-106715| p 2899 N95-32206
PROBLEM SOLVING
Integrals of motion in the two Killing vector reduction of general relativity
|DE95-616281| p 3018 N95-30431
Use of element-by-element preconditioners to solve large scale partially separable optimization problems
|PB95-195772| p 2957 N95-30692
Study of the generalized solutions of n-body type problems with weak forces
|DE95-613381| p 2958 N95-30820
Training metacognitive skills for problem solving
|AD-A290310| p 2959 N95-31002
Pseudo-time methods for constrained optimization problems governed by PDE
|NASA-CR-195081| p 2959 N95-31120
QMR methods in computational fluid dynamics
|DE95-010293| p 2872 N95-31132
Local solutions of harmonical and bi-harmonical equations, universal field equation and self-dual configurations of Yang-Mills fields in four dimensions
|DE95-620521| p 2966 N95-31379
Multipoint quadratic approximation for numerical optimization
|AD-A293837| p 2961 N95-31557
A cognitive architecture for solving ill-defined problems
|AD-A293582| p 2929 N95-31686
PROCESS CONTROL (INDUSTRY)
System identification for robust process control. Nominal models and error bounds
|PB95-197026| p 2839 N95-30777
Network user's guide
|DE95-009185| p 2942 N95-31694
France --- modeling and verification of parallel computer systems
|PB95-208385| p 2949 N95-32371
Synthesis of separation systems: Methods and applications in downstream gas processes
|PB95-208518| p 2798 N95-32372
PROCESSING
Innovative processing of composites for ultra-high temperature applications, book 4
|AD-A290892| p 2786 N95-30867

PROCUREMENT MANAGEMENT
A case study of the teaming concept in the procurement of the V-22 aircraft
| AD-A293770 | p 2752 N95-31578
Report to the Secretary of Defense. Acquisition reform: Comparison of Army's commerical helicopter buy and private sector buys
| GAO/NSIAD-95-54 | p 3021 N95-31659
Report to the Chairman, Legislation and National Security Subcommittee, Committee on Government Operations, House of Representatives. C-17 Aircraft program: Improvements in initial provisioning process
| GAO/NSIAD-94-63 | p 2741 N95-32194
PRODUCT DEVELOPMENT
Feature-based modeling of product families
| PB95-207148 | p 2933 N95-30568
The role of advanced engineering simulation in model-based design
| DE95-008815 | p 2934 N95-30796
National Laboratories: Are their R and D activities related to commercial product development? Report to Congressional Requesters
| GAO/PEMD-95-2 | p 3027 N95-31345
Computational methods for control and optimal design of aerospace systems
| AD-A292861 | p 2751 N95-31451
Initial evaluation of the Oregon State University planetary boundary layer column model for ITWS applications
| AD-A293775 | p 2920 N95-31465
F-200(TM): The new solution for fire protection p 2776 N95-31770
Advanced turbine systems program conceptual design and product development
| DE95-000088 | p 2890 N95-32163
PRODUCTION COSTS
An assessment of the cost of microwave sintering ceramic tiles for armor applications. Phase 2 report
| DE95-010000 | p 2816 N95-31103
Large-area, triple-junction a-Si alloy production scale-up
| DE95-004067 | p 2904 N95-31163
PRODUCTION ENGINEERING
Development of flexible feeder techniques
| PB95-196317 | p 2934 N95-30663
Processing of polymers using supercritical fluids
| AD-A292880 | p 2819 N95-31410
PRODUCTION PLANNING
Feature-based modeling of product families
| PB95-207148 | p 2933 N95-30568
PRODUCTIVITY
Experimental research into usability and organization impact of workflow software
| PB95-197679 | p 2933 N95-30454
Towards increased productivity of algorithm implementation
| AD-A292862 | p 2940 N95-31452
Biomass production by fescue and switchgrass alone and in mixed swards with legumes
| DE95-009137 | p 2909 N95-31612
PROFILOMETERS
A laser-based ice shape profilometer for use in icing wind tunnels
| NASA-TM-106936 | p 2880 N95-30851
PROGRAM VERIFICATION (COMPUTERS)
Validation of the NPARC code for nozzle afterbody flows at transonic speeds
| NASA-TM-106971 | p 2742 N95-30704
An approach to automated reasoning about operational semantics
| AD-A291127 | p 2936 N95-31228
Proceedings of the 19th Annual Software Engineering Workshop
| NASA-CR-189411 | p 2936 N95-31234
Applying program comprehension techniques to improve software inspections p 2937 N95-31241
An experiment to assess the cost-benefits of code inspections in large scale software development p 2937 N95-31242
A process improvement model for software verification and validation p 2938 N95-31243
Experimental control in software reliability certification p 2938 N95-31248
Penelope reference manual: Version 3-3 (C001). Includes Larch/Ada specification manual for sequential Ada (C002)
| AD-A289828 | p 2942 N95-31683
Automatic verification and synthesis of finite-state hard real-time systems
| AD-A291279 | p 2964 N95-32287
France --- modeling and verification of parallel computer systems
| PB95-208385 | p 2949 N95-32371
PROGRAMMERS
A graphical programming language for service robots in semi-structured environments p 2935 N95-30831
Integrated high performance distributed system
| AD-A292821 | p 2947 N95-31445
PROGRAMMING ENVIRONMENTS
Leveraging object-oriented development at Ames p 2938 N95-31244
Integrated high performance distributed system
| AD-A292821 | p 2947 N95-31445
Using process to integrate Software Engineering Environments (Software Technology for Adaptable, Reliable Systems (STARS) program)
| AD-A292816 | p 2946 N95-32290
Integrating a SEE for megaprogramming: Lessons learned (Software Technology for Adaptable, Reliable Systems (STARS) program)
| AD-A292838 | p 2946 N95-32292
PROGRAMMING LANGUAGES
C++ as an introductory programming language
| PB95-195715 | p 2933 N95-30539
A graphical programming language for service robots in semi-structured environments p 2935 N95-30831
Unification of LARCH and Z-based object models to support algebraically-based design refinement: The LARCH perspective
| AD-A289235 | p 2935 N95-30999
An approach to automated reasoning about operational semantics
| AD-A291127 | p 2936 N95-31228
Development of a structured design and programming methodology for expert systems shells utilizing a visual programming language: Application of structured methodology to the MK92 maintenance advisor expert system, performance module prototype
| AD-A289897 | p 2939 N95-31391
Towards increased productivity of algorithm implementation
| AD-A292862 | p 2940 N95-31452
The occurrence of continuation parameters in CPS terms
| AD-A292952 | p 2941 N95-31460
PORK object system programmer's guide
| AD-A293596 | p 2942 N95-31688
Integration issues in modular mission management aid development p 2841 N95-32133
PROJECT MANAGEMENT
A system simulation development project: Leveraging resources through partnerships
| NASA-TM-106962 | p 2753 N95-30514
Domain analysis for the reuse of software development experiences p 2936 N95-31236
Lessons learned in transitioning to an open systems environment p 2938 N95-31245
Unmanned aerial vehicles. 1994 master plan p 2751 N95-31416
Recommended techniques for effective maintainability. A continuous improvement initiative of the NASA Reliability and Maintainability Steering Committee
| NASA-TM-4628 | p 2892 N95-31530
A case study of the teaming concept in the procurement of the V-22 aircraft
| AD-A293770 | p 2752 N95-31578
Software Process Framework. Tool to determine consistency with the CMM (Software Technology for Adaptable, Reliable Systems (STARS) program)
| AD-A292815 | p 2946 N95-32289
PROJECT PLANNING
Defining manually enactable processes using the process definition information organizer templates (Software Technology for Adaptable, Reliable Systems (STARS) program)
| AD-A292854 | p 2946 N95-32293
PROJECTILES
Fast-acting valve for projective launching systems
| AD-D017357 | p 2888 N95-30416
Scaling of cross sections in ion-atom collisions
| DE95-008938 | p 2978 N95-30573
Three-dimensional (3D) large fluid flow computations for US Army applications on KSR-1, CM-200, CM-5, and Cray C-90
| AD-A293125 | p 2869 N95-30889
PROPELLANT ADDITIVES
Oscillatory combustion of aluminized AP/HTPB propellants p 2800 N95-31286
Flame structure studies of neat and NH3 doped H2/N2O flames employing molecular beam mass spectrometry and modeling p 2801 N95-31313
PROPELLANT BINDERS
Laser pyrolysis of HTPB p 2800 N95-31298
A study of gas-phase processes during the deflagration of RDX composite propellants using a triple quadrupole mass spectrometer p 2801 N95-31304
AP reclamation and reuse in RSRM propellant p 2772 N95-31751
Thermoplastic elastomers as a binder in composite propellants
| PB95-211553 | p 2837 N95-32249
PROPELLANT COMBUSTION
Survey of recent Al2O3 droplet size data in solid rocket chambers, nozzles, and plumes p 2770 N95-31195
Viscous heating of liquid layers under intense shear p 2827 N95-31206
Development of a new instrument for rocket engine combustion diagnostics p 2799 N95-31211
Design and testing of an oxidizer-rich preburner p 2799 N95-31212
Unsteady laser augmented combustion of pure oxidizers AP and RDX p 2799 N95-31284
An ignition model for modern double base propellants p 2800 N95-31292
Progress in developing propellant ignition systems based upon electrically conductive polymers p 2800 N95-31300
The oxidation of carbon monoxide by nitrous oxide p 2801 N95-31309
Flame structure studies of neat and NH3 doped H2/N2O flames employing molecular beam mass spectrometry and modeling p 2801 N95-31313
RDX laser-assisted flame structure p 2801 N95-31314
Combustion of LOX with H2(sub g) under subcritical and supercritical conditions p 2797 N95-31717
Effects of gas-phase thermal expansion on the stability of deflagration through a porous energetic material
| DE95-004382 | p 2797 N95-31824
Combustion response to acoustic perturbation in liquid rocket engines p 2770 N95-31972
PROPELLANT DECOMPOSITION
Flame structure studies of neat and NH3 doped H2/N2O flames employing molecular beam mass spectrometry and modeling p 2801 N95-31313
The physical and chemical processes governing CO2 laser-induced pyrolysis and combustion of the solid propellants RDX, ADN, XM39, and M43 p 2836 N95-31531
PROPELLANT TESTS
Pulse forming network in the ETC combustion characterization of plasma augmented solid propellants p 2799 N95-31205
Viscous heating of liquid layers under intense shear p 2827 N95-31206
PROPELLANTS
Analytical instrumentation for environmental research
| AD-A292832 | p 2908 N95-31447
PROPELLERS
Computational modeling of coating integrity effects on impressed current cathodic protection system
| AD-A293256 | p 2815 N95-30894
PROPORTIONAL COUNTERS
Low energy solar neutrino experiments: The Soviet American Gallium Experiment (SAGE)
| DE95-010159 | p 3031 N95-30618
Experimental characterisation of gas microstrip detectors. Part 3: Lifetime characteristics
| PB95-192845 | p 2880 N95-30691
PROPOSALS
Research proposal
| AD-A293207 | p 3032 N95-30899
PROPULSION
A turbulence module for the NPARC code
| NASA-CR-198358 | p 2959 N95-30855
Catapult-launching of the RAFALE design and experimentation p 2752 N95-32008
PROPULSION SYSTEM CONFIGURATIONS
Numerical simulation of ram accelerator performance including transient effects during initiation of combustion and sensitivity studies p 2799 N95-31203
PROPULSION SYSTEM PERFORMANCE
Object-oriented approach for gas turbine engine simulation
| NASA-TM-106970 | p 2754 N95-30594
Investigation of ram accelerator performance capabilities p 2799 N95-31204
Flight assessment of the onboard propulsion system model for the Performance Seeking Control algorithm on an F-15 aircraft
| NASA-TM-4705 | p 2756 N95-31425
Experiment of rocket-ram combined combustor
| NAL-TR-1249 | p 2769 N95-31739
CFD assessment of the pollutant environment from RD-170 propulsion system testing p 2772 N95-31749
PROPULSIVE EFFICIENCY
Investigation of ram accelerator performance capabilities p 2799 N95-31204
PROPYLENE
Composite polymer electrolyte for lithium batteries
| AD-A293924 | p 2820 N95-31514
PROTECTIVE COATINGS
Interfacial studies of coated fiber reinforced glass-ceramic matrix composites
| AD-A290780 | p 2783 N95-30433
High temperature barrier coatings for refractory metals
| NASA-CR-195475 | p 2802 N95-30531

Computational modeling of coating integrity effects on impressed current cathodic protection system
[AD-A293256] p 2815 N95-30894
The impact of microbiologically influenced corrosion on protective polymer coatings
[AD-A288896] p 2816 N95-30997
Brush seal shaft wear resistant coatings
[NASA-CR-198950] p 2889 N95-31382
Comparison of cathodic protection currents on 70/30 copper-nickel and alloy 625 piping systems
[AD-A292953] p 2807 N95-31561
Response of dual-layered structures subjected to shock pressure wave
[AD-A293731] p 2896 N95-31568
Assessment of pollution prevention and control technology for plating operations p 2776 N95-31771
Thin-film sulfuric acid anodizing as a replacement for chromic acid anodizing p 2776 N95-31772
Environmentally regulated aerospace coatings p 2777 N95-31775
Convergent spray process for environmentally friendly coatings p 2777 N95-31776
Robotic weld overlay coatings for erosion control
[DE95-009643] p 2809 N95-32098
Minutes of the fourth annual workshop on chromate replacements in light metal finishing
[DE95-010937] p 2810 N95-32241

PROTECTORS
Releaseable unconstrained inflatable body protector
[AD-D017350] p 2930 N95-30552

PROTEINS
Absorption and ionization spectra of model rubredoxins
[AD-A293668] p 2796 N95-31691

PROTOCOL (COMPUTERS)
Protocols for integrity constraint checking in federated databases
[PB95-197695] p 3022 N95-30456
Holistic analysis of gamma-ray spectra in instrumental neutron activation analysis
[PB95-214458] p 2979 N95-30639
Wide area networking R&D
[AD-A291057] p 2947 N95-30868
Algorithms for categorizing multiprocessor communication under invalidate and update-based coherence protocols
[AD-A290022] p 2947 N95-30930
Client server architecture for multidatabase access. Ingres SQL server
[PB95-192852] p 2947 N95-31051
Gigabit testbed research project
[DE95-010728] p 2945 N95-32270

PROTON BEAMS
Polarized proton beams
[DE95-010843] p 2987 N95-32031
Monte Carlo simulations of muon production
[DE95-009554] p 2988 N95-32063

PROTON IMPACT
Scaling of cross sections in ion-atom collisions
[DE95-008938] p 2978 N95-30573

PROTON SCATTERING
Coulomb correction calculations of pp Bremsstrahlung
[DE95-616349] p 2982 N95-31176

PROTON-PROTON REACTIONS
WW and WZ production at the tevatron
[DE95-011014] p 2981 N95-30970

PROTONS
On explanation of proton electromagnetic form Factor near p (anti p)-threshold from the PS-170 experiment
[DE95-613766] p 2977 N95-30508
Study of cross-tail current carriers in magnetotail p 3005 N95-30804
Experimental results on charge exchange reactions with delta excitations and polarization studies of delta and N(sup *) (1440) resonances
[DE95-614022] p 2981 N95-30913
The superconducting kaon spectrometer
[DE95-010436] p 2982 N95-32159
Spin puzzle in nucleon
[DE95-613654] p 2991 N95-32353

PROTOTYPES
Development of a novel wind lidar, phase 1
[AD-A292703] p 2849 N95-30935
Mobile electric power
[AD-A292721] p 2860 N95-30940
IR materials producibility
[AD-A293330] p 2998 N95-31141
The quad-service satellite transmitting and receiving system for medical supply support: A battlefield interoperability and communications system prototype, volume 2. User documentation
[AD-A292835] p 2851 N95-31448
The quad-service satellite transmitting and receiving system for medical supply support: A battlefield interoperability and communications system prototype, volume 1
[AD-A292836] p 2851 N95-31449
Catapult-launching of the RAFALE design and experimentation p 2752 N95-32008
A programming interface for application-aware adaptation in mobile computing
[AD-A293107] p 2943 N95-32019

PROVING
Plaquette expansion proof and interpretation
[DE95-616282] p 2965 N95-30432
Strange compactification theorem: Infinite processes and the 3-dimensional poincare conjecture 6. Part A
[PB95-207924] p 2965 N95-30504
Extension to higher dimensions of the Jaeschke-Eicker result on the standardized empirical process
[PB95-206868] p 2965 N95-30523
Summary of 1993 Atlantic tropical cyclone activity and verification of author's forecast. A year of unanticipated light hurricane activity and a poor forecast: The expected dissipation of the El Nino did not take place and Caribbean basin surface pressure became quite high p 2918 N95-30842
The occurrence of continuation parameters in CPS terms
[AD-A292952] p 2941 N95-31460
Investigation of cleanliness verification techniques for rocket engine hardware p 2770 N95-31806

PROVISIONING
Report to the Chairman, Legislation and National Security Subcommittee, Committee on Government Operations, House of Representatives. C-17 Aircraft program: Improvements in initial provisioning process
[GAO/NSIAD-94-63] p 2741 N95-32194

PSEUDOMONAS
Degradation of TCE using sequential anaerobic biofilm and aerobic immobilized bed reactor p 2780 N95-31791

PSYCHOLOGICAL TESTS
Selection of Swedish scholastic aptitude test takers as a function of socioeconomic background and ability: Evaluation through follow-up
[PB95-212072] p 3021 N95-30699
Non-comparability of female and male admission test takers: Evaluation through follow-up
[PB95-212080] p 3021 N95-30700
Using computerized neuropsychological testing to assess aviator skills
[AD-A293227] p 2928 N95-30905
Psychological pilot selection in the US Air Force, the Luftwaffe, and the German Aerospace Research Establishment
[AD-A293779] p 2928 N95-31376
Optimizing the long-term retention of skills: Structural and analytic approaches to skill maintenance
[AD-A293798] p 2929 N95-31585

PSYCHOMOTOR PERFORMANCE
Psychological pilot selection in the US Air Force, the Luftwaffe, and the German Aerospace Research Establishment
[AD-A293779] p 2928 N95-31376
Contextual interference effects on acquisition and transfer of a complex motor task
[AD-A293788] p 2929 N95-31583

PUBLIC HEALTH
Particulate air pollution and increased mortality: Biological plausibility for causal relationship
[DE95-006161] p 2909 N95-31703
Combatting urban air pollution through Natural Gas Vehicle (NGV) analysis, testing, and demonstration
[DE95-008300] p 2911 N95-32156

PULSARS
Observations of accreting pulsars
[NASA-CR-198931] p 3028 N95-30469

PULSE AMPLITUDE
Electromyostimulation, circuits and monitoring
[NASA-TM-110741] p 2926 N95-30846

PULSE CODE MODULATION
Computer simulation results for PCM/PM/NRZ receivers in nonideal channels p 2765 N95-32225

PULSE COMMUNICATION
Design and testing of an optimal digital link capable of 14-channel transmission
[AD-A288505] p 3000 N95-31652

PULSE DURATION
Electromyostimulation, circuits and monitoring
[NASA-TM-110741] p 2926 N95-30846
Free electron laser as energy driver for inertial confinement fusion
[DE95-614252] p 2884 N95-30914
Diagnosing high density, fast-evolving plasmas using x-ray lasers
[DE95-010734] p 3006 N95-32028
Infrared and millimeter wave detection using thin films of Pb doped BiSrCaCuO superconductor p 2840 N95-32129

PULSE GENERATORS
Pulse power for high energy density physics experiments
[DE95-010868] p 2992 N95-31232
Basic science with pulsed power and some off-the-wall ideas
[DE95-009486] p 2854 N95-32050
Voltage controlled MESFET pulse shape generator
[DE95-011656] p 2865 N95-32300

PULSE RADAR
Prospects for high accuracy time dissemination and synchronization using coded radar pulses from a low-earth orbiting spacecraft p 2971 N95-32339

PULSE RATE
The HYLIFE-2 inertial fusion energy power plant concept and implications for IFE
[DE95-010561] p 2994 N95-32074

PULSED LASER DEPOSITION
Modeling of thermal, electronic, hydrodynamic, and dynamic deposition processes for pulsed-laser deposition of thin films
[DE95-008906] p 2813 N95-30572
Fabrication and modification of metal nanocluster composites using ion and laser beams
[DE95-009131] p 2784 N95-30731
Substrate heating measurements in pulsed ion beam film deposition
[DE95-010862] p 2818 N95-31377
Ion-Assisted Pulsed Laser Deposition of amorphous tetrahedral-coordinated carbon films
[DE95-010861] p 2885 N95-31394

PULSED LASERS
Morphology and microstructure of (111) crystalline CeO2 films grown on amorphous SiO2 substrates by pulsed-laser ablation
[DE95-008842] p 3009 N95-30542
Reflectivity of plasmas created by high-intensity, ultra-short laser pulses
[DE95-009536] p 3004 N95-30742
Picosecond phase conjugation: New applications, devices, and materials
[AD-A293195] p 3013 N95-30982
Design considerations for a Density-Channel-Guided laser wake-field accelerator
[AD-A292876] p 2884 N95-31190
Theory of unsteady combustion of solids: Investigation of Quasi-steady assumption p 2800 N95-31285
Infrared and millimeter wave detection using thin films of Pb doped BiSrCaCuO superconductor p 2840 N95-32129
Femtosecond, Cr(4+):YAG laser
[DE95-004964] p 2887 N95-32155
The development of a pulsed laser imaging system for natural gas leak detection
[DE95-011407] p 2887 N95-32280

PULSED RADIATION
Numerical studies of nonlinear optical pulse propagation p 2998 N95-31411

PUMPING
Spatial time-series: Pollution pattern recognition under irregular interventions
[AD-A293830] p 2909 N95-31556

PUMPS
Gear pump with reduced fluid-borne noise
[AD-D017362] p 2887 N95-30399
Failure analysis of a repairable system: The case study of a cam-driven reciprocating pump
[AD-A293144] p 2889 N95-30949

PYRIDINES
Electronic structure of Donor-Spacer-Acceptor molecules of potential interest for molecular electronics 4. Geometry and device properties of P3CNQ and Q3CNQ
[AD-A293717] p 2986 N95-31832

PYROELECTRICITY
Large area smart piezoelectric and pyroelectric sensors
[AD-A291487] p 2859 N95-30561
Nonlinear optics in novel composite media
[AD-A293886] p 2999 N95-31542

PYROLYSIS
Laboratory simulated hydrothermal alteration of sedimentary organic matter from Guaymas Basin, Gulf of California
[NASA-CR-198951] p 2914 N95-30865
Synthesis and selected micro-mechanical properties of titanium nitride thin films by the pyrolysis of tetrakis titanium in ammonia
[DE95-010224] p 2818 N95-31187
Laser pyrolysis of HTPB p 2800 N95-31298

The physical and chemical processes governing CO2 laser-induced pyrolysis and combustion of the solid propellants RDX, ADN, XM39, and M43
p 2836 N95-31531
BioFacts: Fueling a stronger economy, thermochemical conversion of biomass
|DE94-006866| p 2905 N95-31822

PYROTECHNICS
A manual for pyrotechnic design, development and qualification
|NASA-TM-110172| p 2766 N95-31358

Q

Q FACTORS
Langasite crystals growth with quality factor Q, that exceeds the Q of quartz, and which are suitable for high-precision resonators
|AD-A293397| p 3013 N95-30969

QUADRATIC EQUATIONS
Multipoint quadratic approximation for numerical optimization
|AD-A293837| p 2961 N95-31557

QUADRATURES
Spectral methods in complex geometries
|PB95-208336| p 2955 N95-30495

QUADRUPOLES
Gravitational-radiation damping of compact binary systems to second post-Newtonian order
|PB95-207882| p 2912 N95-30588
Gravitational waves from inspiralling compact binaries: Energy loss and waveform to second-post-Newtonian order
|PB95-207890| p 2913 N95-30590

QUALITATIVE ANALYSIS
A study of gas-phase processes during the deflagration of RDX composite propellants using a triple quadrupole mass spectrometer p 2801 N95-31304
Contactless characterization of semiconductors using laser-induced surface photo-charge voltage measurements
|AD-A293618| p 2863 N95-31725

QUALITY
The role of advanced engineering simulation in model-based design
|DE95-008815| p 2934 N95-30796

QUALITY CONTROL
Quality in applied science
|PB95-196390| p 2891 N95-30520
Building an experience factory for maintenance
p 2937 N95-31237
Closing the loop on improvement: Packaging experience in the Software Engineering Laboratory
p 2937 N95-31238
Process maturity progress at Motorola Cellular Systems Division p 2937 N95-31239
The Personal Software Process: Downscaling the factory p 2937 N95-31240
An experiment to assess the cost-benefits of code inspections in large scale software development
p 2937 N95-31242
A process improvement model for software verification and validation p 2938 N95-31243
Experimental control in software reliability certification
p 2938 N95-31248
Profile of software engineering within the National Aeronautics and Space Administration (NASA)
p 2939 N95-31252
Quality assurance tendering and awarding contracts
|PB95-197760| p 2891 N95-31362
Management of major system programs and projects. Handbook
|NHB-7120.5| p 3021 N95-31380
Photovoltaic module certification/laboratory accreditation criteria development
|DE95-004063| p 2905 N95-31381
Recommended techniques for effective maintainability. A continuous improvement initiative of the NASA Reliability and Maintainability Steering Committee
|NASA-TM-4628| p 2892 N95-31530

QUANTITATIVE ANALYSIS
A study of gas-phase processes during the deflagration of RDX composite propellants using a triple quadrupole mass spectrometer p 2801 N95-31304
Volumetric and electro analytical techniques for chemical characterization of nuclear grade Ag-In-Cd alloys
|DE95-620664| p 2807 N95-31407
Novel mass spectrometric instrument for gaseous and particulate characterization and monitoring
|DE95-000047| p 2881 N95-31694
Cleaning verification by air/water impingement
p 2782 N95-31805
Investigation of cleanliness verification techniques for rocket engine hardware p 2770 N95-31806
Determination of halogens in a petroleum product by ion chromatography
|DE95-002056| p 2797 N95-31840

QUANTUM CHEMISTRY
Acidity and basicidity of nitro substituted imidazoles
|AD-A293969| p 2836 N95-31526

QUANTUM CHROMODYNAMICS
On the Compton twist-3 asymmetries
|DE95-613627| p 3017 N95-30371
Current issues in perturbative QCD
|DE95-008448| p 2975 N95-30388
Approximate analytic diagonalization of lattice QCD
|DE95-616332| p 3018 N95-30444
Simulation with complex measures
|DE95-616333| p 2955 N95-30445
Theoretical high energy physics
|DE95-003107| p 2991 N95-30527
HERA and the asymptotic behaviour of F2(sup rho)
|PB95-195764| p 2956 N95-30540
Multichannel resonances in coupled channels of meson scattering: Scalar sector
|DE95-613783| p 2981 N95-30912
Hadronic production of B(sub c)-mesons
|DE95-620536| p 2983 N95-31216
Scaling behaviour of leptonic decay constants for heavy quarkonia and heavy mesons
|DE95-620539| p 2983 N95-31218
Double charmed baryons production at B-factory
|DE95-620540| p 2983 N95-31219
Pion-pair production by two photons
|DE95-737162| p 2983 N95-31223
Pion-nucleon and kaon-nucleon scattering lengths in QCD sum rules
|DE95-737278| p 2983 N95-31227
Electromagnetic hadron mass differences and estimation of isotopic symmetry violation parameters of QCD vacuum from quark model
|DE95-613628| p 2985 N95-31621
Spin structure in high energy processes
|DE95-008628| p 2993 N95-31627
Form factor of the process gamma(*) gamma(*) yields pi(sup 0) for small virtuality of one of the photons and QCD sum rules (2): Sum rule
|DE95-613629| p 2988 N95-32078
Applications of chiral symmetry
|DE95-009552| p 2988 N95-32079
A search for jet handedness in hadronic Z-0 decays
|DE95-010099| p 2988 N95-32083
A measurement of quark and gluon jet differences at the Z(sup 0) resonance
|DE95-010666| p 2989 N95-32266
An experimental study of QCD and jets in e(+)e(-) annihilation
|DE95-010667| p 2989 N95-32267
On hadronic production of the B(sub c) meson
|DE95-613726| p 2991 N95-32304
Spin puzzle in nucleon
|DE95-613654| p 2991 N95-32353

QUANTUM EFFICIENCY
Photochemistry of intermolecular C-H bond activation reactions
|DE95-008991| p 2978 N95-30574

QUANTUM ELECTRODYNAMICS
Experiments with highly charged ions up to bare U(sup 92+) on the electron beam ion trap
|DE95-008827| p 2982 N95-31174
Quantum 1/f noise in high technology applications including ultrasmall structures and devices
|AD-A292812| p 2862 N95-31442

QUANTUM ELECTRONICS
Development of germanium-silicon growth technology
|AD-A293199| p 3013 N95-30983
Quantum and nonlinear optics research
|AD-A293879| p 2999 N95-31519
Solid state research
|AD-A293083| p 3015 N95-31826

QUANTUM MECHANICS
Theoretical absorption spectroscopy of high-temperature metal vapors: Model and experiment compared
|AD-A290872| p 2791 N95-30409
Multi-particle correlations in quaternionic quantum systems
|DE95-616271| p 3018 N95-30424
Quantum dynamics in regions of quaternionic curvature
|DE95-616276| p 3018 N95-30426
The Foldy-Wouthuysen transformation
|DE95-616277| p 2976 N95-30427
Dynamics of Current Driven Disordered Josephson Junction Arrays
|DE95-009418| p 3014 N95-31231
Atomic approaches in metastable antiprotonic helium atoms. Reply to Analysis of the lifetimes and fractions of antiprotons trapped in metastable antiprotonic helium states by I. Shimamhura and M. Kimura --- mura
|DE95-737228| p 2986 N95-31658

QUANTUM OPTICS
Quantum and nonlinear optics research
|AD-A293879| p 2999 N95-31519

QUANTUM STATISTICS
The search for the decay of Z boson into two gamma as a test of Bose statistics
|DE95-616373| p 2976 N95-30393
Shnirelman peak in the level spacing statistics
|DE95-623599| p 3019 N95-31276

QUANTUM THEORY
Covariant phase space formulations of superparticles and supersymmetric WZW models
|DE95-616278| p 2964 N95-30428
The solutions of affine and conformal affine Toda field theory
|DE95-616280| p 2965 N95-30430
Two-loop vacuum amplitudes in a non-Abelian gauge theory on S(sub 4)
|DE95-616284| p 3018 N95-30436
Beyond the variational principle in quantum field theory
|DE95-616286| p 3018 N95-30438
Top quark and Higgs boson masses from wormhole physics
|DE95-616384| p 2978 N95-30580
Some functional solutions of the Yang-Baxter equation
|DE95-613584| p 2966 N95-30635
Introduction to the theory of Goyaks: Operator manifold approach to geometry and particle physics
|DE95-613460| p 2980 N95-30740
Light-front dynamics of Chern-Simons systems
|DE95-613467| p 3019 N95-30741
A BRST charge for non-critical W2(s) strings
|DE95-613470| p 3019 N95-30771
Partons and black holes
|DE95-009921| p 3029 N95-31102
Irreducible Green's Functions method in the theory of highly correlated systems
|DE95-614446| p 3019 N95-31186
Quantization of a relativistic particle on the SL(2,R) manifold based on Hamiltonian reduction
|DE95-737163| p 2983 N95-31224
Frobenius algebras and quantum Yang-Baxter equation 2
|PB95-212130| p 2960 N95-31229
Antipodes and integrals in Hopf algebras over rings and quantum Yang-Baxter equation
|PB95-212155| p 2961 N95-31397
Variational optimization in quantum field theory
p 3020 N95-31646
Research progress report
|DE95-010726| p 3030 N95-32269

QUANTUM WELL LASERS
Electron-optical nonlinear interaction in asymmetric quantum-well laser heterostructures
|DE95-613443| p 2883 N95-30609
TV-VI semiconductor quantum well lasers, physics and engineering p 2883 N95-30805
Carrier dynamics and optical properties of GaAs- and InP-based strained quantum well lasers
p 2886 N95-31848

QUANTUM WELLS
Magnetoluminescence characterization of quantum well structures
|DE95-008527| p 3008 N95-30381
Electron-optical nonlinear interaction in asymmetric quantum-well laser heterostructures
|DE95-613443| p 2863 N95-30609
The quantum interference effect in semiconductor space charge layers studied by Feynman path integrals: General formalism and illustrative examples
|DE95-614483| p 3010 N95-30653
Fractal quantum well heterostructures for broadband light emitters
|DE95-009579| p 2860 N95-30707
TV-VI semiconductor quantum well lasers, physics and engineering p 2883 N95-30805
Visible light emitting materials and injection devices
|AD-A292701| p 2786 N95-30934
Development of germanium-silicon growth technology
|AD-A293199| p 3013 N95-30983
Quantum and nonlinear optics research
|AD-A293879| p 2999 N95-31519
Carrier dynamics and optical properties of GaAs- and InP-based strained quantum well lasers
p 2886 N95-31848
Investigation of the basic physics of high efficiency semiconductor hot carrier solar cell
|NASA-CR-198945| p 2906 N95-32212

QUARK MODELS
Large scale periodicity of the universe and baryogenesis
[DE95-613461] p 3028 N95-30366
Phenomenology of the two Higgs doublet sector of a quark-lepton symmetric model
[DE95-616337] p 2976 N95-30446
Instantaneous chiral quark model for relativistic mesons in a hot and dense medium
[DE95-613782] p 2980 N95-30911
Electromagnetic hadron mass differences and estimation of isotopic symmetry violation parameters of QCD vacuum from quark model
[DE95-613628] p 2985 N95-31621

QUARKS
Strange-matter stars
[DE95-008446] p 3028 N95-30361
Dynamical analogy of Cabibbo-Kobayashi-Maskawa matrices
[DE95-613462] p 2975 N95-30367
Current issues in perturbative QCD
[DE95-008448] p 2975 N95-30388
Approximate analytic diagonalization of lattice QCD
[DE95-616332] p 3018 N95-30444
Phenomenology of the two Higgs doublet sector of a quark-lepton symmetric model
[DE95-616337] p 2976 N95-30446
Hadronic production of S-wave and P-wave charmed beauty mesons via heavy quark fragmentation
[DE95-008737] p 2977 N95-30465
Theoretical high energy physics
[DE95-003107] p 2991 N95-30527
Possible reason why leptons are lighter than quarks
[DE95-616383] p 2978 N95-30579
Top quark and Higgs boson masses from wormhole physics
[DE95-616384] p 2978 N95-30580
Introduction to the theory of Goyaks: Operator manifold approach to geometry and particle physics
[DE95-613460] p 2980 N95-30740
Instantaneous chiral quark model for relativistic mesons in a hot and dense medium
[DE95-613782] p 2980 N95-30911
Testing vector boson dominance of electroweak interactions via e(+)e(-) (yields) f-bar f
[DE95-620528] p 2982 N95-31214
Scaling behaviour of leptonic decay constants for heavy quarkonia and heavy mesons
[DE95-620539] p 2983 N95-31218
Electromagnetic hadron mass differences and estimation of isotopic symmetry violation parameters of QCD vacuum from quark model
[DE95-613628] p 2985 N95-31621
SO(8) color as possible origin of generations
[DE95-613560] p 2988 N95-32069
Renormalization group analyses of particle masses in full four-generation fermion condensate scheme
[DE95-613595] p 2988 N95-32070
A search for jet handedness in hadronic Z-0 decays
[DE95-010099] p 2988 N95-32083
A measurement of quark and gluon jet differences at the Z(sup 0) resonance
[DE95-010666] p 2989 N95-32266
Charm photoproduction dynamics
[DE95-009106] p 2990 N95-32303
Thermal rho's in the quark-gluon plasma
[DE95-009543] p 3008 N95-32357

QUARTZ
Metrology of chrome on quartz photomasks using low voltage scanning electron microscopy. Part 1: Physical SEM parameters
[PB95-195780] p 2880 N95-30693

QUATERNIONS
Quantum dynamics in regions of quaternionic curvature
[DE95-616276] p 3018 N95-30426

QUERY LANGUAGES
Extending a multi-set relational algebra to a parallel environment
[PB95-207106] p 3023 N95-30566
Client server architecture for multidatabase access. Ingres SQL server
[PB95-192852] p 2947 N95-31051

QUEUEING THEORY
Analyzing GI/Erlang-r/1 queues
[PB95-197034] p 2949 N95-30400
Fitting discrete distributions on the first two moments
[PB95-197885] p 2950 N95-30462
Symmetric longest queue system
[PB95-197919] p 2950 N95-30808
Workshop on diffusion approximation in communication and stochastic systems theory
[AD-A292672] p 2952 N95-31055
Theory & numerical methods for problems in shape reconstruction and large deviations
[AD-A292674] p 2952 N95-31279
Analysis and modeling of an airport departure process
[AD-A293782] p 2749 N95-31581

QUINOLINE
Electronic structure of Donor-Spacer-Acceptor molecules of potential interest for molecular electronics 4. Geometry and device properties of P3CNQ and Q3CNQ
[AD-A293717] p 2986 N95-31832

R

RADAR APPROACH CONTROL
Integrated terminal weather system (ITWS) demonstration and validation operational test and evaluation
[AD-A293932] p 2749 N95-31521

RADAR ASTRONOMY
The Telecommunications and Data Acquisition Report
[NASA-CR-198911] p 2854 N95-32221

RADAR CORNER REFLECTORS
Physical optics polarization scattering matrix for a right-angle dihedral
[AD-A293036] p 3000 N95-31665

RADAR CROSS SECTIONS
Fast multipole methods for scattering computations
[AD-A291093] p 2848 N95-30869

RADAR DATA
Multisensor data fusion for integrated maritime surveillance p 2842 N95-32135
The application of noncoherent Doppler data types for Deep Space Navigation p 2765 N95-32226

RADAR DETECTION
Unconventional imaging field experiment plan
[AD-A291492] p 2846 N95-30562
Folded compact range development and coherent change detection measurement project
[DE95-009082] p 2853 N95-31628
Adaptive space-time processing for airborne radars based on Doppler pre-processing
[PB95-205464] p 2854 N95-32114

RADAR ECHOES
Point reflector model for the simulation of radar target glint and Doppler phenomena
[PB95-222980] p 2857 N95-32314

RADAR EQUIPMENT
The dynamic range of radar signal generation in the MSS-2 simulation facility
[AD-A293856] p 2857 N95-32259

RADAR IMAGERY
Apparatus and method for producing three-dimensional images
[AD-D017455] p 2847 N95-30727
Functions for processing synthetic aperture radar imagery
[AD-A293895] p 2851 N95-31510
Investigation of ground target detection methods in fully polarimetric wide angle synthetic aperture radar images
[AD-A293922] p 2851 N95-31513
Research in ground-to-air microwave imaging
[AD-A292907] p 2852 N95-31551

RADAR MEASUREMENT
Multiparameter radar measurements of precipitation in complex terrain: Meteorological and hydrological applications
[AD-A290786] p 2918 N95-30403
Middle atmosphere structure and dynamics: Lidar studies at the South Pole, Syowa and Urbana p 2916 N95-31736

RADAR RANGE
The dynamic range of radar signal generation in the MSS-2 simulation facility
[AD-A293856] p 2857 N95-32259

RADAR SCATTERING
Physical optics polarization scattering matrix for a right-angle dihedral
[AD-A293036] p 3000 N95-31665

RADAR SIGNATURES
Fast multipole methods for scattering computations
[AD-A291093] p 2848 N95-30869
Materials with controllable signature properties
[PB95-222964] p 2857 N95-32313

RADAR TARGETS
Unconventional imaging field experiment plan
[AD-A291492] p 2846 N95-30562
Detection of radar targets using higher-order statistics
[AD-D017442] p 2850 N95-31392
Multisensor data fusion for integrated maritime surveillance p 2842 N95-32135
Multiple Target Tracking based on constellation matching and Kalman filter p 2842 N95-32136
Feasibility study concerning an active millimeterwave sensor. Project phase MMS2.1
[PB95-210399] p 2882 N95-32245
The dynamic range of radar signal generation in the MSS-2 simulation facility
[AD-A293856] p 2857 N95-32259
Point reflector model for the simulation of radar target glint and Doppler phenomena
[PB95-222980] p 2857 N95-32314

RADAR TRACKING
Detection of radar targets using higher-order statistics
[AD-D017442] p 2850 N95-31392
Investigation of ground target detection methods in fully polarimetric wide angle synthetic aperture radar images
[AD-A293922] p 2851 N95-31513
Research in ground-to-air microwave imaging
[AD-A292907] p 2852 N95-31551
Multiple Target Tracking based on constellation matching and Kalman filter p 2842 N95-32136
The dynamic range of radar signal generation in the MSS-2 simulation facility
[AD-A293856] p 2857 N95-32259
Point reflector model for the simulation of radar target glint and Doppler phenomena
[PB95-222980] p 2857 N95-32314

RADAR TRANSMISSION
Adaptive space-time processing for airborne radars based on Doppler pre-processing
[PB95-205464] p 2854 N95-32114

RADIAL FLOW
Localization in tungsten heavy alloys subjected to shearing deformations under superimposed high pressures
[AD-A293177] p 2804 N95-30977

RADIANT COOLING
High-temperature oxidation behavior of iridium-rhenium alloys
[NASA-TM-106720] p 2803 N95-30593
Validity of the differential equations for ionization cooling
[DE95-010438] p 2989 N95-32160

RADIANT FLUX DENSITY
Simple model of foam spreading on liquid surfaces
[PB95-211207] p 2838 N95-30630

RADIATION ABSORPTION
Optimization of a thermoelectric IR-detector for low working temperature
[NASA-CR-198933] p 2880 N95-30752
Perpendicular electron heating by absorption of auroral kilometric radiation
[NASA-198815] p 2914 N95-30848

RADIATION BELTS
Low-latitude boundary layer near noon: An open field line model
[ATR-93(7270)-1] p 2914 N95-30773

RADIATION COUNTERS
Sensor Fusion and Nonlinear Prediction for Anomalous Event Detection
[DE95-009429] p 2933 N95-30602
The activities of the high energy physics program
[DE95-010155] p 2991 N95-30615
The design and construction of the muon arm in PHENIX
[DE95-010156] p 2978 N95-30616

RADIATION DAMAGE
Molecular dynamics simulations of high energy cascades in iron
[DE95-010116] p 2982 N95-31104
Microstructural and mechanical property changes in model Fe-Cu alloys
[DE95-010117] p 2805 N95-31105
Cascade damage in the ordered alloy Ni3Al
[DE95-009893] p 2809 N95-32104

RADIATION DETECTORS
Backgrounds and detector performance at a 2 x 2 TeV (mu)(+)(mu)(-) collider
[DE95-009107] p 2992 N95-30800

RADIATION DISTRIBUTION
The radiation conditioned by the 'velocity part' of the electromagnetic field of a moving charge
[DE95-613366] p 2846 N95-30605
Basic study of the pumping of a gamma-ray laser
[AD-A293561] p 2886 N95-31563

RADIATION DOSAGE
Neutron shielding point kernel integral calculation code for personal computer: PKN-pc
[DE95-717876] p 2980 N95-30760
Electromagnetic field exposure dosimeter
[AD-A293191] p 2927 N95-30981

RADIATION EFFECTS
Structural investigation of xenon ion-beam-irradiated glassy carbon
[DE95-616777] p 2977 N95-30474
Amorphization threshold in Si-implanted strained SiGe alloy layers
[DE95-008901] p 2804 N95-30797

Damage dosimetry and embrittlement monitoring of nuclear pressure vessels in real time by magnetic properties measurement
[DE95-011454] p 2894 N95-31254
Cascade damage in the ordered alloy Ni3Al
[DE95-009893] p 2809 N95-32104
Defect configurations in neutron-irradiated U3Si2
[DE95-009896] p 3016 N95-32105
Radiation effects in space: The Clementine 1 mission
[DE95-011513] p 3032 N95-32282
Investigation into the effects of VHF and UHF band radiation on Hewlett-Packard (HP) Cesium Beam Frequency Standards p 2970 N95-32332

RADIATION HARDENING
Microwave coupling into a slotted cavity. Additional results
[PB95-210381] p 2847 N95-30629

RADIATION HAZARDS
Z-scan using a dye laser
[PB95-222923] p 3002 N95-32312

RADIATION MEASUREMENT
Low energy solar neutrino experiments: The Soviet American Gallium Experiment (SAGE)
[DE95-010159] p 3031 N95-30618
History and status of the atmospheric radiation measurement program
[DE95-009951] p 2908 N95-30802
Contamination detection NDE for cleaning process inspection p 2781 N95-31802

RADIATION SHIELDING
Development of BERMUDA: A radiation transport code system. Part 3: A one-dimensional adjoint neutron transport code
[DE95-717875] p 2934 N95-30759
Neutron shielding point kernel integral calculation code for personal computer: PKN-pc
[DE95-717876] p 2980 N95-30760

RADIATION SOURCES
High energy pulsed microwave sources
[AD-A293334] p 2849 N95-31142

RADIATION SPECTRA
Computation of high-altitude hypersonic flow-field radiation p 2743 N95-30843

RADIATION TRANSPORT
Simple model of foam spreading on liquid surfaces
[PB95-211207] p 2838 N95-30630
Development of BERMUDA: A radiation transport code system. Part 3: A one-dimensional adjoint neutron transport code
[DE95-717875] p 2934 N95-30759

RADIATIVE RECOMBINATION
Fractal quantum well heterostructures for broadband light emitters
[DE95-009579] p 2860 N95-30707

RADIATIVE TRANSFER
Proceedings of the 16th Annual Conference on Atmospheric Transmission Models, volume 1
[AD-A293807] p 2915 N95-31575
Proceedings of the 16th Annual Conference on Atmospheric Transmission Models, volume 2
[AD-A293806] p 2916 N95-31604
Brightness temperature simulations for the physical and synoptic interpretation of advanced microwave sounding unit moisture channels p 2921 N95-31721
Preliminary design for Arctic atmospheric radiative transfer experiments
[DE95-009580] p 2917 N95-32080
Use of arm measurements to improve radiative transfer models used in climate models
[NASA-CR-199014] p 2921 N95-32184

RADICALS
Laboratory simulated hydrothermal alteration of sedimentary organic matter from Guaymas Basin, Gulf of California
[NASA-CR-198951] p 2914 N95-30865
Calculated structures and electronic absorption spectroscopy for magnesium phthalocyanine and its anion radical
[AD-A293672] p 2796 N95-31596

RADII
On the string equation at c = 1
[DE95-737161] p 3014 N95-31222

RADIO ANTENNAS
Proceedings of the antenna applications symposium, volume 1
[AD-A293258] p 2848 N95-30895

RADIO ASTRONOMY
A search for interstellar CH3D: Limits to the methane abundance in Orion-KL
[NASA-CR-198932] p 3029 N95-30751
The Telecommunications and Data Acquisition Report
[NASA-CR-198911] p 2854 N95-32221

RADIO COMMUNICATION
Design and testing of an optimal digital link capable of 14-channel transmission
[AD-A288505] p 3000 N95-31652
Residual and suppressed-carrier arraying techniques for deep-space communications p 2856 N95-32235
Digital signal processing in the radio science stability analyzer p 2857 N95-32240
Fast identification of some typical digital modulation schemes
[PB95-211454] p 2857 N95-32247

RADIO EQUIPMENT
High Frequency (HF) upgrade study for the Canadian Regional Operations Control Center (ROCC) AWACS Digital Information Link (RADIL) project
[AD-A293435] p 2850 N95-31367

RADIO FREQUENCIES
Structural, chemical and electronic properties of superconducting thin films and junctions
[AD-A292700] p 3012 N95-30933
Use of a variable frequency source with a single-mode cavity to process ceramic filaments
[DE95-010992] p 2817 N95-31152

RADIO FREQUENCY HEATING
An assessment of the cost of microwave sintering ceramic tiles for armor applications. Phase 2 report
[DE95-010000] p 2816 N95-31103
Dielectric property measurement of zirconia fibers at high temperatures
[DE95-010991] p 2821 N95-31705

RADIO FREQUENCY INTERFERENCE
Interference rejection techniques in a DS spread-spectrum HF radio system
[PB95-211660] p 2846 N95-30479

RADIO NAVIGATION
The Telecommunications and Data Acquisition Report
[NASA-CR-198911] p 2854 N95-32221
Laser retroreflector experiment on NAVSTAR 35 and 36 p 2887 N95-32347

RADIO RECEIVERS
Demodulators for optical fiber interferometers with (3 x 3) outputs
[AD-D017415] p 2995 N95-30402
Signal-processing theory for the TurboRogue receiver
[NASA-CR-198882] p 2846 N95-30581
Guidelines for the design of GPS and LORAN receiver controls and displays
[AD-A293753] p 2749 N95-31572
Computer simulation results for PCM/PM/NRZ receivers in nonideal channels p 2765 N95-32225
Residual and suppressed-carrier arraying techniques for deep-space communications p 2856 N95-32235
Feasibility study concerning an active millimeterwave sensor. Project phase MMS2.1
[PB95-210399] p 2882 N95-32245

RADIO RELAY SYSTEMS
High Frequency (HF) upgrade study for the Canadian Regional Operations Control Center (ROCC) AWACS Digital Information Link (RADIL) project
[AD-A293435] p 2850 N95-31367

RADIO TELEMETRY
Computer simulation results for PCM/PM/NRZ receivers in nonideal channels p 2765 N95-32225

RADIO TRACKING
Determination of the position of Jupiter from radio metric tracking of Voyager 1 p 2854 N95-32222
Laser retroreflector experiment on NAVSTAR 35 and 36 p 2887 N95-32347

RADIO TRANSMISSION
Wavefront simulator for evaluating RF communication array signal processors
[AD-D017372] p 2847 N95-30660

RADIO WAVES
Underdense heating of the ionosphere using oblique high power HF radiowaves p 2917 N95-31951

RADIOACTIVE AGE DETERMINATION
Atomic approaches in metastable antiprotonic helium atoms. Reply to Analysis of the lifetimes and fractions of antiprotons trapped in metastable antiprotonic helium states by I. Shimamhura and M. Kimura --- mura
[DE95-737228] p 2986 N95-31658

RADIOACTIVE ISOTOPES
Faster, cheaper radioanalytical methods
[DE95-009913] p 2797 N95-32061

RADIOACTIVE WASTES
Simulation of airborne electromagnetic measurements in three dimensional environments
[DE95-008546] p 2900 N95-30363
LLW solidification in cement: Effect of dilution
[DE95-010108] p 2798 N95-32091
Waste minimization via preparative scale high performance gel permeation chromatography
[DE95-011797] p 2798 N95-32360

RADIOACTIVITY
Behaviour of polymers in radioactive environments: Effects of dose speed
[DE95-621008] p 2818 N95-31221

RADIOISOTOPE BATTERIES
GPHS-RTGs in support of the Cassini RTG Program
[DE95-010306] p 2768 N95-30674
Welding isotopic heat sources for the cassini mission to Saturn
[DE95-060104] p 2890 N95-32367

RADIOLOGY
Summaries of fiscal year 1994 projects in medical applications and biophysical research
[DE95-010405] p 2925 N95-32040

RADIOMETERS
SeaWiFS technical report series. Volume 28: SeaWiFS algorithms, part 1
[NASA-TM-104566-VOL-28] p 2924 N95-31850

RADIUM
Faster, cheaper radioanalytical methods
[DE95-009913] p 2797 N95-32061

RAILGUN ACCELERATORS
A RASCAL in-bore dynamic analysis of the task B and task C electromagnetic railguns
[AD-A292742] p 2764 N95-30948

RAIN
NASA Tropical Rainfall Measurement Mission (TRMM): Effects of tropical rainfall on upper ocean dynamics, air-sea coupling and hydrologic cycle
[NASA-CR-189437] p 2919 N95-31123

RAIN FORESTS
Comparisons of target detection clutter using data from the 1993 FOPEN experiments
[AD-A293052] p 2852 N95-31606

RAINSTORMS
Multiparameter radar measurements of precipitation in complex terrain: Meteorological and hydrological applications
[AD-A290786] p 2918 N95-30403

RAM ACCELERATORS
The 31st JANNAF Combustion Subcommittee Meeting, volume 1 p 2825 N95-31194
Experiments in a 120-mm ram accelerator including flow visualization p 2799 N95-31202
Numerical simulation of ram accelerator performance including transient effects during initiation of combustion and sensitivity studies p 2799 N95-31203
Investigation of ram accelerator performance capabilities p 2799 N95-31204

RAMAN SPECTRA
Polarized Raman spectroscopy of chemically vapour deposited diamond films
[DE95-616776] p 2815 N95-30791
Fourier Transform (FT) Raman spectroscopy of nitrogen at high pressure
[AD-A293051] p 2796 N95-31670

RAMAN SPECTROSCOPY
Polarized Raman spectroscopy of chemically vapour deposited diamond films
[DE95-616776] p 2815 N95-30791
Fourier Transform (FT) Raman spectroscopy of nitrogen at high pressure
[AD-A293051] p 2796 N95-31670

RAMJET ENGINES
An investigation of the side-dump dual in-line ramjet combustor p 2756 N95-31199
A pulsed liquid fuel ramjet p 2756 N95-31201
Workshop report: Measurement techniques in highly transient, spectrally rich combustion environments p 2799 N95-31208
Experiment of rocket-ram combined combustor
[NAL-TR-1249] p 2769 N95-31739

RAMSAUER EFFECT
Generalized Ramsauer-Townsend minima in heavy-ion induced electron continua
[DE95-010913] p 2989 N95-32120

RANDOM ACCESS MEMORY
High speed random access, Fourier transform holographic associative and high density two-photon three-dimensional optical memories based on bacteriorhodopsin
[AD-A293389] p 2931 N95-30967

RANDOM NOISE
Detection of radar targets using higher-order statistics
[AD-D017442] p 2850 N95-31392
Visual processing of object velocity and acceleration
[AD-A292789] p 2929 N95-31436
Automatic Target Recognition (ATR): Background statistics and the detection of targets in clutter
[AD-A293062] p 2853 N95-31673
Rate considerations in deep space telemetry p 2765 N95-32223
Metafitting: Weight optimization for least-squares fitting of PTTI data p 2971 N95-32340

RANDOM PROCESSES
Development and computer implementation of design/analysis techniques for multilayered composite structures. Probabilistic fiber composite micromechanics
[NASA-CR-198979] p 2930 N95-31134

RANDOM VARIABLES
Extension to higher dimensions of the Jaeschke-Eicker result on the standardized empirical process
[PB95-206868] p 2965 N95-30523

Nonparametric methods for incomplete data in reliability and for changepoints in smooth functions
[AD-A292773] p 2963 N95-31429

RANGE FINDERS
Folded compact range development and coherent change detection measurement project
[DE95-009082] p 2853 N95-31628

RANGEFINDING
Passive range measurement system
[AD-D017344] p 2996 N95-30678
Apparent size passive range method
[AD-D017360] p 2753 N95-31180
Proceedings of the 16th Annual Conference on Atmospheric Transmission Models, volume 1
[AD-A293807] p 2915 N95-31575

RAPID TRANSIT SYSTEMS
Energy storage and alternatives to improve train voltage on a mass transit system
[DE95-010344] p 2906 N95-32090

RARE EARTH ALLOYS
Ultraviolet and visible lasers: Rare earth-doped waveguide devices and non-linear optical extraction techniques
[AD-A293976] p 2885 N95-31528

RARE EARTH ELEMENTS
Lanthanide(III) catalyzed reactions: Structure an d thermodynamics of intermediate complexes, and implications for reactivity
[PB95-197000] p 3019 N95-30775

RARE GASES
Effect of oxygen and decompression bubbles on inert gas washout
[PB95-196556] p 2925 N95-30665

RAREFIED GAS DYNAMICS
Orbiter rarefied-flow reentry measurements from the OARE on STS-62
[NASA-TM-110182] p 2891 N95-30783
The passage from transitional to free molecular plumes p 2871 N95-30994

RATINGS
Decompression illness, observable bubbles. (Session K)
[PB95-195285] p 2926 N95-30511
The relation of handling qualities ratings to aircraft safety p 2746 N95-31067
Prioritization methodology for chemical replacement p 2773 N95-31757

RATIOS
Evaluation of calibration parameters and performance of the video imaging technique of assessing exposure (VITAE system)
[AD-A289023] p 2927 N95-30998

RAY TRACING
Ray trace model of sound propagation in range dependent media
[PB95-211751] p 2973 N95-30481
The effect of ray curvature on Lloyd's mirror fringe estimates and source localisation
[DSTO-TR-0064] p 3001 N95-31745

RDX
Unsteady laser augmented combustion of pure oxidizers AP and RDX p 2799 N95-31284
Modeling of thermal response of filament used in T-jump experiment p 2800 N95-31297
A study of gas-phase processes during the deflagration of RDX composite propellants using a triple quadrupole mass spectrometer p 2801 N95-31304
RDX laser-assisted flame structure p 2801 N95-31314
A study of the gas-phase processes of RDX combustion using a triple quadrupole mass-spectrometer p 2801 N95-31315

REACTING FLOW
Combustion response to acoustic perturbation in liquid rocket engines p 2770 N95-31972
Analysis and modeling of subgrid scalar mixing using numerical data
[NASA-CR-198169] p 2877 N95-31978
Spatially-resolved velocity measurements in steady, high-speed, reacting flows using laser-induced OH fluorescence p 2877 N95-32109
LES, DNS and RANS for the analysis of high-speed turbulent reacting flows
[NASA-CR-199075] p 2878 N95-32219

REACTION BONDING
TEM-examination of ceramic-metal interfaces
[PB95-196531] p 2813 N95-30664

REACTION KINETICS
Orientation of rapid thermally annealed lead zirconate titanate thin films on (111) Pt substrate
[DE95-615232] p 2811 N95-30422
Wettability of boron carbide
[PB95-196358] p 2802 N95-30518
Chemical kinetics and photochemical data for use in stratospheric modeling: Evaluation number 11
[NASA-CR-198863] p 2912 N95-30525
Catalytic reactions of synthesis gas. Part 4: Heterogeneous hydroformylation
[PB95-195558] p 2791 N95-30537
Simulation of chemical kinetics in turbulent natural gas combustion. Volume 2: Experimental studies of nitric oxide production in gas flames
[PB95-196721] p 2791 N95-30541
Applications of SXPS for studying surface structure, reaction mechanisms and kinetics
[DE95-008903] p 2803 N95-30547
Characterization of compressive damage mechanisms in ceramic and polymeric matrix composite materials
[AD-A293171] p 2787 N95-30975
Measurement and analysis related to infrared emissions
[AD-A293296] p 2998 N95-31192
Viscous heating of liquid layers under intense shear p 2827 N95-31206
The 25th International Symposium on Combustion
[AD-A286825] p 2794 N95-31268
An ignition model for modern double base propellants p 2800 N95-31292
Molecular models for nitro compounds p 2831 N95-31293
Observation and characterization of burning surface reaction zones of solid propellants p 2800 N95-31296
An ab initio study of the reaction HNO + NO yields OH + N2O: Preliminary results p 2801 N95-31308
The oxidation of carbon monoxide by nitrous oxide p 2801 N95-31309
The oxidation of carbon monoxide by nitrogen dioxide p 2801 N95-31310
Detailed chemical kinetic modeling of premixed hydrocarbon flames supported by NO2 p 2801 N95-31311
Studies of reactions pertaining to and development of a reduced mechanism for the double base propellant dark zone p 2801 N95-31312
Flame structure studies of neat and NH3 doped H2/N2O flames employing molecular beam mass spectrometry and modeling p 2801 N95-31313
RDX laser-assisted flame structure p 2801 N95-31314
Electron transfer kinetics of self-assembled ferrocene C(12) alkanethiol monolayers on gold electrodes from 125K to 175K
[AD-A292754] p 2984 N95-31427
Consequences of kinetic dispersion on the electrochemistry of an adsorbed redox-active monolayer
[AD-A292794] p 2795 N95-31437
An analysis of gas phase ethanol/water chemistry for diamond CVD
[AD-A293009] p 2795 N95-31473

REACTION PRODUCTS
Electrified microheterogeneous catalysis
[AD-D017446] p 2794 N95-31271
The oxidation of carbon monoxide by nitrogen dioxide p 2801 N95-31310

REACTIVITY
Formation of cavities in Si and their chemisorption of materials
[DE95-009586] p 2980 N95-30708
Numerical computation of one-dimensional detonation waves
[PB95-197950] p 2868 N95-30811
The structure and reactivity of boron and carbon surfaces
[AD-A292804] p 2795 N95-31440

REACTOR DESIGN
The development of the tokamak system technology: A study on the fusion reactor
[DE95-614256] p 3005 N95-31366
Optimal heat transfer design of chemical vapor deposition reactors
[DE95-010997] p 2878 N95-32309

REACTOR MATERIALS
Effects of particle fueling and plasma wall interactions on D3-D discharges
[DE95-009608] p 3003 N95-30612
Evaluation on materials performance of Hastelloy Alloy XR for HTTR uses. 4: Tensile properties of base metals and welded joints
[DE95-721871] p 2804 N95-30761
Microstructural and mechanical property changes in model Fe-Cu alloys
[DE95-010117] p 2805 N95-31105
Volumetric and electro analytical techniques for chemical characterization of nuclear grade Ag-In-Cd alloys
[DE95-620664] p 2807 N95-31407
Development of integrated insulation joint for cooling pipe in tokamak reactor
[DE95-737220] p 3007 N95-32264

REACTOR SAFETY
SHEAT: A computer code for probabilistic seismic hazard analysis, user's manual
[DE95-717874] p 2913 N95-30758

READOUT
Noise signal processor
[AD-D017430] p 2974 N95-30747

REAL TIME OPERATION
Data storage modeling and management for multimedia information systems p 3022 N95-30483
Smart active multiwave sensing with zero background amplitude modulated probes
[DE95-008813] p 2792 N95-30714
Log-polar binocular vision system
[NASA-CR-188375] p 2996 N95-30772
Foundations of technology for constructing highly reliable distributed realtime systems
[AD-A293254] p 2931 N95-30892
Real time correlating operation on diffuse objects
[AD-A293220] p 2997 N95-30901
Airborne ocean water lidar (OWL) real time processor (RTP)
[AD-A293226] p 2848 N95-30904
Application of computer generated holograms to optical transformations
[AD-A293146] p 2880 N95-30921
Making intelligent systems team players. A guide to developing intelligent monitoring systems
[NASA-TM-104807] p 2951 N95-30925
Visible light emitting materials and injection devices
[AD-A292701] p 2786 N95-30934
Development of a novel wind lidar,.phase 1
[AD-A292703] p 2849 N95-30935
New adaptive methods for reconfigurable flight control systems, appendix 1
[AD-A292711] p 2756 N95-30937
A real time method for Fourier transform holographic information storage
[AD-A293186] p 2880 N95-30980
Neural network false alarm filter, volume 1
[AD-A293097] p 2953 N95-31562
Nonparametric recognition of nonrigid motion
[AD-A293630] p 2963 N95-31565
Architecture and implementation of a multi-sensor data fusion demonstration model within the real-time combat system of the Canadian Patrol Frigate p 2842 N95-32139
Automatic verification and synthesis of finite-state hard real-time systems
[AD-A291279] p 2964 N95-32287
The Deep Space Network stability analyzer p 2858 N95-32334
A globally efficient means of distributing UTC time and frequency through GPS p 2970 N95-32335

RECEIVERS
Cascading synchronized chaotic systems
[AD-D017458] p 2860 N95-30748
The quad-service satellite transmitting and receiving system for medical supply support: A battlefield interoperability and communications system prototype, volume 2. User documentation
[AD-A292835] p 2851 N95-31448
The quad-service satellite transmitting and receiving system for medical supply support: A battlefield interoperability and communications system prototype, volume 1
[AD-A292836] p 2851 N95-31449
Development of the Multi-Level Seismic Receiver (MLSR)
[DE95-008823] p 2916 N95-31610
Testing the performance of feedback concatenated decoder with a nonideal receiver p 2856 N95-32231

RECIPROCATION
Linear Motor Free Piston Compressor
[AD-A293452] p 2889 N95-31374

RECLAMATION
AP reclamation and reuse in RSRM propellant p 2772 N95-31751

RECOIL IONS
Kinematical threshold of recoil-ion longitudinal momentum distribution in single ionization of helium by protons and alpha particles
[DE95-010803] p 2990 N95-32271
Recoil longitudinal momentum spectroscopy of electron capture from He by O(7+) and F(8+)
[DE95-010823] p 2990 N95-32274

RECOMBINATION COEFFICIENT
Spectral response of a polycrystalline silicon solar cell
[DE95-614370] p 2903 N95-30723

RECOMBINATION REACTIONS
The junction characteristics and current conduction mechanisms of GaInP2 n(+)p diodes and solar cells
[AD-A290857] p 2902 N95-30408

RECONNAISSANCE
Investigation of ground target detection methods in fully polarimetric wide angle synthetic aperture radar images
[AD-A293922] p 2851 N95-31513
RECONNAISSANCE AIRCRAFT
Unmanned aerial vehicles. 1994 master plan
p 2751 N95-31416
Report to the Chairman, Legislation and National Security Subcommittee, Committee on Government Operations, House of Representatives. Unmanned aerial vehicles: Performance of short-range system still in question
[GAO/NSIAD-94-65] p 2752 N95-32196
RECRYSTALLIZATION
Physical modelling of microstructural evolution during thermomechanical processing of aluminium alloys
[PB95-196341] p 2805 N95-31053
RECTANGULAR PLATES
Studies in non-linear multi-mode responses of harmonically excited rectangular plates with internal resonances p 2895 N95-31331
RECYCLING
Biomass production by fescue and switchgrass alone and in mixed swards with legumes
[DE95-009137] p 2909 N95-31612
Recycling MIL-H-46170 hydraulic fluid to extend fluid service life
[AD-A293035] p 2821 N95-31664
REDUNDANCY
On the kinematic performance of mechanical manipulators operating in the presence of an obstruction
p 2890 N95-31710
REED-SOLOMON CODES
Enhanced decoding for the Galileo low-gain antenna mission: Viterbi redecoding with four decoding stages
p 2855 N95-32230
REFINING
Bravais classes, Voronoie cells, Delone symbols
[PB95-207916] p 3009 N95-30503
Refinement techniques in computer graphics
[PB95-208526] p 2934 N95-30625
REFLECTANCE
State-of-the-art low-cost solar reflector materials
[DE95-000260] p 2902 N95-30526
Reflectivity of plasmas created by high-intensity, ultra-short laser pulses
[DE95-009536] p 3004 N95-30742
REFLECTED WAVES
Reflection and transmission of electromagnetic plane waves from a uniaxial chiro-omega slab
[PB95-206629] p 2853 N95-31649
The effect of ray curvature on Lloyd's mirror fringe estimates and source localisation
[DSTO-TR-0064] p 3001 N95-31745
REFLECTING TELESCOPES
Stratospheric Observatory For Infrared Astronomy (SOFIA). Phase A: System concept description
[NASA-TM-110669] p 3002 N95-32187
REFLECTION
Real time correlating operation on diffuse objects
[AD-A293220] p 2997 N95-30901
REFLECTOMETERS
IPNS neutron scattering instrumentation. A: Existing and planned. B: Possibilities for IPNS upgrade, a 1-MW spallation source
[DE95-004119] p 2985 N95-31616
REFLECTOR ANTENNAS
Proceedings of the antenna applications symposium. volume 2
[AD-A293259] p 2850 N95-31387
DSS-24 microwave holography measurements
p 2857 N95-32239
REFLECTORS
Performance of residual carrier array-feed combining in correlated noise p 2856 N95-32232
Point reflector model for the simulation of radar target glint and Doppler phenomena
[PB95-222980] p 2857 N95-32314
REFRACTIVITY
Effects of molecular structure on the electroactive and optical properties of conjugated rigid-rod polybenzobisazoles
[AD-A292968] p 2819 N95-31467
Quantum and nonlinear optics research
[AD-A293879] p 2999 N95-31519
REFRACTORY COATINGS
High temperature barrier coatings for refractory metals
[NASA-CR-195475] p 2802 N95-30531
REFRACTORY MATERIALS
NASA Lewis Research Center's preheated combustor and materials test facility
[NASA-TM-106676] p 2762 N95-30592
Ultrasonic characterization of fiber-matrix interphasial properties and damage in high-temperature composites
p 2785 N95-30823
Innovative processing of composites for ultra-high temperature applications, book 4
[AD-A290892] p 2786 N95-30867
Innovative processing of composites for ultra-high temperature applications, book 2
[AD-A290890] p 2786 N95-30898
Phthalonitrile prepolymer as high temperature sizing material for composite fibers
[AD-D017447] p 2818 N95-31272
Whisker reinforced glass ceramic
[DE95-010542] p 2823 N95-32305
REFRACTORY METAL ALLOYS
High temperature barrier coatings for refractory metals
[NASA-CR-195475] p 2802 N95-30531
REFRACTORY METALS
High temperature barrier coatings for refractory metals
[NASA-CR-195475] p 2802 N95-30531
REFRIGERANTS
Compatibility of refrigerants and lubricants with motor materials under retrofit conditions
[DE95-010185] p 2814 N95-30767
CFC-replacement by natural working fluids: R&D and industrial challenges within the refrigeration, air conditioning amd heat pump areas
[PB95-195756] p 2815 N95-30871
ARTI Refrigerant Database
[DE95-008336] p 2816 N95-31057
The Oak Ridge Refrigerant Management Program
p 2774 N95-31763
Alternatives to ozone depleting refrigerants in test equipment p 2775 N95-31767
Compatibility of manufacturing process fluids with HFC refrigerants and ester lubricants
[DE95-012152] p 2911 N95-32364
REFRIGERATING
High-temperature superconducting current leads
[DE95-008404] p 2858 N95-30374
Reducing process noise in superconducting helium liquid level probes
[DE95-008956] p 2814 N95-30765
Simultaneous heat and mass transfer in a horizontal tube absorber: Numerical tools for present and future absorber designs
[PB95-196978] p 2869 N95-30872
Construction and performance measurement of a portable thermoacoustic refrigerator demonstration apparatus
[AD-A293265] p 2839 N95-31122
REFRIGERATING MACHINERY
Compatibility of refrigerants and lubricants with motor materials under retrofit conditions
[DE95-010185] p 2814 N95-30767
REFRIGERATORS
Reducing process noise in superconducting helium liquid level probes
[DE95-008956] p 2814 N95-30765
Construction and performance measurement of a portable thermoacoustic refrigerator demonstration apparatus
[AD-A293265] p 2839 N95-31122
Natural gas liquefier for vehicle fuel
[AD-A293619] p 2836 N95-31564
REGENERATORS
Natural gas liquefier for vehicle fuel
[AD-A293619] p 2836 N95-31564
REGRESSION ANALYSIS
Selecting optimal experiments for feedforward multilayer perceptrons
[AD-A290856] p 2949 N95-30406
Modeling F/A-18 flight hour program costs using regression analysis
[AD-A293771] p 2752 N95-31579
The effect of repeatedly sampling an embedded metamodel on the simulation response
[AD-A293783] p 2953 N95-31582
Finite-sample based learning algorithms for feedforward networks
[DE95-009123] p 2941 N95-31631
REGULATIONS
The Oak Ridge Refrigerant Management Program
p 2774 N95-31763
Environmentally regulated aerospace coatings
p 2777 N95-31775
NEIS (NASA Environmental Information System)
p 2783 N95-31811
REINFORCING FIBERS
Interfacial studies of coated fiber reinforced glass-ceramic matrix composites
[AD-A290780] p 2783 N95-30433
The effect of interface properties on nickel base alloy composites
[NASA-CR-198363] p 2785 N95-30787
Effects of hydrostatic pressure on the mechanical behavior of composite materials
[AD-A293162] p 2787 N95-30963
Post-impact fatigue of cross-plied, through-the-thickness reinforced carbon/epoxy composites
[NASA-TM-110625] p 2896 N95-31419
RELATIVISTIC EFFECTS
Relativistic timescale analysis suggests lunar theory revision p 2970 N95-32333
RELATIVISTIC ELECTRON BEAMS
The coupling impedance of a toroidal beam pipe with circular cross section
[DE95-010442] p 2993 N95-31405
RELATIVISTIC PARTICLES
Hamiltonian formulation of two body problem in Wheeler-Feynman electrodynamics
[DE95-620526] p 3019 N95-31193
Quantization of a relativistic particle on the SL(2,R) manifold based on Hamiltonian reduction
[DE95-737163] p 2983 N95-31224
RELATIVISTIC PLASMAS
Perpendicular electron heating by absorption of auroral kilometric radiation
[NASA-198815] p 2914 N95-30848
Instantaneous chiral quark model for relativistic mesons in a hot and dense medium
[DE95-613782] p 2980 N95-30911
RELATIVISTIC THEORY
Relativistic theory for syntonization of clocks in the vicinity of the Earth p 2971 N95-32343
RELATIVITY
Integrals of motion in the two Killing vector reduction of general relativity
[DE95-616281] p 3018 N95-30431
Gravitational waves from inspiralling compact binaries: Energy loss and waveform to second-post-Newtonian order
[PB95-207890] p 2913 N95-30590
Introduction to the theory of Goyaks: Operator manifold approach to geometry and particle physics
[DE95-613460] p 2980 N95-30740
Satellite test of the isotropy of the one-way spe ed of light using ExTRAS p 2973 N95-32349
RELAXATION METHOD (MATHEMATICS)
The one-dimensional model of the off-centre potential of the fluorine ion in the NaBr lattice
[DE95-614310] p 3010 N95-30647
RELIABILITY
Publications of the Fossil Energy Advanced Research and Technology Development Materials Program: April 1, 1993-March 31, 1995
[DE95-009200] p 2903 N95-30745
The role of advanced engineering simulation in model-based design
[DE95-008815] p 2934 N95-30796
Nonparametric methods for incomplete data in reliability and for changepoints in smooth functions
[AD-A292773] p 2963 N95-31429
Recommended techniques for effective maintainability. A continuous improvement initiative of the NASA Reliability and Maintainability Steering Committee
[NASA-TM-4628] p 2892 N95-31530
Data analysis: Naive inductivism
[PB95-212213] p 3026 N95-32254
RELIABILITY ANALYSIS
Probabilistic reliability modeling of fatigue on the H-46 tie bar
[AD-A289926] p 2751 N95-30927
A NASPAC-Based analysis of the delay and cost effects of the western-pacific region preliminary resectorization effort of 1993
[AD-A288696] p 2748 N95-31013
Intelligent finite element submodeling of multichip modules for reliability analysis
[AD-A292911] p 2940 N95-31455
Toward a risk-based approach to the assessment of the surety of information systems
[DE95-008821] p 3025 N95-31662
ASSIST user manual
[NASA-TM-4592] p 2948 N95-32250
RELIABILITY ENGINEERING
Measures of reliability and RCM
[PB95-192985] p 2891 N95-30510
Robust Rocket Engine Concept
[NASA-TM-107010] p 2770 N95-32121
RELIEF VALVES
Navier-Stokes flow field analysis of compressible flow in a high pressure safety relief valve
[NASA-TM-110640] p 2868 N95-30862
REMOTE CONTROL
On-orbit truss structure tele-operation experiment by Engineering Test Satellite-7
[NAL-TR-1246] p 2767 N95-31980
REMOTE SENSING
Simulation of airborne electromagnetic measurements in three dimensional environments
[DE95-008546] p 2900 N95-30363
IR DIAL performance modeling
[DE95-008377] p 2912 N95-30373

Computer vision for detecting and quantifying gamma-ray sources in coded-aperture images
[DE95-008810] p 2900 N95-30472
Weather influence on passive microwave brightness temperatures
[PB95-195384] p 2900 N95-30536
Smart active multiwave sensing with zero background amplitude modulated probes
[DE95-008813] p 2792 N95-30714
Radiometer measurements of sea ice in the Gulf of Bothnia 1992
[PB95-206611] p 2900 N95-30718
SSUSI single sensor auroral E-layer algorithm: Functional description
[AD-A288630] p 2914 N95-31012
Brief review of remote sensing literature pertaining to classification and geostatistics
[AD-A290932] p 2901 N95-31156
Visit to Ionospheric Modeling and Remote Sensing Branch, Phillips Laboratory in Hanscom AFB, MA
[AD-A292339] p 2901 N95-31265
Multiresolution signal and system analysis and the analysis and control of discrete-event dynamic systems
[AD-A292775] p 2851 N95-31430
Emerging applications in probability (Sensor management)
[AD-A292781] p 2749 N95-31433
Proceedings of the 16th Annual Conference on Atmospheric Transmission Models, volume 1
[AD-A293807] p 2915 N95-31575
Millimeter wave radiometer utility study
[AD-A293811] p 2852 N95-31590
Environmental benefits of chemical propulsion p 2772 N95-31750
Surface inspection using FTIR spectroscopy p 2782 N95-31803
Global climatology and variability of potential new production estimated from remote sensing of sea-surface temperature
[NASA-CR-198840] p 2910 N95-31981
Design of an immersion echelle-prism mid-IR spectrograph for chemical remote sensing
[DE95-010729] p 2901 N95-32027
Design of surveillance and multisensor anti-aerial systems p 2841 N95-32134
Multisensor data fusion for integrated maritime surveillance p 2842 N95-32135
The Telecommunications and Data Acquisition Report
[NASA-CR-198911] p 2854 N95-32221

REMOTE SENSORS
SeaWiFS Technical Report Series. Volume 29: SeaWiFS CZCS-type pigment algorithm
[NASA-TM-104566] p 2922 N95-30857
System considerations for efficient communication and storage of MSTI image data
[NASA-CR-198869] p 3024 N95-30858
SeaWiFS technical report series. Volume 28: SeaWiFS algorithms, part 1
[NASA-TM-104566-VOL-28] p 2924 N95-31850
TMD detection and tracking using improved AWACS sensors p 2840 N95-32128
Optimal infrared detector configurations for air target detection p 2841 N95-32130
Acquisition, tracking, pointing and fire control for Ballistic Missile Defense p 2841 N95-32131
Multisensor data fusion for integrated maritime surveillance p 2842 N95-32135
Architecture and implementation of a multi-sensor data fusion demonstration model within the real-time combat system of the Canadian Patrol Frigate p 2842 N95-32139

REMOVAL
Waterjet processes for coating removal p 2777 N95-31779
Environmentally Safe and Effective Processes for Paint Removal
[AGARD-LS-201] p 2843 N95-32165
Overview of paint removal methods p 2843 N95-32166
Paint removal principles p 2843 N95-32167
Background to plastic media blasting p 2843 N95-32168
Dry media blasting with wheat starch p 2843 N95-32169
Water blasting paint removal methods p 2843 N95-32170
Stripping with dry ice p 2844 N95-32172
Aquastrip p 2844 N95-32173
Stripping by laser p 2844 N95-32174
Selective chemical stripping p 2844 N95-32175
Process evaluation p 2845 N95-32180
Standardization work p 2845 N95-32181

RENORMALIZATION GROUP METHODS
Light-front dynamics of Chern-Simons systems
[DE95-613467] p 3019 N95-30741
Renormalization group analyses of particle masses in full four-generation fermion condensate scheme
[DE95-613595] p 2988 N95-32070

REPEATERS
Microwave repeater with broadband active and/or passive isolation control
[AD-D017358] p 2846 N95-30417

REPLACING
Urethane foam process improvements
[DE95-008957] p 2815 N95-30798
CFC-replacement by natural working fluids: R&D and industrial challenges within the refrigeration, air conditioning amd heat pump areas
[PB95-195756] p 2815 N95-30871
A comparison of coating alternatives for US Coast Guard aircraft
[AD-A293270] p 2817 N95-31124
Aerospace Environmental Technology Conference
[NASA-CP-3298] p 2771 N95-31746
Prioritization methodology for chemical replacement p 2773 N95-31757
Evaluating the cost effectiveness of environmental projects: Case studies in aerospace and defense p 2774 N95-31762
The Oak Ridge Refrigerant Management Program p 2774 N95-31763
A water blown urethane insulation for use in cryogenic environments p 2775 N95-31765
Evaluation of HFC 245ca and HFC 236ea as foam blowing agents p 2775 N95-31766
Environmentally safe aviation fuels p 2775 N95-31768
Thin-film sulfuric acid anodizing as a replacement for chromic acid anodizing p 2776 N95-31772
Cadmium plating replacements p 2776 N95-31773
Replacement of corrosion protection chromate primers and paints used in cryogenic applications on the Space Shuttle with wire arc sprayed aluminum coatings p 2776 N95-31774
SSME Main Combustion Chamber (MCC) hot oil dewaxing p 2777 N95-31777
Bicarbonate of soda paint stripping process validation and material characterization p 2777 N95-31778
Evaluation of pressurized water cleaning systems for hardware refurbishment p 2778 N95-31782
Report to the Chairman, Legislation and National Security Subcommittee, Committee on Government Operations, House of Representatives. Tactical aircraft: F-15 replacement is premature as currently planned
[GAO/NSIAD-94-118] p 2964 N95-31987
Liquid natural gas as a transportation fuel in the heavy trucking industry
[DE95-010376] p 2837 N95-32158
Fact sheet for Congressional Committees. Air traffic control: Status of FAA's modernization program
[GAO/RCED-94-167FS] p 2750 N95-32197

REPRODUCTION (COPYING)
Operating system support for distributed multimedia applications: A survey of current research
[PB95-207098] p 2964 N95-30565

REQUIREMENTS
Selective chemical stripping p 2844 N95-32175

RESEARCH
Quality in applied science
[PB95-196390] p 2891 N95-30520
Metascientific problems in safety science
[PB95-196408] p 2838 N95-30521
The activities of the high energy physics program
[DE95-010155] p 2991 N95-30615
Research proposal
[AD-A293207] p 3032 N95-30899
Directory of global environmental sciences in Japan p 2899 N95-31413

RESEARCH AND DEVELOPMENT
A system simulation development project: Leveraging resources through partnerships
[NASA-TM-106962] p 2753 N95-30514
Wide area networking R&D
[AD-A291057] p 2947 N95-30868
Hollow cathode electron gun research and development
[DE95-010262] p 2992 N95-31127
FBIS report: Science and technology. Central Eurasia
[FBIS-UST-95-027] p 2839 N95-31727
FBIS report: Science and technology. Central Eurasia
[FBIS-UST-95-029] p 2863 N95-31728
Air pollution control system research: An iterative approach to developing affordable systems p 2773 N95-31759
Aeronautics and space report of the President
[NASA-TM-110743] p 3028 N95-31979
Microgravity research opportunities for the 1990s
[NASA-CR-199109] p 2838 N95-31983
Solar thermal electric: Program overview, fiscal years 1993-1994
[DE94-000240] p 2906 N95-32058
Report to Congressional Committees. Federal Research: Interim report on the small business innovation research program
[GAO/RCED-95-59] p 3022 N95-32200
Report to the Vice Chairman, Joint Economic Committee, US Congress. Technology transfers: Benefits of cooperative R and D agreements
[GAO/RCED-95-52] p 3027 N95-32201
Laboratory directed research and development report
[DE95-011405] p 3032 N95-32279

RESEARCH FACILITIES
Supplemental multilayer insulation research facility
[NASA-TM-106991] p 2768 N95-30595

RESEARCH MANAGEMENT
Research proposal
[AD-A293207] p 3032 N95-30899
Emerging applications in probability (Sensor management)
[AD-A292781] p 2749 N95-31433
Topics in exploratory and speculative data analysis
[AD-A290505] p 3025 N95-31618
The Oak Ridge Refrigerant Management Program p 2774 N95-31763
Report to Congressional Committees. Federal Research: Interim report on the small business innovation research program
[GAO/RCED-95-59] p 3022 N95-32200

RESEARCH PROJECTS
A system simulation development project: Leveraging resources through partnerships
[NASA-TM-106962] p 2753 N95-30514
Economical analysis relating to the global warming issue
[DE95-764072] p 2908 N95-30677
Sea ice stress research
[AD-A293164] p 2923 N95-30964
National Laboratories: Are their R and D activities related to commercial product development? Report to Congressional Requesters
[GAO/PEMD-95-2] p 3027 N95-31345
Microgravity research opportunities for the 1990s
[NASA-CR-199109] p 2838 N95-31983
The Telecommunications and Data Acquisition Report
[NASA-CR-198911] p 2854 N95-32221
UNLV: Information Science Research Institute
[DE95-011941] p 3027 N95-32362

RESIDUAL GAS
Power oscillator in the tokamaks training
[DE95-616538] p 3003 N95-30473

RESIDUAL STRESS
Residual stresses and stress corrosion cracking in pipe fittings
[DE95-009332] p 2894 N95-31054
Modeling of fiber-reinforced composites incorporating distinct interface properties p 2787 N95-31110
Development of integrated insulation joint for cooling pipe in tokamak reactor
[DE95-737220] p 3007 N95-32264
Residual stress distribution in FeAl weld overlay on steel
[DE95-009178] p 2899 N95-32317

RESIDUES
Observation and characterization of burning surface reaction zones of solid propellants p 2800 N95-31296
Overview of paint removal methods p 2843 N95-32166

RESIN TRANSFER MOLDING
Development of stitched/RTM primary structures for transport aircraft
[NASA-CR-191441] p 2789 N95-31421

RESINS
Characterization and prediction of post-impact fatigue damage in stitched composites p 2785 N95-30826
Faster, cheaper radioanalytical methods
[DE95-009913] p 2797 N95-32061

RESISTANCE HEATING
Electrically heated tube investigation of cooling channel geometry effects
[NASA-TM-106985] p 2768 N95-30856
Modeling of thermal response of filament used in T-jump experiment p 2800 N95-31297
Stability analysis of the TPX toroidal field coil
[DE95-009666] p 2865 N95-32100

RESISTORS
Pre-amplifier with multi-stage feedback
[AD-D017371] p 2859 N95-30659

RESOLVERS
Passive range measurement system
[AD-D017344] p 2996 N95-30678

RESONANCE
The mechanism of particle production process in hadron-nucleon collisions
[DE95-613727] p 2975 N95-30372
Polarisation resonance in X-ray diffraction
[DE95-616727] p 3012 N95-30789

Multichannel resonances in coupled channels of meson scattering: Scalar sector
[DE95-613783] p 2981 N95-30912
Resonance characteristics in the case of the excitation of a monoenergetic beam of free atoms by means of N. F. Ramsey's method
[IFTR-6/1995] p 2993 N95-31336
Aspects of the magnetospheric amplification phenomenon in ducted whistler-mode waves p 2916 N95-31718
Operational characteristics of a 200 C LC parallel resonant circuit
[NASA-TM-106983] p 2864 N95-31742
Polarized proton beams
[DE95-010843] p 2987 N95-32031
Physics goals of a mu(+) mu(-) collider
[DE95-009546] p 2994 N95-32059
Mixing phases of unstable two-level systems
[DE95-613844] p 2989 N95-32151
On the search for exotic hadrons in the experiments with high energy hyperon beam
[DE95-620534] p 2989 N95-32261

RESONANCE SCATTERING
Statistical properties of chaotic scattering with one open channel
[DE95-613370] p 3020 N95-32150

RESONANT FREQUENCIES
Minimizing structural vibrations with Input Shaping (TM)
[NASA-CR-189439] p 2893 N95-30786
Analytic and experimental investigation of rotordynamic response and backward whirl induced by split resonance
[AD-A293639] p 2889 N95-31566
Finite element analysis of smart structures and modal testing of a flexible spacecraft arm
[AD-A293761] p 2890 N95-31576
Detection of the phase shift which accompanies the excitation of an atomic beam by N. F. Ramsey's method
[IFTR-5/1995] p 2986 N95-31818

RESONANT VIBRATION
Dynamical systems as models for flow-induced vibrations
[PB95-206991] p 2869 N95-30956

RESONATORS
Thermoacoustic sound generator
[AD-D017342] p 2973 N95-30413
Langasite crystals growth with quality factor Q, that exceeds the Q of quartz, and which are suitable for high-precision resonators
[AD-A293397] p 3013 N95-30969

RESOURCE ALLOCATION
Dynamic routation in distributed environments
[PB95-197968] p 2847 N95-30812
A microeconomic scheduler for parallel computers
[NASA-CR-198153] p 2932 N95-32046

RESOURCES MANAGEMENT
A system simulation development project: Leveraging resources through partnerships
[NASA-TM-106962] p 2753 N95-30514
Magnesium battery disposal characteristics
[AD-A293053] p 2863 N95-31607
Sustainability protects resources for future generations
[DE95-000285] p 2909 N95-31695
Controller resource management: What can we learn from aircrews?
[DOT/FAA/AM-95/21] p 2750 N95-32186

RESPIRATION
Evaluation of calibration parameters and performance of the video imaging technique of assessing exposure (VITAE system)
[AD-A289023] p 2927 N95-30998

RESPIROMETERS
Analytical instrumentation for environmental research
[AD-A292832] p 2908 N95-31447

RESPONSE TIME (COMPUTERS)
A microeconomic scheduler for parallel computers
[NASA-CR-198153] p 2932 N95-32046

RETENTION (PSYCHOLOGY)
Impact of task properties, data display format and cognitive characteristics on recall performance: A cumulative research investigation p 3025 N95-31334
Optimizing the long-term retention of skills: Structural and analytic approaches to skill maintenance
[AD-A293798] p 2929 N95-31585

RETINA
Laser induced vitreoretinal scarring. Evaluation of causative factors and a therapeutic approach
[AD-A293742] p 2928 N95-31570

RETROREFLECTORS
Laser retroreflector experiment on NAVSTAR 35 and 36 p 2887 N95-32347

REUSABLE ROCKET ENGINES
Robust Rocket Engine Concept
[NASA-TM-107010] p 2770 N95-32121

REVERBERATION
The TEVA experiment cruise report
[AD-A293025] p 2923 N95-31701

REVERSE FIELD PINCH
Lower hybrid accessibility in a large, hot reversed field pinch
[DE95-011001] p 3007 N95-32310

REYNOLDS NUMBER
Heat transfer in shear-free turbulent boundary layers p 2876 N95-31708
Control of unsteady separated flow associated with the dynamic stall of airfoils
[NASA-CR-198972] p 2744 N95-32193

REYNOLDS STRESS
Reynolds stress of localized toroidal modes
[DE95-008750] p 3004 N95-30795
LES, DNS and RANS for the analysis of high-speed turbulent reacting flows
[NASA-CR-199075] p 2878 N95-32219

RHENIUM
Advanced small rocket chambers. Option 3: 110 1bf Ir-Re rocket, volume 1
[NASA-CR-195435-VOL-1] p 2768 N95-31169
Advanced small rocket chambers. Option 3: 110 1bf Ir-Re rocket, volume 2
[NASA-CR-195435-VOL-2] p 2769 N95-31170

RHENIUM ALLOYS
High-temperature oxidation behavior of iridium-rhenium alloys
[NASA-TM-106720] p 2803 N95-30593

RHEOLOGY
Low temperature fabrication from nano-size ceramic powders
[DE95-010995] p 2818 N95-31153
Fluid-film lubrication with an application to piston rings p 2890 N95-32119

RHO-MESONS
Thermal rho's in the quark-gluon plasma
[DE95-009543] p 3008 N95-32357

RHODIUM
Catalytic reactions of synthesis gas. Part 4: Heterogeneous hydroformylation
[PB95-195558] p 2791 N95-30537

RHYTHM (BIOLOGY)
AASERT-92 augmentation of research training in chronobiology: Regulation of the mammalian circadian clock by neurotransmitters
[AD-A288243] p 2925 N95-31144

RIEMANN MANIFOLD
Dressing symmetry of the uniformization solution of Liouville equation
[DE95-613380] p 2956 N95-30607
Multichannel resonances in coupled channels of meson scattering: Scalar sector
[DE95-613783] p 2981 N95-30912
On drawing complicated 3D surfaces
[DE95-619199] p 2939 N95-31257
Ricci-flat Kaehler metrics on symmetric varieties
[DE95-613459] p 2962 N95-32068

RIGID STRUCTURES
Control of mechanical systems with rolling contacts: Applications to robotics p 2889 N95-31332
A simple and efficient procedure for polyhedral assembly partitioning under infinitesimal motions
[DE95-009838] p 2942 N95-31644

RINGS (MATHEMATICS)
Frobenius algebras and quantum Yang-Baxter equation 2
[PB95-212130] p 2960 N95-31229
Antipodes and integrals in Hopf algebras over rings and quantum Yang-Baxter equation
[PB95-212155] p 2961 N95-31397

RISK
Definition of an anti-missile ballistic defense architecture for Europe p 2840 N95-32125

ROBOT ARMS
Log-polar binocular vision system
[NASA-CR-188375] p 2996 N95-30772
Precision manipulation with a dextrous robot hand p 2888 N95-30829

ROBOT CONTROL
Qualitative environmental navigation: Theory and practice --- robot navigation p 2748 N95-30486
Robust position and force tracking control for a robot in contract p 2888 N95-30830
A graphical programming language for service robots in semi-structured environments p 2935 N95-30831
Control of mechanical systems with rolling contacts: Applications to robotics p 2889 N95-31332
Force and vision resolvability for assimilating disparate sensory feedback
[AD-A293581] p 2929 N95-31685

ROBOT DYNAMICS
Control of mechanical systems with rolling contacts: Applications to robotics p 2889 N95-31332

ROBOTICS
Adaptive path planning: Algorithm and analysis
[DE95-008549] p 2950 N95-30463
Log-polar binocular vision system
[NASA-CR-188375] p 2996 N95-30772
Precision manipulation with a dextrous robot hand p 2888 N95-30829
Emerging applications in probability (Sensor management)
[AD-A292781] p 2749 N95-31433
Neural networks for real-time terrain typing
[AD-A293569] p 2953 N95-31540
A simple and efficient procedure for polyhedral assembly partitioning under infinitesimal motions
[DE95-009838] p 2942 N95-31644
Force and vision resolvability for assimilating disparate sensory feedback
[AD-A293581] p 2929 N95-31685
On the kinematic performance of mechanical manipulators operating in the presence of an obstruction p 2890 N95-31710
Robotic weld overlay coatings for erosion control
[DE95-009643] p 2809 N95-32098

ROBOTS
Qualitative environmental navigation: Theory and practice --- robot navigation p 2748 N95-30486
Log-polar binocular vision system
[NASA-CR-188375] p 2996 N95-30772
Robust position and force tracking control for a robot in contract p 2888 N95-30830
A graphical programming language for service robots in semi-structured environments p 2935 N95-30831
Neural networks for real-time terrain typing
[AD-A293569] p 2953 N95-31540
Laboratory robotics: An automated tool for preparing Ion Chromatography calibration standards
[DE95-009441] p 2798 N95-32318

ROBUSTNESS (MATHEMATICS)
System identification for robust process control. Nominal models and error bounds
[PB95-197026] p 2839 N95-30777
Robust position and force tracking control for a robot in contract p 2888 N95-30830
Fourier analysis of a robust multigrid method for convection-diffusion equations
[PB95-197091] p 2958 N95-30835
Advances in robust control
[AD-A291126] p 2952 N95-31266
Robust control: A structured approach to solve aircraft flight control problems p 2758 N95-31995

ROCK MECHANICS
Simulation of fracture in compression using a field-theory model
[DE95-009874] p 2898 N95-32102

ROCKET ENGINE DESIGN
Electrically heated tube investigation of cooling channel geometry effects
[NASA-TM-106985] p 2768 N95-30856
Side force acting on blunted circular cylinder bodies at high angles of attack in supersonic flow
[NAL-TR-1255] p 2744 N95-31741
Robust Rocket Engine Concept
[NASA-TM-107010] p 2770 N95-32121

ROCKET ENGINES
High-temperature oxidation behavior of iridium-rhenium alloys
[NASA-TM-106720] p 2803 N95-30593
Development of a new instrument for rocket engine combustion diagnostics p 2799 N95-31211

ROCKET EXHAUST
The 21st JANNAF Exhaust Plume Technology Meeting, volume 1
[CPIA-PUBL-621-VOL-1] p 2870 N95-30986
Survey of recent Al2O3 droplet size data in solid rocket chambers, nozzles, and plumes p 2770 N95-30987
Atmospheric environmental implications of propulsion systems p 2771 N95-31747
CFD assessment of the pollutant environment from RD-170 propulsion system testing p 2772 N95-31749

ROCKET LAUNCHING
Atmospheric environmental implications of propulsion systems p 2771 N95-31747

ROCKET NOZZLES
Survey of recent Al2O3 droplet size data in solid rocket chambers, nozzles, and plumes p 2770 N95-30987
Advanced small rocket chambers. Option 3: 110 1bf Ir-Re rocket, volume 2
[NASA-CR-195435-VOL-2] p 2769 N95-31170
Survey of recent Al2O3 droplet size data in solid rocket chambers, nozzles, and plumes p 2770 N95-31195
Development of a new instrument for rocket engine combustion diagnostics p 2799 N95-31211
Cleanliness inspection tool for RSRM bond surfaces p 2761 N95-31799

ROCKET PROPELLANTS
Development of a new instrument for rocket engine combustion diagnostics p 2799 N95-31211
ROCKET THRUST
Experiment of rocket-ram combined combustor
|NAL-TR-1249| p 2769 N95-31739
Improved hybrid rocket fuel p 2773 N95-31755
ROCKS
Removal of scattered surface waves from seismic data
|PB95-197802| p 2922 N95-30457
ROCKY MOUNTAINS (NORTH AMERICA)
Simulation of katabatic flow and mountain waves
|DE95-010863| p 2911 N95-32276
RODS
Simultaneity and length of the moving rod
|DE95-613369| p 3017 N95-30364
Einstein's length concept
|DE95-613368| p 3019 N95-30972
ROLLING CONTACT LOADS
Control of mechanical systems with rolling contacts: Applications to robotics p 2889 N95-31332
ROOM TEMPERATURE
Visible light emitting materials and injection devices
|AD-A292701| p 2786 N95-30934
The effect of grain refinement on the room-temperature ductility of as-cast Fe3Al-based alloys
|DE95-010121| p 2805 N95-31107
Composite polymer electrolyte for lithium batteries
|AD-A293924| p 2820 N95-31514
Ultrasensitive fluorescence detection and photophysics in microdroplets
|DE95-010283| p 2798 N95-32086
ROOT-MEAN-SQUARE ERRORS
Towards optimum demodulation of bandwidth-limited and low SNR square-wave subcarrier signals p 2855 N95-32229
ROTARY WINGS
Validation of the helicopter rotor code HERO
|PB95-198040| p 2751 N95-30838
A novel instrumentation system for measurement of helicopter rotor motions and loads data, phase 1
|AD-A293309| p 2751 N95-30923
ROTATING BODIES
Robust fixed-structure control
|AD-A292883| p 2952 N95-30961
ROTATING PLASMAS
Development of a tokamak plasma optimized for stability and confinement
|DE95-009609| p 3003 N95-30641
Stabilization of ballooning modes with sheared toroidal rotation
|DE95-008388| p 3006 N95-31624
Energy spectra of charge-exchange atoms from a rotating plasma
|DE95-614179| p 3006 N95-32054
Wall stabilization of high beta plasmas in D3-D
|DE95-009607| p 3007 N95-32116
ROTATING SHAFTS
Analytic and experimental investigation of rotordynamic response and backward whirl induced by split resonance
|AD-A293639| p 2889 N95-31566
An active magnetic bearing with high T(sub c) superconducting coils and ferromagnetic cores
|NASA-TM-106995| p 2864 N95-31847
ROTATION
Composite structure forming a wear surface
|AD-D017462| p 2785 N95-30749
Stabilization of the resistive shell mode in tokamaks
|DE95-008748| p 3004 N95-30794
Validation of the helicopter rotor code HERO
|PB95-198040| p 2751 N95-30838
A simple and efficient procedure for polyhedral assembly partitioning under infinitesimal motions
|DE95-009838| p 2942 N95-31644
Dynamical analysis of the coriolis effect which causes space disorientation
|NAL-TR-1258| p 2928 N95-31714
ROTOR AERODYNAMICS
A numerical model for dynamic wave rotor analysis
|NASA-TM-106997| p 2754 N95-30617
Axial loads on yawed rotors
|PB95-214193| p 2742 N95-30638
A novel instrumentation system for measurement of helicopter rotor motions and loads data, phase 1
|AD-A293309| p 2751 N95-30923
Digital simulation of wind velocities for wind turbine rotors: General considerations
|PB95-206447| p 2904 N95-31157
ROTOR BLADES (TURBOMACHINERY)
Development of a linearized unsteady Euler analysis for turbomachinery blade rows
|NASA-CR-4677| p 2742 N95-30611
ROTOR DYNAMICS
Numerical simulation of flow in a whirling annular seal and comparison with experiments
|NASA-TM-106961| p 2867 N95-30710
Analytic and experimental investigation of rotordynamic response and backward whirl induced by split resonance
|AD-A293639| p 2889 N95-31566
Vibration reduction in helicopter rotors using an actively controlled partial span trailing edge flap located on the blade p 2762 N95-32111
ROTORS
Wave rotor-enhanced gas turbine engines
|NASA-TM-106998| p 2754 N95-30517
A numerical model for dynamic wave rotor analysis
|NASA-TM-106997| p 2754 N95-30617
Preliminary assessment of combustion modes for internal combustion wave rotors
|NASA-TM-107000| p 2754 N95-30632
Improved modeling of unsteady heat transfer (The first step)
|AD-A292777| p 2874 N95-31432
Application of multigrid computational fluid dynamics (CFD) methods to rotor analysis
|AD-A293012| p 2874 N95-31475
ROUTES
FAA aviation forecasts: Fiscal year 1995-2006
|AD-A293682| p 2741 N95-31598
RUBBER
Evaluation of alternative pavement marking materials
|AD-A292973| p 2763 N95-31468
RUBBER COATINGS
Response of dual-layered structures subjected to shock pressure wave
|AD-A293731| p 2896 N95-31568
RUBIDIUM
The 26th Annual Precise Time and Time Interval (PTTI) Applications and Planning Meeting
|NASA-CP-3302| p 2967 N95-32319
Monte Carlo simulations of precise timekeeping in the Milstar communication satellite system p 2970 N95-32336
SVN 9 End-Of-Life testing p 2767 N95-32345
RUN TIME (COMPUTERS)
The Coprocessor Manager in the BASIS processor system
|PB95-211611| p 2945 N95-32252
RUSSIAN FEDERATION
Mars together and FIRE and ICE: Report of the joint US/Russian technical working groups
|NASA-CR-198864| p 3030 N95-30845
FBIS report: Science and technology. Central Eurasia
|FBIS-UST-95-027| p 2839 N95-31727
FBIS report: Science and technology. Central Eurasia
|FBIS-UST-95-029| p 2863 N95-31728
FBIS report: Science and technology. Central Eurasia
|FBIS-UST-95-028| p 2839 N95-31729
RUSSIAN SPACE PROGRAM
Mir 18 post flight presentation
|NASA-TM-110657| p 2766 N95-30854

S

S MATRIX THEORY
Complex conjugate pairs in stationary Sturmians
|DE95-616279| p 2976 N95-30429
The solutions of affine and conformal affine Toda field theory
|DE95-616280| p 2965 N95-30430
Inelastic plasmon and inter-band electron-scattering potentials for Si from dielectric matrix calculations
|DE95-616778| p 2977 N95-30475
The effect of a non-Hermitian crystal potential on the scattering matrix in reflection electron diffraction
|DE95-616779| p 2977 N95-30476
Physical optics polarization scattering matrix for a right-angle dihedral
|AD-A293036| p 3000 N95-31665
S WAVES
Hadronic production of S-wave and P-wave charmed beauty mesons via heavy quark fragmentation
|DE95-008737| p 2977 N95-30465
A valence-fluctuation mechanism with highly anisotropic S-wave pairing
|DE95-009419| p 3010 N95-30571
SABOT PROJECTILES
A RASCAL in-bore dynamic analysis of the task B and task C electromagnetic railguns
|AD-A292742| p 2764 N95-30948
SACCADIC EYE MOVEMENTS
Simulation of oculomotor post-inhibitory rebound burst firing using a Hodgkin-Huxley model of a neuron
|AD-A293821| p 2927 N95-31552
SAFETY
Recommended techniques for effective maintainability. A continuous improvement initiative of the NASA Reliability and Maintainability Steering Committee
|NASA-TM-4628| p 2892 N95-31530
Data analysis: Naive inductivism
|PB95-212213| p 3026 N95-32254
SAFETY DEVICES
Releaseable unconstrained inflatable body protector
|AD-D017350| p 2930 N95-30552
SAFETY FACTORS
Metascientific problems in safety science
|PB95-196408| p 2838 N95-30521
SAFETY MANAGEMENT
Metascientific problems in safety science
|PB95-196408| p 2838 N95-30521
Generalized implementation of software safety policies p 2939 N95-31249
Fact sheet for Congressional Committees. Air traffic control: Status of FAA's modernization program
|GAO/RCED-94-167FS| p 2750 N95-32197
SALINITY
Ocean mass density calculations from temperature and salinity data
|DSTO-TR-0023| p 2922 N95-30711
The role of the hydrological cycle and the ocean's thermohaline circulation in climate change: A multicomponent climate model study p 2909 N95-31720
SAMPLERS
Novel mass spectrometric instrument for gaseous and particulate characterization and monitoring
|DE95-000047| p 2881 N95-31694
SAMPLES
Standardization of (13)CO2 production procedure from organic matter for mass spectrometric analysis
|DE95-614629| p 2791 N95-30420
SAMPLING
Ultrasonic two probe system for locating and sizing
|AD-D017438| p 2996 N95-30724
Statistical interface for chaotic signal in noise
|AD-A290271| p 2848 N95-30932
Evaluation of calibration parameters and performance of the video imaging technique of assessing exposure (VITAE system)
|AD-A289023| p 2927 N95-30998
SANDWICH STRUCTURES
Design of fibre reinforced composite panels for aerospace applications
|PB95-197851| p 2784 N95-30460
Advanced oxidizers diffusion flames structure p 2801 N95-31307
Influence of layer order and composition on the magnetic anisotropy of ultra-thin Co sandwiches
|DE95-010608| p 2810 N95-32265
SAPPHIRE
Ion implantation and thermal stress resistance of ceramics
|DE95-615349| p 2812 N95-30451
The effect of interface properties on nickel base alloy composites
|NASA-CR-198363| p 2785 N95-30787
Germanate glass ceramic
|AD-D017418| p 2816 N95-31011
SATELLITE ANTENNAS
Proceedings of the antenna applications symposium. volume 2
|AD-A293259| p 2850 N95-31387
SATELLITE COMMUNICATION
STS-70 flight: Day 4
|NASA-TM-110662| p 2764 N95-30877
STS-70 flight: Day 3
|NASA-TM-110661| p 2765 N95-30878
STS-70 flight: Day 2
|NASA-TM-110660| p 2765 N95-30879
Computer interface development for the petite amateur navy satellite (PANSAT) simulator
|AD-A293263| p 2766 N95-31388
The quad-service satellite transmitting and receiving system for medical supply support: A battlefield interoperability and communications system prototype, volume 2. User documentation
|AD-A292835| p 2851 N95-31448
The quad-service satellite transmitting and receiving system for medical supply support: A battlefield interoperability and communications system prototype, volume 1
|AD-A292836| p 2851 N95-31449
Portable digital Satellite News Gathering (SNG) RF terminal using a flat antenna
|NHK-LABS-NOTE-436| p 2853 N95-31744
Information Switching Processor (ISP) contention analysis and control
|NASA-CR-195471| p 2765 N95-31849
Residual and suppressed-carrier arraying techniques for deep-space communications p 2856 N95-32235

SATELLITE CONSTELLATIONS
Fine tuning GPS clock estimation in the MCS
p 2968 N95-32322
SATELLITE IMAGERY
System considerations for efficient communication and storage of MSTI image data
|NASA-CR-198869| p 3024 N95-30858
FISHFINDE: Interactive software package to predict fish locations using satellite image data and fish species behavior rules
|AD-A293394| p 2935 N95-30968
Global Ultraviolet Imager (GUVI) investigation
|NASA-CR-189430| p 2917 N95-31820
SeaWiFS technical report series. Volume 13: Case studies for SeaWiFS calibration and validation, part 1
|NASA-TM-104566-VOL-13| p 2924 N95-32220
Prospects for high accuracy time dissemination and synchronization using coded radar pulses from a low-earth orbiting spacecraft p 2971 N95-32339
SATELLITE NAVIGATION SYSTEMS
A globally efficient means of distributing UTC time and frequency through GPS p 2970 N95-32335
SATELLITE NETWORKS
High accuracy time transfer synchronization
p 2968 N95-32321
SATELLITE OBSERVATION
Satellite multisensor data techniques for sea ice mapping
|AD-A289729| p 2901 N95-31148
Comparison of satellite-derived MSU brightness temperatures and conventionally-derived fields
|AD-A293692| p 2901 N95-31603
SATELLITE-BORNE INSTRUMENTS
Integrated X-ray testing of the electro-optical breadboard model for the XMM reflection grating spectrometer
|DE95-008829| p 2879 N95-30507
The future of space imaging. Report of a community-based study of an advanced camera for the Hubble Space Telescope
|NASA-CR-198818| p 3028 N95-31364
SATURN (PLANET)
Welding isotopic heat sources for the cassini mission to Saturn
|DE95-060104| p 2890 N95-32367
SCALARS
Light-front dynamics of Chern-Simons systems
|DE95-613467| p 3019 N95-30741
Instability of weak vacuum
|DE95-613590| p 2985 N95-31620
Analysis and modeling of subgrid scalar mixing using numerical data
|NASA-CR-198169| p 2877 N95-31978
Harmonic coordinates in the problem on static gravitational and massless scalar fields with a point source
|DE95-623632| p 3020 N95-32295
SCALING
Scaling behaviour of leptonic decay constants for heavy quarkonia and heavy mesons
|DE95-620539| p 2983 N95-31218
SCANNING ELECTRON MICROSCOPY
Direct sublattice imaging of interface dislocation structures in CdTe/GaAs(001)
|DE95-009031| p 3010 N95-30576
Metrology of chrome on quartz photomasks using low voltage scanning electron microscopy. Part 1: Physical SEM parameters
|PB95-195780| p 2880 N95-30693
High aspect ratio metal microstructures and method for preparing the same
|AD-D017463| p 2803 N95-30750
Processing and characterization of nanocrystalline molybdenum disilicide (MoSi2) consolidated by hot isostatic pressing (HIP)
|DE95-010243| p 3012 N95-30756
In situ composites in the aluminum nitride-alumina system
|AD-A293776| p 2789 N95-31509
SCANNING TUNNELING MICROSCOPY
STM studies of clean, CO- and O2-exposed Pt(100)-hex-R0.7 deg
|PB95-195376| p 3009 N95-30535
STM measurements of the interaction of vacancies and steps during low-energy-ion bombardment of Si(001)
|DE95-010935| p 3017 N95-32308
SCARS
Laser induced vitreoretinal scarring. Evaluation of causative factors and a therapeutic approach
|AD-A293742| p 2928 N95-31570
SCATTERING
Apparatus and method for producing three-dimensional images
|AD-D017455| p 2847 N95-30727
Polarisation resonance in X-ray diffraction
|DE95-616727| p 3012 N95-30789
Multichannel resonances in coupled channels of meson scattering: Scalar sector
|DE95-613783| p 2981 N95-30912
Effects of mosaicity on Parametric X-Radiation production
|AD-A293677| p 2985 N95-31597
Two-dimensional Finite Difference Time Domain (FD-TD) model of electromagnetic (EM) scattering from a buried rectangular object
|AD-A293685| p 2852 N95-31601
Removal of the Energy Dependence from the Resolvent Like Energy Dependent Interactions
|DE95-613385| p 2961 N95-31619
SCATTERING AMPLITUDE
On perturbative asymptotic of Regge trajectories
|DE95-613585| p 3018 N95-30636
A compact expression for bilinear combination of Dirac spinors via world tensors
|DE95-619200| p 2960 N95-31258
SCATTERING CROSS SECTIONS
Inversion of the total cross sections for electron-molecule and electron-atom scattering
|DE95-616466| p 2978 N95-30583
Analytic cross sections for collisions of H, H2, He and Li atoms and ions with atoms and molecules
|DE95-722055| p 2979 N95-30654
Fast multipole methods for scattering computations
|AD-A291093| p 2848 N95-30869
SCATTERING FUNCTIONS
The TEVA experiment cruise report
|AD-A293025| p 2923 N95-31701
SCATTEROMETERS
Investigation of microwave backscatter from the air-sea interface
|NASA-CR-198854| p 2851 N95-31457
SCHEDULES
Lessons learned in deploying software estimation technology and tools p 2938 N95-31246
Patient/aircraft forecasting for the strategic aeromedical evacuation lift-bed process
|AD-A293902| p 2747 N95-31512
SCHEDULING
Using case-based reasoning as a Reinforcement Learning framework for optimization with changing criteria
|AD-A293602| p 2953 N95-31654
A microeconomic scheduler for parallel computers
|NASA-CR-198153| p 2932 N95-32046
SCHOOLS
Selection of Swedish scholastic aptitude test takers as a function of socioeconomic background and ability: Evaluation through follow-up
|PB95-212072| p 3021 N95-30699
Non-comparability of female and male admission test takers: Evaluation through follow-up
|PB95-212080| p 3021 N95-30700
SCHROEDINGER EQUATION
Quantum dynamics in regions of quaternionic curvature
|DE95-616276| p 3018 N95-30426
Quasi-periodic solutions of Hamiltonian perturbations of 2D linear Schroedinger equations
|PB95-208443| p 2957 N95-30624
Determination of the symmetry of a non-linear Schroedinger equation
|IFTR-10/1995| p 2960 N95-31339
Fast algorithms for three-dimensional inverse scattering problems
|AD-A293510| p 2852 N95-31537
SCHWARTZ METHOD
Higher Schwarzian operators and combinatorics of Schwarzian derivative
|PB95-208435| p 2957 N95-30623
SCIENTIFIC VISUALIZATION
Management, visualization, and analysis of environmental and geotechnical data
|DE95-000063| p 3026 N95-31823
SCORING
Luminance effects on visual acuity and small letter contrast sensitivity
|AD-A293310| p 2928 N95-31140
SEA FLOOR SPREADING
Studies in marine tectonics: Propagating rifts, depth anomalies and subduction zone anisotropy
p 2923 N95-31719
SEA ICE
Weather influence on passive microwave brightness temperatures
|PB95-195384| p 2900 N95-30536
Radiometer measurements of sea ice in the Gulf of Bothnia 1992
|PB95-206611| p 2900 N95-30718
Sea ice stress research
|AD-A293164| p 2923 N95-30964
Satellite multisensor data techniques for sea ice mapping
|AD-A289729| p 2901 N95-31148
The role of the hydrological cycle and the ocean's thermohaline circulation in climate change: A multicomponent climate model study
p 2909 N95-31720
SEA STATES
The determination of wave group parameters from the resolution of incident and reflected waves
|AD-A293703| p 2924 N95-31829
SEA SURFACE TEMPERATURE
Yellow Sea thermal structure
|AD-A291159| p 2922 N95-30396
Arabian Sea mixed layer dynamics experiment: Mooring deployment cruise report
|AD-A293684| p 2923 N95-31600
Global climatology and variability of potential new production estimated from remote sensing of sea-surface temperature
|NASA-CR-198840| p 2910 N95-31981
SEA WATER
Yellow Sea thermal structure
|AD-A291159| p 2922 N95-30396
Active turbulence control using microelectrodes, permanent magnets in microgrooves
|AD-D017351| p 2867 N95-30553
Ocean mass density calculations from temperature and salinity data
|DSTO-TR-0023| p 2922 N95-30711
The impact of microbiologically influenced corrosion on protective polymer coatings
|AD-A288896| p 2816 N95-30997
Comparison of cathodic protection currents on 70/30 copper-nickel and alloy 625 piping systems
|AD-A292953| p 2807 N95-31561
Carbon dioxide concentrations in surface water and the atmosphere during 1986-1989 NOAA/PMEL cruises in the Pacific and Indian Oceans
|DE95-009659| p 2910 N95-32099
SEALING
Trivalent chromium solutions for sealing anodized aluminum
|AD-D017349| p 2803 N95-30551
SEALS (STOPPERS)
Numerical simulation of flow in a whirling annular seal and comparison with experiments
|NASA-TM-106961| p 2867 N95-30710
Compatibility of Single Hydraulic Fluid with military specification fluids, seals and metallurgy
|AD-A292954| p 2821 N95-31663
SEARCHING
Aspects of the search time in binary search trees modified according to the move-to-root heuristic
|PB95-212148| p 2963 N95-31396
SEATS
Fast-acting valve for projective launching systems
|AD-D017357| p 2888 N95-30416
SECONDARY INJECTION
Enhanced energy release and soot reduction in actively controlled flames p 2799 N95-31200
Pulse forming network in the ETC combustion characterization of plasma augmented solid propellants
p 2799 N95-31205
SECURITY
Requirements for security signalling
|DE95-008714| p 2948 N95-31605
SEDIMENT TRANSPORT
On convective effects in sedimentation of concentrated suspensions with high effective gravity
|TRITA-NA-9316| p 2794 N95-31356
SEDIMENTS
Laboratory simulated hydrothermal alteration of sedimentary organic matter from Guaymas Basin, Gulf of California
|NASA-CR-198951| p 2914 N95-30865
On convective effects in sedimentation of concentrated suspensions with high effective gravity
|TRITA-NA-9316| p 2794 N95-31356
Multiple scatter theory of ocean sediments
|AD-A293951| p 2923 N95-31523
SEISMIC WAVES
Removal of scattered surface waves from seismic data
|PB95-197802| p 2922 N95-30457
Generation of earthquake signals
|PB95-211223| p 2913 N95-30631
Direct and inverse problems in random media
|AD-A293033| p 2850 N95-31280
A seismic data compression system using subband coding p 2857 N95-32238
SEISMOGRAPHS
Fiber optic accelerometer with centrally supported flexural disk
|AD-D017369| p 2879 N95-30658

SEISMOLOGY
Removal of scattered surface waves from seismic data
[PB95-197802] p 2922 N95-30457
Generation of earthquake signals
[PB95-211223] p 2913 N95-30631
Seismic studies of subducted lithosphere p 2915 N95-31335
Development of the Multi-Level Seismic Receiver (MLSR)
[DE95-008823] p 2916 N95-31610

SELECTION
Numerical computation of one-dimensional detonation waves
[PB95-197950] p 2868 N95-30811
Operational parameters and material effects p 2845 N95-32179

SELECTIVE DISSEMINATION OF INFORMATION
Recommendations for protecting National Library of Medicine Computing and Networking Resources
[DE95-011554] p 3026 N95-32285

SELF ALIGNMENT
Photorefractive nonlinear optics
[AD-A292913] p 2999 N95-31458

SELF CONSISTENT FIELDS
Calculated structures and electronic absorption spectroscopy for magnesium phthalocyanine and its anion radical
[AD-A293672] p 2796 N95-31596
Electronic structure of Donor-Spacer-Acceptor molecules of potential interest for molecular electronics III: Geometry and absorption spectrum of CH3-Alpha P3CNQ
[AD-A293662] p 2985 N95-31609

SELF EXCITATION
Control of high Reynolds number round jets p 2876 N95-31733

SELF ORGANIZING SYSTEMS
Aspects of the search time in binary search trees modified according to the move-to-root heuristic
[PB95-212148] p 2963 N95-31396

SEMANTICS
Extending a multi-set relational algebra to a parallel environment
[PB95-207106] p 3023 N95-30566
An approach to automated reasoning about operational semantics
[AD-A291127] p 2936 N95-31228

SEMICONDUCTING FILMS
May multiple inelastic scattering in CBED patterns be removed analytically
[PB95-196333] p 2992 N95-30717

SEMICONDUCTOR DEVICES
Magnetoluminescence characterization of quantum well structures
[DE95-008527] p 3008 N95-30381
Contactless characterization of semiconductors using laser-induced surface photo-charge voltage measurements
[AD-A293618] p 2863 N95-31725

SEMICONDUCTOR DIODES
Picosecond phase conjugation: New applications, devices, and materials
[AD-A293195] p 3013 N95-30982
A 1.94 micrometer laser apparatus, system and method using a thulium-doped yttrium-lithium-fluoride laser crystal pumped with a diode laser
[AD-D017435] p 2884 N95-31213

SEMICONDUCTOR LASERS
Polarization characteristics, control, and modulation of vertical-cavity surface emitting lasers
[DE95-008526] p 2882 N95-30380
Many-body effects in semiconductor lasers
[DE95-008534] p 2883 N95-30390
Extended tuning range semiconductor lasers with sampled gratings p 2883 N95-30498
Optical logic and signal processing using a semiconductor laser diode-based optical bistability device
[AD-A293248] p 2997 N95-30908
Picosecond phase conjugation: New applications, devices, and materials
[AD-A293195] p 3013 N95-30982
A compact and efficient violet laser source
[AD-A292782] p 2885 N95-31434
Optical frequency standards: Hertz-level working standards and their absolute frequency measurement
[AD-A293930] p 2999 N95-31515

SEMICONDUCTORS (MATERIALS)
Magnetoluminescence characterization of quantum well structures
[DE95-008527] p 3008 N95-30381
NIR High-efficiency subwavelength diffractive structures in semiconductors
[DE95-008535] p 3008 N95-30391
Preparation of diisopropyl stibines and use thereof
[AD-D017419] p 2771 N95-30418
Semiconductor nanocrystals formed in SiO2 by ion implantation
[DE95-008900] p 2978 N95-30546
The quantum interference effect in semiconductor space charge layers studied by Feynman path integrals: General formalism and illustrative examples
[DE95-614483] p 3010 N95-30653
Acoustomagnetoelectric effect in a superlattice
[DE95-613445] p 3011 N95-30736
Photophysical properties of opto-electric molecules studied by time-resolved microwave conductivity
[PB95-196994] p 2980 N95-30774
Vertical transport in GaAs/AlGaAs superlattices p 3012 N95-30822
Glass matrix doped with activated luminescent nanocrystalline particles
[AD-D017416] p 2816 N95-31010
Method and apparatus for non-destructively measuring local resistivity of semiconductors
[AD-D017436] p 2862 N95-31343
Nonlinear organized materials for optical devices
[AD-A292809] p 2999 N95-31441
Poisson's ratio for hexagonal crystals
[AD-A293556] p 3015 N95-31539
Nonlinear optics in novel composite media
[AD-A293886] p 2999 N95-31542
Photovoltaic Energy Program overview: Fiscal year 1994
[DE94-011871] p 2905 N95-31661
Operational characteristics of a 200 C LC parallel resonant circuit
[NASA-TM-106983] p 2864 N95-31742
An experimental search for high ZT semiconductors: A survey of the preparation and properties of several alloy systems
[DE95-010232] p 2865 N95-32084
GCMS and FTIR studies of by-product inhibited growth and the rate-limiting step in TEOS-based SiO2 CVD
[DE95-009863] p 3016 N95-32147
Femtosecond, Cr(4+):YAG laser
[DE95-004964] p 2887 N95-32155
Investigation of the basic physics of high efficiency semiconductor hot carrier solar cell
[NASA-CR-198945] p 2906 N95-32212
Materials with controllable signature properties
[PB95-222964] p 2857 N95-32313

SEMISPAN MODELS
Unsteady transonic wind tunnel test on a semispan straked delta wing, oscillating in pitch. Part 1: Description of the model, test setup, data acquisition, and data processing
[AD-A293113] p 2743 N95-30885

SENSITIVITY
Josephson break junction thin film device
[AD-D017343] p 3011 N95-30673
Luminance effects on visual acuity and small letter contrast sensitivity
[AD-A293310] p 2928 N95-31140
Numerical simulation of ram accelerator performance including transient effects during initiation of combustion and sensitivity studies p 2799 N95-31203

SENSORS
Micromachined sensor and actuator research at the Microelectronics Development Laboratory
[DE95-008540] p 2878 N95-30384

SEPARATED FLOW
A turbulence module for the NPARC code
[NASA-CR-198358] p 2959 N95-30855
Vorticity dynamics and control of dynamic stall
[AD-A288658] p 2756 N95-31400
Investigating the use of smart acoustically active surfaces for flow separation control in turbomachinery
[AD-A292819] p 2874 N95-31443

SEPARATION
Synthesis of separation systems: Methods and applications in downstream gas processes
[PB95-208518] p 2798 N95-32372

SEPARATORS
Process for producing hydrophilic polymer membranes
[AD-D017355] p 2811 N95-30415
Reducing process noise in superconducting helium liquid level probes
[DE95-008956] p 2814 N95-30765

SEQUENCING
Automation of the control of acoustic parameters in a digital speech synthesizer
[IFTR-2/1995] p 2850 N95-31357

SERIES EXPANSION
Plaquette expansion proof and interpretation
[DE95-616282] p 2965 N95-30432
Approximate analytic diagonalization of lattice QCD
[DE95-616332] p 3018 N95-30444

SERVICE LIFE
Failure analysis of a repairable system: The case study of a cam-driven reciprocating pump
[AD-A293144] p 2889 N95-30949
Recycling MIL-H-46170 hydraulic fluid to extend fluid service life
[AD-A293035] p 2821 N95-31664
Robust Rocket Engine Concept
[NASA-TM-107010] p 2770 N95-32121

SERVOMECHANISMS
Passive range measurement system
[AD-D017344] p 2996 N95-30678

SET THEORY
Good metric spaces without good parameterizations
[PB95-208427] p 2957 N95-30622

SHAFTS (MACHINE ELEMENTS)
Brush seal shaft wear resistant coatings
[NASA-CR-198950] p 2889 N95-31382

SHALLOW SHELL EQUATIONS
Application of shallow shell stability to plant morphogenesis by Fourier series p 2897 N95-31734

SHALLOW SHELLS
Application of shallow shell stability to plant morphogenesis by Fourier series p 2897 N95-31734

SHALLOW WATER
Yellow Sea thermal structure
[AD-A291159] p 2922 N95-30396
Algorithm comparison and benchmarking using a parallel spectra transform shallow water model
[DE95-009124] p 2913 N95-30683
The TEVA experiment cruise report
[AD-A293025] p 2923 N95-31701

SHAPE MEMORY ALLOYS
Smart material joint band
[AD-D017374] p 2888 N95-30716
Shape memory properties of an iron modified nickel aluminide alloy
[DE95-010223] p 2805 N95-31111

SHAPES
An explanation for the shape of nanoindentation unloading curves based on finite element simulation
[DE95-008905] p 2812 N95-30548
Static behaviour of axially loaded uniplanar and multiplanar tubular x-joints
[PB95-207866] p 2892 N95-30585
A laser-based ice shape profilometer for use in icing wind tunnels
[NASA-TM-106936] p 2880 N95-30851
Theory & numerical methods for problems in shape reconstruction and large deviations
[AD-A292874] p 2952 N95-31279

SHEAR FLOW
Singular eigenfunctions for shearing fluids I
[DE95-008952] p 2868 N95-30763
Shear flow effects on ion thermal transport in tokamaks
[DE95-009115] p 3005 N95-30801
Large eddy simulation of jets using structured upwind numerics p 2871 N95-30993
Study of effect of bubbles on a free-shear layer p 2872 N95-31100
Numerical study of shear-induced heating in high-speed nozzle flow of liquid monopropellant p 2828 N95-31207

SHEAR LAYERS
Study of effect of bubbles on a free-shear layer p 2872 N95-31100

SHEAR PROPERTIES
An evaluation of the Iosipescu specimen for composite materials shear property measurement
[NASA-CR-198755] p 2896 N95-31418

SHEAR STRENGTH
Round-robin validation exercise for plate twist test method
[PB95-208088] p 2812 N95-30487
An evaluation of the Iosipescu specimen for composite materials shear property measurement
[NASA-CR-198755] p 2896 N95-31418

SHEAR STRESS
A turbulence model for steady and unsteady boundary layers in strong pressure gradients p 2868 N95-30840
Effects of hydrostatic pressure on the mechanical behavior of composite materials
[AD-A293162] p 2787 N95-30963
Viscous heating of liquid layers under intense shear p 2827 N95-31206
An evaluation of the Iosipescu specimen for composite materials shear property measurement
[NASA-CR-198755] p 2896 N95-31418

SHEARING
Singular eigenfunctions for shearing fluids I
[DE95-008952] p 2868 N95-30763

SHELL STABILITY
Application of shallow shell stability to plant morphogenesis by Fourier series p 2897 N95-31734

SHELL THEORY
Contributions to the design of neutral cutouts in laminated plates and shells p 2790 N95-32113
SHIP HULLS
Computational modeling of coating integrity effects on impressed current cathodic protection system
[AD-A293256] p 2815 N95-30894
SHIPS
Cloud condensation nuclei measurements in shiptrails
[AD-A293302] p 2919 N95-30951
Shiptracks in the Californian stratus region: Dependency on marine atmospheric boundary layer depth
[AD-A293272] p 2901 N95-31125
Mexico Wind Resource Assessment Project
[DE95-009202] p 2921 N95-31726
Prime power for shipboard high-average power FELs
[AD-A293718] p 2886 N95-31833
SHOCK TESTS
Ion implantation and thermal stress resistance of ceramics
[DE95-615349] p 2812 N95-30451
SHOCK TUBES
Computation of high-altitude hypersonic flow-field radiation p 2743 N95-30843
SHOCK TUNNELS
A numerical study of the starting process in a hypersonic shock tunnel p 2762 N95-30493
SHOCK WAVE INTERACTION
A numerical study of the starting process in a hypersonic shock tunnel p 2762 N95-30493
Numerical simulation of shock/turbulent boundary layer interaction
[NASA-CR-198846] p 2872 N95-31341
Experimental and computational investigation of the tip clearance flow in a transonic axial compressor rotor
[NASA-TM-106711] p 2876 N95-31738
SHOCK WAVES
Numerical simulation of ram accelerator performance including transient effects during initiation of combustion and sensitivity studies p 2799 N95-31203
Numerical simulation of shock/turbulent boundary layer interaction
[NASA-CR-198846] p 2872 N95-31341
A study of numerical solutions of conservation laws
[TRITA-NA-9315] p 2960 N95-31361
Response of dual-layered structures subjected to shock pressure wave
[AD-A293731] p 2896 N95-31568
Effects of cavity bleed and its configuration on aerodynamic characteristics of supersonic internal flow
[NAL-TR-1247] p 2744 N95-31715
Selected problems of the identification of weak double layers in plasma on a background of different aperiodic non-collision structures
[IFTR-4/1995] p 3006 N95-31737
Analysis of plasma measurements for the Geotail mission
[NASA-CR-199074] p 3032 N95-32218
A collisionless shock wave experiment
[DE95-009489] p 3008 N95-32351
SHORT CIRCUIT CURRENTS
Electrical short circuit and current overload tests on aircraft wiring
[AD-A293308] p 2860 N95-30922
SHORT CIRCUITS
Electrical short circuit and current overload tests on aircraft wiring
[AD-A293308] p 2860 N95-30922
SHORT TAKEOFF AIRCRAFT
The control system design methodology of the STOL and maneuver technology demonstrator p 2758 N95-31998
SHORT WAVE RADIATION
Arabian Sea mixed layer dynamics experiment: Mooring deployment cruise report
[AD-A293684] p 2923 N95-31600
SHOULDERS
Erect, neutral and slump sitting postures: A study of the torso linkage system from shoulder to hip joint
[AD-A293239] p 2930 N95-30907
SHRINKAGE
A phenomenological finite element model of part building in the stereolithography process
[DE95-008437] p 2932 N95-30376
Epoxy and acrylate stereolithography resins: In-situ measurements of cure shrinkage and stress relaxation
[DE95-008506] p 2811 N95-30389
Urethane foam process improvements
[DE95-008957] p 2815 N95-30798
SIDE INLETS
An investigation of the side-dump dual in-line ramjet combustor p 2756 N95-31199
SIDESLIP
Transonic aerodynamic characteristics of a proposed wing-body reusable launch vehicle concept
[NASA-TM-108489] p 2742 N95-30712
SIGNAL ANALYSIS
Multiresolution signal and system analysis and the analysis and control of discrete-event dynamic systems
[AD-A292775] p 2851 N95-31430
The Deep Space Network stability analyzer p 2858 N95-32334
SIGNAL ANALYZERS
Wavefront simulator for evaluating RF communication array signal processors
[AD-D017372] p 2847 N95-30660
Noise signal processor
[AD-D017430] p 2974 N95-30747
SIGNAL DETECTION
Generation of earthquake signals
[PB95-211223] p 2913 N95-30631
Optical feature recognition
[AD-A293168] p 2997 N95-30966
Detection of radar targets using higher-order statistics
[AD-D017442] p 2850 N95-31392
Visual processing of object velocity and acceleration
[AD-A292789] p 2929 N95-31436
SIGNAL DETECTORS
Method and system for suppressing noise induced in a fluid medium by a body moving therethrough
[AD-D017339] p 2973 N95-30411
Far field acoustic radiation reduction
[AD-D017452] p 2974 N95-30725
Coherent integrator
[AD-D017422] p 2847 N95-30743
SIGNAL DISTORTION
Rate considerations in deep space telemetry p 2765 N95-32223
SIGNAL ENCODING
A seismic data compression system using subband coding p 2857 N95-32238
SIGNAL PROCESSING
Method and system for suppressing noise induced in a fluid medium by a body moving therethrough
[AD-D017339] p 2973 N95-30411
Microwave repeater with broadband active and/or passive isolation control
[AD-D017358] p 2846 N95-30417
Signal-processing theory for the TurboRogue receiver
[NASA-CR-198882] p 2846 N95-30581
Sensor Fusion and Nonlinear Prediction for Anomalous Event Detection
[DE95-009429] p 2933 N95-30602
Wavefront simulator for evaluating RF communication array signal processors
[AD-D017372] p 2847 N95-30660
Coherent integrator
[AD-D017422] p 2847 N95-30743
Reply-frequency interference/jamming detector
[AD-D017428] p 2847 N95-30746
Noise signal processor
[AD-D017430] p 2974 N95-30747
Airborne ocean water lidar (OWL) real time processor (RTP)
[AD-A293226] p 2848 N95-30904
Advanced signal processing filter
[AD-D017324] p 2848 N95-30917
A novel instrumentation system for measurement of helicopter rotor motions and loads data, phase 1
[AD-A293309] p 2751 N95-30923
Analog preprocessing in a SNS 2 micrometers low-noise CMOS folding ADC
[AD-A293356] p 2849 N95-30954
Microwave electro-optic mixer
[AD-D017328] p 2862 N95-31179
Temporal feature extraction in photorefractive resonators
[AD-A292908] p 2881 N95-31385
Fractional delay waveguide modeling of acoustic tubes
[PB95-206637] p 2975 N95-31650
Automatic Target Recognition (ATR): Background statistics and the detection of targets in clutter
[AD-A293062] p 2853 N95-31673
Neural network based data fusion system
[AD-D017440] p 2953 N95-31692
Neural network based three dimensional ocean modeler
[AD-D017441] p 2953 N95-31693
Design of digital low-pass filters for time-domain recursive filtering of impact acceleration signals
[AD-A293086] p 2864 N95-31842
Adaptive space-time processing for airborne radars based on Doppler pre-processing
[PB95-205464] p 2854 N95-32114
The Telecommunications and Data Acquisition Report
[NASA-CR-198911] p 2854 N95-32221
An efficient implementation of Forward-Backward Least-Mean-Square Adaptive Line Enhancers p 2855 N95-32224
Towards optimum demodulation of bandwidth-limited and low SNR square-wave subcarrier signals p 2855 N95-32229
Testing the performance of feedback concatenated decoder with a nonideal receiver p 2856 N95-32231
Performance of residual carrier array-feed combining in correlated noise p 2856 N95-32232
Residual and suppressed-carrier arraying techniques for deep-space communications p 2856 N95-32235
A high-speed photonic clock and carrier regenerator p 2856 N95-32236
Effects of correlated noise on the full-spectrum combining and complex-symbol combining arraying techniques p 2856 N95-32237
Digital signal processing in the radio science stability analyzer p 2857 N95-32240
SIGNAL RECEPTION
Residual and suppressed-carrier arraying techniques for deep-space communications p 2856 N95-32235
SIGNAL TO NOISE RATIOS
Advanced signal processing filter
[AD-D017324] p 2848 N95-30917
Statistical interface for chaotic signal in noise
[AD-A290271] p 2848 N95-30932
Visual processing of object velocity and acceleration
[AD-A292789] p 2929 N95-31436
Optical frequency standards: Hertz-level working standards and their absolute frequency measurement
[AD-A293930] p 2999 N95-31515
Fast algorithms for three-dimensional inverse scattering problems
[AD-A293510] p 2852 N95-31537
Degradation in finite-harmonic subcarrier demodulation p 2855 N95-32228
Towards optimum demodulation of bandwidth-limited and low SNR square-wave subcarrier signals p 2855 N95-32229
Performance of residual carrier array-feed combining in correlated noise p 2856 N95-32232
Residual and suppressed-carrier arraying techniques for deep-space communications p 2856 N95-32235
SIGNAL TRANSMISSION
Method and system for suppressing noise induced in a fluid medium by a body moving therethrough
[AD-D017339] p 2973 N95-30411
Method and apparatus for locating an acoustic source
[AD-D017347] p 2974 N95-30549
Rate considerations in deep space telemetry p 2765 N95-32223
Fiber optic reference frequency distribution to remote beam waveguide antennas p 2972 N95-32346
(T2L2) Time Transfer by Laser Link p 2887 N95-32348
Satellite test of the isotropy of the one-way spe ed of light using ExTRAS p 2973 N95-32349
SIGNATURES
Far field acoustic radiation reduction
[AD-D017452] p 2974 N95-30725
Singular eigenfunctions for shearing fluids I
[DE95-008952] p 2868 N95-30763
Unification of LARCH and Z-based object models to support algebraically-based design refinement: The LARCH perspective
[AD-A289235] p 2935 N95-30999
Signatures of virtual LSP's at the TEVATRON
[DE95-613798] p 2982 N95-31060
A search for jet handedness in hadronic Z-0 decays
[DE95-010099] p 2988 N95-32083
SILENCERS
An active liner system for jet engine exhaust silencers, phase 1
[AD-A293277] p 2756 N95-31191
SILICA GLASS
Morphology and microstructure of (111) crystalline CeO2 films grown on amorphous SiO2 substrates by pulsed-laser ablation
[DE95-008842] p 3009 N95-30542
SILICATES
Langasite crystals growth with quality factor Q, that exceeds the Q of quartz, and which are suitable for high-precision resonators
[AD-A293397] p 3013 N95-30969
Global climatology and variability of potential new production estimated from remote sensing of sea-surface temperature
[NASA-CR-198840] p 2910 N95-31981
SILICIDES
Processing and characterization of nanocrystalline molybdenum disilicide (MoSi2) consolidated by hot isostatic pressing (HIP)
[DE95-010243] p 3012 N95-30756
An experimental search for high ZT semiconductors: A survey of the preparation and properties of several alloy systems
[DE95-010232] p 2865 N95-32084

Defect configurations in neutron-irradiated U3Si2
[DE95-009896] p 3016 N95-32105

SILICON

Inelastic plasmon and inter-band electron-scattering potentials for Si from dielectric matrix calculations
[DE95-616778] p 2977 N95-30475

Anodically enhanced diffusion in Cu/Ag thin film couples
[DE95-009198] p 2814 N95-30738

Method for laser-assisted silicon etching using halocarbon ambients
[AD-D017426] p 2883 N95-30744

Diamond thin film temperature and heat-flux sensors
[NASA-CR-198859] p 3012 N95-30847

Development of germanium-silicon growth technology
[AD-A293199] p 3013 N95-30983

Opto-electronic components from non-stoichiometric 3-5 materials
[AD-A293206] p 3013 N95-30985

HTS Josephson technology on silicon with application to high speed digital microelectronics
[AD-A288627] p 2861 N95-31147

Photovoltaic Czochralski silicon manufacturing technology improvements
[DE95-004066] p 2904 N95-31162

Synthetic Terrain Imagery for Helmet-Mounted Display. Volume 2: Software design document
[AD-A293611] p 2753 N95-31655

Silicon carbide-silicon heterostructure solar cells
p 2905 N95-31952

Terahertz spectroscopy of silicon micromachined three-dimensional photonic bandgap crystal
[DE95-010233] p 3015 N95-32037

Gelcasting of sintered reaction-bonded silicon nitride for improved mechanical properties
[DE95-010282] p 2822 N95-32085

Suppression of self-interstitials in silicon during ion implantation via in-situ photoexcitation
[DE95-009173] p 3016 N95-32301

STM measurements of the interaction of vacancies and steps during low-energy-ion bombardment of Si(001)
[DE95-010935] p 3017 N95-32308

SILICON ALLOYS

Amorphization threshold in Si-implanted strained SiGe alloy layers
[DE95-008901] p 2804 N95-30797

Comprehensive research on the stability and electronic properties of a-Si:H and a-SiGe:H alloys and devices
[DE95-004088] p 2810 N95-32154

SILICON CARBIDES

Interfacial studies of coated fiber reinforced glass-ceramic matrix composites
[AD-A290780] p 2783 N95-30433

TEM-examination of ceramic-metal interfaces
[PB95-196531] p 2813 N95-30664

Characterization of compressive damage mechanisms in ceramic and polymeric matrix composite materials
[AD-A293171] p 2787 N95-30975

An assessment of the cost of microwave sintering ceramic tiles for armor applications. Phase 2 report
[DE95-010000] p 2816 N95-31103

Band gap measurement of Si(1-x)C(x)/Si (0 less than or equal to x less than or equal to 0.014) alloys using photoluminescence and spectroscopic ellipsometry
[DE95-011020] p 3014 N95-31112

Pseudomorphic heterostructure materials for high performance devices
[AD-A292906] p 2788 N95-31384

Silicon carbide-silicon heterostructure solar cells
p 2905 N95-31952

Influence of fiber content on mechanical performance of SiC-fiber-reinforced reaction-bonded silicon nitride composites
[NASA-TM-110639] p 2790 N95-32060

Low cost fabrication of silicon carbide based ceramics and fiber reinforced composites
[NASA-TM-107001] p 2822 N95-32208

SILICON DIOXIDE

Morphology and microstructure of (111) crystalline CeO2 films grown on amorphous SiO2 substrates by pulsed-laser ablation
[DE95-008842] p 3009 N95-30542

Interface degradation in CAS/Nicalon during elevated temperature aging
[DE95-008843] p 2812 N95-30543

Semiconductor nanocrystals formed in SiO2 by ion implantation
[DE95-008900] p 2978 N95-30546

Mechanisms of enhanced ionic conduction at interfaces in ceramics
[DE95-009125] p 2814 N95-30730

Reflectivity of plasmas created by high-intensity, ultra-short laser pulses
[DE95-009536] p 3004 N95-30742

SILICON FILMS

Band gap measurement of Si(1-x)C(x)/Si (0 less than or equal to x less than or equal to 0.014) alloys using photoluminescence and spectroscopic ellipsometry
[DE95-011020] p 3014 N95-31112

SILICON JUNCTIONS

Spectral response of a polycrystalline silicon solar cell
[DE95-614370] p 2903 N95-30723

Large-area, triple-junction a-Si alloy production scale-up
[DE95-004067] p 2904 N95-31163

SILICON NITRIDES

Interfacial studies of coated fiber reinforced glass-ceramic matrix composites
[AD-A290780] p 2783 N95-30433

Stress relaxation of silicon nitride at elevated temperatures
[DE95-009177] p 2814 N95-30732

Characterization of compressive damage mechanisms in ceramic and polymeric matrix composite materials
[AD-A293171] p 2787 N95-30975

Effect of cyclic loading on the creep performance of silicon nitride
[DE95-010289] p 2894 N95-31131

Life prediction methodology for ceramic components of advanced heat engines. Phase 1: Volume 2. Appendices
[DE95-010806] p 2817 N95-31136

Differences in creep performance of a HIPed silicon nitride in ambient air and inert environments
[DE95-009172] p 2796 N95-31633

Predictions of tensile behavior and strengths of a Si3N4 ceramic at high temperatures based on a viscoplastic model
[DE95-010220] p 2821 N95-32025

Influence of fiber content on mechanical performance of SiC-fiber-reinforced reaction-bonded silicon nitride composites
[NASA-TM-110639] p 2790 N95-32060

Gelcasting of sintered reaction-bonded silicon nitride for improved mechanical properties
[DE95-010282] p 2822 N95-32085

SILICON OXIDES

Innovative processing of composites for ultra-high temperature applications, book 3
[AD-A290891] p 2786 N95-30866

GCMS and FTIR studies of by-product inhibited growth and the rate-limiting step in TEOS-based SiO2 CVD
[DE95-009863] p 3016 N95-32147

Photo-refractive Bi12SiO20: Spatial light modulator
[AD-A293084] p 3001 N95-32153

SILICON POLYMERS

An interpenetrating polymer network for second-order nonlinear optics
[AD-A293019] p 2821 N95-31699

SILICONE RUBBER

Compatibility of Single Hydraulic Fluid with military specification fluids, seals and metallurgy
[AD-A292954] p 2821 N95-31663

SILICONES

Hydrogen sulfide analyzer with protective barrier
[AD-D017412] p 2793 N95-31009

SILVER

State-of-the-art low-cost solar reflector materials
[DE95-000260] p 2902 N95-30526

Anodically enhanced diffusion in Cu/Ag thin film couples
[DE95-009198] p 2814 N95-30738

Optimization of high-temperature superconductor current leads
[DE95-005838] p 2861 N95-30942

SILVER ALLOYS

Optimization of high-temperature superconductor current leads
[DE95-005838] p 2861 N95-30942

Volumetric and electro analytical techniques for chemical characterization of nuclear grade Ag-In-Cd alloys
[DE95-620664] p 2807 N95-31407

Metallurgical and Materials Transactions
[AD-A293617] p 2807 N95-31464

SIMPLEX METHOD

Simplex method for semi-definite programming: Optimization and systems theory
[PB95-212122] p 2934 N95-30792

SIMPLIFICATION

An overview of high-speed networking for workstations
[DE95-009076] p 2947 N95-30577

SIMULATION

Advances in the simulation of toroidal gyro Landau fluid model turbulence
[DE95-008387] p 3003 N95-30359

Finite element simulation of GaAs MESFET's
[PB95-208062] p 3009 N95-30485

A system simulation development project: Leveraging resources through partnerships
[NASA-TM-106962] p 2753 N95-30514

Simulation of chemical kinetics in turbulent natural gas combustion. Volume 2: Experimental studies of nitric oxide production in gas flames
[PB95-196721] p 2791 N95-30541

An explanation for the shape of nanoindentation unloading curves based on finite element simulation
[DE95-008905] p 2812 N95-30548

The role of advanced engineering simulation in model-based design
[DE95-008815] p 2934 N95-30796

Simulation of viscous sintering
[PB95-197109] p 2868 N95-30836

RASSP benchmark 1 executable requirements user's manual
[AD-A290060] p 2935 N95-30931

Self-consistent, 2D simulations of filament propagation in photoconducting switches
[DE95-010794] p 2861 N95-31133

Dynamics of Current Driven Disordered Josephson Junction Arrays
[DE95-009418] p 3014 N95-31231

The development of human behaviour analysis techniques and the development of human factors technologies
[DE95-613356] p 2930 N95-31267

Clouds: Their prediction and simulation
[AD-A292864] p 2920 N95-31453

Large-eddy simulation of turbulent flow using the finite element method
[DE95-009464] p 2875 N95-31591

MPI implementation of PHOENICS: A general purpose computational fluid dynamics code
[DE95-009810] p 2877 N95-32033

SIMULATORS

Wavefront simulator for evaluating RF communication array signal processors
[AD-D017372] p 2847 N95-30660

Computational methods for control and optimal design of aerospace systems
[AD-A292861] p 2751 N95-31451

Hot compression testing of tungsten
[AD-A293683] p 2807 N95-31599

SOSIE: A pragmatic approach to the simulation of Broad Air Defense applied to the theater level
p 2840 N95-32127

Production simulator for wave power plants
[PB95-212262] p 2907 N95-32286

SINE WAVES

Statistical interface for chaotic signal in noise
[AD-A290271] p 2848 N95-30932

SINGLE CHANNEL PER CARRIER TRANSMISSION

Towards optimum demodulation of bandwidth-limited and low SNR square-wave subcarrier signals
p 2855 N95-32229

SINGLE CRYSTALS

Ion implantation and thermal stress resistance of ceramics
[DE95-615349] p 2812 N95-30451

STM studies of clean, CO- and O2-exposed Pt(100)-hex-R0.7 deg
[PB95-195376] p 3009 N95-30535

Josephson break junction thin film device
[AD-D017343] p 3011 N95-30673

Anodically enhanced diffusion in Cu/Ag thin film couples
[DE95-009198] p 2814 N95-30738

New material for high average power infrared generation: QPM-DB GaAs
[AD-A292714] p 2967 N95-30939

Investigations of YBaCuO materials with near-room-temperature resistivity transitions
[AD-A293405] p 3013 N95-31008

Synthesis and selected micro-mechanical properties of titanium nitride thin films by the pyrolysis of tetrakis titanium in ammonia
[DE95-010224] p 2818 N95-31187

Materials for adaptive structural acoustic control, volume 3
[AD-A293446] p 2788 N95-31371

Growth, characterization and device development in monocrystalline diamond films
[AD-A293106] p 3015 N95-32018

On the possibility of a two-state magnetic structure for nanocrystalline chromium
[DE95-009914] p 3015 N95-32062

The pyrochlore-to-perovskite transformation in solution-derived lead zirconate titanate thin films
[DE95-010453] p 2822 N95-32161

STM measurements of the interaction of vacancies and steps during low-energy-ion bombardment of Si(001)
[DE95-010935] p 3017 N95-32308

SINGLE STAGE TO ORBIT VEHICLES
Transonic aerodynamic characteristics of a proposed wing-body reusable launch vehicle concept
| NASA-TM-108489 | p 2742 N95-30712
SINGULAR INTEGRAL EQUATIONS
Numerical solution of a singular integral equation arising from a sequential probability ratio test
| AD-A293463 | p 2963 N95-31375
SINTERING
Simulation of viscous sintering
| PB95-197109 | p 2868 N95-30836
An assessment of the cost of microwave sintering ceramic tiles for armor applications. Phase 2 report
| DE95-010000 | p 2816 N95-31103
In situ composites in the aluminum nitride-alumina system
| AD-A293776 | p 2789 N95-31509
Gelcasting of sintered reaction-bonded silicon nitride for improved mechanical properties
| DE95-010282 | p 2822 N95-32085
SIZE (DIMENSIONS)
Gear pump with reduced fluid-borne noise
| AD-D017362 | p 2887 N95-30399
SIZE DISTRIBUTION
Fabrication and modification of metal nanocluster composites using ion and laser beams
| DE95-009131 | p 2784 N95-30731
Survey of recent Al2O3 droplet size data in solid rocket chambers, nozzles, and plumes p 2770 N95-30987
The Al and A(lc)l2O3 droplet cloud in solid rocket motors p 2770 N95-30988
SIZING MATERIALS
Phthalonitrile prepolymer as high temperature sizing material for composite fibers
| AD-D017447 | p 2818 N95-31272
SKEWNESS
Numerical simulation of the Langevin equation for skewed turbulence
| DE95-009477 | p 2877 N95-32049
SKIN (ANATOMY)
Control of skin blood flow in the neutral zone of human body temperature regulation
| AD-A291499 | p 2926 N95-30563
Evaluation of calibration parameters and performance of the video imaging technique of assessing exposure (VITAE system)
| AD-A289023 | p 2927 N95-30998
SKIN FRICTION
Improved modeling of unsteady heat transfer (The first step)
| AD-A292777 | p 2874 N95-31432
SKIN TEMPERATURE (BIOLOGY)
Control of skin blood flow in the neutral zone of human body temperature regulation
| AD-A291499 | p 2926 N95-30563
SKY RADIATION
Spectral sky background in the IR: Measurements with FTIR
| PB95-222998 | p 2922 N95-32315
SLABS
Seismic studies of subducted lithosphere p 2915 N95-31335
Reflection and transmission of electromagnetic plane waves from a uniaxial chiro-omega slab
| PB95-206629 | p 2853 N95-31649
SLAGS
Shuttle redesigned solid rocket motor aluminum oxide investigations p 2770 N95-30989
SMART STRUCTURES
Large area smart piezoelectric and pyroelectric sensors
| AD-A291487 | p 2859 N95-30561
Smart material joint band
| AD-D017374 | p 2888 N95-30716
Finite element analysis of smart structures and modal testing of a flexible spacecraft arm
| AD-A293761 | p 2890 N95-31576
Structural aspects of active control technology p 2760 N95-32006
Vibration control for precision manufacturing at Sandia National Laboratories
| DE95-009582 | p 2839 N95-32082
SMOKE
Validation of the atmospheric transmission large-area analysis system (ATLAS)
| AD-A293810 | p 2916 N95-31589
SNAKES
Polarized proton beams
| DE95-010843 | p 2987 N95-32031
SNELLEN TESTS
Luminance effects on visual acuity and small letter contrast sensitivity
| AD-A293310 | p 2928 N95-31140
SOBOLEV SPACE
Good metric spaces without good parameterizations
| PB95-208427 | p 2957 N95-30622
SOCIAL FACTORS
The sociology of megaprogramming: Experiences in generating an organizational learning enterprise (Software Technology for Adaptable, Reliable Systems(STARS) program)
| AD-A292998 | p 2946 N95-32294
SODIUM
Membrane transport: A cellular probe of heat stroke
| AD-A293327 | p 2926 N95-30924
SODIUM ALLOYS
NaK pool-boiler solar receiver durability bench test. Volume 2: Metallurgical analysis
| DE95-010338 | p 2905 N95-31640
SODIUM BROMIDES
The one-dimensional model of the off-centre potential of the fluorine ion in the NaBr lattice
| DE95-614310 | p 3010 N95-30647
SODIUM NITRATES
Environmentally compatible solid rocket propellants p 2772 N95-31753
SOFIA (AIRBORNE OBSERVATORY)
Stratospheric Observatory For Infrared Astronomy (SOFIA). Phase A: System concept description
| NASA-TM-110669 | p 3002 N95-32187
SOFTWARE DEVELOPMENT TOOLS
Experimental research into usability and organization impact of workflow software
| PB95-197679 | p 2933 N95-30454
Recommendations for developing portable parallel I/O facilities for scientific applications
| DE95-009384 | p 2947 N95-30578
Summary of technical operations
| AD-A293224 | p 2935 N95-30903
Lessons learned in deploying software estimation technology and tools p 2938 N95-31246
Analysis of symbolic parameter models
| AD-A292916 | p 2940 N95-31459
The Linux operating system: An introduction
| NASA-CR-198178 | p 2932 N95-31988
The Coprocessor Manager in the BASIS processor system
| PB95-211611 | p 2945 N95-32252
Software Process Framework. Tool to determine consistency with the CMM (Software Technology for Adaptable, Reliable Systems (STARS) program)
| AD-A292815 | p 2946 N95-32289
SOFTWARE ENGINEERING
Experimental research into usability and organization impact of workflow software
| PB95-197679 | p 2933 N95-30454
Metrics in method engineering
| PB95-197667 | p 2838 N95-30455
MVP/GMVP: General purpose Monte Carlo codes for neutron and photon transport calculations based on continuous energy and multigroup methods
| DE95-722072 | p 2979 N95-30656
Fast multipole methods for scattering computations
| AD-A291093 | p 2848 N95-30869
Summary of technical operations
| AD-A293224 | p 2935 N95-30903
Operator's handbook: NAWC Software Production Facility
| AD-A290216 | p 2935 N95-31001
An approach to automated reasoning about operational semantics
| AD-A291127 | p 2936 N95-31228
Proceedings of the 19th Annual Software Engineering Workshop
| NASA-CR-189411 | p 2936 N95-31234
Changes and challenges in the Software Engineering Laboratory p 2936 N95-31235
Domain analysis for the reuse of software development experiences p 2936 N95-31236
Building an experience factory for maintenance p 2937 N95-31237
Closing the loop on improvement: Packaging experience in the Software Engineering Laboratory p 2937 N95-31238
Process maturity progress at Motorola Cellular Systems Division p 2937 N95-31239
The Personal Software Process: Downscaling the factory p 2937 N95-31240
An experiment to assess the cost-benefits of code inspections in large scale software development p 2937 N95-31242
A process improvement model for software verification and validation p 2938 N95-31243
Leveraging object-oriented development at Ames p 2938 N95-31244
Lessons learned in transitioning to an open systems environment p 2938 N95-31245
Lessons learned in deploying software estimation technology and tools p 2938 N95-31246
Experience report: Using formal methods for requirements analysis of critical spacecraft software p 2938 N95-31247
Generalized implementation of software safety policies p 2939 N95-31249
A quantitative comparison of corrective and perfective maintenance p 2939 N95-31250
Does software design complexity affect maintenance effort? p 2939 N95-31251
Profile of software engineering within the National Aeronautics and Space Administration (NASA) p 2939 N95-31252
Virtual Reality Software and Technology '94
| AD-A292334 | p 2939 N95-31262
SodaBot: A software agent environment and construction system
| AD-A290056 | p 2939 N95-31277
Development of a structured design and programming methodology for expert systems shells utilizing a visual programming language: Application of structured methodology to the MK92 maintenance advisor expert system, performance module prototype
| AD-A289897 | p 2939 N95-31391
Computational methods for control and optimal design of aerospace systems
| AD-A292861 | p 2751 N95-31451
Synthetic Terrain Imagery for Helmet-Mounted Display. Volume 2: Software design document
| AD-A293611 | p 2753 N95-31655
Proceedings of the 1st Annual Software Engineering Techniques Workshop on Software Reengineering
| AD-A293724 | p 2943 N95-31834
Application of a genetic algorithm to optimize staffing levels in software development
| AD-A293725 | p 2943 N95-31835
Experience with a course on architectures for software systems. Part 2: Educational materials
| AD-A293090 | p 2943 N95-31843
Analysis and extension of model-based software executives
| AD-A293834 | p 2944 N95-32073
Architecture and implementation of a multi-sensor data fusion demonstration model within the real-time combat system of the Canadian Patrol Frigate p 2842 N95-32139
An efficient implementation of Forward-Backward Least-Mean-Square Adaptive Line Enhancers p 2855 N95-32224
User-friendly microcomputer interface with optimization languages AF94-007
| AD-A293184 | p 2932 N95-32257
Software Process Framework. Tool to determine consistency with the CMM (Software Technology for Adaptable, Reliable Systems (STARS) program)
| AD-A292815 | p 2946 N95-32289
Using process to integrate Software Engineering Environments (Software Technology for Adaptable, Reliable Systems (STARS) program)
| AD-A292816 | p 2946 N95-32290
SWSC domain engineering experience (Software Technology for Adaptable, Reliable Systems (STARS) program)
| AD-A292817 | p 2946 N95-32291
Integrating a SEE for megaprogramming: Lessons learned (Software Technology for Adaptable, Reliable Systems (STARS) program)
| AD-A292838 | p 2946 N95-32292
Defining manually enactable processes using the process definition information organizer templates (Software Technology for Adaptable, Reliable Systems (STARS) program)
| AD-A292854 | p 2946 N95-32293
The sociology of megaprogramming: Experiences in generating an organizational learning enterprise (Software Technology for Adaptable, Reliable Systems(STARS) program)
| AD-A292998 | p 2946 N95-32294
SOFTWARE RELIABILITY
Proceedings of the 19th Annual Software Engineering Workshop
| NASA-CR-189411 | p 2936 N95-31234
Applying program comprehension techniques to improve software inspections p 2937 N95-31241
Lessons learned in deploying software estimation technology and tools p 2938 N95-31246
Experience report: Using formal methods for requirements analysis of critical spacecraft software p 2938 N95-31247
Experimental control in software reliability certification p 2938 N95-31248
Generalized implementation of software safety policies p 2939 N95-31249
A quantitative comparison of corrective and perfective maintenance p 2939 N95-31250
SOFTWARE REUSE
Domain analysis for the reuse of software development experiences p 2936 N95-31236

Proceedings of the 1st Annual Software Engineering Techniques Workshop on Software Reengineering
[AD-A293724] p 2943 N95-31834
SWSC domain engineering experience (Software Technology for Adaptable, Reliable Systems (STARS) program)
[AD-A292817] p 2946 N95-32291
Integrating a SEE for megaprogramming: Lessons learned (Software Technology for Adaptable, Reliable Systems (STARS) program)
[AD-A292838] p 2948 N95-32292
Defining manually enactable processes using the process definition information organizer templates (Software Technology for Adaptable, Reliable Systems (STARS) program)
[AD-A292854] p 2946 N95-32293

SOI (SEMICONDUCTORS)
Pseudomorphic heterostructure materials for high performance devices
[AD-A292906] p 2788 N95-31384

SOIL MOISTURE
Field performance of the Walker Branch throughfall displacement experiment
[DE95-008677] p 2908 N95-30793

SOILS
Impact behavior of the active zone within a frozen soil profile
[AD-A292909] p 2915 N95-31386
Biomass production by fescue and switchgrass alone and in mixed swards with legumes
[DE95-009137] p 2909 N95-31612
Faster, cheaper radioanalytical methods
[DE95-009913] p 2797 N95-32061

SOL-GEL PROCESSES
Synthesis of novel precursors for PMN powders and the thin films obtained from them
[DE95-008543] p 2811 N95-30362

SOLAR ACTIVITY
Solar-geophysical data number 604, December 1994. Part 2: (Comprehensive reports). Data for June 1994, and miscellaneous
[PB95-191995] p 3031 N95-30690
Solar-geophysical data number 606, February 1995. Part 1: (Prompt reports). Data for December 1994, January 1995, and late data
[PB95-200853] p 3031 N95-30816
Solar-geophysical data number 606, February 1995. Part 2: (Comprehensive reports). Data for August 1994, and miscellaneous
[PB95-200861] p 3031 N95-30817
Nearly steady flows in GONG prototype data
[NASA-CR-198935] p 2869 N95-30863
Environmental conditions responsible for solar activity
[AD-A292859] p 3031 N95-31450

SOLAR ARRAYS
Space systems environmental interaction studies
[AD-A293826] p 2766 N95-31553

SOLAR CELLS
The junction characteristics and current conduction mechanisms of GaInP2 n(+)p diodes and solar cells
[AD-A290857] p 2902 N95-30408
Spectral response of a polycrystalline silicon solar cell
[DE95-614370] p 2903 N95-30723
InP solar cell development on inexpensive Si substrates
[AD-A293255] p 2903 N95-30893
Photovoltaic Czochralski silicon manufacturing technology improvements
[DE95-004066] p 2904 N95-31162
Large-area, triple-junction a-Si alloy production scale-up
[DE95-004067] p 2904 N95-31163
Investigation of polycrystalline thin film CuInSe2 solar cells based on ZnSe windows
[DE95-004068] p 2904 N95-31164
Silicon carbide-silicon heterostructure solar cells
p 2905 N95-31952
Development of large-area monolithically integrated Silicon-Film(trademark) photovoltaic modules
[DE95-004069] p 2906 N95-32057
Evaluation and analysis survey on new energy introduction, part 3
[DE95-769806] p 2906 N95-32072
Comprehensive research on the stability and electronic properties of a-Si:H and a-SiGe:H alloys and devices
[DE95-004065] p 2810 N95-32154
Investigation of the basic physics of high efficiency semiconductor hot carrier solar cell
[NASA-CR-198945] p 2906 N95-32212

SOLAR COLLECTORS
NaK pool-boiler solar receiver durability bench test. Volume 2: Metallurgical analysis
[DE95-010338] p 2905 N95-31640
Extra focal convective suppressing solar collector
[DE95-010170] p 2907 N95-32288

SOLAR CORONA
XV NSO/Sac Peak Solar workshop
[AD-A292319] p 3030 N95-30482
Mars together and FIRE and ICE: Report of the joint US/Russian technical working groups
[NASA-CR-198864] p 3030 N95-30845
Environmental conditions responsible for solar activity
[AD-A292859] p 3031 N95-31450

SOLAR CORPUSCULAR RADIATION
Radiation effects in space: The Clementine 1 mission
[DE95-011513] p 3032 N95-32282

SOLAR DYNAMIC POWER SYSTEMS
Validation of the FLAGSOL parabolic trough solar power plant performance model
[DE95-000263] p 2903 N95-30887

SOLAR ELECTRONS
HST-FOC observations of a remarkable UV auroral event on Jupiter p 3030 N95-30806

SOLAR ENERGY
Studies of C(60) and C(70) and other fullurenes: Synthesis, derivation, electrochemistry, lubricant properties and new composition materials
[AD-A292726] p 3012 N95-30944

SOLAR ENERGY ABSORBERS
Extra focal convective suppressing solar collector
[DE95-010170] p 2907 N95-32288

SOLAR ENERGY CONVERSION
Data on development of new energy technologies
[DE95-764135] p 2904 N95-31155
Solar thermal electric: Program overview, fiscal years 1993-1994
[DE94-000240] p 2906 N95-32058
Outlook for renewable energy technologies: Assessment of international programs and policies
[DE95-009084] p 2907 N95-32302

SOLAR FLARES
On the relationship between sunspots number and the flare index
[NASA-TM-110643] p 3030 N95-30467
Solar-geophysical data number 604, December 1994. Part 2: (Comprehensive reports). Data for June 1994, and miscellaneous
[PB95-191995] p 3031 N95-30690
Studying the thermal/non-thermal crossover in solar flares
[NASA-CR-189436] p 3031 N95-30785
Solar-geophysical data number 606, February 1995. Part 1: (Prompt reports). Data for December 1994, January 1995, and late data
[PB95-200853] p 3031 N95-30816
Solar-geophysical data number 606, February 1995. Part 2: (Comprehensive reports). Data for August 1994, and miscellaneous
[PB95-200861] p 3031 N95-30817
Environmental conditions responsible for solar activity
[AD-A292859] p 3031 N95-31450

SOLAR FLUX DENSITY
Low energy solar neutrino experiments: The Soviet American Gallium Experiment (SAGE)
[DE95-010159] p 3031 N95-30618

SOLAR GENERATORS
State-of-the-art low-cost solar reflector materials
[DE95-000260] p 2902 N95-30526
Evaluation and analysis survey on new energy introduction, part 3
[DE95-769806] p 2906 N95-32072

SOLAR HEATING
CALORSTOCK 1994: Thermal energy storage. Better economy, environment, technology
[DE95-772422] p 2904 N95-31138

SOLAR MAGNETIC FIELD
Solar-geophysical data number 606, February 1995. Part 1: (Prompt reports). Data for December 1994, January 1995, and late data
[PB95-200853] p 3031 N95-30816

SOLAR NEUTRINOS
Low energy solar neutrino experiments: The Soviet American Gallium Experiment (SAGE)
[DE95-010159] p 3031 N95-30618
The 10th INS Scientific Computational Programs
[DE95-717864] p 2982 N95-31178

SOLAR PHYSICS
XV NSO/Sac Peak Solar workshop
[AD-A292319] p 3030 N95-30482
Solar-geophysical data number 606, February 1995. Part 1: (Prompt reports). Data for December 1994, January 1995, and late data
[PB95-200853] p 3031 N95-30816

SOLAR PROBES
Mars together and FIRE and ICE: Report of the joint US/Russian technical working groups
[NASA-CR-198864] p 3030 N95-30845

SOLAR PROMINENCES
Solar-geophysical data number 604, December 1994. Part 2: (Comprehensive reports). Data for June 1994, and miscellaneous
[PB95-191995] p 3031 N95-30690
Solar-geophysical data number 606, February 1995. Part 2: (Comprehensive reports). Data for August 1994, and miscellaneous
[PB95-200861] p 3031 N95-30817

SOLAR RADIO BURSTS
Solar-geophysical data number 604, December 1994. Part 2: (Comprehensive reports). Data for June 1994, and miscellaneous
[PB95-191995] p 3031 N95-30690
Solar-geophysical data number 606, February 1995. Part 2: (Comprehensive reports). Data for August 1994, and miscellaneous
[PB95-200861] p 3031 N95-30817

SOLAR RADIO EMISSION
Solar-geophysical data number 606, February 1995. Part 1: (Prompt reports). Data for December 1994, January 1995, and late data
[PB95-200853] p 3031 N95-30816

SOLAR REFLECTORS
State-of-the-art low-cost solar reflector materials
[DE95-000260] p 2902 N95-30526
Validation of the FLAGSOL parabolic trough solar power plant performance model
[DE95-000263] p 2903 N95-30887

SOLAR SENSORS
Extra focal convective suppressing solar collector
[DE95-010170] p 2907 N95-32288

SOLAR SPECTRA
XV NSO/Sac Peak Solar workshop
[AD-A292319] p 3030 N95-30482

SOLAR TERRESTRIAL INTERACTIONS
Analysis of plasma measurements for the Geotail mission
[NASA-CR-199074] p 3032 N95-32218

SOLAR THERMAL ELECTRIC POWER PLANTS
Validation of the FLAGSOL parabolic trough solar power plant performance model
[DE95-000263] p 2903 N95-30887
Solar thermal electric: Program overview, fiscal years 1993-1994
[DE94-000240] p 2906 N95-32058

SOLAR WIND
On reflection of Alfven waves in the solar wind
[NASA-TM-110642] p 3031 N95-30582
Mars together and FIRE and ICE: Report of the joint US/Russian technical working groups
[NASA-CR-198864] p 3030 N95-30845
Analysis of plasma measurements for the Geotail mission
[NASA-CR-199074] p 3032 N95-32218

SOLAR X-RAYS
Solar-geophysical data number 604, December 1994. Part 2: (Comprehensive reports). Data for June 1994, and miscellaneous
[PB95-191995] p 3031 N95-30690
Solar-geophysical data number 606, February 1995. Part 2: (Comprehensive reports). Data for August 1994, and miscellaneous
[PB95-200861] p 3031 N95-30817

SOLDERED JOINTS
The 19th Annual Electronics Manufacturing Seminar
[AD-A293067] p 2863 N95-31674

SOLDERING
The 19th Annual Electronics Manufacturing Seminar
[AD-A293067] p 2863 N95-31674

SOLDERS
The 19th Annual Electronics Manufacturing Seminar
[AD-A293067] p 2863 N95-31674

SOLID PHASES
Evidence for electronic energy loss processes stimulating solid phase epitaxial regrowth of spatially isolated amorphous regions in semiconductor systems
[DE95-009892] p 3016 N95-32103

SOLID PROPELLANT COMBUSTION
The 31st JANNAF Combustion Subcommittee Meeting, volume 1 p 2825 N95-31194
Pulse forming network in the ETC combustion characterization of plasma augmented solid propellants p 2799 N95-31205
Workshop report: Measurement techniques in highly transient, spectrally rich combustion environments p 2799 N95-31208
Theory of unsteady combustion of solids: Investigation of Quasi-steady assumption p 2800 N95-31285
Oscillatory combustion of aluminized AP/HTPB propellants p 2800 N95-31286
Characterization of an improved Rijke burner as prelude to measurements of aluminum distributed combustion p 2800 N95-31287
Active control of combustion instability using injection techniques p 2800 N95-31288

Model for defining propellant burn rate performance boundaries p 2800 N95-31290
Survey of US burning rate measurement methods for solid propulsion applications p 2800 N95-31291
Condensed-phase processes during solid propellant combustion. 5: Further observations on depth profiling of burned surfaces of XM39 and M43 propellants p 2800 N95-31295
Observation and characterization of burning surface reaction zones of solid propellants p 2800 N95-31296
Modeling of thermal response of filament used in T-jump experiment p 2800 N95-31297
Assessment of dynamic burning behavior for JA-2 propellant rods p 2800 N95-31299
Measurement of temperatures and OH concentrations of solid propellant flames using absorption spectroscopy p 2801 N95-31302
Species and temperature profiles of propellant flames obtained from FTIR absorption spectroscopy p 2801 N95-31303
Embedded infrared fiber optic absorption studies of nitramine propellant strand burning p 2801 N95-31305
A study of the gas-phase processes of RDX combustion using a triple quadrupole mass-spectrometer p 2801 N95-31315
The physical and chemical processes governing CO2 laser-induced pyrolysis and combustion of the solid propellants RDX, ADN, XM39, and M43 p 2836 N95-31531

SOLID PROPELLANT IGNITION
The 31st JANNAF Combustion Subcommittee Meeting, volume 1 p 2825 N95-31194
Studies of reactions pertaining to and development of a reduced mechanism for the double base propellant dark zone p 2801 N95-31312

SOLID PROPELLANT ROCKET ENGINES
Ageing control no. 3 of propellants for rocket motors RB 27 and RB 28
|PB95-210357| p 2825 N95-30626
Survey of recent Al2O3 droplet size data in solid rocket chambers, nozzles, and plumes p 2770 N95-30987
Shuttle Redesigned Solid Rocket Motor aluminum oxide investigations p 2770 N95-31197
Technology transfer into the solid propulsion industry p 2770 N95-31756
Implementation of environmentally compliant cleaning and insulation bonding for MNASA p 2780 N95-31796
Cleanliness inspection tool for RSRM bond surfaces p 2781 N95-31799

SOLID PROPELLANTS
Pulse forming network in the ETC combustion characterization of plasma augmented solid propellants p 2799 N95-31205
Survey of US burning rate measurement methods for solid propulsion applications p 2800 N95-31291
Measurement of temperatures and OH concentrations of solid propellant flames using absorption spectroscopy p 2801 N95-31302
Improvements in infrared absorption of solid propellant flames p 2801 N95-31306
Advanced oxidizers diffusion flames structure p 2801 N95-31307
The physical and chemical processes governing CO2 laser-induced pyrolysis and combustion of the solid propellants RDX, ADN, XM39, and M43 p 2836 N95-31531

SOLID ROCKET BINDERS
Ageing control no. 3 of propellants for rocket motors RB 27 and RB 28
|PB95-210357| p 2825 N95-30626
Advanced oxidizers diffusion flames structure p 2801 N95-31307

SOLID ROCKET PROPELLANTS
Ageing control no. 3 of propellants for rocket motors RB 27 and RB 28
|PB95-210357| p 2825 N95-30626
The Al and A(lc)l2O3 droplet cloud in solid rocket motors p 2770 N95-30988
Shuttle redesigned solid rocket motor aluminum oxide investigations p 2770 N95-30989
The 31st JANNAF Combustion Subcommittee Meeting, volume 1 p 2825 N95-31194
Experiments in a 120-mm ram accelerator including flow visualization p 2799 N95-31202
Pulse forming network in the ETC combustion characterization of plasma augmented solid propellants p 2799 N95-31205
Workshop report: Measurement techniques in highly transient, spectrally rich combustion environments p 2799 N95-31208
Large deformation failure mechanisms in nonlinear solids
|AD-A293010| p 2896 N95-31474
AP reclamation and reuse in RSRM propellant p 2772 N95-31751
Enhanced alkaline hydrolysis and biodegradability studies of nitrocellulose-bearing missile propellant p 2772 N95-31752
Environmentally compatible solid rocket propellants p 2772 N95-31753
Low acid producing solid propellants p 2773 N95-31754
Thermoplastic elastomers as a binder in composite propellants
|PB95-211553| p 2837 N95-32249

SOLID STATE
Electronic structure of Donor-Spacer-Acceptor molecules of potential interest for molecular electronics III: Geometry and absorption spectrum of CH3-Alpha P3CNQ
|AD-A293662| p 2985 N95-31609
Solid state research
|AD-A293083| p 3015 N95-31826

SOLID STATE LASERS
Diode-pumped, continuously tunable, 2.3 micron CW laser
|AD-D017448| p 2885 N95-31273
Tunable ytterbium-doped solid state laser
|AD-D017449| p 2885 N95-31274
The High Altitude Balloon Experiment demonstration of acquisition, tracking, and pointing technologies (HABE-ATP) p 2841 N95-32132
Laser properties of Yb(3+)-doped Sr5(PO4)3F crystals
|DE95-010686| p 3016 N95-32268

SOLID SURFACES
Application of spin-sensitive electron spectroscopies to investigations of electronic and magnetic properties of solid surfaces and epitaxial systems
|DE95-010154| p 2792 N95-30614

SOLID WASTES
Producing usable fuel from municipal solid waste
|DE95-008405| p 2902 N95-30375

SOLID-SOLID INTERFACES
Interfacial studies of coated fiber reinforced glass-ceramic matrix composites
|AD-A290780| p 2783 N95-30433

SOLIDIFICATION
A phenomenological finite element model of part building in the stereolithography process
|DE95-008437| p 2932 N95-30376
Phase transformations in melt-spun Y-Ba-Cu-O bulk superconductor
|DE95-010237| p 3011 N95-30667
A metallurgical approach toward alloying in rare earth permanent magnet systems
|DE95-010242| p 2966 N95-30668
Fundamental topics in heat transfer through deformable two-phase media p 2874 N95-31532
LLW solidification in cement: Effect of dilution
|DE95-010108| p 2798 N95-32091

SOLIDIFIED GASES
CO2 (dry ice) cleaning system p 2778 N95-31785
Stripping with dry ice p 2844 N95-32172

SOLIDS
Acoustoelastic stress evaluation in metal plate using absolute shear and longitudinal time-of-flight data
|PB95-197810| p 2892 N95-30458
Thermoviscoelastic behaviour of solids
|PB95-196226| p 2784 N95-30694
Large deformation failure mechanisms in nonlinear solids
|AD-A293010| p 2896 N95-31474
Numerical evaluation of three-dimensional crack-tip integrals for layered anisotropic solids p 2898 N95-32191

SOLITARY WAVES
Integrals of motion in the two Killing vector reduction of general relativity
|DE95-616281| p 3018 N95-30431
Numerical studies of nonlinear optical pulse propagation p 2998 N95-31411

SOLUBILITY
Replacement of ozone depleting and toxic chemicals in gravimetric analysis of non-volatile residue p 2780 N95-31793

SOLUTES
Dissolution of eutectic microstructures
|DE95-010244| p 2804 N95-30757

SOLVATION
Processing of polymers using supercritical fluids
|AD-A292880| p 2819 N95-31410

SOLVENT EXTRACTION
Waste minimization via preparative scale high performance gel permeation chromatography
|DE95-011797| p 2798 N95-32380

SOLVENTS
Photochemistry of intermolecular C-H bond activation reactions
|DE95-008991| p 2978 N95-30574
Urethane foam process improvements
|DE95-008957| p 2815 N95-30798
Electron transfer kinetics of self-assembled ferrocene C(12) alkanethiol monolayers on gold electrodes from 125K to 175K
|AD-A292754| p 2984 N95-31427
Consequences of kinetic dispersion on the electrochemistry of an adsorbed redox-active monolayer
|AD-A292794| p 2795 N95-31437
The 19th Annual Electronics Manufacturing Seminar
|AD-A293067| p 2863 N95-31674
Prepsolv (TM): The optimum alternative to 1,1,1-trichloroethane and methyl ethyl ketone for hand-wipe cleaning of aerospace materials p 2774 N95-31764
Cleaning without chlorinated solvents p 2780 N95-31792
Replacement of ozone depleting and toxic chemicals in gravimetric analysis of non-volatile residue p 2780 N95-31793
Evaluation of control parameters for Spray-In-Air (SIA) aqueous cleaning for shuttle RSRM hardware p 2780 N95-31794
Environmentally compatible hand wipe cleaning solvents p 2780 N95-31795
An overview of NASA testing requirements for alternate cleaning solvents used in liquid and gaseous oxygen environments p 2783 N95-31813

SONAR
Calculations of the sound scattering from fluid-filled spherical shell sonar targets
|DSTO-RR-0020| p 2974 N95-31365

SOOT
Enhanced energy release and soot reduction in actively controlled flames p 2799 N95-31200

SORBENTS
Extension of the pore tree model to describe pore interconnectivity
|AD-A290366| p 2793 N95-30971

SOUND DETECTING AND RANGING
Apparatus for producing images acoustically
|AD-D017365| p 2973 N95-30530
Method and apparatus for locating an acoustic source
|AD-D017347| p 2974 N95-30549

SOUND FIELDS
User's manual for the Scanning Fast Field Program (SCAFFIP) EOSAEL version 1.0
|AD-A291445| p 2933 N95-30397
Design of systems for active sound control
|PB95-197869| p 2973 N95-30461
Ray trace model of sound propagation in range dependent media
|PB95-211751| p 2973 N95-30481
Far field acoustic radiation reduction
|AD-D017452| p 2974 N95-30725
Method for extracting forward acoustic wave components from rotating microphone measurements in the inlets of turbofan engines
|NASA-CR-195457| p 2755 N95-30779
Combustion response to acoustic perturbation in liquid rocket engines p 2770 N95-31972

SOUND GENERATORS
Thermoacoustic sound generator
|AD-D017342| p 2973 N95-30413
Method and apparatus for locating an acoustic source
|AD-D017347| p 2974 N95-30549
Solution of the three-dimensional Helmholtz equation with nonlocal boundary conditions
|NASA-TM-110174| p 2974 N95-30850

SOUND PRESSURE
Calculations of the sound scattering from fluid-filled spherical shell sonar targets
|DSTO-RR-0020| p 2974 N95-31365

SOUND PROPAGATION
Ray trace model of sound propagation in range dependent media
|PB95-211751| p 2973 N95-30481
Method for extracting forward, acoustic wave components from rotating microphone measurements in the inlets of turbofan engines
|NASA-CR-195457| p 2755 N95-30779
The effects of large and small scale turbulence on sound propagation in the atmosphere
|AD-A293657| p 2975 N95-31608

SOUND TRANSDUCERS
Investigating the use of smart acoustically active surfaces for flow separation control in turbomachinery
|AD-A292819| p 2874 N95-31443

SOUND TRANSMISSION
Ray trace model of sound propagation in range dependent media
|PB95-211751| p 2973 N95-30481

SOUND WAVES
Method and system for suppressing noise induced in a fluid medium by a body moving therethrough
|AD-D017339| p 2973 N95-30411

Thermoacoustic sound generator
[AD-D017342] p 2973 N95-30413
Apparatus for producing images acoustically
[AD-D017365] p 2973 N95-30530
Method and apparatus for locating an acoustic source
[AD-D017347] p 2974 N95-30549
Energy absorption apparatus
[AD-D017361] p 2814 N95-30715
Far field acoustic radiation reduction
[AD-D017452] p 2974 N95-30725
Acoustomagnetoelectric effect in a superlattice
[DE95-613445] p 3011 N95-30736
Temporal feature extraction in photorefractive resonators
[AD-A292908] p 2881 N95-31385
Acousto-optical frequency shifters in dual-core optical fibres
[AD-A293979] p 2999 N95-31529
The effects of large and small scale turbulence on sound propagation in the atmosphere
[AD-A293657] p 2975 N95-31608

SOUTHERN OSCILLATION
Forecast of Atlantic seasonal hurricane activity for 1994 p 2918 N95-30832
Early August updated forecast of Atlantic seasonal hurricane activity for 1994 p 2919 N95-30844

SPACE BASED RADAR
Guidance and Control for Future Air-Defence Systems
[AGARD-CP-555] p 2839 N95-32123

SPACE CHARGE
The quantum interference effect in semiconductor space charge layers studied by Feynman path integrals: General formalism and illustrative examples
[DE95-614483] p 3010 N95-30653
The coupling impedance of a toroidal beam pipe with circular cross section
[DE95-010442] p 2993 N95-31405

SPACE COMMUNICATION
The Telecommunications and Data Acquisition Report
[NASA-CR-196911] p 2854 N95-32221
Rate considerations in deep space telemetry p 2765 N95-32223
Effects of correlated noise on the full-spectrum combining and complex-symbol combining arraying techniques p 2856 N95-32237

SPACE DEBRIS
Assessment of the NASA orbital debris engineering model
[AD-A293350] p 2766 N95-31143

SPACE EXPLORATION
Aeronautics and space report of the President
[NASA-TM-110743] p 3028 N95-31979

SPACE HEATING (BUILDINGS)
Compatibility of manufacturing process fluids with HFC refrigerants and ester lubricants
[DE95-012152] p 2911 N95-32364

SPACE MISSIONS
Mars together and FIRE and ICE: Report of the joint US/Russian technical working groups
[NASA-CR-198864] p 3030 N95-30845
Mir 18 post flight presentation
[NASA-TM-110657] p 2766 N95-30854

SPACE NAVIGATION
Determination of the position of Jupiter from radio metric tracking of Voyager 1 p 2854 N95-32222
The application of noncoherent Doppler data types for Deep Space Navigation p 2765 N95-32226

SPACE PLASMAS
Operating in the space plasma environment: A spacecraft charging study of the Solar X-ray Imager
[NASA-TM-110644] p 3003 N95-30468
Theoretical high energy physics
[DE95-003107] p 2991 N95-30527
Theory and simulation of electrostatic wave turbulence in the space shuttle-induced plasma environment
[AD-A293467] p 3005 N95-31534

SPACE PROBES
Welding isotopic heat sources for the cassini mission to Saturn
[DE95-060104] p 2890 N95-32367

SPACE SHUTTLE BOOSTERS
Shuttle redesigned solid rocket motor aluminum oxide investigations p 2770 N95-30989
Evaluation of control parameters for Spray-In-Air (SIA) aqueous cleaning for shuttle RSRM hardware p 2780 N95-31794
Environmentally compatible hand wipe cleaning solvents p 2780 N95-31795
Verification of surface preparation for adhesive bonding p 2782 N95-31807

SPACE SHUTTLE MAIN ENGINE
Enhancements to the SSME transfer function modeling code
[NASA-CR-198957] p 2958 N95-30754
Replacement of corrosion protection chromate primers and paints used in cryogenic applications on the Space Shuttle with wire arc sprayed aluminum coatings p 2776 N95-31774
SSME Main Combustion Chamber (MCC) hot oil dewaxing p 2777 N95-31777

SPACE SHUTTLE MISSIONS
Orbiter rarefied-flow reentry measurements from the OARE on STS-62
[NASA-TM-110182] p 2891 N95-30783
STS-71 post flight presentation
[NASA-TM-110658] p 2764 N95-30852
STS-70 flight: Day 8
[NASA-TM-110666] p 2764 N95-30873
STS-70 flight: Day 7
[NASA-TM-110665] p 2764 N95-30874
STS-70 flight: Day 6
[NASA-TM-110664] p 2764 N95-30875
STS-70 flight: Day 5
[NASA-TM-110663] p 2764 N95-30876
STS-70 flight: Day 4
[NASA-TM-110662] p 2764 N95-30877
STS-70 flight: Day 3
[NASA-TM-110661] p 2765 N95-30878
STS-70 flight: Day 2
[NASA-TM-110660] p 2765 N95-30879
STS-70 flight: Day 1
[NASA-TM-110659] p 2765 N95-30880
Space Shuttle Orbiter corrosion history, 1981-1993: A review and analysis of issues involving structures and subsystems
[NASA-TM-104810] p 2810 N95-32183

SPACE SHUTTLE ORBITERS
Orbiter rarefied-flow reentry measurements from the OARE on STS-62
[NASA-TM-110182] p 2891 N95-30783
Theory and simulation of electrostatic wave turbulence in the space shuttle-induced plasma environment
[AD-A293467] p 3005 N95-31534
Space Shuttle Orbiter corrosion history, 1981-1993: A review and analysis of issues involving structures and subsystems
[NASA-TM-104810] p 2810 N95-32183

SPACE SHUTTLE PAYLOADS
STS-71 post flight presentation
[NASA-TM-110658] p 2764 N95-30852
STS-70 flight: Day 7
[NASA-TM-110665] p 2764 N95-30874
STS-70 flight: Day 6
[NASA-TM-110664] p 2764 N95-30875
STS-70 flight: Day 5
[NASA-TM-110663] p 2764 N95-30876
STS-70 flight: Day 4
[NASA-TM-110662] p 2764 N95-30877
STS-70 flight: Day 3
[NASA-TM-110661] p 2765 N95-30878
STS-70 flight: Day 2
[NASA-TM-110660] p 2765 N95-30879
STS-70 flight: Day 1
[NASA-TM-110659] p 2765 N95-30880
Vibration control of spacecrafts and space structures from lift-off to on-orbit environments p 2767 N95-32110

SPACE SHUTTLES
Analysis of stress concentration at holes in components made of 2195 aluminum-lithium
[NASA-TP-3554] p 2893 N95-30613
Mir 18 post flight presentation
[NASA-TM-110657] p 2766 N95-30854
STS-70 flight: Day 8
[NASA-TM-110666] p 2764 N95-30873
STS-70 flight: Day 7
[NASA-TM-110665] p 2764 N95-30874
STS-70 flight: Day 6
[NASA-TM-110664] p 2764 N95-30875
STS-70 flight: Day 5
[NASA-TM-110663] p 2764 N95-30876
STS-70 flight: Day 4
[NASA-TM-110662] p 2764 N95-30877
STS-70 flight: Day 3
[NASA-TM-110661] p 2765 N95-30878
STS-70 flight: Day 2
[NASA-TM-110660] p 2765 N95-30879
The effect of gravity on the deposition of thin films: The physical vapor transport of copper phthalocyanine
[AD-A292997] p 2838 N95-31472

SPACE TRANSPORTATION SYSTEM
STS-70 flight: Day 3
[NASA-TM-110661] p 2765 N95-30878
STS-70 flight: Day 2
[NASA-TM-110660] p 2765 N95-30879

SPACE TRANSPORTATION SYSTEM FLIGHTS
STS-71 post flight presentation
[NASA-TM-110658] p 2764 N95-30852
STS-70 flight: Day 8
[NASA-TM-110666] p 2764 N95-30873
STS-70 flight: Day 7
[NASA-TM-110665] p 2764 N95-30874
STS-70 flight: Day 6
[NASA-TM-110664] p 2764 N95-30875
STS-70 flight: Day 5
[NASA-TM-110663] p 2764 N95-30876
STS-70 flight: Day 4
[NASA-TM-110662] p 2764 N95-30877
STS-70 flight: Day 3
[NASA-TM-110661] p 2765 N95-30878
STS-70 flight: Day 2
[NASA-TM-110660] p 2765 N95-30879
STS-70 flight: Day 1
[NASA-TM-110659] p 2765 N95-30880

SPACE-TIME FUNCTIONS
Quantum dynamics in regions of quaternionic curvature
[DE95-616276] p 3018 N95-30426
The solutions of affine and conformal affine Toda field theory
[DE95-616280] p 2965 N95-30430
Integrals of motion in the two Killing vector reduction of general relativity
[DE95-616281] p 3018 N95-30431
A time stepping coupled finite element-state space modeling environment for synchronous machine performance and design analysis in the ABC frame of reference p 2964 N95-31948

SPACEBORNE ASTRONOMY
HST-FOC observations of a remarkable UV auroral event on Jupiter p 3030 N95-30806
NASA space astronomy update 6
[NASA-CR-197664] p 3028 N95-31099
The future of space imaging. Report of a community-based study of an advanced camera for the Hubble Space Telescope
[NASA-CR-198818] p 3028 N95-31364
Cepheid temperature and the Blazhko effect
[NASA-CR-189433] p 3030 N95-31819

SPACEBORNE EXPERIMENTS
STS-70 flight: Day 7
[NASA-TM-110665] p 2764 N95-30874
STS-70 flight: Day 6
[NASA-TM-110664] p 2764 N95-30875
STS-70 flight: Day 5
[NASA-TM-110663] p 2764 N95-30876
STS-70 flight: Day 4
[NASA-TM-110662] p 2764 N95-30877
STS-70 flight: Day 3
[NASA-TM-110661] p 2765 N95-30878
STS-70 flight: Day 2
[NASA-TM-110660] p 2765 N95-30879
The NASA/JPL Evaluation of Oxygen Interactions with Materials-3 (EOIM-3)
[NASA-CR-198865] p 2796 N95-31660
Satellite test of the isotropy of the one-way speed of light using ExTRAS p 2973 N95-32349

SPACECRAFT
Preventing cracking of anodized coatings
[NASA-TM-104622] p 2839 N95-31690

SPACECRAFT ANTENNAS
Enhanced decoding for the Galileo low-gain antenna mission: Viterbi redecoding with four decoding stages p 2855 N95-32230

SPACECRAFT CHARGING
Operating in the space plasma environment: A spacecraft charging study of the Solar X-ray Imager
[NASA-TM-110644] p 3003 N95-30468

SPACECRAFT CONSTRUCTION MATERIALS
Analysis of stress concentration at holes in components made of 2195 aluminum-lithium
[NASA-TP-3554] p 2893 N95-30613
Effects of thermal and electrical stressing on the breakdown behavior of space wiring
[NASA-CR-198360] p 2768 N95-30860
The NASA/JPL Evaluation of Oxygen Interactions with Materials-3 (EOIM-3)
[NASA-CR-198865] p 2796 N95-31660
Evaluation of static strength of T800H/PMR-15 carbon/polyimide laminates at room temperature and 300 C
[NAL-TR-1254] p 2789 N95-31740
Aerospace Environmental Technology Conference
[NASA-CP-3298] p 2771 N95-31746

SPACECRAFT CONTAMINATION
Vacuum plume backflow and rarefaction p 2871 N95-30995
Replacement of ozone depleting and toxic chemicals in gravimetric analysis of non-volatile residue p 2780 N95-31793
Evaluation of control parameters for Spray-In-Air (SIA) aqueous cleaning for shuttle RSRM hardware p 2780 N95-31794

SPACECRAFT DESIGN
Operating in the space plasma environment: A spacecraft charging study of the Solar X-ray Imager
|NASA-TM-110644| p 3003 N95-30468
GPHS-RTGs in support of the Cassini RTG Program
|DE95-010306| p 2768 N95-30674
Review of Gravity Probe B
|NASA-CR-198959| p 3019 N95-30781
Solid Modeling Aerospace Research Tool (SMART) user's guide, version 2.0
|NASA-TM-4431| p 2940 N95-31420
Side force acting on blunted circular cylinder bodies at high angles of attack in supersonic flow
|NAL-TR-1255| p 2744 N95-31741
Geometric modeling for computer aided design
|NASA-CR-198828| p 2943 N95-31982
SPACECRAFT DOCKING
On-orbit truss structure tele-operation experiment by Engineering Test Satellite-7
|NAL-TR-1246| p 2767 N95-31980
SPACECRAFT LAUNCHING
STS-71 post flight presentation
|NASA-TM-110658| p 2764 N95-30852
STS-70 flight: Day 1
|NASA-TM-110659| p 2765 N95-30880
Environmental benefits of chemical propulsion p 2772 N95-31750
Improved hybrid rocket fuel p 2773 N95-31755
Major weapon system environmental life-cycle cost estimating for Conservation, Cleanup, Compliance and Pollution Prevention (C3P2) p 2774 N95-31761
Vibration control of spacecrafts and space structures from lift-off to on-orbit environments p 2767 N95-32110
SPACECRAFT LUBRICATION
Enhancement of perfluoropolyether boundary lubrication performance: I. Preliminary results
|NASA-TM-106937| p 2813 N95-30621
SPACECRAFT MAINTENANCE
Cleanliness inspection tool for RSRM bond surfaces p 2781 N95-31799
The design and development of a third generation OSEE instrument p 2781 N95-31800
Space Shuttle Orbiter corrosion history, 1981-1993: A review and analysis of issues involving structures and subsystems
|NASA-TM-104810| p 2810 N95-32183
SPACECRAFT ORBITS
Assessment of the NASA orbital debris engineering model
|AD-A293350| p 2766 N95-31143
SPACECRAFT POWER SUPPLIES
GPHS-RTGs in support of the Cassini RTG Program
|DE95-010306| p 2768 N95-30674
SPACECRAFT PROPULSION
Beam-centroid tracking instrument for ion thrusters
|AD-A293654| p 2769 N95-31567
Environmental benefits of chemical propulsion p 2772 N95-31750
SPACECRAFT REENTRY
Orbiter rarefied-flow reentry measurements from the OARE on STS-62
|NASA-TM-110182| p 2891 N95-30783
SPACECRAFT STABILITY
Transonic aerodynamic characteristics of a proposed wing-body reusable launch vehicle concept
|NASA-TM-108489| p 2742 N95-30712
SPACECRAFT STRUCTURES
Control of flexible spacecraft structures using H-infinity wave absorbing control
|AD-A293141| p 2766 N95-30919
Vibration control of spacecrafts and space structures from lift-off to on-orbit environments p 2767 N95-32110
SPACING
Technique to prepare high-reflectance optical fiber Bragg gratings with single exposure in-line or fiber draw tower
|AD-D017445| p 2998 N95-31270
Shnirelman peak in the level spacing statistics
|DE95-623599| p 3019 N95-31276
SPALLATION
IPNS neutron scattering instrumentation. A: Existing and planned. B: Possibilities for IPNS upgrade, a 1-MW spallation source
|DE95-004119| p 2985 N95-31616
SPARE PARTS
Report to the Chairman, Legislation and National Security Subcommittee, Committee on Government Operations, House of Representatives. C-17 Aircraft program: Improvements in initial provisioning process
|GAO/NSIAD-94-63| p 2741 N95-32194
SPATIAL DISTRIBUTION
Geostatistics and hydrology. Part 1: Spatial and temporal variability. Communications of the Sanitary Engineering and Water Management Division
|PB95-206470| p 2900 N95-30819
The Al and A(lc)I2O3 droplet cloud in solid rocket motors p 2770 N95-30988
Nonparametric recognition of nonrigid motion
|AD-A293630| p 2963 N95-31565
Validation of the atmospheric transmission large-area analysis system (ATLAS)
|AD-A293810| p 2916 N95-31589
Two-dimensional Finite Difference Time Domain (FD-TD) model of electromagnetic (EM) scattering from a buried rectangular object
|AD-A293685| p 2852 N95-31601
Image representation using fast algorithms based on the Zak transform
|AD-A293416| p 2942 N95-31684
Non-intrusive combustion diagnostics of premixed hydrocarbon flames using FT-IR spectrometry p 2797 N95-31732
SPATIAL FILTERING
Adaptive space-time processing for airborne radars based on Doppler pre-processing
|PB95-205464| p 2854 N95-32114
SPATIAL RESOLUTION
The land component of the global climate system with adequate spatial resolution
|DE95-009323| p 2908 N95-30686
Reflectivity of plasmas created by high-intensity, ultra-short laser pulses
|DE95-009536| p 3004 N95-30742
SPECIFIC HEAT
On the quasihydrostatic flows of radiatively cooling self-gravitating gas clouds
|DE95-009116| p 3029 N95-30729
SPECIFIC IMPULSE
Experiment of rocket-ram combined combustor
|NAL-TR-1249| p 2769 N95-31739
SPECIFICATIONS
Quality assurance tendering and awarding contracts
|PB95-197760| p 2891 N95-31362
Custom Turnkey Time and Frequency Systems: A structured, expandable approach p 2969 N95-32330
SPECKLE INTERFEROMETRY
Unconventional imaging field experiment plan
|AD-A291492| p 2846 N95-30562
SPECTRA
Analysis on fractals, laplacians on self-similar sets, noncommutative geometry and spectral dimensions
|PB95-208005| p 2956 N95-30556
DEPSCOR92-Wide field spectral imager
|AD-A293079| p 2997 N95-31005
A compact and efficient violet laser source
|AD-A292782| p 2885 N95-31434
Quantum 1/f noise in high technology applications including ultrasmall structures and devices
|AD-A292812| p 2862 N95-31442
Design of an immersion echelle-prism mid-IR spectrograph for chemical remote sensing
|DE95-010729| p 2901 N95-32027
Wavelengths measurements of the He-like krypton K-shell spectrum
|DE95-010264| p 2987 N95-32041
SPECTRAL METHODS
Spectral methods in complex geometries
|PB95-208336| p 2955 N95-30495
Enhancements to the SSME transfer function modeling code
|NASA-CR-198957| p 2958 N95-30754
Numerical stability investigations of processes for solving linear initial value problems
|PB95-207023| p 2959 N95-31183
Spectral element method for numerical simulation of unsteady laminar diffusion flames p 2794 N95-31333
Spectral methods and sum acceleration algorithms
|DE95-009689| p 2941 N95-31630
SPECTRAL SENSITIVITY
Spectral response of a polycrystalline silicon solar cell
|DE95-614370| p 2903 N95-30723
SPECTROGRAPHS
Design of an immersion echelle-prism mid-IR spectrograph for chemical remote sensing
|DE95-010729| p 2901 N95-32027
SPECTROMETERS
Integrated X-ray testing of the electro-optical breadboard model for the XMM reflection grating spectrometer
|DE95-008829| p 2879 N95-30507
The design and construction of the muon arm in PHENIX
|DE95-010156| p 2978 N95-30616
DEPSCOR92-Wide field spectral imager
|AD-A293079| p 2997 N95-31005
IPNS neutron scattering instrumentation. A: Existing and planned. B: Possibilities for IPNS upgrade, a 1-MW spallation source
|DE95-004119| p 2985 N95-31616
Wavelengths measurements of the He-like krypton K-shell spectrum
|DE95-010264| p 2987 N95-32041
High-resolution superconducting x-ray spectrometers with aluminum trapping layers of different thicknesses
|DE95-010253| p 2881 N95-32047
The superconducting kaon spectrometer
|DE95-010436| p 2882 N95-32159
SPECTROSCOPIC ANALYSIS
Modeling of thermal response of filament used in T-jump experiment p 2800 N95-31297
Species and temperature profiles of propellant flames obtained from FTIR absorption spectroscopy p 2801 N95-31303
A study of gas-phase processes during the deflagration of RDX composite propellants using a triple quadrupole mass spectrometer p 2801 N95-31304
Improvements in infrared absorption of solid propellant flames p 2801 N95-31306
Detailed chemical kinetic modeling of premixed hydrocarbon flames supported by NO2 p 2801 N95-31311
RDX laser-assisted flame structure p 2801 N95-31314
A study of the gas-phase processes of RDX combustion using a triple quadrupole mass-spectrometer p 2801 N95-31315
Non-intrusive combustion diagnostics of premixed hydrocarbon flames using FT-IR spectrometry p 2797 N95-31732
SPECTROSCOPY
Conjugated aromatic polyimines. 2. Synthesis, structure, and properties of new aromatic polyazomethines
|AD-A292955| p 2819 N95-31461
A theoretical treatment of the absorption and emission properties of Cu(2) porphyrin
|AD-A293669| p 2795 N95-31595
Contactless characterization of semiconductors using laser-induced surface photo-charge voltage measurements
|AD-A293618| p 2863 N95-31725
On the Jahn-Teller effect of Mn(2+) in zinc-blende ZnS crystal
|AD-A293711| p 2797 N95-31830
Terahertz spectroscopy of silicon micromachined three-dimensional photonic bandgap crystal
|DE95-010233| p 3015 N95-32037
SPECTRUM ANALYSIS
Fabry-Perot interferometer measurement of static temperature and velocity for ASTOVL model tests
|NASA-TM-107014| p 2879 N95-30587
Generation of earthquake signals
|PB95-211223| p 2913 N95-30631
Holistic analysis of gamma-ray spectra in instrumental neutron activation analysis
|PB95-214458| p 2979 N95-30639
Recoil correction in the Dirac-Coulomb problem
|DE95-619241| p 2959 N95-31137
SPEECH
Automation of the control of acoustic parameters in a digital speech synthesizer
|IFTR-2/1995| p 2850 N95-31357
The contextual variance of devoiced fricatives in polish
|IFTR-7/1995| p 2854 N95-32192
SPEED CONTROL
Speed control of an elastic two-mass system: Optimization and systems theory
|PB95-212106| p 2888 N95-30701
SPHERICAL HARMONICS
Nearly steady flows in GONG prototype data
|NASA-CR-198935| p 2869 N95-30863
SPHERICAL SHELLS
Porous spherical shells and microspheres by electrodispersion precipitation
|DE95-009073| p 2815 N95-30799
Calculations of the sound scattering from fluid-filled spherical shell sonar targets
|DSTO-RR-0020| p 2974 N95-31365
SPIN DYNAMICS
Spin structure in high energy processes
|DE95-008628| p 2993 N95-31627
SPINE
Erect, neutral and slump sitting postures: A study of the torso linkage system from shoulder to hip joint
|AD-A293239| p 2930 N95-30907
SPINEL
Germanate glass ceramic
|AD-D017418| p 2816 N95-31011

SPLASHING
Reducing process noise in superconducting helium liquid level probes
| DE95-008956 | p 2814 N95-30765
SPLITTING
Observations of star fracture and longitudinal splitting in BIS 812 EMA and Q1N submarine construction steels
| DSTO-RR-0014 | p 2806 N95-31344
SPRAYED COATINGS
Replacement of corrosion protection chromate primers and paints used in cryogenic applications on the Space Shuttle with wire arc sprayed aluminum coatings
p 2776 N95-31774
SPRAYERS
Demonstration of split-flow ventilation and recirculation as flow-reduction methods in an Air Force paint spray booth, volume 2
| AD-A286808 | p 2762 N95-30926
Convergent spray process for environmentally friendly coatings p 2777 N95-31776
SPRAYING
Demonstration of split-flow ventilation and recirculation as flow-reduction methods in an Air Force paint spray booth, volume 1
| AD-A286807 | p 2763 N95-31101
Icing simulation in the aeropropulsion systems test facility propulsion development test cell C-2
| AD-A293039 | p 2747 N95-31667
A design of experiments test to define critical spray cleaning parameters for Brulin 815 GD and Jettacin cleaners p 2779 N95-31790
Evaluation of control parameters for Spray-In-Air (SIA) aqueous cleaning for shuttle RSRM hardware
p 2780 N95-31794
SPREAD SPECTRUM TRANSMISSION
Interference rejection techniques in a DS spread-spectrum HF radio system
| PB95-211660 | p 2846 N95-30479
SPREADING
Simple model of foam spreading on liquid surfaces
| PB95-211207 | p 2838 N95-30630
SPRINGS (ELASTIC)
Vibration isolation mount with locking means
| AD-D017367 | p 2888 N95-30532
SPUTTERING
Anodically enhanced diffusion in Cu/Ag thin film couples
| DE95-009198 | p 2814 N95-30738
SQUARE WAVES
Scannerless Range Imaging with a square wave
| DE95-009840 | p 2854 N95-32145
SQUARES (MATHEMATICS)
Album of simple perfect squared squares of order 26
| PB95-197398 | p 2954 N95-30401
STABILITY
Fixed modes in quasi-static state feedback decoupling
| PB95-206850 | p 2950 N95-30564
Electron-optical nonlinear interaction in asymmetric quantum-well laser heterostructures
| DE95-613443 | p 2883 N95-30609
Mechanisms of enhanced ionic conduction at interfaces in ceramics
| DE95-009125 | p 2814 N95-30730
Cascading synchronized chaotic systems
| AD-D017458 | p 2860 N95-30748
Stabilization of the resistive shell mode in tokamaks
| DE95-008748 | p 3004 N95-30794
Robust fixed-structure control
| AD-A292883 | p 2952 N95-30961
Electrified microheterogeneous catalysis
| AD-D017446 | p 2794 N95-31271
A compact and efficient violet laser source
| AD-A292782 | p 2865 N95-31434
An analysis of gas phase ethanol/water chemistry for diamond CVD
| AD-A293009 | p 2795 N95-31473
Phase stability, point defects and site preference of FeAl and NiAl with ternary additions
| DE95-009694 | p 3015 N95-31641
Measurements of stability margins and current distribution in large-scale Nb3Sn cable-in-conduit conductors
| DE95-009869 | p 3007 N95-32148
Comprehensive research on the stability and electronic properties of a-Si:H and a-SiGe:H alloys and devices
| DE95-004068 | p 2810 N95-32154
STABILITY DERIVATIVES
Advanced gust management systems: Lessons learned and perspectives p 2759 N95-32002
STABILITY TESTS
Stability analysis of linear control systems with uncertain parameters p 2954 N95-31949
Stability analysis of the TPX toroidal field coil
| DE95-009666 | p 2865 N95-32100
The Deep Space Network stability analyzer
p 2858 N95-32334
STABILIZATION
Stabilization of the resistive shell mode in tokamaks
| DE95-008748 | p 3004 N95-30794
Robust fixed-structure control
| AD-A292883 | p 2952 N95-30961
Global stabilization of nonlinear gyroscopic systems
p 2881 N95-31836
Wall stabilization of high beta plasmas in D3-D
| DE95-009607 | p 3007 N95-32116
STACKS
Thermoacoustic sound generator
| AD-D017342 | p 2973 N95-30413
STAINLESS STEELS
Robotic weld overlay coatings for erosion control
| DE95-009643 | p 2809 N95-32098
Development of integrated insulation joint for cooling pipe in tokamak reactor
| DE95-737220 | p 3007 N95-32264
STANDARD MODEL (PARTICLE PHYSICS)
New tensor interaction and the K(sub L) - K(sub S)mass difference
| DE95-613597 | p 2845 N95-30370
Real Higgs singlet and electroweak phase transition in the standard model
| DE95-616315 | p 2976 N95-30442
Phenomenology of the two Higgs doublet sector of a quark-lepton symmetric model
| DE95-616337 | p 2976 N95-30446
Electroweak flavor-conserving gauge processes: Virtual effects
| DE95-009922 | p 3020 N95-32106
STANDARDIZATION
Standardization of (13)CO2 production procedure from organic matter for mass spectrometric analysis
| DE95-614629 | p 2791 N95-30420
Standardization of surface contamination analysis systems p 2781 N95-31798
Standardization work p 2845 N95-32181
Implementation of a standard format for GPS common view data p 2968 N95-32323
STANDING WAVES
X-ray standing wave interferometry-optics at 1 angstrom with applications to surface and material sciences
| DE95-011453 | p 2998 N95-31114
STAR TRACKERS
Extra focal convective suppressing solar collector
| DE95-010170 | p 2907 N95-32288
STARBURST GALAXIES
Molecular gas in starburst galaxies: Line intensities and physical conditions
| PB95-208021 | p 3029 N95-30569
STARCHES
Dry media blasting with wheat starch
p 2843 N95-32169
Bioremediation of wheat starch media waste
p 2845 N95-32178
STARS
Strange-matter stars
| DE95-008446 | p 3028 N95-30361
STARTING
A numerical study of the starting process in a hypersonic shock tunnel p 2762 N95-30493
STATE ESTIMATION
Neural network based data fusion system
| AD-D017440 | p 2953 N95-31692
Neural network based three dimensional ocean modeler
| AD-D017441 | p 2953 N95-31693
STATIC PRESSURE
Afterbody/nozzle pressure distributions of a twin-tail twin-engine fighter with axisymmetric nozzles at Mach numbers from 0.6 to 1.2
| NASA-TP-3509 | p 2744 N95-31984
STATIC TESTS
Evaluation of static strength of T800H/PMR-15 carbon/polyimide laminates at room temperature and 300 C
| NAL-TR-1254 | p 2789 N95-31740
STATISTICAL ANALYSIS
Thermoviscoelastic behaviour of solids
| PB95-196226 | p 2784 N95-30694
Brief review of remote sensing literature pertaining to classification and geostatistics
| AD-A290932 | p 2901 N95-31156
Detection of radar targets using higher-order statistics
| AD-D017442 | p 2850 N95-31392
Nonparametric methods for incomplete data in reliability and for changepoints in smooth functions
| AD-A292773 | p 2963 N95-31429
Multiresolution signal and system analysis and the analysis and control of discrete-event dynamic systems
| AD-A292775 | p 2851 N95-31430
Investigation of ground target detection methods in fully polarimetric wide angle synthetic aperture radar images
| AD-A293922 | p 2851 N95-31513
Comparison of satellite-derived MSU brightness temperatures and conventionally-derived fields
| AD-A293692 | p 2901 N95-31603
A stochastic difference equation approach to inference with missing data: Some new results
| DE95-010327 | p 2944 N95-32088
A stochastic EM estimator in the presence of missing data: Theory and applications
| DE95-010329 | p 2944 N95-32089
Optimal infrared detector configurations for air target detection p 2841 N95-32130
Objective analysis of oceanic data for Coast Guard trajectory models
| AD-A292884 | p 2924 N95-32363
STATISTICAL DISTRIBUTIONS
Shnirelman peak in the level spacing statistics
| DE95-623599 | p 3019 N95-31276
Statistical properties of chaotic scattering with one open channel
| DE95-613370 | p 3020 N95-32150
STATISTICAL MECHANICS
Gibbs measures and quasi-periodic solutions for nonlinear Hamiltonian partial differential equations
| PB95-207932 | p 2956 N95-30506
STATISTICAL TESTS
Experimental control in software reliability certification
p 2938 N95-31248
A new goodness-of-fit test for the gamma distribution based on sample spacings from complete and censored samples
| AD-A293875 | p 2961 N95-31518
A hypothesis-testing approach to discriminant analysis with mixed categorical and continuous variables when data are missing
| AD-A293714 | p 2964 N95-31831
STEADY FLOW
Axial loads on yawed rotors
| PB95-214193 | p 2742 N95-30638
A turbulence model for steady and unsteady boundary layers in strong pressure gradients p 2868 N95-30840
Selected flows with free surfaces: Streams and drops
| IFTR-3/1995 | p 2876 N95-31817
Spatially-resolved velocity measurements in steady, high-speed, reacting flows using laser-induced OH fluorescence p 2877 N95-32109
STEADY STATE
Development of a tokamak plasma optimized for stability and confinement
| DE95-009609 | p 3003 N95-30641
A theoretical analysis of steady-state photocurrents in simple silicon diodes
| NASA-CR-198885 | p 2859 N95-30651
Robust position and force tracking control for a robot in contract p 2888 N95-30830
Analytic and experimental investigation of rotordynamic response and backward whirl induced by split resonance
| AD-A293639 | p 2889 N95-31566
STEELS
Hydrogen absorption in iron and steel during gas tungsten arc welding
| PB95-197018 | p 2804 N95-30776
Wave propagation in a fluid-loaded homogeneous, transversely isotropic, elastic cylinder of arbitrary thickness
| AD-A292728 | p 2869 N95-30946
The impact of microbiologically influenced corrosion on protective polymer coatings
| AD-A288896 | p 2816 N95-30997
Microstructural and mechanical property changes in model Fe-Cu alloys
| DE95-010117 | p 2805 N95-31105
A study of Damascus steel
| DE95-010127 | p 2809 N95-32023
Validation of favor code linear elastic fracture solutions for finite-length flaw geometries
| DE95-009034 | p 2898 N95-32157
Residual stress distribution in FeAl weld overlay on steel
| DE95-009178 | p 2899 N95-32317
STELLAR ATMOSPHERES
Cepheid temperature and the Blazhko effect
| NASA-CR-189433 | p 3030 N95-31819
STELLAR COMPOSITION
Strange-matter stars
| DE95-008446 | p 3028 N95-30361
STELLAR EVOLUTION
Observations of accreting pulsars
| NASA-CR-198931 | p 3028 N95-30469
STELLAR LUMINOSITY
X-ray performance of the engineering prototype Stellar x-ray polarimeter
| DE95-010268 | p 3028 N95-31129
STELLAR MASS ACCRETION
Observations of accreting pulsars
| NASA-CR-198931 | p 3028 N95-30469

Partons and black holes
[DE95-009921] p 3029 N95-31102
STELLAR MASS EJECTION
Environmental conditions responsible for solar activity
[AD-A292859] p 3031 N95-31450
STELLAR MODELS
On reflection of Alfven waves in the solar wind
[NASA-TM-110642] p 3031 N95-30582
STELLAR OCCULTATION
Relativistic timescale analysis suggests lunar theory revision p 2970 N95-32333
STELLAR RADIATION
Voyager GO program
[NASA-CR-189435] p 3029 N95-31424
STELLAR SPECTRA
Chromospherically active stars. 6: Giants with compact hot companions and the barium star scenario
[NASA-TM-110641] p 3028 N95-30466
Voyager GO program
[NASA-CR-189435] p 3029 N95-31424
STELLAR STRUCTURE
Strange-matter stars
[DE95-008446] p 3028 N95-30361
STELLAR TEMPERATURE
Cepheid temperature and the Blazhko effect
[NASA-CR-189433] p 3030 N95-31819
STEREOCHEMISTRY
Enantioselectivity of quinoprotein alcohol dehydrogenases: Production of enantiomerically pure C3-alcohol synthons
[PB95-196960] p 2771 N95-30734
STEREOSCOPIC VISION
Log-polar binocular vision system
[NASA-CR-188375] p 2996 N95-30772
STIFFNESS
Vibration-damping structural component
[AD-D017376] p 2784 N95-30661
Analysis of variation embedding tests with 17 MM dowel: Densified veneer wood FOREST project, part 7
[PB95-206876] p 2963 N95-30680
An inverse method to measure the axial modulus of composite materials under tension
[AD-A293042] p 2789 N95-31668
STIFFNESS MATRIX
A survey of the core-congruential formulation for geometrically nonlinear TL finite elements
[NASA-CR-199044] p 2944 N95-32203
STILBENE
Conjugated aromatic polyimines. 2. Synthesis, structure, and properties of new aromatic polyazomethines
[AD-A292955] p 2819 N95-31461
STIMULATED EMISSION
Basic study of the pumping of a gamma-ray laser
[AD-A293561] p 2886 N95-31563
The design and development of a third generation OSEE instrument p 2781 N95-31800
Study of surfaces using near infrared optical fiber spectrometry p 2781 N95-31801
STIMULATION
Simulation of oculomotor post-inhibitory rebound burst firing using a Hodgkin-Huxley model of a neuron
[AD-A293821] p 2927 N95-31552
STIRLING CYCLE
Natural gas liquefier for vehicle fuel
[AD-A293619] p 2836 N95-31564
STOCHASTIC PROCESSES
Workshop on diffusion approximation in communication and stochastic systems theory
[AD-A292872] p 2952 N95-31055
Theory & numerical methods for problems in shape reconstruction and large deviations
[AD-A292874] p 2952 N95-31279
Aspects of the search time in binary search trees modified according to the move-to-root heuristic
[PB95-212148] p 2963 N95-31396
Nonlinear time series analysis
[AD-A293841] p 2963 N95-31558
Topics in exploratory and speculative data analysis
[AD-A290505] p 3025 N95-31618
Finite-sample based learning algorithms for feedforward networks
[DE95-009123] p 2941 N95-31631
Stability analysis of linear control systems with uncertain parameters p 2954 N95-31949
A Stochastic EM algorithm for approximating the maximum likelihood estimate
[DE95-010328] p 2943 N95-32044
Estimation in second order dependency model for multivariate binary data
[DE95-010326] p 2944 N95-32087
A stochastic difference equation approach to inference with missing data: Some new results
[DE95-010327] p 2944 N95-32088
A stochastic EM estimator in the presence of missing data: Theory and applications
[DE95-010329] p 2944 N95-32089
STOKES FLOW
Existence of solutions in plane quasistationary stokes flow driven by surface tension
[PB95-197935] p 2868 N95-30810
Simulation of viscous sintering
[PB95-197109] p 2868 N95-30836
STORAGE RINGS (PARTICLE ACCELERATORS)
Beam-beam effects
[DE95-008443] p 2991 N95-30360
HERA and the asymptotic behaviour of F2(sup rho)
[PB95-195764] p 2956 N95-30540
Beam stability at SRRC storage ring
[DE95-010842] p 2995 N95-32260
STORAGE STABILITY
Evaluation of Environmentally Acceptable hydraulic fluids
[AD-A293037] p 2821 N95-31666
STORAGE TANKS
Off-potential measurement systems for impressed current cathodic protection
[AD-A290876] p 2812 N95-30558
STORMS
QTSAW (Quick Typhoon Surge and Waves). Wave information studies of US coastlines
[AD-A293172] p 2919 N95-30976
STOVL AIRCRAFT
Moving base simulation of an integrated flight and propulsion control system for an ejector-augmentor STOVL aircraft in hover
[NASA-TM-108867] p 2750 N95-30646
STRAIN DISTRIBUTION
Stress and strain concentration factors of welded multiplanar joints between square hollow sections
[PB95-208260] p 2892 N95-30492
Seismic studies of subducted lithosphere p 2915 N95-31335
STRAIN ENERGY METHODS
Finite element analysis of damped vibrations of laminated composite plates
[ISBN-0-315-84928-2] p 2789 N95-31731
STRAIN RATE
High strain rate properties and constitutive modeling of glass
[DE95-008434] p 2816 N95-31058
High strain-rate testing of parachute materials
[DE95-009577] p 2897 N95-31614
Influence of strain rate and temperature on the mechanical behavior of iron aluminide-based alloys
[DE95-009426] p 2808 N95-31636
STRAKES
Unsteady transonic wind tunnel test on a semispan straked delta wing, oscillating in pitch. Part 1: Description of the model, test setup, data acquisition, and data processing
[AD-A293113] p 2743 N95-30885
STRANDS
Embedded infrared fiber optic absorption studies of nitramine propellant strand burning p 2801 N95-31305
Industry participation workshop: Chromium electroplating of superconductor strand. Proceedings
[DE95-009629] p 2807 N95-31615
STRATIFICATION
Ocean mass density calculations from temperature and salinity data
[DSTO-TR-0023] p 2922 N95-30711
STRATOCUMULUS CLOUDS
National Institute for Global Environmental Change
[DE95-008333] p 2907 N95-30358
STRATOSPHERE
Chemical kinetics and photochemical data for use in stratospheric modeling: Evaluation number 11
[NASA-CR-198863] p 2912 N95-30525
Forecast of Atlantic seasonal hurricane activity for 1994 p 2918 N95-30832
Early August updated forecast of Atlantic seasonal hurricane activity for 1994 p 2919 N95-30844
Middle atmosphere structure and dynamics: Lidar studies at the South Pole, Syowa and Urbana p 2916 N95-31736
STREAMS
Selected flows with free surfaces: Streams and drops
[IFTR-3/1995] p 2876 N95-31817
STRESS ANALYSIS
Fatigue behaviour of multiplanar tubular joints
[PB95-207874] p 2893 N95-30586
Analysis of stress concentration at holes in components made of 2195 aluminum-lithium
[NASA-TP-3554] p 2893 N95-30613
Response of mechanically fastened composite joints under multiple bypass loads p 2785 N95-30824
Probabilistic reliability modeling of fatigue on the H-46 tie bar
[AD-A289926] p 2751 N95-30927
Sea ice stress research
[AD-A293164] p 2923 N95-30964
An analysis of the cover of a liquid-filled circular container
[IFTR-1/1995] p 2895 N95-31338
Elastic and inelastic micromechanical analysis of functionally graded materials and laminated structures using transformation fields p 2787 N95-31347
Mode I large strain viscoelastic crack behavior in nitrile rubber sheets
[AD-A289984] p 2820 N95-31617
Modeling of stress distributions on the microstructural level in Alloy 600
[DE95-009135] p 2807 N95-31632
A computational procedure for multibody systems including flexible beam dynamics
[NASA-CR-199035] p 2897 N95-31730
Evaluation of static strength of T800H/PMR-15 carbon/polyimide laminates at room temperature and 300 C
[NAL-TR-1254] p 2789 N95-31740
Modeling of grain boundary stresses in Alloy 600
[DE95-009033] p 2808 N95-31825
An extremum principle for the analysis and design of constitutively nonlinear systems p 2898 N95-32112
Residual stress distribution in FeAl weld overlay on steel
[DE95-009178] p 2899 N95-32317
STRESS CONCENTRATION
Stress and strain concentration factors of welded multiplanar joints between square hollow sections
[PB95-208260] p 2892 N95-30492
Fatigue behaviour of multiplanar tubular joints
[PB95-207874] p 2893 N95-30586
Analysis of stress concentration at holes in components made of 2195 aluminum-lithium
[NASA-TP-3554] p 2893 N95-30613
Modeling of stress distributions on the microstructural level in Alloy 600
[DE95-009135] p 2807 N95-31632
STRESS CORROSION
Modeling of grain boundary stresses in Alloy 600
[DE95-009033] p 2808 N95-31825
STRESS CORROSION CRACKING
Residual stresses and stress corrosion cracking in pipe fittings
[DE95-009332] p 2894 N95-31054
Modeling of stress distributions on the microstructural level in Alloy 600
[DE95-009135] p 2807 N95-31632
Modeling of grain boundary stresses in Alloy 600
[DE95-009033] p 2808 N95-31825
STRESS DISTRIBUTION
An evaluation of the Iosipescu specimen for composite materials shear property measurement
[NASA-CR-198755] p 2896 N95-31418
Modeling of stress distributions on the microstructural level in Alloy 600
[DE95-009135] p 2807 N95-31632
Failure mechanisms in composite plates subjected to in-plane compressive loading p 2790 N95-32108
An extremum principle for the analysis and design of constitutively nonlinear systems p 2898 N95-32112
Residual stress distribution in FeAl weld overlay on steel
[DE95-009178] p 2899 N95-32317
STRESS INTENSITY FACTORS
Stress and strain concentration factors of welded multiplanar joints between square hollow sections
[PB95-208260] p 2892 N95-30492
Fourier series methods for cracks in polygonal plates and shells of revolution p 2893 N95-30825
STRESS RELAXATION
Epoxy and acrylate stereolithography resins: In-situ measurements of cure shrinkage and stress relaxation
[DE95-008506] p 2811 N95-30389
Diffraction-line broadening analysis and stress relaxation in thin metal layers
[PB95-213898] p 2893 N95-30634
Stress relaxation of silicon nitride at elevated temperatures
[DE95-009177] p 2814 N95-30732
STRESS WAVES
Response of dual-layered structures subjected to shock pressure wave
[AD-A293731] p 2896 N95-31568
STRESS-STRAIN RELATIONSHIPS
Epoxy and acrylate stereolithography resins: In-situ measurements of cure shrinkage and stress relaxation
[DE95-008506] p 2811 N95-30389
Experimental determination of probability distributions for parameters of a Salem limestone cap plasticity model
[AD-A290878] p 2892 N95-30559
Modeling of fiber-reinforced composites incorporating distinct interface properties p 2787 N95-31110

Impact behavior of the active zone within a frozen soil profile
| AD-A292909 | p 2915 N95-31386
Post-impact fatigue of cross-plied, through-the-thickness reinforced carbon/epoxy composites
| NASA-TM-110625 | p 2896 N95-31419
Multipoint quadratic approximation for numerical optimization
| AD-A293837 | p 2961 N95-31557
Modeling of stress distributions on the microstructural level in Alloy 600
| DE95-009135 | p 2807 N95-31632
Influence of strain rate and temperature on the mechanical behavior of iron aluminide-based alloys
| DE95-009426 | p 2808 N95-31636

STRING THEORY
Covariant phase space formulations of superparticles and supersymmetric WZW models
| DE95-616278 | p 2964 N95-30428
On the string equation at c = 1
| DE95-737161 | p 3014 N95-31222
Non-critical string field theory with non-orientable string interactions
| DE95-737160 | p 3020 N95-31281
Research progress report
| DE95-010726 | p 3030 N95-32269

STRINGS
Theoretical high energy physics
| DE95-003107 | p 2991 N95-30527
A BRST charge for non-critical W2(s) strings
| DE95-613470 | p 3019 N95-30771
On the string equation at c = 1
| DE95-737161 | p 3014 N95-31222
The topological string associated with a simple singularity of type D
| DE95-737229 | p 2983 N95-31225
Non-critical string field theory with non-orientable string interactions
| DE95-737160 | p 3020 N95-31281

STRIPPING
Paint removal principles p 2843 N95-32167
Background to plastic media blasting p 2843 N95-32168
Bioremediation of wheat starch media waste p 2845 N95-32178
Operational parameters and material effects p 2845 N95-32179
Process evaluation p 2845 N95-32180

STRONTIUM
Faster, cheaper radioanalytical methods
| DE95-009913 | p 2797 N95-32061

STRONTIUM COMPOUNDS
Laser properties of Yb(3+)-doped Sr5(PO4)3F crystals
| DE95-010686 | p 3016 N95-32268

STRUCTURAL ANALYSIS
Crystallization of sol-gel derived lead zirconate titanate thin films in argon and oxygen atmospheres
| DE95-615230 | p 3009 N95-30421
Fatigue behaviour of multiplanar tubular joints
| PB95-207874 | p 2893 N95-30586
Development and computer implementation of design/analysis techniques for multilayered composite structures. Probabilistic fiber composite micromechanics
| NASA-CR-198979 | p 2930 N95-31134
The 2nd Japan-US Symposium on Finite Element Methods in Large Scale Computational Fluid Dynamics
| AD-A292337 | p 2960 N95-31264
Modeling multi-beam structures for control p 2895 N95-31346
Multipoint quadratic approximation for numerical optimization
| AD-A293837 | p 2961 N95-31557
Topics in exploratory and speculative data analysis
| AD-A290505 | p 3025 N95-31618
Evaluation of nonlinear structural dynamic responses using a fast-running spring-mass formulation
| DE95-008503 | p 2967 N95-31625
Application of shallow shell stability to plant morphogenesis by Fourier series p 2897 N95-31734
Preservation theorems on finite structures
| DE95-613442 | p 2962 N95-32067
Structural analyses of the JPL Mars Pathfinder impact
| DE95-009581 | p 2767 N95-32081
Validation of favor code linear elastic fracture solutions for finite-length flaw geometries
| DE95-009034 | p 2898 N95-32157
A survey of the core-congruential formulation for geometrically nonlinear TL finite elements
| NASA-CR-199044 | p 2944 N95-32203

STRUCTURAL DESIGN
Structural design using equilibrium programming formulations
| NASA-TM-110175 | p 2893 N95-30682
Failure analysis for polycarbonate transparencies
| AD-A292992 | p 2820 N95-31471
The design and development of a third generation OSEE instrument p 2781 N95-31800
Structural aspects of active control technology p 2760 N95-32006
Contributions to the design of neutral cutouts in laminated plates and shells p 2790 N95-32113
A probabilistic design method applied to smart composite structures
| NASA-TM-106715 | p 2899 N95-32206

STRUCTURAL DESIGN CRITERIA
Selecting optimal experiments for feedforward multilayer perceptrons
| AD-A290856 | p 2949 N95-30406
A probabilistic design method applied to smart composite structures
| NASA-TM-106715 | p 2899 N95-32206

STRUCTURAL ENGINEERING
The 2nd Japan-US Symposium on Finite Element Methods in Large Scale Computational Fluid Dynamics
| AD-A292337 | p 2960 N95-31264

STRUCTURAL FAILURE
Fatigue behaviour of multiplanar tubular joints
| PB95-207874 | p 2893 N95-30586
Failure mechanisms in composite plates subjected to in-plane compressive loading p 2790 N95-32108
Validation of favor code linear elastic fracture solutions for finite-length flaw geometries
| DE95-009034 | p 2898 N95-32157

STRUCTURAL RELIABILITY
Measures of reliability and RCM
| PB95-192985 | p 2891 N95-30510
Analysis of stress concentration at holes in components made of 2195 aluminum-lithium
| NASA-TP-3554 | p 2893 N95-30613
A probabilistic design method applied to smart composite structures
| NASA-TM-106715 | p 2899 N95-32206

STRUCTURAL STABILITY
The determination of wave group parameters from the resolution of incident and reflected waves
| AD-A293703 | p 2924 N95-31829

STRUCTURAL VIBRATION
Minimizing structural vibrations with Input Shaping (TM)
| NASA-CR-189439 | p 2893 N95-30786
Energy flow analysis of coupled structures p 2895 N95-31316
A finite element formulation for the time domain vibration analysis of an elastic-viscoelastic structure p 2895 N95-31318
Studies in non-linear multi-mode responses of harmonically excited rectangular plates with internal resonances p 2895 N95-31331
Nonlinear dynamics and chaotic motions of a singularly perturbed nonlinear viscoelastic beam p 2897 N95-31706
Vibration control for precision manufacturing at Sandia National Laboratories
| DE95-009582 | p 2839 N95-32082
Vibration control of spacecrafts and space structures from lift-off to on-orbit environments p 2767 N95-32110
Vibration reduction in helicopter rotors using an actively controlled partial span trailing edge flap located on the blade p 2762 N95-32111

STRUCTURED PROGRAMMING
An analysis of hierarchical genetic programming
| AD-A293964 | p 2942 N95-31657
Using process to integrate Software Engineering Environments (Software Technology for Adaptable, Reliable Systems (STARS) program)
| AD-A292816 | p 2946 N95-32290
SWSC domain engineering experience (Software Technology for Adaptable, Reliable Systems (STARS) program)
| AD-A292817 | p 2946 N95-32291
Integrating a SEE for megaprogramming: Lessons learned (Software Technology for Adaptable, Reliable Systems (STARS) program)
| AD-A292838 | p 2946 N95-32292
The sociology of megaprogramming: Experiences in generating an organizational learning enterprise (Software Technology for Adaptable, Reliable Systems(STARS) program)
| AD-A292998 | p 2946 N95-32294

STUDENTS
Nonparametric methods for incomplete data in reliability and for changepoints in smooth functions
| AD-A292773 | p 2963 N95-31429
Use of body surface heat patterns for predicting and evaluating acute lower extremity pain among soldiers
| AD-A292829 | p 2927 N95-31446

STUDS (STRUCTURAL MEMBERS)
Coupling stud assembly
| AD-D017335 | p 2887 N95-30387

STURM-LIOUVILLE THEORY
Complex conjugate pairs in stationary Sturmians
| DE95-616279 | p 2976 N95-30429

SUBCRITICAL FLOW
Combustion of LOX with H2(sub g) under subcritical and supercritical conditions p 2757 N95-31717

SUBDUCTION (GEOLOGY)
Seismic studies of subducted lithosphere p 2915 N95-31335
Studies in marine tectonics: Propagating rifts, depth anomalies and subduction zone anisotropy p 2923 N95-31719

SUBGROUPS
Direct subiattice imaging of interface dislocation structures in CdTe/GaAs(001)
| DE95-009031 | p 3010 N95-30576
Phase stability, point defects and site preference of FeAl and NiAl with ternary additions
| DE95-009694 | p 3015 N95-31641

SUBMARINES
Failure analysis of a repairable system: The case study of a cam-driven reciprocating pump
| AD-A293144 | p 2889 N95-30949
Observations of star fracture and longitudinal splitting in BIS 812 EMA and Q1N submarine construction steels
| DSTO-RR-0014 | p 2806 N95-31344

SUBMERGING
Design of an immersion echelle-prism mid-IR spectrograph for chemical remote sensing
| DE95-010729 | p 2901 N95-32027

SUBROUTINE LIBRARIES (COMPUTERS)
Cesar3 MALU library
| PB95-211363 | p 2933 N95-30598

SUBSONIC SPEED
Transonic aerodynamic characteristics of a proposed wing-body reusable launch vehicle concept
| NASA-TM-108489 | p 2742 N95-30712

SUBSTITUTES
Conjugated aromatic polyimines. 2. Synthesis, structure, and properties of new aromatic polyazomethines
| AD-A292955 | p 2819 N95-31461
Assessment of pollution prevention and control technology for plating operations p 2776 N95-31771

SUBSTRATES
Orientation of rapid thermally annealed lead zirconate titanate thin films on (111) Pt substrate
| DE95-615232 | p 2811 N95-30422
Morphology and microstructure of (111) crystalline CeO2 films grown on amorphous SiO2 substrates by pulsed-laser ablation
| DE95-008842 | p 3009 N95-30542
Josephson break junction thin film device
| AD-D017343 | p 3011 N95-30673
Mechanisms of enhanced ionic conduction at interfaces in ceramics
| DE95-009125 | p 2814 N95-30730
Fabrication and modification of metal nanocluster composites using ion and laser beams
| DE95-009131 | p 2784 N95-30731
Anodically enhanced diffusion in Cu/Ag thin film couples
| DE95-009198 | p 2814 N95-30738
High aspect ratio metal microstructures and method for preparing the same
| AD-D017463 | p 2803 N95-30750
Opto-electronic components from non-stoichiometric 3-5 materials
| AD-A293206 | p 3013 N95-30985
IR materials producibility
| AD-A293330 | p 2998 N95-31141
Thin-film edge field emitter device and method of manufacture therefor
| AD-D017453 | p 2862 N95-31275
Substrate heating measurements in pulsed ion beam film deposition
| DE95-010862 | p 2818 N95-31377
Pseudomorphic heterostructure materials for high performance devices
| AD-A292906 | p 2788 N95-31384
Solderability enhancement of copper through chemical etching
| DE95-010514 | p 2806 N95-31406
Plasma source ion implantation of metal ions: Synchronization of cathodic-arc plasma production and target bias pulses
| DE95-009431 | p 3006 N95-31613
High performance YBCO films
| AD-A293045 | p 2863 N95-31669
Silicon carbide-silicon heterostructure solar cells p 2905 N95-31952
Growth, characterization and device development in monocrystalline diamond films
| AD-A293106 | p 3015 N95-32018
Operational parameters and material effects p 2845 N95-32179

SUBSTRUCTURES
Physical modelling of microstructural evolution during thermomechanical processing of aluminium alloys
| PB95-196341 | p 2805 N95-31053
Nonlinear dynamics and chaotic motions of a singularly perturbed nonlinear viscoelastic beam
p 2897 N95-31706
SUCCESS PROJECT
Nonparametric methods for incomplete data in reliability and for changepoints in smooth functions
| AD-A292773 | p 2963 N95-31429
SUDDEN IONOSPHERIC DISTURBANCES
Solar-geophysical data number 606, February 1995. Part 1: (Prompt reports). Data for December 1994, January 1995, and late data
| PB95-200853 | p 3031 N95-30816
SULFIDES
An experimental search for high ZT semiconductors: A survey of the preparation and properties of several alloy systems
| DE95-010232 | p 2865 N95-32084
SULFUR COMPOUNDS
The neutron powder diffraction and acoustic investigations of the NH4SCN phase diagram
| DE95-614372 | p 3009 N95-30419
SULFURIC ACID
Thin-film sulfuric acid anodizing as a replacement for chromic acid anodizing p 2776 N95-31772
SUM RULES
Scaling behaviour of leptonic decay constants for heavy quarkonia and heavy mesons
| DE95-620539 | p 2983 N95-31218
Pion-nucleon and kaon-nucleon scattering lengths in QCD sum rules
| DE95-737278 | p 2983 N95-31227
Form factor of the process gamma(*) gamma(*) yields pi(sup 0) for small virtuality of one of the photons and QCD sum rules (2): Sum rule
| DE95-613629 | p 2988 N95-32078
Supersymmetric magnetic moments sum rules and spontaneous supersymmetry breaking
| DE95-613771 | p 2989 N95-32096
SUMS
Spectral methods and sum acceleration algorithms
| DE95-009689 | p 2941 N95-31630
SUNLIGHT
Monte Carlo code for evaluating the Boundary Layer Illumination and Radiation Balance model (BLIRB)
| AD-A293963 | p 2915 N95-31560
SUNSPOT CYCLE
On the relationship between sunspots number and the flare index
| NASA-TM-110643 | p 3030 N95-30467
SUNSPOTS
On the relationship between sunspots number and the flare index
| NASA-TM-110643 | p 3030 N95-30467
SUPERCOMPUTERS
Algorithm comparison and benchmarking using a parallel spectra transform shallow water model
| DE95-009124 | p 2913 N95-30683
An assessment of worldwide supercomputer usage
| DE95-009879 | p 2932 N95-31645
SUPERCONDUCTING DEVICES
Dynamics of Current Driven Disordered Josephson Junction Arrays
| DE95-009418 | p 3014 N95-31231
Advanced thin-film deposition and physical properties of high-temperature and other novel superconducting materials
| AD-A292798 | p 2795 N95-31439
SUPERCONDUCTING FILMS
Space qualified hybrid superconductor/semiconductor planar oscillator circuit
| NASA-TM-106978 | p 3011 N95-30703
High performance YBCO films
| AD-A293045 | p 2863 N95-31669
SUPERCONDUCTING MAGNETS
An active magnetic bearing with high T(sub c) superconducting coils and ferromagnetic cores
| NASA-TM-106995 | p 2864 N95-31847
Stability analysis of the TPX toroidal field coil
| DE95-009666 | p 2865 N95-32100
SUPERCONDUCTING SUPER COLLIDER
RFQ-DTL matching solutions for different requirements
| DE95-010897 | p 2995 N95-32306
SUPERCONDUCTIVITY
High-temperature superconducting current leads
| DE95-008404 | p 2858 N95-30374
A valence-fluctuation mechanism with highly anisotropic S-wave pairing
| DE95-009419 | p 3010 N95-30571
Reducing process noise in superconducting helium liquid level probes
| DE95-008956 | p 2814 N95-30765
Structural, chemical and electronic properties of superconducting thin films and junctions
| AD-A292700 | p 3012 N95-30933
Optimization of high-temperature superconductor current leads
| DE95-005838 | p 2861 N95-30942
Studies of C(60) and C(70) and other fullurenes: Synthesis, derivation, electrochemistry, lubricant properties and new composition materials
| AD-A292726 | p 3012 N95-30944
Investigations of YBaCuO materials with near-room-temperature resistivity transitions
| AD-A293405 | p 3013 N95-31008
Advanced thin-film deposition and physical properties of high-temperature and other novel superconducting materials
| AD-A292798 | p 2795 N95-31439
High-resolution superconducting x-ray spectrometers with aluminum trapping layers of different thicknesses
| DE95-010253 | p 2881 N95-32047
Measurements of stability margins and current distribution in large-scale Nb3Sn cable-in-conduit conductors
| DE95-009869 | p 3007 N95-32148
The superconducting kaon spectrometer
| DE95-010436 | p 2882 N95-32159
SUPERCONDUCTORS (MATERIALS)
A valence-fluctuation mechanism with highly anisotropic S-wave pairing
| DE95-009419 | p 3010 N95-30571
A simple model for the dc flux transformer in layered superconductors with Josephson coupling
| DE95-614468 | p 2859 N95-30649
Josephson break junction thin film device
| AD-D017343 | p 3011 N95-30673
Minority and majority carrier transport characterization in compound semiconductors
| DE95-010873 | p 3014 N95-31233
Inductively coupled IR staring array based on photofluxonic pixels
| AD-A292784 | p 2998 N95-31435
Advanced thin-film deposition and physical properties of high-temperature and other novel superconducting materials
| AD-A292798 | p 2795 N95-31439
SDIO: Discovering superconducting materials at high temperatures
| AD-A292820 | p 3015 N95-31444
Industry participation workshop: Chromium electroplating of superconductor strand. Proceedings
| DE95-009629 | p 2807 N95-31615
Solution based temperature of Perovskite-type oxide films and powders
| DE95-009089 | p 2820 N95-31629
SUPERCRITICAL AIRFOILS
Control of unsteady separated flow associated with the dynamic stall of airfoils
| NASA-CR-198972 | p 2744 N95-32193
SUPERCRITICAL FLOW
Processing of polymers using supercritical fluids
| AD-A292880 | p 2819 N95-31410
Combustion of LOX with H2(sub g) under subcritical and supercritical conditions p 2797 N95-31717
SUPERCRITICAL FLUIDS
Fischer-tropsch synthesis in supercritical fluids
| DE95-009631 | p 2792 N95-30709
Processing of polymers using supercritical fluids
| AD-A292880 | p 2819 N95-31410
Combustion of LOX with H2(sub g) under subcritical and supercritical conditions p 2797 N95-31717
SUPERCRITICAL PRESSURES
Combustion of LOX with H2(sub g) under subcritical and supercritical conditions p 2797 N95-31717
SUPERHIGH FREQUENCIES
Multiparameter radar measurements of precipitation in complex terrain: Meteorological and hydrological applications
| AD-A290786 | p 2918 N95-30403
X-band magnicon amplifier research at the Naval Research Laboratory
| AD-A293203 | p 3013 N95-30984
High energy pulsed microwave sources
| AD-A293334 | p 2849 N95-31142
Portable digital Satellite News Gathering (SNG) RF terminal using a flat antenna
| NHK-LABS-NOTE-436 | p 2853 N95-31744
Hyperfrequency components
| PB95-208302 | p 2866 N95-32369
SUPERLATTICES
Acoustomagnetoelectric effect in a superlattice
| DE95-613445 | p 3011 N95-30736
Amorphization threshold in Si-implanted strained SiGe alloy layers
| DE95-008901 | p 2804 N95-30797
Vertical transport in GaAs/AlGaAs superlattices
p 3012 N95-30822
Pseudomorphic heterostructure materials for high performance devices
| AD-A292906 | p 2788 N95-31384
SUPERPLASTICITY
Interfacial segregation and deformation of superplastically deformed Al-Mg-Mn alloys
| DE95-009572 | p 2809 N95-32052
SUPERSONIC COMBUSTION
Numerical simulation of ram accelerator performance including transient effects during initiation of combustion and sensitivity studies p 2799 N95-31203
The 25th International Symposium on Combustion
| AD-A286825 | p 2794 N95-31268
SUPERSONIC COMBUSTION RAMJET ENGINES
An experimental study of planar heterogeneous supersonic confined jets
| AD-A290859 | p 2867 N95-30557
The 31st JANNAF Combustion Subcommittee Meeting, volume 1 p 2825 N95-31194
SUPERSONIC DIFFUSERS
Parametrics on 2D Navier-Stokes analysis of a Mach 2.68 bifurcated rectangular mixed-compression inlet
| NASA-TM-107003 | p 2755 N95-30861
SUPERSONIC FLOW
Numerical simulation of shock/turbulent boundary layer interaction
| NASA-CR-198846 | p 2872 N95-31341
Compressible turbulence measurement in low-angle injection into a supersonic flow
| AD-A293836 | p 2874 N95-31516
Effects of cavity bleed and its configuration on aerodynamic characteristics of supersonic internal flow
| NAL-TR-1247 | p 2744 N95-31715
Side force acting on blunted circular cylinder bodies at high angles of attack in supersonic flow
| NAL-TR-1255 | p 2744 N95-31741
SUPERSONIC INLETS
Parametrics on 2D Navier-Stokes analysis of a Mach 2.68 bifurcated rectangular mixed-compression inlet
| NASA-TM-107003 | p 2755 N95-30861
SUPERSONIC JET FLOW
An experimental study of planar heterogeneous supersonic confined jets
| AD-A290859 | p 2867 N95-30557
Spatially-resolved velocity measurements in steady, high-speed, reacting flows using laser-induced OH fluorescence p 2877 N95-32109
SUPERSONIC SPEED
Spatially-resolved velocity measurements in steady, high-speed, reacting flows using laser-induced OH fluorescence p 2877 N95-32109
SUPERSYMMETRY
Covariant phase space formulations of superparticles and supersymmetric WZW models
| DE95-616278 | p 2964 N95-30428
Signatures of virtual LSP's at the TEVATRON
| DE95-613798 | p 2982 N95-31060
Structure formation with majoron supermultiplet
| DE95-613596 | p 2984 N95-31546
Supersymmetric magnetic moments sum rules and spontaneous supersymmetry breaking
| DE95-613771 | p 2989 N95-32096
Research progress report
| DE95-010726 | p 3030 N95-32269
SUPPORT SYSTEMS
Planning board generator. Part 1: Problem instances and types
| PB95-197075 | p 3021 N95-30834
Making intelligent systems team players. A guide to developing intelligent monitoring systems
| NASA-TM-104807 | p 2951 N95-30925
Effectiveness of an electronic performance support system for use with computer-aided design software
| AD-A293757 | p 2941 N95-31573
SURFACE CRACKS
Ion implantation and thermal stress resistance of ceramics
| DE95-615349 | p 2812 N95-30451
SURFACE EMITTING LASERS
Polarization characteristics, control, and modulation of vertical-cavity surface emitting lasers
| DE95-008526 | p 2882 N95-30380
Many-body effects in semiconductor lasers
| DE95-008534 | p 2883 N95-30390
SURFACE ENERGY
Dissolution of eutectic microstructures
| DE95-010244 | p 2804 N95-30757
Transitions, defects, and whiskered microstructures
| AD-A292796 | p 3014 N95-31438
Study of the surface properties of ceramic materials by chromatography
| DE95-011578 | p 2823 N95-32296
SURFACE FINISHING
Solderability enhancement of copper through chemical etching
| DE95-010514 | p 2806 N95-31406

CO2 (dry ice) cleaning system p 2778 N95-31785
QFD analysis of RSRM aqueous cleaners p 2779 N95-31789
A design of experiments test to define critical spray cleaning parameters for Brulin 815 GD and Jettacin cleaners p 2779 N95-31790

SURFACE GEOMETRY
Gear pump with reduced fluid-borne noise
|AD-D017362| p 2887 N95-30399
A theoretical analysis of steady-state photocurrents in simple silicon diodes
|NASA-CR-198885| p 2859 N95-30651
Solid Modeling Aerospace Research Tool (SMART) user's guide, version 2.0
|NASA-TM-4431| p 2940 N95-31420

SURFACE LAYERS
Ion implantation and thermal stress resistance of ceramics
|DE95-615349| p 2812 N95-30451
Structural investigation of xenon ion-beam-irradiated glassy carbon
|DE95-616777| p 2977 N95-30474
Applications of SXPS for studying surface structure, reaction mechanisms and kinetics
|DE95-008903| p 2803 N95-30547
Condensed-phase processes during solid propellant combustion. 5: Further observations on depth profiling of burned surfaces of XM39 and M43 propellants p 2800 N95-31295

SURFACE PROPERTIES
Wettability of boron carbide
|PB95-196358| p 2802 N95-30518
Development of a linearized unsteady Euler analysis for turbomachinery blade rows
|NASA-CR-4677| p 2742 N95-30611
Application of spin-sensitive electron spectroscopies to investigations of electronic and magnetic properties of solid surfaces and epitaxial systems
|DE95-010154| p 2792 N95-30614
Refinement techniques in computer graphics
|PB95-208526| p 2934 N95-30625
Simple model of foam spreading on liquid surfaces
|PB95-211207| p 2838 N95-30630
Condensed-phase processes during solid propellant combustion. 5: Further observations on depth profiling of burned surfaces of XM39 and M43 propellants p 2800 N95-31295
Contactless characterization of semiconductors using laser-induced surface photo-charge voltage measurements
|AD-A293618| p 2863 N95-31725
Surface contamination analysis technology team overview p 2781 N95-31797
Standardization of surface contamination analysis systems p 2781 N95-31798
Study of surfaces using near infrared optical fiber spectrometry p 2781 N95-31801
Contamination detection NDE for cleaning process inspection p 2781 N95-31802
Surface inspection using FTIR spectroscopy p 2782 N95-31803
Verification of surface preparation for adhesive bonding p 2782 N95-31807
Selected flows with free surfaces: Streams and drops
|IFTR-3/1995| p 2876 N95-31817
Operational parameters and material effects p 2845 N95-32179

SURFACE REACTIONS
Observation of a low-binding-energy peak in the 2p core-level photoemission from oxidized Al(111)
|PB95-195350| p 2802 N95-30534
Polarized laser induced holographic surface relief gratings on polymer films
|AD-A293275| p 2817 N95-31126
Theory of unsteady combustion of solids: Investigation of Quasi-steady assumption p 2800 N95-31285
Condensed-phase processes during solid propellant combustion. 5: Further observations on depth profiling of burned surfaces of XM39 and M43 propellants p 2800 N95-31295
Observation and characterization of burning surface reaction zones of solid propellants p 2800 N95-31296
Convoy electron emission from surfaces
|DE95-010298| p 2984 N95-31402
The structure and reactivity of boron and carbon surfaces
|AD-A292804| p 2795 N95-31440
Models of transport, gas-phase and surface chemistry in diamond chemical vapor deposition
|DE95-009861| p 2822 N95-32101
Operational parameters and material effects p 2845 N95-32179

SURFACE ROUGHNESS
The effect of adding roughness and thickness to a transonic axial compressor rotor
|NASA-TM-106958| p 2867 N95-30524
Solderability enhancement of copper through chemical etching
|DE95-010514| p 2806 N95-31406
Cleanliness evaluation of rough surfaces with diffuse IR reflectance p 2782 N95-31804

SURFACE TEMPERATURE
Combustion of LOX with H2(sub g) under subcritical and supercritical conditions p 2797 N95-31717

SURFACE TO AIR MISSILES
Electronic combat and lethal defense suppression p 2842 N95-32140

SURFACE TREATMENT
Laser-induced holographic surface relief gratings on nonlinear optical polymer films
|AD-A293169| p 2997 N95-30973
A centrifuge CO2 pellet cleaning system p 2778 N95-31784
CO2 (dry ice) cleaning system p 2778 N95-31785
Aqueous cleaning and verification processes for precision cleaning of small parts p 2779 N95-31787
Evaluation of control parameters for Spray-In-Air (SIA) aqueous cleaning for shuttle RSRM hardware p 2780 N95-31794
Environmentally compatible hand wipe cleaning solvents p 2780 N95-31795
Implementation of environmentally compliant cleaning and insulation bonding for MNASA p 2780 N95-31796
The role of surface chemical analysis in a study to select replacement processes for TCA vapor degreasing p 2782 N95-31809

SURFACE WATER
Carbon dioxide concentrations in surface water and the atmosphere during 1986-1989 NOAA/PMEL cruises in the Pacific and Indian Oceans
|DE95-009659| p 2910 N95-32099

SURFACE WAVES
Removal of scattered surface waves from seismic data
|PB95-197802| p 2922 N95-30457

SURFACTANTS
On-line surfactant monitoring
|DE95-009417| p 2792 N95-30735
Aqueous cleaning and verification processes for precision cleaning of small parts p 2779 N95-31787

SURGES
Voltage surge suppression power circuits
|AD-D017454| p 2860 N95-30726
QTSAW (Quick Typhoon Surge and Waves). Wave information studies of US coastlines
|AD-A293172| p 2919 N95-30976

SURVEILLANCE
Millimeter wave radiometer utility study
|AD-A293811| p 2852 N95-31590
TMD detection and tracking using improved AWACS sensors p 2840 N95-32128
Optimal infrared detector configurations for air target detection p 2841 N95-32130
Design of surveillance and multisensor anti-aerial systems p 2841 N95-32134
Multisensor data fusion for integrated maritime surveillance p 2842 N95-32135
Multi-sensor data fusion in command and control and the merit of artificial intelligence p 2842 N95-32137

SURVEYS
Operating system support for distributed multimedia applications: A survey of current research
|PB95-207098| p 2964 N95-30565
Survey of recent Al2O3 droplet size data in solid rocket chambers, nozzles, and plumes p 2770 N95-31195
Survey of US burning rate measurement methods for solid propulsion applications p 2800 N95-31291
Initial survey on fracture toughness of commercial Nd2Fe14B
|DE95-009813| p 2808 N95-31643
An experimental search for high ZT semiconductors: A survey of the preparation and properties of several alloy systems
|DE95-010232| p 2865 N95-32084

SWEDEN
Non-comparability of female and male admission test takers: Evaluation through follow-up
|PB95-212080| p 3021 N95-30700
Swedish polar bibliography: A guide to Swedish literature on polar research, 1945-1988 with supplement, 1989-1992
|PB95-208161| p 2902 N95-32115

SWEPT FORWARD WINGS
Flight evaluation of forebody vortex control in post-stall flight p 2752 N95-32003

SWIRLING
Effects of initial conditions on a single jet in crossflow
|NASA-TM-107002| p 2754 N95-30589
Experimental investigation of turbulent particle dispersion in swirling flows
|DLR-FB-94-20| p 2873 N95-31355
A study of Damascus steel
|DE95-010127| p 2809 N95-32023

SWITCHES
Self-consistent, 2D simulations of filament propagation in photoconducting switches
|DE95-010794| p 2861 N95-31133
Information Switching Processor (ISP) contention analysis and control
|NASA-CR-195471| p 2765 N95-31849

SWITCHING
Device for low electric-field induced switching of Langmuir-Blodgett ferroelectric liquid crystal polymer films
|AD-D017457| p 3011 N95-30728
A study of switching behavior in Pb(Zr,Ti)O3 thin films using x-ray diffraction
|DE95-010859| p 2808 N95-31689

SYMBOLS
Bravais classes, Voronoie cells, Delone symbols
|PB95-207916| p 3009 N95-30503

SYMMETRY
The search for the decay of Z boson into two gamma as a test of Bose statistics
|DE95-616373| p 2976 N95-30393
Arithmetic features of rational conformal field theory
|PB95-207908| p 2966 N95-30591
Dressing symmetry of the uniformization solution of Liouville equation
|DE95-613380| p 2956 N95-30607
A BRST charge for non-critical W2(s) strings
|DE95-613470| p 3019 N95-30771
Symmetric longest queue system
|PB95-197919| p 2950 N95-30808
A simplified technique for determining the symmetry groups of non-linear plasma kinetic equations
|IFTR-8/1995| p 2960 N95-31337
Determination of the symmetry of a non-linear Schroedinger equation
|IFTR-10/1995| p 2960 N95-31339
Poisson's ratio for hexagonal crystals
|AD-A293556| p 3015 N95-31539
Spin puzzle in nucleon
|DE95-613654| p 2991 N95-32353

SYNCHRONISM
An overview of high-speed networking for workstations
|DE95-009076| p 2947 N95-30577
Cascading synchronized chaotic systems
|AD-D017458| p 2860 N95-30748
Confederation Verification, Validation, and Accreditation Master Plan (CVVAMP). Technical test plan
|AD-A289717| p 2936 N95-31050
Plasma source ion implantation of metal ions: Synchronization of cathodic-arc plasma production and target bias pulses
|DE95-009431| p 3006 N95-31613
High accuracy time transfer synchronization p 2968 N95-32321
Network time synchronization servers at the US Naval Observatory p 2969 N95-32329
Automated delay measurement system for an Earth station for Two-Way Satellite Time and Frequency Transfer p 2971 N95-32337
Prospects for high accuracy time dissemination and synchronization using coded radar pulses from a low-earth orbiting spacecraft p 2971 N95-32339
(T2L2) Time Transfer by Laser Link p 2887 N95-32348

SYNCHRONOUS MOTORS
A time stepping coupled finite element-state space modeling environment for synchronous machine performance and design analysis in the ABC frame of reference p 2864 N95-31948

SYNCHRONOUS SATELLITES
Using satellites for radar performance monitoring and calibration
|AD-A293809| p 2852 N95-31588

SYNCHROTRON RADIATION
Annual meeting of the Advanced Light Source Users' Association
|DE95-009373| p 3000 N95-31635
Beam stability at SRRC storage ring
|DE95-010842| p 2995 N95-32260
Tune modulation due to synchrotron oscillations and chromaticity, and the dynamic aperture
|DE95-011566| p 2995 N95-32297

SYNCHROTRONS
Background event discrimination in neutron time-of-flight measurements at beams of relativistic nuclei of the JINR synchrotron
|DE95-613006| p 2991 N95-30604
On the use of electronic tilt sensors as angle encoders for synchrotron applications
|DE95-005836| p 2880 N95-30941

Radial mode evolution in longitudinal bunched beam instability
| DE95-010895 | p 2994 N95-32092
The superconducting kaon spectrometer
| DE95-010436 | p 2882 N95-32159

SYNOPTIC METEOROLOGY
Forecast of Atlantic seasonal hurricane activity for 1994 p 2918 N95-30832
Summary of 1993 Atlantic tropical cyclone activity and verification of author's forecast. A year of unanticipated light hurricane activity and a poor forecast: The expected dissipation of the El Nino did not take place and Caribbean basin surface pressure became quite high p 2918 N95-30842
Early August updated forecast of Atlantic seasonal hurricane activity for 1994 p 2919 N95-30844

SYNTAX
Unification of LARCH and Z-based object models to support algebraically-based design refinement: The LARCH perspective
| AD-A289235 | p 2935 N95-30999
The occurrence of continuation parameters in CPS terms
| AD-A292952 | p 2941 N95-31460

SYNTHESIS (CHEMISTRY)
Synthesis of novel precursors for PMN powders and the thin films obtained from them
| DE95-008543 | p 2811 N95-30362
Low temperature synthesis of YBa2Cu3O(8-x) and other crystalline oxides
| AD-D017370 | p 3009 N95-30533
Catalytic reactions of synthesis gas. Part 4: Heterogeneous hydroformylation
| PB95-195558 | p 2791 N95-30537
Design and processing of materials by biomimicking. Sections 1. Publications
| AD-A293852 | p 2820 N95-31559
Novel unsymmetrical polydiacetylenes as materials for second and third order nonlinear optics
| AD-A293020 | p 3001 N95-31700
Synthesis and characterization of nanophase face-centered-cubic titanium
| DE95-009533 | p 2809 N95-32051
Synthesis of separation systems: Methods and applications in downstream gas processes
| PB95-208518 | p 2798 N95-32372

SYNTHESIZERS
Automation of the control of acoustic parameters in a digital speech synthesizer
| IFTR-2/1995 | p 2850 N95-31357
Fractional delay waveguide modeling of acoustic tubes
| PB95-206637 | p 2975 N95-31650

SYNTHETIC APERTURE RADAR
Cesar3 MALU library
| PB95-211363 | p 2933 N95-30598
Apparatus and method for producing three-dimensional images
| AD-D017455 | p 2847 N95-30727
Functions for processing synthetic aperture radar imagery
| AD-A293895 | p 2851 N95-31510
Investigation of ground target detection methods in fully polarimetric wide angle synthetic aperture radar images
| AD-A293922 | p 2851 N95-31513
Comparisons of target detection clutter using data from the 1993 FOPEN experiments
| AD-A293052 | p 2852 N95-31606
Folded compact range development and coherent change detection measurement project
| DE95-009082 | p 2853 N95-31628
Inversion of ERS-1 wavemode spectra. User's and programmer's guide
| PB95-223582 | p 2902 N95-32316
Prospects for high accuracy time dissemination and synchronization using coded radar pulses from a low-earth orbiting spacecraft p 2971 N95-32339

SYNTHETIC ARRAYS
Apparatus and method for producing three-dimensional images
| AD-D017455 | p 2847 N95-30727

SYNTHETIC FUELS
BioFacts: Fueling a stronger economy, global warming and biofuels emissions
| DE94-006884 | p 2910 N95-31821
BioFacts: Fueling a stronger economy, thermochemical conversion of biomass
| DE94-006866 | p 2905 N95-31822

SYNTHETIC RUBBERS
Mode I large strain viscoelastic crack behavior in nitrile rubber sheets
| AD-A289984 | p 2820 N95-31617

SYNTONY
Relativistic theory for syntonization of clocks in the vicinity of the Earth p 2971 N95-32343

SYRIA
A study of Damascus steel
| DE95-010127 | p 2809 N95-32023

SYSTEM FAILURES
Probabilistic reliability modeling of fatigue on the H-46 tie bar
| AD-A289926 | p 2751 N95-30927

SYSTEM IDENTIFICATION
Advanced system identification techniques for wind turbine structures
| DE95-004049 | p 2902 N95-30505
System identification for robust process control. Nominal models and error bounds
| PB95-197026 | p 2839 N95-30777
A two-timescale approach to nonlinear Model Predictive Control
| DE95-000943 | p 2952 N95-31161
Flight test validation of a frequency-based system identification method on an F-15 aircraft
| NASA-TM-4704 | p 2757 N95-31846

SYSTEMS ANALYSIS
Protocols for integrity constraint checking in federated databases
| PB95-197695 | p 3022 N95-30456
Nonlinear dynamical systems: Elements of a complex system analysis
| PB95-211652 | p 2950 N95-30478
System considerations for efficient communication and storage of MSTI image data
| NASA-CR-198869 | p 3024 N95-30858
Centrifugal and axial pump design and off-design performance prediction p 2830 N95-31269
Multiresolution signal and system analysis and the analysis and control of discrete-event dynamic systems
| AD-A292775 | p 2851 N95-31430
Automatic verification and synthesis of finite-state hard real-time systems
| AD-A291279 | p 2964 N95-32287

SYSTEMS ENGINEERING
Learning in an intentional system
| AD-A291158 | p 2949 N95-30395
Metrics in method engineering
| PB95-197687 | p 2838 N95-30455
Specific method for task-based interaction design
| PB95-196440 | p 2929 N95-30522
Precision manipulation with a dextrous robot hand p 2888 N95-30829
An architectural approach to strategic information systems planning for the Office of Naval Intelligence
| AD-A289930 | p 3024 N95-30928
Development of a novel wind lidar, phase 1
| AD-A292703 | p 2849 N95-30935
Recommended techniques for effective maintainability. A continuous improvement initiative of the NASA Reliability and Maintainability Steering Committee
| NASA-TM-4628 | p 2892 N95-31530
Design and testing of an optimal digital link capable of 14-channel transmission
| AD-A288505 | p 3000 N95-31652
Solid state research
| AD-A293083 | p 3015 N95-31826
Automatic flight control system for an unmanned helicopter system design and flight test results p 2759 N95-32004
Digital autopilot design for combat aircraft in ALENIA p 2760 N95-32009
Using a Red Team to devise countermeasures p 2842 N95-32141
Advanced turbine systems program conceptual design and product development
| DE95-000088 | p 2890 N95-32163
Stratospheric Observatory For Infrared Astronomy (SOFIA). Phase A: System concept description
| NASA-TM-110669 | p 3002 N95-32187

SYSTEMS HEALTH MONITORING
Making intelligent systems team players. A guide to developing intelligent monitoring systems
| NASA-TM-104807 | p 2951 N95-30925

SYSTEMS INTEGRATION
The process for addressing the challenges of aircraft pilot coupling p 2745 N95-31063
Adaptiveness in information systems integration p 3025 N95-31348
Experimental Aircraft Programme (EAP): Flight control system design and test p 2760 N95-32010

SYSTEMS SIMULATION
Foundations of technology for constructing highly reliable distributed realtime systems
| AD-A293254 | p 2931 N95-30892
The effect of repeatedly sampling an embedded metamodel on the simulation response
| AD-A293783 | p 2953 N95-31582
Mission critical failure effects analysis using quantitative techniques
| AD-A293098 | p 2864 N95-31844
CALORSTOCK'94. Thermal energy storage. Better economy, environment, technology
| DE95-772421 | p 2907 N95-32368

SYSTEMS STABILITY
Stability analysis of linear control systems with uncertain parameters p 2954 N95-31949

T

TACTILE SENSORS (ROBOTICS)
Precision manipulation with a dextrous robot hand p 2888 N95-30829
Force and vision resolvability for assimilating disparate sensory feedback
| AD-A293581 | p 2929 N95-31685

TAIL ASSEMBLIES
Afterbody/nozzle pressure distributions of a twin-tail twin-engine fighter with axisymmetric nozzles at Mach numbers from 0.6 to 1.2
| NASA-TP-3509 | p 2744 N95-31984

TAKEOFF
Analysis and modeling of an airport departure process
| AD-A293782 | p 2749 N95-31581

TANGENTS
A simple and efficient procedure for polyhedral assembly partitioning under infinitesimal motions
| DE95-009838 | p 2942 N95-31644

TARGET ACQUISITION
Apparent size passive range method
| AD-D017360 | p 2753 N95-31180
Investigation of ground target detection methods in fully polarimetric wide angle synthetic aperture radar images
| AD-A293922 | p 2851 N95-31513
Research in ground-to-air microwave imaging
| AD-A292907 | p 2852 N95-31551
Comparisons of target detection clutter using data from the 1993 FOPEN experiments
| AD-A293052 | p 2852 N95-31606
Optimal infrared detector configurations for air target detection p 2841 N95-32130
Acquisition, tracking, pointing and fire control for Ballistic Missile Defense p 2841 N95-32131
The High Altitude Balloon Experiment demonstration of acquisition, tracking, and pointing technologies (HABE-ATP) p 2841 N95-32132
The dynamic range of radar signal generation in the MSS-2 simulation facility
| AD-A293856 | p 2857 N95-32259

TARGET RECOGNITION
Neurodynamical systems for cognition and target identification
| AD-A293111 | p 2951 N95-30884
Optical feature recognition
| AD-A293168 | p 2997 N95-30966
Detection of radar targets using higher-order statistics
| AD-D017442 | p 2850 N95-31392
Research in ground-to-air microwave imaging
| AD-A292907 | p 2852 N95-31551
Nonlinear time series analysis
| AD-A293841 | p 2963 N95-31558
Automatic Target Recognition (ATR): Background statistics and the detection of targets in clutter
| AD-A293062 | p 2853 N95-31673
Optical correlator optimizations and extensions for automated optical target recognition
| AD-A293013 | p 3000 N95-31697
Analysis of target contrast improvement using polarization filtering in the infrared region
| AD-A293085 | p 3001 N95-31841
Optimal infrared detector configurations for air target detection p 2841 N95-32130

TARGET THICKNESS
Effects of mosaicity on Parametric X-Radiation production
| AD-A293677 | p 2985 N95-31597

TARGETS
Scaling of cross sections in ion-atom collisions
| DE95-008938 | p 2978 N95-30573
Passive range measurement system
| AD-D017344 | p 2996 N95-30678
Reflectivity of plasmas created by high-intensity, ultra-short laser pulses
| DE95-009536 | p 3004 N95-30742
Reply-frequency interference/jamming detector
| AD-D017428 | p 2847 N95-30748
Robust position and force tracking control for a robot in contract p 2888 N95-30830
Calculations of the sound scattering from fluid-filled spherical shell sonar targets
| DSTO-RR-0020 | p 2974 N95-31365
Visual processing of object velocity and acceleration
| AD-A292789 | p 2929 N95-31436

Plasma source ion implantation of metal ions: Synchronization of cathodic-arc plasma production and target bias pulses
[DE95-009431] p 3006 N95-31613
Enhanced brightness x-ray lasers
[DE95-010735] p 2886 N95-32029
The HYLIFE-2 inertial fusion energy power plant concept and implications for IFE
[DE95-010561] p 2994 N95-32074
Acquisition, tracking, pointing and fire control for Ballistic Missile Defense p 2841 N95-32131

TASK COMPLEXITY
A Heuristic and complete planner for the classical mover's problem
[DE95-008440] p 2949 N95-30377
Impact of task properties, data display format and cognitive characteristics on recall performance: A cumulative research investigation p 3025 N95-31334

TASK PLANNING (ROBOTICS)
Computer-aided inspection process definition: Development of an expert planning and programming system for coordinate metrology
[DE95-010411] p 2940 N95-31404

TASKS
Symmetric longest queue system
[PB95-197919] p 2950 N95-30808
The development of human behaviour analysis techniques and the development of human factors technologies
[DE95-613356] p 2930 N95-31267
Using case-based reasoning as a Reinforcement Learning framework for optimization with changing criteria
[AD-A293602] p 2953 N95-31654

TAYLOR SERIES
Derivation of two-dimensional (2-D) conduction equation in generalized coordinates with constant and anisotropic physical properties
[AD-A293896] p 3020 N95-31511

TECHNETIUM ISOTOPES
Faster, cheaper radioanalytical methods
[DE95-009913] p 2797 N95-32061

TECHNICAL WRITING
Closing the loop on improvement: Packaging experience in the Software Engineering Laboratory p 2937 N95-31238
Guidelines for creating and using abbreviations and acronyms
[NASA-CR-198884] p 3025 N95-31713

TECHNOLOGICAL FORECASTING
Sleeping renewable beauty: Will the prince ever come
[PB95-214573] p 2903 N95-30640
Study of Extended Air Defence Post 2000 p 2839 N95-32124

TECHNOLOGIES
FBIS report: Science and technology. Central Eurasia
[FBIS-UST-95-027] p 2839 N95-31727
FBIS report: Science and technology. Central Eurasia
[FBIS-UST-95-029] p 2863 N95-31728

TECHNOLOGY ASSESSMENT
High-temperature superconducting current leads
[DE95-008404] p 2858 N95-30374
State-of-the-art low-cost solar reflector materials
[DE95-000260] p 2902 N95-30526
Sleeping renewable beauty: Will the prince ever come
[PB95-214573] p 2903 N95-30640
Review of Gravity Probe B
[NASA-CR-198959] p 3019 N95-30781
The relation of handling qualities ratings to aircraft safety p 2746 N95-31067
Data on development of new energy technologies
[DE95-764135] p 2904 N95-31155
Workshop report: Measurement techniques in highly transient, spectrally rich combustion environments p 2799 N95-31208
The development of the tokamak system technology: A study on the fusion reactor
[DE95-614256] p 3005 N95-31366
Neural network false alarm filter, volume 1
[AD-A293097] p 2953 N95-31562
An assessment of worldwide supercomputer usage
[DE95-009879] p 2932 N95-31645
The design and development of a third generation OSEE instrument p 2781 N95-31800
Active control technology: Applications and lessons learned
[AGARD-CP-560] p 2757 N95-31989
The potential for microtechnology applications in energy systems: Results of an experts workshop
[DE95-009103] p 2865 N95-32077
Study of Extended Air Defence Post 2000 p 2839 N95-32124
Definition of an anti-missile ballistic defense architecture for Europe p 2840 N95-32125
Possible allied ballistic missile defense systems: Related guidance and control requirements p 2840 N95-32126
Multi-sensor data fusion in command and control and the merit of artificial intelligence p 2842 N95-32137
Electronic combat and lethal defense suppression p 2842 N95-32140

TECHNOLOGY TRANSFER
The Technology Information Environment with Industry (TIE-In): A mechanism for accessing laboratory solutions
[DE95-008542] p 3027 N95-30385
National Laboratories: Are their R and D activities related to commercial product development? Report to Congressional Requesters
[GAO/PEMD-95-2] p 3027 N95-31345
Technology transfer into the solid propulsion industry p 2770 N95-31756
Development of a CFC Critical Area Response (CAR) package p 2783 N95-31814
Report to Congressional Committees. Federal research: Interim report on the pilot technology access program
[GAO/RCED-94-75] p 3022 N95-32195
Report to the Vice Chairman, Joint Economic Committee, US Congress. Technology transfers: Benefits of cooperative R and D agreements
[GAO/RCED-95-52] p 3027 N95-32201
Minutes of the fourth annual workshop on chromate replacements in light metal finishing
[DE95-010937] p 2810 N95-32241

TECHNOLOGY UTILIZATION
Sleeping renewable beauty: Will the prince ever come
[PB95-214573] p 2903 N95-30640
Data on development of new energy technologies
[DE95-764135] p 2904 N95-31155
Lessons learned in transitioning to an open systems environment p 2938 N95-31245
Quantum 1/f noise in high technology applications including ultrasmall structures and devices
[AD-A292812] p 2862 N95-31442
Photovoltaic Energy Program overview: Fiscal year 1994
[DE94-011871] p 2905 N95-31661
Structural aspects of active control technology p 2760 N95-32006
Definition of an anti-missile ballistic defense architecture for Europe p 2840 N95-32125

TECTONICS
Studies in marine tectonics: Propagating rifts, depth anomalies and subduction zone anisotropy p 2923 N95-31719

TELECOMMUNICATION
An overview of high-speed networking for workstations
[DE95-009076] p 2947 N95-30577
Dynamic routation in distributed environments
[PB95-197968] p 2847 N95-30812
JPRS report: Science and technology. Central Eurasia
[JPRS-UST-95-025] p 2771 N95-31360
Dynamic maintenance scheduling for a stochastic telecommunication network: Determination of performance factors
[AD-A293829] p 2852 N95-31555
Custom Turnkey Time and Frequency Systems: A structured, expandable approach p 2969 N95-32330

TELEMETRY
Development of the Multi-Level Seismic Receiver (MLSR)
[DE95-008823] p 2916 N95-31610
Rate considerations in deep space telemetry p 2765 N95-32223
Effects of correlated noise on the full-spectrum combining and complex-symbol combining arraying techniques p 2856 N95-32237

TELEOPERATORS
On-orbit truss structure tele-operation experiment by Engineering Test Satellite-7
[NAL-TR-1246] p 2767 N95-31980

TELEROBOTICS
On-orbit truss structure tele-operation experiment by Engineering Test Satellite-7
[NAL-TR-1246] p 2767 N95-31980

TELESCOPES
Study of different type neutrino oscillations based on neutrino beams from 600 GeV
[DE95-619267] p 2983 N95-31260
Adaptive optics design for the advanced electro-optical system (AEOS)
[AD-A293972] p 2974 N95-31527
The High Altitude Balloon Experiment demonstration of acquisition, tracking, and pointing technologies (HABE-ATP) p 2841 N95-32132

TELEVISION SYSTEMS
Application of computer generated holograms to optical transformations
[AD-A293146] p 2880 N95-30921
Translation workbench for generating subtitles for English TV news
[NHK-435] p 3026 N95-32182

TELLURIDES
Convoy electron emission from surfaces
[DE95-010298] p 2984 N95-31402

TEMPERATURE CONTROL
Control of skin blood flow in the neutral zone of human body temperature regulation
[AD-A291499] p 2926 N95-30563
Supplemental multilayer insulation research facility
[NASA-TM-106991] p 2768 N95-30595

TEMPERATURE DEPENDENCE
Fractal quantum well heterostructures for broadband light emitters
[DE95-009579] p 2860 N95-30707
Hydrostatic extrusion of BSCCO/Ag composite wire
[DE95-007862] p 2805 N95-31121
Hydrogen diffusion and passivation in InGaAlN alloys
[DE95-010889] p 2806 N95-31150
Observations of star fracture and longitudinal splitting in BIS 812 EMA and Q1N submarine construction steels
[DSTO-RR-0014] p 2806 N95-31344
Substrate heating measurements in pulsed ion beam film deposition
[DE95-010862] p 2818 N95-31377
Impact behavior of the active zone within a frozen soil profile
[AD-A292909] p 2915 N95-31386
Differences in creep performance of a HIPed silicon nitride in ambient air and inert environments
[DE95-009172] p 2796 N95-31633
Influence of strain rate and temperature on the mechanical behavior of iron aluminide-based alloys
[DE95-009426] p 2808 N95-31636
Suppression of self-interstitials in silicon during ion implantation via in-situ photoexcitation
[DE95-009173] p 3016 N95-32301
SVN 9 End-Of-Life testing p 2767 N95-32345
Superconducting and normal-state properties of novel materials
[DE95-012368] p 3017 N95-32366

TEMPERATURE DISTRIBUTION
Yellow Sea thermal structure
[AD-A291159] p 2922 N95-30396
Effect of velocity and temperature distribution at the hole exit on film cooling of turbine blades
[NASA-TM-106954] p 2755 N95-30702

TEMPERATURE EFFECTS
Fatigue crack growth behavior of a titanium matrix composite under thermomechanical loading p 2784 N95-30491
Effects of temperature ramp rate during heat treatment on hysteresis loss and critical current density of internal tin processed wires
[DE95-009551] p 2803 N95-30706
May multiple inelastic scattering in CBED patterns be removed analytically
[PB95-196333] p 2992 N95-30717
Evaluation on materials performance of Hastelloy Alloy XR for HTTR uses. 4: Tensile properties of base metals and welded joints
[DE95-721871] p 2804 N95-30761
Calculated coupling efficiency between an elliptical-core optical fiber and an optical waveguide over temperature
[NASA-TM-107005] p 2997 N95-30849
Room temperature fracture and high temperature creep deformation properties of alumina reinforced with 20 vol% particulate niobium
[DE95-010234] p 2815 N95-30897
Membrane transport: A cellular probe of heat stroke
[AD-A293327] p 2926 N95-30924
Performance evaluation of high-temperature superconducting current leads for micro-SMES systems
[DE95-005843] p 2861 N95-30943
Polarized laser induced holographic surface relief gratings on polymer films
[AD-A293275] p 2817 N95-31126
Characterization of an improved Rijke burner as prelude to measurements of aluminum distributed combustion p 2800 N95-31287
Modeling of thermal response of filament used in T-jump experiment p 2800 N95-31297
Hot compression testing of tungsten
[AD-A293683] p 2807 N95-31599
Solution based temperature of Perovskite-type oxide films and powders
[DE95-009089] p 2820 N95-31629
NaK pool-boiler solar receiver durability bench test. Volume 2: Metallurgical analysis
[DE95-010338] p 2905 N95-31640
Evaluation of static strength of T800H/PMR-15 carbon/polyimide laminates at room temperature and 300 C
[NAL-TR-1254] p 2789 N95-31740

Underdense heating of the ionosphere using oblique high power HF radiowaves p 2917 N95-31951
The influence of matrix microstructure and temperature on cyclic deformation and fatigue of particle-reinforced 2219 aluminum p 2808 N95-31974
The influence of microstructure on creep deformation in near-gamma TiAl alloys p 2808 N95-31975
Effects of temperature, frequency, flux density, and excitation waveform on the core loss and dynamic B-H loops of supermalloy
|NASA-TM-106982| p 2865 N95-32207
Influence of storage on the maximal pull-out force of three different optical fibers from three epoxides
|PB95-211777| p 2822 N95-32253

TEMPERATURE GRADIENTS
Thermoacoustic sound generator
|AD-D017342| p 2973 N95-30413
Shear flow effects on ion thermal transport in tokamaks
|DE95-009115| p 3005 N95-30801
Residual stresses and stress corrosion cracking in pipe fittings
|DE95-009332| p 2894 N95-31054
Observations of star fracture and longitudinal splitting in BIS 812 EMA and Q1N submarine construction steels
|DSTO-RR-0014| p 2806 N95-31344

TEMPERATURE MEASUREMENT
Fabry-Perot interferometer measurement of static temperature and velocity for ASTOVL model tests
|NASA-TM-107014| p 2879 N95-30587
Multi-color pyrometer temperature measurement system
|DE95-009825| p 2879 N95-30687
Laser pyrolysis of HTPB p 2800 N95-31298
Measurement of temperatures and OH concentrations of solid propellant flames using absorption spectroscopy p 2801 N95-31302
Non-intrusive combustion diagnostics of premixed hydrocarbon flames using FT-IR spectrometry p 2797 N95-31732
Selected flows with free surfaces: Streams and drops
|IFTR-3/1995| p 2876 N95-31817

TEMPERATURE MEASURING INSTRUMENTS
Diamond thin film temperature and heat-flux sensors
|NASA-CR-198859| p 3012 N95-30847

TEMPERATURE PROFILES
Numerical study of shear-induced heating in high-speed nozzle flow of liquid monopropellant p 2828 N95-31207
Species and temperature profiles of propellant flames obtained from FTIR absorption spectroscopy p 2801 N95-31303
Advanced oxidizers diffusion flames structure p 2801 N95-31307
An efficient numerical procedure for thermohydrodynamic analysis of cavitating bearings
|NASA-CR-195476| p 2878 N95-32210
Film temperatures in the presence of cavitation
|NASA-CR-195481| p 2878 N95-32216

TEMPLATES
Westinghouse Hanford Company Data Management Plan Template, revision 1
|DE95-010046| p 3026 N95-32107

TEMPORAL DISTRIBUTION
Geostatistics and hydrology. Part 1: Spatial and temporal variability. Communications of the Sanitary Engineering and Water Management Division
|PB95-206470| p 2900 N95-30819

TEMPORAL RESOLUTION
Reflectivity of plasmas created by high-intensity, ultra-short laser pulses
|DE95-009536| p 3004 N95-30742
Beam-centroid tracking instrument for ion thrusters
|AD-A293654| p 2769 N95-31567

TENNESSEE
Field performance of the Walker Branch throughfall displacement experiment
|DE95-008677| p 2908 N95-30793

TENSILE CREEP
Differences in creep performance of a HIPed silicon nitride in ambient air and inert environments
|DE95-009172| p 2796 N95-31633

TENSILE DEFORMATION
Ion implantation and thermal stress resistance of ceramics
|DE95-615349| p 2812 N95-30451
Localization in tungsten heavy alloys subjected to shearing deformations under superimposed high pressures
|AD-A293177| p 2804 N95-30977
Predictions of tensile behavior and strengths of a Si3N4 ceramic at high temperatures based on a viscoplastic model
|DE95-010220| p 2821 N95-32025

TENSILE PROPERTIES
Evaluation on materials performance of Hastelloy Alloy XR for HTTR uses. 4: Tensile properties of base metals and welded joints
|DE95-721871| p 2804 N95-30761
Observations of star fracture and longitudinal splitting in BIS 812 EMA and Q1N submarine construction steels
|DSTO-RR-0014| p 2806 N95-31344

TENSILE STRENGTH
Nondestructive testing of ceramic components: Cooperative Research and Development Agreement completion report
|DE95-009510| p 2823 N95-32352

TENSILE STRESS
Stress relaxation of silicon nitride at elevated temperatures
|DE95-009177| p 2814 N95-30732
Differences in creep performance of a HIPed silicon nitride in ambient air and inert environments
|DE95-009172| p 2796 N95-31633
An inverse method to measure the axial modulus of composite materials under tension
|AD-A293042| p 2789 N95-31668

TENSILE TESTS
High strain rate properties and constitutive modeling of glass
|DE95-008434| p 2816 N95-31058
Differences in creep performance of a HIPed silicon nitride in ambient air and inert environments
|DE95-009172| p 2796 N95-31633
Robotic weld overlay coatings for erosion control
|DE95-009643| p 2809 N95-32098
A study of elevated temperature testing techniques for the fatigue behavior of PMCS: Application to T650-35/AMB21
|NASA-TM-106927| p 2791 N95-32209
Metallic multilayers at the nanoscale
|DE95-011534| p 3016 N95-32284

TENSION
Effect of cyclic loading on the creep performance of silicon nitride
|DE95-010289| p 2894 N95-31131

TENSORS
A queer reduction of degrees of freedom
|DE95-613471| p 2964 N95-30369
New tensor interaction and the K(sub L) - K(sub S)mass difference
|DE95-613597| p 2845 N95-30370
New tensor interactions in micron-decay
|DE95-613760| p 2978 N95-30528
The conical singularity and quantum corrections to entropy of black hole
|DE95-613367| p 3029 N95-30606
A compact expression for bilinear combination of Dirac spinors via world tensors
|DE95-619200| p 2960 N95-31258

TERMINAL FACILITIES
The ATC operational evaluation of the prototype integrated terminal weather system (ITWS) at Dallas/Fort Worth and Orlando airports (May-September 1993)
|AD-A293808| p 2921 N95-31587

TERPENES
Prepsolv (TM): The optimum alternative to 1,1,1-trichloroethane and methyl ethyl ketone for hand-wipe cleaning of aerospace materials p 2774 N95-31764

TERRACES (LANDFORMS)
Applications of SXPS for studying surface structure, reaction mechanisms and kinetics
|DE95-008903| p 2803 N95-30547

TERRAIN
Multiparameter radar measurements of precipitation in complex terrain: Meteorological and hydrological applications
|AD-A290786| p 2918 N95-30403
Synthetic Terrain Imagery for Helmet-Mounted Display. Volume 3: Software user's manual
|AD-A293613| p 2753 N95-31463
Synthetic Terrain Imagery for Helmet-Mounted Display. Volume 2: Software design document
|AD-A293611| p 2753 N95-31655
Synthetic Terrain Imagery for Helmet-Mounted Display, volume 1
|AD-A293612| p 2753 N95-31656

TERRAIN ANALYSIS
Neural networks for real-time terrain typing
|AD-A293569| p 2953 N95-31540

TERRESTRIAL RADIATION
Supriolus semi-diurnal variation in the E.R.B.E./outgoing longwave radiation
|NOAA-TR-NESDIS-84| p 2913 N95-30643

TEST FACILITIES
NASA Lewis Research Center's preheated combustor and materials test facility
|NASA-TM-106676| p 2762 N95-30592
Icing simulation in the aeropropulsion systems test facility propulsion development test cell C-2
|AD-A293039| p 2747 N95-31667
Design study of prototype accelerator and MeV test facility for demonstration of 1 MeV, 1 A negative ion beam production
|DE95-737208| p 2995 N95-32262

TEST STANDS
NASA Lewis Research Center's preheated combustor and materials test facility
|NASA-TM-106676| p 2762 N95-30592
Development of a new instrument for rocket engine combustion diagnostics p 2799 N95-31211

TESTING TIME
Computer model to simulate testing at the National Transonic Facility
|NASA-TM-4664| p 2763 N95-32217

TETRAETHYL ORTHOSILICATE
GCMS and FTIR studies of by-product inhibited growth and the rate-limiting step in TEOS-based SiO2 CVD
|DE95-009863| p 3016 N95-32147

TEXTS
An evaluation of an automatic markup system
|DE95-009885| p 3026 N95-32149

TEXTURES
Texture development in aluminium extrusion
|PB95-196598| p 2979 N95-30666
Physical modelling of microstructural evolution during thermomechanical processing of aluminium alloys
|PB95-196341| p 2805 N95-31053
Texture based methods for image analysis: A review
|PB95-211595| p 2945 N95-32251

THALLIUM
Nuclear-spin-dependent parity-nonconserving effects in thallium, lead and bismuth atoms
|DE95-614120| p 2991 N95-32354

THEOREM PROVING
The iteration formula of the Maslov-type index theory with applications to nonlinear Hamiltonian systems
|DE95-613379| p 2957 N95-30676

THEOREMS
Plaquette expansion proof and interpretation
|DE95-616282| p 2965 N95-30432
Strange compactification theorem: Infinite processes and the 3-dimensional poincare conjecture 6. Part A
|PB95-207924| p 2965 N95-30504
4-manifold topology 2: Dwyer's filtration and surgery kernels
|PB95-207940| p 2965 N95-30509
Extension to higher dimensions of the Jaeschke-Eicker result on the standardized empirical process
|PB95-206868| p 2965 N95-30523
The 4-manifold topology 1: Subexponential groups
|PB95-207957| p 2965 N95-30555
Six-vector formalism in electromagnetics of bianisotropic media
|PB95-207130| p 2846 N95-30567
Dressing symmetry of the uniformization solution of Liouville equation
|DE95-613380| p 2956 N95-30607
Barendregt cube with definitions and generalized reduction
|PB95-206793| p 2966 N95-30719
A feedback linearization approach to orbital maneuvers p 2765 N95-30841
Poisson approximation using the Stein-Chen method and coupling: Number of exceedances of a discrete-time-chi-squared process
|PB95-212205| p 2961 N95-31398
Preservation theorems on finite structures
|DE95-613442| p 2962 N95-32067

THEORETICAL PHYSICS
Theoretical high energy physics
|DE95-003107| p 2991 N95-30527
Arithmetic features of rational conformal field theory
|PB95-207908| p 2966 N95-30591
Electrical conductivity study on polythiophenes films
|DE95-614309| p 2813 N95-30645
Abstracts of Annual Physics Conference of Iran
|DE95-611717| p 2768 N95-30881

THEORIES
Formalization of the ramified type theory
|PB95-206785| p 2961 N95-31422

THERMAL ANALYSIS
A metallurgical approach toward alloying in rare earth permanent magnet systems
|DE95-010242| p 2966 N95-30668
Advanced small rocket chambers. Option 3: 110 lbf Ir-Re rocket, volume 2
|NASA-CR-195435-VOL-2| p 2769 N95-31170
Intelligent finite element submodeling of multichip modules for reliability analysis
|AD-A292911| p 2940 N95-31455
Solution based temperature of Perovskite-type oxide films and powders
|DE95-009089| p 2820 N95-31629

An efficient numerical procedure for thermohydrodynamic analysis of cavitating bearings
[NASA-CR-195476] p 2878 N95-32210
Film temperatures in the presence of cavitation
[NASA-CR-195481] p 2878 N95-32216
THERMAL CONTROL COATINGS
High temperature barrier coatings for refractory metals
[NASA-CR-195475] p 2802 N95-30531
THERMAL CYCLING TESTS
Fatigue crack growth behavior of a titanium matrix composite under thermomechanical loading
p 2784 N95-30491
The electrodeposition of low contraction chromium/molybdenum alloys using pulse-reverse plating
[AD-A292727] p 2804 N95-30945
Advanced small rocket chambers. Option 3: 110 lbf Ir-Re rocket, volume 1
[NASA-CR-195435-VOL-1] p 2768 N95-31169
NaK pool-boiler solar receiver durability bench test. Volume 2: Metallurgical analysis
[DE95-010338] p 2905 N95-31640
The influence of matrix microstructure and temperature on cyclic deformation and fatigue of particle-reinforced 2219 aluminum p 2808 N95-31974
THERMAL DECOMPOSITION
Applications of SXPS for studying surface structure, reaction mechanisms and kinetics
[DE95-008903] p 2803 N95-30547
Modeling of thermal response of filament used in T-jump experiment p 2800 N95-31297
The structure and reactivity of boron and carbon surfaces
[AD-A292804] p 2795 N95-31440
THERMAL DIFFUSION
The junction characteristics and current conduction mechanisms of GaInP2 n(+)p diodes and solar cells
[AD-A290857] p 2902 N95-30408
THERMAL EMISSION
Studying the thermal/non-thermal crossover in solar flares
[NASA-CR-189436] p 3031 N95-30785
THERMAL ENERGY
The junction characteristics and current conduction mechanisms of GaInP2 n(+)p diodes and solar cells
[AD-A290857] p 2902 N95-30408
Semiconductor nanocrystals formed in SiO2 by ion implantation
[DE95-008900] p 2978 N95-30546
Fabrication and modification of metal nanocluster composites using ion and laser beams
[DE95-009131] p 2784 N95-30731
CALORSTOCK 1994: Thermal energy storage. Better economy, environment, technology
[DE95-772422] p 2904 N95-31138
THERMAL EXPANSION
Ageing control no. 3 of propellants for rocket motors RB 27 and RB 28
[PB95-210357] p 2825 N95-30626
HTS Josephson technology on silicon with application to high speed digital microelectronics
[AD-A288627] p 2861 N95-31147
Effects of gas-phase thermal expansion on the stability of deflagration through a porous energetic material
[DE95-004382] p 2797 N95-31824
THERMAL FATIGUE
Thermal-mechanical fatigue crack growth in aircraft engine materials
[ISBN-0-315-86543-1] p 2894 N95-31098
The influence of matrix microstructure and temperature on cyclic deformation and fatigue of particle-reinforced 2219 aluminum p 2808 N95-31974
A study of elevated temperature testing techniques for the fatigue behavior of PMCS: Application to T650-35/AMB21
[NASA-TM-106927] p 2791 N95-32209
THERMAL INSULATION
A water blown urethane insulation for use in cryogenic environments p 2775 N95-31765
Evaluation of HFC 245ca and HFC 236ea as foam blowing agents p 2775 N95-31766
Implementation of environmentally compliant cleaning and insulation bonding for MNASA p 2780 N95-31796
Development of integrated insulation joint for cooling pipe in tokamak reactor
[DE95-737220] p 3007 N95-32264
THERMAL MAPPING
Mapping hidden aircraft defects with dual-band infrared computed tomography
[DE95-011531] p 2741 N95-32164
THERMAL PLASMAS
Development of a tokamak plasma optimized for stability and confinement
[DE95-009609] p 3003 N95-30641
THERMAL PROTECTION
High temperature barrier coatings for refractory metals
[NASA-CR-195475] p 2802 N95-30531
A water blown urethane insulation for use in cryogenic environments p 2775 N95-31765
Evaluation of HFC 245ca and HFC 236ea as foam blowing agents p 2775 N95-31766
Convergent spray process for environmentally friendly coatings p 2777 N95-31776
THERMAL RADIATION
Monte Carlo code for evaluating the Boundary Layer Illumination and Radiation Balance model (BLIRB)
[AD-A293963] p 2915 N95-31560
THERMAL RESISTANCE
Ion implantation and thermal stress resistance of ceramics
[DE95-615349] p 2812 N95-30451
THERMAL SHOCK
Ion implantation and thermal stress resistance of ceramics
[DE95-615349] p 2812 N95-30451
THERMAL STABILITY
Nonlinear optical processes in polymer films
[AD-A293384] p 2815 N95-30955
Evaluation of Environmentally Acceptable hydraulic fluids
[AD-A293037] p 2821 N95-31666
THERMAL STRESSES
Ion implantation and thermal stress resistance of ceramics
[DE95-615349] p 2812 N95-30451
Effects of thermal and electrical stressing on the breakdown behavior of space wiring
[NASA-CR-198360] p 2768 N95-30860
Intelligent finite element submodeling of multichip modules for reliability analysis
[AD-A292911] p 2940 N95-31455
Development of integrated insulation joint for cooling pipe in tokamak reactor
[DE95-737220] p 3007 N95-32264
THERMISTORS
Diamond thin film temperature and heat-flux sensors
[NASA-CR-198859] p 3012 N95-30847
THERMOCLINES
Yellow Sea thermal structure
[AD-A291159] p 2922 N95-30396
THERMOCOUPLES
Experimental investigation of the effectiveness of flow-through modules for electronics cooling
[AD-A293284] p 2861 N95-30950
THERMODYNAMIC EFFICIENCY
Natural gas liquefier for vehicle fuel
[AD-A293619] p 2836 N95-31564
THERMODYNAMIC EQUILIBRIUM
Fabrication and modification of metal nanocluster composites using ion and laser beams
[DE95-009131] p 2784 N95-30731
THERMODYNAMIC PROPERTIES
Control of skin blood flow in the neutral zone of human body temperature regulation
[AD-A291499] p 2926 N95-30563
Hydrogen absorption in iron and steel during gas tungsten arc welding
[PB95-197018] p 2804 N95-30776
Germanate glass ceramic
[AD-D017418] p 2816 N95-31011
First-principles approaches to materials stability
[DE95-011533] p 2810 N95-32283
THERMODYNAMICS
Electrochemical vapour deposition of SOFC interconnection materials
[PB95-197844] p 2812 N95-30459
New Fermi-liquid approach for the theory of disordered magnetics
[DE95-613448] p 2967 N95-30739
Lanthanide(III) catalyzed reactions: Structure an d thermodynamics of intermediate complexes, and implications for reactivity
[PB95-197000] p 3019 N95-30775
A proposed phase equilibrium diagram for Pt-Zr system
[DE95-620904] p 2806 N95-31220
Predictions of tensile behavior and strengths of a Si3N4 ceramic at high temperatures based on a viscoplastic model
[DE95-010220] p 2821 N95-32025
THERMOELECTRIC COOLING
Experimental investigation of the effectiveness of flow-through modules for electronics cooling
[AD-A293284] p 2861 N95-30950
THERMOELECTRIC GENERATORS
GPHS-RTGs in support of the Cassini RTG Program
[DE95-010306] p 2768 N95-30674
Welding isotopic heat sources for the cassini mission to Saturn
[DE95-060104] p 2890 N95-32367
THERMOELECTRIC MATERIALS
An experimental search for high ZT semiconductors: A survey of the preparation and properties of several alloy systems
[DE95-010232] p 2865 N95-32084
THERMOELECTRICITY
Optimization of a thermoelectric IR-detector for low working temperature
[NASA-CR-198933] p 2880 N95-30752
THERMOGRAPHY
Use of body surface heat patterns for predicting and evaluating acute lower extremity pain among soldiers
[AD-A292829] p 2927 N95-31446
THERMOGRAVIMETRY
Processing and microstructural evolution of alumina/aluminum alloy and aluminum nitride/aluminum alloy composites by directed melt oxidation
p 2789 N95-31973
THERMOMECHANICAL TREATMENT
A theory for predicting and minimizing the effects of matrix degradation on the thermomechanical properties of general laminates p 2785 N95-30768
Physical modelling of microstructural evolution during thermomechanical processing of aluminium alloys
[PB95-196341] p 2805 N95-31053
Microstructure and aging response of SiCp reinforced A356 Al metal matrix composite subject to post fabrication thermomechanical processing
[AD-A292975] p 2789 N95-31469
THERMOMETERS
Use of body surface heat patterns for predicting and evaluating acute lower extremity pain among soldiers
[AD-A292829] p 2927 N95-31446
THERMONUCLEAR REACTIONS
The 10th INS Scientific Computational Programs
[DE95-717864] p 2982 N95-31178
THERMOPHYSICAL PROPERTIES
CFC-replacement by natural working fluids: R&D and industrial challenges within the refrigeration, air conditioning amd heat pump areas
[PB95-195756] p 2815 N95-30871
THERMOPLASTIC RESINS
Thermoplastic elastomers as a binder in composite propellants
[PB95-211553] p 2837 N95-32249
THERMOPLASTICITY
Thermoplastic elastomers as a binder in composite propellants
[PB95-211553] p 2837 N95-32249
THERMOREGULATION
Control of skin blood flow in the neutral zone of human body temperature regulation
[AD-A291499] p 2926 N95-30563
THERMOSETTING RESINS
Background to plastic media blasting
p 2843 N95-32168
THERMOSPHERE
HST-FOC observations of a remarkable UV auroral event on Jupiter p 3030 N95-30806
SSUSI single sensor auroral E-layer algorithm: Functional description
[AD-A288630] p 2914 N95-31012
Global Ultraviolet Imager (GUVI) investigation
[NASA-CR-189430] p 2917 N95-31820
THERMOVISCOELASTICITY
Thermoviscoelastic behaviour of solids
[PB95-196226] p 2784 N95-30694
THICKNESS
The effect of adding roughness and thickness to a transonic axial compressor rotor
[NASA-TM-106958] p 2867 N95-30524
Wave propagation in a fluid-loaded homogeneous, transversely isotropic, elastic cylinder of arbitrary thickness
[AD-A292728] p 2869 N95-30946
HTS Josephson technology on silicon with application to high speed digital microelectronics
[AD-A288627] p 2861 N95-31147
THIN FILMS
Synthesis of novel precursors for PMN powders and the thin films obtained from them
[DE95-008543] p 2811 N95-30362
Ceramics derived from metal-organic precursors
[AD-A290791] p 2811 N95-30405
Crystallization of sol-gel derived lead zirconate titanate thin films in argon and oxygen atmospheres
[DE95-615230] p 3009 N95-30421
Orientation of rapid thermally annealed lead zirconate titanate thin films on (111) Pt substrate
[DE95-615232] p 2811 N95-30422
Synthesis of carbo-nitride films using high-energy shock plasma deposition
[DE95-615231] p 2811 N95-30450

Morphology and microstructure of (111) crystalline CeO2 films grown on amorphous SiO2 substrates by pulsed-laser ablation
| DE95-008842 | p 3009 N95-30542
Ionic conductivities of lithium phosphorus oxynitride glasses, polycrystals, and thin films
| DE95-008898 | p 2812 N95-30545
Modeling of thermal, electronic, hydrodynamic, and dynamic deposition processes for pulsed-laser deposition of thin films
| DE95-008906 | p 2813 N95-30572
Diffraction-line broadening analysis and stress relaxation in thin metal layers
| PB95-213898 | p 2893 N95-30634
Josephson break junction thin film device
| AD-D017343 | p 3011 N95-30673
Mechanisms of enhanced ionic conduction at interfaces in ceramics
| DE95-009125 | p 2814 N95-30730
A Monte-Carlo model of ionic transport across a solid interface
| DE95-613447 | p 3011 N95-30737
Anodically enhanced diffusion in Cu/Ag thin film couples
| DE95-009198 | p 2814 N95-30738
TV-VI semiconductor quantum well lasers, physics and engineering p 2883 N95-30805
Diamond thin film temperature and heat-flux sensors
| NASA-CR-198859 | p 3012 N95-30847
Structural, chemical and electronic properties of superconducting thin films and junctions
| AD-A292700 | p 3012 N95-30933
High speed random access, Fourier transform holographic associative and high density two-photon three-dimensional optical memories based on bacteriorhodopsin
| AD-A293389 | p 2931 N95-30967
Investigation of polycrystalline thin film CuInSe2 solar cells based on ZnSe windows
| DE95-004068 | p 2904 N95-31164
Cracking during nanoindentation and its use in the measurement of fracture toughness
| DE95-008839 | p 2818 N95-31175
Synthesis and selected micro-mechanical properties of titanium nitride thin films by the pyrolysis of tetrakis titanium in ammonia
| DE95-010224 | p 2818 N95-31187
Molecular nanoclusters as precursors to conductive thin films and crystals
| AD-A290278 | p 3014 N95-31189
Thin-film edge field emitter device and method of manufacture therefor
| AD-D017453 | p 2862 N95-31275
Ion-Assisted Pulsed Laser Deposition of amorphous tetrahedral-coordinated carbon films
| DE95-010861 | p 2885 N95-31394
Intelligent synthetic polymers
| AD-A292905 | p 2819 N95-31395
Deposition and characterization of photoconductive PZT thin films
| ATR-93(8308)-7 | p 2819 N95-31417
Advanced thin-film deposition and physical properties of high-temperature and other novel superconducting materials
| AD-A292798 | p 2795 N95-31439
The structure and reactivity of boron and carbon surfaces
| AD-A292804 | p 2795 N95-31440
The effect of gravity on the deposition of thin films: The physical vapor transport of copper phthalocyanine
| AD-A292997 | p 2838 N95-31472
Characterization of /11'01/ twin dislocation structures in evaporated titanium thin films by HREM
| DE95-615391 | p 2820 N95-31623
A study of switching behavior in Pb(Zr,Ti)O3 thin films using x-ray diffraction
| DE95-010859 | p 2808 N95-31689
Thin-film sulfuric acid anodizing as a replacement for chromic acid anodizing p 2776 N95-31772
A microwave plasma cleaning apparatus p 2779 N95-31786
Spectroscopic ellipsometry as a sensitive monitor of materials contamination p 2782 N95-31808
Microstructure of Al2O3 irradiated with an applied electric field
| DE95-010278 | p 2822 N95-32043
Development of large-area monolithically integrated Silicon-Film(trademark) photovoltaic modules
| DE95-004089 | p 2906 N95-32057
Infrared and millimeter wave detection using thin films of Pb doped BiSrCaCuO superconductor p 2840 N95-32129
The pyrochlore-to-perovskite transformation in solution-derived lead zirconate titanate thin films
| DE95-010453 | p 2822 N95-32161

THIN PLATES
Contributions to the design of neutral cutouts in laminated plates and shells p 2790 N95-32113

THIN WALLED SHELLS
Contributions to the design of neutral cutouts in laminated plates and shells p 2790 N95-32113

THIN WALLS
Performance improvement of composite wings through aeroelastic tailoring and modern control
| AD-A293689 | p 2752 N95-31602

THIOPHENES
Electrical conductivity study on polythiophenes films
| DE95-614309 | p 2813 N95-30645

THOMAS-FERMI MODEL
Low-density ionization behavior
| DE95-009495 | p 2980 N95-30705

THORAX
Erect, neutral and slump sitting postures: A study of the torso linkage system from shoulder to hip joint
| AD-A293239 | p 2930 N95-30907

THREAT EVALUATION
Aerophysics test program 1
| AD-A293890 | p 2963 N95-31543

THREE BODY PROBLEM
The 10th INS Scientific Computational Programs
| DE95-717864 | p 2982 N95-31178

THREE DIMENSIONAL BODIES
On drawing complicated 3D surfaces
| DE95-619199 | p 2939 N95-31257
An investigation of a novel approach to elemental imaging in three dimensions
| DE95-010340 | p 3000 N95-31681

THREE DIMENSIONAL FLOW
Three-D mesh optimization methods for unstructured polyhedra
| DE95-008808 | p 2955 N95-30471
Development of a linearized unsteady Euler analysis for turbomachinery blade rows
| NASA-CR-4677 | p 2742 N95-30611
Solution of the three-dimensional Helmholtz equation with nonlocal boundary conditions
| NASA-TM-110174 | p 2974 N95-30850
Navier-Stokes flow field analysis of compressible flow in a high pressure safety relief valve
| NASA-TM-110640 | p 2868 N95-30862
Three-dimensional (3D) large fluid flow computations for US Army applications on KSR-1, CM-200, CM-5, and Cray C-90
| AD-A293125 | p 2869 N95-30889
Atomization simulations using an Eulerian-VOF-Lagrangian method p 2828 N95-31210
Unsteady flow simulations about moving boundary configurations using dynamic domain decomposition techniques p 2877 N95-31837
Laser anemometer measurements of the three-dimensional rotor flow field in the NASA low-speed centrifugal compressor
| NASA-TP-3527 | p 2756 N95-31985

THREE DIMENSIONAL MODELS
Simulation of airborne electromagnetic measurements in three dimensional environments
| DE95-008546 | p 2900 N95-30363
A phenomenological finite element model of part building in the stereolithography process
| DE95-008437 | p 2932 N95-30376
Numerical simulation of shock/turbulent boundary layer interaction
| NASA-CR-198846 | p 2872 N95-31341
A boundary integral equation approach to three dimensional electromagnetic wave scattering problems p 2853 N95-31839

THRESHOLD CURRENTS
TV-VI semiconductor quantum well lasers, physics and engineering p 2883 N95-30805

THRESHOLDS
Cracking during nanoindentation and its use in the measurement of fracture toughness
| DE95-008839 | p 2818 N95-31175

THRUST AUGMENTATION
Improved hybrid rocket fuel p 2773 N95-31755

THRUST CHAMBERS
Survey of recent Al2O3 droplet size data in solid rocket chambers, nozzles, and plumes p 2770 N95-30987
Advanced small rocket chambers. Option 3: 110 1bf Ir-Re rocket, volume 1
| NASA-CR-195435-VOL-1 | p 2768 N95-31169
Advanced small rocket chambers. Option 3: 110 1bf Ir-Re rocket, volume 2
| NASA-CR-195435-VOL-2 | p 2769 N95-31170
Survey of recent Al2O3 droplet size data in solid rocket chambers, nozzles, and plumes p 2770 N95-31195

THRUST VECTOR CONTROL
Beam-centroid tracking instrument for ion thrusters
| AD-A293654 | p 2769 N95-31567
Flight demonstration of an advanced pitch control law in the VAAC Harrier aircraft p 2760 N95-32012
X-31: A program overview and flight test status p 2753 N95-32013

TIDE POWERED GENERATORS
Production simulator for wave power plants
| PB95-212262 | p 2907 N95-32286

TILT ROTOR AIRCRAFT
Effects of civil tiltrotor service in the northeast corridor on en route airspace loads
| AD-A293586 | p 2747 N95-31687

TIME
Relativistic timescale analysis suggests lunar theory revision p 2970 N95-32333

TIME CONSTANT
Analysis of heads-up display quickening versus handling qualities
| AD-A293797 | p 2753 N95-31584

TIME DEPENDENCE
The interaction of magnetizations with an external electromagnetic field and a time-dependent magnetic Aharonov-Bohm effect
| DE95-613463 | p 2845 N95-30368
Existence of solutions in plane quasistationary stokes flow driven by surface tension
| PB95-197935 | p 2868 N95-30810
Properties of new materials relevant to energy and fuel research
| AD-A289734 | p 2825 N95-31149
Direct and inverse problems in random media
| AD-A293033 | p 2850 N95-31280
Stability prediction with rotational flow effects p 2799 N95-31283
Self-adaptive multilevel methods for fluid flow problems p 2873 N95-31412
Numerical simulation of time dependent viscoelastic fluid flow
| TRITA-NA-9311 | p 2873 N95-31414
The prevention of PIO by design p 2757 N95-31991
Predictions of tensile behavior and strengths of a Si3N4 ceramic at high temperatures based on a viscoplastic model
| DE95-010220 | p 2821 N95-32025

TIME DIVISION MULTIPLEXING
Design and testing of an optimal digital link capable of 14-channel transmission
| AD-A288505 | p 3000 N95-31652

TIME FUNCTIONS
Poisson approximation using the Stein-Chen method and coupling: Number of exceedances of a discrete-time-chi-squared process
| PB95-212205 | p 2961 N95-31398

TIME LAG
SCARLET: DLR rate saturation flight experiment p 2746 N95-31068
The prevention of PIO by design p 2757 N95-31991
High resolution time interval counter p 2969 N95-32331

TIME MEASUREMENT
Burn time measurements of single aluminum particles in steam and carbon dioxide mixtures p 2799 N95-30990
Burn time measurements of single aluminum particles in steam and carbon dioxide mixtures p 2799 N95-31198
The 26th Annual Precise Time and Time Interval (PTTI) Applications and Planning Meeting
| NASA-CP-3302 | p 2967 N95-32319
The 1994 international transatlantic two-way satellite time and frequency transfer experiment: Preliminary results p 2858 N95-32320
High accuracy time transfer synchronization p 2968 N95-32321
European plans for new clocks in space p 2968 N95-32324
Anticipated uncertainty budgets of PRARETIME and T2L2 techniques as applied to ExTRAS p 2968 N95-32326
PTTI applications at the limits of GPS p 2969 N95-32327
Time aspects of the European Complement to GPS: Continental and transatlantic experimental phases p 2969 N95-32328
Network time synchronization servers at the US Naval Observatory p 2969 N95-32329
High resolution time interval counter p 2969 N95-32331
Monte Carlo simulations of precise timekeeping in the Milstar communication satellite system p 2970 N95-32336
Automated delay measurement system for an Earth station for Two-Way Satellite Time and Frequency Transfer p 2971 N95-32337
Study of tropospheric correction for intercontinental GPS common-view time transfer p 2971 N95-32338

Methodologies for steering clocks
p 2971 N95-32341
The effects of clock errors on timescale stability
p 2971 N95-32342
Relativistic theory for syntonization of clocks in the vicinity of the Earth p 2971 N95-32343
(T2L2) Time Transfer by Laser Link
p 2887 N95-32348
Satellite test of the isotropy of the one-way spe ed of light using ExTRAS p 2973 N95-32349

TIME OF FLIGHT SPECTROMETERS
Background event discrimination in neutron time-of-flight measurements at beams of relativistic nuclei of the JINR synchrotron
|DE95-613006| p 2991 N95-30604

TIME RESPONSE
Aspects of the search time in binary search trees modified according to the move-to-root heuristic
|PB95-212148| p 2963 N95-31396

TIME SERIES ANALYSIS
Sensor Fusion and Nonlinear Prediction for Anomalous Event Detection
|DE95-009429| p 2933 N95-30602
Thermoviscoelastic behaviour of solids
|PB95-196226| p 2784 N95-30694
Nonparametric methods for incomplete data in reliability and for changepoints in smooth functions
|AD-A292773| p 2963 N95-31429
Spatial time-series: Pollution pattern recognition under irregular interventions
|AD-A293830| p 2909 N95-31556
Nonlinear time series analysis
|AD-A293841| p 2963 N95-31558
Arabian Sea mixed layer dynamics experiment: Mooring deployment cruise report
|AD-A293684| p 2923 N95-31600

TIME SIGNALS
Ultrasonic two probe system for locating and sizing
|AD-D017438| p 2996 N95-30724
The 1994 international transatlantic two-way satellite time and frequency transfer experiment: Preliminary results p 2858 N95-32320
Implementation of a standard format for GPS common view data p 2968 N95-32323
PTTI applications at the limits of GPS
p 2969 N95-32327
Custom Turnkey Time and Frequency Systems: A structured, expandable approach p 2969 N95-32330
A globally efficient means of distributing UTC time and frequency through GPS p 2970 N95-32335
Prospects for high accuracy time dissemination and synchronization using coded radar pulses from a low-earth orbiting spacecraft p 2971 N95-32339

TIN
Effects of temperature ramp rate during heat treatment on hysteresis loss and critical current density of internal tin processed wires
|DE95-009551| p 2803 N95-30706

TIN ALLOYS
Cadmium plating replacements p 2776 N95-31773
Measurements of stability margins and current distribution in large-scale Nb3Sn cable-in-conduit conductors
|DE95-009869| p 3007 N95-32148

TIN COMPOUNDS
Convoy electron emission from surfaces
|DE95-010298| p 2984 N95-31402

TIN TELLURIDES
Numerical modeling of Bridgman growth of PbSnTe in a magnetic field
|NASA-TM-106996| p 2837 N95-31359

TIP SPEED
Experimental and computational investigation of the tip clearance flow in a transonic axial compressor rotor
|NASA-TM-106711| p 2876 N95-31738

TITAN LAUNCH VEHICLES
Major weapon system environmental life-cycle cost estimating for Conservation, Cleanup, Compliance and Pollution Prevention (C3P2) p 2774 N95-31761

TITANIUM
Characterization of /11'01/ twin dislocation structures in evaporated titanium thin films by HREM
|DE95-615391| p 2820 N95-31623
An experimental search for high ZT semiconductors: A survey of the preparation and properties of several alloy systems
|DE95-010232| p 2865 N95-32084

TITANIUM ALLOYS
Fatigue crack growth behavior of a titanium matrix composite under thermomechanical loading
p 2784 N95-30491
The influence of microstructure on creep deformation in near-gamma TiAl alloys p 2808 N95-31975
Control of interfacial chemistry and mechanical properties in metal/ceramic composites
p 2790 N95-31976
Synthesis and characterization of nanophase face-centered-cubic titanium
|DE95-009533| p 2809 N95-32051
Creep of a fine-grained, fully-lamellar, two-phase TiAl alloy at 760 C
|DE95-009531| p 2810 N95-32272

TITANIUM CARBIDES
A metallurgical approach toward alloying in rare earth permanent magnet systems
|DE95-010242| p 2966 N95-30668

TITANIUM NITRIDES
Synthesis and selected micro-mechanical properties of titanium nitride thin films by the pyrolysis of tetrakis titanium in ammonia
|DE95-010224| p 2818 N95-31187
Self-lubricating, TiN-MoS2 composite coatings produced by simultaneous deposition from Ti((CH3))2N4/NH3/MoF6H2S gas mixture
|DE95-010359| p 2788 N95-31403

TITANIUM OXIDES
Aqueous TiO2 photocatalysis of metal-EDTA complexes
|DE95-011058| p 2793 N95-31113

TOKAMAK DEVICES
Power oscillator in the tokamaks training
|DE95-616538| p 3003 N95-30473
Effects of particle fueling and plasma wall interactions on D3-D discharges
|DE95-009608| p 3003 N95-30612
Development of a tokamak plasma optimized for stability and confinement
|DE95-009609| p 3003 N95-30641
Helium transport and exhaust studies in enhanced confinement regimes in DIII-D
|DE95-009134| p 3004 N95-30685
Stabilization of the resistive shell mode in tokamaks
|DE95-008748| p 3004 N95-30794
Reynolds stress of localized toroidal modes
|DE95-008750| p 3004 N95-30795
Shear flow effects on ion thermal transport in tokamaks
|DE95-009115| p 3005 N95-30801
Development of plasma diagnostics technologies: A study on nuclear fusion reactor
|DE95-614180| p 3005 N95-31004
The development of the tokamak system technology: A study on the fusion reactor
|DE95-614256| p 3005 N95-31366
Stabilization of ballooning modes with sheared toroidal rotation
|DE95-008388| p 3006 N95-31624
Wall stabilization of high beta plasmas in D3-D
|DE95-009607| p 3007 N95-32116
Measurements of stability margins and current distribution in large-scale Nb3Sn cable-in-conduit conductors
|DE95-009869| p 3007 N95-32148
Design study of prototype accelerator and MeV test facility for demonstration of 1 MeV, 1 A negative ion beam production
|DE95-737208| p 2995 N95-32262
Onset of ELMs in JT-60U
|DE95-737209| p 3007 N95-32263
Development of integrated insulation joint for cooling pipe in tokamak reactor
|DE95-737220| p 3007 N95-32264

TOMOGRAPHY
Multiparameter radar measurements of precipitation in complex terrain: Meteorological and hydrological applications
|AD-A290786| p 2918 N95-30403
Impact behavior of the active zone within a frozen soil profile
|AD-A292909| p 2915 N95-31386
A prototype ionospheric tomography system (ITS)
|AD-A293015| p 2916 N95-31698

TOPOGRAPHY
Local fractal dimension estimation
|AD-A293354| p 2959 N95-30953
Visit to Ionospheric Modeling and Remote Sensing Branch, Phillips Laboratory in Hanscom AFB, MA
|AD-A292339| p 2901 N95-31265
Investigation of ground target detection methods in fully polarimetric wide angle synthetic aperture radar images
|AD-A293922| p 2851 N95-31513

TOPOLOGY
Torus bundles and the group cohomology of GL(N,Z)
|PB95-208120| p 2965 N95-30489
4-manifold topology 2: Dwyer's filtration and surgery kernels
|PB95-207940| p 2965 N95-30509
The 4-manifold topology 1: Subexponential groups
|PB95-207957| p 2965 N95-30555
Good metric spaces without good parameterizations
|PB95-208427| p 2957 N95-30622
Co-groups on sequentially complete, locally convex, topological vector spaces in particular on strict LF-spaces
|PB95-206918| p 2966 N95-30681
Interferometry with particles of non-zero rest mass: Topological experiments
|DE95-616244| p 2979 N95-30689
Bifurcations of contracting singular cycles
|DE95-613371| p 2962 N95-32117

TOROIDAL DISCHARGE
The coupling impedance of a toroidal beam pipe with circular cross section
|DE95-010442| p 2993 N95-31405

TOROIDAL PLASMAS
Stability analysis of the TPX toroidal field coil
|DE95-009666| p 2865 N95-32100

TORPEDOES
Smart material joint band
|AD-D017374| p 2888 N95-30716

TORQUE
Speed control of an elastic two-mass system: Optimization and systems theory
|PB95-212106| p 2868 N95-30701
Robust position and force tracking control for a robot in contract p 2888 N95-30830

TORQUE MOTORS
Speed control of an elastic two-mass system: Optimization and systems theory
|PB95-212106| p 2888 N95-30701

TORSION
Static behaviour of axially loaded uniplanar and multiplanar tubular x-joints
|PB95-207866| p 2892 N95-30585

TORSO
Erect, neutral and slump sitting postures: A study of the torso linkage system from shoulder to hip joint
|AD-A293239| p 2930 N95-30907

TOWERS
Static behaviour of axially loaded uniplanar and multiplanar tubular x-joints
|PB95-207866| p 2892 N95-30585
Technique to prepare high-reflectance optical fiber Bragg gratings with single exposure in-line or fiber draw tower
|AD-D017445| p 2998 N95-31270

TOXIC HAZARDS
Hydrogen sulfide analyzer with protective barrier
|AD-D017412| p 2793 N95-31009
Treatment of plastic media waste
p 2844 N95-32177

TOXICITY
Demonstration of split-flow ventilation and recirculation as flow-reduction methods in an Air Force paint spray booth, volume 2
|AD-A286808| p 2762 N95-30926
Particulate air pollution and increased mortality: Biological plausibility for causal relationship
|DE95-006161| p 2909 N95-31703
Atmospheric environmental implications of propulsion systems p 2771 N95-31747
Replacement of ozone depleting and toxic chemicals in gravimetric analysis of non-volatile residue
p 2780 N95-31793
Environmentally Safe and Effective Processes for Paint Removal
|AGARD-LS-201| p 2843 N95-32165
Bioremediation of wheat starch media waste
p 2845 N95-32178

TOXICITY AND SAFETY HAZARD
Enhanced alkaline hydrolysis and biodegradability studies of nitrocellulose-bearing missile propellant
p 2772 N95-31752

TRACE ELEMENTS
Holistic analysis of gamma-ray spectra in instrumental neutron activation analysis
|PB95-214458| p 2979 N95-30639

TRACKING (POSITION)
Passive range measurement system
|AD-D017344| p 2996 N95-30678
Robust position and force tracking control for a robot in contract p 2888 N95-30830
DEPSCOR92-Wide field spectral imager
|AD-A293079| p 2997 N95-31005
Neural network based data fusion system
|AD-D017440| p 2953 N95-31692
Neural network based three dimensional ocean modeler
|AD-D017441| p 2953 N95-31693

TRACKING PROBLEM
A feedback linearization approach to orbital maneuvers p 2765 N95-30841
Multiple Target Tracking based on constellation matching and Kalman filter p 2842 N95-32136

TRACKING RADAR
Using satellites for radar performance monitoring and calibration
| AD-A293809 | p 2852 N95-31588
The Telecommunications and Data Acquisition Report
| NASA-CR-198911 | p 2854 N95-32221
TRADEOFFS
Pressure transducer performance and measurement trade-offs in a transient, high temperature, combustion environment p 2799 N95-31209
TRAFFIC
Algorithms for categorizing multiprocessor communication under invalidate and update-based coherence protocols
| AD-A290022 | p 2947 N95-30930
Energy storage and alternatives to improve train voltage on a mass transit system
| DE95-010344 | p 2906 N95-32090
TRAILING EDGE FLAPS
Vibration reduction in helicopter rotors using an actively controlled partial span trailing edge flap located on the blade p 2762 N95-32111
TRAINING ANALYSIS
Effectiveness of an electronic performance support system for use with computer-aided design software
| AD-A293757 | p 2941 N95-31573
Optimizing the long-term retention of skills: Structural and analytic approaches to skill maintenance
| AD-A293798 | p 2929 N95-31585
TRAINING EVALUATION
Controller resource management: What can we learn from aircrews?
| DOT/FAA/AM-95/21 | p 2750 N95-32186
TRAJECTORIES
Laser Tracker 3: Sandia National Laboratories' third generation laser tracking system
| DE95-008525 | p 2882 N95-30379
Precision manipulation with a dextrous robot hand p 2888 N95-30829
Visual processing of object velocity and acceleration
| AD-A292789 | p 2929 N95-31436
Multiple Target Tracking based on constellation matching and Kalman filter p 2842 N95-32136
TRAJECTORY CONTROL
Design of systems for active sound control
| PB95-197869 | p 2973 N95-30461
TRAJECTORY PLANNING
Adaptive path planning: Algorithm and analysis
| DE95-008549 | p 2950 N95-30463
Qualitative environmental navigation: Theory and practice --- robot navigation p 2748 N95-30486
Objective analysis of oceanic data for Coast Guard trajectory models
| AD-A292884 | p 2924 N95-32363
TRANSDUCERS
Demodulators for optical fiber interferometers with (3 x 3) outputs
| AD-D017415 | p 2995 N95-30402
Apparatus for producing images acoustically
| AD-D017365 | p 2973 N95-30530
Sonic apparatus for degassing liquids
| AD-D017352 | p 2791 N95-30554
Fiber optic interferometric electric field and voltage sensor utilizing and electrostrictive transducer
| AD-D017433 | p 2996 N95-30753
TRANSFER FUNCTIONS
Enhancements to the SSME transfer function modeling code
| NASA-CR-198957 | p 2958 N95-30754
Control of flexible spacecraft structures using H-infinity wave absorbing control
| AD-A293141 | p 2766 N95-30919
Allan deviation computations of a linear frequency synthesizer system using frequency domain techniques p 2972 N95-32344
TRANSFER ORBITS
A feedback linearization approach to orbital maneuvers p 2765 N95-30841
TRANSFORMATIONS (MATHEMATICS)
The Foldy-Wouthuysen transformation
| DE95-616277 | p 2976 N95-30427
Pi1(sup infinity) and infinite simple homotopy type in dimension three: A research announcement
| PB95-196283 | p 2957 N95-30696
TRANSFORMERS
A simple model for the dc flux transformer in layered superconductors with Josephson coupling
| DE95-614468 | p 2859 N95-30649
Plane wave reflection from a uniaxial chiral quarter-wave polarization transformer
| PB95-206512 | p 2849 N95-31159
TRANSIENT RESPONSE
A transient FETI methodology for large-scale parallel implicit computations in structural mechanics
| NASA-CR-199040 | p 2945 N95-32214
TRANSISTOR CIRCUITS
Voltage controlled MESFET pulse shape generator
| DE95-011656 | p 2865 N95-32300
TRANSITION FLOW
The passage from transitional to free molecular plumes p 2871 N95-30994
TRANSITION METALS
A metallurgical approach toward alloying in rare earth permanent magnet systems
| DE95-010242 | p 2966 N95-30668
TRANSITION TEMPERATURE
Structural, chemical and electronic properties of superconducting thin films and junctions
| AD-A292700 | p 3012 N95-30933
TRANSLATING
A simple and efficient procedure for polyhedral assembly partitioning under infinitesimal motions
| DE95-009838 | p 2942 N95-31644
TRANSMISSION
The quad-service satellite transmitting and receiving system for medical supply support: A battlefield interoperability and communications system prototype, volume 2. User documentation
| AD-A292835 | p 2851 N95-31448
The quad-service satellite transmitting and receiving system for medical supply support: A battlefield interoperability and communications system prototype, volume 1
| AD-A292836 | p 2851 N95-31449
TRANSMISSION CIRCUITS
Electromyostimulation, circuits and monitoring
| NASA-TM-110741 | p 2926 N95-30846
TRANSMISSION ELECTRON MICROSCOPY
Semiconductor nanocrystals formed in SiO2 by ion implantation
| DE95-008900 | p 2978 N95-30546
TEM-examination of ceramic-metal interfaces
| PB95-196531 | p 2813 N95-30664
Microstructure and aging response of SiCp reinforced A356 Al metal matrix composite subject to post fabrication thermomechanical processing
| AD-A292975 | p 2789 N95-31469
Amorphization and the effect of implanted ions in SiC
| DE95-009699 | p 2985 N95-31642
Growth, characterization and device development in monocrystalline diamond films
| AD-A293106 | p 3015 N95-32018
TRANSMISSION LINES
HTS Josephson technology on silicon with application to high speed digital microelectronics
| AD-A288627 | p 2861 N95-31147
The 1994 international transatlantic two-way satellite time and frequency transfer experiment: Preliminary results p 2858 N95-32320
TRANSMISSION LOSS
Performance of residual carrier array-feed combining in correlated noise p 2856 N95-32232
TRANSMISSION RATE (COMMUNICATIONS)
Rate considerations in deep space telemetry p 2765 N95-32223
TRANSMITTANCE
Validation of the atmospheric transmission large-area analysis system (ATLAS)
| AD-A293810 | p 2916 N95-31589
TRANSMITTER RECEIVERS
Opto-electronic components from non-stoichiometric 3-5 materials
| AD-A293206 | p 3013 N95-30985
TRANSMITTERS
Apparatus and method for producing three-dimensional images
| AD-D017455 | p 2847 N95-30727
Cascading synchronized chaotic systems
| AD-D017458 | p 2860 N95-30748
TRANSONIC COMPRESSORS
The effect of adding roughness and thickness to a transonic axial compressor rotor
| NASA-TM-106958 | p 2867 N95-30524
Experimental and computational investigation of the tip clearance flow in a transonic axial compressor rotor
| NASA-TM-106711 | p 2876 N95-31738
TRANSONIC SPEED
Validation of the NPARC code for nozzle afterbody flows at transonic speeds
| NASA-TM-106971 | p 2742 N95-30704
Transonic aerodynamic characteristics of a proposed wing-body reusable launch vehicle concept
| NASA-TM-108489 | p 2742 N95-30712
Unsteady transonic wind tunnel test on a semispan straked delta wing, oscillating in pitch. Part 1: Description of the model, test setup, data acquisition, and data processing
| AD-A293113 | p 2743 N95-30885
Afterbody/nozzle pressure distributions of a twin-tail twin-engine fighter with axisymmetric nozzles at Mach numbers from 0.6 to 1.2
| NASA-TP-3509 | p 2744 N95-31984
TRANSONIC WIND TUNNELS
Computer model to simulate testing at the National Transonic Facility
| NASA-TM-4664 | p 2763 N95-32217
TRANSPORT AIRCRAFT
Electrical short circuit and current overload tests on aircraft wiring
| AD-A293308 | p 2860 N95-30922
Report to the Chairman, Legislation and National Security Subcommittee, Committee on Government Operations, House of Representatives. C-17 Aircraft program: Improvements in initial provisioning process
| GAO/NSIAD-94-63 | p 2741 N95-32194
TRANSPORT PROPERTIES
Helium transport and exhaust studies in enhanced confinement regimes in DIII-D
| DE95-009134 | p 3004 N95-30685
A Monte-Carlo model of ionic transport across a solid interface
| DE95-613447 | p 3011 N95-30737
Vertical transport in GaAs/AlGaAs superlattices p 3012 N95-30822
Membrane transport: A cellular probe of heat stroke
| AD-A293327 | p 2926 N95-30924
TRANSPORT THEORY
MVP/GMVP: General purpose Monte Carlo codes for neutron and photon transport calculations based on continuous energy and multigroup methods
| DE95-722072 | p 2979 N95-30656
Development of BERMUDA: A radiation transport code system. Part 3: A one-dimensional adjoint neutron transport code
| DE95-717875 | p 2934 N95-30759
Particle filtration: A comparison between theory and experiment
| DE95-009442 | p 2875 N95-31637
TRAPPED MAGNETIC FIELDS
Study of cross-tail current carriers in magnetotail p 3005 N95-30804
TRAPPED PARTICLES
Advances in the simulation of toroidal gyro Landau fluid model turbulence
| DE95-008387 | p 3003 N95-30359
A study of ion trapping and instability in the Fermilab antiproton accumulator p 2993 N95-31647
The 26th Annual Precise Time and Time Interval (PTTI) Applications and Planning Meeting
| NASA-CP-3302 | p 2967 N95-32319
TRAPPING
Properties of new materials relevant to energy and fuel research
| AD-A289734 | p 2825 N95-31149
A study of ion trapping and instability in the Fermilab antiproton accumulator p 2993 N95-31647
High-resolution superconducting x-ray spectrometers with aluminum trapping layers of different thicknesses
| DE95-010253 | p 2881 N95-32047
TRAPS
Studies of highly charged ions with EBIT and Super-EBIT
| DE95-010251 | p 2967 N95-32038
TRAVELING WAVE AMPLIFIERS
Use of a variable frequency source with a single-mode cavity to process ceramic filaments
| DE95-010992 | p 2817 N95-31152
TRAVELING WAVE MODULATION
Microwave electro-optic mixer
| AD-D017328 | p 2862 N95-31179
TRAVELING WAVE TUBES
High energy pulsed microwave sources
| AD-A293334 | p 2849 N95-31142
TRAVELING WAVES
Numerical computation of one-dimensional detonation waves
| PB95-197950 | p 2868 N95-30811
Control of flexible spacecraft structures using H-infinity wave absorbing control
| AD-A293141 | p 2766 N95-30919
TREES (MATHEMATICS)
Join processing in relational database systems p 3023 N95-30764
Aspects of the search time in binary search trees modified according to the move-to-root heuristic
| PB95-212148 | p 2963 N95-31396
TRELLIS CODING
Minimal trellises for linear block codes and their duals p 2856 N95-32233
Trellis complexity bounds for decoding linear block codes p 2856 N95-32234

TRIANGULATION
Non-critical string field theory with non-orientable string interactions
|DE95-737160| p 3020 N95-31281
TRIAXIAL STRESSES
Effects of hydrostatic pressure on the mechanical behavior of composite materials
|AD-A293162| p 2787 N95-30963
TRIBOLOGY
Synthesis of carbo-nitride films using high-energy shock plasma deposition
|DE95-615231| p 2811 N95-30450
Composite structure forming a wear surface
|AD-D017462| p 2785 N95-30749
Effect of local melting on tribology in metal cutting
|PB95-195392| p 2804 N95-31052
Fluid-film lubrication with an application to piston rings p 2890 N95-32119
TRIGGER CIRCUITS
Implementation of the shower max electron trigger at CDF
|DE95-006684| p 2992 N95-31165
TROPICAL METEOROLOGY
Summary of 1993 Atlantic tropical cyclone activity and verification of author's forecast. A year of unanticipated light hurricane activity and a poor forecast: The expected dissipation of the El Nino did not take place and Caribbean basin surface pressure became quite high p 2918 N95-30842
Early August updated forecast of Atlantic seasonal hurricane activity for 1994 p 2919 N95-30844
NASA Tropical Rainfall Measurement Mission (TRMM): Effects of tropical rainfall on upper ocean dynamics, air-sea coupling and hydrologic cycle
|NASA-CR-189437| p 2919 N95-31123
TROPICAL REGIONS
Comparisons of target detection clutter using data from the 1993 FOPEN experiments
|AD-A293052| p 2852 N95-31606
TROPICAL STORMS
Forecast of Atlantic seasonal hurricane activity for 1994 p 2918 N95-30832
Summary of 1993 Atlantic tropical cyclone activity and verification of author's forecast. A year of unanticipated light hurricane activity and a poor forecast: The expected dissipation of the El Nino did not take place and Caribbean basin surface pressure became quite high p 2918 N95-30842
Early August updated forecast of Atlantic seasonal hurricane activity for 1994 p 2919 N95-30844
LAWS hurricane studies
|NASA-CR-189438| p 2919 N95-31128
TROPOSPHERE
Diagnosis of the kinematics and dynamics of rapidly developing maritime cyclones
|AD-A293919| p 2921 N95-31675
Feasibility of tropospheric water vapor profiling using infrared heterodyne differential absorption lidar
|DE95-009647| p 2917 N95-32142
Study of tropospheric correction for intercontinental GPS common-view time transfer p 2971 N95-32338
TROUGHS
Field performance of the Walker Branch throughfall displacement experiment
|DE95-008677| p 2908 N95-30793
TRUSSES
On-orbit truss structure tele-operation experiment by Engineering Test Satellite-7
|NAL-TR-1246| p 2767 N95-31980
TUNABLE FILTERS
Opto-electronic components from non-stoichiometric 3-5 materials
|AD-A293206| p 3013 N95-30985
TUNABLE LASERS
Extended tuning range semiconductor lasers with sampled gratings p 2883 N95-30498
Diode-pumped, continuously tunable, 2.3 micron CW laser
|AD-D017448| p 2885 N95-31273
Tunable ytterbium-doped solid state laser
|AD-D017449| p 2885 N95-31274
Ultraviolet and visible lasers: Rare earth-doped waveguide devices and non-linear optical extraction techniques
|AD-A293976| p 2885 N95-31528
TUNGSTEN
Hot compression testing of tungsten
|AD-A293683| p 2807 N95-31599
Luminescence properties of ZnWO4:Cr(3+) laser crystals
|AD-A293065| p 2887 N95-32152
TUNGSTEN ALLOYS
Localization in tungsten heavy alloys subjected to shearing deformations under superimposed high pressures
|AD-A293177| p 2804 N95-30977
TUNING
Extended tuning range semiconductor lasers with sampled gratings p 2883 N95-30498
Tunable ytterbium-doped solid state laser
|AD-D017449| p 2885 N95-31274
Fine tuning GPS clock estimation in the MCS p 2968 N95-32322
TUNNEL JUNCTIONS
High-resolution superconducting x-ray spectrometers with aluminum trapping layers of different thicknesses
|DE95-010253| p 2881 N95-32047
TURBINE BLADES
Effect of velocity and temperature distribution at the hole exit on film cooling of turbine blades
|NASA-TM-106954| p 2755 N95-30702
Acceleration potential models PREDICHAT/PREDICDYN applied for calculation of axisymmetric dynamic inflow cases
|PB95-207015| p 2889 N95-30957
Advanced turbine systems program conceptual design and product development
|DE95-000088| p 2890 N95-32163
TURBINE PUMPS
Enhancements to the SSME transfer function modeling code
|NASA-CR-198957| p 2958 N95-30754
Design and testing of an oxidizer-rich preburner p 2799 N95-31212
TURBINE WHEELS
Axial loads on yawed rotors
|PB95-214193| p 2742 N95-30638
TURBINES
Improved modeling of unsteady heat transfer (The first step)
|AD-A292777| p 2874 N95-31432
Advanced turbine systems program conceptual design and product development
|DE95-000088| p 2890 N95-32163
TURBOCOMPRESSORS
The effect of adding roughness and thickness to a transonic axial compressor rotor
|NASA-TM-106958| p 2867 N95-30524
Investigating the use of smart acoustically active surfaces for flow separation control in turbomachinery
|AD-A292819| p 2874 N95-31443
Experimental and computational investigation of the tip clearance flow in a transonic axial compressor rotor
|NASA-TM-106711| p 2876 N95-31738
TURBOFAN ENGINES
Wave rotor-enhanced gas turbine engines
|NASA-TM-106998| p 2754 N95-30517
Method for extracting forward acoustic wave components from rotating microphone measurements in the inlets of turbofan engines
|NASA-CR-195457| p 2755 N95-30779
TURBOJET ENGINE CONTROL
Flight assessment of the onboard propulsion system model for the Performance Seeking Control algorithm on an F-15 aircraft
|NASA-TM-4705| p 2756 N95-31425
TURBOMACHINERY
Investigating the use of smart acoustically active surfaces for flow separation control in turbomachinery
|AD-A292819| p 2874 N95-31443
TURBOSHAFTS
Wave rotor-enhanced gas turbine engines
|NASA-TM-106998| p 2754 N95-30517
TURBULENCE
Method and system for suppressing noise induced in a fluid medium by a body moving therethrough
|AD-D017339| p 2973 N95-30411
Electromagnetically activated compliant wavy-wall
|AD-D017340| p 2866 N95-30412
Small scale turbulence in a plane mixing layer p 2866 N95-30449
Active turbulence control using microelectrodes, permanent magnets in microgrooves
|AD-D017351| p 2867 N95-30553
Method and system for reducing drag on a body moving through a fluid medium
|AD-D017336| p 2867 N95-30672
Hot jet/wake turbulent structure and laser propagaion. Part 1: Jet/wake turbulence modeling p 2871 N95-30991
Hot jet/wake turbulent structure and laser propagation. Part 3: Laser propagation measurements and modeling p 2871 N95-30992
Advanced k-epsilon modeling of heat transfer
|NASA-CR-4679| p 2874 N95-31423
Application of wavelet-filtering techniques to intermittent turbulent and wall pressure events. Part 2. Detection of cluster patterns
|AD-A293805| p 2875 N95-31586
Large-eddy simulation of turbulent flow using the finite element method
|DE95-009464| p 2875 N95-31591
The effects of large and small scale turbulence on sound propagation in the atmosphere
|AD-A293657| p 2975 N95-31608
On the interactions between particles and turbulence in a fully-developed channel flow in air p 2875 N95-31707
Heat transfer in shear-free turbulent boundary layers p 2876 N95-31708
Selected flows with free surfaces: Streams and drops
|IFTR-3/1995| p 2876 N95-31817
Advanced gust management systems: Lessons learned and perspectives p 2759 N95-32002
TURBULENCE EFFECTS
The effects of large and small scale turbulence on sound propagation in the atmosphere
|AD-A293657| p 2975 N95-31608
TURBULENCE MODELS
Validation of the NPARC code for nozzle afterbody flows at transonic speeds
|NASA-TM-106971| p 2742 N95-30704
A turbulence model for steady and unsteady boundary layers in strong pressure gradients p 2868 N95-30840
A turbulence module for the NPARC code
|NASA-CR-198358| p 2959 N95-30855
Parametrics on 2D Navier-Stokes analysis of a Mach 2.68 bifurcated rectangular mixed-compression inlet
|NASA-TM-107003| p 2755 N95-30861
Hot jet/wake turbulent structure and laser propagation. Part 3: Laser propagation measurements and modeling p 2871 N95-30992
Large eddy simulation of jets using structured upwind numerics p 2871 N95-30993
Shear-free turbulent boundary layers p 2873 N95-31349
Large-eddy simulation of turbulent flow using the finite element method
|DE95-009464| p 2875 N95-31591
Analysis and modeling of subgrid scalar mixing using numerical data
|NASA-CR-198169| p 2877 N95-31978
LES, DNS and RANS for the analysis of high-speed turbulent reacting flows
|NASA-CR-199075| p 2878 N95-32219
TURBULENT BOUNDARY LAYER
Active turbulence control using microelectrodes, permanent magnets in microgrooves
|AD-D017351| p 2867 N95-30553
Numerical simulation of shock/turbulent boundary layer interaction
|NASA-CR-198846| p 2872 N95-31341
Shear-free turbulent boundary layers p 2873 N95-31349
Application of wavelet-filtering techniques to intermittent turbulent and wall pressure events. Part 2. Detection of cluster patterns
|AD-A293805| p 2875 N95-31586
Heat transfer in shear-free turbulent boundary layers p 2876 N95-31708
TURBULENT COMBUSTION
A pulsed liquid fuel ramjet p 2756 N95-31201
TURBULENT DIFFUSION
Experimental investigation of turbulent particle dispersion in swirling flows
|DLR-FB-94-20| p 2873 N95-31355
TURBULENT FLOW
Simulation of chemical kinetics in turbulent natural gas combustion. Volume 2: Experimental studies of nitric oxide production in gas flames
|PB95-196721| p 2791 N95-30541
Numerical simulation of flow in a whirling annular seal and comparison with experiments
|NASA-TM-106961| p 2867 N95-30710
A turbulence module for the NPARC code
|NASA-CR-198358| p 2959 N95-30855
A pulsed liquid fuel ramjet p 2756 N95-31201
Role of free-surface boundary conditions and nonlinearities in wave/boundary-layer and wake interaction p 2872 N95-31317
Numerical simulation of shock/turbulent boundary layer interaction
|NASA-CR-198846| p 2872 N95-31341
Advanced k-epsilon modeling of heat transfer
|NASA-CR-4679| p 2874 N95-31423
Improved modeling of unsteady heat transfer (The first step)
|AD-A292777| p 2874 N95-31432
Compressible turbulence measurement in low-angle injection into a supersonic flow
|AD-A293836| p 2874 N95-31516
Application of wavelet-filtering techniques to intermittent turbulent and wall pressure events. Part 2. Detection of cluster patterns
|AD-A293805| p 2875 N95-31586
Large-eddy simulation of turbulent flow using the finite element method
|DE95-009464| p 2875 N95-31591

On the interactions between particles and turbulence in a fully-developed channel flow in air
p 2875 N95-31707
Analysis and modeling of subgrid scalar mixing using numerical data
[NASA-CR-198169] p 2877 N95-31978
LES, DNS and RANS for the analysis of high-speed turbulent reacting flows
[NASA-CR-199075] p 2878 N95-32219

TURBULENT HEAT TRANSFER
Improved modeling of unsteady heat transfer (The first step)
[AD-A292777] p 2874 N95-31432
Heat transfer in shear-free turbulent boundary layers
p 2876 N95-31708

TURBULENT JETS
Hot jet/wake turbulent structure and laser propagaion. Part 1: Jet/wake turbulence modeling
p 2871 N95-30991

TURBULENT MIXING
Experimental investigation of turbulent particle dispersion in swirling flows
[DLR-FB-94-20] p 2873 N95-31355
Analysis and modeling of subgrid scalar mixing using numerical data
[NASA-CR-198169] p 2877 N95-31978

TURBULENT WAKES
Hot jet/wake turbulent structure and laser propagaion. Part 1: Jet/wake turbulence modeling
p 2871 N95-30991

TVD SCHEMES
Improved modeling of unsteady heat transfer (The first step)
[AD-A292777] p 2874 N95-31432

TWISTING
Round-robin validation exercise for plate twist test method
[PB95-208088] p 2812 N95-30487

TWO BODY PROBLEM
Multi-particle correlations in quaternionic quantum systems
[DE95-616271] p 3018 N95-30424
Recoil correction in the Dirac-Coulomb problem
[DE95-619241] p 2959 N95-31137
Hamiltonian formulation of two body problem in Wheeler-Feynman electrodynamics
[DE95-620526] p 3019 N95-31193

TWO DIMENSIONAL BOUNDARY LAYER
Viscous diffusion of vorticity in unsteady wall layers using the diffusion velocity concept
[DE95-008537] p 2866 N95-30383

TWO DIMENSIONAL FLOW
Multigrid convergence acceleration for the 2D Euler equations applied to high-lift systems
[PB95-198081] p 2743 N95-30814
Fourier analysis of a robust multigrid method for convection-diffusion equations
[PB95-197091] p 2958 N95-30835
A turbulence model for steady and unsteady boundary layers in strong pressure gradients p 2868 N95-30840
Parametrics on 2D Navier-Stokes analysis of a Mach 2.68 bifurcated rectangular mixed-compression inlet
[NASA-TM-107003] p 2755 N95-30861
Vorticity dynamics and control of dynamic stall
[AD-A288658] p 2756 N95-31400
Some aspects on the modelling of non-Newtonian fluid flow
[TRITA-NA-9317] p 2873 N95-31415
Numerical solution of the full potential equation using a chimera grid approach
[NASA-TM-110360] p 2744 N95-32188

TWO DIMENSIONAL MODELS
Quasi-periodic solutions of Hamiltonian perturbations of 2D linear Schroedinger equations
[PB95-208443] p 2957 N95-30624
On the theory of hole propagation in an antiferromagnetic background
[DE95-614469] p 3010 N95-30650
Potential integral equations of the 2D Laplace operator in wavelet basis
[TRITA-NA-9401] p 2957 N95-30713
A turbulence model for steady and unsteady boundary layers in strong pressure gradients p 2868 N95-30840
Ferromagnetic Potts model in a magnetic field: Finite lattice extrapolation of the (1 + 1)-dimensional Hamiltonian
[DE95-614447] p 3012 N95-30958
Calculation of a residual mean meridional circulation for a zonal-mean tracer transport model
[DE95-009474] p 2911 N95-32350

TWO PHASE FLOW
The Al and A(lc)l2O3 droplet cloud in solid rocket motors p 2770 N95-30988
Study of effect of bubbles on a free-shear layer
p 2872 N95-31100
The Al and Al2O3 droplet cloud in solid rocket motors
p 2770 N95-31196
Experimental investigation of turbulent particle dispersion in swirling flows
[DLR-FB-94-20] p 2873 N95-31355
On the interactions between particles and turbulence in a fully-developed channel flow in air
p 2875 N95-31707
Effects of gas-phase thermal expansion on the stability of deflagration through a porous energetic material
[DE95-004382] p 2797 N95-31824

TYPHOONS
QTSAW (Quick Typhoon Surge and Waves). Wave information studies of US coastlines
[AD-A293172] p 2919 N95-30976

U

ULTRAHIGH FREQUENCIES
Multiparameter radar measurements of precipitation in complex terrain: Meteorological and hydrological applications
[AD-A290786] p 2918 N95-30403
Comparisons of target detection clutter using data from the 1993 FOPEN experiments
[AD-A293052] p 2852 N95-31606
Investigation into the effects of VHF and UHF band radiation on Hewlett-Packard (HP) Cesium Beam Frequency Standards p 2970 N95-32332

ULTRAHIGH VACUUM
Development of germanium-silicon growth technology
[AD-A293199] p 3013 N95-30983

ULTRASONIC CLEANING
Ultrasonic cleaning: Fundamental theory and application p 2778 N95-31783
Aqueous cleaning and verification processes for precision cleaning of small parts p 2779 N95-31787
Ultrasonic frequency selection for aqueous fine cleaning p 2779 N95-31788
Cleaning without chlorinated solvents
p 2780 N95-31792

ULTRASONIC TESTS
The neutron powder diffraction and acoustic investigations of the NH4SCN phase diagram
[DE95-614372] p 3009 N95-30419
Ultrasonic characterization of fiber-matrix interphasial properties and damage in high-temperature composites
p 2785 N95-30823

ULTRASONICS
Detecting intravascular gas bubbles in ultrasonic images
[PB95-195301] p 2926 N95-30513
Sonic apparatus for degassing liquids
[AD-D017352] p 2791 N95-30554
Ultrasonic cleaning: Fundamental theory and application p 2778 N95-31783
Investigation of cleanliness verification techniques for rocket engine hardware p 2770 N95-31806

ULTRAVIOLET ABSORPTION
RDX laser-assisted flame structure
p 2801 N95-31314

ULTRAVIOLET ASTRONOMY
Chromospherically active stars. 6: Giants with compact hot companions and the barium star scenario
[NASA-TM-110641] p 3028 N95-30466
HST-FOC observations of a remarkable UV auroral event on Jupiter p 3030 N95-30806
NASA space astronomy update 6
[NASA-CR-197664] p 3028 N95-31099

ULTRAVIOLET EMISSION
Surface contamination analysis technology team overview p 2781 N95-31797

ULTRAVIOLET LASERS
Ultraviolet and visible lasers: Rare earth-doped waveguide devices and non-linear optical extraction techniques
[AD-A293976] p 2885 N95-31528

ULTRAVIOLET RADIATION
Voyager GO program
[NASA-CR-189435] p 3029 N95-31424
Contamination detection NDE for cleaning process inspection p 2781 N95-31802

ULTRAVIOLET SPECTRA
Chromospherically active stars. 6: Giants with compact hot companions and the barium star scenario
[NASA-TM-110641] p 3028 N95-30466
Cepheid temperature and the Blazhko effect
[NASA-CR-189433] p 3030 N95-31819

ULTRAVIOLET TELESCOPES
NASA space astronomy update 6
[NASA-CR-197664] p 3028 N95-31099

UNDERGROUND STORAGE
Off-potential measurement systems for impressed current cathodic protection
[AD-A290876] p 2812 N95-30558

UNDERGROUND STRUCTURES
Experimental determination of probability distributions for parameters of a Salem limestone cap plasticity model
[AD-A290878] p 2892 N95-30559
Visit to Ionospheric Modeling and Remote Sensing Branch, Phillips Laboratory in Hanscom AFB, MA
[AD-A292339] p 2901 N95-31265

UNDERWATER ACOUSTICS
Thermoacoustic sound generator
[AD-D017342] p 2973 N95-30413
Ray trace model of sound propagation in range dependent media
[PB95-211751] p 2973 N95-30481
Method and apparatus for locating an acoustic source
[AD-D017347] p 2974 N95-30549
Multiple scatter theory of ocean sediments
[AD-A293951] p 2923 N95-31523
The TEVA experiment cruise report
[AD-A293025] p 2923 N95-31701

UNDERWATER COMMUNICATION
Degradation of blue AlGaN/InGaN/GaN LEDs subjected to high current pulses
[DE95-008824] p 2863 N95-31611

UNDERWATER EXPLOSIONS
Response of dual-layered structures subjected to shock pressure wave
[AD-A293731] p 2896 N95-31568

UNIFORM FLOW
Acceleration potential models PREDICHAT/PREDICDYN applied for calculation of axisymmetric dynamic inflow cases
[PB95-207015] p 2869 N95-30957

UNITED KINGDOM
Integration issues in modular mission management aid development p 2841 N95-32133

UNITED STATES
Mars together and FIRE and ICE: Report of the joint US/Russian technical working groups
[NASA-CR-198864] p 3030 N95-30845
An assessment of worldwide supercompuier usage
[DE95-009879] p 2932 N95-31645
Annual review of aircraft accident data: US general aviation calendar year 1993
[PB95-215828] p 2747 N95-31712
Aeronautics and space report of the President
[NASA-TM-110743] p 3028 N95-31979
Electronic combat and lethal defense suppression
p 2842 N95-32140

UNIVERSAL TIME
Time activities at the BIPM p 2968 N95-32325
A globally efficient means of distributing UTC time and frequency through GPS p 2970 N95-32335

UNIX (OPERATING SYSTEM)
UNIX and PC security in a network environment. UNINETT
[PB95-196291] p 2934 N95-30662
UNIX and PC security in a network environment. LOKALNETT 1993
[PB95-196309] p 2934 N95-30697
Improving data consistency in mobile computing using Isolation-Only Transactions
[AD-A293110] p 2948 N95-32021

UNLOADING
An explanation for the shape of nanoindentation unloading curves based on finite element simulation
[DE95-008905] p 2812 N95-30548
Experimental determination of probability distributions for parameters of a Salem limestone cap plasticity model
[AD-A290878] p 2892 N95-30559

UNSTEADY AERODYNAMICS
Development of a linearized unsteady Euler analysis for turbomachinery blade rows
[NASA-CR-4677] p 2742 N95-30611
Axial loads on yawed rotors
[PB95-214193] p 2742 N95-30638
Validation of the helicopter rotor code HERO
[PB95-198040] p 2751 N95-30838
Unsteady transonic wind tunnel test on a semispan straked delta wing, oscillating in pitch. Part 1: Description of the model, test setup, data acquisition, and data processing
[AD-A293113] p 2743 N95-30885
Unsteady flow simulations about moving boundary configurations using dynamic domain decomposition techniques p 2877 N95-31837
FPCAS3D User's guide: A three dimensional full potential aeroelastic program, version 1
[NASA-CR-198367] p 2899 N95-32205

UNSTEADY FLOW
Viscous diffusion of vorticity in unsteady wall layers using the diffusion velocity concept
[DE95-008537] p 2866 N95-30383
A numerical study of the starting process in a hypersonic shock tunnel p 2762 N95-30493

Electron-optical nonlinear interaction in asymmetric quantum-well laser heterostructures
[DE95-613443] p 2883 N95-30609
A turbulence model for steady and unsteady boundary layers in strong pressure gradients p 2868 N95-30840
Large eddy simulation of jets using structured upwind numerics p 2871 N95-30993
Stability prediction with rotational flow effects p 2799 N95-31283
Spectral element method for numerical simulation of unsteady laminar diffusion flames p 2794 N95-31333
Vorticity dynamics and control of dynamic stall
[AD-A288658] p 2756 N95-31400
Unsteady flow simulations about moving boundary configurations using dynamic domain decomposition techniques p 2877 N95-31837
Control of unsteady separated flow associated with the dynamic stall of airfoils
[NASA-CR-198972] p 2744 N95-32193

UNSTRUCTURED GRIDS (MATHEMATICS)
Multidimensional discretization of conservation laws for unstructured polyhedral grids
[DE95-008796] p 2955 N95-30470
Three-D mesh optimization methods for unstructured polyhedra
[DE95-008808] p 2955 N95-30471

URANIUM
Experiments with highly charged ions up to bare U(sup 92+) on the electron beam ion trap
[DE95-008827] p 2982 N95-31174
Excitation mechanisms of 2s(sub 1/2)-2p(sub 3/2) and 2p(sub 1/2)-2p(sub 3/2)in U(82+) through U(89+)
[DE95-010265] p 2993 N95-32042
Defect configurations in neutron-irradiated U3Si2
[DE95-009896] p 3016 N95-32105

URBAN DEVELOPMENT
Sustainability protects resources for future generations
[DE95-000285] p 2909 N95-31695

URBAN PLANNING
Sustainability protects resources for future generations
[DE95-000285] p 2909 N95-31695

URETHANES
Urethane foam process improvements
[DE95-008957] p 2815 N95-30798
A water blown urethane insulation for use in cryogenic environments p 2775 N95-31765

USER MANUALS (COMPUTER PROGRAMS)
Data management system: User's guide
[DE95-008692] p 3022 N95-30392
User's manual for the Scanning Fast Field Program (SCAFFIP) EOSAEL version 1.0
[AD-A291445] p 2933 N95-30397
MVP/GMVP: General purpose Monte Carlo codes for neutron and photon transport calculations based on continuous energy and multigroup methods
[DE95-722072] p 2979 N95-30656
SHEAT: A computer code for probabilistic seismic hazard analysis, user's manual
[DE95-717874] p 2913 N95-30758
Development of BERMUDA: A radiation transport code system. Part 3: A one-dimensional adjoint neutron transport code
[DE95-717875] p 2934 N95-30759
Neutron shielding point kernel integral calculation code for personal computer: PKN-pc
[DE95-717876] p 2980 N95-30760
RASSP benchmark 1 executable requirements user's manual
[AD-A290060] p 2935 N95-30931
QTSAW (Quick Typhoon Surge and Waves). Wave information studies of US coastlines
[AD-A293172] p 2919 N95-30976
Solid Modeling Aerospace Research Tool (SMART) user's guide, version 2.0
[NASA-TM-4431] p 2940 N95-31420
Synthetic Terrain Imagery for Helmet-Mounted Display. Volume 3: Software user's manual
[AD-A293613] p 2753 N95-31463
Network user's guide
[DE95-009185] p 2942 N95-31634
Penelope reference manual: Version 3-3 (C001). Includes Larch/Ada specification manual for sequential Ada (C002)
[AD-A289628] p 2942 N95-31683
PORK object system programmer's guide
[AD-A293596] p 2942 N95-31688
Operation of the computer model for direct atomic oxygen exposure of Earth satellites
[NASA-CR-198188] p 2767 N95-32189
FPCAS3D User's guide: A three dimensional full potential aeroelastic program, version 1
[NASA-CR-198367] p 2899 N95-32205
Computer model to simulate testing at the National Transonic Facility
[NASA-TM-4664] p 2763 N95-32217
BRUTUS: A program for conversion between image formats
[PB95-211421] p 2945 N95-32246
ASSIST user manual
[NASA-TM-4592] p 2948 N95-32250
Inversion of ERS-1 wavemode spectra. User's and programmer's guide
[PB95-223582] p 2902 N95-32316

USER REQUIREMENTS
RASSP benchmark 1 executable requirements user's manual
[AD-A290060] p 2935 N95-30931
An exploratory survey of information requirements for instrument approach charts
[AD-A293882] p 2749 N95-31520
Scalable ATM encryption
[DE95-009868] p 2948 N95-32065

V

V-22 AIRCRAFT
A case study of the teaming concept in the procurement of the V-22 aircraft
[AD-A293770] p 2752 N95-31578

V/STOL AIRCRAFT
Fabry-Perot interferometer measurement of static temperature and velocity for ASTOVL model tests
[NASA-TM-107014] p 2879 N95-30587

VACANCIES (CRYSTAL DEFECTS)
STM measurements of the interaction of vacancies and steps during low-energy-ion bombardment of Si(001)
[DE95-010935] p 3017 N95-32308

VACUUM
Two-loop vacuum amplitudes in a non-Abelian gauge theory on S(sub 4)
[DE95-616284] p 3018 N95-30436
X-band magnicon amplifier research at the Naval Research Laboratory
[AD-A293203] p 3013 N95-30984
Vacuum plume backflow and rarefaction p 2871 N95-30995

VACUUM CHAMBERS
Supplemental multilayer insulation research facility
[NASA-TM-106991] p 2768 N95-30595

VACUUM DEPOSITION
Development of germanium-silicon growth technology
[AD-A293199] p 3013 N95-30983

VACUUM EFFECTS
Instability of weak vacuum
[DE95-613590] p 2985 N95-31620

VACUUM SYSTEMS
Supplemental multilayer insulation research facility
[NASA-TM-106991] p 2768 N95-30595

VACUUM TESTS
Influence of strain rate and temperature on the mechanical behavior of iron aluminide-based alloys
[DE95-009426] p 2808 N95-31636

VALENCE
A valence-fluctuation mechanism with highly anisotropic S-wave pairing
[DE95-009419] p 3010 N95-30571

VALVES
Fast-acting valve for projective launching systems
[AD-D017357] p 2888 N95-30416

VANADIUM OXIDES
Low-voltage cathodoluminescence of europium-activated yttrium orthovanadate
[DE95-008536] p 3008 N95-30382

VANELESS DIFFUSERS
Laser anemometer measurements of the three-dimensional rotor flow field in the NASA low-speed centrifugal compressor
[NASA-TP-3527] p 2756 N95-31985

VAPOR DEPOSITION
Preparation of diisopropyl stibines and use thereof
[AD-D017419] p 2771 N95-30418
Electrochemical vapour deposition of SOFC interconnection materials
[PB95-197844] p 2812 N95-30459
Polarized Raman spectroscopy of chemically vapour deposited diamond films
[DE95-616776] p 2815 N95-30791
Development of germanium-silicon growth technology
[AD-A293199] p 3013 N95-30983
Synthesis and selected micro-mechanical properties of titanium nitride thin films by the pyrolysis of tetrakis titanium in ammonia
[DE95-010224] p 2818 N95-31187
X-ray diffraction study of clusters in a-tC films
[DE95-010860] p 2794 N95-31393
Self-lubricating, TiN-MoS2 composite coatings produced by simultaneous deposition from Ti((CH3))2N4/NH3/MoF6H2S gas mixture
[DE95-010359] p 2788 N95-31403
An analysis of gas phase ethanol/water chemistry for diamond CVD
[AD-A293009] p 2795 N95-31473
Silicon carbide-silicon heterostructure solar cells p 2905 N95-31952
Models of transport, gas-phase and surface chemistry in diamond chemical vapor deposition
[DE95-009861] p 2822 N95-32101
GCMS and FTIR studies of by-product inhibited growth and the rate-limiting step in TEOS-based SiO2 CVD
[DE95-009863] p 3016 N95-32147
Metallic multilayers at the nanoscale
[DE95-011534] p 3016 N95-32284
Optimal heat transfer design of chemical vapor deposition reactors
[DE95-010997] p 2878 N95-32309

VAPOR PHASES
State resolved dynamics of ion-molecule collisions in a flowing afterglow
[AD-A290895] p 2976 N95-30410
Modeling of thermal, electronic, hydrodynamic, and dynamic deposition processes for pulsed-laser deposition of thin films
[DE95-008906] p 2813 N95-30572
A study of gas-phase processes during the deflagration of RDX composite propellants using a triple quadrupole mass spectrometer p 2801 N95-31304
A study of the gas-phase processes of RDX combustion using a triple quadrupole mass-spectrometer p 2801 N95-31315
An analysis of gas phase ethanol/water chemistry for diamond CVD
[AD-A293009] p 2795 N95-31473
The physical and chemical processes governing CO2 laser-induced pyrolysis and combustion of the solid propellants RDX, ADN, XM39, and M43 p 2836 N95-31531
Effects of gas-phase thermal expansion on the stability of deflagration through a porous energetic material
[DE95-004382] p 2797 N95-31824
Models of transport, gas-phase and surface chemistry in diamond chemical vapor deposition
[DE95-009861] p 2822 N95-32101
GCMS and FTIR studies of by-product inhibited growth and the rate-limiting step in TEOS-based SiO2 CVD
[DE95-009863] p 3016 N95-32147

VAPOR PRESSURE
Replacement of ozone depleting and toxic chemicals in gravimetric analysis of non-volatile residue p 2780 N95-31793

VAPORS
The effect of gravity on the deposition of thin films: The physical vapor transport of copper phthalocyanine
[AD-A292997] p 2838 N95-31472

VARIABILITY
Luminance effects on visual acuity and small letter contrast sensitivity
[AD-A293310] p 2928 N95-31140
Voyager GO program
[NASA-CR-189435] p 3029 N95-31424
Measurements of ionospheric variability
[AD-A293495] p 2915 N95-31535

VARISTORS
Voltage surge suppression power circuits
[AD-D017454] p 2860 N95-30726

VECTOR ANALYSIS
Bifurcations of contracting singular cycles
[DE95-613371] p 2962 N95-32117

VECTOR MESONS
Applications of chiral symmetry
[DE95-009552] p 2988 N95-32079

VECTOR PROCESSING (COMPUTERS)
Cesar3 MALU library
[PB95-211363] p 2933 N95-30598
MVP/GMVP: General purpose Monte Carlo codes for neutron and photon transport calculations based on continuous energy and multigroup methods
[DE95-722072] p 2979 N95-30656

VECTOR SPACES
Co-groups on sequentially complete, locally convex, topological vector spaces in particular on strict LF-spaces
[PB95-206918] p 2966 N95-30681
Exact smooth classification of Hamiltonian vector fields on symplectic 2-manifolds
[DE95-613378] p 2958 N95-30803

VECTORS (MATHEMATICS)
Integrals of motion in the two Killing vector reduction of general relativity
[DE95-616281] p 3018 N95-30431

VEGETATION GROWTH
Application of shallow shell stability to plant morphogenesis by Fourier series p 2897 N95-31734

VEINS
Arterial gas bubbles after decompression in pigs with Patent Foramen Ovale
| PB95-195319 | p 2925 N95-30515
VELOCITY DISTRIBUTION
An experimental and numerical study on the structure and extinction of laminar premixed flames
p 2792 N95-30670
Effect of velocity and temperature distribution at the hole exit on film cooling of turbine blades
| NASA-TM-106954 | p 2755 N95-30702
Assessment of the NASA orbital debris engineering model
| AD-A293350 | p 2766 N95-31143
On the interactions between particles and turbulence in a fully-developed channel flow in air
p 2875 N95-31707
The effect of ray curvature on Lloyd's mirror fringe estimates and source localisation
| DSTO-TR-0064 | p 3001 N95-31745
Laser anemometer measurements of the three-dimensional rotor flow field in the NASA low-speed centrifugal compressor
| NASA-TP-3527 | p 2756 N95-31985
Objective analysis of oceanic data for Coast Guard trajectory models
| AD-A292884 | p 2924 N95-32363
VELOCITY MEASUREMENT
Fabry-Perot interferometer measurement of static temperature and velocity for ASTOVL model tests
| NASA-TM-107014 | p 2879 N95-30587
Laser anemometer measurements of the three-dimensional rotor flow field in the NASA low-speed centrifugal compressor
| NASA-TP-3527 | p 2756 N95-31985
Spatially-resolved velocity measurements in steady, high-speed, reacting flows using laser-induced OH fluorescence p 2877 N95-32109
VENEERS
Analysis of variation embedding tests with 17 MM dowel: Densified veneer wood FOREST project, part 7
| PB95-206876 | p 2963 N95-30680
VENTILATION
Demonstration of split-flow ventilation and recirculation as flow-reduction methods in an Air Force paint spray booth, volume 2
| AD-A286808 | p 2762 N95-30926
Demonstration of split-flow ventilation and recirculation as flow-reduction methods in an Air Force paint spray booth, volume 1
| AD-A286807 | p 2763 N95-31101
VERTICAL DISTRIBUTION
Vertical transport in GaAs/AlGaAs superlattices
p 3012 N95-30822
VERTICAL LANDING
Automatic flight control system for an unmanned helicopter system design and flight test results
p 2759 N95-32004
VERTICAL MOTION SIMULATORS
Moving base simulation of an integrated flight and propulsion control system for an ejector-augmentor STOVL aircraft in hover
| NASA-TM-108867 | p 2750 N95-30646
VERY HIGH FREQUENCIES
Investigation into the effects of VHF and UHF band radiation on Hewlett-Packard (HP) Cesium Beam Frequency Standards p 2970 N95-32332
VERY LARGE SCALE INTEGRATION
System considerations for efficient communication and storage of MSTI image data
| NASA-CR-198869 | p 3024 N95-30858
Decimation of encoding errors in an optimum SNS 2 micron low-noise CMOS ADC
| AD-A293208 | p 2860 N95-30900
Analog preprocessing in a SNS 2 micrometers low-noise CMOS folding ADC
| AD-A293356 | p 2849 N95-30954
VESTIBULES
Physiology and physiopathology of equilibration
| PB95-208328 | p 2926 N95-30494
VHSIC (CIRCUITS)
RASSP benchmark 1 executable requirements user's manual
| AD-A290060 | p 2935 N95-30931
VIBRATION
Low vibration polymeric composite engine
| AD-D017332 | p 2887 N95-30386
Vibration-damping structural component
| AD-D017376 | p 2784 N95-30661
Specific rate coefficients from vibrational overtone activation of 1-methylcyclopropene
| AD-A288755 | p 2793 N95-31014
VIBRATION DAMPING
Computerized design of controllers using data models
| NASA-CR-198921 | p 2950 N95-30655
Vibration-damping structural component
| AD-D017376 | p 2784 N95-30661
Minimizing structural vibrations with Input Shaping (TM)
| NASA-CR-189439 | p 2893 N95-30786
Control of flexible spacecraft structures using H-infinity wave absorbing control
| AD-A293141 | p 2766 N95-30919
Finite element analysis of damped vibrations of laminated composite plates
| ISBN-0-315-84928-2 | p 2789 N95-31731
Vibration control for precision manufacturing at Sandia National Laboratories
| DE95-009582 | p 2839 N95-32082
Vibration control of spacecrafts and space structures from lift-off to on-orbit environments
p 2767 N95-32110
Vibration reduction in helicopter rotors using an actively controlled partial span trailing edge flap located on the blade p 2762 N95-32111
VIBRATION ISOLATORS
Vibration isolation mount with locking means
| AD-D017367 | p 2888 N95-30532
Vibration control of spacecrafts and space structures from lift-off to on-orbit environments
p 2767 N95-32110
VIBRATION MODE
Advanced system identification techniques for wind turbine structures
| DE95-004049 | p 2902 N95-30505
Analytic and experimental investigation of rotordynamic response and backward whirl induced by split resonance
| AD-A293639 | p 2889 N95-31566
VIBRATION TESTS
Analytic and experimental investigation of rotordynamic response and backward whirl induced by split resonance
| AD-A293639 | p 2889 N95-31566
VIBRATIONAL SPECTRA
The theoretical calculation of vibrational circular dichroism spectra
| AD-A293614 | p 2798 N95-32258
VIBRATIONAL STATES
Flow models for the design of a hypersonic iodine vapor wind tunnel nozzle with chemical and vibrational nonequilibrium effects p 2742 N95-30448
Energy transfer dynamics in isolated and colliding highly vibrationally excited molecules
| AD-A293304 | p 2981 N95-30952
Comparison of DSMC predictions with temporally resolved vibrational state measurements in NO
p 2872 N95-30996
VIBRATORY LOADS
Vibration reduction in helicopter rotors using an actively controlled partial span trailing edge flap located on the blade p 2762 N95-32111
VIDEO COMMUNICATION
Multi-dimensional data compression for portable communication
| AD-A292751 | p 2850 N95-31426
VIDEO EQUIPMENT
Apparent size passive range method
| AD-D017360 | p 2753 N95-31180
VIDICONS
Video conferencing using DAVE user's guide
| DE95-010341 | p 2854 N95-32045
VIKING LANDER SPACECRAFT
Structural analyses of the JPL Mars Pathfinder impact
| DE95-009581 | p 2767 N95-32081
VIRTUAL PROPERTIES
Form factor of the process gamma(*) gamma(*) yields pi(sup 0) for small virtuality of one of the photons and QCD sum rules (2): Sum rule
| DE95-613629 | p 2988 N95-32078
VIRTUAL REALITY
Virtual Reality Software and Technology '94
| AD-A292334 | p 2939 N95-31262
Visual tracking of self-occluding articulated objects
| AD-A292894 | p 2928 N95-31383
Design and integration issues of visually-coupled evaluation
| AD-A293521 | p 2931 N95-31538
VISCOELASTIC DAMPING
Vibration-damping structural component
| AD-D017376 | p 2784 N95-30661
A finite element formulation for the time domain vibration analysis of an elastic-viscoelastic structure
p 2895 N95-31318
Finite element analysis of damped vibrations of laminated composite plates
| ISBN-0-315-84928-2 | p 2789 N95-31731
VISCOELASTICITY
A viscoelastic anisotropic wave propagation model for composite cure evaluation p 2786 N95-30839
A finite element formulation for the time domain vibration analysis of an elastic-viscoelastic structure
p 2895 N95-31318
Numerical simulation of time dependent viscoelastic fluid flow
| TRITA-NA-9311 | p 2873 N95-31414
Some aspects on the modelling of non-Newtonian fluid flow
| TRITA-NA-9317 | p 2873 N95-31415
Mode I large strain viscoelastic crack behavior in nitrile rubber sheets
| AD-A289984 | p 2820 N95-31617
Nonlinear dynamics and chaotic motions of a singularly perturbed nonlinear viscoelastic beam
p 2897 N95-31706
VISCOPLASTICITY
Predictions of tensile behavior and strengths of a Si3N4 ceramic at high temperatures based on a viscoplastic model
| DE95-010220 | p 2821 N95-32025
VISCOSITY
Small scale turbulence in a plane mixing layer
p 2866 N95-30449
A study of numerical solutions of conservation laws
| TRITA-NA-9315 | p 2960 N95-31361
Evaluation of Environmentally Acceptable hydraulic fluids
| AD-A293037 | p 2821 N95-31666
VISCOUS FLOW
Viscous diffusion of vorticity in unsteady wall layers using the diffusion velocity concept
| DE95-008537 | p 2866 N95-30383
A numerical study of the starting process in a hypersonic shock tunnel p 2762 N95-30493
Numerical study of shear-induced heating in high-speed nozzle flow of liquid monopropellant
p 2828 N95-31207
VISCOUS FLUIDS
Viscous heating of liquid layers under intense shear
p 2827 N95-31206
VISIBILITY
Visual tracking of self-occluding articulated objects
| AD-A292894 | p 2928 N95-31383
Initial evaluation of the Oregon State University planetary boundary layer column model for ITWS applications
| AD-A293775 | p 2920 N95-31465
Evaluation of alternative pavement marking materials
| AD-A292973 | p 2763 N95-31468
VISIBLE SPECTRUM
Ultraviolet and visible lasers: Rare earth-doped waveguide devices and non-linear optical extraction techniques
| AD-A293976 | p 2885 N95-31528
Cepheid temperature and the Blazhko effect
| NASA-CR-189433 | p 3030 N95-31819
VISION
Laser induced vitreoretinal scarring. Evaluation of causative factors and a therapeutic approach
| AD-A293742 | p 2928 N95-31570
VISUAL ACUITY
Luminance effects on visual acuity and small letter contrast sensitivity
| AD-A293310 | p 2928 N95-31140
VISUAL PERCEPTION
Design and integration issues of visually-coupled evaluation
| AD-A293521 | p 2931 N95-31538
VISUAL PIGMENTS
High speed random access, Fourier transform holographic associative and high density two-photon three-dimensional optical memories based on bacteriorhodopsin
| AD-A293389 | p 2931 N95-30967
VOLATILITY
Air pollution control system research: An iterative approach to developing affordable systems
p 2773 N95-31759
VOLCANOES
Properties of new materials relevant to energy and fuel research
| AD-A289734 | p 2825 N95-31149
VOLTMETERS
Development of a method for measurement of triboelectric charging
| PB95-211322 | p 2859 N95-30633
VOLUMETRIC ANALYSIS
Volumetric and electro analytical techniques for chemical characterization of nuclear grade Ag-In-Cd alloys
| DE95-620664 | p 2807 N95-31407
VON KARMAN EQUATION
Studies in non-linear multi-mode responses of harmonically excited rectangular plates with internal resonances p 2895 N95-31331
VORTEX BREAKDOWN
Numerical investigation into vortical flow about a delta-wing configuration up to incidences at which vortex breakdown occurs in experiment
| PB95-198024 | p 2743 N95-30837

VORTEX GENERATORS
A wind tunnel investigation of the effects of micro-vortex generators and Gurney flaps on the high-lift characteristics of a business jet wing
[NASA-TM-110626] p 2750 N95-30827
VORTEX SHEDDING
Validation of the helicopter rotor code HERO
[PB95-198040] p 2751 N95-30838
VORTICES
Advances in the simulation of toroidal gyro Landau fluid model turbulence
[DE95-008387] p 3003 N95-30359
Small scale turbulence in a plane mixing layer p 2866 N95-30449
A wind tunnel investigation of the effects of micro-vortex generators and Gurney flaps on the high-lift characteristics of a business jet wing
[NASA-TM-110626] p 2750 N95-30827
Navier-Stokes flow field analysis of compressible flow in a high pressure safety relief valve
[NASA-TM-110640] p 2868 N95-30862
Unsteady transonic wind tunnel test on a semispan straked delta wing, oscillating in pitch. Part 1: Description of the model, test setup, data acquisition, and data processing
[AD-A293113] p 2743 N95-30885
Large eddy simulation of jets using structured upwind numerics p 2871 N95-30993
A pulsed liquid fuel ramjet p 2756 N95-31201
Dynamics of Current Driven Disordered Josephson Junction Arrays
[DE95-009418] p 3014 N95-31231
Stability prediction with rotational flow effects p 2799 N95-31283
Inductively coupled IR staring array based on photofluxonic pixels
[AD-A292784] p 2998 N95-31435
Initial evaluation of the Oregon State University planetary boundary layer column model for ITWS applications
[AD-A293775] p 2920 N95-31465
Application of multigrid computational fluid dynamics (CFD) methods to rotor analysis
[AD-A293012] p 2874 N95-31475
Large-eddy simulation of turbulent flow using the finite element method
[DE95-009464] p 2875 N95-31591
The study of flame-vortex interactions using a particle image velocimeter p 2796 N95-31709
Experimental and computational investigation of the tip clearance flow in a transonic axial compressor rotor
[NASA-TM-106711] p 2876 N95-31738
Flight evaluation of forebody vortex control in post-stall flight p 2752 N95-32003
VORTICITY
Viscous diffusion of vorticity in unsteady wall layers using the diffusion velocity concept
[DE95-008537] p 2866 N95-30383
Velocity boundary conditions for vorticity formulations of the incompressible Navier-Stokes equations
[DE95-008715] p 2868 N95-30464
Hot jet/wake turbulent structure and laser propagaion. Part 1: Jet/wake turbulence modeling p 2871 N95-30991
Stability prediction with rotational flow effects p 2799 N95-31283
Vorticity dynamics and control of dynamic stall
[AD-A288658] p 2756 N95-31400
VOWELS
Automation of the control of acoustic parameters in a digital speech synthesizer
[IFTR-2/1995] p 2850 N95-31357
The contextual variance of devoiced fricatives in polish
[IFTR-7/1995] p 2854 N95-32192
VOYAGER PROJECT
Voyager GO program
[NASA-CR-189435] p 3029 N95-31424
VOYAGER 1 SPACECRAFT
Determination of the position of Jupiter from radio metric tracking of Voyager 1 p 2854 N95-32222
VULNERABILITY
Recommendations for protecting National Library of Medicine Computing and Networking Resources
[DE95-011554] p 3026 N95-32285

W

WAFERS
Photovoltaic Czochralski silicon manufacturing technology improvements
[DE95-004066] p 2904 N95-31162
WAKES
Role of free-surface boundary conditions and nonlinearities in wave/boundary-layer and wake interaction p 2872 N95-31317
Initial evaluation of the Oregon State University planetary boundary layer column model for ITWS applications
[AD-A293775] p 2920 N95-31465
Space systems environmental interaction studies
[AD-A293826] p 2766 N95-31553
WALL FLOW
An experimental study of planar heterogeneous supersonic confined jets
[AD-A290859] p 2867 N95-30557
A turbulence model for steady and unsteady boundary layers in strong pressure gradients p 2868 N95-30840
Shear-free turbulent boundary layers p 2873 N95-31349
Experimental and computational investigation of the tip clearance flow in a transonic axial compressor rotor
[NASA-TM-106711] p 2876 N95-31738
WALL PRESSURE
Application of wavelet-filtering techniques to intermittent turbulent and wall pressure events. Part 2. Detection of cluster patterns
[AD-A293805] p 2875 N95-31586
WALL TEMPERATURE
Numerical study of shear-induced heating in high-speed nozzle flow of liquid monopropellant p 2828 N95-31207
WALLS
Viscous diffusion of vorticity in unsteady wall layers using the diffusion velocity concept
[DE95-008537] p 2866 N95-30383
The HYLIFE-2 inertial fusion energy power plant concept and implications for IFE
[DE95-010561] p 2994 N95-32074
WARFARE
Study of Extended Air Defence Post 2000 p 2839 N95-32124
Possible allied ballistic missile defense systems: Related guidance and control requirements p 2840 N95-32126
Design of surveillance and multisensor anti-aerial systems p 2841 N95-32134
Using a Red Team to devise countermeasures p 2842 N95-32141
WARNING SYSTEMS
Time aspects of the European Complement to GPS: Continental and transatlantic experimental phases p 2969 N95-32328
WASHERS (CLEANERS)
Aqueous cleaning and verification processes for precision cleaning of small parts p 2779 N95-31787
WASTE DISPOSAL
Producing usable fuel from municipal solid waste
[DE95-008405] p 2902 N95-30375
Environmental projects. Volume 16: Waste minimization assessment
[NASA-CR-198861] p 2909 N95-31651
Manufacturing waste disposal practices of the chemical propulsion industry p 2771 N95-31748
Enhanced alkaline hydrolysis and biodegradability studies of nitrocellulose-bearing missile propellant p 2772 N95-31752
LLW solidification in cement: Effect of dilution
[DE95-010108] p 2798 N95-32091
WASTE ENERGY UTILIZATION
Publications of the Fossil Energy Advanced Research and Technology Development Materials Program: April 1, 1993-March 31, 1995
[DE95-009200] p 2903 N95-30745
WASTE TREATMENT
Environmental projects. Volume 16: Waste minimization assessment
[NASA-CR-198861] p 2909 N95-31651
Technology transfer into the solid propulsion industry p 2770 N95-31756
Treatment of plastic media waste p 2844 N95-32177
Bioremediation of wheat starch media waste p 2845 N95-32178
Waste minimization via preparative scale high performance gel permeation chromatography
[DE95-011797] p 2798 N95-32360
WASTE UTILIZATION
Producing usable fuel from municipal solid waste
[DE95-008405] p 2902 N95-30375
WASTE WATER
Aqueous TiO2 photocatalysis of metal-EDTA complexes
[DE95-011058] p 2793 N95-31113
WATER
On-line surfactant monitoring
[DE95-009417] p 2792 N95-30735
Field performance of the Walker Branch throughfall displacement experiment
[DE95-008677] p 2908 N95-30793
The impact of microbiologically influenced corrosion on protective polymer coatings
[AD-A268896] p 2816 N95-30997
The oxidation of carbon monoxide by nitrogen dioxide p 2801 N95-31310
Study of melting and freezing processes of water for application to ice thermal energy storage system p 2905 N95-31735
A water blown urethane insulation for use in cryogenic environments p 2775 N95-31765
Waterjet processes for coating removal p 2777 N95-31779
Ultra-high pressure water jetting for coating removal and surface preparation p 2778 N95-31780
Evaluation of pressurized water cleaning systems for hardware refurbishment p 2778 N95-31782
Faster, cheaper radioanalytical methods
[DE95-009913] p 2797 N95-32061
Water blasting paint removal methods p 2843 N95-32170
WATER COLOR
SeaWiFS Technical Report Series. Volume 29: SeaWiFS CZCS-type pigment algorithm
[NASA-TM-104566] p 2922 N95-30857
SeaWiFS technical report series. Volume 13: Case studies for SeaWiFS calibration and validation, part 1
[NASA-TM-104566-VOL-13] p 2924 N95-32220
WATER FLOW
Spatial time-series: Pollution pattern recognition under irregular interventions
[AD-A293830] p 2909 N95-31556
WATER MANAGEMENT
Geostatistics and hydrology. Part 3. Hydro-meteorological network design
[PB95-206462] p 2900 N95-30818
Geostatistics and hydrology. Part 1: Spatial and temporal variability. Communications of the Sanitary Engineering and Water Management Division
[PB95-206470] p 2900 N95-30819
WATER POLLUTION
Spatial time-series: Pollution pattern recognition under irregular interventions
[AD-A293830] p 2909 N95-31556
WATER RESOURCES
Geostatistics and hydrology. Part 3. Hydro-meteorological network design
[PB95-206462] p 2900 N95-30818
WATER RUNOFF
Multiparameter radar measurements of precipitation in complex terrain: Meteorological and hydrological applications
[AD-A290786] p 2918 N95-30403
WATER TREATMENT
Aqueous TiO2 photocatalysis of metal-EDTA complexes
[DE95-011058] p 2793 N95-31113
Water blasting paint removal methods p 2843 N95-32170
WATER TUNNEL TESTS
Study of effect of bubbles on a free-shear layer p 2872 N95-31100
An investigation of the side-dump dual in-line ramjet combustor p 2756 N95-31199
WATER VAPOR
The oxidation of carbon monoxide by nitrous oxide p 2801 N95-31309
Brightness temperature simulations for the physical and synoptic interpretation of advanced microwave sounding unit moisture channels p 2921 N95-31721
Feasibility of tropospheric water vapor profiling using infrared heterodyne differential absorption lidar
[DE95-009647] p 2917 N95-32142
WATER WAVES
The determination of wave group parameters from the resolution of incident and reflected waves
[AD-A293703] p 2924 N95-31829
WATERSHEDS
Field performance of the Walker Branch throughfall displacement experiment
[DE95-008677] p 2908 N95-30793
WATERWAVE ENERGY CONVERSION
Production simulator for wave power plants
[PB95-212262] p 2907 N95-32286
WAVE AMPLIFICATION
Aspects of the magnetospheric amplification phenomenon in ducted whistler-mode waves p 2916 N95-31718
WAVE ATTENUATION
Point reflector model for the simulation of radar target glint and Doppler phenomena
[PB95-222980] p 2857 N95-32314
WAVE DEGRADATION
Degradation in finite-harmonic subcarrier demodulation p 2855 N95-32228
WAVE DIFFRACTION
Reflection and diffraction of atomic de Broglie waves by evanescent laser waves. Bare-state method
[DE95-616458] p 2992 N95-30960

WAVE EQUATIONS
Introduction to the theory of Goyaks: Operator manifold approach to geometry and particle physics
[DE95-613460] p 2980 N95-30740
Calculated coupling efficiency between an elliptical-core optical fiber and an optical waveguide over temperature
[NASA-TM-107005] p 2997 N95-30849
Fast multipole methods for scattering computations
[AD-A291093] p 2848 N95-30869
A study of numerical solutions of conservation laws
[TRITA-NA-9315] p 2960 N95-31361
WAVE EXCITATION
Generation of earthquake signals
[PB95-211223] p 2913 N95-30631
Effects of temperature, frequency, flux density, and excitation waveform on the core loss and dynamic B-H loops of supermalloy
[NASA-TM-106982] p 2865 N95-32207
WAVE FRONTS
Wavefront simulator for evaluating RF communication array signal processors
[AD-D017372] p 2847 N95-30660
WAVE FUNCTIONS
The interaction of magnetizations with an external electromagnetic field and a time-dependent magnetic Aharonov-Bohm effect
[DE95-613463] p 2845 N95-30368
Quantum dynamics in regions of quaternionic curvature
[DE95-616276] p 3018 N95-30426
Schwinger-boson studies of the single hole motion in a 2D quantum antiferromagnet
[DE95-614444] p 3016 N95-32071
WAVE GENERATION
Gravitational waves from inspiralling compact binaries: Energy loss and waveform to second-post-Newtonian order
[PB95-207890] p 2913 N95-30590
WAVE INTERACTION
Modeling and parameterization of gravity wave breaking, interactions, and instability processes in the lower and middle atmosphere
[AD-A292740] p 2914 N95-31278
Role of free-surface boundary conditions and nonlinearities in wave/boundary-layer and wake interaction p 2872 N95-31317
Space systems environmental interaction studies
[AD-A293826] p 2766 N95-31553
WAVE PACKETS
Instability of weakly nonlinear chaotic structures
[DE95-613441] p 2966 N95-32066
WAVE PROPAGATION
Interferometry with particles of non-zero rest mass: Topological experiments
[DE95-616244] p 2979 N95-30689
Propagation and scattering of elastic waves in laminated circular cylinders
[ISBN-0-315-85957-1] p 2848 N95-30828
A viscoelastic anisotropic wave propagation model for composite cure evaluation p 2786 N95-30839
Wave propagation in a fluid-loaded homogeneous, transversely isotropic, elastic cylinder of arbitrary thickness
[AD-A292728] p 2869 N95-30946
Direct and inverse problems in random media
[AD-A293033] p 2850 N95-31280
Numerical studies of nonlinear optical pulse propagation p 2998 N95-31411
Response of dual-layered structures subjected to shock pressure wave
[AD-A293731] p 2896 N95-31568
The effects of large and small scale turbulence on sound propagation in the atmosphere
[AD-A293657] p 2975 N95-31608
WAVE REFLECTION
On reflection of Alfven waves in the solar wind
[NASA-TM-110642] p 3031 N95-30582
Reflection and diffraction of atomic de Broglie waves by evanescent laser waves. Bare-state method
[DE95-616458] p 2992 N95-30960
Plane wave reflection from a uniaxial chiral quarter-wave polarization transformer
[PB95-206512] p 2849 N95-31159
Reflection and transmission of electromagnetic plane waves from a uniaxial chiro-omega slab
[PB95-206629] p 2853 N95-31649
Materials with controllable signature properties
[PB95-222964] p 2857 N95-32313
WAVE SCATTERING
Propagation and scattering of elastic waves in laminated circular cylinders
[ISBN-0-315-85957-1] p 2848 N95-30828
WAVE-PARTICLE INTERACTIONS
Perpendicular electron heating by absorption of auroral kilometric radiation
[NASA-198815] p 2914 N95-30848
Aspects of the magnetospheric amplification phenomenon in ducted whistler-mode waves p 2916 N95-31718
WAVEFORMS
Gravitational waves from inspiralling compact binaries: Energy loss and waveform to second-post-Newtonian order
[PB95-207890] p 2913 N95-30590
Statistical interface for chaotic signal in noise
[AD-A290271] p 2848 N95-30932
Seismic studies of subducted lithosphere p 2915 N95-31335
Effects of temperature, frequency, flux density, and excitation waveform on the core loss and dynamic B-H loops of supermalloy
[NASA-TM-106982] p 2865 N95-32207
WAVEGUIDE ANTENNAS
DSS-24 microwave holography measurements p 2857 N95-32239
Fiber optic reference frequency distribution to remote beam waveguide antennas p 2972 N95-32346
WAVEGUIDES
Fractional delay waveguide modeling of acoustic tubes
[PB95-206637] p 2975 N95-31650
WAVELET ANALYSIS
Potential integral equations of the 2D Laplace operator in wavelet basis
[TRITA-NA-9401] p 2957 N95-30713
Fast algorithms for three-dimensional inverse scattering problems
[AD-A293510] p 2852 N95-31537
Application of wavelet-filtering techniques to intermittent turbulent and wall pressure events. Part 2. Detection of cluster patterns
[AD-A293805] p 2875 N95-31586
WEAK INTERACTIONS (FIELD THEORY)
Dynamical analogy of Cabibbo-Kobayashi-Maskawa matrices
[DE95-613462] p 2975 N95-30367
New tensor interaction and the K(sub L) - K(sub S)mass difference
[DE95-613597] p 2845 N95-30370
Introduction to the theory of Goyaks: Operator manifold approach to geometry and particle physics
[DE95-613460] p 2980 N95-30740
Study of the generalized solutions of n-body type problems with weak forces
[DE95-613381] p 2958 N95-30820
Renormcharges in V-A theories
[DE95-613689] p 2985 N95-31622
WEAPON SYSTEMS
Major weapon system environmental life-cycle cost estimating for Conservation, Cleanup, Compliance and Pollution Prevention (C3P2) p 2774 N95-31761
Vibration control for precision manufacturing at Sandia National Laboratories
[DE95-009582] p 2839 N95-32082
SOSIE: A pragmatic approach to the simulation of Broad Air Defense applied to the theater level p 2840 N95-32127
TMD detection and tracking using improved AWACS sensors p 2840 N95-32128
Infrared and millimeter wave detection using thin films of Pb doped BiSrCaCuO superconductor p 2840 N95-32129
Acquisition, tracking, pointing and fire control for Ballistic Missile Defense p 2841 N95-32131
The High Altitude Balloon Experiment demonstration of acquisition, tracking, and pointing technologies (HABE-ATP) p 2841 N95-32132
Design of surveillance and multisensor anti-aerial systems p 2841 N95-32134
Architecture and implementation of a multi-sensor data fusion demonstration model within the real-time combat system of the Canadian Patrol Frigate p 2842 N95-32139
WEAPONS DELIVERY
Improved altimeter settings for A-10 aircraft
[AD-A293142] p 2753 N95-30920
WEAPONS DEVELOPMENT
A case study of the teaming concept in the procurement of the V-22 aircraft
[AD-A293770] p 2752 N95-31578
Report to the Chairman, Legislation and National Security Subcommittee, Committee on Government Operations, House of Representatives. Unmanned aerial vehicles: Performance of short-range system still in question
[GAO/NSIAD-94-65] p 2752 N95-32196
WEAR
Composite structure forming a wear surface
[AD-D017462] p 2785 N95-30749
WEAR RESISTANCE
Structural investigation of xenon ion-beam-irradiated glassy carbon
[DE95-616777] p 2977 N95-30474
Brush seal shaft wear resistant coatings
[NASA-CR-198950] p 2889 N95-31382
Evaluation of Environmentally Acceptable hydraulic fluids
[AD-A293037] p 2821 N95-31666
WEAR TESTS
Brush seal shaft wear resistant coatings
[NASA-CR-198950] p 2889 N95-31382
WEATHER
Initial evaluation of the Oregon State University planetary boundary layer column model for ITWS applications
[AD-A293775] p 2920 N95-31465
WEATHER FORECASTING
Weather influence on passive microwave brightness temperatures
[PB95-195384] p 2900 N95-30536
Forecast of Atlantic seasonal hurricane activity for 1994 p 2918 N95-30832
Summary of 1993 Atlantic tropical cyclone activity and verification of author's forecast. A year of unanticipated light hurricane activity and a poor forecast: The expected dissipation of the El Nino did not take place and Caribbean basin surface pressure became quite high p 2918 N95-30842
Early August updated forecast of Atlantic seasonal hurricane activity for 1994 p 2919 N95-30844
Offshore next generation weather radar (NEXRAD) OT&E integration and OT&E operational test
[AD-A293223] p 2848 N95-30902
Clouds: Their prediction and simulation
[AD-A292864] p 2920 N95-31453
Integrated terminal weather system (ITWS) demonstration and validation operational test and evaluation
[AD-A293932] p 2749 N95-31521
WEATHER STATIONS
The ATC operational evaluation of the prototype integrated terminal weather system (ITWS) at Dallas/Fort Worth and Orlando airports (May-September 1993)
[AD-A293808] p 2921 N95-31587
WEIBULL DENSITY FUNCTIONS
A new goodness-of-fit test for the gamma distribution based on sample spacings from complete and censored samples
[AD-A293875] p 2961 N95-31518
A Stochastic EM algorithm for approximating the maximum likelihood estimate
[DE95-010328] p 2943 N95-32044
WEIGHTING FUNCTIONS
Metafitting: Weight optimization for least-squares fitting of PTTI data p 2971 N95-32340
WELD TESTS
Advanced small rocket chambers. Option 3: 110 1bf Ir-Re rocket, volume 1
[NASA-CR-195435-VOL-1] p 2768 N95-31169
WELDED JOINTS
Stress and strain concentration factors of welded multiplanar joints between square hollow sections
[PB95-208260] p 2892 N95-30492
Fatigue behaviour of multiplanar tubular joints
[PB95-207874] p 2893 N95-30586
Evaluation on materials performance of Hastelloy Alloy XR for HTTR uses. 4: Tensile properties of base metals and welded joints
[DE95-721871] p 2804 N95-30761
WELDED STRUCTURES
Residual stress distribution in FeAl weld overlay on steel
[DE95-009178] p 2899 N95-32317
WELDING
Coupling stud assembly
[AD-D017335] p 2887 N95-30387
Fatigue behaviour of multiplanar tubular joints
[PB95-207874] p 2893 N95-30586
Residual stresses and stress corrosion cracking in pipe fittings
[DE95-009332] p 2894 N95-31054
Welding isotopic heat sources for the cassini mission to Saturn
[DE95-060104] p 2890 N95-32367
WENTZEL-KRAMER-BRILLOUIN METHOD
On reflection of Alfven waves in the solar wind
[NASA-TM-110642] p 3031 N95-30582
WETTABILITY
Wettability of boron carbide
[PB95-196358] p 2802 N95-30518
WHEAT
Dry media blasting with wheat starch p 2843 N95-32169
Bioremediation of wheat starch media waste p 2845 N95-32178

WHISKER COMPOSITES
Whisker reinforced glass ceramic
[DE95-010542] p 2823 N95-32305
WHISTLERS
Aspects of the magnetospheric amplification phenomenon in ducted whistler-mode waves
p 2916 N95-31718
WHITE LIGHT HOLOGRAPHY
A real time method for Fourier transform holographic information storage
[AD-A293186] p 2880 N95-30980
WHITE NOISE
Generation of earthquake signals
[PB95-211223] p 2913 N95-30631
Automatic Target Recognition (ATR): Background statistics and the detection of targets in clutter
[AD-A293062] p 2853 N95-31673
Rate considerations in deep space telemetry
p 2765 N95-32223
WIND (METEOROLOGY)
Development of a novel wind lidar, phase 1
[AD-A292703] p 2849 N95-30935
Global Ultraviolet Imager (GUVI) investigation
[NASA-CR-189430] p 2917 N95-31820
Simulation of katabatic flow and mountain waves
[DE95-010863] p 2911 N95-32276
WIND EFFECTS
Advanced system identification techniques for wind turbine structures
[DE95-004049] p 2902 N95-30505
WIND MEASUREMENT
Development of a novel wind lidar, phase 1
[AD-A292703] p 2849 N95-30935
LAWS hurricane studies
[NASA-CR-189438] p 2919 N95-31128
Mexico Wind Resource Assessment Project
[DE95-009202] p 2921 N95-31726
WIND SHEAR
Terminal doppler weather radar (TDWR) build 5B operational test and evaluation (OT&E) integration and OT&E operational test plan
[AD-A293251] p 2848 N95-30910
WIND TUNNEL APPARATUS
Flow quality improvements in the NASA Lewis Research Center 9- by 15-foot Low Speed Wind Tunnel
[NASA-CR-195439] p 2763 N95-31653
WIND TUNNEL CALIBRATION
Flow quality improvements in the NASA Lewis Research Center 9- by 15-foot Low Speed Wind Tunnel
[NASA-CR-195439] p 2763 N95-31653
WIND TUNNEL MODELS
A laser-based ice shape profilometer for use in icing wind tunnels
[NASA-TM-106936] p 2880 N95-30851
WIND TUNNEL NOZZLES
Flow models for the design of a hypersonic iodine vapor wind tunnel nozzle with chemical and vibrational nonequilibrium effects p 2742 N95-30448
WIND TUNNEL TESTS
Small scale turbulence in a plane mixing layer
p 2866 N95-30449
An experimental study of planar heterogeneous supersonic confined jets
[AD-A290859] p 2867 N95-30557
Fabry-Perot interferometer measurement of static temperature and velocity for ASTOVL model tests
[NASA-TM-107014] p 2879 N95-30587
Axial loads on yawed rotors
[PB95-214193] p 2742 N95-30638
Transonic aerodynamic characteristics of a proposed wing-body reusable launch vehicle concept
[NASA-TM-108489] p 2742 N95-30712
A wind tunnel investigation of the effects of micro-vortex generators and Gurney flaps on the high-lift characteristics of a business jet wing
[NASA-TM-110626] p 2750 N95-30827
A laser-based ice shape profilometer for use in icing wind tunnels
[NASA-TM-106936] p 2880 N95-30851
Unsteady transonic wind tunnel test on a semispan straked delta wing, oscillating in pitch. Part 1: Description of the model, test setup, data acquisition, and data processing
[AD-A293113] p 2743 N95-30885
Hypervelocity wind tunnel number 9, high Mach number development program
[AD-A289934] p 2743 N95-30929
Hot jet/wake turbulent structure and laser propagation. Part 3: Laser propagation measurements and modeling
p 2871 N95-30992
Afterbody/nozzle pressure distributions of a twin-tail twin-engine fighter with axisymmetric nozzles at Mach numbers from 0.6 to 1.2
[NASA-TP-3509] p 2744 N95-31984
Control of unsteady separated flow associated with the dynamic stall of airfoils
[NASA-CR-198972] p 2744 N95-32193
Computer model to simulate testing at the National Transonic Facility
[NASA-TM-4664] p 2763 N95-32217
WIND TUNNELS
Patterns in the sky: Natural visualization of aircraft flow fields
[NASA-SP-514] p 2741 N95-31000
WIND TURBINES
Advanced system identification techniques for wind turbine structures
[DE95-004049] p 2902 N95-30505
Axial loads on yawed rotors
[PB95-214193] p 2742 N95-30638
Acceleration potential models PREDICHAT/PREDICDYN applied for calculation of axisymmetric dynamic inflow cases
[PB95-207015] p 2869 N95-30957
Digital simulation of wind velocities for wind turbine rotors: General considerations
[PB95-206447] p 2904 N95-31157
Mexico Wind Resource Assessment Project
[DE95-009202] p 2921 N95-31726
WIND VELOCITY
Development of a novel wind lidar, phase 1
[AD-A292703] p 2849 N95-30935
Digital simulation of wind velocities for wind turbine rotors: General considerations
[PB95-206447] p 2904 N95-31157
Validation of special sensor microwave/imager ocean surface wind retrievals in equatorial regions
[AD-A293750] p 2920 N95-31571
Arabian Sea mixed layer dynamics experiment: Mooring deployment cruise report
[AD-A293684] p 2923 N95-31600
WIND VELOCITY MEASUREMENT
Investigation of microwave backscatter from the air-sea interface
[NASA-CR-198854] p 2851 N95-31457
Validation of special sensor microwave/imager ocean surface wind retrievals in equatorial regions
[AD-A293750] p 2920 N95-31571
WINDING
A time stepping coupled finite element-state space modeling environment for synchronous machine performance and design analysis in the ABC frame of reference p 2864 N95-31948
WINDPOWER UTILIZATION
Data on development of new energy technologies
[DE95-764135] p 2904 N95-31155
Mexico Wind Resource Assessment Project
[DE95-009202] p 2921 N95-31726
Outlook for renewable energy technologies: Assessment of international programs and policies
[DE95-009084] p 2907 N95-32302
WING FLAPS
A wind tunnel investigation of the effects of micro-vortex generators and Gurney flaps on the high-lift characteristics of a business jet wing
[NASA-TM-110626] p 2750 N95-30827
WING LOADING
Unsteady transonic wind tunnel test on a semispan straked delta wing, oscillating in pitch. Part 1: Description of the model, test setup, data acquisition, and data processing
[AD-A293113] p 2743 N95-30885
WING OSCILLATIONS
Unsteady transonic wind tunnel test on a semispan straked delta wing, oscillating in pitch. Part 1: Description of the model, test setup, data acquisition, and data processing
[AD-A293113] p 2743 N95-30885
WINGS
Development of stitched/RTM primary structures for transport aircraft
[NASA-CR-191441] p 2789 N95-31421
Performance improvement of composite wings through aeroelastic tailoring and modern control
[AD-A293689] p 2752 N95-31602
A probabilistic design method applied to smart composite structures
[NASA-TM-106715] p 2899 N95-32206
WIRE
High-temperature superconducting current leads
[DE95-008404] p 2858 N95-30374
Smart material joint band
[AD-D017374] p 2888 N95-30716
Hydrostatic extrusion of BSCCO/Ag composite wire
[DE95-007862] p 2805 N95-31121
WIRELESS COMMUNICATION
Multi-dimensional data compression for portable communication
[AD-A292751] p 2850 N95-31426
WOOD
Overview of IEA biomass combustion activities
[PB95-196374] p 2902 N95-30519
Analysis of variation embedding tests with 17 MM dowel: Densified veneer wood FOREST project, part 7
[PB95-206876] p 2963 N95-30680
WOODEN STRUCTURES
Influence of adhesives and bonding techniques on the properties of glued timber-steelplate joints
[PB95-211470] p 2813 N95-30599
WORK-REST CYCLE
Forward rapid rotation shiftwork in USAF air traffic controllers: Sleep, activity, fatigue and mood analyses
[AD-A293448] p 2927 N95-31373
WORKING FLUIDS
CFC-replacement by natural working fluids: R&D and industrial challenges within the refrigeration, air conditioning amd heat pump areas
[PB95-195756] p 2815 N95-30871
WORKSTATIONS
An overview of high-speed networking for workstations
[DE95-009076] p 2947 N95-30577
Synthetic Terrain Imagery for Helmet-Mounted Display. Volume 2: Software design document
[AD-A293611] p 2753 N95-31655
Integration issues in modular mission management aid development p 2841 N95-32133
WOVEN COMPOSITES
Post-impact fatigue of cross-plied, through-the-thickness reinforced carbon/epoxy composites
[NASA-TM-110625] p 2896 N95-31419
A study of elevated temperature testing techniques for the fatigue behavior of PMCS: Application to T650-35/AMB21 .
[NASA-TM-106927] p 2791 N95-32209
WRIST
Precision manipulation with a dextrous robot hand
p 2888 N95-30829

X

X RAY ANALYSIS
An investigation of a novel approach to elemental imaging in three dimensions
[DE95-010340] p 3000 N95-31681
Silicon carbide-silicon heterostructure solar cells
p 2905 N95-31952
X RAY ASTRONOMY
Integrated X-ray testing of the electro-optical breadboard model for the XMM reflection grating spectrometer
[DE95-008829] p 2879 N95-30507
X RAY BINARIES
Observations of accreting pulsars
[NASA-CR-198931] p 3028 N95-30469
X RAY DIFFRACTION
Acoustoelastic stress evaluation in metal plate using absolute shear and longitudinal time-of-flight data
[PB95-197810] p 2892 N95-30458
Diffraction-line broadening analysis and stress relaxation in thin metal layers
[PB95-213898] p 2893 N95-30634
Polarisation resonance in X-ray diffraction
[DE95-616727] p 3012 N95-30789
Residual stresses and stress corrosion cracking in pipe fittings
[DE95-009332] p 2894 N95-31054
X-ray diffraction study of clusters in a-tC films
[DE95-010860] p 2794 N95-31393
In situ composites in the aluminum nitride-alumina system
[AD-A293776] p 2789 N95-31509
Annual meeting of the Advanced Light Source Users' Association
[DE95-009373] p 3000 N95-31635
A study of switching behavior in Pb(Zr,Ti)O3 thin films using x-ray diffraction
[DE95-010859] p 2808 N95-31689
X RAY FLUORESCENCE
Annual meeting of the Advanced Light Source Users' Association
[DE95-009373] p 3000 N95-31635
An investigation of a novel approach to elemental imaging in three dimensions
[DE95-010340] p 3000 N95-31681
X RAY LASERS
Quantum and nonlinear optics research
[AD-A293879] p 2999 N95-31519
Diagnosing high density, fast-evolving plasmas using x-ray lasers
[DE95-010734] p 3006 N95-32028
Enhanced brightness x-ray lasers
[DE95-010735] p 2886 N95-32029

X RAY OPTICS
X-ray standing wave interferometry-optics at 1 angstrom with applications to surface and material sciences
| DE95-011453 | p 2998 N95-31114
Quantum and nonlinear optics research
| AD-A293879 | p 2999 N95-31519
X RAY SOURCES
X-ray performance of the engineering prototype Stellar x-ray polarimeter
| DE95-010268 | p 3028 N95-31129
X RAY SPECTRA
Observations of accreting pulsars
| NASA-CR-198931 | p 3028 N95-30469
X RAY SPECTROSCOPY
Integrated X-ray testing of the electro-optical breadboard model for the XMM reflection grating spectrometer
| DE95-008829 | p 2879 N95-30507
Ionic conductivities of lithium phosphorus oxynitride glasses, polycrystals, and thin films
| DE95-008898 | p 2812 N95-30545
Applications of SXPS for studying surface structure, reaction mechanisms and kinetics
| DE95-008903 | p 2803 N95-30547
Development of plasma diagnostics technologies: A study on nuclear fusion reactor
| DE95-614180 | p 3005 N95-31004
The structure and reactivity of boron and carbon surfaces
| AD-A292804 | p 2795 N95-31440
Annual meeting of the Advanced Light Source Users' Association
| DE95-009373 | p 3000 N95-31635
X RAY TELESCOPES
Operating in the space plasma environment: A spacecraft charging study of the Solar X-ray Imager
| NASA-TM-110644 | p 3003 N95-30468
X RAYS
Integrated X-ray testing of the electro-optical breadboard model for the XMM reflection grating spectrometer
| DE95-008829 | p 2879 N95-30507
Ionic conductivities of lithium phosphorus oxynitride glasses, polycrystals, and thin films
| DE95-008898 | p 2812 N95-30545
Physics and application of high density Z-pinches
| NIFS-PROC-14 | p 3004 N95-30671
Studying the thermal/non-thermal crossover in solar flares
| NASA-CR-189436 | p 3031 N95-30785
X-band magnicon amplifier research at the Naval Research Laboratory
| AD-A293203 | p 3013 N95-30984
X-ray performance of the engineering prototype Stellar x-ray polarimeter
| DE95-010268 | p 3028 N95-31129
Effects of mosaicity on Parametric X-Radiation production
| AD-A293677 | p 2985 N95-31597
An investigation of a novel approach to elemental imaging in three dimensions
| DE95-010340 | p 3000 N95-31681
Enhanced brightness x-ray lasers
| DE95-010735 | p 2886 N95-32029
High-resolution superconducting x-ray spectrometers with aluminum trapping layers of different thicknesses
| DE95-010253 | p 2881 N95-32047
X WING ROTORS
Vibration reduction in helicopter rotors using an actively controlled partial span trailing edge flap located on the blade p 2762 N95-32111
X-29 AIRCRAFT
X-29 flight control system: Lessons learned p 2759 N95-32001
Flight evaluation of forebody vortex control in post-stall flight p 2752 N95-32003
X-31 AIRCRAFT
X-31: A program overview and flight test status p 2753 N95-32013

Y

YAG LASERS
Spotsize measurements of a focused CW Nd: YAG laser
| DE95-007746 | p 2884 N95-31139
Optical frequency standards: Hertz-level working standards and their absolute frequency measurement
| AD-A293930 | p 2999 N95-31515
Femtosecond, Cr(4+):YAG laser
| DE95-004964 | p 2887 N95-32155
Stripping by laser p 2844 N95-32174
YANG-MILLS FIELDS
Local solutions of harmonical and bi-harmonical equations, universal field equation and self-dual configurations of Yang-Mills fields in four dimensions
| DE95-620521 | p 2966 N95-31379
YANG-MILLS THEORY
Local solutions of harmonical and bi-harmonical equations, universal field equation and self-dual configurations of Yang-Mills fields in four dimensions
| DE95-620521 | p 2966 N95-31379
YAW
Axial loads on yawed rotors
| PB95-214193 | p 2742 N95-30638
YBCO SUPERCONDUCTORS
Low temperature synthesis of YBa2Cu3O(8-x) and other crystalline oxides
| AD-D017370 | p 3009 N95-30533
Phase transformations in melt-spun Y-Ba-Cu-O bulk superconductor
| DE95-010237 | p 3011 N95-30667
Space qualified hybrid superconductor/semiconductor planar oscillator circuit
| NASA-TM-106978 | p 3011 N95-30703
Investigations of YBaCuO materials with near-room-temperature resistivity transitions
| AD-A293405 | p 3013 N95-31008
Solution based temperature of Perovskite-type oxide films and powders
| DE95-009089 | p 2820 N95-31629
High performance YBCO films
| AD-A293045 | p 2863 N95-31669
YIELD POINT
New material for high average power infrared generation: QPM-DB GaAs
| AD-A292714 | p 2967 N95-30939
Amorphization and the effect of implanted ions in SiC
| DE95-009699 | p 2985 N95-31642
YIELD STRENGTH
Observations of star fracture and longitudinal splitting in BIS 812 EMA and Q1N submarine construction steels
| DSTO-RR-0014 | p 2806 N95-31344
YLF LASERS
A 1.94 micrometer laser apparatus, system and method using a thulium-doped yttrium-lithium-fluoride laser crystal pumped with a diode laser
| AD-D017435 | p 2884 N95-31213
YTTERBIUM
Laser properties of Yb(3+)-doped Sr5(PO4)3F crystals
| DE95-010686 | p 3016 N95-32268
YTTRIA-STABILIZED ZIRCONIA
Electrochemical vapour deposition of SOFC interconnection materials
| PB95-197844 | p 2812 N95-30459
The effect of interface properties on nickel base alloy composites
| NASA-CR-198363 | p 2785 N95-30787
YTTRIUM
Low-voltage cathodoluminescence of europium-activated yttrium orthovanadate
| DE95-008536 | p 3008 N95-30382
An experimental search for high ZT semiconductors: A survey of the preparation and properties of several alloy systems
| DE95-010232 | p 2865 N95-32084

Z

ZEOLITES
The Wide Field/Planetary Camera 2 (WFPC-2) molecular adsorber
| NASA-CR-198866 | p 2881 N95-31456
Composite polymer electrolyte for lithium batteries
| AD-A293924 | p 2820 N95-31514
ZETA PINCH
Physics and application of high density Z-pinches
| NIFS-PROC-14 | p 3004 N95-30671
Basic science with pulsed power and some off-the-wall ideas
| DE95-009486 | p 2854 N95-32050
ZINC
Luminescence properties of ZnWO4:Cr(3+) laser crystals
| AD-A293065 | p 2887 N95-32152
ZINC ALLOYS
Metallurgical and Materials Transactions
| AD-A293617 | p 2807 N95-31464
Cadmium plating replacements p 2776 N95-31773
Processing and microstructural evolution of alumina/aluminum alloy and aluminum nitride/aluminum alloy composites by directed melt oxidation p 2789 N95-31973
ZINC SELENIDES
Investigation of polycrystalline thin film CuInSe2 solar cells based on ZnSe windows
| DE95-004068 | p 2904 N95-31164
ZINC SULFIDES
Glass matrix doped with activated luminescent nanocrystalline particles
| AD-D017416 | p 2816 N95-31010
Germanate glass ceramic
| AD-D017418 | p 2816 N95-31011
On the Jahn-Teller effect of Mn(2+) in zinc-blende ZnS crystal
| AD-A293711 | p 2797 N95-31830
ZIRCALOYS (TRADEMARK)
Neutronic methods for determination of very low concentrations of hydrogen in metals
| DE95-623967 | p 2807 N95-31409
ZIRCONIUM ALLOYS
A proposed phase equilibrium diagram for Pt-Zr system
| DE95-620904 | p 2806 N95-31220
ZIRCONIUM CARBIDES
A metallurgical approach toward alloying in rare earth permanent magnet systems
| DE95-010242 | p 2966 N95-30668
ZIRCONIUM OXIDES
Dielectric property measurement of zirconia fibers at high temperatures
| DE95-010991 | p 2821 N95-31705
ZONAL FLOW (METEOROLOGY)
Calculation of a residual mean meridional circulation for a zonal-mean tracer transport model
| DE95-009474 | p 2911 N95-32350

Typical Personal Author Index Listing

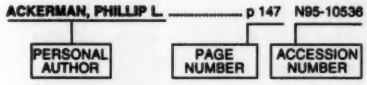

Listings in this index are arranged alphabetically by personal author. The page number helps you locate the citation in the abstract section. The accession number denotes the number by which the citation is identified.

A

AALTO, S. ..... p 3029 N95-30569
AAMOLD, K. ..... p 2934 N95-30663
AARTS, H. ..... p 2879 N95-30507
ABBASCHIAN, REZA ..... p 2786 N95-30866
p 2786 N95-30867
p 2786 N95-30898
ABBATE, A. ..... p 2863 N95-31725
ABBOTT, RONALD T. ..... p 2894 N95-31007
ABDEL-WAHAB, HUSSEIN ..... p 2932 N95-32046
ABE, KIYOHARU ..... p 2913 N95-30758
ABE, TETSUYA ..... p 3007 N95-32264
ABERNATHY, C. R. ..... p 2806 N95-31150
ACKER, JAMES G. ..... p 2924 N95-31850
ADAMS, DANIEL E. ..... p 2771 N95-31748
ADAMS, GEORGE F. ..... p 2831 N95-31293
ADAN, I. J. B. F. ..... p 2949 N95-30400
p 2950 N95-30462
p 2950 N95-30808
ADJEPONG, S. K. ..... p 3011 N95-30736
ADOLPHSEN, C. ..... p 2993 N95-31256
ADUMITROAIE, V. ..... p 2878 N95-32219
AFANASEV, G. N. ..... p 2845 N95-30368
AFONENKO, A. A. ..... p 2883 N95-30609
AGARWALA, VINOD S. ..... p 2803 N95-30551
AGGARWAL, ISHWAR D. ..... p 2816 N95-31011
AGGARWAL, R. ..... p 2931 N95-31130
AHARRAH, RALPH ..... p 2745 N95-31063
AHMED, R. ..... p 2893 N95-30613
AHRENS, L. A. ..... p 2987 N95-32032
AIKEN, JAMES ..... p 2922 N95-30857
AILEY, K. S. ..... p 3015 N95-32018
AJAYI, O. O. ..... p 2813 N95-30621
AJIMURA, S. ..... p 2882 N95-32159
AKGERMAN, A. ..... p 2792 N95-30709
AKLONIS, JOHN J. ..... p 2819 N95-31410
AKPATI, ANTHONY U. ..... p 2777 N95-31777
AKSELSEN, O. M. ..... p 2802 N95-30518
p 2813 N95-30664
ALDSTADT, J. H. ..... p 2797 N95-32061
ALEM, NABIH ..... p 2864 N95-31842
ALFANO, R. R. ..... p 2906 N95-32212
ALI, M. ..... p 2791 N95-30420
ALLAN, DAVID W. ..... p 2970 N95-32335
ALLEN, GALE J. ..... p 2779 N95-31787
ALLEN, L. J. ..... p 2978 N95-30583
p 2980 N95-30790
p 2981 N95-30916
ALLEN, M. T. ..... p 2801 N95-31309
ALLES, W. ..... p 2759 N95-32004
ALLOTEY, F. K. A. ..... p 3011 N95-30736
ALLSUP, GEOFFREY P. ..... p 2923 N95-31600
ALLWINE, DAN ..... p 2950 N95-30655
ALM, I. ..... p 2945 N95-32248
ALTMAN, B. S. ..... p 2967 N95-31625
ALUMBAUGH, D. L. ..... p 2900 N95-30363
ALVARADO, J. S. ..... p 2797 N95-32061
AMALDI, EDOARDO ..... p 2961 N95-31648
AMES, FORREST E. ..... p 2874 N95-31423
AMES, GREGORY H. ..... p 2996 N95-30529
AMIDEI, D. ..... p 2992 N95-31165
AMIS, ERIC J. ..... p 2819 N95-31410
AMOS, K. ..... p 2976 N95-30429
p 2977 N95-30447
p 2978 N95-30583
p 2982 N95-31176
AMPO, YOKO ..... p 2938 N95-31247
AMSDEN, A. A. ..... p 2931 N95-31130
AMUDA, R. ..... p 3013 N95-30959
ANABTAWI, A. ..... p 2765 N95-32225
ANANIKIAN, N. S. ..... p 3011 N95-30722
ANDERSEN, J. N. ..... p 2802 N95-30534
ANDERSON, ALLAN H. ..... p 2935 N95-30931
ANDERSON, DANA Z. ..... p 2881 N95-31385
ANDERSON, DAVID M. ..... p 2772 N95-31750
ANDERSON, GAIL P. ..... p 2915 N95-31575
p 2916 N95-31604
ANDERSON, I. M. ..... p 2803 N95-30733
ANDERSON, R. ..... p 3018 N95-30424
ANDERSON, W. R ..... p 2801 N95-31312
ANDERSON, W. R. ..... p 2801 N95-31313
ANDIARTI, R. ..... p 2950 N95-30564
p 2950 N95-30807
ANDLEIGH, V. K. ..... p 2805 N95-31107
ANDREWS, HAROLD G., II ..... p 3000 N95-31697
ANG, J. A. ..... p 3027 N95-30385
ANGELL, T. S. ..... p 2849 N95-30962
ANGELO, J. E. ..... p 3010 N95-30576
ANTIPIN, D. V. ..... p 2987 N95-32053
AOKI, K. ..... p 2882 N95-32159
APPONI, A. J. ..... p 3029 N95-30751
AREFEV, A. S. ..... p 2983 N95-31260
ARENDALE, W. A. ..... p 2781 N95-31801
ARGE, E. ..... p 2962 N95-32256
ARIAS, D. E. ..... p 2806 N95-31220
ARKLEY, LARRY E. ..... p 2752 N95-31579
ARNOLD, A. ..... p 2949 N95-32371
ARNOLD, G. S. ..... p 2780 N95-31793
ARNOLD, PAUL G. ..... p 2946 N95-32289
ARNONE, ROBERT A. ..... p 2935 N95-30968
ARNZEN, S. ..... p 2879 N95-30600
ARO, M. ..... p 2858 N95-30538
ARRIGO, KEVIN ..... p 2924 N95-31850
ARRIGO, KEVIN R. ..... p 2924 N95-32220
ARRINGTON, E. ALLEN ..... p 2763 N95-31653
ASANOV, R. A. ..... p 3020 N95-32295
ASHVAR, C. S. ..... p 2798 N95-32258
ASKAR, SABRINA ..... p 2863 N95-31611
ASKINS, CHARLES G. ..... p 2998 N95-31270
ASLAM, M. ..... p 3012 N95-30847
ATAMANIUK, B. ..... p 2960 N95-31337
ATHAVALE, M. M. ..... p 2867 N95-30710
ATTAR, MOSHE ..... p 2758 N95-31994
ATWATER, TERRILL ..... p 2863 N95-31607
AU, G. ..... p 2964 N95-30428
AUKRUST, T. ..... p 2979 N95-30666
AUVERMANN, HARRY J. ..... p 2975 N95-31608
AUVINE, B. A. ..... p 2908 N95-30686
AVDEEV, L. V. ..... p 2964 N95-30369
AVENGER, DONALD V. ..... p 2789 N95-31469
AYDEMIR, AHMET ..... p 3004 N95-30794
AYDIN, KULTEGIN ..... p 2918 N95-30403
AYER, J. ..... p 2762 N95-30926
p 2763 N95-31101
AYISTOCK, F. ..... p 2953 N95-31562
AYLSTOCK, F. ..... p 2860 N95-30886
AZAD, HASSAN ..... p 2962 N95-32068
AZGUI, F. ..... p 2881 N95-32047

B

BA, B. ..... p 2903 N95-30723
BAART, DOUGLAS ..... p 2748 N95-31013
BABICH, A. A. ..... p 2984 N95-31547
BABIN, GILBERT ..... p 3025 N95-31348
BABU, G. R. V. ..... p 2780 N95-31791
BACKUS, C. E. ..... p 2905 N95-31381
BAE, Y. W. ..... p 2818 N95-31187
p 2788 N95-31403
BAECKSTROEM, M. ..... p 2847 N95-30629
BAGOT, KEITH W. ..... p 2763 N95-31468
BAILEY, J. E. ..... p 3006 N95-31626
BAILLIE, STEWART W. ..... p 2761 N95-32015
BAIN, D. B. ..... p 2755 N95-30698
BAKER, D. R. ..... p 3003 N95-30612
BAKER, G. A., JR. ..... p 2980 N95-30705
BAKHAREV, T. ..... p 2798 N95-32091
BAKHLE, MILIND A. ..... p 2899 N95-32205
BALKUS, K. J., JR. ..... p 2822 N95-32075
BALLATO, ARTHUR ..... p 3015 N95-31539
BALLESTER, G. ..... p 3030 N95-30806
BALMFORTH, N. J. ..... p 2868 N95-30763
BALTAS, N. ..... p 2877 N95-32033
BANDARU, R. V. ..... p 2791 N95-30541
BANDIN, NORBERTO ..... p 2807 N95-31407
BANE, K. L. F. ..... p 2993 N95-31256
BANG, HA HUY ..... p 2963 N95-30610
BANKS, DARWYN O. ..... p 2952 N95-31517
BAO, Z. ..... p 2854 N95-32114
BARANI, G. ..... p 2841 N95-32130
BARBEE, T. W., JR. ..... p 3006 N95-32028
BARBER, T. E. ..... p 2782 N95-31803
BARENGOLTZ, JACK ..... p 2881 N95-31456
BARESI, LARRY ..... p 2780 N95-31791
BARFKNECHT, A. T. ..... p 2881 N95-32047
BARGER, V. ..... p 2979 N95-30695
p 2994 N95-32059
BARIBEAU, J. M. ..... p 2804 N95-30797
BARIC, A. ..... p 3009 N95-30485
BARIL, C. G. ..... p 2888 N95-30701
BARKER, ROBERT J. ..... p 2861 N95-30979
BARNES, MICHAEL D. ..... p 2798 N95-32086
BARNETT, DONALD M. ..... p 2778 N95-31785
BARRETT, DAVID J. ..... p 2784 N95-30661
BARRON, C. C. ..... p 2878 N95-30384
BARTHOLOMEW, DAVID L. ..... p 2958 N95-30754
BARTLETT, C. S. ..... p 2747 N95-31667
BARTON, DANIEL L. ..... p 2863 N95-31611
BARTRAM, MICHAEL E. ..... p 3016 N95-32147
BASARAN, OSMAN A. ..... p 2815 N95-30799
BASILI, V. R. ..... p 2936 N95-31236
BASILI, VICTOR R. ..... p 2937 N95-31237
BASSIR, A. ..... p 3012 N95-30958
BATEMAN, J. E. ..... p 2880 N95-30691
BATES, BRUCE J. ..... p 2974 N95-30549
BATES, J. B. ..... p 2812 N95-30545
BATES, SUSAN M. ..... p 2974 N95-30549
BATUNIN, A. V. ..... p 2982 N95-31215
BAUCH, A. ..... p 2858 N95-32320
BAUER, JEFFREY E. ..... p 2759 N95-32001
BAUM, CHRISTOPHER C. ..... p 2952 N95-31161
BAUMANN, ERIC D. ..... p 2864 N95-31742
BAUMGARDNER, J. R. ..... p 2931 N95-31130
BAUMONT, FRANCOISE S. ..... p 2858 N95-32320
p 2971 N95-32338
BEACH, R. ..... p 3016 N95-32268
BEARD, RONALD L. ..... p 2887 N95-32347
BEASLEY, M. R. ..... p 2795 N95-31439
BEATRICE, KENNETH J. ..... p 2888 N95-30414
BEAUQUIER, J. ..... p 2949 N95-32371
BEAVIS, D. ..... p 2986 N95-31702
BECKER, C. H. ..... p 2881 N95-31694
BECKER, J. ..... p 2760 N95-32006
BECKER, JOANN F. ..... p 2779 N95-31788
BECKSTEAD, M. W. ..... p 2799 N95-31196
p 2800 N95-31287
p 2800 N95-31292
BECKSTEAD, MERRILL W. ..... p 2799 N95-30990
BEGIN, F. ..... p 2842 N95-32139
BEHEIM, GLENN ..... p 2997 N95-30849
BEHL, WISHVENDER K. ..... p 2905 N95-31554
BEIDAR, K. I. ..... p 2960 N95-31229
p 2961 N95-31397
BEIERSDORFER, P. ..... p 2982 N95-31174
p 2987 N95-32041
p 2993 N95-32042
BELLUATI, PIER LUIGI ..... p 2760 N95-32009
BELONGIE, M. ..... p 2765 N95-32223
p 2855 N95-32230
BELUE, LISA M. ..... p 2949 N95-30406
BEMENT, LAURENCE J. ..... p 2766 N95-31358
BENCH, M. W. ..... p 3016 N95-32103
BENJAFFEL, L. ..... p 3030 N95-30806

BENJAMIN, A. S. ..... p 2967 N95-31625
BENNANI, S. ..... p 2758 N95-31995
BENNETT, ROBERT R. ..... p 2771 N95-31747
p 2773 N95-31754
BENTLEY, J. ..... p 2803 N95-30733
BENYOUSSEF, A. ..... p 3012 N95-30958
BERDING, M. A., SR. ..... p 2998 N95-31141
BEREZHNOJ, A. V. ..... p 2983 N95-31216
BERG, C. ..... p 2802 N95-30534
BERGE, P. ..... p 2809 N95-32023
BERGENE, E. ..... p 3009 N95-30535
BERGER, M. S. ..... p 2994 N95-32059
BERGEY, JOHN ..... p 2943 N95-31834
BERGSTEN, L. ..... p 2859 N95-30596
BERGSTROM, ROBERT W. ..... p 2921 N95-32184
BERHOW, TODD J. ..... p 2839 N95-31122
BERKENBOSCH, A. C. ..... p 2868 N95-30811
BERLINER, MARILYN J. ..... p 2869 N95-30946
BERNSTEIN, DENNIS S. ..... p 2952 N95-30961
BERNSTEIN, L. ..... p 2799 N95-31211
BERRY, ALOK K. ..... p 2862 N95-31343
BERTEAUX, SUSAN S. ..... p 2923 N95-30918
BESHTOEV, KH. M. ..... p 2975 N95-30367
p 2985 N95-31622
BESMANN, T. M. ..... p 2818 N95-31187
p 2788 N95-31403
BEZDELKIN, V. V. ..... p 3013 N95-30969
BEZRUKOV, L. B. ..... p 2983 N95-31260
BHALLA, C. P. ..... p 2989 N95-32120
p 2990 N95-32275
BHANG, H. ..... p 2882 N95-32159
BHASIN, K. B. ..... p 3011 N95-30703
BHASKARAN, S. ..... p 2765 N95-32226
BHATT, R. T. ..... p 2790 N95-32060
BIALASIEWICZ, J. T. ..... p 2902 N95-30505
BIANCHINI, RICARDO ..... p 2947 N95-30930
BICKER, C. J. ..... p 2800 N95-31288
BIERWAGEN, G. ..... p 2810 N95-32241
BIFFLE, J. H. ..... p 2934 N95-30796
BILAL, R. ..... p 2791 N95-30420
BILDSTEN, LARS ..... p 3028 N95-30469
BILLEN, JAMES H. ..... p 2992 N95-31151
BILLUPS, W. E. ..... p 3012 N95-30944
BINER, S. B. ..... p 2897 N95-32024
BINGERT, JOHN F. ..... p 2805 N95-31121
BINGHAM, BARRY L. ..... p 2805 N95-31121
BIONDO, S. J. ..... p 2952 N95-31255
BIRGE, ROBERT R. ..... p 2931 N95-30967
BIRINGEN, SEDAT ..... p 2872 N95-31341
BIRKS, T. A. ..... p 2999 N95-31529
BIRNBAUM, LAWERENCE ..... p 2949 N95-30395
BIRTCHER, R. C. ..... p 3016 N95-32105
BISHOP, ALAN R. ..... p 3014 N95-31231
BISHOP, CHRIS ..... p 2857 N95-32259
BISHOP, WALTON B. ..... p 2847 N95-30746
BISMUT, J. M. ..... p 2965 N95-30489
BISOI, AJAY KUMAR ..... p 2962 N95-32095
BISWAS, R. ..... p 3015 N95-32037
BITSAKIS, NICHOLAS ..... p 2888 N95-30416
BIXLER, J. V. ..... p 2879 N95-30507
BJORDAL, H. ..... p 2933 N95-30598
BLAAUW, M. ..... p 2979 N95-30639
BLACK, J. H. ..... p 3029 N95-30569
BLAIR, D. ..... p 2781 N95-31802
BLAIR, DAVID W. ..... p 2800 N95-31300
BLAIR, S. C. ..... p 2898 N95-32102
BLAKIEWICZ, M. ..... p 2987 N95-32032
BLANCHARD, R. C. ..... p 2891 N95-30783
BLANCHET, L. ..... p 2912 N95-30588
p 2913 N95-30590
BLASCHKE, D. ..... p 2980 N95-30911
BLATT, PAUL ANDREW ..... p 2784 N95-30491
BLAU, P. J. ..... p 2818 N95-31187
p 2788 N95-31403
BLAYLOCK, MICHAEL A. ..... p 2961 N95-31557
BLEIWEISS, MAX P. ..... p 2916 N95-31589
BLEVINS, ELANA ..... p 2775 N95-31765
BLOMSHIELD, FRED S. ..... p 2770 N95-30989
p 2770 N95-31197
p 2800 N95-31288
BLONK, B. ..... p 2922 N95-30457
BLOO, R. ..... p 2966 N95-30719
BLOOM, D. M. ..... p 3015 N95-32037
BLOOMFIELD, DAVID P. ..... p 2860 N95-30940
p 2889 N95-31374
BLOOMFIELD, VALERIE J. ..... p 2860 N95-30940
BOBROWSKI, SOPHIE J. ..... p 2815 N95-30799
BODELL, J. ..... p 2963 N95-31396
BODSON, MARC ..... p 2756 N95-30937
BOERJESSON, A. ..... p 2859 N95-30633
BOERSCHLEIN, DAVID P. ..... p 2948 N95-32250
BOERSMA, P. ..... p 2933 N95-30454
BOGETTI, TRAVIS A. ..... p 2787 N95-30963
BOILY, E. ..... p 2842 N95-32139
BOKHARI, SHAHID H. ..... p 2932 N95-31988
BOLAND, DILLARD E. ..... p 2938 N95-31245
BOLSHAKOV, A. ..... p 2812 N95-30548
BOLSTAD, G. ..... p 2925 N95-30512
BOOTH, R. S. ..... p 3029 N95-30569
BOOTH, T. E. ..... p 2960 N95-31253
BOOTHE, RICHARD E. ..... p 2781 N95-31798
BOOZE, JON A. ..... p 2981 N95-30952
BOPARAI, AMRIT S. ..... p 2798 N95-32360
BORG, A. ..... p 2802 N95-30534
p 3009 N95-30535
BORGSTAHL, RON ..... p 2937 N95-31239
BORSACK, JULIE ..... p 3026 N95-32149
BOSGRA, O. H. ..... p 2758 N95-31995
BOSNYAK, C. P. ..... p 2820 N95-31471
BOSSCHERS, J. ..... p 2751 N95-30838
BOSTAK, J. ..... p 3015 N95-32037
BOSWORTH, JOHN T. ..... p 2759 N95-32001
BOTTKA, NICHOLAS ..... p 2862 N95-31343
BOULANGER, J.-S. ..... p 2971 N95-32340
BOURASSA, R. J. ..... p 2767 N95-32189
BOURGAIN, J. ..... p 2956 N95-30506
p 2957 N95-30624
BOUWER, GERD ..... p 2758 N95-32000
BOUWKAMP, C. J. ..... p 2954 N95-30401
BOYD, JOHN ..... p 2941 N95-31630
BOYER, ERICEFAN T. ..... p 2800 N95-31296
BOYLE, T. J. ..... p 2811 N95-30362
BRACHER, B. H. ..... p 2880 N95-30693
BRADFORD, DANIEL J. ..... p 2772 N95-31753
BRADLEY, BART D. ..... p 2854 N95-32145
BRADLEY, MARTY KEITH ..... p 2742 N95-30448
BRADSHAW, R. W. ..... p 2905 N95-31640
BRAENNLUND, U. ..... p 2934 N95-30792
BRAGIN, S. I. ..... p 3009 N95-30419
BRANAGAN, DANIEL JAMES ..... p 2966 N95-30668
BRAND, SAM ..... p 2747 N95-31454
BRANDOW, B. H. ..... p 3010 N95-30571
BRANDSMA, F. J. ..... p 2743 N95-30837
BRANKOWSKI, J. ..... p 3009 N95-30419
BRANSTETTER, LINDA J. ..... p 2907 N95-32302
BRASEK, THOMAS P. ..... p 2896 N95-31568
BRASKI, D. N. ..... p 2788 N95-31403
BRATKOVSKAYA, E. L. ..... p 2988 N95-32093
BRAUNINGER, H. ..... p 2879 N95-30507
BREAKIRON, LEE A. ..... p 2971 N95-32342
BREHM, P. ..... p 2817 N95-31135
p 2817 N95-31136
BREIDENTHAL, JULIAN C. ..... p 2858 N95-32334
BRENGELMANN, GEORGE L. ..... p 2926 N95-30563
BRENNAN, JOHN ..... p 2783 N95-30433
BREWSTER, M. Q. ..... p 2799 N95-31284
p 2800 N95-31285
p 2800 N95-31286
p 2800 N95-31298
BRIAND, L. C. ..... p 2936 N95-31236
BRIAND, LIONEL ..... p 2937 N95-31237
BRIGUGLIO, EMANUEL ..... p 2846 N95-30417
BRILL, THOMAS B. ..... p 2800 N95-31297
BRINKKEMPER, S. ..... p 3022 N95-30453
p 2838 N95-30455
BRINKMAN, A. C. ..... p 2879 N95-30507
BRINKMAN, R. ..... p 2821 N95-32025
BRINZA, DAVID E. ..... p 2796 N95-31660
BROO, ANDERS ..... p 2985 N95-31609
p 2986 N95-31832
BROOKS, K. G. ..... p 3009 N95-30421
p 2811 N95-30422
BROUGH, A. R. ..... p 2798 N95-32091
BROWN, A. E. ..... p 2795 N95-31593
BROWN, BRUCE ..... p 2985 N95-31616
BROWN, C. W. ..... p 2940 N95-31404
BROWN, DAVID A. ..... p 2879 N95-30658
BROWN, G. V. ..... p 2864 N95-31847
BROWN, J. J., JR. ..... p 2823 N95-32305
BROWN, JAMES W. ..... p 2924 N95-31850
BROWN, JERRY A. ..... p 2775 N95-31769
BROWN, LINCOLN D. ..... p 2914 N95-31012
BROWN, ROBERT A. ..... p 3028 N95-31364
BROWNING, N. D. ..... p 3010 N95-30544
BRUBAKER, J. ..... p 2814 N95-30765
BRUBAKK, A. O. ..... p 2926 N95-30511
p 2925 N95-30512
p 2926 N95-30513
p 2925 N95-30515
p 2925 N95-30665
BRUCE, M. H. ..... p 2998 N95-31192
BRUCH, VICKI L. ..... p 2907 N95-32302
BRUCKNER, A. P. ..... p 2799 N95-31204
BRUEMMER, STEPHEN M. ..... p 2809 N95-32052
BRUMBY, S. P. ..... p 3018 N95-30424
p 3018 N95-30426
BRUNET, M. ..... p 2969 N95-32328
BRYSON, J. W. ..... p 2898 N95-32157
BUCHELNIKOVA, N. S. ..... p 3007 N95-32056
BUCHHEIT, R. G. ..... p 2810 N95-32241
BUCHHOLZ, JOERG J. ..... p 2746 N95-31068
BUCHOLTZ, FRANK ..... p 2996 N95-30753
BUCKINGHAM, WILLIAM M. ..... p 2985 N95-31597
BUCKLES, W. E. ..... p 2861 N95-30943
BUCKLEY, EDWARD ..... p 2930 N95-31399
BUDAI, J. D. ..... p 3009 N95-30542
p 2978 N95-30546
BUESCHER, KEVIN L. ..... p 2952 N95-31161
BUGAJSKI, DAN ..... p 2758 N95-31996
BUI, T. X. ..... p 2809 N95-32104
BUKUR, D. B. ..... p 2792 N95-30709
BULET, BRIAN ..... p 2946 N95-32291
BUNTE, STEVEN W. ..... p 2801 N95-31308
BURCH, I. A. ..... p 2806 N95-31344
BURDEN, H. ..... p 2799 N95-31205
BURGDOERFER, JOACHIM ..... p 2984 N95-31402
BURGESS, FLETCHER ..... p 2777 N95-31779
BURKE, CHRISTOPHER S. ..... p 2791 N95-32209
BURKEN, JOHN J. ..... p 2759 N95-32001
BURKERT, W. ..... p 2879 N95-30507
BURKETT, K. ..... p 2992 N95-31165
BURKHART, SCOTT C. ..... p 2865 N95-32300
BURKOW, T. M. ..... p 2964 N95-30565
BURNS, H. DEWITT ..... p 2781 N95-31797
BURNS, J. A. ..... p 2751 N95-31451
BURNS, JOHN A. ..... p 2960 N95-31319
BURNS, W. K. ..... p 2862 N95-31179
BURRELL, K. H. ..... p 3004 N95-30685
p 3007 N95-32116
BURSILL, L. A. ..... p 3009 N95-30421
p 2811 N95-30422
p 2820 N95-31623
BURTON, D. E. ..... p 2955 N95-30470
BURTON, DONALD E. ..... p 2955 N95-30471
BURTON, LAWRENCE W. ..... p 2764 N95-30948
BUSALACCHI, ANTONIO J. ..... p 2919 N95-31123
BUSBY, MICHAEL R. ..... p 3028 N95-30466
BUTCHER, A. G. ..... p 2800 N95-31294
BYER, ROBERT L. ..... p 2967 N95-30939
BYHEDEN, S. ..... p 2859 N95-30633
BYRUM, K. ..... p 2992 N95-31165

C

CADENE, M. ..... p 2813 N95-30645
CAHILL, PATRICIA ..... p 2860 N95-30922
CAI, TIEQUAN ..... p 2880 N95-30980
CAIMI, RAOUL E. B. ..... p 2782 N95-31805
CAIN, JAMES ..... p 2939 N95-31250
CAIN, R. L. ..... p 2812 N95-30543
CALDWELL, B. D. ..... p 2759 N95-32005
CALHOUN, MALCOLM ..... p 2972 N95-32346
CALLAHAN, JOHN ..... p 2938 N95-31243
CALM, JAMES M. ..... p 2816 N95-31057
CALVERT, JEFFREY M. ..... p 2803 N95-30750
CALVERT, PAUL D. ..... p 2819 N95-31395
CALVERT, THOMAS C. ..... p 2766 N95-31388
CALZETTA, OSVALDO ..... p 2940 N95-31408
CAMERON, CHARLES B. ..... p 2995 N95-30402
CAMPARO, JAMES C. ..... p 2970 N95-32336
CAMPBELL, DAVID H. ..... p 2872 N95-30996
CAMPBELL, JAMES F. ..... p 2741 N95-31000
CAMPBELL, RALPH L. ..... p 2770 N95-31756
CANNON, FRED S. ..... p 2773 N95-31759
CANT, A. ..... p 2936 N95-31228
CANTALLOUBE, H. ..... p 2841 N95-32134
CANTON, L. ..... p 2976 N95-30429
CAPPS, C. D. ..... p 2861 N95-31133
CARLSON, A. L. ..... p 3006 N95-31626
CARLSON, BRAD A. ..... p 2782 N95-31809
CARLSON, DONALD ..... p 2852 N95-31551
CARLSON, PAUL T. ..... p 2903 N95-30745
CARPENTER, D. A. ..... p 2823 N95-32352
CARR, RICHARD D. ..... p 2849 N95-30954
CARROLL, A. ..... p 2986 N95-31702
CARROLL, J. J. ..... p 2886 N95-31563
CARROLL, THOMAS L. ..... p 2860 N95-30748
CARSON, RICHARD F. ..... p 3001 N95-32064
CARSWELL, JAMES R. ..... p 2851 N95-31457
CARTER, MICHAEL T. ..... p 2984 N95-31427
p 2795 N95-31437
CARTER, SUSAN V. ..... p 2901 N95-31390
CASARELLA, MARIO J. ..... p 2875 N95-31586
CATANESE, FABRIZIO ..... p 2956 N95-30608
CAUBLE, R. ..... p 3006 N95-32028
CAUBLE, R. C. ..... p 2886 N95-32029
CAVESTRI, R. C. ..... p 2911 N95-32364
CAVICCHIA, M. A. ..... p 2906 N95-32212
CAYLOR, M. ..... p 2841 N95-32132
CEDERQUIST, JACK N. ..... p 2846 N95-30562
CELESTINA, MARK L. ..... p 2876 N95-31738
CELLIERS, P. ..... p 3006 N95-32028
CHA, Y. S. ..... p 2861 N95-30943
CHABALOWSKI, C. F. ..... p 2798 N95-32258
CHABALOWSKI, CARY F. ..... p 2831 N95-31293
p 2801 N95-31308
CHACHULSKI, ANDRZEJ ..... p 2993 N95-31336
p 2986 N95-31818

CHADSEY, HAROLD ..... p 2971 N95-32341
CHADWICK, JAMES L. ..... p 2798 N95-32318
CHAI, B. H.T. ..... p 3016 N95-32268
CHAIT, ARNON ..... p 2837 N95-31359
CHAKOUMAKOS, B. C. ..... p 2812 N95-30545
CHAKRABARTY, DEEPTO ..... p 3028 N95-30469
CHAKRAVARTI, S. ..... p 2982 N95-31060
CHALK, CHARLES R. ..... p 2746 N95-31072
CHALMER, PAUL D. ..... p 2776 N95-31771
CHALMERS, DAVID ..... p 2968 N95-32321
CHAMBERS, JOSEPH R. ..... p 2741 N95-31000
CHAMBERS, R. S. ..... p 2932 N95-30376
p 2811 N95-30389
CHAMIS, CHRISTOS C. ..... p 2899 N95-32206
CHAN, S. K. ..... p 3016 N95-32105
CHANG, CHAOHSI ..... p 2991 N95-32304
CHANG, H. P. ..... p 2995 N95-32260
CHANG, SEO IL ..... p 2895 N95-31331
CHAO, A. ..... p 3002 N95-32356
CHAO, CHIH-HO ..... p 2954 N95-31838
CHAO, JOSEPH CHIU ..... p 2853 N95-31839
CHAO, ZHANG S. ..... p 2997 N95-30901
CHAPATWALA, KIRIT D. ..... p 2780 N95-31791
CHARETTE, RICK H. ..... p 2973 N95-30530
CHATRENET, D. ..... p 2761 N95-32016
CHEN, C. P. ..... p 2828 N95-31210
CHEN, CHUN ..... p 3010 N95-30644
CHEN, HONG ..... p 2979 N95-30652
CHEN, J. I. ..... p 2821 N95-31699
CHEN, J. R. ..... p 2995 N95-32260
CHEN, J. T. ..... p 3013 N95-31008
CHEN, K. R. ..... p 2813 N95-30572
CHEN, M. ..... p 2908 N95-30686
CHEN, PANG C. ..... p 2949 N95-30377
p 2950 N95-30463
CHEN, T. J. ..... p 2820 N95-31471
CHEN, Y. ..... p 2978 N95-30546
CHEN, YANSONG ..... p 2951 N95-30891
CHEN, YEN-SEN ..... p 2828 N95-31210
p 2772 N95-31749
CHEN, YUOI ..... p 2991 N95-32304
CHENG, Y. ..... p 2995 N95-32260
CHENGJIE, XU ..... p 2997 N95-30909
CHEON, SE WOO ..... p 2930 N95-31267
CHETWYND, JAMES H. ..... p 2915 N95-31575
p 2916 N95-31604
CHEUNG, K. ..... p 2977 N95-30465
CHIANG, I. ..... p 2986 N95-31702
CHIMA, RODRICK V. ..... p 2867 N95-30524
CHIOU, J. C. ..... p 2897 N95-31730
p 2899 N95-32202
CHIRIKOV, B. V. ..... p 3019 N95-31276
CHISHOLM, M. F. ..... p 3010 N95-30544
CHITTUM, C. B. ..... p 2748 N95-31845
CHIU, PEI-CHIH ..... p 2863 N95-31611
CHIZHOV, M. V. ..... p 3028 N95-30366
p 2964 N95-30369
p 2845 N95-30370
p 2978 N95-30528
CHO, PHILLIP EUNG-HO ..... p 2895 N95-31316
CHOI, BYEONG HO ..... p 3005 N95-31004
CHOI, J. ..... p 2976 N95-30442
CHOI, JUNG-EUN ..... p 2872 N95-31317
CHOI, KWANG ..... p 3024 N95-30882
CHOI, WOO KAP ..... p 2911 N95-32350
CHOQUETTE, K. D. ..... p 2882 N95-30380
CHOREY, C. M. ..... p 3011 N95-30703
CHOTIROS, NICHOLAS P. ..... p 2923 N95-31523
CHOUNG, HYUN SUK ..... p 3024 N95-30882
CHOW, W. W. ..... p 2883 N95-30390
p 2860 N95-30707
CHRISS, RANDALL M. ..... p 2756 N95-31985
CHRISTENSEN, ANDREW B. ..... p 2917 N95-31820
CHRISTENSEN, K. ..... p 3016 N95-32301
CHRISTIE, GEORGE M. ..... p 2888 N95-30414
CHRISTODOULATOS, CHRISTOS ..... p 2772 N95-31752
CHU, M. S. ..... p 3007 N95-32116
CHU, YA-CHERNG ..... p 2785 N95-30823
CHUDNOVSKY, A. ..... p 2820 N95-31471
CHUN, E. J. ..... p 2984 N95-31546
CHUNG, SEUNG HO ..... p 3005 N95-31004
CHUNG, SHIRLEY Y. ..... p 2796 N95-31660
CHUNG, WILLIAM W. ..... p 2750 N95-30646
CHURCH, H. W. ..... p 2917 N95-32080
CHURKIN, I. N. ..... p 2987 N95-32053
p 3006 N95-32054
CHURNSIDE, J. H. ..... p 2871 N95-30992
CHYU, M. C. ..... p 2861 N95-30942
CICON, D. E. ..... p 2755 N95-30779
CITURS, KEVIN D. ..... p 2758 N95-31998
CLARK-INGRAM, MARCEIA ..... p 2783 N95-31810
CLARK, DENNIS K. ..... p 2922 N95-30857
CLARK, G. A. ..... p 2900 N95-30472
CLARK, JOSEPH A. ..... p 2974 N95-30725
CLARKE, JERRY ..... p 2869 N95-30889
CLARKE, ROBERT ..... p 2759 N95-32001
CLAYTON, CATHERINE P. ..... p 2780 N95-31795
CLAYTON, EDMUND ..... p 3032 N95-32282
CLEMENS, D. ..... p 2810 N95-32272
CLIFF, E. M. ..... p 2751 N95-31451
CLOUGH, TONY ..... p 2921 N95-32184
COCKE, C. L. ..... p 2990 N95-32274
COEN, MICHAEL H. ..... p 2939 N95-31277
COFFEY, HELEN E. ..... p 3031 N95-30690
p 3031 N95-30816
p 3031 N95-30817
COGGIOLA, M. J. ..... p 2881 N95-31694
COHEN, EDWARD I. ..... p 2785 N95-30749
COIFMAN, RONALD R. ..... p 2848 N95-30869
COLBURN, JOSEPH W. ..... p 2799 N95-31209
COLLINS, C. B. ..... p 2886 N95-31563
COLLINS, GREGG ..... p 2949 N95-30395
COLLINS, MICHAEL ..... p 2909 N95-31612
COLLINS, RICHARD LAURENCE ..... p 2916 N95-31736
COLTRIN, M. E. ..... p 2822 N95-32101
COLUCCI, P. J. ..... p 2878 N95-32219
COLVARD, RICHARD D. ..... p 2752 N95-31578
COMISO, JOSEFINO C. ..... p 2924 N95-32220
CONDIT, ALLEN ..... p 3026 N95-32149
CONDON, STEVEN E. ..... p 2937 N95-31237
CONN, A. R. ..... p 2956 N95-30570
CONNELL, JOHN ..... p 2938 N95-31244
CONNES, A. ..... p 2955 N95-30490
CONNOLLY, J. F. ..... p 2880 N95-30691
CONROY, PAUL J. ..... p 3020 N95-31511
COOK, B. A. ..... p 2865 N95-32084
COOK, BETH ..... p 2783 N95-31811
p 2783 N95-31812
COOK, N. G. W. ..... p 2898 N95-32102
COON, MAX D. ..... p 2923 N95-30964
CORWIN, BILL ..... p 2753 N95-31463
p 2753 N95-31655
p 2753 N95-31656
CORY, MARSHALL G. ..... p 2796 N95-31596
COSBY, STEVE ..... p 2777 N95-31779
COSTA, M. ..... p 2765 N95-32223
COSTELLA, JOHN P. ..... p 2976 N95-30427
COTILLARD, C. ..... p 2840 N95-32126
COTTER, J. E. ..... p 2906 N95-32057
COTTON, W. R. ..... p 2907 N95-30358
p 2920 N95-31453
COUGHLAN, S. DANETTE ..... p 2901 N95-31390
COURTNEY, T. H. ..... p 2802 N95-30404
COVINO-HRBACEK, JOSEPHINE ..... p 3009 N95-30533
CRAIG, W. ..... p 2879 N95-30507
CRAIN, J. S. ..... p 2797 N95-32061
CRAWFORD, KENT ..... p 2985 N95-31616
CRAWFORD, M. H. ..... p 2860 N95-30707
CRAWFORD, TIM ..... p 2774 N95-31760
CRESPI, V. H. ..... p 3017 N95-32366
CRESS, T. ..... p 2908 N95-30802
CRIM, F. F. ..... p 2981 N95-30952
CRISCIONE, MARK ..... p 2937 N95-31239
CRIVELLI, LUIS ..... p 2945 N95-32214
CRIVELLI, LUIS A. ..... p 2944 N95-32203
CRONIN-GOLOMB, MARK ..... p 2999 N95-31458
CROSS, L. ERIC ..... p 2788 N95-31369
p 2788 N95-31370
p 2788 N95-31371
p 2788 N95-31372
CROUT, R. ..... p 2935 N95-30968
CRUBELLATI, RICARDO ..... p 2807 N95-31407
CRUDELE, SCOTT DAVID ..... p 2789 N95-31973
CRUIT, WENDY ..... p 2773 N95-31757
CUCCIO, J. C. ..... p 2817 N95-31135
p 2817 N95-31136
CULVERHOUSE, D. O. ..... p 2999 N95-31529
CUNNINGHAM, A. M., JR. ..... p 2743 N95-30885
CUOMO, FRANK W. ..... p 2996 N95-30679
CURLEE, T. R. ..... p 2816 N95-31103
CURLETT, BRIAN P. ..... p 2754 N95-30594
CURTIN, LARRY S. ..... p 2984 N95-31427
CURTIN, MICHAEL T. ..... p 2817 N95-31152
CUSHNIE, GEORGE C., JR. ..... p 2776 N95-31771
CUTLER, LEONARD S. ..... p 2970 N95-32335

D

DAALAND, O. ..... p 2805 N95-31053
DABUNDO, CHARLES ..... p 2761 N95-32014
DADDIO, RAY E. ..... p 2973 N95-30530
DAEHLEN, M. ..... p 2934 N95-30625
p 2962 N95-32256
DAHL, PETER H. ..... p 2923 N95-31701
DAHLBERG, M. ..... p 2838 N95-30630
DAHLGREN, U. ..... p 2882 N95-32245
DAHMEN, STEPHEN M. ..... p 2940 N95-31420
DAI, YI ..... p 2894 N95-31098
DAIELLO, R. V. ..... p 2905 N95-31381
DALAL, V. ..... p 2810 N95-32154
DAMOUR, T. ..... p 2912 N95-30588
p 2913 N95-30590
DANDY, D. S. ..... p 2822 N95-32101
DANFORTH, STEPHEN C. ..... p 2818 N95-31153
DANIEL, M. ..... p 3013 N95-30959
DANIEL, R. L. ..... p 2776 N95-31774
DANIELL, ROBERT E., JR. ..... p 2914 N95-31012
DANIELS, CHAO FU ..... p 2792 N95-30670
DANIELSON, T. A. ..... p 2787 N95-31146
DANVY, OLIVIER ..... p 2941 N95-31460
DARZI, MICHAEL ..... p 2924 N95-31850
DAS-GUPTA, D. K. ..... p 2859 N95-30561
DAS, P. ..... p 2863 N95-31725
DAS, S. ..... p 2816 N95-31103
DASH, SANDY M. ..... p 2871 N95-30991
p 2871 N95-30993
DASILVA, L. B. ..... p 3006 N95-32028
p 2886 N95-32029
DATTA, A. ..... p 2982 N95-31060
DATYE, ABHAYA K. ..... p 2793 N95-31113
DAVIDSON, J. R. ..... p 2943 N95-32030
DAVIS, ANGELA ..... p 2968 N95-32321
DAVIS, DICK D. ..... p 2969 N95-32331
DAVIS, H. A. ..... p 2818 N95-31377
DAVIS, IAN LANE ..... p 2953 N95-31540
DAVIS, J. A. ..... p 2858 N95-32320
DAVIS, JAMES M. ..... p 2761 N95-32014
DAVIS, LAWRENCE E. ..... p 2782 N95-31809
DAVIS, LAWRENCE JOHN, IV ..... p 2886 N95-31848
DAVIS, MILT W. ..... p 2753 N95-30514
DAVIS, ROBERT F. ..... p 3015 N95-32018
DAVIS, S. EDDIE ..... p 2783 N95-31813
DAVIS, S. J. ..... p 2780 N95-31794
DAVIS, T. ..... p 2960 N95-31264
DAWSON, J. ..... p 2992 N95-31165
DAYDE, M. J. ..... p 2957 N95-30692
DCOSTA, JOSEPH FRANCIS ..... p 2898 N95-32118
DEAN, DAVID L. ..... p 2773 N95-31755
DEANGELIS, CHRIS ..... p 2953 N95-31692
DEANGELIS, CHRIS M. ..... p 2953 N95-31693
DEAS, M. ..... p 2840 N95-32125
p 2840 N95-32127
DEBNAM, WILLIAM J. ..... p 2837 N95-31359
DEBONIS, JAMES R. ..... p 2742 N95-30704
DECAUX, V. ..... p 2987 N95-32041
p 2993 N95-32042
DECKER, F. J. ..... p 2993 N95-31256
DECKER, T. ..... p 2879 N95-30507
DECOCK, K. M. J. ..... p 2743 N95-30814
DEEVI, S. C. ..... p 2803 N95-30575
DEGIORGI, VIRGINIA G. ..... p 2815 N95-30894
DEIMEL, LIONEL ..... p 2937 N95-31241
DEINES, STEVEN D. ..... p 2970 N95-32333
DEJONG, GERRIT ..... p 2971 N95-32337
DELANEY, RICHARD L. ..... p 2951 N95-30890
DELGRANDE, NANCY K. ..... p 2741 N95-32164
DELGUERCIO, M. ..... p 2799 N95-31205
DELL, G. F. ..... p 2994 N95-32243
DELLORCO, P. C. ..... p 2836 N95-32048
p 2837 N95-32355
DEMORE, W. B. ..... p 2912 N95-30525
DEMPSEY, P. J. ..... p 2768 N95-30595
DENALE, ROBERT ..... p 2996 N95-30724
DENBOER, R. G. ..... p 2743 N95-30885
DENBOGGENDE, T. ..... p 2879 N95-30507
DENG, FANG ..... p 2864 N95-31948
DENLINGER, EDGAR J. ..... p 2863 N95-31669
DENNIS, K. W. ..... p 3011 N95-30667
DEPORCEL, L. ..... p 2993 N95-31627
DEPPE, M. W. ..... p 2756 N95-31199
DERENZO, S. E. ..... p 2878 N95-30378
DESMARAIS, KEVIN ..... p 2800 N95-31296
DESPA, F. ..... p 3010 N95-30647
DETOMA, EDOARDO V. ..... p 2971 N95-32339
DEVINE, E. ..... p 2813 N95-30621
DEVLIN, F. J. ..... p 2798 N95-32258
DEVORE, RICHARD C. ..... p 2795 N95-31473
DEVOS, J. C. ..... p 2967 N95-30809
DEWEESE, C. D. ..... p 2780 N95-31794
DEWEESE, C. DARRELL ..... p 2779 N95-31790
p 2780 N95-31796
DEWEESE, CHARLES D. ..... p 2778 N95-31782
DEWS, T. W. ..... p 2823 N95-32352
DEWSON, T. ..... p 2784 N95-30694
DEYOUNG, JAMES A. ..... p 2858 N95-32320
DI, DONG ..... p 2957 N95-30676
DICKENS, ANDREW ..... p 2970 N95-32332
DICKINSON, R. E. ..... p 2908 N95-30686
DICKINSON, STUART C. ..... p 2888 N95-30532
DICKMAN, O. ..... p 2857 N95-32313
DICKSON, T. L. ..... p 2898 N95-32157
DICRISTINA, V. ..... p 2781 N95-31802
DIEBOLT, J. ..... p 2943 N95-32044
DIEBOLT, JEAN ..... p 2944 N95-32068
DIGNAN, MICHAEL ..... p 2756 N95-31191
DILL, DAVID ..... p 2964 N95-32287
DILLARD, TERRY W. ..... p 2778 N95-31782
p 2780 N95-31796

DILORETO, ALDO G. ..... p 2847 N95-30743
DIMIDUK, D. ..... p 2841 N95-32132
DIMOS, D. ..... p 2808 N95-31689
DIMOS, D. B. ..... p 2811 N95-30362
DINARDO, N. J. ..... p 2794 N95-31393
DING, JOW-LIAN ..... p 2821 N95-32025
DINICOLA, ALBERT JOHN ..... p 2898 N95-32191
DIONISIO, C. ..... p 2971 N95-32339
DIRUSSO, E. ..... p 2864 N95-31847
DISALVO, FRANCIS J. ..... p 3015 N95-31444
DIVINEY, WILLIAM ..... p 2848 N95-30902
DIVSALAR, D. ..... p 2855 N95-32227
DIXON, M. ..... p 2947 N95-31051
DOBSON, KIM ..... p 2937 N95-31239
DOCTERS, A. S. ..... p 2818 N95-31221
DOELMAN, N. J. ..... p 2973 N95-30461
DOERR, DONALD F. ..... p 2926 N95-30846
DOERR, ROBERT ..... p 2814 N95-30767
DOGGER, C. S. ..... p 2743 N95-30885
DOHERTY, JOSEPH ..... p 2920 N95-31522
DOI, Y. ..... p 2882 N95-32159
DOKUKIN, E. B. ..... p 2981 N95-30915
DOLAND, JERRY T. ..... p 2937 N95-31238
DOLINAR, JOSEPH F., JR. ..... p 2887 N95-30399
DOLINAR, S. ..... p 2855 N95-32230
p 2856 N95-32231
p 2856 N95-32233
p 2856 N95-32234
DOLS, V. ..... p 3030 N95-30806
DOMAGALA, PIOTR ..... p 2854 N95-32192
DOMINGUEZ, D. ..... p 2859 N95-30649
DOMINGUEZ, DANIEL ..... p 3014 N95-31231
DONAHUE, CHRISTOPHER A. ..... p 2920 N95-31524
DONATO, J. M. ..... p 2813 N95-30572
DONG, J. Q. ..... p 3005 N95-30801
DOORENBOS, ROBERT B. ..... p 2953 N95-31827
DOROBANTU, MIHAI ..... p 2957 N95-30713
DOROKHOV, A. E. ..... p 2985 N95-31621
DORTMANS, P. J. ..... p 2976 N95-30429
p 2977 N95-30447
DOUGLAS, ROB J. ..... p 2969 N95-32327
p 2971 N95-32340
DOWNER, J. D. ..... p 2897 N95-31730
p 2899 N95-32202
DRAGT, J. B. ..... p 2904 N95-31157
DRAKE, J. B. ..... p 2936 N95-31109
DRESIN, D. I. ..... p 3013 N95-30969
DRESKSLER, STEVEN B. ..... p 2747 N95-31454
DREWIEN, C. ..... p 2810 N95-32241
DRIESEN, S. ..... p 2799 N95-31205
DRIVER, MARK A. ..... p 2874 N95-31432
DROGON, KRYSTYNA ..... p 2993 N95-31336
p 2986 N95-31818
DROSSAERS, M. F. J. ..... p 2951 N95-30813
DROZDA, P. M. ..... p 2916 N95-31610
DRUMMOND, C. J. ..... p 2952 N95-31255
DRUMMOND, COLIN K. ..... p 2753 N95-30514
DRYER, F. L. ..... p 2801 N95-31309
p 2801 N95-31310
DUBNICKA, S. ..... p 2984 N95-31548
DUBNICKOVA, A. Z. ..... p 2984 N95-31548
DUBOIS, R. D. ..... p 2978 N95-30573
DUDA, D. ..... p 2907 N95-30358
DUDENHOEFFER, DONALD D. ..... p 2889 N95-30949
DUGDALE, RICHARD C. ..... p 2910 N95-31981
DUIJVESTIJN, A. J. W. ..... p 2954 N95-30401
DUMAN, HUSEYIN ..... p 2961 N95-31518
DUNCAN, A. J. ..... p 2803 N95-30733
DUNCAN, MARK ..... p 2950 N95-30655
DUNNING, F. B. ..... p 2792 N95-30614
DUNWOODIE, C. ..... p 2993 N95-31627
DUPONT, J. N. ..... p 2809 N95-32098
DUPUIS, PAUL ..... p 2952 N95-31055
p 2952 N95-31279
DURBIN, PHILIP F. ..... p 2741 N95-32164
DUSSAULT, DOUGLAS G. ..... p 2973 N95-30530
DUTREY, J.-F. ..... p 2969 N95-32328
DUTTON, S. A. ..... p 2752 N95-31544
DWYER, J. ..... p 3028 N95-31129
DZIUBEK, ROBIN ANN ..... p 3007 N95-32310

E

EASTMAN, J. A. ..... p 3015 N95-32062
EATOUGH, M. O. ..... p 2808 N95-31689
EBISAWA, KATSUMI ..... p 2913 N95-30758
EBMEYER, J. ..... p 2842 N95-32138
ECKARDT, ROBERT C. ..... p 2967 N95-30939
EDEN, J. G. ..... p 2885 N95-31528
EDER, JAMES E. ..... p 2786 N95-30839
EDGE, HARRIS ..... p 2869 N95-30889
EDMONDS, L. ..... p 2859 N95-30651
EDWARDS, H. T. ..... p 2908 N95-30793
EFTEDAL, O. ..... p 2926 N95-30511
p 2926 N95-30513
p 2925 N95-30665
EHARA, TERUMASA ..... p 3026 N95-32182
EHLERS, ROBERT C. ..... p 2762 N95-30592
EINMAHL, J. H. J. ..... p 2965 N95-30523
EINSTEIN, T. L. ..... p 2838 N95-31472
EITTER, JOSEPH J. ..... p 3028 N95-30466
EKEBERG, M. ..... p 2837 N95-32249
EKMAN, ROBERT K. ..... p 2946 N95-32292
EKROOT, L. ..... p 2856 N95-32233
p 2856 N95-32234
EKSTROEM, U. ..... p 2879 N95-30600
ELERIN, L. ..... p 2860 N95-30886
p 2953 N95-31562
ELGERONA, PER-OLOV ..... p 2746 N95-31069
ELGIN, JAMES B. ..... p 2871 N95-30994
ELKHOVSKIJ, A. S. ..... p 2959 N95-31137
ELLINGSON, R. G. ..... p 2917 N95-32080
ELLIOTT, DENNIS L. ..... p 2921 N95-31726
ELLIOTT, S. R. ..... p 2987 N95-32038
ELLIS, JOHN R. ..... p 2791 N95-32209
ELPHIC, RICHARD C. ..... p 2933 N95-30602
ELROD, HAROLD G. ..... p 2878 N95-32216
EMANUEL, M. ..... p 3016 N95-32268
EMMA, P. ..... p 2993 N95-31256
EMMONS, J. R. ..... p 2776 N95-31772
ENDERLE, JOHN D. ..... p 2927 N95-31552
ENDISCH, E. ..... p 2804 N95-30797
ENGEL, B. N. ..... p 2810 N95-32265
ENGELKEN, EDWARD J. ..... p 2927 N95-31552
ENGLER, B. P. ..... p 2916 N95-31610
ENNS, DALE ..... p 2758 N95-31996
EPPING, ANDREAS ..... p 2939 N95-31251
ERENTHAL, ELI ..... p 2758 N95-31994
ERICKSON, M. D. ..... p 2797 N95-32061
ERICSON, B. ..... p 3002 N95-32312
ERIKSON, W. ..... p 2800 N95-31287
ERIKSSON, K. ..... p 2955 N95-30477
p 2956 N95-30500
ERKELENS, L. J. J. ..... p 2748 N95-30815
ERMAK, DONALD L. ..... p 2877 N95-32049
EROKHIN, YU ..... p 3016 N95-32301
ESAIAS, WAYNE E. ..... p 2924 N95-31850
ESFAHANIAN, MOHSEN ..... p 2890 N95-32119
ESKER, D. R. ..... p 2800 N95-31298
ESSIEN, MARCELINO ..... p 2884 N95-31139
ESTEROWITZ, LEON ..... p 2884 N95-31213
p 2885 N95-31273
p 2885 N95-31274
ETT, WILLIAM H. ..... p 2946 N95-32289
p 2946 N95-32290
p 2946 N95-32293
EVANS, KURT B. ..... p 2779 N95-31790
EVANS, ROBERT H. ..... p 2924 N95-31850

F

FALCO, C. M. ..... p 2810 N95-32265
FALEEV, S. V. ..... p 2966 N95-31259
FALK, R. A. ..... p 2861 N95-31133
FANG, F. ..... p 2794 N95-31393
FANG, H. T. ..... p 2817 N95-31135
p 2817 N95-31136
FANG, YUGUANG ..... p 2954 N95-31949
FARE, THOMAS L. ..... p 3011 N95-30728
FARHANGI, S. ..... p 2799 N95-31212
FARHAT, C. ..... p 2767 N95-32204
FARHAT, CHARBEL ..... p 2945 N95-32214
FARHAT, N. H. ..... p 2951 N95-30884
FARWELL, MARK LALON ..... p 3001 N95-31950
FARWELL, S. G. ..... p 2999 N95-31529
FEAGA, A. C. ..... p 2927 N95-30981
FEDOTOV, YU. S. ..... p 2983 N95-31261
FEELY, R. A. ..... p 2910 N95-32099
FEHER, L. ..... p 3019 N95-31226
FEIBELMAN, P. J. ..... p 3017 N95-32307
FEIGELSON, ROPBERT S. ..... p 2967 N95-30939
FEINBERG, JACK ..... p 3013 N95-30982
FEINER, STEVE ..... p 2939 N95-31262
FEINGOLD, G. ..... p 2907 N95-30358
FEINGOLD, RICHARD ..... p 3026 N95-32285
FEKEL, FRANCIS C. ..... p 3028 N95-30466
FELDER, JAMES L. ..... p 2754 N95-30594
FELIPPA, C. A. ..... p 2767 N95-32204
FELIPPA, CARLOS A. ..... p 2944 N95-32203
p 2945 N95-32215
FENG, XIAOPING ..... p 2992 N95-30960
FENG, Z. ..... p 2899 N95-32317
FENNELL, J. F. ..... p 2915 N95-31536
FEO, J. ..... p 2925 N95-32358
FERBER, M. K. ..... p 2814 N95-30732
p 2894 N95-31131
p 2796 N95-31633
FERIA, Y. ..... p 2855 N95-32228
p 2855 N95-32229
p 2856 N95-32231
FERKINHOFF, DAVID J. ..... p 2974 N95-30550
FERNOW, R. C. ..... p 2989 N95-32160
FERNOW, RICHARD C. ..... p 2988 N95-32063
FERRARI, D. ..... p 2945 N95-32270
FERRARIS, J. P. ..... p 2822 N95-32075
FERRAROTTO, P. ..... p 2752 N95-31544
FERRON, J. R. ..... p 3007 N95-32116
FETHEROLF, BARRY LYNN ..... p 2836 N95-31531
FETTIG, R. ..... p 2880 N95-30752
FIELDING, C. ..... p 2760 N95-32012
FIELDS, DAVID ..... p 3000 N95-31672
FIENUP, JAMES R. ..... p 2846 N95-30562
FIFER, R. A. ..... p 2800 N95-31295
FIGIEL, J. J. ..... p 2882 N95-30380
p 2882 N95-30380
FILIPSSON, L. ..... p 2956 N95-30601
FILYUSHKIN, V. ..... p 2917 N95-32080
FINGER, MARK H. ..... p 3028 N95-30469
FINKENTHAL, D. F. ..... p 3004 N95-30685
FINNERTY, ANTHONY E. ..... p 2795 N95-31580
FIRESTONE, ELAINE R. ..... p 2922 N95-30857
p 2924 N95-31850
p 2924 N95-32122
p 2924 N95-32220
FIRESTONE, JAMES K. ..... p 2924 N95-32220
FISHELL, KENNETH A. ..... p 2779 N95-31787
FISHER, M. E. ..... p 2838 N95-31472
FISHER, P. W. ..... p 2778 N95-31784
FISHER, W. M. ..... p 2800 N95-31290
FITZPATRICK, RICHARD ..... p 3004 N95-30794
FITZSIMMONS, M. R. ..... p 3015 N95-32062
FLANDRO, G. A. ..... p 2799 N95-31283
FLEMING, J. G. ..... p 2878 N95-30384
FLEMING, JAMES W. ..... p 2801 N95-31311
FLESNER, R. L. ..... p 2836 N95-32048
p 2837 N95-32355
FLETCHER, S. K. ..... p 3025 N95-31662
FLEYGNAC, D. ..... p 2752 N95-32008
FLICKINGER, WILLIAM F. ..... p 2887 N95-30399
FLIFLET, ARNE W. ..... p 3013 N95-30984
FLOKSTRA, J. ..... p 3023 N95-30566
FLOOK, V. ..... p 2925 N95-30665
FLORO, J. A. ..... p 3014 N95-31112
FLYNN, CHRISTOPHER F. ..... p 2928 N95-30905
p 2928 N95-31376
FLYNN, WILLIAM A. ..... p 2760 N95-32011
FOLKNER, W. M. ..... p 2854 N95-32222
FOLLSTAEDT, D. M. ..... p 2980 N95-30708
FONDA, L. ..... p 2880 N95-31167
FONG, Y. ..... p 2960 N95-31229
p 2961 N95-31397
FOOR, WESLEY E. ..... p 3000 N95-31697
FORSGREN, A. ..... p 2956 N95-30499
FORSHAW, J. R. ..... p 2956 N95-30540
FORSTER, R. A. ..... p 2960 N95-31253
FOSS, JUDITH KATHLEEN ..... p 2866 N95-30449
FOSSUM, ARLO F. ..... p 2892 N95-30559
FOSTER, C. A. ..... p 2778 N95-31784
FOSTER, G. WILLIAM ..... p 2992 N95-30800
FOSTER, I. T. ..... p 2913 N95-30683
FOSTER, TERRY ..... p 2843 N95-32166
p 2843 N95-32168
p 2843 N95-32169
p 2843 N95-32170
p 2844 N95-32171
p 2763 N95-32176
p 2844 N95-32177
p 2845 N95-32179
FOWLER, ALEX JACKSON ..... p 2874 N95-31532
FOWLER, R. F. ..... p 3009 N95-30485
FRALICK, CHARLES R., JR. ..... p 2922 N95-30396
FRANCO-FERREIRA, E. A. ..... p 2890 N95-32367
FRANCO, R. J. ..... p 2916 N95-31610
FRANK, LOUIS A. ..... p 3032 N95-32218
FRANK, M. ..... p 2881 N95-32047
FRANKEL, N. E. ..... p 2967 N95-31177
FRANKEN, L. J. N. ..... p 2847 N95-30812
FRASER, ROBERT S. ..... p 2924 N95-32220
FRASER, STEPHANIE B. ..... p 2747 N95-31687
FRAZIER, GARTH ..... p 2950 N95-30655
FREDRICKS, R. ..... p 3012 N95-30847
FREEDMAN, M. H. ..... p 2965 N95-30509
p 2965 N95-30555
FREEMAN, G. N. ..... p 2871 N95-30995
FREMOUW, E. J. ..... p 2916 N95-31698
FRENCH, JAMES C. ..... p 3023 N95-30619
FRENCH, JONATHAN ..... p 2927 N95-31373
FREYLER, H. ..... p 2842 N95-32138
FREYMAN, TODD ..... p 2801 N95-31302
FRIDAY, K. K. ..... p 3026 N95-32107
FRIDELANCE, PATRICIA ..... p 2887 N95-32348
FRIEBELE, EDWARD J. ..... p 2998 N95-31270
FRIEDMAN, AVNER ..... p 2749 N95-31433
FRIEDMANN, T. A. ..... p 2794 N95-31393
p 2885 N95-31394
FRIESEN, J. A. ..... p 2854 N95-32045
FRIPP, ARCHIBALD L. ..... p 2837 N95-31359

FRISCH, M. J. ..... p 2798 N95-32258
FRITTS, DAVID ..... p 2914 N95-31278
FRITZ, M. D. ..... p 2981 N95-30952
FRITZEMEIER, MARILYN L. ..... p 2770 N95-31806
FRIVIK, P. E. ..... p 2815 N95-30871
FRUEHOLZ, R. P. ..... p 2970 N95-32336
FRY, RONALD S. ..... p 2800 N95-31291
FU, C. L. ..... p 3015 N95-31641
FUCHS, F. JOHN ..... p 2778 N95-31783
FUERSCHBACH, PHILLIP W. ..... p 2884 N95-31139
FUESS, THERESA A. ..... p 2981 N95-30970
FUHRMAN, S. J. ..... p 2768 N95-30864
FUJII, K. ..... p 2994 N95-32059
FUJITA, MASARU ..... p 2853 N95-31744
FUKUDA, T. ..... p 2882 N95-32159
FUNKHOUSER, G. E. ..... p 2748 N95-31845
FURNELL, GRAHAM D. ..... p 2922 N95-30711
FURU, T. ..... p 2805 N95-31053

G

GABRIELSON, THOMAS B. ..... p 2973 N95-30413
GAISER, PETER W. ..... p 2852 N95-31590
GALE, S. L. ..... p 2760 N95-32012
GALIC, J. ..... p 2888 N95-30701
GALLAGHER, R. SCOTT ..... p 2774 N95-31764
GALLARDO, J. C. ..... p 2989 N95-32160
GALLARDO, JUAN C. ..... p 2988 N95-32063
GALMES, JOSE ..... p 2943 N95-31843
GAMMON, R. H. ..... p 2910 N95-32099
GANNAWAY, MARY T. ..... p 2870 N95-30986
p 2825 N95-31194
p 2829 N95-31282
GARBINCIUS, PETER H. ..... p 2990 N95-32303
GAREEV, F. A. ..... p 2981 N95-30913
GARG, VIJAY K. ..... p 2755 N95-30702
GARITO, ANTHONY F. ..... p 2815 N95-30955
GARKUSHA, V. I. ..... p 2983 N95-31261
GARLAN, DAVID ..... p 2943 N95-31843
GARRETT, STEVEN L. ..... p 2995 N95-30402
p 2879 N95-30658
GASKILL, D. K. ..... p 2862 N95-31343
GASSER, E. S. ..... p 2781 N95-31800
GASTELLI, MICHAEL G. ..... p 2791 N95-32209
GATTO, J. L. ..... p 2801 N95-31310
GAUGLER, RAYMOND E. ..... p 2755 N95-30702
GAVRILOV, Y. ..... p 2882 N95-32159
GEBALLE, T. H. ..... p 2795 N95-31439
GEDRIDGE, ROBERT, JR. ..... p 2771 N95-30418
GEERLOF, ARIE ..... p 2771 N95-30734
GEIWITZ, JAMES ..... p 2959 N95-31002
GEMMEN, RANDALL S. ..... p 2792 N95-30762
GENTILE, N. A. ..... p 3021 N95-32359
GEOHEGAN, D. B. ..... p 2813 N95-30572
GEORGE, E. P. ..... p 2805 N95-31106
p 2805 N95-31111
GEORGE, M. H. ..... p 2748 N95-31845
GEORGE, T. G. ..... p 2890 N95-32367
GEORGER, JACQUE H., JR. ..... p 2803 N95-30750
GEORGIADIS, NICHOLAS J. ..... p 2742 N95-30704
GEORGIOU, IOANNIS THEODOROU
p 2897 N95-31706
GERARD, J. C. ..... p 3030 N95-30806
GERDES, D. ..... p 2992 N95-31165
GERI, GEORGE A. ..... p 2942 N95-31684
GERSH, M. ..... p 2799 N95-31211
GERSHCTEJN, S. S. ..... p 2983 N95-31261
GERSTENBERGER, D. C. ..... p 2885 N95-31434
GERTNER, IZIDOR C. ..... p 2942 N95-31684
GETBEHEAD, MARK A. ..... p 3000 N95-31697
GEURTS, E. G. ..... p 2743 N95-30885
GHAFOURIAN, AKBAR ..... p 2770 N95-31972
GIBSON, J. C. ..... p 2757 N95-31991
GIBSON, JOHN C. ..... p 2745 N95-31066
GIESE, J. P. ..... p 2990 N95-32274
GIFFARD, ROBIN P. ..... p 2970 N95-32335
GILARDI, STEPHEN S. ..... p 2814 N95-30715
GILFORD, MICHAEL T. ..... p 2920 N95-31524
GILLESPIE, JOHN W., JR. ..... p 2787 N95-30963
GILLETTE, MARTHA ..... p 2925 N95-31144
GILLIS, J. R. ..... p 2767 N95-32189
GINERIS, DENISE J. ..... p 2901 N95-31148
GIRIMAJI, SHARATH S. ..... p 2877 N95-31978
GIVI, P. ..... p 2878 N95-32219
GLADSTONE, G. R. ..... p 3030 N95-30806
GLASS, J. T. ..... p 3015 N95-32018
GLASS, M. W. ..... p 2866 N95-30464
GLASSER, M. L. ..... p 2954 N95-30425
p 2967 N95-31177
GLENN, RUSSELL D. ..... p 2958 N95-30754
GLENNON, MARY ANN ..... p 2915 N95-31335
GLESENER, JOHN W. ..... p 3014 N95-31269
GLOVER, A. L. ..... p 2779 N95-31786
GNAN, MONIKA ..... p 2928 N95-31376
GOEHNER, R. P. ..... p 3000 N95-31681
GOETTL, BARRY P. ..... p 2929 N95-31583
GOHEEN, KEVIN R. ..... p 2761 N95-32015
GOHIL, P. ..... p 3004 N95-30685
GOLD, DAVID MICHAEL ..... p 3004 N95-30742
GOLD, STEVEN H. ..... p 3013 N95-30984
GOLDBERG, BEN ..... p 2773 N95-31757
GOLDBERG, BENJAMIN E. ..... p 2771 N95-31748
p 2772 N95-31750
GOLDBERG, R. D. ..... p 2804 N95-30797
GOLDEN, D. M. ..... p 2912 N95-30525
GOLDSTEIN, N. ..... p 2799 N95-31211
GONCHAROVA, V. A. ..... p 3009 N95-30419
GONG, KAI F. ..... p 2974 N95-30550
GONGWER, POLLY E. ..... p 2800 N95-31297
GONSALEZ, JOSE C. ..... p 2763 N95-31653
GONZALEZ, EDWARD J. ..... p 2818 N95-31153
GONZALEZ, M. E. ..... p 2818 N95-31221
GOODELL, A. J. ..... p 2813 N95-30621
GOODMAN, P. ..... p 3012 N95-30789
GOODMAN, PETER ..... p 2976 N95-30423
GOODMAN, T. ..... p 2781 N95-31800
GOODS, S. H. ..... p 2905 N95-31640
GOODWIN, G. M. ..... p 2899 N95-32317
GOPAL, RAM DANTURTI ..... p 3023 N95-30764
GOPALAKRISHNAN, G. K. ..... p 2862 N95-31179
GORDON, LESLIE A. ..... p 2967 N95-30939
GORDON, S. P. ..... p 2906 N95-32090
GOTALSKAJA, A. N. ..... p 3013 N95-30969
GOULD, N. I. M. ..... p 2956 N95-30570
p 2957 N95-30692
GOURLEY, P. L. ..... p 2860 N95-30707
GOVONI, D. B. ..... p 2981 N95-30952
GRABBE, S. R. ..... p 2989 N95-32120
p 2990 N95-32275
GRADY, DENNIS E. ..... p 2816 N95-31058
GRANADA, J. R. ..... p 2807 N95-31409
GRANATSTEIN, VICTOR L. ..... p 2861 N95-30979
GRANDE, M. ..... p 2915 N95-31536
GRAVES, RON ..... p 2775 N95-31766
GRAY, G. T. ..... p 2808 N95-31636
GRAY, H. L. ..... p 2964 N95-31831
GRAY, HENRY F. ..... p 2862 N95-31275
p 2862 N95-31342
GRAY, WILLIAM M. ..... p 2918 N95-30832
p 2918 N95-30842
p 2919 N95-30844
GREEN, B. D. ..... p 2998 N95-31192
GREEN, DAVID S. ..... p 2938 N95-31245
GREEN, LEONARD ..... p 2943 N95-31834
GREEN, R. A. ..... p 2879 N95-30687
GREEN, ROBERT ..... p 2953 N95-31692
GREENHALL, C. A. ..... p 2857 N95-32240
GREENHALL, CHARLES A. ..... p 2858 N95-32334
GREENOUGH, C. ..... p 3009 N95-30485
GREFEN, P. ..... p 3022 N95-30456
GREFEN, P. W. P. J. ..... p 3023 N95-30566
GREVE, D. W. ..... p 3013 N95-30983
GRIBAUDO, L. ..... p 2806 N95-31220
GRIBB, T. T. ..... p 2814 N95-30732
GRIFFIN, C. J. ..... p 2955 N95-30445
p 2957 N95-30688
GRIFFIN, DENNIS ..... p 2783 N95-31812
GRIFFIN, P. ..... p 3029 N95-31102
GRIFFITH, D. V. ..... p 2760 N95-32012
GRIMSHAW, ANDREW S. ..... p 3023 N95-30619
GRINEVICH, OLEG ..... p 2793 N95-31014
GROAT, JEFF ..... p 2753 N95-31463
p 2753 N95-31655
p 2753 N95-31656
GRODENT, D. ..... p 3030 N95-30806
GROEBNER, R. J. ..... p 3004 N95-30685
p 3007 N95-32116
GROMNITSKAY ..... p 3009 N95-30419
GRONBECH-JENSEN, NIELS ..... p 3014 N95-31231
GRONG, O. ..... p 2802 N95-30518
p 2813 N95-30664
GROSHART, EARL C. ..... p 2776 N95-31773
GROSJEAN, PAUL D. ..... p 2860 N95-30940
GROSSE, IAN R. ..... p 2940 N95-31455
GROSSMAN, T. ..... p 2785 N95-30787
GROTH, KEITH M. ..... p 2927 N95-30998
GROVES, M. ..... p 2785 N95-30787
GRUBECK, H. ..... p 2857 N95-32314
GRUBER, ARNOLD ..... p 2913 N95-30643
GRUBIN, H. L. ..... p 3013 N95-30985
GRUDA, J. D. ..... p 2967 N95-31625
GRUEDLER, P. ..... p 2971 N95-32338
GRUENBAUM, P. E. ..... p 2767 N95-32189
GRUND, CHRISTIAN J. ..... p 2917 N95-32142
GUCHAIT, M. ..... p 2982 N95-31060
GUESS, T. R. ..... p 2932 N95-30376
p 2811 N95-30389
GUIBAS, L. J. ..... p 2942 N95-31644
GUILINGER, T. R. ..... p 2810 N95-32241
GUILINGER, TERRY R. ..... p 2806 N95-31406
GUILL, FREDERICK C. ..... p 2930 N95-30552
GUIMOND, DAVID P. ..... p 2687 N95-30386
GUIOCHON, GEORGES ..... p 2823 N95-32296
GULDBRANDSEN, P. ..... p 2859 N95-30596
GUNDERSEN, M. A. ..... p 2992 N95-31127
GUNION, J. F. ..... p 2994 N95-32059
GUO, HAN-YING ..... p 2957 N95-30642
GUOHA, SHA ..... p 2885 N95-31389
GURARIE, V. N. ..... p 2811 N95-30450
p 2812 N95-30451
GURSKI, GARY ..... p 2841 N95-32131
GUSTAFSON, GARY B. ..... p 2920 N95-31522
GUTHLEIN, PETER ..... p 2848 N95-30902
p 2848 N95-30910
GUTMARK, E. J. ..... p 2799 N95-31200
p 2756 N95-31201
GUZIK, T. GREGORY ..... p 3032 N95-32282
GWINN, KENNETH W. ..... p 2897 N95-31614
p 2767 N95-32081
GYEKENYESI, ANDREW L. ..... p 2791 N95-32209

H

HAAKE, J. M. ..... p 3023 N95-30496
HAAS, MICHAEL N. ..... p 2777 N95-31778
HACK, HARVEY P. ..... p 2807 N95-31561
HAELLSTROEM, J. ..... p 2858 N95-30538
HAERTEL, CHARMINE ..... p 2750 N95-32186
HAERTEL, GUENTHER F. ..... p 2750 N95-32186
HAFIZI, BAHMAN ..... p 3013 N95-30984
HAGEL, O. J. ..... p 2882 N95-32245
HAGEROTT-CRAWFORD, M. ..... p 2882 N95-30380
HAGERTY, JAMES D. ..... p 2859 N95-30659
HAGLUND, R. F., JR. ..... p 2784 N95-30731
HAGMANN, S. ..... p 2989 N95-32120
p 2990 N95-32275
HAHMANN, A. N. ..... p 2908 N95-30686
HAHN, H. ..... p 2993 N95-31405
HAHN, K.-U. ..... p 2759 N95-32002
HAJI-MAHMOOD, M. S. ..... p 3012 N95-30756
HAKE, K. ..... p 2947 N95-30577
HAKVOORT, R. G. ..... p 2839 N95-30777
HALBGEWACHS, R. D. ..... p 3025 N95-31662
HALE, JEFFREY S. ..... p 2782 N95-31808
HALL, H. K., JR. ..... p 2819 N95-31395
HALL, JOHN ..... p 2999 N95-31515
HALL, R. B. ..... p 2906 N95-32057
HALL, RICHARD L. ..... p 2775 N95-31767
HALLQWIST, N. ..... p 2846 N95-30479
HALPERIN, D. ..... p 2942 N95-31644
HAMAGUCHI, YASUMASA ..... p 2789 N95-31740
HAMELL, ROBERT L. ..... p 2858 N95-32334
HAMILTON, C. P. ..... p 2815 N95-30894
HAMMETT, G. W. ..... p 3003 N95-30359
HAMMOND, R. L. ..... p 2905 N95-31381
HAMMOND, WESLEY ..... p 2774 N95-31761
HAMMOUD, AHMAD ..... p 2768 N95-30860
HAMMOUD, AHMAD N. ..... p 2864 N95-31742
HAMPSON, R. F. ..... p 2912 N95-30525
HAN, EUN SOOK ..... p 3024 N95-30883
HAN, GUOPING ..... p 2991 N95-32304
HAN, L. T. ..... p 2816 N95-30997
HAN, S. H. ..... p 2865 N95-32084
HAN, T. ..... p 2994 N95-32059
HANADA, MASAYA ..... p 2995 N95-32262
HANDEL, PETER H. ..... p 2862 N95-31442
HANKE, DIETRICH ..... p 2746 N95-31071
HANNON, JUDITH A. ..... p 2763 N95-32217
HANSMAN, R. J., JR. ..... p 2749 N95-31520
HANSON-PARR, D. M. ..... p 2799 N95-31200
HANSON-PARR, DONNA ..... p 2801 N95-31307
p 2801 N95-31314
HANSON, P. J. ..... p 2908 N95-30793
HAO, BAI-LIN ..... p 2913 N95-30675
HARBISON, BARRY B. ..... p 2816 N95-31011
HARDESTY, R. MICHAEL ..... p 2917 N95-32142
HARDING, D. S. ..... p 2818 N95-31175
HARGRAVES, C. R. ..... p 2767 N95-32189
HARN, DEUCK HAING ..... p 3024 N95-30882
HARRIMAN, WALTER L. ..... p 2996 N95-30678
p 2753 N95-31180
HARRIS, B. A. ..... p 3018 N95-30436
p 2978 N95-30580
HARRIS, MICHAEL T. ..... p 2815 N95-30799
HARRIS, STACEY A. ..... p 2772 N95-31751
HARTMAN, J. ..... p 2817 N95-31135
p 2817 N95-31136
HASEGAWA, AKIRA ..... p 2934 N95-30759
HASEGAWA, T. ..... p 2882 N95-32159
HASEGAWA, YOJI ..... p 2988 N95-32083
HASHIMOTO, O. ..... p 2882 N95-32159
HASSA, CHRISTOPH ..... p 2873 N95-31355
HASSOON, SALAH ..... p 2793 N95-31014
HASTINGS, DANIEL E. ..... p 3005 N95-31534
HATADA, NOBUKO ..... p 3026 N95-32182
HATAY, FERHAT F. ..... p 2872 N95-31341

HATHAWAY, DAVID H. p 2869 N95-30863
HATHAWAY, MICHAEL D. p 2756 N95-31985
HATTEN, GREGORY E. p 2767 N95-32345
HAUG, S. p 2846 N95-30516
p 2934 N95-30662
p 2934 N95-30697
HAUGE, R. H. p 3012 N95-30944
HAUGEN, BJORN p 2944 N95-32203
HAVERKORT, B. R. p 2847 N95-30812
HAW, R. J. p 2854 N95-32222
HAWKINS, JEFFREY D. p 2901 N95-31148
HAWLEY, ARTHUR V. p 2789 N95-31421
HAYAMI, RICHARD A. p 2963 N95-31543
HAYES, A. H. p 2932 N95-31645
HAYES, JOYCE A. p 2772 N95-31750
HAYES, SUSAN M. p 2815 N95-30799
HAYNES, T. E. p 2804 N95-30797
HE, CHARLES C. p 2839 N95-31690
HE, SHAOWEI p 2997 N95-30908
HEADLEY, T. J. p 2822 N95-32161
HEALEY, ALICE F. p 2929 N95-31585
HEBERT, JOSEPH E. p 2749 N95-31581
HEBERT, MICHEL p 2962 N95-32067
HEFNER, B. p 2781 N95-31800
HEIDBREDER, GLEN R. p 2847 N95-30727
HEINSOHN, ROBERT J. p 2773 N95-31759
HELTSLEY, F. L. p 2884 N95-30906
HENDERSON, R. F. p 2909 N95-31703
HENDRICK, RUSS p 2758 N95-31996
HENDRICKS, R. C. p 2867 N95-30710
HENDRICKSON, C. R. p 2852 N95-31606
HENDRIKS, ROBERT V. p 2775 N95-31766
HENINS, IVARS p 3006 N95-31613
HENRY, GREGORY W. p 3028 N95-30466
HENRY, JOEL p 2939 N95-31250
HENRY, JOHN W. p 2887 N95-30399
HERNANDEZ, JOSE V. p 2933 N95-30602
HERR, JOEL L. p 3003 N95-30468
HERTEL, E. S., JR. p 2816 N95-31058
HESLIN, THOMAS M. p 2839 N95-31690
HESTER, ROGER p 2823 N95-32361
HETZEL, P. p 2858 N95-32320
HEUSCH, C. p 2994 N95-32059
HEWITT, JOHN R. p 2799 N95-31209
HIBBS, ANDREW D. p 2998 N95-31435
HICKMAN, JAMES J. p 2803 N95-30750
HICKMAN, S. R. p 2800 N95-31286
HICKS, DONALD K. p 2941 N95-31573
HIGASHI, A. p 2882 N95-32159
HIGGINS, A. J. p 2799 N95-31204
HIGHLEY, STEVEN R. p 2852 N95-31590
HIGUCHI, MAKOTO p 2804 N95-30761
HILDRETH, M. D. p 2986 N95-31682
HILE, CHERYL VAUGHT p 2998 N95-31411
HILFIKER, JAMES N. p 2782 N95-31808
HILL, STEPHEN C. p 2785 N95-30768
HILLIARD, M. P. p 2927 N95-30981
HILLIER, ANDREW C. p 3014 N95-31189
HILLIS, D. L. p 3004 N95-30685
HILMEN, A. M. p 3009 N95-30535
HINCHLIFFE, I. p 2975 N95-30388
HINDMAN, WARD p 2920 N95-31541
HINEDI, S. p 2856 N95-32235
HINNERICHS, T. D. p 2932 N95-30376
p 2811 N95-30389
HINNERICHS, TERRY p 2839 N95-32082
HINNRICHS, MICHELLE p 3000 N95-31672
HINTZ, J. p 2860 N95-30886
p 2953 N95-31562
HIROSE, HOROAKI p 2796 N95-31596
HIRST, DONALD J. p 2817 N95-31124
HIRUKAWA, HIROHISA p 2942 N95-31644
HJELDE, A. p 2925 N95-30512
HO, C. WING p 2917 N95-31743
HO, DANNY p 2938 N95-31246
HO, HENJEN p 2896 N95-31418
HO, K. M. p 3015 N95-32037
HOCK, VINCENT F. p 2812 N95-30558
HOCKEY, BERNARD p 2818 N95-31153
HODGE, STEVE L. p 2974 N95-30850
HODGKINSON, J. p 2757 N95-31992
HODGKINSON, JOHN p 2746 N95-31067
HOEIER, R. p 2992 N95-30717
HOEIJMAKERS, H. W. M. p 2743 N95-30837
HOENLINGER, H. p 2760 N95-32006
HOFFMAN, A. p 2977 N95-30474
HOFLER, THOMAS J. p 2879 N95-30658
HOGAN, J. T. p 3004 N95-30685
HOH, ROGER H. p 2745 N95-31065
p 2757 N95-31990
HOLDEMAN, J. D. p 2754 N95-30589
p 2755 N95-30698
p 2755 N95-30853
HOLE, D. E. p 2784 N95-30731
HOLLBERG, LEO p 2999 N95-31515
HOLLENBERG, C. L. p 2992 N95-30960
HOLLENBERG, LLOYD C. L. p 2965 N95-30432
p 2965 N95-30435
p 3018 N95-30438
p 3018 N95-30444
HOLLERBACH, K. p 2928 N95-32097
HOLLINGER, JAMES P. p 2852 N95-31590
HOLLNAGEL, E. p 2929 N95-30522
HOLLOWAY, PAUL H. p 2786 N95-30934
HOLMBERG, B. p 2857 N95-32313
HOLMEN, I. M. p 2925 N95-30665
HOLMESTAD, R. p 2992 N95-30717
HOLMQUIST, T. J. p 2816 N95-31058
HOLST, TERRY L. p 2744 N95-32188
HOLT, T. p 2903 N95-30896
HOLTROP, K. L. p 3003 N95-30612
HOLYOAK, KEITH J. p 2929 N95-31686
HOLZHAUSEN, GARY R. p 2880 N95-30941
HOMMERT, P. J. p 2934 N95-30796
HONG, BONG GEUN p 3005 N95-31004
HONG, BONG GUEN p 3005 N95-31366
HONG, W. p 2994 N95-32059
HOOD, CHRISTOPHER p 2774 N95-31761
HOOIJMANS, J. p 2804 N95-30776
HOOKER, STANFORD B. p 2922 N95-30857
p 2924 N95-31850
p 2924 N95-32122
p 2924 N95-32220
HOOVER, CAROL L. p 2930 N95-31401
HOPPE, DAVID p 2777 N95-31779
HOPPE, DAVID T. p 2778 N95-31782
HOPPEL, CHRISTOPHER P. p 2787 N95-30963
HORGAN, CORNELIUS O. p 2896 N95-31474
HORTON, J. A. p 2805 N95-31111
p 2808 N95-31643
HORTON, W. p 3005 N95-30801
HORWITZ, J. L. p 2917 N95-31743
HOSKING, F. MICHAEL p 2806 N95-31406
HOUGAARD, P. p 2929 N95-30522
HOUTZ, WESLEY A. p 2812 N95-30558
HOVENAC, EDWARD A. p 2880 N95-30851
HOWARD, C. J. p 2912 N95-30525
HOWE, HAROLD p 2889 N95-31382
HOWELL, BARBARA F. p 2811 N95-30415
HREHA, MARK A. p 2757 N95-31846
HRYSZKO, M. p 2848 N95-30904
HSEUH, H. C. p 2987 N95-32032
HSIAO, M. C. p 2911 N95-32281
HSU, DAVID S. p 2862 N95-31275
HSU, K. T. p 2995 N95-32260
HU, BAOGANG p 2789 N95-31731
HU, HONG p 2874 N95-31475
HUANG, I.-TE p 2797 N95-31732
HUANG, Y. p 2811 N95-30422
HUANG, YUMING p 2917 N95-31951
HUBBARD, C. R. p 2899 N95-32317
HUBER, ALAN C. p 2766 N95-31553
HUDSON, JAMES G. p 2919 N95-30951
HUGHES, C. p 2781 N95-31801
HUGHES, S. p 2762 N95-30926
p 2763 N95-31101
HUIJBERTS, H. J. C. p 2950 N95-30564
p 2950 N95-30807
HULL, ANDREW J. p 2789 N95-31668
HULL, J. R. p 2861 N95-30942
p 2861 N95-30943
HUMPHERYS, THOMAS W. p 2841 N95-32131
HUNG, CHANG-LI p 2785 N95-30824
HUNN, J. D. p 2822 N95-32043
HUNT, H. B., III p 2934 N95-30603
HUNT, K. p 2799 N95-31212
HUNTLEY, D. R. p 2803 N95-30547
HUNTLEY, M. S., JR. p 2749 N95-31572
HUOTILA, P. p 2858 N95-30480
HURD, W. p 2855 N95-32229
HUSKENS, JURRIAAN p 3019 N95-30775
HUSTAD, J. E. p 2902 N95-30519
HUSTON, ALAN L. p 2816 N95-31010
HUSTON, M. A. p 2908 N95-30793
HUTCHENS, DALE E. p 2778 N95-31782
p 2780 N95-31796
HUTSELL, STEVEN T. p 2968 N95-32322
HWANG, CHUL KEW p 3005 N95-31366
HWANG, CHURL KEW p 3005 N95-31004
HWANG, YONG K. p 2949 N95-30377
HYTOPOULOS, EVANGELOS p 2868 N95-30840

I

IGNATIEV, A. Y. p 2976 N95-30393
ILINCIC, N. p 2801 N95-31312
IMAE, M. p 2971 N95-32338
IMAI, KAZUO p 2853 N95-31744
IMBERT, N. p 2758 N95-31997
IMOILCZYK, JANUSZ p 2850 N95-31357
IN, SANG RYEOL p 3005 N95-31004
IN, SANG RYUL p 3005 N95-31366
INGBER, M. S. p 2866 N95-30464
INOUE, TAKASHI p 2995 N95-32262
INUKAI, THOMAS p 2765 N95-31849
IP, E. H. S. p 2943 N95-32044
p 2944 N95-32089
IP, EDDIE H. S. p 2944 N95-32087
p 2944 N95-32088
IRVING, A. D. p 2784 N95-30694
IRWIN, DENNIS p 2950 N95-30655
IRWIN, R. DENNIS p 2958 N95-30754
ISAYEV, A. A. p 3010 N95-30648
ISONO, TAKAAKI p 3007 N95-32148
ITO, RINSUKE p 2979 N95-30654
IVALDI, CHARLES F. p 2920 N95-31522
IVANOV, O. p 2863 N95-31725
IVEY, LISA R. p 2985 N95-31597
IVORY, M. p 2925 N95-32358
IWASAKI, YOSHIHITO p 2989 N95-32266
IYENGAR, S. S. p 2941 N95-31631
IYER, B. R. p 2912 N95-30588
p 2913 N95-30590
IZRAILEV, F. M. p 3020 N95-32150

J

JACKSON, DARRELL R. p 2923 N95-31701
JACKSON, G. L. p 3003 N95-30612
JACKSON, H. J. p 2857 N95-32239
JACOX, JAMES L. p 2772 N95-31753
JALVING, B. p 2879 N95-30502
p 2748 N95-30597
JAMES, BONNIE F. p 3003 N95-30468
JAMES, RICHARD p 3014 N95-31438
JANKOWSKI, ALAN F. p 2814 N95-30738
p 2809 N95-32051
p 3016 N95-32284
JANSMA, R. M. p 3025 N95-31662
JANSSEN, M. p 2892 N95-30458
JANSSEN, P. p 2847 N95-30812
JANUS, MICHAEL C. p 2792 N95-30762
JAROS, J. A. p 2987 N95-32026
JASSOWSKI, DONALD M. p 2768 N95-31169
p 2769 N95-31170
JAYARAMAN, VIJAYSEKHAR p 2883 N95-30498
JELETIC, KELLYANN F. p 2939 N95-31252
JELSMA, L. p 2792 N95-30714
JENCIC, I. p 3016 N95-32103
JENEKHE, SAMSON A. p 2819 N95-31461
p 2819 N95-31462
p 2819 N95-31466
p 2819 N95-31467
JENSSEN, B. M. p 2925 N95-30515
JEONG, SEUNG HO p 3005 N95-31366
JESTER, T. p 2904 N95-31162
JETTER, M. p 2982 N95-31176
JEWELL, JOHN M. p 2816 N95-31011
JIANG, HONGTAO p 2991 N95-32304
JIANG, X. L. p 3001 N95-31700
JIN, Z. p 2917 N95-32080
JINGCUN, ZANG p 2887 N95-32152
JOE, DAVID A. p 2798 N95-32360
JOE, E. p 2781 N95-31800
JOHANSSON, GUNILLA p 2960 N95-31361
JOHANSSON, H. p 2882 N95-32245
JOHANSSON, L. E. B. p 3029 N95-30569
JOHANSSON, M. p 2857 N95-32247
JOHNSON, CALVIN R. p 2904 N95-30947
JOHNSON, DONALD C. p 2943 N95-31835
JOHNSON, G. R. p 2816 N95-31058
JOHNSON, MADELEINE R. p 2775 N95-31767
JOHNSON, S. A. p 2901 N95-32027
JOHNSON, SALLY C. p 2948 N95-32250
JOHNSON, SPENCER T. p 2778 N95-31780
JOKINEN, T. p 2849 N95-31158
JOKINEN, TAPANI p 2849 N95-31160
p 2849 N95-31181
p 2850 N95-31182
JONAS, F. M. p 2766 N95-31143
JONCKHEERE, R. p 2880 N95-30693
JONES-MEEHAN, J. p 2816 N95-30997
JONES, DENNY A. p 2814 N95-30738
JONES, E. D. p 3008 N95-30381
p 2860 N95-30707
p 3014 N95-31112
JONES, LISA L. p 2782 N95-31805
JONES, MICHAEL E. p 3008 N95-32351
JONES, RANDY K. p 2779 N95-31789
JONES, W. R., JR. p 2813 N95-30621
JOOSTEN, S. p 3022 N95-30453
p 2933 N95-30454
p 2947 N95-30721
JORGENSEN, G. p 2902 N95-30526
JORJADZE, G. p 2983 N95-31224
JOSEFSSON, T. W. p 2977 N95-30475
p 2977 N95-30476

	p 2980	N95-30790
	p 2981	N95-30916
JOSHI, G.	p 3018	N95-30426
JOSHI, G. C.	p 2976	N95-30393
	p 3018	N95-30424
	p 3018	N95-30436
	p 2978	N95-30580
	p 2957	N95-30688
JUN, SONG F.	p 2997	N95-30966
JUNJIE, GAI	p 2997	N95-30909
JUNQING, FAN	p 2997	N95-30909
JUOMPAN, B.	p 2969	N95-32328
JUSTUS, BRIAN C.	p 2816	N95-31010
JUVET, PHILIPPE JEAN-DANIEL	p 2876	N95-31733

K

KAASSCHIETER, E. F.	p 2868	N95-30811
KABACHENKO, V. V.	p 2982	N95-31214
KABANTSEV, A. A.	p 3006	N95-31680
KAKUTA, YOSHIAKI	p 2789	N95-31740
KALINOVSKIJ, YU. L.	p 2980	N95-30911
KALLENBORN, K. J.	p 2776	N95-31772
KALLURI, V.	p 3023	N95-30620
KAMADA, YUTAKA	p 3007	N95-32263
KAMAREDDINE, F.	p 2966	N95-30719
KAMMEYER, MARK E.	p 2875	N95-31586
KANADE, TAKEO	p 2928	N95-31383
KANAI, J.	p 3023	N95-30620
KANE, M.	p 2903	N95-30723
KANG, SIN BOK	p 3024	N95-30883
KANGAS, M. T.	p 2904	N95-31138
	p 2907	N95-32368
KANN, VIGGO	p 2961	N95-31648
KANOPOULOS, NICK	p 2864	N95-31844
KAPITULNIK, A.	p 2795	N95-31439
KAPLAN, ALEXANDER E.	p 2999	N95-31519
KAPLAN, D. B.	p 2991	N95-32365
KAPOOR, RAHUL	p 2864	N95-31844
KARLSSON, M.	p 2945	N95-32246
KARLSSON, T.	p 2822	N95-32253
	p 2857	N95-32313
KASTELLA, KEITH	p 2749	N95-31433
KASUKABE, Y.	p 2820	N95-31623
KATRAGADDA, PRASANNA	p 2940	N95-31455
KATSOGIANNIS, A.	p 2982	N95-31176
KATULKA, G.	p 2799	N95-31205
KATZ, A.	p 2798	N95-32091
KATZ, J.	p 2828	N95-31207
KATZ, R.	p 2945	N95-32270
KATZ, RICHARD A.	p 2973	N95-30411
	p 2867	N95-30672
KAUFMANN, DAVID H.	p 2743	N95-30788
KAVARNOS, GEORGE J.	p 2813	N95-30560
KAWAMURA, MASASHI	p 3007	N95-32264
KAY, STEVEN	p 2848	N95-30932
KEARNEY, D.	p 2903	N95-30887
KEAY, KATHLEEN D.	p 2974	N95-30550
KEBABIAN, P. L.	p 2801	N95-31305
KEEN, JILL M.	p 2779	N95-31790
	p 2780	N95-31796
KEENEY, J. A.	p 2898	N95-32157
KELLAND, JAMES W.	p 2860	N95-30940
KELLER, J. L.	p 2920	N95-31465
KELLER, JAMES F.	p 2761	N95-32014
KELLER, TEDDY M.	p 2818	N95-31272
KELLNER, MARC	p 2946	N95-32293
KELLOGG, G. L.	p 3017	N95-32307
KELLY, ANN M.	p 2805	N95-31121
KELLY, K. C.	p 2910	N95-32099
KEMPEL, LEO CHARLES	p 2847	N95-30669
KEMPKA, S. N.	p 2866	N95-30383
	p 2866	N95-30464
KENDIG, M.	p 2810	N95-32241
KENNEDY, C.	p 2902	N95-30526
KENNEDY, D. C.	p 3020	N95-32106
KENT, SCOTT	p 2946	N95-32292
KENT, STEPHEN D.	p 2798	N95-32360
KENYON, CHRISTOPHER S.	p 2941	N95-31594
KENZAKOWSKI, D. C.	p 2871	N95-30991
KEOLIAN, ROBERT M.	p 2995	N95-30402
KERBEL, G. D.	p 3003	N95-30359
KERSEY, ALAN D.	p 2996	N95-30753
KETTNER, C.	p 3028	N95-30361
KEUM, JONG YONG	p 3024	N95-30882
KEVIL, THOMAS H.	p 2774	N95-31783
KHALIL, S. S.	p 2989	N95-32096
KHAMSEH, AMIR REZA	p 2790	N95-32108
KHAN, HUZOOR H.	p 2958	N95-30821
KHODR, MAJED FOUAD	p 2883	N95-30805
KHORRAM, SHAHLA	p 3012	N95-30822
KHOSLA, PRADEEP K.	p 2929	N95-31685
KHRIPLOVICH, I. B.	p 2991	N95-32354
KHUDIK, V. N.	p 2987	N95-32055
KHVASTUNOV, M. S.	p 3017	N95-30364
	p 3019	N95-30972
KIDA, TAKASHI	p 2767	N95-31980
KIDMAN, D.	p 2752	N95-32007
KIELKOPF, JOHN A.	p 2997	N95-31005
KIELY, A. B.	p 2856	N95-32233
	p 2856	N95-32234
	p 2857	N95-32238
KIEU, T. D.	p 3018	N95-30437
	p 2955	N95-30445
KIEU, TIEN D.	p 3018	N95-30440
KIEU, TIEN DUNG	p 2965	N95-30439
KIGGANS, J. O.	p 2822	N95-32085
KIKUCHI, MITSURU	p 3007	N95-32263
KILCOYNE, S. P.	p 2882	N95-30380
	p 2882	N95-30380
KIM, B. G.	p 2862	N95-31185
KIM, D. Y.	p 2997	N95-30973
	p 2817	N95-31126
KIM, HYEON JEONG	p 3024	N95-30883
KIM, SEONG KYU	p 3005	N95-31004
KIM, SUN JA	p 3024	N95-30882
KIM, SUNG KYU	p 3005	N95-31366
KIM, TAE WHAN	p 3024	N95-30882
KIM, W. H.	p 3001	N95-31700
KIM, YEONG TAEK	p 3024	N95-30883
KIM, YONG-MI	p 2937	N95-31237
KIM, YOUNG MIN	p 3024	N95-30882
KIMMINAU, DONALD F.	p 2747	N95-31512
KIMURA, KENJI	p 2984	N95-31402
KINASHI, YASUHIRO	p 2840	N95-32128
KINDERLEHRER, DAVID	p 3014	N95-31438
KING, BELINDA B.	p 2960	N95-31319
KING, RAYMOND B.	p 2928	N95-30905
KING, RAYMOND E.	p 2928	N95-31376
KINNE, S.	p 2921	N95-32184
KIRILOVA, D. P.	p 3028	N95-30366
KIRK, M. A.	p 3016	N95-32103
	p 2809	N95-32104
KIRK, P. N.	p 2978	N95-30616
KIRKLAND, T. P.	p 2814	N95-30732
	p 2894	N95-31131
	p 2796	N95-31633
KIRKPATRICK, R. J.	p 2798	N95-32091
KIRKWOOD, S.	p 2913	N95-30627
	p 2913	N95-30628
KISELEV, V. V.	p 2983	N95-31218
	p 2983	N95-31219
KISHIMOTO, Y.	p 3005	N95-30801
KIVELAE, S. K.	p 2960	N95-31363
KJELL, G.	p 2913	N95-30631
KLAVUHN, KURT G.	p 2877	N95-32109
KLEINMAN, R. E.	p 2849	N95-30962
KLEPCZYNSKI, WILLIAM J.	p 2858	N95-32320
	p 2971	N95-32338
KLINGLE-WILSON, DIANA L.	p 2749	N95-31521
KLISSURSKA, R.	p 2811	N95-30422
KLUGER, MATTHEW J.	p 2926	N95-30870
KNAELL, KENNETH K.	p 2847	N95-30727
KNAPP, G. S.	p 2880	N95-30941
KNIGHT, JOHN C.	p 2939	N95-31249
KNIO, O. M.	p 2828	N95-31207
KNOWLEN, C.	p 2799	N95-31204
KO, YEONG CHEOL	p 3024	N95-30883
KOBAYASHI, RYOICHI	p 2962	N95-32068
KOCIAN, DEAN F.	p 2931	N95-31538
KOENIG, R.	p 2759	N95-32002
KOHUTH, K. RANDALL	p 2836	N95-31564
KOIKEGAMI, HAJIME	p 2804	N95-30761
KOIVISTO, P. K.	p 2853	N95-31649
KOLB, C. E.	p 2912	N95-30525
KOLLIE, TOM	p 2775	N95-31766
KOMIYAMA, FUMIO	p 2744	N95-31715
KONDO, MASAAKI	p 2913	N95-30758
KONDO, Y.	p 2983	N95-31227
KONDRAGUNTA, CHANDRASEKHARA R.	p 2913	N95-30643
KONONENKO, V. K.	p 2883	N95-30609
KONOSHIMA, S.	p 3003	N95-30612
KONTOTHANASSIS, LEONIDAS	p 2947	N95-30930
KOO, JIRO	p 2928	N95-31714
KOPPANG, PAUL A.	p 2968	N95-32321
KORFISTIS, GEORGE P.	p 2908	N95-31447
KORJACK, THOMAS A.	p 2852	N95-31601
KOROTKIYAN, V. M.	p 3017	N95-30371
KOSZORU, ARTHUR A.	p 2799	N95-31209
KOTEGAWA, HIROSHI	p 2980	N95-30760
KOTELNIKOV, I. A.	p 3006	N95-31679
KOTENG, S.	p 2926	N95-30511
KOUROUS, HELEN E.	p 2879	N95-30587
KOUSEN, KENNETH A.	p 2742	N95-30611
KOVACH, MICHAEL P.	p 2780	N95-31795
KOVALEVSKY, M. YU.	p 3010	N95-30648
	p 2967	N95-30739
KOWALENKO, VICTOR	p 2954	N95-30425
KOWALEWSKI, TOMASZ A.	p 2876	N95-31817
KOZACZEK, K. J.	p 2807	N95-31632
	p 2808	N95-31825
KOZHEVNIKOV, S. V.	p 2981	N95-30915
KOZLOV, G. A.	p 2985	N95-31620
KRAEUTLE, KARL J.	p 2770	N95-30989
	p 2770	N95-31197
KRALL, JONATHAN	p 2884	N95-31190
KRAMER, J. F.	p 2836	N95-32048
	p 2837	N95-32355
KRAMER, M. J.	p 3011	N95-30667
KRASKIEWICZ, J.	p 2984	N95-31548
KRAWCZYK, FRANK L.	p 2992	N95-31151
KREJCIK, P.	p 2993	N95-31256
KRESKOVSKY, J. P.	p 3013	N95-30985
KRISHNAMURTHY, S., SR.	p 2998	N95-31141
KRISTOFERSON, L.	p 2903	N95-30640
KROGSTAD, H. E.	p 2902	N95-32316
KROGULEC, M.	p 3031	N95-30582
KROUGLIKOV, B. S.	p 2958	N95-30803
KRUCZYNSKI, DAVID L.	p 2799	N95-31202
KRUGER, A. A.	p 2798	N95-32091
KRUMKE, S. O.	p 2948	N95-32277
KRUPA, D.	p 2981	N95-30912
KRUPKE, W. F.	p 3016	N95-32268
KUBANTSEV, M. A.	p 2989	N95-32261
KUBIK, ANTHONY	p 2968	N95-32321
KUHNLE, PAUL	p 2972	N95-32346
KUHNLE, PAUL F.	p 2858	N95-32334
KULICK, JOHATHAN D.	p 2875	N95-31707
KULLBERG, E.	p 2746	N95-31069
KULP, THOMAS J.	p 2867	N95-32280
KUMAR, A. H.	p 2787	N95-30978
KUMAR, J.	p 2997	N95-30973
	p 2817	N95-31126
	p 2821	N95-31699
	p 3001	N95-31700
KUMAR, P.	p 2981	N95-31003
KUMAR, SANJEEV	p 2872	N95-31100
KUME, MASAKI	p 2928	N95-31714
KUO, C. C.	p 2995	N95-32260
KUO, K. K.	p 2800	N95-31299
KUO, KENNETH K.	p 2800	N95-31296
	p 2801	N95-31302
KURAEV, E. A.	p 2988	N95-32093
	p 2995	N95-32296
KURATA, YUJI	p 2806	N95-31154
KUROSAWA, NAOHIRO	p 2980	N95-30760
KURTZ, S. R.	p 3008	N95-30381
	p 3014	N95-31112
KURVONEN, L.	p 2900	N95-30718
KURYLO, M. J.	p 2912	N95-30525
KUSTERS, JOHN A.	p 2970	N95-32335
KUZEMSKY, A. L.	p 3010	N95-30650
	p 3019	N95-31186
KWAK, B. S.	p 2812	N95-30545
KWOK, FRANKIE MAN WAI	p 2893	N95-30825
KWON, OKEY	p 2874	N95-31423

L

LAAKKO, T.	p 2933	N95-30568
LAAN, T.	p 2961	N95-31422
LABARCA, RAFAEL	p 2962	N95-32117
LABOV, S. E.	p 2881	N95-32047
LAGERLOEF, GARY	p 2919	N95-31123
LAGERQUIST, B.	p 2846	N95-30479
LAGGAN, WAYNE B.	p 2851	N95-31513
LAGHARI, JAVAID	p 2768	N95-30860
LAHAYE, R. J.	p 3007	N95-32116
LAMIA, WALTER	p 2943	N95-31834
LAMPPA, D. L.	p 2822	N95-32161
LAND, SHERRY A.	p 2951	N95-30925
LANDIS, KENNETH H.	p 2761	N95-32014
LANDIS, LINDA C.	p 2937	N95-31238
LANDSBERG, GREGG	p 2989	N95-32162
LANDSBERG, L. G.	p 2984	N95-31378
	p 2984	N95-31549
	p 2989	N95-32261
LANE, P. A.	p 2817	N95-31108
LANE, S.	p 2815	N95-30897
LANGBECK, B.	p 2934	N95-30663
LANGDON, B.	p 2992	N95-31186
LANGSTON, STEPHEN	p 2804	N95-30945
LANKFORD, JAMES, JR.	p 2787	N95-30975
LAO, L. L.	p 3006	N95-31624
	p 3007	N95-32116
LAPIDUS, M. L.	p 2956	N95-30556
LAPLAZE, D.	p 2813	N95-30645
LARA-CURZIO, E.	p 2814	N95-30732
LARSON, L.	p 2841	N95-32132
LASPINA, HECTOR	p 2807	N95-31407
LASSIG, C. C.	p 2976	N95-30446
LASSILA, ORA	p 2942	N95-31688
LATIF, Z.	p 2791	N95-30420
LATOMBE, J. C.	p 2942	N95-31644
LAVENDER, CURT A.	p 2809	N95-32052
LAW, JULIUS	p 2972	N95-32346

LAWANDY, NABIL M. ..... p 2999 N95-31542
LAWSON, SETH W. ..... p 2780 N95-31796
LAWSON, W. S. ..... p 2861 N95-31133
LAZEEV, B. N. ..... p 3007 N95-32056
LEAR, K. L. ..... p 2882 N95-30380
LEAROYD, C. ..... p 2860 N95-30886
p 2953 N95-31562
LEBOEUF, J. N. ..... p 2813 N95-30572
LEDERER, MELISSA A. ..... p 2743 N95-30929
LEE-GLAUSER, GINA JIMO ..... p 2767 N95-32110
LEE, C. C. ..... p 2816 N95-30997
LEE, CHENG-CHUNG ..... p 3010 N95-30644
LEE, DONG-SEUNG ..... p 2863 N95-31611
LEE, E. ..... p 2992 N95-31166
LEE, EU JIN ..... p 2930 N95-31267
LEE, H. ..... p 3014 N95-31112
LEE, H. S. ..... p 2849 N95-30935
LEE, HAN YEONG ..... p 2930 N95-31267
LEE, J. ..... p 2799 N95-31211
LEE, J. C. ..... p 2995 N95-32260
LEE, JANG-YEON ..... p 2762 N95-30493
LEE, JI HO ..... p 3024 N95-30882
LEE, JONG BOK ..... p 3024 N95-30883
LEE, JUNG WOON ..... p 2930 N95-31267
LEE, KWANG WON ..... p 3005 N95-31004
p 3005 N95-31366
LEE, P. A. ..... p 2933 N95-30539
LEE, R. W. ..... p 2885 N95-31230
LEE, ROBERT E. ..... p 2760 N95-32011
LEE, S. R. ..... p 3014 N95-31112
LEE, SANG-MOO ..... p 2888 N95-30830
LEE, SANGUK ..... p 2765 N95-30841
LEE, SEUNG HEE ..... p 2930 N95-31267
LEE, T. D. ..... p 2991 N95-30527
LEE, W. Y. ..... p 2818 N95-31187
p 2788 N95-31403
LEE, YONG HEE ..... p 2930 N95-31267
LEE, YOUNG JOO ..... p 2801 N95-31304
p 2801 N95-31315
LEEPER, R. J. ..... p 3006 N95-31626
LEES, A. J. ..... p 2978 N95-30574
LEES, DAVID SPENCER ..... p 2935 N95-30831
LEIBENGUTH, R. E. ..... p 2882 N95-30380
LEIF, ROALD N. ..... p 2914 N95-30865
LEIGHTON, D. E. ..... p 2894 N95-31007
LEIJTEN, A. J. M. ..... p 2963 N95-30680
LEMIRE, G. W. ..... p 2801 N95-31313
LEONG, M. Y. ..... p 2755 N95-30853
LEQUEUX, L. ..... p 2752 N95-32008
LERCHENMUELLER, H. J. ..... p 2880 N95-30752
LESCHIUTTA, SIGFRIDO M. ..... p 2968 N95-32324
LESLEY, MICHAEL W. ..... p 2782 N95-31809
LESLIE, DANIEL ..... p 2840 N95-32128
LESZCZYNSKI, FRANCISCO ..... p 2940 N95-31408
LEUCHTNER, R. E. ..... p 2784 N95-30731
LEUNG, HENRY ..... p 2842 N95-32136
LEUNG, M. S. ..... p 2819 N95-31417
LEVIN, B. F. ..... p 2809 N95-32098
LEVINE, S. R. ..... p 2822 N95-32208
LEVIT, ITZAK ..... p 2944 N95-32190
LEWANDOWSKI, WLODZIMIERZ W. p 2971 N95-32338
LEWIS, BRAD J. ..... p 2812 N95-30558
LEWIS, KEITH E. ..... p 2944 N95-32073
LEWIS, M. H. ..... p 2812 N95-30543
LEWIS, PAUL R. ..... p 3001 N95-31745
LEXCELLENT, J. Y. ..... p 2957 N95-30692
LEZNOV, A. N. ..... p 2966 N95-31379
LI, JIAN ..... p 2997 N95-30849
LI, JIAN-MING ..... p 2957 N95-30642
LI, L. ..... p 2997 N95-30973
p 2819 N95-31417
p 2821 N95-31699
LI, LIAN ..... p 2817 N95-31126
LIANG, RANTY H. ..... p 2796 N95-31660
LIAO, C. ..... p 2989 N95-32120
LIAO, G. S. ..... p 2854 N95-32114
LIAW, PAUL ..... p 2828 N95-31210
LIBBY, S. ..... p 3006 N95-32028
LIBERIO, PATRICIA D. ..... p 2775 N95-31768
LIKHODED, A. K. ..... p 2983 N95-31216
p 2983 N95-31219
LIM, J. J. ..... p 3025 N95-31662
LIN, C. D. ..... p 2990 N95-32271
p 2990 N95-32273
LIN, C. K. J. ..... p 2894 N95-31131
LIN, C. T. ..... p 2819 N95-31417
LIN, CATHERINE J. ..... p 2935 N95-30999
LIN, K. K. ..... p 2995 N95-32260
LIN, PENGJU ..... p 2820 N95-31623
LIN, SHENGHIN ..... p 2821 N95-32025
LIN, W. ..... p 2856 N95-32233
p 2856 N95-32234
LINDELL, I. V. ..... p 2846 N95-30567
LINDGREN, M. ..... p 3002 N95-32312
LINK, R. ..... p 2927 N95-30981
LINUSSON, S. ..... p 2955 N95-30477
p 2956 N95-30500
LIPELES, R. A. ..... p 2819 N95-31417
LISCINSKY, D. S. ..... p 2754 N95-30589
LITTLEFIELD, MARIA D. ..... p 2782 N95-31805
LITZINGER, THOMAS A. ..... p 2801 N95-31304
p 2801 N95-31315
LIU, C. L. ..... p 2813 N95-30572
LIU, C. T. ..... p 2805 N95-31106
p 2805 N95-31111
p 2810 N95-32272
LIU, K. C. ..... p 2821 N95-32025
LIU, MATTHEW ..... p 2775 N95-31766
LIU, W. TIMOTHY ..... p 2919 N95-31123
LIU, Y. C. ..... p 2995 N95-32260
LIVSEY, ROBERT A. ..... p 2888 N95-30716
LOEVAS, S. M. ..... p 2900 N95-30536
LOGAN, J. C. ..... p 2787 N95-31146
LOMBARDI, MICHAEL A. ..... p 2969 N95-32331
LOMBARDO, D. C. ..... p 2752 N95-31544
LONG, HOANG NGOC ..... p 2979 N95-30637
LONG, YIMING ..... p 2957 N95-30676
LOPATIN, C. M. ..... p 2816 N95-31058
LOREN, J. ..... p 2847 N95-30629
LORENZO, CARL F. ..... p 2770 N95-32121
LOTT, CHRISTOPHER M. ..... p 2939 N95-31251
LOTT, J. ..... p 2965 N95-30489
LOUER, JOHN W., III ..... p 2920 N95-31524
LOUIS, S. ..... p 2932 N95-31704
LOVE, D. ..... p 2804 N95-30797
LOVEJOY, MICHAEL L. ..... p 3014 N95-31233
LOVELESS, BRUCE F. ..... p 3024 N95-30928
LOWNDES, D. H. ..... p 3009 N95-30542
LU, CHEN ..... p 3005 N95-30804
LU, QI ..... p 2948 N95-32021
LU, YEU-CHERNG ..... p 2800 N95-31296
p 2801 N95-31302
LUBBEN, D. ..... p 2814 N95-30730
LUCAS, B. N. ..... p 2805 N95-31105
LUCKATT, JAMES D. ..... p 2947 N95-30868
LUCKHAM, DAVID C. ..... p 2931 N95-30892
LUHMANN, N. C., JR. ..... p 2881 N95-31828
LUKAS, ROGER B. ..... p 2919 N95-31123
LUN, D. R. ..... p 2978 N95-30583
LUNA, THOMAS D. ..... p 2927 N95-31373
LUND, P. D. ..... p 2904 N95-31138
p 2907 N95-32368
LUNDGREN, E. ..... p 2802 N95-30534
LUNN, P. ..... p 2908 N95-30802
LUNSFORD, JACK H. ..... p 2793 N95-30766
LUO, G. H. ..... p 2995 N95-32260
LUO, Q. ..... p 2936 N95-31109
LUSKIN, MITCHELL ..... p 3014 N95-31438
LUTES, G. ..... p 2856 N95-32236
LUTZ, ROBYN R. ..... p 2938 N95-31247
LYAPIN, V. G. ..... p 2991 N95-30604
LYCAS, JOHN ..... p 2851 N95-31448
p 2851 N95-31449
LYCHE, T. ..... p 2934 N95-30625
LYDERSEN, S. ..... p 2891 N95-30510
LYNN, J. W. ..... p 3015 N95-32062
LYON, ROBERT A., JR. ..... p 2886 N95-31833
LYONS, L. R. ..... p 2914 N95-30773

M

MA, J. P. ..... p 2976 N95-30441
MACAR, F. ..... p 3027 N95-32370
MACARTHUR, DOUG ..... p 2775 N95-31766
MACHIN, G. D. ..... p 3027 N95-30385
MACK, THOMAS ..... p 2941 N95-31573
MACKAY, ROBERT MALCOLM ..... p 2910 N95-31851
MACKENZIE, J. D. ..... p 2806 N95-31150
MADALA, RANGARAO V. ..... p 2921 N95-31577
MADAY, Y. ..... p 2955 N95-30495
MADDEN, TOM ..... p 2793 N95-31113
MAEKITALO, A. ..... p 3021 N95-30700
MAENO, SHUICHI ..... p 2995 N95-32262
MAENTYLAE, M. ..... p 2933 N95-30568
MAESTAS, L. M. ..... p 2810 N95-32241
MAGALLANES, JORGE ..... p 2807 N95-31407
MAGRUDER, R. H., III ..... p 2784 N95-30731
MAHAJAN, S. M. ..... p 3004 N95-30795
MAHDAVI, M. A. ..... p 3004 N95-30685
MAI, PHU V. ..... p 2858 N95-32320
MAINGI, R. ..... p 3003 N95-30612
p 3004 N95-30685
MALAN, PAUL ..... p 2876 N95-31708
MALAVALLON, OLIVIER ..... p 2843 N95-32167
p 2844 N95-32172
p 2844 N95-32173
p 2844 N95-32174
p 2844 N95-32175
p 2845 N95-32178
p 2845 N95-32180
p 2845 N95-32181
MALGHAN, SUBHAS G. ..... p 2818 N95-31153
MALIN, JANE T. ..... p 2951 N95-30925
MALLERY, C. F. ..... p 2801 N95-31303
MALLOY, KEVIN J. ..... p 2863 N95-31611
MALMROS, A. ..... p 2946 N95-32311
MALONE, G. A. ..... p 2802 N95-30531
MALTBY, PETER F. ..... p 2778 N95-31781
MANAK, I. S. ..... p 2883 N95-30609
MANDELBAUM, RICHARD ..... p 2947 N95-30868
MANE, V. ..... p 2994 N95-32242
MANENTE, R. A. ..... p 2878 N95-30378
MANGIACASALE, L. ..... p 2758 N95-31999
MANN, KATHY ..... p 2930 N95-31399
MANN, R. C. ..... p 2941 N95-31631
MANNAMI, MICHIHIKO ..... p 2984 N95-31402
MANOJLOVIC, NENAD ..... p 3018 N95-30431
MANSFEID, F. ..... p 2816 N95-30997
MANTLE, PETER J. ..... p 2839 N95-32124
MARATHE, M. V. ..... p 2934 N95-30603
p 2948 N95-32277
MARCEAU, CARLA ..... p 2942 N95-31683
MARDER, A. R. ..... p 2809 N95-32098
MAREK, E. L. ..... p 3027 N95-30385
MARGOLIS, S. B. ..... p 2797 N95-31824
MARGRAVE, J. L. ..... p 3012 N95-30944
MARIA, J. P. ..... p 2822 N95-32085
MARINELLI, W. J. ..... p 2781 N95-31802
MARLIERE, C. ..... p 2810 N95-32265
MARLIN, DAVE ..... p 2933 N95-30397
MARRERO-RIVERA, M. ..... p 2782 N95-31803
MARRON, JOSEPH C. ..... p 2846 N95-30562
MARRS, ROY D. ..... p 2779 N95-31789
MARSHALL, C. D. ..... p 3016 N95-32268
MARTHINSEN, K. ..... p 2992 N95-30717
MARTIN, CHARLES R. ..... p 2793 N95-30938
MARTIN, JENNIFER R. ..... p 2746 N95-31068
MARTINEZ-MIRANDA, L. J. ..... p 2794 N95-31393
MARTINEZ, DAVID ..... p 2839 N95-32082
MARTINEZ, RADAME ..... p 2848 N95-30902
p 2848 N95-30910
MARTINOLICH, PAUL M. ..... p 2935 N95-30968
MARTUCCIO, MICHELLE THERESE p 2750 N95-30827
MARTURUNKAKUL, S. ..... p 2821 N95-31699
MASINI, G. ..... p 2863 N95-31725
MASOOD, A. ..... p 3012 N95-30847
MASSE, C. E. ..... p 3001 N95-31700
MASSIE, MARK A. ..... p 3000 N95-31672
MATHESON, S. ..... p 3012 N95-30789
MATSUDA, M. ..... p 2976 N95-30393
MATSUMOTO, KOUTAROU ..... p 2767 N95-31980
MATTES, ROBERT A. ..... p 2781 N95-31799
MATTHEIJ, R. M. M. ..... p 2868 N95-30836
MATTHEWS, D. ..... p 2799 N95-31212
MATTINGLY, ALAN CHARLES ..... p 3020 N95-31646
MAUEL, M. ..... p 3007 N95-32116
MAY, DOUGLAS A. ..... p 2901 N95-31148
MAYER, T. ..... p 3014 N95-31112
MAZIASZ, P. J. ..... p 2899 N95-32317
MCCAIN, J. WAYNE ..... p 2783 N95-31814
MCCALLEN, R. C. ..... p 2875 N95-31591
MCCALLUM, R. W. ..... p 3011 N95-30667
MCCANN, GREGORY J. ..... p 2874 N95-31516
MCCARTOR, G. D. ..... p 2964 N95-31831
MCCARTY, G. D. ..... p 2811 N95-30389
MCCLAIN, CHARLES R. ..... p 2924 N95-31850
p 2924 N95-32220
MCCOLLUM, MATTHEW B. ..... p 3003 N95-30468
MCCONNAUGHEY, PAUL ..... p 2772 N95-31749
MCCORMICK, CHARLES ..... p 2823 N95-32361
MCCRORY, J. ..... p 2947 N95-30721
MCCUISH, A. ..... p 2760 N95-32010
MCCULLOCH, D. G. ..... p 2977 N95-30474
MCDONALD, ALLAN J. ..... p 2771 N95-31747
MCELIECE, R. J. ..... p 2856 N95-32233
p 2856 N95-32234
MCGARITY, JOHN O. ..... p 2766 N95-31553
MCGIBBON, A. J. ..... p 3010 N95-30544
p 3010 N95-30576
MCGIBBON, M. M. ..... p 3010 N95-30544
MCGRADY, P. W. ..... p 2942 N95-31634
MCHALE, J. M., JR. ..... p 2820 N95-31629
MCHENRY, MICHAEL E. ..... p 3012 N95-30933
MCINTOSH, ROBERT E. ..... p 2851 N95-31457
MCKAMEY, C. G. ..... p 2805 N95-31107
MCKAY, K. ..... p 2761 N95-32017
MCKEE, SUZANNE ..... p 2929 N95-31436
MCKELLAR, B. H. J. ..... p 2976 N95-30441
MCKELLAR, BRUCE H. J. ..... p 2976 N95-30427
MCKILLIP, ROBERT, JR. ..... p 2751 N95-30923
MCKINLEY, ANGELA DAVIS ..... p 2858 N95-32320
MCLEAN, G. A. ..... p 2748 N95-31845
MCLLREE, A. R. ..... p 2807 N95-31632
p 2808 N95-31825
MCMAHON, JOHN M. ..... p 2885 N95-31274
MCMILLIN, MARK L. ..... p 2940 N95-31420

MCNALLY, P. p 3009 N95-30485
MCNEILL, WALTER, E. p 2750 N95-30646
MCNESBY, K. L. p 2796 N95-31670
MCQUAY, P. p 2894 N95-31263
MCRUER, DUANE T. p 2745 N95-31052
MCWHORTER, ALAN L. p 3015 N95-31826
MEAD, JOEY L. p 2820 N95-31617
MEADE, W. p 2817 N95-31135
p 2817 N95-31136
MEARS, C. A. p 2881 N95-32047
MEDINA, ENRIQUE p 2950 N95-30655
MEERSON, B. p 3029 N95-30729
MEGGED, E. p 3029 N95-30729
MEIROVITCH, LEONARD p 2752 N95-31602
MEISSNER, K. E. p 2860 N95-30707
MELCHER, C. L. p 2878 N95-30378
MELLEGARD, KIRBY D. p 2892 N95-30559
MELTON, GREGORY S. p 2782 N95-31805
MELTZ, B. p 2948 N95-32255
MENG, JAMES C. p 2867 N95-30553
MENG, TERESA H. p 2850 N95-31426
MENIETTI, J. D. p 2914 N95-30848
MENON, M. N. p 2817 N95-31135
p 2817 N95-31136
MENON, VINOD P. p 2793 N95-30938
MENSAH, S. Y. p 3011 N95-30736
MERCER, T. W. p 2794 N95-31393
MERRISH, ARTHUR A. p 3014 N95-31269
MERRITT, BERNARD T. p 2911 N95-32281
MESHCHERYAKOV, G. V. p 2977 N95-30508
MESHCHERYAKOV, V. A. p 2977 N95-30508
p 2981 N95-30912
MEYER, MICHAEL L. p 2768 N95-30856
MEYERS, H. M., III p 2782 N95-31803
MEZA, J. C. p 2962 N95-32076
MEZA, JUAN C. p 2878 N95-32309
MIAO, C. p 2992 N95-31165
MICHEL, E. p 3015 N95-32037
MICHEL, L. p 3009 N95-30503
MICHELMAN, PAUL p 2888 N95-30829
MIDDLETON, DAVID p 2933 N95-30584
MIELKE, THOMAS A. p 2916 N95-31718
MIGNACCA, T. p 2842 N95-32139
MIKS, KATHRYN F. p 2772 N95-31751
MILITELLO, CARMELO p 2945 N95-32215
MILLER, DIANE F. p 3025 N95-31713
MILLER, DOUGLAS S. p 2955 N95-30471
MILLER, H. VINCENT p 2901 N95-31390
MILLER, J. W. p 2964 N95-31831
MILLER, L. H. p 2881 N95-32047
MILLER, M. S. p 2800 N95-31295
MILLER, MARK D. p 2804 N95-30945
MILLER, P. R. p 2980 N95-30790
p 2981 N95-30916
MILLER, R. L. p 3006 N95-31624
MILLER, R. R. p 2800 N95-31290
MILLER, ROGER E. p 2851 N95-31448
p 2851 N95-31449
MILLER, TERRY A. p 2793 N95-30936
MILLION, S. p 2765 N95-32225
p 2856 N95-32235
MILLOTT, THOMAS ALEXANDER p 2762 N95-32111
MILLS, JEFFREY D. p 2791 N95-30409
MILLS, M. J. p 3010 N95-30576
MILOVICH, J. p 3003 N95-30359
MINARIK, STEVEN B. p 2847 N95-30660
MINECK, RAYMOND E. p 2763 N95-32217
MINGJUN, ZHAO p 3001 N95-32153
MINTON, TIMOTHY K. p 2796 N95-31660
MINUS, DONALD K. p 2794 N95-31368
MIRANDA, F. A. p 3011 N95-30703
MIRANIAN, MIHRAN p 2970 N95-32335
p 2971 N95-32338
MIRZABEYGUI, JAHANSHAH p 2768 N95-30881
MITCHA, JENNIFIER L. p 2927 N95-31373
MITCHELL, DAVID G. p 2757 N95-31990
MITCHELL, I. V. p 2804 N95-30797
MITCHELL, JERREL p 2950 N95-30655
MITCHELL, JERREL R. p 2958 N95-30754
MITSUMA, HIDEHIKO p 2789 N95-31740
MITSUMOTO, HIDEO p 2853 N95-31744
MIYAMOTO, KENJI p 2995 N95-32262
MIYAMOTO, T. p 3004 N95-30671
MIZUKAMI, M. p 2755 N95-30861
MLAWER, ELI p 2921 N95-32184
MODIANO, S. H. p 2801 N95-31306
MODINE, F. A. p 2814 N95-30730
MOEN, CHRISTOPHER D. p 2878 N95-32309
MOFFAT, HARRY K. p 3016 N95-32147
MOFFETT, MARK B. p 2814 N95-30715
MOHAIDAT, J. M. p 2906 N95-32212
MOINESTER, M. A. p 2989 N95-32261
MOIR, RALPH W. p 2994 N95-32074
MOKHOV, NIKOLAI V. p 2992 N95-30800
MOLINA, M. J. p 2912 N95-30525
MOLINARI, JOHN p 2919 N95-31128
MONAHAN, PATRICK J. p 2791 N95-30554
MONTAGUE, S. p 2878 N95-30384
MONTEMEZZANI, GERMANO p 2881 N95-31385
MONTENEGRO, E. C. p 2990 N95-32274
p 2990 N95-32275
MONTGOMERY, MATTHEW D. p 2742 N95-30611
MOOG, C. H. p 2950 N95-30564
p 2950 N95-30807
MOON, DARWIN GREGORY p 2785 N95-30826
MOORE, G. J. p 2811 N95-30362
MOORE, GERALD F. p 2922 N95-30857
MOORE, KURT R. p 2933 N95-30602
MOORE, R. L. p 3031 N95-30582
MOORE, SONYA p 2881 N95-31456
MOOREHEAD, T. W. p 3024 N95-30780
MOORHOUSE, DAVID J. p 2758 N95-31998
MORAN, SCOTT J. p 2766 N95-31553
MORAN, WADE W. p 2774 N95-31764
MORE, K. L. p 2788 N95-31403
MOREAU, STEPHANE p 2743 N95-30843
MORENCY, ROGER L. p 2996 N95-30529
MORENO, J. C. p 3006 N95-32028
p 2886 N95-32029
MORETZ, DAVID GAVIN p 3001 N95-31841
MORGAN, D. D. p 2914 N95-30848
MORGAN, D. L., JR. p 2987 N95-32039
MORGAN, J. MURRAY p 2761 N95-32015
MORGAN, JEFF p 2916 N95-31610
MORGAN, M. A. p 2766 N95-31553
MORI, MASAHIRO p 3007 N95-32263
MORI, TAKAMASA p 2979 N95-30656
MORIMATSU, O. p 2983 N95-31227
MORRIS, J. p 2904 N95-31163
MORRIS, J. B. p 2796 N95-31670
MORRIS, VIRGINIA L. p 2777 N95-31775
MORRISON, P. J. p 2868 N95-30763
MORTON, BLAISE p 2952 N95-31266
MOSCOVICI, H. p 2955 N95-30490
MOSES, W. W. p 2878 N95-30378
MOTIWALLA, JUAN p 2939 N95-31262
MOTOVILOV, A. K. p 2961 N95-31619
MOULDER, JOHN F. p 2782 N95-31809
MOVCHAN, A. B. p 3011 N95-30720
MOYER, M. W. p 2823 N95-32352
MROWKA, S. p 3006 N95-32028
MSHELIA, E. D. p 3020 N95-32094
MUELLER, E. p 2880 N95-30752
MUELLER, HANS-GEORG p 2963 N95-31429
MUELLER, M. H. p 3016 N95-32105
MUENCH, ROLF K. p 2887 N95-30386
MUENCHOW, L. p 2980 N95-30911
MUGUIRA, MARITZA R. p 2854 N95-32145
MULDER, E. p 2947 N95-30721
MULDER, J. A. p 2758 N95-31995
MULLEN, KEN I. p 2792 N95-30735
MULLER, BRADLEY MOORE p 2921 N95-31721
MULLINS, D. R. p 2803 N95-30547
MURAD, EDMOND p 2871 N95-30994
MURAKAMI, AKIRA p 2744 N95-31715
MURATA, TAKAO p 2853 N95-31744
MURPHY, JOHN E. p 2976 N95-30423
MURPHY, M. p 3025 N95-31662
MURPHY, P. P. p 2910 N95-32099
MURPHY, R. E. p 2998 N95-31192
MURRAY, ROYCE W. p 2795 N95-31437
MURRAY, W. p 2956 N95-30499
MUSIELAK, Z. E. p 3031 N95-30582
MUSSELMAN, I. H. p 2822 N95-32075
MUTIKAINEN, R. p 2880 N95-30691
MYERS, RODNEY S. p 2782 N95-31807
MYERS, S. M. p 2980 N95-30708
MYKITYSHYN, MARK p 2749 N95-31520

N

NACHEV, I. p 3010 N95-30653
NACHEV, IVO. S. p 3011 N95-30737
NACHTIGAL, N. M. p 2872 N95-31132
NACIRI, JAWAD p 3011 N95-30728
NADOLINK, RICHARD H. p 2866 N95-30412
NAESLUND, T. p 2945 N95-32248
NAHUM, C. p 2841 N95-32134
NAKAGAWA, MASAYUKI p 2979 N95-30656
NAKAJIMA, HAJIME p 2804 N95-30761
p 2806 N95-31154
NAKANE, YOSHIHIRO p 2980 N95-30760
NAKASHIMA, HIROSHI p 2934 N95-30759
NAKATSU, TOSHIO p 3014 N95-31222
p 2983 N95-31225
NALIM, M. RAZI p 2754 N95-30632
NARDONE, STEVEN C. p 2974 N95-30550
NARTKER, T. A. p 3027 N95-32362
NASSTROM, JOHN S. p 2877 N95-32049
NATHAN, G. J. p 2791 N95-30541
NATHEL, H. p 2887 N95-32155
NATION, JOHN A. p 2849 N95-31142
NATKANIEC, I. p 3009 N95-30419
NAU, H. p 2968 N95-32326
NAVEH, NAVA p 2928 N95-31570
NAZARIAN, SOHEIL p 2915 N95-31386
NCNALLY, B. DAVID p 2743 N95-30788
NEAL, EVERETT E. p 2792 N95-30735
NEDERPELT, R. p 2966 N95-30719
NEIHOF, REX A. p 2793 N95-31009
NELHIEBEL, M. p 2845 N95-30368
NELSON, BRADLEY J. p 2929 N95-31685
NELSON, J. F. p 3014 N95-31112
NELSON, J. S. p 3017 N95-32307
NELSON, MARY J. p 2776 N95-31773
NELSON, RANDAL C. p 2963 N95-31585
NELSON, W. D. p 2778 N95-31784
p 2779 N95-31786
NEMANICH, R. J. p 3015 N95-32018
NEMETS, STEVE A. p 2762 N95-30592
NERNEY, S. F. p 3031 N95-30582
NES, E. p 2805 N95-31053
NETEL, H. p 2881 N95-32047
NETZER, D. W. p 2756 N95-31199
NEUBERGER, U. p 2753 N95-32013
NEUFFER, DAVID p 2988 N95-32063
NEVILLE, KELLY J. p 2927 N95-31373
NEWBOLD, B. R. p 2800 N95-31287
NEWMAN, G. A. p 2900 N95-30363
NGUYEN, T. M. p 2855 N95-32224
p 2765 N95-32225
NICHOLS, M. C. p 3000 N95-31681
NICHOLSON, J. Y. p 2891 N95-30783
NICOLAIDES, CLEANTHES A. p 2825 N95-31149
NIEDRA, JANIS M. p 2865 N95-32207
NIEH, T. G. p 2810 N95-32272
NIEMANN, R. C. p 2858 N95-30374
p 2861 N95-30943
NIEMEGEERS, I. G. p 2862 N95-31185
NIEMELAE, M. p 2791 N95-30537
NIILER, PERN P. p 2919 N95-31123
NIKITENKO, YU. V. p 2981 N95-30915
NIKITIN, I. N. p 3019 N95-31193
NIKITIN, L. N. p 2939 N95-31257
NILSEN, J. p 2886 N95-32029
NILSSON, P. p 2922 N95-32315
NIMMO, W. p 2812 N95-30487
NISHINO, Y. p 2983 N95-31227
NISHIO, SATOSHI p 3007 N95-32264
NISHIZAWA, MATSUHIKO p 2793 N95-30938
NIX, DANIEL J. p 2941 N95-31573
NOBLE, BRIAN D. p 2943 N95-32019
NOBLE, JOHN M. p 2933 N95-30397
p 2975 N95-31608
NOBLE, MICHAEL p 2812 N95-30558
NODA, JUNICHI p 2744 N95-31741
NODULMAN, L. p 2992 N95-31165
NOLTEMEIER, H. p 2948 N95-32277
NOONAN, C. A. p 2841 N95-32133
NORDLUND, C. p 2804 N95-30757
NORDQVIST, T. p 2945 N95-32248
NORTON, D. P. p 3009 N95-30542
NORTON, THOMAS S. p 2792 N95-30762
NORTON, W. J. p 2746 N95-31070
NOWAK, IGNACY p 2850 N95-31357
NUGENT, K. W. p 2811 N95-30450
p 2815 N95-30791
NUNN, S. D. p 2822 N95-32085
NUSCA, MICHAEL J. p 2799 N95-31203
NUTT, STEVEN p 2783 N95-30433
NWOSU, KINGSLEY CHUKWUDUM p 3022 N95-30483
NYE, DAVID A. p 2796 N95-31709

O

OAKES, R. E. p 2823 N95-32352
OBLOW, E. M. p 2941 N95-31631
OCKIER, C. J. p 2757 N95-31993
OCONNOR, JOHN C. p 2751 N95-30927
OEGARD, O. p 2929 N95-30522
OERSUND, R. p 2805 N95-31053
OESTREICH, JOHN p 2845 N95-32178
OEZBAY, E. p 3015 N95-32037
OGANESSYAN, K. A. p 3011 N95-30722
OH, BYEONG HOON p 3005 N95-31004
OH, BYUNG HOON p 3005 N95-31366
OH, JOUNG HUN p 3024 N95-30682
OH, S. K. p 2994 N95-32059
OHARA, YOSHIHIRO p 2995 N95-32262
OHLSSON, O. O. p 2902 N95-30375
OHNISHI, YUKIYOSHI p 2989 N95-32267
OHTSUKI, KAZUMASA p 2986 N95-31658
OKUMURA, YOSHIKAZU p 2995 N95-32262
OLARIU, STEPHEN p 2943 N95-31982
OLIVER, MARGARET A. p 2901 N95-31156

OLIVER, W. C. p 2812 N95-30548
p 2805 N95-31105
p 2818 N95-31175
OLSEN, L. C. p 2904 N95-31164
OLSEN, S. p 2800 N95-31287
OLSEN, S. E. p 2799 N95-31198
OLSEN, SHANE E. p 2799 N95-30990
OLSON, C. C. p 2992 N95-31166
OLSON, J. C. p 2818 N95-31377
OLSSON, FREDRIK p 2873 N95-31414
ONO, FUMIEI p 2769 N95-31739
OPAT, G. p 2992 N95-30960
OPAT, GEOFFREY I. p 2979 N95-30689
ORAIFEARTAIGH, L. p 2983 N95-31224
ORAM, TIMOTHY D. p 2753 N95-30920
ORAZI, RICHARD J. p 2883 N95-30744
ORIOL, R. A. p 2935 N95-30968
ORLANDINI, K. A. p 2797 N95-32061
ORLOV, A. V. p 2811 N95-30450
ORME, JOHN S. p 2756 N95-31425
p 2757 N95-31846
OSAHENI, JOHN A. p 2819 N95-31467
OSBORNE, D. H., JR. p 2784 N95-30731
OSGOOD, R. M. p 2902 N95-30505
OSINSKI, LEE MAREK p 2883 N95-31611
OSTERHELD, A. p 2993 N95-32042
OSTERWALD, C. R. p 2905 N95-31381
OSTROM, WILLIAM M. p 2923 N95-31600
OSWALD, R. p 2904 N95-31163
OTTINO, JULIO M. p 3020 N95-31545
OUGOUAG, A. M. p 2894 N95-31254
OUSTERHOUT, J. p 2945 N95-32270
OVER, JIM p 2946 N95-32293
OVERBURY, S. H. p 2803 N95-30547
OWEN, A. KARL p 2753 N95-30514
OWENS, E. C. p 2836 N95-31564
OWENS, LEWIS R., JR. p 2763 N95-32217
OWSIANNY, MARIUSZ p 2850 N95-31357
OZOLS, M. A. p 2936 N95-31228

P

PACKEY, D. J. p 2903 N95-30896
PAIGE, ROBERT p 2940 N95-31452
PAJERSKI, ROSE p 2936 N95-31235
PALACIOS, L. p 3019 N95-30771
PALMA, F. p 2863 N95-31725
PALMER, ROBERT B. p 2988 N95-32063
PALMGREN, S. p 2950 N95-30478
PANJEHSHAHI, E. p 2892 N95-30492
PANKOV, A. A. p 2984 N95-31547
PANLILIO-YAP, NIKKI p 2938 N95-31246
PANNELL, C. N. p 2999 N95-31529
PAPADOPOULOS, G. p 2965 N95-30430
PAPANICOLAOU, GEORGE p 2850 N95-31280
PAPAY, MICHAEL LAWRENCE p 2750 N95-30497
PARESCE, F. p 3030 N95-30806
PARISH, KATHLEEN J. p 2798 N95-32360
PARK, GEUN OK p 2930 N95-31267
PARK, IL-PYUNG p 2748 N95-30486
PARK, JAE CHANG p 2930 N95-31267
PARK, K. C. p 2897 N95-31730
p 2944 N95-32190
p 2899 N95-32202
p 2767 N95-32204
PARK, SOO JIN p 3024 N95-30883
PARKE, MATTHEW C. p 2901 N95-31603
PARR, T. P. p 2799 N95-31200
PARR, TIM p 2801 N95-31307
p 2801 N95-31314
PARRINGTON, RONALD J. p 2894 N95-31054
PARROTT, EDITH p 2762 N95-30592
PARSA, Z. p 2994 N95-32059
PARTHASARATHY, V. p 2814 N95-30732
PARZEN, G. p 2994 N95-32244
p 2995 N95-32297
PASCOLINI, A. p 2882 N95-32159
PASCUAL, X. p 2781 N95-31800
PATEL, NISHEETH p 2869 N95-30689
PATERSON, D. p 3012 N95-30789
PATNAIK, B. K. p 3016 N95-32301
PATRICK, D. p 2886 N95-32143
PATRICK, D. L. p 2882 N95-30379
PATT, FREDERICK S. p 2924 N95-31850
PATTERSON, A. K. p 2752 N95-31544
PATTERSON, J. K. p 2953 N95-31582
PATTERSON, TODD S. p 2852 N95-31555
PAULSEN, T. p 2929 N95-30522
PAUSDER, H.-J. p 2757 N95-31993
PAUSDER, HEINZ-JUERGEN p 2758 N95-32000
PAVER, N. p 2984 N95-31547
PAVLIS, E. C. p 2887 N95-32347
PAXMAN, RICHARD G. p 2846 N95-30562
PAXSON, D. E. p 2754 N95-30617
PAXSON, DANIEL E. p 2754 N95-30517
PAYNE, S. A. p 3016 N95-32268
PEARCE, P. R. p 2858 N95-32320
PEARLSTEIN, FRED p 2803 N95-30551
PEARSON, L. H. p 2782 N95-31804
PEARTON, S. J. p 2806 N95-31150
PECHENIK, ALEXANDER p 2818 N95-31153
PECKERAR, MARTIN C. p 2803 N95-30750
PECORA, LOUIS M. p 2860 N95-30748
PEERY, J. S. p 2866 N95-30464
PEGGS, S. p 2994 N95-32242
p 2994 N95-32243
PELETMINSKY, S. V. p 3010 N95-30648
PENAFIEL, PABLO B. p 2875 N95-31586
PENETRANTE, B. M. p 2911 N95-32281
PENKO, P. F. p 2768 N95-30864
PENNYCOOK, S. J. p 3010 N95-30544
p 3010 N95-30576
PERALTA, A. p 2817 N95-31135
p 2817 N95-31136
PERCEC, V. p 2816 N95-30974
PEREY, D. F. p 2781 N95-31800
PEREZ, IGNACIO M. p 3011 N95-30673
PEROT, JAMES BLAIR p 2873 N95-31349
PERRY, CHRIS E. p 2931 N95-31671
PERRY, MATTHEW p 2864 N95-31842
PERSSON, B. p 2838 N95-30630
PERVUSHIN, V. N. p 2980 N95-30911
PESCE-RODRIGUEZ, R. A. p 2800 N95-31295
PESTOV, Y. N. p 2880 N95-30691
PETERSEN, STEVE p 2840 N95-32128
PETIT, G. p 2971 N95-32343
PETRENKO, A. V. p 2981 N95-30915
PETROVIC, B. G. p 2807 N95-31632
PETTERSSON, A. p 2825 N95-30626
PFALTZ, JOHN L. p 3023 N95-30619
PFEIFFER, SEBASTIAN p 3011 N95-30728
PFEIFLE, TOM W. p 2892 N95-30559
PFENNING, FRANK p 2941 N95-31460
PHAM, T. p 2855 N95-32228
PHANEUF, R. A. p 2979 N95-30654
PHARO, LAWRENCE C., JR. p 2974 N95-30747
PHARR, G. M. p 2812 N95-30548
p 2818 N95-31175
PHILIP, T. p 2879 N95-30687
PHILLIPS, B. SCOTT p 2863 N95-31611
PHILLIPS, CHARLES T. p 2749 N95-32022
PHILLIPS, DICK p 2946 N95-32293
PHILLIPS, M. L. F. p 3008 N95-30382
PHILLIPS, R. J. N. p 2979 N95-30695
PHONG, L. NGO p 2840 N95-32129
PICKRELL, G. R. p 2823 N95-32305
PICORNELL, NIGUEL p 2915 N95-31386
PICRAUX, S. T. p 3014 N95-31112
PIERCE, ROBERT D. p 2850 N95-31392
PIERMARINI, GASPER J. p 2818 N95-31153
PIERSON, LYNDON G. p 2948 N95-31605
PIKE, CHARLES p 2871 N95-30994
PILAFTSIS, A. p 2977 N95-30484
PINTO, JOSEPH F. p 2885 N95-31273
PIQUERAU, A. p 2758 N95-31997
PIROGOV, Y. F. p 2982 N95-31214
PISARSKI, R. D. p 3008 N95-32357
PISARSKI, ROBERT D. p 2988 N95-32079
PISENT, G. p 2976 N95-30429
PLANGETIS, GUS F. p 2887 N95-30387
PLAXTON, SHELDON KENT p 2898 N95-32112
PLICHTA, EDWARD J. p 2905 N95-31554
PLOEGER, E. p 3022 N95-30453
PLOTT, WILLIAM G. p 2861 N95-30950
PLOVNICK, ROSS H. p 2821 N95-31705
PLUCKNETT, K. P. p 2812 N95-30543
POENARU, V. p 2965 N95-30504
POENARU, VALENTIN p 2957 N95-30696
POLANA, RAMPRASAD B. p 2963 N95-31565
POLAT, NEJAT p 3000 N95-31652
POLDERMAN, MICHEL C. p 2971 N95-32337
POLITZER, P. A. p 3003 N95-30641
POLK, THAD p 2940 N95-31459
POLLARA, F. p 2765 N95-32223
p 2855 N95-32227
p 2857 N95-32238
POLLARD, J. E. p 2769 N95-31567
POLLOCK, C. R. p 2887 N95-32155
PONSFORD, A. M. p 2842 N95-32135
POORE, JESSE H. p 2938 N95-31248
POPELAR, J. p 2969 N95-32327
PORCELLO, JOHN p 2848 N95-30902
PORTELLI, JOHN J. p 2974 N95-30747
PORTER, A. p 2937 N95-31242
POTHEN, ALEX p 2932 N95-32046
POULOS, G. S. p 2911 N95-32276
POWANDA, MICHAEL C. p 2926 N95-30870
POWELL, G. L. p 2782 N95-31803
POWELL, H. T. p 3016 N95-32268
POWELL, WILLIAM M. p 2858 N95-32320
p 2968 N95-32321
POWERS, JAMES M. p 2814 N95-30715
POWLESLAND, I. G. p 2752 N95-31544
POZOS, ROBERT S. p 2926 N95-30563
PRABHU, A. N. p 2787 N95-30978
PRAIRIE, MICHAEL R. p 2793 N95-31113
PRAMONO, E. p 2767 N95-32204
PRAWER, S. p 2811 N95-30450
p 2977 N95-30474
p 2815 N95-30791
PREMJI, A. p 2842 N95-32135
PREMORE, R. E. p 2813 N95-30621
PRESS, R. p 2860 N95-30886
p 2953 N95-31562
PRICE, E. W. p 2770 N95-31196
PRICE, ED W. p 2770 N95-30988
PRICE, H. W. p 2903 N95-30887
PRICE, MORGAN p 2943 N95-32019
PRICE, RONALD R. p 2862 N95-31342
PRIDMORE-BROWN, D. C. p 2914 N95-30773
PRINCE, MICHAEL E. p 2779 N95-31790
PRINCE, THOMAS A. p 3026 N95-30469
PROCHKO, AMY E. p 2974 N95-31527
PROKERT, G. p 2868 N95-30810
PROSPERETTI, A. p 2827 N95-31206
PROSPERO, JOSEPH M. p 2918 N95-30782
PROTOPOPESCU, V. p 2941 N95-31631
PROVENZA, A. J. p 2864 N95-31847
PURDY, ELLEN M. p 2821 N95-31663
p 2821 N95-31664
PURETZKY, A. A. p 2813 N95-30572
PURVIS, JOHN A. p 2774 N95-31764
PYKAELAE, M. L. p 2858 N95-30538

Q

QINGHUA, ZHAO p 2997 N95-30909
QIU, CHENGTI p 2870 N95-30965
QUIGLEY, CLAUDIA J. p 2820 N95-31617
QUINTARD, M. p 2875 N95-31592
p 2875 N95-31637

R

RAAB, M. p 2981 N95-31398
RAAEN, S. p 2802 N95-30534
RABIN, JEFF p 2928 N95-31140
RACZKA, R. p 2984 N95-31548
RADHAKRISHNAN, V. p 2934 N95-30603
RADYUSHKIN, A. V. p 2988 N95-32078
RAINSBERGER, R. p 2928 N95-32097
RAISKY, O. Y. p 2906 N95-32212
RAJPOOT, S. p 2994 N95-32059
RAMACHANDRAN, R. p 2991 N95-32353
RAMAN, SETHU p 2921 N95-31577
RAMAN, SHANKAR p 2940 N95-31455
RAMBO, P. W. p 2861 N95-31133
RAMESH, K. T. p 2804 N95-30977
RAMESH, R. p 2808 N95-31689
RAMSEY, J. MICHAEL p 2798 N95-32086
RAND, J. A. p 2906 N95-32057
RANDALL, RICHARD L. p 2946 N95-32290
p 2946 N95-32292
RANDUNSKY, M. B. p 2981 N95-30952
RANGE, R. p 3030 N95-30806
RAO, N. S. V. p 2941 N95-31631
RAPARIA, D. p 2995 N95-32306
RASCH, F. O. p 2804 N95-31052
RATTANAWANGCHAROEN, NIPON p 2848 N95-30828
RAUN, R. L. p 2800 N95-31294
RAVI, J. p 3016 N95-32301
RAVI, S. S. p 2948 N95-32277
RAVISHANKARA, A. R. p 2912 N95-30525
READER, JOSEPH p 3007 N95-32299
READHEAD, MARK p 2974 N95-31365
REANEY, I. M. p 2811 N95-30422
REASS, WILLIAM A. p 3006 N95-31613
REBBERT, MILTON L. p 2803 N95-30750
REDIS, MERCURIOS p 2772 N95-31752
REED, BRIAN D. p 2803 N95-30593
REGAN, AMY H. p 2817 N95-31152
REHDER, JOHN J. p 2940 N95-31420
REHG, JAMES R. p 2928 N95-31383
REINHARDT, KITT C. p 2902 N95-30408
REINHOLD, CARLOS O. p 2984 N95-31402
REINOVSKY, ROBERT E. p 2992 N95-31232
REISENTHEL, PATRICK H. p 2756 N95-31400
REJ, D. J. p 2818 N95-31377
RENCIBIA, P. p 2863 N95-31725
RESING, J. A. C. p 2950 N95-30462
RESS, D. p 3006 N95-32028
RETEL, A. P. p 2743 N95-30885
REUSKEN, A. A. p 2958 N95-30835
REUTERBERG, S. E. p 3021 N95-30699

REYNOLDS, HERBERT M. ..... p 2930 N95-30907
RHEE, IN-SEK ..... p 2821 N95-31666
RIAHI, HASNA ..... p 2958 N95-30820
RICE, B. W. ..... p 3007 N95-32116
RICE, BETSY M. ..... p 2831 N95-31293
p 2801 N95-31308
RICE, P. M. ..... p 2805 N95-31105
RICE, ROBERT F. ..... p 3024 N95-30858
RICHARD, P. ..... p 2989 N95-32120
p 2990 N95-32275
RICHARDS, GEORGE A. ..... p 2792 N95-30762
RICHARDSON, J. W., JR. ..... p 3016 N95-32105
RICHARDSON, JOHN N. ..... p 2984 N95-31427
p 2795 N95-31437
RICHARDSON, W. ..... p 2907 N95-30358
RICHIE, JOSEPH M. ..... p 2748 N95-31013
RICHTER, LUTOSLAWA ..... p 2854 N95-32192
RIDGLEY, MELVIN B. ..... p 2799 N95-31209
RIENTJES, T. H. M. ..... p 2900 N95-30818
p 2900 N95-30819
RIESTER, L. ..... p 2818 N95-31187
RIFKIN, STAN ..... p 2937 N95-31241
RILEY, B. R. ..... p 2768 N95-30864
RIVAS, DAVID R. ..... p 3005 N95-31534
ROBERTS, DONALD E. ..... p 2926 N95-30563
ROBERTS, K. ..... p 2841 N95-32133
ROBERTS, R. G. ..... p 2956 N95-30540
ROBERTS, WILLIAM B. ..... p 2867 N95-30524
ROBERTSON, I. M. ..... p 3016 N95-32103
p 2809 N95-32104
ROBERTSON, J. D. ..... p 2812 N95-30545
ROBINSON, D. W. ..... p 2958 N95-30778
ROBINSON, R. A. ..... p 3015 N95-32062
ROCCA, PATRICK ..... p 2925 N95-30452
ROCHBLATT, D. J. ..... p 2857 N95-32239
ROCHE, C. ..... p 2840 N95-32126
ROCKWAY, J. W. ..... p 2787 N95-31146
RODRIGUES, V. D. ..... p 2990 N95-32271
RODRIGUEZ, FRANCISCO A. ..... p 2887 N95-30399
RODRIGUEZ, J. L. ..... p 2878 N95-30384
ROEDER, J. L. ..... p 2914 N95-30773
p 2915 N95-31536
ROEPKE, G. ..... p 2980 N95-30911
ROGALEV, R. N. ..... p 2960 N95-31258
ROGERS, S. L. ..... p 2836 N95-31470
ROGERS, VICTOR CHARLES ..... p 2890 N95-31710
ROGERS, WILLIAM A. ..... p 2792 N95-30762
ROHLEV, ANTON S. ..... p 2817 N95-31152
ROKHLIN, VLADIMIR ..... p 2848 N95-30869
ROLISON, DEBRA R. ..... p 2794 N95-31271
ROMANOFSKY, R. R. ..... p 3011 N95-30703
ROMEIJN, A. ..... p 2893 N95-30586
RORKE, W. S. ..... p 2906 N95-32090
ROSCA, JUSTINIAN P. ..... p 2942 N95-31657
ROSE, LEO. J. ..... p 2842 N95-32140
ROSE, M. F. ..... p 2904 N95-30947
ROSEN, DAN ..... p 2962 N95-31947
ROSENBERGER, TODD E. ..... p 2799 N95-31208
p 2799 N95-31209
ROSENKRANTZ, D. J. ..... p 2934 N95-30603
ROSENTHAL, PETER ..... p 2861 N95-31147
ROSER, T. ..... p 2987 N95-32031
p 2987 N95-32032
ROSNESS, R. ..... p 2838 N95-30521
p 2929 N95-30522
ROSS, H. ..... p 2753 N95-32013
ROSSI, M. ..... p 2838 N95-30455
ROSSITTO, K. F. ..... p 2757 N95-31992
ROSSOUW, C. J. ..... p 2980 N95-30790
p 2981 N95-30916
ROTMAN, DOUGLAS A. ..... p 2911 N95-32350
ROUTE, ROGER K. ..... p 2967 N95-30939
ROUX, FRANCOIS-XAVIER ..... p 2945 N95-32214
ROUX, O. ..... p 2949 N95-32371
ROWE, GARY K. ..... p 2984 N95-31427
p 2795 N95-31437
ROY, DANIEL M. ..... p 2937 N95-31240
ROYALE, MARK ..... p 2864 N95-31844
ROZGONYI, G. A. ..... p 3016 N95-32301
ROZHKOV, A. A. ..... p 2967 N95-30739
RUBINSTEIN, I. ..... p 2900 N95-30536
RUGGIERO, A. J. ..... p 2792 N95-30714
RUNGTA, R. ..... p 2810 N95-32241
RUSKOV, R. ..... p 2988 N95-32078
RUSSELL, P. J. ..... p 2999 N95-31529
RUSSELL, STEPHEN D. ..... p 2883 N95-30744
RUTH, CARL R. ..... p 2799 N95-31209
RUTKOWSKI, DONNA M. ..... p 2821 N95-31663
p 2821 N95-31664
RUUD, C. O. ..... p 2807 N95-31632
p 2808 N95-31825
RUYTEN, W. M. ..... p 2884 N95-30906
RYE, BARRY J. ..... p 2917 N95-32142
RYNE, ROBERT D. ..... p 2992 N95-31151

S

SABATINI, R. L. ..... p 2803 N95-30706
SABERI, ALI ..... p 2951 N95-30833
SABOLISH, GEORGE ..... p 2938 N95-31243
SACKOS, JOHN T. ..... p 2854 N95-32145
SAHER, D. ..... p 3020 N95-32150
SAITOH, TEIICHIRO ..... p 2804 N95-30761
SAJJAD, M. I. ..... p 2791 N95-30420
SAKAMOTO, HIROSHI ..... p 2769 N95-31739
SAKAMOTO, YUKIO ..... p 2980 N95-30760
SAKATA, KIMIO ..... p 2744 N95-31715
SALDIN, E. L. ..... p 2884 N95-30914
SALEH, ANWAR M. ..... p 2873 N95-31412
SALES, B. C. ..... p 2812 N95-30545
SALITA, MARK ..... p 2770 N95-30987
p 2770 N95-31195
SALOMON, MARK ..... p 2820 N95-31514
SALYER, R. F. ..... p 2756 N95-31199
SAMN, SHERWOOD ..... p 2963 N95-31375
SAMSET, O. ..... p 2902 N95-32316
SAMUELSEN, G. S. ..... p 2755 N95-30853
SANBONGI, SHIGEO ..... p 2789 N95-31740
SANCHEZ, J. A. ..... p 2836 N95-32048
p 2837 N95-32355
SANDEN, R. ..... p 2825 N95-30626
p 2837 N95-32249
SANDER, S. P. ..... p 2912 N95-30525
SANDERS, H. L. ..... p 2776 N95-31774
SANDLIN, GLENN D. ..... p 2852 N95-31590
SANDS, P. D. ..... p 3025 N95-31662
SANNUTI, PEDDAPULLAIAH ..... p 2951 N95-30833
SANTISTEBAN, J. R. ..... p 2807 N95-31409
SARANTSEV, V. P. ..... p 2884 N95-30914
SARIKAYA, MEHMET ..... p 2820 N95-31559
SARKAR, NILANJAN ..... p 2889 N95-31332
SARTENAER, A. ..... p 2956 N95-30570
SARTORI, MICHAEL A. ..... p 2974 N95-30725
SASAKI, MASAKI ..... p 2769 N95-31739
SASIELA, RICHARD J. ..... p 2951 N95-30890
SATO, KAZUO ..... p 2769 N95-31739
SATO, MASAYASU ..... p 3007 N95-32263
SATYANARAYANAN, M. ..... p 2943 N95-32019
p 2948 N95-32021
SAUNDERS, DAVID S. ..... p 2806 N95-31344
SAUNDERS, DAWNN M. ..... p 2795 N95-31580
SAUNDERS, J. D. ..... p 2755 N95-30861
SAUSA, R. C. ..... p 2801 N95-31313
SAVAGE, MARGARET V. ..... p 2926 N95-30563
SAVAGE, S. ..... p 2857 N95-32313
SAVAGE, SAM ..... p 2932 N95-32257
SAVELEVA, N. I. ..... p 3013 N95-30969
SAVELSBERGH, M. W. P. ..... p 3021 N95-30834
SAVION, NAPHTHALI ..... p 2928 N95-31570
SAVOIE, DENNIS L. ..... p 2918 N95-30782
SAVRON, ENDER ..... p 2789 N95-31509
SAYWARD, ELTON G. ..... p 2920 N95-31571
SCALES, E. ..... p 2781 N95-31800
SCARPA, JACK ..... p 2777 N95-31776
SCHADOW, K. C. ..... p 2799 N95-31200
p 2756 N95-31201
SCHAEFER, W. ..... p 2968 N95-32326
SCHAFER, JEFFREY L. ..... p 2860 N95-30900
SCHAFFERS, K. I. ..... p 3016 N95-32268
SCHAICH, P. C. ..... p 2900 N95-30472
SCHANWALD, L. PAUL ..... p 2884 N95-31139
SCHAUBERT, DANIEL H. ..... p 2848 N95-30895
p 2850 N95-31387
SCHAUM, ALAN P. ..... p 3000 N95-31672
SCHECHTER, D. E. ..... p 2778 N95-31784
p 2779 N95-31786
SCHEGOLKOVA, S. N. ..... p 3013 N95-30969
SCHIEBER, BRIAN D. ..... p 2924 N95-32220
SCHIFFMAN, ROBERT L. ..... p 2779 N95-31790
SCHIMMEL, MORRY L. ..... p 2766 N95-31358
SCHKOLNIK, GERARD S. ..... p 2756 N95-31425
p 2757 N95-31846
SCHLANGEN, M. J. ..... p 2852 N95-31606
SCHMIDT, RICHARD E. ..... p 2969 N95-32329
SCHMIDT, S. ..... p 2980 N95-30911
SCHNEIBEL, J. H. ..... p 2808 N95-31643
SCHNEIDER, DIETER ..... p 3004 N95-30769
SCHNEIDER, R. P., JR. ..... p 2882 N95-30380
p 2860 N95-30707
SCHOENMAN, LEONARD ..... p 2768 N95-31169
p 2769 N95-31170
SCHOTT, JOACHIM H. ..... p 3014 N95-31189
SCHRECKENGHOST, DEBRA L. ..... p 2951 N95-30925
SCHROEDER, M. A. ..... p 2800 N95-31295
SCHROEDER, T. B. ..... p 2799 N95-31284
SCHUDDEBOOM, WOUTER ..... p 2980 N95-30774
SCHUKANTZ, J. H. ..... p 2787 N95-31146
SCHULZ, M. ..... p 2914 N95-30773
SCHUTZENHOFER, SCOTT ..... p 2773 N95-31757
SCHUTZENHOFER, SCOTT A. ..... p 2771 N95-31748
SCHWARTZ, A. J. ..... p 2810 N95-32272
SCHWARTZ, MARC N. ..... p 2921 N95-31726
SCHWARTZ, R. A. ..... p 3031 N95-30785
SCHWARZE, GENE E. ..... p 2865 N95-32207
SCHWING, JAMES L. ..... p 2943 N95-31982
SCOTT, COURTNEY C. ..... p 2920 N95-31522
SCOTT, JAMES J. ..... p 2894 N95-31054
SCOTT, JONES M. ..... p 2754 N95-30517
SCOTT, WILLIAM R. ..... p 3011 N95-30673
SCOTTI, STEPHEN J. ..... p 2893 N95-30682
SCRIVEN, GORDON R. ..... p 2871 N95-30995
SEACHOLTZ, RICHARD G. ..... p 2879 N95-30587
SEAGER, C. H. ..... p 3014 N95-31112
SEARS, R. L. ..... p 2905 N95-31381
SEBRING, ROBERT J. ..... p 2805 N95-31121
SECAN, J. A. ..... p 2916 N95-31698
SEHANOBISH, K. ..... p 2820 N95-31471
SEKINE, HIDEO ..... p 2744 N95-31741
SELFRIDGE, GREGORY E. ..... p 2924 N95-31829
SEMERARO, B. D. ..... p 2872 N95-31132
SEMMES, S. ..... p 2957 N95-30622
SENEMEIER, M. ..... p 2785 N95-30787
SENGUPTA, S. K. ..... p 2900 N95-30472
SENNAROGLU, A. ..... p 2887 N95-32155
SENOCAK, EROL ..... p 2790 N95-32113
SENSBURG, O. ..... p 2760 N95-32006
SEOL, S. Y. ..... p 2861 N95-30942
SERDINAK, THOMAS E. ..... p 2896 N95-31419
SERENANDER, T. ..... p 2973 N95-30481
SERGEENKO, M. N. ..... p 3018 N95-30636
SESHADRI, K. ..... p 2801 N95-31312
SETLIFF, LEWIS F. ..... p 2812 N95-30558
SETTER, N. ..... p 2811 N95-30422
SEXTON, DOUGLAS A. ..... p 2883 N95-30744
SGRO, ANTHONY G. ..... p 3008 N95-32351
SHAFFER, WILLIAM A. ..... p 3000 N95-31672
SHAGAM, R. N. ..... p 2811 N95-30389
SHAH, B. ..... p 2856 N95-32235
SHAHBAZIAN, E. ..... p 2842 N95-32139
SHAMAMIAN, VASGEN A. ..... p 2795 N95-31473
SHANG, HUAN-MIN ..... p 2828 N95-31210
SHANHUA, WU ..... p 2887 N95-32152
SHAPIRO, ALAN R. ..... p 2871 N95-30992
SHARLEMANN, E. T. ..... p 2912 N95-30373
SHARPE, JON ..... p 2775 N95-31765
p 2775 N95-31766
SHASHIDAR, RANGANATHAN ... p 3011 N95-30728
SHAW, D. S. ..... p 2976 N95-30443
SHAW, DORIS S. ..... p 2941 N95-31573
SHAW, G. ..... p 2917 N95-32080
SHAW, GARY A. ..... p 2935 N95-30931
SHAW, KEVIN B. ..... p 2901 N95-31390
SHAW, MARY ..... p 2943 N95-31843
SHEEHY, MICHAEL ..... p 2940 N95-31455
SHEKHTMAN, L. I. ..... p 2880 N95-30691
SHEN, JIAN-MIN ..... p 2956 N95-30607
SHEN, STEWART S. ..... p 3007 N95-32148
SHEPELYANSKY, D. L. ..... p 3019 N95-31276
SHER, A. ..... p 2998 N95-31141
SHERER, S. WAYNE ..... p 2946 N95-32289
SHERMAN, RICHARD A. ..... p 2927 N95-31446
SHEVLYAGIN, M. V. ..... p 2983 N95-31216
p 2983 N95-31219
SHI, X. ..... p 2828 N95-31207
SHIAO, MICHAEL C. ..... p 2899 N95-32206
SHIH, MING-HSIN ..... p 2868 N95-30862
SHIH, T.-H. ..... p 2959 N95-30855
SHIHABI, M. ..... p 2856 N95-32235
SHIMOKAWA, TOSHIYUKI ..... p 2789 N95-31740
SHINDO, SIGEMI ..... p 2744 N95-31715
SHINING, YANG ..... p 2997 N95-30901
SHIRAI, TOSHIZO ..... p 2979 N95-30654
SHIVSHANKAR, V. ..... p 2817 N95-31126
SHMUL, MENAHEM ..... p 2758 N95-31994
SHNEJDMILLER, E. A. ..... p 2884 N95-30914
SHOBERG, THOMAS G. ..... p 2923 N95-31719
SHOJI, Y. ..... p 2987 N95-32032
SHONG, WEI-JA ..... p 2894 N95-31254
SHORT, W. ..... p 2903 N95-30896
SHU, SANG MOON ..... p 2930 N95-31267
SHUL, R. J. ..... p 2806 N95-31150
SHUNK, JAMES F. ..... p 2774 N95-31762
SIDHOUM, MOHAMMED ..... p 2772 N95-31752
SIDOROV, ANDREI I. ..... p 2976 N95-30423
SIEGAL, M. P. ..... p 2794 N95-31393
p 2885 N95-31394
SIGMAN, R. K. ..... p 2770 N95-30986
p 2770 N95-31196
SIHVOLA, K. ..... p 2846 N95-30567
SIKKA, V. K. ..... p 2803 N95-30575
p 2810 N95-32272
SILAGADZE, Z. K. ..... p 2988 N95-32069
p 2988 N95-32093
p 2995 N95-32206
SILVER, E. ..... p 3028 N95-31129
SILVESTROV, P. G. ..... p 2966 N95-31259

SIMANDL, R. F. p 2780 N95-31792
SIMMONS, M. L. p 2932 N95-31645
SIMON, HERBERT A. p 2940 N95-31459
SIMONS, GIRARD A. p 2793 N95-30971
SIMPSON, R. L. p 2885 N95-31394
SIMPSON, T. W. p 2804 N95-30797
SIMS, G. D. p 2812 N95-30487
SIMUNOVIC, S. p 2877 N95-32033
SINCLAIR, CRAIG C. p 2939 N95-31252
SINCLAIR, M. B. p 2860 N95-30707
SINGER, NEIL p 2893 N95-30786
SINGH, D. p 2790 N95-32060
SINGH, G. p 2801 N95-31313
SINGH, J. P. p 2790 N95-32060
SINGH, M. p 2822 N95-32208
SINGHOSE, BILL p 2893 N95-30786
SINGSAAS, ALAN L. p 2998 N95-31435
SINHA, N. p 2871 N95-30993
SINHA, SUMON K. p 2874 N95-31443
SINHAROY, A. p 2808 N95-31825
SINKOVITS, ROBERT S. p 2795 N95-31473
SINSHEIMER, F. B. p 2780 N95-31793
SISSON, WARREN G. p 2815 N95-30799
SIVAZLIAN, F. R. p 3015 N95-32018
SIY, H. p 2937 N95-31242
SKOWRONSKI, RAYMUND P. p 2770 N95-31806
SLABOSPITSKIJ, S. R. p 2983 N95-31217
SLANE, STEVE p 2820 N95-31514
SLEEFE, G. E. p 2916 N95-31610
SMALLEY, R. E. p 3012 N95-30944
SMIRNOV, L. S. p 3009 N95-30419
SMITH, A. E. p 2977 N95-30475
p 2977 N95-30476
SMITH, B. K. p 2878 N95-30384
SMITH, BARBARA p 2792 N95-30735
SMITH, C. B. p 2920 N95-31465
SMITH, C. E. p 2755 N95-30698
SMITH, CRAWFORD F. p 2742 N95-30704
SMITH, DENNIS p 2943 N95-31834
SMITH, GARY M. p 2780 N95-31796
SMITH, J. H. p 2878 N95-30384
SMITH, JAMES W. p 2887 N95-30399
SMITH, L. K. p 3016 N95-32268
SMITH, L. L. p 2797 N95-32061
SMITH, LUCY MICHELLE p 2939 N95-31391
SMITH, MYRON p 3029 N95-31424
SMITH, R. A. p 2756 N95-31201
SMITH, R. E. p 3008 N95-30391
p 2745 N95-31062
SMITH, RALPH H. p 2745 N95-31064
SMYRL, N. R. p 2782 N95-31803
SNAIL, KEITH A. p 3014 N95-31269
SNAVELY, DEANNE p 2793 N95-31014
SNAVELY, GEOFF p 2793 N95-31014
SNEAD, L. L. p 2985 N95-31642
SNIEGOWSKI, J. J. p 2878 N95-30384
SOA, DANG VAN p 2979 N95-30637
SOFFER, LOUIS p 2863 N95-31607
SOFRIN, T. G. p 2755 N95-30779
SOGGE, J. p 2798 N95-32372
SOKOL-SUPEL, JOANNA p 2895 N95-31338
SOKOLOV, V. V. p 3020 N95-32150
p 2989 N95-32151
SOLANGI, ATTAULLAH p 2905 N95-31952
SOLEM, JOHNDALE C. p 2854 N95-32050
SOLODUKHIN, S. N. p 3029 N95-30606
SOLOVEV, A. I. p 3009 N95-30419
SON, SANG H. p 3023 N95-30619
SONG, J. Z. p 2817 N95-31135
p 2817 N95-31136
SONG, QIAN p 2997 N95-30908
SONG, WOO SUP p 3005 N95-31366
SONI, BHARAT p 2868 N95-30862
SONNENFROH, D. p 2781 N95-31802
SONNTAG, WILLIAM A. p 2776 N95-31771
SORAN, PATRICK D. p 2792 N95-30735
SORENSEN, K. W. p 2853 N95-31628
SORENSEN, N. ROBERT p 2806 N95-31406
SORNES, P. p 2945 N95-32252
SOULES, DAVID p 2881 N95-31456
SPADAFORA, STEPHEN J. p 2817 N95-31124
SPADY, BLAINE p 2782 N95-31808
SPAEDER, TIMOTHY A. p 2773 N95-31759
SPALDING, D. B. p 2877 N95-32033
SPANGLER, JAN L. p 2940 N95-31420
SPEET, L. J. p 2784 N95-30694
SPENCE, B. p 2964 N95-30428
p 2965 N95-30430
SPENCE, BILL p 3018 N95-30431
SPENCE, PAUL A. p 2878 N95-32309
SPERRY, DAVID J. p 2766 N95-31553
SPIJKER, M. N. p 2959 N95-31184
SPONTARELLI, T. p 2836 N95-32048
p 2837 N95-32355
SPOONER, S. p 2899 N95-32317
SPRAGUE, R. A. p 2915 N95-31535
SPRINGER, A. M. p 2742 N95-30712
SRIVASTAVA, PREM P. p 3019 N95-30741
STAEBLER, G. M. p 3003 N95-30612
STAHL, GEORGE J. p 2860 N95-30726
STALEY, JAMES T. p 2820 N95-31559
STALNAKER, RICHARD p 2800 N95-31288
STALNAKER, RICHARD A. p 2770 N95-30989
p 2770 N95-31197
STAMNES, K. p 2917 N95-32080
STANGE, BERTHA M. p 2793 N95-31113
STANLEY, GARY M. p 2944 N95-32190
STARKOV, A. N. p 2958 N95-30770
STAVNES, MARK p 2768 N95-30860
STAVREV, KRASSIMIR K. p 2795 N95-31595
p 2796 N95-31691
p 2797 N95-31830
STEARNS, R. E. p 2934 N95-30603
STEGEMAN, G. I. p 2999 N95-31441
STEGEMAN, GEORGE p 2884 N95-31145
STEGER, WARREN L. p 2938 N95-31245
STEIN, EARL S. p 2930 N95-31399
STEIN, GUNTER p 2758 N95-31996
STEINBERG, BERNARD D. p 2852 N95-31551
STEINETZ, B. M. p 2867 N95-30710
STEMPLE, JOSEPH Z. p 2794 N95-31271
STEN, T. p 2891 N95-30520
STENBERG, B. p 2837 N95-32249
STEPANOVSKIJ, YU. P. p 2845 N95-30368
STERLING, FRANKLYN D. p 2821 N95-31664
STEVENS, B. p 2907 N95-30358
STEVENS, C. G. p 2901 N95-32027
STEVENS, P. J. p 2798 N95-32258
STEVENSON, JOEL O. p 2806 N95-31406
STEWART, JAMES A. p 2963 N95-31558
STOBIE, I. p 2799 N95-31205
STOCHL, R. J. p 2768 N95-30595
STOCK, THOMAS A. p 2930 N95-31134
STOICA, ION p 2932 N95-32046
STOKES, G. p 2908 N95-30802
STOLIN, A. A. p 2960 N95-31229
p 2961 N95-31397
STOLLER, R. E. p 2982 N95-31104
p 2805 N95-31105
p 2822 N95-32043
STONE, F. D. p 2781 N95-31800
STONEMAN, ROBERT C. p 2884 N95-31213
p 2885 N95-31273
p 2885 N95-31274
STOODT, ROBERT A. p 2888 N95-30716
STOORVOGEL, A. A. p 2951 N95-30833
STORRS, A. p 3030 N95-30806
STORTZ, MICHAEL W. p 2750 N95-30646
STOTTIER, RICHARD H. p 2751 N95-31525
STOYANOV, D. TS. p 2966 N95-30635
STRAIT, E. J. p 3007 N95-32116
STRANE, J. p 3014 N95-31112
STRANGMAN, T. p 2817 N95-31135
p 2817 N95-31136
STRAZISAR, ANTHONY J. p 2867 N95-30524
p 2756 N95-31985
STRELTSOV, V. N. p 2846 N95-30605
STRETCHER, BAXTER p 2848 N95-30902
STRICKLAND, J. H. p 2866 N95-30383
p 2866 N95-30464
STRICKLAND, JOHN W. p 2783 N95-31813
STROKOVSKY, E. A. p 2981 N95-30913
STRONG, RONALD E. p 2766 N95-30919
STROUD, R. J. p 2933 N95-30539
STRUBLE, L. J. p 2798 N95-32091
STRUGALSKI, Z. p 2975 N95-30372
STUBBERUD, P. p 3023 N95-30620
STUBBINS, J. F. p 2894 N95-31254
STURROCK, PETER A. p 3031 N95-31450
SU, TSAN-LIANG p 2772 N95-31752
SU, Z. B. p 3016 N95-32071
SUBRAHMANYAM, V. p 2982 N95-31168
SUCHY, K. p 2846 N95-30567
SUDER, KENNETH L. p 2867 N95-30524
p 2876 N95-31738
SUEMATSU, Y. p 3030 N95-30482
SUENAGA, M. p 2803 N95-30706
SUESS, S. T. p 3031 N95-30582
SULLIVAN, CORNELIUS W. p 2924 N95-32220
SULLIVAN, J. P. p 2794 N95-31393
p 2885 N95-31394
SULLIVAN, MICHAEL J. p 2973 N95-30530
SUMIYOSHI, HIDEKI p 3026 N95-32182
SUN, ELLEN p 2783 N95-30433
SUROVTSEV, YU. S. p 2981 N95-30912
SURYANAARAYANA, KALACHAR p 2817 N95-31115
SUSSKIND, L. p 3029 N95-31102
SUTAY, R. p 2762 N95-30926
p 2763 N95-31101
SUTHAR, JAYANT p 2768 N95-30860
SUTTON, W. H. p 2837 N95-32158
SUZUKI, TAKAO p 2928 N95-31714
SUZUKI, TOMOO p 2934 N95-30759
SVEDIN, J. p 2882 N95-32245
SVENSSON, S. p 3002 N95-32312
SVOBODA, P. p 2903 N95-30887
SWARTZENTRUBER, B. S. p 3017 N95-32308
SWEDENBURG, R. L. p 2842 N95-32141
SWENSON, GARY J. p 2778 N95-31782
SWIFT, CALVIN T. p 2919 N95-31123
SYCARA, KATIA p 2953 N95-31654
SYDNOR, RICHARD p 2967 N95-32319
SYNOWICKI, R. p 2782 N95-31808
SZEBRAT, XAVIER P. p 2747 N95-31687
SZUMSKI, RICHARD GERARD p 2895 N95-31318

T

TAASAN, SHLOMO p 2959 N95-31120
TABATA, TATSUO p 2979 N95-30654
TAGHVA, KAZEM p 3026 N95-32149
TAJIMA, T. p 3029 N95-30729
p 3005 N95-30801
TAKANI, MICHIO p 2913 N95-30758
TAKANO, KOUICHI p 2853 N95-31744
TAKASUGI, K. p 3004 N95-30671
TAKATSU, TAMAO p 2804 N95-30761
TAKEDA, HARUNORI p 2992 N95-31151
TALANOV, V. V. p 2939 N95-31257
TALLANT, D. R. p 2818 N95-31377
p 2885 N95-31394
TAMANOI, H. p 2955 N95-30488
p 2957 N95-30623
TAN, H. H. p 2856 N95-32232
TANAKA, HIDEKI p 3026 N95-32182
TANAKA, SHOJI p 2853 N95-31744
TANAKA, SHUN-ICHI p 2934 N95-30759
TANAKA, TOSHIAKI p 2913 N95-30758
TANG, CHING-JEN p 2801 N95-31304
p 2801 N95-31315
TANG, LI Y. p 2997 N95-30901
TANIS, FREDERICK J., JR. p 2867 N95-30557
TANTER, A. p 2840 N95-32125
p 2840 N95-32127
TAPSCOTT, ROBERT E. p 2747 N95-31569
TARMAN, THOMAS D. p 2948 N95-31605
p 3026 N95-32144
p 2948 N95-32146
TASK, H. L. p 2931 N95-31538
TASNEEM, M. A. p 2791 N95-30420
TATE, ATSUSHI p 2744 N95-31741
TAULBEE, D. B. p 2878 N95-32219
TAUSSIG, DOUGLAS A. p 2998 N95-31435
TAVELLA, PATRIZIA p 2963 N95-32324
TAYLOR, T. S. p 3006 N95-31624
p 3007 N95-32116
TEAFF, D. p 2932 N95-31704
TEAYS, TERRY p 3030 N95-31819
TEICHNER, P. p 2965 N95-30509
p 2965 N95-30555
TELLER, ASTRO p 2943 N95-32020
TENDER, LEONARD M. p 2984 N95-31427
TENTHIJEBOONKKAMP, J. H. M. p 2868 N95-30811
TER-KAZARIAN, G. T. p 2980 N95-30740
TERAZAWA, HIDEZUMI p 2983 N95-31223
TERELST, A. F. M. p 2958 N95-30778
TERYAEV, O. V. p 3017 N95-30371
p 2988 N95-32093
THAGARD, PAUL R. p 2929 N95-31686
THALER, BARRY J. p 2787 N95-30978
THAXTON, ERIC A. p 2782 N95-31805
THOMAS, CLAUDINE p 2968 N95-32323
p 2968 N95-32325
p 2968 N95-32326
THOMAS, J. B. p 2846 N95-30581
THOMAS, N. L. p 2901 N95-32027
THOMAS, VINCENT A. p 3008 N95-32351
THOMAS, W. M. p 2936 N95-31236
THOMPSON, JAMES R. p 3025 N95-31618
THOMPSON, L. M. p 2779 N95-31786
p 2780 N95-31792
THOMPSON, M. O. p 2818 N95-31377
THOMPSON, T. L. p 2836 N95-31470
THOMSON, LAWRENCE J. p 2770 N95-31756
THORNTON, ALFRED J. p 2776 N95-31770
THRONESBERRY, CARROLL p 2951 N95-30925
THUNDAT, T. p 3009 N95-30542
THURSTON, MARLAND p 2774 N95-31761
THYNELL, S. T. p 2800 N95-31299
p 2801 N95-31303
THYNELL, STEFAN T. p 2800 N95-31297
TIAN, ZHIWEI p 2880 N95-30980
TIANJI, WANG p 2997 N95-30901
TIEGS, T. N. p 2822 N95-32085
TINGA, WAYNE R. p 2821 N95-31705
TISSOT, R. G., JR. p 3000 N95-31681

TIWARY, S. N. p 2981 N95-31003
TODD, D. E. p 2908 N95-30793
TODOROV, I. T. p 2966 N95-30591
TOENNESSEN, K. p 2804 N95-31052
TOINT, P. L. p 2956 N95-30570
TOMAC, N. p 2804 N95-31052
TOMAN, C. A. p 2937 N95-31242
TOMITA, KEN-ICHI p 2980 N95-30760
TONON, ALDO p 2760 N95-32009
TOON, O. B. p 2921 N95-32184
TOONEN, B. p 2913 N95-30683
TORRES, FREDDIE p 2894 N95-31054
TORSETHAUGEN, K. p 2907 N95-32286
TORUN, YAGMUR p 2988 N95-32063
TORVUND, T. p 2802 N95-30518
p 2813 N95-30664
TOSHIMA, N. p 2990 N95-32273
TOTH, G. p 2990 N95-32275
TOTTEN, JOHN J. p 2897 N95-31614
TOURDE, R. p 2969 N95-32328
TOWNES, S. p 2855 N95-32228
TOWNSEND, P. D. p 2784 N95-30731
TOYAMA, NOBORU p 2853 N95-31744
TRACY, BARBARA A. p 2919 N95-30976
TRAMMELL, CARMEN J. p 2938 N95-31248
TRAN, TUAN A. p 2979 N95-30637
TRASK, RICHARD P. p 2923 N95-31600
TRAXLER, KATHLEEN M. p 2920 N95-31524
TREBES, J. E. p 3006 N95-32028
TREES, CHARLES C. p 2922 N95-30857
TREHUBENKO, ERIC J. p 2901 N95-31125
TRENARY, MICHAEL p 2795 N95-31440
TRIGEIRO, WILLIAM W. p 2747 N95-31687
TRIPATHY, S. K. p 2997 N95-30973
p 2817 N95-31126
p 2821 N95-31699
TRUE, B. p 2754 N95-30589
TRUMP, JAMES C. p 2890 N95-31576
TRUNZO, RICHARD M. p 2780 N95-31791
TSAI, C. C. p 2779 N95-31786
TSAI, YIFEN p 2798 N95-32360
TSAY, S. C. p 2917 N95-32080
TSIDULKO, YU. A. p 2984 N95-31550
TSUTSUI, I. p 2983 N95-31224
p 3019 N95-31226
TSVETKOV, I. O. p 2991 N95-30604
TUCCHIO, MICHAEL A. p 2888 N95-30716
TUCK, GARY p 2901 N95-31265
TUCKER, H. L. p 2797 N95-31840
TUEGEL, L. p 2799 N95-31212
TUERK, JAMES F. p 2799 N95-31209
TUMA, MARGARET L. p 2997 N95-30849
TURCHI, PATRICE E. A. p 2810 N95-32283
TURNER, GARY S. p 2946 N95-32292
TURNS, S. R. p 2791 N95-30541
TURSKI, A. J. p 2960 N95-31337
TUTTLE, B. A. p 2808 N95-31689
p 2822 N95-32161
TUTTLE, G. p 3015 N95-32037
TVETE, K. p 2933 N95-30501
TYLER, DAVID W. p 2974 N95-31527

U

UDA, G. p 2841 N95-32130
UHLMANN, DONALD R. p 2811 N95-30405
UHRICH, PIERRE J. M. p 2968 N95-32326
p 2969 N95-32328
UHT, J. C. p 2780 N95-31793
ULSTAD, C. p 2900 N95-30536
ULVENSOEN, J. H. p 2802 N95-30518
p 2813 N95-30664
ULYANOV, YU. N. p 2884 N95-30914
UMANATH, NARAYAN S. p 3025 N95-31334
UNDERHILL, K. p 2928 N95-32097
UNDERHILL, LYNN B. p 2946 N95-32294
UPPSAELL, M. p 2945 N95-32251
UPRETY, K. K. p 2859 N95-30649
UPTON, N. K. p 2841 N95-32133
USTAD, A. L. p 2925 N95-30665

V

VAELIMAEKI, V. p 2975 N95-31650
VALENCIAALVARADO, RAUL p 3003 N95-30473
VALETT, JON D. p 2937 N95-31237
VALIN, P. p 2842 N95-32139
VANASSE, G. A. p 2998 N95-31192
VANBLADEL, P. G. p 2784 N95-30460
VANBUSSEL, G. J. W. p 2742 N95-30638
p 2869 N95-30957
VANDENBERG, J. I. p 2743 N95-30837
VANDERBURGH, A. H. P. p 2869 N95-30956
VANDERHOFF, J. A. p 2801 N95-31306
VANDERVEER, G. p 2933 N95-30454
VANDERVEGTE, G. J. p 2892 N95-30585
VANDERWAL, J. p 2950 N95-30808
VANDEVEN, A. A. F. p 2967 N95-30809
VANDEVORST, G. A. L. p 2868 N95-30836
VANDEWIEDE, K. p 3001 N95-31700
VANDIETEN, V. p 2812 N95-30459
VANDIJK, M. J. p 2900 N95-30818
p 2900 N95-30819
VANDORSSELAER, J. L. M. p 2959 N95-31183
VANDRONKELAAR, J. H. p 2748 N95-30815
VANEENIGE, M. J. A. p 2950 N95-30462
VANEIJNDHOVEN, S. J. L. p 2966 N95-30681
VANHOUTUM, C. J. p 2950 N95-30808
VANHOY, D. p 2752 N95-32007
VANLEHN, KURT p 2940 N95-31459
VANLIEMPD, G. p 2847 N95-30812
VARGAS, MARIO p 2880 N95-30851
VARTULI, C. B. p 2806 N95-31150
VASSILAROS, M. G. p 2807 N95-31599
VATN, J. p 3026 N95-32254
VATNE, H. E. p 2979 N95-30666
p 2805 N95-31053
VAUGHAN, J. p 2908 N95-30686
VAVILOV, S. A. p 3011 N95-30720
VAWTER, G. A. p 3008 N95-30391
VAZIRANI, P. p 2856 N95-32237
VEAZIE, DAVID ROBERT p 2787 N95-31110
VECHESLAVOV, V. V. p 2966 N95-32066
VEGA, L. p 2810 N95-32241
VEILLET, CHRISTIAN p 2968 N95-32326
p 2887 N95-32348
VEJVODA, CURTIS E. p 2889 N95-31566
VELEZ, CARLOS p 2821 N95-31666
VELOSO, MANUELA p 2943 N95-32020
VENKATACHALAM, RAVANASAMUDRAM S. p 2811 N95-30415
VER, ISTVAN L. p 2756 N95-31191
VERDON, JOSEPH M. p 2742 N95-30611
VERES, JOSEPH P. p 2830 N95-31289
VERLY, J. G. p 3000 N95-31665
VERMEULEN, A. C. p 2893 N95-30634
VETRANO, JOHN S. p 2809 N95-32052
VICKERS, JOHN H. p 2778 N95-31782
VIDAL, RICHARD C. p 2907 N95-32302
VIITANEN, A. J. p 2849 N95-31159
VIJAYARAGHAVAN, D. p 2878 N95-32210
p 2878 N95-32216
VIK, A. p 2925 N95-30515
VINTON, CLARE p 2773 N95-31758
VISAISOUK, S. p 2844 N95-32171
VISWANATHAN, S. p 2805 N95-31107
VIVEIROS, STEVEN p 2848 N95-30910
VLADIMIROFF, T. p 2832 N95-31301
p 2836 N95-31526
VOECKS, GERALD p 2881 N95-31456
VOGT, GERALD J. p 2817 N95-31152
p 2821 N95-31705
VOGTLIN, G. E. p 2911 N95-32281
VOHRA, SANDEEP T. p 2996 N95-30753
VOIGT, JAMES A. p 2822 N95-32161
VOLKAS, R. R. p 2976 N95-30442
p 2976 N95-30443
p 2976 N95-30446
p 2978 N95-30579
VOLOSOV, V. I. p 3006 N95-32054
VONBERNEWITZ, KAREN p 2821 N95-31666
VONBRENTANO, P. p 2989 N95-32151
VONGERAMB, H. V. p 2982 N95-31176
VONGRUENHAGEN, WOLFGANG p 2758 N95-32000
VOTTA, L. G. p 2937 N95-31242
VREEKE, MARK S. p 2925 N95-30452
VU, BRUCE p 2868 N95-30862
VYLETEL, GREGORY MICHAEL p 2808 N95-31974

W

WADE, J. p 2817 N95-31135
p 2817 N95-31136
WADE, M. R. p 3004 N95-30685
WAELBROECK, F. W. p 3006 N95-31624
WAGANAAR, W. J. p 2818 N95-31377
WAGER, NICHOLAS p 2853 N95-31673
WAGSTAFF, RONALD A. p 2848 N95-30917
WAHLS, RICHARD A. p 2763 N95-32217
WAITE, J. H. p 3030 N95-30806
WAITE, TODD p 2814 N95-30767
WALCHLI, LAWRENCE A. p 2752 N95-32003
WALECH, T. p 2802 N95-30531
WALIGORA, SHARON R. p 2937 N95-31238
WALKER, H. F. p 2940 N95-31431
WALL, MARK A. p 2809 N95-32051
WALLINGFORD, ERROL E. p 2996 N95-30724
WALLMAN, P. H. p 2911 N95-32281
WALTER, GERALD J. p 2776 N95-31770
WALTERS, G. K. p 2792 N95-30614
WALTERS, KENNETH R., SR. p 2920 N95-31524
WALTZ, R. E. p 3003 N95-30359
WAN, A. S. p 3006 N95-32028
p 2886 N95-32029
WAN, CHIH-JIAN p 2881 N95-31836
WAN, HUI p 2880 N95-30980
WANG, B. p 2812 N95-30545
WANG, CHUNXI p 3002 N95-32356
WANG, HANCHING GRANT p 2895 N95-31346
WANG, HSIN-FU p 2790 N95-31976
WANG, HUAXIAO p 2909 N95-31720
WANG, J. N. p 2810 N95-32272
WANG, JANE-LING p 2963 N95-31429
WANG, TEN-SEE p 2868 N95-30862
p 2772 N95-31749
WANG, TIANJI p 2880 N95-30921
WANG, W. B. p 2906 N95-32212
WANG, WEN I. p 2788 N95-31384
WANG, X. L. p 2899 N95-32317
WANG, Y. D. p 2990 N95-32271
p 2990 N95-32273
WARD, MICHAEL D. p 3014 N95-31189
WARMACK, R. J. p 3009 N95-30542
WARREN, M. E. p 3008 N95-30391
WARREN, W. L. p 2808 N95-31689
WARSI, SAIF p 2772 N95-31749
WASSENAAR, REINDER HETTE p 2869 N95-30872
WASSERMAN, H. J. p 2932 N95-31645
WATABIKI, YOSHIYUKI p 3020 N95-31281
WATANABE, KATSUTOSHI p 2804 N95-30761
WATANABE, KAZUHIRO p 2995 N95-32262
WATANABE, MITSUNORI p 2744 N95-31741
WATKINS, F. M. p 2841 N95-32133
WATSON, D. R. p 2815 N95-30798
WATSON, S. J. p 2784 N95-30694
WATSON, T. J. p 2800 N95-31299
WATSON, WILLIE R. p 2974 N95-30850
WATT, A. J. p 2812 N95-30451
WATT, LEWIS C. p 2773 N95-31759
WAY, BRYAN S. p 2923 N95-31600
WAYE, DONALD E. p 2897 N95-31614
WEBB, DAVID p 2783 N95-31812
WEBB, J. S. p 2819 N95-31417
WEBER, B. R. p 2861 N95-30943
WEBER, F. p 3028 N95-30361
WEBSTER, JULIE L. p 2941 N95-31573
WEBSTER, RICHARD p 2901 N95-31156
WEDEVEN, L. D. p 2813 N95-30621
WEDGE, DONNE p 2848 N95-30910
WEEKS, J. D. p 2838 N95-31472
WEFEL, JOHN P. p 3032 N95-32282
WEHRLE, JOHN P. p 2811 N95-30415
WEIDEL, M. p 2759 N95-32004
WEIGEL, M. K. p 3028 N95-30361
WEINMAN, CARL F. R. p 2996 N95-30772
WEISER, P. p 2811 N95-30450
WEISER, P. S. p 2815 N95-30791
WEISS, MARC A. p 2968 N95-32323
WEISS, THOMAS M. p 2921 N95-31587
WEISSHAAR, ANDREAS p 2997 N95-30849
WELCH, C. S. p 2781 N95-31800
WELCH, GERARD E. p 2754 N95-30517
WELLER, ROBERT A. p 2923 N95-31600
WELLMAN, MARK C. p 2959 N95-30953
WELLS, MICHAEL B. p 2915 N95-31560
WENDT, J. R. p 3008 N95-30391
WENG, W. T. p 2994 N95-32092
p 2995 N95-32260
WENGER, LOWELL E. p 3013 N95-31008
WENGER, M. P. p 2859 N95-30561
WENNESON, GREG p 2938 N95-31244
WENNINK, M. p 3021 N95-30834
WERESZCZAK, A. A. p 2814 N95-30732
p 2894 N95-31131
p 2796 N95-31633
WESSEL, RICHARD ALLEN, JR. p 2794 N95-31333
WEST, W. P. p 3003 N95-30612
p 3004 N95-30685
WESTBROOK, CHARLES K. p 2795 N95-31473
WESTPHAL, DOUG p 2921 N95-32184
WHARTENBY, WILLIAM G. p 2914 N95-31012
WHATMOUGH, ROBERT p 2851 N95-31510
WHEATFALL, WALTER L. p 2807 N95-31561
WHEELER, PAUL J. p 2968 N95-32321
WHILLOCK, RAND p 2753 N95-31463
p 2753 N95-31655
p 2753 N95-31656
WHITAKER, A. F. p 2771 N95-31350
p 2771 N95-31748
WHITAKER, S. p 2875 N95-31592
p 2875 N95-31637
WHITBREAD, PAUL p 2851 N95-31510
WHITE, C. W. p 2978 N95-30546
p 2784 N95-30731
p 3016 N95-32301

WHITE, FRANK A., III ..... p 2817 N95-31115
WHITE, K. ..... p 2799 N95-31205
WHITTEN, WILLIAM B. ..... p 2798 N95-32086
WICKERHAUSER, VICTOR ..... p 2848 N95-30869
WICKLUND, A. B. ..... p 2992 N95-31165
WICKWIRE, KENNETH ..... p 2850 N95-31367
WIDDER, J. M. ..... p 2800 N95-31295
WIDMANN, K. ..... p 2987 N95-32041
WIDOM, J. ..... p 3022 N95-30456
WIESERMAN, WILLIAM R. ..... p 2865 N95-32207
WIKA, KEVIN G. ..... p 2939 N95-31249
WILDER, M. C. ..... p 2744 N95-32193
WILLIAMS, J. S. ..... p 2812 N95-30451
WILKEN, B. ..... p 2915 N95-31536
WILKERSON, FRANCES P. ..... p 2910 N95-31981
WILL, C. M. ..... p 2912 N95-30588
WILLEY, ALLAN ..... p 2937 N95-31239
WILLIAMS, BRADLEY A. ..... p 2801 N95-31311
WILLIAMS, CAROL A. ..... p 2970 N95-32333
WILLIAMS, D. M. ..... p 2782 N95-31803
WILLIAMS, F. A. ..... p 2797 N95-31824
WILLIAMS, J. F. ..... p 2894 N95-31254
WILLIAMS, KEVIN L. ..... p 2923 N95-31701
WILLIAMS, W. D. ..... p 2884 N95-30906
WILLIAMSON, D. ..... p 2841 N95-32132
WILLIS, JOHN S. ..... p 2926 N95-30924
WILLSKY, ALAN S. ..... p 2851 N95-31430
WILSON, F. W. ..... p 2920 N95-31465
WILSON, K. J. ..... p 2756 N95-31201
WILSON, L. J. ..... p 3012 N95-30944
WILSON, R. G. ..... p 2806 N95-31150
WILSON, R. H. ..... p 2942 N95-31644
WILSON, ROBERT B. ..... p 3028 N95-30469
WILSON, ROBERT M. ..... p 3030 N95-30467
WING, DAVID J. ..... p 2744 N95-31984
WINGLEE, R. M. ..... p 2914 N95-30848
WINN, DAVID ..... p 2988 N95-32063
WINSKE, DAN ..... p 3008 N95-32351
WINTER, E. M. ..... p 2852 N95-31606
WINTER, J. ..... p 2759 N95-32002
WISEMAN, A. G. ..... p 2912 N95-30588
WITHAM, C. L. ..... p 2881 N95-31694
WITHINGTON, P. M. ..... p 2857 N95-32239
WITHROW, S. P. ..... p 2978 N95-30546
WITTE, N. S. ..... p 2965 N95-30432
p 2965 N95-30435
WOLF, PETER ..... p 2992 N95-30960
p 2968 N95-32326
p 2971 N95-32343
p 2973 N95-32349
WOLFE, W. P. ..... p 2866 N95-30383
WOLINSKI, D. ..... p 2992 N95-31165
WOLTER, S. D. ..... p 3015 N95-32018
WOMACK, MARIA ..... p 3029 N95-30751
WONG, ANDREW K. C. ..... p 2842 N95-32136
WONG, H. K. ..... p 2914 N95-30848
WONG, K. L. ..... p 2990 N95-32274
WONG, R. L. ..... p 2865 N95-32100
WONG, YIU-FAI ..... p 2936 N95-31056
WOOD, B. D. ..... p 2905 N95-31381
WOOD, BLAKE P. ..... p 3006 N95-31613
WOOD, JERRY R. ..... p 2756 N95-31985
WOOD, R. F. ..... p 2813 N95-30572
WOODWARD, ROGER D. ..... p 2769 N95-31716
WOODWARD, W. A. ..... p 2964 N95-31831
WOOLLAM, JOHN A. ..... p 2782 N95-31808
WORKMAN, G. L. ..... p 2781 N95-31801
WORLEY, P. H. ..... p 2913 N95-30683
WORMHOUDT, J. ..... p 2801 N95-31305
WORTH, BRIAN DALY ..... p 2808 N95-31975
WRIGHT, DAVID F. ..... p 2969 N95-32330
WRIGHT, K. ..... p 2785 N95-30787
WRIGHT, SAMUEL A. ..... p 2909 N95-31556
WU, ANDY ..... p 2972 N95-32344
WU, C. Q. ..... p 3016 N95-32071
WU, CHENG-HSIU ..... p 2897 N95-31734
WU, H. ..... p 3011 N95-30667
WU, KE ..... p 2957 N95-30642
WU, W. ..... p 2990 N95-32274
WU, XIANG ..... p 2979 N95-30652
WUEBBLES, DONALD J. ..... p 2911 N95-32350
WYSONG, INGRID J. ..... p 2872 N95-30996
WYSS, G. D. ..... p 3025 N95-31662

X

XIAO, H. ..... p 2816 N95-30997
XIAO, MING-WEN ..... p 3010 N95-30644
XIE, DEREN ..... p 2870 N95-30985
XIONG, JUNJIE ..... p 2941 N95-31533
XU, LIANG ..... p 2921 N95-31577
XU, WANG ..... p 3010 N95-30644

Y

YAGLE, ANDREW E. ..... p 2852 N95-31537
YAMADA, Y. ..... p 2820 N95-31623
YAMAGUCHI, ISAO ..... p 2767 N95-31980
YAMALEEV, R. M. ..... p 3017 N95-30365
YAMAMOTO, MASATAKA ..... p 2789 N95-31740
p 2789 N95-31740
YAMAZAKI, SEIICHIRO ..... p 3007 N95-32264
YAMAZAKI, TOSHIMITSU ..... p 2986 N95-31658
YANG, AN-SHIK ..... p 2797 N95-31717
YANG, CHEN-JEN ..... p 2819 N95-31461
YANG, G. S. ..... p 3012 N95-30847
YANG, S. T. ..... p 2861 N95-30943
YAO, MINWU ..... p 2837 N95-31359
YAO, X. S. ..... p 2856 N95-32236
YASAR, O. ..... p 2931 N95-31130
YATES, K. W. ..... p 2766 N95-31143
YATES, R. K. ..... p 2947 N95-30578
YATSUYANAGI, NOBUYUKI ..... p 2769 N95-31739
YEH, EUENG-NAN ..... p 2924 N95-32220
YEH, H.-G. ..... p 2855 N95-32224
YELTON, DENNIS ..... p 2923 N95-31523
YEN, GUAN-WEI ..... p 2877 N95-31837
YETTER, R. A. ..... p 2801 N95-31309
p 2801 N95-31310
YONG, LIANG ..... p 2905 N95-31735
YONGCHANG, XIE ..... p 2998 N95-31006
YOO, AN NA ..... p 3024 N95-30882
YOON, BYEONG JOO ..... p 3005 N95-31004
YOON, BYUNG JOO ..... p 3005 N95-31366
YOON, JAE SEONG ..... p 3005 N95-31004
YOON, JAE SUNG ..... p 3005 N95-31366
YORKE, J. A. ..... p 2838 N95-31472
YOSHINAGA, TAKASHI ..... p 2744 N95-31741
YOST, FRED G. ..... p 2806 N95-31406
YOST, W. T. ..... p 2781 N95-31800
YOU, H. ..... p 2880 N95-30941
YOUM, I. ..... p 2813 N95-30645
YOUNG, J. F. ..... p 2798 N95-32091
YOUNG, LLOYD M. ..... p 2992 N95-31151
YOUNG, R. A. ..... p 2792 N95-30714
YSTROEM, JACOB ..... p 2794 N95-31356
p 2873 N95-31415
YU, L. ..... p 3016 N95-32071
YUAN, H. ..... p 2827 N95-31206
YUAN, TZU CHIANG ..... p 2977 N95-30465
YUE, MA ..... p 2887 N95-32152
YUEN, JOSEPH H. ..... p 2854 N95-32221
YULIN, LI ..... p 3001 N95-32153
YURA, H. T. ..... p 2883 N95-30394
YUREVICH, V. I. ..... p 2991 N95-30604
YURKOV, M. V. ..... p 2884 N95-30914

Z

ZACHARIA, T. ..... p 2838 N95-30684
p 2931 N95-31130
p 2877 N95-32033
p 2899 N95-32317
ZAEPFEL, T. ..... p 2989 N95-32120
ZAK, B. D. ..... p 2917 N95-32080
ZALIPAEV, V. V. ..... p 3011 N95-30720
ZAVADA, J. M. ..... p 2806 N95-31150
ZAVADIL, K. R. ..... p 2810 N95-32241
ZAWISTOWSKI, JACEK ..... p 2960 N95-31339
ZEBROWSKI, M. A. ..... p 2800 N95-31285
ZELLER, JOACHIM ..... p 2863 N95-31611
ZENG, DAJUN ..... p 2953 N95-31654
ZENG, X. ..... p 2908 N95-30686
ZENO, K. ..... p 2987 N95-32032
ZEPPENFELD, D. ..... p 2979 N95-30695
ZERLAUT, G. A. ..... p 2905 N95-31381
ZERNER, MICHAEL C. ..... p 2795 N95-31595
p 2796 N95-31596
p 2985 N95-31609
p 2796 N95-31691
p 2797 N95-31830
ZHANG, S. Y. ..... p 2986 N95-31832
p 2994 N95-32092
ZHANG, SHU-YU ..... p 2990 N95-32278
ZHANG, VICTOR S. ..... p 2913 N95-30675
ZHANG, Y. ..... p 2969 N95-32331
ZHANG, Y. Z. ..... p 2854 N95-32114
ZHANG, YU-MEI ..... p 3004 N95-30795
ZHANG, YUANCHENG ..... p 2979 N95-30652
ZHAO, WANG ..... p 2997 N95-30908
ZHAO, YIQIANG ..... p 3001 N95-32153
ZHENG, SHANFENG ..... p 2949 N95-30400
ZHOLENTS, A. ..... p 2880 N95-30921
ZHONG, LIN YI ..... p 2991 N95-30360
ZHOU, BANGRONG ..... p 2930 N95-30688
ZHOU, GAN ..... p 2988 N95-32070
p 2881 N95-31385
ZHOU, PING ..... p 2993 N95-31647
ZHOU, YE ..... p 2877 N95-31978
ZHOU, Z. ..... p 2820 N95-31471
ZHU, J. ..... p 2959 N95-30855
ZHU, J. G. ..... p 2978 N95-30546
ZHU, S. ..... p 3009 N95-30542
ZHU, WEILI ..... p 2951 N95-30891
ZIGLER, ARIE ..... p 2884 N95-31190
ZIMMERMAN, F. R. ..... p 2776 N95-31774
ZIMMERMANN, F. ..... p 2993 N95-31256
ZIMMERMANN, H. ..... p 2760 N95-32006
ZINKLE, S. J. ..... p 2806 N95-31188
p 2985 N95-31642
p 2822 N95-32043
ZIOCK, K. ..... p 3028 N95-31129
ZIOCK, K. P. ..... p 2900 N95-30472
ZIRATH, H. ..... p 2882 N95-32245
ZIURYS, L. M. ..... p 3029 N95-30751
ZOLPER, J. C. ..... p 2882 N95-30380
ZORUMSKI, WILLIAM E. ..... p 2974 N95-30850
ZOU, J. ..... p 3015 N95-31641
ZOUROS, T. ..... p 2990 N95-32275
ZUCHOWSKI, KRZYSZTOF ..... p 3006 N95-31737
ZUHR, R. A. ..... p 2812 N95-30545
p 2784 N95-30731
ZUIDGEEST, RENE G. ..... p 2842 N95-32137
ZUIKER, JOSEPH ROBERT ..... p 2787 N95-31347
ZURN, RENA ..... p 2907 N95-32302
ZWILLINGER, DANIEL ..... p 2845 N95-30398

Typical Corporate Source Index Listing

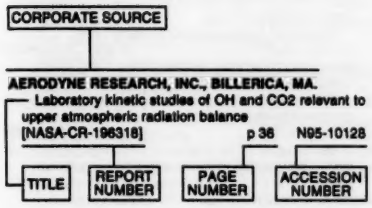

Listings in this index are arranged alphabetically by corporate source. The title of the document provides the user with a brief description of the subject matter. The report number helps to indicate the type of document cited (e.g., NASA report, translation, NASA contractor report). The accession number denotes the number by which the citation is identified. The page number helps you locate the citation in the abstract section. The titles are arranged under each corporate source in ascending accession number order.

A

AC ENGINEERING, INC., HUNTSVILLE, AL.
Standardization of surface contamination analysis systems p 2781 N95-31798

ACADEMY OF SCIENCES (USSR), NOVOSIBIRSK (USSR).
Experimental characterisation of gas microstrip detectors. Part 3: Lifetime characteristics
[PB95-192845] p 2880 N95-30691
Recoil correction in the Dirac-Coulomb problem
[DE95-619241] p 2959 N95-31137
Instanton - antiinstanton interaction and asymptotics of perturbation theory expansion of in double well oscillator
[DE95-619245] p 2966 N95-31259
Removal of impurity ions from a magnetic trap with a two-component plasma on their collision with fast component ions
[DE95-614171] p 2984 N95-31550
Optimization of an expander of a gas-dynamic trap
[DE95-614172] p 3006 N95-31679
Determination of electric and magnetic fields in open trap plasmas by means of atomic-molecular beam hydrogen isotopes
[DE95-614177] p 3006 N95-31680
Calibration of multichannel analyzer of charge-exchange atoms
[DE95-614178] p 2987 N95-32053
Energy spectra of charge-exchange atoms from a rotating plasma
[DE95-614179] p 3006 N95-32054
Longitudinal losses of charged particles from an open configuration with arbitrary beta ratio
[DE95-614187] p 2987 N95-32055
Bernstein-Green-Kruskal wave
[DE95-614201] p 3007 N95-32056
Instability of weakly nonlinear chaotic structures
[DE95-613441] p 2966 N95-32066
SO(8) color as possible origin of generations
[DE95-613560] p 2988 N95-32069
Statistical properties of chaotic scattering with one open channel
[DE95-613370] p 3020 N95-32150
Mixing phases of unstable two-level systems
[DE95-613844] p 2989 N95-32151
Nuclear-spin-dependent parity-nonconserving effects in thallium, lead and bismuth atoms
[DE95-614120] p 2991 N95-32354

ADVANCED FUEL RESEARCH, INC., EAST HARTFORD, CT.
HTS Josephson technology on silicon with application to high speed digital microelectronics
[AD-A288627] p 2861 N95-31147

ADVANCED SCIENTIFIC CONCEPTS, INC., PITTSBURGH, PA.
Training metacognitive skills for problem solving
[AD-A290310] p 2959 N95-31002

ADVISORY GROUP FOR AEROSPACE RESEARCH AND DEVELOPMENT, NEUILLY-SUR-SEINE (FRANCE).
Flight Vehicle Integration Panel Workshop on Pilot Induced Oscillations
[AGARD-AR-335] p 2745 N95-31061
Active control technology: Applications and lessons learned
[AGARD-CP-560] p 2757 N95-31989
Guidance and Control for Future Air-Defence Systems
[AGARD-CP-555] p 2839 N95-32123
Environmentally Safe and Effective Processes for Paint Removal
[AGARD-LS-201] p 2843 N95-32165

AERO OPTICS, INC., ROLLING HILLS ESTATES, CA.
Vacuum plume backflow and rarefaction p 2871 N95-30995

AERODYNE RESEARCH, INC., BILLERICA, MA.
Embedded infrared fiber optic absorption studies of nitramine propellant strand burning p 2801 N95-31305

AERONAUTICA MACCHI S.P.A., VARESE (ITALY).
Control law design using H-infinity and mu-synthesis short-period controller for a tail-airplane p 2758 N95-31999

AEROSPACE CORP., EL SEGUNDO, CA.
Optimum truncation of a Gaussian beam for propagation through atmospheric turbulence
[AD-A291156] p 2883 N95-30394
Oxygen charge state abundance in the inner magnetosphere
[AD-A293497] p 2915 N95-31536
Beam-centroid tracking instrument for ion thrusters
[AD-A293654] p 2769 N95-31567
Replacement of ozone depleting and toxic chemicals in gravimetric analysis of non-volatile residue p 2780 N95-31793
Allan deviation computations of a linear frequency synthesizer system using frequency domain techniques p 2972 N95-32344

AEROSPACE CORP., LOS ANGELES, CA.
Low-latitude boundary layer near noon: An open field line model
[ATR-93(7270)-1] p 2914 N95-30773
Global Ultraviolet Imager (GUVI) investigation
[NASA-CR-189430] p 2917 N95-31820
Monte Carlo simulations of precise timekeeping in the Milstar communication satellite system p 2970 N95-32336

AEROSPATIALE, TOULOUSE (FRANCE).
Flying qualities of civil transport aircraft with electrical flight control p 2761 N95-32016
Paint removal principles p 2843 N95-32167
Stripping with dry ice p 2844 N95-32172
Aquastrip p 2844 N95-32173
Stripping by laser p 2844 N95-32174
Selective chemical stripping p 2844 N95-32175
Bioremediation of wheat starch media waste p 2845 N95-32178
Process evaluation p 2845 N95-32180
Standardization work p 2845 N95-32181

AIR-CONDITIONING AND REFRIGERATION TECHNOLOGY INST., INC., ARLINGTON, VA.
Compatibility of refrigerants and lubricants with motor materials under retrofit conditions
[DE95-010185] p 2814 N95-30767
ARTI Refrigerant Database
[DE95-008336] p 2816 N95-31057
Compatibility of manufacturing process fluids with HFC refrigerants and ester lubricants
[DE95-012152] p 2911 N95-32364

AIR FORCE CIVIL ENGINEERING CENTER, TYNDALL AFB, FL.
Major weapon system environmental life-cycle cost estimating for Conservation, Cleanup, Compliance and Pollution Prevention (C3P2) p 2774 N95-31761

AIR FORCE ENVIRONMENTAL TECHNICAL APPLICATIONS CENTER, SCOTT AFB, IL.
Improved altimeter settings for A-10 aircraft
[AD-A293142] p 2753 N95-30920
Equatorial Africa: A climatological study
[AD-A293956] p 2920 N95-31524
Artificial intelligence techniques for flight test planning, phase 1
[AD-A293962] p 2751 N95-31525

AIR FORCE FLIGHT TEST CENTER, EDWARDS AFB, CA.
Flight test results of the F-16 aircraft modified with axisymmetric vectoring exhaust nozzle p 2752 N95-32007
An investigation of pilot induced oscillation phenomena in digital-flight control systems p 2760 N95-32011

AIR FORCE INST. OF TECH., WRIGHT-PATTERSON AFB, OH.
Selecting optimal experiments for feedforward multilayer perceptrons
[AD-A290856] p 2949 N95-30406
The junction characteristics and current conduction mechanisms of GaInP2 n(+)p diodes and solar cells
[AD-A290857] p 2902 N95-30408
An experimental study of planar heterogeneous supersonic confined jets
[AD-A290859] p 2867 N95-30557
Evaluation of calibration parameters and performance of the video imaging technique of assessing exposure (VITAE system)
[AD-A289023] p 2927 N95-30998
Unification of LARCH and Z-based object models to support algebraically-based design refinement: The LARCH perspective
[AD-A289235] p 2935 N95-30999
Patient/aircraft forecasting for the strategic aeromedical evacuation lift-bed process
[AD-A293902] p 2747 N95-31512
Investigation of ground target detection methods in fully polarimetric wide angle synthetic aperture radar images
[AD-A293922] p 2851 N95-31513
Compressible turbulence measurement in low-angle injection into a supersonic flow
[AD-A293836] p 2874 N95-31516
Acquiring consistent knowledge for Bayesian Forests
[AD-A293858] p 2952 N95-31517
A new goodness-of-fit test for the gamma distribution based on sample spacings from complete and censored samples
[AD-A293875] p 2961 N95-31518
Dynamic maintenance scheduling for a stochastic telecommunication network: Determination of performance factors
[AD-A293829] p 2852 N95-31555
Spatial time-series: Pollution pattern recognition under irregular interventions
[AD-A293830] p 2909 N95-31556
Multipoint quadratic approximation for numerical optimization
[AD-A293837] p 2961 N95-31557
Nonlinear time series analysis
[AD-A293841] p 2963 N95-31558
Analysis and modeling of an airport departure process
[AD-A293782] p 2749 N95-31581
The effect of repeatedly sampling an embedded metamodel on the simulation response
[AD-A293783] p 2953 N95-31582
Analysis of heads-up display quickening versus handling qualities
[AD-A293797] p 2753 N95-31584

Analysis and extension of model-based software executives
[AD-A293834] p 2944 N95-32073

AIR FORCE OFFICE OF SCIENTIFIC RESEARCH, BOLLING AFB, WASHINGTON, DC.
Research proposal
[AD-A293207] p 3032 N95-30899

AIR FORCE SYSTEMS COMMAND, WRIGHT-PATTERSON AFB, OH.
Wide field of view helmet display systems mounted for helicopter simulation
[AD-A293123] p 2930 N95-30888
Multi-valued neural network modified model and its optical realization.
[AD-A293140] p 2951 N95-30891
Real time correlating operation on diffuse objects
[AD-A293220] p 2997 N95-30901
Optical logic and signal processing using a semiconductor laser diode-based optical bistability device
[AD-A293248] p 2997 N95-30908
A study of end-fire coupling of single-mode fiber to Ti: LiNbO3-single-mode planar waveguide
[AD-A293249] p 2997 N95-30909
Application of computer generated holograms to optical transformations
[AD-A293146] p 2880 N95-30921
10 kW heat pipe-heat sink development
[AD-A293167] p 2870 N95-30965
Optical feature recognition
[AD-A293168] p 2997 N95-30966
A real time method for Fourier transform holographic information storage
[AD-A293186] p 2880 N95-30980
Phase object display by using acousto-optical Bragg diffraction
[AD-A293153] p 2998 N95-31006

ALABAMA UNIV., HUNTSVILLE, AL.
Aerophysics test program 1
[AD-A293890] p 2963 N95-31543
Study of surfaces using near infrared optical fiber spectrometry p 2781 N95-31801

ALBANY UNIV., ALBANY, NY.
LAWS hurricane studies
[NASA-CR-189436] p 2919 N95-31128

ALENIA AERONAUTICA, TURIN (ITALY).
Digital autopilot design for combat aircraft in ALENIA p 2760 N95-32009

ALLIED-SIGNAL AEROSPACE CO., KANSAS CITY, MO.
Urethane foam process improvements
[DE95-008957] p 2815 N95-30798
Computer-aided inspection process definition: Development of an expert planning and programming system for coordinate metrology
[DE95-010411] p 2940 N95-31404

ALLIED-SIGNAL CORP., PHOENIX, AZ.
Life prediction methodology for ceramic components of advanced heat engines: Phase 1. Volume 1
[DE95-010805] p 2817 N95-31135
Life prediction methodology for ceramic components of advanced heat engines. Phase 1: Volume 2. Appendices
[DE95-010806] p 2817 N95-31136

ALLISON ENGINE CO., INDIANAPOLIS, IN.
Advanced k-epsilon modeling of heat transfer
[NASA-CR-4579] p 2874 N95-31423
Advanced turbine systems program conceptual design and product development
[DE95-000068] p 2890 N95-32163

AMERICAN SUN CO., BLUE HILL, ME.
Extra focal convective suppressing solar collector
[DE95-010170] p 2907 N95-32288

AMES LAB., IA.
Phase transformations in melt-spun Y-Ba-Cu-O bulk superconductor
[DE95-010237] p 3011 N95-30667
A metallurgical approach toward alloying in rare earth permanent magnet systems
[DE95-010242] p 2966 N95-30668
Processing and characterization of nanocrystalline molybdenum disilicide (MoSi2) consolidated by hot isostatic pressing (HIP)
[DE95-010243] p 3012 N95-30756
Dissolution of eutectic microstructures
[DE95-010244] p 2804 N95-30757
Room temperature fracture and high temperature creep deformation properties of alumina reinforced with 20 vol% particulate niobium
[DE95-010234] p 2815 N95-30897
Magnetic resonance spectroscopy of fullerenes and (pi)-conjugated polymers
[DE95-010131] p 2817 N95-31108
A study of Damascus steel
[DE95-010127] p 2809 N95-32023
A numerical analysis of crack growth in microcracking ceramic and ceramic composites
[DE95-010132] p 2897 N95-32024
An experimental search for high ZT semiconductors: A survey of the preparation and properties of several alloy systems
[DE95-010232] p 2865 N95-32084

AMPTEK, INC., BEDFORD, MA.
Space systems environmental interaction studies
[AD-A293826] p 2766 N95-31553

ANALYTIC POWER CORP., BOSTON, MA.
Mobile electric power
[AD-A292721] p 2860 N95-30940
Linear Motor Free Piston Compressor
[AD-A293452] p 2889 N95-31374

ANALYTICAL METHODS, INC., BELLEVUE, WA.
Survey of recent Al2O3 droplet size data in solid rocket chambers, nozzles, and plumes p 2770 N95-31195

ANALYTICAL METHODS, INC., OGDEN, UT.
Survey of recent Al2O3 droplet size data in solid rocket chambers, nozzles, and plumes p 2770 N95-30987

APPLIED MATHEMATICS, INC., GALES FERRY, CT.
Objective analysis of oceanic data for Coast Guard trajectory models
[AD-A292884] p 2924 N95-32363

ARGONNE NATIONAL LAB., IL.
High-temperature superconducting current leads
[DE95-008404] p 2858 N95-30374
Producing usable fuel from municipal solid waste
[DE95-008405] p 2902 N95-30375
On the use of electronic tilt sensors as angle encoders for synchrotron applications
[DE95-005836] p 2880 N95-30941
Optimization of high-temperature superconductor current leads
[DE95-005838] p 2861 N95-30942
Performance evaluation of high-temperature superconducting current leads for micro-SMES systems
[DE95-005843] p 2861 N95-30943
IPNS neutron scattering instrumentation. A: Existing and planned. B: Possibilities for IPNS upgrade, a 1-MW spallation source
[DE95-004119] p 2985 N95-31616
Influence of fiber content on mechanical performance of SiC-fiber-reinforced reaction-bonded silicon nitride composites
[NASA-TM-110639] p 2790 N95-32060
Faster, cheaper radioanalytical methods
[DE95-009913] p 2797 N95-32061
On the possibility of a two-state magnetic structure for nanocrystalline chromium
[DE95-009914] p 3015 N95-32062
Defect configurations in neutron-irradiated U3Si2
[DE95-009896] p 3016 N95-32105
Combatting urban air pollution through Natural Gas Vehicle (NGV) analysis, testing, and demonstration
[DE95-008300] p 2911 N95-32156
Waste minimization via preparative scale high performance gel permeation chromatography
[DE95-011797] p 2798 N95-32360

ARIZONA UNIV., PHOENIX, AZ.
The land component of the global climate system with adequate spatial resolution
[DE95-009323] p 2908 N95-30686

ARIZONA UNIV., TUCSON, AZ.
Ceramics derived from metal-organic precursors
[AD-A290791] p 2811 N95-30405
Intelligent synthetic polymers
[AD-A292905] p 2819 N95-31395
Influence of layer order and composition on the magnetic anisotropy of ultra-thin Co sandwiches
[DE95-010608] p 2810 N95-32265

ARMSTRONG LAB., BROOKS AFB, TX.
Using computerized neuropsychological testing to assess aviator skills
[AD-A293227] p 2928 N95-30905
Forward rapid rotation shiftwork in USAF air traffic controllers: Sleep, activity, fatigue and mood analyses
[AD-A293448] p 2927 N95-31373
Numerical solution of a singular integral equation arising from a sequential probability ratio test
[AD-A293463] p 2963 N95-31375
Psychological pilot selection in the US Air Force, the Luftwaffe, and the German Aerospace Research Establishment
[AD-A293779] p 2928 N95-31376
Simulation of oculomotor post-inhibitory rebound burst firing using a Hodgkin-Huxley model of a neuron
[AD-A293821] p 2927 N95-31552

ARMY AEROMEDICAL RESEARCH LAB., FORT RUCKER, AL.
Luminance effects on visual acuity and small letter contrast sensitivity
[AD-A293310] p 2928 N95-31140
Design of digital low-pass filters for time-domain recursive filtering of impact acceleration signals
[AD-A293086] p 2864 N95-31842

ARMY ARMAMENT RESEARCH, DEVELOPMENT AND ENGINEERING CENTER, PICATINNY ARSENAL, NJ.
Acidity and basicidity of nitro substituted imidazoles
[AD-A293969] p 2836 N95-31526

ARMY ARMAMENT RESEARCH, DEVELOPMENT AND ENGINEERING CENTER, WATERVLIET, NY.
The electrodeposition of low contraction chromium/molybdenum alloys using pulse-reverse plating
[AD-A292727] p 2804 N95-30945
A simple and accurate technique for monitoring crack growth behavior using a wave form analyzer
[AD-A293161] p 2894 N95-31007
Contactless characterization of semiconductors using laser-induced surface photo-charge voltage measurements
[AD-A293618] p 2863 N95-31725

ARMY COMMUNICATIONS-ELECTRONICS COMMAND, FORT MONMOUTH, NJ.
Magnesium battery disposal characteristics
[AD-A293053] p 2863 N95-31607

ARMY CONSTRUCTION ENGINEERING RESEARCH LAB., CHAMPAIGN, IL.
Off-potential measurement systems for impressed current cathodic protection
[AD-A290876] p 2812 N95-30558
Effectiveness of an electronic performance support system for use with computer-aided design software
[AD-A293757] p 2941 N95-31573

ARMY ENGINEER WATERWAYS EXPERIMENT STATION, VICKSBURG, MS.
QTSAW (Quick Typhoon Surge and Waves). Wave information studies of US coastlines
[AD-A293172] p 2919 N95-30976

ARMY FOREIGN SCIENCE AND TECHNOLOGY CENTER, CHARLOTTESVILLE, VA.
Studies of C(60) and C(70) and other fullurenes: Synthesis, derivation, electrochemistry, lubricant properties and new composition materials
[AD-A292726] p 3012 N95-30944

ARMY RESEARCH LAB., ABERDEEN PROVING GROUND, MD.
Three-dimensional (3D) large fluid flow computations for US Army applications on KSR-1, CM-200, CM-5, and Cray C-90
[AD-A293125] p 2869 N95-30889
A RASCAL in-bore dynamic analysis of the task B and task C electromagnetic railguns
[AD-A292742] p 2764 N95-30948
Effects of hydrostatic pressure on the mechanical behavior of composite materials
[AD-A293162] p 2787 N95-30963
Experiments in a 120-mm ram accelerator including flow visualization p 2799 N95-31202
Numerical simulation of ram accelerator performance including transient effects during initiation of combustion and sensitivity studies p 2799 N95-31203
Pulse forming network in the ETC combustion characterization of plasma augmented solid propellants p 2799 N95-31205
Workshop report: Measurement techniques in highly transient, spectrally rich combustion environments p 2799 N95-31208
Pressure transducer performance and measurement trade-offs in a transient, high temperature, combustion environment p 2799 N95-31209
Molecular models for nitro compounds p 2831 N95-31293
Condensed-phase processes during solid propellant combustion. 5: Further observations on depth profiling of burned surfaces of XM39 and M43 propellants p 2800 N95-31295
Improvements in infrared absorption of solid propellant flames p 2801 N95-31306
An ab initio study of the reaction HNO + NO yields OH + N2O: Preliminary results p 2801 N95-31308
Studies of reactions pertaining to and development of a reduced mechanism for the double base propellant dark zone p 2801 N95-31312
Flame structure studies of neat and NH3 doped H2/N2O flames employing molecular beam mass spectrometry and modeling p 2801 N95-31313
Derivation of two-dimensional (2-D) conduction equation in generalized coordinates with constant and anisotropic physical properties
[AD-A293896] p 3020 N95-31511
Evaluation of halon alternatives in inerting experiments
[AD-A293774] p 2795 N95-31580
Two-dimensional Finite Difference Time Domain (FD-TD) model of electromagnetic (EM) scattering from a buried rectangular object
[AD-A293685] p 2852 N95-31601
Fourier Transform (FT) Raman spectroscopy of nitrogen at high pressure
[AD-A293051] p 2796 N95-31670

The theoretical calculation of vibrational circular dichroism spectra
[AD-A293614] p 2798 N95-32258
ARMY RESEARCH LAB., ADELPHI, MD.
Local fractal dimension estimation
[AD-A293354] p 2959 N95-30953
A two-dimensional finite difference algorithm on the KSR1
[AD-A293576] p 2941 N95-31594
ARMY RESEARCH LAB., FORT MONMOUTH, NJ.
Composite polymer electrolyte for lithium batteries
[AD-A293924] p 2820 N95-31514
Poisson's ratio for hexagonal crystals
[AD-A293556] p 3015 N95-31539
Lithium ion aqueous cells
[AD-A293828] p 2905 N95-31554
ARMY RESEARCH LAB., WATERTOWN, MA.
Mode I large strain viscoelastic crack behavior in nitrile rubber sheets
[AD-A289984] p 2820 N95-31617
ARMY RESEARCH LAB., WHITE SANDS MISSLE RANGE, NM.
User's manual for the Scanning Fast Field Program (SCAFFIP) EOSAEL version 1.0
[AD-A291445] p 2933 N95-30397
Validation of the atmospheric transmission large-area analysis system (ATLAS)
[AD-A293810] p 2916 N95-31589
The effects of large and small scale turbulence on sound propagation in the atmosphere
[AD-A293657] p 2975 N95-31608
ARMY TANK-AUTOMOTIVE COMMAND, WARREN, MI.
Fuel-type classification and parameters prediction by Gas Liquid Chromatography analysis
[AD-A293442] p 2794 N95-31368
ARMY TANK-AUTOMOTIVE RESEARCH AND DEVELOPMENT COMMAND, WARREN, MI.
Compatibility of Single Hydraulic Fluid with military specification fluids, seals and metallurgy
[AD-A292954] p 2821 N95-31663
Recycling MIL-H-46170 hydraulic fluid to extend fluid service life
[AD-A293035] p 2821 N95-31664
Evaluation of Environmentally Acceptable hydraulic fluids
[AD-A293037] p 2821 N95-31666
ARMY TEST AND EVALUATION COMMAND, ABERDEEN PROVING GROUND, MD.
Test operations procedure (TOP) 1-2-512 electromagnetic compatibility tests
[AD-A293758] p 2852 N95-31574
ARNOLD ENGINEERING DEVELOPMENT CENTER, ARNOLD AFS, TN.
Analysis of planar laser-induced fluorescence images obtained during shakedown testing of the AEDC impulse facility
[AD-A293237] p 2884 N95-30906
Icing simulation in the aeropropulsion systems test facility propulsion development test cell C-2
[AD-A293039] p 2747 N95-31667
ASIAN OFFICE OF AEROSPACE RESEARCH AND DEVELOPMENT, APO SAN FRANCISCO, CA.
XV NSO/Sac Peak Solar workshop
[AD-A292319] p 3030 N95-30482
Virtual Reality Software and Technology '94
[AD-A292334] p 2939 N95-31262
The 10th International Conference on the Strength of Materials
[AD-A292335] p 2894 N95-31263
The 2nd Japan-US Symposium on Finite Element Methods in Large Scale Computational Fluid Dynamics
[AD-A292337] p 2960 N95-31264
Visit to Ionospheric Modeling and Remote Sensing Branch, Phillips Laboratory in Hanscom AFB, MA
[AD-A292339] p 2901 N95-31265
ASTROPOWER, INC., NEWARK, DE.
Development of large-area monolithically integrated Silicon-Film(trademark) photovoltaic modules
[DE95-004089] p 2906 N95-32057
ATHENS STATE COLL., AL.
Development of a CFC Critical Area Response (CAR) package p 2783 N95-31814
ATMOSPHERIC AND ENVIRONMENTAL RESEARCH, INC., CAMBRIDGE, MA.
Support of environmental requirements for cloud analysis and archive (SERCAA): Database management facility
[AD-A293938] p 2920 N95-31522
AUBURN UNIV., AL.
A feedback linearization approach to orbital maneuvers p 2765 N95-30841
Prospector 7: Small fuel cells for portable power workshop
[AD-A292729] p 2904 N95-30947

B

BALLISTIC MISSILE DEFENSE ORGANIZATION, WASHINGTON, DC.
System considerations for efficient communication and storage of MSTI image data
[NASA-CR-198869] p 3024 N95-30858
TMD detection and tracking using improved AWACS sensors p 2840 N95-32128
Using a Red Team to devise countermeasures p 2842 N95-32141
BATTELLE MEMORIAL INST., COLUMBUS, OH.
Monte Carlo code for evaluating the Boundary Layer Illumination and Radiation Balance model (BLIRB)
[AD-A293963] p 2915 N95-31560
Alternatives to ozone depleting refrigerants in test equipment p 2775 N95-31767
BAY AREA ENVIRONMENTAL RESEARCH INST., SAN FRANCISCO, CA.
Use of arm measurements to improve radiative transfer models used in climate models
[NASA-CR-199014] p 2921 N95-32184
BBN SYSTEMS AND TECHNOLOGIES CORP., CAMBRIDGE, MA.
An active liner system for jet engine exhaust silencers, phase 1
[AD-A293277] p 2756 N95-31191
Integrated high performance distributed system
[AD-A292821] p 2947 N95-31445
BETTIS ATOMIC POWER LAB., WEST MIFFLIN, PA.
Laboratory robotics: An automated tool for preparing Ion Chromatography calibration standards
[DE95-009441] p 2798 N95-32318
BLACKSTONE CORP., JAMESTOWN, NY.
Ultrasonic cleaning: Fundamental theory and application p 2778 N95-31783
BOEING DEFENSE AND SPACE GROUP, PHILADELPHIA, PA.
Advanced flight control technology achievements at Boeing Helicopters p 2761 N95-32014
BOEING DEFENSE AND SPACE GROUP, SEATTLE, WA.
Cadmium plating replacements p 2776 N95-31773
Operation of the computer model for direct atomic oxygen exposure of Earth satellites
[NASA-CR-198188] p 2767 N95-32189
BOWLING GREEN STATE UNIV., OH.
Specific rate coefficients from vibrational overtone activation of 1-methylcyclopropene
[AD-A288755] p 2793 N95-31014
BRIGHAM YOUNG UNIV., PROVO, UT.
Burn time measurements of single aluminum particles in steam and carbon dioxide mixtures p 2799 N95-30990
Burn time measurements of single aluminum particles in steam and carbon dioxide mixtures p 2799 N95-31198
Characterization of an improved Rijke burner as prelude to measurements of aluminum distributed combustion p 2800 N95-31287
An ignition model for modern double base propellants p 2800 N95-31292
BRISTOL UNIV. (ENGLAND).
Thermoviscoelastic behaviour of solids
[PB95-196226] p 2784 N95-30694
BRITISH AEROSPACE DEFENCE LTD., PRESTON (ENGLAND).
The FCS-structural coupling problem and its solution p 2759 N95-32005
Pilot Induced Oscillation: A report on the AGARD Workshop on PIO p 2761 N95-32017
Integration issues in modular mission management aid development p 2841 N95-32133
BRITISH AEROSPACE DEFENCE LTD., WARTON (ENGLAND).
Experimental Aircraft Programme (EAP): Flight control system design and test p 2760 N95-32010
Flight demonstration of an advanced pitch control law in the VAAC Harrier aircraft p 2760 N95-32012
BROOKHAVEN NATIONAL LAB., UPTON, NY.
Effects of temperature ramp rate during heat treatment on hysteresis loss and critical current density of internal tin processed wires
[DE95-009551] p 2803 N95-30706
The coupling impedance of a toroidal beam pipe with circular cross section
[DE95-010442] p 2993 N95-31405
Long baseline neutrino oscillation experiment at the AGS
[DE95-004378] p 2986 N95-31702
Polarized proton beams
[DE95-010843] p 2987 N95-32031
Observation of intensity dependent losses in Au(15+) beams
[DE95-010845] p 2987 N95-32032
Physics goals of a mu(+) mu(-) collider
[DE95-009548] p 2994 N95-32059
Monte Carlo simulations of muon production
[DE95-009554] p 2988 N95-32063
Applications of chiral symmetry
[DE95-009552] p 2988 N95-32079
Radial mode evolution in longitudinal bunched beam instability
[DE95-010895] p 2994 N95-32092
The superconducting kaon spectrometer
[DE95-010436] p 2882 N95-32159
Validity of the differential equations for ionization cooling
[DE95-010438] p 2989 N95-32160
KRAKEN, a numerical model of RHIC impedances
[DE95-011563] p 2994 N95-32242
Skew chromaticity in large accelerators
[DE95-011564] p 2994 N95-32243
Normal mode tunes for linear coupled motion in six dimensional phase space
[DE95-011565] p 2994 N95-32244
Beam stability at SRRC storage ring
[DE95-010842] p 2995 N95-32260
Review of longitudinal perturbation formalism
[DE95-010894] p 2990 N95-32278
Tune modulation due to synchrotron oscillations and chromaticity, and the dynamic aperture
[DE95-011566] p 2995 N95-32297
RFQ-DTL matching solutions for different requirements
[DE95-010897] p 2995 N95-32306
Thermal rho's in the quark-gluon plasma
[DE95-009543] p 3008 N95-32357
BROWN UNIV., PROVIDENCE, RI.
Workshop on diffusion approximation in communication and stochastic systems theory
[AD-A292572] p 2952 N95-31055
Theory & numerical methods for problems in shape reconstruction and large deviations
[AD-A292874] p 2952 N95-31279
Nonlinear optics in novel composite media
[AD-A293886] p 2999 N95-31542
BUREAU INTERNATIONAL DES POIDS ET MESURES, SEVRES (FRANCE).
Time activities at the BIPM p 2968 N95-32325
Anticipated uncertainty budgets of PRARETIME and T2L2 techniques as applied to ExTRAS p 2968 N95-32326
Study of tropospheric correction for intercontinental GPS common-view time transfer p 2971 N95-32338
Relativistic theory for syntonization of clocks in the vicinity of the Earth p 2971 N95-32343
Satellite test of the isotropy of the one-way spe ed of light using ExTRAS p 2973 N95-32349

C

CALIFORNIA UNIV., BERKELEY, CA.
Research progress report
[DE95-010726] p 3030 N95-32269
Gigabit testbed research project
[DE95-010728] p 2945 N95-32270
CALIFORNIA UNIV., BERKELEY. LAWRENCE BERKELEY LAB, CA.
Beam-beam effects
[DE95-008443] p 2991 N95-30360
Strange-matter stars
[DE95-008446] p 3028 N95-30361
A room temperature LSO/PIN photodiode PET detector module that measures depth of interaction
[DE95-008447] p 2878 N95-30378
Current issues in perturbative QCD
[DE95-008448] p 2975 N95-30388
The art and science of magnet design: Selected notes of Klaus Halbach, volume 2
[DE95-008450] p 2861 N95-31059
Annual meeting of the Advanced Light Source Users' Association
[DE95-009373] p 3000 N95-31635
Superconducting and normal-state properties of novel materials
[DE95-012368] p 3017 N95-32366
CALIFORNIA UNIV., DAVIS, CA.
Nonparametric methods for incomplete data in reliability and for changepoints in smooth functions
[AD-A292773] p 2963 N95-31429
Particle filtration: An analysis using the method of volume averaging
[DE95-009467] p 2875 N95-31592
Particle filtration: A comparison between theory and experiment
[DE95-009442] p 2875 N95-31637
CALIFORNIA UNIV., LOS ANGELES, CA.
Vertical transport in GaAs/AlGaAs superlattices p 3012 N95-30822

Modeling multi-beam structures for control
p 2895 N95-31346
Processing of polymers using supercritical fluids
[AD-A292880] p 2819 N95-31410
A cognitive architecture for solving ill-defined problems
[AD-A293582] p 2929 N95-31686
Stable high-power harmonic gyro-amplifiers
[AD-A293697] p 2881 N95-31628
Vibration reduction in helicopter rotors using an actively controlled partial span trailing edge flap located on the blade p 2762 N95-32111

CALIFORNIA UNIV., SAN DIEGO, CA.
Improved linear dynamic range in externally modulated fiber-optic links p 3001 N95-31950

CALIFORNIA UNIV., SANTA BARBARA, CA.
Extended tuning range semiconductor lasers with sampled gratings p 2883 N95-30498
Study of effect of bubbles on a free-shear layer
p 2872 N95-31100
Processing and microstructural evolution of alumina/aluminum alloy and aluminum nitride/aluminum alloy composites by directed melt oxidation
p 2789 N95-31973

CARNEGIE-MELLON UNIV., PITTSBURGH, PA.
Summary of technical operations
[AD-A293224] p 2935 N95-30903
Structural, chemical and electronic properties of superconducting thin films and junctions
[AD-A292700] p 3012 N95-30933
New adaptive methods for reconfigurable flight control systems, appendix 1
[AD-A292711] p 2756 N95-30937
Development of germanium-silicon growth technology
[AD-A293199] p 3013 N95-30983
Visual tracking of self-occluding articulated objects
[AD-A292894] p 2928 N95-31383
Human-computer interaction (HCI) specialization track Masters of Software Engineering (MSE) program
[AD-A292895] p 2930 N95-31401
The occurrence of continuation parameters in CPS terms
[AD-A292952] p 2941 N95-31460
Metallurgical and Materials Transactions
[AD-A293617] p 2807 N95-31464
Neural networks for real-time terrain typing
[AD-A293569] p 2953 N95-31540
Using case-based reasoning as a Reinforcement Learning framework for optimization with changing criteria
[AD-A293602] p 2953 N95-31654
Force and vision resolvability for assimilating disparate sensory feedback
[AD-A293581] p 2929 N95-31685
PORK object system programmer's guide
[AD-A293596] p 2942 N95-31688
Production matching for large learning systems
[AD-A293105] p 2953 N95-31827
Proceedings of the 1st Annual Software Engineering Techniques Workshop on Software Reengineering
[AD-A293724] p 2943 N95-31834
Experience with a course on architectures for software systems. Part 2: Educational materials
[AD-A293090] p 2943 N95-31843
A programming interface for application-aware adaptation in mobile computing
[AD-A293107] p 2943 N95-32019
PADO: Learning tree structured algorithms for orchestration into an object recognition system
[AD-A293109] p 2943 N95-32020
Improving data consistency in mobile computing using Isolation-Only Transactions
[AD-A293110] p 2948 N95-32021

CASE WESTERN RESERVE UNIV., CLEVELAND, OH.
From molecular to macromolecular liquid crystals
[AD-A293170] p 2816 N95-30974
Spectral element method for numerical simulation of unsteady laminar diffusion flames p 2794 N95-31333
Stability analysis of linear control systems with uncertain parameters p 2954 N95-31949

CATHOLIC UNIV. OF AMERICA, WASHINGTON, DC.
Application of wavelet-filtering techniques to intermittent turbulent and wall pressure events. Part 2. Detection of cluster patterns
[AD-A293805] p 2875 N95-31586

CENTRE EUROPEEN RECHERCHE ET DE FORMATION ADVANCE EN CALCUL SCIENTIFIC, TOULOUSE (FRANCE).
Use of element-by-element preconditioners to solve large scale partially separable optimization problems
[PB95-195772] p 2957 N95-30692

CENTRE NATIONAL DE LA RECHERCHE SCIENTIFIQUE, MARSEILLES (FRANCE).
Temporal information processing mechanisms
[PB95-206344] p 3027 N95-32370

CENTRE NATIONAL DE LA RECHERCHE SCIENTIFIQUE, TOULOUSE (FRANCE).
Use of element-by-element preconditioners to solve large scale partially separable optimization problems
[PB95-195772] p 2957 N95-30692

CENTRUM VOOR REGELEVING EN ONDERZOEK, EDE (NETHERLANDS)
Quality assurance tendering and awarding contracts
[PB95-197760] p 2891 N95-31362

CHALK (CHARLES R.), WILLIAMSVILLE, NY.
Calspan experience of PIO and the effects of rate limiting p 2746 N95-31072

CHALMERS UNIV. OF TECHNOLOGY, GOETEBORG (SWEDEN).
Molecular gas in starburst galaxies: Line intensities and physical conditions
[PB95-208021] p 3029 N95-30569
Feasibility study concerning an active millimeterwave sensor. Project phase MMS2.1
[PB95-210399] p 2882 N95-32245

CHRISTIAN BROTHERS COLL., MEMPHIS, TN.
Improved modeling of unsteady heat transfer (The first step)
[AD-A292777] p 2874 N95-31432

CINCINNATI UNIV., OH.
Artificial neural networks and model-based recognition of 3-D objects from 2-D images p 2954 N95-31838

CITY COLL. OF THE CITY UNIV. OF NEW YORK, NY.
Modern methods in meteorological and oceanographic data acquisition and analyses
[AD-A293884] p 2920 N95-31541
Image representation using fast algorithms based on the Zak transform
[AD-A293416] p 2942 N95-31684
Investigation of the basic physics of high efficiency semiconductor hot carrier solar cell
[NASA-CR-198945] p 2906 N95-32212

CLARKSON UNIV., POTSDAM, NY.
Self-adaptive multilevel methods for fluid flow problems p 2873 N95-31412
A time stepping coupled finite element-state space modeling environment for synchronous machine performance and design analysis in the ABC frame of reference p 2864 N95-31948
Silicon carbide-silicon heterostructure solar cells
p 2905 N95-31952
Vibration control of spacecrafts and space structures from lift-off to on-orbit environments
p 2767 N95-32110

CLEMSON UNIV., SC.
Characterization and prediction of post-impact fatigue damage in stitched composites p 2785 N95-30826

CLEVELAND STATE UNIV., OH.
Development and computer implementation of design/analysis techniques for multilayered composite structures. Probabilistic fiber composite micromechanics
[NASA-CR-198979] p 2930 N95-31134

COLORADO STATE UNIV., FORT COLLINS, CO.
National Institute for Global Environmental Change
[DE95-008333] p 2907 N95-30358
Forecast of Atlantic seasonal hurricane activity for 1994 p 2918 N95-30832
Summary of 1993 Atlantic tropical cyclone activity and verification of author's forecast. A year of unanticipated light hurricane activity and a poor forecast: The expected dissipation of the El Nino did not take place and Caribbean basin surface pressure became quite high
p 2918 N95-30842
Early August updated forecast of Atlantic seasonal hurricane activity for 1994 p 2919 N95-30844
Metal nanotubule membranes with electrochemically switchable ion-transpprt selectivity
[AD-A292712] p 2793 N95-30938
Clouds: Their prediction and simulation
[AD-A292864] p 2920 N95-31453

COLORADO UNIV., BOULDER, CO.
State resolved dynamics of ion-molecule collisions in a flowing afterglow
[AD-A290895] p 2976 N95-30410
Modeling and parameterization of gravity wave breaking, interactions, and instability processes in the lower and middle atmosphere
[AD-A292740] p 2914 N95-31278
Numerical simulation of shock/turbulent boundary layer interaction
[NASA-CR-198846] p 2872 N95-31341
Temporal feature extraction in photorefractive resonators
[AD-A292908] p 2881 N95-31385
Optical frequency standards: Hertz-level working standards and their absolute frequency measurement
[AD-A293930] p 2999 N95-31515
Optimizing the long-term retention of skills: Structural and analytic approaches to skill maintenance
[AD-A293798] p 2929 N95-31585
A computational procedure for multibody systems including flexible beam dynamics
[NASA-CR-199035] p 2897 N95-31730
Combustion response to acoustic perturbation in liquid rocket engines p 2770 N95-31972
Evaluation of discretization procedures for transition elements in adaptive mesh refinement
[NASA-CR-199037] p 2944 N95-32190
Staggered solution procedures for multibody dynamics simulation
[NASA-CR-199034] p 2899 N95-32202
A survey of the core-congruential formulation for geometrically nonlinear TL finite elements
[NASA-CR-199044] p 2944 N95-32203
Computational methods and software systems for dynamics and control of large space structures
[NASA-CR-199036] p 2767 N95-32204
A transient FETI methodology for large-scale parallel implicit computations in structural mechanics
[NASA-CR-199040] p 2945 N95-32214
The individual element test revisited
[NASA-CR-199039] p 2945 N95-32215

COLUMBIA UNIV., NEW YORK, NY.
Qualitative environmental navigation: Theory and practice p 2748 N95-30486
Theoretical high energy physics
[DE95-003107] p 2991 N95-30527
Precision manipulation with a dextrous robot hand
p 2888 N95-30829
Pseudomorphic heterostructure materials for high performance devices
[AD-A292908] p 2788 N95-31384
Numerical evaluation of three-dimensional crack-tip integrals for layered anisotropic solids
p 2898 N95-32191

COLUMBIA UNIV., OLD SAYBROOK, CT.
Film temperatures in the presence of cavitation
[NASA-CR-195481] p 2878 N95-32216

COMBUSTION INST., PITTSBURGH, PA.
The 25th International Symposium on Combustion
[AD-A286825] p 2794 N95-31268

COMISION NACIONAL DE ENERGIA ATOMICA, BUENOS AIRES (ARGENTINA).
A proposed phase equilibrium diagram for Pt-Zr system
[DE95-620904] p 2806 N95-31220
Behaviour of polymers in radioactive environments: Effects of dose speed
[DE95-621008] p 2818 N95-31221
Volumetric and electro analytical techniques for chemical characterization of nuclear grade Ag-In-Cd alloys
[DE95-620664] p 2807 N95-31407

COMISION NACIONAL DE ENERGIA ATOMICA, SAN CARLOS DE BARILOCHE (ARGENTINA).
Development and implementation of a computer facility for nuclear data updating and reactor calculations using personal computers
[DE95-623577] p 2940 N95-31408
Neutronic methods for determination of very low concentrations of hydrogen in metals
[DE95-623967] p 2807 N95-31409

COMMUNICATIONS SATELLITE CORP., CLARKSBURG, MD.
Information Switching Processor (ISP) contention analysis and control
[NASA-CR-195471] p 2765 N95-31849

COMPTROLLER GENERAL OF THE UNITED STATES, WASHINGTON, DC.
Annual report to the Chairman and Ranking Minority Members, House and Senate Committees on Appropriations. Status of open recommendations: Improving operations of federal departments and agencies
[GAO/OP-95-1] p 3022 N95-31986

COMPUTATIONAL PHYSICS, INC., WALTHAM, MA.
SSUSI single sensor auroral E-layer algorithm: Functional description
[AD-A288630] p 2914 N95-31012

COMPUTER RESOURCES INTERNATIONAL A/S (DENMARK).
Specific method for task-based interaction design
[PB95-196440] p 2929 N95-30522

COMPUTER SCIENCES CORP., CALVERTON, MD.
Voyager GO program
[NASA-CR-189435] p 3029 N95-31424
Cepheid temperature and the Blazhko effect
[NASA-CR-189433] p 3030 N95-31819

COMPUTER SCIENCES CORP., LANHAM, MD.
Closing the loop on improvement: Packaging experience in the Software Engineering Laboratory
p 2937 N95-31238
Lessons learned in transitioning to an open systems environment p 2938 N95-31245

CONTINUUM DYNAMICS, INC., PRINCETON, NJ.
A novel instrumentation system for measurement of helicopter rotor motions and loads data, phase 1
[AD-A293309] p 2751 N95-30923
CONVOLVE, INC., ARMONK, NY.
Minimizing structural vibrations with Input Shaping (TM)
[NASA-CR-189439] p 2893 N95-30786
COOPERS AND LYBRAND, HAMBURG (GERMANY).
Does software design complexity affect maintenance effort? p 2939 N95-31251
CORNELL UNIV., ITHACA, NY.
High energy pulsed microwave sources
[AD-A293334] p 2849 N95-31142
SDIO: Discovering superconducting materials at high temperatures
[AD-A292820] p 3015 N95-31444

D

DASSAULT AVIATION, SAINT-CLOUD (FRANCE).
Catapult-launching of the RAFALE design and experimentation p 2752 N95-32008
DAVID SARNOFF RESEARCH CENTER, PRINCETON, NJ.
Ceramic/Metal Composite Circuit-Board-Level Technology for Application Specific Electronic Modules (ASEM's)
[AD-A293183] p 2787 N95-30978
High performance YBCO films
[AD-A293045] p 2863 N95-31669
DAYTON UNIV., OH.
Image representation using fast algorithms based on the Zak transform
[AD-A293416] p 2942 N95-31684
DEFENCE RESEARCH ESTABLISHMENT VALCARTIER, COURCELLETTE (QUEBEC).
Infrared and millimeter wave detection using thin films of Pb doped BiSrCaCuO superconductor p 2840 N95-32129
DEFENCE SCIENCE AND TECHNOLOGY ORGANISATION, CANBERRA (AUSTRALIA).
An approach to automated reasoning about operational semantics
[AD-A291127] p 2936 N95-31228
Functions for processing synthetic aperture radar imagery
[AD-A293895] p 2851 N95-31510
Preparation of S-70A-9 Black Hawk helicopter for flight tests to investigate cause of cracking of inner fuselage panel
[AD-A293891] p 2752 N95-31544
DEFENCE SCIENCE AND TECHNOLOGY ORGANISATION, MELBOURNE (AUSTRALIA).
Ocean mass density calculations from temperature and salinity data
[DSTO-TR-0023] p 2922 N95-30711
Observations of star fracture and longitudinal splitting in BIS 812 EMA and Q1N submarine construction steels
[DSTO-RR-0014] p 2806 N95-31344
Calculations of the sound scattering from fluid-filled spherical shell sonar targets
[DSTO-RR-0020] p 2974 N95-31365
The effect of ray curvature on Lloyd's mirror fringe estimates and source localisation
[DSTO-TR-0064] p 3001 N95-31745
DEFENSE ADVANCED RESEARCH PROJECTS AGENCY, ARLINGTON, VA.
Convergence properties of an augmented lagrangian algorithm for optimization with a combination of general equality and linear constraints
[PB95-208039] p 2956 N95-30570
DELAWARE UNIV., NEWARK, DE.
Inverse and control problems in electromagnetics
[AD-A292993] p 2849 N95-30962
DEPARTMENT OF DEFENSE, FORT MEADE, MD.
Unmanned aerial vehicles. 1994 master plan p 2751 N95-31416
DEPARTMENT OF ENERGY, MORGANTOWN, WV.
Achieving improved cycle efficiency via pressure gain combustors
[DE95-008945] p 2792 N95-30762
DEPARTMENT OF ENERGY, PITTSBURGH, PA.
High-tech controls for energy and environment
[DE95-011702] p 2952 N95-31255
DEPARTMENT OF ENERGY, WASHINGTON, DC.
Minijet veto: A tool for the heavy Higgs search at the LHC
[PB95-196234] p 2979 N95-30695
Global change research: Summaries of research in FY 1994
[DE95-009660] p 2908 N95-30755
History and status of the atmospheric radiation measurement program
[DE95-009951] p 2908 N95-30802
Summaries of fiscal year 1994 projects in medical applications and biophysical research
[DE95-010405] p 2925 N95-32040
DEPARTMENT OF THE AIR FORCE, CALIFORNIA CITY, CA.
Aeroelastic pilot-in-the-loop oscillations p 2746 N95-31070
DEPARTMENT OF THE AIR FORCE, EGLIN AFB, FL.
Electronic combat and lethal defense suppression p 2842 N95-32140
DEPARTMENT OF THE AIR FORCE, WASHINGTON, DC.
Acquisition, tracking, pointing and fire control for Ballistic Missile Defense p 2841 N95-32131
DEPARTMENT OF THE AIR FORCE, WRIGHT-PATTERSON AFB, OH.
Advances in high-power chemical lasers
[AD-A289737] p 2885 N95-31389
Design and integration issues of visually-coupled evaluation
[AD-A293521] p 2931 N95-31538
Vertical impact testing of two helmet-mounted night vision systems
[AD-A293055] p 2931 N95-31671
Environmentally safe aviation fuels p 2775 N95-31768
Luminescence properties of ZnWO4:Cr(3+) laser crystals
[AD-A293065] p 2887 N95-32152
Photo-refractive Bi12SiO20: Spatial light modulator
[AD-A293084] p 3001 N95-32153
DEPARTMENT OF THE NAVY, WASHINGTON, DC.
Low vibration polymeric composite engine
[AD-D017332] p 2887 N95-30386
Coupling stud assembly
[AD-D017335] p 2887 N95-30387
Gear pump with reduced fluid-borne noise
[AD-D017362] p 2887 N95-30399
Demodulators for optical fiber interferometers with (3 x 3) outputs
[AD-D017415] p 2995 N95-30402
Method and system for suppressing noise induced in a fluid medium by a body moving therethrough
[AD-D017339] p 2973 N95-30411
Electromagnetically activated compliant wavy-wall
[AD-D017340] p 2886 N95-30412
Thermoacoustic sound generator
[AD-D017342] p 2973 N95-30413
Locking device for fluid coupling
[AD-D017354] p 2888 N95-30414
Process for producing hydrophilic polymer membranes
[AD-D017355] p 2811 N95-30415
Fast-acting valve for projective launching systems
[AD-D017357] p 2888 N95-30416
Microwave repeater with broadband active and/or passive isolation control
[AD-D017358] p 2846 N95-30417
Preparation of diisopropyl stibines and use thereof
[AD-D017419] p 2771 N95-30418
Passive, multi-channel fiber optic rotary joint assembly
[AD-D017353] p 2996 N95-30529
Apparatus for producing images acoustically
[AD-D017365] p 2973 N95-30530
Vibration isolation mount with locking means
[AD-D017367] p 2888 N95-30532
Low temperature synthesis of YBa2Cu3O(8-x) and other crystalline oxides
[AD-D017370] p 3009 N95-30533
Method and apparatus for locating an acoustic source
[AD-D017347] p 2974 N95-30549
Expert system for assessing accuracy of models of physical phenomena and for selecting alternate models in the presence of noise
[AD-D017348] p 2974 N95-30550
Trivalent chromium solutions for sealing anodized aluminum
[AD-D017349] p 2803 N95-30551
Releaseable unconstrained inflatable body protector
[AD-D017350] p 2930 N95-30552
Active turbulence control using microelectrodes, permanent magnets in microgrooves
[AD-D017351] p 2867 N95-30553
Sonic apparatus for degassing liquids
[AD-D017352] p 2791 N95-30554
Fiber optic accelerometer with centrally supported flexural disk
[AD-D017369] p 2879 N95-30658
Pre-amplifier with multi-stage feedback
[AD-D017371] p 2859 N95-30659
Wavefront simulator for evaluating RF communication array signal processors
[AD-D017372] p 2847 N95-30660
Vibration-damping structural component
[AD-D017376] p 2784 N95-30661
Method and system for reducing drag on a body moving through a fluid medium
[AD-D017336] p 2867 N95-30672
Josephson break junction thin film device
[AD-D017343] p 3011 N95-30673
Passive range measurement system
[AD-D017344] p 2996 N95-30678
Optical fiber pressure sensor for liquid level monitoring
[AD-D017346] p 2996 N95-30679
Energy absorption apparatus
[AD-D017361] p 2814 N95-30715
Smart material joint band
[AD-D017374] p 2888 N95-30716
Ultrasonic two probe system for locating and sizing
[AD-D017438] p 2996 N95-30724
Far field acoustic radiation reduction
[AD-D017452] p 2974 N95-30725
Voltage surge suppression power circuits
[AD-D017454] p 2860 N95-30726
Apparatus and method for producing three-dimensional images
[AD-D017455] p 2847 N95-30727
Device for low electric-field induced switching of Langmuir-Blodgett ferroelectric liquid crystal polymer films
[AD-D017457] p 3011 N95-30728
Coherent integrator
[AD-D017422] p 2847 N95-30743
Method for laser-assisted silicon etching using halocarbon ambients
[AD-D017426] p 2883 N95-30744
Reply-frequency interference/jamming detector
[AD-D017428] p 2847 N95-30746
Noise signal processor
[AD-D017430] p 2974 N95-30747
Cascading synchronized chaotic systems
[AD-D017458] p 2860 N95-30748
Composite structure forming a wear surface
[AD-D017462] p 2785 N95-30749
High aspect ratio metal microstructures and method for preparing the same
[AD-D017463] p 2803 N95-30750
Fiber optic interferometric electric field and voltage sensor utilizing and electrostrictive transducer
[AD-D017433] p 2996 N95-30753
Advanced signal processing filter
[AD-D017324] p 2848 N95-30917
Hydrogen sulfide analyzer with protective barrier
[AD-D017412] p 2793 N95-31009
Glass matrix doped with activated luminescent nanocrystalline particles
[AD-D017416] p 2816 N95-31010
Germanate glass ceramic
[AD-D017418] p 2816 N95-31011
Microwave electro-optic mixer
[AD-D017328] p 2862 N95-31179
Apparent size passive range method
[AD-D017360] p 2753 N95-31180
A 1.94 micrometer laser apparatus, system and method using a thulium-doped yttrium-lithium-fluoride laser crystal pumped with a diode laser
[AD-D017435] p 2884 N95-31213
Method of synthesizing high quality, doped diamond and diamonds and devices obtained therefrom
[AD-D017432] p 3014 N95-31269
Technique to prepare high-reflectance optical fiber Bragg gratings with single exposure in-line or fiber draw tower
[AD-D017445] p 2998 N95-31270
Electrified microheterogeneous catalysis
[AD-D017446] p 2794 N95-31271
Phthalonitrile prepolymer as high temperature sizing material for composite fibers
[AD-D017447] p 2818 N95-31272
Diode-pumped, continuously tunable, 2.3 micron CW laser
[AD-D017448] p 2885 N95-31273
Tunable ytterbium-doped solid state laser
[AD-D017449] p 2885 N95-31274
Thin-film edge field emitter device and method of manufacture therefor
[AD-D017453] p 2862 N95-31275
Method and apparatus for a high resolution, flat panel cathodoluminescent display device
[AD-D017434] p 2862 N95-31342
Method and apparatus for non-destructively measuring local resistivity of semiconductors
[AD-D017436] p 2862 N95-31343
Detection of radar targets using higher-order statistics
[AD-D017442] p 2850 N95-31392
Neural network based data fusion system
[AD-D017440] p 2953 N95-31692
Neural network based three dimensional ocean modeler
[AD-D017441] p 2953 N95-31693
DEUTSCHE AEROSPACE A.G., MUNICH (GERMANY).
X-31: A program overview and flight test status p 2753 N95-32013

DEUTSCHE FORSCHUNGSANSTALT FUER LUFT- UND RAUMFAHRT, BRUNSWICK (GERMANY).
SCARLET: DLR rate saturation flight experiment p 2746 N95-31066
Handling qualities analysis on rate limiting elements in flight control systems p 2746 N95-31071
Experiences with ADS-33 helicopter specification testing and contributions to refinement research p 2757 N95-31993
Model following control for tailoring handling qualities: ACT experience with ATTHeS p 2758 N95-32000
Advanced gust management systems: Lessons learned and perspectives p 2759 N95-32002
DEUTSCHE FORSCHUNGSANSTALT FUER LUFT- UND RAUMFAHRT, COLOGNE (GERMANY).
Experimental investigation of turbulent particle dispersion in swirling flows
[DLR-FB-94-20] p 2873 N95-31355
DEUTSCHE FORSCHUNGSANSTALT FUER LUFT- UND RAUMFAHRT, GOETTINGEN (GERMANY).
Structural aspects of active control technology p 2760 N95-32006
DIRECTION DES RECHERCHES, ETUDES ET TECHNIQUES, PARIS (FRANCE).
Physiology and physiopathology of equilibration
[PB95-208328] p 2926 N95-30494
Spectral methods in complex geometries
[PB95-208336] p 2955 N95-30495
Hyperfrequency components
[PB95-208302] p 2866 N95-32369
DORNIER LUFTFAHRT G.M.B.H., FRIEDRICHSHAFEN (GERMANY).
Automatic flight control system for an unmanned helicopter system design and flight test results p 2759 N95-32004
DREXEL UNIV., PHILADELPHIA, PA.
A viscoelastic anisotropic wave propagation model for composite cure evaluation p 2786 N95-30839
DUKE UNIV., DURHAM, NC.
Fundamental topics in heat transfer through deformable two-phase media p 2874 N95-31532

E

ECOLE CENTRALE DE NANTES (FRANCE).
France
[PB95-208385] p 2949 N95-32371
ECOLE POLYTECHNIQUE, MONTREAL (QUEBEC).
Thermal-mechanical fatigue crack growth in aircraft engine materials
[ISBN-0-315-86543-1] p 2894 N95-31098
EG AND G ENERGY MEASUREMENTS, INC., PLEASANTON, CA.
Numerical simulation of the Langevin equation for skewed turbulence
[DE95-009477] p 2877 N95-32049
ELECTROFORMED NICKEL, INC., HUNTSVILLE, AL.
High temperature barrier coatings for refractory metals
[NASA-CR-195475] p 2802 N95-30531
ELECTRONICS MFG. PRODUCTIVITY FACILITY, INDIANAPOLIS, IN.
The search for CFC alternatives is over?
p 2774 N95-31760
ENGINEERING-SCIENCE, INC., HUNTSVILLE, AL.
Atomization simulations using an Eulerian-VOF-Lagrangian method p 2828 N95-31210
ENVIRONMENTAL PROTECTION AGENCY, RESEARCH TRIANGLE PARK, NC.
Demonstration of split-flow ventilation and recirculation as flow-reduction methods in an Air Force paint spray booth, volume 2
[AD-A286806] p 2762 N95-30926
Demonstration of split-flow ventilation and recirculation as flow-reduction methods in an Air Force paint spray booth, volume 1
[AD-A286807] p 2763 N95-31101
ENVIRONMENTAL RESEARCH INST. OF MICHIGAN, ANN ARBOR, MI.
Unconventional imaging field experiment plan
[AD-A291492] p 2846 N95-30562
ENVIRONMENTAL RESEARCH OFFICE OF THE US ARMY, LONDON (ENGLAND).
Brief review of remote sensing literature pertaining to classification and geostatistics
[AD-A290932] p 2901 N95-31156
ESQUIMALT DEFENCE RESEARCH DETACHMENT, VICTORIA (BRITISH COLUMBIA).
Overview of paint removal methods
p 2843 N95-32166
Background to plastic media blasting
p 2843 N95-32168
Dry media blasting with wheat starch
p 2843 N95-32169
Water blasting paint removal methods
p 2843 N95-32170
Paint removal and surface cleaning using ice particles
p 2844 N95-32171
Facilities used for plastic media blasting
p 2763 N95-32176
Treatment of plastic media waste
p 2844 N95-32177
Operational parameters and material effects
p 2845 N95-32179
EUROPEAN SPACE AGENCY. EUROPEAN SPACE RESEARCH AND TECHNOLOGY CENTER, ESTEC, NOORDWIJK (NETHERLANDS).
Specific method for task-based interaction design
[PB95-196440] p 2929 N95-30522

F

FAST MATHEMATICAL ALGORITHMS AND HARDWARE CORP., HAMDEN, CT.
Fast multipole methods for scattering computations
[AD-A291093] p 2848 N95-30869
FEDERAL AVIATION ADMINISTRATION, ATLANTIC CITY, NJ.
Offshore next generation weather radar (NEXRAD) OT&E integration and OT&E operational test
[AD-A293223] p 2848 N95-30902
Terminal doppler weather radar (TDWR) build 5B operational test and evaluation (OT&E) integration and OT&E operational test plan
[AD-A293251] p 2848 N95-30910
Electrical short circuit and current overload tests on aircraft wiring
[AD-A293308] p 2860 N95-30922
A NASPAC-Based analysis of the delay and cost effects of the western-pacific region preliminary resectorization effort of 1993
[AD-A288696] p 2748 N95-31013
Human factors at the FAA Technical Center: Bibliography
[AD-A288638] p 2930 N95-31399
Evaluation of alternative pavement marking materials
[AD-A292973] p 2763 N95-31468
Chemical options to halons for aircraft use
[AD-A293741] p 2747 N95-31569
The ATC operational evaluation of the prototype integrated terminal weather system (ITWS) at Dallas/Fort Worth and Orlando airports (May-September 1993)
[AD-A293808] p 2921 N95-31587
FEDERAL AVIATION ADMINISTRATION, CAMBRIDGE, MA.
Aviation capacity enhancement plan 1994
[AD-A292758] p 2747 N95-31428
Guidelines for the design of GPS and LORAN receiver controls and displays
[AD-A293753] p 2749 N95-31572
Integration of air traffic databases: A case study
[AD-A293691] p 2749 N95-32022
FEDERAL AVIATION ADMINISTRATION, OKLAHOMA CITY, OK.
Aircraft evacuations through Type-3 exits I: Effects of seat placement at the exit
[DOT/FAA/AM-95/22] p 2748 N95-31845
FEDERAL AVIATION ADMINISTRATION, WASHINGTON, DC.
FAA aviation forecasts: Fiscal year 1995-2006
[AD-A293682] p 2741 N95-31598
FERMI NATIONAL ACCELERATOR LAB., BATAVIA, IL.
Reducing process noise in superconducting helium liquid level probes
[DE95-008956] p 2814 N95-30765
Backgrounds and detector performance at a 2 x 2 TeV (mu)(+)(mu)(-) collider
[DE95-009107] p 2992 N95-30800
WW and WZ production at the tevatron
[DE95-011014] p 2981 N95-30970
Implementation of the shower max electron trigger at CDF
[DE95-006684] p 2992 N95-31165
Search for anomalous ZZ(sub gamma) and Z(sub (gamma, gamma)) couplings with D0
[DE95-010457] p 2989 N95-32162
Charm photoproduction dynamics
[DE95-009106] p 2990 N95-32303
FIAT RESEARCH CENTER, ORBASSANO, TURIN (ITALY).
Prospects for high accuracy time dissemination and synchronization using coded radar pulses from a low-earth orbiting spacecraft p 2971 N95-32339
FLORIDA STATE UNIV., TALLAHASSEE, FL.
Brightness temperature simulations for the physical and synoptic interpretation of advanced microwave sounding unit moisture channels p 2921 N95-31721
FLORIDA UNIV., GAINESVILLE, FL.
Innovative processing of composites for ultra-high temperature applications, book 3
[AD-A290891] p 2786 N95-30866
Innovative processing of composites for ultra-high temperature applications, book 4
[AD-A290892] p 2786 N95-30867
Innovative processing of composites for ultra-high temperature applications, book 2
[AD-A290890] p 2786 N95-30898
Visible light emitting materials and injection devices
[AD-A292701] p 2786 N95-30934
Partons and black holes
[DE95-009921] p 3029 N95-31102
A theoretical treatment of the absorption and emission properties of Cu(2) porphyrin
[AD-A293669] p 2795 N95-31595
Calculated structures and electronic absorption spectroscopy for magnesium phthalocyanine and its anion radical
[AD-A293672] p 2796 N95-31596
Electronic structure of Donor-Spacer-Acceptor molecules of potential interest for molecular electronics III: Geometry and absorption spectrum of CH3-Alpha P3CNQ
[AD-A293662] p 2985 N95-31609
Absorption and ionization spectra of model rubredoxins
[AD-A293668] p 2796 N95-31691
On the Jahn-Teller effect of Mn(2+) in zinc-blende ZnS crystal
[AD-A293711] p 2797 N95-31830
Electronic structure of Donor-Spacer-Acceptor molecules of potential interest for molecular electronics 4. Geometry and device properties of P3CNQ and Q3CNQ
[AD-A293717] p 2986 N95-31832
Electroweak flavor-conserving gauge processes: Virtual effects
[DE95-009922] p 3020 N95-32106
FOREIGN BROADCASTING INFORMATION SERVICE, WASHINGTON, DC.
FBIS report: Science and technology. Central Eurasia
[FBIS-UST-95-027] p 2839 N95-31727
FBIS report: Science and technology. Central Eurasia
[FBIS-UST-95-029] p 2863 N95-31728
FBIS report: Science and technology. Central Eurasia
[FBIS-UST-95-028] p 2839 N95-31729
FORWARD TECHNOLOGY INDUSTRIES, INC., MINNEAPOLIS, MN.
Aqueous cleaning design presentation
p 2778 N95-31781

G

GALAXY SCIENTIFIC CORP., LACKLAND AFB, TX.
Contextual interference effects on acquisition and transfer of a complex motor task
[AD-A293788] p 2929 N95-31583
GENCORP AEROJET, SACRAMENTO, CA.
Advanced small rocket chambers. Option 3: 110 1bf Ir-Re rocket, volume 1
[NASA-CR-195435-VOL-1] p 2788 N95-31169
Advanced small rocket chambers. Option 3: 110 1bf Ir-Re rocket, volume 2
[NASA-CR-195435-VOL-2] p 2789 N95-31170
GENERAL ACCOUNTING OFFICE, WASHINGTON, DC.
National Laboratories: Are their R and D activities related to commercial product development? Report to Congressional Requesters
[GAO/PEMD-95-2] p 3027 N95-31345
Report to the Secretary of Defense. Acquisition reform: Comparison of Army's commerical helicopter buy and private sector buys
[GAO/NSIAD-95-54] p 3021 N95-31659
Report to the Chairman, Legislation and National Security Subcommittee, Committee on Government Operations, House of Representatives. Tactical aircraft: F-15 replacement is premature as currently planned
[GAO/NSIAD-94-118] p 2964 N95-31967
Report to the Chairman, Legislation and National Security Subcommittee, Committee on Government Operations, House of Representatives. C-17 Aircraft program: Improvements in initial provisioning process
[GAO/NSIAD-94-63] p 2741 N95-32194
Report to Congressional Committees. Federal research: Interim report on the pilot technology access program
[GAO/RCED-94-75] p 3022 N95-32195
Report to the Chairman, Legislation and National Security Subcommittee, Committee on Government Operations, House of Representatives. Unmanned aerial vehicles: Performance of short-range system still in question
[GAO/NSIAD-94-65] p 2752 N95-32196
Fact sheet for Congressional Committees. Air traffic control: Status of FAA's modernization program
[GAO/RCED-94-167FS] p 2750 N95-32197

Report to Congressional Committees. Military airlift: C-17 settlement is not a good deal
[GAO/NSIAD-94-141] p 2741 N95-32198
Report to the Chairman, Subcommittee on Transportation and Related Agencies, Committee on Appropriations, House of Representatives. Air traffic control: Status of FAA's plans to close and contract out low-activity towers
[GAO/RCED-94-265] p 2750 N95-32199
Report to Congressional Committees. Federal Research: Interim report on the small business innovation research program
[GAO/RCED-95-59] p 3022 N95-32200
Report to the Vice Chairman, Joint Economic Committee, US Congress. Technology transfers: Benefits of cooperative R and D agreements
[GAO/RCED-95-52] p 3027 N95-32201
Federally funded R and D centers: Executive compensation at the Aerospace Corporation. Report to Congressional requestors
[GAO/NSIAD-95-75] p 3022 N95-32213

GENERAL ATOMICS CO., SAN DIEGO, CA.
Advances in the simulation of toroidal gyro Landau fluid model turbulence
[DE95-008387] p 3003 N95-30359
Effects of particle fueling and plasma wall interactions on D3-D discharges
[DE95-009608] p 3003 N95-30612
Helium transport and exhaust studies in enhanced confinement regimes in DIII-D
[DE95-009134] p 3004 N95-30685
Stabilization of ballooning modes with sheared toroidal rotation
[DE95-008388] p 3006 N95-31624
Wall stabilization of high beta plasmas in D3-D
[DE95-009607] p 3007 N95-32116

GENERAL ATOMICS TECHNOLOGIES CORP., SAN DIEGO, CA.
Development of a tokamak plasma optimized for stability and confinement
[DE95-009609] p 3003 N95-30641

GENERAL ELECTRIC CO., CINCINNATI, OH.
The effect of interface properties on nickel base alloy composites
[NASA-CR-198363] p 2785 N95-30787

GENERAL ELECTRIC CO., SCHENECTADY, NY.
Residual stresses and stress corrosion cracking in pipe fittings
[DE95-009332] p 2894 N95-31054

GEORGIA INST. OF TECH., ATLANTA, GA.
The Al and A(lc)l2O3 droplet cloud in solid rocket motors p 2770 N95-30988
Modeling of fiber-reinforced composites incorporating distinct interface properties p 2787 N95-31110
The Al and Al2O3 droplet cloud in solid rocket motors p 2770 N95-31196
A finite element formulation for the time domain vibration analysis of an elastic-viscoelastic structure p 2895 N95-31318

GEORGIA UNIV., ATHENS, GA.
Membrane transport: A cellular probe of heat stroke
[AD-A293327] p 2926 N95-30924

GESELLSCHAFT FUER MATHEMATIK UND DATENVERARBEITUNG, SAINT AUGUSTIN (GERMANY).
Proceedings of the CSCW 1994 workshop collaborative hypermedia systems
[PB95-208393] p 3023 N95-30496

GIBSON (J. C.), SAINT ANNES (ENGLAND).
Looking for the simple PIO model p 2745 N95-31066
The prevention of PIO by design p 2757 N95-31991

GIE COSYDE, VELIZY-VILLACOUBLAY (FRANCE).
Definition of an anti-missile ballistic defense architecture for Europe p 2840 N95-32125
SOSIE: A pragmatic approach to the simulation of Broad Air Defense applied to the theater level p 2840 N95-32127

GLIDCO ORGANICS CORP., JACKSONVILLE, FL.
Prepsolv (TM): The optimum alternative to 1,1,1-trichloroethane and methyl ethyl ketone for hand-wipe cleaning of aerospace materials p 2774 N95-31764

GOETEBORG UNIV. (SWEDEN).
Selection of Swedish scholastic aptitude test takers as a function of socioeconomic background and ability: Evaluation through follow-up
[PB95-212072] p 3021 N95-30699
Non-comparability of female and male admission test takers: Evaluation through follow-up
[PB95-212080] p 3021 N95-30700

GOSUDARSTVENNYI KOMITET PO ISPOLZOVANIYU ATOMNOI ENERGII, LENINGRAD (USSR).
On drawing complicated 3D surfaces
[DE95-619199] p 2939 N95-31257
A compact expression for bilinear combination of Dirac spinors via world tensors
[DE95-619200] p 2960 N95-31258
Study of different type neutrino oscillations based on neutrino beams from 600 GeV
[DE95-619267] p 2983 N95-31260
On possibility to study neutrino oscillations by detectors located at Gran Sasso (Italy) using beams from 600 GeV UNK-1 machine
[DE95-619268] p 2983 N95-31261

GOSUDARSTVENNYI KOMITET PO ISPOLZOVANIYU ATOMNOI ENERGII, SERPUKHOV (USSR).
Hamiltonian formulation of two body problem in Wheeler-Feynman electrodynamics
[DE95-620526] p 3019 N95-31193
Testing vector boson dominance of electroweak interactions via e(+)e(-) (yields) f-bar f
[DE95-620528] p 2982 N95-31214
Period doubling dynamics in hadron physics: Exact calculations
[DE95-620535] p 2982 N95-31215
Hadronic production of B(sub c)-mesons
[DE95-620536] p 2983 N95-31216
B(sub c)-meson production in hadron-hadron collisions
[DE95-620537] p 2983 N95-31217
Scaling behaviour of leptonic decay constants for heavy quarkonia and heavy mesons
[DE95-620539] p 2983 N95-31218
Double charmed baryons production at B-factory
[DE95-620540] p 2983 N95-31219
Do the narrow cryptoexotic baryon resonances exist?
[DE95-619291] p 2984 N95-31378
Local solutions of harmonical and bi-harmonical equations, universal field equation and self-dual configurations of Yang-Mills fields in four dimensions
[DE95-620521] p 2986 N95-31379
Search for exotic baryons with the SPHINX facility
[DE95-613774] p 2984 N95-31549
On the search for exotic hadrons in the experiments with high energy hyperon beam
[DE95-620534] p 2989 N95-32261

GREAT LAKES CHEMICAL CORP., WEST LAFAYETTE, IN.
F-200(TM): The new solution for fire protection p 2776 N95-31770

H

HAMBURG UNIV. (GERMANY).
The solutions of affine and conformal affine Toda field theory
[DE95-616280] p 2965 N95-30430

HAMPTON UNIV., VA.
Application of multigrid computational fluid dynamics (CFD) methods to rotor analysis
[AD-A293012] p 2874 N95-31475

HARVARD UNIV., CAMBRIDGE, MA.
X-ray standing wave interferometry-optics at 1 angstrom with applications to surface and material sciences
[DE95-011453] p 2998 N95-31114

HEBREW UNIV. OF JERUSALEM, REHOVOT (ISRAEL).
Design considerations for a Density-Channel-Guided laser wake-field accelerator
[AD-A292876] p 2884 N95-31190

HELSINKI UNIV. OF TECHNOLOGY, ESPOO (FINLAND).
Catalytic reactions of synthesis gas. Part 4: Heterogeneous hydroformylation
[PB95-195558] p 2791 N95-30537
Worldwide intercomparison of impulse voltage measuring systems at 600 kV level
[PB95-195574] p 2856 N95-30538
Six-vector formalism in electromagnetics of bianisotropic media
[PB95-207130] p 2846 N95-30567
Feature-based modeling of product families
[PB95-207148] p 2933 N95-30568
Radiometer measurements of sea ice in the Gulf of Bothnia 1992
[PB95-206611] p 2900 N95-30718
Nordic symposium on analysis of electromagnetic transient phenomena using EMTP, part 3
[PB95-206504] p 2849 N95-31158
Plane wave reflection from a uniaxial chiral quarter-wave polarization transformer
[PB95-206512] p 2849 N95-31159
Nordic Symposium on Analysis of Electromagnetic Transient Phenomena Using EMTP, part 2
[PB95-206579] p 2849 N95-31160
Nordic Symposium on Analysis of Electromagnetic Transient Phenomena Using EMTP, part 4
[PB95-206587] p 2849 N95-31181
Nordic Symposium on Analysis of Electromagnetic Transient Phenomena Using EMTP, part 1
[PB95-206595] p 2850 N95-31182
DiffEqlab: A MATLAB based package for studying ordinary differential equations
[PB95-207197] p 2960 N95-31383
Reflection and transmission of electromagnetic plane waves from a uniaxial chiro-omega slab
[PB95-206629] p 2853 N95-31649
Fractional delay waveguide modeling of acoustic tubes
[PB95-206637] p 2975 N95-31650

HELSINKI UNIV. OF TECHNOLOGY, OTANIEMI (FINLAND).
CALORSTOCK 1994: Thermal energy storage. Better economy, environment, technology
[DE95-772422] p 2904 N95-31138
CALORSTOCK'94. Thermal energy storage. Better economy, environment, technology
[DE95-772421] p 2907 N95-32388

HERCULES, INC., MAGNA, UT.
Estimating heat of formation of energetic compounds using corrected semiempirical molecular orbital theory p 2800 N95-31294

HERCULES AEROSPACE CO., MAGNA, UT.
Environmentally compatible solid rocket propellants p 2772 N95-31753

HEWLETT-PACKARD CO., SANTA CLARA, CA.
A globally efficient means of distributing UTC time and frequency through GPS p 2970 N95-32335

HIGH PLAINS ENGINEERING, TEHACHAPI, CA.
Observations on PIO p 2745 N95-31084

HOH AERONAUTICS, INC., LOMITA, CA.
Unified criteria for ACT aircraft longitudinal dynamics p 2745 N95-31065
The role of handling qualities specifications in flight control system design p 2757 N95-31990

HONEYWELL, INC., MINNEAPOLIS, MN.
Advances in robust control
[AD-A291126] p 2952 N95-31266
Dynamic inversion: An evolving methodology for flight control design p 2758 N95-31996

HONEYWELL TECHNOLOGY CENTER, MINNEAPOLIS, MN.
Synthetic Terrain Imagery for Helmet-Mounted Display. Volume 3: Software user's manual
[AD-A293613] p 2753 N95-31463
Synthetic Terrain Imagery for Helmet-Mounted Display. Volume 2: Software design document
[AD-A293611] p 2753 N95-31655
Synthetic Terrain Imagery for Helmet-Mounted Display, volume 1
[AD-A293612] p 2753 N95-31656

HOUSTON UNIV., TX.
Impact of task properties, data display format and cognitive characteristics on recall performance: A cumulative research investigation p 3025 N95-31334

HUGHES STX, INC., EDWARDS AFB, CA.
Comparison of DSMC predictions with temporally resolved vibrational state measurements in NO p 2872 N95-30996

HUGHES STX, INC., LANHAM, MD.
Studying the thermal/non-thermal crossover in solar flares
[NASA-CR-189436] p 3031 N95-30785

HYDRO ALUMINUM A/S, KARMOY (NORWAY).
Physical modelling of microstructural evolution during thermomechanical processing of aluminium alloys
[PB95-196341] p 2805 N95-31053

I

IBM CANADA LAB., NORTH YORK (ONTARIO).
Lessons learned in deploying software estimation technology and tools p 2938 N95-31246

IDAHO NATIONAL ENGINEERING LAB., IDAHO FALLS, ID.
Data management system: User's guide
[DE95-008692] p 3022 N95-30392

ILLINOIS UNIV., CHICAGO, IL.
Failure analysis for polycarbonate transparencies
[AD-A292992] p 2820 N95-31471

ILLINOIS UNIV., URBANA, IL.
AASERT-92 augmentation of research training in chronobiology: Regulation of the mammalian circadian clock by neurotransmitters
[AD-A286243] p 2925 N95-31144
Damage dosimetry and embrittlement monitoring of nuclear pressure vessels in real time by magnetic properties measurement
[DE95-011454] p 2894 N95-31254
Theory of unsteady combustion of solids: Investigation of Quasi-steady assumption p 2800 N95-31285
Oscillatory combustion of aluminized AP/HTPB propellants p 2800 N95-31286
Laser pyrolysis of HTPB p 2800 N95-31298

The structure and reactivity of boron and carbon surfaces
[AD-A292804] p 2795 N95-31440
Ultraviolet and visible lasers: Rare earth-doped waveguide devices and non-linear optical extraction techniques
[AD-A293976] p 2885 N95-31528
Evidence for electronic energy loss processes stimulating solid phase epitaxial regrowth of spatially isolated amorphous regions in semiconductor systems
[DE95-009892] p 3016 N95-32103
Cascade damage in the ordered alloy Ni3Al
[DE95-009893] p 2809 N95-32104

ILLINOIS UNIV., URBANA-CHAMPAIGN, IL.
Seismic studies of subducted lithosphere
p 2915 N95-31335
Middle atmosphere structure and dynamics: Lidar studies at the South Pole, Syowa and Urbana
p 2916 N95-31736

ILLINOIS UNIV. AT URBANA-CHAMPAIGN, SAVOY, IL.
Unsteady laser augmented combustion of pure oxidizers AP and RDX p 2799 N95-31284

INDUSTRIAL MICROELECTRONICS CENTER, LINKOEPING, OESTERGOETLAND (SWEDEN).
Feasibility study concerning an active millimeterwave sensor. Project phase MMS2.1
[PB95-210399] p 2882 N95-32245

INSTITUT DES HAUTES ETUDES SCIENTIFIQUES, BURES-SUR-YVETTE (FRANCE).
Canonical symmetric invariant pairings in vertex operator super algebras and gramians
[PB95-208112] p 2955 N95-30488
Torus bundles and the group cohomology of GL(N,Z)
[PB95-208120] p 2965 N95-30489
Local index formula in noncommutative geometry
[PB95-208146] p 2955 N95-30490
Bravais classes, Voronoie cells, Delone symbols
[PB95-207916] p 3009 N95-30503
Strange compactification theorem: Infinite processes and the 3-dimensional poincare conjecture 6. Part A
[PB95-207924] p 2965 N95-30504
Gibbs measures and quasi-periodic solutions for nonlinear Hamiltonian partial differential equations
[PB95-207932] p 2956 N95-30506
4-manifold topology 2: Dwyer's filtration and surgery kernels
[PB95-207940] p 2965 N95-30509
The 4-manifold topology 1: Subexponential groups
[PB95-207957] p 2965 N95-30555
Analysis on fractals, laplacians on self-similar sets, noncommutative geometry and spectral dimensions
[PB95-208005] p 2956 N95-30556
Gravitational-radiation damping of compact binary systems to second post-Newtonian order
[PB95-207882] p 2912 N95-30588
Gravitational waves from inspiralling compact binaries: Energy loss and waveform to second-post-Newtonian order
[PB95-207890] p 2913 N95-30590
Arithmetic features of rational conformal field theory
[PB95-207908] p 2966 N95-30591
Good metric spaces without good parameterizations
[PB95-208427] p 2957 N95-30622
Higher Schwarzian operators and combinatorics of Schwarzian derivative
[PB95-208435] p 2957 N95-30623
Quasi-periodic solutions of Hamiltonian perturbations of 2D linear Schroedinger equations
[PB95-208443] p 2957 N95-30624
Pi1(sup infinity) and infinite simple homotopy type in dimension three: A research announcement
[PB95-196283] p 2957 N95-30696

INSTITUTE FOR COMPUTER APPLICATIONS IN SCIENCE AND ENGINEERING, HAMPTON, VA.
An executable specification for the message processor in a simple combining network
[NASA-CR-198174] p 2933 N95-30584
Semiannual report
[NASA-CR-198172] p 2931 N95-30657
Pseudo-time methods for constrained optimization problems governed by PDE
[NASA-CR-195081] p 2959 N95-31120
Representation of feedback operators for hyperbolic systems
[NASA-CR-198171] p 2960 N95-31319
Analysis and modeling of subgrid scalar mixing using numerical data
[NASA-CR-198169] p 2877 N95-31978
The Linux operating system: An introduction
[NASA-CR-198178] p 2932 N95-31988
A microeconomic scheduler for parallel computers
[NASA-CR-198153] p 2932 N95-32046

INSTITUTE OF ENERGY ECONOMICS OF JAPAN, (JAPAN).
Economical analysis relating to the global warming issue
[DE95-764072] p 2908 N95-30677

INSTITUTO POLITECNICO NACIONAL, MEXICO CITY (MEXICO).
Power oscillator in the tokamaks training
[DE95-616538] p 3003 N95-30473

INTERFACE, INC., FORT COLLINS, CO.
NASA space astronomy update 6
[NASA-CR-197664] p 3028 N95-31099

INTERNATIONAL CENTRE FOR THEORETICAL PHYSICS, TRIESTE (ITALY).
Dressing symmetry of the uniformization solution of Liouville equation
[DE95-613380] p 2956 N95-30607
Generalized Kummer surfaces and differentiable invariants of Noether-Horikawa surfaces 1
[DE95-613382] p 2956 N95-30608
Electron-optical nonlinear interaction in asymmetric quantum-well laser heterostructures
[DE95-613443] p 2883 N95-30609
Generalized deformed para-Bose oscillator and its coherent states
[DE95-613444] p 2963 N95-30610
Some functional solutions of the Yang-Baxter equation
[DE95-613584] p 2966 N95-30635
On perturbative asymptotic of Regge trajectories
[DE95-613585] p 3018 N95-30636
Electromagnetic-gravitational conversion cross sections in external electromagnetic fields
[DE95-613589] p 2979 N95-30637
Equivalence of two non-commutative geometry approaches
[DE95-613469] p 2957 N95-30642
Alloying effects of Kondo insulators
[DE95-614308] p 3010 N95-30644
Electrical conductivity study on polythiophenes films
[DE95-614309] p 2813 N95-30645
The one-dimensional model of the off-centre potential of the fluorine ion in the NaBr lattice
[DE95-614310] p 3010 N95-30647
Hamiltonian dynamics of the condensed media with spontaneously broken symmetry
[DE95-614448] p 3010 N95-30648
A simple model for the dc flux transformer in layered superconductors with Josephson coupling
[DE95-614468] p 2859 N95-30649
On the theory of hole propagation in an antiferromagnetic background
[DE95-614469] p 3010 N95-30650
Properties of a multichannel resonant-level model
[DE95-614482] p 2979 N95-30652
The quantum interference effect in semiconductor space charge layers studied by Feynman path integrals: General formalism and illustrative examples
[DE95-614483] p 3010 N95-30653
ESAA: Environment for Seismic Activity Analysis
[DE95-612416] p 2913 N95-30675
The iteration formula of the Maslov-type index theory with applications to nonlinear Hamiltonian systems
[DE95-613379] p 2957 N95-30676
Multisite antiferromagnetic Ising spin model: Phase transition through doubling bifurcation
[DE95-614311] p 3011 N95-30722
Spectral response of a polycrystalline silicon solar cell
[DE95-614370] p 2903 N95-30723
Acoustomagnetoelectric effect in a superlattice
[DE95-613445] p 3011 N95-30736
A Monte-Carlo model of ionic transport across a solid interface
[DE95-613447] p 3011 N95-30737
New Fermi-liquid approach for the theory of disordered magnetics
[DE95-613448] p 2967 N95-30739
Introduction to the theory of Goyaks: Operator manifold approach to geometry and particle physics
[DE95-613460] p 2960 N95-30740
Light-front dynamics of Chern-Simons systems
[DE95-613467] p 3019 N95-30741
Around Ratner
[DE95-613377] p 2958 N95-30770
A BRST charge for non-critical W2(s) strings
[DE95-613470] p 3019 N95-30771
Exact smooth classification of Hamiltonian vector fields on symplectic 2-manifolds
[DE95-613378] p 2958 N95-30803
Study of the generalized solutions of n-body type problems with weak forces
[DE95-613381] p 2958 N95-30820
On the degree of approximation by Jackson type operators
[DE95-613383] p 2958 N95-30821
Ferromagnetic Potts model in a magnetic field: Finite lattice extrapolation of the (1 + 1)-dimensional Hamiltonian
[DE95-614447] p 3012 N95-30958
Dynamics of an inhomogeneous anisotropic antiferromagnetic spin chain
[DE95-614449] p 3013 N95-30959
Inner- and outer-shell excitation in lithium isoelectronic sequence
[DE95-614107] p 2981 N95-31003
Signatures of virtual LSP's at the TEVATRON
[DE95-613798] p 2982 N95-31060
Theoretical aspects of electron emission holography
[DE95-614371] p 2880 N95-31167
Effective chiral-spin Hamiltonian for odd-numbered coupled Heisenberg chains
[DE95-614445] p 2982 N95-31168
Irreducible Green's Functions method in the theory of highly correlated systems
[DE95-614446] p 3019 N95-31186
Structure formation with majoron supermultiplet
[DE95-613596] p 2984 N95-31546
Search for new physics indirect effects in e(+)e(-) yields W(+)W(-) at linear colliders with polarized beams
[DE95-613686] p 2984 N95-31547
Unitarization of Koerner-Kuroda model of electromagnetic structure of octet 1/2(+) baryons
[DE95-613765] p 2984 N95-31548
Preservation theorems on finite structures
[DE95-613442] p 2962 N95-32067
Ricci-flat Kaehler metrics on symmetric varieties
[DE95-613459] p 2962 N95-32068
Renormalization group analyses of particle masses in full four-generation fermion condensate scheme
[DE95-613595] p 2988 N95-32070
Schwinger-boson studies of the single hole motion in a 2D quantum antiferromagnet
[DE95-614444] p 3016 N95-32071
Method of normal coordinates in the formulation of a system with dissipation: The harmonic oscillator
[DE95-613372] p 3020 N95-32094
Newton Raphson method, scaling at fractal boundaries and mathematica
[DE95-613374] p 2962 N95-32095
Supersymmetric magnetic moments sum rules and spontaneous supersymmetry breaking
[DE95-613771] p 2989 N95-32096
Bifurcations of contracting singular cycles
[DE95-613371] p 2962 N95-32117
On hadronic production of the B(sub c) meson
[DE95-613726] p 2991 N95-32304
Spin puzzle in nucleon
[DE95-613654] p 2991 N95-32353

INTERUNIVERSITY MICRO-ELECTRONICS CENTER, LEUVEN (BELGIUM).
Metrology of chrome on quartz photomasks using low voltage scanning electron microscopy. Part 1: Physical SEM parameters
[PB95-195780] p 2880 N95-30693

IOWA STATE UNIV. OF SCIENCE AND TECHNOLOGY, AMES, IA.
Study of melting and freezing processes of water for application to ice thermal energy storage system
p 2905 N95-31735
A boundary integral equation approach to three dimensional electromagnetic wave scattering problems
p 2853 N95-31839
Terahertz spectroscopy of silicon micromachined three-dimensional photonic bandgap crystal
[DE95-010233] p 3015 N95-32037

IOWA UNIV., IOWA CITY, IA.
Robust position and force tracking control for a robot in contract p 2888 N95-30830
Perpendicular electron heating by absorption of auroral kilometric radiation
[NASA-198815] p 2914 N95-30848
Role of free-surface boundary conditions and nonlinearities in wave/boundary-layer and wake interaction p 2872 N95-31317
Analysis of plasma measurements for the Geotail mission
[NASA-CR-199074] p 3032 N95-32218

IRANIAN PHYSICS SOCIETY, TEHERAN (IRAN).
Abstracts of Annual Physics Conference of Iran
[DE95-611717] p 2768 N95-30881

ISRAEL AIRCRAFT INDUSTRIES LTD., BEN-GURION AIRPORT (ISRAEL).
Lavi flight control system: Design requirements, development and flight test results p 2758 N95-31994

ISTITUTO ELETTROTECNICO NAZIONALE, TURIN (ITALY).
European plans for new clocks in space
p 2968 N95-32324

J

JAPAN ATOMIC ENERGY RESEARCH INST., TOKYO (JAPAN).
Analytic cross sections for collisions of H, H2, He and Li atoms and ions with atoms and molecules
[DE95-722055] p 2979 N95-30654
MVP/GMVP: General purpose Monte Carlo codes for neutron and photon transport calculations based on continuous energy and multigroup methods
[DE95-722072] p 2979 N95-30656
SHEAT: A computer code for probabilistic seismic hazard analysis, user's manual
[DE95-717874] p 2913 N95-30758
Development of BERMUDA: A radiation transport code system. Part 3: A one-dimensional adjoint neutron transport code
[DE95-717875] p 2934 N95-30759
Neutron shielding point kernel integral calculation code for personal computer: PKN-pc
[DE95-717876] p 2980 N95-30760
Evaluation on materials performance of Hastelloy Alloy XR for HTTR uses. 4: Tensile properties of base metals and welded joints
[DE95-721871] p 2804 N95-30761
Effect of cold work on creep properties of Hastelloy XR
[DE95-722056] p 2806 N95-31154
Design study of prototype accelerator and MeV test facility for demonstration of 1 MeV, 1 A negative ion beam production
[DE95-737208] p 2995 N95-32262
Onset of ELMs in JT-60U
[DE95-737209] p 3007 N95-32263
Development of integrated insulation joint for cooling pipe in tokamak reactor
[DE95-737220] p 3007 N95-32264
JAPAN BROADCASTING CORP., TOKYO (JAPAN).
Portable digital Satellite News Gathering (SNG) RF terminal using a flat antenna
[NHK-LABS-NOTE-436] p 2853 N95-31744
Translation workbench for generating subtitles for English TV news
[NHK-435] p 3026 N95-32182
JAPAN INFORMATION CENTER OF SCIENCE AND TECHNOLOGY, TOKYO (JAPAN).
Directory of global environmental sciences in Japan p 2899 N95-31413
JET EDGE, INC., MINNEAPOLIS, MN.
Ultra-high pressure water jetting for coating removal and surface preparation p 2778 N95-31780
JET PROPULSION LAB., CALIFORNIA INST. OF TECH., PASADENA, CA.
Chemical kinetics and photochemical data for use in stratospheric modeling: Evaluation number 11
[NASA-CR-198863] p 2912 N95-30525
Signal-processing theory for the TurboRogue receiver
[NASA-CR-198882] p 2846 N95-30581
A theoretical analysis of steady-state photocurrents in simple silicon diodes
[NASA-CR-198885] p 2859 N95-30651
Mars together and FIRE and ICE: Report of the joint US/Russian technical working groups
[NASA-CR-198864] p 3030 N95-30845
System considerations for efficient communication and storage of MSTI image data
[NASA-CR-198869] p 3024 N95-30858
JPL Physical Oceanography Distributed Active Archive Center (PO.DAAC) data availability, version 1-94
[NASA-CR-198871] p 2922 N95-30859
Experience report: Using formal methods for requirements analysis of critical spacecraft software p 2938 N95-31247
The Wide Field/Planetary Camera 2 (WFPC-2) molecular adsorber
[NASA-CR-198866] p 2881 N95-31456
Environmental projects. Volume 16: Waste minimization assessment
[NASA-CR-198861] p 2909 N95-31651
The NASA/JPL Evaluation of Oxygen Interactions with Materials-3 (EOIM-3)
[NASA-CR-198865] p 2796 N95-31660
Guidelines for creating and using abbreviations and acronyms
[NASA-CR-198884] p 3025 N95-31713
Degradation of TCE using sequential anaerobic biofilm and aerobic immobilized bed reactor p 2780 N95-31791
The Telecommunications and Data Acquisition Report
[NASA-CR-198911] p 2854 N95-32221
Determination of the position of Jupiter from radio metric tracking of Voyager 1 p 2854 N95-32222
Rate considerations in deep space telemetry p 2765 N95-32223
An efficient implementation of Forward-Backward Least-Mean-Square Adaptive Line Enhancers p 2855 N95-32224
Computer simulation results for PCM/PM/NRZ receivers in nonideal channels p 2765 N95-32225
The application of noncoherent Doppler data types for Deep Space Navigation p 2765 N95-32226
Multiple turbo codes for deep-space communications p 2855 N95-32227
Degradation in finite-harmonic subcarrier demodulation p 2855 N95-32228
Towards optimum demodulation of bandwidth-limited and low SNR square-wave subcarrier signals p 2855 N95-32229
Enhanced decoding for the Galileo low-gain antenna mission: Viterbi redecoding with four decoding stages p 2855 N95-32230
Testing the performance of feedback concatenated decoder with a nonideal receiver p 2856 N95-32231
Performance of residual carrier array-feed combining in correlated noise p 2856 N95-32232
Minimal trellises for linear block codes and their duals p 2856 N95-32233
Trellis complexity bounds for decoding linear block codes p 2856 N95-32234
Residual and suppressed-carrier arraying techniques for deep-space communications p 2856 N95-32235
A high-speed photonic clock and carrier regenerator p 2856 N95-32236
Effects of correlated noise on the full-spectrum combining and complex-symbol combining arraying techniques p 2856 N95-32237
A seismic data compression system using subband coding p 2857 N95-32238
DSS-24 microwave holography measurements p 2857 N95-32239
Digital signal processing in the radio science stability analyzer p 2857 N95-32240
The Deep Space Network stability analyzer p 2858 N95-32334
Fiber optic reference frequency distribution to remote beam waveguide antennas p 2972 N95-32346
JOHNS HOPKINS UNIV., BALTIMORE, MD.
Localization in tungsten heavy alloys subjected to shearing deformations under superimposed high pressures
[AD-A293177] p 2804 N95-30977
Viscous heating of liquid layers under intense shear p 2827 N95-31206
Numerical study of shear-induced heating in high-speed nozzle flow of liquid monopropellant p 2828 N95-31207
Quantum and nonlinear optics research
[AD-A293879] p 2999 N95-31519
JOHNS HOPKINS UNIV., COLUMBIA, MD.
The 21st JANNAF Exhaust Plume Technology Meeting, volume 1
[CPIA-PUBL-621-VOL-1] p 2870 N95-30986
The 31st JANNAF Combustion Subcommittee Meeting, volume 1 p 2825 N95-31194
The 31st JANNAF Combustion Subcommittee Meeting, volume 2
[CPIA-PUBL-620] p 2829 N95-31282
Survey of US burning rate measurement methods for solid propulsion applications p 2800 N95-31291
JOINT INST. FOR NUCLEAR RESEARCH, DUBNA (USSR).
Simultaneity and length of the moving rod
[DE95-613369] p 3017 N95-30364
Elliptic deformed classical mechanics in three-dimensional phase space
[DE95-613384] p 3017 N95-30365
Large scale periodicity of the universe and baryogenesis
[DE95-613461] p 3028 N95-30366
Dynamical analogy of Cabibbo-Kobayashi-Maskawa matrices
[DE95-613462] p 2975 N95-30367
The interaction of magnetizations with an external electromagnetic field and a time-dependent magnetic Aharonov-Bohm effect
[DE95-613463] p 2845 N95-30368
A queer reduction of degrees of freedom
[DE95-613471] p 2964 N95-30369
New tensor interaction and the K(sub L) - K(sub S)mass difference
[DE95-613597] p 2845 N95-30370
On the Compton twist-3 asymmetries
[DE95-613627] p 3017 N95-30371
The mechanism of particle production process in hadron-nucleon collisions
[DE95-613727] p 2975 N95-30372
The neutron powder diffraction and acoustic investigations of the NH4SCN phase diagram
[DE95-614372] p 3009 N95-30419
On explanation of proton electromagnetic form Factor near p (anti p)-threshold from the PS-170 experiment
[DE95-613766] p 2977 N95-30508
New tensor interactions in micron-decay
[DE95-613760] p 2978 N95-30528
Background event discrimination in neutron time-of-flight measurements at beams of relativistic nuclei of the JINR synchrotron
[DE95-613006] p 2991 N95-30604
The radiation conditioned by the 'velocity part' of the electromagnetic field of a moving charge
[DE95-613366] p 2846 N95-30605
The conical singularity and quantum corrections to entropy of black hole
[DE95-613367] p 3029 N95-30606
Instantaneous chiral quark model for relativistic mesons in a hot and dense medium
[DE95-613782] p 2980 N95-30911
Multichannel resonances in coupled channels of meson scattering: Scalar sector
[DE95-613783] p 2981 N95-30912
Experimental results on charge exchange reactions with delta excitations and polarization studies of delta and N(sup *) (1440) resonances
[DE95-614022] p 2981 N95-30913
Free electron laser as energy driver for inertial confinement fusion
[DE95-614252] p 2884 N95-30914
Investigation of Fe3O4 colloid behaviour in a magnetic field by polarized neutron transmission
[DE95-614351] p 2981 N95-30915
Einstein's length concept
[DE95-613368] p 3019 N95-30972
Removal of the Energy Dependence from the Resolvent Like Energy Dependent Interactions
[DE95-613385] p 2961 N95-31619
Instability of weak vacuum
[DE95-613590] p 2985 N95-31620
Electromagnetic hadron mass differences and estimation of isotopic symmetry violation parameters of QCD vacuum from quark model
[DE95-613628] p 2985 N95-31621
Renormcharges in V-A theories
[DE95-613689] p 2985 N95-31622
Form factor of the process gamma(*) gamma(*) yields pi(sup 0) for small virtuality of one of the photons and QCD sum rules (2): Sum rule
[DE95-613629] p 2988 N95-32078
Spin momentum correlation (handedness) in the process of four pion production in the electron-positron collisions
[DE95-613690] p 2988 N95-32093
Harmonic coordinates in the problem on static gravitational and massless scalar fields with a point source
[DE95-623632] p 3020 N95-32295
Radiative corrections to the three quantum annihilation cross section in high energy electron-positron collisions
[DE95-623675] p 2995 N95-32296
JOINT PUBLICATIONS RESEARCH SERVICE, ARLINGTON, VA.
JPRS report: Science and technology. Central Eurasia
[JPRS-UST-95-025] p 2771 N95-31360

K

KANSAS STATE UNIV., MANHATTAN, KS.
Generalized Ramsauer-Townsend minima in heavy-ion induced electron continua
[DE95-010913] p 2989 N95-32120
Kinematical threshold of recoil-ion longitudinal momentum distribution in single ionization of helium by protons and alpha particles
[DE95-010803] p 2990 N95-32271
Ionization of He by highly charged ions at low velocity
[DE95-010815] p 2990 N95-32273
Recoil longitudinal momentum spectroscopy of electron capture from He by O(7+) and F(8+)
[DE95-010823] p 2990 N95-32274
Study of aligned states in ion-atom collisions
[DE95-010825] p 2990 N95-32275
KARLSRUHE UNIV. (GERMANY).
Optimization of a thermoelectric IR-detector for low working temperature
[NASA-CR-198933] p 2880 N95-30752
KENTUCKY UNIV., LEXINGTON, KY.
Biomass production by fescue and switchgrass alone and in mixed swards with legumes
[DE95-009137] p 2909 N95-31612
KOREA CANCER CENTER HOSPITAL, SEOUL (REPUBLIC OF KOREA).
Development of technical information processing systems
[DE95-613311] p 3024 N95-30882

The development of KAERI management information system 2: The development of Time Sheet Management System
[DE95-613355] p 3024 N95-30883
Development of plasma diagnostics technologies: A study on nuclear fusion reactor
[DE95-614180] p 3005 N95-31004
The development of human behaviour analysis techniques and the development of human factors technologies
[DE95-613356] p 2930 N95-31267
The development of the tokamak system technology: A study on the fusion reactor
[DE95-614256] p 3005 N95-31366

L

LABORATOIRE PRIMAIRE DU TEMPS ET DES FREQUENCES, PARIS (FRANCE).
Time aspects of the European Complement to GPS: Continental and transatlantic experimental phases
p 2969 N95-32328

LANTAN, MOSCOW (RUSSIA).
Langasite crystals growth with quality factor Q, that exceeds the Q of quartz, and which are suitable for high-precision resonators
[AD-A293397] p 3013 N95-30969

LAWRENCE LIVERMORE NATIONAL LAB., LIVERMORE, CA.
IR DIAL performance modeling
[DE95-008377] p 2912 N95-30373
Multidimensional discretization of conservation laws for unstructured polyhedral grids
[DE95-008796] p 2955 N95-30470
Three-D mesh optimization methods for unstructured polyhedra
[DE95-008808] p 2955 N95-30471
Computer vision for detecting and quantifying gamma-ray sources in coded-aperture images
[DE95-008810] p 2900 N95-30472
Integrated X-ray testing of the electro-optical breadboard model for the XMM reflection grating spectrometer
[DE95-008829] p 2879 N95-30507
Recommendations for developing portable parallel I/O facilities for scientific applications
[DE95-009364] p 2947 N95-30578
Smart active multiwave sensing with zero background amplitude modulated probes
[DE95-006813] p 2792 N95-30714
Reflectivity of plasmas created by high-intensity, ultra-short laser pulses
[DE95-009536] p 3004 N95-30742
EBIT: Electron Beam Ion Trap V-division experimental physics
[DE95-010207] p 3004 N95-30769
Image enhancement by edge-preserving filtering
[DE95-008077] p 2936 N95-31056
Hollow cathode electron gun research and development
[DE95-010262] p 2992 N95-31127
X-ray performance of the engineering prototype Stellar x-ray polarimeter
[DE95-010268] p 3028 N95-31129
Self-consistent, 2D simulations of filament propagation in photoconducting switches
[DE95-010794] p 2861 N95-31133
Experiments with highly charged ions up to bare U(sup 92+) on the electron beam ion trap
[DE95-008827] p 2982 N95-31174
Future scientific applications for high-energy lasers
[DE95-009380] p 2885 N95-31230
Large-eddy simulation of turbulent flow using the finite element method
[DE95-009464] p 2875 N95-31591
Rationale and summary of methods for determining ultrasonic properties of materials at Lawrence Livermore National Laboratory
[DE95-009475] p 2795 N95-31593
Industry participation workshop: Chromium electroplating of superconductor strand. Proceedings
[DE95-009629] p 2807 N95-31615
Data collection at the Lockheed Santa Cruz facility using midwave hyperspectral imagers
[AD-A293057] p 3000 N95-31672
Class of service in the high performance storage system
[DE95-007959] p 2932 N95-31704
Design of an immersion echelle-prism mid-IR spectrograph for chemical remote sensing
[DE95-010729] p 2901 N95-32027
Diagnosing high density, fast-evolving plasmas using x-ray lasers
[DE95-010734] p 3006 N95-32028
Enhanced brightness x-ray lasers
[DE95-010735] p 2888 N95-32029
Studies of highly charged ions with EBIT and Super-EBIT
[DE95-010251] p 2987 N95-32038
The antiproton-hydrogen atom interaction
[DE95-010252] p 2987 N95-32039
Wavelengths measurements of the He-like krypton K-shell spectrum
[DE95-010264] p 2987 N95-32041
Excitation mechanisms of 2s(sub 1/2)-2p(sub 3/2) and 2p(sub 1/2)-2p(sub 3/2)in U(82+) through U(89+)
[DE95-010265] p 2993 N95-32042
High-resolution superconducting x-ray spectrometers with aluminum trapping layers of different thicknesses
[DE95-010253] p 2881 N95-32047
Numerical simulation of the Langevin equation for skewed turbulence
[DE95-009477] p 2877 N95-32049
Synthesis and characterization of nanophase face-centered-cubic titanium
[DE95-009533] p 2809 N95-32051
The HYLIFE-2 inertial fusion energy power plant concept and implications for IFE
[DE95-010561] p 2994 N95-32074
Automated volumetric grid generation for finite element modeling of human hand joints
[DE95-009575] p 2928 N95-32097
Stability analysis of the TPX toroidal field coil
[DE95-009666] p 2865 N95-32100
Simulation of fracture in compression using a field-theory model
[DE95-009874] p 2898 N95-32102
Wall stabilization of high beta plasmas in D3-D
[DE95-009607] p 3007 N95-32116
Measurements of stability margins and current distribution in large-scale Nb3Sn cable-in-conduit conductors
[DE95-009869] p 3007 N95-32148
Femtosecond, Cr(4+):YAG laser
[DE95-004964] p 2887 N95-32155
Mapping hidden aircraft defects with dual-band infrared computed tomography
[DE95-011531] p 2741 N95-32164
Laser properties of Yb(3+)-doped Sr5(PO4)3F crystals
[DE95-010686] p 3016 N95-32268
Creep of a fine-grained, fully-lamellar, two-phase TiAl alloy at 760 C
[DE95-009531] p 2810 N95-32272
No-thermal plasma processing of VOCs and NO(x) at LLNL
[DE95-011445] p 2911 N95-32281
Radiation effects in space: The Clementine 1 mission
[DE95-011513] p 3032 N95-32282
First-principles approaches to materials stability
[DE95-011533] p 2810 N95-32283
Metallic multilayers at the nanoscale
[DE95-011534] p 3016 N95-32284
Recommendations for protecting National Library of Medicine Computing and Networking Resources
[DE95-011554] p 3026 N95-32285
Voltage controlled MESFET pulse shape generator
[DE95-011656] p 2865 N95-32300
Calculation of a residual mean meridional circulation for a zonal-mean tracer transport model
[DE95-009474] p 2911 N95-32350
Implementation and performance of the pseudoknot problem in Sisal
[DE95-009573] p 2925 N95-32358
Phase transitions and gravitational collapse
[DE95-011732] p 3021 N95-32359

LEEDS METROPOLITAN UNIV., LEEDS (ENGLAND).
Client server architecture for multidatabase access. Ingres SQL server
[PB95-192852] p 2947 N95-31051

LEHIGH UNIV., BETHLEHEM, PA.
Robotic weld overlay coatings for erosion control
[DE95-009643] p 2809 N95-32098

LEIDEN UNIV. (NETHERLANDS).
Numerical stability investigations of processes for solving linear initial value problems
[PB95-207023] p 2959 N95-31183
Effect of the stopping of the Newton iteration in implicit linear multistep methods
[PB95-207056] p 2959 N95-31184

LIEGE UNIV. (BELGIUM).
HST-FOC observations of a remarkable UV auroral event on Jupiter
p 3030 N95-30806

LIGHTWAVE ELECTRONICS CORP., MOUNTAIN VIEW, CA.
A compact and efficient violet laser source
[AD-A292782] p 2885 N95-31434

LOCKHEED CORP., FORT WORTH, TX.
Unsteady transonic wind tunnel test on a semispan straked delta wing, oscillating in pitch. Part 1: Description of the model, test setup, data acquisition, and data processing
[AD-A293113] p 2743 N95-30885

LOGISTICS MANAGEMENT INST., BETHESDA, MD.
The quad-service satellite transmitting and receiving system for medical supply support: A battlefield interoperability and communications system prototype, volume 2. User documentation
[AD-A292835] p 2851 N95-31448
The quad-service satellite transmitting and receiving system for medical supply support: A battlefield interoperability and communications system prototype, volume 1
[AD-A292836] p 2851 N95-31449

LORAL FEDERAL SYSTEMS, GAITHERSBURG, MD.
Software Process Framework. Tool to determine consistency with the CMM (Software Technology for Adaptable, Reliable Systems (STARS) program)
[AD-A292815] p 2946 N95-32289
Using process to integrate Software Engineering Environments (Software Technology for Adaptable, Reliable Systems (STARS) program)
[AD-A292816] p 2946 N95-32290
SWSC domain engineering experience (Software Technology for Adaptable, Reliable Systems (STARS) program)
[AD-A292817] p 2946 N95-32291
Integrating a SEE for megaprogramming: Lessons learned (Software Technology for Adaptable, Reliable Systems (STARS) program)
[AD-A292838] p 2946 N95-32292
Defining manually enactable processes using the process definition information organizer templates (Software Technology for Adaptable, Reliable Systems (STARS) program)
[AD-A292854] p 2946 N95-32293
The sociology of megaprogramming: Experiences in generating an organizational learning enterprise (Software Technology for Adaptable, Reliable Systems(STARS) program)
[AD-A292998] p 2946 N95-32294

LORENTZIAN, INC., NORTH HAVEN, CT.
The theoretical calculation of vibrational circular dichroism spectra
[AD-A293614] p 2798 N95-32258

LOS ALAMOS NATIONAL LAB., NM.
A valence-fluctuation mechanism with highly anisotropic S-wave pairing
[DE95-009419] p 3010 N95-30571
Sensor Fusion and Nonlinear Prediction for Anomalous Event Detection
[DE95-009429] p 2933 N95-30602
Periodically Specified Problems: An Exponential Complexity Gap Between Exact and Approximate Solutions
[DE95-009435] p 2934 N95-30603
Low-density ionization behavior
[DE95-009495] p 2980 N95-30705
On-line surfactant monitoring
[DE95-009417] p 2792 N95-30735
Hydrostatic extrusion of BSCCO/Ag composite wire
[DE95-007862] p 2805 N95-31121
The Los Alamos accelerator code group
[DE95-010989] p 2992 N95-31151
Use of a variable frequency source with a single-mode cavity to process ceramic filaments
[DE95-010992] p 2817 N95-31152
A two-timescale approach to nonlinear Model Predictive Control
[DE95-000943] p 2952 N95-31161
Dynamics of Current Driven Disordered Josephson Junction Arrays
[DE95-009418] p 3014 N95-31231
Pulse power for high energy density physics experiments
[DE95-010868] p 2992 N95-31232
MCNP analyses of criticality calculation results
[DE95-010886] p 2960 N95-31253
Substrate heating measurements in pulsed ion beam film deposition
[DE95-010862] p 2818 N95-31377
Plasma source ion implantation of metal ions: Synchronization of cathodic-arc plasma production and target bias pulses
[DE95-009431] p 3006 N95-31613
Solution based temperature of Perovskite-type oxide films and powders
[DE95-009089] p 2820 N95-31629
Influence of strain rate and temperature on the mechanical behavior of iron aluminide-based alloys
[DE95-009426] p 2808 N95-31636
An assessment of worldwide supercomputer usage
[DE95-009879] p 2932 N95-31645

Dielectric property measurement of zirconia fibers at high temperatures
[DE95-010991] p 2821 N95-31705
Base hydrolysis and hydrothermal processing of PBX-9404 explosive
[DE95-009437] p 2836 N95-32048
Basic science with pulsed power and some off-the-wall ideas
[DE95-009486] p 2854 N95-32050
On the possibility of a two-state magnetic structure for nanocrystalline chromium
[DE95-009914] p 3015 N95-32062
Universal message passing library, or how to writea truly portable code for parallel computers
[PB95-212221] p 2948 N95-32255
Simulation of katabatic flow and mountain waves
[DE95-010863] p 2911 N95-32276
Compact location problems with budget and communication constraints
[DE95-010876] p 2948 N95-32277
A collisionless shock wave experiment
[DE95-009489] p 3008 N95-32351
Base hydrolysis and hydrothermal processing of PBX-9404 explosive
[DE95-009497] p 2837 N95-32355

LOUISIANA STATE UNIV., BATON ROUGE, LA.
The design and construction of the muon arm in PHENIX
[DE95-010156] p 2978 N95-30616
Low energy solar neutrino experiments: The Soviet American Gallium Experiment (SAGE)
[DE95-010159] p 3031 N95-30618

LOUISVILLE UNIV., KY.
DEPSCOR92-Wide field spectral imager
[AD-A293079] p 2997 N95-31005

LOVELACE BIOMEDICAL AND ENVIRONMENTAL RESEARCH INST., ALBUQUERQUE, NM.
Particulate air pollution and increased mortality: Biological plausibility for causal relationship
[DE95-006161] p 2909 N95-31703

LOVELACE SCIENTIFIC RESOURCES, INC., ALBUQUERQUE, NM.
Conference perspective. Neuroimmunomodulation: Stress and immune function
[AD-A291351] p 2926 N95-30870

LUND UNIV. (SWEDEN).
Observation of a low-binding-energy peak in the 2p core-level photoemission from oxidized Al(111)
[PB95-195350] p 2802 N95-30534

M

MADIGAN ARMY MEDICAL CENTER, .TAKOMA, WA.
Use of body surface heat patterns for predicting and evaluating acute lower extremity pain among soldiers
[AD-A292829] p 2927 N95-31446

MANITOBA UNIV., WINNIPEG, MANITOBA (CANADA).
Propagation and scattering of elastic waves in laminated circular cylinders
[ISBN-0-315-85957-1] p 2848 N95-30828

MARTIN MARIETTA ASTRO SPACE, PHILADELPHIA, PA.
GPHS-RTGs in support of the Cassini RTG Program
[DE95-010306] p 2768 N95-30674

MARTIN MARIETTA CORP., HUNTSVILLE, AL.
A water blown urethane insulation for use in cryogenic environments p 2775 N95-31765
Evaluation of HFC 245ca and HFC 236ea as foam blowing agents p 2775 N95-31766

MARTIN MARIETTA ENERGY SYSTEMS, INC., OAK RIDGE, TN.
The Oak Ridge Refrigerant Management Program p 2774 N95-31763
Cleaning without chlorinated solvents p 2780 N95-31792
Surface inspection using FTIR spectroscopy p 2782 N95-31803
Creep of a fine-grained, fully-lamellar, two-phase TiAl alloy at 760 C
[DE95-009531] p 2810 N95-32272

MARYLAND UNIV., COLLEGE PARK, MD.
A numerical study of the starting process in a hypersonic shock tunnel p 2762 N95-30493
Harmonic gyrotron amplifiers and phase-locked oscillators
[AD-A293185] p 2861 N95-30979
Domain analysis for the reuse of software development experiences p 2936 N95-31236
An experiment to assess the cost-benefits of code inspections in large scale software development p 2937 N95-31242
The effect of gravity on the deposition of thin films: The physical vapor transport of copper phthalocyanine
[AD-A292997] p 2838 N95-31472

MASSACHUSETTS INST. OF TECH., CAMBRIDGE, MA.
SodaBot: A software agent environment and construction system
[AD-A290056] p 2939 N95-31277
Multiresolution signal and system analysis and the analysis and control of discrete-event dynamic systems
[AD-A292775] p 2851 N95-31430
An exploratory survey of information requirements for instrument approach charts
[AD-A293882] p 2749 N95-31520
Theory and simulation of electrostatic wave turbulence in the space shuttle-induced plasma environment
[AD-A293467] p 3005 N95-31534

MASSACHUSETTS INST. OF TECH., LEXINGTON, MA.
Machine learning for a toolkit for image mining
[AD-A293137] p 2951 N95-30890
RASSP benchmark 1 executable requirements user's manual
[AD-A290060] p 2935 N95-30931
Initial evaluation of the Oregon State University planetary boundary layer column model for ITWS applications
[AD-A293775] p 2920 N95-31465
Integrated terminal weather system (ITWS) demonstration and validation operational test and evaluation
[AD-A293932] p 2749 N95-31521
Physical optics polarization scattering matrix for a right-angle dihedral
[AD-A293036] p 3000 N95-31665
Solid state research
[AD-A293083] p 3015 N95-31826

MASSACHUSETTS UNIV., AMHERST, MA.
Intelligent finite element submodeling of multichip modules for reliability analysis
[AD-A292911] p 2940 N95-31455
Investigation of microwave backscatter from the air-sea interface
[NASA-CR-198854] p 2851 N95-31457

MASSACHUSETTS UNIV., LOWELL, MA.
Laser-induced holographic surface relief gratings on nonlinear optical polymer films
[AD-A293169] p 2997 N95-30973
Polarized laser induced holographic surface relief gratings on polymer films
[AD-A293275] p 2817 N95-31126
An interpenetrating polymer network for second-order nonlinear optics
[AD-A293019] p 2821 N95-31699
Novel unsymmetrical polydiacetylenes as materials for second and third order nonlinear optics
[AD-A293020] p 3001 N95-31700
Underdense heating of the ionosphere using oblique high power HF radiowaves p 2917 N95-31951

MASTER SYSTEMS, INC., MCLEAN, VA.
Applying program comprehension techniques to improve software inspections p 2937 N95-31241

MATERIALS TECHNOLOGIES OF VIRGINIA, BLACKSBURG, VA.
Whisker reinforced glass ceramic
[DE95-010542] p 2823 N95-32305

MATRA DEFENSE ESPACE, VELIZY-VILLACOUBLAY (FRANCE).
Possible allied ballistic missile defense systems: Related guidance and control requirements p 2840 N95-32126

MCAT INST., SAN JOSE, CA.
Control of unsteady separated flow associated with the dynamic stall of airfoils
[NASA-CR-198972] p 2744 N95-32193

MCDONNELL-DOUGLAS AEROSPACE, HUNTSVILLE, AL.
Improved hybrid rocket fuel p 2773 N95-31755

MCDONNELL-DOUGLAS AEROSPACE, LONG BEACH, CA.
The relation of handling qualities ratings to aircraft safety p 2746 N95-31067
Development of stitched/RTM primary structures for transport aircraft
[NASA-CR-191441] p 2789 N95-31421
The importance of flying qualities design specifications for active control systems p 2757 N95-31992

MCMASTER UNIV., HAMILTON (ONTARIO).
Finite element analysis of damped vibrations of laminated composite plates
[ISBN-0-315-84928-2] p 2789 N95-31731

MELBOURNE UNIV., PARKVILLE (AUSTRALIA).
The search for the decay of Z boson into two gamma as a test of Bose statistics
[DE95-616373] p 2976 N95-30393
Crystallization of sol-gel derived lead zirconate titanate thin films in argon and oxygen atmospheres
[DE95-615230] p 3009 N95-30421
Orientation of rapid thermally annealed lead zirconate titanate thin films on (111) Pt substrate
[DE95-615232] p 2811 N95-30422

Magneto-optical transmission-reflection beam splitter for multi-level atoms
[DE95-616267] p 2976 N95-30423
Multi-particle correlations in quaternionic quantum systems
[DE95-616271] p 3018 N95-30424
Extensions and results from a method for evaluating fractional integrals
[DE95-616272] p 2954 N95-30425
Quantum dynamics in regions of quaternionic curvature
[DE95-616276] p 3018 N95-30426
The Foldy-Wouthuysen transformation
[DE95-616277] p 2976 N95-30427
Covariant phase space formulations of superparticles and supersymmetric WZW models
[DE95-616278] p 2964 N95-30428
Integrals of motion in the two Killing vector reduction of general relativity
[DE95-616281] p 3018 N95-30431
Plaquette expansion proof and interpretation
[DE95-616282] p 2965 N95-30432
A general non-perturbative estimate of the energy density of lattice Hamiltonians
[DE95-616283] p 2965 N95-30435
Two-loop vacuum amplitudes in a non-Abelian gauge theory on S(sub 4)
[DE95-616284] p 3018 N95-30436
What's wrong with anomalous chiral gauge theory?
[DE95-616285] p 3018 N95-30437
Beyond the variational principle in quantum field theory
[DE95-616286] p 3018 N95-30438
Electroweak interactions on the lattice
[DE95-616287] p 2965 N95-30439
Chiral gauge theory in four dimensions
[DE95-616288] p 3018 N95-30440
CP violating effects in e(+) e(-) yields ZH and their optimization
[DE95-616302] p 2976 N95-30441
Real Higgs singlet and electroweak phase transition in the standard model
[DE95-616315] p 2976 N95-30442
Effective Lagrangian approach to the fermion mass problem
[DE95-616316] p 2976 N95-30443
Approximate analytic diagonalization of lattice QCD
[DE95-616332] p 3018 N95-30444
Simulation with complex measures
[DE95-616333] p 2955 N95-30445
Phenomenology of the two Higgs doublet sector of a quark-lepton symmetric model
[DE95-616337] p 2976 N95-30446
Density dependent effective interactions
[DE95-616348] p 2977 N95-30447
Synthesis of carbo-nitride films using high-energy shock plasma deposition
[DE95-615231] p 2811 N95-30450
Ion implantation and thermal stress resistance of ceramics
[DE95-615349] p 2812 N95-30451
Structural investigation of xenon ion-beam-irradiated glassy carbon
[DE95-616777] p 2977 N95-30474
Inelastic plasmon and inter-band electron-scattering potentials for Si from dielectric matrix calculations
[DE95-616778] p 2977 N95-30475
The effect of a non-Hermitian crystal potential on the scattering matrix in reflection electron diffraction
[DE95-616779] p 2977 N95-30476
Possible reason why leptons are lighter than quarks
[DE95-616383] p 2978 N95-30579
Top quark and Higgs boson masses from wormhole physics
[DE95-616384] p 2978 N95-30580
Inversion of the total cross sections for electron-molecule and electron-atom scattering
[DE95-616486] p 2978 N95-30583
Associators in generalized octonionic maps
[DE95-616243] p 2957 N95-30688
Interferometry with particles of non-zero rest mass: Topological experiments
[DE95-616244] p 2979 N95-30689
Polarisation resonance in X-ray diffraction
[DE95-616727] p 3012 N95-30789
Zone axis backscattered electron contrast for fast electrons
[DE95-616775] p 2980 N95-30790
Polarized Raman spectroscopy of chemically vapour deposited diamond films
[DE95-616776] p 2815 N95-30791
K-shell ionization under zone axis electron diffraction conditions
[DE95-616780] p 2981 N95-30918

Reflection and diffraction of atomic de Broglie waves by evanescent laser waves. Bare-state method
[DE95-616458] p 2992 N95-30960
Coulomb correction calculations of pp Bremsstrahlung
[DE95-616349] p 2982 N95-31176
Relativistic non-interacting electron gas in a magnetic field
[DE95-616903] p 2967 N95-31177
Characterization of /11'01/ twin dislocation structures in evaporated titanium thin films by HREM
[DE95-615391] p 2820 N95-31623

MIAMI UNIV., FL.
Aerosol measurements over the Pacific Ocean in support of the IR aerosol backscatter program
[NASA-CR-198925] p 2918 N95-30782

MICHIGAN STATE UNIV., EAST LANSING, MI.
Diamond thin film temperature and heat-flux sensors
[NASA-CR-198850] p 3012 N95-30847
Erect, neutral and slump sitting postures: A study of the torso linkage system from shoulder to hip joint
[AD-A293239] p 2930 N95-30907

MICHIGAN TECHNOLOGICAL UNIV., HOUGHTON, MI.
Mechanical alloying processing with application to structural materials
[AD-A290788] p 2802 N95-30404
An experimental and numerical study on the structure and extinction of laminar premixed flames
p 2792 N95-30670

MICHIGAN UNIV., ANN ARBOR, MI.
Scattering and radiation from cylindrically conformal antennas p 2847 N95-30669
Robust fixed-structure control
[AD-A292883] p 2952 N95-30961
Fast algorithms for three-dimensional inverse scattering problems
[AD-A293510] p 2852 N95-31537
Spectral methods and sum acceleration algorithms
[DE95-009689] p 2941 N95-31630
Global stabilization of nonlinear gyroscopic systems
p 2881 N95-31836
Carrier dynamics and optical properties of GaAs- and InP-based strained quantum well lasers
p 2886 N95-31848
The influence of matrix microstructure and temperature on cyclic deformation and fatigue of particle-reinforced 2219 aluminum p 2808 N95-31974
The influence of microstructure on creep deformation in near-gamma TiAl alloys p 2808 N95-31975
Failure mechanisms in composite plates subjected to in-plane compressive loading p 2790 N95-32108
An extremum principle for the analysis and design of constitutively nonlinear systems p 2898 N95-32112
Contributions to the design of neutral cutouts in laminated plates and shells p 2790 N95-32113

MINNESOTA UNIV., MINNEAPOLIS, MN.
Molecular nanoclusters as precursors to conductive thin films and crystals
[AD-A290278] p 3014 N95-31189
Emerging applications in probability (Sensor management)
[AD-A292781] p 2749 N95-31433
Transitions, defects, and whiskered microstructures
[AD-A292796] p 3014 N95-31438
Control of interfacial chemistry and mechanical properties in metal/ceramic composites
p 2790 N95-31976
A mode decomposition based finite element formulation for the nonlinear dynamics of flexible spatial structures and mechanisms p 2898 N95-32118

MISSISSIPPI STATE UNIV., MISSISSIPPI STATE, MS.
Multi-color pyrometer temperature measurement system
[DE95-009825] p 2879 N95-30687

MISSISSIPPI UNIV., UNIVERSITY, MS.
Investigating the use of smart acoustically active surfaces for flow separation control in turbomachinery
[AD-A292819] p 2874 N95-31443

MISSOURI UNIV., SAINT LOUIS, MO.
Quantum 1/f noise in high technology applications including ultrasmall structures and devices
[AD-A292812] p 2862 N95-31442

MITRE CORP., BEDFORD, MA.
High Frequency (HF) upgrade study for the Canadian Regional Operations Control Center (ROCC) AWACS Digital Information Link (RADIL) project
[AD-A293435] p 2850 N95-31367

MITRE CORP., MCLEAN, VA.
Confederation Verification, Validation, and Accreditation Master Plan (CVVAMP). Technical test plan
[AD-A289717] p 2936 N95-31050
Effects of civil tiltrotor service in the northeast corridor on en route airspace loads
[AD-A293586] p 2747 N95-31687

MONTPELLIER-2 UNIV. (FRANCE)
Universal message passing library, or how to writea truly portable code for parallel computers
[PB95-212221] p 2948 N95-32255

MOTOROLA, INC., ARLINGTON HEIGHTS, IL.
Process maturity progress at Motorola Cellular Systems Division p 2937 N95-31239

N

NARVIK INST. OF TECH., NARVIK (NORWAY).
Effect of local melting on tribology in metal cutting
[PB95-195392] p 2804 N95-31052

NATIONAL ACADEMY OF SCIENCES - NATIONAL RESEARCH COUNCIL, WASHINGTON, DC.
Review of Gravity Probe B
[NASA-CR-198959] p 3019 N95-30781
Microgravity research opportunities for the 1990s
[NASA-CR-199109] p 2838 N95-31983

NATIONAL AERONAUTICS AND SPACE ADMINISTRATION, WASHINGTON, DC.
The process for addressing the challenges of aircraft pilot coupling p 2745 N95-31063
Management of major system programs and projects. Handbook
[NHB-7120.5] p 3021 N95-31380
Recommended techniques for effective maintainability. A continuous improvement initiative of the NASA Reliability and Maintainability Steering Committee
[NASA-TM-4628] p 2892 N95-31530
Aeronautics and space report of the President
[NASA-TM-110743] p 3028 N95-31979

NATIONAL AERONAUTICS AND SPACE ADMINISTRATION. AMES RESEARCH CENTER, MOFFETT FIELD, CA.
Moving base simulation of an integrated flight and propulsion control system for an ejector-augmentor STOVL aircraft in hover
[NASA-TM-108867] p 2750 N95-30646
Flight test evaluation of the Stanford University/United Airlines differential GPS Category 3 automatic landing system
[NASA-TM-110354] p 2743 N95-30788
Leveraging object-oriented development at Ames
p 2938 N95-31244
Use of arm measurements to improve radiative transfer models used in climate models
[NASA-CR-199014] p 2921 N95-32184
Stratospheric Observatory For Infrared Astronomy (SOFIA). Phase A: System concept description
[NASA-TM-110669] p 3002 N95-32187
Numerical solution of the full potential equation using a chimera grid approach
[NASA-TM-110360] p 2744 N95-32188

NATIONAL AERONAUTICS AND SPACE ADMINISTRATION. GODDARD SPACE FLIGHT CENTER, GREENBELT, MD.
SeaWiFS Technical Report Series. Volume 29: SeaWiFS CZCS-type pigment algorithm
[NASA-TM-104566] p 2922 N95-30857
Proceedings of the 19th Annual Software Engineering Workshop
[NASA-CR-189411] p 2936 N95-31234
Changes and challenges in the Software Engineering Laboratory p 2936 N95-31235
Building an experience factory for maintenance
p 2937 N95-31237
Profile of software engineering within the National Aeronautics and Space Administration (NASA)
p 2939 N95-31252
Preventing cracking of anodized coatings
[NASA-TM-104622] p 2839 N95-31690
SeaWiFS technical report series. Volume 28: SeaWiFS algorithms, part 1
[NASA-TM-104566-VOL-28] p 2924 N95-31850
SeaWiFS technical report series. Volume 24: SeaWiFS technical report series cumulative index, volumes 1-23
[NASA-TM-104566-VOL-24] p 2924 N95-32122
SeaWiFS technical report series. Volume 13: Case studies for SeaWiFS calibration and validation, part 1
[NASA-TM-104566-VOL-13] p 2924 N95-32220
The 26th Annual Precise Time and Time Interval (PTTI) Applications and Planning Meeting
[NASA-CP-3302] p 2967 N95-32319
Laser retroreflector experiment on NAVSTAR 35 and 36 p 2887 N95-32347

NATIONAL AERONAUTICS AND SPACE ADMINISTRATION. HUGH L. DRYDEN FLIGHT RESEARCH CENTER, EDWARDS, CA.
Flight assessment of the onboard propulsion system model for the Performance Seeking Control algorithm on an F-15 aircraft
[NASA-TM-4705] p 2756 N95-31425
Flight test validation of a frequency-based system identification method on an F-15 aircraft
[NASA-TM-4704] p 2757 N95-31846
X-29 flight control system: Lessons learned
p 2759 N95-32001

NATIONAL AERONAUTICS AND SPACE ADMINISTRATION. HUGH L. DRYDEN FLIGHT RESEARCH FACILITY, EDWARDS, CA.
PIO: A historical perspective p 2745 N95-31062

NATIONAL AERONAUTICS AND SPACE ADMINISTRATION. JOHN F. KENNEDY SPACE CENTER, COCOA BEACH, FL.
Electromyostimulation, circuits and monitoring
[NASA-TM-110741] p 2926 N95-30846
Aqueous cleaning and verification processes for precision cleaning of small parts p 2779 N95-31787
Cleaning verification by air/water impingement
p 2782 N95-31805

NATIONAL AERONAUTICS AND SPACE ADMINISTRATION. LYNDON B. JOHNSON SPACE CENTER, HOUSTON, TX.
STS-71 post flight presentation
[NASA-TM-110658] p 2764 N95-30852
Mir 18 post flight presentation
[NASA-TM-110657] p 2766 N95-30854
STS-70 flight: Day 8
[NASA-TM-110666] p 2764 N95-30873
STS-70 flight: Day 7
[NASA-TM-110665] p 2764 N95-30874
STS-70 flight: Day 6
[NASA-TM-110664] p 2764 N95-30875
STS-70 flight: Day 5
[NASA-TM-110663] p 2764 N95-30876
STS-70 flight: Day 4
[NASA-TM-110662] p 2764 N95-30877
STS-70 flight: Day 3
[NASA-TM-110661] p 2765 N95-30878
STS-70 flight: Day 2
[NASA-TM-110660] p 2765 N95-30879
STS-70 flight: Day 1
[NASA-TM-110659] p 2765 N95-30880
Making intelligent systems team players. A guide to developing intelligent monitoring systems
[NASA-TM-104807] p 2951 N95-30925
Space Shuttle Orbiter corrosion history, 1981-1993: A review and analysis of issues involving structures and subsystems
[NASA-TM-104810] p 2810 N95-32183

NATIONAL AERONAUTICS AND SPACE ADMINISTRATION. LANGLEY RESEARCH CENTER, HAMPTON, VA.
Structural design using equilibrium programming formulations
[NASA-TM-110175] p 2893 N95-30682
Orbiter rarefied-flow reentry measurements from the OARE on STS-62
[NASA-TM-110182] p 2891 N95-30783
A wind tunnel investigation of the effects of micro-vortex generators and Gurney flaps on the high-lift characteristics of a business jet wing
[NASA-TM-110626] p 2750 N95-30827
Solution of the three-dimensional Helmholtz equation with nonlocal boundary conditions
[NASA-TM-110174] p 2974 N95-30850
Patterns in the sky: Natural visualization of aircraft flow fields
[NASA-SP-514] p 2741 N95-31000
A manual for pyrotechnic design, development and qualification
[NASA-TM-110172] p 2766 N95-31358
Post-impact fatigue of cross-plied, through-the-thickness reinforced carbon/epoxy composites
[NASA-TM-110625] p 2896 N95-31419
Solid Modeling Aerospace Research Tool (SMART) user's guide, version 2.0
[NASA-TM-4431] p 2940 N95-31420
The design and development of a third generation OSEE instrument p 2781 N95-31800
Afterbody/nozzle pressure distributions of a twin-tail twin-engine fighter with axisymmetric nozzles at Mach numbers from 0.6 to 1.2
[NASA-TP-3509] p 2744 N95-31984
Computer model to simulate testing at the National Transonic Facility
[NASA-TM-4664] p 2763 N95-32217
ASSIST user manual
[NASA-TM-4592] p 2948 N95-32250

NATIONAL AERONAUTICS AND SPACE ADMINISTRATION. LEWIS RESEARCH CENTER, CLEVELAND, OH.
A system simulation development project: Leveraging resources through partnerships
[NASA-TM-106962] p 2753 N95-30514
Wave rotor-enhanced gas turbine engines
[NASA-TM-106998] p 2754 N95-30517

The effect of adding roughness and thickness to a transonic axial compressor rotor
[NASA-TM-106958] p 2867 N95-30524
Fabry-Perot interferometer measurement of static temperature and velocity for ASTOVL model tests
[NASA-TM-107014] p 2879 N95-30587
Effects of initial conditions on a single jet in crossflow
[NASA-TM-107002] p 2754 N95-30589
NASA Lewis Research Center's preheated combustor and materials test facility
[NASA-TM-106676] p 2762 N95-30592
High-temperature oxidation behavior of iridium-rhenium alloys
[NASA-TM-106720] p 2803 N95-30593
Object-oriented approach for gas turbine engine simulation
[NASA-TM-106970] p 2754 N95-30594
Supplemental multilayer insulation research facility
[NASA-TM-106991] p 2768 N95-30595
A numerical model for dynamic wave rotor analysis
[NASA-TM-106997] p 2754 N95-30617
Enhancement of perfluoropolyether boundary lubrication performance: I. Preliminary results
[NASA-TM-106937] p 2813 N95-30621
Preliminary assessment of combustion modes for internal combustion wave rotors
[NASA-TM-107000] p 2754 N95-30632
Jet mixing and emission characteristics of transverse jets in annular and cylindrical confined crossflow
[NASA-TM-106976] p 2755 N95-30698
Effect of velocity and temperature distribution at the hole exit on film cooling of turbine blades
[NASA-TM-106954] p 2755 N95-30702
Space qualified hybrid superconductor/semiconductor planar oscillator circuit
[NASA-TM-106978] p 3011 N95-30703
Validation of the NPARC code for nozzle afterbody flows at transonic speeds
[NASA-TM-106971] p 2742 N95-30704
Numerical simulation of flow in a whirling annular seal and comparison with experiments
[NASA-TM-106961] p 2867 N95-30710
Calculated coupling efficiency between an elliptical-core optical fiber and an optical waveguide over temperature
[NASA-TM-107005] p 2997 N95-30849
A laser-based ice shape profilometer for use in icing wind tunnels
[NASA-TM-106936] p 2880 N95-30851
Jet mixing in a reacting cylindrical crossflow
[NASA-TM-106975] p 2755 N95-30853
A turbulence module for the NPARC code
[NASA-CR-198358] p 2959 N95-30855
Electrically heated tube investigation of cooling channel geometry effects
[NASA-TM-106985] p 2768 N95-30856
Parametrics on 2D Navier-Stokes analysis of a Mach 2.68 bifurcated rectangular mixed-compression inlet
[NASA-TM-107003] p 2755 N95-30861
Kinetic theory model predictions compared with low-thrust axisymmetric nozzle plume data
[NASA-CR-198934] p 2768 N95-30864
Centrifugal and axial pump design and off-design performance prediction p 2830 N95-31289
Numerical modeling of Bridgman growth of PbSnTe in a magnetic field
[NASA-TM-106996] p 2837 N95-31359
Experimental and computational investigation of the tip clearance flow in a transonic axial compressor rotor
[NASA-TM-106711] p 2876 N95-31738
Operational characteristics of a 200 C LC parallel resonant circuit
[NASA-TM-106983] p 2864 N95-31742
An active magnetic bearing with high T(sub c) superconducting coils and ferromagnetic cores
[NASA-TM-106995] p 2864 N95-31847
Laser anemometer measurements of the three-dimensional rotor flow field in the NASA low-speed centrifugal compressor
[NASA-TP-3527] p 2756 N95-31985
Influence of fiber content on mechanical performance of SiC-fiber-reinforced reaction-bonded silicon nitride composites
[NASA-TM-110639] p 2790 N95-32060
Robust Rocket Engine Concept
[NASA-TM-107010] p 2770 N95-32121
A probabilistic design method applied to smart composite structures
[NASA-TM-106715] p 2899 N95-32206
Effects of temperature, frequency, flux density, and excitation waveform on the core loss and dynamic B-H loops of supermalloy
[NASA-TM-106982] p 2865 N95-32207
Low cost fabrication of silicon carbide based ceramics and fiber reinforced composites
[NASA-TM-107001] p 2822 N95-32208
A study of elevated temperature testing techniques for the fatigue behavior of PMCS: Application to T650-35/AMB21
[NASA-TM-106927] p 2791 N95-32209

NATIONAL AERONAUTICS AND SPACE ADMINISTRATION. MARSHALL SPACE FLIGHT CENTER, HUNTSVILLE, AL.

Chromospherically active stars. 6: Giants with compact hot companions and the barium star scenario
[NASA-TM-110641] p 3028 N95-30466
On the relationship between sunspots number and the flare index
[NASA-TM-110643] p 3030 N95-30467
Operating in the space plasma environment: A spacecraft charging study of the Solar X-ray Imager
[NASA-TM-110644] p 3003 N95-30468
Observations of accreting pulsars
[NASA-CR-198931] p 3028 N95-30469
On reflection of Alfven waves in the solar wind
[NASA-TM-110642] p 3031 N95-30582
Analysis of stress concentration at holes in components made of 2195 aluminum-lithium
[NASA-TP-3554] p 2893 N95-30613
Transonic aerodynamic characteristics of a proposed wing-body reusable launch vehicle concept
[NASA-TM-106489] p 2742 N95-30712
Space Sciences Laboratory Publications and Presentations
[NASA-TM-108484] p 3024 N95-30780
Navier-Stokes flow field analysis of compressible flow in a high pressure safety relief valve
[NASA-TM-110640] p 2868 N95-30862
Nearly steady flows in GONG prototype data
[NASA-CR-198935] p 2869 N95-30863
Aerospace Environmental Technology Conference: Exectutive summary
[NASA-CP-3297] p 2771 N95-31350
DE-1 observations of polar O(+) stream bulk parameters and comparison with a model of the centrifugally-accelerated polar wind
[NASA-CR-198930] p 2917 N95-31743
Aerospace Environmental Technology Conference
[NASA-CP-3298] p 2771 N95-31746
Manufacturing waste disposal practices of the chemical propulsion industry p 2771 N95-31748
CFD assessment of the pollutant environment from RD-170 propulsion system testing p 2772 N95-31749
Environmental benefits of chemical propulsion p 2772 N95-31750
Prioritization methodology for chemical replacement p 2773 N95-31757
Replacement of corrosion protection chromate primers and paints used in cryogenic applications on the Space Shuttle with wire arc sprayed aluminum coatings p 2776 N95-31774
Waterjet processes for coating removal p 2777 N95-31779
Evaluation of pressurized water cleaning systems for hardware refurbishment p 2778 N95-31782
A design of experiments test to define critical spray cleaning parameters for Brulin 815 GD and Jettacin cleaners p 2779 N95-31790
Evaluation of control parameters for Spray-In-Air (SIA) aqueous cleaning for shuttle RSRM hardware p 2780 N95-31794
Implementation of environmentally compliant cleaning and insulation bonding for MNASA p 2780 N95-31796
Surface contamination analysis technology team overview p 2781 N95-31797
Environmental databases and other computerized information tools p 2783 N95-31810
NEIS (NASA Environmental Information System) p 2783 N95-31811
The effect of environmental initiatives on NASA specifications and standards activities p 2783 N95-31812
An overview of NASA testing requirements for alternate cleaning solvents used in liquid and gaseous oxygen environments p 2783 N95-31813

NATIONAL AEROSPACE LAB., AMSTERDAM (NETHERLANDS).

Multigrid convergence acceleration for the 2D Euler equations applied to high-lift systems
[PB95-198081] p 2743 N95-30814
Development of advanced approach and departure procedures. Failure scenarios
[PB95-198123] p 2748 N95-30815
Validation of the helicopter rotor code HERO
[PB95-198040] p 2751 N95-30838
Multi-sensor data fusion in command and control and the merit of artificial intelligence p 2842 N95-32137

NATIONAL AEROSPACE LAB., TOKYO (JAPAN).

Dynamical analysis of the coriolis effect which causes space disorientation
[NAL-TR-1258] p 2928 N95-31714
Effects of cavity bleed and its configuration on aerodynamic characteristics of supersonic internal flow
[NAL-TR-1247] p 2744 N95-31715
Experiment of rocket-ram combined combustor
[NAL-TR-1249] p 2769 N95-31739
Evaluation of static strength of T800H/PMR-15 carbon/polyimide laminates at room temperature and 300 C
[NAL-TR-1254] p 2789 N95-31740
Side force acting on blunted circular cylinder bodies at high angles of attack in supersonic flow
[NAL-TR-1255] p 2744 N95-31741
On-orbit truss structure tele-operation experiment by Engineering Test Satellite-7
[NAL-TR-1246] p 2767 N95-31980

NATIONAL CENTER FOR MFG. SCIENCES, ANN ARBOR, MI.

National Center for Manufacturing Sciences: Environmentally conscious manufacturing p 2773 N95-31758
Assessment of pollution prevention and control technology for plating operations p 2776 N95-31771

NATIONAL DEFENCE RESEARCH ESTABLISHMENT, LINKOEPING (SWEDEN).

Nonlinear dynamical systems: Elements of a complex system analysis
[PB95-211652] p 2950 N95-30478
Interference rejection techniques in a DS spread-spectrum HF radio system
[PB95-211660] p 2846 N95-30479
Microwave coupling into a slotted cavity. Additional results
[PB95-210381] p 2847 N95-30629
Feasibility study concerning an active millimeterwave sensor. Project phase MMS2.1
[PB95-210399] p 2882 N95-32245
BRUTUS: A program for conversion between image formats
[PB95-211421] p 2945 N95-32246
Fast identification of some typical digital modulation schemes
[PB95-211454] p 2857 N95-32247
Texture based methods for image analysis: A review
[PB95-211595] p 2945 N95-32251
Z-scan using a dye laser
[PB95-222923] p 3002 N95-32312
Point reflector model for the simulation of radar target glint and Doppler phenomena
[PB95-222980] p 2857 N95-32314
Spectral sky background in the IR: Measurements with FTIR
[PB95-222998] p 2922 N95-32315

NATIONAL DEFENCE RESEARCH ESTABLISHMENT, STOCKHOLM (SWEDEN).

Semi-iterative method for estimation of the dipole parameters using the knowledge of the dipole orientation
[PB95-211736] p 2858 N95-30480
Ray trace model of sound propagation in range dependent media
[PB95-211751] p 2973 N95-30481
FOG
[PB95-211546] p 2879 N95-30600
Ageing control no. 3 of propellants for rocket motors RB 27 and RB 28
[PB95-210357] p 2825 N95-30626
Assessment of computer aids during communication exercise 1991
[PB95-211462] p 2945 N95-32248
Thermoplastic elastomers as a binder in composite propellants
[PB95-211553] p 2837 N95-32249
Influence of storage on the maximal pull-out force of three different optical fibers from three epoxides
[PB95-211777] p 2822 N95-32253
Analysis of the final result from the image template matching method with fuzzy logic
[PB95-222915] p 2946 N95-32311
Materials with controllable signature properties
[PB95-222964] p 2857 N95-32313

NATIONAL GEOPHYSICAL DATA CENTER, BOULDER, CO.

Solar-geophysical data number 604, December 1994. Part 2: (Comprehensive reports). Data for June 1994, and miscellaneous
[PB95-191995] p 3031 N95-30690
Solar-geophysical data number 606, February 1995. Part 1: (Prompt reports). Data for December 1994, January 1995, and late data
[PB95-200853] p 3031 N95-30816
Solar-geophysical data number 606, February 1995. Part 2: (Comprehensive reports). Data for August 1994, and miscellaneous
[PB95-200861] p 3031 N95-30817

NATIONAL HELLENIC RESEARCH FOUNDATION, ATHENS (GREECE).
Properties of new materials relevant to energy and fuel research
[AD-A289734] p 2825 N95-31149
NATIONAL INST. FOR FUSION SCIENCE, NAGOYA (JAPAN).
Physics and application of high density Z-pinches
[NIFS-PROC-14] p 3004 N95-30671
NATIONAL INST. OF STANDARDS AND TECHNOLOGY, BOULDER, CO.
Implementation of a standard format for GPS common view data p 2968 N95-32323
NATIONAL INST. OF STANDARDS AND TECHNOLOGY, GAITHERSBURG, MD.
Low temperature fabrication from nano-size ceramic powders
[DE95-010995] p 2818 N95-31153
Measurements of quantum electrodynamic sensitive transitions in Na-like and Cu-like ions
[DE95-011593] p 3007 N95-32299
NATIONAL OCEANIC AND ATMOSPHERIC ADMINISTRATION, BOULDER, CO.
Feasibility of tropospheric water vapor profiling using infrared heterodyne differential absorption lidar
[DE95-009647] p 2917 N95-32142
NATIONAL OCEANIC AND ATMOSPHERIC ADMINISTRATION, WASHINGTON, DC.
Suprious semi-diurnal variation in the E.R.B.E. outgoing longwave radiation
[NOAA-TR-NESDIS-84] p 2913 N95-30643
NATIONAL PHYSICAL LAB., TEDDINGTON (ENGLAND).
Round-robin validation exercise for plate twist test method
[PB95-208088] p 2812 N95-30487
High resolution time interval counter p 2969 N95-32331
NATIONAL RENEWABLE ENERGY LAB., GOLDEN, CO.
Advanced system identification techniques for wind turbine structures
[DE95-004049] p 2902 N95-30505
State-of-the-art low-cost solar reflector materials
[DE95-000260] p 2902 N95-30526
Validation of the FLAGSOL parabolic trough solar power plant performance model
[DE95-000263] p 2903 N95-30887
A manual for the economic evaluation of energy efficiency and renewable energy technologies
[DE95-000211] p 2903 N95-30896
Photovoltaic Czochralski silicon manufacturing technology improvements
[DE95-004066] p 2904 N95-31162
Large-area, triple-junction a-Si alloy production scale-up
[DE95-004067] p 2904 N95-31163
Photovoltaic module certification/laboratory accreditation criteria development
[DE95-004063] p 2905 N95-31381
BioFacts: Fueling a stronger economy. Methanol from biomass, revision 2
[DE95-010302] p 2836 N95-31638
BioFacts: Fueling a stronger economy. Ethanol from biomass, revision 2
[DE95-010304] p 2836 N95-31639
Photovoltaic Energy Program overview: Fiscal year 1994
[DE94-011871] p 2905 N95-31661
Sustainability protects resources for future generations
[DE95-000285] p 2909 N95-31695
Mexico Wind Resource Assessment Project
[DE95-009202] p 2921 N95-31726
BioFacts: Fueling a stronger economy, global warming and biofuels emissions
[DE94-006864] p 2910 N95-31821
BioFacts: Fueling a stronger economy, thermochemical conversion of biomass
[DE94-006866] p 2905 N95-31822
Solar thermal electric: Program overview, fiscal years 1993-1994
[DE94-000240] p 2906 N95-32058
Comprehensive research on the stability and electronic properties of a-Si:H and a-SiGe:H alloys and devices
[DE95-004068] p 2810 N95-32154
NATIONAL RESEARCH COUNCIL OF CANADA, OTTAWA (ONTARIO).
Practical experiences in control systems design using the NCR Bell 205 Airborne Simulator p 2761 N95-32015
PTTI applications at the limits of GPS p 2969 N95-32327
Metafitting: Weight optimization for least-squares fitting of PTTI data p 2971 N95-32340
NATIONAL SERVICE OF METROLOGY, DELFT (NETHERLANDS).
Automated delay measurement system for an Earth station for Two-Way Satellite Time and Frequency Transfer p 2971 N95-32337
NATIONAL TRANSPORTATION SAFETY BOARD, WASHINGTON, DC.
Annual review of aircraft accident data: US general aviation calendar year 1993
[PB95-215828] p 2747 N95-31712
Special investigation report: Safety of the air tour industry in the United States
[PB95-917004] p 2748 N95-32185
NAVAL AIR WARFARE CENTER, ARLINGTON, VA.
Operator's handbook: NAWC Software Production Facility
[AD-A290216] p 2935 N95-31001
NAVAL AIR WARFARE CENTER, CHINA LAKE, CA.
Shuttle redesigned solid rocket motor aluminum oxide investigations p 2770 N95-30989
Shuttle Redesigned Solid Rocket Motor aluminum oxide investigations p 2770 N95-31197
Enhanced energy release and soot reduction in actively controlled flames p 2799 N95-31200
A pulsed liquid fuel ramjet p 2756 N95-31201
Active control of combustion instability using injection techniques p 2800 N95-31288
Advanced oxidizers diffusion flames structure p 2801 N95-31307
RDX laser-assisted flame structure p 2801 N95-31314
The 19th Annual Electronics Manufacturing Seminar
[AD-A293067] p 2863 N95-31674
NAVAL AIR WARFARE CENTER, WARMINSTER, PA.
A comparison of coating alternatives for US Coast Guard aircraft
[AD-A293270] p 2817 N95-31124
NAVAL COMMAND, CONTROL AND OCEAN SURVEILLANCE CENTER, KAILUA, HI.
Comparisons of target detection clutter using data from the 1993 FOPEN experiments
[AD-A293052] p 2852 N95-31606
NAVAL COMMAND, CONTROL AND OCEAN SURVEILLANCE CENTER, SAN DIEGO, CA.
Intermodulation Interference (IMI) testing of composite materials
[AD-A288621] p 2787 N95-31146
Measurements of ionospheric variability
[AD-A293495] p 2915 N95-31535
NAVAL HEALTH RESEARCH CENTER, SAN DIEGO, CA.
Control of skin blood flow in the neutral zone of human body temperature regulation
[AD-A291499] p 2926 N95-30563
NAVAL OBSERVATORY, WASHINGTON, DC.
The 1994 international transatlantic two-way satellite time and frequency transfer experiment: Preliminary results p 2858 N95-32320
High accuracy time transfer synchronization p 2968 N95-32321
Network time synchronization servers at the US Naval Observatory p 2969 N95-32329
Investigation into the effects of VHF and UHF band radiation on Hewlett-Packard (HP) Cesium Beam Frequency Standards p 2970 N95-32332
Methodologies for steering clocks p 2971 N95-32341
The effects of clock errors on timescale stability p 2971 N95-32342
NAVAL POSTGRADUATE SCHOOL, MONTEREY, CA.
Yellow Sea thermal structure
[AD-A291159] p 2922 N95-30396
Decimation of encoding errors in an optimum SNS 2 micron low-noise CMOS ADC
[AD-A293208] p 2860 N95-30900
Control of flexible spacecraft structures using H-infinity wave absorbing control
[AD-A293141] p 2766 N95-30919
Probabilistic reliability modeling of fatigue on the H-46 tie bar
[AD-A289926] p 2751 N95-30927
An architectural approach to strategic information systems planning for the Office of Naval Intelligence
[AD-A289930] p 3024 N95-30928
Failure analysis of a repairable system: The case study of a cam-driven reciprocating pump
[AD-A293144] p 2889 N95-30949
Experimental investigation of the effectiveness of flow-through modules for electronics cooling
[AD-A293284] p 2861 N95-30950
Analog preprocessing in a SNS 2 micrometers low-noise CMOS folding ADC
[AD-A293356] p 2849 N95-30954
Construction and performance measurement of a portable thermoacoustic refrigerator demonstration apparatus
[AD-A293265] p 2839 N95-31122
Shiptracks in the Californian stratus region: Dependency on marine atmospheric boundary layer depth
[AD-A293272] p 2901 N95-31125
An investigation of the side-dump dual in-line ramjet combustor p 2756 N95-31199
Computer interface development for the petite amateur navy satellite (PANSAT) simulator
[AD-A293263] p 2766 N95-31388
Development of a structured design and programming methodology for expert systems shells utilizing a visual programming language: Application of structured methodology to the MK92 maintenance advisor expert system, performance module prototype
[AD-A289897] p 2939 N95-31391
Microstructure and aging response of SiCp reinforced A356 Al metal matrix composite subject to post fabrication thermomechanical processing
[AD-A292975] p 2789 N95-31469
Analytic and experimental investigation of rotordynamic response and backward whirl induced by split resonance
[AD-A293639] p 2889 N95-31566
Response of dual-layered structures subjected to shock pressure wave
[AD-A293731] p 2896 N95-31568
Validation of special sensor microwave/imager ocean surface wind retrievals in equatorial regions
[AD-A293750] p 2920 N95-31571
Finite element analysis of smart structures and modal testing of a flexible spacecraft arm
[AD-A293761] p 2890 N95-31576
A case study of the teaming concept in the procurement of the V-22 aircraft
[AD-A293770] p 2752 N95-31578
Modeling F/A-18 flight hour program costs using regression analysis
[AD-A293771] p 2752 N95-31579
Effects of mosaicity on Parametric X-Radiation production
[AD-A293677] p 2985 N95-31597
Comparison of satellite-derived MSU brightness temperatures and conventionally-derived fields
[AD-A293692] p 2901 N95-31603
Design and testing of an optimal digital link capable of 14-channel transmission
[AD-A288505] p 3000 N95-31652
Automatic Target Recognition (ATR): Background statistics and the detection of targets in clutter
[AD-A293062] p 2853 N95-31673
Prime power for shipboard high-average power FELs
[AD-A293718] p 2886 N95-31833
Application of a genetic algorithm to optimize staffing levels in software development
[AD-A293725] p 2943 N95-31835
Analysis of target contrast improvement using polarization filtering in the infrared region
[AD-A293085] p 3001 N95-31841
NAVAL RESEARCH LAB., BAY SAINT LOUIS, MS.
FISHFINDE: Interactive software package to predict fish locations using satellite image data and fish species behavior rules
[AD-A293394] p 2935 N95-30968
Satellite multisensor data techniques for sea ice mapping
[AD-A289729] p 2901 N95-31148
Digital Mapping Charting and Geodesy Analysis Program technical review of Vector Product Format (VPF)
[AD-A289766] p 2901 N95-31390
NAVAL RESEARCH LAB., MONTEREY, CA.
Environmental support of naval aviation
[AD-A292873] p 2747 N95-31454
NAVAL RESEARCH LAB., WASHINGTON, DC.
Computational modeling of coating integrity effects on impressed current cathodic protection system
[AD-A293256] p 2815 N95-30894
X-band magnicon amplifier research at the Naval Research Laboratory
[AD-A293203] p 3013 N95-30984
Design considerations for a Density-Channel-Guided laser wake-field accelerator
[AD-A292876] p 2884 N95-31190
Detailed chemical kinetic modeling of premixed hydrocarbon flames supported by NO2 p 2801 N95-31311
An analysis of gas phase ethanol/water chemistry for diamond CVD
[AD-A293009] p 2795 N95-31473
A numerical study of the effect of the Gulf Stream and the Appalachian Mountains on Carolina coastal frontogenesis
[AD-A293765] p 2921 N95-31577
Millimeter wave radiometer utility study
[AD-A293811] p 2852 N95-31590

NAVAL SURFACE WARFARE CENTER, BETHESDA, MD.
Comparison of cathodic protection currents on 70/30 copper-nickel and alloy 625 piping systems
[AD-A292953] p 2807 N95-31561
Hot compression testing of tungsten
[AD-A293683] p 2807 N95-31599
NAVAL SURFACE WARFARE CENTER, SILVER SPRING, MD.
Hypervelocity wind tunnel number 9, high Mach number development program
[AD-A289934] p 2743 N95-30929
Electromagnetic field exposure dosimeter
[AD-A293191] p 2927 N95-30981
NAVAL UNDERSEA WARFARE CENTER, NEW LONDON, CT.
Molecular modeling of PMN ceramics
[AD-A290879] p 2813 N95-30560
Wave propagation in a fluid-loaded homogeneous, transversely isotropic, elastic cylinder of arbitrary thickness
[AD-A292728] p 2869 N95-30946
NAVAL UNDERSEA WARFARE CENTER, NEWPORT, RI.
An inverse method to measure the axial modulus of composite materials under tension
[AD-A293042] p 2789 N95-31668
NEBRASKA UNIV., LINCOLN, NE.
Spectroscopic ellipsometry as a sensitive monitor of materials contamination p 2782 N95-31808
NEVADA UNIV., LAS VEGAS, NV.
Adaptive image enhancement of text images that contain touching or broken characters
[DE95-010173] p 3023 N95-30620
An evaluation of an automatic markup system
[DE95-009885] p 3026 N95-32149
UNLV: Information Science Research Institute
[DE95-011941] p 3027 N95-32362
NEVADA UNIV., RENO, NV.
Cloud condensation nuclei measurements in shiptrails
[AD-A293302] p 2919 N95-30951
NEVADA UNIV. SYSTEM, RENO, NV.
Anodically enhanced diffusion in Cu/Ag thin film couples
[DE95-009198] p 2814 N95-30738
NEW ENERGY AND INDUSTRIAL TECHNOLOGY DEVELOPMENT ORGANIZATION, TOKYO (JAPAN).
Data on development of new energy technologies
[DE95-764135] p 2904 N95-31155
Evaluation and analysis survey on new energy introduction, part 3
[DE95-769806] p 2906 N95-32072
NEW HAMPSHIRE UNIV., DURHAM, NH.
Study of cross-tail current carriers in magnetotail p 3005 N95-30804
NEW YORK UNIV., NEW YORK, NY.
Direct and inverse problems in random media
[AD-A293033] p 2850 N95-31280
Towards increased productivity of algorithm implementation
[AD-A292862] p 2940 N95-31452
NEWCASTLE-UPON-TYNE UNIV., NEWCASTLE (ENGLAND).
C++ as an introductory programming language
[PB95-195715] p 2933 N95-30539
NIELSEN ENGINEERING AND RESEARCH, INC., MOUNTAIN VIEW, CA.
Vorticity dynamics and control of dynamic stall
[AD-A288658] p 2756 N95-31400
NORTH ATLANTIC TREATY ORGANIZATION, BRUSSELS (BELGIUM).
Study of Extended Air Defence Post 2000 p 2839 N95-32124
NORTH CAROLINA STATE UNIV., RALEIGH, NC.
Growth, characterization and device development in monocrystalline diamond films
[AD-A293106] p 3015 N95-32018
NORTH CAROLINA UNIV., CHAPEL HILL, NC.
Electron transfer kinetics of self-assembled ferrocene C(12) alkanethiol monolayers on gold electrodes from 125K to 175K
[AD-A292754] p 2984 N95-31427
Consequences of kinetic dispersion on the electrochemistry of an adsorbed redox-active monolayer
[AD-A292794] p 2795 N95-31437
NORTHROP GRUMMAN CORP., PICO RIVERA, CA.
Environmentally regulated aerospace coatings p 2777 N95-31775
NORTHWEST RESEARCH ASSOCIATES, INC., BELLEVUE, WA.
Sea ice stress research
[AD-A293164] p 2923 N95-30964
A prototype ionospheric tomography system (ITS)
[AD-A293015] p 2916 N95-31698
NORTHWESTERN UNIV., CHICAGO, IL.
Numerical studies of nonlinear optical pulse propagation p 2998 N95-31411
A study of ion trapping and instability in the Fermilab antiproton accumulator p 2993 N95-31647
Studies in marine tectonics: Propagating rifts, depth anomalies and subduction zone anisotropy p 2923 N95-31719
The role of the hydrological cycle and the ocean's thermohaline circulation in climate change: A multicomponent climate model study p 2909 N95-31720
NORTHWESTERN UNIV., EVANSTON, IL.
Learning in an intentional system
[AD-A291158] p 2949 N95-30395
Chaos-enhanced transport and aggregation in chaotic flows
[AD-A293892] p 3020 N95-31545
NORWEGIAN DEFENCE RESEARCH ESTABLISHMENT, KJELLER (NORWAY).
BASIS image processor PR5200: Module Common Part
[PB95-212023] p 2933 N95-30501
Results from tests of the Kearfott T16-B Inertial Measurement Unit
[PB95-212031] p 2879 N95-30502
The Coprocessor Manager in the BASIS processor system
[PB95-211611] p 2945 N95-32252
NORWEGIAN HYDRODYNAMIC LABS., TRONDHEIM (NORWAY).
Weather influence on passive microwave brightness temperatures
[PB95-195384] p 2900 N95-30536
NORWEGIAN INST. FOR AIR RESEARCH, KJELLER (NORWAY).
Results from tests of the Honeywell integrated flight management unit
[PB95-211355] p 2748 N95-30597
Cesar3 MALU library
[PB95-211363] p 2933 N95-30598
NOVOSIBIRSK STATE UNIV. (USSR).
Shnirelman peak in the level spacing statistics
[DE95-623599] p 3019 N95-31276
NYMA, INC., BROOK PARK, OH.
Effects of thermal and electrical stressing on the breakdown behavior of space wiring
[NASA-CR-198360] p 2768 N95-30860
Flow quality improvements in the NASA Lewis Research Center 9- by 15-foot Low Speed Wind Tunnel
[NASA-CR-195439] p 2763 N95-31653
Effects of civil tiltrotor service in the northeast corridor on en route airspace loads
[AD-A293586] p 2747 N95-31687
NYSERNET, INC., LIVERPOOL, NY.
Wide area networking R&D
[AD-A291057] p 2947 N95-30868

O

OAK RIDGE NATIONAL LAB., TN.
Morphology and microstructure of (111) crystalline CeO2 films grown on amorphous SiO2 substrates by pulsed-laser ablation
[DE95-008842] p 3009 N95-30542
Interface degradation in CAS/Nicalon during elevated temperature aging
[DE95-008843] p 2812 N95-30543
Direct determination of grain boundary atomic structure in SrTiO3
[DE95-008847] p 3010 N95-30544
Ionic conductivities of lithium phosphorus oxynitride glasses, polycrystals, and thin films
[DE95-008898] p 2812 N95-30545
Semiconductor nanocrystals formed in SiO2 by ion implantation
[DE95-008900] p 2978 N95-30546
Applications of SXPS for studying surface structure, reaction mechanisms and kinetics
[DE95-008903] p 2803 N95-30547
An explanation for the shape of nanoindentation unloading curves based on finite element simulation
[DE95-008905] p 2812 N95-30548
Modeling of thermal, electronic, hydrodynamic, and dynamic deposition processes for pulsed-laser deposition of thin films
[DE95-008906] p 2813 N95-30572
Reaction synthesis of intermetallics
[DE95-009029] p 2803 N95-30575
Direct sublattice imaging of interface dislocation structures in CdTe/GaAs(001)
[DE95-009031] p 3010 N95-30576
An overview of high-speed networking for workstations
[DE95-009076] p 2947 N95-30577
Algorithm comparison and benchmarking using a parallel spectra transform shallow water model
[DE95-009124] p 2913 N95-30683
Advanced computational research in materials processing for design and manufacturing
[DE95-009130] p 2838 N95-30684
Mechanisms of enhanced ionic conduction at interfaces in ceramics
[DE95-009125] p 2814 N95-30730
Fabrication and modification of metal nanocluster composites using ion and laser beams
[DE95-009131] p 2784 N95-30731
Stress relaxation of silicon nitride at elevated temperatures
[DE95-009177] p 2814 N95-30732
Determination of site-occupancies in aluminide intermetallics by ALCHEMI
[DE95-009179] p 2803 N95-30733
Publications of the Fossil Energy Advanced Research and Technology Development Materials Program: April 1, 1993-March 31, 1995
[DE95-009200] p 2903 N95-30745
Field performance of the Walker Branch throughfall displacement experiment
[DE95-008677] p 2908 N95-30793
Amorphization threshold in Si-implanted strained SiGe alloy layers
[DE95-008901] p 2804 N95-30797
Porous spherical shells and microspheres by electrodispersion precipitation
[DE95-009073] p 2815 N95-30799
An assessment of the cost of microwave sintering ceramic tiles for armor applications. Phase 2 report
[DE95-010000] p 2816 N95-31103
Molecular dynamics simulations of high energy cascades in iron
[DE95-010116] p 2982 N95-31104
Microstructural and mechanical property changes in model Fe-Cu alloys
[DE95-010117] p 2805 N95-31105
Review of environmental effects in intermetallics
[DE95-010120] p 2805 N95-31106
The effect of grain refinement on the room-temperature ductility of as-cast Fe3Al-based alloys
[DE95-010121] p 2805 N95-31107
A scalable parallel Strassen's matrix multiply algorithm for distributed memory computers
[DE95-010213] p 2936 N95-31109
Shape memory properties of an iron modified nickel aluminide alloy
[DE95-010223] p 2805 N95-31111
Implementation of KIVA-3 on distributed memory MIMD computers
[DE95-010288] p 2931 N95-31130
Effect of cyclic loading on the creep performance of silicon nitride
[DE95-010289] p 2894 N95-31131
QMR methods in computational fluid dynamics
[DE95-010293] p 2872 N95-31132
Life prediction methodology for ceramic components of advanced heat engines: Phase 1. Volume 1
[DE95-010805] p 2817 N95-31135
Life prediction methodology for ceramic components of advanced heat engines. Phase 1: Volume 2. Appendices
[DE95-010806] p 2817 N95-31136
Low temperature fabrication from nano-size ceramic powders
[DE95-010995] p 2818 N95-31153
Cracking during nanoindentation and its use in the measurement of fracture toughness
[DE95-008839] p 2818 N95-31175
Synthesis and selected micro-mechanical properties of titanium nitride thin films by the pyrolysis of tetrakis titanium in ammonia
[DE95-010224] p 2818 N95-31187
Effect of irradiation spectrum on the microstructure of ion-irradiated Al2O3
[DE95-010225] p 2806 N95-31188
Convoy electron emission from surfaces
[DE95-010298] p 2984 N95-31402
Self-lubricating, TiN-MoS2 composite coatings produced by simultaneous deposition from Ti((CH3))2N4/NH3/MoF6H2S gas mixture
[DE95-010359] p 2788 N95-31403
Biomass production by fescue and switchgrass alone and in mixed swards with legumes
[DE95-009137] p 2909 N95-31612
Finite-sample based learning algorithms for feedforward networks
[DE95-009123] p 2941 N95-31631
Modeling of stress distributions on the microstructural level in Alloy 600
[DE95-009135] p 2807 N95-31632
Differences in creep performance of a HIPed silicon nitride in ambient air and inert environments
[DE95-009172] p 2796 N95-31633

Network user's guide
[DE95-009185] p 2942 N95-31634
Phase stability, point defects and site preference of FeAl and NiAl with ternary additions
[DE95-009694] p 3015 N95-31641
Amorphization and the effect of implanted ions in SiC
[DE95-009699] p 2985 N95-31642
Initial survey on fracture toughness of commercial Nd2Fe14B
[DE95-009813] p 2808 N95-31643
A centrifuge CO2 pellet cleaning system
p 2778 N95-31784
A microwave plasma cleaning apparatus
p 2779 N95-31786
Modeling of grain boundary stresses in Alloy 600
[DE95-009033] p 2808 N95-31825
Predictions of tensile behavior and strengths of a SiN4 ceramic at high temperatures based on a viscoplastic model
[DE95-010220] p 2821 N95-32025
Monte Carlo tests of the ELIPGRID-PC algorithm
[DE95-010811] p 2943 N95-32030
MPI implementation of PHOENICS: A general purpose computational fluid dynamics code
[DE95-009810] p 2877 N95-32033
Microstructure of Al2O3 irradiated with an applied electric field
[DE95-010278] p 2822 N95-32043
Gelcasting of sintered reaction-bonded silicon nitride for improved mechanical properties
[DE95-010282] p 2822 N95-32085
Ultrasensitive fluorescence detection and photophysics in microdroplets
[DE95-010283] p 2798 N95-32086
Carbon dioxide concentrations in surface water and the atmosphere during 1986-1989 NOAA/PMEL cruises in the Pacific and Indian Oceans
[DE95-009659] p 2910 N95-32099
Wall stabilization of high beta plasmas in D3-D
[DE95-009607] p 3007 N95-32116
Validation of favor code linear elastic fracture solutions for finite-length flaw geometries
[DE95-009034] p 2896 N95-32157
Suppression of self-interstitials in silicon during ion implantation via in-situ photoexcitation
[DE95-009173] p 3016 N95-32301
Residual stress distribution in FeAl weld overlay on steel
[DE95-009178] p 2899 N95-32317
Nondestructive testing of ceramic components: Cooperative Research and Development Agreement completion report
[DE95-009510] p 2823 N95-32352

OAK RIDGE Y-12 PLANT, TN.
Determination of halogens in a petroleum product by ion chromatography
[DE95-002056] p 2797 N95-31840

OBSERVATOIRE DE LA COTE D'AZUR, GRASSE (FRANCE).
(T2L2) Time Transfer by Laser Link
p 2887 N95-32348

OFFICE NATIONAL D'ETUDES ET DE RECHERCHES AERONAUTIQUES, PARIS (FRANCE).
Design of surveillance and multisensor anti-aerial systems p 2841 N95-32134

OFFICE NATIONAL D'ETUDES ET DE RECHERCHES AEROSPATIALES, TOULOUSE (FRANCE).
Evaluation of the techniques of fuzzy control for the piloting an aircraft p 2758 N95-31997

OFFICE OF NAVAL RESEARCH, ARLINGTON, VA.
Data collection at the Lockheed Santa Cruz facility using midwave hyperspectral imagers
[AD-A293057] p 3000 N95-31672

OFFICINE GALILEO S.P.A., FLORENCE (ITALY).
Optimal infrared detector configurations for air target detection p 2841 N95-32130

OHIO STATE UNIV., COLUMBUS, OH.
Ultrasonic characterization of fiber-matrix interphasial properties and damage in high-temperature composites
p 2785 N95-30623
The 49th International Symposium on Molecular Spectroscopy
[AD-A292708] p 2793 N95-30936
Fluid-film lubrication: with an application to piston rings
p 2890 N95-32119

OHIO UNIV., ATHENS, OH.
Computerized design of controllers using data models
[NASA-CR-198921] p 2950 N95-30655
Enhancements to the SSME transfer function modeling code
[NASA-CR-198957] p 2958 N95-30754

OKLAHOMA UNIV., NORMAN, OK.
TV-VI semiconductor quantum well lasers, physics and engineering p 2883 N95-30805
Liquid natural gas as a transportation fuel in the heavy trucking industry
[DE95-010376] p 2837 N95-32158

OLD DOMINION UNIV., NORFOLK, VA.
Unsteady flow simulations about moving boundary configurations using dynamic domain decomposition techniques p 2877 N95-31837
Geometric modeling for computer aided design
[NASA-CR-198828] p 2943 N95-31982

OREGON GRADUATE INST. OF SCIENCE AND TECHNOLOGY, BEAVERTON, OR.
The GCRC two-dimensional zonally averaged statistical dynamical climate model: Development, model performance, and climate sensitivity
p 2910 N95-31851

OREGON STATE UNIV., CORVALLIS, OR.
Laboratory simulated hydrothermal alteration of sedimentary organic matter from Guaymas Basin, Gulf of California
[NASA-CR-198951] p 2914 N95-30865
The determination of wave group parameters from the resolution of incident and reflected waves
[AD-A293703] p 2924 N95-31829

ORION INTERNATIONAL TECHNOLOGIES, ALBUQUERQUE, NM.
Assessment of the NASA orbital debris engineering model
[AD-A293350] p 2766 N95-31143

OSLO UNIV. (NORWAY).
Data reduction of piecewise linear curves
[PB95-212270] p 2962 N95-32256

P

PACIFIC ADVANCED TECHNOLOGY, SOLVANG, CA.
Data collection at the Lockheed Santa Cruz facility using midwave hyperspectral imagers
[AD-A293057] p 3000 N95-31672

PACIFIC NORTHWEST LAB., RICHLAND, WA.
Scaling of cross sections in ion-atom collisions
[DE95-008938] p 2978 N95-30573
Interfacial segregation and deformation of superplastically deformed Al-Mg-Mn alloys
[DE95-009572] p 2809 N95-32052
The potential for microtechnology applications in energy systems: Results of an experts workshop
[DE95-009103] p 2865 N95-32077
Laboratory directed research and development report
[DE95-011405] p 3032 N95-32279

PACIFIC-SIERRA RESEARCH CORP., SANTA MONICA, CA.
Airborne ocean water lidar (OWL) real time processor (RTP)
[AD-A293226] p 2848 N95-30904
Hot jet/wake turbulent structure and laser propagation. Part 3: Laser propagation measurements and modeling
p 2871 N95-30992

PADUA UNIV. (ITALY).
Complex conjugate pairs in stationary Sturmians
[DE95-616279] p 2976 N95-30429

PAKISTAN INST. OF NUCLEAR SCIENCE AND TECHNOLOGY, ISLAMABAD.
Standardization of (13)CO2 production procedure from organic matter for mass spectrometric analysis
[DE95-614629] p 2791 N95-30420

PENNSYLVANIA STATE UNIV., ERIE, PA.
A search for interstellar CH3D: Limits to the methane abundance in Orion-KL
[NASA-CR-198932] p 3029 N95-30751

PENNSYLVANIA STATE UNIV., STATE COLLEGE, PA.
Air pollution control system research: An iterative approach to developing affordable systems
p 2773 N95-31759

PENNSYLVANIA STATE UNIV., UNIVERSITY PARK, PA.
Multiparameter radar measurements of precipitation in complex terrain: Meteorological and hydrological applications
[AD-A290786] p 2918 N95-30403
Simulation of chemical kinetics in turbulent natural gas combustion. Volume 2: Experimental studies of nitric oxide production in gas flames
[PB95-196721] p 2791 N95-30541
Observation and characterization of burning surface reaction zones of solid propellants p 2800 N95-31296
Modeling of thermal response of filament used in T-jump experiment p 2800 N95-31297
Assessment of dynamic burning behavior for JA-2 propellant rods p 2800 N95-31299
Measurement of temperatures and OH concentrations of solid propellant flames using absorption spectroscopy
p 2801 N95-31302
Species and temperature profiles of propellant flames obtained from FTIR absorption spectroscopy
p 2801 N95-31303
A study of gas-phase processes during the deflagration of RDX composite propellants using a triple quadrupole mass spectrometer p 2801 N95-31304
A study of the gas-phase processes of RDX combustion using a triple quadrupole mass-spectrometer
p 2801 N95-31315
Materials for adaptive structural acoustic control, volume 1
[AD-A293444] p 2788 N95-31369
Materials for adaptive structural acoustic control, volume 2
[AD-A293445] p 2788 N95-31370
Materials for adaptive structural acoustic control, volume 3
[AD-A293446] p 2788 N95-31371
Materials for adaptive structural acoustic control, volume 4
[AD-A293447] p 2788 N95-31372
The study of flame-vortex interactions using a particle image velocimeter p 2796 N95-31709
Primary atomization of liquid jets issuing from rocket engine coaxial injectors p 2769 N95-31716
Combustion of LOX with H2(sub g) under subcritical and supercritical conditions p 2797 N95-31717
Non-intrusive combustion diagnostics of premixed hydrocarbon flames using FT-IR spectrometry
p 2797 N95-31732

PENNSYLVANIA UNIV., PHILADELPHIA, PA.
Neurodynamical systems for cognition and target identification
[AD-A293111] p 2951 N95-30884
Nonlinear optical processes in polymer films
[AD-A293384] p 2815 N95-30955
Control of mechanical systems with rolling contacts: Applications to robotics p 2889 N95-31332
The physical and chemical processes governing CO2 laser-induced pyrolysis and combustion of the solid propellants RDX, ADN, XM39, and M43
p 2836 N95-31531
Research in ground-to-air microwave imaging
[AD-A292907] p 2852 N95-31551

PHASE FOUR SYSTEMS, INC., HUNTSVILLE, AL.
The dynamic range of radar signal generation in the MSS-2 simulation facility
[AD-A293856] p 2857 N95-32259

PHILLIPS LAB., EDWARDS AFB, CA.
Theoretical absorption spectroscopy of high-temperature metal vapors: Model and experiment compared
[AD-A290872] p 2791 N95-30409
Proceedings of the high energy density matter (HEDM) contractor's conference
[AD-A292988] p 2836 N95-31470

PHILLIPS LAB., HANSCOM AFB, MA.
Proceedings of the 16th Annual Conference on Atmospheric Transmission Models, volume 1
[AD-A293807] p 2915 N95-31575
Proceedings of the 16th Annual Conference on Atmospheric Transmission Models, volume 2
[AD-A293806] p 2916 N95-31604

PHILLIPS LAB., KIRTLAND AFB, NM.
The High Altitude Balloon Experiment demonstration of acquisition, tracking, and pointing technologies (HABE-ATP) p 2841 N95-32132

PHYSICAL SCIENCES, INC., ANDOVER, MA.
Contamination detection NDE for cleaning process inspection p 2781 N95-31802

PICATINNY ARSENAL, DOVER, NJ.
Acidity and basicity of nitro substituted imidazoles
p 2832 N95-31301

PITTSBURGH UNIV., PITTSBURGH, PA.
Analysis of symbolic parameter models
[AD-A292916] p 2940 N95-31459

POLISH ACADEMY OF SCIENCES, WARSAW (POLAND).
Resonance characteristics in the case of the excitation of a monoenergstic beam of free atoms by means of N. F. Ramsey's method
[IFTR-6/1995] p 2993 N95-31336
A simplified technique for determining the symmetry groups of non-linear plasma kinetic equations
[IFTR-8/1995] p 2960 N95-31337
An analysis of the cover of a liquid-filled circular container
[IFTR-1/1995] p 2895 N95-31338
Determination of the symmetry of a non-linear Schroedinger equation
[IFTR-10/1995] p 2960 N95-31339
Automation of the control of acoustic parameters in a digital speech synthesizer
[IFTR-2/1995] p 2850 N95-31357
Selected problems of the identification of weak double layers in plasma on a background of different aperiodic non-collision structures
[IFTR-4/1995] p 3006 N95-31737

Selected flows with free surfaces: Streams and drops
[IFTR-3/1995] p 2876 N95-31817
Detection of the phase shift which accompanies the excitation of an atomic beam by N. F. Ramsey's method
[IFTR-5/1995] p 2986 N95-3181[illegible]
The contextual variance of devoiced fricatives in polish
[IFTR-7/1995] p 2854 N95-32192

PRIMAL SOLUTIONS, INC., PALO ALTO, CA.
User-friendly microcomputer interface with optimization languages AF94-007
[AD-A293184] p 2932 N95-32257

PRINCETON SCIENTIFIC ENTERPRISES, NJ.
Progress in developing propellant ignition systems based upon electrically conductive polymers
p 2800 N95-31300

PRINCETON UNIV., NJ.
The oxidation of carbon monoxide by nitrous oxide
p 2801 N95-31309
The oxidation of carbon monoxide by nitrogen dioxide
p 2801 N95-31310

PURDUE UNIV., WEST LAFAYETTE, IN.
Fatigue crack growth behavior of a titanium matrix composite under thermomechanical loading
p 2784 N95-30491
Energy flow analysis of coupled structures
p 2895 N95-31316
Studies in non-linear multi-mode responses of harmonically excited rectangular plates with internal resonances p 2895 N95-31331
Nonlinear dynamics and chaotic motions of a singularly perturbed nonlinear viscoelastic beam
p 2897 N95-31706

Q

QUANTUM MAGNETICS, INC., SAN DIEGO, CA.
Inductively coupled IR staring array based on photofluxonic pixels
[AD-A292784] p 2998 N95-31435

QUEST INTEGRATED, INC., KENT, WA.
In situ composites in the aluminum nitride-alumina system
[AD-A293776] p 2789 N95-31509

R

RADIOCODE CLOCKS LTD., PENRYN (ENGLAND).
Custom Turnkey Time and Frequency Systems: A structured, expendable approach p 2969 N95-32330

RANGE COMMANDERS COUNCIL, WHITE SANDS MISSILE RANGE, NM.
Using satellites for radar performance monitoring and calibration
[AD-A293809] p 2852 N95-31588

RAYTHEON CANADA LTD., WATERLOO (ONTARIO).
Multisensor data fusion for integrated maritime surveillance p 2842 N95-32135

RAYTHEON CO., BEDFORD, MA.
Neural network false alarm filter, volume 1
[AD-A293097] p 2953 N95-31562

RAYTHEON CO., TEWKSBURY, MA.
Neural network false alarm filter, volume 2
[AD-A293114] p 2860 N95-30886

RE/SPEC, INC., RAPID CITY, SD.
Experimental determination of probability distributions for parameters of a Salem limestone cap plasticity model
[AD-A290878] p 2892 N95-30559

RENSSELAER POLYTECHNIC INST., TROY, NY.
A theory for predicting and minimizing the effects of matrix degradation on the thermomechanical properties of general laminates p 2785 N95-30768
Elastic and inelastic micromechanical analysis of functionally graded materials and laminated structures using transformation fields p 2787 N95-31347
Adaptiveness in information systems integration
p 3025 N95-31348

RESEARCH SCIENCES CORP., LEXINGTON, MA.
Measurement and analysis related to infrared emissions
[AD-A293296] p 2998 N95-31192

RESEARCH TRIANGLE INST., RESEARCH TRIANGLE PARK, NC.
Mission critical failure effects analysis using quantitative techniques
[AD-A293098] p 2864 N95-31844

RHODE ISLAND UNIV., KINGSTON, RI.
Statistical interface for chaotic signal in noise
[AD-A290271] p 2848 N95-30932

RICE UNIV., HOUSTON, TX.
Application of spin-sensitive electron spectroscopies to investigations of electronic and magnetic properties of solid surfaces and epitaxial systems
[DE95-010154] p 2792 N95-30614
Topics in exploratory and speculative data analysis
[AD-A290505] p 3025 N95-31618
Variational optimization in quantum field theory
p 3020 N95-31646

ROCHESTER UNIV., NY.
Algorithms for categorizing multiprocessor communication under invalidate and update-based coherence protocols
[AD-A290022] p 2947 N95-30930
Conjugated aromatic polyimines. 2. Synthesis, structure, and properties of new aromatic polyazomethines
[AD-A292955] p 2819 N95-31461
Excited-state complexes of conjugated polymers: Novel photophysical processes and optoelectronic materials
[AD-A292958] p 2819 N95-31462
Excited-state complexes of conjugated polymers
[AD-A292960] p 2819 N95-31466
Effects of molecular structure on the electroactive and optical properties of conjugated rigid-rod polybenzobisazoles
[AD-A292968] p 2819 N95-31467
Nonparametric recognition of nonrigid motion
[AD-A293630] p 2963 N95-31565
An analysis of hierarchical genetic programming
[AD-A293964] p 2942 N95-31657

ROCKWELL INTERNATIONAL CORP., ALBUQUERQUE, NM.
Adaptive optics design for the advanced electro-optical system (AEOS)
[AD-A293972] p 2974 N95-31527

ROCKWELL INTERNATIONAL CORP., CANOGA PARK, CA.
Design and testing of an oxidizer-rich preburner
p 2799 N95-31212
Thin-film sulfuric acid anodizing as a replacement for chromic acid anodizing p 2776 N95-31772
SSME Main Combustion Chamber (MCC) hot oil dewaxing p 2777 N95-31777
Ultrasonic frequency selection for aqueous fine cleaning p 2779 N95-31788
Investigation of cleanliness verification techniques for rocket engine hardware p 2770 N95-31806

ROCKWELL INTERNATIONAL CORP., CEDAR RAPIDS, IA.
Relativistic timescale analysis suggests lunar theory revision p 2970 N95-32333

ROME LAB., GRIFFISS AFB, NY.
Proceedings of the antenna applications symposium. volume 2
[AD-A293259] p 2850 N95-31387
Optical correlator optimizations and extensions for automated optical target recognition
[AD-A293013] p 3000 N95-31697

ROME LAB., HANSCOM AFB, MA.
Proceedings of the antenna applications symposium, volume 1
[AD-A293258] p 2848 N95-30895

ROYAL INST. OF TECH., STOCKHOLM (SWEDEN).
Size of Fulton's essential set
[PB95-211645] p 2955 N95-30477
Newton methods for large-scale linear inequality-constrained minimization: Optimization and systems theory
[PB95-210332] p 2956 N95-30499
Combination of Fulton's essential set
[PB95-211637] p 2956 N95-30500
Complex mean value interpolation
[PB95-211629] p 2956 N95-30601
Speed control of an elastic two-mass system: Optimization and systems theory
[PB95-212106] p 2888 N95-30701
Potential integral equations of the 2D Laplace operator in wavelet basis
[TRITA-NA-9401] p 2957 N95-30713
Simplex method for semi-definite programming: Optimization and systems theory
[PB95-212122] p 2934 N95-30792
Frobenius algebras and quantum Yang-Baxter equation 2
[PB95-212130] p 2960 N95-31229
On convective effects in sedimentation of concentrated suspensions with high effective gravity
[TRITA-NA-9316] p 2794 N95-31356
A study of numerical solutions of conservation laws
[TRITA-NA-9315] p 2960 N95-31361
Aspects of the search time in binary search trees modified according to the move-to-root heuristic
[PB95-212148] p 2963 N95-31396
Antipodes and integrals in Hopf algebras over rings and quantum Yang-Baxter equation
[PB95-212155] p 2961 N95-31397
Poisson approximation using the Stein-Chen method and coupling: Number of exceedances of a discrete-time-chi-squared process
[PB95-212205] p 2961 N95-31398
Numerical simulation of time dependent viscoelastic fluid flow
[TRITA-NA-9311] p 2873 N95-31414
Some aspects on the modelling of non-Newtonian fluid flow
[TRITA-NA-9317] p 2873 N95-31415
The complexity and approximability of finding maximum feasible subsystems of linear relations
[TRITA-NA-9313] p 2961 N95-31648
Thermoplastic elastomers as a binder in composite propellants
[PB95-211553] p 2837 N95-32249

ROYAL NORWEGIAN COUNCIL FOR SCIENTIFIC AND INDUSTRIAL RESEARCH, OSLO (NORWAY).
Data reduction of piecewise linear curves
[PB95-212270] p 2962 N95-32256

RUTGERS - THE STATE UNIV., NEW BRUNSWICK, NJ.
The remainder form and the cord-slope form in global optimization with interval methods p 2941 N95-31533

RUTHERFORD APPLETON LAB., OXFORD (ENGLAND).
Confronting left-right symmetric models with electroweak precision data at the Z peak
[PB95-208054] p 2977 N95-30484
Finite element simulation of GaAs MESFET's
[PB95-208062] p 3009 N95-30485
HERA and the asymptotic behaviour of F2(sup rho)
[PB95-195764] p 2956 N95-30540
Experimental characterisation of gas microstrip detectors. Part 3: Lifetime characteristics
[PB95-192845] p 2880 N95-30691
Use of element-by-element preconditioners to solve large scale partially separable optimization problems
[PB95-195772] p 2957 N95-30692
Metrology of chrome on quartz photomasks using low voltage scanning electron microscopy. Part 1: Physical SEM parameters
[PB95-195780] p 2880 N95-30693
Thermoviscoelastic behaviour of solids
[PB95-196226] p 2784 N95-30694
Minijet veto: A tool for the heavy Higgs search at the LHC
[PB95-196234] p 2979 N95-30695
Client server architecture for multidatabase access. Ingres SQL server
[PB95-192852] p 2947 N95-31051

S

SAAB-SCANIA, LINKOEPING (SWEDEN).
SAAB experience with PIO p 2746 N95-31069

SAN ANTONIO AIR LOGISTICS CENTER, KELLY AFB, TX.
Bicarbonate of soda paint stripping process validation and material characterization p 2777 N95-31778

SANDIA NATIONAL LABS., ALBUQUERQUE, NM.
Synthesis of novel precursors for PMN powders and the thin films obtained from them
[DE95-008543] p 2811 N95-30362
Simulation of airborne electromagnetic measurements in three dimensional environments
[DE95-008546] p 2900 N95-30363
A phenomenological finite element model of part building in the stereolithography process
[DE95-008437] p 2932 N95-30376
A Heuristic and complete planner for the classical mover's problem
[DE95-008440] p 2949 N95-30377
Laser Tracker 3: Sandia National Laboratories' third generation laser tracking system
[DE95-008525] p 2882 N95-30379
Polarization characteristics, control, and modulation of vertical-cavity surface emitting lasers
[DE95-008526] p 2882 N95-30380
Magnetoluminescence characterization of quantum well structures
[DE95-008527] p 3008 N95-30381
Low-voltage cathodoluminescence of europium-activated yttrium orthovanadate
[DE95-008536] p 3008 N95-30382
Viscous diffusion of vorticity in unsteady wall layers using the diffusion velocity concept
[DE95-008537] p 2866 N95-30383
Micromachined sensor and actuator research at the Microelectronics Development Laboratory
[DE95-008540] p 2878 N95-30384
The Technology Information Environment with Industry (TIE-In): A mechanism for accessing laboratory solutions
[DE95-008542] p 3027 N95-30385
Epoxy and acrylate stereolithography resins: In-situ measurements of cure shrinkage and stress relaxation
[DE95-008506] p 2811 N95-30389

Many-body effects in semiconductor lasers
[DE95-008534] p 2883 N95-30390
NIR High-efficiency subwavelength diffractive structures in semiconductors
[DE95-008535] p 3006 N95-30391
Adaptive path planning: Algorithm and analysis
[DE95-008549] p 2950 N95-30463
Velocity boundary conditions for vorticity formulations of the incompressible Navier-Stokes equations
[DE95-008715] p 2866 N95-30464
Fractal quantum well heterostructures for broadband light emitters
[DE95-009579] p 2860 N95-30707
Formation of cavities in Si and their chemisorption of materials
[DE95-009586] p 2980 N95-30708
The role of advanced engineering simulation in model-based design
[DE95-008815] p 2934 N95-30796
High strain rate properties and constitutive modeling of glass
[DE95-008434] p 2816 N95-31058
Band gap measurement of Si(1-x)C(x)/Si (0 less than or equal to x less than or equal to 0.014) alloys using photoluminescence and spectroscopic ellipsometry
[DE95-011020] p 3014 N95-31112
Aqueous TiO2 photocatalysis of metal-EDTA complexes
[DE95-011058] p 2793 N95-31113
Spotsize measurements of a focused CW Nd: YAG laser
[DE95-007746] p 2884 N95-31139
Hydrogen diffusion and passivation in InGaAlN alloys
[DE95-010689] p 2806 N95-31150
Workshop on transport for a common ion driver
[DE95-007298] p 2992 N95-31166
Minority and majority carrier transport characterization in compound semiconductors
[DE95-010873] p 3014 N95-31233
X-ray diffraction study of clusters in a-tC films
[DE95-010860] p 2794 N95-31393
Ion-Assisted Pulsed Laser Deposition of amorphous tetrahedral-coordinated carbon films
[DE95-010861] p 2885 N95-31394
Solderability enhancement of copper through chemical etching
[DE95-010514] p 2806 N95-31406
Requirements for security signalling
[DE95-008714] p 2948 N95-31605
Development of the Multi-Level Seismic Receiver (MLSR)
[DE95-008823] p 2916 N95-31610
Degradation of blue AlGaN/InGaN/GaN LEDs subjected to high current pulses
[DE95-008824] p 2963 N95-31611
High strain-rate testing of parachute materials
[DE95-009577] p 2897 N95-31614
Evaluation of nonlinear structural dynamic responses using a fast-running spring-mass formulation
[DE95-008503] p 2967 N95-31625
Target diagnostics for intense lithium ion hohlraum experiments on PBFA 2
[DE95-008517] p 3006 N95-31626
Folded compact range development and coherent change detection measurement project
[DE95-009082] p 2853 N95-31628
A simple and efficient procedure for polyhedral assembly partitioning under infinitesimal motions
[DE95-009838] p 2942 N95-31644
Toward a risk-based approach to the assessment of the surety of information systems
[DE95-008821] p 3025 N95-31662
A study of switching behavior in Pb(Zr,Ti)O3 thin films using x-ray diffraction
[DE95-010859] p 2808 N95-31689
Current trends in the packaging of photonic devices
[DE95-009563] p 3001 N95-32064
Scalable ATM encryption
[DE95-009668] p 2948 N95-32065
A modification to the GMRES method for ill-conditioned linear systems
[DE95-010661] p 2962 N95-32076
Preliminary design for Arctic atmospheric radiative transfer experiments
[DE95-009580] p 2917 N95-32080
Structural analyses of the JPL Mars Pathfinder impact
[DE95-009581] p 2767 N95-32081
Vibration control for precision manufacturing at Sandia National Laboratories
[DE95-009582] p 2839 N95-32082
Estimation in second order dependency model for multivariate binary data
[DE95-010326] p 2944 N95-32087
A stochastic difference equation approach to inference with missing data: Some new results
[DE95-010327] p 2944 N95-32088
A stochastic EM estimator in the presence of missing data: Theory and applications
[DE95-010329] p 2944 N95-32089
Energy storage and alternatives to improve train voltage on a mass transit system
[DE95-010344] p 2906 N95-32090
Models of transport, gas-phase and surface chemistry in diamond chemical vapor deposition
[DE95-009861] p 2822 N95-32101
Sandia National Lab's precision laser tracking systems
[DE95-009837] p 2886 N95-32143
Proposed DDS-specific fields for the Generic Authentication Information Element
[DE95-009839] p 3026 N95-32144
Scannerless Range Imaging with a square wave
[DE95-009840] p 2854 N95-32145
A proposed Generic Authentication Information Element
[DE95-009862] p 2948 N95-32146
GCMS and FTIR studies of by-product inhibited growth and the rate-limiting step in TEOS-based SiO2 CVD
[DE95-009863] p 3016 N95-32147
The pyrochlore-to-perovskite transformation in solution-derived lead zirconate titanate thin films
[DE95-010453] p 2822 N95-32161
Minutes of the fourth annual workshop on chromate replacements in light metal finishing
[DE95-010937] p 2810 N95-32241
The development of a pulsed laser imaging system for natural gas leak detection
[DE95-011407] p 2887 N95-32280
Outlook for renewable energy technologies: Assessment of international programs and policies
[DE95-009084] p 2907 N95-32302
Energetics of Pt adsorption on Pt(111)
[DE95-010933] p 3017 N95-32307
STM measurements of the interaction of vacancies and steps during low-energy-ion bombardment of Si(001)
[DE95-010935] p 3017 N95-32308

SANDIA NATIONAL LABS., LIVERMORE, CA.
NaK pool-boiler solar receiver durability bench test. Volume 2: Metallurgical analysis
[DE95-010338] p 2905 N95-31640
An investigation of a novel approach to elemental imaging in three dimensions
[DE95-010340] p 3000 N95-31681
Effects of gas-phase thermal expansion on the stability of deflagration through a porous energetic material
[DE95-004382] p 2797 N95-31824
A Stochastic EM algorithm for approximating the maximum likelihood estimate
[DE95-010328] p 2943 N95-32044
Video conferencing using DAVE user's guide
[DE95-010341] p 2854 N95-32045
Optimal heat transfer design of chemical vapor deposition reactors
[DE95-010997] p 2878 N95-32309

SCIENCE AND ENGINEERING SERVICES, INC., BURTONSVILLE, MD.
Development of a novel wind lidar, phase 1
[AD-A292703] p 2849 N95-30935

SCIENCE APPLICATIONS, INC., BELLEVUE, WA.
NASA Tropical Rainfall Measurement Mission (TRMM): Effects of tropical rainfall on upper ocean dynamics, air-sea coupling and hydrologic cycle
[NASA-CR-189437] p 2919 N95-31123

SCIENCE APPLICATIONS INTERNATIONAL CORP., FORT WASHINGTON, PA.
Hot jet/wake turbulent structure and laser propagaion. Part 1: Jet/wake turbulence modeling
p 2871 N95-30991
Large eddy simulation of jets using structured upwind numerics p 2871 N95-30993

SCIENTIFIC RESEARCH ASSOCIATES, INC., GLASTONBURY, CT.
Opto-electronic components from non-stoichiometric 3-5 materials
[AD-A293206] p 3013 N95-30985

SELSKAPET FOR INDUSTRIELL OG TEKNISK FORSKNING, OSLO (NORWAY).
Refinement techniques in computer graphics
[PB95-208526] p 2934 N95-30625
Data reduction of piecewise linear curves
[PB95-212270] p 2962 N95-32256

SELSKAPET FOR INDUSTRIELL OG TEKNISK FORSKNING, TRONDHEIM (NORWAY).
Measures of reliability and RCM
[PB95-192985] p 2891 N95-30510
Decompression illness, observable bubbles. (Session K)
[PB95-195285] p 2926 N95-30511
Effects of air bubbles on rabbit blood brain barrier
[PB95-195293] p 2925 N95-30512
Detecting intravascular gas bubbles in ultrasonic images
[PB95-195301] p 2926 N95-30513
Arterial gas bubbles after decompression in pigs with Patent Foramen Ovale
[PB95-195319] p 2925 N95-30515
Email: Why and how
[PB95-195327] p 2846 N95-30516
Wettability of boron carbide
[PB95-196358] p 2802 N95-30518
Overview of IEA biomass combustion activities
[PB95-196374] p 2902 N95-30519
Quality in applied science
[PB95-196390] p 2891 N95-30520
Metascientific problems in safety science
[PB95-196408] p 2838 N95-30521
Specific method for task-based interaction design
[PB95-196440] p 2929 N95-30522
Observation of a low-binding-energy peak in the 2p core-level photoemission from oxidized Al(111)
[PB95-195350] p 2802 N95-30534
STM studies of clean, CO- and O2-exposed Pt(100)-hex-R0.7 deg
[PB95-195376] p 3009 N95-30535
Weather influence on passive microwave brightness temperatures
[PB95-195384] p 2900 N95-30536
UNIX and PC security in a network environment. UNINETT
[PB95-196291] p 2934 N95-30662
Development of flexible feeder techniques
[PB95-196317] p 2934 N95-30663
TEM-examination of ceramic-metal interfaces
[PB95-196531] p 2813 N95-30664
Effect of oxygen and decompression bubbles on inert gas washout
[PB95-196556] p 2925 N95-30665
Texture development in aluminium extrusion
[PB95-196598] p 2979 N95-30666
UNIX and PC security in a network environment. LOKALNETT 1993
[PB95-196309] p 2934 N95-30697
May multiple inelastic scattering in CBED patterns be removed analytically
[PB95-196333] p 2992 N95-30717
CFC-replacement by natural working fluids: R&D and industrial challenges within the refrigeration, air conditioning amd heat pump areas
[PB95-195756] p 2815 N95-30871
Effect of local melting on tribology in metal cutting
[PB95-195392] p 2804 N95-31052
Physical modelling of microstructural evolution during thermomechanical processing of aluminium alloys
[PB95-196341] p 2805 N95-31053
Data analysis: Naive inductivism
[PB95-212213] p 3026 N95-32254
Production simulator for wave power plants
[PB95-212262] p 2907 N95-32286
Inversion of ERS-1 wavemode spectra. User's and programmer's guide
[PB95-223582] p 2902 N95-32316
Synthesis of separation systems: Methods and applications in downstream gas processes
[PB95-208518] p 2798 N95-32372

SIEMENS A.G., UNTERSCHLEISSHEIM (GERMANY).
AIDEX: An expert system for aircraft identification
p 2842 N95-32138

SIEMENS SOLAR INDUSTRIES, CAMARILLO, CA.
Photovoltaic Czochralski silicon manufacturing technology improvements
[DE95-004066] p 2904 N95-31162

SIMONS RESEARCH ASSOCIATES, LYNNFIELD, MA.
Extension of the pore tree model to describe pore interconnectivity
[AD-A290366] p 2793 N95-30971

SMITH-KETTLEWELL INST. OF VISUAL SCIENCES, SAN FRANCISCO, CA.
Visual processing of object velocity and acceleration
[AD-A292789] p 2929 N95-31436

SOFTWARE TECHNOLOGY, PROCESS AND PEOPLE, BRADFORD WOODS, PA.
The Personal Software Process: Downscaling the factory p 2937 N95-31240

SOLAREX CORP., NEWTOWN, PA.
Large-area, triple-junction a-Si alloy production scale-up
[DE95-004067] p 2904 N95-31163

SOUTHAMPTON UNIV. (ENGLAND).
Acousto-optical frequency shifters in dual-core optical fibres
[AD-A293979] p 2999 N95-31529

SOUTHERN METHODIST UNIV., DALLAS, TX.
A hypothesis-testing approach to discriminant analysis with mixed categorical and continuous variables when data are missing
[AD-A293714] p 2964 N95-31831

SOUTHWEST RESEARCH INST., SAN ANTONIO, TX.
Characterization of compressive damage mechanisms in ceramic and polymeric matrix composite materials
[AD-A293171] p 2787 N95-30975
Natural gas liquefier for vehicle fuel
[AD-A293619] p 2836 N95-31564
SPACE OPERATIONS SQUADRON (2ND), FALCON AFB, CO.
Fine tuning GPS clock estimation in the MCS
p 2968 N95-32322
SVN 9 End-Of-Life testing p 2767 N95-32345
SPACE TELESCOPE SCIENCE INST., BALTIMORE, MD.
The future of space imaging. Report of a community-based study of an advanced camera for the Hubble Space Telescope
[NASA-CR-198818] p 3026 N95-31364
SPECTRAL SCIENCES, INC., BURLINGTON, MA.
The passage from transitional to free molecular plumes p 2871 N95-30994
Development of a new instrument for rocket engine combustion diagnostics p 2799 N95-31211
SPECTREX, INC., CEDAR GOVE, NJ.
Next generation fire suppressants
p 2775 N95-31769
SPIRE CORP., BEDFORD, MA.
inP solar cell development on inexpensive Si substrates
[AD-A293255] p 2903 N95-30893
SRA TECHNOLOGIES, INC., FALLS CHURCH, VA.
Services to develop, standardize, and validate Polymerase Chain Reaction (PCR) protocols for the detection of leishmaniasis in clinical samples
[AD-A290155] p 2817 N95-31115
SRI INTERNATIONAL CORP., MENLO PARK, CA.
IR materials producibility
[AD-A293330] p 2998 N95-31141
Novel mass spectrometric instrument for gaseous and particulate characterization and monitoring
[DE95-000047] p 2881 N95-31694
STANFORD LINEAR ACCELERATOR CENTER, MENLO PARK, CA
Measurement of the effect of collimator generated wakefields on the beams in the SLC
[DE95-012101] p 2993 N95-31256
Spin structure in high energy processes
[DE95-008628] p 2993 N95-31627
Studies of the strong and electroweak interactions at the Z(sub 0) pole
[DE95-010353] p 2986 N95-31682
A search for jet handedness in hadronic Z-0 decays
[DE95-010099] p 2988 N95-32083
A measurement of quark and gluon jet differences at the Z(sup 0) resonance
[DE95-010666] p 2989 N95-32266
An experimental study of QCD and jets in e(+)e(-) annihilation
[DE95-010667] p 2989 N95-32267
Notes on lie algebraic analysis of achromats
[DE95-009524] p 3002 N95-32356
STANFORD LINEAR ACCELERATOR CENTER, STANFORD, CA.
A search for millicharged particles at SLAC
[DE95-010694] p 2987 N95-32026
STANFORD UNIV., CA.
Response of mechanically fastened composite joints under multiple bypass loads p 2785 N95-30824
Fourier series methods for cracks in polygonal plates and shells of revolution p 2893 N95-30825
A graphical programming language for service robots in semi-structured environments p 2935 N95-30831
Computation of high-altitude hypersonic flow-field radiation p 2743 N95-30843
Foundations of technology for constructing highly reliable distributed realtime systems
[AD-A293254] p 2931 N95-30892
New material for high average power infrared generation: QPM-DB GaAs
[AD-A292714] p 2967 N95-30939
Shear-free turbulent boundary layers
p 2873 N95-31349
Multi-dimensional data compression for portable communication
[AD-A292751] p 2850 N95-31426
Advanced thin-film deposition and physical properties of high-temperature and other novel superconducting materials
[AD-A292798] p 2795 N95-31439
Environmental conditions responsible for solar activity
[AD-A292859] p 3031 N95-31450
On the interactions between particles and turbulence in a fully-developed channel flow in air
p 2875 N95-31707
Heat transfer in shear-free turbulent boundary layers
p 2876 N95-31708
Aspects of the magnetospheric amplification phenomenon in ducted whistler-mode waves
p 2916 N95-31718
Control of high Reynolds number round jets
p 2876 N95-31733
Application of shallow shell stability to plant morphogenesis by Fourier series p 2897 N95-31734
Automatic verification and synthesis of finite-state hard real-time systems
[AD-A291279] p 2964 N95-32287
STATE UNIV. OF NEW YORK, ALBANY, NY.
Diagnosis of the kinematics and dynamics of rapidly developing maritime cyclones
[AD-A293919] p 2921 N95-31675
STATE UNIV. OF NEW YORK, BINGHAMTON, NY.
Photochemistry of intermolecular C-H bond activation reactions
[DE95-008991] p 2978 N95-30574
STATE UNIV. OF NEW YORK, BUFFALO, NY.
Join processing in relational database systems
p 3023 N95-30764
LES, DNS and RANS for the analysis of high-speed turbulent reacting flows
[NASA-CR-199075] p 2878 N95-32219
STEVENS INST. OF TECH., HOBOKEN, NJ.
Analytical instrumentation for environmental research
[AD-A292832] p 2906 N95-31447
Enhanced alkaline hydrolysis and biodegradability studies of nitrocellulose-bearing missile propellant
p 2772 N95-31752
STOCKHOLM ENVIRONMENT INST., STOCKHOLM (SWEDEN).
Sleeping renewable beauty: Will the prince ever come
[PB95-214573] p 2903 N95-30640
STOCKHOLM UNIV. (SWEDEN).
Potential integral equations of the 2D Laplace operator in wavelet basis
[TRITA-NA-9401] p 2957 N95-30713
On convective effects in sedimentation of concentrated suspensions with high effective gravity
[TRITA-NA-9316] p 2794 N95-31358
A study of numerical solutions of conservation laws
[TRITA-NA-9315] p 2960 N95-31361
Numerical simulation of time dependent viscoelastic fluid flow
[TRITA-NA-9311] p 2873 N95-31414
Some aspects on the modelling of non-Newtonian fluid flow
[TRITA-NA-9317] p 2873 N95-31415
The complexity and approximability of finding maximum feasible subsystems of linear relations
[TRITA-NA-9313] p 2961 N95-31648
SVERDRUP TECHNOLOGY, INC., HUNTSVILLE, AL.
Technology transfer into the solid propulsion industry
p 2770 N95-31756
SWEDISH INST. FOR MATERIALS TESTING, BORAS (SWEDEN).
EMC requirements for type approval of marine electronics. Nordtest project 1157-94
[PB95-211330] p 2859 N95-30596
Influence of adhesives and bonding techniques on the properties of glued timber-steelplate joints
[PB95-211470] p 2813 N95-30599
Simple model of foam spreading on liquid surfaces
[PB95-211207] p 2838 N95-30630
Generation of earthquake signals
[PB95-211223] p 2913 N95-30631
Development of a method for measurement of triboelectric charging
[PB95-211322] p 2859 N95-30633
SWEDISH INST. OF SPACE PHYSICS, KIRUNA (SWEDEN).
Kiruna geophysical data. Data summary 94/4-6, April-June 1994
[PB95-210365] p 2913 N95-30627
Kiruna geophysical data. Data summary 94/1-3, January-March 1994
[PB95-210373] p 2913 N95-30628
SWEDISH POLAR RESEARCH SECRETARIAT, STOCKHOLM (SWEDEN).
Swedish polar bibliography: A guide to Swedish literature on polar research, 1945-1988 with supplement, 1989-1992
[PB95-208161] p 2902 N95-32115
SYRACUSE UNIV., NY.
Data storage modeling and management for multimedia information systems p 3022 N95-30483
High speed random access, Fourier transform holographic associative and high density two-photon three-dimensional optical memories based on bacteriorhodopsin
[AD-A293389] p 2931 N95-30967

T

TECHNETICS, INC., DELAND, FL.
Brush seal shaft wear resistant coatings
[NASA-CR-198950] p 2889 N95-31382
TECHNICAL RESEARCH CENTRE OF FINLAND, OULU (FINLAND).
Experimental characterisation of gas microstrip detectors. Part 3: Lifetime characteristics
[PB95-192845] p 2880 N95-30891
TECHNICAL UNIV. OF NORWAY, TRONDHEIM.
Measures of reliability and RCM
[PB95-192985] p 2891 N95-30510
Observation of a low-binding-energy peak in the 2p core-level photoemission from oxidized Al(111)
[PB95-195350] p 2802 N95-30534
STM studies of clean, CO- and O2-exposed Pt(100)-hex-R0.7 deg
[PB95-195376] p 3009 N95-30535
Effect of local melting on tribology in metal cutting
[PB95-195392] p 2804 N95-31052
Physical modelling of microstructural evolution during thermomechanical processing of aluminium alloys
[PB95-196341] p 2805 N95-31053
TECHNISCHE HOGESCHOOL, DELFT (NETHERLANDS).
Static behaviour of axially loaded uniplanar and multiplanar tubular x-joints
[PB95-207866] p 2892 N95-30585
TECHNISCHE UNIV., DELFT (NETHERLANDS).
Removal of scattered surface waves from seismic data
[PB95-197802] p 2922 N95-30457
Acoustoelastic stress evaluation in metal plate using absolute shear and longitudinal time-of-flight data
[PB95-197810] p 2892 N95-30458
Electrochemical vapour deposition of SOFC interconnection materials
[PB95-197844] p 2812 N95-30459
Design of fibre reinforced composite panels for aerospace applications
[PB95-197851] p 2784 N95-30460
Design of systems for active sound control
[PB95-197869] p 2973 N95-30461
Stress and strain concentration factors of welded multiplanar joints between square hollow sections
[PB95-208260] p 2892 N95-30492
Fatigue behaviour of multiplanar tubular joints
[PB95-207874] p 2893 N95-30586
Diffraction-line broadening analysis and stress relaxation in thin metal layers
[PB95-213898] p 2893 N95-30634
Axial loads on yawed rotors
[PB95-214193] p 2742 N95-30638
Holistic analysis of gamma-ray spectra in instrumental neutron activation analysis
[PB95-214458] p 2979 N95-30639
Analysis of variation embedding tests with 17 MM dowel: Densified veneer wood FOREST project, part 7
[PB95-206876] p 2963 N95-30680
Thermoviscoelastic behaviour of solids
[PB95-196226] p 2784 N95-30694
Solvability of a class of hypersingular nonlinear integral equations
[PB95-207031] p 3011 N95-30720
Enantioselectivity of quinoprotein alcohol dehydrogeneses: Production of enantiomerically pure C3-alcohol synthons
[PB95-196960] p 2771 N95-30734
Photophysical properties of opto-electric molecules studied by time-resolved microwave conductivity
[PB95-196994] p 2980 N95-30774
Lanthanide(III) catalyzed reactions: Structure an d thermodynamics of intermediate complexes, and implications for reactivity
[PB95-197000] p 3019 N95-30775
Hydrogen absorption in iron and steel during gas tungsten arc welding
[PB95-197018] p 2804 N95-30776
System identification for robust process control. Nominal models and error bounds
[PB95-197026] p 2839 N95-30777
Geostatistics and hydrology. Part 3. Hydro-meteorological network design
[PB95-206462] p 2900 N95-30818
Geostatistics and hydrology. Part 1: Spatial and temporal variability. Communications of the Sanitary Engineering and Water Management Division
[PB95-206470] p 2900 N95-30819
Numerical investigation into vortical flow about a delta-wing configuration up to incidences at which vortex breakdown occurs in experiment
[PB95-198024] p 2743 N95-30837

Simultaneous heat and mass transfer in a horizontal tube absorber: Numerical tools for present and future absorber designs
[PB95-196978] p 2869 N95-30872
Dynamical systems as models for flow-induced vibrations
[PB95-206991] p 2869 N95-30956
Acceleration potential models PREDICHAT/PREDICDYN applied for calculation of axisymmetric dynamic inflow cases
[PB95-207015] p 2869 N95-30957
Digital simulation of wind velocities for wind turbine rotors: General considerations
[PB95-206447] p 2904 N95-31157
Robust control: A structured approach to solve aircraft flight control problems p 2758 N95-31995

TECHNISCHE UNIV., EINDHOVEN (NETHERLANDS).
Analyzing GI/Erlang-r/1 queues
[PB95-197034] p 2949 N95-30400
Album of simple perfect squared squares of order 26
[PB95-197398] p 2954 N95-30401
Fitting discrete distributions on the first two moments
[PB95-197885] p 2950 N95-30482
Extension to higher dimensions of the Jaeschke-Eicker result on the standardized empirical process
[PB95-206868] p 2965 N95-30523
Fixed modes in quasi-static state feedback decoupling
[PB95-206850] p 2950 N95-30564
Co-groups on sequentially complete, locally convex, topological vector spaces in particular on strict LF-spaces
[PB95-206918] p 2966 N95-30681
Barendregt cube with definitions and generalized reduction
[PB95-206793] p 2966 N95-30719
Reduced heat kernels on nilpotent lie groups
[PB95-206926] p 2958 N95-30778
Generalized controlled invariance for nonlinear systems
[PB95-197901] p 2950 N95-30807
Symmetric longest queue system
[PB95-197919] p 2950 N95-30808
Golden ten equations of motion
[PB95-197927] p 2967 N95-30809
Existence of solutions in plane quasistationary stokes flow driven by surface tension
[PB95-197935] p 2868 N95-30810
Numerical computation of one-dimensional detonation waves
[PB95-197950] p 2868 N95-30811
Dynamic routation in distributed environments
[PB95-197968] p 2847 N95-30812
Noisy-network acceptors
[PB95-197976] p 2951 N95-30813
H(sub 2) optimal controllers with observer based architecture for continuous-time systems: Separation principle
[PB95-197067] p 2951 N95-30833
Planning board generator. Part 1: Problem instances and types
[PB95-197075] p 3021 N95-30834
Fourier analysis of a robust multigrid method for convection-diffusion equations
[PB95-197091] p 2958 N95-30835
Simulation of viscous sintering
[PB95-197109] p 2868 N95-30836
Formalization of the ramified type theory
[PB95-206785] p 2961 N95-31422

TECHNISCHE UNIV., TWENTE (NETHERLANDS).
Contribution of groupware to corporate communication: Towards the horizontal organization
[PB95-197661] p 3022 N95-30453
Experimental research into usability and organization impact of workflow software
[PB95-197679] p 2933 N95-30454
Metrics in method engineering
[PB95-197687] p 2838 N95-30455
Protocols for integrity constraint checking in federated databases
[PB95-197695] p 3022 N95-30456
Operating system support for distributed multimedia applications: A survey of current research
[PB95-207098] p 2964 N95-30565
Extending a multi-set relational algebra to a parallel environment
[PB95-207106] p 3023 N95-30566
Workflow literature guide, version 1
[PB95-207080] p 2947 N95-30721
Effective bandwidth techniques in bufferless and buffered ATM multiplexers
[PB95-207072] p 2862 N95-31185

TEL-AVIV UNIV., RAMAT-AVIV, TEL-AVIV (ISRAEL).
Laser induced vitreoretinal scarring. Evaluation of causative factors and a therapeutic approach
[AD-A293742] p 2928 N95-31570

TENNESSEE STATE UNIV., NASHVILLE, TN.
A quantitative comparison of corrective and perfective maintenance p 2939 N95-31250

TENNESSEE UNIV., CHATTANOOGA, TN.
Experimental control in software reliability certification p 2938 N95-31248

TENNESSEE UNIV., KNOXVILLE, TN.
Study of the surface properties of ceramic materials by chromatography
[DE95-011578] p 2823 N95-32298

TENNESSEE UNIV., TULLAHOMA, TN.
Stability prediction with rotational flow effects p 2799 N95-31283

TEXAS A&M UNIV., COLLEGE STATION, TX.
The activities of the high energy physics program
[DE95-010155] p 2991 N95-30615
Fischer-tropsch synthesis in supercritical fluids
[DE95-009631] p 2792 N95-30709
A study of catalysts and mechanisms in synthesis reactions
[DE95-010177] p 2793 N95-30766

TEXAS UNIV., AUSTIN, TX.
Biosensors based on cross-linking of biotinylated Glucose Oxidase by avidin
[AD-A290439] p 2925 N95-30452
Hadronic production of S-wave and P-wave charmed beauty mesons via heavy quark fragmentation
[DE95-008737] p 2977 N95-30465
On the quasihydrostatic flows of radiatively cooling self-gravitating gas clouds
[DE95-009116] p 3029 N95-30729
Singular eigenfunctions for shearing fluids I
[DE95-008952] p 2868 N95-30763
Stabilization of the resistive shell mode in tokamaks
[DE95-008748] p 3004 N95-30794
Reynolds stress of localized toroidal modes
[DE95-008750] p 3004 N95-30795
Shear flow effects on ion thermal transport in tokamaks
[DE95-009115] p 3005 N95-30801
Multiple scatter theory of ocean sediments
[AD-A293951] p 2923 N95-31523

TEXAS UNIV., EL PASO, TX.
Impact behavior of the active zone within a frozen soil profile
[AD-A292909] p 2915 N95-31386

TEXAS UNIV. AT DALLAS, RICHARDSON, TX.
Basic study of the pumping of a gamma-ray laser
[AD-A293561] p 2886 N95-31563
Tunable composite membranes for gas separations
[DE95-010602] p 2822 N95-32075

THIOKOL CORP., BRIGHAM CITY, UT.
Atmospheric environmental implications of propulsion systems p 2771 N95-31747
AP reclamation and reuse in RSRM propellant p 2772 N95-31751
Low acid producing solid propellants p 2773 N95-31754
QFD analysis of RSRM aqueous cleaners p 2779 N95-31789
Cleanliness evaluation of rough surfaces with diffuse IR reflectance p 2782 N95-31804
The role of surface chemical analysis in a study to select replacement processes for TCA vapor degreasing p 2782 N95-31809

THIOKOL CORP., HUNTSVILLE, AL.
Cleanliness inspection tool for RSRM bond surfaces p 2781 N95-31799

TOKYO UNIV., TANASHI (JAPAN).
The 10th INS Scientific Computational Programs
[DE95-717864] p 2982 N95-31178
On the string equation at c=1
[DE95-737161] p 3014 N95-31222
Pion-pair production by two photons
[DE95-737162] p 2983 N95-31223
Quantization of a relativistic particle on the SL(2,R) manifold based on Hamiltonian reduction
[DE95-737163] p 2983 N95-31224
The topological string associated with a simple singularity of type D
[DE95-737229] p 2983 N95-31225
Global aspects of the WZNW reduction to Toda theories
[DE95-737230] p 3019 N95-31226
Pion-nucleon and kaon-nucleon scattering lengths in QCD sum rules
[DE95-737278] p 2983 N95-31227
Non-critical string field theory with non-orientable string interactions
[DE95-737160] p 3020 N95-31281
Atomic approaches in metastable antiprotonic helium atoms. Reply to Analysis of the lifetimes and fractions of antiprotons trapped in metastable antiprotonic helium states by I. Shimamhura and M. Kimura
[DE95-737228] p 2986 N95-31658

TOLEDO UNIV., OH.
FPCAS3D User's guide: A three dimensional full potential aeroelastic program, version 1
[NASA-CR-198367] p 2899 N95-32205
An efficient numerical procedure for thermohydrodynamic analysis of cavitating bearings
[NASA-CR-195476] p 2878 N95-32210

TOMCO EQUIPMENT CO., LOGANVILLE, GA.
CO2 (dry ice) cleaning system p 2778 N95-31785

TORONTO UNIV. (ONTARIO).
A unified interpretation of singular and near-singular integrals in the boundary element method
[ISBN-0-315-86297-1] p 2962 N95-31947

TRANE CO., LACROSSE, WI.
Compatibility of refrigerants and lubricants with motor materials under retrofit conditions
[DE95-010185] p 2814 N95-30767

TRANSITION RESEARCH, INC., DANBURY, CT.
Log-polar binocular vision system
[NASA-CR-188375] p 2996 N95-30772

TRONDHEIM UNIV. (NORWAY).
Decompression illness, observable bubbles. (Session K)
[PB95-195285] p 2926 N95-30511
Detecting intravascular gas bubbles in ultrasonic images
[PB95-195301] p 2926 N95-30513
Arterial gas bubbles after decompression in pigs with Patent Foramen Ovale
[PB95-195319] p 2925 N95-30515
May multiple inelastic scattering in CBED patterns be removed analytically
[PB95-196333] p 2992 N95-30717

TUFTS UNIV., MEDFORD, MA.
Photorefractive nonlinear optics
[AD-A292913] p 2999 N95-31458

TULSA UNIV., OK.
Controller resource management: What can we learn from aircrews?
[DOT/FAA/AM-95/21] p 2750 N95-32186

U

UNISYS CORP., RESTON, VA.
Penelope reference manual: Version 3-3 (C001). Includes Larch/Ada specification manual for sequential Ada (C002)
[AD-A289828] p 2942 N95-31683

UNISYS GSG CANADA, INC., MONTREAL (QUEBEC).
Architecture and implementation of a multi-sensor data fusion demonstration model within the real-time combat system of the Canadian Patrol Frigate p 2842 N95-32139

UNITED SPACE BOOSTERS, INC., HUNTSVILLE, AL.
Convergent spray process for environmentally friendly coatings p 2777 N95-31776
Environmentally compatible hand wipe cleaning solvents p 2780 N95-31795
Verification of surface preparation for adhesive bonding p 2782 N95-31807

UNITED TECHNOLOGIES CORP., EAST HARTFORD, CT.
Method for extracting forward acoustic wave components from rotating microphone measurements in the inlets of turbofan engines
[NASA-CR-195457] p 2755 N95-30779

UNITED TECHNOLOGIES CORP., HUNTSVILLE, AL.
Evaluating the cost effectiveness of environmental projects: Case studies in aerospace and defense p 2774 N95-31762

UNITED TECHNOLOGIES CORP., SAN JOSE, CA.
Model for defining propellant burn rate performance boundaries p 2800 N95-31290

UNITED TECHNOLOGIES RESEARCH CENTER, EAST HARTFORD, CT.
Interfacial studies of coated fiber reinforced glass-ceramic matrix composites
[AD-A290780] p 2783 N95-30433
Development of a linearized unsteady Euler analysis for turbomachinery blade rows
[NASA-CR-4677] p 2742 N95-30611

UNIVERSITY COLL. OF NORTH WALES, BANGOR (UNITED KINGDOM).
Large area smart piezoelectric and pyroelectric sensors
[AD-A291487] p 2859 N95-30561

UNIVERSITY OF CENTRAL FLORIDA, ORLANDO, FL.
Experimental investigation of optical nonlinearities in conjugated polymers
[AD-A288353] p 2884 N95-31145
Nonlinear organized materials for optical devices
[AD-A292809] p 2999 N95-31441

UNIVERSITY OF NORTHERN ILLINOIS, DE KALB, IL.
Deposition and characterization of photoconductive PZT thin films
[ATR-93(8308)-7] p 2819 N95-31417
UNIVERSITY OF SOUTHERN CALIFORNIA, LOS ANGELES, CA.
Flow models for the design of a hypersonic iodine vapor wind tunnel nozzle with chemical and vibrational nonequilibrium effects p 2742 N95-30448
Small scale turbulence in a plane mixing layer p 2866 N95-30449
Picosecond phase conjugation: New applications, devices, and materials
[AD-A293195] p 3013 N95-30982
The impact of microbiologically influenced corrosion on protective polymer coatings
[AD-A288896] p 2816 N95-30997
On the kinematic performance of mechanical manipulators operating in the presence of an obstruction p 2890 N95-31710
Global climatology and variability of potential new production estimated from remote sensing of sea-surface temperature
[NASA-CR-198840] p 2910 N95-31981
The theoretical calculation of vibrational circular dichroism spectra
[AD-A293614] p 2798 N95-32258
UNIVERSITY OF SOUTHERN MISSISSIPPI, HATTIESBURG, MS.
Responsive copolymers for enhanced petroleum recovery
[DE95-011857] p 2823 N95-32361
UTAH STATE UNIV., LOGAN, UT.
Quasi-Newton updating for large scale nonlinear systems
[AD-A292776] p 2940 N95-31431

V

VIRGINIA POLYTECHNIC INST., BLACKSBURG, VA.
A general inverse design procedure for aerodynamic bodies p 2750 N95-30497
VIRGINIA POLYTECHNIC INST. AND STATE UNIV., BLACKSBURG, VA.
A turbulence model for steady and unsteady boundary layers in strong pressure gradients p 2868 N95-30840
An evaluation of the Iosipescu specimen for composite materials shear property measurement
[NASA-CR-198755] p 2896 N95-31418
Computational methods for control and optimal design of aerospace systems
[AD-A292861] p 2751 N95-31451
Performance improvement of composite wings through aeroelastic tailoring and modern control
[AD-A293689] p 2752 N95-31602
VIRGINIA UNIV., CHARLOTTESVILLE, VA.
Generalized implementation of software safety policies p 2939 N95-31249
Large deformation failure mechanisms in nonlinear solids
[AD-A293010] p 2896 N95-31474
Spatially-resolved velocity measurements in steady, high-speed, reacting flows using laser-induced OH fluorescence p 2877 N95-32109
VIRGINIA UNIV. HOSPITAL, CHARLOTTESVILLE, VA.
Supporting data intensive applications with medium grained parallelism
[DE95-010164] p 3023 N95-30619

W

WASHINGTON STATE UNIV., RICHLAND, WA.
Investigation of polycrystalline thin film CuInSe2 solar cells based on ZnSe windows
[DE95-004068] p 2904 N95-31164
WASHINGTON UNIV., BELLINGHAM, WA.
Electroweak baryogenesis
[DE95-012169] p 2991 N95-32365
WASHINGTON UNIV., SEATTLE, WA.
Investigation of ram accelerator performance capabilities p 2799 N95-31204
Design and processing of materials by biomimicking. Sections 1. Publications
[AD-A293852] p 2820 N95-31559
The TEVA experiment cruise report
[AD-A293025] p 2923 N95-31701
WATERLOO UNIV. (ONTARIO).
Multiple Target Tracking based on constellation matching and Kalman filter p 2842 N95-32136
WAYNE STATE UNIV., DETROIT, MI.
Investigations of YBaCuO materials with near-room-temperature resistivity transitions
[AD-A293405] p 3013 N95-31008
WEST VIRGINIA UNIV., FAIRMONT, WV.
A process improvement model for software verification and validation p 2938 N95-31243
WEST VIRGINIA UNIV., MORGANTOWN, VA.
Management, visualization, and analysis of environmental and geotechnical data
[DE95-000063] p 3026 N95-31823
WESTINGHOUSE HANFORD CO., RICHLAND, WA.
LLW solidification in cement: Effect of dilution
[DE95-010108] p 2798 N95-32091
Westinghouse Hanford Company Data Management Plan Template, revision 1
[DE95-010046] p 3026 N95-32107
Laboratory directed research and development report
[DE95-011405] p 3032 N95-32279
WESTINGHOUSE SAVANNAH RIVER CO., AIKEN, SC.
Welding isotopic heat sources for the cassini mission to Saturn
[DE95-060104] p 2890 N95-32367
WINNIPEG UNIV. (MANITOBA).
Analyzing GI/Erlang-r/1 queues
[PB95-197034] p 2949 N95-30400
WISCONSIN UNIV., MADISON, WI.
Minijet veto: A tool for the heavy Higgs search at the LHC
[PB95-196234] p 2979 N95-30695
Energy transfer dynamics in isolated and colliding highly vibrationally excited molecules
[AD-A293304] p 2981 N95-30952
Lower hybrid accessibility in a large, hot reversed field pinch
[DE95-011001] p 3007 N95-32310
WOODS HOLE OCEANOGRAPHIC INST., MA.
Bibliography of technical reports, 1993
[AD-A292741] p 2923 N95-30918
Arabian Sea mixed layer dynamics experiment: Mooring deployment cruise report
[AD-A293684] p 2923 N95-31600
WRIGHT LAB., WRIGHT-PATTERSON AFB, OH.
The control system design methodology of the STOL and maneuver technology demonstrator p 2758 N95-31998
Flight evaluation of forebody vortex control in post-stall flight p 2752 N95-32003

X

XIDIAN UNIV., XIAN (CHINA).
Adaptive space-time processing for airborne radars based on Doppler pre-processing
[PB95-205464] p 2854 N95-32114

Z

ZWILLINGER AND ASSOCIATES, NEWTON, MA.
Visualization of circuit card electromagnetic fields
[AD-A291491] p 2845 N95-30398

Typical Contract Number Index Listing

AF- AFOSR-0090-93 ..... p 173 N95-10812

CONTRACT NUMBER | PAGE NUMBER | ACCESSION NUMBER

Listings in this index are arranged alphanumerically by contract number. Under each contract number the accession numbers denoting documents that have been produced as a result of research done under that contract are arranged in ascending order. The page number helps to locate the citation in the abstract section. The accession number denotes the number by which the citation is identified.

AF PROJ. ILIR ..... p 2928 N95-30905
AF PROJ. R03-5-B ..... p 2935 N95-30968
AF PROJ. 2103 ..... p 2762 N95-30926
p 2763 N95-31101
AF PROJ. 2305 ..... p 2999 N95-31441
AF PROJ. 2308 ..... p 2791 N95-30409
AF PROJ. 3037 ..... p 2756 N95-31191
AF PROJ. 3054 ..... p 2915 N95-31575
p 2916 N95-31604
AF PROJ. 4600 ..... p 2848 N95-30895
p 2850 N95-31387
p 3000 N95-31697
AF PROJ. 7184 ..... p 2931 N95-31538
AF PROJ. 7755 ..... p 2928 N95-30905
p 2927 N95-31552
AF PROJ. 7930 ..... p 2927 N95-31373
AF-AFOSR-0107-91 ..... p 2999 N95-31542
AF-AFOSR-0152-91 ..... p 2799 N95-30990
p 2799 N95-31198
AF-AFOSR-0180-90 ..... p 2999 N95-31519
AF-AFOSR-0269-91 ..... p 2920 N95-31453
AF-AFOSR-0277-91 ..... p 2849 N95-30962
AF-AFOSR-0281-91 ..... p 2820 N95-31559
AF-AFOSR-0283-91 ..... p 2999 N95-31515
AF-AFOSR-0294-91 ..... p 2940 N95-31431
AF-AFOSR-0297-91 ..... p 2838 N95-31472
AF-AFOSR-0301-91 ..... p 3014 N95-31438
AF-AFOSR-0308-91 ..... p 2940 N95-31452
AF-AFOSR-0319-91 ..... p 3013 N95-31008
AF-AFOSR-0341-91 ..... p 2949 N95-30395
AF-AFOSR-0351-91 ..... p 2752 N95-31602
AF-AFOSR-0354-91 ..... p 2931 N95-30892
AF-AFOSR-0382-91 ..... p 2881 N95-31828
AF-AFOSR-0386-89 ..... p 2963 N95-31429
AF-AFOSR-0387-91 ..... p 2999 N95-31529
AF-AFOSR-0390-91 ..... p 2861 N95-30979
AF-AFOSR-0405-91 ..... p 2825 N95-31149
AF-AFOSR-0410-91 ..... p 2874 N95-31443
AF-AFOSR-0416-89 ..... p 2862 N95-31442
AF-AFOSR-91-0152 ..... p 2800 N95-31287
ARPA ORDER A128 ..... p 2964 N95-31831
ARPA ORDER A840 ..... p 2787 N95-30978
ARPA ORDER 6474 ..... p 2947 N95-30868
ARPA ORDER 6797 ..... p 2947 N95-30868
ARPA ORDER 8100 ..... p 2863 N95-31669
ARPA ORDER 8557 ..... p 2998 N95-31141
ARPA ORDER 8930 ..... p 2947 N95-30930
DA PROJ. 1L1-61102-AH-43 ..... p 2798 N95-32258
DA PROJ. 1L1-61102-AH-45 ..... p 2756 N95-31985
p 2878 N95-32210
DA PROJ. 1L1-62211-A-47-A ..... p 2878 N95-32216
DA PROJ. 1L1-62618-A-1-FL ..... p 3020 N95-31511
DA PROJ. 201-61102-B-74-F ..... p 2929 N95-31585
DA PROJ. 3O1-62787-A8-78 ..... p 2864 N95-31842
DA PROJ. 4A1-62784-AT-41 ..... p 2941 N95-31573
DA PROJ. 4A1-62784A-T41 ..... p 2812 N95-30558
DAAB07-94-C-C009 ..... p 2787 N95-30978
DAAE07-90-C-R059 ..... p 2953 N95-31540
DAAH01-90-C-0833 ..... p 2800 N95-31294
DAAH04-93-C-0053 ..... p 2801 N95-31305
DAAH04-93-G-0057 ..... p 2802 N95-30404
DAAH04-93-G-0413 ..... p 2828 N95-31207
DAAH04-94-C-0075 ..... p 2793 N95-30971
DAAH04-94-G-0422 ..... p 2904 N95-30947
DAAJ02-93-C-0021 ..... p 2874 N95-31475
DAAK70-92-C-0059 ..... p 2836 N95-31564
DAAL01-94-C-0073 ..... p 2800 N95-31300
DAAL03-89-K-0066 ..... p 2852 N95-31551
DAAL03-89-K-0158 ..... p 2918 N95-30403
DAAL03-90-G-0084 ..... p 2801 N95-31312
DAAL03-90-G-0196 ..... p 2915 N95-31386
DAAL03-91-C-0034 ..... p 2915 N95-31560
DAAL03-91-G-0079 ..... p 2804 N95-30977
DAAL03-91-G-0169 ..... p 2819 N95-31395
DAAL03-91-G-0209 ..... p 2951 N95-30884
DAAL03-91-G-0210 ..... p 3025 N95-31618
DAAL03-91-G-0243 ..... p 2999 N95-31458
DAAL03-91-G-0272 ..... p 2929 N95-31685
DAAL03-91-G-0312 ..... p 2881 N95-31385
DAAL03-92-C-0013 ..... p 2756 N95-31400
DAAL03-92-C-0016 ..... p 2889 N95-31374
DAAL03-92-C-0041 ..... p 2860 N95-30940
DAAL03-92-G-0020 ..... p 2800 N95-31299
DAAL03-92-G-0110 ..... p 2799 N95-31204
DAAL03-92-G-0118 ..... p 2800 N95-31296
p 2800 N95-31297
p 2801 N95-31302
p 2801 N95-31303
p 2801 N95-31304
DAAL03-92-G-0186 ..... p 3012 N95-30944
DAAL03-92-G-0281 ..... p 2793 N95-30936
DAAL03-92-G-0400 ..... p 2967 N95-30939
DAAL04-93-G-0364 ..... p 2800 N95-31296
DAAL04-93-G-0409 ..... p 2827 N95-31206
DABT63-91-K-0002 ..... p 2850 N95-31426
DACA76-89-C-0014 ..... p 2953 N95-31540
DAJA45-93-C-0017 ..... p 2859 N95-30561
DAMD17-91-Z-1031 ..... p 2928 N95-31570
DAMD17-92-C-2097 ..... p 2817 N95-31115
DAMD17-93-J-3031 ..... p 2926 N95-30924
DARPA ORDER 7894 ..... p 2648 N95-30869
DARPA ORDER 8103 ..... p 2815 N95-30955
DASG60-89-C-0129 ..... p 2963 N95-31543
DE-AC02-76CH-00016 ..... p 2803 N95-30547
p 2803 N95-30706
p 2993 N95-31405
p 2986 N95-31702
p 2987 N95-32031
p 2987 N95-32032
p 2994 N95-32059
p 2988 N95-32063
p 2988 N95-32079
p 2994 N95-32092
p 2882 N95-32159
p 2989 N95-32160
p 2994 N95-32242
p 2994 N95-32243
p 2994 N95-32244
p 2995 N95-32260
p 2990 N95-32278
p 2995 N95-32297
p 2995 N95-32306
p 3008 N95-32357
DE-AC02-76CH-03000 ..... p 2814 N95-30765
p 2992 N95-30800
p 2981 N95-30970
p 2992 N95-31165
p 2989 N95-32162
p 2990 N95-32303
DE-AC02-76CH-03073 ..... p 3003 N95-30359
DE-AC02-76ER-00881 ..... p 2979 N95-30695
DE-AC02-80ET-15601 ..... p 2879 N95-30687
DE-AC03-76SF-00098 ..... p 2991 N95-30360
p 3028 N95-30361
p 2878 N95-30378
p 2975 N95-30388
p 2861 N95-31059
p 3000 N95-31635
p 3017 N95-32366
DE-AC03-76SF-00515 ..... p 2993 N95-31256
p 2993 N95-31627
p 2986 N95-31682
p 2987 N95-32026
p 2988 N95-32063
p 2988 N95-32083
p 2989 N95-32266
p 2989 N95-32267
p 3002 N95-32356
DE-AC03-89ER-51114 ..... p 3003 N95-30612
p 3003 N95-30641
p 3004 N95-30685
p 3007 N95-32116
DE-AC03-91SF-18852 ..... p 2768 N95-30674
DE-AC04-76DP-00613 ..... p 2815 N95-30798
p 2940 N95-31404
DE-AC04-76DP-00789 ..... p 3004 N95-30685
p 3016 N95-32147
DE-AC04-76EV-01013 ..... p 2909 N95-31703
DE-AC04-94AL-85000 ..... p 2811 N95-30362
p 2900 N95-30363
p 2932 N95-30376
p 2949 N95-30377
p 2882 N95-30379
p 2882 N95-30380
p 3008 N95-30381
p 3008 N95-30382
p 2866 N95-30383
p 2878 N95-30384
p 3027 N95-30385
p 2811 N95-30389
p 2883 N95-30390
p 3008 N95-30391
p 2950 N95-30463
p 2866 N95-30464
p 3010 N95-30576
p 2860 N95-30707
p 2980 N95-30708
p 2934 N95-30796
p 2816 N95-31058
p 3014 N95-31112
p 2793 N95-31113
p 2884 N95-31139
p 2606 N95-31150
p 2992 N95-31166
p 3014 N95-31233
p 2794 N95-31393
p 2885 N95-31394
p 2806 N95-31406
p 2948 N95-31605
p 2916 N95-31610
p 2863 N95-31611
p 2897 N95-31614
p 2967 N95-31625
p 3006 N95-31626
p 2853 N95-31628
p 2905 N95-31640
p 2942 N95-31644
p 3025 N95-31662
p 3000 N95-31681
p 2808 N95-31689
p 2797 N95-31824
p 2943 N95-32044
p 2854 N95-32045
p 3001 N95-32064
p 2948 N95-32065
p 2962 N95-32076
p 2917 N95-32080
p 2767 N95-32081
p 2839 N95-32082
p 2944 N95-32087
p 2944 N95-32088
p 2944 N95-32089
p 2906 N95-32090
p 2822 N95-32101
p 2886 N95-32143
p 3026 N95-32144
p 2854 N95-32145
p 2948 N95-32146
p 3016 N95-32147
p 2822 N95-32161
p 2810 N95-32241
p 2887 N95-32280
p 2907 N95-32302
p 3017 N95-32307
p 3017 N95-32308
p 2878 N95-32309
DE-AC05-76OR-00033 ..... p 2978 N95-30546

DE-AC05-84OR-21400	p 2812	N95-30548
	p 3009	N95-30542
	p 2812	N95-30543
	p 3010	N95-30544
	p 2812	N95-30545
	p 2978	N95-30546
	p 2803	N95-30547
	p 2812	N95-30548
	p 2813	N95-30572
	p 2803	N95-30575
	p 3010	N95-30576
	p 2947	N95-30577
	p 3003	N95-30641
	p 2913	N95-30683
	p 2838	N95-30684
	p 3004	N95-30685
	p 2814	N95-30730
	p 2784	N95-30731
	p 2814	N95-30732
	p 2803	N95-30733
	p 2903	N95-30745
	p 2908	N95-30793
	p 2804	N95-30797
	p 2815	N95-30799
	p 2982	N95-31104
	p 2805	N95-31105
	p 2805	N95-31106
	p 2805	N95-31107
	p 2936	N95-31109
	p 2805	N95-31111
	p 2931	N95-31130
	p 2894	N95-31131
	p 2872	N95-31132
	p 2817	N95-31135
	p 2817	N95-31136
	p 2818	N95-31153
	p 2818	N95-31175
	p 2818	N95-31187
	p 2806	N95-31188
	p 2984	N95-31402
	p 2788	N95-31403
	p 2909	N95-31612
	p 2941	N95-31631
	p 2807	N95-31632
	p 2796	N95-31633
	p 2942	N95-31634
	p 3015	N95-31641
	p 2985	N95-31642
	p 2808	N95-31643
	p 2774	N95-31763
	p 2775	N95-31766
	p 2778	N95-31784
	p 2780	N95-31792
	p 2782	N95-31803
	p 2806	N95-31825
	p 2821	N95-32025
	p 2943	N95-32030
	p 2877	N95-32033
	p 2822	N95-32043
	p 2822	N95-32085
	p 2798	N95-32086
	p 2910	N95-32099
	p 3007	N95-32116
	p 2898	N95-32157
	p 2810	N95-32272
	p 3016	N95-32301
	p 2899	N95-32317
	p 2823	N95-32352
DE-AC05-84OS-21400	p 2797	N95-31840
DE-AC06-76RL-01830	p 2978	N95-30573
	p 2809	N95-32052
	p 2865	N95-32077
DE-AC06-87RL-10930	p 2798	N95-32091
	p 3026	N95-32107
	p 3032	N95-32279
DE-AC07-94ID-13223	p 3022	N95-30392
DE-AC08-93NV-11265	p 2877	N95-32049
DE-AC09-89SR-18035	p 2890	N95-32367
DE-AC11-93PN-38195	p 2798	N95-32318
DE-AC12-76SN-00052	p 2894	N95-31054
DE-AC21-92MC-29116	p 2881	N95-31694
DE-AC21-93MC-29257	p 2890	N95-32163
DE-AC22-92BC-14882	p 2823	N95-32361
DE-AC36-83CH-10093	p 2902	N95-30505
	p 2902	N95-30526
	p 2903	N95-30887
	p 2903	N95-30896
	p 2904	N95-31162
	p 2904	N95-31163
	p 2904	N95-31164
	p 2905	N95-31381
	p 2836	N95-31638
	p 2836	N95-31639
	p 2905	N95-31661
	p 2909	N95-31695
	p 2921	N95-31726
DE-AI03-94ER-61761	p 2910	N95-31821
DE-FC03-90ER-61010	p 2905	N95-31822
DE-FC08-90NV-10872	p 2906	N95-32057
	p 2906	N95-32058
	p 2810	N95-32154
DE-FC08-90NV-10891	p 2917	N95-32142
DE-FC21-92MC-29467	p 2907	N95-30358
DE-FG01-94CE-15599	p 3023	N95-30620
DE-FG01-94CE-15601	p 3026	N95-32149
DE-FG02-85ER-53212	p 3027	N95-32362
DE-FG02-86ER-13491	p 2814	N95-30738
	p 3026	N95-31823
	p 2823	N95-32305
	p 2907	N95-32288
	p 3007	N95-32310
	p 2989	N95-32120
	p 2990	N95-32271
	p 2990	N95-32273
	p 2990	N95-32274
DE-FG02-89ER-14039	p 2990	N95-32275
DE-FG02-89ER-45399	p 2978	N95-30574
DE-FG02-90ER-13030	p 2998	N95-31114
DE-FG02-91CE-23810	p 2894	N95-31254
	p 2814	N95-30767
	p 2816	N95-31057
	p 2911	N95-32364
DE-FG02-91ER-25109	p 2941	N95-31630
DE-FG02-91ER-45439	p 3016	N95-32103
	p 2809	N95-32104
DE-FG02-91ER-61216	p 2908	N95-30686
DE-FG02-92ER-40699	p 2991	N95-30527
DE-FG02-95ER-40896	p 2994	N95-32059
DE-FG03-91ER-40674	p 2994	N95-32059
DE-FG03-92ER-25135	p 2945	N95-32270
DE-FG03-92ER-54150	p 3003	N95-30359
	p 3006	N95-31624
DE-FG03-93ER-40757	p 2977	N95-30465
DE-FG03-93ER-45486	p 2810	N95-32265
DE-FG03-93SF-20143	p 3007	N95-32299
DE-FG05-80ET-53088	p 3029	N95-30729
	p 2868	N95-30763
	p 3004	N95-30794
	p 3004	N95-30795
	p 3005	N95-30801
DE-FG05-86ER-40272	p 3029	N95-31102
	p 3020	N95-32106
DE-FG05-86ER-45233	p 2792	N95-30614
DE-FG05-88ER-13829	p 2793	N95-30766
DE-FG05-88ER-13859	p 2823	N95-32298
DE-FG05-88ER-25063	p 3023	N95-30619
DE-FG05-88ER-40445	p 2978	N95-30616
DE-FG05-88ER-40481	p 3031	N95-30618
DE-FG05-90ER-40559	p 3030	N95-32269
DE-FG05-91ER-40633	p 2991	N95-30615
DE-FG05-94ER-25216	p 2932	N95-32046
DE-FG06-90ER-40561	p 2991	N95-32365
DE-FG22-92PC-92542	p 2809	N95-32098
DE-FG22-92PC-92545	p 2792	N95-30709
DE-FG22-94PC-94222	p 2822	N95-32075
DNA001-92-C-0030	p 2892	N95-30559
DRET-C-94-1021/A000	p 2949	N95-32371
DRET-91/1200A	p 3027	N95-32370
DRET-921438	p 2948	N95-32255
DTFA01-91-Z-02036	p 2920	N95-31465
	p 2749	N95-31521
DTFA01-93-C-0001	p 2747	N95-31687
DTFA02-93-P-7913	p 2750	N95-32186
DTRS57-88-C-0078	p 2749	N95-31520
DTRS57-93-C-00133	p 2924	N95-32363
EPA-DW-899349-75	p 2775	N95-31766
F04701-92-C-0021	p 2780	N95-31793
F04701-93-C-0094	p 2863	N95-30394
	p 2915	N95-31536
F19628-89-C-0001	p 2769	N95-31567
F19628-90-C-0003	p 2850	N95-31367
F19628-90-C-0116	p 2943	N95-31834
F19628-90-K-0021	p 2916	N95-31698
F19628-91-C-0011	p 3005	N95-31534
F19628-91-C-0042	p 2920	N95-31522
F19628-91-C-0103	p 2998	N95-31192
F19628-91-C-0112	p 2914	N95-31012
F19628-91-C-0145	p 2766	N95-31553
F19628-93-C-0129	p 2871	N95-30994
	p 2946	N95-32289
	p 2946	N95-32290
	p 2946	N95-32291
	p 2946	N95-32292
	p 2946	N95-32293
	p 2946	N95-32294
F19628-93-C-0130	p 2942	N95-31683
F19628-93-C-0193	p 2943	N95-32019
	p 2948	N95-32021
F19628-93-C-0199	p 2964	N95-31831
F19628-95-C-0002	p 2951	N95-30890
	p 2935	N95-30931
	p 2920	N95-31465
F29601-89-C-0001	p 3000	N95-31665
F29601-90-C-0068	p 3015	N95-31826
F30602-89-C-0016	p 2766	N95-31143
F30602-90-C-0119	p 2974	N95-31527
F30602-91-C-0016	p 2947	N95-30868
F30602-91-C-0084	p 2942	N95-31688
F30602-92-C-0065	p 2953	N95-31654
F30602-92-C-0102	p 2931	N95-30967
F30602-93-C-0009	p 2860	N95-30886
F30602-93-C-0040	p 2947	N95-31445
F33615-84-C-0507	p 2864	N95-31844
F33615-90-C-0006	p 2940	N95-31455
F33615-92-C-1028	p 2930	N95-30907
F33615-92-C-3405	p 2942	N95-31684
F33615-92-C-3601	p 2871	N95-30992
	p 2820	N95-31471
	p 2753	N95-31463
	p 2753	N95-31655
	p 2753	N95-31656
F33615-98-1-1330	p 2953	N95-31827
F33657-84-C-0247	p 2743	N95-30885
F33657-88-D-2188	p 2885	N95-31389
F41608-94-C-1126	p 2845	N95-30398
F41622-92-D-0006	p 2929	N95-31583
F49620-87-C-0074	p 2944	N95-32203
F49620-91-C-0033	p 2811	N95-30405
F49620-91-C-0034	p 3012	N95-30933
F49620-91-C-0084	p 2848	N95-30869
F49620-91-C-0100	p 2815	N95-30955
F49620-91-1-0279	p 2952	N95-31055
F49620-92-C-0001	p 2783	N95-30433
F49620-92-C-0004	p 2795	N95-31439
F49620-92-C-0007	p 2952	N95-31266
F49620-92-J-0002	p 2851	N95-31430
F49620-92-J-0015	p 3031	N95-31450
F49620-92-J-0022	p 3013	N95-30982
F49620-92-J-0040	p 2981	N95-30952
F49620-92-J-0060	p 3020	N95-31545
F49620-92-J-0072	p 2976	N95-30410
F49620-92-J-0078	p 2751	N95-31451
F49620-92-J-0089	p 2885	N95-31528
F49620-92-J-0098	p 2850	N95-31280
F49620-92-J-0112	p 2896	N95-31474
F49620-92-J-0127	p 2952	N95-30961
F49620-92-J-0138	p 2914	N95-31278
F49620-92-J-0155	p 3013	N95-30983
F49620-92-J-0156	p 2929	N95-31436
F49620-92-J-0179	p 2795	N95-31440
F49620-92-J-0375	p 2799	N95-31204
F49620-92-J-0386	p 2756	N95-30937
F49620-92-J-0415	p 3012	N95-30933
F49620-93-1-0006	p 2848	N95-30932
F49620-93-1-0103	p 2849	N95-31142
F49620-93-1-0264	p 2952	N95-31279
F49620-93-1-0328	p 3015	N95-31444
F49620-93-1-0413	p 2925	N95-31144
F49620-93-1-0554	p 2884	N95-31145
F49620-93-1-0559	p 2997	N95-31005
F49620-93-1-0596	p 2908	N95-31447
F49620-94-C-0032	p 3013	N95-30985
F49620-94-C-0036	p 2885	N95-31434
F49620-94-C-0045	p 2932	N95-32257
F49620-94-C-0052	p 2849	N95-30935
F49620-94-C-0058	p 2998	N95-31435
F49620-94-1-0275	p 2749	N95-31433
F49620-94-1-0292	p 2874	N95-31432
GRI-5086-260-1308	p 2791	N95-30541
GRI-5092-260-2596	p 2791	N95-30541
KBN-3-P401-002-05	p 2854	N95-32192
MDA903-86-K-0297	p 2929	N95-31686
MDA903-90-C-0006	p 2851	N95-31448
	p 2851	N95-31449
MDA903-90-K-0066	p 2929	N95-31585
MDA903-93-C-0109	p 2959	N95-31002
MDA972-92-C-0053	p 2998	N95-31141
MDA972-92-J-1002	p 2943	N95-31843
MDA972-92-J-1012	p 2942	N95-31657
MIPR-90MM052D	p 2927	N95-31446
NAGW-1112	p 2851	N95-31457
NAGW-1919	p 3028	N95-30469
NAGW-2833	p 2914	N95-30865
NAGW-2933	p 3031	N95-30582
NAGW-3065	p 3029	N95-30751
NAGW-3135	p 3028	N95-31364
NAGW-3149	p 2910	N95-31981
NAGW-3969	p 2780	N95-31791
NAG1-1053	p 2896	N95-31418
NAG1-1122	p 2878	N95-32219
NAG1-1123	p 2939	N95-31249
NAG1-1328	p 3012	N95-30847
NAG1-1472	p 2872	N95-31341
NAG1-554	p 2917	N95-31743
NAG1-756	p 2897	N95-31730
	p 2944	N95-32190
	p 2899	N95-32202
	p 2944	N95-32203

	p 2767	N95-32204
	p 2945	N95-32214
	p 2945	N95-32215
NAG3-1096	p 2837	N95-31359
NAG3-1234	p 2899	N95-32205
NAG3-1273	p 2944	N95-32203
NAG3-1345	p 2768	N95-30860
NAG3-1490	p 2906	N95-32212
NAG3-550	p 2930	N95-31134
NAG3-746	p 2768	N95-30864
NAG5-123	p 2936	N95-31236
	p 2937	N95-31242
NAG5-1458	p 3028	N95-30469
NAG5-2102	p 2914	N95-30848
NAG5-2371	p 3032	N95-32218
NAG5-397	p 3028	N95-30466
NAG8-1041	p 2958	N95-30754
NAG8-111	p 3028	N95-30466
NAG8-134	p 2917	N95-31743
NAG8-217	p 2950	N95-30655
NAG8-822	p 2917	N95-31743
NAG8-839	p 3031	N95-30582
NAG8-841	p 2918	N95-30782
NASA ORDER C-78749-C	p 2878	N95-32216
NASA ORDER S-12870-F	p 2919	N95-31128
NASA ORDER S-97229-E	p 3029	N95-31424
NASW-4627	p 3019	N95-30781
	p 2838	N95-31983
NASW-4685	p 2880	N95-30752
NAS1-14101	p 2931	N95-30657
NAS1-14472	p 2931	N95-30657
NAS1-15810	p 2931	N95-30657
NAS1-16394	p 2931	N95-30657
NAS1-17070	p 2931	N95-30657
NAS1-17130	p 2931	N95-30657
NAS1-18107	p 2931	N95-30657
NAS1-18224	p 2767	N95-32189
NAS1-18605	p 2931	N95-30657
NAS1-18862	p 2789	N95-31421
NAS1-19247	p 2767	N95-32189
NAS1-19480	p 2933	N95-30584
	p 2931	N95-30657
	p 2959	N95-31120
	p 2960	N95-31319
	p 2877	N95-31978
	p 2932	N95-31988
	p 2932	N95-32046
NAS1-19570	p 2871	N95-30993
NAS3-25266	p 2876	N95-31738
NAS3-25425	p 2742	N95-30611
NAS3-25644	p 2867	N95-30710
NAS3-25646	p 2768	N95-31169
	p 2769	N95-31170
NAS3-25933	p 2765	N95-31849
NAS3-25950	p 2874	N95-31423
NAS3-26256	p 2802	N95-30531
NAS3-26501	p 2785	N95-30787
NAS3-26618	p 2755	N95-30779
NAS3-27186	p 2762	N95-30592
	p 2742	N95-30704
	p 2880	N95-30851
	p 2768	N95-30860
	p 2763	N95-31653
	p 2864	N95-31742
	p 2899	N95-32206
	p 2865	N95-32207
	p 2822	N95-32208
	p 2791	N95-32209
NAS3-27383	p 2889	N95-31382
NAS5-26555	p 3028	N95-31364
NAS5-31000	p 2967	N95-32319
NAS5-31358	p 2919	N95-31123
NAS5-31845	p 3030	N95-31619
NAS5-32034	p 2893	N95-30786
NAS5-32572	p 2917	N95-31820
NAS5-32584	p 3031	N95-30785
NAS7-1260	p 2912	N95-30525
	p 2846	N95-30581
	p 2859	N95-30651
	p 3030	N95-30845
	p 3024	N95-30858
	p 2881	N95-31456
	p 2909	N95-31651
	p 2796	N95-31660
	p 3025	N95-31713
NAS7-918	p 2922	N95-30859
NAS8-36200	p 2775	N95-31765
	p 2775	N95-31768
NAS8-38100	p 2780	N95-31796
NAS8-38609	p 2781	N95-31801
NAS8-40000	p 2776	N95-31774
NAS8-40148	p 2828	N95-31210
NAS8-40162	p 2799	N95-31211
NAS9-18637	p 2996	N95-30772
NCCW-0040	p 2938	N95-31243
NCC1-99	p 2943	N95-31982
NCC2-637	p 2744	N95-32193
NCC2-817	p 2921	N95-32184
NCC3-208	p 2837	N95-31359
NCC3-291	p 2878	N95-32210
	p 2878	N95-32216
NCC3-370	p 2959	N95-30855
NGT-50559	p 2928	N95-31383
NGT-51184	p 3028	N95-30469
NIVR-01308N	p 2743	N95-30814
NIVR-07302N	p 2743	N95-30837
NR PROJ. RR0-3303	p 2921	N95-31577
NSF ASC-92-17394	p 2944	N95-32203
NSF AST-82-05956	p 3028	N95-30466
NSF AST-86-04324	p 3028	N95-30466
NSF AST-88-19696	p 3028	N95-30466
NSF ATM-91-19580	p 3031	N95-30582
NSF ATM-91-20072	p 2914	N95-30773
NSF CCR-89-03319	p 2934	N95-30603
NSF CCR-89-05296	p 2934	N95-30603
NSF CCR-90-06396	p 2934	N95-30603
NSF CCR-90-24954	p 2932	N95-32046
NSF CCR-92-13427	p 2939	N95-31249
NSF CCR-93-33363	p 2941	N95-31460
NSF CCR-94-06611	p 2934	N95-30603
NSF CTS-91-13151	p 2800	N95-31298
NSF CTS-93-12875	p 2819	N95-31417
NSF HRD-91-04484	p 3028	N95-30466
NSF INT-90-16514	p 3031	N95-30582
NSF IRI-93-57761	p 2939	N95-31277
NSF IRI-94-06481	p 2942	N95-31657
NSF OCE-86-01316	p 2914	N95-30865
NSF OCE-90-02366	p 2914	N95-30865
NUWC PROJ. A10016	p 2813	N95-30560
N00014-82-K-0162	p 2793	N95-30938
N00014-88-K-0141	p 2875	N95-31586
N00014-89-J-1293	p 2770	N95-30988
	p 2770	N95-31196
N00014-89-J-1527	p 2848	N95-30869
N00014-89-J-1828	p 2816	N95-30974
N00014-89-J-3063	p 2819	N95-31410
N00014-90-J-11230	p 2984	N95-31427
N00014-90-J-1148	p 2997	N95-30973
	p 2817	N95-31126
	p 2821	N95-31699
	p 3001	N95-31700
N00014-90-J-1230	p 2795	N95-31437
N00014-90-J-1536	p 2788	N95-31384
N00014-90-J-1608	p 2795	N95-31595
	p 2796	N95-31596
	p 2985	N95-31609
	p 2796	N95-31691
	p 2797	N95-31830
	p 2986	N95-31832
N00014-90-J-1897	p 2852	N95-31537
N00014-90-J-4062	p 2801	N95-31309
	p 2801	N95-31310
N00014-91-C-0001	p 2870	N95-30986
	p 2825	N95-31194
	p 2829	N95-31282
N00014-91-C-0216	p 2863	N95-31669
N00014-91-C-1977	p 2800	N95-31286
N00014-91-J-1529	p 2940	N95-31459
N00014-91-J-1901	p 2964	N95-32287
N00014-91-J-1977	p 2799	N95-31284
	p 2800	N95-31285
	p 2800	N95-31298
N00014-91-J-4038	p 2939	N95-31277
N00014-91-J-4075	p 2786	N95-30866
	p 2786	N95-30867
	p 2786	N95-30898
N00014-91-J-4130	p 2793	N95-31014
N00014-92-C-0027	p 2923	N95-30964
N00014-92-C-0093	p 2787	N95-30975
N00014-92-J-1510	p 2788	N95-31369
	p 2788	N95-31370
	p 2788	N95-31371
	p 2788	N95-31372
N00014-92-J-1532	p 2921	N95-31675
N00014-92-J-1801	p 2947	N95-30930
N00014-92-J-1895	p 2786	N95-30934
N00014-92-WX-24097	p 2801	N95-31307
	p 2801	N95-31314
N00014-93-C-0093	p 2846	N95-30562
N00014-93-I-0437	p 3015	N95-32018
N00014-93-K-2005	p 2886	N95-31563
N00014-93-WX-24268	p 2799	N95-31200
N00014-93-1-0026	p 2807	N95-31464
N00014-93-1-0080	p 2801	N95-31315
N00014-93-1-0221	p 2963	N95-31565
N00014-93-1-0486	p 2920	N95-31541
N00014-93-1-0563	p 3014	N95-31189
N00014-94-C-0261	p 2861	N95-31147
N00014-94-C-0263	p 2789	N95-31509
N00014-94-C-2030	p 2903	N95-30893
N00014-94-WX-2D001	p 2801	N95-31311
N00014-94-1-0026	p 2816	N95-30997
N00014-94-1-0161	p 2923	N95-31600
N00014-94-1-0339	p 2919	N95-30951
N00014-94-1-0438	p 2923	N95-31523
N00014-94-1-0540	p 2819	N95-31461
	p 2819	N95-31462
	p 2819	N95-31466
	p 2819	N95-31467
N00014-95-1-0124	p 2926	N95-30870
N00039-92-C-0100	p 2923	N95-31701
N00123-89-G-0508	p 2924	N95-31829
N00600-94-C-2972	p 2751	N95-31525
N00600-94-C-3087	p 2751	N95-30923
N66269-90-C-0551	p 2848	N95-30904
N68171-94-C-9004	p 3013	N95-30969
N68171-95-C-9007	p 2901	N95-31156
PROJ. FFIE/566/139	p 2945	N95-32252
PROJ. FFIE/633/131.1	p 2748	N95-30597
PROJ. FFIE/654/170	p 2933	N95-30598
PROJ. SOFIA	p 3002	N95-32187
PSR-92-1028-01	p 2871	N95-30991
RTOP 170-38-53-56	p 2869	N95-30863
RTOP 233-01-0C	p 2864	N95-31742
	p 2865	N95-32207
RTOP 233-02-0D	p 2813	N95-30621
RTOP 233-03-02-02	p 2767	N95-32189
RTOP 233-03-02-08-28	p 2796	N95-31660
RTOP 235-01-0A	p 3011	N95-30703
RTOP 242-70-02	p 2802	N95-30531
	p 2867	N95-30710
	p 2768	N95-31169
	p 2769	N95-31170
RTOP 242-80-01-01	p 2891	N95-30783
RTOP 243-30-07	p 2768	N95-30595
RTOP 297-50-00-02	p 2766	N95-31358
RTOP 297-50-00	p 2768	N95-30860
RTOP 314-40-32-10-23	p 2909	N95-31651
RTOP 428-33-07-06-86	p 2922	N95-30859
RTOP 432-20-00	p 2917	N95-31743
RTOP 464-41-04-01-00	p 2912	N95-30525
RTOP 485-15-00-03	p 2881	N95-31456
RTOP 505-59-10-31	p 2763	N95-32217
RTOP 505-59-30-04	p 2744	N95-31984
RTOP 505-59-53	p 2744	N95-32188
RTOP 505-62-10	p 2753	N95-30514
	p 2742	N95-30611
	p 2874	N95-31423
	p 2899	N95-32206
	p 2878	N95-32210
	p 2878	N95-32216
RTOP 505-62-50	p 2879	N95-30587
	p 2754	N95-30617
	p 2997	N95-30849
	p 2770	N95-32121
RTOP 505-62-52	p 2867	N95-30524
	p 2755	N95-30702
	p 2876	N95-31738
	p 2756	N95-31985
RTOP 505-62-82	p 2763	N95-31653
RTOP 505-62-84	p 2762	N95-30592
RTOP 505-63-12	p 2785	N95-30787
RTOP 505-63-5B	p 2864	N95-31847
RTOP 505-63-50-25	p 2974	N95-30850
RTOP 505-64-10-07	p 2948	N95-32250
RTOP 505-64-13	p 2743	N95-30788
RTOP 505-68-00	p 2757	N95-31846
RTOP 505-68-32	p 2750	N95-30646
RTOP 505-69-50	p 2754	N95-30594
RTOP 505-90-5K	p 2959	N95-30855
RTOP 505-90-52-01	p 2933	N95-30584
	p 2931	N95-30657
	p 2959	N95-31120
	p 2960	N95-31319
	p 2877	N95-31978
	p 2932	N95-31988
	p 2932	N95-32046
RTOP 505-90-58	p 2754	N95-30517
	p 2754	N95-30632
RTOP 506-42-31	p 2803	N95-30593
RTOP 506-49-11-01	p 2940	N95-31420
RTOP 506-72-21	p 2765	N95-31849
RTOP 510-02-11-08	p 2789	N95-31421
RTOP 533-02-03	p 2756	N95-31425
RTOP 537-02-00	p 2742	N95-30704
RTOP 537-02-20	p 2755	N95-30853
RTOP 537-02-21	p 2754	N95-30589
	p 2755	N95-30698
RTOP 537-02-22	p 2755	N95-30861
RTOP 537-04-10	p 2822	N95-32208
RTOP 537-06-21-09	p 2893	N95-30682
RTOP 538-03-11	p 2755	N95-30779
RTOP 538-06-14	p 2899	N95-32205
RTOP 538-06-15	p 2791	N95-32209
RTOP 889-21-32	p 3025	N95-31713
RTOP 889-54-49-10-20	p 3024	N95-30858
RTOP 963-35-08	p 2837	N95-31359
SBIR-09.05-8988A	p 2996	N95-30772

SBIR-11.01-4707 ..... p 2802 N95-30531
W-31-109-ENG-38 ..... p 2858 N95-30374
p 2902 N95-30375
p 2880 N95-30941
p 2861 N95-30942
p 2861 N95-30943
p 2985 N95-31616
p 2790 N95-32060
p 2797 N95-32061
p 3015 N95-32062
p 3016 N95-32103
p 2809 N95-32104
p 3016 N95-32105
p 2911 N95-32156
p 2798 N95-32360
W-7405-ENG-36 ..... p 3010 N95-30571
p 2933 N95-30602
p 2934 N95-30603
p 2980 N95-30705
p 2792 N95-30735
p 2805 N95-31121
p 2992 N95-31151
p 2817 N95-31152
p 2952 N95-31161
p 3014 N95-31231
p 2992 N95-31232
p 2960 N95-31253
p 2818 N95-31377
p 3006 N95-31613
p 2820 N95-31629
p 2808 N95-31636
p 2932 N95-31645
p 2821 N95-31705
p 2836 N95-32048
p 2854 N95-32050
p 3015 N95-32062
p 2911 N95-32276
p 2948 N95-32277
p 3032 N95-32282
p 3008 N95-32351
p 2837 N95-32355
W-7405-ENG-48 ..... p 3003 N95-30359
p 2912 N95-30373
p 2955 N95-30470
p 2955 N95-30471
p 2900 N95-30472
p 2879 N95-30507
p 2947 N95-30578
p 3003 N95-30641
p 3004 N95-30685
p 2792 N95-30714
p 3004 N95-30742
p 3004 N95-30769
p 2936 N95-31056
p 2992 N95-31127
p 3026 N95-31129
p 2861 N95-31133
p 2982 N95-31174
p 2885 N95-31230
p 2875 N95-31591
p 2875 N95-31592
p 2795 N95-31593
p 2807 N95-31615
p 2875 N95-31637
p 2932 N95-31704
p 2901 N95-32027
p 3006 N95-32028
p 2886 N95-32029
p 2987 N95-32038
p 2987 N95-32039
p 2987 N95-32041
p 2993 N95-32042
p 2881 N95-32047
p 2877 N95-32049
p 2809 N95-32051
p 2994 N95-32074
p 2928 N95-32097
p 2865 N95-32100
p 2898 N95-32102
p 3007 N95-32116
p 3007 N95-32148
p 2887 N95-32155
p 2741 N95-32164
p 3016 N95-32268
p 2810 N95-32272
p 2911 N95-32281
p 2810 N95-32283
p 3016 N95-32284
p 3026 N95-32285
p 2865 N95-32300
p 2911 N95-32350
p 2925 N95-32358
p 3021 N95-32359
W-7405-ENG-82 ..... p 3011 N95-30667
p 2956 N95-30668
p 3012 N95-30756
p 2804 N95-30757
p 2815 N95-30897
p 2817 N95-31108
p 2809 N95-32023
p 2897 N95-32024
p 3015 N95-32037
p 2865 N95-32084

Typical Report Number Index Listing

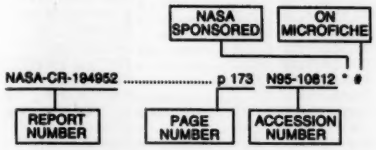

Listings in this index are arranged alphanumerically by report number. The accession number denotes the number by which the citation is identified. The page number helps to locate the citation in the abstract section. An asterisk (*) indicates that the item is a NASA report. A pound sign (#) indicates that the item is available on microfiche.

A-950046 ..... p 2750 N95-30646 * #
A-950066 ..... p 2743 N95-30788 * #
A-950082 ..... p 2744 N95-32188 * #

AD-A286807 ..... p 2783 N95-31101
AD-A286808 ..... p 2762 N95-30926
AD-A286825 ..... p 2794 N95-31268
AD-A288243 ..... p 2925 N95-31144 #
AD-A288353 ..... p 2884 N95-31145 #
AD-A288505 ..... p 3000 N95-31652
AD-A288621 ..... p 2787 N95-31146 #
AD-A288627 ..... p 2861 N95-31147 #
AD-A288630 ..... p 2914 N95-31012 #
AD-A288638 ..... p 2930 N95-31399
AD-A288658 ..... p 2756 N95-31400
AD-A288696 ..... p 2748 N95-31013 #
AD-A288755 ..... p 2793 N95-31014 #
AD-A288896 ..... p 2816 N95-30997 #
AD-A289023 ..... p 2927 N95-30998 #
AD-A289235 ..... p 2935 N95-30999 #
AD-A289717 ..... p 2936 N95-31050 #
AD-A289729 ..... p 2901 N95-31148 #
AD-A289734 ..... p 2825 N95-31149 #
AD-A289737 ..... p 2885 N95-31389 #
AD-A289766 ..... p 2901 N95-31390 #
AD-A289828 ..... p 2942 N95-31683 #
AD-A289897 ..... p 2939 N95-31391 #
AD-A289926 ..... p 2751 N95-30927 #
AD-A289930 ..... p 3024 N95-30928 #
AD-A289934 ..... p 2743 N95-30929 #
AD-A289964 ..... p 2820 N95-31617 #
AD-A290022 ..... p 2947 N95-30930 #
AD-A290056 ..... p 2939 N95-31277 #
AD-A290060 ..... p 2935 N95-30931 #
AD-A290155 ..... p 2817 N95-31115 #
AD-A290216 ..... p 2935 N95-31001 #
AD-A290271 ..... p 2848 N95-30932 #
AD-A290278 ..... p 3014 N95-31189 #
AD-A290310 ..... p 2959 N95-31002 #
AD-A290366 ..... p 2793 N95-30971 #
AD-A290439 ..... p 2925 N95-30452
AD-A290505 ..... p 3025 N95-31618 #
AD-A290780 ..... p 2783 N95-30433 #
AD-A290786 ..... p 2918 N95-30403 #
AD-A290788 ..... p 2802 N95-30404 #
AD-A290791 ..... p 2811 N95-30405 #
AD-A290856 ..... p 2949 N95-30406 #
AD-A290857 ..... p 2902 N95-30408 #
AD-A290859 ..... p 2867 N95-30557 #
AD-A290872 ..... p 2791 N95-30409 #
AD-A290876 ..... p 2812 N95-30558 #
AD-A290878 ..... p 2892 N95-30559 #
AD-A290879 ..... p 2813 N95-30560 #
AD-A290890 ..... p 2786 N95-30896 #
AD-A290891 ..... p 2786 N95-30866 #
AD-A290892 ..... p 2786 N95-30867 #
AD-A290895 ..... p 2976 N95-30410 #
AD-A290932 ..... p 2901 N95-31156
AD-A291057 ..... p 2947 N95-30868 #
AD-A291093 ..... p 2848 N95-30869 #
AD-A291126 ..... p 2952 N95-31266 #
AD-A291127 ..... p 2936 N95-31228 #
AD-A291156 ..... p 2883 N95-30394 #
AD-A291158 ..... p 2949 N95-30395 #
AD-A291159 ..... p 2922 N95-30396 #
AD-A291279 ..... p 2964 N95-32287 #
AD-A291351 ..... p 2926 N95-30870 #
AD-A291445 ..... p 2933 N95-30397 #
AD-A291487 ..... p 2859 N95-30561 #
AD-A291491 ..... p 2845 N95-30398 #
AD-A291492 ..... p 2846 N95-30562 #
AD-A291499 ..... p 2926 N95-30563 #
AD-A292319 ..... p 3030 N95-30482 #
AD-A292334 ..... p 2939 N95-31262 #
AD-A292335 ..... p 2894 N95-31263 #
AD-A292337 ..... p 2960 N95-31264 #
AD-A292339 ..... p 2901 N95-31265 #
AD-A292700 ..... p 3012 N95-30933 #
AD-A292701 ..... p 2786 N95-30934 #
AD-A292703 ..... p 2849 N95-30935 #
AD-A292708 ..... p 2793 N95-30936 #
AD-A292711 ..... p 2756 N95-30937 #
AD-A292712 ..... p 2793 N95-30938 #
AD-A292714 ..... p 2967 N95-30939 #
AD-A292721 ..... p 2860 N95-30940 #
AD-A292726 ..... p 3012 N95-30944 #
AD-A292727 ..... p 2804 N95-30945 #
AD-A292728 ..... p 2869 N95-30946 #
AD-A292729 ..... p 2904 N95-30947 #
AD-A292740 ..... p 2914 N95-31278 #
AD-A292741 ..... p 2923 N95-30918 #
AD-A292742 ..... p 2764 N95-30948 #
AD-A292751 ..... p 2850 N95-31426 #
AD-A292754 ..... p 2984 N95-31427 #
AD-A292758 ..... p 2747 N95-31428 #
AD-A292773 ..... p 2963 N95-31429 #
AD-A292775 ..... p 2851 N95-31430 #
AD-A292776 ..... p 2940 N95-31431 #
AD-A292777 ..... p 2874 N95-31432 #
AD-A292781 ..... p 2749 N95-31433 #
AD-A292782 ..... p 2885 N95-31434 #
AD-A292784 ..... p 2998 N95-31435 #
AD-A292789 ..... p 2929 N95-31436 #
AD-A292794 ..... p 2795 N95-31437 #
AD-A292796 ..... p 3014 N95-31438 #
AD-A292798 ..... p 2795 N95-31439 #
AD-A292804 ..... p 2795 N95-31440 #
AD-A292809 ..... p 2999 N95-31441 #
AD-A292812 ..... p 2862 N95-31442 #
AD-A292815 ..... p 2946 N95-32289 #
AD-A292816 ..... p 2946 N95-32290 #
AD-A292817 ..... p 2946 N95-32291 #
AD-A292819 ..... p 2874 N95-31443 #
AD-A292820 ..... p 3015 N95-31444 #
AD-A292821 ..... p 2947 N95-31445 #
AD-A292829 ..... p 2927 N95-31446 #
AD-A292832 ..... p 2908 N95-31447 #
AD-A292835 ..... p 2851 N95-31448 #
AD-A292836 ..... p 2851 N95-31449 #
AD-A292838 ..... p 2946 N95-32292 #
AD-A292854 ..... p 2946 N95-32293 #
AD-A292859 ..... p 3031 N95-31450 #
AD-A292861 ..... p 2751 N95-31451 #
AD-A292862 ..... p 2940 N95-31452 #
AD-A292864 ..... p 2920 N95-31453 #
AD-A292872 ..... p 2952 N95-31055
AD-A292873 ..... p 2747 N95-31454 #
AD-A292874 ..... p 2952 N95-31279
AD-A292876 ..... p 2884 N95-31190 #
AD-A292880 ..... p 2819 N95-31410 #
AD-A292883 ..... p 2952 N95-30961
AD-A292884 ..... p 2924 N95-32363 #
AD-A292886 ..... p 2889 N95-31382 * #
AD-A292894 ..... p 2928 N95-31383 #
AD-A292895 ..... p 2930 N95-31401 #
AD-A292905 ..... p 2819 N95-31395 #
AD-A292906 ..... p 2788 N95-31384 #
AD-A292907 ..... p 2852 N95-31551 #
AD-A292908 ..... p 2881 N95-31385 #
AD-A292909 ..... p 2915 N95-31386 #
AD-A292911 ..... p 2940 N95-31455 #
AD-A292913 ..... p 2999 N95-31458 #
AD-A292916 ..... p 2940 N95-31459 #
AD-A292952 ..... p 2941 N95-31460 #
AD-A292953 ..... p 2807 N95-31561 #
AD-A292954 ..... p 2821 N95-31683 #
AD-A292955 ..... p 2819 N95-31461 #
AD-A292958 ..... p 2819 N95-31462 #
AD-A292960 ..... p 2819 N95-31466 #
AD-A292968 ..... p 2819 N95-31467 #
AD-A292973 ..... p 2763 N95-31468 #
AD-A292975 ..... p 2789 N95-31469 #
AD-A292988 ..... p 2836 N95-31470 #
AD-A292992 ..... p 2820 N95-31471 #
AD-A292993 ..... p 2849 N95-30962
AD-A292997 ..... p 2838 N95-31472 #
AD-A292998 ..... p 2946 N95-32294 #
AD-A293009 ..... p 2795 N95-31473 #
AD-A293010 ..... p 2896 N95-31474 #
AD-A293012 ..... p 2874 N95-31475 #
AD-A293013 ..... p 3000 N95-31697 #
AD-A293015 ..... p 2916 N95-31698 #
AD-A293019 ..... p 2821 N95-31699 #
AD-A293020 ..... p 3001 N95-31700 #
AD-A293025 ..... p 2923 N95-31701 #
AD-A293033 ..... p 2850 N95-31280
AD-A293035 ..... p 2821 N95-31664 #
AD-A293036 ..... p 3000 N95-31665 #
AD-A293037 ..... p 2821 N95-31666 #
AD-A293039 ..... p 2747 N95-31667 #
AD-A293042 ..... p 2789 N95-31668 #
AD-A293045 ..... p 2863 N95-31669 #
AD-A293051 ..... p 2796 N95-31670 #
AD-A293052 ..... p 2852 N95-31606 #
AD-A293053 ..... p 2863 N95-31607 #
AD-A293055 ..... p 2931 N95-31671 #
AD-A293057 ..... p 3000 N95-31672 #
AD-A293062 ..... p 2853 N95-31673 #
AD-A293065 ..... p 2887 N95-32152 #
AD-A293067 ..... p 2863 N95-31674 #
AD-A293079 ..... p 2997 N95-31005
AD-A293083 ..... p 3015 N95-31826 #
AD-A293084 ..... p 3001 N95-32153 #
AD-A293085 ..... p 3001 N95-31841 #
AD-A293086 ..... p 2864 N95-31842 #
AD-A293090 ..... p 2943 N95-31843 #
AD-A293097 ..... p 2953 N95-31562 #
AD-A293098 ..... p 2864 N95-31844 #
AD-A293105 ..... p 2953 N95-31827 #
AD-A293106 ..... p 3015 N95-32018 #
AD-A293107 ..... p 2943 N95-32019 #
AD-A293109 ..... p 2943 N95-32020 #
AD-A293110 ..... p 2948 N95-32021 #
AD-A293111 ..... p 2951 N95-30884 #
AD-A293113 ..... p 2743 N95-30885 #
AD-A293114 ..... p 2860 N95-30886 #
AD-A293123 ..... p 2930 N95-30888 #
AD-A293125 ..... p 2869 N95-30889 #
AD-A293137 ..... p 2951 N95-30890 #
AD-A293140 ..... p 2951 N95-30891 #
AD-A293141 ..... p 2766 N95-30919 #
AD-A293142 ..... p 2753 N95-30920 #
AD-A293144 ..... p 2889 N95-30949 #
AD-A293146 ..... p 2860 N95-30921 #
AD-A293153 ..... p 2996 N95-31006 #
AD-A293161 ..... p 2894 N95-31007 #
AD-A293162 ..... p 2787 N95-30963 #
AD-A293164 ..... p 2923 N95-30964 #
AD-A293167 ..... p 2870 N95-30965 #
AD-A293168 ..... p 2997 N95-30966 #
AD-A293169 ..... p 2997 N95-30973 #
AD-A293170 ..... p 2816 N95-30974 #
AD-A293171 ..... p 2787 N95-30975 #
AD-A293172 ..... p 2919 N95-30976 #
AD-A293177 ..... p 2804 N95-30977 #
AD-A293183 ..... p 2787 N95-30978 #
AD-A293184 ..... p 2932 N95-32257 #
AD-A293185 ..... p 2861 N95-30979 #
AD-A293186 ..... p 2880 N95-30980 #
AD-A293191 ..... p 2927 N95-30981 #
AD-A293195 ..... p 3013 N95-30982 #

REPORT

AD-A293199 ..... p 3013 N95-30983 #
AD-A293203 ..... p 3013 N95-30984 #
AD-A293206 ..... p 3013 N95-30985 #
AD-A293207 ..... p 3032 N95-30899 #
AD-A293208 ..... p 2860 N95-30900 #
AD-A293220 ..... p 2997 N95-30901 #
AD-A293223 ..... p 2848 N95-30902 #
AD-A293224 ..... p 2935 N95-30903 #
AD-A293226 ..... p 2848 N95-30904 #
AD-A293227 ..... p 2928 N95-30905 #
AD-A293237 ..... p 2884 N95-30906 #
AD-A293239 ..... p 2930 N95-30907 #
AD-A293248 ..... p 2997 N95-30908 #
AD-A293249 ..... p 2997 N95-30909 #
AD-A293251 ..... p 2848 N95-30910 #
AD-A293254 ..... p 2931 N95-30892 #
AD-A293255 ..... p 2903 N95-30893 #
AD-A293256 ..... p 2815 N95-30894 #
AD-A293258 ..... p 2848 N95-30895 #
AD-A293259 ..... p 2850 N95-31387 #
AD-A293263 ..... p 2766 N95-31388 #
AD-A293265 ..... p 2839 N95-31122 #
AD-A293270 ..... p 2817 N95-31124 #
AD-A293272 ..... p 2901 N95-31125 #
AD-A293275 ..... p 2817 N95-31126 #
AD-A293277 ..... p 2756 N95-31191 #
AD-A293284 ..... p 2861 N95-30950 #
AD-A293296 ..... p 2998 N95-31192 #
AD-A293302 ..... p 2919 N95-30951 #
AD-A293304 ..... p 2981 N95-30952 #
AD-A293308 ..... p 2860 N95-30922 #
AD-A293309 ..... p 2751 N95-30923 #
AD-A293310 ..... p 2928 N95-31140 #
AD-A293327 ..... p 2926 N95-30924 #
AD-A293330 ..... p 2998 N95-31141 #
AD-A293334 ..... p 2849 N95-31142 #
AD-A293350 ..... p 2766 N95-31143 #
AD-A293354 ..... p 2959 N95-30953 #
AD-A293356 ..... p 2849 N95-30954 #
AD-A293384 ..... p 2815 N95-30955 #
AD-A293389 ..... p 2931 N95-30967 #
AD-A293394 ..... p 2935 N95-30968 #
AD-A293397 ..... p 3013 N95-30969 #
AD-A293405 ..... p 3013 N95-31008 #
AD-A293416 ..... p 2942 N95-31684 #
AD-A293435 ..... p 2850 N95-31367 #
AD-A293442 ..... p 2794 N95-31368 #
AD-A293444 ..... p 2788 N95-31369 #
AD-A293445 ..... p 2788 N95-31370 #
AD-A293446 ..... p 2788 N95-31371 #
AD-A293447 ..... p 2788 N95-31372 #
AD-A293448 ..... p 2927 N95-31373 #
AD-A293452 ..... p 2889 N95-31374 #
AD-A293463 ..... p 2963 N95-31375 #
AD-A293467 ..... p 3005 N95-31534 #
AD-A293495 ..... p 2915 N95-31535 #
AD-A293497 ..... p 2915 N95-31536 #
AD-A293510 ..... p 2852 N95-31537 #
AD-A293521 ..... p 2931 N95-31538 #
AD-A293556 ..... p 3015 N95-31539 #
AD-A293561 ..... p 2886 N95-31563 #
AD-A293569 ..... p 2953 N95-31540 #
AD-A293576 ..... p 2941 N95-31594
AD-A293581 ..... p 2929 N95-31685 #
AD-A293582 ..... p 2929 N95-31686 #
AD-A293586 ..... p 2747 N95-31687 #
AD-A293596 ..... p 2942 N95-31688 #
AD-A293602 ..... p 2953 N95-31654 #
AD-A293611 ..... p 2753 N95-31655 #
AD-A293612 ..... p 2753 N95-31656 #
AD-A293613 ..... p 2753 N95-31463 #
AD-A293614 ..... p 2798 N95-32258 #
AD-A293617 ..... p 2807 N95-31464 #
AD-A293618 ..... p 2863 N95-31725 #
AD-A293619 ..... p 2836 N95-31564 #
AD-A293630 ..... p 2963 N95-31565
AD-A293639 ..... p 2889 N95-31566 #
AD-A293654 ..... p 2769 N95-31567 #
AD-A293657 ..... p 2975 N95-31608 #
AD-A293662 ..... p 2985 N95-31609 #
AD-A293668 ..... p 2796 N95-31691 #
AD-A293669 ..... p 2795 N95-31595 #
AD-A293672 ..... p 2796 N95-31596 #
AD-A293677 ..... p 2985 N95-31597 #
AD-A293682 ..... p 2741 N95-31598 #
AD-A293683 ..... p 2807 N95-31599 #
AD-A293684 ..... p 2923 N95-31600 #
AD-A293685 ..... p 2852 N95-31601 #
AD-A293689 ..... p 2752 N95-31602 #
AD-A293691 ..... p 2749 N95-32022 #
AD-A293692 ..... p 2901 N95-31603 #
AD-A293697 ..... p 2881 N95-31828 #
AD-A293703 ..... p 2924 N95-31829 #
AD-A293711 ..... p 2797 N95-31830 #
AD-A293714 ..... p 2964 N95-31831 #
AD-A293717 ..... p 2966 N95-31832 #
AD-A293718 ..... p 2886 N95-31833 #
AD-A293724 ..... p 2943 N95-31834 #
AD-A293725 ..... p 2943 N95-31835 #
AD-A293731 ..... p 2896 N95-31566 #
AD-A293741 ..... p 2747 N95-31569 #
AD-A293742 ..... p 2928 N95-31570 #
AD-A293750 ..... p 2920 N95-31571 #
AD-A293753 ..... p 2749 N95-31572 #
AD-A293757 ..... p 2941 N95-31573 #
AD-A293758 ..... p 2852 N95-31574 #
AD-A293761 ..... p 2890 N95-31576 #
AD-A293765 ..... p 2921 N95-31577 #
AD-A293770 ..... p 2752 N95-31578 #
AD-A293771 ..... p 2752 N95-31579 #
AD-A293774 ..... p 2795 N95-31580 #
AD-A293775 ..... p 2920 N95-31465 #
AD-A293776 ..... p 2789 N95-31509 #
AD-A293779 ..... p 2928 N95-31376 #
AD-A293782 ..... p 2749 N95-31581 #
AD-A293783 ..... p 2953 N95-31582 #
AD-A293788 ..... p 2929 N95-31583 #
AD-A293797 ..... p 2753 N95-31584 #
AD-A293798 ..... p 2929 N95-31585 #
AD-A293805 ..... p 2875 N95-31586 #
AD-A293806 ..... p 2916 N95-31604 #
AD-A293807 ..... p 2915 N95-31575 #
AD-A293808 ..... p 2921 N95-31587 #
AD-A293809 ..... p 2852 N95-31588 #
AD-A293810 ..... p 2916 N95-31589 #
AD-A293811 ..... p 2852 N95-31590 #
AD-A293821 ..... p 2927 N95-31552 #
AD-A293826 ..... p 2766 N95-31553 #
AD-A293828 ..... p 2905 N95-31554 #
AD-A293829 ..... p 2852 N95-31555 #
AD-A293830 ..... p 2909 N95-31556 #
AD-A293834 ..... p 2944 N95-32073
AD-A293836 ..... p 2874 N95-31516 #
AD-A293837 ..... p 2961 N95-31557 #
AD-A293841 ..... p 2963 N95-31558 #
AD-A293852 ..... p 2820 N95-31559 #
AD-A293856 ..... p 2857 N95-32259 #
AD-A293858 ..... p 2952 N95-31517 #
AD-A293875 ..... p 2981 N95-31518 #
AD-A293879 ..... p 2999 N95-31519 #
AD-A293882 ..... p 2749 N95-31520 #
AD-A293884 ..... p 2920 N95-31541 #
AD-A293886 ..... p 2999 N95-31542 #
AD-A293890 ..... p 2963 N95-31543 #
AD-A293891 ..... p 2752 N95-31544 #
AD-A293892 ..... p 3020 N95-31545 #
AD-A293895 ..... p 2851 N95-31510 #
AD-A293896 ..... p 3020 N95-31511 #
AD-A293902 ..... p 2747 N95-31512 #
AD-A293919 ..... p 2921 N95-31675 #
AD-A293922 ..... p 2851 N95-31513 #
AD-A293924 ..... p 2820 N95-31514 #
AD-A293930 ..... p 2999 N95-31515 #
AD-A293932 ..... p 2749 N95-31521 #
AD-A293938 ..... p 2920 N95-31522 #
AD-A293951 ..... p 2923 N95-31523 #
AD-A293956 ..... p 2920 N95-31524 #
AD-A293962 ..... p 2751 N95-31525 #
AD-A293963 ..... p 2915 N95-31560 #
AD-A293964 ..... p 2942 N95-31657
AD-A293969 ..... p 2836 N95-31526 #
AD-A293972 ..... p 2974 N95-31527 #
AD-A293976 ..... p 2885 N95-31528 #
AD-A293979 ..... p 2999 N95-31529 #
AD-D017324 ..... p 2848 N95-30917 #
AD-D017328 ..... p 2862 N95-31179 #
AD-D017332 ..... p 2887 N95-30386
AD-D017335 ..... p 2887 N95-30387
AD-D017336 ..... p 2887 N95-30672
AD-D017339 ..... p 2973 N95-30411
AD-D017340 ..... p 2866 N95-30412
AD-D017342 ..... p 2973 N95-30413
AD-D017343 ..... p 3011 N95-30673
AD-D017344 ..... p 2996 N95-30678
AD-D017346 ..... p 2998 N95-30679
AD-D017347 ..... p 2974 N95-30549
AD-D017348 ..... p 2974 N95-30550
AD-D017349 ..... p 2803 N95-30551
AD-D017350 ..... p 2930 N95-30552
AD-D017351 ..... p 2867 N95-30553
AD-D017352 ..... p 2791 N95-30554
AD-D017353 ..... p 2996 N95-30529
AD-D017354 ..... p 2888 N95-30414
AD-D017355 ..... p 2811 N95-30415
AD-D017357 ..... p 2888 N95-30416
AD-D017358 ..... p 2846 N95-30417
AD-D017360 ..... p 2753 N95-31180
AD-D017361 ..... p 2814 N95-30715
AD-D017362 ..... p 2887 N95-30399
AD-D017365 ..... p 2973 N95-30530
AD-D017367 ..... p 2888 N95-30532
AD-D017369 ..... p 2879 N95-30658
AD-D017370 ..... p 3009 N95-30533
AD-D017371 ..... p 2859 N95-30659
AD-D017372 ..... p 2847 N95-30680
AD-D017374 ..... p 2888 N95-30716
AD-D017376 ..... p 2784 N95-30661
AD-D017412 ..... p 2793 N95-31009 #
AD-D017415 ..... p 2995 N95-30402
AD-D017416 ..... p 2816 N95-31010 #
AD-D017418 ..... p 2816 N95-31011 #
AD-D017419 ..... p 2771 N95-30418 #
AD-D017422 ..... p 2847 N95-30743
AD-D017426 ..... p 2883 N95-30744
AD-D017428 ..... p 2847 N95-30746
AD-D017430 ..... p 2974 N95-30747
AD-D017432 ..... p 3014 N95-31269
AD-D017433 ..... p 2996 N95-30753
AD-D017434 ..... p 2862 N95-31342
AD-D017435 ..... p 2884 N95-31213
AD-D017436 ..... p 2862 N95-31343
AD-D017438 ..... p 2996 N95-30724
AD-D017440 ..... p 2953 N95-31692 #
AD-D017441 ..... p 2953 N95-31693 #
AD-D017442 ..... p 2850 N95-31392
AD-D017445 ..... p 2998 N95-31270
AD-D017446 ..... p 2794 N95-31271
AD-D017447 ..... p 2818 N95-31272
AD-D017448 ..... p 2885 N95-31273
AD-D017449 ..... p 2885 N95-31274
AD-D017452 ..... p 2974 N95-30725
AD-D017453 ..... p 2862 N95-31275
AD-D017454 ..... p 2860 N95-30726
AD-D017455 ..... p 2847 N95-30727
AD-D017457 ..... p 3011 N95-30728
AD-D017458 ..... p 2860 N95-30748
AD-D017462 ..... p 2785 N95-30749
AD-D017463 ..... p 2803 N95-30750

AEDC-TR-94-12 ..... p 2747 N95-31667 #
AEDC-TR-94-14 ..... p 2884 N95-30906 #

AF-94-1 ..... p 2849 N95-30935 #

AFIT/CI/CIA-94-130 ..... p 2927 N95-30998 #

AFIT/DS/AA/94-6 ..... p 2867 N95-30557 #

AFIT/DS/ENS/95-01 ..... p 2949 N95-30406 #

AFIT/GA/ENY/95M-1 ..... p 2961 N95-31557 #

AFIT/GAE/ENY/95M-01 ..... p 2753 N95-31584 #
AFIT/GAE/ENY/95M-03 ..... p 2874 N95-31516 #

AFIT/GE/ENG/95M-01 ..... p 2944 N95-32073
AFIT/GE/ENG/95M-02 ..... p 2851 N95-31513 #

AFIT/GOA/ENG/95M-01 ..... p 2963 N95-31558 #

AFIT/GOA/ENS/95M-02 ..... p 2749 N95-31581 #
AFIT/GOA/ENS/95M-04 ..... p 2747 N95-31512 #
AFIT/GOA/ENS/95M-6 ..... p 2953 N95-31582 #

AFIT/GOR/ENC/ENS/95M-08 .... p 2961 N95-31518 #

AFIT/GOR/ENS/95M-14 ..... p 2852 N95-31555 #
AFIT/GOR/ENS/95M-19 ..... p 2909 N95-31556 #

AFIT/GSC/ENG/94D-15 ..... p 2935 N95-30999 #

AFIT/GSO/ENG/95M-01 ..... p 2952 N95-31517 #

AFIT/WSF/ENP/94-05 ..... p 2902 N95-30408 #

AFOSR-94-0093TR ..... p 2884 N95-31145 #
AFOSR-94-0681TR ..... p 2925 N95-31144 #
AFOSR-95-0039TR ..... p 2848 N95-30932 #
AFOSR-95-0068TR ..... p 2976 N95-30410 #
AFOSR-95-0070TR ..... p 2811 N95-30405 #
AFOSR-95-0074TR ..... p 2783 N95-30433 #
AFOSR-95-0087TR ..... p 2949 N95-30395 #
AFOSR-95-0089TR ..... p 2952 N95-31266 #
AFOSR-95-0102TR ..... p 2848 N95-30869 #
AFOSR-95-0139TR ..... p 3015 N95-31444 #
AFOSR-95-0162TR ..... p 3012 N95-30933 #
AFOSR-95-0167TR ..... p 2999 N95-31441 #
AFOSR-95-0168TR ..... p 2795 N95-31440 #
AFOSR-95-0169TR ..... p 2908 N95-31447 #
AFOSR-95-0170TR ..... p 3013 N95-31008 #
AFOSR-95-0173TR ..... p 2795 N95-31439 #
AFOSR-95-0174TR ..... p 2756 N95-30937 #
AFOSR-95-0177TR ..... p 2849 N95-30935 #
AFOSR-95-0178TR ..... p 3014 N95-31438 #
AFOSR-95-0181TR ..... p 2850 N95-31280
AFOSR-95-0182TR ..... p 2896 N95-31474 #
AFOSR-95-0189TR ..... p 2952 N95-31279

AFOSR-95-0190TR ..... p 2952 N95-31055
AFOSR-95-0191TR ..... p 2874 N95-31443 #
AFOSR-95-0192TR ..... p 2874 N95-31432 #
AFOSR-95-0199TR ..... p 2849 N95-30962
AFOSR-95-0202TR ..... p 2952 N95-30961
AFOSR-95-0209TR ..... p 2940 N95-31431 #
AFOSR-95-0217TR ..... p 2914 N95-31278 #
AFOSR-95-0220TR ..... p 2997 N95-31005
AFOSR-95-0221TR ..... p 3031 N95-31450 #
AFOSR-95-0223TR ..... p 2940 N95-31452 #
AFOSR-95-0225TR ..... p 2932 N95-32257 #
AFOSR-95-0226TR ..... p 2838 N95-31472 #
AFOSR-95-0227TR ..... p 2851 N95-31430 #
AFOSR-95-0229TR ..... p 2963 N95-31429 #
AFOSR-95-0232TR ..... p 2849 N95-31142 #
AFOSR-95-0235TR ..... p 2931 N95-30892 #
AFOSR-95-0236TR ..... p 3013 N95-30985 #
AFOSR-95-0238TR ..... p 3013 N95-30982 #
AFOSR-95-0241TR ..... p 2998 N95-31435 #
AFOSR-95-0243TR ..... p 2929 N95-31436 #
AFOSR-95-0250TR ..... p 2861 N95-30979 #
AFOSR-95-0251TR ..... p 2981 N95-30952 #
AFOSR-95-0256TR ..... p 3032 N95-30899 #
AFOSR-95-0319TR ..... p 3020 N95-31545 #
AFOSR-95-0321TR ..... p 2885 N95-31528 #
AFOSR-95-0325TR ..... p 2820 N95-31559 #
AFOSR-95-0326TR ..... p 2752 N95-31602 #
AFOSR-95-0327TR ..... p 2881 N95-31828 #
AFOSR-95-0329TR ..... p 2999 N95-31519 #
AFOSR-95-0331TR ..... p 2999 N95-31542 #
AFOSR-95-0332TR ..... p 2999 N95-31515 #

AF95-1 ..... p 2845 N95-30398 #

AGARD-AR-335 ..... p 2745 N95-31061 #

AGARD-CP-555 ..... p 2839 N95-32123 #
AGARD-CP-560 ..... p 2757 N95-31989 #

AGARD-LS-201 ..... p 2843 N95-32165 #

AI-TR-1493 ..... p 2939 N95-31277 #

AIAA PAPER 95-2361 ..... p 2756 N95-31425 * #
AIAA PAPER 95-2362 ..... p 2757 N95-31846 * #
AIAA PAPER 95-2390 ..... p 2763 N95-31653 * #
AIAA PAPER 95-2500 ..... p 2768 N95-30856 * #
AIAA PAPER 95-2612 ..... p 2959 N95-30855 * #
AIAA PAPER 95-2614 ..... p 2742 N95-30704 * #
AIAA PAPER 95-2799 ..... p 2754 N95-30517 * #
AIAA PAPER 95-2800 ..... p 2754 N95-30617 * #
AIAA PAPER 95-2801 ..... p 2754 N95-30632 * #
AIAA PAPER 95-2995 ..... p 2755 N95-30698 * #
AIAA PAPER 95-2998 ..... p 2754 N95-30589 * #
AIAA PAPER 95-3109 ..... p 2755 N95-30853 * #

AL/AO-PC-1995-0012 ..... p 2927 N95-31552 #

AL/AO-TR-1994-0174 ..... p 2928 N95-30905 #
AL/AO-TR-1995-0003 ..... p 2928 N95-31376 #
AL/AO-TR-1995-0020 ..... p 2963 N95-31375 #

AL/CF-SR-1994-0013 ..... p 2931 N95-31671 #
AL/CF-SR-1995-0004 ..... p 2931 N95-31538 #

AL/CF-TR-1994-0151 ..... p 2930 N95-30907 #
AL/CF-TR-1994-0156 ..... p 2927 N95-31373 #

AL/HR-TP-1994-0034 ..... p 2929 N95-31583 #

AL/HR-TR-1994-0108 ..... p 2942 N95-31684 #

AL/OE-TR-1994-0130 ..... p 2756 N95-31191 #

AMSMI/RD-TR-CR-SS-95-10 ..... p 2857 N95-32259 #

ANL/CMT-ACL/VU-83809 ..... p 2798 N95-32360 #

ANL/ER/CP-84530 ..... p 2797 N95-32061 #

ANL/ES/CP-85156 ..... p 2911 N95-32156 #
ANL/ES/CP-85392 ..... p 2902 N95-30375 #

ANL/ES/PP-85380 ..... p 2858 N95-30374 #

ANL/ET/CP-82190 ..... p 2861 N95-30942 #
ANL/ET/CP-83786 ..... p 2790 N95-32060 * #
ANL/ET/CP-84477 ..... p 2861 N95-30943 #

ANL/IPNS/CP-84859 ..... p 2985 N95-31616 #

ANL/MSD/CP-82825 ..... p 2880 N95-30941 #
ANL/MSD/CP-83382 ..... p 3016 N95-32105 #
ANL/MSD/CP-84769 ..... p 3015 N95-32062 #
ANL/MSD/CP-85466 ..... p 2809 N95-32104 #
ANL/MSD/CP-85469 ..... p 3016 N95-32103 #

AOARD-TR-94-06 ..... p 2960 N95-31264 #
AOARD-TR-94-24 ..... p 2894 N95-31263 #
AOARD-TR-94-30 ..... p 2939 N95-31262 #
AOARD-TR-94-34 ..... p 2901 N95-31265 #
AOARD-TR-94-35 ..... p 3030 N95-30482 #

APL-UW-TM1-95 ..... p 2923 N95-31701 #

AR-008-538 ..... p 2922 N95-30711
AR-008-927 ..... p 3001 N95-31745
AR-008-963 ..... p 2806 N95-31344
AR-008-995 ..... p 2974 N95-31365

ARAED-TR-94-021 ..... p 2836 N95-31526 #

ARCCB-TR-94049 ..... p 2804 N95-30945 #
ARCCB-TR-95001 ..... p 2894 N95-31007 #
ARCCB-TR-95004 ..... p 2863 N95-31725 #

ARI-RN-95-03 ..... p 2959 N95-31002 #
ARI-RN-95-16 ..... p 2929 N95-31585 #
ARI-RN-95-24 ..... p 2929 N95-31686 #

ARL-CR-231 ..... p 2878 N95-32216 * #
ARL-CR-237 ..... p 2878 N95-32210 * #

ARL-MR-213 ..... p 2941 N95-31594
ARL-MR-219 ..... p 3020 N95-31511 #

ARL-TR-282 ..... p 2933 N95-30397 #
ARL-TR-333 ..... p 2756 N95-31985 * #
ARL-TR-422 ..... p 2905 N95-31554 #
ARL-TR-424 ..... p 3015 N95-31539 #
ARL-TR-426 ..... p 2820 N95-31514 #
ARL-TR-513 ..... p 2820 N95-31617 #
ARL-TR-517 ..... p 2959 N95-30953 #
ARL-TR-544 ..... p 2916 N95-31589 #
ARL-TR-565 ..... p 2975 N95-31608 #
ARL-TR-712 ..... p 2869 N95-30889 #
ARL-TR-713 ..... p 2852 N95-31601 #
ARL-TR-718 ..... p 2796 N95-31670 #
ARL-TR-726 ..... p 2764 N95-30948 #
ARL-TR-727 ..... p 2787 N95-30963 #
ARL-TR-732 ..... p 2798 N95-32258 #
ARL-TR-733 ..... p 2795 N95-31580 #
ARL-TR-793 ..... p 2753 N95-30514 * #
ARL-TR-806 ..... p 2754 N95-30517 * #

ARO-25350.15-EL ..... p 2852 N95-31551 #
ARO-26982.10-GS ..... p 2918 N95-30403 #
ARO-28125.9-MA ..... p 2951 N95-30884 #
ARO-28201.1-GS-SAH ..... p 2915 N95-31386 #
ARO-28272.10-MS ..... p 2804 N95-30977 #
ARO-28526.16-PH ..... p 2999 N95-31458 #
ARO-28592.4-PH ..... p 2881 N95-31385 #
ARO-28686.3-MA ..... p 3025 N95-31618 #
ARO-28900.13-MS ..... p 2819 N95-31395 #
ARO-29049.4-EG-S ..... p 2756 N95-31400
ARO-30066.1-CH-SB2 ..... p 2860 N95-30940 #
ARO-30089.1-PH-GF ..... p 2793 N95-30936 #
ARO-30443.1-CH-5 ..... p 2889 N95-31374 #
ARO-30446.1-CH ..... p 3012 N95-30944 #
ARO-30708.3-PH ..... p 2967 N95-30939 #
ARO-30920.9-MS ..... p 2802 N95-30404 #
ARO-32900.2-GS-S ..... p 2793 N95-30971 #
ARO-33865.1-CH-CF ..... p 2904 N95-30947 #

AS-ITP-94-24 ..... p 2991 N95-32304 #

ASC-TR-051-3 ..... p 2959 N95-31002 #

ATC-233 ..... p 2920 N95-31465 #
ATC-234 ..... p 2749 N95-31521 #

ATR-93(7270)-1 ..... p 2914 N95-30773 #
ATR-93(8308)-7 ..... p 2819 N95-31417 #

AWS/FM-95/001 ..... p 2753 N95-30920 #

B-205879 ..... p 3022 N95-31986 #
B-229489 ..... p 2752 N95-32196 #
B-247729 ..... p 2750 N95-32197 #
B-253616 ..... p 3027 N95-32201 #
B-253662 ..... p 2964 N95-31987 #
B-255654 ..... p 3022 N95-32195 #
B-255832 ..... p 2741 N95-32194 #
B-256574 ..... p 3027 N95-31345 #
B-256721 ..... p 2741 N95-32198 #
B-257854 ..... p 2750 N95-32199 #
B-259333 ..... p 3022 N95-32200 #
B-259373 ..... p 3022 N95-32213 #
B-260371 ..... p 3021 N95-31659 #

BBN-7987 ..... p 2947 N95-31445 #

BNL-52459 ..... p 2986 N95-31702 #

BNL-61022 ..... p 2967 N95-32031 #
BNL-61070 ..... p 2994 N95-32092 #
BNL-61071 ..... p 2990 N95-32278 #
BNL-61092 ..... p 2967 N95-32032 #
BNL-61166 ..... p 2994 N95-32242 #
BNL-61167 ..... p 2994 N95-32243 #
BNL-61168 ..... p 2994 N95-32244 #
BNL-61169 ..... p 2995 N95-32297 #
BNL-61181 ..... p 2995 N95-32306 #
BNL-61223 ..... p 2993 N95-31405 #
BNL-61242 ..... p 2803 N95-30706 #
BNL-61547 ..... p 2988 N95-32079 #
BNL-61549 ..... p 3008 N95-32357 #
BNL-61579 ..... p 2989 N95-32160 #
BNL-61581 ..... p 2988 N95-32063 #
BNL-61593 ..... p 2994 N95-32059 #
BNL-61653 ..... p 2882 N95-32159 #
BNL-61719 ..... p 2995 N95-32260 #

BRF1359A ..... p 2765 N95-30880 *
BRF1359B ..... p 2765 N95-30879 *
BRF1359C ..... p 2765 N95-30878 *
BRF1359D ..... p 2764 N95-30877 *
BRF1359E ..... p 2764 N95-30876 *
BRF1359F ..... p 2764 N95-30875 *
BRF1359G ..... p 2764 N95-30874 *
BRF1359H ..... p 2764 N95-30873 *

BUDKERINP-93-93 ..... p 2988 N95-32069 #
BUDKERINP-93-94 ..... p 3020 N95-32150 #
BUDKERINP-93-95 ..... p 2989 N95-32151 #
BUDKERINP-94-24 ..... p 2966 N95-31259 #
BUDKERINP-94-26 ..... p 3019 N95-31276 #
BUDKERINP-94-27 ..... p 2959 N95-31137 #
BUDKERINP-94-53 ..... p 2966 N95-32066 #
BUDKERINP-94-56 ..... p 2991 N95-32354 #

CARDIVNSWC-TR-61-94/14 ..... p 2807 N95-31561 #
CARDIVNSWC-TR-61-94/17 ..... p 2807 N95-31599 #

CBP-131 ..... p 2991 N95-30360

CDI-95-03 ..... p 2751 N95-30923 #

CECOM-TR-94-7 ..... p 2863 N95-31607 #

CERL-FF-95/06 ..... p 2941 N95-31573 #

CERL-TR-FM-94/16 ..... p 2812 N95-30558 #

CMOTT-95-1 ..... p 2959 N95-30855 * #

CMU-CS-94-178 ..... p 2943 N95-31843 #
CMU-CS-94-224 ..... p 2928 N95-31383 #
CMU-CS-95-101 ..... p 2943 N95-32020 #
CMU-CS-95-113 ..... p 2953 N95-31827 #
CMU-CS-95-121 ..... p 2941 N95-31460 #
CMU-CS-95-123 ..... p 2930 N95-31401 #
CMU-CS-95-126 ..... p 2948 N95-32021 #

CMU-RI-TR-95-06 ..... p 2953 N95-31540 #
CMU-RI-TR-95-11 ..... p 2929 N95-31685 #
CMU-RI-TR-95-12 ..... p 2942 N95-31688 #
CMU-RI-TR-95-13 ..... p 2953 N95-31654 #

CMU-SC-95-119 ..... p 2943 N95-32019 #

CMU/SEI-94-SR-008 ..... p 2943 N95-31834 #

CM1198F ..... p 2998 N95-31435 #

CONF-9304146-4 ..... p 2814 N95-30739 #
CONF-930637-16 ..... p 2882 N95-32159 #
CONF-930767 ..... p 2993 N95-31627 #
CONF-9310347 ..... p 2806 N95-31220 #
CONF-9311167 ..... p 2818 N95-31221 #
CONF-9311167 ..... p 2807 N95-31407 #
CONF-9311167 ..... p 2940 N95-31408 #
CONF-9311167 ..... p 2807 N95-31409 #
CONF-940277 ..... p 2908 N95-30802
CONF-9403221-1 ..... p 2987 N95-32039 #
CONF-9404162-18 ..... p 2912 N95-30373 #
CONF-9404162-19 ..... p 2792 N95-30714 #
CONF-9404233-1 ..... p 2890 N95-32367 #
CONF-9404253-1 ..... p 2988 N95-32079 #
CONF-9405308-1 ..... p 2887 N95-32155 #
CONF-940552-35 ..... p 3006 N95-31626 #
CONF-940580-26 ..... p 3003 N95-30612 #
CONF-940593-15 ..... p 3015 N95-32037 #
CONF-940707-1 ..... p 2982 N95-31174 #
CONF-9407123-6 ..... p 2838 N95-30684 #
CONF-940714-53 ..... p 2880 N95-30941 #
CONF-940722-44 ..... p 2992 N95-31185 #
CONF-940722-45 ..... p 3020 N95-32106 #
CONF-940723-36 ..... p 2879 N95-30507 #
CONF-940723-37 ..... p 3028 N95-31129 #

CONF-940723-38 ..... p 2901 N95-32027 #
CONF-940801-VOL-1 ..... p 2907 N95-32368 #
CONF-940801-VOL-2 ..... p 2904 N95-31138 #
CONF-9408156 ..... p 2810 N95-32241 * #
CONF-940816-92 ..... p 2975 N95-30388 #
CONF-9408188-2 ..... p 3029 N95-31102 #
CONF-9408203 ..... p 2768 N95-30881 #
CONF-940829-2 ..... p 2810 N95-32265 #
CONF-940830-4 ..... p 2865 N95-32084 #
CONF-940922-5 ..... p 2967 N95-32036 #
CONF-940922-6 ..... p 2967 N95-32041 #
CONF-940922-7 ..... p 2993 N95-32042 #
CONF-9409226-6 ..... p 2886 N95-32029 #
CONF-9409226-7 ..... p 3006 N95-32028 #
CONF-9409258-7 ..... p 2991 N95-30360
CONF-9409304 ..... p 2992 N95-31166 #
CONF-9409310-2 ..... p 3028 N95-30361 #
CONF-9409314-1 ..... p 2955 N95-30470 #
CONF-9409321-1 ..... p 2894 N95-31054 #
CONF-940933-36 ..... p 3006 N95-31624 #
CONF-941006-5 ..... p 2861 N95-31133 #
CONF-941013-31 ..... p 2861 N95-30942 #
CONF-941013-32 ..... p 2861 N95-30943 #
CONF-941013-33 ..... p 2865 N95-32100 #
CONF-941013-34 ..... p 3011 N95-30667 #
CONF-941013-35 ..... p 2881 N95-32047 #
CONF-9410156-4 ..... p 2900 N95-30472 #
CONF-9410184-7 ..... p 2810 N95-32283 #
CONF-9410192-2 ..... p 3016 N95-32268 #
CONF-9410246 ..... p 3000 N95-31635 #
CONF-9410254-5 ..... p 2955 N95-30471 #
CONF-9410327-1 ..... p 2908 N95-30793 #
CONF-9410330-1 ..... p 2875 N95-31637 #
CONF-9410335 ..... p 2952 N95-31255 #
CONF-941039-5 ..... p 3016 N95-32284 #
CONF-941101-10 ..... p 2994 N95-32074 #
CONF-941101-5 ..... p 3003 N95-30359 #
CONF-941101-7 ..... p 3004 N95-30685 #
CONF-941101-9 ..... p 3007 N95-32116 #
CONF-9411104-3 ..... p 2936 N95-31056 #
CONF-9411173-6 ..... p 2878 N95-30378
CONF-9411174-1 ..... p 2902 N95-30526 #
CONF-9411178-2 ..... p 2913 N95-30683 #
CONF-9411210-1 ..... p 2992 N95-30800 #
CONF-9411210-2 ..... p 2994 N95-32059 #
CONF-9411210-3 ..... p 2988 N95-32063 #
CONF-9411210-4 ..... p 2989 N95-32160 #
CONF-9411214-SUMM ..... p 2911 N95-32156 #
CONF-941129-21 ..... p 2978 N95-30573
CONF-941129-23 ..... p 2984 N95-31402 #
CONF-941144-100 ..... p 2813 N95-30572 #
CONF-941144-102 ..... p 3010 N95-30544 #
CONF-941144-103 ..... p 2812 N95-30545 #
CONF-941144-104 ..... p 2784 N95-30731 #
CONF-941144-105 ..... p 2804 N95-30797 #
CONF-941144-106 ..... p 2818 N95-31175 #
CONF-941144-108 ..... p 2814 N95-30730 #
CONF-941144-110 ..... p 3009 N95-30542 #
CONF-941144-111 ..... p 2803 N95-30575 #
CONF-941144-113 ..... p 3010 N95-30576 #
CONF-941144-115 ..... p 2812 N95-30543 #
CONF-941144-116 ..... p 2815 N95-30799 #
CONF-941144-117 ..... p 2803 N95-30733 #
CONF-941144-118 ..... p 2899 N95-32317 #
CONF-941144-119 ..... p 3016 N95-32301 #
CONF-941144-120 ..... p 2798 N95-32091 #
CONF-941144-126 ..... p 2806 N95-31188 #
CONF-941144-127 ..... p 2818 N95-31187 #
CONF-941144-128 ..... p 2805 N95-31111 #
CONF-941144-129 ..... p 2982 N95-31104 #
CONF-941144-130 ..... p 2805 N95-31105 #
CONF-941144-131 ..... p 2805 N95-31106 #
CONF-941144-132 ..... p 2805 N95-31107 #
CONF-941144-133 ..... p 2822 N95-32043 #
CONF-941144-134 ..... p 2809 N95-32104 #
CONF-941144-135 ..... p 3016 N95-32103 #
CONF-941144-136 ..... p 3016 N95-32105 #
CONF-941144-137 ..... p 2788 N95-31403 #
CONF-941144-138 ..... p 2808 N95-31643 #
CONF-941144-139 ..... p 2985 N95-31642 #
CONF-941144-140 ..... p 2897 N95-32024 #
CONF-941144-141 ..... p 3015 N95-31641 #
CONF-941144-143 ..... p 2885 N95-31394 #
CONF-941144-144 ..... p 2794 N95-31393 #
CONF-941144-145 ..... p 2808 N95-31689 #
CONF-941144-94 ..... p 2803 N95-30547 #
CONF-941144-98 ..... p 2978 N95-30546 #
CONF-941144-99 ..... p 2812 N95-30548 #
CONF-941162-3 ..... p 3003 N95-30641 #
CONF-941210-12 ..... p 2858 N95-30374 #
CONF-941210-13 ..... p 2902 N95-30375 #
CONF-941242 ..... p 2807 N95-31615 #
CONF-941255-3 ..... p 2837 N95-32355 #
CONF-941267-1 ..... p 2822 N95-32161 #
CONF-950117-3 ..... p 3008 N95-30381 #
CONF-950117-4 ..... p 3014 N95-31233 #
CONF-950127-2 ..... p 3008 N95-32357 #
CONF-950129-3 ..... p 2796 N95-31633 #
CONF-950129-4 ..... p 2814 N95-30732 #
CONF-950129-5 ..... p 2790 N95-32060 * #
CONF-950129-6 ..... p 2822 N95-32085 #
CONF-950153-3 ..... p 2917 N95-32080 #
CONF-950158-2 ..... p 2792 N95-30735 #
CONF-950183-1 ..... p 2967 N95-32026 #
CONF-950201-10 ..... p 2809 N95-32051 #
CONF-950201-11 ..... p 2810 N95-32272 #
CONF-950201-12 ..... p 3015 N95-32062 #
CONF-950201-13 ..... p 2809 N95-32052 #
CONF-950201-9 ..... p 2805 N95-31121 #
CONF-950216-115 ..... p 2797 N95-32061 #
CONF-950226-20 ..... p 2884 N95-31139 #
CONF-950226-26 ..... p 2882 N95-30380 #
CONF-950226-27 ..... p 2883 N95-30390 #
CONF-950226-28 ..... p 3008 N95-30391 #
CONF-950226-29 ..... p 3008 N95-30382 #
CONF-950226-31 ..... p 2860 N95-30707 #
CONF-950226-33 ..... p 3026 N95-32149 #
CONF-950226-36 ..... p 2798 N95-32086 #
CONF-950228-4 ..... p 2878 N95-30384 #
CONF-950228-5 ..... p 2839 N95-32082 #
CONF-950242-2 ..... p 2936 N95-31109 #
CONF-950283-1 ..... p 2866 N95-30464 #
CONF-950283-2 ..... p 2866 N95-30383 #
CONF-950285-1 ..... p 2990 N95-32303 #
CONF-950286-1 ..... p 2932 N95-31704 #
CONF-950287-1 ..... p 2989 N95-32162 #
CONF-950287-2 ..... p 2981 N95-30970 #
CONF-950309-5 ..... p 2921 N95-31726 #
CONF-9503109-2 ..... p 3027 N95-30385 #
CONF-9503112-2 ..... p 2934 N95-30796 #
CONF-9503115-1 ..... p 2811 N95-30362 #
CONF-9503121-1 ..... p 2947 N95-30577 #
CONF-9503122-1 ..... p 2934 N95-30603 #
CONF-9503123-1 ..... p 2836 N95-32048 #
CONF-9503124-1 ..... p 3014 N95-31231 #
CONF-9503125-1 ..... p 2980 N95-30708 #
CONF-9503127-1 ..... p 2803 N95-30706 #
CONF-9503127-2 ..... p 3007 N95-32148 #
CONF-9503129-1 ..... p 2948 N95-32065 #
CONF-950336-19 ..... p 2903 N95-30887 #
CONF-950356-1 ..... p 3010 N95-30571 #
CONF-950381-1 ..... p 2877 N95-32049 #
CONF-950389-1 ..... p 2798 N95-32318 #
CONF-950389-2-VUGRAPHS ..... p 2798 N95-32360 #
CONF-950401-1 ..... p 2821 N95-31705 #
CONF-950401-2 ..... p 2817 N95-31152 #
CONF-950412-3 ..... p 2806 N95-31150 #
CONF-950412-4 ..... p 2818 N95-31377 #
CONF-950412-8 ..... p 3014 N95-31112 #
CONF-9504126-1 ..... p 2925 N95-32358 #
CONF-9504132-1 ..... p 2854 N95-32050 #
CONF-9504132-2 ..... p 3008 N95-32351 #
CONF-9504132-3 ..... p 2992 N95-31232 #
CONF-9504135-2 ..... p 2793 N95-31113 #
CONF-9504139-1 ..... p 3026 N95-32144 #
CONF-9504139-2 ..... p 2948 N95-32146 #
CONF-9504139-3 ..... p 2948 N95-31605 #
CONF-9504140-1 ..... p 3001 N95-32064 #
CONF-9504142-1 ..... p 2806 N95-31406 #
CONF-950431-1 ..... p 2877 N95-32033 #
CONF-950431-2 ..... p 2931 N95-31130 #
CONF-950432-2 ..... p 2863 N95-31611 #
CONF-950450-4 ..... p 2900 N95-30363 #
CONF-950472-2 ..... p 2882 N95-30379 #
CONF-950472-4 ..... p 2933 N95-30602 #
CONF-950472-6 ..... p 2854 N95-32145 #
CONF-950494 ..... p 2887 N95-32280 #
CONF-950512-12 ..... p 2987 N95-32031 #
CONF-950512-14 ..... p 2987 N95-32032 #
CONF-950512-21 ..... p 2995 N95-32260 #
CONF-950512-26 ..... p 2992 N95-31151 #
CONF-950512-30 ..... p 2993 N95-31256 #
CONF-950512-40 ..... p 2994 N95-32092 #
CONF-950512-41 ..... p 2990 N95-32278 #
CONF-950512-42 ..... p 2995 N95-32306 #
CONF-950512-59 ..... p 2994 N95-32242 #
CONF-950512-60 ..... p 2994 N95-32243 #
CONF-950512-61 ..... p 2994 N95-32244 #
CONF-950512-62 ..... p 2995 N95-32297 #
CONF-950512-9 ..... p 2993 N95-31405 #
CONF-9505145-2 ..... p 2941 N95-31631 #
CONF-950518-3 ..... p 3016 N95-32147 #
CONF-950518-4 ..... p 2822 N95-32101 #
CONF-9505193-1 ..... p 2949 N95-30377 #
CONF-9505193-3 ..... p 2950 N95-30463 #
CONF-9505193-4 ..... p 2942 N95-31644 #
CONF-9505195-3 ..... p 2960 N95-31253 #
CONF-950537-2 ..... p 2816 N95-31058 #
CONF-950550-2 ..... p 2897 N95-31614 #
CONF-950582-1 ..... p 2767 N95-32081 #
CONF-9506126-2 ..... p 2741 N95-32164 #
CONF-9506145-2 ..... p 2902 N95-30505 #
CONF-9506149-1 ..... p 2811 N95-30389 #
CONF-9506149-2 ..... p 2932 N95-30376 #
CONF-9506170-1 ..... p 2980 N95-30705 #
CONF-9506173-1 ..... p 2928 N95-32097 #
CONF-9506174-1 ..... p 2886 N95-32143 #
CONF-950629-2 ..... p 2792 N95-30762 #
CONF-950629-5 ..... p 2821 N95-32025 #
CONF-950629-6 ..... p 2894 N95-31131 #
CONF-950634-2 ..... p 2872 N95-31132 #
CONF-950646-17 ..... p 2911 N95-32281 #
CONF-950646-1 ..... p 2909 N95-31703 #
CONF-950653-1 ..... p 2952 N95-31161 #
CONF-950655-6 ..... p 2898 N95-32102 #
CONF-950706-10 ..... p 2990 N95-32274 #
CONF-950706-2 ..... p 2990 N95-32273 #
CONF-950706-6 ..... p 2990 N95-32271 #
CONF-950706-7 ..... p 2989 N95-32120 #
CONF-950706-8 ..... p 2990 N95-32275 #
CONF-9507100-1 ..... p 2808 N95-31636 #
CONF-9507120-2 ..... p 2911 N95-32276 #
CONF-950720-1 ..... p 2797 N95-31824 #
CONF-950737-1 ..... p 2797 N95-31840 #
CONF-950740-14 ..... p 3025 N95-31662 #
CONF-950740-16 ..... p 2898 N95-32157 #
CONF-950740-18 ..... p 2807 N95-31632 #
CONF-950740-19 ..... p 2808 N95-31825 #
CONF-950788-2 ..... p 2967 N95-31625 #
CONF-9508113-1 ..... p 2948 N95-32277 #

CPIA-PUBL-620 ..... p 2829 N95-31282
CPIA-PUBL-621-VOL-1 ..... p 2870 N95-30986

CU-CAS-94-08 ..... p 2944 N95-32203 * #

CU-CSSC-90-07 ..... p 2899 N95-32202 * #
CU-CSSC-90-08 ..... p 2897 N95-31730 * #
CU-CSSC-90-17 ..... p 2767 N95-32204 * #
CU-CSSC-91-15 ..... p 2944 N95-32190 * #
CU-CSSC-91-25 ..... p 2945 N95-32215 * #
CU-CSSC-92-15 ..... p 2945 N95-32214 * #

C950028 ..... p 2952 N95-31266 #

DE94-000240 ..... p 2906 N95-32058 #
DE94-006864 ..... p 2910 N95-31821 #
DE94-006866 ..... p 2905 N95-31822 #
DE94-011871 ..... p 2905 N95-31661 #
DE95-000047 ..... p 2881 N95-31694 #
DE95-000063 ..... p 3026 N95-31823 #
DE95-000088 ..... p 2890 N95-32163 #
DE95-000211 ..... p 2903 N95-30896 #
DE95-000260 ..... p 2902 N95-30526 #
DE95-000263 ..... p 2903 N95-30887 #
DE95-000285 ..... p 2909 N95-31695 #
DE95-000943 ..... p 2952 N95-31161 #
DE95-002056 ..... p 2797 N95-31840 #
DE95-003107 ..... p 2991 N95-30527
DE95-004049 ..... p 2902 N95-30505 #
DE95-004063 ..... p 2905 N95-31381 #
DE95-004066 ..... p 2904 N95-31162 #
DE95-004067 ..... p 2904 N95-31163 #
DE95-004068 ..... p 2904 N95-31164 #
DE95-004088 ..... p 2810 N95-32154 #
DE95-004089 ..... p 2906 N95-32057 #
DE95-004119 ..... p 2985 N95-31616 #
DE95-004378 ..... p 2986 N95-31702 #
DE95-004382 ..... p 2797 N95-31824 #
DE95-004984 ..... p 2887 N95-32155 #
DE95-005836 ..... p 2880 N95-30941 #
DE95-005838 ..... p 2861 N95-30942 #
DE95-005843 ..... p 2861 N95-30943 #
DE95-006161 ..... p 2909 N95-31703 #
DE95-006694 ..... p 2992 N95-31165 #
DE95-007298 ..... p 2992 N95-31166 #
DE95-007746 ..... p 2884 N95-31139 #
DE95-007862 ..... p 2805 N95-31121 #
DE95-007959 ..... p 2932 N95-31704 #
DE95-008077 ..... p 2936 N95-31056 #
DE95-008300 ..... p 2911 N95-32156 #
DE95-008333 ..... p 2907 N95-30358
DE95-008336 ..... p 2816 N95-31057 #
DE95-008377 ..... p 2912 N95-30373 #
DE95-008387 ..... p 3003 N95-30359 #
DE95-008388 ..... p 3008 N95-31624 #
DE95-008404 ..... p 2858 N95-30374 #
DE95-008405 ..... p 2902 N95-30375 #
DE95-008434 ..... p 2816 N95-31058 #
DE95-008437 ..... p 2932 N95-30376 #
DE95-008440 ..... p 2949 N95-30377 #
DE95-008443 ..... p 2991 N95-30360
DE95-008446 ..... p 3028 N95-30361 #
DE95-008447 ..... p 2878 N95-30378
DE95-008448 ..... p 2975 N95-30388 #
DE95-008450 ..... p 2861 N95-31059 #
DE95-008503 ..... p 2967 N95-31625 #
DE95-008506 ..... p 2811 N95-30389 #

DE95-006517 ..... p 3006 N95-31626 #
DE95-006525 ..... p 2882 N95-30379 #
DE95-006526 ..... p 2882 N95-30380 #
DE95-006527 ..... p 3008 N95-30381 #
DE95-006534 ..... p 2883 N95-30390 #
DE95-006535 ..... p 3008 N95-30391 #
DE95-006536 ..... p 3006 N95-30382 #
DE95-006537 ..... p 2866 N95-30383 #
DE95-006540 ..... p 2878 N95-30384 #
DE95-006542 ..... p 3027 N95-30385 #
DE95-006543 ..... p 2811 N95-30362 #
DE95-006546 ..... p 2900 N95-30363 #
DE95-006549 ..... p 2950 N95-30463 #
DE95-006628 ..... p 2993 N95-31627 #
DE95-006677 ..... p 2908 N95-30793 #
DE95-006692 ..... p 3022 N95-30392 #
DE95-006714 ..... p 2948 N95-31605 #
DE95-006715 ..... p 2866 N95-30464 #
DE95-006737 ..... p 2977 N95-30465 #
DE95-006748 ..... p 3004 N95-30794 #
DE95-006750 ..... p 3004 N95-30795 #
DE95-006796 ..... p 2955 N95-30470 #
DE95-006808 ..... p 2955 N95-30471 #
DE95-006810 ..... p 2900 N95-30472 #
DE95-006813 ..... p 2792 N95-30714 #
DE95-006815 ..... p 2934 N95-30796 #
DE95-006821 ..... p 3025 N95-31662 #
DE95-006823 ..... p 2916 N95-31610 #
DE95-006824 ..... p 2863 N95-31611 #
DE95-006827 ..... p 2982 N95-31174 #
DE95-006829 ..... p 2879 N95-30507 #
DE95-006839 ..... p 2818 N95-31175 #
DE95-006842 ..... p 3009 N95-30542 #
DE95-006843 ..... p 2812 N95-30543 #
DE95-006847 ..... p 3010 N95-30544 #
DE95-006898 ..... p 2812 N95-30545 #
DE95-006900 ..... p 2978 N95-30546 #
DE95-006901 ..... p 2804 N95-30797 #
DE95-006903 ..... p 2803 N95-30547 #
DE95-006905 ..... p 2812 N95-30548 #
DE95-006906 ..... p 2813 N95-30572 #
DE95-006938 ..... p 2978 N95-30573
DE95-006945 ..... p 2792 N95-30762 #
DE95-006952 ..... p 2868 N95-30763 #
DE95-006956 ..... p 2814 N95-30765 #
DE95-006957 ..... p 2815 N95-30798 #
DE95-006991 ..... p 2978 N95-30574
DE95-009029 ..... p 2803 N95-30575 #
DE95-009031 ..... p 3010 N95-30576 #
DE95-009033 ..... p 2808 N95-31825 #
DE95-009034 ..... p 2898 N95-32157 #
DE95-009073 ..... p 2815 N95-30799 #
DE95-009076 ..... p 2947 N95-30577 #
DE95-009082 ..... p 2853 N95-31628 #
DE95-009084 ..... p 2907 N95-32302 #
DE95-009089 ..... p 2820 N95-31629 #
DE95-009103 ..... p 2865 N95-32077 #
DE95-009106 ..... p 2990 N95-32303 #
DE95-009107 ..... p 2992 N95-30800 #
DE95-009115 ..... p 3005 N95-30801 #
DE95-009116 ..... p 3029 N95-30729 #
DE95-009123 ..... p 2941 N95-31631 #
DE95-009124 ..... p 2913 N95-30683 #
DE95-009125 ..... p 2814 N95-30730 #
DE95-009130 ..... p 2838 N95-30684 #
DE95-009131 ..... p 2784 N95-30731 #
DE95-009134 ..... p 3004 N95-30685 #
DE95-009135 ..... p 2807 N95-31632 #
DE95-009137 ..... p 2909 N95-31612 #
DE95-009172 ..... p 2796 N95-31633 #
DE95-009173 ..... p 3016 N95-32301 #
DE95-009177 ..... p 2814 N95-30732 #
DE95-009178 ..... p 2899 N95-32317 #
DE95-009179 ..... p 2803 N95-30733 #
DE95-009185 ..... p 2942 N95-31634 #
DE95-009198 ..... p 2814 N95-30738 #
DE95-009200 ..... p 2903 N95-30745 #
DE95-009202 ..... p 2921 N95-31726 #
DE95-009323 ..... p 2908 N95-30686
DE95-009332 ..... p 2894 N95-31054 #
DE95-009373 ..... p 3000 N95-31635 #
DE95-009380 ..... p 2885 N95-31230
DE95-009384 ..... p 2947 N95-30578 #
DE95-009417 ..... p 2792 N95-30735 #
DE95-009418 ..... p 3014 N95-31231 #
DE95-009419 ..... p 3010 N95-30571 #
DE95-009426 ..... p 2808 N95-31636 #
DE95-009429 ..... p 2933 N95-30602 #
DE95-009431 ..... p 3006 N95-31613 #
DE95-009435 ..... p 2934 N95-30603 #
DE95-009437 ..... p 2836 N95-32048 #
DE95-009441 ..... p 2798 N95-32318 #
DE95-009442 ..... p 2875 N95-31637 #
DE95-009464 ..... p 2875 N95-31591 #
DE95-009467 ..... p 2875 N95-31592 #
DE95-009474 ..... p 2911 N95-32350 #
DE95-009475 ..... p 2795 N95-31593 #
DE95-009477 ..... p 2877 N95-32049 #
DE95-009486 ..... p 2854 N95-32050 #
DE95-009489 ..... p 3008 N95-32351 #
DE95-009495 ..... p 2980 N95-30705 #
DE95-009497 ..... p 2837 N95-32355 #
DE95-009510 ..... p 2823 N95-32352 #
DE95-009524 ..... p 3002 N95-32356 #
DE95-009531 ..... p 2810 N95-32272 #
DE95-009533 ..... p 2809 N95-32051 #
DE95-009536 ..... p 3004 N95-30742 #
DE95-009543 ..... p 3008 N95-32357 #
DE95-009546 ..... p 2994 N95-32059 #
DE95-009551 ..... p 2803 N95-30706 #
DE95-009552 ..... p 2988 N95-32079 #
DE95-009554 ..... p 2988 N95-32063 #
DE95-009572 ..... p 2809 N95-32052 #
DE95-009573 ..... p 2925 N95-32358 #
DE95-009575 ..... p 2928 N95-32097 #
DE95-009577 ..... p 2897 N95-31614 #
DE95-009579 ..... p 2860 N95-30707 #
DE95-009580 ..... p 2917 N95-32080 #
DE95-009581 ..... p 2767 N95-32081 #
DE95-009582 ..... p 2839 N95-32082 #
DE95-009583 ..... p 3001 N95-32064 #
DE95-009586 ..... p 2980 N95-30708 #
DE95-009607 ..... p 3007 N95-32116 #
DE95-009608 ..... p 3003 N95-30612 #
DE95-009609 ..... p 3003 N95-30641 #
DE95-009629 ..... p 2807 N95-31615 #
DE95-009631 ..... p 2792 N95-30709 #
DE95-009643 ..... p 2809 N95-32098 #
DE95-009647 ..... p 2917 N95-32142 #
DE95-009659 ..... p 2910 N95-32099 #
DE95-009660 ..... p 2908 N95-30755
DE95-009666 ..... p 2865 N95-32100 #
DE95-009689 ..... p 2941 N95-31630 #
DE95-009694 ..... p 3015 N95-31641 #
DE95-009699 ..... p 2985 N95-31642 #
DE95-009810 ..... p 2877 N95-32033 #
DE95-009813 ..... p 2808 N95-31643 #
DE95-009825 ..... p 2879 N95-30687
DE95-009837 ..... p 2886 N95-32143 #
DE95-009838 ..... p 2942 N95-31644 #
DE95-009839 ..... p 3026 N95-32144 #
DE95-009840 ..... p 2854 N95-32145 #
DE95-009861 ..... p 2822 N95-32101 #
DE95-009862 ..... p 2948 N95-32146 #
DE95-009863 ..... p 3016 N95-32147 #
DE95-009868 ..... p 2948 N95-32065 #
DE95-009869 ..... p 3007 N95-32148 #
DE95-009874 ..... p 2898 N95-32102 #
DE95-009879 ..... p 2932 N95-31645 #
DE95-009885 ..... p 3026 N95-32149 #
DE95-009892 ..... p 3016 N95-32103 #
DE95-009893 ..... p 2809 N95-32104 #
DE95-009896 ..... p 3016 N95-32105 #
DE95-009903 ..... p 2790 N95-32060 * #
DE95-009913 ..... p 2797 N95-32061 #
DE95-009914 ..... p 3015 N95-32062 #
DE95-009921 ..... p 3029 N95-31102 #
DE95-009922 ..... p 3020 N95-32106 #
DE95-009951 ..... p 2908 N95-30802
DE95-010000 ..... p 2816 N95-31103 #
DE95-010046 ..... p 3026 N95-32107 #
DE95-010099 ..... p 2988 N95-32083 #
DE95-010108 ..... p 2798 N95-32091 #
DE95-010116 ..... p 2982 N95-31104 #
DE95-010117 ..... p 2805 N95-31105 #
DE95-010120 ..... p 2805 N95-31106 #
DE95-010121 ..... p 2805 N95-31107 #
DE95-010127 ..... p 2809 N95-32023 #
DE95-010131 ..... p 2817 N95-31108 #
DE95-010132 ..... p 2897 N95-32024 #
DE95-010154 ..... p 2792 N95-30614 #
DE95-010155 ..... p 2991 N95-30615 #
DE95-010156 ..... p 2978 N95-30616 #
DE95-010159 ..... p 3031 N95-30618 #
DE95-010164 ..... p 3023 N95-30619 #
DE95-010170 ..... p 2907 N95-32288 #
DE95-010173 ..... p 3023 N95-30620 #
DE95-010177 ..... p 2793 N95-30766 #
DE95-010185 ..... p 2814 N95-30767 #
DE95-010207 ..... p 3004 N95-30769 #
DE95-010213 ..... p 2936 N95-31109 #
DE95-010220 ..... p 2821 N95-32025 #
DE95-010223 ..... p 2805 N95-31111 #
DE95-010224 ..... p 2818 N95-31187 #
DE95-010225 ..... p 2806 N95-31188 #
DE95-010232 ..... p 2865 N95-32084 #
DE95-010233 ..... p 3015 N95-32037 #
DE95-010234 ..... p 2815 N95-30897 #
DE95-010237 ..... p 3011 N95-30667 #
DE95-010242 ..... p 2966 N95-30668 #
DE95-010243 ..... p 3012 N95-30756 #
DE95-010244 ..... p 2804 N95-30757 #
DE95-010251 ..... p 2987 N95-32038 #
DE95-010252 ..... p 2987 N95-32039 #
DE95-010253 ..... p 2881 N95-32047 #
DE95-010262 ..... p 2992 N95-31127 #
DE95-010264 ..... p 2987 N95-32041 #
DE95-010265 ..... p 2993 N95-32042 #
DE95-010268 ..... p 3026 N95-31129 #
DE95-010278 ..... p 2822 N95-32043 #
DE95-010282 ..... p 2622 N95-32085 #
DE95-010283 ..... p 2798 N95-32086 #
DE95-010288 ..... p 2931 N95-31130 #
DE95-010289 ..... p 2894 N95-31131 #
DE95-010293 ..... p 2872 N95-31132 #
DE95-010298 ..... p 2984 N95-31402 #
DE95-010302 ..... p 2836 N95-31638 #
DE95-010304 ..... p 2836 N95-31639 #
DE95-010306 ..... p 2768 N95-30674 #
DE95-010326 ..... p 2944 N95-32087 #
DE95-010327 ..... p 2944 N95-32088 #
DE95-010328 ..... p 2943 N95-32044 #
DE95-010329 ..... p 2944 N95-32089 #
DE95-010338 ..... p 2905 N95-31640 #
DE95-010340 ..... p 3000 N95-31681 #
DE95-010341 ..... p 2854 N95-32045 #
DE95-010344 ..... p 2906 N95-32090 #
DE95-010353 ..... p 2986 N95-31682 #
DE95-010359 ..... p 2788 N95-31403 #
DE95-010376 ..... p 2837 N9E-32158 #
DE95-010405 ..... p 2925 N95-32040 #
DE95-010411 ..... p 2940 N95-31404 #
DE95-010436 ..... p 2882 N95-32159 #
DE95-010438 ..... p 2989 N95-32160 #
DE95-010442 ..... p 2993 N95-31405 #
DE95-010453 ..... p 2822 N95-32161 #
DE95-010457 ..... p 2989 N95-32162 #
DE95-010514 ..... p 2806 N95-31406 #
DE95-010542 ..... p 2823 N95-32305 #
DE95-010561 ..... p 2994 N95-32074 #
DE95-010602 ..... p 2822 N95-32075 #
DE95-010608 ..... p 2810 N95-32265 #
DE95-010661 ..... p 2962 N95-32076 #
DE95-010666 ..... p 2989 N95-32266 #
DE95-010667 ..... p 2989 N95-32267 #
DE95-010686 ..... p 3016 N95-32268 #
DE95-010694 ..... p 2987 N95-32026 #
DE95-010726 ..... p 3030 N95-32269 #
DE95-010728 ..... p 2945 N95-32270 #
DE95-010729 ..... p 2901 N95-32027 #
DE95-010734 ..... p 3006 N95-32028 #
DE95-010735 ..... p 2886 N95-32029 #
DE95-010794 ..... p 2861 N95-31133 #
DE95-010803 ..... p 2990 N95-32271 #
DE95-010805 ..... p 2817 N95-31135 #
DE95-010806 ..... p 2817 N95-31136 #
DE95-010811 ..... p 2943 N95-32030 #
DE95-010815 ..... p 2990 N95-32273 #
DE95-010823 ..... p 2990 N95-32274 #
DE95-010825 ..... p 2990 N95-32275 #
DE95-010842 ..... p 2995 N95-32260 #
DE95-010843 ..... p 2987 N95-32031 #
DE95-010845 ..... p 2987 N95-32032 #
DE95-010859 ..... p 2808 N95-31689 #
DE95-010860 ..... p 2794 N95-31393 #
DE95-010861 ..... p 2885 N95-31394 #
DE95-010862 ..... p 2818 N95-31377 #
DE95-010863 ..... p 2911 N95-32276 #
DE95-010868 ..... p 2992 N95-31232 #
DE95-010873 ..... p 3014 N95-31233 #
DE95-010876 ..... p 2948 N95-32277 #
DE95-010886 ..... p 2960 N95-31253 #
DE95-010889 ..... p 2806 N95-31150 #
DE95-010894 ..... p 2990 N95-32278 #
DE95-010895 ..... p 2994 N95-32092 #
DE95-010897 ..... p 2995 N95-32306 #
DE95-010913 ..... p 2989 N95-32120 #
DE95-010933 ..... p 3017 N95-32307 #
DE95-010935 ..... p 3017 N95-32308 #
DE95-010937 ..... p 2810 N95-32241 #
DE95-010989 ..... p 2992 N95-31151 #
DE95-010991 ..... p 2821 N95-31705 #
DE95-010992 ..... p 2817 N95-31152 #
DE95-010995 ..... p 2818 N95-31153 #
DE95-010997 ..... p 2878 N95-32309 #
DE95-011001 ..... p 3007 N95-32310 #
DE95-011014 ..... p 2981 N95-30970 #
DE95-011020 ..... p 3014 N95-31112 #
DE95-011058 ..... p 2793 N95-31113 #
DE95-011405 ..... p 3032 N95-32279 #
DE95-011407 ..... p 2887 N95-32280 #
DE95-011445 ..... p 2911 N95-32281 #
DE95-011453 ..... p 2908 N95-31114 #
DE95-011454 ..... p 2894 N95-31254 #
DE95-011513 ..... p 3032 N95-32282 #
DE95-011531 ..... p 2741 N95-32164 #
DE95-011533 ..... p 2810 N95-32283 #
DE95-011534 ..... p 3016 N95-32284 #

DE95-011554 ..... p 3026 N95-32285 #
DE95-011563 ..... p 2994 N95-32242 #
DE95-011564 ..... p 2994 N95-32243 #
DE95-011565 ..... p 2994 N95-32244 #
DE95-011566 ..... p 2995 N95-32297 #
DE95-011578 ..... p 2823 N95-32296 #
DE95-011593 ..... p 3007 N95-32299 #
DE95-011656 ..... p 2865 N95-32300 #
DE95-011702 ..... p 2952 N95-31255 #
DE95-011732 ..... p 3021 N95-32359 #
DE95-011797 ..... p 2798 N95-32360 #
DE95-011857 ..... p 2823 N95-32361 #
DE95-011941 ..... p 3027 N95-32362 #
DE95-012101 ..... p 2993 N95-31256 #
DE95-012152 ..... p 2911 N95-32364 #
DE95-012169 ..... p 2991 N95-32365 #
DE95-012368 ..... p 3017 N95-32366 #
DE95-060104 ..... p 2890 N95-32367 #
DE95-611717 ..... p 2768 N95-30881 #
DE95-612416 ..... p 2913 N95-30675 #
DE95-613006 ..... p 2991 N95-30604 #
DE95-613311 ..... p 3024 N95-30882 #
DE95-613355 ..... p 3024 N95-30883 #
DE95-613356 ..... p 2930 N95-31267 #
DE95-613366 ..... p 2846 N95-30605 #
DE95-613367 ..... p 3029 N95-30606 #
DE95-613368 ..... p 3019 N95-30972 #
DE95-613369 ..... p 3017 N95-30364 #
DE95-613370 ..... p 3020 N95-32150 #
DE95-613371 ..... p 2962 N95-32117 #
DE95-613372 ..... p 3020 N95-32094 #
DE95-613374 ..... p 2962 N95-32095 #
DE95-613377 ..... p 2958 N95-30770 #
DE95-613378 ..... p 2958 N95-30803 #
DE95-613379 ..... p 2957 N95-30676 #
DE95-613380 ..... p 2956 N95-30607 #
DE95-613381 ..... p 2958 N95-30820 #
DE95-613382 ..... p 2956 N95-30608 #
DE95-613383 ..... p 2958 N95-30821 #
DE95-613384 ..... p 3017 N95-30365 #
DE95-613385 ..... p 2961 N95-31619 #
DE95-613441 ..... p 2966 N95-32066 #
DE95-613442 ..... p 2962 N95-32067 #
DE95-613443 ..... p 2883 N95-30809 #
DE95-613444 ..... p 2963 N95-30610 #
DE95-613445 ..... p 3011 N95-30736 #
DE95-613447 ..... p 3011 N95-30737 #
DE95-613448 ..... p 2967 N95-30739 #
DE95-613459 ..... p 2962 N95-32068 #
DE95-613460 ..... p 2980 N95-30740 #
DE95-613461 ..... p 3028 N95-30366 #
DE95-613462 ..... p 2975 N95-30367 #
DE95-613463 ..... p 2845 N95-30368 #
DE95-613467 ..... p 3019 N95-30741 #
DE95-613469 ..... p 2957 N95-30642 #
DE95-613470 ..... p 3019 N95-30771 #
DE95-613471 ..... p 2964 N95-30369 #
DE95-613560 ..... p 2968 N95-32069 #
DE95-613584 ..... p 2966 N95-30635 #
DE95-613585 ..... p 3018 N95-30636 #
DE95-613589 ..... p 2979 N95-30637 #
DE95-613590 ..... p 2985 N95-31620 #
DE95-613595 ..... p 2988 N95-32070 #
DE95-613596 ..... p 2984 N95-31546 #
DE95-613597 ..... p 2845 N95-30370 #
DE95-613627 ..... p 3017 N95-30371 #
DE95-613628 ..... p 2985 N95-31621 #
DE95-613629 ..... p 2988 N95-32076 #
DE95-613654 ..... p 2991 N95-32353 #
DE95-613668 ..... p 2984 N95-31547 #
DE95-613669 ..... p 2985 N95-31622 #
DE95-613690 ..... p 2988 N95-32093 #
DE95-613726 ..... p 2991 N95-32304 #
DE95-613727 ..... p 2975 N95-30372 #
DE95-613760 ..... p 2978 N95-30526 #
DE95-613765 ..... p 2984 N95-31548 #
DE95-613766 ..... p 2977 N95-30506 #
DE95-613771 ..... p 2989 N95-32096 #
DE95-613774 ..... p 2984 N95-31549 #
DE95-613782 ..... p 2980 N95-30911 #
DE95-613783 ..... p 2961 N95-30912 #
DE95-613798 ..... p 2982 N95-31060 #
DE95-613844 ..... p 2989 N95-32151 #
DE95-614022 ..... p 2981 N95-30913 #
DE95-614107 ..... p 2981 N95-31003 #
DE95-614120 ..... p 2991 N95-32354 #
DE95-614171 ..... p 2984 N95-31550 #
DE95-614172 ..... p 3006 N95-31679 #
DE95-614177 ..... p 3006 N95-31680 #
DE95-614178 ..... p 2967 N95-32053 #
DE95-614179 ..... p 3006 N95-32054 #
DE95-614180 ..... p 3005 N95-31004 #
DE95-614187 ..... p 2967 N95-32055 #
DE95-614201 ..... p 3007 N95-32056 #
DE95-614252 ..... p 2884 N95-30914 #
DE95-614256 ..... p 3005 N95-31366 #
DE95-614308 ..... p 3010 N95-30644 #
DE95-614309 ..... p 2813 N95-30645 #
DE95-614310 ..... p 3010 N95-30647 #
DE95-614311 ..... p 3011 N95-30722 #
DE95-614351 ..... p 2981 N95-30915 #
DE95-614370 ..... p 2903 N95-30723 #
DE95-614371 ..... p 2880 N95-31167 #
DE95-614372 ..... p 3009 N95-30419 #
DE95-614444 ..... p 3016 N95-32071 #
DE95-614445 ..... p 2982 N95-31168 #
DE95-614446 ..... p 3019 N95-31186 #
DE95-614447 ..... p 3012 N95-30958 #
DE95-614448 ..... p 3010 N95-30648 #
DE95-614449 ..... p 3013 N95-30959 #
DE95-614468 ..... p 2859 N95-30649 #
DE95-614469 ..... p 3010 N95-30650 #
DE95-614482 ..... p 2979 N95-30652 #
DE95-614483 ..... p 3010 N95-30653 #
DE95-614629 ..... p 2791 N95-30420 #
DE95-615230 ..... p 3009 N95-30421 #
DE95-615231 ..... p 2811 N95-30450 #
DE95-615232 ..... p 2811 N95-30422 #
DE95-615349 ..... p 2812 N95-30451 #
DE95-615391 ..... p 2820 N95-31623 #
DE95-616243 ..... p 2957 N95-30688 #
DE95-616244 ..... p 2979 N95-30689 #
DE95-616267 ..... p 2976 N95-30423 #
DE95-616271 ..... p 3018 N95-30424 #
DE95-616272 ..... p 2954 N95-30425 #
DE95-616276 ..... p 3018 N95-30426 #
DE95-616277 ..... p 2976 N95-30427 #
DE95-616278 ..... p 2964 N95-30428 #
DE95-616279 ..... p 2976 N95-30429 #
DE95-616280 ..... p 2965 N95-30430 #
DE95-616281 ..... p 3018 N95-30431 #
DE95-616282 ..... p 2965 N95-30432 #
DE95-616283 ..... p 2965 N95-30435 #
DE95-616284 ..... p 3018 N95-30436 #
DE95-616285 ..... p 3018 N95-30437 #
DE95-616286 ..... p 3018 N95-30438 #
DE95-616287 ..... p 2965 N95-30439 #
DE95-616288 ..... p 3018 N95-30440 #
DE95-616302 ..... p 2976 N95-30441 #
DE95-616315 ..... p 2976 N95-30442 #
DE95-616316 ..... p 2976 N95-30443 #
DE95-616332 ..... p 3018 N95-30444 #
DE95-616333 ..... p 2955 N95-30445 #
DE95-616337 ..... p 2976 N95-30446 #
DE95-616348 ..... p 2977 N95-30447 #
DE95-616349 ..... p 2982 N95-31176 #
DE95-616373 ..... p 2976 N95-30393 #
DE95-616383 ..... p 2978 N95-30579 #
DE95-616384 ..... p 2978 N95-30580 #
DE95-616458 ..... p 2992 N95-30960 #
DE95-616466 ..... p 2978 N95-30583 #
DE95-616538 ..... p 3003 N95-30473 #
DE95-616727 ..... p 3012 N95-30789 #
DE95-616775 ..... p 2980 N95-30790 #
DE95-616776 ..... p 2815 N95-30791 #
DE95-616777 ..... p 2977 N95-30474 #
DE95-616778 ..... p 2977 N95-30475 #
DE95-616779 ..... p 2977 N95-30476 #
DE95-616780 ..... p 2981 N95-30916 #
DE95-616903 ..... p 2967 N95-31177 #
DE95-619199 ..... p 2939 N95-31257 #
DE95-619200 ..... p 2960 N95-31258 #
DE95-619241 ..... p 2959 N95-31137 #
DE95-619245 ..... p 2966 N95-31259 #
DE95-619267 ..... p 2983 N95-31260 #
DE95-619268 ..... p 2983 N95-31261 #
DE95-619291 ..... p 2984 N95-31378 #
DE95-620521 ..... p 2966 N95-31379 #
DE95-620526 ..... p 3019 N95-31193 #
DE95-620528 ..... p 2982 N95-31214 #
DE95-620534 ..... p 2989 N95-32261 #
DE95-620535 ..... p 2982 N95-31215 #
DE95-620536 ..... p 2983 N95-31216 #
DE95-620537 ..... p 2983 N95-31217 #
DE95-620539 ..... p 2983 N95-31218 #
DE95-620540 ..... p 2983 N95-31219 #
DE95-620664 ..... p 2807 N95-31407 #
DE95-620904 ..... p 2806 N95-31220 #
DE95-621008 ..... p 2818 N95-31221 #
DE95-623577 ..... p 2940 N95-31408 #
DE95-623599 ..... p 3019 N95-31276 #
DE95-623632 ..... p 3020 N95-32295 #
DE95-623675 ..... p 2995 N95-32296 #
DE95-623967 ..... p 2807 N95-31409 #
DE95-717864 ..... p 2982 N95-31178 #
DE95-717874 ..... p 2913 N95-30758 #
DE95-717875 ..... p 2934 N95-30759 #
DE95-717876 ..... p 2980 N95-30760 #
DE95-721871 ..... p 2804 N95-30761 #
DE95-722055 ..... p 2979 N95-30654 #
DE95-722056 ..... p 2806 N95-31154 #
DE95-722072 ..... p 2979 N95-30656 #
DE95-737160 ..... p 3020 N95-31281 #
DE95-737161 ..... p 3014 N95-31222 #
DE95-737162 ..... p 2983 N95-31223 #
DE95-737163 ..... p 2983 N95-31224 #
DE95-737208 ..... p 2995 N95-32262 #
DE95-737209 ..... p 3007 N95-32263 #
DE95-737220 ..... p 3007 N95-32264 #
DE95-737228 ..... p 2986 N95-31658 #
DE95-737229 ..... p 2983 N95-31225 #
DE95-737230 ..... p 3019 N95-31226 #
DE95-737278 ..... p 2983 N95-31227 #
DE95-764072 ..... p 2908 N95-30677 #
DE95-764135 ..... p 2904 N95-31155
DE95-769806 ..... p 2906 N95-32072 #
DE95-772421 ..... p 2907 N95-32368 #
DE95-772422 ..... p 2904 N95-31138 #

DIAS-STP-94-22 ..... p 2983 N95-31224 #

DLR-FB-94-20 ..... p 2873 N95-31355 #

DNA-TR-94-39 ..... p 2892 N95-30559 #

DODA-AR-008-799 ..... p 2851 N95-31510 #
DODA-AR-008-926 ..... p 2936 N95-31228 #
DODA-AR-009-205 ..... p 2752 N95-31544 #

DOE/BC-14882/12 ..... p 2823 N95-32361 #
DOE/BC-14971/2 ..... p 2837 N95-32158 #

DOE/CE-15599/T2 ..... p 2823 N95-32305 #
DOE/CE-15601/T1 ..... p 2907 N95-32288 #
DOE/CE-23810/43 ..... p 2911 N95-32364 #
DOE/CE-23810/51B ..... p 2814 N95-30767 #
DOE/CE-23810/51E ..... p 2816 N95-31057 #

DOE/ER-0641T ..... p 2908 N95-30755
DOE/ER-0645 ..... p 2925 N95-32040 #
DOE/ER-13030/T1 ..... p 2894 N95-31254 #
DOE/ER-13491/762 ..... p 2990 N95-32275 #
DOE/ER-13491/764 ..... p 2990 N95-32274 #
DOE/ER-13491/767 ..... p 2989 N95-32120 #
DOE/ER-13491/775 ..... p 2990 N95-32273 #
DOE/ER-13491/777 ..... p 2990 N95-32271 #
DOE/ER-13829/T1 ..... p 2793 N95-30766 #
DOE/ER-13859/T1 ..... p 2823 N95-32298 #
DOE/ER-14039/4 ..... p 2978 N95-30574
DOE/ER-25063/T14 ..... p 3023 N95-30619 #
DOE/ER-25109/T1 ..... p 2841 N95-31630 #
DOE/ER-25135/T1 ..... p 2945 N95-32270 #
DOE/ER-40272/209 ..... p 3029 N95-31102 #
DOE/ER-40272/212 ..... p 3020 N95-32106 #
DOE/ER-40445/46 ..... p 2978 N95-30616 #
DOE/ER-40481/T1 ..... p 3031 N95-30618 #
DOE/ER-40559/T1 ..... p 3030 N95-32269 #
DOE/ER-40561/189 ..... p 2991 N95-32365 #
DOE/ER-40633/3 ..... p 2991 N95-30615 #
DOE/ER-40699/3 ..... p 2991 N95-30527
DOE/ER-40757/060 ..... p 2977 N95-30465 #
DOE/ER-45233/10 ..... p 2792 N95-30614 #
DOE/ER-45399/T2 ..... p 2998 N95-31114 #
DOE/ER-45488/1 ..... p 2810 N95-32265 #
DOE/ER-53212/256 ..... p 3007 N95-32310 #
DOE/ER-61010/T27 ..... p 2907 N95-30358
DOE/ER-61216/3 ..... p 2908 N95-30686
DOE/ER-61761/1 ..... p 2917 N95-32142 #

DOE/ET-15601/T69 ..... p 2879 N95-30687
DOE/ET-53088/691 ..... p 3004 N95-30795 #
DOE/ET-53088/692 ..... p 2868 N95-30763 #
DOE/ET-53088/694 ..... p 3004 N95-30794 #
DOE/ET-53088/697 ..... p 3005 N95-30801 #
DOE/ET-53088/698 ..... p 3029 N95-30729 #

DOE/GO-10095-041 ..... p 2909 N95-31695 #
DOE/GO-10095-082 ..... p 2905 N95-31661 #
DOE/GO-10095-085 ..... p 2906 N95-32058 #

DOE/MC-29116/3956 ..... p 2881 N95-31694 #
DOE/MC-29257/4018 ..... p 2890 N95-32163 #
DOE/MC-29467/3986 ..... p 3026 N95-31823 #

DOE/METC-C/95/7183 ..... p 2792 N95-30762 #

DOE/NV-10872/T176 ..... p 3023 N95-30620 #
DOE/NV-10872/T187 ..... p 3027 N95-32362 #

DOE/PC-92542/T9 ..... p 2809 N95-32098 #
DOE/PC-92545/9 ..... p 2792 N95-30709 #
DOE/PC-94222/1 ..... p 2822 N95-32075 #

DOE/SF-18852/T50 ..... p 2768 N95-30674 #
DOE/SF-20143/T2 ..... p 3007 N95-32299 #

DOT-VNTSC-FAA-94-29 ..... p 2749 N95-32022 #
DOT-VNTSC-FAA-95-7 ..... p 2749 N95-31572 #

DOT/FAA/AM-95/21 ..... p 2750 N95-32186 #
DOT/FAA/AM-95/22 ..... p 2748 N95-31845 #

DOT/FAA/AOR-100/94/008 ..... p 2747 N95-31687 #
DOT/FAA/AOR-100/95-01 ..... p 2749 N95-32022 #

DOT/FAA/ASC-94-1 ..... p 2747 N95-31428 #

DOT/FAA/CT-TN94/49 ..... p 2748 N95-31013 #
DOT/FAA/CT-TN94/50 ..... p 2930 N95-31399
DOT/FAA/CT-TN94/55 ..... p 2860 N95-30922 #
DOT/FAA/CT-TN94/59 ..... p 2848 N95-30910 #
DOT/FAA/CT-TN95/10 ..... p 2848 N95-30902 #
DOT/FAA/CT-TN95/1 ..... p 2921 N95-31587 #

DOT/FAA/CT-94/119 ..... p 2763 N95-31468 #
DOT/FAA/CT-95/9 ..... p 2747 N95-31569 #

DOT/FAA/RD-95-7 ..... p 2749 N95-31572 #

DOTVNTSC-FAA-95/2 ..... p 2749 N95-31520 #

DSTO-RR-0008 ..... p 2936 N95-31228 #
DSTO-RR-0014 ..... p 2806 N95-31344
DSTO-RR-0020 ..... p 2974 N95-31365

DSTO-TN-0004 ..... p 2752 N95-31544 #

DSTO-TR-0023 ..... p 2922 N95-30711
DSTO-TR-0064 ..... p 3001 N95-31745
DSTO-TR-0146 ..... p 2851 N95-31510 #

E-9012 ..... p 2762 N95-30592 * #
E-9076 ..... p 2876 N95-31738 * #
E-9081 ..... p 2899 N95-32206 * #
E-9086 ..... p 2803 N95-30593 * #
E-9216-1 ..... p 2822 N95-32208 * #
E-9390 ..... p 2756 N95-31985 * #
E-9457-VOL-1 ..... p 2768 N95-31169 * #
E-9457-VOL-2 ..... p 2769 N95-31170 * #
E-9465 ..... p 2763 N95-31653 * #
E-9541 ..... p 3011 N95-30703 * #
E-9575 ..... p 2742 N95-30611 * #
E-9577 ..... p 2755 N95-30779 * #
E-9648 ..... p 2791 N95-32209 * #
E-9657 ..... p 2765 N95-31849 * #
E-9664 ..... p 2880 N95-30851 * #
E-9685 ..... p 2813 N95-30621 * #
E-9682 ..... p 2802 N95-30531 * #
E-9692 ..... p 2878 N95-32210 * #
E-9704 ..... p 2755 N95-30702 * #
E-9709 ..... p 2867 N95-30524 * #
E-9713 ..... p 2878 N95-32216 * #
E-9718 ..... p 2753 N95-30514 * #
E-9731 ..... p 2754 N95-30594 * #
E-9732 ..... p 2742 N95-30704 * #
E-9736 ..... p 2755 N95-30853 * #
E-9737 ..... p 2755 N95-30698 * #
E-9745 ..... p 2959 N95-30855 * #
E-9748 ..... p 2874 N95-31423 * #
E-9750 ..... p 2768 N95-30860 * #
E-9751 ..... p 2865 N95-32207 * #
E-9752 ..... p 2864 N95-31742 * #
E-9760 ..... p 2768 N95-30856 * #
E-9766 ..... p 2768 N95-30595 * #
E-9769 ..... p 2785 N95-30787 * #
E-9772 ..... p 2864 N95-31847 * #
E-9773 ..... p 2837 N95-31359 * #
E-9776 ..... p 2754 N95-30617 * #
E-9777 ..... p 2754 N95-30517 * #
E-9779 ..... p 2754 N95-30632 * #
E-9782 ..... p 2754 N95-30589 * #
E-9784 ..... p 2755 N95-30861 * #
E-9787 ..... p 2997 N95-30849 * #
E-9794 ..... p 2770 N95-32121 * #
E-9796 ..... p 2899 N95-32205 * #
E-9799 ..... p 2879 N95-30587 * #

EOARD-TR-95-01 ..... p 2825 N95-31149 #
EOARD-TR-95-09 ..... p 2999 N95-31529 #

EPA/600/R-94/214A ..... p 2763 N95-31101
EPA/600/R-94/214B ..... p 2762 N95-30928

ERP-1168-VOL-1 ..... p 2915 N95-31575 #
ERP-1168-VOL-2 ..... p 2916 N95-31604 #

ESC-TR-94-092 ..... p 3000 N95-31665 #
ESC-TR-94-106 ..... p 3015 N95-31826 #
ESC-TR-94-112 ..... p 2951 N95-30890 #
ESC-TR-94-114 ..... p 2935 N95-30931 #
ESC-TR-95-104 ..... p 2850 N95-31367 #

EUT-94-WSK-02 ..... p 2954 N95-30401 #

FAA-AOR-100-94-012 ..... p 2748 N95-31013 #

FAA-APO-95-1 ..... p 2741 N95-31598 #

FBIS-UST-95-027 ..... p 2839 N95-31727 #
FBIS-UST-95-028 ..... p 2839 N95-31729 #
FBIS-UST-95-029 ..... p 2863 N95-31728 #

FFI/RAPPORT-94/5417 ..... p 2933 N95-30598

FNAL-TM-1929 ..... p 2814 N95-30765 #

FNAL/C-94/150-E ..... p 2992 N95-31165 #
FNAL/C-95/037 ..... p 2992 N95-30800 #
FNAL/C-95/041 ..... p 2990 N95-32303 #
FNAL/C-95/061-E ..... p 2989 N95-32162 #
FNAL/C-95/072-E ..... p 2981 N95-30970 #

FOA-C-20982-2.2 ..... p 2973 N95-30481 #

FOA-R-00047-3.6-SE ..... p 2945 N95-32246
FOA-R-94-00006-3.1-SE ..... p 2945 N95-32251
FOA-R-94-00007-3.2-SE ..... p 2882 N95-32245
FOA-R-94-00011-3.4-SE ..... p 2946 N95-32311
FOA-R-94-00025-3.3-SE ..... p 2857 N95-32314
FOA-R-94-00026-3.1-SE ..... p 2922 N95-32315
FOA-R-94-00029-2.1-SE ..... p 2825 N95-30626
FOA-R-94-00042-3.2-SE ..... p 2847 N95-30629 #
FOA-R-94-00051-3.6-SE ..... p 2857 N95-32247
FOA-R-94-00055-8.4-SE ..... p 2879 N95-30600
FOA-R-94-00056-2.2-SE ..... p 2858 N95-30480
FOA-R-94-00060-3.4-SE ..... p 2950 N95-30478
FOA-R-94-00061-2.1-SE ..... p 2837 N95-32249
FOA-R-94-00065-5.5-SE ..... p 2945 N95-32248
FOA-R-94-00066-3.5-SE ..... p 2846 N95-30479
FOA-R-94-00075-2.5-SE ..... p 2822 N95-32253
FOA-R-95-00093-2.4-SE ..... p 2857 N95-32313

FR001 ..... p 2751 N95-31525 #

F0A-R-94-00021-3.1-SE ..... p 3002 N95-32312

GA-A-21716 ..... p 3003 N95-30612 #
GA-A-21793 ..... p 3006 N95-31624 #
GA-A-21871 ..... p 3003 N95-30359 #
GA-A-21905 ..... p 3004 N95-30685 #
GA-A-21914 ..... p 3007 N95-32116 #
GA-A-21926 ..... p 3003 N95-30641 #

GAO/NSIAD-94-118 ..... p 2964 N95-31987 #
GAO/NSIAD-94-141 ..... p 2741 N95-32198 #
GAO/NSIAD-94-63 ..... p 2741 N95-32194 #
GAO/NSIAD-94-65 ..... p 2752 N95-32196 #
GAO/NSIAD-95-54 ..... p 3021 N95-31659 #
GAO/NSIAD-95-75 ..... p 3022 N95-32213 #

GAO/OP-95-1 ..... p 3022 N95-31986 #

GAO/PEMD-95-2 ..... p 3027 N95-31345 #

GAO/RCED-94-167FS ..... p 2750 N95-32197 #
GAO/RCED-94-265 ..... p 2750 N95-32199 #
GAO/RCED-94-75 ..... p 3022 N95-32195 #
GAO/RCED-95-52 ..... p 3027 N95-32201 #
GAO/RCED-95-59 ..... p 3022 N95-32200 #

GL-5256 ..... p 2967 N95-30939 #

GMD-239 ..... p 3023 N95-30496 #

GRI-94/0421.2 ..... p 2791 N95-30541 #

GRL/9501 ..... p 2886 N95-31563 #

H-2059 ..... p 2757 N95-31846 * #
H-2060 ..... p 2756 N95-31425 * #

HEP-PH-9410306 ..... p 3029 N95-31102 #

HEPPH-9410331 ..... p 2982 N95-31060 #

IASSNS-HEP-94/70 ..... p 3018 N95-30440 #

IC-94/188 ..... p 3020 N95-32094 #
IC-94/225 ..... p 2991 N95-32304 #
IC-94/240 ..... p 2962 N95-32068 #
IC-94/261 ..... p 2991 N95-32353 #
IC-94/268 ..... p 2962 N95-32095 #
IC-94/272 ..... p 3016 N95-32071 #
IC-94/273 ..... p 2962 N95-32067 #
IC-94/277 ..... p 2988 N95-32070 #
IC-94/280 ..... p 2989 N95-32096 #
IC-94/283 ..... p 2913 N95-30675 #
IC-94/284 ..... p 2883 N95-30609 #
IC-94/285 ..... p 2979 N95-30637 #
IC-94/286 ..... p 3010 N95-30644 #
IC-94/288 ..... p 2982 N95-31168 #
IC-94/289 ..... p 2966 N95-30635 #

IC-94/290 ..... p 2980 N95-30740 #
IC-94/291 ..... p 2859 N95-30649 #
IC-94/292 ..... p 3019 N95-31186 #
IC-94/294 ..... p 3012 N95-30958 #
IC-94/295 ..... p 2981 N95-31003 #
IC-94/296 ..... p 2963 N95-30610 #
IC-94/297 ..... p 3010 N95-30650 #
IC-94/298 ..... p 3011 N95-30736 #
IC-94/300 ..... p 2958 N95-30770 #
IC-94/303 ..... p 2982 N95-31060 #
IC-94/304 ..... p 2979 N95-30652 #
IC-94/305 ..... p 3019 N95-30741 #
IC-94/306 ..... p 2984 N95-31546 #
IC-94/314 ..... p 2958 N95-30803 #
IC-94/315 ..... p 2813 N95-30645 #
IC-94/316 ..... p 3010 N95-30647 #
IC-94/318 ..... p 2957 N95-30676 #
IC-94/320 ..... p 3011 N95-30737 #
IC-94/322 ..... p 2957 N95-30642 #
IC-94/324 ..... p 2956 N95-30607 #
IC-94/326 ..... p 3011 N95-30722 #
IC-94/327 ..... p 2984 N95-31547 #
IC-94/329 ..... p 3010 N95-30648 #
IC-94/330 ..... p 2967 N95-30739 #
IC-94/332 ..... p 2958 N95-30820 #
IC-94/333 ..... p 2984 N95-31548 #
IC-94/334 ..... p 3010 N95-30653 #
IC-94/336 ..... p 3019 N95-30771 #
IC-94/337 ..... p 2903 N95-30723 #
IC-94/338 ..... p 3018 N95-30636 #
IC-94/340 ..... p 3013 N95-30959 #
IC-94/341 ..... p 2956 N95-30608 #
IC-94/342 ..... p 2880 N95-31167 #
IC-94/344 ..... p 2958 N95-30821 #

IC/93/366 ..... p 2962 N95-32117 #

ICAM-94-06-03 ..... p 2751 N95-31451 #

ICASE-95-32 ..... p 2959 N95-31120 * #
ICASE-95-33 ..... p 2932 N95-32046 * #
ICASE-95-44 ..... p 2877 N95-31978 * #
ICASE-95-45 ..... p 2960 N95-31319 * #
ICASE-95-47 ..... p 2933 N95-30584 * #
ICASE-95-49 ..... p 2932 N95-31988 * #

ICOMP-95-12 ..... p 2959 N95-30855 * #

IECEC-95-329 ..... p 2865 N95-32207 * #

IEE-SR-257 ..... p 2908 N95-30677 #

IEP-87/822 ..... p 2948 N95-32255

IFSR-691 ..... p 3004 N95-30795 #
IFSR-692 ..... p 2868 N95-30763 #
IFSR-694 ..... p 3004 N95-30794 #
IFSR-697 ..... p 3005 N95-30801 #
IFSR-698 ..... p 3029 N95-30729 #

IFTR-1/1995 ..... p 2895 N95-31338 #
IFTR-10/1995 ..... p 2960 N95-31339 #
IFTR-2/1995 ..... p 2850 N95-31357 #
IFTR-3/1995 ..... p 2876 N95-31817 #
IFTR-4/1995 ..... p 3006 N95-31737 #
IFTR-5/1995 ..... p 2986 N95-31818 #
IFTR-6/1995 ..... p 2993 N95-31336 #
IFTR-7/1995 ..... p 2854 N95-32192 #
IFTR-8/1995 ..... p 2960 N95-31337 #

IFVE-ONF-94-36 ..... p 2983 N95-31260 #

IFVE-93-100 ..... p 2984 N95-31549 #

IHEP-93-100 ..... p 2984 N95-31549 #
IHEP-93-149 ..... p 2984 N95-31378 #
IHEP-94-13 ..... p 3019 N95-31193 #
IHEP-94-19 ..... p 2989 N95-32261 #
IHEP-94-20 ..... p 2982 N95-31215 #
IHEP-94-21 ..... p 2966 N95-31379 #
IHEP-94-23 ..... p 2939 N95-31257 #
IHEP-94-34 ..... p 2983 N95-31261 #
IHEP-94-48 ..... p 2983 N95-31216 #
IHEP-94-4 ..... p 2960 N95-31256 #
IHEP-94-52 ..... p 2982 N95-31214 #
IHEP-94-53 ..... p 2983 N95-31217 #
IHEP-94-56 ..... p 2983 N95-31219 #
IHEP-94-63 ..... p 2983 N95-31218 #

IHES/M/94/67 ..... p 2957 N95-30623
IHES/M/95/11 ..... p 2965 N95-30555 #
IHES/M/95/12 ..... p 2965 N95-30509 #
IHES/M/95/13 ..... p 2956 N95-30506 #
IHES/M/95/14 ..... p 2955 N95-30488 #
IHES/M/95/15 ..... p 2965 N95-30504 #
IHES/M/95/16 ..... p 2965 N95-30489 #

IHES/M/95/19 ..... p 2955 N95-30490 #
IHES/M/95/1 ..... p 2957 N95-30624 #
IHES/M/95/2 ..... p 2957 N95-30622
IHES/M/95/6 ..... p 2957 N95-30696 #
IHES/M/95/9 ..... p 2956 N95-30556 #

IHES/P/94/63 ..... p 3009 N95-30503
IHES/P/95/10 ..... p 2966 N95-30591 #
IHES/P/95/4 ..... p 2912 N95-30588
IHES/P/95/8 ..... p 2913 N95-30590 #

IHK-341-03 ..... p 3031 N95-30785 * #

INEL-94/0121 ..... p 3022 N95-30392 #

INIS-AR-089 ..... p 2806 N95-31220 #
INIS-AR-091 ..... p 2818 N95-31221 #
INIS-AR-093 ..... p 2807 N95-31407 #
INIS-AR-103 ..... p 2940 N95-31408 #
INIS-AR-105 ..... p 2807 N95-31409 #

INIS-MF-14440 ..... p 2768 N95-30881 #
INIS-MF-14453 ..... p 3003 N95-30473 #

INRNE-TH-02/94 ..... p 2966 N95-30635 #

INS-T-528 ..... p 2962 N95-31178 #

INS-1036 ..... p 3020 N95-31281 #
INS-1042 ..... p 2983 N95-31224 #
INS-1043 ..... p 3014 N95-31222 #
INS-1045 ..... p 2983 N95-31223 #
INS-1047 ..... p 2963 N95-31225 #
INS-1048 ..... p 3019 N95-31226 #
INS-1050 ..... p 2986 N95-31658 #
INS-1059 ..... p 2983 N95-31227 #

IS-M-791 ..... p 3015 N95-32037 #
IS-M-810 ..... p 2865 N95-32084 #
IS-M-814 ..... p 3011 N95-30667 #
IS-M-820 ..... p 2897 N95-32024 #

IS-T-1703 ..... p 2809 N95-32023 #
IS-T-1716 ..... p 2815 N95-30897 #
IS-T-1717 ..... p 2817 N95-31108 #
IS-T-1718 ..... p 2804 N95-30757 #
IS-T-1719 ..... p 2966 N95-30668 #
IS-T-1729 ..... p 3012 N95-30756 #

ISBN-0-315-84928-2 ..... p 2789 N95-31731
ISBN-0-315-85957-1 ..... p 2848 N95-30828
ISBN-0-315-86297-1 ..... p 2962 N95-31947
ISBN-0-315-86543-1 ..... p 2894 N95-31098
ISBN-90-370-0109-3 ..... p 2869 N95-30872 #
ISBN-90-370-0114-9 ..... p 2839 N95-30777 #
ISBN-90-407-1071-6 ..... p 2804 N95-30776 #
ISBN-90-407-1075-9 ..... p 2812 N95-30459 #
ISBN-90-407-1084-8 ..... p 2892 N95-30492 #
ISBN-90-507-1055-4 ..... p 2892 N95-30458 #
ISBN-90-6628-186-3 ..... p 2891 N95-31362
ISBN-90-73861-16-0 ..... p 2979 N95-30639 #
ISBN-90-73861-21-7 ..... p 2960 N95-30774 #
ISBN-90-9006731-0 ..... p 2973 N95-30461 #
ISBN-90-9007530-5 ..... p 2893 N95-30634 #
ISBN-90-9007656-5 ..... p 3019 N95-30775 #
ISBN-90-9007838-X ..... p 2784 N95-30460 #
ISBN-90-9007865-7 ..... p 2922 N95-30457 #
ISBN-91-88116-54-9 ..... p 2903 N95-30640 #
ISBN-91-970769-1-0 ..... p 2902 N95-32115 #
ISBN-92-836-0007-X ..... p 2757 N95-31989 #
ISBN-92-836-0008-8 ..... p 2839 N95-32123 #
ISBN-92-836-1013-X ..... p 2745 N95-31061 #
ISBN-92-836-1017-2 ..... p 2843 N95-32165 #
ISBN-951-22-2158-6 ..... p 2975 N95-31650 #
ISBN-951-22-2210-8 ..... p 2849 N95-31159 #
ISBN-951-22-2215-9 ..... p 2853 N95-31649 #
ISBN-951-22-2218-3 ..... p 2846 N95-30567 #
ISBN-951-22-2263-9 ..... p 2960 N95-31363 #
ISBN-951-22-2275-2 ..... p 2900 N95-30718 #
ISBN-951-22-2369-4 ..... p 2791 N95-30537 #

ISTIC-TR-94245 ..... p 2854 N95-32114

IW-93070R ..... p 2904 N95-31157 #
IW-93071R ..... p 2869 N95-30957 #
IW-93073R ..... p 2742 N95-30638 #

IYAF-93-44 ..... p 2984 N95-31550 #
IYAF-93-93 ..... p 2988 N95-32069 #
IYAF-93-94 ..... p 3020 N95-32150 #
IYAF-93-95 ..... p 2989 N95-32151 #
IYAF-93-97 ..... p 3007 N95-32056 #
IYAF-94-24 ..... p 2966 N95-31259 #
IYAF-94-26 ..... p 3019 N95-31276 #
IYAF-94-27 ..... p 2959 N95-31137 #
IYAF-94-33 ..... p 2967 N95-32055 #

IYAF-94-35 ..... p 3006 N95-31680 #
IYAF-94-36 ..... p 2987 N95-32053 #
IYAF-94-53 ..... p 2966 N95-32066 #
IYAF-94-56 ..... p 2991 N95-32354 #
IYAF-94-63 ..... p 3006 N95-31679 #
IYAF-94-67 ..... p 3006 N95-32054 #

JAERI-DATA/CODE-94-002-PT-3 p 2934 N95-30759 #
JAERI-DATA/CODE-94-004 ..... p 2980 N95-30760 #
JAERI-DATA/CODE-94-005 ..... p 2979 N95-30654 #
JAERI-DATA/CODE-94-007 ..... p 2979 N95-30656 #
JAERI-DATA/CODE-94-009 ..... p 2913 N95-30758 #

JAERI-M-94-081-4 ..... p 2804 N95-30761 #

JAERI-RESEARCH-94-004 ..... p 2806 N95-31154 #
JAERI-RESEARCH-94-011 ..... p 3007 N95-32263 #

JAERI-TECH-94-006 ..... p 3007 N95-32264 #
JAERI-TECH-94-007 ..... p 2995 N95-32262 #

JINR-D-2-94-244 ..... p 2846 N95-30605 #

JINR-E-1-94-241 ..... p 2981 N95-30913 #
JINR-E-1-94-294 ..... p 2975 N95-30372 #
JINR-E-14-94-266 ..... p 3009 N95-30419 #
JINR-E-2-94-200 ..... p 3017 N95-30371 #
JINR-E-2-94-221 ..... p 2985 N95-31622 #
JINR-E-2-94-231 ..... p 2985 N95-31621 #
JINR-E-2-94-246 ..... p 3029 N95-30606 #
JINR-E-2-94-248 ..... p 2988 N95-32078 #
JINR-E-2-94-249 ..... p 3017 N95-30365 #
JINR-E-2-94-253 ..... p 2845 N95-30370 #
JINR-E-2-94-254 ..... p 2978 N95-30528 #
JINR-E-2-94-258 ..... p 3028 N95-30366 #
JINR-E-2-94-263 ..... p 2964 N95-30369 #
JINR-E-2-94-293 ..... p 2975 N95-30367 #
JINR-E-2-94-297 ..... p 2845 N95-30368 #
JINR-E-2-94-303 ..... p 2985 N95-31620 #
JINR-E-2-94-307 ..... p 2980 N95-30911 #
JINR-E-2-94-341 ..... p 3020 N95-32295 #
JINR-E-3-94-291 ..... p 2981 N95-30915 #
JINR-E-4-94-234 ..... p 2988 N95-32093 #
JINR-E-5-94-259 ..... p 2961 N95-31619 #
JINR-E-9-94-237 ..... p 2884 N95-30914 #

JINR-R-1-94-239 ..... p 2991 N95-30604 #
JINR-R-2-94-222 ..... p 3019 N95-30972 #
JINR-R-2-94-223 ..... p 3017 N95-30364 #
JINR-R-2-94-243 ..... p 2981 N95-30912 #
JINR-R-2-94-324 ..... p 2995 N95-32296 #
JINR-R-4-94-280 ..... p 2977 N95-30508 #

JPL-PUBL-87-4-VOL-16 ..... p 2909 N95-31651 * #
JPL-PUBL-90-49-REV-5 ..... p 2922 N95-30859 * #
JPL-PUBL-94-001 ..... p 2881 N95-31456 * #
JPL-PUBL-94-16 ..... p 3024 N95-30858 * #
JPL-PUBL-94-26 ..... p 2912 N95-30525 * #
JPL-PUBL-94-29 ..... p 3030 N95-30845 * #
JPL-PUBL-94-31 ..... p 2796 N95-31660 * #
JPL-PUBL-95-06 ..... p 2846 N95-30581 * #
JPL-PUBL-95-10 ..... p 2859 N95-30651 * #
JPL-PUBL-95-9 ..... p 3025 N95-31713 * #

JPL-TDA-42-121 ..... p 2854 N95-32221 * #

JPRS-UST-95-025 ..... p 2771 N95-31360 #

JSC-1510 ..... p 2764 N95-30852 *
JSC-1516 ..... p 2766 N95-30854 *
JSC-27031 ..... p 2810 N95-32183 * #

KAERI/RR-1269/93 ..... p 3024 N95-30882 #
KAERI/RR-1300/93 ..... p 3024 N95-30883 #
KAERI/RR-1339/93 ..... p 2930 N95-31267 #
KAERI/RR-1364/93 ..... p 3005 N95-31366 #
KAERI/RR-1365/93 ..... p 3005 N95-31004 #

KAPL-4798 ..... p 2894 N95-31054 #

KCP-613-5528 ..... p 2940 N95-31404 #
KCP-613-5539 ..... p 2815 N95-30798 #

L-17007 ..... p 2940 N95-31420 * #
L-17407 ..... p 2948 N95-32250 * #
L-17438 ..... p 2744 N95-31984 * #
L-17459 ..... p 2763 N95-32217 * #

LA-UR-94-3256 ..... p 2952 N95-31161 #
LA-UR-95-1074 ..... p 2837 N95-32355 #
LA-UR-95-1082 ..... p 2980 N95-30705 #
LA-UR-95-1097 ..... p 3008 N95-32351 #
LA-UR-95-1110 ..... p 2854 N95-32050 #
LA-UR-95-1159 ..... p 2960 N95-31253 #
LA-UR-95-1206 ..... p 2992 N95-31232 #
LA-UR-95-1260 ..... p 2911 N95-32276 #

LA-UR-95-1281 ..... p 2818 N95-31377 #
LA-UR-95-1293 ..... p 2948 N95-32277 #
LA-UR-95-1440 ..... p 2817 N95-31152 #
LA-UR-95-1452 ..... p 2992 N95-31151 #
LA-UR-95-1459 ..... p 2821 N95-31705 #
LA-UR-95-20 ..... p 2934 N95-30603 #
LA-UR-95-375 ..... p 2932 N95-31645 #
LA-UR-95-654 ..... p 2805 N95-31121 #
LA-UR-95-795 ..... p 2836 N95-32048 #
LA-UR-95-872 ..... p 3006 N95-31613 #
LA-UR-95-883 ..... p 2933 N95-30602 #
LA-UR-95-918 ..... p 2808 N95-31636 #
LA-UR-95-966 ..... p 2792 N95-30735 #
LA-UR-95-967 ..... p 3014 N95-31231 #
LA-UR-95-972 ..... p 3010 N95-30571 #

LA-12625-T ..... p 2820 N95-31629 #

LBL-PUB-755 ..... p 2861 N95-31059 #

LBL-36210 ..... p 3028 N95-30361 #
LBL-36274 ..... p 2878 N95-30378
LBL-36374 ..... p 2975 N95-30388 #
LBL-36500 ..... p 3000 N95-31635 #
LBL-36572 ..... p 2991 N95-30360
LBL-36770 ..... p 3017 N95-32366 #

LC-79-640375 ..... p 3031 N95-30816 #
LC-79-640375 ..... p 3031 N95-30817 #
LC-94-74623 ..... p 2838 N95-31983 * #

LMI-DL205-01R1 ..... p 2851 N95-31448 #
LMI-DL205-01R1 ..... p 2851 N95-31449 #

M-774 ..... p 2771 N95-31350 * #
M-775 ..... p 2771 N95-31746 * #
M-781 ..... p 2893 N95-30613 * #

MCAT-95-09 ..... p 2744 N95-32193 * #

MDC-93K0265 ..... p 2789 N95-31421 * #

MEMO-COSOR-94-30 ..... p 2950 N95-30564 #
MEMO-COSOR-94-31 ..... p 2965 N95-30523 #
MEMO-COSOR-94-33 ..... p 2950 N95-30808 #
MEMO-COSOR-94-34 ..... p 2950 N95-30807 #
MEMO-COSOR-94-36 ..... p 2950 N95-30462 #
MEMO-COSOR-94-37 ..... p 2949 N95-30400 #
MEMO-COSOR-94-41 ..... p 2951 N95-30833 #
MEMO-COSOR-94-42 ..... p 3021 N95-30834 #

MEMO-INF-94-47 ..... p 2862 N95-31185 #
MEMO-INF-94-49 ..... p 2964 N95-30565 #
MEMO-INF-94-50 ..... p 3023 N95-30566 #
MEMO-INF-94-51 ..... p 2947 N95-30721 #
MEMO-INF-94-62 ..... p 2847 N95-30812 #
MEMO-INF-94-63 ..... p 2951 N95-30813 #
MEMO-INF-94-76 ..... p 3022 N95-30453 #
MEMO-INF-94-77 ..... p 2933 N95-30454 #
MEMO-INF-94-79 ..... p 2838 N95-30455 #
MEMO-INF-94-80 ..... p 3022 N95-30456 #

MTR-93B0000141 ..... p 2850 N95-31367 #
MTR-94W0000150 ..... p 2747 N95-31687 #

NAIC-ID(RS)T-0366-94 ..... p 2997 N95-30966 #
NAIC-ID(RS)T-0373-94 ..... p 2997 N95-30901 #
NAIC-ID(RS)T-0379-94 ..... p 2951 N95-30891 #
NAIC-ID(RS)T-0393-94 ..... p 2880 N95-30921 #
NAIC-ID(RS)T-0394-94 ..... p 2880 N95-30980 #
NAIC-ID(RS)T-0396-94 ..... p 3001 N95-32153 #
NAIC-ID(RS)T-0410-94 ..... p 2998 N95-31006 #
NAIC-ID(RS)T-0411-94 ..... p 2997 N95-30908 #
NAIC-ID(RS)T-0414-94 ..... p 2930 N95-30888 #
NAIC-ID(RS)T-0420-94 ..... p 2997 N95-30909 #
NAIC-ID(RS)T-0495-94 ..... p 2870 N95-30965 #
NAIC-ID(RS)T-0496-94 ..... p 2887 N95-32152 #

NAIC-IS(RS)T-0703-94 ..... p 2885 N95-31389 #

NAL-TR-1246 ..... p 2767 N95-31980 #
NAL-TR-1247 ..... p 2744 N95-31715 #
NAL-TR-1249 ..... p 2769 N95-31739 #
NAL-TR-1254 ..... p 2789 N95-31740 #
NAL-TR-1255 ..... p 2744 N95-31741 #
NAL-TR-1258 ..... p 2928 N95-31714 #

NAS 1.15:104566-VOL-13 ..... p 2924 N95-32220 * #
NAS 1.15:104566-VOL-24 ..... p 2924 N95-32122 * #
NAS 1.15:104566-VOL-28 ..... p 2924 N95-31850 * #
NAS 1.15:104566 ..... p 2922 N95-30857 * #
NAS 1.15:104622 ..... p 2839 N95-31690 * #
NAS 1.15:104807 ..... p 2951 N95-30925 * #
NAS 1.15:104810 ..... p 2810 N95-32183 * #
NAS 1.15:106676 ..... p 2762 N95-30592 * #
NAS 1.15:106711 ..... p 2876 N95-31738 * #

NAS 1.15:106715 ..... p 2899 N95-32206 * #
NAS 1.15:106720 ..... p 2803 N95-30593 * #
NAS 1.15:106927 ..... p 2791 N95-32209 * #
NAS 1.15:106936 ..... p 2880 N95-30851 * #
NAS 1.15:106937 ..... p 2813 N95-30821 * #
NAS 1.15:106954 ..... p 2755 N95-30702 * #
NAS 1.15:106958 ..... p 2867 N95-30524 * #
NAS 1.15:106961 ..... p 2867 N95-30710 * #
NAS 1.15:106962 ..... p 2753 N95-30514 * #
NAS 1.15:106970 ..... p 2754 N95-30594 * #
NAS 1.15:106971 ..... p 2742 N95-30704 * #
NAS 1.15:106975 ..... p 2755 N95-30853 * #
NAS 1.15:106976 ..... p 2755 N95-30698 * #
NAS 1.15:106978 ..... p 3011 N95-30703 * #
NAS 1.15:106982 ..... p 2865 N95-32207 * #
NAS 1.15:106983 ..... p 2864 N95-31742 * #
NAS 1.15:106985 ..... p 2768 N95-30856 * #
NAS 1.15:106991 ..... p 2768 N95-30595 * #
NAS 1.15:106995 ..... p 2864 N95-31847 * #
NAS 1.15:106996 ..... p 2837 N95-31359 * #
NAS 1.15:106997 ..... p 2754 N95-30617 * #
NAS 1.15:106998 ..... p 2754 N95-30517 * #
NAS 1.15:107000 ..... p 2754 N95-30632 * #
NAS 1.15:107001 ..... p 2822 N95-32208 * #
NAS 1.15:107002 ..... p 2754 N95-30589 * #
NAS 1.15:107003 ..... p 2755 N95-30861 * #
NAS 1.15:107005 ..... p 2997 N95-30849 * #
NAS 1.15:107010 ..... p 2770 N95-32121 * #
NAS 1.15:107014 ..... p 2879 N95-30587 * #
NAS 1.15:108484 ..... p 3024 N95-30780 * #
NAS 1.15:108489 ..... p 2742 N95-30712 * #
NAS 1.15:108867 ..... p 2750 N95-30646 * #
NAS 1.15:110172 ..... p 2766 N95-31358 * #
NAS 1.15:110174 ..... p 2974 N95-30850 * #
NAS 1.15:110175 ..... p 2893 N95-30682 * #
NAS 1.15:110182 ..... p 2891 N95-30783 * #
NAS 1.15:110354 ..... p 2743 N95-30788 * #
NAS 1.15:110360 ..... p 2744 N95-32188 * #
NAS 1.15:110625 ..... p 2896 N95-31419 * #
NAS 1.15:110626 ..... p 2750 N95-30827 * #
NAS 1.15:110639 ..... p 2790 N95-32060 * #
NAS 1.15:110640 ..... p 2868 N95-30862 * #
NAS 1.15:110642 ..... p 3031 N95-30582 * #
NAS 1.15:110643 ..... p 3030 N95-30467 * #
NAS 1.15:110644 ..... p 3003 N95-30468 * #
NAS 1.15:110669 ..... p 3002 N95-32187 * #
NAS 1.15:110741 ..... p 2926 N95-30848 * #
NAS 1.15:110743 ..... p 3028 N95-31979 * #
NAS 1.15:4431 ..... p 2940 N95-31420 * #
NAS 1.15:4592 ..... p 2948 N95-32250 * #
NAS 1.15:4628 ..... p 2892 N95-31530 * #
NAS 1.15:4664 ..... p 2763 N95-32217 * #
NAS 1.15:4704 ..... p 2757 N95-31846 * #
NAS 1.15:4705 ..... p 2756 N95-31425 * #
NAS 1.18:7120.5 ..... p 3021 N95-31380 * #
NAS 1.21:514 ..... p 2741 N95-31000 * #
NAS 1.26:110641 ..... p 3028 N95-30466 * #
NAS 1.26:188375 ..... p 2996 N95-30772 * #
NAS 1.26:189411 ..... p 2936 N95-31234 * #
NAS 1.26:189430 ..... p 2917 N95-31820 * #
NAS 1.26:189433 ..... p 3030 N95-31819 * #
NAS 1.26:189435 ..... p 3029 N95-31424 * #
NAS 1.26:189436 ..... p 3031 N95-30785 * #
NAS 1.26:189437 ..... p 2919 N95-31123 * #
NAS 1.26:189438 ..... p 2919 N95-31128 * #
NAS 1.26:189439 ..... p 2893 N95-30786 * #
NAS 1.26:191441 ..... p 2789 N95-31421 * #
NAS 1.26:195081 ..... p 2959 N95-31120 * #
NAS 1.26:195435-VOL-1 ..... p 2768 N95-31169 * #
NAS 1.26:195435-VOL-2 ..... p 2769 N95-31170 * #
NAS 1.26:195439 ..... p 2763 N95-31653 * #
NAS 1.26:195457 ..... p 2755 N95-30779 * #
NAS 1.26:195471 ..... p 2765 N95-31849 * #
NAS 1.26:195475 ..... p 2802 N95-30531 * #
NAS 1.26:195476 ..... p 2878 N95-32210 * #
NAS 1.26:195481 ..... p 2878 N95-32216 * #
NAS 1.26:198153 ..... p 2932 N95-32046 * #
NAS 1.26:198169 ..... p 2877 N95-31978 * #
NAS 1.26:198171 ..... p 2960 N95-31319 * #
NAS 1.26:198172 ..... p 2931 N95-30657 * #
NAS 1.26:198174 ..... p 2933 N95-30584 * #
NAS 1.26:198178 ..... p 2932 N95-31988 * #
NAS 1.26:198188 ..... p 2767 N95-32189 * #
NAS 1.26:198358 ..... p 2959 N95-30855 * #
NAS 1.26:198360 ..... p 2768 N95-30860 * #
NAS 1.26:198363 ..... p 2785 N95-30787 * #
NAS 1.26:198367 ..... p 2899 N95-32205 * #
NAS 1.26:198755 ..... p 2896 N95-31418 * #
NAS 1.26:198815 ..... p 2914 N95-30848 * #
NAS 1.26:198818 ..... p 3026 N95-31364 * #
NAS 1.26:198828 ..... p 2943 N95-31982 * #
NAS 1.26:198840 ..... p 2910 N95-31981 * #
NAS 1.26:198846 ..... p 2872 N95-31341 * #
NAS 1.26:198854 ..... p 2851 N95-31457 * #
NAS 1.26:198859 ..... p 3012 N95-30847 * #
NAS 1.26:198861 ..... p 2909 N95-31651 * #
NAS 1.26:198863 ..... p 2912 N95-30525 * #
NAS 1.26:198864 ..... p 3030 N95-30845 * #
NAS 1.26:198865 ..... p 2796 N95-31660 * #
NAS 1.26:198866 ..... p 2881 N95-31456 * #
NAS 1.26:198869 ..... p 3024 N95-30858 * #
NAS 1.26:198871 ..... p 2922 N95-30859 * #
NAS 1.26:198882 ..... p 2846 N95-30581 * #
NAS 1.26:198884 ..... p 3025 N95-31713 * #
NAS 1.26:198885 ..... p 2859 N95-30851 * #
NAS 1.26:198911 ..... p 2854 N95-32221 * #
NAS 1.26:198921 ..... p 2950 N95-30655 * #
NAS 1.26:198925 ..... p 2918 N95-30782 * #
NAS 1.26:198930 ..... p 2917 N95-31743 * #
NAS 1.26:198931 ..... p 3028 N95-30469 * #
NAS 1.26:198932 ..... p 3029 N95-30751 * #
NAS 1.26:198933 ..... p 2880 N95-30752 * #
NAS 1.26:198934 ..... p 2768 N95-30864 * #
NAS 1.26:198935 ..... p 2869 N95-30863 * #
NAS 1.26:198945 ..... p 2906 N95-32212 * #
NAS 1.26:198950 ..... p 2889 N95-31382 * #
NAS 1.26:198951 ..... p 2914 N95-30865 * #
NAS 1.26:198957 ..... p 2958 N95-30754 * #
NAS 1.26:198959 ..... p 3019 N95-30781 * #
NAS 1.26:198972 ..... p 2744 N95-32193 * #
NAS 1.26:198979 ..... p 2930 N95-31134 * #
NAS 1.26:199014 ..... p 2921 N95-32184 * #
NAS 1.26:199034 ..... p 2899 N95-32202 * #
NAS 1.26:199035 ..... p 2897 N95-31730 * #
NAS 1.26:199036 ..... p 2767 N95-32204 * #
NAS 1.26:199037 ..... p 2944 N95-32190 * #
NAS 1.26:199039 ..... p 2945 N95-32215 * #
NAS 1.26:199040 ..... p 2945 N95-32214 * #
NAS 1.26:199044 ..... p 2944 N95-32203 * #
NAS 1.26:199074 ..... p 3032 N95-32218 * #
NAS 1.26:199075 ..... p 2878 N95-32219 * #
NAS 1.26:199109 ..... p 2838 N95-31983 * #
NAS 1.26:4677 ..... p 2742 N95-30611 * #
NAS 1.26:4679 ..... p 2874 N95-31423 * #
NAS 1.55:3297 ..... p 2771 N95-31350 * #
NAS 1.55:3298 ..... p 2771 N95-31746 * #
NAS 1.55:3302 ..... p 2967 N95-32319 * #
NAS 1.60:3509 ..... p 2744 N95-31984 * #
NAS 1.60:3527 ..... p 2756 N95-31985 * #
NAS 1.60:3554 ..... p 2893 N95-30613 * #

NASA-CP-3297 ..... p 2771 N95-31350 * #
NASA-CP-3298 ..... p 2771 N95-31746 * #
NASA-CP-3302 ..... p 2967 N95-32319 * #

NASA-CR-188375 ..... p 2996 N95-30772 * #
NASA-CR-189411 ..... p 2936 N95-31234 * #
NASA-CR-189430 ..... p 2917 N95-31820 * #
NASA-CR-189433 ..... p 3030 N95-31819 * #
NASA-CR-189435 ..... p 3029 N95-31424 * #
NASA-CR-189436 ..... p 3031 N95-30785 * #
NASA-CR-189437 ..... p 2919 N95-31123 * #
NASA-CR-189438 ..... p 2919 N95-31128 * #
NASA-CR-189439 ..... p 2893 N95-30786 * #
NASA-CR-191441 ..... p 2789 N95-31421 * #
NASA-CR-195081 ..... p 2959 N95-31120 * #
NASA-CR-195435-VOL-1 ..... p 2768 N95-31169 * #
NASA-CR-195435-VOL-2 ..... p 2769 N95-31170 * #
NASA-CR-195439 ..... p 2763 N95-31653 * #
NASA-CR-195457 ..... p 2755 N95-30779 * #
NASA-CR-195471 ..... p 2765 N95-31849 * #
NASA-CR-195475 ..... p 2802 N95-30531 * #
NASA-CR-195476 ..... p 2878 N95-32210 * #
NASA-CR-195481 ..... p 2878 N95-32216 * #
NASA-CR-197664 ..... p 3028 N95-31099 * #
NASA-CR-198153 ..... p 2932 N95-32046 * #
NASA-CR-198169 ..... p 2877 N95-31978 * #
NASA-CR-198171 ..... p 2960 N95-31319 * #
NASA-CR-198172 ..... p 2931 N95-30657 * #
NASA-CR-198174 ..... p 2933 N95-30584 * #
NASA-CR-198178 ..... p 2932 N95-31988 * #
NASA-CR-198188 ..... p 2767 N95-32189 * #
NASA-CR-198358 ..... p 2959 N95-30855 * #
NASA-CR-198360 ..... p 2768 N95-30860 * #
NASA-CR-198363 ..... p 2785 N95-30787 * #
NASA-CR-198367 ..... p 2899 N95-32205 * #
NASA-CR-198755 ..... p 2896 N95-31418 * #
NASA-CR-198818 ..... p 3026 N95-31364 * #
NASA-CR-198828 ..... p 2943 N95-31982 * #
NASA-CR-198840 ..... p 2910 N95-31981 * #
NASA-CR-198846 ..... p 2872 N95-31341 * #
NASA-CR-198854 ..... p 2851 N95-31457 * #
NASA-CR-198859 ..... p 3012 N95-30847 * #
NASA-CR-198861 ..... p 2909 N95-31651 * #
NASA-CR-198863 ..... p 2912 N95-30525 * #
NASA-CR-198864 ..... p 3030 N95-30845 * #
NASA-CR-198865 ..... p 2796 N95-31660 * #
NASA-CR-198866 ..... p 2881 N95-31456 * #
NASA-CR-198869 ..... p 3024 N95-30858 * #
NASA-CR-198871 ..... p 2922 N95-30859 * #
NASA-CR-198882 ..... p 2846 N95-30581 * #
NASA-CR-198884 ..... p 3025 N95-31713 * #
NASA-CR-198885 ..... p 2859 N95-30851 * #
NASA-CR-198911 ..... p 2854 N95-32221 * #
NASA-CR-198921 ..... p 2950 N95-30655 * #
NASA-CR-198925 ..... p 2918 N95-30782 * #
NASA-CR-198930 ..... p 2917 N95-31743 * #
NASA-CR-198931 ..... p 3028 N95-30469 * #
NASA-CR-198932 ..... p 3029 N95-30751 * #
NASA-CR-198933 ..... p 2880 N95-30752 * #
NASA-CR-198934 ..... p 2768 N95-30864 * #
NASA-CR-198935 ..... p 2869 N95-30863 * #
NASA-CR-198945 ..... p 2906 N95-32212 * #
NASA-CR-198950 ..... p 2889 N95-31382 * #
NASA-CR-198951 ..... p 2914 N95-30865 * #
NASA-CR-198957 ..... p 2958 N95-30754 * #
NASA-CR-198959 ..... p 3019 N95-30781 * #
NASA-CR-198972 ..... p 2744 N95-32193 * #
NASA-CR-198979 ..... p 2930 N95-31134 * #
NASA-CR-199014 ..... p 2921 N95-32184 * #
NASA-CR-199034 ..... p 2899 N95-32202 * #
NASA-CR-199035 ..... p 2897 N95-31730 * #
NASA-CR-199036 ..... p 2767 N95-32204 * #
NASA-CR-199037 ..... p 2944 N95-32190 * #
NASA-CR-199039 ..... p 2945 N95-32215 * #
NASA-CR-199040 ..... p 2945 N95-32214 * #
NASA-CR-199044 ..... p 2944 N95-32203 * #
NASA-CR-199074 ..... p 3032 N95-32218 * #
NASA-CR-199075 ..... p 2878 N95-32219 * #
NASA-CR-199109 ..... p 2838 N95-31983 * #
NASA-CR-4677 ..... p 2742 N95-30611 * #
NASA-CR-4679 ..... p 2874 N95-31423 * #

NASA-SP-514 ..... p 2741 N95-31000 * #

NASA-TM-104566-VOL-13 ..... p 2924 N95-32220 * #
NASA-TM-104566-VOL-24 ..... p 2924 N95-32122 * #
NASA-TM-104566-VOL-28 ..... p 2924 N95-31850 * #
NASA-TM-104566 ..... p 2922 N95-30857 * #
NASA-TM-104622 ..... p 2839 N95-31690 * #
NASA-TM-104807 ..... p 2951 N95-30925 * #
NASA-TM-104810 ..... p 2810 N95-32183 * #
NASA-TM-106676 ..... p 2762 N95-30592 * #
NASA-TM-106711 ..... p 2876 N95-31738 * #
NASA-TM-106715 ..... p 2899 N95-32206 * #
NASA-TM-106720 ..... p 2803 N95-30593 * #
NASA-TM-106827 ..... p 2791 N95-32209 * #
NASA-TM-106936 ..... p 2880 N95-30851 * #
NASA-TM-106937 ..... p 2813 N95-30821 * #
NASA-TM-106954 ..... p 2755 N95-30702 * #
NASA-TM-106958 ..... p 2867 N95-30524 * #
NASA-TM-106961 ..... p 2867 N95-30710 * #
NASA-TM-106962 ..... p 2753 N95-30514 * #
NASA-TM-106970 ..... p 2754 N95-30594 * #
NASA-TM-106971 ..... p 2742 N95-30704 * #
NASA-TM-106975 ..... p 2755 N95-30853 * #
NASA-TM-106976 ..... p 2755 N95-30698 * #
NASA-TM-106978 ..... p 3011 N95-30703 * #
NASA-TM-106982 ..... p 2865 N95-32207 * #
NASA-TM-106983 ..... p 2864 N95-31742 * #
NASA-TM-106985 ..... p 2768 N95-30856 * #
NASA-TM-106991 ..... p 2768 N95-30595 * #
NASA-TM-106995 ..... p 2864 N95-31847 * #
NASA-TM-106996 ..... p 2837 N95-31359 * #
NASA-TM-106997 ..... p 2754 N95-30617 * #
NASA-TM-106998 ..... p 2754 N95-30517 * #
NASA-TM-107000 ..... p 2754 N95-30632 * #
NASA-TM-107001 ..... p 2822 N95-32208 * #
NASA-TM-107002 ..... p 2754 N95-30589 * #
NASA-TM-107003 ..... p 2755 N95-30861 * #
NASA-TM-107005 ..... p 2997 N95-30849 * #
NASA-TM-107010 ..... p 2770 N95-32121 * #
NASA-TM-107014 ..... p 2879 N95-30587 * #
NASA-TM-108484 ..... p 3024 N95-30780 * #
NASA-TM-108489 ..... p 2742 N95-30712 * #
NASA-TM-108867 ..... p 2750 N95-30646 * #
NASA-TM-110172 ..... p 2766 N95-31358 * #
NASA-TM-110174 ..... p 2974 N95-30850 * #
NASA-TM-110175 ..... p 2893 N95-30682 * #
NASA-TM-110182 ..... p 2891 N95-30783 * #
NASA-TM-110354 ..... p 2743 N95-30788 * #
NASA-TM-110360 ..... p 2744 N95-32188 * #
NASA-TM-110625 ..... p 2896 N95-31419 * #
NASA-TM-110626 ..... p 2750 N95-30827 * #
NASA-TM-110639 ..... p 2790 N95-32060 * #
NASA-TM-110640 ..... p 2868 N95-30862 * #
NASA-TM-110641 ..... p 3028 N95-30466 * #
NASA-TM-110642 ..... p 3031 N95-30582 * #
NASA-TM-110643 ..... p 3030 N95-30467 * #
NASA-TM-110644 ..... p 3003 N95-30468 * #
NASA-TM-110657 ..... p 2786 N95-30854 *
NASA-TM-110658 ..... p 2764 N95-30852 *
NASA-TM-110659 ..... p 2765 N95-30880 *
NASA-TM-110660 ..... p 2765 N95-30879 *
NASA-TM-110661 ..... p 2765 N95-30878 *
NASA-TM-110662 ..... p 2764 N95-30877 *
NASA-TM-110663 ..... p 2764 N95-30876 *
NASA-TM-110664 ..... p 2764 N95-30875 *

NASA-TM-110665 ..... p 2764 N95-30874 *
NASA-TM-110666 ..... p 2764 N95-30873 *
NASA-TM-110669 ..... p 3002 N95-32187 * #
NASA-TM-110741 ..... p 2926 N95-30646 * #
NASA-TM-110743 ..... p 3028 N95-31979 * #
NASA-TM-4431 ..... p 2940 N95-31420 * #
NASA-TM-4592 ..... p 2948 N95-32250 * #
NASA-TM-4628 ..... p 2892 N95-31530 * #
NASA-TM-4664 ..... p 2763 N95-32217 * #
NASA-TM-4704 ..... p 2757 N95-31846 * #
NASA-TM-4705 ..... p 2756 N95-31425 * #

NASA-TP-3509 ..... p 2744 N95-31984 * #
NASA-TP-3527 ..... p 2756 N95-31985 * #
NASA-TP-3554 ..... p 2893 N95-30613 * #

NASA-198815 ..... p 2914 N95-30848 * #

NAWC-WPNS-TP-8242 ..... p 2863 N95-31674 #

NAWCADWAR-95014-43 ..... p 2817 N95-31124 #

NDP-047 ..... p 2910 N95-32099 #

NEAR-TR-482 ..... p 2756 N95-31400

NEDO-P-9320 ..... p 2904 N95-31155
NEDO-P-9327 ..... p 2906 N95-32072 #

NEI-FI-261-VOL-1 ..... p 2907 N95-32368 #
NEI-FI-261-VOL-2 ..... p 2904 N95-31138 #

NHB-7120.5 ..... p 3021 N95-31380 * #

NHK-LABS-NOTE-436 ..... p 2853 N95-31744

NHK-435 ..... p 3026 N95-32182

NHRC-94-27 ..... p 2926 N95-30563 #

NIFS-PROC-14 ..... p 3004 N95-30671 #

NLR-CR-93570L ..... p 2743 N95-30885 #

NLR-TP-93301-U ..... p 2743 N95-30814 #
NLR-TP-93348-U ..... p 2748 N95-30815 #
NLR-TP-93418-U ..... p 2751 N95-30838 #
NLR-TP-93511-U ..... p 2743 N95-30837 #

NOAA-TR-NESDIS-84 ..... p 2913 N95-30643 #

NONP-NASA-VT-95-46007 ..... p 3028 N95-31099 *
NONP-NASA-VT-95-59071 ..... p 2764 N95-30852 *
NONP-NASA-VT-95-59072 ..... p 2766 N95-30854 *
NONP-NASA-VT-95-59164 ..... p 2764 N95-30873 *
NONP-NASA-VT-95-59165 ..... p 2764 N95-30874 *
NONP-NASA-VT-95-59166 ..... p 2764 N95-30875 *
NONP-NASA-VT-95-59167 ..... p 2764 N95-30876 *
NONP-NASA-VT-95-59168 ..... p 2764 N95-30877 *
NONP-NASA-VT-95-59169 ..... p 2765 N95-30878 *
NONP-NASA-VT-95-59170 ..... p 2765 N95-30879 *
NONP-NASA-VT-95-59171 ..... p 2765 N95-30880 *

NPL-DMM(A)156 ..... p 2812 N95-30487

NRA-91-OSSA-07 ..... p 2910 N95-31981 * #

NRAD-TD-2705 ..... p 2787 N95-31146 #
NRAD-TD-2730 ..... p 2915 N95-31535 #

NREL/SP-420-5570-REV-2 ..... p 2836 N95-31638 #
NREL/SP-420-5572-REV-2 ..... p 2836 N95-31639 #
NREL/SP-420-6365 ..... p 2910 N95-31821 #
NREL/SP-420-6379 ..... p 2905 N95-31822 #

NREL/TP-411-7498 ..... p 2904 N95-31162 #
NREL/TP-411-7682 ..... p 2904 N95-31163 #
NREL/TP-411-7695 ..... p 2810 N95-32154 #
NREL/TP-412-7680 ..... p 2905 N95-31381 #
NREL/TP-413-7684 ..... p 2904 N95-31164 #
NREL/TP-413-7702 ..... p 2906 N95-32057 #
NREL/TP-441-7809 ..... p 2921 N95-31726 #
NREL/TP-442-6930 ..... p 2902 N95-30505 #
NREL/TP-462-5173 ..... p 2903 N95-30896 #
NREL/TP-471-7022 ..... p 2902 N95-30526 #
NREL/TP-471-7297 ..... p 2903 N95-30887 #

NRL/FR/7220-95-9774 ..... p 2921 N95-31577 #

NRL/MR/5620-95-7648 ..... p 3000 N95-31672 #
NRL/MR/6380-95/7424 ..... p 2815 N95-30894 #
NRL/MR/6410-95-7662 ..... p 2795 N95-31473 #
NRL/MR/6790-95-7651 ..... p 2884 N95-31190 #
NRL/MR/6793-95-7666 ..... p 3013 N95-30984 #
NRL/MR/7220-95-7652 ..... p 2852 N95-31590 #
NRL/MR/7240-94-7558 ..... p 2901 N95-31148 #

NRL/MR/7420-94-7566 ..... p 2935 N95-30968 #
NRL/MR/7441-94-7539 ..... p 2901 N95-31390 #
NRL/MR/7543-94-7218 ..... p 2747 N95-31454 #

NSWCDD/TR-94/78 ..... p 2927 N95-30981 #
NSWCDD/TR-94/96 ..... p 2743 N95-30929 #

NTSB/ARG-95/01 ..... p 2747 N95-31712 #

NTSB/SIR-95/01 ..... p 2748 N95-32185 #

NUWC-NL-TR-10797 ..... p 2813 N95-30560 #
NUWC-NL-TR-10845 ..... p 2869 N95-30946 #

NUWC-NPT-TR-10801 ..... p 2789 N95-31668 #

NWRA-CR-94-R117 ..... p 2916 N95-31698 #
NWRA-CR-95-R135 ..... p 2923 N95-30964 #

NYSERNET-01 ..... p 2947 N95-30868 #

ORNL-SUB/89-SC674/1/V1 ..... p 2817 N95-31135 #

ORNL/CDIAC-75 ..... p 2910 N95-32099 #

ORNL/FMP-95/2 ..... p 2903 N95-30745 #

ORNL/SUB-88-SC617 ..... p 2909 N95-31612 #
ORNL/SUB-92-22041/02 ..... p 2818 N95-31153 #

ORNL/SUB/89-SC674/1/V2 ..... p 2817 N95-31136 #

ORNL/TM-12867 ..... p 2942 N95-31634 #
ORNL/TM-12896 ..... p 2816 N95-31103 #
ORNL/TM-12899 ..... p 2943 N95-32030 #

OZ-93/20 ..... p 2976 N95-30442 #
OZ-93/21 ..... p 2976 N95-30443 #
OZ-93/25 ..... p 3018 N95-30444 #
OZ-94/11 ..... p 3018 N95-30426 #
OZ-94/6 ..... p 2978 N95-30579 #
OZ-94/8 ..... p 2976 N95-30446 #

PB95-191995 ..... p 3031 N95-30690 #
PB95-192845 ..... p 2880 N95-30691
PB95-192852 ..... p 2947 N95-31051
PB95-192985 ..... p 2891 N95-30510
PB95-195285 ..... p 2926 N95-30511
PB95-195293 ..... p 2925 N95-30512
PB95-195301 ..... p 2926 N95-30513
PB95-195319 ..... p 2925 N95-30515
PB95-195327 ..... p 2846 N95-30516
PB95-195350 ..... p 2802 N95-30534
PB95-195376 ..... p 3009 N95-30535
PB95-195384 ..... p 2900 N95-30536
PB95-195392 ..... p 2804 N95-31052
PB95-195558 ..... p 2791 N95-30537 #
PB95-195574 ..... p 2858 N95-30538 #
PB95-195715 ..... p 2933 N95-30539
PB95-195756 ..... p 2815 N95-30871
PB95-195764 ..... p 2956 N95-30540
PB95-195772 ..... p 2957 N95-30692
PB95-195780 ..... p 2880 N95-30693
PB95-196226 ..... p 2784 N95-30694
PB95-196234 ..... p 2979 N95-30695
PB95-196283 ..... p 2957 N95-30696 #
PB95-196291 ..... p 2934 N95-30662
PB95-196309 ..... p 2934 N95-30697
PB95-196317 ..... p 2934 N95-30663
PB95-196333 ..... p 2992 N95-30717
PB95-196341 ..... p 2805 N95-31053
PB95-196358 ..... p 2802 N95-30518
PB95-196374 ..... p 2902 N95-30519
PB95-196390 ..... p 2891 N95-30520
PB95-196408 ..... p 2838 N95-30521
PB95-196440 ..... p 2929 N95-30522
PB95-196531 ..... p 2813 N95-30664
PB95-196556 ..... p 2925 N95-30665
PB95-196598 ..... p 2979 N95-30666
PB95-196721 ..... p 2791 N95-30541 #
PB95-196960 ..... p 2771 N95-30734 #
PB95-196978 ..... p 2869 N95-30872 #
PB95-196994 ..... p 2980 N95-30774 #
PB95-197000 ..... p 3019 N95-30775 #
PB95-197018 ..... p 2804 N95-30776 #
PB95-197026 ..... p 2839 N95-30777 #
PB95-197034 ..... p 2949 N95-30400 #
PB95-197067 ..... p 2951 N95-30833 #
PB95-197075 ..... p 3021 N95-30834 #
PB95-197091 ..... p 2958 N95-30835 #
PB95-197109 ..... p 2868 N95-30836 #
PB95-197398 ..... p 2954 N95-30401 #
PB95-197661 ..... p 3022 N95-30453 #
PB95-197679 ..... p 2933 N95-30454 #
PB95-197687 ..... p 2838 N95-30455 #
PB95-197695 ..... p 3022 N95-30456 #

PB95-197760 ..... p 2891 N95-31382
PB95-197802 ..... p 2922 N95-30457 #
PB95-197810 ..... p 2892 N95-30458 #
PB95-197844 ..... p 2812 N95-30459 #
PB95-197851 ..... p 2784 N95-30460 #
PB95-197869 ..... p 2973 N95-30461 #
PB95-197885 ..... p 2950 N95-30462 #
PB95-197901 ..... p 2950 N95-30807 #
PB95-197919 ..... p 2950 N95-30808 #
PB95-197927 ..... p 2967 N95-30809 #
PB95-197935 ..... p 2868 N95-30810 #
PB95-197950 ..... p 2868 N95-30811 #
PB95-197968 ..... p 2847 N95-30812 #
PB95-197976 ..... p 2951 N95-30813 #
PB95-198024 ..... p 2743 N95-30837 #
PB95-198040 ..... p 2751 N95-30838 #
PB95-198081 ..... p 2743 N95-30814 #
PB95-198123 ..... p 2748 N95-30815 #
PB95-200853 ..... p 3031 N95-30816 #
PB95-200861 ..... p 3031 N95-30817 #
PB95-205484 ..... p 2854 N95-32114
PB95-206447 ..... p 2904 N95-31157 #
PB95-206462 ..... p 2900 N95-30818 #
PB95-206470 ..... p 2900 N95-30819
PB95-206504 ..... p 2849 N95-31158 #
PB95-206512 ..... p 2849 N95-31159 #
PB95-206579 ..... p 2849 N95-31160 #
PB95-206587 ..... p 2849 N95-31181 #
PB95-206595 ..... p 2850 N95-31182 #
PB95-206611 ..... p 2900 N95-30718 #
PB95-206629 ..... p 2853 N95-31649 #
PB95-206637 ..... p 2975 N95-31650 #
PB95-206785 ..... p 2961 N95-31422 #
PB95-206793 ..... p 2966 N95-30719 #
PB95-206850 ..... p 2950 N95-30564 #
PB95-206868 ..... p 2965 N95-30523 #
PB95-206876 ..... p 2963 N95-30680
PB95-206918 ..... p 2966 N95-30681 #
PB95-206926 ..... p 2958 N95-30778 #
PB95-206991 ..... p 2869 N95-30956
PB95-207015 ..... p 2869 N95-30957 #
PB95-207023 ..... p 2959 N95-31183 #
PB95-207031 ..... p 3011 N95-30720 #
PB95-207056 ..... p 2959 N95-31184 #
PB95-207072 ..... p 2862 N95-31185 #
PB95-207080 ..... p 2947 N95-30721 #
PB95-207098 ..... p 2964 N95-30565 #
PB95-207106 ..... p 3023 N95-30566 #
PB95-207130 ..... p 2846 N95-30567 #
PB95-207148 ..... p 2933 N95-30568 #
PB95-207197 ..... p 2960 N95-31363 #
PB95-207866 ..... p 2892 N95-30585
PB95-207874 ..... p 2893 N95-30586 #
PB95-207882 ..... p 2912 N95-30588
PB95-207890 ..... p 2913 N95-30590 #
PB95-207908 ..... p 2966 N95-30591 #
PB95-207916 ..... p 3009 N95-30503
PB95-207924 ..... p 2965 N95-30504 #
PB95-207932 ..... p 2956 N95-30506 #
PB95-207940 ..... p 2965 N95-30509 #
PB95-207957 ..... p 2965 N95-30555 #
PB95-208005 ..... p 2956 N95-30556 #
PB95-208021 ..... p 3029 N95-30569 #
PB95-208039 ..... p 2956 N95-30570
PB95-208054 ..... p 2977 N95-30484
PB95-208062 ..... p 3009 N95-30485
PB95-208088 ..... p 2812 N95-30487
PB95-208112 ..... p 2955 N95-30488 #
PB95-208120 ..... p 2965 N95-30489 #
PB95-208146 ..... p 2955 N95-30490 #
PB95-208161 ..... p 2902 N95-32115 #
PB95-208260 ..... p 2892 N95-30492 #
PB95-208302 ..... p 2866 N95-32369
PB95-208328 ..... p 2926 N95-30494
PB95-208336 ..... p 2955 N95-30495
PB95-208344 ..... p 3027 N95-32370
PB95-208385 ..... p 2949 N95-32371
PB95-208393 ..... p 3023 N95-30496 #
PB95-208427 ..... p 2957 N95-30622
PB95-208435 ..... p 2957 N95-30623
PB95-208443 ..... p 2957 N95-30624 #
PB95-208518 ..... p 2798 N95-32372
PB95-208526 ..... p 2934 N95-30625
PB95-210332 ..... p 2956 N95-30499 #
PB95-210357 ..... p 2825 N95-30626
PB95-210365 ..... p 2913 N95-30627 #
PB95-210373 ..... p 2913 N95-30628 #
PB95-210381 ..... p 2847 N95-30629 #
PB95-210399 ..... p 2882 N95-32245
PB95-211207 ..... p 2838 N95-30630 #
PB95-211223 ..... p 2913 N95-30631 #
PB95-211322 ..... p 2859 N95-30633
PB95-211330 ..... p 2859 N95-30596 #
PB95-211355 ..... p 2748 N95-30597 #
PB95-211363 ..... p 2933 N95-30598
PB95-211421 ..... p 2945 N95-32246

PB95-211454 ..... p 2857 N95-32247
PB95-211462 ..... p 2945 N95-32248
PB95-211470 ..... p 2813 N95-30599 #
PB95-211546 ..... p 2879 N95-30600
PB95-211553 ..... p 2837 N95-32249
PB95-211595 ..... p 2945 N95-32251
PB95-211611 ..... p 2945 N95-32252
PB95-211629 ..... p 2956 N95-30601 #
PB95-211637 ..... p 2956 N95-30500 #
PB95-211645 ..... p 2955 N95-30477 #
PB95-211652 ..... p 2950 N95-30478
PB95-211660 ..... p 2846 N95-30479
PB95-211736 ..... p 2858 N95-30480
PB95-211751 ..... p 2973 N95-30481 #
PB95-211777 ..... p 2822 N95-32253
PB95-212023 ..... p 2933 N95-30501 #
PB95-212031 ..... p 2879 N95-30502 #
PB95-212072 ..... p 3021 N95-30699 #
PB95-212080 ..... p 3021 N95-30700 #
PB95-212106 ..... p 2888 N95-30701 #
PB95-212122 ..... p 2934 N95-30792 #
PB95-212130 ..... p 2960 N95-31229 #
PB95-212148 ..... p 2963 N95-31396 #
PB95-212155 ..... p 2961 N95-31397 #
PB95-212205 ..... p 2961 N95-31398 #
PB95-212213 ..... p 3026 N95-32254
PB95-212221 ..... p 2948 N95-32255
PB95-212262 ..... p 2907 N95-32286
PB95-212270 ..... p 2962 N95-32256
PB95-213898 ..... p 2893 N95-30634 #
PB95-214193 ..... p 2742 N95-30638 #
PB95-214458 ..... p 2979 N95-30639 #
PB95-214573 ..... p 2903 N95-30640 #
PB95-215828 ..... p 2747 N95-31712 #
PB95-222915 ..... p 2946 N95-32311
PB95-222923 ..... p 3002 N95-32312
PB95-222964 ..... p 2857 N95-32313
PB95-222980 ..... p 2857 N95-32314
PB95-222998 ..... p 2922 N95-32315
PB95-223582 ..... p 2902 N95-32316
PB95-917004 ..... p 2748 N95-32185 #

PINSTECH-RIAD-138 ..... p 2791 N95-30420 #

PL-TR-92-1032 ..... p 2766 N95-31143 #
PL-TR-94-1043 ..... p 2974 N95-31527 #
PL-TR-94-2190 ..... p 2916 N95-31698 #
PL-TR-94-2195 ..... p 2914 N95-31012 #
PL-TR-94-2215 ..... p 2766 N95-31553 #
PL-TR-94-2241 ..... p 2964 N95-31831 #
PL-TR-94-2268 ..... p 2998 N95-31192 #
PL-TR-94-2290 ..... p 2920 N95-31522 #
PL-TR-94-3001 ..... p 2791 N95-30409 #
PL-TR-94-3036 ..... p 2836 N95-31470 #
PL-TR-95-2021 ..... p 3005 N95-31534 #
PL-TR-95-2042 ..... p 2915 N95-31575 #
PL-TR-95-2042 ..... p 2916 N95-31604 #

PNL-SA-24529 ..... p 2978 N95-30573
PNL-SA-26013 ..... p 2809 N95-32052 #

PNL-10458 ..... p 3032 N95-32279 #
PNL-10478 ..... p 2865 N95-32077 #

PSR-2531 ..... p 2848 N95-30904 #

QUEST-TR-650 ..... p 2789 N95-31509 #

R/D-6980-EE-01 ..... p 2859 N95-30561 #
R/D-7152-EE-01 ..... p 3013 N95-30969 #
R/D-7493-EN-01 ..... p 2901 N95-31156

RAL-94-114-PT-3 ..... p 2880 N95-30691
RAL-94-118 ..... p 2947 N95-31051
RAL-94-120 ..... p 2979 N95-30695
RAL-94-124 ..... p 2784 N95-30694
RAL-95-008 ..... p 2956 N95-30540
RAL-95-009 ..... p 2956 N95-30570
RAL-95-010 ..... p 2957 N95-30692
RAL-95-011-PT-1 ..... p 2880 N95-30693
RAL-95-014 ..... p 2977 N95-30484
RAL-95-015 ..... p 3009 N95-30485

RANA-94-15 ..... p 2966 N95-30681 #
RANA-94-16 ..... p 2958 N95-30778 #
RANA-94-17 ..... p 2958 N95-30835 #
RANA-94-19 ..... p 2868 N95-30836 #
RANA-94-21 ..... p 2868 N95-30811 #
RANA-94-23 ..... p 2868 N95-30810 #
RANA-94-24 ..... p 2967 N95-30809 #

RASSP-2 ..... p 2935 N95-30931 #

RCC-296860 ..... p 2852 N95-31588 #

RCHEP-94/13 ..... p 2976 N95-30441 #
RCHEP-94/15 ..... p 3018 N95-30424 #
RCHEP-94/16 ..... p 3018 N95-30437 #
RCHEP-94/17 ..... p 2976 N95-30393 #
RCHEP-94/18 ..... p 3018 N95-30438 #
RCHEP-94/22 ..... p 2965 N95-30439 #
RCHEP-94/23 ..... p 2976 N95-30427 #
RCHEP-94/26 ..... p 3018 N95-30440 #

REPT-06-5035 ..... p 2787 N95-30975 #
REPT-10-21-RR194-207 ..... p 2926 N95-30924 #
REPT-1148-95-04 ..... p 2817 N95-31126 #
REPT-1994-3 ..... p 3015 N95-31826 #
REPT-253200-7-F ..... p 2846 N95-30562 #
REPT-320-6597B ..... p 2919 N95-31128 * #
REPT-56-PT-1 ..... p 2900 N95-30819
REPT-59-PT-3 ..... p 2900 N95-30818 #
REPT-94B00042 ..... p 2924 N95-32220 * #
REPT-95B00083 ..... p 2967 N95-32319 * #
REPT-95B00091-VOL-28 ..... p 2924 N95-31850 * #
REPT-95B00092-VOL-24 ..... p 2924 N95-32122 * #
REPT-95B00096 ..... p 2922 N95-30857 * #
REPT-95B00106 ..... p 2839 N95-31690 * #

RHPU-0428 ..... p 3029 N95-31424 * #
RHPU-0456 ..... p 3030 N95-31819 * #

RL-TR-94-2113 ..... p 2947 N95-30868 #
RL-TR-94-212 ..... p 2864 N95-31844 #
RL-TR-94-216-VOL-2 ..... p 2860 N95-30886 #
RL-TR-94-216 ..... p 2953 N95-31562 #
RL-TR-94-218 ..... p 2940 N95-31455 #
RL-TR-94-220 ..... p 3000 N95-31697 #
RL-TR-94-237 ..... p 2947 N95-31445 #
RL-TR-95-47-VOL-1 ..... p 2848 N95-30895 #
RL-TR-95-47-VOL-2 ..... p 2850 N95-31387 #
RL-TR-95-6 ..... p 2931 N95-30967 #

RSI-0502 ..... p 2892 N95-30559 #

RSS-USA-1 ..... p 2901 N95-31156

R9139-F ..... p 3013 N95-30985 #
R94-970150-3 ..... p 2783 N95-30433 #
R95-970293 ..... p 2742 N95-30611 * #

S-790 ..... p 2951 N95-30925 * #
S-796 ..... p 2810 N95-32183 * #

SAND-93-2577 ..... p 3017 N95-32307 #
SAND-94-0252C ..... p 2884 N95-31139 #
SAND-94-0282C ..... p 3006 N95-31626 #
SAND-94-0854 ..... p 2907 N95-32302 #
SAND-94-1735C ..... p 2866 N95-30464 #
SAND-94-2162 ..... p 2916 N95-31610 #
SAND-94-2169C ..... p 2860 N95-30707 #
SAND-94-2193C ..... p 2878 N95-30384 #
SAND-94-2302C ..... p 2897 N95-31614 #
SAND-94-2324C ..... p 2767 N95-32081 #
SAND-94-2546C ..... p 2900 N95-30363 #
SAND-94-2565C ..... p 2932 N95-30376 #
SAND-94-2569C ..... p 2811 N95-30389 #
SAND-94-2718C ..... p 3014 N95-31112 #
SAND-94-2987C ..... p 2794 N95-31393 #
SAND-94-3010 ..... p 2810 N95-32241 #
SAND-94-3129C ..... p 2942 N95-31644 #
SAND-94-3247C ..... p 2980 N95-30708 #
SAND-94-3279C ..... p 3027 N95-30385 #
SAND-94-8235 ..... p 2905 N95-31640 #
SAND-95-0054C ..... p 3014 N95-31233 #
SAND-95-0085C ..... p 3008 N95-30381 #
SAND-95-0116 ..... p 2992 N95-31166 #
SAND-95-0166C ..... p 2885 N95-31394 #
SAND-95-0241C ..... p 2950 N95-30463 #
SAND-95-0242C ..... p 2949 N95-30377 #
SAND-95-0278C ..... p 2866 N95-30383 #
SAND-95-0322C ..... p 2811 N95-30362 #
SAND-95-0349C ..... p 2967 N95-31625 #
SAND-95-0379C ..... p 2816 N95-31058 #
SAND-95-0389 ..... p 2853 N95-31628 #
SAND-95-0393C ..... p 3008 N95-30382 #
SAND-95-0446C ..... p 3008 N95-30391 #
SAND-95-0455C ..... p 2883 N95-30390 #
SAND-95-0472C ..... p 2882 N95-30379 #
SAND-95-0482C ..... p 2882 N95-30380 #
SAND-95-0486C ..... p 2948 N95-31605 #
SAND-95-0492C ..... p 2934 N95-30796 #
SAND-95-0501C ..... p 3025 N95-31662 #
SAND-95-0504C ..... p 2883 N95-31611 #
SAND-95-0571C ..... p 2917 N95-32080 #
SAND-95-0583C ..... p 2822 N95-32101 #
SAND-95-0588C ..... p 3001 N95-32064 #
SAND-95-0594 ..... p 3017 N95-32308 #
SAND-95-0609C ..... p 2839 N95-32082 #
SAND-95-0661C ..... p 2948 N95-32065 #
SAND-95-0664C ..... p 3016 N95-32147 #
SAND-95-0665C ..... p 2948 N95-32146 #
SAND-95-0666C ..... p 3026 N95-32144 #
SAND-95-0670C ..... p 2886 N95-32143 #
SAND-95-0721C ..... p 2854 N95-32145 #
SAND-95-0734C ..... p 2806 N95-31406 #
SAND-95-0735C ..... p 2822 N95-32161 #
SAND-95-0761C ..... p 2808 N95-31689 #
SAND-95-0763C ..... p 2793 N95-31113 #
SAND-95-0856C ..... p 2806 N95-31150 #
SAND-95-8100 ..... p 2944 N95-32087 #
SAND-95-8101 ..... p 2944 N95-32088 #
SAND-95-8102 ..... p 2943 N95-32044 #
SAND-95-8103 ..... p 2944 N95-32089 #
SAND-95-8210 ..... p 3000 N95-31681 #
SAND-95-8211 ..... p 2854 N95-32045 #
SAND-95-8220 ..... p 2962 N95-32076 #
SAND-95-8222 ..... p 2906 N95-32090 #
SAND-95-8223 ..... p 2878 N95-32309 #
SAND-95-8456C ..... p 2797 N95-31824 #
SAND-95-8561A ..... p 2887 N95-32280 #

SEL-94-006 ..... p 2936 N95-31234 * #

SGD-604-PT-2 ..... p 3031 N95-30690 #
SGD-606-PT-1 ..... p 3031 N95-30616 #
SGD-606-PT-2 ..... p 3031 N95-30617 #

SKS/95/1 ..... p 2874 N95-31443 #

SMC-TR-95-11 ..... p 2915 N95-31536 #
SMC-TR-95-13 ..... p 2769 N95-31567 #
SMC-TR-95-7 ..... p 2883 N95-30394 #

SMU-DS-TR273 ..... p 2964 N95-31831 #

SP-RAPP-1994:34 ..... p 2859 N95-30633
SP-RAPP-1994:39 ..... p 2813 N95-30599 #
SP-RAPP-1994:50 ..... p 2859 N95-30596 #
SP-RAPP-1994:59 ..... p 2913 N95-30631 #
SP-RAPP-94:27 ..... p 2838 N95-30630 #

SR-1 ..... p 2964 N95-31831 #
SR-3 ..... p 2766 N95-31553 #

SRI-3820 ..... p 2998 N95-31141 #

STARS-AC-C001/001/00 ..... p 2942 N95-31683 #

STF10-A94014 ..... p 2902 N95-32316
STF11-A94037 ..... p 2815 N95-30871
STF13-S94001 ..... p 2846 N95-30516
STF13-S94002 ..... p 2934 N95-30662
STF13-S94003 ..... p 2934 N95-30697
STF15-S94007 ..... p 2902 N95-30519
STF19-S94001 ..... p 2992 N95-30717
STF19-S94002 ..... p 3009 N95-30535
STF19-S94004 ..... p 2802 N95-30534
STF21-A94014 ..... p 2798 N95-32372
STF23-A94031 ..... p 2925 N95-30865
STF24-A94044 ..... p 2979 N95-30666
STF24-S94001 ..... p 2802 N95-30518
STF24-S94002 ..... p 2813 N95-30664
STF24-S94003 ..... p 2805 N95-31053
STF30-S94003 ..... p 2804 N95-31052
STF31-A94033 ..... p 2934 N95-30663
STF33-A94042 ..... p 2962 N95-32258
STF33-A94043 ..... p 2934 N95-30625
STF60-A94094 ..... p 2907 N95-32286
STF60-S94005 ..... p 2900 N95-30536
STF75-S93005 ..... p 2891 N95-30510
STF75-S93007 ..... p 2929 N95-30522
STF75-S93039 ..... p 3026 N95-32254
STF75-S93040 ..... p 2891 N95-30520
STF75-S93041 ..... p 2838 N95-30521

SU-GP-93/7-8 ..... p 3018 N95-30431 #

SU-SLAC-PUB-95-6810 ..... p 2987 N95-32026 #
SU-SLAC-PUB-95-6865 ..... p 2993 N95-31256 #

SU-SLAC-R-95-458 ..... p 2966 N95-31682 #
SU-SLAC-R-95-459 ..... p 2966 N95-32083 #
SU-SLAC-R-95-460 ..... p 2989 N95-32266 #
SU-SLAC-R-95-461 ..... p 2989 N95-32267 #

SU-SLAC-444 ..... p 2993 N95-31627 #

SU-SLAC/AP-100 ..... p 3002 N95-32356 #

TARDEC-TR-13619 ..... p 2821 N95-31664 #
TARDEC-TR-13640 ..... p 2821 N95-31666 #
TARDEC-TR-13641 ..... p 2794 N95-31368 #

TFLRF-310 ..... p 2836 N95-31564 #

TKK-SJT-16 ..... p 2858 N95-30538 #

TKK-TKO-B117 ..... p 2933 N95-30566 #

TL-AS-95-94 ..... p 2923 N95-31523 #

TOHOKU-HEP-NOTE-95-06 ..... p 2989 N95-32266 #
TOHOKU-HEP-NOTE-95-07 ..... p 2988 N95-32083 #

TOHOKU-HEP-95-01 ..... p 2989 N95-32266 #
TOHOKU-HEP-95-02 ..... p 2988 N95-32083 #

TOP-1-2-512 ..... p 2852 N95-31574 #

TR-014-1995 ..... p 2925 N95-30452
TR-1008 ..... p 3000 N95-31865 #
TR-100 ..... p 2793 N95-30938 #
TR-1017 ..... p 2951 N95-30890 #
TR-16 ..... p 2793 N95-31014 #
TR-1 ..... p 2816 N95-30997 #
TR-26 ..... p 2985 N95-31609 #
TR-28 ..... p 2986 N95-31832 #
TR-29 ..... p 2797 N95-31830 #
TR-30 ..... p 2795 N95-31595 #
TR-31 ..... p 2796 N95-31691 #
TR-33 ..... p 2796 N95-31596 #
TR-533 ..... p 2947 N95-30930 #
TR-568 ..... p 2942 N95-31657
TR-575 ..... p 2963 N95-31565
TR-5 ..... p 2819 N95-31461 #
TR-63 ..... p 2984 N95-31427 #
TR-66 ..... p 2795 N95-31437 #
TR-6 ..... p 2819 N95-31467 #
TR-7 ..... p 2819 N95-31462 #
TR-8 ..... p 3014 N95-31189 #
TR-8 ..... p 2819 N95-31466 #
TR-94(4507)-1 ..... p 2769 N95-31567 #
TR-94(4925)-2 ..... p 2883 N95-30394 #
TR-95(5940)-4 ..... p 2915 N95-31536 #
TR-95-01 ..... p 2821 N95-31699 #
TR-95-02 ..... p 2997 N95-30973 #
TR-95-03 ..... p 3001 N95-31700 #

TRDEC-TR-13620 ..... p 2821 N95-31663 #

TRITA-MAT-1994-29 ..... p 2888 N95-30701 #
TRITA-MAT-1994-44 ..... p 2956 N95-30499 #
TRITA-MAT-1994-48 ..... p 2963 N95-31396 #
TRITA-MAT-1995-0001 ..... p 2956 N95-30500 #
TRITA-MAT-1995-0002 ..... p 2955 N95-30477 #
TRITA-MAT-1995-0003 ..... p 2956 N95-30601 #
TRITA-MAT-1995-0006 ..... p 2960 N95-31229 #
TRITA-MAT-1995/MS-1 ..... p 2961 N95-31398 #
TRITA-MAT-95/MA-07 ..... p 2961 N95-31397 #

TRITA-NA-9311 ..... p 2873 N95-31414 #
TRITA-NA-9313 ..... p 2961 N95-31648 #
TRITA-NA-9315 ..... p 2960 N95-31361 #
TRITA-NA-9316 ..... p 2794 N95-31356 #
TRITA-NA-9317 ..... p 2873 N95-31415 #
TRITA-NA-9401 ..... p 2957 N95-30713 #

TRITA/MAT-94-47 ..... p 2934 N95-30792 #

TRS-496 ..... p 2933 N95-30539

UAH/ARC-TR-94-07 ..... p 2963 N95-31543 #

UC-405 ..... p 2944 N95-32087 #
UC-405 ..... p 2944 N95-32088 #
UC-414 ..... p 2988 N95-32083 #

UCD-95-4 ..... p 2977 N95-30465 #

UCRL-CR-118231 ..... p 2992 N95-31127 #
UCRL-CR-119438 ..... p 3032 N95-32282 #
UCRL-CR-119484 ..... p 2875 N95-31592 #

UCRL-ID-116054 ..... p 2865 N95-32300 #
UCRL-ID-118223 ..... p 2885 N95-31230
UCRL-ID-118274 ..... p 3004 N95-30769 #
UCRL-ID-116894 ..... p 3026 N95-32285 #
UCRL-ID-119528 ..... p 2947 N95-30578 #
UCRL-ID-119565 ..... p 2911 N95-32350 #
UCRL-ID-119958 ..... p 2795 N95-31593 #

UCRL-JC-116447 ..... p 2810 N95-32283 #
UCRL-JC-116695 ..... p 2936 N95-31056 #
UCRL-JC-116841 ..... p 2886 N95-32029 #
UCRL-JC-116843 ..... p 3006 N95-32026 #
UCRL-JC-116955 ..... p 2861 N95-31133 #
UCRL-JC-116966 ..... p 2865 N95-32100 #
UCRL-JC-117182 ..... p 2987 N95-32038 #
UCRL-JC-117359 ..... p 3016 N95-32268 #
UCRL-JC-117476 ..... p 2900 N95-30472 #
UCRL-JC-118213 ..... p 2879 N95-30507 #
UCRL-JC-118216 ..... p 2987 N95-32039 #
UCRL-JC-118224 ..... p 2901 N95-32027 #

UCRL-JC-118285 ..... p 2912 N95-30373 #
UCRL-JC-118286 ..... p 2792 N95-30714 #
UCRL-JC-118297 ..... p 2982 N95-31174 #
UCRL-JC-118306 ..... p 2955 N95-30470 #
UCRL-JC-118363 ..... p 2993 N95-32042 #
UCRL-JC-118364 ..... p 2987 N95-32041 #
UCRL-JC-118404 ..... p 2877 N95-32049 #
UCRL-JC-118408 ..... p 2887 N95-32155 #
UCRL-JC-118417 ..... p 2898 N95-32102 #
UCRL-JC-118726 ..... p 3028 N95-31129 #
UCRL-JC-118972 ..... p 3016 N95-32284 #
UCRL-JC-119070 ..... p 2994 N95-32074 #
UCRL-JC-119206 ..... p 2955 N95-30471 #
UCRL-JC-119292 ..... p 2881 N95-32047 #
UCRL-JC-119485 ..... p 2875 N95-31637 #
UCRL-JC-119529 ..... p 2925 N95-32358 #
UCRL-JC-119681 ..... p 2810 N95-32272 #
UCRL-JC-119682 ..... p 2809 N95-32051 #
UCRL-JC-119754 ..... p 2932 N95-31704 #
UCRL-JC-119773 ..... p 2928 N95-32097 #
UCRL-JC-120076 ..... p 3007 N95-32148 #
UCRL-JC-120503 ..... p 2911 N95-32281 #
UCRL-JC-120546 ..... p 2741 N95-32164 #

UCRL-LR-114962 ..... p 2875 N95-31591 #
UCRL-LR-117512 ..... p 3004 N95-30742 #
UCRL-LR-118331 ..... p 3021 N95-32359 #

UFIFT-HEP-9413 ..... p 3029 N95-31102 #
UFIFT-HEP-9416 ..... p 3020 N95-32106 #

UM-P-92/84 ..... p 2957 N95-30688 #
UM-P-92/86 ..... p 2820 N95-31623 #
UM-P-93/106 ..... p 3018 N95-30444 #
UM-P-93/107 ..... p 2964 N95-30428 #
UM-P-93/108 ..... p 2955 N95-30445 #
UM-P-93/112 ..... p 2976 N95-30429 #
UM-P-93/117 ..... p 2978 N95-30580 #
UM-P-93/75 ..... p 2965 N95-30430 #
UM-P-93/77 ..... p 3018 N95-30431 #
UM-P-93/80 ..... p 2976 N95-30442 #
UM-P-93/81 ..... p 2976 N95-30443 #
UM-P-93/84 ..... p 2977 N95-30447 #
UM-P-93/87 ..... p 2965 N95-30432 #
UM-P-93/88 ..... p 2982 N95-31176 #
UM-P-93/90 ..... p 2965 N95-30435 #
UM-P-93/91 ..... p 3018 N95-30436 #
UM-P-93/93 ..... p 2812 N95-30451 #
UM-P-93/98 ..... p 3009 N95-30421 #
UM-P-94/09 ..... p 2979 N95-30689 #
UM-P-94/17 ..... p 2992 N95-30960 #
UM-P-94/19 ..... p 2978 N95-30579 #
UM-P-94/21 ..... p 2976 N95-30446 #
UM-P-94/24 ..... p 3018 N95-30426 #
UM-P-94/27 ..... p 2811 N95-30450 #
UM-P-94/34 ..... p 2980 N95-30790 #
UM-P-94/39 ..... p 2811 N95-30422 #
UM-P-94/44 ..... p 3012 N95-30789 #
UM-P-94/45 ..... p 2815 N95-30791 #
UM-P-94/50 ..... p 2976 N95-30441 #
UM-P-94/52 ..... p 2977 N95-30474 #
UM-P-94/54 ..... p 3018 N95-30424 #
UM-P-94/55 ..... p 2977 N95-30475 #
UM-P-94/56 ..... p 2977 N95-30476 #
UM-P-94/57 ..... p 2981 N95-30916 #
UM-P-94/58 ..... p 3018 N95-30437 #
UM-P-94/60 ..... p 2976 N95-30423 #
UM-P-94/63 ..... p 2976 N95-30393 #
UM-P-94/64 ..... p 3018 N95-30438 #
UM-P-94/74 ..... p 2965 N95-30439 #
UM-P-94/76 ..... p 2954 N95-30425 #
UM-P-94/78 ..... p 2976 N95-30427 #
UM-P-94/89 ..... p 2967 N95-31177 #
UM-P-94/93 ..... p 2978 N95-30583 #
UM-P-94/96 ..... p 3018 N95-30440 #

UP-VFRC-11-95 ..... p 2852 N95-31551 #

US-PATENT-APPL-SN-000031 ..... p 2814 N95-30715
US-PATENT-APPL-SN-006544 ..... p 2998 N95-31270
US-PATENT-APPL-SN-010253 ..... p 2884 N95-31213
US-PATENT-APPL-SN-016326 ..... p 2867 N95-30553
US-PATENT-APPL-SN-020939 ..... p 2888 N95-30414
US-PATENT-APPL-SN-025535 ..... p 2784 N95-30661
US-PATENT-APPL-SN-037878 ..... p 2888 N95-30532
US-PATENT-APPL-SN-038364 ..... p 2973 N95-30530
US-PATENT-APPL-SN-040944 ..... p 2862 N95-31275
US-PATENT-APPL-SN-069817 ..... p 2791 N95-30554
US-PATENT-APPL-SN-082645 ..... p 2818 N95-31272
US-PATENT-APPL-SN-094663 ..... p 2753 N95-31180
US-PATENT-APPL-SN-099638 ..... p 2885 N95-31274
US-PATENT-APPL-SN-104682 ..... p 2930 N95-30552
US-PATENT-APPL-SN-104955 ..... p 3009 N95-30533
US-PATENT-APPL-SN-113378 ..... p 2866 N95-30412
US-PATENT-APPL-SN-117512 ..... p 2867 N95-30672
US-PATENT-APPL-SN-117513 ..... p 2973 N95-30411

US-PATENT-APPL-SN-125712 ..... p 2887 N95-30387
US-PATENT-APPL-SN-125715 ..... p 2785 N95-30749
US-PATENT-APPL-SN-127546 ..... p 2887 N95-30386
US-PATENT-APPL-SN-127619 ..... p 2850 N95-31392
US-PATENT-APPL-SN-128289 ..... p 2811 N95-30415
US-PATENT-APPL-SN-128411 ..... p 2974 N95-30725
US-PATENT-APPL-SN-129495 ..... p 2860 N95-30748
US-PATENT-APPL-SN-129499 ..... p 2847 N95-30727
US-PATENT-APPL-SN-129501 ..... p 2887 N95-30399
US-PATENT-APPL-SN-134762 ..... p 2803 N95-30551
US-PATENT-APPL-SN-145352 ..... p 2847 N95-30660
US-PATENT-APPL-SN-147237 ..... p 2974 N95-30549
US-PATENT-APPL-SN-151396 ..... p 2996 N95-30529
US-PATENT-APPL-SN-156752 ..... p 2794 N95-31271
US-PATENT-APPL-SN-159964 ..... p 2771 N95-30418 #
US-PATENT-APPL-SN-163789 ..... p 2879 N95-30658
US-PATENT-APPL-SN-169277 ..... p 2888 N95-30416
US-PATENT-APPL-SN-176373 ..... p 2888 N95-30716
US-PATENT-APPL-SN-199868 ..... p 2996 N95-30679
US-PATENT-APPL-SN-215879 ..... p 2859 N95-30659
US-PATENT-APPL-SN-235844 ..... p 2885 N95-31273
US-PATENT-APPL-SN-258028 ..... p 2862 N95-31179 #
US-PATENT-APPL-SN-314281 ..... p 2848 N95-30917 #
US-PATENT-APPL-SN-321182 ..... p 2783 N95-31009 #
US-PATENT-APPL-SN-324640 ..... p 2953 N95-31693 #
US-PATENT-APPL-SN-324641 ..... p 2953 N95-31692 #
US-PATENT-APPL-SN-367074 ..... p 2816 N95-31011 #
US-PATENT-APPL-SN-371306 ..... p 2816 N95-31010 #
US-PATENT-APPL-SN-378444 ..... p 2974 N95-30747
US-PATENT-APPL-SN-501707 ..... p 2883 N95-30744
US-PATENT-APPL-SN-510976 ..... p 2847 N95-30743
US-PATENT-APPL-SN-617470 ..... p 2847 N95-30746
US-PATENT-APPL-SN-638114 ..... p 2846 N95-30417
US-PATENT-APPL-SN-709901 ..... p 2973 N95-30413
US-PATENT-APPL-SN-747321 ..... p 3014 N95-31269
US-PATENT-APPL-SN-777773 ..... p 3011 N95-30673
US-PATENT-APPL-SN-874403 ..... p 2803 N95-30750
US-PATENT-APPL-SN-889885 ..... p 2862 N95-31342
US-PATENT-APPL-SN-899977 ..... p 2862 N95-31343
US-PATENT-APPL-SN-921863 ..... p 2996 N95-30678
US-PATENT-APPL-SN-931228 ..... p 2995 N95-30402
US-PATENT-APPL-SN-936986 ..... p 2996 N95-30753
US-PATENT-APPL-SN-946716 ..... p 2860 N95-30726
US-PATENT-APPL-SN-966825 ..... p 2996 N95-30724
US-PATENT-APPL-SN-976349 ..... p 2974 N95-30550
US-PATENT-APPL-SN-999619 ..... p 3011 N95-30728

US-PATENT-CLASS-114-67R ..... p 2867 N95-30553
US-PATENT-CLASS-117-88 ..... p 3014 N95-31269
US-PATENT-CLASS-123-546 ..... p 2887 N95-30386
US-PATENT-CLASS-156-693 ..... p 2883 N95-30744
US-PATENT-CLASS-204-275 ..... p 2794 N95-31271
US-PATENT-CLASS-205-203 ..... p 2803 N95-30551
US-PATENT-CLASS-248-550 ..... p 2888 N95-30532
US-PATENT-CLASS-280 ..... p 2930 N95-30552
US-PATENT-CLASS-285-23 ..... p 2888 N95-30716
US-PATENT-CLASS-285-412 ..... p 2887 N95-30387
US-PATENT-CLASS-313-495 ..... p 2862 N95-31342
US-PATENT-CLASS-324-96 ..... p 2996 N95-30753
US-PATENT-CLASS-330-294 ..... p 2859 N95-30659
US-PATENT-CLASS-342-15 ..... p 2846 N95-30417
US-PATENT-CLASS-342-194 ..... p 2850 N95-31392
US-PATENT-CLASS-342-25 ..... p 2847 N95-30727
US-PATENT-CLASS-342-375 ..... p 2847 N95-30660
US-PATENT-CLASS-342-45 ..... p 2847 N95-30746
US-PATENT-CLASS-348-117 ..... p 2996 N95-30678
US-PATENT-CLASS-348-117 ..... p 2753 N95-31180
US-PATENT-CLASS-356-345 ..... p 2995 N95-30402
US-PATENT-CLASS-356-345 ..... p 2879 N95-30658
US-PATENT-CLASS-356-445 ..... p 2862 N95-31343
US-PATENT-CLASS-359-087 ..... p 3011 N95-30728
US-PATENT-CLASS-361-56 ..... p 2860 N95-30726
US-PATENT-CLASS-364-574 ..... p 2974 N95-30550
US-PATENT-CLASS-367-118 ..... p 2974 N95-30549
US-PATENT-CLASS-367-135 ..... p 2974 N95-30747
US-PATENT-CLASS-367-140 ..... p 2973 N95-30413
US-PATENT-CLASS-367-149 ..... p 2996 N95-30679
US-PATENT-CLASS-367-1 ..... p 2866 N95-30412
US-PATENT-CLASS-367-1 ..... p 2867 N95-30672
US-PATENT-CLASS-367-1 ..... p 2974 N95-30725
US-PATENT-CLASS-367-7 ..... p 2973 N95-30530
US-PATENT-CLASS-367-98 ..... p 2847 N95-30743
US-PATENT-CLASS-372-20 ..... p 2885 N95-31273
US-PATENT-CLASS-372-20 ..... p 2885 N95-31274
US-PATENT-CLASS-372-41 ..... p 2884 N95-31213
US-PATENT-CLASS-380-48 ..... p 2860 N95-30748
US-PATENT-CLASS-381-71 ..... p 2973 N95-30411
US-PATENT-CLASS-381-71 ..... p 2814 N95-30715
US-PATENT-CLASS-385-25 ..... p 2996 N95-30529
US-PATENT-CLASS-385-37 ..... p 2998 N95-31270
US-PATENT-CLASS-385-81 ..... p 2888 N95-30414
US-PATENT-CLASS-418-126 ..... p 2887 N95-30399
US-PATENT-CLASS-428-201 ..... p 2784 N95-30661
US-PATENT-CLASS-428-34 ..... p 2785 N95-30749
US-PATENT-CLASS-428-395 ..... p 2818 N95-31272
US-PATENT-CLASS-430-324 ..... p 2803 N95-30750

US-PATENT-CLASS-501-12 ..... p 3009 N95-30533
US-PATENT-CLASS-505-190 ..... p 3011 N95-30673
US-PATENT-CLASS-556-70 ..... p 2771 N95-30418 #
US-PATENT-CLASS-73-602 ..... p 2996 N95-30724
US-PATENT-CLASS-891-810 ..... p 2888 N95-30416
US-PATENT-CLASS-96-175 ..... p 2791 N95-30554

US-PATENT-5-370,087 ..... p 2887 N95-30386
US-PATENT-5,293,261 ..... p 3011 N95-30728
US-PATENT-5,313,266 ..... p 2995 N95-30402
US-PATENT-5,339,087 ..... p 2847 N95-30660
US-PATENT-5,342,737 ..... p 2803 N95-30750
US-PATENT-5,353,260 ..... p 2974 N95-30747
US-PATENT-5,356,936 ..... p 2811 N95-30415
US-PATENT-5,357,484 ..... p 2974 N95-30549
US-PATENT-5,359,574 ..... p 2866 N95-30412
US-PATENT-5,359,663 ..... p 2973 N95-30411
US-PATENT-5,359,951 ..... p 2867 N95-30553
US-PATENT-5,360,325 ..... p 2887 N95-30399
US-PATENT-5,362,098 ..... p 2930 N95-30552
US-PATENT-5,365,490 ..... p 2867 N95-30672
US-PATENT-5,366,198 ..... p 2888 N95-30532
US-PATENT-5,366,254 ..... p 2888 N95-30716
US-PATENT-5,367,333 ..... p 2996 N95-30678
US-PATENT-5,367,496 ..... p 2973 N95-30530
US-PATENT-5,368,344 ..... p 2887 N95-30387
US-PATENT-5,368,914 ..... p 2784 N95-30661
US-PATENT-5,369,485 ..... p 2879 N95-30658
US-PATENT-5,369,625 ..... p 2973 N95-30413
US-PATENT-5,371,257 ..... p 2771 N95-30418 #
US-PATENT-5,371,479 ..... p 2859 N95-30659
US-PATENT-5,371,720 ..... p 2996 N95-30679
US-PATENT-5,371,801 ..... p 2814 N95-30715
US-PATENT-5,371,814 ..... p 2996 N95-30529
US-PATENT-5,372,634 ..... p 2791 N95-30554
US-PATENT-5,373,297 ..... p 2846 N95-30417
US-PATENT-5,373,318 ..... p 2753 N95-31180
US-PATENT-5,373,456 ..... p 2974 N95-30550
US-PATENT-5,374,085 ..... p 2888 N95-30414
US-PATENT-5,374,347 ..... p 2803 N95-30551
US-PATENT-5,375,502 ..... p 2888 N95-30416
US-PATENT-5,376,594 ..... p 3009 N95-30533
US-PATENT-5,376,624 ..... p 3011 N95-30673
US-PATENT-5,378,962 ..... p 2862 N95-31342
US-PATENT-5,379,043 ..... p 2847 N95-30746
US-PATENT-5,379,109 ..... p 2862 N95-31343
US-PATENT-5,379,346 ..... p 2860 N95-30748
US-PATENT-5,381,381 ..... p 2974 N95-30725
US-PATENT-5,381,428 ..... p 2885 N95-31274
US-PATENT-5,381,433 ..... p 2884 N95-31213
US-PATENT-5,381,755 ..... p 3014 N95-31269
US-PATENT-5,382,185 ..... p 2862 N95-31275
US-PATENT-5,383,366 ..... p 2996 N95-30724
US-PATENT-5,385,633 ..... p 2883 N95-30744
US-PATENT-5,388,021 ..... p 2860 N95-30726
US-PATENT-5,388,112 ..... p 2885 N95-31273
US-PATENT-5,389,411 ..... p 2785 N95-30749
US-PATENT-5,389,441 ..... p 2818 N95-31272
US-PATENT-5,390,154 ..... p 2847 N95-30743
US-PATENT-5,394,151 ..... p 2847 N95-30727
US-PATENT-5,396,166 ..... p 2996 N95-30753
US-PATENT-5,400,422 ..... p 2998 N95-31270
US-PATENT-5,402,131 ..... p 2850 N95-31392

USAARL-95-13 ..... p 2864 N95-31842 #
USAARL-95-14 ..... p 2928 N95-31140 #

USAATCOM-TR-94-D-22 ..... p 2874 N95-31475 #

USAFETAC/TN-95/001 ..... p 2920 N95-31524 #

USCG-D-05-95 ..... p 2924 N95-32363 #

UTS-DFT-94-15 ..... p 2984 N95-31547 #

UVA-527437/CS95/101 ..... p 3023 N95-30619 #

WAPD-T-3041 ..... p 2798 N95-32318 #

WES-WIS-31 ..... p 2919 N95-30976 #

WHC-SA-2675 ..... p 2798 N95-32091 #

WHC-SD-GN-UM-30008-REV-1 ... p 3026 N95-32107 #

WHOI-94-31 ..... p 2923 N95-30918 #
WHOI-95-01 ..... p 2923 N95-31600 #

WL-TR-94-3064 ..... p 2820 N95-31471 #
WL-TR-94-3094 ..... p 2743 N95-30885 #
WL-TR-95-3025 ..... p 2753 N95-31656 #
WL-TR-95-3026 ..... p 2753 N95-31655 #
WL-TR-95-3027 ..... p 2753 N95-31463 #

WSRC-MS-93-316P ..... p 2890 N95-32367 #

Y/DK-1043 ..... p 2797 N95-31840 #

Y/DW-1352 ..... p 2823 N95-32352 #

APPENDIX

NASA SCIENTIFIC AND TECHNICAL INFORMATION OFFICE PRODUCTS AND SERVICES

The NASA Scientific and Technical Information (STI) Office provides for the collection and announcement of aerospace-related reports and literature obtained worldwide through agreements and exchanges. The result of the collection is the comprehensive NASA STI Database that covers aeronautics, space, and supporting disciplines.

The STI Database, documents generated or obtained by NASA, and products and services derived from or supporting the database are made available to the NASA research community and to the public. Descriptions and sources of these items are presented in the following pages.

Scientific and Technical Aerospace Reports (STAR) is an abstract journal, listing citations with abstracts for aerospace-related reports obtained from worldwide sources. *STAR* is issued on the first of each month, and announces current documents that have been entered into the NASA STI Database during the previous month. The reports are of the following types:

- NASA, NASA contractor, and NASA grantee reports;
- Reports issued by other U.S. Government agencies, domestic and foreign institutions, universities, and private firms;
- Translations in report form;
- NASA-owned patents and patent applications
- Other U.S. Government agency and foreign patents and patent applications
- Domestic and foreign dissertations and theses.

Journal, book, and conference literature, journal translations, and certain foreign dissertations having the same subject scope as *STAR* are announced in a companion journal, *NASA Open Volumes on Aerospace (NOVA). NOVA* is issued on the 15th of each month and is available from the NASA Center for AeroSpace Information, at the address below.

ELIGIBILITY AND REGISTRATION FOR NASA STI PRODUCTS AND SERVICES

Organizations of the type listed below that have registered with NASA can receive products and services.

- NASA offices and installations, contractors, subcontractors, grantees, and consultants;
- Other U.S. Government agencies and their contractors;
- Libraries in the United States that have arrangements with NASA to maintain collections of NASA documents for public reference;
- Other organizations in the United States having a need for NASA documents in work related to aeronautics and space research;
- Organizations abroad that have established reciprocal documents exchange arrangements with NASA.

The central service points—central points of document acquisition and control within qualified organizations—or individuals are eligible to register for NASA STI products and services. Domestic organizations or individuals may be eligible to receive various classes of NASA publications and services and should address their requests for registration or further information to:

ATTN: Registration Services
NASA Center for AeroSpace Information
800 Elkridge Landing Road
Linthicum Heights, MD 21090-2934
301-621-0390

Organizations abroad should direct requests to:

National Aeronautics and Space Administration
Scientific and Technical Information Office (JT)
International STI Office
Washington, DC 20546-0001
USA
703-271-5640

SUBJECT SCOPE

The subject scope of *STAR* and *NOVA* includes all aspects of aeronautics and space research and development, supporting basic and applied research, and applications. Aerospace aspects of Earth resources, energy development, conservation, oceanography, environmental protection, urban transportation, and other topics of high national priority are also covered.

HOW TO USE *STAR* SUBJECT CATEGORIES

Abstracts in *STAR* are categorized by 10 major subject divisions that are divided further into 76 specific subject categories. The subject divisions and categories are listed in the Table of Contents together with a note for each that defines its scope and provides any cross-references. For example:

> **16 SPACE TRANSPORTATION**
>
> Includes passenger and cargo space transportation, e.g., shuttle operations; and space rescue techniques. For related information see also *03 Air Transportation and Safety* and *18 Spacecraft Design, Testing and Performance*. For space suits see *54 Man/System Technology and Life Support*.

CROSS-REFERENCES

Individual *STAR* abstracts are not ordinarily cross-referenced, except for certain conference reports or book translations that have had separate abstracts written for their component papers or chapters. Citations and abstracts of the components follow immediately after those of the parent document. When the subject content of a component differs sufficiently from the general content of the parent, a cross-reference citation also is printed at the end of the category to which it normally would have been assigned if it were independent.

DOCUMENTS ON MICROFICHE

Documents available on microfiche are designated by a pound sign (#) following the accession number.

LIMITED REPRODUCIBILITY

A note of limited reproducibility appears in the citation, if there are factors affecting the reproducibility of more than 20% of the document. These factors include faint or broken type, color photographs, black and white photographs, foldouts, dot matrix print, or some other factor that limits the reproducibility of the document. This notation also appears on the microfiche header.

NASA PATENTS AND PATENT APPLICATIONS

Patents and patent applications owned by NASA are announced in *STAR* under appropriate subject categories and are referenced in the *STAR* indexes. In the Report Number Index, patents are indexed by the NASA Case Number, and the U.S. Patent Class. Patent applications are indexed by the NASA Case Number and the U.S. Patent Application Serial Number.

Printed copies of patents (which are not microfiched) are available for purchase from the U.S. Patent and Trademark Office.

When ordering patents, the U.S. Patent Number should be used, and payment must be remitted in advance, by money order or check payable to the Commissioner of Patents and Trademarks. Prepaid purchase coupons for ordering are also available from the U.S. Patent and Trademark Office.

NASA patent application specifications are sold in both paper copy and microfiche by the NASA Center for AeroSpace Information (CASI). The N accession number should be used in ordering either paper copy or microfiche from CASI.

The patents and patent applications announced in *STAR* are owned by NASA and are available for royalty-free licensing. Requests for licensing terms and further information should be addressed to:

National Aeronautics and Space Administration
Associate General Counsel for Intellectual Property
Code GP
Washington, DC 20546-0001

SOURCES FOR DOCUMENTS

One or more sources from which a document announced in *STAR* is available to the public is ordinarily given on the last line of the citation. The most commonly indicated sources and their acronyms or abbreviations are listed below, and their addresses are listed on page A-6. If the publication is available from a source other than those listed, the publisher and his address will be displayed on the availability line or in combination with the corporate source line.

Avail: CASI. Sold by the NASA Center for AeroSpace Information. Prices for hard copy (HC) and microfiche (MF) are indicated by a price code following the letters HC or MF in the *STAR* citation. Current values for the price codes are given in the tables on page A-7.

NOTE ON ORDERING DOCUMENTS: When ordering publications from NASA CASI, use the N accession number or other report number. It is also advisable to cite the title and other bibliographic identification.

Avail: SOD (or GPO). Sold by the Superintendent of Documents, U.S. Government Printing Office, in hard copy.

Avail: BLL (formerly NLL): British Library Lending Division, Boston Spa, Wetherby, Yorkshire, England. Photocopies available from this organization at the price shown. (If none is given, inquiry should be addressed to the BLL.)

Avail: DOE Depository Libraries. Organizations in U.S. cities and abroad that maintain collections of Department of Energy reports, usually in microfiche form, are listed in *Energy Research Abstracts*. Services available from the DOE and its depositories are described in a booklet, *DOE Technical Information Center - Its Functions and Services* (TID-4660), which may be obtained without charge from the DOE Technical Information Center.

Avail: ESDU. Pricing information on specific data, computer programs, and details on Engineering Sciences Data Unit (ESDU) topic categories can be obtained from ESDU International Ltd. Requesters in North America should use the Virginia address while all other requesters should use the London address, both of which are on page A-6.

Avail: Fachinformationszentrum Karlsruhe. Gesellschaft für wissenschaftlich-technische Information mbH 76344 Eggenstein-Leopoldshafen, Germany.

Avail: HMSO. Publications of Her Majesty's Stationery Office are sold in the U.S. by Pendragon House, Inc. (PHI), Redwood City, CA. The U.S. price (including a service and mailing charge) is given, or a conversion table may be obtained from PHI.

Avail: Issuing Activity, or Corporate Author, or no indication of availability. Inquiries as to the availability of these documents should be addressed to the organization shown in the citation as the corporate author of the document.

Avail: NASA Public Document Rooms. Documents so indicated may be examined at or purchased from the National Aeronautics and Space Administration (JBD-4), Public Documents Room (Room 1H23), Washington, DC 20546-0001, or public document rooms located at NASA installations, and the NASA Pasadena Office at the Jet Propulsion Laboratory.

Avail: NTIS. Sold by the National Technical Information Service. Initially distributed microfiche under the NTIS SRIM (Selected Research in Microfiche) are available. For information concerning this service, consult the NTIS Subscription Section, Springfield, VA 22161.

Avail: Univ. Microfilms. Documents so indicated are dissertations selected from *Dissertation Abstracts* and are sold by University Microfilms as xerographic copy (HC) and microfilm. All requests should cite the author and the Order Number as they appear in the citation.

Avail: US Patent and Trademark Office. Sold by Commissioner of Patents and Trademarks, U.S. Patent and Trademark Office, at the standard price of $1.50 each, postage free. (See discussion of NASA patents and patent applications on page A-3.)

Avail: (US Sales Only). These foreign documents are available to users within the United States from the National Technical Information Service (NTIS). They are available to users outside the United States through the International Nuclear Information Service (INIS) representative in their country, or by applying directly to the issuing organization.

Avail: USGS. Originals of many reports from the U.S. Geological Survey, which may contain color illustrations, or otherwise may not have the quality of illustrations preserved in the microfiche or facsimile reproduction, may be examined by the public at the libraries of the USGS field offices whose addresses are listed on page A-6. The libraries may be queried concerning the availability of specific documents and the possible utilization of local copying services, such as color reproduction.

FEDERAL DEPOSITORY LIBRARY PROGRAM

In order to provide the general public with greater access to U.S. Government publications, Congress established the Federal Depository Library Program under the Government Printing Office (GPO), with 53 regional depositories responsible for permanent retention of material, inter-library loan, and reference services. At least one copy of nearly every NASA and NASA-sponsored publication, either in printed or microfiche format, is received and retained by the 53 regional depositories. A list of the regional GPO libraries, arranged alphabetically by state, appears on page A-8. These libraries are *not* sales outlets. A local library can contact a regional depository to help locate specific reports, or direct contact may be made by an individual.

PUBLIC COLLECTION OF NASA DOCUMENTS

An extensive collection of NASA and NASA-sponsored publications is maintained by the British Library Lending Division, Boston Spa, Wetherby, Yorkshire, England for public access. The British Library Lending Division also has available many of the non-NASA publications cited in *STAR*. European requesters may purchase facsimile copy or microfiche of NASA and NASA-sponsored documents, those identified by both the symbols # and * from FIZ—Fachinformation Karlsruhe—Bibliographic Service, D-76344 Eggenstein-Leopoldshafen, Germany and TIB—Technische Informationsbibliothek, P.O. Box 60 80, D-30080 Hannover, Germany.

SUBMITTING DOCUMENTS

All users of this abstract service are urged to forward reports to be considered for announcement in *STAR*. This will aid NASA in its efforts to provide the fullest possible coverage of all scientific and technical publications that might support aeronautics and space research and development. If you

usual contract- or grant-reporting channels), please send them for consideration to the NASA Center for AeroSpace Information, 800 Elkridge Landing Road, Linthicum Heights, MD 21090-2934.

Reprints of journal articles, book chapters, and conference papers are also welcome. These will be considered for announcement in *STAR's* companion journal, *NOVA*.

You may specify a particular source to be included in a report announcement if you wish; otherwise the report will be placed on a public sale at the NASA Center for AeroSpace Information. Copyrighted publications will be announced but not distributed or sold.

PURCHASE OF *STAR*

STAR is publicly available on annual subscription from the NASA Center for AeroSpace Information (CASI). 1995 *STAR* subscription prices are $100.00/domestic and $125.00/foreign. Single copy prices: $33.00/domestic, $41.00/foreign.

An annual, cumulative *STAR Index* is also available at $70.00/domestic and foreign.

STAR is available to registered users on annual subscription from the NASA Center for AeroSpace Information, ATTN: Registration Services, 800 Elkridge Landing Road, Linthicum Heights, MD 21090-2934.

ADDRESSES OF ORGANIZATIONS

British Library Lending Division
Boston Spa, Wetherby, Yorkshire
England

Commissioner of Patents and Trademarks
U.S. Patent and Trademark Office
Washington, DC 20231

Department of Energy
Technical Information Center
P.O. Box 62
Oak Ridge, TN 37830

European Space Agency-
Information Retrieval Service ESRIN
Via Galileo Galilei
00044 Frascati (Rome) Italy

Engineering Sciences Data Unit International
P.O. Box 1633
Manassas, VA 22110

Engineering Sciences Data Unit
International, Ltd.
251-259 Regent Street
London, W1R 7AD, England

Fachinformationszentrum Karlsruhe
Gesellschaft für wissenschaftlich-technische
Information mbH
76344 Eggenstein-Leopoldshafen, Germany

Her Majesty's Stationery Office
P.O. Box 569, S.E. 1
London, England

NASA Center for AeroSpace Information
800 Elkridge Landing Road
Linthicum Heights, MD 21090-2934

National Aeronautics and Space Administration
Scientific and Technical Information Office
(JT)
Washington, DC 20546-0001

National Technical Information Service
5285 Port Royal Road
Springfield, VA 22161

Pendragon House, Inc.
899 Broadway Avenue
Redwood City, CA 94063

Superintendent of Documents
U.S. Government Printing Office
Washington, DC 20402

University Microfilms
A Xerox Company
300 North Zeeb Road
Ann Arbor, MI 48106

University Microfilms, Ltd.
Tylers Green
London, England

U.S. Geological Survey Library National Center
MS 950
12201 Sunrise Valley Drive
Reston, VA 22092

U.S. Geological Survey Library
2255 North Gemini Drive
Flagstaff, AZ 86001

U.S. Geological Survey
345 Middlefield Road
Menlo Park, CA 94025

U.S. Geological Survey Library
Box 25046
Denver Federal Center, MS914
Denver, CO 80225

NASA CASI PRICE CODE TABLE

(Effective January 1, 1995)

CASI PRICE CODE	NORTH AMERICAN PRICE	FOREIGN PRICE
A01	$ 6.00	$ 12.00
A02	9.00	18.00
A03	17.50	35.00
A04-A05	19.50	39.00
A06-A09	27.00	54.00
A10-A13	36.50	73.00
A14-A17	44.50	89.00
A18-A21	52.00	104.00
A22-A25	61.00	122.00
A99	Call For Price	Call For Price

IMPORTANT NOTICE

For users not registered at the NASA CASI, prepayment is required. Additionally, a shipping and handling fee of $1.00 per document for delivery within the United States and $9.00 per document for delivery outside the United States is charged.

For users registered at the NASA CASI, document orders may be invoiced at the end of the month, charged against a deposit account, or paid by check or credit card. NASA CASI accepts American Express, Diners' Club, MasterCard, and VISA credit cards. There are no shipping and handling charges. To register at the NASA CASI, please request a registration form through the NASA Access Help Desk at the numbers or addresses below.

RETURN POLICY

Effective June 1, 1995, the NASA Center for AeroSpace Information will gladly replace or make full refund on items you have requested if we have made an error in your order, if the item is defective, or if it was received in damaged condition and you contact us within 30 days of your original request. Just contact our NASA Access Help Desk at the numbers or addresses listed below.

NASA Center for AeroSpace Information
800 Elkridge Landing Road
Linthicum Heights, MD 21090-2934
Telephone: (301) 621-0390
E-mail: help@sti.nasa.gov
Fax: (301) 621-0134

Rev. 5/95

FEDERAL REGIONAL DEPOSITORY LIBRARIES

ALABAMA

AUBURN UNIV. AT MONTGOMERY LIBRARY
Documents Dept.
7300 University Dr.
Montgomery, AL 36117-3596
(205) 244-3650 Fax: (205) 244-0678

UNIV. OF ALABAMA
Amelia Gayle Gorgas Library
Govt. Documents
P.O. Box 870266
Tuscaloosa, AL 35487-0266
(205) 348-6046 Fax: (205) 348-0760

ARIZONA

DEPT. OF LIBRARY, ARCHIVES, AND PUBLIC RECORDS
Research Division
Third Floor, State Capitol
1700 West Washington
Phoenix, AZ 85007
(602) 542-3701 Fax: (602) 542-4400

ARKANSAS

ARKANSAS STATE LIBRARY
State Library Service Section
Documents Service Section
One Capitol Mall
Little Rock, AR 72201-1014
(501) 682-2053 Fax: (501) 682-1529

CALIFORNIA

CALIFORNIA STATE LIBRARY
Govt. Publications Section
P.O. Box 942837 - 914 Capitol Mall
Sacramento, CA 94337-0091
(916) 654-0069 Fax: (916) 654-0241

COLORADO

UNIV. OF COLORADO - BOULDER
Libraries - Govt. Publications
Campus Box 184
Boulder, CO 80309-0184
(303) 492-8834 Fax: (303) 492-1881

DENVER PUBLIC LIBRARY
Govt. Publications Dept. BSG
1357 Broadway
Denver, CO 80203-2165
(303) 640-8846 Fax: (303) 640-8817

CONNECTICUT

CONNECTICUT STATE LIBRARY
231 Capitol Avenue
Hartford, CT 06106
(203) 566-4971 Fax: (203) 566-3322

FLORIDA

UNIV. OF FLORIDA LIBRARIES
Documents Dept.
240 Library West
Gainesville, FL 32611-2048
(904) 392-0366 Fax: (904) 392-7251

GEORGIA

UNIV. OF GEORGIA LIBRARIES
Govt. Documents Dept.
Jackson Street
Athens, GA 30602-1645
(706) 542-8949 Fax: (706) 542-4144

HAWAII

UNIV. OF HAWAII
Hamilton Library
Govt. Documents Collection
2550 The Mall
Honolulu, HI 96822
(808) 948-8230 Fax: (808) 956-5968

IDAHO

UNIV. OF IDAHO LIBRARY
Documents Section
Raybum Street
Moscow, ID 83844-2353
(208) 885-6344 Fax: (208) 885-6817

ILLINOIS

ILLINOIS STATE LIBRARY
Federal Documents Dept.
300 South Second Street
Springfield, IL 62701-1796
(217) 782-7596 Fax: (217) 782-6437

INDIANA

INDIANA STATE LIBRARY
Serials/Documents Section
140 North Senate Avenue
Indianapolis, IN 46204-2296
(317) 232-3679 Fax: (317) 232-3728

IOWA

UNIV. OF IOWA LIBRARIES
Govt. Publications
Washington & Madison Streets
Iowa City, IA 52242-1166
(319) 335-5926 Fax: (319) 335-5900

KANSAS

UNIV. OF KANSAS
Govt. Documents & Maps Library
6001 Malott Hall
Lawrence, KS 66045-2800
(913) 864-4660 Fax: (913) 864-3855

KENTUCKY

UNIV. OF KENTUCKY
King Library South
Govt. Publications/Maps Dept.
Patterson Drive
Lexington, KY 40506-0039
(606) 257-3139 Fax: (606) 257-3139

LOUISIANA

LOUISIANA STATE UNIV.
Middleton Library
Govt. Documents Dept.
Baton Rouge, LA 70803-3312
(504) 388-2570 Fax: (504) 388-6992

LOUISIANA TECHNICAL UNIV.
Prescott Memorial Library
Govt. Documents Dept.
Ruston, LA 71272-0046
(318) 257-4962 Fax: (318) 257-2447

MAINE

UNIV. OF MAINE
Raymond H. Fogler Library
Govt. Documents Dept.
Orono, ME 04469-5729
(207) 581-1673 Fax: (207) 581-1653

MARYLAND

UNIV. OF MARYLAND - COLLEGE PARK
McKeldin Library
Govt. Documents/Maps Unit
College Park, MD 20742
(301) 405-9165 Fax: (301) 314-9416

MASSACHUSETTS

BOSTON PUBLIC LIBRARY
Govt. Documents
666 Boylston Street
Boston, MA 02117-0286
(617) 536-5400, ext. 226
Fax: (617) 536-7758

MICHIGAN

DETROIT PUBLIC LIBRARY
5201 Woodward Avenue
Detroit, MI 48202-4093
(313) 833-1025 Fax: (313) 833-0156

LIBRARY OF MICHIGAN
Govt. Documents Unit
P.O. Box 30007
717 West Allegan Street
Lansing, MI 48909
(517) 373-1300 Fax: (517) 373-3381

MINNESOTA

UNIV. OF MINNESOTA
Govt. Publications
409 Wilson Library
309 19th Avenue South
Minneapolis, MN 55455
(612) 624-5073 Fax: (612) 626-9353

MISSISSIPPI

UNIV. OF MISSISSIPPI
J.D. Williams Library
106 Old Gym Bldg.
University, MS 38677
(601) 232-5857 Fax: (601) 232-7465

MISSOURI

UNIV. OF MISSOURI - COLUMBIA
106B Ellis Library
Govt. Documents Sect.
Columbia, MO 65201-5149
(314) 882-6733 Fax: (314) 882-8044

MONTANA

UNIV. OF MONTANA
Mansfield Library
Documents Division
Missoula, MT 59812-1195
(406) 243-6700 Fax: (406) 243-2060

NEBRASKA

UNIV. OF NEBRASKA - LINCOLN
D.L. Love Memorial Library
Lincoln, NE 68588-0410
(402) 472-2562 Fax: (402) 472-5131

NEVADA

THE UNIV. OF NEVADA LIBRARIES
Business and Govt. Information Center
Reno, NV 89557-0044
(702) 784-6579 Fax: (702) 784-1751

NEW JERSEY

NEWARK PUBLIC LIBRARY
Science Div. - Public Access
P.O. Box 630
Five Washington Street
Newark, NJ 07101-7812
(201) 733-7782 Fax: (201) 733-5648

NEW MEXICO

UNIV. OF NEW MEXICO
General Library
Govt. Information Dept.
Albuquerque, NM 87131-1466
(505) 277-5441 Fax: (505) 277-6019

NEW MEXICO STATE LIBRARY
325 Don Gaspar Avenue
Santa Fe, NM 87503
(505) 827-3824 Fax: (505) 827-3888

NEW YORK

NEW YORK STATE LIBRARY
Cultural Education Center
Documents/Gift & Exchange Section
Empire State Plaza
Albany, NY 12230-0001
(518) 474-5355 Fax: (518) 474-5786

NORTH CAROLINA

UNIV. OF NORTH CAROLINA - CHAPEL HILL
Walter Royal Davis Library
CB 3912, Reference Dept.
Chapel Hill, NC 27514-8890
(919) 962-1151 Fax: (919) 962-4451

NORTH DAKOTA

NORTH DAKOTA STATE UNIV. LIB.
Documents
P.O. Box 5599
Fargo, ND 58105-5599
(701) 237-8886 Fax: (701) 237-7138

UNIV. OF NORTH DAKOTA
Chester Fritz Library
University Station
P.O. Box 9000 - Centennial and University Avenue
Grand Forks, ND 58202-9000
(701) 777-4632 Fax: (701) 777-3319

OHIO

STATE LIBRARY OF OHIO
Documents Dept.
65 South Front Street
Columbus, OH 43215-4163
(614) 644-7051 Fax: (614) 752-9178

OKLAHOMA

OKLAHOMA DEPT. OF LIBRARIES
U.S. Govt. Information Division
200 Northeast 18th Street
Oklahoma City, OK 73105-3298
(405) 521-2502, ext. 253
Fax: (405) 525-7804

OKLAHOMA STATE UNIV.
Edmon Low Library
Stillwater, OK 74078-0375
(405) 744-6546 Fax: (405) 744-5183

OREGON

PORTLAND STATE UNIV.
Branford P. Millar Library
934 Southwest Harrison
Portland, OR 97207-1151
(503) 725-4123 Fax: (503) 725-4524

PENNSYLVANIA

STATE LIBRARY OF PENN.
Govt. Publications Section
116 Walnut & Commonwealth Ave.
Harrisburg, PA 17105-1601
(717) 787-3752 Fax: (717) 783-2070

SOUTH CAROLINA

CLEMSON UNIV.
Robert Muldrow Cooper Library
Public Documents Unit
P.O. Box 343001
Clemson, SC 29634-3001
(803) 656-5174 Fax: (803) 656-3025

UNIV. OF SOUTH CAROLINA
Thomas Cooper Library
Green and Sumter Streets
Columbia, SC 29208
(803) 777-4841 Fax: (803) 777-9503

TENNESSEE

UNIV. OF MEMPHIS LIBRARIES
Govt. Publications Dept.
Memphis, TN 38152-0001
(901) 678-2206 Fax: (901) 678-2511

TEXAS

TEXAS STATE LIBRARY
United States Documents
P.O. Box 12927 - 1201 Brazos
Austin, TX 78701-0001
(512) 463-5455 Fax: (512) 463-5436

TEXAS TECH. UNIV. LIBRARIES
Documents Dept.
Lubbock, TX 79409-0002
(806) 742-2282 Fax: (806) 742-1920

UTAH

UTAH STATE UNIV.
Merrill Library Documents Dept.
Logan, UT 84322-3000
(801) 797-2678 Fax: (801) 797-2677

VIRGINIA

UNIV. OF VIRGINIA
Alderman Library
Govt. Documents
University Ave. & McCormick Rd.
Charlottesville, VA 22903-2498
(804) 824-3133 Fax: (804) 924-4337

WASHINGTON

WASHINGTON STATE LIBRARY
Govt. Publications
P.O. Box 42478
16th and Water Streets
Olympia, WA 98504-2478
(206) 753-4027 Fax: (206) 586-7575

WEST VIRGINIA

WEST VIRGINIA UNIV. LIBRARY
Govt. Documents Section
P.O. Box 6069 - 1549 University Ave.
Morgantown, WV 26506-6069
(304) 293-3051 Fax: (304) 293-6638

WISCONSIN

ST. HIST. SOC. OF WISCONSIN LIBRARY
Govt. Publication Section
816 State Street
Madison, WI 53706
(608) 264-6525 Fax: (608) 264-6520

MILWAUKEE PUBLIC LIBRARY
Documents Division
814 West Wisconsin Avenue
Milwaukee, WI 53233
(414) 286-3073 Fax: (414) 286-8074

*U.S. GOVERNMENT PRINTING OFFICE: 1995-405-129/20013

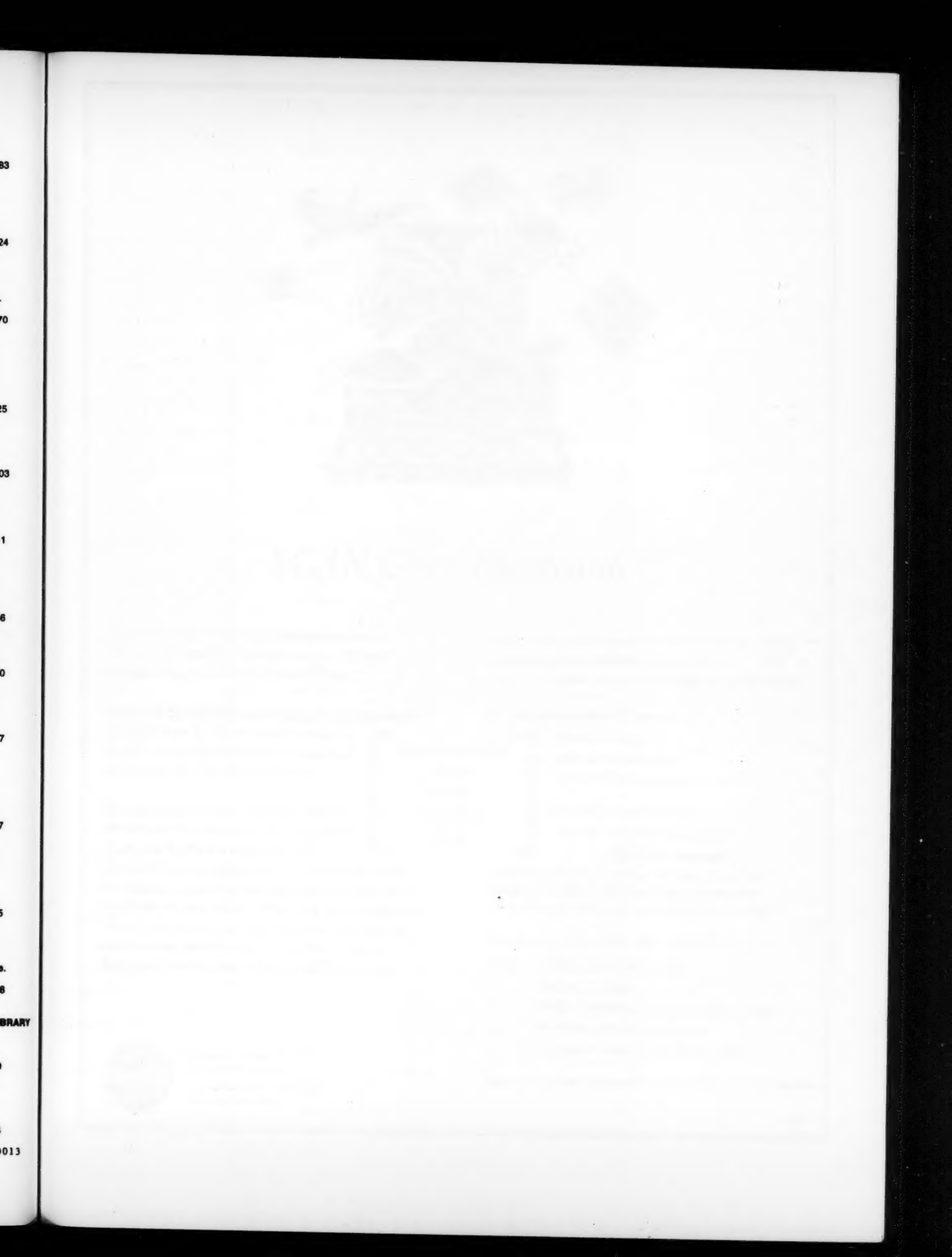

SCAN Goes Electronic!

If you have NASA Mail or if you can access the Internet, you can get biweekly issues of *SCAN* delivered to your desktop absolutely free!

Electronic SCAN takes advantage of computer technology to alert you to the latest aerospace-related, worldwide scientific and technical information that has been published.

No more waiting while the paper copy is printed and mailed to you. You can review *Electronic SCAN* the same day it is released! And you get all 191—or any combination of—subject areas of announcements with abstracts to browse at your leisure. When you locate a publication of interest, you can print the announcement or electronically add it to your publication order list. Start your free access to *Electronic SCAN* today.

Electronic SCAN
Timely
Flexible
Complete
Free!

Over 1,000 announcements of new reports, books, conference proceedings, journal articles . . . and more—delivered to your computer every two weeks.

For instant access via Internet:

ftp.sti.nasa.gov
gopher.sti.nasa.gov
listserv@sti.nasa.gov

For additional information:

e-mail: help@sti.nasa.gov
scan@sti.nasa.gov

(Enter this address on the "To" line. Leave the subject line blank and send. You will receive an automatic reply with instructions in minutes.)

Phone: (301) 621-0390 Fax: (301) 621-0134

Write: NASA Access Help Desk
NASA STI Office
NASA Center for AeroSpace Information
800 Elkridge Landing Road
Linthicum Heights, MD 21090-2934

Home Page: http://www.sti.nasa.gov/STI-homepage.html

National Aeronautics and Space Administration

Scientific and Technical Information Office

7/95

National Aeronautics and
Space Administration
Code JT
Washington, DC 20546-0001